ELSEVIER

Talanta 45 (1997) 1–12

Talanta

New approach to study of spilled crude oils using high resolution GC–MS (SIM) and metastable reaction monitoring GC–MS–MS

D. Munoz [a,b,*], P. Doumenq [a], M. Guiliano [a], F. Jacquot [a], P. Scherrer [b], G. Mille [a]

[a] *Laboratoire de Chimie Analytique de l'Environment, URA CNRS 1409, Case 312, Faculté des Sciences et Techniques de St. Jérôme, 13397 Marseille Cedex 20, France*

[b] *Centre de Recherche TOTAL, Département Analyse, BP 27, 76700 Harfleur, France*

Received 29 January 1996; received in revised form 16 July 1996; accepted 22 July 1996

Abstract

Polycyclic aromatic hydrocarbons (PAHs) and geochemical biomarkers are good environmental markers to study the origin and evolution of an oil spill. To have access to the greatest number of molecular ratios, no fractionation of oil into aliphatic and aromatic compounds is made. Three analytical MS approaches are tested to analyze markers in this total hydrocarbon fraction: classical quadrupole GC–MS, high resolution GC–MS (HR GC–MS) and metastable reaction monitoring GC–MS–MS (MRM GC–MS–MS). This analytical approach is used to follow the evolution of PAHs in petroleum polluted mangrove soils over 8 years by using molecular ratios between polycyclic aromatic hydrocarbons and tri- and tetracyclic terpanes. © 1997 Published by Elsevier Science B.V.

Keywords: Crude oil; Environmental markers; GC–MS; Weathering

1. Introduction

In general, oil is introduced in the environment in a relatively unaltered state, but the identification of oil spilled at sea is limited by the rapid and drastic changes to spilled oil caused by weathering (evaporation, dissolution, oxidation, biodegradation and combined processes). For example, *n*-alkalines, isoprenoids and simple aromatic and heteroatomic compounds can be removed rapidly by these alteration processes. If spills (and the possible sources) cannot be sampled and analyzed very early after their introduction in the environment, the identification becomes impossible. A possible approach is to base the identification and the quantification on components present in the crude oils which are specific for the oil's geological origin and which are more resistant to the weathering process [1–5]. Two classes of compounds are good choices.

Polycyclic aromatic hydrocarbons (PAHs), which are molecules of low volatility and low solubility, are relatively resistant to biodegradation but are involved in photo-oxidation processes [6].

* Corresponding author.

0039-9140/97/$17.00 © 1997 Published by Elsevier Science B.V.
PII S0039-9140(96)02054-1

Table 1
BAL tri- and tetracyclic terpane (Tt and TT) identifications (Fig. 1C)

Peak	Name	Carbon no.
A	13β(H)tricyclic terpane	C19
B	13β(H), 14α(H)tricyclic terpane + bicyclic terpane	C20+C21
C	13β(H), 14α(H)tricyclic terpane	C21
D	13α(H), 14α(H)tricyclic terpane	C21
E	Tricyclic terpane	C22
F	13β(H), 14α(H)tricyclic terpane	C23
G	13β(H), 14α(H)tricyclic terpane	C24
H	13β(H), 14α(H)tricyclic terpanes 17R+17S	C25
I	Tetracyclic terpane	C24
J	13β(H), 14α(H)tricyclic terpanes 17R+17S	C26

Table 3
BAL triaromatic steroid (TA) identifications (Fig. 2D)

Peak no.	Name	Carbon no.
12	Pregnane (ethyl)	C20
13	Methyl-pregnane (2-propyl)	C21
14	Ethyl-pregnanes (2-butyl); epimeric at C20	C22
15	Cholestane 20S	C26
16	Cholestane 20R + ergostane 20S	C26+C27
17	Stigmastane 20S (-24-ethyl cholestane)	C28
18	Ergostane 20R (-24-methylcholestane)	C27
19	Stigmastane 20R (-24-ethyl cholestane)	C28
20	*n*-propyl-cholestane 20S; epimeric at C24	C29

Biomarkers (such as polycyclic terpanes, steranes, diasteranes, mono- and triaromatic steroids), derived from natural precursors, remain unaltered during conversion of sedimented organic material to crude oil (diagenesis, categenesis, etc.). Because of their great stability, biomarkers, already widely used in organic geochemistry [7,8] (exploration, depositional environment, thermal maturity, oil–source and oil–oil correlations, etc.), have also been used to study the origin of an oil pollution in the marine environment [4,6,9,10].

Table 2
BAL monoaromatic steroid (MA) identifications (Fig. 2C)

Peak no.	Name	Carbon no.
1	5β(H), 10β(CH_3)-pregnane	C21
2	5β(H), 10β(CH_3)-20-methyl-pregnane	C22
3	5β(H)-cholestane 20S	C27
4	5β(H)-diacholestane 20S	C27
5	5β(H)-cholestane 20R + 5β(H)-diacholestane 20R	C27
6	5α(H)-cholestane 20S	C27
7	5β(H)-diaergostane 20S	C28
8	5α(H)-cholestane 20R + 5α(H)-ergostane 20S +	C27+
	5β(H)-ergostane 20R + 5β(H)-stigmastane 20S +	C28+
	5β(H)-diastigmastane 20S	C29
9	5α(H)-stigmastane 20S	C29
10	5α(H)-ergostane 20R + 5β(H)-stigmastane 20R +	C28
	5β(H)-diastigmastane 20R	C29
11	5α(H)-stigmastane 20R	C29

Several in vitro and in situ studies have demonstrated that biomarkers and PAHs submitted to environmental conditions, such as in the case of an oil spill, can be altered [11–15]. Thus, they can be considered as good environmental markers to study the origin and the evolution of an oil spill.

The analytical methods now used to study oil spill origin and evolution using markers, generally follow three steps:

- separation of the oil into several fractions (aliphatic, aromatic and polar compounds) b cause of the great number (few thousands) and the low concentration (measured in parts per million) of markers;
- identification of markers by quadrupole GC MS analysis using the selected ion monitoring mode (SIM) and classical mass fragments;
- elaboration of specific molecular ratios between different ions and study of their evolutions.

In this protocol, the aliphatic/aromatic separation is generally achieved with SiO_2/Al_2O_3 open chromatographic columns. This separation technique presents some disadvantages. For example, mono- and triaromatic steroids are then eluted in two different fractions and consequently can not be conjointly used to elaborate ratios. Even with

Table 4
BAL mono-, di- and trimethylphenanthrene identifications (see Figs. 1A and 1B)

Peak no.	Names	Symbols
1	3-monomethylphenanthrene	3-MP
2	2-monomethylphenanthrene	2-MP
3	9- and 4-monomethylphenanthrenes	9- and 4-MP
4	1-monomethylphenanthrene	1-MP
5	3,6-dimethylphenanthrene+2- and 9-ethylphenanthrenes	3,6-DMP+2- and 9-EtP
6	1-ethylphenanthrene	1-EtP
7	2,6- and 3,5-dimethylphenanthrenes	2,6-DMP and 3,5- DMP
8	2,7-dimethylphenanthrene	2,7-DMP
9	1,3-, 2,10-, 3,9- and 3,10-dimethylphenanthrenes	1,3-DMP, 2,10-DMP, 3,9-DMP and 3,10-DMP
10	1,6-, 2,5- and 2,9-dimethylphenanthrenes	1,6-DMP, 2,5-DMP and 2,9-DMP
11	1,7-dimethylphenanthrene	1,7-DMP
12	2,3-dimethylphananthrene	2,3-DMP
13	1,9-, 4,9- and 4,10-dimethylphenanthrenes	1,9-DMP, 4,9-DMP and 4,10-DMP

more rigorous separations, as those obtained by using HPLC [7], a great number of ratios (involving markers which appear in different fractions) become inaccessible.

So we propose, in this work, to operate directly on the "aliphatic plus aromatic" fraction.

2. Experimental

2.1. Hydrocarbon analyses

Hydrocarbons were extracted from wet sediments (50 g) by direct saponification via alkaline hydrolysis. Samples were heated under reflux for 4 h in a mixture of 0.5 N KOH in 95% methanol/toluene (2:1). After the elimination of sediment residue by filtration, the methanol extract was then re-extracted by 3 × 50 ml of toluene. The toluene extracts were combined, washed with pre-extracted salt water, dried over Na_2SO_4, evaporated and weighed on a microbalance (Perkin–Elmer AD 2Z; precision: 0.01 mg) to obtain a total extractable organic matter weight. All or part of the extractable organic matter was dissolved in a *n*-hexane and fractionated. After removal of the saponified compounds by alkaline hydrolysis, the extractable organic matter, and the crude oil, were separated into aliphatic plus aromatic ($F_{1,2}$) and polar (F_3) fractions by Sep-pak plus® (Waters) chromatography using silica gel. Aliphatic plus aromatic hydrocarbons were eluted from the Sep-pak with *n*-hexane (7 ml) then dichloromethane/*n*-hexane (1:1; 12 ml) and polar compounds were obtained using a mixture of dichloromethane/methanol/acetone (5:1:1; 14 ml).

2.2. Analytical conditions

Quadrupole GC–MS analyses (single ion recording, SIR mode) were carried out on a Hewlett–Packard 5989A quadrupole spectrometer (electron energy 70 eV, source temperature 240°C) coupled with a HP 5890 chromatograph equipped with a splitless injector. Separations were achieved using the following conditions: J&W Scientific DB–5–MS (low bleeding) fused silica capillary column (60 m × 0.25 mm, 0.25 μm film thickness), temperature program was started from 50°C and increased initially to 150°C at 40°C min^{-1} and then to 320°C at 4°C min^{-1} (final temperature held for 14 min), helium carrier gas with a constant flow rate of 1 ml min^{-1}. High resolution GC–MS analysis (SIR mode) was carried out using a Hewlett-Packard 5890 gas chromatograph interfected to a VG Autospec high resolution magnetic instrument (double focusing). The gas chromatograph was equipped with a J&W Scientific DB-5-MS (low bleeding) fused silica capillary column (60 m × 0.25 mm, 0.17 μm film thickness). The splitless injector (300°C) is operated in the constant flow mode (helium 1 ml min^{-1}). The temperature pro-

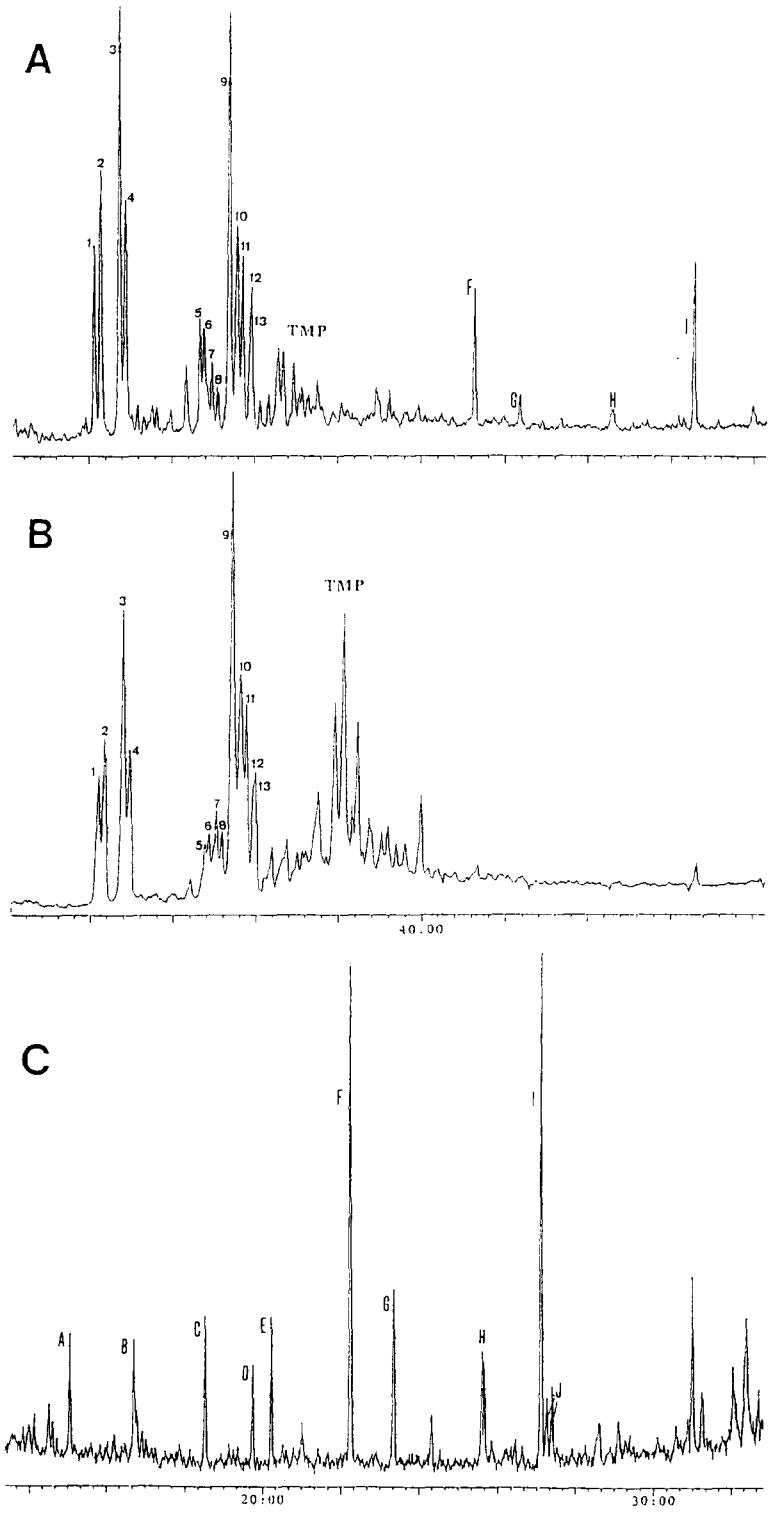

Fig. 1. BAL partial mass fragmentograms for: (A) m/z 191 (tri- and tetracyclic terpanes: Tt + TT); (B) m/z 192, m/z 206, m/z 220 (methyl phenanthrenes: MP, DMP, TMP) from quadrupole GC–MS analysis: (C) m/z 191.18 (Tt and TT) from high resolution GC–MS analysis.

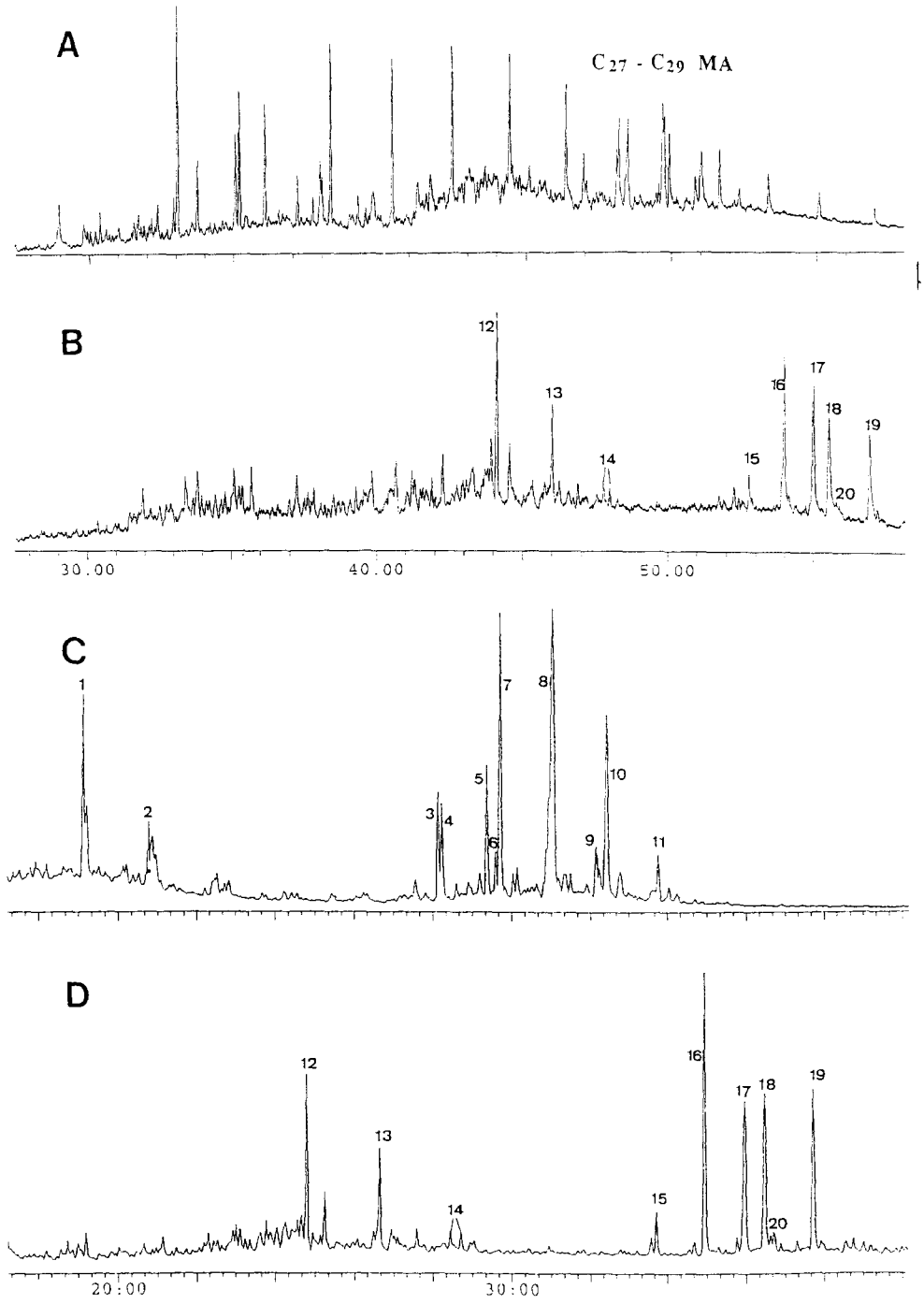

Fig. 2. BAL partial mass fragmentograms for: (A) *m/z* 253 (monoaromatic steroids: MA), (B) *m/z* 231 (triaromatic steroids: TA) from quadrupole GC–MS analysis; (C) *m/z* 253.1956 (MA); (D) *m/z* 231.1174 (TA) from high resolution GC–MS analysis.

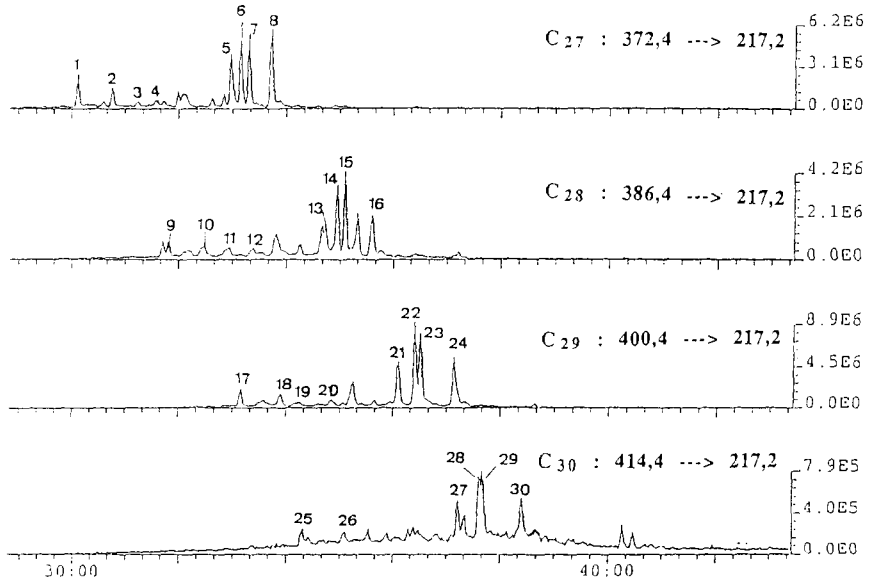

Fig. 3. BAL C_{27}, C_{28}, C_{29} and C_{30} steranes and diasteranes distribution obtained by MRM GC–MS–MS.

gram was started from 50°C and increased initially to 150°C at 40°C min^{-1} (final temperature held for 14 min). Mass spectrometric conditions were: interface temperature, 280°C; source temperature, 240°C; ionization energy, 70 eV. Biomarkers (steranes and diasteranes) present in the $F_{1,2}$ fraction were analyzed with another scanning mode, the MRM mode (metastable reaction monitoring). The chromatographic operating conditions are the same as those described above. Parent ions of steranes and diasteranes were measured at m/z 372.4, m/z 386.4, m/z 400.4, m/z 414.4, respectively, for C_{27}, C_{28}, C_{29} and C_{30} steranes and diasteranes, the major fragment ion being at m/z 271.2

3. Results and discussion

3.1. Advantages and limitations of the different analytical MS approaches

We have seen that if we analyze the $F_{1,2}$ fraction we can gain access to more information. However, in this case, fragmentograms become very complex and the quadrupole GC–MS performance can be illustrated by three examples.

In the analysis of tricyclic and tetracyclic terpanes (respectively, Tt and TT) by m/z 191 ion selection, we observe, in the Tt chromatographic range, an overlapping with the m/z 192 ion resulting from base peaks of monomethylphenanthrenes (MP) and secondary peaks of di- and trimethylphenanthrenes (DMP and TMP) [16] (Fig. 1(A and B)).

To identify monoaromatic steroids (MA) by selecting m/z 253 (Fig. 2A) and triaromatic steroids (TA) by selecting the m/z 231 ion (Fig. 2B), we observe numerous coelutions and the presence of an unresolved complex mixture (UCM), caused by linear and branched alkanes.

In these two cases unambiguous identifications are very difficult. The use of high resolution GC–MS (HR GC–MS) easily makes these identifications by selecting m/z 191.18 (Tt + TT) [17], m/z 253.1956 (MA) and m/z 231.1174 (TA) ions [7,13]. This is illustrated by comparison of Fig. 1(A and C) for Tt and TT (for attributions, see Table 1), by comparison of Fig. 2(A and C) for MA (for attributions, see Table 2) and by comparison of Fig. 2(B and D) for TA (for attributions, see Table 3).

In Fig. 1B, to clearly show the interferences between Tt and MP, DMP and TMP, we have

Table 5
BAL C27–C30 sterane and diasterane identifications (see Fig. 3)

Peak no.	Name	Carbon no.
1	13β(H), 17α(H)-diacholestane 20S	C27
2	13β(H), 17α(H)-diacholestane 20R	C27
3	13α(H), 17β(H)-diacholestane 20S	C27
4	13α(H), 17β(H)-diacholestane 20R	C27
5	5α(H), 14α(H), 17α(H)-cholestane 20S	C27
6	5α(H), 14β(H), 17β(H)-cholestane 20R	C27
7	5α(H), 14β(H), 17β(H)-cholestane 20S	C27
8	5α(H), 14α(H), 17α(H)-cholestane 20R	C27
9	13β(H), 17α(H)-diaergostane 20S	C28
10	13β(H), 17α(H)-diaergostane 20R	C28
11	13α(H), 17β(H)-diaergostane 20S	C28
12	13α(H), 17β(H)-diaergostane 20R	C28
13	5α(H), 14α(H), 17α(H)-erogstane 20S	C28
14	5α(H), 14β(H), 17β(H)-erogstane 20R	C28
15	5α(H), 14β(H), 17β(H)-ergostane 20S	C28
16	5α(H), 14α(H), 17α(H)-ergostane 20R	C28
17	13β(H), 17α(H)-diastigmastane 20S	C29
18	13β(H), 17α(H)-diastigmastane 20R	C29
19	13α(H), 17β(H)-diastigmastane 20S	C29
20	13α(H), 17β(H)-diastigmastane 20R	C29
21	5α(H), 14α(H), 17α(H)-stigmastane 20S	C29
22	5α(H), 14β(H), 17β(H)-stigmastane 20R	C29
23	5α(H), 14β(H), 17β(H)-stigmastane 20S	C29
24	5α(h), 14α(H), 17α(H)-stigmastane 20R	C29
25	13β(H), 17α(H)-dia-24-*n*-propylcholestane 20S	C30
26	13β(H), 17α(H)-dia-24-*n*-propylcholestane 20R	C30
27	5α(H), 14α(H), 17α(H)-24-*n*-propylcholestane 20S	C30
28	5α(H), 14β(H), 17β(H)-24-*n*-propylcholestane 20R	C30
29	5α(H), 14β(H), 17β(H)-24-*n*-propylcholestane 20S	C30
30	5α(H), 14α(H), 17α(H)-24-*n*-propylcholestane 20R	C30

selected, *m/z* 192, 206 and 220 ions to increase the DMP and TMP peak intensities. The identification of methylated phenanthrenes is given in Table 4 [16].

In the case of steranes (St) and diasteranes (DSt), chromatographic coelutions between compounds with exactly the same mass fragments does not allow unambiguous identifications, even with the use of HR GC–MS. We note that this problem is not dependent on the fact that the oil has not been separated into aliphatic and aromatic fractions. To achieve a complete identification a new scanning mode must be used: GC–MS–MS operating in parent mode MRM (metastable reaction monitoring).

The distribution of C_{27}-C_{30} steranes and diasteranes with this technique, given in Fig. 3, is obtained by monitoring parent to daughter ion transitions $M^+ \rightarrow m/z$ 217.2 where M^+ corresponds to molecular ions at *m/z* 372.2, *m/z* 386.2, *m/z* 400.2 and *m/z* 414.2 respectively for C_{27}, C_{28}, C_{29} and C_{30} steranes and diasteranes. Identification of C_{27}–C_{30} steranes and diasteranes are given in Table 5 [7,18].

Nevertheless the use of HR GC–MS or MRM GC–MS–MS is not always necessary to analyze the $F_{1,2}$ fraction. In Table 6, we give the capabilities and the limitations of the quadrupole GC–MS technique to analyze the principal marker families.

So, naphthalene, mono-, di- and trimethylnaphthalenes, fluorene, mono- and dimethylfluorenes, phenanthrene and monomethylphenanthrenes,

Table 6
Capabilities (+) and limitations (−) of quadrupole GC–MS in petroleum markers analysis; comparison with HR GC–MS and GC–MS–MS (MRM)

Compounds and symbols	Quadrupole GC–MS				Interferences and coelutions	Analytical solutions
Napthalene (N), monomethylN (MN) dimethylN (N), trimethylN (TMN)	N 128 +	MN 142 +	DMN 156 +	TMN 170 +	No interference	Quadrupole or high resolution GC–MS
Fluorene (F), monomethyl (MF), dimethylF	F 166 +	MF 180 +	DMF 194 +		Few interferences with linear and branched alkanes (m/z183)	Quadrupole or high resolution GC–MS
Dibenzofuran (DBF), methylDBF (MDBF) dimethylDBF (DMDBF)	DBF 168 −	MDBF 182 −	DMDBF 196 −		Coelutions with linear and branched alkanes (m/z183)	High resolution GC–MS
Nor-hopanes (NH)	NH 177				No interference and light UCM	Quadrupole or high resolution GC MS
Phenanthrene (P), monomethylP (MP), dimethylP (DMP), trimethylP (TMP)	P 178 +	MP 192 +	DMP 206 −	TMP 220 −	Overlapping with C19 to C23 tricyclic terpanes and strong UCM	High resolution GC–MS
Dibenzothiophene (DBT), monomethylDBT (MDBT), dimethylDBT (DMDBT)	DBT 184 −	MDBT 198 +	DMDBT 212 +		Coelutions with linear and branched alkanes (m/z 183) and DBT	High resolution GC–MS
Tricyclic terpanes (Tt)	Tt 191 −				Overlapping with DMP and TMP	High resolution GC–MS
Tetracyclic terpanes (TT)	TT 191 +				Difficult to identify (low abundance)	High resolution GC–MS or MRM
Hopanes (H)	H 191 +				No interference and light UCM	Quadrupole or high resolution GC–MS
Fluoranthene (Fl), pyrene (Py)	Fl 202 −	Py 202 −			Difficult to identify (low abundance in unaltered petroleum)	High resolution GC–MS or MRM
Steranes (St), diasteranes (DSt)	St 217 and 218	Dst 217 and 218			Coelution between families, MRM necessary	MRM
Chrysene (Ch), benzo(a)anthracene (b(a)An)	Ch 228 −	b(a)An 228 −			Difficult to identify (low abundance in unaltered petroleum)	High resolution GC–MS or MRM
Methyl-steranes (MSt)	MSt 231 −				Coelutions with C30 steranes and C30 diasteranes; MRM necessary	MRM
Triaromatic steroids (TA)	TA 231 +				No interference and light UCM	Quadrupole or high resolution GC–MS
Perylene (Pr), benzopyrene (b(e)Py and b(a)Py)	Pr 252 −	b(e)Py 252 −	b(a)Py 252 −		Difficult to identify (low abundance in unaltered petroleum)	High resoution GC MS or MRM
Monoaromatic steroids (MA)	MA 253 −				Coelutions with linear branched alkanes	High resolution GC–MS

mono- and dimethyldibenzothiophenes, nor- hopanes, tetracyclic terpanes, pentacyclic terpanes (hopanes) and triaromatic steroids can be directly analyzed by quadrupole GC–MS.

In Table 7 we give several examples, of molecular ratios characteristic of the origin or the evolution of oil spills, which can be obtained by HR GC–MS or GC–MS–MS (MRM) but not by quadrupole GC–MS.

Table 7
Examples of molecular ratios characteristic of the origin or the evolution of an oil spill obtained by HR GC–MS and GC–MS–MS (MRM)

Indices	High resolution	MRM	Definition
C27 St $\alpha\beta\beta$ R/C29 DSt $\beta\alpha$ S	No	Yes	Origin[b]
C28 St $\alpha\beta\beta$ R/C29 DSt $\alpha\beta$ R	No	Yes	Origin[b]
C28 St $\alpha\beta\beta$ S/C30 St *n*-$\beta\alpha$ R	No	Yes	Origin[b]
C29 St $\alpha\beta\beta$ R/C30 DSt-$\alpha\beta$ S	No	Yes	Origin[b]
C29 St $\alpha\alpha\alpha$ R/C30 St-*n*-$\alpha\alpha\alpha$ S	No	Yes	Origin[b]
C*n* MA/C*m* MA[a]	Yes	No	Evolution
C*n* MA/C*m* TA[a]	Yes	No	Evolution
C19 Tt/C23 Tt	Yes	Yes	Origin[b]
C21 Tt/C22 Tt	Yes	Yes	Origin[b]
Fl/Py	Difficult[c]	Yes	Origin[d]
b(e)Py/b(a)Py	Difficult[c]	Yes	Origin[d]
Ch/b(a)An	Difficult[c]	Yes	Origin[d]

[a] C*n* or C*m* with *n* and *m* as carbon number.
[b] Geologic orgin.
[c] Low abundance in unaltered petroleum.
[d] Biogenic, pyrolytic or anthropogenic origin (see Table 6 for molecular symbol identifications).

Table 8
Gravimetric evolution of hydrocarbon compounds (E.O.M; $F_{1,2}$; F_3) of reference and experimental plots; in g kg^{-1} dry sediment

Plot	E.O.M.	$F_{1,2}$	F_3
Polluted plot			
1987	49.00	42.73	6.27
1994	17.00	5.89	11.11
Reference plot			
1987	10	—	—
1994	9.00	1.41	7.59

—, not determined.

3.2. Application

Mangroves are tropical coastal ecosystems regularly polluted by accidental oil spills. Biodegradation of oil hydrocarbons trapped in a peaty mangrove soil is a very slow process because aerobic microorganism activity is limited [7,19]. In 1986, plots (2 m^2) were delimited and polluted with 5 l m^{-2} of BAL crude oil (Arabian Light) for controlled contamination in a peaty mangrove of Petit-Bourg, Guadeloupe [20,21]. To estimate the evolution of oil alteration, we have analyzed (8 years later) the sediments of these plots (0–20 cm depth).

It is difficult to estimate in situ the real degradation stage of petroleum, because of the conjunction of different organic matter inputs of biogenic, pyrolytic or anthropogenic origins.

In the peaty plot, a regular decrease of total hydrocarbon concentrations (E.O.M.) and saturated plus aromatic fraction ($F_{1,2}$) is observed during the 8 year period from 49 to 17 g kg^{-1} of dry weight sediment (Table 8). On the contrary, an increase of the polar fraction (F_3) is noted. This result shows that the biogenic matter contribution becomes predominant relative to the altered petroleum.

Prince et al. [22] have shown that hopanes were neither generated nor weathered during the cleaning of oil spills and so can be used as an internal standard to evaluate the weathering of more degradable compounds in the crude oil in the environment. In this work, to estimate the PAH evolution, we have chosen tri- and tetracyclic terpanes as internal standards. These markers are indeed very resistant to weathering processes [23–25]. In a preliminary GC–MS analysis we have verified that: (i) the biogenic tri- and tetracyclic terpanes contribution was negligible; (ii) the SIM GC–MS fragmentogram fingerprint (*m/z* 191.18), was conserved through the 8 years of oil alteration; and (iii) using squalene (*m/z* 191.18) as an external standard, the tri- and tetracyclic terpane alteration was negligible compared with aromatic compound degradation.

Table 9
Molecular ratios of PAHs or methyl-PAHs vs. tri- and tetracyclic terpanes characteristic of the evolution of an oil spill (Table 6 for molecular symbol identifications)

PAH compounds	PAH/(TT+Tt) original	PAH/(TT+Tt) degraded	Degradation (%)
N	6.53	0.18	0.69
MN	55.71	0.06	6.05
DMN	233.45	0.50	25.31
F	4.30	0.16	0.45
MF	15.13	0.17	1.63
DMF	26.62	0.35	2.86
DBF	1.36	0.10	0.14
MDBF	3.07	0.04	0.33
DMDBF	4.06	0.01	0.44
P	9.86	0.30	1.04
MP	29.66	0.48	3.17
DMP	41.87	1.98	4.33
DBT	22.60	0.11	2.44
MDBT	66.38	0.25	7.19
DMDBT	121.64	0.03	13.22
MA	4.78	4.59	0.02
TA	9.05	1.52	0.82

Consequently we have elaborated ratios of aromatic or methyl aromatic hydrocarbons vs. tri- and tetracyclic terpanes (Table 9), and calculated the percentage of PAH degradation (Fig. 4).

These results show that:

- methyl PAHs are more degraded than parent homologs;
- degradation decreases with the number of methyl groups;
- degradation, when comparing the different PAH families, decreases as follows: naphthalene > dibenzothiophene > phenanthrene > fluorene > dibenzofuran.

This last result is quite surprising, particularly in the case of dibenzothiophene derivatives, which are considered as very stable geochemical markers for oil-source rock. The mangrove ecosystem is a very unique biotope, containing important quantities of sulfate-reducing bacteria which may degrade sulfur-containing compounds more rapidly than other PAHs.

4. Conclusion

We have tested three analytical methods for analyzing PAHs and biomarkers in a single aliphatic and aromatic fraction. Quadrupole GC–MS remains a useful tool to study many marker families, nevertheless the use of high resolution GC–MS (monoaromatic steroids, tricyclic terpanes etc.) and MRM GC–MS–MS (steranes, diasteranes, methyl-steranes, etc.) is in some cases essential for proper resolution and identification.

To follow hydrocarbon evolution in recent sediments, the use of PAHs is necessary, because they are markers with very different stabilities. So to analyze a low degree of petroleum degradation, a few condensed PAHs (1–3 rings) can be used. On the contrary, in the case of a severe petroleum alteration mono- and triaromatic steroids are better markers.

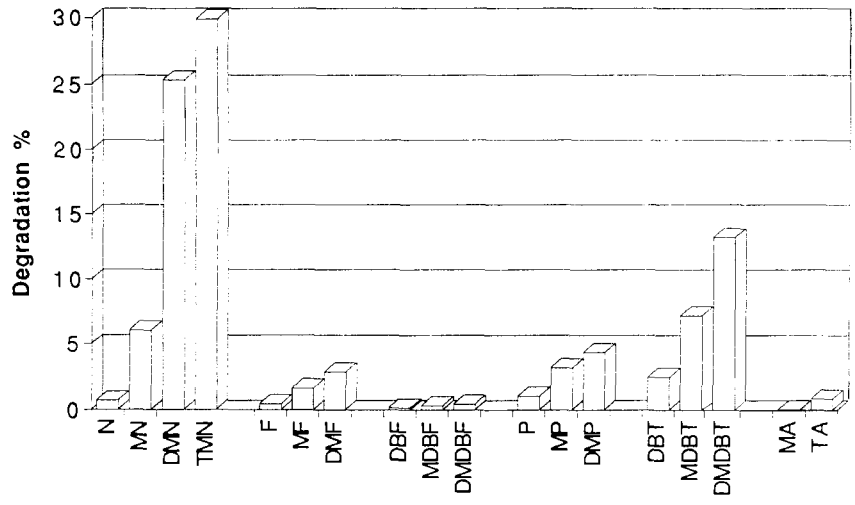

Fig. 4. Degradation (%) of PAHs and methyl PAHs in a BAL-polluted mangrove ecosystem over an eight year period using tri- and tetracyclic terpanes as endogenous internal standards (for compound symbols, Table 6).

Acknowledgements

We thank TOTAL-FRANCE and ADEME (Agence de l'Environnement et de la Maitrise de l'Energie) for their financial support. We are also grateful to M.C. Ehly (TOTAL) for providing high resolution GC–MS facilities and D. Imbert for providing samples.

References

[1] F.D. Hostettler, J.B. Rapp and K.A. Kvenvolden, Mar. Pollut. Bull., 24 (1992) 15.
[2] K.A. Kvenvolden, F.D. Hostettler, J.B. Rapp and P.R. Carlson, Mar. Pollut. Bull., 26 (1993) 24.
[3] Z. Czochanska, C.M. Sheppard, R.J. Weston and A.D. Woolhouse, J. Geol. Geophys., 30 (1987) 1.
[4] F.D. Hostettler, J.B. Rapp and K.A. Kvenvolden, Org. Geochem., 24 (1994) 927.
[5] J.A. William, M. Bjoroy, D.L. Dolcater and J.C. Winters, Org. Geochem. 10 (1985) 451.
[6] F. Brakstad and O. Grahl-Niesen, Mar. Pollut. Bull., 19 (1988) 319.
[7] K.E. Peters and J.M. Moldowan, The Biomarkers Guide. Interpreting Molecular Fossils in Petroleum and Ancient Sediments, Prentice Hall, Englewood Cliffs, NJ, 1993, p. 363.
[8] M. Bjorory, P.W. Brooks and K. Hall, in Bjoroy et al. (Eds.), Advances in organic geochemistry, Proceedings of the 10th International Meeting on Organic Geochemistry, University of Bergen, Norway, 14–18 September 1981, Pitman Press, Bath, London, 1983, p. 87.
[9] T.C. Saucer, J.S. Brown, P.D. Boehm, D.V. Aurand, J. Michel and M.O. Hayes, Mar. Pollut. Bull., 27 (1994) 117.
[10] W.K. Seifert, J.M. Moldowan and G.J. Demaison, Org. Geochem., 6 (1984) 633.
[11] H. Wehner, M. Teschner and K. Bosecker, Org. Geochem., 10 (1986) 463.
[12] M.C. Kennicut, Oil Chem. Pollut., 4 (1988) 89.
[13] A.M. Wardroper, C.F. Hoffmann, J.R. Maxwell, A.J.G. Barwise, N.S. Goodwin and P.J.D. Park, Org. Geochem., 16 (1984) 605.
[14] P. Chosson, J. Connan, D. Dessort and C. Lacanau, in J.M. Moldowan, P. Albrecht and R. Philip (Eds.), Biological Markers in Sediments and Petroleum. Prentice Hall, Englewood Cliffs, NJ, 1992, p. 320.
[15] N.S. Goodwin, P.J. Park and A.P. Rawlinson, in Bjoroy et al. (Eds.), Advances in Organic Geochemistry. Proceedings of the 10th International Meeting on Organic Geochemistry, University of Bergen, Norway, 14–18 September 1981. Pitman, London, 1983, p. 650.
[16] H. Budzinski, Thesis, University of Bordeaux I, France, 1993.
[17] M.I. Chicarelli, F.R. Aquino Nieto and P. Albrecht, Geochim. Cosmochim. Acta, 52 (1988) 1955.
[18] R.P. Philip, J.N. Oung, C.P. Yu and S. Lewis, Org. Geochem., 16 (1990) 1211.
[19] D. Pages, D.W. Maya, J.F. Cooley and E. Sorenson, Oil Spill Conference, IFP Rueil Malmaison, 1979.
[20] P. Scherrer, Thesis, University Paul Sabatier, Toulouse, France, 1988.
[21] P. Scherrer and G. Mille, Mar. Pollut. Bull., 19 (1988) 319.

[22] R.C. Prince, J.R. Lute, C.S. Hsu, C.E. Haith, J.D. Senius, G.J. Dechert, D.L. Elmendorf, G.S. Douglas and E.L. Butler, Environ. Sci. Technol., 28 (1994) 142.
[23] L.H. Lin, G.E. Michael, G. Kovachev, H. Zhu, R.P. Philip and C.A. Lewis, Org. Geochem., 14 (1989) 511.
[24] J.H. Vandermeulen and J.G. Singh, Can. J. Fisheries Aquat. Sci., 51 (1994) 845.
[25] J.G. Palacas, D. Monopolis, C.A. Nicolaou and D.E. Anders, Org. Geochem., 10 (1986) 417.

ELSEVIER

Talanta 45 (1997) 13–17

Talanta

Highly sensitive colour-reaction of nickel with a new chromogenic reagent benzothiaxolyldiazoaminoazobenzene and its application[1]

Shulin Zhao *, Xinquan Xia, Xiangwen Kong, Tiesheng Liu

Department of Polymer Chemical Engineering, Shenyang Institute of Chemical Technology, Shenyang, Liaoning 110021, China

Received 30 August 1996; received in revised form 14 January 1997; accepted 20 January 1997

Abstract

The synthesis of benzothiaxolyldiazoaminoazobenzene (BTDAB) is described, and a simple, rapid and sensitive procedure for spectrophotometric determination of nickel has been developed. At pH 9.4, in the presence of emulsifier *p*-octylpolyethyleneglycol phenylether (OP), the reagent reacts with nickel to form a red 1:3 (metal:ligand) complex. The nickel–BTDAB complex exhibit an adsorption maximum at 550 nm with an apparent molar absorptivity of 1.96×10^5 l mol^{-1} cm^{-1}, Beer's law is obeyed for nickel in the range 0–7 μg per 25 ml. The proposed method has been applied to the determination of nickel in aluminum alloy with satisfactory results. © 1997 Published by Elsevier Science B.V.

Keywords: Benzothiaxolyldiazoaminoazobenzene; Nickel; Spectrophotometry

1. Introduction

Although there are a number of chromogenic reagents proposed for the spectrophotometric determination of nickel [1–8], only a few give high sensitivity and simple operation. Derivatives of triazene have been widely used as spectrophotometric reagents for determination of cadmium, mercury and silver [9]. In 1983, Shen et al. [10], recommended 4′-(*p*-nitrophenyltirazeno) azobenzene as a reagent for the spectrophotometric determination of nickel, the colour reaction has molar absorptivity of the order of 10^5 l mol^{-1} cm^{-1}. In this work, benzothiaxolyldiazoaminoazobenzene (BTDAB), a new derivative of triazene, synthesized in our laboratory, with the following structure

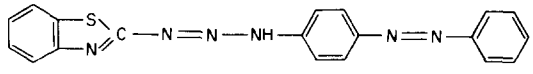

was studied as a chromogenic reagent for the spectrophotometric determination of nickel. It was found that BTDAB also gave a sensitive colour reaction with nickel in borax buffer of pH 9.4, is one of the most sensitive reagent for nickel. In the presence of emulsifier OP, nickel forms a 1:3 (metal:ligand) red complex with BTDAB, its

* Corresponding author. Fax: +86 24 5850082.

[1] Project supported by the Natural Sciences Foundation of Liaoning Province, China.

PII S0039-9140(97)00030-1

apparent molar absorptivity is 1.96×10^5 l mol^{-1} cm^{-1} at 550 nm. Various parameters such as pH, reagent concentrations, equilibration time and interference of foreign ions have been studied. A spectrophotometric method for the determination of nickel has thereby been established and applied to the determination of nickel in aluminum alloy.

2. Experimental

2.1. Apparatus

Absorbance measurements were obtained with a Model 721 spectrophotometer (Shanghai 3rd Analytical Instrument Factory) with a 1-cm cell. The pH measurements were carried out with a Moder pHs-3 pH meter (Shangahi 2nd Analytical Instrument Factory).

2.2. Reagents

2.2.1. Synthesis of BTDAB

First, 1.5 g of 2-aminobenzothiazole was dissolved in 2 ml of ice-cold formic acid, 8 ml of ice-cold distilled water and 5 ml of ice-cold sulfuric acid, 2.5 ml of sodium nitrite (0.7 g) solution was added dropwise and stirred. A yellow diazo-salt solution was prepared by further stirring for 12 h at 0.5°C. The diazo-salt solution was added dropwise with stirring to an ice-cold solution of *p*-aminoazobenzene (2.0 g) in 20 ml of ethanol. The pH value of the mixed solution was adjusted to 3–5 with concentrated sodium carbonate solution. The mixture was stirred in the ice bath for 30 min, then further stirred at 10–15°C for 30 min. After adjusting the pH to 7 with 10% sodium carbonate solution, the mixture was allowed to stand overnight to form a precipitate. The precipitate was separated and recrystallized several times in ethanol. a purified product was obtained from the above procedures (m.p. 156–157°C). Elemental analysis was as follows: calculated, C, 63.70, H 2.91, N 23.34, S 8.95; found, C 63.91, H 4.03, N 23.43, S 8.86%.

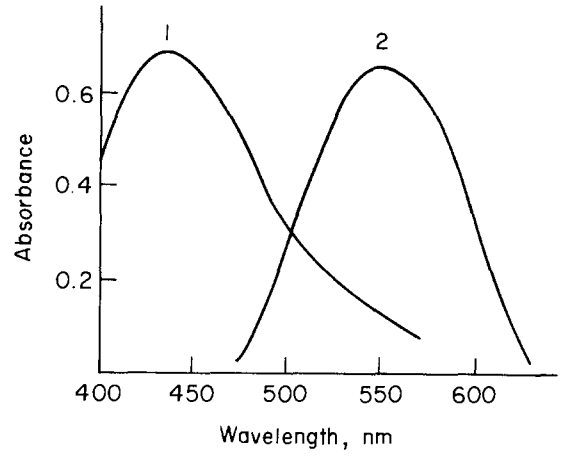

Fig. 1. Absorption spectra of BTDAB and its nickel complex (1) BTDAB against water. (2) Nickel complex against reagent blank.

2.2.2. Standard nickel solution

Dissolve 10 000 g of high purity nickel in 15 ml of 8 M nitric acid, dilute to volume in a 1000 ml calibrated flask and mix well. Dilute further to obtain a 1 μg ml^{-1} working standard solution.

2.2.3. BTDAB solution (0.04%).

Dissolve 0.1 g of BTDAB in 250 ml of ethanol. Emulsifier OP solution (5%). Dissolve 25 ml of emulsifier OP in 475 ml of distilled water.

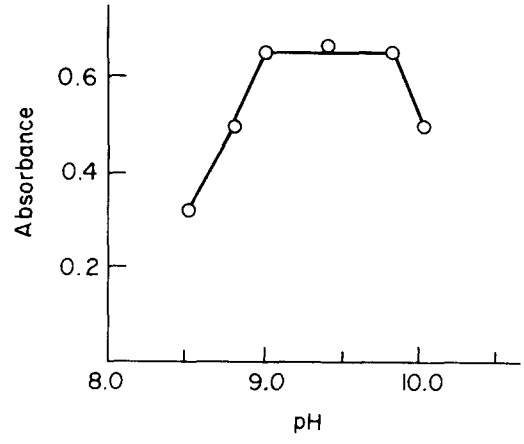

Fig. 2. Effects of pH. Absorbance of complex measured against corresponding reagent blank.

Table 1
Effect of foreign ions on determination of 5 μg of nickel

Ion	Tolerated amount (μg per 25 ml)	Ion	Tolerated amount (μg per 25 ml)
Ca^{2+}	5000	Zr(IV)	20
Mg^{2+}	5000	Ti(IV)	20
Ba^{2+}	5000	Ag^{+}	5
Sr^{2+}	4000	Zn^{2+}	5
La^{3+}	3000	Co^{2+}	2
Bi^{3+}	2000	Cd^{2+}	1
Mn^{2+}	100	Al^{3+}	50[a]
Pb^{2+}	100	Fe^{3+}	50[a]
W(VI)	100	Hg^{2+}	50[b]
Cr(VI)	100	Cu^{2+}	50[b]

[a] In the presence of 100 mg sodium fluoride.
[b] In the presence of 250 mg thiourea.

2.2.4. Borax buffer solution (pH 9.4)

Add dilute sodium hydroxide solution dropwise to a 0.05 M borax solution to the required pH.

All other reagent were of analytical grade.

2.3. Procedure

2.3.1. Procedure for study of the colour reaction of nickel

Transfer a standard solution containing not more than 7 μg of nickel into a 25 ml calibrated flask, add 5 ml of pH 9.4 borax buffer, 4 ml of 5% emulsifier OP solution and 2.0 nl of 0.04% BTDAB solution, dilute to the mark with water, mix and let stand for about 50 min. Measure the absorbance at 550 nm in a 1-cm cell against a reagent blank.

2.3.2. Procedure for the determination of nickel in aluminium alloy

Take an appropriate amount of sample in a 100 ml beaker, add 20 ml of 20% sodium hydroxide and 1 ml of 30% hydrogen peroxide. Heat until the sample has been completely dissolved, then add 5 ml of 50% triethanolamine solution. Heat the solution again to boiling and cool. Filter through a 9-cm slow filter paper, discard the filtrate. Dissolve the precipitate in 6 M hydrochloric acid and evaporate the solution almost to dryness. Cool, add 10 ml of water and boil to dissolve the salts. Cool, transfer the solution into a 100 ml calibrated flask, dilute to the mark with water and mix well. Pipette a portion of sample solution into a 25 nl calibrated flask, add 2 ml of 5% sodium fluoride solution, 5 ml of 5% thiourea solution and complete the determination as above.

3. Results and discussion

3.1. Absorption spectra

The absorption spectra of BTDAB and its nickel complex in the presence of OP at pH 9.4 are shown in Fig. 1. The absorption maximum of the complex is at 550 nm and that of the reagent blank at 435 nm. In the following experiments, the absorbances are measured at 550 nm against a reagent blank.

3.2. Optimum experimental conditions

The influence of pH on the absorbance of the sensitized nickel-BRDAB complex was studied over the range 8.0–11.0. The results obtained are shown in Fig. 2. Maximum and constant absorbance of the complex was obtained in the pH range 9.0–9.8. Therefore, a pH 9.4 was chosen for the determination.

Because BTDAB is only slightly soluble in water, therefore a surfactant was used as a solubilizing agent. In the presence of cationic or anionic surfactants the coloured system give a low ab-

Table 2
Determination of nickel in standard aluminum alloys

Sample	Certified nickel content (%)	Nickel found (%)	R.S.D. (%)	Number of determinations
Aluminum alloy BY2172-1	0.050	0.048	1.2	5
Aluminum alloy BY2125-1	0.093	0.093	1.5	5
Aluminum alloy ZL105A	0.099	0.098	1.7	5

Certified values were obtained by the dimethylglyoxime method.

sorbance, but the presence of a nonionic surfactant the coloured system gives a high absorbance, and emulsifier OP gave a remarkable increase in sensitivity of the nickel complex. In 25 ml of solution, 2–5 ml of 5% OP solution gave a maximum and constant absorbance, so a volume of 4 ml is recommended.

Addition of 4–8 ml of borax buffer was sufficient for pH adjustment. Hence an addition of 5 ml was chosen.

In 25 ml of solution, 1.5–2.8 ml of 0.04% BTDAB solution gave maximum and constant absorbance with 5 μg of nickel. So 2.0 ml of 0.04% BTDAB solution was used in the determination.

At room temperature, the development of colour was completed after 50 min of adding BTDAB with nickel ion, and the absorbance of the coloured complex was stable for at least 24 h.

3.3. Composition of the complex

The ratio of nickel to BTDAB was determined by the equilibrium shifting [11] and Asmus [12] method. A molar ratio of nickel to BTDAB in the complex was found to be 1:3 by both methods.

3.4. Calibration graph

A calibration graph was constructed in the usual way according to the procedure. The regression equation of the curve is given by $A = 0.1338C - 0.0018$, $r = 0.9999$, where A is the absorbance, C is the concentration of nickel in μg per 25 ml and r is the correlation coefficient. Bear's law was obeyed for nickel in the range 0–7 μg per 25 ml. From this straight line, the apparent molar absorptivity coefficient was 1.96×10^5 l mol^{-1} cm^{-1} at 550 nm.

3.5. Effect of diverse ions

The effect of diverse ions on the determination of nickel with BTDAB was studies by adding a know quantity of the desired ion to a solution containing 5 μg nickel which was determined as described in the given procedure and their tolerance limits are listed in Table 1. The tolerance limit of foreign ions was taken as that value which caused an error of not more than ± 5% in the absorbance. For some interfering ions, suitable masking agents were used as indicated in the Table 1.

3.6. Determination of nickel in aluminum alloy

The nickel content of certain aluminum alloy samples was determined by the proposed method. The results of analysis in comparison with the dimethylglyoxime method are given in Table 2, indicating that the method is satisfactory.

4. Conclusion

A comparison of the sensitivity of various methods is shown in Table 3. The data in Table 3 show that BTDAB is one of the most sensitive reagents for the spectrophotometric determination of nickel. The proposed method is simpler and faster than many other methods. It has the advantages of high sensitivity, good selectivity, reproducibility and accuracy.

Table 3
Comparison of spectrophotometric reagents for nickel

Reagent	λ_{max} (nm)	Molar absorptivity (l mol^{-1} cm^{-1})	Ref.
Dimethylglyoxime	445	1.5×10^4	[1]
1-(2-Pyridylazo)-2-naphthol	570	5.0×10^4	[2]
4-(2-Pyridylazo)resorcinol	494	8.1×10^4	[3]
4-(2-Pyridylazo)thymol	610	2.1×10^4	[4]
4-[(2-Methylanabazine)-α-axo]-*p*-cresol	590	2.5×10^4	[5]
4MF2MP	400	1.95×10^4	[6]
5-Br-PADAP	560	1.26×10^5	[7]
3,5-diBr-PAMB	618	1.45×10^5	[8]
Cadion	505	1.0×10^5	[10]
BTDAB	550	1.96×10^5	This work

References

[1] Z. Marczenko, Spectrophotometric Determination of Elements, Horwood, Chichester, 1976, pp. 370–373.
[2] T. Dono, G. Nakagawa, H. Wada, Nippon Kagaku Zasshi 82 (1961) 590.
[3] H. Hoshino, T. Yotsuyanagi, K. Aomura, Anal. Chim. Acta 83 (1976) 317.
[4] T.M. Mirzakasimov, K.Z Rakhmatullaev, Sh.T. Talipov, Uzb. Khim. Zh. 29 (1968) 12.
[5] E.L. Krukovskaya, Sh. T. Talipov, Izv. Akad. Nauk. Kaz. SSR. Ser. Khim. 23 (1973) 10.
[6] Alvaro Lzquierdo, José Carrasco, Analyst 109 (5) (1984) 605.
[7] Wei Fusheng, Qu Peihua, Shen Naikui, Yin Fang, Talanta 28 (1981) 189.
[8] Takeo Katami, Tomokuni Hayakawa et al., Analyst 109 (6) (1984) 731.
[9] Cao Shiti, Li Xu, Fenxi Shiyanshi 6 (4) (1987) 26.
[10] Shen Naikui, Wei Fusheng et al., Mikrochim. Acta 2 (5–6) (1983) 405.
[11] A.E. Pazalev et al., Fact. Lab. 41 (1975) 534.
[12] E. Asmus, Z. Anal. Chem. 178 (1960) 104.

ELSEVIER

Talanta 45 (1997) 19–23

Talanta

Determination of ammonia in ethylene using ion mobility spectrometry

John H. Cross [a,*], Thomas F. Limero [a], James L. Lane [b], Fusheng Wang [c]

[a] *KRUG Life Sciences, Suite 120, 1290 Hercules Drive, Houston, TX 77058, USA*
[b] *Shell Deer Park Chemical Plant, Highway 225, Deer Park, TX 77536, USA*
[c] *Shell Oil Products Company, Westhollow Technology Center, 3333 Highway 6, Houston, TX 77082, USA*

Received 9 October 1996; received in revised form 18 March 1997; accepted 18 March 1997

Abstract

A simple procedure to analyze ammonia in ethylene by ion mobility spectrometry is described. The spectrometer is operated with a silane polymer membrane, ^{63}Ni ion source, $H^+(H_2O)_n$ reactant ion, and nitrogen drift and source gas. Ethylene containing parts per billion (ppb) (v/v) concentrations of ammonia is pulled across the membrane and diffuses into the spectrometer. Preconcentration or preseparation is unnecessary, because the ethylene in the spectrometer has no noticeable effect on the analytical results. Ethylene does not polymerize in the radioactive source. Ethylene's flammability is negated by the nitrogen inside the spectrometer. Response to ammonia concentrations between 200 ppb and 1.5 ppm is near linear, and a detection limit of 25 ppb is calculated. © 1997 Elsevier Science B.V.

Keywords: Ammonia; Analysis; Detection; Determination; Ethylene; Ion mobility spectrometry (IMS)

1. Introduction

Ion mobility spectrometry (IMS) has the sensitivity, selectivity, robustness and operational simplicity necessary for performing analyses in the field. Field monitoring of drugs, chemical warfare agents, and explosives among others are reviewed in a recently published monograph [1], which also provides background information on IMS. The qualities that make IMS attractive for these field analyses are also important considerations for on-line chemical process analysis, and a patent has been issued for an IMS-based process monitor for NH_3 [2]. The patent is licensed to Molecular Analytics, formerly Environmental Technology Group, which has made a process ammonia analyzer commercially available. The major difference between field analyses and process analyses is the sample medium. In field analyses, the samples consist of air drawn from the atmosphere. In process analyses, the samples contain significant fractions of organic chemicals drawn from process equipment such as reactors, pipelines, or stacks. The most specific reports in the literature about using IMS for media other than air regard liquid

* Corresponding author. Tel.: +1 281 4838800; fax: +1 281 4833058; e-mail: jcross@sdpcmail.jcs.nasa.gov.

PII S0039-9140(97)00095-7

chromatography or supercritical fluid chromatography (SFC). For IMS with liquids, the usual, simple radioactive ionization source was abandoned in favor of a more complex corona discharge ionization source [3]. When IMS is used as a SFC detector, the mobility spectra can show drift time effects when the mobile phase is CO_2 or CO_2 with modifiers [4]. Discussions of media effects on IMS can be found in Eiceman and Karpas [5] and St. Louis and Hill [6].

Ion mobility spectrometers operating in the positive mode detect compounds by transfer of a proton from a reactant ion peak (RIP) to the analyte. The RIP in air is the $H^+(H_2O)_n$ ion; dopants can be added to form a different RIP, usually to increase selectivity. Ammonia is detected at parts per billion (ppb) concentrations, because ammonia has a high affinity for protons. Ethylene has a low affinity for protons, but the pi electrons would be expected to interact weakly with them. Thus the effect of large concentrations of ethylene on ammonia detection by IMS are not readily predictable. This paper reports experiments we carried out to assess how well ammonia could be detected in the presence of ethylene.

Three considerations are important for analyzing ammonia in the presence of large concentrations of ethylene. First, ethylene is present in the IMS cell, because a silane polymer membrane in the spectrometer inlet allows ethylene diffusion into the cell. Although the membrane prevents complete mixing and IMS is not very sensitive to ethylene, the quantity passing through the membrane far exceeds the ppb concentrations usually encountered by IMS instruments. Also once in the IMS cell, poor mixing could lead to anomalous effects. For simplicity and accuracy, adding a step to separate the ethylene prior to analysis is undesirable. Second, ethylene's flammability poses a safety issue in a spectrometer as the electrical elements in the cell present a small potential for sparking. Third, radiation can initiate ethylene polymerization [7]. Many IMSs, including the one used here, have ^{63}Ni ionization sources. The beta radiation produced by the nickel source would be unlikely to initiate global polymerization, unlike the deep penetrating (e.g., gamma) radiation reported to be used. Localized polymerization, however, could foul the source, and greatly reduce the spectrometer's performance.

To minimize the potential for fouling and to improve selectivity for ammonia, we began with the nonanone-doping method developed by Eiceman et al. [8] for measuring ammonia in air.

2. Experimental section

We used an E-IMS (Graseby Ionics, Watford, UK), a spectrometer that allows operating conditions to be varied easily. The spectrometer has a polydimethylsilane membrane inlet and chambers for introducing dopants into the drift or source gas. 5-Nonanone (Aldrich Chemical Company, Milwaukee, WI) was doped into the drift gas from an open, test-tube-shaped, 2-ml volumetric flask initially containing 50 μl liquid. Another dopant, acetone, was doped from a Dynacal permeation device (VICI Metronics, Santa Clara, CA; 42 ng min^{-1} at 90°C) at ambient temperature. To eliminate the possibility of combustion in the cell, the drift (220 ml min^{-1}) and source (80 ml min^{-1}) gas was nitrogen; removing oxygen broke the 'fire triangle' of oxidant, fuel and ignition source. The instrument was operated in a hood to remove and dilute exhaust streams safely. The cell temperature was 25°C, and the cell pressure was set 17 mm Hg below ambient.

Mixtures of ammonia in air at 0.4 (5.404 l min^{-1}) and 1.5 ppm (1.468 l min^{-1}) were generated from a permeation device (1.510 μg min^{-1} at 30°C) in a 585 Precision Gas Standards Generator (both from Kin-Tek, LaMarque, TX). The mixtures were delivered through a PTFE tube terminating in a cup placed over the inlet nozzle.

Ethylene with 1.5 ppm NH_3 was prepared by Alphagaz (Walnut Creek, CA) and was used without further analysis. It was dispensed to the E-IMS through stainless steel tubing with needle valves that could divert a portion through 3A molecular sieve to remove the ammonia. This arrangement allowed coarse control of the ammonia concentration between 0 and 1.5 ppm. At the E-IMS inlet, a tee split the flow between the inlet and an exhaust tube open to the atmosphere. One side of the tee was connected to the inlet with a

plastic tube that slipped firmly into the bore of the inlet nozzle, which led to the membrane. A pump on the inlet pulled in the sample across the membrane at roughly 800 ml min^{-1}. Ethylene flow was increased until a flowmeter on the exhaust tube showed a slight positive flow.

Waveforms from the E-IMS were averaged and displayed using Advanced Signal Processing hardware and software (Graseby Ionics). Spectra normally consisted of 32 averages of 640 points collected at 30 kHz after a 2-ms delay. Gating pulses 180 μs long occurred at the rate of 30 Hz. Ammonia concentrations were measured from peak heights taken between two cursors set at nearly the same absolute baseline value. The height of the $H^+(H_2O)_n$ ion peak or protonated nonanone ion peak in air was measured similarly.

3. Results

The spectrum of 1.5 ppm ammonia in ethylene in the nonanone-doped spectrometer (Fig. 1) resembled the pattern described by Eiceman et al. [8]. The only indication of ethylene's presence was a slight enlargement of the usual shoulder upfield of the RIP. Ammonia appeared clearly ($S/N = 12.5$) at a drift time much longer than that of the RIP. The long drift time probably resulted from the size of the ion cluster, since Eiceman et al. [8] found an ammonium ion cluster containing two nonanone molecules. Sensitivity to ammonia, however, was unacceptably low. The peak height

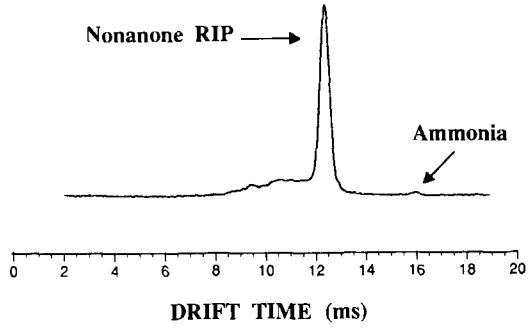

Fig. 1. Spectrum of ammonia in ethylene with 5-nonanone doping. To define the ammonia peak more clearly, 128 waveforms were averaged.

Table 1
Responses to ammonia in ethylene or air in the undoped spectrometer

Ammonia conc.	Peak height
0.0 (v/v ppm in ethylene)	2 ± 1 (mV)[a]
0.1	59 ± 6
0.5	165 ± 4
1.5	524 ± 5
0.4 (ppm in air)	1319 ± 5
1.5	2178 ± 2

[a] Average ± standard deviation of five sequentially collected spectra.

for 1.5 ppm was 24 mV (Table 1), and the RIP showed no depletion.

When the spectrometer was doped with acetone, two broad peaks due to the presence of ethylene were noted. One of these peaks had the same drift time as the ammonia peak, and no further experiments were conducted with acetone doping. But while the preceding result was being established, the spectrometer was exposed repeatedly to ethylene; since no consistent diminution of the RIP after exposure was observed, we concluded the source was not fouling from ethylene polymerization.

Exposing the undoped, 'water chemistry' [$H^+(H_2O)_n$ reactant ion peak] spectrometer to ethylene produced a broad band of partially resolved peaks (Fig. 2(A)). Ammonia appeared as a sharp peak on the small plateau at the furthest upfield part of the band (Fig. 2(B) and (C), drift time = 6.305 ms). The drift time was shorter than that of the nonanone-doped system, because the ammonium ion cluster containing water was presumably smaller. Ammonia was detected at 100 ppb (Fig. 2(B), $S/N = 12$). At 1.5 ppm, the peak remained narrow and well resolved (Fig. 2(C)). The relationship among the four concentrations measured (including 0 ppm) was nearly linear (Table 1). Exposing the undoped E-IMS to ammonia in air produced stronger responses (Table 1) at a drift time of 6.205 ms[1].

[1] The difference of 0.1 ms between drift times in air and nitrogen is a combination of the time resolution, 0.033 ms, in

During undoped experiments, the E-IMS was exposed to ethylene for numerous 5–10 min periods and one period exceeding 30 min. Over the entire period of experimentation, the RIP again showed no diminution after exposure.

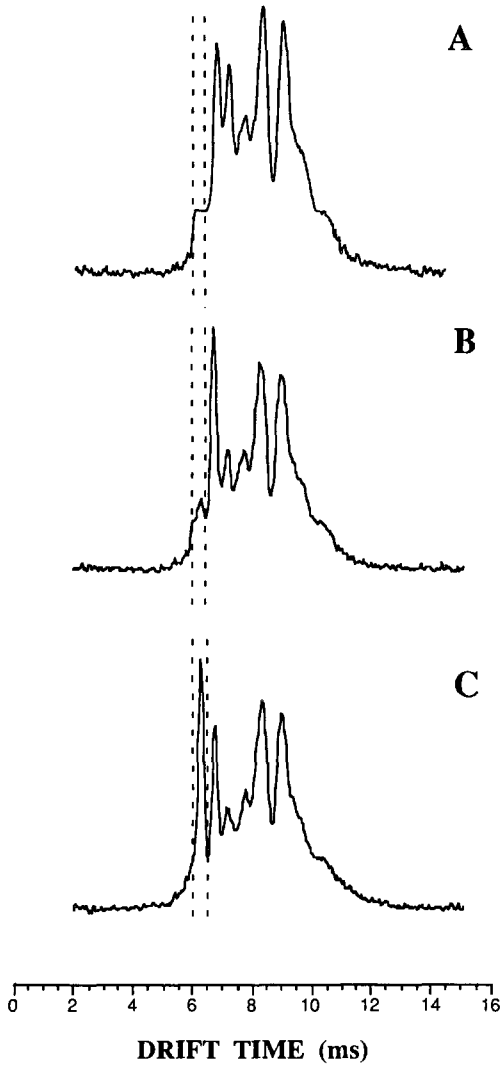

Fig. 2. Spectrum of ammonia in ethylene without a dopant. The vertical pairs of lines bracket the drift time of the ammonia peak. The other peaks are assumed to be clusters of ethylene and the reactant ion peak. (A) 0 ppm; (B) 0.1 ppm; (C) 1.5 ppm.

4. Discussion

The most important reactions in positive-mode IMS are the proton transfers governed by the relative proton affinities of the RIP and other chemicals in the reaction region. The essence of this study was to find a set of conditions that would favor proton transfer to ammonia in the presence of expected large concentrations of ethylene.

Nonanone doping minimizes the effect of ethylene as indicated by the similarity to previous work [8]. Using an open container gives a nonanone concentration higher than normally used for doping in IMS. The IMS response, however, is insufficient to detect ppb concentrations of ammonia, probably because the nonanone competes too well with ammonia for protons. Undoped experiments, in contrast, produce spectra with broad, poorly resolved peaks that suggest formation of numerous weak ethylene-containing clusters undergoing exchange in the drift tube. Since ethylene has a proton affinity lower than water, formation of these ions from the $H^+(H_2O)_n$ RIP indicates (by LeChatelier's principle) high concentrations of ethylene in the drift tube. Nonetheless, ammonia, which has a proton affinity higher than water, competes successfully for protons. In addition, the short drift time of the ammonia ion places it in a part of the spectrum free from interference by the ethylene related ions. Thus, analysis of ppb concentrations of ammonia is possible.

The nearly linear response with concentration (Table 1) shows that the upper limit of sensitivity is greater than 1.5 ppm, because an IMS response is exponential, reaching a plateau at the upper limit of sensitivity. Extrapolation of the signal-to-noise ratio from 100 ppb suggests that the lower limit of detection is 25 ppb. The lower response to ammonia in ethylene versus ammonia in air suggests that competing for protons with high concentrations of ethylene in the cell does reduce the response. The reduction is much less than that caused by nonanone with its much higher proton affinity.

The drift time of ammonia in air was the same as that for ammonia in the mixture of nitrogen

and ethylene in the IMS cell. The mobility equation [9]

$$K = 3q/16N(2\pi/\mu kT)^{1/2}(1+\alpha)/\Omega_D(T)$$

contains two variables that are coincidentally the same for ethylene and nitrogen. The reduced mass, μ, is $mM/(m+M)$ where m is the mass of the ion and M is the mass of the neutral drift gas, 28.0 for both ethylene and nitrogen. N, the number density (molecules/unit volume), is almost identical for nitrogen and ethylene, because the molecular weights and density (1.250 g l^{-1} at STP) [10] are almost equal. These coincidences minimize the effects of operating the IMS with ethylene inside the cell. With another hydrocarbon, the drift time of the ammonia ion would likely depend on the hydrocarbon concentration in the drift tube.

If protons in the ethylene ions are bound loosely to the pi electrons, they could initiate cationic polymerization, which would foul the spectrometer. We noted no cumulative decrease in the RIP after repeated exposures, indicating that the source did not foul appreciably.

In conclusion, analysis of ammonia in ethylene by IMS appears to be relatively simple. No preseparation or preconcentration is required, because crucial mobility parameters for ethylene and nitrogen are equal. The IMS requires no dopant and appears to function safely in spite of ethylene's chemical reactivity.

Acknowledgements

The authors acknowledge the use of equipment and facilities at NASA/Johnson Space Center, Houston, Texas, to conduct this work as a dual technology utilization effort. We also thank Patricia A. Inners for generating the figures from the data.

References

[1] G.A. Eiceman, Z. Karpas, Ion Mobility Spectrometry, CRC Press, Boca Raton, FL, 1994, Ch. 6.
[2] A.T. Bacon, US Patent No. 5,234,838, 1993.
[3] C.B. Shumate, H.H. Hill Jr., Anal. Chem. 61 (1989) 601.
[4] M.A. Morrissey, H.M. Widmer, J. Chromatogr. 552 (1991) 551.
[5] G.A. Eiceman, Z. Karpas, Ion Mobility Spectrometry, CRC Press, Boca Raton, FL, 1994, Ch. 5.
[6] R.H. St. Louis, H.H. Hill Jr., CRC Crit. Rev. Anal. Chem. 21 (1990) 321.
[7] R.A.V. Raff, Ethylene polymers, in: Encyclopedia of Polymer Science and Technology, vol. 6, Wiley, New York, 1967, p. 283.
[8] G.A. Eiceman, M.R. Salazar, M.R. Rodriguez, T.F. Limero, S.W. Beck, J.H. Cross, R. Young, J.T. James, Anal. Chem. 65 (1993) 1696.
[9] E.A. Mason, Ion mobility: its role in plasma chromatography, in: T.W. Carr (Ed.), Plasma Chromatography, Plenum, New York, 1984, p. 50.
[10] S. Budavari (Ed.), The Merck Index, 11th ed., Merck, Rahway, NJ, 1989, pp. 597–598 and 1044.

ELSEVIER

Talanta 45 (1997) 25–33

Talanta

Micellar versus reversed phase liquid chromatography for the determination of desferrioxamine and its chelates with aluminium and iron in uremic serum

P. Menéndez-Fraga [a], E. Blanco-González [b], A. Sanz-Medel [b], J.B. Cannata-Andía [a,*]

[a] *Bone and Mineral Research Unit, Hospital Central de Asturias, Instituto Reina Sofía de Investigación Nefrológica, Oviedo, Spain*
[b] *Department of Physical and Analytical Chemistry, Faculty of Chemistry, University of Oviedo, Oviedo, Spain*

Received 11 September 1996; received in revised form 14 March 1997; accepted 25 March 1997

Abstract

Micellar liquid chromatography with sodium dodecyl sulphate or Brij-35 as surfactants in the mobile phase was evaluated and compared with reversed phase liquid chromatography using conventional acetonitrile-water eluents for the separation and determination of desferrioxamine (DFO) and its complexes with aluminium (AlDFO) and iron (FeDFO) in uremic serum. Reversed phase liquid chromatography proved to be superior in terms of sensitivity and selectivity. The three solutes investigated were separated with a mobile phase of 13% (v/v) acetonitrile/phosphate buffer (5 mM, pH = 3.5) on a C_{18} column and detected by ultraviolet absorption at 210 nm (DFO) and 220 nm (AlDFO and FeDFO). Limits of detection of 0.1 μg ml^{-1} and relative standard deviation of 3–4% were obtained. The recovery from serum samples after ultramicrofiltration was around 90%. The method was applied to the determination of DFO, AlDFO and FeDFO in uremic serum. © 1997 Elsevier Science B.V.

Keywords: Desferrioxamine; Aluminoxamine; Ferrioxamine; Uremic serum; Micellar liquid chromatography; Reversed phase liquid chromatography

1. Introduction

Desferrioxamine (DFO) is a naturally occurring trihydroxamic acid drug widely used for the removal of excess of iron from patients suffering from acute and chronic overload [1]. Since 1980 it has also been used in the diagnosis and treatment of aluminium overload in haemodialysis patients [2,3].

The pharmacological effects of DFO are based on its chelating activity. DFO reacts with Fe (III) and Al (III) to form very stable hexadentate complexes, ferrioxamine (FeDFO) and aluminoxamine (AlDFO) with formation constant values equal to 10^{31} [4] and 10^{22} [5], respectively.

The ability to characterise DFO pharmacokinetics has been hindered by the lack of sufficiently reliable analytical methods for the determination of DFO itself and its chelated forms AlDFO and FeDFO in body fluids [6,7]. The complex chemi-

* Corresponding author. Bone and Mineral Research Unit, Hospital General de Asturias, Julián Clavería s/n, Oviedo 33006, Spain. Tel: 34 8 5106137; fax: 34 8 5106142.

PII S0039-9140(97)00097-0

cal nature of the drug makes it difficult to analyse and only a few quantitative methods of low levels of these three compounds exist. These include colorimetry [8,9], atomic absorption or emission spectrometry [10,11] and high performance liquid chromatography [12–17]. Most of those methods require laborious drug extraction steps. Therefore, the development of simpler, more sensitive, selective and accurate methods for DFO, AlDFO and FeDFO separation and determination is highly desirable.

In recent years interest in micellar liquid chromatography (MLC) has grown steadily [18–20]. The use of micellar mobile phases offer a great variety of possible parameters for regulation and fine-tuning of retention and selectivity [21,22]. The mobile phases are inexpensive, almost non-flammable, biodegradable and they have low toxicity and low pollution impact. Further, anionic and non-ionic micellar mobile phases allow the direct sample injection of biological fluids into the column [23–25]. Unfortunately, MLC has the drawback of producing rather low chromatographic efficiencies [26,27].

In this work MLC has been evaluated and compared with conventional reversed phase HPLC in order to develop a suitable chromatographic method for the separation and determination of DFO, AlDFO and FeDFO in serum of haemodialysis patients.

2. Experimental

2.1. Apparatus

Chromatography was performed using an inert HPLC system constructed from LKB components (LKB Produkter, Bromma, Sweden). It included a Model 2150 high-pressure pump with titanium pump heads, a Model 2152 system controller, a Model 2154-002 injection valve equipped with 25-μl and 200 μl loops of titanium, and a Model 2151 variable-wavelength spectrophotometric detector with a 10-μl flow cell. All connections were made using titanium tubings (LKB, Model 2135-602). Retention times and peak heights were obtained with a recording integrator (LKB, Model 2221).

A model 6K-2401-C pHmeter (Radiometer) and a glass/calomel electrode were used for pH measurements.

Ultramicrofiltration experiments were performed using an Amicon Micropartition system (MPS-1) (Amicon Div., Danvers, MA) fitted with Amicon YM5 membranes (nominal cut-off 5000 Da).

2.2. Reagents

Desferrioxamine mesylate (Desferal) was obtained from Ciba-Geigy (Basle, Switzerland). Ferric chloride, and aluminium chloride atomic absorption spectroscopic standard solutions (Titrisol R) were purchased by Merck (Darmstadt, Germany), the surfactant sodium dodecyl sulphate (SDS, 95% purity) and Polyoxyethylen 23 lauryl ether (Brij-35, solution 30% (w/v)) were purchased from Sigma (Madrid, Spain) and used as received. HPLC grade methanol and acetonitrile were purchased from Teknokroma (Barcelona, Spain). All other chemicals were of the highest analytical grade (Merck). Ultrapure water (specific resistivity 18 MΩ cm^{-1}) was obtained by purifying distilled water in a NANOpure system (Barnstead Co., Boston, MA).

2.3. Clinical samples

Serum pools from healthy volunteers were provided by the Hospital Central de Asturias, in Oviedo, Spain, and serum samples from five uremic patients on regular haemodialysis by the Hospital Camino de Santiago (Ponferrada, Spain). The latter samples were collected at the beginning of the dialysis session and stored at −20°C until analysis. The DFO dose (15 mg kg^{-1}) was diluted in physiological solution and administered, for half-an-hour intravenously, 1 h before the dialysis session.

2.4. Sample handling

Using micellar chromatography the serum samples were spiked with each of the three sought-for solutes and 25 μl injected directly into the chromatographic system.

Using conventional reversed phase liquid chromatography 700 μl aliquots of the serum samples were placed into the ultramicrofiltration cell and them centrifuged at room temperature in an angle-head rotor at 2600 × *g* for 40 min. Then 200 μl of this protein-free ultrafiltrate were finally injected into the column.

2.5. Chromatographic procedures

A stock solution of DFO (10.000 μg ml^{-1}) was made in ultrapure water and stored at 4°C. Working solutions of DFO were subsequently prepared from the stock solution by dilution with the mobile phase or with the pool serum. Similarly, working solutions of FeDFO and AlDFO were prepared by diluting DFO and ferric chloride or aluminium chloride stock solution respectively with mobile phase or pool serum. Aliquots (25 μl) of these standards were injected directly into the micellar HPLC system. In the case of the conventional reversed phase HPLC procedure, the serum-based standards were previously ultrafiltered and 200 μl of the ultrafiltrate injected into the column.

2.5.1. Micellar chromatography

Micellar chromatography was carried out on a surfactant modified Spherisorb ODS-2 column (10 μm, 300 × 4.6 mm I.D., Scharlau, Barcelona, Spain) preceded by a guard-column ODS-TRC-160 (Teknokroma, Barcelona, Spain).

Micellar mobile phases were prepared by dissolving the appropriate amount of SDS in water buffered at pH = 6 with phosphate (0.02 M) or in 5% (v/v) acetonitrile/phosphate buffer (0.02 M) at appropriate pH (3.5–7.5) or Brij-35 in water or in phosphate buffer (10^{-3} M, pH = 7.4). The mobile phases were filtered by passing through a 0.45-μm Nylon filter (Teknokroma, Barcelona, Spain) in an Millipore Model XX1004700 all-glass filter apparatus (Millipore Corp., Badford, MA, USA) and degassed under vacuum prior to use. The column was modified by equilibration with the mobile phase during 1–2 h. Chromatographic studies were carried out at a flow-rate of 0.6 or 1 ml min^{-1} and the wavelength used for the spectrophotometric detection of the solutes investigated was 210 or 220 nm.

2.5.2. Conventional reversed phase liquid chromatography

The separation was performed on a Spherisorb ODS-2 column (10 μm, 250 × 4.0 mm I.D., Teknokroma, Barcelona, Spain) using a 13% (v/v) acetonitrile/phosphate buffer (5 mM, pH = 3.5) as the mobile phase. Isocratic elution was carried out at a flow-rate of 1.5 ml min^{-1} and room temperature. The solutes were detected by ultraviolet absorption at 210 nm for DFO and at 220 nm for AlDFO and FeDFO.

2.6. Precautions to avoid contamination

All materials coming into contact with the samples were tested as potential sources of aluminium or iron exogenous contamination. Reagents or materials which leached any detectable iron or aluminium during the different steps of the analysis were discarded.

To avoid conversion of a certain amount of DFO to FeDFO, presumably through reaction with ferric ions liberated from damp stainless-steel surfaces of the HPLC apparatus [15], an inert chromatographic system was used. In addition, this system and column was very carefully cleaned for metals by pumping a relatively concentrated DFO solution (1.5 mM) in methanol for 12 h at a flow-rate of 0.1 ml min^{-1} before the analytical work.

3. Results and discussion

3.1. Micellar chromatography

On the basis of their pK_a values [28] DFO, AlDFO and FeDFO are positively charged species in the overall pH range (3.5–7.5), due to the protonation of the amine terminal group [29]. Therefore, the most significant mobile phase variables for retention in the present system are surfactant and organic modifier concentrations.

3.1.1. Effect of surfactant concentration

The separation of DFO, AlDFO and FeDFO on a modified C_{18} column with pure micellar mobile phases of SDS (concentration range from

Table 1
Effect of SDS concentration on retention times and capacity factors

SDS (M)	DFO		AlDFO and FeDFO	
	$t_{R\ (min)}$	k'	$t_{R\ (min)}$	k'
0.10	10.58	6.25	19.53	12.38
0.15	7.81	4.35	15.01	9.28
0.20	6.77	3.45	14.98	8.85
0.25	5.80	2.89	11.60	6.78
0.30	5.20	2.48	9.58	5.43

0.1 to 0.3 M) buffered at pH = 6 with phosphate buffer (0.02 M) resulted in excessively high retention times for AlDFO and FeDFO. Thus, in order to lower the retention of these solutes it was necessary to resort to the addition of an organic modifier.

The observed retention variation using a mobile phase containing 5% (v/v) of acetonitrile and different concentrations of SDS delivered at 1 ml min^{-1} is illustrated in Table 1, showing that as the SDS concentration increases retention of all the solutes decreases. Unfortunately, the low efficiency of MLC causes complete overlapping of the AlDFO and FeDFO chromatographic peaks.

3.1.2. Effect of organic modifiers and temperature

In an effort to enhance the efficiency, Dorsey proposed the use of a medium-chain alcohol as an organic modifier and to elevate the column temperature [18]. Therefore both parameters were varied in our system. Results are given in Table 2 showing the effect of different percentages of acetonitrile or 2-propanol in the SDS micellar mobile phase. A decrease in retention times is observed, but the resolution between AlDFO and FeDFO remains unchanged. This situation was not improved but increasing the column temperature from 20 to 50°C.

3.1.3. Effect of mobile-phase pH

Finally, as expected, we verified that the retention times and resolution observed were virtually constant in the 3.5–7.5 pH range assayed.

3.1.4. Effect of surfactant nature

The nature of the surfactant was changed to non-ionic Brij-35. Inversion of the previous elution order occurred but again AlDFO and FeDFO eluted as a single peak over all the range of Brij-35 concentration tested (Table 3). The presence of low percentages (1–10%) of 2-propanol in the Brij-35 micellar mobile phase and also the increase of the column temperature resulted in shortened retention times for all solutes, but again no improvement in chromatographic resolution was observed.

Table 2
Effect of organic modifier on retention times and capacity factors. Mobile phase contained 0.2 M SDS in phosphate buffer 0.02 M, pH = 7.4

Acetonitrile[a] *(%) (v/v)*	DFO		AlDFO and FeDFO	
	$t_{R\ (min)}$	k'	$t_{R\ (min)}$	k'
0	14.61	5.70	–	–
1	12.89	4.30	>26	>9.69
5	11.40	3.67	23.88	8.78
10	10.50	3.26	13.58	4.52
2-propanol[b] *% (v/v)*				
0	9.38	5.01	>24	>14.36
1	6.93	3.52	23.01	14.04
5	5.14	2.27	9.77	5.22
7	4.84	2.08	7.67	3.88

[a]Mobile phase flow-rate, 0.6 ml min^{-1}.
[b]Mobile phase flow-rate, 1 ml min^{-1}.

Table 3
Effect of Brij-35 concentration on retention times and capacity factors. Mobile phase contained Brij-35 in water, flow-rate 1 ml min^{-1}

	AlDFO		FeDFO		DFO	
Brij-35% (w/v)	t_R (min)	k'	t_R (min)	k'	t_R (min)	k'
0.5	11.78	5.43	11.17	5.10	31.62	16.25
1.0	7.05	2.89	6.98	2.85	24.55	12.56
2.0	3.76	1.05	4.07	1.22	12.23	5.68

3.1.5. Chromatographic separation and MLC retention mechanism

The best conditions for separation corresponded to mobile phases consisting of 5% (v/v) acetonitrile/SDS 0.2 M in phosphate buffer (0.02 M, pH = 7.4) or 0.5% (w/v) Brij-35 in phosphate buffer (10^{-3} M, pH = 7.4). Chromatograms of a standard DFO, AlDFO and FeDFO mixture obtained under these conditions are given in Fig. 1 for SDS MLC and Fig. 2 for Brij-35 MLC.

From the above results it is clear that anionic or non-ionic micellar mobile phases allow the isocratic separation of DFO from its complexes AlDFO and FeDFO. Unfortunately separation between these latter two complexes is not achieved.

It is interesting to note that with micellar mobile phases of anionic surfactant SDS, DFO elutes before its complexes while a change in elution was observed with changing to the non-ionic surfactant Brij-35. Using reversed phase liquid chro-

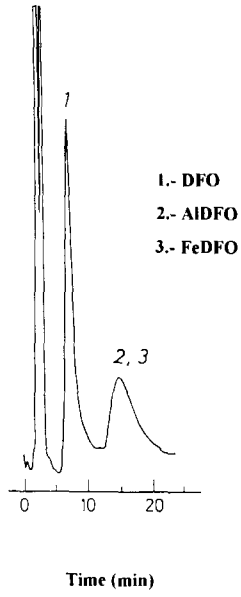

Fig. 1. Chromatograms of a standard mixture containing 239 μg ml^{-1} of DFO, 43.2 μg ml^{-1} of AlDFO and 21.9 μg ml^{-1} of FeDFO. Mobile phase: 5% (v/v) Acetonitrile/0.2 M SDS in phosphate buffer 0.02 M, pH = 7.4. Flow-rate, 1 ml min^{-1}. Detection wavelength, 210 nm.

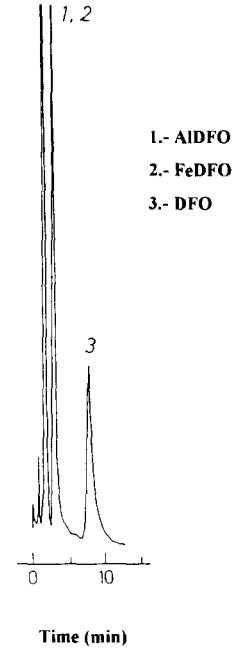

Fig. 2. Chromatograms of a standard mixture containing 239 μg ml^{-1} of DFO, 43.2 μg ml^{-1} of AlDFO and 21.9 μg ml^{-1} of FeDFO. Mobile phase: 0.5% (w/v) Brij-35 in phosphate buffer 10^{-3} M, pH = 7.4. Flow-rate, 1 ml min^{-1}. Detection wavelength, 210 nm.

matography AlDFO and FeDFO are expected to elute faster than DFO, since they have a more compact molecular structure than DFO and thus a smaller contact area on binding to the hydrocarbonaceous stationary phase [12]. It should also be kept in mind that this stationary phase will adsorb surfactant molecules from the mobile phase. When Brij-35 is used as surfactant, this non-ionic surfactant modified stationary phase would allow mainly hydrophobic interactions with the solutes. Consequently, the elution order of the solutes is expected to be the same observed in conventional reversed phase liquid chromatography. Our results (Fig. 2) confirm this mechanism. However, when micellar mobile phases of anionic surfactant SDS are used, electrostatic attractions between the protonated solutes and the modified stationary phase (negatively charged) seem to predominate over the hydrophobic interaction. This fact could explain the observed change in elution order (Fig. 1).

3.1.6. Direct serum injection

An advantage of MLC is the possibility of direct injection of serum. We observed that a direct injection of a serum sample (25 μl injection) in our chromatographic system, with micellar mobile phases, had the drawback of a strong serum matrix band at the beginning of the chromatogram (Fig. 3). This blank signal of serum can overlap the peaks of the compounds to be determined. Optimisation of the mobile phase composition should take into account not only the retention of these compounds, but also the retention of the serum matrix.

Therefore, the effect of varying the concentrations of surfactant and organic modifier in the mobile phase on the serum 'band' profile and its overlapping with DFO peak was investigated.

Increasing concentration of SDS or Brij-35 produced a more rapid elution of the serum components at the solvent front, but in all cases DFO elution occurs on the tail of the serum band. The same chromatographic behaviour was observed by changing the percentage of acetonitrile or 2-propanol. Figs. 3 and 4 illustrate the kind of chromatograms obtained for fresh serum

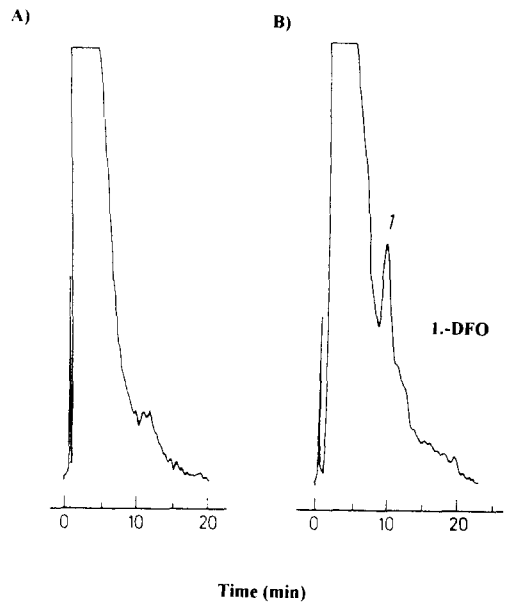

Fig. 3. Chromatograms of serum blank (A) and serum spiked with 60 μg ml^{-1} of DFO (B). Mobile phase contained 5% (v/v) Acetonitrile/0.1 M SDS in phosphate buffer 0.02 M, pH = 7.4. Flow-rate, 1 ml min^{-1}. Detection wavelength, 210 nm.

and serum spiked with DFO under the best conditions (e.g. 5% (v/v) acetonitrile/0.1 M SDS in phosphate buffer 0.02 M, pH = 7.4 (Fig. 3) and 0.5% (w/v) Brij-35 in phosphate buffer 10^{-3} M, pH = 7.4 (Fig. 4). As can be seen, DFO elutes on the tail of the serum matrix band and its peak is clearly observable for qualitative purposes. After adequate subtraction, the measured height was proportional to DFO concentration. Under optimal chromatographic conditions, the detection limits (3 σ_B criterion) of the MLC procedures developed for DFO, using 25 μl injections, were 5.2 μg ml^{-1} at 210 nm with SDS mobile phases and 8.7 μg ml^{-1} at 220 nm with Brij-35 mobile phases. Of course, these detection limits are well above the DFO therapeutic range normally monitored and more sensitivity and accuracy should be desirable even if direct analysis of serum is lost. Thus, reversed phase liquid chromatography as such was tried.

3.2. Conventional reversed phase liquid chromatography

3.2.1. Chromatographic separation

Preliminary experiments were carried out on the effect of variation of organic modifier concentration (acetonitrile), pH and ionic strength of the mobile phase, in order to establish optimal retention times for separation of the three solutes investigated, in an standard mixture, using a C_{18} column.

As shown in Fig. 5, a satisfactory separation for the three solutes studied was achieved with a mobile phase of 13% (v/v) acetonitrile in phosphate buffer (0.02 M, pH = 4) at a flow-rate of 1.0 ml min^{-1}. However, sample pre-treatment of serum was mandatory in this case. Therefore, 'pool' serum samples were ultrafiltrated following the procedure given in Experimental and then the ultrafiltrate was analysed using the above chromatographic conditions. Under these conditions the 'blank' serum ultrafiltrate produced peaks due to different serum components at retention times very close to the sought-for solutes peaks. Therefore, new adjustments of the ionic strength, pH

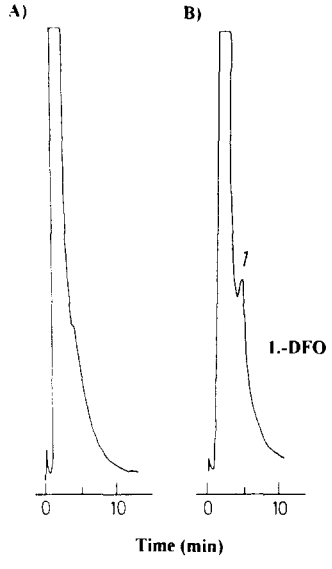

Fig. 4. Chromatograms of serum blank (A) and serum spiked with 50 μg ml^{-1} of DFO (B). Mobile phase contained 0.5% (w/v) Brij-35 in phosphate buffer 10^{-3} M, pH = 7.4. Flow-rate, 1 ml min^{-1}. Detection wavelength, 220 nm.

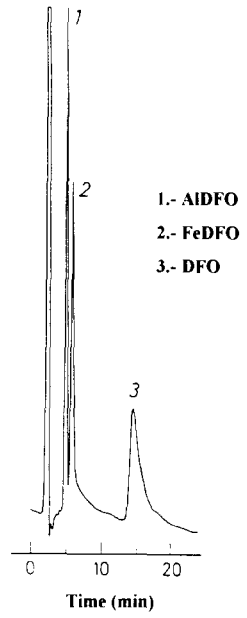

Fig. 5. Chromatograms of a standard mixture containing 18.8 μg ml^{-1} of DFO, 4.3 μg ml^{-1} of AlDFO and 2.2 μg ml^{-1} of FeDFO. Mobile phase: 13% (v/v) Acetonitrile in phosphate buffer 0.02 M, pH = 4. Flow-rate, 1 ml min^{-1}. Detection wavelength, 220 nm.

and flow-rate of the mobile phase were made with this matrix in order to achieve displacement of these solutes peaks from the matrix peaks in the ultrafiltrate. As can be seen in Fig. 6, with a mobile phase of 13% (v/v) acetonitrile/phosphate buffer (5 mM, pH = 3.5) at a flow-rate of 1.5 ml min^{-1}, well-resolved peaks for DFO, AlDFO and FeDFO were eventually obtained for an spiked ultrafiltrate serum sample.

3.2.2. Analytical performance

The efficiency of the ultramicrofiltration procedure was evaluated by studying the recoveries of known amounts of DFO, AlDFO and FeDFO added to samples of serum. Recoveries of the added spikes (estimated from the peak height ratio of a given concentration of the considered solute dissolved in serum and in the mobile phase) ranged from 85 to 95%.

Table 4 summarises the observed analytical figures of merit of the method proposed. The calibration plots were linear over the range tested

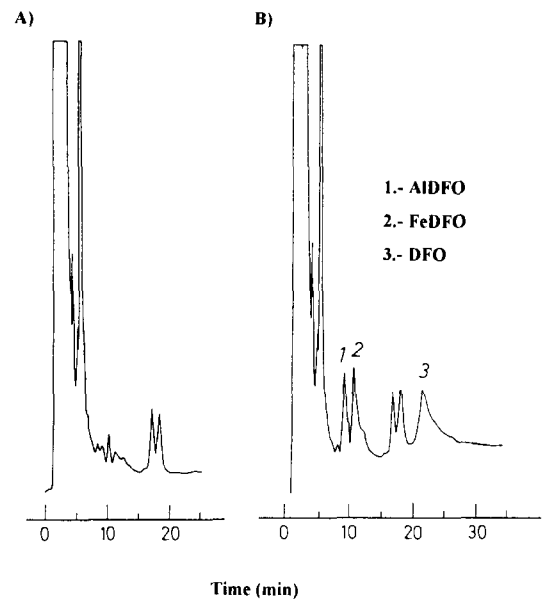

Fig. 6. Chromatograms of ultrafiltrate serum blank (A) and ultrafiltrate serum spiked with 4.4 μg ml^{-1} of DFO, 0.43 μg ml^{-1} of AlDFO and 0.22 μg ml^{-1} of FeDFO (B). Mobile phase: 13% (v/v) Acetonitrile in phosphate buffer 5 mM, pH = 3.5. Flow-rate, 1.5 ml min^{-1}. Detection wavelength, 220 nm (time < 13 min), 210 nm (time > 13 min).

(1–18 μg ml^{-1} of DFO, 0.5–3.3 μg ml^{-1} of AlDFO and 0.3–1.6 μg ml^{-1} of FeDFO). The within-day coefficient of variation was tested by analysing six times a standard mixture of the three solutes in mobile phase at pH = 7.4 (concentrations of 6.8 μg ml^{-1} of DFO, 0.6 μg ml^{-1} of AlDFO and 0.3 μg ml^{-1} of FeDFO). The results given in Table 4 show that the relative standard deviation observed ranged from 3.1 to 4.1% (worst case). The limits of detection (LODs) for spiked ultrafiltrate serum (3 σ_B criterion) and an injected volume of 200 μl, also included in Table 4, are about 0.1 μg ml^{-1}, adequate for monitoring uremic patients undergoing DFO therapy.

Table 5
Serum concentrations (μg ml^{-1}) of DFO, AlDFO and FeDFO after 1 h intravenous injection of 15 mg kg^{-1} of DFO to five patients undergoing haemodialysis

Patient	Compound		
	DFO (μg ml^{-1})	AlDFO (μg ml^{-1})	FeDFO (μg ml^{-1})
1	2.3	0.52	<LOD
2	1.3	1.31	0.18
3	0.7	0.93	<LOD
4	0.6	1.49	0.21
5	11.8	0.66	0.41

3.2.3. Real sample analysis

In order to test the applicability of the developed chromatographic method to clinical samples, blood samples were extracted from five uremic patients who received DFO (15 mg kg^{-1}) by intravenous injection. The corresponding serum samples were analysed with the HPLC method proposed here and the results obtained are given in Table 5 for the five patients. As can be seen, the method proposed could be used to study removal of aluminium with DFO from patients undergoing haemodialysis. The use of this analytical control method for clinical clearance of aluminium from its deposits and target organs (e.g., bone and brain) is presently in progress.

Table 4
Analytical figures of merit of the proposed method for DFO, AlDFO and FeDFO

Compound	Linearity limit (μg ml^{-1})	r^a	RSD%[b]	LOD (μg ml^{-1})	LOD (ng)
DFO	18	0.9972	4.1	0.14	28
AlDFO	3.3	0.9983	3.2	0.10	20
FeDFO	1.6	0.9965	3.1	0.08	16

[a]Correlation coefficient for $n = 4$.
[b]Relative standard deviation for $n = 6$.

4. Conclusions

MLC represents an attractive alternative to conventional reserved phase HPLC for direct serum analysis. The results of this study, however, indicate that MLC does not provide an adequate separation of AlDFO and FeDFO. Direct injection of uremic serum using MLC, avoiding any sample preparation, for the determination of free DFO is possible but proved to be impractical in terms of sensitivity.

Reversed phase conventional HPLC, however, allows the separation and determination of DFO, FeDFO and AlDFO in real uremic serum samples provided that a previous simple ultrafiltration step is performed. It provides a technique adequate to study removal of aluminium in renal failure patients treated with DFO.

Acknowledgements

This study was supported by FICYT (1989–1991) and FiSss 91/0329 (1991–1993). We want to acknowledge the contribution of Jose Luis Fernández Martín (Hospital Central de Asturias, Oviedo, Spain) and Ricardo Mouzo (Hospital Camino de Santiago, Ponferrada, Spain).

References

[1] S. Moeschlin, U. Schnider, N. Engl. J. Med. 269 (1963) 57.
[2] P. Ackrill, A.J. Ralston, J.P. Day, K.C. Hodge, Lancet 2 (1980) 692.
[3] R.A. Yokel, J. Toxicol. Environ. Hlth. 41 (1994) 131.
[4] H. Keberle, Ann. N.Y. Sci. 119 (1964) 758.
[5] G.A. Snow, Biochem. J. 115 (1969) 199.
[6] P. Allain, Y. Mauras, Drugs of Today 28 (1992) 89.
[7] C. Canavese, L. Gurioli, M. D'Amicone, R. Cardelli, F. Caligaris, P. Bongiorno, A. Arnaud, G. Mattiello, M. Marchiori, Nephron 60 (1992) 411.
[8] H.G. Meyer-Brunot, H. Keberle, Biochem. Pharmacol. 16 (1967) 527.
[9] M.J. Pippard, D.K. Johnson, C.A. Finch, Blood 58 (1981) 685.
[10] S. Bourdon, P. Houzé, R. Bourdon, Clin. Chem. 33 (1987) 132.
[11] P.C. D'Haese, L.V. Lamberts, M.E. De Broe, Clin. Chem. 35 (1989) 884.
[12] S.M. Cramer, B. Nathanael, C. Horváth, J. Chromatogr. 295 (1984) 405.
[13] T.P.A. Kruck, W. Kalow, D.R.C. McLachlan, J. Chromatogr. 341 (1985) 123.
[14] G. Matiello, F. Rizzo, R. Zoccolan, M. Andriani, Proc. Eur. Dial. Transplant. Assoc. 3 (1986) 241.
[15] H. Hughes, L.E. Hagen, E.C. Cameron, R.A.L. Sutton, Clin. Chim. Acta 157 (1986) 115.
[16] M.B. Jenny, H.H. Peter, J. Chromatogr. 438 (1988) 433.
[17] S. Sing, R.C. Hider, J.B. Porter, Anal. Biochem. 187 (1990) 212.
[18] M.G. Khaledi, J.K. Strasters, A.H. Rogers, E.D. Breger, Anal. Chem. 62 (1990) 130.
[19] J.R. Torres Lapasió, R.M. Villanueva Camañas, J.M. Sanchís Mallols, M.J. Medina Hernández, M.C. García Alvarez-Coque, J. Chromatogr. 639 (1993) 87.
[20] H. Ding, J. Wang, J.G. Dorsey, J.A. Caruso, J. Chromatogr. 694 (1995) 425.
[21] J.G. Dorsey, Adv. Chromatogr. 27 (1987) 167.
[22] A.S. Kord, M.G. Khaledi, Anal. Chem. 64 (1992) 1894.
[23] P. Menéndez Fraga, E. Blanco González, A. Sanz Medel, Anal. Chim. Acta 212 (1988) 181.
[24] L.J. Cline-Love, J. Fett, J. Pharm. Biomed. Anal. 9 (1991) 323.
[25] I. Carretero, M. Maldonado, J.J. Laserna, E. Bonet, G. Ramis-Ramos, Anal. Chim. Acta 259 (1992) 203.
[26] A. Berthod, M.F. Borgerding, W.L. Hinze, J. Chromatogr. 556 (1991) 263.
[27] R. Bailey, R.M. Cassidy, Anal. Chem. 64 (1992) 2227.
[28] G. Schwarzenbach, K. Schwarzenbach, Helv. Chim. Acta 156 (1963) 1390.
[29] J.B. Porter, E.R. Huehns, R.C. Hider, The development of iron chelating drugs. In: C. Hershko (Ed.), Iron Chelating Therapy, Vol. 2, Ballière Tindall, London, 1989, pp. 257–293.

ELSEVIER

Talanta 45 (1997) 35–38

Talanta

Spectrochemical and thermal analysis of Al-tetrabromophthalate and tetrabromophthalic anhydride. A comparison of methods for determination of aluminium

Lilli Paama [a,*], Hannu Rönkkömäki [b], Paavo Perämäki [b]

[a] *Institute of Chemical Physics, University of Tartu, EE2400 Tartu, Estonia*
[b] *Department of Chemistry, University of Oulu, FIN-9071 Oulu, Finland*

Received 17 January 1997; received in revised form 26 March 1997; accepted 26 March 1997

Abstract

A sequential inductively coupled plasma atomic emission spectrometer (ICP-AES) was used to determine Al content in Al-tetrabromophthalate (Al-TBP). Four emission lines of Al (I) at 309.271, 396.152, 308.215 and 394.401 nm were compared. The microwave mineralisation was carried out by using a two-step digestion procedure and HNO_3-H_2SO_4. The thermal analysis of Al-TBP and tetrabromophthalic anhydride (TBPA) was performed in the air atmosphere. Statistical tests applied (*t*-test, *F*-test) showed no significant differences between the Al results obtained by ICP-AES and thermal method of analysis. © 1997 Elsevier Science B.V.

Keywords: ICP-AES; Al-TBP; TBPA; Microwave mineralisation; Thermal analysis

1. Introduction

Organic halogen flame-retardant compounds such as Al-tetrabromophthalate (Al-TBP), tetrabromophthalic anhydride (TBPA) and decabromodiphenyl oxide (DBDPO) are important chemicals in the manufacture of plastics and textiles [1–3]. The choice of flame retardants is dependent on the nature of the polymer, the method of processing and the proposed service conditions [4].

ICP-AES method with a microwave digestion procedure is one of the most suitable techniques for the determination of aluminium in the different samples [5–8].

The thermogravimetric analysis (TGA) is widely known as a technique for characterizing the degradation mechanism of fire-retardant additives [4,9,10]. Thermal analysis of flame-retardant compounds gives useful information about the thermal behaviour, flammability and volatile compounds formed in the case of fire.

In the present study aluminium content in Al-TBP was determined by ICP-AES and TGA methods. The thermal stability and degradation characteristics of Al-TBP and TBPA were compared by using TGA and mass spectrometry.

* Corresponding author.

PII S0039-9140(97)00106-9

2. Experimental

2.1. ICP-AES analysis of Al-TBP

An inductively coupled plasma atomic emission spectrometer (ICP-AES) was used to determine the Al content in Al-TBP. As Al-TBP was very sparingly soluble material the microwave mineralization was carried out.

2.1.1. Reagents and standard

Al-TBP [$(C_8Br_4O_4)_3Al_2$, Br 64.2%] and TBPA [$C_8Br_4O_3$, Br 68,9%] were grade *pro analysi* (Reagchem. Russia).

The stock solution for ICP-AES, containing 1000 mg l^{-1} of aluminium, was prepared from Al metal (*pro analysi*, Merck). For calibrations, five standards were prepared by serial dilution of stock solution. 65% HNO_3 and 95% H_2SO_4 (Suprapure Merck) were added to the standard solution (2% v/v). For the dilution and the calibration blank, 18 MΩ water was used.

2.1.2. Sample decomposition

As Al-TBP is very sparingly soluble material, the microwave mineralization was carried out in a Milestone MLS 1200 microwave oven. Different digestion programs and mixtures of HNO, H_2O_2, H_2SO_4-H_2O_2 and H_2SO_4-HNO_3 were compared. A two-step digestion procedure using H_2SO_4-HNO_3 and sufficiently high power gave the best results.

Pulverized Al-TBP samples were weighed (0,1 ± 0.0002 g) into the Milestone digestion vessels, type HPV 80 made of PTFE-TFM (polytetrafluorethylene-tetrafluormethoxil). Concentrated sulfuric acid 96% (5 ml) and nitric acid 65% (2 ml) were added and the caps tightened to finger tight only. The vessels (four at a time) were then placed on the microwave oven turntable. The instrument was programmed for 5 min at 20% power and 5 min at 50% power (50% = 425 W) for the first step of digestion. The samples were allowed to cool in a ice and an additional 2 ml aliquout of concentrated nitric acid was added and the vessels were recapped and tightened. A second digestion step was: 4 min at 75% power (75% = 985 W).

The dissolved samples were transferred into a 50-ml volumetric flasks and diluted to the volume with water.

2.1.3. Instrumentation

Analyses were performed using a sequential PU 7000 Philips inductively coupled plasma atomic emission spectrometer. The design of this spectrometer includes a 40.68-MHz free-running oscillator for driving the plasma, an echelle grating for the wavelength separation and a grid nebulizer for the sample aspiration. The spectrometer was equipped with a Gilson 221 Autosampler and Philips P 3230 computer. The ICP operation parameters and measuring wavelengths are summarized in Tables 1 and 2.

2.2. Thermal and mass spectrometric analysis

2.2.1. Instrumentation and procedure

TG and DTG curves were recorded on a Mettler Toledo TA-4000 Thermoanalyser with a Mettler Processor in a temperature range 25–700°C. The sample mass varied between 9 and 10 mg and the samples were weighted in aluminium oxide crucibles (volume 0.07 ml) using a Mettler TG 50 Thermobalance. The dynamic experiments were carried out in air atmosphere with a flow rate 200 ml min^{-1} and heating rate 2°C min^{-1}.

The mass spectra of the decomposition products were recorded using a Kratos NS 80 RF mass spectrometer, employing the direct inlet technique and heating the sample at a rate of 50°C min^{-1}.

Table 1
ICP operating conditions

Injector tube (quartz)	1.50 mm i.d.
Plasma power	1.0 kW
Coolant argon flow	13.0 l min^{-1}
Nebulizer argon pressure	280 kPa (40 psi)
Sample uptake	1.0 ml min^{-1}
Sample read delay	20 s
Autosampler wash delay	15 s
Integration time	3 s
Number of integrations	3

Table 2
Wavelengths, excitation potentials, detection limits (DL) for aluminium and determination of Al in standard solution 10.0 mg l^{-1}

Aluminium line	Wavelength (nm)	Excitation potential (eV)	DL, mg l^{-1}	Found mg l^{-1} [c]	
				$\bar{c} \pm s$	RSD (%)
Al I[a] (1)[b]	309.271	4.009	0.02	10.01 ± 0.03	0.30
Al I (2)	396.152	3.130	0.04	9.83 ± 0.05	0.51
Al I (3)	308.215	4.023	0.03	9.94 ± 0.04	0.40
Al I (4)	394.401	3.144	0.02	9.98 ± 0.05	0.50

[a]I = atom line.
[b]ICP = AES Line Library numbers.
[c]Four replicates.

3. Results and discussion

3.1. ICP-AES analysis

Four emission lines Al I at 309.271, 308.215, 396.152 and 394.401 nm were compared. The Al emission line Al I at 309.271 nm was used for source peaking, to find an optimum viewing position in the ICP discharge and the detection limits (3σ, blanks prepared as samples) were 0.02–0.04 mg l^{-1} (Table 2).

The Al content was determined in standard aluminium samples 10,0 mg Al l^{-1} The precision of the determinations (RSD) ranged from 0.3–0.5% (Table 2). The Al I line at 309.271 nm was used for determination of Al in the Al-TBP. The five aluminium calibration standards were used: 1.0, 5.0, 10.0, 50.0, 100.0 mg l^{-1}. Scan of the measurement lines showed neither background shifts nor sloped background, and therefore background correction was not necessary to perform. The results obtained with ICP-AES are shown in Table 4.

3.2. Thermal and mass spectrometric analysis of Al-TBP and TBPA

The decomposition of Al-TBP and TBPA in the selected temperature range 25–700°C show several DTG peaks in accordance with TG curves. The data of the TA investigations are summarized in Table 3 and Table 4. The mechanism of flame extinguishing of brominated additives is not satisfactorily understood.

To detect reactions taking place, volatile decomposition products were analysed by mass spectrometry, using a direct insertion probe. Aluminiumtetrabromophthalate decomposes in three steps, which are only partly separated. The mass spectra of the decomposition products suggest volatilization of carbon monoxide, carbon dioxide, hydrogen bromide and tetrabromophthalic anhydride. The residue was assumed to be aluminium oxide, (Al_2O_3). The mass spectrometric studies of tetrabromophthalic anhydride revealed that it is only evaporating at 200–320°C.

3.3. A comparison of two methods for the determination of aluminium

The agreement of the results obtained by the two methods were tested by the Student's t (t-test) and F-test [11]. A F-statistic, to test whether the difference between the standard deviations of the two methods is significant, was calculated using the formula:

Table 3
TG data on the decomposition of Al-TBP and TBPA

Sample	Temperature °C		Weight loss (%)
	Range	DTG peak	
Al-TBP	25–295	247.6	17.0
	295–380	344.2	23.4
	380–700	474.4	52.9
	Residue %		6.72 (Al_2O_3)
TBPA	25–400	260.2	100

Table 4
Results of spectrochemical and thermogravimetric determination of aluminium in Al-TBP

Method	Al_2O_3 %, m/m $\bar{x}_{BAR} \pm s$	Al %, m/m $\bar{x} \pm s$	Testing for significance [c]					
			n	s^b	t critical	t calculated	F critical	F calculated
Calculated from formula	6.827	3.614						
ICP-AES[a]	6.82 ± 0.06	3.61 ± 0.03	5	0.041	2.78	2.004	6.59	2.79
TG[a]	6.72 ± 0.09	3.55 ± 0.05	5					

[a]Five replicates.
s^b = pooled value of the standard deviation.
[c]Two-tailed test were used.

$$F = \frac{s_2^2}{s_1^2}$$

Since the standard deviations of the two methods didn't differ significantly, a t-statistic was calculated to compare the mean values $\bar{x}_1$ and $\bar{x}_2$. A t-statistic was calculated using the formula:

$$t = \frac{\bar{x}_1 - \bar{x}_2}{s}\sqrt{\frac{n_1 \cdot n_2}{n_1 + n_2}}$$

,where the pooled standard deviation is obtained by using the equation:

$$s^2 = \frac{(n_1 - 1)S_1^2 + (n_2 - 1)s_2^2}{n_1 + n_2 - 2}$$

Statistical tests applied (Table 4) showed no significant difference in the results of aluminium content in Al-TBP obtained by ICP-AES and thermal method of analyses. ICP-AES and thermogravimetric methods presented are rapid and simple means for the quality controll of the flame-retardant additives and are useful tools for the determination of content of Al-TBP in the different plastics. The thermal and mass spectrometric analyses are useful techniques for the characterizing a degratation mechanism of bromine containing organic flame-retardant compounds.

Acknowledgements

Financical support to Dr L. Paama from Estonian Science Foundation and Estonian Academy of Science is gratefully acknowleged. Thanks to Prof. Risto Laitinen, Head of the Department of Chemistry, University of Oulu for the laboratory and instrumental facilities that were disposal in this study.

References

[1] G. C Tesoro, J. of Polym. Sci. Macromolecular Reviews 13 (1978) 283.
[2] H. Louis, Flame-Retardant Polyamide Fabrics, U.S. Patent 5, 114 (1991) 786.
[3] L. Paama, H. Kokk, U. Mäeorg, Textiles and Composits '92. In: H. Meinander (Ed.), Techn. Research Centre of Finland, Espoo 1992, p. 321.
[4] Thermal Characterization of Polymeric Materials. In: E.A. Turi (Ed.), Academic Press, INC., San Diego, 1981, p. 793.
[5] S. Recknagel, U. Rösick, P. Brätter. J. Anal. At. Spectrom. 9 (1994) 1293.
[6] M.G. Del Monte Tamba, R. Falciani et al., Analyst 119 (1994) 2081.
[7] P.J. Fordham, J.W. Gramshaw, L. Castle et al., J, Anal. At. Spectrom. 10 (1995) 303.
[8] F.E. Smith, E.A. Arsenault, Talanta 43 (1996) 1207.
[9] G. Matuschek, Thermochim. Acta 263 (1995) 59.
[10] Y. Nagasawa, M. Yamamoto, K. Ozawa, Thermochim. Acta 267 (1995) 223.
[11] J.C. Miller, J.N. Miller, Statistics for Analytical Chemistry, Ellis Horwood, UK, 1984, p. 52.

ELSEVIER

Talanta 45 (1997) 39–45

Talanta

Cetylpyridinium chloride micelles as a selective fluorescence quenching solvent media for discriminating between alternant versus nonalternant polycyclic aromatic hydrocarbons

Siddharth Pandey [a], William E. Acree Jr. [a,*], John C. Fetzer [b]

[a] *Department of Chemistry, University of North Texas, Denton, TX 76203-0068, USA*
[b] *Chevron Research and Technology Center, Richmond, California, CA 94802-0627, USA*

Received 18 December 1996; received in revised form 27 March 1997; accepted 27 March 1997

Abstract

Fluorescence behavior of 41 polycyclic aromatic hydrocarbons (PAHs) dissolved in aqueous micellar cetyltrimethylammonium chloride (CTAC) solvent media and in five different cetyltrimethylammonium chloride + cetylpyridinium chloride (CPC) surfactant mixtures is reported. Experimental fluorescence measurements reveal that CPC is a selective fluorescence quenching agent for alternant PAHs. The cetylpyridinium ion effectively quenched emission intensities of the 21 alternant PAHs studied. Emission intensities of nonalternant PAHs, with a few noted exceptions, were unaffected by the presence of CPC in the mixed cationic surfactant micelles. © 1997 Elsevier Science B.V.

Keywords: Cetylpyridinium chloride; Fluorescence quenching; Polycyclic aromatic hydrocarbons; Selective quenching agents

1. Introduction

Reverse-phase liquid chromatographic methods using micellar eluents are becoming increasingly popular in the separation and/or analysis of polycyclic aromatic hydrocarbon (PAH) mixtures [1–5], in part because of lower cost and less toxicity associated with aqueous-surfactant solutions. Published applications include the separation of benzene derivatives and PAHs on an octylsilica column using micellar sodium dodecylsulfate (SDS) and cetyltrimethylammonium bromide (CTAB) mobile phases in both the absence and presence of organic modifiers (methanol, 1-propanol and 1-butanol), PAH separations using a micellar SDS mobile phase and short C_1- and C_4-chain columns, and separation of eleven PAHs in particulate air samples via acetonitrile-aqueous 0.20 molar SDS gradient elusion. Resolution of structurally similar PAHs results largely from differences in the solutes' partitioning behavior between the stationary phase and mobile phase micellar aggregates. Greater sensitivity and lower detection limits in spectrofluorometric determinations are achieved through increased quantum

* Corresponding author. Fax: +1 817 5654318; e-mail: acree@casl.unt.edu

PII S0039-9140(97)00108-2

yields and larger linearity ranges in plots of relative emission intensity versus PAH fluorophore concentration.

Environmentally important PAHs are inherently fluorescent, and sample preconcentration or derivatization is not necessary in many spectrofluorometric determinations. Detection limits at the parts-per-billion level have been reported [6,7]. Spectrofluorometry is more selective than other spectroscopic methods in that the excitation and emission wavelength can be varied independently. An excitation spectrum is obtained by measuring the fluorescence intensity at a fixed emission wavelength as the excitation wavelength is varied, whereas an emission spectrum is recorded by irradiating the solution at a single wavelength and then measuring the intensity as a function of emission wavelengths. While several polycyclic aromatic compounds may absorb at the same excitation wavelength, not all will emit at the wavelength(s) monitored by the detector. Fluorescence determinations do have their limitations, particularly if spectrally interfering substances are present. Unbiased quantification is possible, however, all interferants must be included in the calibration curves.

Utilization of selective fluorescence quenching agents further simplify observed fluorescence spectra by eliminating signals from undesired chemical interferences having only slightly different molecular structures. Sawicki et al. [8,9] introduced selective fluorescence quenching agents to thin-layer chromatographic analysis. Blümer and Zander [10] later extended the ideas to liquid chromatography. The authors noted that both nitromethane and nitrobenzene selectively quenched the fluorescence emission of perylene, dibenzo[*h*,*rst*]pentaphene and dibenzo[*b*,*k*]chrysene dissolved in aqueous-acetonitrile (20:80 percent by volume) mixture. Emission intensities of the three nonalternant PAHs (e.g., naphtho[1,2*b*]fluoranthene, indeno[1,2,3*cd*]pyrene and acenaphthyleno[1,2*k*]fluoranthene) were unaffected by nitromethane addition. Nitromethane (and nitrobenzene to a much lesser extent [11]) is a selective quenching agent for discriminating between alternant versus nonalternant PAHs. Polycyclic aromatic hydrocarbons are classified as alternant PAHs if every alternant carbon atom in the aromatic ring system can be 'starred.' Nonalternant PAHs, on the other hand, would have at least one pair of adjacent starred atoms [12,13].

As part of a seven-year continuing spectroscopic investigation, we [14–33] have reported the fluorescence properties and quenching behavior of numerous PAH6 benzenoids, fluoranthenoids and fluorenoids, methylene-bridged cyclopenta-PAHs, acenaphthylene and acephenanthrylene derivatives, bi-PAHs, and polycyclic aromatic nitrogen heterocycles (PANHs) in organic nonelectrolyte and in aqueous micellar solvent media. In the later studies, we observed that nitromethane quenching selectivity was lost in the case of the four anionic micellar solvent media studied. Nitromethane quenched the fluorescence emission of both alternant and nonalternant PAHs, which is contrary to the 'nitromethane selective quenching rule.' Unexpected fluorescence behavior was found when we extended our studies to include mixed cetyltrimethylammonium chloride (CTAC) and cetylpyridinium chloride (CPC) micelles. We report in this communication the fluorescence behavior of 21 alternant and 20 nonalternant PAHs in the presence of differing concentrations of cetylpyridinium chloride. The 41 PAHs studied are listed in Table 1.

2. Materials and experimental methods

Aqueous micellar cetyltrimethylammonium chloride (Aldrich, circa 7.6×10^{-3} M) solvent media and five different cetyltrimethylammonium chloride + cetylpyridinium chloride (Aldrich, 98%) mixed micellar surfactant solutions were prepared by dissolving the commercial surfactants in doubly deionized water. Synthetic references and/or commercial suppliers for the PAH solutes contained in Table 1 and Table 2 are listed in our earlier papers (for a single source listing see Tucker [28]). Stock solutions were prepared by dissolving the solutes in dichloromethane, and were stored in closed amber glass bottles in the dark to retard any photochemical reactions between the PAH solutes and dichloromethane solvent. Small 25 μl aliquots of each stock solutions

were transferred by Eppendorf pipette into test tubes, allowed to evaporate, and diluted with 10 ml (graduate cylinder) of the micellar solvent media of interest. Solute concentrations were sufficiently dilute (10^{-6} M) so as to prevent excimer formation. All solutions were ultrasonicated, vortexed and allowed to equilibrate for a minimum of 24 h before any spectrofluorometric measurements were made. Experimental results were unaffected by longer equilibration times.

Table 1
List of alternant and nonalternant polycyclic aromatic hydrocarbons examined and their excitation wavelength

Letter	Polycyclic aromatic hydrocarbon	λ_{ex} (nm)
Alternant polycyclic aromatic hydrocarbons		
A	Benzo[*ghi*]perylene	380
B	Benzo[*e*]pyrene	335
C	Pyrene	338
D	Anthracene	340
E	Chrysene	320
F	Benzo[*g*]chrysene	320
G	Perylene	403
H	Triphenylene	300
I	Phenanthrene	300
J	Naphtho[8,1,2*hij*]hexaphene	360
K	Benzo[*vwx*]hexaphene	360
L	Anthranthrene	306
M	Dibenzo[*def,p*]chrysene	310
N	Coronene	334
O	Benzo[*a*]pyrene	350
Alternant polycyclic aromatic hydrocarbon derivatives		
P	1-Methylpyrene	330
Q	2-Methylpyrene	333
R	4-Methylpyrene	320
S	4-Methychrysene	320
T	1-Methylcoronene	340
U	2-Methylanthracene	340
Nonalternant fluoranthenoids and fluorenoids		
V	Naphtho[1,2*b*]fluoranthene	350
W	Benzo[*ghi*]fluoranthene	340
X	Benz [*def*] indeno[1,2,3*hi*]chrysene	406
Y	Benzo[*a*]fluoranthene	406
Z	Naphtho[2,1*k*]benzo[*ghi*]fluoranthene	368
AA	Naphtho[1,2*k*]benzo[*ghi*]fluoranthene	366
AB	Benz [*def*]indeno[1,2,3*qr*]chrysene	408
AC	Dibenzo[*a,e*]fluoranthene	390
AD	Fluoreno[2,3,4,9*defg*]chrysene	315
AE	Benzo[*j*]fluoranthene	315
AF	Dibenzo[*ghi,mno*]fluoranthene	290
AG	Naphtho[2,1*a*]fluoranthene	400
AH	Benzo[*b*]fluoranthene	346
AI	Benzo[*k*]fluoranthene	306
AJ	Naphtho[2,3*b*]fluoranthene	316
Nonalternant fluoranthenoid and fluorenoid derivatives		
AK	1-Methylfluoranthene	360
AL	2-Methylfluoranthene	355
AM	3-Methylfluoranthene	355
AN	7-Methylfluoranthene	357
AO	8-Methylfluoranthene	355

Absorption spectra were recorded on a Milton Roy Spectronic 1001 Plus and a Hewlett-Packard 8450A photodiode-array spectrophotometer in the usual manner. The fluorescence spectra were measured on a Shimadzu RF-5000U spectrofluorimeter with the detector set at high sensitivity. Solutions were excited at the wavelengths listed in Table 1. Fluorescence data were accumulated in a 1 cm^2 quartz cuvette at 21°C (ambient room temperature) with excitation and emission slit width settings of 15 and 3 nm, respectively. The fluorescence spectra represent a single scan which was then solvent blank corrected and verified by repetitive measurements.

Emission intensities associated with the quenching measurements were corrected for primary inner-filtering artifacts and self-absorption arising from the absorption of excitation radiation by cetylpyridinium chloride and the PAH solute, respectively, according to the following expression [34–36]:

$$f_{\text{prim}} = F^{\text{corr}}/F^{\text{obs}} = 2.303A\,(y-x)/[10^{-Ax} - 10^{-Ay}] \quad (1)$$

which differs slightly from the approximate form [37]

$$f_{prim} \approx 10^{0.5A} \quad (2)$$

In the above equations F^{corr} and F^{obs} refer to the corrected and observed fluorescence emission signal, respectively, A is the absorbance per centimeter of pathlength at the excitation wavelength, and x and y denote distances from the boundaries of the interrogation zone to the excitation plane. For many of the fluorescence measurements primary inner-filtering correlations were relatively minor as the observed absorbance was often A cm^{-1}, ≤ 0.05, even in the 300–320 nm spectral region. Significantly larger corrections were re-

Table 2
Relative emission intensities of alternant and nonalternant PAHs dissolved in aqueous micellar (CTAC + CPC) solvent media

Letter[a]	I[b]	II[c]	III[d]	IV[e]	V[f]	VI[g]
Alternant polycyclic aromatic hydrocarbons						
A	738.0	8.1	3.4	3.3	1.3	2.2
B	979.6	39.4	11.1	14.1	4.1	2.0
C	379.6	3.4	2.9	0	0	0
D	137.9	12.2	3.8	3.3	2.1	2.2
E	635.6	23.7	7.6	10.4	2.5	2.2
F	385.7	25.4	8.4	6.0	3.8	3.3
G	1500.0	230.0	90.3	65.2	49.1	38.6
H	615.1	31.7	13.0	10.2	8.1	5.3
I	2000.0	101.6	43.2	26.0	19.6	15.8
J	218.2	59.6	34.5	22.7	7.4	8.0
K	422.6	23.9	16.2	7.4	5.8	6.0
L	586.4	125.6	43.7	34.5	25.5	18.1
M	647.9	30.7	12.9	7.9	7.0	5.8
N	191.3	18.2	17.2	12.2	10.9	13.0
O	1020.0	40.9	13.9	8.8	4.7	3.6
Alternant polycyclic aromatic hydrocarbon derivatives						
P	979.6	12.3	5.4	3.4	3.0	2.6
Q	983.7	7.9	2.7	1.0	0.7	0.5
R	2000.0	40.3	12.4	7.2	4.8	3.9
S	582.3	23.9	8.9	6.1	4.3	3.8
T	129.2	11.3	6.7	3.8	3.2	3.6
U	508.6	82.6	38.8	23.0	16.2	12.5
Nonalternant fluoranthenoids and fluorenoids						
V	742.3	283.3	242.3	213.7	156.4	148.2
W	905.9	914.1	905.9	885.4	860.9	890.9
X	125.6	152.8	168.9	136.4	142.5	118.3
Y	58.3	70.8	56.5	50.6	51.9	63.7
Z	175.8	173.8	171.7	166.6	167.6	167.6
AA	130.6	137.4	148.3	147.1	160.2	144.4
AB	62.2	60.9	62.6	86.9	78.8	77.7
AC	215.7	246.5	219.8	192.7	226.4	242.4
AD	248.9	227.2	218.2	204.1	206.7	197.0
AE	255.7	254.7	250.6	246.5	246.5	247.5
AF	346.5	334.3	320.8	316.7	310.7	310.9
AG	287.4	271.0	271.0	273.1	306.3	301.4
AH	225.0	179.0	160.4	152.3	144.1	138.9
AI	774.8	229.1	142.0	108.7	93.9	90.3
AJ	410.3	122.6	86.7	76.0	90.3	78.0
Nonalternant fluoranthenoid and fluorenoid derivatives						
AK	436.9	383.7	355.0	338.6	322.2	316.1
AL	901.8	856.8	807.6	799.4	803.5	832.2
AM	754.8	742.0	651.1	627.4	635.6	594.6
AN	553.7	484.0	512.7	500.4	488.1	492.2
AO	750.3	725.7	750.3	676.5	733.9	746.2

quired in our earlier studies [14–33] involving nitromethane. Secondary inner-filtering corrections were not necessary. Aqueous micellar CTAC + CPC mixed surfactant solutions were 'optically transparent' in the PAH emission ranges. Computational procedures and interrogation zone dimensions are discussed in greater detail elsewhere [17–19,38,39].

3. Results and discussion

Table 2 summarizes the fluorescence emission intensities of 41 different polycyclic aromatic hydrocarbons dissolved in aqueous micellar cetyltrimethylammonium chloride solvent media and in five binary surfactant mixtures containing differing concentrations of cetylpyridinium chloride. Careful examination of the numerical entries reveals that addition of CPC surfactant lead to a significant decrease in the emission signals of all 21 alternant PAHs studied. Emission intensities of the 20 nonalternant PAHs, with the exception of naphtho[1,2*b*]fluoranthene, benzo[*k*]fluoranthene, benzo[*b*]fluoranthene and naphtho[2,3*b*]fluoranthene, were not affected by CPC. No special significance is given to slight variations in emission intensities, which in all likelihood partly result from the fact that the solutions were prepared using a graduate cylinder. Differences in partitioning behavior of PAHs between bulk aqueous phase and different binary micelles, as well as differences in oxygen solubilities in the six solvent media, may also contribute to part of the observed variation in emission intensities.

Interestingly, of the four nonalternant PAHs whose emission intensities decreased naphtho[2,3*b*]fluoranthene and benzo[k]fluoranthene

[a] Letters refer to the compounds listed in Table 1. [b] Solvent media was circa 7.6×10^{-3} M in cetyltrimethylammonium chloride. [c] Solvent media was circa 7.6×10^{-3} M in cetyltrimethylammonium chloride + circa 2.0×10^{-3} M in cetylpyridinium chloride. [d] Solvent media was circa 7.6×10^{-3} M in cetyltrimethylammonium chloride + circa 4.0×10^{-3} M in cetylpyridinium chloride. [e] Solvent media was circa 7.6×10^{-3} M in cetyltrimethylammonium chloride + circa 6.0×10^{-3} M in cetylpyridinium chloride. [f] Solvent media was circa 7.6×10^{-3} M in cetyltrimethylammonium chloride + circa 8.0×10^{-3} M in cetylpyridinium chloride. [g] Solvent media was circa 7.6×10^{-3} M in cetyltrimethylammonium chloride + circa 1.0×10^{-2} M in cetylpyridinium chloride.

are known exceptions to the nitromethane selective quenching rule. [17,23,40] Both compounds behave as alternant PAHs. Naphtho[1,2*b*]fluoranthene was considered a 'borderline' case in our earlier [17] nitromethane quenching studies performed in both neat acetonitrile and aqueous–acetonitrile (20:80 by volume) solvent mixture. Dreeskamp et al. [40] reported that the fluorescence emission of benzo[*b*]fluoranthene was quenched by nitromethane; however, our measurements [17] in aqueous–acetonitrile solvent mixture after correction for primary inner-filtering could not confirm those authors' observations. Benzo[*b*]fluoranthene may likely be another 'borderline' case where the extent of quenching by nitromethane is small, and depends upon the actual solvent polarity and nitromethane concentration. There is strong correlation between the ability of nitromethane to quench the fluorescence of a given PAH and the PAM's fluorescence behavior in mixed CTAC + CPC mixed micelles. Based upon the 41 PAHs examined we conclude that cetylpyridinium ion, at least in the CTAC + CPC system, selectively quenches the fluorescence emission of alternant PAHs.

Observed similarities in the PAH fluorescence behavior in solutions containing nitromethane and cetylpyridinium chloride is rationalized in terms of the known quenching mechanisms. Zander, Breymann and coworkers [40–43] attributed nitromethane's selectivity to an electron/charge transfer reaction whereby an electron was transferred from the excited PAH fluorophore to nitromethane, which served as the electron acceptor. As argued by the authors, reduction potentials of nonalternant PAHs are generally 0.4 eV more positive than those of alternant PAHs. Quantum mechanical computations show the highest occupied molecular orbital (HOMO) and lowest unoccupied molecular orbital (LUMO) energies of nonalternant PAHs to be lowered against those of alternant PAHs of equal HOMO–LUMO separation. For the electron transfer reaction the change in free energy is expected to be more negative in the case of alternant PAHs. Electron transfer mechanism has been further documented by a $\log k_Q$ versus $E_{1/2(red)}$ Rehm-Weller correlation for the rate of electron transfer in acetonitrile.

A search of the published chemical literature [44–51] reveals that cetylpyridinium chloride/bromide has been used as a fluorescence quenching agent for PAH fluorescence emission numerous times to probe micellar aggregates. The cetylpyridinium ion (CPy^+) is known to be a good electron acceptor. Hashimoto and Thomas [44] established the quenching mechanism as electron transfer based upon an analysis of the time-dependent pyrene fluorescence decay in 0.1 M sodium lauryl sulfate + aqueous–ethylene glycol solvent mixture at both ambient room temperature and 77 K. Malliaris et al. [45] later showed that CPy^+ behaved as an immobile quencher in time-resolved fluorescence quenching studies involving pyrene solubilized in cetylpyridinium chloride + cetyltrimethylammonium chloride mixed micelles. The residence time of CPy^+ inside the micelle was significantly longer than pyrene's fluorescence lifetime. Verela et al. [50] determined the size and aggregation number of sodium dodecylsulfate micelles in the presence of alcohol additives from measured steady-state fluorescence intensities of pyrene as a function of CPC concentration. Velazquez and Costa [51] combined steady-state and transient-state fluorescence methods to deduce aggregation numbers and micellar volumes in mixed sodium decylsulfate and sodium dodecylsulfate micelles based upon the quenching of pyrene fluorescence by CPC. Calculated aggregation numbers and micellar volumes varied between 49 and 65 and between 16.6 and 20 $dm^3\ mol^{-1}$, respectively, depending upon sodium decylsulfate mole fraction. Furthermore, the bimolecular rate constant for the electron transfer interaction was reported to be independent of micellar size.

Only the very recent study by Ayala et al. [52] examined the cetylpyridinium ion's quenching selectivity in regards to alternant versus nonalternant polycyclic aromatic hydrocarbons. The authors' conclusions were based upon a study of the fluorescence behavior of only 14 PAH solutes. Unfortunately, three of the five listed nonalternant PAHs were completely misclassified. Acenaphthene, fluorene and acenaphthylene should be alternant PAHs as none of the five-membered ring systems are aromatic in nature. In fact, acenaphthene and fluorene have two CH_2 and one CH_2 group, respec-

tively, on their five membered ring systems. The only real nonalternant PAHs (fluoranthene and benzo[*b*]fluoranthene) in the Ayala et al. study are known borderline exceptions to the nitromethane selective quenching rule. As shown in Table 2, the selectivity of the cetylpyridinium ion for quenching the fluorescence emission of alternant versus nonalternant PAHs is far better than reported in the earlier Ayala et al. study.

Nitromethane and the cetylpyridinium ion both quench PAH fluorescence emission via an electron transfer mechanism. It is not too surprising, therefore, that a strong correlation exists in regards to the ability of each electron acceptor to selectively quench the fluorescence emission of alternant versus nonalternant polycyclic aromatic hydrocarbons. Discovery of the cetylpyridinium ion as a selective quenching agent is important from a chemical analysis point-of-view. Unlike nitromethane, cetylpyridinium chloride is optically transparent in the excitation spectral region of many of the PAHs. Primary inner-filtering corrections are minimized, and in many cases even eliminated. Additional measurements are planned to ascertain if CPC quenching selectivity extends to anionic surfactant + CPC and nonionic surfactant + CPC solvent media.

Acknowledgements

This work was supported in part by the University of North Texas Research Council.

References

[1] E. Pramauro, E. Pelezetti, Surfactants in Analytical Chemistry: Applications of Organized Amphiphilic Media, Elsevier, Amsterdam, 1996, Chap. 6 and references therein.
[2] M.R. Hadjmohammadi, M.H. Fatemi, J. Liq. Chromatogr. 18 (1995) 2569.
[3] M.N. Kayali, S. Rubio-Barroso, L.M. Polo-Diez, J. Liq. Chromatogr. Rel. Technol. 19 (1996) 759.
[4] M. Angeles Garcia, M. Luisa Mariana, J. Liq. Chromatogr. Rel. Technol. 19 (1996) 1757.
[5] M.N. Kayali, S. Rubio-Barroso, L.M. Polo-Diez, J. Liq. Chromatogr. 17 (1994) 3623.
[6] L.A. Files, J.A. Winefordner, J. Agric. Food Chem. 35 (1987) 471.
[7] J.J.S. Rodriquez, J.H. Garcia, M.M.B. Suarez, A.B. Martin-Lazaro, Lazaro Analyst 118 (1993) 917.
[8] E. Sawicki, T.W. Stanley, W.C. Elbert, Talanta 11 (1964) 1435.
[9] E. Sawicki, W.C. Elbert, T.W. Stanley, J. Chromatogr. 17 (1965) 120.
[10] G.P. Blümer, M. Zander, Fresenius Z. Anal. Chem. 296 (1979) 409.
[11] F.K. Ogasawara, Y. Wang, V.L. McGuffin, Appl. Spectrosc. 49 (1995) 1.
[12] E. Zimmerman, Quantum Mechanics for Organic Chemists, Academic Press, New York, 1975, pp. 145–146.
[13] J. March, Advanced Organic Chemistry: Reactions, Mechanisms and Structure, McGraw-Hill, New York, 1968, pp. 46–48.
[14] S.A. Tucker, H. Darmodjo, W.E. Acree, M. Zander, E.C. Meister, M.J. Tanga, S. Tokita, Appl. Spectrosc. 46 (1992) 1630.
[15] S.A. Tucker, W.E. Acree, C. Upton, Appl. Spectrosc. 47 (1993) 201.
[16] S.A. Tucker, W.E. Acree, C. Upton, Polycyclic Arom. Compds. 3 (1993) 221.
[17] S.A. Tucker, W.E. Acree, B.P. Cho, R.G. Harvey, J.C. Fetzer, Appl. Spectrosc. 45 (1991) 1699.
[18] V.L. Amszi, Y. Cordero, B. Smith, S.A. Tucker, W.E. Acree, C. Yang, E. Abu-Shaqara, R.G. Harvey, Appl. Spectrosc. 46 (1992) 1156.
[19] S.A. Tucker, H. Darmodjo, W.E. Acree, J.C. Fetzer, M. Zander, Appl. Spectrosc. 46 (1992) 1260.
[20] S.A. Tucker, W.E. Acree, Appl. Spectrosc. 46 (1992) 1388.
[21] S.A. Tucker, W.E. Acree, J.C. Fetzer, R.G. Harvey, M.J. Tanga, P.-C. Cheng, L.T. Scott, Appl. Spectrosc. 47 (1993) 715.
[22] S.A. Tucker, H.C. Bates, V.L. Amszi, W.E. Acree, H. Lee, P. Di Raddo, R.G. Harvey, J.C. Fetzer, G. Dyker, Anal. Chim. Acta 278 (1993) 269.
[23] S.A. Tucker, H.C. Bates, W.E. Acree, J.C. Fetzer, Appl. Spectrosc. 47 (1993) 1775.
[24] S.A. Tucker, J.M. Griffin, W.E. Acree, M. Zander, R.H. Mitchell, Appl. Spectrosc. 48 (1994) 458.
[25] S.A. Tucker, J.M. Griffin, W.E. Acree, P.P.J. Mulder, J. Lugtenburg, J. Cornelisse, Analyst 119 (1994) 2129.
[26] S.A. Tucker, J.M. Griffin, W.E. Acree, J.C. Fetzer, M. Zander, O. Reiser, A. De Meijere, I. Murata, Polycyclic Aromat. Compds. 4 (1994) 141.
[27] S.A. Tucker, J.M. Griffin, W.E. Acree, M.J. Tanga, J.E. Bupp, T.K. Tochimoto, J. Lugtenburg, K. Van Haeringen, J. Cornelisse, P.-C. Cheng, L.T. Scott, Polycyclic Aromat. Compds. 4 (1994) 161.
[28] S.A. Tucker, Dissertation, University of North Texas, Denton, Texas, 1994.
[29] J.R. Powell, S. Pandey, B.J. Miller, W.E. Acree, P.E. Hansen, J.C. Fetzer, J. Lumin. 69 (1996) 27.
[30] S. Pandey, W.E. Acree, J.C. Fetzer, Anal. Chim. Acta 324 (1996) 175.

[31] S. Pandey, J.R. Powell, W.E. Acree, B.P. Cho, J. Kum, C. Yang, R.G. Harvey, Polycyclic Aromat. Compds. 12 (1997) 1.
[32] S. Pandey, K.A. Fletcher, J.R. Powell, M.E.R. McHale, A.-S.M. Kauppila, W.E. Acree, J.C. Fetzer, Spectrochim. Acta 57A (1997) 165.
[33] S. Pandey, W.E. Acree, B.P. Cho, J.C. Fetzer, Talanta 44 (1997) 413.
[34] C.A. Parker, W.J. Barnes, Analyst 82 (1957) 606.
[35] J.F. Holland, R.E. Teets, P.M. Kelly, A. Timnick, Anal. Chem. 49 (1977) 706.
[36] M.C. Yappert, J.D. Ingle, Appl. Spectrosc. 43 (1989) 759.
[37] J.R. Lakowicz, Principles of Fluorescence Spectroscopy, Plenum Press, New York, 1983.
[38] S.A. Tucker, W.E. Acree, J.C. Fetzer, J. Jacob, Polycyclic Aromat. Compds. 3 (1992) 1.
[39] S.A. Tucker, V.L. Amszi, W.E. Acree, J. Chem. Educ. 69 (1992) A8.
[40] H. Dreeskamp, E. Koch, M. Zander, Z. Naturforsch. 30A (1975) 1311.
[41] U. Breymann, H. Dreeskamp, E. Koch, M. Zander, Chem. Phys. Lett. 59 (1978) 68.
[42] M. Zander, U. Breymann, H. Dreeskamp, E. Koch, Z. Naturforsch. 32A (1977) 1561.
[43] J. Malkin, Photophysical Properties of Polycyclic Aromatic Compounds, CRC Press, Baco Raton, Florida, 1992, pp. 19–23.
[44] S. Hashimoto, J.K. Thomas, J. Am. Chem. Soc. 105 (1983) 5230.
[45] A. Malliaris, J. Lang, R. Zana, J. Chem. Soc. Faraday Trans. 1 82 (1986) 109.
[46] S. Reekmans, D. Bernik, M. Gehlen, J. van Stam, M. Van der Auweraer, F.C. De Schryver, Langmuir 9 (1993) 2289.
[47] S.C. Bhattacharya, H.T. Das, S.P. Moulik, J. Photochem. Photobiol. 71A (1993) 257.
[48] J. Lang, J. Phys. Chem. 46 (1990) 3734.
[49] D.J. Jobe, R.E. Verrall, B.D. Skalski, Langmuir 9 (1993) 2814.
[50] A.S. Varela, M.I.S. Macho, A.G. Gonzalez, Colloid Polym. Sci. 273 (1995) 876.
[51] M.M. Velazquez, S.M.B. Costa, J. Chem. Soc. Faraday Trans. 86 (1990) 4043.
[52] J.H. Ayala, A.M. Afonso, V. Gonzalez, Talanta 44 (1997) 257.

ELSEVIER

Talanta 45 (1997) 47–55

Talanta

Rapid determination of dissolved organic phosphorus in soil leachates and runoff waters by flow injection analysis with on-line photo-oxidation

D.M.W. Peat [a], I.D. McKelvie [b], G.P. Matthews [a], P.M. Haygarth [c], P.J. Worsfold [a,*]

[a] *Department of Environmental Sciences, Plymouth Environmental Research Centre, University of Plymouth, Drake Circus, Plymouth PL4 8AA, UK*

[b] *Water Studies Centre, Monash University, 900 Dandenong Rd, Caulfield East, Victoria 3145, Australia*

[c] *Institute of Grassland and Environmental Research, North Wyke, Okehampton, Devon EX20 2SB, UK*

Received 16 December 1996; accepted 28 March 1997

Abstract

A rapid method suitable for the determination of dissolved organic phosphorus (DOP) in soil leachates and runoff waters is presented. The flow injection (FI) manifold contains an in-line PTFE reaction coil wrapped around a low power UV lamp and is based on the spectrophotometric determination of dissolved reactive phosphorus (DRP) and mineralised DOP at 690 nm after reduction of phosphomolybdate to molybdenum blue with tin(II) chloride. The linear range was 0–1.5 mg l^{-1} PO_4-P, with a detection limit (3 s) of 7 μg l^{-1} and a sample throughput of 40 h^{-1}. Tolerance to potential matrix interferences in soil pore waters, particularly Al(III), Si(IV), Fe(II) and Fe(III), was achieved using a combination of on-line sample pre-treatment by a strong acid ion exchange column, low photoreactor pH and acid induced control of the kinetics of the molybdenum blue reaction. The results obtained with this manifold were in good agreement with those obtained by a batch spectrophotometric reference method. © 1997 Elsevier Science B.V.

Keywords: Phosphorus speciation; Flow injection; Soil leachate; Photo-oxidation

1. Introduction

Phosphorus in soil water leachate and runoff occurs in both dissolved and particulate forms [1]. The dissolved fraction is defined from an operational standpoint as the fraction that passes through a 0.45-μm filter and typically contains compounds such as orthophosphates, inositol phosphates, nucleic acids, sugars, condensed phosphates and some colloidal phosphorus. Total dissolved phosphorus (TDP) can be operationally divided into phosphorus compounds that are molybdate reactive, i.e., dissolved reactive phosphorus (DRP), and those that are unreactive, including dissolved condensed phosphorus (DCP) and dissolved organic phosphorus (DOP).

The composition of phosphorus species in the operationally defined fractions of soil leachates

* Corresponding author.

PII S0039-9140(97)00105-7

and runoff waters can vary dramatically in a short space of time (minutes) when subjected to a storm or breakthrough event. The molybdenum blue reaction is almost universally used for phosphate determinations but neither batch nor FI based methods are suited to the task of monitoring TDP in such events. Traditional methods for the determination of TDP (and total phosphorus (TP)) involve heating or autoclaving the sample with peroxydisulphate (with or without acid) [2], which can give incomplete recoveries with some samples, and the use of nitric-sulphuric or nitric-sulphuric-perchloric acid mixtures may therefore be required [3]. However these batch methods, although generally accepted as being analytically reliable, involve extensive sample handling and lengthy digestion times (up to 2 h), making them tedious when large numbers of samples need to be analysed.

Most FI methods for the determination of TDP (and TP) involve hydrolysis and thermal oxidation and generally use long digestion reactors (> 10 m), lengthy residence times, high temperatures and elevated pressures in order to mineralise condensed and organic phosphates [4–7]. Such methods are therefore not suitable for in-situ deployment and, in addition, they have a high power consumption and low sample throughput of 10–15 samples h^{-1}.

Ultraviolet (UV) photo-oxidation can be used to mineralise organic matter and has been applied to the determination of DOP [8,9]. Solorzano and Strickland [10] have suggested that because condensed phosphates are not susceptible to UV photo-oxidation, its use provides a basis for differentiating TDP and DOP. However in soil leachates and runoff waters the concentration of condensed phosphates is generally very low (due to rapid biological breakdown) and the difference in concentration between DOP and TDP is therefore negligible.

An FI method for determining DOP in natural waters by photo-oxidation with alkaline peroxydisulphate in a PTFE photoreactor incorporating a low power, medium pressure mercury lamp has been reported by McKelvie et al. [11], but the method was unsuitable for soil waters containing higher concentrations of dissolved aluminium or iron [12]. This paper presents a modification of the above method for the determination of TDP in soil leachates and runoff waters. It involves two strategies for the minimisation of these interferences, viz; pre-treatment of the sample by cation exchange to remove interfering Fe(III) and the use of acidic photo-oxidation conditions. The proposed method was validated against batch analyses performed by independent laboratories at the Water Studies Centre (Caulfield Campus, Melbourne) and the Dairy Research Institute (Ellinbank, Victoria).

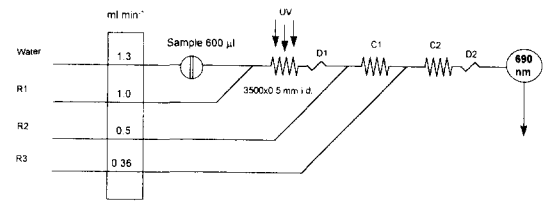

Fig. 1. Flow injection manifold for the FI determination of TDP.

2. Experimental

2.1. Reagents

2.1.1. DOP manifold

The acid peroxydisulphate reagent (R1, as shown in Fig. 1) was prepared by dissolving potassium peroxydisulphate, 50 g l^{-1} (BDH, AnalaR) in 0.12 M H_2SO_4 (BDH, AnalaR). The acid molybdate reagent (R2) was prepared by

Table 1
Recoveries of 1.0 mg l^{-1} standards of model P compounds using on-line acid peroxydisulphate digestion

Model Compound	PO_4-P (mg l^{-1})	RSD (%)
Phytic acid	0.97	0.7
p-nitrophenyl phosphate	1.01	0.6
D-glucose-6′-phosphate	1.01	1.6
o-phosphoryl ethanol	1.02	0.4
Cocarboxylase	0.19	2.1
Tripolyphosphate	0.04	16.2
Orthophosphate	1.00	0.3

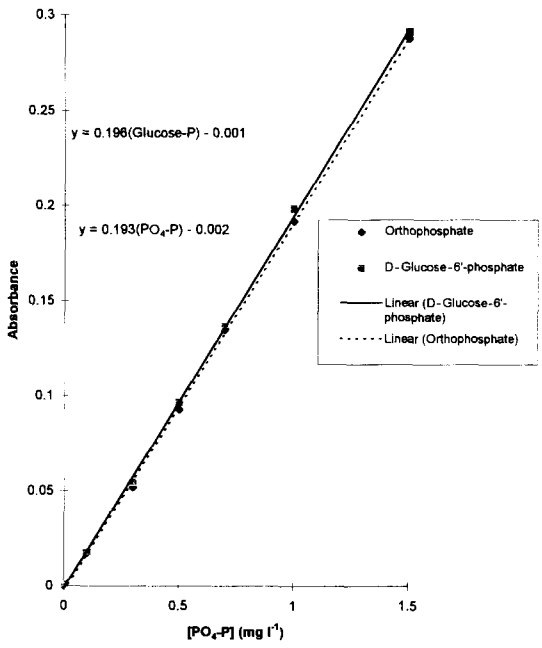

Fig. 2. Linearity of recovery for D-glucose-6′-phosphate.

dissolving ammonium heptamolybdate, 8.1×10^{-3} M (BDH, AnalaR) in 0.41 M H_2SO_4 (BDH, AnalaR). The tin(II) chloride reagent (R3) was prepared by dissolving tin(II) chloride, 8.9×10^{-4} M (May and Baker) and hydrazine sulphate (0.015 M) in 0.41 M H_2SO_4 (BDH, AnalaR).

2.2. Dairy Research Institute (DRI) batch method

Reagent DR1 was 2.5 M sulphuric acid, (AnalaR). Reagent DR2 (potassium antimonyl tartrate solution) was prepared by dissolving 1.3715 g of $K(SbO)C_4H_4O_6.1/2\ H_2O$, (AnalaR) in 500 ml of distilled water. Reagent DR3 (ammonium molybdate solution) was prepared by dissolving 6 g of $(NH_4)_6Mo_7O_{24}.4H_2O$, (AnalaR) in 150 ml of distilled water. Reagent DR4 was ascorbic acid solution (0.01 M), (AnalaR). The combined reagent consisted of 125 ml DR1, 12.5 ml DR2, 37.5 ml DR3 and 75 ml DR4.

2.2.1. Model phosphorus compounds

Model compounds used in the recovery experiments were chosen to represent a range of compound stabilities and functional groups [13], viz., potassium dihydrogen orthophosphate (BDH, Pronalys); sodium tripolyphosphate (Ajax), phytic acid dodecasodium salt hydrate (purity 78%; Aldrich), *p*-nitrophenyl phosphate (purity 99%; Sigma), D-glucose-6′-phosphate (purity 98%; source), cocarboxylase (purity 98%; Sigma), *o*-phosphoryl ethanol (purity 99%; Sigma) and adenosine-5′-triphosphate disodium salt (purity 98%; Sigma).

2.2.2. Interferences

Separate solutions of interfering ions (Al(III), As(V), Ca(II), Fe(II), Fe(III), Si(IV)), were prepared by dilution of the appropriate 1000 mg l^{-1} Spectrosol (BDH) stock solution.

2.3. Instrumentation

2.3.1. DOP Manifold

The manifold used is shown in Fig. 1. PTFE tubing (0.5 mm i.d.) was used throughout and C1 and C2 were mixing coils with lengths of 30 and 60 cm, respectively. Ismatec Mini-S 840 and 820 pumps were used for carrier and reagent delivery, respectively. Sample (600 μl) was injected using a motor driven Rheodyne 5020 injection valve. The UV source was a germicidal U tube (G36 T15 NU, UV Air Pty Ltd, South Australia) that had a major emission line at 254 nm and a power consumption of 40 W, and was housed in a light-tight, fan ventilated box. Oxygen and ozone bubbles formed during photoxidation were removed using two 10 cm lengths of lightly knotted Accurel (S6/2, Enka AG) microporous tubing (D1 and D2). The absorbance was measured with a spectrophotometer (LKB Novaspec) fitted with a 10-mm path length glass flow-through cuvette (75 μl; Starna Pty Ltd) and the output recorded on an analogue chart recorder (ICI Instruments, DP600).

2.3.2. Ion exchange column for sample pre-treatment

The columns were packed with Dowex W50 X8 (BDH) cation exchange resin. The resin was initially cleaned in 10% (v/v) concentrated H_2SO_4 and then flushed with Milli-Q grade water. The columns were regenerated by flushing on-line with

Table 2
Response for Si(IV) standards with zero PO_4-P concentration. Silicon as sodium metasilicate (Na_2SiO_3)

Si(IV) (mg l^{-1})	Response (A.U.)	Equivalent [PO_4-P] (μg l^{-1})	RSD (%)
2	0.000	0.2	–
5	0.003	3.2	39.5
8	0.004	5.7	28.6
10	0.006	8.5	10.1
60	0.011	17.6	10.9

10 ml of 10% (v/v) concentrated sulphuric acid followed by Milli-Q water after each use.

2.3.3. DRI batch method

Samples were autoclaved (Siltex) at 121°C and 200 kPa in borosilicate glass digestion vials (40 ml) with autoclavable PTFE faced, black phenolic solid top screw cap closures. Absorbances were measured using a spectrophotometer (CARY 1E) operated at 880 nm with a 10-mm cuvette.

2.4. DRI procedures

Aliquots (5–20.0 ml) of each water sample containing between 0 and 4 mg l^{-1} phosphorus were pipetted into 40 ml digestion vials. 0.0, 2.5, 5.0, 7.5 and 10.0 ml aliquots of a 2-mg P l^{-1} working standard were pipetted into separate digestion vials. Each vial was diluted to 20.0 ml with distilled water and 5.0 ml of 20% (v/v) sulphuric acid added. Then 0.2 g of ammonium persulphate was added to each vial, the vials capped and the contents mixed by inversion. The sealed vials were transferred to a suitable tray and placed in the autoclave for 60 min. The autoclave was then left for 15 min to allow the vials to cool and return to atmospheric pressure before opening. The volume of 4 M NaOH required to neutralise each digest was determined by adding 1 to 2 drops of phenolphthalein indicator to the vial followed by successive 1.0 ml aliquots of 4 M NaOH, mixing well between additions until the solution just turned pink. 5 ml of the combined colour reagent was added to each vial, mixed well and allowed to stand for a minimum of 30 min before measuring the absorbance of the contents of each vial at 880 nm.

3. Results and discussion

3.1. Optimisation of the FI manifold

Initially the flow rates reported by McKelvie et al. [11] were used (1.3 ml min^{-1}) for the water carrier and peroxydisulphate (R1) streams. Samples were injected into the carrier stream and subsequently merged with the peroxydisulphate stream in order to provide a constant refractive index and hence a stable baseline for the merged streams. The advantage of this approach outweighed the negative effect of on-line sample dilution on the detection limit. In order to minimise sample dilution however the peroxydisulphate concentration was increased to 50 g l^{-1} (the limit of solubility) from 40 g l^{-1} which allowed a decrease in the flow rate of R1 to 1.0 ml min^{-1}, with no loss in oxidation efficiency. To avoid problems with back pressure, the i.d. of the PTFE reactor coil was increased from 0.3 to 0.5 mm with minimal effect on dispersion. The reactor coil was also wrapped around the U shaped lamp in a figure of eight configuration to maximise photochemical efficiency.

3.2. Photo-oxidation and detection chemistry

The principal problem when using alkaline peroxydisulphate photoreactor chemistry is a susceptibility to interference [7] from metal ions, e.g., Al(III), Ca(II), and Fe(III) which form complexes and precipitates with orthophosphate at high pH. Whilst these interfering species are not usually present in sufficient concentrations to cause problems with the analysis of natural waters, they commonly occur at relatively high concentrations

Table 3
As(V) interference in the on-line DOP method with zero PO_4-P concentration

As(V) (mg l^{-1})	Response (A.U.)	Equivalent [PO_4-P] (mg l^{-1})	RSD (%)
0.1	0.006	-0.015	10.2
0.5	0.034	0.063	4.5
1	0.067	0.153	6.8
2	0.167	0.472	0.6

in soil leachates and runoff waters. In order to prevent phosphate-metal complex formation, a low pH photo-oxidation chemistry was used for this work. The formation of bubbles can be more problematic at low pH due to the evolution of CO_2 but this has been overcome in the manifold reported here by improved on-line debubbling using microporous tubing.

The stream entering the photoreactor is acidic, due to the 0.12 M H_2SO_4 initially present, and the acidity of this stream is augmented by the photolysis of peroxydisulphate within the photoreactor:

$$2S_2O_8^{2-} + 2H_2O \xrightarrow{h\nu} 4SO_4^{2-} + O_2 + 4H^+$$

The kinetics of the molybdate detection chemistry are highly susceptible to variations in the concentration of sulphuric acid [14,15] and it has been reported that at concentrations above 0.7 M H_2SO_4 the formation of the heteropoly acid becomes inverse fourth order with respect to acid concentration [16]. The acidity in the peroxydisulphate stream has been compensated by reducing the acidity of the molybdate and reductant streams with respect to those quoted in FI methods which determine DRP in a water carrier stream [17].

3.3. Figures of merit

The linear range and detection limit of the system were determined using orthophosphate standards in the range 0–1.5 mg l^{-1} PO_4-P. The relative standard deviations ($n = 5$) for standards above 0.5 mg l^{-1} were generally $< 1\%$. The reduction in noise compared with the previously reported manifold [11] is attributed to bubble formation causing less serious fragmentation of the flowing stream in the larger diameter photoreactor. The sensitivity of the system was 0.2699 AU per mg l^{-1} PO_4-P and the detection limit was 7 μg l^{-1}, calculated using 3 s ($n = 5$) of the blank signal.

3.4. Recoveries of model phosphorus compounds

Six model compounds were chosen to form a representative range of stabilities of phosphorus compounds found in soil leachates and runoff waters [13], e.g., labile (D-glucose-6′-phosphate (a naturally occurring sugar) and *o*-phosphoryl ethanol) and refractory (phytic acid). Phytic acid is a particularly useful model compound for soil because it is found in a wide range of plant materials such as oil seeds, legumes and cereal grains and is one of the most refractory organic phosphorus compounds [3].

The recoveries for 1.0 mg l^{-1} P in the organic phosphorus model compounds and a 1 mg l^{-1} PO_4-P standard are shown in Table 1. The condensed phosphates, co-carboxylase and tripolyphosphate, gave low recoveries ($< 20\%$) despite the acidic conditions used in the photoreactor. This is attributed to the fact that these compounds are not susceptible to destruction by UV irradiation [10] and did not undergo hydrolysis because the experimental conditions were not sufficiently harsh. Quantitative recoveries for these compounds have only been reported with long exposure times (up to 2 h) and high temperatures (> 110°C) in acidic conditions [8] and in an FI system which combined UV photo-oxidation and thermal digestion [18]. Recoveries for all of the other compounds were quantitative, including phytic acid (97%). Recovery was quantitative for D-glucose-6′-phosphate over the range 0 to 1.5 mg l^{-1} PO_4-P as shown in Fig. 2.

Table 4
Al(III) interference in the determination of 0.5 mg l^{-1} PO_4-P

Al(III) (mg l^{-1})	Response (A.U.)	PO_4-P determined (mg l^{-1})	RSD (%)
0.5	0.174	0.501	0.8
1.0	0.173	0.506	1.6
2.0	0.173	0.506	1.4
10.0	0.171	0.508	1.6

Table 5
Cu(II) and Fe(III) interference in the determination of 1 mg l^{-1} PO_4-P

	Response (A.U.)	[PO_4-P] determined (mg l^{-1})	RSD (%)
Added Cu(II) (mg l^{-1})			
0.5	0.345	0.932	0.6
1.0	0.341	0.909	2.1
2.0	0.315	0.850	0.5
10.0	0.320	0.867	0.5
Added Fe(III) (mg l^{-1})			
0.1	0.390	0.957	0.6
0.5	0.354	0.860	1.1
1	0.319	0.789	0.8
2	0.257	0.686	1.3
10	0.183	0.480	1.4

3.5. Interferences

The determination of organic phosphorus via photo-oxidation and the formation of phosphomolybdenum blue has some potentially serious interferences when applied to the analysis of soil leachates and runoff waters. These can be classified into three types, those that also form molybdate complexes resulting in enhanced absorbance (additive interference), those that form compounds with orthophosphate or organic phosphates and inhibit either the formation of phosphomolybdenum blue or organic compound breakdown (subtractive interference) and those that act as radical scavengers in the photoreactor and hence lower recovery of organic phosphorus (subtractive by radical scavenging).

3.5.1. Additive interferences

Si(IV) forms a complex with molybdate which has a broad band absorbance (λ_{max} 790 nm [19]), which overlaps the 690 nm detection wavelength used in this method, causing an increase in detected peak height and overestimation of phosphorus concentration. This is potentially the most serious interference in the analysis of soil leachates and runoff waters because the Si/P concentration ratio may be as high as 5000 [20]. The rate of formation of the silicon chromophore can be minimised by increasing the acidity to just below the pH at which the rate of formation of phosphomolybdenum blue becomes inverse fourth order with respect to acid concentration i.e. the rate of formation of the silicon molybdate complex is much slower at this acidity and therefore does not interfere within the timescale of an FI determination. Si(IV) standards were therefore analysed using the TDP manifold in order to determine the overestimation of orthophosphate. The results (Table 2) show no significant interference below 8 mg l^{-1} Si(IV), which represents the high end of the concentration range typically found in soil leachates and runoff waters. Even at 60 mg l^{-1} Si(IV) the overestimation is small, being equivalent to 17 μg l^{-1} PO_4-P.

Table 6
Removal of Fe(III) interference on spiked 1 mg l^{-1} PO_4-P standards using ion exchange columns

Fe(III) (mg l^{-1})	[PO_4-P] determined (mg l^{-1})		RSD (%)	
	Small i.d. column	Large i.d. column	Small i.d. column	Large i.d. column
10.0	0.834	0.800	1.1	1.0
3.0	0.869	0.850	0.9	0.6
1.0	0.996	0.997	0.7	0.9
0.5	1.003	0.999	1.6	0.6
0.1	0.998	0.997	0.2	0.3

Table 7
Comparison of DRI batch method with on line FI method

TDP – Batch (μg l^{-1})	RSD (%)	TDP – on-line (μg l^{-1})	RSD (%)
22.4	5.0	21.2	0.0
29.4	5.0	33.0	7.5
49.6	5.0	47.1	14.8

It is well known that arsenate forms an absorbing complex with molybdate [21] which interferes strongly in the determination of phosphate. The molybdenum blue chemistry is so sensitive to arsenate that it is the basis of a spectrophotometric method for its determination [22]. Arsenate standards were analysed using the TDP manifold and Table 3 shows the equivalent PO_4-P response for arsenate standards at various concentrations. For most environmental analyses, the concentration of total arsenic is not sufficiently high to be problematic but care must be taken when heavily polluted waters are analysed [23].

3.5.2. Subtractive interferences

Several ions which commonly occur in soil leachates and runoff waters, i.e. Al(III), Ca(II), Cu(II), Fe(II) and Fe(III), can combine with orthophosphate and some organic species to form complexes and precipitates. Al(III), which is abundant in soil clay minerals [24], is known to cause underestimation of phosphorus concentration by a mechanism that involves the formation of aluminium phosphates at high pH [12]. In the method reported here, there was no reduction in the response for a 0.5-mg l^{-1} PO_4-P standard when spiked with up to 10 mg l^{-1} Al(III) (Table 4) because of the low pH used. This tolerance exceeds the concentration of Al(III) found in most soil leachates and runoff waters. Similarly Ca(II), often present in soils as calcium carbonate, can cause an underestimation of PO_4-P by forming insoluble phosphates. However no reduction in the response for a 0.5-mg l^{-1} PO_4-P standard when spiked with up to 10 mg l^{-1} Ca(II) was observed using the manifold reported here. Fe(II) did not suppress a 1 mg l^{-1} PO_4-P signal at spike concentrations up to 10 mg l^{-1}. Table 5 shows that 0.5 mg l^{-1} Cu(II) and 0.1 mg l^{-1} Fe(III) do however cause suppression of the response for a 1 mg l^{-1} PO_4-P standard. The Cu(II) concentration in soil leachates and runoff waters is usually much less than 0.5 mg l^{-1} [25] and therefore does not represent a serious problem. The binding of Fe(III) to phosphates is well documented, e.g., [26] and, in contrast to Cu(II), is a potentially serious interference in this method.

3.5.3. Subtractive interferences (by radical scavenging mechanism)

Carbonate and bicarbonate ions act as radical scavenging agents [27] which may deplete the number of radicals available to attack organic compounds, thereby resulting in lower organic

compound recovery. The levels of these ions in natural waters are generally not sufficient to affect recovery but problems may be encountered in the analysis of soil and sediment extracts where carbonate or bicarbonate is used as the extractant in combination with alkaline photo-oxidation conditions. The low pH photo-oxidation conditions used in the method reported here eliminates this potential interference by converting carbonate and bicarbonate to carbon dioxide.

3.5.4. Elimination of Fe(III) interference using a cation exchange column

A strong cation exchange column in the H^+ form was introduced as a sample pre-treatment line with the aim of eliminating interference from Fe(III). Two types of packed column geometry were evaluated, a small 1 mm i.d. tube of 45 mm length and a larger 5 mm i.d. tube of 30 mm length. Sample was pumped through both columns at a flow rate of 0.4 ml min^{-1}. For the smaller i.d. column, Fe(III) interference was not observed below 1 mg l^{-1}, as shown in Table 6. The use of a larger i.d. column produced a slightly worse interference threshold for Fe(III), probably due to the formation of preferential flow paths and a shorter residence time in the larger i.d. column. The smaller column was therefore used for the analysis of lake water and soil leachate samples.

3.6. Comparison of on-line and batch methods

Fourteen natural water (lake water) samples were collected from Blackburn Lake, Melbourne, Australia. Filtered samples (0.45 μm) were digested with nitric-sulphuric acid and analysed by a batch method [2] and the proposed FI method for TDP incorporating the 1 mm i.d. ion exchange column. The levels found were all below 40 μg l^{-1} TDP but nonetheless the determined concentrations in thirteen of the samples agreed within experimental error (3 s). The samples were also analysed by a standard FI method for DRP [17] and the results were consistently lower than those obtained for TDP by both methods. Three soil leachate samples from Darnum, West Gibbsland, Australia were also analysed by the batch method and the proposed FI method and there was good agreement for all samples, which covered the range 22–50 μg l^{-1} P, as shown in Table 7.

4. Conclusions

The manifold described is suitable for the determination of TDP in a range of natural waters. A combination of low pH reactor chemistry and an ion exchange column is sufficient to eliminate interferences at concentrations significantly in excess of those likely to be encountered in soil leachates and runoff waters. Sample volume required is low (600 μl), sample throughput is excellent (40 h^{-1}) and the use of a low powered UV lamp and PTFE photoreactor makes the method suitable for field deployment.

Acknowledgements

The Authors would like to thank the Institute of Grassland and Environmental Research (IGER) for financial support, Dr Steve Jarvis (IGER) for his useful comments, the staff of the Water Studies Centre at Monash University for their assistance and Mr David Nash, Dairy Research Institute, Ellinbank, Victoria for his collaboration in the validation phase. PJW would like to thank the NERC for research grant GST/02/587 to support initial studies in this area.

References

[1] I. McKelvie, D.M. Peat, P.J. Worsfold, Anal. Proc. 32 (1995) 437.
[2] A.E. Greenberg, A.E. Greenberg (Eds.), Standard methods for the examination of water and waste water, 18th Ed. 4500-P Phosphorus, 1992, p. 108.
[3] K. Robards, I. McKelvie, R.L. Benson, P.J. Worsfold, N. Blundell, Anal. Chim. Acta 287 (1994) 147.
[4] M. Aoyagi, Y. Yasumasa, A. Nishida, Anal. Chim. Acta 214 (1988) 229.
[5] S. Hinkamp, G. Schwedt, Anal. Chim. Acta 236 (1990) 345.
[6] T. Korenga, K. Okada, Bunseki Kagaku 33 (1984) 683.
[7] K.E. Williams, S.J. Haswell, D.A. Barclay, G. Preston, Analyst 118 (1993) 245.

[8] F.A. Armstrong, S. Tibbitts, J. Marine Biol. Assoc. UK 48 (1968) 143.
[9] A. Henriksen, Analyst 95 (1970) 601.
[10] L. Solorzano, J.D. Strickland, Limnol. Oceanog. 13 (1968) 515.
[11] I. McKelvie, B.T. Hart, Analyst 114 (1989) 1459.
[12] M.D. Ron Vaz, M.C. Edwards, A.C. Shand. M.S. Cresser, Talanta 39 (1992) 1487.
[13] K. Kerouel, A. Aminot, Anal. Chim. Acta 318 (1996) 385.
[14] A.C. Javier, S.R. Crouch, H.V. Malmstadt, Anal. Chem. 40 (1968) 1922.
[15] S.R. Crouch, H.V. Malmstadt, Anal. Chem. 39 (1967) 1089.
[16] J.B. Rodriguez, J.R. Self, P.N. Soltanpour, Soil Sci. Soc. Am. J. 58 (1994) 866.
[17] B. Karlberg, G.E. Pacey, Flow Injection Analysis–A Practical Guide, Elsevier, Amsterdam, 1989, p. 372.
[18] R.L. Benson, I. McKelvie, B.T. Hart, Y.B. Truong, I.C. Hamilton, Anal. Chim. Acta 326 (1996) 29.
[19] B. Rabenlange, A.B. Bendtsen, S.S. Jorgensen, Commun. Soil Sci. Plant Anal. 25 (1994) 3241.
[20] C. Ciavatta, L.V. Antisari, P. Sequi, J. Environ. Quality 19 (1990) 761.
[21] W. Frenzel, F. Titzenthaler, S. Elbel, Talanta 41 (1994) 1965.
[22] H. Onishi, D.J. Elving, J.D. Winefordner (Eds.), Photometric Determination of Traces of Metals. In: Chemical Analysis, Vol. 3, Part IIA, Wiley, New York, 1990.
[23] J.F. Ferguson, J. Gavis, Water Res. 6 (1972) 1259.
[24] M.S. Cresser, K. Killham, T. Edwards, Soil chemistry and its application, Cambridge University Press, 1993, p. 10.
[25] M.S. Cresser, K. Killham, T. Edwards, Soil chemistry and its application, Cambridge University Press, 1993, p. 151.
[26] S. Kuo, E.J. Jellum, Soil Sci. 158 (1994) 124.
[27] D.A. House, Chem. Rev. 62 (1962) 185.

ELSEVIER

Talanta 45 (1997) 57–74

Talanta

Quantitative calibration of vapor levels of TNT, RDX, and PETN using a diffusion generator with gravimetry and ion mobility spectrometry

G.A. Eiceman [a,*], D. Preston [a], G. Tiano [a], J. Rodriguez [a], J.E. Parmeter [b]

[a] *Department of Chemistry and Biochemistry, New Mexico State University, Las Cruces, NM 88003, USA*
[b] *Department 5848, Sandia National Laboratory, Albuquerque, NM 87185-0782, USA*

Received 22 November 1996; received in revised form 31 March 1997; accepted 31 March 1997

Abstract

A prototype generator for creating a continuous stream of explosive vapor was referenced quantitatively both to a standard weight from the National Institute of Standards and Technology (NIST) and to the response of an ion mobility spectrometer. Vapors from solid explosive, in a precision bore glass tube at constant temperature, diffuse into an inert gas flow. Mass output rates were determined by (1) sample temperature, and (2) sample tube dimensions (length and cross-sectional area). A reference to NIST was achieved gravimetrically though a microbalance calibrated with a reference weight; mass output rates were obtained for 2,4,6-trinitrotoluene (TNT), cyclotrimethylenetrinitramine (RDX) and pentaerythritol tetranitrate (PETN) at three or more oven temperatures between 79°C and 150°C. The mass output rate was stable over hundreds of hours of continuous operation and the output was adjustable from a few picograms per second to several nanograms per second through variation of the oven temperature. An independent calibration of the vapor generator for TNT at 79°C using an ion mobility spectrometer matched exactly the gravimetric-based findings. In most instances, measured mass output rates compared favorably with theoretically calculated mass output rates, with discrepancies in a few cases resulting primarily from uncertainties in terms (vapor pressures and diffusion coefficients) used to perform the calculations. Agreement is generally not good for PETN, where molecular decomposition contributed to higher than expected measured mass outputs. © 1997 Elsevier Science B.V.

Keywords: TNT; RDX; PETN; Vapor generator

1. Introduction

Security in mass transportation has been a motivation throughout the last two decades in the development of ultra-trace analytical techniques for monitoring explosives [1]. Several technical approaches to this challenge have been explored and some suitable methods have been placed into operation in field-monitoring venues for screening packages, cargo, or vehicles. In contrast, the screening of humans for explosive residues has

* Corresponding author. Fax: +1 505 6466094; e-mail: geiceman@nmsu.edu

PII S0039-9140(97)00107-0

followed a comparatively slow development and present strategies combine trace chemical detectors with walk-through portals [2,3]. All technologies for field monitoring of explosives, to ensure proper operation, require in-field calibration using a stream of sample vapors of known composition. This is a daunting challenge given the chemical and physical properties of explosives [4], and thus several designs of prospective vapor generators have been described [5–8]. However, these generators have been unsuitable, on the whole, for creating continuous and quantitative vapor levels of explosives with direct links to a primary standard from the National Institute of Standards and Technology (NIST). The goal of the work described here was the creation of an explosive vapor generator with a calibrated mass output and verified explosive vapor purity. A prototype vapor generator was fabricated in which mass losses from a reservoir of explosive were determined gravimetrically with a micro-balance which was calibrated with a standard weight. These results were referenced to findings for TNT only from a second method of calibration which was independent of the gravimetric procedure and was completed at a separate facility. The energies of activation for TNT, RDX, and PETN were determined from mass outputs at several temperatures. Finally, the vapor stream was assayed by ion mobility spectrometry (IMS) and atmospheric pressure chemical ionization mass spectrometry to validate the chemical composition for the mass output studies.

Vapor generators for explosives share common principles which are found in the relationships between temperature and vapor pressure of the chemical as described in Section 2. Discrete mode generators typically involve the thermal desorption of a measured amount of explosive from a surface and are characterized by low cost and convenient operation. Accurate discrete generators have been developed [6]; however, such generators are not capable of producing, quantitatively, continuous vapor streams for extended periods. Such generators also may be prone to systematic errors from uncontrolled losses of material due to variances in desorbing surfaces, thus affecting output stability and reproducibility. The alternative to discrete mode generators is the continuous vapor generator from which the whole flow or only portions may be sampled. In such generators, a small amount of explosive is placed in a sample reservoir, a glass tube in this work, which is thermostatted and placed in a flowing stream of air or nitrogen gas. Under these conditions, the flux of explosive from the generator should be controlled by the sample temperature and by the dimensions of the sample container or glass tube. Under such conditions, even the total amount of explosive in the tube is not important when the distance between the sample and tube end is long enough to be regarded as constant throughout sample losses (as an approximation, the space occupied by the sample should be less than 5% of the total length of the tube). Finally, adsorptive losses to surfaces in such a generator should be negligible after several hours of operation to passivate adsorptive sites. In designs of such generators with pulsed mode sampling, the output rate and pulse time should be independently variable.

In continuous vapor generators, where chemical is contained at the bottom of a glass tube and diluent gas is passed over the open end of the tube, the mass output at steady-state should follow Eq. (1):

$$\text{Output} = \frac{D_a A N_0}{L} \tag{1}$$

where D_a is diffusivity of the explosive in $cm^2\ s^{-1}$, A is cross-sectional area of the sample tube in cm^2, N_0 is vapor phase concentration (in mass/volume, e.g. pg cm^{-3}) at steady-state, and L is length (in cm) of the sample tube. The diffusion coefficient is expected to be proportional to $T^{3/2}$ (in K) and inversely proportional to ambient pressure [9].

2. Theory of vapor generation

Mass transfer or mass output in a vapor generator arises from the chemical potential towards an equilibrium between a solid or liquid in contact with an inert gas flowing over the sample. Mass transfer can be described by the following equations and the subsequent derivations [10]:

$$\Psi_z = -\delta \frac{d\Gamma}{dz} \quad (2)$$

where Ψ_z is the output over variable z, $-\delta$ is a proportionality constant, and $d\Gamma/dz$ is the rate of change with respect to z. Eq. (2) can be arranged to Fick's Law, as in Eq. (3):

$$J^*_{Az} = -D_{AB} \frac{dc_a}{d_z} \quad (3)$$

where J^*_{Az} is the molar flux of component A in the z direction due to molecular diffusion in mol A s^{-1} cm^2, D_{AB} is the molecular diffusivity of the molecule A in the gas B in cm^2 s^{-1}, and c_a is the gas phase concentration of A in mol m^{-3}. The term D_{AB} is the most difficult term to obtain by experiment or calculation and is given in Eq. (4) [9]:

$$D_{AB} = \frac{1.8583 \times 10^{-7} T^{3/2}}{P\sigma^2_{AB}\Omega_{D,AB}(1/M_A + 1/M_B)} \quad (4)$$

where P is absolute pressure in atmospheres, T is temperature in Kelvin, M is molecular weight, σ is average collision diameter, and Ω is collision integral based on the Leonard–Jones potential. A practical method for determining D_{AB} is shown in Eq. (5) [11]:

$$D_{AB} = \frac{1.00 \times 10^{-7} T^{1.75}(1/M_A + 1/M_B)^{1/2}}{P\left[\left(\sum v_a\right)^{1/3} + \left(\sum v_b\right)^{1/3}\right]^2} \quad (5)$$

where Σv is the sum of the structural volume increments for the molecule A and the gas B, as obtained from reference values [9].

In practice, the loss of mass from a vapor generator is obtained in mass versus time plots during continuous operation of the vapor generator. These plots should be linear and provide mass outputs in mass per unit time (e.g. pg s^{-1}) at a specific temperature and specific generator parameters. The plot of ln(mass loss rate) versus $1/T$ should also lead to a linear curve with a slope equal to $-E_a/R$ where E_a is the energy of sublimation or vaporization and R is the universal gas constant.

3. Experimental

3.1. Instrumentation

3.1.1. Vapor generator

A vapor generator, designed and built at Varian (Palo Alto, CA), comprised a sample container, heated block to thermostat the sample container, temperature controllers for all surfaces of the vapor generator, and a gas flow controller as shown in Fig. 1. The sample container was a precision-made glass tube with an inner diameter of 0.47 cm and length of 10 cm; these tubes are commonly available for nuclear magnetic resonance instruments. Gas flow was provided using pressurized nitrogen gas (99.9% purity) and a Model UFC-1020 mass flow control (Unit Instruments, Orange, CA); the nitrogen flow rate was confirmed as 130 ml min^{-1} using a bubble flow meter. Daily variations in flow rate were less than 1 ml min^{-1}. Thermal control of the sample chamber was accomplished through four Omega Engineering Model DP371 series digital temperature controllers (Omegalux, Stamford, CT). The four regions of the generator were equipped with individual controllers as shown in Fig. 1, and included inlet, sample container, diffusion, and outlet regions. Temperature accuracy was better than ± 1.5°C and a single high-precision Omega Engineering temperature meter allowed each region to be monitored to ± 0.01°C. Temperature deviations were estimated as ± 0.05°C.

In one configuration, full sampling of the vapor generator flow, the outlet flow was directed fully into an atmospheric pressure chemical ionization tandem mass spectrometer, a fume hood, or a cold trap. The cold trap was a 50 cm × 6 mm outer diameter × 4 mm inner diameter borosilicate glass tube with U-shape to fit a 1 liter Dewar flask cooled with dry ice and acetone. In a second configuration, a switch box was added to the outlet flow so the vapor stream could be diverted, in a controlled and timed manner, into an ion mobility spectrometer. Any excess flow was vented to a fume hood. This second configuration was called the discrete mode of sampling.

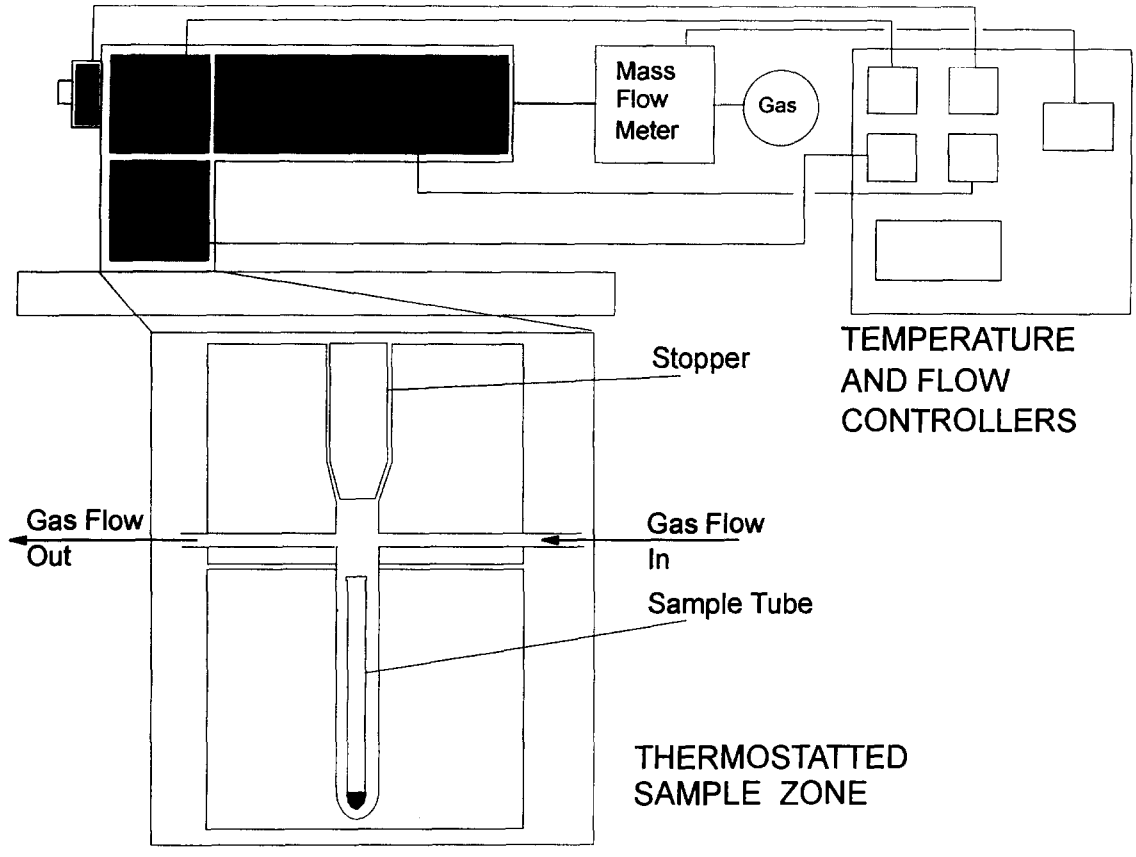

Fig. 1. Schematic representation of the Varian explosives vapor generator. Four zones are independently thermostatted and gas flow is delivered using a mass flow meter. Vapors are swept out of the generator through a heated outlet zone. All inner surfaces are glass.

3.1.2. Microbalance

An AD-6 microbalance (Perkin Elmer, Norwich, CT) was used to determine mass of the sample and container. The scale was operated at ambient conditions and located on a vibration-arrest platform (Eberbach, Ann Arbor, MI). The platform and the scale frame were both grounded through a nearby electrical outlet. The scale electronics were continuously powered for long-term, high stability.

3.1.3. Analytical instruments

Several instruments were utilized to monitor the purity of explosives including a Model 6000 high-performance liquid chromatography (HPLC) system (Waters Associates, Milford, MA), a Model 5890A gas chromatograph (Hewlett-Packard, Avondale, PA), and a Model 5971 gas chromatograph/mass selective detector (Hewlett-Packard). The HPLC system was operated according to a standard method [12] and was equipped with a 25 cm reverse phase column (Supelcosil LC-18; Supelco, Bellefonte, PA), Model 440 absorbance detector (Waters Associates) set to 254 nm wavelength, and an Axxi-Chrom 727 Chromatographic Data Station (Axxiom Chrom., Calabasas, CA). The HPLC system was operated at isocratic solvent conditions with 50% methanol in water at 5 ml min^{-1}. The gas chromatograph was equipped with a flame ionization detector (250°C), automated splitless injector (150–250°C), and 15 m SPB-5 capillary column (Supleco, Bellefonte, PA). The conditions for analysis by gas chromatography (GC) were: initial temperature, 100°C; temperature ramp, 5°C min^{-1}; final temperature, 250°C. The gas chromatograph/mass spectrome-

ter was operated under identical chromatographic conditions. The mass spectrometry (MS) conditions were: initial mass, 45 amu; final mass, 600 amu; scan rate 330 amu s^{-1}. Other conditions were established by default from automatic tuning of the instrument.

A TAGA 6000 tandem mass spectrometer (Sciex, Toronto, Ontario, Canada) was coupled with an ion mobility spectrometer for chemical characterization of the gas stream from the vapor generator. The ion mobility spectrometer was designed and built in-house and was crafted from Series 502-1100 machinable ceramics (Aremco Products, Ossining, NY) with a porcelain drift tube. The drift tube was 7 cm long × 2 cm diameter (Coors Ceramics, Golden, CO) and was connected by flanges to detector and ion source shutter assemblies. The voltage on the complete drift tube was 2.5 kV for a drift region field of 357 V cm^{-1}. The drift gas was bottled nitrogen at 400 ml min^{-1}. Electronics for the ion mobility spectrometer were also designed and constructed in-house and consisted of a high voltage power supply to create the electric field for the drift tube, and a gating pulse unit to inject packets of ions into the drift region. The ion mobility spectrometer was attached to the interface flange of the TAGA 6000 using a Teflon® adapter to the interface assembly of the tandem mass spectrometer in a configuration so that ions from the IMS drift tube would be sampled into the lens assembly of the tandem mass spectrometer. The ion shutters of the IMS drift tube were inactivated (i.e. opened) so maximum ion intensities were delivered into the mass spectrometer. Drift gas flows were unidirectional and were added at the Teflon® adapter. A plenum gas flow protected the pinhole vacuum barrier from contamination and particulate that could block the pinhole and stop ion passage into the MS. Fifty mass spectra scans were averaged to obtain a mass spectrum. The last conducting ring in the drift region was placed at 1400 V and the interface plate was placed at 650 V. Sample was introduced into the ion source region of the IMS drift tube. The ion mobility spectrometer was operated at 160°C and ambient pressure (660 torr). The instrumental parameters for mass identification of ions and for collision induced dissociation with the tandem mass spectrometer were routine values [13].

An ion mobility spectrometer (Model 100; PCP, W. Palm Beach, FL) was used for experiments with the pulse mode sampling of the vapor generator at Sandia National Laboratories in Albuquerque, NM. The drift tube was 8 cm in length and 4.25 in diameter and was equipped with a 10 mCi ^{63}Ni source and methylene chloride reagent gas. The inlet and housing temperatures were both 147°C and the electric field gradient was 375 V cm^{-1}. Other experimental parameters include drift gas flow of 426 ml min^{-1} and carrier gas flow of 20 ml min^{-1}. The vapor generator was operated with specific parameters for these measurements and included the generator temperatures which were, by zone, oven, 79°C; outlet, 86°C; carrier, 79°C; and mixing chamber, 81°C. The flow rate was 174 ml min^{-1} of purified air. Pulse times for sampling the vapor stream were 0–30 s and these were timed manually.

3.2. Materials

3.2.1. Chemicals and solvents

Samples of TNT, RDX, and PETN were obtained from PANTEX (Amarillo, TX) and were batch numbers 86B-002-24728, 94244-DMC 3050-01, and 7119-304M-01, respectively, These explosives were assayed using HPLC, GC, and GC/MS to ascertain the presence of impurities. Explosives were prepared and analyzed as fresh solutions with concentrations of roughly 2 μg μl^{-1}. Trace impurities were found in each sample at comparatively low levels. The amounts of impurities were estimated using a common response factor for all peaks. With this approximation, the TNT was shown (by GC/MS) to be 99.9% or greater in purity; the RDX and PETN were found (by HPLC) to be 95% pure. Nitrogen gas used for the vapor generator was 99.9% purity with approx. 600 ppm humidity and was used without further treatment. Methanol, used in the liquid chromatograph, was HPLC grade (Fisher Scientific, Pittsburgh, PA).

3.3. Procedures

3.3.1. Preparation of sample

Small amounts of sample (PETN, RDX, or TNT) were placed into a sample tube and weighed on a Mettler type H6 analytical scale to make an approximation of the initial mass of sample. Solvent cleaned forceps were used at all times when handling a sample tube and 10–20 mg of sample were placed in the sample tube. The sample tube was placed inside an ordinary test tube to facilitate handling. The tube was tapped slightly on the side with forceps to place the explosive at the bottom of the tube. The sample tube was inserted into the vapor generator through an access port (see Fig. 1) and the port was closed with a glass plug. The vapor generator was operated continuously with pre-set gas flows and temperatures.

3.3.2. Gravimetric determination of sample mass output rates

Measurements of mass output rates for TNT, RDX, and PETN were made continuously from April 1994 to March 1996 and all experiments followed a common plan. That plan involved gravimetric measurements of the sample and container at time intervals after the introduction of the sample tube into the vapor generator. In nearly all instances, the generator was operated for 24–48 h with a sample before the first mass determination was made. This allowed for equilibration of all surfaces where sample vapors flowed and removal of highly volatile impurities, if present, either in the sample or sample tube. After an initial mass reading was obtained, further readings were made on a daily basis or several times a day. Special attention was given to calibrating the microbalance with a NIST standard mass at each weighing and to the manipulation of the sample container for the determination of losses in sample mass.

3.3.3. Microbalance procedures

The sample tube was removed from the vapor generator using stainless steel forceps and the sample tube placed inside a test tube for storage and equilibration to room temperature. Weights totaling 2.400 g (the approximate mass of the sample tube) were loaded using plastic forceps on both pans of the microbalance which was then autotared to 0.000 mg after a period of 30 min. A 10.000 mg calibrating weight (cat. no. 1207; Cahn Instrument Co., ATI Mattson, and Cahn, Madison, WI) was placed on the scale and the scale was allowed to come to rest in about 30 min. Next, one set of tare weights with the calibration weight was removed and replaced by the sample tube which was positioned lengthwise on the scale; the scale was allowed to come to rest and the digital reading was stabilized usually after a few hours. The mass reading was recorded and the sample tube was removed from the scale and returned to the vapor generator; the delay in mass determinations was noted and used to correct total times of operation. The tare and calibration weights were restored to the scale and used to certify scale accuracy to the calibrating weight and thus to an NIST primary standard. If the NIST calibration check varied more than 5 micrograms from the original 10.000 mg setting the weighing was invalidated. Next, the calibrating weight was removed from the scale and the tare weight was verified. If the tare weight varied more than 5 micrograms from the original tare of 0.000 mg, the weighing was invalidated.

3.3.4. Determination of vapor generator mass output rate using IMS

In these experiments, the vapor generator output was diverted into the PCP Model 100 IMS analyzer for time intervals ranging from 5 to 30 s. The resulting signals from these experiments (i.e. product ion intensity versus time) were integrated and plots of vapor output (in arbitrary units) versus pulse time were linear. Calibration of the IMS analyzer was obtained by placing, with a microliter syringe, measured amounts of explosive in acetonitrile solution onto a Pyrex tube (probe). The solvent was evaporated in air and the probe was placed directly into the IMS analyzer where the explosive was evaporated for the measurement. This was completed for mass levels from 0.1 to 1 ng and the resulting linear plot was used to obtain vapor levels from the pulsed mode sampling.

4. Results and discussion

4.1. Gravimetric determination of mass output for TNT, RDX, and PETN

Output in mass against time was observed for explosives in the vapor generator at specific temperatures between 79°C and 150°C; the results are shown in Figs. 2–4 and tabulated in Table 1. In Fig. 2, plots of mass output results are shown for TNT from 79°C to 150°C including replicate experiments at 120°C. The mass output was shown to be linear with time at each temperature and the mass output rates varied from 84 pg s^{-1} at 79°C to 13 ng s^{-1} at 150°C.

Similar results for RDX are plotted in Fig. 3 where mass output rates ranged from 49 ± 12 pg s^{-1} at 110°C to 2.3 ± 0.57 ng s^{-1} at 150°C. The generator temperatures used for RDX were greater than those used with TNT to obtain comparable mass output rates owing to the relatively low vapor pressure of RDX (R. Stimac, personal communication). Although the replicate findings are limited, there was a suggestion that scatter with findings for RDX (RSD of approx. 25%) was greater than that for TNT (RSD of 8% at 120°C). In Fig. 4, mass output results are shown for PETN at 110°C, 120°C, and 125°C including replicate experiments at 110°C. The mass output rates for PETN were also linear with time at each temperature and the mass output rates varied from 170 pg s^{-1} at 100°C to 2.6 ng s^{-1} at 125°C. The vapor pressure for PETN is comparable to RDX and much smaller than TNT (R. Stimac, personal communication). Consequently, the mass output experiments were comparable in duration to the studies with RDX. However, the mass output for PETN at 125°C was extraordinarily large compared to that for RDX at 129°C. Even at 110°C, the mass output for PETN was three to four times greater than that for RDX and at

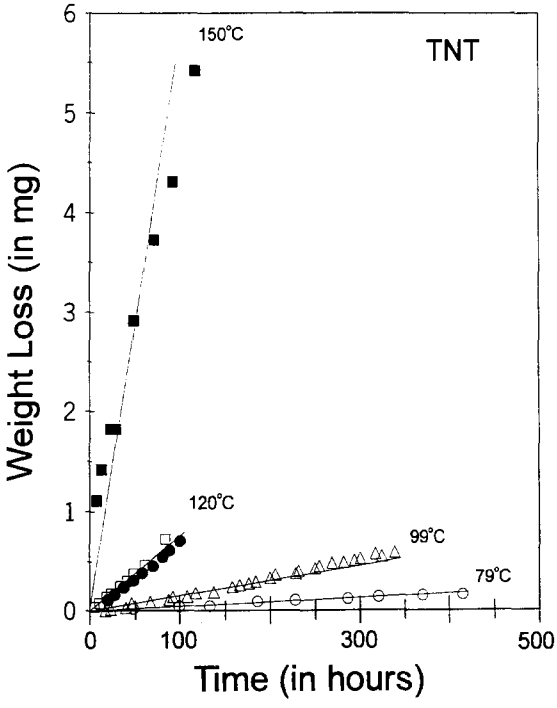

Fig. 2. Mass output for TNT at different temperatures. Each experiment including replicate experiments at a single temperature are given unique symbols: 150°C (■), 120°C (●, □), 99°C (△), 79°C (○).

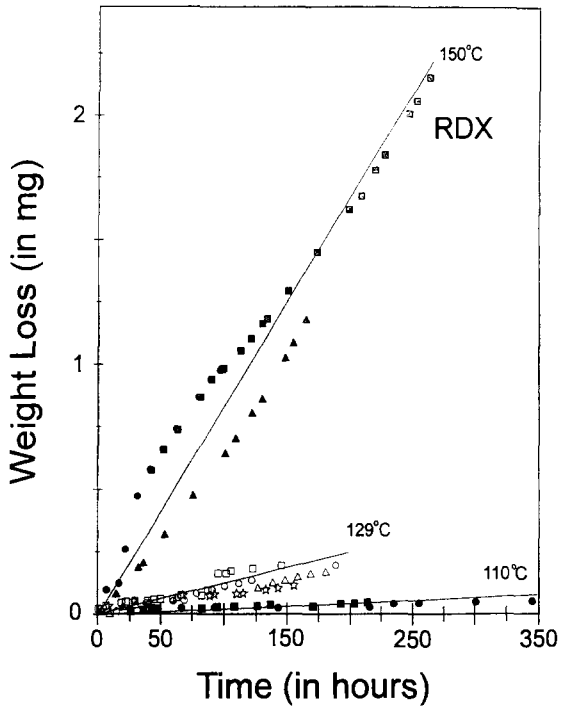

Fig. 3. Mass output for RDX at different temperatures: 150°C (shaded triangle, shaded square, shaded circle), 129°C (△, ☆, ○, □), 110°C (●, ■).

125°C the output for PETN was more than ten times that for the average RDX output at 129°C. These differences suggested that molecular decomposition of PETN was occurring under these conditions.

In Fig. 5, van't Hoff plots (i.e. ln(mass output rate) against $1/RT$) are shown for TNT, RDX, and PETN. Values for the energy of activation (E_a) and the pre-exponential factor (k) were obtained from the curves through regression analysis (see Table 2). The values for E_a and k were 87 kJ mol^{-1} and 34.4 pg s^{-1} for TNT, 131 kJ mol^{-1} and 44.9 pg s^{-1} for RDX, and 233 kJ mol^{-1} and 78.6 pg s^{-1} for PETN. The percent relative standard errors for E_a values were 2.5, 5.9 and 9.9 for TNT, RDX, and PETN, respectively. The percent relative standard errors for the pre-exponential factors were 2.0, 5.2, and 7.2 for TNT, RDX, and PETN, respectively. In short, the relative standard error in the linear regressions was better than 10% for slopes and intercepts in all plots. The most notable feature in Fig. 5 is slope of the plot for PETN (reflected in the E_a value) which was abnormally large compared to those for TNT and RDX. Since the precision for values for Ea was within the range of 10–25%, this difference was not a statistical artifact and can be attributed to chemical decomposition of PETN. This was consistent with the output rates (see above) and literature reports that PETN decomposes above 100°C. Thus, generation of PETN should be reserved to temperatures below 100°C where vapor pressures are very low; however, practical handling of the resulting low mass levels will be difficult.

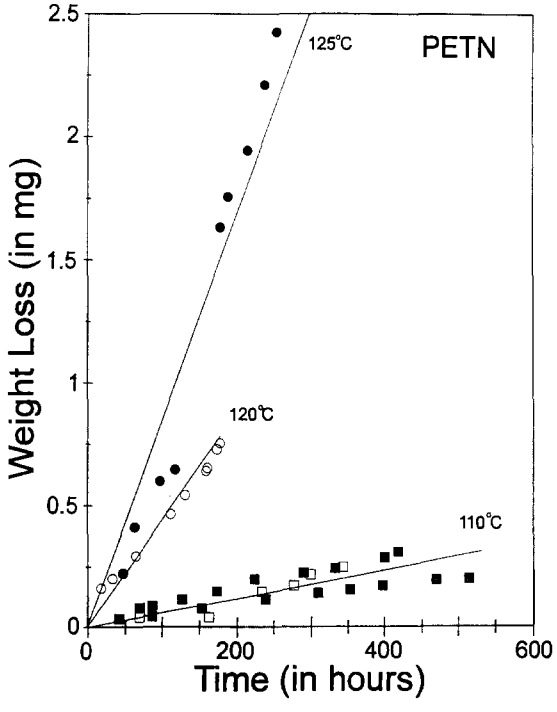

Fig. 4. Mass output for PETN at different temperatures: 125°C (●), 120°C (○), 110°C (□, ▩, ■).

4.2. Vapor generator mass output for TNT using IMS

Results obtained with pulsed mode testing with TNT are shown in Figs. 6–8. In Fig. 6, the integrated results from IMS response versus time are shown for different pulse times with the sample at 79°C. Results are plotted from replicate ($n = 4$) determinations at each pulse time and for 0–30 s pulse times in 5 s increments. The curve was linear and R^2 was 0.991. All points fell on the line within experimental error except points for the pulse time of 5 s, where values were consistently low. This systematic error resulted from the flow switching event. During the first 1–2 s, residual volume in the flow line contains little explosive vapor and this systematic error was particularly evident for the short sampling time of 5 s. Thereafter, the error became negligible.

The calibration of the ion mobility spectrometer using standard solutions and a direct desorption in the IMS drift tube is shown in Fig. 7 for four replicate measurements at each amount of TNT from 0.1 to 0.8 μg. This plot was also linear with $R^2 > 0.98$ and can be used to provide a mass output rate. When combined with the results in Fig. 6, the mass output for TNT was calculated as 85 ± 5 pg s^{-1} and this was in remarkable agreement with the gravimetric-based mass loss experiments. The agreement between two wholly independent methods suggested a robust and reliable performance of the vapor generator under these conditions (TNT at 79°C). Further studies

Table 1
Summary of mass loss for vapor generation of explosives

Explosive	Temperature (°C)	Mass loss (mg)	Time (h)	Mass loss rate (pg s^{-1})
TNT	79	0.126	415.0	84.4
	99	0.604	339.1	495
	120	0.688	84.6	2260
	120	0.732	101.0	2010
	150	5.400	115.7	12960
RDX	110	0.045	215.4	58
	110	0.052	346.4	41
	129	0.197	147.3	372
	129	0.115	156.5	204
	129	0.164	181.6	251
	129	0.199	190.4	289
	150	1.054	98.0	2989
	150	1.124	166.3	1877
	150	2.090	264.3	2197
PETN	110	0.312	417.7	207
	110	0.215	515.7	116
	110	0.239	345.3	192
	120	0.740	177.6	1160
	125	2.350	254.7	2563

at temperatures of 99°C and 120°C were impossible owing to a saturated response of the IMS analyzer at vapor concentrations for those temperatures.

While the chemical integrity of the vapor stream is described in detail in the next section, the ion mobility spectra taken from the pulsed mode sampling studies did not demonstrate any measurable decomposition or contamination of the TNT. Ion mobility spectra are shown in Fig. 9 (frames a–c) in waterfall presentation. In frame A, ion mobility spectra are shown for the background response without TNT vapors directed into the IMS drift tube. Methylene chloride was used as the reagent gas and the intense (off-scale) peak on the left of the spectrum was Cl^-. The remaining two peaks are environmental artifacts that have no apparent consequence in this work. The ion mobility spectrum in frame C, results when TNT from the vapor generator (79°C) is pulsed directly into the ion mobility spectrometer. Identical spectra were obtained (not shown) when vapors from solid TNT at room temperature were presented to the ion mobility spectrometer. The peak that resides between the cursors at 12.05 ms is the parent ion for TNT, a deprotonated M^- species. Noteworthy in this spectrum is the absence of any other peaks that might exist as impurities or decomposition products such as 2,4-dinitrotoluene (shown as a peak at 11.4 ms in the ion mobility spectra in frame b, Fig. 9). This was observed at all temperatures investigated up to 120°C. These findings suggest that TNT is not undergoing significant (i.e. measurable) decomposition and the assay of purity of 99.9% made in this study is consistent with these ion mobility spectra.

4.3. Chemical composition of sample from the vapor generator by IMS/MS

Initial attempts to verify the chemical integrity of sample flow from the vapor generator involved cryogenic trapping of flow with analysis of the trapped material by GC, GC/MS, and HPLC. The results for TNT were of uniformly high quality and demonstrated that the chemical stability of TNT was maintained to temperatures over 150°C

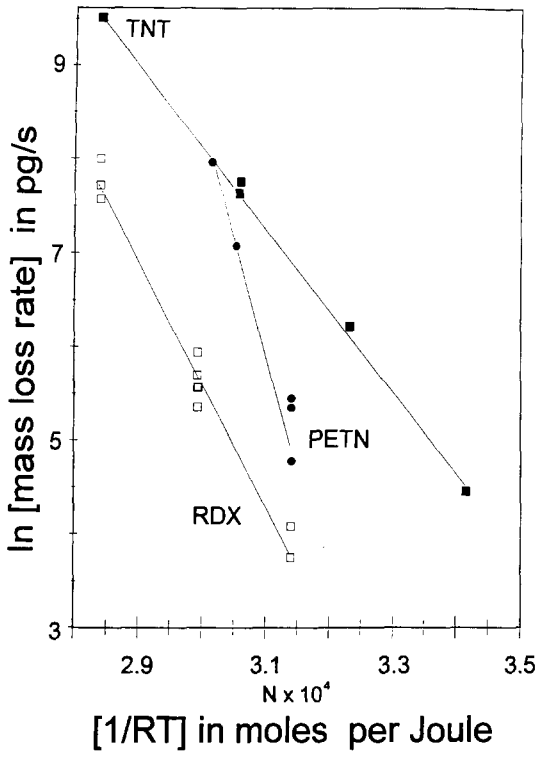

Fig. 5. Plots of ln(mass loss) versus $1/RT$ for TNT (■), RDX (□), and PETN (●).

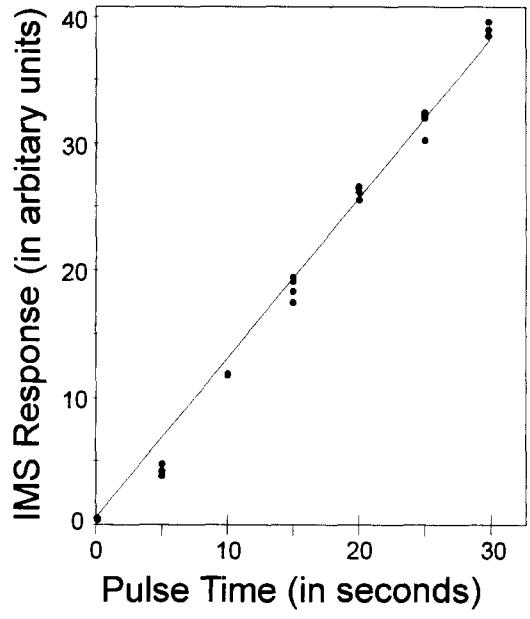

Fig. 6. Plots of IMS response to TNT pulsed from the vapor generator at 79°C. Response was obtained by integrating plots of the peak intensities for the product ion of TNT in the negative mode (see Fig. 8) versus time.

in nitrogen gas. However, the determination of parent peaks and decomposition products for RDX and PETN became problematic and decomposition peaks were not identifiable even though decomposition was noticeable at temperatures of 125°C and above. An ion mobility spectrometer/mass spectrometer was used to probe the degree to which chemical decomposition might have occurred, mindful of the complications that arise from ionization mechanisms at atmospheric pressure. Each explosive was characterized under con-

Table 2
Statistics of regression analysis

	TNT	RDX	PETN
r^2 from linear regression	0.9982	0.9759	0.9709
Root mean square error	0.0922	0.2556	0.2617
Intercept (k)			
Coefficient	34.42	44.93	78.60
Standard error	±0.6712	±2.32	±7.25
Slope (E_a)			
Coefficient	87.52	131.06	233.99
Standard error	±2.15	±7.79	±23.38
F(1,residual)	$F(1,3) = 1664$	$F(1,7) = 283$	$F(1,3) = 100$
P	<0.001	<0.001	0.0021
Upper 95% confidence for slope	94.35	149.05	308.40
Lower 95% confidence for slope	80.69	112.64	159.59

ditions of (1) no reagent gas where the reactant ion was free near-thermal energy electrons and (2) methylene chloride reagent gas where the reactant ion was Cl^- in nitrogen gas with the drift tube at 125°C.

The mass spectra from IMS/MS characterization of TNT from the vapor generator are shown in Fig. 9 and demonstrate an $M-1^-$ species with thermalized electrons (top frame) and a preponderance of $M-1^-$ with Cl^- reagent ions (bottom frame). Small amounts of M^*Cl^- were observed though no impurities such as dinitrotoluene were observed. This was internally consistent with the pulse sampling studies using IMS and with the energy of activation of the van't Hoff plots for TNT. In short, the chemical integrity of TNT through the vapor generator was good with moisture in the nitrogen of approx. 10 ppm.

Results for RDX are shown in Fig. 10 where an abundant ion peak was observed at m/z 258 and minor peaks were observed in the spectrum above baseline. These small peaks could arise from ionization mechanisms and also from minor amounts

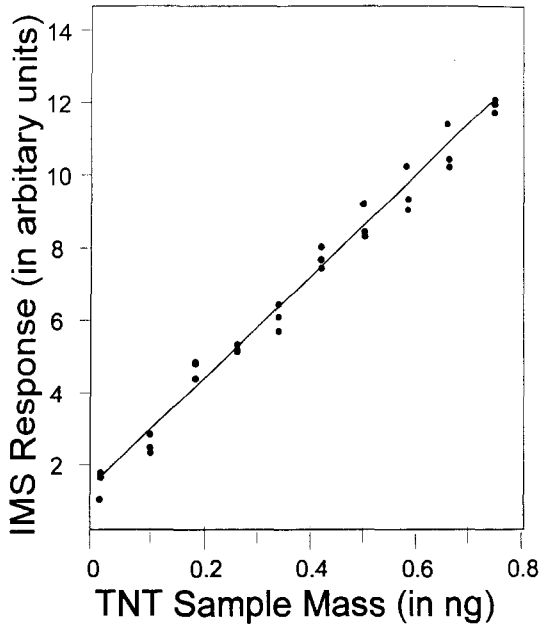

Fig. 7. Plots of IMS response to known amounts of TNT from standard solutions. See legend for Fig. 6.

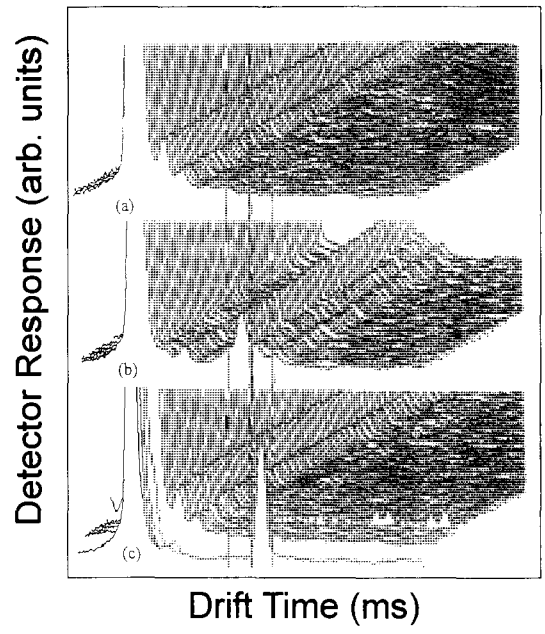

Fig. 8. Plots of IMS spectra in negative polarity from (A) the reagent gas of methylene chloride in nitrogen, (B) a sample of 2,4-DNT placed near the IMS inlet, and (C) vapors of TNT from the vapor generator with pulsed flow. The drift times for the product ions were 11.40 ms for 2,4-DNT (frame B) and 12.05 for TNT (frame C).

of thermal decomposition. The major peak was subjected to collision induced dissociation and was shown to be a cluster of RDX with two molecules of water, that is $M^*(H_2O)_2^-$. The use of chloride as the reactant ion created some minor amounts of fragmentation seen at m/z 89 ($C_2H_4N_2O_2^-$) and the two hydrate cluster of this ion at m/z 125. Nonetheless, the ionization of RDX seemed robust and evidence of weak chemical decomposition was noted in nitrogen at 125°C. This was also internally consistent with the results where the rate of loss was slightly higher than anticipated, possibly due to minor amounts of decomposition.

The mass spectra for PETN with reactant ions of thermal electrons and chloride ions are shown in Fig. 11, top and bottom frames respectively. In the top frame, PETN with thermal electrons showed complex ion species with the largest ion the $M^*NO_3^-$ ion and significant amounts of NO_3^-. The NO_3^- might have come from fragmentation

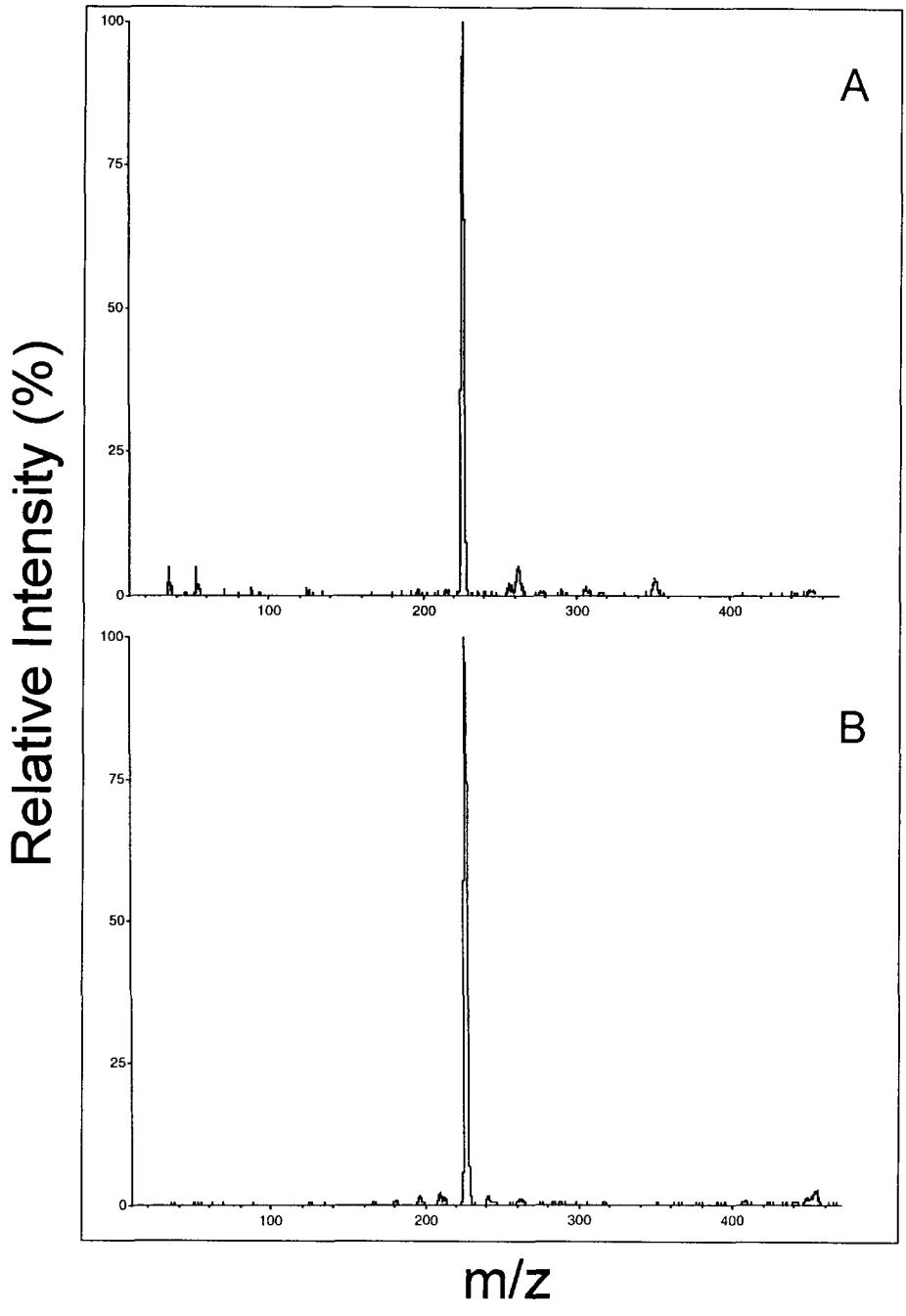

Fig. 9. Mass spectra from IMS/MS characterization of TNT at 1.6 ppm in a continuous stream of nitrogen without (A) and with (B) methylene chloride reagent gas.

of M, though the large intensity of $M^*NO_3^-$ is suggestive, but not proof positive, of thermal decomposition of PETN in the vapor generator. Molecular forms of the chemical are present in abundance in the form of $M^*(H_2O)_n$ and $M^*NO_3^-$ ions, but the large amount of NO_3^-

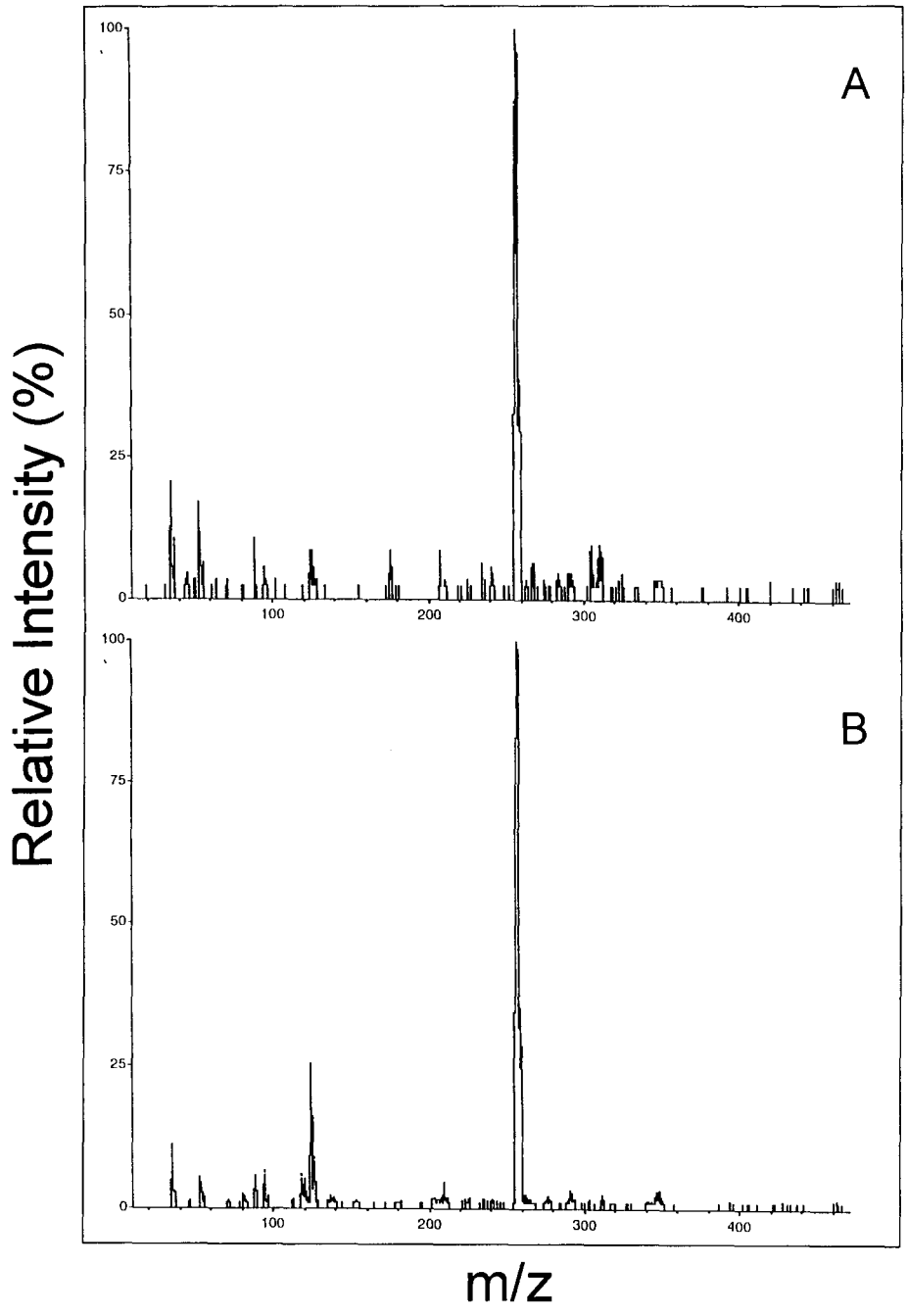

Fig. 10. Mass spectra from IMS/MS characterization of RDX at 1.5 ppm in a continuous flow of nitrogen without (A) and with (B) methylene chloride reagent gas.

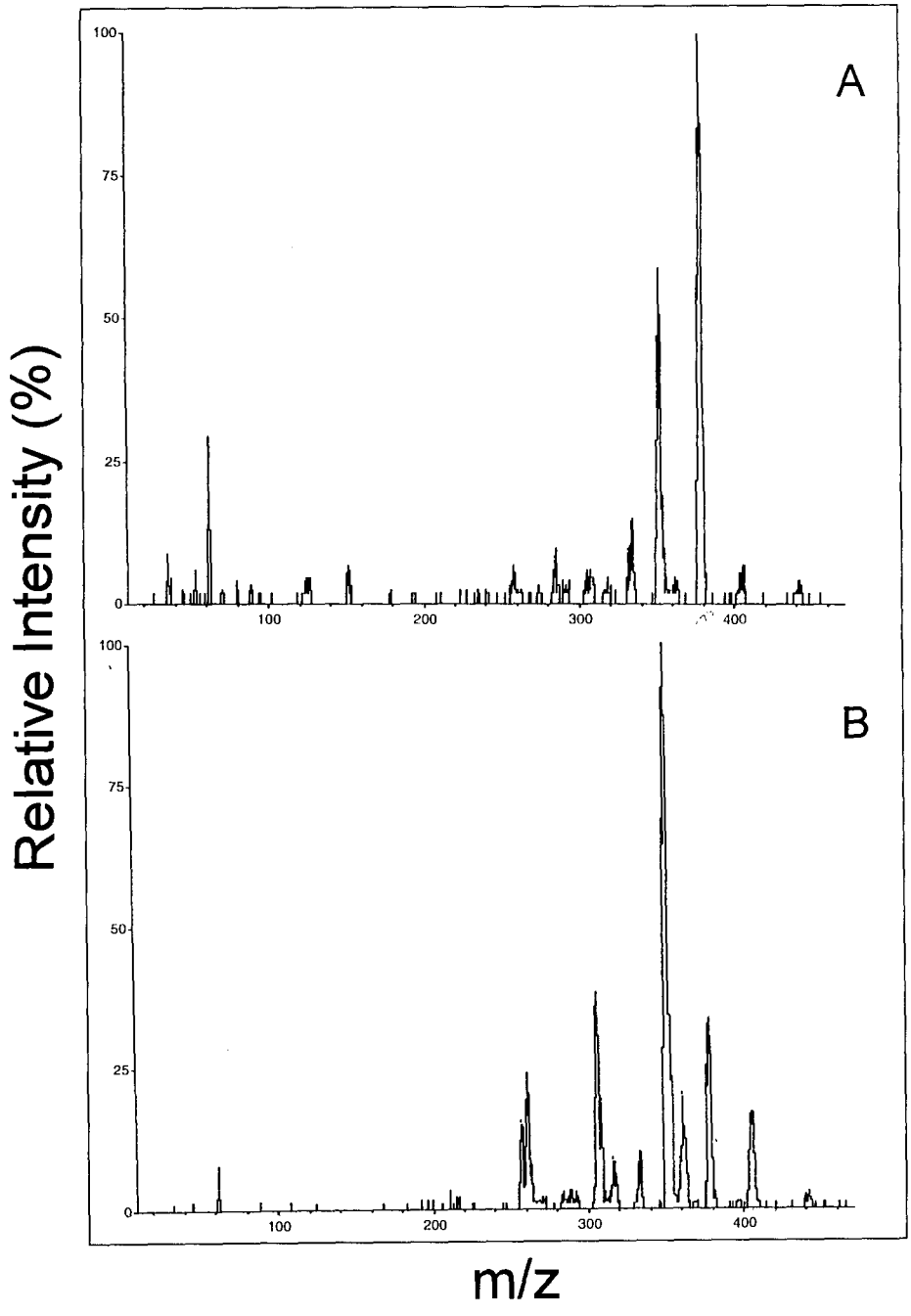

Fig. 11. Mass spectra from IMS/MS characterization of PETN at 1.1 ppm in a continuous flow of nitrogen without (A) and with (B) methylene chloride reagent gas.

Table 3
Calculated values for D_{AB} based on Eq. (4) in text

D_{AB} ($cm^2\ s^{-1}$)	79°C	99°C	110°C	120°C	125°C	129°C	150°C
TNT	0.0982	0.108	0.114	0.119	0.122	0.124	0.135
RDX	0.117	0.129	0.136	0.142	0.145	0.148	0.161
PETN	0.0933	0.103	0.108	0.113	0.116	0.118	0.129

available for reaction with sample vapor to form $M^*NO_3^-$ may have occurred through thermal decomposition of PETN. Thus, these results do not alone prove serious thermal decomposition of PETN in the vapor generator, but certainly are consistent with the extraordinarily large mass loss rates which were attributed to serious thermal decomposition. The use of chloride reactant ions was consistent with the findings using free electrons and significant amounts of autoionized or decomposed fragments were observed as $M-NO_3^-$ and $M-NO_3^-{}^*H_2O$, $M^*NO_2^-$ and $M^*NO_3^-$.

4.4. Models and interpretation of findings

Insight into generator performance can be gained by comparing the experimentally obtained mass output rates with theoretical output rates derived from Eq. (1). Values for D_{AB} used in this equation are derived from Eq. (4) and are listed in Table 3. In Table 4, the experimental and theoretical mass output rates are listed for TNT, RDX, and PETN. The experimental results for TNT agree perfectly with theory at 79°C (see Table 4). The calculated output at 99°C is 21% higher than measured, though this is probably within experimental error, especially considering that there is no replicate data at this temperature. There is more divergence as the temperature is raised: calculated output is too high by a factor of 1.8 at 120°C and by a factor of 3.0 at 150°C. This increasing divergence probably results from increasing error in the theoretical calculation as the temperature is increased. Most notably, the Dionne equation [14] was used to calculate equilibrium vapor density, N_0, for TNT at a given temperature, and this equation was derived based on data obtained between 13°C and 144°C. The experimentally obtained TNT vapor pressures were consistently lower than those obtained from the Dionne equation for temperatures above approximately 120°C. Hence, the N_0 values used to obtain the theoretical estimates are less accurate at 120°C and especially 150°C than at 79°C and 99°C. Increased error in the calculated D_{AB} values could also contribute to the divergence observed at elevated temperatures.

For RDX, the calculated [14] values (Table 4) are consistently low by a factor of 6–8 compared to experimental results. This suggests that the N_0 values obtained from the Dionne equation are systematically low. There is much better agreement between theory and experiment if another equation is used for RDX vapor pressure, one derived recently by Stimac (personal communication; see Table 4, footnote b). Using this equation, agreement is obtained within a factor of 2 at 110°C and 129°C, and agreement within a factor of 2.5 at 150°C. While this is not exact agreement, it is probably as good as can be anticipated for a low vapor pressure molecule, such as RDX, where there may be significant errors in the equations used to calculate vapor pressures. Again, inaccuracies in D_{AB} values could also contribute to the total error. The poor agreement at 150°C compared to lower temperatures could be related to the onset of some decomposition.

For PETN, agreement between theory and experiment is nearly within a factor of 2 at 110°C, but becomes progressively worse as the temperature is raised. This almost surely results from advanced decomposition of the PETN with elevated temperatures, consistent with all experimental results in the present study.

A preliminary examination of the findings in Fig. 5 suggested that the E_a values for TNT and RDX were consistent with a simple and uncomplicated volatilization of chemical. These values were comparable with the heats of vaporization of

Table 4
Calculated mass output for vapor generator and results for experimentally determined values

	Temperature			
	79°C	99°C	120°C	150°C
TNT				
Calculated D_{AB}^{a}	0.0982	0.108	0.119	0.135
Output (calculated)[b]	84.1 pg s^{-1}	601 pg s^{-1}	3.84 ng s^{-1}	39.5 ng s^{-1}
Output (measured)	84.4 pg s^{-1}	495 pg s^{-1}	2.14 ng s^{-1}	13.0 ng s^{-1}
Ratio (calculated/measured)	0.996	1.21	1.79	3.04
RDX (Dionne equation)	110°C	129°C	150°C	
Calculated D_{AB}	0.136	0.148	0.161	
Output (calculated)	6.61 pg s^{-1}	43.0 pg s^{-1}	0.281 ng s^{-1}	
Output (measured)	49.5 pg s^{-1}	279 pg s^{-1}	2.35 ng s^{-1}	
Ratio (calculated/measured)	0.134	0.154	0.120	
RDX (Stimac equation)	110°C	129°C	150°C	
Calculated D_{AB}	0.136	0.148	0.161	
Output (calculated)	31.5 pg s^{-1}	180 pg s^{-1}	1.03 ng s^{-1}	
Output (measured)	49.5 pg s^{-1}	279 pg s^{-1}	2.35 ng s^{-1}	
Ratio (calculated/measured)	0.636	0.645	0.438	
PETN	110°C	120°C	125°C	
Calculated D_{AB}	0.108	0.113	0.116	
Output (calculated)	83.7 pg s^{-1}	0.259 ng s^{-1}	0.447 ng s^{-1}	
Output (measured)	172 pg s^{-1}	1.16 ng s^{-1}	2.56 ng s^{-1}	
Ratio (calculated/measured)	0.487	0.223	0.175	

[a] All D_{AB} values are in cm^2 s^{-1}.
[b] The Stimac equation for RDX vapor pressure is $\log P(\text{RDX,ppt}) = [-6000/T(K)] + 21.945$ (R. Stimac, personal communication). All other calculations utilize the Dionne equations. The Stimac equation for RDX was empirically derived by transferring vapors to an adsorbant surface which was then characterized using an ion mobility spectrometer previously calibrated with quantitative standards. Thus, the equation was made for intact, molecular RDX and not simply the bulk mass of RDX. A preliminary error of only 5% for this method for TNT in comparison to the Dionne equation was used to demonstrate the validity of the approach.

other organic chemicals of similar size and polarity. However, the E_a value for PETN appeared too large for simple volatilization and was large enough to involve the disruption of covalent bonds, i.e. thermal decomposition of PETN. Thus, these E_a values provide further support of molecular instability of PETN.

5. Conclusions

An explosives vapor generator, based on the principles of vapor diffusion from a condensed phase, has been calibrated to a mass standard from NIST. The molecules TNT, RDX, and PETN have been studied and the principal findings for each molecule are:

(1) The generator output of TNT vapor was stable over 400 h of continuous operation and based on mass loss measurements, varies from 84 pg s^{-1} at 79°C to 13 ng s^{-1} at 150°C. An independent calibration of the vapor generator using an ion mobility spectrometer to measure the mass output gave a rate of 85 pg s^{-1} at 79°C, in nearly perfect agreement with the gravimetric results. Theoretical predictions of the TNT mass

output were in excellent agreement with the experimental results for temperatures of 79°C and 99°C, but diverged somewhat at higher temperatures, where the theoretical estimate was a factor of 3 higher than the measured output at 150°C. The cause of this divergence is almost certainly uncertainties in the parameters (vapor pressure, gas phase diffusion coefficient) used to obtain the theoretical estimates at the higher temperatures, rather than problems with the measurements. Chemical assays showed that the vapor produced at 150°C is pure molecular TNT entrained in the carrier gas, without impurities or decomposition products.

(2) Mass loss measurements for RDX also indicated a stable mass output rate for at least 300 h of continuous operation, with the output rate varying from 49 pg s^{-1} at 110°C to 2.4 ng s^{-1} at 150°C. Theoretical estimates of the output rate were a factor of 6–8 lower than the measured outputs if the estimates utilize vapor pressures derived from the Dionne equation [14]; however, values were within a factor of 1.5–2.3 of the measured outputs if the estimates utilize a more recently derived vapor pressure equation for RDX (R. Stimac, personal communication). As in the case of TNT, the vapor output was pure molecular RDX entrained in the carrier gas.

(3) Measured output rates for PETN vary from 170 pg s^{-1} at 110°C to 2.6 ng s^{-1} at 125°C. However, results from IMS/MS studies indicate that in the case of this molecule molecular decomposition is a serious problem; i.e. the vapor output is not pure PETN in the carrier gas but rather contains both PETN and a significant amount of decomposition products. This was supported by a comparison of the measured outputs with theoretical estimates where divergence increased with increases in temperature. The measured output becomes much larger relative to the theoretical estimates at high temperatures, suggesting that the measured mass loss has been inflated due to vaporization of decomposition products that are significantly more volatile than PETN.

These results suggest that the vapor generator is a useful source of vapors for TNT and RDX, but will be of limited utility in performing quantitative experiments with PETN (unless calibration can be performed at very low temperatures where decomposition of PETN is irrelevant).

Acknowledgements

The authors thank James T. Arnold of Varian Associates for technical support and useful discussions regarding the operation of the vapor generator. Others at Sandia National laboratory who contributed to this work include Brady Pompei, James Chapek, Frank Conrad, Chad Custer, David Hannum and Christian Lastoskie. We also thank Robert Stimac of PCP, for making available to us his unpublished data on the temperature dependence of the vapor pressure of RDX. Comments by David Atkinson of Idaho National Engineering Laboratory on the text and by Leigh Murray on statistics were appreciated. This work was funded in part by the United States Department of Energy under contract DE-AC04-94AL-8500. Primary funding came from the Department of Energy Office of Safeguards and Securities and from the Federal Aviation Administration under interagency agreement number DTFA03-95-X-90005.

References

[1] Proceedings of the International Symposium on the Analysis and Detection of Explosives, Quantico, VA, 29–31 March 1983.
[2] J.R. Hobbs, E.P. Conde, Analysis of airflows in personnel screening booths, in: J. Yinon (ed.), Advances in Analysis and Detection of Explosives, Proceedings of the 4th International Symposium on Analysis and Detection of Explosives, 7–10 September 1992, Jerusalem, pp. 437–454.
[3] E.E.A. Bromberg, D. Dussalult, S. MacDonald, W.A. Curby, Vapor generation for use in explosive portal detection devices, in: J. Yinon (ed.), Advances in Analysis and Detection of Explosives, Proceedings of the 4th International Symposium on Analysis and Detection of Explosives, 7–10 September 1992, Jerusalem, pp. 473–484.
[4] T. Urbanski, Chemistry and Technology of Explosives, Pergamon Press, New York, 1964.
[5] P.A. Pella, Anal. Chem. 48 (1976) 1632.
[6] C.S. Giam, L.W. Chang, G.E. Reed, T.L. Holliday, J.M. Budzik, Results from measurements of a portable calibrator for trace levels of RDX, PETN, and TNT using IMS, in: 4th International Workshop on Ion Mobility Spectrometry, Cambridge, UK, 6–9 August 1995.
[7] J.P. Davies, L.G. Blackwood, S.G. Davis, L.D. Goodrich, R.A. Larson, Anal. Chem. 65 (1993) 3004–3009.
[8] D. Atkinson, Vapor generator for explosives, in: 5th International Workshop on Ion Mobility Spectrometry, Jackson Hole, WY, 19–22 August 1996.

[9] P.W. Atkins, Physical Chemistry, Freeman Press, New York, 1986, 657.
[10] C.J. Geankoplis, Transport Processes and Unit Operations, PTR Prentice Hall, Englewood Cliffs, 1993, pp. 381–389.
[11] E.N. Fuller, P.D. Schettler, J.C. Giddings, Ind. Eng. Chem. 58 (1966) 19.
[12] US-Environmental Protection Agency, Method 8330 (revision 0, Nov. 1992), in: Nitroaromatics and Nitramines by HPLC, US-Environmental Protection Agency, 1992.
[13] Z. Karpas, G.A. Eiceman, C.S. Harden, R.E. Ewing, J. Am. Soc. Mass Spectrom. 4 (1993) 507.
[14] B.C. Dionne, D.P. Rounbehehler, E.K. Achter, J.R. Hobbs, D.H. Fine, J. Energ. Mater. 4 (1986) 447–472.

ELSEVIER

Talanta 45 (1997) 75–83

Talanta

Determination of urinary trace elements (As, Hg, Zn, Pb, Se) in patients with Blackfoot disease

Ching-Jyi Horng *, Shinne-Ren Lin

School of Chemistry, Kaohsiung Medical College, Kaohsiung, 80708, Taiwan

Received 23 December 1996; accepted 1 April 1997

Abstract

An endemic peripheral vascular disorder resulting in gangrene of the lower extremities, especially of the feet, is called 'Blackfoot disease (BFD)'. Clinically, the symptoms and signs of Blackfoot disease are similar to those of Buerger's disease. In this study, the objective is to examine the amount of arsenic, mercury, zinc, lead, and selenium in urine samples from BFD patients. After pre-treatment with acids, the samples were digested by means of a microwave oven. The determination of arsenic mercury, zinc, lead and selenium were by hydride atomic absorption spectrometry (HAAS), cold vapor atomic absorption spectrometry (CVAAS), flame atomic absorption spectrometry (FAAS), graphite furnace absorption spectrometry (GFAAS), respectively. The results indicated that urinary arsenic, mercury and lead of the BFD patients were significantly higher than those of the normal controls, while urinary zinc and selenium were significantly lower than those of the normal controls. The possibility that these elements are involved in the etiology of diseases is discussed. © 1997 Elsevier Science B.V.

Keywords: Blackfoot disease; Atomic absorption spectrometry; Trace elements; Urine analysis

1. Introduction

Blackfoot disease (BFD) is an endemic peripheral vascular disease found among the inhabitant of a limited area on the southwestern coast of Taiwan [1], where artesian well water with a high concentration of arsenic has been used for more than 80 years. Clinical manifestations usually progresses from ulceration to black discoloration and then to gangrene [2]. Thus, BFD has been attributed to chronic arsenic poisoning. However, the disease has not yet been reported in arsenic-contaminated areas of other countries. Yeh and How [3] reported that BFD could be divided into two distinct pathological reaction groups: thromboangiitis obliterans (TAO) and arteriosclerosis obliterans (ASO), It had been found that severe lead deposit was accompanied with arsenic accumulation in vascular lesions [4]. Since the zinc levels in hair and plasma are usually subnormal in atherosclerosis [5], the investigation of zinc in the body fluids of BFD patients may be of special interest, whereas selenium has an antagonistic action towards various toxic metals, such as arsenic, mercury, zinc, and lead [6]. Therefore, in addition to examine arsenic as a possible connection with

* Corresponding author.

PII S0039-9140(97)00111-2

the cause of BFD, we plan to explore the possible connection of trace elements such as mercury, zinc, lead, and selenium with the cause of BFD. These toxic metals can sometimes accumulate in various tissues and organs in abnormal concentration. Under such condition, they leads to harmful effects.

The biological monitoring of toxic and heavy metals in urine has become a matter of wide interest as a means of assessing their influence in biological processes [7]. Urine is easily sampled and provides a useful indicator of exposure to toxic and heavy metals. The presence of heavy metals has been known to markedly alter the metabolism and function of some trace elements, such as arsenic, mercury, zinc, lead, and selenium, by competition with binding sites in biological systems. It is also known that these trace elements and their compounds can be toxic if their concentrations exceed certain limits. Thus, the determination of arsenic, mercury, zinc, and selenium in urine appears to be an important clinical screening procedure, The analytical technique chosen was atomic absorption spectrometry (AAS) because of its low cost, ease of sample preparation and determination, sensitivity as well as low interference [8–10]. AAS is also readily available and in place of the more expensive neutron activation or emission spectrometric technique. The optimal conditions for use of FAAS, HAAS, CVASS, and GFAAS techniques will be discussed.

2. Materials and methods

2.1. Apparatus

A GBC system 3000 graphite furnace (GF 3000), hydride generator (HG 3000), and 908 atomic absorption spectrometer were used in this analysis. The HG 3000 continuous-flow hydride generator and the air-acetylene flame for absorption cell heating were used in As analysis, but cold vapor was used in Hg analysis. The GF 3000 includes the PAL 3000 autosampler which will accommodates automatic standard preparation, matrix modification, and calibration of the comparison curve. The 908 double beam spectrometer offering 908 complete report facilities and high speed Ultra-Pulse background correction for accurate correction of sample matrix in the GBC data station. The Photron Super Lamps (for As), and hollow-cathode lamps (for Hg, Zn, Pb, and Se) used for the AA determination were purchased from Photron Pty. (Australia). Elite Software was employed for data analysis. The results were printed by means of a letter-quality Epson LQ-550 printer.

The water was purified by a Millipore plus Milli-Q ultra-pure water system to 18 MΩ resistivity. A Milestone (Bergamo, Italy) microwave system was used for sample digestion. All glassware and polyethylene bottles were thoroughly washed and then soaked overnight in 3 M nitric acid, rinsed with de-ionized water, soaked overnight in 3 M hydrochloric acid and thoroughly rinsed with de-ionized water before use.

2.2. Reagents and standard solutions

All acids and bases used were purchased from Merck and were of Suprapur grade. Other reagents were of analytical grade purity. Water 18.2 MΩ cm^{-1} was de-ionized as previously described.

Sodium borohydride solution: 0.6 (w/v) solution was prepared by dissolving 3.0 g of $NaBH_4$ powder and 3.0 g of NaOH pellets in de-ionized water. The solution was made up to 500 ml, then filtered into an acid-washed 500 ml HG 3000 reagent bottle using a GF/A glass microfibre filter (Whatman International Ltd). (Note: sodium borohydride solutions slowly decomposed during storage. Solution older than 3 to 4 days will severely degrade analytical sensitivity, thus were not used).

Potassium permanganate, mercury free, 5% (w/v): This solution, freshly prepared, daily, is kept in a dark brown bottle to prevent it from decomposing.

Bromate-bromide reagent: A 2-g amount of KBr and 0.56 g $KBrO_3$ were dissolved in 25 ml of de-ionized water, and this solution should be prepared freshly every week [11].

Acid solution: The HG 3000 acid reagent bottle was filled with 500 ml concentrated HCl 30% (w/v).

Stabilizer solution, 0.5% (w/v) $K_2Cr_2O_7$: A 0.5-g amount of $K_2Cr_2O_7$ was dissolved in 100 ml of dilute (65%) HNO_3 (1:1). Then, 1% (v/v) stabilizer was add to all solution for mercury determination and dilute standards in order to ensure stability on storage.

Working standards: Stock solutions containing 1000 ppm of As, Zn, Pb, and Se, respectively, were prepared fresh daily in 2% v/v nitric acid in de-ionized water from Merck Titrisol standard solution (1.000 ± 0.002 g). Magnesium nitrate modifier (for Pb) was prepared from a spectroscopic 1000 μg ml^{-1} magnesium standard to give a concentration of 40 μg ml^{-1} magnesium and nickel nitrate modifier (for Se) was prepared to give a 0.2% Ni solution too.

2.3. Sample pre-treatment

The urine of patients was supplied by the Blackfoot Disease Prevention and Treatment Center. The urine specimens were filtered by means of a 0.45 μm Millipore membrane filter. Concentrated nitric acid (1 ml of acid/dl of urine) was added to aliquots that were stored at 4°C for analysis in 2 weeks or less. If the samples were not analyzed during this period of time, they were frozen and kept at −20°C.

Microwave digestion is particularly suited for rapid preparation of urine samples. In particular, samples that are analyzed by means of AAS or differential pulse anodic stripping voltammetry (DPASV) [12]. For digestion of our samples, 5.0 ml of sample and 10.0 ml of a 1:1 mixture of concentrated hydrochloric acid and nitric acids (5 ml conc. HCl + 5 ml conc. HNO_3) was transferred into a 125 ml pressure-resistant PFTE bottle. The samples were digested either at 300 W for 4 min or at 600 W for 2 min, which was sufficient to remove the interfering matrix within the samples. The resulting solution was digested until a colorless solution was obtained, evaporated almost to dryness to remove excess acid and then diluted with de-ionized water to 25.0 ml.

2.4. Analytical procedures

Air-acetylene FAAS was used to determine Zn, HAAS for As, CVAAS was used for Hg, whereas GFAAS was used for Pb and Se. The determination of arsenic and mercury was using the GBC HG 3000 continuous-flow hydride generator by flow-injection methods. To obtain maximal analytical sensitivity for hydride analysis, this analyte needs to be converted into an appropriate chemical form. Arsenic is normally present in both the tri- and penta-valent oxidation states. The analytical sensitivity of As^{3+} is approximately twice that of As^{5+} using the hydride technique. Before measurement, all As^{5+} present was reduced to As^{3+} by acidifying the samples with concentrated HCl to give an approximately 2 molar solution followed by 0.1% (w/v) KI. Approximately 1 h was allowed for the reduction to proceed to completion at room temperature. Mercury must be present in ionic form for analysis, and the sensitivity is improved in acidified solution. For this work the samples and standards used for Hg analysis were acidified with concentrated HCl to give an approximately 3 molar solution, and 0.1 ml stabilizer and 0.2 ml of bromate-bromide reagent were added and mixed well. Then 5% potassium permanganate solution were added dropwise and shaken until the purple color persisted for at least 15 min. $KMnO_4$ and bromade-bromide reagent was used together in order to obtain the powerful decomposition effect. Standard and blank were the same as procedure for the samples. The method to determine Pb and Se called for addition of modifier to samples and standards. This was performed automatically by the autosampler, thus enabling the sample preparation to be simplified. The sampler was programmed to inject 5.0 μl of 40.0 μg ml^{-1} Mg solution (for Pb) and 10.0 μl of 0.2% Ni solution (for Se). The sample size used was 12 μl and 20 μl and this enabled measurement over a large dynamic range. To determine all of these trace elements, we need to correct the matrix difference between samples and standards. The optimal experimental conditions are summarized in Table 1. To establish the validity of our results we used the Standard Trace Metals 7879 Level II [Analytical

Table 1
Graphite furnace atomic absorption spectrometry (GFAAS) instrumental settings, Pb and Se

Element:	Pb	Se
Wavelength (nm)	283.3	196.0
Lamp current (mA)	8.0	15.0
Slit width (nm)	1.0	2.0
Dry temperature (°C)	120	110
Dry time (ramp/hold, s)	(10/5)	(30/10)
Ashing temperature (°C)	400	700
Ashing time (ramp/hold, s)	(10/5)	(20/5)
Atomization temperature (°C)	2000	2600
Atomization time (ramp/hold, s)	(1.5/2)	(1/2)
Cleaning temperature (°C)	2200	2700
Cleaning time (ramp/hold, s)	(1/1)	(1/2)

Products Group (APG), Belpre, OH, USA], Biological reference materials SRM 2670 urine (Standard Reference Material 2670 Toxic Metals in the freeze-dried urine from NIST) and Seromorm™ Trace Elements Urine (Nycomed Pharma, Norway). All experiments were conducted at room temperature (25°C) following well established laboratory protocols. The analytical performances were evaluated on trace elements. The results obtained after optimization are reported in Table 2.

3. Results and discussion

The clinical onset of the BFD was usually insidious. It may be quite sudden, and almost begins with numbness and tingling or coldness in one or more extremities, usually the feet. Ultimately, rest pain develops and progresses to gangrene [13]. Cancer was the leading cause of deaths in patients with BFD. The causes of death included cancer (18.0%), cardiovascular disease (16.4%), gangrene (13.7%), cerebrovascular disease (11.3%), etc [14]. However, the etiology of the disease is still questionable. The roles of arsenic, mercury, zinc, lead, and selenium are discussed. Thus, the aim of this research was to accomplish the trace elements analysis of urine in a routine clinical laboratory situation. To assess the reliability of these established methods, we evaluated critical factors such as detection limit, range of calibration, cost, accuracy precision, etc. We then applied these methods to determine urinary As, Hg, Zn, Pb, and Se in BFD patients.

3.1. Evaluation of analytical reliability

The precision and accuracy of the analytical methods were ascertained through the use of APG Setpoint Laboratory Standards Trace Metals 7879 Level II, also certified by the USEPA, as according to the instructions. Table 3 shows comparative analytical data of Zn and Pb by AAS (FAAS for

Table 2
Analytical performances of trace elements ($\mu g\,l^{-1}$)[a]

Parameter	Element				
	As	Hg	Zn	Pb	Se
Certified value	480 ± 100	105 ± 8	450	109 ± 4	460 ± 3.0
Measured value	483.6 ± 10.0	101.3 ± 4.3	441.2 ± 7.2	103.4 ± 1.9	462.2 ± 17.3
Sensitivity	0.71	21.6	20.8	31.1	39.8
Dynamic range	0.175–50.2	0.20–263	0.843–1415	0.34–69	0.39–252
Detection limit	0.105	0.12	0.506	0.206	0.234
Precision (% conc.)	2.07 (483.6)	4.25 (101.3)	1.63 (441.2)	1.84 (103.4)	3.7 (462.2)
Accuracy (%)	0.75	−3.52	−1.96	−5.14	0.48
Mean recovery ($\bar{X}$ ± s.d., $n = 6$, %)	96.5 ± 4.0	96.5 ± 4.1	98.0 ± 1.6	94.8 ± 1.7	100.5 ± 3.8

The sensitivity of As, Hg, Zn is expressed by characteristic concentration ($\mu g\,l^{-1}$), whereas, the sensitivity of Pb, Se, by characteristic mass (pg).
[a] 3σ detection limit.

Table 3
Comparative analysis of trace metals 7879 Level II standards by independent analytical techniques[a]

Method	Elements determined ($\mu g\ l^{-1}$)				
	As	Hg	Zn	Pb	Se
HAAS	306.8 ± 7.9				132.1 ± 16.8
CVAAS	–	3.58 ± 0.09	–		
FAAS	–	–	133.2 ± 9.1	–	–
GFAAS	302.7 ± 13.6			220.0 ± 13.6	128.8 ± 5.8
DPASV[b]			139.5 ± 13.6	222.3 ± 18.1	
Certified value	305.6 ± 35.5	3.63 ± 0.53	139.4 ± 11.6	223.4 ± 19.9	123.9 ± 18.5

[a] Each value is the mean ± S.D. of six runs.
[b] Simultaneous determination by DPASV analysis method is required.

Zn, GFAAS for Pb) and DPASV [15] techniques. It also shows data of As and Se by HAAS and GFAAS, and data of Hg by CVAAS by dependent analytical techniques. On the basis of verified analytical reliability of established methods, the more appropriate method was chosen for each trace element. Furthermore, the precision and accuracy of the analytical reliability were confirmed for the SRM 2670 of the four elements (As, Hg, Pb, Se) and Seronorm™ Trace Elements Urine for Zn as shown in Table 4.

3.2. Metal concentration in urine samples

Urine specimens from a total of 32 BFD patients (17 males and 15 females) and 32 healthy normal controls were analyzed by established laboratory methods. The statistical difference between the results of our study and those of others were analyzed by the Mann–Whitney test, using the P-value as a discrimination factor. The sample population showed that BFD is not related to age or sex.

Table 5 shows that the range of urinary arsenic levels in the normal controls was 2.04–31.3 $\mu g\ l^{-1}$, with a mean value of 10.2 ± 7.5 $\mu g\ l^{-1}$, which was not very different from the value of Wang [16] 10.3 ± 5.9 $\mu g\ l^{-1}$, Bencko and Symon [17] 10.9 $\mu g\ l^{-1}$, Stoeppler and Apel [18] 9 $\mu g\ l^{-1}$ and Pan et al. [19] 11.3 ± 4.7 $\mu g\ l^{-1}$ ($P > 0.05$). The range of urinary arsenic level in BFD patient was 7.4–108.1 $\mu g\ l^{-1}$, with a mean value of 32.3 ± 25.9 $\mu g\ l^{-1}$, higher than that of the present normal control ($P < 0.01$). For other BFD patient studies, Wang [16] reported a arsenic level of 10.8 ± 5.8 $\mu g\ l^{-1}$, lower than that of the present mean value ($P < 0.01$). However, Pan et al. [19] reported a arsenic level of 33.6 ± 23.1 $\mu g\ l^{-1}$, which was in good agreement with our present mean value ($P > 0.05$). A total arsenic level in urine of $< 100\ \mu g\ l^{-1}$ was generally considered as normal. In the present work, three BFD patients, i.e. 9.4%, of total sample showed a arsenic level over 100 $\mu g\ l^{-1}$.

Trace element arsenic is toxic and also a chemical carcinogen. Long-term exposure to arsenicals, such as from drinking or from injudicious medications, may result in chronic arsenic poisoning. The clinical features include: chronic nausea, vomiting, diarrhea, peripheral neuropathy, renal damage [20,21], ulceration of the nasal septum, irritation, and a wide variety of skin reactions, including pigmentation, keratosis, and malignant changes. It is well known that hyperpigmentation, keratosis, and cancer are the major manifestations of chronic arsenicism from any source [22], while peripheral circulatory disorder has been reported occasionally in chronic arsenicism [1]. It seems reasonable to assume that arsenic may be the common etiologically factor for skin cancer and BFD [1]. Therefore we do believe that arsenic is still one of the most important factors causing the BFD.

The range of urinary mercury levels for normal control was in the range of 1.5–14.8 $\mu g\ l^{-1}$ with a mean value of 6.2 ± 2.9 $\mu g\ l^{-1}$, which was not

Table 4
Accuracy of biological reference materials SRM 2670 urine (elevated level) and Seronorm™ trace elements urine by independent analytical techniques[a]

Method	Elements determined ($\mu g\ l^{-1}$)				
	SRM 2670				Seronorm™
	As	Hg	Pb	Se	Zn
HAAS	483.6 ± 10.0				
CVAAS		101.3 ± 4.3			
FAAS					441.2 ± 7.2
GFAAS			107.4 ± 5.1	462.2 ± 17.3	
Certified value	480 ± 100	105 ± 8	109 ± 4	460 ± 30	450

Standard Reference Materials 2670 toxic metals in the freeze-dried urine from NIST.
Seronorm™ trace elements urine, Nycomed Pharma, Norway.
[a] Each value is the mean ± S..D of six runs.

very different from the value found by Lo et al., 7.4 ± 2.8 μg l^{-1} [23] ($P > 0.05$), Bourcier et al., 6.9 ± 2.1 μg l^{-1} [24], Pan et al., 5.0 ± 1.8 μg l^{-1} [19] ($P > 0.05$). The urinary mercury levels of the BFD patients was 2.5–22.0 μg l^{-1} with a mean value of 9.9 ± 4.3 μg l^{-1}, higher than that of the present normal control ($P < 0.01$). In a BFD patient study, Pan et al. [19] reported a mercury level of 11.6 ± 5.9 μg l^{-1}, which was in good agreement with our present mean value ($P > 0.05$). The total mercury in urine that is less 20 μg l^{-1} is generally considered as normal. In this work, three BFD patients, i.e. 9.4%, of total samples showed mercury concentration in excess of 20 μg l^{-1}.

In the body, Hg^{+} salts are oxidized by tissues and erythrocytes to highly toxic Hg^{2+}. Hg is retained by liver, kidney, brain, heart, lung, muscle tissues [25]. Depending on the compound, mercury can be locally irritating or corrosive, and damaging to skin and mucous membranes. Mercury toxicity is based on a single basic mechanism: the mercuric ion acting to precipitate protein and to inhibit enzymes containing sulfhydryl groups. Skin lesions due to mercury are more commonly associated with organic (especially mercury fulminate) than with inorganic mercury exposures [26]. In this study, most BFD patients were found to have a higher mercury level than normal controls, which will enhance the toxicity of arsenic to the BFD [27].

The range of urinary zinc levels in normal controls was 240.1–676.9 μg l^{-1}, with a mean value of 427.5 ± 136.9 μg l^{-1}, which was lower than the mean values reported by Pan et al. [28] 766.0 ± 491.2 μg l^{-1} ($P < 0.01$), but was in good agreement with Wang [16] with a mean value of 430.3 ± 257.6 μg l^{-1}, Yieh et al. [29] with a mean value of 464 ± 222 μg l^{-1} and our previous study [2], with a mean value of 420.1 ± 188.9 μg l^{-1} ($P > 0.05$). The urinary zinc level of the BFD patients was 64.9–815.3 μg l^{-1}, with a mean value of 297.7 ± 184.1 μg l^{-1}, lower than that of the present normal control. In other BFD patient studies, Pan et al. [28] reported a zinc level of 582.2 ± 298.4 μg l^{-1} and Wang [16] reported a zinc level of 527.0 ± 310.6 μg l^{-1}, higher than that of the present mean value ($P < 0.01$). However, Lin and Yang [30] reported a mean zinc level of 330 ± 340 μg l^{-1}, our previous study [2] showed 386.9 ± 275.6 μg l^{-1}, and Yieh et al. [29] reported 369 ± 249 μg l^{-1}. All of these are in good agreement with the mean value in the present study ($P > 0.05$).

Zinc is one of the most important metals related to health and also a major constituent of some enzymes in biological activities. Zinc appears to exert beneficial effects on the cardiocirculatory function [31], and its supplements may be beneficial in the prevention of atherosclerosis in BFD. It also has many biologically significant interactions with hormones. Lin and Yang [30]

Table 5
Metal concentrations in urine specimens ($\mu g\ l^{-1}$)[a]

Group	Concentration				
	As	Hg	Zn	Pb	Se
Normal controls	10.2 ± 7.5 (2.04–31.3)	6.2 ± 2.9 (1.5–14.8)	427.5 ± 136.9 (240.1–676.9)	21.5 ± 12.2 (5.18–53.81)	33.2 ± 12.9 (13.0–58.9)
BFD patients	32.3 ± 25.9 (7.4–108.1)	9.9 ± 4.3 (2.5–22.0)	297.7 ± 184.1 (64.9–815.3)	33.5 ± 26.9 (6.54–116.2)	21.2 ± 12.6 (2.2–57.1)
P-value	<0.01 $t = 4.636$	<0.01 $t = 4.036$	<0.01 $t = 3.200$	<0.05 $t = 2.298$	<0.01 $t = 3.764$

[a] Each value is the mean ± S.D. with the range shown in parentheses.

stated that zinc is recognized as an essential factor in wound healing. Poor healing in man is usually a consequence of zinc deficiency [32]. Wound healing of BFD is indeed poor. Zinc deficiency in BFD was reported to result in reduced rate of blood clotting, wound healing, and skin abnormalities [2]. It is also a fact that most of BFD patients in this study had undergone operative amputation.

The range of urinary lead levels in the normal control was 5.18–53.81 $\mu g\ l^{-1}$ with a mean value of 21.5 ± 12.2 $\mu g\ l^{-1}$, which was in good agreement with our previous study [2] 17.4 ± 5.4 $\mu g\ l^{-1}$ ($P > 0.05$) and higher than that of the present normal control ($P < 0.05$). The range of urinary lead level in the BFD patient was 6.54–116.2 $\mu g\ l^{-1}$ with a mean value of 33.5 ± 26.9 $\mu g\ l^{-1}$, which was also in good agreement with our previous work [2] 30.8 ± 30.1 $\mu g\ l^{-1}$ ($P > 0.05$). Normal levels of total lead in urine was less than 80 $\mu g\ l^{-1}$ [33]. In this work, three BFD patients, i. e. 9.4%, of total sample showed a lead level over 80 $\mu g\ l^{-1}$.

Lead can interfere with catalytic ability of enzyme in various metabolic processes. The toxicity of lead includes impaired heme synthesis, kidney, liver, vascular lesions (hypertension and arteriosclerosis), joint involvement (lead arthralgia, myalgia and lead gout), palsy, and lead encephalopathy etc. [26]. In the present study, most BFD patients were found to have a higher lead level than normal controls, which will enhance the toxicity of arsenic to the BFD patients [26], of whom some had suffered from joint involvement and palsy.

The range of urinary selenium levels in normal controls was 13.0–58.9 $\mu g\ l^{-1}$ with a mean value of 33.2 ± 12.9 $\mu g\ l^{-1}$, which was in good agreement with the reported by Yieh et al. [29], 30.8 ± 17.4 $\mu g\ l^{-1}$ ($P > 0.05$). The urinary selenium level of BFD patients was 2.2–57.1 $\mu g\ l^{-1}$ with a mean value of 21.1 ± 12.6 $\mu g\ l^{-1}$, lower than the present normal control. In other BFD patients studies, Yieh et al. [29] reported a selenium level of 23.8 ± 20.2 $\mu g\ l^{-1}$, which was in good agreement with our present mean value ($P > 0.05$). The total selenium in urine that is less than 50 $\mu g\ l^{-1}$ is generally considered as normal. In this work, only one BFD patients, i.e. 3.1%, of total sample showed selenium concentration in excess of 50 $\mu g\ l^{-1}$.

Selenium is a part of some enzymes. Glutathione peroxidase, the enzyme with four atoms of selenium, is a strong indicator of the essential nature of selenium for humans. Selenium acts as an anticancer agent [34], and itself in many oxidative forms is the main factor in protection of cells against lipid peroxidation. Lipid peroxidation has been identified as a damaging reaction that occurs during human lifetime in response to environmental oxidant toxicants and disease [34]. It also has an important role in prevention of cadiovascular diseases and myocardial infarction [30]. Selenium deficiency is a factor in the pathogenesis of ischemic and arteriosclerotic heart disease. The population with lower selenium levels has higher percentages of malignancy, cardiopathy, and some other diseases [35]. In this study, BFD patients with peroxidative damage to cells and tis-

sues which may accelerate the muscle damage and gangrene owing to the deficiency of selenium [30].

Tseng [14] reported that cancer was the leading cause of death in BFD patients (lung cancer 4.2%, hepatoma 3.8%, bladder cancer 2.7%, skin cancer 1.6%, etc.). The mortality of hepatoma in any other areas is lower than that in the endemic area of BFD in Taiwan [30]. Selenium as a supplement to a normal diet which can decrease tumor incidence in animals exposed to known carcinogens. This factor was demonstrated in numerous experiments [30]. Its enzyme glutathione peroxidase together with lipid peroxide and vitamin E are the main factors in protection of cells for oxidative destruction [35].

4. Conclusions

The results showed that the levels of arsenic, mercury, and lead in the BFD patients were significantly higher than those in normal controls. Therefore, we do believe arsenic is still the most important factor causing the BFD. The high lead and mercury level will enhance toxicity of arsenic to the BFD patients. But selenium and zinc were significantly lower than those in the normal controls. Thus, zinc and selenium as a supplement to a normal diet may be beneficial to the BFD patients.

In addition, continuous-flow hydride generation using the GBC HG 3000 and 908 AAS provides a fast and accurate means of analyzing mercury and arsenic by flow-injection methods. Sensitivity and measurement precision are superior to those obtained using conventional batch methods. The determination of lead and selenium were conveniently automated by the use the GBC 908 and the GF 3000 includes the PAL 3000 autosampler. These have a low detection limit and wide dynamic range. We have established the analytical procedure to determine arsenic, mercury, zinc, lead, and selenium in urine by a technique that is not only simpler to follow and less expensive to run but also more rapid and accurate than neutron activation or emission spectrometric technique, thus providing a useful tool to screen large number of individuals that are at risk of exposure to these and perhaps other metals.

Acknowledgements

This research project was supported by a grant from the National Science Council, Taiwan, Republic of China. The authors also thank the Blackfoot Disease Prevention and Treatment Center, Taiwan Provincial Chiayi Hospital for the supply of urine specimens.

References

[1] W.P. Tseng, H.M. Chu, S.W. How, J.M. Fong, C.S. Lin, S. Yeh, J. Natl. Cancer Inst. 40 (1968) 453.
[2] T.C. Pan, C.J. Horng, S.R. Lin, T.H. Lin, C.W. Huang, Biol. Trace Elem. Res. 38 (1993) 233.
[3] S. Yeh, S.W. How, A pathological study on Blackfoot disease in Taiwan, Reports from Institute of Pathology, National Taiwan University 14 (1963) 25.
[4] H.F. Kao, H.Z. Chiang, P.J. Wang, The content of trace heavy metals in vascular lesions patients with Blackfoot disease, Rep. Blackfoot Dis. Res. 39 (1992) 1.
[5] E.J. Underwood. Trace Elements in Human and Animal Nutrition, 4th ed., Academic Press, New York. 1977, p. 219.
[6] H.J. Robberecht, H.A. Deelstra, Talanta 31 (1984) 497.
[7] A.M. Bond, J.B. Reust, Anal. Chim. Acta 162 (1984) 389.
[8] J.A. Fiorino, J.W. Jones, S.G. Capar, Anal. Chem. 48 (1976) 120.
[9] B. Welz, M. Melcher, Atomic Absorption Newslett. 18 (1979) 121.
[10] R.C. Chu, G.P. Barron, A.W. Baumgarner, Anal. Chem. 44 (1972) 1476.
[11] T. Guo, J. Baasner, Anal. Chim. Acta 278 (1993) 189.
[12] R. Blust, A.V. der Linden, W. Decleir, Atomic Spectroscopy 6 (1985) 163.
[13] W.P. Tseng, Blackfoot disease in Taiwan. A 24-year follow-up study, Rep. Blackfoot Dis. Res. 13 (1982) 1.
[14] W.P. Tseng, J. Formosan Med. Assoc. 74 (1975) 37.
[15] C.J. Horng, Analyst 121 (1996) 1511.
[16] C.T. Wang, Eur. J. Clin. Chem. Clin. Biochem. 34 (1996) 493.
[17] V. Bencko, K. Symon, Environ. Res. 13 (1977) 378.
[18] M. Stoeppler, M. Apel, Fresenius' Z. Anal. Chem. 317 (1984) 226.
[19] T.C. Pan, K.C. Huang, T.H. Lin, C.W. Huang, Jpn. J. Toxicol. Environ. Health 39 (1993) 148.
[20] S.M. Lin, Kaohsiung J. Med. Sci. 2 (1986) 100.
[21] J.A. Vale, T.J. Mereditle, A Concise Guide to the Management of Poisoning. Churchill Livingstone, Edinburgh, 3rd ed., 1985, pp. 39–40.
[22] O. Neubaber, Arsenical cancer; a review, Br. J. Cancer 1 (1947) 192–251.
[23] J.M. Lo, J.C. Wei, S.J. Yeh, Anal. Chim. Acta 97 (1978) 311.

[24] D.R. Bourcier, R.P. Sharma, D.B. Drown, Am. Ind. Hyg. Assoc. 43 (1982) 329.
[25] T.W. Clarkson, Mercury poisoning, in S.S. Brown (Ed.), Clinical Chemistry and Chemistry and Chemistry Toxicology of Metals, Elsevier, New York, 1977, pp. 189–200.
[26] Hamilton and Hardy's: Industrial Toxicology Revised by Asher J. Finkel, 4th ed., 1983, pp. 17–144.
[27] Y.L. Huang, MA Thesis, Institute of Medicine, Kaohsiung Medical College, 1992, pp. 1–79.
[28] T.C. Pan, Y.L. Chen, W.J. Wu, C.W. Huang, Jpn. J. Toxicol. Environ. Health 39 (1996) 437.
[29] S.J. Yeh, T.S. Wei, C.N. Kuo, Comparative analysis of trace elements in serum and urine of patients with Blackfoot disease, Rep. Blackfoot Dis. Res. 25 (1986) 18–32.
[30] S.M. Lin, M.H. Yang, Biol. Trace Elem. Res. 15 (1988) 213.
[31] R. Masironi, Nuclear Activation Techniques in the Life Sciences, IAEA, Vienna, 1972, pp. 503–516.
[32] A.S. Prasad, D. Oberleas, Trace Elements in Human Health and Disease, vol. I, Zinc and Copper, Academic Press, New York, 1976, p. 124.
[33] C.J. Menendez-Botet, M.K. Schwartz, Anal. Chem. 63 (1991) 194R.
[34] M. Mikac-Devic, N. Vukelic, K. Kljaic, Biol. Trace Elem. Res. 33 (1992) 87.
[35] M. Mikac-Devic, N. Vukelic, K. Kljaic, Biol. Trace Elem. Res. 36 (1993) 283.

ELSEVIER

Talanta 45 (1997) 85–90

Talanta

Analysis for sulfur as hydrogen sulfide incorporating zirconia pretreatment and preconcentration

Jarrod Wall [a,*], Barry Chiswell [a], Brett Hamilton [a], Cristy Dieckmann [a], Kelvin O'Halloran [b]

[a] *Department of Chemistry, The University of Queensland, St. Lucia, 4072, Australia*
[b] *Centre for Wastewater Treatment, The University of New South Wales, New South Wales, 2052, Australia*

Received 3 February 1997; received in revised form 2 April 1997; accepted 2 April 1997

Abstract

The method of analysis for sulfate by reduction of high oxidation state sulfur to hydrogen sulfide, followed by spectrophotometric analysis, has the advantages of allowing small quantities to be measured and some interfering species to be removed. However, it has been found that acid digested samples cannot be analysed by this method due to destruction of the reduction mixture. A column of zirconium(IV) oxide was successfully used to both, remove interfering ions (H^+, Cl^- and NO_3^-) from a sediment digest, as well as perform preconcentration of sulfate. Recoveries from digests of standard sulfur samples were 101 ± 1%, and from preconcentration solutions 98.8 ± 1.2%. Comparison of results with independent analyses confirmed that not all sulfur species are detected with the same efficiency by the combined zirconia/reduction-spectrophotometric method. © 1997 Elsevier Science B.V.

Keywords: Hydrogen sulfide; Sulfur; Zirconia

1. Introduction

According to Standard Methods [1], of the techniques available for analysis of sulfate, there are two gravimetric procedures, both of which are time-consuming and subject to countless positive and negative interferences. There is also a turbidimetric method which suffers from interference by coloured solutions and requires strict adherence to pH conditions. An automated spectrophotometric method (methylthymol blue) is described but involves more complicated equipment.

Rama Bhat, Eckert and Gibson described a reduction-spectrophotometric method in 1981 [2]. High oxidation states of sulfur, such as sulfate and sulfite, can be reduced to sulfide leading to hydrogen sulfide; tin(II) is oxidized to tin(IV) in the process. The hydrogen sulfide is carried by a stream of nitrogen or argon into a buffered solution containing bis(DMP)copper(II) ions, where DMP is 2,9-dimethyl-1,10-phenanthroline. There it is oxidized with concomitant reduction of the copper(II) to the highly coloured copper(I) complex, having a maximum molar absorptivity of 6.15×10^{-3} l mol^{-1} cm^{-1} at 454 nm. The method was proposed as an Australian Standard

* Corresponding author. Fax: +61 7 38702495.

PII S0039-9140(97)00121-5

for the determination of filterable sulfate in natural waters by spectroscopy [3].

Use of this method for acid digested solid sediment or standard samples does not appear to have been reported, and we have found that the method, when applied to such samples, gave non-reproducible results. It would seem likely that a component of the acid digestion prevents reduction of the sulfur species. A list of interfering ions and approximate concentrations, below which no interference was observed was given by Rama Bhat, Eckert and Gibson [2], and we concluded that the main interfering ions could be chloride and nitrate from the aqua regia used. In particular nitrate, in the presence of strong acid, was thought to be likely to oxidize all of the tin(II) to tin(IV), thereby leaving no tin(II) to reduce high oxidation state sulfur to sulfide.

Zirconia is increasingly being used as a stationary phase in High Performance Liquid Chromatography [4], where it is chosen due to its extreme thermal and chemical stability, its resistance to both alkali and acid, its mechanical durability, and its low cost [5]. Another unique aspect of the chemistry of zirconia is its selectivity for hard Lewis bases, which are small, highly charged species of low polarizability such as fluoride, hydroxide, borate, carbonate, phosphate, sulfate, chromate, tungstate and arsenate [6]. We have utilized this latter property in sample preparation of acid digests of sediments for sulfate analysis. The sulfate has been shown to bind to the zirconia, while the interfering anions of chloride and nitrate pass through the column. The sulfate can then be eluted in a very small volume with base.

2. Experimental

2.1. Reagents

All chemicals were of analytical-reagent grade. Reagent water of resistivity 18 MΩ cm^{-1} was prepared using a Milli-Q system.

2.1.1. Zirconia

Riedel-de Haën zirconium oxide and Judex Chemicals zirconium oxide were used in these experiments; no effective difference in performance was observed.

2.1.2. Standard sulfur-80 mg S l^{-1}

0.3697 g of anhydrous sodium sulfate was dissolved in water. This solution was made up to 1 l in a volumetric flask, to produce a 2.6×10^{-3} M solution (83.5 mg S l^{-1}).

2.1.3. Hydrochloric acid

Of concentrated hydrochloric acid, 75 ml was poured slowly into 150 ml of reagent water. This solution was transferred to a 250 ml volumetric flask and made up to the mark with reagent water to produce a 3 M HCl solution.

2.1.4. Potassium hydroxide

Potassium hydroxide pellets, 28 g were dissolved in water, transferred to a 500 ml volumetric flask and made up to the mark with reagent water. This produced a 1 M KOH solution.

2.1.5. Phenolphthalein solution

Of phenolphthalein, 1 g was dissolved in a mixture of 100 ml reagent water and 100 ml ethanol.

2.1.6. Aqua regia

Digesting acid, 1 l, was prepared by adding 250 ml of concentrated nitric acid with stirring to 750 ml of concentrated hydrochloric acid.

2.1.7. Sediment preparation

Surface sediment (< 10 cm depth) was collected from Lake Manchester, a disused water supply dam west of Brisbane. The sediment was transferred to a large Petri dish and oven dried at 110°C for 48 h.

2.1.8. Reduction-spectrophotometric solutions

All solutions used in the reduction-spectrophotometric method were prepared following the methods described by Rama Bhat, Eckert and Gibson [7], with the following changes based on the Australian Standards Draft [3].

2.1.9. Buffer solution pH 4.0

To prepare approximately 1 l, 815 ml of 0.5 M acetic acid and 185 ml of 0.5 M sodium acetate were mixed. The pH was checked and then adjusted to 4.0 by adding either acetic acid or sodium acetate solution.

2.1.10. Buffer solution pH 4.8

To prepare approximately 1 l, 400 ml of 0.5 M acetic acid and 600 ml of sodium acetate were mixed. The pH was checked and then adjusted to 4.8 by adding either acetic acid or sodium acetate solution.

2.1.11. Copper sulfate

Copper sulfate pentahydrate, 2 g, was dissolved in reagent water and made up to 1 l in a volumetric flask, to yield a 8×10^{-3} M solution.

2.1.12. Trapping reagent

0.15 g of 2,9-dimethyl-1,10-phenanthroline (DMP) hydrochloride (neocuproine hydrochloride) was dissolved in water and transferred to a 1 l volumetric flask. Following this, 25 ml of copper sulfate solution and 125 ml of pH 4.8 buffer solution were added. Finally, the solution was made up to the mark with reagent water. Of this solution, 40 ml, was poured into the second gas washing bottle for each analysis.

2.1.13. Sulfate-30 mg S l^{-1}

Anhydrous sodium sulfate, 0.1337 g was dissolved in water and made up to 1 l in a volumetric flask. The solution produced was 9.41×10^{-4} M or 30.2 mg S l^{-1}.

2.1.14. Cysteine

Cysteine, 0.1129 g was dissolved in water and diluted to 1 l. This produced a 9.32×10^{-4} M or 29.9 mg S l^{-1} solution.

2.1.15. Thiourea

Thiourea, 0.1426 g was dissolved in water, transferred to a 1 l volumetric flask and made up to the mark with reagent water. This produced a 9.37×10^{-4} M or 30.0 mg S l^{-1} solution.

2.1.16. Thiosulfate

Sodium thiosulfate pentahydrate, 0.1177 g, was dissolved in water and diluted to 500 ml in a volumetric flask. This formed a 9.48×10^{-4} M or 60.8 mg S l^{-1} solution.

2.2. Apparatus

2.2.1. Reduction-spectrophotometric apparatus

The reduction-spectrophotometric apparatus was assembled according to the method described by Rama Bhat, Eckert and Gibson [4]. However, after injection of a sample, the trapping reagent was made up in a 100 ml volumetric flask, rather than a 50 ml flask.

2.2.2. Syringe

A Hamilton 1000 μl glass gas tight syringe, with fixed needle was used to inject samples.

2.2.3. Spectrophotometer

The absorbance was measured on a Hewlett-Packard 8450A UV-VIS spectrophotometer using 50 mm glass cells.

2.2.4. Microwave

The microwave oven used to carry out digestions was a model PMO 727, with a rotating carousel. The oven has a variable timing cycle, and on the setting used produces 700 W at 2450 MHz. This equipment unfortunately did not have the facility to measure the temperature of the samples during digestion.

2.2.5. Digestion containers

Teflon FEP (fluorinated ethylene propylene) containers of 125 ml capacity, with Tefzel ETFE (ethylene-tetrafluoro-ethylene copolymer) closures were used in the microwave digestion. To prevent corrosive fumes from entering the microwave, the teflon vessels were housed in a polyethylene container, with a sealed lid during microwaving.

2.2.6. Mechanical shaker

A rotary shaker manufactured by the Department of Chemistry Mechanical Workshop was used.

2.3. Procedure

2.3.1. Column procedure

A 30 cm long glass gravity column, with internal diameter of 1 cm was used in these experiments. A rubber stopper was fitted to the outlet so that it would seal into a vacuum flask. Vacuum below the tap was necessary to move the solution through the column at a reasonable rate. A plug of cotton wool, of depth approximately 2 cm was found to be necessary to prevent the fine particles of zirconia from passing through the sintered glass frit at the bottom of the gravity column.

Approximately 2 g of zirconia was weighed. Water, 10 ml and 5 ml of base were added to form a slurry. This was transferred to the column and allowed to settle. The zirconia was washed with three 10 ml aliquots of 1 M KOH to ensure that any adsorbed sulfate would be displaced. A second wash with 5 ml of 3 M HCl was performed to make the surface sites conducive to binding of sulfate.

After preparing the column, an analyte solution was passed down the column. This was followed by a small volume of water to remove non-bound ions. Then the sulfate was eluted with two 5 ml aliquots of 1 M KOH. The resulting solution was transferred, with washings, to a 25 ml volumetric flask. One drop of phenolphthalein indicator was added, followed by sufficient 3 M HCl to change the indicator from pink to clear to ensure that the hydriodic acid, used as the reducing reagent, retained its efficiency.

Finally, the solution was made up to the mark with reagent water. A sample of this solution was then injected into the reduction-spectrophotometric apparatus for analysis. Between samples, the column was washed with three aliquots of 10 ml of 1 M KOH, followed by 5 ml of 3 M HCl.

2.3.2. Digest with standard solution

Water, 20 ml, was added to a 150 ml beaker, as well as 15 ml of aqua regia, 3 ml of 80 mg S l^{-1} standard was added with mixing by burette and the solution passed down the zirconia column with three water washings of approximately 5 ml each.

2.3.3. Preconcentration

To prepare 100 ml of approximately 1.60 mg l^{-1} sulfur solution, 2 ml of 80 mg S l^{-1} standard was buretted into a 100 ml volumetric flask, which was made up to the mark with reagent water. To ensure the sample was acidic and, therefore more conducive to binding of sulfate to the zirconia, 1 ml of 3 M HCl was pipetted into the flask. The solution was mixed and then transferred quantitatively to the column.

2.3.4. Microwave digestion of sediment

Approximately 1.5 g of dried sediment was accurately weighed into a teflon screw-cap bottle. Aqua regia, 10 ml, was added and the lid tightly closed. The bottle and sample were then microwaved for a total of 15 min. The digest solution was quantitatively transferred to a 25 ml volumetric flask and made up to the mark with washings and reagent water. This solution was then filtered through a 0.45 μm cellulose acetate membrane. Filtered solution, 10 ml was passed down the zirconia column and the remainder was sent for independent analysis.

2.3.5. Shaking digestion of sediment

Approximately 1.5 g of sediment was accurately weighed and transferred to a 250 ml Schott bottle. Following this, 10 ml of aqua regia was pipetted into each bottle. The bottles were placed on a mechanical shaker and left for approximately 5 h. The digest was transferred to a 50 ml volumetric flask and made up to the mark with washings and reagent water. The solution was thoroughly mixed and then vacuum filtered through a 0.45 μm membrane. Of this solution, 20 ml was passed down the column and the remainder was sent for independent analysis.

2.3.6. Shaking digestion of alternative sulfur compounds

Aqua regia, 20 ml, was pipetted into a 250 ml Schott bottle. Then 20 ml of either thiourea, cysteine or thiosulfate were pipetted into the bottle, as well as 10 ml of 30 mg S l^{-1} standard sulfate. Four samples of each solution were prepared. The bottles were then placed on the mechanical shaker and shaken for 5 h. After this

time, approximately 20 ml was sent for independent analysis, and 25 ml was transferred to the zirconia column. The eluted solution was analysed by the reduction-spectrophotometric method.

3. Results and discussion

The recovery of sulfate from a digest composed of standard sulfate was investigated. A solution was prepared to imitate as closely as possible a sediment digest, in terms of pH and concentrations of sulfate, nitrate and chloride. From previous experiments, the concentration of sulfur was approximately 170 μg S g^{-1} sediment. Typically, 1.5–2 g of sediment are weighed out when performing a digest, therefore, 250 μg of sulfur was chosen as the quantity to use in a digest to test recovery. This 250 μg was eluted in a total volume of 25 ml, thus producing a 10 μg S ml^{-1} solution. The mass recovery was extremely close to the expected value, with the average recovery for nine samples being 10.1 ± 0.1 μg sulfur, i.e., $101 \pm 1\%$.

There would also be great benefit if the zirconia column could be used for preconcentration of the sulfate. A volume of 100 ml of 1.67 μg S ml^{-1} solution was passed down the column, eluted and finally diluted to 25 ml to produce a 6.68 μg S l^{-1} solution. Once again the recoveries were very good. The average for nine samples was 6.60 ± 0.08 μg sulfur, i.e., $98.8 \pm 1.2\%$. Given that the reduction-spectrophotometric method has a calculated limit of detection of less than 0.3 μg sulfur, a solution of 3 μg S l^{-1} could be analysed using this preconcentration step. It may be possible to pass down sample volumes greater than 100 ml, thus further improving the detection limit.

Finally, the column was tested for recovery of sulfate from genuine sediment digest samples which had been homogenized and oven-dried. Microwave acid digestions of the sediment sample were performed and the results for sulfate analyses compared with those obtained by independent analysis using ICP-AES on the same digest solutions. The average concentration for six samples by the zirconium column combined with the reduction-spectrophotometric method was 171 ± 15 μg S g^{-1} sediment, while for five of the same samples analysed by ICP-AES the average was 187 ± 13 μg S g^{-1} sediment. From comparison of the results it can be seen that the errors are relatively large, being approximately 14 μg S g^{-1} sediment, regardless of the determination method used. This corresponds to about 8% of the total. However, the concentrations of sulfate in the sediment determined both by the reduction-spectrophotometric method and by ICP-AES are within calculated standard errors of each other. The large error in both results, 8.8 and 6.8% of the totals, respectively, indicated that the microwave digestion procedure was not as reproducible as desired, a possibility that was supported by results from another researcher, who also performed microwave digests and analysed for phosphate using ICP-AES [8].

To investigate whether the poor reproducibility was due to the microwave method, an alternative digestion procedure was used, in which sulfate was extracted from sediment by shaking with aqua regia. The recoveries using this method of digestion were significantly greater and the errors significantly smaller than those of the microwave digestion method, regardless of the method of sulfate analysis used. The calculated concentrations were 300 ± 6 μg S g^{-1} sediment by the zirconia method and 340 ± 2 μg S g^{-1} sediment by independent ICP-AES analysis.

There was a lower result of more than 10% between values obtained by the zirconia/reduction-spectrophotometric method compared with those found by ICP-AES analysis. It has been suggested that the reduction-spectrophotometric method is unable to detect some species containing C–S bonds [3] and to investigate this possibility, solutions of cysteine, thiourea and thiosulfate were prepared, passed down the zirconia column and injected into the reduction mixture. The recovery efficiencies were 0.02% for cysteine, 0.10% for thiourea and 74.2% for thiosulfate, indicating that not all sulfur species would be quantitated by the method. In particular, cysteine and thiourea do not appear to be detected at all by the combined zirconia/reduction-spectrophotometric method.

It was also important to establish whether cysteine, thiourea and thiosulfate are oxidized in a

digest to species that are detected by the reduction-spectrophotometric method. Therefore, a shaking digestion of these solutions was performed. Half of each cysteine and thiourea sample solution was sent for independent analysis, while the other half was analysed by the reduction-spectrophotometric method. The results obtained by the latter method indicate that cysteine and thiourea react with efficiencies of 24.4 ± 5.5 and $97.3 \pm 1.0\%$, respectively. However, the identical samples sent for ICP-AES analysis gave recoveries of 100% for cysteine and 105% for thiourea. A shaking digest of thiosulfate standard produced a recovery of $103 \pm 3\%$ by the zirconia/reduction-spectrophotometric method.

The results show that not all forms of sulfur react in the reduction-spectrophotometric method with the same efficiency, even after performing a digestion and that the ICP-AES analysis detected all forms of sulfur present. This difference may explain the 12% higher value obtained by the ICP-AES analysis compared with the reduction-spectrophotometric method, for the same digestion solution of sediment samples.

4. Conclusion

The results indicate that sulfate can be bound and quantitatively eluted from a column of zirconium(IV) oxide. Recoveries for standard solutions were very close to 100%, with good reproducibility. Also, the eluted solution could be injected into the reduction-spectrophotometric method described by Rama Bhat, Eckert and Gibson [3], without destruction of the reduction mixture. Zirconia is inexpensive, chemically resistant, non-toxic and reusable; one column was used continuously for over 20 samples with no variation in recovery.

Although a gravity column was used in these experiments, a zirconia column may be incorporated into a flow injection analysis (FIA), to achieve semi or full automation. Furthermore, the column may be useful for removing species that interfere in many analyses, for example the removal of protons present in an acid digest that may upset a buffer system being used subsequently in the analysis procedure, or removal of coloured species that interfere with an analysis.

Due to the strong, very specific but reversible associations that zirconia forms with hard Lewis bases, the zirconia column would be expected to be able to quantitatively bind other anions, such as borate, carbonate, phosphate, chromate, tungstate and arsenate, and could be used to preconcentrate these species.

The research also highlighted that the reduction-spectrophotometric method does not detect all sulfur species. This fact is suggested to account for the difference between values obtained by the reduction-spectrophotometric method and the independent ICP-AES analysis.

Acknowledgements

We gratefully acknowledge the Queensland Government Chemical Laboratories for their analyses and Dr Bruce Lowe for his advice on this work.

References

[1] American Public Health Association, American Water Works Association and Water Pollution Control Federation, Standard Methods for the Examination of Water and Wastewater, American Public Health Association, Washington, DC, 16th ed., 1985, pp. 464–470.
[2] S. Rama Bhat, J.M. Eckert, N.A. Gibson, Anal. Chim. Acta 128 (1981) 263.
[3] Standards Australia draft for 'Water-Determination of Filtrable Sulfate-Spectrophotometric Method', Project Number CH/022-0400, June, 1990.
[4] Y. Ghaemi, R.A. Wall, J. Chromatogr. 174 (1979) 51.
[5] J.A. Blackwell, P.W. Carr, J. Chromatogr. 549 (1991) 59.
[6] M.P. Rigney, E.F. Funkenbusch, P.W. Carr, J. Chromatogr. 499 (1990) 291.
[7] S. Rama Bhat, J.M. Eckert, N.A. Gibson, Water, March, 1983, 19.
[8] S.-H. Huang, Determination of Bioavailable Phosphorus by Organic Acid Extraction, M.Sc. Thesis, Department of Chemistry, University of Queensland, 1996.

ELSEVIER

Talanta 45 (1997) 91–104

Talanta

Characterization of an enzyme linked immunosorbent assay for Aflatoxin B_1 based on commercial reagents

Maria Pesavento [b,*], Slavomir Domagala [c], Enrica Baldini [a], Lucia Cucca [a]

[a] *Dipartimento di Chimica Generale, University of Pavia, Pavia, Italy*
[b] *Istituto di Scienze Matematiche, Fisiche e Chimiche, University of Milano, Milano, Italy*
[c] *Department of General and Inorganic Chemistry, University of Lodz, Lodz, Poland*

Received 14 May 1996; received in revised form 3 April 1997; accepted 3 April 1997

Abstract

Two indirect ELISA have been investigated for the determination of Aflatoxin B_1, employing only reagents commercially available, whose composition is not exactly known. In both cases the antigen (Aflatoxin B_1-BSA) was coated to the solid phase (polystyrene microtiter plates). In one procedure the specific antibody was a conjugate with peroxidase, while in the other one it was not conjugated, and a second antibody labelled with alkaline phosphatase was used. A simple model was employed to characterize the equilibria, which is of help also if the exact composition of the immunoreagents is not known, and allows to predict the shape and position of the competition curve. The factors which determine the dynamic range were found to be the affinity constant the complex in the solid and the amount of antigen in the solid, and the affinity constant of the complex in solution phase. Useful aspects of the antigen–antibody complexation equilibria in the solid phase were investigated by ELISA at zero concentration of antigen in solution, obtaining $c_s c^*$ and $K' f_T^n$. The equilibria in solution were studied by competition ELISA, obtaining K, the affinity constant of the antigen–antibody complex in solution. Similar results were obtained with the two procedures, for instance the affinity constant in solution was 2×10^8. A procedure for the determination of Aflatoxin B_1 in food samples was developed. © 1997 Elsevier Science B.V.

Keywords: Affinity constant; Aflatoxin B_1; ELISA; Immunodetermination

1. Introduction

The immunological methods of analysis are becoming more and more important when sensitive, specific and rapid determinations are required, for instance in food and environmental analysis. To this purpose the enzyme linked immunosorbent assays (ELISA) [1] are very interesting, since they allow to perform these determinations also in laboratories not specialized, equipped with the usual instrumentation. In the present work a method for developing and characterizing an ELISA for Aflatoxin B_1 based on commercially available reagents is described. Aflatoxin B_1 is a low molecular weight toxin (PM = 312.3) produced by the fungi Aspergillus Flavus and Aspergillus Parasiticus which grow on foodstuffs like

* Corresponding author.

PII S0039-9140(97)00115-X

peanuts, flour, seeds, and even pepper and other spices. It is very toxic and carcinogenous to man, and its concentration in food and animal feed is strictly limited by law in all the countries. Usually the determination is performed chromatographically, with spectrofluorimetric detection. These methods are not very specific and require an extensive cleaning and confirming procedure. Some immunochemical methods have been proposed [2,3], and a number of kits for the immunoenzymatic determination of Aflatoxin B_1 are commercially available [4–6]. Also the following immunological reagents can be separately obtained on the market: antibody specific to Aflatoxin B_1 (policlonal antibody from rabbit), antibody specific to Aflatoxin B_1 (policlonal antibody from rabbit) conjugate with peroxidase, conjugate Aflatoxin B_1-BSA, conjugate antibody anti-rabbit IgG with alkaline phosphatase (from goat). With such reagents, indirect competitive assays can be worked out, obtained by coating the solid phase with the antigen [7]. There are two different possibilities, since both a specific antibody conjugated with peroxidase and a not-labelled specific antibody are commercially available. In the latter case an antibody anti-rabbit IgG conjugated with an enzyme is then required to label the specific antibody (indirect ELISA with double antibody) [7]. The method with the labelled specific antibody has the advantage of requiring only one incubation, and so is more rapid, while the second one allows to use different enzymes, and to have a higher enzymatic activity of the solid phase, since more than one secondary antibody binds to each primary antibody according to previous suggestions [8].

Generally speaking, the assays developed in the laboratory present some advantages over the commercial kits, mainly a better control of the conditions, which can be selected on the basis of the reagents and instrumentation available, and on the particular problem to face. Of course the reagents must be well characterized in order to be able to develop a useful and controlled procedure. The problem is that the immunoreagents as obtained from the commercial source are usually of unknown composition, and can also be different from batch to batch, both for titer and affinity constant.

In the present paper a method is suggested for characterizing the immunoreagents in view of their use for an ELISA. It is based on a simple model, which takes into account the formation of one antigen–antibody complex in solution and in solid phase. Well known considerations which are widely used for investigating the association equilibria in solution [9], and between different phases, are applied to elucidate the mechanisms involved. The affinity constant in solution is evaluated by an indirect ELISA procedure similar to that previously proposed by Friguet [10]. The affinity constant in the solid, or, more precisely, a quantity related to it, must be known, which is easily determined by an indirect ELISA at zero concentration of antigen in solution. Contrary to what is required in the Friguet procedure, it is not necessary to measure the amount of unbound antibody. Neither the exact amount of antigen coating the solid nor the antibody in solution must be known.

The model here proposed was worked out to help in deciding the best conditions for the ELISA, and in evaluating the dynamic range for the analytical determination when the composition of the immunoreagents is unknown. It is easy to handle, and requires only a limited amount of immunoreagents and of time.

The procedure was applied to the determination of Aflatoxin B_1 in different samples (flour, pepper and peanuts butter), using an ELISA based on reagents commercially available, whose composition is not exactly known neither reproducible from batch to batch.

2. Experimental

2.1. Reagents

All the chemical reagents and solvents were of analytical reagent grade. Aflatoxin B_1 and all other aflatoxins, were obtained from Sigma. The stock solution at concentration of around 100 mg l^{-1} was prepared by weighing the solid and dissolving it in acetonitrile. The following buffers were used: DPBS (Dulbecco Phosphate Buffer Saline, pH = 7.4, containing 0.1% Timerosal

(Sigma)); DPA (DPBS solution added with 1% BSA).

The coating antigen was Aflatoxin B_1-BSA conjugate, containing 8–12 mol of Aflatoxin B_1 per mol of BSA (Sigma). A stock solution of this reagent (around 500 mg l^{-1}) was prepared by dissolving a weighed amount of the solid in DPBS. The stock solution was stored at 4°C, and was further diluted with DPBS immediately before utilization.

Fractionated antiserum developed in rabbit, containing the antibody specific to Aflatoxin B_1 conjugate with horseradish–peroxidase, was obtained from Sigma, and stored in the refrigerator.

Fractionated antiserum containing the antibody specific to Aflatoxin B_1 developed in rabbit, and the affinity isolated antibody to rabbit IgG, from goat, conjugate with alkaline phosphatase were also obtained from Sigma, and stored in the refrigerator at 4°C.

All the antisera were diluted with DPA immediately before utilization. The substrate for horseradish–peroxidase was a solution with the following composition: ABTS (2-2′-azino-bis-(3-ethilbenzthiazoline-6-sulphonic acid, diammonium salt) (Sigma), 0.1% in acetate buffer (0.05 M acetate, pH = 5.1) with $3.4\ 10^{-3}$ M hydrogen peroxide.

The substrate for alkaline phosphatase was: *p*-nitrophenyl phosphate (Sigma), 1% in carbonate buffer (0.1 M Na_2CO_3, 10^{-3} M $MgCl_2$, pH = 9.8).

2.2. Procedures

The assays were performed in polystyrene microtiter plates (Nunc), coated with the antigen by contacting 100 μl of Aflatoxin B_1-BSA in DPBS in each well for at least 16 h at room temperature. Each well was then washed three times with 200 μl of DPBS, and incubated for 1 h at room temperature with 200 μl of DPA, in order to block the residual sorption sites on the walls. The assays were then carried out according to the procedure described in Section 2.2.1 and Section 2.2.2.

All the incubation times for the immunological reactions were selected to reach equilibrium. Each determination was performed at least in triplicate on contiguous wells, and the final medium value of absorbance was considered. For each series an absorbance blank (A_b) was determined by measuring the enzymatic activity of wells not coated with antigen. This depends on the aspecific linking of the antibody to the solid phase. All the absorbances were corrected by subtracting A_b, which never exceeded 0.05–0.2 absorbance units at the label dilution here proposed.

2.2.1. Procedure A (single antibody labelled with peroxidase)

Each activated well was incubated for 1 h at 37°C with 80 μl of DPA, added with the antibody specific to Aflatoxin B_1, horseradish–peroxidase conjugate, and 20 μl of acetonitrile + water (1 + 1). This solution contains Aflatoxin B_1 in the case of competition ELISA. After three times washing with 200 μl of DPA, each well was contacted with 200 μl of the substrate solution for horseradish–peroxidase, and incubated for 15′ at 37°C. Then the substrate solution was sucked out of the well, and transferred to a small volume quartz cuvette with 1 cm optical path, and the absorbance was measured at 405 nm by a usual UV-Vis spectrophotometer (Cary 3, Varian).

2.2.2. Procedure B (double antibody, second antibody labelled with alkaline phosphatase)

Each well was incubated for 3 h at 37°C with 80 μl of DPA, with the antibody specific to Aflatoxin B_1, and 20 μl of acetonitrile + water (1 + 1). This solution contains Aflatoxin B_1 in the case of competition ELISA. After three times washing with 200 μl of DPA, each well was contacted with 100 μl of DPA containing the goat anti rabbit IgG antibody–alkaline phosphatase conjugate, diluted 1:500, and incubated for 1 h at 37°C. After three times washing with 200 μl of DPA, each well was contacted with 200 μl of the substrate solution for alkaline phosphatase and allowed to react for 10 or 20 min at 37°C. Of this solution, 30 μl were transferred to a small volume quartz cuvette with 1 cm optical path where they were added with 1.2 ml of 0.1 M NaOH, which was used to dilute and to stop the enzymatic reaction, and the absorbance was measured at 405 nm, in a UV-Vis spectrophotometer Cary 3, Varian.

3. Theoretical model and calculations

3.1. Characterization of the antibody–antigen complex in the solid phase by ELISA

In the ELISA considered in the present work the immunoreagent fixed to the solid is the antigen (Aflatoxin B_1-BSA), while the second immunoreagent, the antibody, is in solution, (indirect ELISA [7]). In the absence of any antigen in solution, the specific antibody (Ab) combines only to the antigen in the solid phase (T'), according to the equilibrium:

$$\mathrm{Ab} + n\mathrm{T}' \Leftrightarrow \mathrm{AbT}'_n \tag{1}$$

with an affinity constant:

$$K' = \frac{[\mathrm{AbT}'_n]}{[\mathrm{Ab}][\mathrm{T}']^n} \tag{2}$$

where Aflatoxin B_1 is indicated by T, and the antibody by Ab. The prime ' indicates the species in the solid phase, and n can be either 1 or 2, if Ab is a monomeric antibody, as IgG are. Of course different specific antibodies in a policlonal antiserum may have different values of K', however in this treatment it is assumed for simplicity that all the possible antibody–antigen complexes have equal, or very similar, affinity constants. The concentrations in solution are expressed in mol l^{-1} (molarity, M), while those in solid phase in mmol mm^{-2} of solid surface. The total area of coated well will be indicated by w.

Equilibrium 1, and its coefficient 2, is similar to that proposed by Scatchard [9] for the combination of molecules with proteins, and widely used for investigating these equilibria. More recently Friguet proposed the same relationship for the antigen–antibody reaction [10]. Here the unit which combines with the antigen is assumed to be the whole IgG molecule, not the single combination site, since the quantity finally determined in ELISA here considered is the absorbance of the substrate solution (A), which is a measure of the enzymatic activity of the solid phase.

In experiments in which the solid phase activated by sorption of the antigen is contacted with the antibody in solution not containing any antigen, the following mass and absorbance equilibria hold:

$$A = [\mathrm{AbT}'_n]wc^* \tag{3}$$

$$c_{\mathrm{Ab}} = [\mathrm{Ab}] + [\mathrm{AbT}'_n]w/V \tag{4}$$

$$c'_{\mathrm{T}}w = [\mathrm{T}']w + n[\mathrm{AbT}'_n]w \tag{5}$$

where A is the absorbance of the substrate solution at a fixed wavelength, the quantity experimentally determined, and c^* is the proportionality coefficient which relates the final absorbance to the amount of antibody in the solid phase. V is the volume of the antibody solution contacted with the solid. $c'_{\mathrm{T}}w$ is the quantity of antigen actually present in the solid phase, in mmol, which in the present case is known only approximately, since the number of Aflatoxin B_1 moles linked per mole of BSA is not exactly known. If q_{T} is the amount of Aflatoxin B_1-BSA conjugate (in ng), used to activate the solid phase $c'_{\mathrm{T}}w$ is given by

$$c'_{\mathrm{T}}w = q_{\mathrm{T}}f_{\mathrm{T}} \tag{6}$$

Obviously q_{T} is known, since the stock solution of the Aflatoxin B_1-BSA conjugate was prepared by weighing the solid obtained from Sigma. On the contrary f_{T}, the proportionality factor which relates q_{T} to the mmol of Aflatoxin B_1 actually sorbed in the solid phase, is unknown. It accounts also for the possibility that only a fraction of the total conjugate is sorbed onto the face of the well. In the following treatment f_{T} is assumed to be constant in function of different amounts of conjugate sorbed on the well. This was previously demonstrated to be true at least up to a given concentration of protein, which depends on the nature of the protein and of the solid phase [11]. c_{Ab} is the concentration of antibody in the volume V of solution used for the first incubation with the antibody. It is given by the relationship

$$c_{\mathrm{Ab}} = c_{\mathrm{s}}/d \tag{7}$$

where c_{s} is the concentration of Ab in the stock solution, which is unknown, and d is the dilution factor of the antibody. This situation, in which the concentration of the reagents is unknown, is usual in most immunological determinations when commercial reagents are used.

The antigen–antibody complex formation in the solid phase was investigated by performing

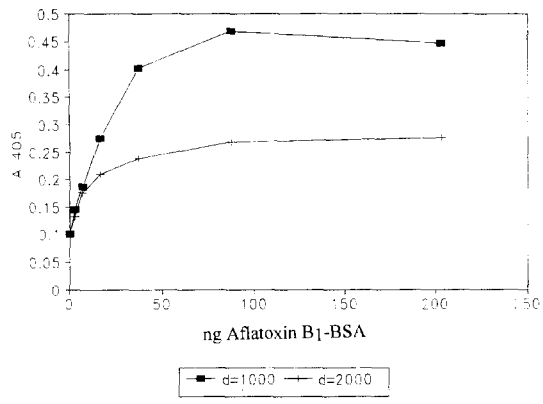

Fig. 1. ELISA at zero concentration of antigen in solution, procedure A. Final absorbance in function of the total amount of conjugate Aflatoxin B_1-BSA used for coating the well (q_T). Dilution of the conjugate specific antibody–peroxidase: ■ $d = 1000$, + $d = 2000$.

series of ELISA at zero concentration of antigen, in which c_{Ab} was kept constant, while the total amount of toxin immobilized in the solid phase ($c'_T w$) was varied, by using different amounts of antigen-BSA conjugate for coating. Curves A versus q_T, like those reported in Fig. 1 and Fig. 2 were obtained. The observed trend can be explained by the following considerations.

If only the complex AbT'_n is formed on the solid the fraction of bound ($B_{Ab} = [AbT'_n]w$) to total

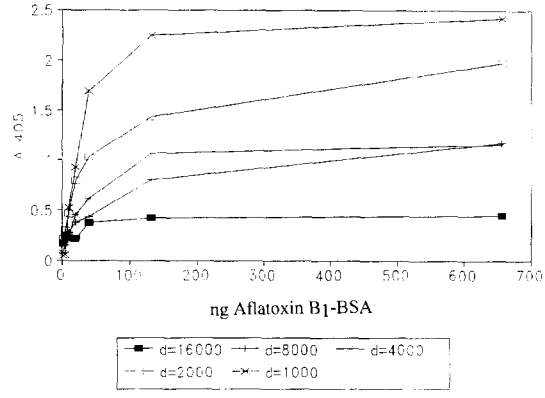

Fig. 2. ELISA at zero concentration of antigen in solution, procedure B. Final absorbance in function of the total amount of conjugate Aflatoxin B_1-BSA used for coating the well (q_T). Dilution of antibody specific to Aflatoxin B_1: ■ $d = 16\,000$, + $d = 8000$, * $d = 4000$, □ $d = 2000$, × $d = 1000$.

($c_{Ab}V = c_s V/d$) antibody is

$$B_{Ab}/c_{Ab}V = \frac{[AbT'_n]w}{[Ab]V + [AbT'_n]w} \tag{8}$$

From Eqs. (2), (3) and (8) the following relationship can be obtained, which relates the final absorbance to the concentration of toxin in the solid phase

$$A = (c_s c^* V/d)\frac{1}{1 + (Vw^{n-1}/K'[T']^n w^n)} \tag{9}$$

From Eq. (9) it can be seen that for low amounts of toxin fixed in the solid ($Vw^{n-1}/K'[T']^n w^n \gg 1$), the absorbance linearly depends on the concentration of free toxin, according to the relation

$$A = (c_s c^* V/d)\frac{K'[T']^n w}{V} \tag{10}$$

On the contrary for high amounts of toxin in the solid ($Vw^{n-1}/K'[T']^n w^n \ll 1$), the absorbance depends only on the amount of antibody, according to the relationship:

$$A = c_s c^* V/d = A_P \tag{11}$$

The constant absorbance obtained at high amounts of antigen in the solid is indicated by A_P, and the quantity $c_s c^*$ can be evaluated from A_P. The concentration of free toxin in the solid [T'] can not be determined in an easy way. If only a small fraction of toxin in the solid is linked to the antibody, which is true when the toxin in present in large excess, or if the affinity constant is low, the following relationship holds, obtained from Eqs. (5) and (6):

$$[T'] = q_T f_T/w \tag{12}$$

By plotting A versus q_T two straight lines should be obtained at very low and very high amount of antigen in the solid, as observed in Fig. 1 and Fig. 2. Their intercept for $n = 1$ is at

$$q_T(i) = (V/K' f_T) \tag{13}$$

which is independent of the amount of antibody.

Notice that this intercept should depend on the amount of antibody if K' were high enough to quantitatively form the complex antigen–antibody. Thus, the hypothesis that only a small

fraction of antigen in the solid is liked to the antibody can be immediately checked by observing if the intercept $q_T(i)$ of the two branches of the curves A versus q_T is independent of the amount of antibody.

The first point is the determination of n in equilibrium 1. Even an approximate value is acceptable since it can be only 1 or 2. This can be easily obtained if $c'_T = [T']$, i.e., that only a negligible amount of toxin is linked to the antibody in the solid. Then Eq. (9) can be transformed in the following logarithmical form

$$\log(A/(c_s c^* V/d - A)) = \log K' f_T^n / w^{1-n} V + n \log q_T \quad (14)$$

which can be used for the simultaneous determination of n and $K' f_T^n / w^{1-n}$. The term to the left can be evaluated if $c_s c^* V/d$ is known, as it is when the plateau value of the absorbance (A_P) is known (Eq. (11)).

It must be clearly kept in mind that Eq. (14) holds if $c'_T = [T']$. If this approximation is suspected not to be true, it is convenient to transform Eq. (9) by taking into account Eqs. (3), (4) and (11). The following relationship is obtained, linear in the parameters, and with two variables:

$$(A^{1-n}/(c_s c^* V/d - A))^{1/n} = (K'/w^{n-1} V)^{1/n} q_T f_T / A - (K'/w^{n-1} V)^{1/n} n\, w/c^* \quad (15)$$

The independent variable is q_T/A, and the dependent one is $(A^{1-n}/(c_s c^* V/d - A))^{1/n}$. It can be evaluated when $c_s c^*$ and n are known. If it is found that the second term to the right in Eq. (15) is near to zero, this means that only a small amount of antigen in the solid is linked to the antibody, i.e., the concentration of free toxin in the solid is equal to the total one.

By this procedure only the quantity $K' f_T$ can be determined, not the individual values of the two quantities K' and f_T. This is however sufficient for characterizing the ELISA procedure.

3.2. Determination of the affinity constant the antibody–antigen complex in solution by competition ELISA

In the presence of antigen in solution (T), the antibody binds also to it according to the equilibrium

$$Ab + mT \Leftrightarrow AbT_m \quad (16)$$

with an affinity constant:

$$K = \frac{[AbT_m]}{[Ab][T]^m} \quad (17)$$

The fraction of antibody linked to the solid phase is given by the relationship

$$B_{Ab}/c_{Ab} V = \frac{[AbT'_n] w}{[AbT'_n] w + [Ab] V + [AbT_m] V} \quad (18)$$

The equilibrium for the formation of the antigen–antibody complex in the solid phase (AbT'_n) is that reported above (Eqs. (1) and (2)). Eq. (18) can be written as following

$$A = (c_s c^* V/d) \frac{1}{1 + (V w^{n-1}/K'[T']^n w^n) + K[T]^m V/K'[T']^n w} \quad (19)$$

In the assay without any antigen in solution, which is always carried out together with the competition experiments, the final absorbance A_d is given by a relationship equal to Eq. (9). Thus, Eq. (19) can be converted in the following relationship

$$1/A = 1/A_d + \frac{K[T]^m V w^{n-1}}{A_d (K'[T']^n w^n + V w^{n-1})} \quad (20)$$

For evaluating m Eq. (20) can be converted in the following logarithmical form

$$\log(A_d/A - 1) = \log K V w^{n-1}/(K'[T']^n w^n + V w^{n-1}) + m \log[T] \quad (21)$$

In solution phase too the concentration of free toxin [T] can not be determined experimentally, but it can be assumed to be equal to the total concentration of antigen, if the affinity constant is low, and the toxin is present in large excess with respect to the antibody, as

$$c_T = [T] + m[AbT_m]. \quad (22)$$

By plotting $\log(A_d/A-1)$ versus $\log c_T$ a straight line should be obtained, with slope m. K can be evaluated, since $K'f_T^n/w^{n-1}$ is known from the experiments in the absence of any antigen in solution, as described above. By this procedure the affinity constant in solution is determined. In principle only one series of ELISA in the presence of antigen is required to obtain this information, if the proper concentration range of the antigen is considered.

3.3. Position of the competition curve and dynamic range

The position of the competition curve can be indicated by the concentration of antigen in solution for which one half of the maximum amount of antibody is linked to the solid ($[T]^m_{(0.5)}$). Here $A/A_d = 0.5$, and thus it is obtained from Eq. (20) that

$$[T]^m_{(0.5)} = \frac{K'[T']^n w^n + Vw^{n-1}}{KVw^{n-1}} \quad (23)$$

It shows that the position of the competition curve is substantially determined by the affinity constant in the solid and in the solution, and by the amount of antigen blocked to the solid phase.

The lower limit for $[T]^m_{(0.5)}$ is given by $1/K$, since here $K'[T']^n w^n$ is negligible with respect to Vw^{n-1}. Of course a decrease in the amount of antigen coating the well causes a decrease in the final signal, and that is the reason why the detection limits depend also on the detection method. It is also seen that by using a higher amount of antigen to coat the wells, the competition curve is shifted towards higher concentration of antigen in solution. The evaluation of $[T]^m_{(0.5)}$ can be done when $K'f_T^n$ and K are known, and the amount of conjugate used for coating the solid has been decided.

Also the range for the competition can be evaluated from Eq. (20). Suppose that the two limiting values for A/A_d are 0.9 and 0.1, respectively for the maximum binding of antibody to the solid phase, and the total competition. To have competition the concentration of the antigen in solution $[T]^m$ should be in the range

$$(10-1)(K'[T']^n w^n + Vw^{n-1})/KVw^{n-1} > [T]^m > (1.111-1)(K'[T']^n w^n + Vw^{n-1})/KVw^{n-1} \quad (24)$$

When $[T]^m$ is higher than $(10-1)(K'[T]^n w^n + Vw^{n-1})/KVw^{n-1}$ there is a total competition, and not any antibody is linked to the solid, while at concentrations lower than $(1.111-1)(K'[T']^n w^n + Vw^{n-1})/KVw^{n-1}$ there is not competition at all. Thus the useful concentration range for the analytical determination should cover about two magnitude orders in concentration, if $m = 1$.

The slope of the standardization curve A/A_d versus $\log c_T$ should be around 0.4.

The amount of antibody seems to be of no importance for determining the position of the competition curve.

4. Results and discussion

4.1. Investigation on the antigen–antibody complex formation in the solid phase and in solution by ELISA

In Fig. 1 and Fig. 2 some curves showing the final absorbance A in function of the amount of Aflatoxin B_1-BSA used to activate the well (q_T, in ng) obtained by ELISA at zero dose of analyte are reported, respectively for procedure A and B. The presence of Aflatoxin B_1-BSA in the solution after coating, and in the washing solutions, was checked by an independent ELISA carried out by procedure B. Not any conjugate was found up to 1000 ng of total conjugate, which seems to be completely sorbed.

For both procedures the curves are composed of two limiting straight lines. Their intercept is seen to be independent of the concentration of antibody, being at around $Q_T(i) = 20$–30 ng in all the experiments carried out at different concentrations of antibody. This indicates that the formation of the complex antigen–antibody (Eq. (1)) is an equilibrium with a low equilibrium coefficient. The value of $K'f_T$ which is obtained from the intercept of the two straight lines, for $n = 1$ and according to Eq. (13), is 4.0×10^{-3}. To have an idea of the value of the formation coefficient K', f_T can be assumed to be 1.4×10^{-10}, the value

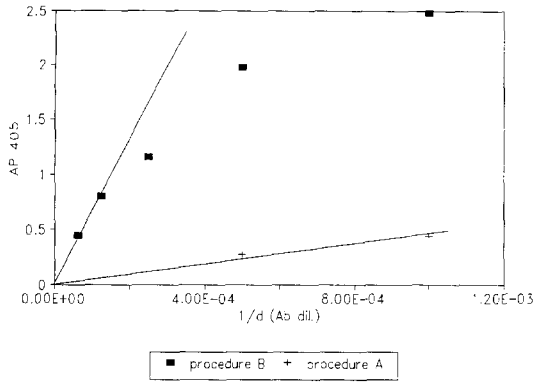

Fig. 3. Limiting value of the absorbance (A_P) at high amount of antigen in the solid phase (ELISA at zero concentration of antigen) in function of the dilution of the specific antibody. Data obtained from Fig. 1 and Fig. 2. + Procedure A. ■ Procedure B.

calculated if exactly 10 mol of Aflatoxin B_1 were linked per mol of BSA, and if all the antigen used for coating was finally linked to the solid. In this case $K' = 2.8 \times 10^7$. Of course if the amount of antigen was exactly known, the coefficient obtained in this way would be the real one. The absorbance at the plateau (A_P) is a function of the antibody dilution, as seen in Fig. 3. On the basis of the simple model outlined above (Eq. (11)) a straight line passing through zero is expected at all the antibody dilutions considered. This is true only at the lowest concentrations of antibody, at low values of $1/d$. At high concentration, the antibody seems not to be completely bound to the solid phase. This can be due to steric reasons. Another explanation can be that not all the Aflatoxin B_1-BSA conjugate sorbed on the well is available for the combination with the antibody, since it is possible that at high amounts of protein its sorption on the well takes place by formation of multilayers [10]. In this case only that antigen belonging to the layer in contact with the solution can react. Here the quantity which limits the final absorbance is the amount of conjugate in the first protein layer.

Whatever is the reason, the value of $c_s c^*$ can be obtained from that part of the curves A_p versus $1/d$ which is a straight line. It is 3.3×10^3 in procedure A and 6.4×10^4 in procedure B. Due to the poor reproducibility, $c_s c^*$ should be determined for each experiment.

The value of n, the moles of toxin linked to each mole of specific antibody in the solid phase, was evaluated by Eq. (14), from which $K' f_T^n / w^{n-1}$ could also be obtained. The results from the data of Fig. 1 and Fig. 2 are reported in Table 1 (Procedure A and Procedure B, with different operators). The average value of n is near to 1. In all the examples considered a straight line was obtained by plotting $\log(A/(c_s c^* V/d - A))$ versus $\log q_T$ according to Eq. (14). This confirms that only a small fraction of toxin in the solid is linked to the antibody.

Once the value of n established ($n = 1$), $K' f_T$ can be calculated at each point, according to Eq. (14). These results too are reported in Table 1. In the case of the procedure B somewhat lower values of $c_s c^*$ were obtained at the highest concentrations of antibody, and also lower values of $K' f_T$. To confirm this point the same kind of determinations were repeated at even higher dilution, using a different incubation time with the alkaline phosphatase substrate. The results, reported in Table 1, confirm that $K' f_T$ is higher and constant in more diluted antibody solution. Of course a higher value of $c_s c^*$ is obtained when a longer incubation time is used. The fact that the affinity constant in the solid obtained by procedure A is only slightly lower than that obtained by procedure B indicates that the combination site for antigen is not affected by the presence of the marker enzyme.

The antigen–antibody complex formation in aqueous solution is characterized by ELISA in the presence of antigen in solution. For fixed amounts of Aflatoxin B_1-BSA in the solid phase and of specific antibody in solution, the final amount of antibody in the solid depends on the amount of Aflatoxin B_1 in solution, being lower when higher amounts of antigen are present, due to the formation of the complex antibody–Aflatoxin B_1 in solution. An example of competition curves obtained with procedure B is shown in Fig. 4, where the final absorbance measured for each well is reported against $\log c_T$ (in $\mu g\ l^{-1}$) of antigen in solution. The three values obtained for each concentration are reported to give an idea of the

Table 1
Complex formation in the solid phase between Aflatoxin B_1-BSA in the solid and the specific antibody in DBA (results obtained by Eq. (14))

	n (S.D.)[a]	$c_x c^{*}$[b]	$K' f_T$
Procedure A			
$d = 2000$, $A_P = 0.276$	1.10(0.10) $R^2 = 0.983$	4.3×10^3	5.34×10^{-3}
$d = 1000$, $A_P = 0.455$	1.36(0.19) $R^2 = 0.970$	4.1×10^3	4.19×10^{-3}
Procedure B	(Operator n.1, 10′ incubation time with substrate)		
$d = 16\,000$, $A_P = 0.447$	0.82(0.19) $R^2 = 0.826$	7.1×10^4	9.23×10^{-3}
$d = 8000$, $A_P = 0.803$	0.55(0.08) $R^2 = 0.972$	6.4×10^4	4.46×10^{-3}
$d = 4000$, $A_P = 1.160$	1.26(0.10) $R^2 = 0.976$	4.6×10^4	2.36×10^{-3}
$d = 2000$, $A_P = 1.578$	0.81(0.03) $R^2 = 0.993$	3.1×10^4	3.30×10^{-3}
$d = 1000$, $A_P = 2.418$	1.74(0.15) $R^2 = 0.971$	3.4×10^4	2.03×10^{-3}
Procedure B	(Operator n.2, 20′ incubation time with substrate)		
$d = 40\,000$, $A_P = 0.905$	0.79(0.15) $R^2 = 0.912$	3.6×10^5	10.9×10^{-3}
$d = 20\,000$, $A_P = 1.793$	0.66(0.07) $R^2 = 0.969$	3.6×10^5	8.95×10^{-3}
$d = 10\,000$, $A_P = 1.316$	0.84(0.06) $R^2 = 0.977$	1.3×10^5	10.3×10^{-3}

[a] Number of antigen moles linked per mole of antibody to form the antigen–antibody complex in the solid.
[b] Obtained from the plateau absorbance A_P.

irreproducibility among the wells. Of course these competition curves can be considered as calibration curves for the determination of Aflatoxin B_1. The second competition curve in Fig. 4 was obtained by the same operator, using exactly the same conditions and the same reagents, but in different days and on a different microplate. This shows that the reproducibility of the calibration curve is poor, and this is the reason why the calibration curve must be repeated for each determination. The reproducibility is much improved if one considers the absorbance relative to that obtained in the same conditions, but at zero concentration of antigen in solution, indicated by A_d. The functions A/A_d versus $\log c_T$ for the data of Fig. 4 are shown in Fig. 5. As an example the same kind of data obtained by procedure A are reported in Fig. 6. All the competition curves obtained in the present work have the same shape.

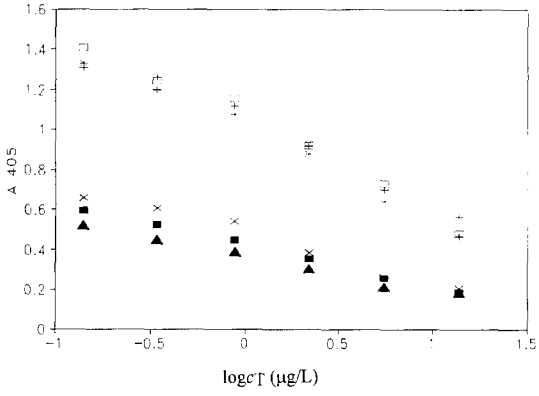

Fig. 4. Competition ELISA curve, procedure B. Two different experiments at the same conditions in different days. Coating: 13 ng of Aflatoxin B_1-BSA per well; $d = 5000$; 20′ incubation time with the substrate.

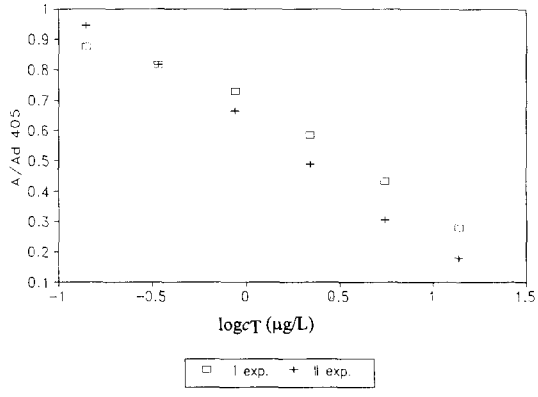

Fig. 5. Competition ELISA curve, procedure B. Ordinates: median absorbance of the three wells at the same concentration of Aflatoxin B_1, relative to that at zero concentration of antigen in solution (A_d). Data obtained from that shown in Fig. 4: □ I experiment, + II experiment.

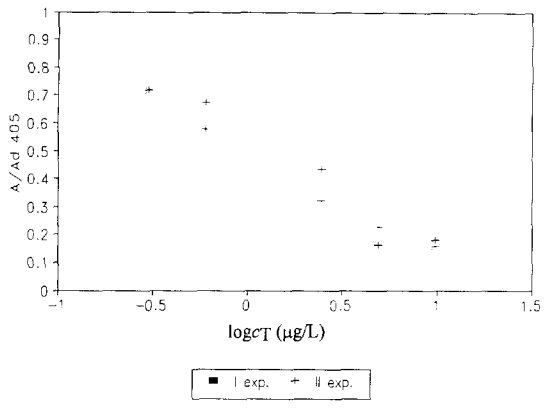

Fig. 6. Competition ELISA curve, procedure A. Ordinates: median absorbance relative to that at zero concentration of antigen in solution (A_d). Coating: 32 ng of Aflatoxin B_1-BSA per well; $d = 1000$.

The dynamic range extends over a concentration range of two magnitude orders, as expected from relationship 24, and the slope is near to the expected value of 0.4.

The results obtained by treating the data of the competition experiments according to Eqs. (20) and (21) are reported in Table 2. The slopes of the straight lines obtained by plotting $\log(A_d/A - 1)$ versus $\log c_T$ (Eq. (21)) are near to 1, so that it is possible to examine the data by Eq. (20) with $m = 1$. The parameters of the straight line obtained by plotting $1/A$ versus c_T (minimum squares method) are given in Table 2. The values of A_d evaluated from the intercept on the ordinates are reported and compared with those obtained experimentally, showing an acceptable agreement. It must be observed again that the values of A_d are very irreproducible. The slopes of the straight lines obtained according to Eq. (20) are reported, together with the values of K calculated. For the first four examples the original data are those of Fig. 5 and Fig. 6. The value of $K'f_T$ was assumed to be that obtained from the direct ELISA, at the particular antibody dilution, as discussed above. The values of K show a good reproducibility, both for procedure A and B, giving an average value of 2×10^8. The similarity of this value in procedure A and B indicates that the site for the combination with the antigen is not affected by the marker enzyme, as previously observed in the case of the complexation in the solid phase.

When $K'f_T$ and K are known, the position of the competition curve can be evaluated in function of the amount of Aflatoxin B_1-BSA sorbed in the well.

From Eq. (23) it is expected that the dynamic range is shifted towards higher concentrations of antigen in solution when the amount of antigen in the solid increases. This is shown in Fig. 7, where two competition curves, obtained respectively by coating with 1 and 13 ng of Aflatoxin B_1-BSA are reported. The values of $[T]_{(0.5)}$ calculated from Eq. (23) were respectively, 0.82 and 1.72 mg l^{-1}, in agreement with those found in the experiments.

Amounts of Aflatoxin B_1-BSA lower than around 1 ng do not have any further effect on the position of the competition curve, since here $[T]_{(0.5)}$ is equal to $1/K = 5 \times 10^{-9}$ M.

On the contrary the dynamic range is expected to be independent of the amount of antibody in the solution phase. This is shown by the data reported in Fig. 8, where the competition curves obtained by coating with 13 ng of Aflatoxin B_1-BSA and different dilutions of specific antibody are reported. The results obtained by treating these data according to Eqs. (20) and (21) are also given in Table 2.

The value of K is important in determining the position of the competition curve. Thus it is expected that in the case of other aflatoxins different from Aflatoxin B_1 the curve is shifted towards higher concentrations of antigen in solution, having probably complexation coefficients with the antibody specific to Aflatoxin B_1 lower than that of Aflatoxin B_1 itself. This is seen in Fig. 9, where the competition curves for Aflatoxin B_1, B_2, G_1 and G_2 are shown. According to the dealer, these aflatoxins are all recognized by the antibody specific to Aflatoxin B_1. As a matter of fact they all compete with the antigen in the solid phase, even if Aflatoxin B_1 is that most strongly bound by its specific antibody. The value of K for the different aflatoxins considered are reported in Table 3. They were calculated by Eq. (20), with $m = 1$, and are around one magnitude order lower than the formation coefficient of Aflatoxin B_1.

Table 2
Competition ELISA for Aflatoxin B_1

	m (S.D.) results obtained from Eq. (21)	Eq. (20) intercept on the ordinates (S.D.) A_d calc. (limits), A_d sper.	Eq. (20) slope (S.D.) K (R^2)
Procedure A, $d = 1000$, $K'f_T = 5 \times 10^{-3}$, Aflatoxin B_1-BSA: 32 ng	0.777 (0.156) $R^2 = 0.860$	5.62(3.98); A_d calc. = 0.178(0.610–0.104); A_d sper. = 0.348	4.43(1.47) × 10^8; K = 2.04 10^8, $R^2 = 0.693$
Procedure A, $d = 1000$, $K'f_T = 5 \times 10^{-3}$, Aflatoxin B_1-BSA: 32 ng	0.748(0.021) $R^2 = 0.998$	4.530(1.062); A_d calc. = 0.221(0.288–0.178); A_d sper. = 0.337	4.51(0.41) × 10^8; K = 2.59 10^8, $R^2 = 0.976$
Procedure B, $d = 10\,000$, $K'f_T = 10 \times 10^{-3}$, Aflatoxin B_1-BSA: 13 ng	0.894(0.142) $R^2 = 0.908$	0.622(0.09); A_d calc. = 1.608(1.879–1.404); A_d sper. = 1.630	5.03(0.34) × 10^8; K = 1.55 × 10^8, $R^2 = 0.982$
Procedure B, $d = 10\,000$, $K'f_T = 10 \times 10^{-3}$, Aflatoxin B_1-BSA: 13 ng	0.917(0.059) $R^2 = 0.983$	2.19(0.35); A_d calc. = 0.457(0.543–0.394); A_d sper. = 0.538	1.91(0.08) × 10^8; K = 2.00 × 10^8, $R^2 = 0.990$
Procedure B, $d = 40\,000$, $K'f_T = 10 \times 10^{-3}$, Aflatoxin B_1-BSA: 13 ng	0.808(0.021) $R^2 = 0.997$	1.86(0.52); A_d calc. = 0.538(0.746–0.420); A_d sper. = 0.728	1.71(0.13) × 10^8; K = 2.27 × 10^8, $R^2 = 0.972$
Procedure B, $d = 10\,000$, $K'f_T = 10 \times 10^{-3}$, Aflatoxin B_1-BSA: 1 ng	0.891(0.038) $R^2 = 0.996$	1.51(0.20); A_d calc. = 0.662(0.763–0.585); A_d sper. = 0.753	3.90(0.13) × 10^8; K = 2.84 × 10^8, $R^2 = 0.997$

Characterization of the antigen–antibody complex formation in solution (DBA) by Eq. (20) and Eq. (21).

4.2. Development of a method for the determination of Aflatoxin B_1 in food samples

As an example an ELISA method is here developed, using procedure B, in which the competition curve should be at a concentration of Aflatoxin B_1 around $[T]_{(0.5)} = 1$ μg l^{-1} (3.2×10^{-9} M) and the detection range is extended from 0.1 to 10 μg l^{-1}. The amount of Aflatoxin B_1-BSA to be used for coating the well, calculated from Eq. (23), is 3.3 ng. The dilution of antibody was selected as low as possible, to have a high final absorbance, but a linear dependence from the antibody concentration. From the data reported in Fig. 3 a dilution of 1:5000 was used. The competition curve experimentally obtained using these conditions is described by the following equation $A/A_d = 0.68(0.06) - 0.43(0.04) \log c_T$(μg l^{-1}) showing that the concentration of Aflatoxin B_1 for which $A/A_d = 0.5$ is at 2.4 μg l^{-1}, near to that expected. The error on the estimated $\log c_T$(μg l^{-1}) is 0.14 units. The lower detection

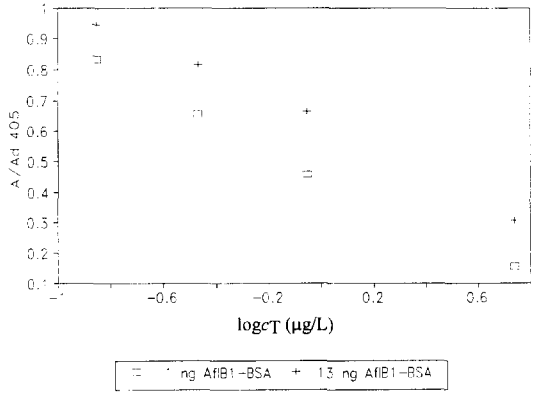

Fig. 7. Effect of the amount of antigen in the solid phase on the dynamic range of the competition ELISA. Procedure B, with $d = 10\,000$; 20′ incubation time with the substrate. Aflatoxin B_1-BSA per well: □ 1 ng; + 13 ng.

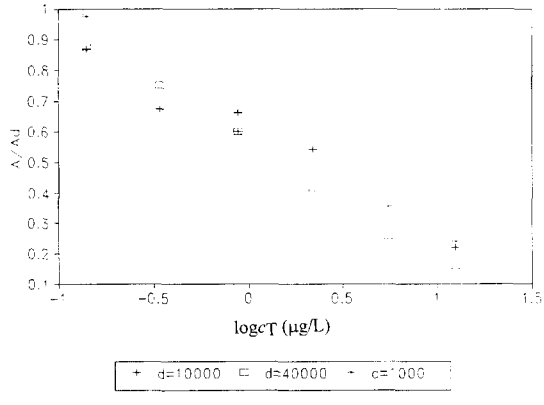

Fig. 8. Effect of the amount of antibody on the dynamic range of the competition ELISA. Procedure B, with 13 ng of Aflatoxin B_1-BSA per well; 20′ incubation time with the substrate. Dilution of antibody: □ $d = 40\,000$, + $d = 10\,000$, * $d = 1000$.

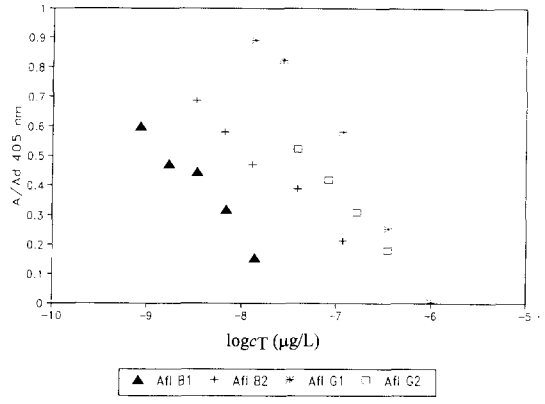

Fig. 9. Competition ELISA for different aflatoxins, using procedure B, with 19 ng of Aflatoxin B_1-BSA per well, $d = 1000$; 10′ incubation time with the substrate.

limit in the final solution is around $\log c_T(\mu g\ l^{-1}) = -0.5$.

Some results obtained by the described procedure are reported in Table 4. Two samples of a certified peanut butter [12] were analyzed by extracting 15 g with 30 ml of acetonitrile + water (1 + 1), for 2 h under stirring in a closed vessel at room temperature. Of the extract, 20 μl were used for the ELISA determination. They were directly added in the well with 80 μl of DPA containing the antibody at the final dilution of 1:5000. The results are the average of three replicates. They are in agreement with the certified value, both for the high and low concentration. The extract was also diluted 1:4 with acetonitrile + water (1 + 1) and immediately analyzed, obtaining a concentration in agreement. Also the recovery was satisfactory.

Table 3
Affinity constants of the complex formed by some different aflatoxins and the antibody specific to Aflatoxin in DBA

	Eq. (20): $1/A = 1/A_{d+}(K[T] V/A_d(K'[T']w+V))$	log K
Aflatoxin B_2	$1/A = 1.79(0.19)+3.15(0.20) \times 10^7\ c_T$ $R^2 = 0.988$	log $K = 7.34$
Aflatoxin G_1	$1/A = 1.27(0.18)+1.26(0.06) \times 10^7\ c_T$ $R^2 = 0.992$	log $K = 7.14$
Aflatoxin G_2	$1/A = 1.17(0.14)+1.21(0.06) \times 10^7\ c_T$ $R^2 = 0.994$	log $K = 7.16$

Results obtained from the data reported in Fig. 9 by using Eq. (20), with $n = 1$ and $m = 1$, and $K'f_T = 2 \times 10^{-3}$.
The error of the estimated parameters is reported in parenthesis.

A wheat flour sample obtained on the market was analyzed after extraction of 15 g with 10 ml of acetonitrile + water (1 + 1). A low, but detectable content of toxin was found. Dilution and recovery were satisfactory. It was noticed that if the extract was analyzed after 7 days storage at 4°C, the toxin was not any more detectable. Not any toxin was found in a barley sample again obtained on the market.

A sample of ground black pepper analyzed in the same way was found to contain 12 μg kg^{-1} of toxin, if the undiluted extract was analyzed, but higher and higher concentrations when the extract was diluted. On the other hand the recovery was also very low. There is evidently some interference which has the effect of lowering the concentration determined. Not any further investigation was carried out to clarify this point. These results are reported to show that even if the immunological reactions are very selective, the possibility of important matrix effects can not be excluded a priori.

5. Conclusions

Theoretical considerations based on widely recognized equilibria concepts, applied to the combination of an antigen with the specific antibody in solution and in the solid phase, with formation of only one kind of complex, showed that the position of the competition curve depends on the amount of antigen-BSA conjugate used for coating the well and on $K'f_T^n$ and on K, which both vary if reagents either from different batches and different commercial sources are used. Thus, they must be individually characterized. Moreover it is possible that different microplates have different sorbing properties towards protein. A complete

Table 4
Concentration of Aflatoxin B_1 in different foodstuffs, determined by procedure B, with 3.3 ng of Aflatoxin B_1-BSA, and antibody diluted 1:5000

Description of the sample	Determination immediately after extraction	Determination immediately after extraction, on the extract diluted	Determination of old extracts	Recovery of additions to the solid sample
Peanut butter, low content, CRM 401, BCR certified reference material, <0.2 μg kg^{-1} Aflatoxin B_1	Not detectable			
Peanut butter, high content, CRM 385, BCR certified reference material, 7.0 μg kg^{-1} Aflatoxin B_1	5.5 μg kg^{-1}	dil 1:4, 7.6 μg kg^{-1}		2.4 μg kg^{-1} added, recovery 85%
Barley (corn)	Not detectable <1 μg kg^{-1}			
Wheat flour	1.3 μg kg^{-1}	dil 1:4, not detectable	After 7 days storing at 4°C: not detectable	1.5 μg kg^{-1} added, recovery 90%
Ground black pepper	12 μg kg^{-1}	dil 1:1, 23 μg kg^{-1}; dil 1:4, 50 μg kg^{-1}		8.0 μg kg^{-1} added, recovery 20%

control of all these points could be a very difficult and time consuming task, and this is probably the reason why not specialized laboratories prefer to use prepacked kits for immunological determinations. However in the present paper it has been shown that it is not necessary to check all these points individually for planning an ELISA experiment. Useful information about the characteristics of the immunoreagents used for an indirect ELISA can be obtained by indirect ELISA at zero concentration of antigen in solution, carried out by keeping constant the amount of specific antibody and by varying the amount of antigen in the solid. This is also true when the exact amount of antigen which actually is sorbed on the solid and that of antibody is not known. The value of $c_s c^*$ for the considered procedure, and the antibody dilutions for which a value of $c_s c^*$ independent of the dilution is obtained, can be easily determined, and used for deciding the proper antibody dilution in the competition experiments. c^* can be evaluated only if c_s is known, which is often not the case when using commercial antisera. However the knowledge of $c_s c^*$ is sufficient for subsequent evaluations. Also the affinity constant of the antigen–antibody complex in the solid can be obtained only if the amount of antigen in the solid is exactly known. If not, the quantity $K' f_T^n$ is determined, which is again sufficient for planning the competition experiments. The antigen–antibody combination in solution can be studied by ELISA experiments in the presence of antigen in solution, and the affinity constant in solution K can be determined if $K' f_T^n$ is known. This can be a convenient method for determining the affinity constant of an antigen–antibody complex.

Then the amount of antigen-BSA conjugate to be used for coating the solid in competition ELISA is selected in function of the desired dynamic range, according to Eqs. (23) and (24) obtained from the model. Possible interferences are also evaluated in function of the affinity constants in solution. A two magnitude order difference in the affinity constants is required to have not any interference.

The characterization method here proposed is simple, requires only a low amount of reagents, and takes the time of 2–3 ELISA. As a matter of

fact two ELISA without competition at two different dilutions of antibody, which can be carried out simultaneously, are necessary for determining $c_s c^*$ and $K' f_T^n$. For each the final absorbance of the substrate solution must be measured at different amount of antigen–BSA up to a value for which a constant absorbance (A_P) is reached. This should be directly proportional to the reciprocal of the antibody dilution d. If it is not, more experiments at lower concentration of antibody must be carried out.

The affinity constant in the solution phase can be calculated from only one ELISA with competition. The treatment of the data is very simple if the total and free concentration of Aflatoxin B_1, both in the solid and in solution, are equal, as it happens in the systems here considered.

Similar results were obtained for the two considered procedures, the indirect ELISA based on the use of only one antibody labelled with peroxidase, and that employing a specific antibody, and a conjugate antibody–alkaline phosphatase. This means that the conjugate specific antibody–peroxidase combines with Aflatoxin B_1, both in solution and in the solid phase, in a way very similar to that of the not conjugated specific antibody, as shown by the values of the respective affinity coefficients.

References

[1] E. Engvall, P. Perlmann, Immunochemistry 8 (1971) 871.
[2] O. El-Nakib, J.J. Petska, F.S. Chu, J. Assoc. Off. Anal. Chem. 64 (1981) 1077.
[3] J.J. Pestka, J. Assoc. Off. Anal. Chem. 71 (1988) 1075.
[4] F.S. Chu, Vet. Human Toxicol. 32 (1990) 42.
[5] L.S. Lee, J. Am. Oil Chem. Soc. 66 (1989) 1398.
[6] A.L. Patey, M. Sharman, R. Wood, J. Gilbert, J. Assoc. Off. Anal. Chem. 72 (1989) 965.
[7] F.S. Chu, Mycotoxins in ecological systems, in: D. Bhatnagar, E.B. Lillehoj, D.K. Arora (Eds.), Handbook of Applied Mycology, Vol. 5, Marcel Dekker, New York, 1992, pp. 87–136.
[8] E. Harlow, D. Lane, Antibodies: A Laboratory Manual, Cold Spring Arbor Laboratories, Cold Spring Arbor, New York.
[9] G. Scatchard, Ann. N.Y. Acad. Sci. 51 (1949) 699.
[10] B. Friguet, A.F. Chaffotte, L. Djavidi-Ohaniance, M.E. Goldberg, J. Immunol. Methods 77 (1985) 305.
[11] L.A. Cantarero, J.E. Butler, J.W. Osborne, Anal. Biochem. 105 (1980) 375.
[12] BCR Information, Reference Materials, CRM 895, 401, Report EUR 13901 en, 1991.

ELSEVIER

Talanta 45 (1997) 105–111

Talanta

Simultaneous spectrofluorimetric determination of 1-naphthylacetic acid and 1-naphthalenacetamide in commercial formulations and soil samples

José Luis Vilchez, Rosario Blanc, Alberto Navalón *

Research Group of Solid-Phase Spectrometry, Department of Analytical Chemistry, University of Granada, E-18071 Granada, Spain

Received 25 November 1996; received in revised form 14 March 1997; accepted 3 April 1997

Abstract

A spectrofluorimetric method for the simultaneous determination of 1-naphthylacetic acid (NAA) and 1-naphthalenacetamide (NAD) was developed. The sample solution containing both analytes was equilibrated with Sephadex QAE A-25 gel by agitation and then only NAA was fixed on gel, while the remaining NAD stayed in the solution. The relative fluorescence intensity of NAA fixed on Sephadex QAE A-25 gel was measured directly after packing the gel beads in a 1-mm silica cell, using a solid-phase attachment. NAD was determined spectrofluorimetrically in the solution. The wavelengths of excitation and emission chosen for the determination of NAA were 280 and 336 nm, respectively, and for NAD determination 222 and 337 nm, respectively. The applicable concentration range was 12–60 ng ml^{-1} for NAA and 6–120 ng ml^{-1} for NAD. The detection limit was 3 ng ml^{-1} for NAA and 2 ng ml^{-1} for NAD. The method was applied satisfactorily to the determination of NAA and NAD in commercial formulations of phytohormones and soil samples. © 1997 Elsevier Science B.V.

Keywords: 1-Naphthylacetic acid (NAA); 1-Naphthalenacetamide (NAD); Phytohormone analysis; Soil analysis; Solid-phase spectrofluorimetry

1. Introduction

1-Naphthylacetic acid (NAA) and 1-naphthalenacetamide (NAD) are naphthalene derivatives widely used as fungicide on fruits and also useful as plant growth regulators to prevent the premature fall of fruits [1,2]. Consequently, trace amounts in soil may be expected coming from agricultural manipulations.

Commercial formulations involving mixtures of NAA, NAD and/or other fungicides are usually found in proprietary brands [2].

Our perusal of publications on these compounds reveals there are no published researches on their simultaneous determination. Probably, this is due to hydrolysis of NAD into NAA. Spectrophotometric determinations of NAA in pineapple fruits down to a limit of detection of 30 ng ml^{-1} were made by Young et al. [3]. Spectrofluorimetry of NAA and NAD in citrics and

* Corresponding author.

PII S0039-9140(97)00116-1

apples up to detection limits of 10 and 25 ng ml^{-1} was reported by Sigrist et al. [4] and García Sanchez et al. [5]. NAA low temperature phosphorescence [6] and at room temperature [7] yielded limits of 2 mg l^{-1}. Gas chromatography (GC) [8,9] with detection limits of 100 ng l^{-1} was used for NAA determination in olives, pears and apples while high-performance liquid chromatography (HPLC) [10–12] was used for NAA in oranges and tangerines with a detection limit of 8 ng ml^{-1} and for NAD in apples down to 10 ng ml^{-1}.

On the other hand, solid-phase spectrofluorimetry (SPF) to measure trace amounts of pesticides in water [13–16] has been found to have several advantages such as: low interference level, low detection limit, high sensitivity and the use of conventional instrumentation.

Here, a method for the simultaneous determination of NAA and NAD using both SPF and conventional spectrofluorimetry in solution is described, and has been applied satisfactorily to commercial formulations of phytohormones and soil samples.

2. Experimental

2.1. Apparatus and software

A Perkin–Elmer LS-5 luminescence spectrometer fitted with accessories described previously [17] was used to perform all spectrofluorimetric measurements, and a variable-angle surface accessory designed and constructed by the authors [17] was also used to carry out the measurements of relative fluorescence intensity (RFI) in gel phase.

A Crison 501 digital pH-meter with a combined glass–saturated calomel electrode and an Agitaser 2000 rotating agitator were also used.

The Statgraphics [18] software package was used for the statistical analysis of data. The lack-of-fit test was applied to check the linearity of the calibration graphs in accordance with the Analytical Methods Committee [19].

2.2. Reagents

All reagents were of analytical-reagent grade unless stated otherwise. Reverse osmosis quality water was used throughout.

Sephadex QAE A-25 dextran type anion-exchange gel (Sigma) was used in the chloride form in the original dry state as obtained from the supplier and without any pre-treatment.

1-Naphthylacetic acid stock solution (0.1 mg ml^{-1}) (Sigma) was prepared by exact weighing and dissolution in absolute ethanol. This solution was stable for at least 1 month. Working solutions were prepared by appropriate dilutions with deionized water.

1-Naphthalenacetamide stock solution (0.1 mg ml^{-1}) (Sigma) was prepared in the same way as described above for NAA stock solution. This solution was stable for at least 1 month. Solutions of lower concentration were obtained by dilution with deionized water.

Buffer solutions of required pH were made from 0.02 M Na_2HPO_4 (Merck) solution and 0.02 M NaH_2PO_4 (Merck) solution.

2.3. Fluorescence measurements

The measured RFI of the gel beads containing NAA and packed in a 1-mm quartz cell was the diffuse transmitted fluorescence emitted from the gel at the unirradiated face of the cell. The optimum angle between the cell plane and the excitation beam was 45° in all instances [17].

The RFI of the solution containing NAD was measured in a standard 1.0 × 1.0 cm quartz cell.

2.4. Basic procedure

An aliquot of the sample solution containing between 120 and 600 ng of NAA and between 60 and 1200 ng of NAD was transferred into a 10-ml calibrated flask containing 1 ml of 0.02 M phosphate buffer solution (pH = 7.0). The solution was diluted to the mark with deionized water. The mixture was then transferred into a 20-ml glass tube with stopper and 50 mg of Sephadex QAE A-25 gel were added. The mixture was shaken mechanically for 3 min. Afterwards, the resin

beads were collected by filtration under suction and with the aid of a pipette, packed into a 1-mm quartz cell together with a small volume (0.2 ml) of the solution. A total of 50 mg of Sephadex QAE A-25 gel was added to the filtrate and then shaken mechanically for 3 min. The new filtrate was collected for the determination of NAD. A blank solution was prepared and treated in the same way as described for the sample. The fluorescence intensities (at 20.0 ± 0.5°C) of the sample and blank were always measured at $\lambda_{em} =$ 336 nm with $\lambda_{ex} = 280$ nm for NAA determination and at $\lambda_{em} = 337$ nm with $\lambda_{ex} = 222$ nm for NAD determination.

Calibration graphs were constructed in the same way using NAA and NAD solutions of known concentrations.

2.5. Treatment of the sample

Fruitone (Etisa): 1.0 g of product was extracted with 100 ml of absolute ethanol assisted with an ultrasonic bath and filtered through Whatman No. 1 filter paper. Then 1 ml of filtrate was diluted with deionized water to 100-ml in a calibrate flask and used for measuring. Aliquots of this solution were taken and treated as described in Section 2.4.

Soils: 3 g of soil sample were extracted with 15 ml of absolute ethanol assisted with an ultrasonic bath during 30 min, filtered through Whatman No. 1 paper and the filtrate was diluted with absolute ethanol to 25-ml in a calibrated flask. An aliquot of this solution was taken and the NAA and NAD contents were determined as described in Section 2.4.

2.6. Distribution measurements

The distribution ratio of NAA fixed on the gel and in solution was studied. For this, 60 ng ml^{-1} of NAA solution was taken and treated as described in Section 2.4. The fluorescence intensity of NAA fixed on the gel and in solution was measured.

The distribution ratio was calculated in the usual way from the initial and equilibrium concentrations in the solution, according to the equation [20]:

$$D = \frac{\dfrac{\text{mmol of analyte fixed gel}}{\text{kg of dry gel}}}{\dfrac{\text{mmol of analyte solution}}{\text{dm}^3 \text{ of solution}}}$$

An average value of $D = 1115$ and a standard deviation of 21 were obtained from five replicates experiments at 60 ng ml^{-1} of initial concentration of NAA.

3. Results and discussion

3.1. Spectral characteristics

NAA and NAD show native fluorescence in aqueous solutions. The wavelengths of excitation and emission are 222 and 336 nm for NAA, and 222 and 337 nm for NAD, respectively (Fig. 1). When NAA is fixed on Sephadex QAE A-25 gel, the maxima of emission and excitation are located at 336 and 280 nm, respectively. On the other hand, NAD is not fixed on this gel (Fig. 2).

3.2. Effect of experimental variables

3.2.1. pH dependence

The influence of pH on the relative fluorescence intensity of both compounds was studied. The results show that the fluorescence emission of NAA fixed on the gel is maximum at pH 5.0–8.0 and of NAD in solution at pH 2.0–9.0. In order to work at the same pH value for the determination of both compounds, a pH of 7.0 was selected as optimum (Fig. 3).

Monohydrogen phosphate/dihydrogen phosphate buffer solution was used as the buffer solution. Since the fluorescence intensity of both compounds decreases with an increase in buffer concentration, a 0.002 M concentration of pH 7.0 buffer was selected to obtain an adequate buffering capacity without excessive loss of sensitivity.

3.2.2. Ethanol percentage

As the stock solutions of both compounds were prepared in absolute ethanol, the effect of this solvent on their relative fluorescence intensity was studied. For both compounds, the relative fluores-

cence intensity remains constant up to an ethanol content of 50% v/v and then decreases when the ethanol content in the medium is increased up to 90% v/v. On the other hand, no shifts in the excitation and emission spectra were observed when the solvent polarity was changed.

3.2.3. Temperature

The RFI dependence of both compounds on temperature is small (-0.5% °C^{-1} between 5 and 70°C for NAA fixed on the gel and -0.7% °C^{-1} for NAD). The RFI decrease with temperature was totally reversible for both compounds. All RFI measurements reported here were performed at 20.0 ± 0.5°C. Since the fixation process was independent of temperature in the range 0–40°C, the fixation of NAA on the gel was carried out at room temperature.

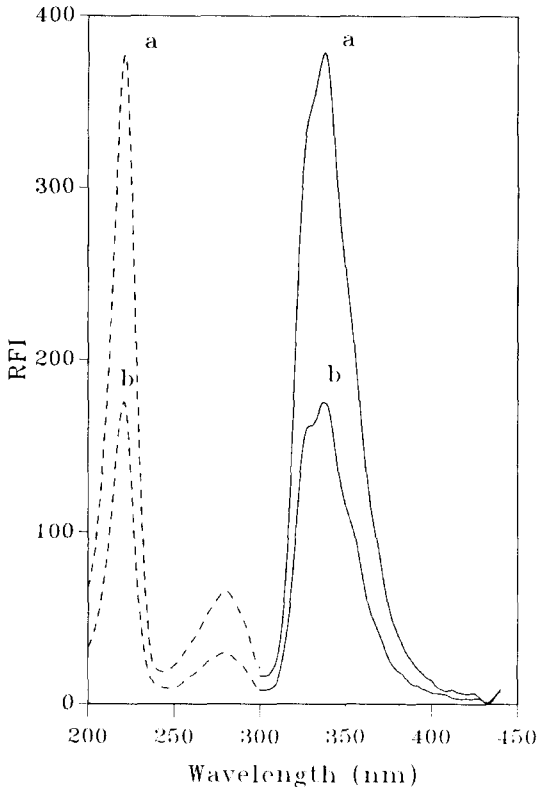

Fig. 1. Excitation (· · ·) and emission (——) spectra in solution of: (a) NAA; (b) NAD. [NAA] = 20 ng ml^{-1}; [NAD] = 20 ng ml^{-1}; pH = 7.0 (phosphate buffer).

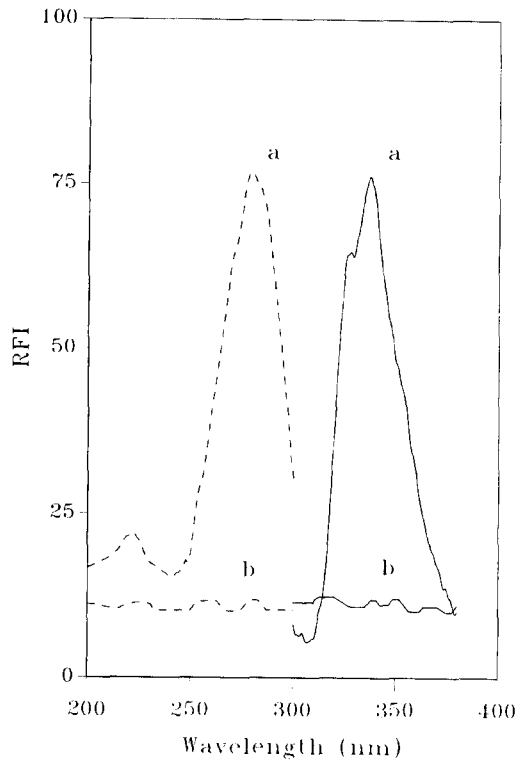

Fig. 2. Excitation (· · ·) and emission (——) spectra in solid phase of: (a) NAA; (b) NAD. [NAA] = 20 ng ml^{-1}; [NAD] = 20 ng ml^{-1}; pH = 7.0 (phosphate buffer).

3.2.4. Other experimental conditions

In the case of NAA fixed on the gel, the stirring time necessary for maximum RFI development was 3 min. Longer times did not result in any improvement. As the use of a large amount of the gel lowered the RFI, only the amount required to fill the cell and facilitate handling, i.e., 50 mg, was used in all measurements.

With regard to the stability of both systems, the RFI remained constant for at least 2 h. The order of addition of the reagents did not affect the results obtained.

3.3. Analytical parameters

The calibration graphs for the samples treated according to the procedure described above are linear for the concentration range 12–60 ng ml^{-1} for NAA and 6–120 ng ml^{-1} for NAD. The

lack-of-fit test [19] was used to check the linearity of the calibration graphs. Two replicates were used for each one of 10 standards prepared to obtain each calibration graph.

The IUPAC detection limits [21] found were 3 ng ml^{-1} for NAA and 2 ng ml^{-1} for NAD, and the quantification limits [22] were 12 and 6 ng ml^{-1} for NAA and NAD, respectively. Clayton's criterion [23] for the determination of the limit detection gave 4 ng ml^{-1} for NAA and 2 ng ml^{-1} for NAD.

The repeatability of the present method and of the packing of the gel in the 1-mm silica cell was also determined. The precision was measured for NAA and NAD concentrations of 30 and 60 ng ml^{-1}, respectively, by performing 10 independent determinations. The relative standard deviations (R.S.D.s) were 4.5 and 1.2% for NAA and NAD, respectively. The precision (R.S.D.) of the packing operation, calculated from 10 measurements, was 1.0% for the NAA fixed on the gel and 0.9% for the gel blank. The precision (R.S.D.) of the fluorescence measurements (noise) was about 0.5% in all instances.

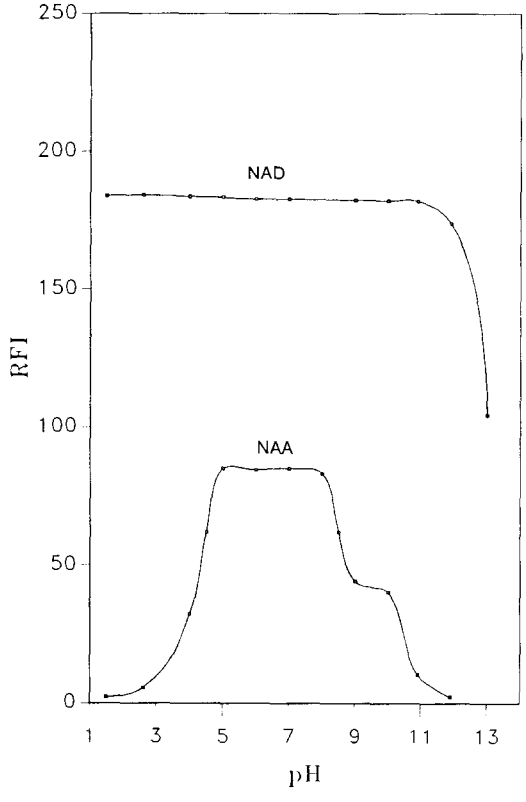

Fig. 3. Curve of variation of RFI vs. pH.

Table 1
Analytical parameters

Parameter	NAA	NAD
Intercept	1.97	12.96
Slope	3.20	6.98
Correlation coefficient	0.999	0.999
P_{lof} (%)[a]	83.6	30.2
Linear dynamic range (ng ml^{-1})	12–60	6–120
Detection limit (ng ml^{-1}):		
IUPAC criterion	3	2
Clayton's criterion[b]	4	2
Quantification limit (ng ml^{-1})	12	6
RSD (%)[c]	4.5	1.2

[a] Probability level of lack-of-fit test.
[b] The value of ($\alpha = 5\%$, $B = 5\%$) is 3.496 for NAA and 3.415 for NAD.
[c] Relative standard deviation for concentrations indicated in the text.

The analytical parameters are summarized in Table 1.

3.4. Applications of the method

The proposed method was applied to the determination of NAA and NAD in a commercial formulation (Fruitone: NAA 0.45% and NAD 1.2%). The sample was prepared as described above. The NAA and NAD determinations in this sample were carried out by using the standard additions method [24]. The reason for the election of the standard additions method was our findings when we used Youden's method [25]. Youden's method estimates the contributions to the fluorescence signal arising from other species different than the analyte constituting the whole matrix (Youden's blank). When applied here, it shows that in the NAD determination there is a matrix effect. Furthermore, the recovery data obtained, 102.2% for NAA and 100.8% for NAD, show good agreement with the composition values indicated by the supplier.

In view of the quality of the results, we applied the method to the determination of NAA and

Table 2
Recovery study of NAA and NAD in soil samples

Sample	NAA (ng ml^{-1})			NAD (ng ml^{-1})		
	Taken	Found[a]	Recovery (%)	Taken	Found[a]	Recovery (%)
Soil 1	10	9.7 ± 0.2	97.0	20	19.2 ± 0.4	96.0
	20	19.8 ± 0.4	99.0	40	39.1 ± 0.2	97.7
	30	29.5 ± 0.4	98.3	60	9.4 ± 0.3	99.0
Soil 2	10	9.9 ± 0.2	99.0	20	19.8 ± 0.3	99.0
	20	20.2 ± 0.3	101.0	40	40.1 ± 0.4	100.2
	30	29.4 ± 0.4	98.0	60	59.2 ± 0.3	98.6

NAA: For soil 1: $R = 98.1$; $s_R = 1.01$; $t(R) = 3.250$ ($P = 8.3\%$); critical value = 4.303 (5%). For soil 2: $R = 99.3$; $s_R = 1.53$; $t(R) = 0.782$ ($P = 50.1\%$); critical value = 4.303 (5%). NAD: For soil 1: $R = 97.6$; $s_R = 1.51$; $t(R) = 2.773$ ($P = 10.9\%$); critical value = 4.303 (5%). For soil 2: $R = 99.3$; $s_R = 0.83$; $t(R) = 1.459$ ($P = 28.1\%$); critical value = 4.303 (5%).
[a] Average value ± standard deviation of six determinations.

NAD in soil samples from the agricultural area near Granada (Spain). We found that the NAA and NAD content in soil samples was smaller than the above stated detection limits. To check the accuracy of the proposed method on the soil samples, a recovery study was carried out also. The soil samples were simultaneously spiked with various amounts of NAA and NAD and the recovery percentages were determined. Table 2 show the results obtained.

3.5. Validation of the method

The validation of the proposed method was carried out using the standard addition methodology [24] with two essential purposes: to check the accuracy and to determine analytes in samples where the analyte–matrix interactions produce an inaccurate result when the standard calibration method is used. For this purpose, we selected the determination of NAA and NAD in the commercial formulation Fruitone.

Three experiments are required to obtain the data set necessary to carry out the statistical protocol: (a) standard calibration (SC) as described above; (b) standard addition calibration (AC), which is obtained by addition of continuous variations of standard at constant sample volume; (c) Youden calibration (YC) with the Youden method, in which a calibration curve is established with continuous variations of sample volume.

By applying linear regression analysis, the slope, the intercept and the regression standard deviation for each curve are calculated. The parameters obtained from these three checkings are reported in Table 3 for NAA and Table 4 for NAD. From the values in Tables 3 and 4, the

Table 3
Numerical values of parameters from SC, AC and YC. Results of analyte content to check accuracy for NAA

Parameter[a]	SC	AC	YC
Calibration			
n	14	5	4
a	1.97	53.78	−4.67
b	3.20	3.01	1453.80
s	5.8367	6.4094	5.9197
s_p	5.9557		
$t(b)$	0.912[b] ($P = 37.6\%$)		
b_p	3.17		
a'	2.81	50.61	
YB			—
Analysis			
C (ng ml^{-1})	18.20	16.16	
	$t(c) = 2.08$ ($P = 5.40\%$)		
	Critical value = 2.12 (5%)		
C sample (%)[c]	0.45	0.40	0.46

[a] n, Number of points for calibration; a, intercept; b, slope; s, regression standard deviation; s_p, pooled regression standard deviation; $t(b)$, t-value for $n_{SC} + n_{AC} - 4$ degrees of freedom at P 1% level; b_p, pooled slope; a', new intercept.
[b] Critical value: 2.95 (1%); P, percentage of Student t-distribution.
[c] Total concentration in the sample.

Table 4
Numerical values of parameters from SC, AC and YC. Results of analyte content to check accuracy for NAD.

Parameter[a]	SC	AC	YC
Calibration			
n	21	4	4
a	12.96	484.67	147.37
b	6.98	6.76	8468.08
s	7.8034	7.5558	10.4829
s_p	7.7802		
$t(b)$	1.23[b] ($P=23.2\%$)		
b_p	6.97		
a'	13.72	478.39	
YB			133.65
Analysis			
C (ng ml^{-1})	47.80	47.49	
	$t(c)=0.51$ ($P=61.5\%$)		
	Critical value = 2.074 (5%)		
C sample (%)[c]	1.19	1.18	1.21

[a] n, Number of points for calibration; a, intercept; b, slope; s, regression standard deviation; s_p, pooled regression standard deviation; $t(b)$, t-value for $n_{SC}+n_{AC}-4$ degrees of freedom at P 1% level; b_p, pooled slope; a', new intercept.
[b] Critical value 2.83 (1%); P, percentage of Student t-distribution.
[c] Total concentration in the sample.

analytes contents of the solution are obtained. The sample contents, calculated from SC, AC and YC, are indicated also. The results from SC and AC are not significantly different, and it can be concluded that the method is accurate. From this study, it can be concluded that the determination of NAA and NAD in Fruitone can be carried out directly by means of SC. However, the Youden's blank should be subtracted from all measurements for NAD determination.

4. Conclusions

A simple and practical spectrofluorimetric method for the simultaneous determination of NAA and NAD in commercial formulations and soil samples from Granada is presented. It was applied with good recovery rates.

References

[1] N.B. Mandava (Ed.), Plant Growth Substances, ACS Series III, American Chemical Society, Washington, DC, 1979.
[2] C. de Liñán, Vademecum de Productos Fitosanitarios y Nutricionales, Ed. Embajadores, Madrid, 1994.
[3] H.Y. Young, S. Shimabukuro, L. Aono, J. Agric. Food Chem. 11 (1963) 132.
[4] R. Sigrist, A. Temperli, J. Hunter, J. Agric. Food Chem. 22 (1974) 568.
[5] F. García Sánchez, C. Cruces Blanco, Mikrochim. Acta II (1989) 49.
[6] L.B. Sanders, J.D. Winefordner, J. Agric. Food Chem. 20 (1972) 166.
[7] J.J. Aaron, E.M. Kaleel, J.D. Winefordner, J. Agric. Food Chem. 27 (1979) 1233.
[8] G. Zweig, D.L. Gutnick, R. Gulli, T.E. Archer, H.T. Hartmann, J. Agric. Food Chem. 12 (1964) 59.
[9] C.A. Bache, D.J. Lisk, M.A. Loos, J. Agric. Food Chem. 47 (1964) 348.
[10] H. Anson Moye, T. Adair Wheaton, J. Agric. Food Chem. 27 (1979) 291.
[11] B. Maiti, R. Desai, T.S. Krishnamoorthy, Analyst 113 (1988) 667.
[12] W.P. Cochrane, M. Lanouette, R. Grant, J. Assoc. Off. Anal. Chem. 63 (1980) 145.
[13] J.L. Vilchez, R. Avidad, A. Navalón, J. Rohand, L.F. Capitán-Vallvey, Int. J. Environ. Anal. Chem. 53 (1993) 139.
[14] J.L. Vilchez, A. Navalón, R. Avidad, J. Rohand, L.F. Capitán-Vallvey, Fresenius J. Anal. Chem. 345 (1993) 716.
[15] F. Capitán, E.J. Alonso, R. Avidad, L.F. Capitán-Vallvey, J.L. Vilchez, Anal. Chem. 65 (1993) 1336.
[16] J.L. Vilchez, R. Avidad, J. Rohand, A. Navalón, L.F. Capitán-Vallvey, Anal. Chim. Acta 282 (1993) 445.
[17] J.L. Vilchez, A. Navalón, R. Avidad, T. García-López, L.F. Capitán-Vallvey, Analyst 118 (1993) 303.
[18] Statgraphics, version 6.0, Manugistics and Statistical Graphics Corporation, USA, 1992.
[19] Analytical Methods Committee, Analyst 119 (1994) 2363.
[20] K. Yoshimura, S. Ohashi, Talanta 25 (1978) 103.
[21] IUPAC, Nomenclature, symbols, units and their usage in spectrochemical analysis, Pure Appl. Chem. 45 (1976) 105.
[22] Guidelines for data acquisition and data quality evaluation in environmental chemistry, Anal. Chem. 52 (1980) 2242.
[23] C.A. Clayton, J.W. Hines, P.D. Elkins, Anal. Chem. 59 (1987) 2506.
[24] L. Cuadros-Rodríguez, A. García-Campaña, F. Alés-Barrero, C. Jiménez-Linares, M. Román-Ceba, J. Assoc. Off. Anal. Chem. 78 (1995) 471.
[25] M.J. Cardone, J. Assoc. Off. Anal. Chem. 66 (1983) 1283.

ELSEVIER

Talanta 45 (1997) 113–118

Talanta

Highly sensitive automatic analysis of polycyclic aromatic hydrocarbons in indoor and outdoor air

Lizhong Zhu [a,*], Yukari Takahashi [b], Takashi Amagai [b], Hidetsuru Matsushita [b]

[a] *Department of Environmental Science, Hangzhou University, Hangzhou 310028, China*

[b] *Division of Environmental Health Science, Graduate School of Nutritional and Environmental Science, University of Shizuoka, Shizuoka 422, Japan*

Received 9 December 1996; received in revised form 19 March 1997; accepted 7 April 1997

Abstract

A method for the quantitation of polycyclic aromatic hydrocarbons (PAHs) in indoor and outdoor air by high-performance liquid chromatography (HPLC) with a spectrofluorometric detection and programmed excitation and emission wavelength pairs is proposed. The mobile phase is a linear gradient of methanol–water. The relative standard deviations ($n=5$) are in the range 0.38–1.7% at concentration levels of 0.69–11.40 ng ml^{-1}. The determination limits ($S/N=10$) are 0.5–15.9 pg. The proposed method was successfully applied to quantitate 12 PAHs in gas phase and particulates in indoor and outdoor air. The recoveries of PAHs from gas phase and particulates were 95.7–117.5 and 94.8–112.4%, respectively. This highly sensitive automatic HPLC analysis for PAHs both in gas phase and particulates can be applied to indoor and outdoor survey. © 1997 Elsevier Science B.V.

Keywords: Polycyclic aromatic hydrocarbons; Fluorescence; Automatic analysis; HPLC; Indoor pollution

1. Introduction

Polycyclic aromatic hydrocarbons(PAHs) are widespread environmental pollutants which are formed in combustion process of carbonaceous materials at high temperature. These combustion sources include emission from automobiles and several natural sources such as forest fires and volcanic eruptions [1]. Indoor air is also contaminated by PAHs which come not only from outdoor air but also from indoor emission sources such as smoking, cooking and heating. Furthermore, peoples spend 80% or more of time in indoors [2]. Indoor air has an important impact on person's well-being. Many of PAHs are known to be carcinogenic and or mutagenic. Because of their biological properties, PAHs existence in the surrounding air has a direct impact on the human population. For example, the lung cancer mortality is increasing in major countries of the world. Thus the analysis of PAHs is a critical element in air pollution monitoring and control. Survey of PAHs levels in indoor and outdoor air is also important as a part of risk assessment and risk management to these chemicals.

* Corresponding author.

PII S0039-9140(97)00109-4

Table 1
Linear gradient of mobile phase

Time	Methanol (%)	Water (%)
0.00	50.0	50.0
5.00	50.0	50.0
5.10	80.0	20.0
20.0	80.0	20.0
30.0	85.0	15.0
40.0	90.0	10.0
40.1	96.0	4.0
50.0	96.0	4.0
50.1	50.0	50.0
60.0	50.0	50.0

Table 2
Excitation and emission wavelength pairs program

PAHs	Times (min)	Ex (nm)	Em (nm)
NAPH, ACEN	0.00	280	324
PHEN	14.60	250	370
AN	16.50	254	400
FLUR	19.00	287	460
PY, 1-Me-PY	21.00	336	394
BaA	30.10	280	387
CHRY	32.00	270	360
BeP	34.00	285	385
BkF, BaP	40.00	296	404

PAHs occur in gas phase and adsorbed on particulates. The analytical techniques usually used for PHAs determination are gas chromatography (GC) with flame ionization detection (FID) or mass spectrometric detection (MS) and high-performance liquid chromatography (HPLC) with UV spectrophotometric or fluorometric detection [3–5]. Reversed-phase high performance liquid chromatography (RP-HPLC) on chemically-bonded octadecyl stationary phase is far the popular liquid chromatographic method for PAHs analysis. The main attraction of RP-HPLC is its unique selectivity for the separation of PAH isomers. In addition, the compatibility of RP-HPLC with gradient elution techniques and the rapid equilibration of these columns to changes in mobile phase composition make RP-HPLC a convenient separation technique. Another major advantage of HPLC is the availability of sensitive and selective dual-monochromator fluorescence detectors. Therefore, the combination of RP-HPLC with fluorescence detection is a reliable method for the quantitative determination of PHAs in environmental samples.

However, difficulties can be encountered with complex matrices and low concentration of PAHs such as environmental tobacco smoke or indoor air. In order to improve the selectivity, fluorescence wavelengths were programmed to enhance the specificity and the selectivity of individual PAHs in the mixture and minimize interferences from coeluting species. Several fluorescence wavelength programs were developed by other research groups to quantitate PAHs [6,7]. However, none of these programs were reported to determine PAHs both in gas phase and in particulates of indoor air samples. Thus, a little of information on PAHs levels indoors was available because the analytical techniques have not met indoor PAHs survey. In order to overcome these difficulties, we have developed a highly sensitive automatic PAHs analysis by HPLC with fluorescence detection and programmed excitation and emission wavelength pairs. The proposed method has been successfully applied to analyze PAHs in gas phase and particulates in indoor and outdoor air.

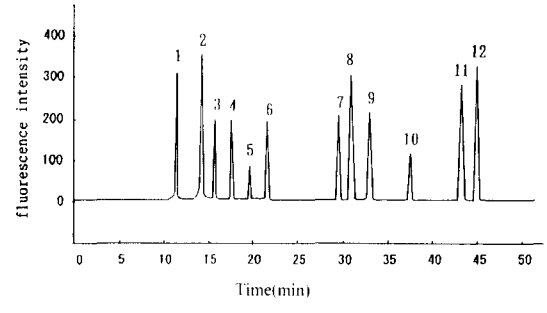

Fig. 1. HPLC chromatogram of PAHs standard solution (100 μl). 1, naphthalene; 2, acenaphthylene; 3, phenanthrene; 4, anthracene; 5, fluoranthene; 6, pyrene; 7, 1-methyl-pyrene; 8, BaA; 9, chrysene; 10, BeP; 11, BkF; 12, BaP.

Table 3
Analytical characteristics

PAHs	Retention time (min)	R.S.D. (%)	Regression coefficient for dose-peak height	R.S.D. (%) for peak height	Determination limit (pg)
NAPH	11.36	0.34	0.999	0.38	15.9
ACEN	14.20	0.36	1.000	0.72	1.0
PHEN	15.70	0.27	0.994	1.70	1.7
AN	17.56	0.23	1.000	0.69	1.0
FLUR	19.71	0.22	0.998	0.36	7.9
PY	21.61	0.18	0.999	1.38	3.5
1-Me-PY	29.53	0.14	0.999	0.62	2.4
BaA	30.93	0.15	0.999	0.55	1.2
CHRY	32.95	0.14	0.999	0.70	2.8
BeP	37.53	0.11	0.999	1.25	14.7
BkF	43.18	0.09	0.999	1.17	1.1
BaP	44.79	0.09	0.997	1.39	0.5

$n = 5$.

2. Experimental

2.1. Apparatus and materials

The HPLC system (Hitachi) consisted of two L-6000 pumps, a AS-2000 autosampler, a column oven, a F-1080 fluorescence detector, a L-5090 degasser, a data processor and a system controller. The pre-column and main column used were Wakosoil-II 5C-18AR, 4.6 ∅ × 30 mm and 4.6 ∅ × 250 mm (Wako Pure Chemical Industrials Ltd), respectively. MP-15CF mini pumps (Shibita Scientific Technology Ltd) were used for air sampling.

2.2. Reagents

In this study, 12 PAHs were selected as target PAHs in consideration of carcinogenicity, mutagenicity and prevalence in indoor and outdoor air. The most are important PAHs in the estimation of emission source of PAHs.

PAHs stock solutions of the standards with concentrations in the range 0.69–11.4 μg ml^{-1} were prepared by dissolving weighed amounts of PAHs in acetonitrile. Standard solution contained naphthalene (NPAH), acenaphthylene (ACEN), phenanthrene (PHEN), anthracene (AN), fluoranthene (FLUR), pyrene (PY), 1-methyl-pyrene (1-Me-PY), benz[*a*]anthracene (BaA), chrysene (CHRY), benzo[*e*]pyrene (BeP), benzo[*k*]fluoranthene (BkF) and benzo[*a*]pyrene (BaP) in the concentration of 0.69–11.4 ng ml^{-1} were prepared by diluting with acetonitrile. Methanol and water were of HPLC-grade (Wako Pure Chemical Industrials Ltd). The other solvents and chemical products were also of HPLC purity.

2.3. Procedure

2.3.1. Air sampling

Indoor and outdoor air were sampled by a low noise small sampler (MP-15CF mini pump) at a flow rate of 1.0 l min^{-1} for 24 h in two homes in Shizuoka, Japan in November, 1996. PAHs in particulates and in gas phase were collected by millipore prefilter (25 mm ∅) [8] and XAD-2 [9,10], respectively.

In prior to HPLC analysis, PAHs in the filters and XAD-2 were separately extracted by sonicated for 20 min. Sample solutions were prepared [8–10] and offered to separation analysis. All sample solutions were filtered through 0.2 μm PTFE filters before separation analysis.

2.3.2. Separation analysis

Separation analysis for 12 PAHs was performed by HPLC system which consisted of pre-column for PAHs condensation and clean-up,

Table 4
Recovery of PAHs from gas phase sample

PAHs	Added amount of PAH to sample solution (ng)	PAH found in gas phase solution (ng)	PAH found in sample solution (ng)	Recovery ± C.V. (%)
NAPH	5.69	73.91	79.85	104.4 ± 7.6
ACEN	2.48	0.53	3.24	109.1 ± 6.5
PHEN	0.97	2.09	3.23	117.5 ± 13.6
AN	0.35	0.04	0.40	102.9 ± 3.9
FLUR	2.36	0.09	2.47	100.8 ± 0.6
PY	2.32	0.12	2.35	95.9 ± 1.6
1-Me-PY	1.66	0.01	1.64	98.2 ± 1.7
BaA	1.83	0.01	1.82	98.6 ± 2.7
CHRY	1.87	0.07	1.88	96.5 ± 1.2
BeP	3.06	-	3.02	98.5 ± 3.1
BkF	1.01	-	1.00	98.0 ± 2.9
BaP	1.16	0.02	1.15	97.0 ± 1.9

main column for PAHs separation, spectrofluorometer, data processor and system controller [8–10]. A sample solution (25–500 ml, usually 100 ml) was injected into the HPLC system by autoinjector and the sample was conveyed by 100% methanol from pump A (0.5 ml min^{-1}), mixed with water from pump B (0.5 ml min^{-1}) by a dynamic mixer and concentrated/cleaned-up on pre-column for 3 min after the injection. After that, the 6-way valve was turned to connect pre-column with main column, PAHs were separated by linear gradient program (Table 1) using methanol and water as mobile phase. Flow rate of the mobile phase was kept at 1.0 ml min^{-1}. Therefore, PAHs in samples were concentrated and cleaned-up in the pre-column, transferred quickly into the separation column, and separated each component, and detected by the computer controlled spectrofluorometer of which excitation and emission wavelengths were automatically set by a time program (Table 2). After 50 min from the injection, the HPLC system was washed with methanol/water (50:50, v/v) for 10 min and returned to the initial condition. Then, next sample was injected automatically to the HPLC system.

3. Results and discussion

3.1. Optimization of chromatographic parameters

Appropriate time for concentrating/cleaning up the sample on pre-column was 3 min. If it took a longer time (more than 4 times), naphthalene in the sample was drained out and the peak of naphthalene disappeared in the HPLC chromatogram.

In order to attain maximum sensitivity, a program to select excitation and emission wavelengths was investigated. The program specified in Table 2 was proposed. Under these experimental conditions, the same wavelength pairs were used to detect naphthalene and acenaphthylene, pyrene and 1-methyl-pyrene, benzo[*k*]fluoranthene and benzo[*a*]pyrene. By linear gradient elution, 12 PAHs including PY and 1-Me-PY, BeP and BaP were successfully separated within 45 min. Fig. 1 shows the HPLC chromatogram of 100 μl PAHs standard solution. The column temperature was 40°C.

3.2. Analytical characteristics

High sensitivity of the present method was achieved by combination use of the highly sensitive spectrofluorometers and the injection system which can inject large amount of sample solution

Table 5
Recovery of PAHs from particulate sample

PAHs	Added amount of PAH to sample solution (ng)	PAH found in particulate solution (ng)	PAH found in sample solution (ng)	Recovery ± C.V. (%)
NAPH	5.69	2.03	7.94	103.9 ± 9.2
ACEN	2.48	0.65	3.28	106.2 ± 6.8
PHEN	0.97	2.77	3.88	112.4 ± 2.4
AN	0.35	0.12	0.51	112.4 ± 7.8
FLUR	2.36	1.59	4.07	105.2 ± 2.4
PY	2.32	1.15	3.37	94.8 ± 2.1
1-Me-PY	1.66	0.08	1.70	97.8 ± 1.6
BaA	1.83	0.50	2.39	103.1 ± 0.6
CHRY	1.87	1.00	2.87	100.2 ± 1.7
BeP	3.06	0.79	3.96	103.6 ± 3.9
BkF	1.01	0.47	1.54	105.6 ± 1.4
BaP	1.16	0.71	1.98	109.5 ± 1.4

(100–500 ml) without and adverse effect in separation characteristics. The method has 50–100 times higher sensitivity than ordinary HPLC analysis. High selectivity in detection of target PAHs was obtained by the use of excitation and emission wavelengths suitable for detection of each target PAHs. The wavelengths were selected in due consideration of excitation and emission spectra of PAHs coeluting with target PAHs in order to eliminate the interference by the coeluting PAHs in quantitative analysis. Simplicity in operation was attained by the introduction of computer system which can control automatically flow rate, mobile phase composition and detection wavelengths. The HPLC system can run without operator, and separation profile and related data were stored in floppy disk. Therefore, the role of the operator is to set sample solutions into the HPLC system and to evaluate the data for qualitative and quantitative analysis.

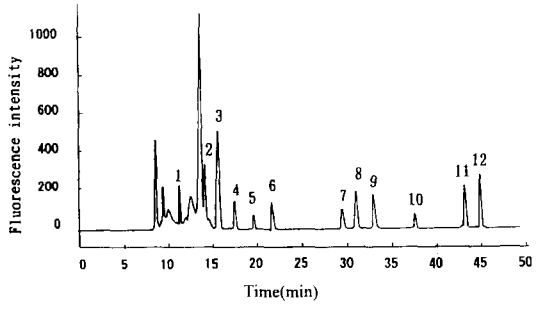

Fig. 2. HPLC chromatogram of PAHs in particulates indoors. 1, naphthalene; 2, acenaphthylene; 3, phenanthrene; 4, anthracene; 5, fluoranthene; 6, pyrene; 7, 1-methyl-pyrene; 8, BaA; 9, chrysene; 10, BeP; 11, BkF; 12, BaP.

The analytical characteristics of proposed method is summarized in Table 3. The new method shows highly repeatability of retention time and high accuracy in PAHs determination. The PAHs concentrations tested were in the range 0.0069–34.12 ng ml^{-1}. Linearity was found in all cases with regression coefficients higher than 0.994. Relative standard deviations (R.S.D., $n = 5$) at PAHs concentration levels of 0.69–11.38 ng ml^{-1} were 0.36–1.70%. Determination limits ($S/N = 10$) were 0.5–15 pg and the limits for most PAHs were less than 5 pg. The determination limit for BaP was the lowest, 0.5 pg. PAHs recoveries are calculated by dividing amount of PAHs found in the sample solutions by amount of PAHs added in the sample solutions. PAHs recoveries from gas phase and particulate samples indoor air were 94.8–117.5% (Tables 4 and 5). The recoveries of most PAHs were within 100 ± 5%. The most of coefficients of variation ($n = 3$) were less than 5%. These results clearly demonstrated that the proposed method was high sensitive and selective for determining PAHs. It suggests strongly usefulness in survey of indoor and outdoor PAHs pollution and assessment of human exposure PAHs.

Table 6
PAHs levels indoor and outdoor air (ng m^{-3})

PAHs	Home 1						Home 2			
	Outdoor		Bedroom		Kitchen room		Outdoor		Living room	
	G	P	G	P	G	P	G	P	G	P
NAPH	353.5	7.59	445.3	0.96	620.2	7.09	323.2	13.09	3100	26.84
ACEN	4.28	0.20	2.36	0.06	4.43	2.28	1.31	0.08	18.64	0.30
PHEN	15.69	12.77	7.47	3.34	17.55	9.68	5.41	5.36	36.81	11.10
AN	0.36	0.55	0.15	0.10	0.30	0.41	0.20	0.30	0.99	0.32
FLUR	1.39	5.95	0.43	2.07	0.74	5.57	1.87	3.67	1.53	6.28
PY	1.98	5.17	0.52	1.67	1.02	4.01	0.68	3.27	2.37	5.70
1-Me-PY	0.41	0.27	0.12	0.11	0.11	0.27	0.06	0.16	0.25	0.29
BaA	0.13	1.35	0.04	0.80	0.04	1.72	0.11	0.64	0.09	1.24
CHRY	0.89	2.33	0.25	1.50	0.28	3.47	0.31	1.37	0.48	2.93
BeP	-	1.44	-	1.30	-	2.75	0.17	0.82	-	2.22
BkF	0.09	0.92	-	0.77	-	1.63	0.08	0.47	-	1.25
BaP	0.10	1.21	0.02	1.22	0.08	2.48	0.12	0.49	0.03	2.16

3.3. Determination of PAHs in indoor air

The proposed chromatographic method was successfully applied to quantitate PAHs in gas phase and particulates of indoor and outdoor. When analyzing PAHs in gas phase,the injection solution volume would be adjusted because of significant difference of PAHs concentration in samples. For example,higher levels of naphthalene and phenanthrene in gas phase samples, the suitable injection volume was 25 ml. Moreover, other PAHs such as BkF and BaP were lower concentration in gas phase, 200 ml of solution were injected into the HPLC system. Usually, a sample of PAHs in gas phase was analyzed twice (25 and 200 ml injection volume). Fig. 2 shows the HPLC chromatogram of PAHs in particulates of indoor air sample, the injection volume is 100 ml.

PAHs levels in indoor and outdoor air showed in Table 6. It was indicated that PAHs levels indoors were generally lower than outdoor, suggesting that PAHs emission from indoor sources are not so high and elimination by sink and adsorption occurred in indoor environment [11]. However, indoor naphthalene concentration of home 2 was much higher than outdoor because of the use of camphor balls to protect against insects. PAHs levels in the kitchen were higher than outdoor because of cooking, especially grilling of fatty fish. Therefore, indoor PAHs levels were related to the resident's life style and living conditions.

References

[1] K. Nikolaou, P. Masclet, G. Mouvier, Sci. Total Environ. 32 (1984) 103.
[2] T. Mori, M. Kikkawa, H. Matsushita, J. Jpn. Soc. Air Pollut. 21 (1986) 446.
[3] K. Peltonem, T. Kuljukka, J. Chromatogr. A 710 (1995) 93.
[4] H.K. Lee, J. Chromatogr. A 710 (1995) 79.
[5] C. Escriva, E. Viana, J.C. Molto, Y. Pico, J. Manes, J. Chromatogr. A 676 (1994) 375.
[6] M.N. Kayali, S. Rubio-Barroso, L.M. Polo-Diez, J. Chromatogr. Sci. 33 (1995) 181.
[7] S.O. Baek, M.E. Goldstone, P.W.W. Kirk, J.N. Lester, R. Perry, Environ. Technol. 12 (1991) 107.
[8] H. Matsushita, Y. Takahashi, S. Azuma, H. Hiroi, T. Amagai, in: G.B. Leslie, K.J. Leslie, J. Huang, Y. Qin (Eds.), Indoor Air Quality in Asia, Lonsdale Press, London, 1994, pp. 236.
[9] Y. Takahashi, T. Amagai, H. Matsushita, in: Proc. 37th Annual Meeting of the Japan Society for Atomospheric Environment, 1996, pp. 425.
[10] Y. Takahashi, PhD Thesis, University of Shizhoka, Shizuoka, 1997.
[11] J.C. Chuang, P.J. Callahan, R.G. Menton, S.M. Gordon, R.G. Lewis, N.K. Wilson, Environ. Sci. Technol. 29 (1995) 494.

ELSEVIER

Talanta 45 (1997) 119–126

Talanta

Application of chelation ion chromatography to the determination of lanthanides in agriculture

Haitao Lu [a], Shifen Mou [b,*], Yan Yan [b], Feng Liu [a], Kean Li [a], Shenyang Tong [a], J.M. Riviello [c]

[a] *College of Chemistry and Molecular Engineering, Peking University, Beijing 100871, China*
[b] *Research Center for Eco-Environmental Sciences, Academia Sinica, P.O. Box 2871, Beijing 100085, China*
[c] *Dionex Corporation, Sunnyvale, CA 94086, USA*

Received 13 December 1996; received in revised form 18 March 1997; accepted 7 April 1997

Abstract

Lanthanides are widely present in soil and plant. In this paper, it is the first time that chelation ion chromatography is applied to analyse lanthanides in a series of samples in agriculture. This technique can eliminate bulk quantity of alkali, alkaline earth metals on chelating concentrator column (MetPac CC-1) and eliminate transition metals on cation exchange column (TMC-1) from complex matrices with ammonium acetate buffer while lanthanides are concentrated. It is shown to be capable of separating and determining all lanthanides on mixed-bed ion exchange column (CS5) in a wide variety of sample types with high accuracy. Elution is carried out with a concentration gradient of oxalic acid (Ox) and diglycolic acid (DGA), coupled with post-column spectrophotometric detection with 4-(2-pyridylazo)resorcinol (PAR) at 520 nm. It can determined ng ml^{-1} scales of lanthanides. The whole run time after sample injection is about 55 min. © 1997 Elsevier Science B.V.

Keywords: Lanthanide; Chelation ion chromatography; On-line sample pretreatment; Complex matrix

1. Introduction

With rapid development of lanthanides production and their widespread application in agriculture, people are even more interested in their effect to human body, environment and yield of crops. It has been reported that lanthanides have less toxicity for human body and environment [1]. When proper concentration of lanthanides is exerted to soil, they can stimulate the growth of plant and improve the yield of crops [2–5]. So, it is important to analyse the content of lanthanides in many fields. However, instrumentation commonly used for lanthanide analysis is relatively expensive and requires skilled operators. Moreover, when matrix concentration is very high, it is required to remove the matrix previously.

* Corresponding author.

PII S0039-9140(97)00110-0

Heberling et al. [6] has successfully separated and determined transition and lanthanide metals in synthetic solution by utilizing a conventional mixed-bed ion exchange column (CS5 column) and a concentration gradient of oxalic acid and diglycolic acid. However, this method could only be used in the samples which had same magnitude level of lanthanides and interferences [7]. Cassidy [8] has shown that high performance liquid chromatography (HPLC) with on-line post-column derivitization could be applied to analyse lanthanides in solution. This method employs a mixture of hydrophobic ion and a complexing eluent to provide rapid separation of lanthanides on ODS column. Al-Shawi et al [9] has reported that the alkali, alkaline earth and transition metals interferences could be eliminated by using Arsenazo III as the derivatizing agent. However, when the content of lanthanides are very low, the samples required to be concentrated. At this time, the concentrated interferences will overload the analytical column. Thus, all these techniques can not be used to real complex samples which contain bulk quantity of alkali, alkaline earth, transition metals and low content of lanthanides. The complex matrices interfere with the separation and determination of trace lanthanides. They must be removed prior to analysis.

Chelation ion chromatography is the new technique which combines on-line analyte concentration and matrix elimination with analytical separation [10–14]. Due to high selectivities of iminodiacetate-based resins towards transition metals and property of the complexes to be kinetically labile, it has been widely used for enrichment of trace lanthanides from complex matrices while alkali, alkaline earth metals are eliminated [15–18]. The sulfonated cation exchanger will eliminate iron, aluminum and other transition metals prior to ion chromatography separation. Chelation ion chromatography is one of the most effective methods which are capable of separating individual lanthanides in complex matrices. In this paper, the method has been systematically applied to determine lanthanides in rare earth fertilizer, soil, the root, stem and leaf of paddy rice.

2. Experimental

2.1. Instrumentation

Chromatographic analyses were carried out by using a metal-free Dionex DX-300 ion chromatography (Dionex Corp., Sunnyvale, CA, U.S.A) equipped with two advanced gradient pumps (AGP), a MetPac CC-1 column (50 × 4 mm, I.D. packed with styrene-based macroporous 12% cross-linked iminodicacetate-functionalized chelating resin, the particle was 20 μm and the capacity of resin was about 0.9 mequiv.), a TMC-1 concentrator column (25 × 3 mm, I.D. containing fully sulfonated PS-DVB cation-exchange resin with high capacity 2.2 mequiv.), an IonPac CG5 Guard column and an IonPac CS5 analytical column (250 × 4.6 mm, I.D., 13 μm bead diameter polystyrene divinylbenzene functionalized with both quaternary ammonium and sulfonate functional groups), a 3.66 ml injection loop and a Dionex variable wavelength detector with a post-column reactor. The MetPac CC-1 and TMC-1 column were used for sample pretreatment. Lanthanides separation was performed on the IonPac CS5 column.

The column was kept at ambient temperature during chromatographic experiment.

Data collection and operation of all components in the system were controlled by Dionex AI-450 chromatographic software interfaced via an ACI-2 advanced computer interface to an AST Power Premium 3/33 computer.

2.2. Chemicals and reagents

Ammonia solution, glacial acetic acid, hydrochloric acid, nitric acid, ammonium acetate, ethanol, lithium chloride and lithium hydroxide monohydrate were of analytical-reagent grade reagents (Peking Chemical Works, Peking, China), perchloric acid, hydrofluoric acid, oxalic acid dehydrate (Ox) and 4-(2-pyridylazo)resorcinol (PAR) were of guaranteed-reagent grade reagents (Peking Chemical Works, Peking, China), pyridine-2,6-dicarboxylic acid (PDCA) was of chromatographic grade reagent (Aldrich, USA), diglycolic acid (DGA) was of chromatographic grade reagent (Fluka).

Working standard solutions were prepared daily by standards (1000 μg ml^{-1}) which were obtained from National Research Centre for Certified Reference (China).

The eluted lanthanides were detected after post-column reaction with PAR (0.8 mM, 1.0 M glacial acetic acid and 3.0 M NH_3) at 520 nm. Flow-rate was 0.7 ml min^{-1}.

All solutions were prepared with pretreated water which was purified with a Milli-Q system (> 18 MΩ, Millipore, Waters Chromatography Devision, Oslo, Norway).

2.3. Samples and sample preparation

Samples used in this study were 'Changle' rare earth fertilizer, soil, the root, stem and leaf of paddy rice (Chinese Science and Technology University).

Rare earth fertilizer sample: It was dissolved and diluted directly by 0. 1 M HNO_3.

Root, stem, leaf and soil samples: 0.3 g of powdered sample was weighted respectively. It was added into a closed polytetrafluoroethyene (PTFE) beaker and wetted with a small amount of water, 5 ml of concentrated nitric acid was added and heated nearly to dryness. Then 20 ml of 50% (w/w) hydrofluoric acid was added and heated to dryness. Furthermore, 5 ml of 60% (w/w) perchloric acid was added to the residue and heated until white fume of perchloric acid appeared. After standing cool, 2 ml of concentrated nitric acid was added and evaporated to dryness again. Finally, the residue was dissolved to 25 ml with 0.1 M HNO_3.

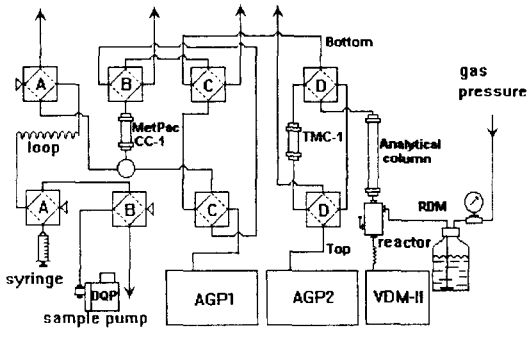

Fig. 1. Scheme of chelation ion chromatography system.

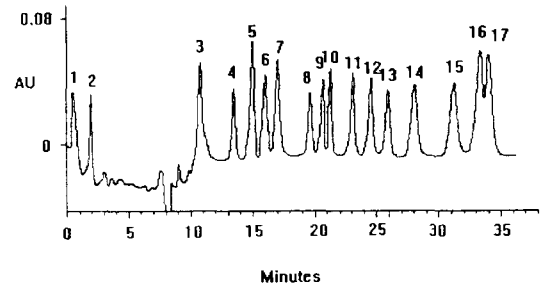

Fig. 2. Chromatogram of lanthanides in synthetic standard solution. Chromatographic conditions: Separator column: IonPac CS5 and CG5; Eluents: (A) water; (B) 0.1 M Ox, 0.19 M LiOH; (C) 0.1 M DGA, 0.19 M LiOH; (D) 0.006 M PDCA, 0.01 M LiOH and 0.05 M LiCl; Gradient: 100% D for 1 min, then 100% A for 3 min, then 40% A, 60% B to 30% A, 70% B in 5 min, then to 59% A, 25% B, 16% C in 9 min, then to 54% A, 25% B, 21% C in 10 min, then to 54% A, 20% B, 26% C in 5 min; Flow Rate: 1.0 ml min^{-1}; Post-column reagent: PAR, 0.7 ml min^{-1}, Detection λ = 520 nm. Peaks: 1 and 2 systemic peaks, 3 = Zn, 4 = La (240 ng ml^{-1}), 5 = Ce (200 ng ml^{-1}), 6 = Pr (96 ng ml^{-1}), 7 = Nd (96 ng ml^{-1}), 8 = Sm (32 ng ml^{-1}), 9 = Eu (32 ng ml^{-1}), 10 = Gd (32 ng ml^{-1}), 11 = Tb (32 ng ml^{-1}), 12 = Dy (32 ng ml^{-1}), 13 = Ho (40 ng ml^{-1}), 14 = Er (32 ng ml^{-1}), 15 = Tm (53.3 ng ml^{-1}), 16 = Yb (64 ng ml^{-1}), 17 = Lu (80 ng ml^{-1}), Al (3.0 mg ml^{-1}), Fe (3.0 mg ml^{-1}), Ca (6.0 mg ml^{-1}), Mg (6.0 mg ml^{-1}), Cu, Ni, Zn, Co, Mn (200 μg ml^{-1}), respectively.

Extracted solution from soil: 20 g soil was weighted and added into a 250 ml beaker. Then, 100 ml of 2.0 M NaAc-HAc (pH 4.8) buffer was added and oscillated (180 rpm) on an oscillator for 30 min. Finally, the solution was filtered with double-lay filter. The filtrate was diluted to 100 ml with buffer solution.

Before injection, each solution needed to be further diluted to a proper concentration within its linear range and filtered through a 0.45-μm filter.

2.4. Experimental procedure

The detailed scheme of chelation ion chromatography system was shown in Fig. 1, AGP1 pretreatment program was entered method file in AI-450 operating software and subsequently down loaded onto AGP1. AGP2 concentration gradient program was entered AGP2 front panel. Elution containers were pressurized with N_2 to 5

Table 1
Lanthanide analytical results of soil sample

Lanthanide	IC ($\mu g\ g^{-1}$)	ICP-MS ($\mu g\ g^{-1}$)	Spiked ($\mu g\ g^{-1}$)	Found ($\mu g\ g^{-1}$)	Recoveries (%)
La	46.84	46.7	30.2	77.76	102.4
Ce	87.52	85.4	24.0	110.2	94.6
Pr	10.38	9.4	13.2	24.66	108.2
Nd	39.21	40.1	11.5	51.3	105.1
Sm	6.87	7.5	4.2	11.32	106
Eu	1.49	1.36	5.8	6.95	94.1
Gd	6.09	6.1	5.0	11.32	104.6
Tb	1.01	0.88	4.6	5.83	104.8
Dy	5.82	5.65	4.4	10.04	96
Ho+Y	71.4	1.02+29	3.7	74.8	92.1
Er	3.2	3.35	5.5	8.59	98
Tm	0.5	0.45	7.6	8.4	104
Yb	3.28	3.01	7.6	11.47	107.8
Lu	0.4.	0.44	11.4	12.61	107.1

$n = 5$.

psi. When operation started, the sample in injection loop was flushed by 0.1 M HNO_3 from sample pump to mixing tee where it was buffered with ammonium acetate solution and entered MetPac CC-1 column. All anions and monovalent cations could not be retained. Following, alkaline earth metals were selectively removed by ammonium acetate buffer further. Then, the residual metals on the MetPac CC-1 column were transferred to TMC-1 column by HCl/EtOH solution, and there rinsed by Ox/HNO_3 solution further. Lanthanides were quantitatively concentrated while iron, aluminum and other transition metals were eluted to the waste. Finally, after AGP1 delivered 0.1 M ammonium nitrate to convert TMC-1 column from hydrogen form to ammonium form, AGP2 delivered PDCA to elute lanthanides from TMC-1 column to CS5 column. Following separation, the lanthanides were eluted by a concentration gradient of Ox and DGA detected photometrically using PAR post-column reagent at 520 nm.

3. Results and discussion

3.1. Matrix elimination and concentration

The first matrix elimination step was performed on MetPac CC-1 column to remove alkali and alkaline earth metals from sample matrix. The MetPac CC-1 column contained macroporous iminodiacetate chelating resin which had very high affinity for transition and lanthanide metals compare to alkali and alkaline earth metals. The higher valency of the metal ion, the stronger bound metal ion was to the resin. Before sample stream passed through MetPac CC-1 column, the sample previously loaded into injection loop was flushed by acid carrier and buffered on-line with 2.0 M ammonium acetate eluent in the pH range of 5–6. All anions and monovalent cations were not retained. By using 2 M ammonium acetate eluent further, alkaline earth metals could be selectively eluted while most transition and all lanthanide metals remained quantitatively bound to the column. Ten mg of Ca could be eluted completely within 5 ml eluent. The other alkaline earth metals had the same results. Changes of flow-rate from 1 to 3 ml min^{-1} did not influence the recoveries of retained metals. Then, the remaining ammonium acetate on MetPac CC-1 column was removed by 0.1 M ammonium nitrate, otherwise, the high concentration of ammonium acetate would crystallize in it.

The selective elimination process proceeded further was to remove the bulk quantity of iron, aluminum and other transition metals on high

capacity TMC-1 concentrator column. It contained fully sulfonated cation exchange resin which had high affinity for multivalent cations. The selective matrix removal was based upon the stable metal chloride complexes in a mixture of 4.0 M hydrochloric acid/65% ethanol eluent. The mixture not only promoted the formation of relatively stable metal chloride complexes, it also decreased the distribution coefficient of the metal complexes on cation exchange resin [10]. It was the effect of high concentration of ethanol that water molecules around the metals were reduced, the forces binding the coordinated hydrated shell and the size of the outer hydration cloud were decreased. As a result, the transition metal chloride complexes formed in the mixture were more stable than that in aqueous system. On the other hand, lanthanides formed less stable metal chloride complexes. Thus, the relatively stable metal chloride complexes of transition metals were selectively removed from TMC-1 column while lanthanides were quantitatively retained and concentrated. Ten mg of transition metals could be eluted within 6 ml eluent. But there were still partial iron and aluminum on the column. Some of them were from the matrix that could not be eluted completely and the others were introduced by eluents. So, they were eluted further by 1.0 M Ox/0.1 M HNO_3 eluent, which existed as $Fe(Ox)_3^{3-}$ and $Al(Ox)_3^{3-}$. The acidity of this eluent (pH 1–2) was very important, or else, the lanthanides would be eluted as $La(Ox)_3^{3-}$. Before the lanthanides were eluted to CS5 column, TMC-1 column must be converted from hydrogen form to ammonium form, otherwise the remaining matrices would interfere the separation of lanthanides. Sometimes, they could overlap the peak of La.

3.2. Chromatographic separation

The separation of lanthanides was accomplished by anion exchange of lanthanide–chelator complexes on mixed-bed IonPac CS5 analysis column. Before starting each analysis, the separation required column equilibration with PDCA eluent. The analytical system equilibrated while sample pretreatment steps were being performed. In this separation, PDCA eluent had two kinds of effects. On one hand, it removed metal contaminants introduced by Ox and DGA eluents from the analysis column, such as iron and aluminum, which existed as $Fe(Ox)_3^{3-}$ and $Al(Ox)_3^{3-}$ bound strongly by the anion exchange sites of the resin. On the other hand, when TMC-1 column was placed on-line with analysis column, PDCA eluted concentrated lanthanides and trace transition metals from TMC-1 column as Metal–PDCA complexes to IonPac CS5 column. Lanthanides formed stable trivalent anionic complexes. Transition metals formed stable divalent anionic complexes which were eluted before lanthanides. But the remaining PDCA on CS5 column would affect the separation and detection of lanthanides. Thus, it must be removed by DI water first. Then lanthanides were separated by using concentration of gradient Ox and DGA eluents. The separation was based on the stability of lanthanide–chelator complexes, the smallest ions formed the strongest complexes and were the least negatively changed. Therefore, when lanthanides was separated by anion exchange with Ox and DGA eluents, the eluent order was from La to Lu.

A series of concentration gradient separating conditions had been tested. From these experiments, an optimum condition was chosen. A typical chromatogram of synthetic standard solution was illustrated in Fig. 2. It was shown that the individual lanthanides peaks were well separated. Although there were bulk quantity of alkali metals, alkaline earth metals, aluminum, iron and other transition metals in the solution, they could not affect the separation and determination of lanthanides.

3.3. Accuracy and detection limit

Under the optimized program, it produced much sharper peaks with good peak separation and excellent calibration curves. All lanthanides had good linearities whose correlation coefficients were greater than 0.998 in the range 15–400 ng

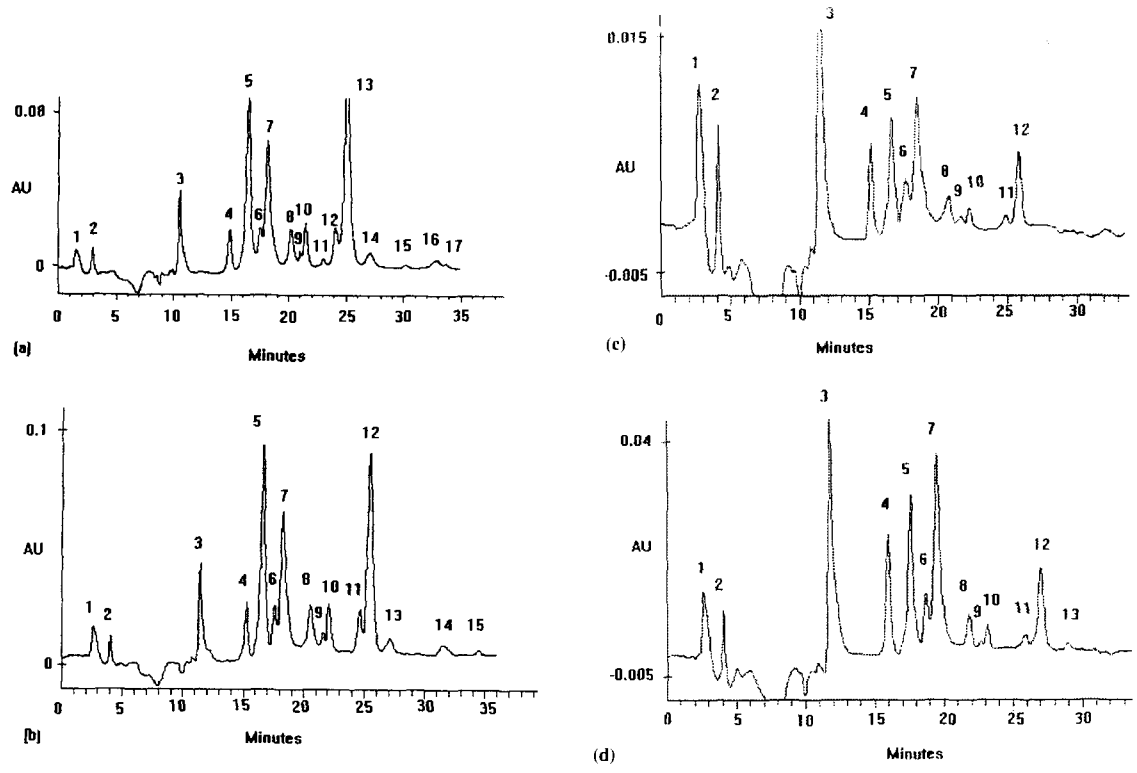

Fig. 3. Chromatogram of lanthanides in a series of samples. (a) Soil, (b) root, (c) stem, (d) leaf. Similar chromatographic conditions to Fig. 2. Peaks: 1 and 2 systemic peaks, 3 = Zn, 4 = La, 5 = Ce, 6 = Pr, 7 = Nd, 8 = Sm, 9 = Eu, 10 = Gd, 11 = Tb, 12 = Dy, 13 = Ho, 14 = Er, 15 = Tm, 16 = Yb, 17 = Lu.

ml^{-1} for La, Ce, 6–120 ng ml^{-1} for Pr, Nd, Yb, Lu, 2–64 ng ml^{-1} for Sm, Eu, Gd, Tb, Dy, Ho and 3–100 ng ml^{-1} for Er, Tm. The R.S.D. based on $> 10 \times$ detection limits concentration ($n = 7$) was found to be in the range of 1.8–5.5%. It was clear from Fig. 2 that the method sensitivity was different among individual lanthanides. The absorbance of light-lanthanides was less than the middle and heavy-lanthanides. The detection limits (signal-to-noise ratio 3:1) of this method from La to Lu were 6.7, 2.7, 1.7, 1.3, 0.7, 0.7, 0.6, 0.7, 0.6, 0.7, 0.9, 1.3, 1.5, and 1.9 ng ml^{-1}, respectively.

3.4. Analysis of sample

As a validation of the analytical technique, soil sample whose lanthanides had been determined previously by ICP-MS was analyzed.. Table 1 showed the comparison. They were averages of three totally independent analyses involving sample digestion and chelation ion chromatography procedure. They were obtained based on the system calibration with our standards. It was found that the IC values were in good agreement with ICP-MS values. All of them had good spiked recoveries. Because of the appreciable overlap between Ho and Y peaks, it was difficult to obtain reliable values for them. Furthermore, it could be seem from Fig. 3(a) that separations between Pr and Nd, Eu and Gd were not well. It was because the concentration of Nd and Gd were bigger than that of Pr and Eu, respectively. So, the peaks of Nd and Gd overlapped partial peaks of Pr and Eu, respectively. Fig. 3(a) also showed that the interference which had been eliminated during the sample pretreatment did not affect the separation and determination any more.

Table 2
Lanthanides analytical results of fertilizer, extracted solution from soil, the root, stem and leaf of paddy rice

Lanthanide	Fertilizer (mg g^{-1})	Extracted solution (μg g^{-1})	Root (μg g^{-1})	Stem (μg g^{-1})	Leaf (μg g^{-1})
La	125	1.427	12.1	3.81	10.0
Ce	38.6	2.324	21.9	1.70	6.01
Pr	17.3	0.347	2.21	0.405	1.36
Nd	41.2	1.671	8.86	1.36	4.49
Sm	2.67	0.407	1.56	0.148	0.412
Eu	0.37	0.104	0.276	0.029	0.101
Gd	0.59	0.498	1.43	0.057	0.25
Tb	N.D.	0.071	0.195	0.02	0.0374
Dy	N.D.	0.353	1.39	0.044	0.148
Ho	N.D.	2.44	7.72	0.318	1.087
Er	N.D.	0.142	0.80	N.D.	0.107
Tm	N.D.	0.0344	0.10	N.D.	N.D.
Yb	N.D.	0.095	0.696	N.D.	N.D.
Lu	N.D.	0.028	N.D.	N.D.	N.D.

N.D., not detected.

System blanks were well below the detection limits for all lanthanides, and there was no indication of any memory effect when a blank was run immediately after a sample with high concentration of lanthanides. These results indicated that the present chelation ion chromatography system is useful for the determination of lanthanides in samples with complex matrices. One of the most important advantage of applying this method was that analytical media could be injected directly for analysis after sample digestion.

The other samples used in this study were rare earth fertilizer, extracted solution from soil, the root, stem and leaf of paddy rice which grew in the soil. Fig. 3(b)–(d) showed some of their chromatograms. It was shown from Table 2 that only dissoluble lanthanides could be absorbed, although the contents of lanthanides in soil was very high, most of them could not be absorbed by paddy rice. It was also seen from Table 2 that the content of dissoluble lanthanides extracted from soil by HAc-NaAc buffer were lower than that in soil greatly. When the dissoluble lanthanides in soil were too low, rare earth fertilizer was needed. Among the root, stem and leaf, the root could absorb and concentrate lanthanides directly from soil, therefore, the contents of lanthanides in it were the highest. The stem delivered lanthanides mainly, therefore, the contents of lanthanides in it were the lowest. Because the paddy rice had not come to its mature period, we had not the datum of grain.

The properties of lanthanides were very similar. But, there were strong light lanthanides enrichment in real samples (e.g. fertilizer, root). So, they could not be determined in a single run. In order to maintain the lanthanides concentration in analyte solution within the linear calibration range and above the detection limit of the method, it was necessary to analyse same sample in different concentration. However, some lanthanides in samples (e.g. leaf, stem) were too low to be determined. If solutions were too thick, the concentration of interference would be too high to be eliminated completely through sample pretreatment and the high concentrated lanthanides would cover the low concentrated lanthanides. All these needed to be studied further in our next work.

4. Summary

The on-line chelation ion chromatography technique performed reliable and accurate analyses of lanthanides in complex matrices. The sample preconcentration and matrix elimination covered a wide range of sample matrix concentration. It was

an extremely versatile technique that the determination of lanthanides was easily adaptable to a wide variety of analytical problems in agriculture.

References

[1] G.X. Xu, Xitu, vol.2, Ch. 17, Beijing, 1995, pp. 386.
[2] P.L. Liu, J.L. Tian, Y.Q. Li, T.J. Ju, J. Chinese Rare Earth Soc. 13 (2) (1995) 155.
[3] H.Z. Liu, Y.D. Li, R. Hao, J. Chinese Rare Earth Soc. 13 (3) (1995) 283.
[4] D.R. Yan, L.D. Zhang, Y.J. Liu, Chinese Rare Earths 17 (4) (1996) 70.
[5] J.T. Zhang, D.F. Cui, Chinese Rare Earths 16 (4) (1995) 60.
[6] S.S. Heberling, J.M. Riviello, S.F. Mou, A.W. Ip, Res. Dev. 29 (9) (1987) 74.
[7] A.W. Al-Shawi, R. Dahl, J. Chromatogr A 671 (1994) 173.
[8] R.M. Cassidy, Chem. Geol. 67 (1988) 185.
[9] A.W. Al-Shawi, R. Dahl, Anal. Chim. Acta 333 (1996) 23.
[10] S.F. Mou, A. Sirirars, J.M. Riviello, Sepu 12 (1994) 166.
[11] A. Sirirars, H.M. Kingston, J.M. Riviello, Anal. Chem. 62 (1990) 1185.
[12] J.M. Riviello, A. Siriraks, R.M. Manake, R. Roehl, U. Alforque, LC/GC 9 (1991) 704.
[13] A. Siriraks, J.M. Riviello, M.P. Harrold, Pittsburg Conf., 1992, p. 1226 (abstract).
[14] Dionex, Technical Note 27.
[15] J.P. Riley, D. Taylor, Anal. Chim. Acta 40 (1968) 479.
[16] S. Hirata, K. Honda, T. Kuamamany, Anal. Chim. Acta 221 (1989) 65.
[17] R.R. Greenberg, H.M. Kingston, J. Radioanal. Chem. 71 (1982) 147.
[18] Y. Liu, J.D. Ingle Jr., Anal. Chem. 61 (1989) 520.

ELSEVIER

Talanta 45 (1997) 127–135

Talanta

Spectrophotometric determination of Sb(III) in Sb(III)/Sb(V) binary mixtures using sodium dodecylsulfate/nonylphenoxy polyethoxyethanol mixed micellar media

Xirong Huang *, Wenjuan Zhang, Shuhua Han, Yongquan Yin, Guiying Xu, Xinqian Wang

Department of Chemistry, Shandong University, Jinan 250100, People's Republic of China

Received 13 November 1996; received in revised form 24 March 1997; accepted 8 April 1997

Abstract

Different micellar media had different effects on the absorption spectra of the complexes of bromopyrogallol red with Sb(III) and Sb(V). The mixed micellar medium composed of 0.7 ml of 0.2% sodium dodecylsulfate (SDS) and 0.3 ml of 2% nonylphenoxypolyethoxyethanol (OP) at 80°C could be used for the sensitive determination of Sb(III) in Sb(III)/Sb(V) binary mixtures. Under the optimal conditions, Beer's Law was obeyed over the range 0.1–2.3 μg ml^{-1} Sb(III) with molar absorptivity at 538 nm being 4.8×10^4 l mol^{-1} cm^{-1} and detection limit 0.04 μg ml^{-1}. For 10 μg Sb(III), more than 100 μg Sb(V) could be tolerated (error < 3%) in the presence of SDS/OP micellar medium as compared with 0.1 μg Sb(V) in the absence of SDS/OP micellar medium. In addition, the sensitivity of Sb(III) in the micellar medium was much higher than that in pure water medium. As compared with conventional extraction spectrometry, the proposed method produced a reproducible result. It did not need the conversion of Sb(III) to Sb(V) and a time-consuming extraction process. A detailed discussion on the selection of surfactants, the effect of temperature, and the role played by the mixed surfactants were also made. © 1997 Elsevier Science B.V.

Keywords: Antimony speciation; Bromopyrogallol red; Mixed micellar media; Spectrophotometry

1. Introduction

Antimony is a toxic element which exists in the aquatic environment in two oxidation states, +3 and +5. It was reported that Sb(III) is more toxic and mobile than Sb(V) [1]. In order to evaluate the toxicity of antimony in the aquatic environment, it is necessary to establish a method which can be used for Sb speciation. However, most of the spectrophotometric methods [2–8] established so far can not be used for the purpose although several atomic absorption spectrometry are available [9–12]. Among a small number of spectrophotometric methods for Sb speciation, the extraction spectrometry [1,13–17] is in the majority. However, this kind of method (with few exceptions [16]) is used merely for Sb(V) determination, that is to say, Sb(III) determination is

* Corresponding author.

PII S0039-9140(97)00114-8

always accompanied by the oxidation of Sb(III) to Sb(V), which leads to errors [13,14]. In addition, the use of toxic organic solvents makes its application to the routine analysis of Sb(III) unpopular.

From the point of view of inorganic chemistry, chemical properties of Sb(III) and Sb(V) must have been different because of their different oxidation states. As a matter of fact, both the peak positions and peak heights of the complexes of bromopyrogallol red (BPR) with Sb(III) and Sb(V) in water medium are different. However, these differences are not big enough to be used for the sensitive determination of Sb(III) in Sb(III)/Sb(V) binary mixtures. Therefore, it is necessary to augment these differences by selecting appropriate reaction reagents [1] or media so that not only Sb(III) could be discriminated from Sb(V) but also Sb(III) could be determined with good sensitivity and accuracy. In this paper, we directed our attention to the selection of media. With the selective determination of Sb(III) as well as use of less toxic media in mind, we chose micelles instead of organic solvents or supercritical fluids [18] as reaction media in that (1) medium properties such as dielectric constant could be continuously varied without changing a solvent, (2) charges on the surface of micelles could have a catalytic effect, and (3) micellar media were less toxic than most organic solvents.

To our knowledge, there seem to be no such reports on the resolution of different oxidation states of a same element based on the influence of micellar media on the spectral features and/or the reactivity of the species involved although several reports have so far been released on kinetic multicomponent determinations based on the effects of micelles on reaction kinetics [19,20].

Based on the influence of micellar media on the absorption spectra of the complexes of Sb(III) and Sb(V) with BPR, we developed a method for the spectrophotometric determination of Sb(III) in Sb(III)/Sb(V) binary mixtures. In addition, a detailed discussion on the selection of surfactants, the effect of temperature, and the role played by the mixed surfactants were also made. All results obtained and discussions made not only laid a solid foundation for the speciation analysis of Sb(III) in real samples, but also made a valuable contribution to the study of the effects of the toxic ion, Sb(III), on large bioaggregates such as membrane because a micellar aggregate formed by ionic and non-ionic surfactants could be regarded as a simplified bioaggregate.

2. Experimental

2.1. Apparatus

The UV-vis absorption spectra were recorded on a Shimadzu UV-240 spectrophotometer using a matched pair of 1 cm quartz cells. The spectrophotometer cell compartment was thermostated by circulating water from its accessories. A shimadzu RF-540 spectrofluorometer with a 1 cm cell was used for fluorescence measurements. The pHs of solutions were measured using a model PHS-2 pH meter.

2.2. Reagents

Unless otherwise stated, all reagents used were of analytical grade and their solutions were prepared by weighing with distilled water as solvent.

The concentration of each reagent was as follows:

1. bromopyrogallol red (BPR), from Merck, 0.01%
2. sodium dodecylsulfate (SDS), from Jining Institute of Chemical Industry, China, 0.2%
3. nonylphenoxypolyethoxyethanol (containing approximately 10 moles of ethylene oxide) (OP), from Wuhan Tongxing Chemical Reagent Plant, China, 2%
4. cetyltrimethylammonium bromide (CTAB), from Jining Institute of Chemical Plant, China, 0.1%
5. Sb(III), as potassium antimony tartrate, 10 μg ml^{-1}
6. Sb(V), as potassium pyroantimonate (Merck), 10 μg ml^{-1}

A 10^{-5} mol l^{-1} pyrene-3-carboxaldehyde (P_y CHO), from Aldrich, was prepared with 0.2% SDS/2% OP (7/3 (V/V)) mixed surfactant solutions.

A buffer solution (pH = 2.0) was prepared by mixing 5.0 ml of 0.2 mol l^{-1} KCl with 10.6 ml of 0.2 mol l^{-1} HCl and finally diluting to 200 ml.

2.3. Procedure

Pipette, in the given order, to a 10 ml colorimetric tube 2.0 ml of 0.01% BPR, 0.3 ml of 2% OP, 0.7 ml of 0.2% SDS, 2.0 ml of the buffer solution (pH = 2.0), and an aliquot of 10 μg ml^{-1} Sb(III) and/or 10 μg ml^{-1} Sb(V); then dilute with distilled water to the mark. Finally, transfer the resulting solution to the thermostated (80°C) cell. After thermal equilibrium (ca. 10 min), record the absorption spectrum against its corresponding blank.

3. Results and discussion

3.1. Selection of surfactants

Three representative surfactants (SF_S), namely, SDS (anionic), CTAB (cationic) and OP (nonionic), were selected for the study. The differences of the spectral features (i.e., the absorbance value of Sb(V)-BPR complex at the absorption maximum of Sb(III)-BPR complex and the peak height of Sb(III)-BPR complex) between Sb(III)-PBR complex and Sb(V)-BPR complex at pH = 2.0 in the presence of a single surfactant or a binary mixture of the above SF_S (concentration of each SF being slightly over its corresponding critical micelle concentration (CMC) [21]) were studied by spectrophotometric technique at various temperatures (from 30–90°C with an interval of 10°C). Preliminary study showed that, in the presence of a single SF, the absorption peak of Sb(III)-BPR complex could not be resolved over the temperature range tested (see Fig. 1, Fig. 2). Of the three binary mixtures, the SDS/CTAB mixture and the CTAB/OP mixture might be unsuitable for the resolution of Sb(III). The differences in the SDS/OP mixed micellar media increased with the increase of the temperature. In addition, at a given temperature (80°C), either increasing the concentration of OP or decreasing the concentration of SDS could augment the differences. So the SDS/OP mixture was chosen for subsequent experiments.

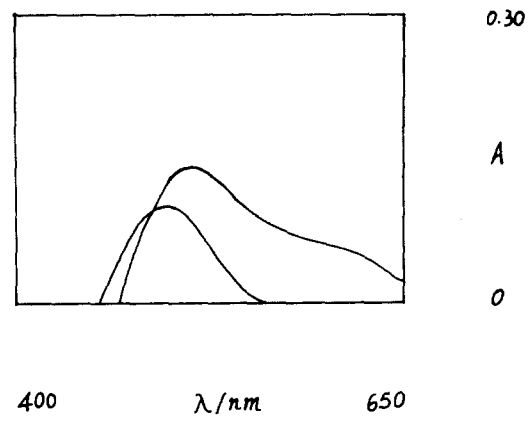

Fig. 1. Absorption spectra of BPR-Sb(III) (right) and BPR-Sb(V) (left) complexes in the presence of a single OP at 80°C (against the reagent blank). The system (10 ml) was composed of 2 ml of 0.01% BPR, 0.5 ml of 0.2% OP, 10 μg Sb, and 1.0 ml of 0.05 mol l^{-1} H_2SO_4.

As is mentioned in the introduction section, Sb(III)/Sb(V) could not be resolved with BPR in water (see Fig. 3). The same was true in a surfactant solution provided the concentration of the surfactant solution was lower than the CMC. A conclusion might be drawn from these results that the interface between the micellar and aqueous

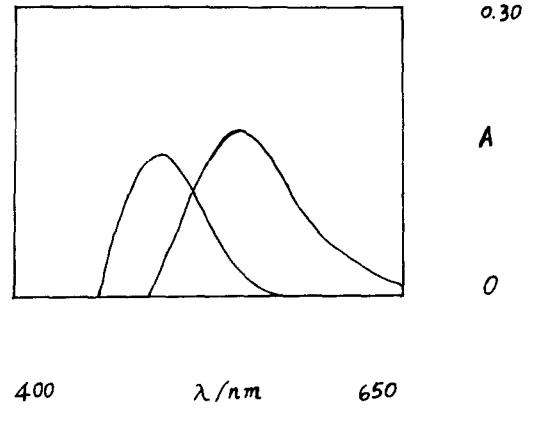

Fig. 2. Absorption sepctra of BPR-Sb(III) (right) and BPR-Sb(V) (left) complexes in the presence of a single SDS at 80°C (against the reagent blank). The system (10 ml) same as in Fig. 1 except that 2.5 ml of 1.0% SDS was used.

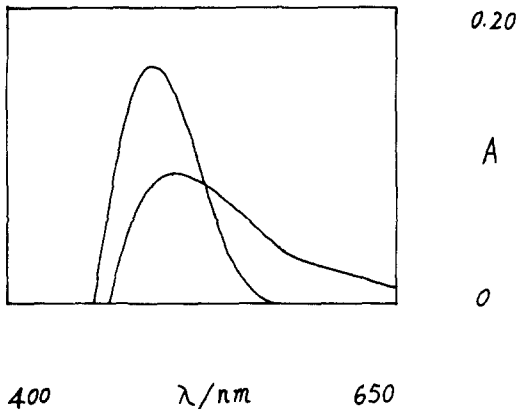

Fig. 3. Absorption spectra of BPR-Sb(III) (right) and BPR-Sb(V) (left) complexes in the absensce of SDS/OP micellar medium at 80°C (against the reagent blank). The system (10 ml was composed of 2.0 ml of 0.01% BPR, 2.0 ml of KCl + HCl buffer solution (pH = 2.0) and 10 μg Sb.

phase could be able to resolve Sb(III) in Sb(III)/Sb(V) binary mixtures (the bulk phase of a micellar system could be regarded as an aqueous phase [21]).

The possible explanation for the above results are as follows. At the reaction pH (2.0), Sb(III) could be present in a certain cationic form (small as it was), while Sb(V) could not. Therefore, a micellar medium with negative charges on micellar surface facilitated the augmentation of the above-mentioned differences. Because of the negative charges on BPR, micelles formed by a single SDS could hardly bind the BPR onto the micellar surface by whether electrostatic or hydrophobic force or both. Addition of OP to SDS could pull the BPR onto the micellar surface by whether electrostatic or hydrophobic force or both. Addition of OP to SDS could pull the BPR to the OP/SDS mixed micellar surface (probably by means of the hydrogen bond between the hydroxyl group on BPR and the oxygen in the polar head group of OP). In addition, OP made it convenient to change the microenvironment of the mixed micellar media (through the change of the aggregation number), this will be discussed in the following section.

3.2. Effect of temperature

The microenvironment provided by micellar surface could be characterized by zeta potential or local dielectric constant. For a given SF (i.e., the type of charge was fixed), it was correlated to the aggregation number of the micelle which could be varied conveniently by changing temperature.

With an increase in temperature, the aggregation number of OP increased in a big margin, especially when the temperature was close to its cloud point (the cloud point of 2% OP was ca. 65°C; addition of SDS made its cloud point increase), while that of SDS decreased a little [21]. Because the molar number of OP under the optimal conditions (see Section 2.3) was approximately twice that of SDS and, what is more, the increase in the aggregation number of the mixed micelle increased as the temperature increased.

3.3. Optimization of the experimental conditions in SDS/OP micellar medium

Conditions for the determination of Sb(III) in Sb(III)/Sb(V) binary mixtures was optimized by changing each experimental variable in turn while keeping all others constant (as in the Section 2.3). Each optimal condition met the following two requirements: (1) the absorbance value of the complex of Sb(V) at the absorption maximum of Sb(III) must be zero, and (2) the absorbance value of the complex of Sb(III) should be maximal.

3.3.1. Composition of the mixed surfactant solution and temperature

Let the total volume of 2% OP + 0.2% SDS be equal to 1.0 ml and change the relative volumes of the OP and the SDS with volume interval being 0.1 ml, then select peak-resolving temperature (PRT). The peak-resolving temperature was here defined as the temperature of water bath (with temperature interval being 5°C) at which the absorbance of the Sb(V) at the absorption maximum of the Sb(III) began to approach to zero. Results showed that when the volumes of 2% OP and 0.2% SDS were both greater than 0.1 ml, the absorption peak of the Sb(III) in different volume ratios could all be resolved. For different volume

ratios, however, the PRT was different (the sensitivity of Sb(III) was also different (see Table 1)). With the increase of the volume of 0.2% SDS, the PRT rose from 75°C (0.2 ml of 0.2% SDS) to 85°C (0.8 ml of 0.2% SDS). Of the different ratios tested, the ratio of 0.3–0.7 (OP to SDS) was the optimal one because in this ratio not only the absorbance of the Sb(V) at the absorption maximum of the Sb(III) (538 nm) was zero (see Fig. 4), but also the sensitivity of the Sb(III) was the highest. The PRT in this ratio was 80 ± 1°C. Further studies demonstrated that in this ratio bath temperature hardly had any influence on the resolution and sensitivity of Sb(III) over the range 80–90°C. However, when bath temperature exceeded 90°C, solutions became turbid (probably because the bath temperature exceeded the cloud point of the mixed SF solution). In addition, for 10 μg Sb(III), small fluctuation in volume (± 0.05 ml) in the vicinity of the optimal ratio caused only $\pm 3\%$ error in absorbance. By the way, the blank solution did not absorb (against water) in the vicinity of the absorption maximum of the Sb(III), which is favourable to the detection limit. One more thing, it is worth a mention, we think, that if the volume ratio of the OP to the SDS equalled 0.15:0.85, both the absorbance of the Sb(V) at the peak of the Sb(III) (550 nm) and that of the Sb(III) at the peak of the Sb(V) (496 nm) were zero (see Fig. 5), which indicates that Sb(III) and Sb(V) could be simultaneously determined in this ratio. We did not optimize this system because the sensitivity of the Sb(III) in this ratio (the sensitivity of Sb(V) was 60% that of Sb(III)) was only approximately half that in the optimal ratio, and, what is more, the zero absorbance point of the Sb(III) at the peak of the Sb(V) was very sensitive to the composition.

Table 1
Effects of the volume of 0.2% SDS on the peak-resolving temperature (PRT), the position of the peak of Sb(III) ($\lambda_{max}^{Sb(III)}$) and the absorbance (A) of Sb(III) at each $\lambda_{max}^{Sb(III)a}$

V_{SDS}, ml	PRT, °C	$\lambda_{max}^{Sb(III)}$, nm	A at $\lambda_{max}^{Sb(III)a}$
0	—	512	0.14
0.1	—	512	0.17
0.2	75	514	0.19
0.3	75	520	0.21
0.4	75	524	0.24
0.5	80	530	0.28
0.6	80	534	0.31
0.7	80	538	0.38
0.8	85	550	0.23
0.9	—	550	0.21
1.0	—	550	0.17

[a] The system was composed of 2.0 ml of 0.01% BPR, 1.0 ml of the mixed (0.2% SDS+2% OP) surfactant solution, 10 μg Sb and 1.0 ml of 0.05 mol l^{-1} H_2SO_4.

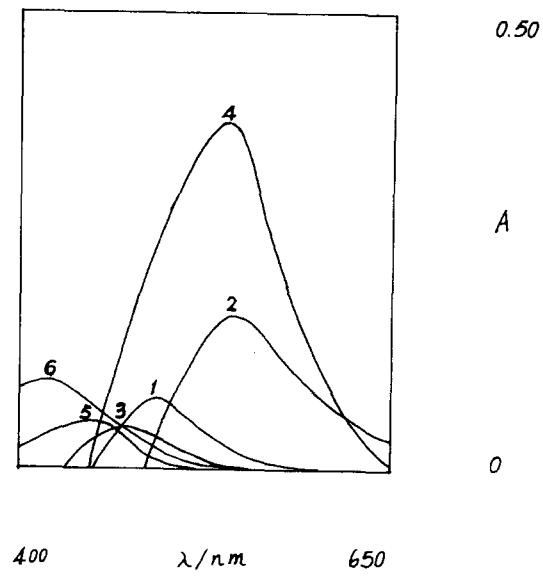

Fig. 4. Effects of temperature on absorption spectra (against corresponding blanks). System: 2.0 ml of 0.01% BPR + 0.3 ml of 2% OP + 0.7 ml of 0.2% SDS + 2.0 ml KCl + HCl buffer solution (pH = 2.0) + 10 μg Sb. Sb(III):2, 4, 6; Sb(V):1, 3, 5. Temperature: 30°C for curves 1, 2; 80°C for curves 3, 4; T > 90°C for curves 5, 6.

3.3.2. *Volume of the mixed SF solution in the optimal ratio*

In the optimal ratio and at PRT (80°C), the optimal volume of the mixed SF solution was 1.0 ± 0.2 ml (relative error $< \pm 3\%$). Deviation from such value resulted in a decrease of the sensitivity of Sb(III). If the volume of the mixed solution was above 1.5 ml or below 0.4 ml, not only the sensitivity of Sb(III) dropped greatly, but also its absorption peak could no longer be well resolved. Under the former volume condition, the

absorption spectra of the Sb(III) and Sb(V) were very similar in peak shape, position and height to curves 6 and 5 in Fig. 4 with the exception that no turbidity occurred. These results indicate that the aggregation number of each micelle, not the number of the micelle, was responsible for the resolution because, theoretically, small increment of the volume of the mixed SF solution could not make the aggregation number change greatly. In other words, it was the zeta potential or local dielectric constant which affected the resolution of the binary mixture.

In order to confirm this deduction, we chose pyrene-3-carboxaldehyde (PyCHO) as fluorescence probe to estimate the polarity at the surface of the SDS/OP mixed micelles (take 1.0 ml the SDS/OP mixed SF solution prepared in the optimal ratio and dilute with water to 10 ml, then keep the final solution at 80°C for 10 min). The main reason why we chose PyCHO, not BPR, as a fluorescence probe, not a UV spectral probe, was that (1) PyCHO was not charged, perturbations of the experimental systems by specific electrostatic charge interactions were expected to be minimal and (2) the solvent-polarity dependence of the fluorescence maxima for PyCHO was established [22]. The fluorescence maximum of the probe under the above condition occurred at approximately 450 nm (the excitation wavelength was 356 nm); the corresponding dielectric constant at the micelle-water interfaces was found to be ca. 35, which was very close to that of the methanol (90%)–water mixture at room temperature [22]. However, if this methanol–water mixture at room temperature instead of the above micellar system at 80°C was used as a medium, Sb(III) could not be well resolved. For 10 μg Sb(III) and 10 μg Sb(V) in this medium, the absorbance value of the Sb(V) at the peak of the Sb(III) was 15% that of the Sb(III). In addition, the sensitivity of Sb(III) decreased by ca. 32%. All these results indicate that, apart from providing an appropriate reaction medium, the SDS/OP mixed micelles also had an additional effects favouring the resolution of the Sb(III)/Sb(V) binary mixtures. This phenomenon might be related to the negative charges on SDS and the oxygen in polyoxyethylene ether chains of OP. Besides its local concentration effect of SDS on Sb(III) (present in a certain cationic form), SDS also had an activating effect on the Sb(III) at the surface by loosing its bonding with solvating water. The nascent Sb(III) (active) intermediate produced could be stabilized by the oxygen 'cage' (like a crown ether) of the polar head groups of OP, favouring its reaction with the BPR at the surface. Of course, the prerequisite of above inference was that the polarity displayed by PyCHO was identical with that experienced by Sb(III)-BPR complex. Research on this aspect are under way.

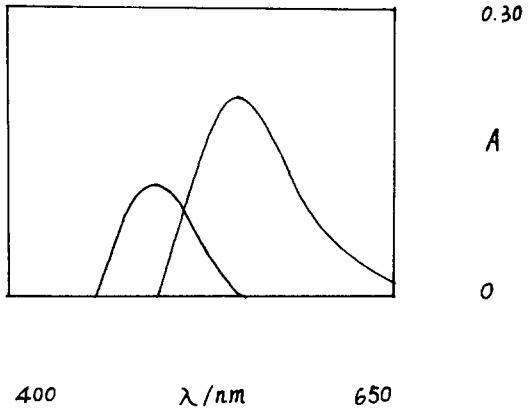

Fig. 5. Absorption spectra of BPR-Sb(III) (right) and BPR-Sb(V) (left) complexes in the presence of SDS/OP micellar medium at a specific composition (0.85/0.15 (V/V)) at 85°C (against the reagent blank). The system same as in Fig. 4 except the composition of the mixed surfactant solution.

3.3.3. Acidity and buffer solution volume

With the decrease of the pH of the system (substitute 0.05 mol l^{-1} H_2SO_4 for the buffer solution, other conditions as in Fig. 4, curves 3, 4), the absorbance of the Sb(III) at 538 nm (its absorption maximum) increased first rapidly then slowly over the pH range 2.6–1.4. However, when pH < 1.8, Sb(V)-BPR complex had a small negative absorption at 538 nm. The optimal pH was 2.0 (pH of the final solution) where 1.0 ml of 0.05 mol l^{-1} H_2SO_4 was added for adjusting the acidity of the system. HCl and HNO_3 with the same acidity as H_2SO_4 had the same effects as H_2SO_4.

Table 2
Recovery assay of Sb(III) in synthetic samples[a]

Composition (μg) Sb(III)+Sb(V)	Found (μg)[b] Sb(III)	RSD (%) Sb(III)	Recovery (%) Sb(III)
10+1	10.0	1.2	100
10+10	10.0	1.1	100
10+100	10.1	1.9	101

[a] Measured under the same conditions as used for the calibration.
[b] Mean of five replicate determinations.

In the vicinity of pH = 2.0, there are four buffering systems available for selection. They are KCl + HCl, NaAc + HCl, glycine + HCl, and sodium citrate + HCl. Of the four buffering systems tested, KCl + HCl was best. The rest had adverse effect in varying degree on the determination of Sb(III) probably because of the complexation of citrate with Sb(III), and the competitive electrostatic adsorption between the protonated-NH_2 group in the glycine and a certain cation of Sb(III) onto the surface of SDS micelles, and the 'salted out' effect of NaAc (because the concentration of NaAc + HCl buffering system was required to be very high). So KCl + HCl was chosen as the buffering system. Its optimal volume was 2.0 ± 0.2 ml.

3.3.4. Volume of 0.01% BPR

Optimization study showed that for 20 μg Sb(III), 2.0 ml of 0.01% BPR was optimum.

3.3.5. Order of addition of the reagents

The order of addition of the reagents was studied. Results demonstrated that the order had a great effect on the absorbance of the Sb(III). BPR and the mixed SF solution must be added before Sb(III). Also it was better that the buffer solution was added before Sb(III). These phenomena further support the explanation described in Section 3.3.1.

3.3.6. Stability of the complex

Under the optimal conditions described in the Section 2.3, the colour reaction was found to be completed in 10 min and the system showed no significant change for up to 2 h.

3.4. Composition of the complex

The composition ratio of the Sb(III)-BPR complex in the SDS/OP mixed micellar media obtained using the mole-ratio method and the method of continuous variations was 2:1 (BPR:Sb(III)), which was different from that (1:1) in pure water [3] and in a single cationic SF solution [4]. This difference may have something to do with the interaction between BPR and the polar head groups of OP.

3.5. Analytical characteristics

Under the optimal conditions, Beer's Law was obeyed over the range 0.1–2.3 μg ml^{-1} Sb(III) with molar absorptivity being 4.8×10^4 mol^{-1} cm^{-1} and detection limit (based on three times the standard deviation of the blank solution) being 0.04 μg ml^{-1}. For 10 μg Sb(III), the relative standard deviation (RSD) of seven replicate determinations was 1.2%.

Compared with other spectrophotometric methods which also used PBR as chromogenic reagents [3–5], our method not only was sensitive but could be used for the selective determination of Sb(III) as well. Although the present method was a little less sensitive than the basic dye extraction spectrometry [1], which was reported lately and considered very sensitive, our method did not need the conversion of Sb(III) to Sb(V) and a time-consuming extraction process.

3.6. Interference study

In order to examine the effects of Sb(V) on the determination of Sb(III), three Sb(III)/Sb(V) bi-

Table 3
Effects of foreign ions on the determination of 10 μg Sb(III) in the presence of 20 μg Sb(V)

Foreign metal ions	Tolerance limits (μg)[a,b]	Foreign non-metal ions (0.1 M)	Tolerance limits (ml)[b]
Pb(II) Cr(III)	200	Fluoride	2
Fe(II)	200	Chloride	2
Al(III) Co(II)	100	Bromide	2
Ni(II) Mn(II)	100	Iodide	1
Cu(II) Zn(II)	50	Nitrate	>2
Mg(II) Ca(II)	50	Sulfate	>2
Hg(II) As(III)	50	Phosphate	2
Mo(VI)	10(100)	Citrate	0.5
Sn(IV)	5(100)	Oxalate	0.5
Fe(III)	5(200)	Ascorbate	1.0
Ti(IV)	5(50)	EDTA	2
Bi(III)	3(20)		

[a] With a relative error being less than ± 5%.
[b] Data in parentheses were obtained in the presence of 0.5 ml of 0.1 M ascorbic acid and 1.0 ml of 0.1 M EDTA. Masking agents were added before interferents.

nary mixtures were selected (see Table 2) as synthetic samples for the recovery assay of Sb(III) in the samples. Results showed at least ten-fold molar excess of Sb(V) with respect to Sb(III) caused no interference. If no surfactant was added, for 10 μg Sb(III), only 0.1 μg Sb(V) was permitted to coexist (relative error < 3%).

Effects of foreign ions on the determination of 10 μg Sb(III) in the presence of 20 μg Sb(V) were also examined separately in this paper (see Table 3). It was obvious that strong oxidizing or reducing agents caused interference because of either decolourization of the BPR or the reduction of Sb(V). Therefore, no extensive research was made for these ions. As we can see from Table 3, interferences of metal ions tested above could be removed with EDTA and ascorbic acid, which made the application of our method to real sample analyses probable.

3.7. Conclusions

(1) Different micellar media had different effects on the absorption spectra of the complexes of Sb(III) and Sb(V) with BPR. Their resolving power depended on the type of charge on the surface of micelles and the aggregation number of micelles. The SDS/OP mixed micellar media could be used for the resolution of Sb(III) in Sb(III)/Sb(V) binary mixtures.

(2) The present method was highly selective; at least ten-fold molar excess of Sb(V) with respect to Sb(III) could be tolerated. As compared with other spectrophotometric methods, our method had many advantages in terms of simplicity, rapidity and sensitivity.

(3) Based on the method, a reproducible results could be obtained because small fluctuations in the bath temperature as well as the composition and the volume of the SDS/OP mixed SF solution had very small effects on the resolution of the binary mixture and the sensitivity of Sb(III).

(4) The order of addition of reaction reagents had great influence on the sensitivity of Sb(III). BPR and the SDS/OP mixed SF media must be added before Sb(III).

(5) Interference study showed that interferences of some foreign metal ions tested could be eliminated with EDTA and ascorbic acid, which made the application of our method to real sample analyses probable.

(6) Preliminary study on the polarity at the micelle-water phase showed that the SDS/OP mixed micellar media had additional effects on the selective and sensitive determination of Sb(III) as compared with organic solvent media which had the same dielectric constant as the SDS/OP micellar media.

Acknowledgements

The authors gratefully acknowledge financial support from the Key Laboratory for Colloid and Interface Chemistry of the State Education Commission, Shandong University, China.

References

[1] M. Sharma, K.S. Patel, Inter. J. Anal. Chem. 50 (1993) 63.
[2] D. Sicilia, S. Rubio, D. Perez-Bendito, Anal. Chem. 64 (1992) 1490.
[3] D.H. Christopher, T.S. West, Talanta 13 (1966) 507.
[4] I. Nemocova, J. Harchovska, J. Mikova, V. Suk, Microchem. J. 30 (1984) 39.
[5] T. Wu, Fenxi Shiyanshi 7 (1988) 32.
[6] N. Lacy, G.D. Christian, J. Ruzicka, Anal. Chim. Acta 224 (1989) 373.
[7] R.W. Ramette, Anal. Chem. 30 (1958) 1185.
[8] H.M. Neuman, J. Am. Chem. Soc. 76 (1954) 2611.
[9] T. Kamada, Y. Yamamoto, Talanta 24 (1977) 330.
[10] M. Yamamoto, K. Urata, Y. Yamamoto, Anal. Lett. 14 (1981) 21.
[11] S. Nakashima, Analyst 105 (1980) 732.
[12] C.H. Chung, E. Iwamoto, M. Yamamoto, Y. Yamamoto, Spectrochim. Acta 39B (1984) 459.
[13] M. Tanaka, M. Kawahara, Bunseki Kagaku 10 (1961) 185.
[14] H. Imai, Bunseki Kagaku 11 (1962) 806.
[15] S. Sato, Talanta 32 (1985) 341.
[16] S. Sato, S. Uchikawa, Anal. Sci. 2 (1986) 47.
[17] A.G. Fogg, C. Burgess, D. Thorburn Burns, Analyst 98 (1973) 347.
[18] J.F. Kauffman, Anal. Chem. 68 (1996) 249A.
[19] D. Sicilia, S. Rubio, D. Perez-Bendito, Anal. Chem. 284 (1993) 149.
[20] X. Huang, N. Jie, W. Zhang, J. Huang, Mikrochim. Acta, in press.
[21] Z. Zhou, T. Gu, J. Ma, Fundamental Colloid Chemistry, Beijing University Press, Beijing, 1987.
[22] K. Kalyanasundaram, J.K. Thomas, J. Phys. Chem. 81 (1977) 2176.

ELSEVIER

Talanta 45 (1997) 137–146

Talanta

Investigation of a flat sheet membrane desolvator for aqueous solvent removal with inductively coupled plasma atomic emission spectrometry

Olujide T. Akinbo, Jon W. Carnahan *

Department of Chemistry, Northern Illinois University, DeKalb, IL 60115, USA

Received 9 December 1996; received in revised form 24 March 1997; accepted 8 April 1997

Abstract

Results obtained from a preliminary investigation of the performance of a flat sheet membrane desolvator (FSMD) utilizing dual hydrophobic polypropylene membranes with an average pore size of 0.05 μm and a 50 ± 5 μm thickness are reported. The membranes have a desolvation area of 241 cm^2. The volume-to-surface area ratio is 0.3 cm. Using the FSMD with an ultrasonic nebulizer (USN), aqueous solvent desolvation efficiencies of greater than 99.9% were obtained at all nebulizer gas flow rates investigated (0.8, 1.2, and 1.8 l min^{-1}). This efficient desolvation occurred when the countercurrent gas flow rate was equal to or slightly greater than the applied nebulizer gas flow rate. Under these conditions preconcentration factors of 18, 44, and 590 were observed with flows of 0.8, 1.2 and 1.8 l min^{-1}, respectively. Operating with countercurrent gas flow rates much higher than the nebulizer gas flow rates leads to a significant reduction in analyte flux, thus increasing detection limits. Depending on the nebulizer and countercurrent gas flow rate conditions, the FSMD contributed between 10–40% to the overall analyte loss in the system. The lowest detection limit observed for aqueous copper with the USN-FSMD system is 0.4 ppb at nebulizer and countercurrent gas flow rates of 1.2 and 1.4 l min^{-1}, respectively. At this nebulizer gas flow rate, replacing the FSMD in the system with a commercial tubular membrane desolvator, MDX100, gave a lowest Cu detection limit of 0.2 ppb at a countercurrent gas flow rate of 1.2 l min^{-1}. These detection limits represents improvements over the 0.7 and 8 ppb obtained with USN and pneumatic nebulization, respectively. © 1997 Elsevier Science B.V.

Keywords: Flat sheet membrane desolvator; Sample introduction; Atomic emission spectrometry; Analyte transport; Preconcentration

1. Introduction

Adverse effects on analytical parameters caused by direct solution nebulization into plasma sources have hindered the realization of the full potential of inductively coupled plasma (ICP) atomic emission and mass spectrometry. When used as the atomization/excitation source in an atomic emission technique, the introduction of solvent adds to the complexity of plasma background spectra. Extinguishment occasionally occurs with low power plasmas [1,2]. Plasma

* Corresponding author.

PII S0039-9140(97)00112-4

cooling, signal reduction, poor detection limits and reduced sensitivity are among other negative effects. These problems are even more pronounced with organic solvents than with aqueous solvents. When a plasma is used as an atomization/ionization source in atomic mass spectrometry, the presence of solvents may cause the formation of molecular ion species which interfere with analyte detection. Typical examples of this phenomenon include the interferences of: $^{40}Ar^{16}O^+$ on $^{56}Fe^+$, $^{35}Cl^{16}O^+$ on $^{51}V^+$ and $^{40}Ar^{35}Cl^+$ on ^{75}As [3–5]. Additionally, $^{238}U^1H^+$ interferes with the determination of ^{239}Pu and $^{232}Th^{16}O^+$ interferes with the determination of ^{248}Cm [6]. Therefore, because of complex spectral background and mass interferences, it is desirable to remove the solvent from the analyte stream prior to plasma introduction.

Various methods for achieving desolvation of the analyte stream prior to analyte introduction into the plasma have been reported in the literature [7–15]. The use of membrane desolvators shows particular promise. Membrane desolvators have the advantages of higher analyte transport efficiency and the capability for greater than 90% desolvation efficiency [5,10]. Gustavsson and coworkers [10,16–18] reported the use of a planar membrane separator. In their report, the separation of solvent from analyte particles was achieved based on the selective solubility of the solvent in the non-porous membrane and also by using a vacuum pump to create a pressure gradient across the membrane, which also helps to drive the transport of the solvent vapor across the membrane to waste. Montaser et al. [19] used a similar membrane separator in combination with a thermospray nebulizer, but these workers used a gas stream to sweep the solvent to waste instead of a vacuum pump. The use of single [20] and multiple [21] tubular membrane desolvation devices have also been reported.

The design of a membrane desolvator plays a major role in its performance. Koropchak et al. [22] have shown that when transporting aerosols through tubes, gravitational settling (in the case of straight tubes) and impaction on the tube walls due to centrifugal forces (in the case of coiled tubes) are factors leading to analyte losses in the tube. Desolvated particles are less prone to settling than undesolvated ones due to their smaller sizes. These workers also reported that longer tubes and/or smaller diameter coils cause greater analyte loss. Also, turbulent flows result in higher analyte losses. The list of factors critical to the performance of a membrane desolvator, therefore, must include the design geometry (i.e. if the membrane is coiled or straight, tubular or planar) and the membrane length and area needed for efficient desolvation. The nature (i.e. porous or nonporous, hydrophilic or hydrophobic) of a membrane will determine the type of transport through the membrane, i.e. whether solvent transport is predominantly by permeation or diffusion [23]. The type of flow (laminar or turbulent) through the desolvator also affects the analyte flux and desolvation efficiency of the system.

Botto and Zhu [20] reported a detailed study of the performance of a tubular membrane desolvator, but no such study has been reported for the flat sheet membrane desolvator (FSMD). In this paper, we report results obtained upon a detailed investigation of the FSMD.

2. Experimental

2.1. Reagents

A 1000 mg l^{-1} Cu^{2+} aqueous stock solution was prepared by dissolving the appropriate amount of $Cu(NO_3)_2 \cdot 6H_2O$ in 1% HNO_3. Other test solutions were prepared by dilution of this stock solution to the desired concentrations using 1% HNO_3.

2.2. Instrumentation

2.2.1. Flat sheet membrane desolvator (fsmd)

The membrane mount is a 3-piece rectangular aluminum block (Fig. 1). The dimensions are: $35 \times 7.4 \times 1.1$ cm for each of the two outer pieces and $35 \times 7.4 \times 0.6$ cm for the central spacer. The spacer has a channel 28 cm long and 4.3 cm wide. Flat sheet microporous polypropylene membranes are placed on either side of the spacer at the interfaces between the spacer and the outer pieces.

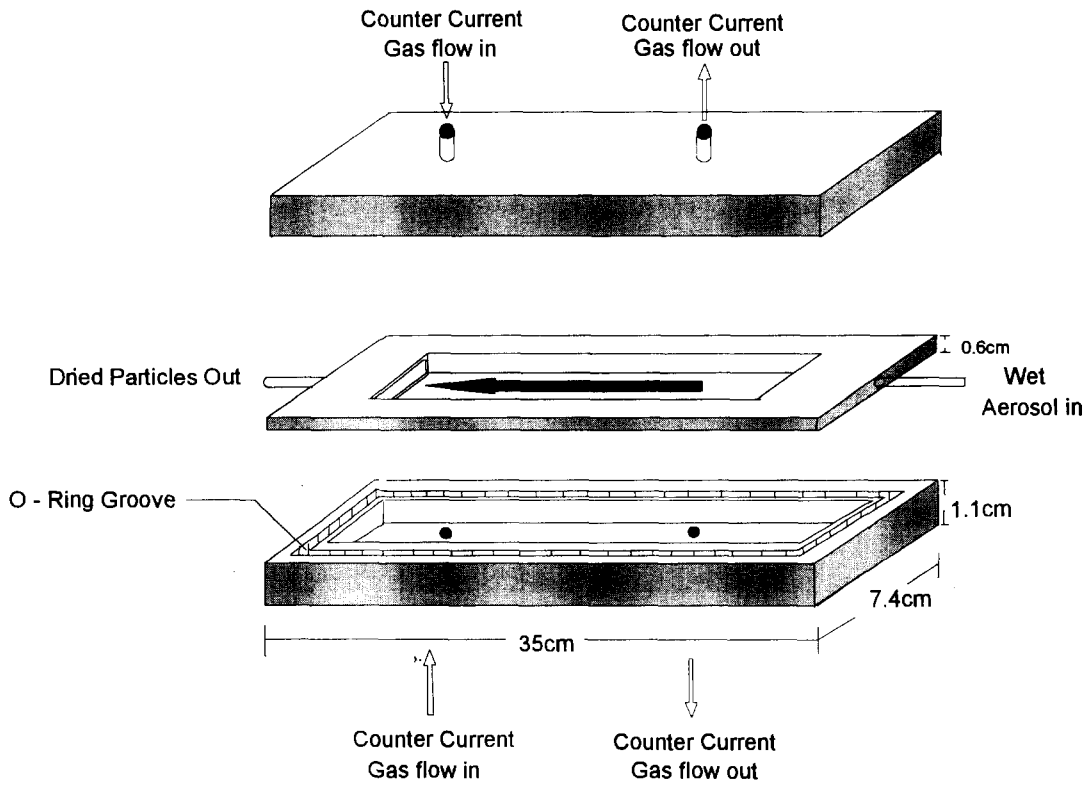

Fig. 1. The flat sheet membrane mount.

The dimensions of the membranes are 30 × 5.6 cm × 50 μm. A seal is made using an O-ring (20.4 cm O.D., 0.334 cm thick) fixed into a rectangular groove on the inner faces of the outer pieces.

The membrane is a polypropylene Celgard® 2402 microporous membrane (Hoechst Celanese Corporation, Charlotte, NC, USA). The polypropylene membrane is hydrophobic. Therefore, aqueous solvent vapor transport through it occurs primarily by diffusion. Other properties of the membrane include: average pore size of 0.05 μm, 38% porosity, and a thickness of 50 ± 5 μm. The membrane mount is held together with 14 stainless steel, 7 × 31 mm, 1 mm per pitch socket head cap screws. The block is wrapped with heating tape and connected to a temperature controller. The temperature controller used for the flat sheet membrane desolvator is a Powermite stepless heat controller (Laboratory Craftsmen Inc., Beloit, WI 53511, USA). In operation, the whole block is heated to a temperature comparable to or higher than the boiling point of the solvent to be removed.

As shown in Fig. 2, the analyte solution is converted to a mist by the ultrasonic nebulizer. Initial desolvation of the stream is done in a water cooled condenser at −5°C. This condensation stage is followed by a heating stage (160°C) for further solvent vaporization and analyte particulate drying. The resultant stream is directed into the central channel of the membrane desolvator (Fig. 3). Ideally, at this stage, the stream is composed of solvent vapor and dry analyte particulates. A dry gas flowing countercurrent to the analyte stream is applied to the outer channels. In the ideal case, only the smaller solvent molecules will diffuse from the central channel through the membrane to the outer channel to be transferred to waste by the countercurrent gas stream. The heavier analyte particulates will be carried by the

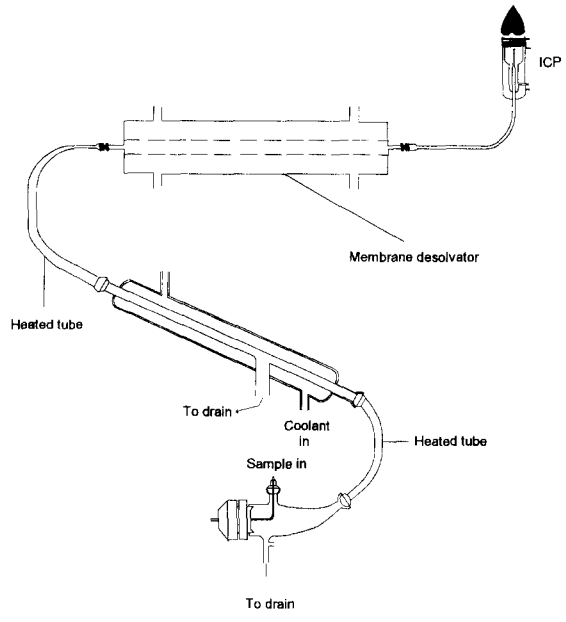

Fig. 2. General system diagram.

central gas stream directly to the plasma. This process enables the transport of dry analyte particles to the plasma.

2.2.2. Additional instrumentation

The nebulizer used in these studies was a CETAC (CETAC Technology Inc., NE, USA) ultrasonic nebulizer model U-5000AT. The tubular membrane desolvator used for comparative studies is the CETAC MDX100 membrane desolvator. The inductively coupled plasma (ICP) spectrometer used in this study is a Plasmaspec Model 2.5 (Leeman Labs Inc., Lowell, MA, USA). The various instrumental operating conditions are either listed in Table 1 or at the appropriate point in Section 3.

2.3. Measurement procedures

2.3.1. Measurement of desolvation efficiency

The desolvation efficiencies at various points in the system were obtained by trapping the solvent vapor/mist in a cold-finger based glass trap condenser cooled at −86°C (using a dry ice-isopropyl alcohol mixture). The solvent was trapped each time for a 30 min duration. The preweighed apparatus was allowed to warm to ambient temperature and weighed. The desolvation efficiency was calculated using the equation:

$$\text{Percent desolvation} = 100 - \frac{SD}{SN}\,100 \qquad (1)$$

where SD is the mass of solvent collected from the outlet of the portion of the system being examined and SN is the mass of solvent collected at the device inlet in a fixed period of time. The nebu-

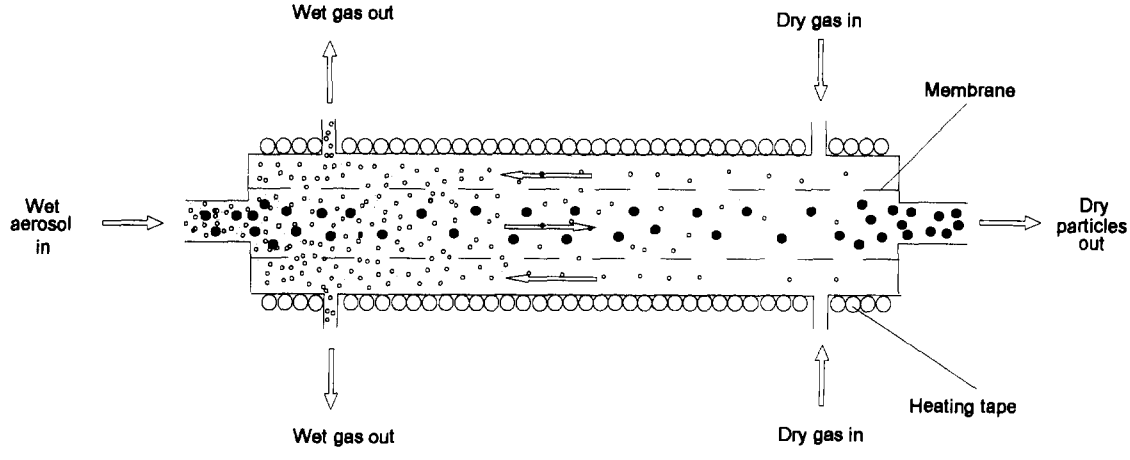

Fig. 3. The desolvation concept showing the fate of the analyte and solvent.

Table 1
Operating conditions for the ICP, USN, and membrane desolvators

ICP	
Power (kW)	1.3
Gas flow rate (l min^{-1})	
Plasma	12
Auxiliary	0.3
Nebulizer	1.2
USN	
Heated tube (°C)	160
Coolant (°C)	−5
Sample uptake rate (ml min^{-1})	1.5
Tubular Desolvator (MDX100)	
Membrane material	Teflon
Membrane dimension	(I.D = 0.5 cm, length = 2 m)
Membrane pore size	1 μm
Membrane body temperature (°C)	160
Countercurrent gas temperature (°C)	160
Flat Sheet Membrane Desolvator (FSMD)	
Membrane material	Polypropylene
Membrane dimension	30 × 5.6 cm × 50 μm
Membrane pore size	0.05 μm
Membrane body temperature (°C)	90
Countercurrent gas temperature (°C)	90

lizer gas flow rate was fixed while the countercurrent gas flow rate was varied from 0 to 2.2 l min^{-1}. This procedure was repeated for each of the three nebulizer gas flow rate settings (0.8, 1.2 and 1.8 l min^{-1}).

2.4. Measurement of analyte transport

The procedure used for obtaining analyte transport information involved collecting analyte at various points in the system (at the spray chamber, condenser, and FSMD outlets). In this procedure, an aqueous solution of 1 mg ml^{-1} Cu^{2+} was nebulized and analyte in the carrier gas flow stream was trapped by bubbling this stream through 15 ml of 1% $HNO_{3\,(aq)}$ in a glass tube for 20 min. The solution was then transferred and diluted to mark in a 50 ml volumetric flask. The diluted solution was analyzed with the ICP using the emission line at 324.75 nm.

2.5. Calculations:

The detection limit was calculated as the concentration of analyte which gave a signal three times the standard deviation of blank (1% $HNO_{3\,(aq)}$). Ten replicate measurements were used for this determination.

The preconcentration factor was calculated using the equation shown below:

$$\text{Preconcentration factor} = \frac{\left(\frac{\text{Analyte flux (mg s}^{-1})}{\text{Solvent flux (ml s}^{-1})}\right)}{\text{Original concentration (mg ml}^{-1})} \quad (2)$$

This factor was used to monitor changes to the concentration of the analyte in the system, and was calculated using analyte and solvent trapped at the outlet of the desolvator under each condition tested.

The sensitivity values were obtained from slopes of calibration plots.

3. Results and discussion

3.1. Desolvation efficiency

The desolvation efficiency trends obtained with the flat sheet membrane desolvator (FSMD) as a function of both the countercurrent gas flow rates (in the range 0–2.2 l min^{-1}) and nebulizer gas flow rates (at 0.8, 1.2 and 1.8 l min^{-1}) are shown in Fig. 4. In each case, the desolvation efficiency increased as the counter-current flow rate was increased from 0 to 2 l min^{-1}. It should be noted that at countercurrent gas flow of 0 l min^{-1} desolvation occurs to some extent. As is always the case, desolvation under this condition is driven by the differences in solvent vapor concentrations on either side of the membrane. However, because the waste solvent is removed only by passive diffusion, this gradient is smaller without a countercurrent flow. The desolvation efficiency reached 99.99% at every nebulizer gas flow rate tested, but the value of the counter current gas flow rate at which this was achieved differed. At nebulizer gas flow rates of 0.8, 1.2 and 1.8 l min^{-1}, the 99.99% desolvation efficiency was at-

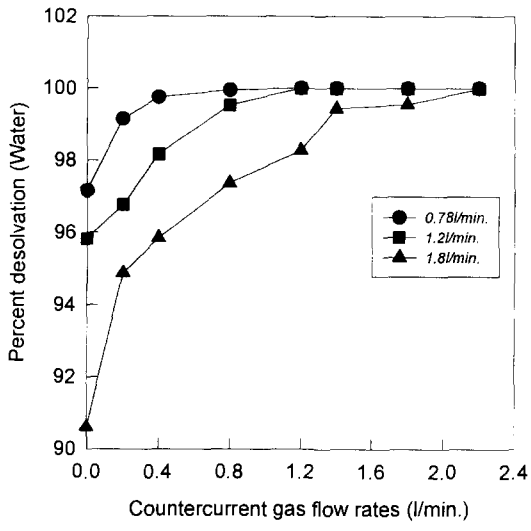

Fig. 4. Desolvation efficiency trends as a function of countercurrent gas flow rates at nebulizer gas flow rates of 0.8, 1.2, and 1.8 l min^{-1}.

tained at counter current gas flow rates of 0.8, 1.2 and 2.2 l min^{-1}, respectively. Higher nebulizer gas flow rates required higher countercurrent flows to facilitate efficient desolvation.

3.2. Analyte transport

3.2.1. Fate of the analyte in the system (USN-FSMD)

With a 1 mg ml^{-1} Cu solution and a sample uptake rate of 1.5 ml min^{-1}, the analyte flux entering the spray chamber is 25 μg s^{-1}. The fate of the analyte through the system (i.e. USN-FSMD) is summarized in Table 2. For this study no countercurrent gas flow was applied to the membrane desolvator. Effects of countercurrent gas flow rate variations on the analyte transport are discussed in the next section. The fraction of the analyte transported through a section of the system was calculated as a ratio of flux-in to flux-out of that section.

In each section of the system, analyte is lost to some extent. Contributions to analyte flux reduction originate from three major sources, viz: losses in the nebulizer/spray chamber section, losses in the condenser due to analyte trapping, and losses in the membrane desolvator due to analyte trapping and/or diffusion of analyte from the central channel to the outer channel where it is swept to waste along with solvent vapor.

As can be seen from Table 2, the major contribution to analyte loss in the entire system is that from the nebulizer/spray chamber section. The fraction of analyte exiting the spray chamber ranged from 2.26% at nebulizer (carrier) gas flow rate of 0.8 l min^{-1} to 5% at a nebulizer gas flow rate of 1.8 l min^{-1}. These fractions are low compared to the 13.4% observed by Tarr et. al. [24] at sample uptake rate of 1.5 ml min^{-1} and analyte transport of 3.35 ± 0.09 μg s^{-1}. These authors also used a 1 mg ml^{-1} analyte solution. It is likely that the difference is due to variations between the systems and the operational conditions. In general, the fraction of analyte exiting the spray chamber increased with nebulizer gas flow rate. It is possible that this is because as the

Table 2
Fate of analyte through USN-Condenser-FSMD

Nebulizer gas flow rate (l min^{-1})	Analyte flux entering the spray chamber (μg s^{-1})	Analyte flux (μg s^{-1}) exiting spray chamber	Analyte flux (μg s^{-1}) exiting condenser	Analyte flux (μg s^{-1}) exiting FSMD[a]
0.80	25.0	0.565 (2.26%)	0.223 (39.5%)	0.012 (5.38%)
1.20	25.0	0.881 (3.52%)	0.283 (32.1%)	0.108 (38.2%)
1.80	25.0	1.25 (5.00%)	0.363 (29.0%)	0.243 (66.9%)

Note: Values in parentheses represent percent analyte transport calculated based on comparison of the analyte flux-in and flux-out at each stage.

[a] Note that this data was collected when no countercurrent gas flow was applied to the FSMD.

nebulizer gas flow rate increased, the residence time of the droplets in the spray chamber decreased, and the time available for coalescing and gravitational settling decreased.

In the double pass condenser, the fraction of analyte transported decreased with increasing nebulizer gas flow rates. This observation is explained by the fact that impaction of the wet aerosol entering the cooled (− 5°C) condenser is probably the dominant analyte loss process. Higher nebulizer gas flow rates increase the probability of impaction.

In the membrane desolvator, the fraction of analyte transported increased with nebulizer gas flow rate. It should be noted that at this stage the aerosol stream is drier and dry aerosols exhibit more efficient transport since these particles are less likely to be lost by impaction than wet aerosols. Also important is the fact that at higher nebulizer gas flow rates, the chances of gravitational settling is reduced. Further studies regarding the position of the desolvator appears to be warranted.

3.2.2. *Effect of countercurrent gas flow rates on analyte transport through the flat sheet membrane desolvator (FSMD)*

Fig. 5 shows the effect of the counter current gas flow rate on the analyte flux through the desolvator at the three nebulizer gas flow rates tested. At nebulizer gas flow rate of 0.8 l min^{-1}. the analyte flux remains almost constant in the counter current gas flow rate range from 0–1.2 l min^{-1} applied. At nebulizer gas flow rates of 1.2 and 1.8 l min^{-1} analyte flux decreased as the counter current gas flow rates were increased. A separate experiment was carried out to determine if the diffusion of countercurrent gas flow through the membrane affected the carrier gas flow rate and if this is the cause for the decrease in analyte flux observed at higher countercurrent gas flow rates. Results from the experiment reveals that the nebulizer gas flow rates (at 0.8, 1.2 and 1.8 l min^{-1}) remained unchanged when counter current gas flow rates in the range 0.2 to 2.2 l min^{-1} were applied to the membrane separator. The reductions in analyte

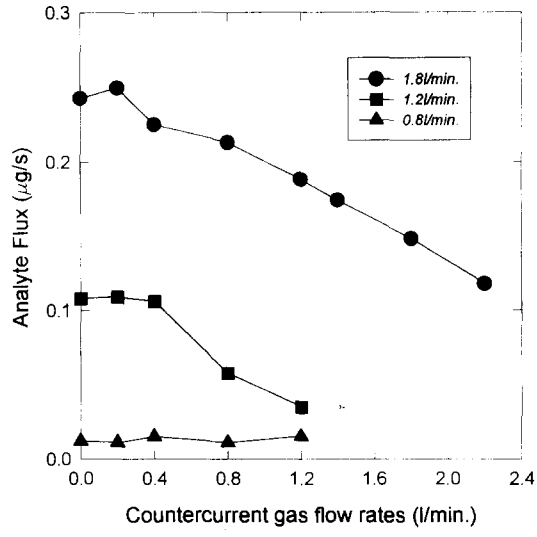

Fig. 5. Effect of countercurrent gas flow rates on analyte flux at nebulizer gas flow rates of 0.8, 1.2 and 1.8 l min^{-1}. Cu emission line at 324.75 nm was used as probe.

fluxes seen at higher countercurrent gas flow rates were therefore not due to changes of the carrier gas flow caused by the countercurrent gas flow. While there are other possible mechanisms by which analytes could be lost in the membrane desolvator, there is no evidence at this time to suggest which might be dominant.

3.3. *Preconcentration factor*

The preconcentration factor is an index for comparing the rate of loss of analyte to the rate of loss of solvent. From Eq. (2), if more solvent is removed than analyte, the ratio in the numerator is high and the preconcentration factor will be high. As an example, at the nebulizer gas flow rate of 1.8 l min^{-1} the highest preconcentration factor of 590 was seen at countercurrent gas flow rate of 2.2 l min^{-1}. This is the region where the lowest analyte flux was observed for that nebulizer gas flow rate. Also, at countercurrent gas flow rate of 1.2 l min^{-1} and nebulizer gas flow rate of 1.2 l min^{-1}, a preconcentration factor of 44 was calculated. These results shows that even though analyte flux decreased at higher countercurrent gas

flow rates there is an advantage of high desolvation efficiency and the fraction of solvent removed was much greater than that of the analyte. The trend for the preconcentration factors as a function of countercurrent gas flow rate is shown in Fig. 6.

3.4. Sensitivity

Measured sensitivities shown in Fig. 7 are the slopes of calibration curves obtained at nebulizer gas flow rate of 1.2 l min^{-1} using the indicated countercurrent gas flow rates. The sensitivities of the USN-FSMD-ICP and USN-MDX100-ICP are normalized to that of the USN-ICP (without a membrane desolvator) which is assigned a value of 100. Again copper was used as the probe analyte. In almost every case the sensitivities of the USN-FSMD-ICP and USN-MDX100-ICP are lower than that of the USN-ICP. This observation is due to analyte losses incurred in the membrane desolvators. However, the sensitivity losses are in the range of approximately 50% or less. It should be noted that these sensitivities are often accompanied by a reduction in background noise as discussed in the next section.

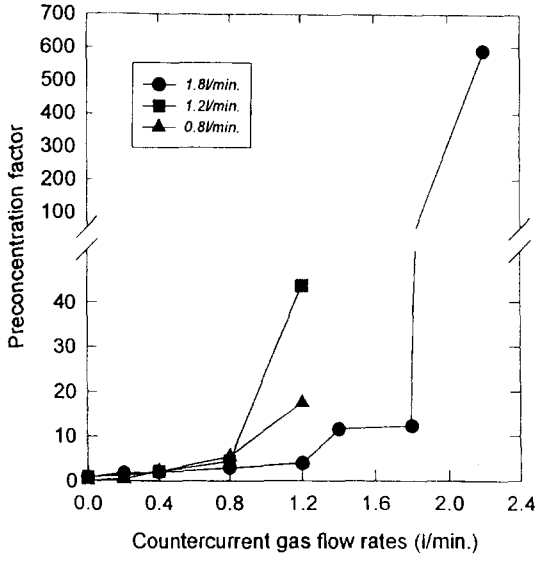

Fig. 6. Preconcentration trends as a function of countercurrent gas flow rates at nebulizer gas flow rates of 0.8, 1.2 and 1.8 l min^{-1}.

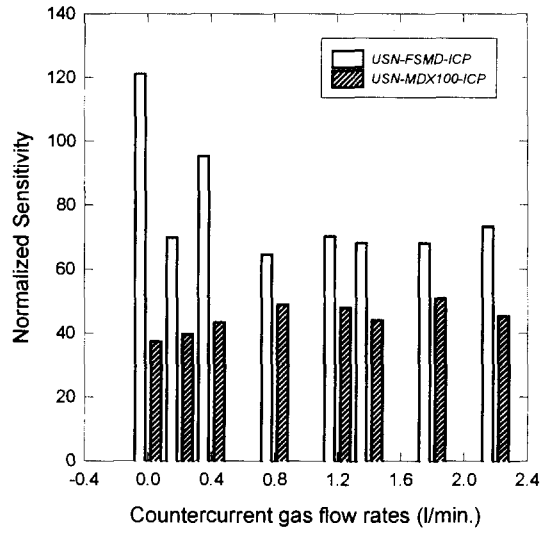

Fig. 7. Effect of the membrane desolvators on the sensitivity of the USN-ICP system. The sensitivities of USN-FSMD-ICP and USN-MDX100-ICP are normalized to the sensitivity of the USN-ICP which was assigned a value of 100.

In each case, the FSMD system exhibits higher sensitivities than the MDX100 system. It is postulated that the cause of this difference is that the analyte spends shorter residence times in the FSMD than the MDX100. Also the design geometry of the FSMD is planar as opposed to the coiled-tube design of the MDX100. These factors may enable higher analyte transport efficiencies with the FSMD.

3.5. Detection limit studies

The detection limit trends for the various system configurations used in this studies are shown in Fig. 8. When the ICP was operated at nebulizer gas flow rate of 1.2 l min^{-1} with the pneumatic (Hilderbrand) nebulizer alone, the detection limit for copper(II) was 8 ppb. However, using the ultrasonic nebulizer at the same nebulizer gas flow rate decreased the detection limit by an order of magnitude to 0.7 ppb. When the flat sheet membrane desolvator was connected on-line (i.e. USN-FSMD-ICP configuration), the detection limit trend showed a minimum of 0.4 ppb at a counter current gas flow rate of 2.2 l min^{-1}. Using the tubular membrane desolvator (i.e. USN-

MDX100-ICP configuration) instead of the FSMD, the detection limit showed a minimum of 0.2 ppb at countercurrent gas flow rate of 1.2 l min^{-1}. Comparing the detection limits observed with the various configurations, at the optimum conditions, the values obtained with USN-FSMD-ICP and USN-MDX100-ICP are not dramatically different.

4. Conclusion

In general, using membrane desolvators in conjunction with the heat-cool-trap desolvation system of the ultrasonic nebulizer enables a high desolvation efficiency of up to 99.99% as demonstrated with the FSMD. However, associated with this high desolvation efficiency is the phenomenon of analyte flux reduction. Despite the analyte flux reduction, operating the systems (USN-FSMD-ICP or USN-MDX100-ICP) at optimal conditions results in detection limits which are lower than those obtained with the USN-ICP system. The optimum condition occurs for both desolvators at points when the countercurrent gas flow rate is equal or is slightly greater than the nebulizer gas flow rate. This result implies that solvents can be removed without impairing analyte detection limits. The advantage this offers is the possibility of the reduction of solvent induced interferences (e.g. hydrides and oxides) in atomic plasma mass spectrometry, and the reduction of molecular background emission in atomic emission spectroscopy. Improvements are expected to be accentuated in applications involving organic solvents, where molecular emission and other effects on the plasma chemistry are more pronounced. With lower power plasmas, which are less tolerant to solvent effects, these advantages may be significant, as well.

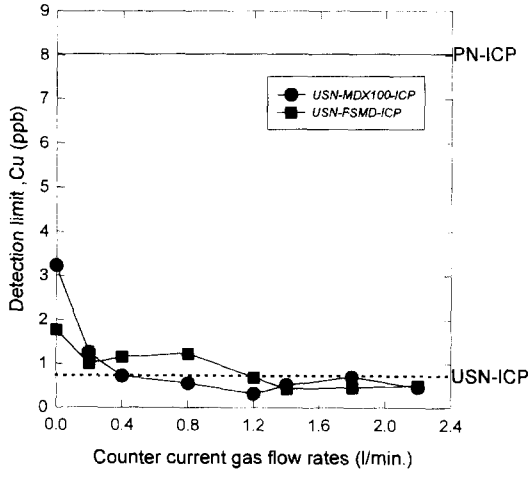

Fig. 8. Detection limit trends obtained with the various system configurations at nebulizer gas flow rate of 1.2 l min^{-1} and different countercurrent gas flow rates.

Despite the differences in the configuration and materials used in the construction of the desolvators, their performances are comparable in terms of detection limits. The FSMD showed better sensitivity than the MDX100 but poorer noise characteristics.

With the observation of high preconcentration factors, high desolvation efficiencies, good sensitivities and low detection limits, the performance of the FSMD is promising. It is rugged, cheap to construct, and easy to assemble. Future studies with the desolvators include desolvation with organic solvent based samples, examinations of metal oxide and hydride ICP-MS interferences, and other solvent induced interferences in plasma optical and mass spectrometry. Additionally studies with low power helium microwave induced plasmas will be conducted to take advantage of the solvent reduction characteristics of the membrane desolvator.

Acknowledgements

The authors will like to acknowledge CETAC Technologies Inc. for technical support and Larry Gregersen of Northern Illinois University for machining the membrane holder.

References

[1] G.K. Webster, J.W. Carnahan, in: P.C. Uden (Ed.), ACS Symposium Ser. 479, ch. 2, p. 31.
[2] K.G. Michlewicz, PhD Thesis, Northern Illinois University, USA, 1987.

[3] C. Pan, G. Zhu, R.F. Browner, J. Anal. Atom. Spectrom. 5 (1990) 537.
[4] R.C. Hutton, A.N. Eaton, J. Anal. Atom. Spectrom. 2 (1987) 595.
[5] H. Tao, A. Miyazaki, J. Anal. Atom. Spectrom. 10 (1995) 1.
[6] J.S. Crain, J.A. Alvarado, J. Anal. Atom. Spectrom. 9 (1994) 1223.
[7] A. Gustavson, Spectrochim. Acta 42B (1987) 113.
[8] L. Zhang, J.W. Carnahan, E. Winans, P.H. Neill, Anal. Chem. 61 (1989) 895.
[9] J. Qinhan, Z. Hangi, W. Ying, Y. Xianglin, W. Yang, J. Anal. Atom. Spectrom. 9 (1994) 851.
[10] A. Gustavson, Spectrochim. Acta 43B (1988) 917.
[11] F.J.M.J. Maessen, G. Kreuning, J. Balke, Spectrochim. Acta 41B (1986) 3.
[12] R.S. Houk, V.A. Fassel, G.D. Flesch, H.J. Svec, A.L. Gray, C.E. Taylor, Anal. Chem. 52 (1980) 2283.
[13] L.C. Alves, M.G. Minnich, G.R. Wiederin, R.S. Houk, J.Anal. Atom. Spectrom. 9 (1994) 399.
[14] J.S. Hill, J. Hartley, L. Ebdon, J. Anal. Atom. Spectrom. 7 (1992) 23.
[15] A. Montaser, H. Tan, I. Ishii, S. Nam, M. Cai, Anal. Chem. 63 (1991) 2660.
[16] K. Backstrom, A. Gustavsson, P. Hietala, Spectrochim. Acta 44B (1989) 1041.
[17] A. Gustavsson, P. Hietala, Spectrochim. Acta 45B (1990) 1103.
[18] J.W. McLaren, J.W. Lam, A. Gustavsson, Spectrochim. Acta 45B (1990) 1091.
[19] A. Montaser, H. Tan, I. Ishii, S. Nam, M. Cai, Anal. Chem. 63 (1991) 2660.
[20] R.I. Botto, J.J. Zhu, J. Anal. Atom. Spectrom. 9 (1994) 905.
[21] H. Tao, A. Miyazaki, J. Anal. Atom. Spectrom. 10 (1995) 1.
[22] A.J. Koropchak, L. Allen, J.M. Davis, Appl. Spectrosc. 46 (1992) 686.
[23] V. Kuban, Crit. Rev. Anal. Chem. 23 (1992) 338.
[24] M.A. Tarr, G. Zhu, R.F. Browner, Spectrochim. Acta 45 (1991) 1424.

ELSEVIER

Talanta 45 (1997) 147–153

Talanta

Simultaneous determination of copper and iron by second derivative spectrophotometry using mixtures of ligands

M. Inés Toral *, Pablo Richter, Cecilia Rodríguez

Department of Chemistry, Faculty of Sciences, University of Chile, P.O. Box 653, Santiago, Chile

Received 10 October 1996; received in revised form 24 March 1997; accepted 8 April 1997

Abstract

A highly sensitive and selective second derivative spectrophotometric method has been developed for the determination of copper and iron in mixtures. The method is based on the separation of the analytes by liquid–liquid extraction as picrate ion pairs. Iron-picrate, reacts in the organic phase of DCE with 5-phenyl-3-(4-phenyl-2-pyridinyl)-1,2,4-triazine (PPT). Similarly the copper-picrate reacts with 2,9-dimethyl-4,7-diphenyl-1,10-phenantroline (bathocuproine). The extracts were evaluated directly by derivative spectrophotometric measurement, using the zero-crossing approach for determination of copper and graphic method for iron. Iron and copper were thus determined in the ranges 8–120 ng ml^{-1} and 8–125 ng ml^{-1}, respectively, in the presence of one another. The detection limits achieved (3σ) were 2.9 ng ml^{-1} of iron and 2.8 ng ml^{-1} of copper. The relative standard deviations were in all instances less than 2.1%. The proposed method was applied to the determination of both analytes in river and tap water and the results were consistent with those provided by the AAS standard method. © 1997 Elsevier Science B.V.

Keywords: Copper; Iron; Spectrophotometry; Ligands

1. Introduction

Microamounts of iron and copper in various substances may be vital or indicative of contamination or malfunction. The chemical properties of these ions makes them essential in different metabolic processes. Consequently, in medical diagnosis and biochemical research in biological, their content in samples such as urine, serum, liver tissue, etc., can be of considerable significance. Moreover, industrial and commercial products may require a knowledge of iron and copper content, because these analytes are included in quality control of these products, including petroleum, alloys, foods, beverages, etc. In this context, simple, sensitive and selective methods for the simultaneous determination of iron and copper are in great demand.

Several spectrophotometric methods have been reported for the determination of these analytes individually, however, relatively few chromogenic

* Corresponding author. Fax: +56 2 2713888.

PII S0039-9140(97)00113-6

reagents are practical for the simultaneous determination of these elements. Cuproinic and ferroinic reagents such as 1,10-phenantroline,2,2′-bipyridine 1,10-phenantroline,2,2′-bipyridine [1], 3-(2-pyridyl)-5,6-diphenyl-1,2,4-triazine [2] and 5-phenyl-3-(4-phenyl-2-pyridinyl)-1,2,4-triazine [3] have been used as chromogens for the simultaneous determination. A common feature of these spectrophotometric methods is that usually the sensitivities are different for each analyte [1–3].

The spectrophotometric resolution of mixtures of copper and iron has been traditionally performed by solving a set of simultaneous equations at two wavelength [4–7] or by sequential procedures [2,8,9], in order to calculate the concentration of each specie in the sample. Other classic spectrophotometric approaches were based on the selective distribution of copper and iron complexes between immiscible phases and on the subsequent absorbance measurement in both phases [4,10].

Derivative spectrophotometry also permits to resolve and determine binary mixtures of constituents [3,11–18]. However, when this approach was used for the simultaneous determination of copper and iron using a common reagent 5-phenyl-3-(4-phenyl-2-pyridinyl)-1,2,4-triazine (PPT), the sensitivities reported for each element were also different [3]. First and second derivative approaches were proposed by Morelli, in which the sensitivities for the analytes are similar. Sensitivities of the derivative approach were considerably lower than the PPT method and its principal disadvantage is the interference of other transition metals [18].

This work reports a method by second derivative extractive-spectrophotometry for the simultaneous determination of copper and iron, using one specific chromogen for each analyte, the 5-phenyl-3-(4-phenyl-2-pyridinyl)-1,2,4-triazine (PPT) for iron and the 2,9-dimethyl-4,7-diphenyl-1,10-phenantroline (bathocuproine) for copper. Picrate was used as counter-ion ligand in order to increase the sensitivity, by ternary complex formation. This method is simple, very sensitive and selective for both analytes and it can be applied in samples of different nature.

2. Experimental

2.1. Apparatus

A Shimadzu UV-160 spectrophotometer with 10 mm cells was used for measurements of the absorbance and derivative absorption spectra. An Orion Research Digital ion-analyzer 701 with glass and saturated calomel electrodes was used for pH determinations.

2.2. Reagents

All reagents were of analytical reagent grade and the solutions were prepared with high-purity water from a Millipore Milli-Q water purification system device.

Standard Copper (II) solution, (Titrisol Merck, 1000 μg ml^{-1}).

Standard Iron (II) solution, (Titrisol Merck, 1000 μg ml^{-1}).

Solutions of 10 μg ml^{-1} of the analytes were prepared by diluting these standard solutions, and other ranges of concentrations were prepared by appropriate dilution.

PPT/bathocuproine solution. A solution containing PPT and Bathocuproine 1×10^{-3} M of each compound, was prepared by dissolving 0.0310 g PPT (Ferrospectron II, Merck) and 0.1805 g bathocuproine (Aldrich) in 100 ml of 1,2-dichloroethane (DCE).

Picric acid solution. A 0.01 M solution was prepared by dissolving 2.2911 g in 1000 ml of water.

Hydroxylamine hydrochloride ($NH_2OH \cdot HCl$) solution. This solution was prepared by dissolving 100 g of the salt in 1000 ml of water.

Sodium acetate–acetic acid buffer (pH 5.0). This solution was prepared by dissolving 164.0 g of sodium acetate (Merck) in 100 ml of water and then was added 64.4 ml of acetic acid (Merck) and diluted to 1000 ml with water.

Foreign ion solutions. Solutions of diverse ions for the interference studies were prepared by dissolving the calculated amount of each compound in order to give 10–1000 μg ml^{-1} solutions of each species. All these solutions were stored in polyethylene containers.

1,2-Dichloroethane (DCE) Extrapure (sp. gr. 1.25).

2.3. Procedure

To an aliquot of sample solution containing less than 12.0 μg of copper and 12.0 μg of iron, respectively, in a 250 ml separating funnel, add 1 ml of acetic–acetate buffer (pH 5.0), 1 ml of 10% $NH_2OH \cdot HCl$ solution, 3 ml of 0.01 M picric acid solution and adjust the total volume to 100 ml. Mix and set aside for 5 min. Then add 5 ml of DCE containing 1×10^{-3} M PPT and 1×10^{-3} M bathocuproine and shake the funnel for 3 min. Allow the phases to separate and run the organic layer into a dry flask. Record the zero-order spectra of the DCE extract over the range from 650 to 450 nm against a reagent blank prepared under the same experimental conditions, using 10-mm cells. Record also the second derivative spectra over the same wavelength range, using $\Delta\lambda = 4.8$ nm.

3. Results and discussion

3.1. Spectral features

Cu(II), in presence of hydroxylamine hydrochloride solution (pH 5.0) and picric acid forms a ion-pair that is extractable into 1,2-dichloroethane containing bathocuproine. The zero-order spectrum of the extract of the Cu(I)–bathocuproine–picrate complex exhibit one band centered at 485 nm, over range of 450–650 mn, corresponding to absorption of Cu(I)–bathocuproine complex (Fig. 1A). Under experimental conditions described above Fe(II) can be extracted as the picrate-iron pair, into organic phase containing PPT in DCE to form Fe (II)–PPT–picrate complex. Under these conditions the extraction and complexation reactions are integrated. The zero-order spectrum of the extract of this complex shows one band centered at 570 nm, over same range of wavelength (Fig. 1B). On the other hand, it was studied the influence of the PPT presence, in DCE phase, on the extraction and formation of the Cu(I)–bathocuproine–picrate complex and it was found that the signal is not modified even when the PPT/bathocuproine ratio was 1:1. The same effect was observed when the Fe(II)–PPT–picrate complex was extracted in presence of the bathocuproine. For this reason, it is possible to assume that the conditional formation constants of the Fe(II)–PPT–picrate and Cu(I)–bathocuproine–picrate complexes are considerable higher than of the Fe(II)–bathocuproine–picrate and of the Cu(I)–PPT–picrate complexes.

When both iron and copper are present in a sample and the PPT and bathocuproine are dissolved in DCE and picric acid are present in the aqueous phase, both analytes are quantitatively extracted, as analyte–chromogen–picrate mixed complexes, into the organic phase. This extraction process permits to both analytes to be separated and preconcentrated by a factor of 20.

The zero-order spectra of both analytes show that only iron could be determined directly between 550–650 nm. However both copper and iron absorb 450–500 nm spectral region, and both ion complexes contribute to the measured absorbance. For this reason, are not possible to reliable direct absorbance measurements for copper determination in mixtures. (Fig. 1C). As derivative spectrophotometry provides additional possibilities, because it enhances the detectability of minor spectral features, this technique was adopted.

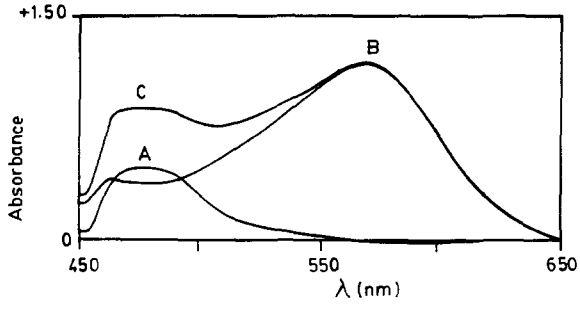

Fig. 1. Absorption spectra of DCE extract of Fe(II)–PPT–picrate, Cu(I)–bathocuproine–picrate complexes and mixtures of these complexes measured against reagent blank. (A) Cu(I)–bathocuproine–picrate, 100 ng ml^{-1}; (B) Fe(II)–PPT–picrate, 100 ng ml^{-1}; (C) Cu(I)–bathocuproine–picrate, 100 ng ml^{-1}; and Fe(II)–PPT–picrate, 100 ng ml^{-1}. All other conditions as in text.

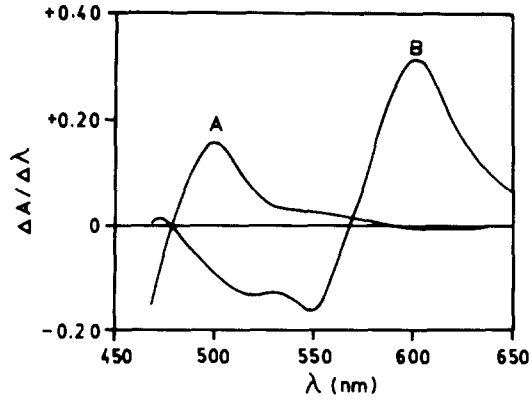

Fig. 2. First derivative spectra of DCE extract of Fe(II)–PPT–picrate, Cu(I)–bathocuproine–picrate complexes and mixtures of these complexes measured against reagent blank. (A) Cu(I)–bathocuproine–picrate, 100 ng ml^{-1}; (B) Fe(II)–PPT–picrate, 100 ng ml^{-1}.

In this context, the first and second derivative spectra of the extracts containing separately the complexes of the Cu(bathocuproine)$_2$ picrate, Fe(PPT)$_3$(picrate)$_2$ were record, respectively. As shown in Figs. 2 and 3, the second derivatives are more resolved for both elements. On the other hand, the second derivative approach is more sensitive, selective and reproducible, which allowed a more reliable determination of both ions. Furthermore, when a $\Delta\lambda = 4.8$ nm value was used

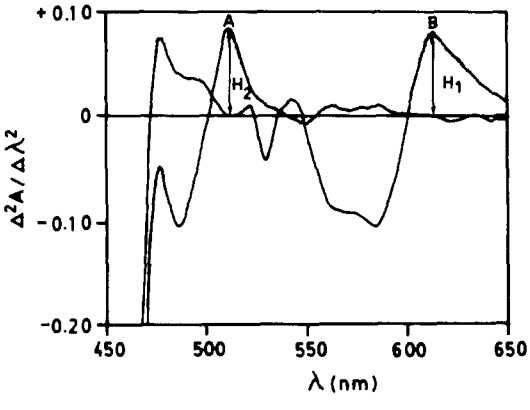

Fig. 3. Second derivative spectra of DCE extract of Fe(II)–PPT–picrate, Cu(I)–bathocuproine–picrate complexes measured against reagent blank. (A) Cu(I)–bathocuproine–picrate, 100 ng ml^{-1}; (B) Fe(II)–PPT–picrate, 100 ng ml^{-1}.

for differentiation, the best spectral resolution and the highest signal/noise ratio were obtained in the determination of both analytes.

Examination of Fig. 3, reveals that the graphical method at 575 and 613 nm can be used for determination of iron, because analytical signals depended only of the absorption of this analyte. However, the peak at 613 nm was selected (H_1), because the band is located more far away that copper absorption, consequently the precision and accuracy are increased and the proposed method is more selectivity. In contrast, the measurement of the second derivative spectrum at an abscissa value of 508 nm, corresponding to the zero crossing point of the second derivative spectrum of Fe(II)–PPT–picrate (H_2) can be used satisfactory for determination of copper.

Higher-order derivatives yield very high yet irreproducible signals. On the other hand the noise increases proportionality with the derivative order. The wavelength speed had no influence on the signal because the differentiation is obtained digitally. Hence a fast value of 480 nm min^{-1} was selected.

3.2. Study of the experimental variables

The chemical and spectral variables were optimized by the univariate method, for each analyte separately. Table 1 shown the range studied and the optimum values found for chemical and spectral variables, together with the working values. Reagent concentrations were selected by taking into account the two analytes and other possible interfering cations that might be present in the sample.

As the determination of each analyte can be performed in a wide pH range, the optimum pH value for simultaneous determination of both species was pH 5.0, which was maintained constant with an acetic acid–acetate buffer.

In the solvent–extraction process the maximum enrichment factor was obtained with an aqueous/organic phase volume ratio of 20. Phase miscibility resulted at phase volume ratios greater than this value.

The order of the derivative and the value of $\Delta\lambda$ were the spectral variables studied, because both

Table 1
Study of variable

Variable	Range studied	Optimum range		Working value
		Copper	Iron	
Chemical				
pH	1.0–13.5	4.0–13.0	3.0–7.0	5.0
PPT solution (10^{-4} M)	0.2–10.0		4.0–10.0	10.0
Bathocuproine (10^{-4} M)	0.1–10.0		4.4–10.0	10.0
Picric acid (1×10^{-2} M [ml])	0.1–3.0	0.7–3.0	0.9–3.0	3.0
Aqueous/organic phase ratio	2–25	2–23	2–24	20
Spectral				
Derivative order	1–4	1–2	1–2	2
$\Delta\lambda$ (nm)	1.6–14.4	3.2–6.4	3.2–6.4	4.8
Wavelength $\Delta\lambda$ (nm)	400–700	505	614	505–614

variables affect the shape and the resolution of the spectra. The best resolution, was obtained working with second-order derivative spectrophotometry and $\Delta\lambda$ value of 4.8 nm. In this conditions the simultaneous determination of copper by the zero crossing method at 508 nm and iron by graphic method at 613 nm is possible.

3.3. Features of the method.

The calibration graphs were obtained by plotting the second-derivative value H_1 for iron and H_2 for copper with $\Delta\lambda = 4.8$ nm, versus the respective analyte concentrations. The linear regression equations and the correlation coefficients calculated for mixtures of both analytes were:

Iron ($\lambda = 613$ nm) $H_1 = 4.9 \times 10^{-4}\ C$ (ppb) $r = 0.999$

Copper ($\lambda = 508$ nm) $H_2 = 4.5 \times 10^{-4}\ C$ (ppb) $r = 0.999$

Where, H values are the analytical signals in derivative unit and C (ppb) corresponds to respective concentration in ng ml^{-1} concentration.

The determination ranges were, between 7.8 and 120 for iron and 7.7–125 ng ml^{-1} for copper. The detection limits calculated by using the 3σ criterion were found to be 2.8 ng ml^{-1} of copper and 2.9 ng ml^{-1} of iron. The reproducibility expressed as variation coefficients for 11 standard samples containing 60 ng ml^{-1} of each analyte were 1.3 and 1.5% for iron and copper, respectively.

3.4. Interference studies.

The effect of diverse foreign ions on the simultaneous determination of copper and iron was examined by adding known quantities of a desired foreign ion to a solution of 40 ng ml^{-1} of both iron and copper, respectively. The tolerance limit was taken as being the amount causing an error $\pm 4\%$ in the signals. As show in Table 2, cationic species were largely tolerated and cobalt was the most serious interferent. EDTA and CN^- interfere negatively by inhibition of the complex formation reactions. According to these tolerance

Table 2
Effect of foreign ions: copper 40 ng ml^{-1} and iron 40ng ml^{-1}

Foreign species	Tolerance limit (ng ml^{-1})
Cations	
K^+, Na^+, Al^{3+}, Mg^{2+}, Ca^{2+}, Sr^{2+}, Mn^{2+}, Zn^{2+}, Cd^{2+}, Hg^{2+}, Bi^{3+}, Cr^{3+}	1.0×10^4
Ni^{2+}, Co^{2+}	4.0×10^4
Anions	
NO_3^-, SO_4^{2-}, Br^-, Cl^-, PO_4^{3-}, NO_2^-	5.0×10^6
Tartrate	1.3×10^6
Oxalate, citrate	1.0×10^4
CN	150
EDTA	100

Table 3
Determination of mixtures of copper and iron in well water

Sample	No.	Found (ppb)[a]			
		Proposed method		A.A.S. Method	
		Iron[b]	Copper[b]	Iron	Copper
River water	1	59.3 (1.9)	12.2 (1.7)	59.5 (2.7)	12.5 (2.6)
	2	60.1 (1.8)	12.3 (1.8)	59.9 (2.6)	12.4 (2.8)
	3	62.1 (1.7)	12.8 (1.9)	62.4 (2.7)	13.7 (2.9)
	4	62.5 (1.9)	12.7 (1.8)	62.7 (2.5)	12.8 (2.7)
Tap water	1	36.7 (1.7)	12.1 (1.7)	36.9 (2.7)	12.0 (2.6)
	2	35.2 (1.8)	13.1 (1.9)	35.6 (2.8)	13.2 (2.7)
	3	34.5 (1.9)	12.2 (1.8)	34.3 (2.7)	12.1 (2.8)
	4	39.6 (1.7)	15.0 (1.9)	39.5 (2.8)	15.4 (2.7)

[a] Average of eight determinations.
[b] R.S.D. and % in parentheses.

limits, the method proposed here is more selective than the most of those reported in the literature for determination of both analytes in mixtures.

3.5. Application of the method

The proposed method was applied to the determination of both analytes in tap and river water. In these type samples, the concentration of the compounds that usually are found, are lower that the tolerance limit of this simultaneous determination (Table 2).

The river water samples were collected at the Maipo river, Chile (in June, 1996). They were instantly drawn through a membrane filter (pore size 0.45 μm) and the samples were preserved by addition of HNO_3 until to reach pH 2.0. The determination of iron and copper of the filtrate was carried out using the proposed method. The tap water samples were collected and analyzed without a previous treatment. The results were quite consistent with those provided by atomic absorption spectrophotometry (Table 3).

4. Conclusions

In this work a simple, sensitive and selective method has been developed for the simultaneous determination of copper and iron by second order derivative spectrophotometry. According to the high selectivity reached, the proposed method can be applicable in a variety of different samples. The high sensitivity of PPT and bathocuproine as chromogenic reagents, combined with the favorable extractability of copper and iron as ternary complexes, facilitate determination of microamount of these elements. An improvement in sensitivity for copper in the determination of copper and iron can be achieved using two specific chromogens.

Acknowledgements

The authors are grateful to the National Fund for Development of Sciences and Technology (FONDECYT), project 1961024 for financial support. Thanks are also extended to Emma Contreras, Felix Blu and Luis Torres of Empresa Metropolitana de Obras Sanitarias EMOS S.A. for facilities given in the comparison of results by AAS.

References

[1] A.A. Schilt, Analytical Applications of 1,10-Phenanthroline and Related Compounds, Pergamon Press, New York, 1969.
[2] A.A. Schilt, P.J. Taylor, Anal. Chem. 42 (1970) 220.

[3] M.I. Toral, P. Richter, Anal. Lett. 28 (1995) 1083.
[4] B. Zak, N. Ressler, Anal. Chem. 28 (1956) 1158.
[5] J.W. Lander, B. Zak, Am. J. Clin. Pathol. 29 (1958) 590.
[6] D. Banerjea, K.K. Tripathi, Anal. Chem. 32 (1960) 1196.
[7] F. de Pablos, J.L. Gómez, F. Pino, Mikrochim. Acta 3 (1985) 327.
[8] I. Singh, M. Poonam, P.S. Kadyan, Talanta 32 (1985) 387.
[9] N.D. Seudeal, R.J. Thibert, B. Zak, Microchem. J. 34 (1986) 131.
[10] D.H. Wilkins, G.F. Smith, Anal. Chim. Acta 39 (1953) 538.
[11] F. Garcia, M. Hernandez, J.C. Marquez, Anal. Chim. Acta 197 (1987) 275.
[12] B. Morelli, Analyst 108 (1983) 1506.
[13] B. Morelli, Anal. Chim. Acta 209 (1988) 175.
[14] M.I. Toral, P. Richter, Talanta 40 (1991) 1405.
[15] P. Levillain, D. Fompeydie, Analusis 14 (1986) 1.
[16] A.I. Jimenez, F. Jimenez, J.J. Arias, Analyst 114 (1989) 93.
[17] M. Blanco, J. Coello, F. Gonzalez, H. Iturriaga, S. Maspoch, Anal. Chim. Acta 226 (1989) 271.
[18] B. Morelli, Analyst 108 (1983) 870.

ELSEVIER

Talanta 45 (1997) 155–165

Talanta

Continuous flow analysis of lead (II) and mercury (II) with substituted diazacrown ionophore membrane electrodes

Xinhao Yang [a], D. Brynn Hibbert [a,*], Peter W. Alexander [b]

[a] *Department of Analytical Chemistry, University of New South Wales, Sydney, NSW 2052, Australia*
[b] *Department of Physical Sciences, University of Tasmania, PO Box 1241, Launceston, Tasmania 7250, Australia*

Received 16 December 1996; received in revised form 8 April 1997; accepted 11 April 1997

Abstract

A novel flow cell for use with ion-selective membrane electrodes is reported in which the carrier stream is drawn through a tube that suppresses the pump noise. PVC membrane electrodes based on 7,16-dithenoyl-1,4,10,13-tetraoxa-7,16-diazacyclooctadecane (DTODC), and 7,16-di-(2-thiopheneacetyl)-1,4,10,13-tetraoxa-7,16-diazacyclooctadecane (DTAODC) for lead (II), and 7,16-dithenyl-1,4,10,13-tetraoxa-7,16-diazacyclooctadecane (DTDC) and 7,16-di-(2-methylquinolyl)-1,4,10,13-tertraoxa-7,16-diazacyclootadecane (DQDC), for mercury (II) were prepared and evaluated. The linear ranges were pPb: 5.5–3.0 (DTODC) and 6.0–2.0 (DTAODC); pHg: 5.5–3.0 (DTDC) and 4.5–2.5 (DQDC). With flow rate of 3 ml min^{-1} the repeatability of measurements was less than 5% RSD ($n = 3$). The system was applied to the determination of lead (II) and mercury (II) in spiked natural water samples. © 1997 Elsevier Science B.V.

Keywords: Ion selective electrode; Ionophore; Heavy metal analysis; Membrane electrode; Flow system

1. Introduction

The increasing demand for industrial process control, biomedical analysis, environmental and pollution monitoring via repetitive determinations of many similar samples has fostered the growing development of continuous analytical methods (CFA, FIA etc.). Potentiometric detectors based on ion-selective electrodes are especially suited to flow measurements because they offer advantages such as high selectivity and sensitivity, good precision, simplicity and low cost [1,2]. These methods make possible direct monitoring of activities or concentrations of selected species without any sample pre-treatment. Some configurations include the construction of solid-state membrane, PVC membrane solid-contact, and liquid-contact flow-through ISEs in which the measuring stream passes across the sensing membrane surface [3–9]. In addition, tubular and sandwich designs have allowed the sensing membrane to become part of the tube and chamber which contains the measuring stream [10–14]. However, electrodes used in flow cells previously reported in the literature have been mostly solid-state membrane and PVC-

* Corresponding author. Fax: +61 2 93856141; e-mail: b.hibbert@unsw.edu.au

PII S0039-9140(97)00122-7

membrane, solid-contact electrodes [3–7]. Conventional PVC-membrane liquid-contact electrodes (i.e., electrodes of the form Reference electrode |Standard solution|Membrane|Test solution| Reference electrode) are often too bulky to be used in narrow-bore flow systems [15,16]. When these types of electrode are used in a flow system, construction of the flow cell is complicated by the flexibility of the PVC membrane [8,9]. Other kinds of ion-selective PVC membrane electrodes based on solid-contact substrates (metallic wire and carbon rod etc.) experience significant drift and exhibit poor adhesion to the substrate surface [17]. The poor adhesion of a PVC membrane in a solid-contact configuration presents a problem with continuous on-line monitoring, when eventually the membrane peels off. Moreover, the thickness of a PVC membrane is difficult to control causing poor reproducibility among electrodes prepared at different times. It is also known that in continuous flow potentiometric analysis, oscillations in the measured potential caused by the use of a peristaltic pump are observed together with electrical noise and interruptions to the signal from air bubbles trapped in the small cell.

The considerable number of publications and commercial products based on PVC-membrane, liquid-contact electrodes are almost all confined to batch analyses, with few reports on their use in flow analysis, despite the many advantages of flow techniques [18]. The controlled hydrodynamics at the membrane surface lead to better reproducibility of signals, faster response, and better lifetimes for electrodes. A down-stream reference electrode also avoids contamination from leaking salt bridge solution. In this study we take advantage of the merits of PVC-membrane liquid-contact electrodes and flow systems, and our work reported here indicates that unless ultra-miniaturisation is necessary these electrodes offer significant advantages in flow systems over PVC-membrane solid-contact electrodes. The elements (lead and mercury) chosen to demonstrate the use of electrodes based on neutral ionophores have not received as much attention as the analysis of alkali metal ions and some anions. As we have reported the synthesis of some ionophores which appear to have selectivity towards lead and mercury [19], the incorporation of these electrodes in the flow system is a logical extension.

We also note that mercury is a significant interferent in the analysis of other heavy metals [19]. The detection of mercury itself may also present a problem, as this metal will often bind so strongly to an ionophore as to poison the electrode surface [20,21]. We have shown that in the batch mode it is possible to measure mercury by the diazacrown ionophores, but the times taken to achieve steady state response were long (20 min [22]). It is hoped that under flow conditions this may be improved.

In this study, electrically neutral ligands, namely diazacrown ether derivatives: 7,16-dithenoyl-1,4,10,13-tetraoxa-7,16-diazacyclooctadecane (DTODC), and 7,16-di-(2-thiopheneacetyl)-1,4,10,13-tetraoxa-7,16-diazacyclooctadecane (DTAODC), and 7,16-dithenyl-1,4,10,13-tetraoxa-7,16-diazacyclooctadecane (DTDC) and 7,16-di-(2-methylquinolyl)-1,4,10,13-tetraoxa-7,16-diazacyclootadecane (DQDC) in PVC membranes were employed as ionophores for the determination of lead (II) and mercury (II). We also report a novel flow arrangement in which the carrier is drawn (instead of being pumped) through the system which incorporates a dampening tube to eliminate pump noise.

The effectiveness of a traditional design of an ISE (with internal reference solution) in a flow cell is compared with a coated wire electrode system.

2. Experimental

2.1. Apparatus

Fig. 1 is a diagram of the flow cell and pulse dampener for elimination of noise. The cell was made from a perspex block (50 × 45 × 25 mm). The indicator ISE was constructed with a 4 mm diameter membrane with internal solution containing 10 mM Cl^- and AgCl|Ag wire reference electrode. A commercial (BAS) Ag|AgCl|Cl^- ref-

erence electrode was positioned 20 mm down stream from the indicator electrode. A plug of cotton wool or Agar gel could be used to separate the reference electrode from the carrier stream. The inlet diameter was 4 mm, and outlet diameter 3 mm. The pulse dampener consisted of a sealed sample tube of diameter 25 mm and height 50 mm.

A Gilson Minipuls variable-speed peristaltic pump was used to draw carrier solution through the electrode assembly. Standard Tygon pump tubing of internal diameters 1.0–3.0 mm was used in the flow system. The reference electrode (Ag|AgCl 0.1 M KCl) was obtained from BAS (Bioanalytical Services, West Lafayette, IN, USA). All potentiometric measurements were made at ambient temperature with an Orion Model SA 720 pH/mV meter and recorded via an amplifier and 12 bit ADC on an Apple (II) computer.

2.2. Chemicals

All chemicals used were of analytical reagent grade. Standard solutions were prepared with Millipore deionised or distilled water. Poly(vinyl chloride) (PVC: high molecular weight type) used as electrode membrane material, 2-nitrophenyl octyl ether (NPOE) used as membrane solvent (plasticiser) and potassium tetrakis (*p*-chlorophenyl) borate (KTpClPB) used as an anion excluder were obtained from Aldrich Chemical 7,16-dithenoyl-1,4,10,13-tetraoxa-7,16-diazacyclooctadecane (DTODC), 7,16-di-2-thiopheneacetyl)-1,4,10,13-tetraoxa-7,16-diazacyclootadecane (DTAODC), 7,16-dithenyl-1,4,10,13-tetraoxa-7,16-diazacyclooctadecane (DTDC) and 7,16-di-(2-methylquinolyl)-1,4,10,13-tetraoxa-7,16-diazacyclootadecane (DQDC) used as the ionophores were synthesised. The procedures of preparation for DTODC, DTAODC, and DTDC have been described earlier [19] and DQDC in [23]. Each of these four ligands were authenticated with ^{1}H nuclear magnetic resonance (NMR), IR spectroscopy, UV spectroscopy, mass spectroscopy and elemental analysis.

All sample solutions were prepared with metal nitrates in Millipore D.I. water and if necessary, pH adjustments were made by the addition of dilute solutions of nitric acid or sodium hydroxide. For calibration, the activities of metal ions were calculated from the extended Debye-Hückel equation [24].

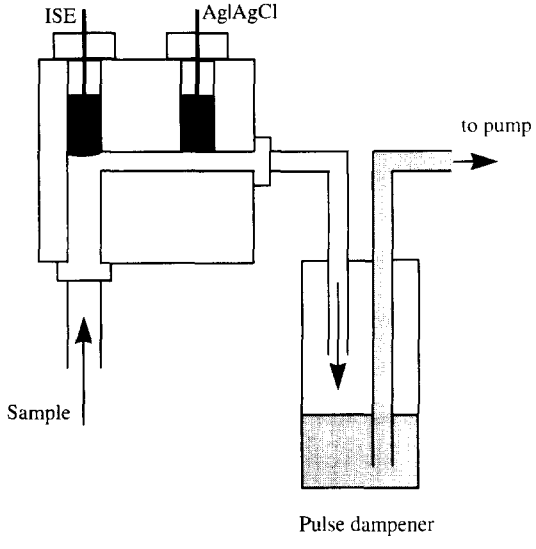

Fig. 1. Schematic diagram of the flow system, showing flow cell and pulse suppressor.

2.3. Preparation of PVC membrane electrodes

The preparation and optimisation of PVC-immobilised ionophore membranes have been described previously [19]. The membrane composition was 3 wt.% ionophore, 30 wt.% PVC, 65–67 wt.% NPOE and half of the number of moles of the ionophore of KTpClPB. A disc of 6 mm diameter of a sheet of the membrane was cut out and attached to the threaded Perspex body by an *O*-ring. The internal standard solutions contained 10 mM metal chlorides. A fresh membrane was conditioned in lead (II) nitrate or mercury (II) nitrate (1 mM) in the cell for about 1 day.

2.4. General measuring procedure

Ionophores DTODC and DTAODC were used to make PVC membranes with 10 mM $Pb(NO_3)_2$

and 10 mM NaCl internal standard solution as sensors for the determination of lead (II) and ionophores of DTDC and DQDC were used to make PVC membranes with 10 mM $CuCl_2$, pH 3 internal standard solution for the determination of mercury (II).

The test solution was drawn at a typical flow-rate of 3 ml min^{-1}. Different concentrations of test solutions were sampled successively until a steady state measurement could be made (about 2–3 min). It was found that bubbles introduced when changing over solutions passed quickly through the system.

The separate solution method (SSM) [25], using solutions of 10 mM nitrates of the interfering cations, was used to estimate selectivity coefficients in the flow system. For lead selectivity coefficients, the pH of all solutions was adjusted to pH 4 except for mercury nitrate and ferric nitrate at pH 2 and 3, respectively. For mercury selectivity coefficients, the pH of all solutions was adjusted to constant pH 3 except for mercury nitrate at pH 2. The flow rate in these experiments was 3 ml min^{-1}.

3. Results and discussion

3.1. Basic properties of the flow cell

The electrochemical flow cell configuration of Fig. 1 which is proposed for ion-selective membrane electrodes with internal reference solution has advantages in steady-state, continuous potentiometric analysis, which can be summarised as follows.

Conventional membrane electrodes with internal reference solution are often too bulky to be used [15,16]. This design accommodates easily the small electrodes used here. The cell volume is not large but still keeps the characteristics of traditional ion-selective membrane electrodes with internal reference solution. The thickness and size of membrane are easily controlled which gives consistent membrane thickness and sensing area. The use of an internal reference electrode with reference solution avoids the signal drift found in solid PVC membrane electrodes [17]. Membrane electrodes of this type also overcome the problem of the poor adhesion of PVC membrane on a solid-contact electrode, which, with continuous flowing carrier, eventually peel off. The size of the flow cell (internal volume about 100 μl) is sufficient not to require a debubbler. Air bubbles are driven out and the working electrode recovered quickly when different test solutions were sampled successively. The cell did not exhibit the noise and random interruptions to electric circuits from air bubbles that become trapped in small cells such as low-volume thin-layer, wall-jet and tubular cells, or from breakage of the thin film of liquid connecting the working electrode with the solution containing the reference electrode in open wall-jet systems [26]. This cell design, having a narrow exit tube, makes use of the flexibility of a PVC membrane to allow the membrane to be convex into the flowing solution. The test solution impinges as a jet onto the convex membrane surface. The dead space is reduced with a high flow rate near the membrane surface. This arrangement improves solution flow in the system [27]. Commercial reference electrodes, because of their bulky size, are usually placed in a beaker of waste solution, generally at a distance 50–100 mm away from the flow-through ISE [3]. In our design it is possible to locate the reference electrode, with a salt bridge if necessary, close to the sensing membrane and downstream (10–20 mm) thus minimising noise [8] and contamination from electrolyte from the reference electrode. The design also allows easy replacement of a membrane.

3.2. Optimisation of continuous flow potentiometric analysis system

In continuous flow systems in which ISEs are used as sensors, oscillations in measuring potential caused by the peristaltic pump are always observed. Some methods for eliminating these baseline oscillations include the addition of a large volume of inert electrolyte, reduction of the length of the tube connecting the ISE with the

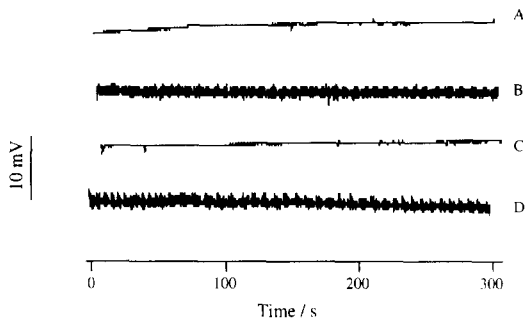

Fig. 2. Recordings of the pulse noise for cells detecting 10^{-4} M Pb^{2+}. A, DTODC membrane electrode with drawing stream through a suppressor; B, DTODC membrane electrode with propelling stream; C, DTAODC membrane electrode with drawing stream through a suppressor; D, DTAODC membrane electrode with propelling stream. Flow rate: 3 ml min^{-1}.

reference electrode and by the choice of the best the diameter of tube based on consideration of streaming potentials [28]. However, one of these solutions is not always possible, e.g., when the electrolyte interferes with the electrode response or if the diameter of tube and the length of tube connecting the ISE with the reference electrode cannot be altered. We incorporated a tube in the line to dampen the pump pulse in order to decrease baseline oscillations. The conventional design of a flow system with the pump propelling solution through the cell was changed to one in which solution is drawn through the cell with a suppressor between flow cell and pump (Fig. 1). For a study of the baseline noise, the analyte was a 10^{-4} M Pb^{2+} solution of pH 5, and DTODC and DTAODC membrane electrodes at a flow rate of 3 ml min^{-1}. Measurements of baseline noise for the conventional flow system without a dampener and the system of Fig. 1 with a suppressor are shown in Fig. 2. It can be seen that for both membranes, the solution propelled through the cell without a suppressor caused noisy baseline potentials (± 2–3 mV), whereas the potential oscillations for the solution drawn through the flowcell with a suppressor were less than ± 1 mV. The optimisation of this flow system significantly decreased the oscillations in the potential caused by the peristaltic pump pulse.

3.3. Determination of Pb^{2+} with DTODC and DTAODC membrane electrodes

With samples containing 10^{-4} and 10^{-3} M Pb^{2+} the steady state response showed a plateau between approximately pH 4 and pH 5.5 (Fig. 3). At high pH the response is affected by formation of metal oxo-hydroxo salts, while acidic conditions caused protonation of the azacrown nitrogens and thus, loss of activity [29].

The response of membrane ISEs, which depend on diffusion processes in the membrane [30], is improved by operation in a flow cell [31–33], and this is confirmed here. The rise in potential of an electrode (E) with time (t) could be modelled by an equation of the form

$$E = \text{const} + s \log_{10}\left(1 - \frac{4}{\pi} e^{-t/\tau}\right) \quad (1)$$

where s is a constant, and τ is the characteristic rise time. Eq. (1) is an approximation to a series expansion that holds for $t > 0.24\tau$ [34]. Such a fit is illustrated in Fig. 4 for the response of a DTAODC membrane electrode to 1 mM Pb^{2+}.

The dependence of the cell response and recovery time on the flow rate was investigated using DTAODC and DTODC membranes with compositions optimised for batch reactions [19]. Both the rise time to a steady state potential and the recovery back to the baseline decreased with increasing flow rate (Fig. 5), although the recovery

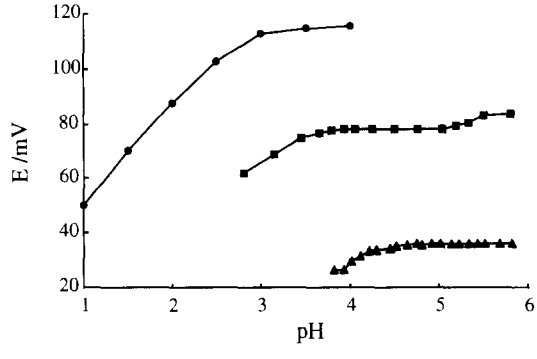

Fig. 3. Variation of the cell response with pH for: DTODC (■) and DTAODC (▲) membrane electrodes responding to 10^{-4} M Pb^{2+}, and DTDC (●) membrane electrode to 10^{-4} M Hg^{2+}. Flow rate: 3 ml min^{-1}.

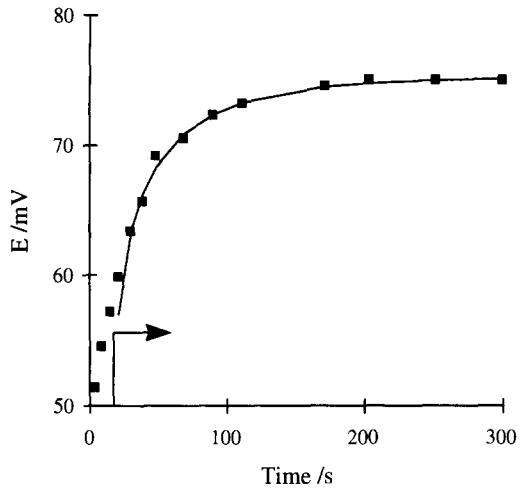

Fig. 4. Dynamic response of a DTAODC membrane electrode to 10^{-3} M Pb^{2+} (■). The line is $E/mV = 75.2 + 16.8 \log_{10}(1 - 4/\pi e^{-t/65.8})$, and the arrow indicates the applicability of the equation ($t > 16$ s).

was slower, a typical effect with complexing membranes. A flow rate of 3 ml min^{-1} was chosen as a suitable compromise between cell response, recovery and sample consumption.

Typical recordings for the analysis of aqueous Pb^{2+} standard solutions using DTODC and

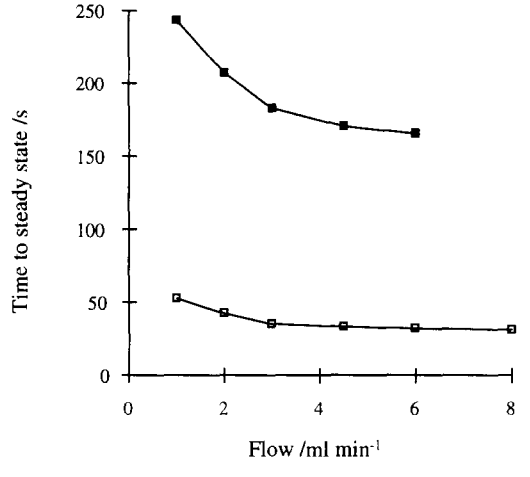

Fig. 5. Dependence of rise time to steady state (●) and recovery time to baseline (■) on the flow rate of a DTAODC membrane electrode. Sample solution: 10^{-4} M Pb^{2+}.

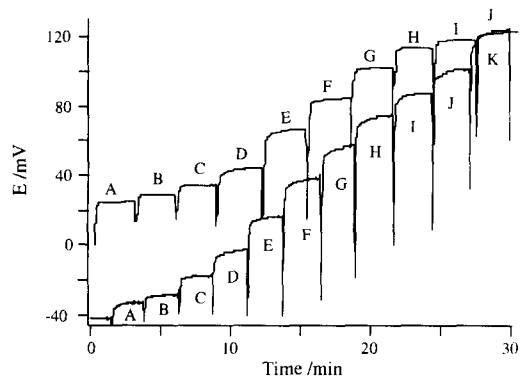

Fig. 6. Potential of a DTODC membrane (upper curve) and a DTOADC membrane (lower curve) in solutions of different concentrations of Pb^{2+}. Flow rate 3 ml min^{-1}. Sample solution: (A) 3×10^{-7} M; (B) 10^{-6} M; (C) 3×10^{-6} M; (D) 10^{-5} M; (E) 3×10^{-5} M; (F) 10^{-4} M; (G) 3×10^{-4} M; (H) 10^{-3} M; (I) 3×10^{-3}; (J) 10^{-2} M; and (K) 10^{-1} M Pb^{2+}.

DTAODC membranes are shown in Fig. 6, and the calibration curves of both membranes are presented in Fig. 7, together with a calibration of a coated wire electrode of the same composition.

Electrode properties such as linear range, slope, detection limit etc. and a comparison between flow and batch systems are summarised in Table 1. It can be seen that performance of both membranes is improved in the flow system. The linear

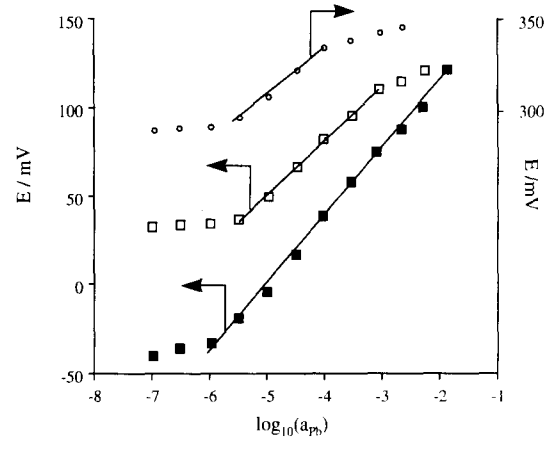

Fig. 7. Calibration graphs for the determination of Pb^{2+}. Flow rate 3 ml min^{-1}. PVC membrane electrodes with internal electrolyte: (●) DTODC, (■) DTAODC, (○) Pt wire electrode coated with PVC membrane of DTODC.

Table 1
Electrode properties of ionophore membrane electrodes in the flow system, in batch mode and of a membrane-coated platinum wire electrode

Parameter	Membrane electrode with internal reference solution				Membrane-coated Pt wire
	Flow system		Batch mode [19]		Flow system
	DTODC	DTAODC	DTODC	DTAODC	DTODC
Linear range (pPb)	5.5–3.0	6.0–2.0	5.0–2.7	5.0–2.0	5.5–4.0
Slope (mV per decade)	31.0	37.7	29.2	28.5	25.9
Coefficient of variation	0.997	0.995	0.998	0.994	0.997
Detection limit (pPb)	6.0	6.3	5.7	5.7	6.0
Working pH range	3.8–5.3	4.0–5.8	4.0–5.5	Not available	Not available

range is wider, the calibration slope is higher and the detection limit is lower for the flow measurements than for the batch measurements. We attribute this improvement to the better performance seen under controlled hydrodynamic conditions as are found in the flow system [31–33]. The performance of the membrane electrode was also superior to that of a coated wire electrode. The linear ranges and slopes of the PVC membrane electrodes with internal reference electrolyte are wider and greater than those of platinum wires coated with the PVC membrane under the same flow conditions. PVC membranes have poor adhesion to a solid substrate surface [17], the surface area of a coated wire is smaller than that our membranes and the surface of the coated wire is not so regular, thus causing fluctuations in the conductivity of the coat with a consequent decrease of measuring sensitivity.

Added to these practical aspects the absence of a properly defined reference potential in a coated wire electrode offers the possibility of drift and instability in the measured potential.

The selectivity of DTODC and DTAODC membranes depends on the chemical nature of the ionophore. We determined that the interference of 14 main cations in the determination of lead (Table 2) is of about same order magnitude as in the batch system [19]. Selectivity data evaluated from batch measurements may be adopted without problems in most cases [30], although caution must be taken when using single solution methods outside the range of the linear response of the electrode.

Table 3 lists the standard deviations and relative standard deviations of five measurements of 10^{-4} M and 10^{-5} M Pb^{2+}. During 5 days continuous use the baseline of a DTODC membrane stayed within ± 1 mV and the slope of the calibration line measured three times during this time has a standard deviation of 0.6 mV decade^{-1}. One membrane was used repeatedly for at least 1 month in this flow system. Membrane ISEs with internal reference solution have longer lifetimes in a flow system than in a batch system [19], and much longer than coated wire electrodes. This arises from the better mechanical properties of membrane ISEs during use and storage.

3.4. Determination of Hg^{2+} with DTDC and DQDC membrane electrodes

A DQDC membrane electrode has been reported for the analysis of mercury (II) [22], but in a batch system the time to achieve steady state was up to 20 min. We have shown [19] that DTDC is not a good ionophore for lead, possibly on account of its amine functionality. The structure of DTDC is, however, similar to that of DQDC and therefore membranes based on these two ionophores were evaluated for the continuous flow analysis of mercury.

The response was sensitive to pH below about pH 3.0 and above pH 4.0, precipitation of mercury hydroxide became significant (Fig. 3). A pH of 3.5 was chosen for the experiments to determine response and calibration parameters (Table 4).

Table 2
Selectivity coefficients of DTDC and DQDC membrane electrodes against Hg^{2+}, and DTODC and DTAODC membrane electrodes against Pb^{2+}

Ionophore	Selectivity coefficient	Cation														
		Mg^{2+}	Ca^{2+}	Ba^{2+}	Cu^{2+}	Zn^{2+}	Cd^{2+}	Pb^{2+} (Hg^{2+})	Ni^{2+}	Co^{2+}	Li^{+}	Na^{+}	K^{+}	Fe^{3+}	Al^{3+}	Ag^{+}
DTDC	$\log K_{Hg,M}$	−4.09	−3.37	−3.43	−4.32	−3.45	−4.23	−3.00	−4.35	−4.37	−2.57	−2.50	−2.45	−4.12	−4.27	+2.50
DQDC	$\log K_{Hg,M}$	−4.76	−4.63	−4.63	−5.44	−3.04	−4.09	−4.42	−4.32	−4.29	−2.79	−2.49	−2.42	−5.77	−5.65	+2.84
DTODC	$\log K_{Pb,M}$	−2.25	−1.98	−1.46	−2.12	−2.35	−2.20	(3.80)	−2.47	−2.34	−0.91	−0.41	−0.13	−2.32	−2.45	
DTAODC	$\log K_{Pb,M}$	−2.64	−2.22	−1.72	−2.11	−2.51	−2.54	(6.60)	−2.79	−2.53	−0.81	−0.79	0.35	−3.00	−2.43	

In the flow system the speed of response of DQDC was improved by a factor of three over that in the batch system [22] while for DTDC membranes in our previous batch experiments a steady state was never completely attained [19]. Rise times to a steady state value for DTDC and DQDC membrane electrodes were 5–6 min (Fig. 8).

Fig. 8 reproduces typical outputs of a DTDC and DQDC electrode in response to a series of solutions containing Hg^{2+}. Calibration graphs for DTDC and DQDC membrane electrodes are presented in Fig. 9 and the characteristics of the electrodes are listed in Table 3. Slopes that are greater than the theoretical 30 mV (decade $[Hg^{2+}])^{-1}$ may be attributed to the formation of mercury (I) complexes (HgX) in the electrode response [22]. The addition of KTpClPB to a membrane can also increase the electrical conductivity [36]. These factors, and the use of a flow system [33] result in greater sensitivity.

It was observed that the addition of $Cu(NO_3)_2$ to the analyte solution helped to condition both membranes and produced a super-Nernstian slope. Addition of 10 mM $Cu(NO_3)_2$ at pH 3.0 increased the slope and linear range compared with the calibration in pH 3.0 carrier alone (Table 3). This parallels recent results by Wroblewski and Brzozka on a lead electrode [35]. Recently Neshkova and Pancheva [37] have suggested that the initial membrane composition does not include mercury, and the fast and reversible formation of a surface complex [36] may be the first step in generating a potential. During this process, copper is drained out of the membrane, thus forming a secondary response to mercury and the observed super-Nernstian slope. For experiments reported here, a 10 mM solution of $HgCl_2$ was used as the internal

Table 3
Means and standard deviations of the potentials of DTODC and DTAODC membrane electrodes

Ionophore	10^{-4} M Pb^{2+}		10^{-5} M Pb^{2+}	
	$\bar{x}$ ($n = 5$) mV^{-1}	RSD %	$\bar{x}$ ($n = 5$) mV^{-1}	RSD %
DTODC	84.3	0.5	50.3	1.4
DTAODC	38.9	1.8	−4.32	7.6

Table 4
Characteristics of DTDC and DQDC membrane electrodes for mercury (II)

	Ionophore					
	DTDC				DQDC	
Electrolyte/pH	H_2O pH 2.5	H_2O pH 3.0	H_2O pH 3.5	10^{-2} M $Cu(NO_3)_2$ pH 3.0	H_2O pH 3.5	10^{-2} M $Cu(NO_3)_2$ pH 3.0
Slope (mV per decade)	39.3	39.8	40.1	75.3	40.2	50.4
Linear range (pPb)	4.0–3.0	4.5–3.0	5.5–3.0	5.0–3.0	4.5–2.5	5.0–3.0
Detection limit (pPb)	4.8	5.2	5.8	5.2	5.0	5.2
Coefficient of variation	0.997	0.993	0.994	0.990	0.991	0.995

filling solution. No great change in the response was observed if 10 mM $Cu(NO_3)_2$ was added.

The selectivity coefficients in Table 2 show that both membranes have good selectivity for mercury (II) against 15 other cations with the exception of silver. We note that silver was also a major interferent against lead when substituted diaza-crowns were used in membrane ISEs.

The mean potentials and standard deviations of five measurements in 10^{-4} M Hg^{2+} solution were for DTDC: 113.8 mV ($s = 0.84$ mV) and for DQDC 213.8 mV ($s = 0.54$ mV). An electrode containing each ionophore was used continuously for 1 month, after which the slope of the response decreased notably, as ionophore leached out of the membrane.

3.5. Determination of Pb^{2+} and Hg^{2+} in spiked water samples

The analytical utility of the four ionophore membrane electrodes in our continuous flow system was assessed by applying DTODC and DTAODC membranes for lead (II) and DTDC and DQDC for mercury (II) in spiked water samples. Four local bore-water samples that were

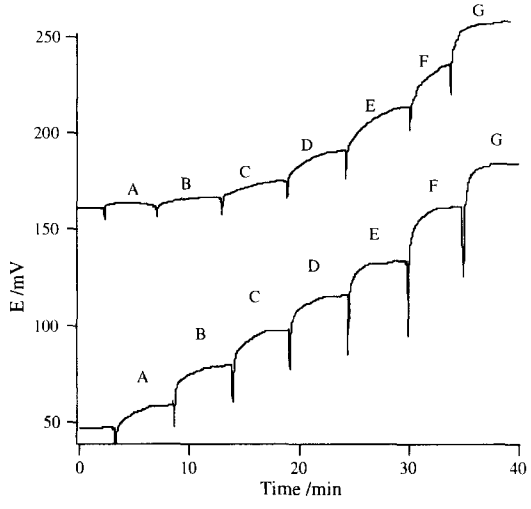

Fig. 8. Potentials of DQDC (lower curve) and DTDC (upper curve) membrane electrodes in solutions of different concentrations of Hg^{2+}. Flow rate 3 ml min^{-1}. Sample solution: (A) 3×10^{-6} M; (B) 10^{-5} M; (C) 3×10^{-5} M; (D) 10^{-4} M; (E) 3×10^{-4} M; (F) 10^{-3} M; and (G) 3×10^{-3} M Hg^{2+}.

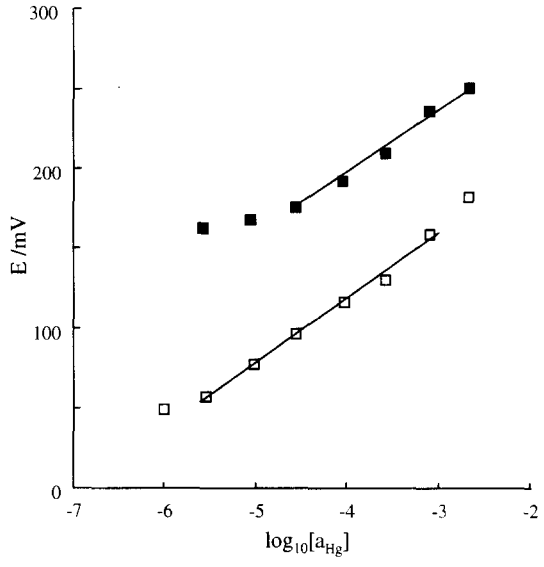

Fig. 9. Calibration plots for the determination of Hg^{2+} at (●) DQDC and (■) DTDC PVC membrane electrodes. Flow rate 3 ml min^{-1}.

Table 5
Analysis of water samples spiked with lead (II) and mercury (II)

Sample	M	M^{2+}/ppm (S.D. $n = 3$) by atomic spectroscopy	M^{2+}/ppm (S.D. $n = 3$) by ISE
Bore (1)	Pb^{2+}	28.0 (ICP) (0.1)	DTAODC 27 (1)
Bore (2)	Pb^{2+}	28.6 (ICP) (0.1)	DTODC 26 (1)
Bore (3)	Pb^{2+}	2.0 (ICP) (0.1)	DTAODC 3.4 (0.3)
Bore (4)	Pb^{2+}	2.1 (ICP) (0.1)	DTODC 2.8 (0.2)
Bore (1)	Hg^{2+}	26.1 (AA) (0.1)	DTDC 23 (1)
Tap	Hg^{2+}	27.5 (AA) (0.1)	DQDC 26 (1)

free from lead (II) and mercury (II) were spiked with approximately 3 or 30 ppm each of lead (II) nitrate and mercury (II) nitrate. The spiked samples were adjusted to pH 4.8–5.0 and pH 3.2–3.5 using dilute nitric acid for the determination of lead (II) and mercury (II), respectively. Although the values for concentrations from the ISEs and spectrometric techniques are within a 95% confidence limit, the small number of samples does not allow a proper comparison. At the lower concentration, the presence of sodium (at about 40 ppm) would add a small component to the ISE potential and so contribute to the over-estimate of the heavy metal concentration (Table 5).

4. Conclusions

We conclude that membrane electrodes based on substituted diazacrowns and used in a continuous flow system are suitable for the analysis of lead and mercury at concentrations in the ppm range. In particular the use of conventional liquid-contact membrane electrodes in flow cells give advantages of greater precision and longer lifetimes of the electrodes. The ionophores chosen have good selectivity for heavy metals, although silver and mercury remain a problem as strong interferents for the diazacrown ionophores. The use of a peristaltic pump to suck solution through a pulse dampener gives a much improved baseline for little extra complexity in the experimental arrangement. We propose this arrangement could be used, for example, in the development of an instrument to analyse the heavy metal content in soils.

References

[1] A.K. Covington, Ion-Selective Electrode Methodology, Vol. 2, CRC Press, Boca Raton, FL, 1979, p. 90.
[2] U. Oesch, D. Ammann, W. Simon, Clin. Chem. 32 (1986) 1448.
[3] T.P. Hadjiioannou, D.S. Papastthopoulos, E.P. Diamandis, in: M. Rubin (Ed.), Computerisation and Automation in Health Facilities, CRC Press, Boca Raton, Fl, 1984, pp. 169–196.
[4] H. Thomson, G.A. Rechnitz, Chem. Instrum. 4 (1972) 239.
[5] E. Wang, S. Kamata, Anal. Chim. Acta 261 (1992) 399.
[6] J. Lexa, K. Stulik, Talanta 38 (1991) 1393.
[7] J.A. Borzitsky, A.V. Dvinin, O.M. Petrukhin, Yu.I. Urusov, Anal. Chim. Acta 258 (1992) 135.
[8] T.K. Christpoulos, E.P. Diamandis, Analyst 112 (1987) 1293.
[9] T.K. Christpoulos, E.P. Diamandis, Anal. Chem. 61 (1989) 504.
[10] M.E. Meyerhoff, P.M. Kovach, J. Chem. Educ. 60 (1983) 766.
[11] S. Alegret, J. Alonso, J. Bartroli, J.M. Paulis, J.L.F.C. Lima, A.A.S.C. Machado, Anal. Chim. Acta 164 (1984) 147.
[12] J.F. van Staden, Anal. Chim. Acta 179 (1986) 407.
[13] A.A.S.C. Machado, Analyst 119 (1994) 2263.
[14] J.L.F.C. Lima, M. Conceicao, B.S.M. Montenegro, J. Alonso-Chamarro, J. Bartroli, J. Garcia-Raurich, Anal. Sci. 8 (1992) 19.
[15] K. Cammann, Fresenius' Z. Anal. Chem. 329 (1988) 691.
[16] T.J. Cardwell, R.W. Catrall, P.C. Hauser, Anal. Chim. Acta 241 (1988) 359.
[17] G.T. Moody, J.M. Slatert, J.D.R. Thomas, Analyst 113 (1988) 103.
[18] A. Izquierodo, M.D. Luque de Castro, Electroanalysis 7 (1995) 505.
[19] X. Yang, N. Kumar, H. Chi, D.B. Hibbert, P. Alexander, Electroanalysis, 1997, in press.
[20] S. Kamata, K. Onoyama, Anal. Chem. 63 (1991) 1295.
[21] E. Malinowska, Z. Brzozka, K. Kasiura, R.J.M. Egerberink, D.N. Rheinhordt, Anal. Chim. Acta 298 (1994) 253.
[22] Z. Brzozka, M. Pietraszkiewicz, Electroanalysis 3 (1991) 855.

[23] M. Pietraszkiewicz, R. Gasiorowski, Z. Brzozka, J. Incl. Phen. Mol. Recogn. Chem. 9 (1990) 239.
[24] H.A. Laitinen, W.E. Harris, Chemical Analysis, McGraw-Hill, NY, 1975, pp. 9–14.
[25] IUPAC Recommendation for Nomenclature of Ion-selective Electrodes, Pure Appl. Chem. 48 (1976) 129.
[26] J. Koryta, K. Stulik, Ion Selective Electrodes, 2nd ed., Cambridge University Press, 1983.
[27] J.G. Schindler, M.V. Gulich, H. Maier, G. Stork, W. Schal, H.-E. Braun, W. Schmid, K.-D. Karaschinski, Fresenius Z. Anal. Chem. 301 (1980) 410.
[28] P. van den Winkel, J. Mertens, D.L. Massart, Anal. Chem. 46 (1979) 1765.
[29] E. Malinowska, Analyst 115 (1990) 1085.
[30] K. Toth, J. Fucsko, E. Lindner, Z.S. Feher, E. Pungor, Anal. Chim. Acta 179 (1986) 359.
[31] J. Mertens, P. van den Winkel, D.L. Massart, Anal. Chem. 48 (1976) 272.
[32] M. Vandeputte, L. Dryon, D.L. Massart, Anal. Chim. Acta 91 (1977) 113.
[33] J. Vesely, D. Weiss, K. Stulik, Analysis with Ion-selective Electrodes, Horwood, Chichester, 1978.
[34] W.E. Morf, W. Simon, Ion-Selective Electrodes Based on Neutral Carriers, in: H. Frieser (Ed.), Ion-Selective Electrodes in Analytical Chemistry, Chapter 3, Plenum Press, New York, 1978.
[35] W. Wroblewski, Z. Brzozka, Anal. Chim. Acta 326 (1996) 163.
[36] M.-T. Lai, J.-S. Shih, Analyst 111 (1986) 891.
[37] M. Neshkova, E. Pancheva, Anal. Chim. Acta 300 (1995) 133.

ELSEVIER

Talanta 45 (1997) 167–180

Talanta

Study of the formation of dye-induced premicellar aggregates and its application to the determination of quaternary ammonium surfactants

Immaculada Casero *, Dolores Sicilia, Soledad Rubio, Dolores Pérez-Bendito

Department of Analytical Chemistry, Faculty of Sciences, University of Córdoba, E-14004 Córdoba, Spain

Received 26 September 1996; received in revised form 24 February 1997; accepted 14 April 1997

Abstract

Formation of dye-induced mixed premicellar aggregates from binary surfactant solutions is proposed for the determination of alkyltrimethylammonium surfactants at the μM level. The Coomassie Brilliant Blue G (CBBG) dye, negatively charged, induces the formation of cationic surfactant aggregates at concentrations far below the cmc. The role of CBBG in the formation of premicelles was studied by using pyrene as a fluorimetric probe. Formation of CBBG-cationic surfactant aggregates of well-defined stoichiometries that depend on the total surfactant concentration added is demonstrated. Also, the influence of analytical parameters affecting the concentration at which a given aggregate is formed was studied. Linear calibrations for alkyltrimethylammonium surfactants were obtained by using different cationic surfactants as titrants; therefore, the previously derived measurement parameter for mixed micelles is applicable to premicellar aggregates as well. © 1997 Elsevier Science B.V.

Keywords: Alkyltrimethylammonium surfactants; Premicellar aggregates; Mixed micelle-based methodology

1. Introduction

There are a host of analytical methods involving micellar media. Most are equilibrium methods based on molecular absorption or emission spectroscopy [1–3], however, surfactants have been increasingly used in dynamic systems involving chromatography [4–6], flow systems [7] and kinetic determinations [8,9] in recent years. Analytical applications of micelles rely on the ability of these organized media to alter the solubilities, pK_a values, chemical equilibria, reaction rates, and mechanisms, spectral distributions and intensities, stereoselectivities, etc., of some chemical processes; the effects result into increased sensitivity and/or selectivity, shorter analysis times and more convenient and inexpensive assays.

Introducing a micelle in a chemical process can have consequences not only on the physicochemical properties of the solutes involved, but also on characteristic parameters of the micelle such as its critical micelle concentration (cmc), aggregation number, micellar structure and shape. Factors influencing these parameters have been studied for

* Corresponding author. Fax: +34 57 218606.

PII S0039-9140(97)00117-3

a long time, and particularly for cmc, considerable effort has been expended to provide adequate mathematical expressions that can satisfactorily account for various dependences of this parameter on different factors [10–13]. Addition of solubilizates (i.e. analytes), in general, lowers the cmc. Ideal mixing between the solubilizate and the aggregated surfactant may in principle be assumed. Accordingly, the cmc value is expected to be reduced by a factor proportional to the mole fraction of the solubilizate in the micelle and this proportionality can be exploited for developing new analytical applications.

Recently, a new approach based on measuring the cmc value of mixed micelles made up of binary surfactant solutions (one of the surfactants being the analyte) was developed by our research group [14]. This methodology has proved useful for determining major non-ionic alkoxylated [14] and anionic alkyl sulphate [15] surfactants; in theory, it could be extended to the determination of any amphiphilic substance capable of forming mixed micelles. Some of the advantages thus obtained in the determination of non-ionic and anionic surfactants include responses that are independent of the molecular weight, sensitivity similar to that afforded by monomer-based methods, high selectivity towards inorganic ions, experimental convenience and expeditiousness. In this work, a new strategy for determining ionic amphiphilic substances with similar sensitivity to that of monomer-based methods was developed. It is based on the formation of dye-rich premicellar aggregates at surfactant concentrations far below their cmc.

Relatively few studies have dealt with solute-surfactant interactions below the cmc. In some cases, surfactants, by themselves are found to associate below their critical micelle concentrations [16–18]. Dimerization is rather a general phenomenon in solutions of amphipathic ions; since this association is presumably favoured by a reduced interfacial energy and hindered by repulsion of charged heads, dimerization is obviously favoured by an expanded chain length [19]. On the other hand, dye-detergent aggregates have been proposed in a number of cases to account for the modified absorption and fluorescence spectra obtained for various dyes below their cmc [20–24]. The many instances reported suggest that surfactant-dye interactions are fairly common among oppositely charged dye-detergent pairs and possible for neutral dyes as well.

The nature of the dyes and their own tendency to aggregate [25–27] must be considered in providing an explanation for such phenomena. Dyes are also amphiphiles in that bulky non-ionic moieties are attached to the ionic groups; however, because they lack long-chain alkyl groups they have weak surface activity and form no micelles in water. Depending on the balance between the hydrophobic and hydrophilic tendencies of any particular dye, increases in dye concentration can lead to stepwise aggregation (i.e. the formation of dimers, trimers, polymers and finally colloids) [28]. If a surfactant is added to such a dye solution at submicellar concentrations, both the surfactant monomer and the dye aggregates can interact to form a special kind of aggregate (a mixed aggregate) at concentrations far below the characteristic cmc of the surfactant. Once the surfactant concentration has closely approached or surpassed the cmc, the dye is eventually incorporated into the micelles.

In this work, the interaction between the dye Coomassie Brilliant Blue G (CBBG), which bears a negative group ($-SO_3^-$), and cationic surfactants [viz. dodecypyridinium chloride (DPC), didodecyldimethylammonium bromide (DDAB), dodecyltrimethylammonium bromide (DTAB) and benzyldimethyldodecylammonium bromide (BDDAB)] were used for the sensitive determination of alkyltrimethylammonium surfactants [viz. dodecyltrimethylammonium bromide (DTAB), tetradecyltrimethyl-ammonium bromide (TTAB) and cetyltrimethyl ammonium bromide (CTAB)]. Formation of CBBG-titrant surfactant and CBBG-titrant surfactant-analyte surfactant mixed aggregates at cationic surfactants concentrations far below their cmc is demonstrated. The dye is assigned a two-fold role in the analytical process: (a) forming associations that induce the formation of premicellar aggregates from monomers of cationic surfactants, and (b) allowing the formation of these premicellar aggregates to be monitored from changes in their spectral features. The

most salient results of this research are discussed below.

2. Experimental

2.1. Apparatus

The equipment used for titrations consisted of a Mettler DL 40 Memotitrator furnished with a 10 ml autoburette, a fan stirrer, a titration vessel and a Mettler GA 14 recorder. The detection unit was a Metrohm 662 spectrophotometer equipped with an inmersion probe. Fluorescence emission spectra for pyrene, which was used as a probe in studying dye-cationic surfactant aggregations, were recorded on a Kontron SFM 25 spectrofluorimeter. Dye-surfactant stoichiometries were determined by using a Hitachi U-2000 spectrophotometer.

2.2. Reagents

Highest grade commercially available reagents were used throughout without further purification. A 6.6×10^{-5} M aqueous solution of Coomassie Brilliant Blue G (CBBG, Sigma) was made by dissolving 0.0575 g of the reagent in 1 l of bidistilled water with sonication for 15 min. Aqueous solutions (1.0×10^{-2} M) of the cationic surfactants dodecylpyridinium chloride (DPC, Merck), didodecyldimethylammonium bromide (DDAB, Fluka), benzyldimethyldodecylammonium bromide (BDDAB, Sigma) dodecyltrimethylammoniumbromide (DTAB, Aldrich), tetradecyltrimethylammonium bromide (TTAB, Aldrich) and cetyltrimethylammonium bromide (CTAB, Serva) were prepared. All were stable for at least 1 week. Working-strength solutions of these surfactants (1.0×10^{-4} M DDAB and BDDAB, and 5.0×10^{-4} M DPC, DTAB, TTAB and CTAB) were prepared daily by appropriate dilution. A pyrene solution (1×10^{-6} M) was made by dissolving 0.0002 g of solid reagent in 1 l of bidistilled water with sonication for 15 min.

2.3. Procedure

In a 50 ml standard flask were placed 15 ml of 6.6×10^{-5} M CBBG solution, an aliquot of standard solution containing alkyltrimethylammonium surfactants and bidistilled water to the mark. This solution, at pH 3–10, was placed in a 100 ml titration vessel and titrated with a cationic surfactant (viz. 5.0×10^{-4} M DPC or DTAB or 1.0×10^{-4} M DDAB or BDDAB) from the burette at a rate of 4 ml min^{-1}. The limits of the linear concentration ranges for the analytes studied (DTAB, TTAB and CTAB) were found to depend on the particular cationic surfactant used as titrant (see Table 1). The stirring rate was set at 250 rpm and the addition autocontrol system at position 1. Titration curves were obtained by recording the absorbance at 680 nm as a function of the titrant volume. The end-point was graphically determined from the intercept of the extrapolated straight line before and after the equivalence point.

The concentration of alkyltrimethylammonium surfactant was determined from the following expression:

$$1 - \frac{C_2^M}{f_2 C_2} = \frac{1}{C_1 f_1} C_1^M \quad (1)$$

which was previously derived for determining surfactants by on formation of mixed micelles [14]. Plotting the parameter $1 - C_2^M/C_2$ as a function of the concentration of alkyltrimethylammonium surfactant (C_1^M) yielded linear calibration graphs (f_2 was unity and f_1 remained unchanged over the C_1^M range considered), which suggest that mixed premicellar aggregates also fit Eq. (1), and their behavior in solution resembles non-ideal mixed micelles. Accordingly, a pre-critical micelle concentration (C*), pcmc, can be defined for the binary mixture of surfactants at concentrations far below the cmc that is a function of the pcmc for the individual surfactants (C_1 and C_2). C_1^M and C_2^M in Eq. (1) denote the concentrations of monomeric surfactant 1 and 2, respectively, and f_1 and f_2 are the activity coefficients for surfactant 1 and 2 in the mixed premicellar aggregate, respectively.

Table 1
Analytical figures of merit of the proposed method for the determination of alkyl quaternary ammonium surfactants

Analyte	Detection limit (μM)	Concentration range (μM)	Intercept ± S.D. × 10^2	Slope ± S.D. (μM^{-1}) × 10^2	r[e]	SEE[f] × 10^2	C_1 (M) × 10^6	C_2/C_1	f_1	f_2
DTAB	0.4[a]	1.0–4.0	1 ± 1	7.3 ± 0.4	0.997	1.2	13 ± 1	0.25	1.15 ± 0.03	0.98 ± 0.01
	1.0[b]	1.0–12.0	−(1 ± 2)	7.6 ± 0.2	0.998	2.5		0.26	1.1 ± 0.1	0.95 ± 0.09
	1.0[c]	1.0–10.0	0 ± 1	4.4 ± 0.2	0.998	1.4		0.69	1.8 ± 0.3	0.9 ± 0.1
	1.0[d]	1.0–10.0	1 ± 1	4.0 ± 0.2	0.995	1.7		1.0	1.8 ± 0.2	0.96 ± 0.09
TTAB	0.2[a]	0.5–4.0	0 ± 1	13.1 ± 0.3	0.9990	1.0	4.2 ± 0.2	0.78	1.9 ± 0.2	1.00 ± 0.03
	0.7[b]	1.0–8.0	0 ± 2	11.9 ± 0.4	0.998	4.3		0.81	2.0 ± 0.2	0.97 ± 0.09
	0.5[c]	0.5-4.0	−(1 ± 2)	15.2 ± 0.7	0.996	1.8		2.14	1.6 ± 0.2	1.1 ± 0.1
	0.3[d]	0.3–4.0	−(2 ± 1)	24.3 ± 0.7	0.997	0.4		3.09	0.99 ± 0.07	1.1 ± 0.1
CTAB	0.3[a]	0.5–4.0	1 ± 1	13.4 ± 0.5	0.997	1.6	3.6 ± 0.3	0.92	2.1 ± 0.2	1.0 ± 0.1
	0.9[b]	1.0–6.0	0 ± 3	13.9 ± 0.8	0.993	4.3		0.94	1.9 ± 0.2	1.1 ± 0.1
	0.2[c]	0.2–1.0	0 ± 1	28.0 ± 0.2	0.9990	1.8		2.5	0.96 ± 0.08	0.9 ± 0.1
	0.04[d]	0.3–1.0	−(1.9 ± 0.1)	32.2 ± 0.5	0.9990	0.4		3.61	0.87 ± 0.09	0.95 ± 0.09

Titrant: [a] BDDAB; C_2(BDDAB) = (3.30 ± 0.02) × 10^{-6} M, [b] DDAB; C_2(DDAB) = (3.4 ± 0.3) × 10^{-6}, [c] DPC; C_2(DPC) = (9.2 ± 1) × 10^{-6} M, [d] DTAB; C_2(DTAB) = (1.3 ± 0.1) × 10^{-5} M, [e] Correlation coefficient, $n = 9$, [f] Standard error of the estimate.

The parameters needed to construct the calibration graph were extracted from titration curves. Thus, the amount of cationic surfactant used in the titration, expressed as a molar concentration, corresponded to the concentration of monomeric cationic surfactant (C_2^M) needed to obtain the pre-critical micelle concentration (pcmc) of the mixed premicellar aggregates (C*). Likewise, the pcmc of cationic single premicellar aggregates (C_2) was determined by performing a similar titration in the absence of alkyltrimetylammonium surfactant from the titration vessel.

3. Results and discussion

3.1. Study of CBBG-cationic surfactants interactions

The dye CBBG has been frequently used for rapid cmc determinations [29]. Its structure is depicted in Fig. 1. The spectral features of this dye were modified by the presence of cationic surfactants. In an aqueous medium, concentrations of these surfactants far below the cmc caused a bathochromic shift in the maximum absorption peak for CBBG from 580 to 620 nm and a considerable increase in the absorbances

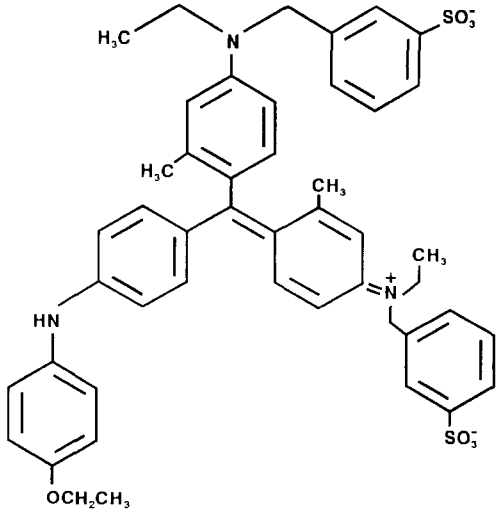

Fig. 1. Structure for Coomassie Brilliant Blue G.

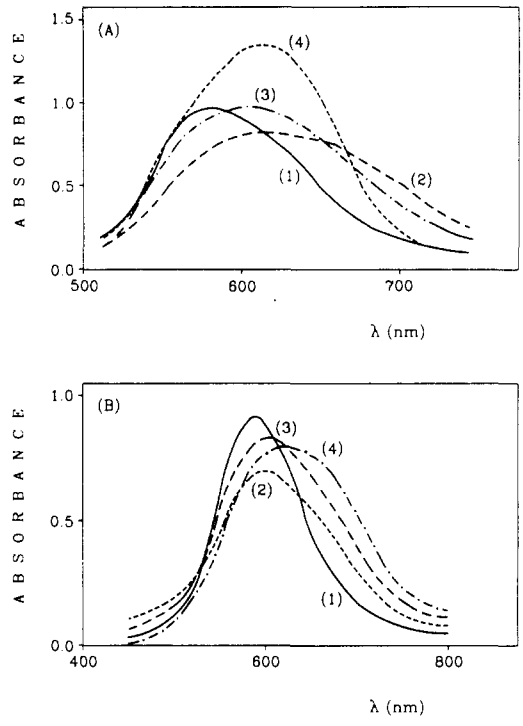

Fig. 2. Spectra for Coomassie Brilliant Blue G (1.98×10^{-5} M) in an aqueous medium (A and B, 1); in the presence of variable concentrations of DPC (A, 2), 1.8×10^{-4} M, (A, 3), 2.0×10^{-3} M, (A, 4) 2.0×10^{-2} M and in the presence of 5.0×10^{-5} M DDAB (B, 2), 1.7×10^{-4} M DTAB (B, 3) and 1.0×10^{-4} M BDDAB (B, 4).

between 660 and 720 nm (e.g. compare curves 1 and 2 for DPC in Fig. 2A). Increasing surfactant concentrations resulted in increased absorbance values at 620 nm and decreased absorbances above 680 nm (Fig. 2A, curve 3); the maximum values at 620 nm were obtained at surfactant concentrations near or above cmc (Fig. 2A, curve 4). Surfactant-induced CBBG spectral changes at surfactant concentrations far below the cmc (lower by about two or three orders of magnitude) were observed for all the cationic surfactant tested as titrants (Fig. 2B).

In order to elucidate the type of interaction between CBBG and cationic surfactants, the occurrence of dye–dye, surfactant–surfactant and dye–surfactant aggregates was investigated. For this purpose, changes in the fluorescence spectrum of pyrene, a proven useful probe for aggregate

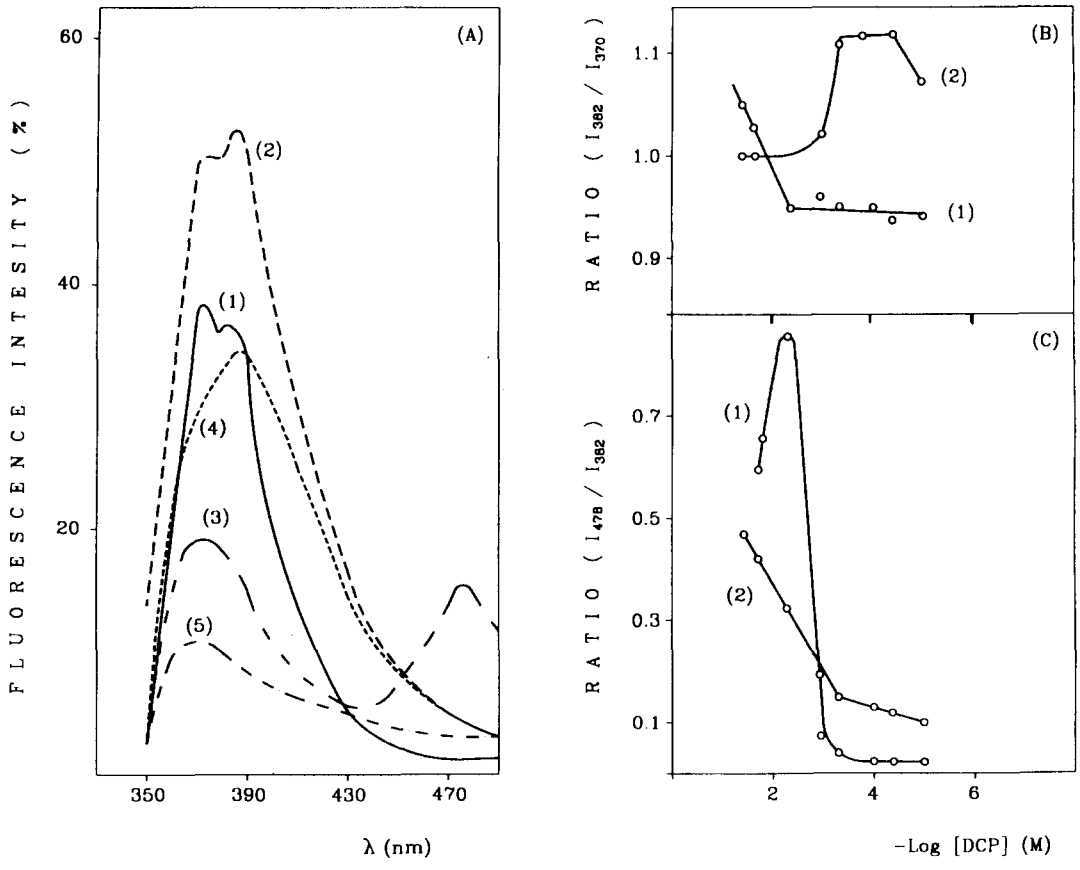

Fig. 3. (A) Fluorescence emission spectra for pyrene (5×10^{-7} M) in an aqueous medium (1) and in the presence of 1.06×10^{-5} M CBBG (2), 5×10^{-3} M DPC (3), 1.06×10^{-5} M CBBG and 5.0×10^{-5} M DPC (4) and 1.06×10^{-5} M CBBG and 5.0×10^{-3} M DPC (5). (B) Ratio of the fluorescence intensity at 382 nm to that at 370 nm and (C) at 478 nm to that at 382 nm, with excitation at 340 nm, as a function of the DPC concentration in the absence (1) and in the presence (2) of 1.06×10^{-5} M CBBG.

formation studies, was used [30,31]. The ratio of the fluorescence intensity at 382 nm to that at 370 nm (the emission peaks for the monomer) has been shown [32] to be a sensitive parameter characterizing the polarity of the microenvironment where pyrene is solubilized, (the I_{382}/I_{370} ratio decreases with increasing medium polarity). On the other hand, excimer formation of pyrene efficiency, expressed as the ratio of the fluorescence intensity of the dimer to that of the monomer, I_E/I_M, or of the fluorescence intensity at 478 nm (emission peak for the excimer) to that at 382 nm, may reflect rearrangement of the hydrocarbon chains of the surfactant molecules during the micelle formation process, i.e. an increased I_E/I_M ratio can be attributed to increased solubilization of pyrene molecules and/or an arrangement conducive to the excimer formation [33,34].

Typical changes in the fluorescence spectrum for pyrene upon addition of CBBG and DPC, which was chosen as a model cationic surfactant for this study, are illustrated in Fig. 3A. The spectral characteristics of pyrene (spectrum 1) were modified by the presence of CBBG (spectrum 2). DPC at submicellar concentrations (up to about 1×10^{-4} M) caused no change in the fluorescence spectrum for pyrene; however, the spectral features of this fluorimetric probe

changed markedly at DPC concentrations near or above cmc (the reported cmc for DPC cmc in water is 1.5×10^{-2} M) (see spectrum 3). It is worth noting that, in the presence of CBBG, addition of DPC caused an abrupt change in the fluorescence spectrum for pyrene at both submicellar and micellar DPC concentrations (spectra 4 and 5, respectively).

Fig. 3B shows the variation of the I_{382}/I_{370} ratio as a function of the surfactant concentration in the absence (1) and presence (2) of CBBG. This ratio was found to increase from 0.96 to 1.05 on adding 1.06×10^{-5} M CBBG to an aqueous solution of pyrene (data not shown in the figure). This increase suggests that CBBG provides a hydrophobic microenvironment for pyrene and that CBBG monomers probably associate to form aggregates in water. No spectral evidence for an interaction between pyrene and DPC in the premicellar region (Fig. 3B, curve 1) could be obtained; the I_{382}/I_{370} ratio did not respond to increasing surfactant concentrations up to the cmc (about 4×10^{-3} M). Any DPC premicellar aggregates, that may have been formed, were apparently not strong enough to affect the ratio, which changed significantly in micellar solutions. On the other hand, evidence for strong association between CBBG and DPC was obtained at surfactant concentrations far below the cmc (Fig. 3B, curve 2). The pyrene environment was more hydrophobic in the presence of CBBG than in its absence, which can reasonably be ascribed to the formation of CBBG-induced premicellar aggregates. These aggregates solubilize or interact further with pyrene molecules.

The results obtained in the study of the excimer formation efficiency of pyrene led to similar conclusions. Fig. 3C shows the I_{478}/I_{382} ratios as a function of the DPC concentration in the absence (curve 1) and presence (curve 2) of CBBG. When the dye was present, a gradual increase in the I_{478}/I_{382} ratio was observed at DPC concentrations below the cmc that suggest the formation of premicellar aggregates which solubilize pyrene molecules and/or arrange them in such a way as to favour the excimer formation. The type of dependence of I_{478}/I_{382} on the DPC concentration provides further evidence for gradual micellization. The occurrence of premicellar aggregates in the absence of CBBG was not apparent from measurements of excimer formation efficiency for pyrene since the fluorescence intensities ratios remained unchanged at submicellar concentrations. Near the cmc, the efficiency was higher in the absence than in the presence of CBBG, as is apparent from spectra 4 and 5 in Fig. 3A, and curves 1 and 2 in Fig. 3C. This suggests that solubilization of pyrene in DPC micelles is more effective in the absence of CBBG, which is logical taking into account that the dye and probe compete for solubilization sites in the micelle.

The possibility of a well-defined stoichiometry of CBBG to DPC was investigated by using the mole-ratio method. Experiments were carried out by mixing increasing DPC concentrations below the cmc (between 0 and 1.8×10^{-4} M) and a constant concentration of dye (1.98×10^{-5} M). Fig. 4A shows the variation of the absorbance at 680 nm as a function of the [DPC]/[CBBG] ratio. The broken line obtained suggests the formation of aggregates of different stoichiometry (between 1:2 and 8:1 DPC:CBBG) in proportion to the DPC concentration. Possible aggregates formed at DPC concentrations above 1.8×10^{-4} M could not be spectrophotometrically investigated because spectral properties of CBBG changed from premicellar to a micellar DPC medium (see Fig. 2A, spectra 2 and 4). These results demonstrate the occurrence of gradual micellization and that CBBG acts as a nucleus from which monomers of DPC associate.

Since the determination of alkyltrimethylammonium surfactants entails the formation of mixed titrant surfactant-analyte surfactant aggregates, the possibility of a well-defined stoichiometry of DPC(titrant) + TTAB(analyte) to CBBG was also investigated. The concentrations of dye and TTAB were constant at 1.98×10^{-5} M and 4×10^{-6} M, respectively, whereas that of DPC was changed between 0 and 2.0×10^{-5} M. Only those aggregates formed in the region of analytical interest were investigated. Fig. 4B shows the formation of premicellar aggregates with DPC + TTAB:CBBG stoichiometries identical with those obtained for DPC:CBBG. Therefore, real CBBG-induced mixed premicellar aggregates are formed at surfactants concentrations far below the cmc.

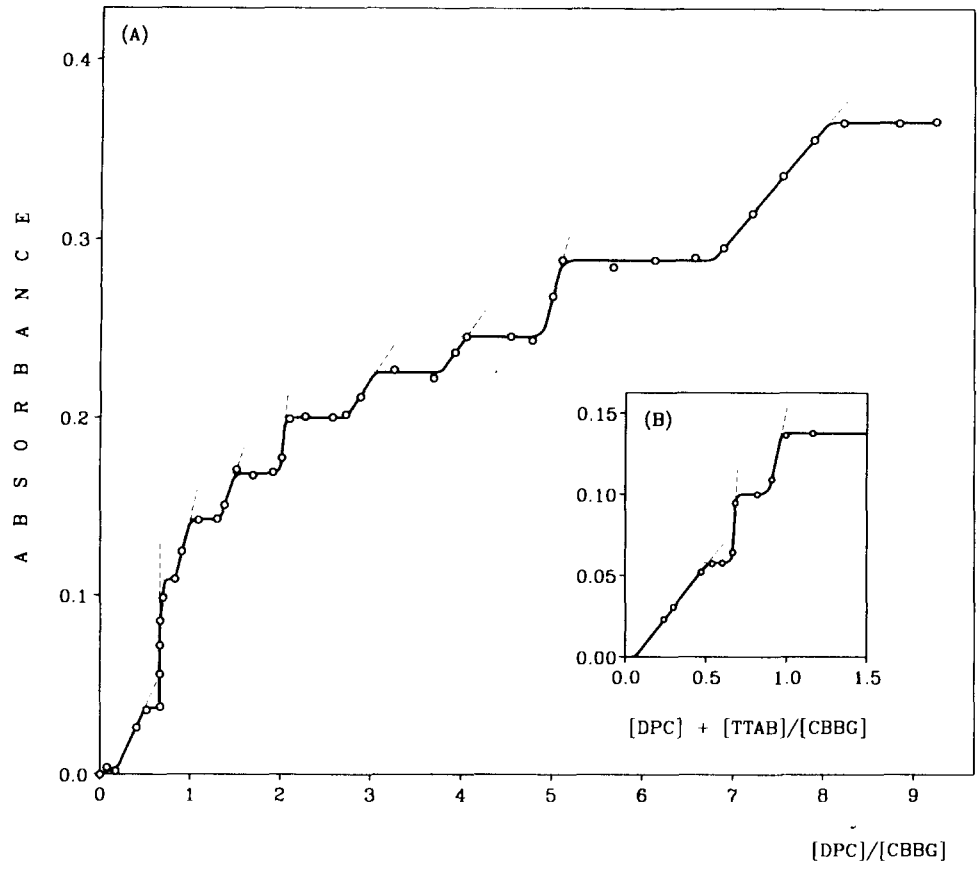

Fig. 4. Variation of the absorbance of Coomassie Brilliant Blue G (1.98×10^{-5} M) at 680 nm as a function of the DPC/CBBG (A) and DPC + TTAB/CBBG (B) molar concentration ratios. [TTAB] = 4×10^{-6} M.

In conclusion, CBBG interacts strongly with DPC, and also presumably with ammonium cationic surfactants; it induces the formation of premicellar aggregates into which cationic monomers are gradually incorporated proportionally as surfactant concentration is increased. Also, cationic micelles are formed that solubilize CBBG. Dye-induced mixed premicellar aggregates are also formed from a binary mixture of surfactants.

In order to determine alkyltrimethylammonium surfactants by formation of mixed premicellar aggregates with cationic surfactants such as DPC, DTAB, DDAB and BDDAB, a continuous plot of the absorbance for CBBG at 680 nm as a function of the volume of cationic surfactant used as titrant was recorded. Fig. 5A shows typical titration curves obtained by using DPC as titrant in the absence (curve 1) and presence of variable TTAB concentrations (curve 2–5). Parameter C_2 and the different C_2^M values can readily be calculated from the volume of titrant (V_2 and V_2^M, respectively) used at the endpoint. Since the premicellar aggregates detected depend on the titrant concentration used, this was selected to ensure maximal sensitivity and precision in the determination of alkyltrimethylammonium surfactans. Under these experimental conditions, the formation of titrant:CBBG or titrant + analyte:CBBG premicellar aggregates of 1:2 and 2:3 stoichiometry were successively recorded (their formation corresponded to the initial curved and linear portions of the titration curves, respectively). When the titrant concentration was high enough for the

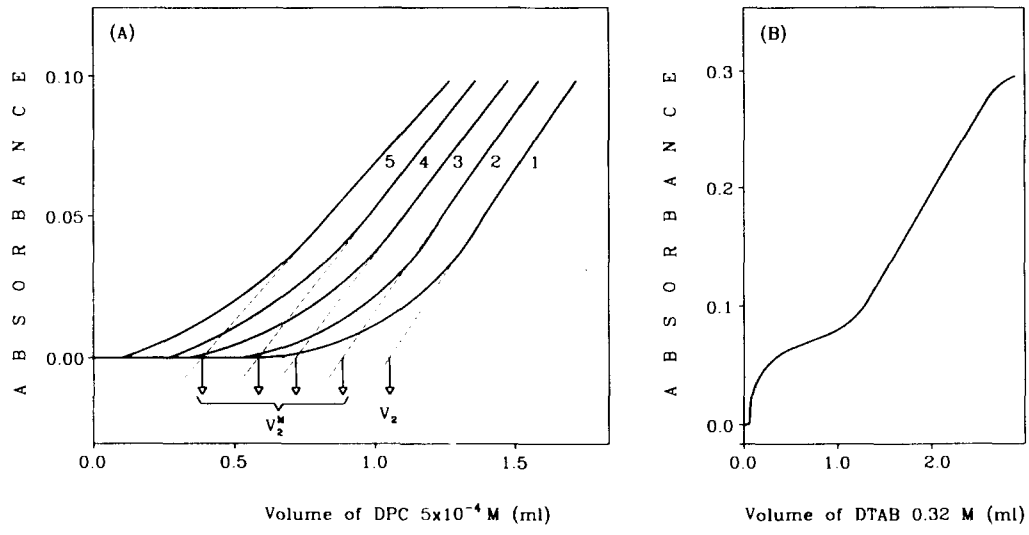

Fig. 5. (A) Variation of the absorbance of Coomassie Brilliant Blue G (1.98×10^{-5} M) at 680 nm as a function of the volume of titrant (5.0×10^{-4} M dodecylpiridinium chloride) added to a titration vessel containing no cationic surfactant (curve 1) or TTAB at a concentration of 1×10^{-6} (curve 2), 2×10^{-6} (curve 3), 3×10^{-6} (curve 4) and 4×10^{-6} M (curve 5). (B) Variation of the absorbance of Coomassie Brilliant Blue G (1.32×10^{-5} M) at 620 nm as a function of the volume of 0.32 M dodecyltrimethyl-ammonium bromide added.

formation of mixed micelles to be detected without dilution effects, the titration curves obtained exhibited two sections corresponding to the formation of mixed premicellar and micellar aggregates, respectively (Fig. 5B).

3.2. Optimization

DPC and TTAB were selected as titrant and analyte, respectively, to optimize the system. Two objectives were considered in selecting the best experimental conditions: (a) the highest possible sensitivity in the determination of the cationic surfactant, and (b) the highest possible precision in determining the titration endpoint. Variables affecting the formation of surfactant aggregates (dye concentration, ionic strength, dielectric constant and temperature) were investigated.

Since CBBG induces micellization of cationic surfactants, increasing concentrations of this dye decreased C_2 and C_2^M throughout the range studied [$(0.4–4) \times 10^{-5}$ M]. Because the decrease was similar in both single (DPC) and mixed (DPC + TTAB) premicellar aggregates, the measurement parameter, $1 - C_2^M/C_2$, remained essentially constant. CBBG concentrations below about 1.3×10^{-5} M proved inadvisable since the absorbance increase as a function of the concentration of cationic surfactant was very small and detracted from precision in the determination of the titration endpoint.

The effect of electrolytes on the formation of both single and mixed premicellar aggregates and on the measurement parameter $1 - C_2^M/C_2$ was examined by using sodium chloride, sodium hydroxide and sulphuric acid. Increasing ionic strength resulted in increasing pcmc values for both single and mixed cationic premicellar aggregates, the increase being independent of the electrolyte used to adjust it (Fig. 6A, C and E). This is logical taking into account that electrolytes can decrease electrostatic interactions between CBBG and cationic surfactants, which, together with hydrophobic interactions, are responsible for the formation of dye-induced premicellar aggregates. The measurement parameter was not altered by addition of NaCl at concentrations between 0 and 1.3×10^{-2} M, but decreased on addition of

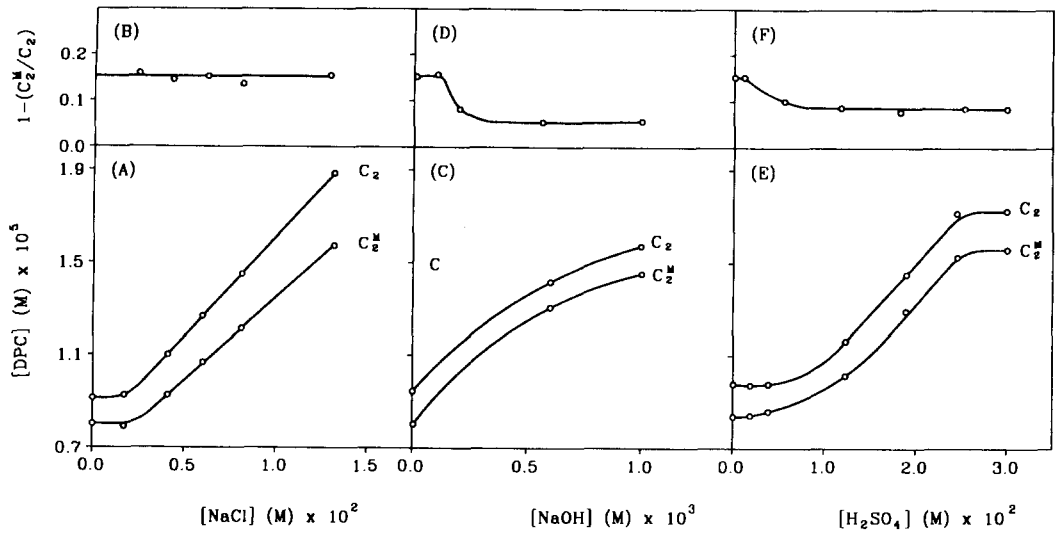

Fig. 6. Influence of the ionic strength on C_2 and C_2^M (A, C, E), and on the measured parameter (B, D, F), studied by adding NaCl (A, B), NaOH (C, D) and H_2SO_4 (E, F). [CBBG] = 1.98×10^{-5} M, [TTAB] = 1×10^{-6} M.

NaOH and H_2SO_4 at concentrations above 1×10^{-4} M (Fig. 6B, D and F, respectively). Addition of NaCl at concentrations above 1.3×10^{-2} M resulted in irreproducibility in C_2 and C_2^M measurements (and hence in the measured parameter). On the other hand, addition of NaCl, NaOH or H_2SO_4 at concentrations higher than 4×10^{-2}, 1×10^{-3} and 3×10^{-2} M, respectively, was inadvisable since the titration curves obtained had ill-defined endpoints owing to the bathochromic shift undergone by CBBG high electrolyte concentrations.

The effect of organic additives on the formation of premicellar aggregates was studied by addition of ethanol at concentrations up to 10%. The alcohol was found not to affect the formation of aggregates in proportions below about 1%; higher contents of this solvent caused a gradual increase in C_2 and C_2^M (Fig. 7A), and a slight decrease in the measurement parameter (Fig. 7B). This is logical since at high bulk phase concentrations, short-chain alcohols decrease the dielectric constant of the aqueous phase. This may increase mutual repulsion of ionic heads in the dye aggregates, thus hindering dye aggregate formation and hence dye–surfactant premicellar aggregate formation.

The temperature, the effect of which was studied between 20 and 55°C, affected the formation of single and mixed premicellar aggregates in a similar way (Fig. 7C). Parameters C_2 and C_2^M did not change between 20 and 35°C, so $1 - C_2^M/C_2$ remained essentially constant over this temperature range. At higher temperatures, pcmc values corresponding to single and mixed premicellar aggregates increased (Fig. 7C) and the measurement parameter decreased in a gradual manner. In addition, the shape of the titration curves changed the exhibited several steps (Fig. 7E, curve 2), and precision in detecting the endpoint suffered as a result. Therefore, increased temperatures hinder the formation of premicellar aggregates by increasing the cationic surfactant concentration needed for DPC to associate.

3.3. Calibration

In order to determine whether the use of dye-induced premicellar aggregates is a useful strategy for determining ionic amphiphilic substances at the same concentration levels as in monomer-based methods, calibration graphs for alkyltrimethyl ammonium surfactants were run by

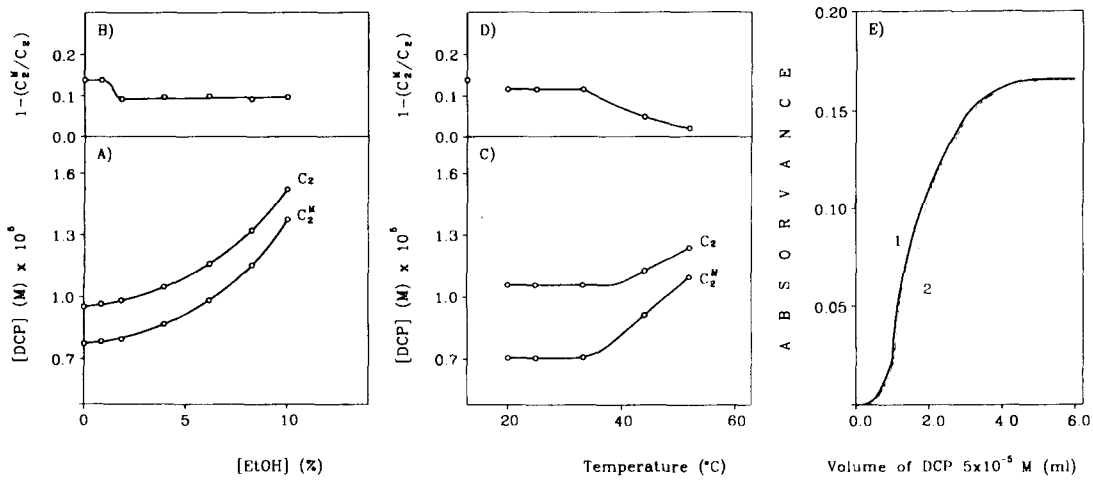

Fig. 7. Influence of the ethanol content on C_2 and C_2^M (A) and on the measured parameter (B). Effect of the temperature on C_2 and C_2^M (C) and on the measured parameter (D). Titration curves (E) obtained at 25°C (1) and 45°C (2). [CBBG] = 1.98×10^{-5} M, [TTAB] = 1×10^{-6} M.

plotting $1 - C_2^M/C_2$ versus the cationic surfactant concentration (C_1^M). The alkyltrimethylammonium surfactants used for this study were C_{12}-, C_{14}- and C_{16}-N^+-$(CH_3)_3$ Br^- (DTAB, TTAB and CTAB, respectively). Table 1 compares the figures of merit of the calibration graphs for these surfactants, run by using DPC, DTAB, DDAB and BDDAB as titrants. Linear calibrations were obtained in all cases (the standard error of the estimate and correlation coefficient varied over the ranges $(0.4–4.3) \times 10^{-2}$ and 0.993–0.9990, respectively); therefore, parameters f_2 and f_1 remained constant over the linear concentration ranges. Likewise, intercept values were not significantly different from zero, so f_2 (the activity coefficient for DPC, DTAB, DDAB and BDDAB in the mixed micelles) was approximately unity, as shown in Table 1. These results prove that, for a binary non-ideal surfactant mixture, the concentration at which a well-defined premicellar aggregate is formed can be expressed as

$$\frac{1}{C^*} = \frac{\alpha}{f_1 C_1} + \frac{1-\alpha}{f_2 C_2} \qquad (2)$$

where α is the mole fraction of surfactant 1 in the total mixed solute and all remaining parameters have the same meaning as in Eq. (1). As a consequence, Eq. (1) which was derived for mixed micelles [14], can be extended to mixed premicellar aggregates.

Using different analytes and titrants for calibration permitted us to draw some preliminary analytical and physico-chemical conclusions. Thus, as with micelles, the sensitivity of the proposed method depends on both C_1 and the C_2/C_1 ratio. Based on Eq. (1), the slope of the calibration curves should increase as C_1 decreases (see Table 1). On the other hand, the C_2/C_1 ratio (which ranged from 0.25 to 3.6 for the analyte-titrant mixtures studied) determines both the absolute value of the calibration slope for a given analyte and the kind of dependence of sensitivity on C_1. For each analyte, the maximum sensitivity is achieved at a C_2/C_1 ratio that is different enough from unity, a C_2 value being at least two or three times higher or lower than C_1 (see Table 1). The dependence of the pre-critical micelle concentration for different analyte-surfactant:titrant surfactant mixtures (C*) on the mole fraction (α) of analyte surfactant (Eq. (2)) is similar to that known for micelles when C_2/C_1 ratios are different from unity (Fig. 8A1 and A3), but changes significantly as the ratio approaches unity (compare curves 1–4 with curve 5, which is typical for micelles, in Fig. 8A2). We found no evidence for the fact that whichever the surfactant used as

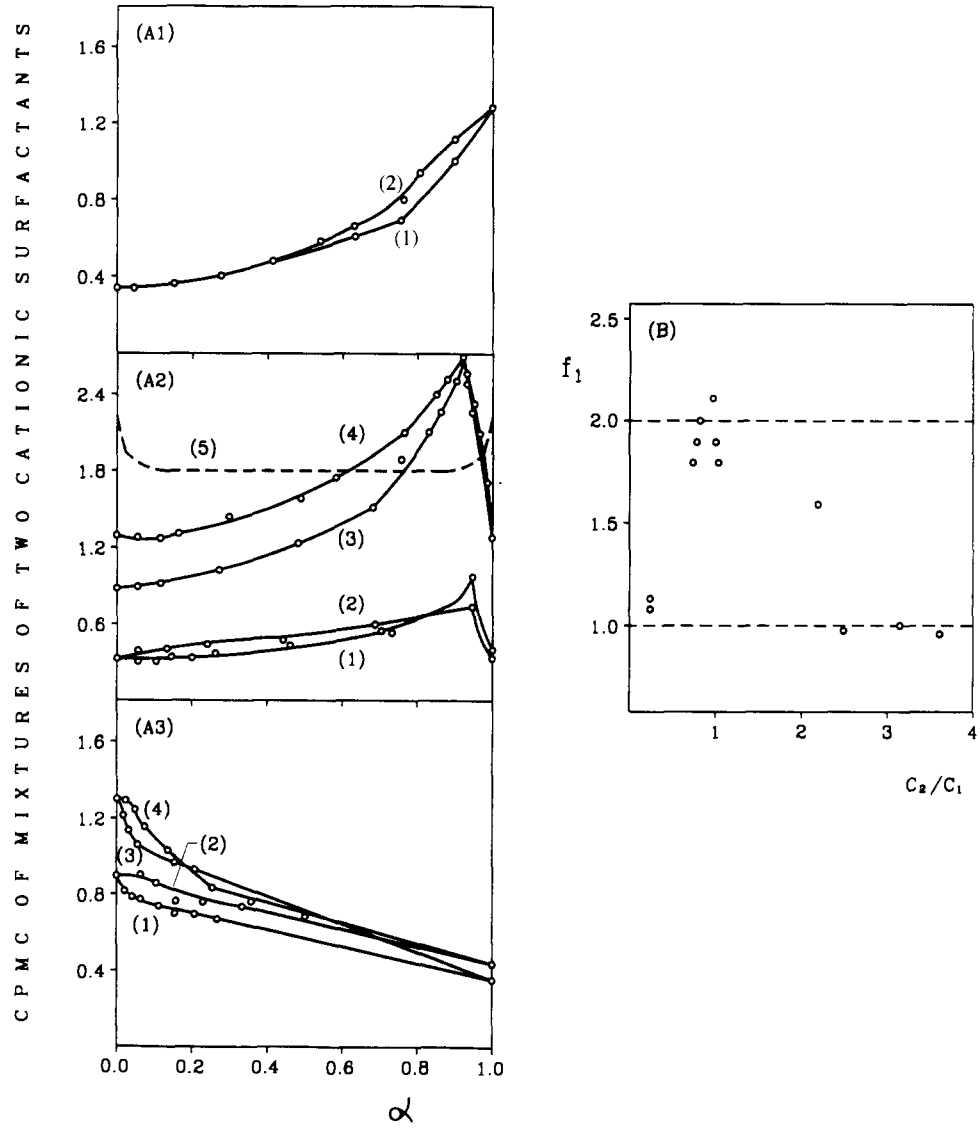

Fig. 8. (A) Dependence of the pre-critical micelle concentration (pcmc) of mixtures of two surfactants (C*) as a function of the mole fraction of the analyte (α) at variable C_2/C_1 ratios (values given in Table 1). (A1) $C_2 < C_1$ (1) DTAB + DDAB, (2) DTAB + BDDAB; (A2) $C_2 \simeq C_1$, (1) TTAB + DDAB, TTAB + BDDAB, CTAB + BDDA, (2) CTAB + DDAB, (3) DTAB + DPC (4) DTAB + DTAB (5) typical dependence of the critical micelle concentration (cmc) on the analyte mole fraction; (A3) $C_2 > C_1$ (1) CTAB + DPC; (2) TTAB + DPC, (3) CTAB + DTAB, (4) TTAB + DTAB. pcmc = C_2 at $\alpha = 0$ and pcmc = C_1 at $\alpha = 1$. (B) Dependence of f_1 on the C_2/C_1 ratio.

titrant, a maximum appeared at analyte mole fractions between 0.9 and 1 at a C_2/C_1 ratio close to unity. From a physico-chemical point of view, it is worth noting that, over the linear analyte concentration range, the C_2/C_1 ratio determines whether the binary association of cationic surfactants to give premicellar aggregates behaves as an ideal ($f_1 \simeq 1$) or non-ideal (f_1 different from unity) surfactant mixture (Fig. 8B).

As noted above, the relative value of C_2 with respect to C_1 also determines the type of dependence of the slope of the calibration curve on C_1.

Linear and exponential dependences were respectively obtained for titrants with pcmc values smaller and greater than C_1 (Fig. 9). Therefore, if a similar response for different alkyltrimethylammonium surfactants is required, a cationic surfactant with as low as possible a pcmc should be used as titrant. On the other hand, as with micelles, maximum responses are obtained for titrants with high pcmc values relative to C_1.

The precision of the proposed method, expressed as relative standard deviation, was 3.3% ($n = 11$) for a concentration of TTABr of 2×10^{-6} M when DPC was used as the titrant.

3.4. Analytical considerations

The results obtained in the determination of alkyltrimetyl ammonium surfactans by formation of dye-induced mixed premicellar aggregates permit us to draw some conclusions regarding the analytical usefulness of these aggregates for determining ionic amphiphilic substances in general and quaternary ammonium surfactants in particular.

Ionic amphiphilic substances generally have cmc values around 10^{-2}–10^{-3} M. In order to make aggregate-based methods competitive with monomer-based methods in terms of sensitivity two requisites should be met: first, the analyte should form a mixed aggregate with the titrant; and second, the concentration at which the analyte forms the correspondent single aggregate (C_1) should be in the micromolar range. Formation of real mixed aggregates is not generally a problem for surfactants of similar or different nature. The second condition, however, calls for strategies providing sufficiently low C_1 values. So far, two alternatives have been proposed by our research group to reduce C_1 by about two or three orders of magnitude, namely addition of a high electrolyte concentration [15] and the approach presented in this paper, which relies on the formation of dye-induced premicellar aggregates. Therefore, it could be of interest to compare the analytical features of the two choices.

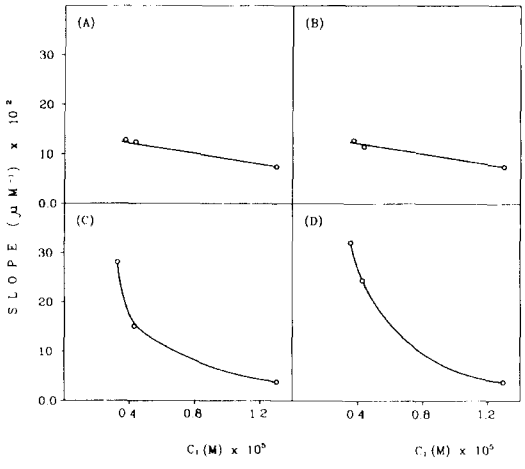

Fig. 9. Dependences obtained between the slope of calibration curves for alkyltrimethyl ammonium surfactants and their pcmc values for different titrants. At $C_2 < C_1$ (A) BDDAB (1.0×10^{-4} M), (B) DDAB (1.0×10^{-4} M). At $C_2 > C_1$ (C) DPC (5.0×10^{-4} M), (D) DTAB (5.0×10^{-4} M).

In terms of sensitivity the two strategies investigated have proved to effectively reduce C_1 in a simple way. In terms of selectivity, formation of micellar aggregates in the presence of high concentrations of inorganic salts permits one to avoid the interference of most inorganic ions having a concomitant effect on monomer-based methods since these are generally based on the extraction of ion-pairs. This enhanced selectivity is an additional advantage of this alternative [15] since the formation of dye-induced premicellar aggregates is more markedly affected by electrolytes and therefore must have a lower selectivity towards inorganic ions. With respect to number of systems to which these strategies can be applied, formation of dye-induced premicellar aggregates are fairly common for oppositely charged dye-detergent pairs and are also possible for neutral surfactants [35], so the number of amphiphilic substances that can be determined by using this alternative is in principle extended. On the other hand, while addition of salts is in principle universally applicable, some problems have been found for given systems that exhibit distorted titration curves at high electrolyte concentrations. This is logical since electrolytes affect the micellar structure. Therefore, the better alternative depends on the particular application.

Anyway, determining the real applicability of dye-induced mixed premicellar aggregates for the

determination of alkyl ammonium surfactants calls for further studies in order to delimit the kinds of sample to which they can advantageously be applied. Research in this direction is currently being conducted our laboratory.

Acknowledgements

The authors gratefully acknowledge financial support from Spain's CICyT (Project No. PB91-0840).

References

[1] W.L. Hinze, in: K.L. Mittal (Ed.), Use of surfactant and micellar systems in analytical chemistry, Solution Chemistry of Surfactants, vol. 1, Plenum, New York, 1979, pp. 79–127.
[2] L.J. Cline Love, J.G. Habarta, J.G. Dorsey, Anal. Chem. 56 (1984) 1133R.
[3] E. Pelizzetti, E. Pramauro, Anal. Chim. Acta 169 (1985) 1.
[4] A. Berthod, J.G. Dorsey, Analusis 16 (1988) 75.
[5] M.G. Khaledi, Trends Anal. Chem. 7 (1988) 293.
[6] W.L. Hinze, Annali Chim. 77 (1987) 167.
[7] B. Moreno Cordero, J.L. Pérez Pavón, J. Hernández Méndez, Quim. Anal. 8 (1989) 231.
[8] D. Pérez-Bendito, S. Rubio, Trends Anal. Chem. 12 (1993) 9.
[9] M. López Carreto, S. Rubio, D. Pérez-Bendito, Analyst 121 (1996) 33R.
[10] S. Puvvada, D. Blankschtein, in: P.M. Holland, D.N. Rubingh (Eds.), Mixed Surfactant Systems, ACS Symposium Series 501, American Chemical Society, Washington, 1992, chapter 5, pp. 96–113.
[11] D.N. Rubingh, in: K.L. Mittal (Ed.), Mixed micelle solutions, Solution Chemistry of Surfactants, vol. 1, Plenum, New York, 1978, pp. 337–354.
[12] P.M. Holland, in: P.M. Holland, D.N. Rubingh (Eds.), Mixed Surfactant Systems, ACS Symposium Series 501, American Chemical Society, Washington, DC, 1992, chapter 2, pp. 31–44.
[13] J.J. Clint, J. Chem. Soc. Faraday Trans. I 71 (1975) 1327.
[14] D. Sicilia, S. Rubio, D. Pérez-Bendito, Anal. Chem. 67 (1995) 1872.
[15] I. Casero, D. Sicilia, S. Rubio, D. Pérez-Bendito, Anal. Chim. Acta. (accepted for publication).
[16] Y. Zimmels, I.J. Lin, J.P. Friend, Colloid Polym. Sci. 253 (1975) 404.
[17] P.J. Mukerjee, J. Phys. Chem. 69 (1965) 2821.
[18] A. Nikolov, G. Martynov, D.J. Exerowa, J. Colloid Interface Sci. 81 (1981) 116.
[19] P.J. Mukerjee, J. Phys. Chem. 62 (1958) 1404.
[20] N. Miyoshi, H. Kiyoaki, I. Yokoyama, G. Tomita, M. Fukuda, Photochem. Photobiol. 47 (1988) 685.
[21] Y. Kusumoto, H. Sato, Chem. Phys. Lett. 68 (1979) 13.
[22] J.H. Baxendale, M.A.J. Rodgers, J. Phys. Chem. 86 (1982) 4906.
[23] A. Sanz-Medel, M.E. Díaz García, Talanta 33 (1986) 255.
[24] J. Rosendorfová, L. Čermáková, Talanta 27 (1980) 705.
[25] P. Mukerjee, A.K. Ghosh, J. Am. Chem. Soc. 92 (1970) 6403.
[26] B.H. Robinson, A. Löffler, G. Schwarz, J. Chem. Soc. Faraday Trans. I 69 (1973) 56.
[27] E.H. Braswell, J. Phys. Chem. 88 (1984) 3653.
[28] R.L. Reeves, M.S. Maggio, S.A. Harkaway, J. Phys. Chem. 83 (1979) 2359.
[29] K.S. Rosenthal, F. Koussale, Anal. Chem. 55 (1983) 1115.
[30] T. Ohyashiki, T. Mohri, Chem. Pharm. Bull. 31 (1983) 1296.
[31] Y. Kusumoto, M. Shizuka, I. Satake, Chem. Lett. 4 (1986) 529.
[32] A. Nakajima, Bull. Chem. Soc. 99 (1977) 2039.
[33] H.J. Pownall, L.C. Smith, J. Am. Chem. Soc. 95 (1973) 3136.
[34] J.M. Vanderkooi, J.M. Gallis, Biochemistry 13 (1974) 4000.
[35] D.C. Barber, R.A. Freitag-Beeston, D.G. Whitten, J. Phys. Chem. 95 (1991) 4074.

ELSEVIER

Talanta 45 (1997) 181–187

Talanta

Study of the interferences in the determination of Pu, Am and Cm in radioactive waste by extraction chromatography

M. Rodríguez [a,*], J.L. Gascón [b], J.A. Suárez [a]

[a] *Instituto Tecnología Nuclear, CIEMAT, Avda. Complutense 22, 28040-Madrid, Spain*
[b] *Dirección de Tecnología, CIEMAT, Avda. Complutense 22, 28040-Madrid, Spain*

Received 14 November 1996; received in revised form 19 February 1997; accepted 14 April 1997

Abstract

This paper describes the experimental studies carried out to determine ^{238}Pu, $^{239/40}Pu$, ^{241}Pu, ^{241}Am, ^{242}Cm and ^{244}Cm in samples from nuclear power plants (mainly spent ion exchange resins and evaporator concentrates) using an organophosphorus compound immobilized on an inert support. These materials are commercially available under the name TRU Resin (for Transuranium Specific) from Eichrom Industries, Darien, IL. An attempt is made to develop a rapid, accurate method of analysis, with minimum waste generation. Standard solutions of Pu and Am and one sample of spent ion exchange resin that contains fission, activation products, Pu, Am and Cm were analyzed to study the separation factors and interferences in the measurement of Pu, Am and Cm isotopes. © 1997 Elsevier Science B.V.

Keywords: α-spectrometry; Extraction chromatography; Radioactive waste and liquid scintillation counting

1. Introduction

In view of increased public attention to radioactive waste disposal and the potential public health effects of releases of radioactive materials to the environment it is necessary to develop accurate and reliable methods for the determination of actinides in the low and medium radioactive wastes that arise from nuclear power plants.

Numerous methods have been described for effecting this separation, among them procedures based on ion exchange [1,2], liquid–liquid extraction [3,4], precipitation [5] and combinations thereof [6,7]. Most of them involve separate rather than simultaneous determinations of these elements. These methods have always been time consuming and involve the use of large amounts of hazardous material.

Therefore, considerable effort has been made to adapt the selective liquid–liquid extraction methods to produce new chromatographic materials. The intention has been to develop a rapid, accurate method of analysis for Pu, Am and Cm, with minimum waste generation. Nowadays the use of extraction chromatography (reversed phase partition chromatography) in the analysis of the actinides has undergone considerable development, and has been applied with good results for the analysis of environmental and biological samples

* Corresponding author. Tel.: +34 1 3466132; fax: +34 1 3466269; e-mail: alcala@ciemat.es

PII S0039-9140(97)00118-5

[8]. The technique uses an inert polymeric support (Amberlite XAD-7) impregnated with a selective extractant (octyl(phenyl)-N,N-diisobutylcarbamoylmethylphosphine oxide (abbreviated CMPO), in tri-*n*-butyl phosphate (TBP). Columns made from this resin selectively adsorb the actinides from acid media. This material is commercially available under the name TRU Resin (for Transuranium Specific) from Eichrom Industries.

This paper describes experimental studies carried out to determine Pu, Am and Cm in samples from nuclear power plants (mainly ion exchange resins and evaporator concentrates) using TRU Resin and on the basis of the data published [9–12] for distribution ratios of actinides in the III, IV, V and VI oxidation states.

2. Experimental method

The method of analysis comprises the following steps:

- The solution is evaporated to dryness once, the plutonium oxidation state is adjusted to III with hidroxylamine hydrochloride.
- The resulting residue is dissolved in 1 M HNO_3, and $NaNO_2$ is added to adjust the plutonium oxidation state to IV.
- TRU Resin (700 mg) was wet-packed in a 10 cm long disposable polyethylene column (empty poly-prep chromatography columns Bio-Rad or equivalent). The column bed volume (c.v.) was 2.0 ml. Gravity flow rates (1–2 ml min^{-1} per cm^{-2}) were employed throughout. Before use the column was washed with 10 ml of 1 M HNO_3,
- the sample solution is transferred to the column,
- the column is rinsed with
  10 c.v. of 1 M HNO_3-0.05 M $NaNO_2$ (Rinse 1–5)
  6 c.v. of 2 M HNO_3-0.5 M $Al(NO_3)_3$ (Rinse 6–8)
  6 c.v. of 1 M HNO_3-0.05 M $NaNO_2$ (Rinse 9–11)
  to remove fission and activation radionuclides and stable elements present,
- 8 M HCl (Rinse 12–17) is added as a crossover to dilute HCl,
- the americium-curium are eluted from the column using 20 c.v. of 2 M HCl,
- the plutonium is eluted from the column using 20 c.v. of 2 M HCl-0.1 M HI,
- the solution of plutonium is divided into two aliquots, one for liquid scintillation counting (LSC) and the other one for electrodeposition as described by Hallstadius [13] followed by α-spectrometry. The α-spectra are taken with 450 mm^2 ion implanted silicon detectors.
- The Am and Cm mixture is electroplated as described above and measured by α-spectrometry.

This separation procedure was applied on standard solutions containing ^{241}Pu and ^{243}Am to determine the chemical yield and to check the efficiency of separation of Pu and Am. Both column rinsing and elution steps were checked and measured by LSC.

Additionally, the procedure was used in the analysis of liquid samples obtained from the destruction of spent ion exchange resins [14] to evaluate the separation of the radionuclides and stable elements that can interfere with the measurement. In this case, ^{236}Pu and ^{243}Am was added to the solutions as tracer to know the chemical yield of the process. The column rinsing and elution steps were checked and measured by γ-ray spectrometry.

Finally, the same spent ion exchange resin sample previously mentioned, was analyzed using anion exchange chromatography [15] to compare the results obtained.

Table 1
Chemical yield of the separation procedure for Pu/Am in a standard solution (results in Bq)

Step	^{241}Pu	^{243}Am
Initial	3.26×10^{2}	1.29×10^{1}
Rinse 1–5	$< 6.93 \times 10^{-2}$	$< 1.70 \times 10^{-2}$
Rinse 6–8	$< 6.93 \times 10^{-2}$	$< 1.70 \times 10^{-2}$
Rinse 9–11	$< 6.93 \times 10^{-2}$	$< 1.70 \times 10^{-2}$
Rinse 12–17	3.67×10^{-1}	4.03×10^{0}
Eluate Am	2.61×10^{1}	8.07×10^{0}
Eluate Pu	1.62×10^{2}	4.17×10^{-2}
%Yield	49	62

Table 2
Selectivity of the separation procedure for Pu/Am/Cm in spent ion exchange resin samples (results in Bq)

Step	^{54}Mn	^{60}Co	^{65}Zn	^{134}Cs	^{137}Cs
Initial	2.47×10^{4}	7.39×10^{4}	2.56×10^{4}	9.77×10^{3}	2.17×10^{4}
Rinse 1–5	1.82×10^{4}	6.14×10^{4}	1.87×10^{4}	7.41×10^{3}	1.80×10^{4}
Rinse 6–8	$<1.45\times10^{0}$	$<1.69\times10^{0}$	$<3.52\times10^{0}$	$<1.38\times10^{0}$	$<2.43\times10^{0}$
Rinse 9–11	$<1.36\times10^{0}$	$<2.14\times10^{0}$	$<4.10\times10^{0}$	$<1.25\times10^{0}$	$<2.43\times10^{0}$
Rinse 12–17	$<1.30\times10^{0}$	$<1.79\times10^{0}$	$<3.52\times10^{0}$	$<1.19\times10^{0}$	$<2.43\times10^{0}$
Eluate Am	$<1.59\times10^{0}$	$<1.64\times10^{0}$	$<3.90\times10^{0}$	$<1.39\times10^{0}$	$<2.43\times10^{0}$
Eluate Pu	$<1.36\times10^{0}$	$<1.77\times10^{0}$	$<1.47\times10^{0}$	$<1.47\times10^{0}$	$<2.43\times10^{0}$

Table 3
Comparison of the results obtained in a spent ion exchange resin by extraction chromatography (EC) and ion exchange chromatography (IC) (results in Bq/g $\pm 2\sigma$)

Method	^{238}Pu	$^{239,40}Pu$	^{241}Pu	^{241}Am	^{242}Cm	^{244}Cm
E.C	40 ± 4	7 ± 1	4143 ± 124	10 ± 1	30 ± 3	13 ± 2
I.C	44 ± 5	7.9 ± 0.8	858 ± 26	6.0 ± 0.4	81 ± 3	33 ± 1

3. Results and discussion

(a) The results obtained with the standard solutions are shown in Table 1. It is observed that this method gives a chemical yield of about 50% for Pu and about 60% for Am. Also it can be seen that when Am is eluted, the Pu found in the solution is about 8% and when Pu is eluted, the Am found in the solution is about 0.32% of the original feed.

(b) The results obtained in the β-γ decontamination of spent ion exchange resins samples are shown in Table 2. It is observed that with 10 c.v. of 1 M HNO_3–0.05 M $NaNO_2$, separations ranging from 73 to 83% are achieved. With another 24 c.v. (6 of 2 M HNO_3–0.5 M $Al(NO_3)_3$, 6 c.v. of 1 M HNO_3–0.05 M $NaNO_2$ and 12 c.v. of 8 M HCl) it is noticed there is no further significant removal of main radionuclides present in the samples. This means that about 25% of the interfering radionuclides still remain in the column. The results indicate that there is a good separation of the interfering radionuclides. These data confirm the selectivity and effectiveness of the separation procedure.

(c) The results of ^{241}Pu and the α emitting Pu, Am and Cm isotopes obtained by both methods: extraction chromatography (EC) and ion exchange chromatography (IC) are shown in Table 3.

Fig. 1 shows the α-spectrum of Pu where it is noticed that there is a good separation of the radionuclides present in the initial sample. The resolution of α-spectra is 33 keV for the Pu peak in terms of the full width at half maximum.

The results obtained by both methods for the ^{238}Pu and $^{239,40}Pu$ are in good agreement considering the experimental errors. The chemical yield of Pu by EC was 50%, as compared to 90% obtained by IC.

^{241}Pu value obtained by EC is higher than that obtained by IC. Fig. 2 shows the plutonium spectra obtained by liquid scintillation counting of the Pu fraction separated by both methods: EC and IC. It is observed that the Pu α-spectra are coincident while the spectra of ^{241}Pu present a great discrepancy, therefore the ^{241}Pu/Pu α ratio does not remain constant (by IC the relation is 11.9 and by EC is 76.9). This implies contamination in the low energy spectrum of other radionuclides present in the sample. Seeing the shape of the spectrum and knowing the different radionuclides present in the samples, it is possible to indicate that the contamination could only be due to ^{54}Mn

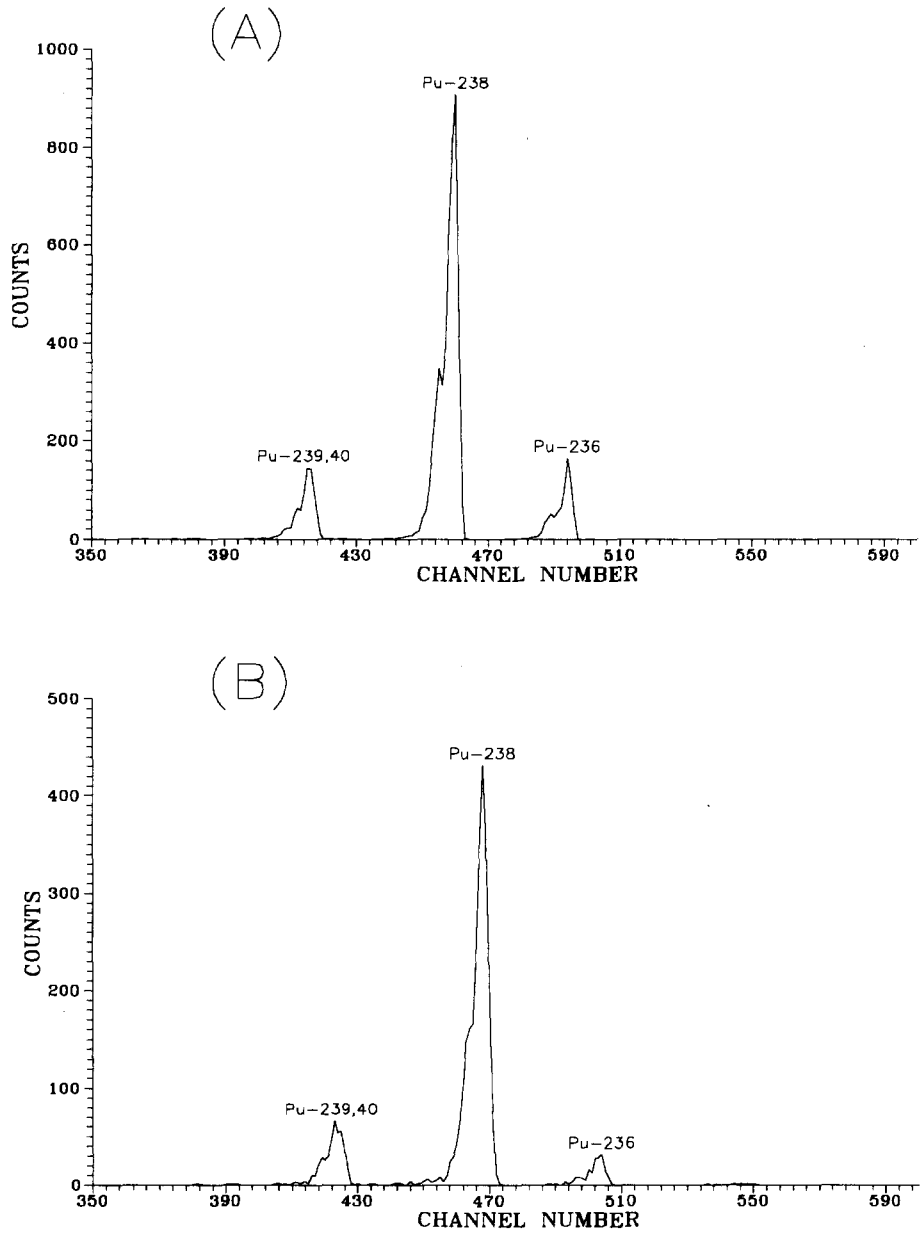

Fig. 1. Spectra of Pu isotopes obtained in the analysis by ion exchange chromatography (A) and extraction chromatography (B).

or ^{55}Fe. However, as it is shown in Table 2, in the samples analyzed, there is a total absence of ^{54}Mn, and for that reason, this radionuclide is not the contributing factor. On the other hand, the sample containing Pu fraction, previously analyzed by LSC, was measured by low energy γ-spectrometry. The γ-spectrum obtained is shown in Fig. 3 where the presence of ^{55}Fe is confirmed. In this case, it is important to note that the Fe(III) distribution ratio is about 100 times lower

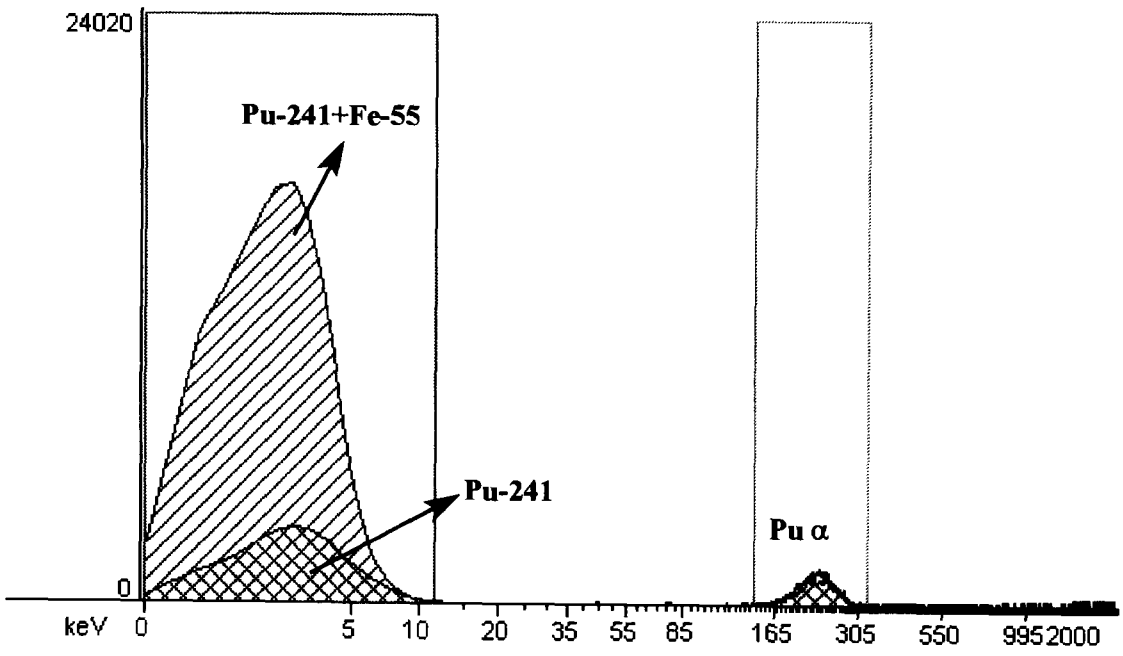

Fig. 2. Spectra of plutonium by liquid scintillation counting of the purified Pu fraction by both methods: anion exchange chromatography and extraction chromatography.

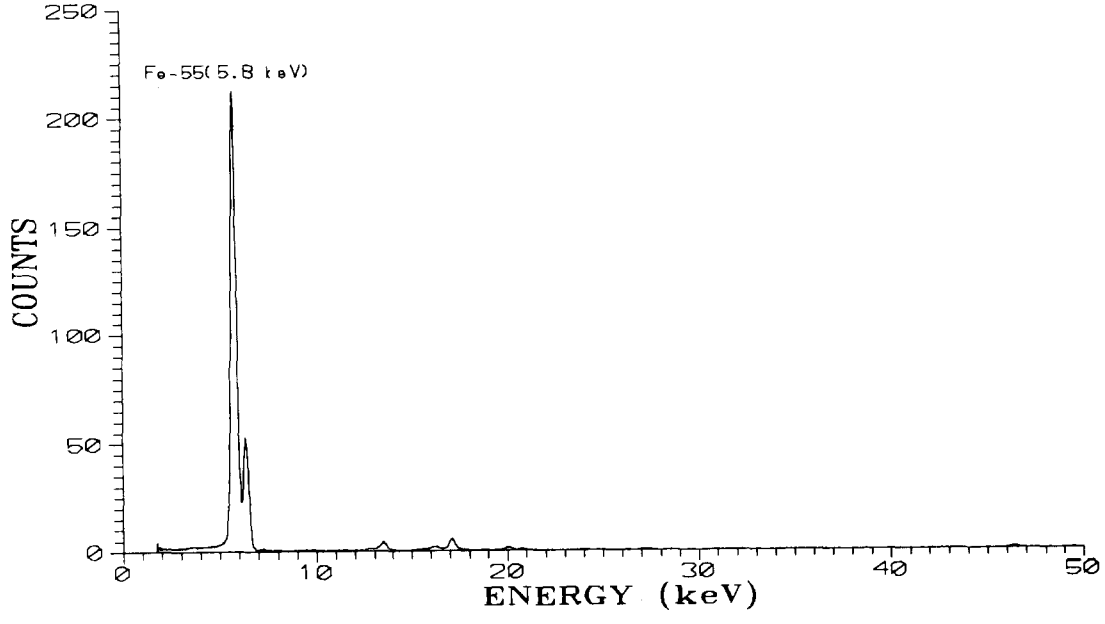

Fig. 3. Spectrum obtained by low energy gamma spectrometry in the purified Pu fraction by extraction chromatography.

than the Am(III) distribution ratio in 1 M HNO_3 medium [8] and the separation factors obtained for ^{55}Fe are higher than 99.31%. In spite of the low percentage (0.69%) of the initial activity

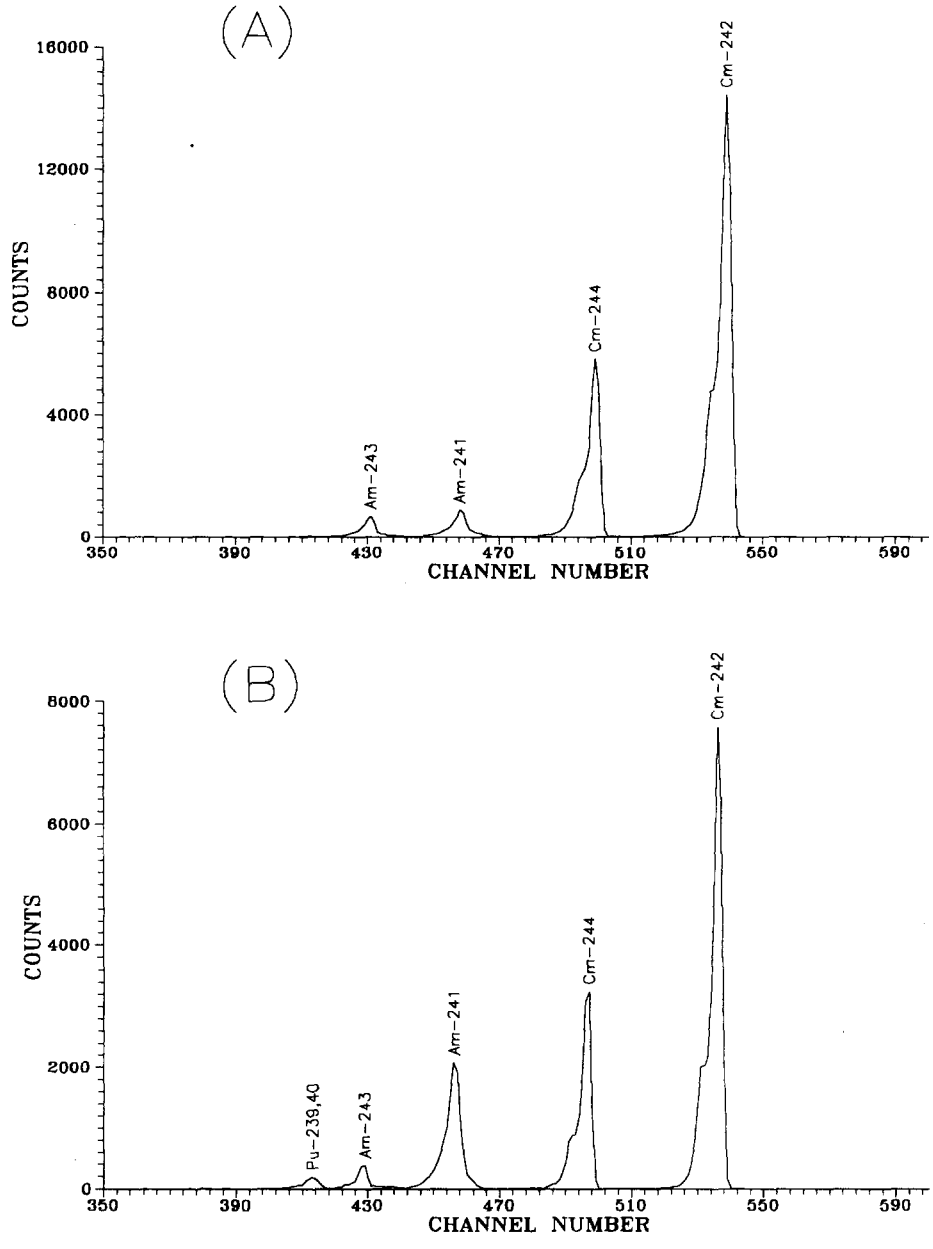

Fig. 4. Spectra of Am and Cm isotopes obtained in the analysis by ion exchange chromatography (A) and extraction chromatography (B).

(about 10^5 Bq/g) of ^{55}Fe that remains in the purified solution of ^{241}Pu, the activity of ^{55}Fe is five times higher than ^{241}Pu activity, therefore ^{55}Fe is the interferent.

With respect to ^{241}Am, the value obtained by EC is higher than that obtained by IC. This is due to the improper separation of Am and Pu as can be seen in the spectrum in Fig. 4. Pu presence can

be seen in the spectra from the $^{239/40}$Pu peak and as a consequence the ^{241}Am and ^{244}Cm peaks will have interference from ^{238}Pu and ^{236}Pu, respectively. The loss of Pu to the Am fraction (8%) may be explained by the presence of a small amount of Pu(III) in the Pu load solution, despite the addition of $NaNO_2$ [16].

Another problem with the use of extraction chromatography is the determination of ^{242}Cm and ^{244}Cm, whose values are lower than that obtained by IC. This is due to the different chemical behaviour of Am and Cm in EC and the use of the ^{243}Am as tracer is not valid to determine the chemical yield of Cm. The chemical yield by EC for Am was 30 and 11% for Cm, while by IC, the chemical yield is higher being for both radionuclides 80%.

Finally, it is possible to indicate that when ^{238}Pu and $^{239/40}$Pu are analyzed by extraction chromatography there is not any interference in the measurement by α-spectrometry, being the method more rapid and generate less waste when compare with another techniques (liquid–liquid extraction, anion exchange chromatography, coprecipitation, etc.). However, the determination of ^{241}Pu, ^{241}Am, ^{242}Cm and ^{244}Cm by extraction chromatography is affected by some interferences and gives incorrect results. The interferences are: ^{55}Fe in the analysis of ^{241}Pu and ^{236}Pu and ^{238}Pu in the analysis of ^{241}Am and ^{244}Cm.

References

[1] A. Yamato, J. Radioanal. Chem. 75 (1–2) (1982) 265–273.
[2] A. Qingjiang Chen, S.P. Aarkrog, H. Nielsen, H. Dahlgaard, K. Nies, Yixuan Yu, K. Mandrup, J. Radioanal. Nucl. Chem. 172 (2) (1993) 281–288.
[3] J.P. Shukla, A. Kumar, R.K. Singh, Radiochimica Acta 60 (1993) 103–107.
[4] S. Zhu, D. Yang, S. Long, Z. Xiao, Radiochimica Acta 65 (1994) 59–61.
[5] J.C. Veselsky, P.C. Kiel, N. Sezginer, J. Radioanal. Chem. 21 (1974) 97.
[6] K. Bunzl, W. Kracke, J. Radioanal. Nucl. Chem. 115 (1) (1987) 13–21.
[7] J.L. Gascón, M. Rodríguez, J.A. Suárez, J. Radioanal. Nucl. Chem. 207 (1) (1996) 63–69.
[8] E.P. Horwitz, R. Chiarizia, M.L. Dietz, H. Diamond, D.M. Nelson, Anal. Chim. Acta 281 (1993) 361–372.
[9] E.P. Horwitz, D.G. Kalina, Solvent Extraction and Ion Exchange 2 (2) (1984) 179.
[10] E.P. Horwitz, D.G. Kalina, H. Diamond, F. Vandergriff, Solvent Extraction and Ion Exchange 3 (1 and 2) (1985) 75.
[11] E.P. Horwitz, R.A. Martin, H. Diamond, L. Kaplan, Solvent Extraction and Ion Exchange 4 (3) (1986) 449.
[12] D.G. Kalina, E.P. Horwitz, Solvent Extraction and Ion Exchange 3 (3) (1985) 235.
[13] L. Hallstadius, Nucl. Instr. Meth. 223 (1984) 266.
[14] J.A. Suárez, M. Rodriguez, J.L. Gascón, Report CIEMAT, ITN/TR-29/SP-91, 1991.
[15] J.L. Gascón, M.L. Aceña, J.A. Suárez, M. Rodríguez, Journal of Alloys and Compounds 213/214 (1994) 557–559.
[16] E.P. Horwitz, M.L. Dietz, D.M. Nelson, J.J. La Rosa, W.D. Fairman, Anal. Chim. Acta 238 (1990) 263–271.

ELSEVIER

Talanta 45 (1997) 189–201

Talanta

Solvent effects on the dissociation reactions of tartaric, maleic and phthalic acids; comparative study and analysis of thermodynamic functions

A.A. Zaghloul *, G.A. El-Naggar, Sh.A. El-Shazly, M.F. Amira

Chemistry Department, Faculty of Science, Alexandria University, Alexandria, Egypt

Received 24 December 1996; received in revised form 25 March 1997; accepted 14 April 1997

Abstract

The first and second dissociation constants of tartaric, maleic and phthalic acids have been determined using EMF method in water–ethanol mixed solvents, over a wide range of solvent composition (0–60 wt% ethanol) at six different temperatures (ranging from 30 to 55°C at intervals of 5°C). The thermodynamic parameters ($\Delta G°$, $\Delta H°$ and $\Delta S°$) for the first and the second ionization reactions were calculated from the well known equations. The results have been discussed in terms of the solute–solvent interactions and were compared with those of malic, malonic and succinic acids in the same mixed solvents. © 1997 Elsevier Science B.V.

Keywords: Dicarboxylic acids; Dissociation constants; EMF Method; Solvent effect on; Thermodynamic parameters

1. Introduction

The ionic dissociation of several monobasic acids in mixed solvents has been extensively documented [1–6]. Such studies elucidated the role of the solvent in acid–base reactions and helped to provide a proper perspective for the interpretation of variety of acid–base reactions in solutions, but there seems to be little similar information about dibasic acids. Therefore, it is not surprising that in recent years much attention has been paid to a quantitative explanation of medium effects on pK values of dicarboxylic acids in mixed solvents [7–15].

The present work is a continuation of our studies [15] on the thermodynamics of acid dissociation reactions in ethyl alcohol–water media, in which the first and second dissociation reactions of maleic, tartaric and phthalic acids were examined in media of varying ethanol compositions up to 60 wt% ethanol which allow for a wide range of dielectric constant. The aim of this work is devoted to: (i) determine the effects of solvent on the dissociation constants of these acids and consequently their associated thermodynamic functions of dissociation; and to (ii) compare the obtained results with those of other dicarboxylic acids in the same mixed solvents [15], this is for better understanding of the dissociation processes occurring in such acids in mixed solvents.

* Corresponding author.

PII S0039-9140(97)00119-7

2. Experimental

The acids (B.D.H. AnalaR) under investigation were recrystallized and dried. The absolute ethyl alcohol used (from Prolabo) was purified as recommended [16]. Stock solutions of HCl (≈ 0.2 m (mole kg^{-1})) were analysed by AgCl weighings, and stock buffer solutions of dicarboxylic acids (H_2L) and Na_2CO_3 (dried at 300°C for 3 h) were made up, by weight, from B.D.H. Analar Samples.

K_1 and K_2 determinations were based on EMF measurements of the cell:glass electrode/HCl (m_1), H_2L (m_2), Na_2CO_3 (m_3)/AgCl(s)/Ag. The practical work has been simplified by adopting a practice [7,8] which prevents movements of the electrode between its calibration and usage. This is preferable to the technique [17,18] of transferring the glass electrode from an HCl solution to an acid ligand solution followed by extrapolation of timed readings to compensate for any EMF drifts. This procedure is considerably faster than that required with a Pt/H_2 electrode where each measurement necessitates refilling with a fresh buffer solution. Moreover several values of K_1 and K_2 could be computed from a single run. The buffer compositions were taken as $[H_2L]$: $[Na_2CO_3] \approx$ 3:1 for K_1 work and 1.2:1 for K_2 work. For phthalic acid, potassium hydrogen phthalate (KHPh) was used with HCl for K_1 determination while KHPh was used with Na_2CO_3 (2:1) for K_2 determination. About 230 g of the required wt% ethyl alcohol (to ± 0.01 g) was weighed into the cell together with sufficient dilute HCl containing the required wt.% ethyl alcohol (≈ 0.035 m) to make ≈ 0.0015–0.0025 m (addition by weight pipette to ± 0.1 mg). With the electrodes in positions, the cell was equilibrated at the desired temperature, the temperature was controlled to ± 0.01°C. This could take up to 3 h, the HCl solution was then given a short stir (≈ 5 s) by a fitted microstirrer and left to settle until EMF (E) was constant (≈ 30 min). Up to six additions of stock buffer were then added by weight pipette. In the first addition about 15 g of the stock buffer solution were added while in the later additions, about 8 g of this solution were added in each case. After each addition the solution was stirred and EMF of the cell then monitored to constancy. The time needed could vary from ≈ 1 h for the first addition for a K_2 series (the point of the greatest EMF change) down to ≈ 15 min for the latter additions and also for all of K_1 series. The constancy of the EMF values was checked by the difference between the first and the last readings which was never more than ± 0.1 mV.

Measurements to ± 0.1 mV were made with a digital pH meter (Beckman 4500 type). The AgCl electrode was made by plating a thin spiral Pt wire with Ag in 0.5% $KAg(CN)_2$ for ≈ 1 h with a 9-V battery followed by electrolysis for AgCl in 0.05 M HCl with a 9-V battery for 20 s.

3. Experiment

The first and second dissociation constant (K_1 and K_2) of three dicarboxylic acids namely: maleic, tartaric and phthalic acids have been determined in ethyl alcohol–water media of varying solvent compositions (0–60 wt% ethyl alcohol) within the temperature range (30–55°C). The expressions used for calculating K_1 and K_2 are,

$$K_1 = [H^+][HL^-]\,\gamma_H\gamma_{HL}/[H_2L] \quad (1)$$

$$K_2 = [H^+][L^{2-}]\,\gamma_L/[HL^-] \quad (2)$$

$$K_{NaL} = [Na^+][L^{2-}]\,\gamma_L/[NaL^-] \quad (3)$$

$$-\log \gamma_i = AZ_i^2[I^{1/2}/(1 + BI^{1/2}) - QI] \quad (4)$$

$$E_{(cell)} = E^o_{(cell)} - k' \log([H^+][Cl^-]\,\gamma_H\gamma_{Cl}) \quad (k' = 2.3026\,RT/F) \quad (5)$$

where I and γ represent ionic strength and activity coefficient, respectively (γ_{H_2L} was negligible i.e., close to 1). The Debye–Huckel constant 'A' was calculated for each temperature and each solvent composition while the constants 'B' and 'Q', the values of which were taken as 1.3 and 0.3, respectively according to data of Monk [7]. Firstly $E^o_{(cell)}$ was calculated from Eq. (4) and Eq. (5) by knowing $E_{(cell)}$ of the diluted HCl solution ($I = [HCl]$). If the stoichiometric molal concentrations of HCl, H_2L and Na_2CO_3 are m_1, m_2 and m_3, respectively, the following equations are used (with Eqs. (1)–(5)) for calculating K_1

$$[H_2L] = m_1 + m_2 - 2m_3 - [H^+] + [L^{2-}] + [NaL^-] \quad (6)$$

$$[HL^-] = m_2 - [H_2L] - [L^{2-}] - [NaL^-] \quad (7)$$

Approximate values of $[H^+]$ on the addition of buffer solution were calculated from Eq. (4) and Eq. (5) with $I = m_1$ followed by use of Eq. (6) and Eq. (7) with $[L^{2-}] = 0$ and $[NaL^-] = 0$ in the first cycle. The subsequent value of I was used to recalculate $[H^+]$ followed by calculation of $[L^{2-}]$ via Eq. (2) with published or estimated values of K_2. $[NaL^-]$ was calculated from Eq. (3) using $K_{NaL} = 0.2$ (approximate value (15) for different runs). If present estimates of K_2 were significantly different the calculations were repeated until the difference between successive values of $[H^+]$ agreed to $\Delta[H^+] \leq 1 \times 10^{-9}$ m, K_1 was then obtained from Eq. (1) and Eq. (4).

For K_2, $[H^+]$ was calculated as described above and then by applying Eq. (8) and Eq. (9) found,

$$[HL^-] = m_1 + 2m_2 - 2m_3 - [H^+] - 2[H_2L] \quad (8)$$

$$[L^{2-}] = m_2 - [H_2L] - [HL^-] - [NaL^-] \quad (9)$$

with $[H_2L] = 0$ and $[NaL^-] = 0$ in the first cycle followed by the use of Eq. (1) and Eq. (3) for calculating $[H_2L]$ and $[NaL^-]$, respectively. K_2 was calculated from Eq. (2) and Eq. (4) when the difference between two successive values of $[H^+]$ agreed to $\Delta[H^+] \leq 1 \times 10^{-9}$ m. All computations were made by means of BASIC programmes with a COMODORE 64 computer.

4. Results and discussion

Table 1 represents some examples of detailed runs, for the studied acids, in different ionic strength and at different experimental conditions. For each run the extrapolated K_1 and K_2 values at zero ionic strength were obtained from the linear least mean square plots of K_1 (or K_2) versus the ionic strength. This method based on extrapolation, for the determination of K_1 and K_2 was used earlier [7–10] and was found to be valid and efficient under different experimental conditions. The computed pK_1 and pK_2 values for different solvent compositions and temperatures are shown in Table 2. It is obvious from. Table 2 that pK_1 and pK_2 values of these acids increase as the composition of ethyl alcohol increases in the ethyl alcohol–water binary mixture. These results are in accordance with Born equation [19] in predicting ionization constants, accordingly the ionization constant should increase as the dielectric constant of the medium increases. Also, the solvent effect on the dissociation constants of weak acids arises mostly due to change in the basicity of the solvent. So far as the effect of solvent change on dissociation constants is concerned, the second dissociation constant is depressed more by changing solvent composition than the first dissociation constant is, since the electrostatic effect due to the negative charge on the first carboxylate ion is more readily transmitted to the seat of second dissociation as the solvent composition increases. The stabilization of the internal hydrogen bond, with increasing solvent composition, increases the dissociation constant K_1 of the uncharged acid and decreases, K_2 of the acid anion, so that the ratios K_1/K_2 increases. The solvent effect on K_1/K_2 ratio appears to be greater in the case of maleic acid where the geometrical structure of this acid plays an important role on the intramolecular hydrogen bond formation.

The distance r (in Å) between the two carboxylic groups of each acid, was calculated under different experimental conditions from Bjerrum's equation [20]

$$\ln\frac{K_1}{4K_2} = \frac{Ne^2}{RTDr}$$

where N is Avogadro's number, e is the electronic charge and D is the dielectric constant. The obtained r's values when presented graphically against the mole fraction of the solvent the correlation was not linear. The good linear correlation has been found between $-\Delta S_2^\circ$ and $1/r$ for the second dissociation reaction of some dicarboxylic acids, as represented in Fig. 1, for 40 and 60 wt% of ethanol (ΔS_2° and $1/r$ values for malic, malonic and succinic acids were taken from ref. [15]). This correlation can be expressed mathematically as,

$$-\Delta S_2^\circ = A + B/r$$

Table 1
Some EMF data for the determination of K_1 and K_2 values of maleic, phthalic and tartaric acids under different experimental conditions

40% EtOH maleic 30°C

$10^3\ m_2 = 1.987 \quad -E_1(\text{mV}) = 304.8$

$10^3\ m_2$	$10^3\ m_3$	$-E_1$ (mV)	$10^3\ I$	$10^8\ K_2$
5.203	4.162	47.6	9.494	2.601
7.785	6.228	32.1	15.076	2.479
10.032	8.026	26.3	19.887	2.496
12.165	9.732	24.2	24.416	2.639
14.613	11.690	22.8	29.572	2.790
17.259	13.807	21.8	35.097	2.931

10% EtOH maleic 55°C

$10^3\ m_1 = 2.063 \quad -E_1(\text{mV}) = 282.0$

$10^3\ m_2$	$10^3\ m_3$	$-E_1$ (mV)	$10^3\ I$	$10^4\ K_1$
10.312	2.574	301.9	10.428	9.532
16.126	4.025	304.2	14.135	9.610
19.848	4.955	306.8	16.842	9.929
24.540	6.126	308.2	19.867	10.251
28.138	6.024	309.1	22.174	10.498
32.688	8.160	310.0	25.060	10.990

30% EtOH maleic 45°C

$10^3\ m_1 = 1.676 \quad -E_1(\text{mV}) = 291.0$

$10^3\ m_2$	$10^3\ m_3$	$-E_1$ (mV)	$10^3\ I$	$10^8\ K_2$
5.219	4.178	41.0	9.821	5.879
7.806	6.250	29.5	15.411	6.036
10.312	8.256	24.7	20.770	6.193
12.562	10.057	22.1	25.540	6.535
14.595	11.684	21.4	29.819	6.859
17.097	13.688	20.2	35.049	7.308

30% EtOH tartaric 45°C

$10^3\ m_1 = 2.257 \quad -E_1(\text{mV}) = 309.9$

$10^3\ m_2$	$10^3\ m_3$	$-E_1$ (mV)	$10^3\ I$	$10^4\ K_1$
10.711	2.674	277.0	6.264	4.305
16.122	4.024	271.7	8.908	4.220
21.794	5.440	268.5	11.756	4.244
27.094	6.763	266.6	14.447	4.260
31.345	7.824	265.6	16.616	4.337
36.504	9.112	264.5	19.250	4.414

40% EtOH tartaric 40°C

$10^3\ m_1 = 2.133 \quad -E_1(\text{mV}) = 314.2$

$10^3\ m_2$	$10^3\ m_3$	$-E_1$ (mV)	10^31	$10^4\ K_1$
10.847	2.708	269.4	5.966	2.206
17.289	4.316	263.6	9.193	2.271
21.591	5.390	261.9	11.385	2.353
26.633	6.648	260.4	13.961	2.423
30.798	7.688	259.5	16.094	2.482
35.623	8.892	258.6	18.565	2.543

50% EtOH tartaric 35°C

$10^3\ m_1 = 1.801 \quad -E_1\ (\text{mV}) = 317.3$

$10^3\ m_2$	$10^3\ m_3$	$-E_1$ (mV)	$10^3\ I$	$10^6\ K_2$
5.238	4.199	180.2	10.154	4.793
7.715	6.185	174.4	15.552	5.638
9.960	7.984	171.0	20.418	6.066
12.156	9.744	169.2	25.258	6.213
14.637	11.733	168.5	30.467	6.714
16.662	13.357	168.0	34.785	6.989

40% EtOH phthalic 30°C

$10^3\ m_1 = 2.016 \quad -E_1\text{mV}) = 307.6$

$10^3\ m_2$	$10^3\ m_3$	$-E_1$ (mV)	$10^3\ I$	$10^4\ K_1$
7.84	2.616	285.0	8.259	30.952
11.97	3.992	284.6	12.299	30.362
16.05	5.352	285.9	16.345	29.855
19 94	6.651	287.7	20.225	29.560
23.63	7.882	289.4	23.992	29.197
26.99	9.002	291.1	27.263	29.089

60% EtOH phthalic 40°C

$10^3\ m_1 = 2.218 \quad -E_1(\text{mV}) = 217.9$

$10^3\ m_2$	$10^3\ m_3$	$-E_1$ (mV)	$10^3\ I$	$10^3\ K_2$
9.09	3.79	92.0	21.969	2.447
13.95	5.81	97.1	34.752	2.868
17.98	7.49	99.2	45.306	3.126
22.15	9.23	100.2	56.136	3.392
26.09	10.87	100.7	66.344	3.632
29.66	12.36	101.0	75.545	3.836

10% EtOH phthalic 55°C

$10^3\ m_1 = 1.983 \quad -E1(\text{mV}) = 280.9$

$10^3\ m_2$	$10^3\ m_3$	$-E_1$ (mV)	$10^3\ I$	$10^4\ K_2$
8.09	2.697	273.4	8.819	64.579
12.25	4.087	276.0	12.890	65.903
15.61	5.202	278.3	16.211	65.939
19.04	6.348	280.6	19.623	66.645
22.61	7.535	283.1	23.172	66.825
26.23	8.742	285.6	26.787	66.902

Table 2
pK_1 and pK_2 values of the studied acids in solvents of different compositions and at different temperatures

wt% EtOH	pK_1						pK_2					
	30°C	35°C	40°C	45°C	50°C	55°C	30°C	35°C	40°C	45°C	50°C	55°C
Maleic												
0	1.97 ± 0.01	1.95 ± 0.01	1.93 ± 0.05	1.90 ± 0.03	1.87 ± 0.02	1.85 ± 0.02	6.24 ± 0.03	6.28 ± 0.03	6.29 ± 0.04	6.30 ± 0.04	6.30 ± 0.03	6.31 ± 0.01
10	2.08 ± 0.01	2.06 ± 0.05	2.07 ± 0.06	2.02 ± 0.09	2.01 ± 0.07	2.00 ± 0.01	6.46 ± 0.01	6.61 ± 0.02	6.63 ± 0.01	6.65 ± 0.02	6.75 ± 0.02	6.86 ± 0.02
30	2.26 ± 0.04	2.00 ± 0.02	1.98 ± 0.02	1.98 ± 0.04	1.93 ± 0.03	2.00 ± 0.06	7.02 ± 0.04	7.14 ± 0.04	7.24 ± 0.06	7 35 ± 0.02	7 44 ± 0.02	7.46 ± 0.01
40	2.42 ± 0.01	2.01 ± 0.02	2.01 ± 0.04	1.99 ± 0.04	1.95 ± 0.06	1.96 ± 0.08	7.67 ± 0.04	7.69 ± 0.03	7.72 ± 0.03	7.74 ± 0.05	7.75 ± 0.09	7.76 ± 0.02
50	2.65 ± 0.02	2.62 ± 0.03	2.60 ± 0.02	2.61 ± 0.06	2.59 ± 0.06	2.56 ± 0.06	8.05 ± 0.03	8.09 ± 0.02	8.11 ± 0.01	8.12 ± 0.02	8.13 ± 0.06	8.15 ± 0.06
60	2.70 ± 0.01	2.67 ± 0.01	2.66 ± 0.05	2.64 ± 0.01	2.63 ± 0.01	2.70 ± 0.01	9 05 ± 0.01	9.07 ± 0.02	9.08 ± 0.01	9.14 ± 0.02	9.14 ± 0.01	9.19 ± 0.00
Tartaric												
0	3.08 ± 0.00	3.03 ± 0.00	3.01 ± 0.01	3.00 ± 0.02	2.97 ± 0.02	2.93 ± 0.03	4.38 ± 0.01	4.37 ± 0.02	4.38 ± 0.00	4.40 ± 0.02	4.40 ± 0.03	4.45 ± 0.02
10	3.40 ± 0.01	3.39 ± 0.00	3.36 ± 0.00	3.32 ± 0.00	3.31 ± 0.01	3.30 ± 0.01	4.49 ± 0.02	4.49 ± 0.01	4.53 ± 0.01	4.56 ± 0.00	4.61 ± 0.01	4.63 ± 0.00
30	3.60 ± 0.02	3.56 ± 0.01	3.52 ± 0.01	3.50 ± 0.01	3.48 ± 0.01	3.44 ± 0.02	4.75 ± 0.01	4.83 ± 0.01	4.89 ± 0.00	4.90 ± 0.00	4.93 ± 0.01	4.94 ± 0.01
40	3.82 ± 0.01	3.80 ± 0.01	3.76 ± 0.01	3.71 ± 0.01	3.66 ± 0.01	3.61 ± 0.01	5.06 ± 0.01	5.23 ± 0.02	5.33 ± 0.02	5.34 ± 0.04	5.35 ± 0.02	5.43 ± 0.06
50	4.13 ± 0.01	4.11 ± 0.01	4.04 ± 0.01	3.98 ± 0.04	3.96 ± 0.01	3.87 ± 0.02	5.32 ± 0.01	5.49 ± 0.02	5.58 ± 0.01	5.65 ± 0.05	5.70 ± 0.03	5.73 ± 0.01
60	4.40 ± 0.01	4.38 ± 0.01	4.38 ± 0.01	4.33 ± 0.01	4.30 ± 0.01	4.30 ± 0.01	8.17 ± 0.08	8.19 ± 0.06	8.24 ± 0.07	8.26 ± 0.07	8.26 ± 0.07	8.30 ± 0.07
Phthalic												
0	2.98 ± 0.00	3.25 ± 0.01	3.28 ± 0.01	3.29 ± 0.00	3.27 ± 0.03	3.27 ± 0.02	5.22 ± 0.00	5.24 ± 0.03	5.25 ± 0.01	5.27 ± 0.02	5.28 ± 0.00	5.34 ± 0.02
10	3.13 ± 0.03	3.13 ± 0.02	3.15 ± 0.01	3.15 ± 0.01	3.16 ± 0.01	3.16 ± 0.01	5.76 ± 0.01	5.78 ± 0.01	5.80 ± 0.02	5.83 ± 0.01	5.85 ± 0.03	5.89 ± 0.01
30	3.18 ± 0.01	3.28 ± 0.02	3.28 ± 0.02	3.33 ± 0.03	3.32 ± 0.01	3.36 ± 0.03	6.66 ± 0.03	6.68 ± 0.02	6.66 ± 0.02	6.74 ± 0.01	6.76 ± 0.06	6.77 ± 0.01
40	3.48 ± 0.03	3.46 ± 0.03	3.46 ± 0.01	3.44 ± 0.01	3.46 ± 0.04	3.47 ± 0.01	7.08 ± 0.02	7.08 ± 0.05	7.07 ± 0.04	7.14 ± 0.03	7.16 ± 0.02	7.17 ± 0.02
50	3.51 ± 0.01	3.53 ± 0.01	3.54 ± 0.03	3.50 ± 0.02	3.59 ± 0.01	3.60 ± 0.01	7.37 ± 0.01	7.36 ± 0.01	7.33 ± 0.01	7.32 ± 0.02	7.30 ± 0.03	7.41 ± 0.05
60	3.71 ± 0.02	3.72 ± 0.01	3.73 ± 0.01	3.75 ± 0.01	3.75 ± 0.02	3.77 ± 0.02	7.93 ± 0.01	7.94 ± 0.01	7.83 ± 0.03	8.02 ± 0.01	7.94 ± 0.01	7.69 ± 0.01

where A and B are empirical constants. According to this empirical correlation as ΔS_2°, for the second ionization reaction, decreases and becomes more negative by solvation from certain acid to another in the series (according to its structure and the interaction of its dicarboxylate anion with the solvent molecules), 'r' decreases consequently. This behaviour can be explained on the basis that solvent molecules in the neighbourhood of the dicarboxylate anion of this acid are acted upon by strong electrostatic forces which restrict their freedom of motion and in the same time such solvent molecules interact with its carboxylate groups causing the decrease of its 'r' value. Thus, this empirical correlation can throw light on the structural variations existing among these acids and their effects on the mode of acid dissociation.

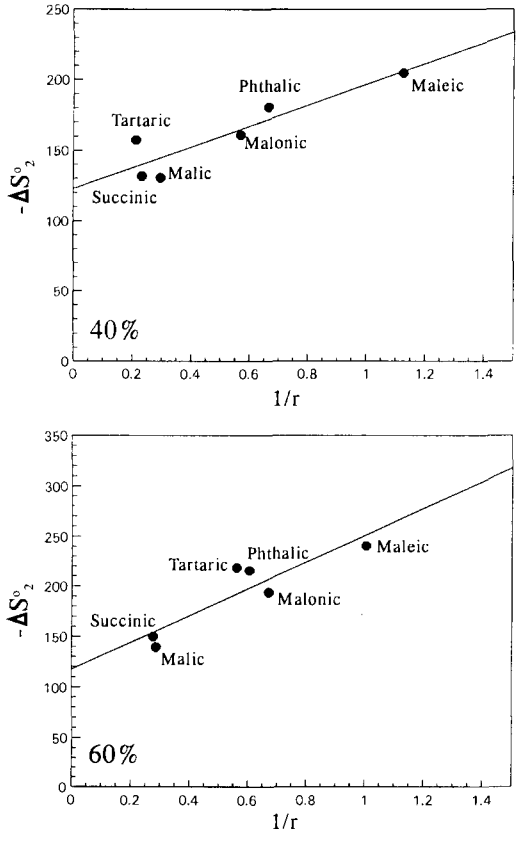

Fig. 1. $-\Delta S_2^\circ - 1/r$ correlation for the second dissociation reaction of dicarboxylic acids in different solvent compositions.

5. Thermodynamics of acid dissociations

The thermodynamic functions for the first and second ionization processes were evaluated from the well-known thermodynamic relations. The plot of pK_1 (or pK_2) versus 1/T gave a straight line for each dicarboxylic acid, which shows that ΔH_1° and ΔH_2° may be treated as sensibly constant over the temperature range studied. The values of these thermodynamic functions for both ionization processes at 40°C are shown in Table 3 together with the respective estimates of the errors while their variation with the mole fraction of ethyl alcohol is shown in Fig. 2 (representative figure for the variation with respect to tartaric and maleic acids). It can be seen from Table 3 and Fig. 2 that ΔG_1° and ΔG_2° have positive values which indicates the preferential stabilization of H_2L in the first dissociation process and of the species HL^- in the second dissociation process, by the mixed solvent. These positive values of ΔG°, for both dissociation processes increase with the increasing of organic content of the solvent mixture. This trend is consistent with the effect of the lowered dielectric constant of the mixed solvent and it is caused by the increase of the electrostatic free energies of the ions produced in the dissociation process. It is interesting to note that the standard entropy of dissociation of these acids becomes steadily more negative with increasing the proportion of ethanol in the solvent mixture as opposed to pure water [21] (except ΔS_1° of maleic acid which showed a maximum). The qualitative explanations of this trend is that the ethyl alcohol–water mixtures are less structured than pure water [21], hence, the species (such as H^+, HL^- and L^{2-}) will orient solvent molecules to a greater extent in ethyl alcohol–water media. Consequently, this greater degree of orientation results in a more negative entropy of dissociation. A useful comparison can be made with the ΔS_1° values for the present work and those obtained for the dicarboxylic acids of ref. [15] (at the same mixed solvents) from which the negative value of ΔS_1° was found to increase in the order: Maleic < Malonic < Tartaric < Malic < Succinic < Phthalic. This trend is primarily because of the electrostatic action on the carboxylic groups, transmitted through CH_2-

Table 3
Thermodynamic parameters for first and second dissociation constants in mixed solvents of variable compositions at 40°C (ΔH°, ΔG° in kJ mol^{-1} and ΔS° in J mol^{-1} K^{-1})

Wt% EtOH	Acid	Tartaric	Maleic	Phthalic	Acid	Tartaric	Maleic	Phthalic
0	ΔH_1°	2.40 ± 0.03	1.93 ± 0.02	−3.10 ± 0.03	$-\Delta H_2^\circ$	18.62 ± 0.04	4.31 ± 0.01	11.53 ± 0.04
	ΔG_1°	18.02 ± 0.05	11.56 ± 0.29	19.65 ± 0.06	ΔG_2°	26.26 ± 0.02	37.72 ± 0.24	31.50 ± 0.06
10	ΔS_1°	49.9 ± 0.2	30.8 ± 0.9	72.7 ± 0.3	$-\Delta S_2^\circ$	143.3 ± 0.2	134.2 ± 0.8	137.4 ± 0.3
	ΔH_1°	2.72 ± 0.04	2.93 ± 0.03	−6.89 ± 0.01	$-\Delta H_2^\circ$	18.37 ± 0.06	10.81 ± 0.12	13.57 ± 0.04
	ΔG_1°	20.21 ± 0.01	12.44 ± 0.36	18.88 ± 0.11	ΔG_2°	27.17 ± 0.03	39.77 ± 0.06	34.78 ± 0.12
	$-\Delta S_1^\circ$	55.8 ± 0.1	30.4 ± 1.2	82.3 ± 0.3	$-\Delta S_2^\circ$	145.4 ± 0.2	161.5 ± 0.4	154.4 ± 0.5
31	ΔH_1°	3.10 ± 0.05	3.51 ± 0.11	−7.69 ± 0.06	$-\Delta H_2^\circ$	18.56 ± 0.07	13.46 ± 0.16	15.19 ± 0.05
	ΔG_1°	21.11 ± 0.06	11.86 ± 0.12	19.63 ± 0.12	ΔG_2°	29.33 ± 0.01	43.38 ± 0.36	39.95 ± 0.12
	$-\Delta S_1^\circ$	57.5 ± 0.2	26.7 ± 0.5	87.3 ± 0.6	$-\Delta S_2^\circ$	152.9 ± 0.2	181.5 ± 1.3	176.1 ± 0.5
40	ΔH_1°	3.66 ± 0.08	1.68 ± 0.17	−11.87 ± 0.01	ΔH_2°	17.31 ± 0.12	17.82 ± 0.03	14.11 ± 0.04
	ΔG_1°	22.57 ± 0.03	11.93 ± 0.24	20.73 ± 0.06	ΔG_2°	31.93 ± 0.12	46.27 ± 0.18	42.41 ± 0.24
	$-\Delta S_1^\circ$	60.4 ± 0.3	32.7 ± 0.9	104.1 ± 0.2	$-\Delta S_2^\circ$	157.3 ± 0.5	204.7 ± 0.6	180.5 ± 0.9
50	ΔH_1°	3.34 ± 0.09	6.85 ± 0.03	−15.51 ± 0.04	$-\Delta H_2^\circ$	17.05 ± 0.14	15.12 ± 0.03	17.38 ± 0.04
	ΔG_1°	24.20 ± 0.05	15.56 ± 0.12	21.20 ± 0.18	ΔG_2°	33.47 ± 0.06	48.63 ± 0.06	43.93 ± 0.06
	$-\Delta S_1^\circ$	66.7 ± 0.3	27.8 ± 0.4	117.2 ± 0.7	$-\Delta S_2^\circ$	161.3 ± 0.5	203.6 ± 0.2	195.8 ± 0.3
60	ΔH_1°	4.30 ± 0.04	8.62 ± 0.03	−16.85 ± 0.02	$-\Delta H_2^\circ$	18.99 ± 0.04	20.82 ± 0.05	20.46 ± 0.11
	ΔG_1°	26.26 ± 0.05	15.97 ± 0.29	22.35 ± 0.06	ΔG_2°	49.37 ± 0.42	54.46 ± 0.06	46.96 ± 0.18
	$-\Delta S_1^\circ$	69.3 ± 0.2	23.5 ± 0.9	125.2 ± 0.3	$-\Delta S_2^\circ$	218.3 ± 1.3	240.4 ± 0.2	215.3 ± 0.9

groups (malonic and succinic) and its hydroxy substituents (malic and tartaric) and is also due to the conjugation effects of maleic and phthalic acids. Moreover, the electrostatic action transmitted through solvent molecules (field effect) also governs these types of interactions and the charged anions of these acids impose order on the surrounding solvent molecules, which in turn interfere with the internal rotation of the alkyl chain of the acid and hence the partial molal entropies of the anions become smaller (relative to the neutral acid), thus ΔS_1° should become correspondingly more negative as the length of the alkyl chain increases, and hence ΔS_1° value of succinic acid is more negative than that of malonic acid which is of smaller chain length. The higher negative ΔS_1° value of succinic acid compared with malic and tartaric acids (same alkyl chain length) can be largely attributed to the hydrogen bonding which mainly exists in malic and tartaric acids. This effect causes a lowering in the basicity of both malate and tartrate mono anions with subsequent decrease of solvation and correspondingly less negative ΔS_1° values compared with succinic acid. The higher conjugation effect acting in the phthalate mono anion compared with maleate mono anion causes more basicity to the former (higher pK_1). Accordingly, the extent of ion solvation should be higher in phthalate mono anion than that of maleate mono anions and consequently, the negative ΔS_1° value of phthalate is the higher, in accordance with the results obtained.

The profile of ΔH° (and ΔS°) mole fraction curves predicts that a compensation effect may be exist between ΔH° and ΔS°. The true explanation of this compensation effect must lie in terms of solvent–solute interaction. Any effect, for example that leads to a stronger binding between the solute species and solvent molecules will lower the enthalpy, it also will lower entropy by restricting the freedom of vibration and rotation of the solvent. Application of more exact theories to these effects leads to the result that they generally will give rise to a fairly exact compensation.

An extrathermodynamic analysis has been examined in the light of ΔH°–ΔS° relationship at different experimental conditions. Fig. 3 repre-

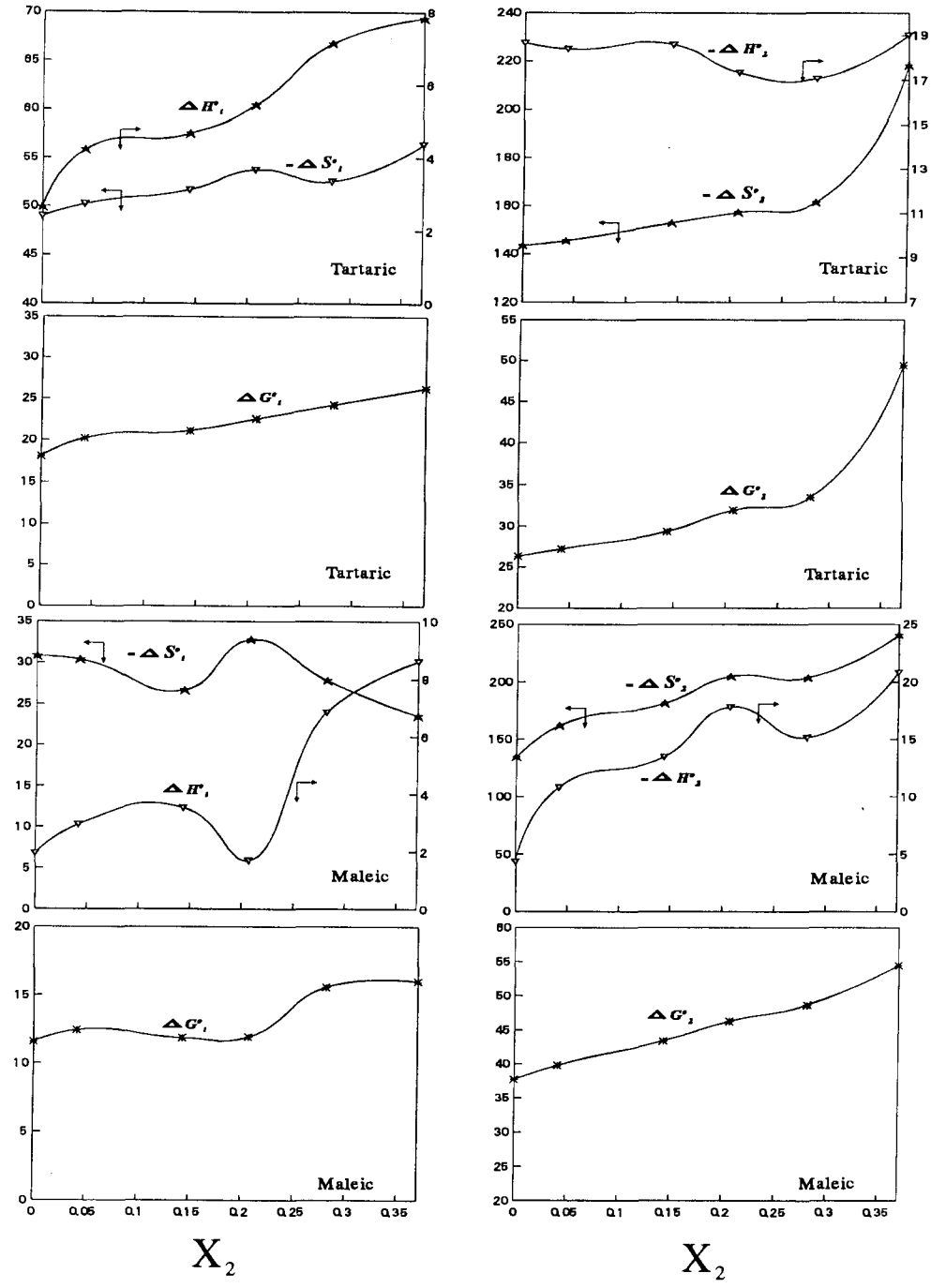

Fig. 2. Variation of ΔG°, ΔH° & $-\Delta S^{\circ}$ with the mole fraction of ethyl alcohol for tartaric and maleic acids at 40°C

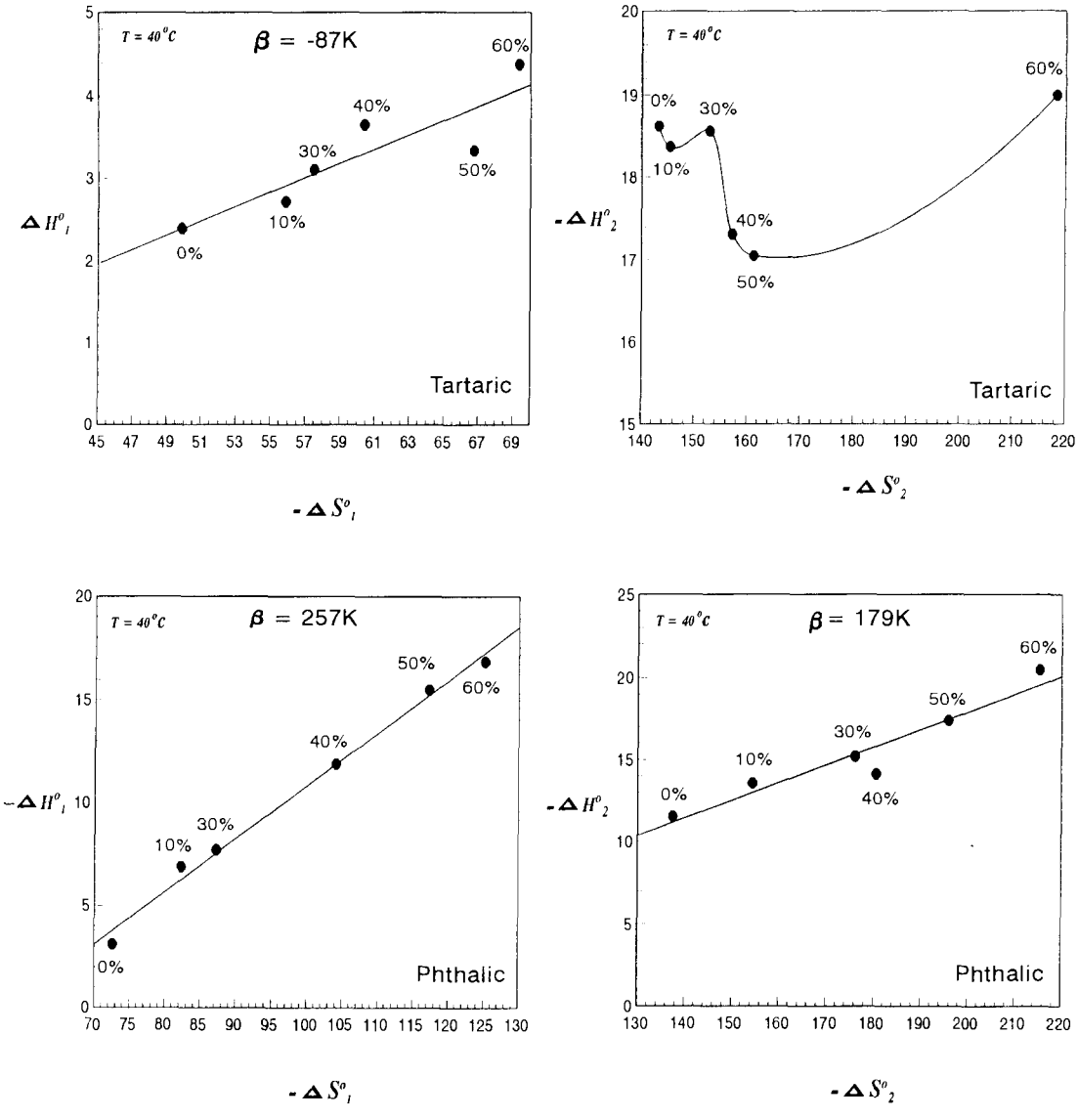

Fig. 3. Isoequilibrium plots for the first and second dissociation reactions of phthalic and tartaric acids.

sents this correlation for tartaric and phthalic acids. This correlation was found to be linear in all cases except for the second dissociation reaction of tartaric acid. Moreover all the linear plots were of positive slopes except the case of tartaric acid (first dissociation process) which gave a negative slope. This abnormal ΔH°–ΔS° behaviour is expected since the most baffling problem in the field of enthalpy–entropy relationship is the interpretation in mixed solvents. Such relationships may be described as approximately linear, as hook shaped and as N-shaped [22]. The value of the positive slope (β/K) obtained in case of both dissociation reactions of maleic and phthalic acids was found to be lower than the experimental temperature indicating

that these dissociation reactions are of entropy controlled type reactions [23] in which the solute solvent interactions play an important role. The negative sign of β (tartaric first dissociation) was observed before by Winstein [24] and was attributed to the complexity of ΔH and ΔS variation with the mole fraction of the organic solvent. This treatment based on the classification of ΔH-ΔS variations into three classes: A, B and C. For class A, both ΔH and ΔS increase; for class B, ΔH decreases while ΔS increases; for C class, both ΔH and ΔS decrease. For classes A and C, the sign of $\delta(\Delta H)/\delta(\Delta S)$ is positive while for class B, the sign is negative. The sign of $\delta\Delta H/\delta\Delta G$ for the three classes A, B and C are $-$, $+$, $+$ while for $\delta\Delta G/\delta\Delta S$ they are $-$, $-$, $+$. Applying the above classification to the present work, the negative sign of β, in case of the first dissociation of tartaric acid, can be now interpreted in term of class B which require further extrathermodynamic analysis of $\Delta G^\circ - \Delta H^\circ$ and $\Delta G^\circ - \Delta S^\circ$ plots, where the signs of their slopes confirm the above requirements for class B (the sign of $\delta\Delta G/\delta\Delta S$ is negative and the sign of $\delta\Delta G/\delta\Delta H$ is positive). Moreover, it is confirmed from such plots that both dissociation reactions of phthalic acid and the second dissociation reaction of maleic acid are belonged to class A, while the first dissociation reaction of maleic acid is of C class. Fig. 4 and Fig. 5 are representative figures for $\Delta G^\circ - \Delta H^\circ$ and $\Delta G^\circ - \Delta S^\circ$ linear correlations in which Fig. 4 represents $\Delta G^\circ - \Delta H^\circ$ correlation for phthalic acid while Fig. 5 represents $\Delta G^\circ - \Delta S^\circ$ correlation for phthalic and maleic acids. Such correlations were predicted in advance as did various electrostatic models for ion-solvent interactions [25,26].

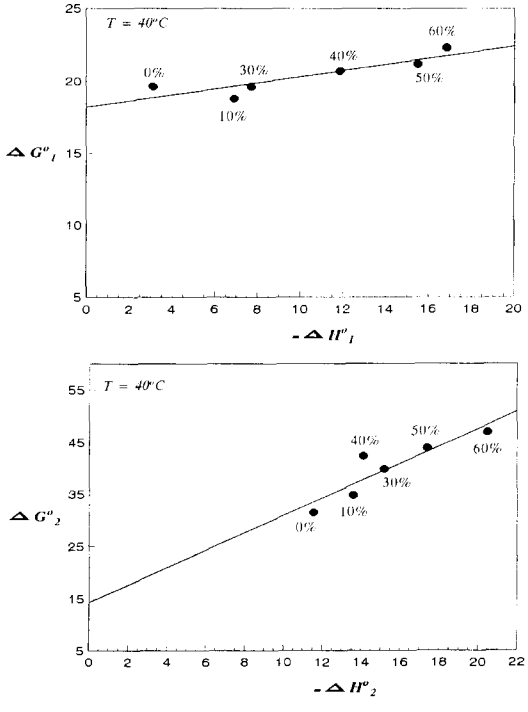

Fig. 4. $\Delta H^\circ - \Delta G^\circ$ correlation for first and second dissociation reactions of phthalic acid.

It was pointed out that if ΔG° and ΔS° are linearly related, it also follows that a linear relation between ΔH° and ΔS° exists, which is verified in most cases of the present work.

It is interesting to test the isoequilibrium correlation among different dicarboxylic acids at fixed solvent compositions. This correlation is shown in Fig. 6 which represents the variation of ΔH_2° with ΔS_2° (ΔH_2° and ΔS_2° values of malic, malonic and succinic acids were taken from ref. [15]). It is clear from Fig. 6 that the correlation is linear in all solvent compositions. It is well known that small changes in the dissociation constants for a series of acids of a common type may arise from parallel changes in ΔH° and ΔS° values which leads to linear relationship between them over a wide range of values for a series. Such parallelism between $\Delta(\Delta H^\circ)$ and $\Delta(\Delta S^\circ)$ among the studied acids at fixed solvent composition for the second dissoci-

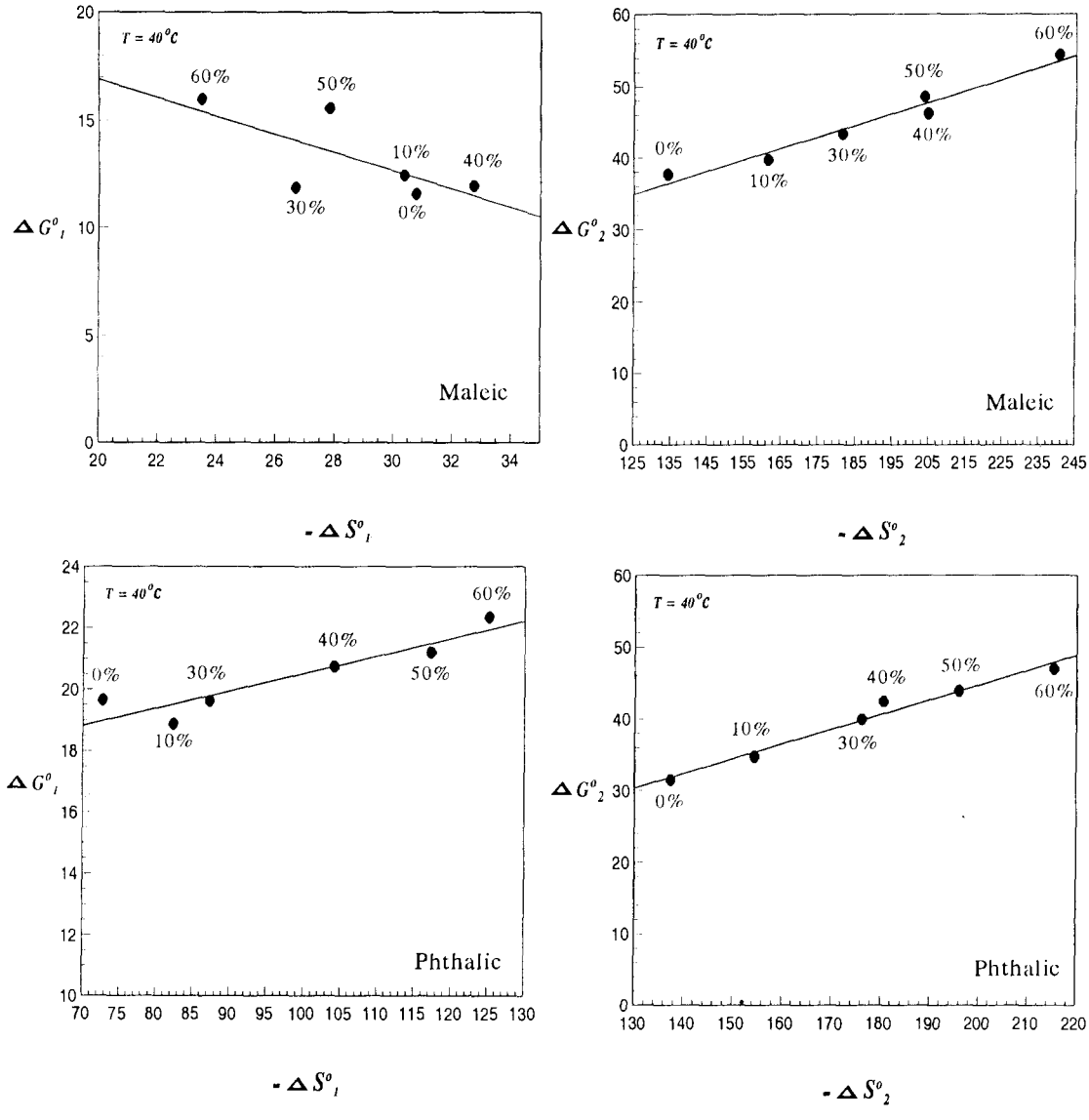

Fig. 5. $\Delta G^\circ - \Delta S^\circ$ correlation for the first and second dissociation reactions of maleic and phthalic acids.

ation reactions corroborates the suggestion that the dissociation reactions of these acids are similar. The isoequilibrium temperature values at different solvent compositions confirm that these reactions are of entropy controlled type except that of 0% composition which is enthalpic controlled one. This correlation was found to be very weak for the first dissociation reaction.

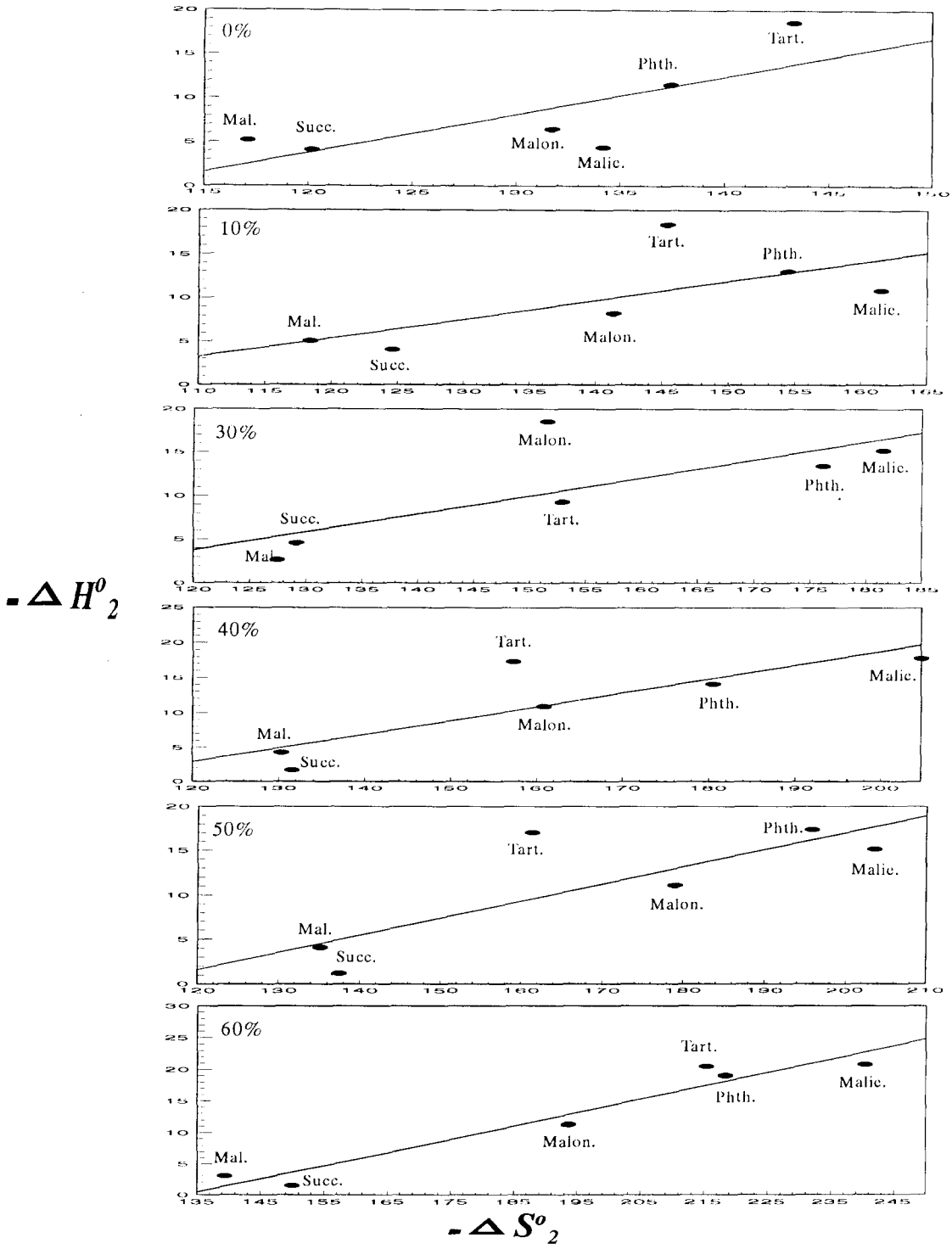

Fig. 6. Isoequilibrium plots for the second dissociation reactions of dicarboxylic acids for different solvent compositions at 40°C

References

[1] M. Mandel, P. Decroly, Trans. Faraday Soc. 56 (1960) 29.
[2] E.F. Calldin, Chem. Rev. 69 (1969) 135.
[3] L.P. Hammet, 1970. Ph. Org. Chem., 2nd edn. McGraw-Hill, New York.
[4] R.P. Bell, 1973. The proton in Chemistry, 2nd edn. Chapman and Hall, London.
[5] W.J. Albery, Ann. Rev. Phys. Chem. 31 (1980) 227.
[6] R.W. Taft, Prog. Phys. Org. Chem. 14 (1982) 247.
[7] C.B. Monk, M.F. Amira, J. Chem. Soc. Faraday Trans. 1 (74) (1978) 1170.
[8] C.B. Monk, M.F. Amira, J. Chem. Soc. Faraday Trans. 76 (1980) 1773.
[9] M.F. Amira, Sh.A. El-Shazly, M.M. Khalil, Thermochim. Acta 115 (1987) 1.
[10] M.T. Mohamed, A.A. Zaghloul, M.F. Amira, Bull. Fac. Sci., Alex. Univ. 31 (B) (1991) 116.
[11] Y. Kondo, W. Sugitani, M. Tokui, J. Chem. Soc. Faraday Trans. 88 (20) (1992) 3019.
[12] G. Papanastasiou, I. Ziogas, Talanta 36 (1989) 977.
[13] J. Barbosa, J.L. Bltran, V. Sanz-Nebot, Anal. Chim. Acta 288 (1994) 271.
[14] A.A. Zaghloul, Afinidad 462 (1996) 123.
[15] A.A. Zaghloul, G.A. El-Naggar, M.F. Amira, Gazz. Ital. 126 (1996) 735.
[16] P.S. Danniel, T.M. Hildebrand, J. Am. Chem. Soc. 44 (1922) 2824.
[17] A. Zielen, J. Phys. Chem. 67 (1963) 1474.
[18] B.M. Low, D.G. Smith, J. Chem. Soc., Faraday Trans. I 69 (1973) 1939.
[19] M. Born, Z. Phys. 1 (1920) 45.
[20] J. Bjerrum, G. Schwarzenbach, L.G. Sillen, 1957. Stability Constants, Chemical Society, London.
[21] E.J. King, J. Am. Chem. Soc. 73 (1951) 155.
[22] H.S. Venkacaraman, C.N. Hinshelwood, J. Chem. Soc., 4986 (1960).
[23] J.E. Leffler, E. Grunwald, Rates and Equilibria of Organic Reactions, Wiley, New York (1963).
[24] S. Winstein, A.H. Fainberg, J. Am. Chem. Soc. 79 (1957) 5937.
[25] E.J. King, Acid-Base Equilibria, Pergamon Press, New York, 1965.
[26] J.J. Christensen, R.M. Izatt, L.D. Hansen, J. Am. Chem. Soc. 89 (1967) 213.

ELSEVIER

Talanta 45 (1997) 203-211

Talanta

Sensitive detection and semiquantitative determination of mercury(II) and lead(II) in aqueous media using polyurethane foam immobilized 1,5-di-(2-fluorophenyl)-3-mercaptoformazan

A.M. Kiwan [a], M.S. El-Shahawi [a,*], S.M. Aldhaheri [a], M.H. Saleh [b]

[a] *Department of Chemistry, Faculty of Science, UAE University, P.O. Box: 17551, Al-Ain, United Arab Emirates*
[b] *Ministry of Health, P.O. Box: 841, Abu Dhabi, United Arab Emirates*

Received 31 January 1997; received in revised form 8 April 1997; accepted 15 April 1997

Abstract

1,5-Di-(2-fluorophenyl)-3-mercaptoformazan (F_2H_2Dz) immobilized and plasticized with tri-n-butylphosphate (TBP) polyurethane foam (PUF) were found suitable for the detection of mercury(II) and lead(II) in extremely dilute aqueous solutions. In batch mode of extraction with immobilized F_2H_2Dz-foam as low as 0.05 and 0.15 μg ml^{-1} of mercury(II) and lead(II), respectively were detected and the colored chelates were found more stable over 72 h. Lower concentrations of these metal ions (≤ 1 ppb) were detected by plasticized F_2H_2Dz-TBP foam packed in column extraction mode. Semiquantitative determination of these metals was also possible using a suitable standard color scale. The effect of diverse ions on the detection of 1 μg mercury(II) and lead(II) by the proposed F_2H_2Dz-foam test was critically investigated. The method was satisfactorily applied for the detection of mercury(II) or lead(II) in natural water samples. © 1997 Elsevier Science B.V.

Keywords: Polyurethane foam; 1,5-Di-(2-fluorophenyl)-3-mercaptoformazan; Mercury(II); Lead(II) detection

1. Introduction

The toxicity of mercury and lead is attributed to their harmful effects on the central nervous system disturbing haem synthesis as well as for causing neuropsychiatric disorders [1,2]. Lead and its compounds have an important role in many industries where small amounts of it are ingested and/or inhaled regularly with food and drink [3,4]. Mercury is a toxic element sparsely distributed in the lithosphere and water where its average concentrations range from 0.08 and 0.80 ppm in igneous and sedimentary rocks, respectively [5]. Natural soils have been found to contain mercury in the range 0.01–0.50 ppm [5].

Dithizone (H_2Dz) reacts with many metals and organometallic ions to form highly colored complexes which are insoluble in water but can be extracted into organic solvents [6–8]. Although this reagent is a sensitive analytical reagent for many metal ions, it is not selective in neutral or

* Corresponding author. Department of Chemistry, Faculty of Science at Damiatta, Mansoura University, Damiatta, Egypt.

PII S0039-9140(97)00120-3

alkaline media. However, its selectivity is enhanced by controlling the pH values, and/or by adding suitable complex forming agents (masking agents) to the aqueous solution [6] and by introducing various substituents in its phenyl rings [7].

The pioneering studies of Braun and Farag [9] on the application of PUF sorbents to trace elements led to the revealing of the potentialities of their special geometrical form: spherical membrane-shaped geometry and to the proposal of their general use in column operations as a substitute for the traditional granular supports in extraction chromatography [9,10]. Open cell PUF immobilizing or anchoring specific chromogenic organic reagents (chromofoams) have been successfully employed for the sensitive detection and semiquantitative determination and collection of several metal ions including Pb^{2+} and Hg^{2+} ions [10–16]. No work has been yet reported on the application of polyurethane foam immobilizing 1,5-di-(2-fluorophenyl)-3-mercaptoformazan, (F_2H_2Dz) for the detection and quantitative collection of mercury(II) and lead(II) in aqueous media. Accordingly, the use of immobilized-polyurethane foam is described here for simple, rapid, and sensitive detection of trace concentrations of mercury and lead.

2. Experimental

2.1. Reagents and materials

All chemicals used were of Analytical Reagent Grade. Open cell polyether based polyurethane foam was supplied by K.G. Schaum (Stoffwerk, Kremsmunster, Austria). Foam cubes of approximately 1 cm^3 were cut from polyurethane foam sheet. The foam material (cubes of ca. 5 mm edge) was washed and dried as previously reported [10]. Stock solutions containing 1.00 mg ml^{-1} of mercury and lead were prepared by dissolving the appropriate amounts of mercury(II) chloride and lead(II) nitrate in deionized water slightly acidified with nitric acid and standardized by EDTA titration. BDH tributylphosphate (TBP) was used without further purification. Series of standard mercury and lead solutions were prepared by dilution with water acidified with few drops of 1 M nitric acid solution.

2.2. Synthesis of 1,5-di-(2-fluorophenyl)-3-mercaptoformazan, (F_2H_2Dz)

The reagent 1,5-di(2-fluorophenyl)-3-mercaptoformazan was prepared by the nitroformazyl method as described elsewhere [7]. The reagents F_2H_2Dz and H_2Dz solutions were prepared separately by dissolving 0.02 g of each reagent in 100 ml dichloromethane. These solutions were kept refrigerated prior to use under acidified aqueous solutions containing 0.2 M sulphuric acid and 0.1 M sodium sulphite. The foam cubes were loaded with F_2H_2Dz or H_2Dz in the presence of sulphur dioxide and were dried as reported by Braun and Farag [11]. The plasticized F_2H_2Dz-TBP or H_2Dz-TBP foams were prepared by mixing the dried foam cubes with the reagents in TBP (0.1% w/v) with efficient stirring for 15 min and dried as reported [11].

2.3. Apparatus

A Shimadzu double beam UV-visible scanning spectrophotometer model UV-2101 PC with 1 cm stoppered quartz cells and a Shimadzu FTIR-8101 Fourier Transform infrared spectrophotometer were used. An Orion pH-meter and glass columns (15 cm height × 10 mm I.D.) were also used.

2.4. General procedures

2.4.1. Batch experiments

To examine the uptake of mercury(II) and lead(II) on 1,5-di(2-fluorophenyl)-3-mercaptoformazan-loaded or plasticized F_2H_2Dz-TBP treated foam, one reagent-loaded foam cube is mixed and shaken with 2–3 ml of the test solution for 2–3 min. A color change of the foam from green to orange-red or pink in the presence of mercury and lead was observed, respectively. For the semiquantitative determination of mercury and lead, a foam color scale is prepared from a series of standard solutions with different concentration of

Table 1
Characteristic absorption i.r. (cm^{-1}) and electronic (nm) spectral data for the reagents F_2H_2Dz and H_2Dz and their mercury(II) and lead(II) chelates in KBr for discs[a]

Compound	Wave number, cm^{-1}					
	υ(N–H)	υ(N=N)	δ(N–H)+(C=N)	υ(N–C–S)	λ_{max} (nm)	$\epsilon \times 10^{-3}$ l mol^{-1} cm^{-1}
F_2H_2Dz	2950 (br)	2380 (w)	1510 (s)	1485 (s)	632	25.3
				1450 (s)	454	23.7
H_2Dz	2960 (br)	2365 (w)	1515 (s)	1505 (s)	615	35.8
				1465 (s)	454	17.9
		1620 (s)	1510 (m)	1490 (s)	484	64.8
$Hg(F_2HDz)_2$	3300 (m)	1590 (m)		1470 (cm)		
		3100 (w)	1540 (s)			
$Pb(F_2HDz)_2$	3340 cm					
	3290 (s)	1615 (s)				
	3085 (w)	1600 (s)	1520 (s)	1495 (s)	521	65.1
		1540 (s)		1475 (s)		
$Hg(HDz)_2$	3210 (cm)					
	3170 (br)	1600 (s)	1510 (s)	1505 (s)	485	71.0
		1570 (s)				
$Pb(HDz)_2$	3280 (m)	1610 (s)	1515 (s)	1510 (s)	518	69.05
	3180 (s)	1564 (vw)				

[a] s = strong, m = medium, w = weak, vw = very weak, sh = shoulder and br = broad.

each metal and the reagent F_2H_2Dz loaded-foam. The concentration of the unknown sample solution was determined by comparison to this scale under the same conditions.

2.4.2. Column experiments

One gram of the F_2H_2Dz-loaded or plasticized F_2H_2Dz-TBP foam in the presence of a acidified aqueous solution of sodium sulphate was homogeneously packed in a glass column by the vacuum method [9,12]. F_2H_2Dz-foam bed in the column was then covered with an acidified aqueous solution of sodium sulphite. A standard series of the metal ion (Hg^{2+} or Pb^{2+}) in 100 ml aqueous solutions at the optimum pH of complex formation was percolated through F_2H_2Dz loaded foam columns at flow rates of 2–3 ml min^{-1}. The aqueous solution of the unknown sample (100 ml) is then passed through the reagent foam column under identical experimental conditions. For the semiquantitative determination of Hg^{2+} or Pb^{2+}, the length of the resulting colored zone foam bed was compared to that of the standard series.

3. Results and discussion

Table 1 summarizes the characteristic infrared frequencies of the solid reagents F_2H_2Dz and H_2Dz along with their mercury(II) and lead(II) complexes. The electronic spectra of the reagents and their complexes with mercury(II) and lead(II) in dichloromethane and in parallelepiped polyurethane foams are also included in Table 1. The electronic spectra of the reagents in dichloromethane showed two well resolved absorption bands in the region of 445–448 and 609–615 nm, whereas their mercury(II) and lead(II) complexes showed well defined single bands in the range 484–521 with slight hypsochromic shift in polyurethane foams. In dichloromethane and polyurethane foams, the introduction of fluorine atoms into the ortho positions of the phenyl nuclei of dithizone leads to small bathochromic shifts in both its bands and also on the values of their relative molar absorptivities compared to dithizone (Table 1). The $\log\epsilon_1$, max decreased to 25.3×10^3 and the $\log\epsilon_2$

max is increased to 23.7×10^3 l mol^{-1} cm^{-1} of F_2H_2Dz compared to H_2Dz in dichloromethane. Since $Hg(HDz)_2$ was found to be tetrahedral [17], the corresponding complex of F_2H_2Dz is most likely tetrahedral.

Considerable interest has been focused on the use of the chromofoam test in batch and dynamic modes for the separation and preconcentration of different metal ions including Hg^{2+} and Pb^{2+} species from aqueous media [9–16]. The immobilization of water insoluble chelating agent within the solid foam combines the advantages of both liquid–liquid and liquid–solid extraction techniques [10]. The immobilized reagent foam combines both the selectivity of the chelating agent and the advantageous rapidity of kinetic process between metal ions in the aqueous solution and the reagent immobilized in the foam membranes [11].

3.1. Detection and semiquantitative determination of mercury(II) with 1,5-di-(2-fluorophenyl)-3-mercaptoformazan

In a weakly acidic solution (pH < 5), 1,5-di-(2-fluorophenyl)-3-mercaptoformazan forms an insoluble orange-red chelate with mercury(II) ions. The complex formed is readily extracted by organic solvents [7] without change in color. This reaction was employed with unloaded foam, F_2H_2Dz-loaded foam and F_2H_2Dz-TBP plasticized foams to detect mercury(II) in the aqueous solution. The reagent F_2H_2Dz is uniformally distributed within the foam cubes and acts as an efficient collector for the mercury(II) present in the aqueous media. The developed colored complex on the foam was easily observed.

On shaking one cube of the unloaded foam with the test solution mixture of the orange-red Hg $(F_2HDz)_2$ complex in a test tube, it was possible to detect as low as 0.15 ppm mercury. The sensitivity of the test was slightly improved to (0.10 ppm) and the color development was achieved in less than 1 min of shaking in the presence of acetate ions. This may be attributed to the ability of acetate ions to act as a coordinating ligand and form a quasi octahedral adduct in the large surface area and the bulk of the polyurethane foam as postulated in Fig. 1. Acetate anion is known to coordinate with the mercury(II) ions and form stable complexes [18,19] as indicated by the values of their stability constants (log $k_1 = 5.55$ and log $\beta_2 = 9.30$). Such unusual octahedral coordination of Hg(II) is known for a number of O-donor ligands [20]. The nitrogen of the urethane or oxygen of the ether linkage of the polyurethane foam under these conditions may also acts as a coordinating ligand towards mercury(II) ions producing a mixed ligand complex [21].

The detection of mercury(II) ions was improved further to 0.05 and 0.01 ppm by employing immobilizing F_2H_2Dz on polyurethane foam and plasticized F_2H_2Dz-TBP foam ion batch extraction mode, respectively. The color of the mercury complex was developed on the plasticized foam faster than in the case of the unplasticized foam where the tri-n-butylphosphate may act as a plasticizer on the foam. The color was also stable for more than 48 h. The plasticizer has a dual purpose [11,12], i.e. it acts as an efficient non-volatile solvent as well as a plasticizer for the foam itself.

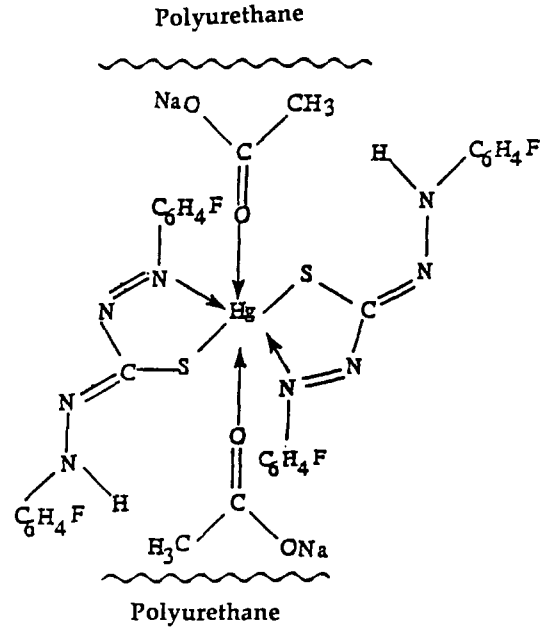

Fig. 1. A postulated structure of the mixed acetate F_2HDz-mercury(II) quasi complex on the polyurethane foam.

Table 2
Comparative sensitivity of batch F_2H_2Dz (a) and H_2Dz (b) for the detection of mercury(II) ions employing polyurethane foams

Method	Amount of Hg^{2+} detected (ppm)		Reference
	(a)	(b)	
Spot test on spot plate	—	5.0	Feigl and Anger, 1972
Unloaded foam in the absence of acetate ions	0.15[a]	0.25[a]	
Unloaded foams in the presence of acetate ions	0.10[a]	0.20	Farag et al., 1987
Immobilized reagent foam in the presence of acetate ions	0.05[a]	0.10	Abou-Elmaty, 1990
Plasticized TBP-reagent foam	0.01[a]	0.10	Abou-Elmaty, 1990

[a] Present work.

This modification increases the mobility of the molecular segments and decreasing the glass transition temperature (Tg) of the system [11]. The mobility of plasticizer molecules within the polymeric network above the Tg is quite high and the individual plasticizer molecules have varying degrees of mobility within the foam matrix [11]. Therefore, the preconcentration and the diffusion rates of chemical species through the micropores and the quasi-spherical membrane structures of the plasticized foam material were found higher than with the unplasticized foams. Obviously, these results (Table 2) are much better than those reported with dithizone [22,23] and the conventional spot test [24].

In aqueous media, the diffusion of mercury(II) species into the micropores of the foam membranes is possibly consistent with the solubility of the $Hg(F_2HDz)$ complex as previously reported for $HFeX_4$ and $HAuX_4$ [25]. The retention of mercury(II) ions on F_2H_2Dz-TBP loaded foams may involve three steps: bulk transport of solute in solution, film transfer involving diffusion of solute through a hypothetical film boundary and diffusion of the solute with the pore volumes of the adsorbent and along pore-wall surfaces to active adsorption sites as reported for cobalt(II) retained on 2-thenoyltrifluoroacetone impregnated on polyurethane foam [26]. Thus, in the TBP-foam, the film and the intraparticle transport are the major factors controlling rates of retention of mercury(II) from solutions by porous sorbents.

The color intensity on the F_2H_2Dz-foam was found to depend on the concentration of mercury(II) in the aqueous solution. Thus a semiquantitative determination of mercury(II) was found possible by comparing the color of the test solution with a standard color scale of the foam cubes prepared with 0.1, 0.5, 1, 5, 10 and 15 ppm mercury(II) in aqueous solution. The proposed foam method was examined for the detection of mercury(II) in natural water spiked with mercury(II) ions and satisfactory results were obtained.

Moreover, the proposed F_2H_2Dz-foam reagent was easily packed in a column for quantitative collection and semiquantitative determination of mercury(II) in extremely dilute aqueous solution. This was achieved by percolating 100 ml of the test solution through the foam column at 2–3 ml min^{-1} flow rate. It was found possible to detect as low as 1 ppb of mercury in of the aqueous solution. This result is much better than that reported (100 ppb) for the detection of mercury(II) ions in aqueous solution with a column packed with jel beads containing dithizone [27]. The length of the colored foam bed was found proportional to the amount of mercury(II) ions present in the aqueous solution. At flow rate > 5 ml/min the colored zone boundary became diffuse. Thus, semi-quantitative determination of mercury(II) in 100 ml aqueous solution was successfully carried out at 2–3 ml/min using a standard color scale covering the range 1–20 ppb of mercury(II) where a linear relationship between the length (cm) of the colored foam zone on the foam column and the mercury(II) concentration was achieved (Fig. 2[1]).

[1] Each point in the figure represents an average of three measurements ± standard deviation.

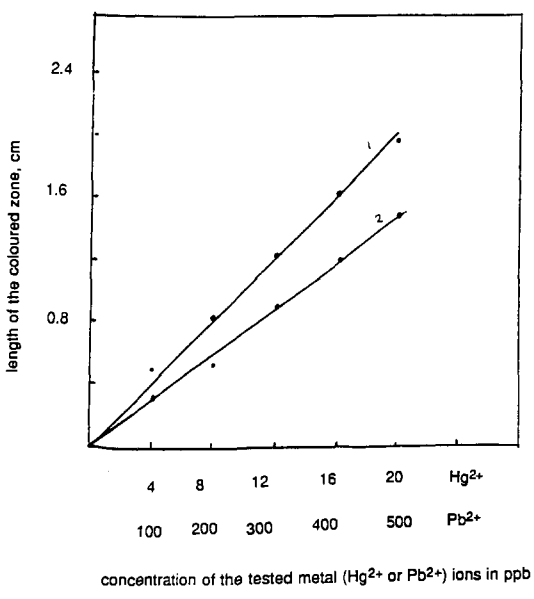

Fig. 2. Relationship between the length of the colored zone foam-bed (mm) on the foam column and the concentrations of mercury(II), 1 or lead(II), 2. Each point in the curve represents an average of three measurements ± SD.

The results obtained with immobilized or plasticized-TBP foam with F_2H_2Dz were found better than those obtained for dithizone (Table 2). The high distribution ratio, log D = 4.45 of $Hg(F_2HDz)_2$ chelate compared to log D = 3.92 of $Hg(HDz)_2$ may account for the higher sensitivity of F_2H_2Dz as compared to H_2Dz towards mercury(II). The values of the D for the complexes $Hg(F_2HDz)_2$ and $Hg(HDz)_2$ retained on the polyurethane foams were calculated employing the equation:

$$D = \frac{\%E}{100 - \%} \times \frac{Vs\ (ml)}{w\ (g)}$$

where E, Vs and W are the percentage of the Hg^{2+} ions extracted from the bulk solution, volume of the tested solution and weight of polyurethane foams, respectively.

The higher molecular weight and the diffusion rates of the chelate $Hg(F_2HDz)_2$ through the thin membrane of the polyurethane foams may be also responsible for enhancing the sensitivity of the F_2H_2Dz towards metal ions as compared to H_2Dz. This behavior is consistent with the general understanding that, the larger the molecular weight of the sorbate the larger the amount of the chelate retained on the non-polar phase when the substances concerned are similar in nature [28]. These findings are parallel to the relevant liquid–liquid extraction data reported by Kiwan and Kassim [7,8] for the higher distribution ratio of F_2H_2Dz and its metal chelates compared to dithizone and its complexes [29,30].

3.2. Detection and semiquantitative determination of lead(II) with 1,5-di(2-fluorophenyl)-3-mercaptoformazan

Lead(II) in aqueous solutions at a concentration as low as 0.10 ppm was easily detected by shaking the test solution with a cube of plasticized F_2H_2Dz-TBP foam, in a batch extraction mode. A comparison between this result (Table 3) and the reported data employing dithizone and other chelating agents [3,15,22–24] shows that the proposed method is more sensitive for the detection of lead(II) than dithizone. Semiquantitative determination of lead(II) was also possible by F_2H_2Dz-

Table 3
Comparative sensitivity of batch F_2H_2Dz (a) and H_2Dz (b) for the detection of lead(II) ions employing polyurethane foams

Method	Amount of Pb^{2+} detected (ppm)		Reference
	(a)	(b)	
Spot test	—	0.80	Feigl and Anger, 1972
Unloaded foam	0.30	0.30	Present work
Immobilized reagent foam	0.15[a]	0.20	Farag et al., 1986
Plasticized TBP-reagent foams	0.01	0.10	Present work

[a] Present work.

Table 4
Detection of 1 μg of mercury and lead with 1,5-di-(2-fluorophenyl)-3-mercaptoformazan immobilized polyurethane foams in the presence of some interfering ions

Ion	Compound added	Tolerance limit[a]		Note
		(a)	(b)	
MnO_4^-	$KMnO_4$	$1:1\times10^3$	$1:1\times10^3$	Add one crystal (~0.5 g) of sodium azide
Formate	Formic acid	$1:1\times10^4$	$1:1\times10^4$	Add bromine water and boil the solution
Bi^{3+}	$Bi(NO_3)_3\cdot7H_2O$	$1:1\times10^3$	$1:1\times10^3$	Add few crystals (~0.5 g) of thiourea
Zn^{2+}	$ZnSO_4$	$1:1x10^4$	$1:1\times10^3$	Add 1 ml of HNO_3 (0.01)
Mn^{2+}	$MnSO_4\cdot4H_2O$	$1:4\times10^3$	$1:1\times10^4$	Add 1 ml of bromine water and boil the solution
Fe^{2+}	$FeSO_4$	$1:5\times10^3$	$1:1\times10^4$	Add one crystal (~0.5 g) of NaF
Fe^{3+}	$FeCl_3$	$1:1\times10^3$	$1:1\times10^3$	Add 1 ml of saturated NaF
Cd^{2+}	$Cd(NO_3)_2$	$1:1\times10^3$	$1:1\times10^2$	Add one crystal (~0.5 g) of thiourea
Cr^{3+}	$Cr(NO_3)\cdot6H_2O$	$1:1\times10^3$	$1:1\times10^4$	Add bromine water and boil the solution
Ni^{2+}	$NiCl_2$	$1:1\times10^3$	$1:1\times10^3$	Add one crystal (~0.5 g) of thiourea
NO_2^-	$NaNO_2$	$1:1\times10^3$	$1:1\times10^3$	Add 1–2 ml of NaF (1 M)
VO_3^-	$(NH_4)\ VO_3$	$1:1\times10^3$	$1:1\times10^3$	Add one crystal (~0.5 g) of NaF

(a) Tolerance limit of the interfering ions towards 1 μg mercury(II) ions.
(b) Tolerance limit of the interfering ions towards 1 μg lead(II) ions.

TBP foam in batch extraction mode using the standard color scale 0.1, 0.5, 1, 5 and 10.0 ppm under the same experimental conditions.

The proposed plasticized F_2H_2Dz foam was employed in column for the quantitative collection of lead(II) in extremely dilute aqueous solution by passing 1 l of the test solution (at pH 4.5–6) through the foam column at 2–5 ml min^{-1} flow rate. As low as 50 ng ml^{-1} of lead(II) ions was easily detected by the proposed procedures. The length of the orange-red colored foam bed was found stable for more than 48 h and proportional to the concentration of lead(II) in the aqueous solution (Fig. 2). These results extend the use of the foam column for the semiquantitative determination of lead(II) ions at the concentration level 50–500 ppb in aqueous media.

3.3. Interference studies

To assess the selectivity of the proposed reagent F_2H_2Dz immobilized polyurethane foam, the detection of mercury(II) or lead(II) by the proposed batch mode was investigated in the presence of various ions. It was found possible to detect as low as 1 μg of Hg^{2+} or Pb^{2+} in the aqueous media in the presence of up to 10 mg of NO_2^-, NO_3^-, SeO_3^{2-}, SeO_4^{2-}, acetate, SO_4^{2-}, F^-, $C_2O_4^{2-}$, IO_3^-, BrO_3^-, $B_4O_7^{2-}$, Ba^{2+}, Ca^{2+}, Mg^{2+}, Mn^{2+}, MoO_4^{2-}, NH_4^+, PO_4^{3-}, WO_4^{2-}, BrO_3^-, IO_4^-, and Li^+. In the presence of some other ions e.g. Cd^{2+}, Fe^{2+}, Fe^{3+}, Pd^{2+}, Cr^{3+}, Bi^{3+}, Mn^{2+}, Cd^{2+}, Zn^{2+}, $S_2O_3^{2-}$, MnO_4^-, NO_2^-, Zn^{2+} and formate, simple modifications of the sample solution were introduced to obtain unambiguous and sensitive detection of Hg and Pb (Table 4). These results also extend the use of the proposed foam test for the detection of Hg and Pb in the different matrices.

3.4. Application of the proposed method

The validity of the proposed method for the detection, semiquantitative and quantitative collection of mercury(II) or lead(II) in natural water was also investigated. A water sample 1 dm^3 acidified to 0.1 mol dm^{-3} sulphuric acid was deaerated by nitrogen gas for at least 15 min and mixed with 10 ml of sodium sulphite (0.1 M). The solution mixture was spiked with 1–10 μg mercury(II) or 50–80 μg lead(II) and was allowed to pass through 0.45 μm Millipore filter. Sodium fluoride (10 ml, 0.1 M) solution was added, and the pH of the final solution was then adjusted to

pH 2.5–3. The solution mixture was percolated through F_2H_2Dz-loaded foam column at 3–5 ml min^{-1}. The length (mm) of the produced red-orange color due to mercury(II) complex or the pink color in the case of lead(II) complex on the foam bed was compared with standard color scales of both metal ions prepared under the same experimental conditions (Fig. 2). Satisfactory results were obtained for the spiked metal ions.

The practical utility of the method for the removal of mercury(II) or lead(II) from water sample was attempted at $2 \leq pH \leq 3$ with F_2H_2Dz-foam packed column (15 cm height × 1.5 cm I.D.). A 0.5 dm^3 aqueous solution containing 1–10 μg of mercury(II) or lead(II) at pH 3–5 were percolated through the F_2H_2Dz-foam column at 3–5 ml min^{-1} flow rate. Analysis of mercury(II) or lead(II) in the effluent solution indicated the absence of mercury(II) or lead(II) and quantitative retention of both metal ions on the foam column.

4. Conclusions

The resilient open cell polyurethane foams plasticized and/or immobilized with some F_2H_2Dz represent an efficient separation and preconcentration medium for mercury(II) and lead(II) in extremely dilute aqueous solutions (ppb level). Foams loaded with 1,5-di-(2-fluorophenyl)-3-mercaptoformazan were found more suitable as compared to dithizone and other chelating agents in the detection, semiquantitative determination and quantitative collection of mercury(II) and lead(II) ions in aqueous media. Further work still remains for improving the selectivity and the utility of the proposed method for the direct spectrophotometric determination of Hg^{2+} or Pb^{2+} on parallelepiped polyurethane foams or by preconcentration of these species from natural and wastewaters on columns packed with F_2H_2Dz-foam followed by elution with selective eluting agent e.g. acetone-HCl (1:3 v/v). The foam sorbents give unique advantage over granular sorbents in rapid, versatile and effective separation of different species from fluid samples. The great potentialities of open cell type resilient polyurethane foam membranes is attributed to their inexpensiveness and the large scale availability all over the world for many industrial applications.

Acknowledgements

The authors would like to thank the UAE University Scientific Council for a research grant provided to one of us (A.M. Kiwan) and the Ministry of Health, U.A.E. for the assistance provided to Mr M.H. Saleh.

References

[1] R. Chakraborty, S.S. Bhattacharya, A.K. Das, Bull. Chem. Soc. Jpn. 66 (1993) 2233.
[2] J.F. de Silva, R.J.P. Williams, The Biological Chemistry of the Elements, Clarendon Press, Oxford, 1993, p. 539.
[3] A.B. Farag, A. El-Waseef, M.H. Abdel Rahman, Acta Chimica Hungarica 122 (1986) 273 and references therein.
[4] G. Somar, H. Aydin, Analyst 110 (1985) 631; S. Landi, F. Fagioli, Anal. Chim. Acta 298 (1994) 363.
[5] H.J.M. Bowen, Environmental Chemistry Academic Press, London, 1979.
[6] Z. Marczenko, Separation and Spectrophotometric Determination of Elements, Ellis Horwood, Chichester, UK, 1986, p. 88.
[7] A.M. Kiwan, A.Y. Kassim, Anal. Chim. Acta 88 (1977) 177.
[8] A.Y. Kassim, Ph.D. Thesis, Kuwait University, Kuwait, 1975.
[9] T. Braun, A.B. Farag, Talanta 22 (1975) 699; T. Braun, A.B. Farag, Anal. Chim. Acta 99 (1978) 1.
[10] S. Palagyi, T. Braun, Radioanal. J. Nucl. Chem. 163 (1992) 69; A. Chow, D. Buksak, Can. J. Chem. 53 (1975) 1373.
[11] T. Braun, A.B. Farag, Anal. Chim. Acta 73 (1974) 301 and references therein; T. Braun, M.N. Abbas, L. Bakos, A. Elet, Anal. Chim. Acta 131 (1981) 311.
[12] T. Braun, J.D. Navratil, A.B. Farag, Polyurethane Foam Sorbents in Separation Science, CRC Press, Boca Raton, FL, 1985.
[13] A.M. El-Wakil, M.S. El-Shahawi, A.B. Farag, Anal. Lett. 23 (1990) 703.
[14] A.B. Farag, E.M. El-Nemma, Int. J. Chem. 3 (1992) 81.
[15] P. Rychlovsky, J. Bily, P. Denkova, Chem. Papers 47 (1993) 233.
[16] Y. Anjaneyulu, R. Maraya, T.H. Rao, Environ. Pollut. 79 (1993) 283.
[17] M. Harding, J. Chem. Soc. (1958) 4136.
[18] D. Panerjea, T.P. Singh, Z. Anorg. Chem. 331 (1964) 225.

[19] Stability Constants Supplement No. 1. Special Publication 25, Chemical Society, London, 1971, p. 114.
[20] N.N. Greenwood, A. Earnshaw, Chemistry of the Elements, Pergamon, London, 1985, p. 1413 and references therein.
[21] A.B. Farag, M.S. El-Shahawi, S. Farrag, Talanta 41 (1994) 617.
[22] A.B. Farag, M.E.M. Hassouna, M.H. Abdel-Rahman, Bull. Chem. Soc. Belg. 96 (1987) 147.
[23] W.M. Abou-Elmaty, M.Sc. Thesis, Mansoura University, Mansoura, Egypt, 1990.
[24] F. Feigl, V. Anger, Spot Tests in Inorganic Analysis, 6th ed., Elsevier, Amsterdam, 1972.
[25] R.D. Oleschuk, A. Chow, 42 (1995) 957; 433 (1996) 1545.
[26] M.M. Saeed, A. Rasheed, N. Ahamed, J. Tolgyessy, Sep. Sci. Technol. 29 (1994) 2143.
[27] Y.K. Lee, K.Ja. Whang, K. Ueno, Talanta 22 (1975) 535.
[28] A.D. Adamson, Physical Chemistry of Surfaces, 2nd ed., Academic Press, New York, 1967.
[29] Calculated from the Stability Constants Data, in: G. Iwantscheff, Das Dithizon und Scine, Anwendung in der Mikro und Spurenanalyse, 2nd ed., Verlag Chemie, Weinhein, 1972.
[30] I.M. Kolthoff, E.B.S. Sandell, E.J. Meehan, S. Bruckenstein, Quntitative Chemical Analysis, Macmillan, London, 1969, p. 352.

ELSEVIER

Talanta 45 (1997) 213–221

Talanta

Physical fractionation of trace and rare earth elements in the sediments of Lake Nasser

S.M.N. Moalla

Chemistry Department, Faculty of Science, Aswan, Egypt

Received 12 November 1996; received in revised form 3 April 1997; accepted 23 April 1997

Abstract

The distribution of major, trace and rare earth elements in bulk, different particle sized and strongly magnetic fractions of Lake Nasser sediments has been investigated. The elements were determined using neutron activation analysis. Statistical data processing indicates good correlation between Th, La and Ce, suggesting that accessory minerals such as monazite may play a role in controlling rare earth elements (REE) in the lake sediments. The highly significant relationship between Al and light-REE accounts for the capability of clay minerals to host these elements. In addition, principle components analysis reflects that there are only four factors which could explain about 90% of the total variance in the lake sediments. The results show also that Al, Th and REE have low contents in the sediment magnetic fraction relative to the corresponding values in the bulk sediments, whereas Fe, Mn, Ti, Co, Cr, Hf, V and Zn have higher concentrations in the same fraction than the corresponding values in the bulk sediments. This may be attributed to their incorporation in Fe–Mn minerals. © 1997 Elsevier Science B.V.

Keywords: Fractionation; Trace elements; Sediment

1. Introduction

Recently the analysis of aquatic sediments has been used to assess the extent and sources of trace element contamination in aquatic environments [1,2]. This approach has some advantages over other methods commonly used, such as analysis of water or aquatic organisms [3]. Sediments have the capacity to accumulate trace elements and other contaminants over time and so give a time-integrated assessment of contamination that may have occurred in the water masses.

In sediments, elements exist in several different forms and are associated with various components [4]. The total element content provides important knowledge about the pollution level, if the background or geochemical composition is known. However, natural or anthropogenic origin of elements is rather difficult to determine.

It is generally recognized that information about the physicochemical forms of the elements is required for understanding their environmental behavior (mobility, pathways, bioavailability). In a water system, the chemical form of an element determines the biological availability and chemical reactivity (sorption/desorption, precipitation/dissociation) towards other components of a system.

PII S0039-9140(97)00123-9

Chemical extraction methods are commonly used in studies of toxic trace element speciation, to elucidate their distribution among the various sediment constituents [5]. However, certain experimental problems with these methods have been recognized, including the possible non-selectivity of extractant and trace element readsorption on active sites, which are possibly formed during the course of extraction [6,7].

It is well known that elements are not homogeneously distributed over the various grain size fractions [8]. Because of the importance of surface reactions in aquatic sediments, it is clear that fine-grained material (clay/silt) has the greatest potential for accumulation of the dissolved trace elements from the water column. On the other hand, the coarse fractions (sand) dominated by quartz components with low metal contents act as a dilution factor for all metals. Magnetism is a property of solids which could be of great interest to study the distribution of transition and rare earth elements in aquatic sediments. Strong magnetism arises from the magnetic moments associated with moving electrons in atoms. Since electron spins tend to pair in atomic and molecular orbitals, the net spin and electronic moment of many materials is zero, and they are nonmagnetic. However, the electrons in the d and f orbitals of transition and rare earth elements are commonly unpaired, so that magnetic properties are generally associated with these elements.

The objective of the present work is to analyse different particle-sized and magnetic fractions, together with bulk sediments, to study the distribution of trace and rare earth elements in Lake Nasser sediments, and furthermore, to elucidate the manner in which such elements are bound to lake sediments. Neutron activation analysis as a non-destructive technique was used to avoid the problems involved with the dissolution of such complex matrix samples, and to avoid any possible contamination through other pretreatment of the samples.

2. Experimental

2.1. Study area

Lake Nasser is about 500 km long, 350 km of which are in Egypt and 150 km in the Sudan (Fig. 1). In southern Egypt and in northern Sudan, major rock formations are the Precambrian basement complex (granites, schists, gneisses) and the Nubian sandstones [9]. The amount of suspended matter carried by the River Nile, and deposited along Lake Nasser, was estimated to be about 100 million tons per year [10].

2.2. Sampling

Ten sediment samples were collected by means of a Peterson grab sampler from the main stream along Lake Nasser in September 1994. The sampling sites were chosen to represent the different sedimentation areas (Fig. 2). The samples were dried at 105°C and representative subsamples were prepared and kept in polyethylene bags.

2.3. Particle size and magnetic fractionation

No chemical dispersive reagent was used prior to particle size fractionation. An initial physical dispersion of the sediment samples was performed by end over end shaking overnight of 150 g sediment with 150 ml deionized water. The suspension was then split using wet sieving and

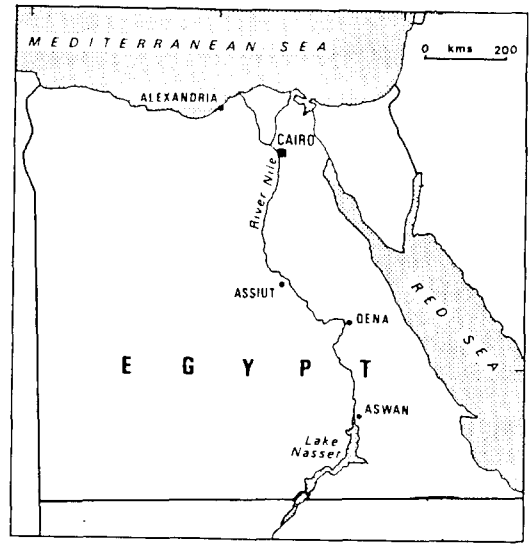

Fig. 1. Location of Lake Nasser.

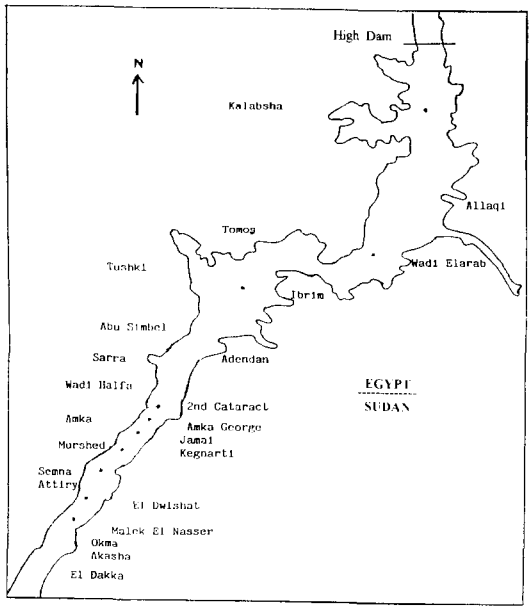

Fig. 2. Location of sample sites in Lake Nasser.

pipette methods [8], into four different sized fractions, <20, 20–32, 32–75 and >75 μm. Then the strongly magnetic fraction phases were extracted from the <20-μm fraction. An appropriate amount of the dried fraction (<20 μm) was suspended in 100 ml of distilled water and separated in an ultrasonic bath using a strong permanent magnet. After drying, the roughly separated fraction was further purified by prolonged whirling with a magnetic stirrer acting from below the clock glass containing the fraction and then removing the magnetic particles attracted to the clock glass placed over the agitated mixture. The separation process is achieved by means of a second strong magnet acting from the above the protecting clock glass. The process was repeated until no more magnetic particles attracted to the lower clock glass.

2.4. X-ray diffraction analysis

X-ray diffraction studies of the magnetic fractions were carried out using a Philips X-ray diffraction unit PW 1050 (Philips, Eindhoven, The Netherlands). The X-ray data obtained coincide with the data of the typical minerals published by the American Society of Testing Materials (ASTM). The relative abundance of detected minerals was estimated by measuring the relative intensity of the characteristic main d-spacing of each mineral.

2.5. Chemical analysis

Al, Hf, Mn, Sc, Ti and V were determined using the short time activation analysis technique. The studied samples were irradiated at a neutron flux of 1.7×10^{12} n·cm^{-2} s^{-1} (Triga Mark II reactor, Atominstitut, Vienna) for 20 and 60 s, respectively, to optimize the irradiation conditions for the investigated elements. The irradiation and counting system consists of a fast transfer system (300 ms) and a high-rate counting high resolution gamma spectroscopy system [11]. For the determination of long-lived nuclides, Ba, Ce, Co, Cr, Cs, Eu, Fe, La, Lu, Rb, Sm, Tb, Th, Yb and Zn, the samples were irradiated for 10 h inside the central thimble of the reactor and gamma activities were measured after 11 days for 2 h. The results were evaluated by means of multi-element reference materials (IAEA-Sediment-SL1, IAEA-Sediment-SL3) and self-prepared standards.

3. Results and discussion

3.1. Physical fractionation

Particle size fractionation shows that the majority of particles (48%) are found in the finest fraction, <20 μm, followed by 32–75 μm (30%), >75 μm (17%) and 20–32 μm (5%).

3.2. Element contents in the different sediment fractions

The results (Table 1) show a slightly increased or nearly equal values of Al, Fe, Ti, Ce, Co, Cr, Eu, Hf, La, Rb, Sm, Yb and Zn concentrations in the finest fraction (F1, <20 μm) with respect to the corresponding values in the bulk sediment.

Table 1
Mean element concentration with standard deviation in bulk and different particle sized and strongly magnetic fractions of Lake Nasser sediments[a]

Element	Bulk	F1 < 20 μm	F2, 20–32 μm	F3, 32–75 μm	F4 > 75 μm	SMF[b]
Al (mg g^{-1})	68 ± 7	73.4 ± 0.4	48.9 ± 0.2	57.4 ± 0.3	55.2 ± 0.3	20 ± 2
Fe	74 ± 8	81.2 ± 1.1	144 ± 3	82 ± 3	47 ± 2	288 ± 22
Mn	1.41 ± 0.28	1.20 ± 0.04	2.10 ± 0.04	1.15 ± 0.03	0.47 ± 0.02	4.0 ± 0.6
Ti	12.3 ± 5.2	19.3 ± 1.3	63 ± 1	25 ± 1	5.7 ± 0.6	93 ± 1
Ba (μg g^{-1})	378 ± 46	312 ± 4	246 ± 34	337 ± 12	527 ± 62	
Ce	91 ± 10	88.1 ± 3.3	94 ± 1	66 ± 6	49 ± 5	38 ± 4
Co	32 ± 5	36.9 ± 0.4	55 ± 1	37 ± 1	27 ± 1	55 ± 4
Cr	120 ± 24	140 ± 1	400 ± 7	269 ± 9	83 ± 3	604 ± 17
Cs	1.84 ± 0.45	1.18 ± 0.27	—	—	—	—
Eu	2.2 ± 0.2	2.20 ± 0.01	2.20 ± 0.05	1.90 ± 0.02	1.4 ± 0.1	1.4 ± 0.1
Hf	6.8 ± 0.9	7.15 ± 0.66	13.8 ± 1.5	7.8 ± 1.2	3.5 ± 0.7	13 ± 1
La	40 ± 4	39.4 ± 0.7	40.4 ± 0.4	28 ± 2	22 ± 2	18 ± 2
Lu	0.69 ± 0.08	0.62 ± 0.05	0.86 ± 0.12	0.61 ± 0.04	0.29 ± 0.03	0.31 ± 0.07
Rb	46 ± 8	47 ± 3	33 ± 2	34 ± 4	48 ± 5	—
Sc	24.0 ± 1.6	18.2 ± 3.9	31 ± 3	18 ± 2	14 ± 3	25.6 ± 1.3
Sm	8.8 ± 0.8	9.2 ± 0.3	9.7 ± 0.1	7.5 ± 0.2	5.4 ± 0.3	4.0 ± 0.6
Tb	2.52 ± 0.36	1.20 ± 0.8	1.26 ± 0.20	0.81 ± 0.17	0.73 ± 0.02	
Th	6.7 ± 0.8	6.1 ± 0.2	6.9 ± 0.3	3.9 ± 0.1	2.6 ± 0.4	4.4 ± 0.7
V	231 ± 37	207 ± 4	560 ± 5	264 ± 4	104 ± 3	1620 ± 51
Yb	2.9 ± 0.3	3.10 ± 0.09	4.2 ± 0.1	3.3 ± 0.1	1.7 ± 0.2	1.1 ± 0.5
Zn	132 ± 51	156 ± 5	116 ± 7	146 ± 30	101 ± 6	221 ± 43

[a] Mean of 10 samples.
[b] SMF, strongly magnetic fraction.

This is possibly attributable to abundance of clay minerals. Because of the importance of surface exchange reactions in lake sediments, it is clear that fine-grained materials (clay/silt) play a great role in element distribution within the lake system. Otherwise, it is well known that amorphous Fe/Mn oxyhydroxides with their association trace elements have great ability to collect on the fine grain size sediments. It was reported that Ce is apparently oxidized to the relatively insoluble +4 valence state and incorporated in the MnO_2 oxide [20].

High values of Fe, Mn, Ti, Co, Cr, Hf, Sc, V and REE were found in the 20–32-μm sediment fraction. This accounts for the existence of these elements as or associated with accessory phases concentrated predominantly in this fraction. Heavy minerals, including iron minerals, dominated by magnetite and ilmenite, titanite, rutile, monazite, zircon, and other heavy minerals, have previously been recognized and identified in the Nile sediments [18]. The high content of Cr could be explained by the existence of ilmenite ($FeTiO_3$) and magnetite (Fe_3O_4). It was reported that Cr^{3+} could substitute Fe^{3+} in the magnetite and Ti^{4+} in the ilmenite, as a result of the similarity in the ionic radii [19]. The high value of vanadium may be attributed to replacing the Fe^{3+}, Cr^{3+}, Ti^{4+} in their bearing minerals [17]. The high abundance of Sc is consistent with the fact that, beside its existence in the ferro-magnesian minerals, much of the Sc is possibly accommodated in the ilmenite and magnetite structure replacing Fe^{3+}. The pronounced increase in Co is also in line with known geochemical behavior of some metals such as Co and Zn to exist in a spinal structure (MFe_2O_4) involving Fe^{3+} and one of these metals having ionic radii favorable for fitting into the tetrahedral sites.

Ba and Rb show higher concentrations in both fine (F1) and coarse (F3 and F4) fractions with respect to the medium fraction, suggesting that these elements exist in the lake sediments associated with clay minerals and as detrital Ba/Rb-bearing phases enriched in the coarse fractions. These observations are in agreement with the fact that during chemical weathering, the elements-associated feldspars (Ca, Na, Rb, Sr and Ba) are strongly fractionated because some elements (Na, Ca) are lost to weathering solution but others (K, Rb, Ba) are retained on the clay minerals [21].

3.3. Magnetic fraction analysis

To illustrate and clarify the role of iron-bearing minerals in the distribution of trace and heavy metals in the lake sediments, strongly magnetic fractions were separated and investigated in comparison with the bulk sediments. The relative abundance of the strongly magnetic fraction in Lake Nasser sediment is in the range of 2.1–7.5%. X-ray diffraction results show that magnetite and ilmenite are the predominant heavy minerals in the magnetic fractions. The results indicate, with exception of Sc, that all elements studied have a pronounced fractionation into two different groups. Al, Th and REE have low concentrations in the sediment magnetic fractions relative to the corresponding values in the bulk sediments. On the other hand, Fe, Mn, Ti, Co, Cr, Hf, V and Zn have higher concentrations in the sediment magnetic fractions than the corresponding values in the bulk sediments. This suggests that Fe-bearing minerals play a significant role in concentrating certain trace and heavy elements in the lake sediment. These findings are consistent with the high abundance of magnetite (Fe_3O_4) and ilmenite ($FeTiO_3$) in the magnetic fraction. From a geochemical point of view, it is well known that Co, Cr, Hf, V and Zn may replace Fe^{3+} (0.64 Å) and Ti^{4+} (0.68 Å), as a result of similarity in the ionic radii in magnetite and ilmenite [19]. The relatively high content of Zn in the magnetic fractions is possibly attributed to the existence of Mn-containing spinels such as (MnZn) Fe_2O_4 and Fe (MnFe)O_4, since pure $ZnFe_2O_4$ is non-magnetic [22].

The low levels of REE and Th in the magnetic fractions support the evidence that these elements are mainly controlled by existence of minor resistant minerals, such as monazite, in the lake sediments. Monazite has a lower magnetic susceptibility than magnetite and ilmenite [22].

Although the study was only conducted on the strongly magnetic fractions, the data obtained gave fairly clear evidence of the relatively significant role of the different sediment components in the distribution of major and trace elements in the sediments of Lake Nasser. Also, the study illustrates the great need to combine the results of the chemical and mineralogical studies to gain clear information about the distribution of elements in a lake system.

3.4. Statistical data analysis of bulk sediments

The statistical data processing of the determined elements was performed using the Minitab program data analysis (Software-package -Standard micro-computer version). The correlation matrix of the analyzed elements is given in Table 2. The results will be discussed in the following sections.

3.5. Correlation between elements

If we consider the sediment samples as objects and analytical data of the measured elements as variables, then the results can be studied by statistical analysis methods, in order to find an internal structure not accessible at first glance. This inter-element correlation matrix was built to find associations between the elements. Fe and Mn show good positive correlation with Ti, Co, V, Sc, Hf, Yb, Tb, Eu and Lu in the bulk lake sediments. This is possibly attributable to accommodation of these elements within detrital Fe- and Mn-bearing minerals. Such behavior is also consistent with the known scavenging role of Fe–Mn oxides [12,13]. The rare earth elements (REE) are often treated as a coherent group of elements in clastic sediments, but this study indicates that in the Lake Nasser sediments the heavy REE (HREE) and light REE (LREE) behave quite differently. Eu, Lu and Tb show perfect positive correlation with

Table 2
Correlation matrix of the determined elements

Al	Fe	Mn	Ti	Ba	Rb	Cs	Cr	Co	V	Sc	Hf	Zn	Ce	Sm	Th	Yb	Th	Eu	Lu	La
Fe	−0.388																			
Mn	−0.532	0.905																		
Ti	−0.873	0.662	0.653																	
Ba	−0.761	0.477	0.614	0.666																
Rb	0.957	−0.188	−0.352	−0.821	−0.789															
Cs	0.725	−0.806	−0.866	−0.701	−0.644	0.586														
Cr	−0.834	0.590	0.606	0.618	0.758	−0.789	−0.785													
Co	−0.506	0.973	0.963	0.658	0.567	−0.312	−0.900	0.664												
V	−0.749	0.853	0.860	0.721	0.701	−0.591	−0.958	0.831	0.920											
Sc	0.108	0.812	0.659	−0.050	0.197	0.260	−0.354	0.228	0.706	0.430										
Hf	−0.459	0.861	0.801	0.433	0.526	−0.315	−0.760	0.718	0.861	0.778	0.649									
Zn	−0.212	−0.446	−0.290	0.386	−0.318	−0.204	0.153	−0.199	0.381	−0.236	−0.629	−0.524								
Ce	0.662	0.280	0.147	−0.552	−0.489	0.811	0.132	−0.504	0.177	−0.152	0.532	0.198	−0.359							
Nd	0.318	0.250	0.236	−0.394	−0.246	0.501	0.025	−0.163	0.235	0.064	0.422	0.127	−0.120	0.599						
Sm	0.448	0.563	0.354	−0.348	−0.315	0.649	−0.052	−0.231	0.422	0.102	0.780	0.422	−0.417	0.904						
Th	0.841	−0.130	−0.306	−0.626	−0.671	0.901	0.568	−0.772	−0.275	−0.543	0.247	−0.180	−0.233	0.871	0.723					
Yb	0.309	0.592	0.553	−0.162	0.069	0.436	−0.219	−0.153	0.522	0.200	0.758	0.472	−0.512	0.799	0.805	0.543				
Tb	−0.209	0.819	0.767	0.310	0.239	−0.014	−0.608	0.360	0.783	0.584	0.688	0.861	−0.323	0.537	0.689	0.167	0.741			
Eu	−0.080	0.901	0.700	0.264	0.195	0.107	−0.576	0.333	0.804	0.603	0.835	0.822	−0.533	0.557	0.780	0.227	0.723	0.883		
Lu	0.048	0.780	0.641	−0.051	0.009	0.277	−0.367	0.225	0.694	0.437	0.861	0.740	−0.445	0.651	0.865	0.343	0.689	0.839	0.847	
La	0.799	0.070	−0.077	−0.627	−0.617	0.902	0.383	−0.666	−0.057	−0.386	0.431	0.006	−0.327	0.959	0.839	0.955	0.677	0.339	0.390	0.531

$P<0.01$, $r=0.708$; $P<0.05$, $r=0.576$.

Table 3
Th and REE concentrations (μg g^{-1}) in selected minerals (the values are means calculated from various sources [16,17])

Element	Mineral					
	Feldspar	Mica	Apatite	Zircon	Allanite	Monazite
La	—	132	—	—	50 300	89 100
Ce	11.6	253	1580	68	71 200	155 500
Nd	3.2	122	1090	23	30 200	67 150
Sm	0.45	23	280	11	7700	24 000
Eu	1.46	1.1	18	0.92	330	460
Yb	0.12	7.9	84	560	410	600
Th	—	—	—	—	—	37 000

Fe and Mn, suggesting their association with Fe–Mn phases. The large dissimilarity between ionic radii of trivalent REE and the major cations of Fe/Mn phases make it more reasonable to consider that the REE are located along basal layers of Fe/Mn-bearing minerals rather than substituting in a specific lattice site. On the other hand, the negative correlation between these HREE and Al suggests that aluminosilicates (clay minerals) act to dilute such elements in the lake sediments. Chemical weathering of the ferro-magnesian and feldspar minerals, bearing such elements, yield clay minerals. Therefore the decrease in these elements is consistent with the increase in Al concentration.

In contrast, Al shows perfect positive correlation with La, Ce and Th, suggesting that clay minerals, especially montmorillonite and kaolinite, can accommodate these elements released from the weathered primary minerals. It was reported that, under progressive chemical weathering, illite and other minerals release REE into the weathering solution [14]. HREE form more soluble complexes than the LREE [15], whereas the latter are preferentially adsorbed onto montmorillonite. The high correlation coefficients between La, Ce and Th, and their higher abundance in the lake sediments could be explained by the occurrence of minor resistant minerals, such as apatite, zircon and monazite. It is well known that monazite contains LREE and Th in such large concentrations that small amounts of it would contribute substantially to the total LREE content of any particular sample.

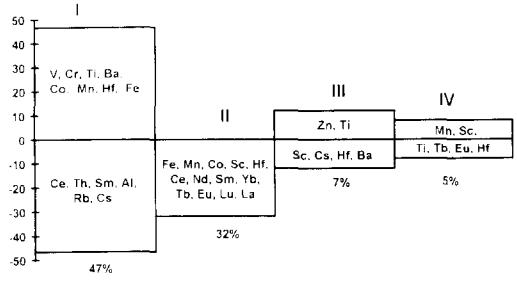

Fig. 3. Diagram showing the major loading of variables on each factor in lake sediments. Numbers I–IV on top of each block refer to the factor number of the group, and values below the block refer to the percentages of variation explained by the factor. Variables having positive loading are given above the horizontal line, and variables having negative loading are given below the horizontal line.

Using the REE abundance in selected minerals (Table 3), calculated from various sources [16,17], the REE concentrations in the Lake Nasser sediments can be easily accounted for by the high abundance of monazite in formations. It was pointed out that the Nile sediments contain large numbers of heavy minerals, including monazite and zircon [18]. These minerals now, and after construction of the High Dam at Aswan, are deposited somewhere in Lake Nasser.

3.6. Principal components analysis (PCA)

The data presented in Table 2 have been studied by means of PCA, a statistical technique for examining relationships between variables. The basic assumption of PCA is that the measured variables can be modeled as a linear combination of other unobserved variables, known as factors.

Ideally, each parameter would be strongly influenced by the mineralogical factor, and only marginally by others, which may represent the weathering, geochemical (major and trace elements), textural and sorting variations.

By extracting the eigenvalues of the correlation matrix, we defined the number of significant factors, the percentage of variance explained by each one of them, and the participation of the old variables in the new ones. There are four significant eigenvalues that explain about 90% of the total variance of results. The PCA groups together related variables into a smaller number of parameters (factors). The positive and negative loadings of related variables in each factor suggest similar or opposite trends. The results of PCA on bulk sediment samples are also expressed in a simplified diagram (Fig. 3) in which each block represents a factor. Variables having positive loadings are written above the horizontal line and variables having negative loadings are written below the horizontal line.

Factor I, which accounts for 47% of the total variance, shows a positive loadings for elements characterized to the ferro-magnesian minerals [19], whereas Al has a negative loading in this factor. Most ferro-magnesian elements (Fe, Mn, Ti, Co, Cr, V, Zn) have negative correlations with Al. This suggests that the ferro-magnesian elements in Nile sediment decrease with increase in the alumino-silicates. The large cations (Rb, Cs), large highly charged cations (Th) and light REE (La, Ce, Sm), all have positive correlations with Al. This indicates that these elements are associated with silicate minerals or quartzose components. These observations support the suggestion that variations of element concentrations in lake Nasser sediments are mainly due to the mineralogical factor.

From the results, it is also apparent that REE contents may primarily be controlled by minor resistant minerals which concentrate the REE, such as monazite, which contribute significantly to the abundance of these elements.

Factor II, which explains 32% of the variation, may be termed as the textural factor. The negative loading in this factor for most studied elements may be attributed to the sorting effect. The hydrodynamic conditions at the time of deposition affect the relative abundances of minerals with different hydraulic properties. Variations in hydraulic behaviour result from differences in the density, size and shape of mineral grains. The third factor, which accounts for 7% of the variance, represents the significant positive loading of Zn and Ti, and negative loading for Sc, Cs, Hf and Ba. This may be explained by assuming that these elements are released by chemical weathering of clays of the illite type. Ba, Sc, Cs and Hf are lost to the weathering solutions, while Ti and Zn are retained on the clay weathering products and carbonate phases. In the fourth factor (5%) Mn and Sc have positive loading, whereas Hf, Eu, Tb and Ti have negative loading. This may indicate that a minor role was played by physico-chemical processes such as sorption and ionic substitution.

Acknowledgements

The author would like to express his thanks to the staff of the Radiochemistry Section, Atominstitut Vienna, for their help during this work. This work was supported by the Austrian Academic exchange service through a scholarship for the author.

References

[1] U. Förstner, W. Salomons, Environ. Technol. Lett. 1 (1980) 494–505.
[2] D. Purves, Trace Element Contamination of the Environment, Elsevier, Amsterdam, 1985.
[3] D. Jaffe, J.K. Walters, Sci. Total Envion. 7 (1977) 1–15.
[4] W.F. Pickering, Crit. Rev. Anal. Chem. 12 (1981) 233–266.
[5] A. Tessier, P.G.C. Campbell, M. Bisson, Anal. Chem. 15 (1979) 844–851.
[6] S. Xiao-Quan, C. Bin, Anal. Chem. 65 (1993) 802–807.
[7] U. Förstner, Int. J. Environ. Anal. Chem. 51 (1993) 5–23.
[8] J. Ducarior, I. Lamy, Analyst 120 (1995) 741–745.
[9] R. Said, The Geology of Egypt, Elsevier, Amsterdam, 1962.
[10] B. Entz, Water-supply Maint. 4 (1980) 63–66.
[11] F. Grass, G.P. Westphal, T. Kasa, Nucl. Geophys. 3 (1987) 253–261.

[12] E.E. Jenne, Am. Chem. Soc. 73 (1968) 337–387.
[13] H.D. Hem, Geochim. Cosmochim. Acta 41 (1977) 527–538.
[14] K.J. Cantrell, R.H. Byrne, Geochim. Cosmochim. Acta 51 (1987) 597–606.
[15] G. Mongelli, Mineral. Petrol. 53 (1995) 103–114.
[16] T.R. Wildeman, Geochim. Cosmochim. Acta 37 (1973) 439–452.
[17] R. Zaghloul, S.S. Ismail, F. Grass, J. Trace Microprobe Tech. 6 (14) (1988) 487–500.
[18] N.M. Shukri, Q. J. Geol. Soc. 105 (1950) 511–534.
[19] K.H. Wedepohl, Handbook of Geochemistry, Springer, New York, 1969.
[20] Z.P. David, Geochim. Cosmochim. Acta 38 (1977) 1007–1022.
[21] E.W. Sawyer, Chem. Geol. 55 (1985) 77–95.
[22] R.C. Weast, Handbook of Chemistry and Physics, CRC Press, 1974.

ELSEVIER

Talanta 45 (1997) 223–225

Talanta

Book reviews

Designing Safer Chemicals, edited by C. DeVito and R.L. Garrett: published by American Chemical Society, Washington, DC, 1996, pp. 254, US $89.95: ISBN 0-8412-3443-4.

This is number 640 in the ACS Symposium Series and is concerned with Green Chemistry for Pollution prevention. The title begs the question 'Safer than what...' but the cover of the book provides the comparison as the structure of benzidine (chemical properties highly desirable for dyestuffs but highly carcinogenic) is shown in red whereas the structure of 2,2′-diethylbenzidine (chemical properties also highly desirable for dyestuffs but considerably less carcinogenic) is shown in green. The book is developed from a symposium sponsored by the Division of Environmental Chemistry, at the 208th National meeting of the American Chemical Society held in Washington, DC, in 1994. Later, in March 1995 president Clinton announced the creation of the Green chemistry Challenge Program and the design of safer chemicals is one of the major components of this Program.

The editors who are with the US Environmental Protection Agency each present a separate chapter giving an overview of the subject. The first of these chapters deals with the history of, and building the foundation for, designing safer chemicals and this is followed by a chapter on toxicological considerations. Relevant Acts of USC, databases and textbooks are all mentioned. These two interesting chapters make an excellent introduction to the topic of green chemistry.

The next seven chapters are succinct and cover some of the methods which may be adopted to produce safer chemicals. These are mechanism-based molecular design related to cancer risk reduction, isosteric replacement of carbon with silicon, retrometabolic concepts, toxicity prediction via prediction of rates of cytochrome-P450-mediated bioactivation, use of computers in toxicology and design, design of biodegradable chemicals, and design of aquatically safer chemicals.

Finally there are three chapters on applications which include relevant examples. These are designing safer nitriles, designing an environmentally safe marine antifoulant, and imine-isocyanate chemistry: new technology for environmentally friendly, high-solids coatings.

All the chapters present interesting and relevant information on aspects of green chemistry and there is an overall subject index. There are some very small changes in letter size and line spacing between chapters but nothing that detracts from the contents. The book is intended for synthetic chemists in industry, academia and government but I consider this book will have a wider appeal—especially to all those involved in environmental chemistry.

P.J. Cox

PII S0039-9140(97)00099-4

Protein and peptide analysis by mass spectrometry, edited by J.R. Chapman: published by Humana, Totowa, 1996, pp. 350, US $69.50: ISBN 0-89603-345-7.

In the Preface to this book, the Editor (John Chapman) warns that 'mass spectrometry offers

ELSEVIER

Talanta 45 (1997) 223–225

Talanta

Book reviews

Designing Safer Chemicals, edited by C. DeVito and R.L. Garrett: published by American Chemical Society, Washington, DC, 1996, pp. 254, US $89.95: ISBN 0-8412-3443-4.

This is number 640 in the ACS Symposium Series and is concerned with Green Chemistry for Pollution prevention. The title begs the question 'Safer than what...' but the cover of the book provides the comparison as the structure of benzidine (chemical properties highly desirable for dyestuffs but highly carcinogenic) is shown in red whereas the structure of 2,2′-diethylbenzidine (chemical properties also highly desirable for dyestuffs but considerably less carcinogenic) is shown in green. The book is developed from a symposium sponsored by the Division of Environmental Chemistry, at the 208th National meeting of the American Chemical Society held in Washington, DC, in 1994. Later, in March 1995 president Clinton announced the creation of the Green chemistry Challenge Program and the design of safer chemicals is one of the major components of this Program.

The editors who are with the US Environmental Protection Agency each present a separate chapter giving an overview of the subject. The first of these chapters deals with the history of, and building the foundation for, designing safer chemicals and this is followed by a chapter on toxicological considerations. Relevant Acts of USC, databases and textbooks are all mentioned. These two interesting chapters make an excellent introduction to the topic of green chemistry.

The next seven chapters are succinct and cover some of the methods which may be adopted to produce safer chemicals. These are mechanism-based molecular design related to cancer risk reduction, isosteric replacement of carbon with silicon, retrometabolic concepts, toxicity prediction via prediction of rates of cytochrome-P450-mediated bioactivation, use of computers in toxicology and design, design of biodegradable chemicals, and design of aquatically safer chemicals.

Finally there are three chapters on applications which include relevant examples. These are designing safer nitriles, designing an environmentally safe marine antifoulant, and imine-isocyanate chemistry: new technology for environmentally friendly, high-solids coatings.

All the chapters present interesting and relevant information on aspects of green chemistry and there is an overall subject index. There are some very small changes in letter size and line spacing between chapters but nothing that detracts from the contents. The book is intended for synthetic chemists in industry, academia and government but I consider this book will have a wider appeal—especially to all those involved in environmental chemistry.

P.J. Cox

PII S0039-9140(97)00099-4

Protein and peptide analysis by mass spectrometry, edited by J.R. Chapman: published by Humana, Totowa, 1996, pp. 350, US $69.50: ISBN 0-89603-345-7.

In the Preface to this book, the Editor (John Chapman) warns that 'mass spectrometry offers

the protein chemist ready access to a wealth of information that is otherwise available only with great difficulty, or perhaps not at all'. I will return to what he said next at the end of this review, but firstly to the contents. The book has 21 chapters written by leading authorities in the field of protein and peptide mass spectrometry and starts with an introductory review by Peter Roepstorff. The areas covered by the book reflect the massive progress that has been made over the past decade, with chapters on ionisation techniques (MALDI, APCI, TS, ESI), LC/MS, the elucidation of peptide/protein structure, the use of database systems for identification, and the analysis of glycoproteins. For a book with so many authors, the Editor is to be congratulated on the consistently high quality of the end product. The accessible style will appeal to the non-expert (even the Biologists amongst us) and to those of us who teach undergraduates about the joys of mass spectrometry.

The book is reasonably priced and all chapters have extensive bibliographies. The appendices (written by the Editor) contain a full list of abbreviations (very useful for the non-expert) and some background information on isotope abundances, peptide fragmentation, etc. Finally, to return to the Preface again. John Chapman warns readers that 'the use of mass spectrometry might become habit forming'. For those of us who are self-confessed addicts of mass spectrometry this book should not be on the shelves of the rehabilitation centre!

B.A. McGraw

PII S0039-9140(97)00100-8

Handbook of chemical and biological sensors, edited by R.F. Taylor and J.S. Schultz: published by the Institute of Physics Publishing, Bristol, 1996: pp. 604: ISBN 0-7503-0323-9: US $279.00.

Sensor science is an inherently interdisciplinary area involving physics, engineering, chemistry and biology. The greatest strength of the Handbook of Chemical and Biological Sensors is its success in bringing together all these areas. It is an edited book with 23 chapters, all by experts in their respective fields. These chapters are generally at the level of an advanced undergraduate text. Their main objective is to present the fundamentals of a particular topic. Important references are cited but these chapters are not reviews.

Several chapters deal with technologies involved in making sensors. For example, there are chapters on integrated surface manufacturing techniques, immobilization methods, methods for modifying surfaces, bilayer lipid membranes and polymers for use in sensors. Other chapters deal with the principles of chemical transduction. These include chapters on physical sensors, photometric transduction, electrochemical transduction and biological recognition elements. Several chapters cover different types of sensors, including solid state, resistive gas sensors, optical sensors, enzyme electrodes and other electrochemical sensors, acoustic sensors and thermal sensors. No important sensor area is slighted. Ancillary topics like microfluidics, flow injection analysis and sensor array calibration are also covered. There are even chapters on biomolecular electronics, an interesting look to the future, and the realities of sensor commercialization.

This reviewer's reaction to the various chapters is probably typical. I found the chapters that covered topics in my area to be simplistic. They did not add to my knowledge. However, the chapters that covered topics unfamiliar to me were excellent introductions to these areas. This is definitely a book that sensor researchers should acquire to increase their breadth rather than their depth of knowledge. Given the broad coverage of principles and topics, it would also be an excellent text for an interdisciplinary course on sensor science provided that the students could recover from the shock of paying $279 for a book.

W.R. Seitz
University of New Hampshire
New Hampshire
New England
USA

PII S0039-9140(97)00101-X

the protein chemist ready access to a wealth of information that is otherwise available only with great difficulty, or perhaps not at all'. I will return to what he said next at the end of this review, but firstly to the contents. The book has 21 chapters written by leading authorities in the field of protein and peptide mass spectrometry and starts with an introductory review by Peter Roepstorff. The areas covered by the book reflect the massive progress that has been made over the past decade, with chapters on ionisation techniques (MALDI, APCI, TS, ESI), LC/MS, the elucidation of peptide/protein structure, the use of database systems for identification, and the analysis of glycoproteins. For a book with so many authors, the Editor is to be congratulated on the consistently high quality of the end product. The accessible style will appeal to the non-expert (even the Biologists amongst us) and to those of us who teach undergraduates about the joys of mass spectrometry.

The book is reasonably priced and all chapters have extensive bibliographies. The appendices (written by the Editor) contain a full list of abbreviations (very useful for the non-expert) and some background information on isotope abundances, peptide fragmentation, etc. Finally, to return to the Preface again. John Chapman warns readers that 'the use of mass spectrometry might become habit forming'. For those of us who are self-confessed addicts of mass spectrometry this book should not be on the shelves of the rehabilitation centre!

B.A. McGraw

PII S0039-9140(97)00100-8

Handbook of chemical and biological sensors, edited by R.F. Taylor and J.S. Schultz: published by the Institute of Physics Publishing, Bristol, 1996: pp. 604: ISBN 0-7503-0323-9: US $279.00.

Sensor science is an inherently interdisciplinary area involving physics, engineering, chemistry and biology. The greatest strength of the Handbook of Chemical and Biological Sensors is its success in bringing together all these areas. It is an edited book with 23 chapters, all by experts in their respective fields. These chapters are generally at the level of an advanced undergraduate text. Their main objective is to present the fundamentals of a particular topic. Important references are cited but these chapters are not reviews.

Several chapters deal with technologies involved in making sensors. For example, there are chapters on integrated surface manufacturing techniques, immobilization methods, methods for modifying surfaces, bilayer lipid membranes and polymers for use in sensors. Other chapters deal with the principles of chemical transduction. These include chapters on physical sensors, photometric transduction, electrochemical transduction and biological recognition elements. Several chapters cover different types of sensors, including solid state, resistive gas sensors, optical sensors, enzyme electrodes and other electrochemical sensors, acoustic sensors and thermal sensors. No important sensor area is slighted. Ancillary topics like microfluidics, flow injection analysis and sensor array calibration are also covered. There are even chapters on biomolecular electronics, an interesting look to the future, and the realities of sensor commercialization.

This reviewer's reaction to the various chapters is probably typical. I found the chapters that covered topics in my area to be simplistic. They did not add to my knowledge. However, the chapters that covered topics unfamiliar to me were excellent introductions to these areas. This is definitely a book that sensor researchers should acquire to increase their breadth rather than their depth of knowledge. Given the broad coverage of principles and topics, it would also be an excellent text for an interdisciplinary course on sensor science provided that the students could recover from the shock of paying $279 for a book.

W.R. Seitz
University of New Hampshire
New Hampshire
New England
USA

PII S0039-9140(97)00101-X

Pharmaceutical and biomedical applications of capillary electrophoresis, edited by S.M. Lunte and D.M. Radzik: published by Elsevier, Oxford, 1996, pp. 511, US $135.00: ISBN 0-08-042014-1.

This text on capillary electrophoresis appears at a time when it will be evaluated against other treatments of the topic already available. Capillary electrophoresis is developing so rapidly that the choice of aspects to be covered and the depth of treatment of these aspects will largely dictate the usefulness of a text. The editors of this volume have succeeded in reaching a good balance. The main theoretical principles and experimental technology are informatively covered and there is indepth coverage of specific application areas in which most readers will find something of relevance.

The editors have arranged this book into three sections each containing several chapters. The first section deals with separation and includes chapters on basic CE theory, modes of separation in a chapter called column technologies and a separate extensive chapter on electrokinetic chromatography. This chapter extends this area beyond the micellar additives to which this technique is often limited. Capillary electrochromatography is dealt with briefly in the chapter on column technologies.

Section 2 contains three chapters which deal respectively, with optical detection, mass spectrometer detection and electrochemical detection methods. These chapters are authoritatively written and the chapter on optical methods contains a wealth of theoretical detail. The CE-MS chapter also includes a considerable coverage of applications. The chapter on electrochemical detection, in contrast, is largely devoted to experimental techniques and interfaces. The applications cited in this last chapter do not live up to the generality of use of electrochemical detection indicated in the introduction and this largely parallels the situation in LC.

The third section of this book, slightly less than half, comprises six separate chapters on different topics. These consist of a single chapter on sample pre-treatment for CE which is of very general use in applications work. There are three chapters on applications to biological species in particular amino acids, proteins and peptides and nucleic acids and oligonucleotides. These are well written overviews of the study of these types of compound by CE and are extensively referenced. Considerably more specialised is the chapter on in vivo CE measurements dealing with microdialysis sampling and single cell analysis. The chapter on CE in pharmaceutical development attempts to place CE in the regulatory framework of drug development. It touches upon, but adds little to, information already discussed with respect to CE although it does contain a short section on chiral separations.

Sections 1 and 2 taken together constitute a valuable addition in themselves to the growing number of texts on CE. The presentation of information is well above that of an introductory text although the basics are adequately covered in Chapter 1. Section 3 will be read selectively depending upon the reader's personal interest. Overall this is one of the most comprehensive texts available on CE theory, practice and applications. All chapters are very well referenced and the book will be a useful source of information for separation scientists and post-graduate students wishing to obtain an overall review of this developing technique.

R.B. Taylor

PII S0039-9140(97)00102-1

ELSEVIER

Talanta 45 (1997) 227–228

Talanta

Announcements

Joint meeting of the Sixth International Symposium on Drug Analysis and the Ninth International Symposium on Pharmaceutical and Biomedical Analysis Brussels, Belgium 11–15 May 1998

Drug analysis '98 is organised by The Belgian Society of Pharmaceutical Sciences. The purpose of Drug Analysis '98 is to bring people together from Industry, Government, Universities, Control Laboratories and Hospitals to discuss the current status of analytical techniques including instrumental applications and theoretical developments.

Topics: the main scientific themes will include;

- Separation of enantiomeric drugs.
- Sample pretreatment and automated analysis
- Recent developments in separation methods
- Techniques for high sensitivity analysis of drugs
- Computer-aided methods
- Method validation, quality assurance and regulatory issues
- Analysis of biotechnology products
- Quality control of bulk drugs and dosage forms
- Bioanalysis of drugs and metabolites.

Second circular and call for papers

The second circular will be sent on request at the above address. It will include guidelines for submission of abstracts, preliminary information about the programme and information about registration and accommodation arrangements.

For further information please contact:

ORGA-MED Congress Office, Essenestraat 77, B-1740 Ternat, Belgium. Tel.: + 32 2 5820852; fax: + 32 2 5825515

PII S0039-9140(97)00104-5

American Microchemical Society 1998, A.A. Benedetti-Pichler Award

The American Microchemical Society seeks nominations for 1998 A.A. Benedetti-Pichler Award in Microchemistry. Nominations and eligibility are not restricted to members of the Society. Nominees from past years are eligible for renomination, although all information, including letters of nomination, should be updated and resubmitted.

The selection of the A.A. Benedetti-Pichler Award recipient is based on service to analytical microchemistry in its broadest sense, which includes research achievements in a wide variety of disciplines of analytical chemistry and chemical measurements. The award also recognizes administration, teaching, or other means that promote the advance of microchemistry.

The nominating documents should include at least three letters of nomination, and a professional summary with a bibliography of publications. The letters of nomination should emphasize the candidate's accomplishments. The deadline for nominations is Friday, October 24, 1997. The award consists of a plaque, and travel expenses to the Fall 1998 Eastern Analytical Symposium and Exposition, at which a symposium will be held in the awardee's honor.**All documents should be sent to:**
Professor Robert G. Michel, Chair, A.A. Benedetti-Pichler Award Committee, c/o Department of Chemistry, University of Conneticut, 215 Glenbrook Road, Storrs, CT 06269 4060, USA. Tel.: +1 860 4863143; e-mail: michel@uconnvm.uconn.edu

Past awardees have been:

1966	J.F. Alicino	1981	P. Flashka
1967	Felix L. Schneider	1982	P. Lott
1968	W. Kirsten	1983	Louis Meites
1969	B.B. Cunningham	1984	B. Zak
1970	Walter C. McCrone	1985	Lockhart 'Buck' Rogers
1971	L.T. Skeggs	1989	K.L. Cheng
1972	L.C. Craig	1990	Peter W. Carr
1974	E. Sawicki	1991	Nicholas Winograd
1975	Petr Zuman	1992	Robert G. Michel
1976	T.S. Ma	1993	Peter C. Uden
1977	George H. Morrison	1994	Isiah M. Warner
1978	Joseph Jordan	1995	Leslie C. Ebdon
1979	A. Steyermark	1996	Daniel W. Armstrong
1980	H. Alber	1997	John G. Dorsey

ELSEVIER

Talanta 45 (1997) 229–235

Talanta

Limits of detection for an AOTF-FFP spectrometer in ICP atomic emission spectroscopy

D.P. Baldwin *, D.S. Zamzow

Ames Laboratory, USDOE, 9 Spedding Hall, Iowa State University, Ames, IA 50011, USA

Received 7 November 1996; accepted 7 November 1996

Abstract

Limits of detection for a number of elements both in air and in argon inductively coupled plasma atomic emission spectroscopy (ICPAES) have been determined using a high-resolution interferometric spectrometer (HiRIS) that consists of an acousto-optic tunable filter, a fiber-optic Fabry-Perot interferometer, and a photon-counting PMT detector. Detection limits using the HiRIS are comparable to those determined using a 1.5 m focal-length grating spectrometer, which has resolution similar to that of the HiRIS. Differences between the two spectrometer systems and the two plasma systems are discussed. The portability and versatility of the HiRIS make it a useful alternative for field or on-line measurements using ICPAES. The high-resolution capabilities allow the HiRIS to replace large grating spectrometers for resolution of isotopic and complex spectra. © 1997 Elsevier Science B.V.

Keywords: Atomic emission spectroscopy; High-resolution spectroscopy; Spectrometer

1. Introduction

High-resolution spectrometers are required in many fields of optical spectroscopy. Inductively coupled plasma atomic emission spectroscopy (ICPAES) is one of these. Although commercial ICPAES systems are routinely used for a wide variety of analytical applications [1], there are a number of situations for which commercial systems lack sufficient resolution to be useful. Most notable among these is the determination of complex mixtures of actinide isotopes, an application for which long focal-length grating spectrometers have previously been used [2–4].

A high-resolution interferometric spectrometer (HiRIS) consisting of two solid-state optical components developed primarily for the communications industry, an acousto-optic tunable filter (AOTF) and a fiber-optic Fabry-Perot (FFP) interferometer, has recently been described for detecting optical emission from an ICP [5]. The AOTF is a TeO_2 crystal coupled to a radio-frequency (RF) acoustic driver. Application of a narrow band of RF power deflects a portion of the selected wavelength interval from a polychromatic light source [6–8], acting as a prefilter to select a narrow band of optical radiation from the ICP. The deflected light is introduced into the FFP, a specialized Fabry-Perot interferometer produced by Micron Optics, Inc. [9,10]. All

* Corresponding author.

PII S0039-9140(97)00143-4

Fabry-Perot interferometers operate on the principle of constructive and destructive interference of light within a linear cavity [11,12]. When the cavity spacing is an integral number of wavelengths, the device transmits light; when the spacing is non-integral, light is reflected back toward the source. Conventional Fabry-Perot interferometers have mirrored coatings on the surfaces of air-spaced optical flats. In contrast, for the FFP, the cavity mirrors are coated directly on the faces of a pair of single-mode fibers [9,10]. Voltage applied to a concentric piezoelectric driver changes the free-air gap between the coated fiber faces, thereby scanning the cavity to produce a high-resolution spectrum. The finesse of FFP interferometers is typically a few hundred to as high as 4000 [13], while that for a conventional bulk optical Fabry-Perot is generally less than 100. The HiRIS, combining AOTF and FFP technologies, has been shown to have high resolution, sufficient for determining hyperfine and isotopic emission lines in ICPAES experiments [5].

The HiRIS system is designed to provide a compact, high-resolution spectrometer for measurements of isotopic abundances of uranium using ICPAES in applications where alternative systems are too large and expensive or are unable to provide the required spectral resolution. These alternatives include large grating spectrometers, at least 1.5 m in focal length, and mass spectrometers. A 1.5 m spectrometer may be too large for applications such as field measurements using ICPAES [14], mobile laboratory settings, process line measurements, and stack monitoring. The prototype HiRIS assembled in this laboratory is less than 0.5 m long and weighs less than 20 pounds, whereas a 1.5 m monochromator weighs several hundred pounds. Although mass spectrometers have sufficient resolution to distinguish U isotopes, most ICPMS systems are incapable of resolving isobaric interferences in mixtures of actinides. Optical spectroscopy using a spectrometer capable of resolving isotopic emission lines (such as the HiRIS) provides a method for determining complex mixtures of actinides, including isobaric interferences. Potential limitations of the HiRIS include a limited tuning range (395–430 nm for the prototype) and some non-linearity in tuning the FFP as discussed in a previous study [5]. However, for the intended use of this system, analytical determination of isotopic abundances of actinides in ICPAES, these limitations are not significant.

In this paper, we will present detection limits for ICPAES in air and argon plasmas using the HiRIS for a number of elements with strong emission lines in the optical range of the HiRIS. We will also determine detection limits for a Czerny-Turner grating spectrometer with similar resolution. We will discuss differences between the air and argon plasmas as well as between the HiRIS and grating systems. Our discussion includes consideration of the impact of the AOTF efficiency on detection limits, the source of noise in the measurements, and the impact of detector choice and spectrometer configuration on the limits of detection.

2. Experimental

The ICP used in these experiments is an RF Power Products HFL 5000D 5 kW, 40.68 MHz system. The ICP is operated using either argon or air as the plasma and sample gases. The operation of this system as an air plasma is described in a previous publication [15]. The operating conditions for the argon plasma are: 16, 1.2, and 0.7 lpm flow in the outer, intermediate, and central channels of a low-flow torch (model 370-71, Precision Glassblowing of Colorado); RF power of 1.1 kW; and an observation height of 15 mm above the load coil. The conditions for the air plasma are: 22, 1.2, and 0.7 lpm flow in the outer, intermediate and central channels; RF power of 2.7 kW; and an observation height of 5 mm. Aqueous solutions are prepared by volumetric dilution of standard solutions (High Purity Standards, Inc.) in 1% nitric or hydrochloric acid diluent. A peristaltic pump is used to deliver these solutions to a CETAC U-5000AT ultrasonic nebulizer at a flow rate of 2.1 ml min^{-1}. Under these conditions, analytes are delivered to the ICP with approximately 15% efficiency as a dry aerosol [15].

The design of the HiRIS system and its resolution performance have been described elsewhere

[5]. The optical and electronic schematic of the HiRIS is shown in Fig. 1. In brief, light from the emission source (ICP) is imaged at an adjustable aperture. This light is re-imaged with a single lens at $f(8)$ through a Brimrose model TEAF-.37-.43 AOTF. The nominal wavelength range for the AOTF is 370–430 nm, and the 3 dB bandwidth is less than 0.6 nm. The AOTF is driven by a Brimrose model PP frequency driver controlled through the parallel port of the data-acquisition personal computer. The deflected beam from the AOTF is re-imaged at 8 × demagnification onto the input face of the single-mode optical fiber of the FFP. This demagnification overfills the acceptance angle of the input fiber, minimizing sensitivity to alignment. The FFP (Micron Optics, Inc.) has a free spectral range of approximately 1500 GHz, a finesse of approximately 200, and a tuning range of 350–440 nm. As described previously [5], below 395 nm the input and output fibers are not single mode. The multiple modes prevent effective use of the high-resolution capabilities of the system below 395 nm. Above 430 nm the reflectance

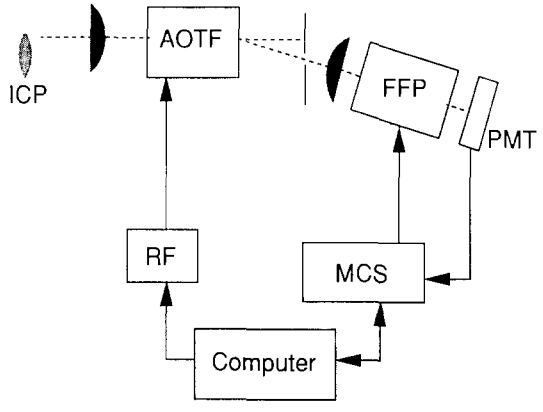

Fig. 1. A block diagram of the experimental apparatus is presented. The emission source is an inductively-coupled plasma (ICP). Light from the plasma is focused through the AOTF and the diffracted beam is reimaged onto the input face of a single mode fiber optic. The fiber optic is at one end of the fiber-optic Fabry-Perot interferometer (FFP). The high resolution transmission is detected by a photon-counting photomultiplier tube (PMT). Data is accumulated using a multichannel scaler, which synchronously scans the FFP. A laboratory computer is used to control the AOTF and the MCS as well as to store and analyze the data.

of the FFP cavity mirrors declines and the resolution of the device is degraded. Therefore, the effective range for the device for high-resolution single-mode operation is 395–430 nm. Within this range, the linewidth is 0.0025–0.005 nm. Tuning of the FFP is accomplished by applying a voltage to the piezoelectric tuning element using a computer-controlled 14-bit digital-to-analog converter. The output of the FFP is detected using a Hamamatsu H6180-01 photon-counting photomultiplier tube assembly. The TTL pulses from the detector are counted using a multichannel scaler (EG&G Turbo-MCS).

Operation of the HiRIS is controlled by a laboratory personal computer running custom software written using LabWindows (National Instruments). This software coordinates selection of the AOTF wavelength (drive frequency), tuning of the FFP cavity, and operation of the multichannel scaler. Applications are included that allow wavelength calibration of the AOTF, spectral data collection, and measurement of the time evolution of a signal. Data are accumulated by obtaining a spectrum of the ICP emission at a fixed AOTF wavelength, selecting a peak position for the FFP, and monitoring the time evolution of signal at that peak wavelength. Limits of detection (LOD), in ppm, are calculated using the formula:

$$\mathrm{LOD} = 3\sigma_b C_s/(I_s - I_b)$$

where C_s is the concentration (ppm) of the standard solution, I_s is the average peak intensity (cps) for the analyte for 30 1-s integrations, I_b is the average background intensity (cps) for 30 1-s integrations, and σ_b is the S.D. (cps) in the background intensity.

The efficiency of the AOTF was measured as a function of wavelength. Laser pulses from an excimer-pumped dye laser were transmitted through an optical fiber bundle to the input of the HiRIS. The laser dye was PBBO, tunable from 390–420 nm. A Glan-Taylor polarizer was placed in front of the AOTF and adjusted to allow only vertically-polarized light to pass through the AOTF. A silicon photodiode was placed in the undeflected laser beam with an ND-3.0 neutral density filter protecting the detector from satura-

Table 1
Limits of detection (LOD) for ICPAES operated using: (I) air as the sample and plasma gas and the high resolution interferometric spectrometer (HiRIS), (II) Ar as the gas and the HiRIS, and (III) Ar and a SOPRA 1.5 m monochromator equipped with a photodiode array detector

Element	Line (nm)	Conc. (ppm)	3σ-LOD (ppm)		
			I	II	III
Al(I)	396.152	100	1.1	1.9	0.55
Ca(II)	396.847	10	0.019	0.013	0.0052
Nd(II)	401.225	100	1.2	1.2	0.59
Th(II)	401.913	100	0.84	0.75	0.72
Mn(I)	403.076	100	0.88	2.4	1.4
Pb(I)	405.783	100	1.6	5.4	5.3
Sr(II)	407.771	10	0.0068	0.0072	0.0033
La(II)	408.672	100	0.14	0.14	0.24
U(II)	409.014	100	3.1	2.9	4.1
Ba(II)	413.066	50	0.48	0.30	0.48
Ce(II)	413.765	100	0.81	0.52	1.1
Y(II)	417.754	10	0.099	0.057	0.14
Ca(I)	422.670	10	0.049	0.17	0.45
Sc(II)	424.683	100	0.015	0.014	0.041

tion. For each wavelength, an ND-0.3 filter was used to check for saturation by placing it in the beam path and checking for 3 dB reduction in signal. The output of the photodiode was integrated and amplified using a Stanford Research Systems gated integrator. The output from the integrator was introduced into an analog-to-digital converter (National Instruments AT-MIO-16F-5). Thirty 1-s integrations were collected for a background (laser beam blocked), signal with the AOTF driver turned off, and signal with the driver power at maximum (~ 2 W). The efficiency of deflection was measured at 5 nm intervals from 395–415 nm. The efficiency for linearly-polarized light varied smoothly from 6% at 395 nm to 44% at 415 nm. A single point was measured at a higher wavelength (441.56 nm) using a continuous-wave HeCd laser and removing the gated integrator from the detection system. The efficiency at this wavelength was 30%. In the following sections we will discuss the impact of this variation in AOTF efficiency on ICPAES limits of detection.

For comparison, detection limits for the same analytical lines were measured for an argon plasma using a 1.5 m monochromator (Sopra, model UHRS 1500), equipped with a 3600 G mm^{-1} grating and a photodiode array (PDA) detector (EG&G model 1453). In previous work, the resolution of this spectrometer was shown to be comparable to that of the HiRIS [5]. The input slit is 25 μm wide, and the output of the spectrometer is passed through a 6 × beam expander and imaged onto the 1024 element array of 2.5 mm × 25 μm diodes. A spectrum is accumulated with the plasma off in order to subtract the dark current from the data. This dark current is typically 330 cps at −5°C (equivalent to 1 million photoelectrons per second) but is stable and constant to ±1 cps. Spectra are accumulated for 30 1-s integrations of the plasma with and without the analyte, and the peak and background intensities and the S.D. of the background are used to calculate the LOD as described above.

3. Results and discussion

The limits of detection determined in this study are shown in Table 1. For each element, the peak wavelength and the concentration of the standard solution are presented along with LOD values for (I) the air plasma ICP using the HiRIS system, (II) the argon plasma using the HiRIS system,

and (III) the argon plasma using the 1.5 m grating spectrometer and a PDA detector. Examination of these results shows that the detection limits for all three combinations are comparable and that no system is best in all cases or dominates the others by as much as a factor of 5 in any instance. However, some valuable information may be obtained from specific comparisons. No significant trend in the ratio of detection limits for the air and argon plasmas (columns I and II) is observed as a function of wavelength. However, four emission lines give detection limits that are markedly superior for the air plasma. These four lines are neutral-atom emission lines, whereas, the others are ion lines. The optical alignment for each of the three configurations is optimized using an ion line, the La 408.672 nm emission line. For a given observation height optimized for ion signals, the air plasma results in more favorable signal levels for atom emission than does the argon plasma. This difference in optimal observation heights is a well-known phenomenon for argon ICP [16], attributed to the depletion of non-ionized atoms at the high temperature region, where ion emission is strongest. For optimal viewing of atoms, one may select a region higher above the load coil where the plasma is cooler, and more of the analyte is in a non-ionized state. In practice, a compromise is achieved between atomic and ionic detection when both are important. However, the plasma temperature in the air ICP is cooler than that for the argon ICP [17], and a higher proportion of atoms are present at the height that is optimal for ion viewing. This is an advantage of air ICP in instances where both atomic and ionic species are being monitored.

A comparison of LOD values for the grating spectrometer and the HiRIS is presented in Fig. 2. The symbols represent the ratios of the LOD for the grating spectrometer to the HiRIS (with respect to the right axis). These points are plotted as a function of the wavelength of the observations. The line in this plot is a fourth-order linear-least-squares fit to the measured AOTF efficiency (for linearly-polarized light). This line is plotted with respect to the left axis in the figure. There is an obvious trend in the ratioed data as a function of wavelength. Below 410 nm, the grating spectrometer has superior detection limits. Between 410 and 425 nm the HiRIS has superior detection limits. Much of this difference is directly attributable to the variable efficiency of the AOTF. When the efficiency is greater than 15% for linearly-polarized light, the detection limit for the HiRIS is superior. Therefore, if an AOTF with efficiency greater than 15% over the entire tuning range of the FFP were used, it is likely that the LOD values for the HiRIS would exceed those of the grating spectrometer. Since the correlation of the two is not perfect, and the data is somewhat scattered, we cannot claim that this would be true in all instances and that no other factors may be involved.

This comparison of the HiRIS and the grating spectrometer is performed under a particular set of conditions, including slit width, integration times, and detectors. An input slit width of 25 μm is used for the grating spectrometer because the resulting resolution is comparable to that of the HiRIS. This slit width is not optimal for best resolution of the spectrometer. Although the output resolution is determined by the width of the PDA elements (25 μm), the 6 × beam expander in front of the PDA would indicate an optimum input slit width of approximately 4 μm. However,

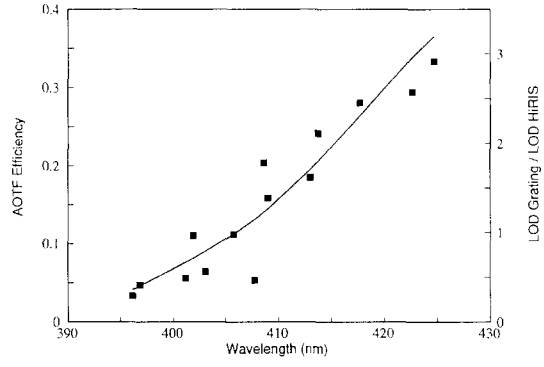

Fig. 2. The line is a fourth-order linear-least-squares fit to measured values of the AOTF efficiency for linearly-polarized laser light. This line is plotted as a function of wavelength versus the left axis. The data points are ratios of detection limits determined using the HiRIS spectrometer and a 1.5 m monochromator. These points are plotted against the right axis. The degradation in sensitivity of the HiRIS at lower wavelengths is largely attributed to the decrease in AOTF effciency at these wavelengths.

setting the slit to 4 μm would provide better resolution at the cost of a significant reduction in sensitivity for the grating spectrometer. A much more meaningful comparison is made possible by matching the resolution for the two systems and comparing sensitivity. In addition, improved instrumental resolution would not be significant, since the temperature- and pressure-broadened emission lines for the ICP are at least as broad as the instrumental bandwidth of the HiRIS.

Use of a PDA detector in these experiments is a choice of convenience. The 0.5 nm wavelength span of the array makes careful optimization of the spectrometer wavelength unnecessary. Comparison of the HiRIS and PDA detection systems is easy because both are designed for integration of timed exposures. However, detection limits using the PDA are predominantly defined by digitization error and the variation in the large dark current inherent in photodiode detectors, whereas the HiRIS photon-counting detection system is essentially shot-noise limited. As stated earlier, the dark current in the PDA is equivalent to approximately 1.5 million photons striking the detector, or approximately 1 million photoelectrons per second. The shot-noise limit for this signal is approximately 1000 photoelectrons or 1/3 of one count. A single count of digitization noise is larger than the shot-noise limit. The background signal (with dark current subtracted) for the PDA measurements is typically 3–5 counts (10 000–15 000 photoelectrons). The shot-noise limit for this background is approximately 100 photoelectrons or 1/30 of one count. Typical S.D. for the PDA background measurements are 0.5–0.9 cps, which is equivalent to the digitization noise. By comparison, the HiRIS detector has a dark current of less than 10 photons per second. The shot-noise limit for this background is approximately 3 photons per second. Typical background levels using the HiRIS are 70–90 (25–40) photons per second including dark current for the argon (air) plasma, and the S.D. are essentially the shot-noise limit of 8–9 (5–6) photons per second. Therefore, by increasing the integration time, the LOD for the PDA system would decrease linearly until the shot-noise limit associated with the dark current became significant. This would occur at an integration time of approximately 2–3 s. On the other hand, the LOD for the HiRIS would still be limited by the shot noise of the background at longer integration times, resulting in only a square-root improvement in detection limit. As a result, the relative detection limit for the PDA compared to the HiRIS could be improved by as much as 70% by increasing the integration time from 1 to 3 s.

If we had selected a PMT detector for the grating spectrometer, we would have had to utilize 25 μm input and output slits in order to obtain a resolution of 0.0025 nm (grating dispersion of 0.10 nm mm^{-1}). This change in detectors would result in a reduction in quantum efficiency of approximately 7 (70% for the PDA and ~ 10% for a PMT). The background levels observed with the PDA would be reduced from approximately 15 000 photoelectrons per second to approximately 2000 photoelectrons per second for the PMT. This background is 25 times larger than that for the HiRIS. Assuming the same resolution, the signal-to-background ratio would be the same for a spectrometer equipped with a PMT and for the HiRIS. Therefore, given 25 times higher signal and background levels for a PMT, we would expect such a system to provide shot-noise limited LODs 5 times better than the HiRIS. However, much of this advantage could be eliminated by the use of a more efficient AOTF in the HiRIS.

Finally, comparing air-plasma detection limits in this work with those reported under similar conditions in a previous study [15] reveals a difference in detection limits of a factor 26 [U(II) and Sr(II)] to 800 [Mn(I)] between the HiRIS and the 0.5 m monochromator with a PDA detector used in that study. It should be noted that the detection limits in this previous study were at significantly poorer resolution (approximately 0.02–0.03 nm compared with 0.0025–0.005 nm) and with a 10 s integration time. At that resolution, interferences by molecular emission in the air ICP are significant and limit the selection of analytical lines. No significant interferences were noted using the HiRIS in the current study.

4. Conclusion

In applications where the resolution of the HiRIS is necessary, such as for resolution of isotopes of actinide elements or resolution of lines that are overlapped by other emission lines in a complex matrix, this system performs as well as comparable grating-based spectrometers. The current system provides LOD values limited by the shot-noise limit of the background. Therefore, the low efficiency of the AOTF in the current system is a limiting factor. The lower cost, rapid tuning afforded by the AOTF, lower weight, and smaller size compared to a 1.5 m grating spectrometer makes this system an attractive option in many field and laboratory applications. In combination with an air-plasma ICP system, this spectrometer is a valuable tool for monitoring of actinides and heavy metals in waste streams and off-gases.

Acknowledgements

The authors would like to thank Dr. Kevin Carney of Argonne National Laboratory—West and Dr. George Miller of Mississippi State University for their support of this work. We would also like to thank Mr. Royce Winge for helpful discussions. This work was funded by Argonne National Laboratory—West and Mississippi State University. Ames Laboratory is operated for the US Department of Energy by Iowa State University under contract No. W-7405-ENG-82.

References

[1] G.A. Meyer, P.N. Keliher, An overview of analysis by inductively coupled plasma-atomic emission spectrometry, in: A. Montaser, D.W. Golightly (Eds.), Inductively Coupled Plasmas in Analytical Atomic Spectrometry, 2nd ed., VCH Publishers, New York, 1992, Chapter 10.

[2] M.C. Edelson, E.L. DeKalb, R.K. Winge, V.A. Fassel, Spectrochim. Acta 41B (1986) 475.

[3] M.C. Edelson, V.A. Fassel, Anal. Chem. 53 (1981) 2345.

[4] M.C. Edelson, High-resolution plasma spectrometry, in: A. Montaser, D.W. Golightly (Eds.), Inductively Coupled Plasmas in Analytical Atomic Spectrometry, 2nd ed., VCH Publishers, New York, 1992, Chapter 7.

[5] D.P. Baldwin, D.S. Zamzow, A.P. D'Silva, Appl. Spectrosc. 50 (1996) 498.

[6] C.D. Tran, Anal. Chem. 64 (1992) 971A.

[7] P.J. Treado, I.W. Levin, E.N. Lewis, Appl. Spectrosc. 46 (1992) 553.

[8] C.D. Tran, R.J. Furlan, J. Lu, Appl. Spectrosc. 48 (1994) 101.

[9] K. Hsu, C. Miller, Photonics Spectra 27 (1993) 135.

[10] C. Miller, Characteristics and Applications of High Performance, Tunable, Fiber Fabry-Perot Filters, the 41st ECTC Conf. Digest, Session X, Atlanta, GA, May, 1991, pp. 489–492.

[11] J.M. Vaughan, The Fabry-Perot Interferometer, Adam Hilger, Bristol, England, 1989.

[12] Burleigh Instruments, Inc., Tech Memo on Fabry-Perot Interferometry, Fishers, NY.

[13] C. Miller, K. Hsu (Micron Optics, Inc., Atlanta, GA), pers. comm.

[14] D.S. Zamzow, D.P. Baldwin, S.J. Weeks, S.J. Bajic, A.P. D'Silva, Environ. Sci. Technol. 28 (1994) 352.

[15] D.P. Baldwin, D.S. Zamzow, A.P. D'Silva, J. Air Waste Manage. Assoc. 45 (1995) 789.

[16] M. Thompson, R.M. Barnes, Analytical performance of inductively coupled plasma-atomic emission spectrometry, in: A. Montaser, D.W. Golightly (Eds.), Inductively Coupled Plasmas in Analytical Atomic Spectrometry, 2nd ed., VCH Publishers, New York, 1992, Chapter 5.

[17] A. Montaser, K.D. Ohls, D.W. Golightly, Inductively coupled plasmas in gases other than argon, in: A. Montaser, D.W. Golightly (Eds.), Inductively Coupled Plasmas in Analytical Atomic Spectrometry, 2nd ed., VCH Publishers, New York, 1992, Chapter 19.

ELSEVIER

Talanta 45 (1997) 237–248

Talanta

Principles and analytical applications of acousto-optic tunable filters, an overview

Chieu D. Tran

Department of Chemistry, Marquette University, P.O. Box 1881, Milwaukee, WI 53201-1881, USA

Received 22 November 1996; accepted 19 February 1997

Abstract

Advantages of acousto-optic tunable filters have been exploited to develop novel analytical instruments which are not feasible otherwise. The instrumentation development and unique features of such AOTF based instruments including the multidimensional fluorimeter, the multiwavelength thermal lens spectrometer, the near-infrared spectrometer based on erbium doped fiber amplifier (EDFA), and detectors for high performance liquid chromatography (HPLC) and flow injection analysis (FIA), will be described. © 1997 Elsevier Science B.V.

1. Introduction

Acousto-optic tunable filter (AOTF) is an all-solid state, electronic dispersive device which is based on the diffraction of light in a crystal [1–9]. Light is diffracted by an acoustic wave because when an acoustic wave propagates in a transparent material, it produces a periodic modulation of the index of refraction (via the elasto-optical effect). This, in turn, will create a moving grating which diffracts portions of an incident light beam. The diffraction process can, therefore, be considered as a transfer of energy and momentum. However, conservation of the energy and momentum must be maintained. The equation for conservation of momentum can be written as [1]:

$$\boldsymbol{k}_d = \boldsymbol{k}_i \pm \boldsymbol{k}_s \quad (1)$$

where $\boldsymbol{k}_i$, $\boldsymbol{k}_d$ and $\boldsymbol{k}_a$ are the wave vector of the incident and diffracted light, and of the phonon.

In the case of the AOTF, the acousto-optic interaction occurs in an anisotropic medium, and the polarization of the diffracted beam is orthogonal to that of the incident beam. The momenta of incident and diffracted photons are:

$$|\boldsymbol{k}_i| = 2\pi n_i/\lambda \quad (2)$$

$$|\boldsymbol{k}_d| = 2\pi n_d/\lambda \quad (3)$$

They are not equal since one is ordinary ray and the other is extraordinary ray (i.e. $n_i \neq n_d$).

In the case of collinear AOTF, the incident and diffracted light beams, and the acoustic beam are all collinear. If the incident light is an extraordinary and the diffracted light is an ordinary ray, the momentum matching condition becomes:

$$\boldsymbol{k}_d = \boldsymbol{k}_i - \boldsymbol{k}_s \quad (4)$$

$$f_s = v_s(n_e - n_o)/\lambda \quad (5)$$

PII S0039-9140(97)00146-X

where $|\boldsymbol{k}_s| = 2\pi f_s/v_s$ and f_s and v_s are the frequency and velocity of the acoustic wave. Eq. (5) can be generalized for all types of AOTFs including the collinear and the noncollinear AOTFs:

$$f_s = \frac{v_s(n_e - n_o)(\sin^4\theta_i + \sin^2 2\theta_i)^{1/2}}{\lambda} \quad (6)$$

where θ_i is the incident angle. When $\theta_i = 90°$ Eq. (6) reduced to Eq. (5), i.e. the case of collinear.

It is thus evidently clear that in an anisotropic crystal, where the phase matching requirement is satisfied, diffraction occurs only under optimal conditions. These conditions are defined by the frequency of the acoustic waves and the wavelength of a particular diffracted light. For a given acoustic frequency, only light whose wavelength satisfies either Eq. (5) or Eq. (6) is diffracted from the crystal. The filter can therefore, be spectrally tuned by changing the frequency of the acoustic waves (i.e. f_s).

Generally, the AOTF is fabricated from an anisotropic TeO_2 crystal and onto it an array of $LiNbO_3$ piezoelectric transducers are bonded. A radio frequency (RF) signal is applied to the transducers which, in turn, generates an acoustic wave propagating through the TeO_2 crystal. These propagating acoustic waves produce a periodic moving grating which will diffract portions of an incident light beam. A light beam propagating as an e-ray is converted into an o-ray and in addition, is spatially separated from the original e-ray by interaction with, and diffraction from, an acoustic wave propagating in the same medium [1–9]. As illustrated in Eq. (6), for a fixed acoustic frequency and sufficiently long interaction length, only a very narrow band of optical frequencies can approximately satisfy the phase matching condition and be diffracted. The wavelength of the diffracted light can therefore, be tuned over large spectral regions by simply changing the frequency of the applied RF signal. The scanning speed of the filter is defined by the speed of the acoustic wave in the crystal, which is on the order of microseconds (μs). As a consequence, compared to conventional gratings, the AOTFs offer such advantages as being all-solid state (contains no moving parts), having rapid scanning ability (μs), wide spectral tuning range and high throughput, allowing high speed random or sequential wavelength access, and giving high resolution (a few angstroms). The AOTF has offered unique means to develop novel instruments which are not possible otherwise. The instrumentation development and unique features of such AOTF based instruments including the multidimensional fluorimeter, the multiwavelength thermal lens spectrometer, the near infra-red spectrometer based on erbium doped fiber amplifier (EDFA), and detectors for high performance liquid chromatography (HPLC) and flow injection analysis (FIA), will be highlighted in this overview.

2. Applications in spectroscopy

2.1. AOTF-based fluorimeter

Fluorescence technique has been demonstrated to be a sensitive method for trace characterization. Since realtime samples are generally mixtures of many different compounds, their analyses usually require measurements of the fluorescence spectra at different excitation wavelengths (because absorption spectra of compounds in the mixture are different). Fluorimeter based on multichannel detection (e.g. videofluorimeter) has been developed to alleviate this time consuming process [10,11]. While the instrument has proven to be a very powerful method for the determination of multicomponent trace chemical species, its applications are still limited because of such factors as high cost, low sensitivity, slow in the data acquisition (the fastest is on the order of milliseconds) and complicated data analysis [10,11]. These limitations can be eliminated if the AOTF is used to develop a new generation multidimension spectrofluorimeter.

As explained above, an incident white light is diffracted by the AOTF into a specific wavelength when a specific RF is applied to it. It is important it realize that the diffracted light needs not be a monochromatic light. Multiwavelength light can be diffracted from the AOTF when more than one RF signals are simultaneously applied into the filter [1–9]. As a consequence, the AOTF can be used as a polychromator. Compared to con-

ventional polychromators, advantages of this electronic AOTF polychromator include its ability to individually amplitude-modulate each wavelength of the diffracted multiwavelength light at different frequency. This is accomplished by individually and sinusoidally modulating each applied RF signal at a different frequency. This feature together with the fast scanning ability make the AOTF to be uniquely suited for the development of a novel, all solid-state, nonmoving parts multidimensional spectrofluorometer.

The schematic diagram of the AOTF based multidimensional fluorimeter is shown in Fig. 1 [2,3]. Two AOTF's were used in this instrument: one for excitation and the other for emission. The first AOTF was used to specifically diffract white incident light into a specific wavelength(s) for excitation. Depending on the needs, the second AOTF (i.e. the emission AOTF) can be used as either a very fast dispersive device or a polychromator. In the first configuration (i.e. the rapid scanning fluorimeter), the sample was excited by a single excitation wavelength; the emitted light was analyzed by the emission AOTF which was scanned very fast. A speed of 4.8 Å μs^{-1} was found to be the fastest speed which the AOTF can be scanned with a reasonable S/N and resolution. With this speed, a spectrum of 150 nm can be measured in 312 μs. Faster scanning is possible, but because of the limitation due to the speed of the acoustic wave, may undesiredly lead to the degradation in the S/N and spectral resolution [2,3]. In the second configuration (i.e. multidimensional fluorimeter), both AOTFs were used as a polychromator. Several different RF signals were simultaneously applied into the first AOTF to provide multiple excitation wavelengths. The emission was simultaneously analyzed at several wavelengths by the emission AOTF. With this configuration, the fluorimeter can be used for the analysis of multicomponent samples, and the maximum number of components it can analyze is, in principle, $a \times b$ where a and b are the number of excitation and emission wavelengths, respectively [3]. In fact, multicomponent samples, e.g. mixtures of rhodamine-B, fluorescein, eosin and 4-(dicyanomethylene)-2-methyl-6-[p(dimethylamino)styryl]-4-H-pyran (DMP) can be simultaneously analyzed at a limit of detection of 10^{-10} M [2,3].

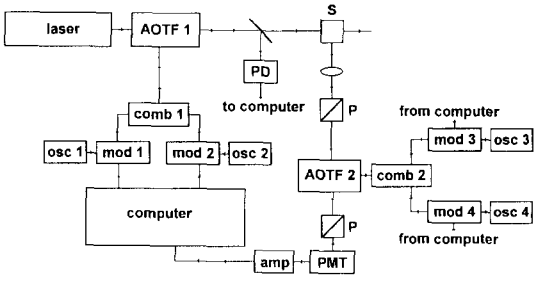

Fig. 1. Schematic diagram of the AOTF based fluorimeter: PD, photodiode; S, sample; P, polarizer; PMT, photomultiplier tube; amp, amplifier; osc, oscillator; mod, modulator; comb, combiner.

2.2. AOTF-based thermal lens spectrophotometer

The fluorescence technique is very sensitive and can be used for the determination of trace chemical species at very low concentration. However, the technique is not applicable to all compounds because only few molecules are fluorescent. Therefore, it is important that a novel technique which has the same sensitivity as the fluorescence technique, but is applicable to non-fluorescent compounds be developed. Thermal lens technique is one of such possibilities.

The thermal lens technique is based on the measurement of the temperature rise that is produced in an illuminated sample by nonradiative relaxation of the energy absorbed from a laser [12–17]. Because the absorbed energy is directly measured in this case, the sensitivity of the technique is similar to that of the fluorescence technique, and is relatively higher than the conventional absorption measurements. In fact it has been calculated and experimentally verified that the sensitivity of the thermal lens technique is 237 times higher than that by conventional absorption techniques, when a laser of only 50 mW power was used for excitation [12–17]. Absorptivities as low as 10^{-7} have been measured using this ultrasensitive technique [12–17]. Potentially, the technique should serve as an excellent method for trace chemical analysis because it has high sensi-

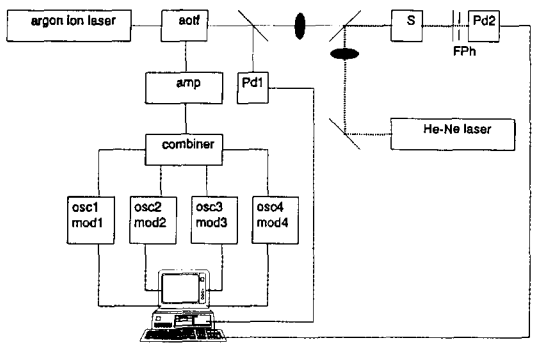

Fig. 2. Schematic diagram of the multiwavelength thermal lens spectrometer based on an AOTF as a polychromator: amp, RF power amplifier; osc, oscillator; mod, sinusoidal modulator; PIN, photodiode; F, interference filter; Ph, pinhole.

tivity, in situ and non-destructive ability, and requires a minimum amount of sample. Unfortunately, its applications to the area of general trace chemical analysis are not so widespread in comparison to other spectrochemical methods. A variety of reasons might account for its limited use, but the most likely one is probably due to the low selectivity. The majority of reported thermal lens spectrometers employ only a single excitation wavelength [12–17], and as a consequence can only be used for the analysis of one component samples. A multiwavelength thermal lens spectrometer is needed to analyze, in realtime, multicomponent samples without any pretreatment. AOTF offers a unique means for the development of the first, all solid state, no-moving part fast scanning multiwavelength thermal lens instrument.

The schematic diagram of the AOTF based multiwavelength thermal lens spectrometer is shown in Fig. 2 [4,18]. This instrument is based on the use of the AOTF as a polychromator. An argon ion laser operated in the multiline mode was used as the light source. This multiwavelength laser beam was converted into the excitation beam with appropriate number of wavelengths by means of a TeO_2 AOTF. In this cased, four different wavelengths were used. They were obtained by simultaneously applying four different RF signals to the AOTF. These RF signals were provided by four different oscillators (oscl, osc2, osc3 and osc4). To differentiate each wavelength from the others, the applied RF's were sinusoidally amplitude modulated at four different frequencies by four modulators (modl, mod2, mod3 and mod4). The four AM modulated RF signals were then combined by means of a combiner, and amplified by a RF power amplifier (amp). The amplified, AM modulated signal was then applied onto the AOTF to enable it to diffract the incident multiline laser beam into beam which has the four different wavelengths. The probe beam, provided by a He-Ne laser, was aligned to overlap with the pump beam at the sample cell by means of a dichroic filter (DF). The heat generated by the sample absorption of the pump beams changes the intensity of the probe beam. The intensity fluctuation of the probe beam was measured by a photodiode (PD2) placed behind a 632.8 nm interference filter (F) and a slit (S). A lens was used to focus the probe beam, and the distance between this lens and the sample was adjusted to give maximum thermal lens signals. The signal intensity, measured as the relative change in the probe beam center intensity, was recorded by a microcomputer through an AD interface board [4,18].

Compared with other multiwavelength thermal lens instruments, this all solid state thermal lens spectrophotometer has advantages which include its ability to simultaneously analyze multicomponent samples in microsecond time scale, without the need for any prior sample preparation. In fact, with this apparatus and with the use of only 12 mW multiwavelength excitation beam, multicomponent samples including mixtures of lanthanide ions (Er^{3+}, Nd^{3+}, Pr^{3+} and Sm^{3+}) can be simultaneously determined with a LOD of 10^{-6} cm^{-1} [18].

2.3. Near infra-red spectrophotometer based on the AOTF and an erbium doped fiber amplifier

The use of the near infra-red spectrometry in chemical analysis has increased significantly in the last few years [15–17,19–25]. The popularity stems from the advantages of the technique, namely its wide applicability, noninvasive and on-line characteristics. Near infra-red region cov-

ers the overtone and combination transitions of the C–H, O–H and N–H groups, and since all organic compounds possess at least one or more of these groups, the technique is applicable to all compounds [19–25]. There is no need for pretreatment of the sample, and since NIR radiation can penetrate a variety of samples, the technique is noninvasive and has proven to be potentially useful for noninvasive, on-line measurements. In fact, NIR technique has been used in industries for on-line measurements for quality control and assurance. However, its applications are not as widely as expected. This may be due to a variety of reasons but the most likely ones are probably due to the limitations on the speed, stability and light throughput of the currently available instruments. To be effectively used as a detector for on-line measurements, the NIR instrument needs to have high and stable light throughput, to suffer no drift in the baseline, and can be rapidly scanned. These impose severe limitations on conventional NIR spectrophotometers because such instruments generally have relatively low and unstable light throughput, suffer some degree of baseline drift, and can only be scanned very slowly. AOTF, with its ability to rapidly scan as well as to control and maintain the intensity of light at a constant level, offers a means to alleviate some of these limitations.

It has been shown recently that stimulated emission can be achieved in a fiber when the fiber is doped with rare earth ions such as Er^{3+}, and optically pumped by an ion laser or YAG laser [26,27]. Now, for the first time, a lasing medium can be confined in a material as flexible and as small (< 10 μm) as a single mode fiber [19,20]. Because of such features, the length of the doped fiber can be adjusted to as long as few kilometers to enable the fiber to have optical output in the range of kilowatts. Furthermore, the doped fiber can be pumped by a high power diode laser fusion-spliced directly into the doped fiber. It is thus, evidently clear that this all-fiber, compact EDFA can provide near infra-red light with highest intensity and widest spectral bandwidth compared to other (cw) near-IR light sources currently available. A novel, compact, all solid state, fast scanning near infra-red spectrophotometer which has no moving part, high and very stable light throughput can, therefore, be developed by use of this EDFA as a light source and AOTF as a dispersive element to scan and control the intensity of the diffracted light. Schematic diagram of such a spectrophotometer is shown in Fig. 3 (with the insert showing the construction of the EDFA). As illustrated, the near infra-red light from the output of the EDFA was dispersed to monochromatic light and spectrally scanned by an AOTF. The RF signal, provided by a driver, was amplitude-modulated at 50 kHz by a home-built modulator and amplified by a RF power amplifier prior to being applied to the AOTF. The light diffracted from the AOTF was split into two beams (i.e. sample and reference beams) by means of a beamsplitter (BS). Intensity of the light in the sample and reference beams was detected by thermo-electrically cooled InGaAs detectors. The output signals from the (reference and sample) detectors which were amplitude modulated at 50 kHz were connected to lock-in amplifiers (Stanford Research Systems Model SR 810) for demodulating and amplifying. The signal from the reference beam can be used either as a reference signal for a double beam spectrophotometer or as a reference signal for the fed-back loop to stabilize the intensity of the light in the sample beam in a manner similar to those used previously [1,4]. The signals from the lock-in amplifiers were then connected to a microcomputer through a 16 bit A/D interface board.

As expected, the sensitivity of this EDFA-AOTF based spectrophotometer is comparable with those of the halogen tungsten lamp-AOTF based instruments. In fact, this spectrophotometer can be used to detect water in ethanol at a limit of detection of 10 ppm. More importantly is its high light throughput. The intensity of this EDFA light source was found to be about 20 times higher than that of 250 W halogen tungsten lamp. As a consequence, it can be used for measurements which are not possible with lamp based instruments. Two measurements were performed to demonstrate this advantage. Shown in Fig. 4 is the intensity of the light transmitted through six sheets of photocopy paper (Cascade X-9000 white paper). As illustrated, because of the high absorp-

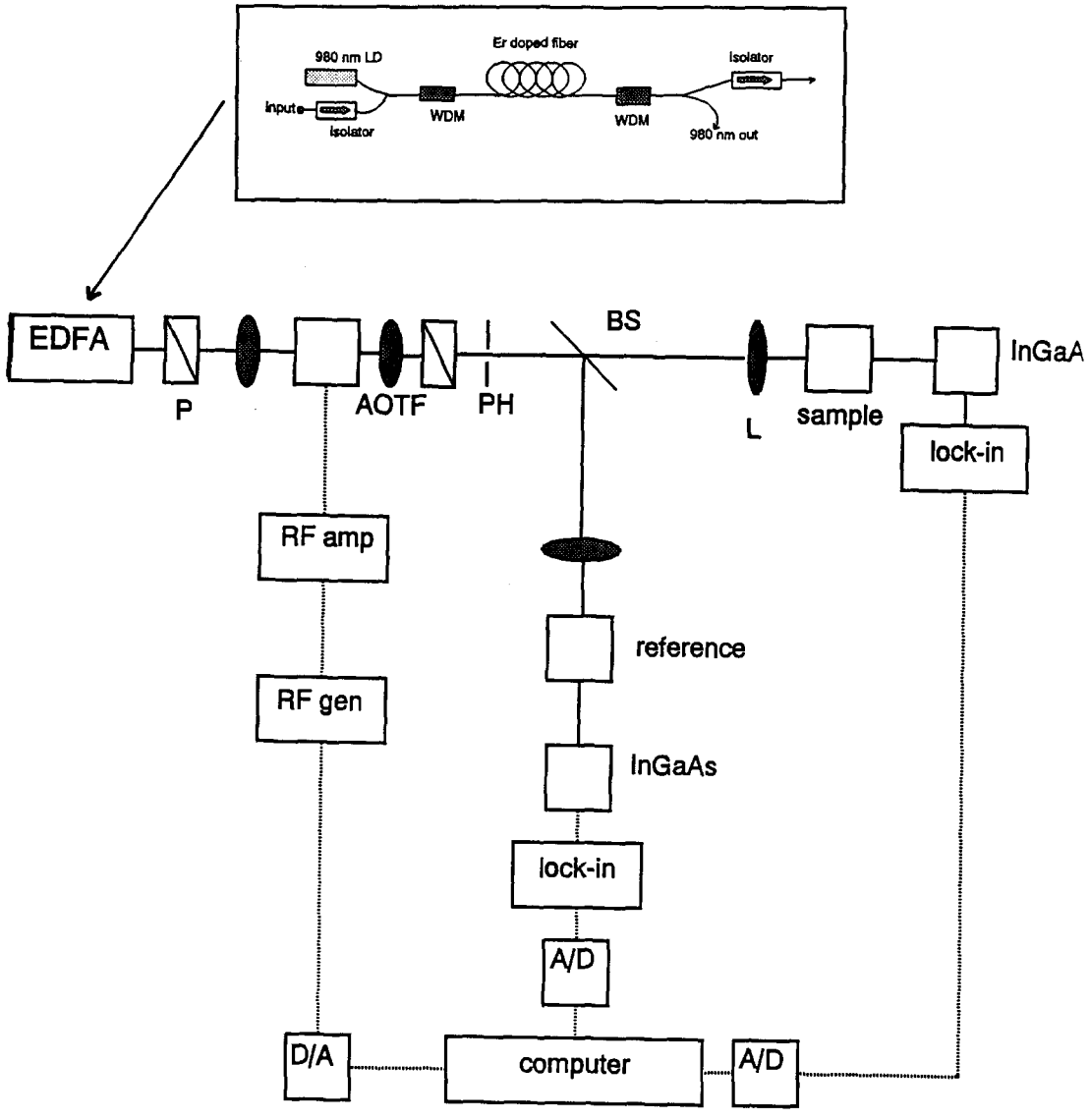

Fig. 3. Schematic diagram of the near infra-red spectrophotometer based on the use of the EDFA as a light source and AOTF as a dispersive element: EDFA, erbium doped fiber amplifier; P, polarizer; AOTF, acousto-optic tunable filter; PH, pinhole; BS, beamsplitter; L, lens; RF amp, RF power amplifier; RF gen, RF generator; InGaAs, detector. Insert: Schematic diagram of the erbium-doped fiber amplifier system: LD, laser diode; WDM, wavelength division multiplexer.

tion (of the papers) and low intensity (of the halogen tungsten lamp) no light was transmitted when the halogen tungsten lamp based spectrophotometer was used. Because of its high intensity, a substantial amount light was transmitted through the papers. In the second measurement which is shown in Fig. 5, it was not possible to use a lamp based spectrometer to measure absorption spectrum of 1.0 M solution of Pr^{3+} in D_2O (in a 2 mm cell) placed after four sheets of photocopy paper (dashed line). Because of its high intensity, substantial amount of EDFA

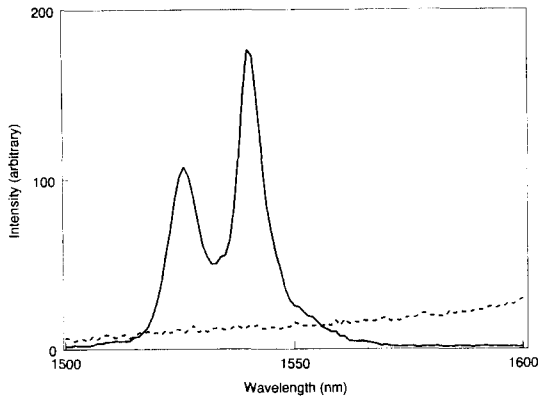

Fig. 4. Relative intensity of the light transmitted through six sheets of paper, measured with a 250 W halogen tungsten lamp based spectrophotometer (– – –), and with the EDFA based spectrophotometer (——).

light was transmitted through the papers and Pr^{3+} solution, and as a consequence, absorption spectrum of the latter can be recorded (Fig. 5, insert). This high throughput advantage is of particular importance in NIR measurements because NIR techniques are often used for measurements in which the signal of interested is very small and riding on top of a very large background signal. As such, it is very difficult, inaccurate and sometimes not possible to perform such measurements with lowlight-throughput spectrophotometers.

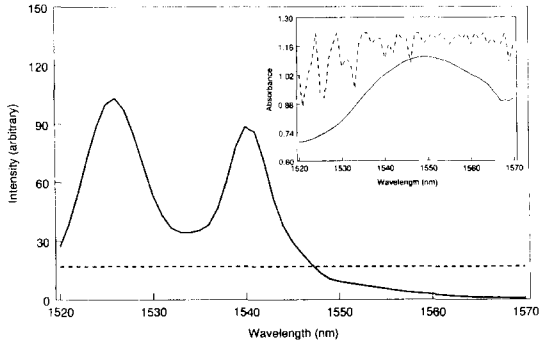

Fig. 5. Relative intensity of the light transmitted through four sheets of paper and 1.0 M solution of Pr^{3+} in D_2O (in a 2 mm pathlength cell), measured with a 250 W halogen tungsten lamp based spectrophotometer (– – –), and with the EDFA based spectrophotometer (——). Insert: spectra of the same sample plotted as absorption spectra.

3. Applications in chemical separations

3.1. AOTF based detector for HPLC

High performance liquid chromatography (HPLC) has increasingly become the technique of choice for chemical separations. As the technique becomes more prevalent the demand for detectors that can provide quantitative as well as qualitative information on the analyse increases.

Variable wavelength absorption detectors are the most widely used detectors for HPLC. However, this type of detector can only be used as a quantitative technique because the qualitative information obtained from this detector is rather limited, namely, it relies on the use of the retention time as the only tool for identification. The development of diode array detectors (DADs) in the early 1980s made it possible to obtain information on peak purity and identity [28]. Specifically, with a DAD based detector, the spectrum obtained for each peak in the chromatogram can be stored, and the subsequent comparison with standard spectra will facilitate the identification of peaks [28]. The optimum wavelength for single wavelength detection can easily be found [28]. Wavelength changes can be programmed to occur at different points in the chromatogram, either to provide maximum sensitivity for peaks, or to edit out unwanted peaks, or both [28]. Unfortunately, in spite of their advantages, DADs still suffer from limitations including their relatively high cost and their low sensitivity (compared to variable and fixed wavelength detectors). It is therefore, of particular importance that a novel detector which has higher sensitivity, low cost and possesses all of the DADs' advantages be developed. The AOTF with its unique features is particularly suited for the development of such a detector. Specifically, with its microsecond scanning speed, the AOTF based detector can rapidly record absorption spectrum of a compound as it elutes from the column. The random access to wavelength(s) makes it possible to change and/or to program the detector to any wavelength(s) to obtain optimal detection. However, different from the DADs, the AOTF-based detector is a single channel detection technique, i.e. it is based on a

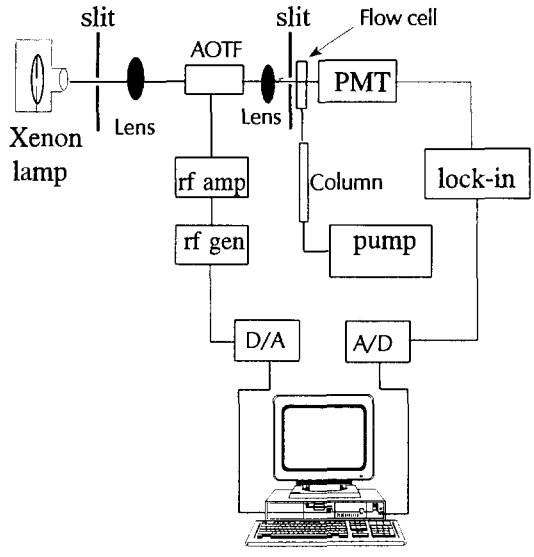

Fig. 6. Schematic diagram of the AOTF based detector for HPLC: PMT, photomultiplier tube; lock-in, lock-in amplifier; RF, RF power amplifier; RF gen, RF signal generator.

photomultiplier tube. Its sensitivity is therefore higher, and its cost is lower than the multichannel detectors (i.e. DADs).

The schematic diagram of the AOTF based detector is shown in Fig. 6. A 150 W xenon arc lamp was used as the light source. Its output radiation which contains UV, and visible light was focussed onto the AOTF by a combination of a reflector, collimator and lens. Acoustic waves will be generated in the AOTF when the RF signal is applied into the filter by a signal generator. To reduce noise and to facilitate the phase sensitive detection the RF signal was sinusoidally modulated at 50 kHz by the microcomputer through the D/A. Prior to being connected to the AOTF, the AM modulated RF signal was amplified to 5 W power by an RF power amplifier. The intensity of the light diffracted from the AOTF was detected by a photomultiplier tube and demodulated (at 50 kHz) by a lock-in amplifier prior to being recorded by a microcomputer.

The chromatographic system consists of an isocratic pump and a sample injector valve equipped with a 40 μl loop. A 250 mm × 4.6 mm I.D. stainless-steel column packed with Nucleosil 5 silica was used. The chromatographic microflow cell used in this study, which has 8 mm path length and 8 μl volume, is similar to that used previously [16].

Shown in Fig. 7 is the three dimensional graph plotting the chromatogram as a function of time and wavelength of a sample which was a mixture of three phenol derivatives, i.e. 4-chloro-, trichloro- and pentachlorophenol. The chromatogram as a function of time was obtained by setting the AOTF at a single wavelength of 292 nm. Absorption spectrum of each compound was measured as it eluted out of the column by rapidly scanning the AOTF. Each single spectrum was obtained by scanning the AOTF for 100 nm (from 250 to 350 nm) and recording 100 points (i.e. 1 point for each nanometer). The setting was selected so that it required 2 ms to record each point. Therefore, the time required to record a single spectrum is 200 ms, and it took 4 s to obtained the spectrum, which is the average of 20 spectra for each compound. However, as evident from the figures, only 60 nm (i.e. from 260 to 320 nm) is required to record the whole spectrum for all three compounds. Therefore, with the optimal setting of 300 μs time constant, 12 dB rolloff, and 2 ms pt^{-1} (on the lock-in amplifier), it requires only 900 ms to obtain an average of 5 spectra which has relatively good S/N.

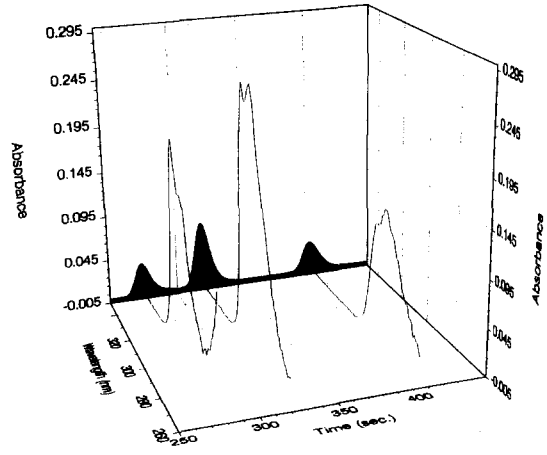

Fig. 7. Three dimensional graph plotting the chromatogram of mixture of pentachloro-, trichloro- and 4-chlorophenol as a function of time and wavelength.

The calibration curve was constructed for each compound over a concentration range of 1.0×10^{-4}–2.0×10^{-3} M using the data obtained when the AOTF was fixed at a single wavelength corresponding to the peak of the absorption spectrum of each compound, i.e. 285, 300 and 306 nm for 4-chloro-, trichloro- and pentachlorophenol, respectively. As expected, good linear relationship was obtained for all three compounds (the correlation coefficients for all three compounds were larger than 0.999). The limits of detection (LODs) defined as twice the peak-to-peak noise of the baseline divided by the slope of the calibration graph, are estimated to be 1.0×10^{-5}, 1.1×10^{-5} and 1.7×10^{-5} M for trichloro-, pentachloro- and 4-chlorophenol, respectively. These LOD values correspond to the mass defectivity of 59, 88 and 65 ng, respectively, and to the absorbance unit of 4.0×10^{-4}. These detections limit are comparable with those found on commercially available (grating or filter based) single wavelength absorption detectors. Particularly, its detectability of 4.0×10^{-4} absorption unit is similar to the value of 3.9×10^{-4} absorbance unit, which we have previously determined for 4-chlorphenol using the Shimadzu model SPD-6AV VU-visible absorption detector [16]. The LOD value of 4.0×10^{-4} AU is much smaller than those obtained using commercially available diode array detectors [28]. This is as expected because the present AOTF based detector is a single channel detection technique, which is more sensitive than the multichannel detection employed in the diode array detectors. Furthermore, the light source used in this AOTF based detector is modulated at 50 kHz (through modulating the applied RF signal) which facilitates the phase lock detection. The S/N is further enhanced by this phase sensitive detection. Other feature which makes this AOTF-based detector more desirable than diode array detectors is its high spectral resolution. Specifically, the resolution of this AOTF-based detector is 0.82 Å at 253 nm [9]. This spectral resolution is much smaller than those of the DAD which are generally on the order of several nanometers [12].

3.2. AOTF based detectors for flow injection analysis

Flow injection analysis (FIA) is among the most widely used methods for automated analysis. Its applications to several fields of chemistry has been demonstrated in recent years [29,30]. Several operational modes of FIA have been realized by appropriately modifying traditional wet chemical methods (dilution, extraction, titration, fast kinetic reactions) into automated flow devices [13,14]. Different types of detectors, including electrochemical, (UV and visible) spectrophotometric, and luminescent, have been applied to the FIA. [29,30]. However, there has not been a FIA detector which is truly universal.

As described in previous section, spectrochemical applications of the near infra-red absorption technique (NIR) has increased significantly in recent years [15]. The popularity stems from advantages of the technique including the wide applicability (all compounds that have C–H, O–H and/or N–H groups have absorption in this spectral region), the possibility of in situ applications (no need for sample pretreatment) and the availability of powerful and effective multivariate statistical methods for data analysis. These features enable the NIR to serve as a universal detector for FIA. However, the detection of FIA by NIR has not been fully exploited. In fact, in there are only two reports describing the utilization of NIR for continuous-flow FIA detection [31,32]. Unfortunately, in these studies, the potentials of the NIR technique have not been fully exploited because they were based on the use of only a single wavelength [31,32]. As a consequence, the multivariate calibration methods cannot be used to analyze data in these studies. This drawback can be overcome by use of an AOTF based NIR detector.

The construction of the AOTF based NIR detector for FIA, shown in Fig. 8, is essentially the same as that of the AOTF based UV-visible detector for HPLC which was described above. The only differences were those of the light source (a 100 W, 12 V halogen tungsten lamp), the AOTF for the NIR region, and a the detector (InGaAs photodiodes)

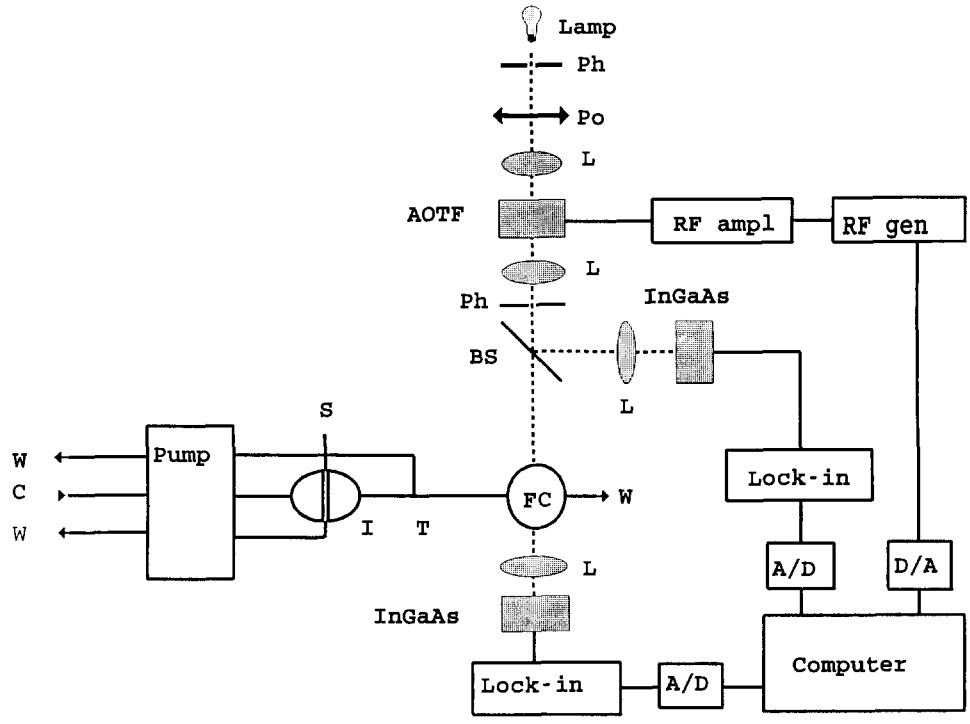

Fig. 8. Near-infra-red-FIA instrument: W, waste; C, carrier; Pump, peristaltic pump; S, sample; I, injector; T, T connector; FC, flow cell; Ph, pinhole; Po, polarizer; L, lens; BS, beamsplitter.

This AOTF based detector covers a near IR region from 1000 to 1600 nm. Because the combination and overtone absorption bands of O–H and C–H groups are in this region, this FIA-AOTF detector can be used for such determinations as water in chloroform, and water and benzene in ethanol. For example, Fig. 9 shows the FIA absorption peak profile (i.e. absorption spectrum as a function of time and wavelength), obtained when a solution of 0.10% (v/v) water was injected into chloroform. It is evident that as the concentration of water in the flow cell increases, there is an increase in the absorption in the 1300–1500 nm region. The can be attributed to the first overtone transition, and the combination of stretching and bending of the O–H group at 1450 and 1180 nm, respectively [17]. The absorption reaches its maximum 12 s after the injection and then starts to decrease. Using the spectra measured 12 s after the injection for different concentrations of water a calibration model based on the partial least square method (PLS) was developed for the determination of water in chloroform. Good correlation was obtained between the con-

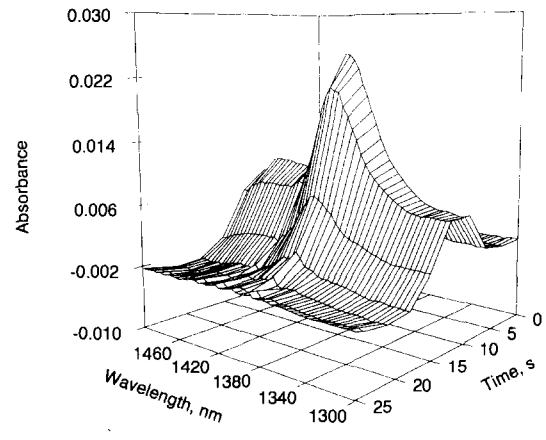

Fig. 9. Absorption (flow cell using chloroform as blank) as a function of time and wavelength after the injection of 0.10% (v/v) water solution in chloroform.

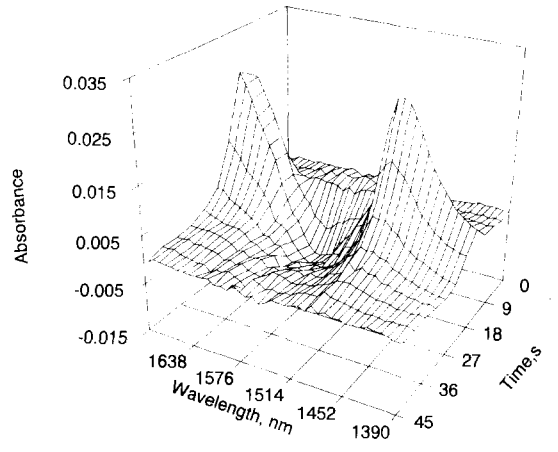

Fig. 10. Absorption (flow cell using ethanol as blank) as a function of time and wavelength measured after the injection of ethanol solution containing 0.6 and 1.5% (v/v) of water and benzene, respectively.

centration of water injected and the concentration of water calculated by the model ($r = 0.99$). The RMSD for this determination was calculated to be 0.002%. The LOD at 1400 nm was found to be 15 ppm of water.

It is possible to sensitively and simultaneously determine the concentrations of water and benzene in ethanol by NIR spectrometry. Fig. 10 shows the absorption measured as a function of time and wavelength after the injection of sample containing 0.6 and 1.5% of water and benzene respectively. As can be seen from the figure, when the sample is passing through the detector between 8 and 26 s there is an increase in the absorption in the 1650–1700 nm and 1390–1500 nm regions (due to absorption of benzene and water, respectively) and a decrease in the 1500–1650 nm region (due to benzene). These spectral profiles are the same to those observed in the previous measurements using the non-flowing 1 cm cuvette (figure not shown). In order to produce a calibration model for the simultaneous determination of benzene and water in ethanol using NIR-FIA technique, 21 samples containing different concentrations of water and benzene were prepared. Each sample was injected four times. Good correlation was obtained between the concentration of water and benzene injected and the concentration of both components calculated by the PLS model (SR = 1450–1496 nm, 1672–1700 nm, 1583–1602 nm; NF = 4 and 3 for water and benzene respectively). The statistical parameters obtained were $r = 0.997$ and RMSD = 0.015% and $r = 0.997$ and RMSD = 0.033% for water and benzene respectively.

In summary, it has been demonstrated that due to its high scanning velocity and wavelength accuracy the AOTF based detector for FIA can measure whole NIR spectra of flowing samples within the time frame required for flow analysis. This allowed the utilization of multivariate statistical methods of analysis, which in turn, increase the sensitivity, accuracy and applicability of the technique. In fact it was possible to perform not only a simple analysis, such as the determination of dryness of organic solvent (i.e. the concentration of water in chloroform) but also a more complex analysis including the simultaneous determination of two component systems (i.e. the concentration of water and benzene in ethanol). For simple one component systems, the LOD of this AOTF-NIR-FIA technique is comparable to that of the FIA spectrophotometry as well as to that of the single wavelength NIR-FIA technique. In this case the advantages of the AOTF-NIR-FIA instrumentation are its sensitivity, automation and wide applicability.

For relatively more complex systems (e.g. two component systems) the advantages become more prevalent. In fact, there is not a method currently available that can be easily coupled with FIA instrument for the sensitive and simultaneous determination of the concentrations of two or more components without any sample pretreatment. The present automated and real-time determination of water and benzene in ethanol is important because ethanol is increasingly being used as a substitute and/or additive to gasoline (i.e. it is important to know the concentrations of water and benzene impurities in such systems).

Acknowledgements

The author wishes to thank his present and former coworkers, whose work is cited in the

references. Acknowledgment is made to the National Institutes of Health for financial support of this work.

References

[1] C.D. Tran, Anal. Chem. 64 (1992) 971A–981A.
[2] C.D. Tran, R.J. Furlan, Anal. Chem. 64 (1992) 2775–2782.
[3] C.D. Tran, R.J. Furlan, Anal. Chem. 65 (1993) 1675–1681.
[4] C.D. Tran, V. Simianu, Anal. Chem. 64 (1992) 1419–1425.
[5] C.D. Tran, J. Lu, Anal. Chim. Acta 314 (1995) 57–66.
[6] M.J. Politi, C.D. Tran, G.H. Gao, J. Phys. Chem. 99 (1995) 14137–14141.
[7] M.S. Baptista, C.D. Tran, G.H. Gao, Anal. Chem. 68 (1996) 971–976.
[8] C.D. Tran, G.H. Gao, Anal. Chem. 68 (1996) 2264–2269.
[9] C. Pasquini, J. Lu, C.D. Tran, S. Smirnov, Anal. Chim. Acta 319 (1996) 315–324.
[10] I.M. Warner, G. Patonay, M.P. Thomas, Anal. Chem. 57 (1985) 463A.
[11] T.T. Ndou, I.M. Warner, Chem. Rev. 91 (1991) 493.
[12] C.D. Tran, Analytical thermal lens spectrometry: past, present and future prospects, in: D. Bicanic (Ed.), Photoacoustic and Photothermal Phenomena III,, Spirnger Verlag, Berlin, 1992, pp. 463–473.
[13] M. Franko, C.D. Tran, Rev. Sci. Instrum. 67 (1996) 1–18.
[14] C.D. Tran, V.I. Grishko, Appl. Spectrosc. 48 (1994) 96–100.
[15] C.D. Tran, V.I. Grishko, Anal. Biochem. 218 (1994) 197–203.
[16] C.D. Tran, G. Huang, V.I. Grishko, Anal. Chim. Acta 299 (1994) 361–369.
[17] C.D. Tran, V.I. Grishko, M.S. Baptista, Appl. Spectrosc. 48 (1994) 833–842.
[18] C.D. Tran, R.J. Furlan, J. Lu, Appl. Spectrosc. 48 (1994) 101–106.
[19] L. Murray, L.A. Cowe, Making Light Work: Advances in Near Infra-red Spectroscopy, VCH Publishing, New York, 1992.
[20] K.L. Hildrum, T. Isaksson, T. Naes, A. Tandberg, Near Infra-Red Spectroscopy, Bridging the Gap between Data Analysis and NIR Applications, Ellis Horwood, Chichester, 1992, chapter 23.
[21] D.A. Burns, E.W. Ciurczak, Handbook of Near-Infrared Analysis, Marcel Dekker, New York, 1992, chapter 3.
[22] G. Patonay, Advances in Near-Infrared Measurements, JAI Press, Greenwich, Connecticut, 1993.
[23] L.G. Weyer, Appl. Spectrosc. Rev. 21 (1985) 1–43.
[24] G. Patonay, M.D. Antoine, Anal. Chem. 63 (1991) 321A–327A.
[25] T. Imasaka, N. Ishibashi, Anal. Chem. 62 (1990) 363A–371A.
[26] A. Bjarklev, Optical Fiber Amplifiers: Design and System Applications, Artech House, Boston, 1993.
[27] E. Desurvire, Erbium-Doped Fiber Amplifiers Principles and Applications, John Wiley, New York, 1994.
[28] L. Huber, S.A. George, Diode Array Detection in HPLC, Marcel Dekker, Inc., New York, 1993.
[29] Z. Fang, Flow Injection Separation and Preconcentration, VCH Press, New York, 1993.
[30] J. Ruzicka, E.H. Hansen, Flow Injection Analysis, 2nd ed., Wiley, New York, 1988.
[31] E.L. Anreus, S. Garrigues, M. Guardia, Fresenius J. Anal. Chem. 351 (1995) 724–728.
[32] S. Garrigues, M. Gallignani, M. Guardia, Anal. Chim. Acta 351 (1993) 259–264.

ELSEVIER

Talanta 45 (1997) 249–255

Talanta

Ion-selective electrode for bismuth(III) in ethylenediamintetraacetate medium

Marcos Fernando de Souza Teixeira, Alexandre Zambon Pinto, Orlando Fatibello-Filho *

Laboratório de Química Analítica, Departamento de Química, Centro de Ciências Exatas e de Tecnologia, Universidade Federal de São Carlos, Caixa Postal 676, 13560-970 São Carlos-SP, Brazil

Received 8 October 1996; received in revised form 21 February 1997; accepted 25 February 1997

Abstract

A coated graphite–epoxy ion-selective electrode for bismuth(III), based on the ion-pair between the $[Bi(EDTA)]^-$ anion and tricaprylylmethylammonium cation (Aliquat 336S) incorporated onto a poly(vinylchloride) (PVC) matrix is constructed. A thin membrane film of this ion-pair, dibutylphthalate (DBPh) or *ortho*-nitrophenyloctylether (*o*-NPOE) in PVC was deposited directly onto a Perspex® tube which contained a graphite–epoxy conductor substrate attached to the end of a glass tube. The coating solution was prepared by dissolving 30% (w/w) of PVC in 10 ml of tetrahydrofuran following addition of 65% (w/w) DBPh or *o*-NPOE and 5% (w/w) of the ionic pair. The effect of pH, EDTA concentration and some cation and anion on the electrode response is investigated. The bismuth(III) ion-selective electrode shows a linear response in the bismuth(III) concentration range from 1.0×10^{-8} to 1.0×10^{-1} mol l^{-1} and 1.0×10^{-7} to 1.0×10^{-1} mol l^{-1} and a slope of 56.8 and 59.2 mV dec.$^{-1}$ for the polymeric membranes containing DBPh and *o*-NPOE, respectively. The lifetime of this electrode was superior to 1 year (over 1600 determinations for each polymeric membrane), with practical detection limits of 6.3×10^{-9} and 4.4×10^{-8} mol l^{-1} with these plasticizers. Application of this electrode with bismuth(III) determination in a stomach anti-acid sample is described. © 1997 Elsevier Science B.V.

Keywords: Coated graphite-epoxy ion-selective electrode; Bismuth(III); Potentiometry

1. Introduction

The determination of bismuth in pharmaceutical compounds is very important, mainly for its control in treatment of patients with gastrointestinal disease. Its determination is routinely performed by gravimetric [1], volumetric [2], spectrophotometric [3] and amperometric [4] methods.

The chemistry of metal complexes has contributed in the development of ion-selective electrodes and amplification in the analysis of multivalent metallic cations species. Ohzeki and Kambara [5] constructed an ion-selective electrode for bismuth(III) based on the ion-pair tri-

* Corresponding author. Fax: +55 16 2748350; E-mail: doff@power.ufscar.br

PII S0039-9140(97)00127-6

octylmethylammonium tetraiodobismuthate incorporated onto a poly(vinylchloride) (PVC) matrix. The sensor was highly sensitive to tetraiodobismuthate(III) in the presence of chloride, iodide and various anions. The response of the electrode was 53 mV dec.$^{-1}$ in the tetraiodobismuthate(III) concentration range of 10^{-5} to 10^{-3} mol l^{-1} in 0.2 mol l^{-1} iodide medium. Also, this electrode was successful when applied in the potentiometric titration of bismuth(III) in iodide solution with EDTA.

The investigation of a coated copper-sensitive electrode to bismuth(III) based on the chlorobismuthate salt of tricaprylymethylammonium immobilized in poly(vinylchloride) has been proposed by Alexander and Joseph [6]. The response of the electrode depends on the degree of complexation of bismuth(III) by chloride, since the slope of 36.5 mV dec.$^{-1}$ is between the monovalent (59.1 mV dec.$^{-1}$) and bivalent (29.5 mV dec.$^{-1}$) species. The disadvantages of this sensor are a high interference of the Hg(II), Zn(II) and Sn(IV) and also the high chloride ion concentration necessary for the complexation of the bismuth(III).

The substitution of the trioctylmethylmmonium by trinonyloctylammonium cation in the preparation of the active material with tetraiodobismuthate(III) was reported by Raklman'ko et al. [7]. The dependence of the electrode responses to iodide concentration limited the linear range from 5.6×10^{-7} to 3.2×10^{-5} mol l^{-1}. On the other hand, Cu(II), Hg(II) and Sn(IV) ions have a strong influence on the electrode potential.

A liquid membrane ion-selective electrode sensitive to bismuth(III) cation was described by Szczepaniak and Ren [8]. A solution of the complex of bismuth(III) with bismuthiol III [5-mercapto-3-(naphthyl-2)-1,3,4-thiadiazolthione-2] was used as liquid ionic exchange in that electrode. The electrode was constructed with a Teflon membrane impregnated with this ionic exchanger and a silver/silver chloride electrode as internal reference electrode in bismuth nitrate solution and potassium chloride. The linear range of the electrode was from 3.2×10^{-10} to 3.2×10^{-7} mol l^{-1} of bismuth(III) solution with a slope of 18.7 mV dec.$^{-1}$. Nevertheless, the Cu(II) and Hg(II) ions interfered strongly in the electrode response.

In the present work, the construction and analytical application of a coated graphite–epoxy ion-selective electrode for the determination of Bi(III) is investigated. The bismuth(III) electrode was constructed with the ionic pair [Bi(EDTA)][Aliquat] (EDTA = Y = ethylenediamintetraacetate anion and Aliquat = tricaprylylmethylammonium) incorporated in a PVC matrix, using the same procedure described by Fatibello-Filho and co-workers [9–11]. The effect of plasticizers (DBPh and *o*-NPOE) in the polymeric membrane, pH, EDTA concentration and some cation and anion on the electrode response was investigated. In addition, the proposed electrode has been successfully used for the determination of bismuth(III) in stomach anti-acid (Brazilian formula).

2. Experimental

2.1. Apparatus

All potentiometric measurements were carried out at 25 ± 0.2°C in a thermostated glass cell with the bismuth(III) ion-selective electrode and a model R684 Analion Ag/AgCl double junction reference electrode (Brazil), both attached to an EA 940 model Orion pH/ion meter (USA) with ± 0.1 mV precision.

The electrochemical cell used for potential measurements was:

Ag|AgCl (s), KCl (1.0 mol l^{-1})

|3.0 mol l^{-1} KNO_3|Test solution|Graphite

–epoxy, PVC membrane

All pH measurements were made with the same pH meter and a 10/402/3092 model Ingold glass membrane electrode (USA). Calibration curves were obtained by the addition of bismuth(III) in EDTA standard solution, at controlled pH, using an E274 model Metrohm microburette, to an EDTA solution at the same pH and ionic strength. In the studies of response time, stability of electrode and life time, the signals were recorded on a two-channel strip-chart recorder (Cole Parmer, model 12020000-USA). A

VARIAN model Gemini AA 12/1475 atomic absorption spectrophotometer was used for the determination of bismuth in the samples.

2.2. Reagents and solutions

All solutions were prepared using Millipore Milli-Q water. Analytical-reagent grade chemicals were used without further purification, unless stated otherwise.

The EDTA tetraneutralized solution (Na_4Y) was prepared by dissolving 14.8896 g of dissodic EDTA ($Na_2C_{10}H_{14}N_2O_8 \cdot 2H_2O$, Merck) salt and 32.0000 g NaOH (Merck) in 200 ml of water. The EDTA tetraneutralized (Na_4Y) solution was used in the preparation of the bismuth(III)–EDTA complex solution.

The 0.5 mol l^{-1} bismuth(III) solution was prepared by dissolving 12.7492 g of $(BiO)_2CO_3$ (Analyticals) with 5 ml of concentrated nitric acid on a hot plate. After dissolution and cooling, this solution was transferred to a 50-ml volumetric flask and the volume completed with Milli-Q water. The solution was standardized by titration with 0.1 mol l^{-1} EDTA standard solution in nitric acid medium (pH ~ 1) using xylene orange [12] as indicator. After that, reference solutions of bismuth(III) in EDTA medium were obtained by suitable dilution of the stock solution, with the appropriate amount of EDTA at several pH values.

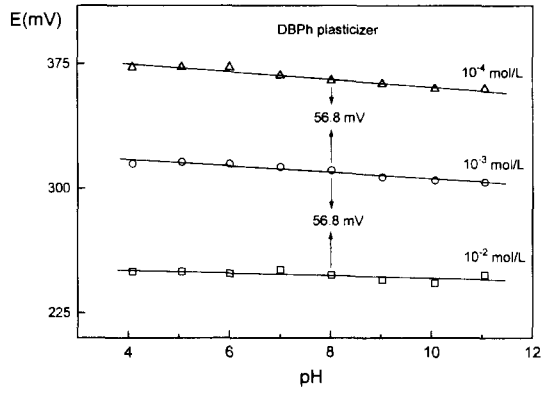

Fig. 1. Effect of pH on the response of the bismuth(III) ion-selective electrode containing the DBPh plasticizer, to Bi(III) concentration: △, 1.0×10^{-4} mol l^{-1}; ○, 1.0×10^{-3} mol l^{-1}; and □, 1.0×10^{-2} mol l^{-1} in 0.25 mol l^{-1} EDTA (Na_4Y) medium, at 25°C.

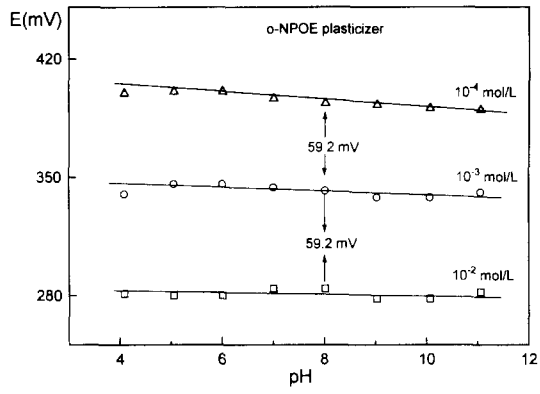

Fig. 2. Effect of pH on the response of the bismuth(III) ion-selective electrode containing the *o*-NPOE plasticizer, to Bi(III) concentration: △, 1.0×10^{-4} mol l^{-1}; ○, 1.0×10^{-3} mol l^{-1}; and □, 1.0×10^{-2} mol l^{-1} in 0.25 mol l^{-1} EDTA (Na_4Y) medium, at 25°C.

Metallic cation solutions at concentration of 10^{-3} mol l^{-1} in 0.25 mol l^{-1} Na_4Y was used in the potentiometric selectivity coefficients determinations.

A 0.1 mol l^{-1} tricaprylylmethylammonium chloride in chloroform was prepared by dissolving 4.0417 g of Aliquat 336S (Aldrich, 99%) in a 100-ml volumetric flask.

High-molecular weight poly(vinylchloride) (PVC, pure grade available from Fluka), tetrahydrofurane (reagent grade, Aldrich), dibutylphthalate (DBPh, Aldrich) and *ortho*-nitrophenyloctylether (*o*-NPOE, Aldrich) were used as received.

2.3. Preparation of the ionic pair

Initially, 50 ml of 0.1 mol l^{-1} bismuth(III) in 0.3 mol l^{-1} EDTA tetraneutralized (Na_4Y) solution was shaken with a 0.1 mol l^{-1} tricaprylylmethylammonium chloride in chloroform for 5 min. The ionic pair [Bi(EDTA)][Aliquat 336S] was extracted in the organic solvent, dried with sodium sulphate, and chloroform was evaporated in a rota-evaporator before being used. The coating solution was prepared by dissolving 30% (w/w) of PVC in 10 ml of tetrahydrofuran (THF)

following the addition of 65% (w/w) DBPh or *o*-NPOE and of 5% (w/w) ionic pair.

2.4. Construction of the coated graphite–epoxy electrode

The coated graphite–epoxy electrodes were constructed as described elsewhere [13,14]. A thin membrane film was prepared embedding ion-pair, dibutylphthalate (DBPh) and PVC (compositions mentioned above) onto an electrically conductive graphite–epoxy support located inside a Perspex® tube using a dropper, then it was dried for 3–4 h. Before use, the electrode was conditioned for 1–2 h by immersion in a 0.01 mol l^{-1} Bi(III) in 0.5 mol l^{-1} EDTA tetraneutralized solution, at working pH (4–10), and finally rinsed with water and 0.5 mol l^{-1} EDTA tetraneutralized solution.

2.5. Sample preparation

For potentiometric determination of bismuth(III) in a stomach anti-acid powder sample (Brazilian formula), an accurately weighed amount (5.00–6.00 g) of solid sample was initially dissolved in 10 ml *aqua-regia* and heated to dryness. After that, the sample was dissolved in 0.25 mol l^{-1} EDTA tetraneutralized solution and was transferred to a 100-ml volumetric flask, and this volume was completed with the same solution. The percentage of mass content of bismuth in this sample was determined by the standard addition method (potentiometry) and by atomic absorption spectroscopy at a wavelength of 223.1 nm.

3. Results and discussion

Several parameters were investigated in order to evaluate the performance of the Bi(III) electrode in terms of membrane composition, reproducibility, response time, calibration curve slopes, selectivity and sample analysis.

The effect of membrane composition (2–10% (w/w) ionic pair) over the response (slope (mV $dec.^{-1}$)) of the Bi(III) ion-selective electrode was initially evaluated in triplicate, at pH 8. The best responses (-56.8 and -59.2 mV $dec.^{-1}$) were

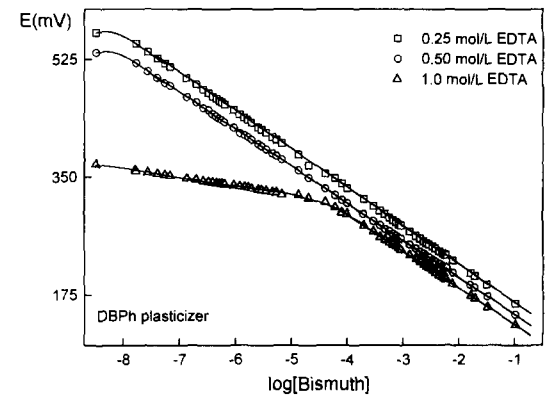

Fig. 3. Effect of Na_4Y concentration on the response of the bismuth(III) ion-selective electrode containing the DBPh plasticizer, to Na_4Y concentration: □, 0.25 mol l^{-1}; ○, 0.50 mol l^{-1}; and △, 1.0 mol l^{-1}, at pH 8.0 and 25°C.

reached for the 5% (w/w) ion-pair; 30% (w/w) PVC and 65% (w/w) DBPh and *o*-NPOE, respectively. The slopes obtained indicate that the electrode preferentially responds to the anionic $[Bi(EDTA)]^-$ species at this pH.

The effect of pH range from 4 to 11 on the response of the bismuth(III) electrode was determined in solutions with 1.0×10^{-4}, 1.0×10^{-3} and 1.0×10^{-2} of Bi(III) in 0.5 mol l^{-1} EDTA tetraneutralized (Na_4Y) solution. The curves presented in Fig. 1 and Fig. 2 show that there are no

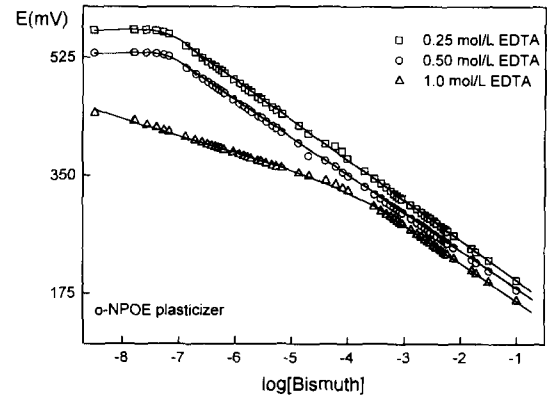

Fig. 4. Effect of Na_4Y concentration on the response of the bismuth(III) ion-selective electrode containing the *o*-NPOE plasticizer, to Na_4Y concentration: □, 0.25 mol l^{-1}; ○, 0.50 mol l^{-1}; and △, 1.0 mol l^{-1}, at pH 8.0 and 25°C.

Table 1
Study of the effect of EDTA (Na_4Y) concentration on the response of the bismuth(III) ion-selective electrode, at pH 8.0

Plasticizer	[EDTA] (mol l^{-1})	Linear range (mol l^{-1})	slope (mV dec.$^{-1}$)	r
DBPh	0.25	1.0×10^{-8}–1.0×10^{-1}	56.8 ± 0.3	0.9998
	0.50	1.0×10^{-8}–1.0×10^{-1}	55.1 ± 0.3	0.9998
	1.0	1.0×10^{-4}–1.0×10^{-1}	54.3 ± 0.3	0.9997
o-NPOE	0.25	1.0×10^{-7}–1.0×10^{-1}	59.2 ± 0.3	0.9993
	0.50	1.0×10^{-7}–1.0×10^{-1}	56.2 ± 0.3	0.9993
	1.0	3.2×10^{-4}–1.0×10^{-1}	55.0 ± 0.4	0.9997

Table 2
Analytical characteristics of the bismuth(III) ion-selective electrode in 0.25 mol l^{-1} EDTA (Na_4Y), at pH 8.0 and 25°C

Plasticizer	Concentration range (mol l^{-1})	Slope (mV dec.$^{-1}$)	Detection limit (mol l^{-1})
DBPh	1.0×10^{-8}–1.0×10^{-1}	56.8 ± 0.3	6.3×10^{-9}
o-NPOE	1.0×10^{-7}–1.0×10^{-1}	59.2 ± 0.3	4.4×10^{-8}

significant variations in the values of potential when the pH of solutions varies between 4 and 11 units. For pH values less than 4 there is a decrease in the potential of the electrode due to the protonation of the EDTA anion. In the pH range of 4–11, $[Bi(EDTA)]^-$ complex does not suffer influence of the medium, which demonstrates that the Bi(III) complex with Na_4Y is sufficiently stable ($K_f = 6.31\times10^{27}$) [2]. As can be seen from the curves presented in Fig. 1 and Fig. 2, the difference in potential is -56.8 mV dec.$^{-1}$ (DBPh) and -59.2 mV dec.$^{-1}$ (*o*-NPOE) between the three bismuth(III) solutions, indicating that the Bi(III) electrodes have a Nernstian response to

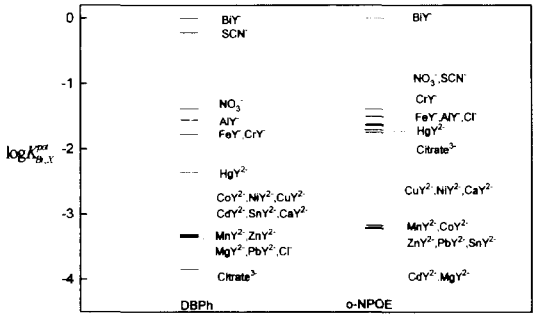

Fig. 5. Potentiometric selectivity coefficient values for the bismuth(III) ion-selective electrodes ($\log K^{pot}_{Bi,X}$) in 0.25 Na_4Y solution, determined by separate methods [14] at 10^{-3} mol l^{-1} concentration of interfering ions (pH 8.0).

$[Bi(EDTA)]^-$ concentration and the equilibrium in the formation of $[Bi(EDTA)]^-$ complex is not influenced by side-reactions with H_3O^+.

Fig. 3 and Fig. 4 show the potential responses of the electrodes at pH 8.0 in three EDTA concentrations (0.25, 0.5 and 1.0 mol l^{-1}) as a function of log[Bi(III)] for each electrode with different plasticizers (DBPh and *o*-NPOE) in the membrane. Table 1 presents the linear range of Bi(III) concentration, slope (mV dec.$^{-1}$), detection limit and the correlation coefficients. The best electrode responses were obtained employing the 0.25 and 0.5 mol l^{-1} Na_4Y solutions. At

Table 3
Determination of bismuth(III) in stomach anti-acid (Salicilato de Bismuto Composto) using the bismuth(III) electrode (containing the *o*-NPOE plasticizer) compared with atomic absorption spectrophotometry

Replicates	Bi/g in samples (mg)		Relative errors (%)
	Spectrophotometry	Potentiometry	
1	37.9	38.4	1.3
2	37.6	38.4	2.1
3	38.2	37.4	−2.1
x	37.9	38.1	
S^2	0.09	0.34	

S, relative standard deviation.

concentrations higher than 0.5 mol l^{-1} Na_4Y, a slope decrease and deviations from linearity of the curves were obtained. At 1.0 mol l^{-1} of EDTA solutions the practical detection limits were 1.0×10^{-4} and 2.5×10^{-4} mol l^{-1}, for DBPh and *o*-NPOE, respectively. In this EDTA concentration the EDTA anion competes with the $[Bi(EDTA)]^-$ specie [7], thus significantly decreasing the potential response of these electrodes.

The determination of the response time t ($\Delta E/\Delta t$) for each electrode was made with the introduction of the electrode in a 1.0×10^{-6} mol l^{-1} bismuth(III) solution in 0.25 mol l^{-1} Na_4Y at pH 8.0 and the time which elapses between the instant when the ISE and reference electrode are brought into contact with this solution and the first instant at which the emf/time slope ($\Delta E/\Delta t$) becomes equal to 0.6 mV min^{-1}. Then, it was added an aliquot of Bi(III) solution in 0.25 mol l^{-1} Na_4Y in a concentration high enough to elevate the concentration of Bi(III) solution for 1.0×10^{-5} mol l^{-1}. The $\Delta E/\Delta t$ was recorded until a variation of 0.6 mV min^{-1} was again recorded. The same procedure was repeated for other concentrations and the response times were 36 and 24 s for the electrode with DBPh and *o*-NPOE plasticizers, respectively, for the 1.0×10^{-6} (initial) and 1.0×10^{-5} mol l^{-1} (final) solutions and of 24 s for both electrodes for the bismuth(III) solution in the concentration alternating from 1.0×10^{-5} to 1.0×10^{-4} mol l^{-1}.

These electrodes showed a useful lifetime of at least 1 year (over 1600 determinations for each polymeric membrane) with a decrease of 5% of their initial potentiometric response at pH 8.

Table 2 shows the mean values (four determinations each) of the response characteristics of the electrodes in 0.25 mol l^{-1} EDTA medium, at pH 8.0 and 25°C.

The effect of some common species on the potential response of the bismuth(III) electrode at pH 8.0 was tested by determining the potentiometric selectivity coefficients of the membrane by the separate solutions method, as described by Lima et al. [14]. In this method, the concentrations of Bi(III) and interfering ion were fixed at 10^{-3} mol l^{-1} in 0.25 mol l^{-1} Na_4Y solution. The values of $K^{pot}_{Bi,X}$ obtained are shown in Fig. 5. These results show good selectivity for all cations and anions solutions tested. The high value of $K^{pot}_{Bi,X}$ obtained for thiocyanate using the electrode containing DBPh plasticizer indicates that this anion is a serious interference to the electrode, while the interference of this anion on the electrode containing the *o*-NPOE was smaller. This interference is due to the lipophilicity [15,16] difference in the plasticizers. As the thiocyanate has lipophilic characteristics, there is a larger interaction of this anion with the polymeric membrane that contains the DBPh plasticizer of smaller dielectric constant.

Table 3 shows the results obtained for bismuth(III) determination in a stomach anti-acid powder sample using potentiometric (standard addition) and atomic absorption spectroscopy methods. The results are in good agreement with those obtained by atomic spectrophotometry and are within an acceptable range of error, indicating that these electrodes can be utilized for a determination of this species in this sample.

4. Conclusions

The bismuth(III) ion-selective electrode which has been developed is easy to make, is of low cost, has a long lifetime, and its good selectivity permits the determination of this metallic cation in stomach anti-acid.

Acknowledgements

Financial support from PADCT/CNPq(process # 620060/91.2) and the scholarship for M.F.S.T. furnished by CAPES (Brazil) are gratefully acknowledged.

References

[1] K. Majumdar, B.R. Singh, Z. Anal. Chem. 154 (1957) 413.

[2] F.J. Welcher, The Analytical Uses of Ethylenediamine Tetraacetic Acid, Van Nostrand Co., New Jersey, 1958, pp. 205–212.

[3] R.N. Wilhite, A.L. Underwood, Anal. Chem. 27 (1955) 1334.
[4] F.J. Welcher, Standard Methods of Chemical Analysis, Van Nostrand Reinhold Co., New York, 1966, pp. 391.
[5] R. Ohzeki, T. Kambara, J. Electroanal. Chem. 88 (1978) 85.
[6] P.W. Alexander, J.P. Joseph, Talanta 28 (1981) 931.
[7] E.M. Rakhman'ko, G.L. Starobinete, A.L. Gulevich, G.A. Tsvirko, N.E. Trofimenko, Zh. Anal. Khim. 40 (1985) 1488.
[8] W. Szczepaniak, M. Ren, Talanta 30 (1983) 945.
[9] O. Fatibello-Filho, M.F.S. Teixeira, A.F. Oliveira, Anal. Lett. 25 (1992) 2187.
[10] M.F.S. Teixeira, P.R. Bueno, O. Fatibello-Filho, Quím. Nova 17 (1994) 124.
[11] M.F.S. Teixeira, O. Fatibello-Filho, J. Braz. Chem. Soc. 4 (1996) 233.
[12] A.I. Vogel, Texbook of Quantitative Chemical Analysis, Longmar Scientific & Technical, New York, 1989, pp. 324.
[13] J.L.F.C. Lima, A.A.S.C. Machado, Analyst 111 (1986) 799.
[14] J.L.F.C. Lima, M. Conceição, B.S.M. Montenegro, A.M.R. Silva, Quím. Anal. 11 (1991) 113.
[15] R. Eugster, T. Rosatzin, B. Rusterholz, B. Aebersold, U. Pedrazza, D. Rüegg, A. Schimid, U.E. Spichiger, W. Simon, Anal. Chim. Acta 289 (1994) 1.
[16] E. Lindner, E. Gráf, Z. Niegreisz, K. Tóth, E. Pungor, R. Buck, Anal. Chem. 60 (1988) 295.

ELSEVIER

Talanta 45 (1997) 257–263

Talanta

The extraction of uranium by amidoximated orlon

S. Katragadda, H.D. Gesser, A. Chow *

Department of Chemistry, University of Manitoba, Winnipeg, Canada R3T 2N2

Received 21 October 1996; received in revised form 24 February 1997; accepted 25 February 1997

Abstract

The nitrile groups in polyacrylonitrile (Orlon™) fabric were converted to amidoxime groups to produce an amidoximated orlon fabric. The amidoximated fabric was evaluated for its ability to extract uranium from aqueous solution with a wide range of temperature and pH values. The conversion of nitrile groups to amidoxime groups was simple and relatively inexpensive. In general, the modified orlon fabric showed superior extractability of uranium at all temperatures and pH values tested when compared to untreated Orlon™ fabric. © 1997 Elsevier Science B.V.

1. Introduction

A number of papers have been published describing the synthesis of macroreticular resins with amidoxime groups [1–3] because of their use in extracting uranium from seawater. The papers describing the synthesis of a sorbent with an amidoxime group, for the most part, involve the incorporation of a nitrile group into a polymer matrix, followed by the conversion of the nitrile group into an amidoxime group by treatment with a solution of hydroxylamine in methanol.

Egawa et al. [4,5] prepared a macroreticular chelating resin containing amidoxime by reacting acrylonitrile–divinyl benzene co-polymer beads with hydroxylamine. Sugasaka et al. [6] synthesized a number of polyacrylamidoxime resins from various copolymers of acrylonitrile and cross-linking agents. Work on fibres has generated wide interest in the last decade because of improvements with respect to flow rate through such a column and the mechanical stability of the fibre. Fibres have been made by radiation-induced graft polymerization of acrylonitrile into polymeric fibres, followed by amidoximation [7,8]. Amidoximation was attained by treating the polyacrylonitrile fibre with hydroxylamine in methanol [6].

It was of interest to determine if the nitrile groups of commonly available materials, such as polyacrylonitrile fabric (e.g. Orlon™), could be converted to amidoxime groups. The modified fabric would then be evaluated for its ability to preconcentrate uranium from aqueous solutions.

Orlon™ is the trade mark for an acrylic fibre that was first introduced into the market in 1950 by E.I. DuPont de Nemours and Co. Inc. Chemically the polymer contains at least 85% by weight of acrylonitrile moieties. The fabric is readily available, inexpensive and shows good chemical and physical/mechanical stability [9]. Preliminary experiments showed that, after amidoximation, the modified Orlon was capable of extracting

* Corresponding author. Fax: +1 204 2750905.

PII S0039-9140(97)00128-8

uranium from aqueous solutions. The Orlon™ fabric, which remained flexible throughout the process of amidoximation, changed colour from white to yellow.

2. Experimental

2.1. Apparatus and reagents

Absorbance measurements for the determination of uranium were made with a Hewlett-Packard Model 8452A diode-array spectrometer. A Markson Science Inc. quartz flow cell with 0.5 cm path length was used for the spectrophotometric analysis. Sample solutions were pumped through the flow cell using a Piper Pump™ Model P10T peristaltic pump.

A Fisher Accumet Model 825MP pH meter was used. Sample solutions were shaken either with a Burrell Wrist-Action Shaker (Burrell Corp., PA, USA) or a Dubnoff Metabolic shaking Incubator (Precision Scientific, IL, USA). Orlon™ cloth was ground to a fine powder using a Wiley™ Mill (Thomas Scientific Apparatus, PA, USA).

The photometric reagent Arsenazo III and hydroxylamine hydrochloride were obtained from Aldrich Co. (WI, USA). Uranyl acetate was obtained from BDH (England). Uranium solutions ranging from 1 to 10 ppm were prepared by successive dilution of a 2000-ppm uranium stock solution which was made from uranyl acetate. All chemicals were of analytical reagent grade and used without further purification. Water was purified by reverse osmosis and a Barnstead Nanopure II system. Orlon™ fabric was manufactured by E.I. DuPont de Nemours and Co. Inc. (DE, USA).

2.2. Analysis

Uranium in solution was determined using a continuous flow spectrophotometric method (CFSM) [10]. Analysis by CFSM involves the simultaneous pumping of 0.006% Arsenazo III in 0.12 M HCl and the uranium solution into a flow mixer to form the Arsenazo III–uranium complex. This complex then enters a quartz flow cell, wherein the absorbance measurements were recorded using a diode-array spectrophotometer.

A wide variety of metal ions react with Arsenazo III (2,2′-(1,8-dihydroxy-3,6-disulphonaphthylene-2,7-bisazo)-bisbenzenearsonic acid, FW 776.37) in weakly acidic to alkaline solutions. Only a few metal ions form highly coloured complex with molar absorptivity greater than 10^5 in strong mineral acid. Arsenazo III has been used widely as a photometric reagent for the analysis of Mg, Zr, U, Th and rare earths [11].

Arsenazo III was used as the preferred choice of chromogenic reagent for the spectrophotometric determination of uranium in the last three decades [12,13]. Uranium forms a 1:1 complex with Arsenazo III in a moderately acidic medium [13,14] and the stability constant for this complex is $\log \beta_1 = 5.42$. The concentration of Arsenazo III was always kept higher than that of uranium for this analysis. The flow rates for uranium solution and Arsenazo III solution were each 8 ml min^{-1} with a combined flowrate of 16 ml min^{-1} from the flow mixer. This flow rate was capable of forcing out air bubbles that often adhered inside the flow cell.

An internal referencing was used to improve the precision of the results by reducing the impact of any changes that may cause a baseline shift due to dust or other particles, air bubbles or a drift in lamp intensity. The absorbance at a reference wavelength (768 nm) on the baseline was subtracted from the absorbance at the analytical wavelength (650 nm). The difference in absorbance was used to obtain a calibration curve and for sample analysis. Uranium standards ranging from 1 to 10 ppm uranium were used to obtain the calibration curve in Fig. 1 using a second order curve fit.

The choice of 0.12 M HCl permitted the analysis of uranium solutions with a wide range of pH values between 1 and 11. Acid concentrations higher than 0.12 M HCl produced larger errors with lower pH uranium solutions, and concentrations lower than 0.12 M HCl resulted in larger errors with higher pH uranium solutions.

2.3. Procedure

Preliminary studies involved the use of unground Orlon™ strips (3 × 10 cm) that were subjected to the amidoximating process. During this procedure, the strips tangled into knots resulting in uneven reaction as seen by the non-uniform change in colour. Powdering the Orlon™ was an easy way to achieve a more consistent reaction on the material for the study of the uptake of uranium from aqueous solution.

Orlon™ cloth was cut into 1 × 1-cm pieces and then ground into a fine powder using a Wiley™ mechanical fabric grinder. The resulting powder passes through a 200 mesh sieve.

Modified Orlon fibres were prepared by treating 30 g of ground Orlon™ fabric with 1 l of amidoximating reagent. This reagent was freshly prepared by dissolving 40 g of hydroxylamine hydrochloride in a 50% (vol/vol) mixture of methanol and water. This solution was adjusted to pH 7.0 by using 2 M KOH solution, and made up to 1 l to give the amidoximating reagent. The mixture of Orlon™ fibres and amidoximating reagent was heated at 40°C with constant stirring under reflux for 12 h. The fibres changed from white to yellow during this process.

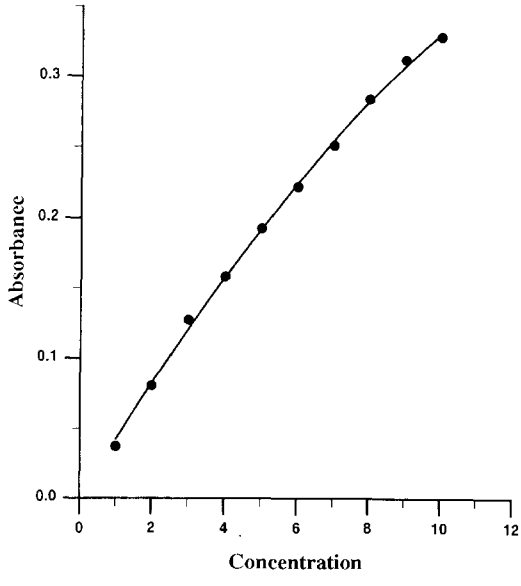

Fig. 1. Calibration graph for uranium standards between 1 and 10 ppm. A 5-mm Markson™ flow cell and 0.006% Arsenazo III in 0.12 M HCl were used.

Preliminary studies with strips indicated that heating the Orlon™ strips at temperatures above 40°C or refluxing for more than 12 h should be avoided as these conditions produced yellow, modified material that was very brittle. The modified Orlon strips obtained, after heating at 40°C with the amidoximating reagent and refluxing for 12 h, were flexible and also retained the physical strength of the unmodified Orlon™ material.

The modified Orlon fibres were removed from the filter paper, soaked in 500 ml of water for 4 h, and the resulting slurry then filtered under vacuum through a Buchner funnel. The fibres were recovered from the filter paper and the complete washing procedure of soaking and filtering was repeated two more times. The fibres were then washed three more times using the same procedure, except for the use of acetone in place of water. This washing procedure should remove impurities that are soluble in water or acetone and any unreacted reagents from the modified Orlon fibres. The clean, powdered fibres were left to dry under vacuum for 4 h to remove traces of acetone. This treatment resulted in a 20% conversion of the nitrile groups in Orlon to amidoxime groups. The percent conversion was calculated using the method described by Lin et al. [2]. Blank Orlon™ fibres, without the addition of hydroxylamine hydrochloride, were prepared in a similar manner to serve as a blank.

The extraction capability of modified Orlon fibre was determined by adding 25 ml of 10 ppm uranium solution to 60-ml screw top Nalgene™ plastic bottles, together with approximately 0.200 ± 0.003 g of dried powdered fibre. The capped bottles were shaken for 5 h in an automatic shaker. The filtered solutions were then analyzed by the continuous flow spectrophotometric method (CFSM) to determine the uranium uptake by the fibres.

The extraction profiles of modified Orlon and blank Orlon™ fibres were studied by equilibrating the fibres with uranium solutions at different temperatures and pH values. Uranium solutions were

adjusted with 2 M HCl or 2 M NaOH solution to pH values between 1.4 and 11.0, and the extraction characteristics studied at different temperatures between 4 and 70°C. Uranium solutions were equilibrated at the required temperature before adding them to the plastic bottles containing the fibres. A Burrell Wrist Action Shaker was used for the shaking of solution with fibres at room temperature (22°C) and at controlled cold room temperature (4°C). At 40 and 70°C, a Dubnoff Metabolic Shaking Incubator equipped with a variable temperature-controlled water bath was used. Temperature measurements were within ± 2°C during the shaking process. Percent extraction was calculated as

$$\%E = 100 \times \frac{(I - F)}{I}$$

Where % E is percent extraction, F is the concentration of uranium left in solution after extraction and I is the concentration of uranium originally available for extraction. I is the concentration of uranium in a solution after it was subjected to the identical filtration, pH and temperature conditions as the fibre sample solution, but without the presence of any fibre.

The concentration of available uranium, rather than the initial concentration (i.e. 10.0 ppm), was used to take into account any precipitation of uranium species which is known to occur at pH > 2. The precipitate is not visible to the naked eye, however, Feldman et al. [15] observed the precipitation of uranyl nitrate at pH > 4.5 by centrifuging the solution. The values for I and F, used in the calculation of %E, are the averages obtained from experiments that were performed in triplicate at the same pH and temperature.

3. Results and discussion

In Fig. 2 it can be seen that modified Orlon at 4°C exhibits a high percent extraction between pH 3 and pH 8 and that the extraction decreases at either end of the pH range. The decrease in percent extraction can be explained by the formation of UO_2Cl_2 and UO_2Cl^+ at pH values below 3 and $UO_2(OH)_3^-$ at pH values above 10 [16]; these species may not be as extractable by this modified Orlon. At higher temperatures, and between pH 3 and 5, it can be seen in Figs. 3–5 that the percent extraction decreases or remains constant with an increase in temperature. This occurs because the amidoxime group is unstable at higher temperatures [17]. At pH 1.4 and 11 the percent extraction increases with temperatures which may be due to the acid/base hydrolysis product of the amidoxime group that are present at the pH. The uranium complexation with the amidoxime will proceed as:

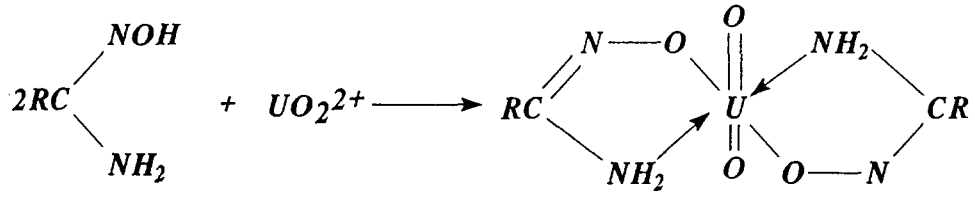

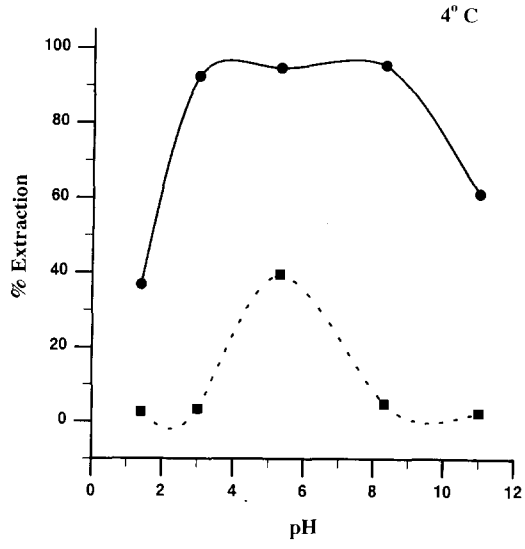

Fig. 2. Comparision of the extraction capability of uranium from aqueous solutions by amidoximated Orlon and blank Orlon™ fibres at 4°C. •, amidoximated Orlon; ■, blank Orlon™.

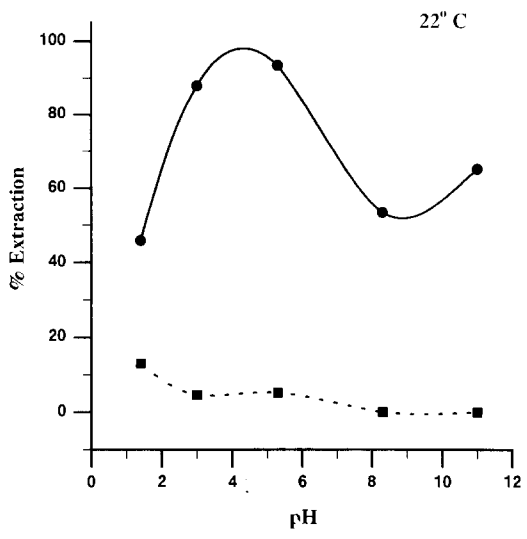

Fig. 3. Comparision of the extraction capability of uranium from aqueous solutions by amidoximated Orlon and blank Orlon™ fibres at 22°C. •, amidoximated Orlon; ■, blank Orlon™.

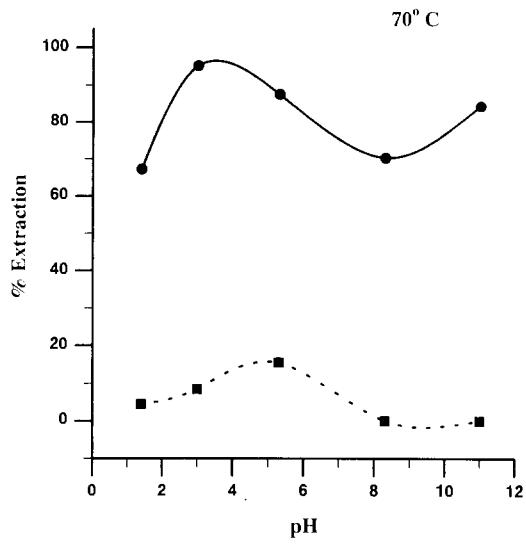

Fig. 5. Comparision of the extraction capability of uranium from aqueous solutions by amidoximated Orlon and blank Orlon™ fibres at 70°C. •, amidoximated Orlon; ■, blank Orlon™.

At lower pH values, acid hydrolysis of the amidoxime group takes place, while at higher pH values base hydrolysis occurs [18]. At pH 8, the percent extraction drops as the temperature increases from 4 to 22°C and then it increases as the temperature rises from 22 to 70°C. The anomaly in the extraction profile at pH 8 at 22°C was not reported earlier and it is our opinion that the initial decrease in percent extraction that was observed between 4 and 22°C was due to the base hydrolysis of the amidoxime group, and the increase in percent extraction that was observed between 22 and 70°C was due to the hydrolysed amidoxime group.

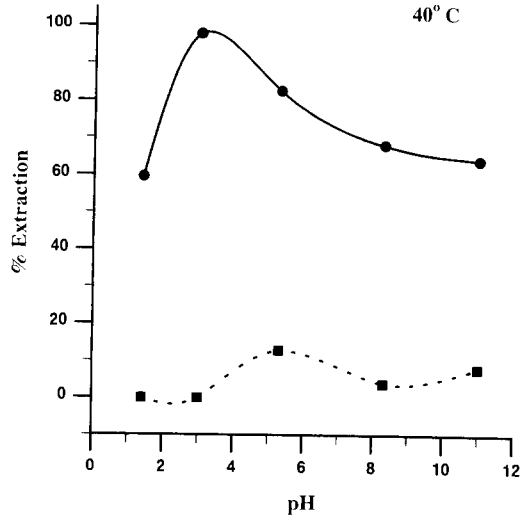

Fig. 4. Comparision of the extraction capability of uranium from aqueous solutions by amidoximated Orlon and blank Orlon™ fibres at 40°C. •, amidoximated Orlon; ■, blank Orlon™.

In Table 1 it can be seen that the maximum extraction from solutions of different pH occurs at different temperatures. At pH 1 and 11 the ideal extraction temperature would be 70°C, and at pH 5.3 and 8.3 the ideal temperature would be 4°C. Experiments beyond 70°C were not undertaken because of difficulties in maintaining the temperature and due to the impracticality of the procedure.

Modified Orlon fibres showed better extraction capability over the wide range of pH and temperature values compared to blank Orlon™ fibres (i.e. without amidoxime transformation) as shown in Table 1. The uncertainty in the percent extrac-

tion by blank Orlon™ fibres at pH 5.3 at 4°C was very high and repeated experiments showed inconsistent results suggesting that the blank Orlon™ fibres may be acting as nucleation sites for the precipitation of uranium at this pH and temperature. Modified Orlon exhibits high extraction between pH 3 and pH 8 at 4°C. At either end of the pH ranges the extraction should be carried out at higher temperature, namely 70°C.

4. Conclusion

Orlon™ was successfully amidoximated by converting the $-C \equiv N$ groups of the Orlon™ fibre into amidoxime groups which are capable of extracting uranium from aqueous solution whose pH ranges between 1.4 and 11. With modified Orlon, high extraction can be obtained at low temperature (i.e. 4°C) for uranium solution where pH ranges between 3 and 8. Similarly at high temperature (i.e. 70°C) for solutions at either end of the pH range. The modified Orlon fibres should be a good sorbent for the sorption of uranium from natural waters as the pH values of natural waters are usually in the range of pH 7 ± 3. These fibres are unique in their ability to extract uranium at low temperature (i.e. 4°C) making it an ideal sorbent for the preconcentration of uranium from natural water systems in cooler regions or during the colder months.

Future investigations should involve the kinetics and mechanism of sorption, and the effects of other elements on the sorption of uranium by modified Orlon in both batch and column experiments. Further developments may be possible using other amidoxime-anchored polymeric materials.

Table 1
Comparison of the extraction capability of amidoximated Orlon with blank Orlon™ for the uptake of uranium for aqueous solutions at various temperature and pH values

pH	Amidoximated Orlon	Blank Orlon™	Temperature (°C)
1.4	36.8 ± 1.4	2.6 ± 2.2	4
3.0	92.4 ± 0.6	3.4 ± 5.6	4
5.3	94.7 ± 0.3	39.5 ± 24.7	4
8.3	95.5 ± 0.2	4.9 ± 1.8	4
11.0	61.3 ± 0.7	2.5 ± 2.2	4
1.4	45.8 ± 1.7	13.0 ± 10.9	22
3.0	87.8 ± 0.8	4.6 ± 4.0	22
5.3	93.1 ± 1.6	5.2 ± 12.3	22
8.3	53.2 ± 3.1	0.0 ± 5.4	22
11.0	64.9 ± 1.7	0.0 ± 2.0	22
1.4	59.5 ± 2.6	0.0 ± 2.4	40
3.0	97.8 ± 0.3	0.0 ± 7.4	40
5.3	82.5 ± 1.1	12.8 ± 4.7	40
8.3	68.0 ± 2.6	3.9 ± 3.6	40
11.0	64.0 ± 2.9	8.0 ± 9.8	40
1.4	67.2 ± 2.0	4.5 ± 3.2	70
3.0	95.1 ± 0.6	8.5 ± 2.8	70
5.3	87.6 ± 1.8	15.5 ± 10.1	70
8.3	70.2 ± 1.1	0.0 ± 3.5	70
11.0	84.4 ± 0.8	0.0 ± 3.9	70

Acknowledgements

The authors acknowledge the financial assistance provided by the Natural Sciences and Engineering Research Council of Canada and Dr. M. King, Faculty of Human Ecology, University of Manitoba, for providing the Orlon™ fabric.

References

[1] C. Kantipuly, S. Katragadda, A. Chow, H.D. Gesser, Talanta 37 (1990) 491.
[2] W. Lin, Y. Lu, H. Zeng, Reactive Polymers 17 (1992) 255.
[3] K. Schwochau, Top. Curr. Chem. 124 (1984) 91.
[4] H. Egawa, H. Harada, T. Nonaka, Nippon Kagaku Kaishi (1980) 1767.
[5] H. Egawa, H. Harada, T. Shuto, Nippon Kagaku Kaishi (1980) 1773.
[6] K. Sugasaka, S. Katoh, N. Takai, H. Takahashi, Y. Umezawa, Sep. Sci. Technol. 16 (1981) 971.
[7] H. Omichi, A. Katakai, T. Sugo, J. Okamoto, Sep. Sci. Technol. 21 (1986) 563.
[8] H. Omichi, A. Katakai, T. Sugo, J. Okamoto, S. Katoh, K. Sakane, K. Sugasaka, T. Itagaki, Sep. Sci. Technol. 22 (1987) 1313.
[9] J. Gordon Cook, Handbook of Textile Fibres, vol. II. Man Made Fibres, Merrow Publishing Co. Ltd., England, 1968.

[10] S. Katragadda, Ph.D. Thesis, University of Manitoba, 1993.
[11] S.B. Savvin, Talanta 8 (1961) 673.
[12] A. Bermejo-Barrera, M.C. Yebra-Biurrun, L.M. Fraga-Trillo, Anal. Chim. Acta 239 (1990) 321.
[13] J.A. Perez-Bustamante, F. Palomares-Delgado, Analyst 96 (1971) 407.
[14] K. Sekine, H. Onishi, Anal. Chim. Acta. 62 (1972) 468.
[15] I. Feldman, W.F. Neuman, J.R. Havill, Report UR-85, 1949; Spectroscopy and Photochemistry of Uranyl Compounds, E. Rabinowitch and R.L. Belford, Pergamon Press Inc., NY, 1964.
[16] R. Djogic, L. Sipos, M. Branica, Limnol Oceanogr. 31 (1986) 1122.
[17] Serva Feinbiochemica G.m.b.H. and Co., Catalog, 1987/88, Heidelberg, Germany.
[18] F.L.M. Schouteden, Makromol. Chem. 24 (1957) 25.

ELSEVIER

Talanta 45 (1997) 265–271

Talanta

Flow injection spectrophotometric determination of nitrate in electrolyte of lead–acid batteries

Fábio R.P. Rocha *, Joaquim A. Nóbrega

Departamento de Química, Universidade Federal de São Carlos, Caixa Postal 676, 13565-905 São Carlos SP, Brazil

Received 28 October 1996; received in revised form 21 February 1997; accepted 25 February 1997

Abstract

Electrolytes of lead–acid batteries can contain several impurities that reduce battery performance and lifetime. Nitrate ions are among these species because they can be reduced to ammonium in the lead electrode. In this work, an analytical method was developed to determine this anion in electrolytes of batteries used in telephone systems, in which nitrate concentration must be lower than 10 mg l^{-1}. The procedure consists in the reduction to nitrite in a copperized cadmium column followed by Griess's modified reaction. Due to the high sensitivity of this methodology, a large dispersion flow diagram (dispersion coefficient = 27.8) was projected. Thus, it was possible to eliminate the Schlieren effect and to obtain a NH_3/NH_4^+ buffer in the sample zone in a suitable pH for reduction reaction (pH $\cong$ 8). Negative interference due to iron(III) was overcome by addition of excess iron (200 mg l^{-1}). A relocatable filter was used to remove iron(III) hydroxide precipitate. This avoided adsorption on the surface of the filings and increase of back pressure. The analytical frequency is 80 measurements/h and the detection limit was estimated as 0.3 mg l^{-1} in a 99.7% confidence level. A 2.2% relative standard deviation was obtained in a repeatability study ($n = 10$) by using a 25 mg l^{-1} nitrate solution in a 3.6 mol l^{-1} sulfuric acid medium. Recoveries from 95.5 to 104% were obtained by spiking 5.00 or 10.0 mg l^{-1} of nitrate in samples of battery electrolyte. © 1997 Elsevier Science B.V.

Keywords: Flow injection spectrophotometry; Lead–acid batteries; Nitrate; Refractive index; Schlieren effect

1. Introduction

Lead–acid batteries are useful devices to produce electrical energy from chemicals. This kind of battery is frequently employed in automobiles, electric vehicles, communication devices and to start engines. In the 1980s, lead–acid batteries represented approximately 60% of the sales of all batteries in the world [1]. The electrolyte in this device is a sulfuric acid solution, with a concentration that depends on both charge state and application of the device. This solution can contain several impurities that affect performance and lifetime of the accumulator. In this sense, nitrate determination is important since this anion can be reduced to ammonium in the negative electrode (Eq. (1)). Thus, the active material of this electrode is consumed without supplying energy through the battery terminals. The formation of lead sulfate was measurable even in the pres-

* Corresponding author. Fax: +55 162 74 8350.

PII S0039-9140(97)00126-4

ence of low concentrations of nitrate [2], such as 10 mg l^{-1}. In addition, ammonium ions produced tend to accumulate during the aging of the battery and they can affect the performance of the device.

$$2\,HNO_3 + 8Pb + 9H_2SO_4 \rightarrow 8PbSO_4 + (NH_4)_2SO_4 + 6H_2O \quad (1)$$

Most of the spectrophotometric methods for determining nitrate can be divided into three groups [3]: (1) nitration or oxidation of organic reagents, (2) measurements in the ultraviolet region, and (3) reduction to nitrite with subsequent determination of the reduced form by diazotization–coupling reactions. The first group involves methodologies that need high concentrations of sulfuric acid, and most of them are subject to interferences from nitrite, chloride and iron(III) ions [3]. The procedures based on measurements of nitrate in the ultraviolet region are very simple but the selectivity is poor. Several ions and organic substances that absorb radiation in the ultraviolet region are interferents [3]. Methods based on the reduction of nitrate are more reliable and selective than others. However, the reduction efficiency is pH dependent, and this must be considered to determine nitrate in the electrolyte of lead–acid batteries.

The procedure based on reduction of nitrate is more easily implemented by using flow injection analysis, since the reduction does not need to be quantitative. In addition, this useful technique for solution management can be explored to a pH adjustment from a previous reduction reaction. However, for relatively concentrated sulfuric acid solutions, the formation of intense refractive index gradients in the sample zone (Schlieren effect) can be troublesome. The usual way to overcome this perturbation is to employ a carrier with physical and chemical characteristics as similar as possible to the samples. However, in some situations this is not a practical alternative, such as the use of a relatively concentrated sulfuric acid solution as carrier for samples of electrolyte of lead–acid batteries.

Some experimental procedures can be used to avoid or to correct the Schlieren effect. An instrumental method based on measurements in two wavelengths was proposed by Zagatto et al. [4]. These measurements must be equally affected by Schlieren effect in both wavelengths, and the molecular absorption process must only occur for one of them. Yamane and Saito [5] employed a flow diagram with injection of a large sample volume. Thus, the central part of the sample zone did not interact with the carrier, and measurements could be made in this region without perturbation. This is an ingenious way to overcome Schlieren effect when there is no limitation in available sample volume and the sampling frequency is not a critical aspect. The use of flow diagrams with large dispersion is the simplest alternative to avoid refractive index gradients, since in these systems the mixture between sample zone and carrier is improved [6]. Thus, a large dispersion flow diagram was investigated to determine nitrate in lead–acid batteries. In spite of the negative effect of dispersion on sensitivity, this procedure permits an adequate pH adjustment for reduction, and this improves the conversion rate of nitrate to nitrite.

2. Experimental

2.1. Apparatus

A peristaltic pump (Ismatec IPC-8) and Tygon tubes (Technicon) were used for fluid propulsion. Polyethylene tubing (0.8 mm i.d.) were used to set up the flow diagram. The absorbance was measured with a 432 Femto (São Paulo, Brazil) spectrophotometer equipped with a glass flow cell with a 0.86-cm optical path. A potentiometer recorder (Cole-Parmer) was used to register the transient signals. For injecting samples, a sliding bar commutator [7] was used. The filtration unit was a glass tube (1 cm; 3 mm i.d.) filled with glass wool.

2.2. Reagents and solutions

All solutions were prepared with analytical reagent grade distilled and deionized water. Sodium nitrate was dried at 110°C for 2 h and used for preparing nitrate stock solution, 1000 mg

l^{-1}. Work solutions were prepared by adequate dilution of this stock. Sulfuric acid additions were made from stock solutions containing 7.2 or 9.0 mol l^{-1}.

Chromogenic reagent (Griess's reagent) was prepared in the concentrations previously established for nitrate determination in natural waters [8], containing 2% (w/v) sulfanilamide and 0.1% (w/v) *N*-1-naphthylethylenediamine dihydrochloride in a 8.5% (v/v) phosphoric acid medium. Cadmium filings were copperized as formerly described [9] and packed into a glass tube (10 cm long; 3 mm i.d.) plugged with glass wool.

Buffer solutions were prepared containing 10, 20 or 25% (w/v) NH_4Cl and 0.5, 1.0, 2.0 or 4.0% (w/v) $Na_2B_4O_7 \cdot 10H_2O$. All solutions contained 0.1% (w/v) Na_2EDTA. Ammonium hydroxide solutions containing 3.0, 4.0, 5.0, 6.0 and 7.0 mol l^{-1} were prepared from a stock solution (12.8 mol l^{-1}) standardized with a hydrochloric acid solution.

For investigating the effect of the iron(III) concentration on the analytical signal, nitrate solutions (10 mg l^{-1}) were prepared containing 2, 5, 10, 15, 20, 50, 100, 200 or 400 mg l^{-1} iron(III) in a 3.6 mol l^{-1} sulfuric acid medium.

Reference nitrate solutions (5.0, 10.0, 15.0, 20.0 and 25.0 mg l^{-1}) were prepared in a medium containing 3.6 mol l^{-1} sulfuric acid and 200 mg l^{-1} iron(III). Samples of electrolytes of lead–acid batteries were spiked with 5.00 or 10.0 mg l^{-1} nitrate. A 2.5×10^{-2} mol l^{-1} sulfuric acid solution was used to dissolve the iron(III) hydroxide precipitate in the system with the relocatable filter.

2.3. Flow diagrams and procedure

The flow diagram of the system with large sample dispersion is shown in Fig. 1. Some experiments were made without the filter (F) and employing only one section of the sliding bar commutator. Since mixing conditions are good, all measurements were made using water as carrier without refractive index perturbations. A 25-μl sample volume was inserted in the carrier by sliding the central part of the commutator. The sample was dispersed in the coil B_1 and confluent streams of ammonium hydroxide and buffer solutions were introduced in the sample zone. The chromogenic reagent was introduced by confluence to the effluent of the cadmium copperized column. Absorbance measurements were made at 535 nm. The relocatable filter was used to remove the iron(III) hydroxide formed when solutions containing Fe^{3+} were processed. After the precipitate removal, the central part of the commutator is again slid and a sulfuric acid solution dissolves the solid in the filter.

3. Results and discussion

For determining nitrate in the electrolytes of lead–acid batteries by reduction to nitrite followed by diazotization–coupling reactions, the pH adjustment in the sample zone before reduction is essential. The merging zones approach was investigated with this purpose. Sample loops were filled with nitrate solutions prepared in 3.6 mol l^{-1} sulfuric acid medium and with an alkaline solution (sodium or ammonium hydroxide). The best sensitivity was obtained with a 5 mol l^{-1} ammonium hydroxide solution, because a buffer was formed in the sample zone with a suitable pH (ca. 8) to nitrite formation from nitrate by copperized cadmium. However, the repeatability was not good (R.S.D. = 13%; $n = 10$) due to the in-

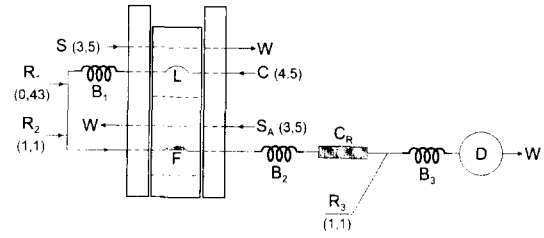

Fig. 1. Flow diagram of the system with large dispersion to nitrate determination. R_1, R_2 and R_3, indicate ammonium hydroxide, buffer and chromogenic reagent solutions, respectively. C, carrier (H_2O). B_1 is a dispersion coil. B_2 and B_3 are coiled reactors (50 and 200 cm, respectively). L, 5-cm sample loop (25 μl). C_R, copperized cadmium column (10 cm, 3 mm i.d.). D, spectrophotometric cell (535 nm). F, filter-glass tube (1 cm; 3 mm i.d.) filled with glass wool. S_A, 0.025 mol l^{-1} sulfuric acid solution. W, waste. The numbers between brackets indicate flow rates in ml min^{-1}. For more details see text.

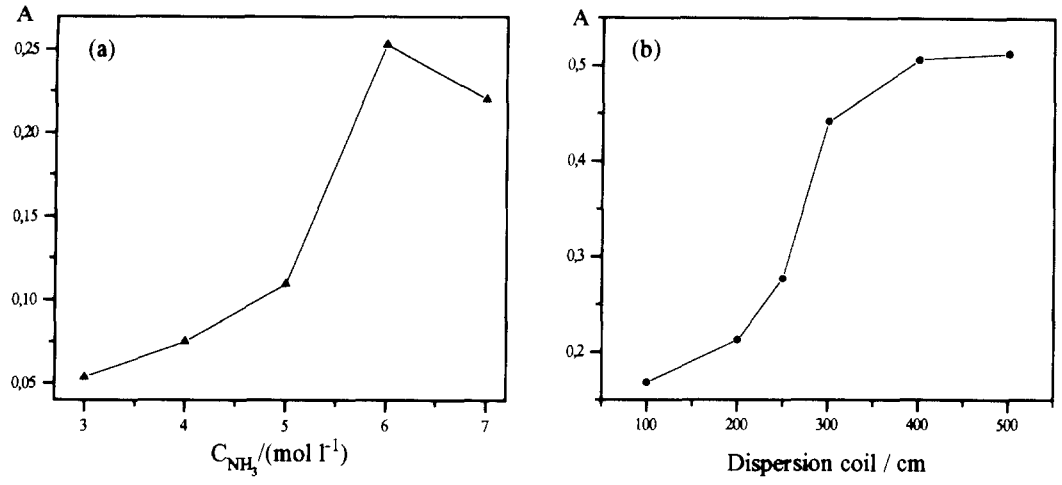

Fig. 2. Effect of (a) ammonium hydroxide concentration ($B_1 = 250$ cm) and (b) dispersion coil (6 mol l^{-1} NH_3) on the absorbance signals of nitrate in 3.6 mol l^{-1} sulfuric acid medium.

tense refractive index gradients in the sample zone and the high concentrations of salts formed by the acid–base reaction. Additionally, air bubbles were formed by the heating produced by the neutralization reaction.

To solve these problems, a large dispersion flow diagram was projected (Fig. 1, without filter F). This consisted in the reduction of the sample volume and employment of a large dispersion coil. Thus, sample zone dispersion was incremented before the confluent stream of ammonium hydroxide. The salt content in the sample zone and the heating produced by the neutralization reaction were decreased. Additionally, mixing conditions were improved and consequently the refractive index gradients were also decreased. With these modifications, a 0.9% relative standard deviation was obtained by using a 10 mg l^{-1} nitrate solution in a 3.6 mol l^{-1} sulfuric acid medium ($n = 10$). In spite of the large dispersion of the sample (dispersion coefficient = 27.8), the sensitivity losses were about 50%, because the reaction conditions (acidity and salt content) for nitrate reduction were improved.

The effects of the ammonium hydroxide concentration and of the length of the dispersion coil (B_1) were investigated, since they affect the acidity gradient in the sample zone and consequently the conversion rate of nitrate to nitrite. The effects of these parameters are not independent and the best concentration of the alkaline solution depends on the length of the dispersion coil employed. Results obtained are shown in Fig. 2. The increase of the sensitivity is due to the pH adjustment for reduction of nitrate by the confluent addition of the alkaline solution (Fig. 2a) or the increase of sample dispersion (Fig. 2b). Relative to the effect of the ammonium hydroxide concentration, it was observed that the sensitivity was increased up to 6 mol l^{-1} solution (250-cm dispersion coil). When higher concentrations were employed with the same length of dispersion coil, the absorbance signal decreased. By maintaining this concentration, the length of the dispersion coil was changed and the best sensitivity was attained at $B_1 = 400$ cm. These parameters were employed in all subsequent studies.

With the formerly established conditions, the absorbance was very dependent on the acidity of the sample injected, and erroneous results were obtained when the sulfuric acid concentration in the samples was out of the 3.0–3.5 mol l^{-1} range. To avoid this inconvenience, the effect of changing the composition of the buffer solution was evaluated. The effect of the ammonium chloride concentration was small for solutions varying

from 10 to 25% (w/v). For a 10% (w/v) NH_4Cl solution, the concentration of the $Na_2B_4O_7 \cdot 10H_20$ was changed from 0.5 to 4.0% (w/v). By using a 1.0% (w/v) tetraborate solution, samples with sulfuric acid concentration in the 3.0–4.5 mol l^{-1} range could be analyzed without errors caused by acid concentration effects. This concentration range is adequate for nitrate determination in samples of electrolyte of lead–acid batteries used in telephone systems.

For investigating the selectivity of the method, five samples were spiked with nitrate (from 2.00 to 8.00 mg l^{-1}, two additions in each one) and the concentrations were determined with the proposed system. For most samples, recoveries varied from 50 to 70%. For investigating the source of this negative error, concentrations of several species that can be found in sulfuric acid electrolytes (Al, Ca, Cd, Cr, Cu, Fe, Mg, Ni, Pb, Sb, Si, Sn and Zn) were estimated by ICP-AES. Most of these metals were not detected in any sample. However, some elements (Al, Ca, Fe and Zn) were present in many samples and the semi-quantitative results are shown in Table 1. Previous studies [9,10] indicated that zinc sulfate, aluminum sulfate, and calcium chloride (1% w/v) did not interfere in the nitrate determination when procedures similar to those proposed were employed. However, discrepant results were observed for iron. According to Henriksen and Selmer-Olsen [9], 1% (w/v) of ferrous sulfate or ferric chloride did not interfere in the nitrate determination. However, 0.5 mg Fe^{3+} l^{-1} caused serious interferences [11], and iron was cited as an

Table 1
Estimated concentrations of some metallic ions in electrolytes from batteries determined by ICP-AES

Sample	C (mg l^{-1})			
	Al	Ca	Fe	Zn
A	2.8	140	7.0	86
B	0.29	9.2	17	2.0
C	0.44	19	29	3.6
D	2.0	89	20	53
E	1.4	90	10	38
F	0.35	8.2	24	1.8

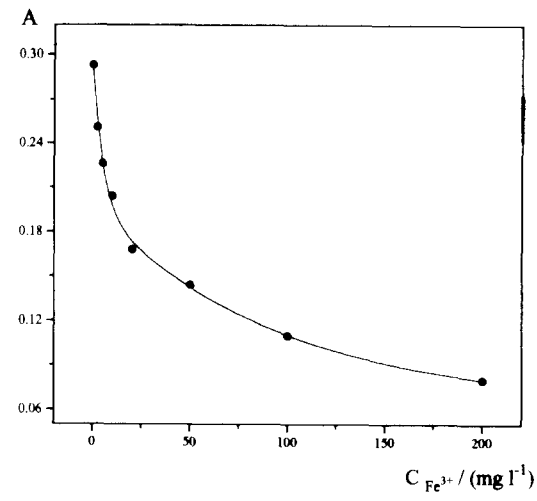

Fig. 3. Effect of iron(III) on the absorbance signals for nitrate (10 mg l^{-1}) in 3.6 mol l^{-1} sulfuric acid medium.

interferent in a standard method to determine nitrate in waters [12]. Thus, the effect of iron on the proposed method was investigated and the results obtained are shown in Fig. 3. It can be observed that the absorbance signal decreased exponentially with the iron concentration. For the concentrations determined in the samples investigated (Table 1), the analytical signal can decrease by up to 45%.

Davison and Woof [13] observed in a batch study employing an analogue procedure that several species caused interference in the determination of nitrate in fresh water. These drawbacks were ascribed to a kinetic effect on the nitrate reduction. In the presence of some concomitants, the reaction rate was reduced and the conversion rate become different to that observed for standard solutions. Probably, the perturbation due to iron(III) was caused by a similar effect. Since the residence time of the sample zone in the cadmium copperized column is very short (less than 8 s), iron(III) present in the samples could be reduced preferentially. Additionally, the nitrite produced could be oxidized by iron(III). Both effects could affect the global conversion rate of nitrate to nitrite.

Several procedures were investigated for eliminating the perturbation caused by iron(III), such

as employment of complexants (EDTA, fluoride, oxalate, phosphoric acid) or reductor agents (ascorbic acid, amalgamated zinc and stannous chloride) to iron(III). In spite of the interference decrement with some of these procedures, none was effective in eliminating it completely. The increase of the residence time in the column and the employment of a higher amount of reductor, as adopted in batch procedures to eliminate these perturbations [13], also produced unsatisfactory results. However, it can be seen in Fig. 3 that the rate of decrement of the analytical signal is less intense to higher concentrations of the ferric ion. This indicates that an addition of an excess of iron could be effective in leveling the perturbation. This was verified by additions of 200 or 400 mg l^{-1} iron(III) in solutions containing 10 mg l^{-1} nitrate in 3.6 mol l^{-1} sulfuric acid and 0, 10, 20 or 50 mg l^{-1} iron(III). Results obtained are shown in Table 2. It can be verified that 200 mg l^{-1} was effective in leveling the perturbation. In spite of the decrease of the absorbance signal, the sensitivity is enough to determine nitrate in electrolytes of lead–acid batteries.

By addition of an excess of the interfering ion, the precipitation of iron(III) hydroxide in the sample zone after the pH adjustment was observed. The adsorption of the precipitate on the surface of the filings affected the reduction efficiency and caused an increase of the back pressure. To avoid this drawback, a filter was inserted in the system (see Fig. 1). The relocalization of this component such as formerly employed [14] was adequate to remove and dissolve the precipitate. Despite the precipitation of iron(III) hydroxide, the remaining iron concentration in the sample zone was enough to level off the perturbation.

Table 2
Effect of iron(III) addition on the interference caused by iron in the absorbance of 10 mg l^{-1} nitrate in 3.6 mol l^{-1} sulfuric acid medium

Iron (sample) (mg l^{-1})	Iron (added) (mg l^{-1})		
	0	200	400
0	0.475 ± 0.004	0.048 ± 0.002	0.006 ± 0.001
10	0.373 ± 0.003	0.049 ± 0.001	0.006 ± 0.001
20	0.321 ± 0.004	0.049 ± 0.001	0.006 ± 0.001
50	0.263 ± 0.001	0.045 ± 0.002	0.006 ± 0.001

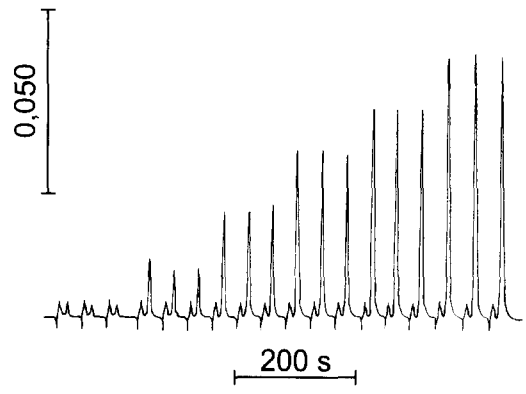

Fig. 4. Absorbance signals obtained for reference nitrate solutions (0, 5.00, 10.0, 15.0, 20.0 and 25.0 mg l^{-1}) in a 3.6 mol l^{-1} sulfuric acid medium. Flow diagram as in Fig. 1.

Nitrate can be properly determined in electrolyte samples containing from 3.0 to 4.5 mol l^{-1} H_2SO_4 without perturbation due to the Schlieren effect by using the system shown in Fig. 1, with a 400-cm dispersion coil (B_1), 6 mol l^{-1} ammonium hydroxide (R_1), and a buffer (10% (w/v) NH_4Cl, 1.0% (w/v) $Na_2B_4O_7 \cdot 10H_2O$) containing 0.1% (w/v) Na_2EDTA. The addition of 200 mg l^{-1} of iron(III) is necessary to level off the perturbation and a relocatable filter is employed to remove the hydroxide precipitate.

Using this system, a repeatability study was performed and a 2.0% relative standard deviation was obtained ($n = 10$) with a solution containing 25 mg l^{-1} nitrate in 3.6 mol l^{-1} sulfuric acid medium. According to the diagram in Fig. 4, the absorbance signal (A) can be related with the concentration (C, mg l^{-1}) by the equation: $A = 0.00286 + 0.00675C$ ($r = 0.999$). The signal distortion observed before the analytical transient signal for nitrate is due to the refractive index gradient caused by the introduction of the sulfuric acid solution remaining in the filter after removal of the precipitate. However, this does not affect the measurements.

The detection limit was estimated in 0.3 mg l^{-1} (99.7% confidence level) and the sampling rate

Table 3
Addition–recovery of nitrate in electrolytes from lead–acid batteries

Sample	Nitrate (mg l^{-1})		Recovery (%)
	Added	Found	
1	5.00	5.00	100
	10.0	9.55	95.5
2	5.00	5.15	103
	10.0	9.91	99.1
3	10.0	10.4	104
4	10.0	9.61	96.1
5	10.0	9.70	97.0

was 80 h^{-1}. An addition–recovery test was performed by spiking samples of electrolyte of lead–acid batteries with 5.00 or 10.0 mg l^{-1} nitrate. The results obtained are shown in Table 3. Recoveries between 95.5 and 104% are adequate to determine nitrate in the samples. Additional studies of accuracy were not possible because standard reference materials or standard reference methods are not available. The comparison with other procedures for nitrate determination was not made, since these could not be directly applied to the electrolyte of batteries or they suffered from lack of selectivity.

4. Conclusions

The proposed method is adequate for rapid determination of nitrate in electrolytes of lead–acid batteries. Interference due to iron(III) was leveled off by addition of excess of the interfering ion, and the iron(III) hydroxide was properly removed and dissolved by using a relocatable filter. A large dispersion flow diagram was effective to eliminate the Schlieren effect, and similar approaches could be used to determine other species in matrices characterized by the presence of high concentrations of concomitants.

Acknowledgements

F.R.P.R. is grateful to CAPES (Coordenadoria de Aperfeiçoamento de Pessoal de Nível Superior) by fellowship. The researchship furnished by CNPq (Conselho Nacional de Desenvolvimento Científico e Tecnológico) to J.A.N. is appreciated. The authors are also grateful to the partial support from FAPESP (Fundação de Amparo à Pesquisa do Estado de São Paulo) and to M.F.N.C. Rosolem (Telebrás-Brazil) for supplying the samples.

References

[1] D. Linden, Handbook of Batteries and Fuel Cells, McGraw-Hill, New York, 1984, p. 14-1.
[2] G.W. Vinal, Storage Batteries, 4th ed., Wiley, New York, 1955, p. 131.
[3] J.W. Williams, Handbook of Anions Determination, Butterworths, London, 1979, p. 127.
[4] E.A.G. Zagatto, M.A.Z. Arruda, A.O. Jacintho, I.L. Mattos, Anal. Chim. Acta 234 (1990) 153.
[5] T. Yamane, M. Saito, Talanta 39 (1992) 215.
[6] E.A.G. Zagatto, B.F. Reis, M. Martinelli, F.J. Krug, H. Bergamin F°, M.F. Giné, Anal. Chim. Acta 198 (1987) 153.
[7] F.J. Krug, H. Bergamin F°, E.A.G. Zagatto, Anal. Chim. Acta 179 (1986) 103.
[8] M.F. Giné, H. Bergamin F°, E.A.G. Zagatto, B.F. Reis, Anal. Chim. Acta 114 (1980) 191.
[9] A. Henriksen, A.R. Selmer-Olsen, Analyst 95 (1970) 514.
[10] M. Okada, H. Miyata, K. Toei, Analyst 104 (1979) 1195.
[11] A. Kojlo, E. Gorodkiewicz, Anal. Chim. Acta 302 (1995) 283.
[12] A.E. Greenberg, L.S. Clesceri, A.D. Eaton, Standard Methods for the Examination of Water and Wastewater, 18th ed., Victor Graphics, Baltimore, 1992, pp. 4–89.
[13] W. Davison, C. Woof, Analyst 104 (1979) 385.
[14] O. Fatibello F°, J.A. Nóbrega, A.J.M. Guaritá-Santos, Talanta 41 (1994) 731.

ELSEVIER

Talanta 45 (1997) 273–278

Talanta

Adsorptive potentiometric stripping analysis of trace tamoxifen at a glassy carbon electrode

Joseph Wang *, Xiaohua Cai, João Roberto Fernandes [1], Mehmet Ozsoz [2], Douglas H. Grant [3]

Department of Chemistry and Biochemistry, New Mexico State University, Las Cruces, New Mexico 88003, USA

Received 14 January 1997; received in revised form 25 February 1997

Abstract

A highly sensitive adsorptive stripping procedure for trace measurement of the anticancer drug tamoxifen is described. The method is based on controlled adsorptive accumulation of the drug at an electrochemically treated glassy carbon electrode, followed by chronopotentiometric measurement of the surface species. The chronopotentiometric operation effectively addresses the large background contribution inherent to the glassy carbon electrode to yield a detection limit of 4×10^{-10} M after 4 min preconcentration. The adsorptive stripping response is evaluated with respect to electrode type and conditioning, accumulation potential and time, stripping current, pH, drug concentration, potential interferences, and other variables. Applicability to urine samples is illustrated. © 1997 Elsevier Science B.V.

Keywords: Tamoxifen; Glassy carbon electrode; Adsorptive stripping voltammetry; Chronopotentiometry

1. Introduction

Tamoxifen Scheme 1 is a nonsteroidal anti-estrogen, used widely for the treatment of hormone-dependent breast cancer [1,2]. It is also used as a preventive agent for healthy women who have a family history of breast cancer. A highly sensitive analytical method for measuring tamoxifen is desired for optimizing its therapy and minimizing side effects. The polarographic behavior of tamoxifen and other triphenylethylene derivatives was elucidated by Fijalek et al. [3], who used it for determining these drugs in pharmaceutical tablets. The oxidation of tamoxifen at a glassy carbon flow detector was exploited for its amperometric monitoring in chromatographic effluents [4].

The present work describes an extremely sensitive adsorptive stripping procedure for trace measurements of tamoxifen. Adsorptive stripping analysis has been shown to be useful for trace measurements of anticancer drugs such as daunorubicin [5] or mitomycin C [6]. Unlike these

* Corresponding author.

[1] Permanent address: Departamento de Química, Universidade Estadual Paulista, Bauru-SP, POB 473, Brazil.

[2] Permanent address: Faculty of Pharmacy, Ege University, Izmir 35100, Turkey.

[3] Permanent address: Department of Chemistry, Mount Allison University, Sackville, NB EOA 3CO, Canada.

PII S0039-9140(97)00129-X

previous voltammetric stripping protocols, the present one relies on the constant-current potentiometric stripping (PSA) mode that effectively corrects for the large background contribution at carbon electrodes. Such coupling of effective adsorptive accumulation of tamoxifen with the sophisticated background correction features of PSA offers convenient quantitation of nanomolar concentrations of tamoxifen. The characteristics and advantages of this stripping potentiometric procedure are reported in the following sections.

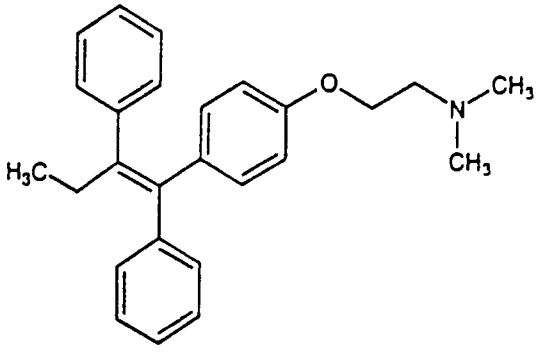

Scheme 1. Structure of Tamoxifen.

2. Experimental section

2.1. Apparatus

Voltammetric measurements were performed with a 264A polarographic analyzer/stripping voltammeter (EG&G/PAR, USA). Parameters for linear scan voltammetry: 50 mV s^{-1} scan rate; +0.2 V initial potential; +1.2 V final potential. Parameters for differential pulse voltammetry (DPV) were: 0.2 s drop time; 50 mV pulse height; scan rate 10 mV s^{-1}; +0.2 V initial potential; +1.2 V final potential. Constant current chronopotentiometic measurements or potentiometric stripping analyses (PSA) were performed with a TraceLab unit (PSU 20, Radiometer, Denmark) interfaced with an IBM PS/2 55SX. Potentials were sampled at a frequency of 30 kHz and the derivative signal (dt/dE) was recorded against the potential. The peak area following baseline fitting was used as the analytical signal.

The three-electrode system consisted of a glassy carbon electrode (GCE), a Ag/AgCl reference electrode (Model RE-1, BAS Inc., W. Lafayette, USA) and a platinum wire auxiliary electrode. The electrodes entered the cell through holes in the Teflon cover.

All measurements were carried out in a 2-ml cell (Kimble Glass Inc., Vineland, NJ, USA). All experiments were conducted at room temperature (22.0 ± 0.5°C).

2.2. Reagents

trans-2-[4-(1,2-Diphenyl-1-butenyl)phenoxy]-*N*,*N*-dimethylethylamine (tamoxifen) (Cat. No. 28,161-1) was received from Aldrich. The stock solution of tamoxifen (2.5 mM) was prepared with methanol and was kept in a refrigerator. Diluted solutions were made with methanol just before use. Britton–Robinson (BR) buffer (0.1 M, pH 4) was prepared with sodium hydroxide and phosphoric, acetic and boric acids. The usual supporting electrolyte was 0.05 M BR buffer containing 20% methanol. Methanol was not used in the blank electrolyte employed during the stripping medium–exchange procedure.

2.3. Procedure

2.3.1. Electrode pretreatment

Before each measurement, the GCE was first polished with 1 μm alumina and rinsed with water; then it was polished with 0.15 μm alumina and rinsed with water, followed by rinsing with ethanol and water. The electrode was anodized at +1.7 V for 1 min in the electrolyte containing tamoxifen.

2.3.2. Adsorptive accumulation

Adsorptive accumulation was performed at −0.1 V for a given time in the same electrolyte solution. The solution was stirred during the accumulation step and was allowed to settle for 5 s before the stripping.

2.3.3. Chronopotentiometric stripping

Chronopotentiometric stripping was performed either in the same electrolyte solution or in the

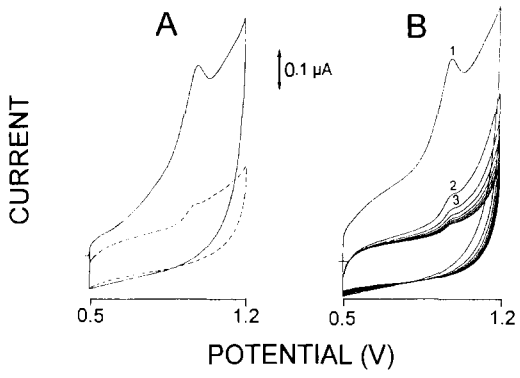

Fig. 1. Cyclic voltammograms for 0.5 μM tamoxifen at the glassy carbon electrode. (A) Response with and without accumulation (solid and dotted lines, respectively); (B) successive runs following the accumulation. Electrolyte, 0.05 M BR buffer (pH 4) containing 20% methanol; electrode pretreatment, 1 min at +1.7 V; accumulation potential and time, −0.1 V and 1 min, respectively; scan rate, 20 mV s^{-1}.

blank electrolyte solution with a stripping current of +10 μA and an initial potential of +0.2 V.

2.4. Analysis of human urine sample

To 1.5 ml fresh human urine, 50 mg fumed silica (0.011 μm, Cat. No S-5380, Sigma) was added. The sample was shaken for 20 min and then was centrifuged (Model 415C, Eppendorf) at 10000 rpm. Supernatant (0.2 ml) was added to the electrochemical cell, along with the electrolyte (0.05 M BR buffer, 20% methanol). Other procedures were as above (the accumulation time being 2 min), and the stripping was carried out in the blank electrolyte solution. The urine sample was spiked with 0.5–2 μM tamoxifen before adding fumed silica.

3. Results and discussion

Fig. 1A (solid line) displays a cyclic voltammogram for 5×10^{-7} M tamoxifen recorded at the glassy carbon electrode after 1 min stirring at −0.1 V. A large definite anodic peak, corresponding to the oxidation of the adsorbed drug, is observed at ca. +0.985 V. No peaks are observed in the cathodic branch, indicating an irreversible redox process. Also shown (as a dotted line) is the analogous response without prior accumulation. A substantially (7-fold) smaller oxidation peak, corresponding to the dissolved species, is observed. Such an anodic signal is attributed to the cyclization reaction to form the corresponding phenanthrene derivative. A similar mechanism was proposed for the oxidation of tamoxifen [3] and related compounds [7] at various electrodes. Fig. 1B shows repetitive cyclic voltammograms for tamoxifen recorded following the 1-min accumulation. Substantially smaller peaks are observed on continued scanning, indicating rapid desorption of the product. Eventually, a stable response, corresponding to the dissolved species (as in Fig. 1A; dotted line) is observed.

The spontaneous adsorption of tamoxifen can be used as an effective preconcentration step, prior to electrochemical measurement, making possible a highly sensitive quantitation. Fig. 2 displays chronopotentiograms obtained at the glassy carbon electrode which has been exposed to a 5 nM tamoxifen solution for times ranging from zero to 2 min (Fig. 2a–e). No response is observed at the nanomolar level unless there is some preconcentration. As the preconcentration period increases, there is a rapid increase in the well-defined oxidation peak (at +0.98 V). As a result, tamoxifen can be readily measured at the nanomolar concentration level. Also shown in Fig. 2 are plots of peak-area vs. preconcentration time for 5 and 50 nM tamoxifen (inset, A and B, respectively). Similar signals were observed after transferring the electrode to a blank solution (following the preconcentration), indicating a very strong adsorption.

The ability to readily measure nanomolar concentrations is attributed not only to the effective preconcentration step, but also to the advanced chronopotentiometric monitoring of the accumulated drug. Fig. 3 (curves b) compare linear-scan (A) and differential-pulse (B) voltammograms, with the corresponding potentiometric stripping response (C). With 100 nM tamoxifen and using 1 min preconcentration, the voltammetric mode is

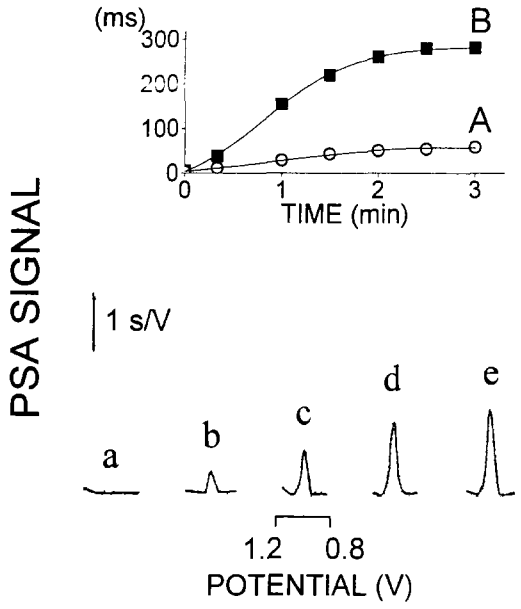

Fig. 2. Chronopotentiograms for 5 nM tamoxifen at the GCE with increasing accumulation time: 0 (a), 0.5 (b), 1 (c), 1.5 (d) and 2 (e) min. Also shown is the effect of accumulation time on PSA signal for 5 (A) and 50 nM (B) tamoxifen. Electrolyte and electrode treatment, as in Fig. 1; accumulation potential: −0.1 V; stripping current: +10 μA.

hardly useful for detecting the accumulated drug, due to the rising background current associated with its extreme peak potential (curves a, A and B). In contrast, the advanced potentiometric stripping operation effectively corrects for this background contribution (C(a)), and results in a

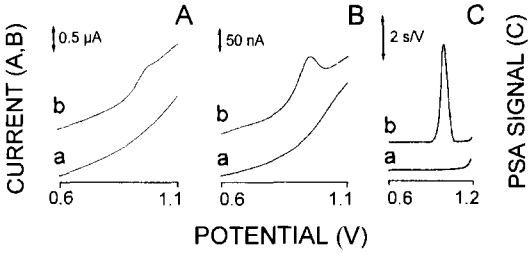

Fig. 3. Linear scan (A), differential pulse (B) voltammograms and chronopotentiogram (C) for 0 (a) and 100 nM (b) tamoxifen at the GCE. Electrolyte and electrode pretreatment, as in Fig. 1; accumulation potential, −0.1 V; scan rate, 50 (A) and 10 (B) mV s^{-1}; pulse height (B), 50 mV; stripping current (C), +10 μA.

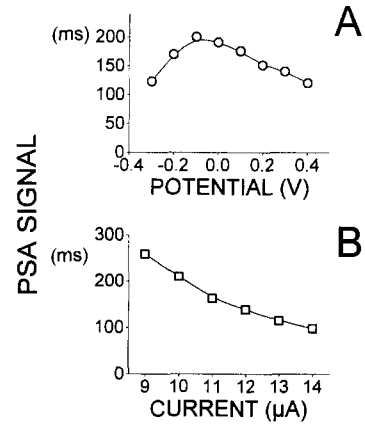

Fig. 4. Effect of accumulation potential (A) and stripping current (B) on the PSA signal of 100 nM tamoxifen at the GCE. Accumulation time, 1 min; other conditions as in Fig. 2.

well-defined adsorptive stripping peak (C(b)). Similar advantages of the adsorptive PSA operation were documented recently in connection with trace analysis of nucleic acids [8].

Various experiments were carried out to find the optimum conditions for adsorptive PSA of tamoxifen. Fig. 4A shows the effect of the accumulation potential upon the PSA peak area. The latter increases upon changing the potential from −0.3 to −0.1 V, but decreases gradually at higher potentials. Fig. 3B shows that the response decreases rapidly upon raising the stripping current between 9 and 14 μA. Both carbon paste and glassy carbon electrodes displayed an attractive adsorptive stripping tamoxifen response. The response of the glassy carbon electrode was improved further (with respect to lowering background contribution and enhancing the stripping signal) by an anodic treatment of its surface. We investigated various parameters of this electrochemical pretreatment and found that a 60-s duration at +1.7 V offers the most favorable signal-to-background characteristics. All subsequent work was carried out using the treated glassy carbon electrode, in view of its more favorable and stable response. Similar results were obtained when the pretreatment was performed in the presence or absence of tamoxifen, The absence of surface passivation following the treatment in

the presence of the drug reflects the rapid desorption of the oxidation product (as expected from the cyclic voltammetric behavior). Solution conditions have also a profound effect upon the response. The latter increases sharply upon raising the pH between 3.2 and 4.0, but decreases rapidly at higher values, with near disappearance at pH 8.0. Whether such pH dependence is due to changes in the electroactivity or adsorptivity of the drug is not clear at this stage. Addition of methanol (at 20% v/v) to the Britton–Robinson pH 4.0 buffer was found essential for maintaining a stable tamoxifen solution (and hence a reproducible response).

Quantitation is based on the dependence of the PSA peak area upon the concentration of the drug. Fig. 5A illustrates the response for successive 20-nM increments in tamoxifen concentration for a 30-s preconcentration period (Fig. 5A(a–e)). Well-defined peaks, whose areas are proportional

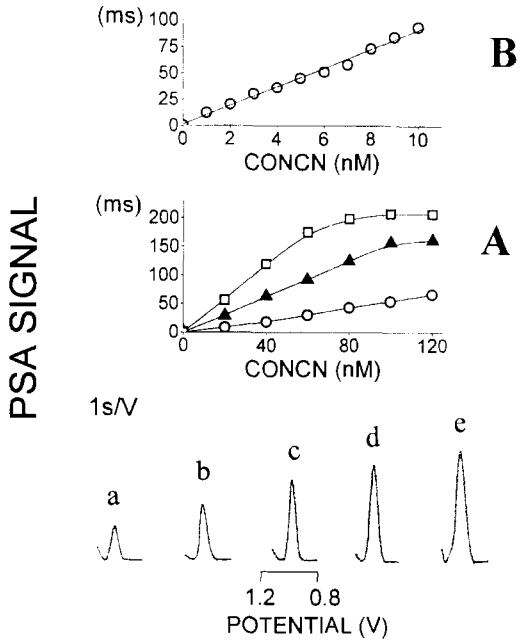

Fig. 5. (A) Chronopotentiograms for 20 (a), 40 (b), 60 (c), 80 (d) and 100 (e) nM tamoxifen following 30 s accumulation. Also shown, calibration plots for 0–120 nM tamoxifen with steps of 20 nM following 15 (○), 30 (▲) and 60 s (□). (B) Calibration plot for 0–10 nM tamoxifen with steps of 1 nM following a 2-min accumulation. Other conditions as in Fig. 2.

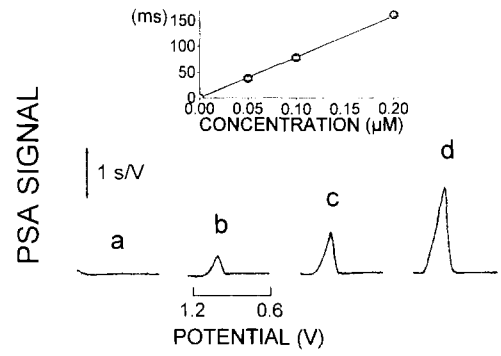

Fig. 6. Chronopotentiograms for a urine sample spiked with 0 (a), 0.5 (b), 1 (c) and 2 (d) μM tamoxifen for 2 min accumulation and stripping in the blank solution (0.05 M BR buffer, pH 4), along with resulting calibration plot (inset). The urine sample was diluted 10-fold with the supporting electrolyte/methanol solution; other conditions as in Fig. 2.

to the drug concentration, are observed. These peaks were a part of a six-point calibration experiment, utilizing preconcentration periods of 15, 30 and 60 s. The resulting calibration plots are also given in Fig. 5A. As expected for processes involving adsorption of the analyte, the response is linear for dilute solutions and/or for short preconcentration periods. While the response following 15-s accumulation is linear over the entire (20–120 nM) range examined, those observed with 30- and 60-s preconcentration times are linear up to 100 and 60 nM, respectively (slopes of linear portions are 0.56, 1.58, and 2.58 ms nM^{-1} for 15, 30, and 60 s accumulation, respectively; correlation coefficients, 0.998, 0.999 and 0.990). Also shown in Fig. 5B is another calibration plot obtained by increasing the tamoxifen level in 1-nM steps and using a 120-s accumulation (Fig. 5B). The response is linear over this 1–10-nM range, with a slope of 8.94 ms nM^{-1} (correlation coefficient, 0.996).

Because of the effective preconcentration of tamoxifen and the background compensation capability of PSA, very low detection limits are obtained with relatively short accumulation times. A detection limit of 0.4 nM tamoxifen was estimated from the signal-to-noise characteristics of the response to 0.6 nM of the drug following a 4-min adsorption ($S/N = 3$; not shown). A series

of eight repetitive measurements of 100 nM tamoxifen was used for estimating the precision (1 min accumulation; not shown). The mean peak area was 278 ms, with a range of 260–292 ms, and a relative standard deviation of 5.3%.

Direct adsorptive stripping assays of urine samples were performed (as shown in Fig. 6). The tamoxifen-free urine sample was spiked with 0.5–2.0 μM of tamoxifen. Well-defined peaks, proportional to the drug concentration, were observed following a 2-min accumulation (Fig. 6b–d). Note that the simple 'fumed-silica' treatment, coupled with simple dilution and medium-exchange protocol, resulted in a flat 'clean' background (Fig. 6a). Indeed, no response was observed for the medium-exchange adsorptive PSA protocol for the common coexisting electroactive interferences ascorbic acid and acetaminophen (both at 0.5 mM; 1 min accumulation; not shown). In contrast, competitive adsorption of uric acid resulted in ca. 20% loss of the 100-nM tamoxifen signal. It also resulted in a uric acid peak (at +0.5 V) that was well separated from the tamoxifen signal. Experiments in 'pure' solutions (with and without the fumed silica) indicated that tamoxifen is not collected by the silica particles.

In conclusion, this work has demonstrated that adsorptive stripping potentiometry is suitable for ultratrace measurements of tamoxifen. Owing to the combination of the sophisticated background fitting of PSA with the spontaneous accumulation of the drug, nanomolar concentrations of tamoxifen can be readily detected at a glassy carbon electrode. Such remarkable sensitivity is sufficient for monitoring clinically relevant concentrations of the drug. It is not clear at this stage whether the method is able to differentiate between the parent drug and its metabolites. While these metabolites appear to be electroactive, they may display significant lower adsorptivity (due to the presence of the hydroxy moiety). Extension to other drugs of triphenylethene derivatives, and improvements of analogous stripping voltammetric schemes for other anticancer drugs [5,6], are expected using similar adsorptive PSA protocols.

Acknowledgements

J.R.F., M.O. and D.H.G. acknowledge fellowships from FAPESP (Brazil), Scientific & Technical Research Council (Turkey) and Mount Allison University (Canada), respectively.

References

[1] M. Gottardis, S.Y. Jiang, M.H. Jeng, V. Jordan, Cancer Res. 49 (1989) 4090.
[2] L. Lerner, V. Jordan, Cancer Res. 50 (1990) 4177.
[3] Z. Fijalek, J. Chodkowski, M. Warona, J. Electroanal. Chem. 226 (1987) 129.
[4] S. Chamart, M. Hanocq, M. Helson, N. Devleeschouwer, G. Leclercq, J. Chromatogr. 496 (1989) 365.
[5] J. Wang, M. Lin, V. Villa, Analyst 112 (1987) 1303.
[6] J. Wang, M. Lin, V. Villa, Anal. Lett. 19 (1986) 2293.
[7] A.J. Bard, J. Phelps, J. Electroanal. Chem. 25 (1970) 2.
[8] J. Wang, X. Cai, C. Jonsson, M. Balakrishnan, Electroanalysis 8 (1996) 20.

ELSEVIER

Talanta 45 (1997) 279–284

Talanta

A compact collinear AOTF Raman spectrometer

Neelam Gupta *, N.F. Fell Jr

Sensors and Electron Devices Directorate, Army Research Laboratory, 2800 Powder Mill Road, Adelphi, MD 20783-1197, USA

Received 3 February 1997; accepted 7 April 1997

Abstract

A compact, lightweight, completely packaged, uncooled, fully-automated collinear acousto-optic tunable-filter (AOTF) based spectrometer has been used to measure Raman spectra of three organic energetic materials (NQ, HMX, and TNT) using argon-ion laser excitation. Even though the resolution of the AOTF spectrometer is modest (7.4 cm^{-1}) and it was not specifically designed for measuring Raman spectra, it has performed impressively. Such an instrument is specially useful for remote sensing and field measurements. In this paper, we will describe this instrument, present the measured Raman spectra and their comparison with the corresponding FT–IR spectra.

Keywords: Acousto-optic tunable-filter; Raman spectra; Organic energetic materials

1. Introduction

Remote detection and monitoring of chemical agents in the field are extremely important spectroscopic applications that require the development of highly sensitive, ruggedized, low-cost, light-weight, compact, and portable analytical instruments. Raman spectra can be used in identifying chemicals with great accuracy, but due to its demanding nature has remained mainly a laboratory technique. Acousto-optic tunable-filter (AOTF) technology is a recent development that can be used to design highly sensitive and robust portable spectrometers which can be used for detection of Raman spectra in a variety of settings. We have used a recently developed compact collinear AOTF spectrometer for detection of Raman spectra of organic energetic materials. Even though, Raman spectra are measured using fairly high resolution instruments, we have obtained impressive results with our small 4-lb. spectrometer.

An AOTF is an electronically tunable phase grating set up in an anisotropic crystal by the propagation of an ultrasonic wave in the crystal. It functions by scattering light from one linear polarization into the other by resonant coupling of the optical wave with the acoustic wave in the crystal, due to the elasto-optic effect. These filters contain no moving parts and offer high-speed wavelength tuning, which can be done sequentially or randomly, depending upon the programmed instructions. The acoustic waves are

* Corresponding author. Tel.: +1 301 3942451; fax: +1 301 3941170; e-mail: NGupta@d1sig.arl.mil

0039-9140/97/$17.00
PII S0039-9140(97)00145-8

generated by the application of a radio frequency (rf) signal to one or more piezo-electric oscillators (transducers) bonded to the crystal. There are two types of AOTFs: collinear cells (for example quartz), where the incident light, the acoustic wave, and the diffracted beam all travel in the same direction; and noncollinear cells (such as tellurium dioxide, TeO_2), in which the incident wave, the acoustic wave, and the diffracted light do not travel in the same direction.

Progress in AOTF technology has been significantly advanced by the progress in the fabrication of high-frequency acoustic transducers and development of materials with excellent acoustic and optical properties and large photoelastic constants. AOTF cells are gradually replacing conventional grating technology in a wide range of applications that require high speed, ruggedness, reproducibility, programmability, and accuracy. AOTFs are lightweight, compact, and very useful for field-portable applications. They have no moving parts, have all solid-state construction, are electronically tuned and are insensitive to vibrations. With moderate spectral resolution, large field of view, and high throughput, they offer high-speed tuning and scanning of wavelengths, with reliable and reproducible operation under computer control. A number of TeO_2 AOTFs are now commercially available.

The performance of AOTFs is primarily limited by the availability of superior materials. To qualify as a candidate for use as an interaction medium for an AOTF, a material must be optically birefringent and transparent in the operating wavelength range of interest, have a low acoustic attenuation in the acoustic frequency range of operation, and have a large AO (acousto-optic) figure of merit. Different materials are used to design AOTF cells for various spectral ranges: crystal quartz is used for the range 255–800 nm (mostly collinear); TeO_2 is used for 350–4500 nm (noncollinear); $CaMoO_4$ is used for 400–4500 nm (collinear); and $LiNbO_3$ is used for 400–4500 nm (collinear). Several excellent review articles are available on AOTF technology in the literature [1–10]. Elsewhere [11–17], AOTFs have been shown to be very powerful tools for all kinds of spectroscopic applications, including absorption, emission, fluorescence, and Raman.

As a result of an ongoing collaboration effort, we presently have a number of collinear quartz AOTF cells and spectrometers operating from the UV to near-IR spectral range (255–800 nm) that were fabricated at the Central Bureau of Unique Instrumentation (CBUI) of the Russian Academy of Sciences in Moscow [6,18]. These instruments are designed primarily for spectral emission and absorption measurements. We are carrying out an extensive program to evaluate these devices for application in the remote detection of chemical and biological agents, using absorption, laser-induced fluorescence, and Raman spectroscopic techniques [11].

We used a visible to near-IR spectrometer to measure the Raman spectra of energetic materials. Raman-scattering measurements are, in general, taken with a specially designed accessory attached to a Fourier transform (FT) spectrometer [19,20]. Since Raman scattering cross sections are very small, they require carefully tailored experimental setup, with very sensitive instruments for detection. This paper presents Raman spectra of three energetic materials—HMX (nitramine cyclotetramethylenetetranitramine), TNT (trinitrotoluene), and NQ (nitroguanidine)—along with a comparison with their respective FT–IR spectra in the range 500–4000 cm^{-1}.

Table 1
Specifications for collinear AOTF spectrometer

Parameter	Value
Spectral range (nm)	400–800
Resolution (nm)	0.1–0.54
Position error (nm)	±0.2
Maximum No. of points	4790
Analog-to-digital conversion range	12 bits
Maximum amplification	15
PMT voltage sensitivity	1:3:9:30
Effective dynamic range (dB)	63
Diameter of aperture (mm)	10
Length of crystal (cm)	15
Field of view (°)	2

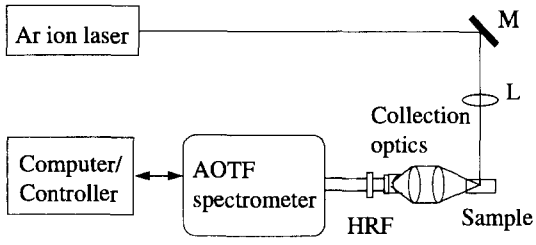

Fig. 1. Optical train for Raman spectroscopy with AOTF spectrometer.

2. Experimental

2.1. AOTF instrument

All the measurements described in this paper were performed with a visible to near-IR collinear AOTF spectrometer developed at CBUI in Moscow [6,18]. The complete instrument system comprises two parts: an optical unit and an electronic controller unit. The optical unit consists of a quartz AOTF cell, a set of crossed polarizers with an extinction ratio of 3×10^5, input/output lenses, and a photomultiplier tube (PMT). The size of this unit is $10 \times 4 \times 1.5$ cubic inches and it weighs slightly less than 4 lb. The electronic controller unit resides inside a standard PC tower, and consists of an rf synthesizer, rf amplifier, PMT power supply, a signal processing unit for the PMT signals, and a PC interface card.

Some of the important operating specifications for this instrument are listed in Table 1. The values for the analog-to-digital converter (ADC), the amplification factor, and the PMT voltage sensitivity are multiplied to define the dynamic range for the instrument, resulting in a value of 1.8432×10^6, or 63 dB. This instrument is approximately two orders of magnitude more sensitive than the older quartz spectrometer designed by CBUI under the name Quartz-4 [7,18]. This sensitivity has been achieved by the use of a novel AOTF cell architecture to minimize undesired acoustic reflections, state-of-the-art integrated electronics chips, and a newly designed PMT. The spectrometer is controlled through a 486 PC. Measurements at each spectral point take 20 ms, and the PMT signal is detected synchronously with the applied rf signal. The rf signal is applied to the AOTF cell for only 5 ms of 'on' time, with 15 ms of 'off' time. An electronic integrator is used to add the PMT signals. During the on time, the signal and background noise are detected by the PMT; during the off time, only the background noise is detected for the first 5 ms. This detection scheme also facilitates the room-temperature operation of the instrument.

2.2. Experimental setup

The Raman experiments described here use the optical train shown in Fig. 1. An argon ion laser operating at 514.45 nm was used for this experiment. A pair of mirrors (M) were used to steer the beam to the sample, and a lens (L) was used to focus the excitation beam on the sample. A set of

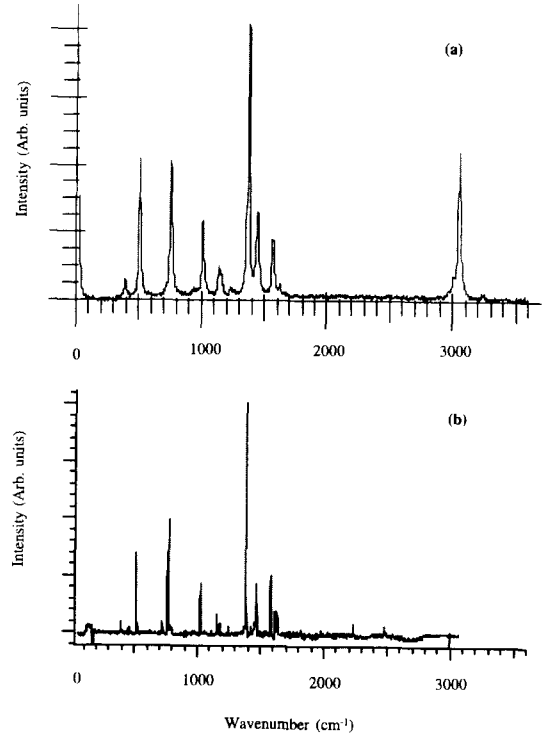

Fig. 2. (a) AOTF Raman spectrum of naphthalene in a capillary tube (amplification 10, accumulations 10, 500 mW, 514.45-nm excitation). (b) FT–Raman spectrum of naphthalene in a capillary tube (400 mW, 1064-nm excitation, 256 co-adds).

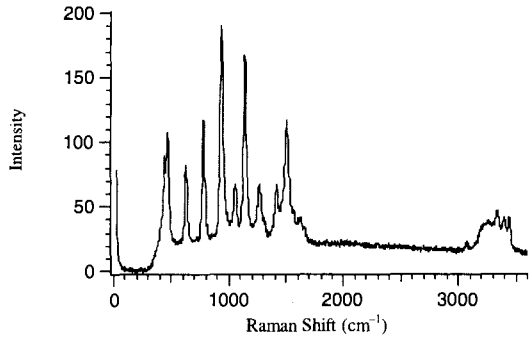

Fig. 3. AOTF Raman spectrum of NQ (accumulations 50, amplification 10).

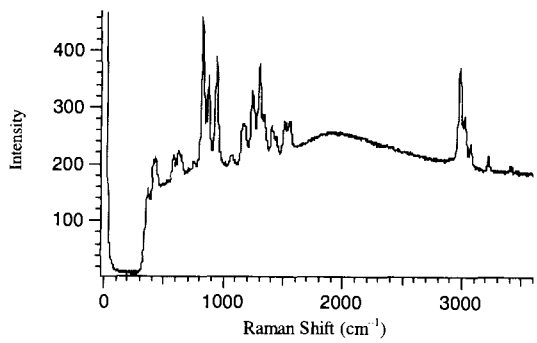

Fig. 4. AOTF Raman spectrum of HMX (accumulations 50, amplification 4).

beam-forming lenses is used to collect, compress, and collimate the scattered Raman photons into the spectrometer. A holographic Rayleigh rejection filter (HRF, Kaiser Optical Systems, Notch-Plus), with a peak rejection ratio of 10^{-6} and an edgewidth of 50 cm^{-1} on the longer wavelength side of the Rayleigh line was used to reduce the strong Rayleigh-scattered light that entered the AOTF spectrometer. We used a glass capillary tube (Fisher Scientific) to hold the sample for solid Raman measurements. In these experiments, the radiation source was a Coherent Innova 70-5 argon ion laser. Depending on the effect of laser heating in the samples, 50 to 500 mW of laser power was used. Raman spectra were collected by scanning the AOTF from 515 to 631.5 nm (or 58 to 3600 cm^{-1}) with 1348 points, the maximum number of points available. Scans took approximately 6 minutes for 10 accumulations and 50 minutes for 50 accumulations. All scans were collected with a PMT setting of 4 (the most sensitive setting), and amplification settings of 4 to 10.

3. Results and discussion

The first experiment we conducted was the collection of a Raman spectrum of an organic powder. We chose naphthalene for this experiment because it has a strong Raman spectrum. In Fig. 2, both the AOTF Raman spectrum and a reference FT–Raman spectrum (taken with a Bomem DA-8.02) are shown for comparison purposes. While the S/N ratio is poorer in the AOTF spectrum, the major peaks are still clearly visible. Data collection time for the AOTF spectrometer was only 6 minutes compared to 20 minutes for the FTR. Extending the accumulation time for the AOTF will clearly improve the S/N ratio. The other factor that is clear from the comparison is the lower resolution of the AOTF (7.4 cm^{-1} for AOTF and 4 cm^{-1} for the FTR). The FTR system does not detect beyond 3050 cm^{-1} because it uses an InGaAs detector [19,20].

The AOTF Raman spectra of three representative energetic materials—NQ, HMX, and TNT (obtained from in-house sources) are shown in Figs. 3–5. HMX and NQ tend to be fairly strong Raman scatterers, while TNT is a weak scatterer. In each case, there is a small, but noticeable, background in the spectrum. The background is due to either fluorescence or heating effects, causing a broad emission under the Raman signal. The background in the HMX spectrum is probably due to fluor escence, since it rises, peaks at approximately

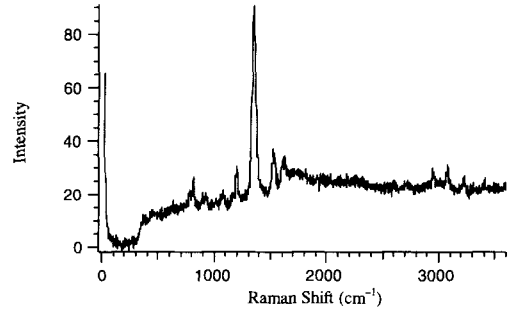

Fig. 5. AOTF Raman spectrum of TNT (accumulations 50, amplification 10).

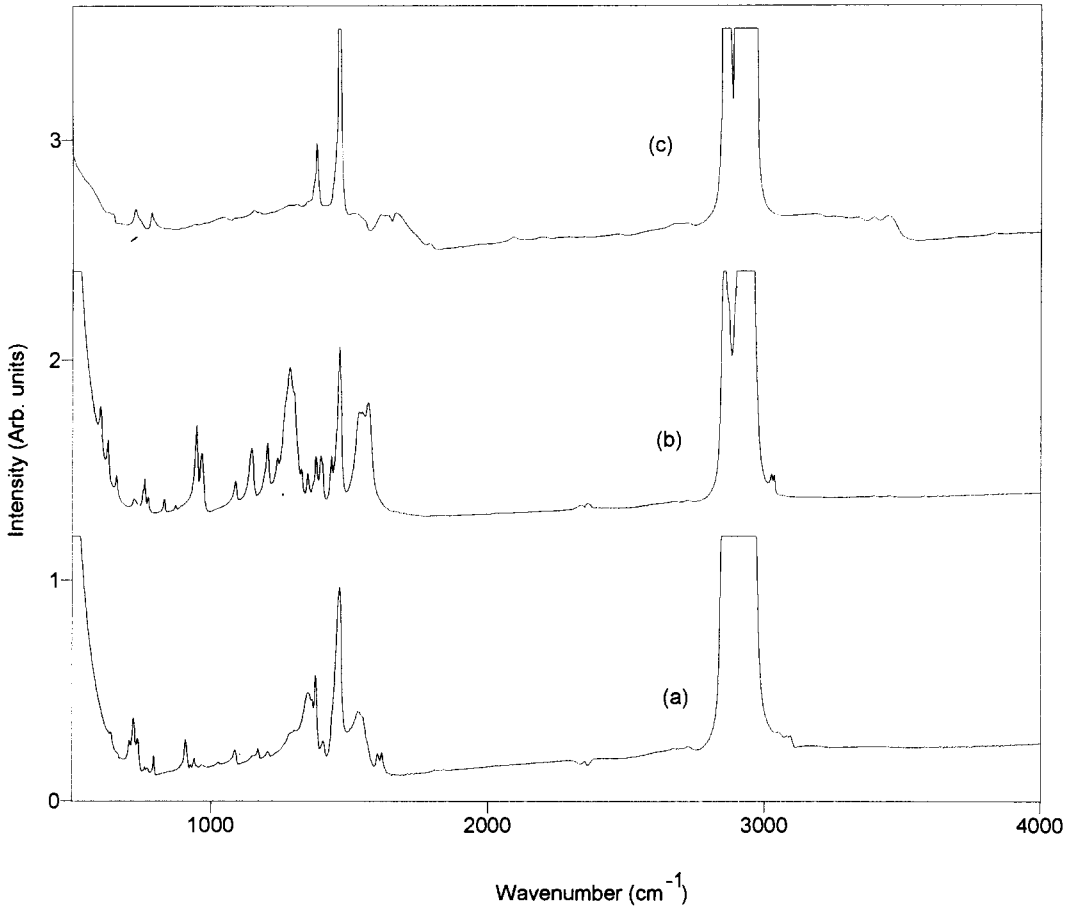

Fig. 6. FT–IR spectra of (a) NQ, (b) HMX, and (c) TNT (accumulations 64).

1943 cm^{-1} or 570.57 nm, then falls. As with the naphthalene spectrum, the peaks correspond to the peaks observed in the FTR spectra, and even though the AOTF spectra have lower resolution, there is sufficient resolution to enable identification of the compounds on the basis of their Raman spectra [19,20].

Fig. 6 shows the measured FT–IR Nujol spectra (standard Nujol peaks are visible in these spectra) of NQ, HMX, and TNT in the range 500–4000 cm^{-1} taken with a Nicolet Magna–IR 550 spectrometer with 4-cm^{-1} resolution. A comparison of the FT–IR and corresponding Raman spectra clearly shows that the peaks in the FT–IR spectra are complementary to those in Raman. The strongest peaks of Raman are a better identifier of these energetic materials than those of the FT–IR. For NQ there are a higher number of better resolved peaks in Raman than in FT–IR, suggesting that Raman may be a better method for identification; for HMX and TNT both Raman and FT–IR have a similar number of resolved peaks. Raman technique has other advantages over FT–IR: it is nondestructive; it does not require any sample preparation; it is relatively insensitive to sample positioning; it is very sensitive to slight differences in molecular structures; it is more suitable for the study of aqueous solutions, because water has a rather weak Raman signal; and in mixtures where IR peaks overlap, Raman peaks can be used for identification of species. Reference 20 has done comparison of the FTR and FT–IR spectra of HMX with similar conclusions.

As shown in Figs. 2–5, the results of using a collinear AOTF spectrometer for measuring Raman spectra are rather impressive, considering that the instrument was not specifically developed for this application. This instrument can be used for fast (less than 1 minute) identification of some chemicals. Another point worth mentioning is the possibility of designing an AOTF with much higher resolution by cascading a number of cells [18]. Design of a collinear AOTF spectrometer, specifically for Raman application is under consideration. AOTF cells and spectrometers in the mid-IR range (2–4 μm) and far-IR range (8–12 μm) are also being developed.

It should also be mentioned that this is the first fully packaged compact collinear AOTF spectrometer system which is very small (10 × 4 × 1.5 cubic inches; 4-lb.); it is very fast (20 ms per spectral point); and has a very high sensitivity (dynamic range 63 dB). The AOTF cell has a relatively high throughput (~30%) and operates without any cooling. All this makes this compact spectrometer a very attractive candidate for field applications and remote sensing.

4. Conclusion

Even though the 400–800 nm spectrometer was not designed specifically for measuring Raman spectra and has a modest resolution (7.4 cm^{-1}), we obtained very impressive results. Raman spectra have been shown to be superior to the FT–IR spectra for identification of energetic chemicals. AOTF spectrometers have no moving parts and are immune to vibrations. They are lightweight, portable, and compact and offer high speed, ruggedness, reproducibility, programmability, and accuracy. The results of our measurements clearly establish the great potential offered by such compact spectrometers, in spite of their modest resolution, for the Raman-scattering measurements in a lab setup, as well as in the field or from an airborne remote sensing platform.

Acknowledgements

The authors would like to thank V.I. Pustovoit for many useful discussions and R. Dahmani for the help in taking the FT–IR spectra. This work was performed while one of the authors, N.F. Fell, Jr., held a National Research Council–U.S. Army Research Laboratory research associateship.

References

[1] R.W. Dixon, IEEE J. Quantum Electron. QE-3 (1967) 85.
[2] S.E. Harris, R.W. Wallace, J. Opt. Soc. Am. 59 (1969) 744.
[3] S.E. Harris, S.T.K. Nieh, D.K. Winslow, Appl. Phys. Let. 17 (1970) 223.
[4] I.C. Chang, Appl. Phys. Let. 25 (1970) 370.
[5] N. Gupta, An AOTF Technology Overview, Proceedings of the First Army Research Laboratory Acousto-Optic Tunable Filter Workshop, ARL-SR-54, March 1997, pp. 11–19.
[6] V.I. Pustovoit, N. Gupta, Collinear Acousto-Optic Spectrometers and Their Applications, Proccedings of the First Army Research Laboratory Acousto-Optic Tunable Filter Workshop, ARL-SR-54, March 1997, pp. 33–44.
[7] A.P. Goutzoulis, D.R. Pepe (Eds.), Design and Fabrication of Acousto-Optic Devices, Marcel Dekker, New York, 1994, p.197.
[8] C.D. Tran, Anal. Chem. 64 (1992) 971A.
[9] N.J. Berg, J.N. Lee (Eds.), Acousto-Optic Signal Processing Theory and Implementation, Marcel Dekker, New York, 1983, p. 139.
[10] I.C. Chang, Proc. SPIE 90 (1976) 12.
[11] N. Gupta, N.F. Fell, Jr., Application of AOTF Technology for Chem/Bio Detection, Proceedings of the First Army Research Laboratory Acousto-Optic Tunable Filter Workshop, ARL-SR-54, March 1997, pp. 137–147.
[12] C.D. Tran, Application of Acousto-Optic Tunable Filters in Analytical Chemistry, Proceedings of the First Army Research Laboratory Acousto-Optic Tunable Filter Workshop, ARL-SR-54, March 1997, pp. 111–136.
[13] S. Medlin, C. Westgate, W. Danley, U. Eschenauer, Solving Process Problems with AOTF-based NIR spectroscopy, Proceedings of the First Army Research Laboratory Acousto-Optic Tunable Filter Workshop, ARL-SR-54, March 1997, pp. 149–163.
[14] D.H. Hueber, C.L. Stevenson, T. Vo-Dinh, Appl. Spectrosc. 49 (1995) 1624.
[15] H.R. Morris, C.F. Hoyt, P.J. Treado, Appl. Spectrosc. 48 (1994) 857.
[16] E.N. Lewis, P.J. Treado, I.W. Levin, Appl. Spectrosc. 47 (1993) 539.
[17] P.J. Treado, I.W. Levin, E.N. Lewis, Appl. Spectrosc. 46 (1992) 1211.
[18] V.I. Pustovoit, V.E. Pozhar, Photon. Optoelectron. 2 (1994) 53.
[19] N.F. Fell, J.M. Widder, S.V. Medlin, J.B. Morris, R.A. Pesce-Rodriguez, K.L. McNesby, J. Raman Spectrosc. 27 (1996) 97.
[20] K.L. McNesby, J.E. Wolfe, J.B. Morris, R.A. Pesce-Rodriguez, J. Raman Spectrosc. 22 (1994) 75.

ELSEVIER

Talanta 45 (1997) 285–289

Talanta

Fluorescence studies of carbocyanines using AOTF

A. George, G. Patonay *

Department of Chemistry, Georgia State University, University Plaza, Atlanta, GA 30303, USA

Received 12 February 1997; accepted 7 April 1997

Abstract

Over the past few years acceptance of acousto-optic devices which can control optical radiation has increased. In this paper the use an acousto-optic tunable filter (AOTF) within an existing spectrofluorometer as a replacement for the excitation monochromator is reported. Long wavelength absorbing carbocyanine dyes that have strong absorption and high quantum yield are used as standards. The major advantage of using an AOTF filter is the wavelength purity and that it can act as a wavelength selector in place of a monochromator. The use of AOTF in place of bandpass filters for removing laser diode side bands is also discussed. © 1997 Elsevier Science B.V.

1. Introduction

In the conventional fluorescence spectrometer the wavelength selection of the incident light is achieved by the use of monochromators or diffraction gratings. These monochromators have moving parts and there is always the possibility of error in the selection of wavelengths. The process requires frequent re-calibration of the spectrometer. Because of these difficulties, there is now a growing interest in alternate technologies such as acousto-optic tunable filters. In the last two decades the development of acousto-optic tunable filters (AOTF) has gained momentum along with new acousto-optic crystal growing methods. AOTF is based on the principle of interaction of optical radiation with sound waves in an anisotropic medium. A detailed description of the theory and principles of AOTF can be found elsewhere [1–5].

AOTF is an electronically tunable bandpass filter with no moving components. The main component of the AOTF is the acousto-optic crystal, where the interaction between the acoustic wave and optical radiation are used to filter a single wavelength from a multi-color or broadband source. The selected wavelength depends on the radio frequency applied to the crystal and wavelength can be changed by changing the frequency. Since there are no moving parts in the AOTF, the selected wavelength is not dependent on the geometry of the device.

There are several reports in the literature about the applications AOTF. In their paper, Kurtz et al. describe the development of a rapid scanning fluorescence spectrometer [6]. They collected the excitation and emission spectra from a fluorescent pH probe in 17 ms with this spectrometer. The excitation and emission spectra in these experiments spanned the region from 450 nm to 550

* Corresponding author.

PII S0039-9140(97)00144-6

nm. Morris, Hoyt and Traedo developed an imaging spectrometer for fluorescence and Raman Microscopy based on AOTF and liquid crystal tunable filters (LCTF) [7]. They concluded that AOTF gives a higher transmittance and spectral range than LCTF, but the imaging quality was inferior.

Tran and Furlan describe a spectrofluorometer based on AOTF for multiple component analysis and rapid scanning [8]. The instrument is portable and capable of measuring a fluorescence spectrum in a few micro seconds. These experiments use two AOTFs, one for specific wavelength excitation and the other as a polychromator on the emission side. The AOTF used for excitation diffracts the fluorescent light and enables them to analyze multiple components in a sample. There are many reports in the literature about the use of AOTF in near-infrared spectroscopy. Eilert and co-workers report the identification of organic components from pre-treated waste water using AOTF-based near-infrared (NIR) spectroscopy [9]. Components are identified by chemometrics and spectral matching with spectral libraries containing calibration spectra. AOTFs are also used in NIR absorption microscopy in combination with an indium antimonide multichannel imaging detector [10]. Most applications of AOTF in NIR are mainly for vibrational studies and not for fluorescence spectroscopy.

In this article, the use of AOTF in an existing fluorometer is discussed. Here the AOTF is used to tune the wavelength of the excitation source that is needed for the fluorescence studies. An advantage of an AOTF is that a pure wavelength can be selected. A problem with laser diodes as excitation sources is that bandpass filters are needed to remove the unwanted side bands. For laser diodes of differing output wavelength, additional filters must be used. Thus, AOTF can be effectively used in place of the filters because of its wavelength selection ability.

2. Experimental

The carbocyanine dyes used for these experiments were 3,3′-diethyloxadicarbocyanine iodide (DODCI), 3,3′-diethylthiadicarbocyanine iodide (DTDCI), and 3,3′-diethyloxatricarbocyanine iodide (DOTCI). All the dyes were obtained from the Eastman Kodak Company of Rochester, New York. All of the sample solutions were prepared in HPLC grade methanol (VWR Scientific, West Chester, PA). Absorbance measurements were performed with a Lambda 20 UV/VIS spectrophotometer (Perkin-Elmer, Connecticut) interfaced to a 486 IBM AT compatible computer equipped with the UV-Winlab data acquisition and analysis software. The concentrations of the samples used in these studies were 5.86×10^{-7} M for DODCI, 6.14×10^{-7} M for DTDCI, and 4.59×10^{-7} M for DOTCI.

The fluorescence experiments were done on an ISS K-2 spectrofluorometer (Champaign, IL). The spectrofluorometer was interfaced to a Gateway-2000 486 computer equipped with ISS K-2 operating software. A 2 mm slit was used in all of the fluorescence experiments. The white light source used in the experiment was a Fiber-Lite, model 190 fiber optic illuminator (Dolan-Jenner Industries, Inc., Woburn, MA). The light source used a general electric, 10.8 V, 30 W bulb for illumination (model EKZ). A 780 nm, 50 mW laser diode was used as an excitation source in some experiments (LaserMax, Rochester, NY).

The commercially available AOTF was obtained from Brimrose Technology of Baltimore, Maryland (Model No. TEAF-0.5–1.0 s). This AOTF operated in the 500–1000 nm wavelength region and used a tellurium oxide crystal. The corresponding drive frequency was 100–180 MHz. A piezoelectric transducer that can convert electrical energy into acoustic energy was attached to a side of the crystal. Acoustic waves were generated when a radio frequency was applied to the transducer. These acoustic waves in turn made the crystal lattice compress and relax alternatively. This caused periodic modulations in the refractive index and provided a moving phase grating. Since the diffraction took place over a large volume, the light diffracted from the AOTF was of one specific wavelength.

A schematic representation of the experimental setup is shown in Fig. 1. The AOTF was placed in front of the light source and the diffracted beam

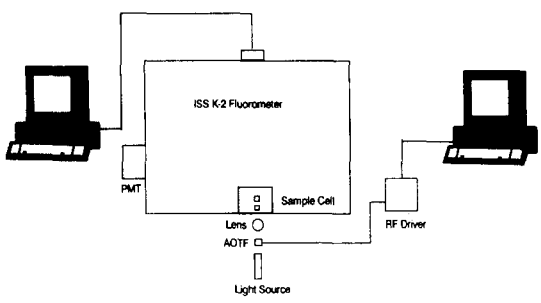

Fig. 1. Schematic representation of the experimental setup.

was focused onto the sample inside the sample compartment of the spectrofluorometer. The light coming out of the Xe-Arc lamp of the fluorometer was completely blocked so as not to interfere with the light from the outside source. The AOTF and the frequency driver were connected to a Zenith 386 computer. The spectra were collected with the computer connected to the spectrofluorometer.

3. Results and discussion

An experiment was performed by placing a scattering solution in the sample compartment and scanning at certain frequencies applied to the AOTF to establish a calibration for the AOTF used in this study. The horizontally polarized beam coming out on the right hand side of the zero order beam was used for this experiment. The peak wavelength of the scattering spectrum gives the wavelength of the light coming out of the AOTF. Fig. 2 shows a linear calibration curve obtained by plotting wavelength versus frequency. The linear fit was suitable for long wavelength dye investigation, where absorption and fluorescence bands are relatively broad.

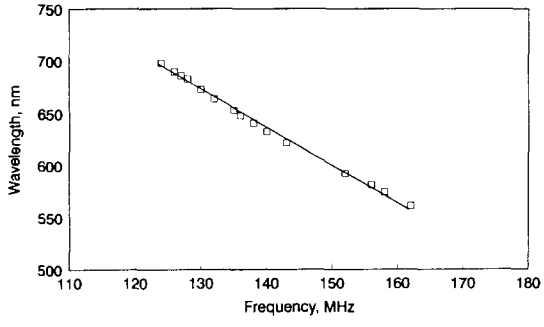

Fig. 2. The wavelength versus frequency calibration curve for the AOTF.

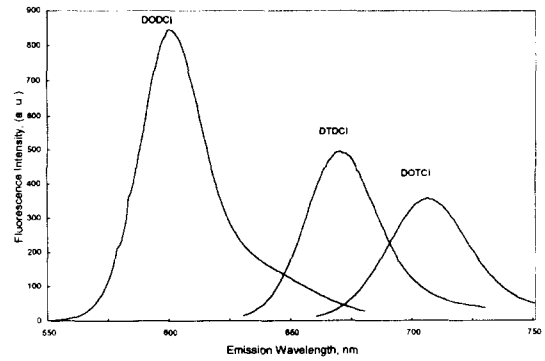

Fig. 3. Fluorescence spectra of DODCI, DTDCI and DOTCI in methanol using excitation monochromator.

The fluorescence spectra of the three dyes used in this study are shown in Fig. 3. These spectra were measured using the existing fluorometer without the use of AOTF and a Xenon-Arc lamp was used as the excitation source. DODCI dissolved in methanol had an absorption and fluorescence maxima at 581 and 600 nm respectively. The dye DTDCI dissolved in methanol had an absorption maximum of 652 nm and a fluorescence maximum of 670 nm. DOTCI in methanol was excited at 683 nm and gave an emission maximum at 706 nm. The next set of experiments

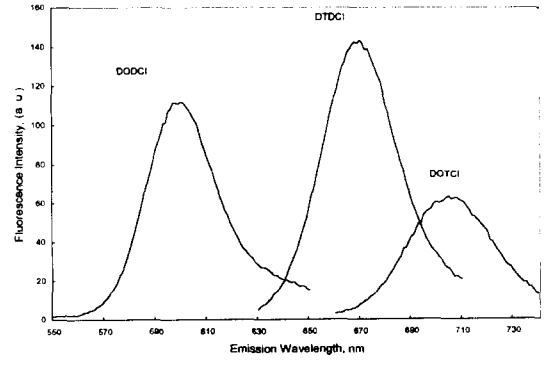

Fig. 4. Fluorescence spectra of DODCI, DTDCI and DOTCI in methanol using AOTF as a wavelength selector.

Table 1
Fluorescence intensities of the dyes DODCI, DTDCI, and DOTCI in methanol at various excitation wavelengths

DODCI		DTDCI		DOTCI	
Wavelength (nm)	Fluorescence intensity (a.u.)	Wavelength (nm)	Fluorescence intensity (a.u.)	Wavelength (nm)	Fluorescence intensity (a.u.)
592	59	664	85	698	41
581	80	652	104	686	54
574	75	641	102	683	57
563	72	633	87	673	56
	—	622	74		—

was performed with the use of an AOTF in place of the monochromator. Fig. 4 shows the fluorescence spectra of DODCI, DTDCI and DOTCI when AOTF was used as the wavelength selector. Different excitation wavelengths were selected by applying certain frequencies to the AOTF. The wavelengths and the corresponding fluorescence intensities for DODCI, DTDCI and DOTCI are shown in Table 1. The spectra are corrected for the concentrations. DOTCI has a quantum yield of 49% in ethanol [11]. The individual spectra are an indication of the quantum yield of the dyes and the throughput efficiency of the AOTF at those emission wavelengths. Fig. 5 is a compilation of the fluorescence spectra of DTDCI at excitation wavelengths 622 nm, 633 nm, and 652 nm, respectively.

All of the experiments were done using the arrangement shown in Fig. 1 and the excitation

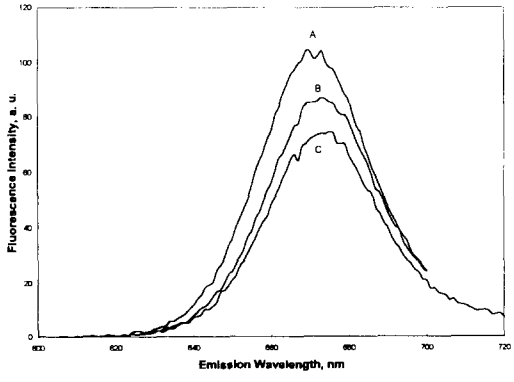

Fig. 5. Fluorescence spectra of DTDCI at excitation wavelengths of (A) 652 nm, (B) 633 nm and (C) 622 nm.

monochromator of the spectrometer was not used whenever the AOTF was in use. These studies show that AOTF can be used in place of monochromators in spectrofluorometers. It is also an effective tool for the fluorescence studies of the carbocyanines in the long wavelength of the electromagnetic spectrum. The fluorescence intensity values shown in Table 1 indicate that the light source used in these experiments was not powerful enough. The addition of a much more powerful light source (e.g. arc lamps) would permit the use of even longer wavelengths.

The second part of this study was designed to verify the usefulness of AOTF as an alternative to bandpass filters for the elimination of unwanted side bands from laser diodes. A 785 nm, 50 mW laser diode was used for this study. The laser beam was passed through an AOTF and the diffracted beam was focused into the sample cell using a lens. A scattering solution was inserted into the sample compartment and the scattering spectrum was taken at different frequencies. The starting frequency was 107.90 MHz and the ending frequency was 109.10 MHz. Spectra were collected at intervals of 0.02 MHz. At the frequency of 108.02 MHz, a peak corresponding to 792 nm was observed. The scattering spectrum is shown in Fig. 6. This peak corresponds to a side band associated with the diode laser and can be observed frequently while using diode lasers [12]. The side band resolution is distorted because the scattered light was measured using an emission monochromator with a 2 nm resolution. The usual practice when using laser diodes is to use an interference filter to remove the side bands. The

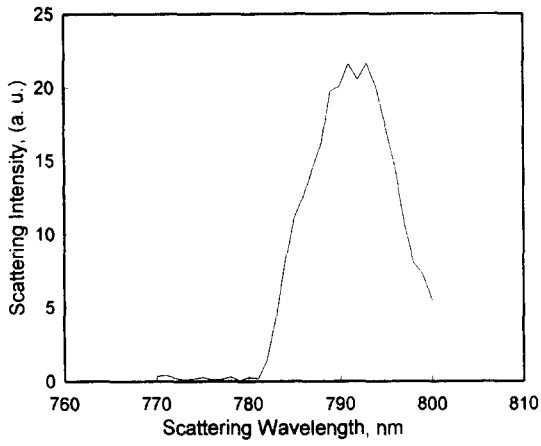

Fig. 6. The scattering spectrum of the laser side band.

main problem with this approach is that the filter needs to be changed when a different laser diode is used. When an AOTF is used in place of the interference filter, a certain frequency can be chosen to give the right wavelength for the laser diode. In this case the correct frequency and the wavelength were 108.74 MHz and 786 nm, respectively.

4. Conclusion

The usefulness of AOTFs in fluorescence spectroscopy of long wavelength absorbing carbocyanine dyes was demonstrated in this study. AOTF can replace the excitation monochromator and allow tuning to any desired wavelength. Since there are no moving parts in an AOTF, only a single calibration is needed if nothing is changed in the instrumentation setup. More studies are needed in the future with a powerful light source to increase the wavelength range into the near-infrared region. It was also demonstrated that AOTF can be used effectively in place of band-pass filters for achieving wavelength purity of laser diodes. It is a better alternative to interference filters, since only one AOTF is needed with laser diodes of different output wavelengths.

References

[1] R.W. Dixon, IEEE J. Quant. Elect. QE-3 (1967) 85.
[2] S.E. Harris, R.W. Wallace, J. Opt. Soc. Am. 59 (1969) 744.
[3] J.A. Kusters, D.A. Wilson, D.L. Hammond, J. Opt. Soc. Am. 64 (1974) 434.
[4] I.C. Chang, App. Phys. Lett. 25 (1974) 370.
[5] C.D. Tran, Anal. Chem. 64 (1992) 971A.
[6] I. Kurtz, R. Dwelle, P. Katzka, Rev. Sci. Instrum. 58 (1987) 1996.
[7] H.R. Morris, C.C. Hoyt, P.J. Traedo, Appl. Spec. 48 (1994) 857.
[8] C.D. Tran, R.J. Furlan, Anal. Chem. 65 (1993) 1675.
[9] A.J. Eilert, W.J. Danley, X. Wang, Adv. Instrum. Control 50 (1995) 87.
[10] P.J. Traedo, I.W. Levin, E.N. Lewis, Appl. Spec. 48 (1994) 607.
[11] Kodak Optical Products Catalog, Eastman Kodak Chemical Company, Rochester, New York.
[12] Laser Diode Users Manual, Sharp Corporation, Japan, 1986.

ELSEVIER

Talanta 45 (1997) 291–296

Talanta

Potentiometric pH sensors based on chemically modified electrodes with electropolymerized metal-tetraaminophthalocyanine

Tian-Fang Kang, Zhong-Yi Xie, He Tang, Guo-Li Shen, Ru-Qin Yu *

Department of Chemistry and Chemical Engineering, Hunan University, Changsha, Hunan 410082, People's Republic of China

Received 16 December 1996; received in revised form 4 April 1997; accepted 11 April 1997

Abstract

Potentiometric pH sensors based on polymer film were prepared by electropolymerization of the monomer nickel(II)-4,4′,4″,4‴-tetraaminophthalocyanine (NiTAPc) or copper(II)-4,4′,4″,4‴-tetraaminophthalocyanine (CuTAPc) on glassy carbon (GC) electrodes. The polymer of metal tetraaminophthalocyanine (*p*-MTAPc) film coated electrodes show a slope of 55 ± 1 mV/pH (at 20°C) and nearly Nernstain potentiometric response to pH over the range of pH 1–13. The electrodes possess good potential reproducibility and high selectivity, and are useful sensing devices in pH determination and end-point indication of acid-base potentiometric titration. © 1997 Elsevier Science B.V.

Keywords: Chemically modified electrode; Metal tetraaminophthalocyanine; pH response; Potentiometry

1. Introduction

In recent years, there has been a growing interest in electropolymerized film chemically modified electrodes and their applications as potentiometric sensors [1,2], in particular as pH sensors [3–9]. The protonation of nitrogen or oxygen atoms in the polymers and ion exchange equilibria between hydrogen ions and exchange sites on the polymer film are expected to impart a pH response to the underlying electrode. Glass membrane electrodes are the most often used pH sensors. However, there are disadvantages such as fragility, high resistance, erosion by hydrofluoric acid solution, etc., limiting the applications of glass electrodes. Compared with traditional glass membrane pH electrodes, the polymer-based pH electrodes have already exhibited a number of advantages, including low resistance, ease of preparation and miniaturization, etc. The electrodes are, therefore, promising alternative analytical devices in certain clinical and biological applications, such as in vivo analysis. Various compounds have been studied as monomers for preparing the electropolymerized film coated pH electrodes, including 1,2-diaminobenzene [3], phenol, 4,4′-diaminobiphenyl [5], etc. Recently, it was reported that electropolymerized cobalt (II) tetrakis(*p*-hydrox-

* Corresponding author.

PII S0039-9140(97)00124-0

yphenyl)porphyrin coated glassy carbon (GC) electrodes or coated indium (tin) oxide glass slides can be used as potentiometric and fiber optic sensors for pH [9]. In our laboratory, pH sensors based on electropolymerized amino derivatives of naphthalene [7] or tetrakis(*p*-aminophenyl)porphrin [8] film modified platinum electrodes were also investigated. Metal phthalocyanine is both chemically and electrochemically stable. Guarr and co-workers have previously reported the electropolymerization of metal phthalocyanine [10]. Very recently, the potentiometric sensors for sulfide [11] and nitrite [12] ions based on electropolymerized cobalt phthalocyanine have been reported. To our best knowledge, however, there is no pH sensor report based on electropolymerized metal phthalocyanine chemically modified electrode. In this paper, nickel(II)-4,4′,4″,4‴-tetraaminophthalocyanine (NiTAPc) or copper(II)-4,4′,4″,4‴-tetraaminophthalocyanine (CuTAPc) was electropolymerized on GC electrodes by cyclic voltammetry. The experimental conditions were optimized. The response characteristics of the polymer of metal tetraaminophthalocyanine (*p*-MTAPc) film coated electrodes toward hydrogen ions were discussed. The electrodes were applied in the pH determination of real samples without any pretreatment.

2. Experimental

2.1. Reagents and apparatus

Nickel(II)-4,4′,4″,4‴-tetraaminophthalocyanine ($C_{32}H_{20}N_{12}Ni$) and copper(II)-4,4′,4″,4‴-tetraaminophthalocyanine ($C_{32}H_{20}N_{12}Cu$) were synthesized according to the procedure described by Achar et al. [13] and characterized by FT-IR and UV/VIS spectrometry. The structure of the metal tetraaminophthalocyanine (MTAPc) was given in Fig. 1. For NiTAPc, FT-IR: 750, 822, 864, 949, 1060, 1090, 1132, 1254, 1312, 1348, 1424, 1483, 1609, 3208,3329 cm^{-1}. UV/VIS (15 M H_2SO_4 aqueous solution medium), maximum adsorption, (log ϵ): 218 (4.81), 300 (4.44), 378 (4.08), 735 (4.45). For CuTAPc, FT-IR: 731, 748, 824, 866, 945, 1053, 1082, 1132, 1256, 1306, 1346, 1410, 1607, 3200, 3321 cm^{-1}. UV/VIS (15 M H_2SO_4 aqueous solution medium), maximum absorption, (log ϵ): 220 (4.91), 298 (4.42), 383 (4.03), 749 (4.01). All the data were in fair agreement with those reported by Achar et al. [13]. Tetra-*n*-butylammonium perchlorate (TBAP) was prepared by the reaction of tetra-*n*-butylammonium bromide with sodium perchlorate. A serious of buffer solutions for the potential-pH measurements were prepared by mixing of 200 mM Na^+, 40 mM PO_4^{3-}, 40 mM $H_2BO_3^-$ and 40 mM acetate with the necessary volume of 2 M orthophosphoric acid or 1 M sodium hydroxide. Solutions with pH below 2.0 was prepared by dissolving appropriate amount of orthophosphoric acid in distilling water. The pH of these solutions was determined with a standard pH glass membrane electrode and a saturated calomel electrode (SCE). All chemicals were of analytical-reagent grade. All solutions were prepared with doubly distilled water.

An EG and G PARC Model 273 potentiostat/galvanostat in conjunction with a Hewlett Packard X-Y recorder was used for the electropolymerization processes. A glassy carbon disc with a diameter of 5 mm (Beijing Institute for Artificial Crystals) or a platinum wire electrode with a diameter of 0.5 mm and a length of 1 cm

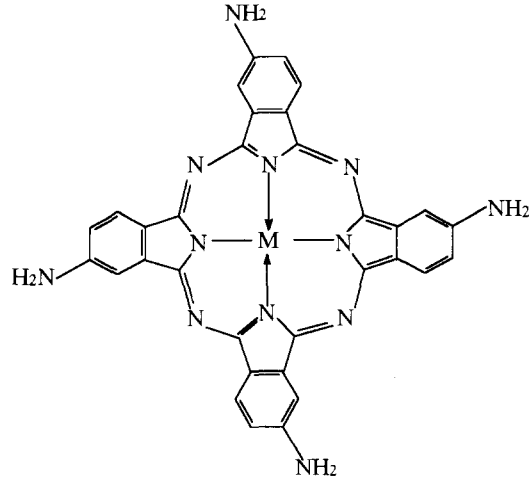

Fig. 1. Structure of M(II)-4,4′,4″,4‴-tetraaminophthalocyanine. M (II) = Nickel (II) or Copper (II).

was used as working electrode, a platinum foil as auxiliary electrode and a SCE as the reference. Potentiometric and pH measurements were performed with a Microprocessor Ionalyzer (Orion Research, Model 910) or PHS-3 pH meter (Shanghai Analytical Instruments). The type 231 glass pH-electrode (Shanghai Electronic Instruments) or *p*-MTAPc film pH-electrodes were used in conjunction with type 217 double-junction reference electrodes (Shanghai Electronic Instruments) with 3 M sodium nitrate solution in their outer compartments. The typical cell used was

Hg, Hg_2Cl_2, KCl (sat.) ‖3 M $NaNO_3$|sample|*p*-MTAPc film|GC surface

A Perkin-Elmer Lambda 17 UV/VIS spectrophotometer, and a Nicolet 510 P FT-IR spectrophotometer were also used to record the electronic spectra and FT-IR spectra, respectively.

2.2. Electrode preparation

The GC electrode was polished to a mirror by using 0.5 μm alumina paste and was then thoroughly ultrasonicated in distilled water before use. The electrode was allowed to air-dry. The GC or platinum wire electrode was placed into a N,N′-dimethylformamide (DMF) solution containing 0.01 M NiTAPc monomer and 0.1 M TBAP employed as the supporting electrolyte. Repetitive cycling (30–40 cycles) from −0.2 to +0.9 V at 200 mV s^{-1} was carried out to generate the polymer film on the surface of the electrode. The electrode was then rinsed with acetone and distilled water and allowed to air-dry. The electrodes were conditioned in 0.1 M phosphate buffer solution (pH 7.0) before and between pH measurements. Cellulose acetate (CA) was used as the material of protective layer. A 1% CA solution was prepared by dissolving CA in a stirred 1:1 mixture of cyclohexanone and acetone. Then 10 μl of the resulting solution was applied onto the polymer of nickel (II) tetraaminophthalocyanine (*p*-NiTAPc) film coated electrode surface and allowed to air-dry for 10 min. The electrode coated with CA was then rinsed thoroughly with distilling water. The protective layer can also be a thin cellulose acetate membrane (Zhejiang Huangyan Biochemical Material Factory). The *p*-NiTAPc modified electrode was shrouded in CA membrane. The membrane was kept close to the *p*-NiTAPc film and was held by a polypropylene ring. The *p*-NiTAPc modified electrode covered with CA membrane was soaked in 0.1 M phosphate buffer (pH 7) for 1 h before use, so that the CA membrane can be swollen by the electrolyte solution. The preparation of polymer of copper (II) tetraaminophthalocyanine (*p*-CuTAPc) film coated electrodes were also performed according to the aforementioned procedure for the preparation of *p*-NiTAPc modified electrodes.

3. Results and discussion

3.1. pH response of the p-MTAPc chemically modified electrodes

The chemically modified electrode and a SCE were immersed into the tested solution to record the potential readings. A set of eight electrodes were used to investigate the effects of the central metal ions in *p*-MTAPc and coated protective layer on the response of the electrodes. It can be seen from the values shown in Table 1 that the use of a protective CA film or membrane does not influence the excellent pH response properties of the *p*-MTAPc coated electrodes. The CA protective layer might be beneficial for extending the electrode lifetime and reducing the interferences from electroactive species. Even the coated CA film is evidently damaged, it can also be conveniently reformed quite easily if it is needed. The response time was less than 1 min. The response time is defined as the period between the time of immersing the pH electrode and reference electrode in the sample solution and the time when a stead-state potential with less than 1 mV min^{-1} change has been achieved.

The potentiometric selectivity coefficients for some cations such as Na^+, K^+, Li^+, and Ca^{2+} were determined by the fix interference method (Table 2). The results showed that the *p*-NiTAPc electrode has high selectivity to hydrogen ion. The effect of anions on the pH response was also

Table 1
Response of different *p*-MTAPc coated electrodes to pH: linear response range, slope, and intercept for Nernstain plots[a]

Electrode	Linear range (pH)	Slope (mV/pH)	Intercept (mV)
p-NiTAPc/GC1[b]	1.0–13.0	55 (1)	−455 (4)
p-NiTAPc/GC2[b]	1.0–12.8	55 (1)	−463 (6)
p-NiTAPc/GC3[c]	1.0–13.0	56 (1)	−458 (5)
p-NiTAPc/GC4[d]	1.0–12.6	55 (2)	−452 (7)
p-NiTAPc/Pt1[b]	1.0–13.0	54 (1)	−446 (6)
p-NiTAPc/Pt2[c]	1.2–12.8	55 (3)	−457 (8)
p-CuTAPc/GC1[b]	1.0–13.0	55 (1)	−450 (3)
p-CuTAPc/GC2[c]	1.0–12.8	56 (1)	−461 (5)

[a] The standard deviation for four measurements is given in parentheses.
[b] Without protective layer.
[c] Coated with CA film.
[d] Covered with CA membrane

tested (Fig. 2). The anion interference was in the sequence of $I^- > SCN^- > Br^- \sim Cl^- > NO_3^-$. The experimental results demonstrate that the anions tested do not interfere with the pH response of the polymetallophthalocyanine modified electrodes except iodide ions. The interference from iodide for the pH response of the *p*-MTAPc coated electrodes was obvious only in the solutions of pH < 3. As pH of sample solution decreases, more and more basic groups in the *p*-MTAPc film are protonated. The positively charged film tends to attract more and more anions to enter the film phase for balancing the electroneutrality condition. The polyatomic anions, such as NO_3^- etc., are sterically unfavorable to enter the molecular cavity of the hydrophobic film due to bigger sizes of them. Among halide anions, iodide is the most hydrophobic one. Therefore, it is possible that the interferences from I^- was mainly caused by the following fact, i.e., the *p*-MTAPc films with three dimensional cross-linking structure are most suitable for iodide ions to enter into and to be held inside the film phases because of the strongly hydrophobic and electrostatic interaction between iodide ions and the protonated films.

The pH response of the chemically modified electrodes can be influenced by the thickness of *p*-MTAPc film. The film thickness was controlled by the number of scans during the repetitive cyclic voltammetric polymerization of the *p*-MTAPc film. It was found that the linear range of pH response increased with the thickness of the film and the influence gradually weakened after the

Table 2
Potentiometric selectivity coefficients of *p*-NiTAPc coated GC electrode for some cations[a]

Ion	Na^+	K^+	Li^+	Ca^{2+}
$\log K^{pot}_{H,M}$	−11.62	−11.42	−10.89	−10.40

[a] The interferant concentration was maintained at the level of 1 M. Mean values of four assays.

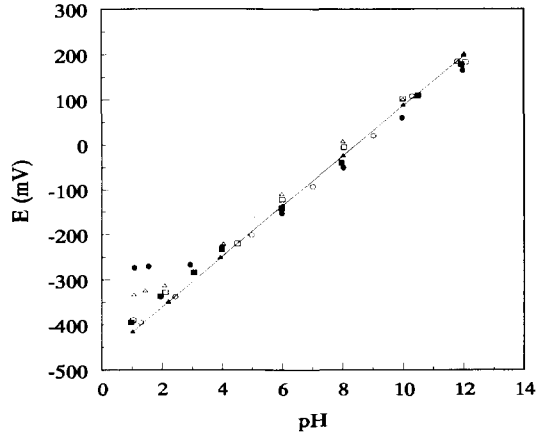

Fig. 2. Effect of concomitant anion in solutions on the potential of the *p*-NiTAPc/GC electrode without interference (▲), with 0.1 M Cl^- (□), 0.1 M Br^- (■), 0.1 M NO^{3-} (○), 0.1 M SCN^- (Δ), and 0.05 M I^- (●).

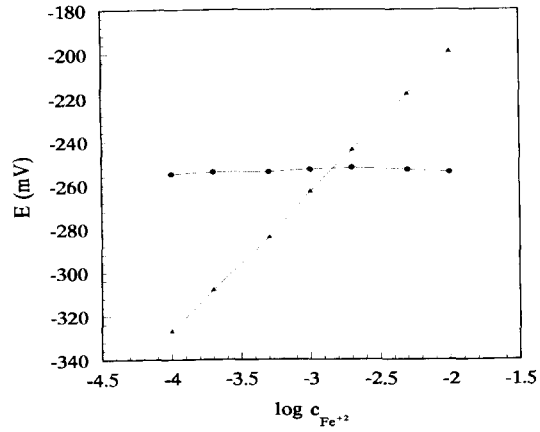

Fig. 3. Effect of Fe^{3+}/Fe^{2+} couple on the potentials of a bare GC electrode (▲) and a *p*-NiTAPc/GC film modified electrode covered with CA membrane (●). Different amount of Fe^{2+} were added into 0.01 M Fe^{3+} solutions of pH 4.0.

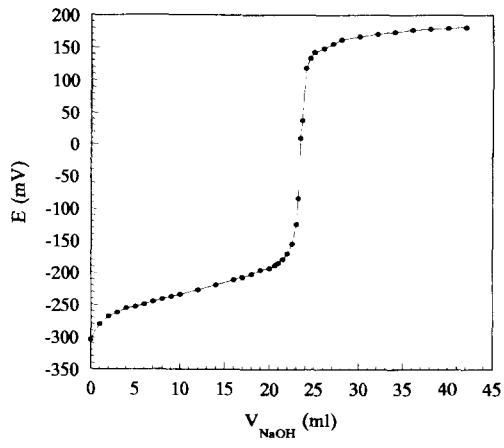

Fig. 4. E-V curve for titration of acetic acid with NaOH using *p*-NiTAPc coated GC electrodes as indicating electrode.

number of scanning exceeded 20 cycles. When the film thickness, however, was thicker than that obtained by 40 cycles of scanning, the pH response properties were no longer improved. So the thickness of the polymer film, i.e., the potential scan cycles, was chosen as 30–40 cycles. The total surface coverage ((Γ^0, mol cm^{-2}) for *p*-NiTAPc film modified electrode obtained with 30–40 cycles was calculated by measuring the area under the accumulated current-voltage curve. The value obtained was 1.6×10^{-9}–1.9×10^{-9} mol cm^{-2}. Based on the estimated concentration of 1.6×10^{-3} mol cm^{-3} monomer units in *p*-NiTAPc [14], the film thickness was estimated to be in the range of 100–120 Å.

Table 3
pH measurements on real samples[a]

Sample	pH readings	
	p-NiTAPc/GC pH electrode	Glass membrane electrode
River water 1	7.53	7.51
River water 2	7.49	7.44
Serum 1	7.51	7.53
Serum 2	7.70	7.76
Serum 3	7.65	7.68

[a] Mean value of four measurements.

The effect of the redox couple Fe^{3+}/Fe^{2+} on the electrode potential was studied (Fig. 3). Different amount of Fe^{2+} were added into a pH 4.0 solution containing 0.01 M Fe^{3+}. There was no substantial change observed in the potential of the *p*-NiTAPc modified electrode covered with CA membrane. Similar phenomena for *p*-CuTAPc modified electrodes covered with CA membrane were also observed. However, the change of the bare GC or platinum wire electrode potential was obvious. The experimental results demonstrate that the CA membrane can effectively resist the interferences from redox couples. The air-dried CA film used to coated the modified electrodes seems to be less effective in preventing the interference of redox couples.

The standard deviation of the electrode potential readings during a period of 3 h in a pH 3.00 solution was 0.8 mV ($n = 20$). An electrode conditioned by soaking in a pH 7.2 buffer solution for at least 1 month did not show obvious loss of performance characteristics.

3.2. Response mechanism

When the *p*-MTAPc coated electrode is brought into contact with an aqueous solution, an interface is formed between the hydrophobic *p*-MTAPc film and the aqueous solution, resulting in an equilibrium distribution of hydrogen ions across the interface. The protonation-deprotona-

tion equilibria of the nitrogen atoms in *p*-MTAPc and the net surplus charge in the vicinity of the nitrogen atoms yield a film potential. Therefore, a potential response is observed for hydrogen ions in aqueous solution. There are three kinds of (in all twelve) nitrogen atoms in each MTAPc monomer. It is possible that different nitrogen atoms in the *p*-MTAPc were responsible for the responses in different pH ranges. Compared with previously reported monomer [3–9] used for preparing polymer film pH sensors, the number of different kinds of nitrogen atoms in MTAPc monomer is the largest, which means that there are more kinds of active sites of pH response in the *p*-MTAPc film. This should be beneficial to the response of *p*-MTAPc coated electrode toward hydrogen ions in a wider pH range. It was found that there was no substantial difference in the response to hydrogen ions between *p*-NiTAPc and *p*-CuTAPc coated electrodes (Table 1). This demonstrates that the central metal ions in the polymer do not have obvious effect on the pH response, though there could be a small difference in axial coordination of the central metal with H_2O or OH^- between the two polymers. Compared with the response of *p*-MTAPc coated electrodes to hydrogen ions, the response of a bare GC electrode to hydrogen ion was not linear and had much less changes with increasing the solution pH values. Thus, the pH response of *p*-MTAPc coated electrodes was mainly caused by the protonation of the nitrogen atoms in the polymer.

3.3. Applications

The pH of two river water samples, three serum samples were measured using the *p*-NiTAPc electrode as the pH sensor. A glass membrane pH electrode was also used for comparison. As can be seen in Table 3, similar pH readings were obtained. The reproducibility of the pH measurements using a *p*-NiTAPc coated GC electrode was studied. The standard deviations for 12 measurements of a serum sample was 0.01 pH for the *p*-NiTAPc coated electrode and 0.008 pH for the glass electrode.

The electrode can be used for end-point indication in acid–base titration. Fig. 4 shows the E-V curve for the 25.00 ml 0.1208 M acetic acid titrated with 0.1063 M sodium hydroxide. The mean of the concentration of acetic acid from five assays obtained with potentiometric titration was 0.1206 M with a standard deviation of 0.0003 M.

4. Conclusion

The experimental results demonstrate that the electropolymerized metallophthalocyanine electrodes show nearly Nernstain potential response to pH over a wide pH range. The electrodes used as pH sensors possess good potential reproducibility and high selectivity and, therefore, are promising in applications of pH determination of real samples, especially biological and clinical samples.

Acknowledgements

The authors thank the financial support from the Natural Science Foundation of China and Education Commission Fund of China.

References

[1] A.E. Karagozler, O.Y. Ataman, A. Galal, Z.-L. Xue, H. Zimmer, H.B. Mark, Anal. Chim. Acta 248 (1991) 163.
[2] R.S. Hutchins, L.G. Bachas, Anal. Chem. 67 (1995) 1654.
[3] H.J. Wieck, A.M. Yacynych, Anal. Chem. 52 (1980) 345.
[4] G. Cheek, C.P. Wales, R.J. Nowak, Anal. Chem. 55 (1983) 381.
[5] Y. Ohnuki, H. Matsuda, T. Ohsaka, N. Oyama, J. Electroanal. Chem. 158 (1983) 55.
[6] L. Jin, Z. Shi, J. Ye, J. Qian, Y. Fang, Anal. Chim. Acta 244 (1991) 165.
[7] S.S. Huang, X.H. Song, H.G. Lin, R.Q. Yu, Mikrochim. Acta 107 (1992) 27.
[8] R. Yuan, Y.-Q. Chai, G.-L. Shen, R.-Q. Yu, Talanta 40 (1993) 1255.
[9] T.L. Blair, J.R. Allen, S. Daunert, L.G. Bachas, Anal. Chem. 65 (1993) 2155.
[10] H. Li, T.F. Guarr, J. Chem. Soc. Chem. Commun., (1989) 832.
[11] Y.-H. Tse, P. Janda, H. Lam, A.B.P. Lever, Anal. Chem. 67 (1995) 981.
[12] J.R. Allen, A. Florido, S.D. Young, S. Daunert, L.G. Bachas, Electroanalysis 7 (1995) 710.
[13] B.N. Achar, G.M. Fohlen, J.A. Parker, J. Keshavayya, Polyhedron 6 (1987) 1463.
[14] X.H. Mu, F.A. Schultz, J. Electroanal. Chem. 361 (1993) 49.

ELSEVIER

Talanta 45 (1997) 297–302

Talanta

A simultaneous packed column supercritical fluid chromatographic method for ibuprofen, chlorzoxazone and acetaminophen in bulk and dosage forms

Viddesh R. Bari [a], U.J. Dhorda [a], M. Sundaresan [b,*]

[a] *Ismail Yusuf College of Science, Jogeshwari (East), Mumbai-60, India*

[b] *C.B. Patel Research Centre For Chemistry and Biological Sciences, 2nd Floor, Mithibai College Building, Vile Parle (West), Mumbai-400 056, India*

Received 24 December 1996; received in revised form 8 April 1997; accepted 18 April 1997

Abstract

A reproducible and efficient method for the separation and estimation of ibuprofen, chlorzoxazone and acetaminophen has been developed using packed column supercritical fluid chromatography (SFC). The separations were performed on an ODS-RP JASCO column employing methanol modified supercritical fluid CO_2 as the mobile phase. The densities and polarities of the mobile phase were optimised from the effects of pressure, temperature and modifier concentration on retention times. In addition a flow programming of the mobile phase helped to obtain better resolution and a faster elution for acetaminophen. The analytes were detected using a uv detector at 254 nm. The study includes a successful attempt at quantitation of the 3 drugs. Chromatographic figures of merit, linear dynamic range, limit of quantitation (LOQ), precision and accuracy etc. were determined to assess the viability of the method. The method has been extended to commercial dosage forms containing all 3 drugs. © 1997 Elsevier Science B.V.

Keywords: Limit of quantitation; Dosage forms; Linear dynamic range

1. Introduction

Packed column supercritical fluid chromatography (SFC) is at present in experimental stages for its applicability to the separation and analysis of drugs and pharmaceuticals. A series of demonstrations of the power of this technique for the rapid separation of psychoactive agents was published by Berger and Wilson [1–3]. This was followed by Bailey et al. [4] who evaluated the separation of 10 β-blockers on a variety of packed columns using SFC. Strobe et al. [5] demonstrated the application of this technique for the determination of felodipine and its potential degradation product in bulk and dosage forms. Several drugs were analysed in serum/plasma solution using this technique [6,7]. Simmons et al. [8] described an SFC/UV method for the determination of phenyl butazone in a commercial tablet. The present paper describes an isobaric and

* Corresponding author. Fax: +91 22 6133400.

PII S0039-9140(97)00153-7

Table 1
Effect of pressure, temperature and modifier concentration on retention times of ibuprofen, chlorzoxazone and acetaminophen

Sr. No.	Modifier conc. % MeOH	Temp.°C	Pressure MPa	Ibuprofen	Chlorzoxazone	Acetaminophen
				(Retention times in min)		
1	9.09	35	7.8	2.93	3.55	10.63
	9.09	35	8.8	2.79	3.38	10.07
	9.09	35	9.8	2.74	3.29	9.68
	9.09	35	14.7	2.65	3.03	8.29
	9.09	35	19.6	2.59	2.93	7.46
2	9.09	35	7.8	2.93	3.55	10.63
	9.09	40	7.8	3.01	3.72	11.39
	9.09	45	7.8	3.28	4.13	12.32
	9.09	55	7.8	2.95	3.61	6.91
3	3.22	35	7.8	3.08	5.35	30.09
	9.09	35	7.8	2.93	3.55	10.63
	11.76	35	7.8	2.61	3.03	7.47
	14.28	35	7.8	2.36	2.70	5.75

Solute concentration: Ibuprofen and chlorzoxazone, 100 ppm; Acetaminophen, 10 ppm; Flow rate (CO_2), 1.5 ml min^{-1}; Injection volume, 20 μl; Column, JASCO RP-C^{18} (250 × 4.6 mm) 10 μm.
Detection by uv detector at 254 nm wavelength.

isothermal separation of ibuprofen, chlorzoxazone and acetaminophen and their simultaneous quantitation in bulk and commercial tablet forms using packed column SFC. Of these drugs ibuprofen and acetaminophen have analgesic and antipyretic properties. The former has in addition anti-inflammatory properties, too. Chlorzoxazone is a centrally acting muscle relaxant that has been claimed to exert an effect primarily at the level of spinal cord and subcortical areas of the brain. These 3 drugs are often administered together in 1 dosage form in cases of painful skeletomuscular spasms. Many high performance liquid chromatography (HPLC) and gas liquid chromatography (GLC) methods are known for the analysis of these drugs, but are not cited here for brevity. This work has been divided into 2 parts: (a) method development and (b) validation.

2. Method development

2.1. Experimental

2.1.1. Reagents and chemicals

HPLC grade methanol was purchased from E. Merck (India). Carbon dioxide gas was obtained from Bombay Carbon Dioxide Co., Mumbai and was 99.9% pure. Samples of ibuprofen, chlorzoxazone and acetaminophen were obtained from reputed U.K. firms with certified copies of analysis. The commercial dosage forms of the 3 drugs in a mixture were obtained locally.

2.1.2. Apparatus

The SFC used was a JASCO-900 series configured with 2 pumps for delivering supercritical fluid and modifier. Pressure could be varied from 7.8 to 34.3 MPa and temperature from 35–85°C. Gas flow rates could be changed from 0.1 to 10 ml min^{-1} and modifiers rates from 0.05 to 10 ml min^{-1}. A rheodyne (model 7125) injection valve with a 20 μl external loop was used. The column used was JASCO-RP-C18 (250 × 4.6 mm) packed with 10 μm particles. Detection was achieved with a multiwavelength uv detector equipped with 5 mm pathlength, 4 μl high pressure flow cell. The detector responses were measured in terms of peak height. The data was processed using Borwin software.

2.1.3. Preparation of standard solutions

Individual solutions of the 3 drugs were prepared by dissolving 100 mg of the respective drugs in 100 ml of methanol and then serially diluting in 10 fold stages to the required concentrations. Mixtures of the drugs were prepared by mixing appropriate volumes of the individual solutions. Wherever necessary mix solutions were evaporated to dryness at 55°C under a stream of nitrogen and then the residue reconstituted in the required volume of the solvent.

2.1.4. Chromatographic experiments

For the preliminary investigations, 20 μl of the solutions were injected into the HPLC system. Analyte elution did not occur with pure CO_2 under the available pressure and temperature conditions and hence the use of a modifier was necessary. Methanol was used as the modifier as it was a good solvent for all the 3 drugs. With each individual drug solution the 3 dof, viz., pressure, temperature and modifier concentration were scanned for a wide range. A review of the data on retention times with change in pressure, temperature and modifier concentration is given in Table 1. The conditions of the experiments are also cited there.

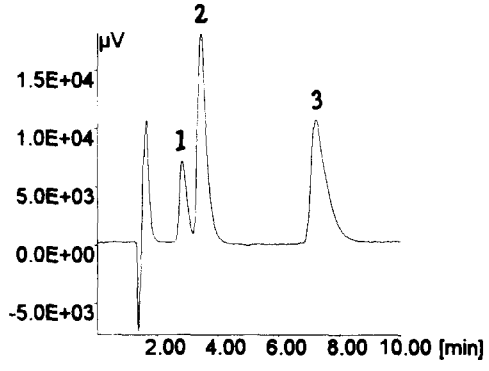

Fig. 1. Typical SFC separation of drugs eluted from a JASCO 250 × 4.6 mm, 10 μm, RP-C18 column under steady state conditions. The conditions were as follows: 0.15 ml min^{-1} of 9.09% modifier (methanol) in CO_2, at 45°C and 7.8 MPa outlet pressure. Modifier concentration held at 9.09% for 4 min when it was changed to 14.28%. Numbered solutes are indicated in the arbitrary mix and the number indicates retention order. (a) Ibuprofen – 2.93 min; (b) Chlorzoxazone – 3.55 min; (c) Acetaminophen – 6.46 min.

3. Results and discussions

Table 1 indicates that for the separation of the 3 drugs, near critical parameters (pressure and temperature) are more ideally suited than higher pressure and temperatures. Pressure has minimal effects on retention times as a 2 fold increase in pressure hardly shifts the retention times of ibuprofen and chlorzoxazone. However, in the case of acetaminophen the elution is faster by at least ~2.5 min. The effect of temperature can also be concluded to have similar behaviour. In the case of acetaminophen the elution is faster by ~4 min when the temperature is raised from 35 to 55°C. This pattern is again revealed with the change in modifier concentration. Acetaminophen is eluted faster than anticipated, the retention times being almost inversely proportional to the modifier concentrations. In order to achieve a selective separation between ibuprofen and chlorzoxazone a modifier concentration of 9.09% is thus required. However acetaminophen under these conditions is slow to elute; an increase of modifier concentration from 9.09 to 14.28% decreases the retention time for acetaminophen from 10.63 to 5.75 min. Thus the isobaric (7.8 MPa) and isothermal (35°C) conditions are suitable for all 3 drugs, while for acetaminophen alone the modifier concentration was changed from 9.09 to 14.28%. The flow rate of the modifier was changed from 0.15 to 0.25 ml min^{-1} after the first 4 min. Thus the best compromise between analysis time and selectivity is obtained from modifier flow programming. A typical chromatogram for the separation of the drugs at the levels of 100 ppm for ibuprofen and chlorzoxazone and 10 ppm for acetaminophen is depicted in Fig. 1, the experimental conditions are given in the caption. The chromatographic figures of merit are given in Table 2.

The present work was done at a reduced pressure of 1.050 and reduced temperature of 1.125. According to Pitzer [9,10] the ideal gas law can be expanded and used for supercritical fluids to relate pressure and density at a given temperature. The same principle can be applied to binary fluids, after the mole fraction of each fluid is taken into consideration as in the modified Han-

Table 2
Chromatographic figures of merit

Name of compounds	HETP	T	K'	N
Ibuprofen	0.0092	1.1	0.86	2704
Chlorzoxazone	0.0069	1.1	1.14	3600
Acetaminophen	0.0031	1.0	3.0	8028

HETP, height equivalent of theoretical plates; T, symmetry factor; K', capacity factor; N, No. of theoretical plates [$N = 16(tr/w)^2$]

derson Brobst-Thomson method [11]. The densities of the supercritical fluid-methanol binary mixtures could then be calculated to be 0.4127 at 9.09% methanol and 0.4342 g ml^{-1} at 14.28%. The change in retention time for acetaminophen from 10.63 to 5.75 min, thus is obviously not due to density changes, but due to production of significant changes in the mobile phase solvent strength [12].

3.1. Validation

Stock solutions of the 3 drugs prepared earlier were used for the quantitation experiments.

For linearity studies 7 different concentrations (1.0, 2.5, 5.0, 10.0, 20.0, 40.0 and 50.0 μg ml^{-1}) in the lower range and 7 different concentrations (50, 100, 200, 300, 500, 750 and 1000 μg ml^{-1}) in the higher range were assayed for ibuprofen. For chlorzoxazone the concentrations assayed were 0.3, 0.6, 1.0, 2.5, 5.0, 7.5 and 15.0 μg ml^{-1} in the lower range. In the higher range solutions containing 15, 30, 60, 120, 180, 240 and 300 μg ml^{-1} were assayed. The concentrations for acetaminophen were 0.05, 0.10, 0.25, 0.50, 1.0, 2.0 and 2.5 μg ml^{-1} and 2.5, 5.0, 10.0, 20.0, 30.0, 40.0 and 50.0 μg ml^{-1} respectively for the lower and higher ranges. The detector response, in peak heights, was linear over the concentration ranges studied. Standard curves were obtained by plotting the drug concentration (μg ml^{-1}) versus peak heights. The data was analysed by a linear least squares regression fit method. The data, when analysed in a single range of concentration, showed slight deviation from the regression line. The S.D. in the intercept values were large, due to the long linear dynamic range of 3 orders. Hence it was decided to analyse the data in 2 ranges. The variation in the slopes and the marginal higher values of the slope in the higher range can be attributed to factors of experimental errors. The respective slopes and intercepts with the S.D. in these values are given in Table 3, together with correlation coefficient and point errors. The S.D. in the intercept values seem to be on the higher side, but the errors affect the actual values only to the extent of 2–3%, as the peak responses are of magnitude.

The limit of quantitation (LOQ) values cited in Table 3 are not figures of merit as they can be further reduced by the proper choice of detection wavelength and injection volumes. Fig. 2 shows 'Log h', where h is the peak height of a mix of all 3 drugs, (100 μg ml^{-1} for ibuprofen and chlorzoxazone and 10 μg ml^{-1} of acetaminophen) on a multiwavelength scale. Fig. 2 shows that the detection limit of ibuprofen can be reduced by a factor of 45 if the detection wavelength is altered from 254 to 220 nm, while for chlorzoxazone it will be 1.2 times. Even for acetaminophen the factor will be 1.3. Accuracies were determined by spiking known concentrations in mixtures and estimating them by the described method. The details are given in Table 4 which shows the relative S.D. are well below 5% which means that the present method can be useful for bulk drug analysis.

3.2. Analysis of tablets

Commercial locally manufactured pharmaceutical dosage forms containing all 3 drugs were then analysed. One tablet weighing 1.0130 gm was disintegrated in 50 ml of methanol in a cylindrical centrifuge tube. The tube was vortexed for 5 min and then centrifuged at $3000 \times g$ for 10 min. From the supernatant solution 1 ml was pipetted out and diluted with methanol to 10 ml. Another 10 fold dilution resulted in a 5000 fold dilution of tablet. From this solution 20 μl was pipetted out and injected into the chromatograph under the conditions given above. The heights of the 3 peaks were measured and related to the values of the slopes and intercepts given in Table 3.

Table 3
Calibration data for SFC/UV of ibuprofen, chlorzoxazone and acetaminophen

Ranges	Ibuprofen		Chlorzoxazone		Acetaminophen	
	1–50 μg	50–1000 μg	0.3–15 μg	15–300 μg	0.05–2.5 μg	2.5–50 μg
Slope *m*	57.4	59.1	187.7	193.5	1140.8	1192.0
Intercept *b*	9.0	−348.8	−7.2	−866.0	13.1	90.0
Correlation coefficient *r*	0.9999	0.9999	0.9999	0.9998	0.9998	0.9999
S.D. of slope Sm	2.33	0.81	0.72	1.38	14.01	15.86
S.D. of intercept Sb	64.70	462.1	4.72	251.26	15.74	481.27
Point error Sy/x	103.6	626.0	9.09	323.0	29.15	619.08

SFC analysis conditions were as follows: 9.09 (v/v) methanol modified CO_2 (at pressure 7.8 MPa, temperature 35°C) as mobile phase; 1.5 ml min^{-1} as flow rate of CO_2; 20 μl injection volume; Column JASCO-RP-C^{18} (250 × 4.6 mm) 10 μ, detection at 254 nm.

Table 4
Recoveries of ibuprofen, chlorzoxazone and acetaminophen from spiked solutions ($n = 5$)

Drug	Spiked quantities (μg ml^{-1})	Found concentration (μg ml^{-1})	R.S.D. ($n = 5$)
Ibuprofen	10	9.98	4.96
	100	101.20	3.25
	500	498.86	0.98
Chlorzoxazone	5	5.06	4.88
	30	29.98	2.75
	180	181.40	1.10
Acetaminophen	1	1.10	3.80
	10	9.96	2.52
	50	49.87	1.23

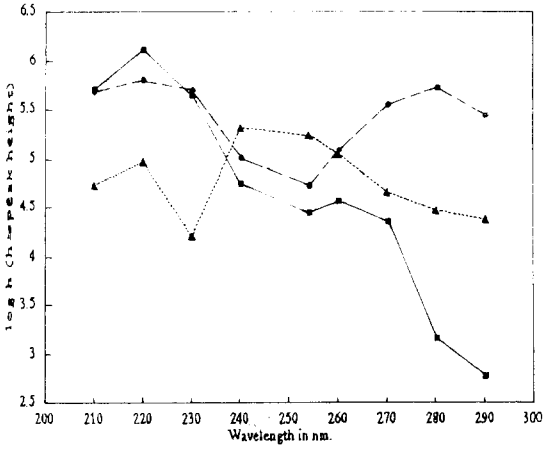

Fig. 2. Log peak responses (height) vs. wavelength. The conditions were as follows: 0.15 ml min^{-1} of 9.09% modifier (methanol) in CO_2, at 45°C and 7.8 MPa outlet pressure. Modifier concentration held at 9.09% for 4 min when it was changed to 14.28%. ■ = Ibuprofen; ● = Chlorzoxazone; △ = Acetaminophen.

The contents of the tablets were found to be the 399.8, 249.5 and 300.8 mg of ibuprofen, chlorzoxazone and acetaminophen, respectively as against 400, 250 and 300 mg stated. The values given above are the mean of 6 replicate measurements. Results indicate that the SFC method can be a viable alternative to HPLC as far as pharmaceutical dosage forms are concerned. At least in this case no interference from excipients was noticed.

4. Conclusions

The work has shown that packed column SFC is suitable for the analysis of drugs and pharmaceuticals. The method can claim low quantifiable limits and is a viable alternative to HPLC. The method obviates the necessity of preparation of mobile phases and can be equally useful as HPLC for analysis of bulk drug and pharmaceutical

dosage forms. Direct extraction of the drugs from the tablet using supercritical fluid extraction also is being attempted.

Acknowledgements

The authors thank Shri. C.P. Kelkar, Director (Admn.), Dr. A.M. Bhagwat, Director, C.B. Patel Research Centre, Mumbai-56, Dr. Devyani Dave, Principal, I.Y. College, Mumbai-60 and co-workers Yagnesh Patel and Indravadan Bhoir for encouragement in carrying out this work.

References

[1] T.A. Berger, W.H. Wilson, J. Pharm. Sci. 83 (1994) 281.
[2] T.A. Berger, W.H. Wilson, J. Pharm. Sci. 83 (1994) 287.
[3] T.A. Berger, W.H. Wilson, J. Pharm. Sci. 84 (1995) 489.
[4] C.J. Bailey, R.J. Ruane, I.D. Wilson, J. Chromatogr. Sci. 32 (1994) 426.
[5] J.T.B. Stobe III, L.T. Tayler, A.L. Howard, D. Ip, M.A. Brooks, J. Pharm. Biomed. Anal. 12 (1994) 1003.
[6] P. Lembke, H.J. Engelhardt, High. Resolut. Chromatogr. 16 (1993) 700.
[7] J.D. Pinkston, C.J. Venkatramani, L.J. Tulich, D.J. Bowling, K.R. Wehmeyer, J. Chromatogr. 622 (1993) 209.
[8] B.R. Simmons, N.K. Jagota, J.T. Stewart, J. Pharm. Biomed. Anal. 13 (1995) 59.
[9] K.S. Pitzer, J. Am. Chem. Soc. 77 (1955) 3427.
[10] K.S. Pitzer, D.E. Lippman, R.F. Curl, C.M. Higgins, D.E. Petersens, J. Am. Chem. Soc. 77 (1955) 3433.
[11] R.C. Reid, J.M. Pransnitz, B.E. Poling, The Properties of Gases and Liquids, 4th ed., McGraw-Hill, N.Y. 1987.
[12] J.J. Langenfeld, S.B. Hawthorne, D.J. Miller, J. Tehrani, Anal. Chem. 64 (1992) 2263.

ELSEVIER

Talanta 45 (1997) 303–307

Talanta

Enhancement of fluorescence of terbium/trimesic acid/cyclodextrin system by zirconate and its application to the determination of terbium

G. Zhao [b], S. Zhao [a], J. Gao [a,*], J. Kang [a], Wu Yang [a]

[a] *Institute of Chemistry, Northwest Normal University, Lanzhou 730070, People's Republic of China*
[b] *Basic Courses of Gansu Agricultural University, Lanzhou 730070, People's Republic of China*

Received 13 January 1997; received in revised form 8 April 1997; accepted 18 April 1997

Abstract

A new approach of fluorescence enhancement for the determination of terbium based on the formation of a new fluorescence system of Tb-TMA-β-CD (benzene-1,3,5-tricarboxylic acid (TMA), β-cyclodextrin (β-CD)) in an aqueous medium of pH 5.0 provided by a HAc-NaAc buffer in the presence of an oxy-acid of transition metal, zirconate acid, is reported. The maximum excitation and emission wavelengths are 301 nm and 545 nm for the terbium complex, respectively. Under the optimal conditions, the method allows the determination of terbium over the range of 0.508–521 ng ml^{-1} with a S.D. of 0.392, and the recovery is in the range of 99.0–100.1%. The emulsion formed by Tb-TMA-β-CD with zirconate acid makes the determinate system more stable than the system of Tb-TMA-β-CD. The proposed method has been employed for the determination of some international standard reference or samples with a good precision (RSD < 1.7%, $n = 5$). © 1997 Elsevier Science B.V.

Keywords: Fluoresence; Benzene-1,3,5-tricarboxylic acid; β-Cyclodextrin

1. Introduction

The fluorescence enhancement [1,2] in the field of analytical determination of rare earth elements has for a long time aroused great interest among scientists because of its lower detection limit and higher sensitivity. Two mechanisms are currently being used to account for the energy transfer which is responsible for the fluorescence enhancement. One of the mechanisms, fluorescence enhancement by intramolecular energy transfer, has been proved by El-Sayed and Bhaumik [3–5] who thought that the energy transfer took place between the ligand and the central ions. In their opinion, the observed emission of lanthanide(III) was not caused by its direct excitation but was due to an internal energy transfer from the ligand to the 4f subshells of the central metal ion. Methods developed from the mechanism mentioned above are extensively applied in the analytical determination because of the high sensitivity. The other mechanism, intermolecular energy transi-

* Corresponding author.

PII S0039-9140(97)00133-1

tion, has been proved by some researchers [6,7], who found that the energy transition took place between two chelates formed by the same ligand with different ions. However, in our recent studies, we have found that the fluorescence intensity of the Tb-TMA-β-CD system can be obviously increased by ZrO_3^{2-}, and some other oxy-ions, such as BiO_3^{3-} and SbO_3^{3-}, have similar properties. We proposed that the mechanism is different from those mentioned in Ref. [3–7]. It should belong to the mechanism of fluorescence enhancement induced by charge transition.

Based on the study of the mechanism of fluorescence enhancement, the aim of the present work was to establish an improved sensitized fluorescent system with high sensitivity, good repeatability and accuracy for the determination of terbium in different artificial samples.

2. Experimental

2.1. Apparatus

All fluorescence intensity measurements were made on a RF-540 fluorescence spectrophotometer (Shimadzu, Japan) equipped with a 150 W Xe arc lamp light source, using 1.0 cm pathlength quartz cells. The excitation and emission slits were both 5 nm in width. The pH measurements were obtained with a SPM-10 pH meter (Shanghai, China), calibrated with buffer solution (pH 4.0 $\pm$ 0.1).

2.2. Reagents

The lanthanide oxides were obtained from the Yuelong chemical plant (Shanghai, China). Analytical reagent grade chemicals as well as distilled, deionized water were used throughout the study.

Stock lanthanide solutions (0.1 M) were prepared by dissolving the appropriate amounts of the corresponding oxides in hot concentrated hydrochloric acid, respectively, and evaporating the solutions to syrup. Then cool them to room temperature, dissolve with water and dilute to the desired volume. A stock solution of Ce^{3+} was obtained by dissolving cerium oxide (purity, 99.99%) in a mixture of sulphuric acid and ammonium sulfate followed by the addition of H_2O_2 to the solution, converting Ce^{4+} to Ce^{3+}. All the stock solutions were standardized with EDTA, using Xylenol Orange as an indicator.

A solution of the chelating agent, TMA (0.0100 M), was prepared by dissolving 0.5250 g of TMA in hot distilled deionized water and then diluting to 250 ml. β-CD aqueous solution was prepared with the same method. A NaAc-HAc solution was used as a buffer (pH 5.0). 0.1 M ZrO^{2+} stock solution was prepared by dissolving 3.2230 g of $ZrOCl_2 \cdot 8H_2O$ in 15 ml concentrated hydrochloric acid and then diluting to 100 ml with distilled, deionized water.

2.3. Procedure

Place solutions to 25 ml calibrated tube as the following order: 1 ml of 1.0000×10^{-5} M Tb^{3+} solution, 2.5 ml of 0.0100 M TMA, 1.5 ml 0.0100 M β-CD, 5 ml of buffer solution and 1.0 ml of 0.1 M ZrO^{2+}. Dilute the mixture solution to 25 ml with distilled deionized water, shake and stand for 10 min at room temperature. Measure the fluorescence intensity at emission wavelength 546 nm in a 1 cm quartz cell, keeping the excitation wavelength at 301 nm. All determining works must be completed in 30 min, if not, the precipitation would appear.

3. Results and discussion

3.1. Fluorescence spectra

We reported the excitation and emission spectra of the fluorescence system formed by Tb^{3+}, TMA, β-CD and ZrO^{2+} solution. ZrO^{2+} transfer into the form of ZrO_3^{2-} in higher pH medium (pH > 1). ZrO_3^{2-} is the main species under the determinate condition. ZrO_3^{2-} can obviously enhance the fluorescence intensity of Tb-TMA-β-CD-ZrO_3^{2-} system, but has no any effect on the position of the characteristic peak of terbium(III) (see Fig. 1). The excitation wavelength was transferred from 260 nm to 301 nm and it was responsible for the maximum absorption of ZrO_3^{2-}. A

intense emission peak of the medium, H_2O, at ca. 397 nm was observed when the excitation wavelength was at 350 nm. The emission peak of water transfer to ca. 413 nm when, the excitation wavelength was at 301 nm. In aqueous medium at room temperature, a 4×10^{-8} M of Tb^{3+} solution does not give any measurable emission in the system of Tb-TMA-β-CD. But the addition of about 400-fold of ZrO_3^{2-} into the system can obtain obviously characteristic peak of Tb^{3+}.

3.2. Effect of the acidity

In order to study the influence of the medium acidity on the formation of the complex, we used 0.1 M NaOH and HCl to adjust the pH of the solutions. As can be seen from Fig. 2, the emission signal remained constant over the pH range 4.65–5.11, so the working pH was adjust to a value within this range. Meanwhile, we investigated the different buffers and found that the buffer consisted of HAc and NaAc affects the fluorescence intensity to the smallest extent. Thus, HAc-NaAc (pH 5.0) buffer solution was used.

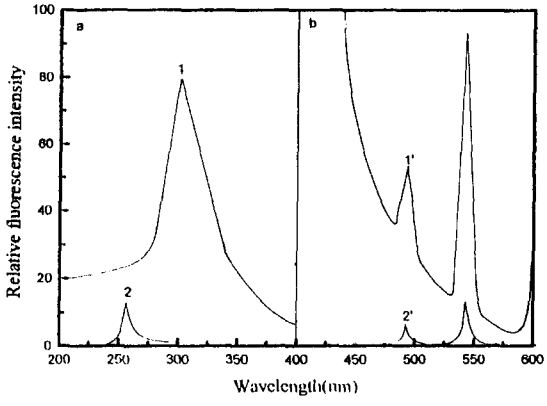

Fig. 1. 1(a): Excitation spectra of the Tb-TMA-Zir-β-CD system. 2(a): Excitation spectra of the Tb-TMA-β-CD system. 1'(b): Emission spectra of the Tb-TMA-Zir-β-CD system. 2'(b): Emission spectra of the Tb-TMA-β-CD system. Tb, 15.80 ng·ml^{-1}, TMA, 1.0×10^{-3} M, Zr, 4.0×10^{-4} M, β-CD, 6×10^{-4} M, pH 5.0.

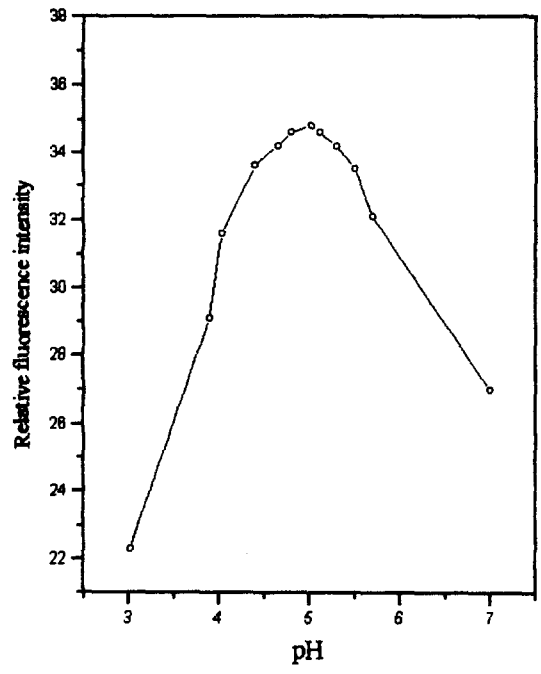

Fig. 2. Effect of pH on the fluorescence intensity of the Tb-TMA-Zi-β-CD system. Tb, 15.80 ng·ml^{-1}, TMA, 1.0×10^{-3} M, Zr, 4.0×10^{-4}, β-CD, 6×10^{-4} M.

From Fig. 2, we can learn that the fluorescence intensity of the system becomes weaker at pH < 4.65 and pH > 5.11. The reason for this is that the protonation of three carboxyl groups of the chelating agent at pH < 4.65 and the intensive hydrolytic action of the trivalence terbium ion at pH > 5.11. Both of which result in a decrease of the chelate concentration, therefore, decrease the fluorescence intensity of the terbium chelate with TMA.

3.3. Effect of the concentration of the chelate agent, TMA

Fig. 3 shows the influence of the TMA concentration on the signal emitted by a solution containing 4×10^{-7} M Tb(III). As can be seen the maximum fluorescence intensity lies between 8×10^{-4}–1.2×10^{-3} M, if less than 8×10^{-4} M or higher than 1.2×10^{-3} M of TMA, the fluorescence intensity starts to decay. A reagent concentration of 1.0×10^{-3} M was thus taken as optimal.

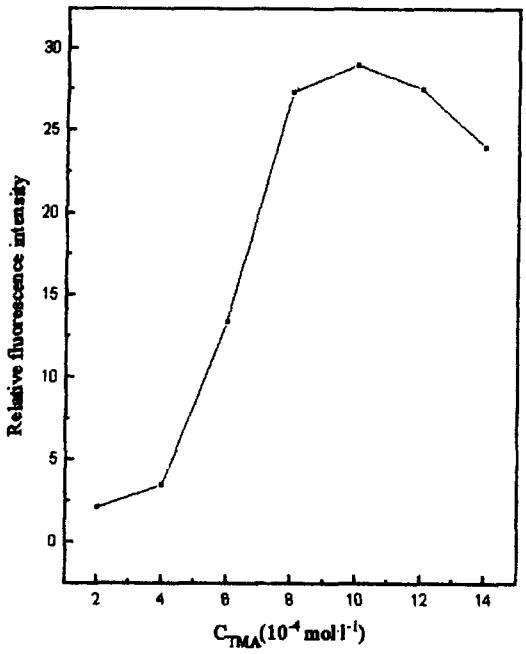

Fig. 3. Effect of the TMA concentration on the fluorescence intensity of the Tb-TMA-Zir-β-CD system. Tb, 15.80 ng·ml^{-1}, Zr, 4.0×10^{-4} M, β-CD, 6×10^{-4} M, pH 5.0.

3.4. Effect of the concentration of β-CD

β-CD takes a important role in this study, it can not only improve stability of the system under the condition of existing with large amounts of other rare earth elements, but also bring about the enhancement of the fluorescence intensity by about 20%. From the experiments, the optimal concentration of β-CD was in the range of 4×10^{-4}–8×10^{-4} M in this system. Hence 6×10^{-4} of β-CD was maintained in this work.

3.5. Effect of time

The effect of the time for the relative fluorescence intensity was studied. The fluorescence intensity reached the maximum value within 10 min and remained stable in the time range of 10–30 min, and then decrease sharply because of the appearance of precipitate.

3.6. Calibration curve

The calibration curve for the determination of terbium is obtained under the optimal experimental conditions. The linear range is from 0.508 to 521 ng·ml^{-1}. The linear equation is $F = 13.5 + 0.0226 \times 10^7 C$ (where F stands for the fluorescence intensity and C represents the molar concentration of terbium), with a linear correlation coefficient (R) 0.999 and a standard deviation (S.D.) 0.392.

3.7. Effect of zirconate acid

The variation in fluorescence intensity was studied as a function of concentration of ZrO_3^{2-}. Under the conditions of a fixed amounts of 1 ml of 1×10^{-5} M terbium, 5 ml of pH 5.0 buffer solution, 1.5 of ml 1×10^{-2} M β-CD, 2.5 ml of 1×10^{-2} M TMA and different amount of ZrO_3^{2-} in 25 ml calibrate tubes. The emulsion can not be formed when the amounts of ZrO_3^{2-} in less than 2.0×10^{-4} M and the enhancement fluorescence can not be observed. On the countary, a obvious quench of the fluorescence was induced when the concentration of ZrO_3^{2-} is more than 1.6×10^{-2} M because of the generation of precipitate. So, in this paper, 4.0×10^{-4} M ZrO_3^{2-} was remained.

3.8. Effect of the foreign ions

In order to determine its selectivity and potential analytical application for Tb(III) in rare earth ores, the influence of various ions on the determination of Tb(III) with the proposed method was studied. The results listed in Table 1 were the tolerated ratio of interferent ions to Tb(III) under which the foreign ions result in no interference (viz, in a deviation less than $\pm$ 4%), the interference can be not negligible over this level.

Table 1
Effect of other rare earth ions

R.E.I	La	Ce	Pr	Nd	Sm	Eu	Gd	Dy	Ho	Er	Tm	Vb	Lu
Tolerated fold	10	15	15	10	25	20	80	25	20	20	25	100	50

Table 2
Analytical results for artificial sample

Sample	Known value (μg ml^{-1})	Determination value (μg ml^{-1})	Average value (μg ml^{-1})	Recovery (%)	RSD (%)
1	1.00	0.97,0.99,0.97,0.99,1.0	0.98	98	1.7
2	5.00	4.81,4.83,4.85,4.88,4.85	4.84	97	0.54

3.9. Determination of the recovery

The results show that the determination of terbium using the proposed method has a good repeatability. The method has been employed for the determination of the artificial synthesized samples 1 and 2 having molar ratios of 50:1 and 25:1 for Yb/Tb, respectively. The analytical results are listed in Table 2.

Yttorfluorite sample was obtained from the rare earth company of bao tou, China. Its component is as follows: La_2O_3 (0.77%), Ce_2O_3 (1.93%), Pr_6O_{11} (0.18%), Nd_2O_3 (0.82%), Sm_2O_3 (0.44%), Eu_2O_3 (0.02%), Gd_2O_3 (0.89%) Tb_4O_7 (0.86%), Dy_2O_3 (0.91%), Ho_2O_3 (0.175%), Er_2O_3 (0.44%), Tm_2O_3 (0.08%), Yb_2O_3 (0.89%), Lu_2O_3 (0.18%), Y_2O_3 (9.63%).

3.10. Effect of fluorescence enhancement

The system of Tb-TMA-β-CD has salient fluorescence properties. When ZrO_3^{2-} solution was added sequentially into the above system, a greater fluorescence enhancement was observed. Some other Oxy-acid ions of transition metals, such as BiO_3^{3-} and SbO_3^{3-}, have the same action for Tb-TMA-β-CD system. The fluorescence enhancement effect of Oxy-acid ions of transition metal, up to now, has not been reported. According to the Ref. [8], we propose that the fluorescence enhancement of this system was mainly caused by three aspects followed:

One or several Tb-TMA chelate molecules was tightly surrounded by many ZrO_3^{2-} and formed an independent little ball. This little ball can protect the fluorescence of terbium from being quenched by hot vibration of water molecules entering into the interior coordinating shell of Tb-TMA chelate. Meanwhile, this ball structure protects the Tb-TMA chelate from copecipitate with coexisting lanthanide chelates, and increases the stability of the determinate system.

All Tb^{3+}, TMA and Tb-TMA surrounded by ZrO_3^{2-} whose concentration is about four hundred times greater than that terbium concentration, may be insufficient proximity in energy level and allow efficient energy transfer, thus, enhanced fluorescence output from Tb^{3+}.

The most important reason, we propose, is that ZrO_3^{2-} has two negative charges. When Tb^{3+} is surrounded tightly by ZrO_3^{2-} anion shell which overlapping with 4f orbit to Tb^{3+} and transferring the charges into 4f orbit of Tb^{3+} from the shell of ZrO_3^{2-}. This transferring action increases the electron density of 4f orbit of terbium, so that the effenciency of the energy transfer was increased and greater fluorescence was emitted.

Acknowledgements

The project was supported in part by a grant from the Educational commission of Gansu Province and National Natural Science Foundation of China.

References

[1] Jinhe Yang, J. Shandong Univ. 21 (42) (1986) 133.
[2] V.L. Ermolaev, E.V. Sveshnikova, T.A. Shakherdev, Russ. Chem. Rev. 45 (1976) 896.
[3] M.A. El-Sayed, M.L. Bhaummik, J. Chem. Phys. 39 (1963) 2391.
[4] J. Gao, G. Zhao, J. Kang, Talanta 42 (1995) 1497.
[5] J. Gao, G. Zhao, J. Kang, C. Li, Analyst 120 (1995) 2081.
[6] Y. Ci, Z. Lan, Anal. Chem. 61 (1989) 1063.
[7] Y. Ci, Z. Lan, Anal. Chim. Acta 212 (1988) 285.
[8] Guozhen Chen, Method of Fluorescence Analysis, 2nd ed., Science Press, Beijing, China, 1990, pp. 50–70.

ELSEVIER

Talanta 45 (1997) 309–315

Talanta

Silica gel-immobilized Eriochrome black-T as a potential solid phase extractor for zinc (II) and magnesium (II) from calcium (II)[1]

Mohamed E. Mahmoud

Chemistry Department, Faculty of Science, Alexandria University, Alexandria, Egypt

Received 24 December 1996; received in revised form 15 April 1997; accepted 21 April 1997

Abstract

The immobilization of silica gel surface with Eriochrome black-T indicator (ERT) for the formation of silica–ERT phase is described. The surface coverage of silica gel, based on carbon and nitrogen analysis of the modified silica gel phase, is 0.38 mmol g^{-1}. The stability towards hydrolysis of silica–ERT phase in different buffer solutions (pH 1–10) is studied and evaluated. The applicability of silica–ERT as a solid phase extractor for Zn(II), Mg(II) and Ca(II) is studied by the batch equilibrium technique and found to show an order similar to the formation constant values of these three metal ions with the indicator. The selectivity of silica–ERT phase towards the extraction of a certain metal ion from a mixture containing only two metal ions is studied by the batch equilibrium technique and exhibited good discrimination orders for Zn(II) and Mg(II) in presence of Ca(II). The results of the column separation and preconcentration studies are consistent with the selectivity behaviour of silica–ERT phase, thus affording reasonable separation of the three studied metal ions. © 1997 Elsevier Science B.V.

Keywords: Eriochrome black-T; Silica–ERT; Immobilization

1. Introduction

Some metal ions are well known for their biological activity in most living systems. Among these essential metals are zinc, calcium and magnesium as major or minor constituents in a large number of biologically important compounds. [1–10] These important biological activities of zinc, calcium and magnesium have prompted many researchers to develop new methods for analysis, separation and preconcentration of these metal ions. A recent study has reported the analysis and separation of calcium and magnesium in sea water by the use of capillary zone electrophoresis in presence of a carrier solution containing EDTA as a complexing agent. [11] Silica gel-immobilized ion exchangers or chelating compounds, on the other hand, are used for preconcentration and separation of many metal ions including zinc, calcium and magnesium ions. Some of such immobilized organic compounds on the surface of silica gel are 8-hydroxyquinoline, [12] mercapto-derivatives, [13] oxine compounds, [14] hydroxy-

[1] Presented in part in the Fourth International Symposium on New Trends in Chemistry – The Role of Analytical Chemistry in National Development. Cairo University, Giza, Egypt. January 4–9, 1997.

PII S0039-9140(97)00132-X

benzoyl derivatives, [15] and some amine compounds. [16]

The selective extraction of a single metal from other interfering metal ion(s) represents a direct challenge for finding the suitable phase capable of exhibiting a sufficient affinity to selectively bind that metal ion. Some of the reported selective phases are those containing crown ethers, [17] γ-aminopropyltrimethoxysilane, [18] oxygen and nitrogen donor macrocyclic compounds, [19] thioaniline derivatives [20] and formylsalicylic acid derivatives. [21,22]

In principle, the formation constant values reported [23] for zinc, magnesium and calcium ions with Eriochrome black-T indicator represent good discrimination order in their chemical binding to the indicator in solution. This property is taken as the basis and guideline for the immobilization of Eriochrome black-T indicator on the surface of silica gel to form a new potential selective solid phase for the extraction, preconcentration and separation of these three metal ions.

2. Experimental

2.1. Chemicals and reagents

Eriochrome black-T indicator and all metal salts were of analytical grade and purchased from Aldrich Chemical Company, Gillingham, England. silica gel (63–200 μm) was purchased from Riedel-Dehaën, Hannover, Germany and 3-chloropropyltrimethoxysilane was received from Aldrich Chemical Company, USA. Organic solvents were dried according to conventional methods.

All solutions were prepared with doubly distilled water and the buffer solutions were prepared from 1.0 M sodium acetate to which different volumes of 1.0 M hydrochloric acid were added and the pH of the resulting solution adjusted with the use of a pH meter.

2.2. Apparatus

The pH measurements were carried out by using the Schott Geräte CG-822 pH meter, which was calibrated against two standard buffer solutions at pH 4.0 and 9.2. Infrared spectra of the silica–ERT phase were obtained from KBr pellets by using a Perkin Elmer 1430 ratio-recording spectrometer. Atomic absorption measurements were performed with a Perkin Elmer 2380 flame atomic absorption spectrophotometer for the determination of Zn(II) and Mg(II), while Ca(II) was determined by the use of a GBC 902 double beam flame atomic absorption spectrophotometer at El-Minia University, El-Minia, Egypt. Elemental analysis of the carbon and nitrogen contents was performed at the microanalytical center at Cairo University, Cairo, Egypt.

2.3. Preparation and stability of the silica-ERT phase

Silica gel was first activated by reflux in conc hydrochloric acid for 4 h to remove any adsorbed metal ions, then filtered, washed repeatedly with doubly distilled water to neutral filtrate and dried in an oven at 160°C for 8 h to remove surface water. 15 g of the dry silica gel were suspended in 300 ml of dry toluene mixed with 25 ml of 3-chloropropyltrimethoxy-silane and refluxed for 20 h. The product (silica–Cl) was filtered off, washed with toluene, alcohol and diethylether and dried artin an oven at 70°C for 6 h. Silica gel-immobilized Eriochrome black-T indicator (silica–ERT) was prepared by the addition of 10 g of dry silica–Cl phase to 4.6 g (10 mmol) of Eriochrome black-T as sodium salt, already dissolved in 400 ml of hot, dry dioxane, and refluxed for 10 h. The resulting phase was filtered, washed with dioxane, alcohol and repeatedly with doubly distilled water until the filtrate showed no trace color of suspended or adsorbed indicator.

The stability of silica–ERT phase in different buffer solutions was investigated by employing the batch equilibrium technique. In this procedure, 0.5 g of the silica–ERT phase was mixed with 50 ml of the selected buffer solution (pH 1–10) in a 100 ml volumetric flask and automatically shaken overnight. The mixture was filtered, washed with another 50 ml portion of the same buffer solution and with doubly distilled water, and dried in an oven at 70°C. 30 mg of the buffered silica–ERT phase were added to a solution of 1.0 ml of 0.1 M Zn(II) or Mg(II) and 9.0

Table 1
Stability of silica–ERT in different buffer solutions determined by the mmol g^{-1} values

pH	Zn(II)		Mg(II)	
	mmol g^{-1}	% phase hydrolysed	mmol g^{-1}	% phase hydrolysed
1.0	0.215	32.8	0.193	34.8
2.0	0.243	24.1	0.222	25.0
3.0	0.278	13.1	0.259	12.5
4.0	0.312	2.5	0.286	3.4
5.0	0.315	1.6	0.290	2.0
6.0	0.320	0.0	0.293	1.0
1.0 M NaOAc	0.320	0.0	0.296	0.0
10.0	0.300	6.3	0.274	7.4

Table 2
Metal capacity values as a function of pH

Buffer pH	Zn(II)		Mg(II)		Ca(II)	
	mmol g^{-1}	std. dev.*	mmol g^{-1}	std. dev.*	mmol g^{-1}	std. dev.*
1.0	0.008	0.001	0.000	0.000	0.000	0.000
2.0	0.012	0.002	0.010	0.001	0.000	0.000
3.0	0.028	0.002	0.035	0.002	0.006	0.002
4.0	0.035	0.003	0.067	0.002	0.015	0.002
5.0	0.172	0.002	0.100	0.003	0.031	0.002
6.0	0.183	0.003	0.127	0.002	0.046	0.003
1.0 M NaOAc	0.320	0.006	0.296	0.004	0.053	0.003
10.0	0.217	0.003	0.065	0.002	0.050	0.003

*$n = 3$

ml of 1.0 M NaOAc, and the mixture was shaken for 30 min by using an automatic shaker. The degree of hydrolysis of silica–ERT phase in different buffer solutions was established from the metal uptake values determined by flame atomic absorption analysis.

2.4. Sorption analysis

2.4.1. Batch experiments

The determination of metal capacity values of the selected metal ions, viz. Zn(II), Ca(II) and Mg(II), as a function of pH of the buffer solution was performed by the addition of 30 mg of the dry silica–ERT phase to a mixture of 1.0 ml of 0.1 M metal ion solution and 9.0 ml of the buffer solution (pH 1–10) in a 50 ml volumetric flask. This mixture was then automatically shaken for 30 min, filtered, washed with 50 ml of doubly distilled water, and the free unextracted metal ion was subjected to further dilution steps in order to meet the requirement of linear dynamic range of each metal ion for atomic absorption analysis. A standard solution was prepared in a similar fashion for the estimation of the metal capacity values.

The selectivity study was also carried out by the batch equilibrium technique via preparation of a mixture containing only the two metal ions (Zn(II)/Ca(II), Zn(II)/Mg(II) or Mg(II)/Ca(II)) in equimolar ratios. 2 ml of these mixtures were buffered with a 25 ml solution of pH 1, 4 and 1.0 M NaOAc and 30 mg of the silica–ERT phase were then added, automatically shaken for 30 min, filtered, washed with 25 ml of the same buffer solution and 40 ml of doubly distilled water, and subjected to further dilution for flame atomic absorption measurement.

Table 3
Selectivity study by the batch equilibrium technique, evaluated by the mmol g^{-1} values of different mixtures

Buffer condition	Zn/Ca		Mg/Ca		Mg/Zn	
	Zn(II)	Ca(II)	Mg(II)	Ca(II)	Mg(II)	Zn(II)
pH 1.0	0.010	0.000	0.002	0.000	0.000	0.009
pH 4.0	0.035	0.009	0.063	0.012	0.040	0.023
1.0 M NaOAc	0.322	0.023	0.290	0.030	0.143	0.192

2.4.2. Column separation and preconcentration

A column similar to that previously reported [24] was filled with a slurry of 100 mg of silica–ERT phase. A 100 ml solution containing a mixture of the two metal ions, ~4–5 ppm each, in 1.0 M NaOAc was passed through the column at a flow rate of 5 ml min^{-1} and the effluent was collected in a 100 ml measuring flask containing 1 ml conc. nitric acid. The adsorbed metal ions were then eluted by successive addition and flow of 100 ml portions of buffer solution (pH 6–1) at a flow rate of 5 ml min^{-1} and received in a 100 ml measuring flask containing 1 ml conc. nitric acid. The metal ion(s) eluted by the influence of the buffer gradient procedure were then determined by flame atomic absorption spectroscopy.

3. Results and discussion

The modification of silica gel surface with Eriochrome black-T indicator is based on the elimination of a sodium chloride molecule from the silica–Cl phase and the indicator to form the CH_2–O_3S bond. The surface coverage of the new silica–ERT phase is determined on the basis of carbon and nitrogen contents as determined by elemental analysis and found to be 0.38 mmol g^{-1}. The suggested structure of silica–ERT phase is confirmed from the infrared analysis and shown below.

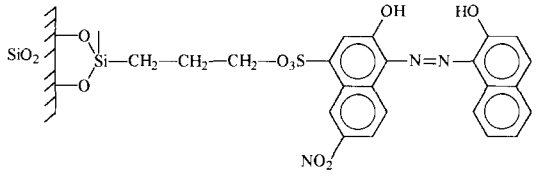

The stability of the silica–ERT phase in different buffer solutions (pH 1–10) was performed in order to identify the degree of hydrolysis of this phase. The procedure is based on overnight equilibration of the phase in presence of the selected buffer solution. This time period is sufficient to force the expected maximum hydrolysis of the phase which is then dried and used to determine the metal uptake (mmol g^{-1}) of Zn(II) and Mg(II) in 1.0 M NaOAc, which were previously found to exhibit the highest metal capacity values, as a measure of the hydrolysis degree of the silica–ERT phase. The results of the stability test are compiled in Table 1 and clearly show a maximum degree of phase hydrolysis at lower pH values (pH 1–3). In moderate pH solutions (pH 4–7), the silica–ERT phase was found to be stable and resistant to hydrolysis, showing only hydrolysis in the range of 0.0–2.0%. The phase was found also to exhibit about 7.5% hydrolysis in presence of pH 10 buffer. Therefore, the applicable and suitable buffer range for silica–ERT phase may be outlined as that of pH 4–7.

The variation in the pH value of the metal ion solution and its influence on the amount adsorbed by silica–ERT phase were studied for the three tested metal ions, Zn(II), Ca(II) and Mg(II). These values are given in Table 2 and reveal that both Zn(II) and Mg(II) are well extracted by silica–ERT phase as 0.320 and 0.295 mmol g^{-1} for the two metal ions, respectively. These two values are considered as a good agreement with the low surface coverage determined for such phase. The influence of pH value of the metal ion solution on the amount adsorbed is also evident in Table 2 and outlined as the appreciable metal

capacity values only at pH > 5, with a maximum metal uptake in presence of 1.0 M NaOAc solution. On the other hand, calcium (II) was found to be the metal ion least extracted by the silica–ERT phase, reaching a maximum mmol g^{-1} value of only 0.053 in presence of 1.0 M NaOAc solution. This trend and behavior of Ca(II) can be used as the guideline basis for selective extraction of Zn(II) or Mg(II) in presence of Ca(II).

The order of metal ion capacity values of the three tested metal ions is Zn(II) > Mg(II) > Ca(II), which shows a good match with the order of formation constant values determined for the same three metal ions with Eriochrome black-T indicator in solution. [23] Thus, we can use the known values of the formation constants to preliminary predict the behavior of silica-immobilized chelating agents towards metal ion binding and extraction in the solid phase conditions. Such discrimination in both sorption order and the formation constant value directed our interest towards the study of selective extraction of Zn(II) or Mg(II) in presence of Ca(II) as an interfering metal ion. Previous studies [22] for the comparison of selective metal ion extraction by both column and batch equilibrium techniques revealed similar behavior of both techniques for low sample volumes, therefore we selected to perform this experiment by only the batch equilibrium technique for simplicity. The results of the selectivity experiment (Table 3) show the evidence for the expected selective extraction of Zn(II) in presence of Ca(II), based on the relatively high mmol g^{-1} values of both Zn(II) and Mg(II) compared to those of Ca (II) at any studied buffer solution. On the other hand, Mg(II) was not selectively extracted from Zn (II) due to the comparable values of mmol g^{-1} of each metal ion at any studied buffer solution.

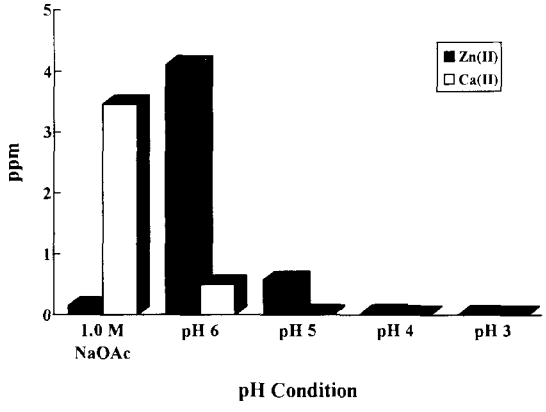

Fig. 1. Column separation and preconcentration of Zn/Ca mixture by buffer gradient.

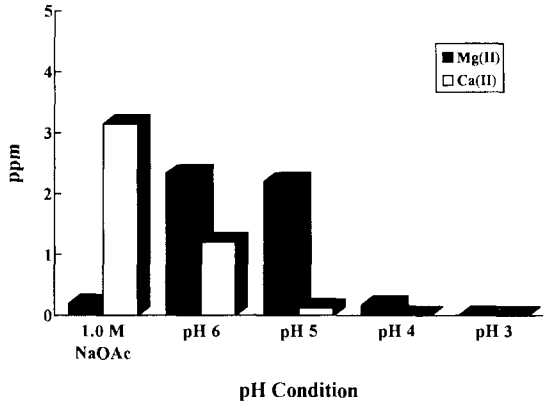

Fig. 2. Column separation and preconcentration of Mg/Ca mixture by buffer gradient.

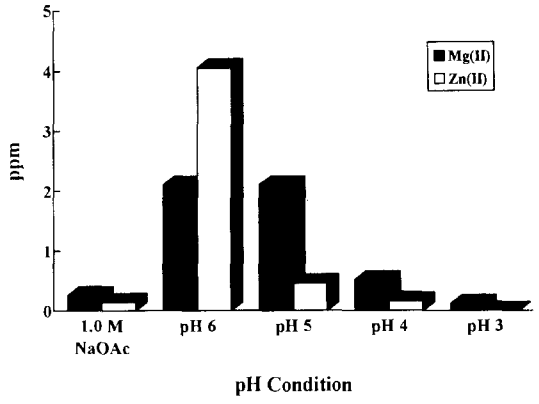

Fig. 3. Column separation and preconcentration of Mg/Zn mixture by buffer gradient.

3.1. Column separation and preconcentration

The absorbed trace metal ions on the surface of silica gel or modified silica gel can be eluted by the use of different acidic or basic solutions, dependent on the stability of such silica phases

Table 4
Column separation and preconcentration of metal ions

Buffer condition	Zn/Ca		Mg/Ca		Mg/Zn	
	Zn(II)	Ca(II)	Mg(II)	Ca(II)	Mg(II)	Zn(II)
1.0 M NaOAc	0.142	3.460	0.190	3.148	0.253	0.140
pH 6.0	4.100	0.501	2.330	1.210	2.100	4.050
pH 5.0	0.572	0.018	2.196	0.122	2.095	0.459
pH 4.0	0.015	0.000	0.164	0.000	0.512	0.160
pH 3.0	0.000	0.000	0.000	0.000	0.113	0.000
pH 2.0	0.000	0.000	0.000	0.000	0.000	0.000
Standard	4.854	4.220	4.816	4.506	4.870	4.733

Values are expressed in ppm and represent the concentration of metal ion eluted by the corresponding buffer solution.

towards elution conditions. In this study, we preferred to use buffer gradient procedure by lowering the pH value of the elution solution, one unit at a time, from pH 7 to 2. Selection of this buffer range is based on the stability results of silica–ERT in different buffer solutions. The results of the preconcentration and separation experiments are shown in Figs. 1–3 and compiled in Table 4. The separation of the Zn/Ca mixture is evident, based on the absorbed ppm values of Ca(II) and Zn(II) ions which proves again the selective behavior of silica–ERT towards Zn(II) preconcentration and extraction in presence of the interfering Ca(II) ion. By gradual lowering of the pH of the elution solution from pH 6 to 4, the retained Zn(II) eluted from the column. Ca(II) was found to be nonadsorbing on the column and eluted at the pH range of 7–6. In the mixture of Mg/Ca, Mg(II) eluted by buffer gradient at pH 6–5 while it was retained on the column in presence of 1.0 M NaOAc, as given in Table 4 and shown in Fig. 2. Lowering the pH value of the elution solution to 3–2 was not of practical importance because all the metal ions in the mixture were found to totally elute above pH 3.

Finally, separation of the mixture containing Mg(II) and Zn(II) by buffer gradient was evident in the range of pH 6–4 with the elution of Zn(II), mainly, in the pH range of 6–5 and Mg(II) in the pH range 6–4, predicting some interference by this unit buffer gradient. In this respect, the separation of Mg(II) from Zn(II) may be enhanced and accomplished by tuning the pH gradient between 6 and 4 for successful and complete separation.

References

[1] H. Sato, Y. Katsube, Clin. Calcium 5 (1995) 936.
[2] R.I. Christopherson, S.D. Lyons, Med. Res. Rev. 10 (1990) 505.
[3] R.E. Kelly, M.I. Mally, D.R. Evans, J. Biol. Chem. 261 (1986) 6073.
[4] T.V. Hambley, R.I. Christopherson, E.S. Zvargulis, Inorg. Chem. 34 (1995) 6550.
[5] X. Wang, W. Chu, F. Lou, C. van Breeman, Biochem. Biophys. Res. Commun. 213 (1995) 1061.
[6] Z. Karim, N. Defontaine, M. Paillard, J. Poggioli, Am. J. Physiol. 269 (1995) 134.
[7] S.-K. Yoo, E.S. Awad, M.A. El-Sayed, J. Phys. Chem. 99 (1995) 11600.
[8] K.W. Koelkebeck, T.W. Odom, Comp. Biochem. Physiol., A: Physiol. 112A (1995) 119.
[9] J.A.T. Pennington, S.A. Schoen, G.D. Salmon, B. Young, R.D. Johnson, R.W. Marts, J. Food Compos. Anal. 8 (1995) 129.
[10] N. Amyard, A. Leyris, C. Monier, H. Frances, R.G. Boulu, J.-G. Henrotte, Magnesium Res. 8 (1995) 5.
[11] K. Fukushi, K. Hiiro, Fresenius Z. Anal. Chem. 356 (1996) 150.
[12] U. Pyell, G. Stork, Fresenius Z. Anal. Chem. 342 (1992) 281.
[13] M. Volkan, O.Y. Ataman, A.G. Howard, Analyst 112 (1987) 1409.
[14] P.Y.T. Chow, F.F. Cantwell, Anal. Chem. 60 (1988) 1569.
[15] T. Seshardi, G. Dietz, H.-J. Haupt, Fresenius Z. Anal. Chem. 319 (1984) 403.
[16] M.E. Mahmoud, Anal. Lett. 29 (1996) 1791.

[17] J.S. Bradshaw, R.L. Bruening, K.E. Karkowiak, B.J. Tarbet, M.L. Bruening, R.M. Izatt, J.J. Christensen, J. Chem. Soc. Chem. Commun. (1988) 812.
[18] A. Tong, Y. Akama, S. Tanaka, Anal. Chim. Acta 230 (1990) 179.
[19] V. Dudler, L.F. Lindoy, D. Sallin, C.W. Schlaepfer, Aust. J. Chem. 40 (1987) 1557.
[20] T. Seshadri, H.-J. Haupt, Anal. Chem. 60 (1988) 47.
[21] M.E. Mahmoud, E.M. Soliman, Talanta 44 (1997) 15.
[22] M.E. Mahmoud, E.M. Soliman, Talanta (1997) in press.
[23] R.M. Smith, A.E. Martell, Critical Stability Constants, vols. 1–6, Plenum, New York, 1974–1989.
[24] R.E. Sturgeon, S.S. Berman, S.N. Willie, J.A. Desaulniers, Anal. Chem. 53 (1981) 2337.

ELSEVIER

Talanta 45 (1997) 317–323

Talanta

Preconcentration of heavy metals ions from aqueous solutions by means of cellulose phosphate: an application in water analysis

P. de Magalhães Padilha [a,*], J. Cesar Rocha [b], J. Celso Moreira [b], J. Theodoro de Sousa Campos [b], C. do Carmo Federici [b]

[a] *Departamento de Química, Instituto de Biociências, UNESP, C.P.-510, Botucatu-SP, 18610-000, Brazil*
[b] *Instituto de Química, UNESP, C.P.-355, Araraquara-SP, 14800-900, Brazil*

Received 24 December 1996; received in revised form 22 April 1997

Abstract

Cellulose phosphate (CELLPHOS) was studied as a collector for analytical preconcentration of traces of Cd(II), Cr(III), Cu(II) and Ni(II) from aqueous sample solution. It has been proved that using chromatographic columns packed with CELLPHOS for preconcentration and 1.0 mol l^{-1} HCl for elution the adsorbed analytes are quantitatively enriched. An enrichment factor of 20 (100 ml sample, 5 ml concentrate) was achieved by this separation procedure, which was applied to a series of water analyses (river, sea, bog water). © 1997 Elsevier Science B.V.

Keywords: Cellulose phosphate; Preconcentration; Heavy metals; Water analysis

1. Introduction

The toxic effects of heavy metals in the biosphere have been demonstrated by a number of studies [1,2]. Since the main sources of heavy metals for humans are water and food, the monitoring of the heavy metals content in natural waters is of paramount importance. For the direct determination of heavy metals in aquatic environments a number of sensitive instrumental methods (e.g. atomic spectroscopy) are available, however, it can suffer from systematic interferences by water constituents. For this reason, a preconcentration step is often necessary before quantifying these analytes. In the last decade the sorption of metal ions on cellulose collectors (modified or not) has been thoroughly studied, in particular the preconcentration of metals ions from both aqueous and non-aqueous mediums[3–6]. According to these studies cellulose collectors for on-line separations provide high distribution coefficients K_d for traces of analytes even in salt solution, multi-element capability and fast separation kinetics [7,8].

In the present study cellulose phosphate (CELLPHOS) already proposed by Schmitt et al. and Brajter et al. [9,10] for the separation of trace metals prefering the complexation with phosphate

* Corresponding author. Fax: +55 14 8213744.

PII S0039-9140(97)00134-3

groups was chosen for flow preconcentration of Cd(II), Cr(III), Cu(II) and Ni(II) from aqueous sample solutions. Firstly, the separation capabilities of CELLPHOS were characterized by both batch experiments and trace/matrix separations in a flow system. The reproducibility and accuracy of the developed flow procedure was another objective of this study. Secondly, a series of analyses in tropical aquatic environments achieved by the combination of the CELLPHOS flow system with flame atomic absorption spectrotometry (FAAS) had to prove the reliability of the collector, but also to characterize the interfering influence of environmental complexants (e.g. humic substances (HS)) contained in organic-rich water samples.

2. Experimental

2.1. Reagents

Cellulose phosphate (CELLPHOS) was prepared according to the Ford and Hall method [11]. This collector had a specific area of 1.96 ± 0.6 m^{-2} g^{-1} and 1.30 ± 0.9 mmols g^{-1} of phosphate groups.

The hydrate chlorides salts of several cations and other reagents were all p.a. grade.

2.2. CELLPHOS specific area determination

It was determined by using the BET method [12] and MICROMERITICS ASAP-200 equipment.

2.3. CELLPHOS phosphates groups determination

The phosphate groups contained in CELLPHOS were determined by the spectrophotometric method of molybdenum blue [13].

2.4. Ion exchange experiments

2.4.1. Kinetics

The time required for attains the exchange equilibria was determined by placing 50 ml of 5.00×10^{-3} mol l^{-1} aqueous solution of the metal ions in various flasks and by shaking them with 0.10 g of CELLPHOS. At appropriate time intervals, the supernatant from each flask was separated and its metal concentration determined by complexometric titration with Na_2EDTA [14].

The amount of metal ion collected by the solid phase was calculated using the following equation:

$$N_f = \frac{N_i - N_s}{m} \quad (1)$$

where N_i represents the initial quantity of metal ions in the solution, and N_s the final quantity of metal ions in the solution equilibrated with the solid phase; m is the CELLPHOS mass used and N_f is the quantity of metal ions collected by CELLPHOS.

2.4.2. Effect of varying the pH

The effect of pH on the exchange of metal ions on CELLPHOS as evaluated in the range of pH 1.0–5.0 varying it by 0.10 mol l^{-1} HCl.

2.4.3. Loading capacity

The loading capacity of the collector CELLPHOS was determined using the batch adsorption method [15]. Different aliquots of standard solutions of each metal chloride, containing 5.00×10^{-3} mol l^{-1} of the studied metals, were diluted to 50 ml samples, and kept at 298 K. To every sample solution 100 mg of CELLPHOS was added and stirred for 60 min under mechanical agitation. After the period of time chosen, CELLPHOS was separated by centrifugation and the metal concentration remaining in the solution was determined by complexometric titration with Na_2EDTA [14]. The quantity of metal ions collected on CELLPHOS was calculated according to Eq. (1).

2.4.4. Salt influence

The influence of dissolved salts on the separation of metal ions by CELLPHOS was evaluated by adding aliquots of 1.00 mol l^{-1} NaCl, $NaNO_3$ or Na_2SO_4 to exchange solutions of metal ions, under the same conditions as described before.

2.5. Preconcentration of analytes

Preconcentration experiments were performed using a glass column of 0.80 cm of inner diameter and 16 cm of height, equipped with a doubled way valve, filled with 2.00 g of CELLPHOS and aprated by a peristaltic pump. Before preconcentration, the CELLPHOS column was washed with 50 ml of 1.00 mol l^{-1} HCl and then with bidistilled water until the chloride ions were completly eluted [16].

To study preconcentration 100 ml of aqueous solutions containing 25 μg l^{-1} of Cd(II), Cr(III), Cu(II) and Ni(II) were passed through the column, at a flow rate of 1.5 ml min^{-1}. Then, the column was washed with 50 ml of bidistilled water followed by 5,10,15,20 and 25 ml of 0.50 mol l^{-1} HCl, respectively, to release the metal ions separated in the CELLPHOS column. The elution efficiency was also studied using an 1.0 mol l^{-1} HCl eluent. All fractions obtained during the elution stage were gathered separately.

Finally the CELLPHOS column was regenerated by passing 50 ml of 1.00 mol l^{-1} HCl and then bidistilled water until complete elution of chloride ions [16].

2.6. Determination by FAAS

The concentration of metal ions gathered from the CELLPHOS column were determined by FAAS according to the standard guidelines of the manufacturers (Spectrometer: VARIAN-INTRALAB AA-1475), chosing resonance lines of sensitivity for Cd, Cr, Cu and Ni [17,18] and deuterium background correction. For the calibration syntetic standard solutions based on 1.0 mol l^{-1} HCl comparable to the samples were used.

2.7. Determinations of metals in natural waters

2.7.1. Pretreatment of water samples

2.7.1.1. Preservation . Samples collected from natural waters were immediately filtrated through 0.45 μm membrane filtration. After acidification (pH < 2.0) with 6.00 mol l^{-1} HNO_3 they were stored in highly purified PE containers.

2.7.1.2. UV digestion. Water samples from organic-rich sources were digested by an oxidizing UV photolysis in the presence of 1% H_2O_2 using a low-pressure Hg-lamp which was integrated into a closed quartz vessel [19].

3. Results and discussion

3.1. Ion exchange experiments

3.1.1. Exchange kinetics

An important aspect for preconcentration is the exchange kinetics governing the separation of analytes from sample solutions. Fig. 1 shows plots of N_f versus time for the separation of Cd(II), Cr(III), Cu(II) and Ni(II) from aqueous solutions. Accordingly, the period of time necessary to reach the exchange equilibrium was about 50 min.

3.1.2. Influence of pH

The influence of the pH value on preconcentration by CELLPHOS is summarized in Fig. 2. This shows that the exchange of metal ions strongly decreases with the acidity of the solution. Obviously, a pH value of 5.0 is optimal for the collection of metal ions. Exchange experiments at pH values higher than 5.0 were not carried out because of the risk of hydrolysis [20].

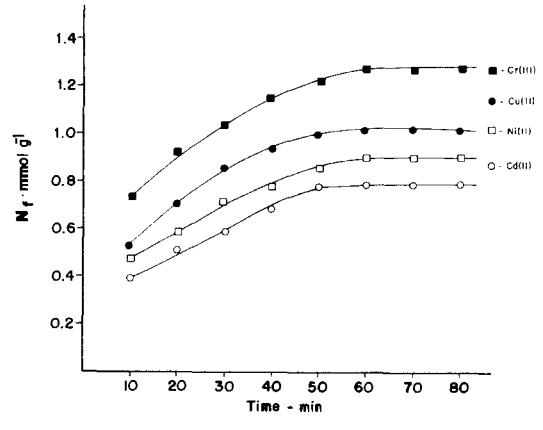

Fig. 1. Metal loading on CELLPHOS (expressed as N_f) as a function of time (100 ml sample, 0.1 g CELLPHOS, pH 5.0, 25°C).

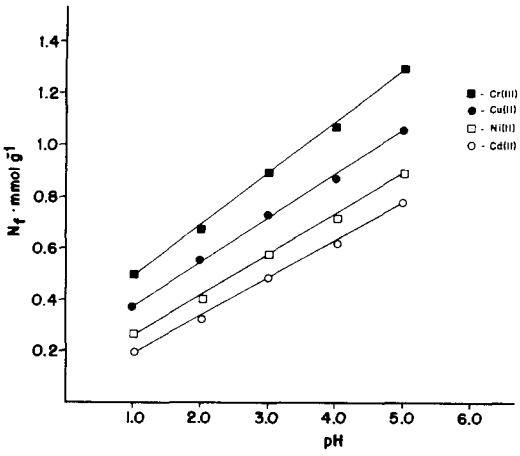

Fig. 2. Metal loading on CELLPHOS as function of the pH (experimental conditions as in Fig. 1).

3.1.3. Loading capacity

The results obtained from exchange experiments with Cd(II), Cr(III), Cu(II) and Ni(II) on CELLPHOS are shown by their loading isotherms in Fig. 3. In these isotherms the term N_f refers to the number of mmol metal ions adsorbed per gram of CELLPHOS, and C represents the final concentration of metal ions in solutions (mmol l^{-1}) at the equilibrium. Based on these isotherms, the following values for the loading capacity of CELLPHOS for metal ions (mmol g^{-1}) were

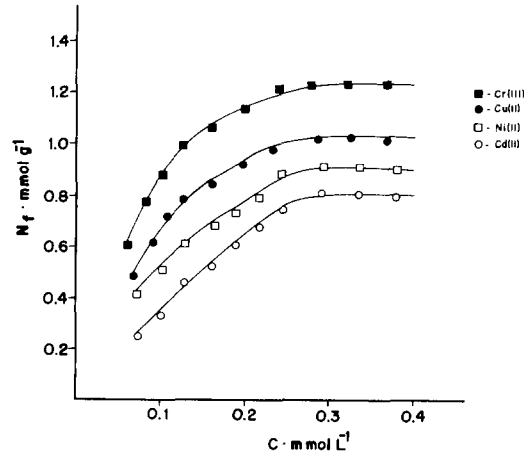

Fig. 3. Loading isotherms of Cd(II), Cr(III), Cu(II) and Ni(II) on CELLPHOS (100 ml sample, pH 5.0, 25°C).

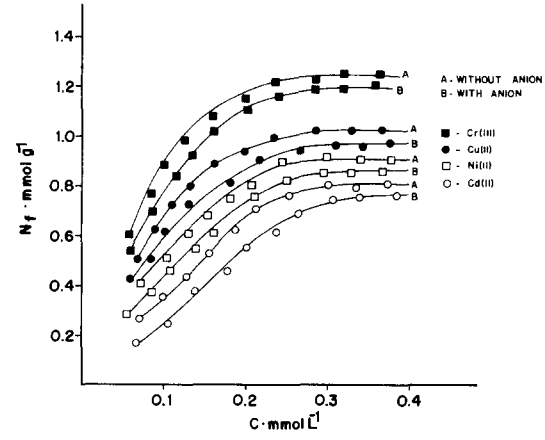

Fig. 4. Loading of Cd(II), Cr(III), Cu(II) and Ni(II) on CELLPHOS in the presence of 1.00 mol l^{-1} of each anion; Cl^-, NO_3^-, SO_4^{2-} (100 ml sample, pH 5.0, 25°C).

found: Cd(II), 0.80; Cr(III), 1.25; Cu(II), 1.10; Ni(II), 0.90.

Comparing the values of N_f^{max} obtained by the functional groups (phosphate groups) of CELLPHOS, the maximum quantity of metal ions separated is comparable to the number of functional groups contained in CELLPHOS (1.30 mmol g^{-1}).

According to this finding, the analytes are bound to the phosphate groups of the CELLPHOS by ion exchange.

3.1.4. Metal distribution coefficients K_d

Multi-element preconcentration by ion exchangers requires collectors offering high distribution coefficients ($K_d > 10^3$) for a variety of analytes described by the Eq. (2):

$$K_d = \frac{C_{exch.}}{C_{sol.}} \quad (2)$$

$C_{exch.}$, analyte bound to the exchanger (mmol g^{-1}); $C_{sol.}$, analyte in solution (mmol ml^{-1})

The separation characteristic of CELLPHOS referring to this aspect is also described in Fig. 3. From the exchange isotherms shown the following distribution coefficients K_d can be derived: Cd(II), 3.5×10^3; Cr(III), 9.0×10^3; Cu(II), 7.5×10^3; Ni(II), 5.0×10^3 (pH 5.0).

Table 1
Recovery of analytes using the CELLPHOS column method and hydrochloric acid solutions as eluent

Concentration of eluent (mol l^{-1})	Volume of eluent (ml)	% Recovery Sr ($n = 3$)			
		Cd(II)	Cr(III)	Cu(II)	Ni(II)
0.50	5.0	99.5 ± 1.8	44.4 ± 1.7	99.3 ± 1.7	99.5 ± 1.6
	10.0	99.2 ± 1.4	67.3 ± 1.8	99.1 ± 1.3	99.3 ± 1.2
	15.0	99.4 ± 1.7	83.2 ± 1.3	99.4 ± 1.2	99.7 ± 1.6
	20.0	99.3 ± 1.8	98.8 ± 1.5	99.5 ± 1.2	99.3 ± 1.4
	25.0	99.5 ± 1.4	99.5 ± 1.7	99.3 ± 1.7	99.6 ± 1.7
1.00	5.0	99.3 ± 1.7	99.1 ± 1.3	99.2 ± 1.3	99.2 ± 1.1
	10.0	99.7 ± 1.9	99.8 ± 1.2	99.7 ± 1.2	99.5 ± 1.7
	15.0	99.6 ± 1.2	99.3 ± 1.7	99.3 ± 1.5	99.2 ± 1.1
	20.0	99.3 ± 1.4	99.2 ± 1.9	99.1 ± 1.2	99.3 ± 1.7
	25.0	99.5 ± 1.1	99.7 ± 1.6	99.6 ± 1.7	99.6 ± 1.8

100 ml sample, 25 μg l^{-1} trace metals.

Accordingly, CELLPHOS is an effective multi-element collector under the experimental condition chosen.

3.1.5. Salt influence

The influence of electrolytes on the preconcentration process is related to their tendency to form complexes with the metal ion to be exchanged. This is shown in Fig. 4, where the influence of competing anions at the concentration level studied (0.10 mol l^{-1} of each anion; Cl^-, NO_3^- and SO_4^{2-}) is relatively weak. Thus, the cation–anion interaction in solution potentially decreasing the transfer of the metal ion from the solution to the solid phase, seems to be of little significance [21].

3.2. Preconcentration of heavy metal ions

The results of recovery experiments using a CELLPHOS column for preconcentration with different volumes and concentrations of diluted HCl for their elution are shown in Table 1.

According to Table 1, 5 ml of 0.25 mol l^{-1} HCl are sufficient to elute almost 100% of Cd(II) Cu(II) and Ni(II), but not of Cr(III). For the recovery of at least 99%, 5 ml 1.0 mol l^{-1} HCl are required. A 20-fold enrichiment is obtained in the concentration of metal ions (100 ml sample, 5 ml concentrate), after the separation procedure.

Comparing the total quantity of analytes collected on CELLPHOS column (2.5×10^{-2} mmol) and its loading capacity (2.0 g CELLPHOS, 2.52 mmol) merely 1% of the capacity is occupied by the exchange process.

3.3. Determination of metals in natural waters

A series of water analyses (selected river, sea, bog water from Brazil) were performed by combining preconcentration in the CELLPHOS flow system with FAAS. The results are summarized in Table 2.

The flow preconcentration was applied for the determination of trace elements in some Brazilan aquatic environments. Apart from the studied analytes (Cd, Cu, Cr) the collector CELLPHOS also provides quantitative recovery of traces of Al, Fe, Mn, Pb and Zn, when pre-supposed interfering aquatic complexants (e.g. HS) are absent. Thus, in undigested sea (Santos coastal-SP/Brazil) and river water (Tiête River, Barra Bonita dam, SP/Brazil) samples the FAAS determinations reveal metal concentration 10–30% lower as compared to the photolyzed samples. This systematic deviation has been attributed to environmental metal species (e.g. inert and/or labile metal complexes of HS) [22] being less accessible for the phosphate groups of the collector. The very strong influence of complexing substances on the preconcentration

Table 2
Preconcentration by the CELLPHOS flow procedure followed by FAAS: different water analyses (with and without UV photolysis, 100 ml sample, $n = 3$)

Metal	μg l^{-1}					
	Tiête River		Sea water		Bog water	
	UV	—	UV	—	UV	—
Al	681 ± 18	525 ± 14	480 ± 15	330 ± 16	540 ± 19	135 ± 14
Cd	8 ± 1.2	5.3 ± 1.5	6 ± 1.3	4.2 ± 1.2	ND	ND
Cu	85 ± 1.6	59 ± 1.3	68 ± 1.5	54 ± 1.6	52 ± 1.4	ND
Cr	18 ± 1.4	16 ± 1.5	12 ± 1.3	10 ± 1.2	25 ± 1.3	ND
Fe	915 ± 16	640 ± 18	620 ± 14	400 ± 15	1100 ± 15	132 ± 16
Mn	512 ± 17	350 ± 14	310 ± 16	250 ± 16	750 ± 18	135 ± 14
Pb	12 ± 1.3	10 ± 1.2	10 ± 1.1	8 ± 1.3	14 ± 1.3	ND
Zn	425 ± 15	290 ± 14	240 ± 15	180 ± 12	460 ± 17	69 ± 13

UV, UV photolysis; —, without UV photolysis; ND, not detected.

procedure is particularly evident in the case of bog water (Lavapés Brook-Botucatu, SP/Brazil) containing high concentrations of HS. Owing to the relatively short contact time in the flow system, only 10% of the heavy metals (in general strongly bound to HS) can be collected by CELLPHOS in the bog water sample without preceding UV photolysis. After UV photolysis, metal ions bound to HS as inert complexes can quantitatively react with phosphate groups of CELLPHOS. These results are in accordance with results obtained by direct determinations with GFAAS (Graphite-furnace AAS) shown in Table 3.

Table 3
Results of different water analysis by GFAA (direct determination, $n = 3$)

Metal	μg l^{-1}		
	Tiête River (UV)	Sea water (UV)	Bog water (UV)
Al	696 ± 20	492 ± 17	552 ± 18
Cd	10 ± 1.8	8 ± 1.1	ND
Cu	93 ± 1.7	72 ± 2.3	48 ± 1.7
Cr	22 ± 1.5	14 ± 1.3	23 ± 1.4
Fe	930 ± 19	632 ± 17	1150 ± 22
Mn	518 ± 16	316 ± 18	742 ± 17
Pb	15 ± 1.7	12 ± 1.4	12 ± 1.3
Zn	431 ± 17	260 ± 11	472 ± 18

UV, UV photolysis; ND, not detected.

4. Conclusions

The CELLPHOS collector provides quantitative analytical recoveries when used for preconcentration of traces of heavy metal in aqueous solutions, even from salt solutions. Thus, CELLPHOS can be proposed as a reliable trace collector in flow systems. Preconcentration by CELLPHOS from waste waters or organic-rich natural waters, however, requires a preceding sample digestion, for instance by a sample oxidizing UV photolysis.

Acknowledgements

The authors wish to thank CAPES, CNPq and FAPESP for the financial support, and Dr Peter Burba (ISAS, Dortmund, Germany) for valuable discussions on the presented results.

References

[1] P.W. Balls, Mar. Pollut. Bull. 20 (1989) 8.
[2] R.D. Wilken, J. Fresenius, Anal. Chem. 342 (1992) 795.
[3] P. Burba, W. Blodorn, Von Wasser 79 (1992) 9.

[4] P. Burba, P.G. Willmer, Fresenius J. Anal. Chem. 324 (1992) 167.
[5] R.A. Jorge, A.P. Chagas, Química Nova 11 (1988) 489.
[6] L.T. Kubota, J.C. Moreira, Y. Gushikem, Analyst 114 (1989) 1385.
[7] S. Caroli, A. Alimonti, F. Petrucci, Zs Horvath, Anal. Chim. Acta 248 (1991) 241.
[8] G. Knapp, et al., Mikrochim Acta 198 (1989) 257.
[9] P.H. Schimitt, J.S. Fritz, Talanta 15 (1968) 515.
[10] K. Brajter, K. Slonawsha, Anal. Chim. Acta 185 (1986) 271.
[11] R.M. Ford, W.P.V.S. Hall, US Patent No. 82.755, 1949.
[12] S. Brunaur, P. Emmet, E. Teller, J. Am. Chem. Soc. 60 (1938) 309.
[13] Z. Marczenko, Spectrophotometric Determination of Elements, Ellis Horwood, Chichester, 1976, pp. 616.
[14] M.P. Padilha, J.T.S Campos, J.C. Moreira, C.C. Federici, Química Nova 18 (1995) 529.
[15] L.T. Kubota, M. Ionashiro, J.C. Moreira, Ecl. Quim. 107 (1988) 70.
[16] A.I. Vogel, A Textbook of Macro and Semimacro Qualitative Inorganic Analysis, Longman, London, 1979, pp. 335.
[17] R.R. Brooks, B.J. Presley, I.R. Kaplan, Talanta 14 (1967) 809.
[18] R.R. Brooks, B.J. Presley, I.R. Kaplan, Anal. Chem. Acta 38 (1967) 221.
[19] P. Burba, P.G. Wilmer, Z. Fresenius, Anal Chem. 311 (1982) 738.
[20] C.F. Baester, R.E. Mesmer, The Hydrolysis of Cations, John Wiley, New York, 1976, pp. 267–274.
[21] P. Lessi, N. Dias L., J.C. Moreira, J.T.S. Campos, Anal. Chim. Acta 327 (1996) 183.
[22] J.C. Rocha, I.A.S. Toscano, P. Burba, Talanta 44 (1997) 69.

ELSEVIER

Talanta 45 (1997) 325–330

Talanta

Direct determination of Fe and Zn in different components of cow milk by FAAS with a high performance nebulizer

P. Bermejo *, R. Dominguez, A. Bermejo

Department of Analytical Chemistry, Nutrition and Bromatology, Faculty of Chemistry, University of Santiago de Compostela. Avda. de las Ciencias, 15706-Santiago de Compostela, Spain

Received 9 December 1996; received in revised form 21 April 1997; accepted 23 April 1997

Abstract

Methods for the direct determination of iron and zinc in different components of cow milk (whole milk, non fat milk and whey milk) by flame atomic absorption spectrometry (FAAS) were performed using two nebulizers (nebulizer of platinum with a glass impact bead and a high performance nebulizer). The non fat milk and the whey milk were obtained by physical procedures (centrifugation and ultracentrifugation) in absence of chemical treatment. A limit of detection of 0.024 and 0.007 μg ml^{-1} for iron and zinc, respectively, were obtained by using a high performance nebulizer. The precision obtained varied between 1.4–4.0% and 0.4–1.9% for iron and zinc, respectively. The accuracy of the methods was studied with the analysis of SRM-1549 and A-11 non fat milk reference materials. The methods were applied to ten cow milk samples. Dates about the distribution of iron and zinc into the different components of cow milk were present. © 1997 Elsevier Science B.V.

Keywords: FAAS; Fe; High performance nebulizer; Milk components; Zn

1. Introduction

The determination of trace element concentrations, in particular, essential elements for human feed such as iron and zinc present a great importance because when these elements reach low levels important diseases such as anemia in the case of iron or enteropatic arcrodermatitis in the case of zinc could be produced.

Due to the low levels of these elements (Fe and Zn) in cow milk samples the use of sensitivity analytical methods for their determinations are necessary. The methods used for this purpose are atomic absorption spectrometry (AAS) using a flame [1,2] or a graphite furnace [3–8] as an atomization system, emission atomic spectrometry (AES) (ICP-AES) [9,10] that allows multielement determinations and neutronic activation [11]. Otherwise, due to the spectral interferences and the high cost of analysis of ICP-AES determination and the difficulties of use in the case of neutronic activation, the AAS methods are the more adequate for this purpose. Good precision, accuracy and reproducibility of AAS methods and the ease and quickness of this analysis make AAS more useful than the other techniques commented above.

* Corresponding author.

PII S0039-9140(97)00125-2

Although, the excellent sensitivity obtained by ETAAS in the direct determination of iron and zinc, its use presents several disadvantages such as the great dilution factor required and the contamination problems related to the iron and zinc determination; thus, the use of FAAS remains an attractive technique. To increase the sensitivity obtained by FAAS, the use of a high sensitivity nebulizer presents an interesting approach. In addition, the analysis time and cost required are lower using FAAS.

To obtain the different component of cow milk, methods based on physical procedures and chemical treatment have been purposed. Different centrifugation procedures for the fat milk separation have been reported. Thus R. García et al. [12] reported $12\,000 \times g$ during 45 min, B. Lönnerdal et al. [13] $10\,000 \times g$ during 30 min, P. Brätter [9] $4000 \times g$ during 10 min at 4°C. To obtain the whey milk, different procedures based on isoelectric precipitation at pH 4.6 [14–17], chemical precipitation [17–19] and physical precipitation methods based on ultracentrifugation to separate the casein micelles and high weight molecular proteins of milk [17,20,21], have been also purposed.

In the present paper, physical procedures for non fat milk and whey milk obtention were studied. Methods for direct determination of iron and zinc in the different components of the cow milk (whole milk, non fat milk and whey milk) using an air/acetilene flame were used.

In addition a comparative study of two nebulizers (high performance nebulizer and platinum nebulizer with a glass impact bead) for the iron and zinc determinations was carried out.

The proposed methods were applied to commercial cow milk samples.

2. Experimental

2.1. Apparatus

Centrifuge Digicen, Orto Alresa and ultracentrifuge L8-M Beckman with a rotor SW-40 were used to obtain non fat milk and whey milk, respectively.

A Perkin-Elmer 5500 atomic absorption spectrophotometer equipped with a Deuterium lamp as a background correction system was used for iron and zinc measurements. Two Perkin-Elmer nebulizers were used, a platinum nebulizer with a glass impact bead and a high performance nebulizer with tantalum capillary and a ceramic impact bead.

Hollow cathode lamps operated at 30 and 15 mA were used for iron and zinc, respectively, that provided resonance lines of 248.3 and 213.9 nm. The spectral bandwidth were 0.2 nm for iron and 0.7 nm for zinc, and an air/acetylene flame was used throughout in both cases.

2.2. Reagents

All solutions were prepared from analytical reagent grade chemicals using ultrapure water, resistivity 18 MΩ cm^{-1} obtained from Milli-Q System of Millipore.

- Iron and zinc stock standard solutions (1000 g l^{-1}) from Merck, Darmstad (Germany).
- Sodium tetrapropylenebenzosulphonate, 5%, Merck, Darmstad (Germany).
- Two non fat milk reference materials, SRM-1549 Nist (USA) and A-11 from the International Atomic Energy Agency, Vienna (Austria) were used.

2.3. Procedure

The iron and zinc determination in the different components of the cow milk was carried out by flame AAS without pretreatment of the sample.

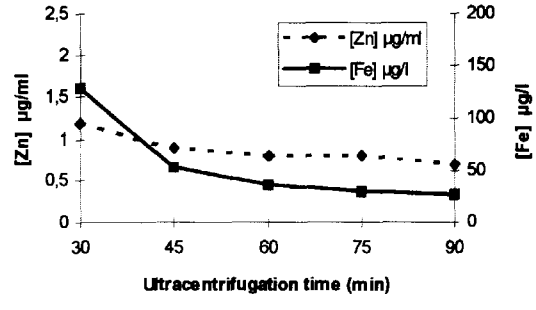

Fig. 1. Optimization of ultracentrifugation time.

Table 1
Calibration and addition equations obtained using two nebulizers corresponding to each component of the cow milk

	Nebulizer of Pt with a glass impact bead		High performance nebulizer	
	Fe	Zn	Fe	Zn
Calibration	A = 0.055 [Fe] + 0.000 r = 0.998	A = 0.440 [Zn] + 0.008 r = 0.999	A = 0.090 [Fe] + 0.000 r = 1.000	A = 0.738 [Zn] + 0.003 r = 1.000
Addition whole milk	A = 0.046 [Fe] + 0.004 r = 0.997	A = 0.362 [Zn] + 0.384 r = 0.999	A = 0.098 [Fe] + 0.012 r = 0.999	A = 0.600 [Zn] + 0.154 r = 0.999
Addition non fat milk	–	A = 0.366 [Zn] + 0.378 r = 0.999	A = 0.100 [Fe] + 0.012 r = 0.999	A = 0.628 [Zn] + 0.163 r = 0.999
Addition whey milk	–	A = 0.415 [Zn] + 0.103 r = 1.000	A = 0.096 [Fe] + 0.001 r = 1.000	A = 0.690 [Zn] + 0.158 r = 0.999

Different dilutions of the cow milk sample were made for each sample.

The non fat milk was obtained by centrifugation at 3200 rpm for 30 min. The fat phase (upper phase) was carefully separated with a glass rod. A dilution of the non fat milk was made for each sample.

The whey milk was obtained by ultracentrifugation at $31\,000 \times g$ and 4°C for 60 min: three phases were obtained, the upper phase (fat) was separated from the intermediate phase (whey milk) and they lower phase (casein micelles and proteins of high molecular weight) was in the bottom of the tube; the whey milk was separated with a micropipette. The whey milk was directly introduced in the nebulizer without dilution.

The whole milk and the non fat milk and whey milk obtained from milk samples were frozen at −4°C until the measurement.

3. Results and discussion

3.1. Fat separation

The fat milk separation was carried out fixing the centrifugation speed (3200 rpm) and varying the centrifugation time between 15 to 120 min with an increase of 15–120 min.

After the centrifugation a liquid phase, nonfat milk, and a solid phase (upper phase) of fat were obtained and the fat was carefully removed using a glass rod.

To obtain the optimum time for total fat separation the iron and zinc concentration of four samples of non fat milk from the same milk sample were centrifugated. The variations of the iron and zinc concentrations in the non fat milk phases were not significant for the different centrifugation times. Therefore, we selected 30 min as optimum time as longer times did not improve the fat separation and increase the time of analysis.

3.2. Whey milk separation

In this paper, a physical method by ultracentrifugation to obtain the whey milk was optimized. For this purpose, a Beckman ultracentrifuge with a SW-40 rotor at $31\,000 \times g$, 4°C temperature with 1 min acceleration and 1 min deceleration times was used.

3.2.1. Optimization of ultracentrifugation time

To optimize the ultracentrifugation time 5 series of six replicates each with the same non fat milk sample were ultracentrifuged using different times in the range of 30–90 min.

As can be seen in Fig. 1, an ultracentrifugation time of 60 min is adequate because with a longer ultracentrifugation times the levels of iron and zinc in the whey milk were constant.

3.2.2. Repeatability of the whey milk

The repeatability of the whey milk preparation was studied by means of the repeatability of the overall procedure, including the whey milk prepa-

Table 2
Sensitivity of the method corresponding to whole milk obtained using two nebulizers

	Nebulizer of Pt with a glass impact bead		High performance nebulizer	
	Fe	Zn	Fe	Zn
LOD ($\mu g\ ml^{-1}$)	0.044	0.011	0.024	0.002
LOQ ($\mu g\ ml^{-1}$)	0.146	0.036	0.081	0.007
Sensitivity ($\mu g\ ml^{-1}$)	0.096	0.024	0.045	0.006

ration and the measurement. Six different whey milk replicates from the same non fat milk sample were measured using the standard addition method for each metal. The RSD obtained were, 7.4 and 5.3% for iron and zinc, respectively.

3.3. Comparison of both nebulizers

The sensitivity was studied using two nebulizers, a platinum nebulizer with a glass impact bead and a high performance nebulizer. The nebulizer has a tantalum capillary and a ceramic impact bead, moreover the body is the unatach plastic, the diameter is bigger and the impact bead is nearest to the venturi, for this the efficiency of the nebulization must be bigger.

With the use of the high performance nebulizer it was not necessary the use of the sodium tetrapropilenebenzosulphonate as an surfactant agent because it is possible to make an important dilution of the sample and then there are no problems with the matrix. Nevertheless for the use of the platinum nebulizer for the whole and non fat milk a surfactant agent was necessary [22] because the milk matrix decreased the nebulization efficiency.

The calibration and standard addition graphs obtained using whole milk, non fat milk and whey milk were studied. Results obtained are shown in Table 1.

The slopes of the calibration and standard addition graphs for both metals were compared by means of the t-test, obtaining slopes related to the calibration and standard addition graphs with statistically significant difference and thus is the use of a standard addition method for Fe and for Zn measurements in all cases including both nebulizers. Otherwise, the difference on the slope values corresponding to the standard addition is necessary using whey milk and the aqueous calibration are less.

When platinum nebulizer with a glass impact bead was used, the standard addition equation using non fat milk and whey milk corresponding to iron determination was not carried out due to the low sensitivity obtained with the use of this nebulizer.

The detectability, expressed through the limit of detection (LOD) and the limit of quantification (LOQ), defined as 3 and 10 S.D. m^{-1} respectively, where S.D. is the standard deviation of 11 replicate measurements of a blank and m is the slope of the addition graph, were studied for both metals and nebulizers. Results are shown in Table 2. On the other hand, sensitivity of a method is usually defined in FAAS as the concentration of analyte that produces an absorbance signal of 0.0044, therefore, sensitivity based on this definition, is also shown in the Table 2.

As can be seen (Table 2), the use of high performance nebulizer give us a high sensitivity for the direct determination of iron and zinc in milk. Thus, a high dilution of samples could be reached avoiding the use of a surfactant agent, then a possible contamination source of the samples is avoided, we have selected the high performance nebulizer as the better approach.

3.4. Analytical performances

The precision of method was studied using whole milk sample, due to the fact that this sample has a more complex matrix than the other components of the cow milk. Thus, the precision

Table 3
Precision corresponding to whole milk obtained for iron and zinc with a high performance nebulizer

	Fe				Zn			
$[]_{add}$ (μg ml^{-1})	0.0	0.1	0.2	0.3	0.0	0.5	1.0	1.5
$[]_{mean}$ (μg ml^{-1})	0.13	0.22	0.32	0.43	3.23	4.72	5.50	7.17
S.D.	0.005	0.003	0.008	0.007	0.017	0.020	0.025	0.139
RSD (%)	4.0	1.4	2.6	1.6	0.5	0.4	0.4	1.9

of the method using a high performance nebulizer, expressed as RSD (%), were obtained for ten analysis of unspiked whole milk and whole milk spiked with 0.5, 1.0 and 1.5 μg ml^{-1} of iron and 0.1, 0.2 and 0.3 of zinc. The results are shown in Table 3. As can be seen a good precision is achieved for both metals.

Due to the fact that a reference material for whole milk and whey milk is not available, the accuracy of the method using a high performance nebulizer was studied through the analysis of a non fat milk reference material with a A-11 control milk of the IAEA with a certified content of 3.65 ± 0.76 μg Fe g^{-1} milk and a SRM-1549 control milk of the NIST with a certified content of 46.1 ± 2.2 μg Zn g^{-1} milk. The results obtained are shown in Table 4. As can be seen good accuracy is achieved for each metal. In addition the accuracy of method was studied through the analytical recovery (Table 5); the analytical recovery of Fe and Zn was close to 100%.

3.5. Application

The levels of iron and zinc related to each component of the cow milk sample (whole milk, non fat milk and whey milk) were determined from ten cow milk samples.

As can be seen (Table 6), for whole milk the levels of iron and zinc varied between 0.22–0.44 and 2.73–7.99 μg ml^{-1}, respectively; for non fat milk varied between 0.10–0.41 μg ml^{-1} and 2.65–4.99 μg ml^{-1}, respectively and for whey milk between 0.01–0.14 μg ml^{-1} and 0.36–0.82 μg ml^{-1}, respectively.

4. Conclusions

A physical procedure for non-fat milk and whey milk obtention, in the absence of chemical treatment, was studied. Methods for the direct determination of iron and zinc in the different components of the cow milk (milk, non fat milk, whey milk) by FAAS with a high performance nebulizer have been developed. The presented methods have adequate sensitivities, accuracies and precision.

The more important advantages of the use of the High Performance Nebulizer are the bigger sensitivity obtained for Zn and Fe. Although in many samples the Zn levels founded are sufficient

Table 4
Accuracy of methods using A-11 (IAEAS) and SRM-1549 (NIST) with a high performer nebulizer

	Fe	Zn
Reference material	A-11 (IAEA)	SRm-1549 (NIST)
Certified value	3.7 ± 0.8 μg Fe g^{-1} milk	46 ± 2 μg Zn g^{-1} milk
Obtained value	3.0 ± 0.2 μg Fe g^{-1} milk	45 ± 1 μg Zn g^{-1} milk

Table 5
Analytical recovery corresponding to whole milk using high performance nebulizer

Fe		Zn	
$[Fe]_{add}$ (μg ml^{-1})	Recovery (%)	$[Zn]_{add}$ (μg ml^{-1})	Recovery (%)
0.1	90.0	0.5	96.0
0.2	105.0	1.0	98.0
0.3	100.0	1.5	100.5

Table 6
Levels of Fe and Zn in different components of milk

Sample no.	Fe (μg ml^{-1})			Zn (μg ml^{-1})		
	Whole milk	Non fat milk	Whey milk	Whole milk	Non fat milk	Whey milk
1	0.27	0.27	0.12	7.03	4.99	0.36
2	0.27	0.23	0.14	7.99	4.80	0.82
3	0.22	0.20	0.08	5.36	4.55	0.44
4	0.24	0.24	0.05	4.34	4.02	0.38
5	0.44	0.29	0.01	5.83	3.77	0.33
6	0.44	0.41	0.03	4.44	3.94	0.43
7	0.41	0.29	0.03	4.82	3.31	0.35
8	0.34	0.18	0.05	4.63	2.65	0.46
9	0.20	0.10	0.04	4.65	3.63	0.42
10	0.44	0.40	0.04	4.34	4.31	0.46

to use the standard nebulization, with the use of the high performance nebulizer it is not necessary the addition of the surfactant agent, in these conditions the procedure is simplified.

A comparison of the iron and zinc level in non fat milk and whey milk show that the major fraction (80 and 78% for iron and zinc, respectively) are present in the non fat milk. For whey milk the level of iron and zinc found were 21.4 and 8.4%, respectively; the majority of the zinc (91.6%) is bounded to high molecular weight proteins separated by ultracentrifugation procedure, while only a 78.6% of iron is bounded to these proteins.

References

[1] S. Arpadhan, D. Stoyanova, Fresenius J. Anal. Chem. 302 (1980) 206.
[2] L. Jorheim, J. AOAC Int. 76 (1993) 798.
[3] R.A. Muzzarelli, C.E. Eugeni, F. Tanfani, G. Garavia, D. Pezzola, Milchwissenschaft 38 (1983) 453.
[4] M.D. Mingorance, M. Lachica, Anal. Lett. 18 (1985) 1519.
[5] M. Oikawa, N. Taguchi, N. Suzuki, K. Kojima, Shokuhin Eiseigakn Zasshi 28 (1987) 180.
[6] D. Wagley, G. Schmiedel, E. Manika, H.J. Ache, At. Spectrosc. 10 (1989) 106.
[7] J. Arnaud, A. Favier, J. Alary, J. Anal. At. Spectrom. 6 (1991) 647.
[8] L. Favretto, D. Vojnovic, B. Campisi, Anal. Chim. Acta 293 (1994) 295.
[9] P. Brätter, B. Gercken, U. Rösick, A. Tomiac, Trace Element Analytical Chemistry in Medicine and Biology, Walter de Gruyter, Berlin, 1988.
[10] K.T. Suzuki, H. Tamagawa, S. Hirano, E. Kobayashi, K. Takahashi, Biol. Trace Element Res. 28 (1991) 109.
[11] V.E. Negretti, S. Recknagel, D. Gawlik, Fresenius J. Anal. Chem. 353 (1995) 137.
[12] R. García, C. Díez, Anal. Bromatol. 1 (1985) 43.
[13] B. Lönnerdal, B. Hoffman, L.S. Hurley, Am. J. Clin. Nutr. 36 (1982) 1170.
[14] K. Julsham, K.J. Andersen, Comp. Biochem. Physiol. 75A (1993) 17.
[15] G.R. Ricci, L.S. Shepard, G. Colovos, N.E. Hester, Anal. Chem. 53 (1981) 610.
[16] F.E. Brinckman, W.R. Blair, K.L. Jewett, W.P. Inverson, J. Chromatogr. Sci. 15 (1977) 493.
[17] P. Bermejo, R. Domínguez, A. Bermejo, Fresenius J. Anal. Chem. 357 (1997) 457.
[18] N. Yoza, J. Oshashi, Anal. Lett. 6 (1973) 595.
[19] K.N. Falchuki, Engl. J. Med. 296 (1977) 1129.
[20] L. Ebdon, S. Hill, P. Hones, J. Anal. Atom. Spectrom. 2 (1987) 205.
[21] L. Ebdon, J.R. Wilkinson, K.W. Jackson, Anal. Chim. Acta 136 (1982) 191.
[22] P. Bermejo, R. Domínguez, R. Soto, A. Bermejo, Analusis 23 (1995) 135.

ELSEVIER

Talanta 45 (1997) 331–341

Talanta

Derivative spectrophotometric determination of copper(II) in non-ionic micellar medium

Narinder Kumar Agnihotri, Vinay Kumar Singh, Har Bhajan Singh *

Department of Chemistry, University of Delhi, Delhi 110007, India

Received 16 October 1996; received in revised form 18 April 1997; accepted 28 April 1997

Abstract

A photometric method for trace analysis of Cu(II) with 1-(2-pyridylazo)-2-naphthol (PAN) in presence of a neutral surfactant, Triton X-100, has been reported in normal and derivative modes. The molar absorption coefficient (ϵ) and Sandell's sensitivity (S) of PAN–Cu(II) complex at 555 nm is 5.21×10^4 l mol^{-1} cm^{-1} and 1.22 ng cm^{-2} respectively. The detection limit of Cu(II) is 4.0 ng ml^{-1} and Beer's law is obeyed in the range 0.08–4.00 μg ml^{-1} of the analyte. Copper content of a number of commercially available alcoholic beverages, biological and standard alloy samples is reported. The results obtained are in excellent agreement with those obtained using AAS. © 1997 Elsevier Science B.V.

Keywords: 1-(2-pyridylazo)-2-naphthol; Surfactant; Micellar medium; Trough depth; Peak height

1. Introduction

A number of analytical methods exist for photometric determination of copper: most commonly used reagents include dithizone, [1–3] dithiocarbamate, [4–6] cuproine, [7,8] cuprizone, [9,10] etc. Copper complex in each case except the last method has to be extracted into an organic solvent (CCl_4, $CHCl_3$, isopentanol etc.). Such solvents are not only toxic but are environment pollutants, [11,12] and have been listed as carcinogens by the Environmental Protection Agency (EPA) [13]. Dithizone, which is one of the most sensitive reagents, not only lacks selectivity but also has limited stability. Cuprizone, has been introduced as a highly sensitive photometric reagent for copper but it is less selective than cuproine reagent [9]. Cuprizone, which forms a water soluble complex with copper in basic medium, has poor sensitivity besides interference due to presence of foreign ions. The methods involving use of sodium diethyldithiocarbamate and cuprizone require prior concentration by ion-exchange method [14]. Although the photometric determination of copper with 1-(2-pyridylazo)-2-naphthol, (PAN) has been reported, both the chromophore and the chelate formed are insoluble in water, and require tedious and time consuming extraction steps before absorbance measurement [15,16]. The selection of a suitable solvent is important for an effective extraction of metal–PAN chelates. Chloroform is most widely

* Corresponding author. Tel.: +91 011 7257794; 7256538.

PII S0039-9140(97)00137-9

used. The extraction is often incomplete with CCl_4, ether and benzene [17].

The high solubilization capacity of surfactants and micellar systems permits modification or development of analytical procedures in which the extraction steps can be avoided and, in many cases, even the sensitivity and selectivity of the procedure is considerably enhanced [18,19]. On the other hand, the use of derivative spectrophotometry offers a useful means of enhancing the sensitivity and selectivity of the method besides convenient solution to well defined analytical problems such as resolution of multi component systems, overcoming interference due to sample turbidity, matrix back ground and enhancement of spectral details [20,21].

In this paper, the complexation reaction between PAN and Cu(II) in the presence of a neutral surfactant, Triton X-100 has been investigated in normal and derivative photometric modes with a view to developing a rapid, reproducible, sensitive and selective spectrophotometric method for the determination of copper(II). The optimized conditions so developed have been employed for the trace determination of copper(II) in certified standard reference materials, alcoholic beverages and biological samples. The sensitivity and the linear range of the developed method has also been compared with the recommended photometric methods. The proposed method is simpler and more sensitive than the methods involving extractive photometric determination with PAN or with dithizone; the latter is one of the most sensitive reagents.

2. Experimental

2.1. Reagents

Aqueous solutions of Cu(II) [25.0 μg ml^{-1}] was prepared from copper(II) sulphate in double distilled water and standardized by known methods. As PAN is insoluble in water, requisite amount (9.36 mg) was first dissolved in minimum amount of dilute sulphuric acid to which was added 4.0 g Triton X-100. The solution was then diluted to the mark with water. All chemicals were of analytical grade purity.

2.2. Instruments

Shimadzu UV-260 recording spectrometer was used for recording normal as well as derivative spectra. All spectra were recorded using 10 mm matched quartz cells with a band width of 2 nm. First and second order derivative spectra were recorded with $\Delta\lambda = 2$ and 4 nm respectively. A ECIL digital pH meter (Model No. 5651) was used for pH measurements. Shimadzu Atomic Absorption Spectrometer (Model AA-640-13) was used to determine copper content.

2.3. Procedure

Absorption spectra (normal and derivative) of the following solutions were recorded, taking water as reference, in order to determine photometric characteristics of the PAN–Cu(II) complex.

Two sets of solutions, one containing 2.50 μg ml^{-1} metal ion and the other without it, and each containing fixed amount of the reagent (2.0×10^{-4} M) and Triton X-100 (2.0% m/v) in the pH range 1.0–9.0, were prepared to determine the optimum pH range of the complexation reaction.

To study the impact of varying surfactant concentration on the absorbance of the PAN–Cu(II) complex, a set of solutions containing increasing amounts of Triton X-100 (0.0–4.0 g), and 2.50 μg ml^{-1} Cu(II) and 2.0×10^{-4} M PAN, at the pH of the maximum complex formation, was prepared.

Effect of varying ligand concentration on the absorbance of the system was investigated by preparing a set of solutions containing 8.0×10^{-6} to 2.0×10^{-4} M of the reagent at optimum pH.

Range of linear proportionality of absorbance of the system with Cu(II) ion concentration has been ascertained based on a set of solutions containing varying amount of the metal ions (0.08–4.0 μg ml^{-1}), 2.0×10^{-4} M PAN, and 2.0% m/v Triton X-100 at pH 6.5, the condition of maximum complex formation.

2.4. Determination of copper in beverage, biological, and standard samples

Appropriate amounts of PAN, Triton X-100, and the metal ions were added to a 10 ml cali-

brated flask to obtain final concentration of 2.0×10^{-4} M, 2.0% (m/v) and 0.08–4.0 μg ml^{-1}, respectively. Absorption spectra was then recorded against water as reference to generate analytical calibration curves in normal mode (λ_{max}, 555 nm) or in first order derivative mode (trough depth at 575 nm) or in second order derivative mode (trough depth at 560 nm or peak height at 590 nm). Citrate (1.0×10^{-3} M) is added to mask Fe(III), wherever necessary. Interference due to the presence of Ni(II) ions is avoided by preparing the calibration curve at 575 nm, the cross-over i.e. iso-differential point of Ni(II)–PAN complex. This technique of generating calibration curves in higher derivative modes has already been successfully utilized by the authors [22]. The sample solutions were diluted, if necessary, in order to bring their absorbance or derivative amplitude values with in the linear range to determine Cu(II) ion concentration using regression equation obtained with standard Cu(II) solutions. Copper content of the standard and the sample was also determined at 324.7 nm using AAS equipped with an air–acetylene flame.

3. Results and discussion

3.1. Effect of pH

Absorption spectra of PAN in non-ionic micellar medium shows a broad peak at 460 nm and a sharp peak at 273 nm. As the pH increases to 5.0, the former shifts to 470 nm while latter reduces to a valley with a simultaneous appearance of a new peak at 300 nm. Though PAN and its copper complex absorb at 555 nm, molar absorption coefficient of the later is much higher than the former. Therefore, relative increase in absorbance of the complex (w.r.t. ligand) was plotted after calculating from the absorbance values of the ligand and complex against water. The complexation commences at pH 3.8 and increases up to pH 6.2. Relative increase in absorbance remains practically constant from pH 6.2–7.0. All subsequent studies have been carried out at 555 nm and optimum pH of 6.5.

3.2. Effect of surfactant

Anionic–sodium laurylsulphate, cationic–cetylpyridinium chloride and cetyltrimethylammonium bromide and non-ionic, Triton X-100 surfactants were investigated to determine their impact on absorption profiles of PAN–Cu(II) complex. Cationic and non-ionic surfactants cause significant change in the optical properties and stabilities of the complex formed. The micellar solutions of cationic surfactants enable formation of several ternary species of different optical properties which are dependent on pH, concentration of the reagent and the surfactant. The relative change in the absorbance on complexation in case of anionic surfactant was low as compared to the cationic and non-ionic surfactants. It is attributed to the inhibition of the complexation reaction between ligand and metal [19]. Maximum increase in absorbance at 555 nm was observed in presence of Triton X-100 as its presence neither shifts equilibrium nor influences ionization of PAN. The absorbance at λ_{max} of the complex shows a sharp increase with increasing Triton X-100 up to 2.0% (m/v) and remains constant between 2.0 and 2.25% (m/v) surfactant concentration. A slight decrease, however, was observed at concentration $> 2.25\%$ (m/v) due to the decrease in the number of chromophores per micelle. The surfactant concentration was kept at 2.0% (m/v), which is greater than its CMC of 3.2×10^{-4} M, during subsequent studies.

3.3. Effect of varying PAN concentration

Absorbance of PAN–Cu(II)–Triton X-100 has been found to increase with increase in the concentration of the ligand. As the ligand absorbs significantly at λ_{max} of the complex, the increase in absorbance is partly due to the increase in the ligand concentration. Absorbance values were, therefore, corrected for the absorption of the uncomplexed ligand and plotted against its molar ratio. The plot shows a sharp increase up to 3.0 (L:M) and remains practically constant up to 25.0. During subsequent studies the ligand concentration was kept between 3 and 25 times the metal concentration wherever possible.

3.4. Effect of varying Cu(II) ion concentration

Absorption of the solutions containing increasing amount of Cu(II) ions and a fixed (but excess) amount of the ligand at 555 nm was plotted against the metal ion concentration in order to obtain the linear range over which the absorbance was proportional to the metal ion concentration. The linear regression analysis between metal ion concentration (μg ml^{-1}), [C] and absorbance at λ_{max} of the complex, $[A]_{max}$ shows excellent fit (Eq. (1)), as evidenced by the value of residue square (Table 1). The linear regression analysis of corrected absorbance, $[A]_{CA}$ (using Eq. (2)) on the metal ion concentration shows a improved linear fit than from uncorrected absorbance values (Table 1).

$$[C] = 1.757[A]_{max} - 3.814 \times 10^{-1} \quad (1)$$

$$[A]_{CA} = [A]_{max} - [(V)_L - R \times (V)_M]\left[\frac{[A]_{max}}{(V)_L}\right] \quad (2)$$

Table 1
Linear regression analysis of Cu(II) ion concentration and absorbance/derivative amplitude in normal/derivative modes

Straight line equation	Regression coefficient
Normal mode	
Absorption at 555 nm	
$[A] = 5.692 \times 10^{-1}$ $[C] + 2.171 \times 10^{-1}$	0.9990[a]
$[A]_{CA} = 6.016 \times 10^{-1}$ $[C] - 4.586 \times 10^{-2}$	0.9994[a]
First derivative mode	
$[TD]_{510\ nm} = 4.081$ $[C] - 4.000 \times 10^{-2}$	0.9984
$[TD]_{575\ nm} = 3.136 \times 10^{1}$ $[C] + 5.360$	0.9985[a]
Second derivative mode	
$[TD]_{560\ nm} = 1.842 \times 10^{1}$ $[C] - 4.133$	0.9945
$[PH]_{590\ nm} = 1.111 \times 10^{1}$ $[C] + 4.320$	0.9947[a]

PH, peak height;
TD, trough depth;
$[A]_{CA}$, corrected absorbance;
[C] concentration of Cu(II) ions (μg ml^{-1}).
[a]Recommended for determination/detection.

where $[[A]_{max}/(V)_L]$ is the ratio of the absorbance at λ_{max} to molar volume of the ligand when there is no metal ion present in the solution and $(V)_M$, the molar volume of the metal ion solution, R, the stoichiometry of the complex and $(V)_L$, the molar volume of the ligand.

The first and second order derivative spectra of the above solutions are also recorded to enhance the spectral profiles of the method (Fig. 1b and c). The first-order derivative spectra is found to be of great value for this system since it provides the λ_{max} of the complex corresponding to the cross-over point at 555 nm. Height of peaks [PH], and depth of the troughs [TD], were measured from the base line of the ligand or zero line and plotted against the metal ion concentration. Relationship between PHs/TDs and metal ion concentration at different wavelengths shows a good linear fit (Table 1) which is useful in determining the analyte in aqueous solutions. The measurements at 575 nm (TD) in first derivative mode and at 590 nm (PH) in second order derivative mode are of great analytical significance. Beer's law is found valid between 0.08 and 4.00 μg ml^{-1} of Cu(II) ions. Molar absorption coefficient (ϵ), specific absorptivity (a) and Sandell's sensitivity (S) of the complex at 555 nm and pH 6.5 are 5.21×10^4 l mol^{-1} cm^{-1}, 0.82 ml g^{-1} cm^{-1} and 1.22 ng cm^{-2} respectively.

3.5. Sensitivity and Detection limits

The sensitivity of the method is defined as calculated analytical sensitivity, $S_A = S_S/m$, where S_S is the standard deviation of the analytical signal at a particular concentration and m, the slope of calibration plot. The detection limit, C_L is defined as the minimum concentration of the analyte that can be measured in a sample processed through the preparative procedure. The detection limit, C_L and limit of quantification, C_Q (i.e. LOQ) of the method in normal as well as in derivative modes, as defined by IUPAC are reported in Table 2 [23]. The LOQ is used to determine the lower limit of the determination range (dynamic range). Precision of the methods was also determined from six replicate concentration measurements on standard solutions. Rela-

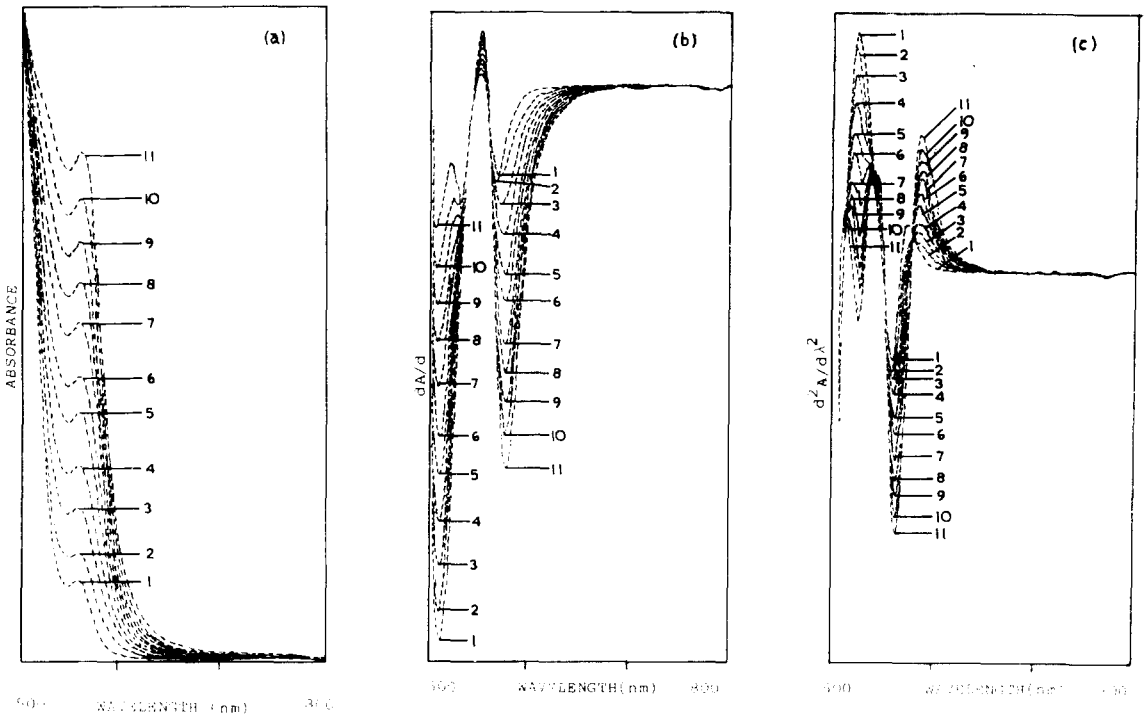

Fig. 1. Absorption spectra of Cu(II)–PAN–Triton X-100 system at pH 6.5. Curve No. 1–2.0×10^{-4} M PAN and 2.0% m/v Triton X-100, Curve Nos. 2–11—increasing amount of Cu(II) ions between 0.25–2.0 μg ml^{-1} and fixed amount of PAN (2.0×10^{-4} M) and 2.0% m/v Triton X-100; (a) Normal mode, (b) first derivative mode and (c) second derivative mode.

tive standard deviation was found to be 1.23 and 1.41% at concentration of 0.10 and 1.8 μg ml^{-1}, respectively. Absorption measurements at 555 nm in the normal mode, and trough depth and peak height at 575 nm and 590 nm respectively in first and second order derivative modes, are recommended for the determination of Cu(II) ions with PAN in the neutral micellar medium. Recommended wavelengths in the derivative modes are based on large dynamic range, better sensitivity and precision (Table 2).

3.6. Composition and Conditional stability constant

Composition of the complex formed under experimental conditions was investigated by Job's method of continuous variations. Plot of absorbance versus mole fraction of the metal ion shows a maximum at 0.33 which corresponds to 1:2 (M:L) ratio in the complex. This is in agreement with the reported composition in organic phase [15,16]. The complex can, therefore, be represented as $Cu(HPAN)_2$, where HPAN denotes monodeprotonated form of the ligand.

Conditional stability constant (k') [24,25] of the complex was calculated assuming the following equilibrium.

$$Cu(II) + 2H_2PAN \rightleftharpoons [Cu(HPAN)_2] + 2H^+$$

Since the solution is dilute and a neutral surfactant is used, concentration is substituted for activity for the purpose of calculation. Average of eight values of k' for PAN–Cu(II) complex are found to be 3.61×10^8 l^2 mol^{-2}.

3.7. Effect of foreign ions

The effect of presence of foreign ions on the trace level determination of Cu(II) in aqueous

Table 2
Photometric characteristics of PAN–Cu(II)–Triton X-100 system

Photometric parameters	Normal mode	First derivative mode (575 nm)	Second derivative mode (590 nm)
Analytical sensitivity, $S_A = S_s/m$, ng ml^{-1}	1.00	3.50	5.50
Detection limit, $C_L(k = 3)$, ng ml^{-1}	6.0	4.0	11.0
Limit of Quantification, $C_Q(k = 10)$, ng ml^{-1}	21.0	13.0	36.0
Linear Dynamic range, ng ml^{-1}	21–4000	13–4000	36–4000
RSD, %($n = 6$)	0.17	0.70	1.09

Table 3
Tolerance limit* of diverse ions on the determination of Cu(II) ions (1.2 μg ml^{-1}) with PAN in neutral micellar medium using Triton X-100

Diverse ions	Amount added(μg)	Remark	Diverse ions	Amount added(μg)	Remark
Cations					
Al(III)	300	—	B(III)	200	—
Ga(III)	100	[a]	Fe(III)	100	[a,b]
Fe(II)	100	[b]	Be(II)	100	—
Ca(II)	3000	—	Mg(II)	3000	—
Pb(II)	500	[a]	Mn(II)	100	[b]
Co(II)	100	[b]	Zn(II)	100	[b]
Cd(II)	100	[b]	Hg(II)	100	[b]
Ni(II)	100	[b]	Tl(I)	800	—
Anions					
Chloride	200	—	Bromide	200	—
Iodide	200	—	Thiocyanate	500	[b]
Ascorbate	400	—	Tartrate	1500	—
Citrate	2000	—	EDTA	100	[c]
Borate	200	—	Acetate	600	—
Cyanate	100	[c]			

* Change in absorbance $\leq 4.0\%$,
[a] masked by citrate,
[b] interferes strongly,
[c] masked the complexation between Cu(II) and PAN.

phase has been investigated in normal as well as the derivative modes to evaluate the analytical utility of the ligand. The criterion for the studies was a $\pm 4.0\%$ change in absorbance for 1.20 μg ml^{-1} of Cu(II) in final 10 ml solution. The amount of foreign ion tolerated (i.e. which changes absorbance by $\leq \pm 4.0\%$) is given in the Table 3; cations of Fe, Co, Cd, Hg, Ni, Mn, and Zn interfere. The complexation reaction between Cu(II) and PAN is completely masked by EDTA and cyanate at low concentration, whereas ascorbic acid, Br^-, Cl^-, I^-, and SCN^- do so at relatively higher concentrations. Though, masking agents such as citrate, phosphate, fluoride and thiocyanate are generally useful to over come interference due to cations, only citrate is found suitable in the present case; presence of 1.0×10^{-3} M of citrate enhances the tolerance limits of Fe(III), Ga(III) and Pb(II) from 100, 100 and 500 μg to ≥ 500, 800, and 1000 μg, respectively.

One of the major cause of interference in the normal mode is the overlap of the spectral profiles of the interfering ion with that of the analyte. This could be overcome in the derivative mode as

Table 4
Comparative evaluation of various photometric reagents for the determination of copper(II)

Reagent	Medium/solvent	λ_{max} (nm)	Molar absorptivity (l mol^{-1} cm^{-1}) × 10^4	Linear range (μg ml^{-1})	Reference
Dithizone	CCl_4	550	4.52	0.4–2.0	[2]
Sodium diethyldithiocarbamate	Acetic acid	430	1.89	—	[6]
Cuproine	1:1 H_2O-DMF/isoamylalcohal	546	0.64	≤10	[7]
Cuprizone	Aqueous	600	1.6	≤4.0	[9]
Dithiocarbamate	Aqueous(β-cyclodextrin)	436	1.3	0–0.6	[12]
Neocuproine	Isoamylalcohal/*n*-hexanol	454	0.79	1.0–10	[26]
Bathocuperione	*n*-hexanol	479	1.42	0.1–40	[27]
Bathocuperione disulphonic acid	Aqueous	483	1.22	—	[28]
Zincon	Zephiramine/$CHCl_3$	625	—	0.2–1.6	[29]
4-(2-Pyridylazo)-resorcinol	Aqueous	535	1.18	0.5–3.0	[30]
Acenaphtho-quinonemonoxime	$CHCl_3$	430	1.33	0.63–2.85	[31]
p-Anisaldehydethiosemicarbazone	Aqueous	402	0.61	0.1–10	[32]
2,4-Dihydroxyacetophenone thiosemicarbazone	Aqueous	360	1.4	1.0–10	[33]
Pyrocatechol violet	Aqueous	620	1.0	0.6–2.5	[34]
4,6-Dihydroxy-2-mercaptopyrimidine	Aqueous	381	—	—; 0.18[a]	[35]
Diphenylcarbazone	MIBK	540	6.30	0.05–1.4	[36]
3-Bromo-2-hydroxy-5-methylacetophenonehydrazone	Aqueous	400	0.48	0.13–2.75	[37]
N-(α-Pyridyl)-2-thioquinaldinamide	Aqueous	520	0.52	0.6–16	[38]
2,4-Dihydroxybenzophenone semicarbazone	Aqueous	355	1.14	0.51–4.06	[39]
1-(2-pyridylazo)-2-naphthol	Ethanol–water	595	—	0.5–3.0	[40]
Dithiocarbamate	CCl_4	436	1.49	—; 0.1173 ± 0.0035[a]	[41]
1-Phenyl-4,4,6-trimethyl(1H,4H)-pyrimidine-2-thiol	Naphthalene/DMF	400	1.3	0.25–3.75	[42]
Cyclopentane-spiro-2′-(1-phenyl-2′,4′-di-thio)-*s*-triazine	DMF, toluene	410	1.08	5.0–50[b]	[43]
3-Thiobenzoyl-1-*p*-tolylthiocarbamide	Toluene	420	1.00	0.5–4.5[b]	[44]
Sodium cyanide	Aqueous	234,242	—	0.55–5.8; 0.13[a]	[45]
1,5-Bis(di-2-pyridylmethylene)thiocarbonohydrazide	DMF	420	2.8	0.1–1.3	[46]
Dithiocarbamate	Aqueous (Hexadecyltrimethylammonium chloride)	436	1.22	—; 0.0406 ± 0.0021[a]	[41]
Dithiocarbamate	Aqueous (Ammonium dodecylsulphate)	434	1.25	—; 0.0544 ± 0.0017[a]	[47]
1-(2-Pyridylazo)-2-naphthol	Aqueous (Triton X-100)	555	5.21	0.08–4.00; 0.004[a]	present work

[a] Detection limit
[b] μg.

overlapping spectral peaks in the normal mode resolve into separate peaks, trough and cross-over (isodifferential) points or zero cross-over points on derivatization. This has been utilized to overcome the interference due to the presence of cations of Co, Cd, Hg, Mn, Ni, and Zn. The Ni(II)–PAN–Triton X-100 complex shows peaks at 530 and 570 nm in normal mode, and a peak at 555 nm, a trough at 585 nm and a cross-over point at 575 nm in first order derivative mode. The measurement of derivative amplitude (trough depth) of Cu(II)–PAN–Triton X-100 complex at 575 nm, the cross-over point of Ni(II) complex in first order derivative mode has been utilized to determine the concentration of Cu(II) ion in presence of Ni(II) ions. Co(II) complex shows peaks at 575 and 625 nm in normal mode, and a trough at 645 nm and cross-over points at 578 and 630 nm in first order derivative mode besides a peak at 655 nm in second order derivative mode. The cross-over point of Co(II) complex at 578 nm in first derivative mode has been utilized to determine Cu(II) ion concentration in presence of Co(II). In addition, the measurement of peak height at 655 nm of Co(II) complex, the zero-crossing point of Cu(II) complex in second order derivative mode has been utilized to determine the concentration of Co(II) ion concentration in presence of Cu(II) without any preseparation and masking.

The interference due to Co(II) and Ni(II) could thus be easily overcome as these ions have well separated absorption maxima, minima and cross-over points from that of the Cu(II)–PAN–Triton X-100 complex in derivative modes.

3.8. Comparison

A comparative evaluation of various spectrophotometric reagents for the determination of copper(II) is given in Table 4. It is observed that in case of the present method using PAN not only the sensitivity is better than the widely used methods but the range of determination is also wider (13–4000 ng ml^{-1} of Cu(II) ions) with a lower detection limit of 4.0 ng ml^{-1}.

4. Analytical applications

The accuracy and applicability of the proposed method were evaluated by its application to various biological and standard alloy samples.

4.1. Determination of Cu(II) in beverages and biological samples

A mixture of beverage (10 ml), nitric acid (10 ml) and hydrogen peroxide (3 ml) was refluxed for

Table 5
Quantitative determination of Cu(II) ions in some beverages and biological samples

Sample No.	Copper found (ppm)[a]	
	Proposed method	AAS
1. Whisky		
A	4.782 ± 0.019	4.776 ± 0.015
B	5.340 ± 0.022	5.356 ± 0.029
C	5.108 ± 0.016	5.128 ± 0.020
D	4.560 ± 0.024	4.562 ± 0.021
2. Rum		
A	9.149 ± 0.034	9.155 ± 0.039
B	8.346 ± 0.025	8.332 ± 0.032
C	7.348 ± 0.030	7.342 ± 0.021
D	8.420 ± 0.023	8.408 ± 0.034
3. Gin		
A	9.318 ± 0.041	9.332 ± 0.066
B	7.245 ± 0.036	7.238 ± 0.040
C	8.024 ± 0.018	8.040 ± 0.026
D	9.028 ± 0.030	9.046 ± 0.038
4. Brandy		
A	4.346 ± 0.039	4.354 ± 0.043
B	3.571 ± 0.028	3.592 ± 0.036
C	4.106 ± 0.032	4.096 ± 0.026
D	4.201 ± 0.041	4.220 ± 0.056
5. Goat Liver		
A	3.742 ± 0.027	3.740 ± 0.038
B	4.562 ± 0.038	4.570 ± 0.048
C	5.658 ± 0.030	5.668 ± 0.021
D	3.842 ± 0.028	3.830 ± 0.040
6. Human hair		
A	0.925 ± 0.006	0.918 ± 0.004
B	0.882 ± 0.007	0.876 ± 0.008
C	0.421 ± 0.011	0.430 ± 0.009
D	0.768 ± 0.003	0.771 ± 0.005

[a] Mean value of six determinations ± S.D.

Table 6
Determination of copper(II) in certified reference materials

Sample	Composition(%)	Copper contents (%)		
		Certified value	Proposed method[a]	AAS[a]
Aluminum alloy, (NKK, 916)	Si 0.410, Fe 0.540, Co 0.030, Mn 0.110, Mg 0.100, Cr 0.050, Ni 0.060, Zn 0.300, Ti 0.100, Sn 0.050, Pb 0.040, V 0.020, Zr 0.050, Bi 0.030, Ca 0.030, Sb 0.010, B 0.0006, Cu 0.270.	0.270	0.271 ± .002	0.271 ± .004
Ni–Cr Steel (JSS, 508-4)	Si 0.28, C 0.38, Cu 0.12, Cr 0.76, P 0.020, N 0.0111, S 0.017, Mo 0.020, Mn 0.49, Ni 3.19.	0.120	0.120 ± .003	0.120 ± .004
Stainless steel, (JSS, 653-7)	C 0.0.068, Si 0.630, Co 0.350, Ni 13.91, Mn 1.72, Cr 22.53, N 0.0276, Cu 0.030.	0.030	0.0305 ± .0029	0.0298 ± .0031
Carbon Steel (JSS, 061-2)	Si 0.260, C 0.64, Cu 0.011, Cr 0.019, Ni 0.019, P 0.010, Mn 0.490, S 0.012, Al 0.034, N 0.0038.	0.011	0.0108 ± .0008	0.0117 ± .0007

[a] Mean value of six determinations ± S.D.

6 h. After digestion, the sample was carefully evaporated to dryness.

Freeze-dried sample of goat liver or washed sample of human hair (washed successively with water and methanol and dried at 110°C for 40 min) was ashed for 12 h at 500–600°C [48]. The residue was dissolved in concentrated nitric acid and evaporated to dryness at a low heating rate.

In both cases, the residue was extracted with distilled water and filtered. Working solutions were prepared by taking a suitable aliquot of the sample and its copper content determined spectrophotometrically and by atomic absorption spectrometry. Both the results are in excellent agreement (Table 5).

4.2. Determination of copper in standard alloys

A 0.1–0.5 g sample of the alloy was dissolved in 10–15 ml of aqua regia by heating on a low flame. After cooling the solution, 3–5 ml hydrogen peroxide (30% v/v) was added and the excess decomposed by heating on a water bath. The solution was evaporated to dryness, residue extracted with distilled water, filtered to remove insoluble components of the alloy and diluted to mark in a calibrated flask. Working solutions were prepared by taking a suitable aliquot of the sample solution. Appropriate amounts of citrate(to mask iron(III)), PAN, and Triton X-100 were added to make the solution 1.0×10^{-3} M, 2.0×10^{-4} M and 2.0% m/v respectively with respect to the added component. The copper ion concentration in the sample solution was then determined at 575 nm, the cross-over point of Ni(II) complex in first order derivative mode, from the calibration graph generated from standard solutions of Cu(II) under identical conditions. The results obtained by the proposed method are found to be in good agreement with those obtained by AAS (Table 6).

5. Conclusion

One of the most important aspects of the present work is the simple and rapid detection and trace level determination of Cu(II) ions as

PAN–Cu(II) complex in an aqueous solution of a neutral surfactant, Triton X-100 in normal as well as in derivative modes. The sensitivity and selectivity of the method was considerably improved by using derivative spectrophotometry. The method does not require tedious and expensive process of solvent extraction, hence avoiding the use of toxic and carcinogenic organic solvents. It provides a high sensitivity with a detection limit of 4.0 ng ml^{-1} and wider determination range of 13–4000 ng ml^{-1}. Compared with the popular photometric methods (using Dithiocarbamate; Limit of detection 40.6 ± 2.1 ppb) [41], and highly sensitive methods such as ICP–AES (Limit of detection 0.5 μg g^{-1} and 0.05–10 μg g^{-1}) [49,50], d.c. plasma emission (Detection limit 0.67 ppm) [51], and AAS (20–200 μg l^{-1}) [52], the method is not only sensitive but also economical (since it is cheaper than ICP–AES, and AAS and does not require any gas or maintenance) and less complicated. The method has been successfully applied for the determination of copper in commercial samples.

Acknowledgements

Financial assistance received from Ministry of Defence, Government of India, New Delhi, through their Grants-in-Aid scheme is gratefully acknowledged.

References

[1] R.W. Geiger, E.B. Sandell, Anal. Chim. Acta 8 (1953) 197.
[2] C.R. Elliott, P.F. Preston, J.H. Thompson, Analyst 84 (1959) 237.
[3] H.M.N.H. Irving, CRC Crit. Rev. Anal. Chem. 8 (1980) 321.
[4] A. Jewsbury, Analyst 78 (1953) 365.
[5] H. Pohl, Anal. Chim. Acta 12 (1955) 54.
[6] M.E.M.S. de Silva, Analyst 99 (1974) 408.
[7] J. Hoste, J. Eeckhout, J. Gillis, Anal. Chim. Acta 9 (1953) 263.
[8] J.P. Riley, P. Sinhaseni, Analyst 83 (1958) 299.
[9] R.E. Peterson, M.E. Bollier, Anal. Chem. 27 (1955) 1195.
[10] C.U. Wetlesen, Anal. Chem. Acta 16 (1957) 268.
[11] The Merck Index, 10th ed., Merck, Rahway, New York, 1983.
[12] Shihe Li, Shengquan Li, A. Chen, Talanta 40 (1993) 1085.
[13] Second Annual Report on Cercinogens, Environmental Protection Agency, NTP 81–43, December, 1981.
[14] B. Tuck, E.M. Osborn, Analyst 85 (1960) 105.
[15] B.F. Pease, M.B. Williams, Anal. Chem. 31 (1959) 1044.
[16] A. Galik, Talanta 16 (1969) 201.
[17] CRC Handbook of Organic Analytical Reagents, CRC Press, Boca Raton, Florida, 1982, p. 188.
[18] E. Pramauro, E. Pelizzetti, Trends in Anal. Chem. 7 (1988) 260.
[19] G.L. McIntire, CRC Cri. Rev. Anal. Chem. 21 (1990) 257.
[20] C.T. Cottrell, Anal. Proc. 19 (1982) 43.
[21] F.S. Rojas, C.B. Ojeda, J.M. Cano Pavon, Talanta 35 (1988) 753.
[22] N.K. Agnihotri, V.K. Singh, H.B. Singh, Analyst 120 (1995) 1809.
[23] IUPAC, Nomenclature, symbols, units and their usage in spectrochemical analysis, Pure Appl. Chem. 45 (1976) 105.
[24] A. Ringbom, J. Chem. Educ. 35 (1958) 282.
[25] L.G. Sillen, A.E. Martell, Stability Constants of Metal Complexes, vol. 1 and vol. 2. Chemical Society, London, 1964, 1971.
[26] G.F. Smith, W.H. McCurdy Jr., Anal. Chem. 24 (1952) 371.
[27] L.G. Borchardt, J.P. Butler, Anal. Chem. 29 (1957) 414.
[28] D. Blair, H. Diehl, Talanta 7 (1961) 174.
[29] M. Sugawara, K. Niiyama, T. Kambara, Bunseki Kagaku 22 (1973) 1219.
[30] M.P. Volkova, B.P. Kolesnikov, V.G. Kossykh, Zh. Anal. Khim. 32 (1977) 2139.
[31] F. Kamil, S.K. Shindhwani, R.P. Singh, Indian J. Chem., A 19 (1980) 609.
[32] K.N. Thimmaiah, H. Sanke Gowda, S. Maqbool Ahmed, Indian J. Chem., A 22 (1983) 690.
[33] K.H. Reddy, K.G. Reddy, K.M.M.S. Prakash, D.V. Reddy, Indian J. Chem., A 23 (1984) 535.
[34] V.K. Reddy, D.V. Reddy, Indian J. Chem., A 21 (1982) 215.
[35] B. Morelli, Analyst 108 (1983) 870.
[36] H.K. Das, J. Indian Chem. Soc. 61 (1984) 182.
[37] K. Lal, S.R. Malhotra, J. Indian Chem. Soc. 60 (1983) 308.
[38] A.K. Chakrabarti, Indian J. Chem., A. 25 (1986) 886.
[39] K.G. Reddy, K.H. Reddy, D.V. Reddy, Indian J. Chem., A. 25 (1986) 982.
[40] A. Gallardo Malgarejo, A. Gallardo Céspedes, J.M. Cano Pavón, Analyst 114 (1989) 109.
[41] M.P. San Andres, M.L. Marina, S. Vera, Talanta 41 (1994) 179.
[42] B.K. Puri, K.W. Jackson, M. Katyal, Mikrochim. Acta 1 (1989) 213.
[43] J.D. Chavan, V.P. Joshi, J. Indian Chem. Soc. 67 (1990) 935.

[44] D.M. Ambhore, A.P. Joshi, J. Indian Chem. Soc. 68 (1991) 175.
[45] W. Naixing, L. Weian, Q. Ping, Talanta 40 (1993) 897.
[46] A.M.G. Rodriguez, A.G. de Torres, J.M. Cano Pavon, C.B. Ojeda, Talanta 40 (1993) 1861.
[47] M.P. San Andres, M.L. Marina, S. Vera, Analyst 120 (1995) 255.
[48] M. Satake, Y. Matsumura, Bunseki Kagaku 26 (1977) 386.
[49] E.H. Van Veen, M.T.C. de Loos-Vollebergt, A.P. Wassink, H. Kalter, Anal. Chem. 64 (1992) 1643.
[50] K. Lobiński, W. Van Borm, J.A.C. Broekaert, P. Tschöpél, G. Tölg, Fresenius J. Anal. Chem. 342 (1992) 563.
[51] S.H. Vien, R.C. Fry, Appl. Spectrosc. 42 (1988) 381.
[52] N. Goyal, P.J. Purohit, A.G. Page, M.D. Shastry, Talanta 39 (1992) 775.

ELSEVIER

Talanta 45 (1997) 343–348

Talanta

A sensitive determination of paraquat by spectrophotometry

M.K. Rai [a,*], Joyce Vanisha Das [b], V.K. Gupta [b]

[a] *Department of Chemistry, Government College of Khairagarh, Distt. Rajnandgaon, M.P. 492881, India*
[b] *School of Studies in Chemistry, Pt. Ravishankar Shukla University, Raipur, M.P. 492010, India*

Received 6 January 1997; received in revised form 21 April 1997; accepted 28 April 1997

Abstract

A sensitive spectrophotometric method for the determination of a widely used herbicide, paraquat using a versatile reducing agent sodium borohydride is described. Paraquat is reduced with sodium borohydride in an alkaline medium to give a blue radical ion with an absorbance maxima at 600 nm. Beer's law is obeyed in the range of 0.05–0.5 μg ml^{-1} of paraquat. The molar absorptivity and Sandell's sensitivity are found to be 2.9×10^5 l mol^{-1} cm^{-1} and 0.0006 μg cm^{-2} respectively. The important analytical parameters and the optimum reaction conditions were evaluated. The method is free from the interference of other commonly used pesticides and metal ions. The method was applied successfully to the determination of paraquat in human samples, such as blood, urine and mother's milk compared to food and environmental samples. © 1997 Elsevier Science B.V.

Keywords: Paraquat; Spectrophotometry; Sodium borohydride

1. Introduction

Paraquat (1,1′dimethyl-4,4′bipyridylium ion) is an extensively used herbicide. It has achieved great prominence because of its wide spectrum of activity against grasses as well as most broad-leaved weed species [1,2]. Paraquat is highly toxic to humans, having been implicated in many deaths [3]. It causes 'paraquat lungs' in which honeycombing of the lungs and hardening of breathing tracts occurs due to development of pulmonary fibrosis caused by retention of ions in the lungs. It is also known to produce 'Parkinsonism' in man [4].

Because of its toxicity and significance, several methods based on different analytical techniques have been reported for the determination of paraquat; i.e. automatic continuous flow spectrometry [5,6], SPE [7], RIA [8], RP-HPLC [9], liquid chromatography [10], ionpair chromatography [11], spectrophotometry [12], etc. Many of the earlier reported spectrophotometric methods are less sensitive and suffer from many drawbacks [13–16], A method for the determination of paraquat using ascorbic acid in an alkaline medium was reported from this laboratory [17]. The method was suitably modified using flow injection analysis, which increased the sensitivity several times [6].

In the present work, a new, sensitive method is reported, where sodium borohydride is used as an

* Corresponding author. Tel.: +91 771 325486, 325948, 546223; fax: +91 771 534283.

PII S0039-9140(97)00136-7

excellent reducing reagent for the reduction of paraquat to form a stable blue coloured free radical ion. The method has a sensitivity of 0.05 μg ml^{-1} of paraquat (range 0.05–0.5 μg ml^{-1}) which is comparable to the flow injection analysis reported earlier [6]. The advantages of the method are primarily the ready availability of sodium borohydride as a simple, versatile, nontoxic reducing agent and the greater stability of the blue free radical ion. During the proposed work, different reagents such as hydrazine, hydroiodic acid, hydrophosphorous acid, hydrophosphite, Zn–HCl and sodium borohydride were tried for the reduction of paraquat. Sodium borohydride was found to be the best, since with sodium borohydride reduction of paraquat was complete, gave maximum absorbance value, good stability and quantitative and reproducible results. With other reducing agents however, the reduction of paraquat was incomplete and the results were neither quantitative nor reproducible. The proposed method was applicable for the determination of paraquat in human samples, food and environmental samples.

2. Experimental

2.1. Apparatus

Varian DMS lOOS UV-Visible spectrophotometer with matched silica cells were used for all spectral measurements and pH measurements were made with Systronics pH meter model 331.

2.2. Reagents

All chemicals used were of AnalaR grade. Double distilled deionized water was used throughout the study.

1. Paraquat (Supplied by ICI India Limited) 1 mg ml^{-1} stock solution of paraquat was prepared in water.
2. A working standard solution was prepared by appropriate dilution of the stock solution.
3. Sodium borohydride (Merck Germany); 1% (w/v) aqueous solution.
4. Sodium hydroxide; 2 M aqueous solution.
5. Ethylenediamine tetraacetic acid disodium salt (EDTA); 5% (w/v) aqueous solution.
6. Sulphuric acid; 9 M aqueous solution.
7. Saturated ammonium chloride solution.
8. Silicagel (BDH) (100–200 mesh). Used for column chromatography.

2.3. Procedure

2.3.1. Procedure for the preparation of calibration graph

To an aliquot of a working standard solution containing 0.5–5.0 μg of paraquat, taken in a calibrated test tube, add 1 ml of 1% aqueous solution of sodium borohydride. Then add 1 ml of 2 M sodium hydroxide. Make up the volume to 10 ml by adding deionized water and keep the test tube in a thermostat maintained at ~35–40°C for 5 min for complete colour development. Measure the absorbance maxima of the blue coloured radical ion obtained at 600 nm against the reagent blank.

2.3.2. Procedure for the determination of paraquat in environmental and food samples. Preparation of column for the extraction of paraquat from samples

Paraquat, being ionic, cannot be extracted using organic solvents. Therefore, a silica gel column was used to separate paraquat from various samples. A 25 ml glass column (9–10 mm in diameter) with a plug of glass wool placed just above the stopcock was used. Silica gel (6 g) was weighed out, packed into the column and then washed with water. A fresh column was used for each experiment.

2.3.3. Determination of paraquat in water

A volume of 100 ml runoff water was collected in PTFE bottles from different agricultural fields where paraquat had been sprayed. The samples were filtered and 1 ml of 5% EDTA was added to each of them to remove various metal ions. They were then allowed to pass through silica gel column at a flow rate of 7 ml min^{-1}. The paraquat was absorbed by the silica gel, which was later eluted by passing 50 ml of saturated ammonium chloride through it at a flow rate of

Table 1
Reproducibility of the method

No. of days	Absorbance[a] at 600 nm
1	0.320
2	0.325
3	0.320
4	0.330
5	0.325
6	0.320
7	0.330

Concentration of paraquat used was 2.0 μg 10 ml^{-1}.
[a] Mean = 0.324; S.D. = ±0.0045; relative S.D. = 1.39%.

about 3 ml min^{-1}. It was collected in a 50 ml calibrated flask and the volume was made up to the mark with water. Then, 5 ml aliquot of this solution was taken and paraquat was determined by the proposed method.

2.3.4. Determination of paraquat in soil

Soil samples were taken from different agricultural fields where paraquat had been used. The sample (25 g) was weighed and ground in a mixer. To the ground sample, 1 ml of 5% EDTA was added, then filtered by adding 150 ml of water using vacuum pump. The filtrate was allowed to pass through silica gel column at a flow rate of 7 ml min^{-1}. Paraquat absorbed by the column was eluted using 50 ml of saturated ammonium chloride at a flow rate of 3 ml min^{-1}. Eluted paraquat was collected in a 50 ml calibrated flask made up to the mark with water. Aliquots of 5 ml were taken and paraquat was determined as described above.

2.3.5. Determination of paraquat in food

Different samples of plant materials like grains, apples, sugarcane foliage, potatoes (25 g of each) were collected from the fields where paraquat had been sprayed. The samples were weighed, macerated and blended in a mixer. Then, 1 ml of 5% EDTA was added to the blended sample and it was extracted using 25 ml of 9 M sulphuric acid. After extraction, the volume of the extract was made up to 150 ml with water and allowed to pass through a silica gel column at a flow rate of 7 ml min^{-1}. The column was washed with 2 × 50 ml of water 2–3 times to remove excess acidity remaining in the column. The absorbed paraquat was eluted by passing 50 ml of saturated ammonium chloride through the column. It was collected in a calibrated flask, made up to the mark and aliquots analysed as described above.

2.3.6. Procedure for the determination of paraquat in human sample

The presence of paraquat has been reported in human samples [18]. Hence, the method was applied for its determination in blood, urine and mother's milk. Samples were taken from people exposed to paraquat during field application. Prior to the determination of paraquat in human samples, 1 ml of 5% EDTA and 1 ml of 1% trichloroacetic acid were added, both to remove interference by various metal ions and for deproteinization respectively [19]. The samples were then centrifuged at 1850 *g* for 10 min. Aliquots were then analysed using the proposed method.

Table 2
Effect of foreign species (Concentration of paraquat 2 μg 10 ml^{-1})

Foreign species	Tolerance limit[a] (μg 10 ml^{-1})	Foreign species	Tolerance limit[a] (μg 10 ml^{-1})
Parathion	25 000	Pb^{2+}	15 000
DDT, BHC	20 000	Mg^{2+}, Zn^{2+}	6000
2, 4-D, 2, 4, 5-T	14 000	Sn^{2+}, PO_4^{3-}	5000
Quinolphos	10 000	Fe^{3+}[b], Fe^{2+}	2500
Carbofuran	3500	Al^{3+}[b]	1500
Kelthane	3000	Cu^{2+}	700

Concentration of paraquat used was 2.0 μg 10 ml^{-1}.
[a] Amount of foreign species that causes ±2% error in absorbance values.
[b] Amount tolerated with 1 ml of 5% EDTA solution.

Table 3
Determination of paraquat in various environmental and food samples

Sample	Paraquat originally found (μg)		Paraquat added (μg)	Total paraquat found (μg)	Difference	Recovery (%)
	Proposed method (*a*)	Reported method [6]	(*b*)	Proposed method (*c*)	(*c*−*a*)	[(*c*−*a*)/*b*] × 100
Water[a]						
A	2.60	2.48	1.0	3.58	0.98	98.00
B	2.35	2.19	2.0	4.34	1.99	99.50
Soil[b]						
A	2.93	2.78	1.0	3.92	0.99	99.00
B	2.12	1.95	2.0	4.09	1.97	98.50
Rice[b]						
A	3.23	3.12	1.0	4.21	0.98	98.00
B	2.58	2.45	2.0	4.55	1.97	98.50
Apple[b]						
A	2.97	2.89	1.0	3.96	0.99	99.00
B	2.85	2.79	2.0	4.80	1.95	97.50
Sugarcane[b]						
A	3.50	3.39	1.0	4.49	0.99	99 00
B	2.96	2.85	2.0	4.95	1.99	99.50
Potato[b]						
A	2.87	2.78	1.0	3.85	0.98	98.00
B	2.53	2.41	2.0	4.48	1.95	97.50

Mean of three replicate analyses.
[a] Size of sample, 100 ml.; [b] Size of sample, 25 g.

3. Results and discussion

3.1. Absorption spectra

The absorption spectra of the blue coloured compound showed maximum absorbance at 600 nm. The reagent blank had negligible absorbance at this wavelength.

3.2. Beer's law and sensitivity

Beer's law is obeyed over the concentration range of 0.5–5.0 μg of paraquat per 10 ml of the final solution (0.05–0.5 μg ml^{-1}) at 600 nm. Paraquat can be detected at levels as low as 0.03 μg ml^{-1} using the proposed method. The molar absorptivity and Sandell's sensitivity were found to be 2.9×10^5 l mol^{-1} cm^{-1} and 0.0006 μg cm^{-2} respectively.

3.3. Reproducibility

Reproducibility of the method was evaluated by replicate analysis of 2.0 μg of paraquat in 10 ml final solution over a period of 7 days (Table 1). The S.D. and relative S.D. of absorbance values were found to be ± 0.0045 and 1.39% respectively.

3.4. Conditions for colour development

Constant and maximum absorbance values were obtained when 1 ml of 1% sodium borohydride solution was used for reduction. The absorbance value was found to decrease when a lesser amount of sodium borohydride was used. The most suitable temperature for full colour development was within the range $\sim$35–40°C. Once the colour had developed, it was found to be

Table 4
Determination of paraquat in human samples

Sample[a]		Paraquat found[b] (μg 10 ml^{-1})	
		Proposed method	Reported method [6]
Blood/serum	A	1.15	1.09
	B	2.08	1.99
	C	1.95	1.82
	D	—	—
	E	1.85	1.71
Urine	A	1.98	1.75
	B	1.52	1.43
	C	2.05	1.97
	D	—	—
	E	—	—
Mother's milk	A	1.25	1.15
	B	1.48	1.40
	C	2.10	2.01
	D	1.99	1.81
	E	1.05	1.99

Samples D and E were taken from a non-exposed person.
[a] Size of sample, 2 ml.
[b] Mean of three replicate analyses.

stable for 12 h. Constant absorbance values were obtained within a pH range of 10–11 and no buffer was required to stabilize the colour. Below and above this pH range, the absorbance value decreased.

3.5. Effect of foreign species

The validity of the method was assessed by investigating the effect of other pesticides and ions in the analysis of paraquat. The tolerance limit values of different foreign species in a solution containing 2 μg 10 ml^{-1} of paraquat are given in Table 2.

Diquat (1,1′-ethylene-2,2′bipyridillium ion), which is structurally related to paraquat, will interfere with the determination of paraquat. However, diquat if present, can be removed by treatment with 0.2 N sodium hydroxide, and there is no loss of paraquat as reported [13,14].

Interference of metal ions such as Fe^{3+} and Al^{3+}, which interfere due to precipitation of hydroxide, was prevented by the addition of 1 ml of 5% EDTA solution prior to the addition of the sodium hydroxide solution [17].

3.6. Application.

The method has been applied satisfactorily to the determination of paraquat in water, soil, grains, fruits, vegetables, blood, urine and mother's milk. The results obtained were in good agreement with the reported method [6] (Tables 3 and 4).

To check the validity of the method, different samples of water, soil, grains, fruits and vegetables were taken. To these samples known amount of paraquat was added and analysed by the proposed as well as reported method [6]. Recovery of about 97–99% was observed (Table 3).

Table 5
Comparison with other spectrophotometric methods

Methods/reference	λ_{max} (nm)	Beer's law range/detection limit (μg ml^{-1})	Remarks
1. Reduction with sodium dithionite [16]	600	4–12	Reagent used is very unstable. Dye stability very poor (5–10 min)
2. Complex with tetra-iodomercurate [13]	400–420	3	Colour development takes 15 min; reagent toxic and expensive
3. Reduction with ascorbic acid [17]	600	1.2–9.6	Less sensitive than the proposed method
4. Reduction with ascorbic acid and potassium iodate [6]	600	0.1–100	Instrumental method using FIA technique
5. Reduction with sodium borohydride (present method)	600	0.05–0.5	Method is simple, selective and sensitive; colour stability is 12 h

3.7. Comparison with other reagents.

Spectrophotometric determination of paraquat with sodium borohydride is reported here as one of the most sensitive methods for the determination of paraquat. This method provides a good alternative to the reported costly, instrumental methods. The advantage of the proposed method is mainly the easy availability of sodium borohydride and greater stability of the blue radical ion. The method has been compared with other published methods and found to be superior to them (Table 5).

Acknowledgements

The authors are thankful to the Head, School of Studies in Chemistry, Pt. Ravishankar Shukla University for providing laboratory facilities. One of them JVD is thankful to C.S.I.R. New Delhi for providing a research grant.

References

[1] H. Martin, Pesticide Manual, Basic Information on the Chemicals used as Active Components of Pesticides, British Crop Protection Council, UK, 1968, pp. 325.
[2] G. Zweig, Pesticides, Plant Growth Regulators and Food Additives, vol. 5, Academic Press, New York, 1967, p. 473.
[3] D. Nigel, This Poisoned Earth, The Truth About Pesticides, Judy Piatkus, London, 1987, p. 5.
[4] V.A. Simon, A. Taylor, J. Chromatogr. 479 (1989) 158.
[5] M. Agudo, A. Rios, M. Valcarcel, Anal. Chim. Acta 28 (1993) 103.
[6] A. Jain, K.K. Verma, A. Townshend, Anal. Chim. Acta. 284 (1993) 275.
[7] N.B. Smith, S. Mathialagan, K.E. Brooks, J. Anal. Toxicol. 17 (1993) 143.
[8] M.R. Bowles, D.W. Eyles, E.C.G.M. Hampson, S.M. Pond, Fundam. Appl. Toxicol. 19 (1992) 375.
[9] M.T. Corasaniti, G. Nistico, J. Chromatogr. 643 (1993) 419.
[10] B.L. Worobey, Pesticide Sci. 18 (1987) 245.
[11] T.L. Kuo, Forensic Sci. Int. 33 (1987) 177.
[12] Official Methods of Analysis, 15th ed., AOAC, Arlington, VA, Sec. 969.09, 1990.
[13] M. Ganesan, S. Natesan, V. Ranganathan, Analyst 104 (1979) 258.
[14] S.P. Yanez, L.M. Polodiez, Talanta 33 (1986) 745.
[15] S.H. Yuen, J.E. Bangness, D. Myles, Analyst 92 (1967) 375.
[16] A. Calderbank, S.H. Yuen, Analyst 90 (1965) 99.
[17] P. Shivhare, V.K. Gupta, Analyst 116 (1991) 391.
[18] T. Malsuoka, J. Okuda, Eisei Kagaku (Japan) 33 (1987) 106.
[19] M. Rai, K.N. Ramachandran, V.K. Gupta, Analyst 1994 (1883) 119.

ELSEVIER

Talanta 45 (1997) 349–355

Talanta

Separation and simultaneous determination of cobalt, nickel and copper with 2-(4-methyl-2-quinolylazo)-5-diethylaminophenol by reversed-phase high-performance liquid chromatography

H. Niwa, T. Yasui, T. Ishizuki, A. Yuchi, H. Yamada, H. Wada *

Laboratory of Analytical Chemistry, Department of Applied Chemistry, Nagoya Institute of Technology, Showa, Nagoya 466, Japan

Received 21 January 1997; received in revised form 21 April 1997; accepted 28 April 1997

Abstract

Performance of six quinolylazo compounds was studied as a pre-column derivatizing reagent for the separation of metal ions in the reversed-phase high-performance liquid chromatography. 2-(4-Methyl-2-quinolylazo)-5-diethylaminophenol (QADP) was suited for the determination of Co, Ni and Cu in the presence of a large amount of Fe. The detection limits under the optimized conditions [stationary phase: L-column ODS; mobile phase: acetone-water (62:38, v/v) containing 0.01 M NH_4SCN and 0.01 M 2-morpholinoethanesulfonic acid-NaOH (pH 6); injection volume: 10 μl] were 0.24 ng for Co, 0.22 for Ni and 0.53 for Cu. This method was successfully applied to the determination of these metal ions in a standard steel sample. © 1997 Elsevier Science B.V.

Keywords: Quinolylazo compounds; Reversed-phase high-performance liquid chromotography; Metal ions

1. Introduction

Reversed-phase high-performance liquid chromatography (RP-HPLC) is one of the separation techniques utilized most frequently. Although it was originally developed for the separation of nonpolar substances, combined use of chemical reactions has expanded its application to the separation of polar or even ionic substances. Metal ions are generally separated as their complexes with some organic chelating reagent [1,2]. In the pre-column derivatization method, no addition of complexing reagents in the mobile phase affords the advantages both in selectivity and sensitivity. Some labile metal complexes may dissociate in the column after separation from an excess ligand [kinetic differentiation mode(KD)-HPLC] [3–5]. If matrix ions form labile complexes, minor components can be determined without any pretreatment. Moreover, lower detection limits are obtained because the baseline in spectrophotometric monitoring is more stable in the absence of free ligands in the mobile phase.

* Corresponding author. Tel.: +81 52 7355211; fax: +81 52 7355247.

PII S0039-9140(97)00135-5

The organic chelating reagents having absorption in a visible range can be favorable pre-column derivatizing reagents, because organic modifiers or buffers have absorption only in the ultraviolet range and do not interfere with the monitoring in the visible range. Thus, heterocyclic azo compounds, reacting with various metal ions and forming stable and intensely colored complexes [6], are promising. They act as a monoanionic tridentate ligand and form neutral or cationic complexes depending upon the electric charges and coordination numbers of metal ions. In a previous work [7], we have studied the HPLC separation of 1-(2-pyridylazo)-2-naphthol (β-PAN) complexes of Fe(II), Co(III), Ni(II) and Cu(II).

In an attempt to enhance the sensitivity of spectrophotometry using heterocyclic azo compounds, several quinolylazo compounds have been synthesized [8–11]. It was actually demonstrated that quinolylazo compounds had larger molar absorptivities than the corresponding pyridylazo compounds. The compound having a diethylamino group at a position para to the azo group, 2-(4-methyl-2-quinolylazo)-5-diethylaminophenol (QADP), especially showed the highest sensitivity and was used for the batchwise spectrophotometric determination of Cd [11]. These reagents, however, have not been used as a pre-column derivatizing reagent.

In this work, we have examined a series of quinolylazo compounds as a pre-column derivatizing reagent to exploit a new chromatographic system having a different selectivity from the conventional ones. Three of the six compounds studied [2-(2-quinolylazo)-1-naphthol (α-QAN), 1-(2-quinolylazo)-2-naphthol (β-QAN) and QADP] had previously been reported as spectrophotometric reagents for metal ions, while the other three [4-methyl-2-(2-quinolylazo) phenol (QAC), 4-methoxy-2-(2-quinolylazo) phenol (QAP-4-OMe) and 2-(4-methyl-2-quinolylazo)-4-methoxyphenol (4′-Me-QAP-4-OMe)] were newly synthesized for this purpose. On the basis of the comparison of the chromatographic behaviors, QADP was applied to the determination of Co, Ni and Cu in a standard steel sample.

2. Experimental

2.1. Apparatus

The liquid chromatograph consisted of a Model CCPD dual pump (resin type, Tosoh, Tokyo, Japan), a Model SVM-6U7 ceramic sample-injection valve with 10 μl sample loop (Sanuki, Tokyo, Japan), a Model MD-915 UV/VIS multiwavelength detector (200–900 nm, Jasco, Tokyo, Japan) and a Model DP-L915 data processing system (Jasco). Two octadecyl-bonded silica gel stationary phases were employed for separation, a Model Kaseisorb LC ODS-300-5 (particle size 5 μm, 4.6 mm i.d. × 250 mm, stainless steel column, Tokyo Kasei, Tokyo, Japan) was used for the study of chromatographic behaviors, and L-column ODS (particle size 5 μm, 4.6 mm i.d. × 250 mm, polyether ether ketone (PEEK) column, Chemical Inspection and Testing Institute, Tokyo, Japan) for sample analysis. The temperature of the column was controlled by a Model 860-CO column oven (Jasco). Teflon® tubing (1.0 mm i.d., GL Sciences, Tokyo, Japan) was used for the connection between the solvent reservoir and the pump, while PEEK tubing (0.25 mm i.d., GL Sciences) for the others. Contamination by metal ions was minimized by utilizing nonmetallic materials for all the parts which may be in contact with the mobile phase. The absorption spectra of the organic phase in solvent extraction were recorded by a Model UV-250 double monochrometer spectrophotometer (Shimadzu, Tokyo, Japan).

2.2. Reagents and materials

α-QAN was prepared by condensation of 2-quinolylhydrazine and napthoquinone [8]. Other compounds were synthesized by the coupling reaction of phenol or naphthol derivatives with 2-quinoline- or 2-lepidinediazonium salt [6,11]. Each crude compound was purified by recrystallization from ethanol. The extraction with chloroform and the flash chromatographic separation with silica-gel or aminopropyl-bonded silica-gel were also carried out for the phenolic derivatives. These reagents were dissolved in ethanol or ace-

tone to give stock solutions. Standard stock solutions (0.01 M, pH 2) of Fe(III), Co(II), Ni(II) and Cu(II) were prepared from the analytical-reagent grade sulfates or nitrates. All other reagents including organic solvents and buffers were of the analytical-reagent grade and used without further purification. Water was purified with a Model Toraypure LV-10 ultra pure water manufacturing device (Toray, Tokyo, Japan).

2.3. Chromatographic procedure

A 1 ml portion of an aqueous solution containing four metal ions (10^{-4} M each) was mixed with 4 ml of a reagent solution (2.5×10^{-4} M). If necessary, the mixture was heated at 80°C for 5 min. An aliquot (10 μl) of the resulting solution was placed on the column via an injection valve. The flow rate of a mobile phase was adjusted to 0.8 ml min^{-1} and the column temperature to 40°C. The absorbance at 400–800 nm was measured. The capacity factors (k') were calculated using the retention time of sodium nitrite as a measure of a void volume (3.34 min for Kaseisorb LC ODS-300-5 and 2.83 min for L-column ODS).

2.4. Recommended procedure for analysis of steel sample

Take a steel sample (0.1–0.2 g) in a beaker, add 20 ml of aqua regia, heat the beaker until the contents become syrupy, then add 10 ml of 5 M hydrochloric acid, and filter off insoluble material using a hardened filter paper (the size of precipitates to be retained: 1 μm). Extract the filtrate three times with methylisobutylketone, and adjust the total volume to 100 ml. Take 1 ml of this solution, add 6 ml of 5×10^{-4} M QADP solution, 1 ml of 30% sodium acetate solution and 1 ml of 0.1 M potassium cyanate. Adjust the total volume to 10 ml and subject it to the chromatographic separation [stationary phase: L-column ODS; mobile phase: acetone-water (62:38, v/v) containing 0.01 M NH_4SCN and 0.01 M 2-morpholinoethanesulfonic acid-NaOH (pH 6); injection volume: 10 μl] and determination using the calibration curves.

3. Results and discussion

3.1. Comparison of derivatizing reagents

Retention of four metal complexes was studied using six quinolylazo compounds as a pre-column derivatizing reagent, a Kaseisorb LC ODS-300-5 column as a stationary phase, and aqueous acetonitrile containing 0.01 M NH_4SCN as a mobile phase. These reagents (uncharged form: HL) form the following complexes with metal ions: $[ML_2]$ for Fe and Ni, $[ML_2]^+$ for Co, and $[ML]^+$ and $[ML_2]$ for Cu; comparable amounts of Co(II) and Fe(III) yielded Co(III) and Fe(II) complexes, respectively. Ammonium thiocyanate was added to control the retention of cationic complexes such as $[CoL_2]^+$ and $[CuL]^+$. The stationary phase showing relatively small retention was adopted to compare the chromatographic behaviors of six reagents. Because of the same reason, acetonitrile was selected as an organic modifier and its content was adjusted so that the Fe(II) complex showing the largest retention was eluted in the 14–18 min region ($k' \simeq 4$) for each ligand; the CH_3CN:H_2O value of 50:50 for QAP-4-OMe, 55:45 for QAC and 4′-Me-QAP-4-OMe, 60:40 for QADP, and 70:30 for α-QAN and β-QAN. The retention profile of complexes is shown in Fig. 1. Copper was not detected with QAC and Fe not with QADP; in the latter case, a small peak was obtained in the absence of NH_4SCN (the retention is shown in a bracket). The absence of peaks for some metal ions will be discussed in the latter sections.

The elusion in QAC, QAP-4-OMe, α-QAN and β-QAN systems proceeded in the following sequence: Cu < Co < HL < Ni < Fe. The k' values for two neutral complexes, $[FeL_2]$ and $[NiL_2]$, in these and 4′-Me-QAP-4-OMe systems resembled to each other. In contrast, the k' value for $[NiL_2]$ in a QADP system was specifically small and thus three metal ions (Co, Ni, Cu) could be separated within a shorter time period. Moreover, iron complexes mainly dissociated in the column and, if survived, were eluted without any overlapping with other complexes. Taking advantage of this specificity, QADP was adopted as a candidate of a derivatizing reagent for the determination of

minor components in steel samples and the experimental conditions were optimized below.

3.2. Effects of column and organic modifier

Fig. 2 shows the effects of a column and an organic modifier on the retention of QADP complexes. The organic contents were similarly adjusted to have all the species eluted within 12 min. Combination of Kaseisorb ODS-300-5 and aqueous acetonitrile afforded good separation in the order of Cu < HL < Ni < Co. Replacement of Kaseisorb ODS-300-5 with L-column ODS and that of aqueous acetonitrile with aqueous acetone selectively reduced the retention of $[CoL_2]^+$ and resulted in rather poor separation between $[CoL_2]^+$ and $[CuL]^+$ and that between $[CoL_2]^+$ and $[NiL_2]$, respectively. Combination of L-column ODS and aqueous acetone, on the other hand, showed another type of good separation in the order of Co < Cu < Ni < HL. The best mobile phase depends on the stationary phase. An L-column ODS, having a higher plate number, was used for subsequent studies in conjunction with aqueous acetone as a mobile phase. The acetone content was optimized to be 62% (v/v) as shown in Fig. 3.

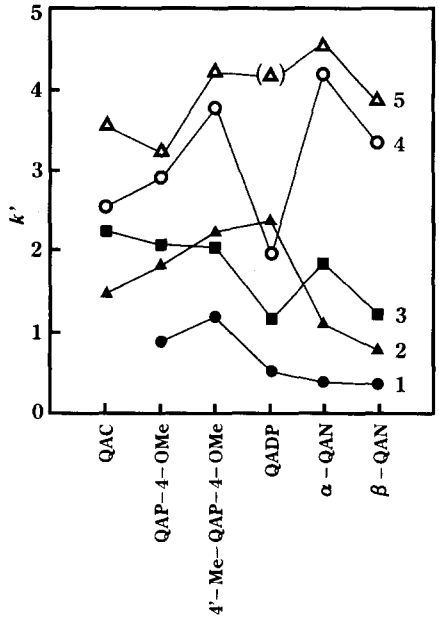

Fig. 1. Retention of complexes of quinolylazo compounds. Column: Kaseisorb ODS-300-5. Mobile phase: acetonitrile-water (QAP-4-OMe: (50:50, v/v); QAC and 4'-Me-QAP-4-OMe (55:45); QADP (60:40); QAN (70:30)) containing 0.01 M NH_4SCN. 1, Cu; 2, Co; 3, HL; 4, Ni, 5, Fe.

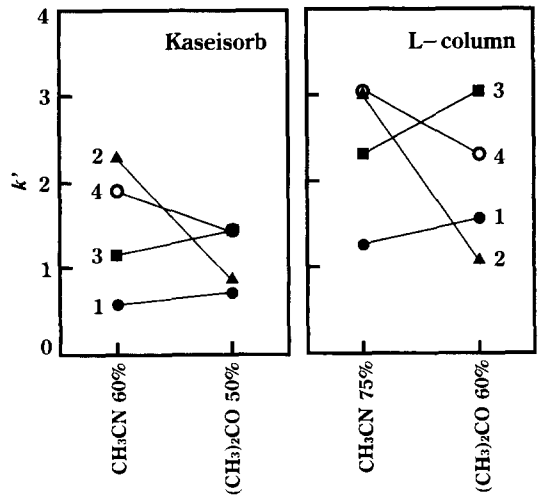

Fig. 2. Effects of column and organic modifier on capacity factors of QADP complexes. Each mobile phase contained 0.01 M NH_4SCN. 1, Cu; 2, Co; 3, HL; 4, Ni.

3.3. Effects of additives

Salts as an additive help the elution of cationic complexes and bring about the partition of ion-

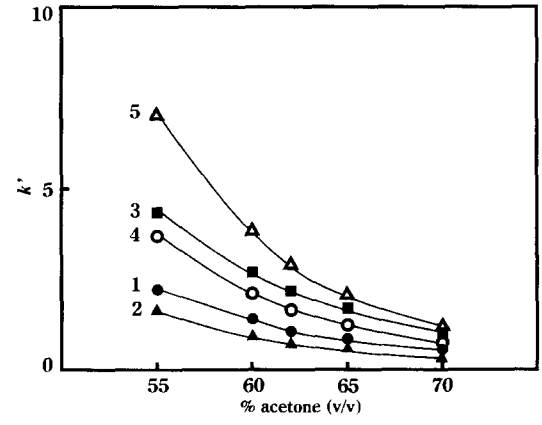

Fig. 3. Effect of acetone contents on capacity factors of QADP complexes. Column: L-column ODS. Each mobile phase contained 0.01 M NH_4SCN. 1, Cu; 2, Co; 3, HL; 4, Ni, 5, Fe.

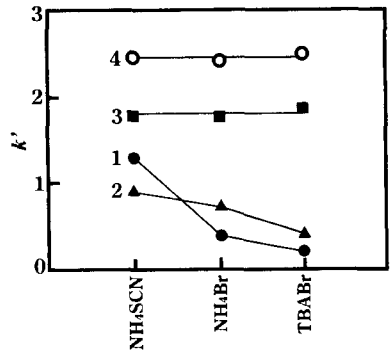

Fig. 4. Effect of additives on capacity factors of QADP complexes. Column: L-column ODS. Mobile phase: acetone-water (62:38, v/v) containing 0.01 M salt. 1, Cu; 2, Co; 3, HL; 4, Ni.

pairs. Anions in salts neutralize the complexes. Inorganic cations preferentially interact with residual silanol groups or lipophillic cations, such as tetraalkylammonium ions, are adsorbed on the stationary phase. All these lead to the reduced interaction of cationic complexes with silanol groups [7,12,13]. Fig. 4 shows the effects of three additives [ammonium thiocyanate (NH_4SCN), ammonium bromide (NH_4Br) and tetrabutylammonium bromide (TBABr); 0.01 M] on the separation of QADP complexes on an L-column ODS using acetone-water (62:38, v/v).

The k' value for $[CoL_2]^+$ using TBABr was actually reduced, compared with that using NH_4Br. When the performance of NH_4SCN and NH_4Br are compared, the k' values for $[CoL_2]^+$ were practically independent of anions, while those of Cu(II) complexes appreciably differed. This is ascribed to the difference in reactivity to form the mixed-ligand complex, [CuLX] (X:Br, SCN). The peak for Cu was not separated sufficiently from the solvent peak with NH_4Br or TBABr, which is not suitable for practical application. Thus, ammonium thiocyanate was the best additive for the QADP system.

The effects of the NH_4SCN concentration on the capacity factors (k') of $[CoL_2]^+$ and $[CuL]^+$ are shown in Fig. 5. The k' value for $[CoL_2]^+$ appreciably varied at $[NH_4SCN] < 0.01$ M. On the other hand, the peak area for Ni decreased with increasing $[NH_4SCN]$ because of the replacement reaction. The concentration was fixed at 0.01 M.

In the pre-column derivatization step using QADP, $[CuL_2]$ as well as $[CuL]^+$ is formed in the presence of an excess ligand. This species is not stable and dissociates to give $[CuL]^+$ after separation from the excess ligand in the column. If the substitution reaction successively proceeds along the column, the peak for Cu may broaden or even disappear (aforementioned for QAC complex). Thiocyanate ion accelerates the replacement reaction to form [CuL(SCN)], giving a sharp peak. Addition of potassium thiocyanate (KSCN) to sample solutions ensured the formation of this type of species but slightly interfered with the formation of Ni complex; potassium cyanate (KCNO) was adopted instead. This ion has a lower coordinating ability than SCN and does not interfere with the complexation of Ni(II) with QADP. The mixed ligand complex of [CuL(-CNO)] formed in the derivatization step, on the other hand, is immediately converted to [CuL(SCN)] in the column.

3.4. Effects of pH

The effect of the mobile phase pH on the chromatographic behavior was studied using 0.01

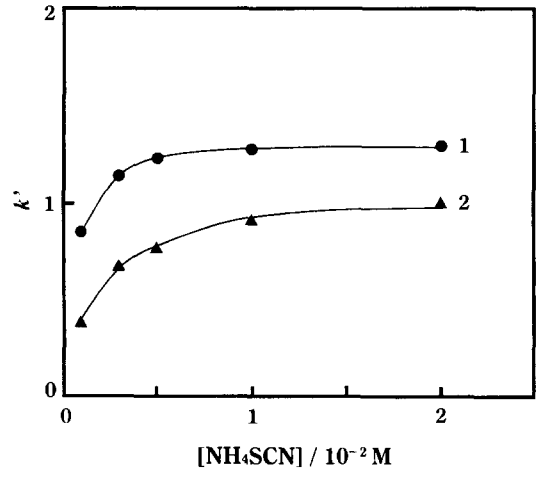

Fig. 5. Effect of NH_4SCN concentration on capacity factors of cationic complexes with QADP. Column: L-column ODS. Mobile phase: acetone-water (62:38, v/v). 1, Cu; 2, Co.

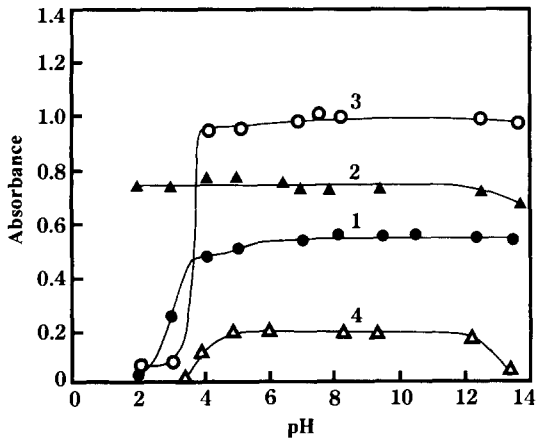

Fig. 6. Effect of pH on the extraction of QADP complexes. Aqueous phase (10 ml) concentration: metal = 1.0×10^{-5} M; QADP = 1.25×10^{-5} M (Cu) or 2.5×10^{-5} M (others); buffer = 0.01 M; KCl = 0.1 M; ascorbic acid = 2.0×10^{-4} M (Fe); $KIO_4 = 4.0 \times 10^{-3}$ M (Co). Organic phase (10 ml): chloroform. Metal, wavelength: (1) Cu, 568 nm; (2) Co, 580 nm; (3) Ni, 547 nm; (4) Fe, 771 nm.

M 2-morpholinoethanesulfonic acid(MES)-NaOH buffer, which is known not to interfere with complexation reactions. In the pH range 4–8, the peak for Fe became higher, while that for Cu showed tailing. To make a compromise between these two conflicting trends, the pH value was fixed at 6 for subsequent studies.

The effect of pH on the extraction of these complexes was also studied as a model for the partition of complexes. Portions of metal (1 ml), reagent, buffer and KCl solutions were placed in a 50 ml centrifuge tube with a screw-cap, diluted to 10 ml, and then extracted with a 10 ml portion of chloroform for 20 min. After phase separation by centrifugation, the absorption spectra of the organic phase were recorded.

The absorbance of the organic phase at the absorption maximum for each metal complex was plotted against the pH value of the aqueous phase (Fig. 6). Nickel and especially Co complexes were stable over a wide pH range. On the other hand, Fe was completely extracted only at pH > 5. This agreed with the chromatographic finding that the peak height for Fe was not reproducible without a buffer; the complex was dissociated after separation from an excess reagent. Cu was extracted as $[CuL]^+$ at pH < 5, while the neutral complex of $[CuL_2]$ also contributed at pH > 5 [11]. In the column, $[CuL_2]$ immediately dissociated to give a sharp peak of $[CuL]^+$ at lower pH, while successively dissociated in the column to cause tailing at higher pH. For the purpose mentioned above, pH was fixed at 6.

3.5. Calibration graphs and analysis of standard steel sample

A series of standard metal solutions ranging 2×10^{-6}–1×10^{-5} M were separated under the optimized conditions [stationary phase: L-column ODS; mobile phase: acetone-water (62:38, v/v) containing 0.01 M NH_4SCN and 0.01 M MES-NaOH (pH 6)] and the maximum absorbance between 400–800 nm was monitored for the eluate using a multiwavelength detector. The calibration graphs for three metal ions were linear over the concentration range examined and the detection limits defined by S/N = 3 were 0.24 ng for Co, 0.22 for Ni and 0.53 for Cu. Comparable performance may be obtained even with the measurement at a fixed wavelength of 552 nm.

This method was applied to the determination of minor components in a standard steel sample [NBS (present NIST) SRM 364] after some pretreatment described in see Section 2. A typical chromatogram is shown Fig. 7. The peak at retention time of 4.7 min was assigned as a vanadium (V) complex of VO_2L; no peaks were observed for the major component of Fe. The analytical results agreed with the recommended values; metal, %

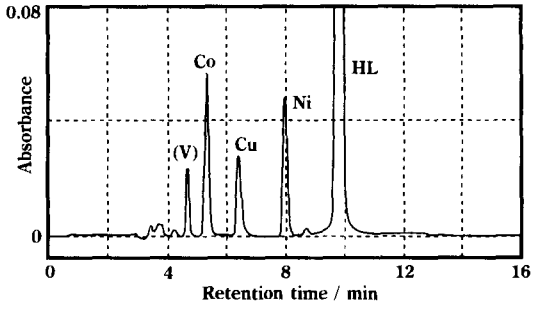

Fig. 7. Typical chromatogram for standard steel sample with QADP. Column: L-column ODS. Mobile phase: acetone/water (62:38, v/v) containing 0.01 M NH_4SCN and 0.01 M MES-NaOH (pH 6). Sample: NBS SRM 364.

found(% certified): Co, 0.145(0.15); Ni, 0.138 (0.144); Cu, 0.231(0.249). The certified values of other elements are Mn, (0.255); V, (0.105); Cr, (0.063); Mo, (0.49); W, (0.10); Ti, (0.24); Zr, (0.068); Nb, (0.157); Ta, (0.11).

Acknowledgements

This work was supported by Grants-in-Aid for Scientific Research (Nos. 06303005 and 08455388) from the Ministry of Education, Science, Sports and Culture of Japan.

References

[1] G. Nickless, J. Chromatogr. 313 (1985) 129.
[2] A.R. Timerbaev, O.M. Petrukhin, Yu.A. Zolotov, Fresenius' Z. Anal. Chem. 327 (1987) 87.
[3] H. Hoshino, T. Yotsuyanagi, Chem. Lett., (1984) 1445.
[4] N. Uehara, M. Kanbayashi, H. Hoshino, T. Yotsuyanagi, Talanta 36 (1989) 1031.
[5] H. Hoshino, K. Nakano, T. Yotsuyanagi, Analyst 115 (1990) 133.
[6] S. Shibata, in: H.A. Flaschka, A.J. Barnard Jr. (Eds.), Chelates in Analytical Chemistry, vol. IV, Marcel Dekker, New York, 1972, pp. 1–232.
[7] T. Yasui, A. Yuchi, H. Yamada, H. Wada, J. Chromatogr. 659 (1994) 359.
[8] A. Kawase, Anal. Chim. Acta 58 (1972) 311.
[9] K. Rakhmatullaev, M.A. Rakhmatullaeva, Sh.T. Talipov, A. Ataev, Zh. Anal. Khim. 27 (1972) 1793.
[10] S.I. Gusev, E.M. Nikolaeva, E.A. Pirozhkova, Zh. Anal. Khim. 30 (1975) 376.
[11] T. Ishizuki, M. Tsuzuki, A. Yuchi, T. Ozawa, H. Wada, G. Nakagawa, Anal. Chim. Acta 272 (1993) 161.
[12] J. Miura, Fresenius' J. Anal. Chem. 344 (1992) 247.
[13] H. Inoue, K. Ito, Microchem. J. 49 (1994) 249.

ELSEVIER

Talanta 45 (1997) 357–369

Talanta

In situ investigation of the ionisation of silica in aqueous ammonia by using a high frequency dielectric method

C. Despas, A. Walcarius, J. Bessière *

Laboratoire de Chimie Physique pour l'Environnement, Unité Mixte de Recherche UMR 9992, CNRS-Université H. Poincaré Nancy I, 405, rue de Vandoeuvre, F-54600 Villers-les-Nancy, France

Received 12 November 1996; received in revised form 8 April 1997; accepted 29 April 1997

Abstract

The reaction of silica gel and Stöber beads of silica with ammonia was studied in aqueous medium using a high frequency dielectric method. Measurements of the complex impedance of silica pulps in both static and dynamic modes were found to be a new rapid, sensitive and non-destructive way for the in situ characterisation of the surface silica ionisation process in aqueous ammonia. The influence of various parameters (field frequency, ionic strength, ammonia concentration) was discussed. The apparent equilibrium constant for the following reaction ($\equiv SiOH) + NH_3 \Leftrightarrow (\equiv SiO^- NH_4^+$) was found to be strongly affected by the degree of dissociation of both silica samples, so that the complete neutralisation was never observed. The porosity of the Stöber silica towards the NH_3 species was demonstrated experimentally through the formation of ($\equiv SiO^- NH_4^+$) entities in the interior of the silica beads. The reversibility of the neutralisation reaction was applied to successive on-column analysis for which the hydrolysis of ammoniated silica was found to be catalysed by the presence of acids. © 1997 Elsevier Science B.V.

Keywords: Silica gel; Stöber silica; Aqueous ammonia; Dielectric sensors; Ionisation; Flow-through cell

1. Introduction

In the fields of environmental chemistry relative to aquatic systems, many efforts have been devoted to the study of mass transfer reactions occurring at the solid–liquid interface because they are responsible for many changes in the water composition [1]. If the surface chemistry of many solids, and especially silica [2], has been thoroughly investigated by using various techniques, most of them were applied under destructive conditions, often in absence of water so that the solid–liquid interface did not exist. It is important, however, to promote the development of non destructive methods for characterising, under in situ conditions, the surface reactivity of solid materials being in direct contact with water in a chemical neighbouring in constant evolution. In this context, the definition of model surfaces (and interfaces) will be of relevant importance, especially regarding the development of new materials for water treatment, separation processes, or soil remediation.

* Corresponding author. Fax: +33 0383 275444; e-mail: Bessiere@ lcpe.cnrs-nancy.Fr

PII S0039-9140(97)00138-0

Silica, one of the major mineral components of sediments, has been largely studied with respect to synthesis, characterisation, solubility, surface modification, polymerisation, adsorption properties [2,3] and successfully applied in catalysis [4] and as stationary phase for chromatographic experiments [5]. However, despite the fact that numerous species of environmental significance (e.g. metal ions) are known to be adsorbed onto silica surfaces, only little information is available dealing with the role of the silica-containing sands, sandstones or diatomaceous earth in the uptake (or release) of pollutants from dilute solutions, the transport of toxic solutes between soils and aquatic media and the influence of surface silica chemistry on these processes [1].

As discussed by Iler [2], the hydroxylated silica surfaces have a point of zero charge of about pH 2 and the concentration of negative charges onto the surface increases slowly from this value to pH 6–7 and then grows rapidly as a consequence of silica ionisation (i.e. transformation of silanol into silanolate groups). Similarly, the adsorption of metal ions on silica has been found to be more efficient with rising pH by neutralising the negative charges on silica [6], demonstrating the importance of the silica ionisation step on the adsorption processes.

Surprisingly, studies dealing with silica ionisation in ammoniacal medium are not widespread, most probably because of the relatively low stability of silica at high pH values [2] and the late occurrence of a detailed description of the overall mechanism responsible for copper adsorption on silica in ammoniacal medium [7,8], more than 50 years after the first report [9] on the fixation of metal ions (nickel and copper) on silica gels in aqueous ammonia. When investigating the equilibria involved in the preparation of copper(II)-modified silica gels in aqueous ammonia, Guyon et al. [7,8] have evaluated the apparent equilibrium constant for the reaction of ammonia with the surface silanol groups of a silica gel. They reported a value of $10^{-0.2}$ obtained by using a computer program able to calculate the reaction constant from experimentally measured equilibrium ammonia concentrations [8]. In a more recent paper, however, Sonnefeld [10] provided both experimental data and theoretical calculations demonstrating the variation of the apparent dissociation constant of acid silanol groups of silica, with the degree of dissociation. When increasing the degree of dissociation of silica (that means increasing the $SiO^-/SiOH$ ratio), the apparent dissociation constant of the remaining silanol groups was found to decrease dramatically, explaining why the direct titration of these silanol groups by a strong base (such as NaOH) did not give a well-defined pH jump that one would expect on the basis of the pK_a value of surface silanol groups at a zero degree of dissociation (6.8 ± 0.2, as determined by Schindler and Kamber [11] at 25°C in 0.1 M $NaClO_4$). Considering these results, the apparent equilibrium constant for the reaction between ammonia and the silanol groups of silica should be affected by the degree of dissociation of these weakly acid groups. To date, all the apparent constants relative to the neutralisation of silica by ammonia were determined from solution analysis, no direct in situ characterisation of the solid substrate (silica) has been reported until now.

The dielectric method at high frequency have been successfully applied for following the adsorption of various inorganic and organic species onto both conductive and non-conductive solid substrates [12–20]. In comparison with the conventional approaches of the adsorption phenomena at the solid–liquid interface (most often studied under destructive conditions), the major advantage of the dielectric technique is its ability to characterise, under in situ conditions, very rapidly and with a great efficiency, a wide range of different adsorption processes, being able to distinguish between a chemical and a physical adsorption. Impedance measurements were then applied to the study of activation and deactivation of blende [14], sphalerite [12,15] or malachite [16] by selected solution-phase ions, to the study of adsorption of organic materials onto galena [18,20] or malachite [19] for mineral flotation purposes. More recently, the high frequency dielectric method was employed for controlling the behaviour of an ion-exchange resin, by means of the complex–impedance variations recorded during the ion exchange reactions [21] following the pioneering works of Hanaï [22,23].

Fundamental principles of the method have been described in details previously [13,14]. Briefly, an alternative current is applied to a capacitive cell containing the decanted pulp and the corresponding complex impedance, Z^*, is measured as a function of the field frequency. According to the Maxwell–Wagner model, Z^* can be converted into a complex permittivity, ϵ^*, allowing the calculation of both dielectric permittivity, ϵ', and dielectric losses, ϵ'' (Eq. (1)).

$$\epsilon^* = \epsilon' - j\epsilon'' \quad (1)$$

These two parameters are indicative of the dielectric changes encountered by the pulp, especially with respect to dipole variations (ϵ') and movement of free charges (ϵ''). The overall response of the pulp results from two different contributions, that of the pure solid and that of the liquid phase. In some simple cases (non porous spherical particles), it was possible to distinguish unambiguously between these contributions by calculating the ϵ' and ϵ'' values of the pure solid, according to the Wagner–Hanaï's equation [22,23].

The present paper aims to demonstrate that the high frequency impedance technique can be applied as a new tool for the in situ characterisation of silica surface ionisation processes in aqueous ammonia. Two kinds of silica will be investigated: a commercially available silica gel and monodispersed silica beads synthesised according a Stöber procedure [24]. The interest of the Stöber silica arises from the unusually low specific surface area (as calculated from BET measurements with N_2), for an amount of hydroxyl groups comparable to that of other silicas. Experiments will be carried out in both static (batch analysis) and dynamic (flow analysis) modes. The influence of frequency, ionic strength and ammonia concentration will be discussed.

2. Experimental

2.1. Materials and reagents

Experiments were carried out by using two different kinds of silica. The chromatographic grade silica gel (Kieselgel 60), obtained from Merck, was characterised by a specific surface area of about 425 ± 25 m^2 g^{-1} and a surface hydroxyl population of 5 OH nm^{-2} [2], corresponding to a concentration of 3.6 mmol OH g^{-1}. The other silica was prepared following the experimental procedure described by Stöber et al. [25] in such conditions that small beads of typically 0.7–0.8 μm in diameter were obtained, with a measured specific surface area of 5 m^2 g^{-1} (N_2) and a concentration of free silanol groups of about 5 mmol OH g^{-1}, as determined by thermogravimetry [24]. These materials will be distinguished in this paper by specifying 'silica gel' and 'Stöber silica', respectively. The ion exchange resin used for comparison purpose was a weakly acid cation exchange resin (Merck) having a maximum capacity of 10 meq g^{-1}.

All chemicals were of analytical reagent grade. Ammonia solutions were freshly prepared before each experiment and isolated from the atmosphere to avoid ammonia evaporation. Sodium nitrate, hydrochloric acid and standard 0.1 M sodium hydroxide (Titrinorm) were purchased from Prolabo and Methyl Red was obtained from Kuhlmann. All solutions were prepared with high purity water (18 MΩ cm^{-1}) from a Millipore Milli-Q water purification system.

2.2. Instrumentation

Batch dielectric experiments were carried out at room temperature and in a frequency ranging from 10^5 to 10^8 Hz, by using the model 4194 A impedance/gain-phase analyser connected to its measurement unit (Hewlett Packard). Typically, measurements were made from decanted pulps in a home-made axial capacitive cell (Fig. 1 A) previously standardised with mercury and pure water. Impedance analysis in flowing stream was performed with the model 4193 A Vector impedance meter (Hewlett Packard) associated with a cylindrical home-made calibrated cell (Fig. 1 B) which can be easily adapted to the chromatographic column (Fig. 1 C).

Raman spectra were obtained at room temperature with the microsonde Raman model T64000 spectrometer (Jobin-Yvon). Decanted silica samples were placed in the laser beam (Argon, 514

nm) with an observation geometry at 180° and the CCD detector was cooled with liquid nitrogen.

2.3. Procedures

In the batch mode, a given amount of silica (typically 1 g silica gel and 0.5 g Stöber silica) was suspended in a defined volume of freshly prepared ammonia solution at a selected concentration. The solution volume was chosen in order to ensure an excess of ammonia with respect to the number of hydroxyl groups introduced by the silica. The mixture was then introduced into the axial capacitive cell, isolated from the external atmosphere by a parafilm (to avoid ammonia evaporation) and allowed to react one hour under constant stirring. After this, the mixture was kept in quiescent conditions for about 15 min and complex impedance measurements were realised from the decanted mineral pulp. The dielectric permittivity and dielectric losses were calculated from these measurements, following the previously described procedure [13,14]. Reproducibility was checked by performing triplicate measurements. Equilibrium ammonia concentrations in solution were determined by acid–base titrations (HCl) and used to calculate the extent of silica ionisation.

For studies realised in the dynamic mode, a chromatographic column (11 mm internal diameter) was filled with 5 g silica, decanted from an aqueous suspension, so that the pulp height in the column was high enough to pass up and down the cylindrical dielectric cell. Before measurement, silica was first conditioned with 0.1 M HCl and then rinsed with water. Solutions were allowed to percolate through the column at an average flow rate of 1 ml min^{-1}, as monitored by a multi-staltic pump (Buchler). Liquid fractions flowing out of the column were collected by using the model Fracto-Mette 200 automatic fraction collector (Buchler) and then analysed by ICP–AES (Plasma 2000, Perkin Elmer) in order to determine the amount of dissolved silica, mainly produced during the flowing stream of alkaline solutions.

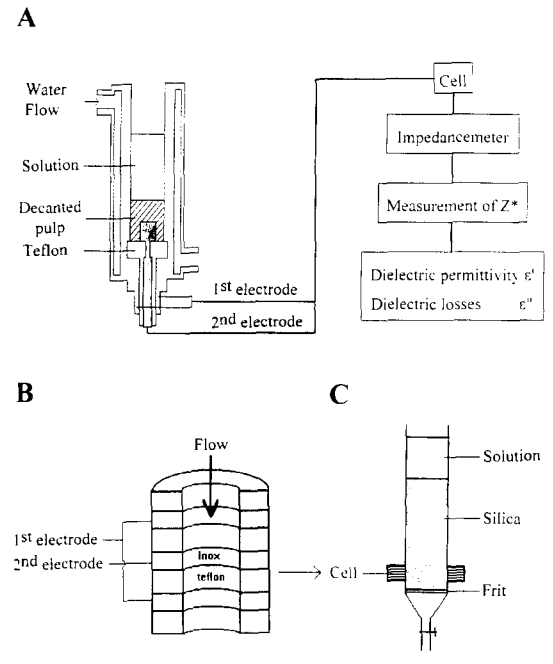

Fig. 1. Schematic representation of the experimental devices: **A** Capacitive axial cell and principle of dielectric measurements; **B** Transversal section of the cylindrical dielectric cell; **C** Chromatographic column with dielectric detector.

3. Results and discussion

3.1. Dielectric characterisation of raw materials

Before starting with the detailed study of the surface reactivity of silica towards NH_3 species, it is important to fully characterise the two different silicas considered in this work. It has been demonstrated previously that the field frequency and the solution ionic strength are significant parameters for the characterisation of mineral pulps [14–16,18–20].

Fig. 2 displays the evolution of the dielectric permittivity, ϵ' (Fig. 2 A), and dielectric losses, ϵ'' (Fig. 2 B), as a function of frequency, for the two kinds of silica studied here. Curves obtained with pure water have been added for comparison purpose. The low ϵ' values are characteristic of electronic insulators [15]. For both silica gel and Stöber silica, ϵ' decreases slowly when increasing frequency up to 20 MHz and remains quite constant in the frequency range 20–100 MHz; the

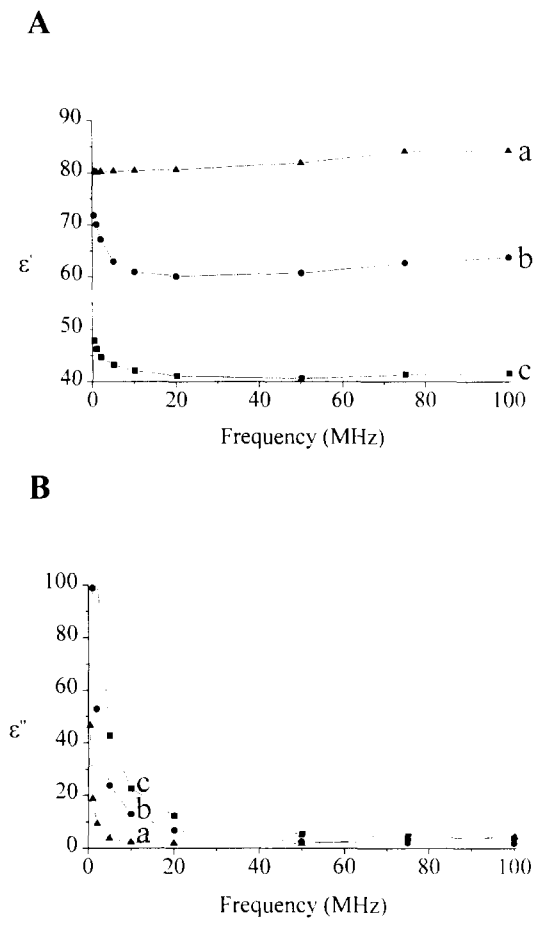

Fig. 2. Influence of the frequency on the dielectric permittivity ϵ' (**A**) and dielectric losses ϵ'' (**B**) for (**a**) distilled water, (**b**) 1.0 g silica gel in equilibrium with 10 ml water and (**c**) 0.5 g Stöber silica in equilibrium with 10 ml water.

permittivity values obtained with the silica gel being however larger than those measured from the Stöber silica, over the entire range of frequency. This allows to distinguish between these two forms of silica and differences in their dielectric properties are most probably due to their different intrinsic structure. Dielectric losses are very low, indicating the absence (or a very low level) of free charged species within the pulp. ϵ'' values are however a little higher than those of water, especially at low frequency. This phenomenon could be explained by the non zero charge of the silica surfaces at the experimental pH of the experiments of Fig. 1 (unbuffered aqueous solution): pH close to 6. At this pH, the surface of silica is negative (point of zero charge at pH of about 2 [2]) and the higher ϵ'' values observed with the silica pulp compared to water alone are due to non zero level of ionic conductivity of the pulp, according to Eq. (2).

$$(\equiv SiOH) \rightleftharpoons (\equiv SiO^-) + H^+ \quad (2)$$

This effect was much more pronounced with the Stöber silica than with silica gel.

The influence of ionic strength upon the dielectric response of silica is described by the results of Table 1. The progressive addition of the electrolyte $NaNO_3$ in the cell did not affect significantly the dielectric permittivity, except that of the Stöber silica at low frequency (1 MHz). As the conductivity of the liquid phase is thought to increase when increasing the ionic strength, it is thus not surprising that the dielectric losses were found to be as higher as stronger was the $NaNO_3$ concentration in the medium. It should be emphasised, however, that this evolution is slightly more dramatic with the Stöber silica than that observed for the silica gel. Indeed, by comparing the values of Table 1, it appears that at each investigated frequency, the ϵ'' values measured in the presence of 0.1 M $NaNO_3$ were 100 times larger than those recorded in pure water for the silica gel and 250 times larger for the Stöber silica. These results indicate different mobilities of the electrolyte ions in the two pulps.

3.2. Silica surface ionisation by reaction with ammonia

3.2.1. Dielectric behaviour of silica in the presence of ammonia—batch analysis

Fig. 3 shows that the addition of ammonia to the silica gel results in a strong variation of the dielectric parameters at any of the investigated frequency. Both ϵ' and ϵ'' were found to increase significantly when replacing pure aqueous silica by the silica + ammonia mixture into the cell. At a frequency of 10 MHz, for example, the dielectric values ϵ' and ϵ'' were respectively 2 and more than 50 times as large in the presence of ammonia as those observed without ammonia. Considering that the dielectric permittivity of aqueous ammo-

Table 1
Dielectric results (dielectric permittivity ϵ' and dielectric losses ϵ'') of 1.0 g silica gel or 0.5 g Stöber silica in equilibrium with 10 ml solution, as a function of the field frequency and the $NaNO_3$ concentration

ϵ' (silica gel)					
Frequency (MHz)	$NaNO_3$ concentration (M)				
	'0'	2.4×10^{-3}	9.6×10^{-3}	5.0×10^{-2}	1.0×10^{-1}
1	70.1	63.4	64.0	67.0	84
5	62.9	60.1	60.2	56.8	60.6
10	60.9	59.1	58.5	55.6	57.5
50	60.7	58.5	58.4	54.5	57.7
ϵ'' (silica gel)					
Frequency (MHz)	$NaNO_3$ concentration (M)				
	'0'	2.4×10^{-3}	9.6×10^{-3}	5.0×10^{-2}	1.0×10^{-1}
1	99	870	1690	5260	10300
5	23.8	176	340	1060	2070
10	12.8	88.9	170	531	1040
50	2.56	18.4	36.1	113	213
ϵ' (Stoëber silica)					
Frequency (MHz)	$NaNO_3$ concentration (M)				
	'0'	5.4×10^{-3}	1.2×10^{-2}	4.9×10^{-2}	1.0×10^{-1}
1	52.5	57.8	64.3	132	312
5	49.8	53.5	54	58	65.9
10	48.7	51.8	51.9	52.3	51.3
50	47.6	49.1	49.3	52.5	56.7
ϵ'' (Stoëber silica)					
Frequency (MHz)	$NaNO_3$ concentration (M)				
	'0'	2.4×10^{-3}	9.6×10^{-3}	5.0×10^{-2}	1.0×10^{-1}
1	144	941	3860	18000	37100
5	30.7	193	788	3640	7390
10	16.4	99.3	399	1830	3690
50	4.45	22.4	84.8	376	735

nia ($\epsilon' = 75$, at 10 MHz) is close to that of pure water and the dielectric losses are relatively low ($\epsilon'' = 169$, at 10 MHz), such increase can be interpreted in terms of a higher conductibility due to the formation of silanolate groups resulting from the acid/base reaction between silanol groups and ammonia (Eq. (3)). This reaction can be evidenced in situ over the entire frequency range 0.4–100 MHz.

$$(\equiv SiOH) + NH_3 \rightleftharpoons (\equiv SiO^- NH_4^+) \quad (3)$$

The effect of silica surface ionisation is more marked by the evolution of ϵ'' values than that of ϵ' (Fig. 3). The strong increases in ϵ'' values are clearly due to the highest conductivity of the medium, indicating the presence of ionic species within the pulp.

Similar behaviour was observed during the alkaline neutralisation of polymeric carboxylate resins. When suspending resin beads into pure water and allowing them to form a decanted pulp, the measured dielectric values ($\epsilon' = 51.4$ and $\epsilon'' = 15.1$, at 10 MHz) corresponding to their molecular form were close to those obtained for silica. On the other hand, when performing the same operation in 5.0×10^{-2} M NH_3, significant increases were observed ($\epsilon' = 474$ and $\epsilon'' = 1060$, at 10 MHz), because of the formation of $RCOO^- NH_4^+$ species (Eq. (4)).

$$(RCOOH) + NH_3 \rightleftharpoons (RCOO^- NH_4^+) \quad (4)$$

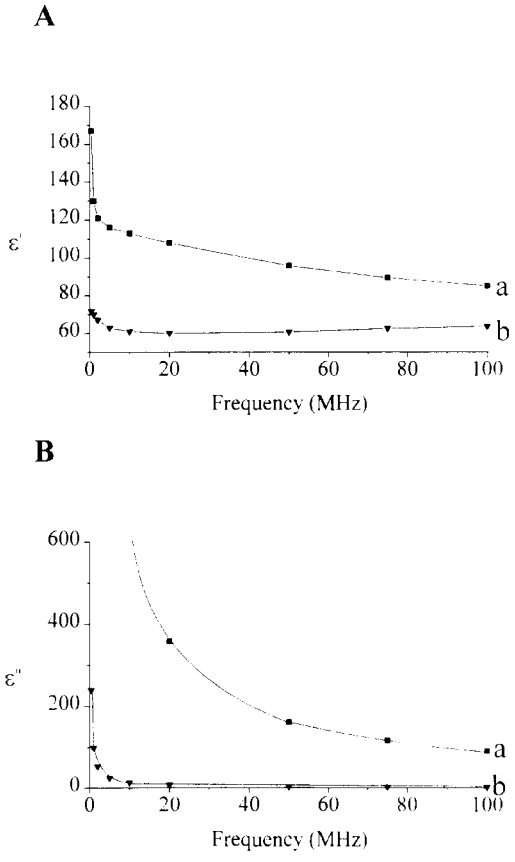

Fig. 3. Influence of the field frequency on the dielectric permittivity ϵ' (**A**) and the dielectric losses ϵ'' (**B**) of 1.0 g silica gel in equilibrium with (**a**) 10 ml 0.46 M NH_3 and (**b**) 10 ml pure water.

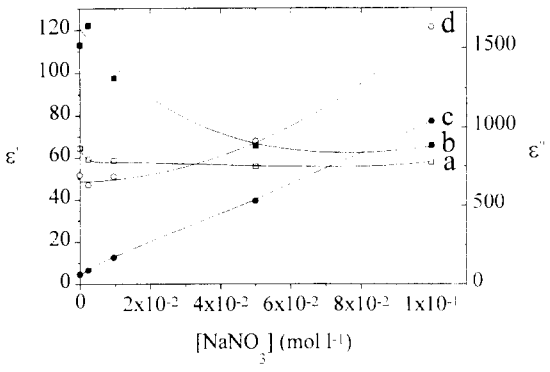

Fig. 4. Influence of the $NaNO_3$ concentration on the dielectric permittivity ϵ' (curves **a** and **b**) and the dielectric losses ϵ'' (curves **c** and **d**) of 1.0 g silica gel in equilibrium with 10 ml of the $NaNO_3$ solution containing 0.46 M NH_3 (curves **b** and **d**) or not (curves **a** and **c**). Field frequency: 10 MHz.

In this case, the nature of the carboxylate-to-ammonium bond is well-known as being of the ionic type [26]. Comparable high ϵ' and ϵ'' values have been also observed with sulfonated resins under their sodium or potassium form, which are ionised structures [21]. By analogy, one can conclude that the chemical bond between ($\equiv SiO^-$) and NH_4^+ is rather ionic than covalent, explaining why the ($\equiv SiO^- NH_4^+$) group appeared as an excellent intermediate for the fixation of metal ions onto silica surfaces in ammoniacal media [27].

In order to assess the ability of the dielectric method to follow the silica ionisation process under in situ conditions, it is very important to study the effect of the ionic strength upon the difference in dielectric behaviour between the two forms of silica surfaces (silanol or silanolate). The results are depicted in Fig. 4 for the silica gel in $NaNO_3$ media, respectively before and after reaction with ammonia. As mentioned above, for pure silica gel, the ionic strength had no effect on ϵ' values and caused ϵ'' to increase linearly with the $NaNO_3$ concentration. With the ionised form of silica ($\equiv SiO^- NH_4^+$), however, the observed evolution was slightly different (Fig. 4). The progressive addition of $NaNO_3$ in the ionised silica pulp resulted in a decrease of its dielectric permittivity, enabling somewhat the distinction between the silanolate and silanol forms of silica, especially at

high ionic strength. Such a behaviour could be explained by the possible ion exchange reaction between ammonium and sodium cations at the silica|water interface. On the other hand, the distinction was still fully accomplished by means of the dielectric losses which appeared to evolve in a parallel direction as a function of the $NaNO_3$ concentration, by maintaining a constant difference between the response of unmodified silica and that of ionised silica.

The occurrence of silanolate groups was also ascertained by Raman spectrometry (spectra not shown). The stretching vibration of silanol groups (unmodified silica) was characterised by a band situated at about 980 cm^{-1} [28]. In the presence of ammonia, however, an additional band appeared at 1015 cm^{-1}, growing as the reaction (Eq. (3)) evolved. This band, more intense than that corresponding to the vibration of silanol groups, was attributed to the vibration of silanolate groups which progressively replaced the silanol being transformed by NH_3. This fully confirms the ionic nature of the $(\equiv SiO^-)-NH_4^+$ bond.

The reaction of ammonia with the Stöber silica was also examined and compared to that with silica gel (Table 2). The first observation is that the ionisation of the Stöber silica in ammoniacal medium can be followed by the proposed high frequency dielectric method. Similarly to what was observed with silica gel, the action of ammonia on the Stöber silica resulted in an increase of both ϵ' and ϵ'' values, compared to those recorded in pure water. This increase was however less than that obtained with silica gel and this phenomenon was as more evident as higher was the field frequency (Table 2): while at 0.4 MHz, the reaction with ammonia caused an increase of the dielectric permittivity of 78% for the Stöber silica and 133% for the silica gel, the same percentages calculated at 100 MHz were respectively 12% and 34%. The same evolution was observed with the dielectric losses. Such a behaviour is directly related to the different structures of the two silicas. As low specific surface area (N_2 adsorption) were reported for the Stöber silica, most probably because the solid is made of micropores and very small channels that water molecules can enter but not nitrogen [28], it appears that the ingress of ammonia within the pore system of the Stöber silica can be somewhat hindered in comparison with the same diffusion process into the silica gel structure (average pore size of about 2 nm). It seems reasonable to ascribe the lower dielectric parameters characteristic of the ionised Stöber silica to the limitation of charge mobility within this confined medium.

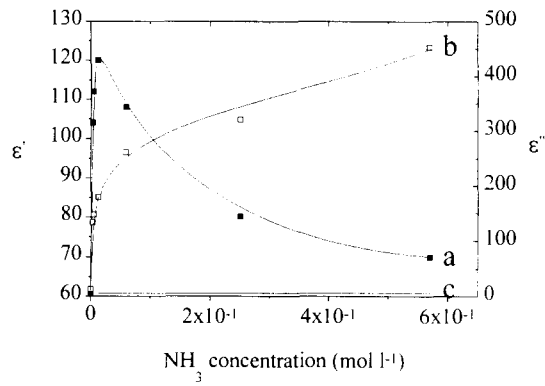

Fig. 5. Influence of the ammonia concentration on the equilibrium values of dielectric permittivity ϵ' (**a**) and the dielectric losses ϵ'' (**b**) of silica gel. The dielectric permittivity ϵ' of silica gel in pure water (**c**) was added for comparison purpose. Field frequency: 10 MHz.

Table 2
Comparison of the dielectric behaviour (dielectric permittivity ϵ' and dielectric losses ϵ'') of 0.5 g Stöber silica and 1.0 g silica gel in the absence or in the presence of 0.46 M NH_3, for three different field frequencies

Experimental conditions	Frequency (MHz)		
	1	10	50
Dielectric permittivity (ϵ')			
Stoëber silica, water	46.2	42.1	40.6
Stoëber silica, NH_3 0.46 M	70.1	51.5	46.9
Silica gel, water	70.1	60.9	60.7
Silica gel, NH_3 0.46 M	130	113	95.9
Dielectric losses (ϵ'')			
Stoëber silica, water	203	22.5	5.39
Stoëber silica, NH_3 0.46 M	3000	306	64.1
Silica gel, water	99	12.8	2.56
Silica gel, NH_3 0.46 M	6840	695	161

Table 3
Titrimetric determination of the amount of silanolate groups (≡SiO^-) formed during the reaction of 1.0 g silica gel or 0.5 g Stöber silica with aqueous ammonia for different initial concentration

Silicas type and mass	Initial NH_3 concentration (M)	Quantity of formed SiO^- (mmol g^{-1})	Deprotonation ratio (%)
Silica gel (1 g)	9.0×10^{-3}	0.5	14
	9.2×10^{-2}	1.4	37
	5.0×10^{-1}	1.8	50
	1.8	2.6	72
Stoëber silica (0.5 g)	10×10^{-2}	0.9	20
	5.6×10^{-2}	1.6	30

Deprotonation ratios, defined as the number of (≡SiO^-) formed divided by the theoretical number of hydroxyl groups (≡SiOH), are also presented.

3.2.2. Influence of the ammonia concentration

As shown in Fig. 5, the concentration of NH_3 in the external solution greatly influences the dielectric response of the silica pulps. All experiments were carried out with the same excess of ammonia with respect to the amount of silanol groups present into the cell (by adapting the volume of the NH_3 solution in conjunction with NH_3 concentration, in order to maintain a constant initial number of NH_3 moles from one experiment to another). As a function of NH_3 concentration, the dielectric permittivity first increases very rapidly up to a ϵ' value of about 120, corresponding to 2×10^{-2} M NH_3, and then decreases slowly for greater ammonia concentrations (Fig. 5, curve a). For all the concentrations investigated here, ϵ' values observed in the presence of ammonia were always greater than those recorded in its absence (Fig. 5, comparison of curves a and c). The evolution of the dielectric losses is totally different: after a rapid increase at low NH_3 concentrations, the ϵ'' values start to level off at concentrations higher than 0.1 M (Fig. 5, curve b). Despite the shape of the curve relative to the ϵ' evolution was not fully understood, the influence of NH_3 concentration on ϵ'' values can be interpreted in detail, as described hereafter.

Table 3 shows that even in large excess of NH_3 (compared to the number of silanol groups), the deprotonation reaction (Eq. (3)) was never completed and that the deprotonation ratio (defined as the number of silanolate groups divided by the theoretical number of surface sites initially under the form of silanol) was greatly affected by the initial ammonia concentration. As larger was the NH_3 concentration, as higher was the deprotonation ratio (Table 3). These results are in perfect agreement with the 65% deprotonation ratio reported by Guyon et al. [8] for silica gel in 1 M aqueous ammonia.

On the basis of the pK_a of both NH_4^+/NH_3 and (≡SiOH)/(≡SiO^-) couples, and assuming that the classical laws of chemical equilibrium could be applied to evaluate the apparent constant for the reaction between silica and ammonia, a value of about 275 should be found to characterise this reaction (Eq. (3)). However, Sonnefeld [10] has shown that the apparent acid constant for silanol groups on spherical silica particles is influenced by the degree of dissociation, the counterion concentration, the surface site density, the intrinsic acid constant (intrinsic pK_a, as determined by Schindler and Kamber [11]) and the particle radius. In the experimental conditions of Table 3, for one selected silica, all these parameters can be considered as constant except the degree of dissociation which is thought to increase as the neutralisation reaction (Eq. (3)) progress. As a consequence, the degree of completion for this reaction between silanol groups and ammonia, symbolised by the deprotonation ratio in Table 3, will be limited by this deprotonation ratio, because the degree of dissociation directly affects a reaction for which the product is under a dissociated form. In such conditions, the equilibrium reaction (Eq. (3)) is thought to be as much more displaced to the right

as lower is the deprotonation ratio. One can define a parameter, K_{app}, as an apparent 'equilibrium' constant for the reaction between surface silanol groups and ammonia, based on the equivalent fractions of (≡SiOH) and ($\equiv SiO^-$) (or ($\equiv SiO^- NH_4^+$)) groups in silica and the equilibrium NH_3 concentration in solution (Eq. (5)).

$$K_{app} = \frac{[\equiv SiO^- NH_4^+]}{[\equiv SiOH] \times [NH_3]} \quad (5)$$

where [≡SiOH] and [$\equiv SiO^- NH_4^+$] refer to the equivalent fractions of (≡SiOH) and ($\equiv SiO^- NH_4^+$), respectively.

In this expression, the bracketed quantities refer to equivalent fractions or concentrations and thus K_{app} represents an apparent constant which is only valid for the given experimental conditions. Using Eq. (5), experimental values of K_{app}, for the neutralisation of silica gel by ammonia, were calculated to be 16, 4.7, 1.1 and 0.55, for deprotonation ratios of respectively 14, 37, 50 and 72%. These values are low in comparison with the theoretical apparent constant calculated on the basis of the pK_a of the NH_4^+/NH_3 and (≡SiOH)/($\equiv SiO^-$) couples (about 275), and decrease as the deprotonation (ionisation) ratio increases, which is consistent with the model of Sonnefeld [10] about the surface acidity of colloidal silica.

Because of the low stability of ammonia solutions (NH_3 evaporation) and ammoniated silica (hydrolysis) the determination of the amount of neutralised silanol groups ($\equiv SiO^- NH_4^+$) is somewhat intricate and must be realised with great care (protection by a parafilm...). Interestingly, the dielectric method provides by means of ϵ'' values a new powerful tool for characterising the extent of the silica surface ionisation process. Indeed, the evolution of ϵ'' with the NH_3 concentration (Fig. 5) is similar to that of the deprotonation ratio with the same quantity (Table 3). The measurement of the dielectric losses from a decanted pulp of silica in aqueous ammonia allows thus the in situ quantitative determination of the deprotonation ratio of silica for different ammonia concentrations (after having determined the relation between ϵ'' and the amount of silanolate groups, of course).

Another interesting feature of Table 3 is the results obtained for the Stöber silica. This material is made of small silica beads of monodisperse size, characterised by an apparently low specific surface area (5 $m^2\ g^{-1}$, as measured by the BET method) and a hydroxyl number of typically 5 mmol OH g^{-1}, as determined by thermogravimetry [24]. On the basis of the measured specific surface area of about 5 $m^2\ g^{-1}$ and the reported average hydroxyl number on a perfect plane silica surface ranging from 4 to 8.5 OH nm^{-2} [2], the maximum concentration of silanol groups theoretically able to react with ammonia (or any other base) should be close to 7×10^{-2} mmol g^{-1}. The results of Table 3 shows that the experimental amounts of fixed ammonia by the Stöber silica were much larger than 7×10^{-2} mmol g^{-1} and were as larger as was the NH_3 concentration, in perfect agreement with the theory discussed above (evolution of K_{app} with the degree of dissociation of silica). This demonstrates unambiguously the porosity of the Stöber silica that did not allow the N_2 adsorption at the interior of its pore and channel system but allow the diffusion and subsequent reaction of NH_3 with the silanol groups inside the silica structure. Considering the concentration of free silanol groups (5 mmol g^{-1}) for an average distribution of 5 OH nm^{-2}, one could estimate the surface area of internal ultramicroporosity in the Stöber particles to be about 600 $m^2\ g^{-1}$. This agrees with the results of Table 3 which indicate the formation of larger amounts of silanolate groups in the case of Stöber beads (compared to silica gel), at the same NH_3 concentration. The accessibility to the pore structure of the Stöber silica is now under study by using bases of different size for which the diffusion within the porous silica should be controlled (or hindered) by the intrinsic size of pores and channels of the Stöber beads. Preliminary results reveal that bases of higher or equal size than that of $(C_2H_5)_3N$ were found to be unable to react with the Stöber silica.

Finally, it is important to remember that the non-complete neutralisation of silanol groups by acid/base reaction has to be taken into account when determining the specific surface area of silica-based materials by titration methods [29–31].

Also, by performing proper calibration, the high frequency dielectric method could be applied as a new, rapid, accurate and non destructive method for the determination of the specific surface area of silica under in situ conditions. For the Stöber silica, this approach should provide higher values than those measured by nitrogen adsorption.

3.2.3. On-column analysis in flowing conditions

All the batch experiments described above have been realised with great care because of the low stability of ammonia solutions due to NH_3 evaporation, intricating somewhat the usually very simple dielectric measurements. An elegant way to overcome this problem is to operate in flow-through conditions so that the silica materials are always contacting a fresh aqueous ammonia solution. The dielectric measurements are then made with the aid of a cylindrical capacitive cell, directly on the silica in equilibrium with the flowing solution. Moreover, the dielectric behaviour of the out-going liquid phase can be monitored at any time, without collecting fractions, by simply mounting another cell at the end of the chromatographic column.

Typical results are depicted in Fig. 6, for three different NH_3 concentrations. The shape of the curves were the same whatever the measured quantity (ϵ' or ϵ'') or the NH_3 concentration. The dielectric values, corresponding first to the raw materials were constant until the ammonia solutions have attained the silica contained in the cylindrical capacitive cell; at this moment, due to the neutralisation reaction (Eq. (3)), ϵ' and ϵ'' values increased rapidly to reach an equilibrium value which remained constant by continuing flowing (Fig. 6). These equilibrium dielectric values are characteristic of the acid/base reaction between silica and ammonia and are the same than those calculated from batch measurements. Obviously, the breakthrough time strongly depends on the NH_3 concentration and therefore on the deprotonation ratio. As illustrated in Fig. 6, as more concentrated was the NH_3 concentration, as smaller was the breakthrough time. But the relation between this breakthrough time (corresponding to a breakthrough volume) with the reagent (NH_3) concentration was not linear, contrarily to what was observed with ion exchange resins for which all the ion exchanging sites were reactive [21] Such a behaviour was explained by the non-completion of the neutralisation reaction, resulting in different deprotonation ratios of silica observed when using solutions of different NH_3 concentration.

By ensuring a constant flow rate and controlling the silica dissolution (by monitoring the soluble silicates by ICP measurements), this dynamic procedure could be used to estimate the

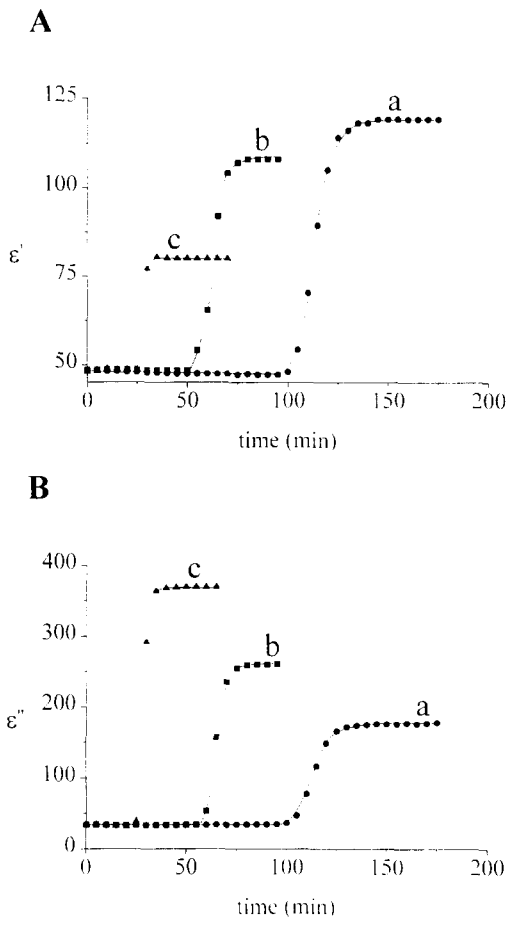

Fig. 6. Evolution of the dielectric permittivity ϵ' (**A**) and the dielectric losses ϵ'' (**B**) of a 5.0 g silica gel column during the flow through of an aqueous ammonia solution. Breakthrough curves for three NH_3 concentrations: 1.2×10^{-2} M (**a**), 5.9×10^{-2} M (**b**) and 2.3×10^{-1} M (**c**). Flow rate: 1 ml min^{-1}. Field frequency: 10 MHz.

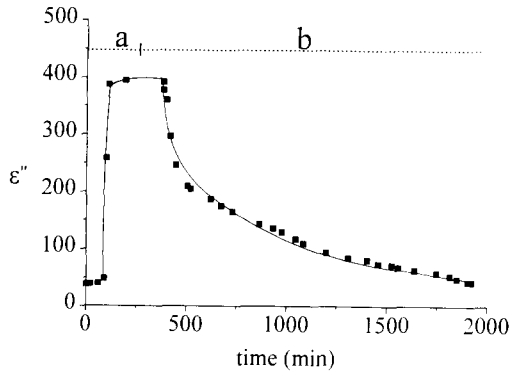

Fig. 7. Evolution of the dielectric losses ϵ'' of a 5.0 g silica gel column during the flow through of (**a**) 5.9×10^{-2} M NH_3 solution and (**b**) pure water, successively. Field frequency: 10 MHz.

amount of silanolate groups formed upon the reaction of silanol with ammonia. In particular, the breakthrough curves obtained by plotting the ϵ'' values as a function of the elution time (Fig. 6, plot B) provide an ideal way to derive the relation between the deprotonation ratio and the dielectric response (ϵ'') measured under in situ conditions.

The ($\equiv SiO^- NH_4^+$) groups were found to be stable only when contacting the ammonia solution in which they were formed and, in agreement with the above results, their stability was as higher as larger was the NH_3 concentration. As a consequence, the ammoniated silica cannot be isolated from its ammonia solution because the washing step should result in the hydrolysis of the ($\equiv SiO^- NH_4^+$) groups. This phenomenon is illustrated in Fig. 7, showing that a water treatment of the ammoniated silica led to the restitution of the starting material ($\equiv SiOH$). Such regeneration step can be accelerated by washing the silica column by an acid solution (HCl) which reacts more rapidly with the silanolate groups than water (data not shown). The silica column can react and can be regenerated several times, demonstrating the major interest of this system, associated with an impedance meter through a cylindrical capacitive cell, for the in situ characterisation of the ionisation of packed particles of silica.

4. Conclusion

The ionisation of surface silanol groups of silica by ammonia can be characterised in situ by high frequency dielectric experiments in both static and dynamic modes. The simple measurement of the complex impedance of a silica pulp allows to distinguish between neutral silica ($\equiv SiOH$) and ammoniated silica ($\equiv SiO^- NH_4^+$), independently of the presence or the absence of salt. Both the silica gel and the Stöber silica were found to produce an amount of ($\equiv SiO^- NH_4^+$) groups as larger as higher was the NH_3 concentration. However, the completion of the neutralisation reaction was never observed, due to the decrease in the apparent equilibrium constant of this reaction with increasing the degree of dissociation of silica. The porosity of the Stöber silica was demonstrated by the observation of ($\equiv SiO^- NH_4^+$) formation in bulk silica beads. Successive analysis can be performed by using flow-through columns of silica which are able to be ammoniated and regenerated several times without apparent deterioration of materials.

Acknowledgements

Prof. A. Burneau (L.C.P.E., Nancy, France) is gratefully acknowledged for providing the stöber silica samples and for the helpful discussions, and A. Labrosse for Stöber synthesis. The authors also thank Dr. B. Humbert for recording the Raman spectra.

References

[1] S.E. Manahan, Environmental Chemistry, 6th ed., Lewis Publishers, CRC Press, Boca Raton, FL, 1994.
[2] R.K. Iler, The Chemistry of Silica, Wiley, New York, 1979.
[3] E.F. Vansant, P. Van der Voort, K.C. Vrancken (Eds.), Characterization and chemical modification of the silica surface, Elsevier, Amsterdam, 1995.
[4] P.J. Heaney, C.T. Prewitt, G.V. Gibbs (Eds.), Silica, Physical Behavior, Geochemistry and Materials Applications, In: P.H. Ribbe (series Ed.), Reviews in Mineralogy, vol. 9, Mineralogical Society of America, Washington, D.C., 1994.

[5] R. Rosset, A. Jardy, J. Caude, Chromatographies en phase liquide et supercritique, Masson, Paris, 1991.
[6] R.O. James, T.W. Healy, J. Coll. Interfac. Sci. 40 (1972) 42–53.
[7] F. Guyon, Thesis, Université Pierre et Marie Curie Paris VI, Paris 1983.
[8] F. Guyon, J. Desbarres, R. Rosset, Anal. Chim. Acta 170 (1985) 311.
[9] G.W. Smith, L.H. Reyerson, J. Am. Chem. Soc. 52 (1930) 2584.
[10] J. Sonnefeld, J. Coll. Interfac. Sci. 155 (1993) 191.
[11] P. Schindler, H.R. Kamber, Helv. Chim. Acta 51 (1968) 1781.
[12] J. Bessière, K. Chlihi, J.M. Thiébaut, Electrochim. Acta 31 (1986) 63.
[13] J. Bessière, J.M. Thiébaut, K. Chlihi, M. El Housni, Ind. Minér. Mines Carrières Tech., aout -sept, 1989, p. 57.
[14] J.M. Thiébaut, K. Chlihi, J. Bessière, G. Roussy, J. Electroanal. Chem. 262 (1989) 131.
[15] J. Bessière, K. Chlihi, J.M. Thiébaut, G. Roussy, Int. J. Miner. Process. 28 (1990) 1.
[16] J. Bessière, M. El Housni, J.J. Prédali, Int. J. Miner. Process. 33 (1991) 165.
[17] E. Benoit, P. Maincent, J. Bessière, Int. J. Pharm. 84 (1992) 283.
[18] J. Bessière, A. Etahiri, Int. J. Miner. Process. 38 (1993) 125.
[19] J. Bessière, M. Khayar, Int. J. Miner. Process. 39 (1993) 107.
[20] J. Bessière, A. Etahiri, Int. J. Miner. Process. 42 (1994) 241.
[21] J. Bessière, A. Kleber, I. Sutapa, M. Perdicakis, Sensors Actuators B26-27 (1995) 411.
[22] T. Hanai, Kolloid Z. 171 (1960) 23.
[23] T. Hanai, Kolloid Z. 175 (1961) 61.
[24] A. Labrosse, A. Burneau, personal communication.
[25] W. Stöber, A. Fink, E. Bohn, J. Coll. Interfac. Sci. 26 (1963) 62.
[26] B. Tremillon, Electrochimie Analytique et Réactions en Solution, tome 1, Masson, Paris, 1993.
[27] G.W. Smith, L.H. Reyerson, J. Phys. Chem. 60 (1956) 1008.
[28] B. Humbert, J. Non-Cryst. Solids 191 (1995) 29.
[29] G.W. Sears Jr., Anal. Chem. 28 (1956) 1981.
[30] W. Cheng, M. McCown, J. Chromatogr. 318 (1985) 173.
[31] T. Takeuchi, T. Miwa, Anal. Chim. Acta 282 (1993) 565.

ELSEVIER

Talanta 45 (1997) 371–377

Talanta

Robotic sample pretreatment–immunoassay determination of chlorpyrifos metabolite (TCP) in soil and fruit

A. Velasco-Arjona [a], J.J. Manclús [b], A. Montoya [b], M.D. Luque de Castro *

[a] *Department of Analytical Chemistry, Faculty of Sciences, University of Córdoba, E-14004 Córdoba, Spain*
[b] *Department of Bioengineering, Polytechnic University of Valencia, E-46022 Valencia, Spain*

Received 24 February 1997; accepted 29 April 1997

Abstract

A fully automated method for leaching of TCP (3,5,6-trichloro-2-pyridinol, the major degradation product of the widely used chlorpyrifos insecticides) from soil and fruit with subsequent determination by ELISA is reported. The automation of the weighing and leaching steps enables unattended development of sample preparation. The determination of the target analyte, traditionally performed by liquid chromatography, has been substituted by specific immunoassay using a non-commercial monoclonal antibody which enables the determination of TCP within the range 0.01–7 ng l^{-1} with an R.S.D. of 8.6%. © 1997 Elsevier Science B.V.

Keywords: Robot; ELISA; 3,5,6-Trichloro-2-pyridinol; Chlorpyrifos; Soil; Fruit

1. Introduction

As a consequence of the widespread use of pesticides, the presence of their residues in both food and the environment has become an important issue in analytical science. There is a growing concern regarding the potential toxicity and/or ecotoxicity of the transformation products associated with these residues, which demands the development of appropriate analytical techniques for their monitoring [1].

3,5,6-Trichloro-2-pyridinol (TCP) is the major degradation product of the insecticide chlorpyrifos [*O,O*-diethyl *O*-(3,5,6-trichloro-2-pyridinyl)-phosphorothioate] and chlorpyrifos-methyl [*O,O*-dimethyl *O*-(3,5,6-trichloro-2-pyridinyl)phosphoro-thioate] as well as the herbicide trichlopyr [[(3,5,6-trichloro-2-pyridinyl)oxy]acetic acid] [2,3]. Both biotic and abiotic transformation processes yield TCP from parent pesticides in environmental and biological compartments. TCP is a polar compound which displays very different physical and chemical properties from the chlorpyrifos insecticides, and therefore exhibits different mobility and persistence in the environment [3]. Most of the existing traditional methods for the determination of this metabolite in solid samples are manual and time-consuming, and in order to reduce analysis times and avoid overloading routine laboratories, should be automated.

* Corresponding author.

PII S0039-9140(97)00140-9

When large numbers of samples have to be analysed, the preliminary operations involved in the analytical process can become very tedious and time-consuming. The steps to be developed in order to obtain the target analyte in solution (namely weighing, leaching or dissolution, filtration or centrifugation, evaporation, etc.) are very difficult to automate, and so require a high degree of human participation. In fact, some of these operations can only be automated by the use of robots. Robotic stations have been used for automation of soil analysis, particularly for sample pretreatment operations, while methods for the determination of volatile compounds [4], pesticides [5], and pH [6] have also been proposed which are based on the use of robots. These methods show the usefulness of this type of automation for processes in which the first steps of the analytical process are the bottleneck, a common occurrence when solid samples are involved.

Immunochemical analysis has been shown to fulfil the analytical requirements for the determination of pesticides and their metabolites, provided that appropriate antibodies are available [7,8]. In this respect, highly specific and sensitive monoclonal antibodies have been obtained and used to develop several immunoassays for the determination of TCP, which have been reported in earlier papers [9,10].

This article describes robotic pretreatments for the leaching of TCP from solid samples (soil and fruit) and subsequent determination of the target analyte by immunoassay.

2. Experimental

2.1. Instruments and apparatus

A robotic station consisting of a Zymate II Plus robot, a System V controller, a printer, all-purpose hand, together with a test tube dispenser, a 16 × 100 mm tube rack, a vibrating motor, a liquid–liquid extraction unit, and a syringe hand with a disposable pipette tip rack were all used. In addition, a Mettler AE balance, a master laboratory station (MLS), a power and event controller (PEC), a dilute and dissolve station (vortex), a Z710 centrifuge and an evaporation station was used (Fig. 1). The System V controller was interfaced to a Netset 286/400 personal computer.

TCP immunoassay was developed in flat bottom polystyrene ELISA plates (Costar High Binding # 3590, Cambridge, MA) and absorbance was read in the dual-wavelength mode (490 nm as test wavelength and 630 nm as reference wavelength) using an ELISA plate reader (Mios, Merck).

2.2. Reagents and solutions

2.2.1. Leaching step

A 3:1, v/v acetone/distilled water solution was used.

2.2.2. TCP immunoassay step

Stock standard solution of TCP (generously supplied by DowElanco) 400 mM in *N,N'*-dimethylformamide (Panreac, Spain) was prepared. The synthesis of the hapten-1, preparation of the HRP (horse-radish peroxidase-1) enzyme tracer, and production of the monoclonal antibody (LIB-MC2) have been described elsewhere [9,10]. Coating buffer containing 50 mM carbonate-bicarbonate (Merck, Darmstadt), pH 5.4 and an aqueous washing solution of 0.15 M NaCl (Merck, Marmstadt) containing 0.05% Tween-20 (Sigma) were also prepared. PBS is the assay buffer, which contains 10 mM phosphate, 139 mM NaCl and 2.7 mM KCl (all from Merck), pH 7.5. PBST is the PBS buffer containing also 0.04% Tween-20 (Sigma). A substrate solution of *o*-phenylendiamine (Merck) 2 mg ml^{-1} containing 0.012% H_2O_2 (Panreac) in 25 mM citrate (Merck), 62 mM sodium phosphate (Merck) buffer, pH 5.4, and a 2.5 M solution of H_2SO_4 (Panreac) were also used.

2.3. Sample pretreatment

2.3.1. Manual procedure

One g of fortified sample is weighed in a test tube and 5 ml of leaching solvent is added. This is stirred for 1 h on a vibrating stirrer before most of the acetone is evaporated on an electrical heating plate at 50°C for 5 min. This loss of weight is

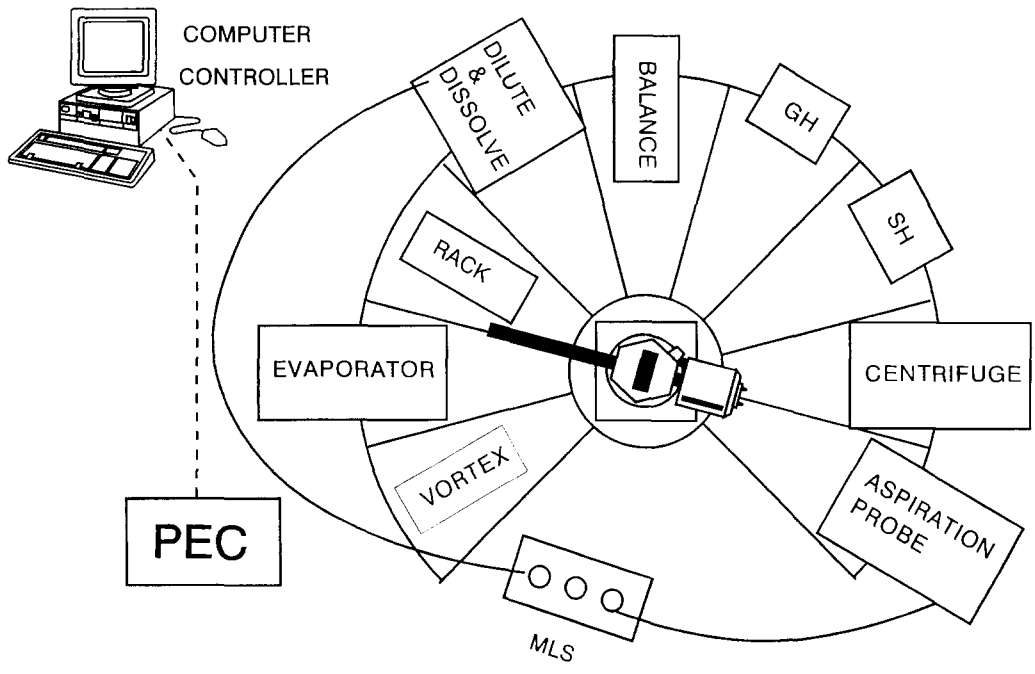

Fig. 1. Robotic station for TCP leaching from soil and fruit. MLS denotes master laboratory station; GH, general hand; SH, syringe hand; PEC, power and even controller.

replaced by an equal weight of phosphate buffer. The sample is then centrifuged at 2000 rpm for 5 min, following which 3 ml of the supernatant is transferred to an empty test tube.

2.3.2. Robotic procedure

With the all-purpose hand, the robot selects an empty centrifuge tube from the test tube dispenser and places it on the balance. Following this it picks up a glass funnel, sets it on the preselected tube and tares the balance. The robot then takes a container with sample, sets it above the funnel placing it against the vibrating motor in order to add ca. 1 g of sample. It puts the container down, takes the funnel off and takes the tube to the dilute and dissolve module where ca. 5 ml of leaching agent (depending on the sample weight) is added. The robot places the tube on the balance again and obtains the weight (P_1). Finally, the robot places the tube in the vortex and repeats these steps until the vortex rack is full, before stirring all the samples for one hour. The robot then places the samples in the evaporator where most of the acetone is evaporated (heating at 50°C for 5 min). After this it takes the samples one by one, weighs them, takes them to the dilute and dissolve unit where PBS is added, places them in the balance again and obtains the new weight P_2. The robot then selects the syringe hand, sucks PBS up from a container and adds it to the tubes in the balance until the weight of acetone evaporated is replaced by an equal weight of PBS. The robot then introduces the samples into the centrifuge where they are centrifuged at 2000 rpm for 5 min. It takes the samples to the test tube rack and sucks up 2 ml of supernatant which is transferred to empty test tubes.

A description of both the peripherals which composes the robotic station and their functions can be found elsewhere [11,12].

2.4. Determination

2.4.1. Preparation of standard solution

An 800-nM TCP solution in PBS is prepared from the 400 mM TCP in *N*,*N*-dimethyl-formamide stock solution. Standards between 160 mg l^{-1} and 2 ng l^{-1} TCP were then prepared by serial dilutions (factor of 5) in PBS. As the assay procedure involved the addition of the same volume of the appropriate HRP-1 concentrations, standards were diluted by a factor of 2. Therefore TCP standards in the final assay ranged from 80 mg l^{-1} to 1 ng l^{-1}.

2.4.2. TCP immunoassay

ELISA plates were coated overnight at room temperature with 100 ml per well of LIB-MC2 MAb solution, washed four times with washing solution before 50 ml per well of standard or sample was added to the antibody-coated plates followed by 50 ml per well of HRP-1 solution. The plates were then incubated for 1 h at room temperature. After washing, the activity of HRP bound to the wells was measured by adding 100 ml per well of H_2SO_4 solution, and the absorbance read in the ELISA plate reader.

2.4.3. Data analysis

Standards and samples were run in triplicate, and the mean absorbance values processed. Standard curves were obtained by plotting absorbance against the logarithm of analyte concentration. Using the Origin software package, sigmoidal competitive curves were fitted to a four-parameter power equation

$$y = \{(A - D)/[1 + (x/C)^B]\} + D$$

where A is the asymptotic maximum (maximum absorbance in the absence of analyte, A_{max}), B is the curve slope at the inflection point, C is the x value at the inflection point (corresponding to analyte concentration giving 50% inhibition of A_{max}, I_{50}), and D is the asymptotic minimum (background signal). Determination of spiked samples was performed by interpolating their mean absorbance values in the standard curve.

3. Results and discussion

The optimisation of variables was focused on the robotic pretreatment step as the determination method had been reported previously [10]. The leaching agent, its volume and the contact-time with the sample while stirring were all studied. Finally, aspects relating to the stability of the analyte were studied as was the effect of the remaining leaching agent on the determination step. All the assays were developed in duplicate using both fruit (apple) and soil (limestone) samples spiked with the analyte.

3.1. Optimisation of the leaching step

Basic, acid and neutral leaching agents consisting of organic–aqueous mixtures were assayed (namely, 9:1 acetone/0.12 N HCl; 20:1 methanol/40% NaOH; and 3:1 acetone/H_2O) [14]. No significant differences in the recovery were obtained (90 ± 6–$92 \pm 6\%$). A 3:1 acetone/water mixture was selected as optimal due to the fact that it has the lowest concentration of organic solvent, which is important as the subsequent quantification step which was proposed in the literature [10] was developed in aqueous medium.

The optimum volume of leaching solution was studied after spiking the samples with 35 ng g^{-1}. The selection of a higher concentration of target analyte in order to encompass any possible concentration in the sample would involve both a higher consumption of extractant and more organic solvent emitted to the atmosphere. Extractant volumes lower than 5 ml yielded incomplete recovery (ca. $73 \pm 5\%$), while a recovery of $93 \pm 6\%$ was obtained with volumes from 5 to 10 ml. When the concentration of TCP in the samples was increased, either a smaller sample amount could be used or the volume of extractant increased.

The stirring time (at a constant speed provided by the vortex station) was studied between 30 and 120 min. The recovery was constant ($93 \pm 6\%$) for 60 min and above.

3.2. Studies of the analyte

Three aspects concerning the stability of the analyte were studied. First the data [13] on stability of the TCP in aqueous solution were checked in order to determine whether pretreated samples could be stored for simultaneous determination. With this aim a solution of 0.01 g l^{-1} of TCP in PBS buffer was prepared, from which a set of three 20-ml aliquots was placed in topace flasks; another similar set were prepared in colourless flasks and both stored in the refrigerator at 4°C. Two similar sets were stored at room temperature in the laboratory. After 1 week it was shown that the concentration in each of the flasks had remained constant.

The method for the determination of TCP previously reported was proposed for aqueous samples [9,10], and so was developed in the absence of organic solvent. As the leaching of the target analyte from solid samples requires the presence of organic solvent (namely 75% acetone), a study was carried out on the influence of this solvent on the subsequent immunodetermination. Duplicate samples containing 3 ng l^{-1} of TCP, PBS buffer if required and acetone concentrations of 0, 1, 20, 40, 60, 80, and 100% were prepared and the immunoassay developed. Poor signals were obtained for acetone contents of 60% or higher. More systematic studies between 40 and 60% organic solvent showed that for concentrations of 45% or less acetone provided similar results. As the pretreated samples contained 75% acetone, a heating/evaporation time of 5 min at 50°C lowered the amount of acetone to below the tolerance level. The complete removal of organic solvent was undesirable for two reasons. Firstly it lengthened the time required for this step, and secondly it increased the possibility of TCP degradation. Once the tolerated acetone concentration in the immunoassay had been checked all the steps involved in the sample pretreatment developed by the robot (a sensorless robot) were taken into account, the step after evaporation was developed as follows: the sample was made to weight rather than volume with PBS buffer, as shown under experimental. Taking into account the densities of both acetone (0.87 g ml^{-1}) and PBS buffer (1.00 g ml^{-1}), and using the two weights before and after evaporation (P_1 and P_2, respectively), the acetone removed was substituted by an equal volume of PBS buffer calculated from the following equation:

$$V_{\text{solution}} = V' - (P_1 - P_2)/0.87 + (P_1 + P_2)$$

where V' is the volume of extractant (ca. 5 ml).

In this way, the results from the samples can be interpolated in the calibration curve run with aqueous standards without any errors other than the R.S.D. of the method.

A final study on the analyte consisted of checking its stability during the evaporation step (5 min at 50°C). Two solutions of 3 ng l^{-1} of TCP were prepared: one of them in 3:1 acetone/water and the other in PBS buffer and a set of three aliquots was taken from each solution. The set from the former solution was subjected to 50°C for 5 min and the solvent removed was substituted by PBS buffer. Both sets of aliquots provided similar results within the range of precision of $\pm 6\%$.

3.3. Determination step

The studies developed in this section involve both the features of the calibration curve and a systematic study of its precision.

The features of the calibration curve were established using the standard solutions, prepared as described under experimental, the values of the parameters A to D of the sigmoidal curve being as follows: $A = 0.523$; $B = 1.046$; $C = 0.261$; $D = 0.007$.

The two extreme portions of the curve yielded high errors as a consequence of its low slope. The central range between 0.01 and 7 ng l^{-1}, which provided an R.S.D. lower than 8.6%, was selected for measurements as optimal range of the calibration curve (ORCC).

The study of the precision of the method was divided into two parts: (a) precision of the determination step (within and between precision of the immunoassay); (b) precision of the pretreatment step as a function of the concentration of the target analyte in both fruit and soil.

For the within precision study, three solutions of TCP were prepared with concentrations in the

Table 1
Comparison of TCP recoveries from solid samples by the robotic and manual methods

Sample	Spiked concentration (ng g^{-1})	Recovery (%)	
		Robotic method	Manual method
Soil (calcareous)			
	0.05	87	90
	0.18	90	89
	0.68	94	91
	2.5	91	88
	9.4	92	93
	35	93	90
	50	91	93
	91	91	89
	165	90	95
	300	87	91
	550	88	89
	1000	88	92
Fruit (apple)			
	0.05	93	90
	0.18	90	91
	0.68	91	95
	2.5	91	93
	9.4	95	95
	35	92	89

centre (3 ng l^{-1}) and extremities (0.01 and 7 ng l^{-1}) of the ORCC. From each solution 11 samples were prepared and monitored. In all three cases an average value of R.S.D. of 7.6% was found.

The between precision study was developed from six solutions with concentration of 3 ng l^{-1} TCP, each of which was used for the preparation of 11 samples. The relative standard deviation obtained was $\pm$ 8.1%.

The reproducibility of the robotic pretreatment step was compared with its manual counterpart. Identical samples of both fruit (TCP concentration between 0.05 and 35 ng g^{-1}) and soil (two TCP concentration ranges: 0.05–35 ng g^{-1} and 0.05–1 mg g^{-1}) were treated by the two procedures, then the solutions obtained subjected to immunoassay. Table 1 lists the results obtained, from which an excellent agreement between the manual and the robotic procedures can be concluded.

3.4. Applicability of the method

In order to check the applicability of the method to different matrices, samples of fruit (namely apple, pear and banana) and soil of different texture and characteristics (limestone, grey and clay) were spiked with the target analyte covering a wide range of concentration (from 0.05 to 35 ng g^{-1}). Each sample was analysed in triplicate. The results obtained are presented in Table 2. Similar recoveries of TCP, close to 100% in most of the cases and in all the types of matrices, proves the excellent performance of the proposed method.

4. Conclusions

The method proposed here dramatically improves the features of both standard and non-standard methods previously reported.

Table 2
Recovery of TCP from different types of soil and fruit

TCP added (ng g^{-1})	TCP recovered (%)					
	Fruit			Soil		
	Apple	Pear	Banana	Calcareous	Grey	Limy
0.05	96 ± 6	90 ± 7	91 ± 7	89 ± 6	92 ± 5	91 ± 6
17	93 ± 4	95 ± 8	91 ± 7	92 ± 5	90 ± 5	94 ± 8
35	90 ± 6	91 ± 7	93 ± 5	91 ± 8	88 ± 3	96 ± 5

With regards to selectivity, the reported method removes the need to carry out some of the unnecessary steps subsequent to leaching as the immunoassay does not require removal of other sample components leached with the analyte, while it is also worth noting that the EPA methods for the determination of TCP in fruit use a number of tedious and time-consuming steps in which the samples are leached, evaporated to dryness, partitioned with organic and aqueous solvents, chromatographed, derivated to a volatile compound which is subjected to GC with MS or electron capture detection [15]. Other non-official methods make use of similar steps and nitrogen detector after GC [16].

In relation to sensitivity, the methods reported so far provide determination limits not lower than 10 ng g^{-1} [14,18] or 50 ng g^{-1} [15–17]. The immunoassay determination lowers this limit to 0.05 ng g^{-1} (5000-times lower!).

In short, the improvement in selectivity of the immunoassay makes it a cheaper and cleaner method, also enabling easy automation.

The sensitivity achieved makes screening methods unnecessary, as ultratraces of the target analyte can be determined with acceptable errors and minimum sample pretreatment.

The implementation in routine laboratories of the overall automation of the determination of TCP in any type of sample requires an automated system for development of the immunoassay step.

Acknowledgements

Comisión Interministerial de Ciencia y Tecnología (CICyT) is thanked for financial support (Project No. PB93-0827). DownElanco and Dr. J.P. Castano (Department of Cell Biology, University of Córdoba) are also thanked for supplying TCP and assay instrumentation, respectively.

References

[1] L. Somasundaram, J.R. Coats, Eds. Pesticide Transformation Products: Fate and Significance in the environment, ACS Symp. Ser. 459. Am. Chem. Soc., Washington, 1991.
[2] K.B. Woodburn, W.R. Gree, H.E. Westerdahl, J. Agric. Food Chem. 41 (1993) 2172.
[3] K.D. Racke, Rev. Environ. Contam. Toxicol. 131 (1993) 1.
[4] M. Markelov, M. Antloga, S.A. Schmidt, in: J.R. Strimaitis, G.L. Hawk (Eds.), Advances in Laboratory Automation Robotic, Zymark Corporation, Hopkinton, MA, 1985, pp. 209.
[5] P.A. Goodwin, in: J.R. Strimaitis, P. Helfrich (Eds.), Advances in Laboratory Automation Robotic, Zymark Corporation, Hopkinton, MA, 1990, pp. 185.
[6] P. Torres, J.A. García-Mesa, M.D. Luque de Castro, M. Valcárcel, Fresenius J. Anal. Chem. 346 (1993) 704.
[7] A. Abad, A. Montoya, J. Agric. Food Chem. 42 (1994) 1818.
[8] J.J. Manclús, J. Primo, A. Montoya, J. Agric. Food Chem. 42 (1994) 1257.
[9] J.J. Manclús, A. Montoya, J. Agric. Food Chem. 44 (1996) 3703.
[10] J.J. Manclús, A. Montoya, J. Agric. Food Chem. 44 (1996) 3710.
[11] A. Velasco-Arjona, M.D. Luque de Castro, Anal. Chim. Acta 333 (1996) 205.
[12] A. Velasco-Arjona, M.D. Luque de Castro, Analyst 122 (1997) 123–128.
[13] W. Reed Green, H.E. Westerdall, J. Agric. Food Chem. 41 (1993) 2172.
[14] DowElanco Europe, Confidential reports.
[15] R.L. McKellar, Pesticide analytical manual 2 (1996) 33.
[16] J.L. Herman, Pesticide analytical manual 2 (1996) 15.
[17] C.R. Mourer, G.L. Hall, W.E. Whitehead, T. Shibamoto, J. Assoc. Off. Anal. Chem. 73 (1990) 294.
[18] Y. Iwata, J.R. O'Neal, J.H. Barkley, T.M. Dinoff, M.E. Düsch, J. Agric. Food Chem. 31 (1983) 603.

ELSEVIER

Talanta 45 (1997) 379–386

Talanta

Multivariate characterization of wine vinegars from the south of Spain according to their metallic content

María I. Guerrero [a,*], Claudia Herce-Pagliai [a], Ana M. Cameán [a], Ana M. Troncoso [a], A. Gustavo González [b]

[a] *Department of Biochemistry, Food Science and Toxicology, University of Seville, 41012 Sevilla, Spain*
[b] *Department of Analytical Chemistry, University of Seville, 41012 Sevilla, Spain*

Received 13 November 1996; received in revised form 29 April 1997; accepted 30 April 1997

Abstract

Forty wine vinegar samples from the south of Spain were analyzed for mineral content. Nine metals (As, Ca, Cu, Fe, K, Mg, Mn, Na and Zn) were chosen as chemical features that may account for the rate of the vinegar fermentation process. Pattern recognition techniques were applied for distinguishing quick and slow processed vinegars. The results obtained indicated an excellent performance in both recalling and prediction ability. © 1997 Elsevier Science B.V.

Keywords: Wine vinegars; Metal determination; Pattern recognition

1. Introduction

Wine vinegar is a greatly appreciated product in wine producing countries, specially in the Mediterranean ones. In others, several raw materials (malt, cider, rice wine, honey, etc.) are used as sources for vinegar production. Given the increasingly important role of vinegars in gastronomy [1], their study is worthwhile.

Wine vinegar is mainly obtained by two different procedures: 'Quick' process, involving submerged cultures and carried out in stainless steel acetators during 24–36 h, and 'Slow' process, encompassing surface cultures and performed in wood tanks during variable periods of time (at least several days) [2]. Furthermore, the substrate for the acetic fermentation is usually quite different; so, quality wines are used for slow acetification and common table wines or, in a lesser extent, wine distillates for quick acetification. Among vinegars made from traditional slow acetification processes, Sherry (Jerez) vinegars are particularly appreciated. They are produced from 'Fino' wines, according to the traditional 'solera' system. Besides Jerez, there are some other zones in the south of Spain that produce wine vinegars following the same process [3], the substrate wine being different according to their origins.

The interest of studying mineral elements in vinegars is due to its potential toxicity, the undesirable phenomena (like precipitations) they can

* Corresponding author.

PII S0039-9140(97)00139-2

arise and the possibility of their use as indicators of origin or technological treatments [4]. Mineral elements have been used to characterize wines of different geographical origin [5,6], although the topic is controversial. The origin of mineral content in vinegars may be due to the natural source of these elements in the grape and wine, the contact with materials during the processes and the contamination from the environment [4]. The characterization of vinegars based on their metallic content has only been studied for the case of the Italian 'Aceto Balsamico Tradizionale di Modena' [7]. The aim of the present paper is to study the utility of mineral elements, like metals, for distinguishing conventional (quick) vinegars from traditional (slow) vinegars.

2. Experimental

2.1. Apparatus

A Perkin-Elmer 3100 atomic absorption spectrometer was used for metal determinations involving flame absorption spectrometry (FAAS) and flame emission spectrometry (FES). For developing hydride generation atomic absorption spectrometry (HG/AAS), a hydride generator system (Perkin-Elmer MSH 10) was fitted to the spectrometer.

2.2. Reagents and solutions

Stock solutions of metal ions were prepared from calcium carbonate, copper metal, zinc metal, iron wire, manganese metal, sodium chloride, potassium chloride and arsenic trioxide (Merck) according to the Perkin-Elmer guidelines. The following stock solutions were used: Ca (500 mg l^{-1}), Fe (1000 mg l^{-1}), K (1000 mg l^{-1}), Mg (1000 mg l^{-1}), Cu (1000 mg l^{-1}), Mn (1000 mg l^{-1}), Na (1000 mg l^{-1}), Zn (500 mg l^{-1}) and As (1000 mg l^{-1}). Working solutions were obtained by suitable dilution from the corresponding stock solution.

Sodium borohydride, potassium iodide, hydrochloric acid, nitric acid and sodium hydroxide were of analytical grade. Milli-Q treated water was used throughout. For hydride generation, the following solution was used: hydrochloric acid 1.5% v/v, potassium iodide 20% w/v, and sodium borohydride 1.4% w/v in sodium hydroxide 3% w/v.

2.3. Analytical procedures

Analytical procedures were the same as appeared in a recent publication [8]. Metals Ca, Cu, Fe, Mg, Mn and Zn were determined from FAAS using an air/acetylene flame, K and Na were determined from FES and As was quantitated by HG/AAS. Major elements (Ca, K, Na and Mg) were determined using external calibration. Minor and trace elements (Cu, Fe, Mn, Zn and As) were quantitated from spiked samples according to the method of standard additions [8].

When sample dilution is performed by using a reaction mixture instead of water, the readout of the mixture (instrumental blank) must be taken into account to evaluate the concentration of unspiked samples. Thus, if the averaged value of the mixture blank is A_0, and the standard addition equation is $y = A + Bx$ (y is the analytical response and x the concentration added), the concentration of metal in the assay solution will be: $x_{a.s.} = (A - A_0)/B$. It is noticeable that A_0 only was significant for As determination. Standard additions must fulfil the condition that the concentration of the maximum spiked sample falls within the linear range of the calibration straight line. All the results were expressed in mg l^{-1} and were the average of triplicate measurements. These results were rounded up to the last figure associated with random error.

2.4. Vinegar samples and data analysis

Forty vinegar samples derived from both slow and quick elaboration methods (labelled as S and Q, respectively) were used for performing this study. Class S (22 samples) consist of: (i) a group of 14 well known genuine vinegars with D.O. trademark (checked denomination and origin) in the production area, obtained from Jerez 'Fino' wines by the traditional 'solera' system, and (ii) a set of eight vinegars collected in other zones of the

south of Spain, as Montilla-Moriles and El Condado. Their elaboration is substantially the same, the substrate wines being from Montilla and El Condado. Class Q (18 samples) includes commercially available vinegars, elaborated by using the quick acetification process from very different wine substrates. All the vinegars were stored in 750 ml glass or PVC bottles at 4–8°C.

Each vinegar sample (object) was considered as an assembly of nine variables (descriptors), namely the concentrations of As, Ca, Cu, Fe, K, Mg, Mn, Na and Zn. Descriptors will be denoted as the chemical symbols of the corresponding element but in capital, as follows: AS, CA, CU, FE, K, MG, MN, NA and ZN. A data matrix whose rows are the vinegar samples and whose columns are the descriptors was built for further multivariate analysis. The pattern recognition tools used in this study involve principal component analysis (PCA) [9,10], cluster analysis (CA) [11,12], linear discriminant analysis (LDA) [13,14], non-parametric K-nearest neighbours method (KNN) [15,16], soft independent modelling of class analogies (SIMCA) [17,18] and artificial neural networks trained by back propagation (BPANN) [19,20]. Outliers (abnormal values) were removed from data matrix according to the Dean and Dixon rejection test [21]. They were declared as missing values and not substituted by means. The Software packages and programs used for calculations were: CSS STATISTICA package from Statsoft for performing PCA, CA and LDA. SIRIUS program was used for SIMCA, WINNN 0.97 package for BPANN and home-made developed software for KNN.

3. Results and discussion

A data matrix X consisting of 40 rows (the vinegar samples) and nine columns (the metal descriptors) is presented in Table 1. Each element x_{ij} of the data matrix is the content in mg l^{-1} of the j-column metal descriptor for the i-row sample considered. Taking into account the number of analyzed samples and the values obtained for skewness and kurtosis statistical parameters, none of the studied metals are normally distributed, and consequently, non-parametric techniques are more suitable for further processing.

At this point, a comparison between the metallic content for both wine vinegars and their substrate wines would be very useful. Unfortunately, the lack of these data for the substrate wines used in quick vinegar elaboration, makes no possible such a comparison. However, the comparison may be focused in slow vinegars produced from substrate wines made by solera systems for which metal data are available [22]. For the sake of comparison, Table 2 shows the average metal content (mg l^{-1}) for the elements considered in our study for slow vinegars and 'Fino' wines. As can be observed, in all cases, the mean values for wine vinegars are higher than for 'Fino' wines. This could be explained by possible increases in solubility and/or corrosion phenomena. Consequently, individual metallic contents seem to be suitable descriptors for wine vinegar characterization since metal increase may be attributed to the elaboration process.

In spite of the a priori knowledge concerning the class membership of studied samples, a preliminary study based on PCA and CA has been carried out.

When PCA was applied to the autoscaled data matrix, four Principal Components (PCs) were extracted according to the Kaiser criterion [10] which explain up to 74% of variance. The communalities of every descriptor was found higher than 0.62. Thus, the true dimensionality of the descriptor space is 4.

Plots of the first principal components, are currently used for visualizing data trends. Nevertheless, as can be observed in Fig. 1, the corresponding scores plot of the studied samples for the two first PCs did not lead to a complete class separation. PC1 and PC2 account for 31.3% and 15.3% of the data variance.

The data matrix was then subjected to a hierarchical agglomerative CA of samples using the selected features. By taking the Euclidean distance as metric and using the Ward's method as amalgamation rule [23], the corresponding dendogram did not indicate a neat separation of categories.

Thus, in order to obtain suitable classification rules for assigning categories to samples, super-

Table 1
Experimental data matrix (mg l^{-1})

CODE		MG	CA	CU	ZN	FE	NA	K	AS	MN
1	Q	61.9	111.9	0.06	0.86	3.82	73.5	629.4	nd	2.56
2	Q	63.7	123.0	0.03	0.71	5.33	130.1	814.4	0.007	3.31
3	Q	69.0	196.6	0.14	1.41		109.6	141.3	0.003	
4	Q	56.0	143.1	0.03	0.58	13.91	77.9	881.3	nd	4.75
5	Q	62.9	120.0	0.04	0.58	4.90	103.3	885.6	0.007	2.54
6	Q	47.8	98.8	0.03	0.41	1.24	149.1	569.4	nd	0.51
7	Q	76.7	149.2	0.09	2.48	12.96	112.0	1132.5	0.006	2.72
8	Q	45.3	80.6	0.02	0.40	6.27	144.0	686.9	0.005	2.72
9	Q	45.9	132.1	0.05	0.84	3.85	62.6	524.4	0.005	1.37
10	Q	83.6	132.1	0.04	0.49	11.61	66.3	1167.5		5.44
11	Q	52.8	56.4	0.02	0.06	3.54	222.4	914.4	0.008	0.15
12	Q	46.7	52.4	0.02	0.18	6.30	327.5	903.8	0.008	1.45
13	Q	69.2	154.2	0.02	0.51	5.24	89.1	1191.3	nd	2.27
14	S	107.8	293.3	0.32	0.55	1.38	156.4	1911.3	0.007	1.20
15	S	108.2	132.1	2.36	6.35	23.08	114.8	1748.1	0.003	0.94
16	S	70.6	152.9	0.46	3.16	19.15	80.4	1231.9	0.012	0.54
17	S	122.6	464.2	1.30	2.98	72.75	212.3	1937.5	0.009	1.79
18	S	229.9	280.8	0.88	5.15	9.03	194.8	3825.0	0.014	3.08
19	S	137.9	88.3	0.15	5.09	9.03	126.6	1675.0	nd	1.89
20	S	104.8	146.7		5.97	9.88	126.6	2005.0	0.003	0.77
21	S	109.9	206.6	3.64	5.12	2.35	113.5	1242.5	0.008	1.81
22	S	76.2	72.5	0.62	1.28	11.78	110.8	1027.5	0.010	1.04
23	S	83.7	76.6	1.67	4.62	11.45	78.9	1551.9	0.008	0.98
24	S	106.1	242.2	6.17	8.56	26.93	140.1	1580.0	0.012	1.31
25	S	107.4	82.7	1.50	5.38	26.63	97.4	2090.0	0.005	1.37
26	S	118.8	119.7	0.29	5.25	6.20	112.0	3455.0	nd	1.99
27	S	158.2	139.5	3.99	0.61	13.90	260.8	813.1	0.022	1.40
28	S	75.7	54.7	0.23	2.70	8.83	67.1	865.0	0.006	
29	S	82.5	51.3	0.43	3.57	9.00	44.3	987.5	nd	0.68
30	S	92.2	101.2	1.21	4.48	4.90	65.4	949.4	0.021	1.23
31	S	103.1	118.9	0.45	2.07	8.45	78.6	2211.9	0.023	0.85
32	S	128.6	239.5	0.07	1.32	40.48	87.9	2785.0	0.005	1.43
33	S	176.9	101.9	0.39		29.23	245.0	3455.0	0.010	2.55
34	S	238.4	89.6	1.22	7.56	29.38	146.5		0.002	3.09
35	S	288.0	26.0	2.71	5.44	15.73	175.4	660.0	nd	3.60
36	Q	55.4	45.8		8.23	12.20	59.1	920.0	0.016	3.13
37	Q	71.8	34.5		3.99	2.13	62.1	1667.5	0.021	3.58
38	Q		47.9		4.97	12.10	76.4	2081.3	0.018	2.96
39	Q	57.9	58.8	0.05	2.18	4.40	65.9	711.9	0.016	2.17
40	Q	90.8	45.8	0.03	2.33	9.53	275.0	799.4	0.016	2.68

nd, not detected.
Holes correspond to missing values or outliers.

vised learning pattern recognition (SLPR) methods were applied.

A preliminary step in SLPR is the feature selection. This was performed according to the Wilks' lambda statistic [24,25] in order to choose the descriptors that best distinguish between classes. The Wilks' lambda statistic for the overall discrimination is computed as the ratio of the determinant of the within-group variance/covariance matrix over the determinant of the total variance/covariance matrix. A partial lambda is computed for each variable as the ratio of Wilks' lambda after adding the respective variable over the Wilks' lambda before adding the variable. A *F*-

Table 2
Average metal contents (mg l^{-1}) for slow vinegars and their typical substrate wines

Metal	Slow vinegars	'Fino' wines from [22]
MG	128	89
CA	149	97
CU	1.4	0.4
ZN	5	1.3
FE	17	4.2
NA	128	46
K	1809	583
AS	0.008	—
MN	1.5	0.7

statistic [26] is computed from the partial lambda values leading to a p-level. The maximum discriminatory power corresponds to minimum p-level values. Wilks' lambda statistic is the current procedure used for feature selection in stepwise LDA. The results of applying the Wilks' lambda statistic is depicted in Table 3. If the true dimensionality of the variable space is 4, then we will select the four most discriminant features, namely, MN, MG, NA and FE. Accordingly, the working data matrix D was obtained from the original data matrix X by deleting the columns corresponding to the non-selected descriptors. Therefore, the matrix D has as dimension 40×4 (40 samples and 4 selected features).

Another prerequisite to be fulfilled for the right application of SLPR methods [27] is that the ratio between the number of samples and the true dimension of the variable space must be greater than three. In our case this ratio is 10, which enables us to directly apply the suitable methodology.

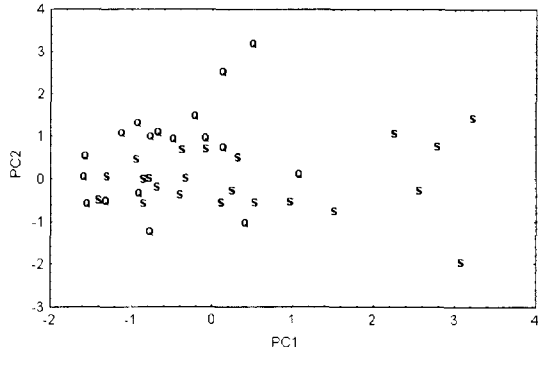

Fig. 1. Scores plot of the vinegar samples using the two first PCs (Q and S stand for samples belonging to the 'quick' and 'slow' classes).

SLPR methods assume that we, a priori, know the class number and the class membership of each sample in the training set. We have 40 vinegar samples consisting of two categories: S (22 samples) and Q (18 samples). The 40 samples were randomly divided into a training set and a prediction set. The percentage of vinegar samples taken for the prediction set was about 25% [28]. Accordingly, the prediction set contains six class S samples and five class Q samples. To suitably validate the recalling rate (goodness of classification in the training set) and the prediction ability (goodness of the classification in the prediction set) of the methods applied, both training and prediction sets were repeated at least ten times for different constitutions. The average of hits (%) in the recalling and prediction obtaining from these ten runs, is taken as a measure of the performance of the classification procedure.

3.1. Classification performance

As indicated above, four SLPR methods have been applied for distinguishing between classes Q and S, namely, KNN, LDA, SIMCA and BPANN. These selected methods are very different in nature. KNN and BPANN are non-parametric methods. According to the non-Gaussian distribution of the variables, non parametric methods were considered the best choice. In the following we describe the different results obtained.

3.1.1. KNN

Before applying KNN, data were autoscaled. The best number of K neighbours is selected from a leave-one-out procedure [27]. Both $K = 1$ and $K = 3$ led to best results. Then learning and prediction sets were applied. In both cases neither false positives nor false negatives were found in recalling/prediction.

Table 3
Results issued from the application of Wilks' lambda statistics for exploring the discriminating power of variables

Variable	Wilks' lambda	Partial lambda	Rao's F	p-Level
MG	0.293	0.577	15.413	0.0008
CA	0.169	1.000	0.004	0.9477
CU	0.177	0.957	0.937	0.3441
ZN	0.175	0.968	0.701	0.4118
FE	0.182	0.929	1.609	0.2185
NA	0.234	0.722	8.074	0.0098
K	0.181	0.936	1.435	0.2443
AS	0.173	0.975	0.533	0.4732
MN	0.296	0.571	15.752	0.0007

3.1.2. BPANN

The architecture selected for BPANN in our studies was $4 \times 3 \times 2$ (plus bias), that is, four neurons in the input layer (corresponding to the four selected descriptors), three neurons in the hidden layer (empirically chosen) and two neurons in the output layer, which corresponds to the two classes S and Q. The target output written in binary form is (1 0) for S and (0 1) for Q. The % Hits is calculated from:

$$\%\ \text{Hits} = 100 \cdot \frac{\sum_{l=1}^{J} \sum_{k=1}^{2} f(\text{out}_{kl} - t_{kl})}{2J} \qquad (1)$$

J being the number of patterns in the training set (recalling) or in the test (prediction) set and f is a function that returns 1 (hit) for arguments less or equal to 0.2 (maximum target error selected) and 0 (fail) otherwise. The objects were previously normalized between 1 and -1. Initial weights were taken randomly between -0.1 and 0.1. Training objects were taken at random. Maximal epochs selected were 1000, learning rate $\eta = 0.2$ and momentum $\mu = 0.5$ were kept constant during training. Always sigmoidal transfer functions were used.

The recalling performance was 100% hits always. In some cases however, a false negative occurred when testing the prediction set, leading to a prediction ability greater than 99%

3.1.3. SIMCA

In our investigation, we perform data autoscaling on each class separately. Then each class was modelled according to the first significant own PCs (issued from NIPALS algorithm [17] according to the cross-validation results). The goodness of fit variance for each class k (k = S or Q), S_k^2 is calculated as the sum of squares of residuals when all training objects are fitted to its PC-model divided by $(4-f)(n-f-1)$ (f is the number of significant PCs for the considered class and n is the number of training objects for the class). In order to construct the k-class envelope, a maximal variance for the class is evaluated according a critical F-test value [18]: $S_{k,max}^2 = F_{crit} S_k^2$. Where F_{crit} if the tabulated value for $4-f$ and $(4-f)(n-f-1)$ degrees of freedom at an α significance level. Any test object may be assayed to belong to k-class by computing the variance when the test object is fitted to the k-class PC-model, S_{test}^2. If $S_{test}^2 > S_{k,max}^2$ then the test object does not belong to class k.

When SIMCA were applied to the training data, both classes Q and S were modelled from zero PCs. In the validation step, recalling performance was of about 89% in average. Prediction ability was of about 82%. SIMCA being a soft modelling procedure, enables us to assess for possible class overlapping. Accordingly we found a high overlapping between the two class boxes. This led to a high amount of false positives for each class in both training and prediction set. All S-objects were classified as belonging to the class Q except for one on average. Similarly, all Q-objects were considered as belonging to class S except for two or three cases depending on the validation run. Thus, SIMCA was unable to achieve the separation of class envelopes.

Table 4
Performance of classification based on Mg, Na and Fe

Method	Recalling (% hits)	Prediction (% hits)	Remarks
KNN	100	100	Normalized data, $K = 1$ and $K = 3$
BPANN	100	99	$4 \times 3 \times 2$, $\mu = 0.5$, $\eta = 0.2$, 1000 epochs, sigmoidal transfer
SIMCA	89	82	High class overlapping
LDA	100	99	Classification based on a posteriori probabilities

3.1.4. LDA

LDA being a parametric technique, perhaps it would seem needless to apply it in situations where the variables do not follow the normal distribution. Nevertheless, these requirements are not absolute and should be regarded as conditions for achieving optimal boundaries between classes. Fisher classification functions were derived and classifications were made according to the a posteriori probabilities. A given object is classified in the class which gives a higher a posteriori probability. In the validation step, the hits (success in classification) in both recalling and prediction were always 100%.

The classification performance attained with the different SLPR methods is summarized in Table 4, with the exception of SIMCA method. Apparently Mg, Fe, Na and Mn seem to be optimal descriptors for distinguishing between class Q and class S vinegars. However, a shadow of doubt remains when we are aware of SIMCA nature. The philosophy of SIMCA embraces the called second level of pattern recognition [29]. Thus, whereas level-1 builds frontiers between classes, level-2 builds boundaries between any class and the rest of the universe. On level-2 pattern recognition works by containing each class in a closed mathematical structure (envelope). The class envelopes are constructed so that an object inside the envelope is considered to be a normal member of the class and an object outside all envelopes are considered an outlier. SIMCA is one of the methods that operates in this second level. Thus, in cases where the classes are non homogeneously distributed, the selection of probability levels for drawing the borderline between each class and the rest of the variable space is crucial and sometimes makes impossible the net separation of class envelopes.

4. Conclusion

The set of studied vinegars can be divided into two groups: slow (S) and quick (Q) vinegars. The difference between these groups arises mainly from the descriptors Mg, Fe, Na and Mn. KNN, LDA and BPANN procedures led to excellent classifications with a percentage of hits in both recalling and prediction of almost 100% always. SIMCA method, however, did not permit the net separation of class envelopes.

References

[1] J. Nieto, M.A. González-Viñas, P. Barba, P.J. Martín-Alvarez, L. Aldave, E. García-Romero, M.D. Cabezudo, Recent progress in wine winegar R&D and some indicators for the future, in: G. Charalambous (Ed.), Food Flavors, Ingredients and Composition, Elsevier, New York, 1993, pp. 469–500.
[2] C. Llaguno, M.C. Polo, La composición química de los vinagres vínicos, in: El vinagre de vino, Consejo Superior de Investigaciones Científicas, Madrid, 1991, pp. 105–131.
[3] M.I. Guerrero, F.J. Heredia, A.M. Troncoso, J. Sci. Food Agric. 66 (1994) 209.
[4] A.M. Troncoso, M. Guzmán, Die Nahrung 32 (1988) 743.
[5] P. Etievant, P. Schlich, J.C. Bouvier, P. Symonds, A. Bertrand, J. Sci. Food Agric. 45 (1988) 25.
[6] M.J. Latorre, C. García-Jares, B. Medina, C. Herrero, J. Agric. Food Chem. 42 (1994) 1451.
[7] F. Conrradini, L. Marcheselli, A. Marchetti, C. Petri, C. Biancardi, J. AOAC Int. 77 (1994) 77.
[8] M.I. Guerrero, C. Herce-Pagliai, A.G. González, F.J. Heredia, A.M. Troncoso, A.M. Cameán, Science des Aliments 16 (1996) 143.
[9] C. Chatefield, A.J. Collins, Introduction to Multivariate Analysis, Chapman&Hall, London, 1980.
[10] E.R. Malinowski, Factor Analysis in Chemistry, Wiley, London, 1991.

[11] D.L. Massart, L. Kaufman, Interpretation of Analytical Data by use of Cluster Analysis, Wiley, New York, 1983.
[12] B. Everitt, Cluster Analysis, Halsted Press, New York, 1974.
[13] P.A. Lachenbruch, Discriminant Analysis, Hafner Press, New York, 1975.
[14] D. Coomans, D.L. Massart, L. Kaufman, Anal. Chim. Acta 112 (1979) 97.
[15] D.L. Massart, A. Dijkstra, L. Kaufman, Evaluation and Optimization of Laboratory Methods and Analytical Procedures, Elsevier, Amsterdam, 1978.
[16] A.M. Harper, D.L. Duewer, B.R. Kowalski, J.L. Fasching, ARTHUR and Experimental data analysis. The heuristic use of a polyalgorythm, in: R.F. Gould (Ed.), Chemometrics: Theory and Application, American Chemical Society, Washington, 1981, p. 14.
[17] S. Wold, M. Sjoström, in: B.R. Kowalski (Ed.), Chemometrics: Theory and Applications, American Chemical Society, Washington, 1977, p. 243.
[18] M.P. Derde, D. Coomans, D.L. Massart, J. AOAC Int. 67 (1984) 721.
[19] J. Zupan, J. Gasteiger, Neural Networks for Chemists, VCH, Weinheim, 1993, pp. 119–148.
[20] J.R. Long, H.T. Mayfield, M.V. Henley, P.R. Kromann, Anal. Chem. 63 (1991) 1256.
[21] J.C. Miller, J.N. Miller, Statistic for Analytical Chemistry, Ellis Horwood, Chichester, 1988.
[22] M. López-Artíguez, A.M. Cameán, M. Repetto, J. AOAC Int. 79 (1996) 1191.
[23] J. Ward, J. Am. Stat. Assoc. 58 (1963) 236.
[24] S.S. Wilks, Biometrika 24 (1932) 471.
[25] G.P. McCabe Jr., Technometrics 17 (1975) 103.
[26] C.R. Rao, Bull. Inst. Int. Stat. 23 (1951) 177.
[27] K. Varmuza, Pattern Recognition in Chemistry, Springer Verlag, Heidelberg, 1980.
[28] M.J. Martín, F. Pablos, A.G. González, Anal. Chim. Acta 320 (1996) 191.
[29] C. Albano, W. Dunn III, U. Edlund, E. Johansson, B. Norden, M. Sjöström, S. Wold, Anal. Chim. Acta 103 (1978) 429.

ELSEVIER

Talanta 45 (1997) 387–395

Talanta

Dicyclohexano 18 crown 6 in butanol–octanol mixture: A promising extractant of Sr(II) from nitric acid medium

Amar Kumar [a], P.K. Mohapatra [b], P.N. Pathak [b], V.K. Manchanda [b,*]

[a] *Waste Management Projects Division, B.A.R.C., Mumbai 400085, India*
[b] *Radiochemistry Division, B.A.R.C., Mumbai 400085, India*

Received 25 November 1996; received in revised form 29 April 1997; accepted 5 May 1997

Abstract

The extraction of strontium from nitric acid medium was investigated employing DCH18C6 in aliphatic alcohols as the diluents. 80% Butanol–20% octanol mixture was found to give higher D_{Sr} values as compared to other alcohols investigated. A linear correlation between the organic phase water content and D_{Sr} was observed, based on which the extraction mechanism was postulated. Effect of anion, cation, extractant concentration, nitric acid concentration and temperature on D_{Sr} was also studied. Conditions for recovery (> 90%) were arrived at and selectivity with respect to other interfering fission products was observed with most of the metal ions studied. © 1997 Elsevier Science B.V.

Keywords: Dicyclohexano 18 crown 6; Butanol–octanol mixture; Sr(II)

1. Introduction

^{90}Sr ($T_{1/2} = 28.5$ years) is one of the important long lived fission products present in high level waste (HLW) solution generated during the reprocessing of spent nuclear fuel. It's cumulative worldwide arisings is estimated at around 10^4 kCi [1]. Due to it's long biological as well as radioactive half lives, it is desirable to separate it from HLW to restrict the personnel radiation exposure during the conditioning of waste and to prevent the thermal deformation of conditioned waste matrix. In addition, there is a growing interest to use ^{90}Sr as a compact power source.

Early extraction procedures for the recovery of ^{90}Sr were based on the use of diethyl hexyl phosphoric acid and chlorinated cobalt dicarbolide as extractants [2–4]. These methods suffered from several drawbacks like a) the need to keep aqueous acidity < 0.1 M, b) high toxicity of diluents employed and c) the use of complexing agents to improve the Sr selectivity. Crown ethers have been employed in recent years by several workers to selectively extract Sr(II) in the presence of actinides and fission products from relatively stronger acidic solution (> 1.0 M) [5]. However, the use of chlorinated hydrocarbons as diluents did not allow any widescale applications of crown ethers in the recovery of ^{90}Sr from HLW solution. Horwitz et al., have investigated dicyclohexano18crown6 (DCH18C6) and it's di-*tert*-

* Corresponding author. Fax: +91 22 5560750.

PII S0039-9140(97)00142-2

butyl derivative (DTBCH18C6) as Sr selective extractants employing a variety of oxygenated aliphatic diluents e.g. alcohols, ketones, carboxylic acids and esters [6]. In contrast to the chlorinated hydrocarbon diluents, it was observed that for the oxygenated diluents the distribution ratio of Sr (D_{Sr}) increases continuously with the increase of nitric acid concentration. A linear correlation was observed between the extraction of Sr and concentration of water in the organic phase. Of the solvents examined, n-octanol was chosen by Horwitz and co-workers in view of it's ability to dissolve large amount of water and rapid phase disengagement rate [7]. Lower homologues of n-octanol viz. n-propanol, n-butanol though superior in terms of water uptake ability, were found unsuitable due to their high miscibility with aqueous phase and poor phase disengagement rate. Similarly, di-*tert*-butyl derivative of DCH18C6 was found to be a better extractant compared to DCH18C6 particularly at ligand concentration >0.05 M which was ascribed to the molecular aggregation phenomenon and the latter was reportedly influenced by the formula weight of the alcohol used as diluent. There is also a need to explore alternate reagent system in view of the prohibitive cost of DTBCH18C6 for (SREX) process application. It was thought of interest therefore to investigate the use of mixture of n-octanol with it's lower homologues viz. n-butanol for the extraction of Sr employing commonly available DCH18C6 under varying conditions of acidity and ligand concentration.

2. Experimental

2.1. Reagents

Cis-DCH18C6 (a mixture of cis–syn–cis and cis–anti–cis), purity $>99\%$ was obtained from Aldrich Chemical Co. U.S.A. DTBDCH18C6 was procured from Eichrom Industries Inc. U.S.A. All other crown ethers were obtained from E. Merck, Germany. A.R. grade solvents viz. n-octanol (Spectrum), n-decanol (Merk), n-hexanol (BDH), n-pentanol (Fluka), n-butanol (Qualigen) and n-propanol (Celanese Corp. U.S.A.) were used as supplied. Karl–Fischer reagent was procured from Qualigen Fine Chemicals, Bombay.

2.2. Extraction of nitric acid

The amount of nitric acid extracted by various diluents was determined volumetrically. Organic phase was pre-equilibrated with equal volume of nitric acid of desired concentration (1–8 M) repeatedly. Known aliquot of the organic phase was titrated with a standard NaOH solution using phenolphthalein as indicator. It was observed that three contacts were sufficient to attain equilibrium concentration of nitric acid in the organic phase. Acid uptake values corresponding to $[HNO_3]_{aq} = 4.05$ M, $V_{aq}/V_{org} = 1.0$; are 1.40 M (one contact), 1.84 M (two contacts), 1.95 M (three contacts).

2.3. Extraction of water

Water uptake in the organic phase was measured by Karl Fischer titration method. Organic phase after pre-equilibration was centrifuged and an aliquot (100 microlitres) was added to moisture free methanol followed by titration with the Karl–Fischer reagent. Water content in the unknown sample was computed from the volume of titrant employing conversion factor obtained earlier with known amount of water content.

2.4. Distribution studies

The dispersion numbers for the diluent mixtures were calculated from the equation:

$$N_{Di} = \frac{1}{t_B}\sqrt{\frac{\Delta Z}{g}} \quad (1)$$

where t_B is the settling time in seconds, ΔZ, the total height of two phases in meters and $g = 9.81$ m sec^{-2}.

The partition coefficient of the ligand DCH18C6 in 80% butanol–20% octanol mixture was estimated by an indirect method. The ligand solution (0.1 M in 80% butanol–20% octanol mixture) was equilibrated with equal volume of 4 M HNO_3. After separation of the phases, the aqueous phase was spiked with $^{85,89}Sr$ tracer and equilibrated with equal volume of the diluent

mixture which contained no ligand. From the D_{Sr} value the ligand concentration (x) can be estimated using a previously constructed calibration line. The partition coefficient is calculated as the quotient of the concentration of the ligand remaining in organic phase (0.1 M $-x$) to that in the aqueous phase (x).

Equal volumes (1 ml each) of pre-equilibrated organic phase and chosen aqueous phase (spiked with $^{85,89}Sr$) were agitated in a thermostated water bath for 30 minutes. It was established earlier that contact time of 10 minutes was sufficient to attain equilibrium (Table 1). Known aliquots (100–300 μl) were withdrawn from two phases after centrifugation. $^{85,89}Sr$ activity was determined using NaI(Tl) detector. D_{Sr} is defined as

$$D_{Sr} = \frac{\text{Counts per minute per unit volume of organic phase}}{\text{Counts per minute per unit volume of aqueous phase}} \quad (2)$$

Distribution experiments were also carried out in the temperature range 10 ± 0.1°C to 50 ± 0.1°C. Sr concentration was maintained in the concentration range of 40–50 ppm during this work.

3. Results and discussion

18 membered crown ethers (cavity radius = 1.45 ± 0.15 Å) have been found to be size selective complexing ligands for Sr^{2+} (ionic radius = 1.13 Å) and are therefore capable of liberating the water molecules associated with the metal ion in aqueous phase [7]. However, the transfer of such cationic crown ether complex species across the interphase necessitates the presence of suitable counter anion in the organic phase [8]. Large volume organophilic anions like picrate, tetraphenyl borate and chloroacetate have been found to be quite effective counter anions in this direction. In addition, ion pair extraction necessitates the use of polar solvents capable of ion solvation.

Table 1
Distribution ratio of Sr^{2+} as a function of the time of equilibration; [DCH18C6] = 0.1 M; $[HNO_3]_{aq}$ = 4.05 M; diluent: 80% butanol–20% octanol

Time of equilibration (minutes)	D_{Sr}
2	6.83
5	7.02
10	7.61
20	7.60
30	7.61
60	7.63

Hard base nature of the nitrate anion (encountered in the high level nuclear waste solution) results in the interaction of large number of water molecules with it in the aqueous phase. To facilitate the transfer of such anions towards the organic phase one needs to provide sufficient chemical energy to liberate these water molecules. Prevalent electrostatic interactions between the strontium crown ether complex (cation) and hydrated nitrate (anion) are too weak for this purpose. As an alternative, oxygenated solvents like alcohols (capable of dissolving water as a consequence of hydrogen bonding) have been employed successfully for the transfer of hydrated nitrate (as counter anion) towards the organic phase. Results obtained during the present work are summarized below.

3.1. The effect of the nature of ligand

To understand the role of crown ether cavity and the nature of substituents, a study was undertaken to determine D_{Sr} values in the presence of various crown ethers under identical experimental conditions. Table 2 shows that except for DTBCH18C6 and DCH18C6, extraction of Sr is poor ($< 5\%$) for all other ligands. Solubility problem was encountered for dibenzo 18 crown 6 and dibenzo 24 crown 8. Inadequate extraction for 12 membered (cavity radius: 0.67 ± 0.07 Å) and 15-membered (cavity radius: 0.97 ± 0.12 Å) ligands substantiate the role of size compatibility in complexation and extraction of Sr. Very high extraction observed for DTBCH18C6 has been attributed to the existence of this ligand as monomer in wide concentration range as against

Table 2
Influence of the nature of the ligand on D_{Sr}, ligand concentration = 0.1 M in n-octanol; aqueous phase: 4.05 M HNO_3

Ligand	D_{Sr}
12Crown4	0.01
15Crown5	0.05
18Crown6	0.03
Benzo15Crown5	<0.01
Dibenzo24crown8[a]	0.02
Dibenzo18Crown6[a]	—
Dicyclohexano18crown6	3.31
Di-*t*-butylcyclohexano18crown6	15.8

[a]Poor dissolution in n-octanol.

the aggregation of DCH18C6 beyond 0.01 M [6]. However, due to the easy availability and relatively low cost of the latter, attempts were made in the present studies to arrive at the suitable conditions which may enable the effective use of the higher concentration of this ligand.

3.2. The effect of the carbon chain length of the aliphatic alcohols

Though several classes of oxygenated solvents have been employed for the extraction of Sr^{2+}, no data is available on the use of such mixed solvents. Presence of TBP in n-octanol has been found to cause decrease in the water activity of the organic phase as well as D_{Sr} in the extraction system Sr^{2+}–1 M HNO_3/0.1 M DCH18C6–TBP–octanol [9]. On the other hand, TBP enhanced the D_{Sr} value in the extraction system Sr^{2+}–2.7 M HNO_3/0.2 M DTBCH18C6–TBP–Isopar L [10]. An attempt has been made in the present work to employ a mixture of 20% n-octanol–80% R–OH (where R represents alkyl group other than C_8H_{17}) as diluent for determining the uptake of water. Table 3 shows that $[HNO_3]_{org}$ and water content of the organic phase increases continuously with the decrease of chain length (R) from $C_{10}H_{21}$ to C_4H_9 which appears to be a consequence of the continuous increase in effective concentration of –OH functional group of alcohols. Thus the uptake of water in organic phase is related to the hydrogen bonding between the water and alcohol molecules. Table 3 also shows that D_{Sr} value increases gradually with the decrease of chain length of R–OH. Experiments with R=C_3H_7 as well as with $\geq$90% C_4H_9–OH content could not be pursued due to sluggish phase disengagement. The dispersion numbers obtained using 80% butanol–20% octanol mixture and 90% butanol–10% octanol mixture were 2.6×10^5 and 1.0×10^5 respectively. $[H_2O]_{org}$ observed for lower proportion of propanol (60%) is too low (6.08 M) to merit consideration of such mixed diluents in this study. Fig. 1 shows the expected continuous increase in $[H_2O]_{org}$ as well as

Table 3
Effect of nature of diluent on $[HNO_3]_{org}$, $[H_2O]_{org}$ and D_{Sr}, [DCH18C6] = 0.1 M; Aqueous phase = 4.05 M HNO_3; 20% n-octanol–80% R–OH.

Diluent (R–OH)	$[HNO_3]_{org}$ (M)	$[H_2O]_{org}$ (M)	D_{Sr}
decanol	0.84	2.58	2.78
octanol	1.10	3.20	3.31
hexanol	1.34	4.90	5.87
pentanol	1.54	6.80	6.45
butanol	2.10	10.40	7.65
90%butanol–10% octanol[a]		12.0	
100% butanol[b]			
80%propanol–20% octanol[b]			
60%propanol–40%octanol		6.08	
40% propanol–60% octanol		3.68	

[a]Phase separation sluggish;
[b]No phase separation.

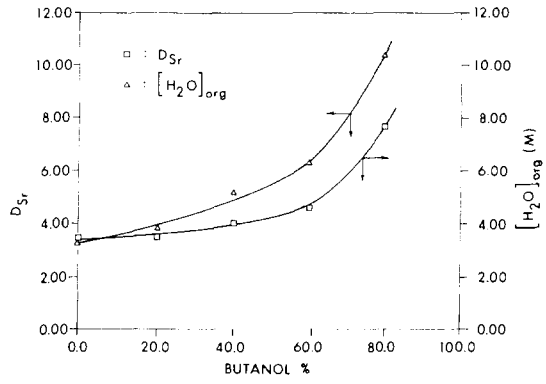

Fig. 1. Distribution ratio of Sr^{2+} and the organic phase water content as a function of increasing butanol content in butanol–octanol mixture; [DCH18C6] = 0.1 M; $[HNO_3]_{aq}$ = 4.05 M.

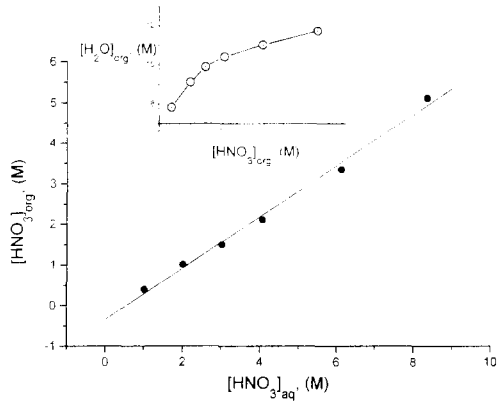

Fig. 2. Nitric acid concentration in the organic phase as a function of aqueous nitric acid concentration; diluent: 80% butanol–20% octanol. Inset: correlation between the organic phase water content and the concentration of nitric acid in the organic phase.

D_{Sr} with increasing proportion of butanol in n-butanol–n-octanol mixture. Due to the increase of D_{Sr} by 2.3 times with 20% n-octanol–80% n-butanol mixture as compared to that in n-octanol, further studies were carried out using the former.

3.3. The effect of $[HNO_3]_{aq}$ concentration

Fig. 2 shows an excellent linear correlation between $[HNO_3]_{org}$ and $[HNO_3]_{aq}$ which suggests that at equilibrium, a little more than half of the

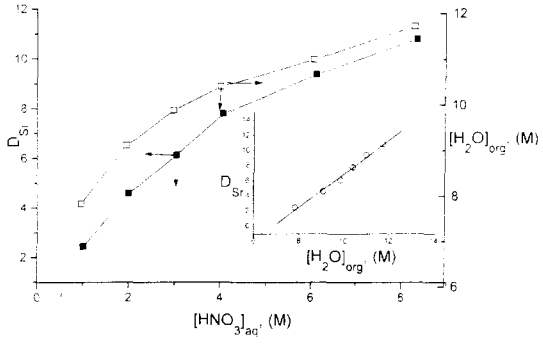

Fig. 3. Distribution ratio of Sr^{2+} and organic phase water content as a function of aqueous nitric acid concentration; [DCH18C6] = 0.1 M; diluent: 80% butanol–20% octanol. Inset: correlation between the distribution ratio of Sr^{2+} and the organic phase water content; [DCH18C6] = 0.1 M; diluent: 80% butanol–20% octanol.

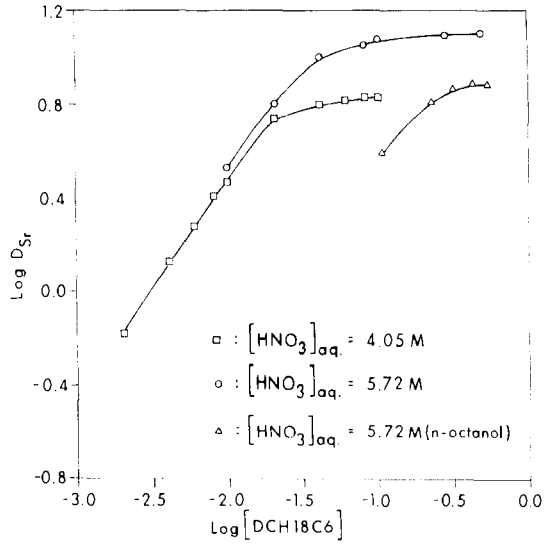

Fig. 4. Distribution ratio of Sr^{2+} as a function of DCH18C6 concentration in the mixed diluent (□,○) and n-octanol (△).

aqueous nitric acid concentration is distributed towards the organic phase. On the other hand, a non-linear relation between $[H_2O]_{org}$ and $[HNO_3]_{org}$ is observed (Fig. 2 inset). The presence of water in the organic phase (4.7 M) is explained on the basis of water solubility in the mixed diluent in the absence of nitric acid. The associated water content does not increase proportionately with increase of $[HNO_3]_{org}$ as the organic phase approaches the limit of water saturation.

Fig. 3 (inset) shows an excellent linear relation between D_{Sr} and $[H_2O]_{org}$ but as expected, no such relation was observed between $[HNO_3]_{aq}$ and $D_{Sr}/[H_2O]_{org}$ (Fig. 3). It appears that during the extraction of Sr, solvation of the species of the type $SrL^{2+}.2\ NO_3(H_2O)_y^-$ is facilitated by the presence of water in the organic phase. It is also evident from Fig. 3 that for [DCH18C6] = 0.1 M, 7 M H_2O is required to be present in the organic phase before the measurable D_{Sr} value is obtained. Few experiments conducted with aqueous phase at pH ~ 6 resulted in $D_{Sr} < 0.001$, as sufficient quantity of nitrate anion and water required for the solvation of $NO_3(H_2O)_y^-$ was not available. It has not been possible to demonstrate nitrate ion dependence of +2 on D_{Sr} either in the present work or by other workers who have carried out similar

studies earlier. This is attributed to the variation in degree of hydration of nitrate ion and it's influence on solvation.

3.4. The effect of the concentration of DCH18C6

Fig. 4 shows log D_{Sr} – log DCH18C6 plots with aqueous nitric acid concentrations at 4.05 M and 5.72 M respectively. Slope of around unity up to [DCH18C6] = 0.01 M suggests that extracted complex involves 1:1 metal ligand species in this concentration range. It is interesting to observe that the slope value decreases when ligand concentration is increased further. Aggregation favoured at higher ligand concentration [12] appears to be influenced by the nature of ligand, solvent as well as concentration of HNO_3. Decreased curvature in the log D_{Sr} – log [DCH18C6] plots at 5.72 M HNO_3 as against that at 4.05 M HNO_3 beyond [DCH18C6] of 3.0×10^{-2} M suggest ligand aggregation to a lesser extent with increased acidity (Fig. 4). Earlier, it has been reported that the presence of methyl- as well as *t*-butyl- groups on dicyclohexano substituents also suppress the aggregation and therefore the latter was preferred for process (SREX) applications for the recovery of ^{90}Sr from the high level waste solutions [7]. Use of mixed diluents also favours the Sr extraction vis-a-vis n-octanol in the ligand concentration range 0.1 M to 0.5 M.

Table 4
Conditional extraction constant (K_{ex}) as a function of ligand concentration and nitric acid concentration under different experimental conditions in 80% butanol–20% octanol mixture

Ligand concentration[a]	K_{ex}	HNO_3 concentration[b]	K_{ex}
0.002	32.24	1.02	160.1
0.004	32.83	2.00	79.4
0.006	31.03	3.00	41.4
0.008	31.41	4.05	28.91
0.01	28.91		
0.02	26.97		
0.04	15.48		
0.08	8.30		
0.1	6.64		

[a] $[HNO_3] = 4.05$ M;
[b] [DCH18C6] = 0.01 M.

Table 5
Influence of $[HCl]_{aq}$ on $[H_2O]_{org}$ and D_{Sr}; [DCH18C6] = 0.1 M

$[HCl]_{aq}$ (M)	$[HCl]_{org}$ (M)	$[H_2O]_{org}$ (M)	D_{Sr}
0.98	0.20	7.20	0.10
1.84	0.47	8.45	0.20
4.00	1.57	12.89	0.53
6.12	3.27	22.32	0.84

As reported by Horwitz et al., [6] the use of the oxygenated aliphatic diluents which favour the uptake of water increase the K_{ex} value defined by Eq. (3).

$$Sr^{2+}_{(aq)} + 2NO^{-}_{3,(aq)} + L_{(org)} + xH_2O_{(org)} \rightleftharpoons SrL^{2+}.2(NO_3)^{-}.xH_2O_{(org)} \quad (3)$$

Table 4 shows the conditional K_{ex} values obtained in the present work under varying experimental conditions. Decrease of K_{ex} with increase of ligand concentration at 4.05 M HNO_3 supports the aggregation hypothesis [12]. In spite of using the mixed diluent, lower K_{ex} value (31.9) compared to the earlier reported value (47.9 by Horwitz et al., [7]) is ascribed as due to the larger $[HNO_3]_{aq}$ in our work. At 1.02 M HNO_3, as expected K_{ex} value is significantly larger in mixed diluent system. Table 4 also shows clearly that K_{ex} values decline sharply with increase of $[HNO_3]_{aq}$ indicating a complex mechanism of extraction involving $[H_2O]_{org}$ as discussed earlier.

3.5. The effect of the nature of the counter anion

It was reported that the extraction of Sr^{2+} is distinctly larger from HNO_3 medium as compared to that from HCl medium in the presence of 0.005 M DCH18C6 and dehydration of the anion does not probably occur in either case [11]. It was observed during the present work (Table 5) that water uptake is much larger for HCl system particularly at higher acidity (≥ 4 M). It was quite surprising to note that D_{Sr} values on the other hand were much lower for HCl system as compared to those for HNO_3 system (Fig. 5). This is contradictory to the linear correlation depicted in Fig. 3. It is possible that large number of water molecules associated with Cl^- causes the ionic

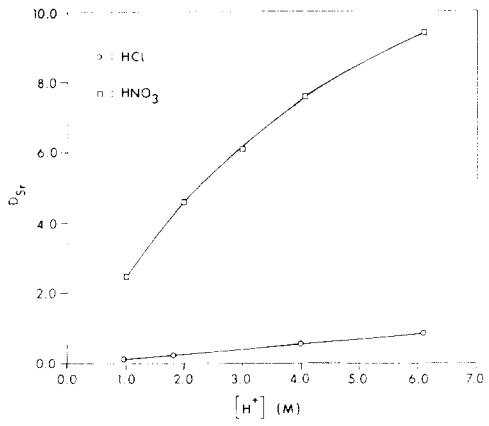

Fig. 5. Distribution ratio of Sr^{2+} as a function of aqueous acidity; [DCH18C6] = 0.1 M; diluent: 80% butanol–20% octanol, (○) HCl, (□) HNO_3.

potential of hydrated chloride anion to be lower than the corresponding nitrate anion thereby affecting the electrostatic interaction (ion pairing energy) between SrL^{2+} and the hydrated chloride ion adversely.

3.6. The effect of foreign cations

It has been reported that based on the salting out principle, the addition of metal nitrates is helpful in increasing D_{Sr} values [5]. During the present study, experiments were conducted in the presence of $Al(NO_3)_3$, $Mg(NO_3)_2$ and

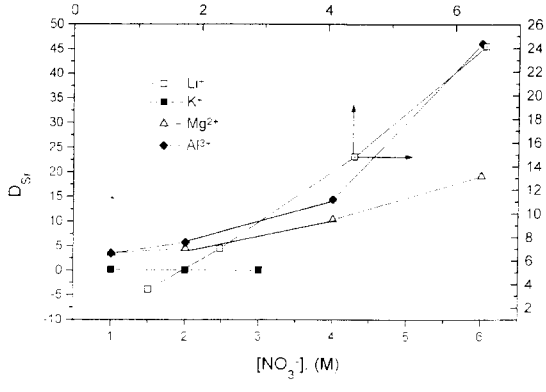

Fig. 6. Effect of inert metal nitrates on the distribution ratio of Sr^{2+}; [DCH18C6] = 0.1 M; diluent: 80% butanol-20% octanol.

Table 6
Effect of temperature on D_{Sr}. [DCH18C6] = 0.1 M; [HNO_3] = 4.0 M

Temperature (K)	D_{Sr}
283.15	8.88
298.15	7.19
308.15	5.57
323.15	4.93

$Li(NO_3)$ and were compared with the results obtained with HNO_3. These salts were chosen in view of smaller ionic radii (0.50 Å–0.65 Å) of the corresponding cations which are non-compatible towards DCH18C6 as compared to Sr^{2+}. Ions such as Na^+ and K^+ which have larger ionic radii (0.95 Å–1.33 Å) compete with Sr^{2+} (1.13 Å) for the ligand. It is interesting to note that in sharp contrast to the behaviour with HNO_3, water uptake is independent of the concentration of salt. Whereas with $LiNO_3$ (range 1.2 M–6.5 M), there is a marginal increase in water uptake from 4.7 M (with distilled water) to 5.4 ± 0.3 M, there was no increase observed in the case of $Mg(NO_3)_2$ and $Al(NO_3)_3$. It appears that these cation hydrates cannot be solvated by the solvent mixture chosen in the present study. However, the decrease of water activity in the aqueous phase caused by the presence of salts appear to facilitate the complexation of Sr^{2+} with DCH18C6 which is reflected in corresponding D_{Sr} values (Fig. 6). On the other hand, in presence of KNO_3 the D_{Sr} values show a decreasing trend with increasing salt concentration. Fig. 6 clearly demonstrates that efficiency of extraction increases with the increase of ionic potential of cations. It is evident that the D_{Sr} values corresponding to 6 M NO_3^- decrease in the order Al^{3+} (2 M) > Li^+ (6 M) > Mg^{2+} (3 M) > H^+ (6 M) ≫ K^+ (6 M, extrapolated data point). Values in brackets show the cation concentration corresponding to 6 M nitrate. This order can be explained considering a) hydration energy and b) concentration of the cation and c) size compatibility of the cation.

Table 7
Stripping behaviour of Sr with varying V_a/V_o as well as with multiple contacts ($V_a/V_o = 1$)

Single contact[a]		Multiple contacts ($V_a/V_o = 1$)[b]	
V_a/V_o	% stripping	Contact No.	% stripping
1	23.4	1st	23.4
2	52.9	2nd	35.3
4	82.8	3rd	33.3
6	92.5		
8	96.6		

[a]Aqueous phase is distilled water;
[b]Organic phase was obtained by contacting 0.1 M DCH18C6 in 80% butanol–20% octanol with $^{85/89}Sr$ tracer in 4.05 M nitric acid

3.7. The effect of temperature

Table 6 gives the extraction data obtained as a function of temperature. The D_{Sr} values decrease with increasing temperature which is in sharp contrast to the extraction behaviour reported with DTBCH18C6 [6] where no change in the D_{Sr} was observed with temperature. The ΔH and ΔS values for the present extraction system were calculated to be -2.81 kcal mol^{-1} and -5.66 cal K^{-1} mol^{-1} respectively suggesting that the free energy change is enthalpic in nature.

Table 8
Comparison of selectivity of 0.01 M DCH18C6 in 80%butanol–20%octanol mixture (D_1, present study) and 0.2 M DTBCH18C6 in n-octanol (D_2, [7])

Fission products	D_1(4 M HNO_3)	D_2(3 M HNO_3)
^{85}Sr	9.49	22
^{137}Cs	0.076	0.04
^{99}Mo	1.24	0.13
^{97}Zr	0.20	0.02
^{140}Ba	1.16	11
^{105}Ru	1.3	0.26
^{147}Nd	<0.01	<0.01
^{141}Ce	<0.01	<0.01
^{140}La	<0.01	<0.01

3.8. Stripping behaviour

Table 7 shows the % stripping of Sr with different org/aq. phase volume ratios. It is required to keep large aqueous (V_a)/organic (V_o) volume ratio (8:1) to strip about 96.6% of Sr. On the other hand, three contacts with 1:1 aq/org. ratio results in ~92% stripping of Sr(II). Poor stripping of Sr(II) is attributed to the large uptake of HNO_3 in the organic phase during forward extraction step. Only a part of $[HNO_3]_{org}$ is transferred towards the aqueous phase in every step. Nitric acid present in the aqueous phase prevents the quantitative stripping of Sr in a single contact. Preliminary experiments carried out during the present study suggest the possibility of removing HNO_3 preferentially over Sr from the stripped aqueous phase using 45% alamine 336–45% dodecane–10% butanol. This reagent mixture is capable of transferring 0.9–1.1 M HNO_3 towards the organic phase ($V_o/V_a = 1$; $[HNO_3]_{aq} = 1$–2 M) without extracting any measurable quantity of Sr. Thus it provides a means of efficient stripping in a Sr recovery process.

3.9. Extraction selectivity

Distribution ratio values measured on various fission products using 0.01 M DCH18C6 in the mixed diluent are shown in Table 8. ^{252}Cf source (spontaneous fission half life = 84.5 years) was used to obtain the fission product activity which was collected on an Al foil. Subsequently the foil was dissolved in 4 M HNO_3 and ^{137}Cs was spiked into it. D_{Sr} is significantly larger than that obtained with pure 4 M HNO_3 due to the presence of $Al(NO_3)_3$. Selectivity of Sr over trivalent lanthanides is excellent, it is fairly good over Cs and only moderate over Zr, Mo, Ba and Ru. Presence of large concentation of Al (10 mg ml^{-1}) appears to influence the absolute as well as the relative D values of various fission products.

3.10. Evaluation as a process solvent

Partition coefficient of DCH18C6 in 80% n-butanol–20% n-octanol is ~33.5 suggesting a loss of ~3% towards the aqueous phase. Similarly,

the loss of diluent towards the aqueous phase is ~ 7% during each equilibration contact. This indeed is a major drawback of the present extraction system for any process application. On the other hand, large enhancement in D_{Sr} is a major advantage. The presence of electrolyte also increases D_{Sr} many fold in the present extraction system which is an additional advantage over the SREX process solvent. Evaluation of this solvent for any large scale process application is necessarily based on these merits and demerits. Additional experiments with multiple contacts under higher loading of Sr need to be performed to evaluate the solvent for process application.

4. Conclusions

DCH18C6 in the mixed diluent (80% butanol–20% octanol) extracts Sr^{2+} from nitric acid medium efficiently by enhancing the water uptake towards the organic phase. Aggregation of the ligand is not observed up to 0.01 M ($[HNO_3]_{aq}$ = 4.05 M). Extraction of Sr from HCl medium is much poorer in spite of significant water uptake. It appears that the mechanism is different in case of extraction from nitrate medium than that from chloride medium. Presence of Al enhances the extraction of Sr significantly. Selectivity of Sr extraction is excellent over lanthanides and Cs but only moderate over Zr, Mo, Ba and Ru.

Acknowledgements

The authors thank Mr. S.D. Mishra, Head, Waste Management Project Division and Mr. N. Govindan for their encouragement and Mr. R.N. Acharya for his help in spectrometry.

References

[1] IAEA Technical Report Series No.356, 1993, p. 5.
[2] B.Ya. Galkin, V.M. Esimantovskii, L.N. Lazarev, R.D. Lyubtsev, V.N. Romanovskii, D.N. Shiahkin, L. Kadlesova, M. Kyrs, I. Rais, P. Selutskii, Int. Solv. Extr. Conf. ISEC '88, Moscow, 1988.
[3] W.W. Schulz, L.A. Bray, Sep. Sci. Tech. 22 (1987) 191.
[4] R.L. Miller, A.B. Pinkerton, P.K. Hurlburt, K.D. Abney, Solv. Extr. Ion Exch. 13 (1995) 813.
[5] E. Blasius, W. Klein, U. Schon, J. Radioanal. Nucl. Chem., Articles 89 (1985) 389.
[6] E.P. Horwitz, M.L. Dietz, D.E. Fisher, Solv. Extr. Ion Exch. 8 (1990) 557.
[7] E.P. Horwitz, M.L. Dietz, D.E. Fisher, Solv. Extr. Ion Exch 9 (1991) 1.
[8] P.K. Mohapatra, V.K. Manchanda, Radiochim. Acta 55 (1991) 193.
[9] E.P. Horwitz, M.L. Dietz, D.E. Fisher, Solv. Extr. Ion Exch 8 (1990) 199.
[10] M.L. Dietz, E.P. Horwitz, R.D. Rogers, Solv. Extr. Ion Exch. 13 (1) (1995) 1.
[11] M.G. Houkins, R.A. Bartsch, Solv. Extr. Ion Exch. 13 (1995) 983.
[12] E.P. Horwitz, M.L. Dietz, D.E. Fisher, Solv. Extr. Ion Exch. 8 (1990) 203.

ELSEVIER

Talanta 45 (1997) 397–404

Talanta

Application of chelate forming resin Amberlite XAD-2–*o*-vanillinthiosemicarbazone to the separation and preconcentration of copper(II), zinc(II) and lead(II)

V.K. Jain *, S.S. Sait, P. Shrivastav, Y.K. Agrawal

Chemistry Department, School of Sciences, Gujarat University, Ahmedabad 380009, India

Received 24 December 1996; received in revised form 1 May 1997; accepted 5 May 1997

Abstract

A very stable chelating resin matrix was synthesized by covalently linking *o*-vanillinthiosemicarbazone (oVTSC) with the benzene ring of the polystyrene-divinylbenzene resin Amberlite XAD-2 through a –N=N– group. The resin was used successfully for the separation and preconcentration of copper(II), zinc(II) and lead(II) prior to their determination by atomic absorption spectrophotometry. The total sorption capacity of the resin was 850, 1500 and 2000 μg g^{-1} of the resin for Cu(II), Zn(II) and Pb(II), respectively. For the quantitative sorption and recovery of Cu(II), Zn(II) and Pb(II), the optimum pH and eluants were pH 2.5–4.0 and 4 M HCl or 2 M HNO_3 for Cu(II), pH 5.5–6.5 and 1.0–2.0 M HCl for Zn(II) and pH 6.0–7.5 and 3 M HCl or 1 M HNO_3 for Pb(II). Both, the uptake and stripping of these metal ions were fairly rapid, indicating a better accessibility of the chelating sites. The $t_{1/2}$ values for Cu(II), Zn(II) and Pb(II) were also determined. Limit of tolerance of some electrolytes like NaCl, NaF, $NaNO_3$, Na_2SO_4 and Na_3PO_4 have been reported. The preconcentration factor for Cu(II), Zn(II) and Pb(II) was 90, 140 and 100 respectively. The method was applied for the determination of Cu(II), Zn(II) and Pb(II) in the water samples collected from Sabarmati river, Ahmedabad, India. © 1997 Elsevier Science B.V.

Keywords: Atomic absorption spectrophotometry; Copper(II); Zinc(II); Lead(II); Chelating resin matrix; Preconcentration

1. Introduction

The main object of much research on chelating resins, is the preparation of insoluble functionalized polymers which can provide more flexible working conditions together with good stability and a high capacity for metal ions [1–5]. For this purpose, ligands already reported, viz. salicylic acid, salicylaldehyde, 2,6-bis(methylthiomethyl)-pyridine, thiourea, dithiozone, alizarin red S etc., known to form stable complexes with metal ions like Mn(II), Fe(III), Cu(II), Zn(II), Pb(II) etc. which are useful in environmental analysis have been attached to polymer resins, especially polystyrene-divinylbenzene [6–11]. This is because

* Corresponding author. Fax: +91 79 6747432.

PII S0039-9140(97)00141-0

such functional polymers are employed, for the preconcentration purposes in trace metal analysis, particularly for water systems [12–14], geological and biochemical samples [15–18] and in chemical catalysis [19].

Several types of chelating resins have been developed by loading various chelating reagents on a polymer matrix through an ion-exchange/$\pi-\pi$ dispersion forces [20–22]. Although these resins have good capacity, but they suffer from less stability. Therefore, it was thought worthwhile to synthesize chelating resin by covalently linking the chelating agent with the commercially available polystyrene-divinylbenzene co-polymer (Amberlite XAD-2) through a –N=N– group [6,10].

Since the sorption characteristics of the metal ions together with the complexation properties of the reagent generally depend upon the size of the chelate ring and the metal atom [23], no. of donor atoms/binding sites on the reagent, type of donor atoms (hard or soft), oxidation state of the metal ion, nature of the solvent, pH of the solvent system etc. As thiosemicarbazones which are known to act as unidentate, bidentate and multidentate chelating agents, its analytical applications have been reviewed [24–26], we have selected *ortho*-vanillinthiosemicarbazone as a chelating agent and hooked it to a solid polymeric support Amberlite XAD-2. oVTSC which has three binding sites as nitrogen, oxygen and sulphur and is expected to form two chelate rings (five and six membered) as shown in Fig. 1, which makes it a more versatile reagent. The thermodynamic parameters and stability constant data of various bivalent metals with oVTSC have already been reported [27].

In this paper, we have described the synthesis of stable chelate forming resin matrix by covalently linking oVTSC with Amberlite XAD-2, which has been recycled many times without affecting its efficiency. This matrix has been studied for its use for the separation and preconcentration of copper(II), zinc(II) and lead(II) prior to their determination by atomic absorption spectrophotometry.

2. Experimental

2.1. Apparatus and reagents

A Shimadzu model AA 680 atomic absorption spectrophotometer with PR-5 graphic printer was used for the determination of metal ions in solution. The pH measurements were made on Systronics digital pH meter model 335. The flow of the liquid through the column was controlled by Miclins Peristaltic pump PP-10.

All chemicals used in this work were of analytical grade of E. Merck or British Drug House, unless otherwise stated. Amberlite XAD-2, surface area 330 $m^2\ g^{-1}$, pore diameter 90 Å and bead size 20–50 mesh was procured from Fluka. Quartz distilled deionised water was used throughout. The *o*-vanillinthiosemicarbazone was prepared as reported in literature [26]. Standard stock solution (1000 ppm) of copper(II), zinc(II) and lead(II) were prepared by dissolving requisite amounts of copper(II) nitrate, zinc(II) nitrate and lead(II) nitrate respectively in double distilled water containing small amounts of corresponding

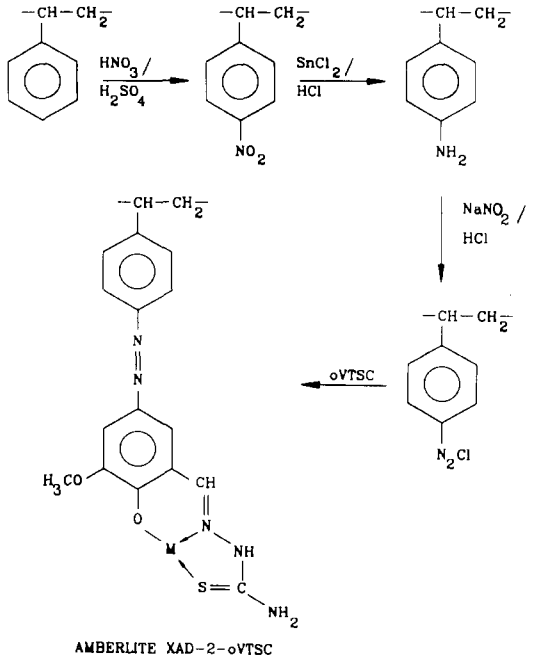

Fig. 1. Schematic representation of reaction sequence.

Table 1
Parameters optimized for sorption and desorption of Cu(II), Zn(II) and Pb(II) on Amberlite-XAD-2–oVTSC resin

No.	Parameters	Metal ions Copper(II)	Zinc(II)	Lead(II)
1.	pH range	2.5–4	5.5–6.5	6.0–7.5
2.	Flow rate (cm^3 min^{-1})	1.5–2.5	2–3	1.5–2.5
3.	Concentration of acid for desorption	4 M HCl or 2 M HNO_3	1–2 M HCl	3 M HCl or 1 M HNO_3
4.	Sorption capacity (μg g^{-1})	850	1500	2000
5.	Preconcentration factor	90	140	100
6.	Average recovery (%)	98	98–99	98–99
7.	Relative standard dediation (%)[a]	2.5	3.2	2.7

[a] Five determinations of 1.5 mg dm^{-3} Cu(II), 1.5 mg dm^{-3} Zn(II) and 1.0 mg dm^{-3} Pb(II).

acid and standardized [28]. The pH adjustments were made with 0.1/0.01 M HCl or NaOH and/or acetate buffers. The glassware used was soaked in 10% HNO_3 for 2 days before use and cleaned repeatedly with double distilled water. The water samples from Sabarmati river were isokinetically collected in clean polyethylene bottles from locations near Sabarmati thermal power station, Ahmedabad.

2.2. Preparation of Amberlite XAD-2–oVTSC resin

A 5-g sample of Amberlite XAD-2 was treated with a nitrating mixture, containing 10 cm^3 of concentrated HNO_3 and 25 cm^3 of concentrated H_2SO_4 and stirred for 1 h at 60°C on an oil bath. The nitrated mixture was poured into ice cold water. It was further filtered, washed repeatedly with distilled water until free from acid and reduced with a mixture of $SnCl_2$ (40 g) in the presence of concentrated HCl (45 cm^3), and ethanol (50 cm^3), and refluxed for 12 h at 90°C. The amino polymer was filtered off and washed with distilled water and 2 M NaOH so as to get the free amino polymer.

The amino polymer was treated with 100 cm^3 of 2 M HCl for 30 min, washed with distilled water to remove excess of HCl, and suspended in 250 cm^3 of ice cold water. It was then diazotized with a 1:1 mixture of 1 M HCl and 1 M $NaNO_2$ by adding 1 cm^3 each time with constant stirring until the reaction mixture showed a permanent blue colour with starch-iodide paper. The diazotized resin was filtered, washed with ice cold water and treated with *o*-vanillinthiosemicarbazone (2.5 g in 350 cm^3 of glacial acetic acid and 150 cm^3 DMF) at 0–3°C for 40 h. The dark brown coloured beads were filtered and washed. The schematic reaction sequence is given in Fig. 1.

2.3. Column procedure for preconcentration and determination of Cu(II), Zn(II) and Pb(II)

A glass column, 5 mm in diameter was packed with 1 g of Amberlite XAD-2–oVTSC resin. It was treated with 20 cm^3 of 4 M HCl and washed with double-distilled water until the resin was free from acid. A suitable aliquot of the solution containing copper(II), zinc(II) or lead(II) in the concentration range 0.020–0.20 ppm was passed through the column after adjusting the appropriate pH with an optimum flow rate (Table 1). The stripping of the metals from the resin was carried out by suitable eluting agents like HCl or HNO_3 (5–15 cm^3). The eluates were collected in a 25-cm^3 volumetric flask, made to volume by double distilled water and aspirated into the flame for atomic absorption spectrophotometric measurements.

The operating conditions of the AAS instrument (previously standardized) for the determination of Cu(II), Zn(II) and Pb(II) were as follows:

	Copper(II)	Zinc(II)	Lead(II)
HC lamp (mA)	5	4	5
Slit (nm)	0.5	0.5	1.0

Wavelength (nm)	324.8	213.9	283.3
Flame	Air–C_2H_2	Air–C_2H_2	Air–C_2H_2
Fuel (l min^{-1})	2.0	2.0	2.0
Oxidant (l min^{-1})	8	8	8
Burner (cm)	10	10	10

3. Results and discussion

3.1. Metal sorption as a function of pH

The pH studies were carried out to find its effect on the degree of metal sorption using the column process. One g of Amberlite XAD-2–oVTSC was packed in a 5-mm diameter column, and a suitable aliquot of metal ion solution [Cu(II), Zn(II) or Pb(II)] was passed with an optimum flow rate at varying pH (Fig. 2). The degree or percentage of metal sorption was calculated by measuring the metal content in supernatant liquid and also by desorbing the resin with eluants like 4 M HCl, 1 M HCl and 1 M HNO_3 for Cu(II), Zn(II) and Pb(II) respectively.

3.2. Effect of flow rate

The degree of metal ion sorption on Amberlite XAD-2–oVTSC was studied by varying the flow rate of the feed solution. It was found that the optimum flow rate for all the three metal ions was 2.0 cm^3 min^{-1}. However at flow rate greater than 3, there was a decrease in percentage sorption (Fig. 3).

3.3. Total sorption capacity

The resin capacity for the sorption of metal ions was determined by the following procedure. First, 1.0 g resin beads were stirred with 250 cm^3 solution of Cu(II), Zn(II) or Pb(II) with a given concentration, at their respective pH and at room temperature (30°C) for 24 h to ensure complete equilibrium. The loading capacity for each metal ion on the resin was calculated from the difference between the metal ion concentration before and after desorption. The data are given in Table 2.

3.4. Kinetics of metal sorption

To determine the rate of loading of Cu(II), Zn(II) and Pb(II) on the resin, batch experiments were carried out under the following conditions: 0.5 g of resin beads were stirred with 250 ml of feed solution containing Cu(II), Zn(II) or Pb(II)

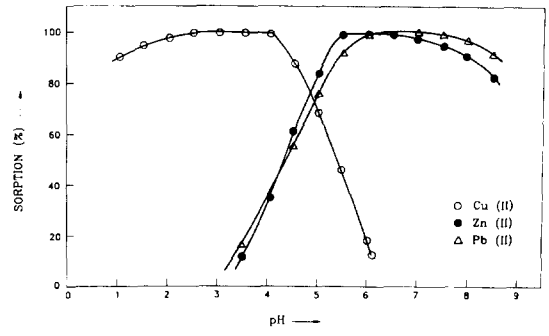

Fig. 2. Effect of pH on the sorption of Cu(II), Zn(II) and Pb(II). Cu(II): 1 ppm, 100 cm^3, eluant 4 M HCl; Zn(II): 2 ppm, 100 cm^3, eluant 2 M HCl; Pb(II): 2 ppm, 100 cm^3, eluant 3 M HCl.

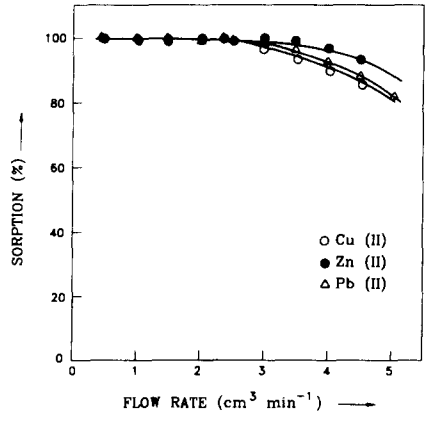

Fig. 3. Variation of percentage sorption with flow rate. Cu(II): 1 ppm, 100 cm^3, pH 3; Zn(II): 2 ppm, 100 cm^3, pH 6; Pb(II): 2 ppm, 100 cm^3, pH 6.5.

Table 2
Binding capacity of Amberlite XAD-2–oVTSC resin for Cu(II), Zn(II) and Pb(II)

Metal ion	Capacity	
	$\mu g\ g^{-1}$ resin	mmol g^{-1} resin
Copper(II)	850	1.34×10^{-2}
Zinc(II)	1500	2.29×10^{-2}
Lead(II)	2000	9.65×10^{-3}

Experimental conditions:
Amberlite XAD-2–oVTSC: 1 g
Copper(II): 10 ppm, 250 cm^3, pH 3
Zinc(II): 10 ppm, 250 cm^3, pH 6
Lead(II): 20 ppm, 250 cm^3, pH 6.5
Temperature: 30°C

at room temperature (30°C). At predetermined intervals, aliquot of 5 cm^3 solution were taken out for analysis. The concentration of metal ions in the supernatant solution was determined by AAS and the amount of metal ions loaded on the resin phase was calculated by mass balance (in $\mu g\ g^{-1}$ resin). The loading half time $t_{1/2}$ defined as the time needed to reach 50% of the resins total loading capacity was estimated from the curves (Fig. 4). The $t_{1/2}$ values obtained were 26, 5 and 11 min for Cu(II), Zn(II) and Pb(II), respectively. The faster uptake of these metal ions on Amberlite XAD-2–oVTSC probably reflects a better accessibility of the metal ions to the chelating sites in the resin.

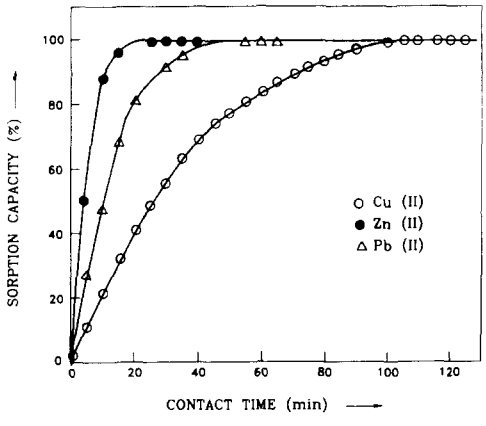

Fig. 4. Kinetics of Cu(II), Zn(II) and Pb(II) binding on Amberlite XAD-2–oVTSC. Cu(II): 10 ppm, 250 cm^3, pH 3; Zn(II): 10 ppm, 250 cm^3, pH 6; Pb(II): 10 ppm, 250 cm^3, pH 6.5. Temperature: 30°C.

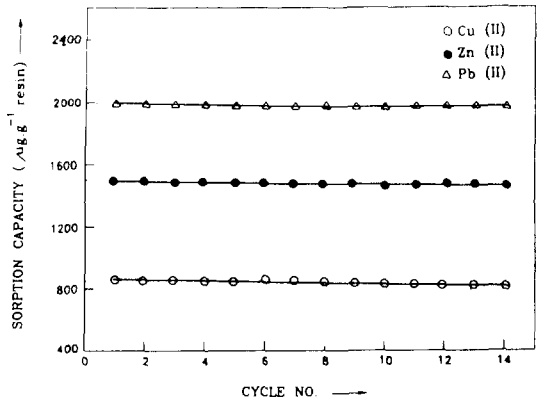

Fig. 5. Evaluation of the stability of Amberlite XAD-2–oVTSC for Cu(II), Zn(II) and Pb(II) loading and elution.

3.5. Resin stability test

To test the resin stability, it was subjected to several loading and elution batch operations. The following conditions were employed for the study: 0.1 g of resin beads were stirred with 5 ppm, 100 cm^3 solution containing Cu(II), Zn(II) or Pb(II) for 24 h at room temperature (30°C). The elution operations were carried out by shaking the resin with 50 ml of suitable eluant for 4 h to ensure complete equilibration. The operating capacity was calculated from the loading and elution tests. The results from both tests agreed within 2–3% error for all the three metal ions (Fig. 5).

3.6. Effect of electrolytes

The effect of various electrolytes like NaCl, NaF, $NaNO_3$, $NaNO_2$, Na_2SO_4 and Na_3PO_4 on the sorption of Cu(II), Zn(II) and Pb(II) with Amberlite XAD-2–oVTSC resin matrix was studied. It was observed that all the electrolytes were tolerated in the concentration range of 0.5–1 M except Na_3PO_4 in which case it was 0.01 M for the sorption of Cu(II), Zn(II) and Pb(II). Their limits of tolerance defined as 1–2% decrease in sorption capacity of the metal ion.

Table 3
Preconcentration factors for Cu(II), Zn(II) and Pb(II)

Metal ion	Volume of solution passed (cm^3)	Concentration (ppb)	Final elution volume (cm^3)	Recovery (%)	Preconcentration factor
Copper(II)	1000	20	11	98	90
Zinc(II)	1000	20	7	99	140
Lead(II)	1000	50	10	98	100

Experimental conditions:
Amberlite XAD-2–oVTSC: 1 g
Copper(II): 20 μg
Zinc(II): 20 μg
Lead(II): 50 μg

The effect of commonly occurring cations in water samples like Fe(II), Fe(III), Co(II), Ni(II) and Mn(II) have been studied on the sorption of Cu(II), Zn(II) and Pb(II) by Amberlite XAD-2–oVTSC. The alkali and alkaline earth metal ions do not effect the recovery of the metal ions upto 250-fold excess; however, the recovery is not complete above this concentration ratio. In the sorption of 10 μg each of Zn(II) and Pb(II), 25 μg Co(II), 25 μg Ni(II), 20 μg Fe(III) and 30 μg Mn(II) did not interfere, whereas Cr(III) and Fe(II) do not show any affinity for the resin. Zn(II) and Pb(II) did not interfere in the determination of Cu(II), as it is sorbed at a lower pH. For 20 μg Cu(II), 100 μg each of Co(II), Ni(II) and Mn(II) did not interfere. The tolerance limit for Fe(III) was however 80 μg.

3.7. Limit of preconcentration and preconcentration factor

Quantitative collection of copper(II), zinc(II) and lead(II) was possible from solutions of concentrations of the order of 20–50 ppb with recovery upto 98–99%. The preconcentration factors for Cu(II), Zn(II) and Pb(II) were found to be 90, 140 and 100, respectively. The results are given in Table 3.

3.8. Applications to analysis of water samples

To check the applicability of the present method for preconcentrating and determining copper(II), zinc(II) and lead(II), the synthesized resin Amberlite XAD-2–oVTSC was subjected to various water sample analysis. Water samples were collected from Sabarmati river, Ahmedabad. For the determination of Cu(II), Zn(II) and Pb(II) by the proposed method, the results are compared by the standard addition technique. In this experiment, 1 l of sample volume was spiked with 1 mg each of Cu(II) and Zn(II) and 5 mg Pb(II) and then determined by AAS. The results were compared with those obtained by passing the same sample volume without spiking through the resin, the data are reported in Table 4, which confirms the utility of the resin as a preconcentrator in the atomic absorption spectrophotometric determination of Cu(II), Zn(II) and Pb(II).

Our investigations also show that Amberlite XAD-2–oVTSC resin can be applied to the separation of copper(II) from zinc(II) and lead(II) based on different pH of sorption (Table 5).

4. Conclusions

The Amberlite XAD-2–oVTSC resin has high sorption capacities for Cu(II), Zn(II) and Pb(II). The sorbed ions can readily be desorbed by common mineral acids. The synthesized resin has the advantage of faster rate of equilibrium, high stability and preconcentration factors. The resin could be recycled many times without affecting its sorption capacity. It has lower matrix interference compared to many other analogous resins re-

Table 4
Determination of Cu(II), Zn(II) and Pb(II) in water samples

Sample	Method	Metal ion					
		Cu(II)		Zn(II)		Pb(II)	
		Amount (ppb)[a]	R.S.D. (%)	Amount (ppb)	R.S.D. (%)	Amount (ppb)	R.S.D. (%)
1. Sabarmati river, Ahmedabad	Amberlite XAD-2 -oVTSC	40	1.1	22	0.9	75	1.1
	Standard addition	45	4.7	26	3.7	81	4.5

Sample volume: 1000 cm^3.
[a] Average of 5 determinations.

Table 5
Separation of copper(II) from zinc(II) and lead(II)

Metal ion	Amount added (mg)	Found (mg)	Recovery of Cu(II) (%)
Zinc(II)	0.10	0.10 ± 0.01	98.5 ± 0.3
	1.0	0.98 ± 0.01	98.3 ± 0.5
	2.0	1.97 ± 0.02	99.0 ± 0.2
Lead(II)	0.10	0.09 ± 0.01	98.5 ± 0.1
	1.0	0.99 ± 0.01	99.9 ± 0.4
	2.0	1.98 ± 0.02	97.5 ± 0.3
Zinc(II) and lead(II)	1.0	0.99 ± 0.01	98.6 ± 0.4
	1.0	0.98 ± 0.01	98.7 ± 0.3

Sample volume: 500 cm^3.
Experimental conditions:
Amberlite-XAD-2-oVTSC: 0.5 g
Copper(II): 20 μg
pH: 3

ported in literature [6,10,22,29]. Since it has negligible affinity for alkali and alkaline earth cations it is highly useful for preconcentration and determination of various metal ions in natural water samples.

Acknowledgements

The financial assistance provided by University Grants Commission (UGC), India is gratefully acknowledged. The authors are indebted to Dr M.M. Sarin, PRL, Ahmedabad for comments and valuable suggestions on this work.

References

[1] C.J. Kantipuly, S. Katragadda, H.D. Gesser, Talanta 37 (1990) 491.
[2] C.J. Kantipuly, A.D. Westland, Talanta 35 (1988) 1.
[3] G.V. Myasoedova, S.B. Savvin, Crit. Rev. Anal. Chem. 17 (1986) 1.
[4] A. Warshawsky, Selective ion exchange polymers, Angew. Macromol Chem. 171 (1982) 109.
[5] A. Warshawsky, Polymeric ligands in hydrometallurgy, in: D.C. Sherrington, P. Hodge (Eds.), Synthesis and Separation using Functional Polymers, Wiley, Chichester, 1988, pp. 325.
[6] R. Saxena, A.K. Singh, D.P.S. Rathore, Analyst 120 (1995) 403.
[7] J. Chwastowska, E. Kosiarska, Talanta 35 (1988) 439.

[8] A. Syamal, M.M. Singh, Ind. J. Chem. 33A (1994) 58.
[9] G. Chessa, G. Marangoni, B. Pitteri, F. Visentin, Reactive Polymers 18 (1992) 7.
[10] R. Saxena, A.K. Singh, S.S. Sambi, Anal. Chim. Acta 295 (1994) 199.
[11] G. Zuo, M. Muhammad, Reactive Polymers 24 (1995) 165.
[12] K. Isshiki, F. Tsuji, T. Kuwamoto, E. Nakamura, Anal. Chem. 59 (1987) 2491.
[13] M.C. Yebra-Biurrum, M.C. Garcia-Dopazo, A. Bermejo-Barrera, M.P. Bermejo-Barrera, Talanta 39 (1992) 671.
[14] C.J. Cheng, T. Akagi, H. Haraguchi, Bull. Chem. Soc. Jpn. 58 (1985) 3229.
[15] A.N. Masi, R.A. Olsima, Talanta 40 (1993) 931.
[16] J.G. Crock, F.E. Lichte, G.G. Riddle, C.L. Beech, Talanta 33 (1986) 601.
[17] M. Soylak, L. Elci, M. Dogan, Talanta 42 (1995) 1513.
[18] I. Chibata, T. Tosa, T. Sato, J. Mol. Catal. 37 (1986) I.
[19] W.T. Ford, Polymeric Reagents and Catalysts, American Chemical Society, Washington, DC, 1986.
[20] A.K. Singh, S.K. Dhingra, Analyst 117 (1992) 889.
[21] K. Brajter, E.D. Zlotorzynska, Analyst 113 (1988) 1571.
[22] S. Hoshi, H. Fujisawa, K. Nakamura, S. Nakata, M. Uto, K. Akatsuka, Talanta 41 (1994) 503.
[23] R.D. Hancock, J. Chem. Edu. 69 (1992) 615.
[24] J.M. Cano Pavon, Microchem. J. 26 (1981) 155.
[25] J.M. Cano Pavon, D.P. Bendito, M. Valcarcel, Quim. Anal. 1 (1982) 118.
[26] B.S. Garg, V.K. Jain, Microchem. J. 38 (1988) 144.
[27] B.S. Garg, V.K. Jain, S.K. Garg, Thermochim. Acta 139 (1989) 375.
[28] A.I. Vogel, A Text Book of Quantitative Inorganic Analysis, 3rd ed., Longmans, London, 1973.
[29] K. Dev, G.N. Rao, Talanta 42 (1995) 591.

ELSEVIER

Talanta 45 (1997) 405–410

Talanta

Reversed flow injection spectrophotometric determination of trace amount of ammonia in natural water by oxidation of ammonia to nitrite

Renmin Liu *, Huaisheng Wang, Ailing Sun, Daojie Liu

Department of Chemistry, Liaocheng Teachers College, Liaocheng, Shandong 252059, People's Republic of China

Received 2 July 1996; received in revised form 7 May 1997; accepted 10 May 1997

Abstract

A new sensitive flow injection method for determination of ammonia in natural water samples have been developed, based on the oxidation of ammonia to nitrite by hypochlorite in the presence of large amount of potassium bromide. The oxidant solution obtained by on-line mixing of hypochlorite and potassium bromide was injected into a water carrier stream, and then mixed with sample stream. Ammonia in the sample solution was oxidized to nitrite. Nitrite was then determined by spectrophotometry with sulfanilamide and *N*-1-naphthylethylenediamine. By reversed injection of the oxidant solution, the interference of nitrite and turbidity of the sample can be removed. The linear range of the method for ammonia is 0.2–12 μM. The proposed method is simple and sensitive. It had been applied to the determination of ammonia in lake water samples. Recoveries of 95–104% were obtained. © 1997 Elsevier Science B.V.

Keywords: Ammonia determination; Reversed flow injection analysis; Spectrophotometry; Ammonia oxidation

1. Introduction

Ammonia is an important micronutrient in the worlds systems. Because ammonia in lake water is readily available to phytoplankton, the concentration of it can be decreased to as low as ppb level [1]. The determination of ammonia in natural water is of significant interest in water evaluation and biological study in water system. Various detection methods and techniques have been used for determining ammonia or ammonium ions, such as ion chromatography [2]; ammonia gas-sensing electrode [3–6]; spectrophotometry [7–11]; fluorometry [12,13] and chemiluminescence [14]. The most common technique used to measure ammonia concentration is the indophenol blue spectrophotometric method. But this method is time-consuming and the sensitivity is low [15]. The ammonia-selective electrode method is widely used for determining ammonia in environmental samples. Unfortunately, this method is susceptible to interference by amines [16] and the electrodes usually have either slow equilibration times or poor sensitivity.

* Corresponding author.

PII S0039-9140(97)00148-3

Richards and Kletsch [17] described an oxidation method, in which ammonia is oxidized to nitrite by hypochlorite in the presence of bromide ion, and then the nitrite is determined by spectrophotometry with sulfanilamide and *N*-1-naphtylethylenediamine. Strickland and Parsons [18], and Truesdale [19] reported modifications. Those method have the disadvantage of being time consuming and some amino acids are determined together with the ammonia. The bromide ion used in these methods is acted as a catalyst [18,19]. Matsunaga and Nishimura [15] reported a modified Richards and Kletsch method in which the oxidation time is reduced to about 1 min from 17 min in Truesdale's method or 3.5 h in Strickland and Parsons' method, and the interference of coexisting amino acids can be eliminated. The sensitivity of this method is very high. Submicrogram amounts of ammonia in fresh water can be determined.

Flow injection analysis (FIA) is a rapid, easily automated method of chemical analysis [20]. Many FIA methods have been developed for ammonia determination in recent years [21–31]. Because the oxidant used in Matsunaga and Nishimura method [15] is unstable (only 1 h) and the toxic arsenite solution was used, no FIA method was based on the oxidation of ammonia to nitrite. Yuan [32] reported a merging zone FIA method for ammonia and nitrite. But the oxidation is not on line.

In this study, a new FIA method for ammonia determination was developed based on the method reported by Matsunaga and Nishimura [15]. The oxidant solution, which is generated by on-line mixing of bromide and hypochlorite solution, was injected into water carrier and then merged with the sample solution. Nitrite produced by the oxidation of ammonia in the sample was measured by spectrophotometry with sulfanilamide and *N*-1-naphthylethylenediamine. The proposed method is sensitive, simple. The problem of oxidant unstable was solved and no arsenite was used. Nitrite and slight turbidity present in the sample have no interference on the determination of ammonia.

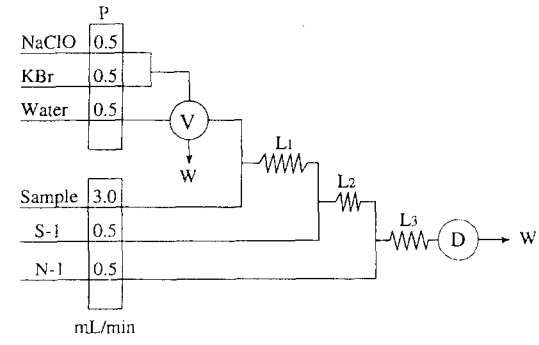

Fig. 1. Schematic diagram of the FIA dystem for determination of ammonia. P, peristaltic pump; V, injection valve; D, detector; L_1, L_2, L_3, reaction tube; S-1, sulfanilamide solution; *N*-1, *N*-1-naphthylethylenediamine solution; W, waste.

2. Experimental

2.1. Reagents

All solutions were prepared with analytical grade chemicals and distilled deionised water.

Ammonium standard solution: a stock solution was prepared by dissolving 107.0 mg of ammonium chloride in 1000 ml of water. Working standard solutions were prepared by diluting the stock solution with water.

Potassium bromide solution: 15% potassium bromide in 4 M sodium hydroxide.

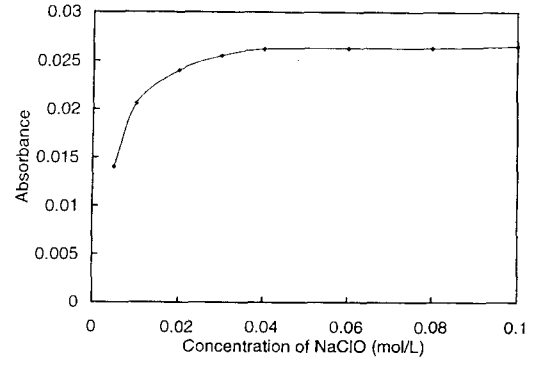

Fig. 2. Influence of concentration of sodium hypochlorite. Other reagents concenration: 15% potassium bromide in 4 M sodium hyroxide; injection volume: 350 μl.

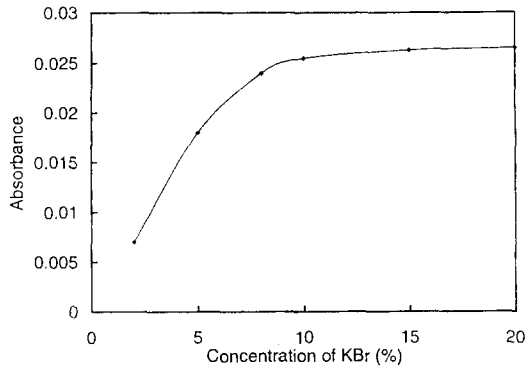

Fig. 3. Influence of concentration of potassium bromide. Other reagents concentration: 0.1 M sodium hypochlorite; the sodium hydroxide in potassium bromide solution is 4 M; injection volume: 350 μl.

Sodium hypochlorite solution: 0.1 M. The concentration was determined by iodimetry.

Sulfanilamide solution: 2 g of sulfanilamide was dissolved in 100 ml of 4 M hydrochloric acid and 1% PVA.

N-1-naphthylethylenediamine solution: 0.1 g of *N*-1-naphthylethylenediamine dihydrochloride in 100 ml of water and stored in amber bottle.

2.2. Apparatus

The FIA system used in this study is shown in Fig. 1. The peristaltic pumps and injection valve

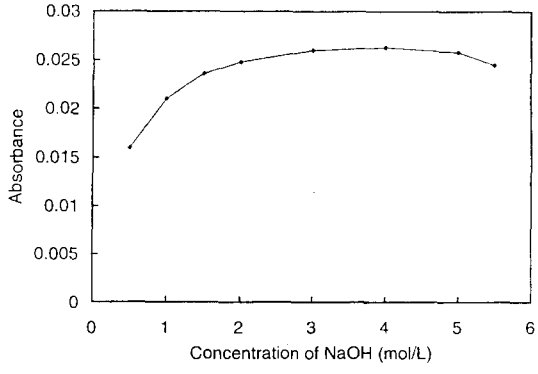

Fig. 4. Influence of sodium hydroxide in potassium bromide solution. Other reagents concentration: 0.1 M sodium hypochlorite; 15% potassium bromide; injection volume: 350 μl.

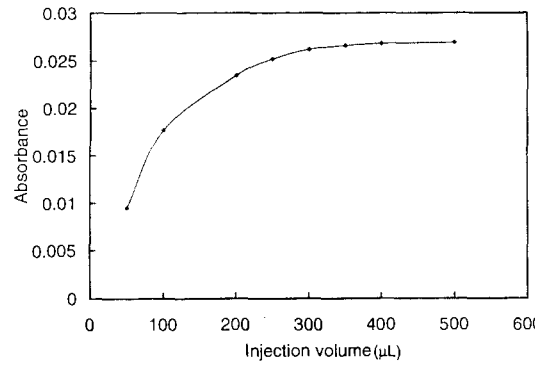

Fig. 5. Influence of injection volume. Reagents concentration: 0.1 M sodium hypochlorite; 15% potassium bromide is 4 M the sodium hydroxide solution.

were supplied by Jiangsu Electroanalytical Instrument Plant. A HP8453A UV-Visible spectrophotometer with a 1 cm flow cell of 18 μl was used as the detector.

2.3. Procedure

The FIA system was connected with PTFE tubing (1.0 mm i.d.) according to the arrangement shown in Fig. 1. The flow rates of all channels were adjusted according to the parameters given in Fig. 1. The absorbance was recorded in the flow cell at 540 nm. The mixture of potassium bromide and sodium hypochloride was injected into carrier stream (water). The peak height is used as the measure of absorbance.

A series of ammonia standard solutions were analyzed by the same procedure. The peak absorbance difference between standard solutions and blank was used for the construction of calibration graph.

3. Results and discussion

3.1. Determination manifold

Sample injection method and oxidant injection method were investigated by changing sample and the oxidant. In sample injection manifold, nitrite in sample solution was determined simulta-

Table 1
Interference of amino acids and urea

Compound	Concentration (μM)	Ammonia added (μM)	Ammonia found[a] (μM)	Recovery (%)
DL-alanine	5.0		0.96	96
L-cystine	5.0		1.03	103
L-glutamic acid	5.0		1.03	103
Glycine	2.0	1.0	0.98	98
L-histidine	5.0		1.01	101
DL-lysine	5.0		1.04	104
L-methionine	5.0		0.98	98
Urea	20		1.07	107

[a] Average value of six determinations.

neously, and the peak height corresponds to the sum of nitrite and ammonia. Nitrite and ammonia can be determined separately, if other channels are added in the FIA system, by using sample injection method. But the turbidity of the sample has a significant effect on the results of determination. In oxidant injection manifold, nitrite and turbidity only affect the altitude of the baseline. They did not affect the peak height corresponds to ammonia. In addition, high sensitivity can be obtained by oxidant injection method. So if only ammonia is needed to be determined, the oxidant injection method is superior to sample injection method.

3.2. Measurement conditions

The measurement conditions, such as reagents concentration, reaction coil length and injection volume, were investigated by measuring 1.0 μM ammonia with the flow rates given in Fig. 1. Fig. 2 shows the effect of concentration of sodium hypochlorite on the determination. It can be seen that the peak absorbance keep almost constant when the concentration of sodium hypochlorite is higher than 0.03 mol l^{-1}. Considering the decomposition of sodium hypochlorite, a 0.1 mol l^{-1} solution was used for all determination. This solution can be used for more than 2 weeks at room temperature. The influence of the concentration of potassium bromide is shown in Fig. 3. Fig. 3 indicates that a constant peak absorbance can be obtained when the concentration of potassium bromide is higher than 10%. So a solution of 15% potassium bromide was used for all determination. The influence of the concentration of sodium hydroxide in potassium bromide solution is shown in Fig. 4. According to these results, a 4 M sodium hydroxide in potassium bromide was used.

The concentration of sulfanilamide and *N*-1-naphthylethylenediamine were also tested. Good results can be obtained with 2% sulfanilamide in 4 M HCl solution and 0.1% *N*-1-naphthylethylenediamine in water. 0.5% PVA was added in the solution of sulfanilamide solution. A white precipitate can be formed when high concentration of sodium hypochlorite is mixed with sulfanilamide without PVA. In addition, the presence of PVA in the solution can increase the rate of color developing. The mixtures of sulfanilamide and *N*-1-naphthylethylenediamine in 10–40% phosphoric acid solutions were also used as the color reagent. But the results were not good.

The influence of the injection volume is shown in Fig. 5. It can be seen that high sensitivity can be obtained with big injection volume. When the injection volume is bigger than 300 μl, the peak absorbance increased very slowly. So a 350 μl sample loop was used for the injection of oxidant solution.

The length of the reaction coils were also investigated. L_1 is the reaction coil for oxidation of ammonia. When it is longer than 450 cm, the peak absorbance keeps constant. So a 500 cm long tube was used as the oxidation reaction coils. L_2 is the reaction coil for nitrite and sulfanilamide. L_3 is the reaction tube for azo-reaction.

Table 2
Results of determination of ammonia in natural water samples

Sample	NH_4^+ found (μM)	NH_4^+ added (μM)	Total NH_4^+ found (μM)	Recovery (%)
Lake water				
1 #	1.68	2.0	3.74	103
2 #	0.82	2.0	2.77	97.5
3 #	3.62	2.0	5.52	95.0
4 #	0.58	2.0	2.66	104

Good results can be obtained with $L_2 = 50$ cm, and $L_3 = 300$ cm.

3.3. Interference

Considerable portion of amino acids are determined together with ammonia in previous oxidation method [19]. The interference of several amino acids on the determination of ammonia was studied by the addition of a certain amount of amino acid to 1.0 μM ammonia standard solution. The interference of urea was also investigated. All the results are shown in Table 1. It can be seen that the tested amino acids and urea have no interference on the determination of ammonia.

The oxidation of nitrite to nitrate with the same oxidant solution and at the same residence time in this FIA system was also investigated by using nitrite solution as the sample. The results indicate that nitrite can not be oxidized to nitrite solution as the sample. The results indicate that nitrite can not be oxidized to nitrate with the same oxidant and at the same residence time in the FIA system used in this experiment.

3.4. Calibration graph

Ammonia standard solutions were analyzed by the proposed method. The calibration graph was constructed according to the difference of peak absorbance between standards and blank. The linear range of the calibration curve is 0.2–12 μM of ammonia. The regression equation of the calibration graph is as follows:

$$\Delta A = 0.0264\,C + 0.0011 \quad r = 0.9996\ (C: \mu M)$$

The detection limit, calculated from the equation with three times the standard deviation of 11 replicate determination of blank water, was 0.072 μM of ammonia.

3.5. Applications

The proposed method had been applied to the determination of ammonia in lake water samples. The recovery of the method was also measured by standard addition of a certain amount of ammonium to the samples. The results are listed in Table 2. The precision of the proposed method was calculated on the basis of the results obtained from seven replicate analyses of the samples listed in Table 2. The relative standard deviations for the samples were 1.1, 1.5, 0.8%, respectively.

References

[1] S. Yamanaka, T. Sono, S. Ichise, Shiga-Kenritsu Eisei Kankyo Senta Shoho 26 (1992) 148.
[2] H. Small, T.S. Stevens, W.C. Bauman, Anal. Chem. 47 (1975) 1801.
[3] D. Midgley, K. Torrance, Analyst 97 (1972) 626.
[4] M.J. Beckett, A.C. Wilson, Water Res. 8 (1974) 333.
[5] T.R. Gilbert, A.M. Clay, Anal. Chem. 45 (1973) 1757.
[6] M.A. Arnold, Anal. Chim. Acta 154 (1983) 33.
[7] J.A. Tellow, A.L. Wilson, Analyst 89 (1964) 453.
[8] J.E. Harwood, A.L. Kuhn, Water Res. 4 (1970) 805.
[9] K. Matsunga, M. Nishimura, Bunseki Kagaku 20 (1971) 993.
[10] Standard methods for the Examination of Water and Waetewater, American Public Health Association, Washington DC, 1985.
[11] P.L. Searle, Analyst 109 (1984) 549.
[12] T. Aoki, S. Uemura, M. Munemori, Anal. Chem. 55 (1983) 1620.
[13] G. Zhang, P.K. Dasgupta, Anal. Chem. 61 (1989) 408.

[14] X. Hu, N. Takenaka, S. Takasuna, M. Kitano, H. Bandow, Y. Maeda, Anal. Chem. 65 (1993) 3489.
[15] K. Matsunaga, M. Nishimura, Anal. Chim. Acta 73 (1974) 204.
[16] M.E. Lopez, G.A. Rechnitz, Anal. Chem. 54 (1982) 2085.
[17] F.A. Richards, R.A. Kletsch, Rescent Researchers in the Fields of Hydrosphere, Atmosphere and Nuclear Geochemistry, Maruzen, Tokyo, 1964, p. 65.
[18] J.D.H. Strickland, T.R. Parsons, Bulletin No. 167, Fisheries Research Board of Canada, 1968, 81 pp.
[19] V.W. Truesdale, Analyst (London) 96 (1971) 584.
[20] J. Ruzicka, E.H. Hansen, Flow-injection Analysis, Wiley, New York, 1981, 207 pp.
[21] H. Filho Bergamin, B.F. Reis, A.O. Jacintho, E.G. Zagatto, Anal. Chim. Acta 117 (1980) 81.
[22] M.E. Meyerhoff, M. Fraticelli Yvonne, Anal. Lett. Part B 14 (1981) 415.
[23] G. Svensson, T. Anfalt, Clin. Chim. Acta 119 (1982) 7.
[24] W.E. Van der Linden, Anal. Chim. Acta 155 (1983) 273.
[25] A.G. Fogg, A.Y. Chamsi, A.A. Barros, J.O. Cabral, Analyst 109 (1984) 901.
[26] T. Aoki, S. Uemura, M. Munemori, Bunseki Kagaku 33 (1984) 505.
[27] P. Martinez-Jimenez, M. Gallego, M. Valcarcel, Anal. Chem. 59 (1987) 69.
[28] G. Zhang, P.K. Dasgupta, Anal. Chem. 61 (1989) 408.
[29] J.R. Clinch, P.J. Worsfold, F.W. Sweeting, Anal. Chim. Acta 214 (1988) 401.
[30] S. Alegret, J. Alonso, J. Bartroli, E. Marlinez-Fabregas, Analyst 114 (1989) 1443.
[31] S. Alegret, J. Alonso, J. Bartroli, M. Del Valle, N. Jaffrezic-Renault, Y. Duvault-Herrera, Anal. Chim. Acta 231 (1990) 53.
[32] Y. Yuan, Fenxi Huaxue 15 (1987) 457.

ELSEVIER

Talanta 45 (1997) 411–416

Talanta

Derivative spectrophotometric determination of iridium after preconcentration of its 1-(2-pyridylazo)-2-naphthol complex on microcrystalline naphthalene

Mohammad Ali Taher [a], Swati Puri [b], R.K. Bansal, Bal Krishan Puri [b,*]

[a] *Department of Chemistry, Shahid Bahonar University, Kerman, Iran*
[b] *Department of Chemistry, Indian Institute of Technology, Hauz Khas, New Delhi 110 016, India*

Received 20 September 1996; received in revised form 7 May 1997; accepted 10 May 1997

Abstract

Iridium is preconcentrated from the large volume of its aqueous solution using 1-(2-pyridylazo-2-naphthol) (PAN) on microcrystalline naphthalene in the pH range of 4.5–6.0. The solid mass after filtration is dissolved with 5 ml of dimethylformamide (DMF) and the metal determined by first derivative spectrophotometry. The detection limit is 20 ppb (signal to noise ratio = 2) and the calibration curve is linear over the concentration range 0.25–75.0 μg in 5 ml of the final DMF solution with a correlation coefficient of 0.9996 and relative standard deviation of ± 1.1%. Various parameters such as the effect of pH, volume of aqueous phase, choice of solvent, reagent and naphthalene concentration, shaking time and interference of a number of metal ions on the determination of trace amount of iridium have been studied in detail to optimize the conditions for its determination in synthetic samples corresponding to various standard alloys and environmental samples. © 1997 Elsevier Science B.V.

Keywords: Iridium; Microcrystalline naphthalene; Derivative spectrophotometry; 1-(2-Pyridylazo)-2-naphthol; Synthetic samples

1. Introduction

Iridium occurs as osmiridium alloy and one of the minor constituents in most platinum metal deposits in North and South America and the Urals. It is commonly used in various jewellery, dental alloys, electrical equipments, corrosion-resistant chemical wares, crucibles for high temperature reactions and extrusion dies for high melting-point glasses. Therefore, highly selective, sensitive, rapid and economical methods are needed for its trace and ultratrace determination. Neutron activation analysis (NAA) [1], atomic absorption spectrometry (AAS) [2], graphite furnace AAS [3,4], inductively coupled plasma atomic emission spectrometry (ICP–AES) [5] may be used for the trace determination of iridium in complex materials, however, these instruments are highly expensive, day to day maintenance is high and not free from various types of interferences [6–9]. A survey of the literature reveals that irid-

* Corresponding author. Fax: +91 11 6862037.

PII S0039-9140(97)00149-5

ium may be determined by zero order spectrophotometry using phenanthrenequinone monoxime [10] ($\epsilon = 2.3 \times 10^4$ l mol^{-1} cm^{-1}) perazine dimalonate [11] ($\epsilon = 9.93 \times 10^3$ l mol^{-1} cm^{-1}), tetrahydrofurfuryl xanthate [12] ($\epsilon = 5.02 \times 10^3$ l mol^{-1} cm^{-1}), 1-phenyl-4,4-6-trimethyl-(1*H*,4*H*)-pyrimidine-2-thiol [13] ($\epsilon = 3.88 \times 10^3$ l mol^{-1} cm^{-1}), thenoyltrifuoroacetone [14] ($\epsilon = 1.26 \times 10^3$ l mol^{-1} cm^{-1}) and 1-(2-pyridylazo)-2-naphthol) [15] ($\epsilon = 1.03 \times 10^4$ l mol^{-1} cm^{-1}). Preconcentration techniques like liquid–liquid extraction or column methods using ion exchange, or various adsorbents may be used for metal ions before their estimation, however these methods are time consuming and have many problems already discussed in our previous communication [16]. The reagent 1-(2-pyridylazo)-2-naphthol reacts with several metal ions to form water insoluble and coloured complexes, and has been widely used in the liquid–liquid extraction zero order spectrophotometric determination of metals [17]. Since this reagent is cheap, sensitive and selective than many of the reagents reported in the literature for the estimation of iridium [10–14]. Therefore, in the present communication, it has been tried for the trace determination of this metal after preconcentration of the metal complex on microcrystalline naphthalene by first order derivative spectrophotometry from a large volume of the aqueous solution of its synthetic samples corresponding to standard alloys and environmental samples. The use of the preconcentration technique and derivative spectrophotometry enhance the sensitivity (signal to signal measurement and free from matrix background) and selectivity (narrow peaks) of the method [18,19]. Metals like platinum or palladium which are normally associated with iridium form complexes with this reagent at room temperature and may interfere in the estimation of this metal, but can be eliminated by pre-extracting them at room temperature since iridium forms 1:2 complex with PAN at high temperature [15] or by the control of pH [17]. Preliminary observations have also revealed that iridium–PAN complex may be extracted into molten naphthalene (0.7–2.5 g) at 90°C in a waterbath [10] and can be determined similarly by the present method but this technique of preconcentration is relatively inconvenient as compared to the present method. The various parameters such as pH, volume of aqueous phase, reagent concentration, amount of naphthalene and interference of a large number of metal ions and anions on the estimation of iridium have been evaluated. The procedure developed has been successfully employed for the trace determination of iridium in various synthetic samples corresponding to standard alloys and environmental samples.

2. Experimental

2.1. Apparatus and reagents

A Shimadzo UV 160 spectrophotometer and a Hitachi UV-Vis model 330 spectrophotometer with a 1.0-cm quartz cells were used. An Elico pH meter was employed for pH measurements. All glassware was washed with mixture of concentrated sulphuric acid and nitric acid (1 + 1) before use. All the reagents used were of analytical grades. The solution of iridium chloride, 1.5500 g was dissolved in 100 ml of 6 M HCl and then diluted it to 1000 ml in a standard flask. This solution was standardized by known methods [20,21] and made 1000 ppm by appropriate dilution. A more dilute solution of iridium can be prepared by diluting the stock solution. A buffer solution of pH ~ 5.5 was prepared by mixing of 0.2 M acetic and 0.2 M sodium acetate solutions in appropriate ratio. A 0.1% solution of 1-(2-pyridylazo)-2-naphthol was prepared in ethanol. Naphthalene was of analytical grade and tested spectrophotometrically before use. A 20% solution of naphthalene in acetone was used. Solution of alkali metal salts (1%) and various metal salts (0.1%) were used to study the interference of anions and cations respectively.

2.2. General procedure

An aliquot of iridium solution (containing 0.25–75 μg) was placed in a 100-ml of an Erlenmeyer flask with tightly fitting stopper. Then 1 ml of 0.1% of the reagent (PAN) was added to it and the mixture was diluted to 30–40 ml with water.

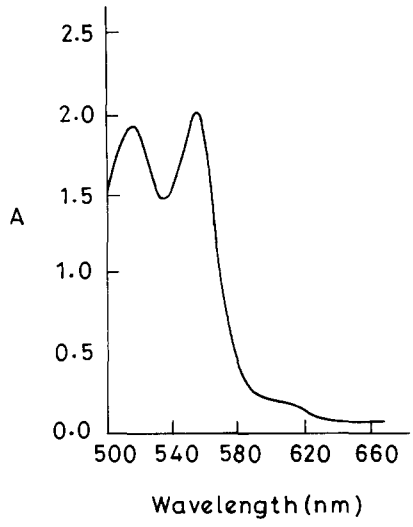

Fig. 1. Zero-order spectrum of Ir–PAN–naphthalene in DMF. Ir: 25 μg; PAN: 1.0 ml (0.1%); pH: 5.5; naphthalene: 2.0 ml (20% in acetone); reference: reagent blank.

The pH was adjusted to ~5.5 with 2 ml of the buffer solution and the solution was heated up to 90°C for 10–15 minutes in a water bath, cooled and allowed to stand for 5 min then, 2 ml of 20% naphthalene solution in acetone was added to it.

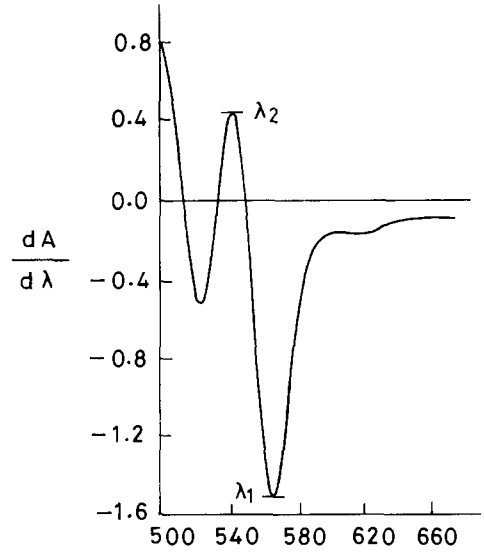

Fig. 2. First-order spectrum of Ir–PAN–naphthalene in DMF. Conditions same as Fig. 1.

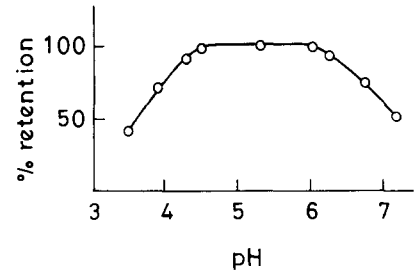

Fig. 3. Effect of pH. Conditions same as Fig. 1.

It was shaken for a few seconds and filtered through a Whatman filter paper No. 1041. The residue was dried in the folds of a filter paper and transferred to the Erlenmeyer flask. The solid mass consisting of the metal complex along with naphthalene was dissolved with 5 ml of dimethylformamide (DMF). Record the first derivative absorption spectra in the range 500–650 nm against a blank solution prepared in the same way. The signal was measured between $\lambda_1 = 565$ and $\lambda_2 = 543$ nm. A calibration curve was prepared by taking various known amounts of iridium under the conditions given above.

3. Results and discussion

3.1. Spectrophotometer measurements

The zero order and first order derivative spectra

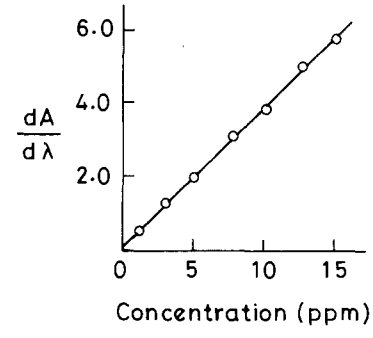

Fig. 4. Calibration curve for Ir by first order spectrophotometry from signal peak to peak measurements between $\lambda_1 = 565$ and $\lambda_2 = 543$ nm ($\Delta\lambda = 10$ nm). Rest of the conditions same as Fig. 2.

of the complex are shown in Figs. 1 and 2. As can be seen, the higher wavelength peaks of the derivative spectra are more significant. Derivative leads to sharper zero-order bands and gives higher signals in the resulting spectra. The characteristics of derivative spectra, such as peak height and noise level depend on the choice of parameters such as order of derivative, scan speed and integration time during recording of the spectra. The optimum parameters were chosen from preliminary experiments. The best results were obtained from first derivative with wavelength interval ($\Delta\lambda$) 10 nm. In the present work a peak to peak method between $\lambda_1 = 565$ and $\lambda_2 = 543$ nm was applied.

3.2. Reaction conditions

These were established with 25 μg of iridium. The adsorption of iridium PAN complexes on microcrystalline naphthalene was found to be a maximum in the pH range 4.5–6.0 (Fig. 3). In subsequent studies, the pH was maintained at approximately 5.5. Addition of 0.5–5.0 ml of the buffer did not effect the retention of iridium and the use of 2.0 ml was recommended. Various amounts of 0.1% alcoholic solution of the reagent were tried. Iridium was quantitatively adsorbed over the range 0.4–4.0 ml of the reagent. Therefore, 1.0 ml of the reagent was recommended in the present study. Various amounts of naphthalene (20% solution of the naphthalene in acetone) were added to the sample solutions keeping other variables constant. It was observed that the signal height remained constant with the addition of 1.0–4.0 ml of 20% naphthalene solution. Therefore, 2.0 ml of 20% naphthalene solution was used in subsequent studies. The effect of shaking time on the adsorption indicated that the signal height re-

Table 1
Effect of foreign salts and metal ions

Salt or iron	Tolerance limit
$CH_3COONa \cdot 3H_2O$,KNO_3	1 g
NH_4Cl, NH_4Br	500 mg
$(NH_4)_2SO_4$	450 mg
Thiourea	600 mg
KI	400 mg
K_2CO_3	100 mg
Sodium potassium tartrate	50 mg
Trisodium citrate, Sodium oxalate	15 mg
KSCN	10 mg
Disodium-EDTA	500 μg
Mn(II)	250 μg
Zn(II), Zr(IV)	300 μg
Al(III), Ca(II), Mg(II)	30 mg
Se(VI), Pb(II)	1 mg
Ga(III), Ni(II), Te(IV)	900 μg
Ti(VI), U(VI), Pd(II), Pt(II)	800 μg
V(V), Rh(III), Ru(III), Os(VIII), Sn(II)	700 μg
Cr(III), Cr(VI)	600 μg
Sb(III)	500 μg
Mo(VI)	100 μg
Fe(III)	100 μg[a,c]
Cu(II)	100 μg[b,c]
Co(II)	100 μg[c]

Iridium: 25.0 μg, total volume ~40 ml.
[a] Masked with 2 ml of 5% NaF solution.
[b] Masked with 0.5 g thiourea and 0.1 g $Na_2S_2O_3$.
[c] Masked with 500 μg by EDTA.

Table 2
Determination of iridium in synthetic mixture corresponding to iridium–rhodium fraction separated from platinum metal concentrates

Concentration (μg ml^{-1})				
Iridium(III) taken	Rhodium(III) added	Osmium(VIII) added	Ruthenium(III) added	Iridium(III)[a]
4	3	2	1	3.95 ± 0.057
12	9	6	3	11.82 ± 0.17
20	15	10	5	19.70 ± 0.32
36	27	18	9	35.45 ± 0.52
40	30	20	10	39.57 ± 0.60

[a] Average of six determination ± standard deviation.

Table 3
Analysis of iridium in synthetic samples

Composition of synthetic sample (μg in 50 ml)	Concentration of iridium (μg in 50 ml) in the synthetic sample	
	Expected value	Found[e]
Ir, 2.0; Cd, 5.0; Cu, 0.5; Ca, 200; Fe, 5.0; Os, 5.0; Mn, 2.5; Ru, 5.0, Mg, 100; Pb, 20; Zn, 10.0; Ni, 2.0; Pd, 5.0; V, 10.0, Rh, 5.0 Pt, 5.0; Al, 118	2.0	1.98 ± 0.030
Ir, 5.5; Ru, 3.0; Cu, 1.0; Ca, 150; Fe, 6.0; Ni, 6.0; Mn, 10.0; Hg, 8.0; Mg, 100; Pb, 25; Zn, 4.0; Tl, 2.0; Pd, 7.0; V, 6.0; Rh, 5.0; Pt, 10.5; Al, 147; Os, 4.0	5.5	5.40 ± 0.08
Ir, 15; Os, 2; Ru, 1.5; Ni, 6.0; Mo, 5.0; Mg, 75; Ca, 74; Cd, 7.0; Hg, 2.5; Bi, 8.0; Zn, 12; Pd, 7.0; V, 11.0; Rh, 10.0; Pt, 10.0; Mn, 3.5;	15.0	14.90 ± 0.21
Ir, 25; Fe, 3.5; As, 6.5; Ca, 120; Mg, 65; Mn, 25; Ru, 3.5; Bi, 16; Mo, 6.5; Sb, 7.5; Hg, 15.0, Pd, 3.5; V, 48.0, Rh, 17.0, Pt, 5.0; Al, 18.0; Os, 15.0; Al, 100;	25.0	24.57 + 0.4

[a] After masking with 0.5 g of thiourea and 0.1 g $Na_2S_2O_3$.
[b] After masking with 2 ml of 5% NaF solution or 500 μg of EDTA.
[c] pH was kept ~6.
[d] The recovery is more than 98%.
[e] Average of six determinations ± standard deviation.

mained constant over a range of 0.5–7.0 min. Therefore, 1.0 min of shaking time was maintained in the present work. The volume of the aqueous phase was varied in the range of 10–700 ml under the optimum conditions, keeping other variable constant. It was observed that the signal height was almost constant up to 200 ml (preconcentration factor of 40). However, for convenience, all the experiments were carried out with 40 ml of the aqueous phase.

3.3. Choice of solvent

A number of solvents were tried to dissolve the metal complex along with naphthalene. Since the solid mass is dissolved in a small volume (3–5 ml) of solvent, it is essential to select a solvent in which the chelate is highly soluble, stable and also sensitive for UV-Vis spectrophotometric measurements. The solid material is insoluble in ordinary organic solvents such as toluene, 1,2-dichloroethane, *n*-hexane, nitrobenzene, isoamyl alcohol, *n*-amyl alcohol, ethyl acetate, methyl isobutyl ketone, chloroform and dioxane, but soluble in dimethylsulfoxide, dimethylformamide (DMF) and propylene carbonate. DMF was preferred because of its high solubility and stability. It was found that 2–3 ml of this solvent was sufficient to dissolve the entire mixture, thus further enhancing the sensitivity of the method.

3.4. Calibration

The calibration curve (Fig. 4) for the determination of iridium was prepared according to the general procedure under the optimum conditions developed above. The detection limits was 20 ppb for iridium at the minimum instrumental settings (signal to noise ratio = 2). The linearity was maintained in the concentration range 0.25–75.0 μg of iridium in the 5 ml of final DMF solution with a correlation factor of 0.9996 and the relative standard deviation ± 1.1%.

3.5. Effect of diverse ions

Various salts and metals ions were added individually to a solution (~ 40 ml) containing 25 μg of iridium and the general procedure was applied. The tolerance limit (error < 3%) is given in Table 1. Among the salts examined, most did not interfere at the gram or milligram level. Among the metal ions studied, many did not interfere even at the milligram level except, Fe(III), Cu(II) and Co(II) but their relatively lower amounts could be tolerated after masking Fe(III) with 2 ml of 5% NaF solution, Cu(II) with 0.5 g of thiourea and

0.1 g of $Na_2S_2O_3$ and Co(II) with 500 μg of EDTA or all the three could be masked with 500 μg of EDTA. Thus the method developed above is fairly selective and sensitive and has been applied to the determination of iridium in various synthetic samples.

3.6. Determination of iridium in iridium–rhodium fraction separated from platinum metal concentrates

Native platinum contains 4% iridium, 3% rhodium, 2% osmium and 1% ruthenium [11], therefore, synthetic mixtures corresponding to this composition was prepared. The final solution was found to contain 4, 3, 2 and 1 μg ml^{-1} of iridium(III), rhodium(III), osmium(VIII) and ruthenium, respectively. An appropriate volume of this solution was taken, pH of the solution was maintained ~ 6 since at this pH platinum and palladium do not interfere. The results of this estimation by the present method is given in Table 2. In general the recovery is more than 98%. The results were counter checked by the methods reported in the literature [10–12].

Synthetic samples were also prepared taking large number of metal ions based upon their interference (Table 1) so that the developed conditions may be used for the determination of iridium in various environmental samples. Synthetic samples containing iridium and other metal ion (Table 3) were prepared in 10 ml of concentration hydrochloric acid and nitric acid (1 + 1) or aqua regia to obtain the desired oxidation state of Ir(III) [10]. The real sample in case available may be decomposed similarly. The final volume was made 50 ml in a standard flask and was taken for the analysis of iridium in the presence of 500 μg of EDTA at pH ~ 6. The results are given in Table 3 which were counter checked with the standard methods reported in the literature [10–12].

References

[1] V. Hodge, M. Stallard, M. Koide, E.D. Goldberg, Anal. Chem. 58 (1986) 616.
[2] S.J. Al-Bazl, A. Chow, Anal. Chem. 53 (1981) 1073.
[3] R. Ivan, Chem. Lesty 84 (1990) 250.
[4] Z. Aneva, Anal. Chim. Acta 236 (1990) 385.
[5] W. Aiharo, M. Mitsuo, Jpn. Chem. Express 5 (1990) 357.
[6] K.W. Jackson, H. Qiao, Anal. Chem. 64 (1992) 50R.
[7] K.W. Jackson, T.M. Mahmmod, Anal. Chem. 66 (1994) 242R.
[8] C.J. Kantipuly, A.D. Westland, Talanta 35 (1988) 1.
[9] A. Ramesh, J. Krishnamacharagulu, L.K. Ravinadranath, S.B. Rao, Analyst 117 (1992) 1037.
[10] A. Wasey, R.K. Bansal, B.K. Puri, Mikrochim. Acta (Wien) 1 (1984) 211.
[11] B. Keshavan, P. Nagaraja, Analyst 110 (1985) 1027.
[12] M.D. Hussain, R.K. Bansal, B.K. Puri, M. Satake, Analyst 110 (1985) 1131.
[13] A. Wasay, B.K. Puri, M. Satake, Analyst 111 (1986) 757.
[14] A.V. Rangnekar, S.M. Khopkar, Chem. Anal. 56 (1967) 84.
[15] J.R. Stokaly, W.D. Jacobs, Anal. Chem. 35 (1963) 149.
[16] M.A. Taher, B.K. Puri, Ann. Chim (Rome) 85 (1995) 183.
[17] A.K. De, R.A. Chalmers, S.M. Khopkar, Solvent Extraction of Metals, Van Nostrand Reinhbold, London, 1970.
[18] S. Shibata, M. Furukawa, K. Goto, Anal. Chim. Acta 65 (1973) 49.
[19] C.T. Cottrel, Anal. Proc. 19 (1982) 43.
[20] R.B. Wilson, W.D. Jacobs, Anal. Chem. 33 (1961) 1650.
[21] F.E. Beamish, The Analytical Chemistry of the Noble Metals, Pergamon Press, Oxford, 1966, pp. 77, 276 and 418.

ELSEVIER

Talanta 45 (1997) 417–424

Talanta

Study of the electro-adsorptive behaviour of the herbicide nitralin by means of voltammetric techniques

A. Arranz, S. Fdez de Betoño, J.M. Moreda, J.F. Arranz *

Departamento de Química Analítica, Facultad de Farmacia, Universidad del País Vasco, Apdo. 450. D.P. 01080. Vitoria, Spain

Received 30 July 1996; received in revised form 14 March 1997; accepted 12 May 1997

Abstract

The electroanalytical behaviour of the herbicide Nitralin has been studied by means of different voltammetric techniques. Nitralin is adsorbed on the mercury electrode and gives 2 reduction waves at -0.6 and -0.7 V versus Ag/AgCl reference electrode, for pH values > 10. The electrochemical process is irreversible and strongly influenced by pH solution. A systematic study of the several instrumental and accumulation variables affecting the stripping response was carried out using square wave (SWV; Osteryoung's method) and differential pulse voltammetry (DPV) as redissolution techniques. The limits of detection were 4.4×10^{-10} mol l^{-1} (AdS-SWV) and 3.5×10^{-11} mol l^{-1} (AdS-DPV), with variation coefficients of 4.17 and 3.90% respectively, at a concentration level of 8×10^{-9} mol l^{-1} ($n = 10$). A method, based on AdS-DPV, for the determination of Nitralin in ground-water is proposed. A detection limit of 8.7×10^{-11} mol l^{-1} (AdS-DPV) was reached in real samples. © 1997 Elsevier Science B.V.

Keywords: Nitralin; Herbicide; Stripping voltammetry; Adsorptive preconcentration

1. Introduction

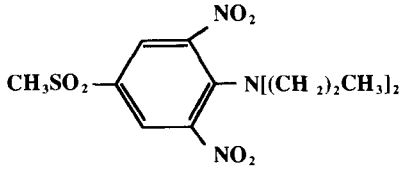

Nitralin is a dinitroaniline frequently used as a selective herbicide in pre-emergency control of annual grasses and many broad-leaved weeds in several crops.

This herbicide is usually determined by means of a variety of techniques such as spectrometry IR, GLC [1] and the capillary gas chromatography [2] with N-P detector (DL 50 pg).

The nitro group in organic compounds are easily reduced at the mercury electrodes. This forms a basis for numerous polarographic and voltammetric studies [3–10]. Whereas, the reduction of 2,6-dinitro-anilines received some attention [11,12] and reductive degradation of some pesticides containing dinitroaniline moiety has been studied [13–15], Nitralin has been investigated only marginally. Its reducibility has been

* Corresponding author.

PII S0039-9140(97)00155-0

reported [11] and a simplex method for the selection of optimum voltammetric parameters for development of an analytical procedure has been described [16].

The aim of the present work is to find optimum conditions for determination of traces of Nitralin in ground-water. The procedure is based on accumulation of Nitralin on the hanging mercury drop electrode (HMDE) followed by its reduction using differential pulse (DPV) or square wave voltammetry (SWV). The effects of analytical variables have been considered and a method to analyze the herbicide in ground-water is proposed. Such procedure is an example of adsorptive stripping voltammetry (AdSV) [17–19], which enables reaching sensitivities comparable or higher than chromatographic techniques.

2. Experimental

2.1. Instruments and reagents

All AdS-voltammetric and polarographic curves were obtained using an Ecochemie pstat 10 voltammetric analyzer and software from Ecochemie model Gpes3. The voltammetric system was linked to a Metohm 663 VA stand, which had a multimode electrode (MME), in the mode (HMDE), as working electrode, with a drop size of 0.52 mm^2. The electrode surface was renewed after each measurement was done. A new drop was formed by dislodging the old one and extruding more mercury. The 3 electrode system was completed by an Ag/AgCl reference electrode and a platinum auxiliary electrode. All measurements were taken at room temperature and a stirring bar provided convective transport during the preconcentration. A Metrohm E-605 pHmeter was used to measure the pH values.

Stock solutions (1.25×10^{-3} mol l^{-1}) of 4-(methyl sulphonyl) 2,6-dinitro-N-N′-dipropylaniline (Planavin or Nitralin) 99′0% (FW 345.37) (Lab. Dr. S. Ehrenstorfer) were prepared by dissolution of the appropriate amount of the herbicide in acetone. The solution was stored under refrigeration and protected from light.

All chemicals employed were of analytical reagent grade (Merck). Buffer stock solutions of various pH values were prepared by adjusting the pH of a mixture of acetic, phosphoric and boric acids, (Britton-Robinson, 0.04 mol l^{-1}) by the addition of sodium hydroxide solution (0.2 mol l^{-1}). All water used was of Milli Q system of Millipore.

3. Voltammetric procedure

The test solution consisting of 25 ml of the supporting electrolyte and 1 ml of sample was added to the cell and degassed with oxygen-free nitrogen for 10 min. The percentage of acetone (4%) was maintained constant in all the samples. The preconcentration potential was applied to the electrode for the selected time period while stirring the solution. The stirring was then stopped and, after a 6 s rest period, a scan to negative direction was initiated, with simultaneous recording of the resulting voltammogram. The redissolution stage was carried out using SWV (Osteryoung's method) or DPV each one with its optimum operational parameters (Table 1). For DC-polarographic experiments a step of 10 mV and an interval time of 0.6 seg. were used.

Table 1
Optimum operation parameters selected for the determination of Nitralin by AdS-DPV and AdS-SWV

Parameters	Units	DPV	SWV
Step	mV	10	10
Pulse amplitude	mV	80	60
Modulation time	ms	20	—
Interval time	s	0.4	—
Frequency	Hz	—	200
pH	B-R buffer	11.5	11.5
Accumulation potential	mV	−375	−375
Accumulation time	s	30	30
Stirring speed	rpm	2500	2500
Rest time	s	6	6

4. Results and discussion

4.1. Cyclic voltammetry

A previous study [16] showed that this herbicide is adsorbed at pH = 8.6 on the mercury electrode. However, there is nothing published about the reversibility and the influence of pH on the Nitralin adsorption process.

The cyclic voltammetric behaviour of a 1×10^{-7} mol l^{-1} Nitralin solution was studied at different pH values in Britton-Robinson buffer and the results are shown in Fig. 1. Repetitive cathodic–anodic cyclic voltammograms were recorded (50 mV s^{-1}) after stirring (2500 rpm) for 30 s at -375 mV (Fig. 1b,c) and without accumulation step (Fig. 1a). The sweep potential started at open circuit voltage (OCV) and the scans were carried out between -1.00 and $+0.15$ V.

For pH over 5.0, 2 cathodic peaks (A and B), probably due to the reduction of 2 nitro groups to the amino group with a 6 electron exchange [20], were observed at the first scan. Subsequent scans exhibit substantially smaller cathodic peaks, indicating a rapid desorption of the herbicide from the electrode surface (Fig. 1a).

On scanning in the anodic direction no oxidation peaks were observed, this behaviour indicates that the reduction of nitro groups is irreversible. Moreover, the absence of an anodic peak of arylhydroxylamine over the whole pH range studied, indicates a possibility of a 6 electrode reduction.

If the cyclic voltammograms are obtained without accumulation, the reduction peaks are smaller than those obtained after a preconcentration stage and the peak potentials are slightly shifted to more anodic potentials because Nitralin is not strongly adsorbed on the electrode (Fig. 1a).

In the voltammograms obtained at pH up to 10, it can be seen that the second wave (B) is sharper and more important than the first one (A) (Fig. 1b). On the contrary, for pH over 10, the principal wave is the first one (A) (Fig. 1c).

A study of the influence of the scan rate on the E_p and I_p, within the range 10–200 mV s^{-1}, was carried out. Plotting $\log i_p$ versus $\log v$, for the second peak ($E_p = -0.472$ V) at pH 8.6, a straight line is obtained which may be expressed

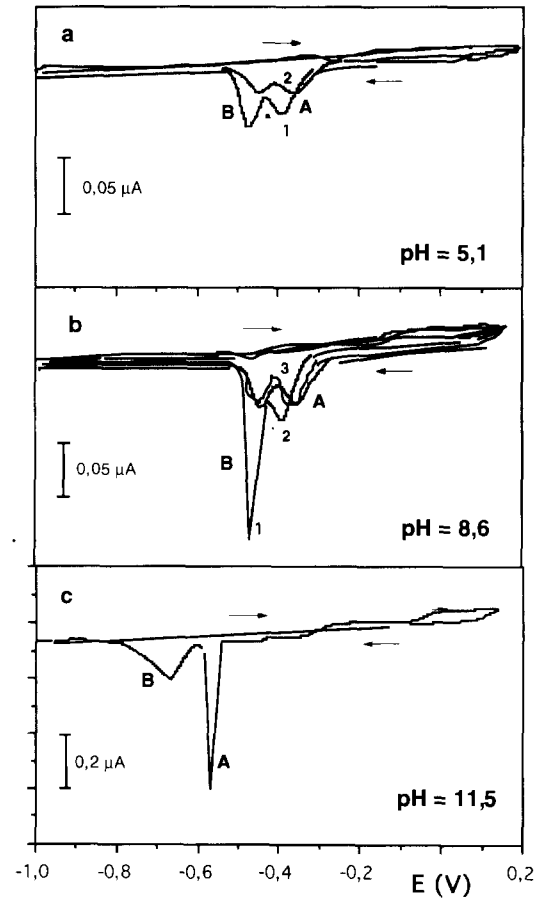

Fig. 1. Cathodic–anodic cyclic voltammograms of Nitralin (1×10^{-7} mol l^{-1}), obtained at different pH values (B-R 0.04 mol l^{-1}). Scan rate 50 mV s^{-1}. (a) pH 5.1; (b) pH 8.6; (c) pH 11.5. (b) and (c) were obtained after an accumulation step. Open circuit voltage (OCV): (a) 0.16 V; (b) 0.13 V; (c) -0.03 V. Scan number: 1, 2 and 3. First wave: A. Second wave: B. For accumulation conditions Table 1.

by the equation: $\log i_p = -0.30 + 0.96 \log v$, ($r = 0.9991$). The slope (0.96) is close to that theoretically expected (1.00) when there is adsorption on the electrode [21].

The peak potential shifts to more negative values on increasing the scan rate and the E_p versus $\log v$ plot shows a linear response according to the equation: $E_p = -0.31 - 6.40 \times 10^{-2} \log v$, ($r = 0.9818$), which confirms its irreversibility.

The dependence of E_p and I_p on the scan speed at high pH values (11.5) was similar to that found at pH 8.6.

4.2. Influence of pH

The influence of pH on the Nitralin polarographic behaviour has been studied by Southwick et al. [11] in the range from 1.5 to 9.2. The reduction process of this herbicide gives rise to a single wave in acidic media, which splits into 2 waves when the pH is increased, but no results are exposed about the behaviour of Nitralin in high alkaline media, which can be very interesting for analytical purposes.

The acidity of a 1×10^{-7} mol l^{-1} Nitralin solution in B-R buffer (0.04 mol l^{-1}) was changed from 1.5 to 12.0 pH. On DP-voltammetry, it is possible to observe 2 waves for pH over 5.0. The potential of both waves shifted to more negative values when the pH of the electrolyte is rised.

Only when AdS-DP-voltammograms were carried out, it was possible to observe the appearance of a single and very intense peak at pH 2.5, diminishing its i_p until the apparition of 2 waves at pH 4, in good agreement with the reported results [11].

When DC-polarography was used, the plot $E_{1/2}$ versus pH (Fig. 2a) shows two clearly different sections which fit straight lines. For the first and second waves according to the equations:

First wave

$$E_{1/2} = -0.05 - 4.33 \times 10^{-2}\,\mathrm{pH}, \quad (n = 7)$$

$$E_{1/2} = -0.50 - 16.07 \times 10^{-4}\,\mathrm{pH}, \quad (n = 4)$$

Second wave:

$$E_{1/2} = -0.14 - 4.62 \times 10^{-2}\,\mathrm{pH}, \quad (n = 7)$$

$$E_{1/2} = -0.65 - 8.44 \times 10^{-4}\,\mathrm{pH}, \quad (n = 4)$$

In the first section and for 2 waves, the slope lessens indicating the participation of protons in the reduction process, while in the second one the peak potential keeps practically constant when pH increases. Therefore, the peak potential is independent of pH in high alkaline solutions.

The intersection points of these straight lines correspond with the polarographic pK′ values of the oxidized forms [22]: $pK'_1 = 10.81 \pm 0.60$ and $pK'_2 = 11.20 \pm 0.59$.

The peak current of both DP-voltammetric peaks was also dependent of pH. The i_p versus pH plot (Fig. 2b) shows that the peak current intensifies with an increase in pH, reaching the maximum i_p in the pH range from 11.0 to 11.6, decreasing for higher pH values. Up to pH close to 9.2, the peak current is smaller for the first wave, being the contrary for pH above these values.

The sharp peaks at pH 8.6 and 11.5 probably indicate a change in adsorption with pH. In Fig. 2b it can be observed that the ratio between i_p for both reduction peaks remains close to 1, indicating transfer of the same number of electrons in two consecutive reduction processes.

The results by DC-polarography for i_{lim} versus pH plot, were very similar to those described above, although in this case, the ratio of 2 wave heights turns over when pH > 10, and the i_{lim} is smaller than the obtained i_p by means of DPV.

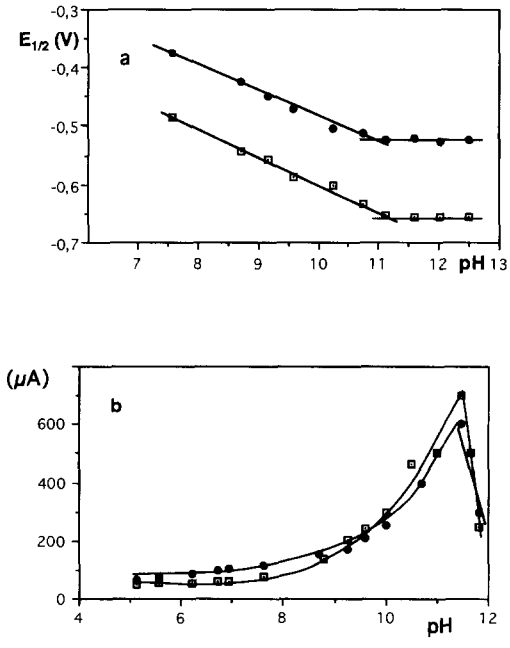

Fig. 2. Influence of pH on: (a) half-wave potential in DC-polarography and (b) peak current in DPV, for a 1×10^{-7} mol l^{-1} Nitralin solution with its optimum working conditions. First wave (●) and second wave (□).

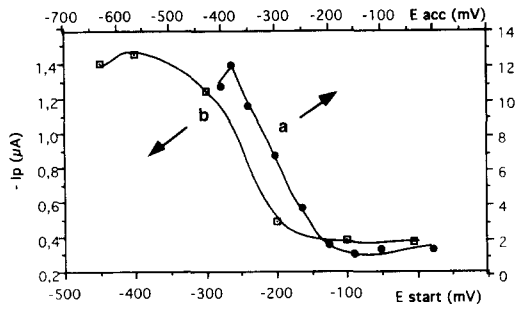

Fig. 3. Influence of the accumulation potential (a) and the start sweep potential (b) on the AdS-SWV peak height for a 4×10^{-6} mol l^{-1} Nitralin solution. For other conditions see Table 1.

Thus, a pH of 11.5 was selected for quantitative determination of the herbicide due to the high peak current and good definition reached for both waves.

4.3. Optimization of redissolution techniques

In order to determine the influence of instrumental parameters of redissolution techniques DPV and SWV on the analytical signals, a 1×10^{-7} mol l^{-1} Nitralin solution was taken and only the variable which was the object of study was modified in each case, the other variables were kept fixed. The results are exposed in Table 1.

4.4. Effect of various parameters on AdSV

The adsorptive properties of Nitralin in alkaline media allow to accumulate it on the HMDE, as a previous step to its polarographic determination, and it is necessary to choose the parameters governing the adsorptive process. The SWV was the redissolution technique selected for this purpose, with its optimum operational parameters (Table 1), and the final concentration of the Nitralin solution tested was 4×10^{-6} mol l^{-1}.

The dependence of the stripping peak current on the preconcentration potential was studied over the range 0.0 to -0.4 V. As can be seen in Fig. 3a, i_p values for Nitralin reach their maximum at -375 mV.

The effect of accumulation time on peak intensity is shown in Fig. 4. It is seen that the optimum preconcentration time before the electrode becomes saturated is 30 s. (1×10^{-8} mol l^{-1}) and 40 s. (4×10^{-9} mol l^{-1}). For the highest concentration range studied, the electrode surface is supersaturated when t_{acc} increases and a thick Nitralin molecules layer is accumulated on the electrode surface, diminishing the electrical conductivity.

The peak current increases by a factor of 6 when the stirring speed is varied in the range from 0 to 2500 rpm and this value was thus selected.

The optimum rest time, which allows the adsorbed substance to homogenize on the electrode surface (0.52 mm^2), was 6 s.

The initial sweep potential was shown to be a significant factor affecting the analytical signal size. As the initial sweep potential is coming close to the accumulation potential, the peak current increases, probably due to a reorientation of the molecules of Nitralin preadsorbed. The initial potential was varied between 0.00 and -0.45 V and better results were achieved when the cathodic scan was performed from a potential close to the accumulation potential (-375 mV), Fig. 3b. Therefore, it was necessary to use the same initial potential in all experiments.

The influence of ionic strength and the temperature on the voltammetric response was studied by means of DPV.

The $NaClO_4$ background solution concentration was shown to be a significant factor affecting negatively the analytical signal. The ionic strength

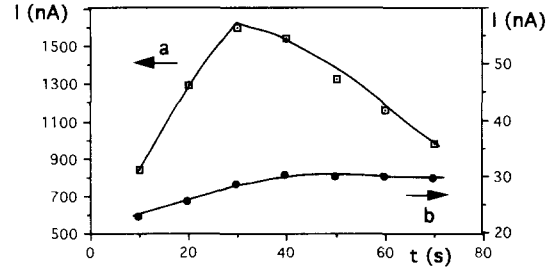

Fig. 4. Influence of the accumulation time on the AdS-SWV peak height for Nitralin solutions: (a) 1×10^{-8} mol l^{-1} and (b) 4×10^{-9} mol l^{-1}. For other conditions see Table 1.

Table 2
Regression data of calibration lines for quantitative determination of Nitralin by means of AdS-DPV and AdS-SWV

	DPV		SWV	
L.R. (mol l^{-1})	$(8\text{-}50)\times10^{-11}$	$(5\text{-}440)\times10^{-10}$	$(4\text{-}100)\times10^{-10}$	$(1\text{-}11)\times10^{-7}$
b	−22.8	−1.7	−9.9	−7.0
a	1.9×10^{-11}	1.2×10^{-2}	-5.8×10^{-9}	3.9×10^{-2}
S_b	0.9	2.8×10^{-2}	0.1	7.4×10^{-2}
S_a	2.5×10^{-10}	5.6×10^{-4}	9.2×10^{-10}	5.7×10^{-3}
S_{yx}	2.7×10^{-10}	1.1×10^{-3}	1.4×10^{-9}	6.6×10^{-3}
r	0.9984	0.9991	0.9993	0.9995
n	5	10	7	10
L.D. (mol l^{-1})	3.5×10^{-11}		4.4×10^{-10}	

L.R.: linear range, b: slope, a: intercept, S_b: S.D. of the slope, S_a: S.D. of the intercept, S_{yx}: error S.D.; r: correlation coefficient, n: data number, L.D.: detection limit.
Optimum operation parameters in Table 1.

was varied, changing the $NaClO_4$ concentration from 0.00 to 0.05 mol l^{-1} in separate samples, the peak intensity decreases on increasing the $NaClO_4$ concentration. On the basis of these results the ionic strength was that adduced by Britton-Robinson buffer (0.04 mol l^{-1}).

When the temperature was changed from 16 to 26°C, the i_p of the two reduction peaks remained constant; decreasing i_p on increasing the temperature until 50°C, probably due to the presence of degradation and hydrolysis processes changing the polarographic behaviour of Nitralin. For this reason, the room temperature was selected for analytical purposes.

The temperature coefficients $[1/(T_2 - T_1)\ln(i_2/i_1)]$ calculated for the first peak in the range 16–44°C were: 0.28% °C^{-1} (16–22°C), 0.27% °C^{-1} (22–26°C), −4.01% °C^{-1} (26–30°C), −1.54% °C^{-1} (30–36°C), −4.76% °C^{-1} (36–40°C), −7.85% °C^{-1} (40–44°C) and −3.54% °C^{-1} (44–50°C) respectively, these random temperature coefficients confirm the adsorptive nature of the reduction process [23].

With these optimum conditions for AdS-DPV and AdS-SWV, exposed in Tables 1 and 2 sharp and well defined reduction peaks at −671 mV and −762 (DPV) and at −652 mV and −752 mV (SWV) were found. In each case, the peak current of the more positive peak is higher than the more negative one.

4.5. Calibration plots and statistical parameters

The influence of the Nitralin concentration on peak current was checked by means of AdS-DPV and AdS-SWV, each one with its optimum operational parameters (Table 1). In both cases, the plot levelled off at higher concentrations, as expected for a process that is limited by adsorption of analyte. Only the results obtained for the first reduction peak, which is the most important, were taken into account.

For AdS-DPV, 2 linear ranges were observed (Table 2): one for concentration below 5×10^{-10} mol l^{-1} and the other for concentrations ranging between 5×10^{-10} and 4.4×10^{-8} mol l^{-1}. The detection limit defined as $a + 3S_{yx}$ [24] was 3.5×10^{-11} mol l^{-1}. Precision, expressed by the variation coefficient, was 3.90% ($n = 10$) for a concentration level of 8×10^{-9} mol l^{-1}.

When AdS-SWV was used, 2 linear ranges were observed also, the first one in the range from 4×10^{-10} to 1×10^{-8} mol l^{-1} and the second one between 1×10^{-8} and 1.1×10^{-7} mol l^{-1} (Table 2), being 4.4×10^{-10} mol l^{-1} the detection limit reached. The reproducibility in terms of variation coefficient was 4.17% ($n = 10$) for a concentration level of 8×10^{-9} mol l^{-1}.

Taking into account the obtained results for regression data of calibration lines exposed in Table 2, it can be said that the DPV is better than SWV to determine Nitralin at trace level because of its lower detection limit, a wider linear range,

better reproducibility and higher sensitivity (slope ratio 2.3).

The variation of Nitralin concentration has also influence on the two E_p obtained, giving rise to a shift of the peak potential towards more anodic values, when the herbicide concentration decreases.

Sometimes, a mixture of Napropamide and Nitralin is used against annual grasses and broad-leaved weeds [25]. In the same experimental conditions, it has been proved that the presence of Napropamide causes no significant changes in the peak potential of the voltammetric reduction waves obtained for Nitralin, due to Napropamide gives a reduction peak at -1.38 V, shifted to more negative potentials than those of the Nitralin ($\Delta E_p = 0.68$ V).

The presence of other herbicides commonly used, as: Isomethiozine, Chloridazone and Metamitron did not interfere in the quantitative determination of Nitralin (-0.47 V) since in our work conditions Isomethiozine does not adsorb on the electrode surface, Chloridazone gives a reduction peak at a different potential (-0.68) and the Metamitron reduction peak (-0.58 V) is overlapped whit the second reduction peak of Nitralin (-0.56 V), which is not used for quantitative purposes. Nevertheless, in presence of these herbicides, the potential of 2 Nitralin reduction peaks shifts to smaller cathodic values.

4.6. Determination of nitralin in spiked ground-water samples

In natural water samples, very low concentration of pesticides can be expected as a result of pollution of aquifers, through leaching and slurry phenomena [26]. For this reason it is necessary to make use of specific and sufficiently sensitive analytical techniques in order to evaluate the adverse effects on the environment.

Direct AdS-DPV assays, under the experimental conditions described in AdSV procedure, were tested to determine Nitralin in ground-water. The ground-water samples were taken from a fountain, which flows under agricultural soil. After the ground-water blank has been recorded, it is spiked at 2 concentration levels 4×10^{-9} and 2×10^{-8} mol l^{-1} and the herbicide determined by means of the standard addition method (Fig. 5). Five determinations were carried out at each concentration, the corresponding recoveries for each one were 101.88% (CV 4.15%) and 100.22% (CV 3.95%) respectively. The reached detection limit in real samples was 8.7×10^{-11} mol l^{-1}.

5. Conclusions

This work demonstrates that highly sensitive voltammetric measurements of Nitralin are feasible using the effective interfacial accumulation and reduction of the herbicide at high pH values on HMDE. DPV is more suitable than SWV as redissolution technique because of its better analytical and statistical characteristics.

In our work conditions, AdS-DPV is 10-fold more sensitive than in weak alkaline media [16]. The method proposed is simpler, faster and more sensitive (0.01 pg ml^{-1}) than the chromatographic method [2], requiring less expensive equipment and less sample preparation.

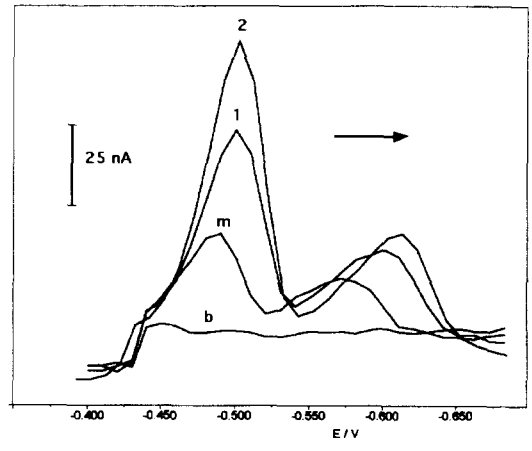

Fig. 5. AdS-DPV-voltammetric curves obtained after a cathodic scan, for the determination of Nitralin in ground-water. (b) blank, (m) ground-water spiked with Nitralin (4×10^{-9} mol l^{-1}), (1) and (2) standard additions of 100 and 200 ml of 1×10^{-6} mol l^{-1} Nitralin solution. For working conditions see Table 1.

Acknowledgements

The authors thank the Departamento de Universidades e Investigacion del Gobierno Vasco for the financial support awarded to this project (PGV 8904). They are also grateful to Angel González Pérez for linguistic revision of the manuscript.

References

[1] Anal. Methods Pestic. Plant Growth Regul. 7 (1973) 625.
[2] R. Deleu, A. Copin, J. High Resolut. Chromatogr. Commun. 5 (1982) 682.
[3] Y.A. Stradinš, Polarography of organic nitrocompounds, Pub. House of the Latvian S.S.S.R., Riga, 1961, p. 165.
[4] W. Kemula, T.M. Krygowski, Nitro compounds, in: A.J. Bard (Ed.), Encyclopedia of Electrochemistry of the Elements, Vol. XIII, M. Dekker, New York, 1973, pp. 77–130.
[5] P. Zuman, Z. Fijalek, D. Dumanović, D. Suznjević, Electroanalysis 4 (1992) 783.
[6] E. Laviron, L. Rouillier, J. Electroanal. Chem. 288 (1990) 165.
[7] E. Laviron, R. Meunierprest, A. Vallat, L. Roullier, R. Lacasse, J. Electroanal. Chem. 341 (1992) 227.
[8] R. Lacasse, R. Meunierprest, E. Laviron, A. Vallat, J. Electroanal. Chem. 359 (1993) 223.
[9] E. Laviron, R. Meunierprest, J. Electroanal. Chem. 375 (1994) 79.
[10] W.F. Smith, P. Tuñón, Quim. Anal. 6 (1987) 337.
[11] L.M. Southwick, G.H. Willis, P.K. Gupta, C.P. Keszthelyi, Anal. Chim. Acta 82 (1976) 29.
[12] L. Holleck, H.J. Exner, Z. Elektrochem. 56 (1952) 677.
[13] G.W. Probst, J.B. Tepe, In: P.C. Kearney, D.D. Kaufman (Eds.), Degradation of Herbicides, Dekker, New York, 1969, p. 255.
[14] G.H. Willis, R.C. Wander, L.M. Southwick, J. Environ. Qual. 3 (1974) 262.
[15] J.F. Parr, S. Smith, Soil Sci. 115 (1973) 55.
[16] A. San Vicente, A. Arranz, J.M. Moreda, J.F. Arranz, Anal. Chim. Acta 298 (1994) 87.
[17] S. Fdez de Betoño, A. Arranz, A. Cid, J.M. Moreda, J.F. Arranz, Quim. Anal. 14 (1995) 112.
[18] R. Kalvoda, M. Kopanica, Pure Appl. Chem. 61 (1989) 112.
[19] J. Wang, Analytical Electrochemistry. VCH, New York, 1994.
[20] M.M. Baizer, H. Lund, Organic Electrochemistry. 2nd ed., Marcel Dekker, New York, 1983.
[21] E. Laviron, L. Rouillier, C. Degrand, J. Electroanal. Chem. 112 (1980) 11.
[22] M. Heyrovský, S. Vavřička, J. Electroanal. Chem. 36 (1972) 203.
[23] L. Meites, Polarographic Techniques, 2nd ed., Wiley, New York, 1965, p. 140.
[24] J.L. Miller, J.N. Miller, Statistics for Analytical Chemistry, 2nd ed., Horwood, London, 1988, p. 103.
[25] C.R. Worthing, S.B. Walker (Eds.), The Pesticide Manual, 9th ed., The British Crop Protection Council, Surrey, 1991.
[26] J.M. Newson, Ground Water Monit. Rev. 5 (1985) 28.

ELSEVIER

Talanta 45 (1997) 425–431

Talanta

Copper(II) complexes of *N*-(phosphonomethyl)glycine in aqueous solution: a thermodynamic and spectrophotometric study

Pier G. Daniele [a,*], Concetta De Stefano [b], Enrico Prenesti [a], Silvio Sammartano [b]

[a] *Dipartimento di Chimica Analitica dell'Università, via Pietro Giuria 5, I-10125 Torino, Italy*
[b] *Dipartimento di Chimica Inorganica, Chimica Analitica e Chimica Fisica dell'Università, Salita Sperone 31, I-98166 Messina (Vill. S. Agata), Italy*

Received 13 February 1997; received in revised form 13 May 1997; accepted 13 May 1997

Abstract

Copper(II) complexes with the herbicide *N*-(phosphonomethyl)glycine (glyphosate) have been investigated in aqueous solution by means of pH-metric measurements at different temperatures, $5 \leq T \leq 45°C$, calorimetry and visible spectrophotometry. Potentiometric data, at all the considered temperatures in the range $2.5 \leq pH \leq 10.5$, can be explained assuming the formation of the species $CuLH^0$, CuL^-, $CuLH_{-1}^{2-}$, CuL_2^{4-} and Cu_2L^+. By using thermodynamic data and calculated electronic spectra for each complex a structural definition is proposed for the different species. Copper(II)–glyphosate complexes are quite stable and must be taken into account in the speciation of natural fluids. © 1997 Elsevier Science B.V.

Keywords: Copper(II); Spectrophotometry; Aqueous solution

1. Introduction

The herbicide activity of *N*-(phosphonomethyl)glycine ($(HO)_2$-PO-CH_2-H_2N^+-CH_2-COOH, glyphosate), is well known and its applications in agriculture are wide. It is a nonselective, non residual, postemergent organophosphorus herbicide which is absorbed by foliage and translocated throughout plants. In soil it is immobilized by colloids and degraded by microorganisms to inoffensive products. The phytotoxic activity arises from inhibition of a specific plant enzyme (enolpyruvyl shikimate-3-phosphate synthase) during the flavonoids synthesis [1]; as a consequence the glyphosate is non-toxic to animals.

Although its structure is particularly interesting, with reference to the possibility of forming coordination compounds with metal ions, few papers deal with this topic, giving only partial contribution to the full understanding of its coordination characteristics in solution [2–7]. In this connection, some relevant aspects can be observed from a careful inspection of glyphosate molecule: (i) the basicity of the glycyl residue

* Corresponding author.

PII S0039-9140(97)00156-2

amino nitrogen might be modified after substitution with a phosphonic group; (ii) both carboxylate and phosphonate groups should be able to form, at the same time, two chelate rings, each of them with the participation of substituted amino nitrogen; (iii) as a consequence, binuclear (homo- and hetero-) complex formation can be favoured, when working in excess of metal ion(s); and (iv) in turn, carboxylate or phosphonate group might be preferentially involved in the complex formation with the different metal ions.

Some previous literature reports show for 1:1 metal to ligand complexes a high stability, if compared with that of the corresponding glycine species and suggest a stronger coordination by glyphosate. Only calcium(II) complexes have been widely investigated [2,4,8,9]. Both the high stability and thermodynamic parameter values obtained for CaL^- species are strongly consistent with the presence of 2 chelate rings involving nitrogen amino group together with negatively charged carboxylate and phosphonate groups, while it seems very likely that proton in $CaHL^0$ species is bound to amino nitrogen. As concerns binuclear complexes, it has been pointed out [9] that in the presence of a calcium(II) excess, a Ca_2L^+ species is formed. Since no structural information is available for other metal ion complexes of glyphosate, our actual contribution gives a better understanding of glyphosate coordination mode in solution regards copper(II) complexes, investigated by means of pH-metric measurements at different temperatures (and consequent determination of thermodynamic parameters), calorimetry and visible spectrophotometry.

2. Experimental

2.1. Chemicals

Glyphosate (H_3L^0) was a Lab. Dr. Ehrenstorfer product (purity > 99.%), used without further purification. Copper(II) nitrate stock solutions were prepared and standardized by means of complexometric titrations with ethylenedinitrilotetraacetate (EDTA), in the presence of the metallochromic indicator murexide. All the solutions were prepared by using deionized and twice distilled water. The ionic strength was adjusted to 0.1 mol dm^{-3} by addition of KNO_3.

2.2. Electromotive force measurements

Potentiometric measurements were performed at 5, 15, 25, 35 and 45°C, and at ionic strength 0.1 mol dm^{-3} (KNO_3) with a Metrohm E-605 potentiometer equipped with a combined glass electrodes. The couple was calibrated in $-\log[H^+]$ units (pH) by means of alkalimetric titrations of nitric acid with standard, carbonate free, potassium hydroxide. The titrations were performed in a stream of purified nitrogen. Temperature control was achieved by a liquid circulation from a thermocryostat (model D1-G Haake). The temperature, the ionic strength and the ionic medium composition of the calibrating solution were the same as the solutions being examined. The concentration range investigated for all temperatures was from 2 to 10 mmol dm^{-3} for C_L (C mean analytical concentrations) with metal to ligand ratios from 3:1 to 1:3. Solutions containing an excess of metal ion were investigated only at 25°C.

2.3. Calorimetric measurements

The calorimetric measurements were performed at 25 ± 0.001°C by using a Tronac titration calorimeter mod. 450. Its accuracy was checked by titrating a TRIS (tris-(hydroxymethyl)aminomethane) buffer with HCl (we found $\Delta H^0 = -47.4 \pm 0.3$ kJ mol^{-1}, in accordance with Grente et al. [10]. ΔH^0 values for copper(II) complexes were obtained by adding $Cu(NO_3)_2 \cdot 3H_2O$ to glyphosate partially or fully neutralized (60–90%) and vice versa. Dilution heat was measured before each experiment.

2.4. Visible spectrophotometric measurements

The visible spectrophotometric determinations were carried out with a Spectracomp 601 Carlo Erba spectrophotometer from 400 to 800 nm, at $t = 25$°C and $I = 0.1$ mol dm^{-3}. The solution being examined was transferred from the poten-

Table 1
Thermodynamic parameters for protonation of glyphosate. I = 0.1 mol dm^{-3}, t = 25°C [9]

Protonation reaction	log K^H	$-\Delta G^0$	$\Delta H^0_{recomm.}$ (kJ mol^{-1})	ΔS^0 (J K^{-1} mol^{-1})	ΔC°_p (kJ K^{-1} mol^{-1})
$H^+ + L^{3-} = HL^{2-}$	10.15	58.0	−27.5	102.5	0.20
$H^+ + HL^{2-} = H_2L^-$	5.46	31.2	1.7	110.5	0.10
$H^+ + H_2L^- = H_3L^\circ$	2.21	12.6	−0.7	40.0	0.10

tiometric to an optical cell (optical path 1.000 cm) using a peristaltic pump. The metal concentration and the metal to ligand ratio were the same with regard to potentiometric determinations.

2.5. Data analysis and calculations

In this ligand, in the absence of metal ions, 4 hydrogen ions per molecule can dissociate, from carboxylic, secondary amino and phosphonate groups. Nevertheless only three protonation constants can be accurately determined, probably corresponding to carboxylate, amino and to one of the phosphonate hydroxyl groups. The stability constants of the complexes for the binary systems are expressed by the general formula: $\beta_{pqr} = [Cu_pL_qH_r]/[Cu]^p[L]^q[H]^r$. The stability constant values have been determined, at each temperature, by means of the program BSTAC [11] which minimizes the error squares sum in electromotive force values and takes into account eventual ionic strength variations among and/or during titrations. The program STACODH has also been used, which minimizes the error squares sum in the value of added volume for each experimental point. This program, in addition to the refinement of formation constants (with eventual variation of ionic strength), takes into account alkalimetric titrations performed at different temperatures and allows a calculation of the values of ΔH^0 (and eventually of ΔC^0_p) as well. In the program STACODH the dependence of formation constants on temperature is described by the equation proposed by Clarke and Glew [12]:

$$\log K_T = \log K_\theta + \frac{1}{2.303R}\left[\Delta H^0_\theta\left(\frac{1}{\theta}-\frac{1}{T}\right) + \Delta C^0_{p,\theta}\left(\frac{\theta}{T}-1+\ln\frac{T}{\theta}\right)\right]$$

where θ is the reference temperature, in this case $\theta = 298.15$ K.

Calorimetric data were analyzed by the computer program ES5CM [13], which minimizes the error squares sum in the reaction heat.

Visible spectrophotometric data were analysed by the MOLEX program which calculates the values of molar absorbant coefficients (ε_λ) of the different complexes by using experimental spectra, analytical concentrations of the reagents and the proposed chemical model (stoichiometric coefficients and known stability constant values of all complexes) as input. After the calculation of the species distribution, electronic spectra are estimated for each complex formed in solution, only assuming the additivity of the absorbance in the investigated concentration range. Neither assumptions on the shape of the curves nor on the nature of electronic transitions are taken into account by the program. In all calculations hydrolysis of cupric ion [14,15] was considered.

3. Results and discussion

3.1. Thermodynamic parameters

The log K^H and ΔH^0 values referred to the ligand protonation were previously determinated [9] by calorimetry and pH-metric measurements at different temperatures and are collected in Table 1. The assignment of a specific site in the

Table 2
Thermodynamic parameters for copper(II) complexes of glyphosate. I = 0.1 mol dm^{-3}, t = 25°C.

Complex	$\log \beta_{pqr}$	$-\Delta G^0$	ΔH^0_{pot} (kJ mol^{-1})	ΔH^0_{cal} (kJ mol^{-1})	$\Delta H^0_{recomm.}$ (kJ mol^{-1})	ΔS^0 (J K^{-1} mol^{-1})	ΔC^0_p (kJ K^{-1} mol^{-1})	λ_{max} (nm)	ε_{max} (dm^3 mol^{-1} cm^{-1})
$CuLH^{\circ}$	15.71 ± 0.03[a]	89.7	−5.5 ± 1.3[a]	−4.5 ± 0.9	−5.0 ± 2[a]	286.3	0.80	745	54
CuL^-	11.80 ± 0.05	67.4	−9.5 ± 2.1	−10.9 ± 1.8	−10.2 ± 2	192.2	0.50	730	60
$CuLH_{-1}^{2-}$	1.89 ± 0.09	10.8	20.4 ± 3.5	—	20.4 ± 4	104.8	0.35	725	62
CuL_2^{4-}	15.86 ± 0.08	90.6	−30.0 ± 3.5	−32.7 ± 4.1	−31.6 ± 4	195.3	0.90	715	68
Cu_2L^+	13.05 ± 0.15	74.5	—	—	—	—	—	745	71

[a] ± 3 (S.D.).

molecule to each of protonation steps was given by Dhansay et al. [16] by NMR spectra (ammonium, first step; phosphonic second step; and carboxylic, third step).

All the potentiometric data obtained from titration of copper(II)–glyphosate mixtures, at different temperatures were refined at the same time with the aim of calculating both the values of formation constants and the enthalpy changes referred to the formation of the different species: 1782 experimental points, pertaining to 53 titration curves, have been taken into account by using the STACODH program. The values of thermodynamic parameters calculated by this refinement are collected in Table 2, together with their experimental error. The ΔC^0_p values must be considered as rough estimates. Since the percent formation is not very high, even in presence of a copper(II) excess, stoichiometric ratios $C_{Cu} > C_{glp}$ were only investigated at 25°C by potentiometry and therefore no ΔH^0 value was determined for Cu_2L^+ species. In Table 3 the values are collected of copper(II) complexes formation constants, calculated at the different temperatures.

Table 3
Values of proton (as $\log K_i^H$)[a] and copper(II) complex formation constants of glyphosate at different temperatures and $I = 0.1$ mol dm^{-3}

T (°C)	5°	15°	25°	35°	45°
$\log K_1^H$	10.52	10.33	10.15	10.00	9.87
$\log K_2^H$	5.45	5.45	5.46	5.47	5.49
$\log K_3^H$	2.23	2.22	2.21	2.21	2.22
$\log \beta_{111}$[b]	15.88	15.77	15.71	15.70	15.76
$\log \beta_{110}$[b]	11.99	11.88	11.80	11.76	11.76
$\log \beta_{11-1}$[b]	1.68	1.77	1.89	2.02	2.16
$\log \beta_{120}$[b]	16.37	16.09	15.86	15.70	15.64

[a] Errors in $\log K_i^H$ are reported in [9].
[b] Errors in $\log \beta_{pqr}$ (see Section 2.5) are very close at all the temperatures (see Table 2).

In Table 2 we have also listed the ΔH^0 values determined by calorimetry. The good agreement between the two sets of values suggests that sometimes the potentiometric measurements at different temperatures can be suitably employed in order to obtain good estimates of enthalpy changes for complex formation reactions. Since errors in the enthalpy change values, obtained using these two techniques are comparable, we report, in Table 2, ΔH^0 recommended values calculated as averages.

3.2. Structural considerations

The analysis of spectrophotometric data, recorded at 25°C, on solutions containing copper(II)–glyphosate mixtures at different pH values (an example of such spectra is reported in Fig. 1a), allowed us to calculate the spectrum of each complex formed in solution. These spectra are drawn in Fig. 1b, while the values of λ_{max} and ε_{max} referred to each complex are listed in Table 2. It can be observed that no species exhibits a λ_{max} value < 700 nm, indicating that a coordination with 2 nitrogen donors in the equatorial plane should never be present in copper(II)–glyphosate complexes [17].

The value of $\log \beta_{110}$ suggests for CuL^- a tridentate character, with the formation of 2 chelate rings. The slightly exothermic value of enthalpy change referred to the reaction $Cu^{2+} + L^{3-} = CuL^-$, low if compared with that determined for the corresponding reaction between copper(II) and

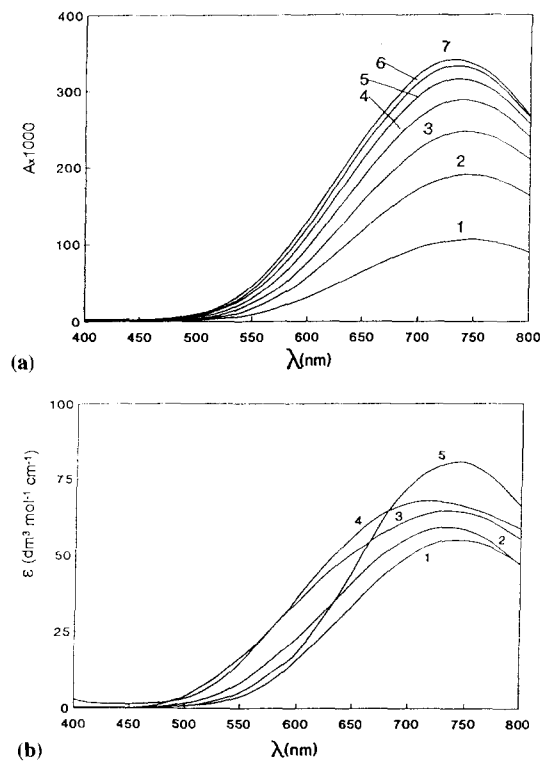

Fig. 1. (a) Visible electronic spectra for copper(II)–glyphosate system recorded on a solution containing $C_{Cu} = 5.85$ and $C_L = 5.90$ mmol dm^{-3} at different pH values: (1) 2.24, (2) 2.76, (3) 3.26, (4) 3.79, (5) 4.27, (6) 4.84, (7) 8.38. (b) Visible electronic spectra calculated for each copper(II) complexes of glyphosate: (1) $CuLH^0$; (2) CuL^-; (3) $CuLH_{-1}^{2-}$; (4) CuL_2^{4-}; (5) Cu_2L^+.

glycine, can be explained by taking into account both the slightly endothermic contribution due to the carboxylate and phosphonate groups and that also the value of enthalpy change obtained for protonation of amino is significantly lower than the one determined for amino group of non N-substituted amino acids. The value of λ_{max} calculated for CuL^- (730 nm, Table 2), though not particularly significant for a structural definition, is nevertheless consistent with coordination by one amino group and two negatively charged donor group (also, X-ray crystal structure confirm this coordination [6]).

The interpretation of all the experimental data regarding $CuLH_{-1}^{2-}$, obtained with the different techniques, is quite unequivocal. Both formation constants and ΔH^0 for the reaction $CuL^- = CuLH_{-1}^{2-} + H^+$ ($\log K = -9.91$ and $\Delta H^0 = 30.6$ kJ mol^{-1}) strongly suggest a hydrolysis reaction [4], which is also confirmed by the visible electronic spectrum calculated (quite similar to that of CuL^-).

The exothermic contribution ($\Delta H^0 = -21.4$ kJ mol^{-1}), calculated for the reaction $CuL^- + L^{3-} = CuL_2^{4-}$ can be explained only if assuming that also the second ligand molecule is coordinated with the involvement of the amino nitrogen, in CuL_2^{4-}. Spectrophotometric data ($\lambda_{max} = 715$ nm) indicate that one of the two nitrogen donors is located in an axial position, probably owing to a steric hindrance. In conclusion, both the values of thermodynamic parameters (ΔG^0 and ΔH^0) and spectrophotometric data strongly suggest that the second ligand molecule is bound to metal ion through the participation of the amino nitrogen in an axial position, with a negatively charged oxygen donor occupying the fourth position in the equatorial plane.

An interpretation of experimental data by means of an unequivocal structure may be more difficult for protonated $CuLH^0$ species. The value of log K for reaction $Cu^{2+} + HL^{2-} = CuLH^0$ can be calculated in two different ways according to whether proton is bound to amino or to negatively charged phosphonate group ($\log K = \log \beta_{111} - \log K_1^H = 5.56$ or $\log K = \log \beta_{111} - \log K_2^H = 10.21$, respectively). Since the value of formation constant referred to the reaction of Cu^{2+} with methylphosphonate is $\log \beta_{110} = 3.52$ [18], the first hypothesis (amino group protonated) requires that copper(II) ion is also coordinated by carboxylate, with the formation of an 8-membered chelate ring. Furthermore, even if, in order to estimate the exothermic contribution due to the binding of copper(II) ion with amino group (ΔH^0_{CuN}), the two slightly endothermic contribution due to phoshonate and carboxylate groups must be subtracted from the value of $\Delta H^0_{110} = -10.2$ (Table 2), it seems likely that the enthalpy change referred to the protonation of amino group (-27.5, Table 1) is more exothermic than the value of ΔH^0_{CuN}, so as it occurs for many other amino compounds [19] (e.g. glycine with $\Delta H^0_{011} = -44.3$ and $\Delta H^0_{110} = -25.$ kJ mol^{-1} and glycyl–glycine with $\Delta H^0_{011} = -44.3$ and $\Delta H^0_{110} = -27.6$ kJ mol^{-1}, at 25°C). As a consequence, if proton is located in the amino group, it

is expected that $\Delta H^0_{111} < \Delta H^0_{110}$ (more exothermic), while in Table 2, ΔH^0_{111} is slightly more endothermic than ΔH^0_{110}. In turn, if the protonation of phosphonate group is assumed, the corresponding value of log $K = 10.21$ (see above) is too high to be consistent with a glycine-like coordination of glyphosate to copper(II). In this case it is necessary to assume a structure in which also the hydrogenphosphonate group is coordinated to copper(II), in addition to amino and carboxylate groups, as proposed by Motekaitis and Martell for $CuLH^-$ complex of iminobis(methylenephosphonic acid) [4]. Between these two hypotheses, the latter seems to be more convincing.

As regards homobinuclear Cu_2L^+ species, only a structure can be proposed, with the formation of two adjacent chelate rings, each of them binding one copper(II) ion.

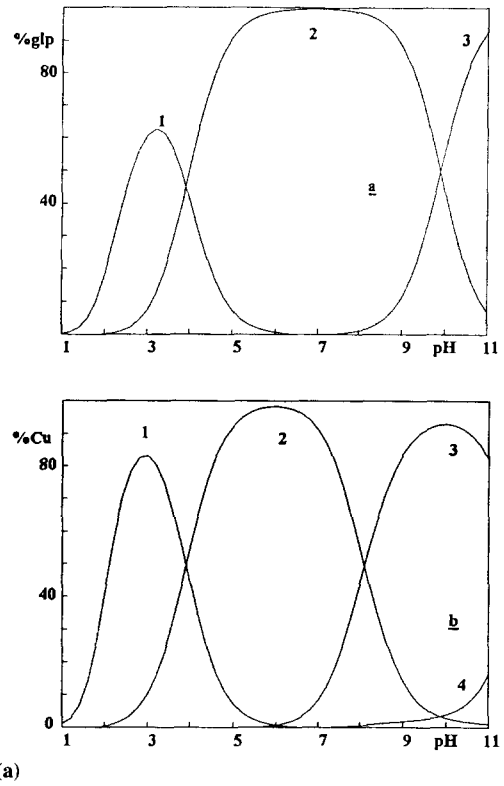

Fig. 2. Distribution of the species vs. pH in the system Cu^{2+} – glyphosate ($T = 25°C$, I = 0.1 mol dm^{-3}). (a) $C_{Cu} = C_{glp} = 5$ mM: 1. Cu(glp)H; 2. Cu(glp); 3. $Cu(glp)H_{-1}$. (b) $C_{Cu} = 5$, $C_{glp} = 15$ mM: 1. Cu(glp)H; 2. Cu(glp); 3. $Cu(glp)_2$; 4. $Cu(glp)H_{-1}$. (c) $C_{Cu} = 15$, $C_{glp} = 5$ mM1: 1. Cu(glp)H; 2. Cu(glp); 3. $Cu_2(glp)$.

3.3. Relevance of copper(II)–glyphosate complexes

As an example, some species distribution plots are drawn in Fig. 2, it is clear the relevance of CuL^- complex (Fig. 2a–c), while in presence of ligand in excess to metal ion also the species CuL_2^{4-} becomes important at high pH values (Fig. 2b). When $C_{Cu} \gg C_{glp}$, the species Cu_2L^+ is formed as well in quite low percentages. Bearing in mind the speciation problems of natural fluids, we note that also trace copper(II) can be complexed by glyphosate in the pH range 5–9.

3.4. Literature comparisons

An examination of the literature data shows a substantial agreement with our results [4,5], as concerns both the species formed in solution and the values of formation constants. The scarce previous structural hypotheses [4,5] are not supported by suitable techniques.

4. Concluding remarks

The tendency of glyphosate to form coordination compounds with metal ions is noticeable. The stability of its complexes, if compared with that of glycine complexes, clearly shows the tridentate character of this ligand. As a consequence of its strong chelating properties, the free ligand should be present in vivo in very low concentrations and

its toxicity should be related to the activity of its metal complexes.

Acknowledgements

We thank MURST and CNR for financial support.

References

[1] H.C. Steinrucken, N. Amrhein, Biochem. Biophys. Res. Commun. 94 (1980) 1207.
[2] H.E. Lundager Madsen, H.H. Christensen, C. Gottlieb-Petersen, Acta Chem. Scand. A32 (1978) 79.
[3] R.L. Glass, J. Agric. Food Chem. 32 (1984) 1249.
[4] R.J. Motekaitis, A.E. Martell, J. Coord. Chem. 14 (1985) 139.
[5] V. Subramaniam, P.E. Hoggard, J. Agric. Food Chem. 36 (1988) 1326.
[6] E.T. Clarke, P.R. Rudolf, A.E. Martell, A. Clearfield, Inorg. Chim. Acta 164 (1989) 59.
[7] M.A. Dhansay, P.W. Linder, J. Coord. Chem. 28 (1993) 133.
[8] P.H. Smith, K.N. Raymond, Inorg. Chem. 27 (1988) 1056.
[9] L. Abate, P. Mineo, C. Rigano, P.G. Daniele, E. Prenesti, C. De Stefano, S. Sammartano, Chem. Spec. Bioavail. 8 (1996) 59.
[10] I. Grente, H. Ots, O. Ginstrup, Acta Chem. Scand. 24 (1970) 1067.
[11] C. De Stefano, P. Mineo, C. Rigano, S. Sammartano, Ann. Chim. (Rome) 83 (1993) 243.
[12] E.C.W. Clarke, D.N. Glew, J. Chem. Soc. Faraday Trans. (1966) 539.
[13] A. De Robertis, C. De Stefano, C. Rigano, Termochim. Acta 138 (1989) 141.
[14] G. Arena, R. Calì, E. Rizzarelli, S. Sammartano, Thermochim. Acta 16 (1976) 315.
[15] A. De Robertis, C. De Stefano, C. Foti, G. Signorino, Talanta, in press.
[16] M.A. Dhansay, P.W. Linder, R.G. Torrington, T.A. Modro, J. Phys. Org. Chem. 3 (1990) 248.
[17] J. Billo, Inorg. Nucl. Chem. Lett. 10 (1974) 613.
[18] M. Wozniak, G. Nowogrocki, Talanta 26 (1979) 381.
[19] R.M. Smith, A.E. Martell, R.J. Motekaitis, NIST Critical Selected Stability Constants of Metal Complexes Database, Version 2.0, U.S. Department of Commerce, Standard Reference Date Program, Gaithensburg, MD 20899, 1995.

ELSEVIER

Talanta 45 (1997) 433–436

Talanta

Adsorptive stripping voltammetric determination of chromium in gallium

M.M. Palrecha, P.K. Mathur *

Analytical Chemistry Division, Bhabha Atomic Research Centre, Mumbai 400 085, India

Received 20 February 1997; received in revised form 12 May 1997; accepted 13 May 1997

Abstract

The electroanalytical chemistry of trace metals has progressed strongly with the development of cathodic stripping voltammetry (CSV) preceded by adsorption collection of organic metal complexes. A sensitive method for the determination of trace amount of chromium in gallium is described. Gallium is dissolved in sodium hydroxide containing hydrogen peroxide. The method is based on the catalytic activity of nitrate ions on the reduction of Cr(III)–TTHA (triethylene tetramine-*N,N,N′,N″,N‴,N‴*-hexaacetic acid) complex. The sensitivity of this method is further improved by adsorption preconcentration of Cr(III)–TTHA complex at a hanging mercury drop electrode (HMDE). The Cr(III) formed at the electrode surface by the reduction of Cr(VI), which is present in the bulk solution, is immediately complexed by TTHA. The adsorbed complex is then reduced at a peak potential of −1.26 V, and the peak height of Cr(III) reduction is measured. The determination limit was restricted by the amount of chromium present in the reagent blank solution. The method is suitable for the determination of chromium at level as low as 0.2 μg g^{-1} (with about 50 mg of sample) and a relative standard deviation of 15%. © 1997 Elsevier Science B.V.

Keywords: Determination; Gallium metal; Adsorptive; Stripping; Voltammetry

1. Introduction

Ultra-pure gallium is of importance in the electronic as well as in semi-conductor devices. It is widely recognised that the variable and often poor quality of semi-insulating substrate is one of the major limitations of the present development.

Chromium plays an important role in the technology of gallium and gallium arsenide. Usually the chromium content is determined by neutron activation analysis [1,2]; coupled with radiochemical separation and measurements. However, this technique is very expensive and quite a long time (5–6 weeks) is required for the measurements. Zeeman atomic absorption spectroscopy for the determination of chromium in gallium arsenide has also been reported [3].

Tanaka and Ito [4] first observed that Cr(III) and Cr(VI) in supporting electrolyte containing EDTA and nitrate ions, give exceptionally high polarographic currents from a catalytic effect caused by reoxidation of the electrolytic Cr(II)–

* Corresponding author. Fax: +91 22 5560750.

PII S0039-9140(97)00150-1

EDTA product. Zarebski [5] observed an outstanding activity of chromium with other polyaminocarboxylic acids such as diethylene triamine-*N*,*N*,*N*′,*N*″,*N*″-pentaacetic acid (DTPA) and *trans*-1,2-diaminocyclohexane-*N*,*N*,*N*′,*N*′-tetraacetic acid (DCTA). Lanza and Taddia [6] has reported differential pulse polarographic method for the determination of chromium in gallium arsenide. The method is suitable for the determination of chromium at levels as low as about 1 μg g^{-1} with about 50 mg Cr sample.

Recently [7–9], a new, more sensitive, voltammetric method is reported for the trace determination of total chromium in various water samples and high purity aluminium. This method is based on the catalytic activity of the nitrate ions on the reduction of the Cr(III)–DTPA or Cr(III)–TTHA (triethylene tetramine hexaacetic acid) complex. The sensitivity of the method is further improved by the adsorptive accumulation of the Cr(III)–TTHA complex at the HMDE.

In the present work, the catalytic cum-adsorptive stripping voltammetric method has been applied for the trace determination of chromium in gallium metal. The various experimental variables like pH, adsorption potential and time were studied to establish optimal conditions.

2. Experimental

A polarographic analyzer EG&G PARC 174A in conjunction with a static mercury drop electrode (SMDE), model 303A, was used to obtain differential pulse voltammograms. The measurements were carried out employing a three electrode system (HMDE indicator, Pt auxiliary and Ag/AgCl reference electrode) under the following experimental conditions: clock time 1 s, pulse height 50 mV, scan rate 5 mV s^{-1}. A digital pH meter was employed for pH measurements. A stock solution of Cr(VI) was prepared by dissolving potassium chromate in deionised water containing 1% H_2SO_4. Aqueous 0.2 M TTHA (Fluka) stock solution was prepared by diluting an equivalent amount of sodium hydroxide (Aristar). Merck Suprapur reagents were used to prepare 1.0 M sodium acetate and 5.0 M sodium nitrate stock solutions. The base solution used for analytical determination contains 0.2 M TTHA, 0.05 M sodium acetate, 0.5 M sodium nitrate in 10 ml sample and the pH was adjusted to 6.2. It is necessary to take a suitable excess of TTHA in addition to the quantity bound by the gallium(III)–TTHA complex.

3. Results and discussions

3.1. Preliminary studies

Aquo complexes of Cr(III) are irreversibly reduced and are not suitable for analytical work. However, some ligands such as EDTA, DTPA and TTHA form strong complexes with Cr(III) in aqueous solution and reduced reversibly, and are, therefore, suitable for voltammetric analysis. In acetate buffer solution of TTHA, chromate ions are reduced in two steps, Cr(VI) to Cr(III) and Cr(III) to Cr(II), as reported in earlier paper [9].

It is well-known that in the presence of nitrate ions, the reduction response of Cr(III)–chelate is noticeably enhanced in classical polarography and in differential pulse polarography as well. To examine this phenomenon, cyclic voltammograms of the reduction of Cr(III)–EDTA, Cr(III)–DTPA and Cr(III)–TTHA complexes have been investigated in the absence and in the presence of nitrate ions (Fig. 1). In the absence of the nitrate ions, Cr(III) chelate undergo a reversible one electron reduction. This is indicated by the difference between the anodic E_a and cathodic E_c peak potentials $[E_a - E_c]$, which is equal to about 60 mV (Fig. 1, curve A). In the presence of the nitrate ions, however, the anodic peak disappears whereas the cathodic peak is enhanced (Fig. 1, curve B). Obviously, the regeneration of the Cr(III)–TTHA complexes by oxidation with the nitrate ions causes an increase of the cathodic peak whereas the depletion of the Cr(II)–TTHA complexes at the electrode is the cause for the absence of the anodic peak according to the following mechanism:

$$\mathrm{Cr(III)} \xrightarrow{e} \mathrm{Cr(II)} \xrightarrow{NO_3^-} \mathrm{Cr(III)}$$

The catalytic action of the nitrate ions was found to be lower in EDTA than in DTPA and TTHA. Moreover, the Cr(III)–EDTA complex does not get adsorbed at the electrode surface, whereas the DTPA and TTHA complexes are found to be adsorbed and hence can be subjected to adsorptive preconcentration.

In an acetate buffer solution of TTHA, chromate ions are reduced in two steps: Cr(VI)–Cr(III) and Cr(III)–Cr(II). The Cr(III) formed at the electrode surface by the reduction of Cr(VI); which is present in the bulk solution is immediately complexed by TTHA. The observed peak current (of the Cr(III)–Cr(II) process) is thus proportional to the bulk concentration of Cr(VI).

3.2. Adsorptive stripping voltammetry

Maximum peak height was obtained between pH 6.1 and 6.3; whereas below pH 4.0 and above pH 8.0 the reduction peak practically vanished. Maximum catalytic current was obtained at 0.5–0.6 M concentration of nitrate ions. The peak current of Cr(III) TTHA complex was found to be maximum following adsorption at −1.0 V. The peak current increased with increasing adsorption time up to 90 s (for 1 ng ml^{-1}) and then levelled off. Therefore, for the determination of Cr in gallium, the following conditions were maintained: pH 6.2; nitrate ion concentration 0.5 M; accumulation potential −1.0 V; accumulation time 60 s; rest time 15 s.

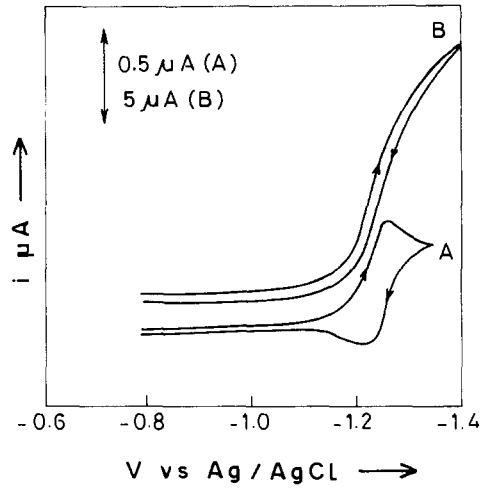

Fig. 1. Cyclic voltammograms of Cr(III)–TTHA. Curve A: 0.4 mM Cr(III), 0.02 M TTHA, 0.1 M CH_3COONa, pH 6.2. Curve B: curve A plus 0.5 M $NaNO_3$.

High purity gallium metal may contain several ultra trace impurities like lead, cadmium, zinc, nickel, iron, thallium, cobalt, copper, titanium, vanadium etc. Most of these impurities form strong complexes with TTHA. Only Pb and Cd–TTHA complexes reduction peaks are very near to Cr(III)–TTHA complex and therefore they may interfere if present in large excess as compared to chromium (about 200 times more than chromium concentration).

3.3. Analytical procedure

Gallium is easily soluble in alkaline solution containing oxidizing agents. Small amount of accurately weighed gallium metal (about 50 mg) was dissolved without difficulty when gently heated with dilute sodium hydroxide (5 ml of 0.1 M) in a teflon beaker containing hydrogen peroxide (1 ml). The mixture was refluxed on a sand bath for about 2 h for ensuring complete oxidation of Cr(III) to Cr(VI) and elimination of peroxide. This was then cooled to room temperature and required amount of base solution (TTHA + acetate buffer + nitrate) was added. The pH of this solution was adjusted to 6.2 ± 0.1 with a few drops of 1 M sodium hydroxide or 1 M nitric acid and the volume was made up to 10 ml. This solution was then transferred quantitatively to the polarographic cell, deaerated for 10 min and adsorption preconcentrated by accumulating at −1.0 V for 1 min. After accumulation, a rest period of 15 s was sufficient to establish diffusion conditions. After the rest period, a differential pulse polarogram was recorded from −1.0 to −1.4 V. Successive 0.1 ml aliquots of 0.1 μg ml^{-1} Cr(VI) standard solutions were added to the cell and the polarograms were recorded after each addition. The peak heights and the blank current were measured and the results were calculated by the standard addition method. The results were then corrected for the chromium contents of the reagent blank (Fig. 2).

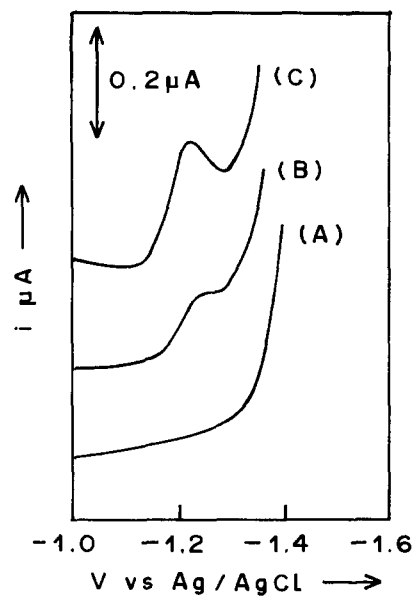

Fig. 2. Adsorptive stripping voltammetry of chromium in a gallium sample. Curve A: reagent blank; curve B: sample; curve C: sample plus standard addition, 10.4 ng ml^{-1}. Media: 0.1 M TTHA, 0.05 M CH_3COONa, 0.5 M $NaNO_3$. Scan rate: 5 mV s^{-1}; modulation amplitude: 50 mV; adsorption potential: −1.0 V (vs. Ag/AgCl); adsorption time: 30 s; rest time: 15 s.

3.4. Validation of the method

Because of the lack of suitable reference samples, analyses of spiked samples were used to assess the accuracy of the proposed procedure. Replicate determinations were made on 50 mg gallium sample spiked with 0.050, 0.100 and 0.200 μg of chromium. The recoveries were 0.048 ± 0.010 (4 results), 0.099 ± 0.016 (4 results) and 0.204 ± 0.012 μg (3 results), respectively.

The method was used satisfactorily to analyse various high purity gallium samples. A typical analysis of two gallium samples supplied by Chemistry Division of BARC yielded Cr contents of 2.9 ± 0.3 and 4.1 ± 0.4 μg g^{-1} (3 results).

On the basis of about 50 mg samples, chromium can be determined by the procedure in gallium samples at level as low as 0.2 μg g^{-1} with a relative standard deviation of 15%. The sensitivity and limit of determination are essentially fixed by the rather high current of the supporting electrolyte at the peak potential. Under these experimental conditions, the blank value of Cr was found to be 0.4 ng ml^{-1} with a deviation of 0.1 ng ml^{-1}. The detection limit (L) can be expressed as $L = \bar{x} \pm 3b$, where $\bar{x}$ is the average blank value and b is the standard deviation of the blank value. The limit of detection, therefore, was computed to be 0.3 ng ml^{-1}; the limit of quantification was 1 ng ml^{-1}.

References

[1] E.E. Nestyurina, A.G. Lototskii, V.B. Ufimtsev, Zuvodsk. Lab. 43 (1979) 437.
[2] S. Agarwal, G. Pinte, S. Mary, J. Radioanal Chem. 38 (1977) 165.
[3] T. Hadeishi, H. Kimura, J. Electrochem. Soc. 126 (1979) 1988.
[4] N. Tanaka, T. Ito, Bull. Chem. Soc. Jpn. 39 (1966) 1043.
[5] J. Zarebski, Chem. Anal. (Warsaw) 22 (1977) 1037.
[6] P. Lanza, M. Taddia, Anal. Chim. Acta 157 (1984) 37.
[7] J. Golimowski, P. Valenta, H.W. Nurnberg, Fresenius Z. Anal. Chem. 322 (1985) 315.
[8] K.M. Sarnaik, M.M. Palrecha, R.G. Dhaneshwar, Electrochemistry 5 (12) (1989) 912.
[9] K.M. Sarnaik, M.M. Palrecha, R.G. Dhaneshwar, Electroanalysis 1 (1989) 469.

ELSEVIER

Talanta 45 (1997) 437–444

Talanta

Studies on complexation and solvent extraction of lanthanides in the presence of diaza-18-crown-6-di-isopropionic acid

Jung Suk Kim *, Chang Heon Lee, Sun Ho Han, Moo Yul Suh

Korea Atomic Energy Research Institute, P.O. Box 105, Yusong, Taejon 305-353, South Korea

Received 22 May 1995; received in revised form 12 May 1997; accepted 13 May 1997

Abstract

Stability constants of some lanthanides with K22DAP (diaza-18-crown-6-diisopropionic acid) were determined by potentiometric titration method. The logarithmic values of these constants for La(III), Nd(III), Sm(III), Gd(III), Tb(III), Dy(III), Er(III), and Lu(III) are 11.14, 11.43, 11.78, 11.74, 11.95, 12.09, 11.49, and 10.88, respectively. Solvent extraction studies were carried out on the K22DAP complexes of La(III), Nd(III) and Lu(III) using TTA (thenoyltrifluoroacetone) as an extractant in different diluents. It appears that nitrobenzene, a diluent with high dielectric constant, favors the extraction of the complexes. Extraction rates of the K22DAP complexes of lanthanides were investigated at pH 5.5 and 8.0 with TTA in chloroform. The rates of extraction are found to be dependent upon the nature of the extracted species. Competitive extractions were carried out to see if selective extractions could be achieved. © 1997 Elsevier Science B.V.

Keywords: Lanthanides; Complexation; Solvent extraction; Diaza-18-crown-6-diisopropionic acid

1. Introduction

Much attention has been paid on the development of ion selective macrocyclic compounds for the separation of lanthanides either as a group or as an element. Crown ethers with ionizable functional groups such as carboxylic acid do not require other counter anion for solvent extraction, because the ligand itself carries the negative charge. In addition, the extraction can be easily carried out even at relatively low pH. These types of ionizable crown ethers have been effectively applied to selective extraction as well as preconcentration of lanthanides from aqueous solutions [1–8].

Various carboxylic acid derivatives of crown ethers shown in Fig. 1 have been synthesized and the thermodynamic and kinetic stabilities of their lanthanide complexes have been determined by a number of authors [7–21]. Diaza-18-crown-6-di-isopropionic acid (K22DAP) was synthesized, and its protonation constants were determined in previous work [22]. The protonation constants($\log k_1 = 9.05$, $\log k_2 = 8.37$, $\log k_3 = 1.88$, $\log k_4 = 0.99$) are similar to those of the structural analogues such as diaza-18-crown-6 (K22) and its derivatives [10,12,15,17].

* Corresponding author.

PII S0039-9140(97)00151-3

In this work, the extraction behavior of the K22DAP complexes with La(III), Nd(III) and Lu(III) using TTA extractant in chloroform was investigated. The stability constants of K22DAP complexes with several lanthanides were measured and compared with those of other structural analogues reported in the literatures. In addition, the extraction studies were carried out in diluents of different dielectric constants to find the nature of extracted species in the system Ln/K22DAP/TTA. The solvent extraction rates of K22DAP–lanthanide(III) complexes were also investigated.

2. Experimental

2.1. Synthesis of ligand

The ligand, diaza-18-crown-6-diisopropionic acid (K22DAP) was synthesized from Kryptofix 22 (Merck), triethylamine (Aldrich), and ethyl-2-bromo-propionate (Aldrich) according to the method of Kulstad and Malmsten with slight modification [10,18–20]. The detailed procedures of synthesis and purification of the ligand K22DAP were described in the previous paper [22].

2.2. Potentiometric titration

The measurement of the stability constants for K22DAP complexes of lanthanides was performed according to the potentiometric titration method described in a previous paper [22]. Standard solution of 0.1060 M $(CH_3)_4NOH$ was prepared by weighing $(CH_3)_4NOH$ in argon atmosphere and dissolving it in carbonate-free deionized water, and then standardized with 0.1018 M HCl. The standard metal solutions having concentrations in the range of 0.0128–0.0153 M were prepared with nitrates or chlorides of lanthanides (Aldrich), and standardized by EDTA complexometric titrations using Arsenazo I as an indicator. $(CH_3)_4NCl$ (Aldrich) recrystallized and purified from a mixture of methanol and acetone was used to adjust ionic strength of both titrant and test solution. The titration system was composed of a water-jacketed titration vessel, a glass electrode, a Ag/AgCl double junction electrode, and a 5-ml microburet containing $(CH_3)_4NOH$ standard solution. The relative potential changes were monitored using a Orion Model 901 microprocessor ionanalyzer. The suitability of the procedure was confirmed by measuring the protonation constants of glycine. All the calculations for E_0 (standard potential of the electrochemical cell) and stability constants were performed with computer programs Magec and Miniquad modified for use of 16-bit personal computer [23].

2.3. Solvent extraction

TTA (Sigma GR grade) was purified by recrystallization from a benzene–hexane mixture. $CH_3COOH/(CH_3)_4NOH$ and Tris [tris(hydroxymethyl)aminomethane]/HCl were employed to prepare buffer solutions of pH 5.5 and 8.0, respectively. $(CH_3)_4NCl$ was used to adjust the ionic strength of aqueous phase. Merck GR grade benzene, chloroform, dichloromethane and nitrobenzene were used as diluents.

2.4. Diluent effect studies

The ionic strength of the aqueous phase containing 2.68×10^{-4} M La(III) and 1.0×10^{-3} M K22DAP was adjusted to 0.2 M in pH 5.5 or 0.4

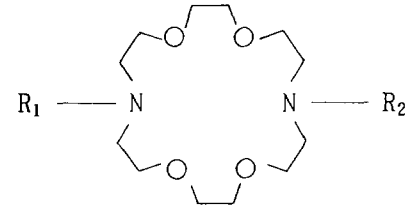

Fig. 1. Structures of K22 derivatives.

	R_1: CH_3	R_2: CH_3
K22DAP:	$-CH-COOH$	$-CH-COOH$
K22:	H	H
K22MA:	H	$-CH_2COOH$
K22DA:	$-CH_2COOH$	$-CH_2COOH$
K22MP:	H	$-CH_2CH_2COOH$
K22DP:	$-CH_2CH_2COOH$	$-CH_2CH_2COOH$

Table 1
Complex stability constants of lanthanides with K22DAP and its analogues

	Log K_{ML}									
	K22DAP[a]	K22DA	K22DP	K22MP	K22MA	K22[b]	K21DA	EDTA	EDDA	18-C-6[c]
La	11.14	12.21	6.18	nm	6.62	6.18	10.11	15.46	7.04	3.29
Nd	11.43	12.21	7.40	nm	7.24		11.60	16.56	8.06	2.44
Sm	11.78	12.12	7.44	nm	7.51		11.72	17.10	8.28	2.03
Gd	11.74	11.93	7.02	nm	7.29		11.66	17.35	8.13	1.32
Tb	11.95	11.70	7.10	nm	7.23		11.52	17.92	8.18	
Dy	12.09	11.57	6.70	nm	7.15		11.55	18.28	8.31	
Er	11.49	11.30	6.20	nm	6.70		11.15	18.83	8.59	
Lu	10.88	10.84	~6	nm	6.01		10.33	19.80	9.09	

$K_{ML} = [ML]/[M][L]$; $\mu = 0.1$; temperature = 25.0 ± 0.1°C; nm, not measurable.
[a] This study (S.D.): La (±0.02), Nd (±0.07), Sm (±0.07), Gd (±0.02), Tb (±0.09), Dy (±0.17), Er (±0.13), Lu (±0.20).
[b] Measured in MeOH/H_2O (95:5 v/v).
[c] Measured in MeOH.

M in pH 8.0. In case of Nd(III) and Lu(III), metal concentration was 2.84×10^{-4} M and 2.66×10^{-4} M, respectively. The concentration of TTA in organic phase was adjusted in the range of 4.0×10^{-4}–8.0×10^{-3} M using different diluents. Seven-ml portion of aqueous phase was equilibrated with equal volume of organic phase in a polyethylene bottle for 12 h on a Burrell wrist action shaker, and stood for 1 h to attain to phase separation. The aqueous phase was then separated carefully, and concentration of Ln(III) was determined by spectrophotometry using Arsenazo III. EDDA (ethylenediamine-*N*,*N*′-diacetic acid) instead of K22DAP was tested as a complexing agent for comparison purpose.

2.5. Extraction rate studies

The Nd(III)–K22DAP aqueous solution mentioned under diluent effect studies was used as such. In case of Lu(III), the concentration was 2.66×10^{-4} M. The concentration of TTA in chloroform was 4.0×10^{-3} or 8.0×10^{-3} M. The concentration of K22DAP in aqueous solution was 1.0×10^{-3} M. A fixed volume of each phase was pipetted into a polyethylene bottle and then equilibrated immediately using a wrist action shaker. The phase contact time for extraction procedure ranged from 2 to 720 min. The aqueous phase was separated promptly and centrifuged for 3–5 min to remove trace chloroform from the aqueous phase. The concentration of Nd(III) or Lu(III) in aqueous phase was determined by spectrophotometry.

In order to observe the extraction behavior of Ln(III) under the competitive extraction conditions, the aqueous phase was prepared with 2.70×10^{-4} M La(III), 3.04×10^{-4} M Nd(III), 3.01×10^{-4} M Sm(III), 2.63×10^{-4} M Gd(III), 3.03×10^{-4} M Tb(III), 2.54×10^{-4} M Er(III), 2.77×10^{-4} M Yb(III), 2.61×10^{-4} M Lu(III) and 8.0×10^{-3} M K22DAP, and the ionic strength was adjusted to 0.2 M in pH 5.5 or 0.4 M in pH 8.0, where organic phase containing 3.2×10^{-2} M TTA in chloroform was then added. The concentration of each lanthanide ion in aqueous phase was determined by inductively coupled plasma atomic emission spectrometry (ICP/AES, Jobin Yvon 38 plus and 50 P).

3. Results and discussion

3.1. Complex stability studies

Potentiometric titration results showed competition between lanthanide ions and protons for binding with the ligand, though the time to reach an equilibrium in titration was somewhat longer for heavy lanthanides. Stability constants of

K22DAP complexes with eight lanthanides are shown in Table 1, together with those of the structural analogues [10,12,15,21,24]. The log K_{ML} values for Ln(III)–K22DAP complexes were found to be in the range 12.09–10.88, and Dy(III) showed maximum stability. The stability constants of Ln(III) complexes with K22DAP are similar to those with K22DA and K21DA. It suggests that the steric effect on complexation is small although K22DAP has a methyl group at α-position of each carboxylic group. The complexation of K22DAP with Ln(III) may be more favorable due to the formation of five membered chelate ring, as compared to that of K22DP which forms six-membered chelate ring [15].

The data show that the complex stability trend for K22DAP is similar to those for K22DP, K22MA, and K21DA rather than that for K22DA. Chang et al. [15] insisted that the complex stability of macrocyclic ligands should be ascribed to the various factors such as macrocyclic effect, chelate ring formation by pendant carboxylate groups, Coulombic interaction between metal ion and pendant carboxylate groups, and alteration of ligand conformation upon complexation, etc. and some of effects may be synergistic. The possible structures of lanthanide complexes of K22 analogues in solution have been suggested in order to discuss the stability of these complexes, some of them are contradictory each other [25,26]. Manchanda et al. [25] suggested an encapsulated model for K22DA and K21DA complexes with lanthanide ions in solution as a possible cause of such difference in stability order.

The trend of stability constants of K22DAP may be interpreted by considering the fitness of metal to crown ether cavity along with the chelate effect of the pendant carboxylic groups. The contribution of the latter increases with increasing atomic number of lanthanides, and that of the former decreases due to lanthanide contraction. Thus, the overall stability of lanthanide complexes of K22 analogues may be governed by these two effects. Although the lighter lanthanides of larger ion size fit better into K22DAP cavity, the lower charge density offsets the advantage of the proper fitness and decreases the stability of complexes. In case of the lantinides in the middle region, which may be effected by the charge density effect rather than their favorable fitness and increases greatly the stability of complexes. For the far heavier lanthanides, it seems that the disadvantage in complexation due to the unfavorable fitness cannot be compensated for by the increase in charge density, thus the stability constants decrease.

IR spectrum of Nd(III)–K22DAP complex recrystallized from ethanol solution of [Nd(III)]/[K22DAP] = 1 showed a very strong absorption band at 1640 cm^{-1} assigned to the antisymmetric υ COO^- vibration. The frequency of υ COO^- and in the complex is the same as the carboxylate ion band in the zwitterion form of crown ether amino acid. However, the spectrum didn't show a strong characteristic CO absorption band at 1740 cm^{-1} which indicates the presence of protonated carboxylic acid groups. The result suggests the electrostatic interaction between the ionized carboxylate groups and the metal ion complexed with K22DAP.

3.2. Solvent extraction studies

3.2.1. Diluent effect studies

The distribution data (Table 2) obtained from the solvent extraction of La(III)–K22DAP complex show that the extraction efficiency varies with different diluents in the order of nitrobenzene > dichloromethane ~ chloroform > benzene. Similar observations have been reported by Chang et al. [6] on the extraction study of some lanthanides

Table 2
Distribution coefficients of La(III) at pH 5.5 and 8.0 in different diluents

Diluent	Dielectric constant (20°C)	D[La(III)]	
		pH 5.5	pH 8.0
Benzene	2.28	0.095	1.799
Chloroform	4.81	0.374	9.341
Dichloromethane	9.08	0.266	9.636
Nitrobenzene	34.82	6.299	12.295

[La] = 2.68×10^{-4} M, [TTA] = 4.0×10^{-3} M, [K22DAP] = 1.0×10^{-3} M, $\mu = 0.2$ (pH 5.5), $\mu = 0.4$ (pH 8.0).

Table 3
Slope of log D vs. log [TTA] for extraction at pH 8.0 in different diluents

Diluent	Log D/Log [TTA]			
	K22DAP		EDDA	
	La	Nd	Lu	Nd
Chloroform	1.0	1.2	2.0	2.2
Nitrobenzene	1.2		0.9	

[La] = 2.68×10^{-4} M, [Nd] = 2.84×10^{-4} M, [Lu] = 2.66×10^{-4} M, [TTA] = 4.0×10^{-4}–8.0×10^{-3} M, [K22DAP] = 1.0×10^{-3} M, [EDDA] = 2.84×10^{-3} M, $\mu = 0.4$.

into different diluents using K21DA, K22DA and TTA. They suggested that the lanthanides are extracted by forming ion pairs due to the favorable solvation energy of the ions in the diluents of high dielectric constant.

Extraction studies were carried out at various concentrations of TTA in chloroform or nitrobenzene, with a fixed concentration of K22DAP and lanthanide ions in the aqueous phase of pH 8.0. Slope values of log D versus log [TTA] for La(III), Nd(III), and Lu(III) obtained by least squares method are given in Table 3. The values for La(III) and Nd(III) in both diluents are around 1.0, which suggests that the extracted species are predominantly ternary complexes of the type Ln(K22DAP)TTA. The values for Lu(III) vary with different diluents, however, Lu(III) has a tendency to form a ternary complex in diluent with the higher dielectric constant. Slope value for extraction of Nd(III) in the presence of EDDA at pH 8.0 is similar to those in the presence of EDDA or K22DAP at pH 5.5 [22]. This result indicates that the binary species, $Nd(TTA)_3$ forms predominantly due to weak complexation of Nd(III) with EDDA.

3.2.2. Extraction rate studies

It is well known that the extraction of Ln(III) ions at pH 5.5 using TTA without any other complexing agents reaches equilibrium rapidly, because the $Ln(TTA)_3$ complexes are readily formed from the hydrated Ln(III) ions. On the other hand, in the presence of aqueous complexing agents, such as K22DA, K21DA and K22DAP, the extracted species at pH 5.5 was binary species, $Ln(TTA)_3$ predominantly [4,6,22]. Chang et al. [7] have reported that the presence of K22DA or K21DA in the aqueous phase resulted in vastly different extraction rates for different lanthanides. Therefore, K22DAP was expected to give a similar solvent extraction behavior for lanthanides. Fig. 2 shows the % extraction for Nd(III) and Lu(III) ions into chloroform from the aqueous phase of pH 5.5 as a function of equilibration time (phase contact time). The results suggest that the dissociation of $Nd(K22DAP)^+$ complex species for the formation of $Ln(TTA)_3$ is much faster than that for $Lu(K22DAP)^+$ complex. This is attributed to that the rate determining step for the extraction at pH 5.5 is the dissociation of the $Ln(K22DAP)^+$ complex species which is known to be much slower because the formation of Ln–TTA complex species is much faster. Higher TTA concentration in the organic phase increases the extraction efficiency but not necessary the extraction rate. Fig. 3 shows the % extraction for Nd(III) and Lu(III) at pH 8.0 as a function of time. The slope values of log D versus log $[TTA]_0$ revealed that the extracted species in chloroform from an aqueous phase at pH 8.0 containing K22DAP are predominantly ternary species, Ln(K22DAP)TTA for La(III) and

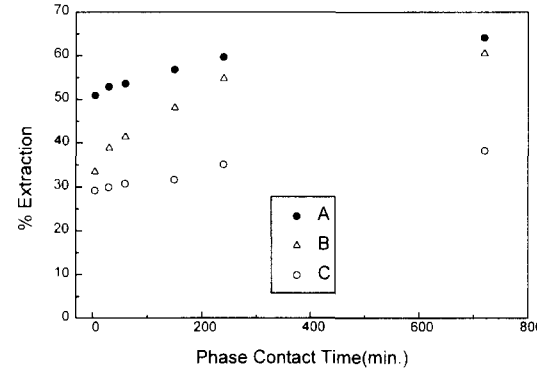

Fig. 2. Percentage extraction of Nd(III) and Lu(III) as a function of time at pH 5.5. A: [Nd] = 2.84×10^{-4} M, $[TTA]_0 = 8.0 \times 10^{-3}$ M, [K22DAP] = 1.0×10^{-3} M; B: [Lu] = 2.66×10^{-4} M, $[TTA]_0 = 4.0 \times 10^{-3}$ M, [K22DAP] = 1.0×10^{-3} M; C: [Nd] = 2.84×10^{-4} M, $[TTA]_0 = 4.0 \times 10^{-3}$ M, [K22DAP] = 1.0×10^{-3} M.

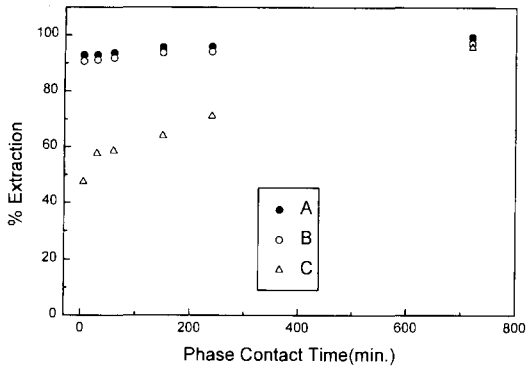

Fig. 3. Percentage extraction of Nd(III) and Lu(III) as a function of time at pH 8.0. A: $[Nd] = 2.84 \times 10^{-4}$ M, $[TTA]_0 = 8.0 \times 10^{-3}$ M, $[K22DAP] = 1.0 \times 10^{-3}$ M; B: $[Nd] = 2.84 \times 10^{-4}$ M, $[TTA]_0 = 4.0 \times 10^{-3}$ M, $[K22DAP] = 1.0 \times 10^{-3}$ M; C: $[Lu] = 2.66 \times 10^{-4}$ M, $[TTA]_0 = 4.0 \times 10^{-3}$ M, $[K22DAP] = 1.0 \times 10^{-3}$ M.

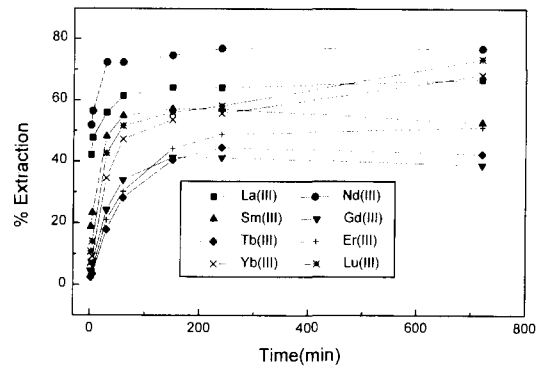

Fig. 4. Variation of % extraction of Ln(III) from a mixture containing eight lanthanide ions as a function of time at pH 5.5. $[TTA]_0 = 3.2 \times 10^{-2}$ M, $[K22DAP] = 8.0 \times 10^{-3}$ M, $[La] = 2.70 \times 10^{-4}$ M, $[Nd] = 3.04 \times 10^{-4}$ M, $[Sm] = 3.01 \times 10^{-4}$ M, $[Gd] = 2.63 \times 10^{-4}$ M, $[Tb] = 3.03 \times 10^{-4}$ M, $[Er] = 2.54 \times 10^{-4}$ M, $[Yb] = 2.77 \times 10^{-4}$ M, $[Lu] = 2.61 \times 10^{-4}$ M.

Nd(III) ions and a mixture of $Lu(TTA)_3$ and Lu(K22DAP)TTA for Lu(III). Extraction of ternary species only requires the formation of bonds between $Ln(K22DAP)^+$ and TTA^-, followed by the transfer of the formed neutral species into the organic phase. The rate of bond formation between $Ln(K22DAP)^+$ and TTA^- is determined by the dissociation rate of a coordinated water molecule, which is fast. Nd(III) is extracted mostly as ternary species Nd(K22DAP)TTA and its extraction reaches equilibrium in less than 2 min [7]. On the other hand, the extraction of Lu(III) took more than fours hours to reach equilibrium. This slow extraction is attributed to the fact that the extracted species are a mixture of binary and ternary, $Lu(TTA)_3$ and Lu(K22DAP)TTA. The extraction of binary species, $Lu(TTA)_3$ is slow due to the slow dissociation of $Lu(K22DAP)^+$ prior to formation of binary species [7]. Thus, these extraction behaviors suggest that the light lanthanides with smaller distribution coefficients can be selectively extracted from lanthanide mixtures by controlling the phase contact time.

Competitive extraction experiments were carried out to determine that extraction selectivities could be achieved. The experiments were carried out with TTA in chloroform for the aqueous phases containing K22DAP and eight lanthanide ions, i.e. La(III), Nd(III), Sm(III), Gd(III), Tb(III), Er(III), Yb(III) and Lu(III) at pH 5.5 and 8.0. The variation of extraction rates in competitive extraction appears to be different from those of individual extraction experiments. Fig. 4 shows the % extraction curves for the eight lanthanides at pH 5.5 in the presence of K22DAP. The results show that the rates of La(III) and Nd(III) extraction are faster and those of Lu(III) and Yb(III)

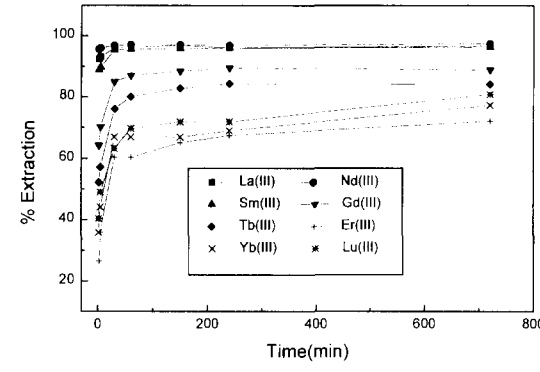

Fig. 5. Variation of % extraction of Ln(III) from a mixture containing eight lanthanide ions a function of time at pH 8.0. $[TTA]_0 = 3.2 \times 10^{-2}$ M, $[K22DAP] = 8.0 \times 10^{-3}$ M, $[La] = 2.70 \times 10^{-4}$ M, $[Nd] = 3.04 \times 10^{-4}$ M, $[Sm] = 3.01 \times 10^{-4}$ M, $[Gd] = 2.63 \times 10^{-4}$ M, $[Tb] = 3.03 \times 10^{-4}$ M, $[Er] = 2.54 \times 10^{-4}$ M, $[Yb] = 2.77 \times 10^{-4}$ M, $[Lu] = 2.61 \times 10^{-4}$ M.

Table 4
Separation factor values of competitive extraction at pH 5.5

Phase contact time (min)	Lu/Yb	Lu/Er	Lu/Tb	Lu/Gd	Lu/Sm	Lu/Nd	Lu/La
2	1.57	5.04	4.84	2.47	0.52	0.11	0.17
720	1.29	2.66	3.77	4.38	2.51	0.83	1.37

$[TTA]_0 = 3.2 \times 10^{-2}$ M, $[K22DAP] = 8.0 \times 10^{-3}$ M, $[La] = 2.70 \times 10^{-4}$ M, $[Nd] = 3.04 \times 10^{-4}$ M, $[Sm] = 3.01 \times 10^{-4}$ M, $[Gd] = 2.63 \times 10^{-4}$ M, $[Tb] = 3.03 \times 10^{-4}$ M, $[Er] = 2.54 \times 10^{-4}$ M, $[Yb] = 2.77 \times 10^{-4}$ M, $[Lu] = 2.61 \times 10^{-4}$ M.

Table 5
Separation factor values of competitive extraction at pH 8.0

Phase contact time (min)	Lu/Yb	Lu/Er	Lu/Tb	Lu/Gd	Lu/Sm	Lu/Nd	Lu/La
2	1.21	1.87	0.62	0.38	0.08	0.03	0.05
720	1.24	1.63	0.79	0.53	0.16	0.11	0.14

$[TTA]_0 = 3.2 \times 10^{-2}$ M, $[K22DAP] = 8.0 \times 10^{-3}$ M, $[La] = 2.70 \times 10^{-4}$ M, $[Nd] = 3.04 \times 10^{-4}$ M, $[Sm] = 3.01 \times 10^{-4}$ M, $[Gd] = 2.63 \times 10^{-4}$ M, $[Tb] = 3.03 \times 10^{-4}$ M, $[Er] = 2.54 \times 10^{-4}$ M, $[Yb] = 2.77 \times 10^{-4}$ M, $[Lu] = 2.61 \times 10^{-4}$ M.

are slower for competitive extraction. Fig. 5 shows the extraction curves at pH 8.0 in the presence of eight lanthanides and K22DAP. The extraction efficiencies for eight lanthanide ions at pH 8.0 in the presence of K22DAP are higher than those at pH 5.5. The extraction rates for La(III), Nd(III), and Sm(III) appear to be much faster than those for Er(III), Yb(III) and Lu(III). It seems clear that the extraction rates for heavier lanthanides are slower than those for lighter lanthanides due to the slow dissociation of LnL^+ complexes.

The separation factor values in competitive extraction at pH 5.5 and pH 8.0 using 2 min of phase contact time as well as 12 h (equilibrium) are given in Tables 4 and 5. The separation factor values of Lu/Nd and Lu/La are much lower compared to Lu/Yb and Lu/Er at short phase contact time, i.e. 2 min, at pH 8.0 under competitive extraction. Thus, the selective separation of light lanthanides from a mixture containing heavy lanthanides may be realized by the solvent extraction of short phase contact time.

References

[1] J. Tang, C.M. Wai, Anal. Chem. 58 (1986) 3233.
[2] J. Tang, C.M. Wai, Analyst 114 (1989) 451.
[3] J. Tang, C.M. Wai, Talanta 36 (1989) 1129.
[4] V.K. Manchanda, C.A. Chang, Anal. Chem. 58 (1986) 2269.
[5] V.K. Manchanda, C.A. Chang, Anal. Chem. 59 (1987) 813.
[6] V.K. Manchanda, C.A. Chang, J. Peng, Solvent Extr. Ion Exch. 6 (1988) 835.
[7] C.A. Chang, V.K. Manchanda, J. Peng, Solvent Extr. Ion Exch. 7 (1989) 413.
[8] C.A. Chang, V.K. Manchanda, J. Peng, Inorg. Chim. Acta 130 (1987) 117.
[9] C.A. Chang, V.O. Ochaya, V.C. Sekhar, J. Chem. Soc. Chem. Commun. (1985) 1724.
[10] C.A. Chang, M.E. Rowland, Inorg. Chem. 22 (1983) 3866.
[11] C.A. Chang, B.S. Garg, V.K. Manchanda, V.O. Ochaya, V.C. Sekhar, Inorg. Chim. Acta 115 (1986) 101.
[12] C.A. Chang, V.O. Ochaya, Inorg. Chem. 25 (1986) 355.
[13] V.C. Sekhar, C.A. Chang, Inorg. Chem. 25 (1986) 2061.
[14] C.A. Chang, V.C. Sekhar, Inorg. Chem. 26 (1987) 1981.
[15] C.A. Chang, P.H. Chang, V.K. Manchanda, S.P. Kasprzyk, Inorg. Chem. 27 (1988) 3786.
[16] V.K. Manchanda, P.K. Mohapatra, Polyhedron 9 (1990) 2455.
[17] M. Takagi, M. Tazaki, K. Ueno, Chem. Lett. (1978) 1179.
[18] S. Kulstad, L.A. Malmsten, Acta Chem. Scand. B 33 (1979) 469.
[19] R.A. Kolinski, J. Mrozinski, Polyhedron 2 (1983) 1217.
[20] S.P. Kasprzyk, R.G. Wilkins, Inorg. Chem. 27 (1988) 1834.
[21] R.M. Izatt, J.D. Lamb, J.J. Christensen, B.L. Haymore, J. Am. Chem. Soc. 99 (1977) 8344.
[22] J.S. Kim, C.H. Lee, S.H. Han, M.Y. Suh, T.Y. Eom, J.H. Park, J. Korean Chem. Soc. 36 (1992) 840.

[23] D.J. Leggett, Computational Methods for the Determination of Formation Constant, ch. 3 and 5, Plenum Press, New York, 1985.
[24] S.P. Sinha, Complexes of the Rare Earths, ch. 5, Pergamon Press, London, 1966.
[25] V.K. Manchanda, P.K. Mohapatra, C. Zhu, R.M. Izatt, J. Chem. Soc. Dalton Trans. (1995) 1583.
[26] R.C. Holz, S.L. Klakamp, C.A. Chang, W.D. Horrocks Jr., Inorg. Chem. 29 (1990) 2651.

ELSEVIER

Talanta 45 (1997) 445–450

Talanta

Determination of passive-sampled sulphur dioxide in ambient air as sulphate ion by flow injection analysis with an in-line reaction column

Yi Yang [1,a], Xin-Xiang Zhang [2,a], Takashi Korenaga [a,*], Keiro Higuchi [b]

[a] *Faculty of Integrated Arts and Sciences, University of Tokushima, Tokushima 770, Japan*
[b] *Tokyo Kasei Kogyo Co. Ltd., 6-15-9, Toshima, Kita-Ku, Tokyo 114, Japan*

Received 19 February 1997; received in revised form 13 May 1997; accepted 14 May 1997

Abstract

A modified FIA method was developed for the determination of sulphur dioxide (SO_2) in ambient air collected by a passive sampler. SO_2 was oxidized by hydrogen peroxide and determined as sulphate ion in solution. Barium–dimethylsulfoazo-III complex was used as spectrophotometric reagent. A $BaSO_4$-immobilized in-line reaction column was introduced into the flow system to increase the sensitivity and reproducibility. An in-line cation exchange column was used to eliminate triethanolamine, which was used as the absorbent reagent in the passive sampler. Sulphate ions can be analyzed in the range of 0.08–10.00 mg l^{-1} with the R.S.D. less than 1.6% at the rate of 15 samples h^{-1}. It was satisfactory to apply this method to the analysis of sulphur dioxide in ambient air and the results agreed with those obtained by ion chromatography. © 1997 Elsevier Science B.V.

Keywords: Sulphur dioxide in air; In-line reaction column; FIA; Passive sampler

1. Introduction

Along with the development of industry and society, environmental pollution, particularly air pollution, is becoming a worldwide problem. The emission of sulphur dioxide (SO_2) by the burning of fuel, especially coal, is largely responsible for the air pollution. SO_2 is a main component of 'acid rain' which has a serious effect on the ecological system. It can also cause diseases of the human respiratory system.

Reliable knowledge of individual exposure to SO_2 or outdoor/indoor air environment measurements is an important parameter in air pollution and environmental hygienic studies. Different sampling methods have been applied in the collection of air samples. The active sampler is not convenient especially in the measurement of personal exposure because a battery is needed to make the pump work. On the contrary, the pas-

* Corresponding author.
[1] Visiting scientist from Department of Applied Chemistry, Beijing University of Chemical Technology, Beijing 100029, China.
[2] Visiting scientist from Department of Chemistry, Peking University, Beijing 100871, China.

PII S0039-9140(97)00152-5

sive sampler does not need a pump. It is compact, light, inexpensive, nonhazardous, and easily used without disturbing daily human activity [1]. Such samplers are suitable for the simultaneous multipoint determinations, which are frequently required in large-scale studies such as personal/environmental exposure study and outdoor/indoor air pollution monitoring [2,3].

Generally, the passive-sampled SO_2 was oxidized by hydrogen peroxide and determined as sulphate ion in solution. Several methods have been reported for the analysis of sulphate ion [4–7]. Ion chromatography (IC) is a common method for determination of sulphate ion. However it takes 15–20 min for one sample analysis, and the durability of the ion exchange column remains a problem.

Flow injection methods for the analysis of sulphate ion were reported by some authors. Barium–dimethylsulfoazo-III complex was used as the spectrophotometric reagent. The reagent solution or the carrier solution was saturated with $BaSO_4$ to obtain high sensitivity and good reproducibility [8,9]. In this paper a $BaSO_4$ – immobilized reaction column was used instead of the saturated $BaSO_4$ solution. The sensitivity, reproducibility and analysis rate were improved as expected. The developed method was successfully used in the analysis of sulphur dioxide in ambient air collected by passive samplers.

2. Experimental

2.1. Reagents

All reagents used were analytical-reagent grade. Barium–dimethylsulfonazo-III (2,7-bis[(4-methyl-2-sulfophenyl)azo]-1,8-dihydroxy-naphthalene-3,6-disulfonic acid, disodium salt; Dojindo Laboratories, Japan) complex was used as the spectrophotometric reagent. The reagent solution was prepared as follows: add 5.6 ml of 10^{-2} M dimethylsulfonazo-III, 3.9 ml of 10^{-2} M $BaCl_2$, 5 ml of 1.0 M KNO_3, 20 ml of 1.0 M chloroacetic acid–sodium chloroacetate buffer, and 800 ml of ethanol into a 1000-ml flask. Then dilute to the mark with distilled water. Standard sulphate solution was prepared from sodium sulphate.

2.2. Apparatus

The FIA apparatus, consisted of a double plunger pump (PU-5000, Sanuki, Japan), a spectrophotometer (UV-150-02, Shimadzu, Japan) equipped with a flow-through cell (10-mm light path, 18-μl inner volume), a multirange recorder (Nippon Denshi Kagaku Model U-228) and an auto sampler (Atto Model SJ-1700), an in-line reaction column (150 × 2.2 mm I.D.; Tokyo Kasei Kogyo Co., Ltd. Japan), was used. A column (50 × 5 mm I.D.) filled with cation exchange resin (Dowex 50W-X8, 100–200 mesh, H form; Muromachi Kagaku Kogyo, Japan) was placed after the injection valve to eliminate triethanolamine (TEA). The schematic diagram used in this work is shown in Fig. 1. The flow system was connected by 0.5 mm I.D. polytetrafluoroethylene (PTFE) tube.

An ion chromatographic analyzer (PIA-1000, Shimadzu, Japan) containing a pump, an ion exchange column (Shim-pack IC-A3 (S), 150 × 2 mm I.D.), and an electric conductivity detector was also used for sulphate ion analysis.

2.3. Procedure

2.3.1. Sampling method

The badge-type SO_2 passive samplers (Toyo Roshi Kaisha, Ltd, Japan) were used to collect SO_2 in ambient air. The structure of the sampler is

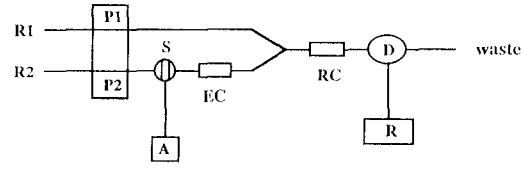

Fig. 1. Schematic diagram of the FIA system. R1: reagent solution, flow rate 0.30 ml min^{-1}; R2: water carrier solution, flow rate 0.30 ml min^{-1}; P1, P2: double plunger pump; S: sampling valve; A: auto injector; EC: cation ion exchange column; RC: in-line reaction column; D: spectrophotometer, 662 nm; R: multirange recorder.

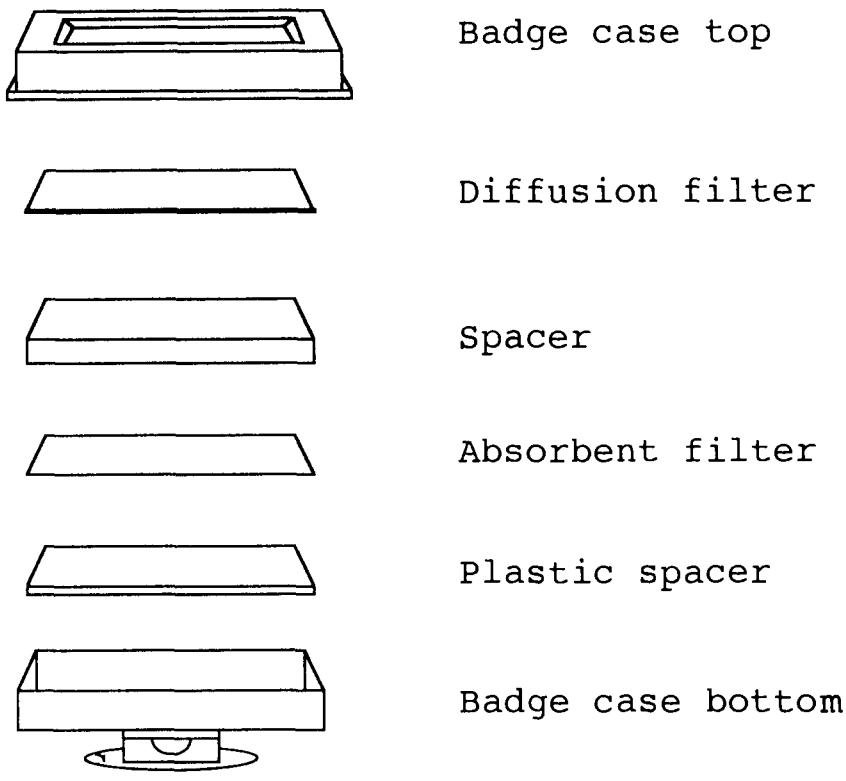

Fig. 2. Structure of a typical SO_2 passive sampler.

shown in Fig. 2. It consisted of a diffusion zone and an absorbent zone in a badge case. The diffusion zone, composed of a multilayer polytetrafluoroethylene-like membrane filter, was used to avoid the fluctuation caused by turbulent flow of wind. The absorbent zone was a filter paper impregnated with TEA solution as absorbent reagent.

The passive sampler was taken from the sealed aluminum pouch filled with nitrogen and put in the sampling place (indoor and/or outdoor). Care was taken to protect it from rain while sampling. After being exposed to air for a certain time, the sampler was returned to the original pouch. The pouch was sealed with adhesive tape.

The sample solution was prepared as follows: The absorbent filter was taken out and immersed in 10 ml of H_2O_2 solution (0.1%). SO_2 absorbed by TEA was oxidized to SO_4^{2-} by H_2O_2. The solution obtained was stored in a sealed vial and kept in a refrigerator before analysis.

2.3.2. Preparation of the reaction column

The glass beads (∅ 0.4 mm) were treated with 1.0 M NaOH solution at 40°C for 3 h and washed with distilled water. The treated glass beads were then immersed in $BaSO_4$ suspension solution overnight to immobilize $BaSO_4$ on the surface of the glass beads. After washing with distilled water and drying, the $BaSO_4$-immobilized glass beads were packed in a glass tube (150 × 2.2 mm I.D.).

2.3.3. Analytical methods

For FIA analysis, sample solutions containing sulphate ion were injected into the carrier stream by the automatic sample injector at 4-min intervals. The reagent solution and carrier (distilled water) were delivered by the double plunger

pump. The two streams merged and reacted in the reaction column. The decrease of absorbance caused by the dissociation of the barium–dimethylsulfonazo-III complex was measured at 662 nm with the spectrophotometer.

For IC analysis, the eluent containing 8.0 mM *p*-hydroxybenzoic acid and 3.2 mM bis-Tris was used. The ion exchange column was equilibrated with the eluent at the flow rate of 0.2 ml min^{-1} for 20 min. After eliminating TEA with cation-exchange resin the sample solution was injected into the system and the results were calculated from peak areas.

3. Results and discussion

3.1. Effect of the reaction column

As we know, it is difficult to acquire good reproducibility with a precipitation reaction in FIA system. Reasons include heterogenous precipitation reaction in the thin PTFE tube and the low rate for the precipitate formation.

Sulphate ion reacts with barium–dimethylsulfonazo-III complex in aqueous medium and forms $BaSO_4$ precipitate. The reaction rate is very slow. It takes about 1 h to reach equilibrium in batch system. The kinetic curve based upon the decrease of the absorbance at 662 nm is shown in Fig. 3. It is useful for designing an FIA system. In our previous experiment a long reaction coil and low

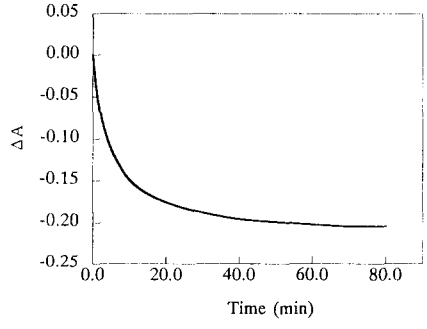

Fig. 3. Kinetic curve of the reaction between Ba–dimethylsulfonazo-III complex and sulphate ion in batch system; 2 ml of reagent solution plus 2 ml of sulphate ion solution (2 mg l^{-1}).

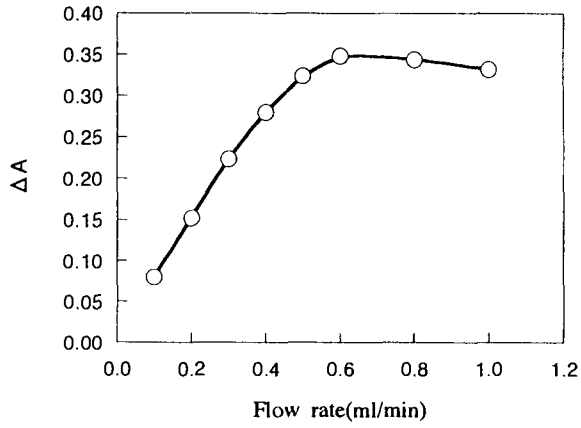

Fig. 4. Effect of flow rate. Concentration of SO_4^{2-}: 4 mg l^{-1}; injection volume: 200 μl.

flow rate were used in FIA system to obtain longer residence time. High concentration of dimethyl sulfoxide (DMSO) in the reagent solution was used to improve the precipitation behaviour. It was also reported that using a saturated $BaSO_4$ solution as carrier which contained enough crystal nuclei could induce the formation of the precipitate[8]. In this paper, a $BaSO_4$-immobilized reaction column was introduced instead of the long reaction coil and the saturated $BaSO_4$ solution. The column not only provides crystal nuclei, but can be regarded as a packed tube. The packed reactor is most effective for promoting radial mass transfer. Glass beads in the column can increase radial dispersion and reduce axial dispersion of the sample zone. It offers easy reaction of sample with reagent so that a long residence time is not necessary. The flow rate was tested in the range of 0.1–1.0 ml min^{-1} with 4 mg ml^{-1} of sulphate ion. As shown in Fig. 4, the sensitivity increased as the increase of the flow rate when the flow rate was changed from 0.1 to 0.6 ml min^{-1}. When the flow rate was lower the sensitivity was lower and peak broadening was serious because of axial dispersion. When the flow rate was higher than 0.6 ml min^{-1} the peak height decreased and the noise increased as the flow rate increased. The flow rate was fixed at 0.6 ml min^{-1} for further research.

With the use of the $BaSO_4$-immobilized column the sensitivity of detection was enhanced and the

reproducibility was greatly improved. Moreover, the preparation of the carrier solution was simplified.

The sensitivity of the reaction column decreased only 3% after 80 samples had been analyzed. It was found better to wash the column with distilled water daily after analysis to recover the activity of the column.

3.2. Effect of injection volume

Three injection coils with injection volumes of 50, 100 and 200 μl were tested at a flow rate of 0.6 ml min^{-1} and with a 2 mg l^{-1} solution of sulphate ion. The peak height increased with the increase of injection volume. A volume of 200 μl was chosen to meet the need of the air sample analysis because the concentration of SO_2 in air was low.

3.3. Interference

As reported in a previous paper [8], univalent ions up to mg-level did not interfere with the determination of sulphate. Ca^{2+} interfered seriously. It was found that when TEA was used as the absorbent in the SO_2 passive sampler it interfered with the determination seriously. When such a kind of sample was analyzed by IC, the sample solution had to be treated with cation exchange resin to eliminate TEA. That made the analysis procedure quite complicated. Even if the cation exchange cartridge could be used during the sample injection, it is a poor economy. In this paper, an ion exchange column (5 × 50 mm) with cation exchange resin was placed just after the sample injection valve to eliminate TEA. The sample solution was, therefore, injected into the FIA system directly without pretreatment. The results showed that the interference of TEA could be eliminated effectively. The column could be used for analysis of more than 500 samples before regeneration. With the use of the on-line exchange column the analysis procedure was simplified and the analytical rate was increased.

3.4. Calibration curve and reproducibility

The calibration curve of sulphate ion was acquired under optimized conditions. The linearity was in the range of 0.08–10 mg l^{-1} with a correlation coefficient of 0.999. The equation was $y = 0.001 + 0.054x$, where y was the absorbance and x was the concentration of sulphate in sample solution (mg l^{-1}). The detection limit was 0.08 mg l^{-1} of the sulphate ion (S.N.R. = 3), which is equal to 4.64 μl Nm^{-3} of SO_2 in air. The relative standard deviation (R.S.D.) was 1.6% for ten replicate injections of 1.0 mg l^{-1} of sulphate ion.

3.5. Application

The present method was applied to the analysis of SO_2 in ambient air. The passive sampler was used to collect air samples from Beijing, China. The samples were processed and analyzed as mentioned in Section 2.3.

The relationship between the concentration of SO_2 in air (μl Nm^{-3}) and the concentration of sulphate ion determined in sample solution was obtained by wind tunnel exposure experiments using standard SO_2 gas [1]. The equation was as follow:

$$y = 58.0x \quad (1)$$

where x was the concentration of SO_4^{2-} detected in the sample solution (mg l^{-1}). The results agreed satisfactorily with those obtained by the IC method (Table 1).

With the introduction of the $BaSO_4$-immobilized in-line reaction column, the reproducibility and the sensitivity of the analysis were improved and the analytical rate was substantially increased. This method can be widely used in daily monitoring systems, especially for the monitoring of indoor/outdoor environment and personal exposure because the maintenance of the instruments and operation process are simple and the reliability is good.

Table 1
Analytical results of SO_2 in ambient air in Beijing, China

Sample number	Sampling date (1996)	$[SO_4^{2-}]$ Found (mg l^{-1})		SO_2 in air (μl Nm^{-3})	
		FIA	IC	FIA	IC
Indoor-1	Oct. 30	0.211	0.236	12.2	13.7
Indoor-2	Oct. 31	0.200	0.190	11.6	11.0
Indoor-3	Nov. 1	0.573	0.532	33.2	30.8
Outdoor-1	Oct. 29	0.226	0.250	13.1	14.5
Outdoor-2	Oct. 30	0.427	0.428	24.8	24.8
Outdoor-3	Oct. 31	0.635	0.605	36.8	35.1
Outdoor-4	Oct. 31	0.731	0.809	42.4	46.9
Outdoor-5	Nov. 1	0.750	0.694	43.5	40.2
Outdoor-6	Nov. 2	1.500	1.480	87.0	85.8
Outdoor-7	Nov. 2	1.154	1.030	66.7	59.7

One of the authors (T.K.) is grateful for partial financial support from Grant-in-Aids (06558079, 07044171, 07650982) given by the Ministry of Education, Science and Culture, Japan. X. Zhang thanks the financial support from the Japanese Society for the Promotion of Sciences (P 96115). Y. Yang is supported by the International Cultural Exchange Foundation of University of Tokushima.

References

[1] Y. Yanagisawa, H. Nishimura, Environ. Int. 8 (1982) 235.
[2] R.D. Treitman, P.B. Ryan, D.P. Harlos, M.L. Soczek, Y. Yanagisawa, J.D. Spengler, I.H. Billick, Monitoring methods for toxics in the atmosphere, in: W.L. Zielinski, Jr., W.D. Dorko (Eds.), ASTM STP 1052, American Society for Testing and Materials, Philadelphia, 1990.
[3] E. Yamada, D. Yoshida, L. Hu, T. Yamada, Bunseki Kagaku 45 (1996) 1083.
[4] F.J. Krug, E.A.G. Zagatto, B.F. Reis, O.F. Bahia, A.O. Jacintho, S.S. Jorgensen, Anal. Chim. Acta 145 (1983) 179.
[5] T. Korenaga, Y. Yokota, K. Okada, T. Takahashi, T. Moriwake, Bunseki Kagaku 39 (1990) T29.
[6] T. Korenaga, K. Okada, T. Takahashi, T. Moriwake, Bunseki Kagaku 39 (1990) T129.
[7] T. Tang, H. Huang, Anal. Chem. 67 (1995) 2299.
[8] O. Kondo, H. Miyata, K. Toei, Anal. Chim. Acta 134 (1982) 353.
[9] S. Nakashima, M. Yagi, M. Zenki, M. Doi, K. Toei, Fresenius Z. Anal. Chem. 317 (1984) 29.

ELSEVIER

Talanta 45 (1997) 451–462

Talanta

Redox method for the determination of stability constants of some trivalent metal complexes

Rita Delgado [a,b,*], M. do Carmo Figueira [a], Sandra Quintino [a]

[a] *Instituto de Tecnologia Química e Biológica, Rua da Quinta Grande, 6, Apartado 127, 2780 Oeiras, Portugal*
[b] *Instituto Superior Técnico, 1096 Lisboa codex, Portugal*

Received 15 January 1997; received in revised form 13 May 1997; accepted 16 May 1997

Abstract

Stability constants determination of very stable metal complexes using the redox method, based on the equilibrium of Fe^{3+}/Fe^{2+} followed by a couple of platinum/reference electrodes, was undertaken and tested to complexes of some trivalent metal ions with well known polyaminopolycarboxymethylated linear ligands (edta, nta, cdta, dtpa and ttha) and also to some new macrocyclic ligands. SUPERQUAD program was used for the calculations, after adaptation of the experimental data. The method proved to be very useful for Fe^{3+} and In^{3+} complexes, if no polynuclear complexes are formed or/and if the kinetics of the complexation reaction is not very slow. However, for the Ga^{3+} complexes the applicability of this method is very limited and the competition with OH^- using the displacement reaction which occurs at pH higher than 6 with formation of $Ga(OH)_4^-$ seems to give more accurate results. A complete data of stability constants for the case of the complexes of ttha with In^{3+} is given. © 1997 Elsevier Science B.V.

Keywords: Stability constants determination; Polyaminopolycarboxymethylated ligands; Complexes of trivalent metal ions; pH-Potentiometric methods; Redox method

1. Introduction

In the last few decades the search of new ligands having high selectivity for some metal ions and/or very high thermodynamic stability has been very intense owing to their possible applications in medicine, in the treatment of metal intoxications in cases of metal poisoning, as contrast-enhancing agents in magnetic resonance imaging (MRI), or as radiopharmaceuticals for diagnostic or therapeutical uses [1–4]. Iron(III) is an interesting example of the first case, because although an essential component of the body, it becomes toxic when in excess and the treatment of iron overload diseases such as β-thalassemia (Cooley's anemia) is usually made by chelation therapy [3,5,6]. Lanthanides or radionuclides complexes of the ligands are used in the last applications mentioned. Radionuclides chosen are generally ^{67}Ga, ^{68}Ga, ^{64}Cu and ^{111}In, between others [7]. For safety reasons, the premature release of those metal ions in the body should be

* Corresponding author.

PII S0039-9140(97)00157-4

prevented, as they are toxic elements and can be accumulated in the liver, bone, and bone marrow. The stability of the complex in vivo and its integrity in the biological medium, are the first conditions to be accomplished if these applications are desired. So the complexes should have high stability constants, and should not dissociate or transfer to thermodynamic competing ligands present in biological media, such as albumin or transferrin [4,5,8].

In this work we are specifically interested in analysing the cases of the Fe^{3+}, Ga^{3+} and In^{3+} complexes, which are very important in the above described applications.

The determination of very high values of stability constants has led usually to critical problems, because in most cases the pH-potentiometric techniques (titrations using a strong base to neutralise the protons released by the formation of the complex and followed by a couple of glass/reference electrodes) can not be applied, as the complex is already formed at very low pH values. Sometimes it is possible to determine the constants by UV-vis spectroscopic methods, if the complex has an absorption band which reasonably change with the variation of the pH of the solution. For Fe^{3+} complexes this is generally the situation, but not for Ga^{3+} or In^{3+}. In those cases, competition methods are frequently used for the determination of the stability constants, by another ligand or metal ion, following the competition by pH-potentiometric or spectrophotometric methods [9–12]. The Ga^{3+} complexes present, in general, an exclusive situation as the stability constant can be determined taking into account the competition or displacement reaction which occurs at pH higher than 6 [10–12]:

$$GaL^{3-x} + 4OH^- \rightleftharpoons Ga(OH)_4^- + L^{x-}$$

However, the competition methods have, usually, very slow kinetics and preclude computer aided potentiometric methods, so batch techniques are necessary. In this case each point of the titration is prepared in a separated vial, which is left to equilibrate at the desired temperature to constant pH value. It is a very tedious, expensive and time consuming technique, because the vials require time for stabilisation, the pH or absorbance values need to be read several times to check the stabilisation and large amounts of ligands are required.

In our search for other methods of determination of this kind of constants we examined the redox method introduced by Schrøder [13] and developed by Bottari and Anderegg [14] and Harju [15], after the work of Stráfelda [16]. This last author has titrated several metal ions complexometrically by measuring redox potentials with a couple of platinum/reference electrodes and the other authors have applied the same technique for the calculation of stability constants. However, only Anderegg et al. [14] have developed the method for the determination of stability constants of complexes with a second metal ion, different from Fe^{3+}. Curiously this method has not been used in recent publications.

In the present work we have tested this redox method for the determination of stability constants of the complexes of well known polyaminopolycarboxymethylated ligands and also of some new macrocyclic compounds (see Scheme 1) with some trivalent metal ions, we have updated the technique and the calculations. The results are compiled, and analysed in comparison with data from the literature.

The method proved to be very useful for Fe^{3+} and In^{3+}, when no polynuclear complexes are formed or when the kinetics of the complexation reaction is not very slow, but the applications for Ga^{3+} complexes are very limited.

For simplicity the charges of the completely deprotonated forms of the ligands will generally be omitted in the text.

2. Experimental

2.1. Reagents

The non-cyclic ligands used were obtained commercially and used without further purification: K_2H_2edta (dipotassium ethylenedinitrilotetraacetate), H_4cdta (*trans*-1,2-cyclohexylenedinitrilotetraacetic acid), H_5dtpa (diethylenetrinitrilopentaacetic acid) and H_3nta (nitrilotriacetic acid) from Fluka, H_6ttha (triethylenetetranitrilohexaacetic acid) from Merck. The macrocyclic ligands

1,4,7,10-tetraazacyclo-dodecane-1,4,7,10-tetra-acetic acid (H_4dota), 3,11-diacetate-7-methyl-3,7,11,17-tetraazabicyclo[11.3.1]hepta-deca-1(17), 13,15-triene acid ($H_2ac_2Mepy14$), and 3,6,9-tri-acetic-3,6,9,15-tetraazabicyclo [9.3.1]pentadeca-1(15),11,13-triene acid (H_3ac_3py12), were synthesised and purified in our laboratory by previously reported procedures [17–19]. All the other chemicals were of reagent grade and used as supplied without further purification.

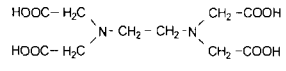

H_4 edta

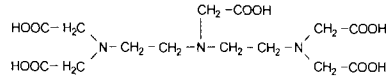

H_5 dtpa

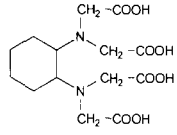

H_4 cdta

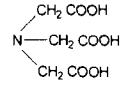

H_3 nta

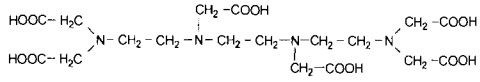

H_6 ttha

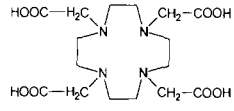

H_4 dota

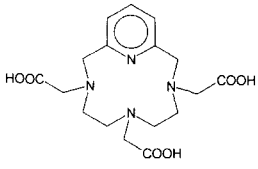

H_3ac_3py12

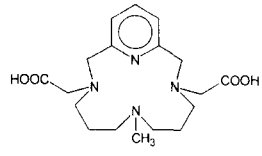

$H_2ac_2Mepy14$

Scheme 1.

2.2. Potentiometric measurements

2.2.1. Reagents and solutions

Metal ion solutions were prepared at about 0.025 M from the nitrate salts of the metals, of analytical grade (from Aldrich), with demineralised water (obtained by a Millipore/Milli-Q system) and were standardised by titration with K_2H_2edta [20]. A backtitration with a standard solution of $ZnSO_4$ was necessary for Ga^{3+}. The solutions of the trivalent metal ions were kept in excess of nitric acid in order to prevent hydrolysis. Fe^{2+} was used in the form of ammonium iron(II) sulfate, weighed in the exact amount and thrown directly into the potentiometric cell. Solutions of the ligands, used as titrants, were prepared in a large range of concentrations, from about 1.7×10^{-3} to 1.1×10^{-1} M. Carbonate-free solutions of KOH, used for calibrations and pH-potentiometric titrations, having the glass electrode as an indicator, were prepared by dilution of a commercial ampoule of Titrisol (Merck) analytical concentrate with demineralised water under a stream of purified nitrogen gas. These solutions were standardised by titration with 0.100 M nitric acid and discarded when the percentage of carbonate was about 0.5% of the total concentration of base present. The nitric acid was prepared by dilution of a commercial ampoule of Titrisol and used without standardisation.

2.2.2. Equipment and work conditions

For the redox potentiometric titrations an Orion 720A measuring instrument was used. This instrument is provided with two channels, in one of them an Orion-Ross 81-02 combined electrode was plugged in and, in the other, a Metrohm platinum electrode and an Orion 90-05 Ag/AgCl reference electrode were connected. A Wilhelm-type salt bridge [21] containing 0.10 M KNO_3 solution was used to separate the reference electrode from the working-cell. The described system allows the measurement of $[H^+]$ values in the first channel and the emf corresponding to the $[Fe^{3+}]/[Fe^{2+}]$ ratio in solution, in the second one. A 50 ml glass-jacketed titration cell completely sealed from the atmosphere was used and the temperature was controlled using a Grant W6 thermostat

(25.0 ± 0.1°C) by circulation of thermostated water through the jacketed cell. Atmospheric CO_2 was excluded during the titration by passing purified Argon across the top of the experimental solution in the reaction cell and the titrant, one of the ligands, was added through a capillary tip at the surface of the solution by a Crison microBu 2031 burette. The ionic strength of the solutions was kept at 0.10 M with KNO_3.

For the pH-potentiometric titrations the same instrument was used but now coupled with an Orion 91-01 glass electrode and an Orion 90-05 Ag/AgCl reference electrode. The standard base (or acid) was added by a Metrohm Dosimat 665 burette. A Wilhelm-type salt bridge [21] containing 0.10 M KNO_3 solution was also used and the ionic strength of the solutions was also kept at 0.10 M with KNO_3. All the other conditions were identical to those already described for the redox titrations. In this case an automatic process of acquisition of data was used.

2.2.3. Measurements

The hydrogen ion concentration, $[H^+]$, of the solutions was determined by the measurement of the emf of the cell, $E_1 = E_1'^\circ + Q_1 \times \log [H^+] + E_j$, in the first channel. $E_1'^\circ$ and Q_1 were obtained by previous calibration, titrating a standard solution of known hydrogen-ion concentration at the same ionic strength, using the values of the acid range. The liquid-junction potential, $E_j = j_H[H^+] + j_{OH^-}[OH^-]$, whose constants j_H and j_{OH} were determined by an acid/base titration of concentrated solutions [21,22] was found to be -148.5 $[H^+]$ in the experimental conditions used. The term pH is defined as $-\log[H^+]$ and the value of $K_W = ([H^+][OH^-])$, was determined from data obtained in the alkaline range of the calibration, considering E'° and Q valid for the entire pH range, and found equal to $10^{-13.80}$. The $[Fe^{3+}]$ of the solutions was determined by the emf of the cell, second channel, $E_2 = E_2'^\circ + Q_2 \times \log[Fe^{3+}]/[Fe^{2+}]$, for a constant concentration of Fe^{2+}, being $E_2'^\circ$ and Q_2 determined by a previous calibration using standard solutions of Fe^{3+} and Fe^{2+}, at the same ionic strength.

A typical redox equilibrium measurement was made on 25.00 ml of $\cong 1.8 \times 10^{-3}$ M Fe^{3+} solution, 17.5 mg of $Fe(SO_4)_2(NH_4)_2$, a certain amount of KNO_3 1.5 M (to obtain the desired 0.10 M ionic strength) and enough HNO_3 to start with a pH value of about 2. Measurements were also made with ten times diluted concentration obtaining the same final stability constants.

The pH-potentiometric equilibrium measurements were made on 20.00 ml of ligand solutions $\cong 2.50 \times 10^{-3}$ M, diluted to a final volume of 30.00 ml, first in the absence of metal ions (to determine protonation constants) and then in the presence of each metal ion for which the C_L:C_M ratios were 2:1, 1:1 or 1:2. The E_1 data were taken after additions of 0.025 or 0.050 ml increments of standard 0.100 M KOH solution, and after stabilisation in this direction, equilibrium was then approached from the other direction by adding standard 0.100 M nitric acid solution.

In the cases of competition reactions (with an additional metal ion in solution) the equilibrium was slower to attain. It was necessary to wait 15–30 min in each point of the titration in the range where the competition reaction took place.

2.2.4. Calculation of equilibrium constants

Protonation constants,

$$K_i^H = \frac{[H_iL]}{[H_{i-1}L][H]}$$

were calculated by fitting the potentiometric data obtained for the free ligand to the SUPERQUAD program [23]. Stability constants of the various species formed in solution were obtained from the experimental data corresponding to the various titrations with the same system with also the aid of the SUPERQUAD program, having previously corrected the emf values (E_2) obtained experimentally. The corrected values used (E_2') are equal to $E_2 + Q \times \log[Fe^{2+}]$, having taken into account the dilution of Fe^{2+} in the solution. Both potential values, E_1 and corrected E_2, were incorporated in the file for the SUPERQUAD program for each point of the titration. The initial computations were obtained in the form of overall stability constants, $\beta_{M_mH_hL_l}$,

$$\beta_{M_mH_hL_l} = \frac{[M_mH_hL_l]}{[M]^m[L]^l[H]^h}$$

Mononuclear species, ML, MHL or MH_2L, were found and also the binuclear species M_2L in the case of the ligand ttha. Differences, in log units, between the values β_{MHL} (or $\beta_{ML\text{-}H}$, or β_{M_2L}) and β_{ML} provide the stepwise protonation constants. The errors quoted are the standard deviations of the overall stability constants given directly by the program. In the case of the stepwise constants the standard deviations were determined by the normal propagation rules and do not represent the total experimental errors.

The protonation constants were obtained from 80–120 experimental points (two titration curves for each ligand). The stability constants of Fe^{3+} were obtained from 156 (for the cdta) to 207 (for the edta) experimental points (four to five titration curves), for Ga^{3+} from 97 (for edta) to 160 (for cdta) experimental points (three to four titration curves) and for In^{3+} were obtained from 81 (for dtpa) to 174 (for ttha) points (three titration curves).

2.2.5. Hydrolysis species of the trivalent metal ions

The trivalent metal ions studied in this work form easily hydrolytic species in aqueous solution whose constants are the object of some discrepancies in the literature. We have used the values listed before and considered more reliable [11,12,18,19].

3. Results and discussion

The method used in the present work for the determination of very high stability constants values, such as those of the complexes of some polyaminopolycarboxylate ligands with trivalent metal ions, was developed before for Fe^{3+} [13,15] and for this and other metal ions [14]. We have undertaken and adapted it to the more powerful methods of calculation of nowadays. The accuracy of the revised method was tested by studying some known cases of the literature, such as the Ga^{3+}, Fe^{3+} and In^{3+} complexes of edta, dtpa, cdta, nta and ttha. Also the complex formed by a divalent metal ion, Cu^{2+}-edta, was studied. To obtain a complete model for the systems analysed, with good precision in the values of the constants, we have modified the data in such a way that the SUPERQUAD program could be used. The authors that have used this redox method earlier have made some approximations to calculate the final constants by the existing means of computation. As the titrations in this method are performed at low pH (about 2), to obtain the model taking into account all the species which can be justified by the principles of co-ordination chemistry, including protonated, non-protonated and hydroxo species and indeed binuclear species for the case of ttha, it was also necessary to add to the datafile for the SUPERQUAD program other titrations performed in different conditions. In Table 2 the values of stability constants obtained in this work are summarised and, also, the corresponding values from the literature. In Table 1 we present the values of protonation constants of the ligands studied redetermined in our experimental conditions, except those below 2 (log units), for which potentiometric techniques are not adequate, we have used reference values (Table 1).

The literature values mentioned on Table 2 are supplied by the two available databases [24,25]. In the Martell et al. database [24] only one value is indicated for each species and each ionic strength, selected by the authors, but in the IUPAC database [25] all the values from the literature are compiled. From this last database we selected the values obtained in aqueous solution and in experimental conditions similar to ours, same ionic strength and temperature and, when possible, the same medium. The references for the values selected can be seen below the Table 2 and are exactly in the same form as in the IUPAC database, where only two or three of the authors names are indicated.

As can be seen in Table 2 there is an enormous dispersion of data in the literature, but our results are always in the range of the values available and when there is more than one similar result obtained by several authors using different techniques, which makes those data more reliable, the stability constants determined in this work are in close agreement with them, as in the cases of the

Table 1
Protonation constants (K_i^H) of the ligands

Ligand	log K_1^H	log K_2^H	log K_3^H	log K_4^H	log K_5^H	log K_6^H	log K_7^H	log K_8^H
edta	10.22(2)	6.16(1)	2.71(1)	2.0(1)				
	10.19[a]	6.13[a]	2.69[a]	2.0[a]	(1.5)[a]			
dtpa	10.52(1)	8.56(1)	4.31(7)	2.804(1)	2.22(2)			
	10.48[a]	8.60[a]	4.28[a]	2.6[a]	2.0[a]	(1.6)[a]	(0.7)[a]	
cdta	—	6.09(1)	3.53(1)	2.56(2)	—			
	12.30[a]	6.12[a]	3.49[a]	2.40[a]	1.60[a]			
nta	9.70(1)	2.52(2)	1.90(9)					
	9.67[a]	2.51[a]	(1.8)[a]	(1.0)[a]				
ttha	10.63(5)	9.46(2)	6.11(3)	4.04(4)	2.75(4)	2.34(7)		
	10.62[a]	9.49[a]	6.10[a]	4.06[a]	2.75[a]	2.3[a]	(1.8)[a]	(1.5)
ac_3py12	10.90[b]	7.11[b]	3.88[b]	2.27[b]				
$ac_2Mepy14$	10.72[c]	7.74[c]	4.05[c]	1.8[c]				

$T = 25.0$°C; $I = 0.1$ M KNO_3.
[a] 25.0°C, 0.10 M in K^+ salt as electrolyte, [23].
[b] 25.0°C; 0.10 M $(CH_3)_4NNO_3$ [18].
[c] 25.0°C; 0.10 M $(CH_3)_4NNO_3$ [19].

Fe^{3+} and In^{3+} complexes of edta and dtpa, or the Fe^{3+} complexes of cdta and nta. The stability constant of the ML complex of In^{3+} with cdta we obtained is slightly higher than the values from the literature, but our value was based on four titrations, two 1:1 pH-potentiometric titrations and two redox ones with different concentrations of the reagents. For edta we have tried the determination of the constants of its complexes with Cu^{2+} and although the value for the ML species is slightly higher than the values of the literature this system could be studied by this method.

Ttha is the most complicated case and the least studied as it has ten donor atoms and a great tendency to form binuclear complexes, M_2L. In this species the octahedral co-ordination sphere of each metal ion will be completed with one molecule of H_2O, forming species $M_2L(OH_2)_2$. These water molecules are directly co-ordinated and strongly bound to the metal ion, dissociating at very low pHs to form the species $M_2L(OH)_2$. This species was referred before for some of the complexes of ttha, namely those of Al^{3+} and of Fe^{3+} [24,25], and observed in the X-ray diffraction structure of the gallium complex of ttha ($Ga_2(OH)_2(ttha)Na_2(H_2O)_6.2H_2O$), which exhibits a Ga-O short distance for the hydroxyl directly bound to the metal ion [26]. The system is difficult to study because six to eight species have to be considered to determine stability constants. The redox titration curves show two inflexion points, in the first plateau M_2L species are formed and in the second one MH_2L and MHL species exist (L being ttha). Coupling the data of these titrations with pH-potentiometric titrations in the ratios 1:1 and 2:1 (M:L) it was possible to determine all the constants referred in Table 2. The stability constants of the 1:1 complexes of Fe^{3+} are in the range of those determined before, but our value for the M_2L species is lower than that indicated by Harju [15], who has made some approximations to achieve the values for the constants of this complicated system. However we found also hydroxo species of the type $M_2L(OH)$ whose constant was not determined before. For the In^{3+} complexes we have found a model similar to that of the Fe^{3+} one, the redox titration has also two inflexions, both species Fe_2L and In_2L coexisting before the first inflexion and FeH_2L, FeHL and InHL forming in the second part. The complete model for the In^{3+} complexes of ttha was determined for the first time in the present work. On the basis of our calculations the program SUPERQUAD only converges well for homobinuclear species. Heterobinuclear complexes are excluded.

Table 2
Stability constants (β_{ML}) of Fe^{3+}, Ga^{3+} and In^{3+} complexes with several polyaminopolycarboxylic acids

Ligand	Equilibrium quotient	Fe^{3+}	Ga^{3+}	In^{3+}	Cu^{2+}
edta	[ML]/[M][L]	**25.10(5)**; 25.1[a,d]; 24.23[e]; 23.75[f]; 25.42[g]	**22.01(8)**; -*; 21.0[a]; 20.27[h]; 20.5[i]; 21.1[d]; 21.7[j,k]; 20.90[l]	**25.09(5)**; 24.9[a]; 23.06[m]; 25.62[n]; 25.3[d]; 20.71[l]	**19.23(8)**; 18.78[a]; 18.79[h]; 18.87[o]; 19.19[p]; 19.00[q]; 18.7[r]
	[MHL]/[ML][H]	**1.88(3)**; (1.3)[a]; 1.36[b]; 1.2[d]; 1.29[e]	**2.30(5)**; (1.8)[a]; 1.91[i]; 1.83[d]; 1.7[k]	**1.90(5)**; (1.5)[a]; 1.5[d]	**3.06(8)**; 3.1[a]; 2.95[h]; 3.0[o]; 3.28[p]
	[ML]/[MLOH][H]	**7.53(7)**; 7.37[a]; 7.49[b]; 7.4[c]; 7.3[d]	**5.57(9)**; 5.58[a]; 5.44[d]; 5.52[k]	**8.36(6)**; 8.49[a]; 8.47[d]	**11.33(9)**
	[MLOH]/[$ML(OH)_2$][H]	—	—	**10.80(8)**	
dtpa	[ML]/[M][L]	**27.74(8)**; 28.0[a]; 28.6[s]; 27.50[t]; 27.3[d]; 28.7[u]	**25.11(3); 24.24(7)***; 24.3[a]; 23.0[i]; 25.54[d]; 26.84[v]; 28.1[w]; 23.32[k]	**29.48(4)**; 29.3[a]; 28.42[x]; 29.0[d]; 29.6[y]	
	[MHL]/[ML][H]	**3.37(2)**; 3.56[a,s]; 2.56[t]; 3.58[d]	**4.06(4)**; 4.16[a,k]; 3.92[i]; 4.35[d]	—	
	[MH_2L]/[MHL][H]	—	**1.81(9)**	—	
	[ML]/[MLOH][H]	**pp**; 9.68[a,s]; 9.9[d]	**7.1(1)**; 7.51[a,k]; 7.28[d]	**pp**; 11.9[a]; 11.74[d]	
cdta	[ML]/[M][L]	**28.70(2)**; 30.0[a]; 27.48[z]; 28.05[d]; 29.49[g]	**(24.38); 23.06(6)***; 22.8[a]; 22.91[h]; 22.5[i]; 23.10[d]; 22.34[k]	**29.37(2)**; 28.8[a]; 25.05[m]; 28.74[d]	
	[MHL]/[ML][H]	**1.91(2)**	**2.08(4)**; 2.7[a,k]; 2.43[i]	**1.36(6)**	
	[ML]/[MLOH][H]	**9.51(7)**; 9.70[a]	**6.8(1)**; 7.48[a,k]; 7.34[d]	**8.78(3)**; 8.80[a,d]	
nta	[ML]/[M][L]	**16.06(1)**; 15.9[a]; 15.87[b]; 16.26[d]; 15.91[aa]; 16.33[bb]; 14,78[cc]			
	[MHL]/[ML][H]	– ; 6.8[a]; 0.89[cc]			
	[ML]/[MLOH][H]	**3.75(7)**; (4.1)[a]; 4.08[b]; 3.98[bb]			
	[MLOH]/[$ML(OH)_2$][H]	**7.4(1)**; (7.8)[a]; 7.77[b]			

Table 2 (continued)

Ligand	Equilibrium quotient	Fe^{3+}	Ga^{3+}	In^{3+}	Cu^{2+}
ttha	[ML]/[M][L]	**27.66(4)**; 26.8[a,dd]; 29.4[ee]	**27.75(7)***[gg]; 28.21[a]; 15.1[hh]	**26.88(6)**; 26.6[a]	
	[MHL]/[ML][H]	**7.49(2)**; 7.55[a]; 7.60[dd]; 7.51[ee]	**4.8(1)**[gg]; 5.30[a]; 4.52[hh]	**7.30(3)**	
	$[MH_2L]/[MHL][H]$	**2.05(2)**; 2.68[a]; 2.75[dd]; 2.60[ee]	**3.9(1)**[gg]; 3.96[a]; 3.54[hh]	**2.33(4)**	
	[ML]/[MLOH][H]	—; 9.6[a,ee]	**9.43(4)**[gg]; 9.64[a]	—	
	$[MLOH]/[ML(OH)_2][H]$	—; 10.3[a,ee]	—	—	
	$[M_2L]/[ML][M]$	**12.13(2)**; 13.7[a,dd]	**12.40(9)**[gg]; 10.0[hh]	**9.0(1)**	
	$[M_2L]/[M_2L(OH)][H]$	**2.11(3)**	**3.25(9)**[gg]	**4.2(1)**	
	$[M_2L]/[M_2L(OH)_2][H]^2$	**5.91(5)**; 6.4[a]; 7.0[dd]; 6.6[ff]	**7.46(7)**[gg]	—	
ac_3py12	[ML]/[M][L]	21.77(5)[ii]	—	21.42(7)[ii]	
	[MHL]/[ML][H]				
	[ML]/[MLOH][H]				
$ac_2Mepy14$	[ML]/[M][L]	20.64(6)[ij]			
	[MHL]/[ML][H]				
	[ML]/[MLOH][H]				

In bold the values obtained in this work.

$T = 25°C$; $I = 0.10$ M KNO_3.

[a] 0.10 M; 25°C; [24]; All the other values in this table were taken from [25]. When not mentioned we have used our value of K_w for conversions.

[b] 0.10 M KCl, 20°C; G. Schwarzenbach, J. Heller, Helv. Chim. Acta, 34 (1951) 576, 1889.

[c] 0.10 M KNO_3, 25°C; R. Skochdopole, S. Chaberek, J. Inorg. Nucl. Chem., 11 (1959) 222.

[d] 0.10 M $NaClO_4$; 20°C; Ref. [14].

[e] 0.0 M; 20°C; M. Beck, S. Gorog, J. Inorg. Nucl. Chem., 12 (1960) 353.

[f] 0.10 M (?); 19°C; N. Zhirnova, K. Astakhov, S. Barkov, Zhur. Phys. Khim., 41 (1967) 366 (710).

[g] 0.20 M (?); 20°C; O. Borggaard, Acta Chem. Scand., 26 (1972) 393.

[h] 0.10 M KNO_3; 20°C; G. Schwarzenbach, R. Gut, G. Anderegg, Helv. Chim. Acta, 37 (1954) 937.

[i] 0.10 M KNO_3; 20°C; T. Moeller and S. Chu, J. Inorg. Nucl. Chem., 28 (1966) 153.

[j] 0.01 M $NaClO_4$; 20°C; T. Chernova, K. Astakhov, S. Barkov, Zhur. Phys. Khim., 43 (1969) 617.

[k] 0.10 M KNO_3; 25°C; Ref. [9].

[l] 0.10 M $NaClO_4$; 20°C; N. Skorik, A. Artish, Zhur. Neorg. Khim., 30 (1985) 1994 (1130).

Table 2 (continued)

[m] 0.50 M (?); D. Ryabchikov, I. Marov, Y. Ko-min, Zhur. Neorg. Khim., 8 (1963) 326 (641).
[n] (?) 21°C; N. Zhirnova, K. Astakhov, S. Barkov, Zhur. Phys. Khim., 39 (1965) 647 (1224), 952, 1489.
[o] 0.10 M KNO_3; 25°C; A. Brunetti, G. Nancollas, P. Smith, J. Am. Chem. Soc., 91 (1969) 4680.
[p] 0.10 M KNO_3; 25°C; E. Bauman, J. Inorg. Nucl. Chem., 36 (1974) 1827.
[q] 0.10 M KNO_3; 25°C; G. Anderegg, N. Podder et al., J. Coord. Chem., 4 (1975) 267.
[r] 0.10 M KNO_3; 25°C; J. Felcman, J. da Silva, Talanta, 30 (1983) 565.
[s] 0.10 M KNO_3; 25°C; V. Vandegaer, S. Chaberek, A. Frost, J. Inorg. Nucl. Chem., 11 (1959) 210.
[t] 0.10 M (?), 20°C; G. Anderegg, P. Nageli, F. Muller et al., Helv. Chim. Acta, 42 (1959) 827.
[u] 0.10 M $NaClO_4$; 25°C; V. Pal'chevski, T. L'vova et al., Koord. Khim., 11 (1985) 237.
[v] ? 20°C; T. Chernova, K. Astakhov, S. Barkov, Zhur. Phys. Khim., 44 (1970) 8, 1883.
[w] 0.10 M $NaClO_4$; 25°C; T. Nozaki, K. Kasuga, Nippon Kagaku Kaishi, (1973) 2117.
[x] (?) 19°C; N. Zhirnova, K. Astakhov, S. Barkov, Zhur. Phys. Khim., 40 (1966) 222 (417).
[y] 0.10 M $NaClO_4$; 25°C; T. Nozaki, K. Kasuga, K. Koshiba, Nippon Kagaku Kaishi, (1972) 568.
[z] ? M; 20°C; M. Beck, S. Gorog, Acta Chim. Acad. Sci. Hung., 22 (1960) 159.
[aa] 0.10 M $NaClO_4$; 20°C; J. Stary, Anal. Chim. Acta, 28 (1963) 132.
[bb] 0.50 M $NaNO_3$; 25°C; M. Morin, J. Scharff, Anal. Chim. Acta, 66 (1973) 113.
[cc] 1.00 M $NaClO_4$; 25°C; G. Anderegg, Inorg. Chim. Acta, 121 (1986) 229.
[dd] 0.10 M KNO_3; 25°C; Ref. [15].
[ee] 0.10 M $NaClO_4$; 25°C; Ref. [13].
[ff] 0.10 M KNO_3; 25°C; T.A. Bohigian, Jr., A.E. Martell, J. Inorg. Nucl. Chem., 29 (1967) 453.
[gg] 0.10 M KNO_3; 25°C; Ref. [26].
[hh] 0.10 M KNO_3; 25°C; A. Yingst, A. Martell, J. Am. Chem. Soc., 91 (1969) 6927.
[ii] 0.10 M $(CH_3)_4NNO_3$; 25°C; Ref. [18].
[jj] 0.10 M KNO_3; 25°C; Ref. [19].
* [26], values obtained by a direct method using competion with OH^-.

All the systems involving Ga^{3+}, except that of edta, have led to problems in this redox method and sometimes it was impossible to determine the stability constants, as for cdta. We have compared the results of the redox method for this type of systems with those obtained by the method developed by Martell et al. [10]. In this last method the stability constants for the Ga^{3+} complexes are calculated taking into account the competition reaction with OH^- ions, as described in the introduction. In general, if no precipitation occurs for higher values of pH (where this competition reaction takes place, usually pH > 6) and if stabilisation of each point of the titration is achieved (generally, this competition is slow) good values of constants are obtained. We have studied three cases in the present work: with edta, the redox titration gives results comparable with those from the literature, and the Martell method was impossible to use as precipitation has occurred for higher pHs values; in the dtpa case the redox titration gives a higher value than that of the Martell method but we consider the last value more reliable as the stabilisation was very difficult to attain in the former method; finally, for cdta it was impossible to obtain a good value using the redox method because there was no stabilisation of the potential in the part of the titration curve where the gallium(III) complex is being formed. With the few points apparently stabilised we obtained a constant which is higher than that given by Martell's method, whose value is similar to those found in the literature.

Included in Table 2 are the constants of the Fe^{3+} of two new ligands, ac_3py12 and $ac_2Mepy14$, and also for In^{3+} with the first ligand, determined by the method described here, already published [18,19], which have provided good results. We have tried some other systems involving macrocyclic ligands, such as dota and others, but without good results. In the last cases we did not have an inflexion point and we think that the formation of polynuclear species is the possible explanation of those drawbacks.

4. Conclusions

To obtain good values of stability constants with the redox method described in this work some conditions need to be fulfilled:

1. The concentration of Fe^{2+} must be constant during the titration. This means that the values of the stability constants of the complexes of the ligand in study with Fe^{2+} ought to be much lower than those of the complexes of the same ligand with Fe^{3+} (and also of the In^{3+} or Ga^{3+} complexes if values for the complexes of those metal ions are desired), to prevent the formation of complexes with Fe^{2+}. Also, for the same reason, it is necessary to work at a very low pH value. The complexes of Fe^{2+} are impossible to take into account using the SUPERQUAD program, because the E_2 potential will be function of two variables: the concentrations of Fe^{2+} and Fe^{3+}. It is convenient to test the coherence of the final results using a program such as SPE [27] to determine the concentration of all the species in solution at the pH of work, with the complete model found and including the complexes formed by the ligand with Fe^{2+}, to verify the constancy of the $[Fe^{2+}]$ in solution. In Table 3 are collected the values of stability constants of Fe^{2+} with the ligands studied in the present work, taken from the literature.
2. The complexation reaction has to be sufficiently fast, to prevent the oxidation of the Fe^{2+}, even if the solution is under argon it can occur. This is the main problem for the reactions involving Ga^{3+} as the competition is in general a slow process and at the same time a certain amount of Fe^{2+} should be oxidised, increasing the value of the constant determined.
3. In the competitive reactions with two metal ions (Fe^{3+}/In^{3+} or Fe^{3+}/Ga^{3+}) the first system works very well in all the cases we have checked. The second one has given good results only when edta is used. We have examined other systems without success. The constants for the Ga^{3+} complexes are usually lower than that of the Fe^{3+} ones and so the formation of the Ga^{3+} complex occurs after

Table 3
Stability constants of the complexes of the ligands studied with Fe^{2+} [a]

Equilibrium quotient	edta	dtpa	cdta	nta	ttha
[ML]/[M] [L]	14.30	16.4	18.90	8.83	17.0
[MHL]/[ML] [H]	2.71	5.35	2.70	1.9	8.56
$[MH_2L]/[MHL]$ [H]	—	—	—	—	3.8
[ML]/[MLOH][H]	—	8.79	—	10.6	8.82
$[MLOH]/[ML(OH)_2][H]$	—	9.43	—	—	9.61
$[M_2L]/[ML]$ [M]	—	3.1	—	3.97	9.36
$[M_2L]/[M_2L(OH)][H]$	—	—	—	—	8.53
$[M_2L]/[M_2L(OH)_2]$ $[H]^2$	—	—	—	—	17.15

$T = 25.0$°C; $I = 0.1$ M KNO_3.
[a] Values from [24].

that of the Fe^{3+}, in a second plateau, and for the majority of the cases stabilisation of the E_2 potential is not reached in the region of the formation of the Ga^{3+} complex. For the In^{3+} systems studied in the present work the constants of the complexes with this metal ion and with Fe^{3+} are very similar and so both complexes are formed at the same time and titration curves present only one inflexion point. Probably similar problems to those exhibited by the Ga^{3+} systems will occur if both complexes have different values of stability constants.

4. If only ML species are formed the results given directly by the redox method are straightforward. However if protonated species are present some ambiguity in the results arises, as the program can converge for the species ML and also MHL for different values and does not accept both. The way to achieve a correct model for the system is to couple data of one or more pH-potentiometric titrations in varied metal to ligand ratios (1:1 or 2:1 or 1:2, depending of the complexity of the system), in the same medium, to the redox data.

In conclusion it can be said that this method is very attractive for the determination of stability constants of complexes of Fe^{3+} and, in most cases, of the In^{3+} complexes. For instance, it was impossible to determine the constants for the ttha system, both for Fe^{3+} or In^{3+}, if this method was not undertaken, because we could not find good ligands to perform competitive reactions.

Acknowledgements

The authors acknowledge the financial support from Junta Nacional de Investigação Científica e Tecnológica and PRAXIS XXI program (Project n. PRAXIS/2/2.1/QUI/17/94). One of us (MCF) thanks the material support from Instituto de Biologia Experimental e Tecnológica (IBET).

References

[1] P.M. May, R.A. Bulman, in: G.P. Ellis (Ed.), Progress in Medicinal Chemistry, 1983, 20, p. 225.
[2] R.A. Bulman, Struct. Bonding 67 (1987) 91.
[3] A.E. Martell, Biol. Trace Element Res. 21 (1989) 295.
[4] V. Alexander, Chem. Rev. 95 (1995) 273.
[5] C.G. Pitt, A.E. Martell, ACS Symp. Ser. 140 (1980) 279.
[6] A.E. Martell, R.J. Motekaitis, I. Murase, L.F. Sala, R. Stoldt, C.Y. Ng, H. Rosenkrantz, J.J. Metterville, Inorg. Chim. Acta 138 (1987) 215.
[7] D. Parker, Chem. Soc. Rev., 19 (1990) 271, also Chem. Br., October (1994) 818.
[8] R. Delgado, Rev. Port. Quím. 2 (1995) 18.
[9] W.R. Harris, A.E. Martell, Inorg. Chem. 15 (1976) 713.
[10] R.J. Motekaitis, A.E. Martell, Inorg. Chem. 19 (1980) 1646.
[11] R. Delgado, Y. Sun, R.J. Motekaitis, A.E. Martell, Inorg. Chem. 32 (1993) 3320.
[12] C.F.G.C. Geraldes, R. Delgado, A.M. Urbano, J. Costa, F. Jasanada, F. Nepveu, J. Chem. Soc., Dalton Trans. (1995) 327.
[13] K.H. Shrøder, Acta Chem. Scand. 19 (1965) 1797.
[14] E. Bottari, G. Anderegg, Helv. Chim. Acta 50 (1967) 2349.

[15] L. Harju, Anal. Chim. Acta 50 (1970) 475.
[16] F. Sfráfelda, M. Karlík, J. Matousek, Collection Czech. Chem. Commun. 19 (1965) 1797.
[17] (a) R. Delgado, J.J.R. Fraústo da Silva, Talanta, 29 (1982) 815; (b) S. Chaves, R. Delgado, J.J.R. Fraústo da Silva, Talanta, 39 (1992) 249.
[18] R. Delgado, S. Quintino, M. Teixeira, A. Zhang, J. Chem. Soc. Dalton Trans. (1997) 55.
[19] J. Costa, R. Delgado, M.C. Figueira, R.T. Henriques, M. Teixeira, J. Chem. Soc. Dalton Trans. (1997) 65.
[20] G. Schwarzenbach, H. Flaschka, Complexometric Titrations, Methuen, London, 1969.
[21] H.S. Rossotti, Talanta 21 (1974) 809.
[22] L. Pehrsson, F. Ingman, A. Johansson, Talanta 23 (1976) 769.
[23] P. Gans, A. Sabatini, A. Vacca, J. Chem. Soc. Dalton Trans. (1985) 1195.
[24] R.M. Smith, A.E. Martell, R.J. Motekaitis, Nist Critical Stability Constants of Metal Complexes Database, US Department of Commerce, Gaithersburg, 1993.
[25] L.D. Pettit, H.K. J. Powell, IUPAC Stability Constants Database, Academic Software, Timble, 1993.
[26] B. Achour, J. Costa, R. Delgado, E. Garrigues, C.F.G.C. Geraldes, N. Korber, F. Nepveu, M.I. Prata, submitted.
[27] A.E. Martell, R.J. Motekaitis, Determination and Use of Stability Constants, 2nd ed., VCH, New York, 1992.

ELSEVIER

Talanta 45 (1997) 463–471

Talanta

Determination of equilibrium constants of strong acidic ion exchange resins by potentiometric titrations

Gregorio Borge *, Juan M. Madariaga

Kimika Analitikoaren Departamentua, Euskal Herriko Unibertsitatea, UPV/EHU, 644 PK, E-48 080 Bilbao, Spain

Received 5 December 1996; received in revised form 25 April 1997; accepted 21 May 1997

Abstract

A new method for the determination of ion exchange equilibrium constants is developed. A technique based in the application of potentiometric titrations is used in the study of non selective strong acidic resins. Potentiometric titrations are carried out without constant ionic strength, so a mathematical treatment is developed in order to take into account the estimation of the activity coefficients and the liquid junction potentials. The ion exchange thermodynamic equilibrium constants for two resins, Dowex CM-15 and Dowex C650, between the proton form and the alkaline metals at 25°C are given. © 1997 Elsevier Science B.V.

Keywords: Ion exchange equilibrium constants; Potentiometry; Ionic strength; Methods of calculation

1. Introduction

The determination of ion exchange equilibrium constants is usually performed by means of two experimental methodologies: (a) the batch method: known samples of the resin are equilibrated with a known volume of a solution containing the ions under study; after equilibration, at least the aqueous phase is analysed. (b) The column method: the ion exchanger is introduced in a column and a solution of known concentration containing the ions under study is passed through the column; equilibration is reached when the concentration of the ions in the effluent and in the initial solution are the same. In order to analyse the resin phase, the exchanged ions are displaced by means of an excess of a third ion. A solution containing all the exchanged ions is obtained and analysed.

Both experimental methods are adequate if the equilibrium situation is assured. This requirement is related to the kinetics of the ion exchange processes: in the batch methodology, equilibration times are usually large, whereas using columns, important volumes of solution and low fluxes are necessary. However, both are expensive methodologies, if the necessary amount of chemicals, time and subsequent analyses are taken into account.

Potentiometric titration is a technique widely used in the field of solution equilibria and it has been successfully applied in the study of equilibria between two phases [1–3]. Nevertheless, the appli-

* Corresponding author.

PII S0039-9140(97)00158-6

cation of this methodology in the determination of ion exchange equilibria constants is very scarce [4]. This is due to some problems of, a priori, difficult solution:

(a) This methodology makes it impossible to analyse the resin phase in each experimental point, so mass balance equations must be solved in order to know the concentrations in the resin. This calculation can be biased if possible adsorption phenomena change the volumes of the solutions and the swelling of the resins are not properly taken into account [5].

(b) The study of non highly selective ion exchange resins cannot be performed using the so called constant ionic medium method, since the ionic medium is not an inert species for the ion exchanger. On the other hand, the constant ionic medium method is very practical in the potentiometric titration technique, since its use reduces the values of the liquid junction potential and allows the estimation of this value by means of simple equations [6]. The constant ionic medium method can be used only if highly selective ion exchangers are studied, so equilibria with ions of the medium do not take place. This is the case of some chelating resins [7–9]. Moreover, activity coefficients can be considered constant if a constant ionic medium is used.

In this work, the ion exchange equilibrium constants of two non selective cationic resins are determined for the systems $H^+ - M^+$, where M = Li, Na, K, Rb, Cs by means of the potentiometric titration technique. A calculation method is developed in order to consider the peculiarities of the application of the technique to ion exchangers: the variation of the activity coefficients is taken into account directly in the molar scale by means of the Modified Bromley's Methodology (MBM) [10–12]; the estimation of the liquid junction potential in potentiometric titrations is performed using the recent modifications of the Falkenhagen model [13,14] for the estimation of conductivities and that of the Henderson equation [15,16] for the liquid junction potentials; determination of the densities of the resins is performed in order to estimate the volume change of the aqueous phase; finally, the activity coefficients of the species in the resin phase are estimated by means of the Wilson model [17,18] which proposes a direct mathematical dependence of the activity coefficient of the species in the resin phase with its concentration.

2. Experimental

Dowex CM-15 (macroporous, 15% DVB) and Dowex C650 (monosphere, 10% DVB) are strong acidic resins with sulphonate as the active group. Both were washed with water and treated with HCl (Normaslov, 35%) to excess in order to assure the proton form. Resins were finally washed with water and kept completely swollen. Swollen resin was weighed after air drying for the experimental work.

The resins were characterized following methods described elsewhere [19,20] for the determination of the densities in the proton and alkaline forms and the water content ($28.1 \pm 0.9\%$ for Dowex CM-15 and $28.6 \pm 1.0\%$ for Dowex C650). Table 1 collects the values obtained for the densities of the resins.

The exchange capacity was determined following two different methods: (a) a batch method: 0.6–1.4 g of resin were equilibrated with different volumes of known solutions of MOH (M = Li, Na, K); after equilibration, the pH of the aqueous phase was measured (Radiometer PHM84 Research pH-meter with a combined Ingold electrode) and plotted versus the number of millimoles of added MOH. (b) a potentiometric titration method: known amounts of the resin and of a HCl solution were titrated with solutions of MOH (M = Li, Na, K, Rb, Cs); the emf value was measured with a glass electrode. Hydroxide solutions were prepared from $LiOH \cdot H_2O$ (Fluka BioChemika Mikroselect, 99.5%), NaOH (Merck, p.a., ACS), KOH (Merck, p.a., ACS, ISO), RbOH (Janssen, 99.9%) and CsOH (Aldrich, 99.9%). HCl (Fluka, p.a.) was used in the titrations. All solutions were prepared in MilliQ water. The inflection point of the obtained plots yields the value of the exchange capacity for both techniques. Results are collected in Table 2. Results given by both techniques are coincident within experimental uncertainty.

Table 1
Densities of the resins

Resin	Form	Dry resin density $\rho_{A,d}$ [a] (g cm^{-3})	Swollen resin density $\rho_{A,s}$ [b] (g cm^{-3})	Density of the volume change of the solution ρ_B [c] (g cm^{-3})
Dowex CM-15	H	0.620 ± 0.005	0.562 ± 0.003	1.29 ± 0.02
	Li	0.644 ± 0.004	0.614 ± 0.006	1.32 ± 0.02
	Na	0.675 ± 0.004	0.629 ± 0.003	1.36 ± 0.01
	K	0.709 ± 0.005	0.603 ± 0.002	1.47 ± 0.01
	Rb	0.802 ± 0.006	0.689 ± 0.006	1.68 ± 0.05
	Cs	0.882 ± 0.006	0.826 ± 0.005	1.84 ± 0.03
Dowex C650	H	0.739 ± 0.006	0.552 ± 0.002	1.31 ± 0.02
	Li	0.775 ± 0.004	0.552 ± 0.005	1.35 ± 0.01
	Na	0.797 ± 0.006	0.646 ± 0.004	1.41 ± 0.01
	K	0.817 ± 0.009	0.684 ± 0.003	1.46 ± 0.02
	Rb	0.920 ± 0.014	0.795 ± 0.004	1.67 ± 0.05
	Cs	1.048 ± 0.008	0.855 ± 0.007	1.82 ± 0.05

[a] $\rho_{A,d}$ = grams of dry resin/cm^3 of dry resin.
[b] $\rho_{A,s}$ = grams of dry resin/cm^3 of swollen resin.
[c] ρ_B = grams of dry resin/cm^3 of water and resin-cm^3 of water added.

The potentiometric titrations performed for the determination of the ion exchange equilibrium constants were carried out by measuring the emf of the following electrochemical cell:

$$\text{Ag/AgCl/MCl 0.1 M, AgCl sat.//MCl}\underset{(1)}{\text{0.1 M}}\text{//}\underset{(2)}{\text{test solution}}\text{/G.E.} \quad (1)$$

Double junction reference electrodes Ag/AgCl Metrohm 6.0726.100 and glass electrodes Metrohm 6.0101.000 were used. The test solution was a known amount between 0.10 and 0.80 g of resin in the proton form in 75 cm^3 of MilliQ water, which was titrated with MCl 0.4 mol dm^{-3} solutions. The titrations were performed for M = Li, Na, K, Rb and Cs. The metal in the reference electrode and in the titrant solutions were the same in every case. Titrant, bridge and reference electrode internal solutions were prepared from LiCl (Fluka, BioChemika Mikroselect), NaCl (Merck, p.a., ACS, ISO), KCl (Merck, p.a., ACS), RbCl (Merck, p.a.) and CsCl (Merck, p.a.).

Table 2
Ion exchange capacity of the resins

Resin	Method used	Counterions	q_{max} (mmol g^{-1})
Dowex CM-15	Batch	Li, Na, K	3.43 ± 0.03
Dowex CM-15	Titrations	Li, Na, K, Rb, Cs	3.44 ± 0.12
Dowex C650	Batch	Li, Na, K	3.46 ± 0.03
Dowex C650	Titrations	Li, Na, K, Rb, Cs	3.40 ± 0.07

Titrations were carried out using an automated system developed in this laboratory [21] and a thermostatic bath at 25.0 ± 0.1°C. The signals from the electrodes, preamplified by an operational amplifier in order to adequate the electric signal, were measured by a Hewlett-Packard HP-E1326B voltameter incorporated into the VXI data acquisition system connected to the computer. Previous experiments showed that equilibrium was reached (i.e., emf value did not change) after 20 min approximately, so an equilibration time of 30 min for each point was considered and when the standard deviation of the emf over about 6 min was less than ± 0.04 mV an instruction for new addition was given by the computer to the burette. Addition of the titrants was performed using Metrohm 665 automatic burettes connected to the computer via an RS-232C interface. Each titration took around 40 h and all of them were carried out at least three times.

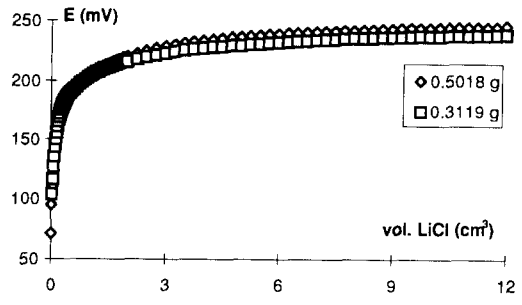

Fig. 1. Potentiometric titrations obtained for the H^+-Li^+ system in Dowex CM-15. The legend indicates the grams of the resin in the proton form.

3. Results and data treatment

As an example, Fig. 1 shows the profiles of two of the titrations obtained for the H^+-Li^+ ion exchange system in Dowex CM-15. The same kind of representations were obtained for the rest of the systems studied.

The mathematical treatment was developed taking into account the following points:

3.1. Correction of the solution volume

The measurement of the emf must be corrected taking into account the decrease of the volume of the aqueous phase due to the swelling of the resin. The correction was performed by means of the densities of the resins in the different forms (see definitions in Table 1). For each H^+-M^+ system, the mean values of the densities $\rho_{A,d}$, $\rho_{A,s}$ and ρ_B for both ions were used for obtaining the value of the volume in each experimental point of the titration.

3.2. Activity coefficients

Activity coefficients of the species in the aqueous phase were estimated by means of the Modified Bromley's Methodology (MBM). The MBM allows the estimation of the activity coefficients of an ion by means of the following equations

$$\log \gamma_M = -\frac{A(z_M)^2 I^{1/2}}{1+I^{1/2}} = \sum_X \left(\dot{B}_{MX} \frac{(|z_M|+|z_X|)^2}{4} [X] \right) \quad (2)$$

$$\dot{B}_{MX} = \frac{(0.06+0.6B_{MX})|z_M z_X|}{[1+(1.5/|z_M z_X|)\, I]^2} + B_{MX} \quad (3)$$

where B_{MX} is the interaction parameter of the MBM between the cation M and the anion X and it is reported directly in the molar scale, so the activity coefficients can be estimated in this scale. The B_{MX} values used in this work are 0.163 (MX = HCl), 0.142 (LiCl), 0.071 (NaCl), 0.038 (KCl), 0.034 (RbCl), and 0.012 (CsCl) [11]. Values are given in $dm^3\ mol^{-1}$.

Activity coefficients of the species in the resin phase were estimated using the Wilson model. This is the only model in the bibliography which uses interaction parameters and the concentration of the species in the resin phase for the estimation of the activity coefficients. The Wilson model is suitable for the resolution of the systems. In this case, the equations of the Wilson model for the estimation of the activity coefficients of the species H and M in the resin phase are

$$\ln f_H = 1 - \ln(\overline{x_H} + \overline{x_M}\lambda_{HM}) - \left(\frac{\overline{x_H}}{\overline{x_H} + \overline{x_M}\lambda_{HM}} + \frac{\overline{x_M}\lambda_{MH}}{\overline{x_H}\lambda_{MH} + \overline{x_M}} \right) \quad (4)$$

$$\ln f_M = 1 - \ln(\overline{x_H}\lambda_{MH} + \overline{x_M}) - \left(\frac{\overline{x_H}\lambda_{HM}}{\overline{x_H} + \overline{x_M}\lambda_{HM}} + \frac{\overline{x_M}}{\overline{x_H}\lambda_{MH} + \overline{x_M}} \right) \quad (5)$$

The interaction parameters λ_{HM} and λ_{MH} are estimated together with the thermodynamic equilibrium constants, since no information in the literature about these systems has been found. The Wilson model has been recently applied in the determination of ion exchange equilibrium constants and in the prediction of multicomponent systems [18,22,23].

3.3. Mass balances

There is just one equilibrium (the ion exchange one) in the systems under study, so the solution of the mass balance equations is quite simple. In

fact, this simplicity allows the mathematical solution of the complete system. Mass balance equations can be written as follows:

proton: $$q_{max}g_{res} + h_0v_0 = q_Hg_{res} + [H^+]v_{tot} \quad (6)$$

metal: $$c_{MCl}v = q_Mg_{res} + [M^+]v_{tot} \quad (7)$$

resin: $$q_{max} = q_H + q_M \quad (8)$$

chloride: $$c_{MCl}v + h_0v_0 = [Cl^-]v_{tot} \quad (9)$$

where v is the volume of the titrant added, v_0 is the initial volume in aqueous phase (corrected with the values of the densities), v_{tot} is the total volume and q_i is the number of moles of the i species in the resin phase per gram. h_0 is the initial concentration of protons in the solutions.

Eqs. (6)–(9) can be rearranged so the values of $[Cl^-]$, $[M^+]$, q_H and q_M can be expressed as a function of the proton concentration. The other quantities are known, except h_0.

3.4. Estimation of the liquid junction potential

The emf measured value is related to the concentration of the species in solution by means of Eq. (10)

$$E = E^0 + g \log \{H^+\} + E_j \quad (10)$$

where E^0 is the standard potential of the electrochemical cell which must be calculated for each titration. The liquid junction term (E_j) cannot be estimated using the classical equations proposed by Biedermann or Rossotti, since ionic strength is not kept constant throughout the titrations. The E_j value is thus estimated by means of a recently developed model for the estimation of the diffusion potential [16]. This model is based on the Henderson equation and it uses the values of the activities of the ions instead of those of the concentrations. Eq. (11) is therefore used in this work:

$$E = E^0 + g \log \{H^+\} - g \frac{\sum_i (z_i/|z_i|)\, \lambda_i(\{i\}_2 - \{i\}_1)}{\sum_i |z_i|\, \lambda_i(\{i\}_2 - \{i\}_1)} \log \frac{\sum_i |z_i|\, \lambda_i \{i\}_2}{\sum_i |z_i|\, \lambda_i \{i\}_1} \quad (11)$$

Numbers 1 and 2 refer to the reference electrode and test solutions, respectively, as expressed in the electrochemical cell (1).

The conductivities of the ions in Eq. (11) are estimated using the so called Extended Falkenhagen's Equation [14,16]. Activity coefficients are estimated using the MBM. Therefore, Eq. (11) can be used for the resolution of the system since the parameters of the Falkenhagen and Bromley models are known.

3.5. Estimation of the initial proton concentrations (h_0) in solution

A cationic ion exchange resin in the proton form which has been pretreated with an acid gives a slightly acidic pH in solution, although an exhaustive washing with water is performed. In the experimental part of this work, it was observed that the initial points of each titration showed a slightly acidic emf value between 60 and 130 mV. This emf value varied depending on the resin and the amount of resin, but it was checked that there was no direct relationship.

If this emf initial value is taken into account within the general model for the interpretation of the potentiometric data of this work, an initial value of the proton concentration could be obtained. This value should be small, but it is not due to ion exchange phenomena; it can be proposed that their presence is due to the pretreatment with HCl. The value must be considered since it can be important in the first points in the titrations: the proton concentrations obtained because of the ion exchange equilibrium in these points are still low. It is supposed that the counterion of these initial protons in solution is chloride because the resin was always pretreated with HCl. This is contained in the mass balance equation of chloride in Eq. (9).

The h_0 value can be obtained from Eq. (11) if the initial solution of each titration is considered as a very dilute one (in fact, only MilliQ water was equilibrated with the resin in the initial point). In this case, activity coefficients of the species are equal to the unity and the conductivities are the limiting ones collected in the bibliography [24]. In these situations, Eq. (11) can be

rearranged, so the following expression is obtained:

$$\log h_0 = \frac{\frac{E-E^0}{g} + \frac{\lambda^0_M - \lambda^0_{Cl}}{\lambda^0_M + \lambda^0_{Cl}} \times \log \frac{\lambda^0_H + \lambda^0_{Cl}}{[MCl]_{ref}\,\gamma^{ref}_M(\lambda^0_M + \lambda^0_{Cl})}}{1 - \frac{\lambda^0_M - \lambda^0_{Cl}}{\lambda^0_M + \lambda^0_{Cl}}} \quad (12)$$

where E is the experimental emf value of the first point in each titration (no MCl is added yet) and the term 'ref' is referred to the bridge solution in the electrochemical cell in expression (1).

3.6. Calculation of the ion exchange equilibrium constant

The mathematical treatment was carried out minimizing the value of the quadratic sum of absolute errors in the potential, i.e.,

$$U_{abs} = \sum_{i=1}^{N_p} (E_{calc,i} - E_{exp,i})^2 \quad (13)$$

where N_p is the number of experimental points.

$E_{cal,i}$ is estimated following Eq. (11). Activity coefficients and conductivities in the electrode reference solution can be estimated by means of the MBM and the Extended Falkenhagen's Equation. In the test solution, activity coefficients and conductivities of the ions depend on the concentration of H^+, Cl^- and M^+. Concentrations of Cl^- and M^+ can be expressed as a function of $[H^+]$ and E^0, using the mass balances equations and the dependence $h_0 = f(E^0)$ in Eq. (12).

The equilibrium in the titration cell and the corresponding equilibrium constant are:

$$\overline{RH} + M^+ \rightleftharpoons \overline{RM} + H^+ \quad (14)$$

$${}^0K^M_H = \frac{[H^+](\gamma_H)(\overline{x_M})(f_M)}{(x_H)(f_H)[M^+](\gamma_M)} \quad (15)$$

Molar fractions, $[M^+]$, and the activity coefficients in both the aqueous and resin phases can be expressed as a function of $[H^+]$ and h_0, using the mass balances in equations and the expressions of the activity coefficients. Therefore, all the variables in Eq. (15) can be expressed as a function of $[H^+]$ and the parameters to be calculated, ${}^0K^M_H$, E^0, λ_{HM} and λ_{MH}. Rearranging terms:

$$y = {}^0K^M_H(\overline{x_H})(f_H)[M^+](\gamma_M) - [H^+](\gamma_H)(\overline{x_M})(f_M) = 0 \quad (16)$$

The values of $[H^+]$ can be obtained solving the roots of Eq. (16), i.e., obtaining the values of $[H^+]$ which fulfill the condition $y = 0$. Initial values of the parameters of the system are proposed and the equation is resolved. Once the proton concentration is known, $E_{calc,i}$ can be calculated and U_{abs} is obtained. If this value is not the minimum, new values of the parameters are proposed and the calculation is repeated.

The Nlreg program, which permits the resolution of iterative calculations, was used in order to perform the calculations. The parameters were calculated taking into account all the valid titrations for each system. Results of the fits (values of the thermodynamic equilibrium constant, the Wilson parameters and the statistical results) for Dowex CM-15 and Dowex C650 are collected in Table 3. Values of E^0 are not collected since they varied for the different titrations. As an example, Fig. 2 shows the distribution of errors for the system H^+–Cs^+ in Dowex C650. These kind of distributions were obtained for all the systems under study.

4. Discussion

A new method for the determination of ion exchange thermodynamic equilibrium constants is presented in this work. The method is based in the potentiometric titration technique and a mathematical treatment is developed in order to consider the variation of the ionic strength along the titration.

In addition to the technique used, this methodology presents an important difference in comparison with the more classical ones: no isotherms are obtained in the experimentation. Experimental points of different total concentrations and ionic strengths are studied throughout a titration, thus it is shown that the obtention of isotherms is not strictly necessary for the determination of ion exchange equilibrium constants.

In this sense, the value of the so-called equilibrium quotient, which is defined in Eq. (17), is

Table 3
Thermodynamic equilibrium constants and Wilson parameters for the H^+-M^+ ion exchange system in Dowex CM-15

Resin	M^+	${}^0K_H^M$	λ_{HM}	λ_{MH}	N_p	σ_{tot} [a]
Dowex CM-15	Li^+	0.94 ± 0.05	1.10 ± 0.05	0.05 ± 0.03	110	0.57
	Na^+	5.6 ± 0.7	0.70 ± 0.04	1.3 ± 0.3	76	0.40
	K^+	4.7 ± 0.5	0.02 ± 0.03	3.0 ± 0.1	110	0.22
	Rb^+	1.5 ± 0.2	3.0 ± 0.7	0.3 ± 0.1	81	0.18
	Cs^+	2.1 ± 0.2	3.0 ± 0.6	0.6 ± 0.2	110	0.59
Dowex C650	Li^+	0.62 ± 0.05	1	1	110	0.60
	Na^+	2.9 ± 0.6	1.24 ± 0.05	0.002 ± 0.01	99	0.47
	K^+	2.3 ± 0.3	2.17 ± 0.08	0.04 ± 0.1	94	0.30
	Rb^+	3.4 ± 0.2	1.3 ± 0.3	0.3 ± 0.1	55	0.44
	Cs^+	2.6 ± 0.4	0.8 ± 0.2	3.9 ± 0.7	131	0.70

[a] $\sigma_{TOT} = \sqrt{U_{abs}/(N_p - N_k)}$; $U_{abs} = \Sigma_{i=1}^{N_p} (E_{calc,i} - E_{exp,i})^2$.
N_p = number of points; N_k = number of parameters.

not known directly from the experimental results. Thus, the thermodynamic equilibrium constant cannot be obtained with this experiment if ion exchange models based in the use of the equilibrium quotient (the three-parameter model [25] or that based in the Gaines and Thomas' integral [26]) are used. It is therefore necessary to use the Wilson model.

$$K_H^M = {}^0K_H^M \frac{f_H}{f_M} = \frac{[H^+](\gamma_H)(\overline{x_M})}{(\overline{x_H})[M^+](\gamma_M)} \quad (17)$$

In the bibliography it is assumed that the selectivity of an ion exchanger decreases with the hydrated ionic radius, although exceptions are usual [19]. The selectivity of the ion exchangers is usually represented by the equilibrium quotient of the system as defined in Eq. (17). In this work, the equilibrium quotient of the systems can be calculated from the values of the thermodynamic equilibrium constants and the Wilson parameters collected in Table 3. Fig. 3 shows the representation of the calculated equilibrium quotient for the

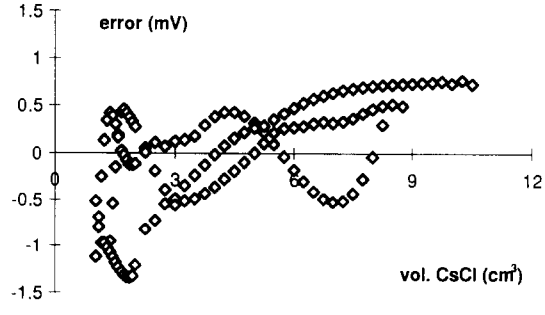

Fig. 2. Distribution of absolute errors for the titrations of Dowex CM-15 (a) and Dowex C650 (b) in the proton form with CsCl.

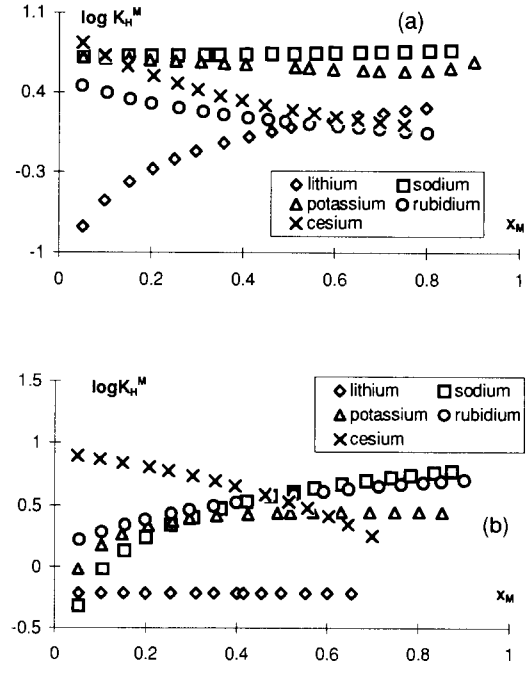

Fig. 3. Equilibrium quotient versus metal concentration in the resin phase for H^+-M^+ equilibria in Dowex CM-15 (a) and Dowex C650 (b).

H^+-M^+ ion exchange equilibria in Dowex CM-15 and Dowex C650 versus the metal molar fraction in resin. Plots in Fig. 3 would be those obtained experimentally following the usual batch methodologies collected in the literature for the determination of ion exchange thermodynamic equilibrium constants. The variation of the equilibrium quotient with the metal concentration in the resin phase shows that the selectivity depends strongly on composition and activity coefficients of species, since these are the variables present in Eq. (17).

Therefore, conclusions on selectivity of the resins should be established taking into account the values of the thermodynamic equilibrium constants and the characteristics of the resin. The thermodynamic equilibrium constant is a very practical value for a general methodology in ion exchange: it is not possible to determine equilibrium quotients in all the situations, so the determination of the selectivity in given conditions can be more rapidly performed from the values of the thermodynamic equilibrium constants and the parameters for the estimation of the activity coefficients.

Fig. 3 includes an ideal system, the H^+-Li^+ one in Dowex C650. The numerical treatment gave no acceptable results for the systems if the values of λ_{HLi} and λ_{LiH} varied, so they were taken as the unity. In this case, the resin phase shows an ideal behaviour, since activity coefficients of the species in the resin phase are 1.

Table 3 shows that the errors in the Wilson parameters are usually higher than those obtained for the equilibrium constants. The more direct influence of ${}^0K_H^M$ in the calculations performed, as it can be seen in Eq. (16), allows a better definition of this value. On the other hand, λ_{HM} and λ_{MH} are related to the ideal behaviour of the resin, which is shown when the resin is pure. Because of this, the best experimental data for a good determination of the Wilson parameters are those obtained when the molar fraction of the metal in the resin is next to 0 or 1. Unfortunately, obtaining of such data is experimentally difficult.

Table 4 collects the values found in the literature for the Wilson parameters for H^+-M^+ systems in strong acidic cation resins with sulphonate as the active group. The number of parameters is quite small for comparations with the results obtained here. The Wilson parameters obtained in this work show some trends, e.g., lithium, sodium and potassium λ_{HM} parameters decrease whereas λ_{MH} parameters increase in Dowex CM-15, but rubidium and cesium do not follow the trend. More experimental work on other systems should be necessary in order to ascertain some relationships between the values of the Wilson parameters and the ions under study.

Table 4
Wilson parameters values in the literature for strong acidic sulphonate resins

Resin	System	λ_{ij}	λ_{ji}	Reference
Lewatit SP120	H–Na	0.43	2.28	[27]
Dowex HCR-3	H–Na	0.70	1.24	[23]
Dowex HCR-3	H–K	0.0487	4.1491	[23]

As a general conclusion, it should be stressed that ten ion exchange experimental systems have been resolved by means of the potentiometric titration technique. The applicability of the technique has been proved, and time and chemicals have been easily saved.

5. List of symbols

A	0.511 at 25°C
B_{MX}	Interaction parameter of the MBM
$\dot{B}_{MX}$	Intermediate term in the MBM
c_{MCl}	Concentration of the titrant solution
E	Emf value of the electrochemical cell
E^0	Standard potential of the electrochemical cell
E_{calc}	Calculated emf value
E_{exp}	Experimental emf value
E_j	Liquid junction potential
f_i	Activity coefficient of i in the resin phase
g	59.16 mV
G.E.	Glass electrode
g_{res}	Resin weight
h_0	Initial concentration proton
I	Ionic strength
K_H^M	Equilibrium quotient

$^0K_H^M$	Ion exchange thermodynamic equilibrium constant between H^+ and M^+
N_k	Number of parameters
N_p	Number of points
q_i	Moles of *Ri* per resin gram
q_{max}	Ion exchange capacity of the resin
U_{abs}	Quadratic sum of absolute errors
v_{tot}	Total volume of titration
x_i	Molar fraction of *i* in the resin phase
y	Function of the constant equilibrium
z_i	Charge of *i*
γ_i	Activity coefficient of *i* in aqueous phase
γ_i^{ref}	Activity coefficient of *i* in reference electrode solution
λ_i	Molar conductivity of *i*
λ_i^0	Limit conductivity of *i*
λ_{ij}	Wilson parameter between *i* and *j* in the resin phase
$\rho_{A,d}$	Dry resin density
$\rho_{A,s}$	Swollen resin density
ρ_B	Solution volume change density
σ_{tot}	Standard deviation of the fit

Acknowledgements

This research was supported by the European Union (project LIFE 94/E/A121/E/01409/PVA). Gregorio Borge is grateful for the Scholarship granted to him by the Basque Government.

References

[1] H. Rossotti, The Study of Ionic Equilibria, An Introduction, Longman, New York, 1978, p. 19.
[2] M. Meloun, J. Havel, E. Högfeldt, Computation of Solution Equilibria: A Guide to Methods in Potentiometry, Extraction and Spectrophotometry, Ellis Horwood, Chichester, 1988.
[3] A. Rios, G. Arana, N. Etxebarria, L.A. Fernández, Talanta 43 (1996) 11.
[4] E. Högfeldt, Acta Chem. Scand. 6 (1952) 610.
[5] F. Helfferich, Ion Exchange, McGraw-Hill, New York, 1962, pp. 229–242.
[6] G. Biedermann, L.G. Sillén, Arkiv Kemi 5 (1953) 425.
[7] M. Meloun, E. Högfeldt, Talanta 41 (1994) 217.
[8] N.V. Jarvis, J.M. Wagener, Talanta 41 (1994) 747.
[9] N.V. Jarvis, J.M. Wagener, R.D. Hancock, Solv. Extr. Ion Exch. 13 (1995) 591.
[10] L.A. Bromley, AIChE J. 19 (1973) 313.
[11] G. Borge, R. Castaño, M.P. Carril, M.S. Corbillón, J.M. Madariaga, Fluid Phase Equilibria 121 (1996) 85.
[12] G. Borge, N. Etxebarria, L.A. Fernández, M.A. Olazabal, J.M. Madariaga, Fluid Phase Equilibria 121 (1996) 99.
[13] H. Falkenhagen, M. Leist, G. Kelbg, Ann. Phys. 6 (1952) 51.
[14] A. De Diego, A. Usobiaga, J.M. Madariaga, J. Electroanal. Chem. (1997) (in press).
[15] P. Henderson, Z. Physik. Chem. 63 (1908) 325.
[16] G. Borge, J.M. Madariaga, J. Electroanal. Chem. (1997) (in press).
[17] G.M. Wilson, J. Am. Chem. Soc. 86 (1964) 127.
[18] M.A. Mehablia, D.C. Shallcross, G.W. Stevens, Solv. Extr. Ion Exch. 14 (1996) 309.
[19] M. Marhol, Ion Exchangers in Analytical Chemistry, Their Properties and Use in Inorganic Chemistry, Elsevier, Amsterdam, 1982, 93, pp. 33–34.
[20] M. Iborra, C. Fité, J. Tejero, F. Cunnill, J.F. Izquierdo, React. Polym. 21 (1993) 65.
[21] R. Cazallas, L.A. Fernández, N. Etxebarria, J.M. Madariaga, Lab. Robotics Autom. 5 (1993) 161.
[22] D.C. Shallcross, C.C. Herrmann, B.J. McCoy, Chem. Eng. Sci. 43 (1988) 279.
[23] M.A. Mehablia, D.C. Shallcross, G.W. Stevens, Chem. Eng. Sci. 49 (1994) 2277.
[24] R.A. Robinson, R.H. Stokes, Electrolyte Solutions, Butterworths, Londres, 1965, pp. 133–173.
[25] E. Högfeldt, A three-parameter model for summarizing data in ion exchange, in: J.A. Marinsky, Y. Marcus (Eds.), Ion Exchange and Solvent Extraction, vol. 11, Marcel Dekker, New York, 1993, pp. 109–150.
[26] G.L. Gaines, H.C. Thomas, J. Chem. Phys. 21 (1953) 714.
[27] G. Vázquez, R. Méndez, R. Blázquez, An. Quím. A. 81 (1985) 135.

ELSEVIER

Talanta 45 (1997) 473–476

Talanta

Announcements

Eighth Annual Meeting of Setac-Europe: Interfaces in Environmental Chemistry and Toxicology

Bordeaux, France
April 1998

The Annual Meeting of SETAC-Europe provides a forum for scientific communication among professionals in academia, government, business and other segments of society involved in the various fields of fundamental and applied research in environmental toxicology and chemistry.

The meeting will focus on the important role of interfaces and boundaries in environmental toxicology and chemistry. For example, at the global scale, biogeochemical cycles of metals and organic contaminants are heavily influenced by the exchange capacities at the interfaces between oceans and atmosphere, estuaries and coastal waters, and soil and freshwater systems, etc. At the organism or cell levels, interactions between toxic substances and biological barriers control the bioaccumulation processes and the structural and functional perturbations.

As the main theme of the meeting a number of carefully structured sessions will focus on the role and importance of interfaces and boundaries at the various levels from global to molecular.

To serve the broader interests of the participants of the SETAC-Europe Annual Meeting, platform and poster sessions will address a wide variety of environmental topics.

General topics:

- Environmental toxicology
- Environmental chemistry and geochemistry
- Ecological risk assessment
- Environmental policy
- Life-cycle assessment

Located in the heart of the conference centre, parallel sessions and poster area, an exhibition will allow consultants, industrial companies, service suppliers, equipment manufacturers and publishers to present their activities, equipment and know-how.

For further details, please contact:

SETAC-Europe, Av. E. Mounier 83, Box 1, 1200 Brussels, Belgium. Fax: +322 770 5386

PII S0039-9140(97)00147-1

20th International Symposium on Capillary Chromatography
Riva del Garda, Italy
25–29 May 1998

The program will consist of:

- Review papers by leading scientists in the field covering the latest developments
- Key note lectures by young scientists
- Contributed papers presented in poster sessions
- Discussion sessions to stimulate intense scientific exchange
- Workshop seminars presenting the latest developments in commercial instrumentation
- Exhibition

Authors intending to submit papers for the symposium should send a 300 word abstract no later than December 15, 1997. Abstracts should be sent to Professor Dr P. Sandra, at the address below.

Topics covered are:

Techniques

- Column
- Sample preparation
- Sampling systems
- Capillary gas chromatography
- Micro liquid chromatography
- Supercritical fluid extraction and chromatography
- Electromigration methods
- Field flow fractionation
- Coupled and multidimensional techniques
- Hyphenated techniques
- Trace analysis

Applications

- Environmental applications
- Energy, petrochemistry and industrial applications
- Biomedical and pharmaceutical applications
- Analysis of natural products, food, flavours and fragrances

For further details please contact: The Central Organization: Professor P. Sandra, I.O.P.M.S., Kennedypark 20, B-8500 Kortrijk, Belgium. Tel.: +32 56 204960; fax: +32 56 204859; e-mail: ric.sandra@ven.be or the Local Organization: Dr S. Trestianu, Thermo Quest Italia SpA, Strada Rivoltana, I-20 090 Rodano (Milano), Italy. Tel.: +39 2 95059299; fax: +39 2 95059389; e-mail: sorin.trestianu@ceinstruments.it

HPCE '98: High Performance Capillary Electrophoresis and Related Microscale Techniques
Orlando, FL, USA
31 January–5 February 1988

Technical Program

1. Advances in CE and CEC:
   - enantiomeric separations
   - sample multiplexing
   - on-line preconcentration
   - polymer matrices
   - novel stationary phases
   - new buffer systems
2. Microscale analytical techniques:
   - chemical arrays
   - microchip-based analysis
   - microfabrication techniques
   - nl samples
   - microscale MS
   - CE/MS
3. Solutions to analytical problems in:
   - industrial labs
   - protein chemistry
   - clinical chemistry
   - environmental analysis
   - pharmaceuticals
   - DNA analysis
   - method validation
   - immunology
   - mutational analysis

Student travel grants

Undergraduate and graduate students presenting papers at HPCE '98 will be eligible for travel grants including waived registration fee and/or a cash award. No more than two grant requests will be considered per research group. Letters of application are due September 1, 1997. Each must be accompanied by a letter of support from the faculty research advisor and a copy of the submitted abstract.

Call for papers

Abstracts are due September 1, 1997. Abstracts received after September 1 but before December 15, 1997 will be considered for late-breaking lecture and poster sessions.

Presented papers will be reviewed for publication in a special volume of the Journal of Chromatography. Manuscripts are due by February 3, 1998.

For further details contact:

Shirley E. Schlessinger, Symposium Manager HPCE '98, Suite 1015, 400 East Randolph Drive, Chicago IL 60601, USA. Tel.: +1 312 5272011; fax: +1 312 5273437; website: http://www.hpl.hp.com/casss/hpce98

HPLC '98: 22nd International Symposium on High Performance Liquid Phase Separations and Related Techniques
St. Louis, MO, USA
3–8 May 1988

This will be the most important and inclusive meeting of the year for industrial academic and government scientists who want to be at the forefront of their separations field.

Scientific program

The Organizers have outlined a strong program that includes the foremost international and domestic speakers. This includes the entire scope of high resolution liquid phase separations and related techniques. Some of the broad categories to be covered:

- Liquid chromatography
- Electrophoretic separations
- Hyphenated techniques (including MS, NMR and IR)
- Pharmaceutical separations
- Chiral separations
- Environmental separations
- Petrochemical separations
- Chemical industry
- Separations
- Preparative separations
- New detection methods
- Data analysis, treatment and handling
- Miniaturization
- Government and Regulatory
- Much more

Call for papers: We encourage the submission of abstracts covering all aspects of liquid-based separation techniques. There will be oral presentations in both plenary and parallel sessions, workshops, and informal discussions. Most importantly, there will be prominently featured poster presentations which frequently contain the newest and most novel research.

Abstract deadline: October 31, 1997.

Proceedings: Papers accepted for presentation at HPLC '98 will be peer reviewed for publication in an internationally recognized journal.

For further details please contact:

Janet Cunningham, HPLC '98 Symposium, c/o Barr Enterprises, PO Box 279, Walkersville, MD 21 793, USA. Tel.: + 1 301 8983772; fax: + 1 301 8985596; e-mail: janetbarr@aol.com

ELSEVIER

Talanta 45 (1998) 477–484

Talanta

On-line coupling of gas diffusion to capillary electrophoresis

Petr Kuban, Bo Karlberg *

Department of Analytical Chemistry, Stockholm University, S-10 691 Stockholm, Sweden

Received 3 February 1997; received in revised form 18 April 1997; accepted 18 April 1997

Abstract

On-line gas diffusion has been coupled to a capillary electrophoresis system (CE) via a specially designed interface. The sample is merged with a modifying solution, e.g., a strong acid, in a flow system to transform the analytes of interest into their respective gaseous forms. These transformed, gaseous analytes permeate through a PTFE membrane into an acceptor stream comprising of a tris–buffer. The continuously flowing acceptor stream is led into an injector forming an integrated part of a flow injection analysis (FIA) system. The sample receiving carrier stream in the FIA system, a chromate buffer, brings the sample, 50 μl, to the FIA-CE interface into which one end of a separation capillary has been inserted. A small portion of the injected sample enters the capillary (electrokinetic injection) and separation takes place. A UV detector is placed at the other capillary end and a run potential of 25 kV is applied to two platinum electrodes positioned in the flow system. Multiple sample injections can be performed in one uninterrupted electrophoretic run. A typical sampling frequency is 15 h^{-1}; each run may result in quantitation of at least five anions. The overall repeatability is in the range 1.8–3.6% (RSD). The technique has been applied to the analysis of real samples such as soft drinks, vinegar and wine. Selective discrimination of anions which are unable to form volatile species is accomplished. No off-line sample pre-treatment is needed. © 1998 Elsevier Science B.V.

Keywords: Anions; Capillary electrophoresis; Gas diffusion

1. Introduction

Capillary electrophoresis (CE) has attained great interest in the last decades because of its high resolution, speed of analysis and low consumption of sample and running buffer [1–3]. However, problems encountered with complicated sample matrices still limit its applicability as a routine method. Off-line sample pre-treatment steps such as extraction, filtration, centrifugation, or dilution have to be performed prior to the injection into the separation system. The total analytical scheme then becomes tedious and may even yield inaccurate results.

Gas diffusion carried out in flow systems is commonly applied in the analysis of a wide range of samples, in particular environmental and food samples. Unfortunately, such wet-chemistry flow systems are seldom designed to determine more than one analyte at a time. Simultaneous determinations of several analytes require sophisticated devices including several detectors and complicated manifold schemes. From this point of view,

* Corresponding author. Fax: +46 8 156391; e-mail: bkarlberg@anchem.su.se

PII S0039-9140(97)00131-8

the on-line coupling of gas diffusion to some kind of separation technique has several advantages among which can be mentioned the improved economy of the total analytical procedure. Devices and methods for sample pre-treatment combined with chromatography have been described, for instance on-line preconcentration techniques for liquid chromatography [4,5]. However, problems occurring when coupling on-line sample pre-treatment with CE still restrict its versatile application. A few promising attempts to couple CE to some kind of automated sample pre-treatment technique have been made, including solid phase extraction [6,7] and dialysis [8]. Bao and Dasgupta [9] showed that it is possible to combine dialysis and gas diffusion with CE. They used a narrow bore tubular membrane as a joint for two fused silica capillary segments. The distance between the capillary ends and the inner diameter of the tubular membrane defined the acceptor phase volume. The donor solution, i.e., the sample, was pumped on the outside of the membrane for a pre-defined time and the subsequent separation was performed in the capillary. The technique was used for the analysis of wastewater, blood and gaseous mixtures. The sampling frequency was in this case limited by the total time elapsing from the start of the preconcentration step to the end of the separation step.

In the present paper on-line coupling of gas diffusion to a CE system is described. A specially designed interface [10] in a flow injection analysis (FIA) system was modified and used. The developed technique enables multiple injections of several samples without interrupting the applied high voltage. Typical applications include simultaneous determinations of several analytes in food samples. No off-line sample pre-treatment steps are required. A similar technique has been developed for on-line dialysis [11].

2. Experimental

2.1. Chemicals

All chemicals were of analytical grade. Stock solutions, 10 000 ppm, of both inorganic and organic anions were obtained from the corresponding sodium salts by dilution with deionised water, except for sodium fumarate, which was prepared from fumaric acid by adding a stoichiometric amount of NaOH. Two electrolyte solutions were used, both containing 6 mmol l^{-1} potassium chromate and 3 mmol l^{-1} boric acid but with addition of either 23 μM CTAB (cetyltrimethylammonium bromide) at pH 8.75 (electrolyte I) or 30 μmol l^{-1} CTAB at pH 8.0 (electrolyte II). The pH of the electrolytes was adjusted by addition of 0.1 mol l^{-1} NaOH. Sulphuric acid, 1 mol l^{-1}, was used for conversion of the analytes to their respective gaseous species.

2.2. Instrumental

2.2.1. The FIA system

An eight channel peristaltic pump (Gilson, France) was employed for continuous delivery of the electrolyte and for pumping acceptor and donor solutions. A constant rotation speed of the pump was applied; different flow rates were obtained by an appropriate choice of PVC pump tubings. The injection valve, furnished with a 50 μl sample loop, was operationally controlled through a FIAstar 5020 unit (Perstorp Analytical, Sweden). All parts of the FIA manifold were connected via PTFE tubings, 0.7 mm i.d. A planar Celgard 2500 PTFE membrane was sandwiched between the two halves of a Tecator 5106 Dialysis module (Perstorp Analytical, Sweden). The two halves had matching flow channel lengths of 50 cm. The membrane was exchanged when it became permeable for H_2SO_4 from the donor solution.

2.2.2. The FIA-CE interface

The FIA-CE interface previously presented by Kuban et al. [10] was slightly modified and used for sample introduction into the separation capillary of the CE part of the system. In essence, the modification comprised of bending the platinum electrode slightly so that it was positioned at an angle of 45° in the flowing stream, see Fig. 1.

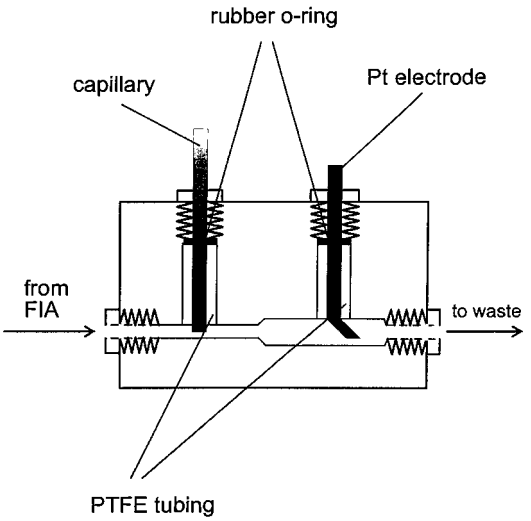

Fig. 1. Schematic view of the FIA-CE interface.

2.2.3. The CE part

The CE part of the system was housed in a home-made plexiglass box equipped with a safety lock on the access door which turned off the high voltage if the box was opened during an electrophoretic run. The CE system consisted of a high voltage supply (Series 320, Bertan Associates, Hicksville, NY, USA) applying a run potential of 25 kV to the two platinum electrodes positioned as shown in Fig. 2 (Pt_1 and Pt_2). A 50 μm i.d., 375 μm o.d. polyimide coated capillary (Polymicro Technologies, Phoenix, AZ, USA) was used, having a total length of 80 cm. The distance between the injection and detection sites was 45 cm.

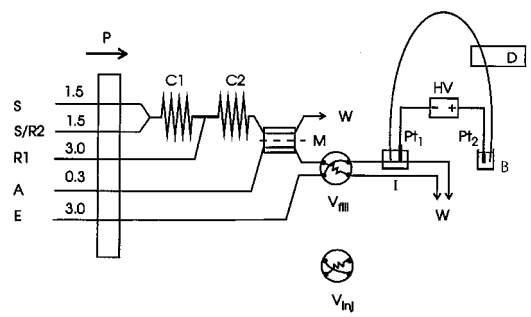

Fig. 2. Working principle of the gas diffusion-CE system. P, perstaltic pump; S, sample; R2, sodium hydroxide (optional solution); R1, sulphuric acid; A, acceptor solution; E, electrolyte solution; C1 and C2, reaction coils (60 cm, 0.5 mm i.d.); W, waste; M, gas diffusion membrane; Pt_1 and Pt_2, platinum electrodes; HV, high voltage supply; D, detector; I, FIA-CE interface; B, buffer solution. V_{fill} shows injector in fill position, V_{inj} in inject position.

2.2.4. Detection

A CV[4] UV-visible detector (ISCO, Lincoln, NE, USA) was operated in an indirect UV detection mode at 372 nm (chromate electrolyte buffer). Electropherograms were registered using an ELDS 900 laboratory data system (Chromatography Data Systems, Kungshög, Sweden) on an IBM personal computer.

2.3. Principle

Fig. 2 shows the complete gas diffusion FIA-CE system. The sample (S) was normally introduced via two lines into a coil (C1) and then mixed with the acid modifier (R1) in a reaction coil (C2). The conditions were chosen so that all of the analytes of interest were transformed into their gaseous forms. The gaseous species could subsequently penetrate the PTFE membrane (M) when passing by. Upon entering the acceptor solution (A) the gaseous analytes were converted back to their respective ionic forms. The acceptor phase carried the ionic analytes to the injector (position V_{fill}). When the injection loop had been filled with a representative sample, the injector was switched to the inject position (V_{inj}) and a discrete sample volume of 50 μl was injected into the electrolyte stream (E) and brought to the interface (I). The sample plug passed by the end of the separation capillary placed in the FIA-CE interface and a small fraction was electrokinetically introduced into the capillary. The separated analytes finally reached the detector (D) placed at some distance from the capillary outlet. This outlet was immersed in a receiving solution in a beaker (B).

If a second reagent was required for the purpose of treating the sample with an optional reagent, one of the two introduction lines normally intended for the sample could be used for such a reagent (R2), see Fig. 2.

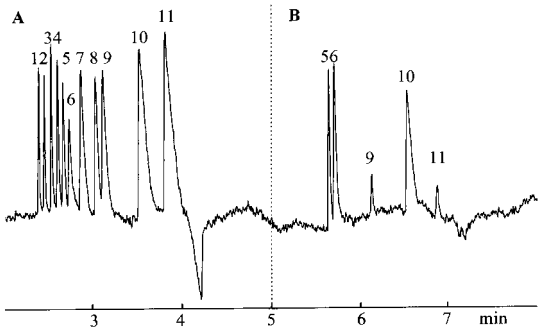

Fig. 3. Separation of a model anion solution (A) without and (B) with gas diffusion. Conditions: electrolyte I (chromate); 25 kV; acceptor solution: 5 mmol l^{-1} tris. The injection valve was actuated at $t=0$ (A) and at $t=3$ min (B). Peaks: 1, $S_2O_3^{2-}$; 2, Cl^-; 3, SO_4^{2-}; 4, NO_3^-; 5, HS^-; 6, SO_3^{2-}; 7, citrate; 8, fumarate; 9, formate; 10, HCO_3^-; 11, acetate. Flow rates according to Fig. 2.

3. Results and discussion

3.1. Separation of a model anion mixture

Fig. 3A shows the separation of 11 anions originating from a model solution directly introduced as solution A in the system (see Fig. 2), i.e., no gas diffusion was performed. Thus, the model solution was directly filled into the injection valve being in position V_{fill}. The injector was switched to position V_{inj} whereby an exact volume of the model solution was inserted into the electrolyte E. The analyte introduction into the capillary, the analyte separation and the detection were performed as described in Section 2 above. The same model solution was then subjected to gas diffusion. Consequently, it was pumped as solution S into the system through the two lines S and S/R2 as shown in Fig. 2. The acid modifier, 1 mol l^{-1} H_2SO_4, was pumped as solution R1. The S and R1 solutions were mixed in coil C2 whereby volatile analytes were formed which diffused through the membrane M into acceptor solution A. Injection of the A solution, now containing the analytes in the form of back-converted anions, took place and the ions were separated and detected in the capillary as previously described. The resulting electropherogram is shown in Fig. 3B. All the peaks in Fig. 3 have been produced in one electrophoretic run and by using electrolyte I. Concentrations of the anions ranged from 10 to 100 ppm, although, in the case of gas diffusion, second injection in Fig. 3, the concentration of formate and acetate had to be increased to 500 ppm since the corresponding acids to these ions exhibit a low membrane penetration. As can be seen in Fig. 3 only some of the anions originally present in the model mixture can be transformed to gaseous species capable of penetrating the membrane. Thiosulphate disproportionates in acidic media to sulphur dioxide and elemental sulphur according to

$$S_2O_3^{2-} + 2H^+ \rightarrow SO_2(g) + S(s) + H_2O$$

This causes an increase in the SO_3^{2-} peak. High concentrations of thiosulphate produce large quantities of elemental sulphur which may lead to membrane fouling. The thiosulphate anion was therefore excluded from further studies.

When chromate is used as a carrier electrolyte the negative system peak usually appears far enough from the separated anions if the pH of the electrolyte is kept at about 8.0. However, HS^- and SO_3^{2-} do not separate completely at this pH value; the pH value has to be increased further to promote the dissociation of HS^-. The system peak then migrates into the area of the separated anions causing problems with both the separation and the quantitation of some of the analytes. By decreasing the concentration of the electroosmotic flow modifier, CTAB, the system peak can be removed from the analyte peak region. Electrolyte I containing 6 mmol l^{-1} potassium chromate, 3 mmol l^{-1} boric acid and 23 μmol l^{-1} CTAB at pH 8.75 was found to be suitable for accomplishing baseline separation of all ions in the model mixture, also allowing quantitation of all the selected anions.

3.2. Optimisation of the flow conditions

The Codex 2.5 Software was used to create the experimental design for flow conditions optimisation. A three level full factorial design was created. The acceptor and the donor flow rates were chosen as variables and the sensitivity as the response. The sensitivity was correlated to the

areas of the HS^- and the SO_3^{2-} peaks. Response surface plots revealed that the acceptor flow rate should be kept as low as possible while the donor flow rate should be as high as possible. No significant difference was observed between con- and counter-current flow arrangements. Concurrent flow mode was finally chosen since the membrane over-pressure then became satisfactorily low. The selected flow rates for the donor and the acceptor phases were 0.3 and 3 ml min^{-1}, respectively.

3.3. Choice of the composition of the donor and acceptor phases

Studies were performed to evaluate the effect of the sulphuric acid concentration on the transformation of analytes from anions to gaseous species. The transformation efficiency was evaluated by comparing the peak areas for the HS^- and SO_3^{2-} anions obtained at the various experimental conditions. The concentration of sulphuric acid was changed within the interval 0.1–1.0 mol l^{-1}. Only slight increases in peak areas were observed when increasing the concentration of H_2SO_4 from 0.1 to 0.7 mol l^{-1}, while a constant response was observed in the range of 0.7–1.0 mol l^{-1}. An acid concentration of 1 mol l^{-1} was therefore selected in all subsequent experiments.

In the acceptor phase the gaseous analytes are converted back to their respective anions. In order to accomplish a complete conversion it is required that the pH of the acceptor phase is sufficiently high. Furthermore, the acceptor phase must have a high buffering capacity. A portion of the acceptor solution is injected into the electrolyte solution. Thus, it is necessary that these two solutions are 'compatible', i.e., no chemical reactions should take place in the two interface areas bracketing the injected acceptor solution plug.

The electropherograms in Fig. 4 have been obtained by using different acceptor solutions. Water and chromate electrolytes are less suitable acceptor solutions, see electropherograms A and B in Fig. 4. These solutions are not able to completely absorb the gaseous species originating from weak acid anions such as carbonate and hydrogen sulphide. Borate and tris–buffers, on the other hand, are more advantageous in this

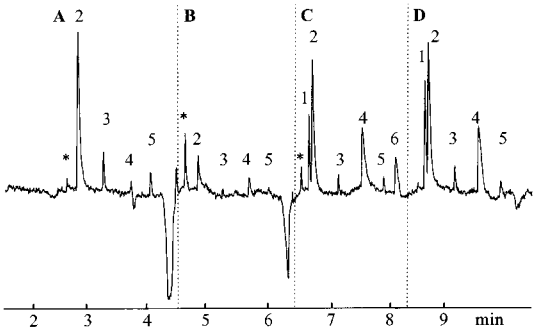

Fig. 4. Effect of different acceptor solutions: A, H_2O; B, chromate (electrolyte I); C, 3 mmol l^{-1} borate; D, 5 mmol l^{-1} tris. Conditions were the same as in Fig. 3. Valve actuations at $t = 0$, 2, 4 and 6 min. Peaks: 1, HS^-; 2, SO_3^{2-}; 3, formate; 4, HCO_3^-; 5, acetate; 6, borate.

respect, see electropherograms C and D in Fig. 4. However, a small peak of borate appears when the borate buffer is chosen as acceptor phase. This peak may interfere with acetate. Consequently, 5 mmol l^{-1} tris was preferred as the acceptor phase in all the subsequent experiments.

3.4. Repeatability and gas diffusion yield

Repeatability of the gas diffusion FIA-CE system was evaluated by continuously subjecting a standard solution of five anions to gas diffusion. During this procedure the acceptor solution was repeatedly injected into the electrolyte. Fig. 5 shows the repeatability of five such consecutive injections. The maximum number of injections

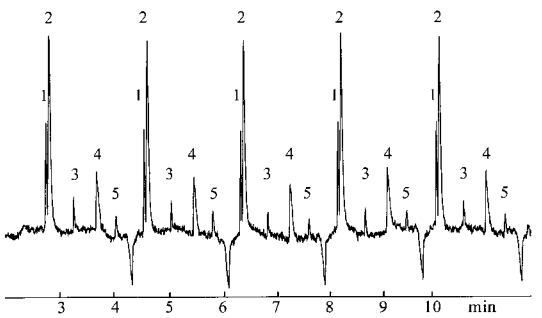

Fig. 5. Repeatability of the gas diffusion procedure, five consecutive injections (1.75 min interval). Conditions as in Fig. 3.

Table 1
Repeatability of peak area, and migration time (t_M), and gas diffusion (GD) yield of the GD-CE technique, $n = 8$

Anion	Peak area RSD, %	t_M RSD, %	Gas diffusion yield, %
HS^-	3.4	0.29	95
SO_3^{2-}	2.7	0.35	110
Formate	2.1	0.44	1
HCO_3^-	1.8	0.43	40
Acetate	3.6	0.34	1

that can be made in one uninterrupted electrophoretic run is five since the appearance of the first negative peak occurs 12 min after the first injection. However, the repeatability data presented in Table 1 originate from eight independent runs, i.e., each commenced gas diffusion process was concluded by only one injection of the acceptor solution. Table 1 also shows the repeatability of the various migration times and gas diffusion yields. The latter is defined as the ratio between the peak area obtained for the analyte subjected to gas diffusion and corresponding peak area obtained without gas diffusion, i.e., direct injection of sample into the electrolyte. Gas diffusion yields are significantly higher for inorganic anions than for organic anions, such as formate or acetate. This discrimination effect observed for organic anions benefits the determination of low levels of sulphite in the presence of large amounts of acetate, see the results for vinegar samples presented below.

3.5. Real samples

Table 2 shows analytical results obtained for some real samples. Carbonate was determined in three different soft drink and beer samples, and calibration solutions of carbonate were used for the quantitation. The obtained results were verified by an independent method (titration). Results from the simultaneous determinations of acetate and sulphite in vinegar are also given in Table 2. In Fig. 6 some typical electropherograms obtained for the vinegar samples are depicted. Sulphite is present in apple and white wine based vinegar to which it is added to prevent oxidation which may occur during storage.

Table 2
Quantitation of some analytes in soft drinks, beer and vinegar samples

Sample	HCO_3^-(g l^{-1})	SO_3^{2-} (mg l^{-1})	Acetate (g l^{-1})
Apple cider	0.27	—	—
Coca-Cola	1.86	—	—
Beer	2.48	—	—
Common vinegar	—	n.d.	217
Apple cider vinegar	—	82.0	177
White wine vinegar	—	32.5	170
Red wine vinegar	—	n.d.	170

The electropherogram in Fig. 7 indicates the possibility of simultaneous determination of free SO_2, carbonate and acetate in wine samples. By employing 1 mol l^{-1} sodium hydroxide as an optional reagent (R2), see Fig. 2, total SO_2 can also be determined simply by introducing the wine samples directly. No manual, off-line pre-treatment is required. Note that no physical redesign of the manifold is required. Fig. 8 shows some typical electropherograms and in Table 3 the analytical results are given. The analyte concentrations were calculated by using the internal standard method; formate was used as an internal

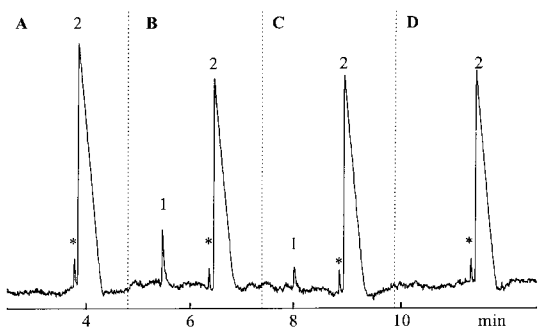

Fig. 6. Determination of acetic acid and sulphur dioxide in vinegar. Conditions: electrolyte II (chromate); 25 kV; acceptor solution: 5 mmol l^{-1} tris. Samples: A, common vinegar; B, apple cider vinegar; C, white wine vinegar; and D, red wine vinegar. Valve actuations at $t = 0$, 2.5, 5 and 7.5 min. Peaks: 1, SO_3^{2-}; 2, acetate; *, carbonate present in the acceptor phase.

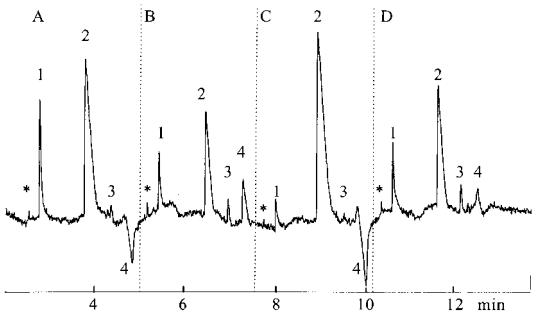

Fig. 7. Determination of carbonate and free SO_2 in wine samples. Valve actuations at $t = 0$, 2.5, 5 and 7.5 min. Peaks: 1, SO_3^{2-}; 2, HCO_3^-; 3, acetate; *, SO_4^{2-}. Samples: A, white wine 1; B, white wine 2; C, red wine 1; D, red wine 2. Conditions as in Fig. 3.

standard for this application. Some sulphate ions penetrate the gas diffusion membrane (marked with asterisks in Fig. 7 and Fig. 8). The sulphate peaks also appeared when the calibration solutions were run. However, no sulphate could be found in standard solutions and samples which were introduced directly into the system thus not being subjected to gas diffusion. The amounts of free and total SO_2 vary with the type of wine. None of the wine samples exceeded the maximum allowed limits for free and total SO_2.

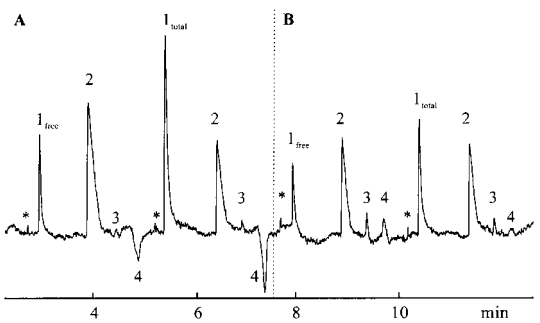

Fig. 8. Determination of free and total SO_2 in wine. Valve actuations at $t = 0$, 2.5, 5 and 7.5 min. Peaks: 1, SO_3^{2-}; 2, HCO_3^-; 3, acetate; 4, system peak; *, SO_4^{2-}. Samples: A, white wine 1; B, white wine 2. Conditions as in Fig. 3.

Table 3
Determination of SO_2 and acetate in wine samples

Sample	SO_2 (ppm)		CO_2 (ppm)	Acetate (ppm)
	Free	Total		
White wine 1	26.3	164.1	276.6	314.2
White wine 2	9.6	104.7	43.8	467.6
Red wine 1	12.1	62.5	50.2	510.1
Red wine 2	9.7	48.8	306.0	454.8

4. Conclusions

On-line gas diffusion coupled to CE in a flow arrangement is a suitable technique for automated pre-treatment of samples having a complicated matrix composition. Sulphite, carbonate and acetate are of particular interest since they are often present in food samples; sulphite is added to the food as an antioxidant, carbonate is present in almost all aqueous solutions, and acetate can be found in wine or vinegar since it is formed when ethanol is oxidised. The determination of all these three analytes in one uninterrupted electrophoretic run has been possible with the developed technique. The sampling throughput is comparable to that of a conventional FIA system designed for the determination of one analyte only. The technique should have a large potential for process analysis and monitoring. Future work will be directed to the integration and optimisation of further types of pre-treatment procedures.

References

[1] F. Foret, L. Krivankova, P. Bocek, Capillary Zone Electrophoresis, VCH, Weinheim, 1993.
[2] P. Jandik, G. Bonn, Capillary electrophoresis of small molecules and ions, VCH, New York, 1993.
[3] K.D. Altria, Capillary electrophoresis guidebook, Humana Press, Totowa, New Jersey, USA, 1996.
[4] N.C. Van de Merbel, J.J. Hageman, U.A.T. Brinkmann, J. Chromatogr. 634 (1993) 1.
[5] U.A.T. Brinkman, J. Chromatogr. 665 (1994) 217.
[6] A.J. Tomlinson, L.M. Benson, N.A. Guzman, S. Naylor, J. Chromatogr. 744 (1996) 3.
[7] A.J. Tomlinson, L.M. Benson, W.D. Braddock, R.P. Oda, S. Naylor, J. High Resolut. Chromatogr. 18 (1995) 381.

[8] B.L. Hogan, S.M. Lunte, J.F. Stobaugh, C.E. Lunte, Anal. Chem. 66 (1994) 596.
[9] L. Bao, P.K. Dasgupta, Anal. Chem. 64 (1992) 991.
[10] P. Kuban, A. Engström, J.C. Olsson, G. Thorsen, R. Tryzell, B. Karlberg, Anal. Chim. Acta. 337 (1997) 117.
[11] P. Kuban, B. Karlberg, Anal. Chem. 69 (1997) 1169.

ELSEVIER

Talanta 45 (1998) 485–492

Talanta

Incorporation of electrodialysers into the conduits of FIA systems: enhancement of the mass transfer of chloride anions through passive neutral membranes[1]

J.F. van Staden *, C.J. Hattingh

Department of Chemistry, University of Pretoria, Pretoria 0002, South Africa

Received 15 January 1997; received in revised form 28 April 1997; accepted 29 April 1997

Abstract

The viability of electrodialysis (ED) for the enhancement of mass transfer through passive neutral membranes in a flow injection system was investigated. A Spectrapore and Technicon type C membrane were evaluated using chloride anions as analyte. Both membranes showed an increase in mass transfer and the proposed electrodialyser/FIA system was applied for the determination of chloride in industrial effluents with results that compared very well with a standard titration procedure. © 1998 Elsevier Science B.V.

Keywords: Chloride; Electrodialysis; Passive neutral membranes; Flow injection analysis

1. Introduction

The technique of mass transfer in on-line analytical dialysers has been employed in continuous flow systems with gas-diffusion and dialysis membranes for many years, particularly in routine clinical laboratories. There are a number of thorough and authoritative reviews of the early history of membrane science and all the details are not repeated here. One of the milestones in this regard is a review by Lonsdale [1] on the growth of membrane technology up to 1982.

Dialysis is a technique based on a diffusion process which involves the selective separation of sample species through a semi-permeable membrane. The technique can be divided into passive dialysis and active (or Donnan) dialysis. The classification of dialysis processes as passive or active (Donnan) depends on the nature of the membrane [2,3]. In the passive process a neutral membrane differentiates between separations on a molecular scale with a preciseness of molecular order allowing species within a given range of molecular mass to diffuse across a neutral membrane. In active (Donnan) dialysis, ions with a given type of charge are transferred across an ion-exchange membrane. Passive dialysis is a highly efficient molecular filter, but is inefficient in terms of solute diffusion rates across a semi-permeable mem-

* Corresponding author. Fax: +27 12 432863.

[1] Presented at the Eighth International Conference on Flow Injection Analysis (ICFIA '97), held in Orlando, Florida, January 12–16, 1997.

PII S0039-9140(97)00179-3

brane with an efficiency of only about 0–7% [4]. It is possible to increase the diffusion rate by increasing the ratio of membrane surface area to sample volume. This can be done by designing a dialyser system with a maximum ratio of membrane surface area to sample volume. In flow injection dialyser systems a very small sample plug is injected into a carrier donor stream which fulfil these optimum conditions. Passive dialysis is, however, only suitable for controllable dilution.

Active or Donnan dialysis is a promising technique for the preconcentration, recovery and speciation of ionic species, but with a limitation in the amount of mass transfer of species through the membrane. Cox et al. [5,6] have worked for many years on sample preparation on an analytical scale using Donnan dialysis, employing the technique for matrix normalization [5] and sample preconcentration [6].

As the name implies, electrodialysis (ED) is a dialytic process in which an applied electric field is used to force ions through a membrane [1]. The main driving force which impels ions through the membrane is the potential gradient across the two sides of the membrane. So far, ion separation is affected through the use of selectively ion-permeable membranes. In practical ED, many selective membranes are placed perpendicularly in the path of the electrical field. In all the research work reported to date [1,7–9], conventional ED utilized ion-exchange membranes. ED with ion-exchange membranes was also utilized as suppressors in ion chromatography [10,11] and for electrodialytic neutralization of samples prior to analysis in ion chromatography [12,13]. The electrodialyser units described by Cooper et al. [7] were designed with three compartments: a feed solution containing the sample was placed in a channel between a cation exchange membrane on the one side and an anion exchange membrane on the other side. Ions from the sample channel permeate under the influence of an electric field to the respective corresponding acceptor channels.

ED is also a membrane-based separation technique that is appealing because of its capability to deionize one stream while concentrating the electrolytes in another stream. ED therefore produces a purified stream that can either be discharged or reused and a concentrated electrolyte stream that can be disposed of or processed for reclamation of the dissolved salt. In most of these electrodialyser units, cation- and anion-permeable ion-exchange membranes were arranged in an alternating pattern. The series of cells became alternately diluting and concentrating compartments when a direct current was passed through the system. These stacks were mostly employed in desalination systems and industrial applications. Some applications of ED include [1,8,9], desalination of brackish waters, desalting of whey and stabilisation of wine, purification of protein solutions, recovery of metals from plating of rinse waters, recovery of acids, recovery of heavy metals from mining mill processes and the treatment of cooling-tower blowdown for water recovery and effluent volume reduction.

A literature survey showed that, to date, ED has only been exploited to a limited extent in flow injection systems. ED has been reported for the separation of alanine and aspartic acid [14] and for extraction of ephedrine from spiked plasma [15]. Kittsteiner-Eberle et al. [16] reported an application for the separation of leucine from ketoleucine during flow injection analysis with leucine dehydrogenase. The selectivity for L-amino acids in flow injection analysis was enhanced using ED with amino acid oxidation [7]. Conventional ED configurations [8] using cation and anion exchange membranes were mainly employed in all the applications to date.

Although there is a perception in certain circles [12], that passive dialysis through a neutral membrane is a slow process requiring a large volume of sample, it has been reported [2,3,17], that membrane separation with passive dialysis is one of the most successful separation techniques in flow analysis. In fact, the passive process involving neutral membranes forms the backbone in most routine clinical laboratories worldwide in flow systems. One of the disadvantages of passive dialysis is, however, that it results in severe sample dilution. It is, however, possible to design an electrodialyser unit with only two compartments where a passive neutral membrane is incorporated between only two channels (a donor and an acceptor) of the conduits of an FIA system, using

the same dialyser configuration as in conventional dialysis. By using this concept it is possible to enhance the transfer of certain sample components through a passive neutral membrane. Previous results [18] showed that diffusion through the Technicon type C membrane (pore size 4–6 nm) is more rapid than diffusion through the Spectrapore membrane (MW cut-off 6000–8000, pore size 2.5–4 nm) under normal passive dialysis conditions in flow systems and these two neutral membrane types were therefore chosen for this study.

The most reliable way of evaluating the transfer of selected sample components through these two types of membranes in an electrodialyser flow injection setup is through the study of the actual percent dialysis of solutes of known size under the same conditions. This paper therefore deals with the incorporation of a passive (neutral) membrane as part of an electrodialyser unit into the conduits of a flow injection system, studying the permeability of chloride as the selected anion.

2. Experimental

2.1. Reagents and solutions

All reagents were prepared from analytical grade chemicals unless otherwise specified. Deionized water from a Modulab system (Continental Water Systems, San Antonio, TX) was used for dilution. The water was tested for traces of chloride before use. All solutions were degassed before measurement with a water vacuum pump system. The main solutions were prepared as follows:

2.2. Standard chloride solution

A standard stock chloride solution containing 10 000 mg l^{-1} was prepared by dissolving 32.97 g of dried sodium chloride in water and diluting to 2 l with de-ionized water. Working standard solutions were prepared by appropriate dilutions to cover the working ranges as discussed in the text.

2.3. Colour reagent

The colour reagent was prepared by dissolving 1.26 g of mercury(II)thiocyanate in 300 ml of methanol, 1 l of de-ionized water was added and shaken to mix well. 10 ml concentrated nitric acid (specific gravity 1.42) and 31 g $Fe(NO_3)_3 \cdot 9\ H_2O$ were added, dissolved and diluted to 2 l with deionized water. The colour reagent was filtered if necessary. The reagent is stable for several months at room temperature if stored in a dark bottle.

2.4. Instrumentation

The FIA system (Fig. 1) used in this work, was composed from the following components: a six-roller Cenco peristaltic pump rotating at 10 rpm, a Valco (Houston, Texas) 10-port electrically actuated injection valve with a sample loop of 70 μl, reaction manifold system and a laboratory-made electrodialyser. The electrodialyser used was a slightly modified version of the dialyser previously described by van Staden [18,19]. The semi-tubular grooves in both the top and bottom parts were 0.6×0.6 mm in internal diameter and imbedded on both sides of the membrane, forming the outer wall of the grooves, were two electrodes as illustrated in Fig. 2. A Leader LPS 156 potentiostat was used to apply the d.c. potential. For current and potential measurements a Prema 5000 integrating multimeter was used. Two different passive membranes were used namely, a Spectrapore membrane (MW cut-off 6000–8000, pore size 2.5–4 nm, thickness 0.031 mm) and a Technicon type C membrane (pore size 4–6 nm, thickness 0.015 mm). Tygon tubing (0.76 mm id) was used

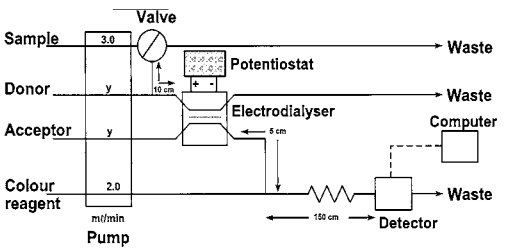

Fig. 1. Schematic flow diagram of the electrodialyser/flow injection system for the determination of chloride.

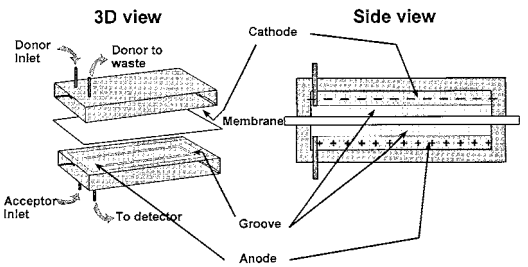

Fig. 2. A 3-D and side view of the electrodialyser unit.

to construct the manifold system. The detector used was a Unicam 8625 UV/VIS spectrophotometer equipped with a 10 mm Hellma-type flow-through cell (volume 80 ml). The spectrophotometer and the injection valve were coupled to a personal computer equipped with the FlowTEK program [20].

2.5. Flow system

The flow system used is depicted in Fig. 1. Sample solutions were drawn up into a 70 μl sample loop of the Valco valve from where it was injected into the carrier donor stream and transported into the electrodialyser. Analytes in the sample donor stream were electrodialysed under the influence of an applied d.c. potential through the passive neutral membrane to the acceptor channel. The electrodialysate ions were swept from the electrodialyser unit and mixed with iron(III)/mercury(II)thiocyanate chromogenic reagent in the reaction manifold system. This colour reaction product was then transported to the spectrophotometer for measurement at a wavelength of 480 nm.

Data acquisition and device control were achieved using a PC30-B interface board (Eagle Electric, Cape Town, South Africa) and an assembled distribution board (MINTEK, Randburg, South Africa). The FlowTEK [20] software package (obtainable from MINTEK) for computer-aided flow-analysis was used throughout for device control and data acquisition. All the data given (mean height values) are the average of 10 replications.

3. Results and discussion

In order to enhance the mass transfer of chloride anions through the passive neutral membrane as an accurate and precise measurable product, optimum system conditions are of critical importance in the design and operation of the electrodialyser/flow injection system. The first main target of the investigation was to draw the maximum amount of chloride ions across the neutral membrane into the conduits of the acceptor channel by applying a d.c. potential gradient across the two sides of the membrane. The second goal was to prevent any of the electrodialysate chloride ions to come into contact with the anode obviating any side-reactions which might involve the chloride anions. This was done optimising the acceptor stream flow rate in order to flush the anions immediately towards the reaction manifold. Research in this work was therefore concentrated on the design of the electrodialyser unit and optimisation of the flow rates of the donor and acceptor streams and the applied potential over the membrane.

3.1. Applied potential

The sensitivity and reproducibility of the electrodialysed chloride analyte sample plugs in the electrodialyser unit depend on the potential gradient applied on the system. The applied potential was therefore evaluated using the detector signal for response and %RSD as indicators. The d.c. potential was varied between 0 and 27 V for both membranes, while the flow rates in the donor and acceptor streams were kept constant at 1.6 ml min^{-1}. The results in Fig. 3 revealed that the precision at low applied potentials was poor (RSD $>8\%$ for the Technicon membrane and $>13\%$ for the Spectrapore membrane), indicating that the contribution of detectable chloride ions drawn through the neutral membrane was unstable. As the applied voltage was increased to 6.8 V, the %RSD decreased significantly, reaching an optimum value of 2.8% for the Spectrapore membrane and 1.9% for the Technicon membrane. It can be assumed that the majority of electrodialysate chloride ions were drawn into the core of

the acceptor stream and that the anode electrode had a minor influence at the applied potential of 6.8 V. It is furthermore apparent that there is a slight increase of the %RSD from very low voltages (6.8 V) to higher voltages (27 V) in both the membranes. This is probably due to the stronger attraction forces exerted on the chloride anions from the anode resulting in a loss of anions from the main acceptor stream and also to possible electrode reactions. The precision of the Spectrapore membrane deteriorated faster than the precision of the Technicon membrane with the increase of applied voltage above 6.8 V. The results in Fig. 3 also showed an increase in peak height when the applied potential was increased from 0 to 24 V. The results in Fig. 3 revealed that the peak height of the Technicon membrane increases faster than the peak height of the Spectrapore membrane when the applied potential was increased from 0 to 24 V. This is probably due to the larger pore size and smaller thickness of the Technicon membrane. The increase in peak height of the Technicon membrane flattened off for applied potentials larger than 24 V. It is therefore clear from these results that the Technicon membrane is, by far, more superior than the Spectrapore membrane in the ED/FIA system. It is also clear from the results that it should be possible to apply any potential between 6.8 and 18 V for the Technicon membrane, depending on the requirements of a specific application (working range used and precision required).

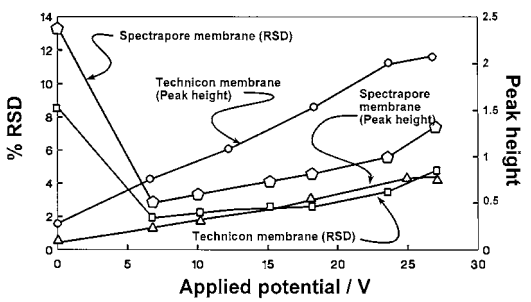

Fig. 3. Evaluation of response and relative S.D. as a function of the applied potential for both membranes.

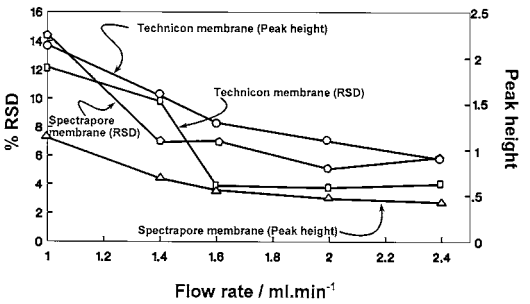

Fig. 4. Evaluation of response and relative S.D. as a function of the flow rate for both membranes.

3.2. Flow rates of the donor and acceptor streams

The main purpose of flow rate of the acceptor stream was to flush the dialysate chloride anions immediately as they emerged from the membrane to the reaction manifold and to prevent any anions to reach the anode. Evaluation of the flow rates of both the donor and acceptor streams revealed that the best results were obtained with the flow rates of both streams in the same direction when applied in the continuous mode. Sensitivity and precision were used as indicators in the optimisation of the flow rates. In all the experimental work done, the same flow rate was applied for both the donor and acceptor streams. During these experiments the applied potential was kept constant at 15 V while the flow rates of the donor and acceptor streams were varied. The influence of the flow rates, for both membranes, was first compared on the basis of %RSD, as illustrated in Fig. 4. It is clear from the results that the precision deteriorated remarkably for flow rates below 1.4 ml min^{-1} for the Spectrapore membrane and for flow rates below 1.6 ml min^{-1} for the Technicon membrane. It is obvious that at low flow rates the dialysate chloride ions tended to move through the core of the acceptor stream and were able to reach the anode where possible electrode reactions could cause sufficient disturbance to increase the %RSD. Another contribution to this increase is the irregular flow patterns at lower flow rates. The precision improved at higher flow rates with the best precision obtained at a flow rate of 2 ml min^{-1} for both membranes. If one

looks at the peak height versus the flow rate (Fig. 4), the best response was obtained with flow rates of 1 ml min^{-1} for both membranes. A possible explanation for the decrease in sensitivity with higher flow rates was that although the flux of ions across the neutral membrane under the influence of the applied electric field remained the same, it could not match the influence of the higher flow rate with dilution effect on the dialysate anions in the acceptor channel of the FIA system. It is also clear from the results in Fig. 4 that the response of the Technicon membrane are by far better than that of the Spectrapore membrane. The best compromise between sensitivity and precision for employment of the proposed electrodialyser/FIA system was obtained with a flow rate of 1.6 ml min^{-1} for the Technicon membrane and 2.0 ml min^{-1} for the Spectrapore membrane. The proposed electrodialyser/FIA system is, however, very flexible and it is therefore possible to use the influence of donor and acceptor stream flow rates to apply the system in other analyte concentration ranges when required.

3.3. Interferences

The following ions (Br^-, I^- and NH) were found to have an influence on the response of chloride ions in the ED/flow injection system. It was found that bromide and iodide ions interfered positively with the determination of chloride, starting at levels as low as the detection limit for chloride. An evaluation revealed that the bromide and the iodide interfered whether they were injected into the donor or the acceptor streams. The conclusion of this was that the bromide and iodide being anions, experienced the same driving force exerted by the applied potential than the chloride ions. Additionally, however, the main interference was that the bromide and iodide ions also reacted with iron(III)/mercury(II)thiocyanate chromogenic reagent to give coloured reaction products absorbing at the same wavelength as the colour product from the chloride ions. The influence of ammonia/ammonium ion is illustrated in Fig. 5. The interference of ammonia depends on the type of compound used. When ammonium hydroxide was used as the primary source of ammonia, ammonia interfered when even very low concentrations of ammonia were injected into the donor stream of Technicon membrane as seen from Fig. 5A. Interference also started at a concentration of 0.011 mol l^{-1} when the Spectrapore membrane (Fig. 5B) was used. Gas and molecular diffusion was probably the main cause for this interference as the ammonium cations were not drawn to the anode. Two factors contributed to this: the total effective cross-sectional area of pores available for gas and molecular diffusion were big enough to allow for the ammonia/ammonium ions to diffuse through the passive neutral membranes. Secondly, the thinner Technicon membrane was probably responsible for the ammonium acetate to diffuse through the membrane, whereas the Spectrapore membrane was just thick enough to prevent diffusion through the membrane even at higher concentrations, as is evident in Fig. 5B. The ammonia/ammonium ion that diffused through both membranes had a buffer effect on the acidic colour reagent. The influence of the buffer effect can be reduced by increasing the amount of HNO_3 used in the colour reagent about five to 10 times.

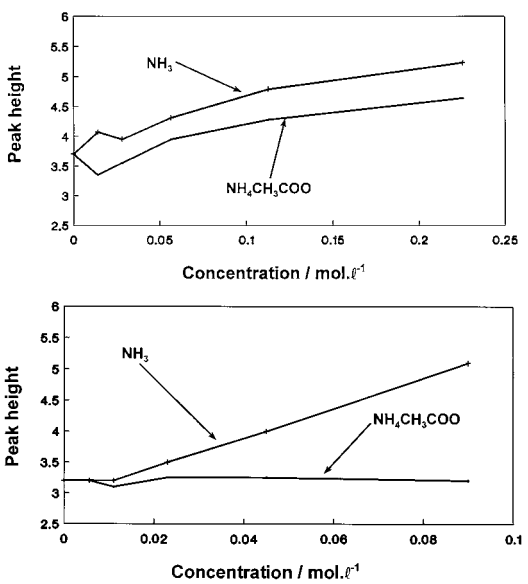

Fig. 5. Influence of interferences. (A) Technicon membrane and (B) Spectrapore membrane.

Table 1
Comparison of the performance of the Spectrapore and Technicon membranes in the electrodialyser/flow injection system

Parameter	Spectrapore membrane	Technicon membrane
% Dialysis	10	37
Runs h^{-1}	26	23
Experimental time (s)	140	160
Sample interaction (%)	0.23	0.32
Linear range (mg l^{-1})	400–3200	200–1200
Applied potential (V)	15	15
Flow rate (ml min^{-1})	2.0	1.6

3.4. Calibration and comparison of the Spectrapore and Technicon membranes.

A comparison between the performances of Spectrapore and Technicon membranes in the electrodialyser/flow injection system depicted in Fig. 1, is outlined in Table 1. The linearity of the electrodialyser/FIA system for the determination of chloride was evaluated under optimum running conditions for both membranes (2.0 ml min^{-1} and 1.6 ml min^{-1} for the Spectrapore and Technicon membranes respectively with an applied potential of 15 V for both membranes). As can be seen from Table 1, the linear range for the Spectrapore membrane was between 400 and 3200 mg l^{-1} with the straight line equation $y = 0.002039x - 0.8556$ and $r^2 = 0.9974$. The linear range for Technicon membrane was found to be between 200 and 1200 mg l^{-1} with the equation for the straight line $y = 0.003975x - 0.2557$ and $r^2 = 0.9941$. The mass transfer was increased to 10 and 37% for the Spectrapore and Technicon membrane respectively, which was a remarkable improvement on the values possible with conventional dialysis. Sample interaction was 0.23% for the Spectrapore membrane and 0.32% for the Technicon membrane at sample frequencies of 26 and 23 samples per hour respectively. These sample interactions are neglible.

3.5. Samples

Real samples from industrial effluents were analysed with the proposed ED/FIA system. The results obtained for both membranes were compared with the results obtained from a standard titration method for the determination of chloride. The results, as shown in Table 2, revealed a good correlation between the ED/FIA system and the standard titration procedure.

4. Conclusion

The aim of the project was to investigate the viability of ED in the enhancement of mass transfer over passive neutral membranes in FIA systems. Chloride anions were selected to evaluate the electrodialyser/FIA system. The system proved to be very successful and it was possible to retain all the advantages of passive dialysis in flow systems, but at the same time, increase mass transfer through the membrane. The flexibility of the ED/FIA system is also shown by variation in the working range to fit a specific application, a commodity that was possible with alteration in the applied voltage and flow rates of the donor and acceptor streams.

Table 2
Comparison of the results of a number of samples as determined with the Spectrapore and Technicon membranes in the electrodialyser/flow injection system and a standard titration procedure

Sample	Spectrapore membrane	Technicon membrane	Standard titration procedure
1	1054	1060	1063
2	435	444	439
3	2004	2007[a]	1997

Chloride concentrations given as mg l^{-1}.
[a] Diluted to fall within the linear range.

References

[1] H.K. Lonsdale, J. Membr. Sci. 10 (1982) 81.
[2] M. Valcarcel, M.D. Luque de Castro, Non-chromatographic continuous separation techniques, Royal Society of Chemistry, London, 1991.
[3] J.F. van Staden, Fresenius J. Anal. Chem. 352 (1995) 271.
[4] L. Grimsrud, A.L. Babb, Chem. Eng. Progr. Symp. Ser. 19 (1966) 62–66.
[5] J.A. Cox, Z. Twardowski, Anal. Chim. Acta 119 (1980) 39.
[6] J.A. Cox, E. Dabek-Zlotorzynska, R. Saari, N. Tanaka, Analyst (London) 113 (1988) 1401.
[7] J.C. Cooper, J. Danzer, H.-L. Schmidt, Anal. Chim. Acta 282 (1993) 369.
[8] K.S. Spiegler, Principles of Desalination, Academic Press, London, 1966.
[9] J.J. Schoeman, Electrodialysis of salts, acids and bases by electro-osmotic pumping. PhD-thesis, University of Pretoria, 1992.
[10] D.L. Strong, P.K. Dasgupta, Anal. Chem. 61 (1989) 939.
[11] S. Rabin, J. Stillian, V. Barreto, K. Friedman, M. Toofan, J. Chromatogr. 640 (1993) 97.
[12] P.R. Haddad, S. Laksana, R.G. Simons, J. Chromatogr. 640 (1993) 135.
[13] P.R. Haddad, S. Laksana, J. Chromatogr. 671 (1994) 131.
[14] H. Strathmann, H. Chmiel, Chem.-Ing.-Tech. 56 (1984) 214.
[15] A.J.J. Debets, W.Th. Kok, K.-P. Hupe, U.A.Th. Brinkman, Chromatographia 30 (1990) 361.
[16] R. Kittsteiner-Eberle, I. Ogbomo, H.-L. Schmidt, Biosensors 4 (1989) 75.
[17] Z. Fang, Flow injection separation and preconcentration, VCH, Weinheim, 1993.
[18] J.F. van Staden, A. van Rensburg, Analyst 115 (1990) 1049.
[19] J.F. van Staden, Anal. Chim. Acta 261 (1992) 453.
[20] G.D. Marshall, J.F. van Staden, Anal. Instr. 20 (1992) 79.

.

ELSEVIER

Talanta 45 (1998) 493–505

Talanta

ByT-FAS (Bypass trapped-flow analysis system)

Kent K. Stewart *, Stephen W. Hillard

Department of Biochemistry, VPI&SU, Blacksburg, VA 24061-0308, USA

Received 27 February 1997; received in revised form 25 April 1997; accepted 29 April 1997

Abstract

A new semi-automated flow analysis system called bypass trapped flow analysis system (ByT-FAS), is described. ByT-FAS gives an analyst the ability to inject sample and reagent volumes of 50–100 μl or more, into flowing streams and attain physical steady state concentrations in the detection cell within a few seconds (< 1 min) after the insertion of the sample and/or reagent. After physical steady state is attained, the system flow is diverted around the detection cell and the reaction mixture is trapped in the detector. The concentration of the analyte and the reagent in the detection cell can be readily computed from knowledge of the original concentrations of the analyte sample and reagents and knowledge of the flow rates of the streams propelling the analyte and the reagents. ByT-FAS was demonstrated to be useful for direct measurements of analytes in liquid solutions and for assays which utilize equilibrium and/or kinetic chemistries to create measurable product(s) using ultraviolet/visible spectrophotometry. Enzyme activities and fundamental enzyme kinetic parameters (K_Ms, K_Is, k_{cat}s, etc.) were determined directly. The ByT-FAS instrumentation, as described, can be used interchangeably for either equilibrium or kinetic assays. It is believed that this new type of instrumentation will be of significant use for the analytical chemical, biochemical, molecular biology, biotechnology, environmental, pharmaceutical and medical communities. © 1998 Elsevier Science B.V.

Keywords: Detection cell; Physical steady state; Analyte

1. Introduction

In recent years the life sciences have made impressive advancements in their ability to determine the chemical structures of genetic determinants, modify those structures and/or the control the activity of those structures. Significant advancements have been made for the insertion of modified genetic material into living organisms to alter the metabolism and synthetic activity of the modified organisms. These advances have permeated and changed almost all aspects of the life sciences. Many of the genetic modifications are aimed at the modification of enzyme activities, either by changing the fundamental kinetic parameters (K_Ms, K_Is, k_{cat}s, etc.) of a given enzyme or, by changing the total amount of the enzyme produced by a living organism. Those in the life sciences need sensitive and specific analyt-

* Corresponding author. Present address: Department of Chemistry and Biochemistry, A5300, University of Texas, Austin, TX 78712. Fax: +1 512 4581078; e-mail: kkstewart@mail.utexas.edu

PII S0039-9140(97)00178-1

ical tools to measure these changes in the activities of given enzymes. Furthermore, most of the genetic modification studies generate large numbers of modified organisms and tools are needed that will permit through-puts of hundreds of samples per day.

Determination of the fundamental kinetic parameters (K_Ms, K_Is, k_{cat}s, etc.) of given enzymes requires that the concentrations of the enzymes, substrates, reagents and products be known with certainty[1]. Traditional manual methods, where reactants of known volumes and concentrations were added to a reaction vessel and the product formation (or reactant loss) was observed over time, have been used for the determination of the fundamental kinetic parameters. The traditional manual assays are tedious, time consuming and labor intensive. Typical reaction volumes are 3 ml and typical volumes of the assayed enzymes ranged from 50 to 250 μl. Measurement times are typically 1–15 min.

Traditional stopped-flow systems also permit knowledge of the concentrations of the enzymes, substrates and reagents in the reaction mixture. These traditional stopped-flow systems (used for the determination of the kinetic parameters of rapid reactions) utilize the rapid expulsion of syringes ($\sim$2 ml each) containing analyte and reagents into the detection chamber. The rapid reading systems for the stopped-flow systems was on the order of 0.03 s/point with the first point taken $\approx$0.03 s after mixing, (e.g. see review by Gibson [1]). Typical stopped-flow systems have the disadvantages that each assay required relatively large sample and reagent volumes ($\sim$2 ml each), sample through-put was relatively slow since the system had to be drained, syringes recharged between each assay and the equipment required for these assays was usually expensive.

Flow injection analysis (FIA) [2–5] and stopped-flow FIA [6,7] systems have the desired ease of use and through put for enzyme assays. However, traditional FIA systems do not attain physical steady state[2] in the detector under normal conditions of analysis and sometimes do not have the necessary assay sensitivity due to the limited reaction times ($<$60 s). The added reaction times resulting from stopped-flow FIA systems [6,7] can solve the problems of limited reaction time, however even the traditional stopped-flow FIA systems do not attain physical steady state in the detector under normal conditions of analysis. The problems of dispersion that result from laminar flow in flow injection systems are of such magnitude that we do not know of any published practical FIA system which permits measurement of small volumes ($<$500 μl) of undiluted sample. One of the premises of our studies was that a system design was needed in which some portion of the sample/reagent boluses did reach physical steady state and were not diluted by laminar dispersion (Fig. 1).

We report our studies on the development of a new semi-automated sample handling system called bypass-trapped-flow analysis system (ByT-FAS). This system uses small sample volumes (50–100 μl) and is designed to permit the acquisition of physical steady state in the detector. Thus the analyst can compute the concentrations of the analyte, reagents and products at the detection cell from knowledge of the original concentrations

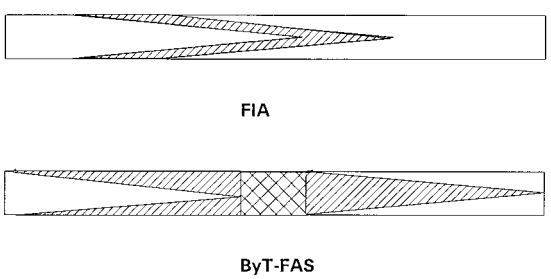

Fig. 1. Diagrammatic representations of concentration profiles in FIA and ByT-FAS. The slashed region [//] represents a region where the concentration profile is determined by laminar flow. In this region the reactant concentrations vary with time, molecular diffusion constants and radial distance from the edge of the tubing. In the cross hatched region, the reactant concentrations are independent of the time, molecular diffusion constants and radial distance from the edge of the tubing. In the cross hatched region, the reactant concentrations can be computed directly from the knowledge of the initial reactant concentrations and the flow rates of the different flow streams.

[1] Knowledge of only the ratios of their concentrations (as may be available from traditional FIA systems) is not adequate.

[2] At physical steady state the concentration of reactants and products are not affected by laminar dispersion and their concentrations prior to any chemical reaction are a function of their original concentrations and the flow rates of the various streams in the flowing system.

of the analyte sample and reagents and knowledge of the flow rates of the streams propelling the analyte and reagents. ByT-FAS can be used for those assays which utilize kinetic and/or equilibrium chemistries to create measurable product(s) in liquid solutions. Enzyme activities and fundamental enzyme kinetic parameters (K_Ms, K_Is, k_{cat}s, etc.) can be determined directly. It is believed that this new instrumentation may be of significant use for the analytical communities in the life sciences.

1.1. Background

The studies of Vanderslice et al. [8,9] indicate that in a straight tube and sample volumes $< 20\%$ of the system volume, the volume of a sample bolus is a function of the flow rate, the tube radius and length and an inverse function of chemical diffusion constant of the molecules of concern as shown in Eq. (1).

$$\text{Peak volume} = q^{0.36} * r^2 [L]^{0.64} / D^{0.036} \quad (1)$$

where q is the flow rate in ml min^{-1}, r is the radius in centimeters, L is the reaction coil length in centimeters and D is the chemical diffusion constant for the molecule of concern.

Thus, given our goal to minimize sample dilution at the detector, small radius and short length reaction tubing was needed. However, in the case of colorimetric reactions, the need for an adequate reaction time for colorimetric reactions would suggest lengthening the reaction coil or reducing the flow rate. The conventional wisdom has been to lengthen the reaction coil. Thus there was a conflict between the needs to minimize the system parameters to minimize the laminar dispersion and the need to lengthen the reaction coil so that there was sufficient time for the chemical reactions to occur. As will be seen, we eventually used a trapped flow system with essentially no reaction coil.

It seemed intuitive that the use of larger sample volumes would eventually lead to a steady state condition in the detector. Thus we asked "How much sample volume would need to be injected to attain steady state concentrations in the detector?" In a preliminary approximation using Eq. (1) and assuming the system volume equals $\pi r^2 L$, the ratio of the peak volume to system volume is approximately that shown in Eq. (2).

$$\text{Ratio} = 11.3[q/L]^{0.36} D^{-0.036} \quad (2)$$

Several preliminary calculations using Eq. (2) demonstrated that for reasonably small volume systems of straight tubes, flow rates of 10–0.1 ml min^{-1}, reaction coil lengths of 1–20 cm and diffusion coefficients common to most biochemical compounds, the peak volume was always larger than the system volume for flow injection systems. The ratios of peak volume to system volume varied with the system parameters and ranged from about 1.8 to 28. The results of these calculations clearly demonstrate the difficulties of attaining steady state in FIA systems. In our attempts to attain steady state at the detector with low volume samples (< 100 μl), we built systems with very small diameter fittings and tubing, short lengths of tubing and disrupted the laminar flow wherever possible by using knotted or braided tubing.

2. Experimental section

2.1. Reagents

Chemical reagents were purchased from Fisher Scientific or Sigma.

2.2. Colorimetric assays

Standard colorimetric protein assays (biuret [10], bromo-cresol green [11] and bicinchoninic acid [12]) were used. The reagents were prepared as described in the cited references. The assays used for alkaline phosphatase [13,14] measured the rate of hydrolysis of *p*-nirtrophenyl phosphate in 1 mM $MgSO_4$, 0.1 mM $ZnSO_4$, pH 10–50 mM glycine buffer by measuring the change in absorption at 400 nm.

2.3. ByT-FAS components

The pump used in the system was a double head, 10 μl stroke Sanuki (Tokyo, Japan) Series

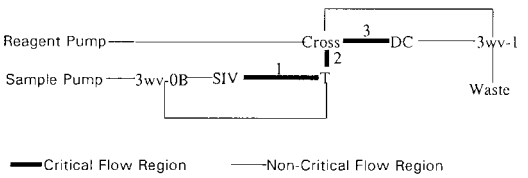

Fig. 2. Diagrammatic representation of a single sample insertion valve ByT-FAS. The tubing numbered 1, 2 and 3 had 0.5 mm i.d. The other tubing had 0.8 mm i.d. Abbreviations: 3WV, three-way valve; SIV, sample injection valve; DC, detector cell; T, a tee tubing connection; Cross, a cross tubing connector.

DMX Model DMX2300-T. For these experiments, each pump head was set to deliver a flow rate of 0.5 ml min^{-1}. The computer controlled 3-way valves (3WV) used in the system were from NResearch P/N 225T033 3 watt 115VDC. Standard six port chromatography sample injection valves (SIV) were used for both sample and reagent introduction (Rheodyne Model 7010). Braided thin wall Teflon tubing 100 or 200 μl sample loops were used. The tubing used between the points of sample and reagent injection and the detector cell was also braided. Larger Teflon tubing (0.8 mm i.d.) was used outside the critical flow system. An 8 μl Helma flow cell with a 1 cm path length was used with a Gilford Model 260 spectrophotometer with a thermostated cell compartment.

2.4. ByT-FAS design

Two ByT-FAS flow systems are shown schematically in Figs. 2 and 3. The single SIV ByT-FAS system (Fig. 2) consisted of carrier and reagent reservoirs, a two piston pump, two 3WV, one SIV, 0.25–0.5 mm i.d. tubing, small bore 'T's (0.5 mm i.d.), a small bore cross (0.5 mm i.d.), a low volume flow through cell, a spectrophotometric detector, a flow meter, miscellaneous low volume fittings and a waste container. The sample loops in the sample injection values were braided as was the short connecting tubing between the cross and the detector cell. The two SIVs ByT-FAS system (Fig. 3) had an additional injection valve for reagent injection and an additional 3WV for control of the bypass around the reagent SIV. The initial ByT-FAS systems used a double-head, alternating stroke HPLC pump with 10 μl delivered per stoke. One head delivered the carrier stream and the other the reagent stream. Thus the flow rates of each stream were approximately equal. Equal flow rates in a ByT-FAS system are equivalent to equal volumes in a manual assay system. ByT-FAS systems with equal carrier and reagent flow rates do not mimic most manual assays in which the volumes of the analyte and the reagents frequently differ by as much as tenfold. The use of differential flow rates is discussed by Hillard and Stewart [15,16]. The carrier stream solution used in each experiment was the same buffer as that used to prepare the sample and reagent solutions.

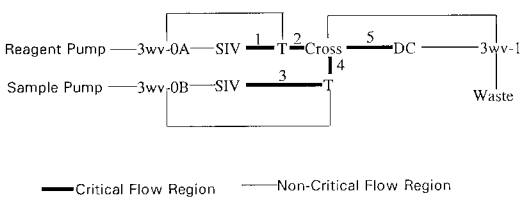

Fig. 3. Diagrammatic representation of a double sample insertion valve ByT-FAS. The tubing numbered 1, 2, 3, 4 and 5 had 0.5 mm i.d. The other tubing had 0.8 mm i.d. Abbreviations: 3WV, three-way valve; SIV, sample injection valve; DC, detector cell; T, a tee tubing connection; Cross, a cross tubing connector.

We define the section of the ByT-FAS system between the beginning of the sample loops on the sample and reagent injection valves through the 'Tees' and 'Crosses' and through the detector cell as the 'critical flow region'. For it is in this portion of the ByT-FAS system that any dispersion or dilution of the sample bolus will result in dilution and/or dispersion of the sample in the detector cell. For that reason, only low volume and small diameter components are used and tubing lengths are kept to a minimum.

Timing control is a crucial part of ByT-FAS operation. The time course of a ByT-FAS assay is described as having four major periods: load, inject, detection and flush. ByT-FAS systems are designed so that differing parts of the critical flow region are in the route of liquid flow at each of the four major time periods (Table 1 and Fig. 4).

Table 1
Time course of a ByT-FAS assay system

Time period	Operation	Critical flow component in or out of flow		
		SIV	SIV-sample loop	Detector
Load	Sample loading			
	Load sample loop	Bypass	Load	In stream
	Sample loop loaded	Bypass	Inject	In stream
	Reagent loading			
	Load reagent loop	Bypass	Load	In stream
	Reagent loop loaded	Bypass	Inject	In stream
Inject	Sample (reagent) injection	In stream	Inject	In stream
Detection	Acquire data	In stream	Inject	Bypass
Flush	Wash out system	In stream	Inject	In stream

At the beginning (Load) the ByT-FAS system flow goes around the SIV and through the detector cell. In this time period the sample and reagent are loaded into their respective SIV which are in their load positions. After the sample loops are loaded, the SIV are manually switched to the inject position. In the inject time period, the system flow is switched to go through the SIV by electronically switching the 3-way valves upstream (3WV-0s) of the SIVs. During this phase of a ByT-FAS run, the sample and reagent travel through the system, meet at the cross, mix and this mixture travels into and through the detector flow cell. If the sample size is large enough and the ByT-FAS system has a sufficiently small volume and the appropriate geometry, then the concentration of a portion of the mixture bolus will reach physical steady-state. When a physical steady-state is reached, the 3-way valve downstream (3WV-1) of the detector flow cell is fired to begin the detection time period. The sample-reagent mixture is trapped in the detector flow cell and the flow of the ByT-FAS system goes around the detector flow cell. After a sufficient number of data points have been taken, the 3WV-1 is fired again and the entire system is flushed out during the 'flush' time period. By the end of the flush time period the entire system, including the sample and reagent loops, has been flushed of all sample and is ready for another sample.

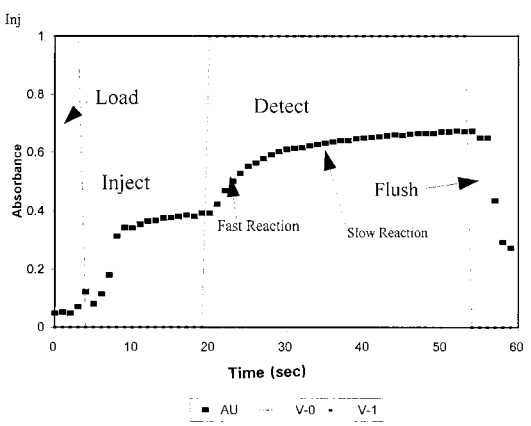

Fig. 4. The stages of ByT-FAS operation. See Table 1 and the text for details.

The needed length of each time period is dependent upon ByT-FAS system volume and geometry, the carrier stream flow rate, the reagent stream flow rate, the assay chemistry reaction rates, sample and reagent molecular weights and the amount of data smoothing needed for the assay. Thus different assays and different analytes may require different ByT-FAS time period durations.

2.5. Computerized system control and data acquisition

The ByT-FAS system's electronically controlled 3WV and the Gilford Model 260 spectrophotometric detector output were both interfaced to an IBM compatible XT computer. The spectrophotometer was interfaced via a Data Translation 2805

board and LabTech Notebook version 6.0 was used for data acquisition and system control. The 3WV firing were programmed using a binary ASCII file. The duration of each ByT-FAS time period was predetermined by the injection of model compounds for the assay. The data generated from a sample run was written by LabTech Notebook to an ASCII file which was then imported into a spreadsheet for analysis. Quattro Pro version 4.0 (Borland, St. Louis, MO) was used for data analysis.

2.6. Effect of reaction coil length

In the preliminary studies, the system described in Fig. 2 was constructed except braided reaction coils (0.5 mm i.d.) of various lengths were placed between the cross [4] and the sample flow cell [6]. The colorimetric determination of bovine serum albumin with biuret [10] was used as a model assay because the molecular weight of bovine serum albumin is about that of medium sized enzymes (~ 60 Kd) and the reagent components have relatively low molecular weights (< 0.5 Kd). Thus such a reaction system should model a typical enzyme-substrate reaction mixture.

2.7. Effect of analyte molecular weight

A system similar to that described in Fig. 2 was used. Two hundred microliter samples of solutions of DNP-glutamic acid, hemoglobin and blue dextran were separately injected into the system and their concentration was measured spectrophotometrically at 405 nm, 405 and 650 nm respectively. The system was operated in a FIA manner and the 3WV were not actuated.

2.8. No reaction—concentration measurements

Hemoglobin (Sigma) solutions between the range of 0.015 and 0.2 mg ml^{-1} were prepared in duplicate in 0.05 M NaCl. Each solution's absorbance at 405 nm was then measured using both the ByT-FAS system as shown in Fig. 2 and normal manual procedures. Standard curves for hemoglobin concentration were then generated from the ByT-FAS and manually produced data. The standard curves were compared for R^2, sensitivity and detection limits.

2.9. Colorimetric equilibrium measurements

The bromo-cresol green method for determining protein content in solution was used for the colorimetric equilibrium measurements. The manual method [17] dilutes the sample with bromo-cresol green reagent in a 1:2 ratio. Since the ByT-FAS system described here, mixes the sample with reagent in a 1:1 ratio, a modified bromo-cresol green reagent was prepared so that the ratio of sample concentrations to reagent concentrations at the point of detection would be the same for both methods. The manual method was then modified to use the same bromo-cresol green reagent by changing the mixing ratio of sample to reagent of 1:1 as well. Thus a direct comparison of the two methods is possible. Solutions of bovine serum albumin (Sigma) ranging from 0.05 to 2.0 mg ml^{-1} were prepared in duplicate in 0.05 M NaCl. The bromo-cresol green reagent was modified as follows; 133 mg bromo-cresol green (Sigma), 2.66 gm NaOH, 13.07 gm succinate, 2.0 gm Brij 35, to 1 l of distilled water, adjusted pH to 4.05. Each bovine serum albumin sample was assayed using ByT-FAS system shown in Fig. 2 and manually by adding an equal volume of bromo-cresol green reagent. The standard curves were compared for R^2, sensitivity and detection limits. The manual method was based upon a 30 min reaction time at 37°C and the ByT-FAS analyses data were obtained at the points where the reaction mixture had reached equilibrium. The ByT-FAS flow cell was thermostatted at 37°C.

2.10. Kinetic determination of protein content using the bicinchinoninic acid

The micro version of the bicinchinoninic acid (BCA) assay [12] for determining protein content in solution was used as a kinetic assay for bovine serum albumin at 1 mg ml^{-1} and at 0.1 mg ml^{-1} 0.05 M NaCl. The carrier solution was 0.05 m NaCl. The total system flow rate was 1 ml min^{-1}; 1/2 carrier, 1/2 reagent. The detection cell was thermostatted at 37°C. The slopes of the kinetic

assays were determined for that portion of the reaction curve where the rate of reaction was not changing with time (i.e. the $R^2 > 0.99$).

2.11. Determination of the kinetic attributes of alkaline phosphatase

A comparison of the ByT-FAS system to manual methods for determination of the kinetics of enzymes was investigated using the alkaline phosphatase enzyme assay. The reaction rate was measured spectrophotometrically at 400 nm by the production of phenolate ion from the hydrolysis of substrate *p*-nitrophenyl-phosphate (*p*-NPP). All solutions were prepared in 0.1% bovine serum albumin to block enzyme binding to either cuvettes or ByT-FAS system components. Enzyme velocity as a function of substrate concentration was measured using concentrations of *p*-NPP from 0.5 to 2.0 mM. The final concentration of alkaline phosphatase used in the reaction was 10 ugm ml^{-1}. Michaelis-Menten and Lineweaver-Burk plots were generated for comparison from the ByT-FAS system shown in Fig. 3 and the traditional manual methodology. The standard curves were compared for R^2, sensitivity and detection limits. The enzyme turnover numbers and Michaelis constants were computed from the Lineweaver-Burk plots of the ByT-FAS and manual data with Quattro-Pro.

3. Results

3.1. Preliminary studies

Preliminary studies of FIA systems were designed to examine the effect of reaction coil length on the peak maximum in a colorimetric assay of a medium molecular weight protein. Four reaction coil systems were examined; no reaction coil, a 1 m 0.5 mm i.d. reaction coil, a 1 m 0.8 mm i.d. reaction coil and a 4 m 0.8 mm i.d. reaction coil. The results are shown graphically in Fig. 5. As expected, the peak maximum of the product of the biuret assay of bovine serum albumin occurred at a later and later time as the reaction tubing volume was increased by either increasing

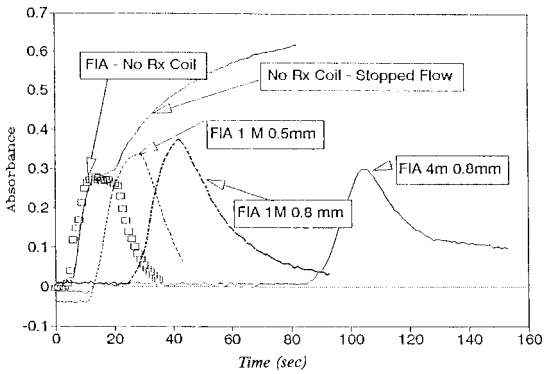

Fig. 5. Effect of reaction coil length and diameter on the signal from a biuret determination of bovine serum albumin. The dimensions given are the length and the diameter of the FIA reaction coil used in the assay.

the radius or by increasing the tubing length. However, the peak height did not always increase as the system volume was increased. It did increase with the addition of the 1 m 0.5 mm i.d. reaction coil and with the increased diameter of the 1 m reaction coil to 0.8 mm i.d. reaction coil but the peak height resulting from a 4 m 0.8 mm i.d. reaction coil was lower than that of the 1 m reaction coils. Clearly, the dilution effects of laminar dispersion were greater than any increases in absorbance resulting from the longer reaction time. The use of stopped-flow with no reaction coil yielded the highest absorbance of any of the reaction coil systems shown in Fig. 5.

Other preliminary studies of FIA system designs (data not shown) gave physical steady state concentrations of the injected analyte in the detector when 100 μl volumes were injected into carrier streams which were pumped at 0.5–2 ml min^{-1}. When physical steady state was achieved, the analyte concentrations at the detector cell were easily calculated from a knowledge of the system flow rates and the initial concentrations. However, the portion of the time the signal was at physical steady state was a small portion of the time that the analyte was in the detector. Larger sample volumes increased the time that the reaction mixture remained at steady state, but only if the sample loop was braided and had a sufficiently small diameter. Higher flow rates de-

creased the time to steady state but made it less likely steady state was ever achieved. While these FIA systems demonstrated the feasibility of attaining physical steady state concentrations using reasonable sample volumes, these traditional FIA systems did not seem practical for routine analyses. Several problems were anticipated, e.g. a significant amount of sensitivity would be lost for reactions which took more than 12 s to come to equilibrium. If there were only 2–3 s for signal acquisition, significant signal noise could be expected from both electronic and flow sources. Mixing appeared to be a problem and in some cases saw-toothed signals were obtained as the analyte moved through the detector. The results of these preliminary studies lead us to believe that it would be difficult to achieved our objectives of being able to make absolute measurements and increase assay sensitivity with a traditional FIA system. Instead we investigated the potential of a trapped flow–no reaction coil system. The final design of the system is shown in Fig. 2 for a ByT-FAS system for injection of the analyte and in Fig. 3 for the injection of the analyte and reagent. The time course for a typical ByT-FAS assay system is shown in Fig. 4. The time course for a fast equilibrium reaction is shown in Fig. 6

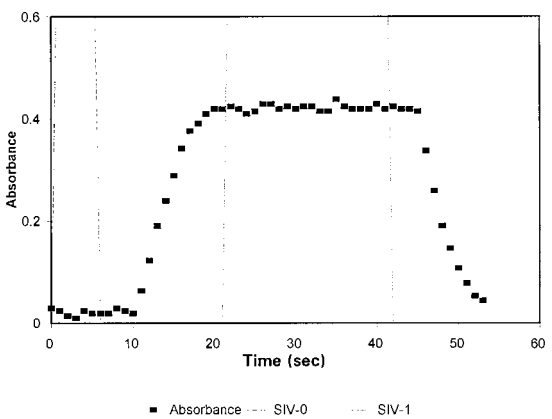

Fig. 6. A typical output of a ByT-FAS analysis of a reaction system that is in chemical equilibrium in the detector cell. Three-way valve 0 was activated to divert the flow around the sample injection valve from 0 to 6 s and the three-way valve 1 was activated to divert the flow around the detector from 21 to 42 s.

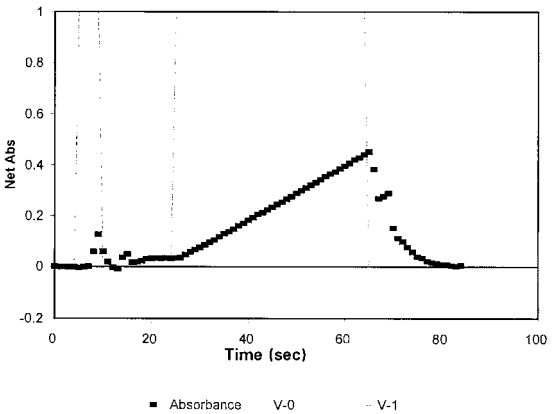

Fig. 7. A typical output of a ByT-FAS kinetic analysis. This is the output of a bromo-cresol green assay of 1.0 mg ml^{-1} of bovine serum albumin. See Fig. 9 for the comparable output of the same assay of a 0.1 mg ml^{-1} of bovine serum albumin. Three-way valve 0 was activated to divert the flow around the sample injection valve from 3 to 9 s and the three-way valve 1 was activated to divert the flow around the detector from 22 to 63 s.

and the time course for a kinetic assay is shown in Fig. 7.

3.2. Effect of analyte molecular weight

The outputs for the injection of 100 μl samples of solutions of DNP-glutamic acid, hemoglobin and blue dextran in a no-reaction coil FIA system are shown in Fig. 8. Note that the theoretical values of 50% of original concentration were

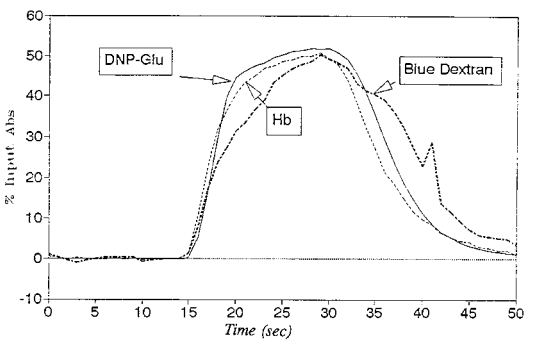

Fig. 8. Flow patterns by analyte molecular weight. The ByT-FAS system was used in a FIA operation mode. DNP-GLU is dinitropheny glutamic acid ($mw = 341$ Da), Hb is hemoglobin ($mw = 66$ kDa) and blue dextran ($mw = \sim 1000$ kDa).

Table 2
Comparison of manual and ByT-FAS assay results for direct measurements

	Direct hemoglobin assay	
	Manual	ByT-FAS
LOD (mg ml^{-1})	0.0056	0.0039
R^2	0.999335	0.999674
Linear range (mg ml^{-1})	0.0056–0.2	0.0039–0.2

achieved with the injection of the DNP-glutamic acid ($mw = 341$ Da) and hemoglobin ($mw = 66$ kDa) and perhaps with the blue dextran ($mw = \sim$ 1000 kDa). The data for the DNP-glutamic acid and hemoglobin clearly demonstrate that theoretical steady state conditions can be attained with a low-volume critical flow region and low–medium analyte molecular weights. Clearly the peak shape changes with analyte molecular weight and the higher the molecular weight the longer it takes for the output to come to steady state and the shorter the time it remains at steady state.

3.3. No reaction—concentration measurements

The data for the assay of the concentrations of hemoglobin at 405 nm are shown in Table 2. The manual and ByT-FAS methodologies clearly yield identical results in these assays.

3.4. Equilibrium colorimetric assays

The data for the assay of bovine serum albumin with bromo-cresol green are shown in Table 3. The manual and ByT-FAS methodologies clearly yield identical results in these assays.

Table 3
Comparison of manual and ByT-FAS assay results for reactions at chemical equilibrium

	BCG assay of BSA	
	Manual	ByT-FAS
LOD (mg ml^{-1})	0.015	0.012
R^2	0.999047	0.999373
Linear range (mg ml^{-1})	0.015–1	0.012–1

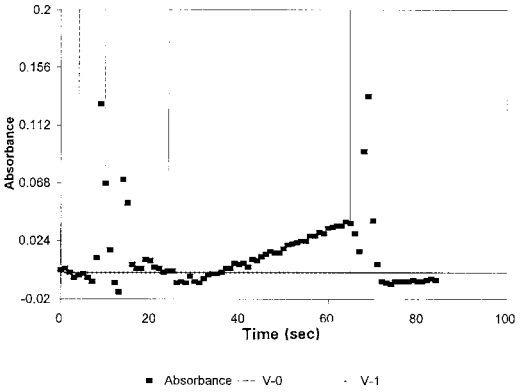

Fig. 9. The output of a ByT-FAS kinetic analysis of a bromo-cresol green assay of a 0.1 mg ml^{-1} of bovine serum albumin. Note the noise when the SIVs are fired. Three-way valve 0 was activated to divert the flow around the sample injection valve from 3 to 9 s and the three-way valve 1 was activated to divert the flow around the detector from 22 to 63 s.

3.5. Kinetic measurements

The time courses of the kinetic assays of 1 and 0.1 mg ml^{-1} bovine serum albumin samples as assayed by the BCA method are shown in Figs. 7 and 9, respectively. The data from these runs is given in Table 4. The data from replicate determinations on two separate days of the kinetic constants V_{max} and K_M of alkaline phosphatase by ByT-FAS and manual assay are shown in Table 5.

4. Discussion

The studies on the effect of analyte molecular weight clearly suggest that the DNP-glutamic acid

Table 4
Evaluation of kinetic BCA determination of bovine serum albumin

BSA concentration	1 mg ml^{-1}	0.1 mg ml^{-1}
R^2	0.9968	0.9982
Number of observations	40	34
Degrees of freedom	39	32
y-intercept	0	−0.0075
Slope (AU s^{-1})	0.111	0.0131
SD of slope (AU s^{-1})	0.00047	0.00024

Table 5
Evaluation of kinetic constants of alkaline phosphatase with *p*-NPP using ByT-FAS and manual techniques

	Day 1		Day 2	
	$K_m \pm$ s.d. (mM)	$V_{max} \pm$ s.d. (μmol min^{-1} mg^{-1})	$K_m \pm$ s.d. (mM)	$V_{max} \pm$ s.d. (μmol min^{-1} mg^{-1})
Manual	0.27 ± 0.051	17 ± 1.0	0.26 ± 0.060	16.0 ± 0.38
ByT-FAS	0.26 ± 0.005	17 ± 0.09	0.28 ± 0.020	16.6 ± 0.26

and hemoglobin solutions reached physical steady state conditions. The peak shape changes with analyte molecular weight and the higher the molecular weight the longer it takes for the output to come to steady state. These data demonstrate that the molecular size of the analyte can have significant effects on the output of an FIA assay system and that molecular sizes need to be taken into account when developing ByT-FAS systems. In every case, the time to physical steady state for individual ByT-FAS designs and reactants must be determined by calibration of individual ByT-FAS and reactants combinations by injecting components of molecular weights which were similar to those of the reactants so that the time to reach steady state could be accurately determined. The firing of 3WV-1 was then set so that it would occur after the reactant mixture had reached physical steady state in the detector cell.

A comparison of the data for the direct determination of hemoglobin concentrations clearly show that manual analysis and the ByT-FAS analysis give the same results. The ByT-FAS analysis required less sample. If a diode spectrophotometer was used as a detector for ByT-FAS, then the entire spectrum of a sample could be taken using less sample (~ 100 μl) than the 1 or 3 ml required for traditional spectrophotometric analysis. A comparison of the data for the direct determination of bovine serum albumin with bromo-cresol green shows that manual analyses and ByT-FAS analyses give the same results. The ByT-FAS analysis required less sample and less manual manipulation. The ByT-FAS kinetic analyses of 0.1 and 1 mg ml^{-1} bovine serum albumin gave the expected 10 fold difference in rates between the two samples. Although this analysis could be readily done by traditional stop flow analysis, it would be quite difficult to do in a manual mode given the speed of the reaction. Since the reaction was done in a stopped-flow mode, post reaction analysis of the data permitted the separation of the system noise from the product signal. The post analysis data analysis also permitted selecting the linear portion of the reaction curve for the determination of the reaction rate.

The results of the replicate determinations on two separate days of the kinetic constants (K_M, V_{MAX}) of alkaline phosphatase by ByT-FAS and manual assay, clearly show that the direct ByT-FAS determinations of these kinetic parameters were directly comparable to those determined in the traditional manual mode. The ByT-FAS analyses had smaller S.D., were easier to do and took less time per analysis. Others have used FIA systems for the determination of the kinetic constants of an enzyme, (see Hirano et al. [19]), by doing the enzyme reactions in a fixed volume container and then measuring the product formation at given times with flow injection analysis. However, we believe that this is the first demonstration of direct measurement of kinetic constants of an enzyme in an FIA type system.

4.1. Basic concepts of ByT-FAS design

These experiments have led to the development of the following concepts as being important in the design and operation of ByT-FAS.

4.1.1. Critical flow region

The critical portion of the ByT-FAS system are the components starting at the sample loops in the injection valves and ending at the exit of the

detector cell. This part of the ByT-FAS is defined as the critical flow region. It is essential that short lengths of small i.d. tubing (0.5 mm or less), low volume connectors and fittings, small i.d. low volume 'T's and 'Crosses' and small i.d.-low volume sample insertion valves be used in this region. Additionally we found it important to use braided small i.d. tubing as the sample loops in the sample and reagent insertion valves and to use a braided small i.d. tubing as a mixer past the cross and prior to the detector cell. In essence, the reaction coil was eliminated and the reaction took place in the detector cell. Eliminating the reaction coil did reduce the back pressure of the system however because of the small bore tubing used in our ByT-FAS, the back pressure was still about 30 PSI. The use of small critical flow regions permitted the attainment of steady state with sample volumes of 50–100 μl with analytes of molecular weights up to about 60 000. The time to physical steady state varied with the construction of the system, the flow rates of the pumps and the molecular weight of the analyte. Under these conditions the concentration of the analyte in the flow cell could be computed from knowledge of the concentration of inserted analyte sample and the flow rates of each stream as shown in Eq. (3)

$$CS_{det} = C^{*}_{org} CS\ Flow/[(CS\ Flow) + (RS\ Flow)] \quad (3)$$

Where CS_{det} is the steady state concentration of the analyte at the detector, C_{org} is the original concentration of the analyte as placed in the sample loop of the SIV; CS Flow is the flow rate of the carrier stream and RS Flow is the flow rate of the reagent stream.

Since steady state concentrations of the analyte were achieved for only a few seconds, we used a stopped-flow system to give the opportunity for longer reaction times and for better signal acquisition and averaging.

4.1.2. Trapped flow at the detector

Trapped-flow operations were designed for two parts of the system: the sample and/or reagent injection valve(s) and the detector cell. The flow-controlling valves were placed outside the critical flow region. This idea of placing the flow controlling valves outside the critical flow region has been previously reported for multiple column gas chromatography by Deans [18]. The placement of the 3WVs outside the critical flow region permitted use of standard 3WVs since the volume of these valves did not play a role in the dispersion within the critical flow region. Furthermore, with the use of diverted flow we were able to maintain a quite constant flow rate from the pumps. In our hands, when stopped-flow was achieved by turning the pumps on and off, the flow rates were erratic for an initial period after the pumps were turned on. This problem was averted when we diverted the liquid flow.

4.1.3. Computerized data acquisition and system control

The use of computerized data acquisition and system control gave precision to flow handling and data acquisition not normally found with manual operations. Significant advantages in precision of time of injection, time to steady state, signal measurements and the generalized ease of data handling were gained by the use of computerized data acquisition and system control. The general advantages of computerized valve control and automated data acquisition included the precise ability to trap the plateau region of the injected bolus in a reproducible manner in the detection flow cell, leading to better control of reaction conditions and the post run ability to screen out injection and pump noise. Since the reaction mixture was trapped in the detector cell, it could be brought to a fixed temperature using a thermostatted flow cell. The acquisition of results could be delayed until the reaction reached the desired temperature or alternately the data could be edited post run to permit the analysis of only those data which were taken at constant temperature. Among other things, such a thermostatted system reduced the optical noise created by the refractive index differences caused by solvent streams of different temperatures.

4.1.4. Single system

The ByT-FAS systems as shown in Figs. 1 and 2 could be used interchangeably for either equi-

librium or kinetic assays. The physical components of the system did not need changing, only the post analysis data manipulation was changed to fit the type of analysis, kinetic or equilibrium.

4.2. Analyte and reagent injection

It is frequently the case that high reagent costs preclude the feasibility of continuously pumping the reagent in the reagent stream. The ByT-FAS system shown in Fig. 3 was designed to permit the injection of both the analyte and the reagent thus, significantly reducing the required volume and cost of the reagent. Several experiments (data not shown) indicate that such a double injection system was quite feasible as long as the plumbing of the system was adjusted so that both the analyte and reagent reached physical steady state at the same time in the detector. Such adjustments were empirical and the final layout depended upon the characteristics of the solutes and analytes as well as the plumbing of the ByT-FAS system. This type ByT-FAS instrumentation is explored further in the accompanying papers by Hillard and Stewart.

4.3. Pumps and detectors

The initial successful ByT-FAS systems used a double-head, alternating stroke HPLC pump with 10 μl delivered per stoke. One head delivered the carrier stream and the other the reagent stream. ByT-FAS systems with equal carrier and reagent flow rates do not mimic most manual assays in which the volumes of the analyte and the reagents frequently differ by as much as tenfold. The use of ByT-FAS with variable independent flows is also discussed in the accompanying papers by Hillard and Stewart. We believe that the ByT-FAS system could use any HPLC, FIA, or other continuous flow detector as long as the mixing volume of the detector cell was quite small. The use of fluorescent and chemi-luminescent detection systems for ByT-FAS is discussed in the accompanying papers by Hillard and Stewart.

5. Summary

We believe that the results presented above clearly demonstrate that ByT-FAS gives an analyst the ability to inject sample and reagent volumes of 50–100 μl (or more) into flowing streams and attain physical steady state concentrations in the detection cell within a few seconds (<1 min) after the insertion of the sample and/or reagent. The concentration of the analyte and the reagent at the detection cell can be readily computed from knowledge of the original concentrations of the analyte sample and reagents and the flow rates of the streams propelling the analyte and the reagents. Using the bypass trapped concept to achieve a stopped-flow situation, ByT-FAS was demonstrated to be useful for direct measurements of analytes in liquid solutions and for assays which utilize kinetic and/or equilibrium chemistries to create measurable product(s) using ultraviolet/visible spectrophotometry. Enzyme activities and fundamental enzyme kinetic parameters (M_Is, k_{cat}s, K_Is, etc.) were determined directly. It is believed that this new instrumentation will be of significant use for the analytical chemical, biochemical, molecular biology, biotechnology, environmental, pharmaceutical and medical communities.

Acknowledgements

We gratefully acknowledge the donation of a pump from the Sanuki Instrument Company (Tokyo, Japan)

References

[1] Q.H. Gibson, in: K. Kustin (Ed.), S.P. Colowick, N.O. Kaplan (Series Eds.), Methods in Enzymology, vol. 16, 1969, pp. 187–228.
[2] J. Růžička, E. Hansen, Flow Injection Analysis, Wiley, New York, 1981.
[3] K.K. Stewart, Anal. Chem. 55 (1983) 931A.
[4] M. Valcarcel, M.D. Luque de Castro, Flow Injection Analysis— Principles and Applications, Wiley, New York, 1987.

[5] J.L. Burguera (Ed.), Flow Injection Atomic Spectroscopy, Marcel Dekker, New York, 1989.
[6] J. Růžička, Anal. Chim. Acta 261 (1992) 3.
[7] G.D. Christian, J. Růžička, Anal. Chim. Acta 261 (1992) 11.
[8] J.T. Vanderslice, K.K. Stewart, A.G. Rosenfeld, D.J. Higgs, Talanta 28 (1981) 11.
[9] J.T. Vanderslice, A.G. Rosenfeld, G.R. Beecher, Anal. Chim. Acta 179 (1986) 119.
[10] C.R. Shideler, K.K. Stewart, J. Crump, M.R. Wills, J. Savory, B.W. Renoe, Clin. Chem. 26 (1980) 1454.
[11] B.W. Renoe, K.K. Stewart, G.R. Beecher, M.R. Wills, J. Savory, Clin. Chem. 26 (1980) 331.
[12] P.K. Smith, R.I. Krohn, G.T. Hermanson, A.K. Mallia, F.H. Gartner, M.D. Provenzano, E.K. Fujimoto, N.M. Goeke, B.J. Olson, D.C. Klenk, Anal. Biochem. 150 (1985) 76.
[13] O.H Lowry, in: P.D. Boyer (Ed.), The Enzymes, vol. 4, Academic Press, New York, 1957, pp. 371–372.
[14] E. Harlow, D. Lane, Antibodies—A Laboratory Manual, Cold Spring Harbor Laboratory, 680, 1988.
[15] S.W. Hillard, K.K. Stewart, Talanta, this issue.
[16] S.W. Hillard, K.K. Stewart, Talanta, this issue.
[17] F.L. Rodkey, Clin. Chem. 11 (1965) 488.
[18] D.R. Deans, J. Chromatogr. 203 (1981) 19–28.
[19] H. Hirano, Y. Baba, N. Yoza, S. Ohashi, Anal. Chim. Acta 179 (1986) 209.

.

ELSEVIER

Talanta 45 (1998) 507–512

Talanta

A bypass trapped-flow analysis system evaluation of enzyme kinetic parameters with a coupled enzyme assay and fluorescence detection

Stephen W. Hillard *, Kent K. Stewart

Department of Biochemistry and Anaerobic Microbiology, Virginia Polytechnic Institute and State University, 304 Engel Hall, Blacksburg, VA 24060, USA

Received 4 March 1997; received in revised form 5 May 1997; accepted 5 May 1997

Abstract

The newly developed flow instrument, bypass trapped-flow analysis system (ByT-FAS), was used to perform enzyme assays and generate data for evaluation of an enzyme's kinetic parameters. The enzyme assay was yeast hexokinase coupled to glucose-6-phosphate dehydrogenase and the production of reduced NADPH was monitored fluorometrically. The kinetic parameters of hexokinase that were evaluated with the system were the apparent K_m's of the substrates glucose and ATP, and the K_i of the competitive inhibitor for ATP, ADP. The ByT-FAS generated data were comparable to other manually derived published values of the kinetic constants for hexokinase and validates the utility of the ByT-FAS system for making absolute enzyme measurements. The semi-automated ByT-FAS system can perform analyses more rapidly than manual assay techniques with less manual manipulation and smaller sample and/or reagent volumes. © 1998 Elsevier Science B.V.

Keywords: Instrumentation; Enzyme kinetics; FIA; ByT-FAS

Many important, and routinely performed biochemical assays still require the use of manual methods that are labor intensive and time consuming, not to mention expensive. Some attempts have been made at automating these assays [1–4], but to date no system has generally adopted by the biochemical community. We believe that if a satisfactory system were developed, then many biochemical assays would be run in an automated or semi-automated mode. Flow injection analysis (FIA) would seem to be an appropriate technique however it has not been generally accepted by the biochemical community. We believe that this lack of acceptance is due to the lower sensitivity of FIA systems caused by the short reaction times and the inherent laminar dilution of the analyte and the lack of knowledge about exact concentrations of the enzyme, reagents and products at the point of detection in FIA.

Bypass trapped-flow analysis system (ByT-FAS) is a newly developed and recently described [5] flow system which we believe holds potential

* Corresponding author.

PII S0039-9140(97)00180-X

for application and automation of biochemical assays that absolutely required manual techniques in the past. A properly designed ByT-FAS gives an analyst the ability to use analyte sample volumes of 50–200 μl and reagent volumes of approximately the same size and inject these into flowing streams and attain physical steady state concentrations in the detection cell within a few seconds (less than a minute) after the insertion of the sample and/or reagent. After physical steady state is attained, the system flow is diverted around the detection cell and the reaction mixture is trapped in the detection cell. The concentration of the analyte and the reagent in the detection cell can be readily computed from knowledge of the original concentrations of the analyte sample and reagent The amount of time of entrapment for a analyte and its reagent is predetermined and is a complex function of the system geometry, component molecular diffusion coefficients, and flow characteristics as well as the desired assay sensitivity and/or sample throughput. The duration of trapping sample is completely dependent upon the assay goal and the chemistry being monitored but can range from seconds to hours to days.

The objective of this paper is to demonstrate the use of a ByT-FAS system for the determination of fundamental enzyme kinetic parameters using a coupled enzyme assay and a fluorometric detection system. To obtain meaningful enzyme kinetic data from a coupled enzyme assay, the reaction conditions must be manipulated to pseudo-first order with respect to the enzyme and substrates under investigation. Higher order reaction kinetics would not produce useful enzyme kinetic data, and therefore were not investigated with ByT-FAS in this paper.

The coupled enzyme assay used hexokinase and glucose-6-phosphate dehydrogenase with the velocity of the reaction monitored by the change in fluorescence of the reduced analyte NADPH. The velocity of the reaction as function of the concentrations of hexokinase, glucose, ATP, and ATP in the presence of ADP was evaluated using the ByT-FAS flow system. The data were then utilized to obtain the kinetic parameters of hexokinase as a function of glucose, ATP, and ADP with hexokinase concentrations. These data were then compared to literature values obtained by manual assays of the enzyme.

1. Materials and methods

1.1. Instrumentation

The concepts of the ByT-FAS instrumentation are presented in the accompanying manuscript [5] in this edition of *Talanta*. All determinations of hexokinase velocity using the coupled enzyme reaction were performed with the ByT-FAS flow system as shown in Fig. 1. Enzyme and substrates were loaded into the reagent and sample injection valves (SIVs) respectively (Rheodyne, Cotati, CA). Two hundred microliters of each were injected into the system per run for analysis. The flow rate of the system was determined at the point of waste collection to be 1 ml min^{-1}. The contribution of each pump head to the total flow rate was calibrated using the slopes of an analyte's standard curve injected in both SIVs compared with each SIV independently. It was determined that the reagent (enzyme) pump head is responsible for 52.8% of the total flow while the sample (substrate) pump head accounted for the remaining 47.2%. Exact knowledge of the contri-

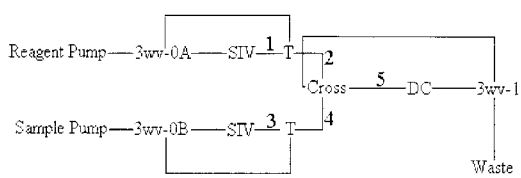

Fig. 1. Schematic diagram of a ByT-FAS flow system. Approximately equal flow rates are used for both the sample (47.2% of total flow) and reagent (52.8% of total flow) carrier flow streams. Total system flow rate is 1 ml min^{-1}. Critical flow area comprised of tubing sections 1, 2, 3, 4, (0.25 mm i.d. by 5 cm) and 5 (0.25 mm i.d. by 12 cm, braided mixing coil), T's (0.5 mm i.d.), Cross (0.5 mm i.d.), and Detector Cell (DC, 0.45 mm i.d. by 2 cm). Injected sample loop volume 150 μl. Injected reagent loop volume 200 μl. 3WV-0A, three way valve for reagent injection valve; 3WV-0B, three way valve for sample injection valve; SIV, standard six port injection valve; T, three way intersection (0.5 mm i.d.); Cross, four way intersection (0.5 mm i.d.); DC, detector flow cell; 3WV-1, three way valve controlling bypass flow.

bution of each pump head to the total flow rate is critical in determining the absolute concentrations of enzyme and substrate at the point of detection and evaluating kinetic data. The ByT-FAS system was coupled directly to an HPLC fluorometric detection system (McPherson model FL-748, Acton, MA) without any reconfiguration of the flow patterns used in ByT-FAS. The fluorometer flow cell was 5 μl in volume and contained the largest i.d. of any part of the system at approximately 0.8 mm.

1.2. Sample insertion and system control

Samples were manually loaded into the sample loops of the SIVs by aspiration before the start of each run. After initiation of each run, the samples were inserted into the system by manual movement of the SIV from loading to injection mode. System flow and timing was controlled by an IBM compatible 386sx16 computer with the program LabTech Notebook version 6.0. (Laboratory Technologies, Wilmington, MA). Flow patterns through the system were directed by the firing of three, three-way valves (3-WVs)(NResearch, Maplewood, NJ) at different times during the course of a sample run (see Fig. 1.). Data acquisition during a run was mediated by LabTech notebook employing a Data Translation 2805 card interfaced to the detector. Each sample run's data was stored in its own *.prn file and directly imported into a Quattro pro spreadsheet for analysis. See the accompanying manuscript for more details of the ByT-FAS instrumentation.

1.3. Reagents

Unless otherwise stated, all reagents were purchased from Sigma (St. Louis, MO). Glucose was purchased from Fisher (Fairlawn, NJ). All enzyme and substrate solutions were prepared and assayed in 50 mM MOPS (3-[*N*-Morpholino]propanesulfonic acid) buffer and 1 mM $MgCl_2$ at pH 7.4. The source of hexokinase and glucose-6-phosphate dehydrogenase (G6PDH) used in all assays was yeast (Catalog # s, H-4502, and G-8878 respectively). $NADP^+$, ATP, and ADP were also used as substrates or inhibitors in the assays of hexokinase with ByT- FAS instrumentation (Catalog # s, N-3886, A-9187, and A-2754 respectively). Because the ByT-FAS system employs small i.d. tubing, all sample and reagent solutions were filtered at 0.8 μm before use.

The assay of hexokinase concentration on reaction velocity was performed on a range of hexokinase concentrations of 0.5–5.0 units ml^{-1} injected. The concentrations of G6PDH and all substrates in the reaction were fixed at 5 units ml^{-1} and 5 mM respectively. For this assay all reaction components except hexokinase were mixed together and injected as the reagent. Hexokinase was injected alone as the sample.

The velocity of hexokinase as a function of glucose concentration was performed over a range of glucose from 25 μM to 2.5 mM injected. Hexokinase and G6PDH were fixed at 1 and 3.5 units ml^{-1} injected respectively. The injected concentrations of $NADP^+$ and ATP were both 7.5 mM. The reagent for this assay was the mixture of both enzymes and $NADP^+$ and ATP while the sample (glucose) was injected alone.

The velocity of hexokinase as a function of ATP concentration was performed over a range of ATP from 0.16 to 1.2 mM injected. Hexokinase and G6PDH were fixed at 1 and 3.5 units ml^{-1} injected respectively. The injected concentrations of $NADP^+$ and glucose were both 5 mM. The reagent for this assay was the mixture of both enzymes and $NADP^+$ and glucose while the sample (ATP) was injected alone.

The assay of hexokinase velocity as function of ATP concentration in the presence of the competitive inhibitor ADP was performed on a range of ATP from 0.3 to 1.5 mM injected in the presence of ADP at 0, 1, 2, and 3 mM injected. The reagent for this experiment was comprised of both enzymes and the substrates $NADP^+$ and glucose. The concentrations of the reagent species were 1 and 3.5 units ml^{-1} of hexokinase and G6PDH respectively with 5 mM $NADP^+$ and glucose. The ATP was prepared in its concentration range with the presence of the different amounts of ADP. The ATP/ADP mixture was then injected as the sample. The determination of the kinetic parameters was done with commercial computer programs based upon the work of Cleland. [6]

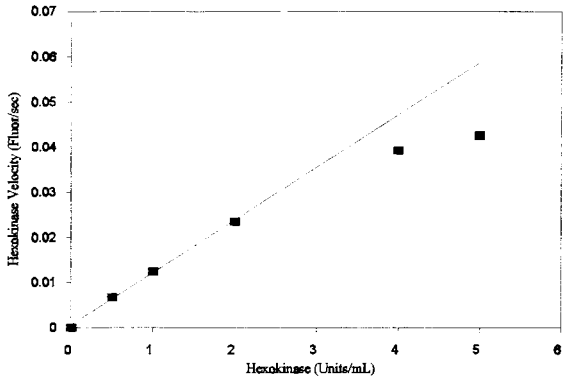

Fig. 2. Hexokinase velocity as a function of hexokinase concentration. Elucidation of the ratio of hexokinase to coupling enzyme (glucose-6-phosphate dehydrogenase) to achieve a pseudo-first order reaction rate with respect to hexokinase. Glucose-6-phosphate dehydrogenase concentration held constant at 5 units ml^{-1}. To determine the hexokinase velocity under pseudo-first order conditions, the coupling enzyme to hexokinase concentration ratio must be at least 2.5/1.

The velocity of each enzyme reaction was monitored fluorometrically by the production of NADPH. Because Michaelis–Menten kinetics requires initial enzyme velocity measurements, the rate of NADPH degradation in the detector cell under initial velocity conditions is not a factor in these experiments.

2. Results

In order to make the reaction catalyzed by hexokinase the rate limiting step in the coupled enzyme system, which is necessary for obtaining meaningful enzyme kinetic parameter data, and insure that the reaction was working properly, the velocity of the reaction as a function of hexokinase concentration with fixed amounts of substrate and G6PDH was determined. A plot of the data from this experiment is shown in Fig. 2. From this graph it was determined that the ratio of G6PDH to hexokinase in units ml^{-1} injected necessary to obtain a pseudo-first order response with respect to hexokinase concentration was 2.5/1. From this data, and as added insurance that the rate of NADPH production is dependent solely upon the amount of hexokinase in the assay, all future assays of enzyme velocity with the various substrates were conducted at a ratio of 5/1. It is economically feasible to do this because of the small sample and reagent volume requirements necessary to run an assay on ByT-FAS.

2.1. Kinetic constants

Using the ByT-FAS flow system, initial velocities for the hexokinase analyses at different concentrations of its substrates, glucose and ATP were determined. Shown in Fig. 3 are ByT-FAS raw data traces for the assay of hexokinase velocity at different levels of glucose present in the detector cell. All glucose concentration runs are plotted on the same graph for comparison. Lineweaver–Burk plots of $1/v$ versus 1/glucose μM^{-1} and 1/ATP μM^{-1} are shown in Figs. 4 and 5 respectively. The inhibition of initial velocities for the hexokinase analyses were determined at differing concentrations of ADP (a competitive inhibitor of hexokinase). Fig. 5 shows the

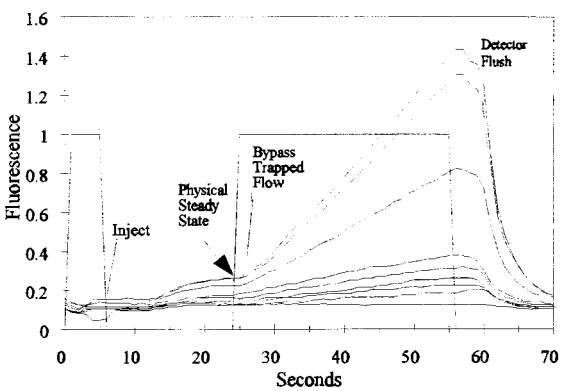

Fig. 3. ByT-FAS raw data traces of hexokinase velocity with increasing glucose concentrations. Sample and reagent are both injected simultaneously under no flow conditions at 6 s. At 24 s, physical steady state bolus profile is trapped in the detector cell. The system flow is sent on a bypass around the trapped flow in the detector cell (see Figure 1). The enzyme kinetic reaction is monitored fluorometrically until 56 s. The reaction mixture is flushed. Enzyme velocity is calculated by regression analysis of the data between 35 and 50 s. The enzyme velocities are plotted versus glucose concentration at the point of detection. Increasing line slope corresponds to larger glucose concentration.

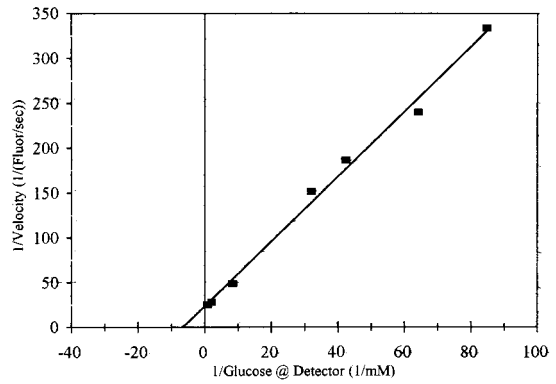

Fig. 4. Lineweaver–Burk plot of hexokinase velocity as a function of glucose concentration. K_m of glucose with hexokinase calculated as the negative reciprocal of the x-intercept ($-1/K_m$).

Lineweaver–Burk plot of these data. These plots depict a classical competitive inhibition pattern of ADP in the presence ATP.

All of the hexokinase kinetic parameters calculated from the data generated by the ByT-FAS instrumentation were comparable to known literature values. The ByT-FAS determined apparent K_m's of glucose and ATP are 0.138 ± 0.002 mM and 0.269 ± 0.02 mM respectively. These apparent K_m values agree well with cited literature values of 0.1 and 0.17 mM for glucose and 0.2 mM for ATP [7,8]. The apparent K_i for ADP as a competitive inhibitor for ATP using the ByT-FAS data was calculated to be 1.2 mM $\pm 7.4\%$ while a literature value for the constant is 1.14 mM [8].

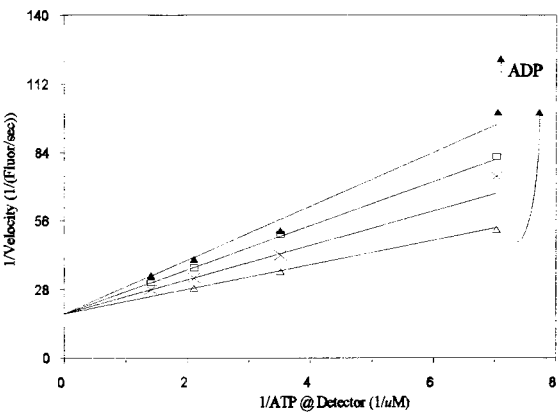

Fig. 5. Lineweaver–Burk plot of ADP inhibition of ATP with hexokinase. Determinations of the K_m for ATP with hexokinase and the K_i for ADP on ATP. Δ-0 mM ADP, × -0.47 mM ADP, □-0.95 mM ADP, ▲-1.42 mM ADP. $NADP^+$ at 5 mM in all assays.

3. Discussion

Our objective in performing these experiments was to demonstrate that the ByT-FAS flow system could perform coupled enzyme reactions with multiple substrates and generate the same kinetic constants as the classical manual assays. The results of these experiments serves to validate that ByT-FAS does what it was designed to do, produce accurate results with less labor intensive methods of manipulating samples and acquiring data on biological solutions. We believe that the ByT-FAS instrumentation can be used for almost any kind of enzyme measurement that may be necessary and that the resulting data will be directly comparable to those acquired by the classical slower manual assays. ByT-FAS's design has other advantages. Its small critical flow volume makes sample and reagent consumption for each analysis reasonably small (currently as low as 50 μl injected). Not only does this make all assays performed on ByT-FAS less expensive, but experiments with valuable samples that would otherwise be prohibitive to perform, may be feasible with the system. Since ByT-FAS is semi-automated, there is less manual manipulation of samples per assay than other techniques. As a result, it is more time efficient. A typical ByT-FAS enzyme sample run, such as those the ones used to produce the data reported in this paper, took approximately 1 min per assay. For research that requires the screening of hundreds or thousands of samples, ByT-FAS potentially has the capability to provide the biochemical and molecular biological researcher with a power tool with high sample throughput.

We believe that this is the first report of the direct determination of fundamental enzyme kinetic parameters for coupled enzyme assays us-

ing flow injection type instrumentation at physical steady state at the point of detection. The use of short, small diameter connecting tubing, braided samples loops and connecting tubing, and small volume fluorescence flow through detector was crucial to the success of the ByT-FAS for these analyses.

We trust that the biochemical community will find that ByT-FAS is a useful new tool for virtually any wet chemistry methodology or detection system.

.

References

[1] K.K. Stewart, G.R. Beecher, P.E. Hare, Fed. Proc. Fed. Am. Soc. Biochem. 33 (1974) 1429.
[2] J. Růžička, E.H. Hansen, Anal. Chim. Acta 78 (1975) 145.
[3] L.T. Skeggs, Am. J. Clin. Pathol. 13 (1957) 451.
[4] N.G. Anderson, Science 166 (1969) 317.
[5] K.K. Stewart, S.W. Hillard, Talanta (1997) this issue.
[6] W.W. Cleland, Biochim. Biophys. Acta 67 (1963) 104.
[7] H.J. Fromm, V. Zewe, J. Biol. Chem. 237 (1962) 3027.
[8] T.E. Barman, Enzyme Handbook, Springer, New York, 1969, p. 377.

ELSEVIER

Talanta 45 (1998) 513–518

Talanta

Bypass trapped flow analysis system (ByT-FAS) used in application: quantitative chemiluminescent detection of whole intact *E. coli* cell genetic transcription levels via induction of luciferase with tetracycline

Stephen W. Hillard *, Kent K. Stewart [1]

Department of Biochemistry and Anaerobic Microbiology, Virginia Polytechnic Institute and State University, 304 Engel Hall, Blacksburg, Virginia 24 060, USA

Received 4 March 1997; received in revised form 5 May 1997; accepted 5 May 1997

Abstract

Bypass trapped flow analysis system (ByT-FAS) is a new trapped flow apparatus designed to perform chemical measurements with flow injection systems at physical steady state using small volumes (10–150 μl) of injected sample and reagent. We have used a micro-volume version of ByT-FAS instrumentation with a chemiluminescent detection system to quantitate the protein transcription levels of transformed whole intact *E. coli* cells. The cells were transformed using a firefly luciferase encoding plasmid with a tetracycline inducible promoter. Luciferase synthesis was induced in *E. coli* cells containing multiple copies of this plasmid by different levels of tetracycline in the growth media. The level of induction was determined by measuring the velocity of luciferase enzyme per absorbance unit of the injected culture. The micro-volume ByT-FAS instrumentation permitted the rapid determination of the level of induced luciferase and was significantly faster than the traditional quantitative determination of genetic transcription levels. The micro-volume ByT-FAS assays also used significantly lower amounts of the expensive substrate luciferin. This is the first reported use of ByT-FAS for the detection and analyses of transformed cells. ByT-FAS with chemiluminescent detection has the potential of being a useful tool for the rapid analyses of promoter DNA sequences, promoters, and transcription repressors in whole intact bacterial cells by molecular biologists and biochemists. © 1998 Published by Elsevier Science B.V.

Keywords: Flow injection cytometry; Chemiluminescent whole *E. Coli* transcription assay

1. Introduction

Biochemists, molecular biologists, and biotechnologists frequently study changes in promoter sequences, transcription inducers and repressors, and growth media additives for their impact on

* Corresponding author.

[1] Present address. Department of Chemistry and Biochemistry, Mail code A5300, University of Texas at Austin, Austin, Texas 78 712. E-mail: kkstewert@mail..utexas.edu

PII S0039-9140(97)00181-1

the level of transcription of a certain gene. The laboratory standard quantitative procedure for elucidating the level of gene transcription in a cell is the method by Miller. [1] The general procedure for this assay relies on the amount of ß-galactosidase serving as the reporter enzyme that has been produced from a certain induced gene transcription. A basic version of the procedure is described:

1. Prepare overnight cultures with different assay variable grown at 37°C.
2. Dilute cells 1/100 into same media that they were grown in.
3. Grow diluted cells about 2 h at room temperature until A_{600} is 0.7.
4. Set cells on ice.
5. Spin down 1.5 ml of each culture and resuspend in 1 ml of assay buffer and place back on ice.
6. Dilute cells 1/6 into assay buffer and take absorbance of cells at A_{578}.Assay for ß-galactosidase
7. Place X μl of cells in assay buffer, plus 20 μl of 0.10% SDS, plus 10 μl of 2N NaOH, plus assay buffer to 800 μl total volume.
8. Incubate at 28–30°C for 10 min for cell lysis.
9. Add 160 μl of 4 mg ml^{-1} ONPG (*o*-nitrophenyl galactoside) at time = 0.
10. Add 400 μl of 1 M Na_2CO_3 after about 10–15 min and yellow color has developed. Time is stopped.
11. Spin down assay mixture to remove cell debris for 2 min.
12. Read absorbance at 420 nm.

Using this method, approximately 30–50 overnight cultures can be assayed in one full day.

Recently, a plasmid containing the firefly luciferase gene has been constructed and inserted into *E. coli*. This recombinant *E. coli* strain was obtained as a gift from the laboratory of Dr Timothy J. Larson (Virginia Tech, Biochemistry). This strain of *E. coli* contains a plasmid with kanamycin resistance and a gene for firefly luciferase under the transcription control of tetracycline. It has an origin of replication site that allows approximately 80–100 copies of the plasmid per cell. We decided to use this plasmid to evaluate the ability of our micro-ByT-FAS instrumentation to detect transformed whole cells and develop a simple assay for these transformed whole cells by injection into ByT-FAS. The level of luciferase gene transcription under a tetracycline inducible promoter was then quantitated with ByT-FAS using chemiluminescent detection.

ByT-FAS is a new stopped flow system conceptualized and designed in the late 1980s by Kent K. Stewart. [2] ByT-FAS is currently designed to enable the performance of semi-automated continuous flow analysis of wet chemistry assays using small sample volumes while circumventing the diluting affects of laminar dispersion. The initial design of the instrument was demonstrated to be successful by Kent Stewart with a UV/VIS spectrophotometric detection cell. [3] In this paper, ByT-FAS is applied to the analysis of whole intact bacterial cells using chemiluminescent detection.

2. Materials and methods

2.1. Instrumentation

All analyses of the luciferase activities of the different *E. coli* cell cultures were performed with the ByT-FAS flow system as shown in Fig. 1 (see

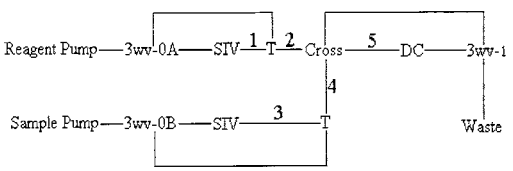

Fig. 1. Schematic diagram of a ByT-FAS flow system. Reagent to sample carrier flow stream ratio of 10:1 (reagent stream = 90.9% and sample stream = 9.1% of total system flow). Total system flow rate is 0.22 ml min^{-1}. Critical flow area comprised of tubing sections 1, 2, 3, 4 (0.127 mm i.d. by 5 cm) and 5 (0.127 mm i.d. by 12 cm, braided mixing coil), T's (0.5 mm i.d.), Cross (0.5 mm i.d.), and Detector Cell (DC, 0.45 mm i.d. by 2 cm). Injected sample loop volume 25 μl and braided. Injected reagent loop volume 150 μl and braided. 3wv-0A-three way valve for reagent injection valve, 3wv-0B- three way valve for sample injection valve, SIV; standard six port injection valve, T-three way intersection (0.5 mm i.d.), cross-four way intersection (0.5 mm i.d.), DC- detector flow cell, 3wv-1-three way valve controlling bypass flow.

accompanying manuscripts in this copy of Talanta for more on ByT-FAS operation). The ByT-FAS critical flow region was made from short lengths of small bore tubing, typically 0.127 mm i.d[2]. The reagent to sample carrier stream flow ratio was 10/1 and the total flow rate of the system determined at the point of waste collection was 0.22 ml min^{-1}. Lennox broth liquid media was used as the sample and reagent carrier flow streams. The ByT-FAS system was coupled directly to an HPLC fluorometric detection system (McPherson model FL-748, Acton, MA) without the light source turned on to serve as a chemiluminometer. The fluorometer flow cell contained the largest internal diameter of any part of the system at approximately 0.45 mm. Solutions containing the cells or the substrate were manually loaded into the sample loops of the SIV (sample insertion valve) by aspiration before the start of each run. After initiation of each run, the samples were inserted into the system by manual movement of the SIV from loading to injection mode under no flow conditions (sample and reagent loops bypass, see Fig. 1). System flow and timing was controlled by an IBM compatible 386s × 16 computer with the program LabTech Notebook™ version 6.0. (Laboratory Technologies Corporation, Wilmington, MA). Flow patterns through the system were directed by the firing of three, three-way valves (3-WVs) at different times during the course of a sample run (NResearch, Maplewood, N.J.). Data acquisition during a run was mediated by LabTech ™ notebook employing a Data Translation 2805 card interfaced to the detector. Each sample run's data was stored in its own file and directly imported into a Quattro Pro™ spreadsheet for analysis.

2.2. Reagents

All laboratory chemicals were purchased from Sigma (St. Louis, MO). The recombinant *E. coli* strain was obtained as a gift from Dr Timothy Larson (Virginia Tech, Department of Biochemistry). The bacterial strain was sustained on Lennox broth (LB) Agar (20 gm l^{-1} LB, 15 gm l^{-1} Agar) plates containing 50 μg ml^{-1} filter sterilized kanamycin by reinoculation every 2–3 weeks. The kanamycin resistance on the plasmid insured that only *E. coli* cells that received a copy of the plasmid would survive. This procedure was used to ensure the cell culture remained homogeneous and pure.

An outline of the assay method to determine the level of luciferase gene transcription using ByT-FAS is:

1. Grow overnight cultures at 37°C with different levels of tetracycline.
2. Cool the cultures to room temperature for 2 h.
3. Dilute each culture to an approximate absorbance of 0.1 AU at 600 nm versus an LB blank.
4. Load 150 μl of diluted culture into the reagent side of ByT-FAS and 25 μl 1 mM luciferin substrate into the sample side of ByT-FAS; run the ByT-FAS analysis.
5. Analyze the resulting data.

The details are as follows. The *E. coli* strain level of genetic transcription of luciferase was assayed was follows. Four tubes of 5 ml LB broth were prepared each containing 50 μg ml^{-1} kanamycin. The tubes were then individually added with and 0, 50, 75, and 100 ng ml^{-1} tetracycline. One colony of *E. coli* was picked from the LB agar plate using an autoclaved P-200 pipette tip and dropped in the LB broth using aseptic technique for each tube. The cultures were incubated for growth overnight at 37°C under continuous shaking. After overnight incubation (16 h), the tubes were removed from 37°C and set at room temperature (20°C) for approximately 2 h. The cooled cultures were then diluted 1/25 into fresh LB broth and measured for their absorbance at 600 nm versus an LB broth blank. The cell cultures were diluted to give an approximate absorbance of 0.1 AU at 600nm and the diluted cells were then injected into ByT-FAS which mixed the cells with the substrate luciferin. The cells were loaded into the reagent side of the system with a reagent coil loop of 150 μl. Luciferin at 1 mM dissolved in water was loaded into the sample side of the system using a sample coil loop of 25 μl.

[2] See the accompanying manuscripts by Stewart and Hillard and Hillard and Stewart for a more complete description of the critical flow region.

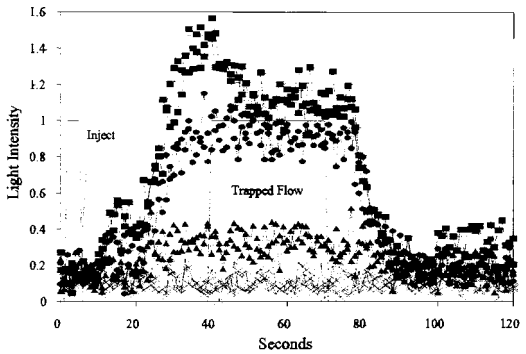

Fig. 2. Raw data traces of diluted *E. Coli* overnight cultures as function of tetracycline induction of luciferase. Four overnight cultures of *E. coli* containing the luciferase plasmid were grown overnight with different levels of tetracycline added to the growth media. The overnight cultures were diluted into fresh LB media to an approximate absorbance (600 nm) reading of 0.1. Each culture, 150 μl, was injected in the reagent side of ByT-FAS. Of 1 mM luciferin, 25 μl, was injected in the sample side. Raw data traces of injected cultures contain the following amounts of tetracycline in the overnight growth media: X-0 ng ml^{-1}, ▲-50 ng ml^{-1}, ○-75 ng ml^{-1}, ▩-100 ng ml^{-1} tetracycline.

The reagent and sample carrier stream solution was LB broth. The ByT-FAS analysis was then run.

3. Results

The chemiluminescent ByT-FAS raw data traces of the different tetracycline induction concentrations are shown in Fig. 2. The duplicate sets of lines and symbols correspond to the amount of tetracycline in the overnight culture for each injected culture. Increasing light signal corresponds to higher concentrations of tetracycline and more luciferase transcribed per AU_{600nm}. The raw data traces contain substantial detector noise as a result of the increased sensitivity needed to detect light production from inside the cells.

Because light is a transient product of the luciferase catalyzed reaction with ATP, luciferin, and O_2, there is not an accumulation of detectable product as there is in traditional absorption spectroscopy [4]. However, the light intensity signal can be summed as if the light were accumulating. This gives the total amount of light produced per culture during the trapped phase of the ByT-FAS run. The summed light intensities of the raw data traces during the trapped phase of the run are shown in Fig. 3. When the light intensities are summed, the excessive detector noise visible in the raw data traces shown in Fig. 2 is significantly reduced. To determine an average rate of light production for each cell culture, regression analyses of the summed light intensities shown in Fig. 3 were performed between 45 and 70 s in the run. All such regression analyses had an R^2 value of 0.99 or higher These rates of light production from the slope of the regression analysis were then normalized to the amount of bacteria in the culture that produced the rate of light production by dividing the rate of luciferase light production by the absorbance (600 nm) of each diluted cell culture. The standard curve of luciferase velocity per injected AU_{600nm} versus tetracycline concentration in the overnight growth media is shown in Fig. 4. The standard response curve ($Y = 0.226X - 8.98$, regression line)) has an R^2 value of 0.991.

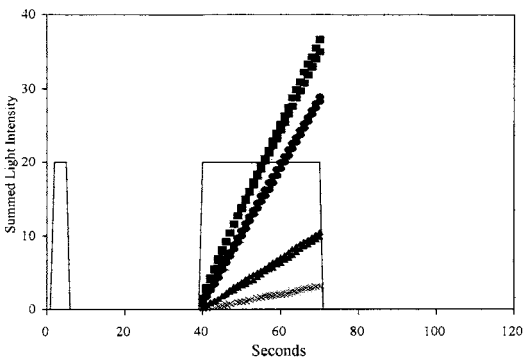

Fig. 3. Trapped flow summed light intensities to determine a luciferase rate of light production. From Fig. 2 it is not easy to calculate a rate of light production for luciferase. Since light is a transient product of the enzyme luciferase, a summation of the light signal would provide a cumulative total of light produced. The linear lines ($R^2 > 0.99$) can then be used for regression analysis to determine a rate of luciferase light production. The pairs of lines correspond to the summed light signals of each overnight culture during the trapped flow period of the ByT-FAS run. The different symbols represent the different cultures with tetracycline in the overnight growth media as follows: X-0 ng ml^{-1}; ▲-50 ng ml^{-1}; •-75 ng ml^{-1}; ▩-100 ng ml^{-1} tetracycline.

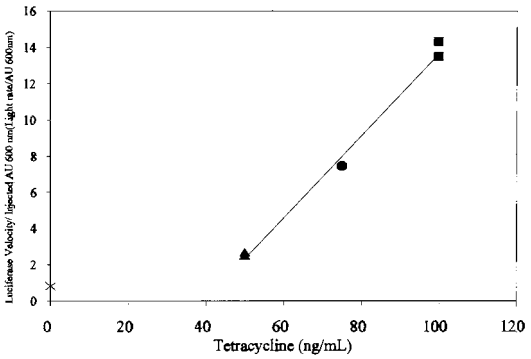

Fig. 4. Standard response curve of luciferase velocity per AU_{600nm} versus tetracycline concentration in the overnight growth media. From Fig. 3 a regression analysis of each summed light intensity is taken between 45 and 70 s. This establishes a rate of light production (photons s^{-1}) by luciferase. The rate of light production is then normalized for each cell culture by dividing the absorbance at 600 nm into the luciferase velocity. Once the luciferase velocities have been described by the number of bacteria assayed (based upon AU_{600nm}), the data are plotted versus the tetracycline concentration in the overnight growth media. The standard response curve has an R^2 value of 0.991. The different symbols represent the different cultures with tetracycline in the overnight growth media as follows: X-0 ng ml^{-1}, ▲-50 ng ml^{-1}, •-75 ng ml^{-1}, ▩-100 ng ml^{-1} tetracycline.

Physical steady state signals for the injected whole cell cultures was not verified in these experiments. However, the ByT-FAS system still had adequate sensitivity for the analysis of luciferase in the whole cells.

4. Discussion

Recently, flow injection analysis has been applied to the analysis of injected cells and this new field has been called flow injection cytometry (cytoanalysis) [5,6]. Significant effort has been directed towards the coupling of a flow injection system to measurement of cell cultures for on-line monitoring of microbial activity, intracellular enzyme activities, and metabolite concentrations in the culture [7–9]. For the on-line monitoring of intracellular enzyme activities, this flow injection system employed an on-line cell disintegration mechanism through the action of ultrasonic and glass microbial-mixer mills [7,10]. In addition to the cell disintegration device, the flow injection manifold also contained a membrane device to separate the cell debris and the released enzyme from the disintegrated sample solution. The enzyme activities were then measured.

Our objective in performing these experiments was to demonstrate that the ByT-FAS flow system could perform assays of genetic transcription levels using whole *E coli* cell cultures with chemiluminescence detection. This was accomplished. Under our conditions it would appear that the potential sample throughput for the total analysis of transformed cells can be well over 100 per day. It is believed that this is an operationally simpler assay system for studying genetic transcription which might have broad appeal. Obviously more work is needed before our technique might be considered as a routine assay procedure. Still, we suggest that the small volume ByT-FAS system has the potential of being a less expensive, and less labor intensive methodology for the analysis of bacterial genetic transcription levels.

5. Conclusion

This is the first reported use of ByT-FAS for the detection and analyses of transformed cells. However, FIA has been applied to the analysis of recombinant *E coli* cells. [8] ByT-FAS with chemiluminescent detection has the potential of being a useful tool for the rapid analyses of promoter DNA sequences, promoters, and transcription repressors in whole intact bacterial cells by molecular biologists and biochemists. Thus, we believe the techniques and instrumentation described above, add a new dimension to the analysis of bacterial cells with flowing systems. Furthermore, there appear to be many potential applications of such an assay system for the fields of molecular genetics, biotechnology, and bioremediation for fast and sensitive analysis of new promoter DNA sequences, altered promoters, transcription repressors, and environmental toxins.

References

[1] J.H. Miller, Experiments in Molecular Genetics, Cold Spring Harbor, New York, 1972, pp. 352.
[2] K.K. Stewart, Personal communication, 1992.
[3] K.K. Stewart, S.W. Hillard, Talanta, this issue, 1997.
[4] S.E. Brolin, G. Wettermark, Bioluminescence Analysis, Weinheim, New York, 1992.
[5] J. Růžička, Analyst, 119 (1994) 1925.
[6] W. Lindberg, J. Růžička, G.D., Christian, Cytometry, 14 (1993) 230.
[7] K. Steube, U. Spohn, Anal. Chim. Acta 287 (1994) 235.
[8] T. Ding, U. Bilitewski, R.D. Schmid, D.J. Korz, E.A. Sander, J. Biotechnol. 27 (1993) 143.
[9] Y.L. Huang, S.Y. Li, B.A.A. Dremel, U. Bilitewski, R.D. Schmid, J. Biotechnol. 18 (1991) 161.
[10] K. Steube, U. Spohn, J. Biotechnol. 33 (1994) 221.

ELSEVIER

Talanta 45 (1998) 519–529

Talanta

Decisive problems of zone-circulating flow injection analysis and its solution[1]

Yoshio Narusawa *, Yuichi Miyamae

Department of Chemistry, College of Science, Rikkyo (St. Paul's) University, 3-34-1, Nishi-Ikebukuro, Toshima-ku, Tokyo 171, Japan

Received 27 February 1997; received in revised form 15 May 1997; accepted 20 June 1997

Abstract

Although experiment and computer analysis of zone-circulating flow injection analysis (ZCFIA) data have been investigated, there are still some essential problems inherent to ZCFIA. Computer program of high dimensional modified simplex method was used for resolving peaks of ZCFIA damped response curves. Peaks are resolved on the basis of the criterion that each area of the peak surrounded by the curve and the abscissa is equal, because each sample zone circulates repeatedly in the manifold in equal volume. As a result, the peaks of the damped response curve have been resolved into each component and the curve obtained by summing these components has been proved to be equal to the original response curve. By following up the data analysis of ZCFIA, it was found that there were many conflicts in the manual analysis of data by Li. At least, the dispersion in a flow system should not be investigated by ZCFIA, and it might be studied by the single-line manifold of FIA. © 1998 Elsevier Science B.V.

Keywords: Zone-circulating flow injection analysis; Single-line manifold flow injection analysis; Axial dispersion coefficient

1. Introduction

Yu [1] studied the dispersion of a solute injected into a round tube, and Daskopoulos and Lenhoff [2] studied the axial dispersion coefficient in laminar flow. Vrentas and Vrentas [3] developed an asymptotic solution for the dispersion, Mansour [4] solved an exact, closed-form solution of a mathematical model, and Shankar and Lenhoff [5] pointed out that the axial dispersion of an impulse tracer was caused by the interaction of radial diffusion.

In relation to flow injection analysis (FIA), Vanderslice et al. [6] derived expressions for the dispersion, and Ramsing et al. [7] proposed the study on the highly reproducible concentration gradients formed between an injected sample zone and the carrier stream in FIA for titration. Reijn et al. [8] studied the dispersion of an injected sample zone caused by transport phenomena in most FIA systems, Betteridge et al. [9] studied

* Corresponding author. Fax: +81 3 59923434; e-mail: narusawa@rikkyo.ac.jp

[1] Partly presented at the 8th International Conference on Flow Injection Analysis, ICFIA97/JAFIA held in Orlando, Florida, January 12–16, 1997.

PII S0039-9140(97)00200-2

dispersion and chemical reaction in a single-channel FIA system modeled by a random walk method, and Wentzell et al. [10] also investigated the evaluation of dispersion profiles by using random walk simulation in FIA. Zagatto et al. [11] reported that the addition of a confluent stream increased the mean length of the sample zone and simultaneously decreased the involved concentrations. Kolev and Pungor [12] investigated single-line FIA systems with two types of reactor with different dispersion characteristics. Stone and Tyson [13] studied the application of two models based on the stirred mixing tanks, the well stirred tank and the two tanks in parallel models. Van Staden [14,15] investigated the response time phenomena of coated open-tubular solid state silver halide selective electrodes and their influence on sample dispersion in FIA.

The problem of the dispersion in a flow system is essential. Update investigations have been performed by many researchers [16–19] in the world, but it is difficult for us to say that all have been resolved. In fact, earlier theoretical treatment of dispersion by Taylor [20] has led to the recent investigation by Korenaga [21], who published the review on the convection-diffusion phenomena. The present authors made efforts to obtain the data in relation to dispersion problems in the conventional FIA manifold because Korenaga focused on the ideal apparatus which was far from the reality. Recently, Kolev [22] reported the review on the dispersion and diffusion in a flow system.

Although the technique of zone-circulating manifold itself was used by Rios et al., [23] they did not apply the technique to the investigation of dispersion phenomena. Li and Narusawa [24] proposed the name ZCFIA, in which they described the technique by connecting the outlet of the single-line manifold to the inlet. By this technique, Li and Narusawa [24] suggested solutions to the complex relationships among dispersion coefficient, length of coil, flow-rate, residence time of the sample zone, and so on. However, our laboratory has come to recognise there are still some problems in ZCFIA. First, there is room for doubt, because of the arbitrariness in the manual analysis of ZCFIA damped response curves in the former study. In subsequent studies, the present authors pursued the problems of dispersion and diffusion in a flow system, and identified limitations quite well by trying data analysis of ZCFIA with the computer analysis technique [25–27]. In the present analyses defects in ZCFIA were found not only in theory and experiment, but also in technique of the original analysis.

One of the purposes of this paper is to show the composition of damped response curves of ZCFIA. The others are to point out that the manual analysis [24] cannot be used to discuss the dispersion and diffusion in a flow system, and to propose ways of solving the problems.

2. Theoretical aspects

ZCFIA has an advantage in that a lot of information is obtained, because the sample zone circulates hermetically in a closed system under the same condition in length of the coil. At the same time, however, it has many disadvantages because of the problems of overlapping of a sample zone owing to repeated circulation of the sample zone and of agitation of a laminar flow in many places of the manifold, such as the joint, flow-through cell, peristaltic pump, sample-loop valve, and so on. One of the most important defects is that the definition of dispersion by Ruzicka and Hansen [28] should not be applied to ZCFIA. Even if the estimation of the parameters has been accomplished for quantitative discussion, ZCFIA is still inadequate to discuss dispersion, because there is no simple way to appreciate parameters exactly in relation to dispersion owing to the overlapping of the sample zone.

Problems are described in the following.

2.1. Overlapping of the sample zone

Overlapping of the sample zone was pointed out by Joelsson and Ivaska [29] for the sequential injection analysis (SIA). Essentially the overlapping is different from our problem, which has already been pointed out by the present authors in the previous paper [27]. In ZCFIA, this overlapping of the sample zone is inevitable. When the

sample zone circulates repeatedly in the closed manifold like ZCFIA, the front of sample zone overtakes the delayed part of the same zone again and again, because the laminar flow of inner zone propagates faster than outer zone. Relations of these circumstances is shown in Fig. 1, in which pump, cell, valve, as well as the diffusion effect

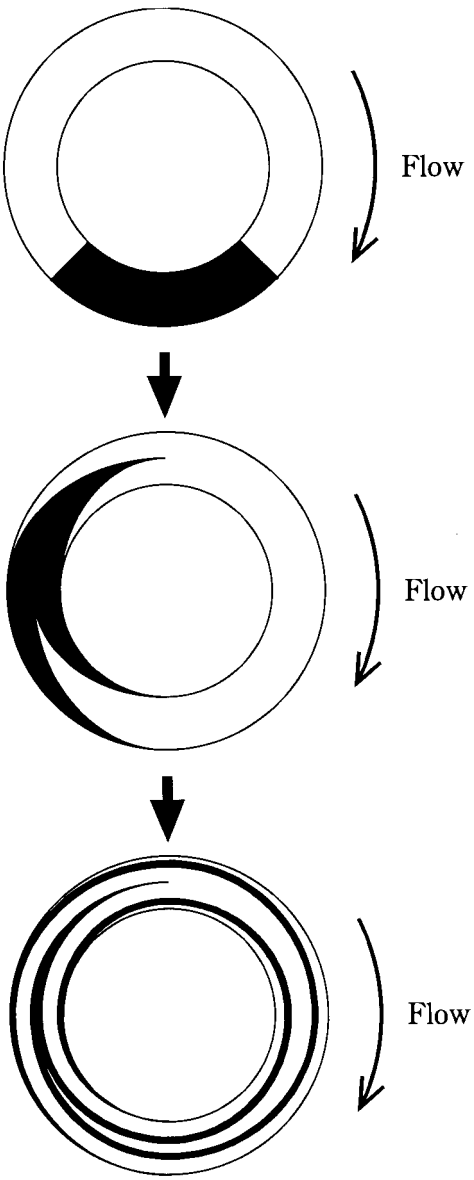

Fig. 1. Schematic diagram of overlapping of sample zone.

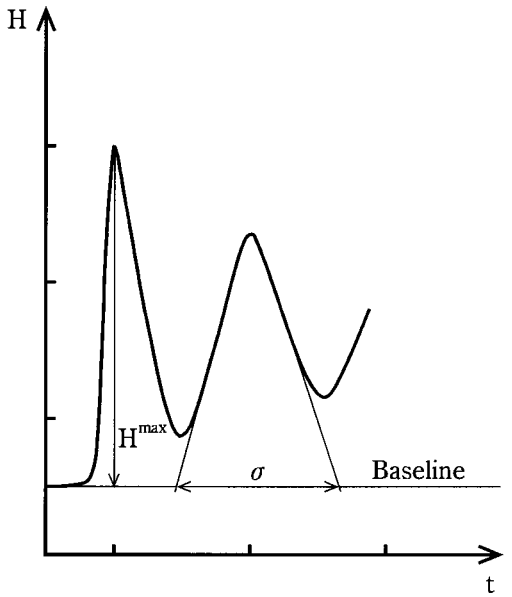

Fig. 2. Definition of signal height H^{max} and peak width σ.

were neglected. Of course, in case of single-line manifold of FIA, this overlapping doesn't take place, because the sample zone is detected only once in a flow-through cell.

It is noted that damped response signals of ZCFIA do not drop to the baseline as shown in Fig. 2. The overlapping signal is expected from the figure, because cross-over of peaks appears. Moreover, the overlapping signal becomes more and more pronounced in the later stage of the curve. This leads to a conclusion of an error in the application of the definition of Ruzicka and Hansen [28] to the analysis of ZCFIA data. Therefore, the dispersion in relation to signal heights described in the previous papers by Li and Narusawa [24,30,31] should be defined as 'the degree of dilution', and in order to obtain the radial dispersion, signal height free from overlapping should be estimated by any means.

2.2. Assembly involving reactor tube, peristaltic pump tube, and flow-through cell tube

Agitation for the laminar flow condition by the assembly involving reactor tube, peristaltic pump tube, and flow-through cell tube seemed to be

very important, and it should not be passed over. There is a difference between inner diameters in reactor tube and flow-through cell tube, one is 1.0 mm and the other is 0.5 mm, in which the sample zone circulates repeatedly in ZCFIA.

In the previous papers [24,30,31], Li used the manifold of the reaction coil of 1 mm in inner diameter and 2 m in length. Simple calculation of the volume shows to be 1570 μl ($l = dm^3$) for the reaction coil part. Moreover, in the closed system there are some dead-volumes in various parts and amounts to ca. 2000 μl as a whole. If 100 μl of the sample volume is diluted completely in the system, the degree of dilution becomes ca. 20. In those papers, [24,30,31] almost all the dispersion degrees were denoted to be ca. 16, which corresponded to the uppermost limit. This means that signal does not attenuate, but converges to some constant value. Therefore, the overlapping effect is serious in ZCFIA, and any discussions of radial dispersion and axial dispersion, including radial diffusion and axial diffusion have no meaning at all in reference to the basis of data without removing the overlapping effect in the data analysis.

2.3. Construction of flow-through cell

The flow-through cell is shown in Fig. 3. Since the flow-through cell itself is complex in construction, agitation for laminar flow of the sample zone occurs, and an ambiguity is brought about in analyzing the dispersion phenomenon. This is significant in ZCFIA and should not be neglected, because the sample zone passes through the flow-through cell repeatedly. The light path of the cell is 10 mm in length and 1 mm in inner diameter. Both the inlet and the outlet of the cell are connected to the short length tube of 0.5 mm inner diameter. Differences in inner diameter like these caused the laminar flow to agitate, especially for ZCFIA.

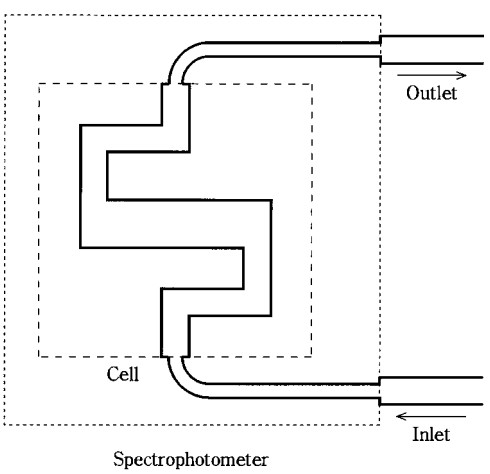

Fig. 3. Construction of flow-through cell for spectrophotometer.

2.4. Handling of peristaltic pump

Peristaltic pump is inadequate for the measurement of dispersion phenomenon in ZCFIA, because a stripping off and a serious agitation of the sample zone occur during repeated passage of it through the pump. The dead volume and the stripping off effect in this portion cannot be neglected in ZCFIA.

2.5. Relation between radial dispersion and axial dispersion

All of the graphs in this section are qualitatively expressed, because the graphs are not obtained by the simulation with the real data. Therefore, any units and numerical values were omitted in all graphs. In the previous paper [31], Li defined the radial dispersion and the axial dispersion shown in Fig. 2 and showed the analyzed values in the table (Table 1 [31]). As shown in Fig. 2, for the peak area surrounded by both the tangent lines of the response curve and the abscissa, the triangle approximation holds. Since dispersion is reciprocally proportional to the peak height, the peak area is proportional to σ/D. Calculated values of σ/D from data at the flow-rate 3.80 ml/min (Table 1[31]) are 0.54 and 2.05 for the length at 100 and 1700 cm, respectively. Although the area must be essentially the same in a flow of ZCFIA, the area in 1700 cm is 3.8 times as large in comparison to the area in 100 cm. This means that the effect must be taken into consideration, because the last peak area of the signal is 280% as large as the first, in spite of the equality in area. This value is

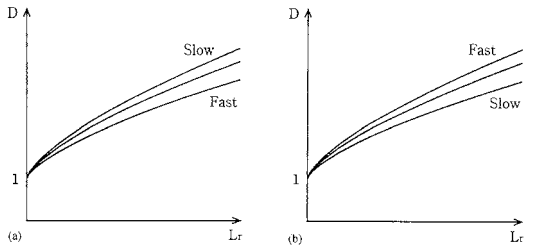

Fig. 4. Relationship between radial dispersion D and coil length L_r at various flow-rate. (a) Result of ZCFIA, (b) Prediction by the present theory.

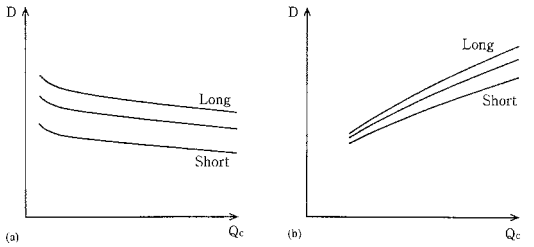

Fig. 5. Relationship between radial dispersion D and flow-rate Q_c at various coil length. (a) Result of ZCFIA, (b) Prediction by the present theory.

not a measuring error. That's why ZCFIA is suggested to be essentially inadequate in both theory and technique for analyzing the dispersion phenomena. As shown by the schematic diagram in Fig. 1, the change in sample zone is essential and the overlapping effect of the sample zone should be corrected in analyzing the ZCFIA data.

Fig. 4 shows the curves for ZCFIA, in which Fig. 4(a) (Fig. 8 [24,30]) is for the original ZCFIA and Fig. 4(b) is for the present theory. In Fig. 4(a) and (b), the relations between D versus L_r are contrary in relation to the flow-rate Q_c. This reversal phenomenon is interpreted as the result of the neglect of the overlapping effect in the original analysis of ZCFIA data in Fig. 4(a). It will be described in detail later. In case of the same length of coil, dispersion must be more pronounced in high flow-rate than in low flow-rate [28]. However, in case of considerably low flow-rate, the effect of radial diffusion [26] takes place in the direction to reduce the radial dispersion. Therefore, it will be difficult to analyze the dispersion precisely without any correction for the diffusion.

Fig. 5 shows the curves for ZCFIA, in which Fig. 5(a) (Fig. 9 [24,30]) is for the original ZCFIA and Fig. 5(b) is for the present theory. These relations are totally different in shape: Fig. 5(a) is downward in the right-hand side but on the contrary, Fig. 5(b) is upward in the right-hand side. This discrepancy once again can explain the neglect of the overlapping effect in ZCFIA. A matter of course, the results of Fig. 4(a) and Fig. 5(a) for the original ZCFIA are compatible and those of Fig. 4(b) and Fig. 5(b) for the present theory are also compatible. However, the relation between the dispersion and the flow-rate in case of the original ZCFIA (Fig. 5(a)) is not acceptable, because there is a general rule that the dispersion increases as the flow-rate increases irrespective of the reaction coil length, if the coil length is constant [28]. When the flow-rate approaches infinitely zero, the dispersion approaches unity without limit. Circumstances in the limit will not be clear. In fact, Korenaga [21] pointed out that the diffusion plays important role in ultra-low flow-rate.

Fig. 6 shows the curves for ZCFIA, in which Fig. 6(a) (cf. Fig. 3[31]) represents the original ZCFIA and Fig. 6(b) the present theory. These relations are totally different in shape: Fig. 6(a) is upward extraordinarily in the right-hand side, while Fig. 6(b) is upward in the right-hand side, but it reaches the uppermost limit. The phenomenon for ZCFIA is also due to the overestimation of σ, especially in the later stage of the curve.

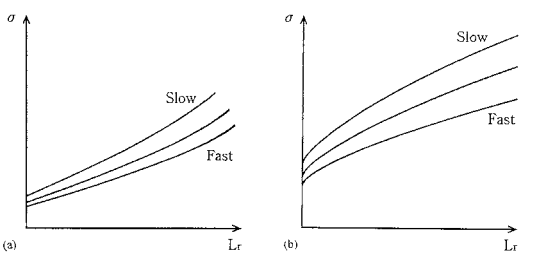

Fig. 6. Relationship between peak width σ and coil length L_r at various flow-rate. (a) Result of ZCFIA, (b) Prediction by the present theory.

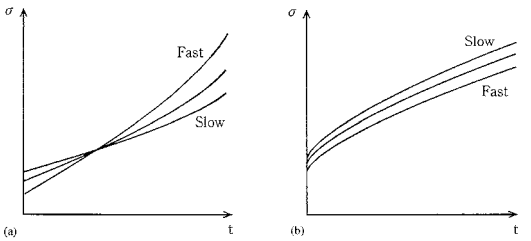

Fig. 7. Relationship between peak width σ and residence time t at various flow-rate. (a) Result of ZCFIA, (b) Prediction by the present theory.

Fig. 7 shows the curves for ZCFIA, in which Fig. 7(a) (cf. Fig. 4 [31]) represents the original ZCFIA and Fig. 7(b) the present theory. The relations in Fig. 7(a) and (b) are essentially similar to the relations of Fig. 6(a) and (b), except for the inverse relation in the later stage of the curve and the cross point in the middle stage of the curve in Fig. 7(a). This discrepancy is explained by the neglect of the overlapping effect in the original analysis of ZCFIA data. As a matter of fact, the results of Fig. 6(a) and Fig. 7(a) for the original ZCFIA are compatible and those of Fig. 6(b) and Fig. 7(b) for the present theory are again compatible. However, the results for the original ZCFIA (cf. Fig. 6(a) and Fig. 7(a)) are not acceptable without the consideration of the overlapping effect.

3. Experimental

The sample was potassium dichromate, the injected volume was 100 μl, and the length of the coil and the inner diameter were 2 m and 1 mm, respectively. Absorbance was measured at 440 nm [24]. In a preliminary investigation by a single-line FIA manifold, we use the 4-channel peristaltic pump of Denki Kagaku Keiki. There is no trouble for the peristaltic pump in the single-line manifold, but there is a problem in ZCFIA, because sample zone circulates repeatedly through the pump. ZCFIA data were taken into the file as binary data with the computer (NEC PC-9801RA) by using the chromatocorder 12 (Scientific Instruments). Data acquisition was performed by the program 'EXT' accompanied by the SIC chromatocorder 12. Every one datum of the binary data was composed of every three bytes, hence the data were denoted from 1 to FFFFFF as hexadecimal, and from 1 to 16777216 as decimal. The data were transferred to ASCII data for further computer analysis on the MS-DOS. Transference to the ASCII data was performed with the UBASIC program [32] developed by ourselves. For the model for the dispersion, we referred to the previous papers [26,27], and for the separation of overlapped peaks, the UBASIC program of modified simplex method with high dimensional optimization approach [33] developed by ourselves was used. Computer analysis was performed by the following sequences: load data, peak detection, set of initial parameters, optimization processes, and finish. Resolution of peaks and optimization of the curve were made on the basis of the criterion that each area of the peak is equal. There are two parameters, height and position, and six parameters for the peak-shape common to each peak. If the number of the peak is assumed to be P, there are $2P+6$ parameters for each peak. In front of the peak, the function was defined by Gaussian and Linear, and in rear of the peak, it was defined by Gaussian and Lorentzian. Therefore, the curve represented in Fig. 2 is considered to be asymmetrical in shape. These were optimized so as to be minimized to an infinitesimally small value at the same time, on the basis of the criterion that each peak was equal in area. UBASIC program can afford both speed and precision, which was already tested in the previous paper [32].

4. Results and discussion

Calibration between pump speed and flow-rate is not obtained essentially in ZCFIA, because the volume of the sample flowed is observed in an open system of the circuit. Therefore, the relation was obtained by the data acquired with the computer. The relation of the pump scale versus the flow-rate was obtained by the intervals of peak to peak. The flow-rate was calculated as the volume of the system to be ca. 2000 μl, including the

volumes of the flow-through cell tube and the peristaltic pump tube. The range of the flow-rate was obtained to be 1.2–8.7 ml/min under the pump speed scale of 5–75 at five intervals, and 85 and 95. The linearity was good enough and slope, intercept, and linear regression coefficient were 0.0802, 0.993, and 0.9993, respectively.

Recently, Korenaga [21] pointed out in his review on the convection-diffusion phenomena that there were several problems for analyzing dispersion phenomena by using the conventional FIA apparatus: for example, pump for sample delivery, sample injection loop, reactor tube, flow-through cell with detector, and so on.

Several equations have been already proposed [24,30,31]. If the time requires to travel the flow-through cell without dispersion θ_t (s), the following relation is obtained:

$$\theta_t = S_v/Q_c = 0.10\ \mathrm{cm^3} Q_c^{-1}\ (\mathrm{cm^3 s^{-1}}) \quad (1)$$

where S_v and Q_c are the volume of the sample zone and the flow-rate, respectively.

For the discussion of dispersion, following equations and parameters are good enough to be cited. The peak height and axial dispersion were defined in the previous paper [26]. D and D_A, refer to Table 2 [26,27].

$$D = K_1 L_r^{\mu_1} Q_c^{\mu_2} + 1 \quad (2)$$

$$K_1 = 0.349,\ \mu_1 = 0.558,\ \mu_2 = -0.222$$

$$D_A = K_4 L_r^{\mu'_1} Q_c^{\mu'_2} + \theta_t \quad (3)$$

$$K_4 = 0.045,\ \mu'_1 = 1.01,\ \mu'_2 = -1.46$$

In Eq. (2), L_r is proportional to the residence time t, hence the relationship of D versus t are schematically expressed in Fig. 8, because μ_1 is smaller than unity. The larger the flow-rate becomes, the larger the dispersion is, when the residence time t is the same.

This tendency is the same as that of in Li and Narusawa (Fig. 11 [24]). On the other hand, Fig. 7(a) and (b) are totally different from each other, and this discrepancy comes from the characteristics of ZCFIA. As σ is the width on the chart, the flow-rate must be multiplied in order to obtain the axial dispersion. By this transformation, we obtain curves of D_A versus t (Fig. 5 [27]). This result

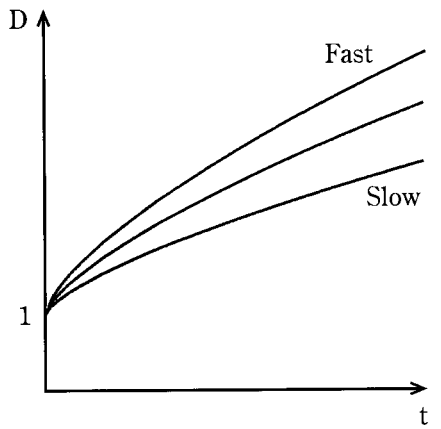

Fig. 8. Relationship between radial dispersion D and residence time t at various flow-rate.

is shown by the curve predicted with the theory in line, except for the slope of curves. The present theory predicts μ'_1 in Eq. (3) to be less than unity as predicted from Fig. 7(b). Although Li predicted for μ'_1 to be significantly larger than unity, because the curves of σ versus t were remarkably upward in the right-hand side. However, μ'_1 was obtained to be 1.01 by the computer-aided simulation of ZCFIA data (Table 2 [27]). This means that μ'_1 could not be predicted correctly to be smaller than unity by the original ZCFIA theory.

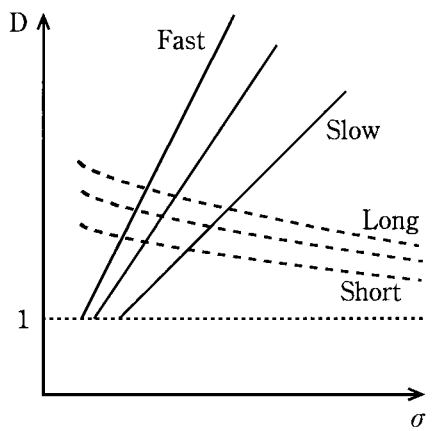

Fig. 9. Relationship between radial dispersion D and peak width σ. Solid line: Effect of flow-rate, Dotted line: Effect of coil length.

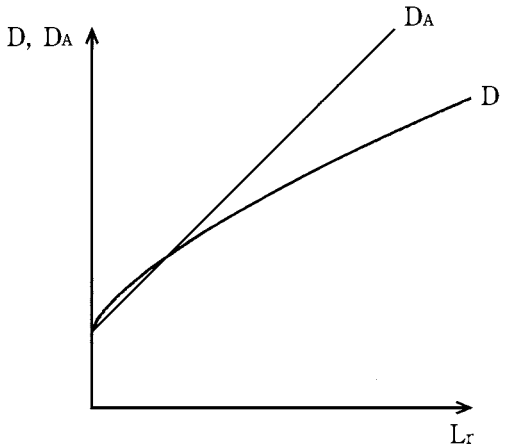

Fig. 10. Relationship among radial dispersion D, axial dispersion D_A and coil length L_r. Curve D_A versus L_r is calculated from $\mu'_1 = 1.01$ in Eq. (3) (see text). Curve D versus L_r is the same as Fig. 4(b).

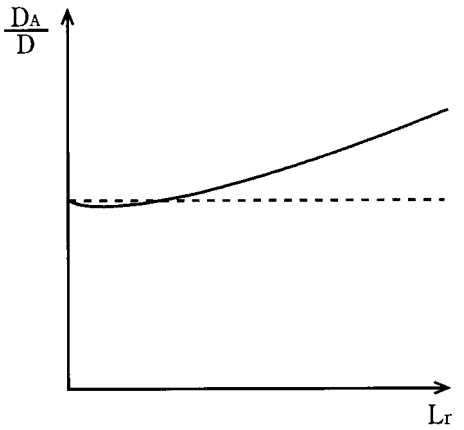

Fig. 11. Relationship between ratio of axial dispersion D_A to radial dispersion D and coil length L_r. Solid line: Result from computer-aided simulation (cf. [26] and [27]), Dotted line: Prediction of present theory.

The relationships between D versus σ with the flow-rate are shown in Fig. 9. Solid line curves are shown in linear lines in relation to the flow-rate; it holds on the basis of the criterion that the area of each peak is just the same, because the volume of the sample zone is constant (cf. Section 5). Relationships of D versus σ along with the coil length are shown in dotted line in Fig. 9. Dispersion is observed pronounced for the longer coil than the shorter coil under the same σ value. At the same time, the slower the flow-rate becomes, the smaller the dispersion D becomes and the larger the width σ becomes, if the coil length is constant. In case of extremely fast flow-rate, D becomes extremely large and σ becomes zero; which means that the signal width can't be observed, because it is vital that the chart recorder does not move. In this case, it will be meaningless to discuss the dispersion problem, because the condition of laminar flow will not hold.

Therefore, the relations among D, D_A and L_r are shown in Fig. 10. The relation between D and L_r was the same as that of Fig. 4(b), and linear relation between D_A and L_r at constant Q_c was obtained from $\mu'_1 = 1.01$, which was calculated by the computer-aided analysis [27] of ZCFIA data. As a result, a curve upward in the right-hand side should be obtained from the computer-aided simulation [26,27] of ZCFIA data as shown in solid line in Fig. 11. On the other hand, the present theory predicts the relation parallel to the abscissa as shown by the dotted line in Fig. 11, because areas of the sample zone must be constant on the basis of the criterion mentioned above.

Axial dispersion expressed in width of the chart σ versus the flow-rate Q_c is shown in Fig. 12. The required time for the sample zone to pass through the cell is reciprocally proportional to the flow-

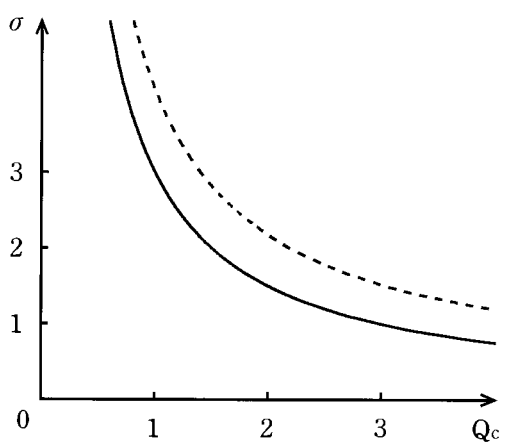

Fig. 12. Relationship between peak width σ and flow-rate Q_c. Solid line: Without the dispersion, Dotted line: With the dispersion.

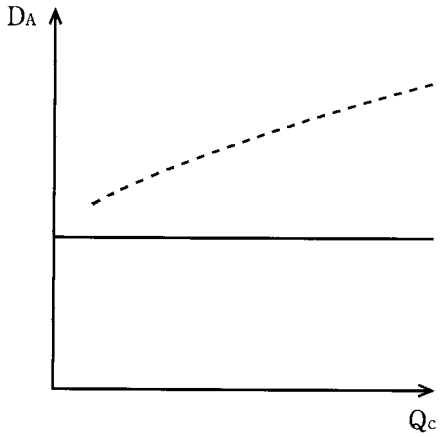

Fig. 13. Relationship between axial dispersion D_A and flow-rate Q_c. Solid line: Without the dispersion, Dotted line: With the dispersion.

rate. Solid line expresses the curve of sample zone not being accompanied by the dispersion. The time to path through the cell might change according to the flow-rate, but the pattern of the curve would be the same as shown in dotted line. In order to discuss the axial dispersion, we must use the parameter D_A indifferent to the chart width. By using this parameter, the relation of D_A versus Q_c is obtained as shown in Fig. 13. Solid line expresses the curve of the sample zone not being accompanied by the dispersion, because the sample zone propagates in a plug flow without any change in absorbance and D_A is directly proportional to D under the condition of the equality in area. Dotted line represents the curve being accompanied by the dispersion, because D_A denotes the same tendency to D (cf. Fig. 5(b)). According to the original ZCFIA prediction of Eq. (3), D_A must decrease as the flow-rate increases at constant coil length. This is the completely opposite direction to the present prediction. The cause of the problems is the neglected overlapping effect of the sample zone (cf. Fig. 4 [31]) by Li. This is the key point to the discrepancy. That's why the definition of Ruzicka and Hansen [28] is unadaptable for discussing the dispersion with ZCFIA data. In 1985, Rios et al. [23] already proposed the zone circulating manifold, and the signals in their paper showed that the response curves did not attenuate, because the sample zone was diluted to a constant value. Under these circumstances at the last stage of the measurement, dispersion phenomena were not observed (cf. Fig. 3 [23]). This is perfectly explained to be the dilution effect with the results under various conditions: if the sample volume and the coil length are constant, the greater the flow-rate becomes, the more dense the damped response curve becomes, and the signal converges to a constant value; if the sample volume and the flow-rate are constant, the greater the coil length becomes, the wider the damped response curve becomes, and the signal converges to the lesser value; if the coil length and the flow-rate are constant, the higher the concentration of sample becomes, the more intense the signal becomes, but the interval does not change.

Fig. 14 shows the composite curve of the peak-waves obtained by the simulation using the computer program. The composite curve well explains the shape of the damped response curve of ZC-FIA. Fig. 15 shows one of the results resolving a response curve of ZCFIA by the high dimensional modified simplex method. It is found that the signals are well resolved, and the composite curve reproduces the original curve well. In this instance, it is obvious that the third peak is already suffered from overlapping of the sample zone.

It should be emphasized again that the manual analysis of Li for ZCFIA data erroneously appreciates the radial dispersion to a small extent and the axial dispersion to an extremely large extent. It does not exaggerate to say that ZCFIA should

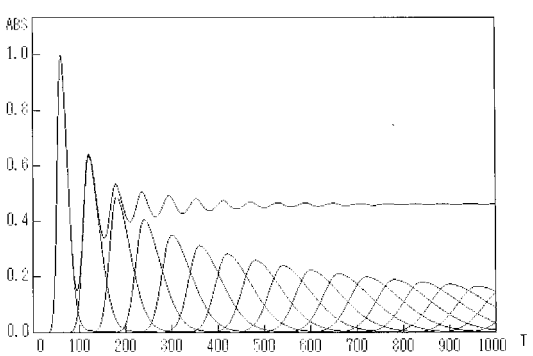

Fig. 14. Schematic representation of ZCFIA signal.

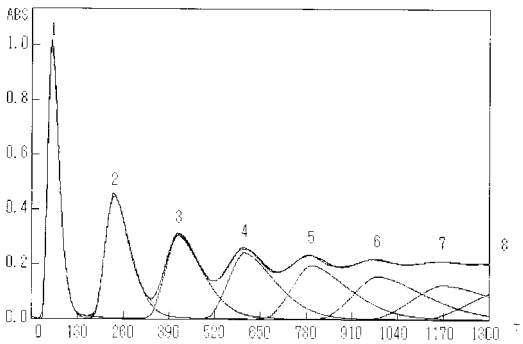

Fig. 15. Peak separation of ZCFIA signal. PS (pump scale): 70 (see text).

not be trusted for discussing the dispersion problem in a flow system, not only flow-injection analysis field, but also almost all related fields of flow system; such as gas chromatography, liquid chromatography, ion chromatography and so on. Therefore, any conclusions deduced from ZCFIA are not trustworthy. For the reasons mentioned above, it was found that the analysis of ZCFIA data would not bring any significant contributions to fluid dynamics. From these consideration, ZCFIA should be completely inadequate to discuss any dispersion problems. This means that ZCFIA may be fully imperfect in both theory and technique.

5. Conclusions

It was found that the manual analysis of Li for ZCFIA data erroneously appreciated the radial dispersion to a small extent and the axial dispersion to an extremely large extent, because the overlapping effect of the sample zone was not taken into consideration. It should be said that ZCFIA can't be trusted for discussing dispersion problems in a flow system, not only flow-injection analysis field, but also almost all related fields of flow system; such as gas chromatography, liquid chromatography, ion chromatography, and so on, if the correction of the overlapping effect is not carried out as precisely as possible. Therefore, any conclusions deduced from ZCFIA are not trustworthy, and do not bring any significant contributions to the fluid dynamics, because the flow-rate cannot be obtained exactly as a principle. Moreover, it is completely incorrect to discuss any dispersion problems at present. This means that ZCFIA is fully imperfect in both theory and technique, if the modification compatible to the fluid dynamics is not carried out explicitly. The present authors have made every effort to develop the theory and improve the technique in order to solve the problems of ZCFIA.

Acknowledgements

The authors thank Ken Takahashi for his assistance in part of the experiment, Rikkyo (St. Paul's) University for 'Kenkyu Shorei Joseikin (Research Fellowship Foundation) in 1996', and the Nomura Micro-Science Co. for supplying ultra-pure water.

References

[1] J.S. Yu, J. Appl. Mech. 48 (1981) 217.
[2] P. Daskopoulos, A.M. Lenhoff, AIChE J. 34 (1988) 2052.
[3] J.S. Vrentas, C.M. Vrentas, AIChE J. 34 (1988) 1423.
[4] A.R. Mansour, Sep. Sci. Technol. 24 (1989) 1437.
[5] A. Shankar, A.M. Lenhoff, AIChE J. 35 (1989) 2048.
[6] J.T. Vanderslice, K.K. Stewart, A. Rosenfeld, H. Gregory, J. Darla, Talanta 28 (1981) 11.
[7] A.U. Ramsing, J. Ruzicka, E.H. Hansen, Anal. Chim. Acta 129 (1981) 1.
[8] J.M. Reijn, H. Poppe, W.E. van der Linden, Anal. Chem. 56 (1984) 943.
[9] D. Betteridge, C.Z. Marczewski, A.P. Wade, Anal. Chim. Acta 165 (1984) 227.
[10] P.D. Wentzell, M.R. Bowdridge, E.L. Taylor, C. MacDonald, Anal. Chim. Acta 278 (1993) 293.
[11] E.A.G. Zagatto, B.F. Reis, M. Martinelli, F.J. Krug, F.H. Bergamin, M.F. Gine, Anal. Chim. Acta 198 (1987) 153.
[12] S.D. Kolev, E. Pungor, Anal. Chim. Acta 208 (1988) 117.
[13] D.C. Stone, J.F. Tyson, Analyst (London) 112 (1987) 515; 114 (1989) 1453.
[14] J.F. van Staden, Analyst (London) 117 (1992) 51.
[15] J.F. van Staden, Anal. Chim. Acta 261 (1992) 381.
[16] H. Ma, Yankuang Ceshi, 11 (1992) 273, 280 (in Chinese).
[17] N. Wu, D. Zhou, Fenxi Huaxue 23 (1995) 6 (in Chinese).
[18] J. Li, G. Liu, H. Ma, T. Korenaga, Anal. Chim. Acta 310 (1995) 329.

[19] G.-W. Zhou, Z. Liu, Gaodeng Xuexiao Huaxue Xuebao 16 (1995) 1186 (in Chinese).
[20] G. Taylor, Proc. R. Soc. (London) A219 (1953) 186; 225 (1954) 473.
[21] T. Korenaga, BUNSEKI 2 (1995) 145 (in Japanese) and references cited therein.
[22] S.D. Kolev, Anal. Chim. Acta 308 (1995) 36.
[23] A. Rios, M.D. Luque de Castro, M. Valcarcel, Anal. Chem. 57 (1985) 1803.
[24] Y.-S. Li, Y. Narusawa, Anal. Chim. Acta 289 (1994) 355.
[25] Y. Narusawa, Y. Miyamae, J. Chem. Software 2 (1994) 1.
[26] Y. Narusawa, Y. Miyamae, Anal. Chim. Acta 296 (1994) 129.
[27] Y. Narusawa, Y. Miyamae, Anal. Chim. Acta 309 (1995) 227.
[28] J. Ruzicka, E.H. Hansen, Flow Injection Analysis, second ed., Wiley, New York, 1988.
[29] A. Joelsson, A. Ivaska, Kem. Tidskr. 105 (1993) 20, 24 (in Swedish).
[30] Y.-S. Li, Y. Narusawa, J. Flow Injection Anal. 10 (1993) 66 (in Japanese).
[31] Y.-S. Li, Y. Narusawa, J. Flow Injection Anal. 11 (1994) 68 (in Japanese).
[32] Y. Narusawa, Y. Miyamae, J. Chem. Software 1 (1993) 99 (in Japanese).
[33] Y. Miyamae, C.-L. Zhang, Y. Narusawa, J. Chem. Software 2 (1995) 159 (in Japanese).

ELSEVIER

Talanta 45 (1998) 531–542

Talanta

On-line cryogenic trapping with microwave heating for the determination and speciation of arsenic by flow injection/hydride generation/atomic absorption spectrometry

J.L. Burguera *, M. Burguera, C. Rivas, P. Carrero

Venezuelan Andean Institute for Chemical Research (IVAIQUIM), Faculty of Sciences, University of Los Andes, P.O. Box 542, Mérida, Venezuela

Received 4 February 1997; received in revised form 12 June 1997; accepted 13 June 1997

Abstract

An on-line flow injection-hydride generation/atomic absorption spectrometry method was developed for the preconcentration and selective determination of inorganic arsenic [As(III) and As(V)] and its methylated species. The separation of the arsenic species was performed by an automated pH-selective arsines generation technique, using sodium tetrahydroborate(III) as reductant. Each arsine was cryogenically trapped in a PTFE coil, knotted and sealed inside another wider diameter tube, through which liquid nitrogen was suctioned by negative pressure. Then, based on their different boiling points, the arsine species were selectively liberated by using a heating cycle of microwave radiation, followed by atomic absorption detection. A sample solution aliquot mixed with 1% citric acid was used for the determination of As(III) alone, while a second sample aliquot mixed with 2 mol l^{-1} nitric acid was used for the quantitative determination of total inorganic arsenic, monomethylarsonic acid and dimethylarsinic acid. Based on 10 ml sample, the detection limits lie within the range 20–60 ng As l^{-1}, which are sufficiently low to detect the arsines-forming species in natural waters. These values are negatively affected by the reagents purity and background noise due to flame flickering, but the sensitivity can substantially be improved by increasing sample size or running several consecutive reactions. © 1998 Elsevier Science B.V.

Keywords: Arsenic speciation; Cryogenic trapping; Microwave heating; Flow injection; Hydride generation; Atomic absorption spectrometry; Automated analysis

1. Introduction

Arsenic is one of the elements which, because of its abundance in the environment, its known toxicity for living organisms and its complex bio- and geochemistry is of particular concern and interest for scientists working in different fields. It is of special importance to study some aquatic ecosystems, where, depending on the specific conditions of the water bodies (pH, salinity, redox potential, temperature, presence of microorganisms, etc.), arsenic may exist in different oxidation states (As(III) and As(V)) or organic forms [1,2]. It is thought that As(V) as a phosphate analog is

* Corresponding author. Fax: + 58 74 401286.

PII S0039-9140(97)00189-6

Table 1
Some physical constants[a] of the arsenicals studied

Compound	pK	α_0 at pH 1[b]	α_0 at pH 4[b]	Volatile product	Boiling point (°C)
Arsenous acid [As(III)] ($HAsO_2$)	9.23	1.00	1.00	AsH_3	−55
Arsenic acid [As(V)] (H_3AsO_4)	2.25	0.95	0.017	AsH_3	−55
Monomethylarsonic acid (MMAA) [$(CH_3AsO(OH)_2$]	2.60	0.98	0.038	CH_3AsH_2	2
Dimethylarsinic acid (DMAA) [$(CH_3)_2AsO(OH)$]	6.19	1.00	1.00	$(CH_3)_2AsH$	35.6

[a] Values taken from references.

[b] $\alpha_0 = [H^+]/[H^+] + K_1$

is the fraction of undissociated arsenic species at equilibrium, where K_1 is the first dissociation constant of the acids and $[H^+]$ is the hydrogen ion concentration.

readily taken by aquatic organisms and transformed into simple methylated species: monomethylarsonic acid (MMAA) and dimethylarsinic acid (DMAA). Due to biotransformation processes, these species are frequently detected not only in the aquatic biota, but also in marine and freshwater systems [1]. Thus, although the total concentration of the element is useful to know, the individual determination of the different species is more relevant. However, when such a problem has to be solved, the analytical chemists are faced with very difficult tasks in assuring the acquisition of accurate data, since spontaneous changes in species distribution may occur in time, leading to erroneous results and of course to misleading conclusions.

For the determination of arsenic species in water samples, where the concentrations are usually below 1 μg l^{-1}, whatever the method, one or more preconcentration steps may be always necessary, while to differentiate between species it is more common, though possibly more time consuming to use a separation technique. Most workers have successfully used high performance liquid chromatography (HPLC) [3–5] and ion exchange [6–8], followed by arsines generation with inductively coupled plasma atomic emission spectrometry (ICP) or atomic absorption spectrometry (AAS) detection [2]. In general, these techniques are time consuming and involve tedious procedures to separate the individual species. Selective generation of the arsines followed by their freeze trapping and sequential volatilization prior to the determination of the analyte by AAS [9,10] or other methods [11], have proved to be more simple and sensitive. This is the bases of the speciation procedure developed in this study.

It is well documented that trivalent and pentavalent arsenic show different behavior in the generation process due to kinetic discrimination. In the batch arrangements this difference is not very pronounced and provided selected experimental conditions in flowing systems, mainly in flow injection (FI) only As(III) is reduced, probably because the As(V) reaction is too slow [12,13]. This effect could be reduced or even eliminated by using long reaction coils [14]. This approach is not generally recommended since it increases the total time of analysis and could result in increased interferences [15]. Differentiation between the two valence states is made possible using pH selective arsine generation technique and carefully controlling the experimental conditions for the generation of the volatile species. Not only inorganic, but also some organic containing arsenic compounds, namely MMAA and DMAA are reduced to the corresponding arsines (Table 1) by sodium tetrahydroborate in acidic media. Thus, they may contribute to the apparent yield of arsine if the generator is connected directly to the atomizer, so

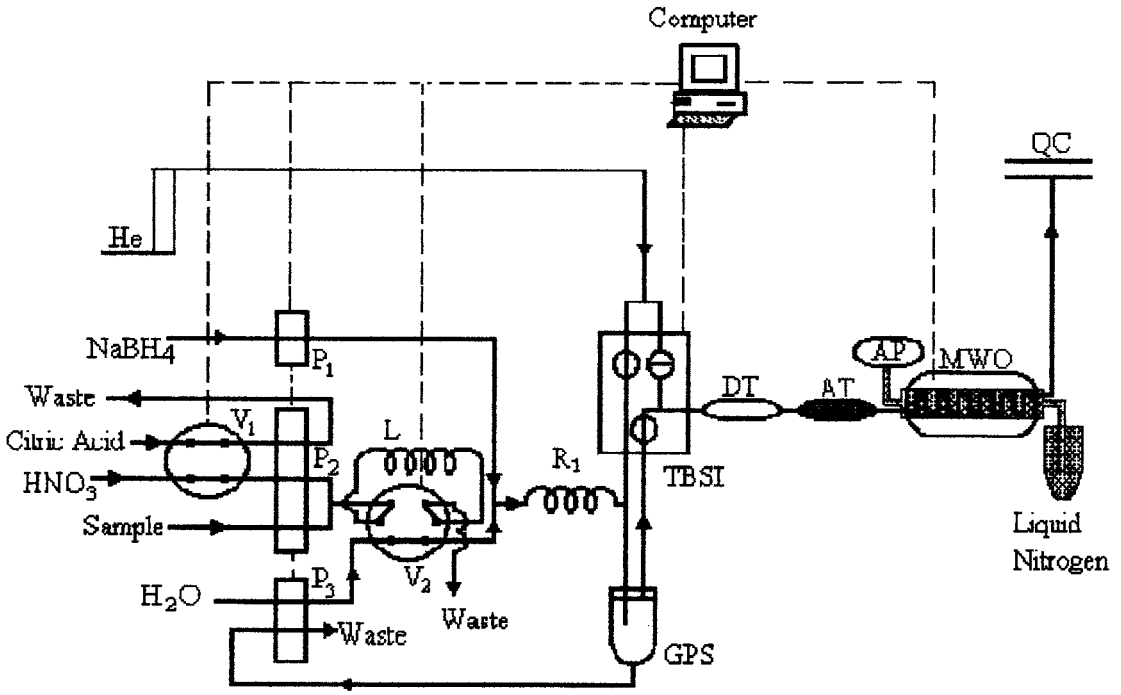

Fig. 1. Schematic diagram of the FI-Hg-AAS system used for the determination of arsenic species with on-line cryogenic trapping and volatilization with MW heating. The system is shown in the sample and nitric acid loading position for the determination of total inorganic arsenic, MMAA and DMAA.

that inorganic arsenic concentration will be overestimated.

This paper describes an automated method that utilizes an ingenious trapping procedure for the separation and preconcentration of four arsenic species by first trapping and then selectively volatilizing them prior to AAS analysis. For the first time microwave (MW) energy was used to selectively volatilize the trapped species.

2. Experimental

2.1. Apparatus

The experimental assembly used in this work is schematically shown in Fig. 1. It consists on three Ismatec IPC peristaltic pumps (P_1–P_3) and two Latek TMW injectors, one 4-way, (V_1), and the other 6-way, (V_2), used to choose the acidic solutions for HG and to inject the acidic mixture, respectively. P_1, P_2 and V_2 are synchronized in such a way that to avoid excess $NaBH_4$ and acidified sample being carried to waste. It also includes a time based solenoid injector (TBSI) [16] used to distribute the He gas in the system, a gas phase separator (GPS) recently described elsewhere [17], a drying tube for water vapors (DT), an NaOH trap for acid vapors and CO_2 (AT), a cryogenic trap (CT) located inside a domestic Panasonic programmable microwave oven (MWO) and a quartz cell (QC) aligned in the light path of a Varian arsenic lamp. A Varian, Model 1475 atomic absorption spectrometer linked to a TDK 286 personal computer, which controls the whole system, was capable of measuring both peak height and peak area values. All determinations were made at least in triplicate under the optimized experimental operating parameters given in Table 2.

To remove water vapors and reagents mist, a drying tube (DT) made of polypropylene, 5 cm

long, 1.0 cm i.d., was filled with Drierite® as desiccant; the carbon dioxide and acid vapors absorber (AT) was a 5 cm long, 1.0 cm i.d., polypropylene tubing partly filled with small sodium hydroxide beads, Becker analyzed® reagent of 0.4–0.5 cm of diameter. Both were incorporated to the experimental arrangement as shown in Fig. 1.

The CT, made from PTFE 1.0 m long, 0.8 mm i.d., was sealed in a knotted form inside a polystyrene tube 1.0 m long, 0.5 cm i.d., through which liquid nitrogen was suctioned by negative pressure produced by an IWAKI air pump (AP), Model AP-115 operated at a maximum flow of 15 l min^{-1}. This produces a vacuum of 450 mm Hg, enough to almost fill the polystyrene tubing with liquid nitrogen.

In order to assure proper active sites on the QC surface during the atomization step, the cell was periodically cleaned with concentrated hydrofluoric acid as recommended in the literature [18]. The pH was measured with a Metrohm Herisau Titriskop, Model E 516. Helium used to maintain a stable baseline and to carry the hydrides to the QC, introduced in the system by alternating the positions of the TBSI, was from AGA, which certifies a purity of 99.99%. The removal of the liquid from the GPS, as well as the washing procedure were controlled by P_3 maintained in operation during the entire process.

Table 2
Operating conditions of the on-line arrangements

Wavelength	193.7 nm
Band width	0.5 nm
Lamp	Varian (5 mA)
Quarts cell (QC)	15 cm path length × 8 mm i.d.
Flame	Air/acetylene (12.0/1.5 l min^{-1})
Hellium flow rate	
Direct to QC	250 ml min^{-1}
Through GPS	250 ml min^{-1}
Reductant	
Concentration	2% (w/v) in 0.1 mol l^{-1} NaOH
Flow rate	1 ml min^{-1}
Acids	
Concentration	
Citric acid[a]	1% (w/v)
Nitric acid[b]	2 mol l^{-1}
Flow rate	5 ml min^{-1}
Sample flow rate	5 ml min^{-1}
P_1 activation time	1 min
P_2 activation time	2 min
Trapping coil length	1 m
MWO power	700 W

[a] For the selective determination of As(III).[b]For MMAA, DMAA and total inorganic arsenic determination.

2.2. Reagents

Standard solutions (1000 mg As l^{-1}) of arsenite, arsenate, MMAA and DMAA as well as reductant solutions were prepared as indicated elsewhere [8]. Freshly prepared solution of sodium tetrahydroborate(III) [2.0% (w/v) in sodium hydroxide 0.2% (w/v)] was used throughout. High purity mineral acids (HCl, $HClO_4$, H_2SO_4, HNO_3 and H_3PO_4), commercially available from Merck, were submitted to a purification process [19]. The organic acids (formic, acetic, oxalic, citric, tartaric and trichloracetic), tested for the generation of the hydrides were also analytical grade reagents from Merck. High purity deionized water (18 M cm^{-1}) was used throughout to prepare all the solutions. The glass- and plastic-ware used for the preparation and storage of solutions was precleaned by soaking in nitric acid and rinsed with water. Solutions containing potential interferents were prepared from chloride or nitrate salts. All chemicals, after preparation were degassed by bubbling through a flow of nitrogen and then, were kept in closed dispenser bottles to avoid absorption of carbon dioxide from air.

The buffers considered in this study were: acetic acid-acetate (1 mol l^{-1}) (pH range 1.0–5.0), citric acid-citrate (5 + 1 sodium citrate 1 mol l^{-1} + citric acid 10% (m/v)) for a pH range 5.5–6.0 and phosphoric acid-phosphate (pH range 5.5–8.5), prepared as indicated in the literature [20].

2.3. Samples

For the analysis of arsenic species in water samples, special care must be taken on the design of the sampling protocol to avoid losses or changes between species. The sampling scheme adopted in this study was as follows: river and trout fishery waters were collected at each sampling site using a 1l high density polyethylene

bottle, which was rinsed several times with the sample in an attempt to saturate adsorption sites on the vessel walls. The representative sample was taken at last from that site; where possible, the sample was taken from below the surface. The bottles were filled to the brim with the samples to avoid any air space, were transported to the laboratory without any additives and were kept refrigerated (4°C) until the analysis was carried out.

2.4. Procedure

The procedure consists on various steps concerning arsines generation and cryogenic trapping followed by selective volatilization and detection, as described below.

2.4.1. Procedure 1. Determination of total inorganic arsenic, MMAA and DMAA.

Arsines generation starts when valve V_1 and pump P_2 are activated for 160 s to deliver sample and nitric acid solutions to fill the loop (L) of V_2. At the same time, P_1 is activated to deliver a volume of reductant. The reaction takes place in R_1 and is completed in the GPS. The volume of $NaBH_4$ is controlled by the P_1 tubing diameter and its time of activation. Concomitantly with the activation of V_1 and P_2, the air pump is turned on to fill in the polystyrene tubing inside the MWO with liquid nitrogen. As the reaction takes place, the TBSI changes position to deviate the flow of helium through the GPS in order to help the sweeping of the volatile products (AsH_3 from As(III) and As(V) and the corresponding arsines of MMAA and DMAA) to CT. The H_2 evolved as by-product of the reaction, passes directly to the QC (its boiling point is -295°C), water vapors are retained in DT, CO_2 and acid vapors are absorbed in AT and the arsines are freezed in CT. The selective volatilization of the arsines trapped is the most critical step of all. It is carried out by activating the MWO for 5 min at its maximum power setting (700 W), while the carrier gas flows continuously and the signal is recorded. During the whole process, P_3 is activated and consecutively it performs several functions: it removes liquid waste from the GPS, allows the transport of the acidified sample from the loop towards the GPS, and also performs the washing procedure. The latest is always carried out between samples and consists of flowing water through the sample channel for 30 s to flush away the last traces of the previous sample, thus avoiding inter-samples contamination and/or memory effects.

2.4.2. Procedure 2. Determination of As(III)

Arsine from As(III) was selectively generated from a solution aliquot mixed with 1% citric acid, which was introduced by activating V_1 to an alternate position, and the signal was obtained following the procedure 1.

The amount of As(V) is determined by arithmetic difference between the responses of total inorganic arsenic obtained in procedure 1 and As(III) obtained in procedure 2.

3. Results and discussion

3.1. Preliminary considerations

Although the generation and atomization conditions for the determination of these arsenic species have been previously studied [8], the peculiarity of the system proposed here demand for an exhaustive optimization of all experimental variables. The parameters controlling each step of the analytical process have been optimized under the criteria of providing the best sensitivity, resolution and reproducibility as well as good recoveries for the analyte measurement in the samples. During the development of the analytical method the concentration of the arsenic species in the test solutions was maintained at 1 g l^{-1}, which based on 10 ml sample volume, makes 10 ng of arsenic injected.

It was clearly demonstrated some time ago that the reduction reactions for arsines generation are not only pH dependent, but also related to the pKa values of each arsenic acid [21]. From the physical constants values given in Table 1 it is obvious that As(III) and DMAA will be reduced over a wide pH range, while the other species over a narrower range. This behavior, added to the fact that each compound form a different arsine, each with a different boiling point, makes possible

their selective volatilization under controlled reaction conditions.

3.2. Effect of acids type and concentration

Different types of acids as well as concentrations are described in the literature to reduce arsenic species with $NaBH_4$. The conclusions are sometimes contradictory depending on the scope of research being carried out as well as on the experimental assembly and reaction conditions, although kinetic factors or mixing dynamics appears to be the most reasonable explanation.

In order to find the appropriate acidic system, which will avoid strong pH variations during the mixing of samples with the alkaline reductant, a series of mineral (HCl, H_2SO_4, HNO_3, $HClO_4$, and H_3PO_4) and organic (formic, acetic, oxalic, citric, tartaric and trichloracetic) acids were tested. Some of these solutions have shown promising selectivity for the arsenic species studied, but independent of the acid type, we found that when the pH was higher than 8.5 there was no vigorous hydrogen evolution such as occurs at lower pH values, and consequently no response was obtained from any of the arsenic species.

The effect of varying the mineral acids concentration on the responses from the four As species was studied. All but phosphoric acid affect similarly the responses on changing acid type and concentration in the range studied. The results obtained, clearly show that concentrations of 2 mol l^{-1} and lower, allow the evolution of arsines from all species to almost identical extents. At higher concentrations, the responses from As(III) and As(V) increased, reaching rapidly a constant value, while the other species (MMAA and DMAA) experienced a marked decay. Furthermore, in highly acidic solutions the effervescence due to hydrogen generation also increases causing splashing of solution droplets on the GPS walls and cap. Water vapor and/or reagents mist might condense on the transfer lines and consequently can trap the analyte gases and then release them slowly causing loss in sensitivity and memory effects. To reduce the amount of moisture into the drying tube and thus avoiding its frequent changing, the acid concentration was kept as low as the experiment requirements allowed it. In orthophosphoric acid the two organic species showed a slight increase in sensitivity, although never reached the values obtained in 2 mol l^{-1} of the other mineral acids. Therefore, this acid was not used for further studies. Below 2 mol l^{-1} of any other mineral acid studied, it is possible to determine total arsenic in direct transfer systems, without the need of sample digestion prior to analysis. It is also possible to speciate MMAA, DMAA and total inorganic arsenic in arrangements like the one described in this paper. The literature abounds with papers where HCl is generally used, although it was repeatedly reported that its vapors cause devitrification of the QC [17]. There is also some controversy on the use of H_2SO_4. Anderson and co-workers [21] found that at concentrations above 0.1 mol l^{-1} the signals for all species decayed considerably, behavior attributed to a series of factors including rapid reductant decomposition at higher acid concentrations, sulfate interference or unknown characteristics of degassing. This explanation is not at all convincing because it is not based on any experimental data. However, some other authors proposed its use below 2 mol l^{-1} [22]. Above that concentration it was found to produce disproportionation in the analysis of DMAA. It is also well known that perchloric acid is not recommended unless special fume hoods are available. Based on the results shown in Fig. 2(a), and on the considerations made above, we are entitled to recommend the use of nitric acid for the speciation and quantitation of MMAA, DMAA and total inorganic arsenic, although in our system, sulfuric acid also provides good recoveries for all species.

Since both inorganic As species yield the same hydride, it was necessary to search for a different acidic media which would differentiate between As(III) and As(V), thus allowing their speciation. It was interesting to find that in all organic acids tasted, there was a great difference between the As(III) and As(V) responses. The generation of the arsines from As(III) and DMAA is essentially independent on the acidity of the reaction media in formic, tartaric and acetic acids, while the signals from As(V) and MMAA become negligible especially in acetic, oxalic and citric acids. It

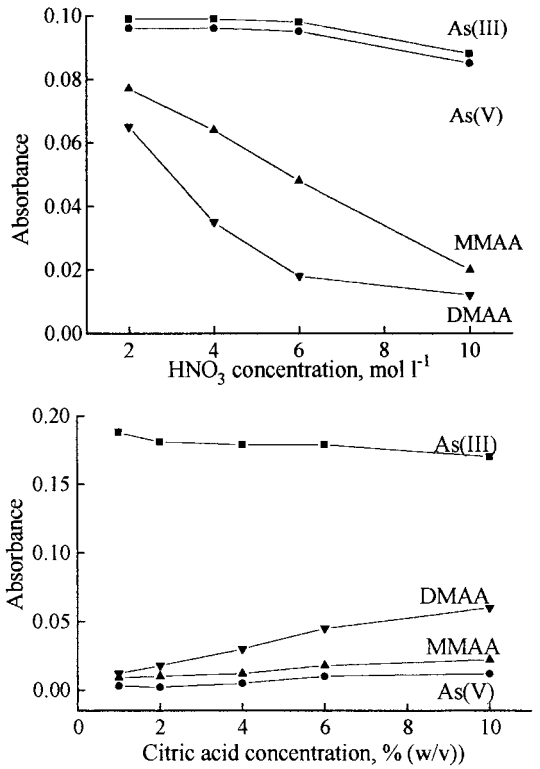

Fig. 2. Effect of inorganic acids (a–e), organic acids (f–j) and buffer systems (k–n) on the absorbance signals from 10 ng As of each arsenic species; other conditions as specified in Table 2.

appears that in these media, the rate of the reduction reaction of As(V) to As(III) decreases until it eventually becomes much slower than the rate of hydrolysis of $NaBH_4$ under the same conditions [23]. To avoid any positive contribution from As(V) in the determination of As(III), 1% citric acid (Fig. 2b) is recommended for further studies in order to differentiate As(III) from As(V).

The instrumental parameters and the acids type and concentration used for further work are listed in Table 2.

3.3. Effect of reductant

Sodium tetrahydroborate(III) has been chosen as the obvious reducing agent for the synthesis of the arsines in the FI system described in this paper. The decomposition reaction of this reagent in acidic media is completed within a fraction of a second and its rate increases when the pH decreases. This means that the formation of the hydrides is even faster and apparently $NaBH_4$ has sufficient life to effect the reduction of the arsenic compounds [24]. However, the separation of the hydrides from the liquid phase takes much more time. In our system, the mixing process is carried out in such a way that there is no decomposition of $NaBH_4$ prior to its reaction with the analyte. There is a limitation on the optimization of the reductant flow rate and concentration due to the generation of excess hydrogen which causes variations on the signal-to-background ratios (S/B). Above a concentration of 3% (w/v) of reductant, the background absorption suddenly increased, possibly owing to the burning H_2 inside the QC, while a concentration lower than 0.5% (w/v) produces small S/B ratios for all species. The optimum $NaBH_4$ concentration was thus chosen to be 2% (w/v).

3.4. Effect of volumes and flow rates

The volumes of sample, acids and reductant are controlled by the flow rates delivered by P_1 and P_2 and by their time of operation. The system allows equivalent standard or sample and acid volumes to be mixed in the loop. The volume of the acidified sample is thus limited by the loop capacity which it was chosen to allow a maximum volume of 10 ml to be carried to the GPS each time. By varying the flow rate of P_2 from 1 to 15 ml min^{-1}, and operating it for 1 min, the response increased continuously as a consequence of increasing the amount of analyte in the GPS. However, if an adequate control of the time is carried out, in order to introduce the same amount of analyte, the flow rates of sample and acids had no effect at all, up to 7 ml min^{-1}. However, for higher flow rates, the reproducibility deteriorated, probably due to an inefficient mixing of both solutions with the reductant in R_1 and in the GPS. For the reasons discussed above, we have chosen a flow rate of 5 ml min^{-1} for P_2. Also a variation in the reductant volume up to 4 ml, had no effect on the absorbance values, but a bigger volume produced unpaired results due to

increased effervescence caused by violent hydrogen production. A volume of $NaBH_4$ of 1 ml was considered appropriate for complete reaction.

3.5. Effect of carrier gas

Helium was used in two parts of the system: (a) to maintain a stable baseline and (b) to carry the generated arsines from the GPS to the cryogenic trap and to transfer the collected hydrides, once they have been revolatilized, to the atomizer.

The baseline was stabilized by continually passing a flow of 250 ml min^{-1} of He to the QC through the TBSI. The flow of He meant to transport the arsines to the trap is also aided by the hydrogen by-product. Once the acidity of the reaction media and the reductant concentration were optimized, the carrier flow rate was no longer critical, but, both flows have to be equal to avoid problems of the gas reverse movement due to pressure-built in the system.

The flow of He used to transfer the volatilized arsines to the QC is more critical since it affects the residence time of the analyte in the atomizer and also the separation effectiveness. The effect of altering the carrier gas flow rate in a range as wide as possible (20–1000 ml min^{-1}) shows that for high flow rates (>500 ml min^{-1}) the hydrides are carried out too quickly, resulting in a loss of resolution and decrease in sensitivity. This is logical because the larger is the flow rate the lesser is the residence time of the analyte in the atomizer. At low flow rates (<50 ml min^{-1}) the signals gave good reproducibility, but distorted and broadened peaks were obtained with consequent loss in resolution.

A compromise had to be made in choosing 250 ml min^{-1} as optimum carrier gas flow rate to transport the arsines to the QC.

3.6. Microwave-aided selective volatilization

As the generated hydrides are collected in the freezing trap, the precision of the analysis will only be affected by an efficient energy absorption as MW pass into the trapped arsines and their proper transfer to the QC. Polystyrene and PTFE tubing used for housing the liquid nitrogen and to trap the hydrides, respectively, are good insulators and effectively transparent to microwaves. In this case, heat through the coils walls becomes insignificant. As liquid nitrogen is also transparent to the radiation, only the trapped, frozen products will be heated and selectively volatilized from the coil. In order to obtain good reproducibility and reasonable resolution of the results, the different experimental sequences have to be strictly coordinated and carried out at specific time intervals. Typical output signals obtained from the HG-AAS system are shown in Fig. 3. The selective volatilization profiles were similar when the arsenic compounds were present individually or in admixture. The volatilization times were 90, 180 and 235 s for dimethylarsine, methylarsine and arsine, respectively. The higher sensitivity for all species was obtained at maximum power setting (700 W) of the MWO, because the signals rapidly decay at lower power settings; no signals were obtained for none of the species at 75% of the MWO power, probably because of an insufficient sample heating, thus resulting in no vaporization of the arsines. Therefore, this parameter was excluded from those experimentally optimized in this work.

In previous works, cryogenically trapped arsines were evolved upon worming, in order of their boiling points or according to their volatility [10,11]. However, this was not the case in this work, probably because the separation is carried out using MW energy at a given frequency, which heats the trapped hydrides by dipole rotation, being quite different from the conventional conductive heating. The sequence of arsines evolution could be due to the contribution of two mechanisms: (1) to the absorption of MW energy as it passes into the sample, depending mainly on the dielectric constant of each compound and (2) to the dipole size which affects the penetration depth of the MW energy; the larger the molecular size of the dipole, the more it is penetrated by the MW energy. It is obvious that the major contribution of these two mechanisms of heating is dominated by dipole rotation, and the heating time is shorter for those molecules with higher dielectric constant. However, the efficacy of heating by dipole rotation depends here upon the samples charac-

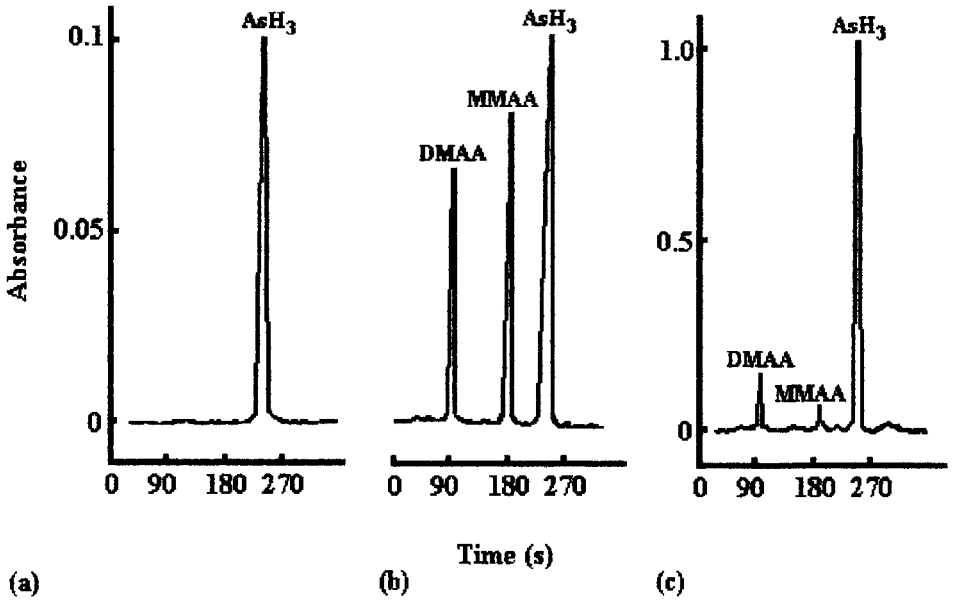

Fig. 3. Analytical signals obtained from inorganic arsenic (5 ng each) and its methylated species (10 ng each) using (a) 2 mol l^{-1} nitric acid and (b) 1% w/v citric acid. (c) This shows the responses from a trout fishery sample. The experimental conditions were as specified in Table 2.

teristics, in particular the inherent mobility of each trapped species without ionic migration as it is the case of the heating pattern of any ionic solution.

Other aspects of the proposed system, which have been studied, are the trapping coil length and its arrangement inside the freezing tube into the MWO. Many coil length were assessed (0.7–2.0 m), but no difference in signal and arsines separation performance were observed. Trapping coils longer than 3 m caused substantial dispersion, resulting in a decrease in sensitivity and deterioration of the resolution. On the other hand, for tubing length shorter than 0.7 m, the signals decreased due to a poor trapping efficiency. The efficiency of the hydrides collected and the resolution were better in a knitted tube than in a straight one of the same length and inner diameter. Thus, it was proposed to use a 1 m long trapping coil which assured a relatively high sensitivity and reasonable good resolution for all the arsenic species studied.

3.7. Analytical figures of merit

Under the optimal experimental conditions outlined in Table 2, the AAS signals were measured and the concentrations of As(III), As(V), MMAA and DMAA were calculated against the individual arsenic species standard curves, which in all cases were linear up to 50 ng. The sensitivity values (slopes of the calibration curves), the lower limits of the linear range, the detection limits (DL, expressed as twice the background standard deviation) and the reproducibility values are given in Table 3.

The relative standard deviation (R.S.D.%) was calculated from the responses obtained by consecutively injecting 10-times a solution containing the four species at concentrations corresponding approximately to 5-times the lower limit. The precision of measurements at the 1 g l^{-1} level was around 1.5% for all species.

The accuracy of the proposed procedure was tasted on the bases of % recovery calculated for a trout fishery water sample spiked with the four

Table 3
Analytical characteristics

Compound	Slope (10^{-2})	Lower limit[a] (ng)	Detection limit[a] (ng)	R.S.D.[b] (%)
As(III)	0.99	0.50	0.20	2.5
As(V)	0.98	0.60	0.24	2.8
MMAA	0.90	0.80	0.35	3.5
DMAA	0.80	1.50	0.60	3.8

[a] Calculated for 10 ml total sample volume.
[b] Obtained for a concentration 5-times higher than the lower limit ($n = 10$).

compounds at two concentration levels: 5- and 10-times the corresponding DL. The mean values obtained are given in Table 4. Substantial amounts of the species were recovered, thus enabling this method to be used for the analysis of real samples. The accuracy was further tested by determining: (1) the different species of arsenic in a certified water sample and (2) the sum of all arsenic species (ΣAs) were compared with those obtained by ETAAS [25], where owing to the analytical difficulties in quantifying low arsenic concentrations, the technique of standard additions was adopted. The ΣAs agreed well with the As(T) and with the certified values of two water samples (Table 5), which is another indication of satisfactory accuracy of the proposed method. However, the lack of materials which certify the arsenic species and the poor sensitivity of available alternative methods for detection of such low concentrations of arsenic species, made further studies on the accuracy of our procedure impossible.

The analytical parameters obtained in this work show that the methodology here proposed is sensitive, precise and accurate. The DL were as good as, or better than those previously obtained in manually operated systems using arsines trapping techniques [9–11]. However, these fitures (Table 3) could be further improved due to the possibility of preconcentration of the products by using a bigger volume or running several consecutive reactions. Several consecutive reactions have been carried out, thus achieving preconcentration of the species for those samples with extremely low arsenic species content (e.g. MMAA concentration in the sample from the trout fishery). For samples with arsenic content over the linear working range, dilution is avoided by reducing the operating time of the P_2, thus introducing less amount of analyte in the system.

Table 4
Mean recovery values (%) for trout fishery water samples[a] spiked with the four arsenic species

Compound	Concentration level[b]		
	DL × 5	DL × 10	Total mean recovery (%)
As(III)	83.5 ± 6	93.4 ± 4	88.5
As(V)	100.9 ± 4	96.8 ± 3	98.9
MMAA	102.0 ± 5	99.0 ± 3	100.5
DMAA	98.9 ± 5	100.4 ± 4	99.7

[a] Endogenous values as in Table 5.
[b] Analysis in triplicate for the species at each level.

3.8. Applications

The concentrations of total arsenic in most natural water systems are reported [26,27] to be in the range 0.1–1.0 μg l^{-1}. However, in different parts of the world, the levels of arsenic are two and even three orders of magnitude higher than that of most natural waters consumed by man [28,29]. Such is the case, for example, of the drinking water consumed in Cordoba, Argentina [30], where the arsenic levels are as high as 1400 g l^{-1}, while in the shallow tubewells in South Bengal, India [7,28,29], the levels are from 60 to 58/000 g l^{-1}. It is also reported [31] that mineral waters may contain up to 50-times and hot springs up to 300-times more arsenic than the normal background level. In an attempt to protect aquatic life as well as to establish a control over the implications of arsenic concentrations for public health, different international organiza-

Table 5
Arsenic content in different types of water

Sample	As(III)	Arsenic concentration (μg l^{-1})[a]			ΣAs	As(T)[b]
		As(V)	MMAA	DMAA		
River water						
1	1.20 ± 0.02	4.20 ± 0.09	—	—	5.40	5.41 ± 0.20
2	1.35 ± 0.03	4.90 ± 0.10	—	—	6.25	6.22 ± 0.20
Trout fishery	1.90 ± 0.4	8.50 ± 0.20	0.70 ± 0.01	1.80 ± 0.05	12.90	13.0 ± 0.30
HPS certified sample[c]	57.27 ± 0.43	24.73 ± 0.30	—	—	82.00	81.20 ± 0.50
NIST certified sample[d]	34.76 ± 0.30	16.38 ± 0.20	—	—	51.14	48.70 ± 0.20

[a] Results expressed as $X \pm St/\sqrt{n}$ ($n = 5$).
[b] Determined by ETAAS.
[c] Certified value for HPS certified reference material. Trace metals in drinking water = 80.0 ± 4.0 μg l^{-1}.
[d] ™NIST SRM 1643b, Trace elements in water. Reference value = 49 ng g^{-1}.

tions recommended the permissible dissolved total arsenic concentration in natural waters, between 8 and 50 g l^{-1}.

The analytical procedures optimized in this work have been used for the quantitation of four arsenic species in different type of water samples: river waters and samples from a trout fishery. The range of arsenic concentrations of these water samples provided an opportunity to apply our procedure to the analysis of real samples.

The results shown in Table 5 are in general agreement with those reported in the literature [27,32]. In the aquatic environment, arsenic is found predominantly in the inorganic form with As(V) being thermodynamically stable. This is the case for the turbulent high mountains river waters analyzed here, where the oxidation processes are favored under aerobic conditions. None of the methylated species was detected in river waters, despite the reports that these species can represent a considerable fraction of the total arsenic present [27,32]. The low temperatures of these waters may inhibit the biological formation of such species. In the sample from the trout fishery the dominant species were As(V) and DMAA. The presence of methylated species in this sample might be attributed to unidentified biological mediation; some authors have concluded that arsenate is taken up by phytoplankton and subsequently converted to MMAA and DMAA, probably as part of a detoxification mechanism, and replaced back into the water column [33–35]. Both, MMAA and DMAA are stable species in the aquatic environment, but their production and distribution in oxic surface waters is a fluid process that is seasonably dependent. A systematic, long-term sampling should be undertaken in order to reach solid, well-fundamented conclusions regarding the natural processes in such water bodies.

4. Conclusions

The development of the selective preconcentration technique proved to be a powerful tool for the determination of extremely low arsenic levels in water samples. One of the attractions of our procedure was the simplicity of the equipment which allowed high efficiency of analyte introduction, ease of preconcentration and the possibility of speciation.

Using the manifold described in this paper the risk of contamination and volatilization losses are drastically reduced since the system is completely closed and all operations are performed on-line. The analysis is carried out with optimum sensitivity due to the preconcentration in the cryogenic trap, which allow the analyte to be conveyed to the atomizer in a much higher yield than is ever attained in conventional HG. This makes the method attractive for application to matrices with low arsenic content like the different types of waters. Other benefits are the increased speed of analysis compared to similar procedures, the use

of microwave energy to volatilize the hydrides added to the facility to optimize the system since fewer parameters are involved.

This system also affords the intimate mixing of reagents with better pH control; it appears to be much more tolerant to elements which normally interfere in the hydride generation and provides the opportunity to elegantly eliminate volatile reaction by-products.

Automation of the whole procedure, from sample loading to data report leads to enhanced sensitivity, precision and accuracy compared to manual methods.

Acknowledgements

The authors appreciate financial support from BID-CONICIT (Banco Interamericano de Desarrollo-Consejo Nacional de Investigaciones Científicas y Tecnológicas), Project QF-46.

References

[1] A.C. Aurillo, R.P. Mason, H.F. Hemond, Environ. Sci. Technol. 28 (1994) 577.
[2] M. Burguera, J.L. Burguera, Talanta (1997) in press.
[3] Ch-Jev Hwang, S-Jen Jiang, Anal. Chim. Acta 289 (1994) 205.
[4] X-Chun Le, W.R. Cullen, K.J. Reimer, Talanta 41 (1994) 495.
[5] M.A. Lòpez-Gonzalvez, M.M. Gòmez, C. Càmara, M.A. Palacios, J. Anal. At. Spectrom. 9 (1994) 291.
[6] O. Jimenez de Blas, V. Gonzalez, R. Seisdedos Rodriguez, J. Hernandez Méndez, J. AOAC Int. 77 (1994) 241.
[7] A. Chatterjee, D. Das, D.K. Mandal, T.R. Chowdhury, G. Samanta, D. Chakraborti, Analyst 120 (1995) 643.
[8] J.L. Burguera, M. Burguera, C. Rivas, P. Carrero, C. Rondón, M.R. Brunetto, Quim. Anal. (1997) in press.
[9] P.H. Masscheleyn, R.D. Delaune, W.H. Patrick Jr., J. Environ. Qual. 20 (1991) 96.
[10] A.G. Howard, S.D.W. Comber, Mikrochim. Acta 109 (1992) 27.
[11] P. Michel, B. Averty, V. Colandini, Mikrochim. Acta 109 (1992) 35.
[12] M.S. Mohan, R.A. Zingaro, P. Micks, P.J. Clark, Int. J. Environ. Anal. Chem. 11 (1982) 175.
[13] J. van Elteren, H.A. Das, C.L. De Ligny, J. Agterdenbos, D. Bax, J. Radioanal. Nucl. Chem. Articles 179 (1994) 211.
[14] S.C. Pinillos, J. Sanz Asensio, J. Galbán Bernal, Anal. Chim. Acta 300 (1995) 321.
[15] B. Welz, M. Sucmanová, Analyst 118 (1993) 1425.
[16] P. Carrero, J.L. Burguera, M. Burguera, C. Rivas, Talanta 40 (1993) 1967.
[17] M. Burguera, J.L. Burguera, C. Rivas, P. Carrero, M.R. Brunetto, M. Gallignani, Anal. Chim. Acta 308 (1995) 339.
[18] S. McIntosh, Perkin-Elmer Technical Summary, Order no. TSAA-17.
[19] Z. Li, N. Zhe-Ming, S. Xiao-Quan, Spectrochim. Acta 44B (1989) 339.
[20] C. Luca, The pH and Its Applications (Rom), 2nd ed., Editura Tecnica, Bucuresti, Romania, 1973.
[21] R.K. Anderson, M. Thompson, E. Culbard, Analyst 111 (1986) 1143.
[22] G. Rauret, R. Rubio, A. Padró, Fresenius J. Anal. Chem. 340 (1991) 157.
[23] J. Aggett, A.C. Aspell, Analyst 101 (1976) 341.
[24] J. Agterdenbos, D. Bax, Fresenius J. Anal. Chem. 323 (1986) 783.
[25] M.E. Soares, B.L. Bastos, M. Ferreira, Analyst 120 (1995) 2367.
[26] A. Leonard, in: E. Merian (Ed.), Metals and their Compounds in the Environment: Occurrence, Analysis and Biological Relevance, VCH, New York, 1991.
[27] W.R. Cullen, K.J. Reimer, Chem. Rev. 89 (1989) 713.
[28] A. Chatterjee, D. Das, D. Chakraborti, Environ. Pollut. 80 (1993) 57.
[29] A. Chatterjee, D. Das, D.K. Mandal, T.R. Chowdhury, G. Samanta, D. Chakraborti, Analyst 120 (1995) 925.
[30] R.M. Bergoglio, Prensa Med. Argent. 51 (1964) 994.
[31] H.G. Seiler, H. Sigel (Eds.), Handbook on Toxicity of Inorganic Compounds, Marcel Dekker, New York, 1988.
[32] L.E. Hunt, A.G. Howard, Marine Pollut. Bull. 28 (1994) 33.
[33] M.O. Andreae, in: P.J. Craig (Ed.), Organometallic Compounds in the Environment, Wiley, New York, 1986.
[34] M.O. Andeae, Deep-Sea Res. 25 (1978) 391.
[35] M.O. Andeae, Arsenic: industrial, biomedical and environmental perspectives., in: W.H. Lederer, R.J. Fensterheim (Eds.), Proceedings of the Arsenic Symposium, 1981, Van Nostrand, New York, 1983.

.

ELSEVIER

Talanta 45 (1998) 543–548

Talanta

New phase separator for extraction-spectrophotometric determination of anionic surfactants with Malachite Green by flow injection analysis

Tadao Sakai [a,*], Hiromasa Harada [a], Xiaoqin Liu [a], Nobuo Ura [a], Kenji Takeyoshi [b], Kunihiko Sugimoto [b]

[a] *Department of Applied Chemistry, Aichi Institute of Technology, Yachigusa, Yakusa-cho, Toyota 470-03, Japan*
[b] *Tokai Technical Centre, Inokoishi, Meito-ku, Nagoya 465, Japan*

Received 3 March 1997; received in revised form 25 March 1997

Abstract

A simple flow injection spectrophotometric method for the determination of anionic surfactants in river water was studied. A three-channel flow system was assembled. The distilled water as a carrier and 5×10^{-5} mol l^{-1} Malachite Green (MG) dissolved in 0.1 mol l^{-1} CH_3COONa-CH_3COOH buffer solution (pH 5) were delivered at 1.94 ml min^{-1}. The mixed solvent (toluene + methylisobutyl ketone (MIBK) = 1 + 1) was pumped at 0.78 ml min^{-1}. Other conditions were the extraction coil 0.5 mm i.d. × 3 m, the reaction temperature 20°C and the sample size 200 μl. The calibration graph was linear in the range 0.1–0.4 ppm at 626 nm. The detection limit (S/N = 3) was 18 ppb and a sample frequency of 20 h^{-1} was attained. The relative standard deviation ($n = 7$) for 0.4 ppm standard sodium dodecylsulfate (SDS) solutions was 1.1%. And also, new phase separator with a convenient connector was designed. This Fl method was applied to the determination of anionic surfactants in river water. © 1998 Elsevier Science B.V.

Keywords: Anionic surfactants; Malachite Green; Mixed solvent; New phase separator; Solvent extraction

1. Introduction

In both Standard Methods for the Examination of Water and Waste Water [1] and Japanese Industrial Standards [2], the solvent extraction of ion-associates formed between Methylene Blue and anionic surfactants is recommended, however, the batchwise method is time-consuming and terrible. Because the method needs three times extractions and washing the extract and also large amounts of toxic chloroform are consumed. Recently, an extraction-spectrophotometric method with Ethyl Violet proposed by Motomizu et al. [3] is adopted in Japanese Industrial Standards [4]. The method needs only a single extraction and it has advantages on sensitivity and simplicity. On the other hand, flow injection analysis (FIA) developed by Ruzicka and Hansen [5] is a very versatile and practical technique. The technique has been widely used in industrial, environmental,

* Corresponding author. Fax: +81 565 480076.

PII S0039-9140(97)00096-9

clinical and pharmaceutical analyses because the method permits automatic, rapid and sensitive analysis compared with the batchwise method.

In 1978, Karlberg and Thelander [6] introduced solvent extraction utilizing a T-piece glass fitting and a teflon fibre string to the FIA and also, at the same time, Kina et al. [7] have reported ultramicro solvent extraction and fluorimetry based on Fl method. Since then, many solvent extraction-FIA systems and several phase separators have been reported. Kawase et al. [8] reported a solvent extraction-FIA using a phase separator with a poly (tetrafluoroethylene) (PTFE) porous membrane and Nord et al. [9] have tested several membrane phase separators designed newly. Motomizu et al. [10] have also compared several phase segmentors and separators and extraction systems in FIA have been investigated, however, there are some problems with long-term continuous runs and permeation of a small amount of water during measurements. It is difficult to maintain the hydrophobicity of membrane for a long time and to prevent leakage of aqueous phase. Recently, the novel extraction systems without segmentation and phase separation have been reported [11,12].

On the other hand, Manzoori and Miyazaki [13] used two phase separators to remove completely the remaining trace moisture in the organic phase and to obtain only pure organic phase by the second separator for the fluoride determination with ICP/AES. To dissolve the problem, a newly designed phase separator with double membranes has been proposed by Sakai et al. [14].

In this paper, we discuss the function of improved separator with a convenient connection and of the back pressure coils and application to the anionic surfactants assay with Malachite Green and the mixed solvent of (toluene + MIBK = 1 + 1) by flow injection analysis.

2. Experimental

2.1. Apparatus

A Hitachi U-3000 spectrophotometer was used with 10 mm light-path cells for absorption measurements. A Horiba M-8L pH meter with a glass electrode was used to measure the pHs. A Taiyo Mini 80 thermostat was used for controlling the extraction temperature.

2.2. Reagents

2.2.1. Malachite green (MG)

Malachite Green, 0.258 g (Katayama Chemical Industries, Osaka) was dissolved in 250 ml of buffer solution (pH 5) to make a 1×10^{-3} mol l^{-1} solution.

2.2.2. Sodium dodecylsulfate (SDS)

1.02 g of sodium dodecylsulfate (purity 98%, Katayama Chemical Industries) was dissolved in 1000 ml of distilled water to make a 1000 ppm solution.

2.2.3. Buffer solution (pH 5)

Sodium acetate, 8.2 g and 3.4 ml of acetic acid were dissolved in an adequate amount of distilled water and the pH was exactly adjusted to pH 5 by adding 3 mol l^{-1} sodium hydroxide.

2.2.4. Extracting solvents

Extracting solvents (toluene + MIBK = 2 + 1, 1 + 1 and 1 + 2) were prepared to mix an adequate volume of toluene and MIBK (Kanto Chemicals, Tokyo).

2.2.5. Batchwise procedure

Mix 5 ml of 10 ppm SDS, 1 ml of 1×10^{-3} mol l^{-1} MG and 5 ml of buffer solution (pH 5) in a 25 ml calibrated flask and dilute to the mark with distilled water. Transfer the mixture into a 100 ml separating funnel and shake with 5 ml of the mixed solvent (toluene + MIBK = 1 + 1). After separation of the organic layer, measure the absorbance of the organic phase at 626 nm against water or reagent blank as a reference.

2.2.6. Procedure for Fl method

A diagram of the flow system used is shown in Fig. 1. The absorbance was measured at 626 nm with a Soma Optics (Tokyo) S-3250 double-beam spectrophotometer with 10 mm micro flow cell (8 μl) and recorded as peak-shaped signals using a

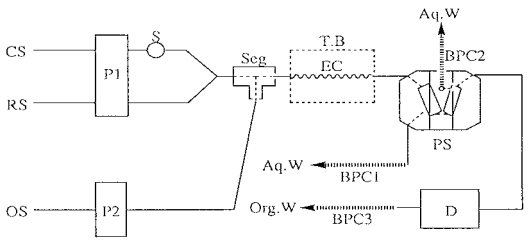

Fig. 1. Flow diagram for the determination of SDS. CS, carrier (distilled water); RS, MG solution (1×10^{-5} mol l^{-1}) dissolved in buffer (pH 5); OS, (toluene + MIBK = 1 + 1); P1, double-plunger pump; P2, single-plunger pump; S, sample injection, 200 μl; seg, sementor; EC, extraction coil (0.5 mm i.d. × 3 m); TB, thermostat bath (20°C); PS, double-membrane phase separator; D, detector ($\lambda = 626$ nm); BPC1, 2, 3, back pressure coil (0.25 mm i.d. × 1, 6, 0.5 m); Aq. W, aqueous phase waste; org. W, organic phase waste.

Shimadzu R-II recorder. A double-plunger micro pump (Sanuki Kogyo, DM2U-1026, Tokyo) and a single-plunger micro pump (Hitachi L-6000, Tokyo) were used for delivering the carrier, the reagent solution (MG) and extracting solvent at 1.94 ml min^{-1} and 0.78 ml min^{-1}. The samples were injected into the carrier stream with a six-way injection valve (dead volume, 80 μl) to which a volume control loop was attached. Flow lines were made of poly(tetrafluoroethylene)(PTFE) tubing (0.5 mm i.d.) except for the back pressure coil (0.25 mm i.d.).

3. Results and discussion

3.1. Improved phase separators and line connector

Motomizu et al. [15] and Sakai [16] have obtained good results using a phase separator with a sloped groove (membrane chamber depth 2 mm, width 2 mm) with PTFE membrane (0.8 μm pore size) for analyses of anionic surfactants and quaternary ammonium salts. However, when trace moisture penetrates the membrane and passes through the flow cell by the fatigue and stopping of the porous membrane and by changing the stream pressure, we have some terrible works on washing the lines and cell. To prevent the permeation of aqueous phase into the cell and to obtain a pure organic phase, double membrane phase separator was designed and the function was investigated on an ion associate formed between berberine cation and perchlorate anion [14]. In this work, the MG-SDS ion association system which causes the deposit and adsorption on the membrane (0.5 μm) was investigated. In the previous paper [16], the needle valve was used to obtain a 97% recovery of organic phase, however, it is difficult to maintain a constant recovery every time. The volumes of aqueous and organic phases which were conducted to W_1 (waste 1), W_2 and W_3 in Fig. 2(a) were compared by varying the

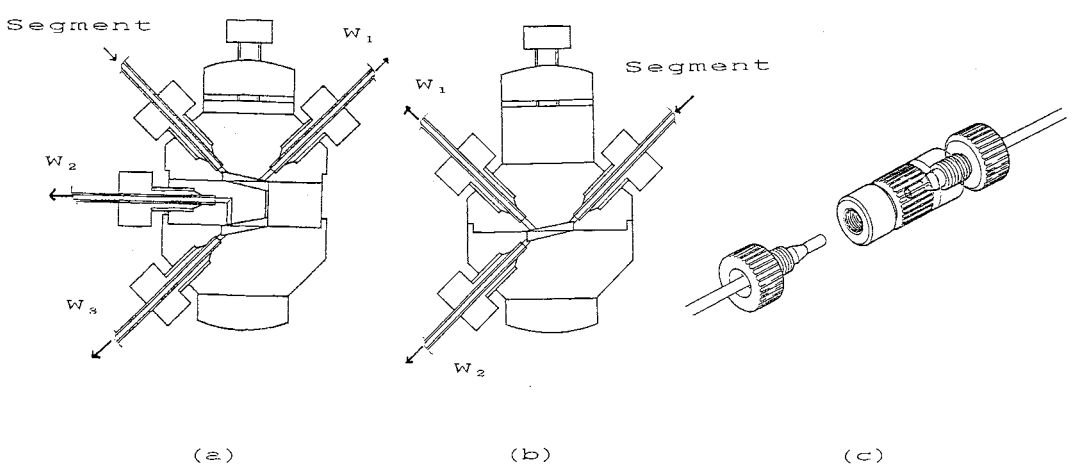

Fig. 2. Phase separators and connector of lines W_1, W_2, W_3: exit of waste.

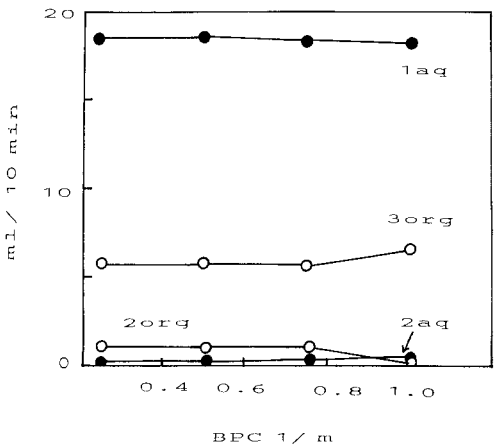

Fig. 3. Effect of BPC1 length sample: 200 μl; MG, 1×10^{-5} mol^{-1}; buffer, pH 5; extraction coil, 0.5 m i.d. × 3 m; temperature, 20°C; flow rate, P_1 1.94 ml min^{-1}, P_2 0.78 ml min^{-1}; $\lambda = 626$ nm; solvent, (toluene + MIBK = 1 + 1); BPC2, 6 m; BPC3, 0.5 m.

back pressure coils (BPC1, BPC2 and BPC3 in Fig. 1). The results are shown in Fig. 3, Fig. 4 and Fig. 5. Curves 1 aq and 1 org refer to the aqueous and organic phases exhausted to W_1, 2 aq and 2 org, to W_2 and 3 org, to W_3. The back pressure coil 2(BPC2) and the coil 3(BPC3) were fixed to 6 and 0.5 m, the BPC1 length was varied in the range 0.2–1 m and the volumes of aqueous and organic phases conducted to each exit for 10 min were measured. The (toluene + MIBK = 1 + 1) was used as an extracting solvent. The results are

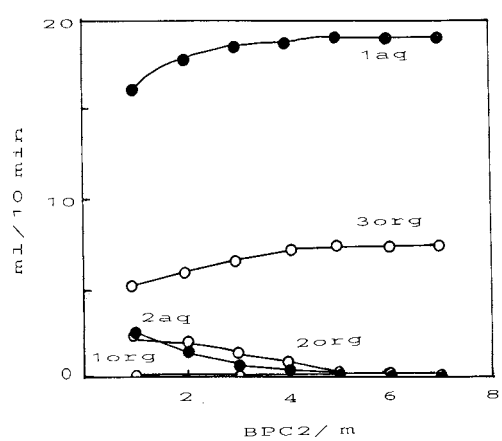

Fig. 4. Effect of BPC2, BPC1, 1 m; BPC3, 0.5 m.

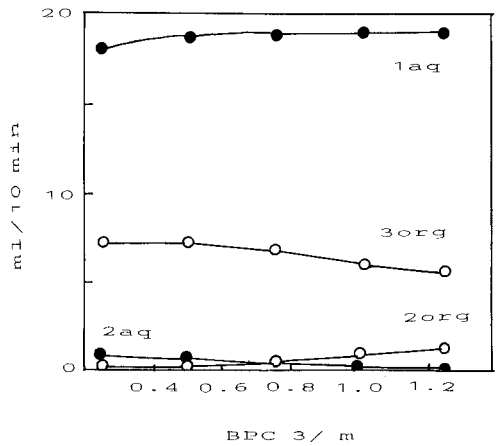

Fig. 5. Effect of BPC3, BPC1, 1 m; PBC2, 6 m.

shown in Fig. 3. When the BPC1 was 1 m, the recovery of 3 org increased and that of 2 org decreased. On the other hand, the volume of 1 aq was constant and that of 2 aq was extremely small. The 1 m length of BPC1 was chosen. The BPC1 and BPC3 were fixed to 1 m and 0.5 m and BPC2 was varied in the range 1–7 m. When the length was over 5 m, the volume of 3 org were constant and largest. On the contrary, that of 2 org decreased and were almost zero (Fig. 4). The 6 m length of BPC2 was used. In addition, after the BPC1 and BPC2 were fixed to 1 and 6 m, the BPC3 was varied in the range 0.25–1.25 m. When BPC3 was less than 0.5 m, about 94% recovery of 3 org was obtained (Fig. 5). When the length was over 0.75 m, the volume of 3 org decreased gradually and that of 2 org increased. As a result, BPC1 1 m, BPC2 6 m and BPC3 0.5 m were chosen in the system. However, when solvents having different specific gravity are chosen, each back pressure coil length has to be determined to get higher recovery of 3 org. The separator was available for continuous runs for 7 h without exchanging the membranes. And also, the jointing devices which the tubes can connect easily was designed as shown in Fig. 2(a, b and c).

3.2. Experimental variables

3.2.1. Batchwise method

As shown in Fig. 6, absorption maximum of

MG-SDS associates occurred at 626 nm. When the mixed solvent (toluene + MIBK = 1 + 1) was used, the reagent blank was almost zero. Molar absorptivity was about 70 000 l mol^{-1} per cm. The effect of pH on the extraction of MG-SDS associate was examined in the pH range 3–9. A pH 5 was chosen.

3.2.2. Fl method

The effect of MG concentration on the colour development was examined. MG($1-10 \times 10^{-5}$ mol l^{-1}) were added to 0.25 ppm SDS. Addition over 1×10^{-5} mol l^{-1} of MG gave the highest and constant peak height. The effect of the extraction coil length was examined in the range 1–7 m. The largest peak height was obtained in the range 1–5 m. A 3 m extraction coil was used. When the coil was 7 m, the height decreased because of dispersion of the extracts.

3.3. Extracting solvent

Mixed solvents such as (1,2-dichloroethane + benzene = 1 + 1), (dichlorobenzene + benzene = 1 + 1) and (chlorobenzene + benzene = 1 + 1) were tested for the cationic dyes-anionic surfactants ion pair extraction systems [15]. However, the use of these halogen organic solvents is controlled to depress water and air pollutants. In this work, the mixed solvents (toluene + MIBK = 1 + 1, 1 + 2 and 2 + 1) were investigated for the MG-SDS associates. Fig. 7 shows the flow signals with different composition mixtures. The (toluene + MIBK = 1 + 1) gave the highest and constant peaks (Fig. 7a). Although the (toluene + MIBK = 2 + 1) gave stable and reproducible signals ($n = 8$, RSD = 1.1%), sensitivity decreased (Fig. 7b). When the (toluene + MIBK = 1 + 2) was used, the larger disorder of both signals and base lines was observed.

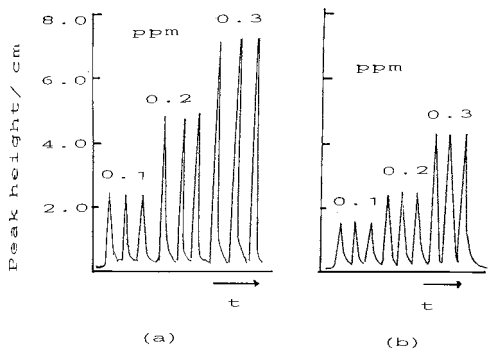

Fig. 7. Flow signals by different composition solvents. (a) (toluene + MIBK = 1 + 1); (b) (toluene + MIBK = 2 + 1).

3.4. Calibration graph

The calibration graph obtained in the extraction-Fl system showed a good linear relationship over the range 0.1–0.4 ppm SDS when 200 μl of the standard solution was injected. The RSD ($n = 7$)

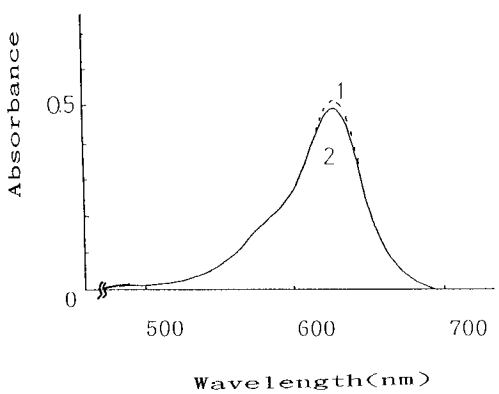

Fig. 6. Absorption spectra of MG-SDS associates. SDS, 2 ppm; MG, 4×10^{-5} mol l^{-1}; pH, 5; solvent, (toluene + MIBK = 1 + 1); (1) reference water, (2) reference reagent blank.

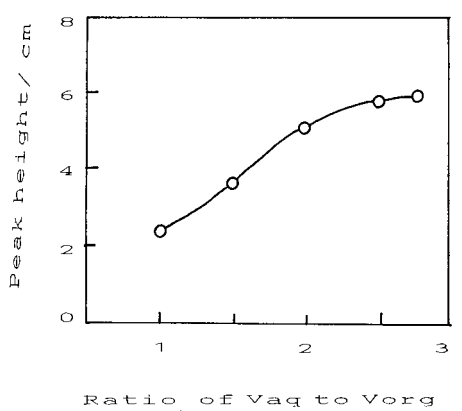

Fig. 8. Effect of the ratio of aqueous to organic phase volume SDS, 0.25 ppm; sample, 200 μl; solvent, toluene + MIBK = 1 + 1.

Table 1
Determination of anionic surfactants in river water

Sample	Anionic surfactants, ppm[a]	
	This work	Methylene Blue method [2]
Yada river (Nagoya)		
Kariyado bridge	1.88	2.0
Shinyashiki bridge	0.30	0.30
Seto river (Nagoya)	2.83	2.95

[a] Average of two determinations.

was 1.1% for 0.4 ppm SDS. The detection limit (S/N = 3) was 18 ppb. Sampling frequency was 20 h^{-1}.

3.5. Concentrated effect by solvent extraction

The flow rates of three streams were varied from 0.5–2.25 ml min^{-1}. The flow rates of the carrier and the reagent stream were identical. The results obtained are shown in Fig. 8. The peak height increased with an increase of the ratio of the aqueous phase to the organic phase (V aq/V org). When the ratio was over about 2.5, the peak height was largest and constant. In this system, the flow rate of pump 1 was 1.94 ml min^{-1} and that of pump 2 was 0.78 ml min^{-1}.

3.6. Determination of anionic surfactants in river water

By using the flow system in Fig. 1, anionic surfactants present in river water were determined. River water samples were filtered with a glass filter to remove any solid substances. After appropriate dilution, the sample (200 μl) was injected. The results obtained are shown in Table 1. The results by this method are in good agreement with those obtained by the Methylene Blue batchwise method [2].

References

[1] Standard Methods for the Examination of Water and Waste Water, 14th Ed., American Public Health Association, Washington DC, 1975, pp. 600.
[2] Japanese Industrial Standards, JIS K0102, Japanese Standard Association, Tokyo, 1974.
[3] S. Motomizu, S. Fujiwara, A. Fujiwara, K. Toei, Anal. Chem. 54 (1982) 392.
[4] Japanese Industrial Standards, JIS K0102, Japanese Standard Association, Tokyo, 1993.
[5] J. Ruzicka, E.H. Hansen, Anal. Chim. Acta 78 (1975) 145.
[6] B. Karlberg, S. Thelander, Anal. Chim. Acta 98 (1978) 1.
[7] K. Kina, K. Shiraishi, N. Ishibashi, Talanta 25 (1978) 295.
[8] J. Kawase, A. Nakae, M. Yamanaka, Anal. Chem. 51 (1979) 1640.
[9] L. Nord, B. Karlberg, Anal. Chim. Acta 118 (1980) 285.
[10] S. Motomizu, M. Oshima, Analyst 112 (1987) 295.
[11] F. Canete, A. Rios, M.D.L. Castro, M. Valcarcel, Anal. Chem. 60 (1988) 2354.
[12] Y. Luo, R. Al-Othman, J. Ruzicka, G.D. Christian, Analyst 2121 (1996) 601.
[13] J.L. Manzoori, A. Miyazaki, Anal. Chem. 62 (1990) 2457.
[14] T. Sakai, Y.S. Chung, N. Ohno, Anal. Chim. Acta 276 (1993) 127.
[15] S. Motomizu, M. Oshima, T. Kuroda, Analyst 113 (1988) 747.
[16] T. Sakai, Analyst 116 (1991) 187.

ELSEVIER

Talanta 45 (1998) 549–555

Talanta

Catalytic determination of silver(I) by extractive flow injection analysis[1]

Hideyuki Itabashi *, Masaaki Takahata, Hiroshi Kawamoto, Hideo Akaiwa

Department of Applied Chemistry, Faculty of Engineering, Gunma University, Kiryu, Gunma 376, Japan

Received 26 February 1997; received in revised form 10 April 1997; accepted 10 April 1997

Abstract

A new catalytic method for the determination of silver(I) was developed based on a metal exchange reaction between ethylenediaminetetraacetatomercury(II) (Hg^{II}-EDTA) in the aqueous phase and bis(diethyldithiocarbamato)copper(II) (Cu^{II}-DDTC) in the organic phase. This exchange reaction (Cu^{II}-$DDTC_{org}$ + Hg^{II}-EDTA → Hg^{II}-$DDTC_{org}$ + Cu^{II}-EDTA, where org denotes the organic phase) was observed to proceed slowly and the Cu^{II}-DDTC complex transferred quantitatively to Hg^{II}-complex in the organic phase in the equilibrium state. In this system, silver(I) acts as the catalyst and can be determined by measuring the decrease in the absorbance of the Cu^{II}-DDTC complex ($\lambda_{max} = 435$ nm). The reaction was applied to the extractive flow injection analysis of silver(I). The present method allows the determination of silver(I) at 10^{-7} mol dm^{-3} level with the sampling frequency of 30 h^{-1}. The relative standard deviation of 0.28% ($n = 10$) was obtained at 4.0×10^{-7} mol dm^{-3} of silver(I). © 1998 Elsevier Science B.V.

Keywords: Catalytic determination; Flow injection analysis; Solvent extraction; Silver(I)

1. Introduction

Kinetic methods of analysis based on catalytic reactions have been widely used in trace analysis of metal ions because of their extremely high sensitivities [1,2]. Indicator reactions for catalytic methods are classified into two types on the basis of the reaction mechanism [3]: one is a redox reaction and the other is an exchange reaction with coordination compounds. In the case of redox reactions, many catalytic methods have been developed and applied to trace analysis of metal ions [4]. However, the usefulness of the method is limited to some metal ions having two or more oxidation states such as manganese, iron, cobalt etc. On the other hand, a catalytic method using exchange reactions with coordination compounds may be applied to determine metal ions which do not act as catalysts in redox reaction systems [5]. In this category, only a few methods have been developed.

* Corresponding author. Fax: +81 277301300; e-mail: itabashi@cc.gunma-u.ac.jp

[1] Presented at the Eighth International Conference on Flow Injection Analysis (ICFIA '97), held in Orlando, FL, USA, January 12–16, 1997.

PII S0039-9140(97)00130-6

For the above purpose, solvent extraction seems to be appropriate because an extraction reaction, including ligand exchange, can easily be designed based on the principle of Hard and Soft Acids and Bases (HSAB) [6].

A new catalytic method for the determination of some metal ions based on solvent extraction has been developed based on this principle. This paper describes the principle of the proposed method and its application to the extractive FIA of silver(I).

2. Experimental

2.1. Reagents

A stock solution of copper(II) (1.0×10^{-2} mol dm^{-3}) was prepared by dissolving 2.50 g of copper(II) sulfate pentahydrate in 1 dm^3 of 5.0×10^{-2} mol sulfuric acid. A stock solution of mercury(II) (2.0×10^{-2} mol dm^{-3}) was prepared by dissolving 3.43 g of mercury(II) nitrate in 500 cm^3 of 1.0×10^{-2} mol dm^{-3} nitric acid, and was standardized by ethylenediaminetetraacetic acid (EDTA). Stock solutions of diethyldithiocarbamic acid (DDTC) and EDTA were prepared by dissolving an appropriate amount of diethyldithiocarbamic acid sodium salt and ethylenediaminetetraacetic acid disodium salt in water. A stock chloroform solution containing 1.0×10^{-4} mol dm^{-3} of bis(diethyldithiocarbamato)copper(II) (Cu^{II}-DDTC) complex was prepared as follows; 200 cm^3 of an aqueous solution containing 1.0×10^{-3} mol dm^{-3} copper(II), pH adjusted to 6.5, was added to an equal volume of chloroform solution containing 2.0×10^{-4} mol dm^{-3} DDTC in a separator funnel. The mixture was shaken vigorously for 1 h. After the phases were allowed to separate, the organic phase was stored in the refrigerator.

All reagents used were of analytical grade and were used without further purification. The water used to prepare the reagent was obtained from a Milli-Q water purification system (Millipore Co.).

2.2. Apparatus

A Hitachi (Model U-2000 A) spectrophotometer with a 10-mm glass cell was used for measuring the absorption spectrum. A Fisher Scientific (Accumet pH meter 15) and an Iwaki (KM-type) shaker were used for pH measurements and shaking of the separator funnels, respectively.

A schematic flow diagram for the determination of silver(I) is shown in Fig. 1. Two double micro plunger pumps (Sanuki Kogyo, DMX-2200-T) were used for propelling the reagent and carrier solutions. Sample solutions were injected by six-way rotary valve (Sanuki Kogyo SVM-6M2) into the carrier stream. A phase separator (Sanuki Kogyo) with porous PTFE membrane (0.8 μm pore size) was used [7]. The flow lines were made of PTFE tubing (0.5 mm i.d.) and connectors. The absorbance was measured at 435 nm with a Soma Kogaku S-3250 spectrophotometer with a 10-mm micro flow cell (8 μl) and was recorded on a Hitachi Model 056 recorder.

2.3. Procedure

Batch procedure: 10 cm^3 of an aqueous solution containing 1.0×10^{-4} mol dm^{-3} ethylenediaminetetraacetatomercury(II) (Hg^{II}-EDTA) complex, 1.0×10^{-2} mol dm^{-3} 3-morpholinopro-

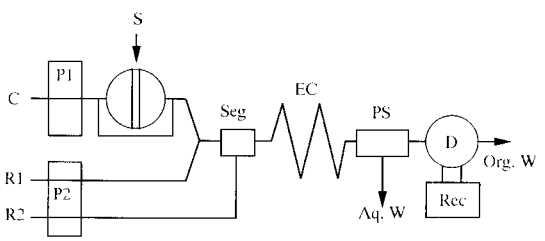

Fig. 1. Schematic diagram of flow injection system. C, Carrier solution (1.0×10^{-2} mol dm^{-3} HNO_3); R1, 4.0×10^{-3} mol dm^{-3} Hg^{II}-EDTA solution containing 0.2 mol dm^{-3} MES buffer (pH = 6.0); R2, 1.0×10^{-4} mol dm^{-3} Cu^{II}-DDTC chloroform solution; P1, pump (1.2 cm^3 min^{-1}); P2, pump (0.6 cm^3 min^{-1}); S, sample injector (sample volume 400 μl); Seg, segmentor (T-connector); EC, extraction coil (10 m long, 0.5 mm i.d.); PS, phase separator; D, spectrophotometer with an 8-μl flow cell (435 nm); Rec, recorder; Aq.W, aqueous phase waste; Org.W, organic phase waste.

panesulfonic acid (MOPS) buffer and 10^{-5}–10^{-6} mol dm^{-3} level metal ions was taken in a separator funnel. An equal volume of chloroform solution containing 1.0×10^{-4} mol dm^{-3} Cu^{II}-DDTC complex was added, and the mixture was shaken vigorously for a definite time. After the phases were allowed to separate, the absorbance of the organic phase was measured. A pH of the aqueous phase was also measured by using a glass electrode. All experiments were carried out at room temperature (ca. 293 K).

Flow injection procedure: a 1.0×10^{-2} mol dm^{-3} nitric acid carrier solution (C) was pumped at a flow rate 1.2 cm^3 min^{-1}. A 4.0×10^{-3} mol dm^{-3} Hg^{II}-EDTA solution containing 0.2 mol dm^{-3} 2-morpholinoethanesulfonic acid (MES) buffer (pH = 6.0) in reservoir R1 and a 1.0×10^{-4} mol dm^{-3} Cu^{II}-DDTC chloroform solution in reservoir R2 were pumped at a flow rate 0.6 cm^3 min^{-1}. A sample solution (400 μl) containing silver(I) was injected into the carrier stream. The metal exchange reaction was catalyzed by silver(I) in the extraction coil (10 m long). After the phases were separated by phase separator, the absorbance of the organic phase was monitored continuously at 435 nm.

3. Principle

Indicator reaction of the proposed method is represented as follows:

$$MR_{org} + M'L \rightleftarrows M'R_{org} + ML \quad (1)$$

where org denotes the organic phase and M, M′, R, L represent a hard metal ion, a soft metal ion, a soft extractant and a hard water-soluble ligand, respectively. Based on the HSAB principle, reaction Eq. (1) proceeds quantitatively to right hand side. In this case, the addition of a small amount of harder metal ion (C) than M′ into the aqueous phase will induce the following reactions:

$$M'L + C \rightarrow CL + M' \quad (2)$$

$$MR_{org} + M' \rightarrow M'R_{org} + M \quad (3)$$

$$M'L + M \rightarrow ML + M' \quad (4)$$

If reactions (Eqs. (2)–(4)) are faster than reaction Eq. (1), reaction Eq. (1) is accelerated catalytically by adding C. Similarly, when a softer metal ion (C′) than M is added into the aqueous phase, reactions Eq. (4) and Eq. (3) are induced by reaction Eq. (5).

$$MR_{org} + C' \rightarrow M + C'R_{org} \quad (5)$$

Consequently, by the addition of C or C′ into the aqueous phase, reaction Eq. (1) is accelerated, and catalytic determination of C or C′ may be feasible by monitoring the formation rate of $M'R_{org}$ or ML complex or the decreasing rate of MR_{org} or M′L complex.

To confirm the feasibility of the above method, copper(II), mercury(II), DDTC and EDTA were selected as a harder metal ion, a softer metal ion, a soft extractant and a hard water-soluble ligand, respectively.

$$Cu^{II}\text{-}DDTC_{org} + Hg^{II}\text{-}EDTA \rightleftarrows Hg^{II}\text{-}DDTC_{org} + Cu^{II}\text{-}EDTA \quad (6)$$

A decrease in the concentration of Cu^{II}-$DDTC_{org}$ was monitored by measuring the absorbance of the organic phase.

4. Results and discussion

Absorption spectra of the organic phase at the shaking time 0 to 100 min are shown in Fig. 2(a). In this case, a free metal ion is not added to the aqueous phase. Absorbance of Cu^{II}-DDTC decreases with increasing shaking time. Reaction (6) is observed to proceed slowly in the forward direction, and the reaction does not reach the equilibrium even though the mixture is shaken for 100 min. On the other hand, when free copper(II) is added to the aqueous phase, the reaction becomes very fast, the absorption spectrum of Cu^{II}-DDTC disappears within 40 s (Fig. 2(b)). Similar results were obtained by adding mercury(II) to the aqueous phase. By using the above catalytic role of copper(II) and mercury(II), the trace determination of these metals becomes feasible.

The effect of pH on the proposed reaction was examined by measuring the absorbance (435 nm)

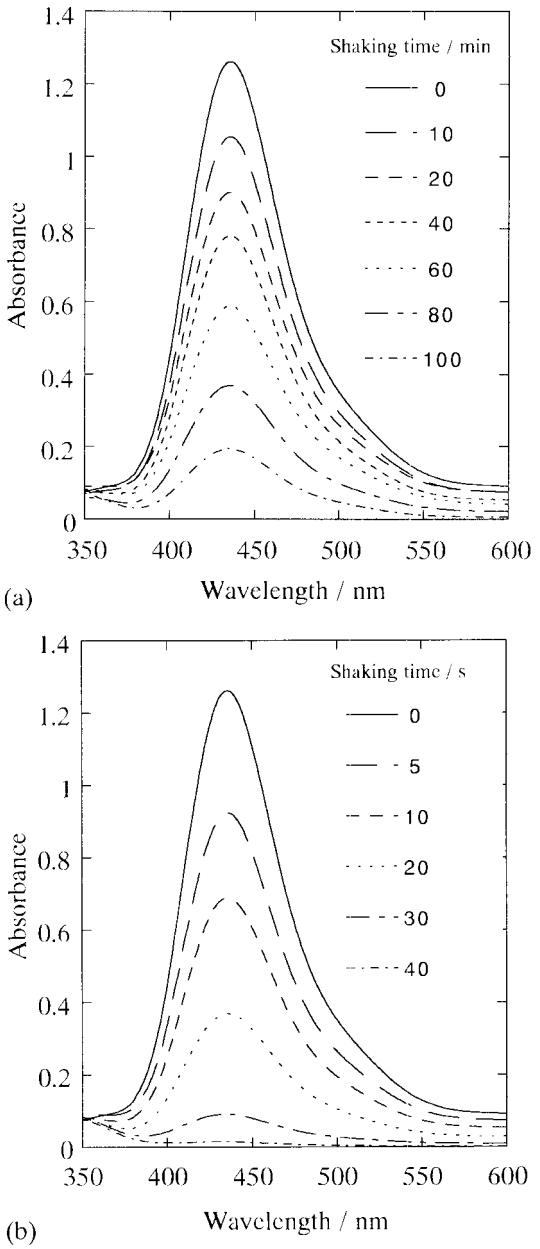

Fig. 2. Absorption spectra of the organic phase at various shaking times. (a), in the absence of free metal ion (pH = 6.9); (b), in the presence of 3.9×10^{-5} mol dm^{-3} copper(II) (pH = 6.8).

of the organic phase at the shaking time of 60 s. The results are shown in Fig. 3. The absorbance in the absence of a free metal ion is almost constant in the pH range 6–11, whereas in the presence of 3.0×10^{-5} mol dm^{-3} copper(II), it rapidly decreases in the pH region lower than 8. A pH of 6.0 was selected for the procedure because the difference in the absorbance between the absence and the presence of free copper(II) became a maximum at around pH 6.

The effect of some metal ions on the proposed reaction was examined to investigate how a metal ion acts as a catalyst. In this case, concentration of a metal ion in the aqueous phase was adjusted to be 6.5×10^{-6} mol dm^{-3}, and the absorbance of the organic phase at the shaking time of 15 min was measured. As a result, Na(I), Mg(II), K(I), Ca(II), Ti(IV), V(V), Cr(VI) and Sr(II) were inactive whereas Al(III), Mn(II), Fe(II), Co(II), Ni(II), Cu(II), Zn(II), Ag(I), Cd(II), Hg(II) and Pb(II) acted as a catalyst.

To examine the catalytic action of these metal ions more precisely, an observed rate constant for the reaction was measured. The observed rate constant was estimated as follows: assuming that the reaction rate is the first order with respect to the concentration of Cu^{II}-$DDTC_{org}$, the reaction rate (v) is defined as

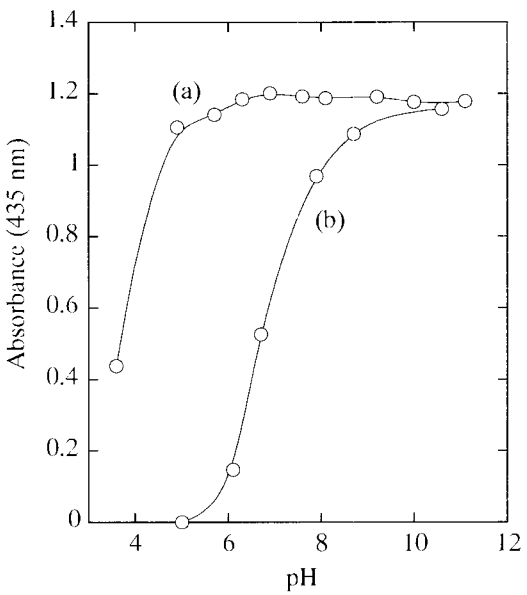

Fig. 3. Effect of pH for the proposed reaction. (a), in the absence of free metal ion; (b), in the presence of 3.0×10^{-5} mol dm^{-3} copper(II).

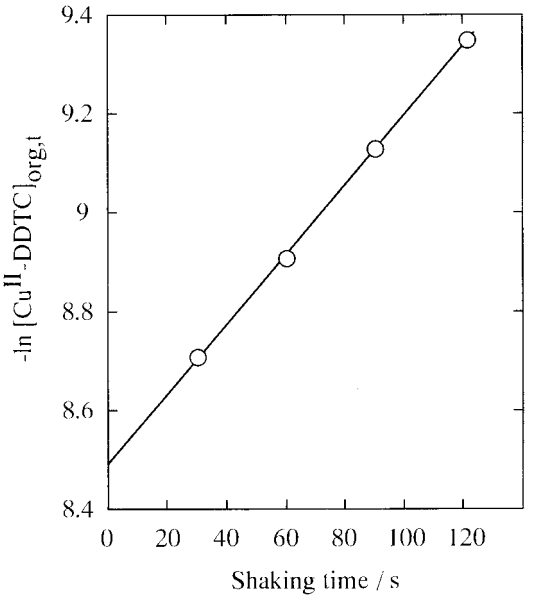

Fig. 4. A plot of $-\ln[Cu^{II}\text{-}DDTC]_{org,\,t}$ against shaking time in the presence of 2.0×10^{-5} mol dm^{-3} cobalt(II).

$$v = -\frac{d[Cu^{II}\text{-}DDTC]_{org}}{dt}$$

$$= k_{obsd}[Cu^{II}\text{-}DDTC]_{org} \quad (7)$$

where k_{obsd} represents the observed rate constant. Integration results in

$$-\ln[Cu^{II}\text{-}DDTC]_{org,\,t}$$

$$= -\ln[Cu^{II}\text{-}DDTC]_{org,\,t=0} + k_{obsd}t \quad (8)$$

where the subscript t represents shaking time. According to Eq. (8), a plot of $-\ln[Cu^{II}\text{-}DDTC]_{org,\,t}$ against shaking time t should give a straight line having a slope of k_{obsd}. Fig. 4 shows an example of the plot when 2.0×10^{-5} mol dm^{-3} cobalt(II) was added into the aqueous phase. The plots fall on a straight line, indicating the validity of Eq. (8). By adding other metal ions to the aqueous phase, straight lines were also obtained. The k_{obsd} values for each metal ion obtained by the plot are summarized in Table 1. As can be seen from Table 1, silver(I) acts as the most effective catalyst for the reaction system, the value is about one thousand times as large as the value in the absence of free metal ions.

Table 1
k_{obsd} values for each metal ion

Metal ion*	k_{obsd} s^{-1}
none	3.00×10^{-4}
Ag(I)	2.76×10^{-1}
Cu(II)	8.27×10^{-2}
Hg(II)	7.30×10^{-2}
Pb(II)	2.10×10^{-2}
Cd(II)	1.84×10^{-2}
Zn(II)	1.33×10^{-2}
Fe(II)	1.24×10^{-2}
Co(II)	7.00×10^{-3}
Ni(II)	4.23×10^{-3}
Al(III)	2.50×10^{-3}

*2.0×10^{-5} mol dm^{-3}

From these experimental results, we selected silver(I) as a catalyst and developed extractive FIA of silver(I). Based on the batch investigation, reaction condition at pH 6.0 and the concentration of Cu^{II}-DDTC 1.0×10^{-4} mol dm^{-3} were selected. Here, the effect of Hg^{II}-EDTA concentration, the flow rate of pump 2 and the extraction coil length were examined.

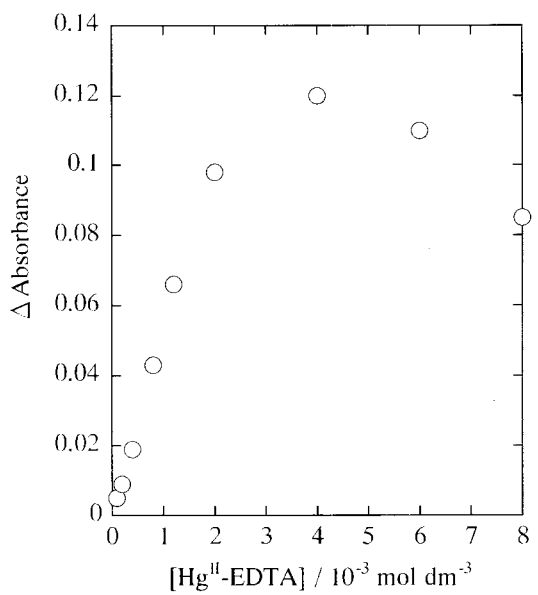

Fig. 5. Effect of Hg^{II}-EDTA concentration on the FIA peak heights for silver(I). $[Ag^{I}]$, 5.0×10^{-7} mol dm^{-3}; extraction coil length, 3 m. Other conditions as in Fig. 1.

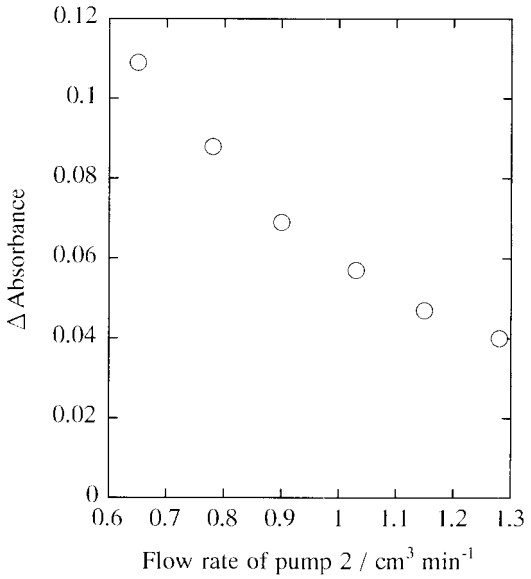

Fig. 6. Effect of flow rate of pump 2 on the FIA peak heights for silver(I). [Ag^{I}], 5.0×10^{-7} mol dm^{-3}; extraction coil length, 3 m. Other conditions as in Fig. 1.

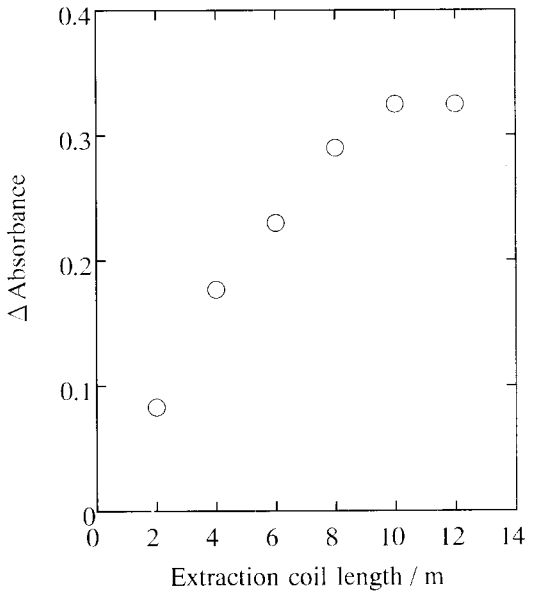

Fig. 7. Effect of extraction coil length on the FIA peak heights for silver(I). [Ag^{I}], 5.0×10^{-7} mol dm^{-3}. Conditions as in Fig. 1.

The effect of Hg^{II}-EDTA concentration was examined within the range 1.0×10^{-4}–8.0×10^{-3} mol dm^{-3} (Fig. 5). The height of FIA peaks increased with the increasing concentration and showed maximum at the concentration of 4.0×10^{-3} mol dm^{-3}. Therefore, 4.0×10^{-3} mol dm^{-3} Hg^{II}-EDTA was chosen for the procedure. The effect of flow rate of pump 2 was then examined, keeping the flow rate of pump1 constant (1.2 cm^3 min^{-1}) (Fig. 6). The height of FIA peaks increased with a decrease in the flow rate of pump 2, because the ratio of the aqueous phase to the organic phase increased with a decrease in the flow rate of pump 2. However, the baseline became unstable at the flow rate below 0.6 cm^3 min^{-1} because the blank reaction proceeds with decreasing the flow rate. Hence, the flow rate of pump 2 was adjusted to be about 0.6 cm^3 min^{-1}. The effect of the extraction coil length was also studied (Fig. 7). The height of FIA peaks increased with an increase in the extraction coil length and showed maximum at an extraction coil length longer than 10 m. In this system, a 10 m coil was used considering the frequency of sample injection.

Finally, a calibration curve was prepared by using the flow system shown in Fig. 1. Typical flow signals for silver(I) at the 10^{-7} mol dm^{-3} level are shown in Fig. 8. The baseline is stable, and the determination of 30 samples per hour can be possible. The relative standard deviation for ten injection of 4.0×10^{-7} mol dm^{-3} silver(I)

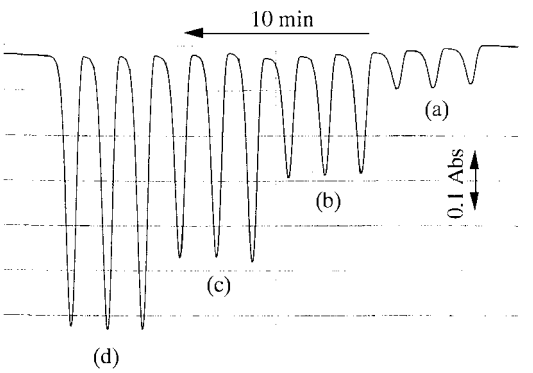

Fig. 8. Flow signals of silver(I). [Ag^{I}] ($\times 10^{-7}$ mol dm^{-3}) (a), 2.0; (b), 4.0; (c), 6.0; (d), 8.0. Conditions as in Fig. 1.

was 0.28%. The detection limit was 1×10^{-7} mol dm^{-3}.

5. Conclusions

A new catalytic method for the determination of some metal ions was developed based on solvent extraction, and it was applied to FIA of silver(I). As a result, the determination of silver(I) at 10^{-7} mol dm^{-3} level could be feasible. This reaction system will also be applied to the determination of some metal ions other than silver(I).

References

[1] H.A. Mottola, Kinetic Aspects of Analytical Chemistry, Wiley, New York, 1988.
[2] D. Perez-Bendito, M. Silva, Kinetic Methods in Analytical Chemistry, Horwood, Chichester, 1988.
[3] H. Muller, CRC Crit. Rev. Anal. Chem. 13 (1982) 313.
[4] H.A. Mottola, D. Perez-Bendito, Anal. Chem. 66 (1994) 131R.
[5] P.R. Bontchev, Talanta 17 (1970) 499.
[6] M. Tanaka, Youbaityusyutsu no Kagaku (Solvent Extraction Chemistry) (in Japanese), Kyouritsu, Tokyo, 1977.
[7] S. Motomizu, M. Oshima, Analyst 112 (1987) 295.

ELSEVIER

Talanta 45 (1998) 557–563

Talanta

Development of an amperometric biosensor based on acetylcholine esterase covalently bound to a new support material

Masoud Khayyami [a], Maria Teresa Pérez Pita [1,b], Nuria Peña Garcia [b], Gillis Johansson [c], Bengt Danielsson [a], Per-Olof Larsson [a,*]

[a] *Department of Pure and Applied Biochemistry, Centre for Chemistry and Chemical Engineering, Lund University, S-221 00 Lund, Sweden*

[b] *TMS CHEM AB, Ideon S-223 70 Lund, Sweden*

[c] *Department of Analytical Chemistry, Centre for Chemistry and Chemical Engineering, Lund University, S-221 00 Lund, Sweden*

Received 24 March 1997; received in revised form 5 May 1997; accepted 7 May 1997

Abstract

A new type of amperometric biosensor based on immobilised acetylcholine esterase was designed and constructed. The enzyme was immobilised on a flow-through working electrode, which was prepared from reticulated vitreous carbon (RVC) or from a composite material consisting of RVC and superporous agarose. The sensor was operated in FIA mode using acetylthiocholine as a substrate. The sensor responded to inhibitors such as paraoxon—10^{-9} mol was detected by the sensor in a non-optimised configuration. The practical lifetime of the sensor was at least 1 month. © 1998 Elsevier Science B.V.

Keywords: RVC-electrode; Biosensor; Acetylcholine esterase; Acetylthiocholine; Amperometric; Thiocholine; Mediator; Superporous agarose gel

1. Introduction

During the last decades, there has been an ever growing requirement for the detection of very small concentrations of different organic compounds, especially those dangerous to the environment and those with pharmacological applications. Biosensors are useful for such applications thanks to their high sensitivity and specificity [1], their ease of use and compact size as well as their avoidance of the use of radioactivity [2]. Acetylcholine esterase (AChE) is one of the most investigated enzymes, because of its great importance in the transducing of neuronal signals. There are two different aims of using acetylcholine esterase as a biocatalytic element in biosensors. The measurement of acetylcholine for

* Corresponding author. Tel.: +46 46 2228263; fax: +46 46 2224611: e-mail: Per-Olof.Larsson@tbiokem.lth.se

[1] Present address: Department of Analytical Chemistry, Faculty of Chemistry, Universidad Complutense de Madrid, 280 40 Madrid, Spain.

PII S0039-9140(97)00182-3

clinical purposes on one hand, and the determination of certain pesticides on the other.

For the first purpose, most previous amperometric sensors have combined the action of acetylcholine esterase with choline oxidase. The product of the first enzyme choline, is not electrochemically measurable. However, the oxidase reacts with choline, and in the process consumes oxygen and produces hydrogen peroxide, both of which are easily monitored [3].

Determination of pesticides, for example, organophosphates such as paraoxon, parathion, malathion and pirimiphos has become a major topic in agricultural chemistry and in environmental control. These pesticides efficiently inhibit acetylcholine esterase and are therefore easily detected by sensors based on this enzyme. Since substrate determination is not the issue in this case, monitoring of electroactive products, like thiocholine, is widely employed.

This paper describes a new electrode material for amperometric sensors, a composite of reticulated vitreous carbon (RVC) and superporous agarose. The composite has several favourable properties such as high binding capacity for enzymes and good flow properties.

2. Experimental

2.1. Chemicals

Acetylcholine esterase (AChE, E.C, 3.1.1.7) type VI-S from electric eel (specific activity 270 U mg^{-1} protein), acetylthiocholine iodide (ATC), 1-cyclohexyl-3-(2-morpholinoethyl) carbodiimide metho-*p*-toluenesulfonate, paraoxon (diethyl-*p*-nitrophenyl phosphate) and Meldola Blue (8-dimethylamino-2,3-benzophenoxazine) were from Sigma Chemical, St Louis, MO. Reticulated vitreous carbon (RVC) porosity grade 100 s (pore size nominally 0.25 mm) was obtained from Energy Research and Generation, Oakland, CA.

2.2. Pretreatment of the RVC material

RVC cylinders (1.5 × 0.50 cm) were cut from a block of RVC material, soaked in 6 M HCl for about one hour, washed with distilled water until the wash became neutral and then soaked in dry methanol for 2 h. Finally, the cylinders were dried in an oven at 110°C overnight.

2.3. Immobilisation of acetylcholine esterase on RVC

The pretreated RVC cylinder was fitted into a glass tube provided with flow adaptors. 10 ml of 0.05 M acetate buffer (pH 5.1), containing 40 mg ml^{-1} of 1-cyclohexyl-3-(2-morpholinoethyl) carbodiimide metho-*p*-toluenesulfonate, was pumped through the system at a flow rate of 0.2 ml min^{-1} for 150 min, in order to activate the RVC surface. Then, the RVC electrode was washed with cold acetate buffer at a flow rate of 1.2 ml min^{-1} for 30 min.

The immobilisation was carried out by circulating the enzyme (3.8 mg AChE in 5 ml of cold buffer) at 0.2 ml min^{-1} through the activated RVC cylinder for 3 h at 0–5°C. Finally, the RVC electrode was rinsed with cold 0.1 M phosphate buffer, pH 7.5 for 5 min.

2.4. Preparation of agarose-RVC composite

A pretreated RVC cylinder was fitted into a glass tube provided with adapters for connecting to a syringe or a pump. Agarose emulsion was prepared in the following way: 20 ml of agarose solution (6% w/v, 60°C) was mixed with 10 ml cyclohexane (60°C), containing 0.6 ml Tween 80 surfactant. The mixture was emulsified by stirring at 1200 rpm for 2 min. Warm agarose emulsion, 10 ml, was injected into the RVC cylinder kept at 50°C. The emulsion was then allowed to gel at room temperature. Subsequently, the organic phase was washed away by pumping first 50% ethanol and then water through the column. The composite cylinder was removed from the glass cylinder and its ends trimmed 1 mm with a razor blade in order to remove any excess of superporous agarose gel.

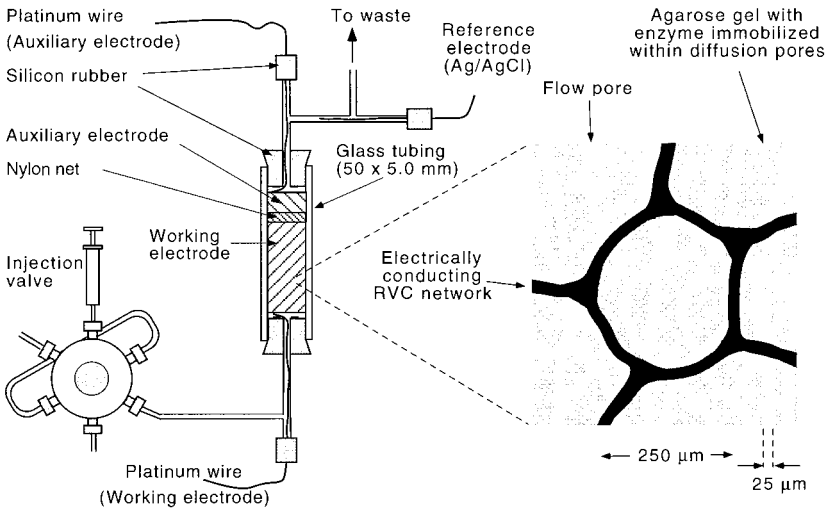

Fig. 1. Biosensor design. The working electrode was made either of reticulated vitreous carbon (RVC) coated with immobilised acetylcholine esterase or of reticulated vitreous carbon together with superporous agarose gel (RVC-agarose composite), containing immobilised acetylcholine esterase. The magnified part shows the principle structure of the RVC-agarose composite. The electrode was operated in a FLA arrangement. The transporting buffer contained the mediator Meldola Blue. When the electrode was used for pesticide determination the transporting buffer also contained the substrate acetylthiocholine. Further details in the text.

2.5. Immobilisation of AChE on RVC-agarose composite

The RVC-agarose composite cylinder was again fitted into a glass tube connected to a syringe and placed in an ice bath. The cylinder was washed by injecting 20 ml of 2 M potassium phosphate buffer, pH 12.1. Activation was then commenced by injecting 10 ml of a cyanogen bromide solution through the cylinder. The cyanogen bromide solution was prepared immediately before injection by mixing a solution of 400 mg BrCN dissolved in 1 ml of acetonitrile with 9 ml of cold 2 M potassium phosphate buffer, pH 12.1. The injection of cyanogen bromide lasted for 3 min. After an additional 2 min the activated composite cylinder was washed with cold water, about 50 ml. Finally, the cylinder was washed with cold 0.05 M phosphate buffer pH 7.6 [4].

A solution of cold 0.05 M phosphate buffer pH 7.2, containing acetylcholine esterase (1.5 mg per 15 ml), was first rapidly pumped through the column for 5 min and then slowly circulated through the column overnight in the cold room. The column was finally washed with 0.05 M phosphate buffer, pH 7.2.

2.6. Biosensor design

The biosensor device is shown in Fig. 1. An RVC cylinder (1.5×0.50 cm) or an RVC-agarose composite cylinder (1.5×0.50 cm), both containing immobilised enzyme) was used as working electrode and was fitted into a precision bore glass tube (5.0×0.50 cm). An Ag/AgCl electrode placed downstream was used as a reference electrode and an uncoated RVC cylinder was used as counter electrode. The biosensor was operated in a FIA mode. Samples (100 µl) were injected via a valve and transported with 0.1 M sodium phosphate buffer, pH 7.0, containing dissolved 5 µM Meldola Blue, pumped by a peristaltic pump. The electrodes were attached to a potentiostat (Model MA 5410; Chemel, Lund, Sweden) and the response to the injected samples was registered on a recorder.

3. Results and discussion

3.1. Mechanism

Since the sensor described here was ultimately destined for the detection of AChE inhibitors, such as pesticides or other neurotoxic compounds, an artificial substrate, acetylthiocholine, with suitable properties was chosen. The product generated by the enzyme, thiocholine, is electrochemically active and is usually detected amperometrically at 800 mV [5–7]. However, a lower working potential is advantageous to minimize unwanted contributions to the signal from other electroactive compounds that might be present in a sample. To this end the mediator Meldola Blue was considered, since it had been shown to function efficiently in other biosensors [8,9]. Initial experiments also showed that the mediator oxidised thiol compounds as evidenced by the rapid bleaching of the colour of the mediator. Subsequent use in biosensor operation (usually at 250 mV) confirmed the usefulness of the mediator. Thus, it is suggested that the product of the enzymatic reaction, thiocholine, reacts with the mediator Meldola Blue, present also within the diffusion layer of the electrode. The reduced mediator subsequently migrates to the surface of the working electrode, where it is reoxidised electrochemically.

3.2. Sensor properties

3.2.1. RVC electrodes

Reticulated vitreous carbon (RVC) is an open pore material with many advantages, such as high electrical conductivity, high mechanical rigidity, comparatively large surface area and low pressure drop to fluid flow. Another favourable property of RVC is its low background current when used as electrode material [10]. Here, we have used the RVC for biosensor applications in two configurations: (a) as a single electrode element, where the enzyme acetylcholine esterase was immobilised directly onto the RVC surface or (b) as a composite electrode where the RVC was integrated with a superporous agarose gel structure, the latter carrying the immobilised enzyme. The special properties of the RVC-agarose composite are described under a separate heading below.

3.2.2. Mediator—oxidation potential

Reduced Meldola Blue can be oxidised at potentials as low as -100 mV [8]. To speed up the rate of oxidation the acetylcholine esterase biosensor was usually run at a higher potential, in fact all of the experiments described here were carried out at $+250$ mV. At this potential background interference could be somewhat higher. However, interference from the iodide ions present as counter ions in the substrate (acetylthiocholine iodide), was not observed since iodide oxidation requires a higher operating potential. The concentration of Meldola Blue was kept low, 5 μM. Higher concentration of mediator would probably have improved the signal but at the cost of a higher background level, as shown earlier with other electrodes [11,12].

3.2.3. The pH-profile

The pH profile of the sensor was investigated (Fig. 2). As is evident from the figure the sensor response was not at all sensitive to moderate changes of pH (6.5–8.5). A pH of 7 was selected for further work. The very flat pH profile obtained suggests that the rate limiting step was not the enzymatic conversion. Otherwise a more pronounced pH optimum around pH 7, the optimum for free enzyme, would be expected [13,14]. Other

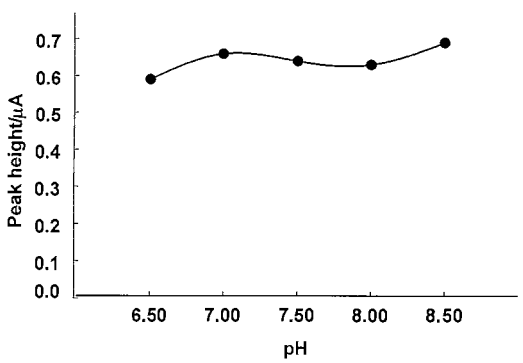

Fig. 2. Biosensor pH-optimum. The biosensor based on RVC coated with immobilised acetylcholine esterase was operated at different pH values by varying the transporting buffer (phosphate buffer with pH adjusted as indicated).

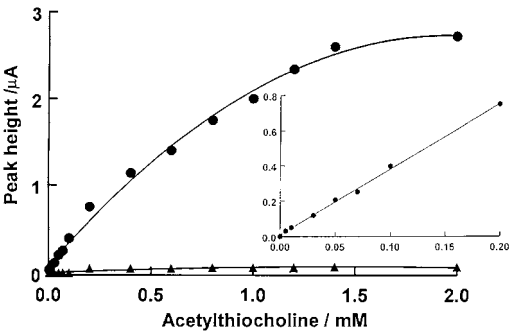

Fig. 3. Biosensor substrate response. The biosensor was based on RVC coated with immobilised acetylcholine esterase. The acetylthiocholine substrate (0.10 ml) at the concentration shown was injected and the response recorded.

related sensor constructions have shown a clearer pH optimum around 7.

3.2.4. Flow rate

The effect of the flow rate was briefly studied. The current at + 250 mV resulting from acetylthiocholine hydrolysis decreased when the flow rate increased (data not shown). Low flow rates however result in low sample throughput and as a compromise 1 ml min^{-1} was chosen, which permitted up to 38 samples per hour to be analysed.

3.2.5. Substrate response curves

Fig. 3 shows calibration curves for acetylthiocholine ranging from 5 to 2000 μM. The current reached a plateau at 2 mM and did not change when the acetylthiocholine concentration was increased to 10 mM. The coefficient of variation was 3–4% for multiple injections of acetylthiocholine when tested in the concentration range 550 μM. A blank electrode without enzyme was also prepared and its response to various levels of acetylthiocholine is also displayed in Fig. 3.

3.2.6. Electrode stability

The electrode stability is described by Fig. 4. The electrode response was tested intermittently over a 1 month period and on each occasion 20–25 samples were injected, i.e. a total of about 250 samples. During the period the response gradually diminished, although at a very slow rate. Thus, after 1 month the response was still 60% of the original, a stability that should be satisfactory for most applications.

3.3. Special properties of RVC-agarose composite electrode

The biosensor based on enzyme-coated RVC as described above gave a satisfactory signal strength. However, the total surface area available for binding could in some situations be a limiting factor. For example, if a very high signal level is desired, a higher load of enzyme is necessary. To this end a modified biosensor was prepared, in which the RVC was supplemented with superporous agarose. Fig. 1 gives an approximate view of the design of the composite electrode material. As can be seen the working electrode now contained three continuous phases, the electrically conducting RVC, the 25 μm flow pores (determined under the microscope) through which the injected sample was pumped and the agarose phase with its 300 A diffusion pores in which the enzyme was immobilised.

The superporous agarose integrated in the RVC structure is a new type of material that may be prepared as discrete particles for chromatographic use [15] or as continuous beds in a number of physical shapes [16].

The composition of the RVC-agarose composite electrode was such that about 60% of its volume consisted of agarose gel. Thus, the elec-

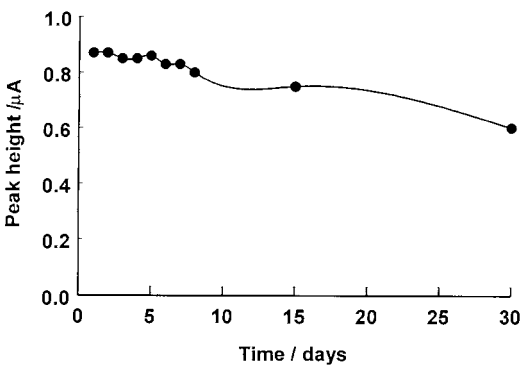

Fig. 4. Biosensor stability. The biosensor was based on RVC coated with immobilised acetylcholine esterase. At the times indicated the biosensor response to substrate was checked as in Fig. 3.

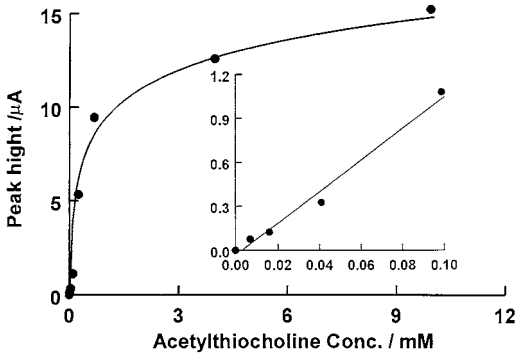

Fig. 5. Substrate response for RVC-agarose composite electrode. The electrode was based on RVC containing superporous agarose with immobilised acetylcholine esterase. The acetylthiocholine substrate (0.10 ml) at the concentration shown was injected and the response recorded.

trode offered ample volume for attachment of immobilised acetylcholine esterase. Tests of residual activity after immobilisation indicated almost complete immobilisation, i.e. the composite electrode contained up to 1.5 mg of enzyme, corresponding to up to 400 I.U. of enzyme activity. In comparison, carbodiimide-activated RVC bound much less enzyme. Direct measurement of the protein coating was not possible due to the very low protein amount. However, geometrical calculations indicated a maximum binding capacity of 0.01 mg of enzyme, i.e. less than 1% of the value ascribed to the RVC composite. The calculations were based on the known surface area of RVC (67 $cm^2\ cm^{-3}$; the manufacturer) and the assumption that the surface area was completely covered by acetylcholine esterase molecules.

Fig. 5 shows that the composite electrode gave a high signal level and that the calibration curve was reasonably linear up to almost 1 mM of acetylthiocholine. The response (peak height) for the composite electrode compared with the electrode without superporous agarose (Fig. 3) was about twice as high at low substrate concentrations but more than five times as large at higher substrate concentrations, indicative of the higher amount of enzyme present. Calculations of the coulometric yield indicated that it was up to ten times as high for the composite electrode as for the RVC electrode, reaching a level of about 10% under the conditions employed in the described experiments (flow rate, Meldola blue concentration etc.).

One disadvantage of using the composite gel electrode was that the response peaks became slightly broader, about 50% broader than in the absence of agarose. This can easily be explained by the comparatively slow diffusion within the agarose gel for the reactants, thiocholine and Meldola Blue (reduced and oxidised forms). As expected the biosensor response decreased when the flow rate was increased from 0.3 to 1.5 ml min^{-1} (data not shown), supporting the assumption that the signal was limited by reactant diffusion rate. The useful lifetime of the composite electrode was about 1 month.

3.4. Determination of pesticide

The RVC-agarose composite sensor was tested for the determination of the pesticide paraoxon. The analysis was set up in a competitive FIA configuration, i.e. the pesticide samples were injected in a stream containing the substrate acetylthiocholine. The substrate concentration was 0.4 mM, i.e. around the Km level. [6,7]. This mode of analysis does not favour very sensitive pesticide detection for several reasons. The flow system will limit the contact time for the inhibitor and the presence of substrate will competitively protect the enzyme. Also, the comparatively large amount of enzyme present in the composite electrode will require a larger amount of inhibitor for a clearly observable decrease in activity. Advantages on the other hand include a fairly rapid analysis and possibilities of repeated use (the pesticide binds essentially irreversibly). Fig. 6 shows that inhibitor concentrations down to 10 μM in 100 μl, i.e. 1 nmol of paraoxon in the sample, could be detected. The detection limit at three times the noise level was 0.5 nmol. The general requirements for pesticide detection in EU is 0.1 $\mu g\ l^{-1}$ of any single compound or 0.5 $\mu g\ l^{-1}$ for all pesticides together. Our lower limit corresponds to 1.4 mg l^{-1} However, it could easily be lowered, simply by increasing the injection volume and by gearing the test protocol towards higher sensitivity, e.g., by manipulating flow rates and the substrate concentration.

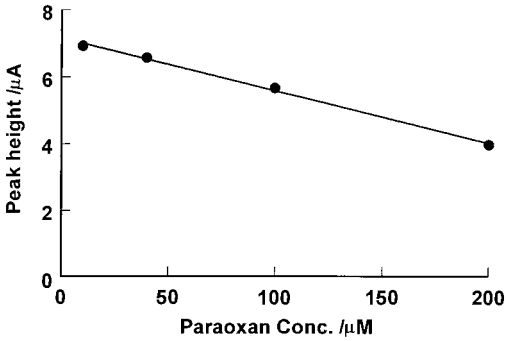

Fig. 6. Pesticide determination with RVC-agarose composite electrode. The analysis was carried out in a continuous, competitive FIA mode. The transporting buffer contained besides the electron mediator the substrate acetylthiocholine (0.4 mM). Samples of paraoxon (0.1 ml) at the concentrations indicated were injected and the decreased response level was recorded.

4. Conclusion

The biosensor described here allowed sensitive detection of acetylthiocholine and of the pesticide paraoxon. The operational stability was very satisfactory. The flow-through electrode based on RVC-superporous agarose composite permitted high catalyst loading, which could be of interest also in other sensors.

Acknowledgements

We gratefully acknowledge the efficient help of Ms Anne Persson and Ms Andrea Unger with the paraoxon measurements, fruitful discussion with Per-Erik Gustavsson regarding superporous agarose, the linguistic advice of Dr Richard Ansell, and the financial support given by The Swedish Research Council for Engineering Sciences, The Swedish Natural Research Council and WITEC, Sweden.

References

[1] M.P. Byfield, R.A. Abuknesha, Biosens. Bioelectron. 9 (4) (1994) 373.
[2] R.S. Sethi, Biosens. Bioelectron. 9 (3) (1994) 243.
[3] B.L. Ruiz, E. Dempsey, C. Hua, M.R. Smyth, Anal. Chim. Acta 273 (1993) 425.
[4] J. Porath, R. Axen, Methods Enzymol. 44 (1976) 19.
[5] M.K. Halbert, R.P. Baldwin, Anal. Chem. 57 (1985) 591.
[6] M. Stoytcheva, Electroanalysis 6 (1995) 560.
[7] M. Stoytcheva, Electroanalysis 7 (1995) 660.
[8] L. Gorton, A. Torstensson, H. Jaegfeldt, G. Johansson, J. Electroanal. Chem. 161 (1984) 103.
[9] B. Persson, L. Gorton, J. Electroanal. Chem. 292 (1990) 115.
[10] J. Wang, Electrochim. Acta 26 (1981).
[11] M. Khayyami, G. Johansson, D. Kriz, B. Xie, P.-O. Larsson, B. Danielsson, Talanta 43 (1996) 957.
[12] M. Khayyami, N.P. Garcia, P.-O. Larsson, B. Danielsson, G. Johansson, Electroanalysis 9 (1996) 523.
[13] P. Skládal, Anal. Chim. Acta 252 (1991) 11.
[14] J. Kulys, E.J. D'Costa, Biosens. Bioelectron. 6 (1991) 109.
[15] P.-E. Gustavsson, P.-O. Larsson, J. Chromatogr. A 734 (1996) 231.
[16] P.-O. Larsson, Swedish patent application 9 200 827-5.

ELSEVIER

Talanta 45 (1998) 565–573

Talanta

Potentiometric flow injection determination of amylase activity by using hexacyanoferrate(III)-hexacyanoferrate(II) potential buffer

Hiroki Ohura [a], Toshihiko Imato [b,*], Yasukazu Asano [c], Sumio Yamasaki [a]

[a] *Department of Industrial Chemistry, Faculty of Engineering, Kyushu Sangyo University, Matsugadai, Higashi-ku, Fukuoka 813, Japan*

[b] *Department of Chemical Sciences and Technology, Faculty of Engineering, Kyushu University, Hakozaki, Higashi-ku, Fukuoka 812, Japan*

[c] *DKK Corporation, Kitamachi, Kichijoji, Musashino, Tokyo 180, Japan*

Received 3 April 1997; received in revised form 15 August 1997; accepted 18 August 1997

Abstract

A highly sensitive potentiometric flow injection determination of amylase activity was carried out, utilizing a redox reaction of hexacyanoferrate(III) in alkaline media with reducing sugar as product of the enzymatic hydrolysis reaction of starch with amylase. The analytical method is based on the potential change detection of a flow-through type redox electrode detector due to the composition change of a $[Fe(CN)_6]^{3-}$–$[Fe(CN)_6]^{4-}$ potential buffer solution, which is caused by the redox reaction with the product of the enzymatic reaction. A linear relationship exists between the potential change (peak height) and the activity of amylase. Amylase of a wide activity range from 2.5×10^{-2} to 1.2×10^{-4} U ml^{-1} can be determined by the changing the concentrations of the $[Fe(CN)_6]^{3-}$–$[Fe(CN)_6]^{4-}$ potential buffer from 10^{-3} to 10^{-5} M. The lower detection limit of amylase activity is 6.0×10^{-5} U ml^{-1}. The sampling rate and relative standard deviation are 15 h^{-1} and 0.9% ($n = 5$) for 3.8×10^{-3} U ml^{-1} of amylase. The present method was successfully applied to determine amylase activity in real samples (commercial digestive medicines) with an accuracy of 4% compared with analytical results obtained using the present method with those achieved using the conventional titration method. © 1998 Elsevier Science B.V.

Keywords: Flow-injection; Amylase activity; $[Fe(CN)_6]^{3-}$–$[Fe(CN)_6]^{4-}$ potential buffer; Digestive medicine

1. Introduction

An accurate and rapid method for determination of amylase activity in digestive medicines has been requested from process and quality control in the pharmaceutical industry. Some standard official testing methods [1] for amylase activity, regulated by the pharmacopoeia of Japan are based on an iodide–thiosulphate titration modified Somogyi method and a spectrophotometric method, where the amount of product of

* Corresponding author. Fax: +81 92 6424134; e-mail: imato@cstf.kyushu-u.ac.jp

PII S0039-9140(97)00303-2

the enzyme reaction of starch with amylase in unit reaction time is determined. The enzyme reactions are carried out at 37°C, pH 5.0 for 10 min. One of these methods is conducted using the procedure illustrated in Scheme 1. The same procedure is required for blank solutions as well as the sample solution. The official methods provide good accuracy but are cumbersome as well as time-consuming requiring about 40 min for the determination of one sample. A promising approach for a more rapid and simpler operation is the application of flow-injection analysis (FIA) techniques [2]. Spectrophotometric determination of fungel α-amylase activity using flow injection analysis has been reported for *Aspergillus oryzae* fermentations [3]. The method is based on the spectrophotometric measurement of residual starch by formation of an iodine complex, after degradation of starch by the enzyme. Nikolelis et al. [4] has reported the flow injection determination method of amylase using an enzymatic catalyzed reaction yielding glucose as a product, and an electrochemical oxygen detector with a three-electrode amperometric system. This method has been applied to real samples such as blood serum—for amylase. The limit of detection for amylase activity is 0.357 U ml^{-1}.

We have reported a highly sensitive potentiometric flow injection determination of reducing sugars using a $[Fe(CN)_6]^{3-}$–$[Fe(CN)_6]^{4-}$ potential buffer solution [5]. The analytical method is based on the detection of change in the composition of potential buffer solution due to a reaction of reducing sugar with $[Fe(CN)_6]^{3-}$ using a flow-through type redox electrode. The advantages of the present potentiometric method are (1) the electrode potential is very stable since the electrode is immersed in a well-defined potential buffer, (2) samples with a wide concentration range are determinable by appropriately selecting the concentration of the buffer solution. For example, the detection limit was 1×10^{-7} M for glucose and the measurable concentration range of reducing sugars was wide from 1×10^{-7} M to ca. 0.1 M by appropriately changing the concentration of the potential buffer solution and injection volume [7]. If our FIA method is adapted to determine the reducing sugar generated by the enzyme reaction of amylase with starch, activity of amylase is expected to be determined rapidly and with high sensitivity.

In this paper, we describe an application of our FIA method to determine amylase activity and demonstrate the usefulness of this method for real samples of digestive medicines.

2. Experimental

2.1. Reagents and preparation of solutions

Soluble starch was purchased from Wako and was used after drying. Biodiastase 1000, which is the commercial name of α-amylase (EC 3.2.1.1) from *Aspergillus oryzae*, was donated from Amano Pharmaceutical, and was used as the standard amylase reagent without purification. Digestive medicines containing biodiastase produced by five pharmaceutical companies in Japan, A, B, C, D and E, were purchased from local drug stores. Other reagents were of analytical grade and used as received.

A 1% (w/v%) of starch solution was substrate for amylase and prepared according to the procedure of the Japanese Pharmacopoeia Official Testing Method [1]: Dried soluble starch (1 g) was added to ca. 25 ml of 0.4 N sodium hydroxide solution until the solution became a paste-like solution. After heating the solution for 3 min and cooling to room temperature, the solution was neutralized with a 2 N hydrochloric acid solution and was then adjusted to pH 5.0 by acetate buffer solution. The solution was finally made up 100 ml in a volumetric flask with deionized water. Concentration (molarity) of the starch solution was defined as the weight of starch per litre divided by the molecular weight of the monomer unit (glucose). A standard solution of α-amylase was prepared by dissolving 10 mg of biodiastase 1000 with 500 ml of a 0.1 M acetate buffer (pH 5.0) solution containing 6 mM $CaCl_2$ and 20 mM NaCl. The addition of $CaCl_2$ and NaCl to the amylase solution stabilizes enzyme activity. Decrease in activity by self-decomposition was less than 3% in 3 days when stored in a refrigerator. Amylase activity was determined using the official

method shown in Scheme 1. One unit of amylase activity was defined as the amount of enzyme that yielded reducing sugar equivalent to 1 mg of reducing sugar from starch min^{-1} at pH 5.0 and 37°C g^{-1} of solid-amylase. Activity of standard α-amylase solution was 9.2×10^3 U g^{-1} (0.184 U ml^{-1}) and was used as a stock solution. The sample solutions were prepared by dissolving 0.473, 0.561, 0.350, 0.463 and 0.325 g, which are the weights of one tablet of digestive medicines obtained from A, B, C, D and E pharmaceutical, respectively, with 500 ml of the same buffer solution used in the above standard solution. Amylase activity, U g-$tablet^{-1}$ (U ml^{-1}), of the digestive medicines from A, B, C, D and E pharmaceutical, respectively, were determined using the official method as being 1.8×10^2 (0.168), 1.1×10^2 (0.248), 4.1×10^2 (0.288), 5.5×10^2 (0.256) and 0.98×10^2 (0.064), respectively. These solutions were stored in a refrigerator as stock solutions. In the FIA method, the stock solution was diluted with the above buffer solution so as to measure activity using the flow system. A stock potential buffer solution consists of 0.1 M $[Fe(CN)_6]^{3-}$, 0.1 M $[Fe(CN)_6]^{4-}$ and NaOH was prepared according to the procedure previously described [5]. For the sake of simplicity, this buffer is abbreviated to 0.1 M $[Fe(CN)_6]^{3-}$–$[Fe(CN)_6]^{4-}$ potential buffer solution. Buffer solutions of different concentrations were prepared by serial dilution of the stock solution with deionized water.

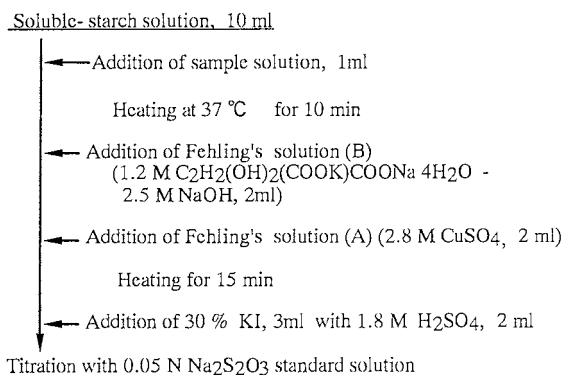

Scheme 1. Procedure of the official method (modified Somogyi method).

2.2. Apparatus

The flow-injection apparatus consisted of a peristaltic pump (Model Minipuls 2, Gilson), a six-way valve (HPV-6, GLC Science) with a loop for sample injection (sample volume 140 μl), a flow-through type redox electrode detector which has a platinum-plate electrode and a silver/silver chloride reference electrode (DKK) and a potentiometer (IOC 10, DKK) for measuring the potential of the electrode detector. The potential signal of the detector was fed to a recorder (Model EPR221E, Toa Electronics). The manifold was constructed with Teflon tubing (0.5 mm i.d.) throughout.

2.3. Procedure

The flow system consists of three streams, a carrier stream of water (C.S.), a stream of starch solution ($R.S._1$) and a stream of $[Fe(CN)_6]^{3-}$–$[Fe(CN)_6]^{4-}$ potential buffer solution ($R.S._2$), as shown in Fig. 1(A). A sample solution containing amylase is injected into the carrier stream and merges with the stream of starch solution at the confluence point (C_1). The starch is catalytically hydrolyzed by amylase to generate reducing sugar in the reaction tube ($R.C._1$). This mixed stream is subsequently merged with the stream of potential buffer at the confluent point (C_2) and the reducing sugar is oxidized by $[Fe(CN)_6]^{3-}$ the potential buffer in a reaction coil ($R.C._2$), which changes the composition of the potential buffer solution. The composition change is detected by the redox electrode detector located downstream. The potential change of the detector is measured using the potentiometer and a peak-shaped signal is recorded. Since the reaction time of the injected sample in $R.C._1$ is kept strictly constant by controlling the pumping rate of solutions, the amount of reducing sugar generated in $R.C._1$ is related to

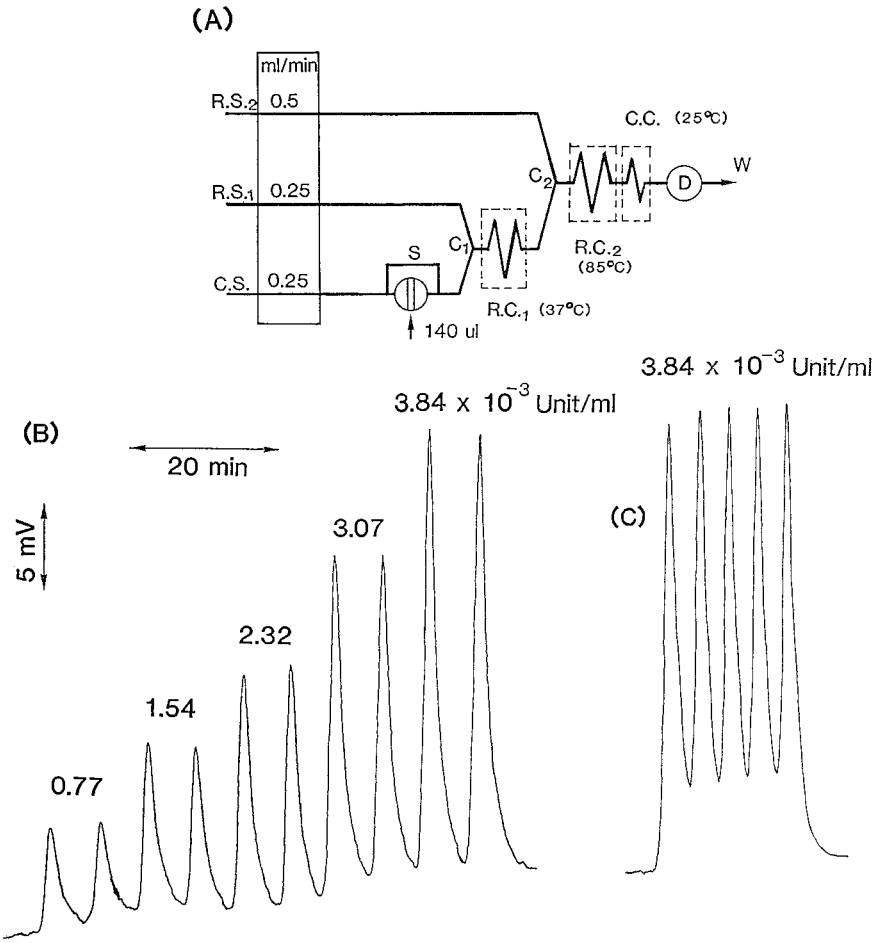

Fig. 1. Schematic diagram of FIA for amylase and analytical peak. (A) Flow injection system: C.S., carrier stream (water); $R.S._1$, reagent stream 1(10 mM soluble-starch (pH 5.0); $R.S._2$, reagent stream 2 (1×10^{-4} M $[Fe(CN)_6]^{3-}$-1×10^{-4} M, $[Fe(CN)_6]^{4-}$, 0.6 M NaOH); P, peristaltic pump; $R.C._1$, reaction coil 1 (5 m × 0.5 mm i.d.); $R.C._2$, reaction coil 2 (12 m × 0.5 mm i.d.); C.C., cooling coil (2 m × 0.5 mm i.d.); D, redox electrode detector; C_1 and C_2, confluence points; length of tube between S and C_1, 50 cm × 0.5 mm i.d. (B) Calibration peaks injected every 6 min. (C) Repeated peaks of 3.84×10^{-3} U ml^{-1} amylase injected every 4 min.

amylase activity, and the peak height of the potential signal is proportional to amylase activity. Amylase activity is determined from the calibration curve based on peak heights. The standard operational parameters for the determination of amylase activity are given in Fig. 1(A), which were optimized by experiments. The flow rates of CS, RS_1 and RS_2 are set up at 0.25, 0.25 and 0.5 ml min^{-1}, respectively, for the sake of dispersion suppression of the sample zone and completion of the redox reaction between reducing sugar and $[Fe(CN)_6]^{3-}$ in $R.C._2$. Usually the sample solution was injected every 6 min, except for examination of the effect of its time interval on peak heights. It took about 6 min from sample injection to detect a peak maximum. The average residence times of the sample in $R.C._1$ and $R.C._2$ were ca. 2 min and ca. 2.5 min, respectively. The temperatures of $R.C._1$ and $R.C._2$ were maintained at 37 and 85°C, respectively.

The Michaelis parameters, K_m and V_m were calculated from the Lineweaver–Burk plot using data obtained from batchwise experiments.

2.4. Analytical method

Determination of amylase activity by the FIA method, involved the two following reactions, enzymatic reaction of amylase with starch as a substrate depicted in Eq. (1) and the oxidation reaction of reducing sugar by $[Fe(CN)_6]^{3-}$ expressed by Eq. (2)

$$\text{starch} + H_2O \xrightarrow{\text{amylase}} \text{reducing sugar} \quad (1)$$

$$\text{reducing sugar} + n[Fe(CN)_6]^{3-} \xrightarrow{OH^-} n[Fe(CN)_6]^{4-} + \text{oxidation products} \quad (2)$$

where n is the number of moles of $[Fe(CN)_6]^{3-}$ required to oxidize a mole of reducing sugar [6].

When the reaction of reducing sugar with $[Fe(CN)_6]^{3-}$ in the potential buffer solution goes to completion according to Eq. (2), the potential change (ΔE) (peak height) of the redox electrode is expressed by the following equation, which is derived from the Nernst equation [7]:

$$\Delta E/\text{mV} = -59 \log\{1 - n[\text{reducing sugar}]/[Fe(CN)_6]_o^{3-}\} / \{1 + n[\text{reducing sugar}]/[Fe(CN)_6]_o^{4-}\} \quad (3)$$

where [reducing sugar] is the concentration of reducing sugar produced from starch by Eq. (1), and $[Fe(CN)_6]_o^{3-}$ and $[Fe(CN)_6]_o^{4-}$ are the initial concentrations of $[Fe(CN)_6]^{3-}$ and $[Fe(CN)_6]^{4-}$ in the potential buffer solution, respectively. The amylase activity is determined from peak heights and the calibration curve which is obtained from the standard solution of injected amylase. The linear relationship between ΔE and amylase activity of the standard solution, exists where ΔE is less than 25 mV, according to Eq. (3).

3. Results and discussion

3.1. Determination of amylase activity of standard solution using the official method

The determination of amylase activity of the standard solution was performed according to the official method shown in Scheme 1. This method is a modified Somogyi method. The enzyme reaction with amylase was determined using an iodine/thiosulphate titration method. At first, the activity of the sample solution prepared by diluting the standard solution was measured under reaction conditions at different concentrations of starch. The results are shown in Fig. 2. The amylase activity proportionally increased with concentration of starch solution up to 2 mM and became constant at concentrations higher than 10 mM. This constant value was 0.184 U ml^{-1}. This identical activity irrespective of starch concentration at higher concentrations than 10 mM indicates that this enzyme reaction obeys a law of zero-order reaction.

Fig. 3 shows the Lineweaver–Burk plot for hydrolysis of starch by amylase calculated from the data of Fig. 2. A good linear relationship with a correlation coefficient of 0.99 was observed between the inverse of amylase activity and the inverse of starch concentration. From Fig. 3, K_m and V_m values of 2.2 mM and 0.224 U ml^{-1} min^{-1} were obtained, respectively. This K_m value for amylase from *Aspergillus oryzae* was almost the same as that obtained for amylase from *Pseudomonas stutzeri* ($K_m = 1.6$ mM) as determined by Sakano et al. [8].

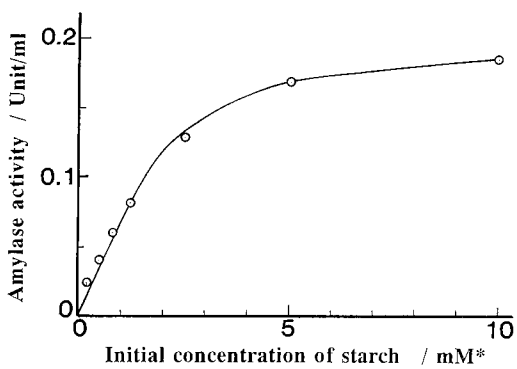

Fig. 2. Relationship between amylase activity and concentration of starch solution. Conditions: starch solution; 10 ml of 0.25–10mM starch solution, amylase solution: 1 ml of 20 mg l^{-1} amylase.

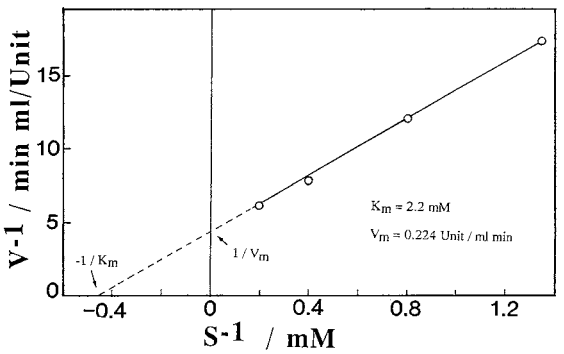

Fig. 3. Lineweaver–Burk plot for the hydrolysis reaction of starch by amylase. V, amylase activity; S, concentration of starch; K_m, Michaelis constant obtained at the intercept of the extrapolated line with the abscissa; V_m, maximum activity obtained at the intercept of the extrapolated line with the ordinate.

3.2. Optimization of analytical procedure of flow system

The concentration of sodium hydroxide in the potential buffer and temperature in the reaction coil (R.C.$_2$) are expected to have an affect on the reaction of reducing sugar with $[Fe(CN)_6]^{3-}$ i.e. on the sensitivity of amylase activity determination. The effects of sodium hydroxide concentration in the potential buffer and reaction temperature on the peak height were examined—1×10^{-4} M potential buffer solution was used in the flow system without the stream of R.S.$_1$ in Fig. 1. Moreover, the effect of reaction time on the reactivity between $[Fe(CN)_6]^{3-}$ in the potential buffer and reducing sugar in the R.C.$_2$ was examined at different residense times of the sample zone by changing flow rates of C.S., R.S.$_1$ and R.S.$_2$. Since maltose is the main product of starch hydrolysis by amylase in neutral media [9], maltose was used as reducing sugar sample for optimization of the flow system. The concentration of the maltose sample solution injected was 5×10^{-6} M. No peak was detected for the potential buffer containing sodium hydroxide at concentrations below 0.05 M. A peak was detected at 0.1 M sodium hydroxide and the peak height increased with increasing concentration of sodium hydroxide. The peak height was almost constant in the concentration range of 0.6 M–1 M. Above 1 M, however, the peak became broad. This may be due to the increase in viscosity of the mixed solution of R.S.$_1$ and R.S.$_2$ caused by generation of a gel of starch in the reaction coil (R.C.$_2$).

No peak was observed when the temperature of the R.C.$_2$ was below 40°C. Above 50°C, the peak height gradually increased and approached a constant value of about 80°C. The baseline potential was observed to shift more or less to the negative potential side, when temperature was over 90°C. This may be due to $[Fe(CN)_6]^{3-}$ in the potential buffer which is partially reduced to $[Fe(CN)_6]^{4-}$ by heating. Thus, the potential buffer solution containing 0.6 M sodium hydroxide and the R.C.$_2$ kept at 85°C were used in subsequent experiments.

The peak height was also dependent on the reaction time (residence time of the sample zone in R.C.$_2$) in the oxidation reaction of maltose by $[Fe(CN)_6]^{3-}$. The peak height gradually increased with increasing reaction time until about 2.5 min and then reached an almost constant value, when 1×10^{-3} M potential buffer solution containing 0.6 M NaOH was used. This indicates that the reaction between maltose and $[Fe(CN)_6]^{3-}$ finishes in about 2.5 min. The response potential (ΔE) at a reaction time of 2.5 min was 19.0 mV, and this value corresponded to the n value which was equal to 7.1 as calculated from Eq. (3). This means that 7 mol of $[Fe(CN)_6]^{3-}$ are consumed in the oxidation of 1 mol of maltose under the above reaction conditions. This n value was slightly larger than that reported by Gupta (4–6 mol) obtained under reaction conditions in an ammoniacal medium [10]. Therefore, the flow system shown in Fig. 1(A) was decided to be the reaction time in the R.C.$_2$ of 2.5 min.

3.3. Determination of amylase in digestive medicines

The standard amylase solutions at different activity, determined previously using the official method, were injected into the carrier stream of the flow system shown in Fig. 1(A) to obtain the calibration curve. In this case, the concentrations of starch in the stream of R.S.$_1$ was varied to

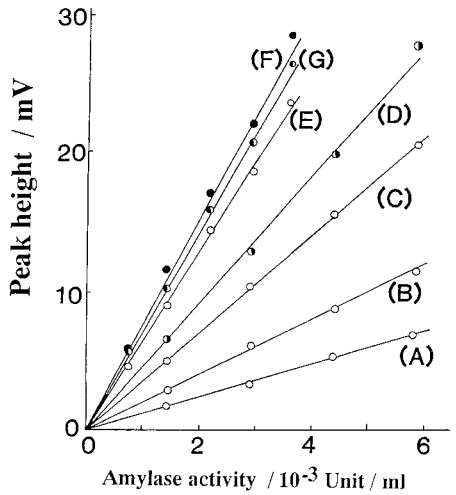

Fig. 4. Relationship between peak heights and amylase activities. Starch concentration (mM): (A), 0.5; (B), 1.25; (C), 2.5; (D), 5.0; (E), 10.0; (F), 15.0; (G), 20.0.

examine the concentration dependence on sensitivity, i.e. the slope of the calibration curve. As shown in Fig. 4, a linear relationships exists between the peak height and the amylase activity in the range from 1×10^{-3} U ml^{-1} to 6×10^{-3} U ml^{-1} when the 1×10^{-4} M potential buffer solution was used. The sensitivity, however, increased with increasing starch concentrations up to 10 mM and was almost constant above 10 mM. Above 30 mM, the sensitivity decreased slightly and the peak became broad. The dependence of starch concentration on sensitivity was similar to that the amylase activity observed in Fig. 2. Table 1 lists the amylase activity obtained using the official method and the sensitivity obtained by the FIA system at different starch concentrations.

The typical flow injection peaks with calibration (curve (E) in Fig. 4) are shown in Fig. 1(B). The shape of the peak was broad and the peak width is about twice that compared with the peak width obtained using the same FIA manifold using the stream of water instead of the starch solution in R.S.$_1$. The drifts of baseline potentials were less than 3 mV h^{-1}. The baseline potential drift for the determination of reducing sugars using the similar FIA manifold without the stream of the starch solution was 0.8 mV h^{-1} [5,7]. Therefore the larger baseline potential drift of the present case may be due to the use of starch solution. FIA peaks for repeated injection of a sample of 3.8×10^{-3} U ml^{-1} amylase ($n = 5$) every 4 min are shown in Fig. 1(C) and the relative standard deviation is 0.9% for their peak heights. The repeated injection every 4 min causes 5% positive error due to the overlapping of adjacent peaks in comparison with repeated injections every 6 min. The determination of 15 samples h^{-1} was possible with good reproducibility using the proposed FIA method.

The sensitivity of the proposed FIA method defined as peak height per activity (slope of the calibration curve, mV U^{-1} ml^{-1}) depended on the concentration of potential buffer, as estimated

Table 1
Dependence of amylase activity and sensitivity on starch concentration

Starch Concentration (mM)	Activity[a] (U ml^{-1})	Relative activity[b]	Sensitivity[c] ($\times 10^3$ mV^{-1} U^{-1} ml^{-1})	Relative sensitivity[d]
0.5	0.04	0.22	1.15	0.16
1.25	0.08	0.44	1.99	0.28
2.5	0.128	0.70	3.47	0.49
5.0	0.168	0.91	4.69	0.66
10.0	0.184	1.0	6.70	0.94
15.0	0.184	1.0	7.48	1.05
20.0	0.184	1.0	7.14	1.0

[a] Amylase activity was obtained by the official method (Fig. 2).
[b] Normalized by the acitivity above the starch concentration of 10.0 mM
[c] Sensitivity was obtained using the FIA method (Fig. 4).
[d] Normalized by the sensitivity at the starch concentration of 20.0 mM

Table 2
Effect of potential buffer concentration on sensitivity and measurable concentration range of amylase

Concentration of the buffer (M)	Sensitivity (mV^{-1} U^{-1} ml^{-1})	Measurable concentration range (U ml^{-1})
1×10^{-3}	1.0×10^{3}	$(0.5–2.5)\times10^{-2}$
1×10^{-4}	6.6×10^{3}	$(0.8–3.8)\times10^{-3}$
5×10^{-5}	9.9×10^{3}	$(0.5–2.5)\times10^{-3}$
1×10^{-5}	3.9×10^{4}	$(1.2–6.0)\times10^{-4}$

from maltose sensitivity to potential buffer concentration. As shown in Table 2, the sensitivity increased by two order of magnitude when the concentration decreased from 10^{-3} M to 10^{-5} M, although the oxidation rate of reducing sugar by $[Fe(CN)_6]^{3-}$ is slower in the case of dilute buffer solution. When a 1×10^{-5} M potential buffer was used, the lower detection limit of amylase activity was 6.0×10^{-5} U ml^{-1}, and this is ca. 200 fold higher in comparison with the sensitivity obtained using other flow methods [3].

The proposed FIA method was applied to the determination of amylase in digestive medicines from five pharmaceutical companies, A, B, C, D and E. The sample solutions of the medicines, whose activities were determined previously using the official method, were injected into the flow system in Fig. 1(A). The amylase activity in the digestive medicine was determined by a peak height observed using the calibration curve obtained using the standard amylase solution. The correlation of analytical results using the official and FIA methods is shown in Fig. 5. From Fig. 5, the regression line expressed by $Y=1.04X-(1.17\times10^{-4})$ with a correlation factor of 0.99 was obtained for all digestive medicines. The amylase content (mg g-$tablet^{-1}$) in the digestive medicine calculated using the official method and the proposed method are listed in Table 3. The analytical results obtained by the proposed method is in agreement with those obtained using the official method within relative error of 4.5–8.7%. The proposed FIA system using $[Fe(CN)_6]^{3-}$–$[Fe(CN)_6]^{4-}$ potential buffer can

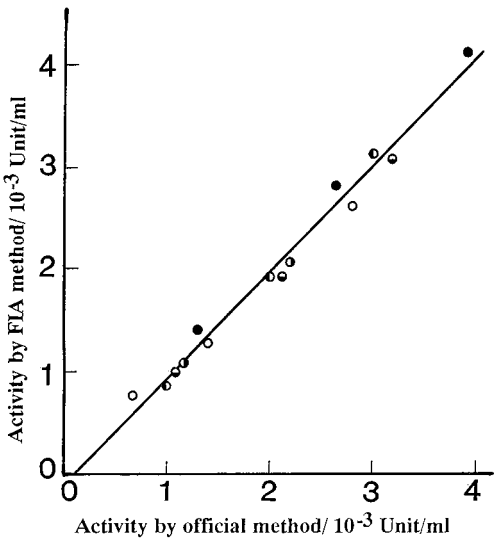

Fig. 5. Comparison between amylase activities obtained using the FIA method and the official method on various commerical digestive medicines. ○: A, ●: B, ◑: C, ◐: D, ◒, E. The solid line is the regression line. The circles are the results of the digestive medicines.

be applied to the determination of amylase in digestive medicines.

In conclusion, the proposed FIA method using a combination of $[Fe(CN)_6]^{3-}$–$[Fe(CN)_6]^{4-}$ potential buffer and the redox electrode detector was more sensitive than other flow methods [3,4], and was successfully applied to the determination of amylase in real samples of digestive medicines. Amylase in a wide activity range between two orders of magnitude was measured by selecting concentrations of potential buffer

Table 3
Determination of the amylase content in digestive medicines

Pharmaceutical company	Amylase content, mg g-$tablet^{-1}$	
	Official method	FIA method
A	19.3	18.0
B	12.0	12.7
C	44.7	41.6
D	60.1	57.4
E	10.3	9.4

from 10^{-3} M to 10^{-5} M. We did not examine the interference from redox species. Some redox species must exist, which cause some interfering response to the redox electrode detector. Serious interference was not observed in the digestive medicine that was examined in this paper. Therefore, at this stage, applicability of the proposed method is limited to types of samples used in this study.

Acknowledgements

The authors are grateful to Mr. Nomura of Amano Pharmaceutical for his kind donation of the standard amylase (Biodiastase 1000) sample used in this work.

References

[1] The Japanese Pharmacopoeia 13th Technical Information, Yakugyo Jiho, 1966, p. 102.
[2] J. Ruzicka, E.H. Hansen, Flow-Injection Analysis, Wiley, New York, 1981.
[3] P.W. Hansen, Anal. Chim. Acta 158 (1984) 375.
[4] D.P. Nikolelis, H.A. Mottola, Anal. Chem. 50 (1978) 1665.
[5] H. Ohura, T. Imato, Y. Asano, S. Yamasaki, N. Ishibashi, Bunseki Kagaku 35 (1986) 807.
[6] J.D. Roberts, M.C. Casserio, Basic Principles of Organic Chemistry, Benjamin, New York, 1965, p. 618.
[7] H. Ohura, T. Imato, S. Yamaski, N. Ishibashi, Anal. Sci. 3 (1987) 453.
[8] Y. Sakano, Y. Kashiwagi, T. Kobayashi, Agric. Biol. Chem. 46 (1982) 639.
[9] F. Scheller, F. Schobert, Biosensors, Elsevier, Amsterdam, 1992.
[10] K.C. Gupta, A. Sharma, V.D. Misra, Tetrahedron 37 (1981) 2887.

ELSEVIER

Talanta 45 (1998) 575–581

Talanta

Flow injection analysis for residual chlorine using Pb(II) ion-selective electrode detector

Aki Sakai [a], Akihide Hemmi [a], Hiromitsu Hachiya [a], Fumie Kobayashi [a], Satoshi Ito [a], Yasukazu Asano [a], Toshihiko Imato [b,*], Yoshito Fushinuki [c], Isao Taniguchi [d]

[a] *R&D Division, DKK Corporation, Kitamachi, Kichijoji, Musashino 180, Japan*
[b] *Kyushu University, Hakozaki, Higashi-ku, Fukuoka 812, Japan*
[c] *Scientific Investigation Research Laboratory, Kagoshima Pref. Police HQ, Kamoike-shinmachi, Kagoshima 892, Japan*
[d] *Kumamoto University, Kurokami, Kumamoto 860, Japan*

Received 7 April 1997; received in revised form 28 August 1997; accepted 28 August 1997

Abstract

A simple flow injection analysis (FIA) system for residual chlorine in tap water has been developed by using a Pb(II) ion-selective electrode (ISE) detector. The method is based on a specific response of the Pb(II)-ISE to residual chlorine. The FIA system consists of a millivolt meter, a peristaltic pump, a Pb(II)-ISE detector and a recorder. A linear working curve between peak height and concentration of residual chlorine was obtained from 0.1 to 1 mg l^{-1} for the developed FIA system. The relative standard deviation for repeated injections of a 0.2 mg l^{-1} residual chlorine sample was 2%. The regression line and its correlation factor between the conventional *o*-tolidine colorimetric method and the present method were $Y = 0.75X + 0.17$ and 0.967, respectively, for this determination.

Keywords: Flow injection analysis; Residual chlorine; Pb(II) ion-selective electrode detector; Tap water

1. Introduction

Liquid-chlorine and sodium hypochlorite are widely used as industrial disinfectants and bleaches. In particular, residual chlorine plays an important role in the purification of tap water because of its strong disinfectant properties and lifetime in solution. The concentration of residual chlorine in tap water in the final stage of water purification is generally regulated to 0.1–1 mg l^{-1} in order to maintain sterilizing power [1,2].

A colorimetric method using diethyl-*p*-phenylene diamine, a coulometric titration method and iodometry have been adopted as the standard testing method for industrial water (Japanese Industrial Standard) [3] as well as for the analysis of municipal water (Japan Water

* Corresponding author. Dept of Chem. Systems Eng., Kyushu University Graduate School of Engineering, Hakozaki, Higashi-ku, Fukuoka Pref., 812 Japan. E-mail: imato@cstf.kyushu-u.ac.jp

0039-9140/98/$19.00
PII S0039-9140(97)00299-3

Works Association). All these methods are indirect methods which use reagents, such as *o*-toluidine and iodide to react with residual chlorine which is then determined by colorimetry and titrimetry. Since residual chlorine is unstable in water, a chemical sensor method represents a highly desirable analytical method for such an unstable species, since such analytical results can be obtained by simply immersing a sensor probe in an appropriate sample solution.

Chemical sensor methods for residual chlorine based on amperometry [4] and potentiometry [5,6] have been reported. The principle involved for the response of sensors to residual chlorine is an indirect method. Namely, in both cases, a redox reaction of residual chlorine with iodide is used to detect residual chlorine.

We recently discovered that a Pb(II) ion-selective electrode (ISE) responds to residual chlorine in a specific manner during our investigation of substances which interfere with the Pb(II)-ISE. Based on our findings, we recommended the use ascorbic acid for the determination of Pb(II) ion in tap water in order to eliminate interference from residual chlorine [7].

Utilizing the above interference characteristics of residual chlorine to the Pb(II)-ISE, we developed a direct potentiometric method for the determination of residual chlorine by using the Pb(II)-ISE in a batch-beaker system [8]. However, the reproducibility of the determination, using the batch-beaker system was not good because residual chlorine is easily vaporized in this system, which is exposed to air. The low level of reproducibility of the batch-beaker system was also thought to be due to conversion of the residual chlorine to chlorine, hypochloric acid and hypochlorite ion, depending on the pH of the sample solution [9,10].

Chemical analysis by flow injection analysis (FIA) has numerous advantages, such as the use of a small sample volume, low load to waste-water, it is environmentally friendly, its simplicity, its high analytical throughput, high sensitivity, stability and selectivity, its ease of handling, and the fact that the analyses can be carried out by moderately trained personnel. Therefore, FIA would be expected to be the most promising technique for wet chemical analysis and would be expected to survive and grow into a powerful analytical method [11–14]. One advantage of FIA is its capability for analysis in a closed system. This suggests that FIA would be suitable for the analysis of unstable samples, such as residual chlorine, and would improve reproducibility as well as the accuracy of wet chemical analysis, which is often done using a batch system.

We predict that the reproducibility of the Pb(II)-ISE method for residual chlorine would be much improved over the batch-beaker system, using an FIA system. In this paper, we wish to report an FIA method for the determination of residual chlorine using our previously reported method [7] based on the specific response of the Pb(II)-ISE to residual chlorine.

2. Experimental

2.1. Reagents

All chemicals used were of analytical reagent grade. Deionized water was treated with a membrane filter (pore size, 0.45 μm), which gave an electrical conductivity of less than 0.1 μS/cm, and was used throughout the work. A standard solution of residual chlorine was prepared by diluting a sodium hypochlorite stock solution (available chlorine, 8.5–13.5%) with an appropriate amount of deionized water, and was used after standardizing by titration with a 0.1 mol l^{-1} potassium thiosulfate solution prior to each run.

2.2. Apparatus

A millivolt meter (DKK Model IOL-50), a Pb(II)-ISE (DKK Model EL 7180) and a double-junction reference electrode (DKK Model 4083: 1 M KNO_3 outer solution, 3 M KCl inner solution, Ag/AgCl inner electrode, glass sleeve–liquid junction) were used for the investigation in the batch-beaker system. An iodide-ISE (DKK Model EL 7060), a Cu(II)-ISE (DKK Model EL 7140), a Cd(II)-ISE (DKK Model EL 7120), an Ag(I)-ISE (DKK Model EL 7080) and a Pt electrode (DKK Model EL 6154) were used in the batch-beaker

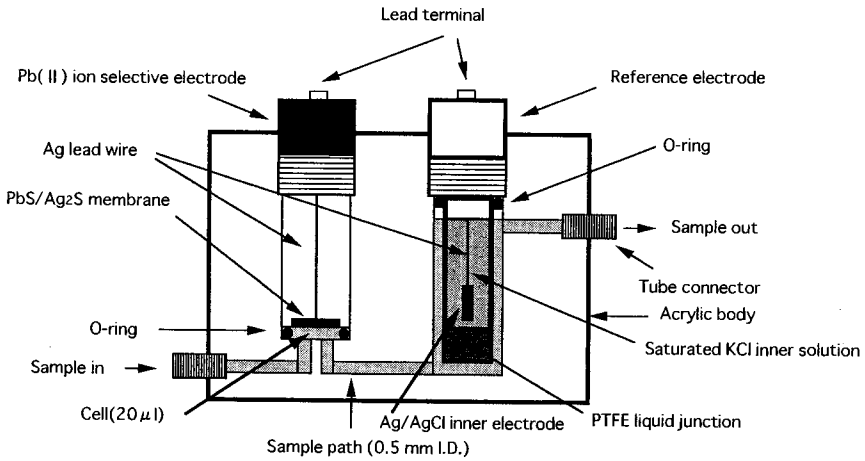

Fig. 1. Pb(II) ion-selective electrode detector for residual chlorine.

system to compare the response behavior of the Pb(II)-ISE to residual chlorine.

2.3. Fabrication of the Pb(II)-ISE detector

The Pb(II)-ISE detector for FIA is schematically shown in Fig. 1. The detector was fabricated by assembling a Pb(II)-ISE (DKK Model 7181: size, 12 × 50 mm (O.D. × length)) and a reference electrode (DKK Model 4401, PTFE single liquid junction; size, 12 × 60 mm (O.D. × length); surface area of liquid junction, 4.8 cm^2) specially designed for flow analysis [15]. A body of the flow cell was fabricated from acrylic resin (size, 50 × 80 × 40 mm ($h \times w \times d$)). The effective volume of the flow cell was ca. 20 μl.

2.4. FIA system with the Pb(II)-ISE detector

As shown in Fig. 2, a two-channel FIA system was constructed from a peristaltic pump (Alitea AB, XV type, Sweden), an injector (Rheodyne, 7125, USA), the Pb(II)-ISE detector, the millivolt meter and a recorder (Sekonic, 250-F, Japan). The flow rate of the reagent and water streams was 0.9 ml min^{-1}. The 700-cm long mixing coil (0.5 mm I.D.) from the confluence point to the detector was determined experimentally. A 1 mol l^{-1} potassium nitrate solution, adjusted to pH 6.0 with 0.15 mol l^{-1} sodium acetate was used as the reagent solution for the FIA system. One hundred μl of a sample solution buffered at pH 6.0 with 0.15 mol l^{-1} sodium acetate were injected into the water stream, and this stream was merged with the reagent stream. The mixed stream was then transported to the detector after passing through the mixing coil. The potential of the detector was measured with the millivolt meter and its potential signal fed to the recorder. The concentration of residual chlorine was determined by the change of the detector, which was observed as a peak-shaped signal (FIA signal) on the recorder.

3. Results and discussion

3.1. Batch system study

3.1.1. Response of Pb(II)-ISE to residual chlorine in the bath-beaker system

As described above, the presence of residual chlorine in a sample of Pb(II) caused a large positive error for the determination of Pb(II) by the Pb(II)-ISE. To clarify the reasons why the Pb(II)-ISE showed a response to residual chlorine, we compared the potential of the response of Ag(I)-, Cu(II)-, Cd(II)- and I-ISEs, whose sensing membrane consisted mainly of Ag_2S, to residual chlorine. As shown in Fig. 3, the Cu(II)- and Cd(II)-ISEs exhibit response to residual chlorine

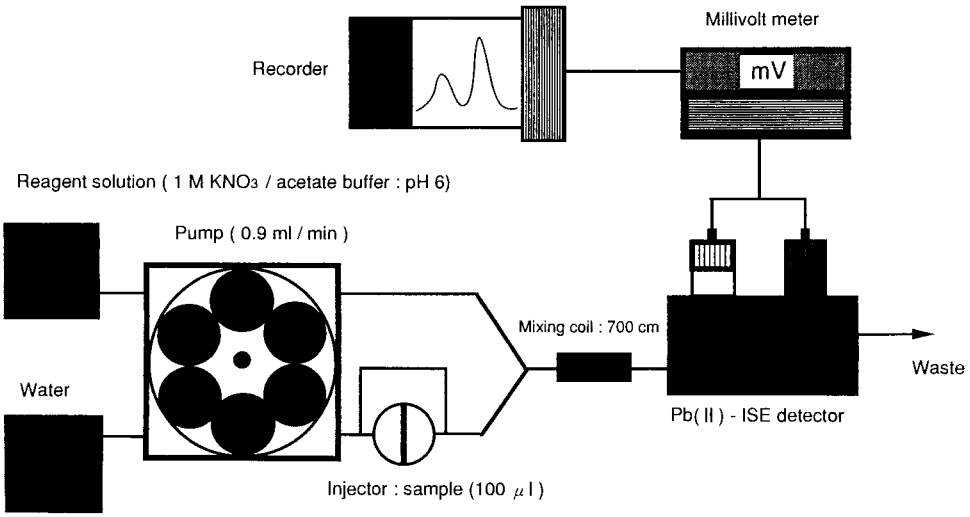

Fig. 2. Potentiometric flow injection system for residual chlorine.

similar to the Pb(II)-ISE, whereas the Ag(I)- and I-ISEs showed no response. This result indicates that transition metal sulfides, Pb(II)S, Cd(II)S and Cu(II)S, which are contained in the sensing membrane of the ISEs, appear to play a role in the response to residual chlorine.

The response mechanism of the Pb(II)-ISE to residual chlorine is not clear at this stage of the study. However, one possible explanation is that

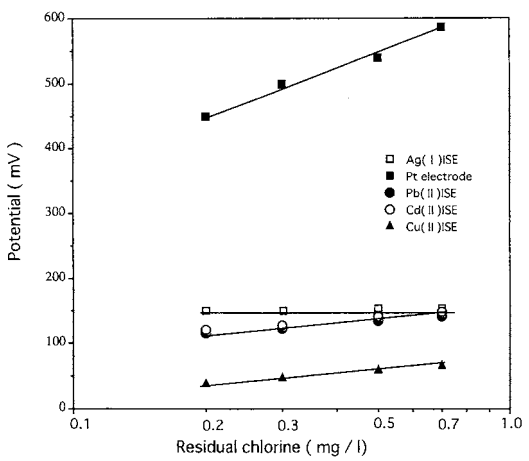

Fig. 3. Comparison of response to residual chlorine for the ISE and Pt electrode in the batch system.

the response of the Pb(II)-ISE to residual chlorine may arise from the oxidation of sulfide to sulfate at the surface of the Pb(II)S/Ag_2S membrane by residual chlorine. Since the electric conduction through the sensing membrane of the Pb(II)-ISE and the other ISE, the sensing membrane of which consists of Ag_2S, is mainly governed by a silver ion conduction mechanism, these electrodes generally do not show a direct response to redox species, compared with the metal electrode, in which the electric conduction is governed by an electron conduction mechanism. Based on the silver ion conduction mechanism, the potential of the Pb(II)-ISE is known to be determined by the activity of silver ion at the surface of the PbS/Ag_2S membrane, which is related to the precipitation equilibrium shown in Eq. (1)

$$Ag_2S = 2Ag^+ + S^{2-},\ PbS = Pb^{2+} + S^{2-} \qquad (1)$$

If residual chlorine oxidizes S^{2-} at the surface of the membrane of the Pb(II)-ISE to SO_4^{2-}, the reaction of which is known to occur in an aqueous solution [9], the activity of the silver ion at the surface of the electrode membrane increases according to the equilibria shown in Eq. (1), and thus the Pb(II)-ISE would show a positive response to residual chlorine. The Ag(I)-ISE also

should show a response to residual chlorine, since the above oxidation reaction also occurs at the surface of the Ag(I)-ISE. However, as shown in Fig. 3, the Ag(I)-ISE shows no detectable response. The sulfide concentration at the surface of the Pb(II)-, Cu(II)- and Cd(II)-ISEs are estimated to be higher than that of the Ag(I)-ISE, judging from the values of the solubility product of the metal sulfide. The difference in the response of the Pb(II)-ISE to residual chlorine from that of the Ag(I)-ISE may be due to a difference in the concentration of sulfide at the surface of the electrodes. In addition, the transition metal sulfides, which are added to the sensing membrane, may have an effect on the oxidation of sulfide with residual chlorine.

Furthermore, we compared the response of the Pb(II)-ISE to residual chlorine to that of a Pt electrode, in which the sensing membrane is an electron conductor. As shown in Fig. 3, the potential of the Pt electrode is proportional to the logarithmic concentration of residual chlorine as well as the Pb(II)-ISE. However, the slope of the potential change against the concentration for the Pb(II)-ISE (50 mV/decade) is smaller than that for the Pt electrode (100 mV/decade).

3.1.2. Response time

The response time of the Pb(II)-ISE was examined by changing the residual chlorine concentration from 0.1 to 1 mg l^{-1} in the batch system. The time required to attain 90% of equilibrium (90% response time) was less than 10 s for the Pb(II)-ISE, while it was more than 1 min for the Pt electrode. The recovery time of the Pb(II)-ISE, which was measured by replacing the sample solution with the 0.1 mg l^{-1} residual chlorine solution, was also shorter than that of the Pt electrode. The Pb(II)-ISE was found to be superior to the Pt electrode with respect to response time and memory effect.

3.1.3. Selectivity

The selectivity of the present method for the determination of residual chlorine was studied for several substances, which often coexist in tap water, in the batch system. The Pb(II)-ISE showed no response to common cations and anions such as Na^+, K^+, Zn^{2+}, Ca^{2+}, SO_4^{2-}, Cl^-, F^-, NO_3^- CO_3^{2-} and F^-. The levels of Pb^{2+}, Cd^{2+} and Cu^{2+} in tap water are mandated by law in Japan [16] to be less than 0.05, 0.01 and 1 mg l^{-1}, respectively. The potential responses of the Pb(II)-ISE to Pb^{2+}, Cd^{2+} and Cu^{2+} are shown in Fig. 4, together with the response to residual chlorine. A concentration of 0.05 mg l^{-1} Pb(II) is lower than the detection limit of the Pb(II)-ISE. Indeed, no interference from Pb(II) and Cd(II) in the concentration range of 0.1 $^{-1}$ mg l^{-1} was observed during the determination of 0.1 mg l^{-1} of residual chlorine in the FIA system. In addition, the potential response to Cu(II) is nearly the same as for residual chlorine, as shown in Fig. 4. Indeed, the presence of Cu(II) at a concentration of 0.1 mg l^{-1} gave an error of 100% for the determination of 0.1–1 mg l^{-1} residual chlorine in the FIA system. Therefore, Cu(II) must be eliminated from the sample prior to the determination of residual chlorine.

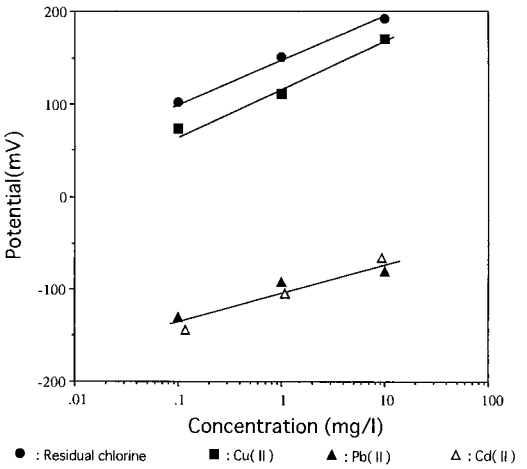

Fig. 4. Effect of heavy metal ions on the potential of the Pb(II)-ISE in the batch system.

We also investigated the effect of redox compounds such as $KMnO_4$, H_2O_2, $Na_2S_2O_3$ and L-ascorbic acid on the electrode potentials of the Pb(II)-ISE in the batch system. The results are shown in Fig. 5, which show that the response potential of the Pb(II)-ISE to $KMnO_4$ is higher than that to residual chlorine, even at a concentration of 10^{-6} mol l^{-1}, and the potential slope

of 121 mV/decade for $KMnO_4$ is larger than the 50 mV/decade for residual chlorine. This indicates that the presence of $KMnO_4$ at concentrations as low as 0.1 mg l^{-1} (10^{-6} mol l^{-1}) interferes with the determination of residual chlorine at a level of 0.05 mg l^{-1} (10^{-6} mol l^{-1}). However, the potentials of the Pb(II)-ISE to H_2O_2, $Na_2S_2O_3$ and L-ascorbic acid are much lower than that to residual chlorine in the concentration range from 10^{-6} to 10^{-3} mol l^{-1}, as shown in Fig. 5. This suggests that the above three reducing compounds do not respond to the Pb(II)-ISE directly, but they do not coexist in the residual chlorine sample because of a redox reaction with residual chlorine. Since the presence of $KMnO_4$ and other redox compounds in tap water is, in most cases, unrealistic, interference from these compounds would not be a problem in the analysis of tap water.

3.1.4. pH effect

The potential response of the Pb(II)-ISE to 1 mg ml^{-1} residual chlorine solution over the pH range from 3 to 10 was examined. The electrode potential was nearly the same from pH 5 to 8, while the potential increased for pH values below pH 5 and the potential decreased with an increase in pH above pH 8. As a result, the reagent solution was adjusted to pH 6.0 prior to use in the FIA system.

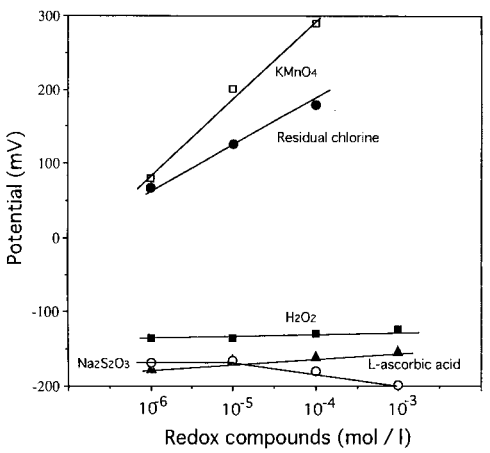

Fig. 5. Effect of redox compounds on the potential of the Pb(II)-ISE in the batch system.

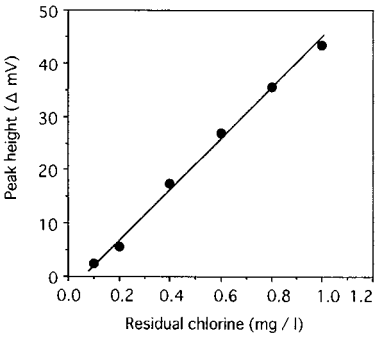

Fig. 6. Calibration curve for residual chlorine for the FIA system. Regression line, $Y = 46.82X - 2.23$; correlation factor, 0.996.

3.2. Examination of the FIA system

3.2.1. Calibration curve for residual chlorine

The relationship between the concentration of standard solutions of residual chlorine (0.1–1.0 mg l^{-1}) and FIA signals (the peak heights) was investigated by using the FIA system shown in Fig. 2, for which the conditions were determined by a comparison of the batch and FIA systems. A linear calibration curve was obtained for the range of 0.1–1.0 mg l^{-1} of residual chlorine as shown in Fig. 6 and which had a slope of 46.8 mV/mg l^{-1} for the entire range. As shown in Figs. 4 and 5, the potential response of the Pb(II)-ISE is linear to the logarithmic concentration of residual chlorine with the slope of 50 mV/decade. However, the peak height obtained in the FIA system was proportional to the concentration of residual chlorine. This may be due to the fact that the sample injected in the FIA system is dispersed in the 700-cm long mixing coil. The lower detection limit was 0.01 mg l^{-1} at a S/N ratio of 3.

3.2.2. Reproducibility of FIA signals and related performance

The relative standard deviation of the FIA signals was 2.0% for five injections of the same sample which contained 0.2 mg l^{-1} of residual chlorine (Fig. 7). The sampling rate was approximately 15 per hour and the drift of baseline potential was less than 0.6 mV h^{-1}.

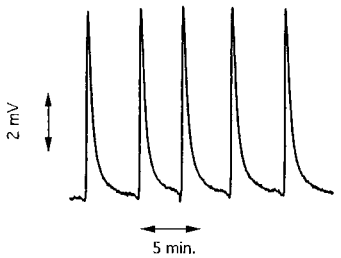

Fig. 7. FIA signals for residual chlorine obtained with the Pb(II)-ISE detector. Residual chlorine, 0.2 mg l^{-1}.

3.3. Correlation between the FIA method and Japanese Industrial Standard

The present FIA system was applied to the determination of residual chlorine in six tap water samples. The analytical results obtained by the FIA method were compared with those obtained by the conventional Japanese Industrial Standard method (*o*-tolidine colorimetric method). The correlation of analytical results between the two methods is reasonably good, as shown in Fig. 8. From this figure, the regression line expressed by $Y = 0.75X - 0.17$ and a correlation factor of 0.967 were obtained. This indicates that the present FIA system with the Pb(II)-ISE detector can be used for the determination of residual chlorine in tap water.

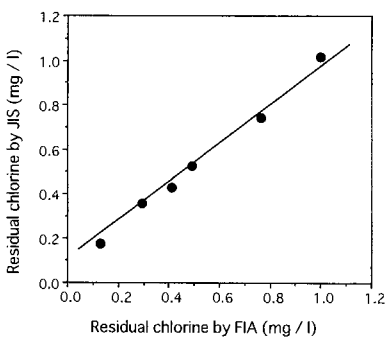

Fig. 8. Correlation between the JIS method and the FIA method for the determination of residual chlorine. Regression line, $Y = 0.75X + 0.17$; correlation factor, 0.967.

4. Conclusion

We have developed the simple FIA system in conjunction with the Pb(II)-ISE detector for the determination of residual chlorine by using the specific response of the Pb(II)-ISE to residual chlorine. The response mechanism of the Pb(II)-ISE to residual chlorine is interesting, but unclear at the present stage. Reproducibility was improved from 7 to 2% CV utilizing the FIA closed system, compared with the batch system. The present FIA system for the determination of residual chlorine has the advantages of stability, simplicity, low cost, ease of maintenance, saving of regents, ease of use and no need of heavily trained experts in the field of chemical analysis. However, this system was affected by MnO_4^- and Cu(II) ions for samples containing more than 0.1 and 1 mg l^{-1}, respectively. Therefore, for such samples, an elimination procedure must be combined in the present system.

References

[1] C.T. Butterfield, E. Wattie, Public Health Reports 3 (1948) 934.
[2] APHA, AWWA, WCCF, Standard Method for the Examination of Water and Wastewater, 16th ed., 1985.
[3] JIS K 0101, Testing Method for Industrial Water, Japan Standard Association, 1994, pp. 50–60.
[4] J.S. Beach Jr., M.I. Beach, Prog. Water Tech. 9 (1977) 97.
[5] US Patent 4,049,382, 1977.
[6] L.P. Lester, G.J. Moody, J.W. Frazer, Anal. Chem. 50 (1978) 465.
[7] Instruction Manual for Pb(II) ion-selective electrode, DKK Corporation, 1987, p. 24.
[8] Y. Asano, S. Ito, F. Kobayashi, Ann. Meet Jpn. Soc. Anal. Chem. Abstr. 28 (1979) 729.
[9] G. Charlot, L'analyse qualitative et les reactins en solution, Part II, Ch. 12, 1957, Masson et C. Editeures (Paris).
[10] G.C. White, Handbook of Chlorination, Norstrand Reinhold Company, 1972.
[11] J. Ruzika, J. Flow Injection Anal. 10 (1993) 164.
[12] G.D. Christian, Biologie prospective, Compies rendus du 8 Collogue de Pont. a Mousson, in: M.-M. Galteau, G. Siest, J. Henny (Eds.), John Libbey Eurtext, Paris, 1993, 7–12.
[13] J. Ruzika, Analyst 119 (1994) 1925.
[14] G.D. Christian, Analyst 119 (1994) 2309.
[15] S. Ito, H. Hachiya, K. Baba, Y. Asano, H. Wada, Talanta 42 (1995) 1685.
[16] The Ministerial Ordinance on Standards of Water Quality (21st), Edited by The Ministry of Welfare, Japan, 1992.

ELSEVIER

Talanta 45 (1998) 583–589

Talanta

Continuous flow system for the determination of trace vanadium in natural waters utilizing in-line preconcentration/separation coupled with catalytic photometric detection[1]

Takeshi Yamane *, Yoshie Osada, Miho Suzuki

Department of Chemistry, Faculty of Education, Yamanashi University, Takeda-4, Kofu 400, Japan

Received 31 March 1997; received in revised form 10 June 1997; accepted 12 June 1997

Abstract

A sensitive and rapid method is presented for the determination of vanadium at ng to sub-ng ml^{-1} levels in natural waters, in which in-line preconcentration/separation is directly coupled with catalytic detection of vanadium in a flow-injection system. Vanadium was adsorbed on a small column packed with Sephadex G-25 gel and desorbed with a small volume of 0.010 M HCl. The catalytic action of vanadium on the oxidation of chromotropic acid (1,8-dihydroxy-3,6-naphthalenedisulphonic acid) by bromate in pH 3.8 buffered media was used in the sensitive determination of vanadium. Effective preconcentration/separation of trace vanadium can be achieved from Fe(III), Cu(II) and a large excess of sodium chloride in seawater sample. A linear calibration using a 5 m sample loop was obtained for vanadium in the range 0–2.5 ng ml^{-1}. The limit of detection was 0.02 ng ml^{-1} and the relative standard deviation was 1.2% for 1.0 ng ml^{-1} vanadium ($n = 5$). The present FIA system is rapid and sensitive and can be readily applied to river water and coastal seawater samples. © 1998 Published by Elsevier Science B.V.

Keywords: Catalytic photometric detection; Flow injection system; Trace vanadium; River water and seawater; Sephadex gel

1. Introduction

The determination of vanadium in natural waters is of interest in biochemical, geochemical and environmental studies. Its low concentration at around 1 ng ml^{-1} in most natural waters and high salt content especially in seawater generally requires the preconcentration and/or preseparation techniques, thus determination becomes complicated, laborious and time-consuming. Ion-exchange (including chelate formation) [1–6], solvent extraction [7,8], precipitation [9,10], and high performance liquid chromatography [11] have been used for such pretreatment of samples.

* Corresponding author. Fax.: +81 552208183; e-mail: yamane@grape.kkb.yamanashi.ac.jp

[1] Presented at the Eighth International Conference on Flow Injection Analysis (ICFIA 1997), held in Orlando, FL. USA. January 12–16, 1997.

PII S0039-9140(97)00188-4

Most detection techniques such as spectrophotometry [1,10], atomic absorption spectrometry (AAS) [7,8], inductively coupled plasma atomic emission spectrometry (ICP-AES) [6], X-ray fluorescence spectrometry [9], catalytic method [2,12–14] and neutron activation analysis [3,4] used so far for vanadium determination in natural waters lack the necessary sensitivity and/or selectivity without pretreatment.

An ion-exchange technique is widely used for preconcentration/separation of trace metals but is not always satisfactory for the purpose of seawater analysis because the sodium chloride matrix causes a lowering of distribution coefficients of metals and thus limits the volume of sample solution that can be used for preconcentration.

Sephadex gels, cross-linked dextran, are of interest owing to their unique affinity properties for such elements as boron, tungsten, molybdenum and vanadium forming oxo-anions, their potential analytical significance has been studied [15–19]. Yoshimura et al. [20] used a Sephadex G-25 gel for separation and preconcentration of traces of vanadium (V) from geochemical samples before determination by spectrophotometry with 4-(2-pyridylazo)resorcinol(PAR). The method requires considerable time and is laborious, because the procedure is operated manually and batchwise. Large sample volumes were needed to determine ng ml^{-1} level of vanadium in natural waters because the sensitivity of the PAR spectrophotometry used was not favorable.

Catalytic methods of analysis have been recognized as an important means for achieving enhanced sensitivity using inexpensive apparatus, owing to the chemical amplification principle [21]. Dynamic measurements, however, are usually required and some variables affecting quantitative measurements must be precisely controlled. Flow injection analysis (FIA), a rapidly growing analytical system which is expected to promote automation of chemical analysis, has proven to be well suited to catalytic methods of analysis as FIA has inherent dynamic characteristics [22]. In addition, it has a great advantage of permitting in-line preconcentration and separation, further improving analytical sensitivity and selectivity [23].

In this paper we report a novel FIA method for the determination of trace levels (ng ml^{-1} to sub ng ml^{-1} range) of vanadium in natural waters. A Sephadex gel column was examined for in-line preconcentration/separation of trace vanadium which should be directly coupled with catalytic detection based on the oxidation of chromotropic acid by bromate in a continuous flow system. Detailed investigations were made to establish the optimal conditions for both in-line preconcentration/separation and catalytic detection of vanadium. The proposed FIA system was satisfactorily applied to the determination of vanadium in river water and seawater samples.

2. Experimental

2.1. Chemicals and solutions

All chemicals used were of reagent-grade (Wako, Osaka, Japan), unless otherwise specified.

Standard solutions of vanadium were prepared from a 100 μg ml^{-1} certified standard solution by suitable dilution.

A working chromotropic acid solution (5.5×10^{-2} M) was prepared by dissolving 4.01 g of the reagent in water, followed by the addition of 20 ml acetate buffer solution (2.0 M CH_3COOH-0.25 M CH_3COONa, pH 3.8), a dilution to 200 ml was made with water.

A potassium bromate solution (1.2×10^{-1} M) was prepared by dissolving the reagent in water.

Acetate buffer solution (2.0 M CH_3COOH-0.25 M CH_3COONa, pH 3.8) was prepared by mixing 45.6 ml of 8.8 M acetic acid solution and 50 ml of 1.0 M sodium acetate solution with dilution to 200 ml with water.

The artificial seawater sample was prepared by dissolving NaCl (11.70g), $CaCl_2 \cdot 2H_2O$ (0.70 g), $MgCl_2 \cdot 6H_2O$ (5.30 g), and Na_2SO_4 (1.90 g) in 500 ml of water, it was used immediately after preparation.

2.2. FIA manifold and general procedure

The FIA manifold schematically shown in Fig. 1 was constructed using PTFE tubing (0.5 mm

i.d.) and all components (unions, endfittings, and valves) in contact with solution were made of PTFE, Daiflon, or ceramics. The preconcentration/separation column (SE) was prepared by slurry packing the Sephadex G-25 gel (20–80 μm particle size, purchased from Farmacia Biotech AB, Uppusara, Sweden) into a borosilicate glass column (4 mm i.d., 7 cm long). A Tokyo Rikakikai Model LP-1000 pump (metal-free type) and a Sanuki Kogyo Model DM2M-1024 pump was used.

The sample solution buffered by the addition of pH 3.8 acetate buffer solution is injected using valve S with a 5 m sample loop (0.5 mm i.d.) and passed through the column SC. Six minutes after the sample injection, 0.010 M HCl was injected via valve E with a 2.5 m loop (0.5 mm i.d. tubing) to desorb the vanadium. The desorbed vanadium is mixed downstream with R1 and R2 reagent solutions and catalyzes the oxidation of chromotropic acid by bromate as the mixed solution moves through the RC to the detector. The absorbance change is monitored at 430 nm and the recorded peak height is linearly related to the vanadium concentration.

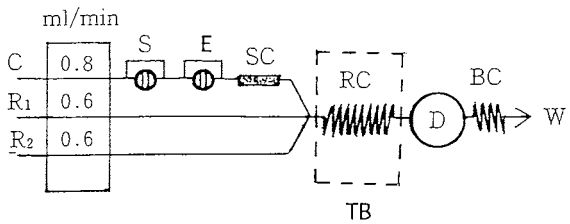

Fig. 1. Schematic FIA diagram for trace vanadium determination using in-line preconcentration/preseparation directly coupled with catalytic detection: C, carrier(0.02 M CH_3COOH-0.0025 M CH_3COONa, pH 3.8); R1, (5.5×10^{-2} M chromotropic acid solution with 0.2 M CH_3COOH-0.025 M CH_3COONa, pH 3.8); R2, 0.12 M potassium bromate solution; SC, separation column (Sephadex G-25 gel, 4 mm i.d., 7 cm long); S, sample loop (0.5 mm i.d., 5 m long); E, desorbing acid solution (0.010 M HCl, 0.5 mm i.d., 2.5 m long); RC, reaction coil (0.5 mm i.d., 20 m long); TB, temperature controlled bath (35°C); D, spectrophotometric detection (430 nm); BC, back pressure coil (0.5 mm i.d., 10 m long); W, waste.

3. Results and discussion

3.1. Catalytic detection of vanadium in a continuous flow system

In the catalytic detection of vanadium, the reaction conditions were similar to earlier work [24] but significant modifications of the manifold were made in the present study. Specifically a carrier stream was introduced to transport the sample solution (or analyte vanadium) in a carrier separate from the streams of the reagent solution. A 5.5×10^{-2} M chromotropic acid solution and a 20 m reaction coil were also used in place of 2.2×10^{-2} M and a 3 m coil, so as to improve detection sensitivity. The increase in absorbance due to the catalyzed reaction is measured at 430 nm and the recorded peak shape signal directly relates to vanadium concentration. Although catalytic detection is very sensitive, suitable preconcentration/separation is required in order to determine ng ml^{-1} to sub ng ml^{-1} levels of vanadium in natural waters without possible interference from the matrix sodium chloride and coexisting ions such as iron and copper. The FIA manifold was designed and constructed so that catalytic detection can be directly coupled with in-line preconcentration/separation of vanadium using a Sephadex gel column.

3.2. Preconcentration/separation by Sephadex column

The effect of pH on the adsorption of vanadium on a Sephadex gel column was investigated to find the conditions necessary for quantitative preconcentration from seawater. The flow system (Fig. 1) with a 100 cm sample loop was used for this purpose with the injection of 1.0 ng ml^{-1} vanadium standard solution.

Fig. 2 shows the peak height for desorbed vanadium after adsorption from sample solutions and adjusted to different pH values. The carrier solution was also adjusted to the same pH as the sample solution. A maximum adsorption of vanadium was observed from the sample solutions buffered from pH 3.6 to 4.7 with acetate buffer solution. The concentration of acetate buffer solu-

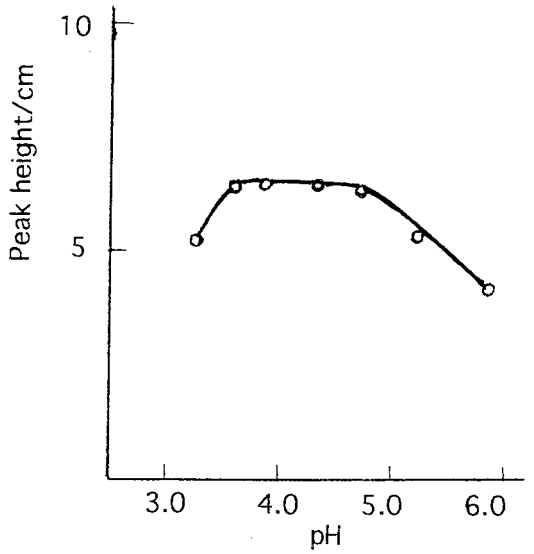

Fig. 2. Effect of sample solution pH on the peak height which is directly related to the adsorption efficiency for 1.0 ng ml^{-1} vanadium.

tion (pH 3.8) in the range 0.01 M CH_3COOH-0.00125 M CH_3COONa-0.10 M CH_3COOH-0.0125 M CH_3COONa did not significantly affect vanadium adsorption. The acetate buffer solution (0.02 M CH_3COOH-0.0025 M CH_3COONa, pH 3.8) was used as carrier solution and added to the sample solution before preconcentration. Addition of sodium chloride at concentrations up to 4.0 M had no significant effect on the adsorption of vanadium. This is a very important and desirable observation because it demonstrate the applicability of the Sephadex gel column for seawater analysis.

The adsorbability of iron and copper on the Sephadex column which interferes in the catalytic detection of trace vanadium must be determined. Fig. 3 shows the elution behavior of V(V), Fe(III) and Cu(II) using the acetate buffer solution (pH 3.8) as eluent (carrier). The metals in the effluent were continuously detected by PAR spectrophotometry. Vanadium once adsorbed on the column was found to be eluted by further addition of eluent (carrier) the beginning of elution being approximately 10 min after injection, while Fe(III) and Cu(II) were eluted prior to vanadium. This shows that the distribution coefficient of V(V) is not very large and suggests the possible separation of V(V) from Fe(III) and Cu(II) by desorbing vanadium after elution of such metals. In fact, the injection of 0.010 M HCl in order to desorb vanadium was found to minimize the effect of Fe(III) and Cu(II) on vanadium determination as shown later. Fe(III) in the absence of fluoride resulted in different elution as compared with Fe(III) in the presence of fluoride, though Fe(III) in both cases eluted faster almost at the void volume. The tailing peak observed in the former is probably due to the weak affinity of

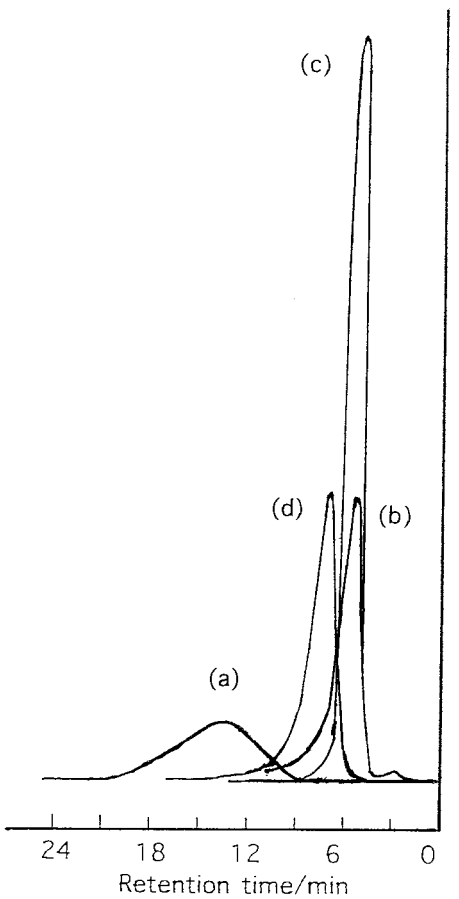

Fig. 3. Elution behaviors of (a) 0.1 μg ml^{-1} V(V) solution, (b) 0.1 μg ml^{-1} Fe(III) solution (c) 0.1 μg ml^{-1} Fe(III) solution in the presence of 100 μg ml^{-1} F^-, and (d) 0.1 μg ml^{-1} Cu(II) solution.

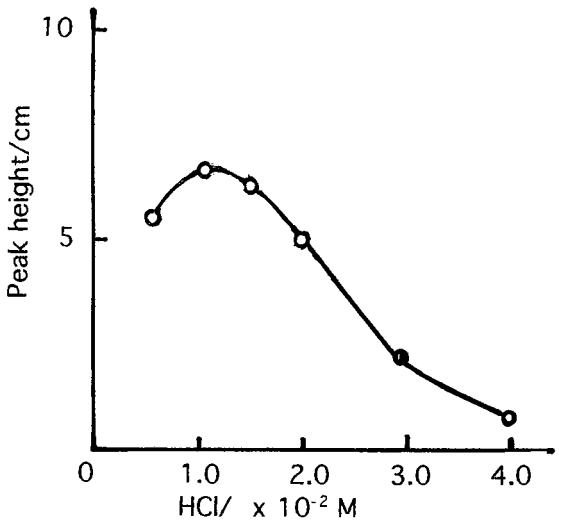

Fig. 4. Dependence of peak height for 1.0 ng ml^{-1} vanadium adsorbed with 5 m sample loop on the concentration of HCl (as desorbing agent using 2.5 m loop).

Sephadex gel for partially hydrolyzed Fe(III) and the sharp elution of Fe(III) in the presence of fluoride is due to the decreased affinity of Sephadex gel for the formed Fe(III)-fluoro complex.

Yoshimura et al. [20] showed that Sephadex gel desorbs vanadium reversibly in 0.12 M HCl. Preliminary experiments have shown that HCl added to the catalyzed reaction system significantly influenced detection sensitivity. The effect of HCl concentration on the signal intensity for 1.0 ng ml^{-1} vanadium was examined using a 2.5 m loop, as described in the study of elution behavior. The highest signal response was observed at 0.010 M as shown in Fig. 4. The lower peak height at decreased HCl concentration is probably due to insufficient desorption of vanadium. Whereas increased HCl concentration (<0.010 M) seems sufficient to desorb vanadium quantitatively using a single desorbing run as will be described, a steady decrease in the peak height was found when the HCl concentration increased. This could be attributed to the fact that when the HCl is merged with the reaction mixture after desorption of vanadium, the optimum conditions for vanadium-catalyzed chromotropic acid-bromate reaction are disturbed and result in deterioration of the detection sensitivity. At conditions and the procedure described in Section 2.2, V(IV) showed similar adsorption and elution behavior to that of V(V).

Experiments have shown that HCl at 0.010 M in the sample solution using a 2.5 m loop only causes a little deterioration of the catalytic sensitivity for vanadium but was sufficient to quantitatively elute vanadium with recovery in excess of 97%.

The effect of sample volume on the peak height was studied by injecting 1.0 ng ml^{-1} vanadium solution in the presence of excess sodium chloride (2.0 M) with sample loops of different length. The peak height for vanadium increased linearly as the sample loop length increased up to 9 m. The sensitivity of vanadium determination can be improved by preconcentration introducing a larger sample volume even in the presence of 2.0 M sodium chloride. Preconcentration with sample loops longer than 9 m was not studied because the sensitivity of catalytic detection used in this study seemed sufficient to determine vanadium encountered in most natural waters.

3.3. Calibration graph

A typical calibration graph obtained using a 5 m sample loop (994 μl) and synthetic seawater sample solutions buffered at pH 3.8 showed a linear response of peak height vs. vanadium concentration in the range 0–2.5 ng ml^{-1} with the equation $Y=6.65X$ with a correlation coefficient of 0.999 (Y, peak height in cm and X, vanadium concentration in ng ml^{-1}). The slope was almost identical to that obtained for aliquots of standard vanadium solutions. For sample injections with a 5 m sample loop (994 μl), the relative standard deviation for 1.0 ng ml^{-1} vanadium was 1.2% ($n=5$) and the limit of detection (defined as the concentration giving a signal three times the standard deviation of blank signal) was 0.02 ng ml^{-1}. Sensitivity can be improved by using a larger sample volume injection.

3.4. Interferences

The effect of diverse ions on the determination of 1.0 ng ml^{-1} vanadium was examined according

to Section 2.2. No significant interference was observed by the following ions (μg ml^{-1}), Fe(II,III) (0.3), Cu(II) (0.5), Al(III) (1.0), Zn(II) (1.0), Ni(II) (5.0), Mn(II) (5.0), Co(II) (0.5), Mo(VI) (0.1), Cr(VI) (1.0), Cr(III) (5), Pb(II) (1.0), Ag(I) (1.0), Cd(II) (1.0), Se(IV) (5.0), As(III) (1.0), Br^- (100), F^- (100), I^- (10), HPO_4^{2-} (5.0). Relative errors less than $\pm 5\%$ were considered tolerable. The interferences from Fe(III) and Cu(II) at a few μg ml^{-1} levels could be eliminated by the addition of 2.0×10^{-4} M *N*-(Dithiocarboxy)sarcosine in the sample solution. Iron could also be masked in the presence of 100 μg ml^{-1} F^- because adsorption of Fe(III) on the Sephadex column was minimized by forming the Fe(III)-fluoro complex as described above.

As shown in these results, most of the ions did not interfere with the determination of vanadium when present in a 300 fold excess. The results of artificial seawater analysis containing 1.0 ng ml^{-1} vanadium showed that the major ions of Na^+, Ca^{2+}, Mg^{2+}, Cl^-, SO_4^{2-} existing in seawater do not affect determination when present in a large excess.

Thus the method is free from interference by diverse ions commonly found in natural waters.

3.5. Analysis of sea and river water samples

The proposed method was applied to the determination of vanadium in coastal seawaters, ground water and river water. In order to evaluate possible effects from other coexisting components, the recovery of known amounts of vanadium added to the sample solutions was also studied. Fig. 5 shows typical signal traces for these analysis using a 5 m sample loop (994 μl) injection. These results are summarized in Table 1 and show good reproducibility with relative standard deviations lower than 2% and satisfactory recoveries $>96\%$. The results obtained for coastal seawater are similar to independent results for coastal seawater previously reported [1,2,8,20]. Discrimination between V(IV) and V(V) could not be achieved due to the adsorption properties of Sephadex gel. Thus vanadium determined using the present FIA system should be the sum of V(IV) and V(V).

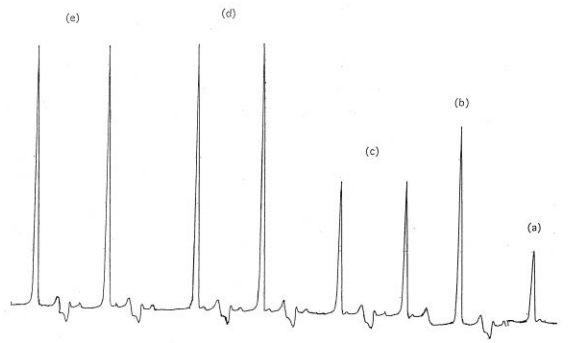

Fig. 5. Typical signal traces for (a) river water, (b) seawater, (c) 1.0 ng ml^{-1} vanadium standard solution, (d) 2.0 ng ml^{-1} vanadium standard solution and (e) seawater spiked with 0.50 ng ml^{-1} vanadium by the present FIA system using a 5 m sample loop injection.

4. Conclusions

AAS and ICP-AES are the most widely used detection methods for various metals in environmental samples but often lack necessary sensitivity in the determination of vanadium in natural waters and are subject to matrix effects such as

Table 1
Analysis of natural waters by the present FIA system

Sample	V added (ng ml^{-1})	V found (ng ml^{-1})	Recovery (%)
Seawater A		$1.49 \pm 0.01_4$ ($n=5$)	
	0.50	1.98	98.0
	0.50	1.97	96.0
	1.00	2.49	100.0
	1.00	2.48	98.0
Seawater B		$1.46 \pm 0.02_4$ ($n=5$)	
River water		$0.52 \pm 0.01_5$ ($n=3$)	
Underground		$0.22 \pm 0.00_5$ ($n=3$)	

Seawaters A and B were both 1996 coastal samples from Izu in Shizuoka Pref. and from Sado in Niigata Pref. respectively, in Japan.
River water and underground water were 1996 samples from Arakawa, Yamanashi Pref. and from Nasu, Tochigi Pref. respectively, in Japan.

salinity. Matrix interferences from seawater can be suppressed by the addition of ascorbic acid in the determination of some metals by flameless AAS [25] but the detection limit of 18 ng ml^{-1} vanadium using this technique was insufficient in seawater sample applications. Very sensitive HPLC methods [11] and catalytic methods [26] have been reported for determination of total vanadium in natural waters with detection limits of 0.026 and 0.08 ng ml^{-1}, respectively. However, both methods may cause contamination problems and lower analytical precision. The catalytic method is not always applicable to seawater analysis, no further study was found regarding the effect of salinity. Most recently Kasahara et al. [6] have reported the ICP-AES method which allows the determination of sub ng ml^{-1} levels of vanadium in river water. The method was operated batchwise and required a 100-fold preconcentration using synthesized silica-gel immobilized 8-quinolinol from 1.0 l of a large sample for attaining necessary sensitivity.

As described in the present study, in-line preconcentration/separation using a Sephadex gel column directly combined with catalytic photometric detection in a flow injection system has shown to provide a sensitive and reliable analytical method for the determination of traces of vanadium in natural waters. It should be noted that the present FIA method is so sensitive even with only a 994 μl sample and selective that it can readily be applied to seawater analysis without effecting the matrix salt. Moreover, the present FIA system offers many advantages over other methods mentioned above with respect to simplicity and sensitivity. The analysis is achieved in a continuous and nearly closed system without instrumental and operational complexity which minimizes potential contamination and operator error. An analysis time of about 9 min, good reproducibility and a relatively small sample volume are additional advantages.

.

Acknowledgements

The authors are grateful to The Salt Science Research Foundation for supporting this work (9507).

References

[1] T. Kiriyama, R. Kuroda, Anal. Chim. Acta 62 (1972) 464.
[2] T. Fukasawa, T. Yamane, Anal. Chim. Acta 88 (1972) 147.
[3] K.D. Linstedt, P. Kruger, Anal. Chem. 42 (1970) 113.
[4] R.G. Greenberg, H.M. Kingston, Anal. Chem. 55 (1983) 1160.
[5] B. Patel, S.J. Haswell, R. Grzeskowik, J. Anal. Spectrosc. 4 (1989) 195.
[6] I. Kasahara, N. Takayama, H. Yamamoto, K. Sakurai, S. Taguchi, Bunseki Kagaku 45 (1997) 211.
[7] Y.K. Chau, K. Lum-Shue-Chan, Anal. Chim. Acta 50 (1970) 201.
[8] Y. Shijyo, Y. Kimura, T. Shimizu, K. Sakai, Bunseki Kagaku 32 (1983) E285.
[9] K. Hirayama, D.E. Leyden, Anal. Chim. Acta 188 (1986) 1.
[10] K.M. Chan, J.P. Riley, Anal. Chim. Acta 34 (1966) 337.
[11] J. Miura, Anal. Chem. 62 (1990) 1424.
[12] S. Nakano, M. Tago, T. Kawashima, Anal. Sci. 5 (1989) 69.
[13] M.J. Fishman, M.W. Skougstad, Anal. Chem. 36 (1964) 1643.
[14] Q. Weiguo, Anal. Chem. 55 (1983) 2043.
[15] S. Karayannis, H.M. Ortner, H. Spitzy, Talanta 19 (1972) 903.
[16] H.M. Ortner, H. Krainer, H. Dalmonego, J. Chromatogr. 82 (1973) 249.
[17] H.M. Ortner, H. Dalmonego, J. Chromatogr. 89 (1974) 287.
[18] H.M. Ortner, Anal. Chem. 47 (1975) 162.
[19] K. Yoshimura, R. Kiriyama, R. Kariya, T. Tarutani, Anal. Chim. Acta 109 (1979) 115.
[20] K. Yoshimura, H. Kaji, E. Yamaguchi, T. Tarutani, Anal. Chim. Acta 130 (1981) 345.
[21] H.A. Mottola, Kinetic Aspects of Analytical Chemistry, Wiley, New York, 1988.
[22] T. Yamane, J. Flow Inject. Anal. 3 (1986) 77.
[23] T. Yamane, K. Koshino, Talanta 43 (1996) 963.
[24] T. Yamane, T. Fukasawa, Anal. Chim. Acta 119 (1980) 389.
[25] M. Tominaga, K. Bansho, Y. Umezaki, Anal. Chim. Acta 169 (1985) 171.
[26] Ashraf, A. Mohamed, M. Iwatsuki, T. Fukasawa, M.F. El-Shahat, Analyst 120 (1995) 2281.

ELSEVIER

Talanta 45 (1998) 591–599

Talanta

The flow analysis database on the World Wide Web

Stuart J. Chalk *

Department of Natural Sciences, University of North Florida, Jacksonville, FL 32224, USA

Received 13 March 1997; received in revised form 17 June 1997; accepted 18 June 1997

Abstract

The field of flow injection analysis (FIA) is growing rapidly because much applied research is being conducted around the world. This creates a great need for information dissemination across the globe to keep researchers up to date on current research trends. With the internet becoming the tool for global communication, it seems appropriate that support of the growth in FIA should be via this medium. Thus, the flow analysis database (FAD) has been developed as a central resource for bibliographic information on the area of FIA and flow analysis in general. © 1998 Elsevier Science B.V.

Keywords: Flow analysis; Database; World Wide Web

1. Introduction

In 1975, the grandfather's of flow injection analysis, Jaromir Ruzicka and Elo Hansen published a paper showing that segmenting flowing streams with air was not necessary for reproducible analysis [1]. Today, flow injection analysis (FIA), sequential injection analysis (SIA) and flow cytometry have extended nearly every instrumental analytical technique by improving detection limits and broadening the range of samples that can be analyzed. There seems to be no end to the versatility and applicability of this simple, yet increasingly sophisticated technology.

Solutions to analytical problems are being found all over the world using flow analysis techniques. Research groups in many countries are pushing the forefront of this technology and present their results to the world at conferences such as Flow Analysis and the International Conference on Flow Injection Analysis. Also, in journals such as Analytica Chimica Acta, the Journal of Flow Injection Analysis and Analytical Chemistry. Yet, a large portion of flow analysis research is published in less well known journals, at smaller conferences and in company reports and as a result is not generally available.

The current estimates of publications in flow analysis show that the area is still growing rapidly despite its maturity. Fig. 1 shows yearly totals of publications and cumulative totals of publications collected by this author since 1990. However, it is very likely that this is a low estimate of the total number of publications because flow analysis research extends over a large number of different disciplines such as agriculture, pharmaceuticals,

* E-mail: schalk@unf.edu

PII S0039-9140(97)00195-1

medicine, biochemistry, petrochemicals, brewing, as well as chemistry. Also, there has been no formal definition of what technologies come under the umbrella of flow analysis. It seems that the time is right to address both these issues and bring information about flow analysis techniques into one central resource. The obvious vehicle for this is the internet.

There is probably no one in the analytical community who has not heard of the internet. The explosive growth of the information superhighway has mimicked the rapidity of the home computer revolution. The idea that every place in the world can be linked by a single, yet distributed, computer network has grasped the world's attention and promises to bring us together as a planet. Today, everyone connected can find information on any particular subject and more importantly can share information with the world from their home computer. There seems to be no limit as to what one can do with this system, given the caveats of time, money and bandwidth (see the advances in the internet at the World Wide Web consortium [2]).

The World Wide Web (WWW) is a large part of the success of the internet. Based on the hypertext markup language (HTML), pages of information can be transmitted, within seconds, from servers anywhere in the world. The system works because the pages are small and in plain text allowing anybody to write and easily distribute them. Over the last few years the number of computers serving WWW pages has grown exponentially [3] (Fig. 2) and this will only continue with the recent release of software for serving pages from personal computers [4,5]. As of 26 February, 1997 Alta Vista, one of the many indices of the WWW, listed over 31 million individual web pages. By the time this paper goes to press this will probably be close to 40 million.

Bringing together the need for better information transfer and the ease of worldwide publication on the WWW, this paper presents the flow analysis database (FAD—http://schalk.as.unf.edu/fad.html) a fast searchable database of publications being made available at the University of North Florida. The features, scope and future directions of the database will be discussed in this paper.

2. Computer setup

2.1. Database search facility

The FAD is served from an Apple (Cupertino, CA) Macintosh Performa 5215 CD personal computer with 40 MB RAM. The web server software is WebCenter 1.0b3 by Social Engineering, (http://www.slaphappy.com/). The engine used (an asynchronous common gateway interface (acgi) application) to search the tab delimited text database is Webdataserver.acgi 1.3 from Aardvark Software (Studio City, CA). The text document that acts as the database is produced by exporting bibliographic information from EndNote Plus 2.3 from Niles & Associates, Inc. (Berkeley, CA).

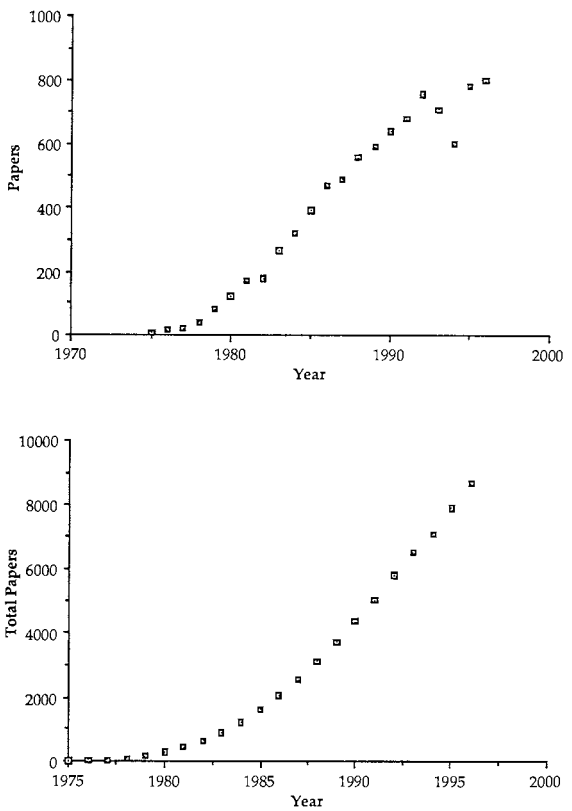

Fig. 1. Yearly and cumulative growth of publications in the area of flow analysis.

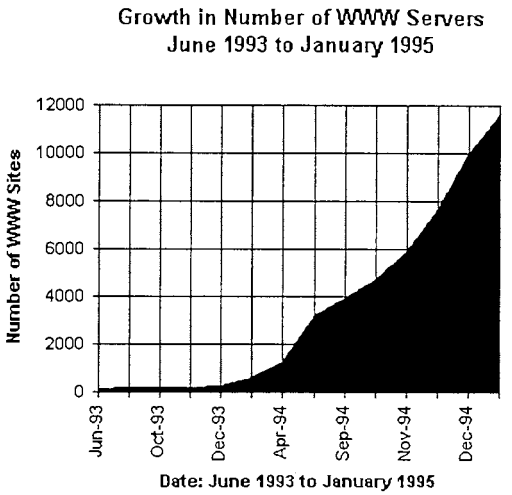

Fig. 2. The growth of World Wide Web servers from 1993 to 1995.

2.2. Listserver

The flow analysis list server is being run using the PowerPC version of Macjordomo 1.08 rev B by Leuca Software (Ithica, NY). The Apple Internet Mail Server 1.1.1 (Apple) is used to serve email to and from the list.

3. Features

The FAD currently contains over 1600 entries to papers, books, reports, thesis, conference presentations and patents dating up to 1985. By the time this paper comes out this number should be close to 8000. The scope of publications contains anything pertinent to flow analysis and therefore includes entries on FIA, SIA, flow cytometry (some), and post column derivatization in chromatography (both liquid and ion). It currently does not include information on air segmented flow analysis because of the different mechanisms of mixing. The scope, however, is not set in stone and this author would be happy to receive any comments regarding additions or deletions that readers feel would be appropriate to the database.

With such a large amount of information, the key to producing a useful resource is organization. This is achieved by separating important information into discrete fields that can be searched independently. Table 1 shows the fields that can be currently searched in the FAD. Not only does this make the process of finding relevant information easy, it speeds up the search process, important when the search engine gets a large number of requests at the same time.

3.1. Basic search (http://schalk.as.unf.edu/basic.html)

This page (Fig. 3) allows simple, single field searches of the analyte, author and keyword fields. Entering the search term in a text box and clicking on the appropriate submit query button results in a page displaying relevant entries. Fig. 4 shows the entries found for a search of mercury in the analyte field. If this number is greater than 100 only the first 100 will be retrieved and a link to the rest of the entries is served within that page.

Each entry is listed as a summary of the title and the bibliographic reference. Clicking on the entry number links to the database to retrieve the entire database record for that entry (Fig. 5). This information can be downloaded to the users hard drive within whichever browser is being used.

3.2. Advanced search (http://schalk.as.unf.edu/advsearch.html)

A more sophisticated search facility is available on the advance search page (Fig. 6). Each of the fields in the database can be searched for up to three separate terms. These are logically ORed together when the search is performed. The year field also has a facility to search a range of years that are entered. If terms are entered in more than

Table 1
Searchable fields in the flow analysis database

Publication type	Journal	Authors
Title	Volume	Issue
Page	Analytes	Matrices
Techniques	Language	Address
FA Terms		

Basic Search

Select the field you wish to search and enter search string. Click on the links to see indices of terms used in the indicated fields

Analyte search (Analytes)
Search Term: mercury Submit Query

Author search (Authors)
Search Term: Submit Query

FATerm search (FAterms)
Search Term: Submit Query

Thanks to the contributors to this database.

Last updated March 14, 1997 SJC
© Copyright, University of North Florida, 1997

Fig. 3. The flow analysis database basic search page.

one field the search is performed as a logical AND and only those entries that contain all terms are returned. This is probably the most useful part of the FAD where users can search for analytes in specific matrices, maybe even analyzed by only one technique. Fig. 7 shows the results of a search for arsenic and selenium analyzed by atomic absorption. In all cases the results are returned chronologically, with the most recent articles last. Access to the individual reference information is via the same mechanism as for the basic search page.

3.3. Term indexes

On both of the search pages, links are available to view indexes of terms used in each of the fields. These lists are generated from EndNote Plus and are used in putting together the database entries. Thus, they are the definitive guide to searching fields. Table 2 shows a portion of the terms in the analyte field index. Every effort has been made to include as much pertinent information as possible. Thus, if the paper contains the analysis of different species of arsenic they are all included in the analyte field as separate entries. This makes the database much more useful as users can look specifically for what they are interested in, yet it also allows generic searching. In a similar fashion the matrices and technique fields have terms that are as descriptive as possible.

The journal field term index provides additional information. Each of the journals is listed with its full title, the approved abbreviation, the city of

Search Results

There are 22 references matching your criteria. Matches 1 to 22 are displayed.

If you find any information in error, or missing, please contact FIAWeb (see below) and it will be updated immediately

256 *Continuous monitoring of heavy metals in industrial waste waters*
Anal. Chim. Acta, **1980** 114() 303-310

277 *Continuous-flow, isotope-dilution method for studies of adsorption behaviour of metal ions*
Anal. Chim. Acta, **1980** 116(2) 275-287

373 *Evaluation of n-app for the underpotential deposition of mercury on gold by flow injection coulometry*
Anal. Chem., **1981** 53() 1855

374 *The determination of mercury at trace levels by flow injection analysis with electrochemical detection*
Diss. Abstr. Int., **1981** 41B() 3021

380 *Enzyme reactors in analytical detection systems. Theory and applications*
Lund University, **1981** Ph.D.()

411 *Continuous-flow cold-vapor atomic-absorption determination of mercury*
Anal. Chem., **1981** 53(13) 2030-2033

412 *Determination and on-site sampling of inorganic and organic mercury in aqeous samples with enzyme reactors*
Anal. Chim. Acta, **1981** 125() 45-53

437 *Original papers by younger research workers*
Anal. Proc., **1981** 18(2) 60-73

476 *Determination of metal ions in a flow-through electrochemical cell porous electrodes*
Zh. Anal. Khim., **1981** 36(9) 1692-1695

Fig. 4. Search results page from the flow analysis database.

publication and the common acronym for the journal. Each journal is entered in the database using the abbreviation, but if no abbreviation is known (or needed) the full title of the journal/publication is used.

Lastly, the FATerms field provides specific flow analysis terms. This is the language of flow techniques that everyone in this area is familiar with, which will grow as the area grows.

4. Future directions

4.1. The flow analysis database

After initial development of the database the ideas for additions and changes have been numerous. The following are some features planned for the FAD.

Requested reference #411

If you find any information in error or missing please contact FIA Web (see below) and it will be updated immediately

Reference type: Journal Article
Title: Continuous-flow cold-vapor atomic-absorption determination of mercury
Author(s): Oda, C.E. and Ingle, J.D.
Reference: Anal. Chem., **1981** 53(13), 2030-2033
Language: English
Analytes: Mercury
Matrices: Water, potable
Techniques: Spectrophotometry, atomic absorption, cold vapor
FATerms:
Address: Oregon State Univ., Dept. Chem., Corvallis, OR 97331 USA

Search completed on 5/27/97 2:08 PM using *Web Data Server 1.3*
Return to the Basic or Advanced search pages.

Comments on this search are welcome, and should be directed to Stuart Chalk
Last updated March 14, 1997 SJC

Fig. 5. Typical reference page from the flow analysis database.

- Transfer to mainframe: In the next 6 months the site will be transferred to a campus mainframe at the University of North Florida. This will make the response faster and provide better reliability both in terms of downtime and file backup.
- Incorporation of HTML 3.0: The site will be upgraded to use HTML frames as soon as possible. This will make it easier to see the search and the results on the same 'page'.
- Email of search results: Currently, the proposed search facility is only available to those users that have web access. This will be expanded to all users with email capability to allow searches to be submitted and the results returned, via email messages. This function will be announced on the listserver (see below) when it becomes available.
- Return of multiple selected references: At the present time it is only possible to see the full text entry from one reference at a time. This will be enhanced so that multiple references can be selected and then returned as one single page.
- Email addresses/mailto links: Addition of another field to each entry will contain the current email address (mailto link) of the primary (and maybe secondary) author. This would make it easy to request reprints and ask questions.
- Research groups link: Yet another field could have an HTML link to the home page of the research group that published the paper.

Some more long term, and ambitious ideas, are

- Addition of author abstracts: One aspect that would enhance the information available at the site would be to have authors of papers, books, and theses write short personal abstracts of the publication. This would be added to each entry and would give significant information about the scope and applicability of the publication.

Advanced Search

Use this to search for term(s) in a the fields indicated. For each field (except the year) you can enter up to three keywords which will be logically ORed. Keywords in different fields are ANDed together. For the year you can either enter a specific year, or a range of years.

Click on the links below to see indices of terms used in the indicated fields

Analytes Authors Techniques Journals FATerms Language Matrices

Title:			
Author:			
Journal:			
Year:	Only:	Range:	to
Analyte:	arsenic	selenium	
Matrix:			
Technique:	atomic absorption		
FATerm:			

Submit Query

Last updated March 14, 1997 SJC

Fig. 6. The flow analysis database advanced search page.

- Links to previous references: Eventually, as the database becomes more complete, addition of links to references cited in each publication could be added and linked to its entry in the database.
- Journal information: Finally the journal index will be continually updated and will be expanded to include the mailing address, the email address of the editor and a link to the any on-line information about the journal.

4.2. Listserver

At the 1997 ICFIA meeting, where the FAD was first announced, participants were also interested in starting up a listserver on flow analysis. Since that meeting, this has been added and can be subscribed to by sending an email message to macjordomo@schalk.as.unf.edu. In the body of the message include the line 'Subscribe fialist First_Name Last_Name'. Once subscribed to, the list sending email to fialist@schalk.as.unf.edu will send a message to all the subscribers. Again, this will be transitioned to a university computer in the near future and subscribers to the list will be told about the change at that time.

4.3. Web site

In addition to the database, the site at UNF contains other information related to flow analysis technology. This includes links to flow analysis

Search Results

There are 15 references matching your criteria. Matches 1 to 15 are displayed.

If you find any information in error, or missing, please contact FIAWeb (see below) and it will be updated immediately

189 *Design considerations for an automated hydride-evolution system based on continuous-flow principles*
J. Autom. Chem., **1980** 2(3) 134-138

731 *Ultra-trace-level detection of arsenic and selenium using a commercially available hydride generator with atomic-absorption detection*
J. Autom. Chem., **1983** 5(4) 193-196

835 *Effect of continuous pre-reduction by heating with potassium iodide and hydrochloric acid for determining total arsenic by continuous hydride generation - atomic-absorption spectrometry using sodium tetrahydroborate reduction*
Bunseki Kagaku, **1983** 32(6) 357-361

859 *An automated hydride generation atomic absorption spectrometric method for the determination of total arsenic in raw and potable waters*
Water Res. Cent., **1983** ()

876 *Wet-digestion method for determination of total arsenic in marine organisms. 2. Digestion method of marine organisms for determination of total arsenic by atomic-absorption spectrometry*
Bunseki Kagaku, **1983** 32(8) E259-E264

877 *Wet-digestion method for determination of total arsenic in marine organisms. 1. Study on wet-digestion method for determination of total arsenic in marine organisms by continuous-flow arsine generation and atomic-absorption spectrometry using some model compounds*
Bunseki Kagaku, **1983** 32(6) E171-E176

884 *Development and comparison of methods for the determination of selenium in biological tissues and/or fluids*
Acta Cient. Venez., **1983** 34() 449

Fig. 7. Advanced search results page from the flow analysis database.

research groups, information about conferences, links to suppliers of flow analysis equipment, theory of flow analysis methodology and reports of standard methods based on flow analysis. Any useful suggestions on other information should be addressed to the author by either regular or electronic mail.

5. Conclusion

There is no doubt that this facility will help information dissemination for the flow analysis community. The vehicle of the WWW is powerful at providing up-to-date information for a global audience. How much it will help will largely de-

Table 2
Part of the analyte field term index

Amines	Amines, aromatic	Amines, primary, total
Amines, secondary	Amino acids	Amino acids, D
Amino acids, thiols	Aminoacylase	Aminoglycosides
Ammonia	Ammonium	Ammonium ion
Ammonium, nitrogen	Amoxycillin	Ampicillin
Amylase	Anilide	Aniline
Anions	Anions, inorganic	Anisole
Antibiotics, β-lactam	Antimony	Arginine
Aromatic, 2-hydroxy acids	Arsenate	Arsenic
Arsenic(III)	Arsenic(V)	Arsenic, total
Arsenobetaine	Arsine	Ascorbic acid

pend on researchers in the area. This is a worldwide project initiated at the University of North Florida, however without the help of the FA community it cannot reach its potential as the ultimate resource, so I encourage everyone to contribute to the database no matter how small.

References

[1] J. Ruzicka, E.H. Hansen, Anal. Chim. Acta 79 (1975) 145.
[2] http://www.w3.org/pub/WWW/, March 4, 1997
[3] http://www.rhythm.com/ ~ bpowell/Atlas/Ch1.htm, February 26th, 1997
[4] http://www.microsoft.com/msdownload/personalweb/00000.htm Microsoft's personal webserver software, March 7, 1997
[5] http://pws.hhg.apple.com/ Apple Computer's personal web server software, March 3, 1997

ELSEVIER

Talanta 45 (1998) 603–612

Talanta

Membrane preconcentration-capillary electrophoresis tandem mass spectrometry (mPC–CE–MS/MS) in the sequence analysis of biologically derived peptides

Stephen Naylor [a,b,*], Andy J. Tomlinson [a]

[a] *Biomedical Mass Spectrometry Facility and Department of Biochemistry and Molecular Biology, Guggenheim CL C009B, Mayo Clinic/Foundation, Rochester, MN 55905, USA*

[b] *Department of Pharmacology and Clinical Pharmacology Unit, Guggenheim CL C009B, Mayo Clinic/Foundation, Rochester, MN 55905, USA*

Received 5 February 1997; received in revised form 2 June 1997; accepted 4 June 1997

Abstract

We demonstrate the use of membrane preconcentration capillary electrophoresis tandem mass spectrometry (mPC–CE–MS/MS) for sequencing peptides at the sub-100 femtomole level. In particular by loading the mPC–CE cartridge off-line with a pressurized bomb apparatus, 100 μl solutions can be loaded in <5 min. Furthermore, mPC–CE–MS in conjunction with on-line transient isotachophoresis carried out in 25 μm i.d. capillaries results in enhanced resolution and theoretical plate values as compared to convention 50–75 μm i.d. capillaries. We show that this is a powerful new approach in the sequencing of biologically derived compounds from complex mixtures such as MHC class I peptides. © 1998 Elsevier Science B.V.

Keywords: mPC–CE–MS/MS; Sequence analysis; Biologically derived peptides

1. Introduction

Capillary electrophoresis (CE) separations are performed in narrow bore capillaries (~5–100 μm i.d.). A high voltage (5–30 kV) is applied across the capillary, and analytes are separated based (to a first approximation) on their different charge-to-mass ratios [1,2]. CE is characterized by low solvent consumption (nl–μl per run), and minimal sample loss due to the small volume (1–2 μl) and surface area of the capillary. However, the small, finite volume of the CE capillary also leads to poor concentration limits of detection (CLOD). This fact has proved to be a major limitation of CE in the analysis of many analyte mixtures [3,4] since resolution and separation efficiency are compromised when sample injection of $>$~1.5–2% of the CE capillary volume are attempted [5]. Hence, analysis of sample volumes of only ~1–100 nl are common in CE. This dramatically contrasts with the ~1–100 μl injections carried out in capillary HPLC. Therefore, while it is recognized that both CE and HPLC offer orthogonal modes to sepa-

* Corresponding author. Tel.: +1 507 2845220; fax: +1 507 2848433; e-mail: naylor.stephen@mayo.edu

PII S0039-9140(97)00186-0

rate analyte mixtures, the latter is often the method of choice for many mixtures that contain low concentrations of analytes.

The same poor CLOD is also present for the on-line CE–MS analysis of mixtures. The development of CE–MS was pioneered independently by Smith using a coaxial sheath liquid approach [6,7] and by Henion who developed the liquid junction interface [8,9]. Since the first report of on-line CE–MS, it has undergone considerable development in both instrumentation and applications and was the subject of a recent review [10]. However, only introduction of sample onto the CE capillary using transient isotachophoresis (tITP) has been explored in terms of attempting to improve CLOD in CE–MS [11,12]. This injection technique is ultimately implemented as the voltage is applied across the CE capillary which subsequently results in focusing of the injected analyte zone. This is brought about due to the faster mobilities of ions in the leading and trailing buffer zones sandwiching the analyte zone. However, even under optimal conditions this approach only allows sample volumes of ~1 μl to be introduced onto the CE capillary.

A practical solution to poor CLOD in CE was pioneered by Guzman [13] who described the use of on-line analyte concentration. This approach has subsequently been developed by us and other groups and was recently reviewed [3,4]. Typically, most groups have utilized a small bed (~1–2 mm) of HPLC solid phase or immobilized antibodies covalently attached to solid phase at the inlet of the CE capillary. It is clear that the use of a suitable adsorptive phase at the inlet of the CE capillary solves some of the major limitations of CE and CE–MS by substantially improving CLOD. In addition, sample contaminants (e.g. matrix components or chemical reagents) can be pre-eluted and washed from the phase prior to analyte elution and analysis. Such on-line sample cleanup reduces sample handling which usually results in improved analyte recoveries. However, we and others have shown compromised CE performance when using a solid phase packing material at the capillary inlet [14–20]. This has been attributed to an increased back pressure that reduces hydrodynamic flow within the CE capillary. In addition, as ion flow is impaired by the solid phase, electroosmotic flow (EOF) can be reduced leading to variable analyte migration times. We have also previously reported that large volumes of organic solvent required to remove analytes from the solid phase within the CE capillary can also lead to reduced EOF. These factors can result in the broadening of analyte zones, compromised resolution, and loss of separation efficiency [21,22].

In attempting to design and construct a new preconcentration-CE approach, factors that would decrease or remove all of the potential problems associated with the solid phase PC–CE capillary were considered. Hence, we have found that by minimizing the volume of the adsorptive phase and using an appropriate coated/impregnated membrane, it is possible to reduce the volume of elution solvent required for efficient removal of analytes from the phase. Therefore, adverse effects due to the presence of large volumes of organic solvent on CE performance can be significantly reduced. For convenience, the membrane is installed in a Teflon cartridge system, as shown in Fig. 1 [15]. This facilitates the ready removal of the cartridge to allow CE capillary cleaning/conditioning and activation of the adsorptive membrane, and we term this approach membrane PC–CE (mPC–CE).

The mPC–CE cartridge is also compatible with on-line CE–MS (mPC–CE–MS) [16,17,23]. In our case we use the coaxial flow electrospray interface (ESI) configuration previously described by Smith [6,7], and this is also shown schematically in Fig. 1. Optimal configuration conditions for this CE–ESI–MS interface, as well as means to enhance sensitivity limits have been reported elsewhere [24,25]. In this work we describe the rapid loading of the mPC–CE cartridge with subsequent analysis by mPC–CE–MS. Furthermore, we demonstrate the efficacy of this approach in the sequence analysis of biologically derived MHC class I peptides by mPC–CE–tandem MS (mPC–CE–MS/MS).

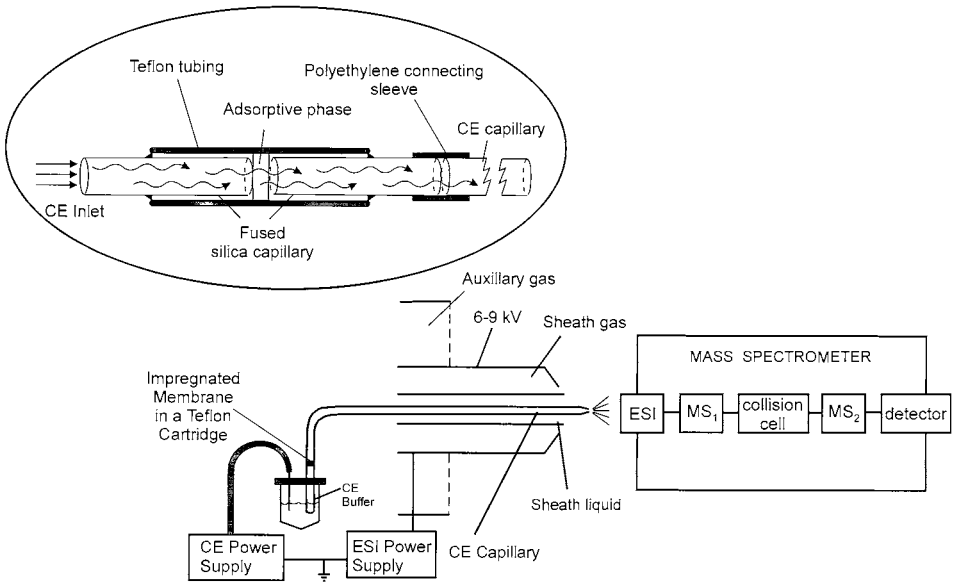

Fig. 1. Schematic of mPC–CE–MS using a Finnigan MAT ESI interface source. The mPC–CE cartridge is shown magnified for clarity (not to scale).

2. Experimental

2.1. Chemicals and materials

Acetic acid (99.9% + grade) was obtained from Aldrich (Milwaukee, WI). Ammonium acetate (99.9% + grade), ammonium hydroxide, and potassium hydroxide were purchased from Sigma (St. Louis, MO). HPLC grade isopropanol, methanol, and water were obtained from Baxter (Minneapolis, MN). The peptide mixture containing angiotensin II, bombesin, bradykinin, luteinizing hormone releasing hormone (LHRH), α-melanocyte stimulating hormone (α-MSH), leucine enkephalin, methionine enkephalin, oxytocin and thyrotropin releasing hormone (TRH) was obtained from Bio-Rad (Richmond, CA). Polymeric styrene-divinyl benzene copolymer (SDB) Empore™ membranes (3M, St. Paul, MN) were obtained Varian (Harbor City, CA). Polyimide-coated fused silica capillary tubing was purchased from Polymicro (Phoenix, AZ). Teflon tubing was obtained from Chromtech (Apple Valley, MN).

2.2. mPC–CE–MS

The CE capillary used in these experiments was prepared from uncoated fused silica tubing pretreated with potassium methoxide, methanol, and CE separation buffer 2 mM ammonium acetate:1% acetic acid in water, pH 2.9). mPC–CE–MS studies were conducted using a cartridge system containing an SDB membrane at the inlet of the CE capillary. The construction of this cartridge was as described previously [16,17]. The dimensions of this capillary were 25 μm i.d. × 70 cm in length. SDB mPC cartridges were activated by washing with methanol (150 μl) and CE separation buffer (150 μl) prior to use by means of a pressurized bomb apparatus (see Fig. 2). Samples were loaded onto the mPC cartridge and cleanup was effected (with CE separation buffer), prior to final construction of the mPC–CE capillary, using the same pressurized bomb apparatus. The mPC–CE capillary was washed with CE separation buffer after installation of the mPC cartridge, containing an off-line loaded sample, to ensure continuity of this solution throughout the mPC–CE capillary. This also ensures the removal of gas

bubbles that may be introduced into the CE capillary during cartridge installation. Analytes were eluted from the hydrophobic SDB membrane with a solution of methanol:water (80:20 v/v). Moving boundary tITP conditions were developed, after analyte elution from the membrane, using a leading stacking buffer (LSB) of 0.1–5% ammonium hydroxide and a trailing stacking buffer (TSB) of CE separation buffer.

All analyses were performed using a Beckman P/ACE 2100 CE (Fullerton, CA) modified with a Beckman-MS adapter kit for operation with a mass spectrometer and coupled to a Reason Technology 486 personal computer (Rochester, MN) with system control by System Gold software

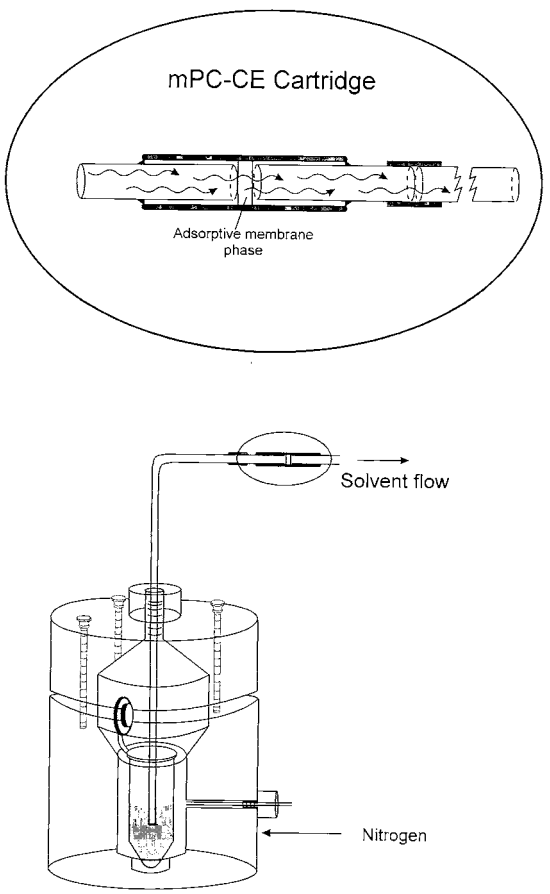

Fig. 2. A schematic diagram of the pressurized bomb apparatus used to load samples onto an mPC-cartridge prior to assembly of the mPC–CE capillary.

(Beckman). A Finnigan MAT 95Q (Bremen, Germany) of EBQ_1Q_2 configuration (where Q_1 is an rf-only octapole collision cell and Q_2 is a quadrupole mass filter) was used throughout. A Finnigan MAT electrospray ion source was used in positive ion mode. This source employs a spray needle that is floated to voltage (typically 3–5 kV) referenced to the accelerating voltage and a heated metal capillary (225°C). A sheath gas was not used during these studies. The mPC–CE capillary was interfaced to this ion source using a sheath liquid consisting of isopropanol:water:acetic acid (60:40:1 v/v/v) at a flow rate of 3 μl min^{-1}. The mass spectrometer was operated at a resolution of ~1000 and a scan range of 300–1300 Da at a speed of 2 s $decade^{-1}$ for mPC–CE–MS studies. A scan range of 60–1000 Da at a speed of 0.4 s/100 amu, and a xenon collision gas pressure of 2×10^{-5} mbar and a ramped collision energy of 18–26 eV was used during mPC–CE–MS/MS experiments.

2.3. Preparation of HPLC fractions of MHC class I peptides for mPC–CE–MS

EL-4 cells (3×109) were lysed with CHAPS and nuclei and membranes were pelleted and the lysate subsequently treated as described previously [26]. After filtration of the MHC class I peptide mixture through a 3 kDa membrane, the filtrate containing MHC class I peptides was subjected to reversed phase HPLC using a Shimadzu HPLC Instrument and a Vydac C-18 300 Å 5 μm column (4.6×250 mm). Peptide separations were achieved using a mobile phase gradient of A: 0.06% TFA/H_2O and B: 0.052% TFA in CH_3CN. A solvent gradient of 2% A → 37.5% B (0–60 min); 37.5 → 75% B (60–90 min); and 75 → 98% B (90–105 min) was used at a flow rate of 500 μl min^{-1}. Fractions were collected based upon their UV response at 214 nm. These were subjected to removal of the organic solvent and reduced to ~50 μl total volume, under vacuum. Subsequently, these samples were then diluted with ~100 μl of CE separation buffer (2 mM NH_4OAc) in 1% acetic acid. Approximately 50–100 μl volumes of the MHC class I fractions were then loaded onto the mPC–CE cartridge before final capillary assembly as described above.

3. Results and discussion

3.1. mPC–CE

The overall goal in developing mPC–CE was to ensure that the preconcentration cartridge did not adversely effect CE and CE–MS performance. Hence, we found that minimizing the volume of the adsorptive phase by using an appropriately impregnated membrane made it possible to reduce the volume of elution solvent required for efficient removal of analytes from the phase [14,16]. Therefore, adverse effects due to the presence of large volumes of organic solvent on CE performance could be overcome. As noted previously, for convenience the membrane was installed in a Teflon cartridge system, as shown in Fig. 1. This facilitates the ready removal of the cartridge to allow CE capillary cleaning/conditioning and activation of the adsorptive membrane. The high loading capacity of such membranes makes it possible to load large volumes (~60–100 μl) prior to CE or CE–MS analysis [16]. However, the small bed volume greatly enhances analyte recoveries using a reduced volume of organic elution solvent. Furthermore, sample cleanup prior to CE–MS analysis is possible. This is particularly important for many samples derived from body fluids such as urine, where the presence of high salt concentrations can dramatically effect CE analyte separations by degrading the efficiency of contemporary CE stacking and focusing procedures. One final advantage of mPC–CE is that a higher flow rate through the capillary is possible since impedance to flow is minimized. This ultimately leads to faster analysis times and analyte migration time are also more reproducible.

3.2. mPC–tITP–CE–MS

The use of mPC–CE–MS in the analysis of dilute synthetic peptide mixtures has recently been demonstrated [16,17]. However, in order to efficiently remove peptides from the adsorptive membrane, an elution solvent that contains some water (e.g. 80:20 v/v methanol:H_2O) is necessary. Furthermore, optimal peptide recovery is achieved only when >50 nl of such a solvent mixture is used [17]. This relatively large volume of elution solvent, along with the inefficient analyte stacking that occurs, results in some peak broadening and loss of analyte resolution. Therefore, the use of moving-boundary tITP, in conjunction with mPC–CE–MS, was attempted, *after* the peptides were eluted from the adsorptive membrane. In this case, moving-boundary tITP conditions are used to stack analyte zones and also aid the dispersion of the organic elution solvent. It is effected by elution of the peptides from the membrane between zones of a LSB, typically 0.1–5% NH_4OH in water, and a TSB, typically 1% acetic acid in water or CE separation buffer, and this has been described in detail elsewhere [16].

We have shown that baseline resolution of a nine peptide mixture consisting of angiotensin II, bombesin, bradykinin, LHRH, α-MSH, leucine-enkephalin, methionine-enkephalin, oxytocin and TRH was possible using mPC–CE–MS [16]. The separation was carried out using a 50 μm i.d. fused silica capillary and, in conjunction with tITP (LSB–0.1% NH_4OH; TSB–1% acetic acid), 'theoretic' plate values of 1.5×10^5–2.6×10^6 were possible.

3.3. mPC–tITP–CE–MS in 25 μm i.d. capillaries

Previous studies have shown that considerable enhancement of CE–MS sensitivity is obtained by use of capillaries with a reduced internal diameter [27,28]. However, use of such small volume capillaries often exacerbates the problems associated with poor CE concentration sensitivity. Ultimately, only ultra-small sample injection volumes, sometimes as low as a few picoliters, can be analyzed without degradation of CE performance. This limitation has been overcome by the advent of mPC–CE technology since it is possible to use the impregnated membrane to trap analytes at the inlet of the CE capillary. Using such approaches, sample volumes (typically 1–200 μl) that greatly exceed the total volume of the CE capillary can be routinely analyzed. Hence, by careful consideration of the chromatographic properties of the adsorptive phase, analytes of low concentration within a complex sample matrix can be extracted

and preconcentrated to a level that leads to their detection by CE–UV, CE–LIF, or, indeed, CE–MS. Furthermore, the use of a narrow bore (< 25 μm i.d.) mPC–CE–MS capillary extends the utility of this technology for the detection of analytes of low concentration (e.g. MHC class I peptides) by enhancing MS sensitivity.

Initially, the use of mPC–CE and mPC–CE–MS with reduced diameter capillaries presented a significant challenge. The flow rate in a 25 μm i.d. mPC–CE capillary is only ~120–150 nl min^{-1}. Hence the introduction of 100 μl of sample into such a capillary would take in excess of 13 h. This time constraint is further exaggerated by washing the mPC–CE capillary with at least 50 μl of CE separation buffer to effect sample cleanup. However, the removable mPC–CE cartridge design lends itself to sample loading and cleanup with CE separation buffer prior to its installation onto the CE capillary.

We have previously described the use of a pressurized bomb apparatus to introduce biological samples onto a microcolumn of solid phase packing material before final analysis by electrospray-MS (ESI–MS) [29]. We have extended this concept and used the bomb apparatus to preload and clean up samples on the mPC-cartridge (see Fig. 2) prior to analysis by mPC–CE–MS. Eppendorf tubes of either analyte solutions (1–100 μl) or washing solvents are contained in a Perspex pressured bomb and subjected to ~40–60 psi of pressure. This effects transfer of the contents of the Eppendorf tube via a fused silica capillary (75 μm i.d. × 360 μm o.d.) through the mPC–CE cartridge. Typically, at such a pressure, approximately 100 μl of solution can be passed through the mPC–CE cartridge in less than 5 min.

It should be noted that the bi-directional flow of analyte solution and solvents through the mPC-cartridge is important since it has been our experience that sample loaded in the opposite direction to which analytes are eluted into the CE capillary yields a more optimal performance than those introduced in the forward direction. This we believe is due, at least in part, to the fact that analyte adsorption is at the surface of the membrane with minimal penetration. Thus, provided the membrane does not become saturated during this process, analytes are eluted by the leading edge of the elution solvent. This leads to efficient analyte removal from the membrane and results in a less diffuse analyte zone within the mPC–CE capillary even before electrophoretic mobilization is commenced. A further advantage of reversing the solvent flow through the mPC–CE capillary is the removal of sample-originated particulates from this device prior to its installation onto the CE capillary. This aids the reproducibility of mPC–CE(MS) performances and tends to overcome issues of irreproducible EOF due to the erratic hydrodynamic flow that have been reported for solid phase preconcentration techniques [14,20]. Additionally, the reduced tendency for clogging of the membrane by particulates extends the life of the mPC-cartridge.

A second challenge regarding optimal performance of mPC–CE(MS) in narrow bore capillaries is the development of efficient moving boundary tITP conditions for analyte focusing at the onset of electrophoresis. For example, moving boundary tITP conditions that yield optimal mPC–CE(MS) performance for peptide analysis in a 50 μm i.d. mPC–CE capillary are a LSB of 0.1% ammonium hydroxide in water and an acidic TSB which is typically the CE separation buffer [16]. If these conditions were used in a 25 μm i.d. mPC–CE capillary, the process of introducing LSB, elution solvent, and TSB into the capillary would tend to completely fill this narrow bore capillary and change the separation characteristics of the developed CE separation strategy. However, increasing the concentration of LSB to 1% ammonium hydroxide in water ensures that efficient moving boundary tITP conditions can be developed with a smaller volume of this reagent. Increasing the concentration of LSB still further to 5% ammonium hydroxide in water can further improve the focusing of peptide zones. This result, shown in Fig. 3, indicates improved separation efficiency through enhanced signal:noise ratios and more narrow peak widths for the nine peptide component mixture described earlier using a 50 μm i.d. capillary.

In addition to the effects induced by the LSB, we have observed a dependence of mPC–CE(MS) performance on the volume of TSB. Indeed, it is

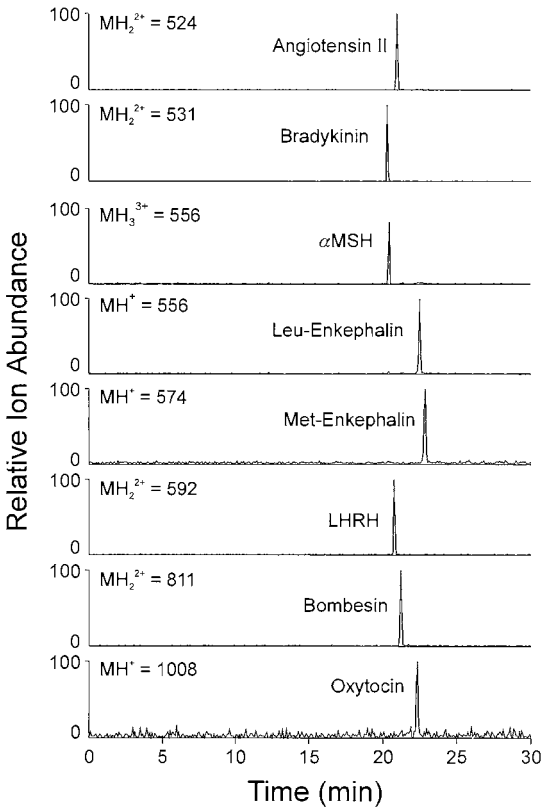

Fig. 3. Ion electropherogram of an mPC–tITP–CE–MS analysis of the BioRad nine peptide mixture using a Beckman P/ACE 2100 CE connected to a MAT 95Q mass spectrometer. The separation buffer used was 2 mM NH_4OAc:1% acetic acid in a 25 μm i.d. × 70 cm uncoated fused silica capillary. CE capillary voltage was 25 kV, and the LSB was 1% NH_4OH (60 nl) and the TSB was 1% acetic acid (70 nl). Peptides were eluted from the SDS membrane using 80:20 MeOH:H_2O (70 nl).

clear from our studies that the analyte elution zone needs to be pushed a reasonable distance away from the membrane to achieve optimal performance. We have attributed this result, at least in part, to a potential for analyte to readsorb onto the hydrophobic membrane if their mobility is towards the back edge of the elution zone (inlet of the mPC–CE capillary) at the onset of electrophoresis. In our experience, typical volumes of LSB:elution solvent:TSB used in a 25 μm i.d. mPC–CE capillary are in a ratio of 1:1:1.5 (corresponding to absolute volumes of ~60:60:90 nl of these reagents). We have found there is a slight difference, however, due to a slight difference of hydrodynamic flow properties of each mPC-cartridge, we have found, for optimal performance, it is necessary to systematically evaluate the volume ratios of each of these reagents when used for the first time in a newly prepared mPC–CE capillary.

3.4. mPC–tITP–CE–MS/MS

The ultimate goal of peptide analysis is primary sequence determination. In this regard MS/MS affords both high sensitivity, and the most appropriate method for structural characterization of subpicomole amounts of peptide on-line with chromatographic separation techniques. Therefore, we recently investigated the use of mPC–tITP–CE–MS/MS for sequencing synthetic peptides present in a mixture at the low femtomole (< 100 fmol) amounts [17].

Initial studies indicated that subtle changes in collision cell parameters led to substantial changes in product ion spectra. These changes appeared to be much greater for the analysis of low femtomole amounts of peptide than is normally observed at higher picomole amounts. This prompted us to systematically investigate the effects of all collision cell parameters on product ion spectra obtained on less than 100 femtomoles of peptide, and this has been reported in detail elsewhere [17]. Briefly, we evaluated type of target gas, collision gas pressure and energy, as well as the effect of CE capillary i.d. on the production efficiency of product ions formed in the collision induced dissociation (CID) process occurring in the collision cell. Xenon was the preferred target gas due to its larger atomic radius. This results in a sizable increase in yield of product ions detected at MS_2 as compared to a smaller gas such as argon or helium [17]. A collision gas pressure of 2×10^{-5} mbar was found to minimize product ion scatter within the collision cell, but maximize product ion formation and transmission. It was found that small variations in collision energy (5–10 eV) could result in substantial differences in both the type and abundance of product ions formed in the CID process of low femtomole amounts of peptide. Therefore, we suggest that a ramping of collision energy between 18–26 eV for doubly

charged peptides (MH_2^{2+}) in the mass range ~450–600 Da is optimal. Finally, we demonstrated that a significant improvement (~fourfold) enhancement in signal:noise occurred for product ion spectra using a 25 μm i.d. versus 50 μm i.d. CE capillary.

3.5. mPC–tITP–CE–MS/MS of biologically derived peptides

A major stimulus behind the development of mPC–CE–MS and mPC–CE–MS/MS was to sequence biologically significant MHC class I peptides. This area of research was pioneered by Hunt [30] and has been shown to exhibit considerable analytical challenges. First, it has been noted that MHC class I glycoproteins can bind in excess of 10 000 structurally unique peptides. These immunologically significant peptides are only extracted at extremely low concentrations (10^{-15}–10^{-18} M) from 10^8–10^{10} cells. Furthermore, only a few of these peptides that are presented at the cell surface by the MHC class I glycoprotein exhibit antigenic activity, and most of them are of unknown sequence.

The strategy we have developed for characterizing and ultimately sequencing biologically derived MHC class I peptides has been reported in detail elsewhere [26]. In brief, HPLC fractions were collected and subjected to removal of the acetonitrile under vacuum. Resultant peptide solutions (~40–70 μl) were *diluted* with CE separation buffer (2 mM NH_4OAc:1% acetic acid, pH 2.9) to a final volume of ~150 μl. An aliquot of this solution (50 μl) was then subjected to mPC–tITP–CE–MS for determination of the peptide molecular mass. Off-line sample loading and cleanup (with CE separation buffer) were used, since the flow rate in the 25 μm i.d. mPC–CE capillary was only 120–150 nl min^{-1}. On-line loading of 50 μl of sample in this capillary would take up to 5.5 h. However, the flow rate achieved in an mPC cartridge loaded off-line can be much higher, since these devices can withstand relatively high pressures (~60 psi). Furthermore, system back pressure is also reduced, and up to 100 μl of sample can often be loaded off-line in < 5 min, thus significantly reducing analysis time.

In a specific example, approximately 50 μl of diluted HPLC fraction MHC class I peptides isolated from a K^b immunoprecipitation of EL-4 mouse cells were pressure loaded via the bomb apparatus onto a mPC–CE cartridge containing a preactivated SDB impregnated membrane. Subsequently, the cartridge was reversed, reinstalled onto the pressurized bomb apparatus, and washed with CE separation buffer (50 μl). The total loading and washing took < 5 min. After connecting the mPC–CE cartridge to the CE capillary, the assembled mPC–CE capillary was washed with CE separation buffer (10 min). During this process the flow rate of CE separation buffer through the capillary was measured using a microflow meter made from a 10 μl syringe. The measured flow rate (~127 nl min^{-1}) was used to estimate the volumes of elution reagents used during this analysis. Next, the peptides retained by the mPC-cartridge were eluted with ~40 nl of a solution of 80:20 MeOH:H_2O between a ~20 nl of LSB (1% NH_4OH) and ~80 nl of TSB (CE separation buffer) and subjected to mPC–CE–MS. This resulted in the detection and separation of four doubly charged responses ($MH_2^{2+} = 450.1$, 469.1,498.2 and 605.7) all of which were within the expected molecular weight range for MHC class I peptides (data not shown). Following this molecular weight screening, the remaining 100 μl of the prepared fraction were loaded as described above and subjected to mPC–CE–MS/MS using conditions that were developed for synthetic peptide mixtures [17]. As an example, the doubly charged ion at m/z 469.1 was subjected to CID using xenon as the collision gas. An abundant 'y' series of ions at m/z 838.4 (y_7) 724.4 (y_6), 625.3 (y_5), 510.3 (y_4), 347.2 (y_3), and 260.2 (y_2), as well as a partial 'b' series at m/z 806.4 (b_7), 678.3 (b_6), 410.2 (b_4^0), and 214.1 (b_2) suggested a sequence assignment of VNVDYSKX (X represents I or L). The data was also searched against the Seaquest database search algorithm developed by Yates [31]. This peptide was ranked with the highest priority score. Nevertheless, while the MS/MS data correlates well with the peptide sequence, we are in the process of preparing a synthetic peptide. We will subsequently subject this to mPC–CE–MS/MS analysis and compare it with the data

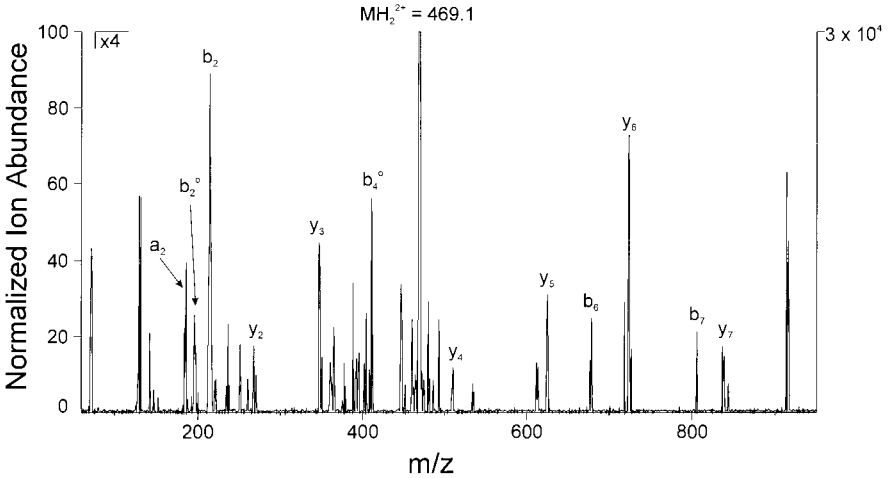

Fig. 4. mPC–tITP–CE–MS/MS analysis of an MHC class I peptide with a detected molecular ion of $MH_2^{2+} = 469.1$. All conditions as for Figure 3 except collision gas was xenon at a pressure of 2×10^{-5} mbar, ramped collision energy was 18–24 eV, scan range was 60–100 Da at 0.4 s/100 amu.

obtained for the biologically derived peptide in order to verify the accuracy of the sequence determined Fig. 4.

4. Conclusions

mPC–CE and mPC–CE–MS strategies are currently under continual refinement. In the present study, while we recommend the use of a narrow bore (≤ 25 μm i.d.) capillary for high sensitivity mPC–CE–MS studies, we show that use of such capillaries yields two potential limitations of this approach. First, the flow rate in these capillaries is extremely low, often < 150 nl min^{-1}. Therefore, on-line loading of large sample volumes, up to 100 μl, is inherently time consuming and often impractical. However, utilizing the removable design of the mPC-cartridge, we have demonstrated the viability of loading large sample volumes prior to final assembly of the mPC–CE capillary. Indeed, the use of this strategy tends to prolong the life of the mPC-cartridge since sample loading and cleanup is achieved by solution flow in opposite directions. Hence, particulates that originate from sample solutions are flushed from the mPC-cartridge prior to its installation onto the CE capillary. Furthermore, this action tends to prevent blocking of narrow bore mPC–CE capillary and improve the reproducibility of mPC–CE(MS) analyses.

A potential second limitation of mPC–CE(MS) analyses in narrow bore capillaries was the development of efficient moving boundary tITP conditions after analyte elution from the mPC–CE cartridge at the onset of electrophoresis. Reagent concentrations and volumes that are optimal for larger bore capillaries tend to completely fill a capillary of smaller internal diameter. Therefore, we have reported moving boundary tITP conditions for use with narrow bore capillaries and have demonstrated that increasing the concentration of LSB allows the use of a smaller volume of this reagent. Furthermore, we have found that the volume of TSB (typically a small volume of CE separation buffer) is more critical in the small i.d. capillaries. It is apparently advantageous to move the zone of eluted analytes a reasonable distance away from the membrane. We have attributed this, at least in part, to a tendency for analytes to readsorb onto the membrane if their initial migration is towards the back edge of the elution solvent zone which is close to the membrane. We report a typical volume ratio for LSB:elution solvent:TSB is 1:1:1.5, which corresponds to actual reagent volumes of 60:60:90 nl, respectively,

but suggest that these conditions require optimization (with a standard mixture of peptides) for each newly prepared mPC–CE capillary. However, we have found a well-optimized mPC–CE capillary yields reproducible performance on a weekly basis.

Finally, we have demonstrated the efficacy of the modified mPC–CE–MS approach with narrow bore capillaries for characterizing biologically derived MHC class I peptides. In a specific example, showed the detection of four doubly charged responses that were suspected to be MHC class I peptides in an HPLC fraction isolated from a K^b immunoprecipitation of mouse EL-4 cells. Furthermore, we demonstrated the power of mPC–CE–MS/MS in conjunction with database searching of the acquired data for structurally characterizing these important molecules of the immune system.

Acknowledgements

We thank Mrs. Diana Ayerhart for her help in preparing this manuscript. We thank Finnigan MAT, Beckman Instruments, and Mayo Foundation for their support of this work.

References

[1] N.A. Guzman (Ed.), Capillary Electrophoresis Technology. Marcel Dekker, New York, 1993, p. 634.
[2] R. Weinberger, Practical Capillary Electrophoresis. Academic Press, San Diego, 1993, p. 312.
[3] A.J. Tomlinson, N.A. Guzman, S. Naylor, J. Cap. Elec. 2 (1995) 247.
[4] A.J. Tomlinson, L.M. Benson, N.A. Guzman, S. Naylor, J. Chromatogr. A. 744 (1996) 3.
[5] J. Cai, Z. El Rassi, J. Liq. Chromatogr. 15 (1992) 1179.
[6] R.D. Smith, J.A. Olivares, N.T. Nguyen, H.R. Udseth, Anal. Chem. 60 (1988) 436.
[7] R.D. Smith, J.A. Loo, C.J. Barinaga, C.G. Edmonds, H.R. Udseth, J. Chromatogr. 480 (1989) 211.
[8] E.D. Lee, W. Mueck, J.D. Henion, T.R. Covey, J. Chromatogr. 458 (1988) 313.
[9] I.M. Johannson, E.C. Huang, J.D. Henion, J. Zweigenbaum, J. Chromatogr. 554 (1991) 311.
[10] J. Cai, J.D. Henion, J. Chromatogr. A. 703 (1995) 667.
[11] L.M. Benson, A.J. Tomlinson, J.M. Reid, D.L. Walker, M.M. Ames, S. Naylor, J. High Resol. Chromatogr. 16 (1993) 324.
[12] M.H. Lamoree, N.J. Reinhoud, U.R. Tjaden, W.M.A. Niessen, J. Van der Greef, Biol. Mass Spectrom. 23 (1994) 339.
[13] N.A. Guzman, M.A. Trebilcock, J.P. Advis, J. Liq. Chromatogr. 14 (1991) 997.
[14] A.J. Tomlinson, L.M. Benson, R.P. Oda, W.D. Braddock, B.L. Riggs, J.A. Katzmann, S. Naylor, J. Cap. Elec. 2 (1995) 97.
[15] A.J. Tomlinson, L.M. Benson, W.D. Braddock, R.P. Oda, S. Naylor, J. High Resol. Chromatogr. 18 (1995) 381.
[16] A.J. Tomlinson, S. Naylor, J. Cap. Elec. 2 (1995) 225.
[17] A.J. Tomlinson, S. Naylor, J. Liq. Chromatogr. 18 (1995) 3591.
[18] A.J. Tomlinson, L.M. Benson, R.P. Oda, W.D. Braddock, M.A. Strausbauch, P.J. Wettstein, S. Naylor, J. High Resol. Chromatogr. 17 (1994) 669.
[19] A.J. Tomlinson, W.D. Braddock, L.M. Benson, R.P. Oda, S. Naylor, J. Chromatogr. B Biomed. Appl. 669 (1995) 67.
[20] A.J.J. Debets, M. Mazereeuw, W.H. Voogt, D.J. van Iperen, H. Lingeman, K.-P. Hupe, U.A.T. Brinkman, J. Chromatogr. 608 (1992) 151.
[21] A.J. Tomlinson, L.M. Benson, S. Naylor, LC-GC 12 (1994) 122.
[22] A.J. Tomlinson, L.M. Benson, S. Naylor, Am. Lab. 26 (1994) 29.
[23] A.J. Tomlinson, S. Naylor, J. High Resol. Chromatogr. 18 (1995) 384.
[24] A.J. Tomlinson, L.M. Benson, S. Naylor, J. Cap. Elec. 1 (1994) 127.
[25] K.L. Johnson, A.J. Tomlinson, S. Naylor, Rapid Commun. Mass Spectrom. 10 (1996) 1159.
[26] A.J. Tomlinson, S. Jameson, S. Naylor, J. Chromatogr. A. 744 (1996) 273.
[27] J.H. Wahl, D.C. Gale, R.D. Smith, J. Chromatogr. 659 (1994) 217.
[28] J.H. Wahl, D.R. Goodlett, H.R. Odseth, R.D. Smith, Anal. Chem. 64 (1992) 3194.
[29] C. Czaja, R. Litwiller, A.J. Tomlinson, S. Naylor, P. Tavares, J. LeGall, J.J.G. Moura, I. Moura, F. Rusnak, J. Biol. Chem. 270 (1995) 20273.
[30] D.F. Hunt, R.A. Henderson, J. Shabanowitz, K. Sakaguchi, H. Michel, N. Sevilir, A.L. Cox, E. Appella, V.H. Engelhard, Science 255 (1992) 1261.
[31] J.R. Yates, J.K. Eng, A.L. McCormack, D. Schieltz, Anal. Chem. 67 (1995) 1426.

.

ELSEVIER

Talanta 45 (1998) 613–618

Talanta

Fluorescence detection in short capillary and chip using a variable wavelength epi-fluorescence microscope

Y. Zhang [a], H.K. Lee [a], S.F.Y. Li [b,*]

[a] *Department of Chemistry, National University of Singapore, Kent Ridge Crescent, Singapore 119260, Singapore*
[b] *Department of Chemistry and Institute of Materials Research and Engineering, National University of Singapore, Kent Ridge Crescent, Singapore 119260, Singapore*

Received 5 February 1997; received in revised form 13 May 1997; accepted 14 May 1997

Abstract

Fast, efficient separation of five free acid forms of porphyrins was achieved in a short capillary and a chip, respectively. The capillary was 6 cm long from injection end to detector with an electric field strength of 214 V cm^{-1}. Separations were performed within 5 min. A glass microchip device was fabricated using standard photolithographic procedures and chemical wet etching. The channels were sealed using a direct bonding technique. For a separation length of 2.8 cm with electric field strength of 500 V cm^{-1}, electrophoretic separations with baseline resolution were achieved in less than 2 min. A variable wavelength epi-fluorescence microscope was used as an on-column detector. © 1998 Elsevier Science B.V.

Keywords: Capillary electrophoresis; Chip; Epi-fluorescence microscope; Short capillary

1. Introduction

Capillary electrophoresis (CE) has been well known as a rapid, highly efficient separation technique [1,2]. Many applications based on this technique have been developed since the 1980s. CE is now gaining popularity as an alternative analytical tool for biotechnology, process control, and the environmental and medical sciences [3,4]. Several models of CE instruments are commercially available now. A logical development of the instrumentation for performing chemical analyses is to combine all sample handling and measurement steps into a small package incorporating a high level of automation [4,5]. The miniaturization of the CE system would be valuable in helping to meet the increasing needs for novel and routine analytical applications.

Recently, several groups have performed separation of fluorescent dyes [6–9], metal ions [10], oligonucleotides [11,12], amino acid [5,10,13,14], DNA restriction fragments [15,16] and DNA sequencing fragments [17] in a fabricated CE devices on glass or silica chips. The analysis time was decreased significantly due to the application of high electric field strengths to short separation length. Consequently, band dispersion could be

* Corresponding author. Tel.: +65 7722681; fax: +65 7791691.

PII S0039-9140(97)00291-9

reduced by minimizing longitudinal dispersion of the analyte as well as by decreasing both injection and detection volumes. Joule heating problems were avoided by the efficient dissipation capability of the glass chips. Another major advantage of this approach is that multiple channels of identical geometry are easily generated on a single substrate, which would help to meet the requirement of multiple biochemical samples analysis in parallel [9,11,15,18].

In this paper, fast separation of five free acid forms of porphyrins were performed in both short capillary and chip under low applied potential. Compared with traditional CE, analyses time was significantly decreased.

2. Experimental

2.1. Instrumental

A lamp-based fluorescence detection system was used as described previously [19]. Briefly, the microscope and accessories used was a Nikon Labophot-2A episcopic fluorescence microscope (Nikon, Tokyo, Japan). The excitation lamp was a 100 W high-pressure mercury lamp. A filter block with the excitation filter (EX 510–560 nm), the dichroic mirror (DM 580 nm) and the barrier filter (BA 590 nm) was used for the detection of rhodamine B and eosin yellowish. For the porphyrins, a 405 nm excitation filter was used instead. The fluorescence emission was collected with a Nikon CF N Plan Achromat ELWD long working distance objective (5.08–6.84 mm), magnification 40; numerical aperture 0.55. A Hamamatsu silicon photodiode with a built-in amplifier (Model HC220-21, Hamamatsu, Japan) was attached to the trinocular housing of the microscope. A Shimadzu integrator (C-R6A Chromatopac, Shimadzu, Japan) was used for signal recording. A home-made light-proof box was used to cover the entire light sensitive area. A high voltage power supply (Spellman High Voltage Electronics, Plainview, NY) was used for injection and separation.

2.2. Reagents

Sodium tetraborate, sodium dihydrogen phosphate and sodium dodecyl sulphate (SDS) were purchased from Fluka (Buchs, Switzerland). CAPS (3-cyclohexylamino-1-propanesulfonic acid), Rhodamine B, eosin yellowish (2′,4′,5′,7′-tetrabromofluorescein disodium salt) and protoporphyrin IX were obtained from Sigma (St. Louis, MO). Hexacarbosylporphyrin I, heptacarboxylporphyrin I and uroporphyrin I were obtained from Porphyrin Products (Logan, UT), coproporphyrin I was from Aldrich (Milwaukee, WI). All the buffer solutions were prepared in Millipore water and were sonicated and filtered with 0.2 μm pore size nylon filters (Poretics, USA) before use.

2.3. Capillary and chip

The fused silica capillary was obtained from Polymicro Technologies (Phoenix, AZ). The total length of the capillary is 14 cm. The distance from injection end to the detection window is 6 cm. Two 50 μm plastic vials were used as buffer reservoirs. The two ends of the capillary were inserted into the reservoirs through the holes made on the side by a syringe needle, while the electrodes were immersed into the buffer from the top of the plastic vials. The capillary and reservoirs were mounted onto the microscope's XY stage holder.

The glass structures were fabricated using standard photolithographic and wet chemical etching techniques described previously [15]. Fig. 1 shows the layout and dimensions of the channels. Fifteen

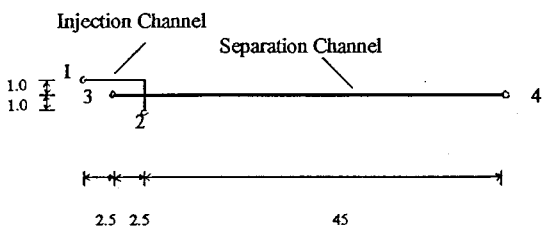

Fig. 1. Layout and dimensions of microfabricated channels. The separation channel is 50 μm wide; the injection channel is 30 μm wide; all the channels are 8 μm deep; access holes are 1 mm in diameter. The dimensions shown are in mm.

channels were etched in a 100 mm × 80 mm × 1.5 mm Hoya borosilicate glass (Hoya, Japan). A metal etched mask was used. The micromachined substrate and the cover were joined using a direct bonding technique. Four holes were drilled through the top plate to contact four of the channels. After bonding, pipette tips were inserted into these holes to form small reservoirs. Prior to thermal bonding, the top plate with holes and etched bottom plate were submerged in hot H_2SO_4–H_2O_2 for 10 min, rinsed thoroughly with Milipore water, and then the surface were hydrolyzed in dilute NH_4OH solution, rinsed again with Milipore water and dried with N_2 gas. Subsequently, the pair of glass plates were annealed in a model 2-525 programmable furnace (Barkmeyer, USA). The temperature program was as follows: 20°C min^{-1} to 500°C for 1 h, 550°C for 0.5 h, and 620°C for 2–3 h, 550°C for 1 h, followed by natural cooling of the furnace to room temperature. When some regions (especially in the channel area) were not totally bonded, this cycle needed to be repeated about 3–4 times to eliminate bonding defects [20].

2.4. Electrophoresis procedures

Hydrodynamic injection was employed in the short capillary at a height difference of 14 cm. The power supply for the separation was operated at 3 kV relative to ground.

Before use, the fabricated channels were washed with H_2SO_4–H_2O_2 (5 min), water (5 min), NaOH (2 min), water (2 min) and electrolyte solution (10 min) by introducing a drop of solution into one of the four holes with a microsyringe. After the channels were filled with the solution hydrodynamically, the solution was flushed away through a pipette tip connected to a nitrogen gas cylinder. The pressure used was less than 20 psi. The buffer composition for the separation of the porphyrins was [19]: 40 mmol l^{-1} CAPS, pH 10.8, 20 mmol l^{-1} SDS, 8% dimethyl formamide (DMF). After the channels were filled with buffer solution, pipette tips were inserted into the four holes to form reservoirs into which buffer and Pt electrodes were placed. In this paper, reservoir 1 was filled with the sample, the rest were filled with separation buffer. About 1 kV potential was applied between reservoirs 1 and 2 to drive the samples into the channels. Separation was carried out between reservoirs 3 and 4 under 2.5 kV. The distance from the injection cross to the detection window was 2.8 cm.

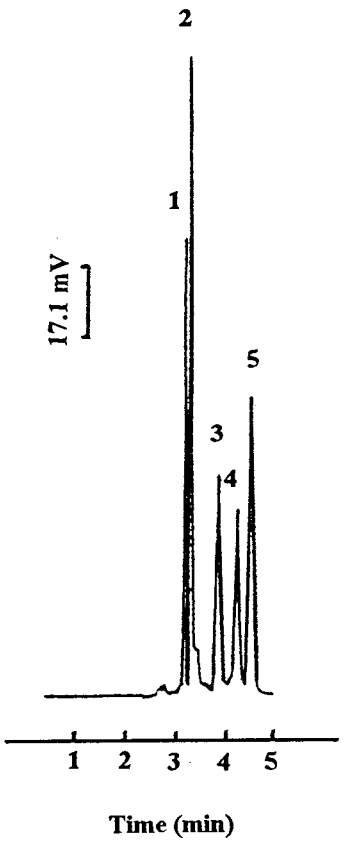

Fig. 2. Electropherogram obtained for free acid forms of porphyrins using a short capillary. Buffer: 20 mmol l^{-1} SDS, 8% dimethylformamide, 40 mmol l^{-1} CAPS, pH 10.8; capillary: 50 μm i.d. × 14 cm (effective length 6 cm); voltage: 3 kV; detection: excitation wavelength 405 nm, emission wavelength 590 nm; injection: hydrodynamic injection for 10 s. Peaks identities: 1, coproporphyrin I; 2, protoporphyrin IX; 3, hexacarboxylporphyrin I; 4, heptacarboxylporphyrin I; 5, uroporphyrin. Concentration of each peak is around 5 μmol l^{-1}.

3. Results and discussion

Fig. 2 shows the electropherogram of five free acid forms of porphyrins using the short capillary. Baseline separation was achieved within 5 min. Good reproducibility was observed when the injection amount was carefully controlled. Table 1 shows the statistical data for the run-to-run reproducibility of migration times.

All the porphyrin sample solutions were prepared in DMF because of their high hydrophobicity. A significant effect of the injection amount on the separation has been observed. When samples were introduced into the capillary hydrodynamically, the concentration of DMF of the sample band was much higher than that of the buffer solution, which tended to cause a disturbance of the micelles [21] in the separation buffer near the injection end of the capillary. As a result, when the injection amount increased, the migration times of porphyrins decreased and the resolution of peaks decreased. In a long capillary, this effect can be diminished to some extend after a relative long migration time, while in a short capillary, this effect becomes more critical and the injection amount needs to be controlled to a minimum value in order to obtain an acceptable resolution.

A typical electropherogram obtained in a chip for rhodamine B and eosin yellowish is illustrated in Fig. 3. Complete separation was achieved within 30 s. Fig. 4. shows the rapid separation of five free acid forms of porphyrin.

Table 1
Reproducibility of migration times using a non-gel sieving buffer

Peak number	Porphyrin	Migration time (min) (mean $\pm$ S.D., $n = 5$)
1	Coproporphyrin I	3.145 ± 0.018
2	Protoporphyrin IX	3.283 ± 0.025
3	Hexacarboxyl-porphyrin I	3.897 ± 0.010
4	Heptacarboxyl-porphyrin I	4.343 ± 0.025
5	Uroporphyrin	4.659 ± 0.036

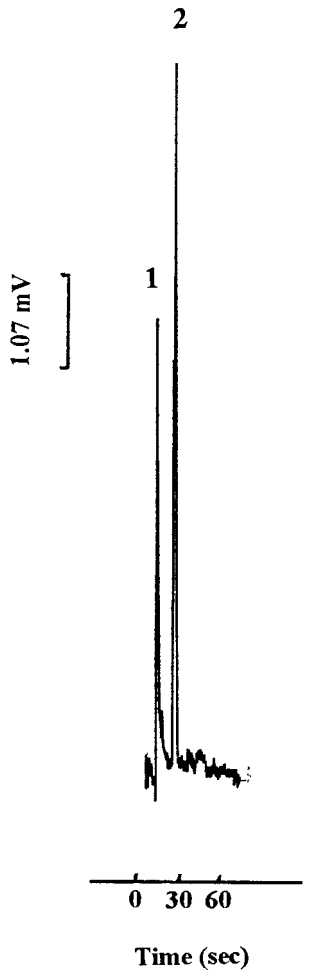

Fig. 3. The electropherogram obtained for a mixture of rhodamine B and eosin yellowish using a glass chip. Peaks identities: 1, rodamine B 6.7×10^{-6} mol l^{-1}; 2, eosin yellowish, 1.4×10^{-4} mol l^{-1}. Buffer: 0.05 mol l^{-1} phosphate, 0.025 mol l^{-1} borate, pH 7.01; separation channel: 50×8 μm $\times$ 4.5 cm (effective length 2.8 cm); injection: 1 kV, 4 s; running: 2.5 kV; detection: excitation wavelength 510–560 nm, emission wavelength $>$ 590 nm.

The floating model for sample injection [10,11,15,17] was used in both separations of dyes and porphyrins. The sample was introduced into the channel by applying a potential of 1 kV for 4 s between reservoirs 1 and 2, while the separation channel was left floating. Then the dyes and porphyrins were separated by applying a potential difference between reservoirs 3 and 4 with reser-

voirs 1 and 2 floating. Compared with that for the dyes, the separation baseline of porphyrins is less stable. Frequently, shortly after the appearance of five peaks the baseline started to drift and remained at a high level. We attribute this phenomena to the adsorption of porphyrins and the leakage of sample from the injection channel to the separation channel. Harrison et al. reported that control of the potential at only the buffer and waste reservoirs during separation led to ≈3–4% leakage from the sample channel in the case of fluorescein dye [13]. To alleviate this problem, a potential should be maintained in reservoirs 1 and 2 during separation to drive the mobile phase back away from the injection cross. This is the so called pinched sample loading method [9,18,21], in which potentials are applied to reservoirs 1, 2 and 4 during injection and thereby plug shape and leakage are controlled. The adsorption problem was solved by washing the channel when required with a strong detergent (10 min), water (5 min), H_2SO_4–H_2O_2 (5 min), water (5 min), and nitrogen gas (1 min). Through the microscope, some colored tiny spots could be seen at the inner wall of the channel near the injection cross. They may correspond to aggregates of porphyrins or particles with porphyrins adsorbed onto them. They were washed away through the above procedure.

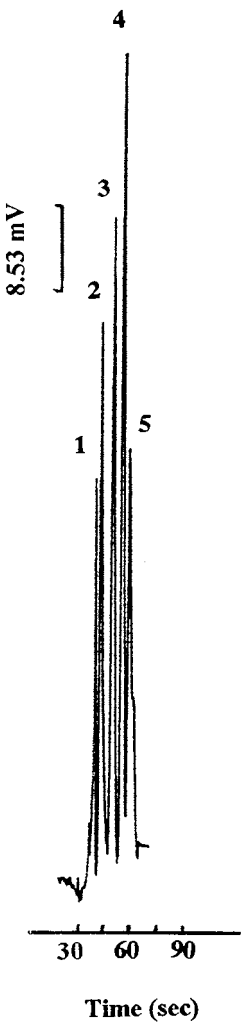

Fig. 4. The electropherogram obtained for a mixture of porphyrins using a glass chip. The concentration of each peak is around 0.15 mmol l^{-1}. Buffer composition and detection are the same as in Fig. 2; separation channel, peak identities, injection and running conditions are the same as in Fig. 3.

Compared with the separation obtained in the capillary, the sensitivity obtained in the chip under a lamp-base detector was lower. The detection limit for the porphyrin separation in the short capillary was 10^{-8} M, only 10^{-5} M could be reached in the case of the microchip (S/N of 3). These values were the direct consequence of the reduction in the light path. There were other important factors that contributed in increasing the background noise and decreased the sensitivity as a result. Scattered light and leakage of the sample at the T junction are among these factors. The background noise generated was measured experimentally. In the case of the capillary for an injected plug of 0.98 nl of 5 μM of rhodamine B solution, we obtained a S/N ratio of 166. In the case of the chip for a 0.56 nl plug the S/N ratio was 45. Proportionally the S/N ratio for the microchip was smaller, thus explaining in part the decrease in sensitivity.

4. Conclusion

In the present study we report the rapid separation of porphyrins in a short capillary and the first successful separation of porphyrins in a micromachined planar glass chip. The most important advantage of the chip-based method com-

pared with the CE separations using a capillary is the shorter separation times obtainable. The analysis time was decreased significantly due to the application of high electric fields across short separation lengths. The main disadvantage of the chip-based method is the lower sensitivity obtained. Nevertheless, it is expected that detection sensitivity could be enhanced by concentrating the sample through stacking [22], controlling the injection channel potentials during separation to eliminate leakage, or by using better optics, a brighter source and a more sensitive photon detector.

Acknowledgements

The authors would like to thank the National University of Singapore for financial assistance and Isabel Rodríguez for her help with the editing.

References

[1] J.W. Jorgenson, K.D. Lukacs, Anal. Chem. 53 (1981) 1298.
[2] J.W. Jorgenson, K.D. Lukacs, Anal. Chem. 218 (1981) 209.
[3] S.F.Y. Li, Capillary Electrophoresis-Principles, Practice and Applications, Elsevier, Amsterdam, 1991.
[4] C.S. Effenhauser, A. Manz, H.M. Widmer, Anal. Chem. 65 (1993) 2637.
[5] S.C. Jacobson, J.M. Ramsey, Electrophoresis 16 (1995) 481.
[6] D.J. Harrison, Z.H. Fan, K. Seiler, Anal. Chem. Acta 283 (1993) 361.
[7] K. Seiler, D. J Harrison, A. Manz, Anal. Chem. 65 (1993) 361.
[8] N. Burggraf, A. Manz, E. Verpoorte, C. Effenhauser, H.M. Widmer, Sens. Actuators B 20 (1994) 103.
[9] S.C. Jacobson, R. Hergenröder, L.B. Koutny, J.M. Ramsey, Anal. Chem. 66 (1994) 1114.
[10] S.C. Jacobson, A.W. Moore, J.M. Ramsey, Anal. Chem. 67 (1995) 2059.
[11] C.S. Effenhauser, A. Paulus, A. Manz, H.M. Widner, Anal. Chem. 66 (1994) 2949.
[12] C.S. Effenhauser, A. Manz, H.M. Widmer, Anal. Chem. 67 (1995) 2284.
[13] D.J. Harrison, K. Fluri, K. Seiler, Z.H. Fan, C.S. Effenhauser, A. Manz, Science 261 (1993) 895.
[14] Z.H. Fan, D.J. Harrison, Anal. Chem. 66 (1994) 177.
[15] A.T. Woolley, R.A. Mathies, Proc. Natl. Acad. Sci. USA 91 (1994) 11348.
[16] S.C. Jacobson, J.M. Ramsey, Anal. Chem. 68 (1996) 720.
[17] A.T. Woolley, R.A. Mathies, Anal. Chem. 67 (1995) 3676.
[18] L.B. Koutny, D. Schmalzing, T.A. Taylor, M. Fuchs, Anal. Chem. 68 (1996) 18.
[19] K.T. Chan, Y.J. Yao, C.L. Ng, S.F.Y. Li, J. Fresenius, Anal. Chem. 349 (1994) 487.
[20] D.J. Harrison, A. Manz, Z.H. Fan, H. Lüdi, H.M. Widmer, Anal. Chem. 64 (1992) 1926.
[21] S.C. Jacobson, R. Hergenröder, L.B. Koutny, R.J. Warmack, J.M. Ramsey, Anal. Chem. 66 (1994) 1107.
[22] S.C. Jacobson, J.M. Ramsey, Electrophoresis 16 (1995) 481.

.

ELSEVIER

Talanta 45 (1998) 619–629

Talanta

Analysis of leachable and total trace metals in air particulate matters by capillary electrophoresis

Ying-Sing Fung *, Kap-Man Lau, Ho-Shan Tung

Department of Chemistry, The University of Hong Kong, Pokfulam Road, Hong Kong, Hong Kong

Received 28 January 1997; received in revised form 9 July 1997; accepted 9 July 1997

Abstract

A new analytical procedure was developed for simultaneous determination of ammonium, leachable and total metals in fine and coarse air particulate matters using a new capillary electrophoresis (CE) procedure, with a new buffer system containing 10 mM histidine, 2 mM 18-crown-6 and 8 mM lactic acids with pH adjusted to 4.0. A two complexes system, 18-crown-6 ether and lactic acid, was developed to solve the co-migration problem of NH_4^+ and K^+ and to give satisfactory separation of transition metals. Satisfactory separation and quantitation of NH_4^+, K^+, Ca^{2+}, Na^+, Mg^{2+} and Zn^{2+} were obtained using the CE procedure developed for both leachable and total metals in coarse (10–3 μm) and fine (<3 μm) air particulate matters. Wide working ranges (ppb to ppm range) and sensitive detection limits (ppb) were obtained for the cations investigated. The reliability was established by parallel method comparison with the ICP-AES method. The analytical procedure developed is shown to provide a quick, sensitive, precise and economic method for simultaneous determination of ammonium, leachable and total metals in air particulate matters. © 1998 Elsevier Science B.V.

Keywords: Air particulate matters; Cation analysis; Capillary electrophoresis; Trace analysis

1. Introduction

Analysis of chemical composition of air particulate matters has recently become important for environmental monitoring, due to the health impact of respirable particulate matters in the range of 1–10 μm sizes and the need to apportion the major sources of air particulate matters at receptor sites with high population density [1–3]. For industries with emission of particulate matters with toxic metals or other harmful substances, it is mandatory to monitor the chemical content of the particulate matters for occupational health protection [4,5]. With regard to health considerations, the major pollutants of concern are trace metal contents in air particulate matters.

There are two major groups of air particulate matters, one from the weathering of soil and the other from anthropogenic sources. The former are normally large in size and the latter are very small and generally less than 3 μm in diameter. Those smaller than 10 μm will give the biggest health effect, as they cannot be removed from the body's own defense mechanism once respired into the

* Corresponding author. Fax: +852 25482132.

PII S0039-9140(97)00283-X

lung. Thus, using a high volume sampler equipped with a cascade input impactor with 10 μm cutoff and a series of impactors with suitable size fractionation, it is able to sample air particulate matters in different sizes and to provide information on the relative importance of man-made and natural sources of the air particles sampled.

The content of trace metals present in air particulate matters can be divided into two types, those leached out by deionised water and those containing both soluble and insoluble forms of the same metal—the total metal content. The leachable ones are mostly coming from sea aerosols, secondary pollutants or industrial discharge. The insoluble ones are mostly coming from crustal sources or combustion products. The ratio of leachable to total metal content provides information on the source of pollutants collected at a given sampling site. Combining the information about the particle size and the leachable/total form of chemicals in air particulate matters with chemical analysis, will assist the interpretation of the results obtained, with regard to the health effect and the apportionment of major air pollution sources at given receptor sites. Due to the need to analyze a lot of samples, with regard to their particle size, water solubility and total metal contents, a fast and economic analytical method, requiring simultaneous determination of as many metals as possible in a single run, is needed.

The most common methods for trace metal analysis in air particulate matters are Inductively Coupled Plasma-Atomic Emission Spectroscopy (ICP-AES) [6], Inductively Coupled Plasma-Mass Spectrometry (ICP-MS) [7], Direct Current (DC) arc emission spectroscopy [8–10], Particle Induced X-ray Emission (PIXE) [11–14], X-ray Fluorescence (XRF) [15,16], Instrumental Neutron Activation Analysis (INAA) [17] and Ion Chromatography (IC) [18,19]. Many of these methods require expensive equipment such as ICP-MS, PIXE, XRF and INAA. The ICP-AES method, though providing simultaneous determination of trace metals, is high in operational costs and cannot analyze NH_4^+, an important cation to assess the extent of secondary pollution. Different columns are needed in IC to analyze NH_4^+, alkali or transition metals and a long running time is required for the IC column. All these lead to a lot of labour and time to analyze a given set of air particulate samples.

The recent advance in capillary electrophoresis provides a promising technique for the above analyses. It features high separation efficiency, good reproducibility, fast analysis and low consumption of electrolytes and samples [20–24]. Moreover, the capital and operating costs are significantly lower, since neither bulky equipment nor costly columns are needed in addition to low consumption of chemical reagents during CE separation. Upon careful selection and optimization of the background electrolyte (BGE), it is possible to provide a method for simultaneous determination of both NH_4^+, alkali and transition metals in a single CE run. Moreover, both total and leachable forms of the metal can be analyzed using the BGE developed.

In the present work, a new CE procedure was developed to analyze the most common metal and ammonium cations present in air particulate matters in leachable and total form collected, using a high volume sampler equipped with a PM10 inlet. The selection of BGE, the optimization of the analytical parameters, the reliability and the applicability of the procedure developed will be given and discussed.

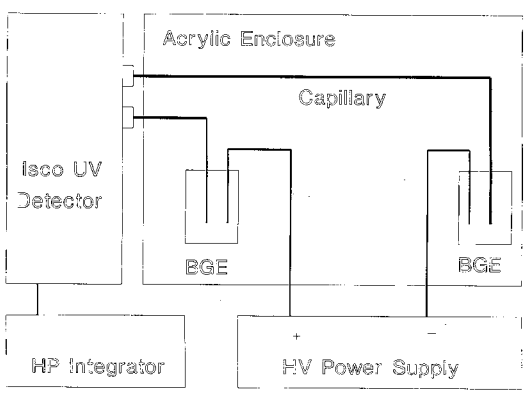

Fig. 1. Schematic diagram of the capillary electrophoresis system (HV power supply: Spellman 30 kV constant voltage supply; Detector: ISCO CE variable-wavelength detector; Recorder: HP3396A integrator; Capillary: 65 cm × 75 μm i.d. uncoated fused-silica capillary).

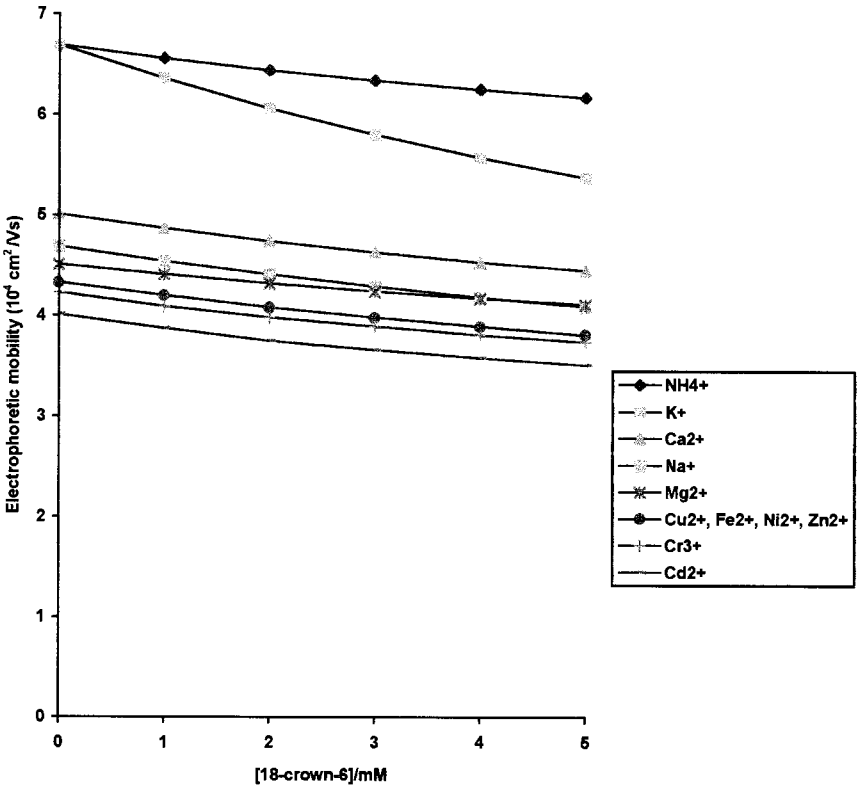

Fig. 2. The effect of using 18-crown-6 alone on the differential electrophoretic mobility of the cations present in air particulate matters. [M] = 2 ppm, [NH_4^+] = 2 ppm and BGE: 10 mM histidine (pH 4.65).

2. Experimental

2.1. Equipment and apparatus

The CZE system comprised of a Spellman (model CZE1000R) 30 kV constant voltage supply with reversible polarity, an uncoated fused-silica capillary (65 × 75 μm i.d.) with a capillary filling/washing apparatus, an ISCO CV4 variable-wavelength detector, and a HP3396A integrator. A schematic diagram of the setup is shown in Fig. 1.

The ICP-AES system consists of a Perkin-Elmer Optima 3000DV ICP-OES spectrophotometer equipped with a standard torch assembly, a conventional cross flow nebulizer and a Perkin Elmer AS-90 autosampler.

2.2. Reagents and samples

All solutions were prepared by weighing and dissolving given amounts of analytical or equivalent reagent grade chemicals in doubly quartz-distilled water, prior to making up to volume in 100 ml volumetric flasks. Nitrate salts of the metals were used as the standards. The ammonium standard was made up of ammonium nitrate. All the background electrolytes (BGEs) and standards were prepared daily by dilution from stock solutions, filtering through a 0.45 μm cellulose membrane filter and degassing under vacuum prior to use.

The air particulate matters were collected at a sampling site situated at the roof-top of a building inside the University, at a height of ~40 m above the nearest busy road, so as to sample particulate

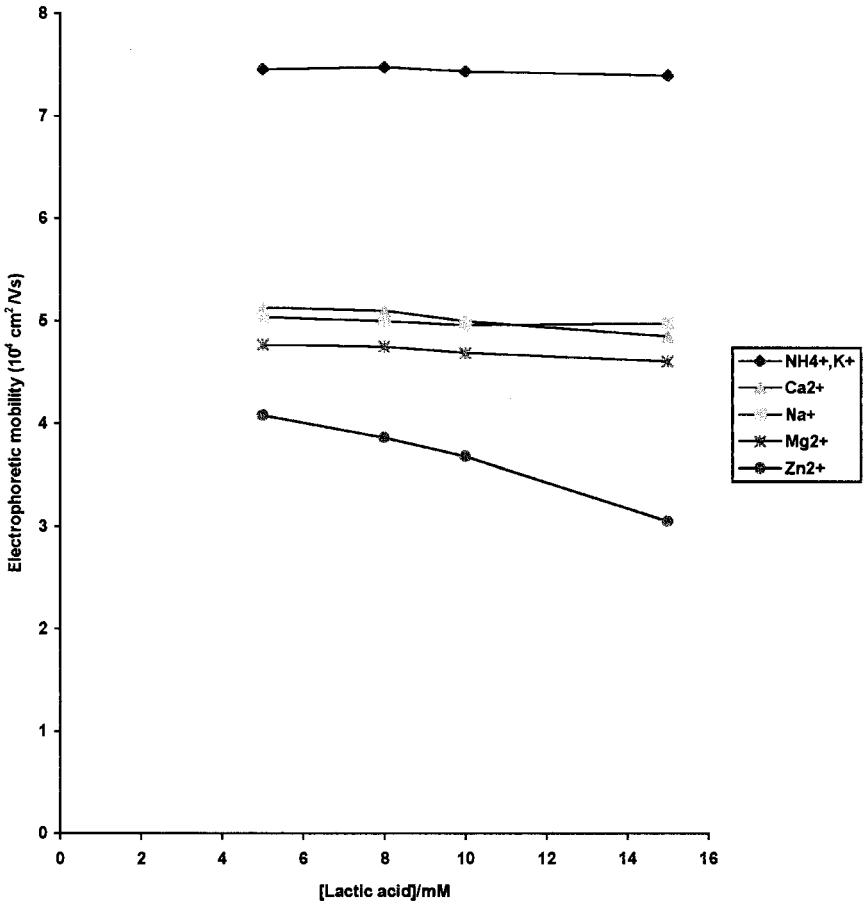

Fig. 3. The effect of using lactic acid alone on the differential electrophoretic mobility of the cations present in air particulate matters. [M] = 2 ppm, [NH_4^+] = 2 ppm and BGE: 10 mM histidine (pH 4.65).

matters coming through a longer distance. The Andersen high volume sampler with a 10 μm inlet (Model 1200 PM-10 Sampling Inlet, Anderson) was used to collect the samples over a 24 h period with a flowrate of 40 ft^3 per min. Typically, 55 mg of air particulate matters were collected during each sampling period. The filters (Whatman 41) were conditioned in a humidity controlled chamber (Relative humidity kept at $40 \pm 0.5\%$) for 24 h prior to weighing and they were stored in a refrigerator at $-18°C$ prior to analysis.

2.3. Procedures

All samples and standard solutions were filtered through a 0.45 μm filter prior to analysis. The capillary column obtained from Yongnian Fibre Optic Factory was used directly without coating. Hydrodynamic sampling was performed by gravity created by the height difference between the two ends of the capillary inserted into the two BGE vials. The high voltage used for the CE run was controlled by the Spellman high voltage power supply.

Prior to use, new capillaries were treated with the following wash cycles in sequence, each for 10 min duration: (1) 1 M NaOH, (2) 0.1 M NaOH, (3) deionised water, (4) electrophoretic buffer. For daily conditioning of cleaned capillaries, the first cycle was omitted. Between two consecutive

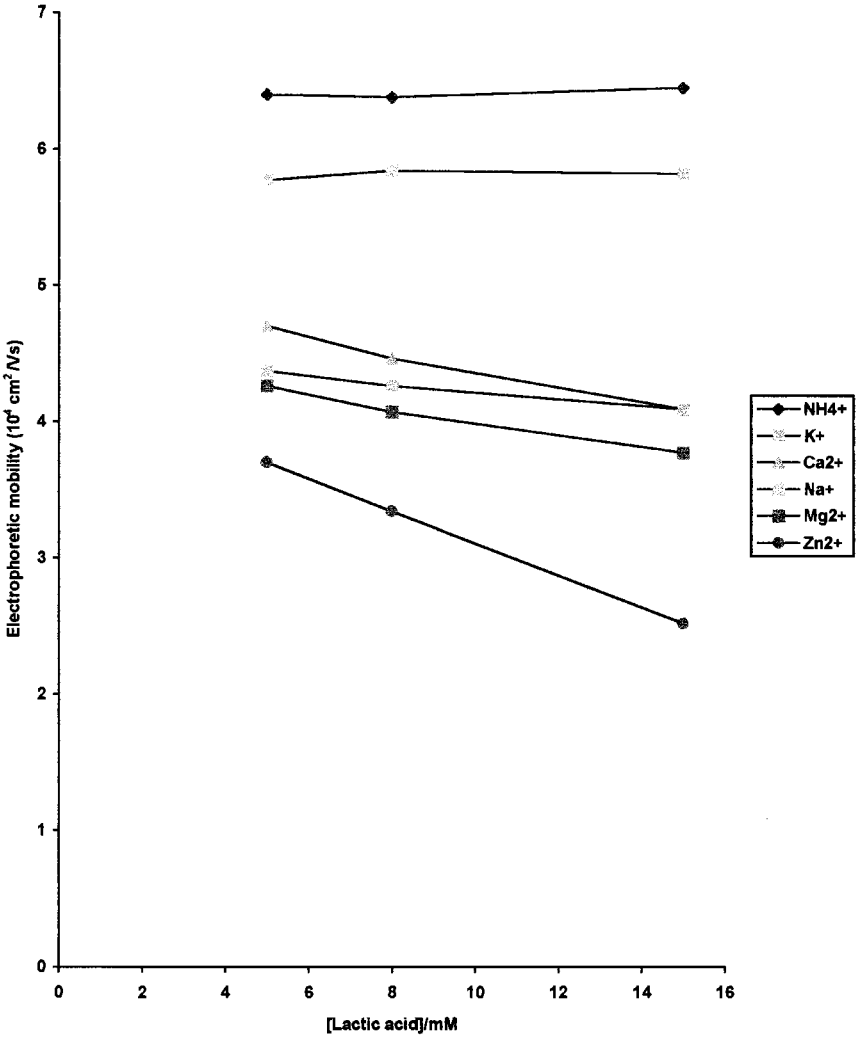

Fig. 4. The effect of combined use of lactic acid and 18-crown-6 ether on the differential electrophoretic mobility of the cations present in air particulate matters. [M] = 2 ppm, [NH_4^+] = 2 ppm and BGE: 10 mM histidine and 2 mM 18-crown-6 (pH 4.65).

analyses, the capillary was rinsed with deionised water (2 min) and then with the electrophoretic buffer (3 min) to improve the reproducibility of the electroosmotic flow and migration time.

For ICP-AES analysis, the RF power was set at 1300 W and the argon gas flowrates for the nebulizer, auxiliary and plasma flow were controlled at 0.8, 1.0 and 15 l min^{-1}. respectively, whereas the sample flow was kept constant at 1.3 ml min^{-1}. Peak area was used for quantitation. Auto Integration (2–20 s) was used, with both read and rinse delay set at 45 s.

For the measurement of molar absorptivity, 0.1 mM UV-absorbing cations (except gramine with a concentration of 0.05 mM) were used. The absorption spectra were recorded by a Shimadzu model UV-240 UV-Visible Spectrophotometer and the molar absorptivities were calculated based on single point calibration and Lambert-Beer's law.

The electrophoretic mobility (μ_{ep}) of the cations were determined under the same run with correction for electroosmotic flow (μ_{eo}) using the following formula [25]:

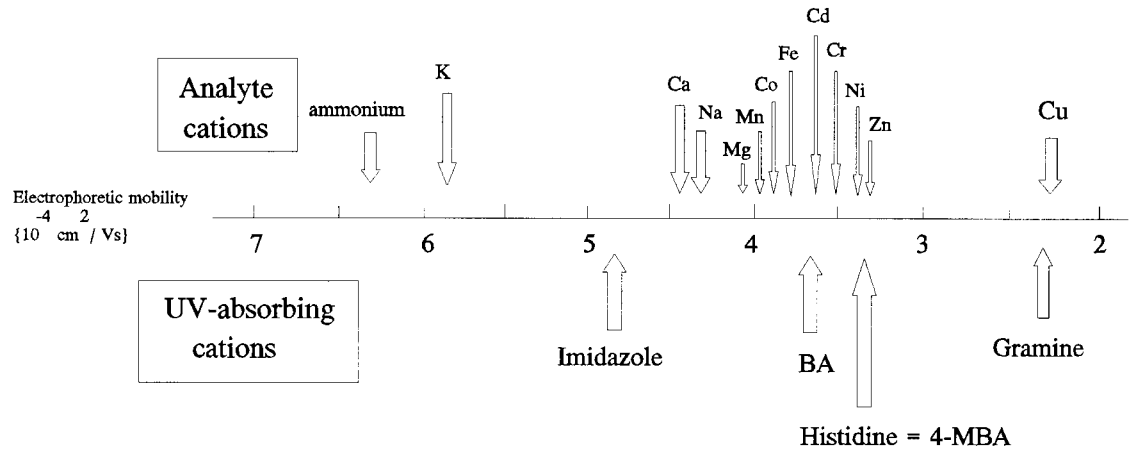

Fig. 5. The electrophoretic mobilities of common UV-absorbing cations and analyte cations.

$$\mu_{ep} = \frac{L_d L_t}{V}\left(\frac{1}{t_m} - \frac{1}{t_o}\right)$$

where L_d is the length of the capillary from the inlet to the detector, L_t is the total length of the capillary, V the applied voltage, t_m the migration time of the cation and t_o the migration time of a neutral marker (water).

3. Results and discussion

3.1. Composition of background electrolyte

The cations present in air particulate matters can be divided into two groups [1–3,26,27]. The first group consists of the ammonium ions, the alkali and the alkali-earth metal cations. They are normally present in higher concentration in the range of parts-per-thousand to percentage levels. The second groups are transition metal ions. They are normally present in ppm levels in air particulate matters. The major problem facing the separation of the first group of metal ions is the co-migration problem between NH_4^+ and K^+ and the problems for the second group of metal ions are the separation of a large group of metal ions and the high sensitivity required for detecting low level metal concentrations.

Weston et al. [28] had increased the pH of the BGE to 7, to solve the co-migration problem of NH_4^+ and K^+. Unfortunately, many transition metal cations form insoluble metal hydroxides at high pH and thus, this method cannot be used for the present work.

Another method to solve the co-migration problem is the addition of complexing agents to the BGE. These complexing agents can selectively modify the mobility of the metal cations due to the formation of metal complexes of different stability inside the capillary. This CE separation mode was first proposed by Foret et al. [29] for the separation of 14 lanthanide cations with the aid of hydroxyisobutyric acid (HIBA) as a complexing agent. Suitable complexing agents including acetic, glycolic, lactic, phthalic, oxalic, malonic, succinic, malic, tartaric and citric acids had been studied for their effect on the selectivity of metal ions, especially for the transition metals[30,31]. However, none of these complexing agents mentioned above can solve the co-migration problem of NH_4^+ and K^+ at the working pH.

Bachmann et al. [32] had successfully utilized a 18-crown-6 ether to separate NH_4^+ and K^+. However, the ether added cannot separate some of transition metals (Cu^{2+}, Mn^{2+}, Fe^{2+}, Ni^{2+}, Co^{2+}, Zn^{2+}) commonly found in the air particulate matters. Shi and Fritz [33] had used a lactic acid/crown ether system to separate NH_4^+ from K^+. Methanol was added to solve the problem of

interference of a large Na^+ concentration on trace analysis of metals like Ca^{2+}, Mg^{2+}, Sr^{2+} and Ba^{2+}. As the two buffer systems gave a promising BGE to separate cations present in air particulate matters, a combination of lactic acid and 18-crown-6 ether buffer systems was investigated in the present work with an aim to obtain a buffer system capable of simultaneous separation of ammonium, alkali, alkaline earth and transition metals present in air particulate matters.

The effect of using 18-crown-6 ether alone to separate ammonium, alkaline metals and transition metals are shown in Fig. 2. Although the separation between NH_4^+ and K^+ can be improved by increasing the concentration of 18-crown-6 ether, the transitional metals such as Cu, Fe, Ni and Zn give the same mobility from 0 to 5 mM 18-crown-6 ether. The use of lactic acid alone led to the co-migration problem of NH_4^+ and K^+ (Fig. 3). However, the combined use of lactic acid and 18-crown-6 ether gave a satisfactory differentiation in mobility between ammonium, alkali, alkali earth and transition metals commonly found in air particulate matters (Fig. 4).

Table 1
The molar absorbtivities of common UV-absorbing cations

Carrier electrolyte	Molar absorptivity at 214 nm (cm^{-1} mol^{-1} l)
Imidazole	5000
Benzylamine (BA)	4300
Histidine	6400
4-Methylbenzylamine (4-MBA)	6000
Gramine	25 000

Table 2
The effect of pH on electrophoretic mobility of the cations present in air particulate matters

Analyte cations	Electrophoretic mobilities (10^{-4} cm^2/Vs)	
	pH 4.0	pH 4.7
NH_4^+	6.4	6.4
K^+	5.7	5.8
Ca^{2+}	4.6	4.4
Na^+	4.4	4.3
Mg^{2+}	4.2	4.1
Zn^{2+}	3.7	3.4
Mn^{2+}	4.1	4.0
Co^{2+}	4.0	3.8
Fe^{2+}	3.9	3.7
Cd^{2+}	3.8	3.6
Cr^{3+}	3.8	3.5
Ni^{2+}	3.8	3.4
Cu^{2+}	2.9	2.2

BGE: 10 mM histidine, 8 mM lactic acid and 2 mM 18-crown-6.

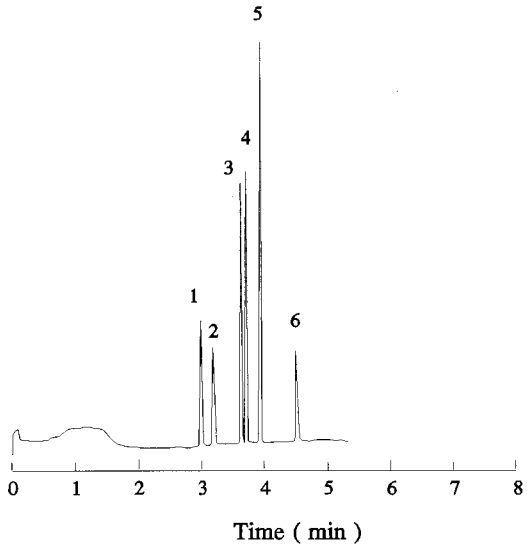

Fig. 6. The separation of a standard cation mixture. Conditions: BGE: 10 mM histidine, 2 mM 18-crown-6 and 8 mM lactic acid at pH 4.0; capillary: 65 cm × 0.05 mm i.d. fused silica; run: +20 kV; current: 9 uA; injection: 8 cm for 20 s; detection: 214 nm. Cation standards: 10 ppm each. 1, ammonium; 2, potassium; 3, calcium; 4, sodium; 5, magnesium; 6, zinc.

3.2. Optimization of operational parameters

To provide a good separation and a sensitive detection for cations using indirect photometric detection, UV-absorbing cations have to be added to the BGE with suitable mobility, preferably in the middle of the analyte cations to reduce fronting and tailing, and with high molar absorptivity so as to enhance the sensitivity of the method. Foret et al. [29] utilized indirect UV detection to separate 14 lanthanide cations by CE,

Table 3
The analytical parameters of the cations determined

Cations	RSD in:		Limit of detection (ppb)[a]	Correlation coefficient in linearity test[b]	Separation efficiency N[c]
	Migration time/% (10 ppm, $n=3$)	Peak area/% (10 ppm, $n=3$)			
NH_4^+	0.42	3.2	140	0.999	62 500
K^+	0.39	7.6	210	0.997	66 700
Na^+	0.35	4.1	125	0.982	45 700
Mg^{2+}	0.33	4.7	80	0.998	99 600
Ca^{2+}	0.31	3.3	80	0.999	129 600
Zn^{2+}	0.34	6.2	250	0.999	230 000

[a] S/N = 2 for LOD; injection 8 cm for 20 s.
[b] 2 ppm–30 ppm, $n=3$.
[c] $N = 5.54\ (t_m/W_{0.5})^2$, where t_m is the migration time for the cation and $W_{0.5}$ is the half height peak width.

with the aid of creatinine as a UV-absorbing cation. Beck and Engelhardt [34] investigated the use of several BGEs for indirect UV-detection and found that imidazole was suitable for the separation of metal ions, amines and amino alcohols. Suitable UV-absorbing cations include *N*,*N*-dimethylbenzylamine, *p*-toluidine and 4-methylbenzylamine had been reported in the literature [35].

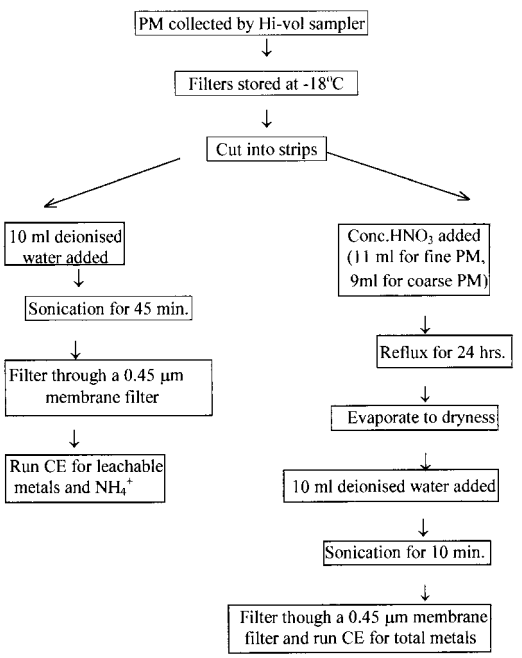

Fig. 7. Flowchart for sample preparation of air particulate matters (PM).

The electrophoretic mobilities of the analyte cations and the common UV-absorbing cations (determined in 10 mM acetate buffer at pH 4.65) are given in Fig. 5. The molar absorptivities for UV-absorbing cations are listed in Table 1. The results suggest that histidine is a suitable UV-absorbing cation, as it gives a high molar absorptivity at 214 nm and its electrophoretic mobility is in the middle of the set of analyte cations of interest.

The effect of pH on the electrophoretic mobility of cations present in air particulate matters is shown in Table 2. The best separation was obtained at pH 4.65, which gave a better separation of ammonium, alkali, alkali earth and transition metals commonly found in air particulate matters. However, better separation of Ca^{2+} and Na^+ were obtained at pH 4.0. Thus, the BGE was buffered at pH 4.0.

The electropherogram for the separation of a standard cation mixture is given in Fig. 6, indicating well resolved peaks for the cations investigated and with no system or other peaks in the electropherogram. The analytical parameters of the cations determined by the optimized CE procedure is shown in Table 3, which shows that the limits of detection for all cations are in the ppb range, wide working ranges from ppb to ppm and good separation efficiency.

Table 4
The working ranges and detection limits for the CE procedure developed for ammonium and metal cation analysis in air particulate matters

Cations	Detection limit (ppm)				Working range (ppt)[a]			
	Leachable		Total		Leachable		Total	
	Coarse	Fine	Coarse	Fine	Coarse	Fine	Coarse	Fine
NH_4^+	535	428	535	856	1.07–115	0.86–91.7	1.07–115	1.72–183
K^+	802	642	802	1280	1.94–115	1.28–91.7	1.94–115	2.56–183
Ca^{2+}	369	296	369	591	0.61–115	0.48–91.7	0.61–115	0.96–183
Na^+	577	462	577	923	0.95–115	0.76–91.7	0.95–115	1.52–183
Mg^{2+}	369	296	369	591	0.61–115	0.48–91.7	0.61–115	0.96–183
Zn^{2+}	955	765	955	1530	1.91–115	1.53–91.7	1.91–115	3.06–183

[a] ppt, Parts-per-thousand.

3.3. Reliability and applicability study

The flowchart for the application of the CE procedure developed for the analysis of leachable and total metals in air particulate matters is given in Fig. 7, which is applicable for analyzing both fine (< 3 μm) and coarse (> 3 μm) air particulate matters. The detection limits and working ranges for analyzing air particulate matters are given in Table 4, which indicate satisfactory working ranges and sensitive detection limits for the cations studied.

The electropherograms for the field samples are shown in Figs. 8 and 9 for the leachable and total metals ions present in the air particulate matters. For leachable cations, a well resolved electropherogram was obtained (Fig. 8) with stable baseline. All the peaks are within the quantitation range for a single CE run, including NH_4^+, K^+, Ca^{2+}, Na^+ and Mg^{2+}. The zinc peak (peak 6) is relatively small and tends to be variable amongst samples collected in different dates. For total metal analysis, the electropherogram shows a more noisy baseline and the appearance of a system peak (peak S, Fig. 9). This is related to the residual nitric acid left behind after evaporation or some oxidation products coming from the air particulate matters upon oxidation by nitric acid. However, all the peaks are resolved and the total metal content can be determined from the electropherogram.

To test the reliability of the procedure developed, parallel method determination of total metals in air particulate matters was performed using ICP-AES as the alternative method. The

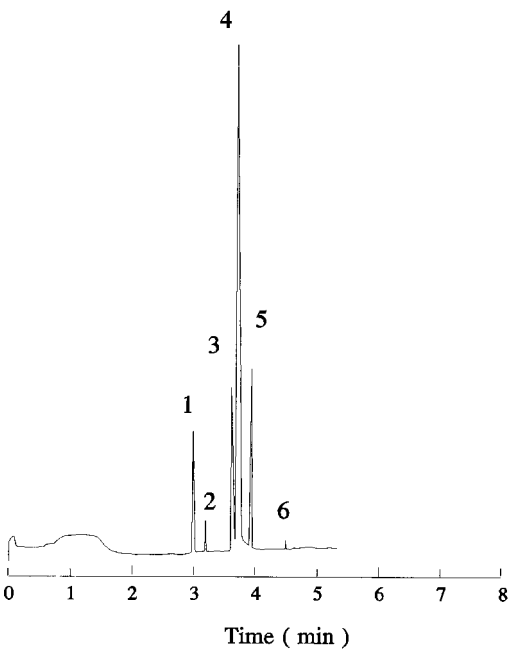

Fig. 8. A typical electropherogram showing the separation of leachable cations in a field sample of air particulate matters. Conditions: BGE: 10 mM histidine, 2 mM 18-crown-6 and 8 mM lactic acid at pH 4.0; capillary: 65 cm × 0.05 mm i.d. fused silica; run: + 20 kV; current: 9 uA; injection: 8 cm for 20 s; detection: 214 nm. Migration order: 1, ammonium; 2, potassium; 3, calcium; 4, sodium; 5, magnesium; and 6, zinc.

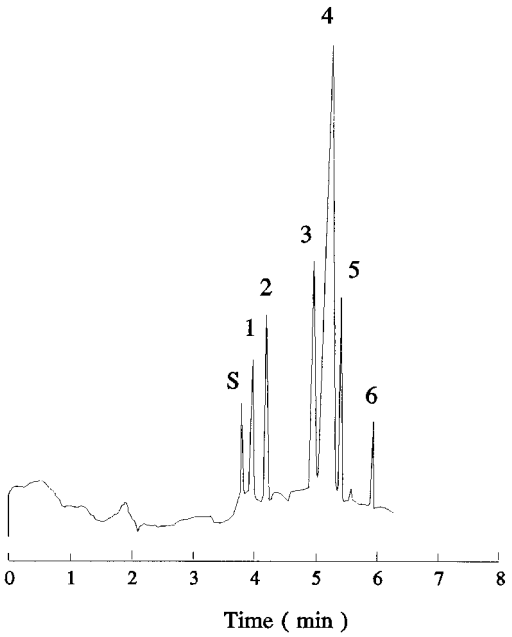

Fig. 9. A typical electropherogram showing the separation of cations in a field sample of air particulate matters after acid digestion. Conditions: BGE: 10 mM histidine, 2 mM 18-crown-6 and 8 mM lactic acid at pH 4.0; capillary: 65 cm × 0.075 mm i.d. fused silica; run: +15 kV; current: 8 uA; injection: 8 cm for 20 s; detection: 214 nm. Migration order: S, system peak; 1, ammonium; 2, potassium; 3, calcium; 4, sodium; 5, magnesium; and 6, zinc.

results obtained are shown in Table 5, which indicate a better precision of the CE procedure as compared to the ICP-AES method. Using the *t*-test, the computed *t* value (0.197) is within the statistical *t* value (2.78) for 4 DF. Thus, no statistical significant difference was obtained using the two methods for the determination of cations in air particulate matters at 95% CI.

4. Conclusion

A new analytical procedure was developed for simultaneous determination of ammonium, leachable and total metal content of fine and coarse air particulate matters, using a CE method developed for such analysis. A two complexes system using 18-crown-6 ether and lactic acid were developed to solve the co-migration problem of NH_4^+ and K^+ and provide the capability of separating transition metals. Satisfactory separation and quantitation of NH_4^+, K^+, Ca^{2+}, Na^+, Mg^{2+} and Zn^{2+} were obtained using the CE procedure developed for both leachable and total metals in air particulate matters. Satisfactory working ranges (ppb to ppm) and sensitive detection limits (ppb) were obtained for the cations investigated. The reliability was established by parallel method comparison with the ICP-AES method. The analytical procedure developed is shown to provide a quick, sensitive, precise and economic method for simultaneous determination of ammonium, leachable and total metals in air particulate matters.

Table 5
Parallel method determination of total metals in air particulate samples using CE/ICP-AES

Metal cations	Found by CE[a] (mg/l)	Found by ICP-AES[a] (mg/l)
K^+	12.43 ± 1.39	14.13 ± 5.72
Ca^{2+}	18.30 ± 2.59	19.73 ± 2.66
Na^+	35.82 ± 3.10	37.43 ± 5.50
Mg^{2+}	3.69 ± 0.37	4.08 ± 0.93
Zn^{2+}	3.27 ± 1.03	3.51 ± 1.02

[a] Data are given as mean ± 2 SD, $n = 3$.

Acknowledgements

We would like to acknowledge the financial support of the Hong Kong Research Grants Council and the Hong Kong University Research Grants Committee for the above work.

References

[1] R.F. Pueschel, Atmospheric aerosols, in: H.B. Singh (Ed.), Composition, Chemistry and Climate of the Atmosphere, Van Nostrand Reinhold, New York, 1995, pp. 120–175.
[2] Y.S. Fung, L.W.Y. Wong, Atmos. Environ. 29 (1995) 2041.
[3] G.M. Hidy, Aerosols—An Industrial and Environmental Science, Academic Press, Orlando, FL, 1984, pp. 580–645.

[4] I. Barker, J. Barker (Eds.), Clean Air Around the World— The Law and Practice of Air Pollution Control in 14 Countries and in 5 Continents, IUAPPA, Brighton, UK, 1988.
[5] A. Parker (Ed.), Industrial Air Pollution Handbook, McGraw-Hill, London, 1977, pp. 67–99.
[6] J.P. Lodge, Jr (Ed.), Methods of Air Sampling and Analysis, 3rd edn., Lewis, Chelsea, Michigan, 1989, pp. 89–92.
[7] C.F. Wang, J.Y. Yang, C.H. Ke, Anal. Chim. Acta 320 (1996) 207.
[8] J. Reednick, Am. Lab. 11 (1979) 127.
[9] C.D. Keirs, T.J. Vickers, Appl. Spectrosc. 31 (1977) 273.
[10] J.A.C. Broekaert, Anal. Chim. Acta 196 (1987) 1.
[11] T.A. Cahill, P.J. Feeney, R.A. Eldred, Nucl. Instrum. Methods B22 (1987) 344.
[12] E. Bombelka, F.W. Richter, H. Ries, U. Watjen, Nucl. Instrum. Methods B3 (1984) 296.
[13] R.A. Eldred, T.A. Cahill, P.J. Feeney, Nucl. Instrum. Methods B22 (1987) 289.
[14] H.O. Lannefors, H.C. Hansson, L. Granat, Atmos. Environ. 17 (1983) 87.
[15] E. Merian (Ed.), Metals and Their Compounds in the Environment: Occurrence, Analysis and Biological Relevance, VCH, Weinheim, 1991.
[16] T.A. Cahill, P.J. Freeney, M.L. Pitchford, R.A. Eldred, P.J. Feeney, L.L. Ashbaugh, Atmos. Environ. 15 (1981) 2017.
[17] R. Dams, J.A. Robbins, K.A. Rahn, J.W. Winchester, Anal. Chem. 42 (1970) 861.
[18] D.T. Gjerde, J.S. Fritz, G. Schmuckler, J. Chromatogr. 187 (1980) 35.
[19] Y.S. Fung, W.M. Tam, J. Environ. Sci. 3 (1991) 29.
[20] P.E. Jackson, P.R. Haddad, Trends Anal. Chem. 12 (1993) 231.
[21] J. Romano, W.R. Jones, R.J. Jandik, P. Jackson, J. Chromatogr. 546 (1991) 411.
[22] P. Jandik, W.R. Jones, R. Pfeifer, Am. Lab. 23 (1991) 40.
[23] G. Bondonx, W.R. Jones, R.J. Jandik, J. Chromatogr. 602 (1992) 79.
[24] P.K. Dasgupta, L. Bao, Anal. Chem. 65 (1993) 1003.
[25] S.C. Smith, J.K. Strasters, M.G. Khaledi, J. Chromatogr. 539 (1991) 57.
[26] Y.S. Fung, L.W.Y. Wong, Proceedings of the International Conference on Sustainable Development Strategies and Global/Regional/Local Impacts on Atm. Composition and Climate, Delhi, India, Jan. 1993, vol. XV, pp. 213–216.
[27] Y. S. Fung, L.W.Y. Wong, C.J. Muskett, Proceedings of the POLMET 88 International Conference on Pollution in the Urban and Metropolitan Environment, Hong Kong, Nov. 1988, vol. I, pp. 321–326.
[28] A. Weston, P.R. Brown, W.R. Jandik, W.R. Jones, A.L. Heckenberg, J.Chromatogr. 593 (1992) 289.
[29] F. Foret, S. Fanali, A. Nardi, P. Bocek, Electrophoresis 11 (1990) 780.
[30] Y. Shi, J.S. Fritz, J. Chromatogr. 640 (1993) 473.
[31] T.I. Lin, Y.H. Lee, Y.C. Chen, J. Chromatogr. 654 (1993) 167.
[32] K. Bachmann, J. Boden, I. Haumann, J. Chromatogr. 626 (1992) 259.
[33] Y. Shi, J.S. Fritz, J. Chromatogr. A 671 (1994) 429.
[34] W. Beck, H. Engelhardt, Chromatographia 33 (1992) 313.
[35] M. Chen, R.M. Cassidy, J. Chromatogr. 640 (1993) 425.

.

ELSEVIER

Talanta 45 (1998) 631–639

Talanta

Quantitative analysis of pesticides by capillary column high performance liquid chromatography combined with solid-phase extraction

Wuping Liu, Hian Kee Lee *

Department of Chemistry, National University of Singapore, Kent Ridge, Singapore 119260, Singapore

Received 5 February 1997; received in revised form 13 May 1997; accepted 14 May 1997

Abstract

High performance liquid chromatography (HPLC) combined with solid-phase extraction was reported on, for simultaneous analysis of pesticides in this work. The separation of 12 pesticides was achieved on a C_{18} capillary column with gradient elution. Sub-microlitre injection volume of the samples and a U-shaped 35 nl flow cell were used to improve the separation and detection. In addition, the method used C_{18} solid-phase extraction disks to allow a 250-fold enrichment of the pesticides from fortified water and apple samples. The calculated detection limits range was 0.15–0.8 μg/l. Under the optimal extraction conditions, recoveries of 85–107% for most of the pesticides at 1.0–10.0 μg/l level, were obtained. © 1998 Elsevier Science B.V.

Keywords: Capillary column; HPLC; Solid-phase extraction; Pesticides

1. Introduction

Gas chromatography (GC) and high performance liquid chromatography (HPLC) are the two most commonly used approaches for the analysis of pesticides [1,2]. HPLC has found its application for pesticides with ultraviolet (UV) or fluorescent properties [3,4], especially for those that can't be directly analysed by GC [5]. At present, many of the HPLC systems use conventional columns (with an inner diameter (i.d.) of 4.6 mm). Because of this, when compared with capillary GC, HPLC exhibits lower separation efficiency; besides, the extracolumn peak broadening from the μl-scale detection cells and dead volume after the column compromises the chromatography. Efforts to overcome these drawbacks have been made by developing columns with smaller i.d. and packing materials size. It has been reported that the miniaturised columns possess many advantages [6], including higher column efficiencies, improved detection performance, various benefits of drastically reduced flow rates and the ability to work with smaller samples and solvents. In recent years, following the use of narrow-bore (2.0 < i.d. < 4.6 mm) and micro-bore columns (0.5–2.0 mm i.d.) [7,8], capillary (180 or

* Corresponding author. Tel.: +65 7756666; fax: +65 7791691; e-mail: chmleehk@leonis.nus.sg

PII S0039-9140(97)00298-1

300 μm i.d.) and nano-bore columns (50, 75 or 100 μm i.d.) packed with 3 μm packing materials have become commercially available. Another improvement for detection limits was achieved through changing the flow cell shape and decreasing its inner volume [9,10]. The combination of capillary columns and nano-volume flow cells has lead to the appearance of micro-HPLC systems of high separation efficiency and detection sensitivity. However, very few applications have been found referring to capillary or nano-column HPLC [11].

Owing to their very low residual amount in environmental matrices, in most cases, and the interferences from the samples, direct analysis of pesticides is usually difficult, whether by GC or HPLC. As a result, extraction and preconcentration procedures are necessary before chromatographic analysis. Many approaches have been developed in this area [12,13]. A substantially new approach is solid-phase extraction (SPE) [14]. It offers many advantages, and has been successfully adapted to environmental water analysis, although its advantages have not yet been fully realised in the isolation of pesticide residues from all matrices [15]. To date, both techniques—cartridges and disks, are used in SPE, while the latter is relatively new. With the advantages of permitting higher flow-rate, shorter extraction time, not getting plugged and occurrence of channeling [14,16], extraction disks have been used as an alternative to the former and have been described in some studies [17,18]. Very recently, SPE microextraction (SPME), a preconcentration approach usually limited to GC, has been used by Jinno et al. [8] and combined with micro-column HPLC for the preconcentration and analysis of pesticides in environmental water samples.

Our purpose in the present study was to explore the potential of analysing pesticides by a capillary-HPLC system combined with SPE. The separation of multi-pesticides including insecticides, herbicides and fungicides was achieved on a capillary C_{18} column with gradient elution. High sensitivity and low detection limits were obtained by a uniquely designed capillary flow cell and a submicrolitre injection volume. Combined with SPE for preconcentration, the performance of this method in real sample analysis was evaluated using fortified water and apple samples.

2. Experimental

2.1. Reagents and standards

The mobile phase was composed of acetonitrile (MeCN) and water; HPLC-grade MeCN and methanol, analytical-grade acetone, tetrahydrofuran and ethyl acetate were purchased from J.T. Baker Chemicals (Phillipburg, NJ). Naphthalene, biphenyl, anthrancene and fluoranthene were also of analytical-grade and supplied by Aldrich Chemical (Milwaukee, WI).

All pesticides were supplied by Supelco (Bellefonte, PA). They were dissolved in methanol at 1 mg ml^{-1} concentrations as stock solutions. A mixture containing 1–5 μg ml^{-1} of each pesticide in methanol was prepared from the stock solutions and used as the working solution. In order to avoid the influence on the results from the possible degradation of pesticides, the working solution was freshly prepared everyday. Deionised water, with typical resistivity higher than 18 mΩ cm^{-1} was produced on a Milli-Q system (Bedford, MA).

2.2. Instrumentation

Chromatography was carried out with two JASCO PU-980 (Tokyo, Japan) pumps, a 5 μl loop Rheodyne (Cotati, CA) 3493 injector valve, a Waters 746 (Milford, MA) integrator and an Applied Biosystems 785A (Foster City, CA) variable wavelength UV-vis programmable absorbance detector (operated at 220 nm) equipped with a LC Packings (San Francisco, CA) capillary flow cell (75 μm i.d./280 μm o.d. × 8mm). An Upchurch (Oak Harbor, WA) T-shape solvent mixer with a 2 μl dwell volume was used as part of the gradient elution system. An LC Packings ACURATE flow rate processor (with a split ratio 1:70) was connected to the solvent mixer to generate an eluent of 3–4 μl min^{-1} flow rate. The column was an LC Packings capillary C_{18} column (3 μm particle size, 150 × 0.18 mm i.d.). The

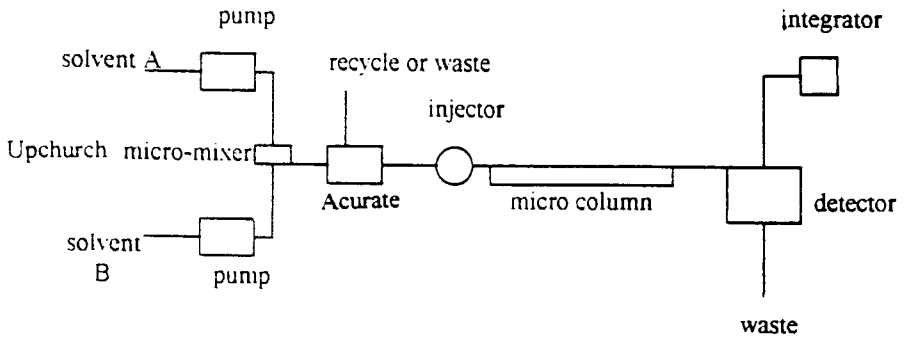

Fig. 1. Schematic of the capillary column HPLC system.

analyses were performed with a 0.25 μl injection volume at room temperature. Gradient elution, combining both the solvent and flow rate programmes as shown in Figs. 2–4, was used for the separation of all components.

A Millipore (Bedford, MA) 25 mm filtration apparatus equipped with J.T. Baker (Phillipsburg, NJ) 25 mm disks of octyl-bonded silica was used for the extraction of samples.

2.3. Extraction procedures

SPE disks were preconditioned by washing with successive volumes of 10 ml of elution solvent, methanol and water. A thin layer of water was allowed to remain above the disk after preconditioning to prevent it from drying out. Sample solutions (250 ml) were then loaded by pouring gradually and extraction was carried out at a rate of 10–20 ml min^{-1}. Although its influence on the recoveries of pesticides was negligible when the preconcentration speed as above was used, it should be noted that much higher or lower speeds were not appropriate for preconcentration because (a) the recoveries of the early eluting compounds, i.e. simazine, fensulfothion and isoprocarb, have been found to deteriorate at much higher preconcentation speeds, or (b) the preconcentration procedure would be very long at much lower speeds, e.g. >50 min at 5.0 ml min^{-1}. Sample volumes of 500 ml, or larger, were also tried to obtain higher enrichment fold. In order to avoid the loss of recovery for simazine when larger sample volumes were used, 250 ml volumes were finally chosen as the maximum sample volume in the present study. After preconcentration, the retained solutes in the disk were eluted, at ≈ 0.5 ml min^{-1}, with successive aliquots of 1.0 ml methanol, 2×1.0 ml acetone and 1.0 ml methanol. The effluent was collected into a graduated conical tube and concentrated, under a stream of nitrogen, to near dryness. The sample was then re-dissolved into 1.0 ml methanol, and a 0.25 μl aliquot was injected into the HPLC for analysis.

2.4. Sample preparation

2.4.1. Spiked water samples

Spiked water samples were prepared by dissolving 10–40 μl standard solutions in deionised or tap water to give a 250 ml volume. Methanol (1–2 ml) was also added to the sample solution as a solid-phase wetting agent [15].

2.4.2. Fortification of apple samples

Finely chopped apples (10 g) were homogenised with 30 ml of a mixture of acetone/ethyl acetate/methanol (21/7.5/1.5). At the same time, 1.00–10.0 μg l^{-1} of each pesticide were added and the sample was allowed to stand at room temperature for 12 h. The sample mixture was first filtered through a 6 cm Buchner filter. After washing the residual jar with 10 ml methanol, the collected solution underwent further pretreatment with a #4 sinter funnel. Then, the bulk of the filtrate was removed under a gentle stream of nitrogen gas, and diluted to 250 ml with deionised water.

Further extraction, enrichment and analysis were conducted according to the procedures listed in Section 2.3.

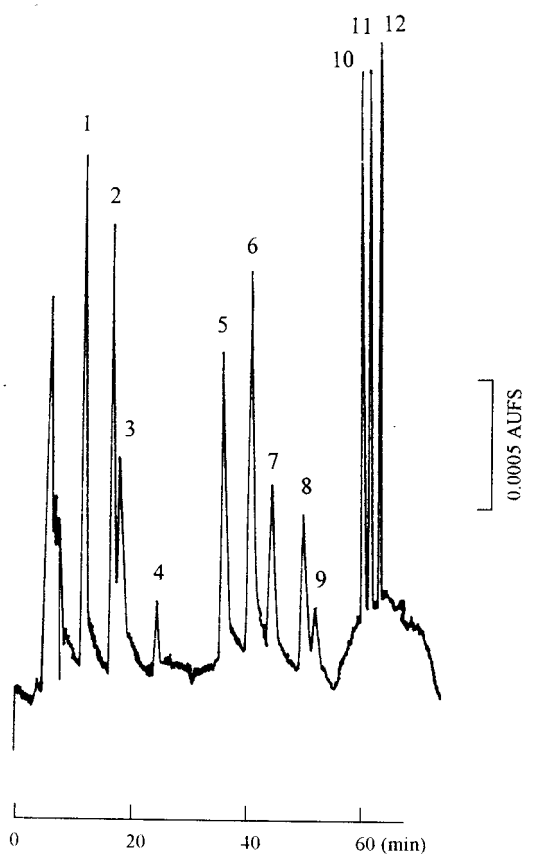

Fig. 2. Chromatogram of 12 pesticides in simulated sample. Column: LC Packings C_{18} (3 μm, 0.18 × 150 mm); detection, 220 nm, U shape flow cell; injection, 0.5 μl; temperature, ambient. Gradient of flow rate: 3 μl min^{-1}, 0.1–42 min; 3 μl min^{-1} at 42 min to 4 μl min^{-1} at 44 min, 4 μl min^{-1} after 44 min. Mobile phase: A, 90/10 MeCN/water, B, 45/55 MeCN/water. Gradient of A: 0.1–5.0 min, 1%; 5.0–10 min, 1–10%; 10–15 min, 10–30%; 15–20 min, 30–40%; 20–25 min, 40–50%; 25–30 min, 50–45%; 30–40 min, 45%; 40–45 min, 45–50%; 45–50 min, 50–80%; 50–55 min, 80–85%; 55–60 min, 85–95%; after 60 min, 95%. Peaks (injection concentration): 1, simazine (1.0 μg ml^{-1}); 2, fensulfothion (4.0 μg ml^{-1}); 3, isoprocarb (2.0 μg ml^{-1}); 4, fenobucarb (1.5 μg ml^{-1}); 5, chlorothalonil (2.0 μg ml^{-1}); 6, etridiazole (1.0 μg ml^{-1}); 7, mepronil (0.75 μg ml^{-1}); 8, pronamide (3.0 μg ml^{-1}); 9, mecoprop (1.0 μg ml^{-1}); 10, bensulide (3.0 μg ml^{-1}); 11, isofenphos (1.5 μg ml^{-1}); 12, terbutol (1.5 μg ml^{-1}).

3. Results and discussion

3.1. HPLC system

The column efficiency was first evaluated by using 70/30 MeCN/water mixture as mobile phase. The highest plate number of 150 000 m^{-1} was obtained with naphthalene, biphenyl, anthracene and fluoranthene as standard compounds. This value was nearly two and a half times higher than conventional HPLC columns. Because of its μm scale i.d and 3 μm packings size, the column allowed a very low flow rate and consumes only 1–10 μl solvent min^{-1}. In addition, by the use of a flow rate processor between the pumps (with a practical output of > 0.01 ml min^{-1}) and injector, a highly accurate and reproducible microflow could be generated for satisfactory analysis. Simultaneously, a U-shaped capillary flow cell was used with the UV-vis detector. Because of its extremely small cell volume (35 nl), virtually no dead volume was generated and higher sensitivity could be obtained for analysis. The schematic of the whole system in the present work is depicted in Fig. 1.

3.2. Separation of pesticides

Preliminary separation of the pesticides was conducted with an isocratic gradient. Both MeCN/water and MeOH/water mixtures were used as the mobile phase. The effects of MeCN and MeOH concentration on the separation and determination of the pesticides were studied. Results showed that methanol was not as an appropriate organic solvent as MeCN in this case because it resulted in worse peak shapes and longer elution time.

Because baseline separation of the pesticides could not be achieved by isocratic elution, gradient elution was adopted using the MeCN/water system. To optimise the separation, different elution methods were compared. Results showed that 12 pesticides were simultaneously resolved with the combination of flow rate and solvent gradient method. A typical chromatogram is illustrated in Fig. 2. As can be seen, most of the pesticides were baseline separated within 65 min. Other than the

Table 1
Calibration equations ($y = a + bx$), linear ranges, RSD values (4 replicates) and detection limits ($s/n = 3$) of the pesticides

Pesticide	a($\times 10^5$)	b($\times 10^6$)	r^2	Linear range[a]	RSD (%)		Detection limit (μg l^{-1})	
				(μg l^{-1})	water	apple	No SPE	SPE[b]
Simazine	5.538	9.851	0.9978	0.4–40.0	8.4	10.7	34	0.15 (37.5[c])
Fensulfothion	−1.863	2.074	0.9989	2.0–100	6.6	7.9	170	0.80 (200)
Isoprocarb	3.524	4.686	0.9974	2.0–100	6.8	8.0	75	0.30 (75.0)
Fenobucarb	−0.334	0.835	0.9984	2.4–120	4.3	4.1	124	0.65 (163)
Chlorothalonil	0.766	9.320	0.9986	0.4–20	4.1	4.8	49	0.19 (47.5)
Etridiazole	0.013	3.801	0.9994	1.6–48	4.2	5.5	110	0.43 (107)
Mepronil	2.491	8.516	0.9918	1.0–16	5.3	6.9	44	0.18 (45.0)
Pronamide	−9.919	6.492	0.9897	3.0–60	6.7	10.1	165	0.76 (190)
Mecoprop	1.332	2.325	0.9885	4.0–100	7.1	10.3	135	0.74 (185)
Bensulide	19.78	1.677	0.9993	2.4–60	5.8	7.1	132	0.64 (160)
Isofenphos	2.104	3.018	0.9984	1.0–40.0	5.1	6.0	107	0.52 (130)
Terbutol	9.737	2.703	0.9991	1.0–40.0	5.5	6.6	120	0.58 (145)

[a] With preconcentration, upper limits are not the maximum.
[b] 250-fold enrichment.
[c] femtograms, 0.25 μl injection.

extra peak dispersion of the analytes with the increase in elution time, very narrow and sharp peaks were observed for the last three pesticides. This was attributed to the rapid increase of MeCN concentration during a short period of time (50–95% within 15 min). Independent experiments have shown that the mixing of MeCN and water is a heat-absorbing process and will cause a decrease in temperature of the solution and its environment. When this happens inside the column, it will conceivably result in the decrease of the thermal movement of the solute molecules, and hence, peak dispersion.

Table 2
Mean recoveries, R ($n = 3$), of the pesticides in water and apple samples by solid-phase extraction

Pesticide	Fortified concentrations	Recovery[a] (%)								
	(μg l^{-1})	A_1	A_2	B_1	B_2	C_1	C_2	D_1	D_2	E[b]
Simazine	1.0	70.2	72.6	88.6	88.3	72.9	73.2	91.6	92.0	102.8
Fensulfothin	4.0	83.6	85.1	75.3	76.2	80.6	79.4	86.1	86.5	88.2
Isoprocarb	6.0	78.2	80.1	91.7	92.0	84.0	86.6	92.9	94.1	105.0
Fenobucarb	10. 0	84.4	84.4	95.1	93.2	88.0	90.8	101.9	103.2	94.6
Chlorothalonil	2.0	88.3	89.0	92.5	93.3	91.0	90.8	95.8	96.9	107.1
Etridiazole	4.0	101.8	99.6	98.9	102.2	106.0	102.4	97.8	99.1	105.0
Mepronil	3.0	82.3	84.9	86.7	90.1	83.0	84.1	86.3	89.7	87.2
Pronamide	7.5	26.6	26.2	8.49	10.3	13.5	15.0	41.2	43.7	36.9
Mecoprop	10. 0	69.4	71.0	18.5	20.0	26.7	30.1	45.5	50.9	39.2
Bensulide	3.0	77.0	79.0	72.3	75.3	83.3	83.0	86.8	88.1	84.9
Isofenphos	2.0	62.7	63.1	63.0	61.6	76.1	77.7	88.4	92.8	94.7
Terbutol	2.0	77.3	79.0	77.6	73.1	83.0	85.5	91.5	90.8	89.2

[a] A, ethyl acetate 1.0 ml (×3)+methanol 1.0 ml; B, methanol 1.0 ml (×3)+ethyl acetate 1.0 ml; C, acetone 1.0 ml (×3)+methanol 1.0 ml; D, methanol 1.0 ml+acetone 1.0 ml (×2)+methanol 1.0 ml. Subscript 1, tap water; subscript 2, deionised water.
[b] E, fortification of apple samples, elution condition is the same as D.

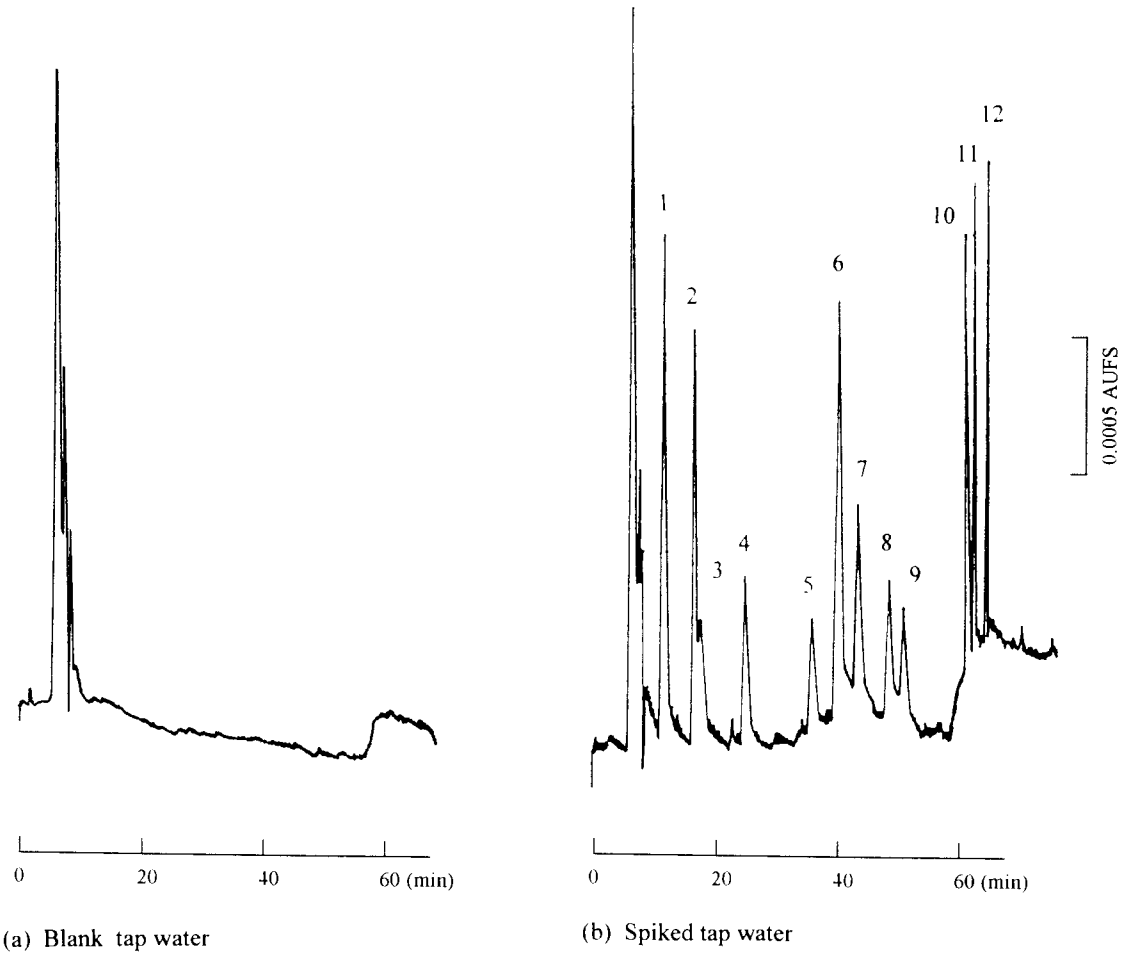

Fig. 3. Chromatogram of pesticides in spiked tap water sample: all the conditions and peaks are the same as shown in Fig. 2, concentrations of pesticides listed in Table 2.

In order to shorten the analytical time, additives as methanol and ethyl acetate were added to the mobile phase. While ethyl acetate slightly improved the separation between the critical peaks with the decrease of sensitivity, methanol was less effective.

3.3. Quantitative analysis of pesticides

The linearity of the pesticide calibration plots were checked by injecting 0.25 μl of the analytes after preconcentration with different concentrations (0.4–120 $\mu g\,l^{-1}$). The data of peak areas were processed by a statistical package for linear regression. The calibration equations, linear ranges and detection limits for pesticides are listed in Table 1. The relative standard deviation (RSD) values for pesticides in tap water and apple samples are also summarised in Table 1. A trend of higher RSD values for pesticides in apple samples than those in tap water could possibly due to the relatively more complicated sample matrix of the former.

3.4. Recovery experiments and choice of optimal extraction conditions

The pesticides were spiked into deionised water for recovery studies. The pesticide concentrations

in the water were kept constant throughout, and the results (means of three analyses) are listed in Table 2. In the analysis of real-life samples, environmental matrices are different from one another. As a consequence, great attention should be paid to the choice of appropriate eluents and eluting order to ensure satisfactory extraction and recoveries. In the present study, methanol, acetone, ethyl acetate, acetonitrile and tetrahydrofuran were used as the organic components in the eluents. Acetonitrile and tetrahydrofuran gave poor recoveries and were not used for further study.

Fig. 4. Chromatogram of pesticides in fortified apple sample: all the conditions and peaks are the same as shown in Fig. 2, concentrations of pesticides listed in Table 2.

In order to optimise the SPE procedures, different eluents methods were studied with deionised and tap water samples. From the results listed in Table 2, the recoveries obtained from the both matrices are similar. Besides, the use of methanol followed by ethyl acetate or acetone for the elution increased the recoveries of most pesticides. However, the recoveries of pronamide and mecoprop were lower than the others. Reasons for these are still not very clear. A possible explanation is that they were not stable during the extraction and analytical process. For example, the acetylenic bond in pronamide is reactive and can undergo hydrolysis.

Figs. 3 and 4 are typical chromatograms of spiked tap water and fortified apple samples. As can be seen, separation was achieved for most of the pesticides. Corresponding results in Table 2 show that satisfactory recoveries were obtained for Simazine, fensulfothion, isoprocarb, fenobucarb, chlorothalonil, etridiazole, mepronil, bensulide, isofenphos and terbutol. For the analysis of apple sample, a drifting baseline was observed (Fig. 4).

Some key aspects of different HPLC systems for the analysis of pesticides in spiked water, fruits and vegetables are listed in Table 3. The capillary HPLC exhibits comparable detection limits with the best results of capillary GC (with electron capture, nitrogen-phosphorus and flame-photometric detection) (detection limit of 0.2–150 $\mu g\ l^{-1}$) [20], and capillary GC–MS (detection limit of 0.1 $\mu g\ l^{-1}$) [21]. In comparison with other HPLC systems, the present method consumes the least sample and solvent.

4. Conclusions

The combination of capillary column HPLC and SPE provides an effective method for the determination of trace pesticides. Satisfactory separation of different kinds of pesticides was achieved on a 180 μm i.d. capillary column

Table 3
Comparison among different HPLC methods for the analysis of pesticides

Method/detector	Column (mm; μm)[a]	Extraction/enrichment	Injection volume (μl)	Flow rate (ml min^{-1})	Detection limit (μg l^{-1})	Reference
HPLC/UV, U-shaped flow cell	150 × 0.18; 3	SPE/C_{18}	0.25	0.003	0.15–0.8	present work
HPLC/UV	250 × 1.5; —	SPME/polyacrylate	1.0	0.100	0.10–5[b]	[8]
HPLC/Diode-array UV	100 × 2.1; 5	1000-fold	25	0.350	0.02	[7]
	250 × 4.6; 5	SPE/C_8	100	1.000	6–20	[3]
HPLC/Fluorescence	250 × 4.6; 5	MSPD/C_{18}	200	1.000	20	[19]

UV, ultraviolet detection; SPE, solid-phase extraction; SPME, solid-phase micro-extraction; MSPD, matrix solid-phase dispersion.
[a] Length × i.d.; particle size.
[b] ppb.

packed with 3 μm C_{18} stationary phase. Detection limits at picogram levels were obtained with direct injection (250 nl) and a zero dead volume flow cell. Further improvement in detection limits (down to the femtogram levels) could be accomplished by employing SPE.

Acknowledgements

The authors thank the National University of Singapore for financial support.

References

[1] C.M. Torres, Y. Picó, M.J. Redondo, J. Mañes, J. Chromatogr. A719 (1996) 95–103.
[2] J. Tekel, S. Hatrik, J. Chromatogr. A754 (1996) 397.
[3] P. Cabras, C. Tuberoso, M. Melis, M.G. Martini, J. Agric. Food Chem. 40 (1992) 817.
[4] S.M. Lee, M.L. Papathakis, H.M.C. Feng, G.F. Hunter, J.E. Carr, Fresenius J. Anal. Chem. 339 (1991) 376.
[5] R.J. Bushway, J. Chromatogr. 457 (1988) 437.
[6] M. Novotny, Anal. Chem. 60 (1988) 500A.
[7] A. Gretzfeld-Hüsgen, R. Schuster, HPLC for Environmental Analysis, Hewlett-Packard Company, France, 1994, pp. 75.
[8] K. Jinno, T. Muramatsu, Y. Saito, Y. Kiso, S. Magdic, J. Pawliszyn, J. Chromatogr. A754 (1996) 137.
[9] M. Janecek, F. Foret, K. Slais, P. Bocek, Chromatographia 25 (1988) 815.
[10] J.P. Chervet, M. Ursein, J.P. Salzmann, R.W. Vannoort, LC-GC 7 (1989) 514.
[11] LC Packings Instruction Manual, San Francisco, USA, 1994, pp. 24.
[12] G. Font, J. Mañes, J.C. Moltó, Y. Picó, J. Chromatogr. 642 (1993) 135.
[13] M.C. Hennion, Trend Anal. Chem. 10 (1993) 317.
[14] A. Balinova, J. Chromatogr. A754 (1996) 125.
[15] E. Viana, M.J. Redondo, G. Font, J.C. Moltó, J. Chromatogr. A733 (1996) 267.
[16] T. McDonnell, H. Rosenfeld, J. Chromatogr. 629 (1993) 41.
[17] S. Chirón, D. Barceló, J. Chromatogr. 645 (1993) 125.
[18] J.S. Salau, R. Alonso, G. Batlló, D. Barceló, Anal. Chim. Acta 293 (1994) 109.
[19] S.C. Stafford, W. Lin, J. Agric. Food Chem. 40 (1992) 1026.
[20] L. Kodencki, Z. Arpad, I. Gardi, A. Ambrus, L. Gyorfi, G. Reese, W. Ebing, J. Assoc. Off. Anal. Chem. 75 (1992) 53.
[21] M.S. Mills, E.M. Thurman, Anal. Chem. 64 (1992) 1985.

.

ELSEVIER

Talanta 45 (1998) 641–656

Talanta

Development and validation of analytical methodology using capillary electrophoresis for separation and determination of anions in rainwater

Ying-Sing Fung *, Kap-Man Lau

Department of Chemistry, Hong Kong University, Pokfulam Road, Hong Kong, Hong Kong

Received 28 January 1997; received in revised form 9 July 1997; accepted 9 July 1997

Abstract

A new capillary electrophoresis (CE) procedure was developed for simultaneous determination of both organic and inorganic anions in rain water using a background electrolyte (BGE) containing 5 mM molybdate, 0.15 mM CTAH, 0.01% PVA and 5 mM Tris buffer to adjust pH at 7.9. Under optimised conditions, good repeatability (RSD for sulphate in migration time = 0.36% and peak area = 4.2%), low detection limit (2 ppb for chloride) and satisfactory working range (50 ppb–20 ppm for hydrodynamic injection, 10 ppb–3 ppm for electrokinetic injection for chloride) were obtained. The reliability of the CE procedure developed was established by satisfactory recovery tests and good agreement of results obtained by both the CE and ion chromatography (IC) methods. The procedure developed had been successfully applied for field monitoring of rainwater showing good repeatability and capability of detecting trace anions at ppb levels beyond the IC working range. Thus, the new CE procedure developed provides a quick, sensitive, economic and reliable method to meet the need for the simultaneous determination of both organic and inorganic anions in the acid rain monitoring programme. © 1998 Elsevier Science B.V.

Keywords: Acid rain; Anion analysis; Capillary electrophoresis; Organic anion analysis; Trace analysis

1. Introduction

Acidic deposition has recently become one of the most important global environmental concerns for air pollution. Frequent analyses of chemical composition of rainwater is needed to assess the major sources of distant and local air pollutants, to quantify the extent of acidic deposition, and to identify hidden problems in areas with alkaline air particulate matters neutralising the acidity of the rainwater. However, due to the need to trace the source of air pollutants by mapping the change of pollutant concentrations spatially and temporally, a large number of samples have to be analysed at trace (ppb to ppt) levels at numerous sampling sites.

Thus, a sensitive analytical method with fast sample throughput using equipment with low capital and operational cost is needed for the acid rain monitoring programme.

* Corresponding author. Tel.: +852 25482132.

PII S0039-9140(97)00284-1

In addition to the analysis of anions in rainwater, increasing attention has been paid recently to the analysis of organic acids in rainwater [1–3]. They were formed as a result of photochemical reaction in the atmosphere. Recent increase in the use of CFC substitutes degradable in the atmosphere has led to the increase of organic acids in rainwater. Thus, methods to monitor organic acid anions present in the rainwater are needed. The most common inorganic anions of interest for rainwater analysis are: chloride, sulphate, nitrate, fluoride, phosphate and carbonate. For organic acid anions, formate and acetate have been detected in rainwater [4].

The traditional analytical method [5] employed for rainwater analysis is ion chromatography (IC). The major problems facing the use of IC are: (1) high operational and capital cost; (2) insufficient sensitivity for some of the anions needed to be analysed in rainwater; (3) different columns are needed for the separation and quantitation of different anions and organic acids. The recently developed non-suppressed Ion Chromatography may provide a cheaper method for analysis [6,7]. However, the sensitivity for anion analysis is less as compared to the suppressed IC and the method is not sensitive enough to analyse anions of interest present in rainwater at ppb to sub-ppb levels.

The recent advance in capillary electrophoresis (CE) provides a promising technique for the above analyses. It features high separation efficiency, good reproducibility, fast analysis and low consumption of electrolytes and samples [8–12]. Moreover, the capital and operational costs are significantly lower since neither bulky equipment nor costly columns are needed in addition to low consumption of chemical reagents during CE runs. Due to the low ionic sample matrix of rainwater, the stacking technique can be used for sample introduction so as to increase the sensitivity of the method for analysis of anions at ppb to sub-ppb levels. Upon proper selection of background electrolyte (BGE) with suitable mobility and careful adjustment of the electroosmotic flow, it is possible to separate and quantify both anions and organic acids in a single CE run.

To provide a suitable separation for anions, the CE BGE has to satisfy the following three requirements. Firstly, the electroosmotic flow (EOF) has to be reversed or suppressed in order to minimize the time of analysis. Secondly, the mobility of the UV-absorbing anions has to be matched with the analyte anions in order to reduce fronting and tailing of the analyte CE peaks. Thirdly, the molar absorptivity of the UV-absorbing anions should be as high as possible so as to provide a sensitive means of indirectly photometric detection of the analyte anions when they reach the detector window. Although other means of detection such as on-column conductivity detection has been used for CE detection [13,14], indirect photometric detection method is the most popular method for anion determination due to

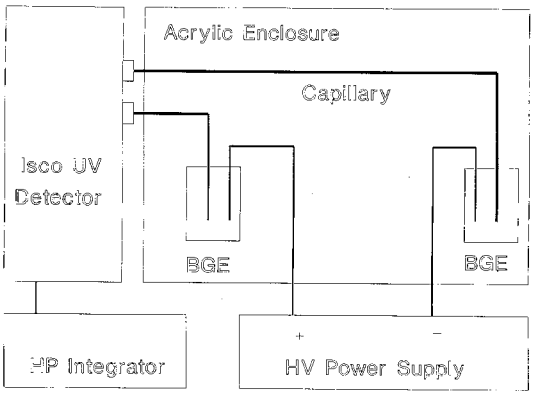

Fig. 1. Schematic diagram of the CE system (HV Power Supply: Spellman 30 kV constant voltage supply; Detector: ISCO CE variable-wavelength detector; Recorder: HP 3396A integrator; Capillary: 65 cm × 75 μm i.d. uncoated fused silica capillary).

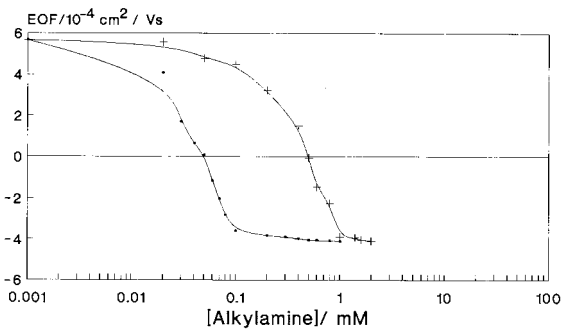

Fig. 2. The effect of alkylamine on EOF (BGE = 3 mM molybdate at pH 6.8).

Table 1
The molar absorptivities of common UV-absorbing anions

UV-absorbing anions	Molar absorptivity ($1\ mol^{-1}\ cm^{-1}$)
Chromate	3180 (254 nm)
Vanadate	4250 (254 nm)
Molybdate	5650 (230 nm)
Pyromellitate (PMA)	7065 (254 nm)
Trimellitate (BTA)	7147 (254 nm)
Phthalate	4750 (230 nm)
Benzoate	4800 (230 nm)

its universal response to most of the anions and the availability of commercial instrumentation with suitable sensitivity.

A large variety of UV-absorbing anions have been investigated for indirect photometric detection of anions after CE separation since the successful introduction of chromate and tetradecyltrimethylammonium bromide (TTAB) with UV detection at 254 nm as a commercial chemical reagent kit marketed by Waters for the analysis of fast moving simple inorganic anions [15]. Subsequently, various organic anions [16] have been developed for the analysis of slower moving anions. The optimization of indirect UV detection and the investigation of different injection techniques for CE separation of anions have been studied previously [17–19]. Compared to other UV-absorbing anions, chromate provided a good mobility match for highly mobile anions such as chloride, sulphate and nitrate [20]. The use of aromatic anions such as benzoate [9], phthalate [21], trimellitate [22,23], pyromellitate [24], 2,6-naphthalene-dicarboxylate [25] and naphthalene mono-, di and trisulfonates [26] as UV-absorbing anions for indirect detection of inorganic anions had been reported and discussed [26,27]. Phthalate at pH 6.5 gave the best detection limits. However, aromatic monocarboxylic acids provided a better mobility match for some less mobile anions such as fluoride and in particular for organic acids [20]. Out of the various anions investigated, the most common UV-absorbing anions within the range of mobilities of analyte anions of interest for rainwater analysis are: chromate, PMA, molybdate, BTA, vanadate, phthalate and benzoate.

For the application of CE for inorganic and organic anions analysis in rainwater, little work has been reported in the literature. Dichromate had been used as the UV-absorbing anion for the analysis of anions in rain water by CE [28], however, the sensitivity is limited to sub-ppm level even electrokinetic sampling method was used. No CE BGE system has been developed for the separation and quantitation of both inorganic and organic anions of interest in rainwater in a single CE run. This paper will describe the development of a new CE procedure for simultaneous determination of both organic and inorganic anions in rainwater using a new BGE system. The composition of the BGE developed, the optimisation of the operational parameters and the investigation of the reliability and applicability of the analytical procedure developed will be reported and discussed.

2. Experimental

2.1. Equipment and apparatus

The CZE system comprised of a Spellman (model CZE1000R) 30 kV constant voltage supply with reversible polarity, an uncoated fused-silica capillary (65 cm × 75 μm i.d.) with a capillary filling/washing apparatus, an ISCO CV4 variable-wavelength detector, and a HP3396A integrator. The apparatus was put in a room with temperature regulated at 24°C by a centralised air-conditioned system and the capillary was fixed in an acrylic enclosure together with a small fan for generating air movement to achieve quick thermal equilibrium. A schematic diagram of the setup is shown in Fig. 1.

The non-suppressed IC system used in previous studies [6,7,29–32] consisted of an isocratic pump (Gilson pump, model 805), a low pulse damper, a high pressure injection valve (Model 7125, Rheodyne), a 100 ml sampling loop, a variable wavelength detector (Spectro-Monitor 3100, Milton Roy) and a Hitachi (model QPD54) strip chart recorder. A guard column packed with PRP-1 resin (25 mm l. × 4.6 mm i.d.) was used to protect the analytical column (Hamilton PRP-X100, 150 mm l. × 4.6 mm i.d.).

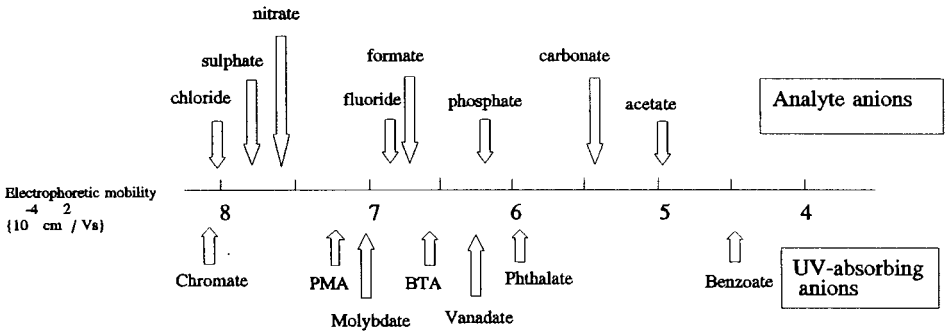

Fig. 3. The electrophoretic mobilities of common UV-absorbing anions and analyte anions.

2.2. Reagents and samples

All solutions were prepared by weighing and dissolving given amounts of analytical or equivalent reagent grade chemicals in doubly quartz-distilled water prior to making up to volume in 100 ml volumetric flasks. Potassium salts were used for chloride, sulphate, nitrate, fluoride, carbonate and formate, whereas sodium salts were used for molybdate and acetate. All the background electrolytes (BGEs) and standards were prepared daily by dilution from stock solutions, filtering through a 0.45 mm cellulose membrane filter and degassing under vacuum prior to use. Cetyltrimethylammonium hydroxide (CTAH) was prepared from cetyltrimethylammonium bromide (CTAB) by exchanging bromide with hydroxide in a solution of 1 mM CTAB with the ion exchanger Amberlite IRA-904 (Serva, Heidelberg, Germany).

The rain sampler was placed at a sampling site on the rooftop of a building at the Shatin valley, New Territories, Hong Kong on February 18, 1994 to collect rainwater in a 1 l polyethylene bottle through a 30 cm diameter polyethylene funnel mounted 1 m away from the roof surface. The sampler was normally covered to cut off dry deposition and was opened only at the start of a rain. The rain samples collected were stored in polyethylene bottles and placed inside a refrigerator at 4°C. The polyethylene bottle was cleaned by washing with doubly quartz-distilled water prior to next sampling.

2.3. Procedures

All samples and standard solutions were filtered through a 0.45 μm filter prior to analysis. For CE separation, 5 mM tris(hydroxyl)aminomethane (Tris buffer) was used as the buffer solution with pH adjusted by 2-hydroxyisobutyric acid or lithium hydroxide. The electrophoretic mobilities of analyte and UV-absorbing anions were determined under the BGE of 2 mM phosphate at pH 11.0. The capillary column obtained from the Yongnian Fibre Optic Factory was used directly without coating. Hydrodynamic sampling was performed by gravity created by the height difference between the two ends of the capillary inserted into the two BGE vials. The high voltage used for electrokinetic injection and for CE run was controlled by the Spellman high voltage power supply.

For IC separation, the non-suppressed system used in previous studies [6,7,29–32] was used. A sample containing 2 mM potassium hydrogen phthalate (pH 5.0) was used as the eluent which was passed through a 0.45 μm nylon 66 membrane filter and degassed under vacuum prior to use. To reduce the reaction of eluent with atmospheric CO_2, a glass tube packed with Carbosorb AS (6–12 mesh) was attached to the eluent container as a guard column. The eluent flow rate was kept constant at 1.5 ml min^{-1} and the wavelength of the detector was set at 205 nm throughout the study.

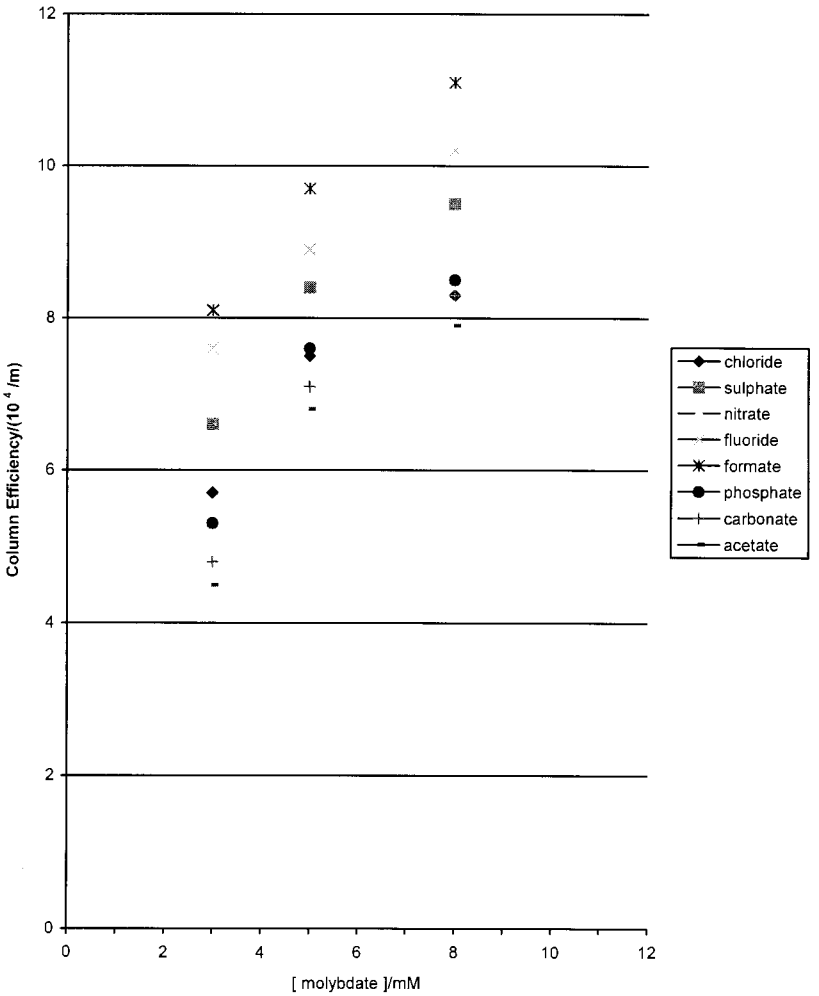

Fig. 4. The effect of molybdate concentration on the separation efficiency.

3. Results and discussion

3.1. Composition of background electrolyte

In order to increase the speed for the separation of anions, the EOF has to be reversed. The most effective way to manipulate the EOF is the addition of a quaternary amine EOF modifier in the electrolyte [33], such as tetradecyltrimethylammonium hydroxide (TTAH) and CTAH. CTAH is more effective to reverse the EOF as compared to TTAH at all the concentrations under investigation (Fig. 2) due to its longer alkyl chain. Thus, CTAH was selected as the EOF modifier. The Tris buffer was added to the BGE to provide stabilization against pH change and to reduce the baseline noise.

To provide a good separation and a sensitive method to quantify both organic and inorganic anions in rainwater using indirect photometric detection, UV-absorbing anions with suitable mobility amongst the analyte anions have to be added to the BGE to reduce fronting and tailing.

Its molar absorptivity should be as high as possible so as to enhance the sensitivity of the method. Moreover, it must be stable upon storage

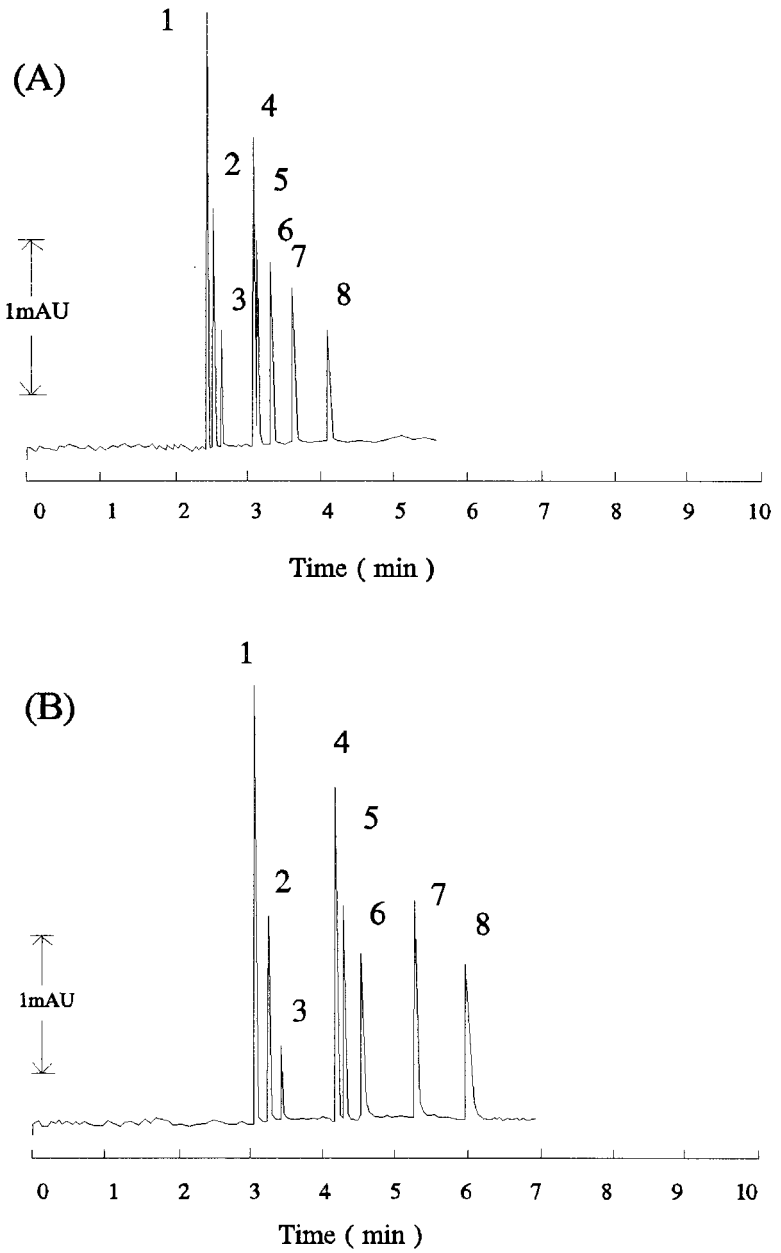

Fig. 5. The effect of PVA on the separation of a standard anion mixture. Conditions: (A) BGE: 5 mM Molybdate, 0.15 mM CTAH, 5 mM Tris buffer at pH 7.9; Capillary: 65 cm × 0.075 mm i.d. fused silica; Run: −20 kV; Current: 12 μA; Injection: 8 cm for 20 s; Detection: 230 nm. (B) same as (A) except 0.01% PVA in BGE and Current: 10 μA. Anion standards: 2 ppm each: 1 = chloride; 2 = sulphate; 3 = nitrate; 4 = fluoride; 5 = formate; 6 = phosphate; 7 = carbonate; 8 = acetate.

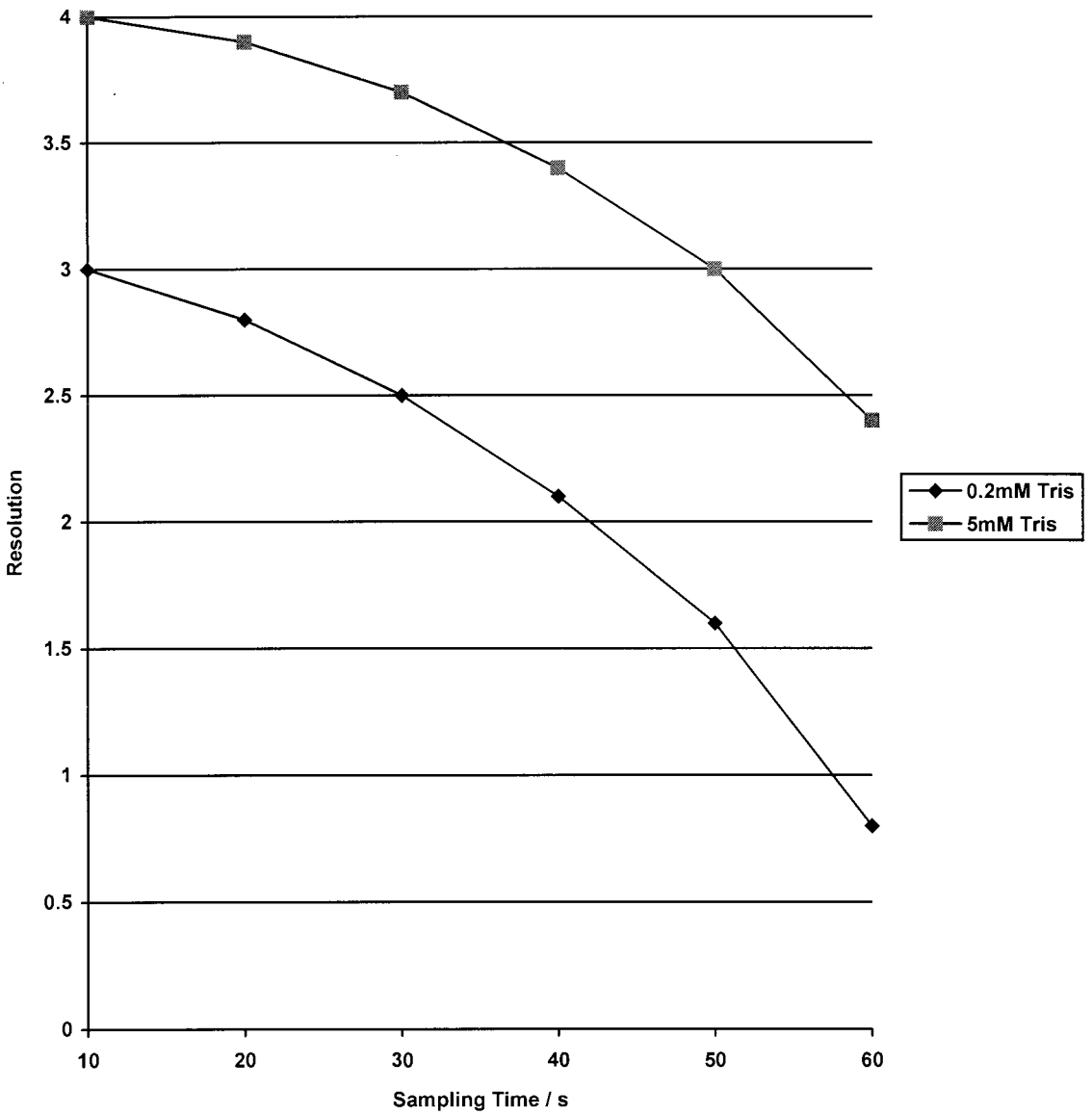

Fig. 6. The effect of sampling time on the resolution of 5 ppm of formate and fluoride at different Tris buffer concentration. Tris buffer concentration: ◆ = 0.2 mM, ■ = 5 mM.

and continuous analysis so as to obtain repeatable results. The molar absorptivities of the common UV-absorbing anions are given in Table 1 and results for the electrophoretic mobilities of UV-absorbing anions determined in 2 mM phosphate buffer at pH 11 and analyte anions in molybdate buffer are shown in Fig. 3.

The commercially available chromate system, though showing good separation of high mobility inorganic anions from chloride to phosphate, is not a stable BGE system for routine anion analysis in rainwater. Jones [34] had commented that if fluoride and phosphate started to co-migrate, the electrolyte should be replenished. In other studies,

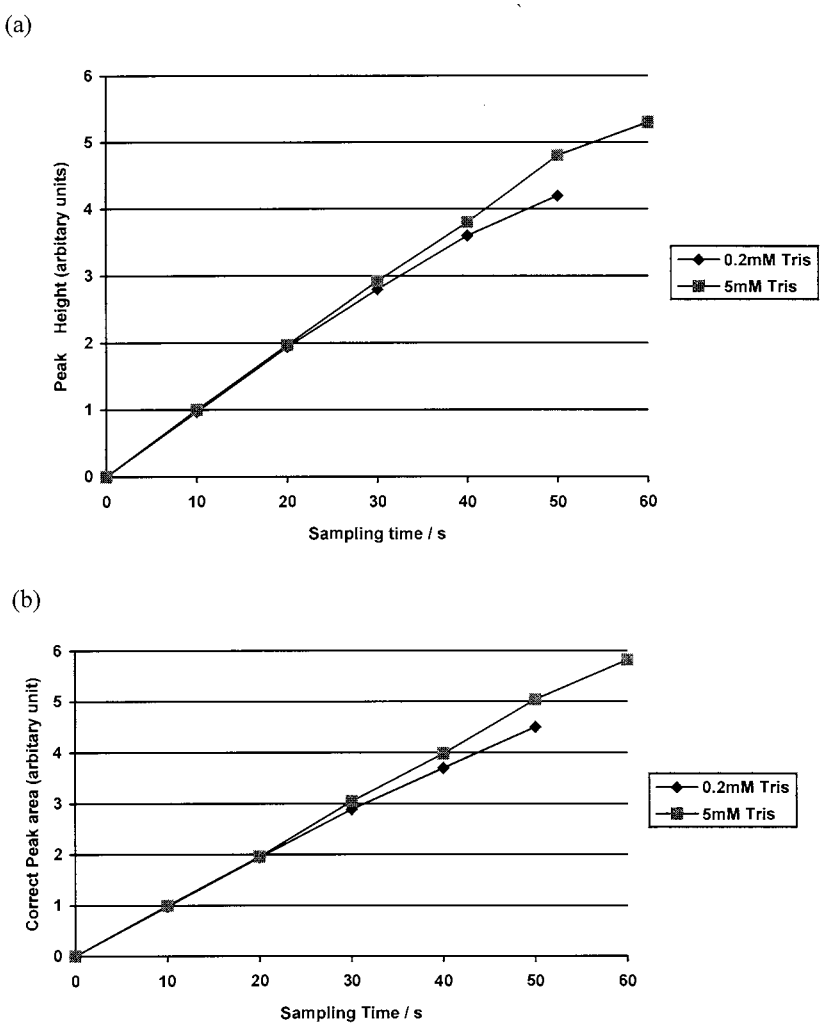

Fig. 7. The effect of sampling time on sensitivity for determining 5 ppm fluoride at different Tris buffer concentrations. (a = peak height, b = corrected peak area, Tris buffer concentration: ◆ = 0.2 mM, ■ = 5 mM).

the migration times were found steadily reduced upon aging of the chromate buffer [35]. In the present work, as indicated by the ranking of mobility given in Fig. 3, chromate is too fast for the slow moving organic anions. This will lead to poor resolution and tailing of CE peaks for the organic anions. Also, the molar absorptivity of chromate is the lowest compared to other UV-absorbing anions (Table 1).

Beside showing low molar absorptivity (Table 1), phthalate and benzoate are having significantly lower mobilities and are thus not suitable for the separation and detection of fast moving anions (Fig. 2). Thus, pyromellitate (PMA), molybdate, trimellitate (BTA) and vanadate are within the range of mobility suitable for rainwater analysis. However, vanadate and PMA were found to form white precipitates with cationic surfactants (e.g. CTAH and TTAH). Thus, less effective EOF modifiers such as hexamethonium hydroxide [24] or diethylenetriamine [36] have to be used in the vanadate and PMA system, giving undesirable long analysis time (migration time for fluoride = 11 min). Comparing molybdate and BTA, molyb-

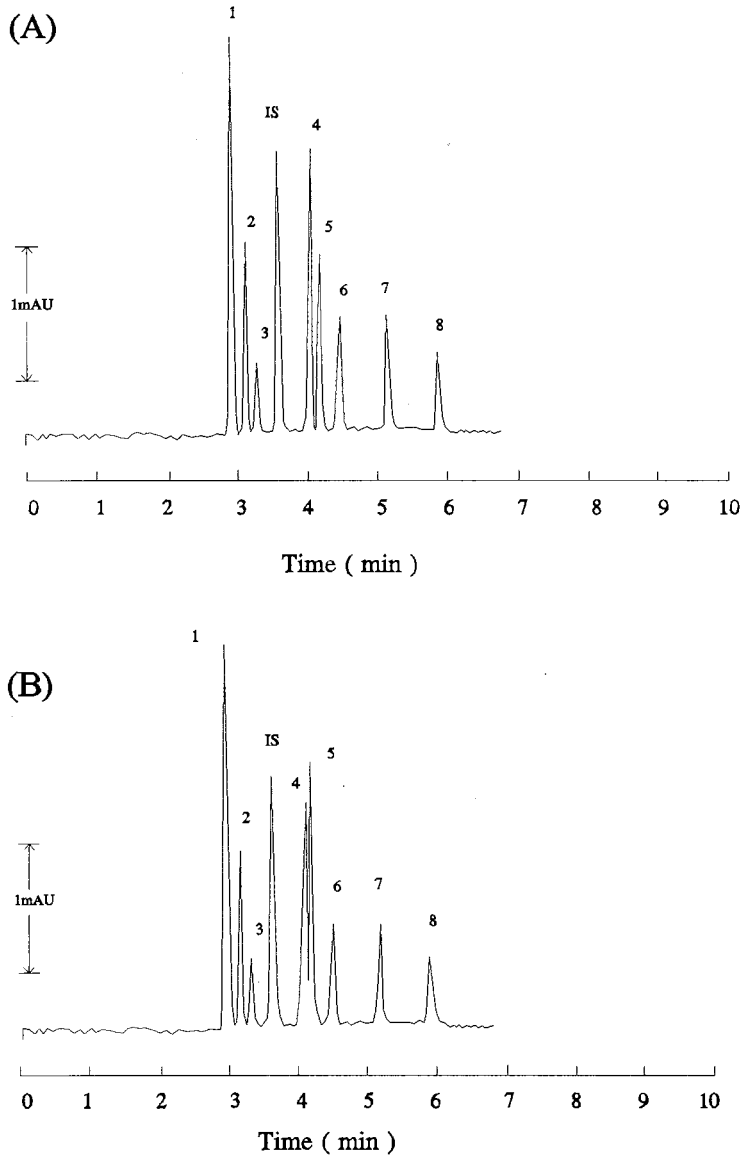

Fig. 8. The effect of injection voltage on the separation of a standard anion mixture. Conditions: (A) BGE: 5 mM Molybdate, 0.15 mM CTAH, 0.01% PVA and 5 mM Tris Buffer at pH = 7.9; Capillary: 65 cm × 0.075 mm i.d. fused silica; Run: − 20 kV; Injection; − 3 kV for 20 s; Detection: 230 nm; Current: 10 μA. (B) same as (A) except injection at − 20 kV for 3 s. Anion standards: 200 ppb each: 1 = chloride; 2 = sulphate; 3 = nitrate; 4 = fluoride; 5 = formate; 6 = phosphate; 7 = carbonate; 8 = acetate and IS = internal standard (chlorate, 500 ppb).

date is preferred due to its higher mobility, showing a better match with the mobilities of the analyte anions and its good chemical stability as compared to the organic BTA acid anions. Moreover, molybdate has a broad range of UV absorption similar to chromate, thus allowing fine adjustment of the absorption wavelength in case of sample matrix interference. Thus, molybdate

Table 2
Comparison of the analytical parameters using the hydrodynamic and electrokinetic sampling method for the analysis of common anions

Anions		Cl^-	SO_4^{2-}	NO_3^-	F^-	HCO_2^-	HPO_4^{2-}	HCO_3^-	CH_3COO^-
(1) Precision/RSD									
Hydrodynamic sampling[a]	Migration time/%	0.45	0.36	0.41	0.81	0.76	1.2	2.3	1.5
	Peak area/%	6.5	4.2	6.0	7.2	7.6	4.5	5.2	4.8
	Peak height/%	5.3	4.1	5.8	6.5	5.9	4.8	5.6	5.2
Electrokinetic sampling[b]	Migration time/%	0.63	0.52	0.59	1.21	1.13	2.8	3.1	2.9
	Peak area/%	7.1	5.9	6.3	7.8	8.3	5.8	6.6	5.8
	Peak height/%	5.9	4.6	5.3	6.8	6.5	5.1	7.1	6.2
(2) Detection Limit									
Hydrodynamic sampling/ppb		11	40	73	10	48	52	75	98
Electrokinetic sampling/ppb		2	8	16	2	10	12	16	20
(3) Working range									
Hydrodynamic sampling	Range/ppm	0.05–20	0.2–20	0.2–20	0.05–10	0.2–10	0.2–20	0.4–20	0.4–20
	R	0.996	0.997	0.995	0.991	0.992	0.994	0.993	0.991
Electrokinetic sampling	Range/ppb	10 –3000	30 –3000	50 –3000	10 –1000	40 –1000	40 –3000	50 –3000	50–3000
	R	0.994	0.994	0.992	0.990	0.990	0.991	0.992	0.991

(1) Precision: [a] 8 cm for 20 s, 2 ppm anion standard, $n = 5$; [b] -3 kV for 20 s, 200 ppb anion standard, $n = 5$.
(2) Detection limit: minimum detectable concentration at S/N = 2 (peak height); 20 s EK sampling at -3 kV; 60 s HD sampling at 8 cm.
(3) Working range: 20 s EK sampling at -3 kV, $n = 5$; 60 s HD sampling at 8 cm, $n = 5$.
R = correlation coefficient for linearity test.

was selected as the UV-absorbing anion for the optimisation of the BGE system.

3.2. Optimisation of operational parameters

The pH of the BGE was found to exert a strong effect on the migration time. The pH of the BGE controls the EOF and the mobility of anions of weak acids such as phosphate and carbonate.

It is better to use pH above 6.5 for faster analysis as the pK_{a1} of carbonate is 6.35. However, at pH 8.2, carbonate will co-migrate with phosphate and at pH 8.7 phosphate will overlap with formate. Thus, the pH of the BGE was kept at 7.9 to provide satisfactory separation of the analyte anions in rainwater.

The concentration of molybdate was found to exert a strong effect on peak height and separation efficiency. No analyte peak was observed when the molybdate concentration was less than 0.01 mM. Broad analyte peaks were observed when the molybdate concentration was between 0.01 to 1 mM. In general, S/N tends to be double with the increase in molybdate concentration from 3 to 5 mM, giving sharper peaks and better resolution. However, at concentrations greater than 5 mM molybdate, a downward trend in S/N ratio is evident. This decrease in S/N is due to the increase in the noise with increasing concentration of UV-absorbing anion.

The effect of the concentration of molybdate on the separation efficiency is shown in Fig. 4. In general, the separation efficiency of different an-

ions is inversely proportional to the difference of their mobilities with the molybdate BGE (Fig. 3), with higher efficiency for smaller mobility difference. The increase of the molybdate concentration leads to the increase in the separation efficiency for all anions. However, the extent of the increase is different for different anions (Fig. 4), with more for phosphate and less for chloride at higher molybdate concentration, leading to the reverse of their order of efficiency from 3–8 mM molybdate. Moreover, the joule heating effect is also increased rapidly at higher molybdate concentration, leading to the increase of the baseline noise. Thus, the optimum concentration of 5 mM is chosen. It is a compromise between sensitivity (S/N ratio) and resolution.

For indirect photometric detection, it had been shown [37] that lowering the concentration of UV-absorbing anions led to lower detection limit due to the more stable background signal. However, it also leads to reduced dynamic range at a given transfer ratio. As sensitivity is an important issue for rainwater analysis, a low UV-absorbing anion concentration is used to lower the detection limit together with a high Tris buffer concentration (5 mM) so as to make a BGE with high ionic strength in order to exercise the preconcentrating stacking effect for the low ionic rainwater samples.

Fig. 5A shows a typical electropherogram of a mixture of the analyte of interest (2 ppm of each analyte) in the BGE at pH 7.9. Most of the anions could be separated in less than 5 min. However, fluoride and formate could not be baseline-resolved. Upon the addition of 0.01% polyvinyl alcohol (PVA) to the BGE, all the analyte anions were found to be baseline-resolved in less than 6.5 min (Fig. 5B). Increasing the concentration of PVA in BGE, there is no further improvement in the separation between formate and fluoride but at the expense of increase in the analysis time. Thus, 0.01% PVA was used as a BGE additive for anion analysis in rainwater.

For sample introduction, two injection modes, the hydrodynamic and electrokinetic sampling, were studied. For hydrodynamic sampling, the effect of the sampling time on the resolution and sensitivity of the method was shown in Figs. 6 and 7. Corrected peak area (peak area/migration time) calculated from integrator results was used as a quantitative parameter to study the effect of different sampling times normalised using chlorate as the internal standard. This is to compensate for the increase in the migration time due to the increase of sampling time as results of the isotachophoretic effect for samples with low ionic content [38]. Alternatively, the constant current mode can be used to minimise this sample zone effect. The most critical separation between fluoride and formate was used to test the separation efficiency.

The resolution between fluoride and formate was found to decrease at longer sampling time and lower Tris buffer concentration (Fig. 6). It was degraded from 4.0 to 2.4 as the sampling time was increased from 10 to 60 s at 5 mM Tris buffer due to the increase in the sample zone. The sensitivity was found to increase with longer sampling times (Fig. 7). However, due to the increase in the sample zone, the use of sampling times longer than 60 s led to poor separation between formate and fluoride. The use of high Tris buffer concentration (5 mM) was found to give a slight improvement in the peak height and peak area. However, the linearity of sampling time to the analytical signal was found to extend over a longer sampling time at a higher Tris buffer concentration. With a compromise between resolution and sensitivity, a sampling of 60 s was adopted with the use of 5 mM Tris buffer in the BGE, as the stacking effect of the components in the capillary was enhanced with more concentrated BGE [39].

As the amount of injected analyte was found to depend on the mobility of the anions and the ionic strength of the sample solution during electrokinetic sampling, chlorate was used as the internal standard so that better quantitation results could be achieved. Moreover, the amount of solute injected by electrokinetic sampling, w, is given by the following [40]:

$$w = \frac{(\mu_{ep} + \mu_{eo})\pi r^2 V_i t_i}{L} C$$

where μ_{ep} is the electrophoretic mobility of the sample molecule, μ_{eo} is the electroosmotic mobil-

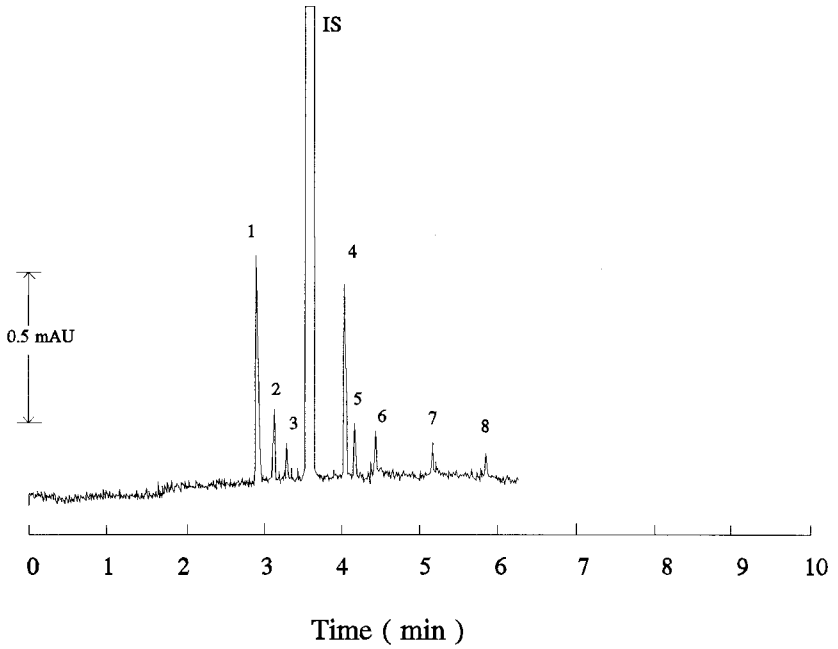

Fig. 9. The electropherogram of the eight standard anion mixture near the limit of detection using the electokinetic sampling. Conditions: BGE: 5 mM Molybdate, 0.15 mM CTAH, 0.01% PVA and 5 mM Tris buffer at pH 7.9; Capillary: 65 cm × 0.075 mm i.d. fused silica; Run: −20 kV; Injection: −3 kV for 20 s; Detection: 230 nm; Current: 10 μA. Anion standards: 20 ppb each: 1 = chloride; 2 = sulphate; 3 = nitrate; 4 = fluoride; 5 = formate; 6 = phosphate; 7 = carbonate; 8 = acetate and IS = internal standard (chlorate, 500 ppb).

ity of the sample solution, V_i is the injection voltage, L is the length of the column, r is the radius of the capillary and C is the sample concentration.

Thus, the quantity of the sample injected during electrokinetic injection can be controlled through the injection time t_i and the injection voltage V_i. However, too high an injection voltage can adversely affect the resolution of some analytes. This effect is shown in Fig. 8. The electropherograms in Fig. 8A and 8B were obtained under identical conditions except for the injection voltage, which was 3 kV for 20 s in Fig. 8A and 20 kV for 3 s in Fig. 8B. In the electropherogram Fig. 8B, overlapping of formate and fluoride was found to occur. Thus, a lower injection voltage (3 kV) and a longer injection time (20 s) was used during electrokinetic sampling. Direct sample electrokinetic injection is used in the present work, as its sensitivity is sufficient for the intended application and a simple system is preferred to handle a large number of samples for chemical analysis.

The analytical parameters using the hydrodynamic and electrokinetic sampling methods were compared in Table 2. Both injection modes provided excellent precision for the migration time. Good precision was obtained for both peak height and peak area for most analyte anions. However, the corrected peak area was shown to be a better quantitative parameter than the use of peak height. In general, the precision in the hydrodynamic sampling is better than that in the electrokinetic sampling even though both of them have used chlorate as the internal standard. However, for detection limit, electrokinetic sampling is better than hydrodynamic sampling. The electropherogram showing the determination of a standard mixture of eight anions at concentrations close to their detection limits using electrokinetic sampling is given in Fig. 9 whereas that of using hydrodynamic sampling is shown in Fig. 10. For working range, hydrodynamic sampling covers a longer range at the upper end, whereas electrokinetic

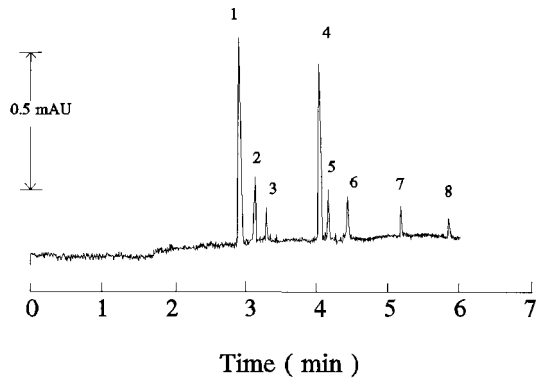

Fig. 10. The electropherogram of the eight standard anion mixture near the limit of detection using the hydrodynamic sampling. Conditions: BGE: 5 mM Molybdate, 0.15 mM CTAH, 0.01% PVA and 5 mM Tris buffer at pH 7.9; Capillary: 65 cm × 0.075 mm i.d. fused silica; Run: −20 kV; Injection: 8 cm for 60 s; Detection: 230 nm; Current: 10 μA. Anion standards: 200 ppb each: 1 = chloride; 2 = sulphate; 3 = nitrate; 4 = fluoride; 5 = formate; 6 = phosphate; 7 = carbonate; 8 = acetate.

sampling extends an order of magnitude at the lower end. Thus, both sampling methods can be used to lengthen the working range so as to cover a wider concentration range for the application of the method for minor and trace anion analysis in rainwater.

3.3. Reliability and applicability study

The reliability of the CE procedure developed for chemical analysis of rainwater was established by the recovery test of spiked samples and by comparison of results with the established IC method for rain samples collected during field work. The results on the recoveries of various anions added to rain water samples are given in Table 3, which indicate that better than 90% recoveries were obtained for all the analyte anions under investigation. The results obtained using the IC and CE techniques are compared and given in Table 4. Using the matched pair t-test method [41], the computed t value (0.898) is within the statistical t-value (3.182) for 4 d.f. Thus, no statistically significant difference was obtained using the two methods for the determination of anions in rainwater samples at 95% confidence level.

The CE procedure developed was applied for a field monitoring programme at the Shatin valley, a new town with more than a million people built in the New Territories, Hong Kong, at a geographical area with potential temperature inversion. The chromatograms of a typical rain water sample showing the nitrate, chloride and sulphate peaks is given in Fig. 11 whereas that for carbonate determination is given in Fig. 12. A typical electropherogram using electrokinetic sampling for the determination of trace anions in rain water such as fluoride and acetate is given in Fig. 13. In

Table 3
Recovery of various anions added to rain water samples

Analytes	Present (mg l^{-1})	Added (mg l^{-1})	Found[a] (mg l^{-1})	Recovery (%)
Chloride[b]	0.43	0.5	0.86	97
Sulphate[b]	2.45	0.5	2.77	94
Nitrate[b]	1.24	0.5	1.65	95
Fluoride[c]	0.01	0.1	0.10	91
Formate[c]	ND	0.1	0.09	90
Phosphate[c]	ND	0.1	0.09	90
Carbonate[b]	2.50	0.5	2.79	93
Acetate[c]	0.05	0.1	0.14	93

ND = Not detected.
[a] $n = 5$.
[b] Determined by hydrodynamic sampling (8 cm for 60 s).
[c] Determined by electrokinetic sampling (3 kV for 20 s).

Table 4
Parallel method determination of rainwater samples using CE and IC

Analyte	Found by CE (mg l^{-1})[a]	Found by IC (mg l^{-1})
Chloride[b]	0.43 ± 0.06	0.46 ± 0.05
Sulphate[b]	2.45 ± 0.30	2.60 ± 0.28
Nitrate[b]	1.24 ± 0.21	1.18 ± 0.19
Fluoride[c]	0.01 ± 0.003	ND
Formate[c]	ND	ND
Phosphate[c]	ND	ND
Carbonate[b]	2.50 ± 0.39	2.61 ± 0.36
Acetate[c]	0.05 ± 0.03	ND

ND = Not detected
[a] $n = 5$.
[b] Determined by hydrodynamic sampling (8 cm for 60 s).
[c] Determined by electrokinetic sampling (3 kV for 20 s).

order to normalise the migration time and peak area for anion determination, 500 ppb chlorate was added to the rain sample as the internal standard. Six out of the eight common organic and inorganic anions were found with detectable concentrations in the field sample. Good separation was obtained, showing no fronting or tailing of the CE peaks. However, the fluoride (peak 4) and acetate (peak 6) peaks were found much lower in concentration as compared to other anions. Thus, for major anions at ppm levels such as

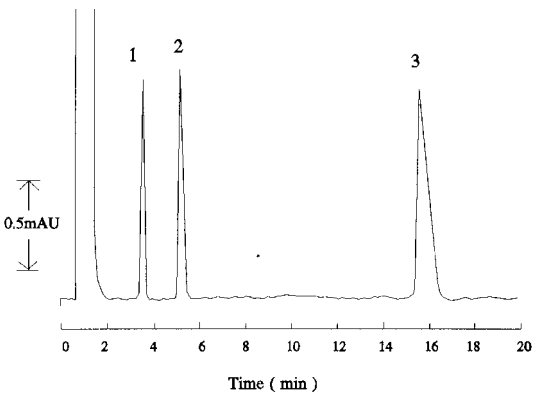

Fig. 11. The chromatogram of a typical rain water sample. Conditions: Eluent: 2 mM KHP at pH = 5.0; flowrate = 1.5 ml min^{-1}; detection wavelength = 272 nm; sample volume = 0.100 ml; column = PRP-X100. Peaks: S = system peak; 1 = chloride; 2 = nitrate; 3 = sulphate.

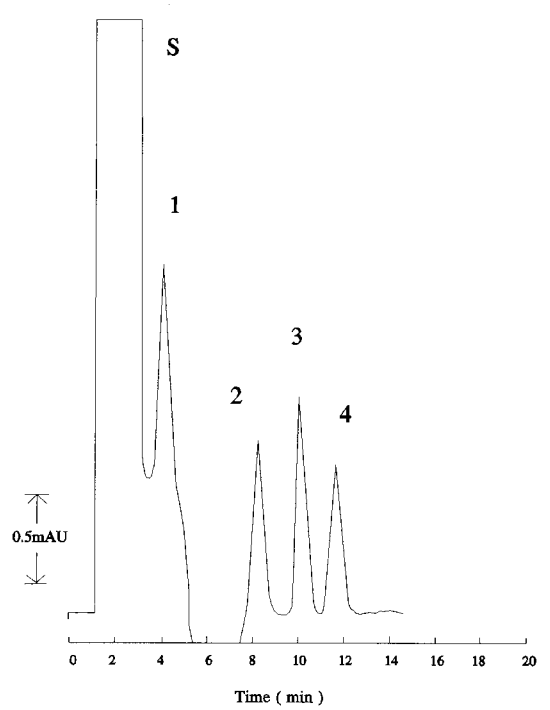

Fig. 12. The chromatogram for the determination of carbonate in a typical rain water sample. Conditions: Eluent: 0.6 mM KHP at pH = 9.5; flowrate = 1 ml min^{-1}; detection wavelength = 272 nm; sample volume = 0.100 ml; column = PRP-X100. Peaks: S = system peak; 1 = chloride; 2 = nitrate; 3 = carbonate; 4 = sulphate.

chloride, sulphate, carbonate and nitrate, a 60 s hydrodynamic sampling at 8 cm was used for sampling introduction and a typical electropherogram was shown in Fig. 14 whereas a 20 s electrokinetic sampling at 3 kV was used to stacking the trace anions (< 200 ppb) such as fluoride and acetate prior to their separation and quantitation. The results for the field monitoring work were given in Fig. 15, which show satisfactory repeatability for all the anions determined. The major anions such as chloride, sulphate and nitrate were checked against the IC method, giving same results within statistical variation (Table 4). Many trace anions detected by CE were found beyond the detection limit of the IC system. This illustrates the very high sensitivity of the CE procedure using stacking technique for trace anion analysis.

4. Conclusion

A new CE procedure was developed for simultaneous determination of both organic and inorganic anions in rainwater using a BGE containing 5 mM molybdate as a UV-absorbing anion, 0.15 mM CTAH as an EOF modifier, 0.01% PVA as an additive to solve the co-migration problem of fluoride and formate, and 5 mM Tris buffer to adjust pH at 7.9.

The results obtained in the present study demonstrate the feasibility and advantages of using CE for the analysis of both organic and inorganic anions in rainwater. The corrected peak area was shown to be a better quantitative parameter than the use of the peak height. The use of longer injection time in hydrodynamic injection was shown to increase the sensitivity of the method but suffered the loss of efficiency and resolution of the separation. Thus, 60 s was adopted for hydrodynamic injection. The use of electromigration injection technique was shown to enhance the sensitivity of the method though suffered less precision of results and biased sampling due to sample matrix. Under optimised conditions, good repeatability (RSD for sulphate in migration time = 0.36% and peak area = 4.2%), low detection limit (2 ppb for chloride) and satisfactory working range (50 ppb–20 ppm for hydrodynamic injection, 10 ppb–3 ppm for electrokinetic injection for chloride) were obtained.

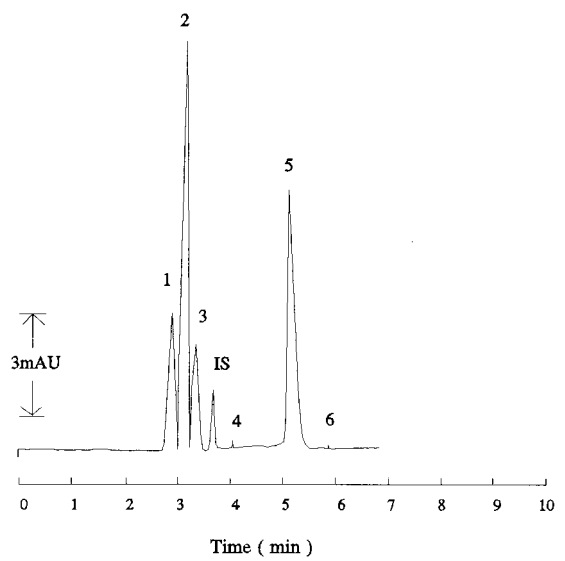

Fig. 13. The electropherogram of a typical rain water sample using electrokinetic sampling. Conditions: BGE: 5 mM Molybdate, 0.15 mM CTAH, 0.01% PVA and 5 mM Tris buffer at pH 7.9; Capillary: 65 cm × 0.075 mm i.d. fused silica; Run: −20 kV; Current: 10 μA; Injection: −3 kV for 20 s. Migration order: 1 = chloride; 2 = sulphate; 3 = nitrate; 4 = fluoride; 5 = carbonate; 6 = acetate and IS = internal standard (chlorate, 500 ppb).

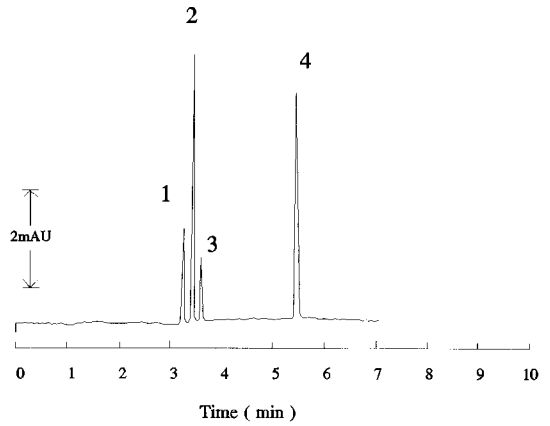

Fig. 14. The electropherogram of a typical rain water sample using hydrodynamic sampling for major anion determination. Conditions: BGE: 5 mM Molybdate, 0.15 mM CTAH, 5 mM Tris buffer at pH 7.9; Capillary: 65 cm × 0.075 mm i.d. fused silica; Run: −20 kV; Current: 10 μA; Injection: 8 cm for 60 s; Detection: 230 nm. Migration order: 1 = chloride; 2 = sulphate; 3 = nitrate; 4 = carbonate.

The reliability of the CE procedure developed was established by satisfactory recovery tests and parallel determination with closely matching results for all the analyte anions. It has been successfully applied for a field monitoring programme showing good repeatability and capability of detecting trace anions at ppb levels beyond the IC working range. In summary, CE was shown to provide a quick, sensitive, economic and reliable method for simultaneous determination of both organic and inorganic anions in the acid rain monitoring programme.

Acknowledgements

We would like to acknowledge the financial support of the Hong Kong Research Grants

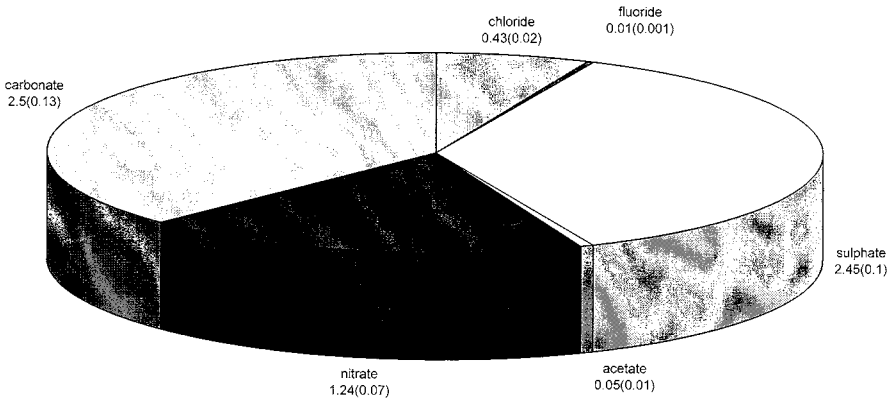

Fig. 15. The anion composition of rainwater collected in the Shatin new town, New Territories, Hong Kong. (Results given as mean SD for $n = 5$).

Council and the Hong Kong University Research Grants Committee for the above work.

References

[1] J.M. Hales, Acidic precipitation, in: H.B. Singh (Ed.), Composition, Chemistry and Climate of the Atmosphere, Van Nostrand Reinhold, New York, 1995, pp. 443–479.
[2] P.S.P. Rao, G.A. Momin, P.D. Safai, A.G. Pillai, L.T. Khemani, Atmos. Environ. 29 (1995) 2025.
[3] T.E. Graedel, D.T. Hawkins, L.D. Claxton, Atmospheric Chemical Compounds—Sources, Occurrence and Bioassay, Academic Press, London, 1986, pp. 315–341.
[4] H.E. Jeffries, Photochemical air pollution, in: H.B. Singh (Ed.), Composition, Chemistry and Climate of the Atmosphere, Van Nostrand Reinhold, New York, 1995, pp. 308–348.
[5] L.E.T. Topol, M. Levon, J. Flanagan, R.J. Schwall, A.E. Jackson, Quality assurance manual for precipitation systems, EPA/600/4-82-042a, US Environmental Protection Agency: Research Triangel park, NC, USA, 1983.
[6] Y.S. Fung, W.M. Tam, Anal. Chim. Acta 326 (1996) 67.
[7] Y.S. Fung, Zucheng Wu, K.L. Dao, Anal. Chem. 68 (1996) 2186.
[8] P.E. Jackson, P.R. Haddad, Trends Anal. Chem. 12 (1993) 231.
[9] J. Romano, W.R. Jones, R.J. Jandik, P. Jackson, J. Chromatogr. 546 (1991) 411.
[10] P. Jandik, W.R. Jones, R. Pfeifer, Am. Lab. 23 (1991) 40.
[11] G. Bondonx, W.R. Jones, R.J. Jandik, J. Chromatogr. 602 (1992) 79.
[12] P.K. Dasgupta, L. Bao, Anal. Chem. 65 (1993) 1003.
[13] F. Foret, M. Deml, V. Kahle, P. Bocek, Electrophoresis 7 (1986) 430.
[14] X. Huang, J.A. Luckey, M.J. Gorden, R.W. Zare, Anal. Chem 61 (1989) 766.
[15] B.J. Wildman, P.E. Jackson, W.R. Jones, P.G. Alden, J. Chromatogr. 546 (1991) 459.
[16] W.R. Jones, R.J. Jandik, J. Chromatogr. 608 (1992) 385.
[17] W.R. Jones, J. Chromatogr. 640 (1993) 387.
[18] J.B. Nair, C.G. Izzo, J. Chromatogr. A 640 (1993) 445.
[19] S.A. Oehrle, J. Chromatogr. A 671 (1994) 383.
[20] P. Jandik, W.R. Jones, J. Chromatogr. 546 (1991) 431.
[21] S.P.D. Lalljie, J. Vindevogel, P. Sandra, J. Chromatogr. A 652 (1993) 563.
[22] S.M. Consins, P.R. Haddad, W. Buchberger, J. Chromatogr. A 671 (1994) 397.
[23] W. Buchhberger, S.M. Consins, P.R. Haddad, Trends Anal. Chem. 13 (1994) 313.
[24] M.P. Harrold, M.J. Wojtusik, J. Riviello, P. Henson, J. Chromatogr. 640 (1993) 463.
[25] E. Dabek-Zlotorzynska, J.F. Dlonhy, J. Chromatogr. A 671 (1994) 389.
[26] S.A. Shamsi, N.D. Danielson, Anal. Chem. 66 (1994) 375.
[27] Y. Ma, R. Zhang, J. Chromatogr. 625 (1992) 341.
[28] H.L. Nguyen, S.L. Tamisier-Karolak, M. Czok, R. Laugier, P. Cardot, Analusis 23 (1995) 82.
[29] Y.S. Fung, K.L. Dao, Anal. Chim. Acta 300 (1995) 207.
[30] Y.S. Fung, K.L. Dao, Anal. Chim. Acta 334 (1996) 51.
[31] Y.S. Fung, K.L. Dao, Anal. Chim. Acta 309 (1995) 173.
[32] Y.S. Fung, K.L. Dao, Anal. Chim. Acta 315 (1995) 347.
[33] C.A. Lucy, R.S. Underhill, Anal. Chem. 68 (1996) 300.
[34] W.R. Jones, Electrophoretic capillary ion analysis, in: J.P. Landers (Ed.), Handbook of Capillary Electrophoresis, 1st ed., CRC Press, Boca Raton, FL, 1994, pp. 209–223.
[35] R. Stahl, J. Chromatogr. A 686 (1994) 143.
[36] L. Kelly, R.J. Nelson, J. Liq. Chromatogr. 16 (1993) 2103.
[37] E.S. Yeung, Acc. Chem. Res. 22 (1989) 125.
[38] D.S. Burgi, Anal. Chem. 65 (1993) 3726.
[39] D.S. Burgi, R.L. Chien, Anal. Chem. 63 (1991) 2042.
[40] P.E. Jackson, P.R. Haddad, J. Chromatogr. 640 (1993) 481.
[41] E.L. Bauer, A Statistical Manual for Chemists, 2nd ed., Academic Press, New York, 1971, 65 pp.

ELSEVIER

Talanta 45 (1998) 657–661

Talanta

Measurement of nitrate and chlorate in swimming pool water by capillary zone electrophoresis

P. Wang [a], S.F.Y. Li [b], H.K. Lee [a,*]

[a] *Department of Chemistry, National University of Singapore, Kent Ridge, Singapore 119260, Singapore*
[b] *Department of Chemistry and Institute of Materials Research and Engineering, National University of Singapore, Kent Ridge, Singapore 119260, Singapore*

Received 5 February 1997; accepted 31 March 1997

Abstract

Capillary zone electrophoresis (CZE) of nitrate and chlorate in swimming pool water are described. Nitrate and chlorate were determined simultaneously with an indirect detection method in an electrolyte containing 10 mM chromate and 0.1 mM cetyltrimethylammonium bromide (CTAB). Where chloride concentration was so high that nitrate could not be determined satisfactorily because of interference, a direct detection technology was developed in which 10 mM sulfate and 0.1 mM CTAB were used as the buffer. The wavelength for indirect detection was 254 nm and 214 nm for direct detection. Relative standard deviations of the quantification of nitrate and chlorate in real samples were below 6%. The detection limits were 7 μg ml^{-1} for chlorate, and 4 μg ml^{-1} (indirect detection) and 0.4 μg ml^{-1} (direct detection) for nitrate. © 1998 Elsevier Science B.V.

Keywords: Nitrate; Chlorate; Capillary zone electrophoresis; Water analysis

1. Introduction

Water analysis has an important place in the chemical analysis of environmental samples. The development of, and improvement in, methods for the analysis of water is a major task of analytical chemists. This is especially so since each type of water has its own specific constituents and any one procedure may not be completely amenable to different water-types.

Swimming pool water should basically have the quality of drinking water. Swimming pool water generally has a higher concentration of chloride because chlorine or hypochlorous acid is the principal sterilizing agent used in such water. Because of the nature of its usage, it is desirable that swimming pool water be analyzed regularly to monitor its quality.

According to the US National Interim Primary Drinking Water Regulations [1], the nitrate nitrogen level should be below 10 μg ml^{-1}. That is to say, the nitrate concentration should be below 45 μg ml^{-1}. No standard has been published for chlorate in drinking water.

* Corresponding author. Tel.: +65 7756666; fax: +65 7791691.

PII S0039-9140(97)00296-8

The principal methods for the analysis of nitrate in swimming pool water include colorimetry [2,3], titrimetry [2], ion-specific electrode electroanalysis [2] and ion chromatography (IC) [4]. Chlorate can be determined by iodometry [3] or by IC [4]. However, the high chloride content and free chlorine usually interferes with the determination of nitrate in the above chemical analysis methods; the former must be precipitated before determination [2]. These operations are time-consuming and are not suitable for automated analysis of large numbers of samples. IC is a powerful method for the analysis of anions in water [5]. However, nitrate and chlorate cannot be easily separated on IC columns because their interaction with ion exchangers are very similar. Nitrate can be determined by UV detection at 215 nm at which chlorate has little absorbance, thus minimize the interference posed by the later [4]. Mobile phase IC (MPIC) has been used to determine both ions [4]. In this method, 10% acetonitrile must be added to the eluent.

In this communication, a new method for the simultaneous determination of nitrate and chlorate in swimming pool water by capillary zone electrophoresis (CZE) is described. Another more sensitive method for the analysis of trace nitrate by CZE is also described. This method is useful where chloride levels are so high as to cause interference with nitrate analysis. In general, the methods reported are simple, fast, reproducible and require no volatile organic solvent.

2. Experimental

2.1. Reagents

Sodium nitrate, sodium chlorate, sodium chromate and anhydrous sodium sulfate were obtained from Fluka (Switzerland). Cetyltrimethylammonium bromide (CTAB) was purchased from Aldrich Chemical (Milwaukee, WI). All solutions were prepared using water purified by a Barnstead NANOpure system (Dubuque, IA).

The buffer used in the indirect CZE was prepared by diluting 1 ml 100 mM sodium chromate and 0.1 ml of 10 mM CTAB to 10 ml total volume (pH = 9.4). The buffer used in the direct CZE was prepared by diluting 1 ml of 100 mM sodium sulfate and 0.1 ml of 10 mM CTAB to 10 ml total volume (pH = 5.2). These working electrolytes were replaced daily.

The standard nitrate and chlorate storage solutions (each 1000 μg ml^{-1}) were prepared by dissolving the appropriate amounts of the corresponding sodium salts in deionized water.

All the above solutions were filtered through 0.45 μm membrane filters before use.

2.2. Apparatus

A Lauerlabs CE system (Emmen, The Netherlands) equipped with a Bischoff (Leonberg, Germany) model 1000 UV detector and a Shimadzu

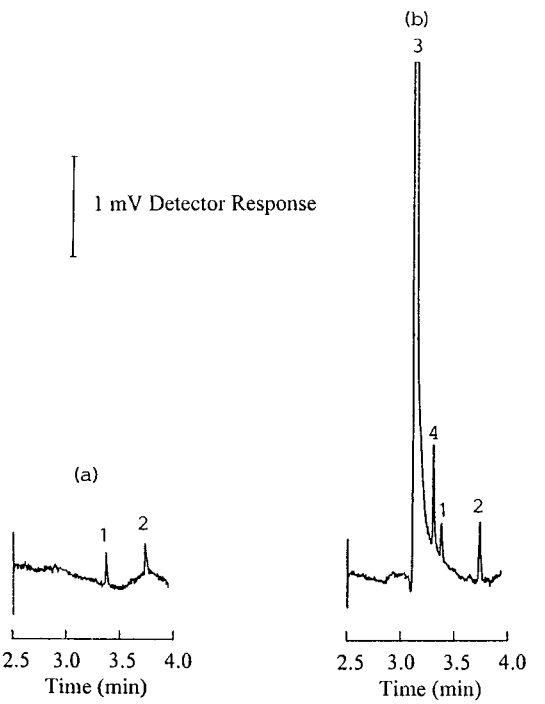

Fig. 1. Electropherograms of (a) standard anions by indirect detection. Peaks: 1 = nitrate; 2 = chlorate. (b) A real swimming pool water sample by indirect detection. Peaks: 1 = nitrate; 2 = chlorate; 3 = chloride; 4 = sulfate. Separation conditions: 10 mM chromate and 0.1 mM CTAB (pH = 9.4), − 20 kV, 65 cm × 50 μm fused silica (52 cm to detector), 254 nm, 0.1 min injection time under 50 mbar, ambient temperature.

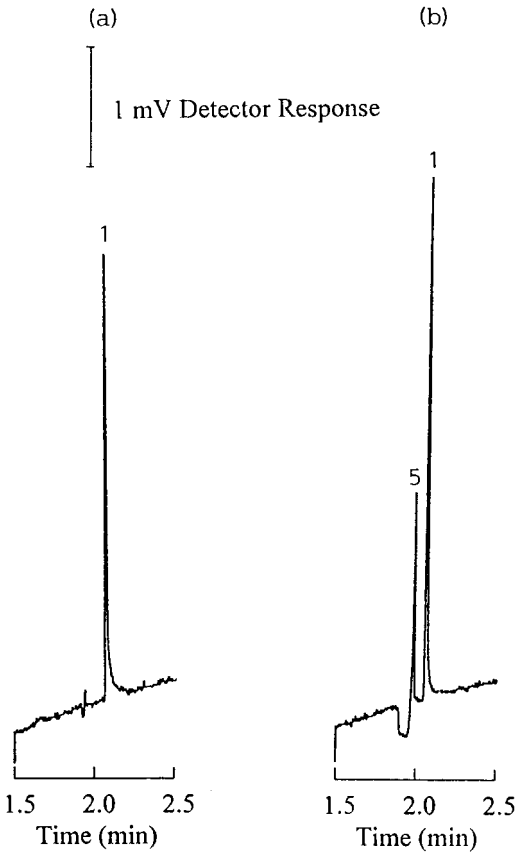

Fig. 2. Electropherograms of (a) standard anions by direct detection. Peak: 1 = nitrate. (b) A real sample by direct detection. Peaks: 1 = nitrate; 5 = not identified. Separation conditions: 10 mM sulfate and 0.1 mM CTAB (pH = 5.2), − 20 kV, 65 cm × 50 ηm fused silica (52 cm to detector), 214 nm, 0.1 min injection time under 50 mbar, ambient temperature.

(Tokyo, Japan) C-R6A integrator were used in this study.

A 65 cm × 50 μm i.d. uncoated fused-silica capillary with the detection window placed 52 cm from the injection end was used. The voltage was set at 20 kV (negative mode). The detector was set at 254 and 214 nm for the indirect and direct modes, respectively. Hydrostatic injection was realized in 0.1 min under a pressure of 50 mbar. All experiments were carried out at ambient temperature (22–25°C).

3. Results and discussion

3.1. Analytical conditions

Because of the high ratio of the concentration of chloride to nitrate and chlorate, analytical conditions must be chosen carefully in order to determine nitrate and chlorate simultaneously by indirect detection. A series of solutions which contained 10 mM chromate and 0.1 mM CTAB with different pH values, adjusted by 0.1 M NaOH or 0.1 M H_2SO_4, were used as buffer solutions. A buffer at pH = 9 gave the best results. Fig. 1a shows the electropherogram of a standard solution of nitrate and chlorate, while Fig. 1b is an electropherogram of a real swimming pool water sample.

As shown in Fig. 1b, the nitrate peak is much smaller than that of chloride. Greater sensitivity and accuracy for nitrate analysis could be achieved by direct detection, in which nitrate was monitored at 214 nm. Direct detection is easy to perform, because chloride, sulfate and chlorate have little response at 214 nm whereas nitrate has a strong absorbance signal. Except for the change of buffer from chromate to sulfate and wavelength from 254 to 214 nm, the other conditions for direct detection method were the same as those for the indirect method. The time needed to re-equilibrate the column was very short. The column was rinsed for 10 min by water under

Table 1
Quantitative results for nitrate and chlorate in water from three open-air swimming pools

Sample	*n*	Chlorate (μg ml^{-1})	Nitrate (by indirect detection) (μg ml^{-1})	Nitrate (by direct detection) (μg ml^{-1})
1	3	14.5 ± 0.40	8.78 ± 0.31	9.98 ± 0.12
2	3	22.3 ± 0.58	18.2 ± 0.44	17.3 ± 0.21
3	3	12.6 ± 0.33	24.1 ± 0.68	23.3 ± 0.23

Table 2
Recoveries of nitrate and chlorate from a real sample

Analyte	*n*	Added (μg ml^{-1})	Found (μg ml^{-1})	Recovery (%)
Chlorate	3	5.0	5.53 ± 0.17	111
		15.0	15.5 ± 0.32	104
		25.0	25.7 ± 0.66	103
Nitrate (by indirect detection)	3	5.0	4.36 ± 0.16	87.2
		15.0	15.1 ± 0.45	101
		25.0	25.7 ± 0.92	103
Nitrate (by direct detection)	3	2.0	2.06 ± 0.03	103
		6.0	5.69 ± 0.08	94.8
		10.0	9.98 ± 0.09	99.8

pressure (2000 mbar), and then for another 10 min with sulfate buffer. Fig. 2a shows an electropherogram of standard nitrate and Fig. 2b a typical electropherogram of swimming pool water, both obtained by the direct detection method.

3.2. Quantification

As shown in Fig. 2, the peak tailing in the standard nitrate solution was more significant than that in the sample. This is probably due to the difference in conductivity between the standard and the real samples. In order to eliminate this matrix effect, the quantitative method of standard additions was used in the chlorate and nitrate analyses. The linear equations for one of the real samples, which were constructed by adding standard solutions with different concentrations of chlorate or nitrate to the sample, are as follows:

chlorate (added range: 0–25 μg ml^{-1})

$y = 21.32x + 314.0 \qquad R^2 = 0.9939$

nitrate (indirect method, added range: 0–25 μg ml^{-1})

$y = 47.02x + 465.9 \qquad R^2 = 0.9917$

nitrate (direct method, added range: 0–10 μg ml^{-1})

$y = 370.9x + 1043 \qquad R^2 = 0.9943$

where y is the peak height, and x is the concentration (μg ml^{-1}). The negative intercepts of the above regression lines represent the amount of the corresponding analytes in the sample.

Samples from three open-air swimming pools were analyzed using the above quantification method. The results are listed in Table 1.

3.3. Recovery, precision and detection limits

The results of recovery tests are shown in Table 2. The mean recoveries of nitrate and chlorate added to swimming pool water were 87.2–103 and 103–111%, respectively.

The intra- and inter-assay precisions were evaluated as coefficients of variation (C.V.) which are listed in Table 3. The values were all less than 6%.

The detection limits were 7 μg ml^{-1} for chlorate, and 4 μg ml^{-1} for nitrate by the indirect

Table 3
The precision of the methods

Analyte	*n*	Intra-day C.V. (%)	Inter-day C.V. (%)
Chlorate	5	3.1	5.1
Nitrate (by indirect detection)	5	4.2	5.5
Nitrate (by direct detection)	5	1.6	2.2

method and 0.4 μg ml^{-1} by the direct method, when the signal-to-noise ratio was 3:1.

4. Conclusion

This paper demonstrates the use of CZE-based methods for the analysis of nitrate and chlorate in swimming pool water. The two anions of interest may be separated and determined simultaneously even if the chloride content in the real sample is much higher than each of the two ions. Trace amounts of nitrate can be analyzed by a direct detection method without any interference. The CZE methods are convenient, sensitive, reproducible and require no pernicious volatile organic solvent. CZE can be used in the routine monitoring of these pollutants in swimming pool water.

Acknowledgements

The authors thank the National University of Singapore for financial support.

References

[1] National Interim Primary Drinking Water Regulation, US EPA Publication No. 570/9-76-003, 1976.
[2] K. Holl, Water—Examination Assessment Conditioning Chemistry Bacteriology Biology, Walter de Gruyter, Berlin, Germany, 1972, 389 pp.
[3] J.A. Beech, R. Diaz, C. Ordaz, B. Palomeque, Am. J. Public Health 70 (1980) 79.
[4] E.L. Johnson, K.K. Haak, Liquid Chromatography in Environmental Analysis, Humana, Clifton, NJ, 1983, 291 pp.
[5] O.A. Shpigun, Y.A. Zolotov, Ion Chromatography in Water Analysis, Ellis Horwood, Chichester, UK, 1988, 188 pp.

ELSEVIER

Talanta 45 (1998) 663–671

Talanta

Application of capillary electrophoresis to process monitoring in the manufacturing of semisynthetic penicillins

H.B. Wan [a], J. Liu [a], K.C. Ang [a], S.F.Y. Li [b,*]

[a] *CE Resources Pte Ltd, Innovation Centre, National University of Singapore, Singapore 119260, Singapore*
[b] *Department of Chemistry, National University of Singapore, Institute of Materials Research and Engineering, 10 Kent Ridge Crescent, Singapore 119260, Singapore*

Received 5 February 1997; received in revised form 22 May 1997; accepted 23 May 1997

Abstract

Application of capillary electrophoresis to monitoring the concentration of material penicillin and the intermediates in the manufacturing process of semisynthetic penicillins was investigated. Factors affecting the precision of analysis were screened and optimised by orthogonal array designs. Compared to conventional HPLC methods, the capillary electrophoresis method gives better resolution and faster sample throughput. Other advantages of the capillary electrophoresis method over HPLC methods include much less consumption of buffer solution and the absence of organic solvents in the analysis. © 1998 Elsevier Science B.V.

1. Introduction

The penicillins are a group of antibiotics produced wholly or in part as microbial metabolites. As shown in Fig. 1, all penicillins contain a common bicyclic nucleus consisting of fused β-lactam and thiazolidine rings with different acylamino side chains at the C-6 position. There are two basic processes for the production of penicillins. One is by growing a penicillin mould in the presence of proper side chain precursor (fermentation process) and the other is by acylation of 6-amino penicillanic acid (6-APA). Penicillins produced by the second process are called semisynthetic penicillins. The chemical reactions in the process of semisynthetic penicillins are shown in Fig. 2. In the first step, a penicillin produced by fermentation process is hydrolysed under the catalysis of an enzyme to produce 6-APA which contains the common bicyclic nucleus of penicillin. In the second step, the 6-APA is acylated with different acyl groups to give different semisynthetic penicillins.

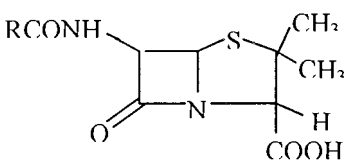

Fig. 1. Chemical structure of penicillins.

* Corresponding author. Tel.: +65 7722681; fax: +65 7782987.

PII S0039-9140(97)00293-2

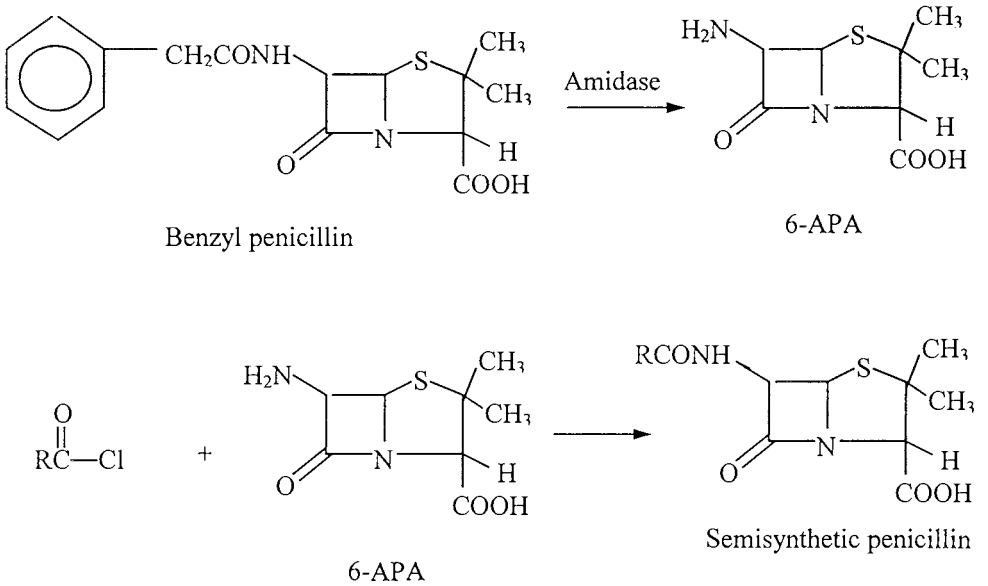

Fig. 2. Chemical reactions in manufacturing semisynthetic penicillins.

The monitoring of concentration of the material penicillin in the process is very important. If the reaction is terminated too early, a certain amount of material penicillin will be wasted. If the reaction is terminated too late, degradation of 6-APA will become significant, giving lower product purity and production yield. Currently, liquid chromatography is the predominant method for process monitoring of penicillins. Capillary electrophoresis is a relatively new but very promising analytical technique. It provides an alternative or complementary option for HPLC. Although in the past few years many investigations on the application of capillary electrophoresis to pharmaceutical analysis have been published, there have been few studies on routine process monitoring [1,2]. The present work investigates the application of capillary electrophoresis to process monitoring in the manufacture of semisynthetic penicillins. This paper also demonstrate the application of statistical experimental designs to the optimisation of analytical conditions.

2. Experimental

2.1. Chemicals

Disodium hydrogen phosphate (electrophoresis reagent) and phenylacetic acid (chemical reagent) were purchased from Sigma (St. Louis, MO). Sodium tetraborate anhydrous with purity above 99% were purchased from Fluka (Buchs, Switzerland). Water used for sample dilution and buffer preparation was obtained from a Nanopure ultrapure water system (Barnstead/Thermolyne, Dubuque, IA). Benzyl penicillin (Pen G), 6-amino penicillanic acid (6-APA) and the amidase beads for catalysis of Pen G hydrolysis were gifts from Beecham Pharmaceuticals, Singapore.

2.2. Preparation of process samples

Process samples for evaluation of the analytical methods were produced following conventional industrial process which involves mixing Pen G solution with amidase beads at 37°C while maintaining the pH at 8.0 by addition of sodium

hydroxide solution. The reaction solution (sometimes called enzymation solution) was sampled at different reaction stages and diluted 50–100 times with water prior to instrumental analysis.

2.3. Instrumentation

Capillary electrophoresis was performed on a Model 270A capillary electrophoresis system (Applied Biosystems, Foster City, CA) equipped with a 30-kV power supply and a UV spectrophotometric detector connected to a data acquisition system. Typical conditions for capillary electrophoresis analysis: fused silica capillary column, 43 cm total length/24 cm effective length/50 μm I.D.; running buffer, 30 mM tetraborate (natural pH 9.2); applied voltage, 15 kV; column oven temperature, 30°C; injection, hydrodynamic/1 s at 12.7 cmHg pressure difference (equivalent to an injection volume of about 6 nl).

3. Results and discussion

3.1. Selection of conditions for capillary electrophoresis separations

Since both Pen G and its reaction products exist as anions at pH above 7, and the difference in molecular size among the analytes is rather large, free solution capillary electrophoresis should be sufficient for a complete separation. The initial conditions were selected by rule of thumb. The final conditions for the separation was selected after comparing the effects of running buffer (borate and phosphate), the pH of running buffer (7.5 and 9.4), the concentration of the electrolyte (10, 20, and 40 mM) and the length of the column (55 cm total length/43 cm effective length and 50 cm total length/38 cm effective length). Figs. 3–6 show the resultant electropherograms under different conditions. Sodium tetraborate gave sharper peaks than disodium hydrogen phosphate as running buffer at the same molarity, though the analytes had shorter migration times in the latter case (Fig. 3). Reducing the electrolyte pH from 9.4 to 7.5 adversely affected the shape of peaks (Fig. 4). Higher electrolyte concentrations tended to give narrower peaks although the migration times of analytes were longer. The migration time can be reduced considerably by using a shorter capillary column. The effect of column length on the migration time under similar voltage and buffer conditions can be calculated using the following equation:

$$\frac{t_2}{t_1} = \frac{l_2 L_2}{l_1 L_1}$$

where l is the effective length of capillary column and L is the total length of the capillary column. As shown in Fig. 6, the migration time of the last peak (phenyl acetic acid) was reduced from 9.81 to 6.98 min when the capillary was reduced by 5 cm at the sample inlet end. In the later experiments, sodium tetraborate at 30 mM was used as running buffer. The length of capillary was reduced further to 43 cm total length/23 cm effective length to cut the analysis time. Under the selected conditions, benzyl penicillin and the two reaction products were well separated. The migration time for the last peak was 5 min (Fig. 7).

3.2. Conditions for column rinse prior to electrophoresis

The effects of type of rinsing solution and time of rinse on the repeatability of migration times were investigated. A 5-min rinse with 0.1 M NaOH solution prior to rinse with running buffer improved the reproducibility of migration time considerably. The best reproducibility of migration time was obtained when 1.5% H_3PO_4 was used for the first rinse. A relative standard deviation (RSD) on migration time of 0.42% was obtained from ten consecutive electrophoresis runs when a 4-min rinse with phosphoric acid and a 5-min running buffer rinse were adopted prior to each electrophoresis run.

3.3. Optimisation of variables for precision of analysis

In process monitoring, the speed and the reproducibility of analysis are of the most concern. The precision of a capillary electrophoresis analysis may be affected by many variables such as those

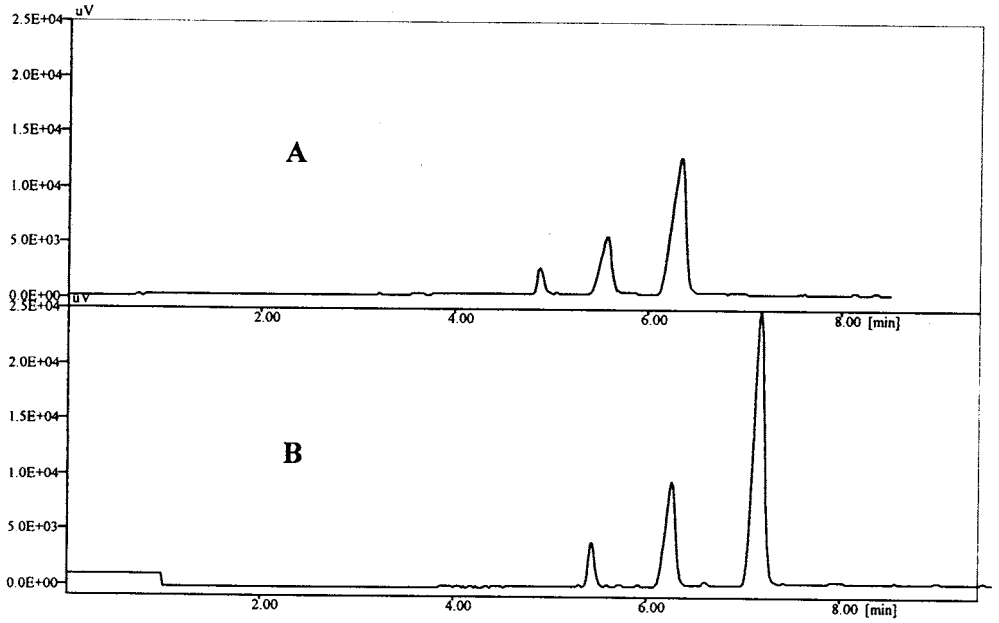

Fig. 3. Effect of electrolytes on the separation of benzyl penicillin (Pen G), 6-APA, and phenyl acetic acid. (A) 20 mM Na_2PO_4 (pH 9.0); (B) 20 mM borate (pH 8.9). Injection, 10 s/10 cm by gravity; capillary column, fused silica/55 cm total length/43 cm effective length/50 μm I.D.; voltage, 15 kV; UV detection, 210 nm.

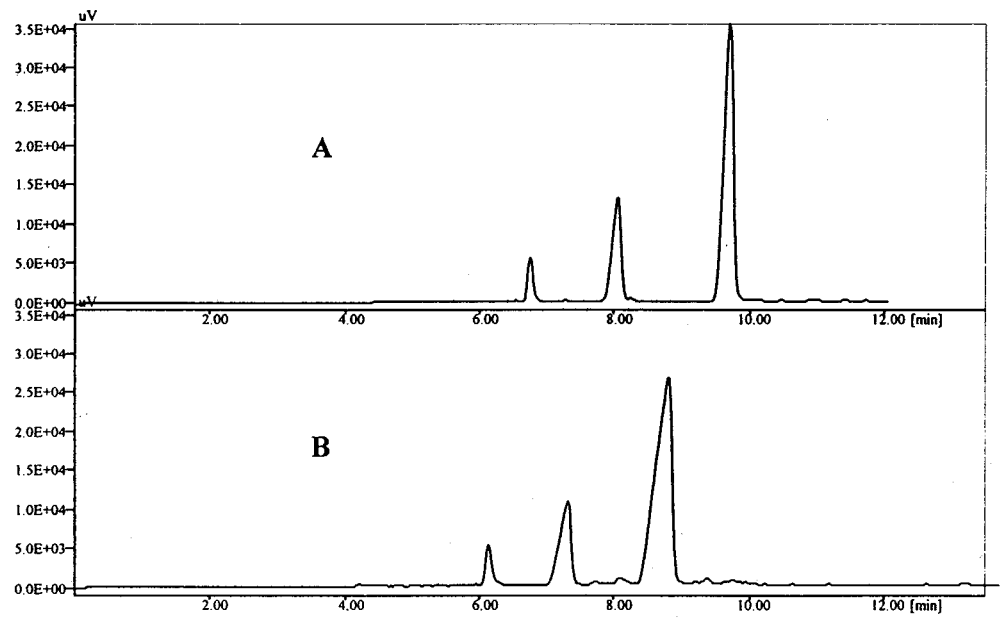

Fig. 4. Effect of pH on the separation of Pen G, 6-APA and phenyl acetic acid. (A) 40 mM borate (pH 9.4) as running buffer; (B) 40 mM borate + H_3PO_4 (pH 7.5) as running buffer. Other conditions of electrophoresis were the same as described in Fig. 3.

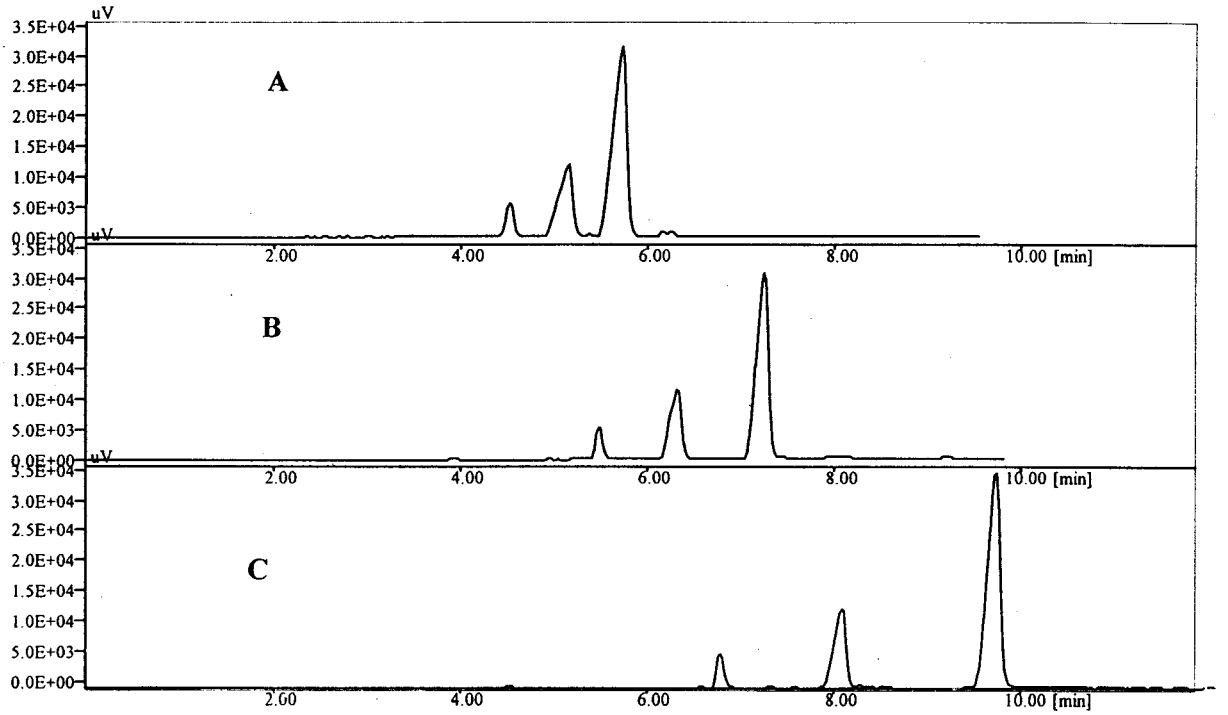

Fig. 5. Effect of electrolyte concentration on the separation of Pen G, 6-APA, and phenyl acetic acid. (A) 10 mM borate as running buffer; (B) 20 mM borate as running buffer; (C) 40 mM borate as running buffer. Other conditions of electrophoresis were the same as described in Fig. 3.

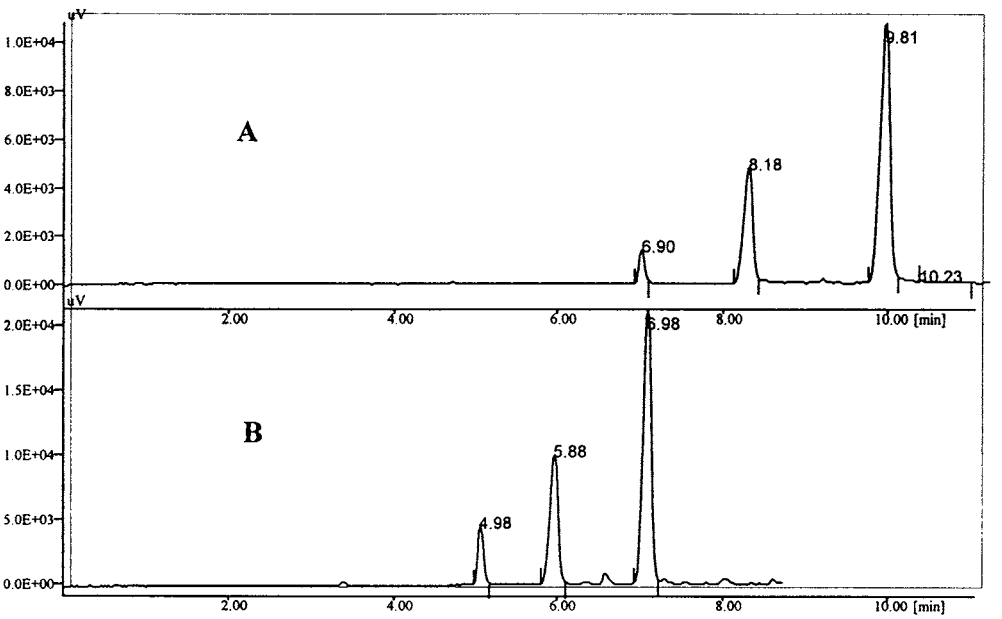

Fig. 6. Effect of capillary length on the migration time. (A) Capillary with 55 cm total length/43 cm effective length; (B) capillary with 50 cm total length/38 cm effective length. Other conditions of electrophoresis were the same as described in Fig. 3.

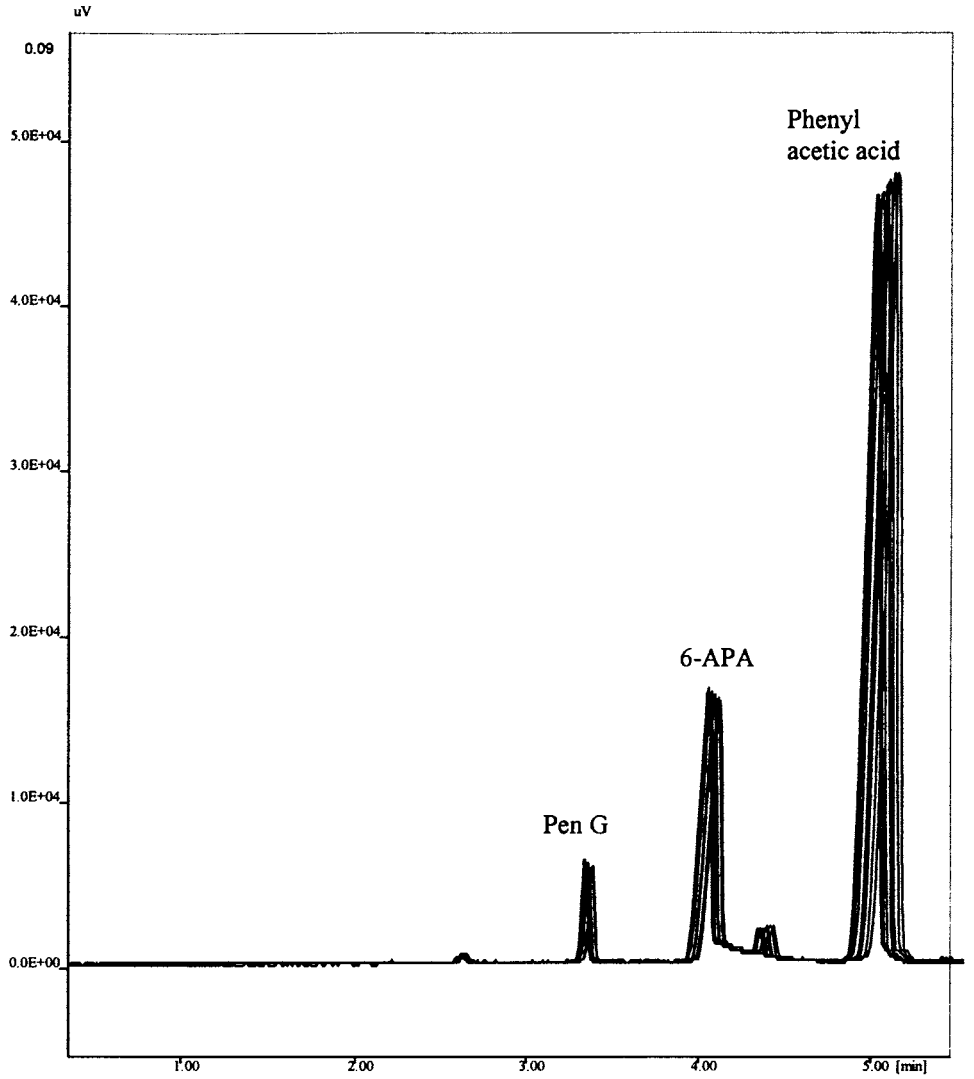

Fig. 7. Electropherograms of eight consecutive CE runs of one sample under the optimised conditions. CE conditions: capillary column, 43 cm total length/24 cm effective length/50 μm I.D.; running buffer, 30 mM borate; voltage, 15 kV; column oven temperature, 30°C; injection, hydrodynamic/1 s at 12.7 cmHg pressure difference; UV detection, 210 nm.

affecting the amount of injection (pressure difference, viscosity of sample, temperature, accuracy of timing, etc.), those affecting the reproducibility of CE runs (rinse cycle, sample properties, injection amount, degree of depletion of the running buffer, stability of instrument control, etc.), and those affecting accuracy of integration (peak recognition criteria and sampling speed). The effects of these variables may be investigated by trial and error methods, one-variable-at-a-time methods, or statistically designed method (e.g. factorial designs and orthogonal array designs). The trial and error methods can work well only if the experimenter is experienced and the number of variables is small. One-variable-at-a-time method can give conclusive results but requires large number of experiments and is difficult to study interactions between variables. When the

Table 1
An orthogonal array matrix for experimental design

Experiment	Columns						
	1	2	3	4	5	6	7
1	1	1	1	1	1	1	1
2	1	1	1	2	2	2	2
3	1	2	2	1	1	2	2
4	1	2	2	2	2	1	1
5	2	1	2	1	2	1	2
6	2	1	2	2	1	2	1
7	2	2	1	1	2	2	1
8	2	2	1	2	1	1	2

number of variables is large, methods based on statistically designed experiments are the most efficient choice. They can give more reliable results with much less experiments in comparison with the other two types of methods.

In the present work, orthogonal array designs were used to examine the effects of variables. In orthogonal array designs, orthogonal array matrices are used to arrange experiments whose results can then be analysed by using a common mathematical procedure. In an orthogonal array matrix, different combinations of numbers from any two columns have equal appearance frequency. Here 'orthogonal' means balanced. Although the mathematics behind this method may be complicated, the principle of the method is simple, that is to separate the effects of the variables by arranging the experiments in a balanced way. This method was applied to the optimisation of chromatographic separation and solid-phase extraction [3,4]. Table 1 is an orthogonal array matrix. Each row of the matrix represents an experiment and each column can be used to test a variable at two levels. This matrix indicates that seven variables at most can be tested by doing eight experiments. Normally four or five variables are tested by using such a matrix since some columns have to be used to test the interaction effects between the variables. The arrangement of the variables into the matrix follows the triangular table shown in Table 2. For example, if variable A is assigned to column 1 and variable B is assigned to column 2, the interaction effect between A and B should be assigned to column 3 as shown in the triangular table.

Table 2
Triangular table for arranging the interactions between each two columns

Column number	Column number					
	2	3	4	5	6	7
1	3	2	5	4	7	6
2		1	6	7	4	5
3			7	6	5	4
4				1	2	3
5					3	2
6						1

In the present investigation, four variables which may affect the precision of analysis were tested. The selection of these variables and the ranges for each variable were based on previous knowledge and experience of capillary electrophoresis (Table 3). Table 4 shows the arrangement of the experiments for testing the four variables. The arrangement follows the orthogonal array matrix given in Table 1. For each experiment, four consecutive capillary electrophoresis analysis were performed using the conditions for each experiment as indicated in Table 4. The relative standard deviation (RSD) of peak area for each experiment was calculated and used to assess the precision of the analysis. The results of the eight experiments are give in Table 5. The average RSD for each variable at the two levels were calculated from the experiment results according to the arrangement given in Table 4. For example, the variable rinse solution was set at level 1 in experiments 1, 3, 5, and 7, the average RSD for this variable at level 1 is calculated from experiments 1, 3, 5, and 7: $(2.98 + 1.24 + 4.05 + 0.36)/4 = 2.16$ (%). The effect for each variable is then calculated following the equation:

$$\text{Variable effect} = (\text{average RSD at level 1} - \text{average RSD at level 2})^2$$

A variable with a larger variable effect means it is more critical to the precision of analysis. The results of variable effects and the average RSD are shown in Table 6. Although the critical variables can be identified by a statistical procedure

Table 3
Variables tested by orthogonal array design for optimisation of analysis repeatability

Test level	Variables			Sampling time (s)
	Filtration of buffer	Time of second rinse (min)	Solution for first rinse	
1	Filtered buffer	5	0.1 M NaOH	1.0
2	Not filtered	10	1.5% H_3PO_4	1.4

Table 4
Experiment arrangement according to the orthogonal array matrix in Table 1

Experiment	Variables						
	Filtration of buffer	Time for the second rinse (min)	3[a]	Solution for first rinse	5[b]	6[c]	Sampling time (s)
1	Filtered	5	1	0.1 M NaOH	1	1	1.0
2	Filtered	5	1	1.5% H_3PO_4	2	2	1.4
3	Filtered	10	2	0.1 M NaOH	1	2	1.4
4	Filtered	10	2	1.5% H_3PO_4	2	1	1.0
5	Not filtered	5	2	0.1 M NaOH	2	1	1.4
6	Not filtered	5	2	1.5% H_3PO_4	1	2	1.0
7	Not filtered	10	1	0.1 M NaOH	2	2	1.0
8	Not filtered	10	1	1.5% H_3PO_4	1	1	1.4

[a] Column 3 is left for the interaction between variables assigned to columns 1 and 2.
[b] Column 5 is left for the interaction between the variables assigned to columns 1 and 4.
[c] Column 6 is left for interaction between variables assigned to columns 2 and 4.

such as *F*-test, a visual observation of the variable effects is sufficient in many cases. The results in Table 6 indicate that the sampling time, the solution for the first rinse, and the time for the second rinse with running buffer are critical variables. Table 6 also shows a significant interaction effect between the solution for first rinse and the time for the second rinse (column 6, variable effect = 1.93). Therefore, the effects of the two interactive variables are analysed separately. The results are given as follows:

When 0.1 M NaOH is used for first rinse the effect of the time of the second rinse is very critical; the average RSD is 3.52% with a 5-min second rinse and 0.80% with a 10-min second rinse. When 1.5% H_3PO_4 is used for the first rinse, the effect of time of the second rinse is not critical; the average RSD is 1.19% with a 5-min second rinse and 1.26% with a 10-min second rinse.

3.4. Summary of the optimisation results

Based on the analysis of the eight experiments, the following conditions were selected for analysis of penicillin in the process solution:

1. Use 1.5% phosphoric acid for the first capillary rinse,

Table 5
Results of the eight experiments

Experiment number	1	2	3	4	5	6	7	8
RSD (%)	2.98	1.62	1.24	1.05	4.05	0.76	0.36	1.46

Table 6
The average RSD for tested variables at each level and the effects of the variables

	Average RSD (%)						
	Filtration of buffer	Time for the second rinse	Column 3	Solution for first rinse	Column 5	Column 6	Sampling time
Level 1	1.72	2.35	1.61	2.16	1.61	2.39	1.29
Level 2	1.66	1.03	1.78	1.22	1.77	1.00	2.09
Effect[a]	0.0036	1.74	0.029	0.88	0.026	1.93	0.64

[a] Effect = (RSD at level 1 − RSD at level 2)^2.

2. Set the time of the second rinse with running buffer at 5 min,
3. Set the sampling time at 1 s.

Ten consecutive electrophoresis runs were performed under the selected conditions. The RSD was 2.2%. Another eight consecutive electrophoresis runs on another day gave a RSD of 2.1%. Such repeatability is as good as that of HPLC. The electropherograms of the eight CE runs are shown in an overlapped form in Fig. 7.

4. Conclusions

Capillary electrophoresis can be used for process monitoring in the manufacturing of semisynthetic penicillins. It has two notable advantages over HPLC: one is the absence of organic solvents and the other is much less consumption of running buffer. Less than 1 l of running buffer is sufficient for 1 week of analysis, saving much time in buffer preparation. This work also demonstrated the successful application of orthogonal array designs to the optimisation of capillary electrophoresis analysis. In the present work, a RSD of 2.1–2.2% in peak area was achieved. More variables may be tested by another round of experiments if better repeatability is required.

References

[1] P. Emaldi, S. Fapanni, A. Baldini, J. Chromatogr. 711 (1995) 339.
[2] S.F.Y. Li, C.L. Ng, C.P. Ong, Pharmaceutical analysis by capillary electrophoresis, in: P.R. Brown, E. Grushka (Eds.), Advances in Chromatography, Marcel Dekker, New York, 1995, pp. 199–257.
[3] H.B. Wan, W.G. Lan, M.K. Wong, C.Y. Mok, Anal. Chim. Acta 289 (1994) 371.
[4] H.B. Wan, W.G. Lan, M.K. Wong, C.Y. Mok, Y.H. Poh, J. Chromatogr. 677 (1994) 255.

ELSEVIER

Talanta 45 (1998) 673–681

Talanta

Detection of apolipoprotein E genotypes by capillary electrophoresis[1]

Evelyn S.C. Koay [a,b,*], Mingde Zhu [c], Tim Wehr [c], M.L. Choong [a], M.C. Khaw [b], S.K. Sethi [a,b], T.C. Aw [a,b]

[a] *Department of Pathology, National University of Singapore, Kent Ridge, Singapore 119260, Singapore*
[b] *Department of Laboratory Medicine, National University Hospital, Singapore 119074, Singapore*
[c] *Bio-Rad Laboratories, 2000 Alfred Nobel Drive, Hercules, CA 94547, USA*

Received 10 April 1997; received in revised form 21 July 1997; accepted 23 July 1997

Abstract

The apolipoprotein E (apo-E) genotype of an individual is of significant relevance in the associated risk of developing cardiovascular disease and late-onset Alzheimer's disease. Detection of the six common apo-E genotypes is based on the restriction fragment length polymorphisms (RFLPs) arising from the abolition or creation of *Hha*I restriction sites within an amplified target DNA sequence of the apo-E gene. Genomic DNA was extracted from leukocytes, a 230 bp target sequence within the apo-E gene was amplified by polymerase chain reaction (PCR) and digested with *Hha*I, and the restricted DNA fragments separated by capillary electrophoresis (CE). This was performed on the BioFocus™ 3000 automated CE system equipped with an experimental laser-induced fluorescence (LIF) detector (Bio-Rad Laboratories, Hercules, CA), using capillaries (27 cm length, 75 μm i.d.) coated internally with polyaminoacryloylethoxyethanol. The analysis buffer (2 × Tris borate–EDTA, pH 8.3) was supplemented with a proprietary sieving polymer and 0.05 μM thiazole orange six. Samples were injected electrophoretically. Separations were carried out at 40°C under constant voltage, and the emitted fluorescence detected at 515 nm. Restriction fragment lengths of the cleaved PCR products were estimated from the migration times, with a 20/100 bp ladder (Bio-Rad Laboratories 20/100 bp molecular ruler) serving as reference. Six different reproducible patterns were obtained for the six common apo-E genotypes, with good resolution of the component restriction fragments. The calculated sizes of the separated peaks closely corresponded with the predicted restricted fragment lengths for each specific genotype. We believe this is the first published report demonstrating the feasibility of automating the post-PCR detection of the apo-E RFLPs[2]. This methodology overcomes the most labour-intensive step in apo-E genotyping, thus making it amenable to routine clinical application. © 1998 Elsevier Science B.V.

Keywords: Apolipoprotein E; Capillary electrophoresis; Restriction fragment length polymorphisms

* Corresponding author: Tel.: + 65 7724564; fax: + 65 7780671; e-mail: patkoaye@nus.sg

[1] Establishments where the work was done: Department of Laboratory Medicine, National University Hospital, 5 Lower Kent Ridge Road, Singapore 119074 and Bio-Rad Laboratories, 2000 Alfred Nobel Drive, Hercules, CA 94547, USA.

[2] Since submission of this manuscript another paper has been published on the same subject, Clinical Chemistry 43 (1997) 1321.

PII S0039-9140(97)00286-5

1. Introduction

Detection of polymorphic loci or mutations in native target DNA sequences is frequently required in the diagnosis of human diseases at the molecular level [1,2]. Although the polymerase chain reaction (PCR) technology has significantly advanced the identification and quantification of nucleotide sequences [3,4], the complexity of conventional methods for post-PCR product detection such as hybridisation and slab gel electrophoresis, has severely limited the application of molecular techniques in clinical diagnosis.

Capillary electrophoresis (CE) has proven to be a powerful analytical tool for high resolution separation of double-stranded DNA (dsDNA) molecules and PCR products [5–11]. With CE, polymer solutions, known as 'entangled polymer networks' [5,6], simulate the pore structure of a gel and serve as excellent sieving media for separation of DNA fragments and oligonucleotides. In essence, the negatively charged DNA molecules, during migration towards the anode, must also navigate through this 'physical' gel matrix. Smaller fragments will be able to move through the matrix with greater speed whilst passage of the larger fragments is more hindered. This enables separation based on molecular mass to be achieved. While soluble polymers act as sieving media when incorporated into the buffer, they may also be covalently attached to the capillary wall to reduce the electroendosmotic flow (EOF) in fused silica capillaries to negligible levels [12]. In this study, the capillaries were covalently coated with polyaminoacryloylethoxyethanol (polyAAEE) to reduce EOF, and a proprietary polymer additive was used as a sieving medium in the analysis buffer.

Linear polymers, such as low- or zero-crosslinked polyacrylamide, polyethylene glycol, and methylcellulose derivatives [7], as buffer additives, have allowed for high-resolution separations within a narrow DNA size range. Using this approach, Del Principe et al. [8] showed, in their study of a fragment of the dystrophin gene, that CE is an effective tool for carrier detection and prenatal diagnosis of X-linked recessive disorders. McCord et al. [9,10] applied this technology to forensic applications. CE has also been shown to be of some use in the analysis of larger DNA fragments [6,11]. Much work remains to be done in the testing and development of novel, innovative sieving matrices with different selectivities.

The high sensitivity afforded by fluorescence detection has also been utilised to attain high resolution separations in the case of samples with very low analyte concentrations or very small sample volumes. Both diode lasers and lasers which operate in the deep ultraviolet (UV) are increasingly used in CE systems to provide excitation sources for laser-induced fluorescence (LIF) detection. Using both absorbance detection and LIF detection modes, McCord et al. [9,10] demonstrated the simplicity of post-PCR RFLP analysis by CE-LIF, with observed detection limits in the 500 ng/l range. Current detection limits extend to picomolar or attomolar concentrations of fluorescent labels or native fluorescent compounds [13,14].

The availability of automated systems combining advanced CE technology and LIF detection, e.g. P/ACE™ 5000 (Beckman Instruments, Fullerton, CA) and BioFocus™ 3000 (Bio-Rad Laboratories, Hercules, CA) CE systems provides the means to achieve fast, high-efficiency separations of DNA fragments, using minute amounts of samples. The resolution limit for the separation of DNA fragments with the present technology is ≈ 3 bp, but with the development of novel sieving matrices, achieving unit base resolution is within reach.

The structural apo-E gene locus on chromosome 19q is polymorphic, with three different co-dominant alleles—$\varepsilon 2$, $\varepsilon 3$, and $\varepsilon 4$, giving rise to three homozygous—$\varepsilon 2\varepsilon 2$, $\varepsilon 3\varepsilon 3$, and $\varepsilon 4\varepsilon 4$, and three heterozygous—$\varepsilon 2\varepsilon 3$, $\varepsilon 2\varepsilon 4$, and $\varepsilon 3\varepsilon 4$ genotypes, with varying frequencies [15]. The translated protein products of $\varepsilon 2$, $\varepsilon 3$, and $\varepsilon 4$ are called apolipoprotein E2, E3 and E4, respectively. This polymorphism arises from single base changes resulting in amino acid substitutions involving cysteine and arginine at residues 112 and 158. Apo-E, a constituent of triglyceride-rich lipoproteins such as chylomicrons and very low density lipoproteins (VLDL), is the recognition ligand for both the chylomicron remnant receptor and

the low density lipoprotein (LDL) receptor. The different apo-E variants are known to differentially influence clearance of plasma triglyceride-rich lipoproteins, via receptor-mediated endocytosis, and the presence of either $\varepsilon 2$ or $\varepsilon 4$ (in single or double dose) in lieu of the wild-type $\varepsilon 3$ allele, contributes to the atherogenic profile of an individual [16,17]. Inheritance of the $\varepsilon 4$ allele has also been shown to be associated with significantly higher risk of having late-onset familial Alzheimer's disease [18]. Determination of the apo-E genotype will thus enhance the assessment of patients for associated risk of coronary heart disease or late-onset familial Alzheimer's disease [16,19].

We explored the feasibility of using CE-LIF as a direct and automated post-PCR detection system for apo-E genotypes. In this paper we report the use of an automated CE-LIF system, coated capillaries and a sieving buffer with a mono-intercalating fluorescent dye to produce rapid, high-resolution separations of the restriction fragment length polymorphisms (RFLPs) of the six common apo-E genotypes. In addition, we also showed that sample desalting in conjunction with electrophoretic sample injection result in more efficient separations, with fewer non-specific interfering peaks and less background noise.

2. Experimental

2.1. Preparation of DNA samples

Genomic DNA was extracted from leukocytes (EDTA- or Heparin-anticoagulated blood), as previously described [20]. The DNA pellet was reconstituted in Tris–EDTA buffer (10 mM Tris–HCl, 0.1 mM EDTA, pH 8.0) to a final concentration of about 300 ng/μl and stored at −70°C. To date, we have a stock of more than 1200 DNA samples collected from both healthy volunteers and patients.

2.2. PCR amplification and HhaI digestion of PCR products

A 230-base target sequence of the apo-E gene was amplified by PCR, as described by Hixson and Vernier [21], with slight modification. The sequences of the two primers are 5′-ACA-GAATTCGCCCCGGCCTGGTACAC-3′ (F4) and 5′-TAAGCTTGGCACGGCTGTCCAAGG-A-3′ (F6). The PCR reaction mixture (final volume = 30 μl) contained 600 ng DNA, 50 pmol of each primer, 10% DMSO, 200 μM dNTP mix, 1.5 mM $MgCl_2$ and 1 U Taq DNA polymerase (Promega, Madison, WI) in a reaction buffer supplied by the same manufacturer. The reaction mixture was heated to 95°C for 5 min, followed by 30 cycles of 95°C (30 s), 60°C (1 min) and 72°C (1 min). The amplified PCR products were digested for 2 h or overnight at 37°C with 4 U of *Hha*I (Amersham, UK). The cleaved PCR products were diluted 10-fold with 0.4 mM Tris borate–EDTA buffer (EDTA 0.01mM, pH 8.0), and the RFLPs subsequently analysed by CE. It is recommended that the PCR-amplified products be desalted, purified and concentrated by diatomacious earth size-selective binding using the Prep-A-Gene™ DNA Purification System (Bio-Rad Laboratories) prior to restriction, dilution and CE analysis. This is to reduce the high salt content and to remove excess primers, and polymerised primer-dimers which, when present, will give rise to confounding non-specific peaks (see Section 3).

2.2.1. DNA molecular weight markers

A 20/100 bp ladder (Bio-Rad 20/100 bp Molecular Ruler) was not desalted but diluted 100-fold with the Tris borate–EDTA diluent prior to injection into the CE system.

2.3. Buffer system

The analysis buffer was 2 × TBE (178 mM Tris borate, 4 mM EDTA, pH 8.3). This buffer was supplemented with a proprietary sieving polymer and 0.05 μM thiazole orange six (TO6). The nature of the sieving polymer is undisclosed as the buffer is part of a commercial kit for the separation of double stranded DNA fragments (Bio-Rad Laboratories). The TO6 dye was added shortly prior to use and the buffer filtered to remove particulates and degassed by sonication.

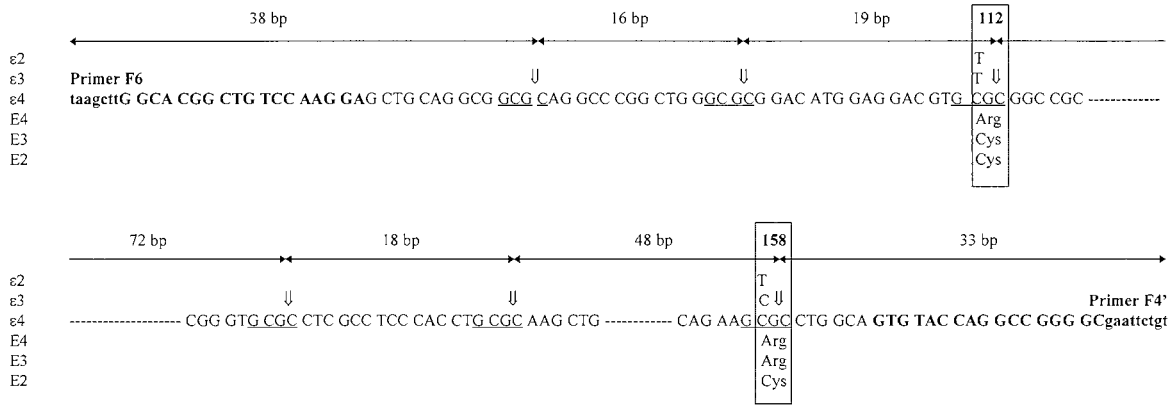

Fig. 1. DNA sequences of amplified regions of the apo-E gene encoding common apo-E genotypes and locations of *Hha*I restriction sites. The sequences of amplification primers (F6 and F4′, the reverse complement of F4) are shown in bold; only the nucleotides printed in upper case letters are part of the apo-E gene sequence. Nucleotide changes that distinguish the ε2, ε3 and ε4 alleles at codons 112 and 158 and the resultant amino acid substitutions are highlighted (within the boxes); substitution of a T by a C creates an *Hha*I restriction site and vice versa. The cleavage sites for the *Hha*I restriction enzyme in the ε4 sequence are underlined and marked by vertical arrows, and the lengths of the resulting restriction fragments are indicated by the horizontal arrows as being (from left to right) 38, 16, 19, 72, 18, 48 and 33 bp. Only the 38, 16 and 18 bp fragments are common to all apo-E genotypes. Homozygous ε2ε2 samples will have, in addition to these shared fragments, 91 and 81 bp fragments reflecting the absence of cleavage sites at 112cys and 158cys. A homozygous ε3ε3 sample will contain, besides the shared fragments, the 91 bp (no cleavage site at 112cys) and two other fragments of 48 and 33 bp, from cleavage at the *Hha*I site at 158arg. RFLPs from heterozygous genotypes (ε2ε3, ε2ε4 and ε3ε4) will show combinations of both sets of RFLPs of each allele. The smaller fragments below 30 bp do not appear in the electrophoretograms in Figs. 2–5.

2.4. The CE system

All CE separations were performed on a Bio-Focus 3000™ automated CE system equipped with an experimental LIF detector (Bio-Rad Laboratories). Surface-modified fused silica capillaries (75 μm i.d., 27 cm length, 19.5 cm effective length) were used for all analyses. These capillaries were coated internally with a linear polymer, polyAAEE, to suppress EOF. The capillary cassette was maintained at 40°C with flowing water as coolant. Prior to a run, it was purged with run buffer for 60 s at 100 psi, and the capillary and high voltage electrode surfaces were rinsed with water to prevent carryover of the viscous sieving buffer into the sample solution. Sample injection was performed electrophoretically at 3.5 kV for 10 s. Separations within the coated capillary were carried out under constant voltage (3 kV) with negative (inlet)-to-positive (detector) polarity (reversed polarity mode). Detection was achieved by excitation at 488 nm using an argon ion laser and emitted fluorescence was collected at 515 nm. Typically, CE runs take 10–15 min per sample.

Migration times were determined and post-run analysis of data was performed using the BioFocus™ integration software. Restriction fragment lengths (in bp) were estimated by comparison with a 20/100 bp ladder (Bio-Rad 20/100 bp Molecular Ruler) diluted 100-fold with the Tris borate–EDTA diluent. Tracings of the molecular weight marker were superimposed on those of the samples using the BioFocus™ integration software for this purpose.

3. Results and discussion

3.1. DNA restriction fragment analysis

Six unique patterns with good resolution of the component fragments were obtained for the six apo-E genotypes. The positions and the number

of peaks obtained were characteristic of each apo-E genotype and the patterns were reproducible. The characteristic patterns are based on the RFLPs arising from the abolition or creation of *Hha*I restriction sites within the 244-base amplified DNA sequence (Fig. 1). Substitution of a T by a C creates an *Hha*I restriction site and vice versa.

Fig. 2 is the CE resolution pattern of the DNA from an individual with an apo-$\varepsilon3\varepsilon3$ genotype. It is an example of a typical run obtained when the CE sieving buffer system was applied to an *Hha*I-cleaved PCR-amplified sample which was not 'cleaned' prior to injection. Due to materials used in the PCR process, the sample had a relatively high salt content and contained several non-specific low molecular weight materials (see below), which required removal in order to obtain higher detectability and peak efficiency. The apo-$\varepsilon3\varepsilon3$ genotype is the most common of the six genotypes, occurring with a frequency of 68.8% in the Singaporean population (Koay et al., data submitted for publication). The others, in decreasing order of frequency, are $\varepsilon3\varepsilon4$ (17.0%), $\varepsilon2\varepsilon3$ (10.2%), $\varepsilon2\varepsilon4$ (2.3%), $\varepsilon2\varepsilon4$ (1.3%), and $\varepsilon2\varepsilon2$ (0.4%).

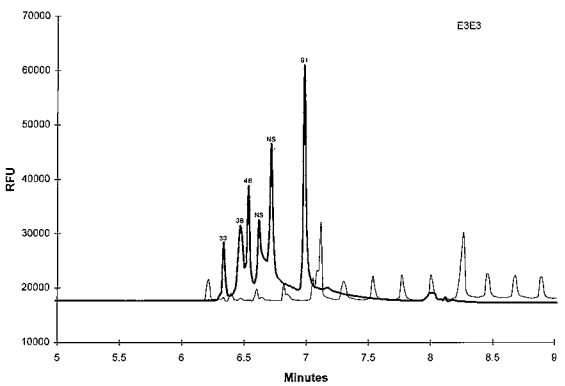

Fig. 2. The CE resolution of the restriction fragments of an 'untreated' DNA sample from an individual with the apo-$\varepsilon3\varepsilon3$ genotype. The restricted PCR-amplified products were diluted 10-fold with 0.4 mM TBE, pH 8.0 and injected electrophoretically at 3.5 kV for 10 s. Separation was performed in a 75 μm (i.d) × 27 cm polyAAEE-coated capillary, using a 2 × TBE buffer containing a proprietary linear polymer and 0.05 μM TO6 dye, pH 8.3. Detection of emitted fluorescence was at 515 nm on a BioFocus™ 3000 CE system fitted with an experimental LIF detector. Restriction fragment lengths are 91, 48, 38 and 33 bp; the two peaks with migration times between 6.6 and 6.8 min represent non-specific impurities (see text and Fig. 3 for explanation). Peaks of component restriction fragments in Figs. 2–5 are identified by fragment size (number of bp); the two non-specific peaks are labelled NS.

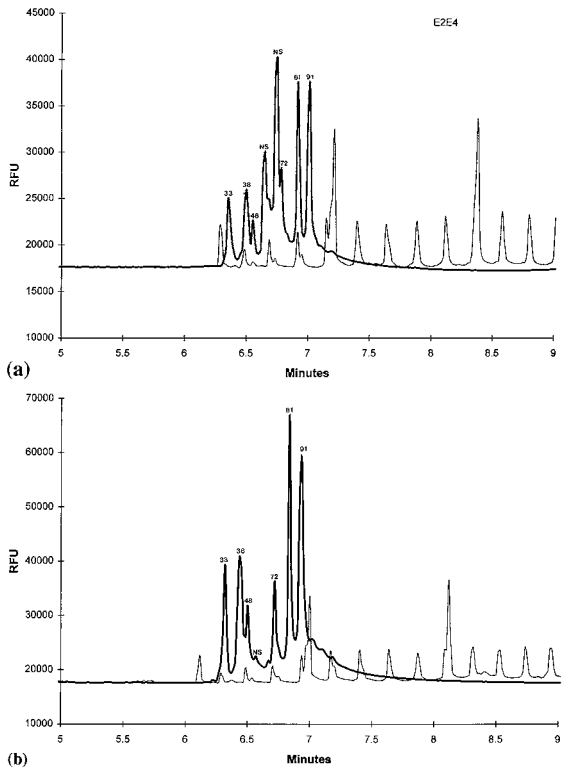

Fig. 3. CE resolution of two aliquots of PCR-amplified products from an individual with apo-$\varepsilon2\varepsilon4$ genotype. The two electrophoretograms, (a) and (b), from consecutive runs, demonstrate the effect of a clean-up step using the Prep-A-Gene DNA Purification System (Bio-Rad Laboratories) on the PCR products. (a) The CE pattern for an untreated aliquot and (b) that of a treated aliquot. Run conditions were as in Fig. 2. The peaks resolved are typical of RFLPs derived from the apo-$\varepsilon2\varepsilon4$ genotype, with restriction fragment lengths of 91, 81, 72, 48, 38 and 33 bp. In (a) the two NS peaks with migration times of ≈6.6 and 6.8 min are the major non-specific 'contaminants' peaks. In (b) they have been effectively removed (see text for explanation). Removal of buffer salts, primers, primer-dimers and other impurities resulted in a slight shift in the migration times of the restriction fragments.

Fig. 3(a) shows the more complex high-resolution separation pattern of an individual with a heterozygous $\varepsilon2\varepsilon4$ genotype. In both Figs. 2 and 3(a), two extra non-specific peaks were detected, with migration times of ≈6.6 and 6.8 min. The same two peaks are also evident in the CE data (Fig. 4) from a negative control which was not

'pre-cleaned'. The negative control data indicates that PCR products which are not treated with the Prep-A-Gene™ protocol contain lower molecular weight materials such as single-stranded primers, dNTPs, and primer-dimers. The latter, in particular, may co-migrate with, or close to, a PCR fragment of interest, due to their sizes (≈ 50 bp). As shown in Fig. 3(b), the Prep-A-Gene™ procedure removes the two major non-specific peaks as well as other minor components. Fig. 3(a) and 3(b) are results from the same DNA sample, processed in the same manner but omitting the Prep-A-Gene step in one instance (Fig. 3(a)) and processing the duplicate sample through this clean-up step (Fig. 3(b)).

Fig. 5 shows the characteristic CE patterns of the $\varepsilon 2\varepsilon 2$ (Fig. 5(a)), $\varepsilon 4\varepsilon 4$ (Fig. 5(b)), $\varepsilon 2\varepsilon 3$ (Fig. 5(c)), and $\varepsilon 3\varepsilon 4$ (Fig. 5(d)) genotypes. None of these samples were 'cleaned' using the Prep-A-Gene DNA purification system.

In Figs. 2–5, the separation profiles of the various PCR products and the negative control were shown with an overlay of the separation pattern of the 20/100 bp ladder molecular weight marker. This facilitates estimation of the sizes of the various restriction fragments represented by the peaks. Fig. 6 shows the migration times of DNA fragments in the size range of 33–91 bp. The estimated sizes of the component restriction fragments of six samples representing all six apo-E genotypes are plotted on the x-axis (mean $\pm$ SD). We first constructed a calibration curve

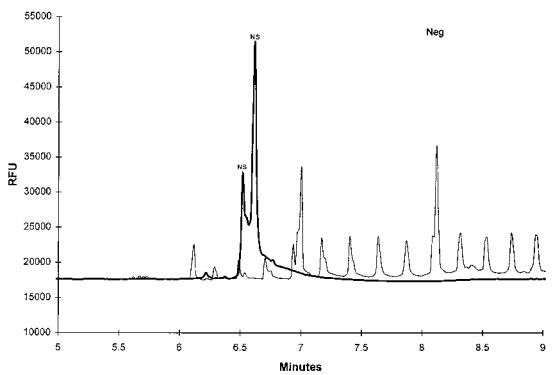

Fig. 4. The CE profile of an 'untreated' negative control sample. Two major non-specific (NS) 'contaminants' peaks are clearly evident. Run conditions were as in Fig. 2.

based on the known sizes of the 20/100 ladder fragments and their relative migration times, and used it to calculate the apo-E restriction fragment lengths from their measured migration times. The linear relationship obtained in Fig. 6 confirms that calculated sizes of the separated peaks closely corresponded to the expected (predicted) sizes of the component fragments of the RFLP for each specific apo-E genotype. Thus CE can be used to replace the more labour-intensive polyacrylamide gel electrophoresis (PAGE) in the post-PCR identification of the RFLPs for each specific apo-E genotypes.

3.2. Method optimisation

The classic separation technique for DNA fragments or oligonucleotides employs slab gel electrophoresis followed by stain or probe detection. While this has been accepted as a standard method in the molecular biology field, several drawbacks exist. Because slab gel electrophoresis is time-consuming, labour-intensive, and difficult to quantitate, much less to automate, CE becomes an attractive alternative to the standard method. In the separation of double-stranded DNA fragments, such as those found in the analysis of PCR products and DNA restriction digests, mobility is independent of molecular weight under free solution conditions [22]. A sieving mechanism is required to separate components having the same mass-to-charge ratio. Non-crosslinked, linear polyacrylamide has been used in classical electrophoresis for DNA separations [23]. Zhu et al. [12] showed, with CE, that linear polymers could also be used as buffer additives to act as molecular sieves for the separation of protein and DNA fragments.

By selecting polymer additives of various average molecular weights and varying their concentration, a separation system similar to gel electrophoresis is created in which resolution can be optimised for a particular DNA size range [5]. The DNA restriction fragments obtained after *Hha*I cleavage of the PCR-amplified products in our apo-E genotyping procedure range in size from 16 to 91 bp. To resolve these small molecular weight components efficiently, we experi-

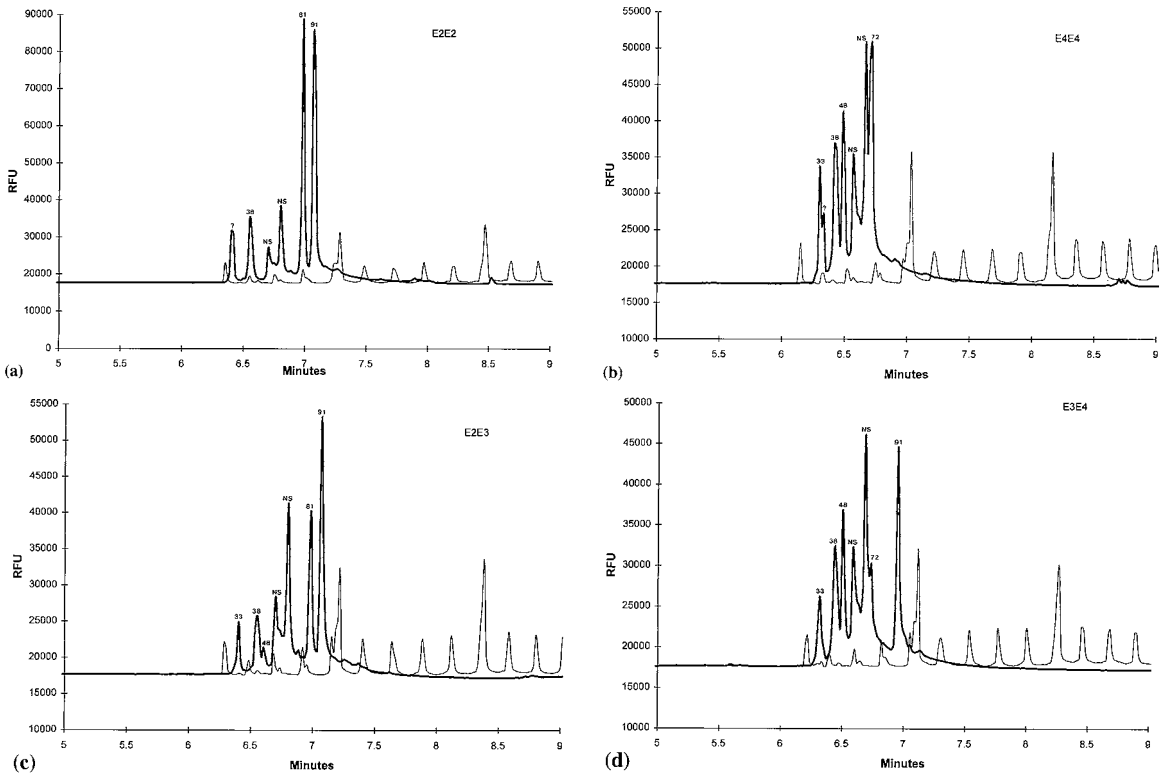

Fig. 5. CE separation profiles of four common apo-E genotypes: $\varepsilon 2\varepsilon 2$, $\varepsilon 4\varepsilon 4$, $\varepsilon 2\varepsilon 3$ and $\varepsilon 3\varepsilon 4$. The PCR products were not treated to remove buffer constituents, primers and polymerised primer-dimers. The latter gave rise to the 'non-specific' (NS) peaks between 6.6 and 6.8 min migration times. Run conditions were as in Fig. 2. The characteristic RFLPs, with the restriction fragments (in bp), in ascending order of migration times, are: a, apo-$\varepsilon 2\varepsilon 2$ (38, NS, NS, 81, 91)*; b, apo-$\varepsilon 4\varepsilon 4$ (33, 38, 48, NS, NS, 72); c, apo-$\varepsilon 2\varepsilon 3$ (33, 38, 48, NS, NS, 81, 91); d, apo-$\varepsilon 3\varepsilon 4$ (33, 38, 48, NS, NS, 72, 91). In all cases, smaller fragments of < 20 bp were not detectable. * An additional peak, with migration time of ≈ 6.3 min, was observed. As it corresponded with a fragment size of ≈ 25 bp, it was probably caused by an excess of the two primers used in the PCR amplification.

mented with various polymer additives, arriving at a proprietary polymer with proper sieving properties for resolution of the apo-E restriction fragments. Resolution was further improved by the elimination of EOF using capillaries, whose internal wall surfaces were covalently coated with polyAAEE.

For a specific size range, analysis times can be shortened by using a shorter capillary, an increase in field strength, or both. This occurs at the expense of some resolution (data not shown). Higher fields generate more Joule heat, leading to impaired separation performance. This poser may be partially resolved through the use of capillaries with smaller internal diameters (25–50 μm in lieu of 75–100 μm) which would permit higher fields and less Joule heat generation. However, the use of very small capillaries (25–50 μm i.d.) is not practical in our situation, as sample detectability is sacrificed.

From the data presented above, it is obvious that the cleaning-up step will remove much of the relatively high salt content of the PCR reaction buffer as well as other non-specific interfering materials. However, because of the reproducible and characteristic RFLPs for the six common apo-E genotypes, it is a moot point whether the additional expense and effort is worthwhile in

routine, non-quantitative apo-E genotyping, provided the results are interpreted alongside an intra-batch run of a negative control treated in identical manner to the samples.

We have demonstrated excellent separation efficiency using optimised sieving buffers and appropriately coated capillaries for the DNA restriction fragments generated from our apo-E genotyping protocol. Our results demonstrate the feasibility of using the CE-LIF combination for automated post-PCR detection of apo-E genotypes, making it possible to routinely carry out this molecular diagnosis in a clinical laboratory setting. This CE system enables the post-PCR separation step of the apo-E genotyping to be automated and results in a substantial reduction of analysis time when compared with the standard separation methods of PAGE and other slab gel electrophoresis. It provides yet another example to a rapidly growing list demonstrating the vast potential of CE systems for automating a variety of diagnostic, clinical and forensic applications at the molecular level, including DNA restriction fragment mapping and PCR product analysis.

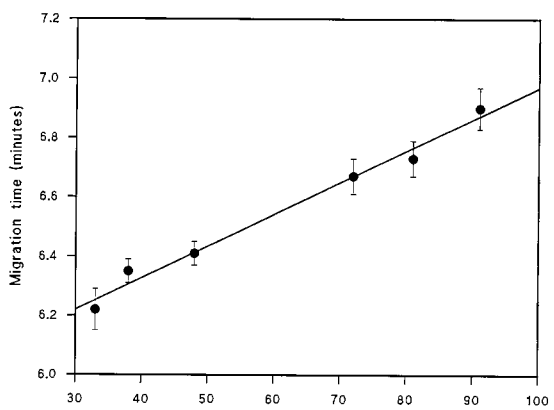

Fig. 6. Relationship between the restriction fragment lengths obtained from all 6 apo-E genotypes shown in Figs. 2 and 3 and Fig. 5, and their relative migration times. Calculation of the estimated fragment sizes (lengths) was based on a calibration plot of the migration times vs. known sizes of the 20/100 bp ladder (Bio-Rad Laboratories 20/100 bp Molecular Ruler). The means ± SD are plotted. See text for explanation.

Acknowledgements

The authors gratefully acknowledge the provision of research grants by the National Medical Research Council, Singapore (RP # 0940357) and the Singapore Totalizator Board to E.S.C. Koay, which enabled this project to be funded. We are very grateful to Mr Tong Ping Heng, Regional Manager, Pacific-ASEAN, and Miss Veronica C.N. Tok, Product Manager, Bio-Rad Laboratories (Singapore) Pte, for their assistance and unstinting support in coordinating specimen transportation and other communications between the Singaporean and USA co-workers of this project.

References

[1] D.J. Weatherall, The New Genetics and Clinical Practice, 3rd ed., Oxford University Press, Oxford, 1991, pp. 1–3.
[2] R. Elles, An overview of clinical molecular genetics, in: R. Elles (Ed.), Molecular Diagnosis of Genetic Diseases, Humana Press, Totowa, 1996, pp. 1–16.
[3] F.L. Kiechle, Diagnostic molecular pathology in the 21st century, in: D.H. Farkas (Ed.), DNA Technology, Clinics in Laboratory Medicine, Vol. 16 (1), Saunders, Philadelphia, PA, 1996, pp. 213–222.
[4] A.A. Killeen, Quantitation of nucleic acids, in: D.H. Farkas (Ed.), DNA Technology in the Clinical Laboratory, Clinics in Laboratory Medicine, Vol. 17 (1), Saunders, Philadelphia, PA, 1997, pp. 1–20.
[5] H.E. Schwartz, K.J. Ulfelder, F.J. Sunzeri, M.P. Busch, R.G. Brownlee, J. Chromatogr. 559 (1991) 267.
[6] D.N. Heiger, A.S. Cohen, B.L. Karger, J. Chromatogr. 516 (1990) 33.
[7] K.J. Ulfelder, H.E. Schwartz, J.M. Hall, F.J. Sunzeri, Anal. Biochem. 200 (1992) 260.
[8] D. Del Principe, M.P. Iampieri, D. Germani, A. Menchelli, G. Novelli, B. Dallapiccola, J. Chromatogr. 638 (1993) 277.
[9] B.R. McCord, J.M. Jung, E.A. Holleran, J. Liq. Chromatogr. 16 (1993) 1963.
[10] B.R. McCord, D.M. McClure, J.M. Jung, J. Chromatogr. 652 (1993) 75.
[11] M. Strege, A. Lagu, Anal. Chem. 63 (1991) 1233.
[12] M. Zhu, D.L. Hansen, S. Burd, F. Gannon, J. Chromatogr. 480 (1989) 311.
[13] T. Higashijima, T. Fuchigami, T. Imasaka, N. Ishibashi, Anal. Chem. 64 (1992) 711.
[14] T.T. Lee, E.S. Yeung, J. Chromatogr. 595 (1992) 319.

[15] K.H. Weisgraber, S.C. Rall Jr., R.W. Mahley, J. Biol. Chem. 260 (1981) 6240.
[16] J.H. Contoise, B.A. Anamani, G.F. Tsongalis, The underlying molecular mechanism of apolipoprotein E polymorphism, in: D.H. Farkas (Ed.), DNA Technology, Clinics in Laboratory Medicine, Vol. 16 (1), Saunders, Philadelphia, PA, 1996, pp. 105–123.
[17] P. DeKnijff, A.M. van den Maagdenberg, R.R. Frants, et al., Hum. Mutat. 4 (1994) 178.
[18] W.J. Strittmatter, A.M. Saunders, D. Schmechel, et al., Proc. Natl. Acad. Sci. USA 90 (1993) 1977.
[19] G. Siest, T. Pillot, A. Regis-Bailly, B. Leininger-Muller, J. Steinmetz, M.M. Galteau, S. Visvikis, Clin. Chem. 41 (1995) 1068.
[20] S.A. Miller, D.D. Dykes, H.F. Polesky, Nucleic Acids Res. 16 (1988) 1215.
[21] J.E. Hixson, D.T. Vernier, J. Lipid Res. 31 (1990) 545.
[22] N.C. Stellwagen, Electrophoresis of DNA in agarose and polyacrylamide gels, in: A. Chrambach, M.J. Dunn, B.J. Radola (Ed.), Advances in Electrophoresis, Vol. 1, VCH, New York, 1987, pp. 177–228.
[23] H.J. Bode, Anal. Biochem. 83 (1977) 364.

ELSEVIER

Talanta 45 (1998) 683–691

Talanta

Capillary electrophoresis separation of *p*-sulfonated calix[*n*]arenes, $n = 4, 6, 8$

I. Rodriguez [a], H.K. Lee [a], S.F.Y. Li [b,*]

[a] *Department of Chemistry, National University of Singapore, Kent Ridge Crescent, Singapore 119260, Singapore*
[b] *Department of Chemistry and Institute of Materials Research and Engineering, National University of Singapore, Kent Ridge Crescent, Singapore 119260, Singapore*

Received 5 February 1997; received in revised form 13 May 1997; accepted 14 May 1997

Abstract

The CE separation of *p*-sulfonated calix[*n*]arenes, where $n = 4$, 6 and 8, was investigated. Under positive potential conditions optimum separation was found to be borate buffer modified with sodium dodecyl sulfate. Under these conditions separation was achieved in less than 10 min. The effect on the separation of the addition of divalent cations: Mg^{2+}, Ca^{2+} and Ba^{2+} was studied. *p*-Sulfonatedcalixarenes were detected in the anodic side of the capillary. There was an improvement in the reproducibility and analysis time although efficiency did not improve significantly. © 1998 Elsevier Science B.V.

Keywords: Capillary electrophoresis separation; *p*-sulfonated calix[*n*]arenes; Divalent cations

1. Introduction

Calixarenes are cavity-shaped oligomers which are obtained from the condensation of *p*-ter-butylphenol and formaldehyde [1]. The name calixarene [2] is due to the cone conformation adopted by the smallest oligomers, *p*-ter-butylcalix[4]arene and *p*-ter-butylcalix[5]arene. In order to maximize their intramolecular hydrogen bond, when the number of phenol units increase, the structures become flatter.

The growing interest in calixarenes derives from their ability to reversibly include small molecules and ions. There is an extensive complexation reported of the parent calixarenes in solid state [3] and in solution [4]. Calixarenes can act as host of neutral organic molecules [5] as well as selectively complexate metal cations such as cesium [6], calcium and lantanides [7] and organic cations such as amines [8,9]. The high interest in these compounds is also due to their large accessibility from inexpensive and readily available starting materials. Accordingly, the chemistry of calixarenes is widely investigated to explore new aspects and applications of their chemistry.

The use of parent calixarene in selective complexation of metal cations is severely limited by their low solubility in organic solvents and water. Therefore, it has been of particular interest to

* Corresponding author. Tel.: +65 874 2681; fax: +65 779 1691.

PII S0039-9140(97)00292-0

synthesize water soluble calixarenes and special derivatives whose complexing capabilities are more pronounced [10,11]. The first water soluble calixarenes were synthesized by Ungaro and coworkers [12] who prepared carboxylcalixarenes and Shinkai et al. [13] who prepared sulfonatocalixarenes. Recently, amino [14], nitro [15], phosphonato [16] calixarenes have been synthesized. The synthesis of these functionalized water soluble derivatives have enabled the study of the complexing capabilities of the calixarenes in solution and the development of new applications as catalyst, ligands and host molecules [17].

Sulfonated calixarenes have been used in capillary electrophoresis to modify selectivities for the separation of benzenediols and chlorophenols [18]. The separation of *p*-sulfonated calixarenes (4, 6 and 8) has been reported previously [19]. The separation was based on the reversal of the EOF by the use of different concentrations of Mg^{2+}.

In this study we investigated the separation of three *p*-sulfonated calixarenes, i.e. 4, 6 and 8, under conditions of positive and negative potential upon the addition of different cations: Mg^{2+}, Ca^{2+} and Ba^{2+}.

2. Experimental

p-Sulfonated calix[*n*]arenes standards (SCX[*n*], $n = 4,6,8$) were synthesized by literature methods (University of Western Australia). Water purified with Millipore System (Millipore, Bedford, MA, USA) was used to prepare buffers for CE. All chemicals were of analytical reagent grade. CE under positive potential conditions was carried out on a laboratory built system. A Spellman power supply was used (Painview, New York, USA). Peaks were detected with a Shimadzu (Kyoto, Japan) spectrophotometer (model SPD-6A). Injection was performed hydrodynamically for 10 s at a height difference of 10 cm. Experiments requiring negative potential were carried out in an Applied Biosystems Model 270A capillary electrophoresis system (Foster City, CA, USA). Injection was performed hydrodynamically by vacuum (12.7 cmHg) for 1 s. Data was processed on a Shimadzu (Kyoto, Japan) Chromatopac CR6A integrator. A fused-silica capillary (Polymicro Technologies, Phoenix, AZ, USA) of 50 μm ID, 30 cm effective length and 50 cm total length was used as separation column. New capillaries were pretreated by rinsing with 0.1 M NaOH for 5 min, rinsing with water for 2 min and buffer for 5 min before injection. Due to some adsorption of the SCX[*n*] in the positive potential conditions, between runs the capillary was washed with hot water for 10 min followed by buffer for 5 min. During the experiments carried out with negative potential operating conditions, in order to obtain good reproducibility, the capillary was initially equilibrated for 30 min with the running buffer and between runs was regenerated with buffer for 5 min. Calixarenes standards were dissolved in the running buffer ($\sim 10^{-4}$ M) which was composed of 25 mM boric acid and 25 mM sodium borate (pH 9). The applied electric field was 18 kV. All the analyses were conducted at room temperature (22°C). Experiments were performed in triplicate to ensure reproducibility.

3. Results and discussion

3.1. Positive potential conditions

SCX[*n*] bear the negative charge of the ionized sulfonated groups and in addition, further ionization of the phenolic OH groups can be expected. The acidities of these groups are determined by the system of intramolecular hydrogen bonds. The pK_{a1} value of SCX[4] is considerably reduced in comparison with the pK_a values of the corresponding linear phenols. Subsequent ionization occurs at a higher pH [20]. The pK_a of the SCX[4] has been determined [21] to be: $pK_{a1} = 3.26$, $pK_{a2} = 11.8$, $pK_{a3} = 12.8$ and $pK_{a4} = 14$. The reduction of the pK_{a1} is less for SCX[6] and SXC[8] and their pK_a values are comparable with those of the linear oligomers [20]. The values for SCX[6] were calculated [22] to be: $pK_{a1} < 1$, $pK_{a2} = 3$, $pK_{a3} = 4$ and $pK_{a4} > 11$. The values of SCX[8] have not been found in literature.

Therefore, at the working pH (i.e. pH = 9), SCX[*n*] are expected to carry negative charges (i.e. $SCX[4]^{5-}$ and $SCX[6]^{9-}$). Initial experiments

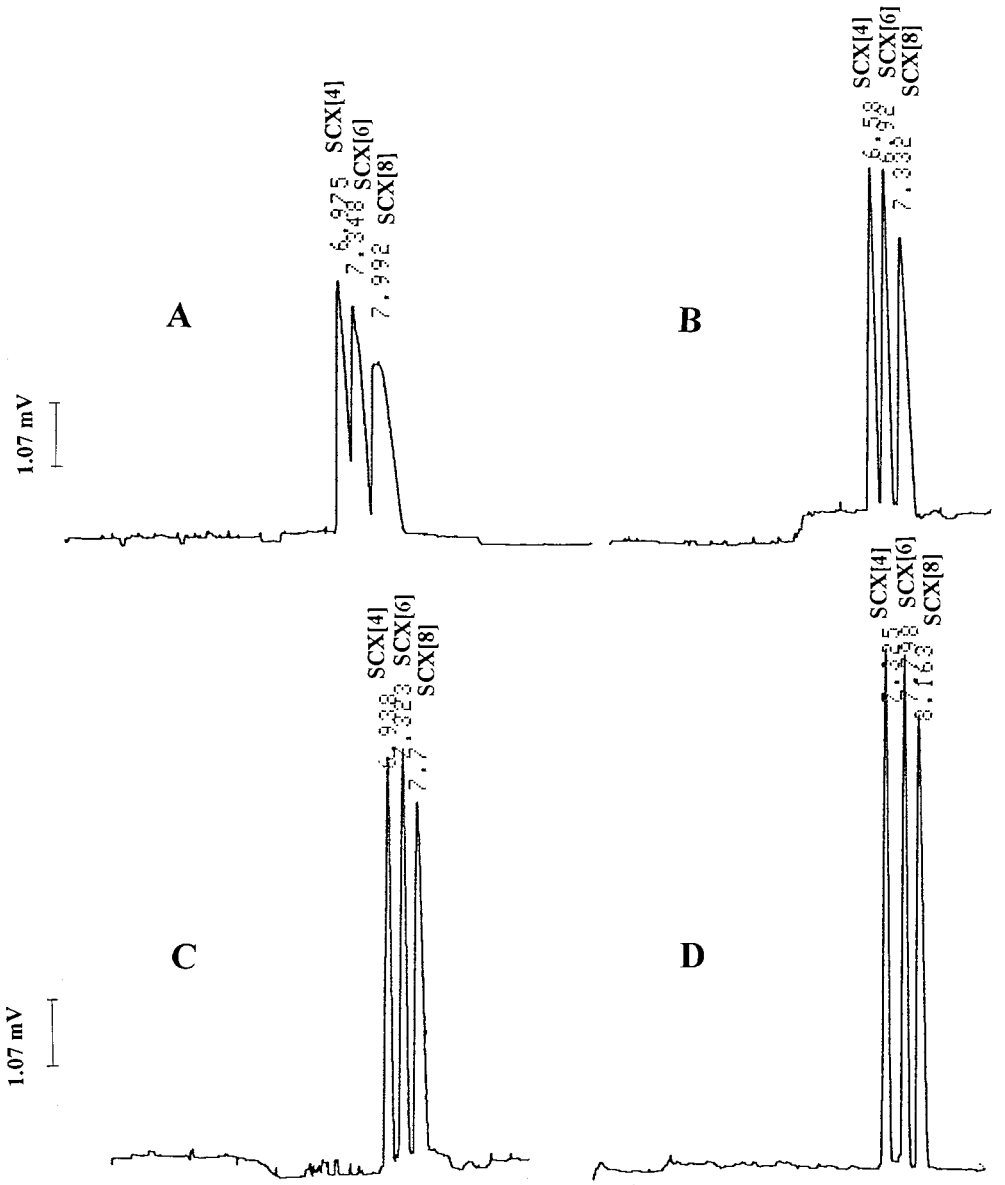

Fig. 1. Capillary electrophoresis separation of *p*-sulfonated calix[*n*]arenes, $n = 4$, 6, 8. Buffer: 25 mM boric acid/25 mM sodium borate, pH 9; separation capillary: 50 μm ID × 45 cm total length (effective length 30 cm); applied voltage: 18 kV; UV detection, 215 nm. Concentration of each peak is $\sim 10^{-4}$ M. (A Without addition of SDS; (B) with addition of 25 mM SDS; (C) with addition of 50 mM SDS; (D) with addition of 75 mM SDS.

showed that using the following buffer conditions: 25 mM boric acid/25 mM sodium borate, baseline separation could not be achieved and the SCX[*n*] showed very broad peaks. The electropherogram of the mixture of calixarenes under these conditions is shown in Fig. 1A. The migration order is tetramer, hexamer and octamer with a total migration time of 10 min. The negatively charged

SCX[n] detected on the cathode side are carried against their electrophoretic mobility by a strong EOF at pH 9 and separated by differences of charge to mass ratio. To improve resolution the effect of the addition of different concentrations of SDS was tested. 25 mM of SDS provided satisfactory separation of the SCX[n] with a relatively short analysis time (see Fig. 1B). These results indicate that there is solubilization and/or hydrophobic interaction of the analytes with the micelles. On the other hand, it should be noted that the migration times of the SCX[n] decreased slightly. The reason may be that the SCX[n] being solubilized by the micelles experienced an increase in mobility towards the cathode due to the fact that the micellar phase had a mobility towards the cathode higher than that for the analytes. As can be seen in Fig. 2, the peak of micellar marker, Sudan III has a shorter migration time than the analytes. Addition of 50 mM of SDS was be still more effective for complete separation of the SCX[n] and improvement of the peak shape (see Fig. 1C). With additions of SDS to 75 and 100 mM, further improvement in the resolution and peak shape of all the three compounds was obtained (see Fig. 1D). SDS (100 mM) was used in subsequent experiments for maximum efficiency and resolution (see Fig. 2). The results showed that as we increased the concentration of SDS from 25 to 100 mM, SCX[n] experienced an increase in migration time, which related to the increase in volume of the micellar phase [23], resulted in an improvement in resolution and peak shape.

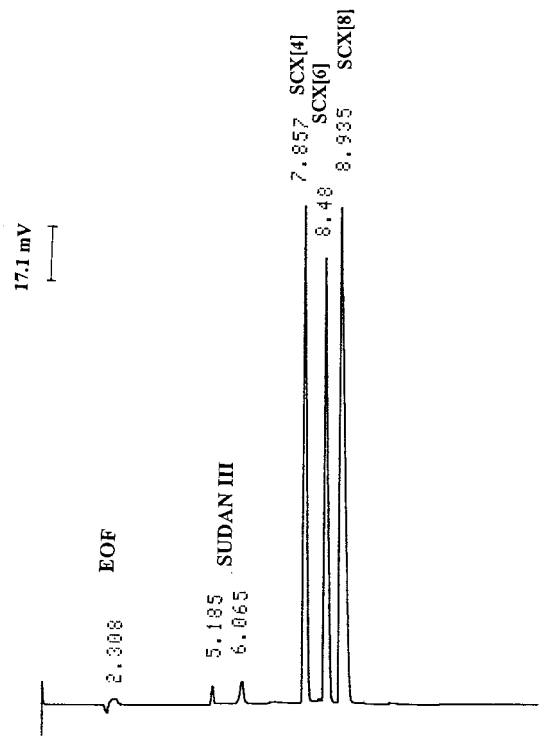

Fig. 2. Capillary electrophoresis separation of p-sulfonated calix[n]arenes, $n=4$, 6, 8. Buffer: 25 mM boric acid/25 mM sodium borate/100 mM SDS pH 9; separation capillary: 50 μm ID × 50 cm total length (effective length 30 cm); applied voltage: −18 kV; UV detection, 215 nm. Concentration of each peak is $\sim 10^{-4}$ M.

The mobility of the analytes in MEKC is a weighted average of the electroosmotic and micellar mobilities as determined by the capacity factor k'. If expressed in terms of migration times [24]:

$$k' = \frac{t_R - t_0}{t_0(1 - t_R/t_{mc})}$$

were t_R is the migration time of the analyte in presence of the micelles, t_0 is the migration time of an unretained solute and t_{mc} is the migration time of the micelles. For the purpose of obtaining t_{mc} we used Sudan III. As can be seen in Fig. 2, the marker migrates faster than the analytes. This result was confirmed by using quinine as micelle tracer [25]. The migration times of the analytes beyond the micelle window indicated that the SCX[n] anions were retarded by their electrophoretic attraction towards the anode. In our system, where the migration times of the SCX[n] in the absence of the micelles are longer than those in presence of the micelles, and the analytes migrates after the micelle phase, the use of these values results in k' values which are positive and higher for the smaller concentration of SDS used. These values are unrealistic since migration times would be expected to increase with the addition of SDS. Therefore, we calculated k' using t_0 as the migration time of the EOF. Methanol was used as neutral marker. The results are shown in Fig. 3. The k' values obtained were negative and increased linearly with the concentration of surfac-

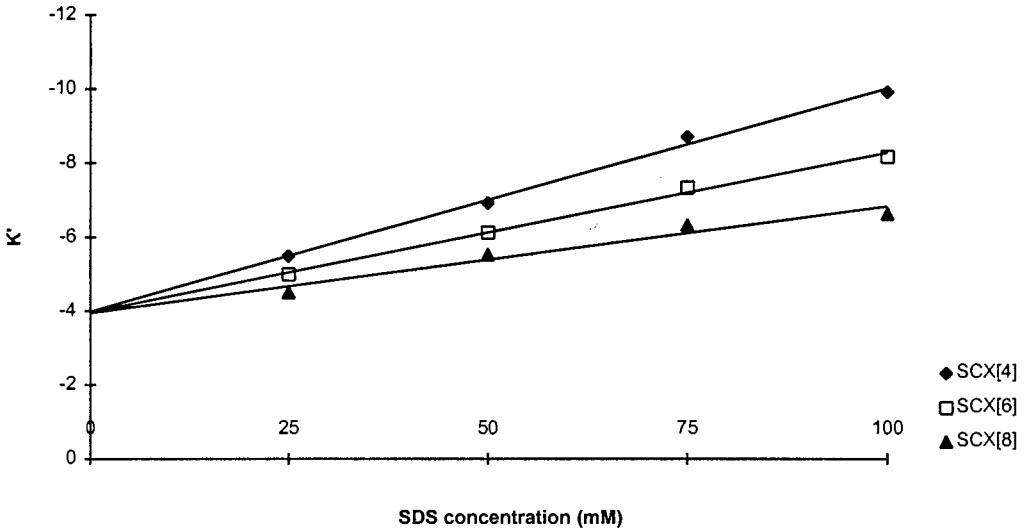

Fig. 3. Variation of capacity factor, k', of p-sulfonated calixarenes as function of SDS concentration.

tant (in absolute value). As we discussed before when we increased the concentration of SDS the resolution between each pairs of SCX[n] was increased.

Other parameters affecting the separation were evaluated. We tested three different buffers of pH 8, 9 and 10. The results are shown in Fig. 4. As we increased the pH from 8 to 10 the ionic strength increased drastically and the mobility of the EOF experienced a decrease (data not shown). Of these three variables, i.e. ionic strength, pH and EOF, ionic strength played the most important part in the separation. At pH 8 satisfactory separation between the pair SCX[4] and SCX[6] could not be achieved. At pH 10 the ionic strength was excessively high giving rise to very high currents and irreproducible results. At pH 9 we obtained a stable current of 54 μA and therefore this pH was chosen for subsequent experiments.

With respect to buffer concentration optimal resolution was observed with boric/borate combination at concentrations of 25 mM and above. The lowest acceptable buffer concentration of 25 mM was chosen in order to shorten analysis time and to reduce the current and therefore Joule heating effect.

3.2. Negative potential conditions

Buffer metal cations have been used in CE to control the EOF and to improve separation of some compounds [26–28]. We investigated the use of Ca^{2+}, Mg^{2+}, Ba^{2+} and Al^{3+}, as additives to the buffer system: boric acid/borate (pH 9) used in the previous experiments.

EOF mobility can be altered through modifications of the zeta potential of the capillary wall after adsorption of positive charges at the negatively charged silica surface. When positive charges are adsorbed to the silica wall, its zeta potential and thus the EOF decreases. At higher concentrations the surface charge can be inverted resulting in an EOF towards the anode due to excess of solvated anions [29]. This effect has usually been achieved by the use of cationic surfactants [30], polymer cations, such as polybrene [31], or alkyltrimethylammonium salts [32]. Honda et al. [33] used 100 mM calcium acetate to reverse the EOF and to improve the separation of derivatives of carbohydrates. Brechel et al. [34] studied the effect on the EOF of different concentrations of Zn, Al and Ba salts in fused silica capillaries at different pH. In their work they demonstrated the dependence of the zeta potential

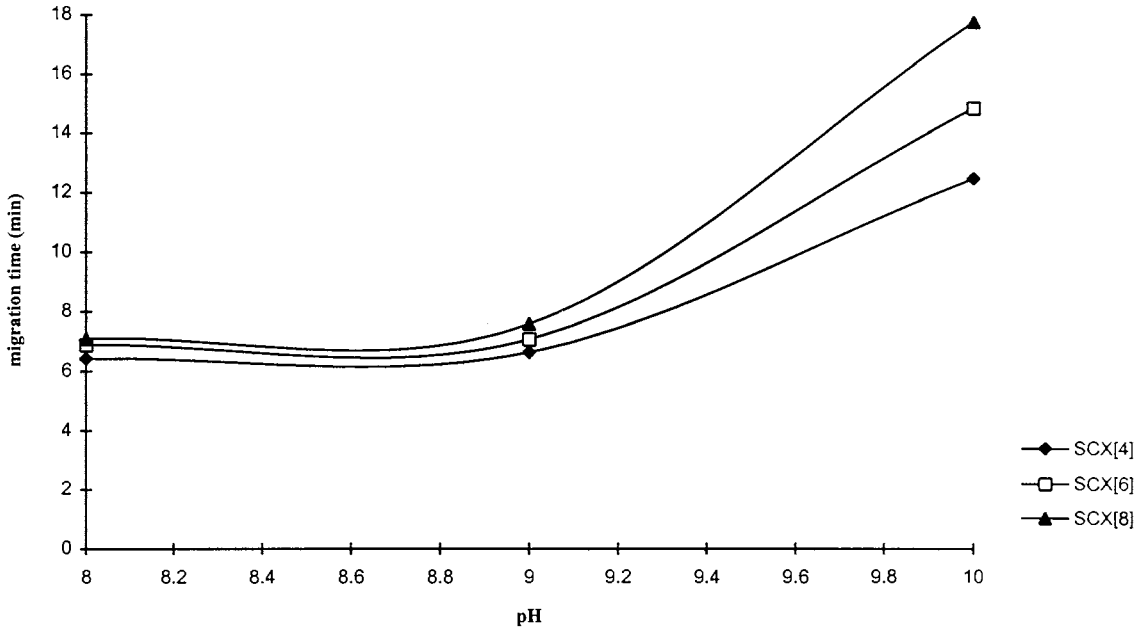

Fig. 4. Variation of the migration time of *p*-sulfonated calixarenes as function of the buffer pH.

on the concentration on the metal cation, they concluded that barium salts were effective agents for the control of the EOF and there was no charge reversal at barium concentrations up to 32 mM although the effect of the ions was more pronounced at higher pH. After the addition of the cations to the buffer, SCX[*n*] were detected on the anode side operating with negative polarity. Aluminium was an exception, for which no results were obtained either in positive or negative polarity within an analysis time of 50 min and studies were not pursued any further. The electrophorograms of the SCX[*n*] obtained after the addition of 10 mM of $BaCl_2$, $MgCl_2$ and $CaCl_2$ can be seen in Fig. 5A, B and C, respectively. From these results we can infer that the cations might have either reversed the EOF or decreased it to a very low value. We could not detect the EOF with dimethylformamide, as well as mesityl oxide as neutral markers. Therefore, we switched the polarity of the electric field to positive and we obtained the peak corresponding to the EOF which gave a relatively low value of 1.8×10^{-4} $cm^2\ s^{-1}\ V^{-1}$, indicating that the EOF had not been reversed. The SCX[*n*] migrated towards the anode due to their high electrophoretic mobilities and against a small EOF.

After switching the polarity of the electric field, the order of migration remained the same, i.e. SCX[4], SCX[6] and then SCX[8]. Experiments carried out with CTAB showed a reversal of the migration order, i.e. SCX[8], SCX[6] and SCX[4]. There could be a special interaction between the SCX[*n*] and the cations to account for this observation. The extensive complexation of SCX[*n*] reported in solid state and in solution suggests that the SCX[*n*] may complex with the metal cations. According to their complexing capabilities the migration times would decrease as association increase since the negative charges of the SCX[*n*] would be neutralized by the positively charged cations.

The three cations, Ba^{2+}, Mg^{2+} and Ca^{2+}, gave similar results in terms of migration time. It is likely that the effect of the cations studied could be masked to some extent by the higher Na^+ concentration in the buffer. Nevertheless, there was a small increase in the order $Ba < Mg < Ca$,

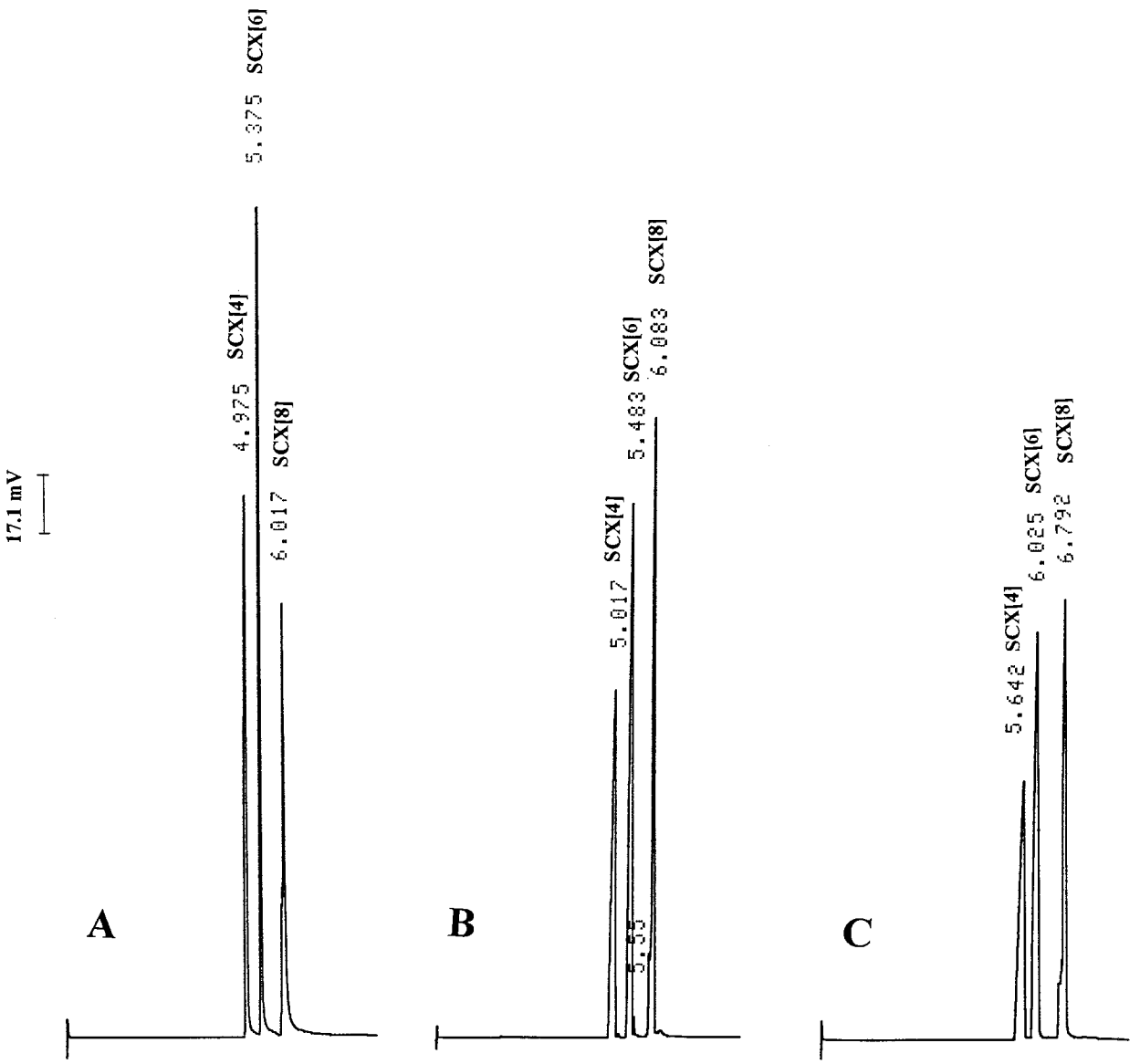

Fig. 5. Capillary electrophoresis separation of *p*-sulfonated calix[*n*]arenes, $n = 4$, 6, 8. Buffer: 25 mM boric acid/25 mM sodium borate, pH 9, separation tube: 50 μm ID × 50 cm total length (effective length 30 cm); applied voltage: − 18kV; UV detection, 215 nm. Concentration of each peak is $\times 10^{-4}$ M. (A) With addition of 10 mM $BaCl_2$; (B) with addition of 10 mM $MgCl_2$ (C) with addition of 10 mM $CaCl_2$.

Table 1
Relative Standard Deviations ($n = 5$) for the migration time (MT) for buffers containing different types of additives

	RSD			
	SDS	Mg	Ba	Ca
SCX[4]	0.42	0.08	0.23	0.25
SCX[6]	0.24	0.07	0.32	0.47
SCX[8]	0.54	0.07	0.36	0.42

and the peak shape became broader in the same order suggesting that the complexation efficiency would increase.

3.3. Detection limit and reproducibility

The detection limits were 9.7×10^{-7}, 7.7×10^{-7} and 8.6×10^{-7} M for SCX[4], SCX[6] and SCX[8], respectively, for the buffer containing $MgCl_2$. Results obtained using SDS as additive indicated detection limits on the same order. With these low detection limits [19], CZE or MEKC can be used to detect SCX[n] as impurities in various samples, e.g. a batch of synthesis/production.

The reproducibility of the results for different buffer compositions were determined by performing five repetitive analysis of the SCX[n] standard solution and calculated as %RSD for the migration time and area. The values are shown in Tables 1 and 2. The buffer system containing Mg^{2+} gave highly reproducible results. The values obtained for Ca^{2+} and Ba^{2+} were also good. In general the reproducibility was dependent on the equilibration time of the capillary. We obtained less reproducible results with the SDS buffer system although they were still acceptable ($< 0.5\%$). The reason for these results may be due to some adsorption to the capillary wall experimented by the SCX[n]. Interaction of calixarenes with silanol groups of a reverse phase packing have been reported before [35]. In these results we should also take into account the fact that the instrumentation used for these experiments was home-built and as a result, less precise than the experiments carried out using negative polarity when a commercial instrument was used.

Table 2
Relative Standard Deviations ($n = 5$) for peak area (PA) for buffers containing different types of additives

	RSD			
	SDS	Mg	Ba	Ca
SCX[4]	2.03	1.45	1.97	1.20
SCX[6]	3.65	1.53	1.85	1.91
SCX[8]	3.48	0.93	2.10	1.42

Acknowledgements

The authors would like to thank Dr R. Trengove and Mr. B.F. Graham for supplying the *p*-sufonated calixarenes standards and the National University of Singapore for the financial assistance.

References

[1] C.D. Gutsche, in: J. Vicens, V. Böhmer (Eds.), Calixarenes. A Versatile Class of Macrocycic Compounds, Kluwer, Dordrecht, 1991, pp. 3–37.
[2] C.D. Gutsche, B. Dhawan, K. Hyun No, R. Muthukrishnan, J. Am. Chem. Soc. 103 (1981) 3782.
[3] G.D. Andreetti, in: J. Vicens, V. Böhmer (Eds.), Calixarenes. A Versatile Class of Macrocycic Compounds, Kluwer, Dordrecht, 1991, pp. 87–123.
[4] C.D. Gutsche, in: J.F. Stoddart (Ed.), Calixarenes, Monographs in Supramolecular Chemistry, Royal Society of Chemistry, Cambridge, 1989, pp. 149–185.
[5] L.J. Bauer, C.D. Gutsche, J. Am. Chem. Soc. 107 (1985) 6063.
[6] S.R. Izatt, R.T. Hawkins, J.J. Christensen, R.M. Izatt, J. Am. Chem. Soc. 107 (1985) 63–66.
[7] J.M. Harrowfield, M.I. Ogden, W.R. Richmond, A.H. White, J. Chem. Soc., Dalton Trans. 8 (1991) 2153.
[8] C.D. Gutsche, M. Iqbal, I. Alam, J. Am. Chem. Soc. 109 (1987) 4314.
[9] J.M. Harrowfield, W.R. Richmond, A.N. Sobolev, J. Vicens, Z. Asfari, J.M. Harrowfield (Eds.), Calixarenes 50th Anniversary, Kluwer, Dordrecht, 1995, pp. 257–277.
[10] R. Ungaro, A. Pochini, in: J. Vicens, V. Böhmer (Eds.), Calixarenes. A Versatile Class of Macrocycic Compounds, Kluwer, Dordrecht, 1991, pp. 127–147.
[11] M.J. Schwing, M.A. McKervey, in: J. Vicens, V. Böhmer (Eds.), Calixarenes. A Versatile Class of Macrocycic Compounds, Kluwer, Dordrecht, 1991, pp. 149–172.

[12] A. Arduini, A. Pochini, S. Reverberi, R. Ungaro, J. Chem. Soc., Chem. Commun. 15 (1984) 981.
[13] S. Shinkai, S. Mori, H. Koreishi, T. Tsubaki, O. Manabe, J. Am. Chem. Soc. 108 (1986) 2409.
[14] C.D. Gutsche, J.A. Jevine, P.K. Sujeeth, J. Org. Chem. 50 (1985) 5802.
[15] S. Shinkai, T. Tsubaki, T. Sone, O. Manabe, Tetrahedron Lett. 26 (1985) 3343.
[16] T. Arimura, T. Nagasaki, S. Shinkai, T. Matsuda, J. Org. Chem. 54 (1989) 3766.
[17] S. Shinkai, in: J. Vicens, V. Böhmer (Eds.), Calixarenes. A Versatile Class of Macrocycic Compounds, Kluwer, Dordrecht, 1991, pp. 173–198.
[18] D. Shohat, E. Grushka, Anal. Chem. 66 (1994) 747.
[19] Y. Zhang, I.M. Warner, J. Chromatogr. A 688 (1994) 293.
[20] V. Böhmer, Angew. Chem. Int. Ed. Engl. 34 (1995) 713.
[21] I. Yoshida, N. Yamamoto, F. Sagara, D. Ishii, K. Ueno, S. Shinkai, Bull. Chem. Soc. Jpn. 65 (1992) 1012.
[22] S. Shinkai, Pure Appl. Chem. 58 (1986) 1523.
[23] S. Terabe, K. Otsuka, T. Ando, Anal. Chem. 57 (1985) 834.
[24] J.H. Knox, J. Chromatogr. A 680 (1994) 3.
[25] J. Vindevogel, P. Sandra, Introduction to Micellar Electrokinetic Chromatography, Hüthig, Heidelberg, 1992.
[26] A.S. Cohen, S. Terabe, J.A. Smith, B.L. Karger, Anal. Chem. 59 (1987) 1021.
[27] S. Fujiwara, S. Honda, Anal. Chem. 58 (1986) 1811.
[28] S. Chen, D. Pietrzyk, Anal. Chem. 65 (1993) 2770.
[29] S.F.Y. Li, Capillary Electrophoresis, Principles, Practice and Applications, Elsevier, Amsterdam, 1991.
[30] C.A. Lucy, R.S. Underhill, Anal. Chem. 68 (1996) 300.
[31] S. Terabe, T. Isemura, Anal Chem. 62 (1990) 652.
[32] T. Kaneta, S. Tanaka, H. Yoshida, J. Chromatogr. 538 (1991) 385.
[33] S. Honda, J. Chromatogr. 588 (1991) 327.
[34] R. Brechtel, W. Hohmann, H. Rüdiger, H. Wätzig, J. Chromatogr. A 716 (1995) 97.
[35] I. Rodriguez, B.F. Graham, R.D. Trengove, S.F.Y. Li, J. Liq. Chrom. Rel. Technol. 20 (1997) 1197.

.

ELSEVIER

Talanta 45 (1998) 693–701

Talanta

Purification of metallothionein proteins from the crab, *Portunus pelagicus*—selectivity of hydrophobic interaction chromatography

Siau Gek Ang *, Peng Siong Chong

Department of Chemistry, National University of Singapore, Lower Kent Ridge Road, Singapore 119260, Singapore

Received 5 February 1997; received in revised form 1 August 1997; accepted 4 August 1997

Abstract

Both hydrophobic interaction chromatography (HIC) and ion-exchange chromatography (IEC) are commonly used for the purification of proteins as their mild elution conditions preclude the dangers of denaturation. Of the two methods, IEC which fractionates proteins on the basis of charge differences, exhibits a higher selectivity. In the case of the metallothionein (MT) proteins, the charge states of the proteins are very susceptible to change due to oxidation of the abundant thiol groups. This complicates fractionation with IEC. Separation using HIC, on the other hand, is based on the exposed hydrophobic groups, which remain relatively intact if the tertiary structure of the proteins is not disrupted. In this work, the successful isolation of two MT isoforms from the tropical crab species, *Portunus pelagicus*, using HIC serves to demonstrate the high selectivity of this technique, in addition to the fact that it is indifferent to the state of oxidation of the MT proteins during the purification procedure. © 1997 Elsevier Science B.V.

Keywords: Hydrophobic interaction chromatography; Ion-exchange chromatography; Metallothioneins; Isoforms; *Portunus pelagicus*

1. 1. Introduction

Metallothioneins (MTs) are a group of low molecular weight metal-binding proteins that contain abundant cysteinyl residues (20–30% of the total amino acid composition). Since the discovery of cadmium binding MTs in the equine kidney [1], it has been generally assumed that these proteins play a central role in metal homeostasis and detoxification in living organisms. These proposed functions were supported by evidence revealed in earlier studies [2–5]. At the Second International Meeting on 'Metallothioneins and Other Low Molecular Weight Binding Proteins' in Zurich, 1985 [6], the decision was made to place all proteins that shared the above mentioned features into three classes. Class I MTs are known to exist in isoforms with physical properties that exhibit only minor differences. Hence, ion exchange chromatography would be a suitable technique to fractionate these proteins on the basis of its high selectivity.

Ion exchange chromatography is based on the reversible adsorption of charged solutes to immobilized ion exchange groups of reverse charge. At a given pH, the net charge of various biological

* Corresponding author. Fax: +65 778 0671

PII S0039-9140(97)00263-4

molecules can deviate considerably leading to varying degrees of interaction between these molecules and the ion exchanger. Further manipulation of factors such as the salt content and the pH of the buffers used accounts for the unsurpassed resolving power of ion exchange chromatography in low pressure LC.

In the course of our purification work on MTs from the crustaceans *Portunus pelagicus*, we had discovered that oxidation of the abundant cysteinyl residues in these proteins led to the generation of several species with different charge states. Hence, fractionation via charge difference was found not to be reliable. Though Olafson et al [7] has reported the separation of two naturally occurring MT isoforms namely MTI and MTII from the crab species, *Scylla serrata* by means of ion exchange, work carried out by our team [8,9] has illustrated that this result was only possible with freshly obtained material. Oxidation on prolonged storage of material was seen in the form of a complex ion exchange chromatogram with numerous overlaying peaks. Reducing agents such as 2-mercaptoethanol and dithiothreitol (DTT) are recommended by some workers to be added to running buffers, [10–13] but their use serves only to retard the oxidation process. In this study, an alternative physical property of the proteins has been employed to effect fractionation.

For any given protein, there always exists some exposed hydrophobic sites on its surface [14,15]. These sites are maintained by the molecular tertiary structure and are relatively stable if the structure is not disrupted. Hydrophobic interaction chromatography utilizes the differences in these sites that exist between proteins to bring about their separation. In this work, MT isoforms were isolated from a tropical marine crab species, *Portunus pelagicus* by means of two purification routes; first, a widely used protocol which employed ion exchange chromatography and second, a new procedure designed in this work that utilized hydrophobic interaction chromatography. From the results obtained, a comparison of the two techniques was made.

Recently, HPLC reverse phase columns are increasingly being used for the isolation of metallothioneins [16,17]. High resolution and rapid isolation are advantages offered by this method [8]. However small sample size capacity on HPLC analytical columns makes HIC an attractive alternative for bulk isolation of metallothioneins.

2. Experimental

2.1. Chromatographic Techniques

Hepatopancreas tissue was harvested from crabs that were reared in tanks of copper spiked seawater for 5 days. The tissues were homogenized in reducing buffer and centrifuged at $25\,000 \times g$ to remove insoluble matter. DTT (Sigma) was used to provide the reducing condition while a pH of 8.6 was maintained in the homogenizing buffer by 0.02 M Tris–HCl (Sigma). To reduce the loss of MT proteins due to proteinase action, a proteinase inhibitor, phenylmethanesulfonyl fluoride (PMSF, 0.1 mM) was also added to the buffer. Homogenization of the tissue was carried out at 40°C to minimize denaturation of protein by the heat generated.

After centrifugation, the clear supernatant obtained was divided into four portions and from these, two lots were processed within 3 days. These materials were labeled as A3. One lot of A3 material was processed by first eluting through a Sephadex G50 (Pharmacia, Uppsala) gel column for a further clean up before fractionation was carried out on an anion-exchanger column packed with DEAE-Sephacel (Pharmacia). To the second lot of A3 sample, 2.0 M ammonium sulfate (BDH AR grade, UK) was added to precipitate out the large molecular weight proteins. The contents were then spun down and the clear solution was subsequently loaded onto a hydrophobic interaction gel column. Butyl Sepharose 4B (Pharmacia) was used as the packing material. The absence of charged groups in this gel is an important factor for its selection. Furthermore, its high binding capacity which permits heavy loading and its rigidity that allows a rapid flow rate to be sustained are ideal properties of the gel for working with MTs.

The remaining two lots of samples, designated as A7 were stored at -200°C under a reducing

environment provided by 0.1 M DTT with an inert nitrogen atmosphere for 7 days. After this period, the two samples were processed separately as detailed for the previous two samples.

NaCl (0.01 M) was used as the starting buffer on the IEC column and the concentration was increased to 0.4 M over 8 h. For the HIC, an 8 h reverse salt gradient was used starting with 2.0 M ammonium sulfate and reducing to 0.0 M. A pH of 8.6 was maintained for all IEC buffers by 0.02 M Tris–HCl. Due to the tendency of the ammonium ion to be replaced and lost in alkaline pH conditions, the pH of the HIC eluents was hence adjusted to 7.0. As usual, a reducing environment was maintained by 50 mM DTT for all the chromatographic runs.

Fractions collected from the IEC column were first checked for copper using the Shimadzu AA670 flame absorption spectrophotometer. Selected fractions were then pooled and concentrated by freeze drying for desalting on a Sephadex G25 column. Acetic acid (1%) was used as eluent for the desalting. In the mild acidic medium, thiol groups in the MT proteins are protonated and hence are protected from oxidation[18]. For freeze drying, a Buchi rotary evaporator with dry ice–ethanol mixture in the cold finger was used. High vacuum was provided by an Edward RV8 pump.

Due to the presence of large quantities of salt in the HIC fractions, that results in clogging of the burner head in the AAS flame spectrophotometer after a short period of usage (thereby introducing large fluctuations in the readings obtained), a modification was applied to the method for checking the metal content. From each of the fractions to be analyzed, an aliquot was pipetted out and diluted 10-fold with water before the measurement was carried out on the Perkin Elmer graphite furnace spectrophotometer. To desalt the HIC material, relevant fractions were pooled and concentrated by freeze drying. When the water was slowly removed, the increasing ammonium sulfate concentration would eventually cause the proteins in solution to precipitate out. The precipitated proteins were spun down on a bench top centrifuge and the pellet was reconstituted in 1% acetic acid for loading onto the desalting column.

2.2. One dimensional SDS-PAGE

Proteins that were purified from fresh material (without storage) using the ion exchange column were checked with 1-D SDS-PAGE for homogeneity prior to amino acid composition analysis. Since the molecular weight of MTs lies in the range of $6 \times 10^3 - 10 \times 10^3$, electrophoretic gels that can fractionate low molecular weight proteins and peptides were casted based on the method developed by Guilian [19]. In this protocol, the gel is made pliable by casting a 20% gel with only 0.5% cross linking. In addition, 10% glycerol was added to increase the viscosity of the gel so as to retard migration of proteins through the latter. Gels were casted on the BioRad (USA) MiniProtean set and the running time took approximately an hour. About 10 min of power supply at 220 V was used to stack the proteins and this was followed by 45–50 min of running at a constant voltage of 200 V. The resulting gels were visualized using Commassie Blue G250 staining.

2.3. Pyridylethylation and amino acid analysis

Modification of the cysteinyl residues in a protein is vital prior to acid hydrolysis as this would prevent their destruction under extreme conditions. To achieve alkylation, 4-vinylpyridine (Merck) was used. About 1 mg of purified protein was dissolved in 100 μl of 6 M guanidine–HCl (Sigma). Five molar excess of DTT over the total thiol group in the protein was added before the contents were incubated at 500°C for 30 min. 4-vinylpyridine was next added in an amount twice that of the DTT used. The reaction was allowed to proceed at room temperature in the dark for no more than 2 h. Following that, the reaction was halted by the addition of 10–20 μl of concentrated HCl and the contents were desalted on a Sephadex G25 column using 1% acetic acid as buffer.

Hydrolysis of the desalted modified protein was carried out in vacuo with 6 N HCl at 1500°C for about 1 h. The hydrolysate obtained was analyzed on a Waters PicoTag™ system. The information obtained serves to confirm the existence of the

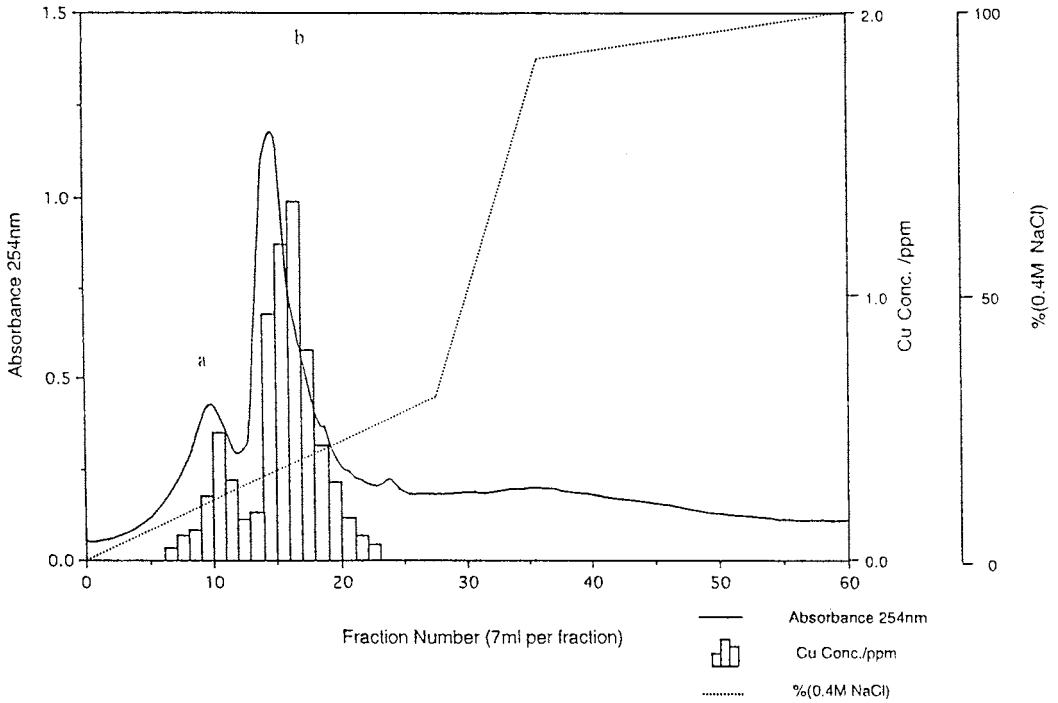

Fig. 1. Anionic exchanger chromatogram of fresh supernantant after gel filtration.

MT isoforms in the crab, *Portunus pelagicus* and helped in the identification of these MT proteins in the purification with HIC. Since the modified cysteine would be released in the hydrolysis as β-pyridylethyl cysteine (PE-Cys), a small amount of this compound was synthesized employing a procedure previously reported [20]. PE-Cys (0.05 μmole) was added to the mixture of amino acid standards.

3. Results and discussion

3.1. Evidence for MT isoforms in the crab species, Portunus pelagicus

Fig. 1 shows the ion-exchange chromatographic profile that was obtained for the fresh material collected from the gel filtration column. Two well defined peaks (*a* and *b*) were revealed which are likely to contain the two MT isoforms from *Portunus pelagicus*. This deduction was made based firstly on the high level of copper detected for the corresponding fractions with flame AAS. Secondly, the molecular weights of the proteins from these two peaks when checked with 1-D gels (Fig. 3) were found to be between 6–10 K. These values corresponded to the reported MT molecular weights of less than 10 K [21]. The third piece of supportive evidence concerns the amino acid composition results listed in Table 1. For the two proteins processed from the IEC peaks (*a* and *b*), the cysteinyl content analyzed were 32 and 29% respectively of the total amino acid composition. These values correlated well with the figures reported for MTs. Moreover, there is an absence of aromatic residues in the proteins analyzed which agreed with another known characteristic feature of the MTs.

Table 1
Amino acid composition of desalted and alkylated proteins from both IEC and HIC runs

Amino acid	a	b	I	II	III	IV
Asx	3	5	5	3	5	3
Glx	8	7	7	8	7	8
Ser	7	5	5	7	5	7
Gly	2	3	3	2	3	2
Arg	1	2	2	1	2	1
Thr	3	3	3	3	3	3
Ala	5	4	4	5	4	5
Pro	4	6	6	4	5	4
Val	2	3	3	3	3	3
Cys[a]	22	20	19	22	20	21
Leu	3	3	3	2	3	3
Lys	7	7	4	4	3	4
Total residue	67	68	64	64	63	64

[a] Cysteine residue was quantified as β-pyridylethyl cysteine.

3.2. Efficiency of HIC in processing oxidized MT samples

The profile for the HIC run of the fresh A3 sample is illustrated in Fig. 2 with the amino acid composition of the proteins purified from the peaks marked I and II listed in Table 1. The IEC and HIC profiles of the samples that were stored before processing are shown in Figs. 4 and 5 respectively. In spite of the measures that were taken (see Section 2.1), oxidation of the A7 sample was evident from the drastic difference seen in the IEC profiles shown in Figs. 1 and 4. Several additional peaks were observed in the later part of the chromatogram in Fig. 4 and these peaks possibly contain the oxidized species. As deduced from the position of these peaks, the oxidized material was negatively charged compared with native MTs. Negative charges could be contributed by the exposed thiol groups of the cysteinyl residues in the MTs upon detachment from some of the metal ions. Although deprotonated sulfhydryl groups are likely to become involved in either inter or intramolecular disulfide linkages, some of these could be in unfavorable orientations and therefore retain their charged states under the alkaline conditions of the eluent buffer. Nevertheless, not all the metal ions would be lost

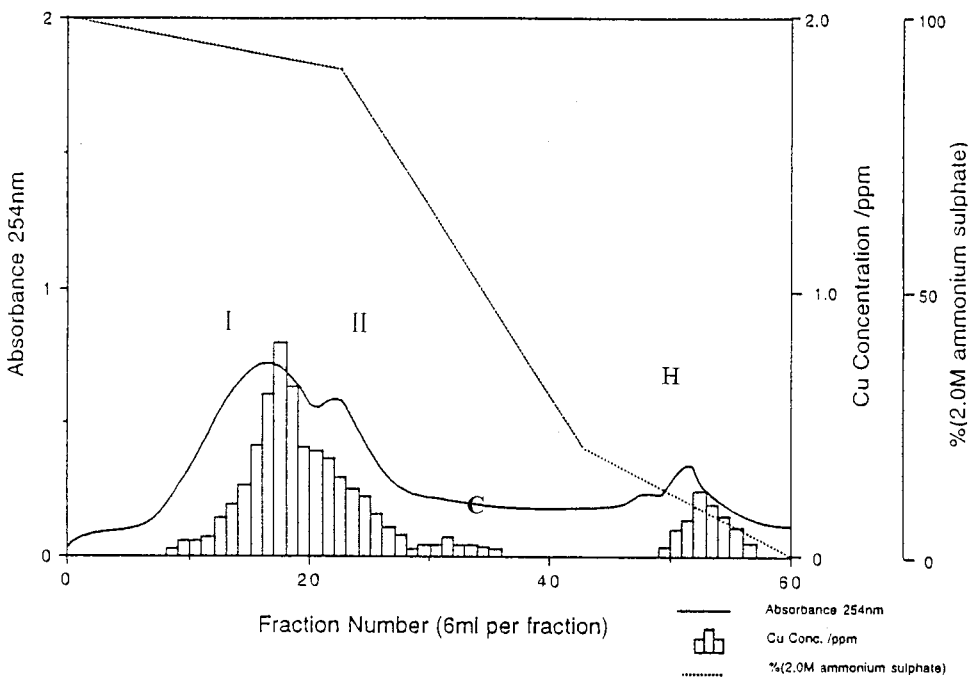

Fig. 2. Hydrophobic interaction chromatographic profile for fresh supernatant (without storage).

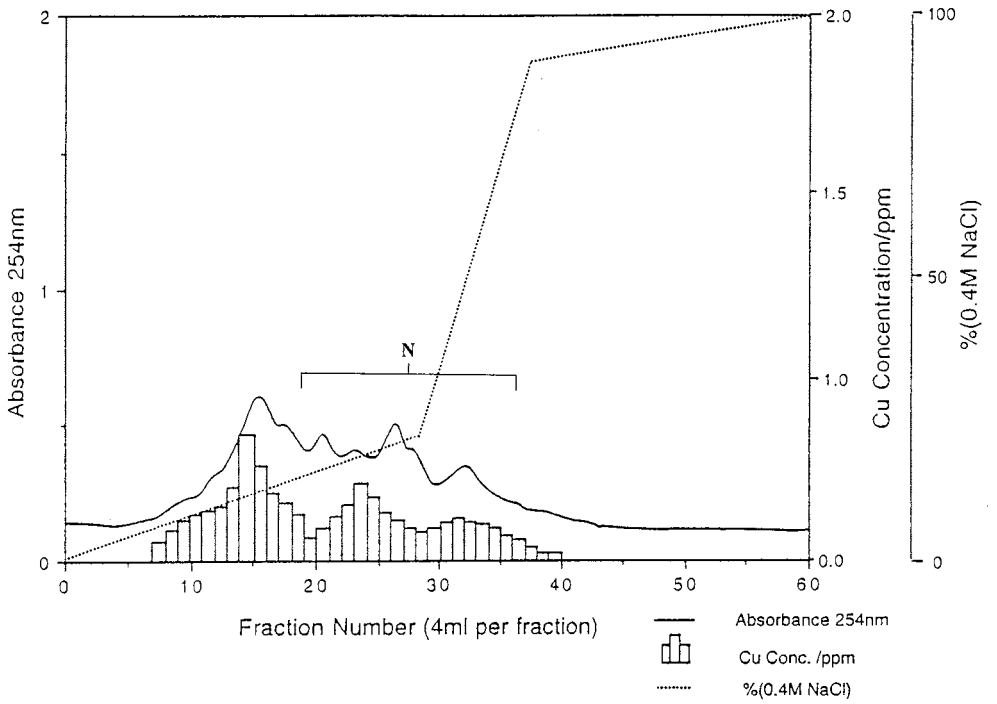

Fig. 3. Anionic exchanger chromatogram for oxidised material after cleanup with Sephadex G50 column.

unless under extremely acidic pH conditions, especially in the case of copper ions [21]. The metal ions remaining in the proteins accounted for the substantial levels of copper that were detected in the fractions corresponding to the extra peaks in Fig. 4 marked N.

In our study, we have observed that the IEC profile in Fig. 4 was not reproducible among different batches of A7 samples. In contrast, little change was noticed between the two profiles of the HIC. One feature to note was the absorbance of the peaks, I–IV which varied inversely with those of the peaks labeled H in Figs. 2 and 4. Aggregated MT species were suspected to be found in peak H as the hydrophobicity of these larger molecules was expected to be higher. Evidence supporting this deduction came from the increased absorbance of peak H for oxidized samples and this was reduced with DTT treatment (data not shown). Unlike the IE chromatograms, similar UV absorbance traces were obtained for all the HIC runs involving oxidized samples. This demonstrated that the hydrophobicity of the MT proteins remains relatively unaffected by the extent of oxidation and hence confirmed the suitability of the HIC technique for the purification process in this work.

3.3. Resolution of the two MT isoforms on the HIC column

Despite the selectivity exhibited by HIC towards the polymerized oxidized proteins, the two distinct copper peaks that were obtained using the IEC (see Fig. 1) were not observed on both the profiles in Figs. 2 and 4. UV detection has however revealed the presence of at least two components represented by the I/III and II/IV peaks. Materials were taken separately from these peaks for alkylation and subsequently analyzed for amino acid composition (see Table 1). By comparing the results in Table 1 for proteins purified by the two chromatographic techniques, the close match between values of column a and II, and between b and I indicates a reverse elution order for the MT isoforms for the two chromatographic

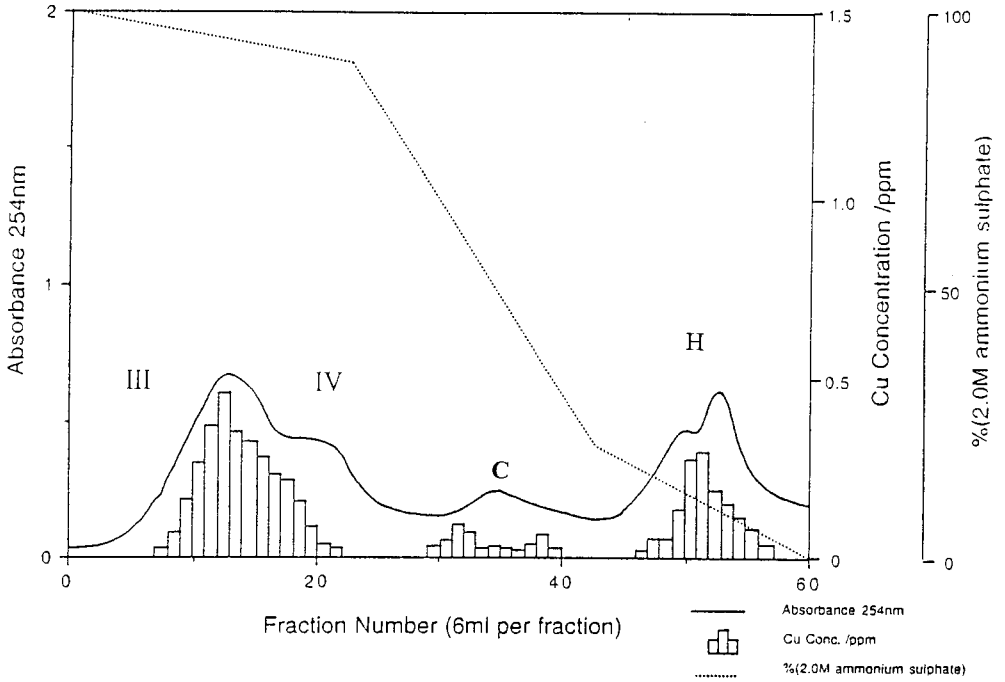

Fig. 4. Hydrophobic interaction chromatographic profile for oxidised material.

columns. Furthermore, a good separation of the two isoforms was achieved on the HIC column. This was indicated by the relatively pure isoforms obtained from each of the two HIC peaks in Figs. 2 and 4 to yield the results in Table 1.

3.4. HIC as a possible replacement for the traditional two step (gel filtration and ion exchange) purification protocol

Besides the capability of handling oxidized samples and the good resolution achieved between the two MT isoforms, other advantages for using HIC were observed. For example, precipitation of large molecular weight proteinaceous compounds by the addition of 2.0 M ammonium sulfate during the loading of the HIC column has also simplified the purification by omitting the gel filtration step. On the other hand, the gel filtration which requires up to at least 16 h of run time is an essential step commonly associated with the use of IE column. The other copper containing protein, superoxide dismutase (SOD), which is not precipitated by the ammonium sulfate solution, is separated from the MT proteins on the HIC chromatogram. This protein appeared as a small copper peak marked C positioned after the second UV peak in both Figs. 2 and 4. Using IEC, SOD is a common contaminant in the MT samples as illustrated by the results in Fig. 3 (SDS-PAGE). Other substances found in the supernatant consist of some short peptides, amino acids and non-proteinaceous compounds such as the zinc ligands reported by Wong et al [22] which do not seem to bind onto the gel during loading. These low molecular weight compounds would normally be removed during the pre-running wash with the starting buffer. Hence the various observations described above justified the omission of the gel filtration step.

4. Conclusion

With HIC, we have succeeded in purifying oxidized MTs with a small limitation posed by aggregated molecules. Since MTs are known to polymerize more readily in concentrated solution,

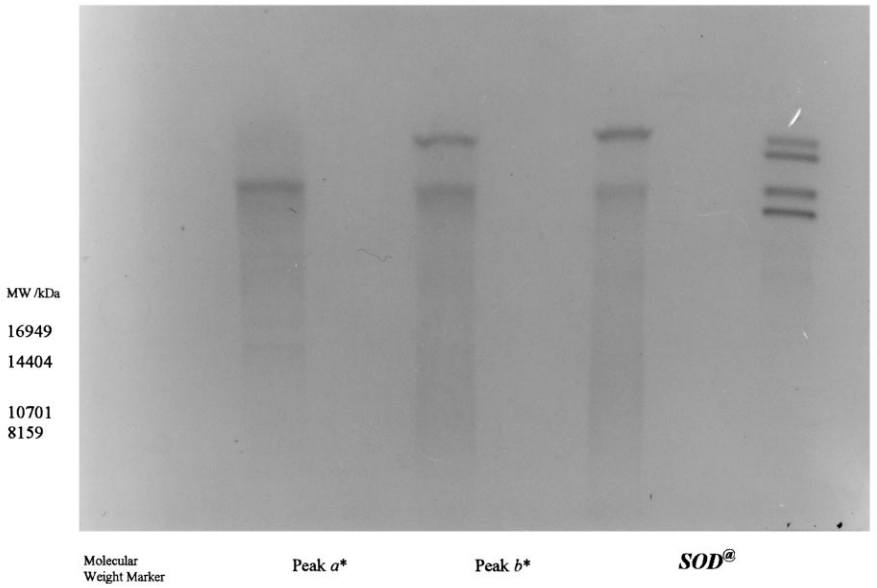

Fig. 5. Purity check by one dimensional SDS-PAGE for desalted A3 material collected from anionic exchanger column. *Refer to Fig. 1 for designation. @A common contaminant suspected to be superoxide dismutase. The material for this band was taken from Sephadex G50 fractions that corresponded to a molecular weight of $>10^4$ and the amino acid composition results obtained for this sample revealed non-MT characteristics (i.e. low cysteinyl content and the presence of aromatic residues).

by avoiding this and by carrying out rapid purification using the HIC, production of these aggregated species can be drastically reduced. Furthermore, with the use of HIC, excess DTT can be added to salvage the polymerized proteins. Conversely, this procedure is unlikely to work for the IEC, the reason being that even if the disulfide bonds were to be reduced, the permanent loss of the metal prevents the restoration of the original charge state in these proteins. Regarding HIC, if the native configuration is not disrupted and the hydrophobic regions are not altered, fractionation remains possible. This method was subsequently modified and employed for our later work involving the isolation of MTs from another species of crustaceans, *Thenus orientalis* [23].

As well as its effectiveness in processing oxidized samples, the use of HIC had also helped to shorten considerably the whole isolation process in this study by eliminating the need for the gel filtration step. Nonetheless, the utility of HIC would be of more value not by replacing it but in complementing gel filtration and ion exchange chromatography. Hence, HIC adds a new dimension to the spectrum of separatory techniques needed to handle the ever demanding need for fractionating the widening array of biological molecules being discovered.

References

[1] M. Margoshes, B.L. Vallee, J. Am. Chem. Soc. 79 (1957) 4813.
[2] A.O. Udom, F.O. Brady, Biochem. J. 187 (1980) 329.
[3] W.J. Langston, M.J. Bebianno, M. Zhou, Mar. Environ. Res. 28 (1989) 195.
[4] H.E. Rugstad, T. Norseth, Nature (London) 257 (1975) 136–137.
[5] L. Cai, J. Koropatnick, M.G. Cherian, Chem.-Biol. Interact. 96 (1995) 143–155.
[6] B.A. Fowler, C.E. Hildebrand, Y. Kojima, M. Webb, Experientia Suppl. 52 (1987) 19.
[7] R.W. Olafson, K.G. Boto, R.G. Sim, Comp. Biochem. Physiol. 62B (1979) 407–416.

[8] S.G. Ang, V.W.T. Wong, J. Lig. Chromatogr. 1414 (1991) 2647–2663.
[9] S.G. Ang, V.W.T. Wong, J. Chromatogr. 599 (1992) 21–24.
[10] D.T. Minkel, K. Poulsen, S. Wielgus, C.F. Shaw, D.H. Petering, Biochem J. 191 (1980) 475.
[11] J. Overnell, Comp. Biochem. Physiol. 77C (2) (1977) 245–248.
[12] V.W.T. Wong, P.S. Rainbow, Comp. Biochem. Physiol. 85A (1986) 159.
[13] M.J. Stillman, C.F. Shaw, K.T. Suzuki (Eds.), Metallothionein-Synthesis, Structure and Properties of Metallothioneins, Phytochelatins and Metal Thiolate Complexes, VCH Publisher, 1992, pp. 29.
[14] L. Brand, J.R. Gohlke, Ann. Rev. Biochem. 41 (1972) 704–706.
[15] I.M. Klotz, Arch. Biochem. Biophys. 138 (1970) 704–706.
[16] B. Berger, P.E. Hunziker, C.R. Hauer, N. Birchler, R. Dallinger, Biochem. J. 311 (1995) 951–957.
[17] P.E. Hunziker, P. Kaur, M. Wan, A. Kanzig, Biochem. J. 306 (1995) 265–270.
[18] M.J. Stillman, C.F. Shaw, K.T. Suzuki (Eds.), Metallothionein-Synthesis, Structure and Properties of Metallothioneins, Phytochelatins and Metal Thiolate Complexes, VCH Publisher, 1992, pp. 204.
[19] G.G. Giulian, Fed Proc. 44 (1985) 686.
[20] J.B.C. Findlay, M.J. Geisow (Eds.), Protein Sequencing-a practical approach, JRL Press, Oxford, 1989, pp. 22.
[21] D. Hamer, Metallothionein, Annu. Rev. Biochem. 55 (1986) 913–951.
[22] V.W.T. Wong, P.S. Rainbow, Comp. Biochem. Physiol. 87C (1) (1987) 203–209.
[23] S.G. Ang and P.S. Chong, unpublished results.

.

ELSEVIER

Talanta 45 (1998) 703–711

Talanta

Determination of lead in blood by hydrodynamic voltammetry in a flow injection system with wall-jet detector

S. Jaenicke [a,*], R.M. Sabarathinam [1,a], B. Fleet [b], H. Gunasingham [b]

[a] *Department of Chemistry, National University of Singapore, Kent Ridge, Singapore 119260, Singapore*
[b] *Eutech Cybernetics Pte Ltd., 55 Ayer Rajah Crescent, Singapore 139949, Singapore*

Received 3 February 1997; received in revised form 2 June 1997; accepted 4 June 1997

Abstract

Lead is one of the most widely distributed toxic heavy metals in the environment. It is a cumulative poison, affecting the brain and nervous system. The threshold between the normal lead level and the level where physiological effects become manifest is relatively narrow. It is therefore desirable to screen exposed populations in order to identify the danger in time. The lead concentration in the blood is a measure to the total amount of lead in the body. A fast, accurate and cheap method for the determination of lead in blood is therefore needed. The conventional method used to determine lead in blood is atomic absorption. Electrochemical methods like stripping voltammetry combine high analytical sensitivity with relatively low cost for the equipment; however, electrode preparation is critical for the success of an analysis, and highly skilled personnel are needed. We describe an automated electrochemical method, using flow injection analysis with a wall-jet detector. Lead is released from its binding site in the blood by ion exchange and quantified by stripping voltammetry with a mercury film electrode (MFE). The method allows for the detection of 0.05 ppm Pb^{2+} with an accuracy of about 10%. Electrode poisoning by proteins from the blood can be effectively suppressed when a MFE modified with a Nafion®-membrane coating is used. Such modified electrodes can be activated in the solution without further treatment, and used for more than 100 analyses before they have to be replaced. A solid matrix MFE with a Nafion®-membrane and all necessary chemicals for mercury film formation and lead release has been developed. Such electrodes are discussed as disposable electrodes for a portable blood lead detector. © 1998 Elsevier Science B.V.

Keywords: Blood analysis; Lead; Wall-jet cell; Anodic stripping voltammetry; Mercury film electrode

1. Introduction

Environmental lead poisoning [1] is the most common among all heavy metal poisonings. The toxicological problems of lead have long been of concern in the industrialised countries, but only recently has the problem emerged in Asia and the developing countries, where over two billion peo-

* Corresponding author. Fax: +65 7791691; e-mail: chmsj@leonis.nus.sg

[1] Present address: Central Electrochemical Research Institute, Karaikudi 623006, India

PII S0039-9140(97)00297-X

ple are exposed to lead pollution. The largest part of the environmental lead is released from leaded gasoline with 86% of all the lead emitted into the atmosphere originating from automobile exhausts. Other sources of lead are paints, food containers, pewter, lead glass and lead water pipes.

Chronic lead poisoning is characterised by neurological defects, renal tubular dysfunction, anemia and damage to the central nervous system, causing lead encephalopathy and neuropathy. In children, chronic lead poisoning has been associated with behavioral problems, intellectual impairment and hyperactivity [2].

The biochemical effects of lead have been critically reviewed by Vallee and Ulmer [3]. Lead causes a decrease in the rate of globulin and haem synthesis. Symptoms of lead poisoning include renal insufficiency, colic, constipation and other gastrointestinal effects. It also affects the reproductive system, resulting in sterility, abortions, still birth and neonatal deaths. The accepted tolerance limit is a blood lead concentration of 0.4 μg ml^{-1} for adults [4] and 0.1 μg ml^{-1} for children and adolescents [5].

Atmospheric lead levels range from 0.4 to 7.6 μg m^{-3} in cities, depending on the motor traffic density [6]. Most of the lead originates from the exhaust fumes of vehicles burning petrol containing lead alkyl additives. The exposure in rural areas is generally much lower. Lead fallout from the atmosphere can be incorporated into vegetable crops and rain water. Surface water used for domestic purposes and especially water from lead-lined tanks and pipes have been found to contain lead levels up to 55 μg l^{-1} [7]. The total daily lead intake from food and beverages by human adults ranges from 200 to 350 μg day^{-1}. Approximately 10% of the lead intake is absorbed through the gastrointestinal tract. Lead is more easily absorbed via the lungs than through the digestive system. Lead-containing aerosols like those resulting from burning leaded gasoline, therefore, pose a more severe health problem than other lead sources. Once absorbed, lead is distributed between the blood, soft tissues and the skeleton. The residence time of lead in blood and soft tissues is ≈ 4–6 weeks and in bones as long as 30 years. Over 70% of the body lead is retained in the skeletal system. The transfer of lead between the various systems, such as the blood, the soft tissues and the bones, results in a non-linear relationship between exposure and the concentration of lead in blood. Blood lead levels tend to saturate with increasing exposure.

The direct determination of lead in blood is complicated by the presence of matrix components, such as red blood cells, haemoglobin and erythrocyte protoporphyrin which may suppress or mask the signal. The wet or dry ashing procedures reported [8,9] for the blood lead analysis are time consuming and require relatively large volumes of blood for a single determination. Irradiation techniques for the release of bound lead in blood have been reported by Bately et al. [10]. Atomic absorption spectrophotometry (AAS) is widely used for the analysis of lead in blood. Sensitive flameless atomic absorption techniques have been developed which involve electrothermal heating of the sample in an graphite oven or tantalum boat to produce atomic lead vapor. Costantini [11] compared flameless atomic absorption spectrometry and anodic stripping voltammetry for the determination of blood lead.

Anodic stripping voltammetry is an established method for trace metal analysis. The technique is gaining increasing popularity for the analysis of trace metals in body fluids because of its inherent sensitivity and significantly lower cost of instrumentation. In addition to sensitivity and economy, anodic stripping voltammetry has several other advantages. Three to five trace elements can be determined by anodic stripping voltammetry in a single run whereas in ordinary atomic absorption, only one element can be quantified at a time. The determination can be done with little pretreatment and without separation steps. Several attempts have therefore been made to apply this technique to the analysis of lead in blood [12–14].

Sample pretreatment procedures for the effective release of the lead from its binding sites in the red blood cells have been reviewed [15]. The methods include acid digestion with a mixture of perchloric acid, nitric acid and sulfuric acid, irradiation, low temperature ashing, digestion under pressure, and dilution with a decomplexing agent.

The digestion used to destroy the organic matter and to release the bonded lead from its binding sites is time consuming, and the added reagents may introduce metals at concentrations which exceed those present in the original sample. To avoid digestion, direct methods have been tried by a number of workers [16,17]. The main interference in the case of blood lead analysis stems from the presence of organic matter in the sample. Complexed lead is electrochemically inactive. It has to be made available for analysis by acidification or by addition of a release agent. Proteins and other organic compounds tend to adsorb at the mercury electrode where they interfere with the transfer of metal ions through the interface during the deposition and stripping step. This results in reduced peak currents and a shift in peak potential. To avoid this interference, it has been proposed to cover the electrode with a permselective polymeric coating [18–21].

1.1. Anodic stripping voltammetry techniques

Anodic stripping voltammetry was initially developed using a hanging mercury drop electrode. Recently, the mercury film electrode has gained popularity because it offers a higher surface-to-volume ratio than the mercury drop. Therefore, diffusion of ions from the bulk of the film to the electrode surface is very fast, resulting in sharper stripping peaks and increased resolution. Glassy carbon is the ideal support for mercury films because of its hardness, good electrical conductivity, high hydrogen overpotential, and chemical inertness. Mercury films on glassy carbon are usually prepared either in situ or by preplating. For in situ preparation, mercury ions are added to the sample to be analysed and the film is formed while the metal ions of interest are simultaneously deposited. Preplated mercury films are deposited onto the glassy carbon from a mercury plating solution before the electrode is transferred into the sample solution. This method is superior to the use of in situ mercury films because it allows for better control over the film properties. The same preplated mercury film can be used for several determinations.

The high sensitivity of stripping voltammetry is the result of the electrolytic preconcentration step. Metal ions from the solution are reduced at constant potential and dissolved into the mercury film. All dissolved metal atoms are reoxidised during the stripping step, using a potential ramp. Different metallic species can be identified by the appearance potential of their stripping peak. The accuracy of the method depends on the reproducibility of the preconcentration step. Commonly, a hydrodynamic situation is set up where the flux of the electroactive analyte to the working electrode is maintained under well developed convective diffusion [22]. This can be attained by vigorous stirring of the solution, rotating the electrode [23], use of arrays of microelectrodes [24] or flowing the electrolyte past the electrode surface. The latter is utilised in the wall-jet cell [25], which is specially suitable for on-line monitoring and complete automation of the measurement.

1.2. The wall-jet detector

Hydrodynamic voltammetry requires an optimised electrode configuration and cell design with well defined hydrodynamic characteristics, low dead volume, constant effective electrode area, as well as ease of construction and maintenance [26]. The wall-jet cell fulfills all these requirements. For well developed wall-jet conditions, the hydrodynamic cell has to be dimensioned so that:

1. There is no breakage in the jet of the electrolyte coming from the inlet until it impinges on the surface of the working electrode.
2. The inlet jet nozzle should be located outside of the hydrodynamic boundary layer. Similarly the nozzle body, the counter electrode and the reference electrode should not be so close to the working electrode that the boundary layer is disturbed.
3. The diameter of the jet delivered from the nozzle should be negligible compared with the electrode diameter. Usually, a ratio $a/r > 10$ is considered sufficient.

In this work, several attempts are described to improve detection of lead in blood samples by anodic stripping. In order to minimise handling and operator interference, a flow injection ar-

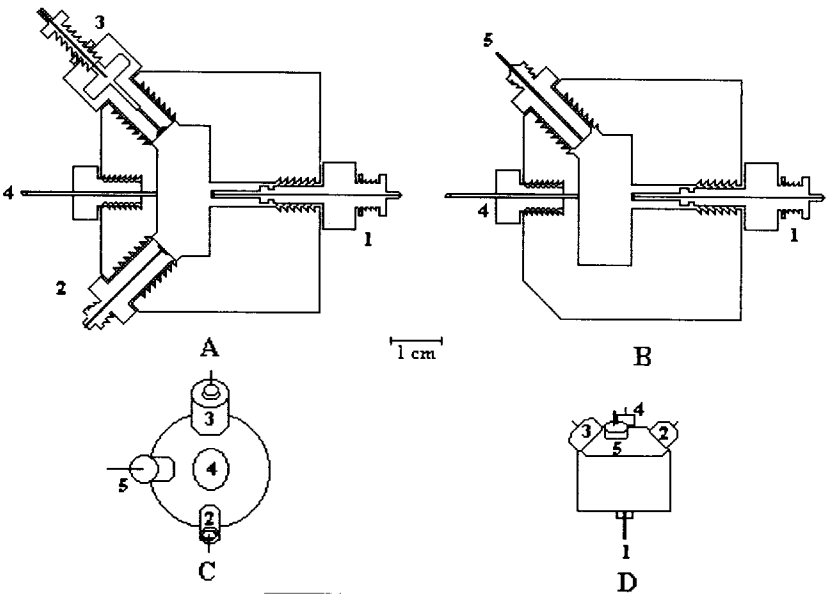

Fig. 1. Schematic of the wall-jet cell: A, B side elevation; C top view; D perspective view; 1, working electrode; 2, counter electrode; 3, reference electrode; 4, wall-jet nozzle; 5, liquid out.

rangement is proposed. In this mode, the polished electrode is mounted in the wall-jet cell. A mercury film is deposited by flushing a Hg^{2+}-containing solution through the cell at a cathodic potential. Blood samples are diluted 1:15 with a release agent, which contains Cr^{3+}, Ca^{2+}, and hydroxylamine. They are ultrasonicated with the release agent for 2 min, and injected. A further development is a glassy carbon electrode, which is coated with a Nafion®-membrane, in which Hg^{2+} is incorporated. The mercury film is formed in situ by reducing the mercury ions after the electrode is installed in the cell. A prototype for a disposable electrode has been tested, where both Hg^{2+} for the mercury film formation and Cr^{3+} as release agent are incorporated into the Nafion®-membrane. This electrode is simply inserted into the cell, and a computer program controls the timing for film plating, sample preconcentration, and stripping. The blood sample has only to be diluted with supporting electrolyte before an aliquot is injected into the wall-jet cell. Since the Cr^{3+} will be removed from the membrane by ion exchange, this modified electrode can only be used for a limited number of analyses, but it simplifies the experimental set-up because both the Hg^{2+} plating solution and the release agent are eliminated from the experiment.

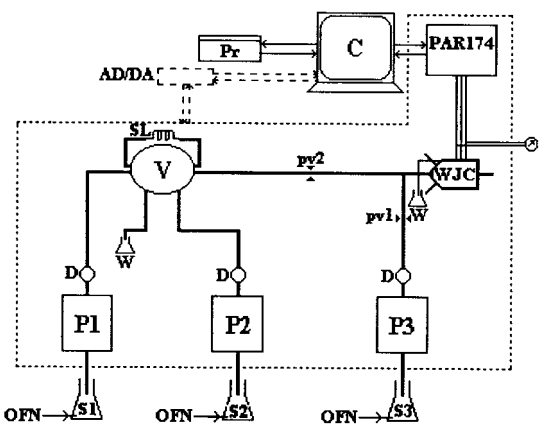

Fig. 2. Automated set-up for flow injection and detection by stripping voltammetry: C computer; D pulse dampeners; P1, P2, P3 pumps; PV1, PV2 pinch valves; S1, supporting electrolyte; S2, blood sample in release agent (1:15); S3, Hg^{2+} plating solution; V Sampling valve with SL sample loop (100 μl); WJC wall-jet cell.

Table 1
Peak currents obtained with different release agents (μA)

Pb^{2+} (μg ml^{-1})	0.05	0.10	0.15	0.20	0.25
Without EDTA	0.215	0.420	0.650	0.840	1.028
With EDTA and release agent 1	0.163	0.336	0.530	0.739	0.954
With EDTA and release agent 2	0.064	0.159	0.265	0.369	0.463

Sample is $Pb(NO_3)_2$ in supporting electrolyte; release agent 1 is 0.04 M Cr^{3+} and 0.08 M Ca^{2+}, release agent 2 is 0.1 M perchloric acid

2. Experimental

Fig. 1 shows the wall-jet cell used in this study. The cell is manufactured from perspex with an internal volume of ≈ 4 cm^3. The working electrode is a glassy-carbon disc 3.0 mm diameter and 2.0 mm thickness (Tokai, Tokyo) which was press-fitted in a teflon holder using an epoxy resin seal. The electrode was prepared by first polishing with abrasive paper (# 1200) followed by a final polish using 0.3 μm diamond paste until a mirror finish was obtained. A graphite disc (Johnson Matthey) with the same dimension as that of the working electrode was used as counter electrode. The reference electrode was a |Ag|AgCl|saturated KCl| cell with a 'Dycor' polymer frit (Princeton Applied Research) as a liquid junction. The flow-injection assembly consists of the wall-jet cell and the necessary valves to switch between plating solution and the supporting electrolyte, and to inject the sample (Fig. 2). The timing sequence for the pumps, valves and voltametric cycles are computer controlled. All voltammetric experiments were performed using a PAR model 174A polarographic analyser, which had been modified for remote control.

Millipore Milli-Q system purified water was used for all reagent preparation. Standard solutions of Hg^{2+} and Pb^{2+} with a concentration of 1000 μg ml^{-1} were obtained from BDH. The supporting electrolyte, KNO_3/HNO_3 (0.1 M/0.005 M), was prepared from analytical grade reagents and purged with oxygen-free nitrogen for at least 20 min before use. Samples, standards and plating solutions were prepared from the stock solutions by diluting with de-aerated supporting electrolyte solution. All glassware and sample containers were soaked with 1 + 1 nitric acid overnight and thoroughly rinsed with purified water before use.

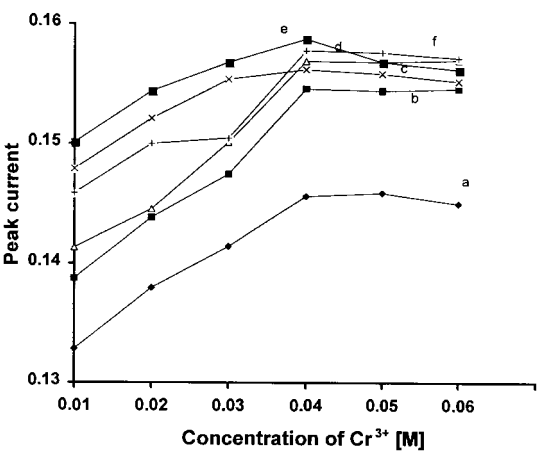

Fig. 3. The effect of the Cr^{3+} and Ca^{2+} concentration on the stripping peak: lead 0.05 μg ml^{-1}; EDTA 10 mM ml^{-1}. Calcium concentration: (◆) 0.0 M; (■) 0.02 M; (x) 0.04 M; (△) 0.06 M; (■) 0.08 M; (+) 0.10 M.

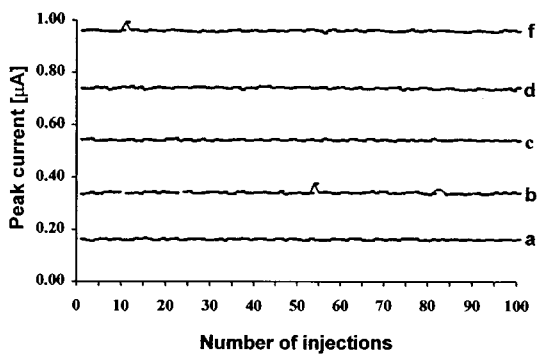

Fig. 4. Electrode stability and repeatability for the detection of complexed lead in the presence of release agent. Lead concentration: (a) 0.05 μg ml^{-1}; (b) 0.1 μg ml^{-1}; (c) 0.15 μg ml^{-1}; (d) 0.2 μg ml^{-1}; (e) 0.25 μg ml^{-1}.

Nafion®-modified electrodes were prepared as described by Dalangin [21]. A mercury(II)acetate solution (10 mg ml^{-1}) was prepared by dissolving the required amount of the salt in absolute ethanol and acidifying it with 100 μl of conc. acetic acid. A 5% Nafion® solution in a mixture of lower aliphatic alcohols + 10% water was obtained from Aldrich. The coating mixture consisted of 20 vol% mercury acetate solution and 20 vol% Nafion® solution made up to volume with absolute alcohol. The required volumes of stock mercury(II)acetate and Nafion® solutions were measured out with micro pipettes, mixed in a vial with a screw cap, and sonicated to produce a homogeneous mixture. Five microlitres of this solution were used to coat a freshly polished glassy carbon electrode. The solvent was allowed to evaporate slowly (inside an inverted beaker) to form a pinhole-free coating. For the chromium/mercury-modified electrodes, 50 ml of a stock solution containing mercury acetate (10 mg ml^{-1}) and chromium trichloride (0.04 M) was prepared by dissolving the required amounts of the respective salts in absolute alcohol and acidifying with 100 μl of conc. acetic acid.

Prior to use, the electrode was activated as follows: the electrodes were inserted, and the wall-jet cell was filled with supporting electrolyte. The pumps were switched off and a potential of −1.0 volts (vs. Ag/AgCl) was applied for 5 min. Thereafter, the electrolyte was allowed to flow again while holding the potential at 0.0 V (vs. Ag/AgCl) for 2 min. The electrode was then ready for analysis.

3. Results and discussion

Experiments were conducted with the MFE as well as with the Nafion®- and Nafion®/Cr^{3+}-modified electrodes. With each electrode, the stripping current was measured as a function of the Pb^{2+} concentration for (1) a reference containing only the measured amount of Pb^{2+} in supporting electrolyte, (2) the same solutions but with added EDTA, (3) Pb^{2+} solutions with EDTA and a Cr^{3+}/Ca^{2+} release agent, and (4) Pb^{2+} solutions with EDTA and perchloric acid.

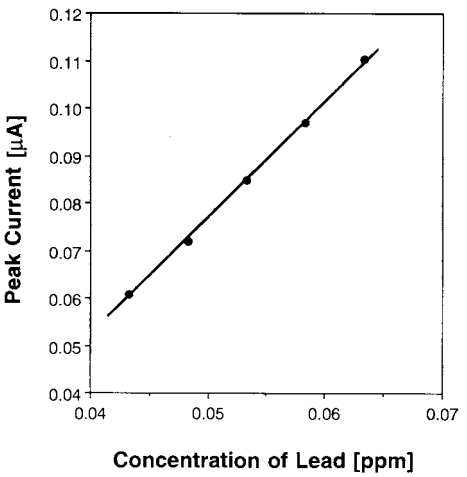

Fig. 5. Stripping signal vs. lead concentration in spiked whole blood samples measured with a bare mercury film electrode.

All reported peak currents are the average of three successive injections. Samples with Pb^{2+}/EDTA were used to simulate the complex formation in blood. These samples without release agent show no distinct stripping signal. Linear calibration plots over the concentration range 0.05–0.25 μg ml^{-1} Pb were obtained in all other cases. The results are shown in the Table 1. A whole blood standard (SERONOM; certified analysis 0.383 μg/ml) was used to validate the experimental results. The linear regression with the Cr^{3+}/Ca^{2+} releasing agent is given by: $Y = 3.086X - 0.09236$ (X in ppm and Y in μA) with a correlation coefficient of 0.9996, while for complexing agent/perchloric acid system, $Y = 2.1X - 1.1$, with rather poor reproducibility during repetitive analysis.

The concentration of perchloric acid was varied from 0.5 to 2%. The stripping current increases with increasing acid concentrations up to 1%, but remains almost constant at higher acid concentration. However, the recovery of the lead is below 30%. The Cr^{3+}/Ca^{2+} release agent gave a considerably higher rate of recovery. The composition of the releasing agent was investigated. A concentration range of 0.01–0.06 M for Cr^{3+} and of 0.0–0.1 M for Ca^{2+} was examined. The complexed lead concentration was 0.05 μg ml^{-1}. The peak current increases with increasing concentration of Cr^{3+} and Ca^{2+} and reaches a maximum

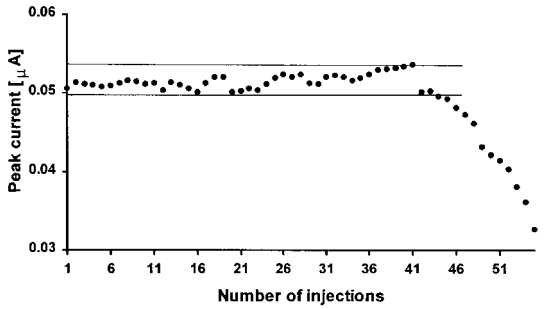

Fig. 6. Repeatability of a bare mercury film electrode for successive injections of whole blood samples in release agent (0.04 M Cr^{3+}; 0.08 M Ca^{2+})

at a concentration ratio of 0.04 and 0.08 M, respectively (Fig. 3). Cr^{3+} alone is capable of releasing lead but at a lower efficiency, whereas Ca^{2+} exerts an synergistic effect but by itself is not very effective in releasing Pb^{2+}. The optimum concentration was found to be 0.04 M Cr^{3+} and 0.08 M Ca^{2+}. This concentration was used in all subsequent experiments. The recovery i_p/i_p^o, where i_p is the stripping current of the sample and i_p^o that of the blank, was around 80%.

The excellent stability and reproducibility of the mercury film electrode is shown in Fig. 4. The signal remained constant for over 100 successive injections of the EDTA/Pb^{2+} complex with releasing agent present.

After optimising the system with the EDTA-complexed lead, measurements were taken on whole blood samples. For an unspiked sample, a stripping peak current of 0.050 μA was obtained, corresponding to a recovery of 60.4%. The dependence of the peak currents on the lead concentration in spiked samples is shown in Fig. 5. The calibration curves are linear over the selected concentration range. However, the recovery of lead varies from 60%, at low lead concentrations, to 81% at high concentrations. In spite of this, the results were highly reproducible. It is possible that the Pb^{2+} added for spiking is less strongly bound and therefore more readily available for the analysis than the lead originally present in the blood. The useful life of the electrode was studied with repeated injections of unspiked blood samples. Reproducible results were obtained up to about 40 injections. Thereafter, the mercury film appears to be affected and the signal decreases (Fig. 6).

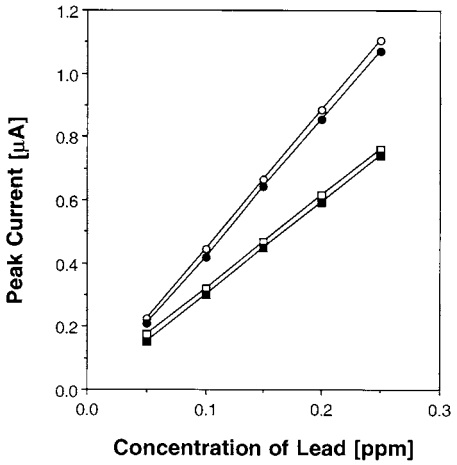

Fig. 7. Calibration plots for the modified electrodes with lead/EDTA and whole blood samples: (○) Nafion®-modified electrode; Pb^{2+}/EDTA, (●) Cr^{3+}/Nafion®-modified electrode; Pb^{2+}/EDTA, (□) Nafion®-modified electrode; spiked whole blood, (■) Cr^{3+}/Nafion®-modified electrode; spiked whole blood.

It was anticipated that the problem of surface contamination from the organic components in the blood could be reduced when Nafion® film-modified electrodes were used. The dependence of

Table 2
Recovery rate of lead from blood samples using different modified electrodes

Type of electrode	Peak current (μA)	Amount recovered[a] (μg ml^{-1})	%	RSD
Bare MFE	0.0501	0.231	60.4	5.1
Nafion®-modified electrode	0.0491	0.226	59.1	4.9
Nafion®/Cr^{3+}-modified electrode	0.0479	0.221	57.7	3.6

RSD, relative standard deviation based on four independent measurements
[a] 0.383 mg ml^{-1} Pb in original blood; samples were diluted 15:1 with release agent or supporting electrolyte

the stripping peak current, i_p, on the concentration was studied using both types of modified electrodes. In the case of mercury acetate/Nafion®-modified electrode, the sample was added together with the metal releasing agent and injected onto the modified electrode. However, for the chromium/mercury-modified electrode, the sample diluted with the supporting electrolyte was directly injected onto the modified electrode. Peak currents obtained are listed in Table 2. Fig. 7 shows calibration graphs for different samples with Nafion®-modified electrodes. Lead recovery from an unspiked sample of SERONOM blood of 59.1% was obtained with the Nafion®-modified electrode in the presence of added release agent. The yield was 57.7% with the chromium/Nafion®-modified electrode without additional release agent. These values are almost the same as those found with the bare MFE. Chromium ions incorporated into the mercury/Nafion®-modified electrode are indeed capable of releasing lead from its binding site. The peak currents, recovery rate and relative SD are also given in Table 2.

The long-term stability of the modified electrodes was studied using multiple injections of the unspiked blood sample. Fig. 8 shows the repeatability of the electrodes. Whereas the Nafion®-modified electrode shows good stability and is not affected up to at least 50 injections, the Cr^{3+}-modified electrode shows decreasing recovery after about ten injections. Obviously, the Cr^{3+} is leached out of the electrode by the supporting electrolyte. However, the experiment proves that at the given Cr^{3+} concentration within the membrane, lead release is almost as high as during prolonged sonication with the release agent in a separate processing step.

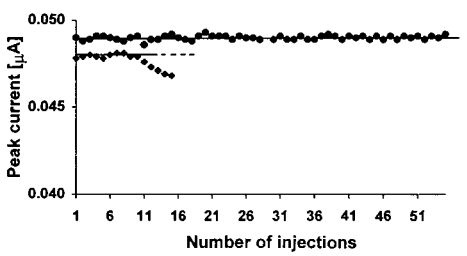

Fig. 8. Repeatability study of the modified mercury film electrode: (●) Nafion®-modified electrode (with release agent), (◆) Cr^{3+}/Nafion®-modified electrode (no release agent). Seronom whole blood with Pb 0.383 µg ml^{-1}; dilution factor 15:1.

4. Conclusions

Repeatability studies show that Nafion®-modified electrodes were superior to simple mercury-film electrodes for the analysis of lead in whole blood, since accumulation of surface contaminants is effectively suppressed. In the case of the chromium/mercury electrode, the repeatability was initially very good, but after about ten successive injections, the peak current begins to slowly decrease. Even though the sensitivity of the bare mercury film electrode is slightly higher than that of the modified electrodes, the Nafion®-modified electrode has better precision. The Nafion®/Cr^{3+}-modified electrode gives satisfactory performance only for a limited number of analyses. However, this type of modified electrode may find applications as a disposable electrode in portable instruments, since the mercury film is generated in situ and no additional release agents are required. The results provide valuable experimental data towards the ultimate goal of preparing a solid matrix blood–lead sensor device.

References

[1] J.J. Breen, C. Stroup (Eds.), Lead Poisoning, Lewis Publishers, CRC Press, Boca Raton, FA, 1995.
[2] A.T. Philip, B. Gerson, Clin. Lab. Med. 14 (1994) 423; 651.
[3] B.L. Vallee, D.D. Ulmer, Annu. Rev. Biochem. 41 (1972) 91.
[4] National Academy of Sciences (USA) Report, Comm. Biol. Effects. Atomos. Pollutants, 1971.
[5] P.A. Baghurst, A.J. McMichael, N.R. Wiggs, G.V. Vimpani, E.F. Robertson, R.J. Roberts, S.L. Tong, New Engl. J. Med. 327 (1992) 1279.
[6] R.M. Hicks, Chem.-Biol. Interact. 5 (1972) 361.
[7] W.H. Durum, J. Haffty, USA Geol. Surr. Circ. 445, 1961.
[8] A.A. Cernik, Br. J. Ind. Med. 24 (1967) 289.
[9] P.P. Donovan, D.T. Feeley, Analyst 94 (1969) 879.
[10] G.E. Batley, Y.J. Farrar, Anal. Chem. Acta 99 (1978) 283.

[11] S. Costantini, R. Giordano, M. Rabbiani, Microchem. J. 35 (1987) 70.
[12] D. Jagner, M. Joseffon, S. Westerlund, K. Aren, Anal. Chem. 53 (1981) 1406.
[13] L. Almestrand, D. Jagner, L. Renman, Anal. Chim. Acta 193 (1989) 71.
[14] H. Huiliang, D. Jagner, L. Renman, Anal. Chim. Acta 207 (1988) 17.
[15] J. Wang, J. Electroanal. Chem. 139 (1982) 225.
[16] L. Almestrand, M. Betti, C. Hua, D. Jagner, L. Renman, Anal. Chim. Acta 209 (1988) 339.
[17] P.J.S. Barbeira, L.H. Mazo, N.R. Stradiotto, Analyst 120 (1995) 1647.
[18] B. Hoyer, T.M. Florence, Anal. Chem. 59 (1987) 2839.
[19] J. Wang, L.D. Hutchins-Kumar, Anal. Chem. 58 (1986) 402.
[20] R.B. Smart, E.E. Stewart, Environ. Sci. Technol. 19 (1985) 137.
[21] R.R. Dalangin, H. Gunasingham, Anal. Chim. Acta 291 (1994) 81.
[22] H. Gunasingham, B. Fleet, in: A.J. Bard (Ed.) Electroanalytical Chemistry: A Series of Advances, vol. 16, Marcel Dekker, New York and Basel 1989, 8.
[23] T.R. Copeland, J.H. Christie, R.A. Osteryoung, R.K. Skogerboe, Anal. Chem. 45 (1973) 2171.
[24] B.J. Feldman, A. D'Alessandro, J.D. Osterloh, B.H. Hata, Clin. Chem. 41 (1995) 557.
[25] B. Fleet, C.J. Little, J. Chromatogr. Sci. 12 (1974) 747.
[26] H. Gunasingham, B. Fleet, Anal. Chem. 55 (1983) 1409.

.

ELSEVIER

Talanta 45 (1998) 713–719

Talanta

The degree of deacetylation of chitosan: advocating the first derivative UV-spectrophotometry method of determination

Su Ching Tan [b], Eugene Khor [a,*], Teck Koon Tan [b], Sek Man Wong [b]

[a] *Department of Chemistry, The National University of Singapore, 10 Kent Ridge, Singapore 119260, Singapore*
[b] *School of Biological Sciences, The National University of Singapore, 10 Kent Ridge, Singapore 119260, Singapore*

Received 5 February 1997; received in revised form 24 July 1997; accepted 28 July 1997

Abstract

The degree of deacetylation (DD) is increasingly becoming an important property for chitosan, as it determines how the biopolymer can be applied. Therefore, a simple, rapid and reliable method of determining the DD for chitosan is essential. In this report, the DD of chitosan was determined by nuclear magnetic resonance (NMR), linear potentiometric titration (LPT), ninhydrin test and first derivative UV-spectrophotometry (1DUVS). The DD was calculated on a per mol basis instead of on a per mass basis. This is important as the molecular weights of *N*-acetyl-D-glucosamine and D-glucosamine are different. By converting the mass of *N*-acetyl-D-glucosamine and D-glucosamine into mols and calculating for the percentage of D-glucosamine present in the chitosan sample, a more accurate estimation of the DD can be obtained. Of the four methods, there is good correlation between 1DUVS and NMR. The concentration of chitosan solution for 1DUVS analysis was standardised as 0.1000 mg chitosan per ml of 0.0100 M acetic acid solution. The presence of D-glucosamine was corrected for by a reference curve for *N*-acetyl-D-glucosamine. 1DUVS is easy to perform, sensitive and the interference of other contaminants to the results is minimal compared with the other three methods. Therefore, we advocate 1DUVS to be used as the standard methods for routine determination of DD of chitosan. © 1998 Elsevier Science B.V.

Keywords: Chitosan; Degree of deacetylation; First derivative UV-spectrophotometry

1. Introduction

Over the past 30 years, chitosan, the (β-1,4)-linked D-glucosamine derivative of the polysaccharide chitin, has been extensively advanced as a promising renewable polymeric material. Wide ranging applications in many areas for chitosan include wastewater treatment, food, agriculture, cosmetic/personal care and biotechnological and pharmaceutical industries [1]. While chitosan has lived up to some of these expectations, significant barriers to its broader usage exist. These include supply cost, variability in quality and poor methods of characterisation of its properties [2]. One of the more important property is the degree of deacetylation (DD), which determines whether the biopolymer is chitin or chitosan. The arbitrary

* Corresponding author. Tel.: +65 7722836; fax: +65 7791691; e-mail: chmkhor@nus.edu.sg

PII S0039-9140(97)00288-9

DD of ≥ 40 defining chitosan [3], plays an important role in defining the use of chitosan as DD influences the physical, chemical and biological properties of chitosan such as the tensile strength of films [4], ability to chelate metal ions [5] and immunoadjuvant activity [6,7].

Many methods have been used to determine the DD of chitosan. These include infrared spectroscopy (IR) [8–10], near infrared spectroscopy (NIR) [11], UV-spectrophotometry [12], first derivative UV-spectrophotometry (1DUVS) [13], colloidal titration [14], linear potentiometric titration (LPT) [15], enzymatic determination [16], nuclear magnetic resonance (NMR) [17], ninhydrin test [18] and circular dichroism measurements [19]. The choice of method appears to be arbitrary and often does not correlate well with others [12]. A standard method used to determine the DD of chitosan that satisfies the producers and end users is essential, if the wider exploitation of chitosan is to be realised. A standard method has to be simple, rapid, cost effective and reliable yet tolerate the presence of impurities, especially protein, a common contaminant. From our survey, the use of the 1DUVS as proposed by Muzzarelli and Rocchetti is the simplest and most convenient among all the presently available methods. The 1DUVS method requires only very small amounts of sample and relies on simple reagents and instrumentation. In addition, the results obtained from 1DUVS are reasonably independent of protein contamination. Therefore, we wish to advocate the use of 1DUVS as the standard method for determining the DD of chitosan.

In this paper, we have evaluated and refined the 1DUVS method. The DD of commercial and purified commercial chitosan were determined and the results compared with those of NMR, LPT and ninhydrin test.

2. Materials and methods

Chitosan was obtained from Fluka (Switzerland) and Tokyo Kasei (Japan). D-Glucosamine (GlcN) and *N*-acetyl-D-glucosamine (GlcNAc) were obtained from Sigma (USA). All other chemicals were of reagent grade.

2.1. Purification of chitosan

Chitosan (4.0 g) and 160 ml of 40% (w/v) NaOH were placed in a 500 ml round bottom flask. $NaBH_4$ (0.05 g) was added and the suspension was refluxed, with stirring, at 95°C for 4 h. The suspension was cooled, the residue retained by filtration and washed with distilled water until the pH of the filtrate was same as the pH of distilled water. The residue was submitted to another round of reflux. The residue retained from the second round of reflux was dissolved in 250 ml of a 2% acetic acid solution. The chitosan solution was centrifuged at $16\,000 \times g$ for 5 min and the supernatant retained. Chitosan was then precipitated from the supernatant by increasing the pH (to pH 8–9) with 1 N NaOH. The suspension was centrifuged at $16\,000 \times$ g for 5 min and the chitosan pellet retained. The chitosan was washed with distilled water until the pH of the supernatant was the same as the pH of distilled water. The chitosan was finally washed once with 95% ethanol and freeze dried.

2.2. Calculation of the degree of deacetylation of chitosan

Besides NMR, the DD in all methods were calculated on a per mol basis instead of on a per mass basis. This is important as the molecular weights of chitin (acetylated form of chitosan) and chitosan are different. By converting the mass of chitin and chitosan into mols and calculating for the percentage of chitosan present in the sample, a more accurate estimation of the DD is realised.

2.3. Nuclear magnetic resonance [17]

A chitosan sample was dissolved in CD_3COOD/D_2O solution and the NMR spectrum (300 MHz) was obtained at 90°C (Bruker; Model ACF 300). The DD of the chitosan was determined by the formula below.

$$\mathrm{DD} = \left[1 - \left(\frac{1/3I_{\mathrm{CH_3}}}{1/6I_{\mathrm{H_2-H_6}}}\right)\right] \times 100,$$

Table 1
Degree of deacetylation of commercial chitosan measured by first derivative spectrophotometry, nuclear magnetic resonance, linear potentiometric titration and ninhydrin test

Chitosan sample		Fluka	Kasei	Purified Kasei
Degree of Deacetylation (%)	First derivative uv-spectrophotometry	85.82 ± 0.51	82.66 ± 0.74	98.08 ± 0.03
	Nuclear magnetic resonance	82.20*	N/A	N/A
	Linear potentiometric titration	75.00 ± 0.41	73.29 ± 0.62	89.25 ± 0.38
	Ninhydrin test	51.01 ± 1.88	44.92 ± 1.75	55.41 ± 2.91

* No replicate was done.

where I_{CH_3} is the integral intensity of CH_3 and $I_{H_2-H_6}$ is the summation integral intensities of H_2, H_3, H_4, H_5, H_6 and $H_{6'}$.

2.4. Linear potentiometric titration [15]

The determination of DD by LPT was a modification of the method of Ke and Chen. Chitosan (0.20–0.25 g) was dissolved in 20 ml of standardised 0.10 N HCl (to give a non-viscous solution) and diluted with 10 ml of distilled water. The pH of the solution was adjusted to ≈ 2 with standard 0.01 M NaOH and taken as the start point. Under continuous stirring, 1 ml of standard NaOH (0.5 ml for purified chitosan) was added, allowed to equilibrate and the pH recorded. This sequence was repeated until the pH reached a value of 3. A value of $f(x)$ of the corresponding volume of NaOH added was calculated using the following formula:

$$f(x) = \left(\frac{V_0 + V}{N_B}\right) \times ([H^+] - [OH^-]),$$

where V_0 is the volume of chitosan solution (ml); V is the volume of NaOH added (ml); N_B is the concentration of NaOH (N); $[H^+]$ is the concentration of H^+ (M); $[OH^-]$ is the concentration of OH^- (M).The linear titration curve was obtained by plotting $f(x)$ vs. the corresponding volume of NaOH. The volume of NaOH at the end point of the titration, V_e, was estimated by extrapolating the linear titration curve to the x-axis. The DD of the chitosan sample was calculated using the following formula. Five replicates were performed for each sample.

$$DD(\%) = \varnothing / [(W - 161\varnothing) / 204 + \varnothing] \times 100,$$

where $\varnothing = (N_A V_A - N_B V_e)/1000$; N_A is the concentration of HCl (N); V_A is the volume of HCl (ml); N_B is the concentration of NaOH (N); V_e is the volume of NaOH at the end point (ml); W is the sample mass (g).

2.5. Ninhydrin test [18]

Ninhydrin test is another test which estimates the amount of chitosan by direct detection of the $-NH_2$ group on the glycoside repeat unit of chitosan. Standard solutions were prepared by pipetting 0.1, 0.2, 0.3, 0.4, and 0.5 ml of GlcN solution (0.1 mg ml^{-1} 2% acetic acid) into separate test tubes. Acetic/acetate buffer (0.5 ml; pH 5.5, 4 M) was added to each tube and the volume adjusted to 1 ml with distilled water. Finally, 2 ml of ninhydrin reagent (250 ml acetic/acetate buffer, pH 5.5, 4 M, 20 g ninhydrin, 3 g hydrindantin, 750 ml methyl cellosolve) were added to each tube and the solution heated in a boiling water bath for 10 min. The solution was allowed to cool for 15 min before the UV absorbance at 570 nm of each solution was recorded. The calibration curve was obtained by plotting the absorbance against the concentration of standard solutions. Sample solutions consisted of 0.5 ml of chitosan solution (0.1 mg ml^{-1} 2% acetic acid) to which was added the buffer, topped up with distilled water and the ninhydrin reagents. The solution was heated as above and the absorbance value recorded. The amount of chitosan in the sample was estimated and the DD of the chitosan samples were determined by the formula below. Five replicates were performed for each sample.

$$DD = \varnothing / [\,(W - 161\varnothing) / 204 + \varnothing\,] \times 100,$$

where $\varnothing$ is the amount of GlcN determined/161 and W is the sample mass.

2.6. First derivative UV-spectrophotometry [13]

UV-vis absorption spectra were obtained using a Shimadzu 1601 UV-vis spectrophotometer. The zero crossing point (ZCP) was determined by superimposing the first derivative spectra of 0.0100, 0.0200 and 0.0300 M of acetic acid solutions at 203 nm.

2.6.1. Calibration curve

Solutions of 0.0050–0.0500 mg of GlcNAc per ml of 0.0100 M acetic acid solution were prepared and their first derivative spectra obtained. Each concentration had five replicates. The spectra of 0.0100, 0.0200 and 0.0300 M of acetic acid solutions were superimposed and the vertical distance from ZCP to each GlcNAc solution spectrum, H, was measured (mm). A linear calibration curve was obtained by plotting the H values against the corresponding GlcNAc concentration.

2.6.2. Correction of the effect of D-glucosamine on H values

As proposed by Muzzarelli and Rocchetti, the presence of GlcN may give rise to a larger H value for GlcNAc than expected. Therefore, a reference curve for correcting this discrepancy was necessary. A 0.1000 mg GlcNAc per ml 0.0100 M acetic acid solution was prepared and varying amounts of GlcN was dissolved in the GlcNAc solution to give a series of different percentages of GlcNAc solutions (w/w). The H values of the pure GlcNAc solution, H_1, and the H values of the solutions of different percentages of GlcNAc, H_2, were measured. The reference curve was obtained by plotting H_1/H_2 vs. the corresponding GlcNAc percentage.

2.6.3. Determination of the DD of chitosan

Freeze-dried chitosan samples (0.0100 g) were dissolved in 10 ml of 0.1000 M acetic acid solution and topped up to 100 ml with distilled water. Five replicates were performed for each sample. The H values of the chitosan samples were measured and the contribution due to GlcNAc was obtained from the calibration curve. The DD of the samples were determined by the formula:

$$\mathrm{DD} = 100 - [A \,/\, (W - 204A) \,/\, 161 + A] \times 100),$$

where A is the amount of GlcNAc determined/204 and W is the mass of chitosan sample used.

3. Results and discussion

In the estimation of the DD, methods which assess the amine or acetyl amine groups on the glycoside unit of chitosan directly would be preferred. Methods such as circular dichroism, NMR, GPC and thermogravimetry are not suitable for routine purposes because of the cost, specialist considerations and sophistication which renders them more appropriate for research purposes. Elemental analysis has long been the common method to ascertain the DD of chitosan. The method requires very pure samples for accurate estimation. This is not often attainable in the extraction of chitin and chitosan from shellfish. Furthermore, the hygroscopic nature of chitosan will always include water in the derivation of the empirical formula. IR and NIR spectroscopy are methods that are also commonly used. However, they are primarily a solid state method and may not be appealing because variations can be found in the results obtained using different baselines [8–11]. Different baselines have been suggested for samples with different ranges of DD [6] but the choice of the baseline is debatable, especially when its range for individual samples are unknown. Therefore, we feel that IR and NIR are not suitable as standard methods to determine the DD of chitosan. Thus the choice of the standard method to determine the DD on a routine basis appears to rest on a solutions based approach. In dilute solutions, it is expected that the amine group would be at its most accessible for optimum quantification.

We have reviewed four solution based methods and are advocating the use of 1DUVS. Table 1 presents the results of the DD obtained from NMR, LPT, ninhydrin test and 1DUVS. The DD of 1DUVS, LPT and ninhydrin methods do not correlate well with each other. Of the four meth-

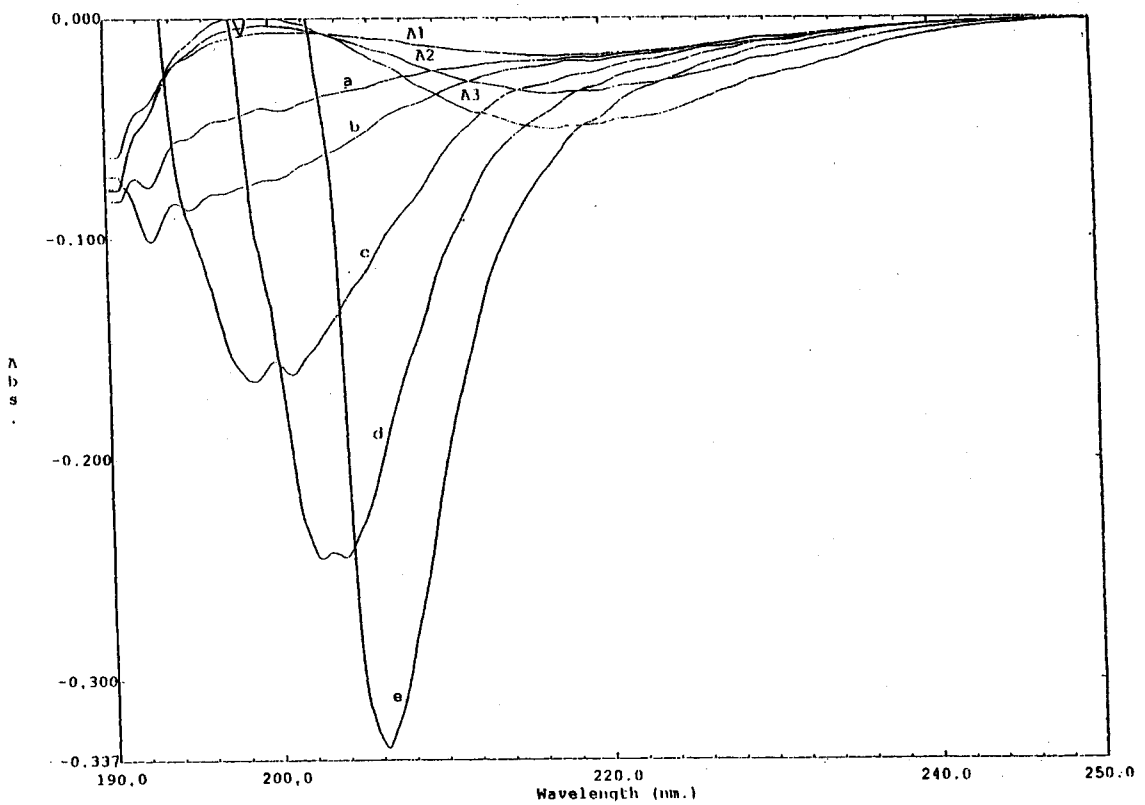

Fig. 1. First derivative UV-spectra for various concentrations of chitosan solutions. A1, 0.01 M acetic acid solution; A2, 0.02 M acetic acid solution; A3, 0.03 M acetic acid solution; a, 0.05 mg chitosan/0.01 M acetic acid solution; b, 0.10 mg chitosan/0.01 M acetic acid solution; c, 0.25 mg chitosan/0.01 M acetic acid solution; d, 0.50 mg chitosan/0.01 M acetic acid solution; e, 1.00 mg chitosan/0.01 M acetic acid solution.

ods, we believe that the results obtained by 1DUVS are the closest to the actual DD of the chitosan samples. This is because the results from NMR, LPT and ninhydrin test may be affected by the presence of protein contaminants, which is commonly present in crude chitosan samples. The maximum UV absorbance of proteins is typically at the wavelength 280 nm, far enough from 203 nm, the wavelength at which the H value was measured. Therefore, the interference from the proteinaceous contaminant in the sample to the results obtained by 1DUVS is kept at a minimal level.

Although the result from NMR correlates well with 1DUVS, 1DUVS has several advantages over the NMR method. The most important is 1DUVS can tolerate a higher level of proteinaceous contaminants. Second, chitosan samples used for NMR has to be dissolved in deuterated solvent (CD_3COOH/D_2O) which is usually more expensive than the solvent (CH_3COOH/H_2O) used in 1DUVS. Last, the cost of NMR instrumentation is typically prohibitive compared with UV-spectrophotometry for the small producer.

The advantage of using ninhydrin test is that a very small amount of chitosan is required. However, the values of DD obtained were the lowest among the three methods compared. There was a large difference between the results obtained by ninhydrin test and other methods. This may be attributed to the fading of colour intensity of the sample solution with time, after the boiling process. This decolourisation was observed visually about 30 min after the boiling process and there-

fore, contribute to errors in the absorbance values [16]. The procedure of this method is also relatively more complicated than LPT and 1DUVS as the ninhydrin reagent needs to be freshly prepared for each test. Furthermore, the ninhydrin reagent is carcinogenic and extra precautions in handling are necessary. Finally, since the chemical basis for the ninhydrin test is reaction with the amine group, the presence of protein (which also contains amines) in the sample may adversely interfere with the results.

LPT is easier to perform than the ninhydrin test and the results are often more consistent. Unlike the traditional potentiometric titration, the analyte is not titrated all the way to its end point. Therefore, interference from the precipitation of chitosan is avoided. The equipment and reagent used in LPT are also simple and readily available in a chemistry laboratory. The major source of error for LPT is the reliability of the pH measurement. The results from LPT are very dependent on the $[H^+]$ and $[OH^-]$ concentrations in the analyte as the pH measured directly affects the DD determined. The amine and thiol groups in amino acids will affect the $[H^+]$ concentration of the analyte, and therefore, the presence of protein contaminant can also be a major interference.

1DUVS is very sensitive for GlcNAc detection, the detectable concentration of GlcNAc in 0.01 M acetic acid solution was found to be as low as 0.0005 mg ml^{-1}. The concentration of the chitosan sample solution to be used for analysis was standardised as 0.1000 mg chitosan per ml of acetic acid solution. This permitted a wider range of DD (0–50%) to be ascertained based on the calibration plot ranging from 0.0050 to 0.0500 mg GlcNAc per ml acetic acid solution. In this range, the plot was linear and obeyed Beer's law. This is contrary to the concentration of 1 mg chitosan per ml of acetic acid solution used by Muzzarelli and Rocchetti [13]. Using this concentration, only DD in the range 0–5% can be determined, which is quite narrow. The dip of the 1DUVS spectrum of chitosan solution is shifted to the right with increasing chitosan concentration (Fig. 1). If the concentration of chitosan solution is too high, the dip of its first derivative spectrum may be shifted beyond the valid range. Therefore, high concentrations of chitosan solution for analyses are to be avoided as it would require more sample which may add more experimental errors whenever dilutions are made. Chitosan solutions of too low concentrations are also not advisable as this may also incur larger experimental errors.

The reference curve for the correction of the effect of GlcN on the *H* value is shown in Fig. 2. Muzzarelli and Rocchetti showed that the presence of GlcN contributes to the *H* value, when the GlcNAc to GlcN ratio is below 0.11 (GlcNAc is less than 10%). However, our results showed that even when the GlcNAc is 20%, contributions of the GlcN to the *H* value is also present. The discrepancy between our data and that of Muzzarelli and Rocchetti may lie in the sensitivity of the UV-spectrophotometer used. Therefore, our current data suggests that corrections up to 20% are necessary.

Based on the results we obtained, the DD of chitosan determined, varied with the methods used. Each of these methods has its own advantages and disadvantages. Therefore, it is difficult to tell which method has given us the most accurate results. However, all of them did show the relative DD between different chitosan samples. Up to date there is still no standard method for

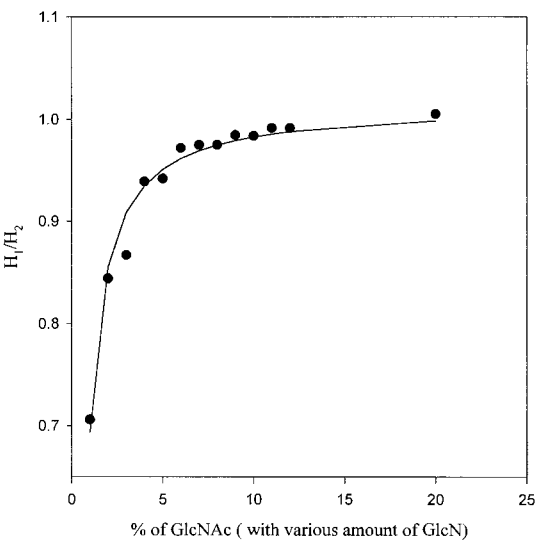

Fig. 2. Correction curve for GlcNac determination.

the determination of DD of chitosan yet. We advocate 1DUVS to be used as the standard method for routine determination of the DD of chitosan due to its high sensitivity, minimal interference of results from contaminants and easy to be performed.

Acknowledgements

The authors acknowledge the National University of Singapore for financial sponsorship of this work (RP 920633) and the award of a research scholarship for S.C. Tan.

References

[1] P.A. Sandford, Chitosan: commercial uses and potential application, in G. Skjak, T. Anthonsen, P. Sandford (Eds.), Chitin and Chitosan: Sources, Chemistry, Biochemistry, Physical Properties and Applications, Elesevier, New York, 1988, pp. 51–69.
[2] Chitin and Chitosan: Specialty Polymers for Food, Medicine and Industry, Technical Insights, Engelwood, NJ.
[3] M.G. Peters, Applications and environmental aspects of chitin and chitosan, J. Mat. Sci.–Pure Appl. Chem. A32 (1995) 629–640.
[4] S. Mima, M. Miya, R. Iwamoto, S. Yoshikawa, Highly deacetylated chitosan and its properties, J. Appl. Polym. Sci. 28 (1983) 1909–1917.
[5] H. Miyoshi, K. Shimahara, K. Watanabe, K. Onodera, Characterisation of some fungal chitosans, Biosci. Biotech. Biochem. 56 (1992) 1901–1905.
[6] K. Nishimura, S. Nishimura, N. Nishi, I. Saiki, S. Tokura, I. Azuma, Immunological activity of chitin and its derivatives, Vaccine 2 (1984) 93–99.
[7] K. Nishimura, S. Nishimura, N. Nishi, F. Numata, Y. Tone, S. Tokura, I. Azuma, Adjuvant activity of chitin derivatives in mice and guinea-pigs, Vaccine 3 (1985) 379–384.
[8] A. Baxter, M. Dillon, K.D.A. Taylor, G.A.F. Roberts, Improved method for IR determination of the degree of *N*-acetylation of chitosan, Int. J. Biol. Macromol. 14 (1992) 166–169.
[9] A. Domard, U. Rinaudo, Preparation and characterisation of fully deacetylated chitosan, Int. J. Biol. Macromol. 5 (1983) 49–52.
[10] T. Sannan, K. Kurita, K. Ogura, Y. Iwakura, Studies on chitin: 7. IR spectroscopy determination of degree of deacetylation, Polym. 19 (1978) 458–459.
[11] T.D. Rathke, S.M. Hudson, Determination of the degree of *N*-deacetylation in chitin and chitosan as well as their monomer sugar ratios by near infrared spectroscopy, J. Polym. Sci. 31 (1993) 749–753.
[12] S. Aiba, Studies on chitosan: 1. Determination of the degree of *N*-acetylation of chitosan by ultraviolet spectrophotometry and gel permeation chromatography, Int. J. Biol. Macromol. 8 (1986) 173–176.
[13] R.A.A. Muzzarelli, R. Rochetti, Determination of the degree of acetylation of chitosan by first derivative ultraviolet spectrophotometry, Carbohydr. Polym. 5 (1985) 461–472.
[14] H. Terayama, Method of colloid titration (a new titration between polymer ions), J. Polym. Sci. 8 (1952) 243–253.
[15] H. Ke, Q. Chen, Potentiometric titration of chitosan by linear method, Huaxue Tongbao 10 (1990) 44–46.
[16] F. Nanjo, R. Katsumi, K. Sakai, Enzymatic method for determination of the deacetylation of chitosan, Anal. Biochem. 193 (1991) 164–167.
[17] A. Hiral, H. Odani, A. Nakajima, Determination of degree of deacetylation of chitosan by ^{1}H NMR spectroscopy, Polym. Bull. 26 (1991) 87–94.
[18] E. Curotto, F. Aros, Quantitative determination of chitosan and the percentage of free amino groups, Anal. Biochem. 211 (1993) 240–241.
[19] A. Domard, Determination of *N*-acetyl content in chitosan samples by cd measurements, Int. J. Biol. Macromol. 9 (1987) 333–336.

.

ELSEVIER

Talanta 45 (1998) 721–726

Talanta

Effect of the composition of Nafion deposition solutions on the ion-exchange properties of the Nafion films by quartz crystal microbalance sensor (QCM)

Guizhu Zhao, Hardy Chan, Sam F.Y. Li *

Department of Chemistry, National University of Singapore, Singapore 119260, Singapore

Received 4 February 1997; received in revised form 4 June 1997; accepted 10 June 1997

Abstract

A quartz crystal microbalance (QCM) sensor system was employed to investigate the properties of Nafion films on a gold surface supported on a quartz-crystal as a function of the water content in the deposition solutions (0.5% Nafion in mixed ethanol/water). The rates of loading and unloading of the complex ion $Ru(bpy)_3^{2+}$ through Nafion films were measured. A linear dependence of the frequency changes on the percentage of water in the deposition solution was observed for both loading and unloading. The ion-exchange distribution coefficients for Nafion films from various deposition solutions were calculated. We concluded that films cast from solutions of higher water content had more 'open' structures which allowed faster diffusion of ions. This conclusion was further supported by the results of SEM experiments. © 1998 Elsevier Science B.V.

Keywords: Nafion; Ion-exchange; Quartz crystal microbalance sensor

1. Introduction

Nafion deposited on electrode surfaces is one of the most extensively investigated polyelectrolyte coating systems that have been employed to modify the behaviour of electrodes [1–13]. Much effort was devoted to study the morphology, transport properties, and mechanical characteristics [14–17] of these polymers.

There is ample evidence which suggests that Nafion shows remarkable affinity for hydrophobic cations [3,4,18–21]. These polymers can engage in strong hydrophobic interactions with organic cations and, hence, hydrophobic organic cations are preferentially incorporated into the microdomain around the polymer chains [21]. The hydrophobic organic cation, i.e. Tris (2,2′-dipyridine) ruthenium dichloride ($Ru(bpy)_3\ Cl_2$) was employed to investigate the properties of Nafion films.

Striebel et al. studied the effect of humidity level during film deposition on the properties of the films [22]. They evaporated ethanolic solutions of Nafion on electrodes under a glass cover, which also contained either pure water ('wet-cured

* Corresponding author. Fax.: + 65 7791691; e-mail: chmlifys@leonis.nus.sg

PII S0039-9140(97)00187-2

films') or P_2O_5 desiccant ('dry-cured films'), and tested the permeability of $Ru(bpy)_3^{2+}$ in the films. It turned out that loading of $Ru(bpy)_3^{2+}$ ions was much faster into the wet-cured films than into the dry-cured films. Rubinstein and co-workers studied the composition of the Nafion deposition solution and its effect on the properties of the resultant films and the modes of binding and diffusion of $Ru(bpy)_3^{2+}$ in these films [23].

All these studies used electrochemical methods and coulometry was performed to monitor the amount of hydrophobic organic cations incorporated into Nafion films. However, in coulometry some organic cations may be trapped in regions inaccessible to electrochemical oxidation or diffuse to the electrolyte solution owing to the solution contact during the coulometric experiment [24].

The quartz-crystal microbalance (QCM) is presently finding considerable application as a probe of interfacial processes [25–28]. In this report, we describe the use of the quartz crystal microbalance in combination with ellipsometry and scanning electron microscope (SEM) to study the properties of Nafion films on a gold surface supported on a quartz crystal as a function of the water content in the deposition solutions.

2. Experimental

2.1. Chemicals and apparatus

A solution of 5% Nafion (Fluka, Switzerland) was diluted 10 times with ethanol and water. Tris (2,2′-dipyridine) Ruthenium dichloride was purchased from Sigma (St. Louis, USA). All chemicals were analytical grade. Water was from a Milli-Q purification system.

The QCM system was completed with a frequency oscillator, a faraday cage, and a remote probe unit from Elchema (Elchema, Potsdam, New York). AT-cut quartz crystals (10.00 MHz) were purchased from International crystal Manufacturing Inc. (Oklahoma, OK). Gold electrodes were deposited in a keyhole pattern on both sides of the crystals and the total area exposed to the solution was $\sim$ 0.2 cm^2. The sensitivity of the system was calculated to be 0.9 ng Hz^{-1}.

2.2. Film deposition

Coating of the electrode was carried out by applying a drop of 1 μl Nafion solution (0.5% w/v in mixed ethanol-water) on the center of the gold electrode, followed by room-temperature evaporation of the solvent in an environment of 25°C and 70% humidity. Special attention was paid to maintain the areas of the coatings to be the same (0.03 cm^2). The thickness of the film was 50 nm as determined by ellipsometry. The amount of the incorporated $Ru(bpy)_3^{2+}$ in the films was determined by the frequency difference and its concentration was calculated from the 'effective' volume of the film.

2.3. Procedures and calculations

The resulting coating was soaked in 0.02 phosphate buffer solution to obtain a background frequency shift, which would be subtracted from the total value. The electrode was transferred to a 0.5 mM $Ru(bpy)_3^{2+}$ solution for loading. It was saturated within 1 min, i.e. the film was loaded with the maximum quantity of $Ru(bpy)_3^{2+}$ species that can be accommodated on the basis of electroneutrality requirements. It was then removed from the loading solution, rinsed and transferred to the background solution for unloading. The mass change during loading Δm (g) can be calculated from the corrected frequency shift ΔF (Hz) of the AT-cut, shear-mode QCM using [29,30]

$$\Delta m = \frac{-A(\rho_q \mu_q)^{0.5}}{2F_0^2}\Delta F = -1.6 \times 10^{-10}\Delta F \qquad (1)$$

where F_0 is the oscillation frequency of the uncoated quartz crystal (10.00 MHz), A the coating area on the electrode (0.03 cm^2), ρ_q the density of quartz (2.65 g cm^{-3}), and μ_q its shear modulus (2.59×10^{11} dyn cm^{-2}). In agreement with Eq. (1), QCM calibrations indicated that a decrease in frequency (ΔF) of 1 Hz corresponded to an increase in electrode mass (Δm) of 0.16 ± 0.01 ng. This ratio ($\Delta F/\Delta m$) was subsequently employed to calculate Δm.

We express the extent of the exchange of the $Ru(bpy)_3^{2+}$ for Na^+ in the Nafion film in terms of a distribution coefficient, k_D, which is the equi-

librium coefficient for the hypothetical partition reaction

$$M^{n+}_{aq} \Leftrightarrow M^{n+}_{film} \quad (2)$$

and is given by $k_D = [M^{n+}]_{film}/[M^{n+}]_{aq}$.

The film concentrations were calculated from the mass of $Ru(bpy)_3^{2+}$ loaded and the calculated film volume. The mass of ejected Na^+ ions should be considered when calculating the actual loading mass of $Ru(bpy)_3^{2+}$ [31]. The Na^+ ions are in the hydrated forms and the hydration number is 7 [32].

3. Results and discussion

3.1. Loading and unloading

The conversion of a Nafion film to the $Ru(bpy)_3^{2+}$ form ('loading') was carried out by soaking the coated electrode in a phosphate buffer solution of $Ru(bpy)_3^{2+}$ dichloride. Two parameters seem to govern the rate of complex incorporation: the rate of material supply to the film-solution interface and the rate of mass-transport in the polymer.

When the coated electrode was immersed in an unstirred solution of the complex, the rate of material supply was limited by diffusion in the solution. Stirring the solution accelerated significantly the incorporation rate, which increased with speed of stirring up to a saturation point (Fig. 1). The stirring was carried out by a magnetic stirring hot plate (Heidolph MR3001) from ITS company. A film deposited from 20% H_2O Nafion solution reached the saturation point when the stirring speed was up to 600 min^{-1}.

Since the rate of complex incorporation in a quiescent solution is limited primarily by mass transport in the solution, it does not demonstrate fully the effect of film structure. Therefore, loading and unloading experiments were performed at fast enough stirring speed (over 600 min^{-1}, as indicated in Fig. 1).

The rate of permeation (and transport) in the polymer was found to be dependent upon the nature of the specific film. As noted above, coating of the electrode was carried out upon applying 1 μl of Nafion solution (0.5% w/v) in mixed ethanol-water onto the surface, followed by room temperature evaporation of the solvent. It was found that the composition of the depositing solvent, i.e. the $EtOH/H_2O$ ratio, strongly affected the rate of permeation. Nafion solutions that contained higher amounts of water appeared to form more 'open' films, allowing more facile incorporation of the complex. Results of a set of measurements, carried out in a solution of 0.5 mM $Ru(bpy)_3^{2+}$ in 0.02 M phosphate buffer solution, are shown in Fig. 2. Films were prepared from Nafion solutions with water content ranging from 10 to 90%. QCM response of incorporated $Ru(bpy)_3^{2+}$ were recorded at time intervals of 10 s, showing the growth of the complex concentration in the polymer. Plots of the loading rates of the different films presented as frequency shift vs. time, are shown in Fig. 2. There is a clear correlation between the frequency shift at a certain time and the percentage of water in the depositing Nafion solution. Measurements taken after 20 s of loading show a linear relationship between frequency shift and percentage of H_2O in the deposition solution, as shown in Fig. 3.

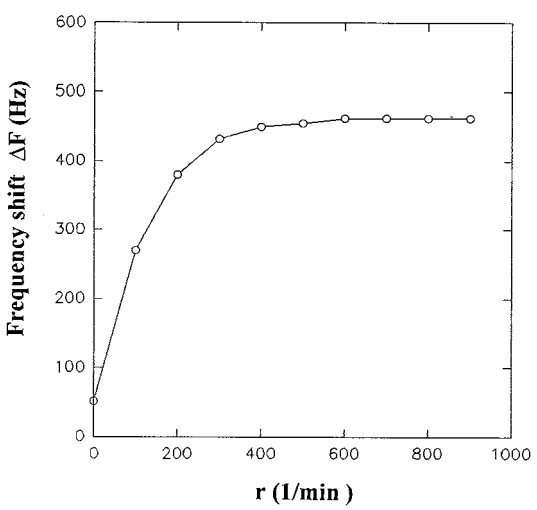

Fig. 1. Loading curve for QCM/Nafion (deposited from $EtOH/H_2O$ 80:20) in 0.5 mM $Ru(bpy)_3^{2+}$ in 0.02 M phosphate buffer solution taken after 20 s, with increasing stirring speed.

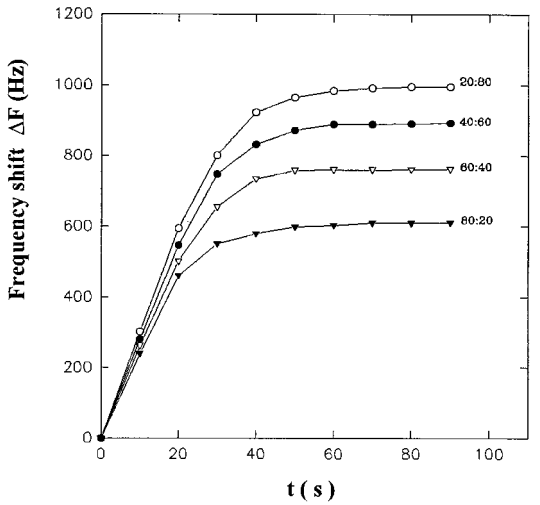

Fig. 2. Loading curves for QCM/Nafion in vigorous enough stirring solution of 0.5 mM $Ru(bpy)_3^{2+}$ in 0.02 M phosphate buffer solution, as a function of the water content of the Nafion deposition solution. The compositions of the Nafion deposition solutions are marked (as $EtOH:H_2O$).

The rate of unloading of Nafion films in the background solution was also monitored. Unloading of complex ions from the film in the background solution indicated ion exchange with

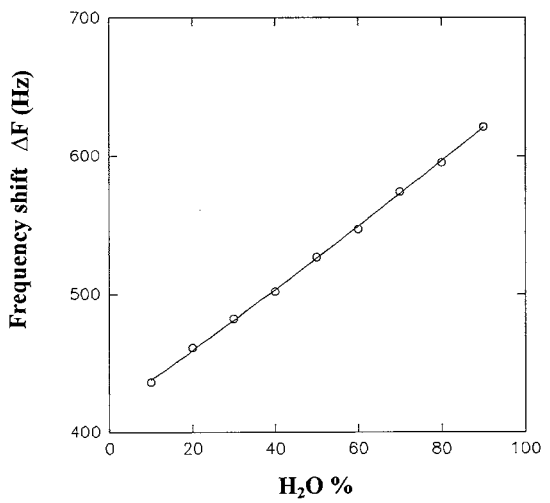

Fig. 3. Loading curves for QCM/Nafion in vigorous enough stirring solution of 0.5 mM $Ru(bpy)_3^{2+}$ in 0.02 M phosphate buffer solution taken after 20 s, as a function of the water percentage of the Nafion deposition solution.

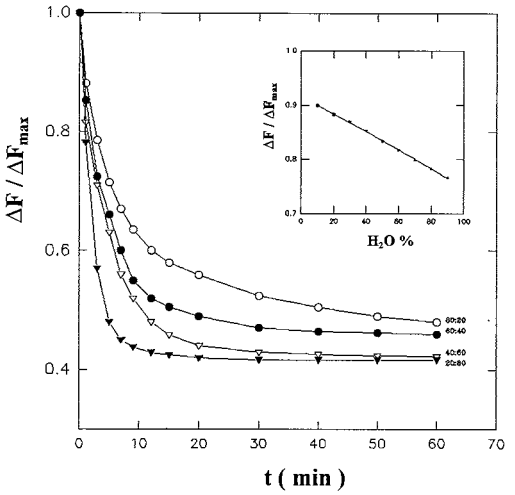

Fig. 4. Unloading curves for $Ru(bpy)_3^{2+}$ from QCM/Nafion in a vigorously stirred 0.02 M phosphate buffer solution. The compositions of the deposition solutions are marked (as $EtOH:H_2O$). Insert: loss of $Ru(bpy)_3^{2+}$ after 1 min unloading, as a function of water content in the deposition solution.

cations of the supporting electrolyte (in the present case, Na^+). The electrode was removed from the loading solution, rinsed, and transferred to a pure 0.02 M phosphate buffer solution which was fully stirred. The stirring was aimed at minimising mass-transport limitations in the solution, i.e. accumulation of the complex near the solution/film interface, which would slow the process. A continuous decrease in frequency shifts was observed, as shown in Fig. 4. The unloading was fast at the beginning and then slowed down until it practically stopped, at $\sim 40\%$ of the initial frequency shift (frequency shifts in Fig. 4 were normalised to the initial value, ΔF_{max}).

Here, too, the correlation between the rate of transport in the polymer and the composition of the deposition solutions was clearly shown. A plot of the normalised frequency shift taken after 1 min vs. the water content in the deposition solution showed a linear relationship (Fig. 4, insert), a behaviour rather similar to that observed during loading.

We assume that the higher rates of loading observed with films deposited from Nafion solutions of higher water content are due to the more

Table 1
Ion-exchange distribution coefficients, k_D, of Nafion films from deposition solutions of various water contents

Solvent EtOH:H_2O	80:20	60:40	60:40	20:80
k_D	2.60×10^6	3.26×10^6	3.79×10^6	4.24×10^6

open structure of these films. This is caused by a different organisation of the side chains, resulting from higher solvating of the sulfonic groups by water molecules and/or due to longer evaporation times of the more water rich mixtures. Thus, in the more open film the ionic clusters might be larger and the interconnecting channels might be wider, which would enhance the diffusion.

3.2. Distribution coefficients in various films

Since the extent of the exchange of the $Ru(bpy)_3^{2+}$ for Na^+ in the Nafion film can be characterised by the equilibrium coefficient for the partition reaction, it was of interest to calculate the distribution coefficients of the Nafion films from different deposition solutions to show their ion-exchange properties. The results are summarised in Table 1.

These coefficients were calculated from the points on the plateau parts of the loading curves (see Fig. 2).The complex concentration in the film was determined by the frequency shift (Section 2).

3.3. Scanning electron microscope (SEM) experiments

The above assumed dependence of the open structure of the Nafion film on the water content of the deposition solution was further confirmed by SEM micrographs. Fig. 5(a–c) show the structures of the Nafion films formed from three different deposition solutions where the water content was 20, 40 and 80%, respectively. The surface of the Nafion film was magnified 3600 times here. More open structure of the film was observed as the water content of the deposition solution was increased from 20 to 80%. It can be seen that the SEM results are in good agreement with the conclusions from QCM experiments.

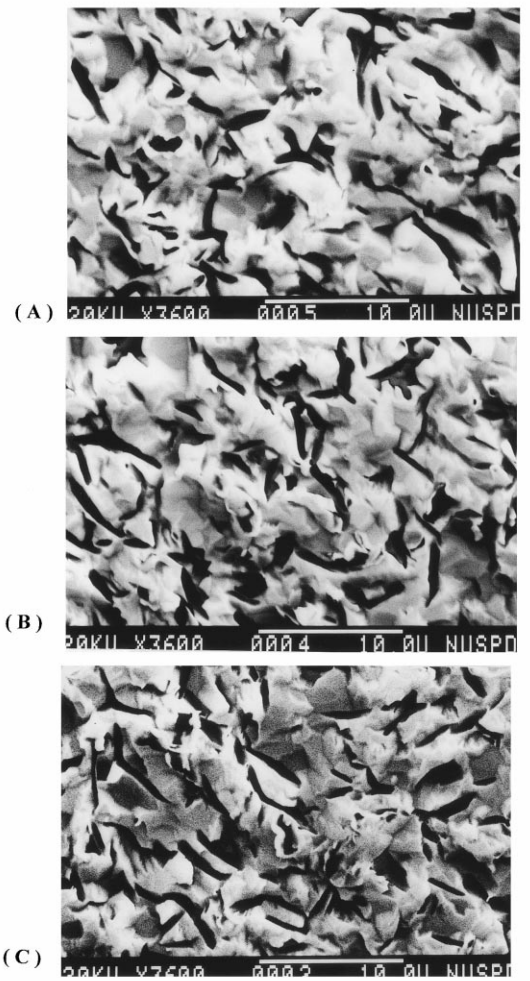

Fig. 5. Scanning electron microscope (SEM) micrographs of Nafion films formed from deposition solutions of various water contents. (A) 20%. (B) 40%. (C) 80%. The surface of the Nafion film was magnified 3600 times.

4. Conclusion

It was found that the composition of the depositing solvent, i.e. the EtOH:H_2O ratio, strongly affected the rate of permeation of the hydrophobic cation, i.e. $Ru(bpy)_3^{2+}$. Nafion solutions that contain higher amounts of water appear to form more 'open' films, allowing more facile incorporation of the complex. There is a clear linear relationship between the frequency shift at a certain time and the percentage of water in the depositing Nafion solution. A similar linear relationship was observed during unloading. The results from QCM experiments were further confirmed by the conclusions from SEM micrographs.

Acknowledgements

We thank Ms Hua of the Department of Physics of NUS for the SEM experiments and Dr Z.Q. Gao for helpful discussions.

References

[1] I. Rubinstein, A.J. Bard, J. Am. Chem. Soc. 102 (1980) 6641.
[2] T.P. Henning, H.S. White, A.J. Bard, J. Am. Chem. Soc. 103 (1981) 3937.
[3] H.S. White, J. Leddy, A.J. Bard, J. Am. Chem. Soc. 104 (1982) 4811.
[4] C.R. Martin, I. Rubinstein, A.J. Bard, J. Am. Chem. Soc. 104 (1982) 4817.
[5] D.A. Butry, F.C. Anson, J. Electroanal. Chem. 130 (1981) 333.
[6] D.A. Buttry, F.C. Anson, J. Am. Chem. Soc. 105 (1983) 685.
[7] M.N. Szentirmay, C.R. Martin, Anal. Chem. 56 (1984) 1898.
[8] D.A. Buttry, F.C. Anson, J. Am. Chem. Soc. 106 (1984) 59.
[9] D.A. Buttry, J.M. Saveant, F.C. Anson, J. Phys. Chem. 88 (1984) 3086.
[10] F.C. Anson, J.M. Saveant, Y.M. Tsou, J. Electroanal. Chem. 178 (1984) 113.
[11] M. Sharp, J. Electroanal. Chem. 230 (1987) 109.
[12] W.J. Vining, T.J. Meyer, J. Electroanal. Chem. 237 (1987) 191.
[13] M. Sharp, B. Lindholm, E.L. Lind, J. Electroanal. Chem. 274 (1989) 35.
[14] W. Grot, Chem. Ing. Tech. 50 (1978) 299.
[15] R.S. Yeo, J. McBreen, G. Kissel, F. Kulesa, S. Srinivasan, J. Appl. Electrochem. 10 (1980) 741.
[16] F.G. Will, J. Electrochem. Soc. 126 (1979) 35.
[17] R.S. Yeo, D.T. Chin, J. Electrochem. Soc. 127 (1980) 549.
[18] D.A. Buttry, F.C. Anson, J. Am. Chem. Soc. 104 (1982) 4824.
[19] C.R. Martin, H.L. Freiser, Anal. Chem. 53 (1981) 902.
[20] C.R. Martin, K.J. Dollard, J. Electroanal. Chem. Interfacial Electrochem. 159 (1983) 127.
[21] N.E. Prieto, C.R. Martin, J. Electrochem. Soc. 131 (1984) 751.
[22] K.A. Striebel, G.G. Scherer, O. Haas, J. Electroanal. Chem. 304 (1991) 289.
[23] Z. Porat, I. Rubinstein, B. Zinger, J. Electrochem. Soc. 140 (1995) 2501.
[24] Z. Gao, A. Ivaska, Anal. Chim. Acta 184 (1993) 393.
[25] M.R. Deakin, D.A. Buttry, Anal. Chem. 61 (1989) 1147A.
[26] R. Schumacher, Angew. Chem. Int. Ed. Engl. 29 (1990) 329.
[27] M.D. Ward, D.A. Buttry, Science 249 (1990) 1000.
[28] D.A. Buttry, in: A.J. Bard (Ed.), Electroanal Chemistry, Vol. 17, Marcel Dekker, New York, 1991, p. 1.
[29] R. Ebersole, D.M. Ward, J. Am. Chem. Soc. 110 (1988) 8623.
[30] G.Z. Sauerbrey, Z. Phys. 155 (1959) 206.
[31] M. Shin, E. Kim, J. Kwak, I.C. Jeon, J. Electroanal. Chem. 394 (1995) 87.
[32] G. Inzelt, J. Electroanal. Chem. 287 (1990) 171.

.

ELSEVIER

Talanta 45 (1998) 727–733

Talanta

Organic vapor detection by quartz crystal microbalance modified with mixed multilayer Langmuir–Blodgett Films

S. Zhang [a], Z.K. Chen [a], G.W. Bao [a], Sam F.Y. Li [a,b,*]

[a] *Department of Chemistry, National University of Singapore, 10 Kent Ridge Crescent, Singapore 119260, Singapore*
[b] *Institute of Materials Research and Engineering, National University of Singapore, 10 Kent Ridge Crescent, Singapore 119260, Singapore*

Received 5 February 1997; received in revised form 25 July 1997; accepted 28 July 1997

Abstract

Mixed chloroform solution of Polysiloxane PS-264 and stearic acid was made into multilayer Langmuir–Blodgett (LB) films on the surface of quartz crystal microbalance (QCM). The condition for forming mixed multilayer LB films is discussed in this paper. In addition, PS-264, stearic acid and their mixture (molar ratio 1:1) were coated on the surface of QCM sensors by a spin coating method. The above modified crystals were exposed to different concentrations of various organic vapors, including related chlorinated hydrocarbons and alcohol vapors. The results of frequency changes corresponding to concentration change of the above vapors were compared. The linear regression coefficients of the QCM with LB film had better values ($0.9881 < R < 0.9981$) than QCM with spin-coated films. The sensitivity between analytes/coating was interpreted in terms of solubility interactions. For the more polar organic vapors investigated, even at the same concentration, frequency changes of the QCM with LB films were somewhat larger, especially for chloroform and dichloromethane. However, the sensitivity of many organic vapors investigated on the mixed multilayer LB films is similar to the spin-coated films of mixture and PS-264, except that chloroform and dichloromethane only were sensed with much higher sensitivity on the mixed monolayer. The sensitivity of the QCM spin-coated with the mixture of PS-264 and stearic acid was between mixed LB films and PS-264 for many organic vapors investigated. In this study, the surface morphologies of the uncoated and coated QCM were characterized by atom force microscopy (AFM). © 1998 Elsevier Science B.V.

Keywords: Quartz crystal microbalance sensor; Detection of organic vapors; LB films; Sensitivity AFM

1. Introduction

The application of quartz crystal microbalance (QCM) devices for sensing chemical vapors was first described by Sauerbrey [1] and later by King [2], and has remained an active research field since then [3,4]. The principle and application for detecting vapors by means of QCM has been reviewed by several researchers [5,6]. To first approximation, the frequency change (ΔF) caused by adsorption or absorption of mass (ΔM) follows the Sauerbrey equation:

* Corresponding author. Tel.: +65 8742681; fax: +65 7791691; e-mail: chmlifys@leonis.nus.sg

PII S0039-9140(97)00287-7

$$\Delta F = -2.3 \times 10^6 F_0^2 \Delta M/A$$

Where, F_0 is the fundamental frequency for the 10 MHz Au-coated AT-cut QCM and A is the gold electrode area. Based on this concept, the polymer coating applied on the surface of QCM should be rigid and thin [7,8], and the initial frequency F_0 should be low compared to that of surface acoustic wave (SAW) sensors, so that the QCM responding to the vapors can be treated as a nearly ideal gravimetric detector [9]. The interaction between polymer coating and detected organic vapors can be explained in terms of bulk dissolution of organic molecules in the polymer layers [10], such as dispersion interaction, polarizability, dipolarity and hydrogen-bond basicity or acidity. In recent years, there has been increasing interest in methods for applying polymer coatings on the surface of the QCM, such as spin coating [11], ion plasma [12] and Langmuir-Blodgett (LB) [13] techniques. Among these methods, sensors with organic thin films made by the LB technique is one of the most promising methods, because it is a way to guarantee that the relationship between frequency change corresponding to the change of number of monolayer is in good linear range [14–16]. The work area of aromatic LB films has been connected with gas sensors, particularly for oxidising and reducing acidic and basic gases [17,18]. The gas molecules bind to the film molecules, creating charge carrier which are detected by measuring the film conductivity. The speed of response of LB film sensors of this type is much higher than those of films of similar materials made by conventional film-forming. In addition, rapid and totally reversible responses were obtained in less than 30 s for the 45 layer CuPccp gas sensor to ammonia vapor [19].

The polymer coating studied in this paper is polysiloxane PS-264. This material has some fluid property and is not easy to form stable monolayer on the surface of the water, and so cannot form multilayer LB films on its own. However, Kuhn et al. [20] pointed out the concept of using a molecular assembly technique to make mixed monolayers—of dyes and fatty acids—depending on the mixing ratio of the two components. William R. Barger [19] found that higher quality CuPccp LB films could be transferred from the film balance to the device substrate if the monolayer film consisted of a 1:1 mixture (by molar weight) of CuPccp and stearyl alcohol. Multilayer films prepared from pure CuPccp could not be transferred to the device substrate with high reproducibility. This concept was also employed to form mixed multilayer films consisting of PS-264 and stearic acid.

In the present paper, the surface of the QCM was modified with the two-components mixed multilayer LB films technique, and spin coating of PS-264, stearic acid as well as the mixture of PS-264 and stearic acid, respectively. Subsequently, the coated QCMs were exposed to different concentrations of various organic vapors, such as tetrachloroethane, tetrachloroethylene, dichloromethane, chloroform, propan-1-*ol*, propan-2-*ol* and acetone. The frequency changes corresponding to different concentrations of the above vapors investigated showed satisfactory linear relationships. The sensitivity of the different coating-modified on the surface of the QCM to different vapors investigated was explained in terms of the solubility interactions. The surface morphologies of the uncoated and coated QCM were studied by using atomic force microscopy (AFM).

2. Experimental

2.1. Materials

PS-264 [Copolymer of 92–96% polydimethylsiloxane, 3–7% diphenylsiloxane and 0.5–1% methylvinylsiloxane], stearic acid and detected organic chemicals including tetrachloroethane, tetrachloroethylene, dichloromethane, chloroform, propan-1-*ol*, propan-2-*ol* and acetone were obtained from Fluka (Chemie AG, Buchs, Switzerland) and 10 MHz quartz crystals with gold electrodes were bought from International Crystal Manufacturing (Oklahoma City, OK). The subphase water was deionized water from a Millipore system and the resistivity of the water was greater than 18 MΩ.

2.2. Frequency measurements

The experimental set-up of the QCM gas sensor system has been described elsewhere [21]. The frequency output from a home made QCM oscillator was measured with a Hewlett Packard 53131A universal counter.

2.3. Procedure of making LB films on the QCM

The mixture of Polysiloxane PS-264 and stearic acid (molar ratio 1:1) was dissolved in chloroform ($\approx 0.1\%$ weight/volume). The crystals were previously treated with certain siloxane. All LB films depositions on the quartz were performed at room temperature (22 ± 0.2°C) on a NIMA LB Trough 622 (Coventry, England) with an area of 1200 cm^2. A sample containing 1 ul of the above in a mixture chloroform solution in the microsyringe needle was injected in deionized water and the monolayers spread on the surface of the subphase of water. The compression speed for all the monolayers was controlled at 5 mm min^{-1}. The different number of mixed multilayers were deposited on the surface of the QCM under the pressure of 30 mN m^{-1}, and its deposition mode [22] was x-type. The frequency changes caused by deposition of LB films were measured.

2.4. Spinning coating on the QCM

PS-264 and stearic acids were prepared in chloroform solution ($\approx$ 0.1% weight/volume). Chloroform solutions of PS-264, stearic acid and the above mixture for making LB films were dropped on both sides of the QCM, respectively, first spinned at a rate of 400 rpm for 5 min and then at 2000 rpm for 30 s. The desired frequency change was controlled at about 2000 ± 75 Hz.

2.5. Surface morphology of the QCM

The surface morphologies of the uncoated and coated QCM were characterized with a TMX 1010 Explorer AFM (Topometrix, Santa Clana, CA), operated in the non-contact mode.

3. Results and discussion

3.1. Formation of mixed multilayer LB films

The isotherm for surface pressure (π) vs. area (A) per molecular repeat unit for the mixed LB layer consisting of PS-264 and stearic acid is shown in Fig. 1. The limiting areas per molecule for the mixed compounds before the collapse was determined to be approximately 27 $Å^2$ $molecule^{-1}$ by extrapolation of the rising portion of the π–A diagram. Based on the π–A diagram, it should be possible to form multilayers of the mixed compounds from the plateau region with low surface area/molecule. The diagram also indicates that the monolayers are not stable. A total of 5, 10, 15 and 20 multilayer LB films were made on the surface of the QCM according to x-type deposition. Fig. 2 shows the relationship between the frequency change caused by the deposited LB films and the number of mixed multilayer LB films ($R = 0.9992$). Because the x-type deposition method with all heads up is usually not very stable [14], every certain number of LB films made should be repeated three times.

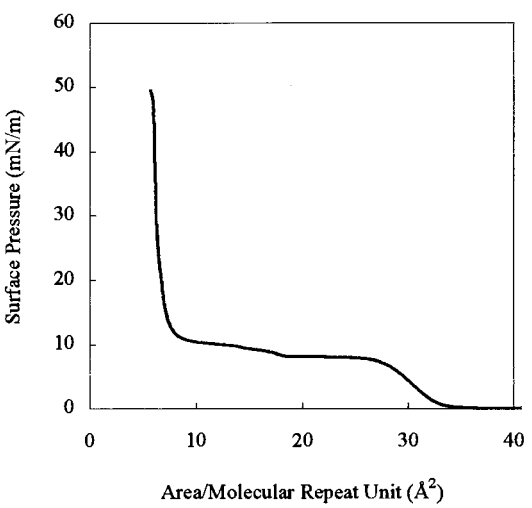

Fig. 1. Plot of surface pressure vs. area per molecule (adsorption isotherm) for mixed LB films consisting of PS-264 and stearic acid.

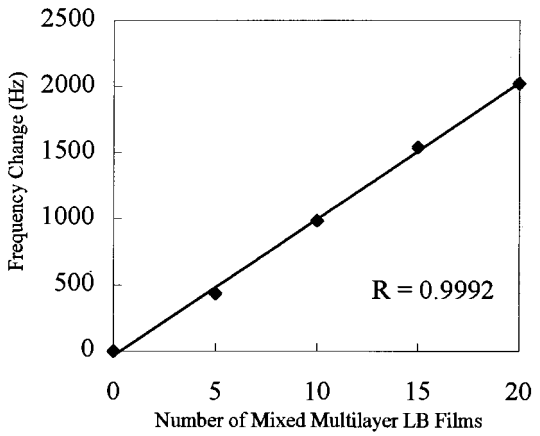

Fig. 2. Plot of frequency shifts vs. number of mixed multilayer LB films on the QCM.

3.2. Relationship between frequency and concentration change

The results of frequency shift vs. vapor concentration change are shown in Fig. 3. The frequency change caused by mixed LB films (◇), PS-264 (□) stearic acid (Δ) and mixture (×) of PS-264 and stearic acid with spin coating procedures were 1945.72, 2035.93, 2070.87 and 2143.64 Hz, respectively. Satisfactory linear relationships were obtained for analyte/LB films ($0.9881 < R < 0.9981$), analyte/PS-264 ($0.9852 < R < 0.9941$) and analyte/mixture of PS-264 and stearic acid ($0.9829 < R < 0.9969$). From Fig. 3, it can be seen that there are different sensitivities between the mixed monolayer films and siloxane polymer alone, to the same organic vapors detected. For the more polar organic vapors investigated, frequency changes of the QCM with LB films exhibited larger values than QCM with spin-coated PS-264 and mixture of PS-264 and stearic acid as shown in Fig. 3a, c, d, e and g. Thus, it is implied that the mixed film is somewhat 'better'. The polysiloxane PS-264 is almost nonpolar because this polymer contains 92–96% nonpolar polydimethylsiloxane. For all the organic vapors investigated, dispersion interaction between polysiloxane/analytes takes an important role. Due to the change in the functional group (3 ~ 7% diphenylsiloxane), PS-264 has a very weak polarizability. Nonpolar molecules, such as C_2Cl_4 and $C_2H_2Cl_4$, interacted with PS-264 via dipole/induced dipole, where the polarizability of the aromatic ring arises from π-electrons. For the polar molecules, such as dichloromethane, chloroform, propan-1-*ol*, propan-2-*ol* and acetone, the interaction between polar molecules/polarizable coating might also take place. In fact, different solubility reactions between the coating/analytes might have resulted in different sensitivites. From Fig. 3c and d, it is also observed that the PS-264 in the mixed multilayer LB films and their mixture with spin coating method have much higher sensitivities to select and to sense the chloroform and dichloromethane organic vapors. For other vapors, the sensitivities on mixed multilayer LB films and PS-264 films exhibited little difference. The reason being that the polymer siloxane by itself is almost nonpolar, whereas the mixed monolayer material has basic carboxylic groups, which could interact with chloroform and dichloromethane by way of two vapors by hydrogen bonds. From Fig. 3 it is also concluded that the sensitivities on the mixture films by spin coating were between LB films and PS-264. Furthermore, it is also observed that the QCM coated with stearic acid had very low frequency change corresponding to concentration change of the vapors, and are therefore expected to be less sensitive. This can be explained by the fact that the stearic acid film is crystalline, and so has less sorption capacity than an amorphous material like siloxane polymer, or polymer-containing mixed film. On the other hand, the polysiloxane PS-264 cannot form LB films, the introduction of stearic acid can help to form LB films [23].

3.3. Surface morphology characterization of the QCM

It is known that the mass of coating plays an important role on the frequency response of the sensor [1,2]. Ljubinka et al. [24] once pointed out that the last layers of coating made significant contribution to the generation of the total response. The advantage of the LB films method is that exact control of the frequency change can be more readily achieved. On the other hand, for the

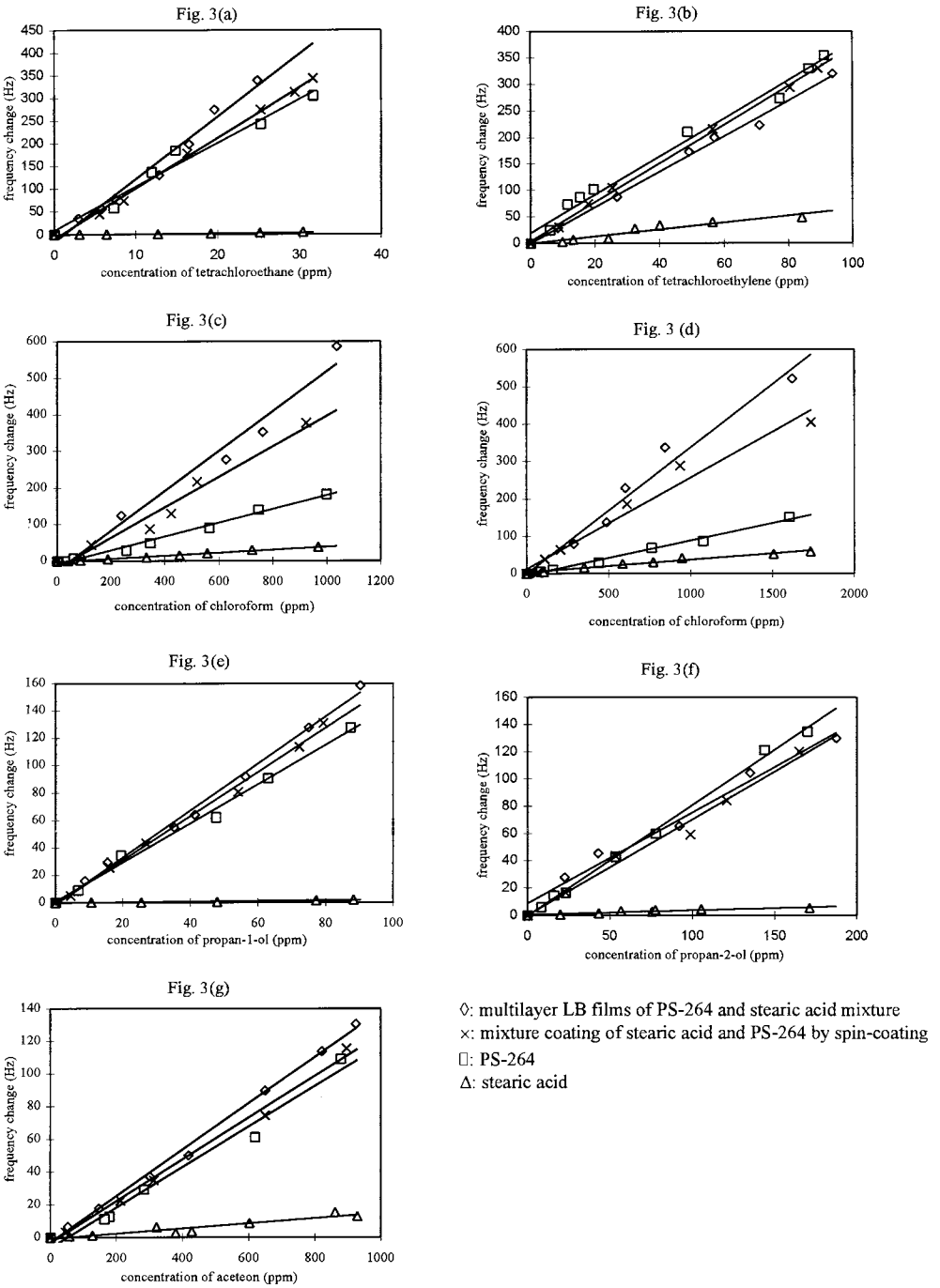

Fig. 3. Plot of frequency shifts vs. concentration changes of organic vapors at room temperature (23.8°C). ◇: QCM with 20 layer LB films; □: QCM with PS-264; Δ QCM with stearic acid; × : mixture of stearic acid and PS-264 by spin coating method.

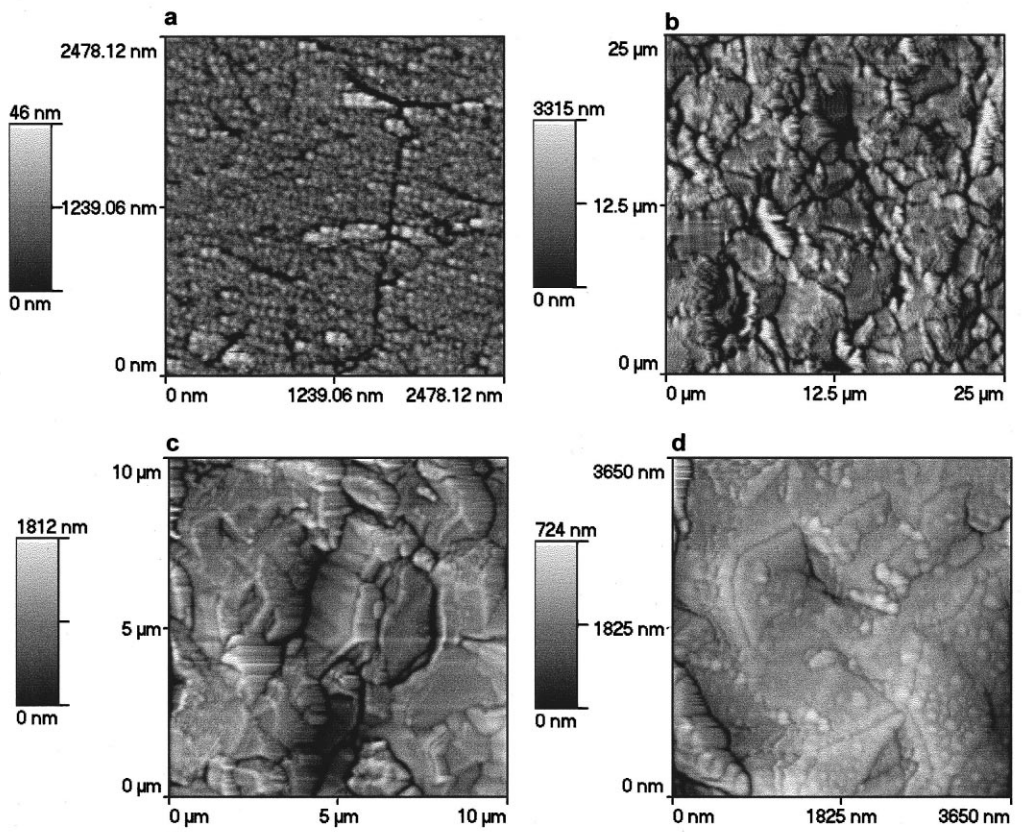

Fig. 4. AFM images of the uncoated QCM and coated QCM. (a) 2500 × 2500 nm region; (b) 25 × 25 μm AFM images of 20-layer LB films on QCM; (c) 10 μm × μm, enlarged area of the middle of (b); (d) 3650 × 3650 nm, enlarged area of the upper left of the (c).

spin-coated method, it is not easy to guarantee the same frequency change by the coating every time.

Fig. 4a illustrates the image of the uncoated gold surface of QCM obtained by AFM. It shows that the gold surface consists of small grains, cracks and channels. Fig. 4b–d exhibits the surface morphology of the QCM coated with 20-layer LB films, obtained at different scan sizes. Deposited stearic acid forms very rugged films on the top of the gold surface. Large irregular grains with different sizes and shapes can be clearly seen. Fig. 4d reveals some superimposed fine grains on the particles, which we believe, correspond to capillary interactions between the tip and the thin liquid films of the PS-246 covering the surfaces of the large particles. As far as LB films are concerned, such irregularity is undesirable and further improvement is needed. Therefore, the spreading of the PS-264 on the stearic acid grain and in the boundary areas matters at these points. As indicated in Fig. 4d, it seems that the surface is not thoroughly coated with PS-264. This could be one of the reasons that the sensitivity and selectivity are not very much improved by the LB films. Also, the stability of x-type LB films should be considered.

4. Conclusion

QCM sensors modified by mixed multilayer LB films could be used to detect organic solvent vapors. Frequency shifts vs. concentration changes of the vapors studied exhibit satisfactory linear relationships. The mechanism affecting sen-

sitivity and selectivity was correlated with solubility interactions, such as dispersion interactions, polarizability and hydrogen bond acidity. There are some different sensitivities between the mixed monolayer LB films, the siloxane polymer alone and their mixture by spin coating method. Chloroform and dichloromethane are sensed with much higher sensitivity on both the mixed monolayer LB films and normal spin coating method. The frequency change vs. concentration of organic vapors for the LB films coated sensors had a little larger value than that of QCM with PS-264 and mixture coating to the tetrachloroethane, propan-1-*ol*, propan-2-*ol* and acetone. The surface morphology of the QCM coated with LB films possesses some cavities and an irregular structure. The control of LB films for gas sensors needs further improvement.

Acknowledgements

The authors would like to thank the National University of Singapore for financial assistance.

References

[1] G. Sauerbrey, Z. Phys. 155 (1959) 206.
[2] W.H. King Jr., Anal. Chem. 36 (1964) 1735.
[3] J. Hlavay, G.G. Guilbault, Anal. Chem. 60 (1988) 2142.
[4] J. Hartmann, J. Auge, P. Hauptmann, Sensors and Actuators B 19 (1–3) (1994) 429.
[5] J.W. Grate, S.J. Martin, R.M. White, Anal. Chem. 65 (1993) 940A and 987A.
[6] G.Harsanji, Polymer Films in Sensor Applications, Technomic, LA, 1996, 140 pp.
[7] S.J. Martin, G.C. Frye, S.D. Senturia, Anal. Chem. 66 (1994) 2201.
[8] V.E. Cranstatt, S.J. Martin, J. Appl. Phys. 75 (3) (1994) 301.
[9] S.J. Martin, G.C. Frye, Ultrasonic Symposium Proceedings, IEEE, New York, 1991, 393 pp.
[10] J.W. Crate, M.H. Abraham, Sensors and Actuators B 3 (1991) 85.
[11] M. Haug, K.D. Bchierbaum, G. Gauglitz, W. Göpel, Sensors and Actuators B 11 (1993) 383.
[12] M.E. Dominguez, J. Liu, R.L. Curiale, E.J. Poziomek, Anal. Lett. 28 (6) (1995) 945.
[13] V. Tsionsky, E. Gileadi, Langmuir 10 (1994) 2830.
[14] I.R. Peterson, J. Phys. D: Appl. Phys. 23 (1990) 379.
[15] B. Holcroft, G.G. Roberts, Thin Solid Films 160 (1988) 445.
[16] F. Makoto, S. Lyong, Mol. Cryst. Liq. Cryst. 227 (1993) 325.
[17] S. Baker, M.C. Petty, G.G. Roberts, M.V. Twigg, Thin Solid Films 99 (1983) 33.
[18] W.R. Barger, A.W. Snow, H. Wohltjen, N.L. Javis, Thin Solid Films 133 (1985) 197.
[19] H. Wohltjen, W.R. Barger, A.W. Snow, N. Lynnjarivs, IEEE Trans. Electron Devices, ED- 32 (7) (1985) 1170.
[20] V.K. Agarwal, Phys. Today 6 (1988) 40.
[21] S. Zhang, Sam F.Y. Li, Analyst 121 (11) (1996) 1721.
[22] T. Richardson, Chem. Br. 12 (1989) 1218.
[23] M.C. Petty, Langmuir–Blodgett Films an Introduction, Cambridge University Press, Cambridge CB2, NY, 48 pp.
[24] V.R. Ljiubinka, S. Strbac, Anal. Chim. Acta 313 (1995) 83.

.

ELSEVIER

Talanta 45 (1998) 735–738

Talanta

Characterization and third-order optical nonlinearities of uniform surface-modified CdS nanoparticles

M.Y. Han [a,*], L.M. Gan [a], W. Huang [a], C.H. Chew [a], B.S. Zou [a], C.H. Quek [a], G.Q. Xu [a], W. Ji [b], X.J. Zhang [b], S.C. Ng [b]

[a] *Department of Chemistry, National University of Singapore, Singapore 119260, Singapore*
[b] *Department of Physics, National University of Singapore, Singapore 119260, Singapore*

Received 5 February 1997; received in revised form 21 April 1997; accepted 28 April 1997

Abstract

Size-controlled uniform surface-capped CdS nanoparticles were readily prepared by an improved inverse microemulsion technique using hexanethiol as co-surfactant. The third-order optical nonlinearities were studied for the first time by newly-developed Z-scan technique, from which the enhanced nonlinear optical responses were observed after heat-treatment. © 1998 Elsevier Science B.V.

Keywords: Nanoparticles; Z-scan technique; Optical nonlinearities

1. Introduction

Extensive investigations of the third-order optical nonlinearities of a new class of nanometer-sized semiconductor materials have demonstrated new physics and potential applications [1]. The large nonlinear optical responses of nanometer-sized particles are suggested to be based on the quantum and dielectric confinement effects. In the present work, a newly-developed Z-scan technique was used to measure the optical nonlinearities of the surface-capped CdS nanoparticles. The Z-scan technique is a sensitive and simple method enabling easy separation of the nonlinear absorption and refraction in solution system using a combined nonlinear transmittance and beam distortion [2]. A transparent inverse microemulsion is an appropriate system for the Z-scan measurements because it is thermodynamically stable, isotropic dispersion of surfactant-coated and stabilized water in an oil phase [3].

In this report, the surface-capped R-CdS (R: $C_6H_{13}S-$) nanoparticles were prepared by an improved inverse microemulsion technique using hexanethiol as co-surfactant. The IR and TEM results indicate that the monodispersed R-CdS nanoparticles with purely modified surfaces can be readily prepared by this method. The third-order optical nonresonant nonlinearities were measured by the Z-scan technique at a wavelength of 532 nm, which permitted observation of the en-

* Corresponding author. Fax: +65 7791691; e-mail: chmhanmy@leonis.nus.sg

PII S0039-9140(97)00289-0

hanced nonlinear optical responses for the sample after reflux.

2. Experimental

2.1. Reagents

Sodium bis(2-ethylhexyl) sulfosuccinate (AOT, purchased from Fluka, $>98\%$ purity) was purified in petroleum ether. Cadmium nitrate tetrahydrate (Merck, 99%), $(NH_4)_2S$ (Merck, 20 wt% solution in water) and Hexanethiol (Merck, $>97\%$) were used without further purification. Tetrahydrofuran (A.R. grade) and Heptane (A.R. Grade) were used as purchased from J.T. Baker. Water was purified by a Milli-Q system.

2.2. Preparation of the surface-modified CdS nanoparticles

R-CdS nanoparticles were prepared in an inverse microemulsion containing three common components, i.e. 18 wt% surfactant AOT/co-surfactant hexanethiol (molar ratio = 1:5), 76 wt% heptane and 6 wt% 0.1 M $(NH_4)_2S$ aqueous solution. Another aqueous solution of 0.1 M $Cd(NO_3)_2$ with 1.25 times the weight of $(NH_4)_2S$ aqueous solution was added to the microemulsion upon vigorous stirring, where a light yellow transparent solution of CdS nanoparticles was formed immediately. After 10 min, the mixed solution changed from initially transparent to slightly turbid and finally completely turbid after several hours.

The solution was then divided into two equal portions. One portion was allowed to stand for several hours, the nanoparticles flocculated completely and colourless transparent upper layer appeared. After recovery by pouring out the upper layer, the resulting yellow powder was washed for several times with heptane so as to remove the residual surfactant replaced by co-surfactant in solution. The purified powder was evacuated to remove the heptane (S_I), then it was immediately dissolved into THF to form a transparent solution. The other portion of nanoparticle solution was refluxed overnight in order to remove water in micelles and replace residual AOT surfactant completely, which can induce strong surface modification at the surface of CdS nanoparticles. The rest of the procedure was identical to that used in the first part, the powder (S_{II}) can be dissolved completely in THF within half an hour. All the operations were carried out under nitrogen atmosphere.

2.3. Nonlinear optical measurements

The R-CdS nanoparticles (S_I and S_{II}) in heptane were put into a 1-mm-thick quartz cuvette for the optical measurements. Their nonlinear optical properties were investigated with linearly polarized pulses ($\lambda = 532$ nm; pulse width = 25 ps) from a picosecond mode-locked frequency-doubled Nd:YAG laser [4]. The spatial profiles of the optical pulses were nearly Gaussian, and the laser beam was focused onto the samples with 25 cm focal length. The spot radius of the laser pulses at the cuvette was 35 ± 5 μm. Both incident and transmitted laser pulses were monitored simultaneously by a calibrated beam and two energy detectors which were linked to a computer by the IEEE interface as shown in Fig. 1. The nonlinear optical properties of the samples were manifested by moving the samples along the axis of the incident beam (i.e. z-direction) with respect to the focal point (Z-scan). We have tested the apparatus with the standard reference of CS_2 [5].

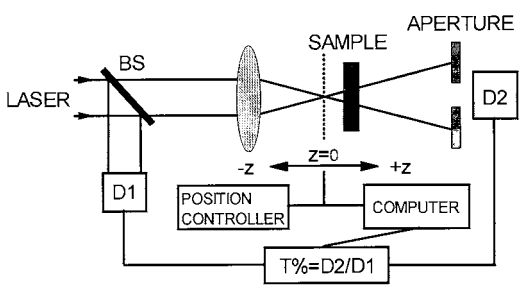

Fig. 1. Schematic diagram of the experimental setup for Z-scan measurements in which the energy ratio is recorded as a function of the sample position z. The abbreviations are: BS, beam splitter; D1 and D2, energy detectors.

3. Results and discussion

3.1. Characterization of the surface-modified CdS nanoparticles

The IR spectra were measured in order to characterize hexanethiol-capped R-CdS nanoparticles. The presence of a capping reagent on the surface of the CdS nanoparticles was supported by an IR absorption peak assigned to the C–S stretching (700 cm^{-1}). In addition, the IR analysis does not evidence the presence of residual AOT on R-CdS nanoparticles (S_{II}) whose IR absorption peaks are assigned to $-SO_3Na$ (1000, 1100–1300 cm^{-1}) and –C=O (1740 cm^{-1}). These results show that the surface of the R-CdS nanoparticles is covered only with the capping reagent. A direct observation of R-CdS by TEM exhibits that the particle size of S_{II} is about 3 nm in diameter. The above results indicate that the CdS nanoparticles with narrow-size distribution and purely modified surfaces were readily prepared with the microemulsion technique using co-surfactant hexanethiol.

3.2. The advantages of the preparation of the surface-modified CdS nanoparticles by microemulsion technique using co-surfactant as capping reagent

The preparation of the surface-capped CdS particles using a modified method was first reported by Steigerwald et al. [6]. During the reaction of Cd^{2+} with $S(TMS)_2$ in an AOT/H_2O/heptane reversed-micelle solution, the surface of the resulting CdS microcrystallites was stabilized in situ by PhS(TMS) or RS(TMS) by adding its heptane solution to the CdS nanoparticles solution. The IR spectra demonstrated that the CdS nanoparticles were covered not only by the capping reagent, but also by a small amount of residual AOT [7].

In this experiment, the surface capping reagent hexanethiol was regarded as co-surfactant in the inverse microemulsion, and used simultaneously with surfactant AOT to prepare surface modified CdS nanoparticles. This is an effective way to modify the surface of CdS nanoparticles by hexanethiol because the co-surfactant chemisorbed uniformly on the surface of the particles. Of course, it is crucial that the molar ratio of Cd^{2+} to S^{2-} is larger than 1:1, which can maintain enough amount of Cd^{2+} ions on the surface of the nanoparticles to react with hexanethiol. The above discussion indicates that the microemulsion technique using co-surfactant hexanethiol is an effective method to prepare R-CdS nanoparticles with uniform modified surfaces.

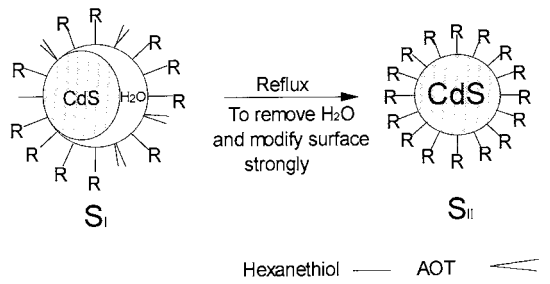

Fig. 2. Schematic illustration for the formation of strong surface modified CdS nanoparticles during reflux.

3.3. The influence of heat-treatment of the CdS nanoparticles on their optical nonlinearities

Electron diffraction patterns demonstrate that both S_I and S_{II} are microcrystallites. This manifests that the contribution of reflux is mainly to remove water from micelles and enhance the effect of the surface modification of CdS nanoparticles Fig. 2.

S_I and S_{II} were dissolved in THF at low concentrations (1 mg cm^{-3}). There is no significant difference between their electronic absorption spectra. Their third-order optical nonlinearities at a nonresonant wavelength was characterized by the Z-scan technique. The open aperture Z-scan measurements of the nonlinear optical absorption shown in Fig. 3 were carried out with 25 ps duration laser pulses at 532 nm. The nonlinear optical absorption comes from the two-photon absorption of the samples. From the best fit, we obtain two-photon absorption coefficients β of 6.0×10^{-11} and 1.9×10^{-10} cm W^{-1} or an imaginary third-order susceptibility $Im\chi^{(3)}$ of 2.6×10^{-22} and 8.2×10^{-22} m^2 V^{-2} for S_I and S_{II}, respectively. The nonlinear absoprtion coefficient

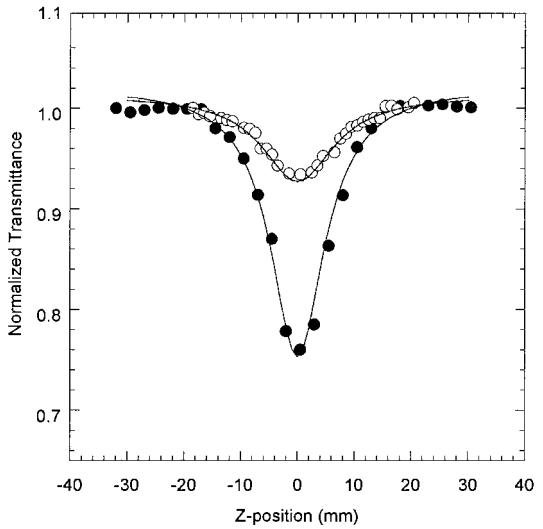

Fig. 3. The open aperture Z-scan data for S_I (○) and its crystallized product S_{II} (●) in THF at 532 nm with 25 ps duration laser pulses, 10 Hz repetition rate and I ($Z = 0$) being 40 GW cm^{-2}. The dotted lines are the experimental results, and the solid curves are a theoretical fitting based on the theory in the literature [2]. The optical length is 1 mm.

of S_{II} is close to the data found for the Cd(Se, Te) nanoparticles in glass [8]. The nonlinear optical absorption of the S_{II} is twice stronger than that of the initial S_I. The results show that the nonlinear optical responses of the R-CdS nanoparticles are enhanced by reflux.

The results can be explained by the difference in their surface properties of the CdS nanoparticles and the microenvironment (Fig. 2). First, the nonlinear polarizability of water at 532 nm laser excitation is very small [9], and the presence of surface-adsorbed water at the surface of CdS nanoparticles (S_I) can form an effective relaxation tunnel for the excited states of the CdS nanoparticles due to dipolar polarization. They make it complicated for the nonlinear responses of this system whose nonlinear optical absorption is due to the interactions of the CdS-water system in the microenvironment. On the other hand, water around CdS nanoparticles decreases the contribution of the dielectric confinement effect [10], which is mainly from the modification of hydrocarbon-chains. After the complete extraction of water in micelles by heat-treatment, the crystallized S_{II} (Fig. 2) possesses stronger modified surface at which most of the hexanethiol molecules are incorporated with the cadmium ions. This enhances its dielectric confinement effect, i.e. increases the excited state life of the R-CdS nanoparticles, and leads further to the increment of two-photon absorption [11]. Thus the more stable excitation state of S_{II} without water can generate enhanced nonlinear optical responses as compared with S_I.

Acknowledgements

This project is financially in part supported by the National University of Singapore, and M.Y. Han wishes to thank the National Science and Technology Board for a postdoctoral fellowship.

References

[1] A.D. Yoffe, Adv. Phys. 42 (1993) 173.
[2] M. Sheik-Bahae, A.A. Said, T.H. Wei, D.J. Hagan, E.W. Van Stryland, IEEE J. Quantum Electron. 26 (1990) 760.
[3] A. Bellocq, D. Roux, in: S.E. Friberg, P. Bothorel (Eds.), Microemulsions: Structure and Dynamics, CRC Press, Boca Raton, FL, 1987.
[4] S. Shi, W. Ji, S.H. Tang, J.P. Lang, X.Q. Xin, J. Am. Chem. Soc. 116 (1994) 3615.
[5] W. Ji, H.J. Du, S.H. Tang, S. Shi, J. Opt. Soc. Am. B12 (1995) 876.
[6] M.L. Steigerwald, A.P. Alivisatos, J.M. Gibson, T.D. Harris, R. Kortan, A.J. Muller, A.M. Thayer, T.M. Duncan, D.C. Douglass, L.E. Brus, J. Am. Chem. Soc. 110 (1988) 3046.
[7] S. Yanagida, T. Ogata, A. Shindo, H. Hosokawa, H. Mori, T. Sakata, Y. Wada, Bull. Chem. Soc. Jpn. 68 (1995) 752.
[8] D. Cotter, M.G. Burt, R.J. Manning, Phys. Rev. Lett. 68 (1992) 1200.
[9] Z. Blaszczak, M. Farhoud, J. Mol. Liq. 68 (1996) 157.
[10] T. Takagahara, Phys. Rev. B 39 (1989) 10206.
[11] Y. Nosaka, K. Tanaka, N. Fujii, J. Appl. Polymer Sci. 47 (1993) 1773.

.

ELSEVIER

Talanta 45 (1998) 739–749

Talanta

Temperature programmed decomposition (TPDE) of $[Mo(CO)_6]$ on metal oxide supports: a novel tool to elucidate surface acidity and surface-mediated reactions

W.L. Loh, S. Jaenicke *, G.K. Chuah, H.G. Ang

Department of Chemistry, National University of Singapore, Kent Ridge Crescent, Singapore 119260, Singapore

Received 5 February 1997; received in revised form 13 May 1997; accepted 14 May 1997

Abstract

A novel technique, the temperature programmed decomposition (TPDE) of $[Mo(CO)_6]$, has been developed to examine surface acid/base properties. In particular, the nucleophility of different surface hydroxyl groups can be quantified with this method, and it is found that the activation energy for decarbonylation of the carbonyl complex correlates well with the field strength of the metal cations in the support. Activation energies are derived from the CO peak maxima in the TPDE spectra by means of the Redhead equation. TPDE is also used to probe surface-mediated reactions of metal carbonyls. The technique enables identification of intermediates formed during the thermal decomposition process. Comparison with simulated TPDE spectra provides evidence for cluster formation during decarbonylation. By quantifying the amounts of CO and H_2 generated during the TPDE reaction, the surface concentration of the adsorbed species and the oxidation state of the central atom can be deduced at any given temperature. © 1998 Elsevier Science B.V.

Keywords: Temperature programmed decomposition; $[Mo(CO)_6]$; Surface reactions; Surface acidity

1. Introduction

The study of surface-mediated reactions is of considerable interest because surfaces reduce the dimensionality of a reaction and can open new reaction pathways by directing the stereochemistry of the adsorbed complex. The surface may also play the role of a 'macroligand' and help to stabilise reaction intermediates. The idea of a surface adopting the role of a ligand has been introduced by Ugo et al. [1] who pioneered the field of 'surface organometallic chemistry'. The presence of a surface can alter the conditions required for certain reactions. For example, high pressure is no longer needed to effect the formation of polynuclear carbonyl clusters when surface adsorbed reactants are used. Surface properties such as the acid/base character play an important role in determining the path of a reaction, directing the route towards decomposition or cluster formation. In order to gain an insight into the

* Corresponding author. Fax: +65 7791691; e-mail: chmsj@leonis.nus.sg

PII S0039-9140(97)00290-7

chemistry of acid/base catalysed reactions, it is necessary to characterise the acid/base sites on the surface. Traditionally, acid sites have been determined by the adsorption of basic molecules like ammonia or pyridine [2]. However, the strong basicity of these probe molecules causes an interaction even with the weakest acid sites. This makes their interaction with the surface acid sites rather unspecific. The use of a much weaker basic probe, carbon monoxide, which adsorbs on Lewis acid sites at the surface of metal oxides has been introduced by Knözinger [3]. The interaction of metal carbonyls such as $[Mo(CO)_6]$ on a surface has been proposed as an alternative probe for surface properties [4,5]. This probe molecule offers a number of advantages. It is easy to handle and the reactions take place well above room temperature. The spherical symmetry of the molecule with a van der Waals radius of about 0.45 nm enables surface features to be explored at a scale relevant to catalytic transformations of most substrates.

In this paper, we describe the temperature programmed decomposition (TPDE) of molybdenum carbonyl, $[Mo(CO)_6]$, on different metal oxides, and the interpretation of the spectra in terms of surface properties. The technique allows for the determination of the acid/base properties of a material; in particular, the nucleophility of different surface hydroxyl groups can be compared. It is also possible to identify intermediates formed during thermal reaction. Hence, the reaction pathway can be deduced. The TPDE spectrum provides evidence for cluster formation as an early step of the aggregation to larger metal particles. The activation energy for CO decarbonylation can be determined from the temperature of the CO peak maxima in the TPDE spectrum using the Redhead equation. Finally, through accurate quantitative analysis of the amount of CO and H_2 generated during the TPDE analysis, the coverage of the adsorbed metal species on the support and the oxidation state of the metal can be elucidated.

TPDE or TPD (temperature programmed desorption) can be used to study the kinetics of adsorbate desorption, decomposition, surface catalysed reactions of adsorbates and a reactive gas in the carrier gas stream as well as reaction between co-adsorbates [6]. This technique is commonly applied in surface science and catalysis to determine surface coverage of adsorbates and to determine adsorption energies [7].

Thermal desorption is the removal of adsorbed particles from a surface by heating. The temperature dependence of the surface coverage θ can be described by an Arrhenius-type expression, the Polanyi–Wigner equation [8].

$$r(\theta) = -\mathrm{d}\theta/\mathrm{d}t = \nu(\theta)\theta^n \exp\{-E(\theta)/RT\} \quad (1)$$

where $r(\theta)$ is the rate of desorption; $\nu(\theta)$ is the pre-exponential factor of desorption; θ is the adsorbate coverage; $E(\theta)$ is the (coverage dependent) activation energy of desorption; t is time; n is the order of desorption; R is the gas constant; and T is the temperature; for a linear ramp $T = T_0 + \beta t$ where β is the heating rate. Differentiation of the Polanyi–Wigner equation gives

$$E/RT_m^2 = \nu/\beta \exp(-E/RT_m) \quad (2)$$

for coverage-independent desorption parameters and first order kinetics, where T_m is the temperature at peak maximum where $\mathrm{d}r/\mathrm{d}T = 0$.

Redhead showed that for a first-order desorption, the temperature at peak maximum, T_m, is directly related to the desorption energy E. For a wide range of ν and β, this relation can be approximated as:

$$E = RT_m[\ln(\nu T_m/\beta) - 3.64] \quad (3)$$

Deviation of the above equation from the analytically correct Eq. (2) are within 1.5% if ν/β falls between 10^8 and 10^{13} K^{-1}. This equation is frequently applied to determine E from a single spectrum. It is then necessary to assume a value for the preexponential factor. Throughout this study, we take ν ($\approx kT/h$) $= 10^{13}$ s^{-1}. The calculated activation energy changes by less than 10% if the value of ν assumed is a factor of ten higher or lower than 10^{13} s^{-1}. It is in principle possible to obtain an experimental value for ν by conducting experiments at different heating rates β. However, with the present set-up, the heating rate can only be varied by a factor of four (between 5 and 20 K min^{-1}), not enough to give reliable values for the pre-exponential factor. The value 10^{13} s^{-1} leads to an dissociation energy for the first CO

from the adsorbed [$Mo(CO)_6$] complex which is somewhat lower than the value determined in the gas phase. This is consistent with the picture that the formation of the surface bond will lead to a labilization of the metal-CO bond in the complex.

In this work, we show that the elimination of CO from a metal carbonyl complex can be treated with the same formalism as the thermal desorption of an adsorbate from a surface site. The initial surface coverage with metal carbonyl complexes is low so it is unlikely that the thermal decomposition of the complex is influenced by other adsorbed molecules. Thus we can assume that desorption follows first-order kinetics. The narrow width of the desorption signal notably on partially dehydroxylated silica is consistent with a single first-order reaction. The influence of surface heterogeneity on the bond energies within the complex is negligible. The Redhead expression is used to obtain activation energies for the decarbonylation reactions. More complicated desorption spectra can be deconvoluted into individual CO-dissociation signals with the assumption that the reaction proceeds through successive elimination of one CO molecule after the other from the complex.

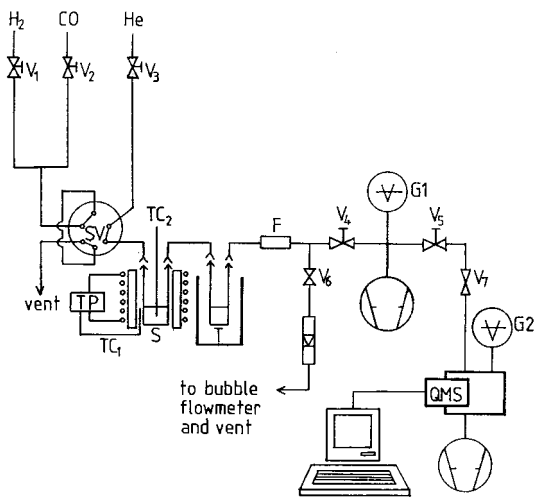

Fig. 1. Schematic diagram of the apparatus used for TPDE; F, 5 μm filter; G_1, G_2, pressure gauges; QMS, quadrupole mass spectrometer; S, sample; SV, sampling valve; T, trap; TC_1, TC_2, thermocouples; TP, temperature programmer; V_1–V_6, fine-metering valves; and V_7, metal-bellow valve (Nupro).

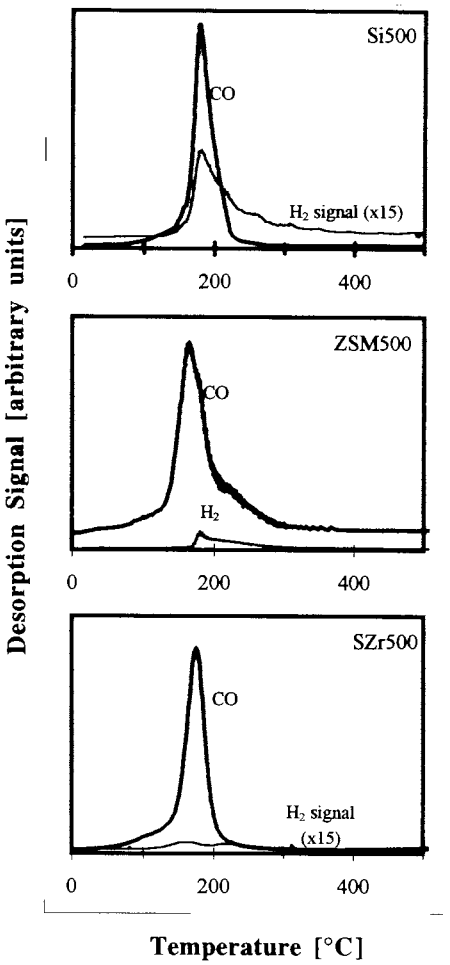

Fig. 2. TPDE of [$Mo(CO)_6$] on acidic supports; pretreatment 500°C; heating ramp 20°C min^{-1}. Si, silica; ZSM, H-ZSM-5 molecular sieve; $SZrO_2$, sulphated zirconia.

2. Experimental

A number of different inorganic oxide supports with widely different acidity, namely alumina, magnesia, zinc oxide, silica, H-ZSM-5, zirconia and sulphated zirconia have been examined. Zinc oxide and zirconia are prepared by the precipitation of respective salt solutions [9] and zirconia was sulphated as described by Vedrine et al. [10]. H-ZSM-5 with a Si/Al ratio of 14 was obtained from PQ Corporation and Al_2O_3 was from Degussa. The other materials were from Merck. Sur-

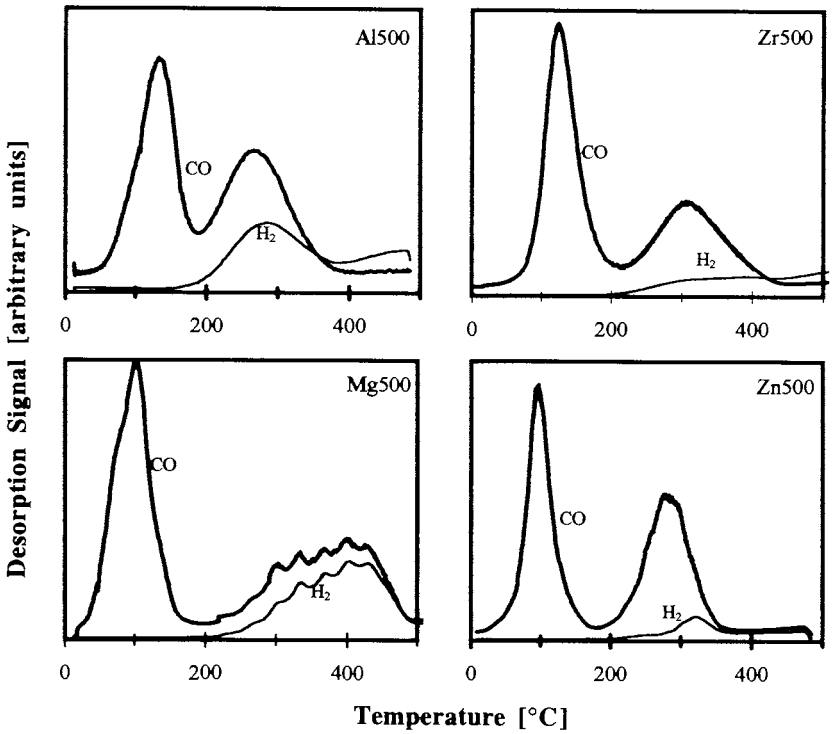

Fig. 3. TPDE of $[Mo(CO)_6]$ on ZnO, MgO, Al_2O_3 and ZrO_2; pretreatment 500°C; heating ramp 20°C min^{-1}.

face areas were determined by single point nitrogen adsorption (Micromeritics Flowsorb 2300). For TPDE, the support (0.5 g) was placed in a quartz reactor cell and pre-treated to temperatures of 500, 800 or 1000°C for 2–3 h. The experimental set-up for TPDE is shown in Fig. 1. A quartz reaction cell (25 ml volume) is placed inside a temperature-programmed clam-shell oven. A continuous sweep of helium gas is passed over the sample and removes all desorbed species. The evolved gases are swept by the carrier He flow through a differentially pumped interface into a quadrupole mass spectrometer (Hiden Analytical) for analysis and quantitation.

About 6 mg of $[Mo(CO)_6]$ was dissolved in 2 ml freshly distilled pentane and injected through a septum onto the pre-treated support with the sample cell cooled in ice. All operations were performed under a continuous flow of dry helium. Removal of the pentane solvent was achieved over a period of about 2–3 h. The solvent was recovered in a cold trap placed downstream of the reactor. The amount of $[Mo(CO)_6]$ sublimed with the solvent was quantified by its characteristic UV absorption at 290 nm. After the impregnated support was completely depleted of solvent, the cold trap was exchanged with a U-tube of lesser volume to reduce peak broadening and the time lag between desorption in the reaction cell and detection in the mass spectrometer. The U-tube was cooled to dry ice temperature to remove all condensable components from the gas stream so that only the permanent gases, hydrogen and CO reached the analyser. A temperature controller/programmer (Eurotherm) was used to achieve a linear ramp of 20°C min^{-1} during the TPDE reaction.

During experiments with fully dehydroxylated supports which are obtained by pre-treating to 1000°C, it is absolutely essential to strictly exclude any moisture, as even traces of moisture will rehydroxylate the support during cooling from the

pre-treatment temperature or during impregnation and solvent purging. The high purity helium carrier gas was very carefully dried by passing it through a column of freshly activated molecular sieve before it entered the reactor. This was checked by monitoring for mass 18 (H_2O) in the quadrupole mass spectrometer. With the molecular sieve trap in place, the water signal decreased by a factor of three to a value indistinguishable from the background signal in the mass spectrometer ($2 \cdot 10^{-11}$ mbar). Immersing the molecular sieve in liquid nitrogen did not lower the signal any further. Hence, it is concluded that the molecular sieve trap is sufficient to ensure a moisture-free carrier flow through the set-up.

Despite thorough drying of the carrier gas, the TPDE of $[Mo(CO)_6]$ on fully dehydroxylated alumina pre-treated at 1000°C still shows a hydrogen signal below 500°C. In order to ensure that this hydrogen was evolved from the surface-mediated reaction between the $[Mo(CO)_6]$ and residual surface OH-groups, and was not caused by other sources like moisture getting into the system when the $[Mo(CO)_6]$ solution was injected, or from a reaction between the hydrocarbon solvent with the highly activated surface, a number of blank runs were performed. For this, the alumina support was pre-treated as before, pure distilled pentane was injected and purged dry. Thereafter, a TPDE was run with the mass spectrometer set to detect masses 2 and 28 for hydrogen and CO, respectively. In these experiments, neither hydrogen nor CO was detected. In another experiment, the cold bath was removed from the trap, the support was pre-treated in a similar manner, and mass 18 was observed. No increase in the water signal was recorded during reheating of the support. It has therefore to be concluded that the small amount of hydrogen evolved stems indeed from the reaction of the decarbonylated molybdenum with residual surface -OH groups.

In order to quantify the amount of evolved gas, the instrument was calibrated after each run by injecting a known volume of the gas into the reactor, using a 6-port Valco valve with a 250 μl sample loop.

3. Results and discussions

3.1. Nature of supports

TPDE of $[Mo(CO)_6]$ on acidic supports such as silica, H-ZSM-5 or sulphated zirconia which had been pre-treated to 500°C shows a single CO decomposition peak occurring at temperatures above 150°C (Fig. 2). The temperature range over which decarbonylation takes place is narrow. The TPDE spectrum is consistent with consecutive first order reactions, where the first CO loss is rate determining, with the other five CO being lost successively, each with a dissociation energy equal or slightly less than that of the first eliminated CO.

In contrast, on more basic supports like magnesia, zinc oxide, zirconia and alumina, the CO evolution shows two peaks of approximately equal area (Fig. 3). CO is lost from the complex at a lower temperature, ≈ 100°C, over these supports as compared with the acidic supports. The 6 CO of $[Mo(CO)_6]$ are now eliminated in two steps

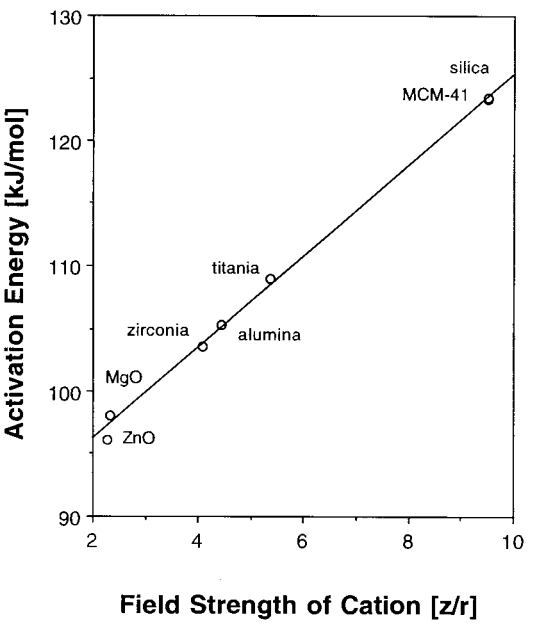

Fig. 4. E_{act} for the loss of the first CO from $[Mo(CO)_6]$ adsorbed on different supports against z/r (nm^{-1}). All supports were pretreated to 500°C.

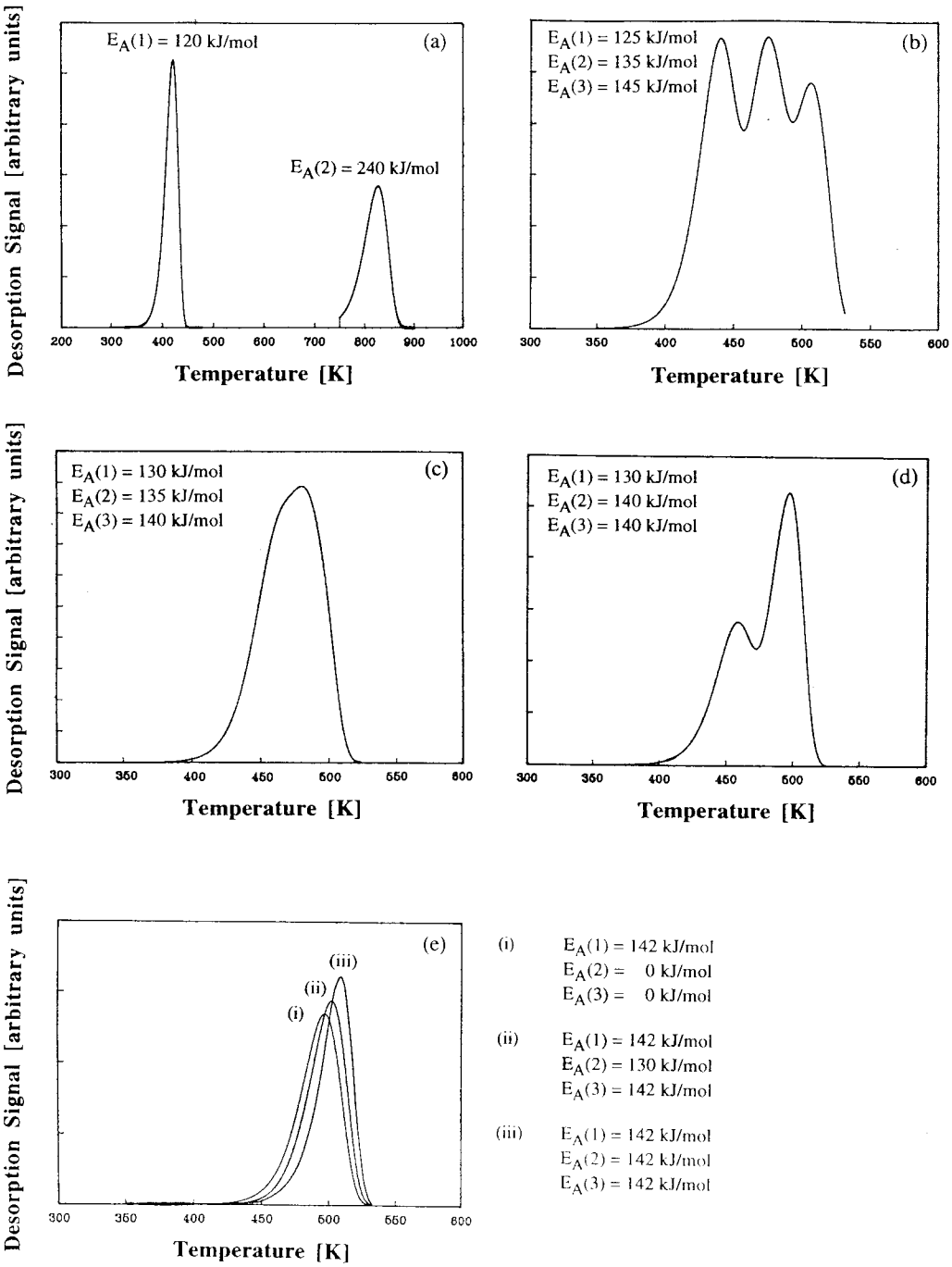

Fig. 5. Simulated TPDE curves for the successive loss of CO with different activation energies.

of three CO each, indicating that a tricarbonyl intermediate, $[Mo(CO)_3]$ads, can be stabilised on the basic supports. Only upon heating to temperatures above 200°C are the 3 remaining CO eliminated, generating metallic molybdenum, or by reaction with surface -OH groups, molybdenum oxides. Thus, the nature of the support, acidic or basic, determines the pathway of decomposition. This can be clearly seen using TPDE which also identifies intermediates formed during the surface-mediated reaction.

From the desorption temperatures, the activation energy for CO elimination from $[Mo(CO)_6]$ can be calculated using the Redhead equation. Over basic supports, the activation energy for the first CO loss is $\approx 96–105$ kJ mol^{-1} while for acidic supports, higher activation energies of $\approx$ 120 kJ mol^{-1} are encountered. With a slower heating rate of 5°C min^{-1} instead of 20°C min^{-1}, the desorption spectrum becomes broader and the peak maximum shifts to lower temperature. However, the activation energy calculated was the same within 1.5%.

The surface hydroxyl concentration for various supports after heating to different temperatures has been determined [11]. A support which has been pretreated to 500°C still has a considerable amount of hydroxyl groups present at the surface, hence it can be considered to be only partially dehydroxylated. It has been proposed that the mechanism for the decomposition of $[Mo(CO)_6]$ over a partially dehydroxylated surface involves surface hydroxyl groups [12,13]. These hydroxyl groups act as ligands which coordinate to the molybdenum centre, where they replace the CO groups. Hence the mechanism is a ligand substitution reaction. To be an effective ligand, the oxygen of the hydroxyl groups must donate electrons from its lone pair into the empty d-orbitals of the molybdenum atom. The ability of the oxygen lone pairs to act as donors (nucleophility) is affected by the field strength of the neighbouring metal cation, i.e. the basicity of the support. The field strength at a metal cation is given as z/r, where z is the ionic charge of the cation, and r its ionic radius (nm) in the appropriate co-ordination sphere. A plot of activation energy versus z/r is linear (Fig. 4), showing a good correlation between the two parameters [14]. Hence, hydroxyl groups which are good nucleophiles can easily replace the CO from $Mo(CO)_6$, lowering the activation energy for decomposition. Hydroxyl groups next to a cation of high nuclear charge are less nucleophilic. For this case, a higher temperature for the initial CO evolution is observed. Hence, the thermal decomposition of $[Mo(CO)_6]$ provides a method to measure the surface basicity.

3.2. Mechanism of decomposition

In order to gain further insights into the decomposition mechanism, we simulated the desorption

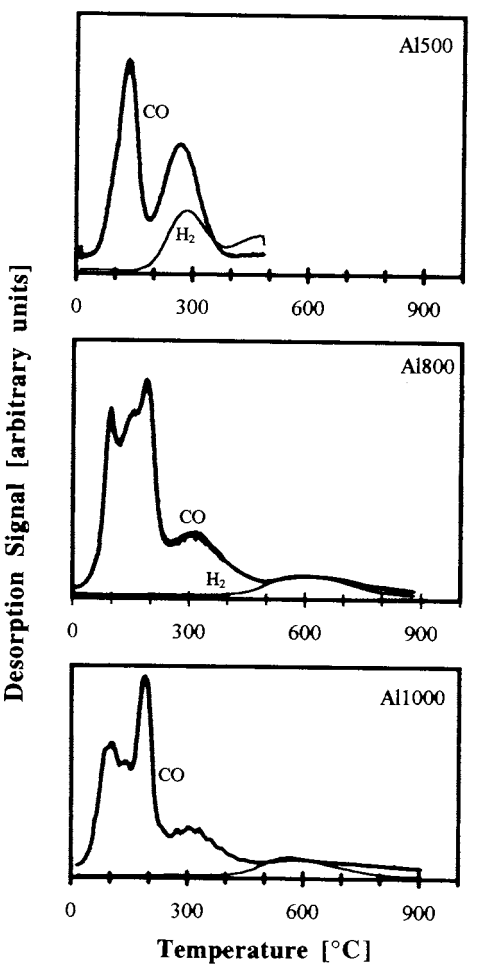

Fig. 6. TPDE of $[Mo(CO)_6]$ on alumina pretreated to 500, 800 and 1000°C; heating ramp 20°C min^{-1}.

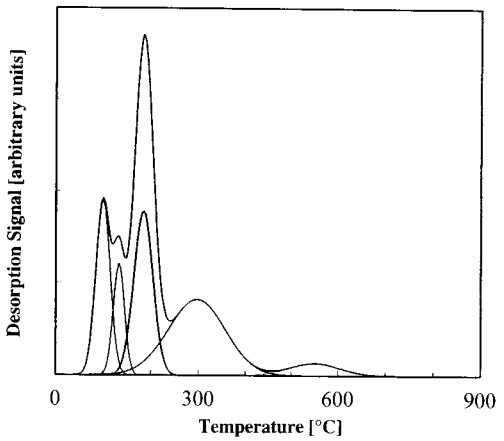

Fig. 7. Deconvolution of the TPDE signal for $[Mo(CO)_6]$ on alumina pretreated to 1000°C.

spectra for a number of situations with successive CO-dissociation steps. The TPDE spectra for $[Mo(CO)_6]$ on acidic supports like silica, H-ZSM-5 and sulphated zirconia are narrow and agree with the model of a single first order reaction. It is therefore assumed that the much broader signals observed with the more basic supports do not arise from surface heterogeneity, but are rather due to the kinetics of the thermal decomposition of the adsorbed complex. In order to gain insight into the mechanism of the decarbonylation reaction, we generated TPDE spectra by computer simulation. For this, the system of six successive first-order reactions was solved numerically for different activation energies. A single-step first order reaction results in a typical asymmetric desorption signal (Fig. 5a). The signal from a reaction with a higher activation energy appears at a higher temperature and is broader than that of a process with a lower activation energy. However, the dimensionless parameter, f = [full width at half maximum]/[peak temperature], is almost invariant with a value of 0.067. Fig. 5b–d simulate the loss of 3 successive CO. In the case where the activation energies of the successive steps increase by more than 10 kJ mol^{-1}, well resolved peaks are seen (Fig. 5b). If the successive decarbonylation increases in activation energy by 5 kJ mol^{-1} or less, the individual peaks coalesce into a single broad signal (Fig. 5c). This is observed for the TPDE of $[Mo(CO)_6]$ on partially dehydroxylated basic supports alumina, ZnO, MgO and zirconia (Fig. 3). In the case of two successive decomposition reactions with somewhat increasing activation energy which are followed by steps with equal or lower activation energy, a shoulder develops on the low temperature side (Fig. 5d). The simulation in Fig. 5e illustrates that: (i) if the first dissociation step is rate determining, followed by two successive fast CO decarbonylation steps, the resultant spectrum will resemble that of a single first order reaction; (ii) if the activation energy for the second dissociation step is smaller in magnitude than the first and third, the peak will sharpen; (iii) if all three steps have identical activation energies, the peak sharpens and shifts simultaneously to higher temperature, while the f parameter is smallest, $f = 0.055$, a decrease of 20% relative to a simple first order reaction. This mechanism describes the $[Mo(CO)_6]$ decomposition on silica pre-treated to 500°C (Fig. 1) where the measured f value is 0.058. Considering that back-mixing in the reactor and transfer lines contributes to broadening of the observed signal, the actual signal should be even narrower. Thus, we propose that the decarbonylation of $[Mo(CO)_6]$ on silica proceeds by successive removal of the 6 CO, where the activation energy for each step is of comparable magnitude. Careful line-shape analysis thus enables one to obtain additional information with regard to the different activation energies for the case of sequential reactions.

3.3. Effect of degree of hydroxylation

All support have been pre-treated to 500, 800 and 1000°C to investigate the effect of surface dehydroxylation on the decomposition stoichiometry and reaction pathway. The sample code used here is MXXX where M is the chemical symbol of the support cation and XXX refers to the pre-treatment temperature. For alumina as support, the TPDE spectra change drastically upon dehydroxylation (Fig. 6). The spectrum of Al500 consists of two CO peaks of approximately equal area. This reveals that the intermediate $[Mo(CO)_3]$ads is formed. The spectra for Al800 and Al1000 however consist of a series of overlap-

ping peaks. Deconvolution of the CO signal into individual components can be carried out in such a way that each deconvoluted peak represents one or more CO and the total area corresponds to a multiple of six. Integral values for every deconvoluted peak can only be obtained if a total number of 24 CO is assumed for both Al800 and Al1000. This implies that 4 $[Mo(CO)_6]$ are involved, which form clusters by CO elimination during the surface assisted TPDE reaction. This clustering effect is not surprising and is a necessary step towards the formation of metallic particles from mononuclear complex [15]. A deconvoluted spectrum for Al1000 is shown in Fig. 7. The series of narrow peaks corresponds to the elimination of 4, 2, 5 and 5 CO, followed by a much broader band corresponding to 7 CO and finally 1 CO. The narrow peaks represent CO decomposition from well-defined surface-adsorbed carbonyl or subcarbonyl species. The especially sharp band at about 180°C arises from the five successive CO elimination steps from subcarbonyl species as they cluster together. These successive CO elimination reactions have activation energies which are very close to one another. The broad band corresponding to the loss of 7 CO indicates CO losses from a larger cluster entity, where different coordination sites lead to a range of binding energies. These larger entities are possibly already metallic aggregates which are still covered with CO. The last CO is evolved over a very large temperature range and is attributed to a reaction between a carbidic carbon and a surface oxygen species [16] similar to the reaction proposed for the high temperature desorption signal seen on metallic tungsten and molybdenum [17,18]. Analysis of TPDE spectrum with the aid of simulated spectra thus provides an insight into the steps during surface-mediated clustering of metal carbonyl or subcarbonyl complexes. Clustering is observed only on the basic supports but not on acidic ones like silica. Other basic supports which had been dehydroxylated to 800°C or higher also promote cluster formation. Cluster formation can also be observed on partially dehydroxylated alumina when the initial loading of $[Mo(CO)_6]$ is very high (Fig. 8). Obviously, a high (Mo/surface OH) ratio is necessary for cluster formation. This is the case on dehydroxylated surfaces where the number of OH-groups is small, as well as on a partially dehydroxylated surface for high Mo coverage.

Dehydroxylation of the more acidic supports like silica and H-ZSM-5 does not promote cluster

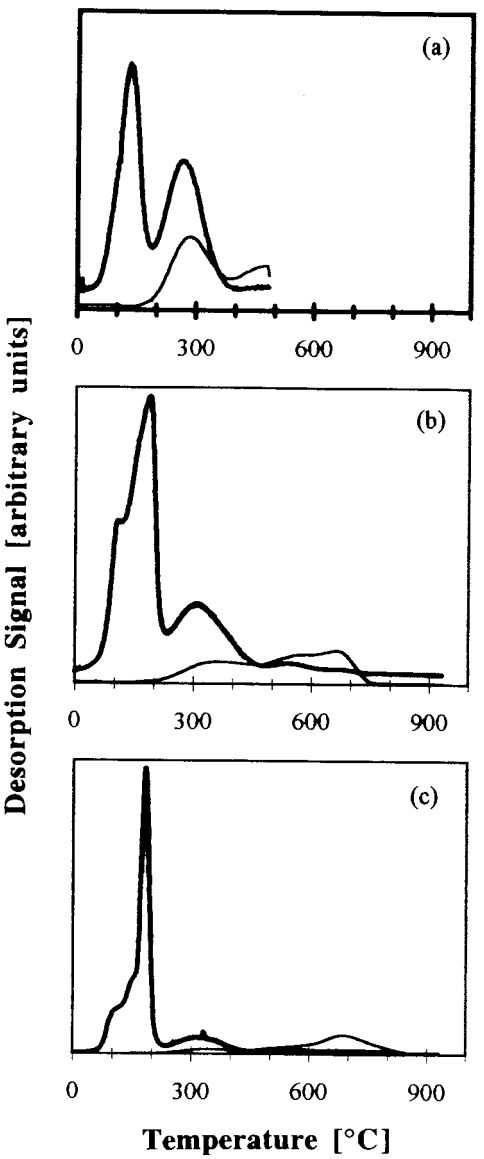

Fig. 8. TPDE of $[Mo(CO)_6]$ on alumina at different Mo coverage; pretreatment temperature: 500°C, heating ramp: 20°C min^{-1}, (a) 0.14 Mo nm^{-2}; (b) 0.32 Mo nm^{-2}; (c) 0.55 Mo nm^{-2}.

Table 1
Experimentally determined molybdenum oxidation number as a function of the ratio surface-OH:Mo

Pretreatment temperature (°C)	Surface-OH [nm^{-2}][a]	Mo [nm^{-2}]	OH/Mo	Mo O.N.[b]
500	3.1	0.14	22.1	3.4
500	3.1	0.16	19.4	2.9
500	3.1	0.32	9.69	1.52
500	3.1	0.35	8.86	1.72
500	3.1	0.55	5.60	0.75
800	0.6	0.21	2.86	0.6
1000	0.1	0.15	0.67	0.3
1000	0.1	0.19	0.53	0.2
1000	0.1	0.37	0.27	0.12
1000	0.1	0.55	0.18	0.08
1000	0.1	0.58	0.17	0.05

[a] Values from Iwasawa [11].
[b] Oxidation number determined from the integrated hydrogen evolution signal up to 500°C.

formation. Even after pre-treatment at 1000°C, the TPDE profile remains a single, narrow CO peak with maximum above 150°C, consistent with the elimination of 6 CO, where the activation energy for each successive step is within ± 5 kJ mol^{-1} from that of the first step.

The coverage of Mo on the support is quantified assuming each Mo evolves a total of 6 CO. Complete decarbonylation of the carbonyl complex does not necessarily lead to metallic Mo, because the hydroxyl groups on the surface can react with the adsorbed subcarbonyl during thermal decomposition to produce hydrogen and Mo^{n+}. Thus, through the quantitation of the amount of hydrogen evolved, we can also deduce the extent of oxidation of Mo. Table 1 tabulates the Mo oxidation state at 500°C together with the hydroxylation of the alumina support. It is found that the extent of oxidation is proportional to the OH:Mo ratio. Thus, it is expected that metallic Mo particles can only form on supports which are completely depleted of OH groups, or at a very high Mo coverage.

4. Conclusion

TPDE can be used to study the surface-mediated thermal decomposition reaction of $[Mo(CO)_6]$. It can identify the formation of intermediates, if any, during the thermal decomposition reaction. It is able to give an insight into the reaction mechanism and provides evidence for the formation of clusters. The TPDE profile is highly sensitive to the type of surface, with the temperature of decarbonylation being dependent on the nucleophility of the surface hydroxyl groups. Hence, this reaction constitutes a novel tool to gauge the basicity of the surface. The dissociation energy of CO from the complexes $[Mo(CO)_x]$ads can be calculated using the Redhead equation. The evolution of hydrogen during TPDE is a clear indication that after the removal of all CO groups, not metallic molybdenum, but an oxidised species is obtained, where the final oxidation state depends on the number of hydroxyl groups initially present on the surface.

Acknowledgements

This research was supported by NUS research grant RP940602. We thank the PQ Corporation for the donation of H-ZSM-5.

References

[1] D. Roberto, E. Cariati, R. Psaro, R. Ugo, Organometallics 13 (1994) 734.
[2] K. Tanabe, M. Misono, Y. Ono, H. Hattori, New Solid Acids and Bases, Elsevier, Amsterdam, 1989, p. 5.

[3] H. Knözinger, P. Ratnasamy, Catal. Rev. Sci. Eng. 17 (1978) 31.
[4] A. Brenner, R.L. Burwell Jr., J. Catal. 52 (1978) 353.
[5] J. Goldwasser, S.M. Fang, M. Houalla, W.K. Hall, J. Catal. 115 (1989) 34.
[6] J.L. Falconer, J.A. Schwarz, Catal. Rev. Sci. Eng. 25 (1983) 141.
[7] A.M. de Jong, J.W. Niemantsverdriet, Surf. Sci. 233 (1990) 355.
[8] R.J. Cvetanovic, Y. Amenomiya, Catal. Rev. Sci. Eng. 6 (1) (1972) 21.
[9] R. Srinivasan, D. Taulbee, B.H. Davis, Catal. Lett. 9 (1991) 1.
[10] F.R. Chen, G. Coudurier, J.-F. Joly, J.C. Vedrine, J. Catal. 143 (1993) 616.
[11] Y. Iwasawa, Tailored Metal Catalysts, Reidel, Hingham, M.A., USA, 1986, p. 16.
[12] M. Laniecki, R.L. Burwell Jr., J. Colloid Interface Sci. 75 (1980) 95.
[13] K.P. Reddy, T.L. Brown, J. Am. Chem. Soc. 117 (1995) 2845.
[14] H.G. Ang, K.S. Chan, G.K. Chuah, S. Jaenicke, S.K. Neo, J. Chem. Soc. Dalton Trans. (1995) 3753.
[15] H.G. Ang, G.K. Chuah, S. Jaenicke, W.L. Loh, J. Chem. Soc. Dalton Trans. 1997, 1243.
[16] J.S. Lee, M. Boudart, Jpn. J. Appl. Phys. 32 (1993) 472.
[17] B.E. Nieuwenhuys, Surf. Sci. 126 (1983) 307.
[18] G. Broden, T.N. Rhodin, C. Brucker, R. Benbow, C. Hurych, Surf. Sci. 59 (1976) 593.

ELSEVIER

Talanta 45 (1998) 751–757

Talanta

Characterization of atomic force microscopy (AFM) tip shapes by scanning hydrothermally deposited ZnO thin films

G.W. Bao, S.F.Y. Li *

Department of Chemistry and Institute of Material Research and Engineering, National University of Singapore, 10 Kent Ridge Crescent, Singapore 119260, Singapore

Received 5 February 1997; accepted 27 May 1997

Abstract

Direct observation of tip shapes by atomic force microscopy (AFM) has been achieved using spike-like crystallites in ZnO thin films deposited on microscope glass slides by the hydrothermal deposition technique. Three types of AFM tips, e.g. standard Si_3N_4 tips, a broken silicon supertip and a noncontact silicon tip were examined and the acquired images for these tips show that ZnO crystallites are good samples to image commonly used AFM tips. The most obvious characteristic of this method is that it is easy for every chemical laboratory to access. © 1998 Elsevier Science B.V.

Keywords: Atomic force microscopy; ZnO thin films; Tip shapes

1. Introduction

The atomic force microscope (AFM), developed by Binnig et al. [1], has become a widely used tool for investigating surfaces with high spatial resolution. Due to its large dynamical range, the AFM has been used to analyze surfaces and interfaces on various levels ranging from atomic resolution to more technological applications such as imaging nanofabricated semiconductor structures.

One basic problem common to the AFM technique is the shape of the tip which determines the resolution and affects the images of the structures, because in AFM the tip geometry convolutes with the shapes of samples [2–5]. Therefore, for better understanding of AFM images, there is a great need for characterization of the shapes of the tips since the different forces involved in AFM depend on the actual tip shape [6–9].

A direct imaging of the tip geometry using AFM itself has been discussed in some reports [10–15]. To make an in situ measurement of the tip, one should image a surface with structures that are sharper than the probing tip, giving, in the ideal case with delta function peaks protruding from the surface, an image of the probing tip. Montelius used InP columns fabricated using aerosol and dry etching techniques to successfully image the Si_3N_4 tip shape [12]. Atamny presented a direct imaging of AFM Si_3N_4 tip shape using a

* Corresponding author. Tel.: +65 7722681; fax: +65 7791691; e-mail: chmlifys@leonis.nus.sg

PII S0039-9140(97)00294-4

sharp pin-like feature present on copper films deposited by metal organic chemical vapor deposition (MOCVD) [14]. Bogdanov fabricated two-dimensional arrays of very sharp tips with e-beam evaporation of metals to calibrate the lateral motion of the scanner [15]. Sheiko [16] used high temperature treated (305) surfaces of a $SrTiO_3$ single crystal with an automatically defined saw-tooth morphology to inspect the mesoscopic shape of the tip shape by recording defined saw-tooth morphologies of $SrTiO_3$ surfaces. Although acceptable for making sharp structures on the surfaces, these methods are usually complicated and rarely accessible to every scanning force microscopy laboratories. Typically the radius of an AFM tip is taken from manufacturer's specifications or, rarely, measured by scanning electron microscopy (SEM) [17]. The application of SEM, nevertheless, requires a conductive coating that would be awkward to remove before using the silicon nitride tips as AFM tips and, therefore, is likely to destroy the tips.

In this paper we present a direct observation of AFM tip shape utilizing a new method for preparing samples with much sharper structures than the tip itself. Zinc oxide thin films prepared by hydrothermal deposition technique were used as samples for characterizing AFM tips. With this method it is possible to map tip images and thereby, to determine the radii of curvature of the tips. The method presented here is the easiest compared to published techniques and is readily accessible in every chemical laboratory.

2. Experimental

2.1. Fabrication of ZnO films

The film deposition method we used was the same as described by Saeed [18]. Zinc oxide thin films were grown onto glass microscope slides from solution containing zinc acetate (0.02 M), and ethylenediamine (0.06 M). The initial pH value of the solution was around 8 and was raised to 10–11 by the addition of a small amount of 0.5 NaOH. Glass microscope slides were treated in 50% H_3PO_4 solution at boiling point for 30 min, rinsed with DI water and acetone and then immersed into the reaction bath. The reaction mixture was maintained in a water bath at 50°C for 1 h for deposition. After that the substrates were taken out, washed with distilled water and spin dried for use. To visualize the morphology of prepared ZnO thin films, SEM experiments were conducted on gold-coated ZnO films.

2.2. Acquiring AFM tip images

The surfaces of ZnO thin films were scanned using a commercial AFM instrument (TMX 1010 Explorer, Topometrix, Santa Clara, CA) equipped with a 100 μm scanner. Three types of tips were used in this study, e.g. standard Si_3N_4 tips with cantilever force constant of 0.03 N m^{-1} as indicated by the manufacturer, a silicon supertip, and noncontact silicon tips with cantilever force constant in the range of 40–55 N m^{-1} (also as indicated by the manufacturer). The so called 'supertip' has a very sharp silicon needle at the apex of a pyramidal base mounted on the V-shaped cantilever (see Fig. 3d). The sharp needle of the supertip in this work had been broken before it was imaged. This tip was a good sample to examine if our method could reveal some features of a spoiled tip. Because the force constant of the noncontact tip cantilever is very high, ZnO films were totally destroyed by the tip when operations were conducted in contact mode. In this case, noncontact mode was used to image the triangular conical tip. This mode was also used to image the supertip in order to compare with contact mode results. All experiments were carried out in ambient condition with temperature $\approx$ 22–24°C and RH $\approx$ 55%.

3. Results and discussion

Fig. 1 is the SEM micrograph of ZnO thin films on glass microscope slide prepared by the hydrothermal deposition technique. It can be seen that the films consists of hexagonal columnar crystallites nearly of the same size. A large number of the crystallites oriented perpendicular or nearly perpendicular to the substrate, forming pin

arrays in the films parallel to the substrate normal. As estimated with the SEM micrograph, the lateral dimensions of these crystallites were around 0.15 μm , much smaller than the tip geometrical sizes. So these spiky crystallites could serve as samples to image the tip shape inverse to the normal imaging process.

Fig. 2 shows the SEM micrograph and the AFM images of the standard Si_3N_4 tip over the ZnO film. The AFM image (Fig. 2b) consists entirely of pyramid-shaped features, which correspond to the tip shapes. No spiky hexagonal pin shaped features relating to ZnO crystallites were revealed. The feature sizes, i.e. height and width, are not uniform due to the fact that not all ZnO crystallites were oriented to the substrate normal and that the vertical heights of the crystallite columns protruding upwards are not equal. It should also be noted that the apexes of the pyramidal features are very sharp (the data will be given below), indicating that the apexes of the tip and ZnO crystallites in the films are both very sharp. The spiky geometry of the ZnO crystallite columns is very important for the accurate characterization of AFM tip shapes.

Fig. 3 represents the supertip images acquired in contact and noncontact modes. As is obvious from the pictures, the features in these images appear to be truncated pyramids with flat terraces at the apexes on which the supersharp needle had

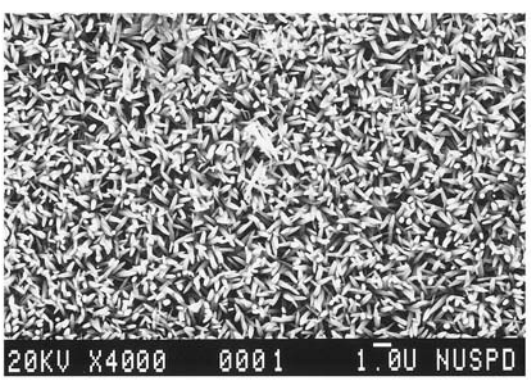

Fig. 1. SEM micrograph of ZnO thin film prepared by hydrothermal deposition showing a large number of the spike-like crystallites oriented normal to the substrate.

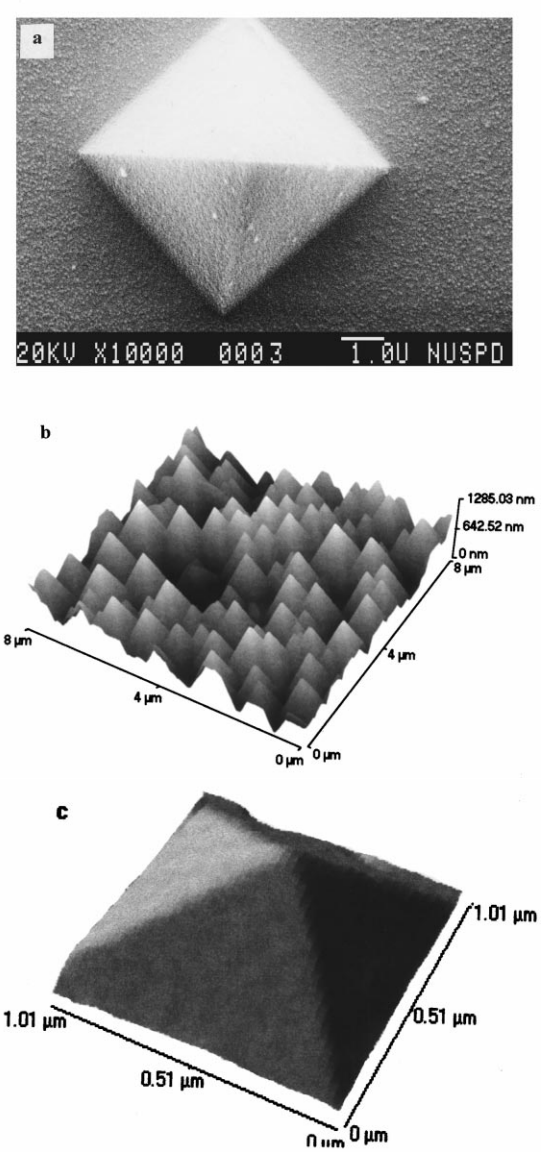

Fig. 2. Standard Si_3N_4 tip images. (a) SEM micrograph of Si_3N_4 tip. The dimensions of the tip are 5 μm in width and length; (b) AFM image of the tip consisting entirely of the tip pyramids. Note the sharp apex of the feature, which indicates the sharpness of both the tip and the crystallite apex; (c) single tip image obtained by zooming in on (b)

stood before it was broken as mentioned previously. In fact, what was imaged was the base of the supertip. Regular pyramidal shapes showed up as the upper parts of the features while the lower parts appeared to be covered. These par-

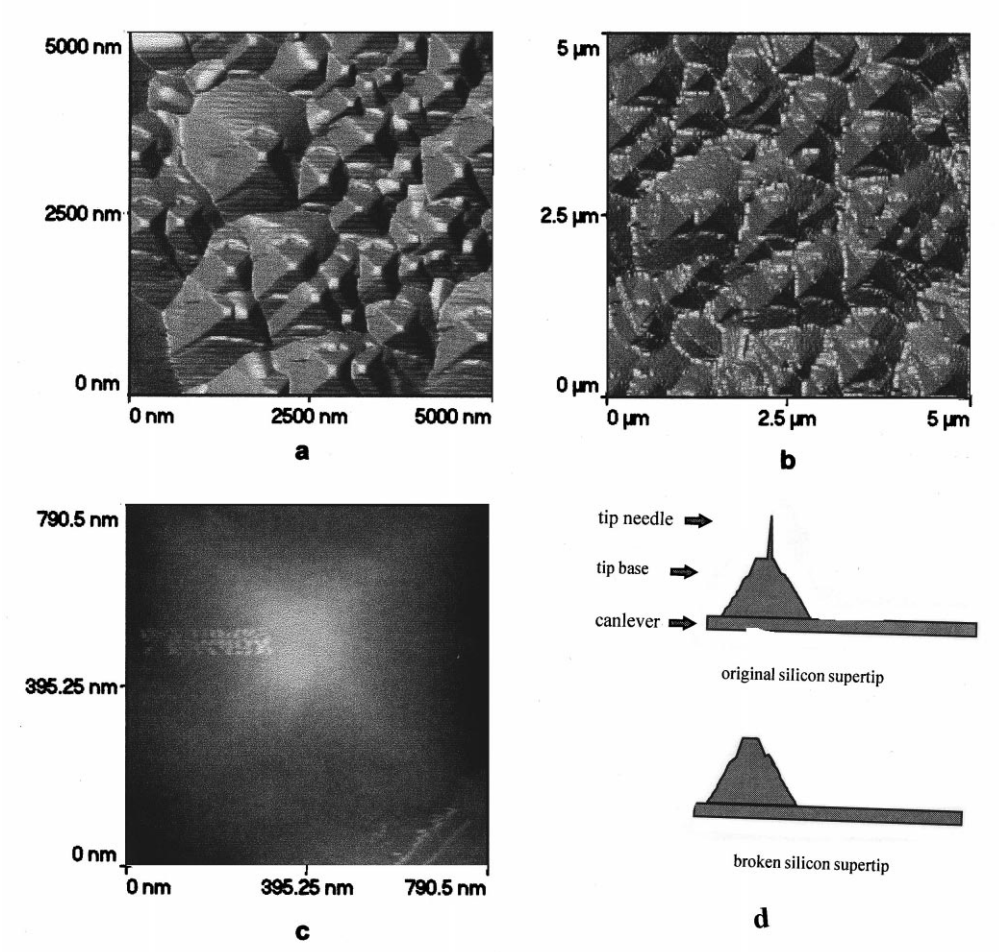

Fig. 3. Images for the broken supertip showing the tip base in truncated pyramidal shape. Note the flat terrace on top of the feature and the covered structure of the lower half of the feature. (a) Tip image obtained in contact mode; (b) tip image obtained in noncontact mode; (c) tip image obtained by scanning the tip over single vertical crystallite in noncontact mode. Note the bright round spot, corresponding to the broken scar of the tip needle; (d) a diagram of the supertip.

tially covered pyramidal features, reproducible at different locations and in different imaging modes, reflected structures positioned on the tip possibly resulting from the microfabrication process of the tip, rather than the consequence of the tip-sample convolution. Further measurements indicated that the slopes of the pyramids in Fig. 3 were smaller than that of the standard Si_3N_4 tip as shown in the preceding image. If the supertip base took a perfect pyramidal shape, the pyramidal shape like the standard Si_3N_4 tip should have been imaged. It was, nevertheless, obviously not the case. Fig. 3c is an image of a single tip obtained by scanning the supertip over one vertical ZnO crystallite in noncontact mode. On the rectangular shaped flat terrace at the apex of the feature, a round bright spot, corresponding the broken scar of the tip needle, can be distinguished. The diameter of the scar was measured to be 70–80 nm, representing the end diameter of the broken silicon needle positioning on the pyramidal tip base apex. Both facts, the partially covered pyramidal feature and the scar of the broken tip, demonstrate that the ZnO thin films

prepared with the hydrothermal deposition method can be used to conduct reverse imaging, in which a surface with delta-functionlike features is used to image the shape of objects on the AFM tip [12].

Apart from soft tips such as the standard Si_3N_4 tips, stiff tips like the noncontact silicon tip could also be imaged using the hydrothermally deposited ZnO films. Because of the high stiffness of the noncontact silicon tips, the ZnO films were destroyed when operation was conducted in contact mode and no image could be acquired. In noncontact mode the triangular conical shape of the tip was successfully imaged, as shown in Fig. 4. The SEM micrograph of the same tip is also presented for comparison (Fig. 4a). The AFM image obtained represents the forehead of the tip considering that the lateral dimensions of the tip are large, around 7 μm as estimated from Fig. 4a.

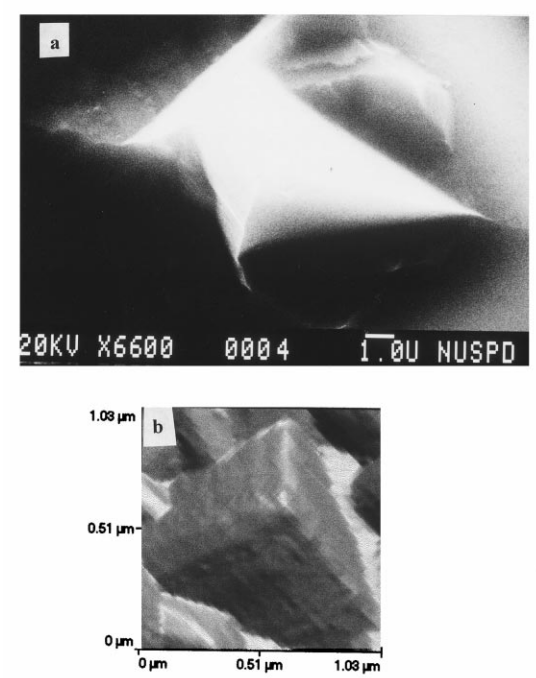

Fig. 4. Triangular conical tip images. (a) SEM micrograph of the noncontact tip showing irregular triangular conical shape; (b) AFM image of the tip apex obtained in noncontact mode.

It is known that geometrical shape of tip apexes are the key factors determining the image resolution [2–4]. For the purpose of characterizing such shapes, AFM images of the tips are very useful because tip characterization can be operated in situ and tip dimensions can be accurately measured on the nanometer scale, which are inaccessible by other analytical techniques. With the images obtained, line measurements for the apexes of the three types of tips were conducted and the results are shown in Fig. 5. We took the cross-section at a relatively flat segment in the profile of a tip apex as the tip apex diameter. As measured, the standard Si_3N_4 tip used in this work had a very small apex diameter of around 30 nm. The Si_3N_4 tips we used were actually new tips and no noticeable damage was made before this experiment. The flat terrace at the apex of the supertip base was measured to be 70×100 nm in length $\times$ width. The triangular conical silicon tip was a used one but still had a small apex diameter of around 60 nm. The angles between the tip sloping planes and the cantilever base could also be defined from the cross section profiles of the tip images. The measurement results indicated that the triangular conical shape of the silicon tip had steeper sloping planes than the pyramid of the standard Si_3N_4 tip. Approximately, these angles ranged from 70–80° for the former, and 50–60° for the latter, varying from plane to plane.

Zinc oxide commonly exists in the hexagonal (wurtzite) form [19]. Although hydrothermally deposited ZnO films are not preferentially oriented [18,20], the growth of the crystallites at low temperatures such as 50°C, is heterogeneous, resulting in pin-like crystallites with high aspect ratios. Although it is impossible to make all these pin-like particles stand parallel to the substrate normal by hydrothermal deposition, the samples prepared by this method are still suitable to be used for imaging AFM tip shape due to the fact that there are a lot of particles normal to the substrate and that the foreheads of the particles are in spike shapes with diameter less than 30 nm, as revealed by standard Si_3N_4 tip image (Fig. 5).

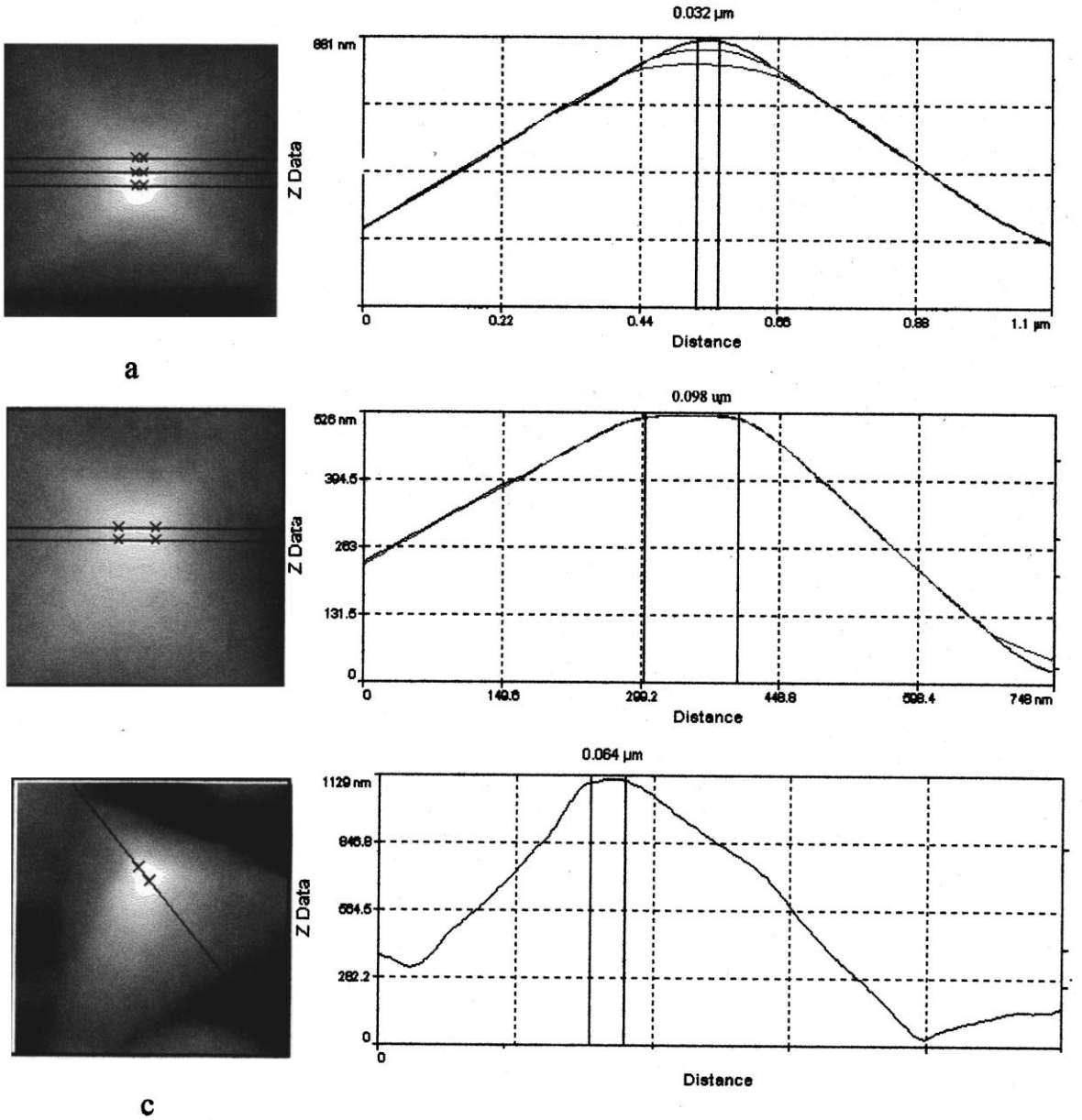

Fig. 5. Cross section profiles of the three different tips and measurements of the apex diameter of the tips. (a) standard Si_3N_4; (b) broken supertip base; (c) triangular conical tip.

4. Conclusion

Hydrothermal deposition technique is the easiest method to prepare thin films. We used this method to successfully obtain ZnO thin films with a large number of spiky crystallites aligning normal to the substrate at low temperatures of 50°C. These spike-like crystallites with an apex radius of less than 30 nm and an aspect ratio of more than 1:20 are suitable for imaging tip shape by AFM

itself. Three different types of commonly used AFM tips were examined and clear-cut tip images were obtained. For stiff cantilever tips, noncontact mode of the AFM could be used to avoid the sample destruction by the tip and the tip shape could still be imaged. Moreover, some structures positioning on the tip could also be imaged, which were useful to pick out spoiled tips in AFM experiments.

Acknowledgements

We thank Ms Hua of the Department of Physics of NUS for the SEM work and Mr L. Zhou for helpful discussions.

References

[1] G. Binnig, C.F. Quate, Ch. Gerber, Phys. Rev. Lett. 56 (1986) 930.
[2] Ph. Niedermann, O. Fisher, J. Microsc. 152 (1988) 93.
[3] J.P. Pelz, R.H. Koch, Phys. Rev. B41 (1990) 1212.
[4] D. Keller, Surf. Sci. 353 (1991) 253.
[5] K.L. Westra, A.W. Mitchell, D.J. Thomson, J. Appl. Phys. 74 (1993) 3608.
[6] E. Tekman, S. Ciraci, J. Phys. Condens. Matter 3 (1991) 2613.
[7] U. Landman, W.D. Luedtke, N.A. Burnhan, R.J. Colton, Science 248 (1990) 454.
[8] U. Hartmann, J. Vac. Sci. Technol. A8 (1990) 411.
[9] A. Wadas, P. Grutter, Phys. Rev. B39 (1989) 12013.
[10] G.F.A. van de Walle, H. van Kempen, P. Wyder, Surf. Sci. 167 (1986) L219.
[11] L. Hellemans, K. Waeyaert, F. Hennau, L. Stockman, I. Heyvaert, Ch. van Heesendonck, J. Vac. Sci. Technol. B9 (1991) 1309.
[12] L. Montelius, J.O. Tegenfeldt, Appl. Phys. Lett. 62 (1993) 2628.
[13] F. Jensen, Rev. Sci. Instrum. 64 (1993) 2595.
[14] F. Atamny, A. Baiker, Surf. Sci. 323 (1995) L314.
[15] A.L. Bogdanov, D. Erts, B. Nilsson, H. Olin, J. Vac. Sci. Technol. B12 (1994) 3681.
[16] S.S. Sheiko, M. Moller, E.M.C.M. Reuvekamp, H.W. Zandbergen, Phys. Rev. B48 (1993) 5675.
[17] J.L. Hutter, J. Bechhoefer, Rev. Sci. Instrum. 64 (1993) 1863.
[18] T. Saeed, P. O'Brien, Thin Solid Films 271 (1995) 35.
[19] J. Auld, D.J. Houlton, A.C. Jones, S.A. Rushworth, M.A. Malik, P. O'Brien, G.W. Critchlow, J. Mater. Chem. 4 (1994) 1249.
[20] D. Ravindra, J.K. Sharma, J. Appl. Phys. 58 (1985) 838.

.

ELSEVIER

Talanta 45 (1998) 759–766

Talanta

Synthesis, characterization and sensing application of novel semiconductor oxides

G.-J. Li, S. Kawi *

Department of Chemical Engineering, National University of Singapore, 10 Kent Ridge Crescent, Singapore 119260, Singapore

Received 5 February 1997; received in revised form 27 May 1997; accepted 28 May 1997

Abstract

Mesoporous SnO_2 with high surface areas were synthesized using a cationic surfactant (*N*-cetyl-*N*,*N*,*N*-trimethylammonium bromide) as a synthetic template. Acidity of the starting synthesis slurry was used as one of the controlling parameters for the synthesis. After the SnO_2 was synthesized at pH 7.15, it was calcined at 723 K for 10 h in air. It had a BET surface area of 156.8 $m^2\ g^{-1}$ with a pore diameter of 38.4 Å. Infrared spectroscopy (FTIR) and thermal analysis techniques (thermogravimetry and differential thermal analysis) showed that the surfactant was incorporated in the mesopores of SnO_2 and calcination in air at 673–723 K was needed to remove the surfactant completely from the mesopores. The effects of SnO_2 surface area on its gas sensing properties were also investigated. It was observed that SnO_2 with higher surface areas had much higher sensitivities to hydrogen at 573 K. © 1998 Elsevier Science B.V.

Keywords: Mesoporous SnO_2; Gas sensor; MCM-41; Surfactant template

1. Introduction

Since the successful synthesis of MCM-41 [1], great efforts were made to synthesize mesoporous oxide materials other than silica. The syntheses of mesoporous materials of tungsten, molybdenum, iron, lead oxides [2], TiO_2 [3], SnO_2 [3] and ZrO_2 [4,5] were reported recently. However, the mesoporous structures of most materials, except MCM-41, easily collapsed once the surfactants were removed by thermal treatment or by liquid extraction; hence this greatly limits the applications of such materials.

Tin dioxide is widely used in many research areas, such as catalysts for oxidation [6,7] and selective hydrogenation [8] of organics, solid state semiconductor sensors for reducing gases, [9,10] and starting materials for making indium-tin oxide transparent conductive glasses [11]. As a semiconductor gas sensor, SnO_2 shows high sensitivity to many reducing gases, such as H_2, CO, and alcohol. SnO_2-based gas sensors are widely used to detect reducing gases, such as in gas leak alarms, in pollutant emission control, and in alcohol concentration monitoring, and they have revealed the potential to be used as gas detectors for analytical equipments, such as gas chromatographic detectors [12].

* Corresponding author. Tel.: +65 8746312; fax: +65 7791936; e-mail: CHEKAWIS@NUS.SG

PII S0039-9140(97)00295-6

When reducing gases are contacted with SnO_2 at proper temperatures, the oxygen species, such as O^- or O_2^-, on SnO_2 surfaces are removed through the reaction with the gases, inducing an increase of the conductance of SnO_2. The response of the increase of conductance or the decrease of resistance is used to detect the gas concentrations in certain circumstances. Since the reaction between surface oxygen species and the reducing gases is of importance for gas sensitivity, it is believed that sensor sensitivity can be improved by increasing the sensor surface areas, which will provide more surface sites for more oxygen to be adsorbed and contacted with the gases.

To improve the sensing properties, SnO_2 is generally prepared by the sol-gel method [13–15] using alkoxides (or other inorganic salts in some cases) as starting precursors and by thin film techniques. However, the preparation procedure by the sol-gel method is quite complicated and it is difficult to control the experimental conditions. In accordance with the syntheses of MCM-41 and MCM-like materials, one may consider that, using a similar synthetic strategy, mesoporous SnO_2 with a high surface area is possible to synthesize. Ulagappan et al. [3] recently reported the syntheses of mesoporous SnO_2 using an anionic surfactant as a synthetic template; however, the mesoporous structures of their SnO_2, which was characterized by XRD and atomic force microscopy, could not be maintained once the surfactants were removed and no surface area data for the resulting material was reported.

Here we report, for the first time, the synthesis of thermally-stable mesoporous SnO_2 using a cationic surfactant as a synthetic template and sodium stannate as the starting inorganic precursors. The resulting SnO_2 was calcined at 673–723 K to remove the surfactants completely from the mesopores, as shown by FTIR and thermal analysis techniques. The surface areas of the resulting materials were systematically varied by controlling the acidity of the starting slurry. The effects of surface areas on gas sensing sensitivities was systematically investigated using these materials at high temperatures.

2. Experimental

2.1. Synthesis procedure of mesoporous SnO_2

The chemicals used in the synthesis of mesoporous SnO_2 were $Na_2SnO_3 \cdot 3H_2O$ (British Drug House), *N*-cetyl-*N*,*N*,*N*-trimethylammonium bromide, and an aqueous solution of HCl. A typical preparation procedure of mesoporous SnO_2 is described as follows.

To an aqueous solution of $Na_2SnO_3 \cdot 3H_2O$ (0.34 M, 25 g) was added an aqueous solution of *N*-cetyl-*N*,*N*,*N*-trimethylammonium bromide (0.55 M, 25 g). The combined solution (pH 11.7) was stirred at 298 K for 10 min. An aqueous solution of HCl was then slowly added in drops to the solution under constant stirring. A sticky slurry was obtained when the pH value of the solution mixture was adjusted to about 11.2. Additional HCl solution was added to reach the desired pH values in the range of 1.7–9.0. The resultant slurry was then transferred into a polypropylene bottle (125 cm^3) and sealed. The reaction mixture was then thermally and statically treated at 369 K for 72 h. After the mixture was cooled down, the solid sample was filtered or centrifuged followed with repeated washing by deionized water. The white powder was then dried at 323 K overnight. To remove the surfactants from the as-synthesized samples, calcination was carried out at 723 K for 10 h with a ramping rate of 1 K min^{-1} in air. The samples were denoted SN2–SN7 as listed in Table 1.

For comparison, a sample without surfactant treatment was also prepared by adding HCl aqueous solution to $Na_2SnO_3 \cdot 3H_2O$ to adjust its pH to 7.0. The precipitate was filtered and washed using the same procedure as for the surfactant treated samples. This sample is denoted as SN1.

2.2. Infrared spectroscopy

Infrared spectra of mesoporous SnO_2 samples before and after calcination were recorded on a Shimadzu FTIR 8101M spectrometer at a resolution of 4 cm^{-1}. Samples were mixed and ground with KBr followed by pressing into pellets for IR measurement in the range of 400–4000 cm^{-1}.

Table 1
Synthesis of mesoporous SnO_2 materials with different starting mixture compositions

Label	Initial pH	Sn:CTMABr molar ratio[a]	Thermal treatment temperature (K)	Thermal treatment time (h)
SN1	7.0	1:0	—	—
SN2	9.2	1:0.8	369	70
SN3	11.0	1:1.6	369	72
SN4	9.0	1:1.6	369	72
SN5	7.1	1:1.6	369	72
SN6	4.9	1:1.6	369	72
SN7	1.7	1:1.6	369	72

[a] CTMABr, *N*-cetyl-*N*,*N*,*N*-trimethylammonium bromide.

2.3. Thermal analyses

Thermogravimetry (TGA) and differential thermal analysis (DTA) were performed on a Shimadzu TGA-50 and a Shimadzu DTA-50, respectively. The experiments were carried out in an air flow (60 ml min^{-1}) with a temperature rising rate of 20 K min^{-1} from 298 K up to 1173 K.

2.4. N_2 adsorption

An adsorption study of the calcined SnO_2 was performed on a Quantachrome NOVA 1000 analyzer using N_2 at liquid nitrogen temperature as an adsorbate. Samples (0.02–0.1 g) were treated in flowing N_2 at 573 K for 1 h prior to the adsorption measurement. Adsorption and desorption isotherms were obtained continuously in the partial pressure range 0.05–0.95. The surface area was determined by a multi-point BET method using the adsorption data in the partial pressure range 0.05–0.25. The desorption isotherm was used to determine the pore size distribution using the BJH method.

2.5. Fabrication of sensor elements and measurements of H_2 sensing properties

As-synthesized SnO_2 powders were pressed into 13-mm-diameter pellets and calcined at 723 K for 10 h in order to simultaneously remove the surfactants from the mesopores and sinter the samples. Subsequently, two Pt wire (0.2 mm diameter) electrodes were formed on both sides of each pellet by applying silver paste onto them and followed with curing at 423 K for 1 h. The sensing elements were then mounted into a specially designed quartz cell. Hydrogen concentration was controlled by adjusting the flow rate ratio of H_2 (5% volume in N_2) and air. The sample was first heated at the rate of 5 K min^{-1} from 298 K to 723 K and then cooled down to the desired temperatures for gas sensing measurement. The changes of resistance of the samples were recorded on a Keithley 6517 electrometer by applying a constant voltage (2 V) across the sensor elements. Data were collected and processed on a personal computer connected to the electrometer. The sensitivity of a sensor is expressed as the ratio of the resistance in air to that in reducing gases ($S = R_{air}/R_{gas}$).

3. Results and discussion

3.1. FTIR spectroscopy

Fig. 1 shows the FTIR spectra of SN5 before and after calcination. Before calcination (Fig. 1a), IR bands of surfactants are obviously seen. The bands at 2920 and 2850 cm^{-1} are due to the asymmetric and symmetric C–H stretching vibrations [16] of the hydrocarbon chains of the surfactant (CTMA) incorporated in the sample, while the sharp bands in the range of 1450–1500 cm^{-1} are attributed to the deformation of $-CH_2-$ and $-CH_3$ [16] of the incorporated surfactants. Other surfactant treated samples also gave similar results. The results are in good agreement with

those reported by Hudson et al. [5] on mesoporous ZrO_2. The existence of these bands shows direct evidence of the incorporation of surfactant cation (CTMA) in the mesopores of the as-synthesized samples. After calcination in air at 723 K for 10 h, all these bands due to CTMA disappeared, indicating the complete removal of the surfactant from the mesopores of SnO_2. The broad band between 3200–3600 cm^{-1} and the band centered at 1640 cm^{-1} observed on both as-synthesized and calcined samples are assigned to O–H stretching and deformation vibrations of weak-bound water. The bands between 400–800 cm^{-1} are attributed to the framework vibrations of tin oxide [7].

3.2. Thermal analysis

In the syntheses of mesoporous materials using surfactants as templates, TGA and DTA are widely used to characterize the procedure of surfactant removal. Fig. 2 shows the TGA and DTA results of SN5 in air. The weight loss of water at the lower temperature range (<450 K) was about 4.5%. When the treatment temperature reached about 450 K, the weight loss due to the removal of surfactant began. The surfactants were almost completely removed at about 723 K, which is in accordance with the IR data shown in Fig. 1. The DTA curve of SN5 has two sharp exothermic peaks centered at 600 and 680 K and a shoulder exothermic peak below 700 K, all of which correspond to the three steps in weight loss between 450–723 K shown in the TGA curve. Surfactant-

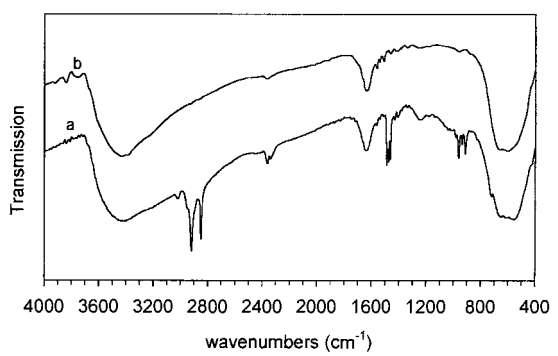

Fig. 1. FTIR spectra of SN5 (a) before and (b) after calcination.

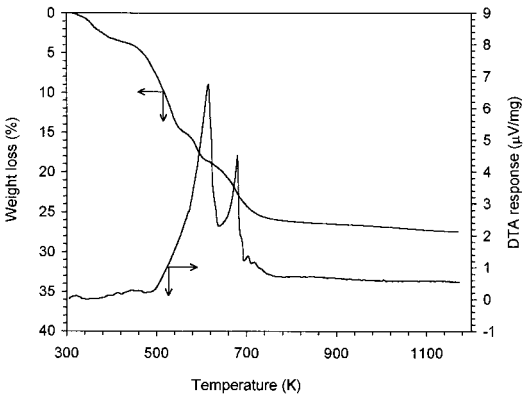

Fig. 2. TGA and DTA profiles of SN5 in flowing air with a heating rate of 20 K min^{-1}.

containing mesoporous ZrO_2 gave similar results [4,5]. Similar TGA and DTA patterns were observed for SN2, SN3, SN4, and SN6 samples. Only one step in weight loss of 5% due to surfactant removal was observed for SN7, reflecting the smaller amount of surfactant incorporated in the sample. For sample SN1, which was prepared by the conventional precipitating method, only one step in weight loss due to water and a corresponding endothermic peak were observed below 500 K.

From the weight loss of water and surfactant (23 wt.% in total), the composition of the as-synthesized SN5 is calculated as $SnO_2 \cdot 0.17CTMA \cdot 0.58H_2O$. Compared to the initial ratio of Sn to surfactant (1:1.6) in the starting slurry as listed in Table 1, only a small part of the surfactant is incorporated in the mesopores of hydrous tin oxide. The surfactant amount incorporated in the as-synthesized SN5 ($CTMA/SnO_2 = 0.17$) is similar to that incorporated in the as-synthesized Si–Al–MCM-41 [1] ($CTMA/(SiO_2 + Al_2O_3) = 0.2$) and in mesoporous ZrO_2 [5] ($CTMA/ZrO_2 = 0.14$), implying strongly that there is an analogy of mesoporous structures between these as-synthesized materials prepared from a similar surfactant synthesis strategy.

3.3. N_2 adsorption

To get information about the surface areas and porosities of the calcined samples, an adsorption

study was performed at 77 K using N_2 as the adsorbate. As shown by FTIR and TGA data that the surfactants were completely removed from the mesopores of SnO_2 at 723 K, all samples were calcined at 723 K for 10 h before adsorption. Adsorption and desorption isotherms of SN1 and SN5 are shown in Fig. 3. Both samples have type IV isotherms which are typical for mesoporous materials [17]. The adsorption at low P/P^0 for SN5 is due to the monolayer adsorption of N_2 on the wall of mesopores and on the external surfaces of SnO_2 particles, while the sharp increase started at $P/P^0 = 0.5$ is due to the filling of the mesopores. After the pores were filled, no more adsorption was further observed, indicating saturation of N_2 adsorption in this narrow range of partial pressures and the uniformity of the pores. The adsorption amount of N_2 on SN1 is much smaller than that on SN5, indicating that SN1 has a much lower surface area than SN5. The surface areas calculated by the multi-point BET method and the pore volumes of the different samples are listed in Table 2. The highest surface area of 156.8 $m^2\ g^{-1}$ is derived from sample SN5. As the surface area of SnO_2 decreased sharply between 573 and 773 K, less than 30% of the initial surface area was maintained for SnO_2 calcined at 723 K [6,13]. To our knowledge, the SnO_2 surface area of 156.8 $m^2\ g^{-1}$, as shown by SN5, is the largest ever reported for SnO_2 calcined at 723 K.

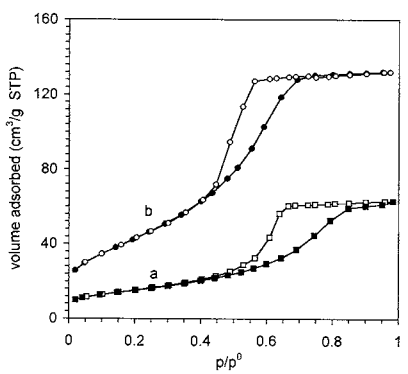

Fig. 3. N_2 adsorption and desorption isotherms of (a) SN1 and (b) SN5 (filled mark, adsorption; empty mark, desorption) calcined at 723 K for 10 h.

Table 2
BET surface areas and total pore volumes of SnO_2 samples calcined at 723 K

Samples	BET surface area ($m^2\ g^{-1}$)	Total pore volume ($cm^3\ g^{-1}$)
SN1	54.0	0.10
SN2	95.3	0.16
SN3	72.6	0.12
SN4	111.4	0.19
SN5	156.8	0.21
SN6	109.2	0.23
SN7	86.8	0.12

Desorption isotherms were used to calculate the pore size distributions using the [BJH] method developed by Barrett et al. [18]. Fig. 4 plots the BJH pore size distributions of SN1 and SN5 for pores smaller than 200 Å in diameter. The narrow pore diameter distribution centred at about 40 Å and the higher pore volume of SN5 compared with those of SN1 suggest the uniformity of the mesoporous structures of SnO_2. For surfactant-treated samples having lower surface areas, larger mesopores were observed. The existence of the uniform mesopores for calcined samples implies that at least part of the mesoporous structures of the as-synthesized samples were still maintained when the surfactants were thermally removed. Similar results were also reported for ZrO_2–surfactant systems [5]. It was reported that the destruction of the mesoporous structure happened during the removal of the surfactant from the

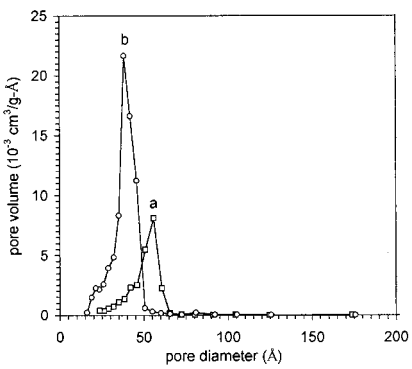

Fig. 4. BJH pore size distributions of (a) SN1 and (b) SN5 calcined at 723 K for 10 h.

mesoporous materials containing no Si and Al [2,3].

The data shown in Tables 1 and 2 show that the acidity of the starting synthesis mixtures substantially affect the surface areas of the final products. An optimal pH value exists for preparing samples with high surface areas. The highest surface area was obtained for sample SN5 synthesized with a starting pH of about 7.

For the synthesis of Si-MCM41, it is suggested that anionic SiO^- groups are needed for charge compensation of the quaternary ammonium cations [19]. In this study, SnO_3^{2-} or $HSnO_3^-$ may be the counter anions of $CTMA^+$ to form hydrous SnO_2 layers around the surfactant micelles [1]. The precipitate of hydrous SnO_2 formed by increasing acidity of Na_2SnO_3 solution equilibrates with the dissolved ions of SnO_3^{2-} and $HSnO_3^-$. Under proper conditions where surfactants form micelles, SnO_3^{2-} and $HSnO_3^-$ in the solution will be located around the surfactants by chemically connecting with the subsequent formation of SnO_3^{2-} and $HSnO_3^-$ from the dissolution of hydrous SnO_2. If the pH is too low, the equilibrium concentrations of SnO_3^{2-} and $HSnO_3^-$ will be low, resulting in the formation of minute SnO_2 around surfactant micelles. This is supported by the TGA data for SN7, where only 5% of the surfactant was found to exist on the sample. At high pH values, a small amount of hydrous SnO_2 will be formed and it is difficult to get stable layers of these hydrous SnO_2 around surfactant micelles. Thus an optimal pH value exists for the synthesis.

3.4. Gas-sensing characteristics

Gas sensing properties of semiconductor oxides are generally concerned with the changes of electrical properties due to the concentration changes of the surface bound oxygen species. To study the effects of surface areas on the sensitivities of SnO_2, H_2 was used as a probing gas to compare sensitivity changes on samples with different surface areas at 573 K. Fig. 5 shows the changes of resistance of SN5 pellet at 573 K in dry air and in 500 ppm H_2, which was a typical sensing condition for all the samples in this study. After the resistance of the sample became stable, 500 ppm of H_2 was introduced into the sensor cell by mixing a H_2–N_2 flow with air. When the sample was contacted with H_2, its resistance decreased quickly from R_{air} and stabilized to R_{gas} in several minutes. About 90% of resistance change ($R_{air} - R_{gas}$) was achieved within the first 1.5 min of response time. When the H_2 was switched off, the resistance returning from R_{gas} to R_{air} was much slower. Generally more than 10 min were needed to reach R_{air} for most samples.

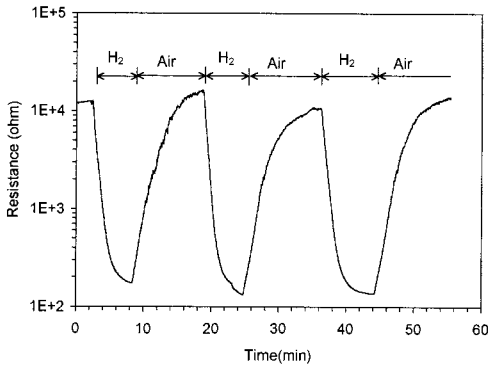

Fig. 5. Response transients of a SN5 sensor to switching on and off of 500 ppm H_2 in air at 573 K.

Fig. 6 shows the relationship between the sensitivity in 500 ppm H_2 at 573 K versus the surface areas of the SnO_2 sensors. It is very interesting to notice that higher sensitivities were observed with

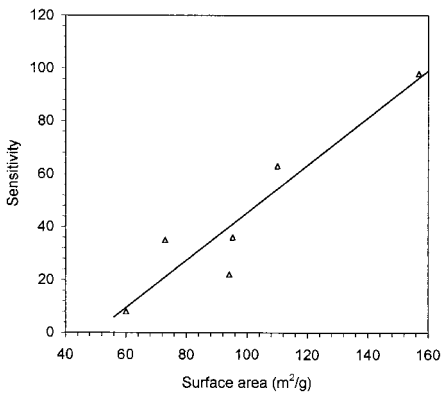

Fig. 6. Relationship between the surface areas of SnO_2 sensors and their sensitivities to 500 ppm H_2 in air at 573 K.

sensors having higher surface areas. The linear relationship shows clearly the linear dependence of the sensitivity on the surface area of the sensor. This phenomena is not surprising as it is well known that surface oxygen anions, such as O^- or O^{2-} adsorbed on n-type semiconductor oxide surfaces, act as surface acceptors, accepting electrons and diminishing the surface conductivity [10,20]. Reductant gas sensitivity of n-type semiconductor oxides, such as SnO_2, arises from the increase of conductivity due to the surface reaction between reducing gases with the surface oxygen anions. A higher surface area of SnO_2 means more surface adsorption sites or surface oxygen anions are available to react with the reducing gases. Consequently, SnO_2 having the higher surface areas are more sensitive to the surrounding gas atmosphere.

Yamazoe and colleagues [21,22] studied the effects of grain size on the gas sensitivity of SnO_2 and they concluded that sensitivity increases strongly as grain size decreases for both CO and H_2. Their results are in agreement with ours as smaller grain sizes provide higher surface areas. The surface area effects on gas sensing properties for SnO_2 modified by sulfuric acid were also studied by Keshavaraja et al. [23], however, maximum sensitivity to reducing gases (such as CO, NH_3 and alcohol) was not observed for the sensor with the highest surface area as the increasing content of sulfuric acid substantially affected the sensing properties.

The correlation of sensitivity with the concentration of H_2 on sensors with different surface areas is shown in Fig. 7. A nice linear relationship between sensitivity and H_2 concentration was observed on all sensors at H_2 concentration lower than 1500 ppm, reflecting the systematic changes of SnO_2 conductivity with reducing gas concentration. The slope of the linear relationship gets steeper as the surface area of the sensors gets larger. The results suggest that the mesoporous high-surface-area SnO_2 synthesized in this study may be a good sensor model to detect very low concentrations of reducing gases.

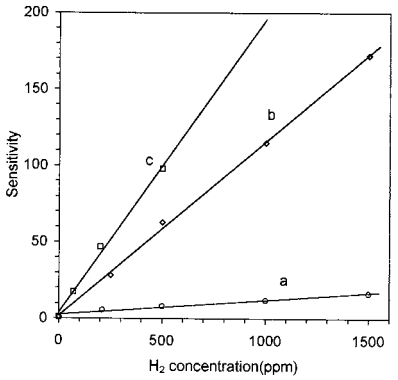

Fig. 7. Relationship between the sensitivity of (a) SN1, (b) SN6, and (c) SN5 sensors and H_2 concentration at 573 K.

4. Conclusions

Mesoporous SnO_2 with high surface areas were synthesized using *N*-cetyl-*N*,*N*,*N*-trimethylammonium cations as a synthetic template and by controlling the acidities of the starting reaction mixtures and the thermal treatment conditions. FTIR and thermal analysis data gave direct evidence for the incorporation of surfactant cations in the mesopores of the as-synthesized samples. Calcination in air at 723 K completely removed the incorporated surfactant from the mesopores of SnO_2. Acidity of the synthesis mixture is an important controlling factor for the optimal synthesis of high surface area SnO_2. The highest surface area of 156.8 $m^2\ g^{-1}$ was derived from a sample prepared under a pH of 7.1. Using H_2 as a probing gas, higher sensitivities were found on samples having higher surface areas. A linear relationship between H_2 concentration and sensitivity was also observed for all the sensors. These results imply that there are potential applications for these high surface area SnO_2 as highly sensitive sensors for the measurement of reducing gases at very low concentrations.

Acknowledgements

The present study was supported by the National University of Singapore (RP 950669) and the Process Analysis and Optimization (PAO) Enterprise.

References

[1] J.S. Beck, J.C. 1263Vartuli, W.J. Roth, et al., J. Am. Chem. Soc. 114 (1992) 10834.
[2] U. Ciesla, D. Demuth, R. Leon et al., J. Chem. Soc., Chem. Commun. (1994) 1387.
[3] N. Ulagappan, C.N.R. Rao, J. Chem. Soc., Chem. Commun. (1996) 1685.
[4] J.S. Reddy, A. Sayari, Catal. Lett. 38 (1996) 219.
[5] M.J. Hudson, J.A. Knowles, J. Mater. Chem. 6 (1996) 89.
[6] M.J. Fuller, M.E. Warwick, J. Catal. 29 (1973) 441.
[7] F. Sala, F. Trifiro, J. Catal. 34 (1974) 68.
[8] G.J. Li, T. Li, Y.D. Xu, J. Chem. Soc., Chem. Commun. (1996) 497.
[9] T. Seiyama, A. Kato, K. Fujishi, M. Nagatani, Anal. Chem. 34 (1962) 1502.
[10] T. Seiyama, in: T. Seiyama (Ed.), Chemical Sensors—Current State and Future Outlook in Chemical Sensor Technology, vol. 1, Kodansha, Tokyo, 1988, pp. 1–38.
[11] J.C. Manifacier, Thin Solid Films 90 (1982) 297.
[12] N. Barsan, R. Ionescu, Sens. Actuators B 19 (1994) 470.
[13] N.L. Wu, L.F. Wu, Y.C. Yang, S.J. Huang, J. Mater. Res. 11 (1996) 813.
[14] E.W. Giesekke, H.S. Gutowsky, P. Kirrov, H.A. Laitinen, Inorg. Chem. 6 (1967) 1294.
[15] R.S. Hiratsuka, S.H. Pulcinelli, C.V. Santilli, J. Non-Cryst. Solids 121 (1990) 76.
[16] L.J. Bellamy, The Infrared Spectra of Complex Molecules, 3rd ed., vol. 1, Chapman Hall, New York, 1975.
[17] S. Lowell, J.E. Shields, Powder Surface Area and Porosity, 2nd ed., Chapman Hall, London, 1984.
[18] E.P. Barrett, L.G. Joyner, P.P. Halenda, J. Am. Chem. Soc. 73 (1951) 373.
[19] C.Y. Chen, S.L. Burkett, H.X. Li, M.E. Davis, Microporous Mater. 2 (1993) 27.
[20] T.G. Nenov, S.P. Yordanov, Ceramic Sensors—Technolory and Applications, Technomic, Lancaster, 1996.
[21] N. Yamazoe, N. Miura, Some basic aspects of semiconductor gas sensors, in: S. Yamauchi (Ed.), Chemical Sensor Technology, vol. 4, Kodansha, Tokyo, 1992, pp. 19–42.
[22] C.N. Xu, J. Tamaki, N. Miura, N. Yamazoe, Sens. Actuators B 3 (1991) 147.
[23] A. Keshavaraja, B.S. Jayashri, A.V. Ramaswamy, K. Vijayamohanan, Sens. Actuators B 23 (1995) 75.

.

ELSEVIER

Talanta 45 (1998) 767–773

Talanta

AFM imaging and characterization of latex particles formed by copolymerization of styrene and poly(ethylene oxide) macromonomer

P.-C. Zhang [a], J. Liu [a], C.H. Chew [a], L.M. Gan [a], S.F.Y. Li [b,*]

[a] *Department of Chemistry, National University of Singapore, 10 Kent Ridge Crescent, Singapore 119260, Singapore*
[b] *Institute of Materials Research and Engineering and Department of Chemistry, National University of Singapore, 10 Kent Ridge Crescent, Singapore 119260, Singapore*

Received 5 February 1997; received in revised form 6 August 1997; accepted 11 August 1997

Abstract

A new type of latex particle was prepared by copolymerization of styrene and poly(ethylene oxide) macromonomer. By controlling the concentration of styrene in reaction mixtures, several latexes with different grain sizes were obtained. The packing patterns of the latex films as well as shapes and sizes of the latex particles were measured with atomic force microscopy (AFM). AFM images revealed that the grain sizes of the latexes increase with increasing concentration of styrene. At a higher styrene concentration (10 wt%), the latex showed a rather homogenous distribution of grain sizes. Lateral force microscopy (LFM) was used to reveal frictional features of latex particles. Contact and non-contact mode AFM were employed to image the same sample of the latex films. The results show that AFM working in non-contact mode can be used to effectively eliminate the horizontal-line-like artifacts, which may obscure AFM images. © 1998 Elsevier Science B.V.

Keywords: ATM imaging; Latex particles; Copolymerization; Styrene; Poly(ethylene oxide)

1. Introduction

Since the publications on macromonomers by ICI group [1] and Milkovich [2–4], numerous studies have been done on the preparation of well-defined graft copolymers. A number of poly(ethylene oxide) (PEO) macromonomers have also been synthesized and copolymerized with conventional monomers [5–10].

One of the most interesting features of PEO macromonomers is their amphiphilic nature. Moreover, the macromonomer can readily be modified to consist of a polymerizable end group, such as methacrylate (MA) or *p*-vinylbenzyl ether (VB). The general representations for these modified macromonomers are R-PEO-MA-n and R-PEO-VB-n respectively. These macromonomers have been successfully homopolymerized [11,12] and dispersionally copolymerized [13,14] in dispersion systems by Ito and coworkers. Owing to the existence of hydrophillic PEO and hydropho-

* Corresponding author. Tel.: +65 772 2681; fax: +65 779 1691.

PII S0039-9140(97)00264-6

bic R and polymerizable end groups, MA or VB, the PEO macromonomers can undergo unusually rapid homopolymerization in water due to their organization into micelles. A new type of amphiphilic PEO macromonomer (PEO-R-MA-n) with a polymerizable group attached to a rather long hydrophobic segment ($R = C_{11}$) has been reported recently [15]. The rate of its polymerization in water (within 30 min) was extremely rapid as compared with its solution polymerization in benzene (days).

The invention of scanning tunneling microscope (STM) [16] has led to a revolution in surface science, due to the extremely high resolution of this microscope. Based on STM, several scanning probe microscopes (SPMs) have been developed in the past few years, such as the atomic force microscope (AFM), [17] lateral force microscope (LFM) [18], magnetic force microscope (MFM) [19] and photon scanning tunneling microscope (PSTM) [20]. Amongst these microscopes, AFM has attracted most attention for studying polymeric materials because it can image both conducting and non-conducting samples. AFM has several advantages: (1) ability to image samples under different environmental conditions, i.e. vacuum, air and solution, with high resolution, (2) direct imaging of sample surface structures without staining or shadowing, and (3) providing local structural information in real space. SPM studies on morphologies of several bulk [21] and thin-film [22–25] polymer surfaces have been reported in recent years. In addition, AFM has been used to study effects of aging and annealing of polystyrene latex film [26] and effect of surfactant postadded to latex dispersion on film formation [27,28]. In this work, the shapes, sizes and packing patterns of the latex particles prepared by copolymerization of PEO-R-MA-n and styrene at different styrene concentrations are characterized directly by AFM.

2. Experimental section

2.1. Apparatus

The AFM experiments were performed on a TMX Explorer SPM (TopoMetrix, Santa Clara, CA). Constant force images were recorded in the repulsive mode under ambient conditions. Si_3N_4 cantilevers with V-shape tips were used for measurement in the contact mode. The cantilevers used were supplied by the microscope manufacturer, and had a nominal force constant of 0.032 Nm^{-1}. The force applied with the AFM tip was ≤ 10 nN. From time to time checks were performed to ensure that the set point was stable, and still at the same location of the force curve to ensure that the applied force was kept as low as possible. In order to reduce the normal and shear forces applied to the specimen by the tip, non-contact mode was used particularly for the imaging of small size latex particles. These measurements were performed in air using single-member cantilevers of nominal force constant 0.4–1.5 Nm^{-1}. In this mode, the cantilever was oscillated in a vertical direction near its resonant frequency. The lateral dragging effect in the non-contact mode was much reduced. No filtering was applied to the feedback signal or the images unless stated otherwise. All structures shown in the AFM images were independent of scanning frequency, scanning direction, and x-y range.

2.2. Materials

Styrene was distilled under vacuum before use. Potassium persulfate (KPS) from Fluka (Fuch, Switzerland) was recrystallized from pure water.

Table 1
Emulsion copolymerization of styrene (M_1) and PEO-R-MA-40 (M_2)[a]

Latex sample	M_2	$[M_1/M_2]$ (mol/mol)	St (M_1) (wt%)
SM1	PEO-R-MA-40	198.81	15.3
SM2	PEO-R-MA-40	140.03	10.78
SM3	PEO-R-MA-40	75.19	5.79

[a] Total weight of emulsion: 50 g, PEO-R-MA-40: 1.5 wt%, KSP: 0.5 mM, temperature: 60°C, conversion: nearly 100%.

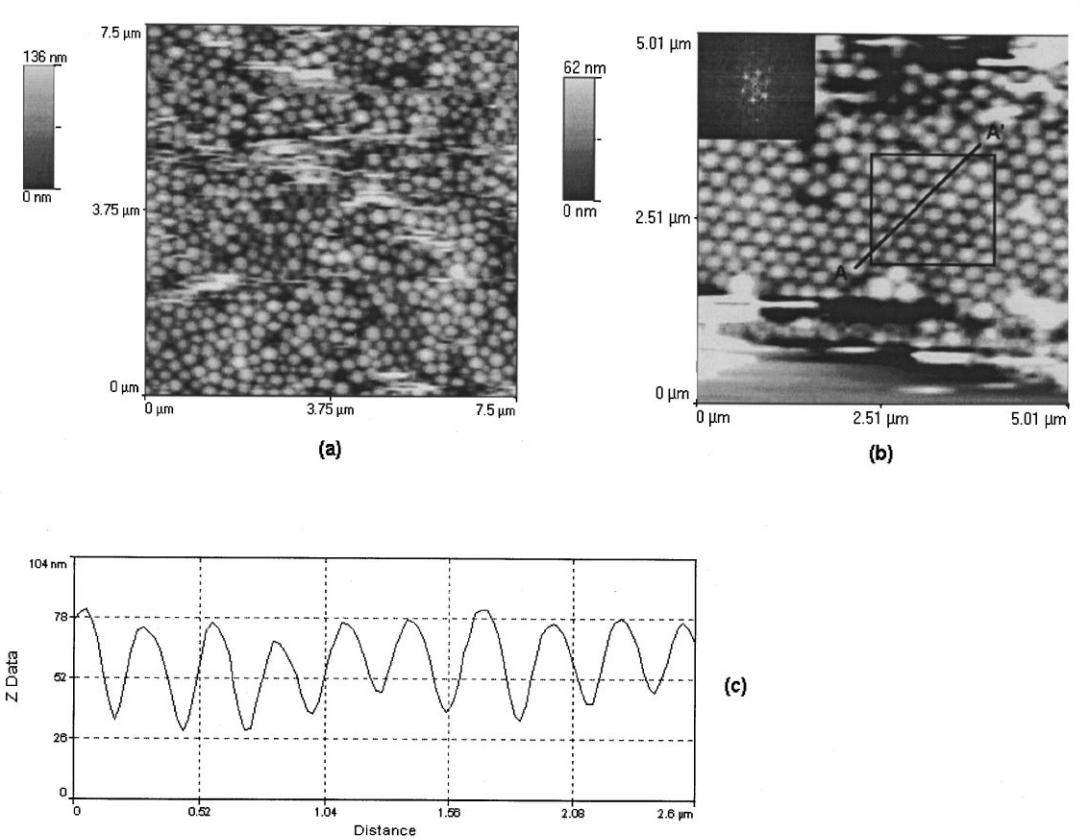

Fig. 1. AFM images of SM1 latex particles. (a) Disordered close packed regions; (b) hexagonal close packed region; (c) cross-sectional profile along AA′ direction in (b). The AFM images were obtained in contact mode.

Water was purified by distillation. PEO-R-MA-n ($n = 40$) was prepared and characterized as described elsewhere [15]. The copolymerization of PEO-R-MA-40 with styrene (ST) was carried out by using KPS as the initiator under nitrogen atmosphere. The copolymerization was undertaken at 60°C with magnetic stirring around 700 rpm for 8 h. Several latexes (SM1, SM2, SM3) were prepared with the composition shown in Table 1. Two drops of the obtained products were diluted to 2 ml with water, then a drop of the diluted solution was placed on the freshly cleaved mica plate which was allowed to air-dry at room temperature for more than 4 h. Subsequently, the formed films were imaged with AFM under ambient conditions.

3. Results and discussion

AFM imaging of the various latex films reveals abundant information such as packing patterns, packing defects and grain diameter. All images are displayed in the gray scale, such that dark regions correspond to areas of lower height than light regions.

A packing layer of SM1 latex particles formed after air-drying is shown in Fig. 1a. Most of the area exhibits disordered arrangements, but some regions indicate regular one-dimensional linear ordered arrangement composed of several, to ten or more particles. Rather spherical latex particles are shown in Fig. 1b and they are arranged in a hexagonally packed structure. The Fourier trans-

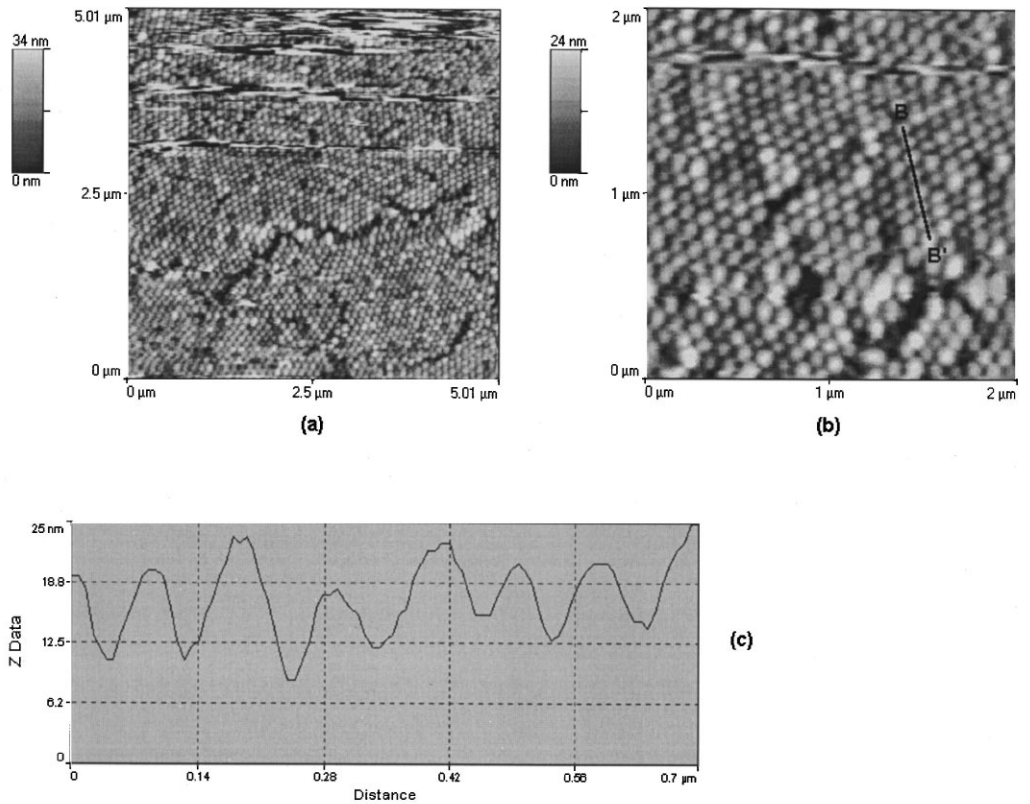

Fig. 2. AFM images of SM2 latex particles. (a) 5 μm × 5 μm; (b) 2 μm × 2 μm; (c) cross-sectional profile along BB′ direction in (b). The AFM images were obtained in contact mode.

formation of the selected rectangular region gives a pattern as shown at the top-left corner of the figure, which provides further evidence for the hexagonal structure. A few hole-like packing defects are also seen (Fig. 1a). However, some light horizontal lines that partially obscure much of this scan always appear in the AFM images. They were due to a characteristic imaging artifact similar to the previous observation of polystyrene latex film without annealing treatment [26]. It seems probable that a few smaller molecules (unpolymerized monomer or surfactant molecules) are adsorbed on the surface of some of the latex particles. They may be removed by the tip owing to the strong interactions between tip and sample which cause surface damage of the latex particles so that the light horizontal lines are formed.

The diameters of the latex particles were measured by the cross-sectional profile along the AA′ direction as shown in Fig. 1c. This profile shows the peak-to-peak distance is in the range of 270–280 nm. The narrow size distributions of these latex particles indicate that copolymerization of PEO-R-MA-40 with styrene forms uniform latex particles. Similarly, the height change of peak-to-trough was also measured by the cross-sectional profile. Since the irregular corrugation might perturb the determination of the height, it was avoided by taking the cross-section along the direction of several particles that had approximately the same alignment.

A large area of the close-packed layer of sample SM2 can be seen from Fig. 2a. Some areas exhibit regular one-dimensional arrangement. The surface of the packing multilayer is smooth, though some

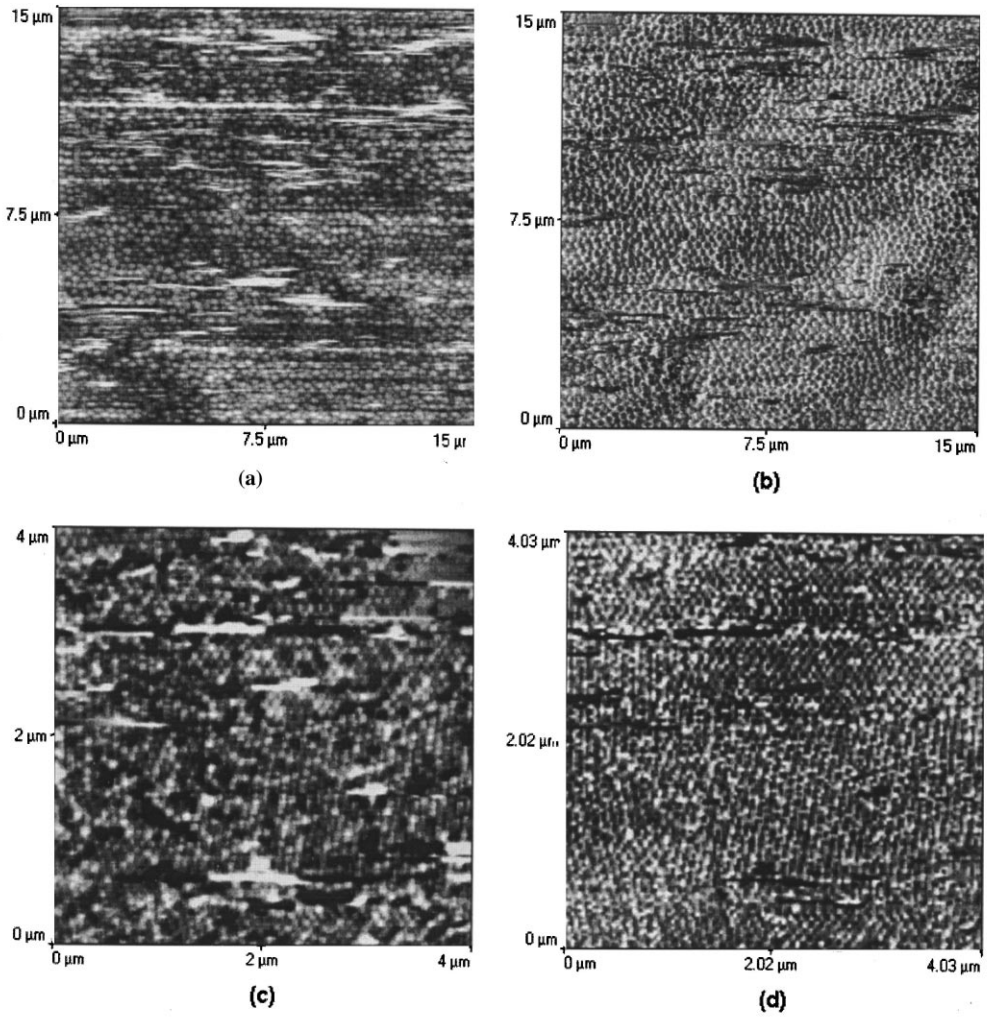

Fig. 3. AFM and LFM images of latex particles. (a) and (b) are AFM and LFM images of SM1 latex particles, respectively. (c) and (d) are AFM and LFM images of SM2 latex particles.

cracks or hole-like defects are also observed. A higher magnification image is shown in Fig. 2b. The grain sizes of these latex particles can be measured by a cross-sectional profile alone BB′ direction, which is shown in Fig. 2c. The peak-to-peak distances are almost the same. A significant peak-to-valley periodic change is visible in Fig. 2c. The profile shows that SM2 particles have relative homogenous distribution of grain sizes ranging from 85 to 100 nm, which are smaller than those of SM1 particles. This is consistent with the fact that sample SM2 consisted of lower amount of styrene than that of sample SM1.

Besides the morphologies of the latex particles, their surface frictional features are also examined. This information may be used to evaluate the homogeneity of surface properties of individual particles in different regions. The packing layers of the latex particles can be measured simultaneously by AFM and LFM. For the SM1 packing layers as shown in Fig. 3a (AFM) and Fig. 3b (LFM), the latex particles in different regions

exhibit different frictional features. The difference might be attributed to the inhomogeneity of surface state of individual particles formed during polymerization. The different extent of dryness of individual particles might be another reason for the difference. The AFM and LFM images of SM2 sample are shown in Fig. 3c and d respectively. The LFM image indicates that the frictional features of the particles in different regions are inhomogenous, similar to the case of SM1 particles.

The horizontal lines in contact mode images were always observed in all latex samples and the quality of the AFM images became progressively worse with a decrease of scan size. Considering the case of SM3 with small grain size, a clear image was seldom captured by contact mode AFM during many attempts at scanning. Individual particles are very difficult to distinguish in the contact mode, owing to the existence of the horizontal lines. These lines may be caused by a little amount of unpolymerized monomers on the surface of latex particles or some salts of small molecules deposited on the surface of latex particles. When a relatively small region is scanned, strong interactions between tip and sample surface cause surface damage of latex particles and contamination of the tip, resulting in formation of some horizontal lines and reduction of resolution. In fact, these artifacts like horizontal lines have been observed in other latex particles systems [26].

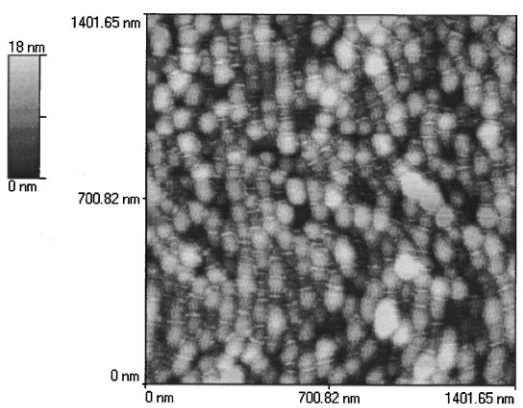

Fig. 4. AFM image of SM3 latex particles. The AFM images were obtained in non-contact mode.

When the same sample was imaged in non-contact mode, these artifacts could be eliminated effectively as shown in Fig. 4. These particles are seen to be in the form of close-packed structures and only a few hole-like packing defects are detected. These particles exhibit globular or ellipsoidal shape. The grain sizes of most of the particles are in the range of 60–80 nm. Zooming into higher magnification for all samples, a clear image without any artifacts could be obtained. This shows that AFM working in non-contact mode is more suitable for the measurement of latex particles than in contact mode.

4. Conclusions

A new type of latex particles with nanoscale size can be prepared by copolymerization of styrene and PEO-R-MA-40. The sizes of the particles can be well controlled by adjusting appropriate molar ratio of styrene and PEO-R-MA-40 as shown in Table 1. The latex particles prepared under different conditions can be imaged directly by AFM without staining and shadowing. Topographical AFM images reveal the shapes and sizes of the particles and their relationships to preparation conditions. LFM images may be used to reveal surface properties of individual particles, which is difficult to measure by other techniques. Non-contact AFM is potentially a powerful tool for characterizing small-size latex particles, capable of providing nanometer scale resolution without causing damage to the surface of the particles.

Acknowledgements

This work was supported by the National University of Singapore.

References

[1] J. Walbridge, in: K.E.J. Barret (Ed.), Dispersion Polymerization in Organic Media, Wiley, London, 1975, Chapter 3.
[2] R. Milkovich, M.T. Chiang, USP 3,786, 1974, 116.

[3] G.O. Schultz, R. Milkovich, J. Appl. Polym. Sci. 27 (1982) 4773.
[4] G.O. Schultz, R. Milkovich, J. Polym. Sci., Polym. Chem. Ed. 22 (1984) 1633.
[5] S. Kobayashi, T. Mizutani, M. Kaku, Saegusa, T. Polym. Bull. 8 (1993) 169.
[6] T. Suzuki, T. Tomono, J. Polym. Sci., Polym. Chem., Ed. 22 (1993) 2829.
[7] D.W. Xia, J. Smid, J. Polym. Sci., Polym. Lett., Ed. 22 (1984) 617.
[8] I. Nwankwo, D.W. Xia, J. Smid, J. Polym. Sci., Part B: Polym Phys. 26 (1988) 581.
[9] Y. Tsukahara, K. Ito, H.-C. Tasi, Y. Yamashita, J. Polym. Sci., Part A: Polym. Chem., Ed. 27 (1989) 1099.
[10] K. Ito, in: M.K. Mishra (Ed.) Macromolecular Design, Frontier, New York, 1994, Chapter 4,
[11] K. Ito, K. Tanaka, H. Tanaka, G. Imai, S. Kawaguchi, S. Itsuno, Macromolecules 24 (1991) 2348.
[12] K. Ito, K. Hashimura, S. Itsuno, E. Yamada, Macromolecules 24 (1991) 3977.
[13] K. Ito, S. Yokoyama, F. Arakawa, Polym. Bull. 16 (1986) 345.
[14] S. Kawaguchi, M.A. Winrick, K. Ito, Macromolecules 28 (1995) 1159.
[15] J. Liu, C.H. Chew, L.M. Gan, J. Macromol. Sci., A-Pure Appl. Chem. A33 (3) (1996) 337.
[16] G. Binnig, H. Rohrer, Helv. Phys. Acta. 55 (1982) 726.
[17] G. Binnig, C.F. Quate, C. Gerber, Phys. Rev. Lett. 56 (1986) 930.
[18] L.A. Wenzler, T. Han, R.S. Bryner, T.P. Beebe, Rev. Sci. Instrum. 65 (1994) 85.
[19] A. Kikukawa, S. Hosaka, Y. Honda, S. Tanaka, Appl. Phys. Lett. 61 (1992) 2607.
[20] T.L. Ferrell, S.L. Sharp, R.J. Warmack, Ultramicroscopy 42 (1992) 408.
[21] T. Kajiyama, I. Ohki, K. Tanaka, S.-R. Ge, A. Takahara, Proc. Jpn. Acad. 71 (1995) 75.
[22] V.V. Tsukruk, M.D. Foster, D.H. Reneker, A. Schmidt, H. Wu, W. Knoll, Macromolecules 27 (1994) 1274.
[23] V.V. Tsukruk, M.D. Foster, D.H. Reneker, A. Schmidt, W. Knoll, Langmuir 9 (1993) 3538.
[24] T. Hayashi, H. Yamamura, T. Nishi, M. Kakimoto, Polymer 33 (1992) 3751.
[25] Yu. Moiseev, V. Panov, S. Savinov, I. Yaminsky, P. Todua, D. Znamensky, Ultramicroscopy 42–44 (1992) 304.
[26] A. Goudy, M.L. Gee, S. Biggs, S. Underwood, Langmuir 11 (1995) 4454.
[27] D. Juhue, J. Lang, Collids Surfaces A: Physicochem. Eng. Aspects 87 (1994) 177.
[28] D. Juhue, J. Lang, Langmuir 9 (1993) 792.

ELSEVIER

Talanta 45 (1998) 777–786

Talanta

Gas chromatography study of the adsorption of refrigerating fluids on microporous solid adsorbents

A. Adell *, J. Petrissans

Laboratoire de Chimie Physique, Université Montpellier II, Montpellier, France

Received 22 May 1996; received in revised form 12 February 1997; accepted 13 February 1997

Abstract

Adsorption isotherms for microporous solids have been determined by elution gas chromatography. Adsorbents are of 'molecular sieves' type; their utilization in affinity thermal machines is envisaged. These machines work in a relatively high domain of pressure for the adsorbate, so the chromatographic technique is generally inadequate for their study. The possibility of increasing the maximal pressures reached by chromatography has been investigated in relation with: the carrier gas flow rate, the length and width of columns, the injected adsorbate mass. This study has been made for different solid adsorbents (zeolite 4A and 13X, silica gel), in different shapes (small stick, pellet, powder), and with different adsorbates (water, methanol, ethanol). In the most favorable conditions that have been derived, the qualities of the chromatographic method, rapidity, simplicity and large range of measures, appear well fitted to the search of this kind of isotherms which does not require a great accuracy. © 1998 Published by Elsevier Science B.V.

Keywords: Elution peak profile; Gas chromatography; Solid adsorption thermal machines

1. Introduction

Gas chromatography has been used for studying different solid-gas couples which have been thought to set in working chemical affinity thermal machines. These machines—heat pumps, refrigerators, energy storing devices—can work with low temperature heat sources such as: waste energy of industrial processes, solar or geothermal energies, etc. They are the subject of investigations in the saving of energy programs [1]. They may be a substitute solution for compression machines which work with C.F.C. fluids prejudicial to the atmospheric ozone. The utilization of adsorbents in chemical affinity thermal machines enables the deletion of the mechanical compressor. Two working periods occur in these machines: a period of desorption of the adsorbate from the adsorbent at high temperature and high vapour pressure, and a period of readsorption with a low temperature and a low pressure. According to the use which is made (refrigerating machine, heat pump or energy storage apparatus), the values of temperature and pressure can reach different levels.

* Corresponding author.

PII S0039-9140(97)00060-X

For optimizing or sizing the machine, it is necessary to evaluate previously its theoretical performances. For that, it is necessary to ascertain a certain number of physico-chemical parameters such as, isosteres, heat and entropy of adsorption. These parameters can be deduced from adsorption isotherm curves. These isotherms must be obtained in physical conditions that must be the most similar to those envisaged for the working of the machine. These isotherms have been obtained using the 'elution peak profile' chromatographic method. The analysis of the chromatographic signal has allowed us to deduce the isotherms using a graphic procedure first presented by Glueckauff [2]. This method has been developing for nearly 20 years [3].

The range of maximal temperatures attainable to commercial chromatographs is sufficient for simulating the conditions of desorption in the different cases of utilization of the machine, when this machine is driven with energy sources like solar energy. These temperatures rise by between 80 and 150°C. The minimal temperatures corresponding to adsorption (between 30 and 50°C) also are attainable to chromatographs. However, the chromatographic experiments carried at these minimal temperatures, have posed some practical problems due to the fact that the duration of the signal, which gets longer when the temperature decreases, can become excessive. It has then become necessary to adjust the value of the flow rate of the carrier gas according to the length of the column.

For the vapour pressures of the adsorbate, the experimental limitations occur at the level of the lowest pressures obtained for low temperatures and also at the level of the highest pressures for high temperatures. For the low temperatures, the adsorbed vapour comes from a cold source: either an evaporator when the system works as refrigerator, or a cold ambient source when the working is as heat pump or storage apparatus. This vapour is found at a relatively weak pressure. For example, for water used as refrigerating fluid, this pressure can vary from 0.2 Torr for freezing, to 20 Torr for heat pumps used for housing. This range of pressure is easily reached by the chromatographic method. A limitation can appear for low pressures at the level of the inflexion point which appears in the isotherms of microporous solid adsorbents. For such solids, the isotherms are generally of the type V of the B.E.T. classification. The change of concavity of the isotherm at the inflexion point (change from type III to type I) causes a topling of the diffuse edge of the chromatographic peak between the left side and the right side. This zone of change of the diffuse edge is difficult to exploit, although the graphical method is yet theoretically applicable. This is more often masked, or little noticeable, with the type of products which we have tested. It occurs for very low pressures, lesser than the threshold of practical usefulness and so it has not been considered when we have drawn our isotherm curves.

For the high temperatures associated with the highest pressures, an important problem has appeared. In this case, the vapour is extracted at a relatively high temperature which corresponds either to the temperature of the condenser (refrigerating), or to the temperature of the premises to be heated (heat pump or storage device); for example this is the case for water vapour, which evolves between a range of pressures from 25 to 120 Torr. These pressures have been difficult to obtain experimentally in standard conditions of use of the chromatograph. Indeed, one of the major inconveniences of the elution method which we have used, in comparison with the method of continuous injection, is that the level of the maximal pressure which is reached by the isotherm is not mastered a priori. When the adsorbate advances in the column, there is a progressive widening of the zone reached by the adsorbate. This widening comes from the fact that the speed of propagation of high concentrations and low concentrations is different. This widening corresponds to a decrease in the maximal concentration, and therefore in the maximal pressure, which is the consequence of the mass conservation law. Thus, the principal objective of experiments has consisted in studying the influence of different factors upon the maximum value reached by the pressures of the adsorbate vapours at the exit of the chromatographic column. These factors are: length and diameters of the column, mass of the injected adsorbate, physical state of solid adsorbents and flow rate of the carrier gas.

A preliminary focus of the method has seemed desirable for highlighting out the distinctive features of our utilization.

2. Focus on the method

2.1. General presentation of the method

There are two principal ways for obtaining chromatograms:

- One method undertakes continuous injections of adsorbate in the carrier gas to create a concentration step at the entry of the column filled with the solid adsorbent (frontal analysis and equilibrium chromatography).
- The other method undertakes discontinuous injections of a given mass of adsorbate (analysis of the diffuse edge of the elution peak).

Also, there exist two ways for deducing the isotherms from chromatograms:

- One method deduces several points which enable one to draw the isotherm from the interpretation of only one chromatogram (elution peak profile and analysis of the front of the step).
- The other method takes into account several chromatograms obtained in the same temperature conditions, while varying either the injected quantity (elution peak maximum), or the height of the concentration step (equilibrium chromatography). One chromatogram enables one, in this case, to draw only one point of the isotherm.

The advantages of the chromatographic method, in comparison with the static methods (thermogravimetry and volumetry), are well known. It is a quick and simple method which does not need to work under vacuum. It is easy to change the products. One can get a large range of measurements for the pressures of the adsorbate vapours and, in particular, it is possible to have access to the range of very weak pressures because of the great sensitivity of the chromatographic detectors.

An important inconvenience of the method is the lack of the reliability of certain obtained isotherms. This reliability is estimated by the comparison of the obtained results with the results given by classical methods. Sometimes it may be necessary to make some reference experiments. This reliability which can be very good in some cases, particularly in equilibrium chromatography, is linked to the validity of certain simplifying hypotheses necessary for the calculus of the isotherm points. These simplifications produce some systematic errors. The validity of these hypotheses depends upon the operating conditions (flow rate and nature of the carrier gas, dimensions of the column, temperatures and pressures level). But also it depends upon the nature and the state of the products (adsorption—desorption cycle without hysteresis, homogeneity of the adsorbent surfaces, no 'swelling' adsorbent, good permeability, good diffusivity in micropores, good thermal transfers). An important effort, theoretical as well as experimental, has been carried out to better specify the general conditions of the validity of the method and the corrections to add to the interpretation of the chromatograms.

Because of the mentioned advantages, it has appeared that the chromatographic method was well fitted to our problem, that is the study of adsorption properties of couples of 'molecular sieves—refrigerating fluids' type. These couples present in the studied domain, an adsorption—desorption cycle almost without hysteresis; this cycle essentially incorporates an adsorption of physical type without swelling of the network. During a thermal cycle of a chemical affinity machine, the pressure of vapours can vary in an important ratio, about 10^3, which strong corresponds to the possibilities of investigation of the method. When it is envisaged to use such couples in affinity machines, it is necessary to determine the mass of adsorbate adsorbed by the adsorbent in function of two parameters, the temperature and the filling ratio of the pores. These two parameters are imposed by the working conditions envisaged for the machine. The chromatographic method, simple and quick, then, enables one to envisage a lot of working situation models by means of a reduced experimental effort.

2.2. Description of the method

The theoretical works of Wilson [4] on chromatography have allowed one to link the form of chromatograms to the adsorption isotherms law (direct problem). De Vault [5], while going deeply into the calculus of Wilson, has evoked the possibility of upsetting the problem by deducing the adsorption isotherms from the chromatographic results (inverse problem). However, it is Glueckauff [2] who has proposed the practical means for reaching this result. An historical account and a bibliography of these preliminary studies are given in Ref. [6].

The Glueckauff method is a graphic method which allows one to draw the adsorption isotherm, point by point, from some parameters directly measured on the chromatogram. Some simplifying hypotheses are necessary: 'hypotheses of ideality' linked to the processus occuring in the column and hypotheses linked to the operating conditions [7]. In particular, one of the hypotheses used in our calculus concerns the shape of the injected feed band at the entry of the column. It has been assumed that this shape is similar to a 'δ' function, that is, its width Δt tends to zero and its height tends to a maximum value which may reach the concentration of saturation c_s in the case of an important injected mass. This hypothesis leads to a constant value for the dead time t_m which becomes independent of c, because all the concentrations between 0 and c_s are present at the same time at the entry of the column, either for

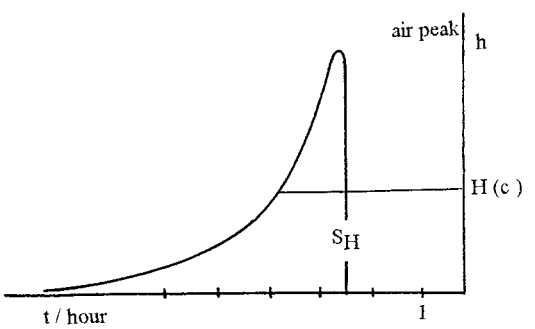

Fig. 1. Chromatogram of silica gel (powder)– water $T = 60$°C, $L = 50$ cm, $\Phi = 3/8$ inch, $\omega = 2.5$ ccs^{-1}, $m = 0.5$ ml.

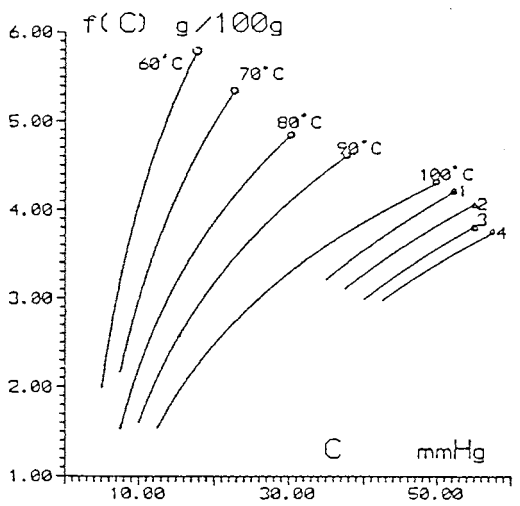

Fig. 2. Isotherms from 60 to 100°C silica gel (powder)—water, $L = 50$ cm, $\Phi = 3/8$ inch, $\omega = 2.5$ cc s^{-1}, $m = 0.500$ ml. 1-Isotherms 100°C deduced from the chromatogram using formulas Eq. (4) and Eq. (5), 2-isotherm 100°C given by the manufacturer of the silica gel. 3-Isotherm 100°C deduced from [14], 4-isotherm 100°C deduced in [13].

increasing or decreasing concentrations. This hypothesis seems quite justified in analysis chromatography where the injected masses are lowest. In the 'elution peak profile' method, the injected mass is necessary more important. In some of our experimentations, the duration Δt of the feed band may exceed 7 min and the feed band's shape is probably very far from the 'δ' shape. However we have conserved the hypothesis of an instantaneous injection (a constant t_m) because the retention time was always greater than 7 h whatever c is (see Fig. 1) and so the variations of t_m were considered to be negligible in comparison of the retention time t_{Rc}(c).

With these hypotheses, the local mass balance and the relations between partial derivatives lead to the differential equation of the direct problem:

$$1/\left[\frac{\partial x}{\partial t}\right]_c = \left(\frac{1-\tau}{\omega}q\right)\left(\frac{da}{dc}\right) + \frac{\tau q}{\omega} \qquad (1)$$

The notations which we have used are those given by Saint-Yriex [8].

t: time starting at the injection instant.

x: distance from the column entry.

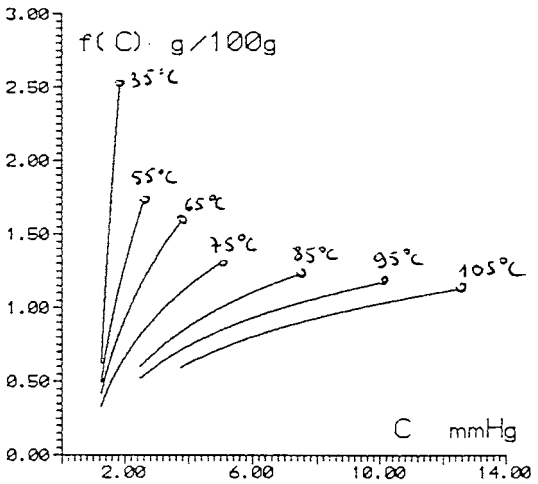

Fig. 3. Isotherms from 35 to 105°C silica gel (grain)—water $L = 1$ m, $\Phi = 3/8$ inch, $\omega = 2.5$ cc s^{-1}, $m = 0.250$ ml.

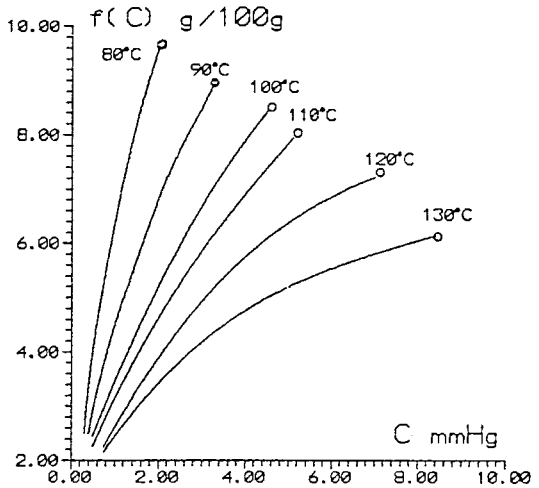

Fig. 5. Isotherms from 80 to 130°C zeolite 13X (pellet)—water, $L = 25$ cm, $\omega = 2.5$ cc s^{-1}, $\Phi = 3/8$ inch, $m = 0.350$ m.

$a(x,t) = a(c)$: mass adsorbed by a volume unity of adsorbent.

$c(x,t)$: adsorbate concentration in the moving phase.

w: flow rate of the moving phase measured at the column temperature.

q: area of the section of the column.

τ: part of the section of the column filled with the moving phase.

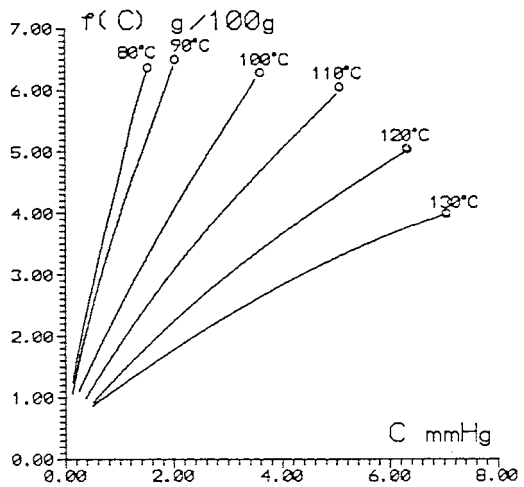

Fig. 4. Iostherms from 80 to 130°C zeolite 4A (pellet)—water, $L = 25$ cm, $\omega = 2.5$ cc s^{-1}, $\Phi = 3/8$ inch, $m = 0.250$ ml.

The term

$$\left(\frac{\partial x}{\partial t}\right)_c$$

of Eq. (1) represents the speed of propagation of the 'front of concentration c' in the column; it is an experimentally attainable quantity because it is linked to the retention time t_{Rc}. We have:

$$\left(\frac{\partial x}{\partial t}\right)_c = \frac{L}{t_{Rc}},$$

where L is the column length. According to the concavity of the isotherm, da/dc may be creasing or decreasing and it is respectively the small or the important concentrations which are the fastest, and so, which will lead to a chromatogram with a diffuse edge ahead or backhead on the recording paper. This feature makes the chromatographic method inadequate for the study of the inverse problem in adsorption phenomenons that present a certain hysteresis.

From the Eq. (1) the integral equation of the inverse problem is deduced, by introducing the dead time of the column:

$$t_m = \frac{\tau q L}{\omega}$$

$$a(c) = \int_0^c \frac{\mathrm{d}a}{\mathrm{d}c}\,\mathrm{d}c = \frac{\omega}{(1-\tau)qL}\int_0^c (t_R - t_m)\,\mathrm{d}c \qquad (2)$$

A point of the isotherm, which gives the adsorbed mass per mass unity of adsorbent $f(c)$, corresponds then, to:

$$f(c) = \frac{a(c)(1-\tau)q}{g} = \frac{\omega R^*}{gu} \int_0^H l_0(h)\,\mathrm{d}h \qquad (3)$$

where R^* is the detector constant, h is the height of the signal read on the chromatogram, $l_0(h)$ is the length measured on the chromatogram of the time of apparition of the point of the diffuse edge corresponding to a height h with the origin at the air peak, g is the mass of adsorbent present in the column, u is the speed of the unwinding of the recording paper, and

$$\int_0^H l_0(h)\,\mathrm{d}h = S_H$$

is the area of the surface limited by the base line, the air peak line, the line drown at the height H and the diffuse edge (see Fig. 1).

The detector constant R^* is determined from the total mass m of the injected adsorbate:

$$R^* = \frac{mu}{S_{\text{peak}}}$$

where S_{peak} is the total area situated under the chromatographic peak. Numerous works have been carried out to take into account the deviations from the ideal situation (sorption effect [9], compressibility coefficient [10], deviation from perfect gas law [11]).

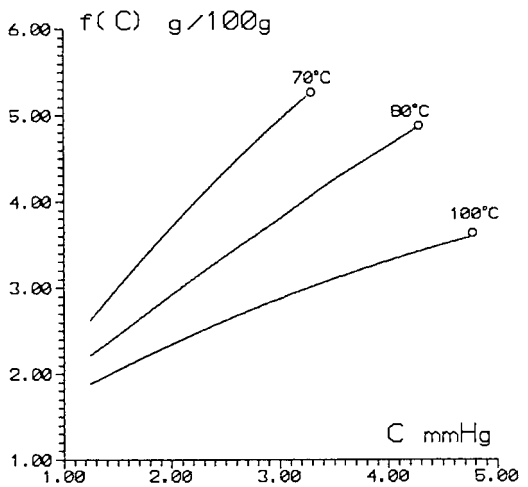

Fig. 6. Isotherms 70, 80 and 100°C silica gel (grain)—ethanol, $L = 50$ cm, $\Phi = 3/8$ inch, $\omega = 2.5$ cc s^{-1}, $m = 0.500$ ml.

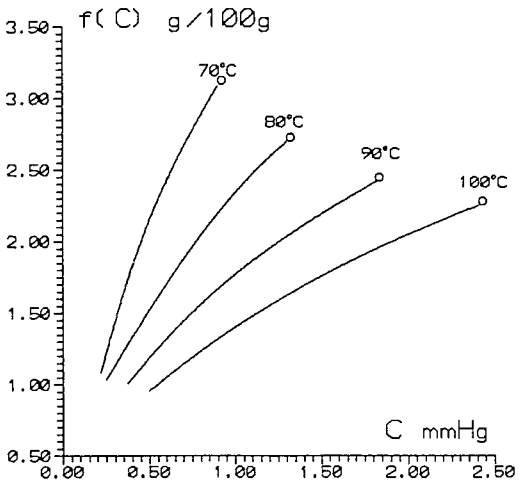

Fig. 7. Isotherms from 70 to 100°C silica gel (grain)—methanol, $L = 25$ cm, $\Phi = 3/8$ inch, $\omega = 2.5$ cc s^{-1}, $m = 0.200$ ml.

Conder and Purnell [12] have given a formula for the local balance, which takes into account these three types of correction and which leads to the true retention time $t_R(c)$:

$$t_R(c) = \frac{1}{j^*\bar{\omega}}\left[\tau qL + j^*\frac{P_e}{P_s}V_{inj} + j^*V_{\text{det}} + (1-\tau)qL(1-Aj^*y_S)\left(\frac{\partial a}{\partial c}\right)_{P=\bar{P}}\right] \qquad (4)$$

where $\bar{\omega}$ and $\bar{P}$ are, respectively, a flow rate and a pressure 'suitably averaged'.

j^* and A are corrective coefficients which depend on the pressure drop, the concentration and the deviation from the perfect gas law, y_s is the molar fraction of the adsorbate at the concentration c in the column exit conditions, P_e and P_s are, respectively, the pressures at the entry and at the exit of the column. The first three terms inside the brackets correspond to the retention time of a non adsorbable gas. The true retention volume measured at the column exit, is:

$$V_R(c) = \bar{\omega} t_R$$

When the adsorption isotherms are searched for, the essential difficulty in the utilization of a corrected formula of type Eq. (4), comes from considering the effects of sorption because, of course, the adsorbed quantities are unknown. It is possible to proceed by iteration, beginning with a simplified formula without sorption effect. One uses the partition coefficient K of the adsorbate between solid and gaseous phases. If the influence of the variation of K is supposed negligible, the corrected mean flow rate of the formula Eq. (4) in function of the flow rate ω of the carrier gas measured experimentally at the exit of the column, becomes:

$$\bar{\omega} = \frac{(1 + K(1 - \tau/\tau))\omega}{1 + K((1 - \tau/\tau))(1 - y_S j)}$$

where j is the compressibility factor of James-Martin [8].

$$j = 3/2 \frac{(P_e/P_S)^2 - 1}{(P_e/P_S)^3 - 1}.$$

Then the values of A, P, and j^* can be taken approximately equal to:

$$A = 1;\ j^* = j;\ P = P_S\left[4/3 \frac{(P_e/P_S)^3 - 1}{(P_e/P_S)^4 - 1}\right] \quad (5)$$

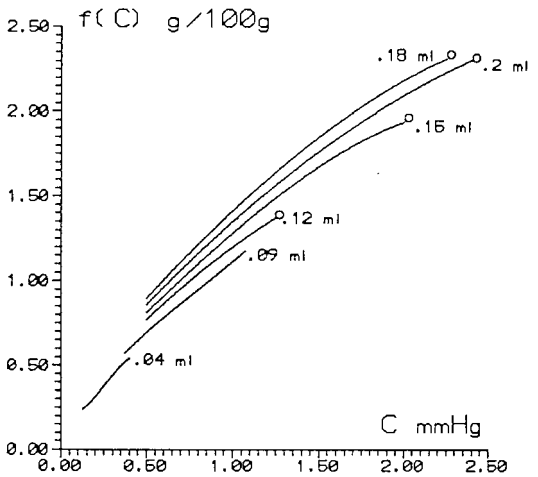

Fig. 8. Isotherms 100°C silica gel (grain)—methanol, $L = 25$ cm, $\Phi = 3/8$ inch, $\omega = 2.5$ cc s^{-1}, $m = 40$, 90, 120, 150, 180 and 200 μl.

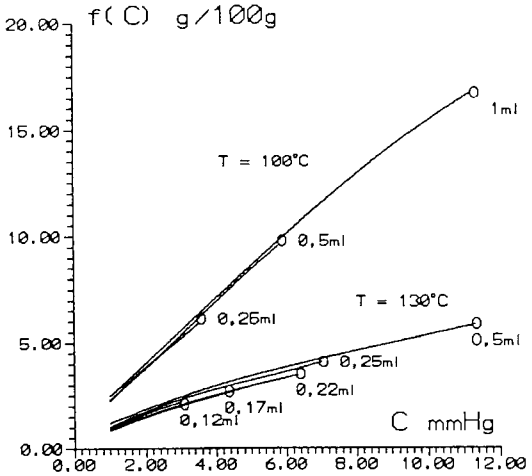

Fig. 9. Isotherms 100 and 130°C zeolite 4A (pellet)—water, $L = 25$ cm, $\Phi = 3/8$ inch, $\omega = 2.5$ cc s^{-1}, $T = 130$°C, $m = 120$, 170, 220, 250, 500 μl, $T = 100$°C, $m = 250$, 500 and 1000 μl.

From Eq. (4) and Eq. (5), the corrected differential equation of the inverse problem, is deduced:

$$(\partial a/\partial c)_{P_S} = Z(c) t_R(c) \quad (6)$$

where t_R corresponds to the chromatographic curve and $Z(c)$ is a function given by Eq. (4) and Eq. (5). To determine the isotherm $a(c, P_S)$, one first draws, the simplified isotherm $a(c)$ which gives the partition coefficient $K(c)$, and so which enables one the integration of Eq. (6). With the help of a data acquisition system, it is possible to program directly the integration of the Eq. (6) following an iterative method. The application of the corrected formula Eq. (6) to our chromatographic experimental curves in the case of the isotherm 100°C for the couple water vapour—microporous silica gel for pressures greater than 40 Torr, leads to a difference of 10% in comparison with the result given by the simplified formula Eq. (3). The difference between the simplified isotherm and the value given by the manufacturer of the silica gel, is about 20%. This difference corresponds to a change of 5°C of the isotherm. For the same adsorption couple, but with another type of silica gel produced by another manufacturer, the extreme differences also reach nearly 20% [13,14] (see Fig. 2). So, it does not seem

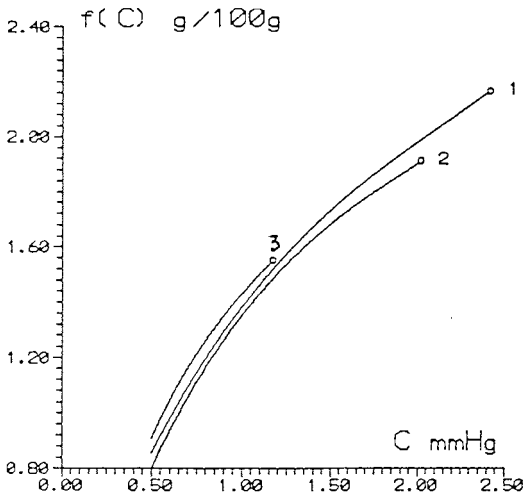

Fig. 10. Isotherms 100°C silica gel (grain)—methanol, $\omega = 2.5$ cc s^{-1}, $\Phi = 3/8$ inch, $m = 0.200$ ml, $L = 25$ cm (1), 50 cm (2), 10 cm (3).

essential to utilize a corrected formula such as Eq. (6), when the aim of the work is to conduct a preliminary study of a machine draft, as was the case of our work.

The search for the best operating conditions in the Glueckauff method is closely linked to the satisfaction of the hypotheses of ideality. These

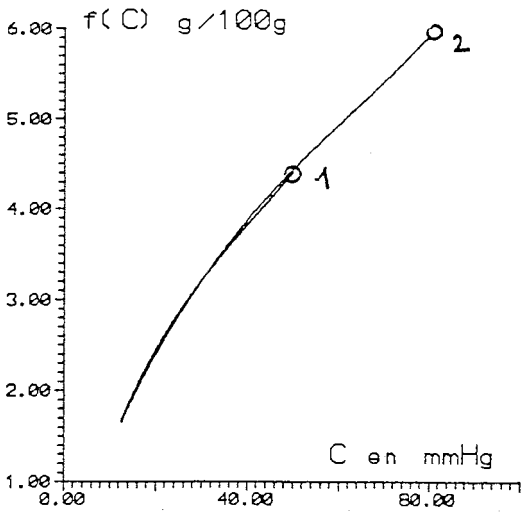

Fig. 11. Isotherms 100°C silica gel (powder)-water, $L = 50$ cm, $\omega = 2.5$ cc s^{-1}, $m = 0.500$ ml, $\Phi = 3/8$ inch (1), 1/8 inch (2).

conditions differ from the ones which are searched for in analysis or preparative chromatography. A discussion of the optimal conditions of the use of adsorption chromatography is given in Refs. [6] and [7].

3. Experimentation

3.1. Products and apparatuses

The chromatograph is of DELCI 'serial 30' type, with a catharometric detector. We have used nitrogen as the carrier gas. Three lengths of column have been tested: 25, 50 and 100 cm; the columns have two diameters: 1/8 and 3/8 inch. The adsorbate has been injected in a discontinuous way, with quantities varying from 40 to 1000 μl. Three adsorbates have been tested: water, methanol and ethanol (MERCK). The adsorbents tested are solids of 'molecular sieves' type: zeolite 4A and 13X, and microporous silica gel (CECA). The adsorbents were used in powder form (diameter lesser than 0.1 mm for the zeolites and lesser than 0.5 mm for the silica gel), in small sticks form (2.5 mm) and pellet form (1.5 mm) for the zeolites and grain form (diameter lesser than 2 mm) for silica gel. The temperatures of experiments have extended from 35 to 130°C. The concentration of adsorbate (linked to the partial pressure) has directly been evaluated in mmHg. The isotherm curves which are presented, have been obtained with the help of a computer, by smoothing the curves of the experimental points deduced graphically from chromatograms using the simplified formula Eq. (3).

3.2. Experimental conditions

As a consequence of the applied aspect of our work and the fact that we have been particularly interested in the domain of high pressures of the adsorbate vapour, a great accuracy was not justified. The standard quality of the utilized products, without any preliminary treatment, was sufficient to this accuracy. Among the chromatographic methods, the elution peak profile one, is

the most convenient and the quickest. Yet, it is the one which gives the less accurate results, especially for high pressures. So it was necessary to work as closely as possible to the most favourable operating conditions:

- pressure drops concerning the column, lesser than 10%, to avoid the variations of the flow rate due to the variations of the pressure.
- length of the column either sufficiently short to minimize the pressure drops and the effect of the various diffusions, and sufficiently long so that the chromatogram may be as spread as possible.
- appropriate flow rate of the carrier gas (between 1 and 5 cc s^{-1}), on one hand to get a stable signal of the detector in a reasonable time and on the other hand to avoid a too weak flow rate which favours diffusion and a too strong flow rate one consequence of which is to put the mass transfer process out of equilibrium.
- the detector has conserved a linear response in all the studied domains with a precision of 1%.

4. Results and discussion

4.1. Isotherms charts (see Figs. 2–7)

The adsorption isotherms of water vapour on silica gel in powder form, have been drawn. The value of the maximal concentration obtained experimentally for each isotherm is represented by a little circle. For the isotherm 100°C, a comparison has been made with the corrected isotherm deduced from the chromatogram using formulas Eq. (4) and Eq. (6) and with the isotherm given by the manufacturer of the silica gel and other isotherms given by different authors for other types of silica gel.

The maximum of the obtained values varies in an approximately linear way in function of the injected quantities (Figs. 8 and 9).

4.1.1. Influence of the dimensions of the column

A noticeable increasing of the maximal concentration is observed when the length of the column decreases (Fig. 10). A reduction of the maximal concentration is seen when the diameter of the column increases (Fig. 11).

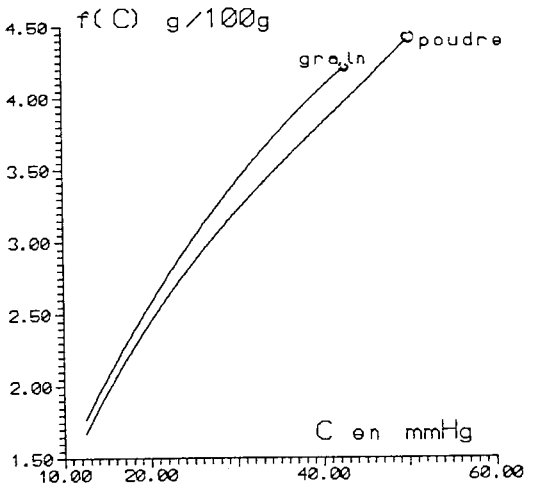

Fig. 12. Isotherms 100°C silica gel (powder (1), grain (2))-water, $L = 50$ cm, $\Phi = 3/8$ inch, $\omega = 2.5$ cc s^{-1}, $m = 0.500$ ml.

4.1.2. Influence of the physical state of the adsorbent and of the flow rate of the carrier gas

A small increasing of the maximal concentration is observed when going from an adsorbent in grain form to an adsorbent in powder form (Fig. 12). The variation of the flow rate of the carrier gas from 1 to 5 cc s^{-1} has no noticeable influence on the value of the maximum concentration of the adsorbate at the column exit (Fig. 13).

4.1.3. General discussion

The isotherm charts of Fig. 2, Fig. 3, Fig. 4, Fig. 5 and Fig. 6 show that the maximal values reached by the concentrations, are insufficient to include all the operating situations of a chemical affinity machine which works with these adsorption couples, in particular for working during the desorption period with a high temperature condenser. The study of the influence of different factors on the level of the maximal concentrations, which has been shown in Fig. 7, Fig. 8, Fig. 9, Fig. 10, Fig. 11, Fig. 12 and Fig. 13, has allowed one to specify the best operating conditions. In the case of the couple silica gel-water, these conditions are: length of the column $L = 25$

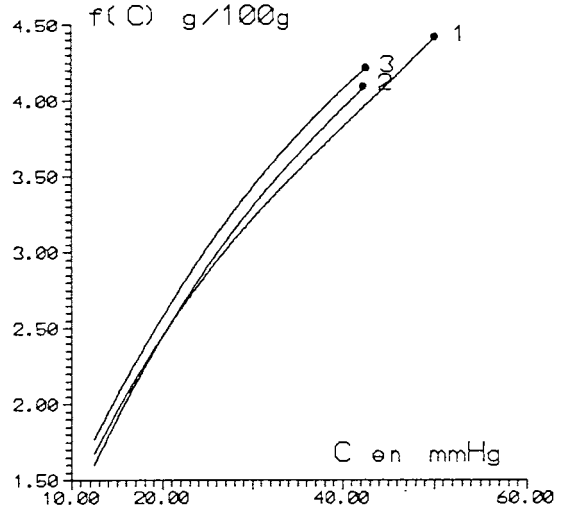

Fig. 13. Isotherms 100°C silica gel (powder)-water, $L = 50$ cm, $\Phi = 3/8$ inch, $m = 0.500$ ml, $\omega = 2.5$ cc s^{-1} (1), 5 cc s^{-1} (2), 1 cc s^{-1} (3).

cm, diameter $\Phi = 1/8$ inch, flow rate of nitrogen $\omega = 2.5$ cc s^{-1}, injected mass $m = 500$ µl, the adsorbent in powder form.

5. Conclusion

We have obtained isotherms of adsorption for couples, microporous solid-refrigerant, using the chromatographic method termed 'elution peak profile'. These isotherms allow the calculation of the theoretical performances of a solid adsorption thermal machine working with these couples. For studying all the working situations of the machine, it has been necessary to broaden the field of application of this chromatographic method. A study of the influence of different factors on the level of the maximal pressures reached by the adsorbate vapours at the exit of the column, has been made. Thus, the influences of the flow rate of the carrier gas, the length and width of the column, the mass of the injected adsorbate, have been studied. This study has been made for different adsorbents (zeolite 13X and 4A, silica gel) under several shapes (small stick, pellet, powder, grain) and different adsorbates (water, ethanol, methanol). For the utilized chromatograph, the highest level of pressure has been reached in the following conditions: length of column 25 cm, width 1/8 inch, injected mass 500 µl, nitrogen flow rate 2.5 cc s^{-1}, the adsorbent in a powder form. In these conditions, the isotherms obtained allow one to envisage all of the scenarios of the working of a thermal machine utilized as refrigerator, heat pump or energy storage apparatus, and this, whatever the ambient conditions. We have shown that a standard chromatograph, without particular additions, is able to give the awaited results with a precision sufficient for a preliminary overall study of a project of machine. In addition, the qualities of the chromatographic techniques, speediness, simplicity and large domain of measure have proved very adequate to such studies. To make the definitive dimensional of a particular machine, it seems desirable to use a more precise chromatographic method such as 'equilibrium chromatography'. Also it is necessary to consider the different corrections such as those given in formulas Eq. (4), Eq. (5) and Eq. (6), especially for the high pressures.

References

[1] A. Adell, S. Gromb, Int. J. Refrigeration 9 (1986) 308.
[2] E. Glueckauff, Nature 156 (1945) 748.
[3] A.V. Kiselev, Physical Chemistry: Modern Problems, Khimiya Publishers, Moscow, 1980, p. 180. D.M. Ruthven, Principles of Adsorption and Adsorption processes, Wiley, New York, 1984, p. 184.
[4] J.N. Wilson, J. Am. Soc. 62 (1940) 1583.
[5] D. de Vault, J. Am. Soc. 65 (1943) 532.
[6] J.F.K. Huber, R.G. Gerritse, J. Chromatogr. 58 (1971) 137.
[7] J.R. Conder and C.L. Young, Measurement by Gas Chromatography, Wiley, Chichester, 1979.
[8] A. Saint-Yriex, Bull. Soc. Chim., 1965, 3407.
[9] E. Wicke, Angew. Chem., B19 (1947) 15. C.H. Bosanquet and G.O. Morgan, D.H. Desty (Ed.), Vapour Phase Chromatography, Butterworth, London, 1957.
[10] A.T. James, A.J.P. Martin, Biochem. J. 50 (1952) 679.
[11] D.H. Everett, Trans. Faraday Soc., 61 (1965) 1637. D.E Martire, D.C. Locke, Anal. Chem. 37 (1965) 144.
[12] J.R. Conder, J.H. Purnell, Trans. Faraday Soc. 64 (1968) 3100.
[13] D.W. Breck, Zeolite Molecular Sieves, Wiley, New York, 1974.
[14] R.M. Barrer, J.C. Bratt, J. Phys. Chem. Solid 12 (1959) 130.

ELSEVIER

Talanta 45 (1998) 787–793

Talanta

Electrochemical studies of NiTMpyP and interaction with DNA

Feng Qu [a], Nan-Qiang Li [a,*], Yu-Yang Jiang [b]

[a] *Department of Chemistry, Peking University, Beijing 100 871, People's Republic of China*
[b] *Department of Chemistry, Tsinghua University, Beijing 100 871, People's Republic of China*

Received 30 January 1997; received in revised form 1 May 1997; accepted 8 May 1997

Abstract

In this paper, cyclic voltammetry, linear sweep voltammetry and chronocoulometry in connection with the hang mercury drop electrode were used to study NiTMpyP and its mixture with DNA. The reduction of NiTMpyP in our experimental conditions involves in 4e reduction of TMpyP. NiTMpyP interacting with DNA forms electrochemically non-active complex DNA-2NiTMpyP, which can not be reduced on the Hg electrode. The peak potential of NiTMpyP does not shift and its electrochemical kinetic parameters indicate no significant change in the presence of DNA. However, the reduction current of NiTMpyP decreases obviously due to the formation of DNA-2NiTMpyP, which implies its equilibrium concentration decreases when DNA was mixed. The decrease of peak current is proportional to DNA concentration, which can be applied to estimate DNA concentration. © 1998 Published by Elsevier Science B.V.

Keywords: DNA; Electrochemical; NiTMpyP

1. Introduction

The study of interaction of nucleic acid with small molecules has been an active research field for recent years. The interaction of porphyrins and metalloporphyrins with DNA has attracted considerable interest due to two main reasons. First, the two basic modes of porphyrin binding to DNA (intercalation and outside binding) can be used as models for the DNA binding of anti-cancer drugs [1,2]. Also, it has been found that porphyrins can inhibit HIV-1, the virus responsible for AIDS [3]. Until recently, the majority of reports have concentrated on meso-tetra (4-*N*-methyl-pyridyl) porphine (TMpyP) and its metal derivatives by spectroscopic methods [4–9]. Practically, porphyrins and metalloporphyrins have been studied extensively by electrochemical methods because of their better electrochemical activity and some of these species play vital role in biological processes [10–16]. However, the papers about DNA interacting with porphyrins by means of electrochemical methods were seldom found in literature [17,18], and voltammetry in connection with Hg electrode has never been seen. In this paper, the electrochemical investigations of NiTMpyP and interaction with DNA are re-

* Corresponding author. Fax: +86 10 62751708.

PII S0039-9140(97)00154-9

ported. Based on the fact, the decrease of peak current of NiTMpyP when DNA was mixed, it could be applied to determine DNA. Electrochemical method is useful to determine DNA concentration, especially, when some substance show UV absorbance near 260 nm, where the bases of DNA show absorbance too. So, our work should be a good complementation to spectroscopic in determination of DNA and other approaches to interaction of metalloporphyrins with DNA.

2. Experimental

2.1. Reagents

Calf thymus DNA(CTDNA), yeast RNA(YRNA) adenosine monophosphate (AMP) were purchased from Beijing Baitai Biochemistry Technology Company. Fish sperm DNA(FS-DNA) was purchased from New Jersey (USA). The stock solution of CTDNA, FSDNA and YRNA were prepared by directly dissolving them in triply distilled water from an all-quartz still. Their concentrations were determined by the absorbance at 260 nm in 0.1 M NaCl. NiTMpyP was obtained by the method of Hou [15]. 0.1 MHAc-NaAc was used as buffer solution. Unless otherwise stated, the DNA in the following section represents CTDNA.

2.2. Apparatus

Cyclic voltammetry, linear sweep voltammetry and chronocoulometry experiments were carried out using a PAR model 273 Potentiostat–Galvanostat with PAR Model 303 Static Mercury Drop Electrode (SMDE). The electrode was used in a HMDE mode. The real electrode surface area was 0.0218 cm^2, calculated from the weight of a large number of mercury drops. An Ag–AgCl electrode was used as the reference electrode and a platinum wire as the counter electrode. The Shimadzu Model UV-265 spectrophotometer was used for spectrophotometric determinations.

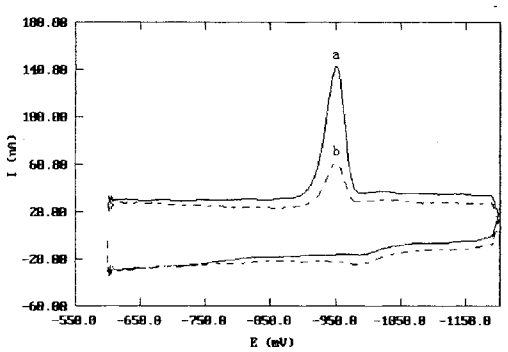

Fig. 1. Cyclic voltammograms of NiTMpyP (a) 1×10^{-6} M and (b) mixture of 1×10^{-6} M NiTMpyP with 2×10^{-6} M DNA. Background electrolytes 0.1 M HAc–NaAc, pH 5.8; accumulation time $t_A = 2$ s; accumulation potential $E_A = -0.6$ V; switching potential $E_{SW} = -1.2$ V; scan rate 0.2 V s^{-1}.

3. Results

3.1. Electrochemical behavior of NiTMpyP

The cyclic voltammograms (Fig. 1) shows the reduction of NiTMpyP at -0.94 V is irreversible. The longer the accumulation time t_A, the larger the peak current I_p (Fig. 2) and the larger the reduction charge amount Q (Fig. 3) of NiTMpyP, which means NiTMpyP is absorbed on Hg electrode. When t_A is longer enough, reaching 90 s, the E_p shifts positively (Fig. 2(d)), I_p and Q de-

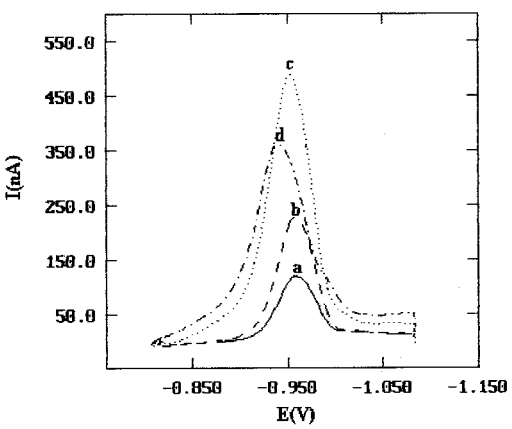

Fig. 2. Linear sweep voltammograms of 1×10^{-6} M NiTMpyP at different accumulation time t_A: (a) 2 s, (b) 10 s, (c) 60 s, (d) 90 s, $E_A = -0.8$ V, scan rate 0.2 V s^{-1}.

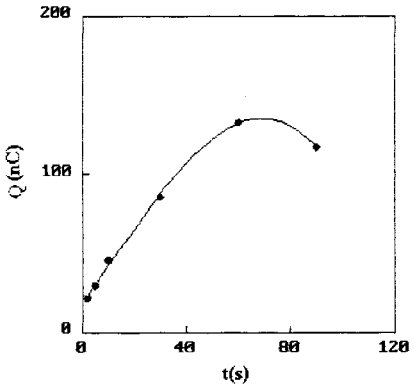

Fig. 3. Dependence of Q on the accumulation time t_A. Other conditions were the same as in Fig. 2.

crease, which means the state of adsorbed NiTMpyP on Hg electrode has changed due to the long time's adsorbance. In our following experiments, $t_A = 2$ s is chosen.

We select 0.1 M HAc–NaAc pH 5.8 as the buffer solution because there is the largest reduction current in solution within a pH range from 4.9 to 9.3. In acid solution, the reduction potential of NiTMpyP shifts linearly in negative direction with the increase of pH, $E_p(V) = -0.62-0.065$ pH, which means the reduction of NiTMpyP involves proton reaction.

In NiTMpyP, Ni^{2+} as the center metal ion in porphyrin TMpyP. Both Ni^{2+} and TMpyP can be reduced possibly. Hou [11] has reported that NiTMPyP can be reduced at -1.0 V (vs. Ag–AgCl) in ammoniacal buffer solution (pH = 9). He suggested the reduction may be attributed to six-electron transfer reduction of both Ni^{2+} and TMpyP in the complex. Two in six electrons belong to Ni^{2+} reduced to Ni, the other four electrons belong to the reduction of TMpyP. Due to the different experiment condition, the n value might be varied in our system.

The chronocoulometric method is suitable for determining the diffusion coefficient D, electron transfer number n of a reactant or the electrode area A, according to the formula given by Anson [19]

$$Q = \frac{2nFAC\,(Dt)^{1/2}}{\pi^{1/2}} + Q_{dl} + Q_{ads} \quad (1)$$

Q_{dl} is double-layer charge (integration of charging current), Q_{ads} the faradaic component due to the reduction of adsorbed species. From the slope of the linear relationship between Q and $t^{1/2}$, the D (diffusion coefficient) and n can be determined if the C (concentration) and A (surface area of Hg drop) are known. The D of NiTMpyP and TMpyP can be assumed as the same as that of FeTMpyP, which is 2.5×10^{-6} $cm^2\ s^{-1}$ [20], then from the slopes of NiTMpyP and TMpyP, electron transfer number $n = 4$ can be determined (Table 1). Fig. 4 shows the plot of Q versus $t^{1/2}$ of NiTMpyP and TMpyP. In our experiments, the step potential $-0.8--1.2$ V and $-0.1--0.8$ V are chosen, respectively, for they can be reduced completely. The slope of TMpyP is two times larger than that of NiTMpyP (Fig. 4) also the concentration of TMpyP is two times higher than that of NiTMpyP, so their n value should be equal. This result is consistent with that calculated (Table 1). Therefore, we believe that, in acid solution, the reduction of 4e of NiTMpyP at -0.94 V does not belong to the center ion Ni^{2+}, but the ligand TMpyP.

Our experiment results show the electrode reaction of NiTMpyP is irreversible (see Fig. 1) surface (see Fig. 2) electrochemical reaction and the reactant is strongly adsorbed. According to Laviron's equation [21–23]:

$$E_p = E^{0\prime} + \frac{RT}{\alpha nF}\ln\frac{RTk_s}{\alpha nF} - \frac{RT}{\alpha nF}\ln v \quad (2)$$

where α is the transfer coefficient, k_s the standard rate constant of the surface reaction, v the scan rate and $E^{0\prime}$ the formal potential. According to Eq. (2), the plot of E_p versus $\ln v$ should be linear. From its slope, the αn value can be determined, and from the intercept, the k_s can be calculated, if the value of $E^{0\prime}$ is known. The value of $E^{0\prime}$ in Eq. (2) can be determined from intercept of E_p versus v plot on the ordinate by extrapolating the line to $v = 0$. Fig. 5 and Fig. 6 are plots E_p versus $\ln v$ and E_p versus v, respectively, from slope (-0.01247), intercept (-0.9786 V) and $E^{0\prime}$ (-0.93 V), $\alpha = 0.52$, $k_s = 1.63$ s^{-1} were obtained.

Table 1
Determination of n value

$C_{NiTMpyP}$ (10^{-6} M)	Slope ($\mu C\ s^{-1/2}$)	n	C_{TMpyP} (10^{-6} M)	Slope ($\mu C\ s^{-1/2}$)	n
3.0	0.0494	4.3	3.0	0.0426	3.8
4.0	0.0588	3.9	4.0	0.0583	3.9
5.0	0.0786	4.1	5.0	0.0728	3.9

3.2. Studies of the mixture of NiTMpyP and DNA

When DNA was mixed in NiTMpyP, the 434 nm Soret maximum for NiTMpyP with DNA arises from a red shift of 417 nm four-coordinate species [4]. From resonance Raman spectra reported by Nils Blom [7], the bands that are characteristic of both four and six coordinate NiTMpyP can be observed, and they also observed relative intensity changes of these bands when the NiTMpyP is reacted with DNA [7]. In our experiments, the reduction current of NiTMpyP decreases obviously. However, reduction potential E_p does not shift (Fig. 1) and no new reduction peak is found between -0.1 and -1.3 V. This means the electrochemically non-active complex DNA-mNiTMPyP is formed. Because NiTMpyP may combine with DNA in the mode of either intercalation or outside binding, it is difficult for NiTMpyP in the complex to contact with the surface of Hg electrode, and it cannot be reduced at Hg electrode, so the complex is electrochemically non-active. However, the formation of complex results in the decrease of equilibrium concentration of NiTMpyP in solution, so the decrease of reduction current. With the continual increase of DNA concentration, reduction peak of DNA appears at -1.4 V which caused by reduction of A and C bases in DNA (Fig. 7(a, b)).

At our experimental condition, such a short accumulation time and low NiTMpyP and DNA concentration, Hg electrode surface cannot be covered totally by NiTMpyP and NiTMpyP–DNA. From Fig. 7, we can see when 5×10^{-6} MDNA (a), 1.5×10^{-5} M DNA (b) was added in 3×10^{-6} M NiTMpyP solution, respectively, $t_A = 2$ s, with DNA concentration increase, I_p of DNA increase but I_p of NiTMpyP decrease. When t_A increases from 2 s to 10 s, both the peak current of NiTMpyP and DNA increase (Fig.

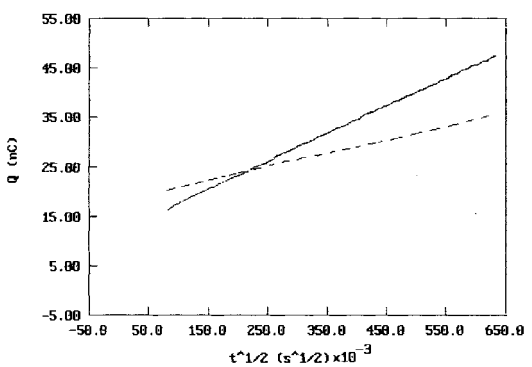

Fig. 4. Chronocoulometric dependence of charge on the square root of time for—4×10^{-6} M TMpyP, potential step -0.1– -0.8 V; - - - 2×10^{-6} M NiTMPyP, potential step: -0.8– -1.2 V.

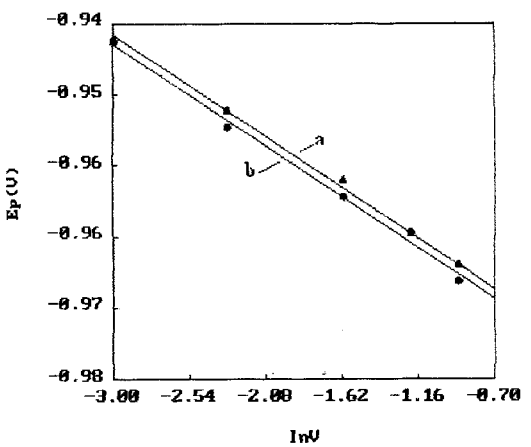

Fig. 5. Semilogarithmic dependence of the peak potential E_p on the potential scan rate ln v: for (a) 1×10^{-6} M NiTMpyP pH 5.8; (b) a + 1×10^{-6} M DNA.

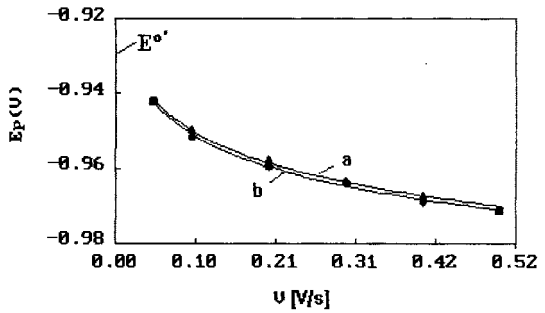

Fig. 6. Dependence of the peak potential E_p on the potential scan rate v for: (a) 1×10^{-6} M NiTMpyP pH 5.8; (b) a + 1×10^{-6} M DNA.

7(b, c)) which manifest that under our experiment conditions, when accumulation time is 2 s, the decrease of current of NiTMpyP is not due to the displacement by adsorbed DNA.

The α of NiTMpyP mixed with DNA is 0.52, while the k_s was estimated to be 1.58 s^{-1} from Fig. 5 and Fig. 6 (slope -0.01249, intercept -0.979 V, $E^{0\prime}$ -0.93 V). Comparing with those of NiTMpyP (0.52, 1.63 s^{-1}), no obvious change can be found, which implies that the reactant is still NiTMpyP but complex DNA-mNiTMpyP.

3.3. The determination of combined number

With reference to the method of Li [24], it is assumed that DNA and NiTMpyP only produce a complex DNA-mNiTMpyP

$$\text{DNA} + \text{mNiTMpyP} \Leftrightarrow \text{DNA} - \text{mNiTMpyP}$$

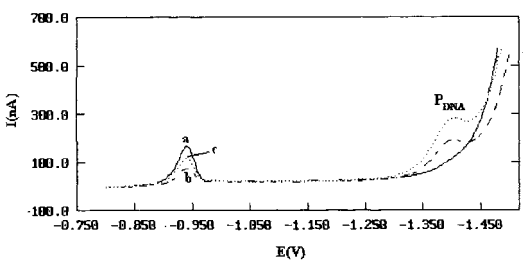

Fig. 7. Linear sweep voltammograms for: (a) 3×10^{-6} M NiTMpyP + 5×10^{-6} M DNA, $t_A = 2$ s; (b) 3×10^{-6} M NiTMpyP + 1.5×10^{-5} M DNA, $t_A = 2$ s; (c) 3×10^{-6} M NiTMpyP + 1.5×10^{-5} M DNA, $t_A = 10$ s.

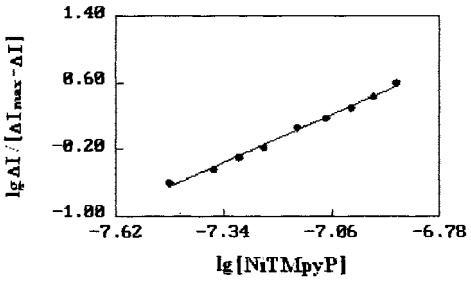

Fig. 8. Relationship between $\lg[\Delta I/(\Delta I_{max} - \Delta I)]$ and lg[NiTMpyP].

The condition formation constant is as follows

$$\beta_s = \frac{[\text{DNA} - \text{mNiTMpyP}]}{[\text{NiTMpyP}]^m[\text{DNA}]} \tag{3}$$

and the following equations can be deduced

$$\Delta I_{MAX} = k' C_{DNA} \tag{4}$$

$$\Delta I = k'[\text{DNA} - \text{mNiTMpyP}] \tag{5}$$

$$[\text{DNA}] + [\text{DNA} - \text{mNiTMpyP}] = C_{DNA} \tag{6}$$

$$\Delta I_{max} - \Delta I = k'(C_{DNA} - [\text{DNA} - \text{mNiTMpyP}]) \tag{7}$$

$$\Delta I_{max} - \Delta I = k'[\text{DNA}] \tag{8}$$

Put Eqs. (5) and (8) into Eq. (3), we have

$$\lg \frac{\Delta I}{\Delta I_{max} - \Delta I} = \lg \beta_s + m \lg[\text{NiTMpyP}] \tag{9}$$

$$\frac{1}{\Delta I} = \frac{1}{\Delta I_{max}} + \frac{1}{\beta_s \cdot \Delta I_{max}} \times \frac{1}{[\text{NiTMpyP}]^m} \tag{10}$$

If DNA and NiTMpyP form a complex, then $\lg(\Delta I/\Delta I_{max} - \Delta I) - \lg\{\text{NiTMpyP}]$ becomes linear with the slope of m. The results of $m = 2$ and $\lg \beta_s = 14.16$ were obtained from Fig. 8, which means that only one compound is formed. To Eq. (10), we assume $m = 1, 2, 3$, plot $(1/\Delta I) - (1/[\text{NiTMpyP}]^m)$, if ΔI_{max} calculated is approximate to the experiment data ΔI_{max} 37.5, the assumptive value of m is reasonable,

Table 2
Results of sample determination

Samples	Added (10^{-6} M)	Found (10^{-6} M)	Recoveries (%)	RSD ($n=5$) (%)
CTDNA	2	2.05	102.5	1.9
FSDNA	2	2.18	109	3.2
CTDNA+FSDNA	2+2	4.06	101.5	2.7
FSDNA+AMP+YRNA	2+15+9.63	1.97	98.5	1.9
1		2.67		2.4
2		6.19		1.6

(a) $m=1$ $\Delta I_{max}=176.8$ $\lg \beta_s=5.1$ $r=0.9968$
(b) $m=2$ $\Delta I_{max}=40.7$ $\lg \beta_s=14.32$ $r=0.9925$
(c) $m=3$ $\Delta I_{max}=30.4$ $\lg \beta_s=19.02$ $r=0.9613$

Based on the data above, for 40.7 is the nearest value of 37.5, m can be determined to be 2, and $\lg \beta_s=14.32$ is nearly identical to the experimental data $\lg \beta_s=14.16$.

3.4. Analytical application

Adding DNA in NiTMpyP solution results in the decrease of I_p of NiTMpyP, which can be applied to DNA concentration determination. According to our experiment, $t_A=2$ s is chosen which can save experimental time, 0.2–0.5 V s^{-1} scan rate leads to a good peak shape of NiTMpyP which is suitable to determine its current. When DNA was added in 2×10^{-6} M NiTMpyP, $t_A=2$ s, 0.2 V s^{-1} scan rate, the I_p of NiTMpyP decreases linearly with DNA concentration from 5×10^{-7} to 1×10^{-5} M. Linear regression equation $I_p=-0.043\ C+0.408$ (I_p μA, C 10^{-6} M), correlation coefficient $r=0.9988$. Small amounts of bovine serum albumin BSA ($<6\times10^{-7}$ M) does not disturb the determination of NiTMpyP. When the AMP concentration and YRNA concentration was as high as eight times and five times that of DNA respectively, no interference was observed. Plasmide DNA sample 1 and sample 2 were obtained from *E. coli* Ju 109 (prepared by Department of Chemistry, Tsinghua University) by method of J. Sambrook [25]. Samples 1 and 2 were determined after diluting 10 times. Other samples were synthetic samples. Table 2 shows the results of samples determination. The determination results in Table 3 show consistence by two kinds of method, UV-Spectroscopy (UV-S) and Electrochemical Method (ECM), which means the ECM is suitable to DNA concentration determination. Electrochemical methods have special advantage when the substances which can interact with DNA show UV absorbance near 260 nm, which will disturb the absorbance value of bases of DNA. Until now, we have not found the reports about DNA concentration determination using metalloporphyrins by method of spectroscopy of electrochemistry.

Table 3
Comparison of determination results by UV-S and ECM method

Samples	Added (10^{-6} M)	Found (UV-S) (10^{-6} M)	Found (ECM) (10^{-6} M)
1		2.58	2.67
2		6.12	6.19
CTDNA	2	2.07	2.05
FSDNA	2	2.09	2.18
CTDNA+FSDNA	2+2	4.16	4.06

Acknowledgements

This project was jointly supported by No. 9 400 120 of the Foundation of Doctoral Program of the State Commission of Education and No. 29 575 192 of the National Natural Science Foundation of China.

References

[1] L.G. Marzilli, New J. Chem. 14 (1990) 409.
[2] M.J. Waring, Annu. Rev. Biochem. 50 (1981) 159.
[3] J.L. Sessler, M.J. Cyr, V. Lynch, J. Am. Chem. Soc. 112 (1990) 2810.
[4] R.F. Pasternack, E.J. Gibbs, J.J. Villafranca, Biochemistry 22 (1983) 2406 and 22 (1983) 5409.
[5] R.F. Pasternack, E.J. Gibbs, J. Am. Chem. Soc. 107 (1985) 8179.
[6] J.M. Kelly, M.J. Murphy, Nucleic Acids Res. 13 (1) (1985) 167.
[7] N. Blom, J. Odo, K. Nakamoto, D.P. Strommen, J. Phys. Chem. 90 (1986) 2847.
[8] K.T. Yue, M.F. Lin, Inorg. Chem. 30 (1991) 3214.
[9] B.P. Hudson, J. Soe, D.J. Berger, J. Am. Chem. Soc. 114 (1992) 8997.
[10] J.E. Falk, Porphyrins and Metalloporphyrins, Elsevier, Amsterdam, 1964.
[11] J.H. Zagal, Coordination Chem. Rev. 119 (1992) 89.
[12] A. Zwase, A. Igarashi, Electrochem. Acta. 38 (1993) 689.
[13] D. Dolphin, The Porphyrins, Vol. 5, Academic Press, New York, 1978.
[14] Q.K. Zhuang, X.X. Gao, Electrochim. Acta 40 (8) (1995) 959.
[15] J.M. Hou, X.X. Gao, Chem. J. Chin. Univ. 15 (8) (1994) 1136.
[16] C. Zhou, Y.M. Ni, X.X. Gao, Chin. Sci. Bull. 22 (1990) 1717.
[17] A.J. Bard, Pure Appl. Chem. 64 (2) (1992) 185.
[18] M. Rodriguez, A.J. Bard, Inorg. Chem. 31 (1992) 1129.
[19] F.C. Anson, Anal. Chem. 36 (1964) 932.
[20] P.A. Forshey, T. Kuwana, Inorg. Chem. 29 (1981) 693.
[21] E. Laviron, J. Electroanal. Chem. 52 (1974) 355.
[22] E. Laviron, J. Electroanal. Chem. 101 (1979) 19.
[23] A.J. Bard, L.R. Faulkner, Electrochemical Methods, Foundamentals and Applications, Wiley, New York, 1980, p. 525.
[24] N.Q. Li, J. Min, FenXiHuaXue 17 (4) (1989) 346.
[25] J. Sambrook, E.F. Fritsch, T. Manicatis, Molecular Cloning, A Laboratory Manual, 2nd ed., Cold Spring Harbor, New York, 1989, p. 58.

.

ELSEVIER

Talanta 45 (1998) 795–799

Talanta

Spectrophotometric determination of astemizole

Chilukuri S.P. Sastry *, Petla Y. Naidu

Foods and Drugs Laboratories, School of Chemistry, Andhra University, Visakhapatnam 530 003, India

Received 4 November 1996; received in revised form 13 May 1997; accepted 14 May 1997

Abstract

Four simple and sensitive spectrophotometric methods for the determination of astemizole (AZ) in pure samples and pharmaceutical formulations are described. They are based on the oxidation of astemizole with excess *N*-bormosuccinimide (NBS) and determination of the unconsumed NBS with, metol-sulphanilamide (method A, λ_{max}: 520 nm) or celestine blue (method B, λ_{max}: 540 nm); or by the reduction of Folin-ciocalteu reagent (method C, λ_{max}: 720 nm); or by the formation of a chloroform-soluble, coloured ion-association complex between the drug and azocarmine G (AG) at pH 1.5 (method D, λ_{max}; 540 nm). The results obtained are reproducible with a coefficient of variation of less than 1.0%. © 1998 Elsevier Science B.V.

Keywords: Astemizole; Methods; Spectrophotometric

1. Introduction

Astemizole (AZ) is chemically 1-(4-fluorobenzyl-2 {[1-(4-methoxyphenethyl)-4-piperidyl]-amino}-benzimidazole. It antagonizes the effects of histamine on peripheral H_1-receptor. Astemizole is not official in any of the pharmacopoeia. Literature mentions only a few methods such as non-aqueous [1], UV spectrophotometric [1], HPLC [1–3] and radio immuno assay [4] methods for its determination in biological fluids and formulations. Although visible spectrophotometric methods are the instrumental methods of choice commonly used in industrial laboratories, for their simplicity, selectivity and sensitivity there is not even a single report so far for the determination of astemizole. Therefore, the need for a fast, low cost and selective method is obvious, especially for routine quality control analysis of pharmaceutical products containing astemizole.

This paper describes the development of sensitive and rapid spectrophotometric methods using *N*-bromosuccinimide [5,6], Folin-Ciocalteau reagent [7] and azocarmine G [8], which have been found to be satisfactory for the determination of astemizole in pure and pharmaceutical formulations.

2. Experimental

2.1. Apparatus

A Milton-Roy spectronic 1201 spectrophotometer with 1 cm matched glass cells was used for all

* Corresponding author. Fax: +91 891 555547.

PII S0039-9140(97)00160-4

the absorbance measurements. An Elico digital model LI-120 pH meter was used for pH measurements.

2.2. Reagents and solutions

All chemicals were of analytical or pharmacopoeial grade and doubly distilled water was used throughout.

Aqueous solutions of NBS (Loba, 4.94×10^{-3} M), SA (Wilson Labs: 1.16×10^{-2} M), metol (Loba 8.71×10^{-3} M) and acetic acid (Loba: 8.76×10^{-1} M) were prepared for method A. Aqueous solutions of NBS (Loba, 100 μg ml^{-1}), celestine Blue (E-Gurr, 100 μg ml^{-1}) and hydrochloric acid (BDH, 5 M) were prepared for method B. Aqueous solutions for sodium hydroxide (E. merck, 3 M) and commercially available Folin-ciocalteu (Loba: 2N) reagent were used for method C. Aqueous solution of AG (E. Gurr, 3.50×10^{-3} M) was prepared for method D. A pH 1.5 buffer solution was prepared by mixing 33.8 ml of 0.1 M glycine solution (Loba: 7.507 g of glycine + 5.85 g of NaCl, dissolved in 1 l of water) and 66.2 ml of 0.1 M HCl.

2.3. Preparation of standard drug solution

Stock solutions of AZ (1 mg ml^{-1}) were prepared by dissolving 100 mg of AZ in 0.1 M HCl (methods A&B) or 1,4-Dioxan (method C) or chloroform (method D). The working standards were prepared by suitable dilution of the stock solution with distilled water (method A, 100 μg ml^{-1}; method B, 20 μg ml^{-1}) or 1,4-dioxan (method C, 200 μg ml^{-1}) or chloroform (method D, 20 μg ml^{-1}).

2.4. Preparation of sample solution

An amount of powdered tablet or of suspension equivalent to 100 mg of astemizole was extracted with chloroform (4×10 ml), the combined extracts were evaporated on a steam-bath and the residue was treated as for preparation of standard drug solution.

3. Procedures

Method A: in to a series of 25 ml graduated test tubes containing aliquots of AZ Solution, 1.0 ml each of acetic acid and NBS were added and the total volume in each tube was made upto 10 ml with distilled water and kept for 20 min at room temperature ($28 \pm 5°$). Then 1.0 ml of metol solution and after 2 min 2.0 ml of SA was added, and the volume was made upto the mark with distilled water. The absorbances were measured against distilled water at 520 nm during the stability period of 10–30 min. A blank experiment was also carried out omitting the drug. The decrease in the absorbance corresponding to AZ was obtained by subtracting the test from the blank. The amount of AZ was calculated from a calibration curve prepared from 1.0–3.5 ml portions of 100 μg ml^{-1} AZ standard solution.

Method B: in to a series of 25 ml graduated test tubes containing aliquots of AZ solution, 1.25 ml of 5 M HCl and 2.5 ml of NBS were added and the volume was made upto 15 ml with distilled water. After 10 min, 10 ml of CB was added and mixed thoroughly and the absorbances were measured at 540 nm against distilled water within the stability period (5–60 min). Blank was prepared appropriately. The decrease in absorbance corresponding to consumed NBS and in turn, to drug concentration, was obtained by subtracting the absorbance of the blank solution from that of the test solution. The calibration graph was drawn by plotting the decrease in the absorbance of the dye (CB) against the amount of drug. The amount of AZ was calculated from a calibration curve prepared from 1.0–6.0 ml portions of 20 μg ml^{-1} AZ standard solution.

Method C: into a series of 25 ml graduated test tubes containing aliquots of AZ solution, 1.0 ml of F-C reagent and 5.0 ml of NaOH solution were added successively and kept aside for 10 min at laboratory temperature (28 ± 5°C). The solution in each tube was made upto the mark with distilled water and the absorbance of

Table 1
Optical characteristics, precision and accuracy

Parameters	Methods			
	A	B	C	D
λ_{max} (nm)	520	540	720	540
Beer's law limits (μg ml^{-1})	4.0–14.0	0.4–4.0	0.8–8.0	1.0–10.0
Detection limits (μg ml^{-1})	0.129	0.025	0.038	0.042
Molar absorptivity (1 mol^{-1} cm^{-1})	1.16×10^{4}	7.09×10^{4}	3.74×10^{4}	3.34×10^{4}
Sandell's sensitivity (μg Cm^{-2} per 0.001 absorbance unit)	0.040	0.006	0.011	0.013
Regression equation (Y)[a]				
Slope (b)	2.40×10^{-2}	1.55×10^{-1}	8.79×10^{-2}	7.28×10^{-2}
Std. dev. on slope (Sb)	7.99×10^{-5}	5.58×10^{-4}	2.58×10^{-4}	4.62×10^{-4}
Intercept (a)	7.14×10^{-4}	2.0×10^{-4}	-1.0×10^{-4}	-2.10×10^{-4}
Standard deviation on intercept (Sa)	6.39×10^{-3}	1.74×10^{-3}	1.37×10^{-3}	3.06×10^{-3}
Standard error of estimation (Se)	8.45×10^{-4}	1.87×10^{-3}	1.30×10^{-3}	2.92×10^{-3}
Correlation coefficient (r)	0.9999	0.9999	0.9999	0.9999
Relative standard deviation (%)[b]	0.86	0.38	0.25	0.37
% Range of error[b] (95% confidence limit)	0.91	0.40	0.27	0.39

[a] $Y=a+bc$ where C is concentration in μg ml^{-1} and Y in absorbance units.
[b] Six replicate samples (concentrations of 8.0, 3.2, 6.4 and 6.0 μg ml^{-1} of the drug for methods A, B, C and D, respectively).

the solution was measured at 720 nm against reagent blank prepared simultaneously within the stability period (5 min–5 h). The amount of AZ was calculated from a calibration curve prepared from 0.2–2.2 ml portions of 200 μg ml^{-1} AZ standard solution.

Method D: aliquots of the drug solution were placed in a series of 125 ml separating funnels. Then 6.0 ml of buffer solution (pH 1.5) and 2.0 ml of AG solution were added to each funnel. The total volume of aqueous layer in each funnel was brought to 15 ml with water. To each separating funnel sufficient chloroform was added to make the final volume of the organic layer to 10 ml. The solutions were shaken and allowed to stand for clear separation of the two phases. The absorbance of the separated chloroform layer was measured at 540 nm against a reagent blank. The stability of the coloured complex in the chloroform layer was 10 h. The amount of AZ was calculated from a calibration graph prepared from 0.5–5.0 ml portions of 20 μg ml^{-1} AZ standard solution.

4. Results and discussion

The experimental conditions were established by varying one variable at a time (OVAT) [9] and observing its effect on the absorbance of the coloured species.

Method A or B: involves two stages oxidation of AZ by NBS [first stage] and estimation of unconsumed NBS with metol-SA (method A) or CB (method B) [Second stage]. In the first stage for the oxidation of Astemizole, use of 0.5–1.5 ml CH_3COOH, 0.5–1.5 ml of NBS and a waiting period of 10–30 min (method A) or 1.0–2.0 ml of 5 M HCl, 2.0–3.0 ml of NBS and a waiting period of 5–15 min (method B) were found necessary. In the second stage, 0.5–1.5 ml of metol solution and 1.5–2.5 ml of SA solution (method A) or 8–12 ml of celestine blue (Method B) solution were found optimal. The intermittent waiting period prior to the addition of SA was 1–3 min (method A) or CB was 3–6 (method B).

In method C, 0.8–1.2 ml of Folin-Ciocalteu reagent and 4–6 ml of 3 M sodium hydroxide

Table 2
Assay and recovery of astemizole in pharmaceutica formulations

Pharmaceutical formulations	Labelled amount (mg)	Amount found* (mg)				Found by reference[a] method	Recovery by proposed methods[b]%			
		Proposed methods								
		A	B	C	D		A	B	C	D
Tablets I (LUPIN)	10	9.98 ± 0.05 $t = 0.66$, $F = 2.07$	10.03 ± 0.08 $t = 1.87$, $F = 1.10$	9.99 ± 0.08 $t = 1.88$, $F = 1.97$	10.01 ± 0.11 $t = 1.79$, $F = 1.97$	9.98 ± 0.08	99.7 ± 0.5	100.2 ± 0.5	99.5 ± 0.9	99.9 ± 0.4
Tablets II (TORRENT)	10	9.97 ± 0.05 $t = 0.28$, $F = 1.98$	9.89 ± 0.15 $t = 1.41$, $F = 4.66$	9.95 ± 0.09 $t = 0.19$, $F = 1.37$	9.99 ± 0.04 $t = 0.69$, $F = 3{,}69$	9.96 ± 0.07	99.3 ± 0.4	98.8 ± 0.6	99.3 ± 0.4	99.6 ± 0.2
Suspension I (TORRENT)	60	59.9 ± 0.33 $t = 0.45$, $F = 1.25$	60.2 ± 0.49 $t = 1.27$, $F = 1.84$	59.9 ± 0.53 $t = 0.62$, $F = 2.11$	60.1 ± 0.67 $t = 0.16$, $F = 3.27$	60.08 ± 0.37	$99./8 \pm 0.8$	100.0 ± 0.9	99.4 ± 0.7	100.2 ± 1.2
Suspension II (MICRONOVA)	60	59.8 ± 0.30 $t = 0.11$, $F = 1.36$	59.6 ± 0.78 $t = 0.82$, $F = 4.97$	59.7 ± 0.55 $t = 0.18$, $F = 2.54$	59.8 ± 0.49 $t = 0.31$, $F = 2.01$	59.823 ± 0.35	99.5 ± 0.7	99.0 ± 0.3	99.2 ± 0.6	99.4 ± 0.4

I&II, formulations that are manufactured by two different pharmaceutical companies.

* Average $\pm$ standard deviation of six determinations; the t- and F-values refer to comparison of the proposed method with the reference method. Theoretical values at 95% confidence limits $F = 5.05$; $t = 2.57$.

[a] UV reference method.

[b] Recovery of 10 mg added to the pharmaceutical formulations (average of three determination).

were found to give maximum colour intensity. The order of addition however was found not to have significant effect.

In method D, in order to establish the optimum pH range, astemizole was allowed to react with AG in aqueous solutions buffered to pH 1.0–3.0 and the complex formed was extracted into chloroform for measurement. Constant absorbances were obtained over the pH range 1.2–1.7 in glycine buffer. Hence a pH of 1.5 was used. A 1.5–2.5 ml portion of AG solution was found to be optimal, shaking times of 1.5–4.0 min produced constant absorbance, hence a shaking time of 2.0 min was selected for use. A ratio of 1.5:1 of aqueous to chloroform phases was required for efficient extraction of the coloured species.

4.1. Analytical data

The optical characteristics and figures of merit are given in Table 1. The values obtained by the proposed methods and a reference method [1] for formulations are compared in Table 2, together with the results of recovery experiments.

5. Conclusions

A significant advantage of visible spectrophotometric method is that it can be applied to the determination of individual compounds in a multicomponent mixture. The instrument is simple and is not of high cost. The importance lies in the chemical reactions upon which the procedures are based rather than upon the sophistication of the instrument. In the present study, astemizole was determined (Method A–D) successfully as pure compound as well as component in representative pharmaceutical formulations by exploiting different functional groups present. The ingredients usually present in the pharmaceutical formulations of astemizole did not interfere in the proposed methods. Thus the proposed methods are simple, rapid and sensitive ($B > C > D > A$) and can be used in the routine determination of pharmaceutical formulations depending upon the need of specific situation.

References

[1] R.T. Sane, P.K. Aruna, S.A. Renu, S.R. Shallesh, Indian Drugs 30 (4) (1993) 156.
[2] R. Woestenborghs, L. Embrechts, J. Heykants, J. Chromatogr. Biomed. Appl. 29 (J. Chromatogr. 278) (1983) 359.
[3] G.s. Sadana, A.J. Potdar, Indian Drugs 2 (1989) 140.
[4] R. Woestenborghs, I. Geuens, M. Michiels, R. Hendriks, J. Heykants, Drug Dev. Res. 8 (1–4) (1986) 63.
[5] C.S.P. Sastry, B.S. Reddy, B.G. Rao, Indian J. Pharm. Sci. 43 (1981) 118.
[6] C.S.P. Sastry, K.R. Srinivas, K.M.M. Krishna Prasad, Mikrochim. Acta 122 (1996) 77.
[7] O. Folin, D. Ciocalteu, J. Biol. Chem. 73 (1927) 627.
[8] C.S.P. Sastry, P.Y. Naidu, Mikrochimica. Acta (1997).
[9] D.L. Massart, B.G.M. Vandeginste, S.N. Deming, Y. Michotte, L. Kaufman, Chemometrics; A Test book, Amsterdam, Elsevier, 1988, pp. 80, 293.

ELSEVIER

Talanta 45 (1998) 801–806

Talanta

Elimination of hydrofluoric acid interference in the determination of antimony by the hydride generation technique

A. D'Ulivo [a,*], L. Lampugnani [a], D. Faraci [a], D.L. Tsalev [a,c], R. Zamboni [b]

[a] *C.N.R., Istituto di Chimica Analitica Strumentale, Via Risorgimento 35, 56126 Pisa, Italy*
[b] *Università di Pisa, Dipartimento di Chimica e Chimica Industriale, Via Risorgimento 35, 56126 Pisa, Italy*
[c] *Faculty of Chemistry, University of Sofia, Sofia, Bulgaria*

Received 31 December 1996; received in revised form 22 April 1997; accepted 14 May 1997

Abstract

For the determination of antimony by hydride generation techniques a pretreatment procedure has been developed for the reduction of Sb(V) to Sb(III) in order to remove the effect of hydrofluoric acid which strongly interferes with the reduction of pentavalent antimony to the trivalent state. It is based on the combined action of L-cysteine and boric acid at 80°C. The pretreatment is effective in both nitric and hydrochloric acid media. Quantitative recoveries are obtained in less than 60 min. Under these conditions antimony is reduced to the trivalent state in acid media containing both nitric and hydrochloric acid. The method has been applied to the determination of total antimony in certified reference materials of sediments after pressurized microwave digestion with HNO_3-HCl-HF. Good agreement is obtained by using both analytical techniques: continuous flow hydride generation atomic fluorescence spectrometry and flow injection electrothermal atomic absorption spectrometry with in-situ trapping of stibine in a graphite atomizer. © 1998 Elsevier Science B.V.

Keywords: Antimony determination; Hydride generation; Hydrofluoric acid interference; L-cysteine and boric acid effect; Sediment analysis

1. Introduction

In the determination of antimony by hydride generation technique, the presence of hydrofluoric acid is a serious source of interference [1,2]. Hydrofluoric acid suppresses the stibine generation from Sb(V), but not from Sb(III), even at concentration as low as 0.02 mol l^{-1}. Furthermore, Petrick and Krivan [2] found that the most common prereducing agents like KI or KI-ascorbic acid failed to reduce Sb(V) to Sb(III) at room temperature, neither was KI useful at 95°C. The addition of boric acid aimed at complexing the fluoride ions was not effective, either. The only suitable prereduction method found was KI-ascorbic acid at 95°C, however some limitations have been reported under particular experimental conditions and no applications to real samples have been attempted.

* Corresponding author. Fax: +39 50 502589; e-mail: dulivo@icas.pi.cnr.it

PII S0039-9140(97)00171-9

The use of L-cysteine as prereducing and masking agent is well know [3,4]. Recently it was found that L-cysteine is able to remove interferences arising from some particular acid mixtures containing nitric acid [5]. In this paper is proposed a simple and reliable method for elimination of the HF interference on Sb(V) based on the effect of L-cysteine at 80°C in the presence of boric acid, with applications to the determination of total antimony to sediment certified reference materials by using two different hydride generation atomic spectrometric techniques.

2. Experimental

2.1. Reagents

Standard solutions of Sb(III) were prepared by serial dilutions of 1 mg ml^{-1} stock solution containing Sb(III) in the form of $SbCl_3$ (Carlo Erba, Normex®) in 3 mol l^{-1} hydrochloric acid. Standard solution of Sb(V) were prepared immediately before use by oxidation with potassium bromate at room temperature.

A stock solution of 5% m/v $NaBH_4$ was prepared by dissolving the solid reagent (BDH, Reagent for Atomic Spectroscopy) in 0.3% m/v NaOH and filtering it through a 0.45 μm membrane. A 0.1% working solution was prepared daily by dilution and adjusting the final NaOH concentration to 0.3% m/v.

A 10% m/v L-cysteine (Fluka Biochemika) stock solution was prepared in 0.05 mol l^{-1} HCl. This solution was stable for up to 2 weeks at room temperature. All other chemicals were of analytical-reagent grade. Water purified with a Milli-Q system (Millipore) was used in all the operations.

2.2. Antimony determination

A continuous flow hydride generation system coupled with non dispersive atomic fluorescence spectrometric detection (HGAFS) was employed for antimony determination during the optimization studies on trivalent antimony recoveries. The system has been described previously [5]. Determinations of antimony in sediment digests were performed both with the above described HGAFS system and by in-situ trapping of stibine in a graphite atomizer (HG-ETAAS). The integrated platform of the graphite furnace was permanently modified by a Zr-Ir treatment, as detailed elsewhere [6]. For the latter method, a Perkin-Elmer Model 4100ZL atomic absorption spectrometer with transverse-heated graphite atomiser and longitudinal Zeeman-effect background correction were employed. In the case of HG-ETAAS, stibine was generated by using a FIAS-400 flow-injection system. Experimental details on FI-HG-ETAAS coupling are reported elsewhere [7].

2.3. Certified reference materials

Sediment certified reference materials (CRMs) were obtained from the National Research Council of Canada (Ottawa, Canada), viz. Marine Sediment Reference Material (MESS-1 and BCSS-1) and from Institute of Reference Materials and Measurements, Commission of the European Communities (Geel, Belgium), viz., Estuarine Sediment (CRM-277) and River Sediment (CRM-320).

2.4. Sample decomposition

Digestion procedures for antimony standard solution and for sediments (0.1–0.2 g) were carried out in Parr Teflon bombs (Model 4782) for microwave digestion.

Reversed aqua regia (HNO_3-HCl, 3:1, 4 ml) containing different amount of 50% w/v hydrofluoric acid up to a maximum of 1 ml was used in all cases. The bombs were microwave heated at 850 W for 1 min followed by 1 min at 0 W. The cycle was repeated ten times. After cooling, the contents of each bomb were transferred to a 50 ml polyethylene calibrated flask containing 5 ml of the L-cysteine solution and 10 ml of 2.5% m/v H_3BO_3 and diluted to the mark with 1 mol l^{-1} HCl. A pre-reduction step was then carried out in a water bath at 80°C for 60 min. Aliquots of 10 ml of the resulting solution were transferred to 25 ml polyethylene calibrated flasks containing

2.5 ml of the L-cysteine solution. For the quantification of Sb in sediments, the standard addition method was employed, unless otherwise specified.

3. Results and discussion

3.1. Removal of fluoride interference

The interference of fluorides on the reduction of Sb(V), both to the trivalent state and to stibine with $NaBH_4$, could be explained by the formation of fluoro complexes of the type [2]

$$SbO(OH)_3 \overset{HF}{\rightleftharpoons} [SbF_n(OH)_{6-n}]^- \ (n = 0,1,..6) \quad (1)$$

In a previous paper [5] it has been observed that the simultaneous addition of hydrofluoric acid and L-cysteine to a Sb(V) solution produced only moderate interference effects on the determination of antimony by hydride generation. This indicates that L-cysteine was able to reduce Sb(V) to Sb(III) in the presence of fluorides. The same was not true if the addition of the L-cysteine was made a few minutes later, i.e. to Sb(V) solution already containing hydrofluoric acid.

The reduction of Sb(V) to Sb(III) with L-cysteine, by analogy with the behaviour of arsenic [8,9] leads to the formation of thiol-antimony(III) compounds (thiolates) according with reaction:

$$SbO(OH)_3 + 5RSH \rightarrow Sb(S-R)_3 + RS-SR + 4H_2O \quad (2)$$

The behaviour of Sb(V) in the presence of HF and L-cysteine described above, could be explained assuming a competition between reactions, Eq. (1) and Eq. (2).

We have tried to verify whether the competition between these two processes is influenced by the temperature. After treatment of a standard solutions of Sb(V) (4 ng ml^{-1}) with different amount of hydrofluoric acid (final concentration in the range of 0.023–0.23 mol l^{-1}), the addition of 1% L-cysteine was not able to recover the antimony at any hydrofluoric acid concentration neither in hydrochloric or nitric acid media nor in their mixtures (total acidity in the range of 1–2 mol l^{-1}). After heating at 80°C for 60 min, quantitative recoveries were obtained in hydrochloric acid and in nitric-hydrochloric acid media, but not in nitric acid media only. The depressive effect of nitric acid and the positive effect of hydrochloric acid could be related to the competition of chloride ions with fluorides in the complexation of Sb(V), while nitrate ions cannot exerts any complexing action.

Boric acid, which complexes the fluorides according to the reaction:

$$H_3BO_3 + 4HF \rightleftharpoons BF_4^- + H_3O^+ + 2H_2O \quad (3)$$

was not able to remove fluoride interference as reported by Petrick and Krivan [2]. In the present work, boric acid was added to sample digests in order to avoid attack of glassware parts of hydride generation apparatus. It was observed that when it was added before the prereduction step together with L-cysteine, it allowed improved recoveries also in nitric acid medium.

From the above preliminary studies had become evident that numerous experimental parameters play a role in the quantitative reduction of Sb(V) to Sb(III) in the presence of hydrofluoric acid. The prereduction step required a careful optimization of the experimental parameters as reported in the next section.

3.2. Optimization of prereduction step

The recovery of Sb(III), $Y(\%)$, was systematically investigated as a function of different experimental parameters (Table 1). A total of 124 independent experiments were performed. The results are fitted with a polynomial function containing linear and squared terms:

Table 1
Parameters employed in the analysis of variance

Parameters	Values
Acidity (HCl-HNO_3) (mol l^{-1})	(1:0), (2:0), (0:1), (0:2), (1:1)
L-cysteine (% m/v)	1
HF (mol l^{-1})	0, 0.023, 0.06, 0.12, 0.23
H_3BO_3 (mol l^{-1})	0, 0.08, 0.16
Temperature (°C)	25, 60, 70, 80
Time (min)	0, 15, 30, 60, 90

Table 2
Results of model fitting

Independent variable	Coefficient	S.D.	Significance level (*P*-value)*
Temp.	0.64	0.21	0.0033
[HCl]	8.52	3.05	0.0063
$[HNO_3]$	−14.02	7.67	0.0702
$[H_3BO_3]$	835.40	85.65	0.0000
[HF]	−124.58	19.76	0.0000
$[H_3BO_3]\cdot$temp.	−8.64	1.36	0.0000
Time·temp.	0.00894	0.0034	0.0101
Time·$[HNO_3]$	0.0854	0.128	0.5075

$R^2 = 0.9380$; 124 observations fitted.
* for difference with respect to zero.

$$Y(\%) = f(\text{time, temperature, [HCl], } [HNO_3], [H_3BO_3], \text{[HF]})$$

For the evaluation of the results it was used the ANOVA (analysis of variance), a statistical technique capable of estimating, on the base of a set of experiments performed according a plan of experimental design (see Table 1), the significance of various factors and their interaction on measurements. More details about ANOVA can be found elsewhere [10,11]. The results of model fitting ANOVA are given in Table 2 and Table 3, respectively, for the most significant terms. Determination of Sb in sediments certified reference material is given in Table 4.

From Table 2 can be inferred that the model was able to explain about 94% of the total variance ($R^2 = 0.9380$) and that all the independent variables considered, except time·$[HNO_3]$, were significantly different from zero at a level better than 90% ($P < 0.1$). The negative coefficients imply that the relevant variable contributes to depress the yield.

From Table 3, the ANOVA brings to the conclusions that again the variable time·$[HNO_3]$, but also the variable $[HNO_3]$, have a low descriptive power in modelling the recovery of Sb(III). Indeed their *P*-values are greater than 0.5 and 0.2, respectively, in the *F*-ratio test. All the remaining six parameters, having a *P*-value ≤ 0.0000, appear to have a significant descriptive power.

It is interesting to note that while the boric acid concentration and temperature contribute positively to the yield, the squared terms containing both these variables can contribute to a dramatic decrease of the yield.

Table 3
Analysis of variance for the fitted model

Independent variable	Σx^2	df	*F*-ratio	Significance value (*P*-value)
Temp.	505 479.446	1	1586.62	0.0000
[HCl]	29 812.992	1	93.58	0.0000
$[HNO_3]$	431.423	1	1.35	0.2469
$[H_3BO_3]$	13 704.922	1	43.02	0.0000
[HF]	15 682.804	1	49.23	0.0000
$[H_3BO_3]\cdot$temp.	15 583.003	1	49.81	0.0000
Time·temp.	13 894.190	1	43.61	0.0000
Time·$[HNO_3]$	140.795	1	0.44	0.5146
Model	594 729.576	8	—	—

Table 4
Determination of Sb in sediments certified reference materials

Sample	Certified (μg g^{-1})	Found (μg g^{-1})	
		HGAFS	HG-ETAAS
BCSS-1	0.59 ± 006	0.63 ± 0.04^{a}	$0.63 \pm 0.04^{a,b}$
			$0.57 \pm 0.01^{b,d}$
			$0.57 \pm 0.02^{a,d}$
MESS-1	0.73 ± 0.08	0.77 ± 0.04^{a}	0.74 ± 0.02^{a}
			0.73 ± 0.09^{b}
CRM-320	(0.6)[c]	0.46 ± 0.02^{a}	$0.53 \pm 0.06^{a,b}$
CRM-277	(4.0)[c]	3.5 ± 0.06^{a}	3.3 ± 0.02^{a}

[a] standard additions; [b] calibration graph; [c] information value only; [d] independent set of measurements.

From the above results a straight forward choice can not be made of working conditions giving a maximum yield. Indeed, different sets of experimental conditions can be used to obtain quantitative recoveries. A rational choice would be to employ relatively mild conditions to allow quantitative recoveries of antimony within 60 min. Thus, the optimized experimental conditions were: digestion time 60 min, temperature 80°C, concentration of reagents 0.08 mol l^{-1} H_3BO_3 and 1% L-cysteine. These conditions were further verified and the results are illustrated in Fig. 1. The simultaneous presence of boric acid and L-cysteine allows obtaining quantitative recoveries independently of acid mixture composition (including HNO_3 alone) as well as of hydrofluoric acid concentration.

3.3. Sediment analysis

Several authors mentioned that aqua regia or reversed aqua regia are the most suitable acid mixtures in order to obtain quantitative extraction of antimony from sediments, soils, sludges and geological materials [12,13]. This extraction, however, gives acceptable results only in some cases, e.g. when digests are not allowed to stay in contact with the undissolved silica residues. Otherwise with digests aged for several hours or overnight, recoveries were lower (within 45 and 75%) and precision was dramatically impaired to RSDs as high as 50%.

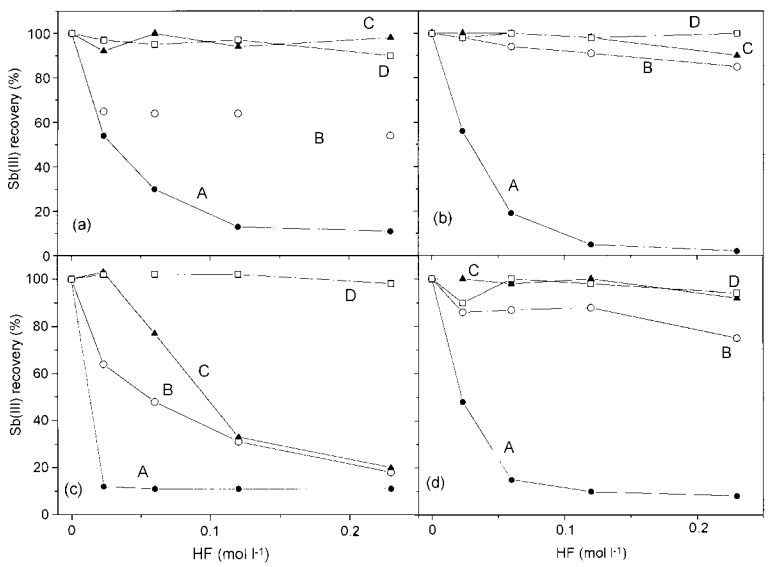

Fig. 1. Reduction of Sb(V) to Sb(III) with 1% L-cysteine in the presence of different concentration of hydrofluoric acid and under different experimental conditions. Reaction time 60 min. Reaction media (a) HCl 2 mol l^{-1}; (b) HNO_3 1 mol l^{-1} + HCl 1 mol l^{-1}; (c) HNO_3 2 mol l^{-1}; (d) HNO_3 0.35 mol l^{-1} + HCl 1 mol l^{-1}. Different curves are referred to (A) no boric acid, temp. 25°C; (B) boric acid 0.08 mol l^{-1}, temp. 25°C; (C) no boric acid, temp. 80°C; (D) boric acid 0.08 mol l^{-1}, temp. 80°C.

Therefore, the complete dissolution approach with HF-containing acid mixtures was considered more reliable.

The digestion procedure with reversed aqua regia plus HF was tested in analyses of several sediment CRMs: MESS-1, BCSS-1, CRM-320 and CRM-277.

For the MESS-1 and BCSS-1 samples, the results are in good agreement with certified values using both HGAFS and HG-ETAAS.

For CRM-320 and CRM-277 sediments information values only are given by the manufacturer for total antimony level. In this case recoveries appear to be relatively low, 76 and 87%, respectively, by using HGAFS. The results obtained by HG-ETAAS are in good agreement with those obtained by HGAFS. The above discrepancy is not easy to explain. Even if an assumption is made about the occurrence of some residual interference from hydrofluoric acid, it seems unlikely that such interference takes place only with this kind of sediments.

It is worth mentioning that the standard addition method of calibration cannot be avoided in HGAFS technique. The HG-ETAAS method gives accurate results using both modes: calibration curve and standard additions. This more favourable performance may be due to the fact that in HG-ETAAS are employed higher dilution factors and, moreover, some possible sources of interferences such as liquid-phase kinetics effects, transport and atomization interferences are better tolerated.

4. Conclusion

Quantitative decomposition of sediments for total antimony determination can be achieved only in the presence of hydrofluoric acid. Interference of hydrofluoric acid can be then eliminated by performing prereduction to Sb(III) with mixtures of L-cysteine and boric acid at 80°C for less than 1 h. Hydride generation AFS and AAS determinations in sediment digests are sensitive and reliable.

Acknowledgements

Technical assistance of Mr Marco Mascherpa of C.N.R, Istituto di Chimica Analitica Strumentale is gratefully acknowledged. Financial support to D.L.T. by the Consiglio Nazionale delle Ricerche, Istituto di Chimica Analitica Strumentale, Pisa, is gratefully acknowledged. This work was supported in part by the Ministry of University, Scientific Research and Technology (Progetto Speciale Sistema Lagunare Veneziano), Italy. R. Zamboni thanks the CNR, National Commitee for the Environment and Habitat Technologies, Italy, for the financial support.

References

[1] K. Tsujii, Anal. Lett. 14 (1981) 181.
[2] K. Petrick, V. Krivan, Anal. Chem. 59 (1987) 2476.
[3] H. Chen, I.D. Brindle, S. Zheng, Analyst 117 (1992) 1603.
[4] B. Welz, M. Šucmanová, Analyst 118 (1993) 1417.
[5] A. D'Ulivo, L. Lampugnani, G. Pellegrini, R. Zamboni, J. Anal. At. Spectrom. 10 (1995) 969.
[6] D.L. Tsalev, A. D'Ulivo, L. Lampugnani, M. Di Marco, R. Zamboni, J. Anal. At. Spectrom. 10 (1995) 1003.
[7] D.L. Tsalev, A. D'Ulivo, L. Lampugnani, M. Di Marco, R. Zamboni, J. Anal. At. Spectrom. 11 (1996) 979.
[8] X.-C. Le, W.R. Cullen, K. Reimer, Anal. Chim. Acta 285 (1994) 277.
[9] H. Haraguchi, A. Takatsu, Spectrochim. Acta Part B 42 (1987) 235.
[10] D.L. Massart, B.G.M. Vandeghinste, S.N. Deming, Y. Michotte, L. Kaufman, Chemometrics: A Textbook, Elsevier, Amsterdam, 1988, pp. 59–74.
[11] R. Caulcutt, R. Boddy, Statistics for Analytical Chemists, Chapman and Hall, London, pp. 126–197.
[12] A. Kuldvere, Analyst 114 (1989) 125.
[13] A.D. Hewitt, J.H. Cragin, Environ. Sci. Technol. 25 (1991) 986.

ELSEVIER

Talanta 45 (1998) 807–815

Talanta

Direct electrothermal atomic absorption spectrometry determination of nickel in sea water using multiple hot injection and Zeeman correction

Pilar Bermejo-Barrera *, Jorge Moreda-Piñeiro, Antonio Moreda-Piñeiro, Adela Bermejo-Barrera

Department of Analytical Chemistry, Nutrition and Bromatology, Faculty of Chemistry, University of Santiago de Compostela, Avenida de las Ciencias s/n, 15 706 Santiago de Compostela, Spain

Received 21 February 1997; received in revised form 13 May 1997; accepted 21 May 1997

Abstract

Methods for the direct determination of Ni in sea water samples by ETAAS were developed using Zeeman effect background correction system (ZEBC) and a multi-injection technique. A mass of palladium nitrate of 2.5 μg (for an injection volume of 100 μl) was used as chemical modifier. The optimum pyrolysis and atomization temperatures were 1700 and 2100°C, respectively. The characteristic mass (m_0) and characteristic concentration (C_0), precision and accuracy were studied for different injection volumes (20, 100 and 200 μl). For an injection volume of 100 μl (five 20 μl aliquot) of sample the accuracy analysis of different certified materials (saline and non saline water) was agreeable. The total time of the proposed procedure is 6 min. A m_0 and C_0 of 34.5 pg and 0.3 μg l^{-1}, respectively were obtained for this injection volume (100 μl). Finally, interferences from major and minor components of sea water was studied.

Keywords: Nickel; Sea water; ETAAS; Multiple injection; Hot injection; Zeeman correction

1. Introduction

Nickel enters to aquatic system from dissolution of rocks and soils from biological cycles, from atmospheric fallout and specially from industrial process and water disposal [1]. The determination of nickel in coastal sea waters is being increasing in contamination studies due to the need to guarantee a good quality of the sea water for several uses. Thus, nickel is enclosed in the european directive (79/923/CEE) [2] relative to quality of water used to keep molluscs [2].

Electrothermal atomic absorption spectrometry (ETAAS) was used for the direct determination of traces of nickel in several water samples [3–10]. However, considerable difficulties can be encountered in the direct determination of nickel in sea water, owing to the concentration is minute. Sea water contains 0.1–0.5 μl Ni l^{-1} (mainly in form of Ni^{2+} cation and of chloro and carbonato-com-

* Corresponding author.

PII S0039-9140(97)00159-8

Table 1
Nickel determination in sea water by ET-AAS

Preconcentration	Background corrector	Chemical modifier	LOD	Reference
No	Zeeman	$Mg(NO_3)_2$	—	[7]
No	Zeeman	NH_4NO_3	—	[8]
No (signal summation)	Zeeman	No	2.4 μg l^{-1}	[10]
Complexation with DEDC, extraction into Freon-TF and reextraction into diluted nitric acid	—	No	—	[11]
Complexation with APDC and dithizone and extraction into $CHCl_3$	Zeeman	No	0.25 μg l^{-1}	[13]
Complexation with DEDC and extraction into chloro-toluene	—	No	0.09 μg l^{-1}	[14]
Complexation with APDC and extraction into 1,1,1 trichloroethane	D_2	No	0.5 μg l^{-1}	[15]
Complexation with DEDC and extraction into CCl_4	D_2	No	250 pg	[16]
Complexation with 1,1,1-trifluoro-4-mercapto-4-(2-thienyl) but -3-en-2-one-TOPO and extraction into cyclohexene	—	—	—	[17]
Complexation with APDC/NaDEDC extraction into DIBK and reextraction with Pd	Zeeman	Pd	—	[19]
Reductive precipitation by Na-tetrahydroborate	Zeeman	Pd	6 ng l^{-1a}	[22]
Adsorption on Chelex-100, elution HNO_3	—	No	—	[25]
Adsorption on Chelex-100	—	No	20.0 ng l^{-1b}	[26]
Adsorption on silica inmobilzed 8-hydroxyquinoline	D_2	No	—	[27]
Adsorption on Poliorgs VII sorbent	Zeeman	No	—	[28]
Adsorption on unicellular green chlorella algae	D_2	No	—	[30]
Adsorption on Chelamine chelating resin with pentamine ligands	Zeeman	No	18 ng l^{-1a}	[31]
This work, single injection (20 μl)	Zeeman	Pd	1.0 μg l^{-1}	
This work, multiple injection (100 μl)	Zeeman	Pd	0.2 μg l^{-1}/2.6ng l^{-1a}/1.7 ng l^{-1b}	

[a] LOD = 3 S.D. (three times the standard deviation (S.D.) of 11 replicates of the blank of the addition graph).
[b] LOD = 2 S.D. (two times the standard deviation (S.D.) of 11 replicates of the blank of the addition graph).

plexes), this concentration are lower at the surface and higher in greater depth [1]. Occasionally sea water contain much higher nickel concentration owing to nickel pollution of water. Thus, several authors use previous preconcentration procedures (extractive, coprecipitation and ion exchange methods) that allow an increase on sensitivity of nickel determination by ETAAS [11–33]. These procedures used for the nickel determination in sea water samples are summarized in Table 1.

However, these methods consume time and are associated with the risk of contamination. Therefore the direct determination of nickel in sea water reached by using multi-injection technique remains of great interest.

In the present work by using chemical modification and Zeeman effect background correction, a preconcentration of the nickel into the graphite tube using a multi-injection technique is developed. The method optimized was applied to the direct nickel determination in several references materials and in sea water samples. The results were compared with obtained with a deuterium arc background correction with a conventional atomizer (DABC).

2. Experimental

2.1. Apparatus

A Perkin-Elmer Zeeman 4100 ZL atomic absorption spectrometer equipped with an AS-71 autosampler and a Perkin-Elmer 1100B atomic

Table 2
Graphite furnace temperature programme and spectrometer operating conditions

Step	Temperature (°C)	Ramp time(s)	Hold time(s)	Argon flow (ml min^{-1})
Drying	130	1	5	300
	150	5	30	300
Pyrolysis	1700	10	10	300
Atomization	2100	0	3	0 (read)
Cleaning	2600	1	3	300

Ni hollow cathode lamp: wavelength, 232.0 nm; lamp current, 25 mA; spectral bandwidth: 0.2 nm; integration time, 3s. Peak area measurements. Transverse heated graphite atomizer (THGA) with integrated platform.

absorption spectrometer equipped with HGA-700 and an autosampler AS-70 were used for nickel determination. The spectrometer operating conditions are shown in Table 2.

2.2. Reagents

All the solutions were prepared from analytical-reagent grade chemicals using ultrapure water, resistivity 18 MΩ cm^{-1}, which was obtained by a Milli-Q water purification system (Millipore). Nickel nitrate stock standard solution, 1.000 g l^{-1}; supplied by Merck (Darmstadt, Germany). Palladium nitrate stock standard solution, 3.000 g l^{-1}; obtained from palladium supplied by Aldrich, prepared according to the procedure of Welz et al. [34]. Synthetic sea water samples of high 72.8‰ (SSWI) and low 34.2‰ (SSWII) salinity, prepared according to [35–37]. Certified water materials, saline (NASS-4, supplied by the Research Council of Canada and CRM-403, supplied by the Commission of the European Communities) and non saline (IAEA/W-4 supplied by the International Atomic Energy Agency and SLRS-2 supplied by the Research Council of Canada) were used to achieved to accuracy of the method. Argon N-50 purity (99.999%), use as sheath gas for the atomizer and to purge internally was obtained from SEO (Madrid, Spain).

2.3. Procedure for sample collection

Sea water samples were collected from coastal surface water from Galicia (north west, Spain) in 100 ml glass bottles, the samples were acidified with 100 μl of concentrated nitric acid [38], this brings a $pH < 1.6$ avoiding the adsorption of nickel onto the glass bottle walls.

2.4. Procedure

A portion of the sea water sample, 600 μl, with appropriate volumes of palladium nitrate solution, to get concentrations of 25 mg l^{-1}, was transferred into the autosampler cup, then it was completed to 1 ml and stirred before measurements. A volume of 20 μl was injected into the atomizer five times inserting a drying step between each injection. Sequential dry-ash-atomizer-clean programme (Table 2) of the graphite furnace was run and the integrated absorbance recorded. The graphite tube can be cycled with this procedure around 700 times. The total time of the proposed procedure is 6 min, around ten samples per h.

3. Results and discussion

3.1. Optimum conditions

Experiments were carried out to determine the optimum temperatures and times for the drying, pyrolysis and atomization steps for solutions prepared from 600 μl of the sea water sample diluted to 1 ml, spiked with 40 μg l^{-1} of Ni^{2+} and the adequate concentration of palladium nitrate as chemical modifier.

The drying step was optimized to reach a satisfactory drying of 100 (five 20 μl aliquots) of sample, then two drying steps required.

The pyrolysis curves obtained for Ni^{2+} aqueous standard solution (40 μg l^{-1}), synthetic

sea water samples (SSWI and SSWII) and real sea water sample spiked with 40 μg l^{-1} of Ni^{2+}, are shown in Fig. 1. In these experiments, the atomization temperatures was 2100°C. On the other hand, the atomization curves are also shown in Fig. 1 for the same solutions, being 1600°C the pyrolysis temperatures used for all cases. As we can see, the nickel absorbance signal remains constant until 1600°C for aqueous standard solution, real and synthetic sea water samples. The optimum atomization temperatures was 2100°C. The ramp and hold times of the pyrolysis step were also optimized. Results show a great nickel absorbance signal for low ramp rates and hold times a non-tolerable background absorbance was obtained when the bulk of salts from sea water are volatilized in the atomization step. Loss of nickel was observed during the pyrolysis step for ramp and hold times bigger than 10 s.

The background signal obtained for real sea water samples were kept as small than 0.030 and 0.130 s. When an injection volume of 20 and 100 μl were used respectively. For an injection volume of 200 μl, the background signal was 0.250 s. These background signals can be easily corrected using Zeeman effect background correction technique. For injection volumes of 100 and 200 μl, the introduction of intermediate pyrolysis steps among each injection gives us a considerable reduction of the background signal with a poor sensitivity.

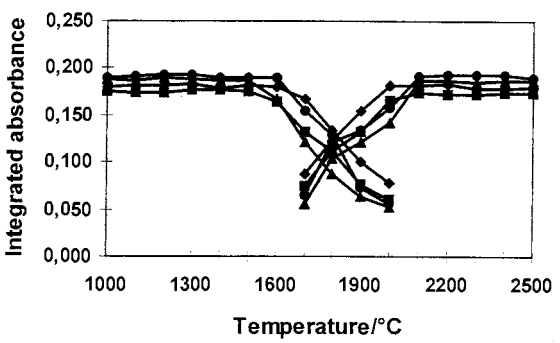

Fig. 1. Pyrolysis (left) and atomization (right) curves obtained for aqueous standard solution of 40 μg l^{-1} of Ni^{2+} (◆), synthetic sea water samples of high (▲) and low (■) salinity ans real sea water sample (●) spiked with Ni^{2+} (40 μg l^{-1}).

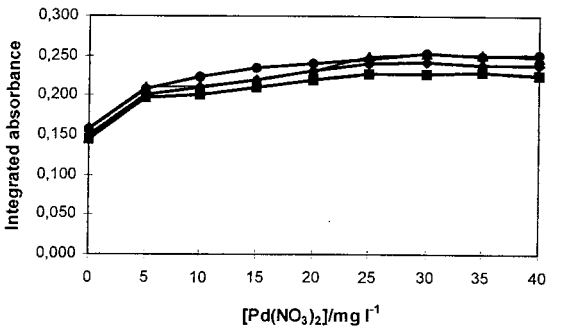

Fig. 2. Dependence of nickel absorbance signal with the amount of palladium nitrate for Ni^{2+} aqueous standard (◆), synthetic sea water of high (▲) and low (■) salinity, and real sea water sample (●).

Although the refractory behaviour of nickel, chemical modification is necessary due to the high salts concentration in the graphite tube achieved by the multi-injection technique. Among the different chemical modifiers proposed for nickel determination in sea water, palladium nitrate provide more consistent performances than the use of other chemical modifiers [39]. Thus, the effect of various amounts of palladium nitrate (0–40 mg l^{-1}) on nickel absorbance signal was studied with a nickel aqueous standard solution, synthetic sea water samples of high and low salinity and real sea water samples spiked with 40 mg l^{-1} of Ni^{2+}. As it can be seen in Fig. 2, the nickel absorbance signal is gradually increased up to 20 mg l^{-1} of $Pd(NO_3)_2$,(for experiments on nickel aqueous standard solution and synthetic sea water sample of low salinity) and to 25 mg l^{-1} of $Pd(NO_3)_2$, for experiments on synthetic sea water samples of high salinity and real sea water samples. Then the nickel absorbance signal remains constant in case of concentrations of $Pd(NO_3)_2$ higher than 20 and 25 mg l^{-1}, respectively.

3.2. Use of a multi-injection technique

The direct determination of nickel in sea water using palladium nitrate as chemical modifier were carried out and the analytical performances for different injection volumes (20, 100 and 200 μl) were studied. Table 2 shows the graphite furnace

Table 3
Calibration and standard addition graphs with different injection volumes

Injection volume (μl)	Aqueous calibration	Calibration SSWII	Calibration SSWI	Standard addition
20	$Q_A = 0.013 + 2.5\ 10^{-3}$ [Ni]	$Q_A = 0.005 + 2.2\ 10^{-3}$ [Ni]	$Q_A = 0.003 + 2.1\ 10^{-3}$ [Ni]	$Q_A = 0.021 + 2.3\ 10^{-3}$ [Ni]
100	$Q_A = 0.006 + 0.011$ [Ni]	$Q_A = 0.012 + 0.012$ [Ni]	$Q_A = 0.013 + 0.021$ [Ni]	$Q_A = 0.018 + 0.013$ [Ni]
200	$Q_A = 0.015 + 0.020$ [Ni]	$Q_A = 0.021 + 0.031$ [Ni]	—[a]	$Q_A = 0.023 + 0.027$ [Ni]

[a] Non-tolerable background signal.

temperature programme used for different injection volumes. The injection of a volume of 100 and 200 μl into the atomizer was reached by the injection of five times 20 and 40 μl aliquots of sea water solution, inserting a drying step among each injection. To reach a satisfactory drying of 40 μl of the sea water solution, a hot injection technique was required. It was found that a hot injection temperature of 120°C was enough to achieve an efficient drying. In addition, a lower pipette speed (40%) was used to increase the drying.

3.2.1. Calibration and addition graphs

Calibration graphs related to synthetic sea water samples (SSWI and SSWII) and nickel aqueous standard solutions were performed for each injection volume. The standard addition method was applied over the same range of concentrations using a real sea water sample. The equations obtained are shown in Table 3, where Q_A is integrated absorbance and [Ni] is the Ni concentration in μg l^{-1}. As it can be seen, the equations corresponding to the two synthetic sea waters, the nickel aqueous standard solution and the real sea water sample show a similar slope for an injection volume of 20 μl when t-test for a confidence level of 95% [40] was applied. Some matrix effect was observed for high salinity for an injection volume of 100 μl. For an injection volume of 200 μl differences on slopes values obtained were important.

Therefore, we can conclude that the calibration curve using aqueous standard solutions could be used for analysis of sea water over all salinities when an injection volume of 20 μl was used. The standard addition method is required for the determination of nickel in sea water of high salinity and an injection volume of 100 μl and for real and synthetic sea water samples when the injection volume was increased to 200 μl.

Table 4
Sensitivity, within-batch precision and recovery corresponding to different injection volumes

Injection volume (μl)	m_0 (pg)	C_0 (μg l^{-1})	LOD (μg l^{-1})	LOQ (μg l^{-1})	[Ni] added (μg l^{-1})	RSD (%)	Analytical recovery (%)
20	38 ± 2	1.9	1.0	3.3	0	9.6	—
					25	8.3	100 ± 3
					50	4.9	103 ± 2
					100	1.6	106 ± 3
100	34 ± 3	0.30	0.2	0.7	0	7.8	—
					10	4.3	103 ± 6
					20	3.5	105 ± 7
					40	2.3	109 ± 8
200	33 ± 4	0.17	0.1	0.3	0	9.5	—
					5	6.5	110 ± 7
					10	4.3	109 ± 9
					20	3.6	107 ± 8

Table 5
Analysis of reference materials corresponding to different injections volumes

Injection volume	SLRS-2	IAEA/W-4	NASS-4	CRM-403
(μl)	1.03 ± 0.10 (μg l^{-1})	2–4 (μg l^{-1})	0.228 ± 0.009 (μg l^{-1})	256.0 ± 21.2 (μg kg^{-1})
20	—	3.2 ± 0.5	—	—
100	0.9 ± 0.06	2.8 ± 0.6	0.232 ± 0.07	267.0 ± 29.2
200	1.1 ± 0.07	3.1 ± 0.6	0.287 ± 0.09	353.6 ± 38.5

Finally, for an injection volume of 200 μl, the calibration equations using synthetic sea water of high salinity could not be obtained due to the insufficient removal of salts. This originates a non-tolerable background signal due to the radiation scattering cause by the residual salt matrix. For this reason, the analysis of sea water of high salinity is not possible using injection volumes of 200 μl.

3.2.2. Sensitivity

The sensitivity of the methods corresponding to each injection volume was studied through two parameters: characteristic mass (m_0) and characteristic concentration (C_0). The limit of detection (LOD) and the limit of quantification (LOQ) [41] were also studied. By performing the necessary measurements, the results for these parameters are shown in Table 4.

Table 6
Effect of different major and minor components of sea water on nickel absorbance signal for a sea water sample spiked with 40 μg l^{-1} of nickel

Interferent	Added as	Interferent concentration added (g l^{-1})	Typical levels of interferent [42] (g l^{-1})	Absorbance signal variation (%)
Cl^-	HCl	20	19.5	−8.2
	NaCl	20	19.5	−9.6
	KCl	20	19.5	−11.7
SO_4^{2-}	H_2SO_4	3	2.7	+2.4
	Na_2SO_4	3	2.7	+0.3
	K_2SO_4	3	2.7	+4.5
HCO_3^-	$NaHCO_3$	0.2	0.15	−9.0
F^-	KF	2×10^{-3}	1.3×10^{-3}	−8.3
$H_2PO_4^-$	NaH_2PO_4	1×10^{-3}	3×10^{-4}	−0.1
IO_3^-	KIO_3	1×10^{-3}	5×10^{-5}	−2.8
NO_3^-	HNO_3	5×10^{-3}	4×10^{-3}	+3.5
MoO_4^{2-}	$(NH_4)_2MoO_4$	1×10^{-3}	1×10^{-5}	−3.4
BO_3^{3-}	H_3BO_3	5×10^{-3}	4.5×10^{-3}	−4.9
SiO_3^{2-}	SiO_3^{2-}	0.2	0.12	[a]
Na^+	NaCl	13	10.8	−9.6
	$NaNO_3$	13	10.8	+6.9
K^+	KCl	3	0.4	−4.7
Mg^{2+}	$MgCl_2$	1.5	1.3	+2.1
	$Mg(NO_3)_2$	1.5	1.3	−7.6
Ca^{2+}	$CaCl_2$	0.4	0.4	+6.9
	$Ca(NO_3)_2$	0.4	0.4	−2.1
Li^+	$LiNO_3$	1×10^{-3}	2×10^{-4}	+0.7

The injection volume was 100 μl.
[a] Non tolerable background signal.

3.2.3. Precision

The within-batch precision of the method obtained for 11 replicates of four sea water samples spiked with different nickel concentrations was investigated for each volume injected. As can be seen (Table 4) a poor precision is achieved for large injection volume. However, the precision is good, RSD values lower than 10%, for all concentration tested, all injection volumes.

3.2.4. Accuracy

The accuracy was obtained analysing two sea water reference material CRM-403 (salinity between 34.6–34.8‰) and NASS-4 (salinity of 31.3‰) with a certified nickel content of 256.0 ± 21.2 ng kg^{-1} and 0.228 ± 0.009 μg l^{-1}, respectively, and a non saline reference material SLRS-2 (riverine water) and IAEA/W-4 (simulated fresh water) with a certified concentration of 1.03 ± 0.10 and 2–4 μg l^{-1}, respectively. The result are show in Table 5. As it can be seen, the increase on the injection volume (200 μl) produces a loss of accuracy. For an injection volume of 20 μl the analysis of CRM-403, NASS-4 and SLRS-2 were not possible due to the high detection limit obtained for this injection volume.

On the other hand, the accuracy was also studied through the analytical recovery. Values of this parameter corresponding to each injection volume are shown in Table 4 where analytical recoveries close to 100% was obtained for all cases.

3.3. Interferences study of major and minor components of the sea water

The effects of major and minor components of the sea water were investigated for an injection volume of 100 μl. Different amounts of the species showed in Table 6 were added to a real sea water sample at a concentration higher than its found in sea water samples [42]. As it can be seen in Table 6, the interferences from major and minor components of the sea water are lower. The higher interferences was obtained for chloride and sodium ions ($+8.2$–11.7%) and for SiO_3^{2-}, for which a non-tolerable background signal was obtained.

3.4. Comparison of the results obtained using deuterium arc background correction with a conventional graphite atomizer (DABC)

The optimum pyrolysis and atomization temperatures achieved using DABC were 1700 and 2600°C. The difference in the atomization temperature is due to the poor efficiency of heating (in comparison with transverse heating) obtained with a conventional graphite atomizer.

For an injection volume of 20 μl no matrix effect were observed. Otherwise for an injection volume of 100 and 200 μl matrix effects were observed for high and low salinity, respectively. In addition the accuracy obtained using the saline reference materials (NASS-4 and CRM-403) were poor even for an injection volume of 100 μl. This fact is due to poor background correction achieved with deuterium arc. For non saline waters (IAEA/W-4 and SLRS), the results obtained are a good agreement with certified values.

The detection limits obtained for 20, 100 and 200 μl were 0.50, 0.13 and 0.07 μg l^{-1}, respectively. As can be seen, the sensitivity using the ZEBC design was lower than DABC design. This fact is due to the atomizer design that affect adversely the spectral absorption as expressed from Beer's law, the length of the graphite tube is 28 mm for DABC and 18 mm for ZEBC design.

Table 7
Nickel levels in several sea water samples[a]

Sample	[Ni] ± S.D. (μg l^{-1})	R.S.D (%)
1	1.0 ± 0.02	2.1
2	1.6 ± 0.03	1.8
3	0.3 ± 0.02	5.2
4	0.7 ± 0.02	3.4
5	0.6 ± 0.02	3.1

[a] $n = 4$

4. Application

The method, by using Zeeman effect background correction, palladium nitrate as chemical modifiers and a multi-injection technique (100 μl) were applied to the determination of nickel in sea

water from Galician coast (North-Western, Spain). A calibration method using synthetic sea water of low salinity (SSWII) was used. The nickel concentration obtained are given in the Table 7, together with the R.S.D.s. The values obtained, between 0.3 and 1.6 μg l^{-1}.

5. Conclusions

The methods for the nickel determination in sea water by ETAAS are summarized in Table 1. As can be seen, by using the multi-injection technique the detection limit achieved are similar or smaller than obtained by the mentioned preconcentration procedures. On the other hand, the use of Zeeman effect background correction and matrix modification allow an efficiently matrix removal and background correction. The sample manipulation, risk of contamination and time consumed associated to conventional preconcentration procedures are considerably reduced.

The results of this work show that nickel can be directly determined in sea water with accuracy and precision using ETAAS with Zeeman effect background corrector and chemical modification with palladium nitrate. A detection limit of 1.0 μg l^{-1} with an injection volume of 20 μl is obtained. The matrix interferences are completely removed, thus, a calibration curve using deionized water can be use for analysis. The detection limit can reduced to 0.2 μg l^{-1} using a multi-injection technique (100 μl) and using the standard addition method.

References

[1] E. Merian (Ed.), Metals and their Compounds in the Environment, VCH, New York, 1991, II.22, 1101.
[2] Directive of the council of 10 November 1979, (79/923/CEE), relative to quality of the water use to keep mollusc, Off. J. Eur. Comm. No. L 281, 1979.
[3] T. Kempf, M. Sonneborn, Mikrochim. Acta, II (5–6) (1983) 445.
[4] D.C. Manning, W. Slavin, Appl. Spectrosc. 37 (1983) 1.
[5] J. Aggett, Analyst 108 (1983) 808.
[6] K.R. Sperling, B. Bahr, Fresenius'Z. Anal. Chem. 314 (1983) 760.
[7] Z. Grobenski, R. Lehmann, B. Radziuk, U. Voellkopf, At. Spectrosc. 5 (1984) 87.
[8] W. Calmano, W. Ahlf, T. Schilling, Fresenius' Z. Anal. Chem. 323 (1986) 865.
[9] M. Hoenig, P. Van Hoeyweghen, A.M. De Kersabiec, Analusis 16 (1988) 18.
[10] H. Berndt, G. Schaldach, Fresenius'J. Anal. Chem. 336 (1990) 567.
[11] L.-G. Danielsson, B. Magnusson, S. Westerlund, K. Zhang, Anal. Chim. Acta 144 (1982) 183.
[12] I. Gustavsson, L. Hansson, Int. J. Environ. Anal. Chem. 17 (1984) 57.
[13] A.M. De Kersabiec, G. Blanc, M. Pinta, Fresenius'Z. Anal. Chem. 322 (1985) 731.
[14] Y. Shijo, T. Shimizu, K. Sakai, Anal. Sci. 1 (1985) 479.
[15] S.C. Apte, A.M. Gunn, Anal. Chim. Acta 193 (1987) 147.
[16] D. Chakraborti, F. Adams, W. Van Mol, K.J. Irgolic, Anal. Chim. Acta 196 (1987) 23.
[17] K. Ueda, K. Kubo, V. Yoshimura, Y. Yamamoto, Bull. Chem. Soc. Jpn. 61 (1988) 2791.
[18] Y. Shijo, T. Shimizu, T. Tsunoda, T. Shiquan, M. Suzuki, Anal. Chim. Acta 242 (1991) 209.
[19] S. Sachsenberg, T. Klenke, W.E. Kumbein, E. Zeeck, Fresenius'J. Anal. Chem. 342 (1992) 163.
[20] R. Boniforti, R. Ferraroli, P. Frigieri, D. Heltai, G. Gueirazza, Anal. Chim. Acta 162 (1984) 33.
[21] S. Nakashima, M. Yagi, Anal. Lett. 17 (1984) 1693.
[22] S. Nakashima, R.E. Sturgeon, S.N. Willie, S.S. Berman, Anal. Chim. Acta 207 (1988) 291.
[23] M. Hirade, Z.-S. Chen, H. Kawaguchi, Anal. Sci. 7 (1991) 65.
[24] T. Nakamura, H. Oka, M. Ishii, J. Sato, Analyst 119 (1994) 1397.
[25] L.-G. Danielsson, B. Magnusson, K. Zhang, At. Spectrosc. 3 (1982) 39.
[26] R. Boniforti, R. Ferraroli, P. Frigieri, D. Heltai, G. Queirazza, Anal. Chim. Acta 162 (1984) 33.
[27] S. Nakashima, R.E. Sturgeon, S.N. Willie, S.S. Berman, Fresenius'Z Anal. Chem. 330 (1988) 592.
[28] G.R. Ishmiyarova, N.I. Shcherbinina, E.M. Sedykh, G.V. Myasoedova, E.K. Vul'fson, Zh. Anal. Khim. 43 (1988) 1981.
[29] S.-C. Pai, Anal. Chim. Acta 211 (1988) 271.
[30] M. Shengjun, J.A. Holcombe, Talanta 38 (1991) 503.
[31] S. Blain, P. Appriou, H. Handel, Anal. Chim. Acta 272 (1993) 91.
[32] C.L. Chakrabarti, Y. Lu, J. Cheng, M.H. Back, W.H. Schroeder, Anal. Chim. Acta 276 (1993) 47.
[33] E.M. Sedykh, Yu.G. Tatsy, G.R. Ishmiyarova, M.M. Ostronova, At. Spectrosc. 15 (1994) 245.
[34] B. Welz, G. Schlemmer, J.R. Mudakavi, J. Anal. At. Spectrom. 3 (1988) 695.
[35] L. Ciaccio (Ed.), Water and Water Pollution, Vol. 1, Dekker, New York, 1971.
[36] K. Grasshoft (Ed.), Methods of Sea Water Analysis. Verlag Chemie, Weinheim, 1976.

[37] D.C. Baxter, W. Frech, Anal. Chim. Acta 225 (1989) 175.
[38] S.N. Willie, R.E. Sturgeon, S.S. Berman, Anal. Chem. 55 (1983) 981.
[39] P. Bermejo-Barrera, J. Moreda-Piñeiro, A. Moreda-Piñeiro, A. Bermejo-Barrera, Quim. Anal. 15 (1996) 249.
[40] J.C. Miller, J.N. Miller, Statistics for Analytical Chemistry, Wiley, New York, 1984.
[41] L. Keith, W. Crummett, J. Deegan, R. Libby, J. Taylor, G. Wentler, Anal. Chem. 55 (1983) 2210.
[42] F.J. Millero, M.L. Sohn, Chemical Oceanography, CRC Press, Boca Raton, Florida, 1992.

ELSEVIER

Talanta 45 (1998) 817–827

Talanta

On the role of solvent in acid–base equilibria of diuretics in acetonitrile–water mixed solvents

J. Barbosa [a,*], D. Barrón [a], J.L. Beltrán [a], S. Butí [b]

[a] *Department of Analytical Chemistry, Universitat de Barcelona, Avda. Diagonal, 647, 08028 Barcelona, Spain*
[b] *Department of Chemical Engineering, Universitat Politécnica de Catalunya, Av. V. Balaguer, s/n, 08800 Vilanova i la Geltrú, Barcelona, Spain*

Received 7 January 1997; received in revised form 21 May 1997; accepted 23 May 1997

Abstract

The dissociation constants of representative loop (furosemide), thiazide (chlorthiazide and trichlormethiazide) and potassium sparing (amiloride) diuretics in 10, 30, 40, 50 and 70% (w/w) acetonitrile–water mixtures at 298.15 K were determined, in accordance with IUPAC procedures. The variation in pK_a values over the whole composition range can be explained by preferential solvation and the structural features in acetonitrile–water mixtures. Correlations between pK_a values and various bulk and solvatochromic properties of the solvents were calculated. The linear solvation energy relationship (LSER) method was applied. The resulting equations allowed us to calculate pK_a values for the diuretics studied in any acetonitrile–water mixture up to 70% (w/w) and should help to clarify the acid–base behaviour of diuretics in the widely-used acetonitrile–water mixed solvents. © 1998 Elsevier Science B.V.

Keywords: Preferential solvation; Linear solvation energy relationship; pK values; Acetonitrile–water mixtures; Diuretics

1. Introduction

Diuretics are widely used in the treatment of congestive heart failure and hypertension [1]. Most increase urinary potassium excretion and can cause hypokalemia in patients taking them for a prolonged period, either covertly or on prescription. Diuretics are also used to enable athletes to lose weight quickly so that they can be included in lower weight categories in certain sports (e.g. weightlifting, judo or taekwondo) and to dilute a urine specimen in a deliberate attempt to avoid detection during the drug test [2]. For this reason, the Medical Commission of the International Olympic Committee has banned diuretics. During the Olympic games in Seoul, four athletes tested positively for the loop diuretic furosemide.

Liquid chromatography (LC) is widely used for the separation and determination of diuretics, which are generally unchanged on excretion [3]. The optimization of chromatographic selectivity can be achieved by taking into account the ionization constant and the capacity factors of the ionized and non-ionized forms of the analytes [4].

* Correspondence address. Tel.: + 34 3 4021279; fax: + 34 3 4021233.

PII S0039-9140(97)00167-7

Acetonitrile is a widely-used organic modifier in LC. Recently, the linear solvation energy relationship (LSER) based on the Kamlet-Taft multiparameter scales [5,6] has been used to predict the retention of a series of peptides [7], anabolic steroids [8,9] and quinolones [10], using acetonitrile–water mixtures as mobile phase. However, this approach only permits the optimization of the content of the organic modifier in the mobile phase, but provides no information about the pH of this phase, which is important in understanding the retention process [11].

The difficulties encountered in measuring the pH and in obtaining pK values in acetonitrile–water mixtures have led to the use of pH measurements and analyte pK values obtained in aqueous medium for predicting analyte behaviour in acetonitrile–water mobile phases used in LC. However, acetonitrile is an aprotic dipolar solvent with a relatively high dielectric constant ($\epsilon = 36.2$), $pK_{ap} = 33.6$ [12,13] and weaker solvatochromic characteristics than water, polarity/polarizability, $\pi^* = 0.75$, hydrogen bond acidity, $\alpha = 0.19$ and hydrogen bond basicity, $\beta = 0.31$ [14]. Thus, acetonitrile is a weaker solvent than water.

In a previous study [15] pH values were assigned to primary standard buffer solutions for the standardization of potentiometric sensors in acetonitrile–water mixtures, in accordance with the NIST multiprimary standard scale [16]. pH can thus be measured in these media as it can in water [17]. However, the few pK_a values for acetonitrile–water mixtures reported in the literature [11,18–20] differ substantially from those found in water. The addition of acetonitrile as an organic modifier increases the magnitude and range of pH measurements and ionization constants in a complex way [11,21] as was proved in a previous paper in which a series of quinolones have been studied [19]. Consequently, the pH required to maximize the retention of solutes by ion suppression might differ from that predicted when taking into account the pH and pK_a values in aqueous media. Thus, the study of the acid–base behaviour of analytes in acetonitrile–water media might be very important in predicting the influence of pH on retention and selectivity in LC.

The aim of this study is to determine the pK_a values of four diuretics in 10, 30, 40, 50 and 70% (w/w) acetonitrile–water mixtures in accordance with IUPAC procedures [11]. The diuretics chosen include compounds with different molecular structures and physico-chemical properties: furosemide, an acidic loop diuretic compound; chlorthiazide and trichlormethiazide, weakly acidic compounds of the major thiazide group; and amiloride, a basic potassium sparing diuretic. The pK_a values obtained, over the whole composition range studied, can be explained by the preferential solvation of ionizable compounds in acetonitrile–water mixtures. The results are discussed in terms of the average macroscopic properties of the mixed solvents and the possible variation in microheterogeneity of the solvation shells around the solute. Relationships between pK_a and various bulk properties (such as the dielectric constant) were examined and the linear solvation energy relationship (LSER) method [22] was used to correlate pK_a values with solvent polarity/polarizability (π^*), solvent hydrogen bond donating acidity (α) and solvent hydrogen bond accepting basicity (β). The equations obtained allowed us to calculate pK_a values of diuretics in any acetonitrile–water mixture up to 70% (w/w) and to determine the acid–base behaviour of these substances in acetonitrile–water media.

2. Experimental

2.1. Apparatus

Potentiometric measurements were performed with a Crison micropH 2002 meter, equipped with a Crison-Ingold 102623015 glass electrode and an Ag/AgCl reference electrode prepared according to the electrolytic method [13] and directly immersed in the solution to avoid residual liquid junction potential. The glass electrode was stored in water when not in use and soaked for 15–20 min in acetonitrile–water before potentiometric measurement.

The reference electrode was stable for 3 months and throughout this time the standard potential in

each solvent, E°, remained essentially constant (standard deviation, $s < 0.6$ mV). The electrode system was standardized each time the solvent medium was changed, and the constancy of E° values was ensured by means of periodic calibrations. The stabilization criterion for emf readings was 0.2 mV within 2 min; if stabilization was not achieved after 10 min (in the zone near of equivalence points), more titrant was added. The system gave stable, reproducible potentials within 4 min. The potentiometric measurements were performed in a double-walled vessel maintained at 25 ± 0.1°C by circulating water. The titrant was added from a Metrohm Dosimat 665 autoburette. The potentiometric system was controlled automatically with a PC microcomputer.

2.2. Reagents

Analytical reagent grade chemicals were used unless otherwise indicated.

All solutions were prepared by mixing double-distilled freshly boiled water whose conductivity did not exceed 0.05 μS cm^{-1} and acetonitrile (Merck, chromatography grade).

Potassium hydroxide (0.1 M) working solutions were obtained by diluting a concentrated solution (1 M, Merck), prepared with an ion-exchange resin to avoid carbonation, and were standardized volumetrically against potassium hydrogen phthalate using phenolphthalein as indicator. The concentration of KOH solution was 0.02 M when using 70% (w/w) acetonitrile–water because of its low solubility in this medium. HCl 0.05 M solutions were prepared by diluting the commercial reagent (Merck, 25%).

Furosemide, chlorothiazide, trichlormethiazide and amiloride (hydrochloride) were supplied by Sigma.

2.3. Procedures

The pK_a values of the diuretics were determined by titration of appropriate solutions of acid species in 10, 30, 40, 50 and 70% (w/w) acetonitrile–water mixtures using potassium hydroxide solutions in the same mixture as titrant and approximately 7×10^{-3} M KCl solution for the correct response of the electrode system. For amiloride, which is a basic diuretic, an excess of HCl solution was added so that it was fully protonated at the beginning of the titration.

pK_a values were obtained from systematic measurements of the emf of the cell:

$$\mathrm{Pt|Ag|AgCl|HA + A + KCl\ in\ acetonitrile - water|GE}$$

where HA and A are the acidic and basic species involved in the dissociation equilibrium studied. The emf, E, of this cell is directly related to the activities of the hydrogen and chloride ions in solution:

$$E = E^{\circ} + g \log(a_{H^+} \cdot a_{Cl^-}) \quad (1)$$

where E°, the standard emf of the cell, was determined as in a previous study [13] and g is the Nernst coefficient.

The dissociation constant for these species could be expressed as:

$$K = \frac{c_A \gamma_A c_{H^+} \gamma_{H^+}}{c_{HA} \gamma_{HA}} \quad (2)$$

Thus, the equation that gives pK_a is:

$$pK_a = \frac{E^{\circ} - E}{g} + \log \frac{c_{HA} \gamma_{HA} c_{Cl^-} \gamma_{Cl^-}}{c_A \gamma_A} \quad (3)$$

where c_{HA} and c_A are the molar concentrations of acidic and basic species, c_{Cl^-} is the molar concentration of the mixed electrolyte KCl and γ_x is the molar activity coefficient of species x.

In the case of furosemide, for which $pK < 5$, computation of c_{HA} and c_A values required knowledge of c_{H^+}, which is in turn a function of the molar activity coefficient γ, which could be calculated using the Debye-Hückel equation:

$$p\gamma_{Cl^-} = \frac{AI^{1/2}}{(1 + a_o B I^{1/2})} \quad (4)$$

where A and B are the Debye-Hückel constants, a_o is the ion size parameter in the solvent mixture and I is the ionic strength. Values of A and $a_o B$ at 25°C at different percentages of acetonitrile in all mixtures with water have been reported in previous studies [13,23].

Calculation of $p\gamma_{Cl^-}$ requires knowledge of the ionic strength I of the HA + A + KCl mixed electrolyte solution. I is a function of the c_{H^+}, which is expressed by:

$$pc_{H^+} = \frac{E^o - E}{g} - pc_{Cl^-} - p(\gamma_{H^+}\gamma_{Cl^-}) \quad (5)$$

Thus, determination of pK_a values requires an iterative cycle for each point of the potentiometric titration at which E is measured. The calculation begins with $I = c_A + c_{Cl^-}$ and γ_{Cl^-} values are obtained, using the Debye-Hückel equation, for their subsequent use in obtaining pc_{H^+} values and a better value of I and so on, until the constancy of I values is obtained.

The difference between the two ionization constants of amiloride is small and the second ionization equilibrium of the diuretics took place in very alkaline conditions. Thus, the calculations were carried out with the program written in PASCAL, PKPOT [23]. The least-squares PKPOT program allows the determination of thermodynamic acid–base constants, in aqueous and non-aqueous media, taking into account the activity coefficients of the species. These mathematical procedures also permit the determination of pK_a values in overlapping ranges ($pK_i - pK_j < 2$) and dissociation constants in very alkaline conditions. The procedures are based on the postulation of a chemical model, i.e. of an initial set of species defined by their stoichiometric coefficients and formation constants, which are then refined by least-squares minimization.

3. Results and discussion

Emf measurements for the cell were taken at different concentrations of acidic, HA, and basic, A, species of diuretics in 10, 30, 40, 50 and 70% (w/w) acetonitrile–water solvent. For each diuretic in each solvent mixture studied, from four to six series of measurements were performed, for a total of 1600 independent measurements over the solvent interval explored. To simplify the tabulation, and as an example, one series of measurements for one titration of trichlormethiazide in 30% (w/w) acetonitrile–water using KOH solution in the same solvent as titrant is given in Table 1, where V_o is the initial volume of solution (ml), V_e the equivalence volumes, [KOH] the titrant concentration, [KCl] the initial KCl concentration, and E^o the standard emf of the cell, previously standardized. For each volume of titrant added, V, the emf value, E, was measured. [H_2A] is the concentration of acidic species, [HA^-] the concentration of intermediate species, [A^{2-}] the concentration of basic species and [K^+], [Cl^-] and [H^+] the concentrations of potassium, chloride and hydrogen ions at each point of the titration. The calculations were made using the program written in PASCAL, the PKPOT previously reported [24].

Table 2 shows the ionization constant values determined for the series of four diuretics studied in 10, 30, 40, 50 and 70% (w/w) acetonitrile–water mixtures and the respective standard deviation, s, together with the pK_a values in water previously reported [21].

As is shown in Table 2, all diuretics studied have two pK_a values corresponding to two acid–base functional groups. Values obtained for furosemide, the loop diuretic, are consistent with the protolytic equilibrium of carboxylic acid which occurs in acid media and the dissociation of the sulphonamide group (Fig. 1) under alkaline conditions [25]. The pK_2 of chlorthiazide and trichlormethiazide (Fig. 1) are similar to the values of furosemide and can be assigned to the dissociation of the sulphonamide group. Thus, the pK_1 of these diuretics could be assigned to the other ionizable hydrogen, as shown in Fig. 1.

The reaction of amiloride with hydrochloric acid is equimolar: from potentiometric titrations of amiloride hydrochloride solutions or amiloride with an excess of HCl solutions with KOH, the same results are obtained. Thus, pK_1 corresponds to the deprotonation of the aliphatic amino group and pK_2 to the ionization of the amide functional group.

The few pK_a values of diuretics cited in the literature correspond to values in water and are shown in Table 2 [26]. However, other data in the literature, such as $pK_1 = 8.6$ for trichlormethi-

Table 1
pK values of trichlormethiazide in 30% (w/w) acetonitrile–water

V_o (ml)	V_e (ml)		[KCl] (M)	[KOH] (M)	E^o (mV)		
20	1.80	3.60	6.79e-3	0.0196	423.3		
V (ml)	E (mV)	$[K^+]$	$[Cl^-]$	$[H^+]$	$[H_2A]$	$[HA^-]$	$[A^{2-}]$
0.10	−111.24	6.85e-3	6.76e-3	1.64e-7	1.64e-3	1.55e-4	1.60e-8
0.20	−125.94	6.92e-3	6.72e-3	9.48e-8	1.53e-3	2.52e-4	4.48e-8
0.30	−136.40	6.98e-3	6.69e-3	6.42e-8	1.43e-3	3.47e-4	9.15e-8
0.40	−144.80	7.04e-3	6.65e-3	4.68e-8	1.32e-3	4.41e-4	1.60e-7
0.50	−151.92	7.10e-3	6.62e-3	3.57e-8	1.22e-3	5.34e-4	2.54e-7
0.60	−158.40	7.16e-3	6.59e-3	2.80e-8	1.12e-3	6.26e-4	3.81e-7
0.70	−164.40	7.22e-3	6.56e-3	2.22e-8	1.02e-3	7.18e-4	5.50e-7
0.80	−170.22	7.28e-3	6.53e-3	1.79e-8	9.21e-4	8.08e-4	7.72e-7
0.90	−175.92	7.34e-3	6.49e-3	1.44e-8	8.23e-4	8.97e-4	1.07e-6
1.00	−181.66	7.40e-3	6.47e-3	1.16e-8	7.27e-4	9.86e-4	1.46e-6
1.10	−187.60	7.46e-3	6.44e-3	9.23e-9	6.31e-4	1.07e-3	1.99e-6
1.20	−193.98	7.52e-3	6.41e-3	7.27e-9	5.36e-4	1.16e-3	2.74e-6
1.30	−200.90	7.57e-3	6.38e-3	5.60e-9	4.43e-4	1.24e-3	3.82e-6
1.40	−208.60	7.63e-3	6.35e-3	4.17e-9	3.51e-4	1.33e-3	5.48e-6
1.50	−217.70	7.68e-3	6.32e-3	2.93e-9	2.61e-4	1.40e-3	8.27e-6
1.60	−229.28	7.74e-3	6.29e-3	1.87e-9	1.75e-4	1.48e-3	1.37e-5
1.65	−236.40	7.77e-3	6.27e-3	1.40e-9	1.34e-4	1.51e-3	1.86e-5
1.70	−244.90	7.80e-3	6.26e-3	1.00e-9	9.74e-5	1.53e-3	2.65e-5
1.75	−254.72	7.82e-3	6.24e-3	6.74e-10	6.62e-5	1.55e-3	3.98e-5
1.80	−265.60	7.85e-3	6.23e-3	4.42e-10	4.33e-5	1.55e-3	6.08e-5
1.90	−286.00	7.90e-3	6.20e-3	2.12e-10	2.01e-5	1.50e-3	1.23e-4
2.00	−300.74	7.96e-3	6.17e-3	1.26e-10	1.13e-5	1.43e-3	1.98e-4
2.10	−311.50	8.01e-3	6.14e-3	8.51e-11	7.22e-6	1.34e-3	2.77e-4
2.20	−319.76	8.06e-3	6.12e-3	6.24e-11	4.95e-6	1.26e-3	3.55e-4
2.30	−326.46	8.11e-3	6.09e-3	4.79e-11	3.55e-6	1.18e-3	4.33e-4
2.40	−332.00	8.16e-3	6.06e-3	3.80e-11	2.61e-6	1.09e-3	5.09e-4
2.50	−336.84	8.21e-3	6.04e-3	3.07e-11	1.95e-6	1.01e-3	5.84e-4
2.60	−341.06	8.26e-3	6.01e-3	2.52e-11	1.47e-6	9.33e-4	6.58e-4
2.70	−345.10	8.31e-3	5.98e-3	2.09e-11	1.12e-6	8.55e-4	7.29e-4
2.80	−348.76	8.36e-3	5.96e-3	1.75e-11	8.51e-7	7.80e-4	7.97e-4
2.90	−352.12	8.41e-3	5.93e-3	1.47e-11	6.48e-7	7.07e-4	8.63e-4
2.95	−353.72	8.44e-3	5.92e-3	1.35e-11	5.65e-7	6.72e-4	8.95e-4
3.00	−355.22	8.46e-3	5.90e-3	1.24e-11	4.92e-7	6.38e-4	9.26e-4
		$pK_1 = 7.90$		$pK_2 = 10.96$			

azide, differ considerably and the methods used for their determination are not adequately described (temperature, solvent media, ionic strength, etc.) and they are therefore omitted from Table 2.

The extrapolation of pK values in water to acetonitrile–water mixtures is not linear (Table 2). This table shows that it is difficult to interpret the variations of pK_1 and pK_2 of diuretics according to the percentage of acetonitrile in the mixtures.

However, pK_a values corresponding to the dissociation of an acid functional group such as carboxylic, sulphonamide or amide vary in line with the percentage of acetonitrile, unlike the protonation behaviour of amine nitrogens of amiloride. For dissociation of acid functional groups, differences as large as 2 units in pK values are obtained by changing the percentage of acetonitrile from 10% (w/w) to 70% (w/w), while pK_a values corresponding to the deprotonation of

Table 2
pK values of diuretics in acetonitrile–water mixtures up to 70% (w/w) at 298.15 K (values in parentheses are standard deviation, $30<n<60$)

Diuretic		% (w/w) acetonitrile					
		0	10	30	40	50	70
Furosemide	pK_1	3.9	4.52(0.04)	4.87(0.02)	5.25(0.03)	5.58(0.01)	6.41(0.02)
	pK_2	—	10.1(0.09)	10.29(0.1)	11.01(0.07)	11.27(0.1)	12.29(0.05)
Chlorthiazide	pK_1	6.7	6.95(0.01)	7.14(0.03)	7.35(0.01)	7.62(0.01)	8.25(0.04)
	pK_2	9.5	9.72(0.04)	9.82(0.2)	10.27(0.5)	10.95(0.2)	11.27(0.6)
Trichlormethiazide	pK_1	—	7.30(0.02)	7.93(0.01)	8.30(0.02)	8.83(0.04)	9.46(0.05)
	pK_2	—	10.0(0.1)	10.62(0.5)	11.35(0.1)	11.61(0.2)	12.44(0.03)
Amiloride	pK_1		8.37(0.01)	8.90(0.05)	9.04(0.03)	9.28(0.03)	9.67(0.05)
	pK_2		10.57(0.3)	10.93(0.3)	11.56(0.1)	12.34(0.2)	12.76(0.3)

amine nitrogens show only minor changes in the same range of compositions.

The standard free energy of dissociation comprises of two terms: an electrostatic one, which can be estimated by the Born equation [27] and a non-electrostatic one, which includes specific solute–solvent interaction. When the electrostatic effects predominate, then in accordance with the Born equation:

$$\Delta \mathrm{p}K = \frac{121.6n}{\bar{r}}\left(\frac{1}{\epsilon} - 0.0128\right) \quad (6)$$

the plot of pK_a versus $1/\epsilon$ should give a straight line. In this equation, $\bar{r}$ is the common radius of the ions, ϵ is the dielectric constant of the hydroorganic mixture, $n=2$, for HA,A pairs of the charge type $A^o \leftrightarrow B^-$, $n=4$ for the charge type $A^- \leftrightarrow B^{2-}$ and $n=0$ for the charge type $A^+ \leftrightarrow B^o$.

The variation of pK_1 and pK_2 values of the four diuretics studied with the reciprocal of the dielectric constant of the medium is shown in Fig. 2. As the above equation predicts, for the dissociation of the sulphonamide group of furosemide, chlorthiazide and trichlormethiazide, electrostatic interactions overwhelm the specific solvation because charges are created ($HA \leftrightarrow H^+ + A^-$) as is shown in Fig. 1. Hence the correlations between these pK_1 values and $1/\epsilon$ are linear with correlation coefficients greater than 0.99. However, in dissociation of the monocharged cation acid of amiloride, there is no change in the number of charges ($HA^+ \leftrightarrow H^+ + A$) and the dissociation depends only on the solvation of the different species by the solvents of the mixture. In this case the correlation between pK_1 values of amiloride and $1/\epsilon$ is poor and the slope describing its variation has the lowest numerical value. Moreover, as is shown in Fig. 2, the variation of pK_2 values assigned to the dissociation of sulphonamide and amide groups versus $1/\epsilon$ is linear with correlation coefficients greater than 0.99 and with the greatest slope values, as is predicted by Eq. (6).

Furthermore, in acetonitrile–water mixtures $1/\epsilon$ and x_{AN} (the molar fraction of acetonitrile) are related by means of $1/\epsilon = 1.26\times10^{-2} + 1.73\times10^{-2}x$, where the correlation coefficient of the equation is 0.9999. Thus, Eq. (6) becomes $\mathrm{p}K = A' + B'x$. The variation of the pK values of diuretics studied versus x_{AN} are shown in Fig. 3. As expected, the poorest correlation coefficients and the lowest slope are obtained for pK_1 of amiloride. The other pK_1 and pK_2 values obtained are linearly correlated with $1/\epsilon$ with $r>0.99$.

Although pK values of diuretics obtained in acetonitrile–water mixtures increase with the percentage of acetonitrile, they are lower than expected considering the high pK values expected in acetonitrile alone [28]. The variation in the pK_a values of diuretics in acetonitrile–water mixtures might be explained by the existence of preferential solvation in these media [21] and is probably related to the structural features of these mixtures [29]. Preferential solvation in acetonitrile–water

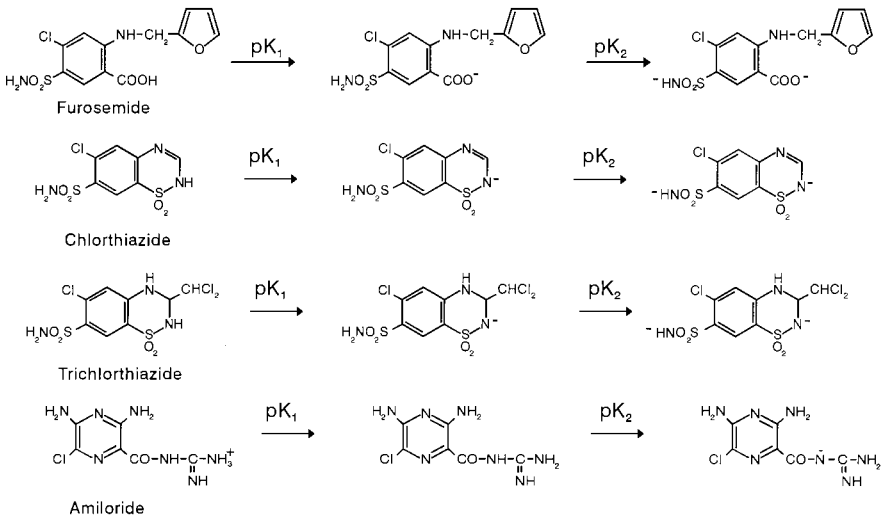

Fig. 1. Protolytic equilibria of diuretics.

mixtures produces lower pK values than expected when the preferred solvent is water. The composition of the immediate surroundings of a solute may differ from that of the bulk mixture. Preferential solvation is attributable to an excess or a deficiency of molecules of one of the solvents in these surroundings [30]. If the solute displays no preference for the solvent molecules, the solvent composition in the cybotactic zone, in the immediate neighbourhood of the solute, is the same as in the bulk. For such cases:

$$pK_s = x_1 pK_{s_1} + x_2 pK_{s_2} \quad (7)$$

where pK_s is the pK value in the mixture and pK_{s_1} and pK_{s_2} represent the pK values in acetonitrile and water, respectively. The deviation from the ideal dependence on the composition of the mix-

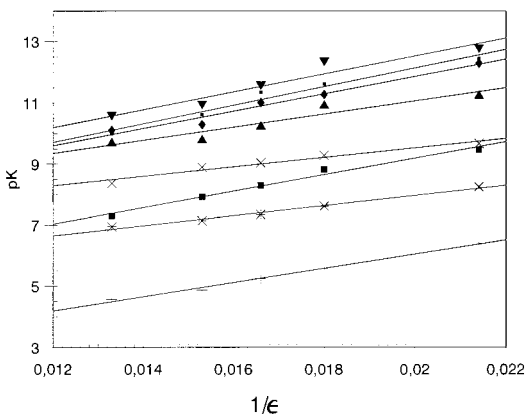

Fig. 2. pK_1 and pK_2 values of diuretics versus $1/\epsilon$ up to 70% (w/w). +, pK_1 of furosemide; *, pK_1 of chlorthiazide; ■, pK_1 of trichlormethiazide; ×, pK_1 of amiloride; ◆, pK_2 of furosemide; ▲, pK_2 of chlorthiazide; ■, pK_2 of trichlormethiazide; ▼, pK_2 of amiloride.

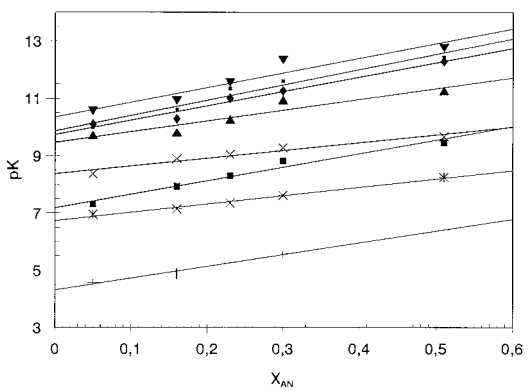

Fig. 3. pK_1 and pK_2 values of diuretics versus x_{AN} up to 70% (w/w). +, pK_1 of furosemide; *, pK_1 of chlorthiazide; ■, pK_1 of trichlormethiazide; ×, pK_1 of amiloride; ◆, pK_2 of furosemide; ▲, pK_2 of chlorthiazide; ■, pK_2 of trichlormethiazide; ▼, pK_2 of amiloride.

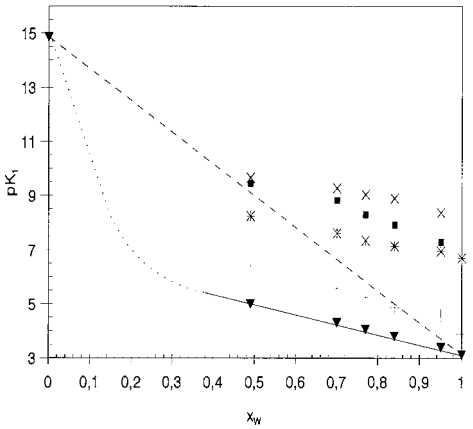

Fig. 4. pK_1 versus mole fraction of water, x_W, in acetonitrile–water mixtures. +, furosemide; *, chlorthiazide; ■, trichlormethiazide; ×, amiloride; ▼, citric acid. The dashed straight lines correspond to the ideal variation of the pK_1 values for the citric acid.

ture indicates that the solvent composition in the neighbourhood of the solute may differ from that in the bulk.

In the water-rich region of acetonitrile–water mixtures ($x_{AN} \leq 0.15$) and in the microheterogeneity region ($0.15 \leq x \leq 0.75$), solvation by water is preferred [21], which might explain the small increase in pK values of diuretics when the percentage of acetonitrile increases, Table 2. This is consistent with reported values of preferential solvation, δ_W, of hydrogen ions by water in acetonitrile–water mixtures [21]. In these regions ($x_{AN} \leq 0.75$) the solutes are preferentially solvated by water and variations of pK_a values are small. At $x_{AN} \geq 0.75$ the number of water clusters is low, and water–acetonitrile interactions that could be discounted in the middle range now become important [31–34]. This may be considered as a region in which preferential solvation by water decreases [21].

pK_a values of diuretics in acetonitrile neat solvent are not known, but pK_1 and pK_2 values of citric acid have been determined in previous studies [19] over the whole composition range of acetonitrile–water mixtures. Fig. 4 shows pK_1 of citric acid as a function of x_W, the bulk mole fraction of water. The deviation from the ideal dependence on the composition of the mixture to lower pK values indicates preferential solvation by water. Fig. 4 also shows the variation of the pK_1 values of the diuretics studied versus x_W for comparison. The pK_1 values obtained differ but are lower than the theoretical ones because of the preferential solvation of the electrolytes by water. A concave variation of pK versus x_W may be expected with an inflexion point at $x_W = 0.25$, where preferential solvation by water is maximal [21].

It remains unclear whether solvatochromic parameters would be valid to act as stand-ins for generalised solutes in binary solvent mixtures with regard to the properties they are supposed to measure. Preferential solvation in such mixtures may interfere more seriously with the ability of indicators to act as stand-ins for generalised solutes than in the case of single solvents. Progress has been made [31,35] and although this problem has not been solved unequivocally, these investigations provide significant evidence that the solvatochromic parameters seem to have general validity.

Table 3
Linear solvation energy relationships for pK_1 and pK_2 values of diuretics

Diuretic	Multiparametric equation	r
Furosemide	$pK_1 = 26.15 - 1.93\alpha - 22.11\beta - 5.85\pi^*$	0.9994
	$pK_2 = -9.48 + 22.94\alpha + 32.45\beta - 21.19\pi^*$	0.98
Chlorthiazide	$pK_1 = 28.66 - 3.43\alpha - 25.38\beta - 2.75\pi^*$	0.9999
	$pK_2 = -36.42 + 30.28\alpha + 68.16\beta - 23.25\pi^*$	0.998
Trichlormethiazide	$pK_1 = 5.42 + 7.17\alpha + 13.58\beta - 12.31\pi^*$	0.993
	$pK_2 = -6.65 + 8.12\alpha + 17.35\beta - 13.92\pi^*$	0.995
Amiloride	$pK_1 = 20.48 - 3.65\alpha - 8.71\beta - 2.86\pi^*$	0.9990
	$pK_2 = -46.02 + 35.49\alpha + 86.90\beta - 28.76\pi^*$	0.9993

Table 4
Relationships between pK values of diuretics and weight, w, and volume, v, percentages of acetonitrile

Diuretic	Multiparametric equation	r
Furosemide	$pK_1 = 3.95 + 5.33e\text{-}2w$	0.995
	$- 8.96e\text{-}4w^2 + 9.13e\text{-}6w^3$	
	$pK_1 = 3.93 + 4.83e\text{-}2v$	0.996
	$- 8.33e\text{-}4v^2 + 8.22e\text{-}6v^3$	
	$pK_2 = 10.43 - 5.52e\text{-}2w$	0.992
	$+ 2.26e\text{-}3w^2 - 1.56e\text{-}5w^3$	
	$pK_2 = 10.61 - 6.50e\text{-}2v$	0.993
	$+ 2.05e\text{-}3v^2 - 1.19e\text{-}5v^3$	
Chlorthiazide	$pK_1 = 6.72 + 1.89e\text{-}2w$	0.997
	$- 2.34e\text{-}4w^2 + 3.95e\text{-}6w^3$	
	$pK_1 = 6.72 + 1.82e\text{-}2v$	0.998
	$- 3.04e\text{-}4v^2 + 4.32e\text{-}6v^3$	
	$pK_2 = 9.60 - 2.20e\text{-}2w$	0.976
	$+ 1.53e\text{-}3w^2 - 1.23e\text{-}5w^3$	
	$pK_2 = 9.58 - 1.57e\text{-}2v$	0.973
	$+ 9.76e\text{-}4v^2 - 6.18e\text{-}6v^3$	
Trichlorthiazide	$pK_1 = 7.28 - 1.09e\text{-}2w$	0.999
	$+ 1.39e\text{-}3w^2 - 1.13e\text{-}5w^3$	
	$pK_1 = 7.38 - 0.02v + 1.29e\text{-}3v^2$	0.999
	$- 8.63e\text{-}6v^3$	
	$pK_2 = 9.90 - 3.44e\text{-}3w$	0.995
	$+ 1.34e\text{-}3w^2 - 1.10e\text{-}5w^3$	
	$pK_2 = 10.05 - 2.10e\text{-}2v$	0.995
	$+ 1.42e\text{-}3v^2 - 9.65e\text{-}6v^3$	
Amiloride	$pK_1 = 8.02 + 3.94e\text{-}2w$	0.999
	$- 4.60e\text{-}4w^2 - 3.33e\text{-}6w^3$	
	$pK_1 = 7.98 + 3.55e\text{-}2v$	0.999
	$- 4.01e\text{-}4v^2 + 2.97e\text{-}6v^3$	
	$pK_2 = 11.45 - 0.13w + 5.17e\text{-}3w^2$	0.999
	$- 4.25e\text{-}5w^3$	
	$pK_2 = 11.85 - 0.16v + 4.88e\text{-}3v^2$	0.999
	$- 3.48e\text{-}5v^3$	

It is therefore of interest to examine the correlation between dissociation pK values of electrolytes with the most significant solvent properties (polarity and hydrogen bond properties) in order to determine the influence of each property on the dissociation process.

Taft, Kamlet and co-workers proposed the use of solvatochromic parameters in order to evaluate solute–solvent interactions for many Gibbs free energy-related properties, including dissociation constants of protonated bases in water [22,36], through correlation analysis, and linear solvation energy relationships (LSER). Recently, application of the method to dissociation of some electrolytes in 1,4-dioxane–water [37,38] and 2-methylpropan-2-ol–water mixtures [39] has been investigated.

The number of terms in the equation used to correlate the studied property, depends on the significance of the solute–solvent interactions. When the property studied refers to a single solute in multiple solvents, the general equation is usually expressed as [40]:

$$XYZ = (XYZ)_o + h\delta_H^2 + s\pi^* + a\alpha + b\beta \quad (8)$$

where XYZ is the free energy-related property, $(XYZ)_o$ is the value of this property for the same solute in a hypothetical solvent for which $\alpha = \beta = \pi^* = 0$, δ_H is the Hildebrand solubility parameter, which accounts for the cavity term, π^* measures the solvent polarity/polarizability, α measures the solvent hydrogen bond donor capability, β measures the solvent hydrogen bond acceptor capability and s, a and b are the susceptibilities of the solute property studied to changes in π^*, α and β, respectively.

When the property being correlated is the dissociation pK_a values in mixtures with the same solvents, the appropriate form of Eq. (8) would be:

$$pK = pK_o + s\pi^* + a\alpha + b\beta \quad (9)$$

This equation can include additional terms or some of its terms can be equal to zero, depending on the series of solutes being described [41].

In this study, several attempts were made to find the best form of Taft-Kamlet equation to describe the variation of pK values of diuretics in acetonitrile–water mixtures. All possible combinations of solvatochromic parameters were tested. The best fit was obtained when the three solvatochromic parameters π^* [31,42], α [31,43] and β [31,44] were used, providing the general equations in Table 3. The high coefficient in the β terms for pK values (Table 3) compared with the α and π^* terms confirmed the overriding dependence of the

pK_1 and pK_2 values of diuretics on the hydrogen bond accepting basicity of the solvent for the whole range of composition studied, up to 70% (w/w) of acetonitrile. The *s* coefficients were found to be negative for pK_a values, which means that an increase in the polarity of the mixed solvent decreases the pK_a value. Thus, an increase in the polarity increases the solvation of ions and, therefore, the dissociation. From the linear solvation energy relationships obtained (Table 3) the pK_a values of diuretics can be determined in any acetonitrile–water mixture up to 70% (w/w) acetonitrile. From a practical point of view, it is of great interest to apply multiple regression analysis to the whole set of pK_a values of diuretics and the usual concentration by volume % (v/v), *v*, and weight % (w/w), *w*, as the intercept variables. In these cases the third-order polynomials shown in Table 4 were obtained. The equations given in Tables 3 and 4 enable us to determine the pK_1 and pK_2 values of the diuretics studied in any binary solvent acetonitrile–water mixture up to 70% (w/w) acetonitrile and, thus, permit the interpretation of their acid–base behaviour in these widely-used hydroorganic mixtures.

Acknowledgements

Financial support of this project by Comissionat per a Universitats i Recerca (Ref. 1995SGR 00458) is gratefully acknowledge.

References

[1] J.W. Bridges, L.F. Chasseaud, Progress in Drug Metabolism, vol. 7, J. Wiley & Sons, New York, 1983, p. 58.
[2] S.J. Park, H.S. Pyo, Y.J. Kim, M.S. Kim, J. Park, J. Anal. Toxicol. 14 (1990) 84.
[3] R. Ventura, T. Nadal, P. Alcalde, J.A. Pascual, J. Segura, J. Chromatogr. A 655 (1993) 233.
[4] P.J. Shoenmakers, S. Molle, C.M.G. Hayes, L.M. Hunk, Anal. Chim. Acta 250 (1991) 1.
[5] J.H. Park, P.W. Carr, M.H. Abraham, R.W. Taft, R.M. Doherty, M.J. Doherty, Chromatographia 25 (1988) 373.
[6] P.W. Carr, R.M. Doherty, M.J. Kamlet, R.W. Taft, W. Melander, C. Horwáth, Anal. Chem. 58 (1986) 2694.
[7] J. Barbosa, V. Sanz-Nebot, I. Toro, J. Chromatogr. A 725 (1995) 249.
[8] D. Barrón, J.A. Pascual, J. Segura, J. Barbosa, Chromatographia 41 (1995) 573.
[9] D. Barrón, J. Barbosa, J.A. Pascual, J. Segura, J. Mass Spectrom. 31 (1996) 309.
[10] J. Barbosa, R. Bergés, V. Sanz-Nebot, J. Chromatogr. A 719 (1996) 27.
[11] J. Barbosa, D. Barrón, R. Bergés, V. Sanz-Nebot, I. Toro, J. Chem. Soc. Faraday Trans. I 93 (1997) 1915.
[12] J. Barbosa, V. Sanz-Nebot, Talanta 36 (1989) 837.
[13] J. Barbosa, V. Sanz-Nebot, Anal. Chim. Acta 244 (1991) 183.
[14] C. Reichardt, Solvent and Solvent Effects in Organic Chemistry, 2nd ed., V.C.H. Vorlagsgesellscheff, Weinheim, 1988.
[15] J. Barbosa, V. Sanz-Nebot, Fresenius J. Anal. Chem. 353 (1995) 148.
[16] F.G.K. Baucke, R. Naumann, C. Alexander-Weber, Anal. Chem. 65 (1993) 3244.
[17] A.K. Covington, R.G. Bates, R.A. Durst, Pure Appl. Chem. 57 (1985) 531.
[18] J. Barbosa, J.L. Beltran, V. Sanz-Nebot, Anal. Chim. Acta 288 (1994) 271.
[19] J. Barbosa, R. Bergés, I. Toro, V. Sanz-Nebot, Talanta 44 (1997) 1271.
[20] L. Pillai, R.D. Boss, M.S. Greenberg, J. Sol. Chem. 8 (1979) 625.
[21] J. Barbosa, V. Sanz-Nebot, J. Chem. Soc. Faraday Trans. 90 (1994) 3287.
[22] M.J. Kamlet, J.L.M. Abboud, M.H. Abraham, R.W. Taft, J. Org. Chem. 48 (1983) 2877.
[23] J. Barbosa, V. Sanz-Nebot, Mikrochim. Acta 116 (1994) 131.
[24] J. Barbosa, D. Barrón, J.L. Beltrán, V. Sanz-Nebot, Anal. Chim. Acta 317 (1995) 75.
[25] S. Rondinini, P.R. Mussini, T. Mussini, Pure Appl. Chem. 59 (1987) 1549.
[26] A.C. Moffat, J.V. Jackson, M.S. Moss, B. Widdop (Eds.), Clarke's Isolation and Identificacion of Drugs in Pharmaceuticals, Body Fluids and Post-mortem Material, 2nd ed., The Pharmaceutical Press, London, 1986.
[27] R.G. Bates, Determination of pH: Theory and Practice, J. Wiley & Sons, Inc., New York, 1964.
[28] I.M. Kolthoff, Anal. Chem. 46 (1974) 1992.
[29] A.J. Easteal, L.A.J.J. Woolf, Chem. Thermodyn. 20 (1988) 693.
[30] Y. Marcus, J. Chem. Soc. Faraday Trans. 85 (1989) 381.
[31] Y. Marcus, Y. Migron, J. Phys. Chem. 95 (1991) 400.
[32] A.K. Covington, R.G. Bates, R.A. Durst, Pure Appl. Chem. 57 (1985) 531.
[33] T. Mussini, P. Longhi, P. Giammario, Chim. Ind. (Milan) 53 (1971) 1124.
[34] H. Kovacs, A. Laarksonen, J. Am. Chem. Soc. 113 (1991) 5596.
[35] Y. Migron, Y. Marcus, J. Chem. Soc. Faraday Trans. 87 (1991) 1339.

[36] M.J. Kamlet, J.F. Gal, P.C. Maria, R.W. Taft, J. Chem. Soc. Perkin Trans. 2 (1985) 1583.
[37] E. Casassas, G. Fonrodona, A. De Juan, R. Tauler, Chemometr. Intell. Lab. Syst. 12 (1991) 29.
[38] E. Casassas, N. Dominguez, G. Fonrodona, A. De Juan, Anal. Chim. Acta 283 (1993) 548.
[39] E. Bosch, F. Rived, M. Rosés, J. Phys. Org. Chem. 7 (1994) 696.
[40] J. Alcamí, O. Mó, M. Yañez, J.L.M. Abboud, J. Phys. Org. Chem. 4 (1991) 177.
[41] M.J. Kamlet, R.W. Taft, Acta Chem. Scand. Ser. B 39 (1985) 611.
[42] W.J. Cheong, P.W. Carr, Anal. Chem. 60 (1988) 820.
[43] J.H. Park, M.D. Jang, D.S. Kim, P.W. Carr, J. Chromatogr. 513 (1990) 107.
[44] T.M. Krygowsky, P.K. Wrona, V. Zielkowska, C. Reichardt, Tetrahedron 41 (1985) 4519.

ELSEVIER

Talanta 45 (1998) 829–834

Talanta

Use of time-resolved lanthanide-sensitized luminescence for the kinetic determination of *p*-aminobenzoic acid

S. Panadero *, A. Gómez-Hens, D. Pérez-Bendito

Department of Analytical Chemistry, Faculty of Sciences, University of Córdoba E-14004, Córdaba, Spain

Received 24 March 1997; received in revised form 26 May 1997; accepted 26 May 1997

Abstract

Lanthanide-sensitized luminescence was for the first time used to develop a simple kinetic method for the determination of *p*-aminobenzoic acid. The method is based on the formation of a complex with terbium(III) in the presence of trioctylphosphine oxide as synergistic agent and Triton X-100 as micellar medium. The high initial rate of the complex formation required the use of stopped-flow mixing technique in order to make kinetic measurements which, in addition, allows the method to be automated. Its analytical features compare very favourably with those described by using solid-surface room temperature phosphorescence in terms of rapidity, precision and selectivity. The initial rate is obtained within only 0.2 s after the reactants are mixed, which allows ready application of the proposed method to routine analyses. The calibration graph is linear over the range 0.08–4.0 μg ml^{-1} *p*-aminobenzoic acid and the detection limit is 0.02 μg ml^{-1}. The relative standard deviation is close to 2%. The kinetic methodology avoids the effect of the sample matrix allowing the direct determination of this compound in pharmaceutical preparations. Analytical recoveries ranged between 98.6 and 113.0%. © 1998 Elsevier Science B.V.

Keywords: Kinetic method; *p*-Aminobenzoic acid; Lanthanide-sensitized luminescence; Stopped-flow technique; Pharmaceutical samples

1. Introduction

The advent of the different modalities of room temperature phosphorimetry (RTP) (solid-surface RTP, micelle-stabilized RTP and sensitized RTP) resulted in an increase in analytical interest of this technique because the methods usually show low detection limits and high selectivity [1]. However, although these modalities have been successfully employed in a variety of analytical situations, their general use has been limited owing to different causes: solid-surface RTP involves several steps which are relatively time consuming; only few compounds show a high phosphorescence signal in solution even in the presence of a surfactant and, also, few compounds act as efficient energy acceptors. In addition, the removal of oxygen in the latter two cases is always a necessary requirement.

An approach which can be considered as a special sort of sensitized phosphorescence is lanthanide-sensitized luminescence, where an in-

* Corresponding author.

PII S0039-9140(97)00169-0

tramolecular energy transfer process occurs through the excited triplet state of the ligand to the emitting level of the lanthanide ion. The features of this process (large Stokes shift, narrow emission band and long lifetime) make it very suitable for analytical purposes and the drawbacks of the other phosphorimetric alternatives are avoided. Thus, although the most efficient energy acceptors between the lanthanide ions are terbium(III) and europium(III), they form stable complexes with numerous organic compounds. The reactions are very fast and the removal of oxygen is not required. A difference between the use of lanthanide ions as energy acceptors rather than compounds such as biacetyl and 1,4-dibromonaphthalene is that in the latter case the energy transfer is intermolecular, which accounts for the lower efficiency than in the former instance.

p-Aminobenzoic acid (PABA) has been extensively examined and used as a model compound for RTP studies. In all instances, solid-surface RTP has been used by assaying filter paper [2–12] and sodium acetate [13–16] as supports and by adding heavy atoms [8,10], surfactants [10], cyclodextrins [11] and polyacrylic acid [4] to improve the phosphorescence signal. Although the methods reported generally show good sensitivity and selectivity, they require time-consuming steps to minimize the background phosphorescence of the substrate [5], placement of the sample on the support and drying of the adsorbed sample prior to the measurement step [6]. It is well-known that moisture is one of the main concomitants which can diminish the phosphorescence signal, although this effect seems to be less marked when sodium acetate is used as support [13,14]. However, filter paper is the most widely used solid surface for inducing RTP.

In order to avoid these manual steps which make this technique very dependent on random errors and frequently result in poor reproducibility, the feasibility of using flow injection as a continuous sample introduction method for solid-surface RTP was studied and applied to the determination of PABA [12]. A two-nebulizer system was used to spray the heavy-atom and analyte solutions separately onto the moving filter-paper strip and the measurements were obtained in a continuous mode by using a kinetic program. The detection limit obtained was 371 ng ml^{-1}, which was higher than those reported by using manual methods; this was ascribed to the shorter drying times used giving rise to greater quenching by moisture. Also, the noise caused by the motion of the paper and the possible concentration fluctuations induced by the peristaltic flow could have been some of the reasons for the variations observed in the measurements, resulting in a reproducibility close to 13%.

This paper describes a direct method for PABA determination in solution based on its capability of forming a luminescent complex with terbium(III) in the presence of Triton X-100 and trioctylphosphine oxide (TOPO). Although the luminescence lifetime of this system is shorter than the phosphorescence lifetime of PABA [8,14], it is sufficiently long to allow the use of the phosphorescence measurement mode. Thus, this is the first liquid phosphorimetric determination of PABA. The analytical features of the method improve those reported by using solid-surface RTP in terms of rapidity, precision and selectivity. The use of kinetic methodology in conjunction with the stopped-flow mixing technique facilitates automation of the method and its application to the analysis of real samples.

2. Experimental

2.1. Instrumentation

All measurements were made on a Perkin-Elmer Model LS-50 luminescence spectrometer fitted with a stopped-flow module [17] supplied by Quimi-Sur Instrumentation. The instrument was controlled with a Hewlett-Packard Vectra Computer. Reaction rate data were obtained by using the Kinetic Obey application program. The observation cell of the stopped-flow module had a path length of 1.0 cm and the excitation and emission slits were adjusted to provide a 15-nm band pass. The delay and gate times selected for the time-resolved mode were 0.03 and 3.0 ms, respectively. The temperatures of the solutions in the stopped-

flow module and cell compartment were kept constant at 18°C by circulating water from a thermostated tank.

2.2. Reagents

All chemicals used were of analytical-reagent grade. A 100-μg ml^{-1} stock solution of PABA (Sigma) was prepared in distilled water. A 0.01 M terbium(III) aqueous solution was prepared by dissolving the appropriate amount of $Tb(NO_3)_3 \cdot 5H_2O$ (Sigma). A 2×10^{-3} M stock solution of TOPO was prepared in 1% aqueous Triton X-100. A hexamine (hexamethylenetetramine) buffer solution (0.7 M, pH 6.0) was also used.

2.3. Procedure

A solution containing terbium(III) (2×10^{-3} M), TOPO (1.8×10^{-4} M), Triton X-100 (0.1%) and hexamine buffer (2×10^{-2} M, pH 6.0) was used to fill one of the two 10-ml reservoir syringes. The other 10-ml syringe was filled with a solution containing PABA standard solution (0.08–4.0 μg ml^{-1}) and the same buffer concentration. In each run, 0.15 ml of each solution was mixed in the mixing chamber. Measurements were obtained at λ_{ex} 295 nm and λ_{em} 545 nm by using the phosphorescence mode, with delay and gate times of 0.03 and 3.0 ms, respectively. The kinetic curve was monitored during ca. 1–2 s. All measurements were carried out at 18°C. Data were processed by linear regression using a microcomputer, furnished with a program for application of the initial-rate method (Kinetic Obey). The initial rate was determined in ca. 0.2 s and each standard or sample was assayed in triplicate. The blank signal was found to be negligible.

2.3.1. Determination of PABA in pharmaceutical formulations

Liquid samples were appropriately diluted with distilled water to obtain a PABA concentration level within the linear range of the calibration graph. Solid samples were analysed by weighing and powdering individually six tablets or capsules of each sample, transferring the powder into a 50 ml-volumetric flask and diluting to volume with ethanol. The suspension was shaken for 1–2 min in an ultrasonic bath and then filtered. A volume of the diluted solution from the liquid samples or the filtrate from the solid samples was treated as described above.

3. Results and discussion

In order to study the capability of PABA to form luminescent complexes with lanthanide ions, terbium(III) and europium(III) were assayed. Only an intense luminescence signal was obtained with the former when the excitation wavelength used was that corresponding to the maximum absorption of PABA (285 nm). This signal showed the typical emission bands of terbium(III) at 490, 545 and 580 nm; the second band was the most intense.

The luminescence lifetime obtained for the PABA–terbium(III) complex was 0.5 ms, shorter than those reported for PABA in solid-surface RTP. The phosphorescence lifetime of PABA adsorbed on sodium acetate was close to 1 s [15] and those reported on several filter papers ranged from 2.2 to 690 ms [8]. In spite of these differences, luminescence measurements could be obtained in solution by using the time-resolved mode with delay and gating times of 0.03 and 3 ms, respectively. Under these conditions, the luminescence values obtained were higher than those obtained by the fluorescence mode.

With the aim of minimizing radiationless deactivation processes, the effect of several micellar solutions and synergistic agents was studied. The effect of cationic, anionic and non-ionic surfactants on the PABA–terbium(III) system was very different. By using the time-resolved mode, CTAB did not modify the spectral features, but SDS and Triton X-100 slightly decreased the luminescence signal. In addition, the excitation spectrum of the system changed in the presence of Triton X-100 and exhibited a 10-nm red shift, similar to the change observed in the excitation spectrum obtained for PABA alone, by using the fluorescence mode. This behaviour suggests that PABA is associated in some particular way with this surfac-

tant as this effect was not observed by changing Triton X-100 with other non-ionic surfactants such as Brij or Polydocanol. The effect of several synergistic agents in the system, namely EDTA, 1,10-phenanthroline and tri-*n*-octylphosphine oxide (TOPO), was studied in the absence and presence of Triton X-100. While EDTA and 1,10-phenanthroline decreased the luminescence signal, TOPO did not affect the luminescence signal in the absence of Triton X-100 but notably increased it in the presence of the surfactant. The kinetic curve obtained under these conditions showed a high initial rate, better than those obtained in the absence of TOPO and Triton X-100, and required the use of the stopped-flow mixing technique as the reaction was developed in about 1 s. The study of the distribution of the reactants between the two syringes of the module showed that the best results are obtained when terbium(III) is placed together with TOPO and Triton X-100 in one syringe and PABA in the other.

3.1. Effect of variables

The variables involved in the proposed kinetic method were optimized by the univariate method. All concentrations stated are the initial concentrations in the syringes (twice the actual concentration in the reaction mixture at time zero after mixing). Each kinetic result was the average of three measurements.

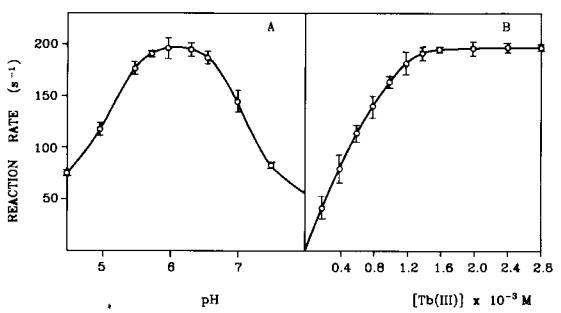

Fig. 1. Effect of pH (A) and terbium(III) concentration (B) on the system. [PABA] = 3 μg ml^{-1}; [terbium(III)] = 1.5×10^{-3} M; [TOPO] = 10^{-4} M; [Triton X-100] = 0.1%. A 2×10^{-2} M hexamine buffer, pH 6, was used in (B).

The effect of pH on the system is shown in Fig. 1A. This variable was studied by adjusting the pH of each solution in the syringes, which allowed the same value to be adjusted in the mixing chamber (as checked in the waste). The initial rate was pH independent over the range 5.6–6.5. Several buffer solutions (ammonium acetate, Tris, imidazole and hexamine) were used to adjust the pH. The highest initial rate values were obtained by using hexamine buffer solution, with 2×10^{-2} M being the optimum concentration. Fig. 1B shows the effect of terbium(III) concentration on the initial rate, which was independent of this variable over the range from 1.6×10^{-3} M to at least 3.0×10^{-3} M. Because TOPO is soluble in Triton X-100, the effect of TOPO concentration was studied while the concentration of Triton X-100 (0.1%) remained constant. The initial rate was independent of TOPO concentration over the range 1.4×10^{-4} to 2.0×10^{-4} M. The highest initial rate values were obtained when the Triton X-100 concentration ranged from 0.07 to 0.12%, which was higher than the critical micelle concentration of this surfactant (0.018%). Finally, increasing temperatures in the range 10–20°C did not affect the initial rate, but it decreased the rate at higher temperatures. A temperature of 18°C was selected.

The initial slopes of the luminescence versus time curves for solutions containing different concentrations of PABA revealed the reaction to be first order in PABA. Under optimum conditions, the other reactants showed a pseudo-zero-order dependence; thus the simple kinetic equation $v = k$[PABA] is proposed, where v is the rate of formation of the complex and k is the conditional rate constant.

3.2. Figures of merit of the proposed method

The kinetic curves obtained for different concentrations of PABA, with excitation and emission wavelengths of 295 and 545 nm, respectively, were processed by the initial rate method. The calibration graph was linear over the range 0.08–4.0 μg ml^{-1} and conformed to the equation v (s^{-1}) = 61.7 ± 1.6[PABA (μg ml^{-1})] + 11.9 ± 3.6, with a Pearson's correlation coefficient (r) of

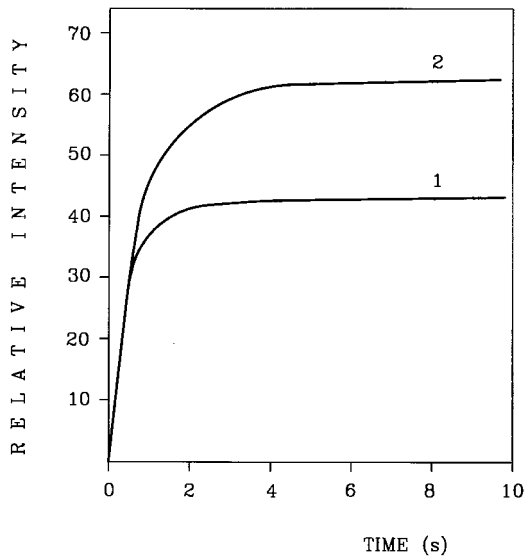

Fig. 2. Effect of the sample matrix on the kinetic curves obtained for the PABA system. Curve 1 was obtained from sample 2 (see Table 1), which was diluted up to a final 0.5 μg ml^{-1} PABA concentration; curve 2 corresponds to a standard solution containing 0.5 μg ml^{-1} PABA. [terbium(III)] = 2×10^{-3} M; [TOPO] = 1.8×10^{-4} M; [Triton X-100] = 0.1%; [hexamine buffer] = 2×10^{-2} M.

0.998 ($n = 8$) and a standard estimated error of 5.8. The detection limit, calculated according to IUPAC recommendations [18], was 0.02 μg ml^{-1}. This value is similar to that reported for PABA in solid-surface RTP by using filter paper, thallium(I) and SDS [10], and lower than that reported on filter paper but by using sodium iodide (60 ng/ml) [8]. Also, the detection limit obtained in the flow injection method reported for PABA determination [12], where the measurements were obtained by using kinetic methodology, was higher (371 ng ml^{-1}) than the value obtained here by the kinetic stopped-flow method.

The precision of the method was studied at two PABA concentrations, viz, 0.2 and 2.0 μg ml^{-1}; the relative standard deviations obtained ($n = 11$) were 2.7 and 1.8%, respectively. These results were similar to that obtained in solid-surface RTP by using sodium acetate as support [13], but notably improved the values reported by using filter paper as support, which are close to 13% [8,12].

Table 1
Determination of PABA in pharmaceutical preparations

Sample[a]	PABA content (mg)	
	Certified	Found[b]
1	50	50 ± 1
2	50	50 ± 5
3	200	200 ± 3
4	500	512 ± 26

[a]Trade mark, manufacturers' names and compositions of samples: (1) Pantenil (La Química Médica, S.A.); solution: 110 ml distilled water, 100 ml alcohol; 1 g D-calcium pantothenate, 0.05 g PABA, 0.022 g $HgCl_2$, 0.2 ml lavender essence. (2) Complidermol (Medea, S.A.); per capsule: 150 μg biotin, 5000 IU vitamin A palmitate, 25 mg calcium pantothenate, 25 mg *meso*-inositol, 50 mg PABA, 25 mg pyridoxine chlorhydrate, 25 μg hydroxocobalamin acetate, 50 mg L-phenylalanine, excipient. (3) Tri-hachemina (Medea, S.A.); injectable ampoule: 0.2 g PABA (sodium salt), 0.05 g *meso*-inosite, 0.003 g pantothenic acid (sodium salt), 2 ml bi-distilled water c.s.p. (4) Hachemina fuerte; per tablet: 0.5 g PABA, excipient.
[b]Average of six determinations ± SD.

3.3. Applications

PABA is used in cutaneous alterations such as alopecia and is present in several pharmaceutical preparations, alone or together with other compounds such as pantothenic acid and *meso*-inositol. The proposed kinetic method for PABA determination was applied to the analysis of several pharmaceutical samples. While the slope of the kinetic curves was not affected by the presence of other sample constituents, the equilibrium signal was modified by them (Fig. 2). This behaviour shows that kinetic methodology improves the selectivity in the analysis of real samples as data are obtained at the start of the reaction. The results obtained are summarized in Table 1. For solid samples, each result is the average of six determinations of six different tablets or capsules of each sample. Recoveries were determined by adding different amounts of PABA to each sample and subtracting the results obtained for similarly prepared pharmaceutical to which no PABA was added. Table 2 summarizes the results obtained; as can be seen, the recovery ranged from 98.6 to 113.0%. The lightly high recoveries obtained for

Table 2
Recovery of PABA from pharmaceutical preparations

Sample[a]	Added ($\mu g\ ml^{-1}$)	Found[b] ($\mu g\ ml^{-1}$)	Recovery (%)
1	0.5	0.56 ± 0.05	113.0
	1.0	1.07 ± 0.07	106.8
	2.0	2.1 ± 0.3	103.1
2	0.5	0.56 ± 0.05	111.6
	1.0	1.02 ± 0.07	102.1
	2.0	2.04 ± 0.09	102.1
3	0.5	0.54 ± 0.04	108.6
	1.0	1.00 ± 0.07	99.7
	2.0	2.07 ± 0.03	103.4
4	0.5	0.50 ± 0.03	100.0
	1.0	0.99 ± 0.09	98.6
	2.0	2.1 ± 0.1	103.1

[a]See Table 1.
[b]Average of six determinations $\pm$ SD.

0.5 $\mu g\ ml^{-1}$ in samples 1, 2 and 3 could be ascribed to the presence of pantothenate.

4. Conclusions

The results obtained show the usefulness of lanthanide-sensitized luminescence for the determination of PABA in solution, which avoids some of the drawbacks of numerous methods reported for PABA by using solid-surface RTP. Although the equilibrium of the PABA-terbium(III) system is rapidly reached, the use of kinetic methodology is justified in order to apply directly the method to the analysis of real samples, avoiding the effect of the sample matrix. Stopped-flow mixing technique allows determination of reproducible values of the fast initial rate of this system and provides a very simple means of accomplishing automation in routine analyses involving phosphorescence measurements.

Acknowledgements

The authors are grateful to the CICyT (Comisión Interministerial de Ciencia y Tecnología) for financial support (Grant No. PB91-0840).

References

[1] R.J. Hurtubise, Phosphorimetry: Theory, Instrumentation and Applications, VCH Publishers Inc., New York, 1990.
[2] M.W. Warren II, J.P. Avery, H.V. Malmstadt, Anal. Chem. 54 (1982) 1853.
[3] J.L. Ward, R.P. Bateh, J.D. Winefordner, Analyst 107 (1982) 335.
[4] V.P. Senthilnathan, S.M. Ramasamy, R.J. Hurtubise, Anal. Chim. Acta 157 (1984) 203.
[5] D.L. McAleese, R.B. Dunlap, Anal. Chem. 56 (1984) 600.
[6] D.L. McAleese, R.B. Dunlap, Anal. Chim. Acta 162 (1984) 431.
[7] H.T. Karnes, S.G. Shulman, J.D. Winefordner, Anal. Chim. Acta 164 (1984) 257.
[8] G. Scharf, B.W. Smith, J.D. Winefordner, Anal. Chem. 57 (1985) 1230.
[9] W.J. Long, R.C. Norin, S.Y. Su, Anal. Chem. 57 (1985) 2873.
[10] M.C. García Alvarez-Coque, G. Ramis Ramos, A.M. O'Reilly, J.D. Winefordner, Anal. Chim. Acta 204 (1988) 247.
[11] A.M. Alak, N. Contolini, T. Vo-Dinh, Anal. Chim. Acta 217 (1989) 171.
[12] A.D. Campiglia, A. Berthod, J.D. Winefordner, Anal. Chim. Acta 231 (1990) 289.
[13] R.M.A. von Wandruszka, R.J. Hurtubise, Anal. Chem. 48 (1976) 1784.
[14] R.M.A. von Wandruszka, R.J. Hurtubise, Anal. Chem. 49 (1977) 2164.
[15] S.M. Ramasamy, R.J. Hurtubise, Anal. Chem. 59 (1987) 432.
[16] S.M. Ramasamy, R.J. Hurtubise, Anal. Chem. 59 (1987) 2144.
[17] A. Loriguillo, M. Silva, D. Pérez-Bendito, Anal. Chim. Acta 199 (1987) 29.
[18] G.L. Long, J.D. Winefordner, Anal. Chem. 55 (1983) 712A.

.

ELSEVIER

Talanta 45 (1998) 835–842

Talanta

Flow injection spectrophotometric determination of boron in ceramic materials

S. Sanchez-Ramos, M.J. Medina-Hernández, S. Sagrado *

Departamento de Química Analítica. Facultad de Farmacia, Universitat de València, C/Vicent A. Estellés s.n., E-46100, Burjassot (València), Spain

Received 23 January 1997; received in revised form 14 May 1997; accepted 30 May 1997

Abstract

A flow injection spectrophotometric method for the determination of boron in ceramic materials is described. The method is based on spectrophotometric measurement of the decrease in the pH produced by the reaction between boric acid and mannitol in the presence of an acid-base indicator. A bichannel FI (flow injection) manifold in which the sample solutions were injected into deionized water (at pH 5.4) and the stream was later merged with the reagent stream (a mannitol solution containing 1×10^{-4} mol l^{-1} bromocresol green at pH 5.4), was used. Transient signals were monitored at 616 nm. A theoretical model which describes the dependence between the absorbance values and boric acid concentration is presented. The model predicts a non linear dependence between the absorbance or increment in absorbance and the boric acid concentration. In contrast, the model predicts a linear dependence between the inverse of the absorbance values and the boric acid concentration. The calibration graphs ($1/A$ vs μg ml^{-1} B_2O_3) were linear over the range 1–30 μg ml^{-1} of B_2O_3. The relative standard deviations were 0.7 and 0.4% for 4 and 8 μg ml^{-1} of B_2O_3, respectively. The limit of detection was 0.02 μg ml^{-1} of B_2O_3 (3σ criterium). The method was used to determine boron in nine ceramic materials with very different nominal boron compositions. The results were compared with those obtained using a potentiometric titration method as reference method. No significant differences (at 95% probability level) were found between the proposed and reference methods. The method is rapid, reliable, precise and free of interferences. © 1998 Elsevier Science B.V.

Keywords: Boron; Ceramic materials; Flow injection spectrophotometric determination

1. Introduction

Borate chemicals and boric acid have a wide variety of industrial applications. Borax, ulexite and colemanite are principally used in the ceramics industry for manufacturing borosilicate and similar glasses. The presence of boric oxide in these glasses facilities the dissolution of metallic oxides and produces a decrease in the melting point of the frits. Boric oxide also influences both the refractive index and the coefficient of expansion [1]. The control of impurities of boron in other materials is also important.

Boron is one of the chemical elements that is difficult to determine. Several analytical methods

* Corresponding author.

PII S0039-9140(97)00173-2

for determining boric acid in ceramic materials have been proposed, including atomic absorption spectroscopy [2,3], atomic emission spectroscopy with inductively coupled plasma (ICP) [4,5], X-ray fluorescence [6] and UV-Vis spectrophotometry [1,7]. Atomic absorption techniques have low sensitivity (the detection limits are ranged from 150 to 200 μg ml^{-1} of B_2O_3), and several problems related to the matrix and interference effects [2,3] have been reported. ICP emission spectroscopy gives accurate and precise results, but has several drawbacks, the most important being it is expensive. Several spectrophotometric methods using selective and sensitive reagents, e.g. curcumin, carmine, methylene blue and azomethine H have been used. In most cases, borate distillation, elimination of interferences and strict control of reaction conditions are required [1,7]. The flow injection (FI) methodology with spectrophotometric detection has been proposed for the determination of boric acid in waters [8–10], plants and soils [11,12] and pharmaceuticals [13,14]. No references have been found related to the FI determination of boron in ceramic materials.

The most precise, reliable and generally useful method for the determination of boron is the titration of boric acid with a standard base [1]. Boric acid is too weak (the logarithm of the protonation constant, log K_1 is 9.2) to be titrated directly with a standard base solution. However, it forms strongly acidic complexes with certain polyalcohols (i.e. glycerine, mannitol, sorbitol) that can be very precisely titrated. The mannitol-borate system has been the one most extensively studied. The method has been used to determine very small amounts of boron as well as macro amounts. It has usually been used as a reference method to evaluate the accuracy and reproducibility of other methods [3,4]. However, a typical problem of this method is the presence of transition-metal cations, which precipitate upon the addition of a base. The pH changes involved in the boric acid-polyalcohol reaction have been used in a FI method [14] and a FI pseudo-titration [13] to determine boric acid in pharmaceutical preparations.

In this paper an automated procedure for determining boron in ceramic materials is proposed. It is based on continuous-flow spectrophotometric measurement of the decrease in pH produced by the reaction between mannitol and boric acid in the presence of bromocresol green. The method has been applied to the determination of boron in ceramic raw materials, ceramic frits and ceramic pigments with very different nominal boron concentrations and a considerable variation in physical and chemical properties. The differences between the proposed and the potentiometric titration method (reference method) are also evaluated.

2. Experimental

2.1. Apparatus

A pH meter (MichropH 2000, Crison, Barcelona) and a diode-array spectrophotometer (Model 8452A, Hewlett-Packard, Palo Alto, CA) connected to a Vectra computer via an HPIB protocol (Hewlett-Packard) were used. The FI assembly was built using a peristaltic pump (Model Minipuls 2, Gilson, Middleton, WI) an injection valve (model 5020, Rheodyne, Berkeley, CA), a 18 μl flow-cell (model 178012-QS, Hellma, Mülheim/Baden) and 0.5 mm i.d. PTFE tubes.

2.2. Reagents

All chemicals were of analytical-reagent grade. E-pure deionized water (Barnstead Sybron, MA) was used throughout to prepare the solutions. Stock solutions of bromocresol green (Panreac, Barcelona, Spain) 1×10^{-3} mol l^{-1} were prepared by dissolving 0.17 g in 0.25 l of water. Solutions of mannitol (Merck, Darmstad, Germany) 0.75 mol l^{-1} containing 1×10^{-4} mol l^{-1} of indicator were prepared by dissolving 68.3 g of the solid in about 400 ml of water, adding 50 ml of indicator stock solution and diluting to 500 ml with water. The pH of the solution was adjusted to 5.4 using diluted HCl solutions.

2.3. Standard solutions

Stock standard solutions of boric acid (5×10^{-3} mol l^{-1}) were prepared by dissolving 0.31 g of boric acid (Merck, Darmstadt) in 1.0 l of water. Working standard solutions were prepared by appropriate dilution of the stock standard solution in the range 3×10^{-5}–3×10^{-3} mol l^{-1} (equivalent to 1–100 μg ml^{-1} of B_2O_3). The pH of the working standard solutions was previously adjusted to 5.4.

2.4. Stock sample solutions

Ceramic raw materials were dried at 40°C for 12 h and finely ground to pass completely through a 200 mesh. A total of 2–3 g of sample were weighed and transferred to a 250 ml vessel, and 70–80 ml of 10% (v/v) HCl solution were added. The mixture was boiled for 1 min, then left in a thermostatic bath for 1 h at 70–80°C. After that, the sample solution was filtered through a 40 Whatman filter and diluted with deionized water in a 250 ml calibrated flask.

Ceramic frits and pigments were dried at 110°C and finely ground to pass completely through a 200 mesh. A total of 0.2–1.2 g of sample were mixed in a platinum crucible (or nickel crucible if the samples contained Pb) with a 7-fold amount of Na_2CO_3/ZnO (2:1). The mixture was heated and placed in a muffle furnace at 900°C for 10 min. The synterized samples were transferred to a porcelain capsule and 100 ml of hot deionized water were added. The mixture was filtered through a 40 Whatman filter and centrifuged if necessary, and the resulting solution was diluted with deionized water in a 250 ml calibrated flask.

2.5. Procedures

2.5.1. Potentiometric titration method

To obtain precise results, two potentiometric titrations were performed for each sample. First, the residual acidity of each sample was evaluated by titrating 50 ml of the samples with 0.1 mol l^{-1} NaOH in order to determine the pH of the equivalence point. Second, the pH of 50 ml of the raw material solutions was adjusted to the pH of the equivalence point with the aid of a diluted NaOH solution. After that, 10 g of mannitol were added and the sample was titrated with a standardized 0.5 mol l^{-1} NaOH solution.

For the analysis of the ceramic frits and pigments, 50 ml of the sample solutions were previously neutralized with HCl and filtered or centrifuged if neccesary. Then, 5–10 ml of 20% $BaCl_2$ solution were added to the solution in order to precipitate sulphate, chromate, aluminate and silicate anions. After settling for one hour, the solution was filtered. The filtrate was neutralized with HCl (1:1) to a methyl red (adding a small excess), boiled for 5 min to remove the CO_2 and filtered if necessary. After cooling, the solution was titrated as in the former case.

2.5.2. FI method

Adequate aliquots of stock sample solutions were taken and diluted to obtain a boric acid concentration in the range 3×10^{-5}–3×10^{-4} mol l^{-1}. The pH of the samples was previously adjusted to 5.4 using a pH meter. In the case of ceramic frits and pigments solutions, the aliquots were previously boiled in acidic media for 5 min in order to eliminate the carbonic acid system. Fig. 1 shows a scheme of the manifold designed to determine boron in ceramic materials. A total volume of 200 μl of the sample solutions were injected into deionized water at pH 5.4 (channel C), and the stream was later merged with the reagent stream containing the mannitol-bromocresol green solution at pH 5.4 (channel R). Transient signals were monitored at 616 nm. Other FI conditions were: flow rate 2.7 ml min^{-1} and 300 cm reaction coil.

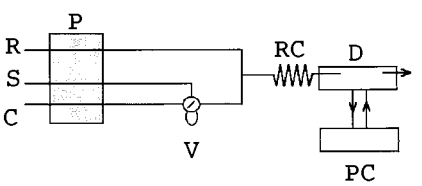

Fig. 1. Schematic diagram of the FI system. C, carrier stream (deionized water at pH 5.4); R, reagent stream (0.75 mol l^{-1} mannitol and 1×10^{-4} mol l^{-1} bromocresol green solution at pH 5.4); P, pump; S, sample solution; V, injection valve (200 μl); RC, reaction coil (300 cm); d, detector (616 nm); PC, computer.

3. Results and discussion

3.1. Theoretical model

Polyhydroxy compounds (mannitol, sorbitol, glycerine) form stable complexes with the borate anion, producing an increase in the ionization of the acid, thus decreasing the pH of the solution. The exact nature of the polyalcohol-borate complexes and attendant equilibria reactions has often been the subject of controversy [1]. However, when polyalcohols (LH_2) are present in relatively large excess in diluted solutions of boric acid the reaction is:

$$H_3BO_3 + 2LH_2 \rightarrow H^+ + L_2B^-$$

Let us suppose that we have a solution of a bicoloured acid-base indicator, HI, with a protonation constant, K_I, in a C_I analytical concentration. In the presence of a relatively large excess of the polyhydroxy compound, the absorbance value at a given wavelength (A_λ) can be expressed as a function of the boric acid concentration according to the expression:

$$A_\lambda = \varepsilon_{HI,\lambda} C_I \frac{K_I[[H^+] + C_{H_3BO_3}]}{1 + K_I[[H^+] + C_{H_3BO_3}]} + \varepsilon_{I^-,\lambda} C_I \frac{1}{1 + K_I[[H^+] + C_{H_3BO_3}]} \quad (1)$$

where $\epsilon_{HI,\lambda}$ and $\epsilon_{I,\lambda}$ are the molar absorptivities for the species HI and I^- at this wavelength and C_{H3BO3} is the boric acid concentration and $[H^+]$ corresponds to the initial pH value.

Usually, when an indicator is used to monitor the pH changes in a flow injection system, the difference between the initial and final absorbance values is used as analytical signal. These increments could be calculated by:

$$\Delta A_\lambda = (\varepsilon_{I^-,\lambda} - \varepsilon_{HI,\lambda}) C_I \frac{K_I C_{H_3BO_3}}{(1 + K_I[H^+])\,(1 + K_I[[H^+] + C_{H_3BO_3}])} \quad (2)$$

As can be observed, Eq. (1) and Eq. (2) indicate that the relationships between the absorbance or ΔA at a selected wavelength and the boric acid concentration are not linear. However, in some conditions linear relationships can be obtained. First, for low boric acid concentrations, the term $K_I C_{H3BO3}$ in the denominator of Eq. (1) and Eq. (2) could be negligible, and these equations should then provide an apparent linear relationship. Second, if the molar absorptivity of the basic form of the indicator at the selected wavelength is significantly higher than the molar absorptivity of the corresponding acidic form, the first term of Eq. (2) could be negligible. In this case, the inverse of the absorbance becomes:

$$\frac{1}{A_\lambda} = \frac{1 + K_I[H^+]}{\varepsilon_{I^-,\lambda} C_I} + \frac{K_I C_{H_3BO_3}}{\varepsilon_{I^-,\lambda} C_I} \quad (3)$$

Eq. (3) indicates that the relationship between the inverse of the absorbance values and the boric acid concentration is linear. In order to confirm these conclusions, standard solutions of boric acid ranging from 3×10^{-5} to 3×10^{-3} mol l^{-1} (equivalent to 1–100 μg ml^{-1} of B_2O_3) were injected into the FI assembly using bromocresol green as indicator. The experimental behaviour observed was in agreement with the theoretical conclusions. Although a slight deviation from the linearity was observed in plot $1/A$ vs μg ml^{-1} of B_2O_3 at high B_2O_3 concentrations (Fig. 2), useful linear relationship in the range 1–30 μg ml^{-1} was

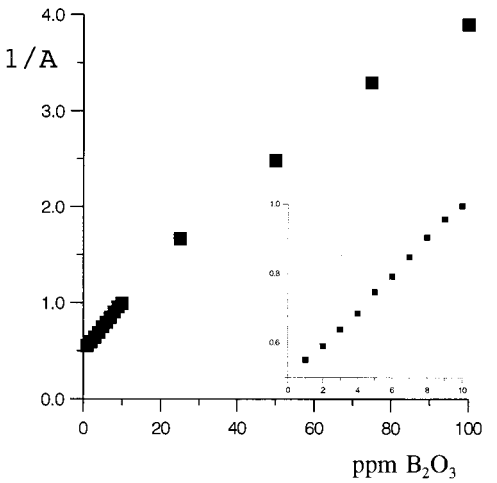

Fig. 2. Dependence between the inverse of the absorbance at 616 nm and the concentration of boric oxide in the conditions of Fig. 1. Bromocresol green was used as the indicator.

obtained (relative difference between estimated and observed signal lower than 3%). In contrast, the linear relationships found using Eq. (1) and Eq. (2) were only satisfactory in the range 1–4 μg ml^{-1} of B_2O_3.

3.2. Selection of the indicator

The protonation constant of the indicator should be adequate to measure the pH changes of the solution. These changes should occur between 6 (pH of the mannitol solution) and 3.5 (the minimum pH obtained after the mannitol-borate reaction). Therefore, $\log K_I$ values in the range 4.5–5.5 should be adequate. On the other hand, Eq. (2) indicates that the sensitivity depends on the difference between the molar absorptivities of the basic and acidic forms of the indicator. In addition, in order to satisfy the condition that leads to the Eq. (3), the molar absorptivity of the acidic form of the indicator at the working wavelength should be as low as possible. Therefore, these considerations should be taken account in selecting the indicator. Bromocresol green ($\log K_I = 4.9$) was found to be the most favourable indicator. At 616 nm (the wavelength of maximum absorption of the basic form of the indicator) the molar absorptivity was 3.7×10^4 mol l^{-1} cm^{-1}. At this wavelength, the molar absorptivity of the acidic form was 2.04×10^2 mol l^{-1} cm^{-1}.

3.3. Selection of manifold and optimization

Two FI manifolds were assayed. First, a monochannel manifold was used in which boric acid solutions containing the indicator at pH 5.4 were injected into a carrier stream containing the mannitol solution with the same concentration of indicator and pH. Second, a bichannel FI manifold was studied. In this case only the mannitol solution contained the indicator. Boric acid solutions were injected into a carrier stream of deionized water at pH 5.4. This solution merged in a T union with the mannitol-indicator solution (Fig. 1). Although in both cases, adequate linear $1/A$ vs μg ml^{-1} B_2O_3 relationships were obtained, the bichannel FI manifold showed more repeatable signals due to the smaller contribution of the refractive index to the signal. In addition, it does not require extra preparation of the samples, while the monochannel assembly requires the addition of a constant indicator concentration to all solutions.

Chemical (pH, bromocresol green concentration, and mannitol concentration) and FI (sample volume, reagent flow-rates and reaction coil length) variables were optimized with the aid of boric acid standard solutions. First, the concentration of the mannitol in channel R was optimized. As can be expected, the absorbance values at 616 nm increased as the mannitol concentration increased from 0.1 to 0.75 mol l^{-1}. Maximal signals were obtained by using a 0.75 mol l^{-1} mannitol concentration (due to the low solubility of mannitol in water, a more concentrated solution could not be prepared). The sensitivity of the procedure increased when the indicator concentration increased in the range 5×10^{-5}–5×10^{-4} mol l^{-1}, but the initial absorbance values did the same, as predicted by Eq. (3) and Eq. (2), respectively. An adequate compromise between sensitivity and the initial absorbance value was obtained using a 1×10^{-4} M bromocresol green concentration. The pH of the mannitol-indicator solution was adjusted to 5.4 with 0.01 M HCl (upper limit of the transition pH interval of the indicator). In these conditions the initial absorbance values were around 2.

The range of FI variables studies were: flow rate 0.5–2.7 ml min^{-1}, injection volume 100–500 μl, and reactor length 100–500 cm. The selected values among those which lead to a good compromise between sensitivity (peak height), reproducibility (coefficient of variation), sample passage (peak width) and peak shape (conditions which produce double peak were excluded) were: 2.7 ml min^{-1}, 200 μl and 300 cm, respectively. These parameters were used to establish the analytical features of the FI procedure.

3.4. Analytical data

The calibration curve of boric acid, expressed as B_2O_3, was obtained by triplicate injections of standard solutions with a concentration of the

compound varying from 1 to 10 μg ml^{-1} of B_2O_3. The inverse of the absorbance values and the increment of absorbance values at 616 nm were used as dependent variables. The presence of outliers, normality of residuals (Kolmogoroff test), homogeneity of variances (Cochran and Bartlett tests) and validity of the linear model (lack-of-fit test) were studied in agreement with the suggestions reported by Sarabia and Ortiz [15]. In all cases the significance levels found assure the validity of the regression models. Table 1 shows regression statistics for the calibration curves. The regression coefficient and the standard error of the regressions values, as well as the values of the residual variance to the variance modelled by regression ratio (F), indicated that the use of the inverse of the absorbance is preferable as dependent variable, in accordance with Eq. (3) and Fig. 2, and it was therefore selected.

Injections of blank solutions did not produce significant analytical signals. The limit of detection (LOD, 3σ criterium) calculated from the S.D. of 5-fold injections of a 1 μg ml^{-1} boric acid solution was 0.02 μg ml^{-1} of B_2O_3, and the LOD estimated from the S.D. of the intercept and the slope of the calibration curve was 0.58 μg ml^{-1} of B_2O_3. The repeatability was evaluated by means of repetitive injections ($n = 11$) of B_2O_3 solutions at two levels of concentration, 4.0 and 8 μg ml^{-1}. The relative standard deviations were 0.68 and 0.41%, respectively.

Table 1
Regression statistics for the calibration curves of boric oxide using (1) inverse absorbance values and (2) increment absorbance values at 616 nm as dependent variables

Parameter	1	2
Slope ± ts[a]	$(5.16 \pm 0.15) \times 10^{-2}$	$(8.5 \pm 1.1) \times 10^{-2}$
Intercept ± ts[a]	$(48.5 \pm 1.0) \times 10^{-2}$	$(9 \pm 7) \times 10^{-2}$
S.E. of regression	0.005	0.04
r	0.999_4	0.9_9
F	6064	327
n	10	10

r, correlation coefficient; F, the ratio between the residual variance and the variance modelled by regression; n, number of points.
[a] The confidence intervals (ts) were calculated at a 95% probability level.

3.5. Analysis of ceramic materials

The proposed method was applied to determine boric acid in nine ceramic materials with a wide variety of compositions. Samples were kindly donated by different Spanish ceramic manufactures. Table 2 shows the composition of the samples declared by the manufactures (routine quality control). Samples 1–3 (colemanite, ulexite and borax) are used in the ceramics industry as raw materials; samples 4–8 are ceramic frits and sample no. 9 is a ceramic pigment.

The boric acid content was obtained by injecting the sample solutions into the FI manifold in triplicate. Samples were also analyzed by the potentiometric titration method (see Section 2). This method is considered the reference method for the analysis of boric acid in this kind of materials. Table 3 shows the results obtained when these methods were used. As can be observed the results obtained by the proposed procedure and the potentiometric method coincide closely with the declared contents (Table 2). The B_2O_3 contents obtained by the proposed procedure were plotted against those obtained by the potentiometric method. The equation of the fitted straight line together with the confidence interval of the parameters (95% probability level) was:

$$\%\, B_2O_3\,(FI\ method) = 0.0\ (\pm 0.3) + 1.006\ (\pm 0.011)\ \%\, B_2O_3\ \text{(potentiometric method)},$$

$r^2 = 0.9998$, F ratio = 43253. The intercept and the slope values were significantly equal to zero and to unity, respectively, which reveals the absence of systematic errors. In addition, the paired t-test and the Wilcoxon test (2-tailed) [16] were also applied to compare the results given in Table 3. The statistics calculated ($t_{cal} = 1.67 < t_{95,8} = 2.30$ and $t_{cal} = 10.5 > t_{95} = 6$, respectively) indicated that the methods were not significantly different at the 95% probability level in the range of boric acid studied (40–1.7%).

Table 2
Composition of analyzed samples (in percentage)

	1	2	3	4	5	6	7	8	9
SiO_2	3.96	4.30	—	11.70	26.56	40.20	54.10	40.90	32.32
Al_2O_3	<0.03	0.10	—	—	—	9.50	12.10	6.53	0.13
B_2O_3	43.30	37.90	38.00	18.75	17.01	23.90	3.65	1.79	1.85
Fe_2O_3	0.04	0.03	—	—	—	0.18	0.16	—	0.17
CaO	26.90	17.70	—	—	—	9.62	12.40	0.77	—
MgO	1.49	1.65	—	—	—	0.90	0.35	0.14	—
Na_2O	0.01	5.69	16.95	—	—	4.48	0.31	1.03[a]	5.26
K_2O	<0.01	0.02	—	—	—	0.99	1.67	[a]	0.04
TiO_2	<0.01	0.02	—	—	—	0.10	0.06	—	5.62
ZrO_2	—	—	—	—	—	<0.01	<0.01	7.3	3.48
BaO	—	—	—	—	—	8.84	7.80	—	—
Li_2O	—	—	—	—	—	0.71	0.93	—	—
PbO	—	—	—	68.45	42.23	0.07	0.29	38.83	37.90
V_2O_5	—	—	—	—	—	—	—	—	13.20
ZnO	—	—	—	—	—	0.09	4.81	1.05	—
SrO	0.95	0.70	—	—	—	—	—	—	—
As_2O_3	<0.01	2.02	—	—	—	—	—	—	—
LOI[b]	24.02	32.00	45.00	—	13.2	—	—	—	—

Samples 1–3 are ceramic raw materials, samples 4–8 ceramics frits and sample 9 is a ceramic pigment.
[a] Sum Na_2O+K_2O.
[b] Loss of calcination.

The proposed FI method for the determination of boric acid ceramic materials presents a series of advantages concerning the reference potentiometric method: The determination of boric acid is rapid (1 min for sample). The sample preparation is less time consuming. The proposed method has no potential interferents. The possible interferents could be compounds (i.e. carbonate) which can buffer the solution or cations (i.e. Pb, Zn) which may precipitate at the working pH. The carbonic acid system has been eliminated by boiling the sample solution in acidic media during its treatment. Pb, Zn and other transition metals do not precipitate at the working pH range (5.4–4.4). Finally, the use of Na_2CO_3/ZnO as disgregant eliminates the silica by formation of sodium zinc silicate which precipitates. Finally, the FI method could be easily automated with the purpose of implementing it in routine analysis.

Table 3
Determination of boron in ceramic materials expressed as % B_2O_3

Sample	Potentiometric method ($n=3$)	FI-spectrophotometric method ($n=3$)
1	43.6 ± 0.3	43.5 ± 0.2
2	38.0 ± 0.5	38.3 ± 0.2
3	37.3 ± 0.3	37.9 ± 0.1
4	18.7 ± 0.3	18.8 ± 0.3
5	17.27 ± 0.03	17.2 ± 0.2
6	24.15 ± 0.04	24.36 ± 0.06
7	4.1 ± 0.3	4.09 ± 0.05
8	1.5 ± 0.2	1.66 ± 0.08
9	1.71 ± 0.05	1.65 ± 0.02

On the other hand, the proposed method has an LOD (20 ppb B_2O_3) similar to the ICP method [17] (16 ppb) and lower than the one obtained by atomic absorption (48 ppm) and potentiometric methods [1] (2.5%; 120 ppm according to the described procedure). Dynamic ranges are comparable for the proposed FI and ICP methods (1–30 ppm and 3–160 ppm, respectively). These results indicate that the proposed method has adequate analytical features in relation to those methods, besides its simplicity and availability.

References

[1] R.S. Braun, W.E. Chambers, Teatrise on Analytical Chemistry, part II, Analytical Chemistry of Inorganic and Organic Compounds, vol. 10, John Wiley, New York, 1978.
[2] W.P. Kilroy, C.T. Moyniham, Anal. Chim. Acta 83 (1976) 389.
[3] B.E. Andrew, Ceramic Bull. 55 (1976) 583.
[4] M.F. Barba, F.J. Valle, L'Industrie Ceramique 38 (1984) 389.
[5] J.N. Walsh, R.A. Howe, Appl. Geochem. 1 (1986) 161.
[6] S. Uhling, L. Müller, 3rd Euro-Ceramics 3 (1993) 1037.
[7] R. Ruggeri, Anal. Chim. Acta 29 (1961) 145.
[8] T. Lussier, R. Gilbert, J. Hubert, Anal. Chem. 64 (1992) 2201.
[9] S. Motomizu, M. Oshima, Z. Jun, Anal. Chim. Acta 251 (1991) 269.
[10] K. Toei, S. Motomizu, M. Oshima, M. Onoda, Bunseki-Kagaku 35 (1986) 344.
[11] D. Chem, F. Lazaro, M.D. Luque de Castro, M. Valcarcel, Anal. Chim. Acta 226 (1989) 221.
[12] J.C. De Andrade, M. Ferreira, N. Baccan, O.C. Bataglia, Analyst 113 (1988) 289.
[13] I.P. Anagnostopoulou, M.A. Koupparis, J. Pharm. Sci. 74 (1985) 886.
[14] K. Nose, M. Zenki, Analyst 114 (1991) 711.
[15] L. Sarabia, M.C. Ortiz, Trends Anal. Chem. 13 (1994) 1.
[16] D.L. Massart, M.P. Derde, Y. Michotte, L. Kaufman, Balance—A Program to Compare Two Series of Measurements, Elsevier, Amsterdam, 1984.
[17] American Public Health Association, Standard Methods for the Examination of Water and Wastewater, XVIII ed., American Public Health Association, Washington, 1992.

.

ELSEVIER

Talanta 45 (1998) 843–850

Talanta

Voltammetric determination of copper in water samples digested by ozone

Ž. Filipović-Kovačević [a,*], L. Sipos [b]

[a] *Faculty of Food Technology and Biotechnology, University of Zagreb, Zagreb, Croatia*
[b] *Faculty of Chemical Engineering and Technology, University of Zagreb, Zagreb, Croatia*

Received 29 March 1995; received in revised form 3 June 1997; accepted 3 June 1997

Abstract

The applicability of ozone as a digestion agent in voltammetric trace metal analysis of water samples was investigated. It was shown that ozone efficiently destroys dissolved organic matter, causing a significant decrease of the concentration of surface active substances in the sample, thus enabling voltammetric measurements. Ozonolysis times of 30 and 60 min were sufficient for the treatment of river water and biologically treated wastewater samples, depending on their organic load, prior to voltammetric determination of copper using a solid gold electrode. © 1998 Elsevier Science B.V.

Keywords: Ozone; Sample digestion; Voltammetry; Copper

1. Introduction

Electroanalytical techniques such as polarography, differential pulse polarography and related techniques can be successfully applied to the determination of low concentrations of copper and other heavy metals [1–3].

In electroanalytical techniques, organic matter and/or surface active substances are generally unfavorable due to interferences with or hindering of the electrode process [4]. Sample digestion is necessary prior to trace metal determinations. Wet acid digestion of aquatic samples is one of the most efficient processes; however, it is time consuming and there is contamination risk by the chemicals used. The application of ozone seems to have advantages in this respect.

It was namely found that ozone used for sample treatment, prior to anodic stripping voltammetry (ASV), is very effective and remarkably active in destroying naturally organic compounds [5]. An extensive study of the applicability of ozone as oxidant of organic sequestering agents in water prior to determination of trace metals by ASV has already been published [6]. It was generally concluded that adsorption of surface active compounds seems to be the limiting factor in the analysis of natural samples by ASV, even when applying ozonolysis for the preparation of samples prior to the analysis [6].

In the present paper, ozonolysis as a water sample treatment procedure was studied with re-

* Corresponding author.

PII S0039-9140(97)00174-4

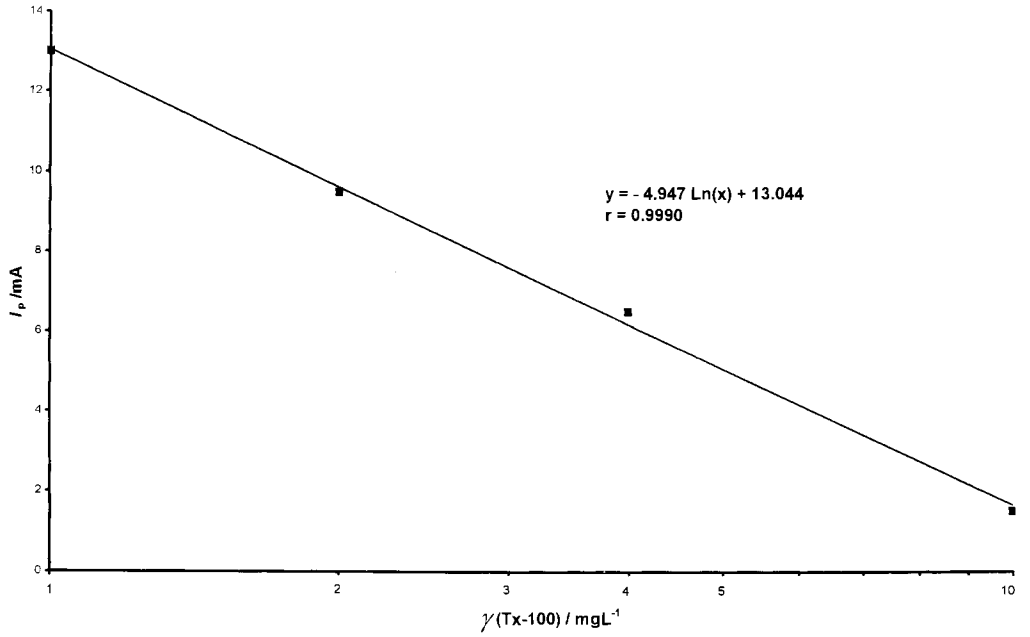

Fig. 1. Calibration curve for Triton X-100 in a supporting electrolyte containing NaCl and $HgCl_2$.

spect to its oxidizing ability of organic matter present in surface and wastewater samples. Moreover, the role of ozonolysis of samples was studied. It was shown that ozone mainly affect elimination of surface active properties of organic matter, rather than destroying it.

The use of ozonization as a water sample pretreatment procedure for electroanalytical determination of copper on gold electrode is described and compared with the conventional wet digestion treatment.

2. Experimental

2.1. Apparatus

A home-made ozone generator with maximum ozone production of 80 mg h^{-1} was used. The ozone production cell consists of a 400 mm long ($\phi = 10$) Pyrex glass tubing coated with aluminum foil and with a 400 mm long ($\phi = 2$) stainless-steel rod placed inside, concentrically, along the axes of the glass tubing. High purity oxygen was passed through the cell at controlled flow rates. The aluminum foil and the stainless-steel rod were used as electrodes. The high voltage applied between the electrodes, necessary for ozone production, was generated by an electronic circuitry described elsewhere [7].

The amount of ozone produced was controlled by the frequency of the high voltage generator and its concentration was quantitatively determined by the KI method [8].

Voltammetric measurements were performed using the polarographic analyzer PAR 264A (EG and G PAR, USA) connected with an XY recorder PL 3 (Lloyd, UK). A three electrode electrochemical cell was used. The dropping mercury electrode (DME) and a gold electrode were used as working electrodes, the saturated calomel electrode (SCE) as reference electrode and Pt wire as auxiliary electrode.

The total organic carbon (TOC) values were determined in acidified (pH = 2) samples using the Carbon Analyzer Model 1555, Ionics, Incorporated.

2.2. Sample collection

Water samples were collected and stored in a way usual for trace metal analysis [9] as follows:

The samples were taken manually, using polyethylene gloves, into 1 l polyethylene bottles scrupulously cleaned [10] and then wrapped into two polyethylene bags. From cleaning to sampling, the bottles were filled with pure water, acidified to pH = 2 with hydrochloric acid. The samples were stored at − 20°C until the analysis.

Water samples of the river Sava in the vicinity of Zagreb were taken for a part of our experiments.

The other experiments were made using treated wastewater samples. They were taken from the effluent of the wastewater treatment plant of the yeast-production industry in Koprivnica. The treatment plant uses the one-stage aerobic activated sludge process.

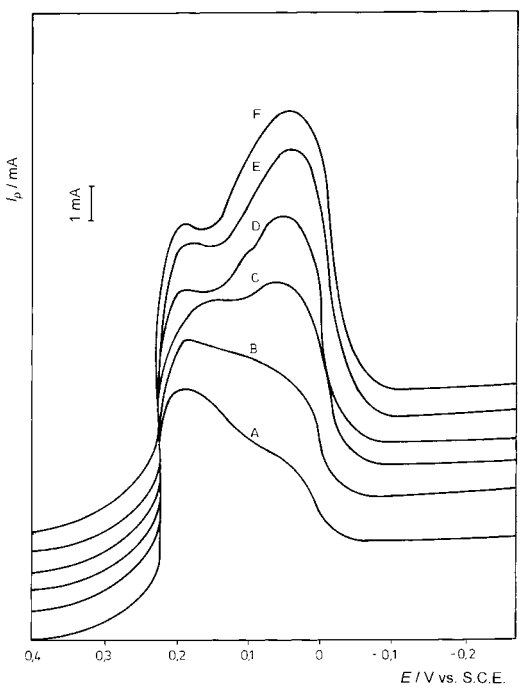

Fig. 2. Polarographic maxima of the oxygen reduction wave of a river water sample in dependence on the ozonolysis time. Curves A–F represent ozonolysis times of 0, 5, 10, 15, 30 and 60 min, respectively.

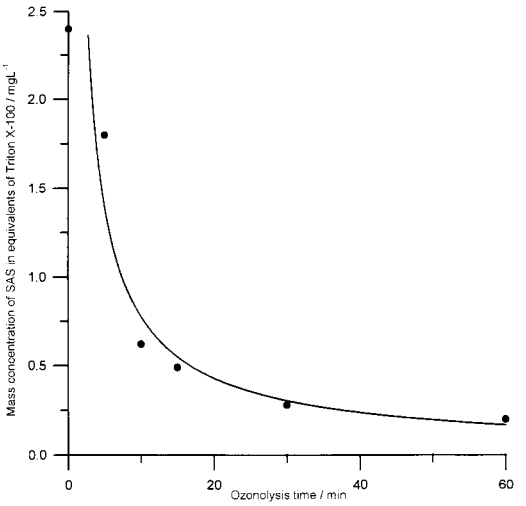

Fig. 3. The change of concentration of surface active substances in river water (in equivalents of Triton X-100) with ozonolysis time.

2.3. Sample digestion

Analytical grade chemicals (Merck) and deionized water (Millipore Q system) were used throughout. For wet digestion, 'Suprapure' nitric acid (Merck) was used.

Wet digestion of the samples (20 ml vol.) was performed with 1–2 ml of HNO_3 in a quartz vessel (approximately 100 ml), placed in an aluminum heating block (temperature 210°C). The sample was evaporated until the appearance of a solid residue, treated with a few drops of 30% H_2O_2 until disappearance of its color and, finally, the residue was dissolved in 10 ml of water prior to the voltammetric measurement. This procedure took approximately 60 min.

The ozone treatment was usually performed with 20 ml of sample, placed in thermostated quartz tubings (vol. of 100 ml) under a controlled ozone flow (78 mg h^{-1} O_3).

After ozone treatment, the samples were ordinarily deaerated in the voltammetric cell to eliminate oxygen and the remaining ozone from the solution.

2.4. Determination of surface active substances (SAS)

The procedure described elsewhere [11] was used as follows: into 50 ml of sample 1 ml $HgCl_2$ solution (c = 0.1 M) and 5 ml saturated NaCl solution was added, well mixed and the polarogram of the oxygen wave was recorded in a potential range from +0.4 to −0.2 V vs. SCE. The height of the polarographic maxima that appeared at +0.1 V vs. SCE was measured. The concentration of SAS was determined using calibration curves obtained by standard Triton X-100 solutions.

In the case of ozonolysis, the samples were left to equilibrate with air for a few hours before the determination of SAS.

2.5. Voltammetric determination of copper

In digested samples (pH = 2), copper was determined by anodic stripping voltammetry (ASV) using a gold electrode [1]. The copper was deposited on a stationary gold disc electrode at −0.2 V vs. SCE for 5 min, and the copper response was recorded in DPASV mode in the potential range of −0.2 to +0.5 V vs. SCE. The solution was mixed during the deposition time with a Teflon coated magnetic stirring bar. The standard addition technique was applied. Prior to each measurement, the gold electrode were activated electrochemically in 0.1 M $HClO_4$ solution containing 2.5 mM HCl (medium exchange). The activation was performed by polarizing it to +1.7 V for 6 min and subsequently to +0.7 V for 1 min. Activation of the electrode was also necessary before each standard addition.

3. Results and discussion

Organic matter present in aquatic samples may disturb the electroanalytical determination of trace metals. Organic matter may act as a complexing agent for trace metals, changing the kinetics of the electrode process. On the other side, organic matter may act as a surface active substance adsorbing on the electrode surface and hindering the electrode processes during both the deposition and stripping steps. Solid electrodes such as gold, graphite, etc. are extremely sensitive to surface active substances. Independently of the complexing and/or surface active properties of the dissolved organic matter, significant errors in electroanalytical determinations of trace metals may occur. Thus, elimination of organic matter itself, or its complexing and surface active properties, is necessary prior to voltammetric measurements. It is known that ozone, as a strong oxidizing agent, tends to oxidize inorganic substances into their highest oxidation states, while organic substances are disintegrated to CO_2 and H_2O [12].

The effect of ozone on the surface active properties of the dissolved organic matter, though noticed, was not the subject of detailed study.

Electoanalytical techniques [11] seem to be an ideal tool for measuring the surface active properties of dissolved organic matter in the case of ozonolysis. Measurement of the polarographic maxima is one of the simplest techniques for this purpose [13]; hence, it was applied in this work for the investigation of the effect of ozone on the surface active properties of organic matter.

Triton X-100 is commonly used as standard solution for the determination of SAS [11]. Fig. 1 shows the calibration curve for Triton X-100 in the supporting electrolyte containing NaCl and $HgCl_2$. Thus, using the calibration curves obtained, the concentration of SAS in water samples, as equivalents of Triton X-100, can be determined. Excellent linearity was found between the height of the polarographic maxima and the log of the concentration of Triton X-100 in the concentration range 1–10 mg l^{-1}.

Fig. 2 shows the relation between the height of the polarographic maxima and the ozonolysis time in a river water sample. It is interesting to note that a similar curve shape was obtained by ozonolysis in a solution of Triton X-100, indicating decreasing surface active properties at the ozonolyzed Triton X-100.

By increasing the time of ozonolysis, the height of polarographic maxima of the oxygen reduction wave increases, indicating a decrease of the concentration of SAS in river water samples, as shown in Fig. 3. One can conclude that, using

Table 1
Results of copper determinations ($\gamma(Cu) \times 10^6$ mg l^{-1}) in a yeast wastewater sample (COD = 5.25 g l^{-1} O_2) digested under different conditions

Digestion		Sample dilution ratio											
Procedure	Time (min)	1:0				1:5				1:10			
		$\gamma(Cu) \times 10^6$		COD	TOC	$\gamma(Cu) \times 10^6$		COD	TOC	$\gamma(Cu) \times 10^6$		COD	TOC
		mg l^{-1}	σ_{n-1}	g l^{-1} O_2	g l^{-1} C	mg l^{-1}	σ_{n-1}	g l^{-1} O_2	g l^{-1} C	mg l^{-1}	σ_{n-1}	g l^{-1} O_2	g $^{-1}$ C
Ozonolysis	0			5.25	2.52			2.50	2.56			2.30	2.80
	30	3.0	0.137	5.05	2.50	9.0	0.057	2.70	2.56	10.0	0.165	2.50	2.80
	60	5.9	0.155	5.25	2.54	10.0	0.192	2.80	2.56			2.50	2.70
	120	7.2	1.114	5.20	2.52			2.65	2.56			2.40	2.70
	240	8.8	0.099										
Wet		10.0	0.471			10.3	0.242			10.0	0.157		

Ten parallel samples were analyzed.
Confidence level 95%.

Table 2
Results of copper determination ($\gamma(Cu) \times 10^6$ mg l^{-1}) in a river water sample determined by different digestion procedures

Digestion procedure	$\gamma(Cu) \times 10^6$ mg l^{-1}	σ_{n-1}	V (%)
Without digestion	0.0034	0.0005	15.7
Wet digestion	0.0048	0.0006	13.7
Ozonolysis 30 min	0.0048	0.0006	13.0

Five parallel samples were analyzed.

ozone as a sample treatment agent, the concentration of SAS can be decreased to practically negligible amounts. Evidently, the surface active properties of the sample drastically decrease in the first ten min. of ozonolysis.

The question arises what is the product of ozonolysis? According to the literature data, the main final product of ozonolysis should be CO_2 and H_2O [12]. Our experiments are not in agreement with such a conclusion.

The COD values (measured by permanganate consumption) of samples did not decrease to the expected extent. Typically, in the river water samples, with permanganate consumption in the range 1–6 mg l^{-1} O_2, only 50% of COD elimination was achieved.

In the case of the yeast industry wastewater, no significant decrease of COD values was noticed (Table 1). Moreover, the total organic carbon (TOC) values were also practically unaffected by ozonolysis (Table 1). These experiments indicate that products of ozonolysis are certainly not CO_2 and H_2O, but some substances with minor surface active properties enabling the application of electroanalytical techniques.

The question arises: under which conditions could ozone be applied in combination with the voltammetric determination of copper in river water and biologically treated wastewater? To find the answer to this question, determination of copper using a solid gold electrode and the voltammetric technique was applied in ozonized samples under different conditions.

A series of seven measurements show that surface waters like river water, with a relatively low

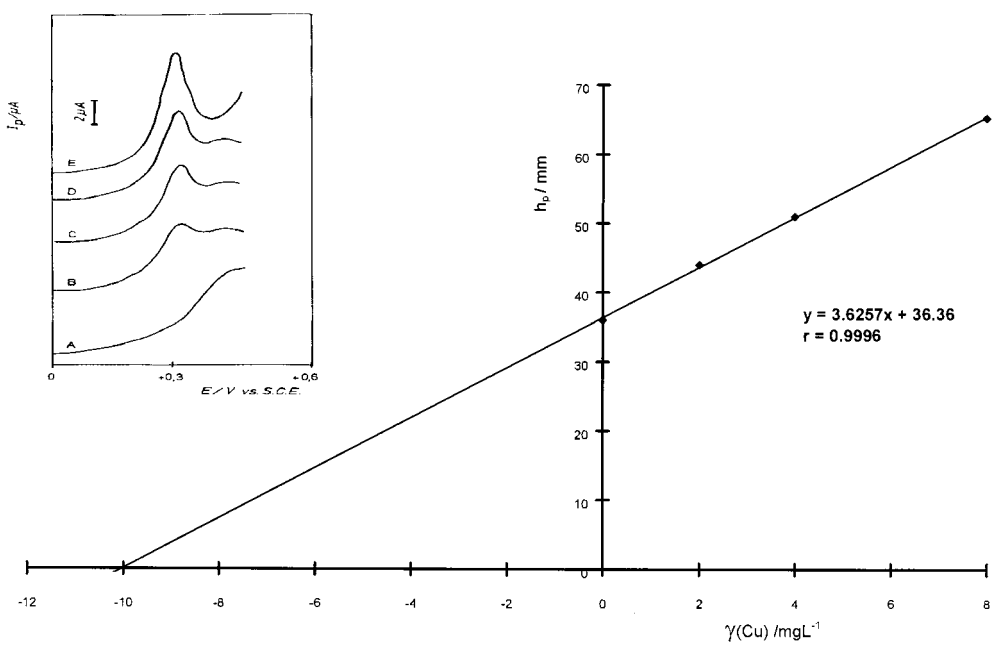

Fig. 4. Typical voltammograms and calibration curve of copper in a yeast wastewater sample. Curves: A, without ozone treatment; B, C, D ozone treatments for 30, 60 and 120 min, respectively; E as curve D after addition of 6 μg l^{-1} copper.

Table 3
Results of copper determination ($\gamma(Cu) \times 10^6$/mg l^{-1}) under different conditions in a sample of biologically treated water (COD = 1.4 g l^{-1} O_2)

Temperature (°C)	Digestion procedure							
	Ozonolysis							
	Time of ozonolysis (min)						Wet digestion	
	0		30		60			
	γ(Cu)	σ_{n-1}	γ(Cu)	σ_{n-1}	γ(Cu)	σ_{n-1}	γ(Cu)	σ_{n-1}
—	0.3	0.059						
2			1.9	0.100	2.5	0.212		
18			2.4	0.158	2.8	0.148	3.3	0.393
37			2.6	0.360	3.3	0.283		
57			2.6	0.217	3.3	0.424		

Five parallel samples were analyzed.

organic load, can be successfully treated with ozone prior to voltammetric determination. Agreement between the copper concentration in ozonized and wet digested samples was obtained. Ozonolysis time of 30 min was usually sufficient (Table 2).

Experiments showed that copper could not be determined by the voltammetric technique on a gold electrode in a yeast wastewater sample without any treatment (Curve A, Fig. 4). However, by increasing the ozone treatment times, and sample dilution well defined stripping voltammetric curves of copper appeared (Curves B–E). To define the proper sample treatment conditions by ozone, a series of measurements were performed and the results obtained were compared with wet digestion. Namely, electroanalytical analysis combined with wet digestion was many times compared with other available techniques [2,3]. Thus, comparison of the wet digestion technique with other techniques, was outside of the frame of this paper.

Raw wastewater samples (COD = 5.4 g l^{-1} O_2), ozonized for as long as 240 min, were not sufficient to obtain the results of wet digestion (Table 1). By diluting the wastewater samples in ratios 1:5 and 1:10 with deionized water, the sufficient ozonolysis time was decreased to 60 and 30 min, respectively, and thus an agreement between the results of wet digestion and ozonolysis was obtained.

In contrast to raw wastewater, biologically treated wastewater (COD = 1.4 g l^{-1} O_2) could be sufficiently distracted by ozone without dilution. Moreover, the results of experiments at different temperatures and ozonolysis times show that the latter takes 60 min and can be performed at room temperature (Table 3). Thus, no significant difference (proven by the t-test at 95% confidence level) was noticed between copper concentrations in ozonolyzed and wet digested samples under such conditions. This was not the case of ozonolysis at 2°C and/or ozonolysis times of 30 min, thus indicating insufficient ozonolysis efficiency. The efficiency of ozonolysis at 2°C was significantly lower than those at 18, 37 and 57°C.

4. Conclusion

Ozone seems to be an efficient digestion agent for the treatment of river water and biologically treated wastewater samples prior to copper determination by anodic stripping voltammetry (ASV).

Using ozone as a sample treatment agent, the interference from SAS in ASV determination of

copper is decreased to practically negligible extend.

Ozonolysis times of 30 and 60 min were sufficient for the treatment of river water and biologically treated wastewater samples, respectively, depending on their organic load, prior to voltammetric determination of copper using a solid gold electrode. However, raw wastewater samples have to be diluted in the ratios of 1:5 and 1:10 to complete ozonolysis in 60 or 30 min, respectively.

Acknowledgements

The authors express their thanks to Krešimir Košutić, Mr.Sc. (Faculty of Chemical Engineering and Technology, University of Zagreb, Croatia) for determinations of the total organic carbon in wastewater samples.

References

[1] L. Sipos, J. Golimowski, P. Valenta, H.W. Nürnberg, Fresenius Z. Anal. Chem. 1 (1979) 298.
[2] D. Martinčić, H.W. Nürnberg, M. Stoeppler, M. Branica, Thalasia Jugosl. 16 (1980) 297.
[3] M. Stoeppler, P. Valenta, H.W. Nürnberg, Fresenius Z. Anal. Chem. 22 (1979) 297.
[4] M. Plavšić, B. Čosović, Anal. Chim. Acta. 284 (1994) 539.
[5] R.G. Clem, A.F. Sciamanna, Anal. Chem. 47 (1975) 276.
[6] R.G. Clem, A.T. Hodgson, Anal. Chem. 50 (1978) 102.
[7] H. Everding, Elektronishes Zundsystem reduziert schadliche Abgase, Elektronik (1976) Heft 1, 61.
[8] F.J. Welcher (Ed.), Standard Methods of Chemical Analysis, vol. 2, part B, Van Nostrand, New York, 1962, p. 2461.
[9] H.W. Nürenberg, L. Mart, H. Rützel, L. Sipos, Chem. Geol. 40 (1983) 116.
[10] L. Mart, Fresenius Z. Anal. Chem. 296 (1979) 350.
[11] B. Čosović, V. Žutic, Z. Kozarac, Croatica Chemica Acta 50 (1977) 229.
[12] W.H. Glaze, J.W. Kang, D.H. Chapin, Ozone: Sci. Eng. 9 (1987) 335.
[13] V. Žutić, B. Ćosović, Z. Kozarac, J. Electroanal. Chem. 78 (1977) 113.

ELSEVIER

Talanta 45 (1998) 851–856

Talanta

The electrochemical copolymerization of 3,4-dihydroxybenzoic acid and aniline at microdisk gold electrode and its amperometric determination for ascorbic acid

Jian-Jun Sun, Dong-Mei Zhou, Hui-Qun Fang, Hong-Yuan Chen *

Department of Chemistry, State Key Laboratory of Coordination Chemistry, Nanjing University, Nanjing, 210093, People's Republic of China

Received 7 February 1997; received in revised form 2 June 1997; accepted 4 June 1997

Abstract

The electrochemical copolymerization of 3,4-dihydroxybenzoic acid (3,4-DHBA) and aniline was carried out at microdisk gold electrodes by means of cyclic voltammetric sweep. The polymer obtained on the electrode shows good electrochemical activity and high stability even though in neutral and weakly basic media. It was found that the response current of ascorbic acid was greatly enhanced at this composite polymer electrode. Moreover, the anodic overpotential was significantly reduced for about 200 mV (vs. SCE) compared with that obtained at bare gold electrodes. The electrode exhibits a rapid current response (less than 2 s) and a high sensitivity (0.21 AM^{-1} cm^{-2}). The dependence of response currents on the concentration of ascorbic acid was linear in the range of 1.0×10^{-4}–1.0×10^{-2} M. In addition this composite polymer modified electrode exhibits a high electrode stability for a long-term use. © 1998 Elsevier Science B.V.

Keywords: Microelectrode; Copolymerization; Aniline; 3,4-Dihydroxybenzoic acid; Ascorbic acid; Catalysis; Amperometric determination

1. Introduction

Ascorbic acid has been extensively studied because of its significance in bioelectrochemistry, neurochemistry and clinical diagnostics' applications [1]. The oxidation of ascorbic acid at conventional electrodes is well documented and is known to proceed via two consecutive one-electron transfer processes involving the participation of a radical anion intermediate to form dehydro-L-ascorbic acid. This species subsequently undergoes a hydration reaction characteristic of carbonyl groups to form an electroinactive product.

The catalytic oxidation of ascorbic acid has been obtained at many mediator-modified electrodes [2–6]. However, most of them still suffered from the pollution of ascorbic acid due to its adsorption on the electrode surface, especially at inorganic film modified ones.

* Corresponding author. Fax: +86 25 3317761.

PII S0039-9140(97)00183-5

Polymer modified electrodes have been widely used for the immobilization of mediators or enzymes by their matrix structure, electrocatalysis of biological molecules and the construction of molecular devices, etc. [7–11]. Usually, polymer modified electrodes exhibited a good stability and catalytic effects resulted from their three-dimensional mediator distribution. The conductive polymers such as polyaniline, polypyrrole, polythiophene as well as their derivatives have been used for constructing various biosensors.

Polyaniline has been studied extensively because of its high stability and conductivity. It was well known that the polyaniline could be electrochemically polymerized easily in acid media. Protons would participate in the redox process of polyaniline. However, as pH of the media increased above 4 the polymer would lose its electrochemical activity [12]. This has greatly limited its application in biological sample's analysis.

Recently, Bartlett [13] obtained the polyaniline-poly(vinylsulfonate) composite film that exhibited an off/on switching response when it was exposed to NADH at pH 7.0. The reduction of the oxidized form of polyaniline(pernigraniline) in the composite film by reacting with NADH in pH 7.0 buffer solution brought about a switch in the conductivity of devices. The negative charged PVS, which was doped into polyaniline, could provide protons for the nitrogen atom of linear structure of polyaniline and led this composite film to work in neutral media. Karyakin et al. [14,15] also reported that the copolymerization of aniline with *m*-aminobenzoic acid or metrillic acid could exhibit a wide pH-range electroactivity even in basic solution. However, the application of this composite polymer in neutral media has not been reported.

The application of microelectrode to the studies of neurotransmitters, which has been pioneered by Adams, to monitor the concentration of neurotransmitters in the central nerve system (CNS) has had a special impact [16]. The advantages of microelectrode include fast-response time, small size, high mass transportation flux and low IR drop [17–19]. They could be further developed for constructing miniaturized biosensors and used for the in-vivo analysis.

Here, the copolymerization of 3,4-DHBA with aniline in acid media was obtained. It was found that the resulted polymer was self-doped one that exhibited a stable electroactivity even in neutral and weakly basic media. It suggested that 3,4-DHBA in oxidized state could react with the radicals of aniline and produce a composite polymer. Because of the presence of -COOH and -OH groups in the polymer structure, a self-doped composite polymer was obtained. Moreover, the catalysis of ascorbic acid could be obtained at this polymer modified electrode. As a consequence, such a miniaturized biosensor could be further developed for the clinical applications.

2. Experimental

2.1. Reagents and materials

Dopamine was purchased from Fluka AG (Switzerland). Ascorbic acid was obtained from the Shanghai Biochemistry Research Institute. Aniline was distilled before use. All the other reagents were analytical grade. Water used in experiments was twice-quartz-distilled. The phosphate buffer was made of 1.0×10^{-2} M $K_2HPO_4 + KH_2PO_4$ and 0.2 M KCl.

2.2. Apparatus

Electrochemical experiments were carried out with a BAS-100B Electrochemical Analyzer equipped with a PA-1 Preamplifier (BAS, USA) which was used to amplify the current and to filter out noise. A microdisk gold electrode (ø50 μm) was used as working electrode. The auxiliary electrode and the reference one were a platinum wire and a saturated calomel electrode, respectively. The test solution was deaerated by high pure nitrogen before experiments and experiments were all performed under nitrogen atmosphere. The experimental temperature was controlled at 20 ± 0.5°C.

2.3. Procedure

The copolymerization of 3,4-DHBA and aniline was carried out in 0.5 M sulfuric acid by cyclic voltammetric sweeping from -200 to 850 mV at a scan rate of 50 mV s^{-1}. Amperometric determination of ascorbic acid was performed in phosphate buffer at a constant potential.

3. Results and discussion

3.1. The electrochemical copolymerization of 3,4-DHBA and aniline

The electrochemical copolymerization of aniline with 3,4-DHBA by cyclic voltammetry was depicted in Fig. 1. It can be seen that there were two couples of peaks, denoted as electrocouple I and electrocouple II, situated at about 0.12 and 0.47 V, respectively, and also a sharp peak, peak III, at about 0.7 V. It is shown that at the very beginning of the polymerization there was no peaks appeared in the voltammograms but nucleation process of aniline on the electrode surface (point IV in Fig. 1). Several cycles later, the peak values of I, II and III began to increase. The peak potential of peak III shifted negative with the increase of the cycling number, and it might correspond to the oxidation process of 3,4-DHBA by polyaniline, and relate to an electrocatalytic mechanism for the peak potential of III was less than that of the oxidation of 3,4-DHBA at a bare gold electrode (ca. 0.83 V, see also Fig. 2).

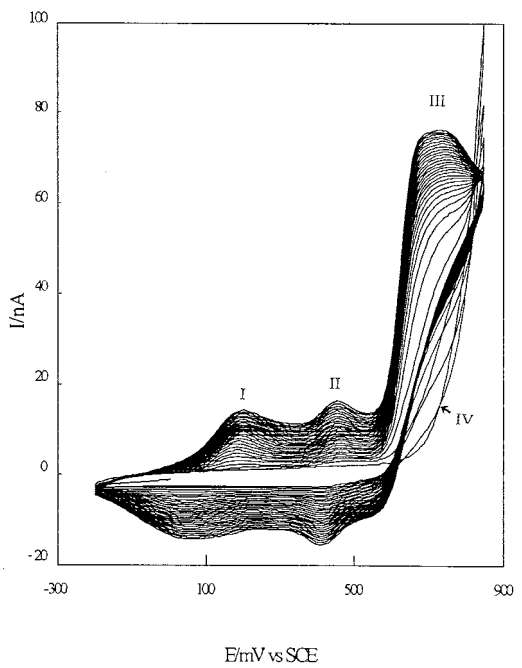

Fig. 1. The cyclic voltammograms at the microdisk gold electrode with 50 mV s^{-1} in 0.5 M H_2SO_4 containing 0.1 M aniline and 5×10^{-3} M 3,4-dihydroxybenzoic acid.

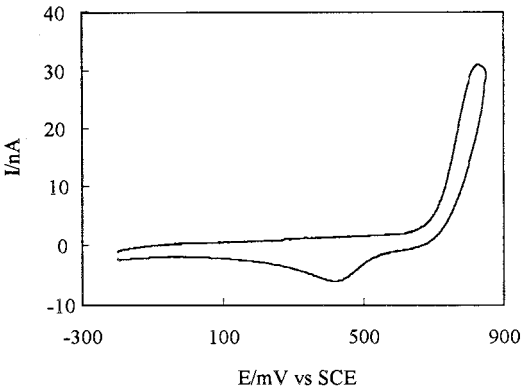

Fig. 2. The cyclic voltammograms at the microdisk gold electrode with 50 mV s^{-1} in 0.5 M H_2SO_4 containing 5×10^{-3} M 3,4-dihydroxybenzoic acid.

The structure of electrocouple II in Fig. 1 was very different from that in the voltammograms of the polymerization of aniline itself, the former had higher peak strength and larger peak area. In the process of aniline polymerization; the peak appeared at ca. 0.5 V might be ascribed to the formation of the oligomer in the film [20,21]. Whereas in the case of the copolymerization of aniline with 3,4-DHBA, the electrocouple II might ascribe not only to the formation of the oligomer of aniline itself but also to that of aniline with 3,4-DHBA. As a mater of fact, the oxidized form of 3,4-DHBA was electrophilic (see also scheme 1 in [22]), and it could react with the radicals of nucleophilic *N*-atoms in the chain of polyaniline. The products of this reaction might incorporate into the copolymerized film.

3.2. Characteristics of the composite polymer modified electrode

Fig. 3 showed the voltammograms of the modified electrode in neutral media. There was an electrocouple appeared in the range of − 500–550 mV and its electroactivity did not decrease under the continuously sweeping. It was well known that polyaniline would lose its electroactivity easily at pH values above 4 because there were not enough protons in the media to be doped in the pores of the film to hold the charge equilibrium during the oxidation process. In the present case, the function groups of 3,4-DHBA incorporated in the film, such as -COOH and -OH, could donor protons to the nitrogen atoms of the linear structure of the polymer and cause the polymer hold electroactivity in neutral media.

When this composite polymer modified electrode was cyclically swept in neutral media with different scan rates, it exhibited that the current response was linear with the square root of scan rates. Meanwhile, the anodic and cathodic potential would shift toward positive and negative direction with the increasing scan rates, respectively. In lower scan rates, the couple was more reversible compared with that obtained at higher scan rates. Moreover, the cathodic potential had a larger change. This suggested that the reduction of this composite film was rather difficult. During the process of reduction the film would store the negative charged ions in its pores for keeping its charge equilibrium. With the increase of the pHs, this phenomenon could be further observed.

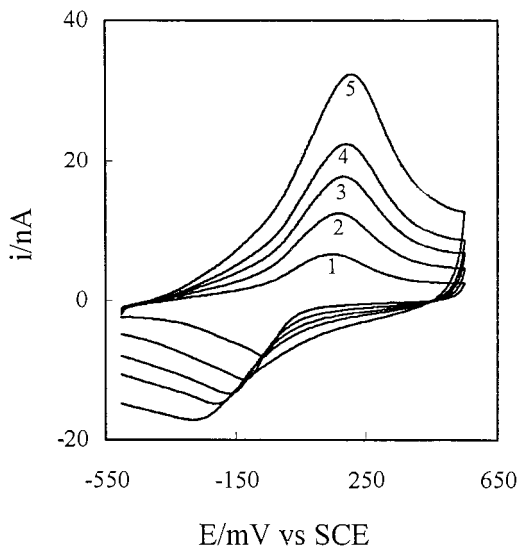

Fig. 3. The cyclic voltammograms at the composite polymer modified electrode in pH 7.0 buffer solution at the scan rate: (1) 10; (2) 30; (3) 50; (4) 70 and (5) 9O mV s^{-1}.

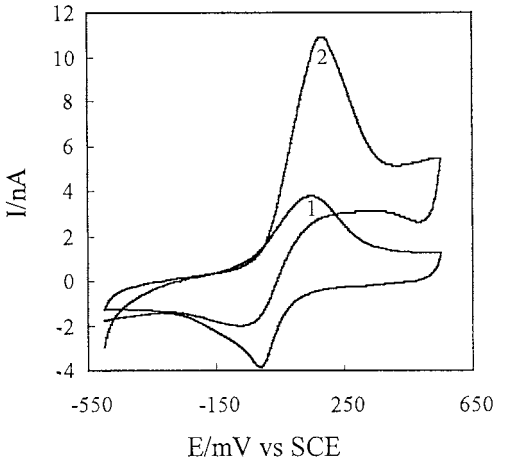

Fig. 4. The cyclic voltammograms at the composite polymer modified electrode in pH 7.0 buffer solution at a scan rate of 10 mV s^{-1} in (a) absence and (b) presence of 2.0×10^{-3} M ascorbic acid.

3.3. Electrocatalytic oxidation of ascorbic acid at the modified electrode

Fig. 4 showed that the cyclic voltammograms which was obtained at the composite polymer modified microelectrode in the absence and presence of 2.0×10^{-3} M ascorbic acid. With the addition of ascorbic acid, the anodic peak currents increased significantly. The anodic overpotential was reduced for 200 mV compared with that obtained at bare gold electrodes. This large increase of oxidation currents might not be due to the doping of ascorbic acid into the copolymer because its concentration was very smaller than that of the other anions in the support media. It might be ascribed to the fact that ascorbic acid diffused to the electrode surface, reacted with the electroactive couple of the copolymer and resulted in a current increase.

The dependence of the catalytic peak currents on the square root of the scan rates was linear. It meant that the electrode process was a semi-infinite diffusion one rather than a surface reaction one. When this modified electrode was swept in ascorbic acid solution for a long time, no pollution phenomenon was observed. Thus, it is promising for further developing biosensors due to its easy-fabrication and stability.

The positive-charged dopamine was used as a probe for the feature examination of the copolymer films. The results showed that dopamine could not be catalyzed at the film. It suggested that this film was positive-charged and repulsive to dopamine because of the identical charge.

3.4. The effects of pH on the catalytic oxidation of ascorbic acid

Fig. 5 depicts the dependence of catalytic currents on the pHs of the media. It is shown that the current responses decreased with the pHs increased from 5.0–9.0. The ratios of the current responses at pH 7.0 and pH 8.0 to that at pH 5.0 were about 0.3 and 0.14, respectively, and at pH 9.0, it became zero. Thus, this electrode could not be used in the media of the pHs over 8.5 and could be used in neutral media for the detection

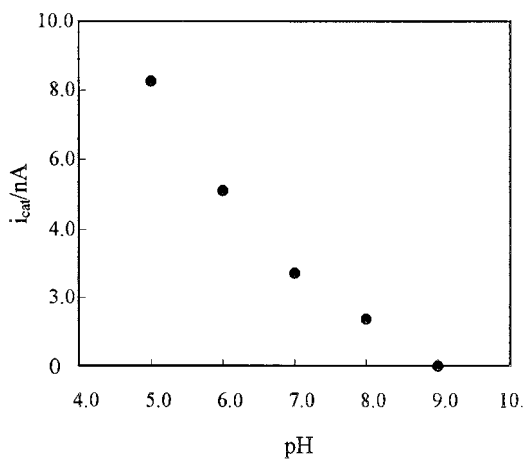

Fig. 5. The dependence of catalytic currents on pH from CVs in 2.0×10^{-3} M ascorbic acid phosphate buffer solution at scan rate of 10 mV s^{-1}.

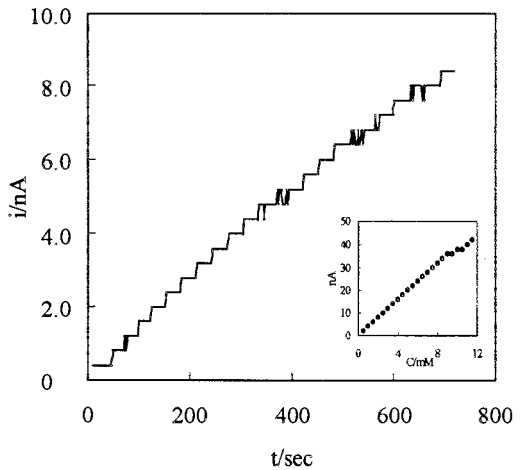

Fig. 6. Dynamic response of the composite polymer modified electrode to successive addition of ascorbic acid in 0.1 mM steps at a constant potential of 0.2 V vs. SCE in pH 7.0 buffer solution. Insertion: the corresponding calibration curve.

of ascorbic acid. It should be noted that the catalytic currents were seriously influenced by the pHs of the media. Hence the pHs of the media have to be controlled carefully in the measurements.

3.5. The determination of ascorbic acid

Steady-state amperometric determination of ascorbic acid had been carried out at a constant potential to demonstrate the analytical usefulness of the electrode as an ascorbic acid sensor. Fig. 6 depicts a typical trace of the steady-state current response of the electrode. After the addition of ascorbic acid stock solution, the oxidation current rose steeply to reach a stable value within ca. 2 s. Hence the electrode exhibited a short current response time and could be used in the case of rapid determination of ascorbic acid.

The calibration curve of the electrode response to ascorbic acid is depicted in the insertion of Fig. 6. The current responses were linear with the concentration of ascorbic acid in the range of 1.0×10^{-4}–1.0×10^{-2} M. The detection limit was 5.0×10^{-5} M at a signal-to-noise ratio of 3. The sensitivity of the electrode was estimated from the calibration curve to be 4 nA mM^{-1} or 0.21 AM^{-1} cm^{-2}.

3.6. The stability of this self-doped polymer modified electrode

This modified electrode exhibited a high stability whenever it was placed in dry state or in phosphate buffer solutions at 4°C. No loss of electroactivity of the electrode was found for the continuously cyclically sweep for 500 cycles. Over ten successive assays of 0.1 mM ascorbic acid, the relative standard deviation was ca. 1.4%. The electrode was also not deteriorated even for long a month.

4. Conclusions

The copolymerization of 3,4-DHBA and aniline may be easily carried out using cyclic voltammetry. This composite polymer modified electrode exhibits a good electrochemical activity even in neutral and weakly basic solutions. It was found that this electroactive polymer could act as mediators for the catalytic oxidation of ascorbic acid. The amperometric determination of ascorbic acid had been carried out at a constant potential. The electrode exhibits a rapid current response (less than 2 s) and a high sensitivity (0.21 AM^{-1} cm^{-2}). Moreover, the linear response current was achieved in a concentration range from 1.0×10^{-4}–1.0×10^{-2} M. This composite polymer modified electrode could be developed for the construction of miniaturized biosensors to the amperometric determination of ascorbic acid.

Acknowledgements

This project was supported by the National Natural Science Foundation of China and the Found of the National Education Committee of China.

References

[1] L.R. Faulkner, Chem. Eng. News 62 (1984) 28.
[2] A.P. Doherty, M.A. Stanley, J.G. Vos, Analyst 120 (1995) 2371.
[3] A.-M. Yu, D.-M. Sun, H.-Y. Gu, H.-Y. Chen, Anal. Lett. 29 (1996) 2633.
[4] K.N. Kuo, R.W. Murray, J. Electroanal. Chem. 132 (1982) 37.
[5] J. Facci, R.W. Murray, Anal. Chem. 54 (1982) 772.
[6] C. Ueda, D.C.-S. Tse, T. Kuwana, Anal. Chem. 54 (1982) 850.
[7] J. Ye, R.P. Baldwin, J.W. Schlager, Electroanalysis 1 (1989) 133.
[8] S. Dong, Z. Sun, Z. Lu, J. Chem. Soc. Chem. Commun. (1988) 993.
[9] B.L. Wheeler, G. Caple, A. Henderson, J. Francis, K. Cantrell, S. Vogel, S. Grey, D. Russell, J. Electrochem. Soc. 136 (1989) 2769.
[10] Y. Kang, M.-H. Lee, S.B. Rhee, Synth. Met. 52 (1992) 319.
[11] T. Tatsuma, M. Gondaria, T. Watanabe, Anal. Chem. 64 (1992) 1183.
[12] T. Hirai, S. Kuwabata, H. Yoneyama, J. Chem. Soc. Faraday Trans. I 85 (1989) 969.
[13] P.N. Bartlett, J.H. Wang, E.N.K. Wallace, J. Chem. Soc. Chem. Commun. (1996) 359.
[14] A.A. Karyakin, A.K. Strakhova, A.K. Yatsimirsky, J. Electroanal. Chem. 371 (1994) 259.
[15] A.A. Karyakin, I.A. Maltsev, L.V. Lukachova, J. Electroanal. Chem. 402 (1996) 217.
[16] R.N. Adams, Anal. Chem. 48 (1976) 1126A.
[17] R.J. Forster, Chem. Soc. Rev. 23 (1994) 289.
[18] E. Csoregi, L. Gorton, G. Marko-Varga, Anal. Chim. Acta. 273 (1993) 59.
[19] M. Fleischman, S. Pons, D.R. Robinson, Schmidt, Ultramicroelectrodes, Datatech Systems, Morganton, NC, 1987.
[20] D.E. Stilwell, S.-M. Park, J. Electrochem. Soc. 135 (1988) 2254.
[21] S. Dong, D. Zhang, Z. Li, Chin. Chem. Lett. 3 (1992) 29.
[22] F. Pariente, F. Tobalina, M. Darder, E. Lorenzo, H.D. Abruna, Anal. Chem. 68 (1996) 3135.

.

ELSEVIER

Talanta 45 (1998) 857–864

Talanta

Preconcentration of trace elements on a support impregnated with sodium diethyldithiocarbamate prior to their determination by inductively coupled plasma-atomic emission spectrometry

D. Atanasova [a,*], V. Stefanova [a], E. Russeva [b]

[a] *Plovdiv University, Centre of Analytical Chemistry and Applied Spectroscopy, 24 Tsar Assen St., 4000 Plovdiv, Bulgaria*
[b] *Institute of General and Inorganic Chemistry, Bulgarian Academy of Sciences, 1113 Sofia, Bulgaria*

Received 5 February 1997; received in revised form 22 May 1997; accepted 5 June 1997

Abstract

A procedure is developed for determination of As, Co, Se, Cr, Pb, Zn, Cu, Mn, Cd, Sb, and Sn in water by ICP-AES analysis of alcohol eluates after pre-concentration of the samples. The pre-concentration is performed on a sodium diethyldithiocarbamate supported soft polyurethane foam. The sorbed elements are subsequently eluted with 1-propanol and the alcohol eluates are analysed by ICP-AES. A eight-fold concentration is achieved. An increased sensitivity in the analysis of propanol–water (30:70, v/v) solution is established as compared with aqueous solutions. The strongest effect is observed for As, Se, Pb, Cr, Sn, and Cd-increasing is more than twice. For other elements the matrix influence is by a factor of 1.45 (Cu), 1.36 (Sb), 2.08 (Zn). The method is applied to the analysis of natural water samples. © 1998 Elsevier Science B.V.

Keywords: Preconcentration; Sodium diethyldithiocarbamate; ICP-AES analysis; Water

1. Introduction

ICP-AES analysis of heavy and toxic elements in ecological samples suffers from a relatively low sensitivity. This drawback can be overcome by a combination of a suitable pre-concentration technique with subsequent ICP-AES determination. Among known pre-concentration methods solvent extraction, co-precipitation and various chromatographic techniques seem to be the most advantageous [1–4,6,7]. Their application to ICP-AES [9–17] helps to avoid matrix interference and provides low detection limits in analysis of real samples as well.

The majority of known preconcentration techniques makes use of organic solvents. Investigations of the aerosol characteristics in nebulization of organic solutions in ICP-AES have revealed an increased efficiency of the analyte transfer to the plasma. On the other hand the increase in evaporation of the organic solvent from the surface of the aerosol droplets charges the plasma with a large amount of molecular vapors, the latter causing a destabilization of the discharge and changes

* Corresponding author.

PII S0039-9140(97)00175-6

in excitation conditions [8]. Avery et al. [4] studied the behaviour of methanol solutions (methanol: water = 50:50, v/v) and succeeded in eliminating the effect of the solvent by applying a DIN introduction system. The effect of the organic matrix can be surmounted using desolvatation or back extraction with strong acid solutions as well [5,12].

The present paper aims at developing a method for a group preconcentration of toxic metals in waters and their subsequent ICP-AES determination. The preconcentration is performed on a sodium diethyldithiocarbamate supported soft polyurethane foam. The sorbed elements are subsequently eluted with 1-propanol. The propanol eluates are further analysed by ICP-EAS.

2. Experimental

2.1. Apparatus

A 'Spectroflame' atomic emission spectrometer (Spectro Analytical Instruments, Germany) was used throughout the experiments. The characteristics of the instrument were as follows:

- three optical systems: six channel vacuum polychromator, 12 channel air polychromator, air monochromator 200–480 nm;
- high frequency generator 27.12 MHz with a maximum power of 2.5 kW;
- Three argon flows quartz plasma torch;
- Meinhard type nebulizer.

The optimized operating parameters are listed in Table 1.

Reagents of AR grade and redistilled water (RDW) were used throughout. Stock solutions (1000 mg l^{-1}) of all studied elements (see Table 1) from Fluka were used. The working solutions (2 mg l^{-1}) were prepared by dilution with RDW. The solutions of hydrolizable elements were acidified to pH = 1 with nitric acid.

1-Propanol from E. Merck was used without additional purification.

Sodium diethyldithiocarbamate (Na-DTC) -E. Merck, Germany, was used. Its purity was additionally checked by ICP-AES.

2.2. Procedures

2.2.1. Preparation of chromatographic columns

Medical syringes (20 ml) were used as columns. The support was prepared from soft polyurethane foam as follows: 1 cm thick segments with diameter of 2.5 m (diameter of the segments should be same as the diameter of the syringe) were cut. The segments were soaked in 0.1 mol l^{-1} nitric acid overnight, then thoroughly washed with RDW until neutral reaction and air-dried. The syringes were then filled with the air-dried segments. Chromatographic columns comprise 8–9 separate segments. Portions of solid Na-DTC (total amount of 2.5 g) were spread between the segments. This amount of the complex forming agent is necessary to retain the studied elements in 50 ml sample. Prior to passing next 50 ml aliquots additional 2.5 g of solid Na-DTC were introduced into the column.

2.2.2. Sorption studies

Portions of the working solutions of the elements were sucked in the column and allowed to interact for 30 min. The liquid phase was then sucked out and analysed against blank.

Table 1
ICP-AES operating parameters

Incident power	1.5 kW	
Nebulizer pressure	2.2 bar	
Plasma gas	16 l min^{-1}	
Auxiliary gas	3.5 l min^{-1}	
Sample flow rate	1.0 ml min^{-1}	
Observation height	14 mm	
Wavelength (nm)/ type of optic system	As (VP) 193.76;	Cd (M) 214.42;
	Se (VP) 196.09;	Sb (M) 217.56;
	Zn (P) 213.856	Co (M) 228.60;
	Mn (P) 257.610	Cr (M) 284.324;
	Cu (P) 324.75	Sn (M) 283.99;
	Pb (M) 220.34	BG corr.(−0.028/+0.38)

VP, vacuum polychromator; P, air polychromator; M, monochromator. The figures in brackets point to the two side background corrections of the Pb line.

2.2.3. Elution studies

Elution was carried out with 50 ml of 1-propanol as follows:

The piston was taken away and 20 ml of propanol were introduced into the column. Then the piston was put in and the liquid sucked out into a 50 ml calibrated flask. The next portions were sucked with the piston and sucked out into the flask to a total volume of 50 ml. Aliquots, 8 ml, of the combined propanol eluates were diluted to 25 ml with RDW and subjected to ICP-AES analysis.

2.2.4. Preconcentration of trace elements in natural waters

Aliquots of the water sample, 100–200 ml (the analysed waters have been preliminarily conserved with nitric acid—0.5% v/v of conc. HNO_3) were passed through chromatographic columns (pistons have been taken away). The sorbed metal ions were eluted with 10 ml of 1-propanol. The eluates were diluted to 30 ml with RDW and subjected to analysis.

2.2.5. Calibration

Standard solutions of the elements containing 0.1, 0.4, 1.0, 2.0 and 4.0 mg l^{-1} were prepared from the stock standard monoelement solutions (As, Co, Se, Cr, Pb, Zn, Cu, Mn, Cd, Sb, and Sn) by dilution with a propanol eluate of a blank. The latter was diluted to 30:70, v/v propanol–water with RDW.

3. Results and discussion

The trace elements As, Co, Se, Cr, Pb, Zn, Cu, Mn, Cd, Sb and Sn were pre-concentrated through sorption on Na-DTC supported soft polyuretane foam.

3.1. Chromatographic support

A number of carriers have been studied, such as silica gel, cotton, cellulose and soft polyurethane foam. The latter was chosen to suit the best the purpose of the present paper and was used in all further investigations.

The optimum amount of the chelate forming reagent ensuring quantitative sorption of the studied elements was established. It is known that Na-DTC is easily soluble in water, hence, it was expected that part of it should be eluted while passing aqueous solutions of the elements through the column. It was established that the optimum amount of Na-DTC depends on the volume of the sample passing through the column.

Investigations were carried out with solid Na-DTC (from 0.5 to 20 g) spread between the polyurethane foam segments (see Section 2). It was established that 5 g of solid Na-DTC was sufficient to provide quantitative retention of 200 μg of each element in 100 ml sample.

The effect of the pH on the sorption was studied in the range $pH = 1–6$. The pH range was selected having in mind that Na-DTC is destroyed in acid medium on one hand and some of the studied elements are hydrolysed in alkaline medium on the other. The samples were adjusted to the desired pH value with nitric acid and then passed through the columns. The results obtained are shown in Fig. 1. In the range $1 < pH < 2$ the retention of all studied elements exceeds 95%. Beyond pH 2 the retention decreases to a different extent depending on the element.

Under established optimum conditions an eight-fold concentration was achieved.

3.2. Eluent

The choice of the eluent was a difficult problem because of the limitation of the ICP to tolerate organic solvents. In addition, the eluent should not destroy the polyuretane foam. Among organic solvents alcohols seem to answer these requirements. The ability of ICP to tolerate organic solvents depends on the evaporation factors of the matrix [8]. The plasma tolerance to the alcohols decreases in the order butanol > propanol > ethanol > methanol with a fixed flow rate in accordance with their boiling points. The ICP-AES Spectro instrument is not equipped with additional solvent trap between the spray chamber and the plasma torch and a free running RF generator. That is why it was not possible to perform elution with methanol and ethanol. The

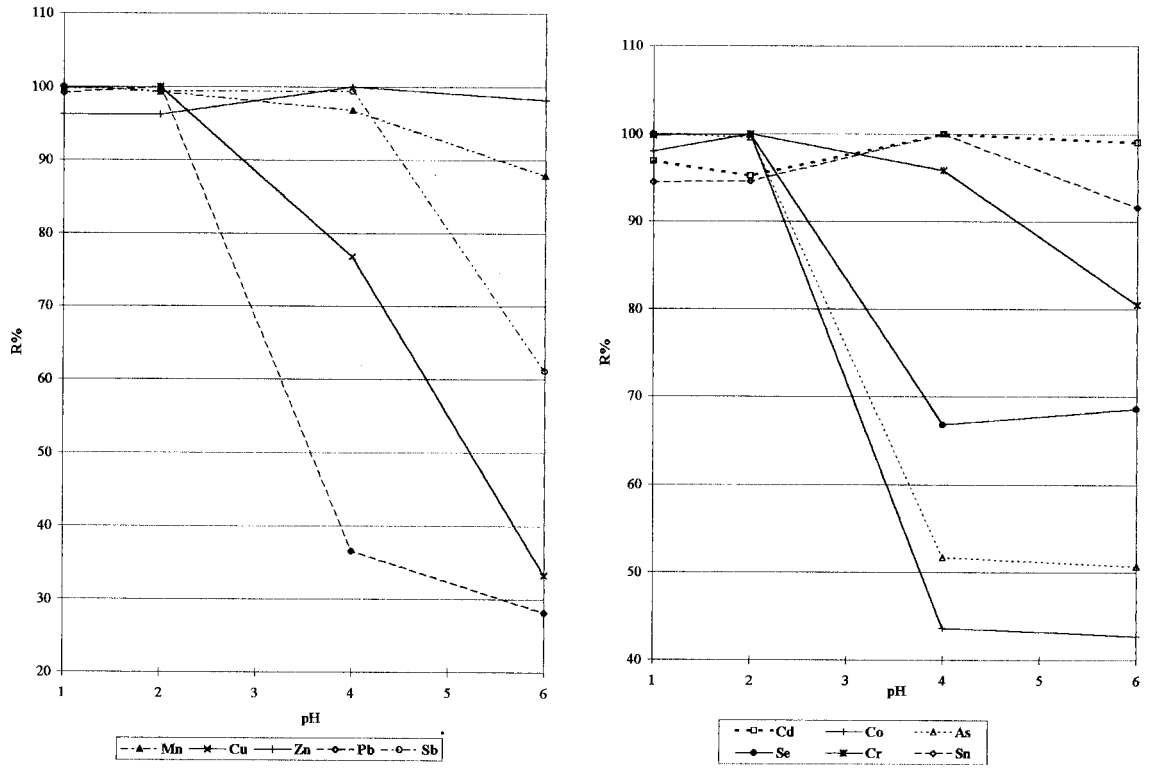

Fig. 1. Effect of pH on the retention (R%) of elements on Na-DTC supported soft polyuretane foam: a. Mn, Cu, Zn, Pb, Sb; b. Cd, Co, As, Se, Cr, Sn.

plasma torch becomes unstable when the methanol content is higher than 15% and ethanol content exceeds 20%. The following alcohols were tested as eluents: 1-propanol, *i*-propanol, butanol, *i*-butanol and 1-pentanol. It was established that when water–alcohol solutions were introduced into ICP it is preferable to apply higher flow rates and incident power as compared with aqueous solutions. The increase in alcohol content of the solutions made the plasma discharge narrower and causes an expansion of the central channel. The C_2 molecular band emission typical of organics appeared around the base of the plasma, while the periphery of the toroid and tail of the discharge coloured by violet cyan emission. Our experiments showed that the plasma became unstable on introducing solutions exceeding 20% of ethanol and 30% of propanol and *i*-propanol.

The cleaning time of the spray chamber from alcohol vapours was increased to 3 min. On the other hand it was impossible to reduce the alcohol concentration since further dilution of the eluates caused precipitation of the dithiocarbamate complexes.

Elution with longer chain alcohols appeared to be unsuitable. The best eluent is 1-propanol. Investigations showed that propanol:water mixtures (30:70 v/v) aspirated into the plasma with a conventional nebulization system did not affect significantly the discharge stability. On the other hand 99.5% propanol provided quantitative elution of the sorbed chelate complexes and the eluates were stable for 12 days. Lower concentration of propanol should be avoided in order to prevent precipitation of the dithiocarbamate complexes. Hence, the retained dithiocarbamate complexes were eluted with pure propanol and the eluates were further diluted to 30% v/v propanol prior to analysis.

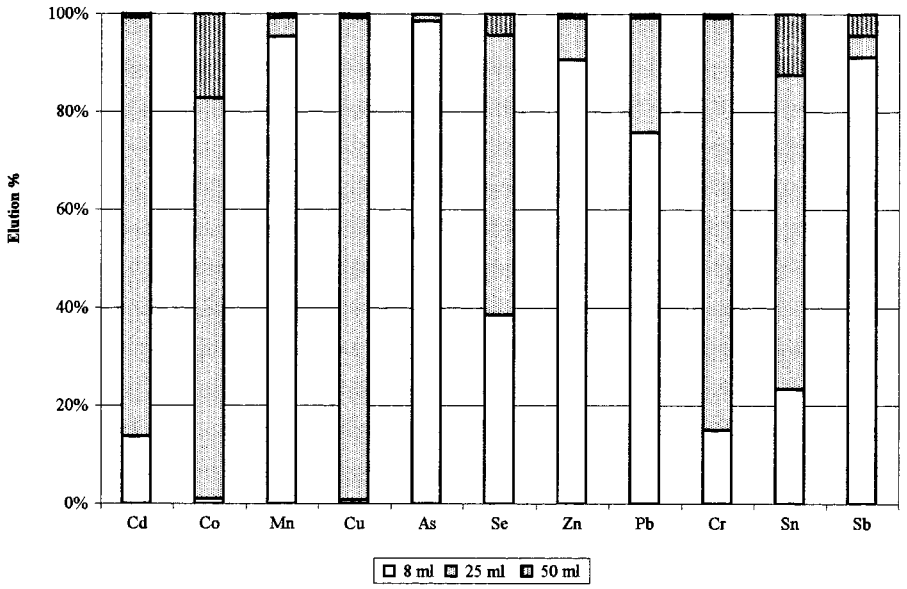

Fig. 2. Effect of eluent volume on the elution of sorbed elements (total amount of each element 400 μg).

The effect of the volume of the eluent has been studied as well. The experiments were carried out as follows. Known amount of each element was retained on the support. The elution was performed with three different portions of propanol—8, 25 and 50 ml, respectively. The eluates were collected separately and analysed after dilution. The percentage of the eluted element in each eluate was calculated. Fig. 2 illustrates the results of elution experiments. The first 8 ml portion of propanol eluted about 80% of Mn, As, Zn, Sb and Pb, 40% of Se and only 10–20% of Cd, Cr and Sn. It is recommended to use 50 ml of propanol to ensure complete elution of all elements, but if trace amounts are analysed, 25 ml of propanol are quite enough for elution.

3.3. ICP-AES determination. Optimization of the operating parameters

The effect of Na-DTC on the background of the element emission lines was studied. The background signals of the selected lines were recorded in the presence of Na-DTC and compared with that in RDW (see Fig. 3). It was established that Na-DTC (5–50 mg l^{-1}) does not affect significantly the background signal for Co, Cd, Pb, Sb and Sn (the change is below 10%). The most significant are changes in the background emission for As, Mn, Se, Cu, Cr and Zn—between 20 and 50%. No definite relationship between Na-DTC concentration and background signal could be derived. It was established that the presence of alcohol enhances the background signals by a factor of 2–5 as compared with aqueous solutions. The enhancement is the most for the lines in the near UV range of the spectrum. BG change decreases with longer wavelength and is the least for antimony and copper lines—by factor of 2.

The simultaneous presence of Na-DTC and propanol changes the background against pure water–alcohol solutions of the As, Zn and Mn lines only. The change is, however, negligible as compared with the effect of the alcohol itself.

The results obtained revealed that in order to reduce the matrix induced change of the background emission the calibration should be performed with standard solutions containing the same amounts of Na-DTC and propanol as that in the analysed samples. The line of Pb 220.35 nm needs a double-side background correction.

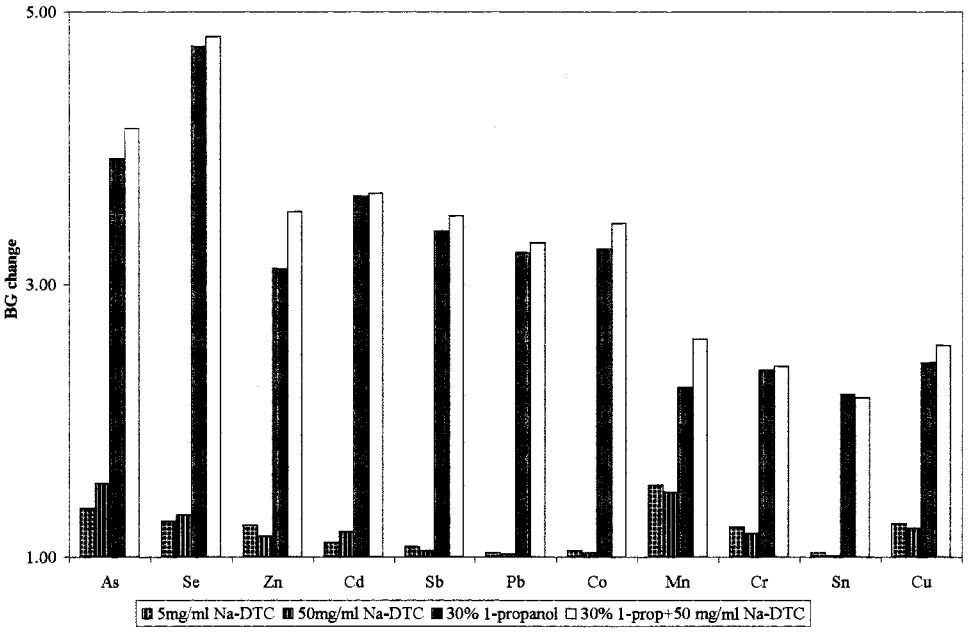

Fig. 3. Matrix induced change of the background emission on Na-DTC and 1-propanol normalised to RDW.

The matrix effect was studied by comparing the signals produced by aqueous standard solutions of the elements and alcohol standard solutions (30% v/v propanol) containing varying amounts of Na-DTC (see Fig. 4). It is seen that the presence of the propanol matrix causes a signal increase for all studied elements. In the case of column loading with 0.5 g Na-DTC the sensitivity increase is by a factor of 1.17 (Sb), 1.45 (Cu), 2.8 (Zn) and 3.77 (Se), respectively. The effect of

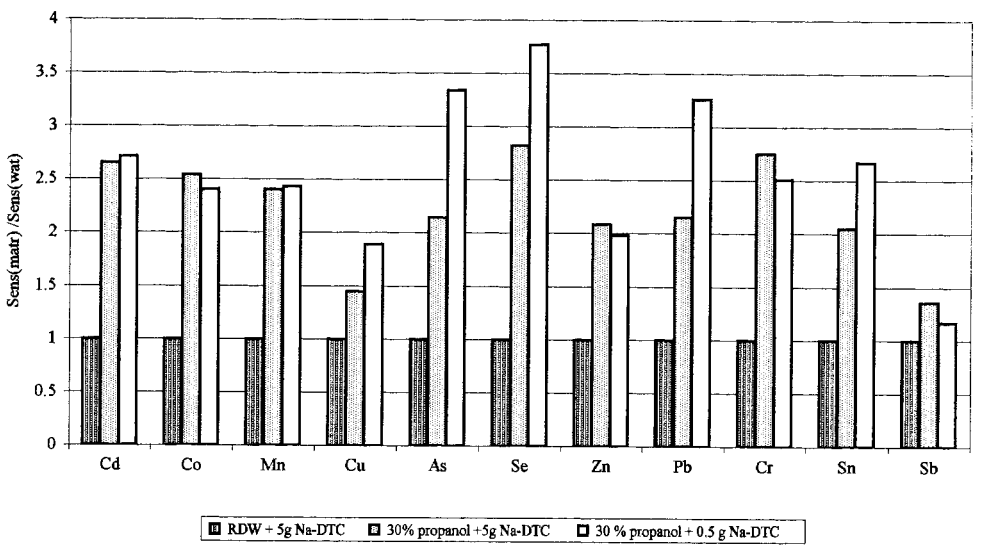

Fig. 4. Sensitivity of the ICP-AES analysis of propanol–water eluates containing dithiocarbamates of the studied elements.

Table 2
Limits of determination (DL) of 11 elements with eight-fold concentration of the initial sample and ICP-AES analysis

Element	Cu	Zn	As	Se	Pb	Cd
DL (mg l^{-1})	0.01	0.008	0.08	0.12	0.015	0.003
Element	Co	Mn	Cr	Sn	Sb	
DL (mg l^{-1})	0.02	0.005	0.004	0.02	0.16	

(Six replicates and k = 6).

$$DL(mg\,l^{-1}) = \frac{6.SD_{blank}.EDF.V_{eluent}}{Senitivity.F_{preconc}}$$

where DL, limits of determination; $S.D._{blank}$, standard deviation of blank solution (ten repeats); Sensitivity, $m = dI_{em}/dc$; V_{eluent}, eluent volume (25 ml); EDF, eluent dilution factor (3.25); $F_{preconc}$, preconcentetion factor (8).

matrix was eliminated by a suitable calibration (see Section 2).

The effect of water matrix elements was studied. No spectral interference was observed.

In Table 2 are presented the calculated absolute limits of determination for 11 elements with eight-fold concentration of the initial samples.

The developed procedure was applied in the analysis of natural water samples. The results obtained are compared with these from ICP-MS analysis (Table 3).

4. Conclusions

A procedure for preconcentration of 11 elements on a soft polyuretane foam loaded with sodium diethylditiocarbamate was developed. The retained elements were eluted with 1-propanol. The eluates were diluted to 30% v/v and analysed by ICP-AES. The optimum parameters of ICP-AES analysis of alcohol eluates were established. The sensitivity for Se, As and Pb was increased by a factor of 3, and for Cr, Sn, Cd, Co and Mn by a factor of 2.5, as compared with analysis of aqueous solutions.

A method for a group (11 elements) preconcentration of toxic metals in natural waters and ICP-AES determination is developed. It is based on complex formation with a sodium diethyldithiocarbamate supported soft polyurethane foam. The sorbed helate complexes are subsequently eluted with 1-propanol. The method was applied for multielemental analysis with eight-fold concentration of the initial samples.

Table 3
Microelement content (mg l^{-1}) in natural water (probability 95%, four replicates)

Element	Natural water-Plovdiv (mg l^{-1})		Natural water-Sadovo (mg l^{-1})	
	Present method	ICP-MS	Present method	ICP-MS
Cu	0.06 ± 0.008	0.063 ± 0.005	<0.01	0.009 ± 0.0007
Zn	0.79 ± 0.01	0.81 ± 0.007	0.48 ± 0.01	0.46 ± 0.006
Mn	0.03 ± 0.002	0.032 ± 0.0005	<0.005	0.004 ± 0.0005
As	<0.08	0.014 ± 0.0015	<0.08	0.003 ± 0.0003
Se	<0.12	0.011 ± 0.0012	<0.12	<0.01
Pb	<0.015	0.007 ± 0.0003	<0.015	0.01 ± 0.0008
Cr	0.008 ± 0.002	0.006 ± 0.008	<0.04	<0.002
Sb	<0.16	0.003 ± 0.0004	<0.16	<0.002
Sn	0.02 ± 0.002	0.021 ± 0.002	<0.02	<0.002
Cd	<0.003	0.001 ± 0.00016	<0.003	<0.001
Co	<0.02	0.002 ± 0.0003	<0.02	<0.001

References

[1] Z. Horvath, A. Lasztity, R.M. Barnes, Spectrochim. Acta Rev. 14 (1991) 45.
[2] F. Laborda, M.T.C. de Loos-Vollebregt, L. de Galan, Spectrochim. Acta 46B (6–7) (1991) 1089.
[3] P. Schramel, L.Q. Xu, Fresenius J. Anal. Chem. 343 (4) (1992) 373.
[4] T.W. Avery, Ch. Chakrabarty, J.J. Thompson, Appl. Spectrosc. 44 (1990) 1690.
[5] J.M. Lo, Y.P. Lin, K.S. Lin, Anal. Sci. 7 (1991) 455.
[6] P. MacCarthy, R.W. Klusman, S.W. Cowling, Am. Chem. Soc. (1991) 301R.
[7] L.Q. Xu, P. Schramel, Fresenius J. Anal. Chem. 342 (1–2) (1992) 179.
[8] F.J.M.J. Maessen, G. Kreuning, J. Blake, Spectrochim. Acta 41B (1986) 3.
[9] H. Ogura, K. Oguma, Microchem. J. 49 (2–3) (1994) 220.
[10] S.F. Durrant, A. Krushevska, D. Amarasiriwrdena, M.D. Argentine, S. Romonguesnier, R.M. Barnes, J. Anal. At. Spectrom. 9 (3) (1994) 199.
[11] K. Hirayama, T. Sekine, N. Unohara, Bunseki Kagaku 13 (12) (1994) 1065.
[12] A. Alexandrova, S. Arpadjan, Anal. Chim. Acta 307 (1) (1995) 71.
[13] R. Rattray, E.D. Salin, J. Anal. At. Spectrom. 10 (12) (1995) 1053.
[14] G.V. Myasoedova, N.I. Shcherbinina, O.N. Grebneva, Anal. Sci. 11 (1) (1995) 181.
[15] O.N. Grebneva, N.M. Kuzmin, G.I. Tsysin, Y.A. Zolotov, Spectrochim. Acta 51B (11) (1996) 1417.
[16] X.J. Li, P. Shramel, H.Z. Wang, P. Grill, A. Kettrup, Fresenius J. Anal. Chem. 356 (1) (1996) 52.
[17] B. Fairman, A. Sanzmedel, Fresenius J. Anal. Chem. 355 (7–8) (1996) 757.

ELSEVIER

Talanta 45 (1998) 865–873

Talanta

Electrochemical and thermodynamic studies of the ion-pair formation of chloropentamminecobalt(III) ion in ethyl alcohol-water media containing different dicarboxylate ligands

A.A. Zaghloul [a,*], G.A. El-Naggar [b], S.B. Abuo Ali [b]

[a] *Chemistry Department, Faculty of Science, Alexandria University, Alexandria, Egypt*
[b] *Chemistry Department, Faculty of Education, Alexandria University, Alexandria, Egypt*

Received 10 January 1997; received in revised form 15 May 1997; accepted 6 June 1997

Abstract

The ion-pair dissociation constants, K_D, of the ion-pair formed between chloropentamminecobalt(III) ion (CpX^{2+}) and a variety of dicarboxylate ligands, have been determined from EMF measurements of a cell composed of glass and calomel electrodes. Measurements were made in water and in aqueous binary mixtures of ethyl alcohol, over a wide range of solvent composition (0–60 wt% ethyl alcohol), at six different temperatures (ranging from 30 to 55°C at intervals of 5°C). The thermodynamic parameters of association ΔG^0_{ass}, ΔH^0_{ass} and ΔS^0_{ass} have been calculated and discussed. $\Delta H^0_{ass}-\Delta S^0_{ass}$, $\Delta S^0_{ass}-\Delta S^0_{1(or\ 2)}$, $\Delta G^0_{ass}-G^0_{1(or\ 2)}$ and $\Delta H^0_{ass}-\Delta H^0_{1(or\ 2)}$ correlations among different solvent media and different dicarboxylate ligands were examined (where 1 and 2 denote the first and the second dissociation reactions of the studied dicarboxylic acids). The pK_D value has been correlated with the dielectric constant of the medium according to Born's equation. © 1998 Elsevier Science B.V.

Keywords: Ion-pair; Ethyl alcohol; Dicarboxylate ligands

1. Introduction

In continuation of our studies on ion-pairing between chloropentamminecobalt(III) ion (CpX^{2+}) and a variety of dicarboxylate anions from EMF measurements in 10% ethanol, 10% dioxane, 10% acetone and 20% ethylene glycol [1–5], we have now extended these studies to mixed solvent media of varying dielectric constant to test electrostatic theories of ion association with a view to investigating changes in the solvation of ions as one solvent replaces another and simply to broaden the field of study of ion association. The present investigation deals with a study of ion-pairs formed between (CpX^{2+}) ion with six different types of dicarboxylate anions (L^{2-}) namely: succinate, malate, tartrate, malonate, maleate and phthalate which have different reactivities toward ion-pair formation with complex cation or with metal ions [6,7]. Measurements were made, at different temperatures, by EMF method in ethyl alcohol–water media of different

* Corresponding author.

PII S0039-9140(97)00176-8

compositions (0–60 wt% ethyl alcohol), which allow for a wide range of dielectric constant. This study is likely to enable us to determine the effects of solvent on ion-pair formation and consequently of the thermodynamics of ion association and hence can add useful information to the field of study of the ion-pairing effects which finds important applications in many branches of science.

2. Experimental

The warm saturated solution of $CpXCl_2$ prepared by the published method [8] was filtered while still warm and the residue first washed thoroughly with 2 N hydrochloric acid, then with EtOH and Et_2O and the salt was then dried at 70°C. The dicarboxylic acids, used in the study, were recrystallised and dried. The absolute ethyl alcohol used (from Prolabo) was purified as recommended [9]. Stock buffer solutions made of the dicarboxylic acids (H_2L) and Na_2CO_3 (dried at 300°C for 3 h) were prepared by weight from B.D.H., AnalaR samples.

The ion-pair dissociation constant determinations were based on EMF measurements of the cell: glass electrode/H_2L (m_1), Na_2CO_3 (m_2), complex salt (m_3)/sat. KCl calomel electrode; where m_1, m_2 and m_3 are the molal concentrations of the dicarboxylic acid, Na_2CO_3 and the complex salt, respectively. Measurements for each ion-pairing dicarboxylate ligand were made at six different temperatures (ranging from 30 to 55°C at intervals of 5°C), in six media of different solvent compositions, in which the ethyl alcohol content was varied from zero to 60 wt%.

For the determination of the ion-pair dissociation constant the glass electrode was soaked for several hours in the cell containing the desired buffer solution of the dicarboxylate ligand and of known wt% of ethyl alcohol, at the desired temperature. The temperature was controlled to $\pm$ 0.01°C. The EMF readings were taken until constancy for at least 1–2 h in order to determine the EMF of the cell and from which the standard potential of the cell, E^0, was calculated. The complex salt was added in 3–4 additions of 0.1–0.15 g portions. After each addition the solution was stirred using an electric stirrer with a polyethylene rod. The EMF reading was recorded after stability for several minutes. Usually 15–30 min were sufficient to obtain steady readings for complete run. The complex salt was added in small quantities by weight to minimize the aquation errors since it had been pointed [6] that the EMF method is only suitable when measurements are made in small fractions of the half-lives of the reactions. The dissociation constants of $CpX^{2+}...L^{2-}$ were, therefore, determined since the chloro complex cation had an aquation half-life of ≈ 19 hours at 25°C and this method of measuring K_D required <1 h. Measurements to ± 0.1 mV were made with a digital pH meter (Beckmann 4500 type). The potentiometric glass electrode technique was at least as precise as those obtained by other methods. Monk [10] has compared the data available for some Co(III) ion-pairs and indicated the unsuspected features or experimental uncertainties involved in the various systems.

3. Results and discussion

The calculations of the thermodynamic ion-pair dissociation constants (K_D) were based on the following equations:

(a) Before adding complex salt (calculation of E^0):

$$K_1 = [H^+][HL^-]f_1^2/[H_2L] \quad (1)$$

$$K_2 = [H^+][L^{2-}]f_2/[HL^-] \quad (2)$$

$$E = E^0 - k' \log [H^+]f_1 \quad (3)$$

$k' = 2.3026\ RT/F$, $f =$ activity coefficient and assuming $f_H = f_{HL} = f_1$

$$I = 0.5([H^+] + [HL^-] + 4[L^{2-}] + 2m_2) \quad (4)$$

where I is the ionic strength.

$$-\log f_i = AZ_i^2[I^{1/2}/(1 + 1.3I^{1/2}) - 0.3I] \quad (5)$$

$A =$ Deby-Hückel constant; (A) was calculated for each temperature (T) and for each solvent composition of dielectric constant (D) according to the equation $A = 1.823 \times 10^6/(DT)^{3/2}$

$$[HL^-] = 2m_1 - 2m_2 - [H^+] - 2[H_2L] \quad (6)$$

$$[L^{2-}] = m_1 - [HL^-] - [H_2L] \quad (7)$$

(b) After adding the complex salt (calculation of K_D):

$$I = 0.5([H^+] + [HL^-] + 4[L^{2-}] + 4[CpX^{2+}] + 2m_2 + 2m_3) \quad (8)$$

$$[CpXL] = m_1 - [H_2L] - [HL^-] - [L^{2-}] \quad (9)$$

$$[CpX^{2+}] = m_3 - [CpXL] \quad (10)$$

$$K_D = [L^{2-}][CpX^{2+}]f_2^2/[CpXL] \quad (11)$$

E^0 was computed from Eq. (3) after determining f_1 from Eq. (4) by the method of successive approximations. The free-hydrogen ion concentration can thus be estimated from Eq. (3). Eq. (1), Eq. (2) and Eq. (6) together with Eq. (8)–Eq. (11) were used to calculate K_D also by the successive approximation method. A basic computer program was designed for this purpose. Some examples of the present work are shown in Table 1, which collects some EMF data for the ion-pairs formed under different experimental conditions. For each run the different K'_D values for different complex salt concentrations (m_3) were calculated. The average values of K'_D for different experimental conditions are listed in Table 2 as K_D. It is clear from this table that K_D values of the ion-pair decrease as the content of ethyl alcohol increases in the ethyl alcohol–water binary mixture, which means that the extent of association between the cation (CpX^{2+}) and the dicarboxylate anion (L^{2-}) increases with increasing ethyl alcohol content in the mixed solvent. This trend of changing K_D with solvent composition seems to result from structural factors in ethyl alcohol–water medium [11], as the possibility of a rapidly changing solvent structure and the dielectric constant in the zone of solvent surrounding the ions, also the effective sizes of the solvated ions due to the replacement of aqueous hydrates by organic solvates. Moreover, it can be seen from Table 2 that for the same dicarboxylate buffer and the same solvent composition, the value of K_D decreases with increasing temperature. This marked decrease of K_D for all dicarboxylate buffers under investigation needs some thermodynamic analysis of the obtained data.

3.1. Thermodynamics of the ion-pair formation reaction

Good straight lines were obtained when pK_{ass} ($K_{ass} = 1/K_D$) versus $1/T$ was plotted for each dicarboxylate buffer at a certain wt% of ethyl alcohol. ΔH^0_{ass} was computed from the slope of each line while the other thermodynamic parameters ΔG^0_{ass} and ΔS^0_{ass} were computed from the well known thermodynamic Eq. (12) and Eq. (13).

Table 1
Examples for the determination of the ion-pair dissociation constant (K'_D) in dicarboxylate buffers at different ethanol compositions and at different temperatures

10^3 m_3	$-E$ (mV)	10^3 CpXL	10^3 K'_D
0% EtOH Succinic 50°C			
$10^3m_1 = 37.6$	$10^3m_2 = 28.06$	$-E_1$ (mV) = 161.3	
8.882	162.8	6.560	4.13
13.438	164.7	7.714	3.51
17.964	166.4	8.734	3.81
22.359	167.8	9.552	3.81
30% EtOH Malic 40°C			
$10^3m_1 = 37.6$	$10^3m_2 = 28.07$	$-E_1$ (mV) = 165.9	
12.622	178.5	5.245	8.52
16.662	179.0	5.491	8.79
20.843	179.9	5.602	8.16
60% EtOH Tartaric 35°C			
$10^3m_1 = 37.6$	$10^3m_2 = 28.07$	$-E_1$ (mV) = 149.5	
4.321	156.9	2.003	2.32
8.481	159.8	3.408	2.74
12.627	160.6	3.697	3.58
10% EtOH Malonic 55°C			
$10^3m_1 = 37.6$	$10^3m_2 = 28.07$	$-E_1$ (mV) = 145.1	
4.185	152.5	1.834	2.38
8.292	155.4	3.143	2.82
12.514	158.4	4.437	2.87
16.718	160.3	5.144	2.69
40% EtOH Maleic 45°C			
$10^3m_1 = 37.6$	$10^3m_2 = 28.06$	$-E_1$ (mV) = 13.6	
4.171	21.6	2.779	1.33
12.329	31.8	7.302	1.13
16.336	32.6	7.460	1.58
20.548	33.9	7.831	2.08
50% EtOH Phthalic 30°C			
$10^3m_1 = 30.1$	$10^3m_2 = 11.23$	$-E_1$ (mV) = 35.0	
7.861	43.2	6.911	1.44
11.612	45.8	8.096	1.63
15.637	47.0	8.480	1.67
20.049	48.0	8.765	1.83

Table 2
The average values of the ion-pair dissociation constants (K_D) at different experimental conditions

T°C	EtOH (wt%)					
	0	10	30	40	50	60
	Succinic 10^3 K_D					
30	5.18 ± 0.38	4.27 ± 0.57	4.16 ± 0.63	3.86 ± 0.13	3.43 ± 0.80	3.12 ± 0.13
35	4.75 ± 0.61	3.70 ± 0.31	3.48 ± 0.38	3.22 ± 0.10	3.14 ± 0.10	3.02 ± 0.66
40	4.39 ± 0.51	3.64 ± 0.29	3.15 ± 0.66	2.75 ± 0.69	2.79 ± 0.72	2.88 ± 0.63
45	3.93 ± 0.10	3.56 ± 0.31	2.86 ± 0.48	2.68 ± 0.54	2.69 ± 0.80	2.82 ± 0.78
50	3.82 ± 0.21	3.55 ± 0.45	2.60 ± 0.29	2.59 ± 0.88	2.40 ± 0.77	2.68 ± 0.12
55	3.61 ± 0.27	3.46 ± 0.20	2.54 ± 0.39	2.25 ± 0.71	2.54 ± 0.55	2.39 ± 0.60
	Malonic 10^3 K_D					
30	6.87 ± 0.85	4.96 ± 0.26	4.22 ± 0.71	3.42 ± 0.68	3.20 ± 0.77	2.40 ± 0.78
35	7.62 ± 0.23	3.74 ± 0.38	4.14 ± 0.67	3.15 ± 0.91	2.96 ± 0.45	1.92 ± 0.78
40	7.56 ± 0.59	3.62 ± 0.28	3.31 ± 0.46	2.97 ± 0.42	2.81 ± 0.61	1.74 ± 0.68
45	7.22 ± 0.16	3.15 ± 0.15	2.77 ± 0.47	2.87 ± 0.49	2.70 ± 0.43	1.44 ± 0.34
50	7.14 ± 0.03	2.92 ± 0.03	2.46 ± 0.20	2.39 ± 0.57	2.34 ± 0.55	1.42 ± 0.35
55	6.65 ± 0.37	2.69 ± 0.18		2.29 ± 0.58	2.27 ± 0.83	1.38 ± 0.16
	Malic 10^3 K_D					
30	11.41 ± 0.33	10.48 ± 0.19	9.10 ± 0.43	8.29 ± 0.62	7.31 ± 0.39	6.23 ± 0.46
35	10.16 ± 0.41	10.05 ± 0.55	8.75 ± 0.47	7.43 ± 0.78	6.65 ± 0.51	6.20 ± 0.57
40	9.92 ± 0.54	8.83 ± 0.29	8.49 ± 0.26	6.71 ± 0.88	5.40 ± 0.70	5.27 ± 0.02
45	9.62 ± 0.31	7.75 ± 0.80	7.44 ± 0.12	6.56 ± 0.50	5.12 ± 0.45	4.65 ± 0.32
50	9.46 ± 0.56	7.23 ± 0.69	7.01 ± 0.37	6.01 ± 0.29	4.07 ± 0.46	4.60 ± 0.11
55	8.52 ± 0.51	6.96 ± 0.18	6.70 ± 0.12	5.32 ± 0.56	3.66 ± 0.56	3.94 ± 0.73
	Maleic 10^3 K_D					
30	4.88 ± 0.74	3.54 ± 0.09	2.09 ± 0.34	1.81 ± 0.39	2.03 ± 0.64	2.03 ± 0.64
35	4.75 ± 0.22	3.47 ± 0.11	2.01 ± 0.51	1.68 ± 0.18	1.93 ± 0.78	1.85 ± 0.41
40	4.51 ± 0.32	3.07 ± 0.52	1.92 ± 0.49	1.55 ± 0.35	1.85 ± 0.46	1.64 ± 0.42
45	4.31 ± 0.28	2.82 ± 0.20	1.72 ± 0.17	1.53 ± 0.35	1.57 ± 0.38	1.52 ± 0.41
50	4.05 ± 0.32	2.50 ± 0.10	1.59 ± 0.13	1.42 ± 0.23	1.46 ± 0.16	1.45 ± 0.18
55	3.76 ± 0.15	2.15 ± 0.09	1.46 ± 0.30	1.28 ± 0.33	1.25 ± 0.17	1.11 ± 0.11
	Tartaric 10^3 K_D					
30	5.62 ± 0.72	4.88 ± 0.21	3.25 ± 0.44	3.03 ± 0.67	3.00 ± 0.64	2.99 ± 0.04
35	5.33 ± 0.66	4.70 ± 0.32	3.24 ± 0.51	3.01 ± 0.55	2.98 ± 0.59	2.88 ± 0.52
40	4.64 ± 0.35	4.61 ± 0.06	3.16 ± 0.57	2.96 ± 0.11	2.89 ± 0.10	2.83 ± 0.45
45	4.00 ± 0.60	4.31 ± 0.55	3.07 ± 0.22	2.81 ± 0.20	2.79 ± 0.47	2.75 ± 0.51
50	3.60 ± 0.78	3.75 ± 0.26	2.98 ± 0.44	2.63 ± 0.72	2.73 ± 0.43	2.62 ± 0.46
55	2.96 ± 0.76	2.75 ± 0.57	2.84 ± 0.42	2.59 ± 0.60	2.46 ± 0.51	2.15 ± 0.36
	Phthalic 10^3 K_D					
30	1.78 ± 0.23	1.33 ± 0.14	1.48 ± 0.31	1.24 ± 0.46	1.64 ± 0.15	2.01 ± 0.66
35	1.67 ± 0.31	1.19 ± 0.10	1.29 ± 0.08	1.18 ± 0.46	1.45 ± 0.13	1.99 ± 0.58
40	1.55 ± 0.20	1.11 ± 0.43	1.11 ± 0.20	0.90 ± 0.34	0.90 ± 0.08	1.05 ± 0.18
45	1.48 ± 0.23	1.06 ± 0.54	1.07 ± 0.19	0.72 ± 0.39	1.02 ± 0.18	1.05 ± 0.16
50	1.41 ± 0.23	1.08 ± 0.52	1.00 ± 0.07	0.59 ± 0.09	0.77 ± 0.04	1.00 ± 0.17
55	1.33 ± 0.39	1.03 ± 0.58	0.96 ± 0.16	0.35 ± 0.12	0.60 ± 0.10	1.00 ± 0.22

$$\Delta G^0_{ass} = -RT \ln K_{ass} \quad (12)$$

$$\Delta S^0_{ass} = (\Delta H^0_{ass} - \Delta G^0_{ass})/T \quad (13)$$

Table 3 represents these thermodynamic parameters at 45°C together with their estimates of errors. It is clear from Table 3 that the most

Table 3
The thermodynamic parameters ΔH^0_{ass}, ΔG^0_{ass} and ΔS^0_{ass} for the ion-pair association constant K_{ass} in different ethanol compositions and at 45°C (ΔH^0_{ass}, ΔG^0_{ass} in kJ mol^{-1}, ΔS^0_{ass} in J mol^{-1} K^{-1})

EtOH (wt%)	Acid	Succinic	Malic	Tartaric	Malonic	Maleic	Phthalic
0	ΔH^0_{ass}	12.19 ± 0.09	11.90 ± 0.05	11.77 ± 0.03	17.99 ± 0.02	12.63 ± 0.02	19.90 ± 0.04
	$-\Delta G^0_{ass}$	14.64 ± 0.66	12.28 ± 0.09	14.60 ± 0.38	13.04 ± 0.06	14.40 ± 0.18	17.22 ± 0.43
	ΔS^0_{ass}	84.37 ± 2.10	76.03 ± 0.32	82.91 ± 1.20	97.55 ± 0.20	84.90 ± 0.59	116.70 ± 1.38
10	ΔH^0_{ass}	13.86 ± 0.03	14.93 ± 0.05	13.59 ± 0.03	18.60 ± 0.05	13.32 ± 0.02	20.06 ± 0.02
	$-\Delta G^0_{ass}$	14.91 ± 0.22	12.85 ± 0.26	14.40 ± 0.59	15.52 ± 0.12	15.52 ± 0.18	18.10 ± 2.16
	ΔS^0_{ass}	90.43 ± 0.71	87.33 ± 0.85	87.99 ± 1.86	106.55 ± 0.43	90.68 ± 0.63	119.90 ± 6.79
30	ΔH^0_{ass}	14.35 ± 0.02	12.73 ± 0.04	14.35 ± 0.07	18.91 ± 0.04	14.08 ± 0.10	20.10 ± 0.02
	$-\Delta G^0_{ass}$	15.49 ± 0.43	12.96 ± 0.04	15.29 ± 0.19	15.10 ± 0.36	16.38 ± 0.27	18.07 ± 0.49
	ΔS^0_{ass}	93.81 ± 1.36	80.75 ± 0.18	93.21 ± 0.65	106.91 ± 1.15	97.20 ± 0.92	119.90 ± 1.56
40	ΔH^0_{ass}	15.31 ± 0.03	13.61 ± 0.09	15.00 ± 0.08	18.40 ± 0.05	14.39 ± 0.07	20.29 ± 0.01
	$-\Delta G^0_{ass}$	15.65 ± 0.50	13.29 ± 0.20	15.53 ± 0.18	15.48 ± 0.46	17.13 ± 0.59	19.12 ± 1.33
	ΔS^0_{ass}	97.34 ± 1.59	84.57 ± 0.70	95.99 ± 0.65	106.50 ± 1.46	99.11 ± 1.88	123.80 ± 4.19
50	ΔH^0_{ass}	16.27 ± 0.02	13.97 ± 0.03	15.12 ± 0.07	18.56 ± 0.03	16.08 ± 0.06	20.38 ± 0.03
	$-\Delta G^0_{ass}$	15.64 ± 0.81	13.94 ± 0.23	15.55 ± 0.44	15.64 ± 0.45	17.07 ± 0.68	18.21 ± 0.46
	ΔS^0_{ass}	100.32 ± 2.55	87.76 ± 0.76	96.42 ± 1.40	107.51 ± 1.44	104.22 ± 1.49	121.30 ± 1.45
60	ΔH^0_{ass}	16.84 ± 0.06	15.69 ± 0.03	15.73 ± 0.04	18.32 ± 0.06	17.99 ± 0.03	20.36 ± 0.07
	$-\Delta G^0_{ass}$	15.52 ± 0.77	14.20 ± 0.17	15.59 ± 0.53	17.29 ± 0.60	16.69 ± 0.77	18.12 ± 0.42
	ΔS^0_{ass}	101.74 ± 2.44	93.98 ± 0.56	98.46 ± 1.66	111.95 ± 1.92	110.76 ± 2.45	121.00 ± 1.33

probable trend in ΔG^0_{ass} values in the studied buffers (for different experimental conditions) is malate < succinate < tartrate < malonate < maleate < phthalate. The high stability of maleate and phthalate ion-pairs is presumably due to the high concentration of charge available on the negatively charged oxygen atom due to delocalization from benzene ring in phthalate and conjugation in maleate, while the trend of stability in the other ion-pairs can be explained on the basis of ring formation between the complex cation and dicarboxylate anion, in which the stability increases with decreasing ring size [12]. Malonate ion-pair is of smaller chain length than the other ion pairs and therefore it is more stable. The increased stability of tartrate ion-pairs relative to those of succinate and malate (same chain length) is due to ring formation through the 2-hydroxyl groups. The same trend of stability of dicarboxylate ion-pairing ligands was matched before in aqueous [13] and mixed organic solvents [7]. Moreover, it can be seen from Table 3 that ΔG^0_{ass} tends to be more negative as the ethyl alcohol content increases in the mixture (0–60 wt%) indicating the increased stability of the ion-pair in that direction, while ΔH^0_{ass} becomes more positive as the organic co-solvent concentration increases in the medium indicating greater energy requirements accompanying the association reaction through dehydration of ions and reflects the greater extent of ion-pair formation in these media. The entropy of association, ΔS^0_{ass}, for all studied dicarboxylate ligands, is positive and arises from the association of the oppositely charged ions. There is an entropy change favouring ion-pair formation. Frank and Evans [14] suggested that ions in solution order water molecules around them to form an 'iceberg', the process being similar to the localised freezing of a liquid and ion-pair formation tends to break down this 'iceberg' structure. Thus, the decreased orientation of solvent molecules leads to a positive entropy change. The magnitude of the positive ΔS^0_{ass} value depends on the extent of both charge neutralization occurring when the ions associate and ion hydration. The order of increase of ΔS^0_{ass} among the different dicarboxy-

late ligands is malate < tartrate < succinate < maleate < malonate < phthalate. It has been shown [15] that for a series of ion-pairs with a common cation, a corresponding linear correlation exists between the entropy of dissociation and the hydration entropy of the anion. In addition, for a series with a common anion, a corresponding linear relationship exists between the entropy of dissociation and the hydration entropy of the cation. Such regularities have been found for both the bivalent metal-EDTA complexes and for the much weaker association of the alkaline earth metals with formate or acetate or the hexamine-cobaltic ion with Cl^-, Br^- and I^-. George [16] has generalized this further and shown that the equation:

$$\Delta S^0 = \Delta S_i + \text{constant}$$

applies to a considerable number of series of ion-pairs, where ΔS_i is the hydration entropy of the ion not common to the series. Each series has its own characteristic constant. In the present investigation this correlation has not been given because the values of the entropy of hydration of the different dicarboxylate anions in ethyl alcohol–water media are not available. However a new correlation has been found between the entropy of association ΔS^0_{ass} and the entropy of either first or second acid dissociation reactions ($\Delta S^0_{1(or\ 2)}$) of the studied acids at different solvent compositions ($\Delta S^0_{1(or\ 2)}$ values were taken from [17]). This correlation was a good one and can take the following empirical formula

$$\Delta S^0_{ass} = a + b\ \Delta S^0_{1(or\ 2)}$$

Also a similar correlation was found to exist for different dicarboxylate ion-pairing ligand at fixed solvent compositions. This correlation is shown in Fig. 1, for the first dissociation reaction in both cases. The values of the empirical constants a and b depend on the type of acid ligand and also on the solvent composition. The parallelism between $\Delta(\Delta S^0_{ass})$ and $\Delta(\Delta S^0_{1(or\ 2)})$ for either different solvent compositions or different types of dicarboxylate ion-pairing ligand is probably related to ion-solvation where the controlled factor is the reorientation of the hydration shell of both free complex ion and ion-pair and also of dicarboxylate anion. The isoequilibrium plot of ΔH^0_{ass} against ΔS^0_{ass} was found to fit the dicarboxylate ion-pairing ligand series at 40°C (at fixed solvent composition) in one straight line with a positive slope. The computed isoequilibrium temperature, β, for different solvent compositions were found to be much lower than that of the experimental temperature (313 K) indicating that these ion-pair reactions are entropy controlled ones. The same results were found for the isoequilibrium plots of one dicarboxylate type at different solvent compositions as shown in Fig. 2.

3.2. Linear free energy like relationship

It is well known that when a series of reactions involves only a single reaction mechanism, there is a trend for rate constants to increase monotonically with equilibrium constants and in some cases this trend even takes the form of an accurate linear relationship between the quantities ΔG^*

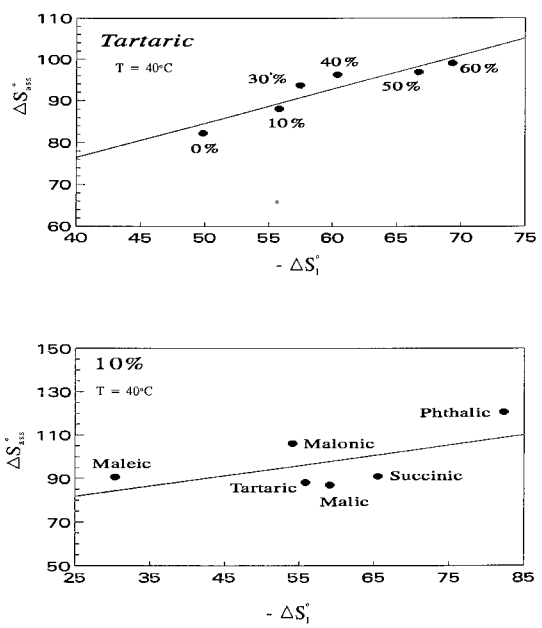

Fig. 1. ΔS_{ass}–ΔS^0_1 correlation for tartaric acid in different solvent compositions and in 10 wt% ethanol for different dicarboxylate ligands.

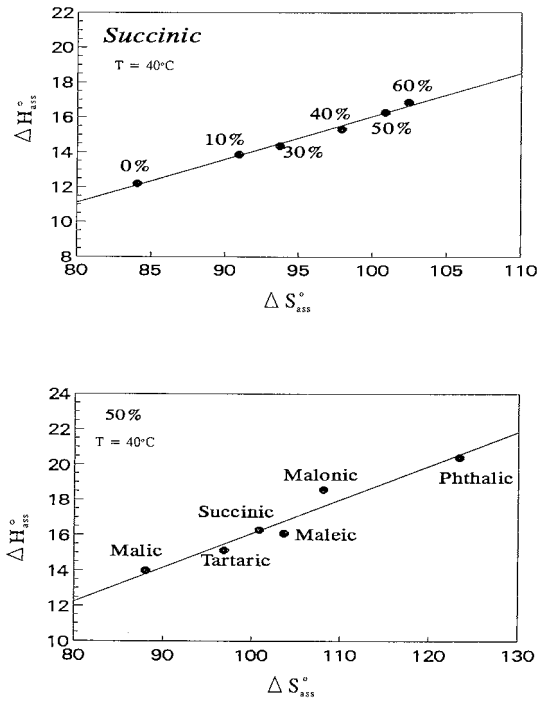

Fig. 2. ΔH^0_{ass}–ΔS^0_{ass} correlation for succinic acid in different solvent compositions and in 50 wt% ethanol for different dicarboxylate ligands.

and ΔG^0. In the present work we aimed to examine a new linear free energy like relationship among the dicarboxylate series under investigation which is ΔG^0_{ass}–$\Delta G^0_{1(or\ 2)}$ correlation. This correlation was found to be linear for the different dicarboxylates at fixed solvent composition or for one dicarboxylate type at different solvent compositions and Fig. 3 shows this correlation in both cases. This linear correlation takes the form:

$$\Delta G^0_{ass} = b\ \Delta G_{1(or\ 2)} + a$$

where a and b are empirical constants, their values are varied from one plot to another. This obtained linear free energy relationship represented by the above empirical equation can be considered as LFE like relationship which relates ΔG^0_{ass} for the ion-pair formation reaction with $\Delta G^0_{1(or\ 2)}$ for the acid dissociation ($\Delta G^0_{1(or\ 2)}$ values were taken from [17]). In light of the above discussions, the parallelism between ΔG^0_{ass} and $\Delta G^0_{1(or\ 2)}$ for all studied dicarboxylate ligands is strong evidence that the dicarboxylate anion, lying close to the line, form an electrostatic ion-pair in which the anion is localized in its interaction with the complex cation. The position taken up by the anion is across the back edge of the octahedron in such a way that π-bonding with t_{2g} orbitals is possible.

Moreover, ΔH^0_{ass} was found to be linearly correlated with $\Delta H^0_{1(or\ 2)}$ [17] for all studied dicarboxylate ligands and for all compositions. These linear correlations existing among ΔG^0_{ass}–$\Delta G^0_{1(or\ 2)}$ and ΔS^0_{ass}–$\Delta S^0_{1(or\ 2)}$. Also, the parallelism between ΔH^0_{ass} and $\Delta H^0_{1(or\ 2)}$ is attributed to ion solvation process.

3.3. Effect of dielectric constant

Fig. 4 shows the linear dependence of pK_{ass} on $1/D$ (D values were taken from Ref. [18]) for different dicarboxylate ion-pairing ligand which gives linear correlation in accordance with Born's equation [19].

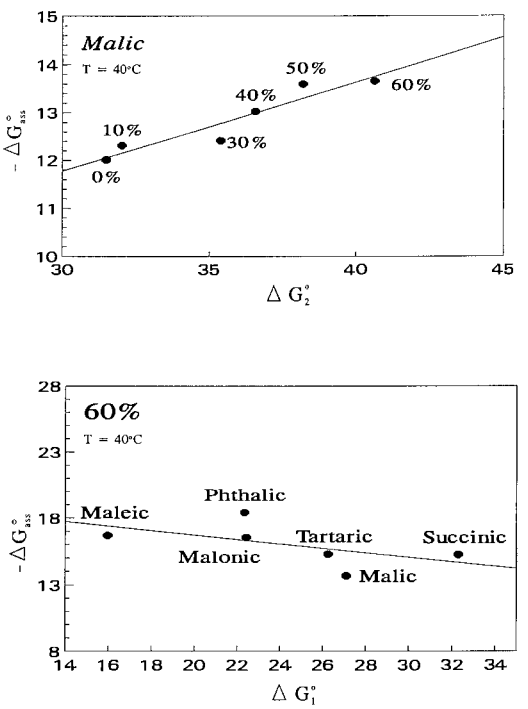

Fig. 3. ΔG^0_{ass}–ΔG^0_2 correlation for malic acid in different solvent compositions and ΔG^0_{ass}–ΔG^0_1 correlation in 60 wt% ethanol for different dicarboxylate ligands.

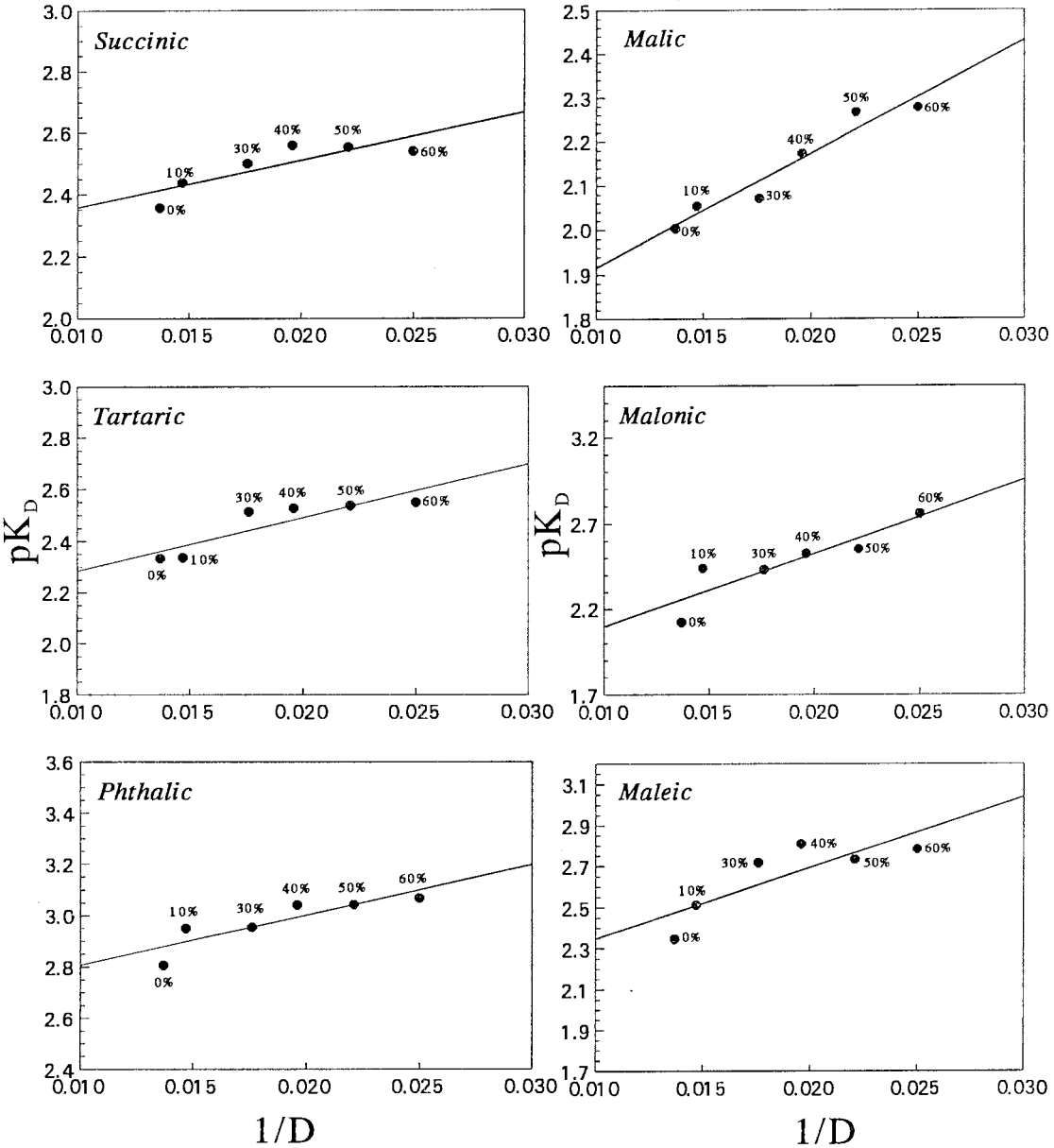

Fig. 4. pK_D-1/D correlation for the ion-pair association reaction of dicarboxylic acids in different solvent compositions at 40°C.

$$pK_D = \frac{\Delta G^0_{n.e.s}}{2.303\,RT} + \frac{Ne^2}{4.606\,RTD}(1/r^+ - 1/r^-)$$

where r^+ and r^- are the radii of the complex cation and ion-pairing ligand respectively. It was found from Fig. 4, that the lines obtained have intercepts which differ slightly from each other and the average value of the intercept is 2.20 which represents the non-electrostatic part of the free energy of association, but they have different

slopes because the slope is varied only with the radius of dicarboxylate anion (the cation is common):

$$\text{Slope}\ (b) = \frac{\text{Ne}^2}{4.606\ RT}\,(1/r^+ - 1/r^-)$$

Substituting of the constants e, N and R at 40°C we can find

$$1/r^- = 1/r^+ - 8.64 \times 10^5.b$$

Assuming the value of r^+ $(r_{\text{NH}_3} + r_{\text{CoIII}})$ to be 2.23×10^{-8} cm [20]. The above equation takes the form,

$$1/r^- = 4.48 \times 10^7 - 8.64 \times 10^5 b$$

The obtained values of $r-$ are 3.17, 4.41, 3.70, 12.99, 6.71 and 3.88 Å for succinate, malate, tartrate, malonate, maleate and phthalate ion-pairing ligands, respectively. It is seen that those values are reliable (except that of malonate which is of a higher value) and indicate that there is a sort of specific solvation of this ligand existing in ethanol–water medium.

References

[1] M.F. Amira, Sh.A. El-Shazly, M.M. Khalil, F.M. Abdel-Halim, Trans. Met. Chem. 11 (1986) 72.

[2] M.F. Amira, K.Z. Ismail, A.A. Zaghloul, Proceedings of the International Conference on Coordinate Chemistry, Athens, Greece, 1986, p. 546.

[3] Sh.A. El-Shazly, M.T. Mohamed, A.A. Zaghloul, M.F. Amira, Bull. Fac. Sci. A32 (1992) 46.

[4] M.F. Amira, Sh.A. El-Shazly, M.M. Khalil, Proceedings of the International Conference on Coordinate Chemistry, Athens, Greece, 1986, p. 545.

[5] Sh.A. El-Shazly, N.H. El-Hammamy, M.F. Amira, A.S. Babaqi, M.T. Mohamed, Gazz. Chim. Ital. 122 (1992) 335.

[6] D.W. Archer, D.A. East, C.B. Monk, J. Chem. Soc. A (1965) 720.

[7] M.F. Amira, P. Carpenter, C.B. Monk, J. Chem. Soc. Dalton. Trans. (1980) 1726.

[8] E.C. Rochow, Inorg. Synth. 6 (1960) 138.

[9] P.S. Danniel, T.M. Hildebrand, J. Am. Chem. Soc. 44 (1922) 2824.

[10] C.B. Monk, J. Chem. Soc., (1965) 245.

[11] M.J. Blandamer, J. Burgess, Quat. Rev. 4 (1) (1975) 55.

[12] H. Irring, R.J. Williams, D.J. Ferret, A.E. Williams, J. Chem. Soc. (1954) 3494.

[13] M.B. Campbell, M.R. Wendt, C.B. Monk, J. Chem. Soc., Dalton Trans. (1972) 1714.

[14] H.S. Frank, M.W. Evans, J. Chem. Phys. 13 (1945) 507.

[15] G.H. Nancollas, Quat. Rev. 14 (1960) 402.

[16] J.H.B. George, J. Am. Chem. Soc. 81 (1959) 5530.

[17] A.A. Zaghloul, G.A. El-Naggar, M.F. Amira, Gazz. Chim. Ital. 126 (1996) 735.

[18] G. Åkerlof, J. Am. Chem. Soc. 54 (1932) 4125.

[19] M. Born, Z. Phys. 1 (1920) 45.

[20] C.B. Monk, Electrolytic Dissociation, Academic Press, London and New York, 1961, p. 257.

.

ELSEVIER

Talanta 45 (1998) 875–882

Talanta

Sulphuric acid influence on liquid–liquid extraction of Co(II) and Zn(II) by MIBK from NH_4SCN medium

M. Avila Rodríguez *, J.A. Barrón Zambrano, A. Alatorre Ordaz, R. Navarro Mendoza, T.I. Saucedo Medina

Instituto de Investigaciones Científicas, Universidad de Guanajuato, Cerro de la Venada s/n, 36040 Guanajuato, Mexico

Received 4 April 1997; received in revised form 9 June 1997; accepted 10 June 1997

Abstract

Liquid–liquid extraction of Co(II) and Zn(II) by methylisobutylcetone (MIBK) has been studied systematically from NH_4SCN/H_2SO_4 media. The influence of sulphuric acid concentration on the percentage of extraction of Co(II) and Zn(II) has been discussed. It is shown that sulphuric acid concentration has not the same effect on distribution curves of Co(II) and Zn(II). Thus, it is possible to have a separation of Zn(II) of Co(II) when $[NH_4SCN]$ is 0.5 mol l^{-1} and $[H_2SO_4]$ is about 2 mol l^{-1}. Under these conditions the separation factor ($S_{Zn/Co}$) is around 580. The results are treated in terms of thermodynamic activities in aqueous phase, to determine the composition of the extracted complexes ($M:SCN^-$) and to discuss the extraction mechanism. © 1998 Published by Elsevier Science B.V.

Keywords: Thermodynamic; Liquid–liquid; Sulphuric acid

1. Introduction

During the hydrometallurgical process for the obtaining of zinc, in the metallurgical plant METMEX, Peñoles (Torreon, Mexico), solid wastes are generated. These wastes present concentrations of $\approx 3.5\%$ in weight of cobalt. One of the characteristics of these solid wastes is the high concentration of zinc (46.5% in weight). Thus, its commercialization is difficult. This is why it is necessary to diminish the zinc concentration, so the value of the product can be increased. Liquid–liquid extraction is a good option to attain this objective, since it is a versatile technique and easily implemented at an industrial level.

There are different extraction systems reported in the literature, for cobalt and for zinc, using extractants of different nature [1–6]. Some of the extractants reported are Cyanex 302 (bis(2,4,4-trimethylpentyl)thiophosphinic acid) [1], Cyanex 272 (bis(2,4,4-trimethylpentyl)phosphinic acid) [7], D2EHPA (bis(ethilhexylphosphinic)acid) [5], as well as methylisobutylketone (MIBK) [6]. The use of an extraction system that allows an efficient separation of these two metallic ions depends in good measure on the characteristics of the medium from which the extraction will be made. Since the Co(II) and Zn(II) solutions are obtained from a solid leaching, the acid concentration in

* Corresponding author.

PII S0039-9140(97)00177-X

the aqueous solution is high. Therefore it is convenient to use an extractant with solvating properties to attain the separation of Co(II) from Zn(II), rather than an extractant with ionic exchange properties, as DEHPA, Cyanex 302 and Cyanex 272. Ketones are a good choice for their solvatation ability, due to the basic properties of the oxygen atom, as well as their chemical stability and low solubility in water. Among the ketones that have been used for liquid–liquid extraction, MIBK has been largely employed for the extraction of metallic complexes, both at a large scale as in analysis at the laboratory [8–11].

Many metal ions can be extracted with MIBK as anionic complexes, together with ions H^+ and other cations, as Na^+ or NH_4^+ [6,12,13]. The information found in the literature shows that Co(II) is extracted by MIBK from a thiocyanate medium [6]. The extraction of cobalt thiocyanates has been used at an industrial level for their separation from nickel [6]. On the other hand, the extraction of Zn(II) can also be made from these kind of media, in which the affinity of MIBK towards the zinc is important. This is a limiting factor in the Co(II)/Zn(II) separation, for it diminishes the selectivity of the extraction system. Therefore, in this work, a systematic study of the extraction of Co(II) and Zn(II) by MIBK in thiocyanate medium has been made, in the presence of sulphuric acid. The distribution curves of these two ionic metals have been obtained, with and without sulphuric acid and the influence of this acid in the extraction process has been analysed. The results have been treated in terms of the activity coefficients of the species (calculated with the CALCACT program) in aqueous phase, with the purpose of explaining the extraction mechanism of Co(II) and Zn(II).

2. Experimental

The reagents used were all analytical grade. The volumes of the organic phase (V_{org}) and the aqueous phase (V_{aq}), for the extraction and stripping, were always of 10 ml. The organic phase contained only undiluted MIBK (purity of 98%). The aqueous phase consisted of the metal ion to be extracted, as well as NH_4SCN and H_2SO_4, in different concentrations. When the concentration of sulphuric acid was higher than 2 M, the decomposition of NH_4CSN was observed. The solutions (aqueous phase/organic phase) were shaken with a (Cole Palmer 51502) ping pong shaker at 150 rpm at 25°C for 2 h, which is enough time to reach equilibrium. Once equilibrium is attained, the phases are separated and the concentration of the metal ion in the aqueous phase is determined with a (Perkin–Elmer 3110) atomic absorption spectrometer. The concentration of the metal ions in the organic phase were calculated by mass balance. The concentrations H_2SO_4 extracted by the MIBK was determinated by potentiometric titration (Titrino 716, Metrohm) with NaOH 0.1 M. The concentration of the water extracted to the organic phase was determinated by the Karl–Ficher method with a Titrino 701 titrator (Metrohm).

The values of the activity of water (a_{H_2O}) in NH_4SCN and H_2SO_4 are those reported by Covington and Matheson [14] and Staples [15], respectively. In the case of the mixed NH_4SCN/H_2SO_4 media, the values of (a_{H_2O}) were calculated using the CALCACT programme. This programme was written in Quick Basic. It allows us to obtain the activity coefficients (based on Mikulin's relationship) of the different electrolytes of a solution and the activity of water (based on Zadonvskii's rule) for the same solution.

3. Results and discussion

3.1. Distribution curves of Co(II) and Zn(II) from NH_4SCN and NH_4CSN/H_2SO_4 media

The extraction results of Co(II) and Zn(II) by MIBK from NH_4SCN medium are presented in Fig. 1, in which the percentage of extraction (%E) of Co(II) and Zn(II) are presented, as a function of NH_4SCN concentration.

In Fig. 1 we can see that the %E of both metals increase depending on the concentration of NH_4SCN. The extraction of Zn(II) (curve 1, Fig. 1) is almost quantitative when the NH_4SCN concentrations are close to 0.2 M. Concerning Co(II)

(curve 2, Fig. 1), the %E are close to 100% when the SCN^- concentration is about 1.5 M.

This behaviour can be explained if the extraction of both metallic ions is considered as an extraction that occurs through a solvation process. In fact, the increase in the SCN^- ion concentration leads to the formation of complexes that can be extracted from the organic phase by the MIBK. The nature of the complexes extracted will be discussed later on.

The separation of these two metallic ions can be considered using the separation factor ($S_{Zn(II)/Co(II)}$), which is defined by the ratio of the distribution coefficients (D_M) of Zn(II) and Co(II):

$$S_{Zn(II)/Co(II)} = \frac{D_{Zn(II)}}{D_{Co(II)}} \quad (1)$$

where

$$D_M = \frac{\bar{M}}{[M]}$$

[M] and [$\bar{M}$] represent the concentrations of metal ion in the aqueous phase and in the organic phase, respectively.

When the value of $S_{Zn(II)/Co(II)}$ moves away from 1, the possibility of reaching an efficient separation increases. The maximum separation factor obtained is equal to 44.98 (Table 1), but in this condition the concentration of Zn(II) in the organic phase is not higher than 70%. This means that the quantitative separation of these two cations cannot be achieved in only one step.

Table 1
Values of $D_{Co(II)}$, $D_{Zn(II)}$ and $S_{Zn(II)/Co(II)}$ at different concentrations of NH_4SCN

[NH_4SCN] (M)	$D_{Co(II)}$	$D_{Zn(II)}$	$S_{Zn(II)/Co(II)}$
0.1	0.048	2.1595	44.98
0.2	1.1655	11.5	9.87
0.25	2.159	22.8	10.56
0.4	5.13	39	7.60
0.6	11.5	60	5.21
1	22.8095	74.8	3.28
1.5	34	81.98	2.41

The effect of sulphuric acid in the extraction of Co(II) and Zn(II) is shown in Figs. 2 and 3, in which the variation of %E as a function of the concentration of NH_4SCN has been graphed, for different concentrations of sulphuric acid (1 and 2 M).

The analysis of Figs. 2 and 3 indicates that the presence of H_2SO_4 plays a role in the %E of

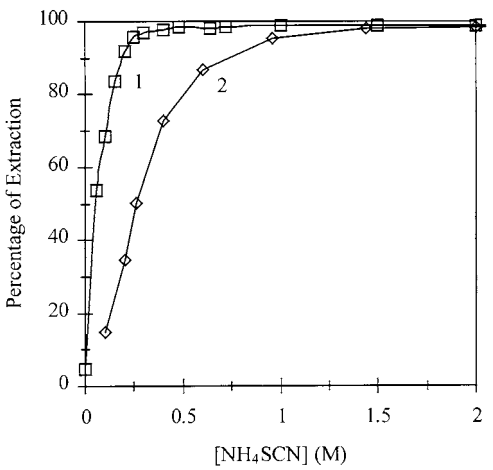

Fig. 1. Percentage of extraction of (1) Zn(II) and (2) Co(II) (considered separately) at equilibrium, at 25 ± 2°C, as a function of NH_4SCN concentration by MIBK (98%). Phase ratio = 1. [Zn(II)] and [Co(II)] were initially 10^{-3} M.

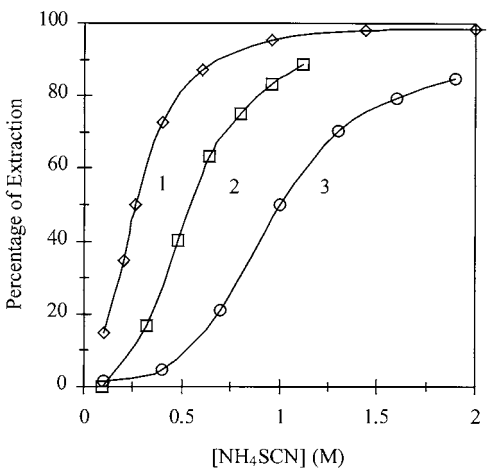

Fig. 2. Percentage of extraction of Co(II) at equilibrium, at 25 ± 2°C, as a function of NH_4SCN concentration by MIBK (98%), in absence (1) and presence of H_2SO_4 1 M (2) and 2 M (3). Phase ratio = 1. [Co(II)] was initially 10^{-3} M.

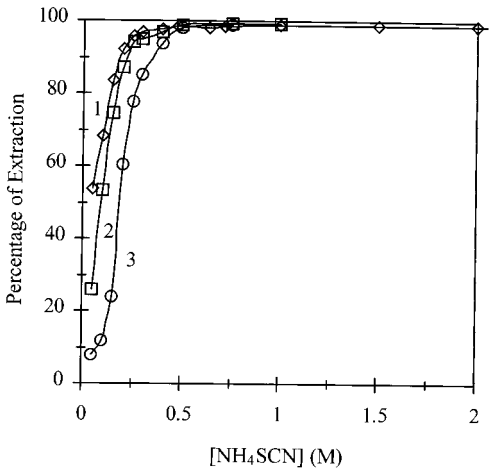

Fig. 3. Percentage of extraction of Zn(II) at equilibrium, at 25 ± 2°C, as a function of NH_4SCN concentration by MIBK (98%), in absence (1) and presence of H_2SO_4 1 M (2) and 2 M (3). Phase ratio = 1. [Zn(II)] was initially 10^{-3} M.

Co(II) and Zn(II). This influence is observed by the displacement of these curves towards higher values of thiocyanate ions concentration, which means that the %E are decreased. When the H_2SO_4 concentration is 2 M, the extraction curves are displaced even more towards higher values of NH_4SCN concentration. This phenomenon is clearer in the extraction of Co(II). Thus, in H_2SO_4 2 M medium it is easier to find better conditions for an efficient separation, since it is possible to obtain higher $S_{Zn(II)/Co(II)}$ values (Table 2). For instance, for a NH_4SCN concentration of 0.5 M, the separation factor is 7.6 without H_2SO_4 (Table 1) and 577.25 with H_2SO_4 (Table 2). In these conditions almost 99% of Zn(II) is in the organic phase, while 92% of Co(II) is in the aqueous phase. This shows that the presence of H_2SO_4 enhances the separation of Zn(II) from Co(II) in NH_4SCN medium, using MIBK.

Table 2
Values of $D_{Co(II)}$, $D_{Zn(II)}$ and $S_{Zn(II)/Co(II)}$ at different concentrations of NH_4SCN in presence of H_2SO_4 2 M

[NH_4SCN] (M)	$D_{Co(II)}$	$D_{zn(II)}$	$S_{Co/Zn}$
0.1	0.015	0.13	8.93
0.4	0.049	15.06	310.01
0.5	0.087	50.20	577.25
0.7	0.266	100.51	377.39

3.2. Thermodynamic study of the extraction of Co(II) and Zn(II) by the MIBK in SCN^- medium, in the presence of H_2SO_4

The extraction of Co(II) and Zn(II) by the MIBK is carried out by a solvation mechanism. In this kind of extraction the %E increases with the NH_4SCN concentration. In these conditions the activity of water diminishes, this promotes the variation of the activity coefficients of the different species found in the medium. The presence of H_2SO_4 enhances also changes in the activity of water and in the activity coefficients of the electrolytes (Table 3). For the study of this extraction system, it is necessary to consider the activity coefficients or the activities of the different species that participate in the process.

The reaction of extraction of Co(II) by the MIBK can be written as follows:

$$Co(SCN)_2 + nNH_4^+ + nSCN^- + mH_2O + p\overline{MIBK} \Leftrightarrow \overline{Co(SCN)_{(2+n)}mH_2OpMIBKnNH_4} \quad (2)$$

The species with overbars are those that are found in the organic phase.

This reaction is based on the existence of the species $Co(SCN)_2$, considering that this species is present in apppreciable concentration for all the range of SCN^- concentrations studied, as we can see in the species distribution diagram shown in Fig. 4.

The thermodynamic constant of extraction is written in this way:

$$K^0_{ext} = \frac{a_{\overline{Co(SCN)_{2+n}mH_2OpMIBKnNH_4}}}{a_{Co(SCN)_2} a^n_{SCN^-}\ a^n_{NH_4^+} a^m_{H_2O} a^{\overline{p}}_{\overline{MIBK}}} \quad (3)$$

where a represents the activity of the different species in the aqueous and organic phases.

It is possible to introduce the activity coefficients of the metallic complexes, both in the aqueous and organic phases, in Eq. (3).

Table 3
Values of the activity of water (a_{H_2O}) in the absence and in the presence of sulphuric acid. The values in the mixed media were calculated with the assistance of the CALCACT programme.

[NH_4SCN] (M)	γ_{NH_4SCN} in absence of H_2SO_4	a_{H_2O} in absence of H_2SO_4	γ_{NH_4SCN} in presence of H_2SO_4 2 M	a_{H_2O} in presence of H_2SO_4 2 M
0.1	0.7725	0.9922	0.2543	0.9565
0.2	0.7241	0.9848	0.2676	0.9478
0.4	0.6762	0.9803	0.2924	0.9387
0.6	0.6500	0.9549	0.3145	0.9290
0.96	0.6240	0.9278	0.3494	0.9152
2.0	0.5992	0.88470	0.4293	0.7909

$$K^0_{ext} = \frac{\gamma_{\overline{Co(SCN)_{(2+n)}mH_2OpMIBKnNH_4}}}{\gamma_{Co(SCN)_2}} \frac{\overline{[Co(SCN)_{(2+n)}mH_2OpMIBKnNH_4]}}{[Co(SCN_2)]\, a^n_{SCN^-} a^n_{NH_4^+} a^m_{H_2O} a^{\overline{p}}_{MIBK}} \quad (4)$$

With the aim of simplifying the treatment of the system of extraction, we consider that the variation of the activity coefficients of the complex in the organic phase and in the aqueous phase is similar, since these complexes have no charge. Thus, it is possible to obtain an apparent extraction constant K_{ext} which takes into consideration the ratio $\gamma_{\overline{Co(SCN)_{(2+n)}mH_2OpMIBKnNH_4}}/\gamma_{Co(SCN)_2}$. The apparent extraction constant is:

$$K_{ext} = \frac{\overline{[Co(SCN)_{(2+n)}mH_2OpMIBKnNH_4]}}{[Co(SCN)_2] a_{NH_4SCN} a^m_{H_2O} a^{\overline{p}}_{MIBK}} \quad (5)$$

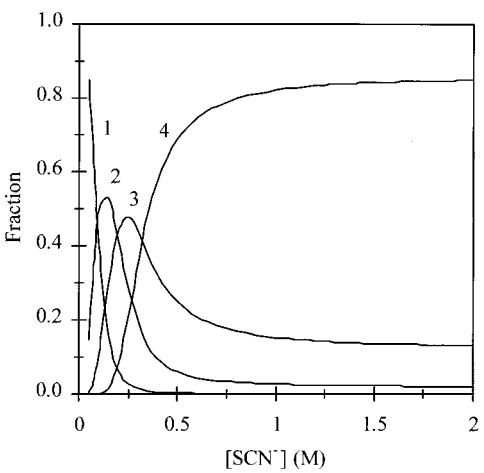

Fig. 4. Distribution plot of the species of the system Co(II)/SCN^-, calculated with the constants shown in Table 4. (1) Co^{2+}, (2) $Co(SCN)^+$, (3) $Co(SCN)_2$, (4) $Co(SCN)_4^{2-}$.

where:

$$a_{NH_4SCN} = a_{NH_4^+} a_{SCN^-}$$

In the other hand, the distribution coefficient is defined in the following way:

$$D = \frac{\overline{[Co(II)]}}{[Co(II)]} \quad (6)$$

where [Co(II)] and $\overline{[Co(II)]}$ represent the total concentration of the metallic ion in the aqueous and the organic phase, respectively.

If the predominance of only one complex is considered in the organic phase, then:

$$\overline{[Co(II)]} = \overline{[Co(SCN)_{(2+n)}mH_2OpMIBKnNH_4]} \quad (7)$$

In the case of the aqueous phase we have:

$$[Co(II)] = [Co^{2+}] + \sum_i [Co(SCN)_i^{(2-i)}] + \ldots \quad (8)$$

The presence of the different complex species of Co(II) and SCN^-, in the aqueous phase, have an effect on the equilibrium of the extraction of the $Co(SCN)_2$, for which it is necessary to introduce the complexation coefficient $\alpha_{Co(SCN)_2}$, which is defined as follows:

$$\alpha_{Co(SCN)_2} = \frac{1}{\beta_2[SCN^-]^2} + \frac{\beta_1}{\beta_2[SCN^-]} + \frac{\beta_3}{\beta_2}[SCN^-] \quad (9)$$

where, β_i is the overall formation constant of $Co(SCN)_i$ complex.

Table 4
Values of the overall formation constants used in the systems Co(II)/SCN^- and Zn(II)/SCN^- [16]

System	Constant	Conditions
Co(II)/SCN^-	$\log \beta_1 = 1.59$	Extrapolated to ionic strength $I = 0$ as reported in [17]
	$\log \beta_2 = 2.41$	
	$\log \beta_4 = 3.25$	
Zn(II)/SCN^-	$\log \beta_1 = 1.33$	Extrapolated to ionic strength $I = 0$
	$\log \beta_2 = 1.91$	
	$\log \beta_3 = 2.0$	
	$\log \beta_4 = 1.63$	

This $\alpha_{Co(SCN)_2}$ depends on the concentrations of the thiocyanate ion and does not take into consideration the effect on the medium (salting-out effect), which is caused by the existance of important concentrations of electrolytes in the aqueous phase (NH_4SCN and H_2SO_4). In order to have a function that can take into consideration this phenomenon, it is necessary to know the SCN^- ion activity values, the problem is that this is thermodynamically impossible. Since it is possible to obtain from the literature the value for a_{NH_4SCN}, we can calculate the approximate value of a_{SCN^-} in the following way:

$$a^*_{SCN^-} = \sqrt{a_{NH_4SCN}} \tag{10}$$

The [SCN^-] can be replaced by the previous term in Eq. (9) to give:

$$\alpha^*_{Co(SCN)_2} = \frac{1}{\beta_2 a^{*2}_{SCN^-}} + \frac{\beta_1}{\beta_2 a^*_{SCN^-}} + \frac{\beta_3}{\beta_2} a^*_{SCN^-} + \ldots \tag{11}$$

This equation does depend upon the changes of the thiocyanate ion activity coefficients, which are due to the effect of the medium. The values of β used to calculate the complexation coefficient are shown in Table 4.

When the term $\alpha^*_{Co(SCN)_2}$ and the distribution coefficient are introduced in Eq. (5), we have:

$$K_{ext} = D_{Co(II)} \frac{\alpha^*_{Co(SCN)_2}}{a_{NH_4SCN} a^m_{H_2O} a^p_{\overline{MIBK}}} \tag{12}$$

Equation 12 can be rearranged in the logarithmic form in the following manner:

$$\log D_{Co(II)} + \log \alpha^*_{Co(SCN)_2} = \log K_{ext} + p \log a_{\overline{MIBK}} + n \log a_{NH_4SCN} + m \log a_{H_2O} \tag{13}$$

When the extraction of Co(II) is carried out with concentrated MIBK, this can be considered as a pure solvent and the value of $a_{\overline{MIBK}}$ will be equal to one. Eq. (13) will then take the following form:

$$\log D_{Co(II)} + \log \alpha^*_{Co(SCN)_2} = \log K_{ext} + n \log a_{NH_4SCN} + m \log a_{H_2O} \tag{14}$$

This equation matches one of a straight line with slope equal to 1, that depends on the values of n and m, which represent the number of molecules of SCN^- and H_2O involved in the extraction process. Different values of n and m were tested, searching for the best correlation of the data, in the case of the extraction of Co(II) in absence of H_2SO_4.

The results obtained for n and m equal to 3 show that the data fit appropriately in a straight line with slope close to one ($y = 2.78 + 1.01x$, $R^2 = 0.992$). This indicates that the ratio for Co:SCN^-:H_2O is 1:3:3. The correlation of the experimental data suggests that the hypothesis made, as a result of the thermodynamic treatment of the system of extraction, are satisfactory. The value of the apparent extraction constant, obtained from the ordinate, is $K_{ext} = 10^{2.78}$.

The same thermodynamic treatment was made for the extraction of Co(II), using MIBK in NH_4SCN medium, in the presence of H_2SO_4. The aim of this study was to ratify the limits of the proposed model. These results are shown in Fig. 5, in which the variation of $\log D_{Co(II)} + \log \alpha^*_{Co(SCN)_2}$ as a function of $3 \log a_{NH_4SCN} + 3 \log a_{H_2O}$ has been plotted, in the presence of H_2SO_4 1, 1.5 and 2 M. In Fig. 5, the results obtained in absence of sulphuric acid have been included. The activity values of NH_4SCN and H_2SO_4 have been calculated with the assistance of the CALCACT program, which allows us to calculate the activity coefficients of electrolytes in a three component solution.

The analysis of Fig. 5 shows that the slopes of the straight lines obtained are similar (for H_2SO_4 1 M and 1.5 M the slope is 0.93 and 1.03 and for H_2SO_4 2 M, the slope is 1.12), when the stoichiometric ratio of the extracted complex ($Co:SCN^-:H_2O$) in the organic phase is 1:3:3. Moreover, for the extraction of Co(II) in presence of H_2SO_4 1 M and 1.5 M, the apparent extraction constant value $K_{ext} = 10^{2.59}$ and $K_{ext} = 10^{2.64}$, respectively are very close to the one obtained in the extraction of this same cation in the absence of H_2SO_4 ($K_{ext} = 10^{2.78}$). This findings indicate that the thermodynamic treatment that has been developed takes into consideration, in an appropriate way, the effect of the sulphuric acid present in the medium. Nevertheless, when the concentration of sulphuric acid is 2 M, the straight line that is plotted does not match with the other three. The different behaviour can be explained if we take into consideration the beginning of decomposition of NH_4SCN by the presence of high concentrations H_2SO_4.

Fig. 6 shows the results obtained for the Zn(II) extraction, in the study of $\log D_{Zn(II)} + \log \alpha^*_{Zn(SCN)_2}$ as a function of $n \log a_{NH_4SCN} + m \log a_{H_2O}$, when $n = 2$ and $m = 4$, in the absence of H_2SO_4 and in the presence of H_2SO_4 1 and 2 M.

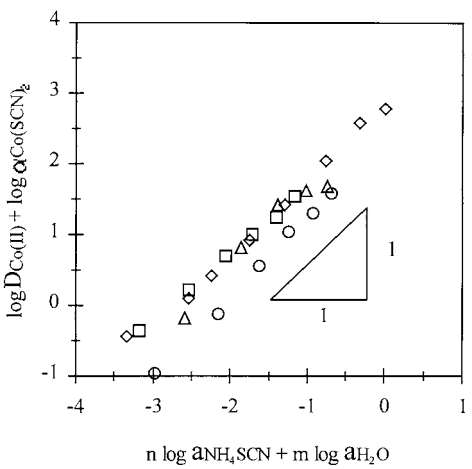

Fig. 5. Plot of $\log D_{Co(II)} + \log \alpha_{Co(SCN)_2}$ vs. $n \log a_{NH_4SCN} + m \log a_{H_2O}$, in the case of the extraction of Co(II) (initially 10^{-3} M) by MIBK (98%) from NH_4SCN (◇), NH_4SCN/H_2SO_4 1 M (□), 1.5 M (△), 2 M (○) media. It is assumed that $m = n = 3$.

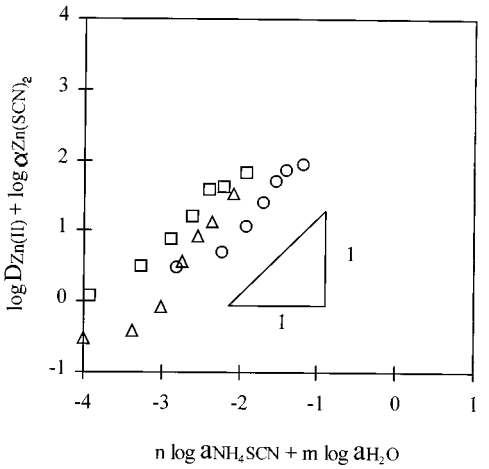

Fig. 6. Plot of $\log D_{Zn(II)} + \log \alpha_{Zn(SCN)_2}$ vs. $n \log a_{NH_4SCN} + m \log a_{H_2O}$, in the case of the extraction of Zn(II) (initially 10^{-3} M) by MIBK (98%) from NH_4SCN (○), NH_4SCN/H_2SO_4 1 M (□) and 2 M (△) media. It is assumed that $m = 4$ and $n = 2$.

In Fig. 6 it is possible to see that the data do not follow the same tendency, both in absence and in presence of sulphuric acid. This behaviour suggests the presence of several Zn(II) solvates in the organic phase. This means that the extraction process may not be represented by only one equilibrium. Then, it is not possible to appreciate the influence of the medium in the extraction of Zn(II) by the MIBK, using the thermodynamic model that has been developed.

Even though this model is rather simple, it considers the effects of the medium for the extraction of Co(II) by the MIBK from SCN^- medium, for H_2SO_4 concentrations up to 1.5 M.

4. Conclusions

The separation process of Co(II) from Zn(II) by the MIBK in amonium thiocyanate medium is highly improved when it is realized in the presence of sulphuric acid. The highest separation factor obtained in this medium is around 580, when the SCN^- and H_2SO_4 concentrations are 0.5 and 2 M, respectively.

The extraction mechanism of both ions is carried out by a solvation process. The extraction

model that has been developed, has allowed us to explain the effect of the medium, induced by the presence of H_2SO_4 in the extraction system, for the extraction of Co(II) by the MIBK.

Acknowledgements

The authors thank Dr Shafia Súcar Súccar for her help in preparing this manuscript. This study was financed by CONACYT as part of project 3177-A.

References

[1] Z. Hubicki, H. Hubicka, Hydrometallurgy 40 (1996) 65.
[2] K.C. Sole, J.B. Hiskey, Hydrometallurgy 30 (1992) 345.
[3] M. Avila-Rodríguez, G. Cote, D. Bauer, Solv. Extr. Ion Exch. 10 (1992) 811.
[4] A. Almela, M.P. Elizalde, Hydrometallurgy 37 (1995) 47.
[5] W.A. Rickelton, R.J. Boyle, Solv. Extr. Ion Exch. 8 (1990) 783.
[6] I.V. Pyanitskii, Analytical Chemistry of Cobalt, 1a de., Arbor-Humphrey, Israel, 1969, p. 48.
[7] B.K. Tait, Hydrometallurgy 32 (1993) 365.
[8] T.F. Brown, L.K. Zeringue, Commun. Soil. Sci. Plant Anal. 22 (1991) 399.
[9] E.Y. Tserovski, S. Arpadzhan, D.L. Tsalev, Spectrosc. Lett. 25 (1992) 693.
[10] M. Akhoond, A.A. Ensafi, A. Massoumi, A. Safavi, Microchem. J. 45 (1992) 365.
[11] A.K. Chakrabarti, J. Inst. Chem. (India) 63 (1991) 177.
[12] A.K. Chakrabarti, J. Inst. Chem. (India) 63 (1991) 145.
[13] M. Kauppinen, K. Smolander, Anal. Chim. Acta 285 (1994) 45.
[14] A.K. Covington, R.A. Matheson, J. Sol. Chem. 6 (1977) 263.
[15] B.R. Staples, J. Phys. Chem. Ref. Data 10 (1981) 779.
[16] E. Högfelt, Stability Constants of Metal-Ion Complexes, Part A. Inorganic Ligands, IUPAC Chemical Data Series, No. 21, Pergamon, Oxford, 1982.
[17] P.W. Linder, K. Murray, Talanta 29 (1982) 377.

.

ELSEVIER

Talanta 45 (1998) 883–890

Talanta

Accelerated dynamic leaching of iron from soil with on-line derivatization and integrated concentration–detection

M.M. Jiménez-Carmona *, M.P. da Silva [1], M.D. Luque de Castro

Department of Analytical Chemistry, Faculty of Sciences, University of Córdoba, E-14004, Córdoba, Spain

Received 26 November 1996; received in revised form 24 February 1997; accepted 10 June 1997

Abstract

A module for continuous high pressure–temperature leaching is proposed. The overall approach involves the coupling of an extractor with a continuous-flow manifold where the analyte forms a complex with SCN^-, which is driven to a flow-cell packed with a suitable material for retention and continuous monitoring of this process which in turn is a way for indirect monitoring of the leaching kinetics. The approach has been used for the determination of iron in soil after leaching and derivatization. The sensitivity of the method (ng level) and the short time required (only 15 min versus 24 h for leaching and 30 min for the measurement step required by the conventional method), together with its precision (RSD less than 9%) makes this method an excellent alternative to the conventional procedure. © 1998 Elsevier Science B.V.

Keywords: Accelerated leaching; Iron; Soil; Integrated retention–detection

1. Introduction

The pretreatment of solid samples is the Aquilles' heel of analytical processes as this is the most time consuming, diversified and tedious step. A number of energy sources have been proposed in the last few years with the aim of shortening the time required for pretreatment. Thus, ultrasounds [1–3], microwaves irradiation both mono- [4–6] and multimode versions [7,8] in open and closed vessels have been used with excellent results. Supercritical fluid extraction using different fluids as extractants but preferably SC–CO_2, modified [9,10] or not [11,12], has resulted to be an excellent alternative, particularly when non-polar and medium polar analytes are involved. Liquid water at high temperature and pressure seems to be an advantageous alternative to other solid sample pretreatments, particularly when the analytes to be removed are polar or ionic. A major shortcoming of the last approach is the high dilution undergone by the extracted analytes, which require to be concentrated after monitoring [13–15]. Lasers are very energetic sources for helping solid sample pretreatment such as leaching [16], desorption [17] and ablation [18,19], but the high cost of the equipment makes their general use forbidden.

* Corresponding author.

[1] address: Department of Analytical Chemistry and Instrumental Analysis, Faculty of Sciences, UAM, E-28049, Madrid, Spain.

PII S0039-9140(97)00185-9

In order to circumvent the problems inherent to the use of water as leaching agent, we have coupled a subcritical-water extractor to a continuous flow manifold (FI) and photometric detector furnished with a flow-cell packed with exchanger material for the analysis of iron in soil. The aim of this coupling has been to achieve continuous concentration–detection of the target analyte, thus showing when the leaching step is finished.

2. Experimental

2.1. Instruments

A Knauer 64 HPLC pump with digital flow-rate and pressure readouts was used in order to impel the leaching agent.

The extractor used is a prototype designed and patented by Salvador and Merchán [20], consisting of a stainless steel cylindrical extraction chamber (8 cm in length and 3 mm i.d.), and closed with two screw caps at either end that permit the circulation of the leaching fluid through them. Both screw caps also contain stainless steel filter plates (2 μm in thickness and 1/4″ i.d.) to ensure that the solid sample will remain in the leaching chamber. This chamber, together with a stainless steel preheater, is located in an oven which can work up to 300°C. This variable was controlled using a Toho TC-22 temperature controller.

A cooler system (consisting of a coil coupled to an Ultraterm 6000383 P-Selecta recirculation bath) was used in order to cool the fluid from the oven to a temperature close to 25°C before entering the flow manifold. The outlet of this coil was coupled to a home-made variable restrictor in order to control the pressure in the leaching chamber. The leaching agent leaving the restrictor was collected in a debubbler which avoided the arrival of bubbles to the detector. The collector was laboratory made from a glass test-tube (9.5 cm in length and 1.3 mm i.d.) with Teflon tubing (0.8 mm i.d.) fitted at its bottom. This device drove the solution from the debubbler to the flow manifold.

A Gilson Minitpuls-3 low-pressure peristaltic pump, two Rheodyne 5041 low-pressure injection valves (one of them acting as a switching valve) and Teflon tubing of 0.8 mm i.d. were used to build the flow manifold, which was connected to a Unicam 8625 UV-visible spectrophotometer furnished with a Hellma 178.52QS flow-cell (1.5 mm path length, 25 μl inner volume) containing the anion exchanger, and connected to a Kipp-Zonne recorder.

2.2. Materials

Stock standard solution of Fe (1 g l^{-1}) was prepared by dissolving the pure metal (Merck) in 1:5 HNO_3–H_2O. The anion exchanger was a Dowex-1 resin (Merck) with a mesh size of 200 and a cross-linkage of two. The derivatizing solution was prepared by dissolving 0.5 M ammonium thiocyanate (Merck) in 0.5 M hydrochloric acid. An aqueous solution of 0.2 M sodium fluoride and 0.3 M ammonium thiocyanate (both from Merck) was used as eluent.

Diatomaceous earth (Sigma) was used as matrix in the leaching step for optimization of the extraction variables.

Bidistilled degassed water purified through a Milli-Q deionizing unit (Millipore) was used as leaching agent.

2.3. Preparation of the reaction–detection unit

The resin was first cleaned with Milli-Q water and then conditioned by triplicate treatment with 4 M hydrochloric acid, 2 M sodium hydroxide, Milli-Q water and 4 M hydrochloric acid, which converted the resin into the chloride form [21]. In order to pack the flow-cell, the outlet of a Hellma cell (25 μl capacity) was packed with glass wool to avoid washout of the resin. The cell itself was packed with resin up to 0.9 cm from the bottom, so that the light beam passed through the upper part of the packed material. The resin required a 5-min interval with the solution flowing through the cell for proper packing.

2.4. Preparation of the spiked matrix for the optimization of the leaching variables

The solid matrix (0.13 g of diatomaceous earth) was spiked with 200 μl of a 2500 ng ml^{-1} Fe(III) solution. After support-solution homogenization, the mixture was introduced into the leaching chamber aided by a funnel.

2.5. Procedures for the determination of iron in soil

2.5.1. Standard procedure

The soil was dried and mixed with water. The suspension thus obtained was stirred for 24 h. The extract was filtered through paper and the analyte (Fe) was determined by AAS using a suitable standard. The result was expressed as μg g^{-1} (ppm).

2.5.2. Automated procedure

The method was developed using the assembly shown in Fig. 1, based on the coupling of the leaching and the retention–detection approaches, as follows: degassed Milli-Q water stored in a reservoir is impelled by the HPLC pump to the oven, where it reaches the preheater and passes through the 1-ml leaching chamber which contains 0.13 g of the soil–diatomaceous earth mixture. The leached Fe is cooled in the refrigerant at 25°C and, after passing the debubbler, is mixed at point M with the reagent solution (0.5 M ammonium thiocyanate-0.5 M hydrochloric acid). The Fe(III)-thiocyanate complex formed in the mixing coil (L, 60 cm in length, 0.5 mm i.d.) is retained on a Dowex 1X2-200 anion exchanger located in the flow-cell, and monitored spectrophotometrically ($\lambda = 480$ nm). After leaching, the valve SV is switched so that the thiocyanate complex is quickly eluted both by formation of the iron-fluoride complex and ionic displacement from the resin.

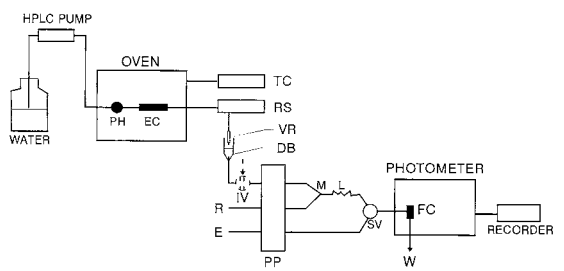

Fig. 1. On-line coupling of a subcritical water extractor with a FI manifold and an integrated retention–detection unit for the determination of iron in soils. PH, preheater; EC, leaching chamber; TC, temperature controller; RS, refrigerant system; VR, variable restrictor; DB, debubbler; R, reagent; E, eluent; PP, peristaltic pump; M, mixing point; L, mixing coil; SV, selecting valve; IV, injection valve; FC, flow-cell; W, waste.

3. Results and discussion

A preliminary study was performed in order to establish the optimum approach to be used with the double aim of concentrating the diluted analyte from the leaching chamber and monitoring the leaching kinetics. Two continuous approaches were tested:

3.0.1. Continuous percolation

Continuous percolation of the solution emerging from the leaching chamber through the conventional photometric cell containing an immiscible solvent with a dissolved complexing agent (CCl_4-ditizone). A two-tube system inside the photometric cell was used according to Agudo et al. [22]. One of the tubes came from the FI system and reached the bottom of the cell thus enabling maximum percolation of the leaching solution. The other tube had one of its ends ca. 2 mm above the level of the organic solvent and the other connected to a pump tubing in order to aspirate the aqueous phase after percolation. The light beam passed through the organic phase and monitored the formation of the Fe-ditizone complex. The enrichment of the organic solution in the analyte was not favourable due to the small value of the formation constant of the Fe-ditizone complex [determination range of Fe(III) in an aqueous solution at the μg ml^{-1} level]. After completion of the leaching step, when the recording reached a plateau, the photometric cell was manually washed with HNO_3 and then rinsed thoroughly with distilled water.

Table 1
Optimisation of variables

Step	Variable	Range studied	Optimum value
Detection	Height of resin, cm	0–1.2	0.9
Complex formation	[NH_4SCN], M	0.3–0.6	0.5
	[HCl], M	0.1–1.0	0.5
Elution	[NaF], M	0.1–0.3	0.2
	[NH_4SCN], M	0.2–0.4	0.3
Transport	Length of L, cm	15–120	60
	Sample volume, ml	0.5–1.2	1.0
	Flow-rate, ml min^{-1}	1.0–4.0	4.0
Leaching	Temperature, °C	50–250	250
	Pressure, bar	0–350	100
	Flow-rate, ml min^{-1}	1.0–4.0	4.0

3.0.2. Continuous retention–detection

Continuous retention–detection based on, i) merging of the solution from the leaching chamber with a stream of SCN^- in acidic medium, which yielded the red complex along the coil between the restrictor outlet and the detector [15,23] (see Fig. 1), according to the reaction:

$$Fe^{3+} + 4SCN^- = Fe(SCN)_4^- \qquad K_f = 10^{0.8} \quad (1)$$

ii) retention of the complex on an ion-exchanger material packed in the flow-cell, with continuous detection of the in situ concentrated product:

$$[Fe(SCN)_4^-]_{solution} = [Fe(SCN)_4^-]_{resin} \quad (2)$$

After completion of the leaching step (that is, when the recording of the process reached a plateau) a selecting valve enabled to remove the retained complex in an automatic way by displacement of the former ligand (SCN^-) by F^-, which provided a stronger complex with Fe(III), according to the reaction:

$$[Fe(SCN)_4^-]_{resin} + F^- = FeF^{2+} + 4SCN^-$$

$$K_{f(FeF)} = 10^{5.2} \quad (3)$$

This approach enabled the determination of Fe(III) from a solution at the ng ml^{-1} level. This was the approach selected for the development of the method due to the higher sensitivity and automation it provided.

3.1. Optimization of variables

The experimental variables were optimized in order to maximize recovery of Fe in a time interval as short as possible. The univariate method was used for this purpose. Ranges over which the effect of the variables were studied and the optimum values found are shown in Table 1.

3.1.1. Detection variables

A Dowex 1 resin (mesh size 200, cross-linkage 2) was selected as solid support in the flow-cell as proposed by Lázaro et al. [2]. The support level in the flow-cell was a key variable: once it is packed with the resin, the light beam must cross through the upper part of the packed resin, as close to the surface as possible, but without surpassing the support–solution interphase. A resin layer of 0.9 cm (from the bottom) was the optimal as it provided the highest analytical signal for the iron-thiocyanate complex. When the packed material bed was higher, the complex was retained first in the resin region above the light beam (and the analytical signal was small); with lower levels the light beam passed through the solution only, so the concentration effect was not detected.

3.1.2. Complex formation

The concentration of NH_4SCN in the solution was studied in the range 0.3–0.6 M, and the highest signal was obtained for 0.5 M. The HCl

concentration in the reagent solution was studied between 0.1–1.0 M. The signal increased with increased HCl concentration, but levelled off above 0.5 M. Thus, a 0.5 M NH_4SCN-0.5 M HCl solution was used as colour-former reagent.

3.1.3. Elution variables

Fluoride was used as eluent by displacing SCN^-, thus given rise to a catonic complex which was not retained by the resin. A 0.2 M solution provided an instantaneous elution. The solution was also 0.3 M in NH_4SCN in order to keep constant the ionic strength between the detection and elution steps, thus avoiding changes in the resin swelling.

3.1.4. Transport variables

The flow-rate of the continuous manifold was adjusted at that of the dynamic extractor in all instances by using either pump tubes of different inner diameter or different rotation speed of the peristaltic pump. After fixing the flow-rate, the residence time of the extract–reagent mixture in the manifold, and thus the development of the derivatizing reaction, was a function of the reactor length. Once optimized, the flow manifold in Fig. 1 was modified with an additional valve (dashed lines in Fig. 1), which was used for establishment of the analytical signal corresponding to a 100% leaching. With this aim, an amount of iron equal to that to be introduced into the extraction chamber and mixed with the solid matrix (diatomaceous earth) was inserted through the injection valve. The signal thus obtained corresponded to a 100% recovery of the analyte leached as checked by the following experiment: the same amount of Fe(III) was diluted to 0.5, 0.7, 1.0, and 2.5 ml and injected into the FI manifold. The same absorbance was obtained in the plateaux corresponding to the different dilutions of the analyte, thus proving that the kinetics of the retention step is fast enough and the Eq. (2) is rapidly established.

3.1.5. Leaching variables

Once the working conditions in the flow manifold were established, the optimization of the variables affecting the leaching step was carried out, using as sample diatomaceous earth spiked with the iron solution. The variables studied concerned to both those of the leaching agent (temperature, pressure and composition of the leacher), and dynamic variables (leaching time and flow-rate of the leaching agent).

After optimization of each variable its optimal value was selected for further experiments. The leaching-time was always kept shorter than that providing a 100% recovery of the analyte in order to detect improvements of the leaching process when the values of the variables were changed.

3.1.6. Temperature

The effect of water temperature (at a constant flow-rate of 4 ml min^{-1} and a pressure of ca. 100 bar) is shown in Table 2. Triplicate extractions were performed for 10 min each, and values of 50, 100, 200 and 250°C were assayed. The increase in temperature resulted in increased recovery through the range studied. The highest analytical signal was obtained at 250°C, so this value was selected as optimum.

3.1.7. Pressure

To determine the effect of this variable, a home-made variable restrictor was used, whose diameter was modified manually. This device allows the pressure in the leaching chamber to be modified. Leachings were performed at a flow-rate of 4 ml min^{-1}, a leaching time of 10 min and a constant temperature of 250°C. Values of 2, 100 and 220 bar were assayed and the recoveries obtained were 23, 76 and 78%, respectively. The

Table 2
Effect of temperature in the recovery of iron from diatomaceous earth[a]

Temperature, °C	%Recovery	SD*
50	18.2	2.4
100	30.8	0.7
150	61.6	2.2
200	71.8	6.4
250	79.8	5.8

[a] Working conditions: pressure, 100 bar; water flow-rate, 4 ml min^{-1}; leaching time, 10 min.
* $n = 3$.

presence of steam, at 2 bar, decreased the recovery drastically, but when the water was liquid (100 and 220 bar) the small increase in density due to the increase of the pressure had not significant influence on the recovery. So, a value of 100 bar was chosen for the development of the method.

3.1.8. Flow-rate

10-min leachings were performed at a constant temperature and pressure of 250°C and 100 bar, respectively, using values of flow-rate of 1, 2, 3 and 4 ml min^{-1}. The recoveries obtained were 28, 55, 78 and 95%, respectively, so a flow-rate of 4 ml min^{-1} was selected.

3.1.9. Composition of the leaching solution

Two leaching aqueous solutions (0.5 M CH_3COONH_4 and 0.5 M NH_4SCN) were tested under the optimal working conditions with the aim of accelerate the removal of the analyte as compared with the use of pure water as leaching agent. The use of acetate was unfeasible in the proposed approach as the complex formed between this anion and the analyte is more stable than that with SCN^- ($K_{f[(CH3COO)3Fe]} = 10^{8.7}$ versus $K_{fFe(SCN)4-} = 10^{5.2}$). There was no displacement reaction along the dynamic manifold, so no response in the detection system at 480 nm (maximum of the Fe-SCN^-) was obtained. On the other hand, when the SCN^- solution was used as leacher the signal was higher than that obtained for the same amount of iron inserted through the injection valve. This fact was probably due to the high temperature in the leaching system (250°C) which favoured the formation of the Fe-SCN^- complex with respect to the equilibrium reached in the flow-manifold, where the iron was injected at room temperature in the calibration step. Thus, none of the leaching agents could be used, and water was the agent selected.

3.1.10. Leaching-time

The recovery of iron from diatomaceous earth under optimal working conditions was quantitative (99.8%) when the leaching-time was 15 min, so this value was selected for the development of the method.

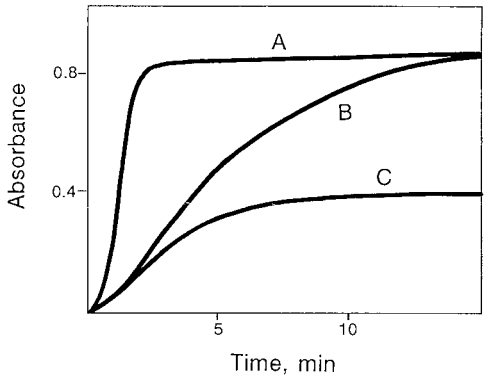

Fig. 2. Analytical signals obtained for (A) direct injection of 500 ng of Fe(III) in the FI system. (B) leaching of 500 ng of Fe(III) added to 0.13 g of diatomaceous earth under optimum working conditions. (C) leaching of 220 ng of Fe(III) from a soil.

3.2. Features of the method

The calibration graph was run by injecting in duplicate standard solutions into the flow manifold. The range of linearity is 80–600 ng of Fe, the equation obtained is $Y = 1.53 \times 10^{-2} + 0.95m$ (where Y is the absorbance on the plateau and m is the mass of Fe in μg), and the regression coefficient is 0.9995. The proposed method has a good sensitivity, with detection and determination limits of 50 and 80 ng ml^{-1}, respectively.

The repeatability, expressed as RSD, of both the detection system and the overall process was studied. The precision of the flow-manifold used for derivatization–concentration–detection was obtained by injecting standard solutions of 200 ng ml^{-1} Fe(III). The RSD was 1.62% for $n = 13$. The precision of the overall method (leaching and sensor system) was tested by leaching 500 ng of Fe(III) added to 0.13 g of diatomaceous earth under the optimal working conditions. The average recovery thus obtained was 99.8%, and the RSD was 3.69% for $n = 6$.

The recordings obtained by direct injection of 500 ng of the analyte into the FI manifold and that obtained after leaching of 500 ng of iron spiked on diatomaceous earth are shown in Fig. 2, curves A and B, respectively. As can be seen, the leaching kinetics of the process is showed by the

rising portion of the curve whose slope is less sharp than that obtained by injecting the same amount of the target analyte in a 200 μl volume (also the injected analyte reached the detector within a shorter time). Fig. 2 also shows that the leaching is complete after 15-min as the same final absorbance is obtained in both cases.

3.3. Application of the method

The performance of the proposed method was tested by applying it to the analyses of five soils from Laguna de la Vaca, Huelva (South-West, Spain), whose contents in Fe were previously determined by the manual standard method as described under experimental. As the concentration of Fe found was at the μg ml^{-1} level, a previous dilution was required in order to fit the concentration to the linear range of the method. With this purpose, the suitable amount of soil was mixed with inert support (diatomaceous earth). The recording provided by one of these samples is shown in Fig. 2C. The results obtained, in comparison with those provided by the manual method and the SD for each sample are shown in Table 3. The results obtained by both methods were similar and the precision was quite good, particularly at the lower concentration level.

4. Conclusions

A new method is proposed for the analysis of iron from soils, which enables a dramatic decrease of the pretreatment time. The accelerated dynamic leaching of the analyte was accomplished using liquid water at high temperature and pressure. In this way, a leaching-time of 15 min, versus 24 h of the standard method, was achieved. The advantage of dynamic versus static-closed vessel leaching is a faster, complete removal of the analyte as the sample always is in contact with clean extractant thus displacing the analyte- matrix/analyte-extractant equilibrium to the latter. A major drawback of dynamic leaching (namely, the higher analyte dilution) is circumvented by a concentration step integrated with the detection which, in addition, enables the kinetics of the leaching step to be monitored. The excellent agreement of the results obtained as compared with those provided by the standard manual method certified its usefulness as an alternative to its time consuming manual counterpart.

Table 3
Determination of Fe in soil (concentration of Fe in μg g^{-1})

Soil	Standard method	Proposed method $\pm$SD*
1	11.3	11.8 ± 0.3
2	15.1	15.7 ± 0.7
3	33.5	32.4 ± 1.3
4	37.9	39.1 ± 2.1
5	68.2	70.8 ± 6.2

* $n = 3$

Acknowledgements

The Comisión Interministerial de Ciencia y Tecnología (CICyT) is thanked for financial support (Project No. PB95-1265).

References

[1] P. Linares, F. Lázaro, M.D. Luque de Castro, M. Valcárcel, J. Autom. Chem. 10 (1988) 88.
[2] F. Lázaro, M.D. Luque de Castro, M. Valcárcel, Anal. Chim. Acta 242 (1991) 283.
[3] T.F. Jenkins, C.L. Grant, Anal. Chem. 59 (1987) 1326.
[4] L.I. Pleskach, E.P. Ezhova, G.D. Chirkova, Zh. Anal. Khim. 45 (6) (1990) 1092.
[5] P. Torres, E. Ballesteros, M.D. Luque de Castro, Anal. Chim. Acta 308 (1995) 371.
[6] D.W. Bryce, A. Izquierdo, M.D. Luque de Castro, Anal. Chim. Acta 324 (1996) 69.
[7] J. Paré, U.S. Patent 5 002 784, 26 March 1991.
[8] V. López-Ávila, R. Young, N. Teplitsky, J. Ass. Anal. Chem. Int. 79 (1996) 142.
[9] M.D. Luque de Castro, M.T. Tena, Trends Anal. Chem. 15 (1) (1996) 32.
[10] K. Sugiyama, J. Chromatogr. 332 (1985) 17.
[11] A. Izquierdo, M.T. Tena, M.D. Luque de Castro, M. Valcárcel, Chromatographia 42 (1996) 206.
[12] M.T. Tena, M.D. Luque de Castro, M. Valcárcel, Anal. Chem. 68 (1996) 2386.
[13] S.B. Hawthorne, Y. Yang, D.J. Miller, Anal. Chem. 66 (1994) 2912.

[14] Y. Yang, S. Bowadt, S.B. Hawthorne, D.J. Miller, Anal. Chem. 67 (1995) 4571.
[15] M.M. Jiménez-Carmona, M.D. Luque de Castro, Anal. Chim. Acta 342 (1997) 215.
[16] B.K. Zuev, L.E. Kordonskii, I.L. Skbyabin, Zh. Anal. Khim. 46 (7) (1991) 1268.
[17] L.J. Kovalenko, C.R. Maeching, S.J. Chemett, J.M. Philippoz, R.N. Zare, Anal. Chem. 64 (1992) 682.
[18] M.A. Shannon, X.L. Mao, A. Fernández, W.T. Chan, R.E. Russo, Anal. Chem. 67 (1995) 4522.
[19] S. Nakamura, Y. Ito, K. Sone, H. Hiraga, K. Kaneko, Anal. Chem. 68 (1996) 2981.
[20] F. Salvador and M.D. Merchán, USA Patent 5 400 642, 1995.
[21] M. Marhol, Ion Exchangers in Analytical Chemistry, Elsevier, Amsterdam, 1982, p. 85.
[22] M. Agudo, A. Ríos, M. Valcárcel, Anal. Chem. 65 (1993) 2941.
[23] M. Valcárcel, M.D. Luque de Castro, Flow-through (Bio)chemical Sensors, Elsevier, Amsterdam, 1994.

.

ELSEVIER

Talanta 45 (1998) 891–898

Talanta

PEG-modified glucose oxidase immobilized on a PVA cryogel membrane for amperometric biosensor applications

Lucio Doretti [a,*], Daniela Ferrara [a], Paola Gattolin [a], Silvano Lora [b], Franco Schiavon [c], Francesco M. Veronese [c]

[a] *Ufficio Sicurezza e Prevenzione del CNR, Corso Stati Uniti 4, 35127 Padova, Italy*
[b] *Istituto di Fotochimica e Radiazioni d'Alta Energia del CNR, Sezione di Legnaro, Via Romea 4, 35020 Legnaro (Padova), Italy*
[c] *Dipartimento di Scienze Farmaceutiche, Università di Padova, Via Marzolo 5, 35131 Padova, Italy*

Received 14 February 1997; received in revised form 10 June 1997; accepted 12 June 1997

Abstract

Poly(ethylene glycol)-modified glucose oxidase was immobilized in a poly(vinyl alcohol) cryogel membrane, obtained by a freezing–thawing cyclic process, to obtain a suitable amperometric glucose sensor. The covalent linkage between PEG and GOD molecule improved the physical immobilization of enzyme in the polymeric matrix, by decreasing its loss in time. Sensor behaviour was evaluated electrochemically with a hydrogen peroxide electrode. The glucose content in standard solutions was determined and linear calibration curves in the 5×10^{-5}–5×10^{-3} mol l^{-1} range were obtained. The kinetic parameters in the immobilized system were evaluated and analytical characteristics of sensor, including stability and influence of pH and temperature, were determined. © 1998 Elsevier Science B.V.

Keywords: Biosensors; Glucose oxidase; PEG-modified glucose oxidase; PVA cryogel

1. Introduction

Enzyme-based amperometric sensors are being used in an increasing number of clinical, environmental and biotechnological applications.

Generally, physical entrapment of enzyme molecules in polymeric membranes is one of the most advantageous methods because it is rapid and simple, the retained activity is high and no chemical bonds are required.

Pursuing our interest for biocompatible membrane electrodes, recently we immobilized glucose oxidase (GOD) in poly(vinyl alcohol) (PVA) cryogels obtained by freezing–thawing cyclic processing [1].

Poly(vinyl alcohol) is a biocompatible polymer [2], that is considered an appropriate matrix for sensor preparation.

Several authors demonstrated the possibility of immobilizing enzymes in PVA matrices by means of different methods (cross-linking with aromatic tri-isocyanates, gamma or UV irradiation etc.) and realized suitable biosensors [3–9].

The method proposed in the previous paper [1] for enzyme immobilization in PVA hydrogels was characterized by the absence of chemical initiators

* Corresponding author. Fax: + 39 49 8295662.

PII S0039-9140(97)00191-4

or cross-linking agents that could leave residual materials dangerous in biological applications. The subjection of aqueous PVA solutions to several freezing–thawing cycles led to reinforced gels owing to the densification of the macromolecular structure [10,11]. The chains were physically cross-linked by semi-permanent entanglements, molecular associations or crystallites.

GOD immobilized in PVA cryogel membranes was used to assemble an amperometric sensor measuring hydrogen peroxide produced in the enzymatic reaction.

The obtained biosensor showed good performances concerning response time, magnitude of electrochemical signal and linear range, but the membranes kept under control for a two month period showed an enzyme leakage of about 5–10% with respect to the activity measured before use. This kind of leakage had no effect on analytical performances, but it could perhaps be a problem when proposing the biocompatibility of the system.

In order to improve the characteristics of biocompatibility so as to prevent all the enzyme leakage, poly(ethylene glycol)-modified glucose oxidase was immobilized in a PVA cryogel membrane.

Poly(ethylene glycol) may be covalently bound to proteins by means the end chain terminating hydroxylic groups that are properly activated to react with nucleophiles in proteins, usually available amino groups [12–14].

Once bound to proteins the PEG chains create a hydrophilic water cloud that prevents the approach of proteolytic enzymes as well as antibodies or immunocompetent cells.

This procedure reduces the immunogenicity of the enzyme and may helpfully reduce the protein leakage for the possible interconnecting twisting of PEG on PVA chains.

An amperometric sensor was constructed by using PEG-modified GOD immobilized in PVA membranes obtained by freezing–thawing cyclic process; the parameters that could affect the electrode performances were evaluated and compared with those of the sensor that used unmodified enzyme immobilized in the same PVA matrix.

2. Experimental

2.1. Reagents

Glucose oxidase (EC 1.1.3.4, type II-S from *Aspergillus niger*, 18 000 U g^{-1} solid), peroxidase (POD, EC 1.11.1.7, type VI from Horseradish, 250 purpurogallin U mg^{-1} solid), 4-aminoantipyrine, β-glucose, ascorbic acid, uric acid and acetaminophen were obtained from Sigma (St. Louis, MO). Stock solutions were prepared in bi-distilled water or buffer solution and stored in the dark at 4°C. Glucose solutions were allowed to mutarotate overnight at room temperature before use.

PVA with a MW = 124 000–186 000 and a degree of hydrolysis of 99% was purchased from Aldrich Chemie (Stenheim, Germany) and used without further purification.

Monomethoxypoly(ethylene glycol)-norleucine (PEG-Nleu) with an average MW = 5000 was obtained from Shearwater Pol. (Huntsville, USA).

Nafion perfluorinated ion-exchange resin (5% m/v in a mixture of lower aliphatic alcohols and 10% water), from Aldrich Chemie, was used as supplied.

All other analytical grade chemicals were purchased from Carlo Erba (Milano, Italy) or Merck (Darmstadt, Germany).

Control serum was manufactured by Technicon Instruments (Tarrytown, USA) and marketed by Bayer Diagnostics (Oreq-Tournai, Belgium).

2.2. Apparatus

The determination of hydrogen peroxide was performed in an electrochemical cell with a working volume of 20 ml, in a three-electrode configuration. The three electrodes were connected to an AMEL (Milano, Italy) 559 model potentiostat. A saturated calomel electrode and a platinum foil with a large surface area were used as the reference and counter electrode, respectively. All the experiments were carried out in a temperature-controlled cell using a Haake F3-C thermostatic bath.

Spectrophotometric measurements were carried out with a Hitachi U-3200 spectrophotometer equipped with a 1 cm thermostated cell.

The ultrafiltration was performed by means of an apparatus purchased from Amicon Italia (Passirana di Rho, Milano, Italy) equipped with a XM 30 membrane.

The separation and purification of the obtained PEG-GOD conjugates were carried out with a Pharmacia FPLC system (Pharmacia LKB Biotechnology, Uppsala, Sweden), equipped with a Superose 12 gel filtration column (2 × 50 cm, 100 ml h^{-1}).

2.3. GOD modification by PEG

Glucose oxidase (13.4 mg) was dissolved in a 0.2 M borate buffer (2 ml) at pH 8.0 and 49 mg of monomethoxypoly(ethylene glycol)-norleucine activated at the carboxylic group as hydroxysuccinimidyl ester were added in small portions. The mixture was maintained at room temperature for 12 h to complete the reaction and then transferred to an ultrafiltration apparatus. The solution was diluted with 10 ml of water and concentrated to about 1 ml under N_2 pressure; 10 ml of water were added to the residual solution that was concentrated again. This procedure was repeated three times. The concentrated and purified solution was finally chromatographed in a gel filtration column and the eluate was assayed at 280 nm for protein elution, with an iodine assay for the polymer [15] and for enzymatic activity for the conjugate.

The peak where protein and polymer were contemporaneously eluted was pooled and the enzymatic activity, protein and polymer concentration were evaluated. The modified GOD was maintained in a lyophylized state.

2.4. GOD immobilization and sensor preparation

PVA cryogel preparation and GOD immobilization were carried out as previously described [1]. An aqueous solution of 15% PVA in 0.1 M phosphate buffer at pH 6.0 was heated at 90°C to achieve complete polymer dissolution. When the solution had cooled to 30–35°C the appropriate amount of PEG-modified GOD (10 U g^{-1} of polymer solution) dissolved in few microliters of buffer was added. Polyethylene vials (5 mm i.d.) filled with the viscous honey-like solution were sonicated, left at −25°C for 16 h and then thawed at 4°C for 8 h. This process was repeated five times, finally the resulting sponge-like material was cooled at −20°C and sliced into about 120 μm discs with a microtome. The discs were carefully washed four times with a 0.1 M phosphate buffer (20 ml, pH 6.0) for 12 h at 4°C.

The working electrode was a platinum wire (0.5 mm diameter) sealed in a glass tube and polished with alumina powder to ensure a flat surface. A membrane disc, placed on the electrode surface and fixed with a Teflon cap having a 3 mm hole, formed the active sensor. When not in use the membranes were stored at 4°C in 0.1 M phosphate buffer at pH 6.0 or in a dry state.

2.5. Measurements of enzyme activity

Free glucose oxidase activity was determined as follows. The assay mixture containing 2 ml glucose solution (0.1 M in phosphate buffer, pH 6.0), 20 μl 4-aminoantipyrine solution (1% m/v), 40 μl of phenol solution (1% m/v), 100 μl POD (100 U purpurogallin U ml^{-1}) was incubated at 25°C for 5 min in a spectrophotometer. The reaction was initiated by the addition of an appropriate amount of the enzyme and the absorbance value was read at 500 nm. The apparent activity of the immobilized enzyme was determined by dipping a membrane in the above solution and incubating for 1 min, stirring at 25°C. After removing of the membrane, activity was calculated from the absorbance value at 500 nm.

3. Electrochemical measurements

Glucose determination was carried out electrochemically by measuring the hydrogen peroxide production as a result of the enzymatic reaction. This was done by immersing the sensor in stirred 0.1 M phosphate buffer at pH 6.0 and applying an oxidative potential of +600 mV against a saturated calomel electrode. When the background current had stabilized, an appropriate amount of substrate solution was introduced to give a preselected concentration. All measure-

ments were carried out using a thermostated bath at 25°C, unless otherwise mentioned.

4. Results and discussion

The described procedure produces a matrix of a physically cross-linked polymer containing uncrossed-linked polymer and water. The porous, hydrophilic and permeable membranes had interesting mechanical characteristics and could be handled easily; their properties were in detail described in the paper previously reported [1].

GOD immobilized in this matrix gave an amperometric sensor with good performance concerning response time, electrode response and linear range, but the membranes showed, in the long period, a slight leakage of enzyme compromising the biocompatibility of the system [1].

In order to improve the characteristics of biocompatibility, glucose oxidase modified with monomethoxypoly(ethylene glycol) was immobilized in PVA cryogel.

Activated PEG in a slight basic aqueous solution reacts specifically with strong nucleophiles in proteins, namely α-amino and ε-amino groups of lysine.

The reaction was carried out under mild basic conditions which were enough to speed up the aminolysis without inactivating the polymer reactive groups by hydrolysis.

Fig. 1A reports the elution pattern of the reaction product after the extensive ultrafiltration. As can be seen from the comparison with the elution pattern of unmodified glucose oxidase (Fig. 1B) all the enzyme is modified by PEG under the reported conditions, while only a small amount of unreacted PEG with low molecular weight is present. This, however, can be completely separated by gel filtration. The superimposable elution pattern of protein peak as revealed by iodine reaction indicates that eluted protein is enzymatically active and PEG is bound to it.

The evaluation of the number of bound PEG chains in the conjugate material present in the pooled peak, was carried out by the presence of norleucine, that is very useful for analytical purposes [16]. In the present case the amino acid composition, after acid hydrolysis, showed nine Nleu residues per protein molecule. This value indicated that nine PEG molecules were present in the conjugate.

Generally, the modification degree can be estimated by a colorimetric method based on the decrease in the number of amino groups following PEG binding [17]; this method uses the reactivity of these groups towards trinitrobenzene sulfonate. In this case, the number of the amino groups in GOD resulted apparently higher after modification. There is no plausible explanation for this behaviour which seemed to indicate that some masked amino groups came to light upon PEG binding, and thus available for the reaction with the colorimetric reagent.

The PEG binding was accompanied by the lowering of GOD enzymatic activity that droped to about 70–75% of the starting value.

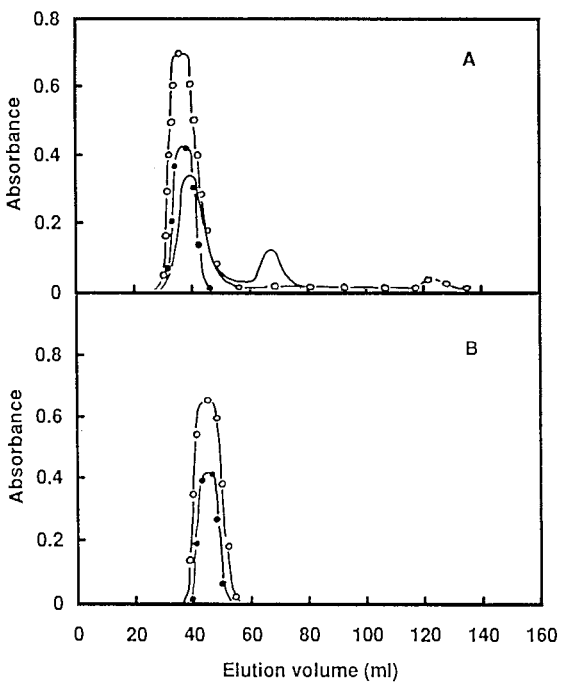

Fig. 1. (A) Elution pattern from a gel filtration column of the reaction product of glucose oxidase with activated PEG-Nleu. The eluate was analysed by reading at 280 nm (○) to detect the elution of the protein, by iodine reaction (——) to detect the PEG and by enzymatic activity (●). (B) Elution pattern of unmodified glucose oxidase. The eluate was analysed as in A.

Decrease in enzyme activity is a common phenomenon in enzyme conjugation to polymer and is usually interpreted, either as the minor modification in the enzyme tertiary structure that may be reflected in the distortion of amino acid residues involved in catalysis, or in the reduced binding of the substrate following a decrease in the positive charge of amino groups in acylation by PEG. In case of GOD, the first explanation seems to hold because glucose is a neutral molecule and would not be influenced by any charge modification on the enzyme surface. Losses in enzyme activity, generally observed in the modification of enzymes that are active towards larger molecular weight substrates, are instead interpreted on the basis of hindering the substrate's approaching the active site [18]. This however is not the case of GOD since glucose, because its size, may easily diffuse through PEG chains.

In order to measure the apparent activity of truly fixed PEG-modified GOD and to determine the percentage leakage from the gel, the following method was used. Some just sliced membranes were assayed for enzyme activity and then several membranes with a total weight of about 0.5 g were washed with a phosphate buffer (10 ml, pH 6.0) for 24 h, then the washing solution was assayed for enzyme activity. This process was repeated eight times, using the same matrix sample. After the last washing, the matrix was also assayed for apparent enzyme activity.

As shown in Fig. 2 with a PEG-modified enzyme loading of 10 U g^{-1} of polymeric solution, about 40% of the activity introduced passed into solution with the first two washings and about 45% was really fixed permanently in the matrix. It must be emphasized that the sum of activities measured in the washings and in the matrix was less than that introduced and this could be due to several reasons. First of all a reduction of about 10% of the original activity could be attributed to the freezing-thawing cyclic process; in fact, aqueous solutions of enzyme under the same experimental conditions showed an analogous decrease in enzyme activity. Secondly, the spectrophotometric determination of the activity in the polymeric matrix was difficult owing to the uncertain weight evaluation of the membrane due to the water uptake during swelling in solution and also a possible error in the absorbance measurement due to the partial adhesion of quinoneimine dye to the membrane surface.

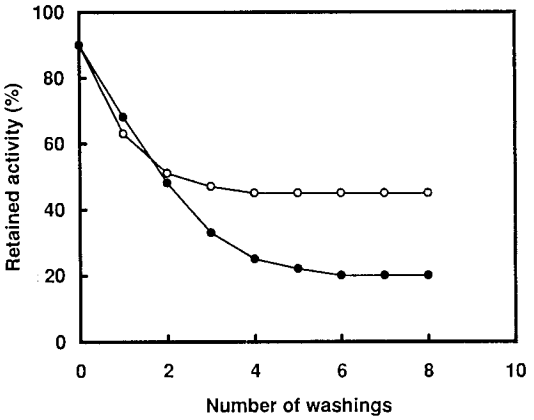

Fig. 2. Activity retention curves for the immobilized enzyme after repeated washings. (○) PEG-modified GOD, 10 U g^{-1} loading; (●) unmodified GOD, 10 U g^{-1} loading.

It is interesting to note that with an unmodified enzyme loading of 10 U g^{-1} the amount really fixed was only 20%.

Moreover some membranes (about 0.5 g) stored in a buffer solution (20 ml) after four washings and kept under control for eight weeks showed no enzyme leakage, whereas the same matrices with native GOD showed an enzyme leaking of about 5–10% after a two month period with respect to the activity measured in the matrix after six washings [1].

In PVA gel formation the gel reinforcement is believed to be caused by mechanisms involving hydrogen bonding and polymer crystallite formation [10]. The improved immobilization of PEG-modified enzyme suggests that the side chains of PEG get stuck among the physical cross-linked chains of the cryogel.

A further observation must be made with regard to the extent of modification that corresponds to an increase in GOD molecular weight of about 50 000 Da. Due to the flexibility of PEG chains that are highly hydrated and extended towards the water, widening the protein molecule, the final Stokes's radius of the conjugate may be very high.

All the following measurements were carried out with membranes obtained from a PEG-Nleu-modified enzyme loading of 10 U g^{-1} of polymer and washed four times with buffer solutions so that all unfixed GOD had been rinsed out.

The apparent activity of immobilized GOD in measured membranes (120 μm thickness and 5 mm diameter) used for the amperometric analysis was about 60 mU cm^{-2}. A typical calibration curve for glucose standard solutions, measured by anodic oxidation of H_2O_2, is shown in Fig. 3. The linearity was verified in the 5×10^{-5}–5×10^{-3} M range with a linear regression equation of $y = 0.044x - 0.002$, $R^2 = 0.9992$, where y was the current (μA) and x was the substrate concentration (mmol l^{-1}). A detection limit of 3×10^{-5} M was estimated with a signal-to-noise ratio > 3. The relative standard deviation for five replicate determinations of 1 mM glucose solution was $< 3\%$.

The electrochemical behaviour of this PEG-GOD-modified electrode was similar to that assembled with native enzyme immobilized in PVA cryogel [1]. The slope of the resulting calibration graph in the linear range, and hence the sensitivity, was 0.044 μA l $mmol^{-1}$. This lower response with respect to the reported sensor (0.141 μA l $mmol^{-1}$) was ascribed to the lower immobilized activity (60 mU cm^{-2} instead of 150 mU cm^{-2}).

The effect of substances which might interfere with the response of the electrode was examined.

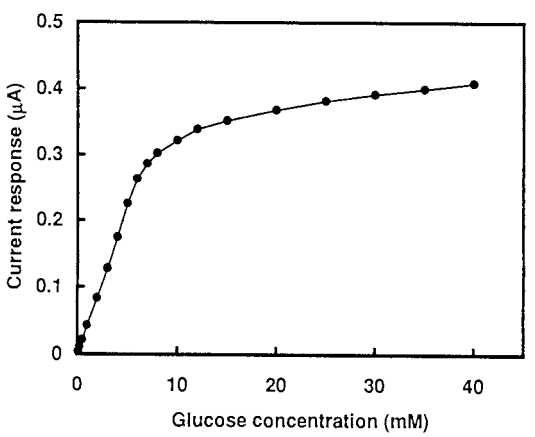

Fig. 3. Calibration graph for glucose obtained at pH 6.0 and 25°C.

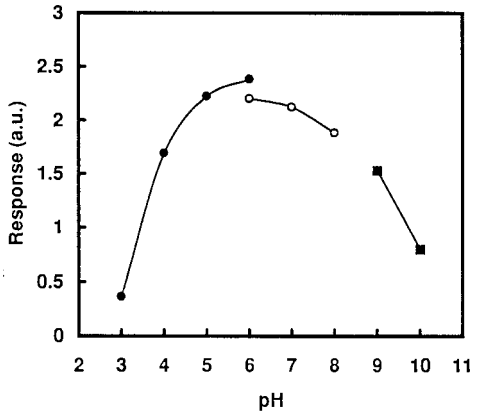

Fig. 4. Dependence of biosensor response on pH in 1 mM glucose solution at 25°C. (●) 0.1 M citrate, (○) 0.1 M phosphate and (■) 0.1 M carbonate buffer.

Ascorbate (0.25 mM), urate (0.15 mM) and acetaminophen (0.15 mM), three common interferents in biological samples, showed currents of 30, 10 and 40 nA respectively. After the electrode was covered with a Nafion film (about 150 μg) the responses to ascorbate, urate and acetaminophen were reduced to 3%, zero and 12% respectively. The sensitivity of the sensor to glucose was lowered of about 15%. This is probably due to the restricted diffusivity of hydrogen peroxide to the electrode surface owing to the presence of the additional film.

The sensor was characterized with regard to pH and temperature.

The pH effect was evaluated by using 0.1 M different buffers (citrate, phosphate and carbonate) with pH values ranging from 3.0 to 10.0. The results are shown in Fig. 4, each point being the mean of three determinations. The optimum pH was found at 6.0, while the free GOD shows a maximum acrivity around pH 5.5 [19,20]; this typical shift towards more alkaline values upon immobilization procedure may be ascribed to the interaction between the matrix and PEG-modified enzyme. A phosphate buffer (0.1 M pH 6.0) was selected for all the other experiments.

Fig. 5 shows the trend of the response as a function of temperature. The response increased gradually with a temperature increase from 15 to

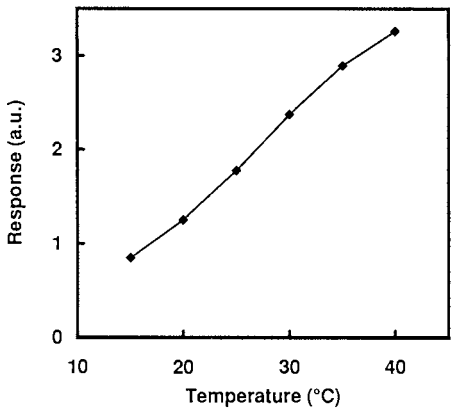

Fig. 5. Dependence of biosensor response on temperature in 1 mM glucose solution, pH 6.0.

40°C. In this range no irreversible modification to the system was observed; measurements carried out at 25°C with the same electrode again showed the original signal.

The glucose response curve can be described by the Michaelis–Menten equation expressed in the electrochemical Hanes form:

$$C/i = (C + Km_{(app)})/i_{max}$$

where C is the glucose concentration, i the steady-state current, i_{max} the maximum steady-state current and $Km_{(app)}$ the apparent Michaelis–Menten constant.

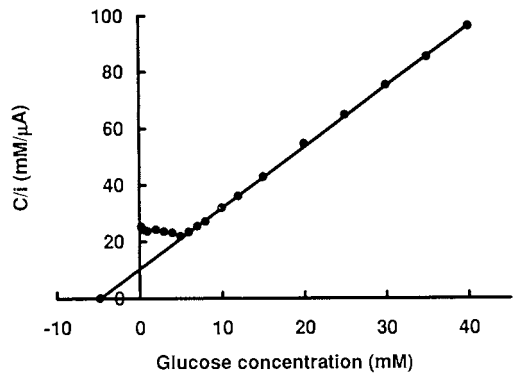

Fig. 6. Hanes plot of the calibration data for a glucose oxidase electrode.

The linear portion of the curve (Fig. 6), corresponding to the response in the kinetic regime, gave a value of 4.8 mM for $Km_{(app)}$ ($-x$ intercept) and 0.464 μA for i_{max} (reciprocal of the slope).

As was observed for the previously reported sensor utilizing native GOD, the apparent Michaelis–Menten constant calculated was also very low. The apparent Km obtained from Lineweaver–Burk double-reciprocal plots for the free native and PEG-modified glucose oxidase at 25°C in 0.1 M phosphate buffer (pH 6.0) was 30 mM for both enzyme types.

The high water content and hydroxyl groups in the polymer provides microenvironmental conditions that are particularly favourable for glucose oxidase.

The poor linearity observed in Fig. 6 seems to indicate diffusional limitations for lower glucose concentrations.

A low value for the apparent Michaelis–Menten constant implies more favourable conditions for GOD activity, but lowers the upper limit of the linear response range.

Since the response is modulated by the mass-transport through the membrane, the electrode signal is considerably influenced by the thickness of the enzyme layer. The electrode signal of ten membranes with the same diameter, average weight and presumably the same thickness showed a relative standard deviation less than 5%.

The response time was within 120 s and it remained unchanged for the entire life of the membranes.

In order to examine the long term stability of the enzyme membranes, they were stored in phosphate buffer (0.1 M, pH 6.0) at 4°C or in the dry state. In this latter case, the membranes, after rinsing with a buffer, were dried at 25°C and then stored at 4°C in a dessicator. Before being used they were equilibrated in a phosphate buffer for 1 h at room temperature. After 2 months, in both cases, the electrode signal decreased by about 5% in comparison with the initial value measured at a single concentration in the linear response range.

As it was observed in the previous paper [1], physical immobilization procedures are always connected with protein leakage on long term stor-

age, especially if there are modifications of ionic strength or pH values.

In the case of PEG-modified GOD, four washings seem to be enough to remove all the enzyme adsorbed and not permanently fixed on the polymer and the membranes stored in a buffer solution for eight weeks showed no enzyme leakage.

The electrode was finally successfully tested to determine glucose in a control serum. The results compared to those obtained for the same sample by the enzymatic-spectrophotometric method generally used in routine biomedical analysis are as follows.

Nominal value of serum = 4.17 mmol l^{-1} (scattering range 3.67–4.67 mmol l^{-1}); mean value found by spectrophotometric method (triplicate) = 3.85 ± 0.04 mmol l^{-1}; mean value found by amperometric method (triplicate) = 3.92 ± 0.08 mmol l^{-1}.

5. Conclusions

This work confirms the result that PVA cryogel obtained by a cyclic freezing-thawing process is a suitable material for the immobilization of GOD on an electrode surface.

The PEG-modification of glucose oxidase was found to produce a better immobilization on a polymeric matrix than unmodified enzyme, since the membranes show no enzyme leakage after a long period of storage.

Moreover the PEG chains bonded to enzyme create an hydrophilic water cloud that could prevent the approach of proteolytic enzymes or antibodies with the resulting reduction of the immunogenicity of the system.

The response time and other electrochemical characteristics of the biosensor are similar to those of sensor utilizing native GOD.

.

References

[1] L. Doretti, D. Ferrara, P. Gattolin, S. Lora, Talanta 44 (1997) 859.
[2] N. Minoura, in: T. Tsuruta, T. Hayashi, K. Kataoka, K. Ishihara, Y. Kimura (Eds.), Biomedical Applications of Polymeric Materials, CRC Press, Boca Raton, 1993 and references therein.
[3] K. Hajizadeh, H.B. Halsall, W.R. Heineman, Talanta 38 (1991) 37.
[4] C. Galiatsatos, C. Ikariyama, J.E. Mark, W.R. Heineman, Biosens. Bioelectron. 5 (1990) 47.
[5] K. Hajizadeh, H.B. Halsall, W.R. Heineman, Anal. Chim. Acta 423 (1991) 23.
[6] K. Imai, T. Shiomi, K. Uchida, M. Miya, Biotechnol. Bioeng. 28 (1986) 1721.
[7] Q. Deng, Y. Guo, S. Dong, Anal. Chim. Acta 319 (1996) 71.
[8] H. Lin, J. Qian, Y. Lin, T. Yu, J. Deng, Bioelectrochem. Bioenerg. 39 (1996) 303.
[9] K. Matsumoto, H. Mizuguchi, K. Ichimura, Kobunshi Ronbunshu 41 (1984) 221; Chem. Abstract 101 (1984) 86528s.
[10] N.A. Peppas, S.R. Stauffer, J. Control. Release 16 (1991) 305.
[11] S.R. Stauffer, N.A. Peppas, Polymer 33 (1992) 3932.
[12] S. Zilipski, C. Lee, in: J.M. Harris (Ed.), Poly(Ethylene Glycol) Chemistry: Biotechnical and Biomedical Applications, Plenum Press, New York, 1992, p. 347.
[13] F.M. Veronese, P. Caliceti, O. Schiavon, L. Sartore, in: J.M. Harris (Ed.), Poly(Ethylene Glycol) Chemistry: Biotechnical and Biomedical Applications, Plenum Press, New York, 1992, p. 127.
[14] C. Monfardini, O. Schiavon, P. Caliceti, M. Morpurgo, J.M. Harris, F.M. Veronese, Bioconjugate Chem. 6 (1995) 62.
[15] E.C. Sims, T.J. Snafe, Anal. Biochem. 107 (1980) 60.
[16] L. Sartore, P. Caliceti, O. Schiavon, C. Monfardini, F.M. Veronese, Appl. Biochem. Biotech. 31 (1991) 213.
[17] S.L. Snyder, P.Z. Sabacinsky, Anal. Biochem. 64 (1975) 284.
[18] P. Caliceti, O. Schiavon, L. Sartore, C. Monfardini, F.M. Veronese, J. Bioact. Compatible Polym. 8 (1993) 41.
[19] R. Wilson, A.P.F. Turner, Biosens. Bioelectron. 7 (1992) 165.
[20] G.G. Guibault, G.J. Lubrano, Anal. Chim. Acta 64 (1973) 439.

ELSEVIER

Talanta 45 (1998) 899–907

Talanta

Simultaneous fluorometric determination of nalidixic acid and 7-hydroxymethylnalidixic acid by partial least squares calibration

Isabel Durán Merás *, Arsenio Muñoz de la Peña, María Isabel Rodriguez Cáceres, Francisco Salinas López

Department of Analytical Chemistry, University of Extremadura, 06071, Badajoz, Spain

Received 3 March 1997; received in revised form 3 June 1997; accepted 12 June 1997

Abstract

The resolution of binary mixtures of nalidixic acid (NA) and 7-hydroxymethylnalidixic acid (OH–NA) has been accomplished by partial least squares (PLS) and principal component regression (PCR) multivariate calibration. The method of determination is based on the fluorescence emission of these compounds in the presence of γ-cyclodextrin (γ-CD). The formation of the inclusion compounds gives rise to an increase of the fluorescence emission compared to aqueous solution. The total luminescence information of the compounds has been used to optimize the spectral data set to perform the calibration. A comparison between the predictive ability of three multivariate calibration methods, PLS-1, PLS-2 and PCR, on three spectral data sets, excitation, emission and synchronous spectra has been performed. The PLS-1 method, applied to the emission spectra, has been selected as optimum. The proposed method has been applied to the simultaneous determination of NA and OH–NA in urine. Recovery values from urine samples containing (NA) and (OH–NA) range from 91 to 103% (mean 97%), and from 92 to 105% (mean 99%), respectively. © 1998 Elsevier Science B.V.

Keywords: Nalidixic acid; 7-Hydroxymethylnalidixic acid; Fluorometry; Partial least squares

1. Introduction

Nalidixic acid (NA) and 7-hydroxymethylnalidixic acid (OH–NA) are synthetic chemotherapic derivatives of the quinolonic acid. OH–NA is the major metabolite of NA, in man and animals. McChesney et al. [1] found that between 80–94% of the total NA excreted, is eliminated as OH–NA. Both compounds are antibacterial agents, and have been extensively used in the treatment of Gram-negative urinary tract infections [2]. They are also widely used for the prevention and treatment of infection diseases cultured fish. Almost all the studies about their form of action have been made with NA, and the results point to their influence on the DNA replication in the sensible microorganisms, being the urine their major via of elimination [3]. In patients under

* Corresponding author.

PII S0039-9140(97)00184-7

treatment with these compounds, adverse reactions involving the gastro-intestinal tract (nausea, vomiting), the skin or the central nervous system, have been observed in a relatively high proportion (5–10%). The determination of these compounds in serum, plasma and urine usually involves fluorometric methods [1,4–7], and HPLC methods with UV detection [8–11].

The use of mathematical algorithms formerly employed in other branches of science, has boosted advances in analytical determination methods, by processing the information typically produced by the instrumentation. First-order multivariate calibration methods, such as the classical least-squares (CLS), principal component regression (PCR) and partial least-squares (PLS) methods [12], have so far been the most frequently used for treating first-order data. UV-Visible absorption spectra have been frequently used as data for multicomponent analysis [13–16]. However, only an small number of methods have been described in which fluorescence data are used for multicomponent analysis, by these approaches [17].

For the first time, Lindberg et al. [18] applied PLS calibration to emission fluorescence data for the determination of humic acid and ligninsulfonate. Martens et al. [19–21] applied PLS calibration to a combination of several emission scans, for the determination of three botanical components. Jones et al. [22] reported the use of excitation, emission and synchronous spectra for the determination of acyclovir and guanine, applying several multivariate calibration methods. Sanchez Peña et al. [23] applied PLS to the analysis of binary mixtures of sulfonamides by photochemically-induced fluorometry.

Recently, we reported on the resolution of ternary mixtures of salicylic acid and two of its main urinary metabolites, by PLS [24,25], and on the analysis of binary mixtures of salicylic acid and diflunisal in serum samples, by combination of synchronous fluorometry with PLS calibration [26].

Previously, we have studied the inclusion complexes formed between NA and OH–NA with γ-cyclodextrin [5,27]. The investigation of the luminescent characteristics of the inclusion complexes was performed and, in both cases, an enhancement of fluorescence was observed upon inclusion.

In the present study, a method is reported for the simultaneous determination of NA and its principal metabolite, OH–NA, in urine samples, by combination of fluorescence emission spectra and PLS-1 multivariate calibration.

2. Experimental

2.1. Apparatus

Fluorescence measurements were made on an SLM Aminco Bowman, Series 2, luminescence instrument, equipped with a 150 W continuous Xenon lamp, interfaced by a GPIB card and driver with a PC 386-microcomputer. Data acquisition and data analysis were performed by the use of AB2 software, Version 1.40, running under OS/2 2.0. The excitation and emission slits were maintained at 8 and 4 nm, respectively. The scan rate of the monochromators was maintained at 10 nm s^{-1} in recording conventional spectra, and at 30 nm s^{-1} when recording three-dimensional excitation–emission spectra. All measurements were performed in 10 mm quartz cells, at 10°C, by use of a thermostatic cell holder and a Selecta Model Frigiterm thermostatic bath.

2.2. Software

The GRAMS-386 Level I Version 2.0 software package, with the PLS plus Version 2.1G application software [28], were used for the statistical treatment of the data, and the application of the PLS and PCR factor analysis based multivariate calibration methods. The digitized spectra, acquired with the Series 2 luminescence instrument, were converted to ASCII XY format with the converter included in the AB2 software, and imported to the GRAMS 386 program through the included ASCII XY converter. A converter program, running in BASIC, developed by us, was used to transform the bidimensional files, in ASCII XY format, to the software package SURFER for Windows [29], to obtain the three-

dimensional excitation–emission matrices presented as contour plots. The contour plots, in the two dimensions of excitation and emission, are generated by linking points of equal fluorescence intensity to form the contour map.

2.3. Reagents

Stock solutions of nalidixic acid (Sigma), and 7-hydroxymethylnalidixic acid (Sanofi-Wintrop) containing 100 μg ml^{-1}, were prepared in water. Stock aqueous solutions of γ-cyclodextrin (Sigma) 4×10^{-2} M, were prepared by dissolving 1.30 g of γ-cyclodextrin in 25 ml volumetric flasks. Purified liquid chromatography grade water (Labconco Waterpro PS) was used.

2.4. Procedure for the simultaneous determination in urine

Dilute spiked urine samples ten times with distilled, deionized water. Place a known volume of diluted urine (10 ml) into a separating funnel, and adjust the pH to 2.5–3.0 with HCl. Extract with 10 ml of chloroform by shaking for 3 min. Take 8 ml of the organic phase and evaporate to dryness. Dissolve the residue in water, transfer it into a 25 ml calibrated flask and dilute to volume with water. For the analysis, transfer an aliquot of this solution into a 3 ml cell, add 470 μl of 4×10^{-2} M γ-CD and 100 μl of 0.2 M HCl. Dilute the solution with water to a final volume of 3 ml. Record the fluorescence emission spectra between 300 and 420 nm, and use it as the analytical signal to make the calibration. Perform the PLS-1 calibration, with a calibration set of 18 samples, containing NA and OH–NA in the concentration ranges indicated in Table 1. Apply the optimized calibration matrix, calculated by application of the PLS-1 method, to analyze the emission spectra of the problem samples, and determine the concentrations of NA and OH–NA in the urine samples.

3. Results and discussion

Preliminary studies indicated that these antibiotics form inclusion complexes with γ-CD, and that, in both cases, enhancements on the fluorescence emission were produced [5,27]. In those studies, the influence of the pH, order of addition of the reagents, γ-CD concentration, and instrumental variables were optimized for both compounds. The study of the complex between NA and γ-CD has been performed at 357 nm, exciting at 314 nm. A 6.26×10^{-3} M concentration of γ-CD and a pH of 2.8 were selected as optimum. A method for the spectrofluorometric determination of NA was proposed, with an application range between 0.1 and 2 μg ml^{-1}, and with a detection limit of 14 ng ml^{-1}. The wavelengths for the study of the complex OH–NA: γ-CD were $\lambda_{ex} = 258$ nm and $\lambda_{em} = 363$ nm. A concentration of 6.32×10^{-3} M of γ-CD and a pH = 2.0 were selected as optimum The proposed method for the determination of OH–NA presents an application range between 0.1 and 4 μg ml^{-1} and a detection limit of 20 ng ml^{-1}.

The overlap between spectra can be best examined collecting a total luminescence spectrum of each of the compounds, in the form of an emission-excitation matrix (EEM). The EEMS were

Table 1
Composition of the different mixtures used in the calibration set for the determination of NA and OH–NA by PLS and PCR methods

Calibration set	NA μg ml^{-1}	OH–NA μg ml^{-1}
1	0.00	1.50
2	1.28	0.00
3	0.00	0.00
4	1.29	0.50
5	1.29	0.70
6	1.29	0.90
7	1.29	1.20
8	1.29	1.50
9	0.52	1.30
10	0.71	1.30
11	0.90	1.30
12	1.23	1.30
13	1.49	1.30
14	0.52	1.20
15	0.71	0.50
16	0.81	0.50
17	0.90	0.60
18	1.10	0.80

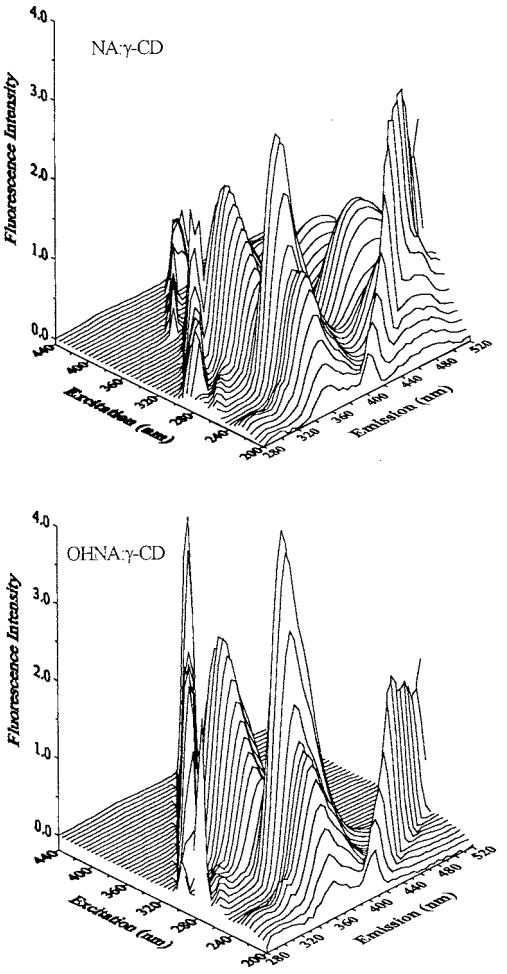

Fig. 1. Total luminescence spectra of the inclusion complexes of NA and OH–NA with γ-cyclodextrin. Each horizontal slice represents a separate emission scan with a fixed excitation wavelength.

collected by scanning the emission spectrum, between 280 and 520 nm, at increments of the excitation wavelength of 4 nm, between 200 and 440 nm. The total luminescence spectra of each of the antibiotics are represented in Fig. 1.

Fig. 2 shows the contour plots corresponding to the complexes. The two small diagonal bands of excitation–emission are coursed by stray light from first and second order grating effects. The scanning paths selected to perform the calibration are represented in the contour plots as solid lines. They were selected as compromise values to pass as close as possible near the maxima of the two complexes of the mixture. The emission spectrum was recorded maintaining constantly an excitation wavelength of 258 nm, the excitation spectrum at an emission wavelength of 360 nm, and the synchronous path was scanned with a wavelength difference between the emission and excitation wavelengths of 102 nm. The corresponding spectra are represented in Fig. 3.

3.1. Matrix of calibration and selection of the spectral zones for the analysis

To perform the determination, PLS-1, PLS-2 and PCR methods were evaluated for the resolution of the mixture, and a comparative study of the three chemometric approaches was undertaken. The two methods employed (PLS and PCR) decompose (or factor) the data matrix in different ways. PLS performs the spectral factoring trying to account for the spectral variation, while assuming that the new basis vectors relate to

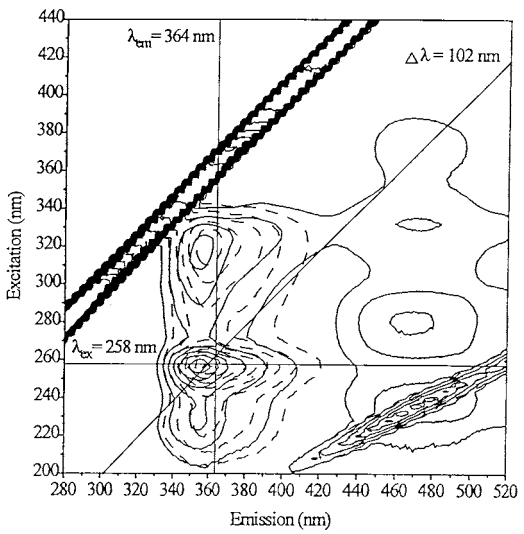

Fig. 2. Contours plots of the total fluorescence spectra of NA: γ-CD (——) and OH–NA: γ-CD (- - -) complexes. The selected paths for scanning the excitation ($\lambda_{em} = 360$ nm), emission ($\lambda_{ex} = 258$ nm) and synchronous ($\Delta\lambda = 102$ nm) spectra are shown by the solid lines slicing the data matrix.

the calibration concentrations. When the PLS method is used to calibrate a simple chemical constituent at a time, it is termed PLS-1, while for the calibration of several constituents simultaneously it is called PLS-2 regression. PCR, on the other hand, performs the factoring of the spectral data matrix without using information about the concentrations.

In addition, three different data sets, the emission spectra, the excitation spectra, and the synchronous spectra were evaluated to perform the determination. The two components mixture presents a difficult resolution problem, because of the similarities between the spectra, as can be observed on Fig. 2.

To establish a quantitative model for the system, 18 calibration samples containing different amounts of NA and OH–NA, were prepared. The concentration of each antibiotic was varied between 0.00 and 1.50 μg ml^{-1}, through the calibration matrix (Table 1).

The only pre-processing applied to the data was mean-centering. This pretreatment involves calculating the average spectrum of all training spectra, and subtracting this result from every spectrum. In addition, the mean concentration value for each component is calculated and subtracted from the concentration of every samples. This removes any offset from the data and tends to scale the data such that the mathematics of the spectral decomposition perform better.

The spectral regions between 200 and 300 nm for the excitation spectra, between 330 and 420 nm for the emission spectra, and between 280/382 and 450/552 for the synchronous spectra, were selected for the analysis, because these are the zones with the maximum spectral information from the mixture components. This implies working with 101, 91 and 171 experimental points per spectra, respectively, as the spectra were digitized each nanometer.

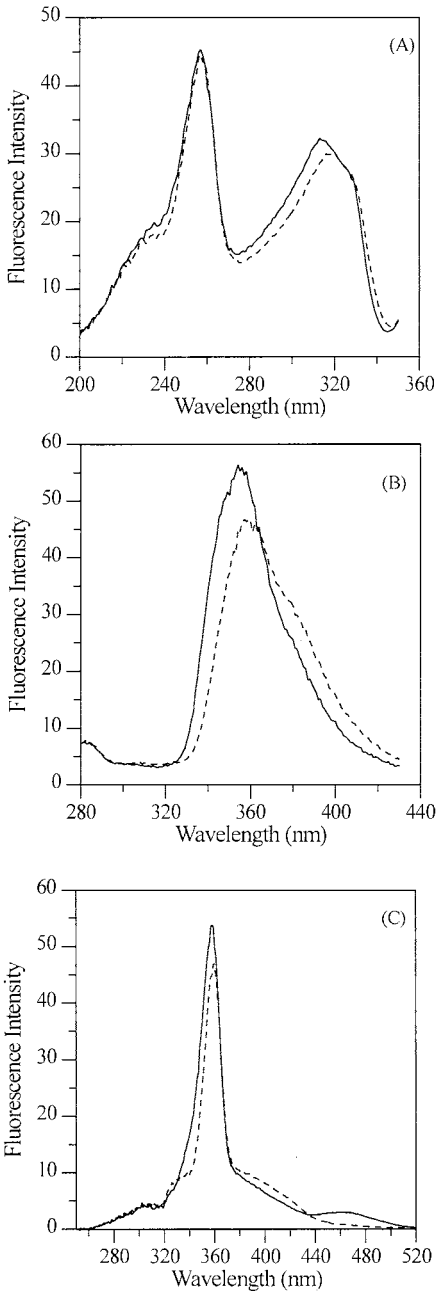

Fig. 3. A) Excitation ($\lambda_{em} = 360$ nm), B) Emission ($\lambda_{ex} = 258$ nm) and C) Synchronous ($\Delta\lambda = 102$ nm) spectra data sets selected for the determination of NA and OH–NA, by PCR and PLS methods.

3.2. Selection of the optimum number of factors and statistical parameters

The selection of the number of principal components or factors, to be used in the calibration with the PLS and PCR algorithms, is very important in order to achieve the best predictions.

Table 2
Statistical parameters of the PLS and PCR methods using the three spectral data sets

Component	Method	Excitation		Emission		Synchronous	
		RSEP(%)	R	RSEP(%)	R	RSEP(%)	R
NA	PLS-1	12 (4)	0.9648	4 (2)	0.9939	13 (3)	0.9517
	PLS-2	12 (4)	0.9680	5 (3)	0.9924	13 (3)	0.9521
	PCR	12 (5)	0.9629	5 (3)	0.9908	13 (3)	0.9524
OH–NA	PLS-1	8 (5)	0.9805	5 (3)	0.9919	5 (3)	0.9913
	PLS-2	12 (4)	0.9632	6 (3)	0.9915	5 (3)	0.9914
	PCR	11 (5)	0.9681	6 (3)	0.9909	5 (3)	0.9913

Values in parentheses correspond to the number of factors used in prediction.

To select the number of factors in the PLS and PCR algorithms, in order to model the system without overfitting the concentration data, cross-validation, leaving out one sample at a time, was used. Cross-validation consists of systematically removing one of the observations in turn, and using only the remaining observations for construction of latent factors, and regression on the latent factors. The predicted concentrations were compared with the known concentrations of the compounds in each calibration sample, and the predicted error sum of squares (PRESS) was calculated. The PRESS was calculated in the same manner, each time a new factor was added to the PLS or PCR models. To select the optimum number of factors, the criterium proposed by Haaland and Thomas was used [30,31].

When using the emission or the synchronous spectra data set, the optimum number of factors was three for PLS-2 and PCR methods. In PLS-1, cross-validation is performed with respect to the number of factors affecting the prediction of each of the compounds individually, and three factors for each acid were found. For the excitation spectra data set, the optimum number of factors was four for the PLS-2 method, and five for the PCR method. For PLS-1, values of four for NA and five for OH–NA were found as the optimum number of factors.

Once the optimal number of PLS or PCR factors is determined, it is necessary to perform the final calibration, using all the calibration samples with the optimal number of factors.

3.3. Statistical parameters

Known concentrations of all tested samples, included in the calibration matrix, were compared with the predicted concentrations by cross-validation, for the three methods, and for the three spectral data sets employed. In order to compare the quality of the results obtained with the different calibration models used, the relative standard deviations for the error of prediction (RSEP), for each analyte in the sample set, were calculated [34]:

$$\mathrm{RSEP}(\%) = \sqrt{\frac{\sum_{1}^{n}(c_{\mathrm{found}} - c_{\mathrm{added}})^2}{\sum_{1}^{n} c_{\mathrm{added}}^2}}$$

where c_{found} is the concentration calculated, c_{added} is the concentration present in the mixture, and n is the number of samples in the calibration set. The values obtained are summarized in Table 2.

It can be observed that the values for RSEP are not significantly different for PLS-1, PLS-2 and PCR methods. These results are in agreement with findings by other workers in different systems [16,32,33]. However, slightly better results were found with PLS-1 than with PLS-2 or PCR. This is in agreement with a detailed study of comparison of several multivariate calibration methods for quantitative analysis, in which the authors recommended the use of PLS-1. They found empirically that PLS-1 often exhibits better predictive properties than PCR and PLS-2, in analyzing real samples [31]. In consequence the

Table 3
Recovery of NA and OH–NA in mixtures, by PLS-1 multivariate calibration, using the three spectral data sets

Added μg ml^{-1}		Found, μg ml^{-1}											
		Excitation				Emission				Synchronous			
NA	OH–NA	NA	%Rec	OH–NA	%Rec	NA	%Rec	OH–NA	%Rec	NA	%Rec	OH–NA	%Rec
0.647	0.800	0.622	96	0.824	103	0.645	99	0.734	92	0.604	93	0.719	90
1.035	0.500	0.839	81	0.572	114	0.923	89	0.541	108	0.903	87	0.446	89
1.293	1.400	1.190	92	1.464	104	1.264	98	1.298	93	1.291	99	1.345	96
1.422	0.500	1.233	87	0.602	120	1.352	95	0.550	110	1.322	93	0.491	98
1.000	0.518	1.067	107	0.629	121	1.077	108	0.587	113	1.108	108	0.633	122
2.011	1.036	2.150	107	1.356	131	2.069	103	1.123	108	2.269	113	1.270	122

methods for quantitative analysis, in which the authors recommended the use of PLS-1. They found empirically that PLS-1 often exhibits better predictive properties than PCR and PLS-2, in analyzing real samples [31]. In consequence the PLS-1 algorithm, that performs PLS analysis one component at a time, has been selected to perform the determination. On the other hand, from the results in Table 2, we can follow that RSEP values for the emission spectra were much lower than the RSEP values obtained for the excitation or synchronous spectra.

In addition, the values of the correlation coefficient (R), which is an indication of the quality of all the data to a straight line, were calculated. They were virtually the same in the three approaches (PLS-1, PLS-2 and PCR) used for the two components. In all instances, the better values for R were obtained when the emission spectra were used for the calibration.

To evaluate the predictive ability of the method, the PLS-1 calibration model was applied to the three spectral data sets, for a series of problem mixtures, selected in the same concentration ranges used in the calibration set. The results obtained are summarized in Table 3.

In accordance with the statistical data obtained by internal cross-validation, the better results for the prediction were obtained when using the emission spectral data set as the analytical signal. In consequence, this spectral data set was selected for the application of the method to urine samples. The reason of this becomes evident from the observation of the three spectra data set profiles for the two components (Fig. 3). The overlapping of NA and OH–NA is smaller in the emission spectra, than in the excitation and synchronous spectra.

As we can see in Table 1, the minimun concentration tested for each analyte was 0.5 μg ml^{-1}.

3.4. Application of the method to urine samples

The proposed method has been applied to the determination of NA and OH–NA in human urine samples, spiked with these antibiotics. For the application of the method, urine samples, obtained from different sources, were spiked by adding different quantities of stock aqueous solutions of NA (8.81×10^{-4} M) and OH–NA (3.70×10^{-4} M), to obtain analyte concentrations within or above the therapeutic range (25–50 μg ml^{-1}) [6]. The urine samples were diluted ten times and the proposed method was then applied as described in the Procedure Section.

The percentages of recoveries found, by application of the PLS-1 calibration method to the emission spectral data, are shown in Table 4. Three spectra of three different samples, at the same concentration, were used for each concentration level included in Table 4. As can be seen, the agreement between calculated and experimental values was good. The mean recovery was 97% for NA and 99% for OH–NA.

Table 4
Recovery of NA and OH–NA added to human urine by PLS-1 calibration

Added (μg ml^{-1})		Found (μg ml^{-1})[a]			
NA	OH–NA	NA	Recovery ± SD[b] %	OH–NA	Recovery ± SD[b] %
27.7	15.0	27.0	97 ± 1	15.8	105 ± 2
30.5	19.3	31.2	102 ± 1	20.1	104 ± 1
38.5	38.5	35.1	91 ± 1	35.5	92 ± 2
38.5	19.3	35.9	93 ± 1	18.5	96 ± 1
48.6	25.0	49.0	101 ± 1	25.8	103 ± 1
55.5	30.8	52.5	94 ± 2	30.5	99 ± 2
76.4	38.5	75.6	99 ± 1	37.8	98 ± 1

[a] Mean of three determinations.
[b] SD: Standard deviation.

4. Conclusions

The results obtained in this work allow us to conclude that both components of the binary mixture are accurately determined by fluorescence spectroscopy, in combination with PLS calibration. The proposed method allows the direct determination of both analytes simultaneously, without needing a previous separation step.

The total luminescence information contained in the three-dimensional excitation–emission matrices allows the selection of the most suitable spectral data set, to perform the multivariate calibration. When comparing the results obtained by PCR, PLS-1 and PLS-2 methods, slightly better results have been obtained with PLS-1 than with PLS-2 and PCR. The selection of the spectral data set composed of the emission spectrum was the optimum path for NA and OH–NA quantification. The NA and OH–NA mixtures, in a wide range of ratios, were resolved, and the prediction of each analyte concentration, yielded RSEP values of 4% for NA and 5% for OH–NA. Human urine samples containing different quantities of NA and OH–NA, were resolved by using the proposed PLS-1 multivariate calibration method, and recoveries of 97% for NA and 99% for OH–NA were obtained.

Acknowledgements

The authors are grateful to the DGICYT (Project PB95-1141) and to the Consejeria de Educación y Juventud de la Comunidad de Extremadura (Project EIA94-36) for finantial support. Sanofi-Wintrop (Barcelona, Spain) is also acknowledged for supplying the 7-hydroxymethylnalidixic acid used in this study.

References

[1] E.W. McChesney, E.J. Froelich, G.Y. Lesher, A.V.R. Craim, D. Rossi, Toxicol. Appl. Pharmacol. 6 (1964) 292.
[2] R. Gleckman, S. Alvarez, D.W. Joubert, S.J. Mathews, Am. J. Hosp. Pharm. 36 (1979) 1071.
[3] D. Dámaso, M. Moreno-López, R.M. Daza, Antibióticos y quimioterápicos antibacterianos, Uso clínico, Ed. Grutesa, Madrid, 1984.
[4] R. Staroscik, J. Sulkowska, Acta Pol. Pharm. 30 (1973) 499.
[5] I. Durán Merás, A. Muñoz de la Peña, F. Salinas López, I. Rodriguez Cáceres, Analyst 119 (1994) 1215.
[6] S. Panadero, A. Gómez-Hens, D. Pérez Bendito, Anal. Chim. Acta 303 (1995) 39.
[7] J.A. Murillo Pulgarín, A. Alañón Molina, P. Fernández López, Talanta 43 (1996) 431.
[8] L. Shargel, R.F. Koss, A.V.R. Crain, V.J. Boyle, J. Pharm. Sci. 62 (1973) 1452.
[9] R.H.A. Sorel, H. Roseboom, J. Chromatogr. 162 (1979) 461.
[10] R.H.A. Sorel, A. Hulshoff, C. Snellman, J. Chromatogr. 129 (1980) 129.

[11] G. Cuisinaud, N. Ferry, M. Seccia, N. Bernard, J. Sassard, J. Chromatogr. 181 (1980) 399.
[12] H. Martens, T. Naes, Multivariate Calibration, Wiley, Chichester, 1991.
[13] A. Espinosa Mansilla, A. Muñoz de la Peña, F. Salinas, A. Zamoro, Anal. Chim. Acta 258 (1992) 47.
[14] A. Espinosa Mansilla, A. Muñoz de la Peña, F. Salinas, M. Martínez Galera, Anal. Chim. Acta 276 (1993) 141.
[15] I. Durán Merás, A. Espinosa Mansilla, F. Salinas, Analyst 120 (1995) 2567.
[16] I. Durán Merás, A. Muñoz de la Peña, A. Espinosa Mansilla, F. Salinas, Analyst 118 (1993) 807.
[17] L. Norgaard, Talanta 42 (1995) 1305.
[18] W. Lindberg, J.A. Persson, S. Wold, Anal. Chem. 55 (1983) 643.
[19] S.Aa. Jensen, L. Munck, H. Martens, Cereal Chem. 59 (1982) 477.
[20] S.Aa. Jensen, H. Martens, Cereal Chem. 60 (1983) 172.
[21] B. Pedersen, H. Martens, Multivariate calibration of fluorescence data, in: L. Munck (Ed.), Fluorescence Analysis in Foods, Longman, Essex, 1989, ch. 13.
[22] R. Jones, T.J. Coomber, J.P. McCormick, A.F. Fell, B.J. Clark, Anal. Proc. 25 (1988) 381.
[23] M. Sanchez Peña, A. Muñoz de la Peña, F. Salinas López, M.C. Mahedero, J.J. Aaron, Analyst 119 (1994) 1177.
[24] A. Muñoz de la Peña, I. Durán Merás, M.D. Moreno, F. Salinas, M. Martínez Galera, Fresenius J. Anal. Chem. 351 (1995) 571.
[25] A. Muñoz de la Peña, I. Durán Merás, M.D. Moreno, F. Salinas, M. Martínez Galera, Fresenius J. Anal. Chem. 353 (1995) 221.
[26] A. Muñoz de la Peña, M.D. Moreno, I. Durán Merás, F. Salinas, Talanta 43 (1996) 1349.
[27] I. Durán Merás, A. Muñoz de la Peña, F. Salinas López, I. Rodriguez Cáceres, Applied Spectroscopy 51 (1997) 684.
[28] GRAMS-386 Software Package, Version 2.0 and Add-on Application PLS plus Version 2.1G, Galactic Industries, Salem, NH, 1993.
[29] SURFER for Windows Software Package, Version 5.0, Golden Software, Golden, CO, 1993.
[30] D.M. Haaland, E.V. Thomas, Anal. Chem. 60 (1988) 1193.
[31] D.M. Haaland, E.V. Thomas, Anal. Chem. 60 (1988) 1202.
[32] P. MacLaurin, P.J. Worsfold, M. Crane, P. Norman, Anal. Proc. 29 (1992) 65.
[33] D.M. Haaland, E.V. Thomas, Anal. Chem. 62 (1990) 1091.
[34] M. Blanco, J. Coello, F. González, H. Iturriaga, S. Maspoch, A.R. Puigdoménech, Talanta 43 (1996) 1489.

.

ELSEVIER

Talanta 45 (1998) 909–915

Talanta

Extraction of lead(II) with cyanex 302 and its spectrophotometric determination with PAR

Anant P. Argekar *, Ashok K. Shetty

Analytical Laboratory, Department of Chemistry, The Institute of Science, 15, Madam Cama Road, Bombay 400 032, India

Received 10 January 1997; received in revised form 9 June 1997; accepted 16 June 1997

Abstract

A method is developed for the extraction of lead(II) from an aqueous solution of pH 2.1–8.3 with cyanex 302 [bis(2,4,4-trimethylpentyl monothiophosphinic acid)] in toluene as an extractant. Lead(II) was stripped with 0.1 mol dm^{-3} nitric acid and determined spectrophotometrically with PAR. The method is most sensitive and permits the separation of lead(II) from binary mixtures containing commonly associated metal ions. The method is applicable for the separation and determination of lead in alloys and environmental samples. © 1998 Elsevier Science B.V.

Keywords: Extractant; Lead; Spectrophotometry

1. Introduction

Lead and its compounds are hazardous because the poison is cumulative and its toxic effects are many and severe [1]. Atomic absorption spectrometry and atomic emission spectrometry are used for routine trace analysis of lead especially for environmental samples. However, spectrophotometric methods are versatile and economical particularly for developing countries. A large number of spectrophotometric methods for the trace analysis of lead are available as shown in Table 1. Dithizone, sodium diethyl dithiocarbamate, arzenazo-TB, 1-(2-thiazolylazo-2-naphthol), monothiothenoyltrifluoro acetone and pyridine-2-acetaldehyde salicyloylhydrazone are not suitable for trace analysis of lead due to low sensitivity. Malachite green, but rhodamine B and 4-(2-pyridylazo)resorcinol (PAR) are sensitive but a large number of cations interfere.

PAR method is suitable for routine spectrophotometric analysis of lead due to its rapidity and sensitivity and also because it does not require any organic solvents. However, cadmium, cobalt, copper, silver, mercury, nickel and zinc metals interfere in this method. Therefore in order to increase the selectivity a reliable separation technique like solvent extraction is necessary before the spectrophotometric determination of lead by PAR.

Literature survey shows various solvent extraction methods for the separation and preconcentration of lead. Different reagents such as amberlite LA-1 [10], tributyl phosphate [11], thio-2-theonyltrifluroacetone [12], dibutylsulphoxide [13], trioctylamine [14], alamine 336 [15], aliquat 336 [16],

* Corresponding author.

PII S0039-9140(97)00192-6

Table 1
Review of spectrophotometric methods for determination of lead(II)

Reagent	Phase	λ_{max} (nm)	ε	Remarks	Reference
Dithizone	CCl_4	520	25 000	Light sensitive Hg. 11, Fe interfere	[2]
Sodium diethyl dithiocarbamate	CCl_4	435	13 000	—	[3]
Arsenazo-TB	Aqueous	620	20 000	Th, Tl, U interfere	[3]
1-(2-thiazol-ylazo-2) -naphthol	Aqueous	575	17 000	Mn, Fe, Co, M, Zn, tartrate, EDTA interfere	[4]
Malachite green	Toluene	642	41 000	Ca, Hg, Sb, Bi Co, Sn, Tl, interfere	[5]
Monothiothenoyl trifluoro acetone	C_6H_6	384	26 000	Equilibration time 30 min. Ni, Ca, Co, Cu, Zn, Pd, interfere	[6]
Butylrhodamine-B	C_6H_6	570	59 000	Hg, In, Bi Tl, Ag, interfere	[7]
Pyridine-2-acetaldehyde salicyloyhydrozone	$CHCl_3$	380	19 300	Saltingout agent used	[8]
PAR	Aqueous	520	43 000	Ag, Cd, Co, Cu, Hg, Ni Zn, interfere	[9]

mesityl oxide [17], triphenylphosphine oxide [18], 2-ethylhexylphosphoric acid monoester [19] have been reported for extraction of lead. However the existing methods suffer from limitations such as longer extraction time [10,15], critical pH [12], incomplete extraction [10,15], use of salting out agents [11] and co-extraction of commonly associated ions [11–14,17,18]. Although [bis(2,4,4-trimethylpentyl monothiophosphinic acid)] (cyanex 302) has been used to study the extraction behaviour of some metal ions [20–26], there has been no detailed study on the use of this reagent for the extractive separation of lead. In the present work, a new method for the solvent extraction separation of lead(II) with cyanex 302 into toluene has been developed and the lead thus, separated was stripped into HNO_3 for its spectrophotometric determination by PAR from binary mixtures, alloys and environmental samples.

2. Experimental

2.1. Apparatus

GBC 902 Atomic absorption spectrometer (GBC, Australia), a UV-VIS 160A Shrmadzu spectrophotometer and a Control Dynamics pH meter were used.

2.2. Reagents

Stock solution of lead(II) was prepared by dissolving 2.0 g of lead nitrate in 250 ml of distilled water containing 0.5 ml of concentrated nitric acid. The solution was standardized complexometrically using EDTA [27] and working solutions of lower concentration were prepared by suitable dilutions.

A 0.1 mol dm^{-3} stock solution of cyanex 302 [bis(2,4,4-trimethylpentyl monothiophosphinic acid)] was prepared by dissolving the reagent in toluene. The stock solution was diluted wherever necessary.

A 0.1% aqueous solution of 4-(2-pyridylazo) resorcinol (PAR) was used for the spectrophotometric determination of lead.

All other reagents used were of analytical reagent grade.

2.3. General procedure

An aliquot of solution containing lead(II) was taken and its pH was adjusted to 5.0 with dilute nitric acid and ammonium hydroxide. The total volume was made to 25 ml, transferred to a separatory funnel and shaken with 5 ml of 0.005 mol cyanex 302 for 1 min. After separating the two phases, lead was back extracted from the

organic phase by shaking with 10 ml of 0.1 mol nitric acid and estimated either by atomic absorption spectrometry or spectrophotometrically with PAR [9].

3. Results and discussion

3.1. Extraction as a function of pH

Lead(II) was extracted in the pH range of 1.0–10.0 with 5×10^{-3} mol dm^{-3} cyanex 302 in toluene. The extraction was quantitative between pH 2.1 and 8.3. Hence all extractions were carried out at pH 5.0 (Fig. 1).

3.2. Extraction as a function of cyanex 302 concentration

Lead(II) was extracted with varying concentrations of cyanex 302 (1×10^{-2}–1×10^{-4} mol dm^{-3}) in toluene at the fixed pH of 5.0. The extraction was quantitative with 5×10^{-3} mol dm^{-3} (Fig. 2).

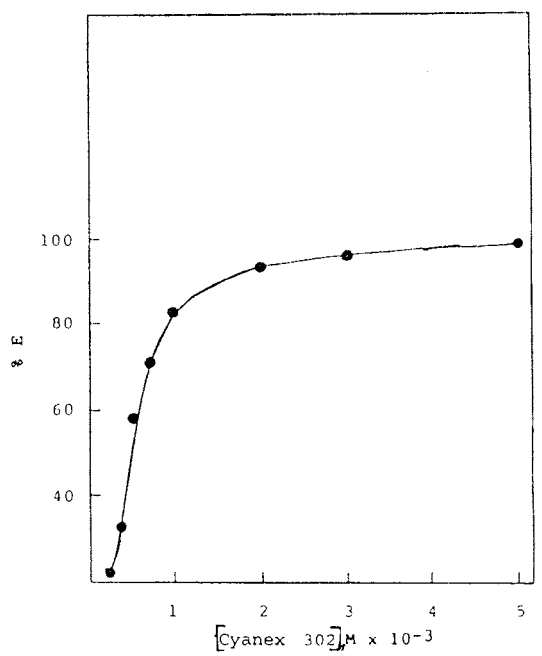

Fig. 1. Effect of pH on extraction; Pb = 50 μg, Cyanex 302 = 5×10^{-3} mol l^{-1}.

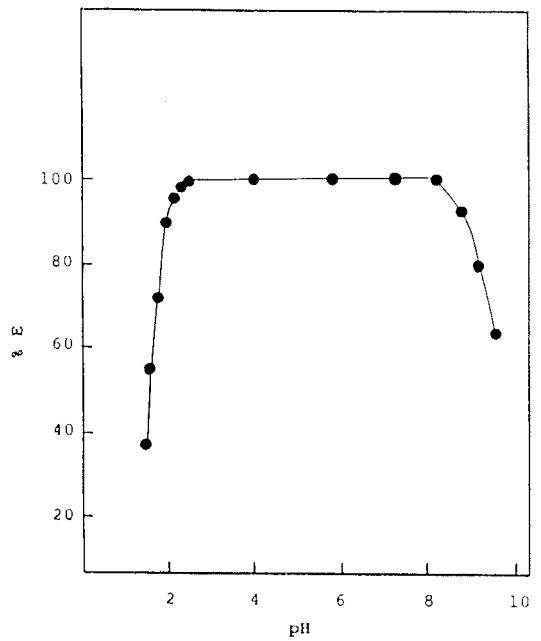

Fig. 2. Effect of Cyanex concentration on percentage extractions; Pb = 50 μg; pH = 5.0

3.3. Extraction with various diluents

Lead(II) was extracted with 0.005 mol cyanex 302 in different solvents. The percentage extraction in toluene, xylene, benzene, carbon tetrachloride and chloroform are 99.7, 97.2, 92.6 85.2 and 76.3 respectively. Hence toluene was selected as a solvent for cyanex 302 for further studies.

Table 2
Effect of diverse ions on extraction of 50 μg of lead(II)

Tolerance limit μg	Diverse ions
7500	Ba(II), Ca(II), Al(III)
6000	Mg(II), Sr(II), Al(m), Cr, NO_3
5000	Ti(IV), V(V), Cr(VI), W(VI), Sb(II) thiosulphate, oxalate
3500	Sn(II), Bi(III), As(III), SO_4^{2-}, Mn(II), citrate, tartarate
2000	Mo(VI), Cu(II), cyanide
1000	Co(II), Ni(II), Fe(III), Cd(II)
500	Zn(II)

Table 3
Separation of lead(II) from binary mixtures

Separation no.	Composition (μg)	Recovery of Pb(II) (%)	Relative standard deviation (%)	Recovery of added ion (%)[a]	Relative standard deviation (%)	Estimation procedure for added ions and their references
1.	Pb(II), (40); Sn(II), (500);	99.5	0.76	99.1	0.83	Spectrophotometrically with pyrocatechol violet [28]
2.	Pb(II), (40); Sb(III), (200);	99.6	0.48	99.8	1.01	Spectrophotometrically with KI [29]
3.	Pb(II), (40); Bi(III), (200);	99.2	0.91	99.5	0.85	Spectrophotometrically with thioruea [2]
4.	Pb(II), (40); Cr(VI), (150);	99.8	0.29	99.6	1.23	Spectrophotometrically with diphenyl carbazide [29]
5.	Pb(II), (40); V(V), (150);	99.4	0.85	99.2	0.56	Spectrophotometrically with hydrogen peroxide [29]
6.	Pb(II), (40); Ti(IV), (200);	99.7	0.46	99.8	0.72	Spectrophotometrically with hydrogen peroxide [29]
7.	Pb(II), (40); Cu(II), (500);	99.4	0.39	99.0	0.97	Spectrophotometrically with EDTA after decomposing, organic layer [27]
8.	Pb(II), (40); Fe(III), (50);	99.5	0.88	99.3	1.09	Spectrophotometrically with thiocyanate [29]
9.	Pb(II), (40); Zn(II), (200);	99.1	1.06	99.4	0.65	Spectrophotometrically with PAR [29]

[a] Average of five determinations.

Table 4
Determination of lead in non ferrous alloys

Separation no.	Sample and its composition	Certified Value	Amount found by AAS (%)	Amount found by proposed method[a] (%)	Coefficient of variation (%)
1.	Leaded gun-metal (BCS 183/4) Cu 84.0; Pb 3.15; Fe 0.05; Bi 0.005; Ni 1.0; Sb 0.23; S 0.11; Zn 3.47; As 0.13	3.15	3.15	3.13	0.85
2.	Leaded bronze (BCS 364) Cu 80.6; Ni 0.28; As 0.065; Fe 0.002; Bi 0.007; Sb 0.181; P 0.056; Co 0.002 Pb 9.35; Zn 0.13	9.25	9.24	9.21	0.44
3.	Tin base whitemeal (BCS 178/2) Sn 82.2; Sb 9.45; Cu 4.58; Pb 3.18; Ni 0.17; As 0.15; Cd 0.14; Bi 0.11; Zn 0.04	3.18	3.18	3.17	0.94

[a] Average of five determinations.

3.4. Effect of shaking time

The shaking time for extraction was varied from 15 to 180 s. The minimum shaking time required for quantitative extraction of lead(II) was 1 min.

3.5. Nature of the extracted species

The nature of the extracted species was determined by plotting log [D] against log [cyanex 302] at fixed pH of 5.0, where [D] denotes the distribution ratio of lead(II) between the two phases and [cyanex 302] is the reagent concentration in the organic phase. The slope was 1.9. Therefore probable composition of the extractable species is $2R_2P(S)OH + Pb2^+ = = [R_2P(S)O]_2Pb + 2H^+$

3.6. Effect of diverse ions

Various amounts of diverse ions were added to a solution containing a fixed amount of lead (50 μg). The recommended procedure was then followed for the extraction and determination of lead ions. The tolerance limit was set at the amount of diverse ions required to cause a $\pm 2\%$ error in the recovery of lead. The results are as given in Table 2.

3.7. Separation of lead(II) from binary mixtures

The separation of lead(II) from its binary mixtures with Sn(IV), Bi(m), Sb(m), V(V), Ti(IV), Cr(VI), Cu(II), Zn(II) and Fe(III) were carried out by the proposed method and the results are as shown in Table 3. Under the optimum conditions of the extraction of lead(II), metal ions such as Sn(IV), Sb(III), Bi(m), V(V), Il(IV) and Cr(VI) are not extracted and hence remain quantitatively in the aqueous phase. Fe(m), Zn(II) and Cu(II) are extracted with cyanex 302 under the extraction conditions of lead(II). Fe(m), Zn(II) and Cu(II) are not stripped with 0.1 mol HNO_3 whereas Pb(II) is stripped quantitatively. Thus,

Table 5
Determination of lead in industrial wastewater samples

Sample	Amount found by present method[a] ($\mu g\ ml^{-1}$)	Coefficient of variation (%)	Amount found by AAS ($\mu g\ ml^{-1}$)
Waste water			
A	3.9	0.21	3.8
B	0.8	0.39	0.8
C	4.7	0.16	4.6

[a] Average of five determinations.

separation of Pb(II) from these metals is achieved. Fe(m) and Zn(II) are recovered by stripping into 2 and 4 mol dm^{-3} HCl whereas Cu(II) remains in the organic phase which after decomposing can be estimated.

3.8. Determination of lead in non-ferrous alloys

Alloy (0.1 g) was dissolved in 5 ml of concentrated nitric acid. The solution was evaporated to dryness. The residue was dissolved in 5 mol dm^{-3} nitric acid, any metastannic acid was filtered off and the filtrate was washed with hot dilute nitric acid and finally with hot water. The filtrate was and ted to 100 ml with distilled water. An aliquot portion of each alloy was taken for extraction and determination of lead by the recommended procedure (Table 4).

3.9. Determination of lead in industrial wastewater samples

Waste industrial water samples were procured from Maharashtra Water Pollution Control Board, New Bombay (India) and were directly used without any pretreatment of the samples for the content of lead by the proposed procedure. The results obtained are shown in Table 5.

Thus, cyanex 302 can be effectively employed for the selective separation of lead and its spectrophotometric determination with PAR in binary mixtures, alloys and environmental samples. The important feature of this method is that the cyanex 302 in toluene used for extractive separation of lead can be re-used after stripping except when copper is present.

Acknowledgements

The authors are grateful to CYNAMID Cynamid Canada, Canada for their generous gift of Cyanex reagents.

References

[1] R. Renner, Environ. Sci. Technol. 29 (1995) 256.
[2] E.B. Sandell, Colorimetric Determination of Trace Metals, 3rd ed., Inter Science, New York, 1958.
[3] L.C. Willemsons, Handbook of Lead Chemicals, Project LC-116, International Lead Zinc Research Organisation, New York, 1986.
[4] G.V. Ralkaiah, M.C. Eshwar, Indian J. Technol. 23 (1985) 157.
[5] P.P. Kisch, Ya.R. Bazel, I.S. Balog, Zh. Anal. Khirn. 39 (1984) 820.
[6] T. Hongo, A.O. Azaki, L. Terada, T. Kiba, Fresenius Z. Anal. Chem. 331 (1988) 647.
[7] P.P. Kisch, Ya.R. Bazel, I.S. Balog, Zh. Anal. Khim. 39 (1984) 1052.
[8] M.N. Bale, D.P. Dave, A.D. Sawant, Talanta 42 (1995) 1291.
[9] R.M. Dangell, T.S. West, P. Young, Talanta 12 (1965) 583.
[10] T. Suzuki, T. Sotobayasi, Jpn. Analyst 12 (1964) 910.
[11] A.A. Yadav, S.M. Khopkar, Talanta 18 (1971) 833.
[12] S.B. Akki, S.M. Khopkar, Bull. Chem. Soc. Jpn. 45 (1972) 167.
[13] J.W.O. Laughlin, T.P. O'Brien, Talanta 12 (1975) 597.
[14] Ya.B. Spivakov, V.I. Lebedev, V.M. Shkiner, N. Krivenkova, T.S. Plotnikova, I.P. Kharlamov, Yu.A. Zolotov, Zh. Anal. Khim. 31 (1976) 757.
[15] C.W. McDonald, M.M. Mahayani, M. Kanjo, Sepn. Sci. Technol. 13 (1978) 429.
[16] V.V. Mudshingikar, V.M. Shinde, Indian J. Chem. 13 (A) (1984) 539.
[17] B. Raman, V.M. Shinde, Bull. Chem. Soc. Jpn. 62 (1989) 3679.
[18] J. Wang, Huaxue Tongbao 7 (1986) 37.

[19] J. Zhang, Z. Li, H. Huang, Z. Hu, L. Zhu, Feuxi Huaxue 19 (1991) 677.
[20] L. Steiner, X. Miaolin, S. Hartland, Process. Metall. 7B (1992) 1175.
[21] D. Dreisinger, P. Westsells, J.A. King, C. Patel, Australas. Inst. Min. Mettall. 7 (93) (1993) 357.
[22] B.K. Tait, Hydrometallurgy 32 (1993) 365.
[23] K.C. Sole, T.L. Ferguson, J.B. Brent, Solvent Extr. Ion Exch. 12 (5) (1994) 541.
[24] T. Kakoi, M. Goto, F. Nakashio, Solvent Extr. Ion Exch. 12 (3) (1994) 541.
[25] A.P. Argekar, A.K. Shetty, Anal. Sci. 13 (1997) 132.
[26] A.P. Argekar, A.K. Shetty, Indian J. Chem. (in press).
[27] A.I. Vogel, A Text book of Quantitative Inorganic Analysis, Longmans, London, 1961.
[28] W.S. Ross, J.C. White, Anal. Chem. 33 (1961) 421.
[29] Z. Marczenko, Spectrophotometric Determination of Elements, Ellis Horwood, Chichester, 1976.

ELSEVIER

Talanta 45 (1998) 917–923

Talanta

Highly sensitive detection of L-glutamate by on-line amperometric micro-flow analysis based on enzymatic substrate recycling

Toshio Yao [a,*], Seita Suzuki [a], Taketoshi Nakahara [a], Hirohito Nishino [b]

[a] *Department of Applied Chemistry, College of Engineering, and Research Institute for Advanced Science and Technology, Osaka Prefecture University, Gakuencho, Sakai, Osaka 599, Japan*
[b] *Eicom Ltd., 24-2 Shimotoba-Enmenda, Fushimi, Kyoto 612, Japan*

Received 15 January 1997; received in revised form 11 June 1997; accepted 16 June 1997

Abstract

A highly selective and sensitive on-line monitoring system is proposed for amperometric assay of trace amounts of L-glutamate. The system includes a microdialysis probe, immobilized enzyme reactor, and poly(1,2-diaminobenzene)-coated platinum electrode. The enzyme reactor prepared by the co-immobilization of L-glutamate oxidase and glutamate dehydrogenase are here employed to enhance the sensitivity of L-glutamate as an on-line amplifier based on the substrate recycling. The L-glutamate in the dialysate from the probe are recycled enzymatically during passage through the reactor in the presence of sufficient amounts of NADH and oxygen to produce a large amount of hydrogen peroxide, which is detected if selectively at a downstream poly(1,2-diaminobenzene)-coated platinum electrode without interference from oxidizable species such as L-ascorbate in the sample and NADH added to the carrier buffer. The cycle is also initiated with 2-oxoglutarate, and so saccharopine dehydrogenase reactor is positioned in series before the amplifier reactor to remove 2-oxoglutarate in the dialysate. By the present method, L-glutamate is selectively assayed with a 160-fold increase in sensitivity compared with the unamplified responses. The detection limit is 0.5×10^{-7} M of L-glutamate. © 1998 Elsevier Science B.V.

Keywords: Amperometric detection; Microdialysis probe; Enzyme reactor; L-Glutamate; Substrate recycling

1. Introduction

Microdialysis is a sampling technique for in vivo assay and has been applied in pharmacological and behavioral studies of brain neurotransmitters. The dialysate collected by a given time interval is assayed by LC [1–4], but the time resolution of the assay is not sufficient for real-time monitoring. We reported before a continuous flow system which makes possible on-time real-time monitoring of glucose, L-glutamate, and acetylcholine [5]. This method is based on the use of microdialysis probe in combination with an immobilized enzyme reactor. A similar attempt has been achieved for the on-line monitoring of glucose by the use of an enzyme electrode [6,7].

* Corresponding author. Fax: +81 722 593340.

PII S0039-9140(97)00193-8

However, these method was not sufficient in the sensitivity for the in vivo monitoring of trace amounts (less than 10^{-6} M) of L-glutamate which is one of the important neurotransmitters in the central nervous system.

An interesting approach has been done to enhance the sensitivity of the flow system with enzyme reactor. That is based on the use of the enzyme reactor involving amplification by substrate recycling. The substrate is recycled by choosing a combination of coupled enzymes such that the product of the first enzyme-catalysed reaction is the substrate for the second enzymes. Such a principle has been applied to the highly sensitive detection of a variety of substrates e.g. glucose [8], NAD coenzymes [9–11], L-glutamate [12], phosphate [13], and L-lactate [14–16].

In this paper, we describe the highly selective and sensitive detection of L-glutamate using a co-immobilized L-glutamate oxidase/glutamate dehydrogenase reactor as an on-line amplifier in an amperometric micro-flow system with a microdialysis probe. In addition, a poly(1,2-diaminobenzene)-coated platinum electrode was also used as the highly selective detector of hydrogen peroxide generated enzymatically as an end product, without electrochemical interferences from NADH and L-ascorbate. As a result, this method permitted the on-line and real-time measurements of trace amounts of L-glutamate in microdialysate.

2. Experimental

2.1. Materials

Distilled water purified with the use of a Millipore Milli Q system (Nippon Millipore, Tokyo) was used throughout. L-Glutamate oxidase (E.C. 1.4.3.11, 24.9 U mg^{-1} of protein from *Streptomyces* sp.) was obtained from Yamasa Shoyu (Chiba), glutamate dehydrogenase (E.C. 1.4.1.3, 90 U mg^{-1} of protein from beef liver) and NADH were from Oriental Yeast (Tokyo), and saccharopine dehydrogenase (E.C. 1.5.1.7, 68 U mg^{-1} of protein from bakers yeast) was from Sigma (St. Louis, MO). They were used as received. L-Glutamic acid, 2-oxoglutaric acid, L-lysine, 1,2-diaminobenzene, and glutaraldehyde (20% solution) were obtained from Wako (Osaka). All other chemicals were of analytical reagent grade. Controlled-pore glass (aminopropyl CPG; mean pore size, 527 Å; particle size 200–400 mesh) was obtained from CPG (Fairfield, NJ) and was used as a support material for enzyme immobilization. The phosphate buffers were prepared from ammonium dihydrogenphosphate. The artificial physiological fluid (Ringer's solution) was prepared from NaCl (147 mM), KCI (4 mM), $CaCl_2$ (1.2 mM), and $MgCl_2$ (1.0 mM).

2.2. Preparation of immobilized enzyme reactors

Aminopropyl CPG was packed into three PTFE coils (20×0.5 mm i.d.) furnished with small nylon nets (350 mesh) at each end. They were activated by circulating 4%(v/v) glutaraldehyde solution into the CPG as previously described [11]. After washing with distilled water for 1 h, each of the enzymes was loaded onto each reactor by pumping at 3 μl min^{-1} the 0.1 M, pH 7.0, sodium phosphate buffer (500 μl) containing glutamate oxidase (0.6 U) or saccharopine dehydrogenase (6.8 U) or a couple of glutamate oxidase (0.18 U) and glutamate dehydrogenase (5.2 U). The excess of enzymes and the residual aldehyde groups on the CPG were removed by washing with glycine buffer (0.1 M, pH 7.5) for 2 h. Three PTFE enzyme reactors were stored at ca 4°C in the buffer used for the immobilization when not in use.

2.3. Apparatus and procedure

The microdialysis flow-system used in this work is outlined in Fig. 1. Microdialysis probe was gift from Eicom (Kyoto). The design was as follows; a regenerated cellulose dialysis fiber (o.d. 220 μm, i.d. 200 μm; molecular cut-off approximately 50 000) is inserted into a fused silica tube (o.d. 470 μm, i.d. 350 μm) and glued in the interior of the silica tube leaving an active length of 3 mm. Another two fused silica tube (o.d. 150 μm, i.d. 75 μm) inserted from the upper end is served as the

inlet and outlet, and the upper end of the probe and the fiber tip are sealed with epoxy cement.

The apparatus consisted of a two-channel microsyringe pump (Eicom EP-60), an electrochemical detector with potentiostat and thin-layer flow-cell (Eicom ECD-300), and a strip chart recorder (Hitachi 056). The electrode assembly of the thin-layer flow-cell consisted of a platinum disk (3 mm in diameter) as working electrode, a silver-silver chloride reference electrode, and a stainless steel tube as an auxiliary electrode. The platinum disk was coated with the poly(1,2-diaminobenzene) film by the electropolymerization of 1,2-diaminobenzene according to the previously described procedure [17] and used as the working electrode in this work. A constant potential (+ 0.6 V versus Ag/AgCl) was applied to the polymer film-coated electrode and the current was recorded.

The L-glutamate oxidase immobilized PTFE reactor was used in the flow system without amplification (Fig. 1A), while a saccharopine dehydrogenase immobilized PTFE reactor and a L-glutamate oxidase/glutamate dehydrogenase co-immobilized PTFE reactor positioned in series were used in the flow system with amplification (Fig. 1B). All the parts were connected with PTFE coil (i.d. 0.1 mm). In both systems, Ringer's solution was pumped at a constant flow

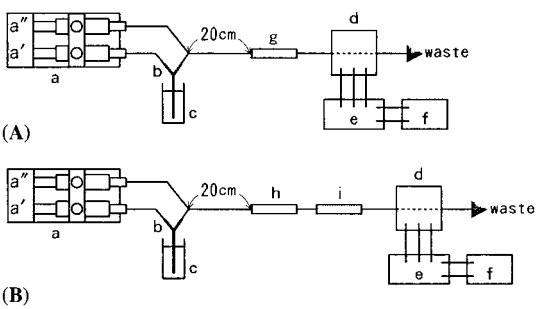

Fig. 1. Schematic diagram of microdialysis system without (A) and with amplification (B). (a) Two-channel microsyringe pump; (b) microdialysis probe; (c) sample solution; (d) amperometric detector [poly (1,2-diaminobenzene) film-coated platinum electrode]; (e) potentiostat; (f) recorder; (g) L-glutamate oxidase immobilized PTFE reactor; (h) saccharopine dehydrogenase immobilized PTFE reactor; (i) L-glutamate oxidase/glutamate dehydrogenase co-immobilized PTFE reactor.

into a dialysis probe with a microsyringe pump a′. The carrier optimized for each flow system (0.1 M, pH 7.5, sodium phosphate buffer for Fig. 1A; 0.1 M, pH 7.5, ammonium phosphate buffer containing 3 mM NADH and 3 mM L-lysine for Fig. 1B) was also pumped at a constant flow with a microsyringe pump a″. The analyse in the dialysate from the probe was carried into the enzyme reactor and then produced enzymatically the hydrogen peroxide which could be detected selectively by a downstream poly(1,2-diaminobenzene) film-coated platinum electrode. The steady-state current obtained was related to the L-glutamate concentration in the sample solution.

3. Results and discussion

3.1. Micro flow system without amplification

In this work, the L-glutamate oxidase immobilized PTFE reactor was positioned in the line shown in Fig. 1A. As an optimum buffer, 0.1 M phosphate buffer at pH 7.5 was selected [18] and pumped with pump a″. When the flow rate of the Ringer's solution and the buffer kept constant at 2 and 4 μl min^{-1} respectively, a linear calibration plot for L-glutamate was obtained over 2×10^{-6}–5×10^{-3} M; the slope, the y intercept, and the linear correlation coefficient were 181 nA mM^{-1}, 0.01 nA, and 0.999. Also, over the concentration range of the linear calibration plot the conversion efficiency of L-glutamate to hydrogen peroxide was ca. 100%. The detectable concentration was 1×10^{-6} M ($S/N = 3$).

3.2. Micro flow system with amplification

In this work, L-glutamate oxidase/glutamate dehydrogenase coimmobilized PTFE reactor was used for the amplification of L-glutamate. The operating principle of this enzyme reactor is shown schematically in Fig. 2. On passage through this enzyme reactor, coupled enzymes (L-glutamate oxidase and glutamate dehydrogenase) permit the recycling of L-glutamate in the presence of excess of NADH, oxygen, and ammonium in the carrier solution. Thus, for every L-

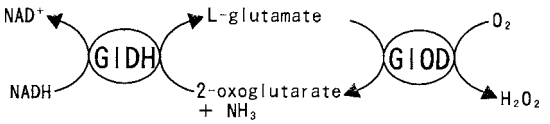

Fig. 2. Enzymatic recycling model of L-glutamate in the L-glutamate oxidase (GlOD)/glutamate dehydrogenase (GIDH) co-immobilized reactor, under the conditions in the presence of excess of NADH, oxygen, and ammonium.

glutamate molecule a number of oxygen molecules are converted to a large amount of hydrogen peroxide, which can be detected amperometrically. However, the cycle can also be initiated with 2-oxoglutarate. Therefore, the presence of 2-oxoglutarate interferes with the measurement of L-glutamate. Because of this, saccharopine dehydrogenase immobilized PTFE reactor was inserted in series before the L-glutamate oxidase/glutamate dehydrogenase co-immobilized reactor to remove 2-oxoglutarate in the dialysate according to Eq. (1).

$$\text{2-oxoglutarate} + \text{L-lysine} + \text{NADH} \xrightarrow{\text{saccharopine dehydrogenase}} \text{saccharopine} + \text{NAD}^+ \quad (1)$$

Experiments were first conducted to establish the optimum pH for the L-glutamate oxidase/glutamate dehydrogenase PTFE reactor. Ammonium phosphate (0.1 M) of various pH values containing 3 mM NADH was used as the carrier buffer, because the presence of NADH, oxygen, and ammonium is necessary for the substrate recycling (see Fig. 2). The buffer and Ringer's solution was pumped at same flow rate (2 μl min^{-1}), and then the probe was immersed in the same buffer containing 1×10^{-5} M L-glutamate and a steady-state current was recorded. Maximum response to L-glutamate was obtained at pH 7.0–7.5. At pH values below 6.5, the amplified current decreased. At pH values above 8.0, phosphate ion in the buffer reacted to produce insoluble calcium phosphate with calcium ion in Ringer's solution; this was responsible for the closing of PTFE coil. Therefore, 0.1 M ammonium phosphate at pH 7.2 was selected throughout as the optimum buffer.

When the NADH concentration in the buffer was increased from 0 to 1 mM as shown in Fig. 3, the sensitivity to L-glutamate was increased about 200 times. This indicates that the recycling of L-glutamate occurs effectively between the coupled enzymes in the presence of NADH and ammonium, because oxygen is dissolved in the buffer and Ringer's solution. However, the increase was only slight at higher concentration of NADH, probably because of limited oxygen in the solution. The saccharopine dehydrogenase immobilized PTFE reactor needs NADH as well and furthermore L-lysine to decompose 2-oxoglutarate according to Eq. (1). Therefore, the concentration of L-lysine in the buffer was raised from 0 to 5 mM, keeping the concentration of NADH constant at 3 mM. As shown in Fig. 4, the increase of the L-lysine concentration led to the decrease of the response current to 2-oxoglutarate. At the L-lysine concentration more than 3 mM, more than 95% of 2-oxoglutarate could be decomposed to saccharopine. Therefore, 0.1 M ammonium phosphate buffer (pH 7.2) containing 3 mM NADH and 5 mM L-lysine was selected as the optimum buffer for both enzyme reactors.

In this work, hydrogen peroxide generated in the enzyme reactor was detected by a poly(1,2-diaminobenzene) film-coated platinum electrode. If a bare platinum electrode without surface modification was used as the detector of hydrogen peroxide, a large background current was caused by

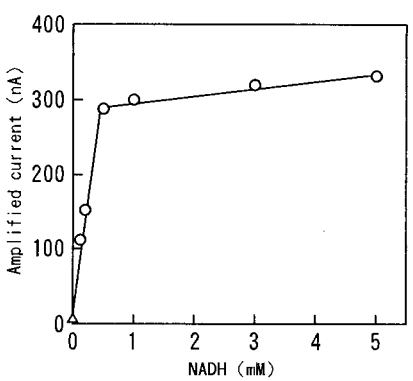

Fig. 3. Effect of NADH concentration in the carrier buffer on amplified current for 1×10^{-5} M L-glutamate. Δ, without NADH.

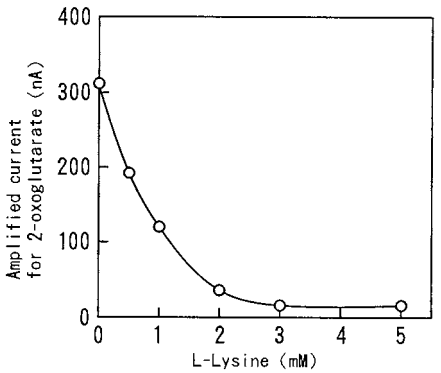

Fig. 4. Effect of L-lysine concentration in the carrier buffer on the enzymatic decomposition of 2-oxoglutarate in the saccharopine dehydrogenase immobilized reactor: sample, 1×10^{-5} M 2-oxoglutarate; carrier buffer, 0.1 M ammonium phosphate buffer (pH 7.2) held constant NADH concentration at 3 mM. The carrier buffer and Ringer's solution were pumped at same flow rate (2 μl min^{-1}).

the direct oxidation of NADH in the buffer at an applied potential of 0.6 V versus Ag/AgCl. Because of this large background current, the bare platinum electrode was essentially not capable of detecting the hydrogen peroxide generated in the enzyme reactor. In contrast, the poly(1,2-diaminobenzene) film-coated platinum electrode gave a small base-line current, even in the presence of 3 mM NADH in the buffer. This means that the poly(1,2-diaminobenzene) film blocks the access of NADH in the buffer to the electrode surface. Similarly, this modified electrode blocks the access of oxidizable interferents such as L-ascorbate, urate, and L-cysteine at concentration below 2 mM to the electrode surface. In addition to this, the response current of this modified electrode to hydrogen peroxide was decreased to 42% of that obtained at bare electrode. From these results it is apparent that the poly(1,2-diaminobenzene) film-coated platinum electrode prevents NADH in the carrier buffer and oxidizable interferents such as L-ascorbate from reaching the electrode surface and selectively allows hydrogen peroxide to penetrate into the film. Consequently, this modified electrode was very useful as an amperometric detector that responds selectively to hydrogen peroxide produced enzymatically in the L-glutamate oxidase/glutamate dehydrogenase reactor, in spite of the presence of excess NADH in the carrier buffer.

When the flow rate was increased, keeping the ratio (1:1) of the flow rate of the Ringer's solution and the buffer constant, the permeability of L-glutamate into the probe was decreased and the amplification factor decreased as well (Table 1). The decrease of the amplification factor can be related to the residence time of the analyte in the reactor (that is, the turnover numbers of recycling). When the flow rate of the Ringer's solution and the buffer was 1 μl min^{-1}, respectively, the amplified current for L-glutamate was greatest. However, the time required to reach steady-state response after the immersion of the probe in the L-glutamate solution was too long (ca. 23 min). Therefore, the Ringer's solution and buffer were pumped at the same flow rate of 2 μl min^{-1}, because this provided relatively good sensitivity (amplification factor of 160) and reasonable response times (or delay time of 10.5 min).

Fig. 5 shows log–log calibration graphs for L-glutamate with and without NADH in the buffer. In the absence of NADH in the buffer, the response depended linearly on the L-glutamate concentration between 5×10^{-6} and 1×10^{-3} M. The presence of 3 mM NADH in the buffer, however, resulted in an immensely increased signal. The calibration graph for the amplified response was linear over the range 0.8×10^{-7}–2×10^{-5} M L-glutamate. In this region, the L-glutamate response was amplified by a factor of about 160. However, the presence of NADH in the carrier buffer caused higher noise level compared with the case of the absence of NADH. Because of this, the detection limit was 0.5×10^{-7} M ($S/N = 3$), which was a higher value compared with that expected from amplification factor. The relative standard deviations for seven replicate measurements were 5.1% for 5×10^{-6} M L-glutamate. This result indicates that substrate recycling can be a useful method for increasing the sensitivity of microdialysis flow system with immobilized enzyme reactors.

Three immobilized enzyme reactors used in this work were used repeatedly to confirm the instability with time. The L-glutamate oxidase and saccharopine dehydrogenase immobilized reactors

Table 1
Effect of flow rate on steady-state signal for L-glutamate

Flow rate (μl min^{-1})	Signal current (nA)			Amplification factor	Permiability[c] (%)	Time[d] (min)
Ringer's solution	Buffer	No amplified[a]	Amplified[b]			
1	1	244	583	239	12.3	23.3
2	2	200	321	161	7.8	10.5
3	3	163	177	109	6.4	7.5

[a] No amplified current for 1×10^{-3} M L-glutamate (in the absence of NADH in the buffer).
[b] Amplified current for 1×10^{-5} M L-glutamate (in the presence of 3 mM NADH in the buffer).
[c] Calculated from the ratio of no amplified current for L-glutamate obtained at the systems with and without probe.
[d] The time required to reach the steady-state current.

retained the sufficient enzyme activities which could enable complete enzymatic conversion even after repetitive use (about 3 h per day) for 40 days. However, the L-glutamate oxidase/glutamate dehydrogenase co-immobilized reactor was inferior to other two enzyme reactors in the long-term stability; after repetitive use (about 3 h per day) for 20 days its enzyme activity decreased rapidly. Similarly, the poly(1,2-diaminobenzene) film-coated platinum electrode was used repeatedly to confirm the long term stability; even after use for 3 weeks, it was stable enough to use, but after that lost its desired properties gradually.

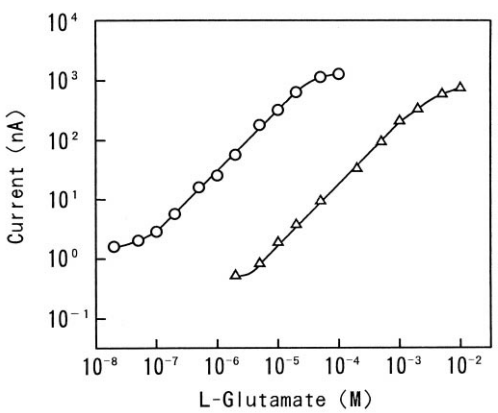

Fig. 5. Calibration graphs for L-glutamate: (○) Amplified current (obtained in the presence of NADH); (△) no amplified current (obtained in the absence of NADH). The carrier buffer [0.1 M ammonium phosphate buffer (pH 7.2) containing 3 mM NADH and 5 mM L-lysine] and Ringer's solution were pumped at 2 μl min^{-1} in the flow system shown in Fig. 1(B).

4. Conclusions

The present microdialysis flow system, with the poly(1,2-diaminobenzene) film-coated platinum electrode as an amperometric detector and L-glutamate oxidase/glutamate dehydrogenase coimmobilized reactor involving amplification, was found to be useful for the highly sensitive detection of L-glutamate, without a pronounced increase in the base-line currents due to direct oxidation of NADH in the carrier stream. Also, saccharopine dehydrogenase immobilized reactor was used to eliminate 2-oxoglutarate which interfered with the measurement of L-glutamate, by inserting in series before the L-glutamate oxidase/glutamate dehydrogenase coimmobilized reactor. As a result, the present continuous flow method was useful for highly selective and sensitive detection of L-glutamate, by recycling only L-glutamate in the reactor involving amplification.

This method will be applied for the in vivo monitoring of trace amounts of L-glutamate in the dialysate e.g. in rat brain; details of this will be reported in the near future.

Acknowledgements

The author (T.Y.) wishes to express his appreciation to the Ministry of Education, Science and Culture of Japan (No.07640814), for Scientific Research for partial financial support of this research project.

References

[1] W.H. Church, J.B. Justice Jr., Anal. Chem. 59 (1987) 712.
[2] C.E. Lunte, D.O. Scott, P.T. Kissinger, Anal. Chem. 63 (1991) 773A.
[3] B.H.C. Westerink, Trends Anal. Chem. 11 (1992) 176.
[4] M.T. Diaz, D.O. Scott, G.E. Lunte, Anal. Chem. 64 (1992) 806.
[5] T. Yao, S. Suzuki, H. Nishino, T. Nakahara, Electroanalysis 7 (1995) 1114.
[6] D. Moscone, M. Pasini, M. Mascini, Talanta 39 (1992) 1039.
[7] E. Zilkha, A. Koshy, T.P. Obrenovitch, H.P. Bennetto, L. Symon, Anal. Lett. 27 (1994) 453.
[8] F. Schubert, D. Kirstein, K.L. Schroder, F.W. Scheller, Anal. Chim. Acta 169 (1985) 391.
[9] T. Yao, N. Kobayashi, T. Wasa, Anal. Chim. Acta 248 (1991) 345.
[10] K. Kronkvist, K. Wallentin, G. Johansson, Anal. Chim. Acta 290 (1994) 335.
[11] T. Yao, H. Ogawa, T. Nakahara, Talanta 42 (1995) 1297.
[12] T. Yao, N. Kobayashi, T. Wasa, Electroanalysis 2 (1990) 563.
[13] T. Yao, N. Kobayashi, T. Wasa, Anal. Chim. Acta 238 (1990) 339.
[14] M.V. Asouzu, W.K. Nonidez, M.H. Ho, Anal. Chem. 62 (1990) 708.
[15] T. Yao, N. Kobayashi, T. Wasa, Electroanalysis 3 (1991) 493.
[16] E.H. Hansen, L. Norgaad, M. Pedersen, Talanta 38 (1991) 275.
[17] T. Yao, M. Satomura, T. Nakahara, Anal. Chim. Acta 296 (1994) 271.
[18] T. Yao, N. Kobayashi, T. Wasa, Anal. Chim. Acta 231 (1990) 121.

ELSEVIER

Talanta 45 (1998) 925–930

Talanta

An extraction study of gallium, indium and thallium using TPASO as an extractant

Santosh V. Vartak, Vijay M. Shinde *

Analytical Laboratory, Department of Chemistry, The Institute of Science, 15, Madam Cama Road, Mumbai 400 032, India

Received 13 March 1997; received in revised form 13 June 1997; accepted 16 June 1997

Abstract

A method is proposed for the extraction and individual separation of trivalent gallium, indium and thallium from salicylate media using triphenylarsine oxide dissolved in toluene as an extractant. The optimum extraction conditions are evaluated and described. The extracted metal ions are stripped and estimated spectrophotometrically following complexation with 4-(2-pyridylazo) resorcinol. A possible mechanism of the extraction is discussed. The method permits rapid and precise individual separation of gallium (III), indium (III) and thallium (III) and is applicable to the analysis of alloy samples. © 1998 Elsevier Science B.V.

Keywords: Extraction; Separation; TPASO

1. Introduction

Gallium, indium and thallium are industrially important metals and hence their separation and purification is desired. Various neutral extractants such as tributyl phosphate [1], mesityl oxide [2], tributylphosphine oxide [3] and trioctylphosphine oxide [3] have been reported for the extraction of gallium, indium and thallium. But these methods suffer from drawbacks such as longer extraction periods [1,3], use of salting out agents [1,2], scrubbing [1], critical temperature control [3] and multiple extraction. Triphenylphosphine oxide [4] and tris-(2-ethylhexyl) phosphate [5] have also been explored as potential extractants for trivalent gallium, indium and thallium in our laboratory.

Triphenylarsine oxide, being more basic than corresponding phosphine oxide appears to form stronger bonds with metals. It has already been used in our laboratory for the extraction studies of Ti, Zr, Hf [6]; Zn, Cd, Hg; U, Th and Bi, Te. An extension of this study showed that triphenylarsine oxide permits individual separation of trivalent gallium, indium and thallium from salicylate media. The method is simple, precise, free from above mentioned drawbacks and is applicable to the estimation of gallium, indium and thallium from alloy samples.

* Corresponding author.

PII S0039-9140(97)00197-5

Table 1
Optimum extraction conditions for trivalent gallium, indium and thallium

Metal ion	Sodium salicylate	pH	[TPASO]	Shaking period	Estimation procedure	Stripping solution
Ga (III)	5×10^{-2}	5.5–6.5	10 ml of 0.15% in toluene		2×5 ml	
5–20 μg	6.25×10^{-2}			40	Ammonium hydroxide	PAR
In (III)	6.25×10^{2}	5.0–5.5	5 ml of 0.5% in toluene			
5–20 μg	7.5×10^{-2}			40	2×5 ml water	PAR
TI (III)	6.25×10^{-3}	3.0–3.5	5 ml of 0.3% in toluene			PAR
5–50 μg	-1.25×10^{-2}			50	2×5 ml acetate buffer	

2. Experimental

2.1. Apparatus

Absorbance and pH measurements were taken on Shimadzu UV-VIS 160 A spectrophotometer and Control Dynamics digital pH meter with combined glass electrode, respectively.

2.2. Reagents and chemicals

Stock solutions of gallium (III) and indium (III) were prepared by dissolving gallium trichloride (7.7 g) and indium trichloride (4.2 g) (Aldrich), respectively, in 250 ml distilled water containing 0.5 M hydrochloric acid. The stock solution of thallium was prepared by dissolving 6.5 g of thallous nitrate (BDH) in 500 ml of distilled water containing 1 M nitric acid. The solutions were standardised complexometrically [7,8] and diluted to obtain required concentration.

In the test solution, thallium (I) was oxidised to thallium (III) by adding a few drops of bromine water, warmed to remove excess of bromine, cooled and used for extraction.

A sodium acetate buffer solution was prepared by dissolving 17.2 g of sodium acetate trihydrate in 400 ml of distilled water, adding 17 ml of glacial acetic acid and diluting to 1 l.

Triphenylarsine oxide (TPASO) (99.8% purum manufactured by Fluka, Switzerland) dissolved in toluene was used as an extractant. All other chemicals used were of analytical reagent grade.

2.3. General extraction procedure

To an aliquot of solution (25 ml) containing microgram amounts of gallium (III), indium (III) and thallium (III), sodium salicylate was added to obtain the desired molarity. The pH of the solution was suitably adjusted with 0.1 N sodium hydroxide and hydrochloric acid solutions. The solution was then extracted for the required period with triphenylarsine oxide dissolved in toluene. (The optimum extraction conditions are reported in Table 1). After the phase separation, the metal ions were stripped from the TPASO

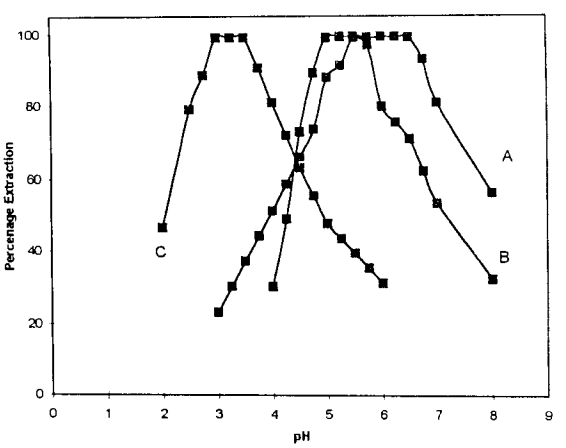

Fig. 1. Effect of pH on the extraction of trivalent gallium (A) (at 5×10^{-2} M sodium salicylate and 10 ml of 0.15% TPASO), indium (B) (at 6.25×10^{-2} M sodium salicylate and 5 ml of 0.5% TPASO) and thallium (C) (at 6.25×10^{-3} M sodium salicylate and 5 ml of 0.3% TPASO).

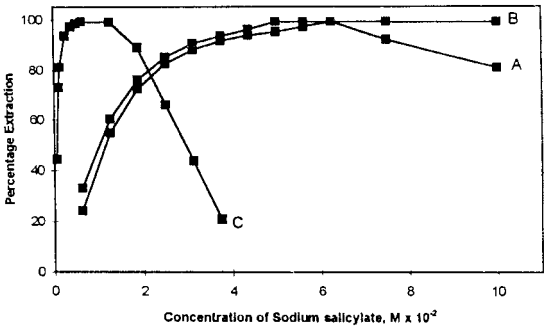

Fig. 2. Effect of sodium salicylate concentration on the extraction of trivalent gallium (A) (at pH 6.5 and 10 ml of 0.15% TPAS0), indium (B) (at pH 5.0 and 5 ml of 0.5% TPASO) and thallium (C) (at pH 3.0 and 5 ml of 0.3% TPAS0).

phase with appropriate stripping solutions and estimated spectrophotometrically in the aqueous phase with 4-(2-pyridylazo) resorcinol (PAR) as follows.

For gallium (III), 1 ml of aqueous solution of 0.05% PAR was added, pH was adjusted to 5.0–6.0 with 0.1 N sodium hydroxide and hydrochloric acid and absorbance was measured at 500 nm against reagent blank prepared analogously.

For indium (III), 1 ml of aqueous solution of 0.1% PAR was added, pH was adjusted to 6.0–7.5 and the absorbance was measured at 510 nm against reagent blank prepared analogously.

For thallium (III), 1 ml of aqueous solution of 0.1% PAR was added, pH was adjusted to 3.5–4.5 with 0.1 N sodium hydroxide and hydrochloric acid solutions and the absorbance was measured at 520 nm against the reagent blank prepared analogously.

The recoveries of trivalent gallium, indium and thallium were computed from the calibration plots.

3. Results and discussion

TPASO do not extract gallium (III), indium (III) and thallium (III) from free acids solutions. This behaviour is similar to that observed with trioctylarsine oxide [9] and may be due to formation of $(TPASOH)^+$ which has high stability and is favoured at high acidities. The extraction of gallium, indium and thallium, with salicylate media is however feasible, possibly because it controls the hydrogen ion concentration. The aromatic group in salicylate and its ability to form neutral ion pair complexes are also the probable reasons of TPASO to extract gallium (III), indium (III) and thallium (III) from salicylate solution.

The extraction was studied at various pH (1.5–8.0), sodium salicylate (5×10^{-4}–1×10^{-1} M) and TPASO concentration (0.01–0.5%) to establish the optimum conditions for the quantitative extraction of gallium (III), indium (III) and thal-

Table 2
Effect of foreign ions

Foreign ion	Tolerance limit (μg)		
	Ga (III) 10 μg	In (III) 10 μg	TI (III) 40 μg
Zn (II)	250	250	600
Cd (II)	300	200	450
Hg (II)	350	400	600
Cu (II)	300	200	200
Pb (II)	150	200	150
Mn (II)	250	200	300
Re (VII)	400	400	400
Cr (VI)	200	200	250
Mo (VI)	400	400	750
W (VI)	300	300	600
Ti (IV)	150	150	200
V (V)	350	250	450
Ni (II)	250	250	300
Co (II)	300	400	300
Mg (II)	600	700	600
Al (III)	600	600	800
Bi (III)	—	—	—
Sb (III)	250	200	350
Fe (III)	200	200	250
Te (IV)	100	150	100
EDTA	—	—	—
SCN^-	200	150	400
Citrate	100	150	250
Tartarate	100	100	300
Oxallate	200	150	200
$S_2O_3^{2-}$	200	200	400

Gallium (III), aqueous phase—salicylate 5×10^{-2} M, pH 5.5–6.5; organic phase—10 ml of 0.15% TPASO in toluene.
Indium (III), aqueous phase—salicylate 6.25×10^{-2} M, pH 5.0–5.5; organic phase—5 ml of 0.5% TPASO in toluene.
Thallium (III), aqueous phase—salicylate 6.25×10^{-3} M, pH 3.0–3.5; organic phase—5 ml of 0.3% TPASO in toluene.

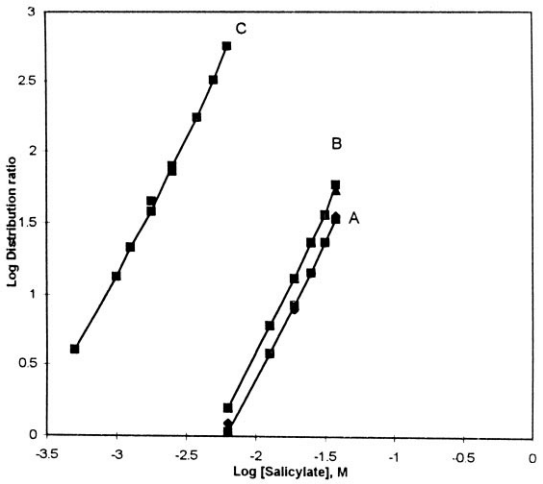

Fig. 3. Plots of log of distribution ratio vs. log of salicylate concentration for trivalent gallium (A) (at fixed pH 6.5 and 10 ml of 0.15% TPASO), indium (B) (at fixed pH 5.0 and 5 ml of 0.5% TPASO) and thallium (C) (at fixed pH 3.0 and 5 ml of 0.3% TPASO).

lium (III) (Fig. 1 and Fig. 2). The quantitative extraction of gallium, indium and thallium occurs at pH 5.5–6.5, 5.0–5.5 and 3.0–3.5, respectively, when extracted from 5×10^{-2}–6.25×10^{-2} M, 6.25×10^{-2}–7.5×10^{-2} M and from 0.62×10^{-2}–1.25×10^{-2} M sodium salicylate solution.

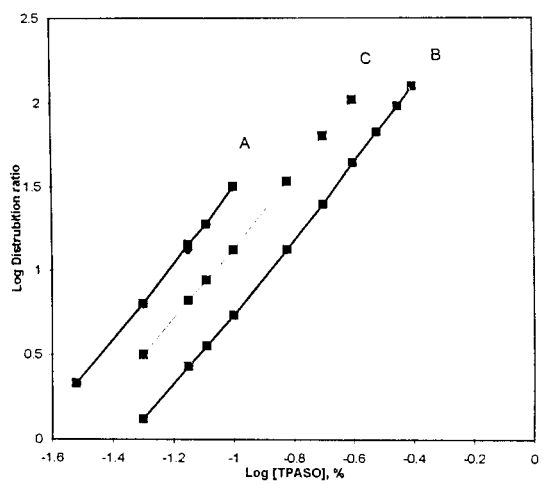

Fig. 4. Plots of log of distribution ratio vs. log of TPASO concentration for trivalent gallium (A) (at fixed pH 6.5 and 5×10^{-2} M sodium salicylate), indium (B) (at fixed pH 5.0 and 6.25×10^{-2} M sodium salicylate) and thallium (C) (at fixed pH 3.0 and 6.25×10^{-3} M sodium salicylate).

Variation in shaking period showed that a shaking period of 40 s was adequate for the quantitative extraction of gallium (III) and indium (III) whereas that of 50 s was adequate for thallium (III). Prolonged shaking had no adverse effect.

The suitability of diluents was investigated using solvents such as toluene, xylene, benzene, chloroform and carbon tetrachloride. The extraction was incomplete with other diluents except toluene and xylene. Toluene gives quick and better phase separation and hence used for the further extraction studies.

Of the various stripping agents tried for the back extraction of gallium (III), indium (III) and thallium (III) from TPASO phase, 0.5–1.0 M nitric acid and ammonium hydroxide stripped gallium quantitatively. The stripping of indium (III) and thallium (III) were feasible with water and acetate buffer, respectively.

The results in the Table 2 show the effect of various diverse ions on the extraction and determination of gallium (III), indium (III) and thallium (III) by the recommended procedure.

3.1. Nature of extracted species

An attempt is made to ascertain the composition of the extracted species using log–log plots (Fig. 3 and Fig. 4). A plot of log of distribution ratio versus log of salicylate concentration at fixed pH and TPASO concentration gave slopes of 2.0, 2.1 and 2.0 for trivalent gallium, indium and thallium, respectively. The observed slopes indicate the ratio of metal to salicylate is 1:2. Similarly plot of log of distribution ratio versus log TPASO concentration at fixed pH and salicylate concentration gave slopes of 1.98, 2.0 and 1.96 for gallium (III), indium (III) and thallium (III), respectively. This show that two TPASO molecules are associated with each metal ion. Therefore, the probable extraction mechanism is

$$M^{+3}_{aq} + Sal^{2-}_{aq} \rightleftharpoons MSal^{+}_{aq}$$

$$MSal^{+}_{aq} + Hsal^{-}_{aq} \rightleftharpoons [MSal^{+}HSal^{-}]_{aq}$$

$$[MSal^{+}Hsal^{-}]_{aq} + 2\,TPASO_{org} \rightleftharpoons [MSal^{+} HSal^{-}]2\,TPASO_{org}$$

Table 3
Estimation of gallium, indium, thallium in ternary mixtures

Analysis number	Mixture (μg)	Recovery[a] %	Coefficient of variation %
1	Ga, 10; In, 10; TI, 50	Ga, 99.0; In, 99.0; TI, 99.2	Ga, 0.21; In, 0.13; TI, 0.1
2	Ga, 20; In, 10; TI, 40	Ga, 99.2; In, 99.0; TI, 99.1	Ga, 0.19; In, 0.2; TI, 0.19
3	Ga, 10; In, 20; TI, 40	Ga, 99.0; In, 99.1; TI, 99.0	Ga, 0.23; In, 0.17; TI, 0.13

[a] Average of triplicate analysis.

The ion pair complex formed with salicylate is solvated by TPASO. Which is being more basic supplants water molecules and renders the species hydrophobic, thus favouring extraction into the organic phase.

3.2. Individual separation of trivalent gallium, indium and thallium

The method permits individual separation of trivalent gallium, indium and thallium at tracer concentrations. A mixture of gallium (III), indium (III) and thallium (III) from 0.625×10^{-2} M sodium salicylate solution adjusted to pH 3.0 was extracted for 50 s with 5 ml of 0.3% TPASO in toluene. This transfers thallium (III) quantitatively into TPASO phase retaining gallium (III) and indium (III) in aqueous phase. Thallium (III) from TPASO phase is stripped with acetate buffer and determined spectrophotometrically with PAR. The aqueous phase containing gallium and indium was first evaporated to lesser volume and then sufficient amount of sodium salicylate was added to make the concentration 6.25×10^{-2} M: adjust pH to 6.0 and extract for 40 s with 10 ml of 0.15% TPASO in toluene. This transfers gallium quantitatively in the TPASO phase along with indium (III) (40%). The co-extracted indium (III) was selectively stripped with water, mixed with the aqueous phase containing major portion of unextracted indium (III) and estimated spectrophotometrically with PAR. Gallium (III) is finally stripped with 1 N ammonium hydroxide from TPASO phase and determined spectrophotometrically with PAR. The recoveries of the metals from ternary mixtures were greater than 99.0%. The complete separation and estimation takes 20 min. Results are reported in Table 3.

3.3. Analysis of alloy samples

A 1 g amount of each alloy was dissolved in 3 ml of aqua regia, evaporated to incipient dryness and diluted to 100 ml. An aliquot of each sample solution is then analysed by the proposed method for the estimation of trivalent gallium, indium and thallium. The recoveries are greater than 99.0% The results are reported in Table 4.

Table 4
Analysis of alloy samples

Composition (%)	% Recovery*			Coefficient of variation %		
	Ga (III)	In (III)	TI (III)	Ga (III)	In (III)	TI (III)
Mg, 0.87; Si, 0.65 In, 0.14: Mn, 0.50 Ti, 0.65; Zn, 0.87 Al, 96.3; +1 mg TI	99.0	99.1	99.0	0.19	0.2	0.17
Mg, 0.25, Si, 0.10 Ga, 0.05; Mn, 1.5 Ti, 1.5; Zn, 1.5 Al, 94.0; +1 mg TI	99.2	99.0	99.1	0.12	0.17	0.15

* Average of triplicate analysis.

Acknowledgements

The financial assistance to this project by Council of Scientific and Industrial Research (CSIR, New Delhi, India) is gratefully acknowledged.

References

[1] A.K. De, A.K. Sen, Talanta 19 (1967) 629.
[2] M.B. Chavan, V.M. Shinde, Sep. Sci. 8 (1973) 285.
[3] N. Oldrich, M. Jiri, K. Jiri, Collect. Czech. Chem. Commun. 46 (1981) 1906.
[4] S.M. Kakade, V.M. Shinde, Analyst 118 (1993) 1449.
[5] D.C. Nambiar, J.S. Gaudh, V.M. Shinde, Talanta 41 (1994) 1951.
[6] D.C. Nambiar, N.G. Bhilare, V.M. Shinde, Anal. Lett. 30 (1) (1997).
[7] A.I. Vogel, A Textbook of Quantitative Inorganic Analysis, 3rd ed., Longman, London, 1961.
[8] F.J. Welcher, The Analytical Uses of Ethylendiaminetetra Acetic Acid, 1st ed., Van Norstrand, New York, 1961.
[9] K. Irgolic, R.A. Zingaro, D.E. Linder, J. Inorg. Nucl. Chem. 30 (1968) 1941.

ELSEVIER

Talanta 45 (1998) 931–934

Talanta

The ionic product of water in highly concentrated sodium perchlorate solutions

M.L. Turonek *, G.T. Hefter, P.M. May

Department of Chemistry and Mineral Science, Murdoch University, Murdoch, WA 6150, Australia

Received 15 April 1997; accepted 17 June 1997

Abstract

The ionic product of water, $pK_w = -\log[H^+][OH^-]$, has been determined in aqueous solutions of sodium perchlorate over the concentration range of 1.0–8.0 M at 25°C from high-precision potentiometric titrations carried out in cells with liquid junction using both glass and hydrogen electrodes. The glass electrode results are systematically lower probably as a result of interference by Na^+ ions. © 1998 Elsevier Science B.V.

Keywords: Sodium perchlorate; High-precision potentiometric titrations; Glass electrode; Hydrogen electrode

1. Introduction

The detailed study of thermodynamic parameters of highly concentrated mixed electrolyte solutions is of direct relevance to a wide variety of chemical systems of geochemical or industrial interest. Models for such systems aim to describe the change in chemical speciation over a wide range of temperature, pressure, concentration and composition. These models depend on equilibrium parameters extracted from simple systems. Sodium perchlorate is of special interest because of its high aqueous solubility and its broad use as an inert supporting electrolyte for maintaining ionic concentrations such that activity coefficients remain virtually constant.

Accurate values of the ionic product of water, pK_w:

$$H_2O \rightleftharpoons H^+_{(aq)} + OH^-_{(aq)}$$

$$K_w = [H^+_{(aq)}][OH^-_{(aq)}]$$

are required for the estimation of activity coefficient changes, liquid junction potentials, and metal-ligand formation constants as part of our continuing thermodynamic investigations of chemical equilibria in concentrated electrolytes. In particular, we need systematic and internally-consistent measurements of pK_w for a wide range of ionic media. Data for the ionic product of water, pK_w, in this medium [1–10] are scarce, however, above $I = 4$ M. Accordingly, new determinations of the ionic product of water at 25°C have been made in aqueous solutions of sodium perchlorate over the concentration range 1.0–8.0 M by application of glass- and hydrogen-electrode potentiometry.

* Corresponding author.

PII S0039-9140(97)00199-9

2. Experimental

2.1. Materials

Sodium perchlorate monohydrate, $NaClO_4.H_2O$, (BDH AnalaR, 99.0% purity) was used as received, with a water content determined by thermogravimetric analysis to be 11.99% (theor. 12.83%). The titrant was prepared from commercial volumetric ampoules of sodium hydroxide (BDH Convol) and the acid solutions were prepared from concentrated perchloric acid (70% w/w aqueous solution, analytical grade, Ajax Chemicals) and standardised volumetrically against NaOH (BDH Convol) using methyl orange indicator. All solutions were made up with Millipore Milli-Q water that had been boiled and purged with high purity nitrogen to remove oxygen and carbon dioxide. Gran analyses of the potentiometric titrations indicated that the solutions were essentially carbonate free (accounting for less than 0.2% of the total alkalinity).

2.2. Apparatus and procedure

The ionic product of water was determined by potentiometric titration of $HClO_4$ (0.020 M) dissolved in $NaClO_4$ (c-0.020 M) with NaOH (0.1 M) in $NaClO_4$ (c M). Measurements were carried out over the ionic strength range of $1.00 \leq c \leq 8.00$ M. All the titrations were performed using Ag/AgCl electrodes of in-house construction, together with either a glass electrode (Metrohm, model 6.0101.000) or a hydrogen electrode (prepared and used as described previously [11]) in a standard jacketed glass cell using the high precision automated titration system developed in our laboratories. Where glass electrode potentiometry was used the solutions were blanketed by high purity nitrogen delivered through a carbon dioxide trap and a pre-humidifier containing a solution of the sodium perchlorate at the concentration of interest. Where the hydrogen electrode was used ultra-high purity hydrogen gas (CIG) was delivered to the cell via thick-walled copper tubing to a pre-humidifier. The cell was tightly sealed to minimize contamination by atmospheric oxygen and carbon dioxide. The burettes were Metrohm 665 Dosimat (calibrated precision $\pm 0.1\%$) driven by an IBM PC computer. All volumetric glassware was A-grade and calibrated. The cell emf was measured to ± 0.1 mV by high impedance digital voltmeters of in-house construction, interfaced with the computer. The temperature in the cells was maintained at 25.0 ± 0.02°C by use of a circulator thermostat (Heto Birkerød Denmark, model 04 PT 623). Temperatures were monitored with a thermistor calibrated against a quartz crystal thermometer (Hewlett Packard, Model HP2804A).

The cells used for the titrations may be represented schematically as:

$$\mathrm{Ag} \mid \mathrm{AgCl(s)} \mid \mathrm{5\ M\ NaCl(aq)} \underset{E_{j1}}{\|} \mathrm{5\ M\ NaCl(aq)} \underset{E_{j2}}{\|} x\mathrm{HX},(c-x)\mathrm{MX} \mid \mathrm{HE} \quad (1)$$

where HE represents a hydrogen ion-responsive glass (GE) or platinum (H_2(g)/Pt) electrode, and E_{j1} and E_{j2} are liquid junction potentials. E_{j1} is essentially constant and may be incorporated into the potential E_{ref} of the silver-silver chloride reference electrode. The potential of the cell is then:

$$E_{cell} = E_{HE} - E_{ref} - E_{j2} \quad (2)$$

If it is assumed that throughout the course of a titration that E_{ref}, E_{j2}, the activity coefficients of the trace species of interest (H^+ and OH^-), and the hydrogen fugacity (pressure) are constant, then it is readily shown by the usual methods of electrochemical thermodynamics that, at 25°C, the relationship between the cell potential and the hydrogen ion concentration is:

$$E_{cell}/\mathrm{mV} = E^{0\prime}/\mathrm{mV} + 59.16 \log([H^+]/\mathrm{M}) \quad (3)$$

where $E^{0\prime}$ is the 'formal' cell potential, which includes the standard cell potential, the liquid junction potential E_{j2}, and activity coefficient and hydrogen fugacity terms.

The resulting emf data Eq. (3) were collected from 4–8 titrations for each sodium perchlorate concentration of interest and evaluated by least-squares analysis with respect to either the values of the cell potential (to obtain an estimate of the formal potential) or of the concentration of H^+ ions (to obtain an estimate of pK_w). The least-squares optimizations were made using the ESTA

suite of computer programs [12–14]. Gran-plots were calculated for each titration to evaluate the degree of carbonate contamination and the general condition of the electrochemical cell.

3. Results and discussion

Despite the high solubility of $NaClO_4$ and its widespread use as a supporting electrolyte for equilibrium constant measurements, there is an absence of reliable literature data for pK_w measured in the high background ionic strength range above 4.0 M. To our knowledge, this work is the first determination of the ionic product of water in sodium perchlorate in the ionic strength range above 5 M. The results of the least-squares analyses of the emf data are collected in Table 1. The stated precisions in parentheses refer to the internal consistency of the titration data; the real errors in the equilibrium constant (pK_w) are generally an order of magnitude greater than the internal precision [14]. In Fig. 1, our experimental results for pK_w in aqueous $NaClO_4$ are plotted against ionic strength, together with selected data from the literature. It is noteworthy that the hydrogen electrode results of Carpéni et al. [10] and Fischer and Byé [6] lie reasonably close to the same curve as the present HE values, although the agreement is not as good as observed previously for NaCl solutions [11]. This may reflect the presence of minor impurities in the notoriously difficult to purify $NaClO_4$. Similarly the glass electrode results of Näsänen and Meriläinen [5] match our own findings.

Table 1
The ionic product of water, pK_w, in aqueous sodium perchlorate at 298.15 K and 1 atm[a]

I (M)	pK_w (HE)	OBJT/10^{-1}	pK_w (GE)	OBJT/10^{-8}
1.0	13.7706 (7)	0.5	13.7709 (5)	0.3
2.0	13.9597 (4)	0.5	13.9374 (4)	0.5
4.0	14.5161 (8)	2.9	14.4465 (3)	0.3
6.0	15.2234 (7)	1.9	15.1295 (6)	1.8
8.0	15.9396 (8)	2.0	15.9653 (7)	1.7

[a] HE, hydrogen electrode; GE, glass electrode; OBJT, objective function [12–14]. Numbers in parentheses indicate the standard deviation in the last decimal place quoted.

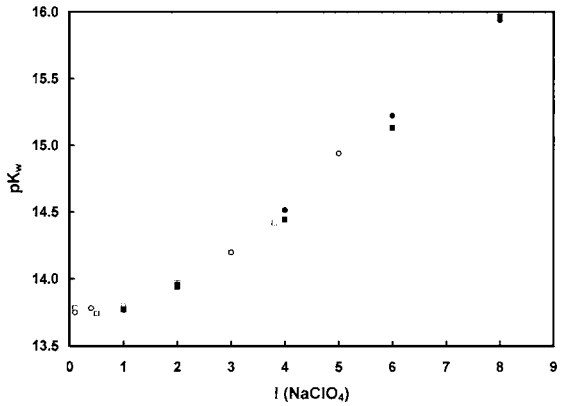

Fig. 1. Ionic product of water in sodium perchlorate at 25°C: □ [6] (HE); ○ [10] (HE); ◥ this work (GE); ● this work (HE).

It is apparent from Fig. 1 that there is a systematically increasing difference between the glass and hydrogen electrode results as the ionic strength increases up to 6.0 M. Although small, these differences are outside the experimental error (Table 1). Similar results were observed by us in NaCl media (up to $I = 5.0$ M) and have been tentatively ascribed to interference of Na^+ with the glass membrane as no such effect is observed in KCl, at least up to the solubility limit.

In 8.0 M $NaClO_4$ the difference between the results obtained from the two electrodes virtually disappears. The reasons for this are unclear at present. Comparison of the slopes $S\ (= \Delta pK_w/\Delta I)$ of the GE and HE curves in Fig. 1 at first sight suggests this convergence may be due to a decline in the HE performance. Thus, S_{GE} increases smoothly over the entire ionic strength range whereas S_{HE} increases initially but eventually becomes constant (i.e. pK_w become linearly dependent on I). However, a linear relationship (between log K_{HF} and I) has also been observed for the similar equilibrium:

$$HF_{(aq)} \rightleftharpoons H^+_{(aq)} + F^-_{(aq)}$$

obtained from a fluoride ion-selective electrode measurements over the same concentration range in $NaClO_4$ media [15]. It should also be noted

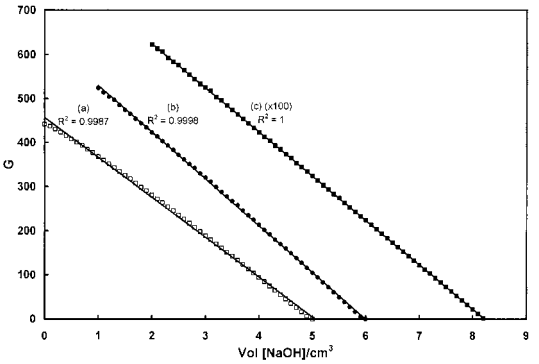

Fig. 2. Performance of glass electrodes as measured by Gran plots ($G = 10^{E/59.16}(V_0 + V)$, where E is the cell potential (mV), V_0 is the initial volume of the solution, and V is the volume of added titrant). (a) Electrode soaked in 0.02 M $HClO_4$ and $I = 8$M ($NaClO_4$) (□); (b) electrode soaked in 0.02 M $HClO_4$ and $I = 1.0$ M ($NaClO_4$) for 36 h (●); (c) electrode soaked in 1 mM HCl in $I = 1.0$ M ($NaClO_4$) (◥). Note: Gran plots refer to strong acid-strong base titrations in: (a,b) 8 M $NaClO_4$; (c) 1 M $NaClO_4$. The data points (●) and (◥) are offset by 1 and 2 cm^3, respectively for purposes of clarity.

that if the convergence of results at $I = 8.0$ M is due to a decline in performance of either or both electrodes, any such deterioration is not reflected in the objective function values or the standard deviations listed in Table 1.

With respect to the glass electrode there is clear evidence of a degradation in performance at very high $NaClO_4$ concentrations. Gran plots in the acidic region of the titration (Fig. 2, curve (a)) are clearly curved, which indicates that the glass electrode response is not Nernstian. This behaviour is in marked contrast to what we routinely observed in more dilute electrolte solutions (Fig. 2, curve (c)). Such behaviour first becomes apparent in 4.0 M $NaClO_4$ solutions but is increasingly marked when $c \geq 6.0$ M.

Our customary protocol in using glass electrodes for equilibrium constant measurements in concentrated electrolyte solutions is to store the electrode between titrations in 1 mM H^+ and 1.0 M NaCl or in the medium of interest. Electrodes are always 'rested' in such solutions for at least 16 h before re-use. This minimises any 'shock' to the membrane when it is placed in a test solution and helps to shorten stabilisation times. It appears that this protocol is unsatisfactory for very concentrated electrolyte solutions, at least in $NaClO_4$, possibly due to the dehydration of the glass membrane induced by the very low water activity. The electrode response can be improved to a satisfactory level, as indicated by a return to linearity in the Gran plot, by allowing the glass electrode to soak in a solution of 0.02 M $HClO_4$ and 1.0 M $NaClO_4$ for 36 h before and after each titration to 'recuperate' (Fig. 2, curve (b)).

Although some problems associated with loss of platinum black have occasionally been observed, especially in acid solution, the behaviour of carefully prepared hydrogen electrodes at these concentrations appears normal. For the present work, our hydrogen electrodes were always stored in 0.02 M $HClO_4$ and 1.0 M $NaClO_4$ for at least 24 h before re-use.

Acknowledgements

This work was funded by the Australian alumina industry through the Australian Mineral Industry Research Association Project P380B and a collaborative grant from the Australian Research Council.

References

[1] A. Ågren, Acta Chem. Scand. 9 (1955) 39.
[2] N. Ingri, G. Lagerstrom, M. Frydman, L.G. Sillén, Acta Chem. Scand. 11 (1957) 1034.
[3] G. Lagerström, Acta Chem. Scand. 13 (1959) 722.
[4] B. Carell, Å. Olin, Acta Chem. Scand. 14 (1960) 1999.
[5] R. Näsänen, P. Meriläinen, Suom. Kem B33 (1960) 149.
[6] R. Fischer, J. Byé, Bull. Soc. Chim. Fr. (1964) 2920.
[7] P.N. Kovalenko, K.N. Bagdasarov, Zh. Neorg. Khim. 10 (1965) 1624.
[8] G. Anderegg, Helv. Chim. Acta 50 (1967) 2333.
[9] H. Persson, Acta Chem. Scand. 25 (1971) 543.
[10] G. Carpéni, E. Boitard, R. Pilard, S. Poize, N. Sabiani, J. Chim. Phys. 69 (1973) 1445.
[11] I. Kron, S.L. Marshall, P.M. May, G.T. Hefter, E. Koenigsberger, Monatsh. Chem. 126 (1995) 819.
[12] P.M. May, K. Murray, D.R. Williams, Talanta 35 (1988) 825.
[13] P.M. May, K. Murray, Talanta 35 (1988) 927.
[14] P.M. May, K. Murray, Talanta 35 (1988) 933.
[15] G.T. Hefter, J. Solution Chem. 11 (1982) 45.

ELSEVIER

Talanta 45 (1998) 935–946

Talanta

Highly precise Re–Os dating for molybdenite using alkaline fusion and NTIMS

Richard Markey [a,*], Holly Stein [a,b], John Morgan [a]

[a] *AIRIE Group, Department of Earth Resources, Colorado State University, Fort Collins, CO 80523-1482, USA*
[b] *US Geological Survey, 910 National Center, Reston, VA 20192, USA*

Received 21 May 1997; received in revised form 18 June 1997; accepted 19 June 1997

Abstract

The technique described in this paper represents the modification and combination of two previously existing methods, alkaline fusion and negative thermal ion mass spectrometry (NTIMS). We have used this technique to analyze repeatedly a homogeneous molybdenite powder used as a reference standard in our laboratory. Analyses were made over a period of 18 months, using four different calibrations of two different spike solutions. The age of this standard reproduces at a level of $\pm 0.13\%$. Each individual age analysis carries an uncertainty of about 0.4% that includes the uncertainty in the decay constant for ^{187}Re. This new level of resolution has allowed us to recognize real differences in ages for two grain-size populations of molybdenite from some Archean samples. © 1998 Elsevier Science B.V.

Keywords: Alkaline fusion; Molybdenite; Negative thermal ion mass spectrometry

1. Introduction

In recent years there has been a surge of interest in directly dating ore deposits by dating the ore minerals themselves. Molybdenite has been of particular interest because it is a relatively common ore mineral and is ideally suited for analysis by the Re–Os method: molybdenite typically contains tens to hundreds of ppm Re (up to weight percent [1]), while essentially excluding Os from its structure during formation [2].

Several workers have dated molybdenite by the Re–Os method. The Re–Os dating scheme was developed for molybdenite by Herr and coworkers [3,4] and has been sporadically applied to molybdenites ever since. Until recently, attempts were hampered by insensitivity of the instruments used for analysis, uncertainties in the value of the decay constant for ^{185}Re, difficulties in isotopically equilibrating the sample with the spike, or Os loss during the chemical procedure.

Recent advances both in instrumentation and in chemical procedure have overcome these difficulties, and it is now possible to routinely produce accurate, precise age determinations on molybdenite (e.g. Ref. [5]). Suzuki and coworkers

* Corresponding author. Tel.: +1 970 4913789; fax: +1 970 4916307; e-mail: rmarkey@CNR.colostate.edu.

PII S0039-9140(97)00198-7

[6] use a microwave acid digestion technique in PTFE vessels with potassium dichromate as an oxidizer, followed by distillation of Os without further addition of oxidant. Their method seems to give good results, although Walker [7] has noted that OsO_4 can diffuse through PTFE when heated for prolonged periods of time. Shirey and Walker [8] developed a Carius tube technique for digestion and isotopic equilibration of samples, although to our knowledge this technique has not yet been applied to molybdenite. Another common digestion technique is alkali fusion with Na_2O_2 [9]. This is the basic technique which we have modified for dating molybdenite.

There are two analytical techniques currently used for analysis of Re and Os: inductively coupled plasma mass spectrometry (ICP-MS) and negative thermal ion mass spectrometry (NTIMS). Of the two, NTIMS provides greater precision for measuring Re and Os isotopic ratios.

Significant advances have also been made in the determination of the decay constant for ^{187}Re. Lindner et al. [10] determined a decay constant for ^{187}Re of 1.64×10^{-11} year^{-1}, with an uncertainty of $\pm 3\%$. Recently, Smoliar et al. [11] at the University of Maryland (UMD) redetermined the value of $\lambda^{187}Re$ based on the slope of the Re–Os isochron for IIIA meteorites. They report a value of $\lambda^{187}Re = 1.666 \times 10^{-11}$ year^{-1} with a nominal uncertainty of $\pm 0.31\%$ for analyses using spike solutions calibrated with their own standards, but an uncertainty of $\pm 1.02\%$ for the value in general because of systematic errors introduced by the lack of stoichiometry in the Os standard materials. The Os spike used in our laboratory has the same isotopic composition as the one used by UMD, and we share Re and Os standard solutions with UMD; therefore, we can take advantage of the smaller $\pm 0.31\%$ uncertainty in $\lambda^{187}Re$ in our age calculations. Shen et al. [12] have independently calculated a nearly identical value for the decay constant (1.66×10^{-11} year^{-1}) using a different Os spike and a different Os calibration standard, thereby further validating the 1.666×10^{-11} year^{-1} value for $\lambda^{187}Re$.

We describe in detail the technique we use and present data from replicate analyses of several different molybdenite samples. Using a double-fusion, double-distillation technique, coupled with NTIMS, we are able to replicate the age of our laboratory standard to $\pm 0.13\%$; and using the precise value for $\lambda^{187}Re$, individual ages carry an uncertainty of about 0.4%. This represents a new level of precision and reproducibility for the Re–Os analysis of molybdenite.

2. Experimental

2.1. Sample material and preparation

Molybdenite powder HLP-5 is from a carbonatite vein-type molybdenum–(lead)–uranium deposit in the Jinduicheng–Huanglongpu area of Shaanxi Province, China [13]. Ore mined from an exploratory adit was treated by froth flotation to yield about 500 kg of molybdenite concentrate; 2 kg of this material was processed further for analysis. The residues from the flotation process were removed from the sample by repeated washing in ethanol. After drying, the sample was milled and mixed repeatedly, to give a clean and homogeneous powder. We received a 30 g split of this powder. Chemical analysis of this powder by atomic absorption is presented in Table 1.

Other molybdenite samples are typical-sized mineral separates prepared by heavy liquid separation and hand picking. They range in size from multi-millimeter chunks to approximately 150 mesh.

Table 1
Atomic absorption analysis of molybdenite powder HLP-5

	%
Fe	1.62
Cu	0.063
Pb	1.59
Ca	1.88
K	0.27
Zn	0.036
Na	0.418
Al	0.25
Mn	0.011
Mg	0.024
Insoluble	6.78
Gravimetric Mo	43.89
Oil and water content	0.545

Table 2
Isotopic composition of spikes used for analysis. Osmium spike composition data from Ref. [14]

	Isotope	Atomic abundance (%)
P-series Re spike	^{185}Re	97.40
	^{187}Re	2.60
S-series Os spike	^{186}Os	0.0207
	^{187}Os	0.0235
	^{188}Os	0.5033
	^{189}Os	0.9535
	^{190}Os	96.57
	^{192}Os	1.902

2.2. Spikes and materials

Enriched ^{185}Re and ^{190}Os powders were purchased from Oak Ridge National Laboratory. Isotopic compositions for the spikes are listed in Table 2. The detailed procedure for making the spike and standard solutions are described in Morgan and Walker [9]. Briefly, the ^{185}Re spike powder was dissolved in redistilled HNO_3. The HNO_3 was removed by repeated heating with concentrated HCl, and the stock solution was made up in 6 N HCl. The ^{190}Os spike powder was fused with NaOH and Na_2O_2, and the Os collected by distillation and trapping in concentrated HBr. The HBr solution was evaporated to near-dryness, and the stock solution was made up in 1 N HCl.

Spikes were calibrated against standard solutions of normal isotopic composition. The Re calibration standard was made from zone-refined Re metal, and the Os calibration standard was made from ammonium hexachlorosmate [14]. The Re standard is accurate within the weighing errors, but the stoichiometry of the Os standards in use today is probably accurate to no better than about 1% [12,14]. Our spike calibrations are shown in Table 3. Both Re and Os calibration standards are the same actual solutions as those used by the UMD group [11].

Filaments for mass spectrometry are made from platinum wire which has been rolled into ribbon approximately 0.035 mm thick and 0.5 mm wide, at the Department of Terrestrial Magnetism of the Carnegie Institution (DTM), with rollers that are used only for platinum. Before being cut to length and mounted on filament posts, the Pt is cleaned by fusion with potassium pyrosulfate (J.T. Baker acid flux grade) in a silica crucible at 700°C for 3 h [14]. The solidified potassium pyrosulfate is then removed by boiling with several batches of ultrapure water. The Pt is placed into a Teflon bomb with 6 N HNO_3, capped tightly, and placed in a 105°C oven for several hours. The ribbon is rinsed repeatedly with ultrapure water and dried. Loading blanks are approximately 2 pg Re and undetectable Os.

2.3. Apparatus

2.3.1. Distillation

We use a distillation apparatus similar to that of Morgan and Walker [9]. The only modification to the glassware is that the transfer tube is detachable from the head at a ground glass joint projecting from the top of the head, which provides for easier cleaning (Fig. 1). We use a six-place electric heating mantle assembly with individual temperature controls (Glascol). Prior to the acquisition of the individually controlled mantle unit, samples were run in batches of three and the temperature of the individual boiling flasks was controlled by selectively covering or uncovering the flasks with aluminum foil as needed. A stream of compressed air is introduced into the distillation apparatus through a manifold equipped with six needle valves to individually control air flow to each vessel.

2.3.2. Anion exchange columns

Anion exchange columns are prepared by cutting off the top of 3.5 ml single use plastic transfer pipettes. Bottles of anion exchange resin (Biorad AG 1-X8, 200–400 mesh, chloride form) are batch-cleaned twice in 1.5–2.0 l of 8 N HNO_3, reconverted to the chloride form, and dried to about 25 wt% moisture. Roughly 0.25 g of resin (0.18–0.2 g dry wt.) is slurried with water and sandwiched between two plugs of quartz wool, forming a 1.5 cm resin column with a volume of roughly 0.3 ml. The resin in the column is again cleaned in sequence with 3 ml H_2O, 1 ml of 0.8 N

Table 3
Calibration data for spikes used in this study. Data for Os spike calibrations from Ref. [14]

	Mix	Standard	Spk/Std	Conc. (ng g^{-1})	
Re spikes					
P-2: 3/27/95	RB-1	RD3	4.3	4367.01	
	RB-2	RD3	8.6	4359.97	Mean = 4362 ng g^{-1}
	RB-3	RD3	5.6	4359.45	$2\sigma_m$ = 4.9 (0.11%)
P-2: 1/23/96	SC-1	RD3	4.7	4382.28	
	SC-2	RD3	8.5	4388.04	Mean = 4386 ng g^{-1}
	SC-3	RD3	5.7	4387.01	$2\sigma_m$ = 3.5 (0.08%)
P-4: 2/8/96	SC-10	RD3	2.8	2790.85	
	SC-11	RD3	5.3	2791.60	Mean = 2795 ng g^{-1}
	SC-12	RD3	10.7	2803.46	$2\sigma_m$ = 8.2 (0.29%)
P-4: 7/15/96	SC-31	RD2	1.9	2805.51	
	SC-32	RD2	3.7	2797.03	Mean = 2801 ng g^{-1}
	SC-33	RD2	4.8	2799.24	$2\sigma_m$ = 4.4 (0.18%)
Os spike					
S-II (1992 calibration)	Mix 4	B2	1.0	236.1	
	Mix 5	B2	2.0	236.5	
	Mix 6	B2	4.0	235.9	
S-II (1994 calibration)	Mix 1	B1	0.9	235.1	
	Mix 2	B1	2.4	236.1	
	Mix 3	B1	4.8	234.6	
	Mix 4	B2	1.0	235.3	
	Mix 5	B2	2.5	234.9	Mean = 235.4 ng g^{-1}
	Mix 6	B2	4.9	234.0	$2\sigma_m$ = 0.5 (0.23%)

HNO_3, 5 ml of 4 N HNO_3 and conditioned with 1 ml of 2 N H_2SO_4, followed by 1 ml of 5 N H_2SO_4 just prior to loading the sample.

2.3.3. Mass spectrometry

Isotope ratios were measured using a NBS-type, 12-inch radius, 90° magnetic sector mass spectrometer configured for NTIMS. The instrument is outfitted with both a Faraday cup and an electron multiplier, though for the results reported here only the Faraday cup collector was used. The nominal accelerating voltage is set at 7.155 kV, and the various peaks are measured by varying the field strength of the magnet. Peaks are measured for 6 s each, with an 8 s pause after switching peaks.

For Re, at least two blocks of data comprising 10 scans each were cumulated. A smoothing routine was applied for the calculation of ratios, resulting in 18 ratios per 10 scan block. Isotope dilution determinations were carried out using 2σ cumulative data from the analysis. For Os, 2σ cumulative data were used from at least two blocks of 26 scans each, using a similar smoothing routine for the calculation of ratios. Richard Walker (UMD) and Mary Horan (DTM) provided the original mass-spectrometer software, from which our current molybdenite program was modified.

Total analytical blanks are less than 100 pg for Re, less than 15 pg for common Os, and less than 3 pg for ^{187}Os. These blanks are insignificant relative to the sample Re and ^{187}Os concentrations. The Os blank levels are significant, however, with regard to common Os concentrations in molybdenites; but common Os is insignificant relative to the amount of radiogenic ^{187}Os in molybdenite.

2.4. Procedure

The chemical procedure used for molybdenite has been adapted from Morgan and Walker [9]. Sample digestion and spike-sample equilibration is achieved by alkaline fusion and oxidation with Na_2O_2. Osmium is separated and purified by double distillation, and Re is separated by anion-exchange chromatography [15].

2.4.1. Set-up and fusion

An amount of Re spike solution appropriate for the sample is carefully weighed into a clean, dry, oxidized, 35 ml Zr crucible. The crucible is placed on a warm hot plate (~ 50°C) and the spike is evaporated to dryness. Osmium spike solution is added immediately upon cooling, and similarly allowed to slowly evaporate to dryness on a warm hot plate. Care is taken to remove the crucibles from the hot plate as soon as the solutions have evaporated, as the Re- and Os-bearing residue may be affected by continued heating in the absence of stabilizing alkali.

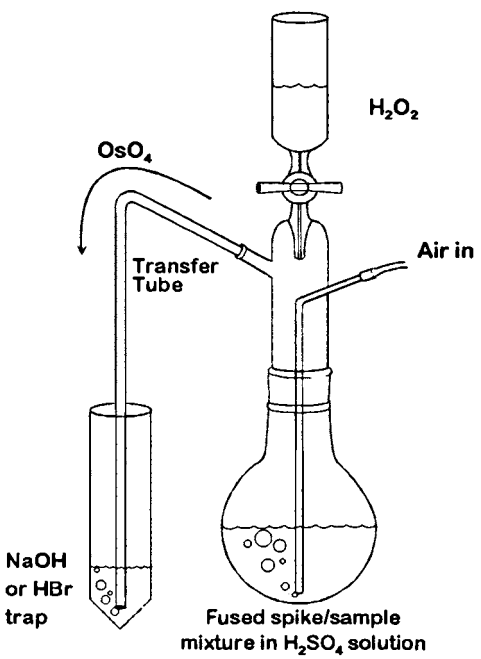

Fig. 1. Apparatus for distillation of Os.

The molybdenite samples are then weighed and added to the crucibles. Sample size depends on the estimated Re and Os abundances and age of the sample. We use samples ranging in size from 10 to 200 mg.

Roughly 1 g of NaOH (Baker Analyzed) is added to the crucibles, followed by about 1 ml H_2O to dissolve. Molybdenite powder and small flakes tend to float in this alkali solution. The crucibles are placed on a warm hot plate and the NaOH solution is slowly evaporated to dryness. A careful attempt is made to try to wet the grains and submerge them in the NaOH solution, but total success is not critical since all grains will be covered in the alkali when dryness is attained. This step ensures that Re and Os from both sources (spike and sample) are effectively smothered in NaOH before being subjected to high temperatures in the furnace during the subsequent fusion step.

Roughly 3.3 g NaOH are added to the crucibles, for a total of 4–4.25 g NaOH in each. The crucibles are covered and placed on a fused silica tray in a muffle furnace set at 350°C. Every 20 min during the 1 h fusion, the crucibles are removed from the furnace and vigorously swirled until the contents freeze. Likewise, the temperature is increased in 25°C increments twice during this hour to a final temperature of 400°C. During this first fusion, the sample and spike are dissolved in the molten alkali, and the two become thoroughly mixed. Larger flakes of the sample often remain undissolved until the temperature reaches 375°C, and are frequently observed to float unwetted on the surface of the melt. Coarser-grained samples may cause spattering on the underside of the lid, inhibiting isotopic equilibration between sample and spike. For this reason, use of coarse-grained samples (> 2–3 mm) is discouraged. It is not recommended that crucibles smaller than 35 ml be used for the quantities of reagents described in this paper, since smaller crucibles do not provide enough room for swirling or allow for possible NaOH 'creep' up the sides of the crucible when drying down on the hot plate.

After cooling, roughly 4 g of Na_2O_2 (Mallinckrodt) are added and the crucibles are placed into the furnace, now set at 550°C. Again, the

crucibles are swirled until the contents freeze and the temperature is increased 25°C every 20 min for 1 h until a final temperature of 600°C is reached. This second fusion step homogenizes Re and Os from spike and sample, and ensures that Re and Os from both sources are equilibrated at the same high oxidation states [16]. The crucibles are cooled for a few minutes in the open room, and are then placed in a dessicator and allowed to cool to room temperature.

2.4.2. Dissolution and acidification

The lid to the crucible is rinsed with a light stream of H_2O into a 400 ml PTFE beaker. The crucible itself is placed into the beaker, which is then covered with a Teflon watchglass. If the crucible lid was considerably spattered during sample dissolution, it may also be placed into the beaker (next to the crucible). Then 20 ml H_2O is poured directly into the crucible, and the beaker is quickly covered with the Teflon watchglass. Dissolution of the fusion product is allowed to continue to completion. In some cases (large or impure samples), the dissolution reaction may be rapid and vigorous. In other cases dissolution is slow, and the beaker may be placed on a warm hot plate to speed dissolution of the fusion cake. After dissolution, the bottom side of the watchglass is carefully rinsed into the beaker. The contents of the beaker are transferred into a 125 ml boiling flask resting in an ice bath.

Then 5 ml of 1:1 H_2SO_4 are added to the crucible, and then swirled around within the beaker. This solution is slowly and carefully poured down the inside surface of the boiling flask so as not to generate reaction heat too quickly within the flask. The crucible and beaker are washed with a further 25 ml of 1:1 H_2SO_4 in two batches; these are also added to the boiling flask. The final acidity of the solution in the boiling flask is about 5 N H_2SO_4.

2.4.3. Separation Os by distillation

The boiling flask is fitted with a distillation head and placed in an electric heating mantle. About 4–5 ml of 30% H_2O_2 (Baker Ultrex) are added to the flask through the stopcock at the top of the head. The transfer tube of the apparatus is immersed into a trap of 10 ml of 6 N NaOH in a conical centrifuge tube cooled in ice, and then connected to the distillation head (Fig. 1). A stream of air is introduced into the H_2SO_4 solution at a rate such that a few bubbles per second are produced in the trap. This stream of air helps to transfer the Os (as volatile OsO_4) into the NaOH trap. The heating mantle is turned to a high setting until the decomposition of the peroxide is initiated, at which point the mantle can be turned down to about 105°C. Initial reaction with the peroxide can be vigorous, and care must be taken at first to keep the solution from boiling over into the Os trap. The temperature is maintained such that the middle of the sloping portion of the transfer tube is kept quite warm to the touch, but no liquid condensate is transferred into the trap. Distillation proceeds for 2 h, adding H_2O_2 dropwise as necessary to maintain a slightly carbonated appearance in the flask solution. In contrast to the case with most other sulfides and meteorite samples, reaction of the peroxide with the H_2SO_4 solution containing a pure molybdenite sample is typically slow and smooth (with the exception of the first initial reaction, when the 4–5 ml of 30% H_2O_2 are directly added to the flask). For most molybdneites, the 4–5 ml of peroxide added at the beginning are enough to maintain oxidizing conditions (manifested by the slightly carbonated appearance of the solution) for the entire 2 h of the distillation. At most, an additional 4–5 ml of H_2O_2 might be necessary.

After the first distillation, a small aliquot of the Re-containing pot solution is added to anion-exchange columns (described in the following section), the boiling flask is thoroughly rinsed with H_2O, and the contents of the NaOH trap are transferred back to the flask. The centrifuge tube is rinsed with a small squirt of ultrapure H_2O, and these washings are also collected in the boiling flask. The flask is placed in ice, and the contents of the flask are acidified with 25 ml of 1:1 H_2SO_4. The second distillation proceeds as above, except that 7 ml H_2O_2 is used for all samples, and the Os is trapped in 5 ml quadruple-distilled HBr (SeaStar). This second distillation is allowed to proceed for 1.5 h.

Following the distillation, the Os-bearing HBr trap is removed from the ice, sealed with Parafilm, and allowed to stand for a few hours at room temperature before transferring the contents to a conical-bottom Savillex teflon vial (precleaned in hot HNO_3). The Os-bearing HBr is then evaporated to dryness under a heat lamp.

2.4.4. Separation of Re by anion exchange

Residuum from the first distillation is cooled to room temperature in the boiling flask. Because of the high concentration of Re in molybdenite, only a small aliquot of this solution is needed to provide enough Re for mass spectrometric analysis. Consequently, only about 1 ml of the flask solution is applied to the columns (prepared as described above). An additional 2 ml is reserved for any potential future need or re-runs, and the remaining 50+ ml are discarded. Molybdenum and tungsten are stripped from the columns with 10 ml of 1 N HCl and the Re is subsequently eluted with 4.25 ml of 4 N HNO_3 (the first 0.25 ml of the eluant are discarded). In most cases this single column procedure provides a clean enough separation for mass spectrometric analysis. Occasionally, a similarly prepared clean-up column is used. An amount of eluant equivalent to 2 ng of the added spike Re is dried down in a round-bottom Savillex vial and the rest is discarded.

2.5. Mass spectrometry

For Os analysis, the dried residue is redissolved in 10 μl HBr for loading onto a Pt filament. The filament load is then dried under a heat lamp. For the results reported in this paper, two techniques were used for Os analysis. In earlier runs, a fraction of the sample equivalent to 25–50 ng of the added Os spike was loaded onto a Pt filament, and the Os was reduced to the metal from the hexabromosmate by slow heating to approximately 750°C at a pressure of less than 2×10^{-7} torr (either in an NBS-model degasser or in the mass spectrometer itself). About 25 μg of Ba as $Ba(NO_3)_2$ were applied to the filament to aid in the formation of negative ions [17]. For later runs, a fraction of sample equivalent to about 10 ng of spike Os was loaded onto a Pt filament and dried. About 25 μg of Ba as $Ba(OH)_2$ were then loaded directly onto the sample and dried [18]. This latter procedure has the advantages of requiring less Os for the analysis, eliminating a time-consuming step in the procedure (Os reduction), and producing a more predictable and stronger ion signal for measurement.

Analyses were made at a filament temperature of 860–960°C. Extra-dry oxygen was introduced into the source area through a precision leak valve. Total pressure in the source was maintained at about 4×10^{-7} torr, while pressure in the flight tube remained in the 10^{-9} torr range. Peaks were measured at 235, 238 and 240 AMU ($^{187}OsO_3$, $^{190}OsO_3$, and $^{192}OsO_3$, respectively). Correction for oxygen-isotopic effects were made on-line. Possible isobaric interferences on the measured peaks due to other ionic species were monitored at masses 233 ($^{185}ReO_3$), 243 ($^{195}PtO_3$) and 231 ($^{183}WO_3$). No correction was made for mass fractionation, noting that the analyses reported here were all made using the Faraday cup.

For Re analysis, the sample residue was redissolved in 3 N HCl, and about 1 ng Re was loaded onto the filament, about 13 μg Ba as $Ba(NO_3)_2$ were applied, and the filament was inserted into the mass spectrometer. Analyses were made at a pressure of less than 2×10^{-7} torr, with a filament temperature of 860–900°C. Peaks were measured at 249 and 251 AMU ($^{185}ReO_4$ and $^{187}ReO_4$, respectively). Again, no correction was made for mass fractionation while using the Faraday cup.

2.5.1. Data reduction

Rhenium and osmium concentrations are determined by isotope dilution. We measure three masses for Os, from which we calculate both the $^{187}Os/^{190}Os$ and the $^{190}Os/^{192}Os$ of the mixture. Using a three-isotope dilution equation for Os, it is possible to estimate the concentration of common Os and precisely determine the radiogenic ^{187}Os concentration. To calculate both of these quantities, we assume a $^{187}Os/^{188}Os$ for common Os of 0.12. Note that the choice of $^{187}Os/^{188}Os$ for the common Os has essentially no effect on age determinations, given the minuscule concentrations of common Os relative to that of radiogenic

Os in these molybdenites [5]. Note also that the common Os calculated in this study is very approximate because of the difficulty in precisely measuring $^{190}Os/^{192}Os$ (~ 50 due to our ^{190}Os spike). Also, in contrast to radiogenic ^{187}Os and the age, the common Os calculation is sensitive to the actual $^{187}Os/^{188}Os$ of the common Os and the size and composition of the Os blank. Re concentrations are readily calculated from the $^{185}Re/^{187}Re$ of the spike–sample mixture.

Stated errors include instrumental uncertainty in the measurement of the ratios, error magnification associated with spiking [19], uncertainty in spike calibration (Table 3) and, for the age determination, uncertainty in the decay constant for ^{187}Re [11]. Because of the essentially mono-isotopic nature of Os in molybdenite (nearly all ^{187}Os) and of our Os spike (nearly all ^{190}Os), the error magnification is insignificant for the determination of ^{187}Os concentration for molybdenites. Essentially, most of the quoted error in both the Re and Os concentrations is from the uncertainty in the Re and Os spike calibrations, and weighing errors for spikes and sample. The weighing error of the sample does not contribute to the uncertainty on the ages.

3. Results and discussion

Molybdenite powder HLP-5 is used as an internal reference standard in our laboratory. Table 4 shows the results of all 19 non-experimental runs carried out over the course of 18 months using two different Re spike solutions. The mean and standard deviation of the calculated ages are 221.0 ± 1.0 Ma (0.4%); but because the distribution of the data is not purely Gaussian, the reproducibility inherent in the technique is perhaps better described by the median and mean absolute deviation (MAD) of 221.3 ± 0.24 Ma (0.13%). Concentration data for Re and ^{187}Os are reproducible to within 0.81 and 0.85%, respectively.

Data for typical mineral separates (i.e. not powders) are somewhat less reproducible, probably reflecting minor inhomogeneities in the sample material (Tables 5 and 6). Reproducibilities in the ages for these samples are 0.5–1.3% for three replicates per sample. Concentration data are reproducible to within 1.9–7.4% for Re and 1.5–7.3% for ^{187}Os. Sample weighing errors probably contribute somewhat to the variability in the concentration data but do not affect the uncertainty on the calculated age. The uncertainty for each individual age determination is approximately 0.4%, this includes the 0.31% uncertainty in the decay constant for ^{187}Re.

Table 4
Replicate analyses for the homogeneous molybdenite powder HLP-5. Uncertainties on concentration data and individual age determinations are 2σ standard deviations

Run #	Total Re (ppm)	^{187}Os (ppb)	Age (Ma)
M-34	278.1 ± 1.22	645 ± 3.2	221.1 ± 0.90
M-35	285.3 ± 1.09	662 ± 2.9	221.1 ± 0.90
M-36	289.1 ± 1.19	672 ± 3.0	221.6 ± 0.93
M-37	281.8 ± 1.16	656 ± 3.0	221.1 ± 0.91
M-38	284.4 ± 1.14	662 ± 3.0	222.0 ± 0.92
M-39	282.7 ± 1.17	657 ± 3.1	221.5 ± 0.90
M-60	284.5 ± 1.17	661 ± 3.1	221.5 ± 0.91
M-76	282.0 ± 1.17	654 ± 3.1	221.0 ± 0.89
M-79	286.4 ± 0.93	660 ± 2.6	219.7 ± 0.88
M-87	283.9 ± 1.20	662 ± 3.2	221.0 ± 0.88
M-104	284.5 ± 1.67	661 ± 3.7	222.2 ± 1.09
M-106	283.7 ± 1.56	657 ± 3.4	220.8 ± 1.08
M-107	287.0 ± 1.40	657 ± 3.0	218.0 ± 1.07
M-109	285.3 ± 2.05	661 ± 4.6	220.7 ± 1.09
M-112	286.4 ± 1.48	658 ± 3.2	219.1 ± 1.07
M-124	285.7 ± 1.41	660 ± 3.1	220.4 ± 1.08
M-141	283.7 ± 1.24	659 ± 3.1	221.3 ± 0.96
M-143	282.8 ± 1.23	657 ± 3.0	221.5 ± 0.97
M-148	286.9 ± 1.22	667 ± 3.0	221.5 ± 0.96

Mean age, 221.0 Ma; Standard deviation (1σ), 1.0 Ma (0.4%). Median age, 221.3 Ma; Mean absolute deviation, 0.24 Ma (0.13%)

For fine- and coarse-grained fractions of some Archean molybdenite samples, we noticed a reproducible difference in not only Re and Os concentrations but also ages (Table 5). To test whether these variations were real (geologic) or an artifact of grain-size bias in our analytical method, we took a coarse-grained (mm-size) Proterozoic molybdenite sample with a less complicated geologic history, chopped it up with a razor blade, and sieved it into three very different grain-size fractions. Table 6 shows that all three grain sizes yield virtually identical ages, illustrating that analytical results are not dependent on

Table 5
Replicate analyses for coarse- and fine-grained fractions of Archean molybdenites A34 and A950. Stated errors for each analysis are 2σ standard deviations

Sample	Run #	Total Re (ppm)	^{187}Os (ppb)		Age (Ma)
A34 MA fg	M-40	10.887 ± 0.026	294.9 ± 0.9		2533 ± 11
A34 MA fg	M-41	11.297 ± 0.026	303.8 ± 0.9		2515 ± 10
A34 MA fg	M-45	11.14 ± 0.027	299.0 ± 0.9		2510 ± 10
				Mean:	2519 ± 12 (0.5%)
A34 MA cg	M-42	20.954 ± 0.045	595.8 ± 1.8		2656 ± 11
A34 MA cg	M-43	18.915 ± 0.069	534.4 ± 2.2		2639 ± 11
				Mean:	2648 ± 12 (0.5%)
A950 cg	M-49	95.79 ± 0.22	2790 ± 8.5		2719 ± 11
A950 cg	M-54	97.00 ± 0.21	2771 ± 8.1		2668 ± 11
A950 cg	M-57	98.97 ± 0.85	2863 ± 25.3		2701 ± 11
				Mean:	2696 ± 26 (1.0%)
A950 fg	M-48	57.826 ± 0.133	1608 ± 5.0		2599 ± 11
A950 fg	M-50	52.256 ± 0.214	1470 ± 6.6		2627 ± 11
A950 fg	M-56	60.503 ± 0.248	1699 ± 7.8		2624 ± 11
				Mean:	2617 ± 15 (0.6%)

grain size of the sample. We conclude that the data in Table 5 represents real geologic information: these coarse–fine pairs represent two different populations of molybdenite that formed at two different times in these samples. The technique described in this paper permits resolution of real geologic events closely spaced in time. These events would not be resolvable at lower levels of analytical precision.

3.1. Observations

Initial attempts at Re–Os analysis in our laboratory using the unmodified technique of Morgan and Walker [9] gave erratic results. After making a few modifications to their technique, we were able to obtain reproducible results (Fig. 2). The modifications, seemingly minor, were critical for working with molybdenite, a mineral with unique surficial properties.

We switched from Morgan and Walker's [9] three-fusion method (spikes first fused with NaOH before addition of sample) to a two-fusion method, where sample and NaOH are added immediately after the spikes are dried. In doing this, spikes and sample are mixed in the first fusion, decreasing the possibility for spike/sample fractionation. As another precaution, we also vigorously swirl the molten mixture periodically during the fusions until the mixture hardens. This is done at regular intervals, and serves to speed dissolution of the sample in the NaOH melt and to more thoroughly homogenize the spike/sample mixture. One seemingly minor but surprisingly significant observation we made is that initial dry-down of the osmium spike in the crucibles is critically sensitive to the composition of the atmosphere in which the drying takes place. For early experiments, spikes were dried at one end of tha exhaust hood in which the HNO_3 bath used for cleaning the glassware also resided. This bath was cool and covered with a watchglass during spike dry-down. Nevertheless, the presence of the covered HNO_3 bath was apparently occasionally enough to cause some loss of ^{190}Os spike: these early experiments produced erratic and anomalously old ages.

3.2. Re spikes: non-ideal behavior

Our principle Re spike was prepared from a highly concentrated stock solution (P-1). Our original working preparation (P-2) contained 4362 ± 4 ng g^{-1} Re (Table 3). This P-2 spike yielded excellent results, but its relatively low concentration meant that spike amounts in excess of 1 g were necessary for optimum spiking of

Table 6
Data for replicates of additional samples

Sample	Run #	Total Re (ppm)	^{187}Os (ppb)		Age (Ma)
SW93-PK4 cg	M-55	170.0 ± 0.3	3240 ± 9		1793 ± 8
SW93-PK4 mg	M-59	176.2 ± 1.6	3348 ± 32		1787 ± 7
SW93-PK4 fg	M-58	183.5 ± 1.5	3489 ± 30		1789 ± 7
				Mean $\pm$ SD:	1790 ± 3 (0.17%)
A996B	M-46	23.73 ± 0.09	710 ± 3		2790 ± 11
A996B	M-52	23.21 ± 0.05	695 ± 2		2792 ± 11
A996B	M-53	23.01 ± 0.05	692 ± 2		2806 ± 11
				Mean $\pm$ SD:	2796 ± 9 (0.3%)

The three grain-size fractions for Proterozoic molybdenite SW93-PK4 were produced by chopping millimeter-sized molybdenite grains with a razor blade and sieving. These fractions represent a single geologic population in the rock. This experiment indicates that there is no laboratory bias in analyzing different grain sizes of molybdenite. Archean molybdenite A996B is from a sample with a single grain-size population of molybdenite. Stated errors for each analysis are 2σ standard deviations.

many molybdenite samples. Several attempts were made to spike samples using highly concentrated Re spikes.

A dilution of the original P-1 stock solution was made (P-5), having a concentration of 36.791 ± 0.019 μg g^{-1}. Runs made using this new solution gave wildly erratic and always high values for the Re content of HLP-5. After obtaining these spurious results, we recalibrated P-5 and confirmed that the concentration of the spike was not an issue.

Suspecting that the Re species in the P-series stock solution had changed, we made a stock solution (RS-1) from a new batch of ^{185}Re powder. A dilution (RS-2) was made and calibrated at 41.867 ± 0.025 μg g^{-1}. Again, the results for HLP-5 were erratic and high by roughly a factor of two. Adding 0.2 ml of 30% H_2O_2 to the Re spike before dry-down (to oxidize the Re species in solution) provided no improvement, nor did an initial spike fusion with NaOH prior to addition of sample (as in Ref. [9]). A third dilution, this time in 1 N HCl (RS-2a; 45.610 ± 0.005 μg g^{-1}), was made, under the supposition that the high concentration of Re was complexing intractably with the high concentration of chloride in the 6 N HCl. This made no improvement in the HLP-5 analyses either.

Periodically during our experiments with the concentrated spikes, we made check runs with the last milliliters of the original spike (P-2). These continued to produce good results, as did runs using a more dilute Re spike solution (P-4; 2795 ± 4 ng g^{-1}) made from the same original P-1 stock solution (Table 3). With these less-concentrated spikes, however, larger quantities of spike are necessary, and Re-rich samples are often slightly underspiked, increasing the error magnifier component of the uncertainty for the Re concentration. (On the other hand, Re ratios of slightly underspiked samples are closer to unity, and therefore are more precisely measured on the mass spectrometer; furthermore, gram quantities of spike can be precisely weighed, minimizing weighing error.)

The non-ideal behavior of concentrated Re spikes in our laboratory remains somewhat perplexing (although such behavior has been observed in other laboratories; Du, personal communication, 1995). Considering that the procedure for spike calibration is very similar to that for sample analysis, it is puzzling why the calibration runs are so highly precise and reproducible, while runs using concentrated spikes with molybdenite are not. One possibly significant difference between the two procedures is that, for calibration runs, the spike and standard solutions are mixed together before the first dry-down, resulting in only one dry-down step. In contrast, for sample runs, the Re spike is dried down, then Os spike is added and dried, subjecting the spike Re in the crucible to heat twice. This may in some way adversely affect the Re from the concentrated spike, making it in part unavailable to the rest of the chemical procedure.

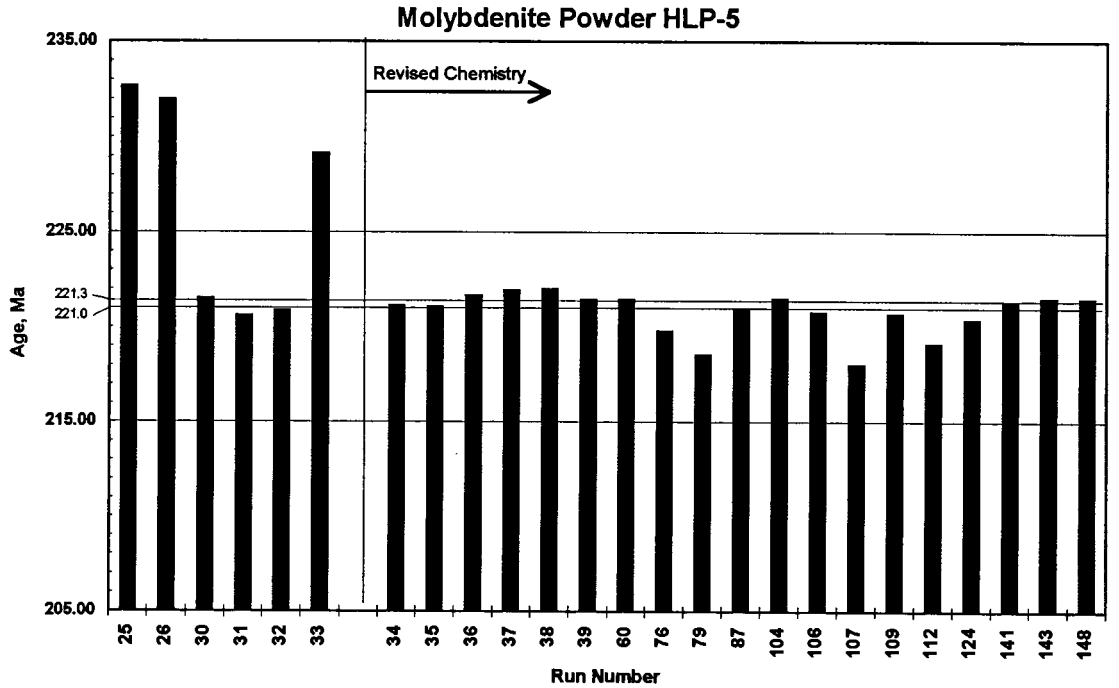

Fig. 2. Histogram illustrating the improvement in reproducibility of our method after revising the chemical procedure described in Ref. [9]. All analyses are for HLP-5.

There are several possibilities for circumventing this apparent non-ideal behavior of the concentrated Re spike. One possibility is to reverse the spiking order, putting the Os spike dry-down ahead of that for the Re spike, although this might adversely affect the behavior of the Os spike. Our experience has shown Os to be generally more sensitive than the Re in situations where loss can occur. Another possibility is to mix the Re and Os spikes together prior to dry-down. For this, spikes should be weighed into a closeable vessel and subsequently transferred into the crucibles in order to avoid potentially large errors due to evaporation during weighing. Alternatively, batches of mixed Re–Os spikes could be prepared and calibrated [11], with different Re–Os ratios to accommodate samples of different ages. This method would provide the added benefit of effectively removing the spike weighing errors from the age calculation. Finally, sample digestion by Carius tube [8] avoids the issue of spike dry-down altogether.

It is noteworthy that McCandless [20] uses a highly concentrated Re spike solution (213.88 μg g^{-1}) with a spiking and digestion method otherwise similar to our own and reports no difficulties with non-ideal behavior. Significantly, the spike used in that study was in a medium of 8 N HNO_3 rather than in HCl, as is used in our laboratory. It is possible that the HNO_3 maintains the Re as a species that behaves ideally over a greater range of concentrations than does HCl. Rhenium spikes in HNO_3 would not be suitable for making mixed Re–Os spikes, however, since the Os would be rapidly oxidized and lost from the solution.

4. Summary

The technique described in this paper represents the modification and combination of two previously existing methods, alkaline fusion and NTIMS. This method results in a new level of precision and reproducibility in the Re–Os analy-

sis of molybdenite. This new level of resolution has allowed us to recognize real geologic events in the ages of some Archean molybdenite samples.

Precision in the individual age determinations is typically about 0.4%. This high precision is in part derived from the fact that our spikes are calibrated against the same standard solutions as those of Smoliar et al. [11], and therefore we use the low 0.31% uncertainty for the ^{187}Re decay constant.

Acknowledgements

Many individuals contributed to this work. We thank Du Andao and Sun Yali for providing the HLP-5 molybdenite powder, Steve Dall for providing the AA analysis of HLP-5, Olavi Kouvo for providing size fractions of Archean molybdenites, Krister Sundblad and Martti Lehtinen for the Proterozoic molybdenite sample, Phil Baedecker for preparing the P-series Re spike stock solution and the P-2 dilution, Mary Horan and Rich Walker for the mass spectrometry software and assistance in its adaptation for molybdenite. We also gratefully acknowledge BHP Minerals International, in particular Noel White, Chief Geologist, for providing critical operating funds at the time this work was carried out.

References

[1] M. Fleischer, Econ. Geol. 55 (1959) 607–609.
[2] J.W. Morgan, J.F. Lovering, R.J. Ford, J. Geol. Soc. Aust. 15 (1968) 189–194.
[3] W. Herr, E.P. Wölfe, E. Kopp, in: Radioactive Dating and Methods of Low-Level Counting, International Atomic Energy Agency, Vienna, 1967, pp. 499–508.
[4] B. Hirt, W. Herr, W. Hoffmeister, in: Radioactive Dating, International Atomic Energy Agency, Vienna, 1963, pp. 35–43.
[5] H.J. Stein, K. Sundblad, R.J. Markey, J.W. Morgan, G. Motuza, Miner. Depos., in press (1998).
[6] K. Suzuki, Q. Lu, H. Shimuzu, A. Masuda, Analyst 117 (1992) 1151–1156.
[7] R.J. Walker, Anal. Chem. 60 (1988) 1231–1234.
[8] S.B. Shirey, R.J. Walker, Anal. Chem. 34 (1995) 2136–2141.
[9] J.W. Morgan, R.J. Walker, Anal. Chim. Acta 222 (1989) 291–300.
[10] M. Lindner, D.A. Leich, G.T. Russ, J.M. Bazan, R.J. Borg, Geochim. Cosmochim. Acta 53 (1989) 1597–1606.
[11] M.I. Smoliar, R.J. Walker, J.W. Morgan, Science 271 (1996) 1099–1102.
[12] J.J. Shen, D.A. Papanastassiou, G.J. Wasserburg, Geochim. Cosmochim. Acta 60 (1996) 2887–2900.
[13] H.J. Stein, R.J. Markey, J.W. Morgan, A. Du Andao, S. Yali, Econ. Geol. (special issue), accepted.
[14] J.W. Morgan, M.F. Horan, R.J. Walker, J.N. Grossman, Cosmochim. Acta 59 (1995) 2331–2344.
[15] J.W. Morgan, D.W. Golightly, A.F. Dorzapf, Talanta 38 (1991) 259–265.
[16] J.W. Morgan, Anal. Chim. Acta 32 (1965) 8–16.
[17] R.A. Creaser, D.A. Papanastassiou, G.J. Wasserburg, Geochim. Cosmochim. Acta 55 (1991) 397–401.
[18] J. Volkening, T. Walczyk, K. Heumann, Int. J. Mass Spec. Ion Proc. 105 (1991) 147–159.
[19] K. Heumann, in: F. Adams, R. Gijbels, R. Van Grieken, (Eds.), Inorganic Mass Spectrometry, Wiley Interscience, New York, 1988, pp. 301–376.
[20] T.E. McCandless, Evaluation of the rhenium–osmium geochronometer and its application to base metal porphyry mineralization, Ph.D. Thesis, University of Arizona, Tucson, AZ, 1994, 92 pp.

.

ELSEVIER

Talanta 45 (1998) 947–950

Talanta

Studies on the absorption spectra of aqueous L-tyrosine and its dissociation equilibria

Jia-Zhen Yang *, Zi-Fu Zhang

Department of Chemistry, Liaoning University, Shenyang 110036, People's Republic of China

Received 26 March 1997; received in revised form 11 June 1997; accepted 23 June 1997

Abstract

The UV absorption spectra of aqueous tyrosine at various total ionic strengths were measured at known pH values at 298.2 ± 0.2 K. The standard third dissociation constant of tyrosine was determined from the spectra by linear extrapolation and polynomial approximation. The results obtained from both methods are in good agreement within experimental error. © 1998 Elsevier Science B.V.

Keywords: Absorption spectra; Isosbestic point; Dissociation constant; Pitzer's equation; L-tyrosine

1. Introduction

Considerable attention has been devoted to the thermodynamics properties of aqueous amino acid solutions which interests life science, biochemistry and chemical thermodynamics [1–3]. This work reported on the study of the dissociation equilibria of tyrosine in aqueous solution by its characteristic absorption spectrum. The two isosbestic points in the spectra were used to determine the third standard dissociation constant of tyrosine at 298.15 K, which is difficult to measure by electrochemical methods because usual chemical methods and electrochemical methods to measure the dissociation of weak electrolyte often can not distinguish between ion-pair and molecule dissociation. However, using UV spectra to measure the degree of dissociation one may draw a distinction between an ion pair and molecule because their absorption spectra are different from each other.

2. Experimental

2.0.1. Chemicals

Water was doubly deionized. Tyrosine of CP grade was recrystallized twice from water–ethanol mixed solvent and was dried under reduced pressure. NaCl and borax were of GR grade and were dried for 3 h before use. Sodium dihydrogen phosphate, disodium hydrogen phosphate and sodium hydroxide of AR grade were used without further purification. A series of buffer solutions with constant ionic strength and various pH values were prepared. NaCl was used to adjust the

* Corresponding author.

PII S0039-9140(97)00194-X

solution to various constant total ionic strength, I, from 0.05 to 2.0 mol kg^{-1} as run solutions. The molarity of tyrosine in each run solution was the same with $m = 1.0 \times 10^{-4}$ mol kg^{-1}.

2.0.2. Experimental procedure

The absorption spectra of aqueous tyrosine solutions at various total ionic strength were measured by a UV-240 spectrophotometer using 10 mm cells at 298.15 ± 0.2 K. The pH value of each run solution was measured by a an Orion EA-940 Ionometer at 298.5 ± 0.2 K.

3. Results and discussion

The absorption spectra of aqueous tyrosine solutions were plotted over 250–340 nm at each constant total ionic strength 0.05, 0.1, 0.2, 0.6, 0.8, 1.1, 1.4, 1.7, 2.0 mol kg^{-1}. Fig. 1 is a spectrum of aqueous tyrosine solution at constant total ionic strength $I = 0.1$ mol kg^{-1}. The other spectra at different total ionic strength are similar to Fig. 1 with two isosbestic points which are in good agreement with literature values of wavelength $\lambda_1 = 267.0$ nm and $\lambda_2 = 277.5$ nm [4]. The wavelength values of the two isosbestic points and the maximum absorption peaks in acid solution and in alkaline solution are listed in Table 2. We can see from Table 2 that bathochromic shifts of the maximum absorption peaks in alkaline and acid solution and the isosbestic points do not appear on the absorption spectra of the aqueous tyrosine solutions. This is different from the results of our former paper [5,6].

3.1. True dissociation degree of tyrosine

The second isosbestic point, $\lambda_2 = 277.5$ nm, on the absorption spectrum corresponds to the third dissociation equilibrium of tyrosine, that is, the deprotonation of the phenolic anion of tyrosine:

$$\begin{aligned} &HR^- = H^+ + R^{2-} \\ &K_3^\circ = a_{H+}\,(m_2/m_1)\,(\gamma_2/\gamma_1) \end{aligned} \quad (1)$$

here K_3° is the third standard dissociation constant, HR^- and R^{2-} are $HOC_6H_4CH_2$–$CH(NH_2)COO^-$ and $^-OC_6H_4CH_2$–$CH(NH_2)COO^-$, m_1, m_2 and γ_1, γ_2 are their molalities and activity coefficients, respectively, a_H is activity of the ion H^+. In Eq. (1),

$$m_2/m_1 = \alpha/(1-\alpha) \quad (2)$$

where α is the true third dissociation degree which is calculated according to Eq. (3) [7]

$$\alpha = (D - D_1)/(D_2 - D_1) \quad (3)$$

where D_1, D_2, and D are the absorbances of three solutions of the same molality of tyrosine measured in a cell of the same pathlength. D_1 refers to a solution of the lowest pH, D_2 to a solution of the highest pH and D to one of intermediate pH, in which a is the true third degree of dissociation. The values of D_1, D_2 and D were obtained from the absorption spectra. Using Eq. (3), the values

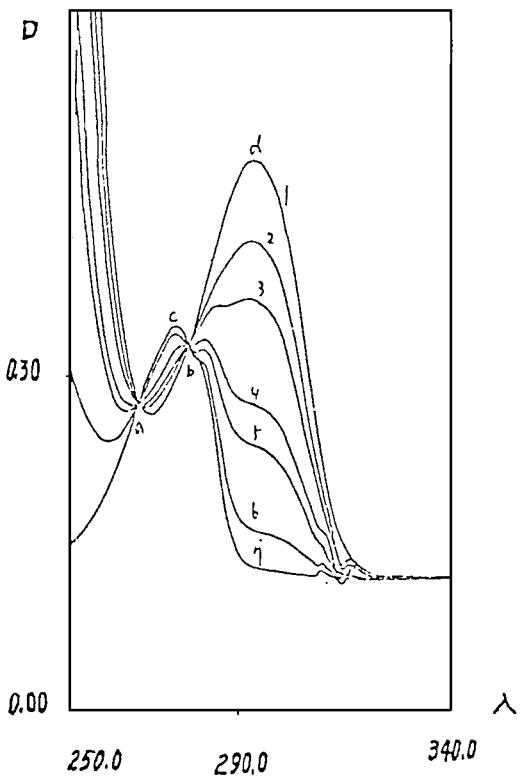

Fig. 1. Absorption spectra of L-tyrosine at 298.2 ± 0.2 K at constant total ionic strength, 0.1 mol kg^{-1}, and various pH values (from top to bottom): (1) 11.832, (2) 10.356, (3) 0.863, (4) 9.602, (6) 9.362, (6) 8.647, (7) 4.806. D means absorbance.

Table 1
The values of dissociation degree α of L-tyrosine and pH of run solution

I/mol kg^{-1}	pH	α	l/mol k^{-1}	pH	α
0.05	9.981	0.5889	0.8	9.207	0.2435
0.05	9.778	0.4774	0.8	8.201	0.0587
0.05	9.604	0.3866	1.1	9.934	0.7530
0.05	9.369	0.3019	1.1	9.523	0.4799
0.05	8.088	0.4310	1.1	9.263	0.3434
0.1	10.356	0.7682	1.1	8.997	0.2229
0.1	9.868	0.5465	1.1	a.328	0.0341
0.1	0.602	0.4101	1.4	9.842	0.6494
0.1	9.362	0.2996	1.4	9.511	0.4073
0.1	8.647	0.1209	1.4	9.288	0.3417
0.2	10.060	0.7085	1.4	9.034	0.2411
0.2	9.783	0.5502	1.4	8.841	0.0725
0.2	9.606	0.4326	1.7	9.621	0.5360
0.2	9.313	0.3130	1.7	9.346	0.3964
0.2	8.630	0.1285	1.7	9.110	0.2962
0.5	10.069	0.8680	1.7	8.901	0.2050
0.5	9.754	0.6220	1.7	8.198	0.0631
0.5	9.530	0.4840	2.0	9.491	0.5163
0.5	9.258	0.3360	2.0	9.210	0.3462
0.5	8.331	0.1200	2.0	9.062	0.2617
0.8	9.939	0.6995	2.0	8.852	0.2021
0.8	9.734	0.4893	2.0	0.098	0.0116
0.8	9.499	0.3644			

of α were calculated and are listed in Table 1. In calculation of α, this suggests that absorption at the peak in acid solution is due to anion HR^- and at the peak in alkaline solution is due to the anion R^{2-}, at the second isosbestic point, λ_2, the extinction coefficients of the two species, HR^- and R^{2-}, are equal, and the two species can be mixed in any proportion (at constant total morality of tyrosine) without change in absorption (Table 2).

3.2. Linear extrapolation to determine the value of K_2°

It is proposed that the ionic strength of the supporting electrolyte equals the total ionic strength, I, in each run solution. Thus, the activity coefficients, γ_2 and γ_1, might be represented using the extended Debye–Hückel equation. Then the working equation of extrapolation can be obtained:

$$pK' = pH - \log[\alpha/(1-\alpha)] + 3A\ (\rho I/c^\circ)^{1/2} /[1 + Ba^\circ(\rho I/c^\circ)^{1/2} = pK_3^\circ - b(I/m^\circ) \quad (4)$$

where ρ is the density of the run solution, $c^\circ = 1$ mol dm^{-3}, $m^\circ = 1$ mol kg^{-1}, pK' is the extrapolated function which can be calculated from experimental results, A and B are Debye–Hückel parameters. Using a linear least squares program, regression of pK' against ionic strength, I, yields a good straight line, the intercept of the line is pK_3°. In the extrapolation, several possible values of ion size parameter, a°, were employed. The best value of a° was chosen when it associated with the smallest standard deviation of the linear regression, that is $a^\circ =$ 0.70 nm, for which standard deviation of $s =$ 0.06, for a $pK_3^\circ = 10.05$, which compares well with 10.07 in literature [8].

Table 2
Wavelength of peak acid and alkaline solution and wavelength of isosbestic points on the absorption spectra of L-tyrosine

I	0.05	0.1	0.2	0.5	0.8	1.1	1.4	1.7	2.0
a	266.2	266.7	266.9	266.4	267.0	267.1	266.5	286.9	266.7
b	277.9	277.6	277.8	277.5	277.0	277.2	277.0	277.1	277.5
c	274.4	274.0	270.0	274.4	274.7	274.6	274.5	274.0	274.4
d	293.1	298.2	293.0	293.1	293.1	293.0	298.0	298.1	292.9

a, first isosbestic point; b, second isosbestic point; c, in acidic solution; d, in basic solution.

3.3. Polynomial approximation to determine K_3°

The polynomial approximation proposed on the basis of Pitzer's electrolyte solution theory [9] in Yang's paper [3] was applied to determine pK_3° of tyrosine from the absorption spectra. It was assumed that: (1) the interaction of HR^- and R^{2-} with supporting electrolyte, NaCl, are only considered; (2) the total ionic strength of each run solution equals to the molality of NaCl; (3) mixed parameters Φ_{ij} and Ψ_{ijk} in Pitzer's theory [9] are regarded as independent of ionic strength so that the working equation of the polynomial approximation is obtained:

$$\begin{aligned} pK' &= pH - \log[\alpha/(1-\alpha)] - 3f^{\upsilon}/\ln 10 \\ &\quad - 3(m/m^\circ)^2\,\beta^{(1)}_{NaCl}S_2/\ln 10 \\ &= pK_3 + 2(m/m) \\ &\quad (\beta^{(0)}_{NaHR} - \beta^{(0)}_{NaHR} + \Phi_{RCl} - \Phi_{RHCl})/\ln 10 \\ &\quad + 2\{m/m^\circ\}\ S_1\cdot(\beta^{(1)}_{NaR} - \beta^{(1)}_{NaHR})/\ln 10 \\ &\quad + \{m/m^\circ\}^2 \\ &\quad \cdot(C_{NaR} + \psi_{NaRCl} + C_{NaCl} - C_{NaHRCl})/\ln 10 \end{aligned} \tag{5}$$

$$f^{\gamma} = -A_{\varphi}[(I/m^\circ)_{1/2}/\{1 + 1.2\,(I/m^\circ)_{1/2}\} + (2/1.2)\ln\{1 + 1.2\,(I/m^\circ)^{1/2}\}] \tag{6}$$

$$S_1 + 2\{1 - [1 + 2\,(I/m^\circ)^{1/2}]\exp[-2(I/m^\circ)^{1/2}]\}/[4(I/m^\circ)] \tag{7}$$

$$S_2 + 2\{-1 + [1 + 2\,(I/m^\circ)^{1/2} + 2(I/m^\circ)]\exp[-2(I/m^\circ)^{1/2}]\}/[4(I/m^\circ)^2] \tag{8}$$

.

In Eqs. (5)–(8), the meaning of other symbols is the same as those in [9]. The extrapolation function, pK', may be calculated from experimental results and the values of Pitzer's parameters [9]. Using a polynomial approximation program according to the working Eq. (5), the regression yields a value of $pK_3^\circ = 10.07$ with standard deviation $s = 0.04$. The values of pK_3° obtained from both methods are in good agreement within experimental error.

Acknowledgements

This project was supported by the National Natural Science Foundation of China.

References

[1] W.-B. Liu, J.-J. Wang, C.-L. Wang, J.-S. Lu, Acta Physico-Chim. Sin. 8 (1992) 742.
[2] Z.-A. Zhu, Y.-Z. Wang, R.-T. Chen, Acta Physico-Chim. Sin. 3 (1987) 67.
[3] J.-Z. Yang, D.-Y. Men, et al., J. Phys. Chem. 53 (1989) 7251.
[4] D. Shugra, Biochemistry 25 (1952) 140.
[5] Z.-F. Zhang, J.-Z. Yang, Acta Physico-Chim. Sin. 9 (1993) 668.
[6] J.-Z. Yang, L.-T. Zhang, et al., Chem. J. Chin. Univ. 11 (1990) 180.
[7] Z.-Q. Huang, The Introduction to Electolyte Solution Theory, 2nd ed., Beijing, Science Press, 1983, p. 143.
[8] R. Barker, Organic Chemistry of Biological Compounds, CRC, New York, 1971, pp. 56–57.
[9] K.S. Pitzer, in: K.S. Pitzer (Ed.), Activity Coefficents in Electrolyte Solution, 2nd ed., CRC Press, Boca Raton, FL, 1991, p. 75.

ELSEVIER

Talanta 45 (1998) 951–956

Talanta

Benzoquinone modified electrode for sensing NADH and ascorbic acid

A.S.N. Murthy *, Jyotsna Sharma

Department of Chemistry, Indian Institute of Technology, New Delhi, 110 016, India

Received 3 March 1997; received in revised form 18 June 1997; accepted 24 June 1997

Abstract

A benzoquinone modified basal plane pyrolytic graphite electrode shows electrocatalytic activity for the oxidation of NADH and ascorbic acid in phosphate buffer (pH 7.3). The modified electrode shows a linear variation of catalytic current with concentration in the range 1–10 mM for both NADH and ascorbic acid. The rate constants have been estimated from the surface coverage data. © 1998 Elsevier Science B.V.

Keywords: Ascorbic acid; NADH; Benzoquinone; Cyclic voltammetry; Sensors

1. Introduction

The electrochemical oxidation of reduced nicotinamide adenine dinucleotide (NADH) to NAD^+ is of considerable interest in the development of amperometric biosensors for NAD^+ dependent dehydrogenases [1,2]. The direct oxidation of NADH at solid electrodes occurs at considerable overpotentials (1.1 V at carbon [1,2] and 1.3 V at Pt electrodes [1,2] and involves radical intermediates which cause electrode fouling. An approach based on the surface immobilised redox functionalities has been employed in an effort to accelerate the kinetics of NADH oxidation and the subject has been reviewed [1,2]. Investigations by Matsue et al. [3] have shown that the oxidation peak current in the voltammograms of ferrocene derivatives increases on addition of NADH with a simultaneous decrease of reduction peak current. The NADH oxidation occurs at ~0.4 V vs. SCE. Recently, a tetracyanoquinodimethane (TCNQ) modifed edge plane pyrolytic graphite (EPG) electrode [4,5] has shown electrocatalytic activity for NADH oxidation (0.38 V vs. Ag/AgCl) at pH 7.0. The rate of the reaction between adsorbed TCNQ and NADH in solution has been estimated to be of the order of $10^6\ M^{-1}\ s^{-1}$. Using NADH oxidase as an enzyme, McNeil et al. [6] have shown that it catalyses the oxidation of NADH in the presence of dioxygen as a natural electron acceptor or ferrocene derivatives as artificial electron acceptors. The enzyme diaphorase (Dp) acts as a catalyst for NADH oxidation and an amperometric determination of NADH at an immobilised Dp

* Corresponding author. Fax: +91 11 6862037; e-mail: murthy@chemistry.iitd.ernet.in

PII S0039-9140(97)00201-4

electrode was reported with ferrocenyl methanol as a mediator at ~0.2 V vs. SCE. Methylene green and meldola blue have also been employed as mediators [7]. Electrodes modified with poly(3-methyl thiophene) [8] exhibit NADH oxidation at 0.45 V vs. Ag/AgCl as compared to 0.65 V at the unmodified electrodes. The redox polymer of 3,4-dihydroxybenzaldehyde on a glassy carbon electrode (GCE) [9] exhibits electrocatalytic behaviour towards NADH oxidation (at 0.25 V vs. SCE) at pH 7.0 with a linear calibration for NADH in the concentration range of 1–6 mM. This modified electrode serves as an aldehyde biosensor [10].

L-ascorbic acid (AH_2) (vitamin C) is an extremely important molecule with a unique electrochemical role to play [11]. Petersson [12] has found that ferrocene modified Pt electrode mediated the oxidation of AH_2 electrocatalytically at ~0.40 V vs. SCE at pH 2.0. The catalytic current depends on the concentration of AH_2 in the range 0–0.06 mM. Palladium dispersed carbon paste electrode (CPE) [13] and ruthenium and platinum dispersed ultrathin carbon films [14] have been shown to enhance the electron transfer rates with oxidation occurring at ~0.4 V vs. Ag/AgCl. Recently, Murthy and Anita [15] have demonstrated that an EPG electrode modified with TCNQ lowered the potential for the oxidation of AH_2 to ~0.0 V vs. Ag/AgCl at pH 7.0. Kulys and D'Costa [16] have prepared TCNQ modified graphite based strip type sensors and found that they can be operated in the 50–100 mV vs. Ag/AgCl range for the determination of AH_2. The linear range was extended to 7.2 mM at an operating potential of 100 mV. A tetrathiafulvalene (TTF) modified CPE [17] was also observed to enhance the oxidation of AH_2 at ~0.25 V. The upper limit for the detection of AH_2 was, however, up to 1 mM only. Employing Pt microdisk electrodes modified with polyvinylferrocene and prussian blue, Dong and Che [18,19] have noted that AH_2 can be electrocatalytically oxidised at ~0.3 V vs. SCE. A carbon fibre micro disk electrode modified by electrodeposition with copper heptacyanonitrosyl ferrate [20] has similarly shown an ability to catalyse the oxidation of AH_2 at ~0.2 V vs. SCE. A linear response upto 6 mM was observed.

Although the electrocatalytic oxidation of NADH by *o*-quinones has been established [1,2], it is interesting that the oxidation has not been examined with *p*-quinone derivatives. We, therefore, considered to examine the viability of a basic *p*-quinone (e.g. *p*-benzoquinone) for the oxidation of NADH and AH_2. In this study, a simple method of modifying a basal plane pyrolytic graphite (BPG) electrode with benzoquinone (Q) is described and used to investigate the oxidation of NADH and AH_2.

2. Experimental

2.1. Reagents

NADH (Extra Pure for Biochemistry, SRL, India) and Ascorbic acid (A.R., S.D. Fine, India) were used without further purification. Benzoquinone (Aldrich) was recrystalised from *n*-hexane. All measurements were carried out in 0.2 M phosphate (K_2HPO_4 and KH_2PO_4) buffer, pH 7.3. To prevent any competitive oxidation by dissolved O_2, all solutions were thoroughly deoxygenated by purging with N_2 (highest purity).

2.2. Apparatus

Cyclic voltammetry experiments were performed in a three electrode electrochemical cell with a working volume of 5 ml using BAS voltammograph (CV27) with a *X*–*Y*–*t* chart recorder (Model No. MF 8050 F). Basal plane pyrolytic graphite working electrode (from Le Carbone Lorraine, France) was polished with 600 grit SiC paper and 1 μM diamond paste. Its area was determined by chronoamperometry using 2 mM $K_4[Fe(CN)_6]$ solution containing 1 M KCl. The diffusion coefficient for ferrocyanide is 0.65×10^{-5} cm^2 s^{-1}. The potential was stepped from 0 to 800 mV for 30 s. The area calculated using the Cottrell equation was found to be 0.183 cm^2. The area is actually a geometrical area of a disc electrode with flat surface. This area (A) was used subsequently for surface coverage calculation. All potentials were referred to the Ag/AgCl reference electrode. A Pt wire was used as an auxiliary electrode.

2.3. Immobilisation procedure

Benzoquinone (Q) was adsorbed on the BPG electrode according to the procedure described by Hu and Turner [21] with a minor modification. The BPG electrode was dipped in a solution of 200 mM Q in propanol for about 3 h at room temperature. It was then allowed to dry for 30 min, washed with phosphate buffer and stored in the same at 4°C.

3. Results and discussion

The cyclic voltammogram (CV) of Q modified BPG electrode in phosphate buffer (pH 7.3) shows E_{pa} and E_{pc} values at 0.15 and 0.08 V respectively (Fig. 1). The peaks, show a linear variation with scan rate (inset Fig. 1), characteristic of a surface modified electrode. The CVs were stable without change of either current or potential for a period of 48 h. The immobilisation procedure is such that a multilayer of quinone is formed on the electrode surface. The stability for the first 48 h of cycling may be due to the slow depletion of the outer layers which are not electrically linked to the graphite surface. An approximate estimate of the surface coverage of the electrode by Q was made by adopting the method used by Sharp et al. [22]. According to this method, the peak current is related to the surface coverage by the relation

$$i_{Pa} = \frac{n^2F^2A\Gamma\upsilon}{4RT} \quad (1)$$

where n represents the number of electrons involved in the reaction, A (cm^2) is the area of the electrode, Γ (mol cm^{-2}) is the surface coverage and other symbols have their usual significance. The calculated surface coverage is based on depositions carried out with three separate electrodes and the values are not very different from each other. The average surface coverage was found to be 6.5×10^{-10} mol cm^{-2}. This method was successfully employed by Sharp et al. [22] for ferrocene modified electrode and by us [4,5].

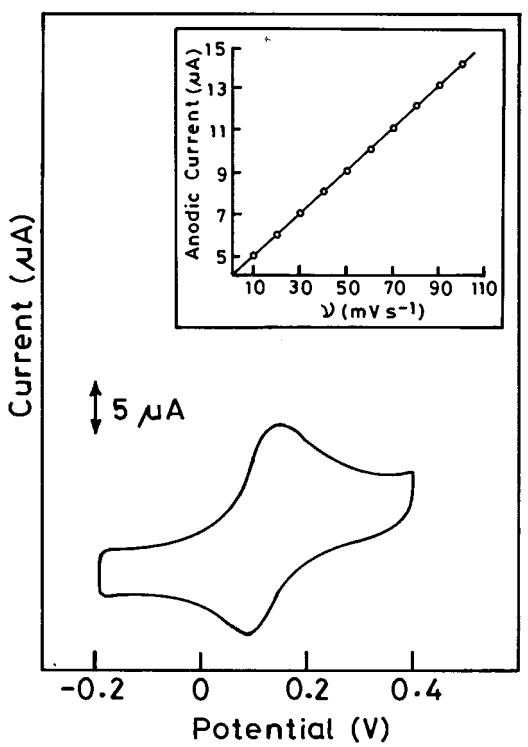

Fig. 1. Cyclic voltammogram of benzoquinone (Q) modified BPG electrode in phosphate buffer, pH 7.3. Scan speed: 25 mV s^{-1}; Plot of anodic peak current vs. scan rate for a Q modified BPG elctrode in background electrolyte (inset).

3.1. Electrocatalytic oxidation of NADH

The electro-oxidation of NADH at conventional metal electrodes requires a high overpotential (~1.0 V) and proceeds through the formation of a radical intermediate. NADH gets oxidised to NAD. which couples to form a dimer yielding NAD^+. We found, at the unmodified BPG electrode, that the oxidation of NADH occurs at 0.52 V. The CV of the Q-modified BPG electrode in the presence of NADH is shown in Fig. 2. The oxidation of NADH is accompanied by an increase in the anodic peak current at 0.15V vs. Ag/AgCl. The observed increase can be explained by assuming that NADH diffuses upto the electrode surface and reduces the Q produced electrochemically. The overall reaction scheme can be represented as

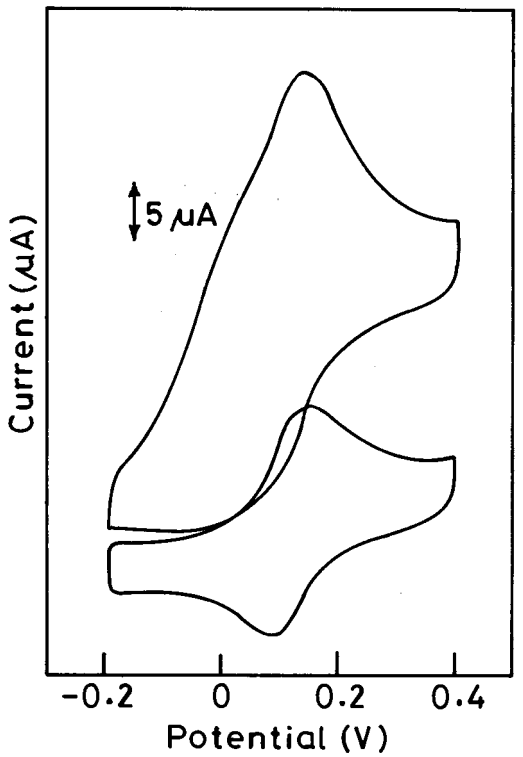

Fig. 2. (a) Cyclic voltammogram of Q modified BPG electrode in phosphate buffer, pH 7.3. (b) as in (a) with 8 mM NADH; Scan Rate: 25 mV s^{-1}.

$$Q + 2NADH \rightarrow 2NAD^+ + H_2Q + 2e^- \quad (2)$$

$$H_2Q \Leftrightarrow BQ + 2H^+ + 2e^- \quad (3)$$

$$\text{Net: } NADH \rightarrow NAD^+ + H^+ + 2e^- \quad (4)$$

The measured amperometric current (at 0.15 V) for different concentrations of NADH at Q modified electrode varies in the range 1–10 mM (Fig. 3). Each measurement is an average of three values from three different electrodes. A straight line was obtained by linear regression analysis and the correlation coefficient (r) was found to be 0.992 [$y = 0.2x + 0.02$]. The apparent Michaelis Menten constant, K'_m is found to be 10 mM (Table 1).

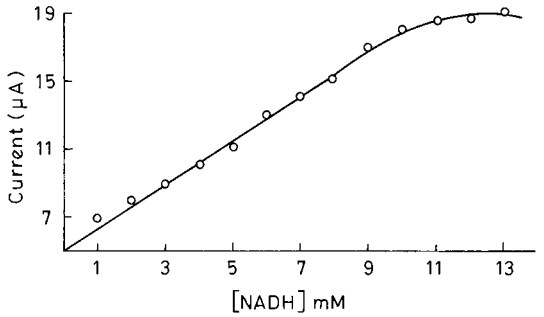

Fig. 3. Variation of catalytic current with concentration of NADH (Scan speed 25 mV s^{-1}).

3.2. Kinetic aspects

We attempted to determine the approximate rate of the reaction (k) (Eq. (2)) from an analysis of CVs assuming k to be fast. Andrieux and Saveant [23] have analysed the CVs in the framework of a model of redox chemically modified electrode. Based on extensive computations, a working curve showing the relationship between numerical values of $i_p/nFA(DnFv/RT)^{1/2}C$ and $\log[k\Gamma/(DnFv/RT)^{1/2}]$ (Fig. 1 of [23]) is given. Here n represents the number of electrons involved in the reaction, A (cm^2) is the area of the electrode, C is the bulk concentration (of NADH), D is the diffusion coefficient (of NADH) and other parameters have their usual significance. The value of k can thus be calculated from such a working curve. For the Q modified electrode, an analysis of the CVs has given an average value for the ratio $i_p/nFA(DnFv/RT)^{1/2}C$ to be 0.359. Using this value and Fig. 1 of [23] the rate constant, k for the reaction Eq. (2) was calculated to be 2.9×10^6 M^{-1} s^{-1} (Table 1). Here, the diffusion of NADH to the electrode surface may limit the overall heterogeneous electron transfer between NADH and the adsorbed quinone. Mass

Table 1
Kinetic constants

	K'_m (mM)	k (M^{-1} s^{-1})
NADH	10	2.9×10^6
Ascorbic acid	10	3.2×10^7

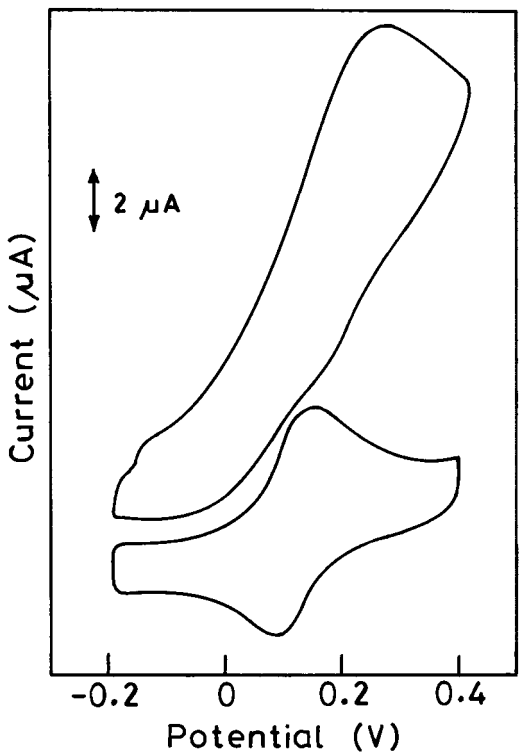

Fig. 4. (a) Cyclic voltammogram of Q modified BPG electrode in phosphate buffer, pH 7.3. (b) as in (a) with 5 mM AH_2; Scan Rate: 25 mV s^{-1}.

transport limitation may not thus give a clear picture of the true kinetics. The value of the rate constant is in fair agreement with the values reported for NADH oxidation at other modified electrodes [1,2,5].

3.3. Electrocatalytic oxidation of ascorbic acid (AH_2)

The AH_2 oxidation at the unmodified BPG electrode occurs at ~0.3 V. The CV of Q modified BPG electrode in the presence of AH_2 is shown in Fig. 4. The increase in the anodic peak current at 0.2 V vs. Ag/AgCl with a simultaneous decrease in the cathodic peak current is indicative of the reaction between the surface bound Q and the dissolved AH_2. The electrocatalytic mechanism can be written as

$$Q + AH_2 \rightarrow A + H_2Q \quad (5)$$

$$H_2Q \rightleftharpoons Q + 2H^+ + 2e^- \quad (6)$$

$$\text{Net: } AH_2 \rightarrow A + 2H^+ + 2e^- \quad (7)$$

The observed catalytic current varies with AH_2 concentration in the range 1–10 mM. A straight line was obtained by linear regression analysis and the correlation coefficient (r) was found to be 0.996 [$y = 0.15x + 0.015$]. The apparent Michaelis Menten constant, K'_m is found to be 10 mM (Table 1).

3.4. Kinetic aspects

The surface coverage was calculated using Eq. (1) and was found to be 7.8×10^{-10} mol cm^{-2}. An approximate estimate of rate of the reaction Eq. (5) was made by using the method of Andrieux and Saveant [23] which relates the peak current with the concentration. With the value of 0.396 for the constant, the rate constant, k for the reaction Eq. (5) was calculated to be 3.2×10^7 M^{-1} s^{-1} (Table 1). This value may be compared with the range of values 7.1×10^6–5.7×10^7 M^{-1} s^{-1} reported in the literature for prussian blue modifed electrode [19] and 1.5×10^7 M^{-1} s^{-1} for polyvinylferrocene modified electrode [18] for AH_2 oxidation.

4. Conclusions

The results reported in this investigation conclusively demonstrate that an electrode modified with a p-quinone can be effectively used for sensing NADH and AH_2 with concentrations extending up to 10 mM. The electrode preparation is simple and does not require chemical modification.

Acknowledgements

Jyotsna Sharma is thankful to the University Grants Commission for the award of a fellowship.

References

[1] W. Schuhmann, H.L. Schmidt, Amperometric Biosensors for substrates of oxidases and dehydrogenases, in: A.P.F. Turner (Ed.), Advances in Biosensors, vol. 2, Jai Press, London, 1992, pp. 79–130.
[2] M.F. Cardosi, A.P.F. Turner, Mediated electrochemistry: a practical approach to biosensing, in: A.P.F. Turner (Ed). Advances in Biosensors, Vol. 1, Jai Press, London, 1991, pp. 125–169.
[3] T. Matsue, M. Suda, I. Uchida, T. Kato, U. Akiba, T. Osa, J. Electroanal. Chem. 234 (1987) 163.
[4] A.S.N. Murthy, Anita, Bioelectrochem. Bioenerg. 33 (1994) 71.
[5] A.S.N. Murthy, Anita, R.L. Gupta, Anal. Chim. Acta 289 (1994) 43.
[6] C.J. McNeil, J.A. Spoors, D. Cocco, J.M. Cooper, J.V. Bannister, Anal. Chem. 61 (1989) 25.
[7] J. Kulys, G. Gleixner, W. Schuhmann, H.L. Schmidt, Electroanalysis 5 (1993) 201.
[8] N.F. Atta, A. Galal, A.E. Karagozler, G.C. Russell, H. Zimmer, J.F. Rubinson, H.B. Mark, J. Chem. Soc. Chem. Commun. (1990) 1347.
[9] F. Pariente, E. Lorenzo, H.D. Abruna, Anal. Chem. 66 (1994) 4337.
[10] F. Pariente, E. Lorenzo, F. Tobalina, H.D. Abruna, Anal. Chem. 67 (1995) 3936.
[11] G. Dryhurst (Ed.), Electrochemistry of Biological Molecules, Academic Press, New York, 1977.
[12] M. Petersson, Anal. Chim. Acta 187 (1986) 333.
[13] J. Wang, N. Naser, L. Angnes, H. Wu, L. Chen, Anal. Chem. 64 (1992) 1285.
[14] J. Wang, P.V.A. Pamidi, C.L. Renschler, C. White, J. Electroanal. Chem. 404 (1996) 137.
[15] A.S.N. Murthy, Anita, Biosensors Bioelectron. 9 (1994) 439.
[16] J. Kulys, E.J. D'Costa, Anal. Chim. Acta 243 (1991) 173.
[17] A.S.N. Murthy, Anita, Biosensors Bioelectron. 11 (1996) 191.
[18] S. Dong, G. Che, J. Electroanal. Chem. 309 (1991) 103.
[19] S. Dong, G. Che, J. Electroanal. Chem. 315 (1991) 191.
[20] Z. Gao, A. Ivaska, T. Zha, G. Wang, P. Li, Z. Zhao, Talanta 40 (1993) 399.
[21] J. Hu, A.P.F. Turner, Anal. Lett. 24 (1991) 15.
[22] M. Sharp, M. Petersson, K. Edstrom, J. Electroanal. Chem. 95 (1979) 123.
[23] C.P. Andrieux, J.M. Saveant, J. Electroanal. Chem. 93 (1978) 163.

.

ELSEVIER

Talanta 45 (1998) 957–961

Talanta

Rapid and selective method for the spectrophotometric determination of nickel naphthenate in gasoline in a microemulsion

Qin Wei *, Bin Du

Department of Applied Chemistry, Shandong Institute of Building Materials, Jinan 250022, People's Republic of China

Received 24 March 1997; received in revised form 18 June 1997; accepted 24 June 1997

Abstract

A new method for the spectrophotometric determination of nickel naphthenate in gasoline in a microemulsion was developed. PAN reacts with nickel(II) forming a red complex with composition 1:2 (metal to ligand) nickel(II)-PAN and absorption maximum at 568 nm. Nickel naphthenate in gasoline can be determined with PAN in a microemulsion, in the pH range 3.0 ~ 10.0 with a molar absorptivity of 4.8×10^4 l mol^{-1} cm^{-1}. Beer's law was obeyed up to 0.8 mg l^{-1} of nickel(II) in the microemulsion system. The interference of Cu^{2+}, Fe^{3+}, Mn^{2+}, Pb^{2+} and Zn^{2+} can be eliminated by adding 0.5 ml of a mixed masking agent. The method is rapid, simple and highly selective. © 1998 Elsevier Science B.V.

Keywords: Nickel naphthenate; Gasoline; Microemulsion; Spectrophotometry

1. Introduction

In order to apply gasoline to various uses, certain amounts of organometallic additives are often added to gasoline to improve its properties. The most commonly encountered additive elements in gasoline are lead, manganese, barium, copper, nickel and zinc [1–7]. For examples, nickel naphthenate and copper naphthenate are added to gasoline as anti-static agents. Alkyl lead compounds and methylcyclopentadienyl manganese tricarbonyl are added to gasoline as anti-knock agents. The control of the additive concentrations is important in the control of the physical and chemical properties of gasoline. The methods commonly used for the determination of additive elements are spectrophotometry with chromogenic reagents after extraction, dry ashing and wet digestion. These methods are time consuming and the loss of volatile elements or compounds possible. In this work, we have solved the above problems by adding emulgent-OP(*p*-octyl polyethylene glycol phenyl ether), *n*-butanol and water into gasoline to form microemulsion systems.

Microemulsions are transparent or translucent, low viscosity and homogeneous stable systems consisting of water, oil, surfactant and cosurfac-

* Corresponding author. Fax: +86 531 7963172.

PII S0039-9140(97)00196-3

tant, spontaneously formed at appropriate ratios. According to their different compositions, microemulsion systems can be divided into three types: the O/W (oil in water) type, the W/O (water in oil) type and the BC (bicontinuous) type. Particle diameters of the disperse phase in microemulsion systems are between 0.01 and 0.1 μm, and the oil–water interfacial tensions are less than 10^{-5} N m^{-1}. Microemulsion systems have great stability, are mixable with oil, water in certain concentration ranges. They have strong solubilization power to organic and inorganic substances [8]. Nickel(II) can be determined spectrophotometrically by using 1-(2-pyridylazo)-2-naphthol (PAN) in the presence of emulgent-OP [9,10]. In the work described here, the microemulsion system consisting of gasoline (or *n*-heptane), emulgent-OP, *n*-butanol, water was prepared and tested as a medium for the spectrophotometric determination of nickel naphthenate in gasoline with 1-(2-pyridylazo)-2-naphthol (PAN). In the microemulsion, 1-(2-pyridylazo)-2-naphthol (PAN) reacts instantaneously with nickel to form a red 1:2 (Ni-PAN) complex. The Ni-PAN complex exhibits an absorption maximum at 568 nm with a molar absorption of 4.8×10^4 l mol^{-1} cm^{-1}. Beer's law was obeyed up to 0.8 mg l^{-1} of nickel(II) in the microemulsion system and the color system was stable for no less than 3 weeks. The proposed method has been successfully applied to the spectrophotometric determination of nickel naphthenate (anti-static agent) in gasoline, and has the advantages of high selectivity, rapidity and simplicity without further extraction, dry ashing or wet digestion.

2. Experimental

2.1. Apparatus and reagents

A Shimadzu spectrophotometer, model UV-3000, with 1cm matched glass and silica cells was used for absorbance measurements. A model PHS-25 pH meter was used for pH measurements. Calibrated glassware was used for volumetric measurements. All glassware and polythene bottles were acid washed with a solution containing 2 mol l^{-1} HNO_3 and 1.5 mol l^{-1} HCl and rinsed with doubly distilled water.

All solvents and reagents were of analytical-reagent grade unless otherwise stated. Emulgent-OP (*p*-octyl polyethylene glycol phenyl ether) was supplied by Shandong Institute of Chemicals and PAN [1-(2-pyridylazo)-2-naphthol] was supplied by Shanghai Reagent Chemicals. Doubly distilled water was used throughout.

Nickel(II) stock standard solution was prepared by dissolving 1.00 g of nickel in 30 ml of water containing 15 ml of nitric acid by warming, cooling and diluting with water to 1000 ml in a calibrated flask. This solution contains 1.0 mg ml^{-1} of nickel(II). Working standards were prepared daily by appropriate dilution of the stock solution.

A butanol solution of PAN (0.05% w/v) was prepared by dissolving 0.05 g of PAN in 100 ml butanol.

Acetate buffer solution (pH 4.3) was prepared by mixing 42.3g of sodium acetate and 80 ml of glacial acetic acid and diluting to 1000 ml with doubly distilled water.

Stock standard solutions of diverse ions.

Mixed masking agent solution was prepared by mixing 5 g of potassium pyrophosphate, 25 g of citric acid and 10 g of thiourea and diluting to 100 ml with doubly distilled water.

2.2. Procedure for the determination of nickel naphthenate in gasoline

A 6.25 ml gasoline sample containing upto 20 μg nickel(II) was placed in 25 ml calibrated flask, 4.25 ml *n*-butanol, 8.75 ml emulgent-OP, 2.0 ml 0.05% PAN butanolic solution and 0.5 ml acetate buffer solution (pH 4.3) were added. The solution was diluted to mark with water. All solutions were placed with microburette. After being shaken for 1 min, the microemulsion system of the gasoline sample was obtained. The absorbance was measured at 568 nm in a 1 cm cell against a reagent blank.

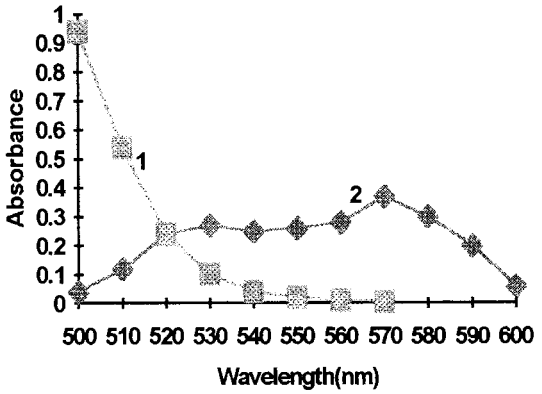

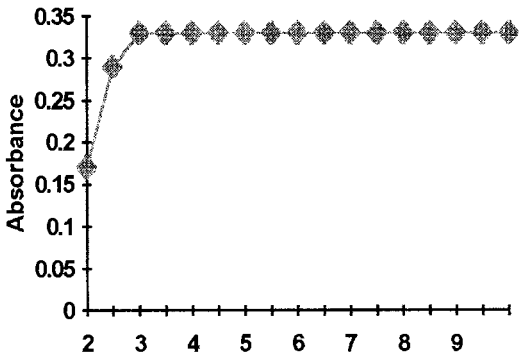

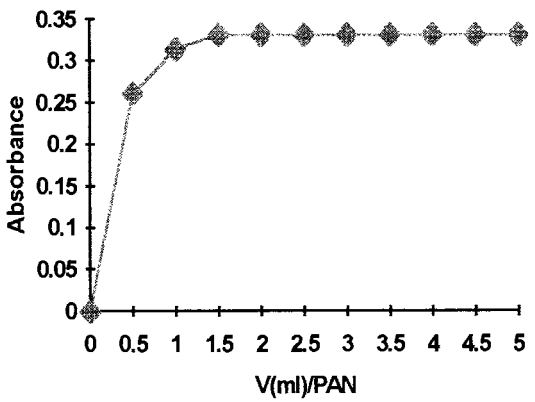

Fig. 1. The absorption spectra of: (1) PAN against water; (2) Ni(II)-PAN against PAN.
Fig. 2. pH effect on the Ni(II)-PAN system.
Fig. 3. Effect of reagent concentration.

Table 1
Tolerance limits in the spectrophotometric determination of nickel(II) with PAN

Ion	Amount tolerated (μg)	Ion	Amount tolerated (μg)
Ca^{2+}	1000	Zr(IV)	100
Mg^{2+}	1000	Bi^{3+}	40
$Fe3^{+}$ [a]	100	Cu^{2+} [a]	100
Al^{3+}	50	Cr^{3+}	100
Zn^{2+} [a]	500	Cr(VI)	300
Mn^{2+}	200	Si(IV)	300
Pb^{2+} [a]	80		

[a] Masking with 0.5 ml of mixed masking agent solution.

2.3. Procedure for preparing standard solutions

A 6.25 ml *n*-heptane (or octane, nonane) was placed in 25 ml calibrated flask, 4.25 ml *n*-butanol, 8.75 ml emulgent-OP, 2.0 ml 0.05% PAN butanolic solution and 0.5 ml acetate buffer solution (pH 4.3) were added. Then standard solution of nickel(II) in needed volume was added, the solution was diluted to mark with water. All solutions were placed with microburette. After being shaken for 1 min, the standard microemulsion system of nickel was obtained. The absorbance was measured at 568 nm in a 1 cm cell against a reagent blank.

3. Results and discussion

3.1. Spectral characteristics

The absorption spectrum of the Ni-PAN red complex was recorded in the range of 500 ~ 600 nm, (Fig. 1). The Ni-PAN red complex showed an absorption maxima at 568 nm against the reagent blank. Hence 568 nm was chosen for further studies.

3.2. Effect of varying reaction conditions

3.2.1. Effect of pH

The effect of pH for maximum absorbance was studied by adjusting the pH of the aqueous phase in the range of 2.0 ~ 12.0 in the standard microe-

Table 2
Analytical results of gasoline samples and standard addition recovery experiments

Samples (gasoline)	AAS value (μg/ml)	This work value (μg/ml, $n=7$)	Relative standard deviation (%)	Ni^{2+} added (μg)	Rate of recovery (%, $n=7$)
1	0.52	0.51	2.3	5.0	99.5
2	0.79	0.81	1.2	5.0	102
3	1.12	1.10	2.9	5.0	105
4	2.23	2.30	0.80	5.0	103

mulsion system containing 0.4 μg ml^{-1} of nickel as reported in the procedure for preparing standard solution. The results show (Fig. 2) that the optimum pH required for formation of Ni-PAN red complex is $3.0 \sim 10.0$, the pH 4.3 was chosen for further studies.

3.2.2. Effect of reagent concentration

Fig. 3. shows the effect of reagent concentration on the formation of Ni-pan red complex. The results show that the optimum reagent concentration required for formation of Ni-PAN red complex is $1.0 \sim 5.0$ ml. Hence 2.0 ml PAN butanolic solution was chosen for further studies. The optimum reaction condition was not affected by the order of addition of reagents.

3.2.3. Choice of alkanes

Gasoline is a type of alkane mixture system mostly consisting of $7 \sim 9$ carbons. The influence of alkanes on formation of the Ni-PAN red complex was studied. In the experiments, the standard microemulsion systems containing 0.4 μg ml^{-1} of nickel(II) were prepared using *n*-heptane, octane and nonane as oil phases respectively. The results showed that the variations of absorbance were less than 3.0%. Hence, the *n*-heptane (or octane, nonane) was chosen as the oil phase in place of gasoline for further studies.

3.2.4. Rate of reaction and stability of the complex

In the standard microemulsion system, the formation of the Ni-PAN red complex was instantaneous and the absorbance of the red complex remained almost constant for no less than 3 weeks.

3.2.5. Calibration graph

Under the optimal reaction conditions the absorbance follows beer's law in the range of $0 \sim 0.8$ mg l^{-1} of nickel(II) in the microemulsion system. The molar absorptivity was found to be 4.8×10^4 l mol^{-1} cm^{-1}.

The corresponding regression equation and coefficient of correlation were: $A = 0.030 + 0.810C$ $(mg \cdot l^{-1})$; $r = 0.999$

3.2.6. Stoichiometry of the complex

The slope ratio method was used in establishing the composition of the Ni-PAN red complex. The method indicated a 1:2 complex of nickel to PAN.

3.2.7. Interference

The selectivity of the proposed method was investigated by the analysis of samples containing 10 μg of nickel(II) in the presence of various amounts of diverse ions (Table 1). A maximum error of 5% in the absorbance reading was considered tolerable. The tolerance limit of various ions is given in Table 1. The interference of Cu^{2+}, Fe^{3+},Pb^{2+} and Zn^{2+} was eliminated by masking with 0.5 ml of mixed masking agent solution.

4. Applications

The proposed method was applied to nickel determination in several gasoline samples. In this work, standard addition recovery experiments were conducted. The results are summarized in Table 2.

5. Conclusions

Analysis of several gasoline samples indicated that the procedure for nickel naphthenate determination in gasoline provides accurate and precise results. This simple and fast method presented satisfactory selectivity, and can be applied to other oil samples.

References

[1] Q. Wei, B. Du, Z.H. Du, Fenxi Huaxue 22 (1994) 971.
[2] Q. Wei, B. Du, D.B. Hui, X. Shen, Fenxi Huaxue 22 (1994) 423.
[3] Q. Wei, B. Du, D.B. Hui, Fenxi Huaxue 22 (1994) 1132.
[4] G.C. Evetett, T.S. West, R.W. Williams, Anal. Chim. Acta. 70 (1974) 204.
[5] M.D. Dupuis, H.H. Hill, Anal. Chem. 51 (1979) 292.
[6] J.W. Hwang, Anal. Chem. 44 (1972) 22A.
[7] W.A. Aue, B. Millier, X.Y. Sun, Anal. Chem. 62 (1990) 2453.
[8] M.J. Schwuger, K. Stickdorn, R. Schmäcker, Chem. Rev. 95 (1995) 849.
[9] W.B. Qi, K.T. Fu, Fenxi Huaxue 9 (1981) 697.
[10] W.B. Qi, Chem. J. Chinese Universities 2 (1981) 385.

.

ELSEVIER

Talanta 45 (1998) 963–968

Talanta

Transport of Cu(II) with hydroxamic acid through a liquid membrane

Kanji Kubo *, Junko Kubo, Chifumi Kaminaga, Tadamitsu Sakurai

Department of Applied Chemistry, Faculty of Engineering, Kanagawa University, Kanagawa-ku, Yokohama, 221, Japan

Received 24 April 1997; received in revised form 18 June 1997; accepted 24 June 1997

Abstract

N-Hydroxy-*N*-naphthylbenzamides (**3**) were synthesized for examining their ability to extract and transport Cu(II) through a liquid membrane. The transport was proton-driven and was capable of moving metal ions 'up-hill'. Thus, it was possible to follow the transfer of Cu(II) from the aqueous source phase to the organic layer and from the organic layer to the receiving phase. The *N*-hydroxy-*N*-(2-naphthyl)benzamide (**3b**) carrier displayed much more remarkable selectivity for Cu(II) compared with *N*-hydroxy-*N*-(1-naphthyl)benzamide (**3a**). This difference in selectivity was explained in terms of the stability of the Cu(II) complex in chloroform. © 1998 Elsevier Science B.V.

Keywords: Transport; Cu(II); Hydroxamic acid; Liquid membrane

1. Introduction

The isolation of *N*-hydroxyoxamic acid from the reaction products of diethyloxalate and hydroxylamine attracted much attention to the chemistry of hydroxamic acids [1]. The complexation of metal ions with hydroxamic acids constitutes the basis of many analytical determinations [2,3]. A beautiful purple color of the Fe(III) and Cu(II) complexes enabled sensitive qualitative and quantitative determinations of carboxylic acids and their derivatives. Liquid membrane methods [4–6] are useful for assessing the partitioning of metal into and out of organic phases and are of considerable importance in medicine, water purification, and metallurgy. A liquid membrane, (which consists of an organic solvent placed at the bottom of a U-tube), has been widely used in order to study ion transport from one water compartment to the other, a process requiring, of course, passage through the chloroform barrier.

A few studies [7] regarding metal ion transport with hydroxamic acid derivatives such as *N*-hydroxy-*N*-phenylbenzamide (BPA) and *N*-hydroxy-*N*-phenylcinnamamide through liquid membranes have been reported. In this paper, we will describe the synthesis and properties of *N*-hydroxy-*N*-naphthylbenzamide (**3**) that serves as an effective transporting agent of Cu(II) through a liquid membrane.

* Corresponding author. Tel.: +81 45 4815661; fax: +81 45 4816594; e-mail: can@kamome.cc.kanagawa-u.ac.jp

PII S0039-9140(97)00202-6

2. Experimental

Elemental analyses were performed by Perkin Elmer PE2400 series II CHNS/O analyzer. The melting points were obtained with a Yanagimoto Micro Melting Point Apparatus and were uncorrected. The NMR spectra were measured on a JEOL JNM-500 Model spectrometer in $CDCl_3$; the chemical shifts are expressed by an δ unit using tetramethylsilane as an internal standard. The IR spectra were recorded on a Hitachi Model 270-30 infrared spectrometer with KBr disks for crystalline compounds. The UV spectra were measured using a Shimadzu Model UV-2200 spectrophotometer.

2.1. Synthesis of *N*-benzoyl-*N*-naphthylhydroxylamines (**3**)

Nitronaphthalene **1** (0.02 mol, 5.18 g) was dissolved in 1:1 v/v ethanol/1,2-dichloroethane (50 cm^3) and was cooled to 0°C. Raney nickel (type W-4; 1.0 g) was added by stirring into the solution. Then, 80% hydrazine hydrate solution (2.0 cm^3, 0.064 mol) was added drop by drop, taking care to maintain the reaction temperature below 10°C. The complete (or nearly complete) nitronaphthalene conversion was confirmed by TLC analyses on silica gel using benzene as an eluent. The catalyst was removed by filtration. The solvent was evaporated and the residue was recrystallized from benzene to yield *N*-naphthylhydroxylamines. The residue of the *N*-arylhydroxylamine (which was obtained by the evaporation of solvents in the above procedure) was redissolved in benzene (40 cm^3) and was washed with ice-cold water (20 cm^3). This mixture was added with stirring into a previously cooled solution (0°C) of 5% sodium hydrogencarbonate in water (60 cm^3). Benzoyl chloride (4.98 g, 0.03 mol) in benzene (30 cm^3) was added drop by drop to the well-stirred mixture in about 0.5 h, taking care to maintain the temperature of the reaction below 5°C. The mixture was stirred for a further 2 h at 0–5°C. The benzene layer was separated and the aqueous layer was extracted with benzene (30 cm^3). The combined benzene extract was washed with water (40 cm^3) and then with 10% sodium hydroxide solution (150 cm^3). The aqueous alkaline solution was separated and acidified with a 10% hydrochloric acid solution when the *N*-hydroxy-*N*-naphthylbenzamide were separated from the solution. The obtained crystals were purified by column chromatography over silica gel (70–230 mesh, Merck) using hexane and benzene as the eluent. Recrystallization from ethyl acetate or ethanol gave analytically pure samples with the following physical properties.

N-hydroxy-*N*-(1-naphthyl)benzamide (**3a**): Colorless crystals, mp 166.0–167.0°C. ^{1}H NMR δ = 7.13 (2H, dd, J = 7.9, 7.6 Hz), 7.23 (1H, d, J = 7.0 Hz), 7.28 (1H, dd, J = 7.6, 7.0 Hz), 7.32 (1H, t, J = 7.9 Hz), 7.37 (2H, d, J = 7.0 Hz), 7.58 (1H, dd, J = 8.2, 7.0 Hz), 7.66 (1H, dd, J = 8.2, 7.0 Hz), 7.87 (1H, d, J = 8.2 Hz), 7.90 (1H, d, J = 8.2 Hz), 8.23 (1H, d, J = 8.2 Hz), and 9.30 (1H, bs). ^{13}C NMR δ = 123.2, 125.2, 127.0, 127.5, 127.8, 128.1 (2C), 128.36, 128.42 (2C), 130.4, 130.5, 131.1, 131.6, 134.4, 135.8, 167.0. IR ν 714, 771, 912, 972, 1407, 1449, 1596, 1629, 2866, 3052, 3448 cm^{-1}. Found: C, 77.71%; H, 5.47%; N, 5.27%. Calcd for $C_{17}H_{13}NO_2$: C, 77.55%; H, 4.98%; N, 5.32%.

N-hydroxy-*N*-(2-naphthyl)benzamide (**3b**): Colorless crystals, mp 139.0–141.5°C. ^{1}H NMR δ = 7.22–7.25 (2H, m), 7.31 (1H, dd, J = 8.9, 2.1 Hz), 7.35 (1H, tt, J = 7.0, 2.1 Hz), 7.45–7.51 (4H, m), 7.69 (1H, d, J = 2.1 Hz), 7.71 (1H, dd, J = 7.0, 2.1 Hz), 7.75 (1H, d, J = 8.9 Hz), 7.80 (1H, d, J = 8.2 Hz), 9.23 (1H, bs). ^{13}C NMR δ = 123.7, 124.5, 126.9, 127.0, 127.7, 128.2, 128.3, 128.9 (2C), 129.1 (2C), 131.1, 132.0, 132.4, 133.1, 136.7, 165.3. IR ν 654, 678, 696, 717, 747, 789, 831, 864, 1053, 1128, 1161, 1254, 1422, 1452, 1509, 1572, 1590, 1611, 2920, 3052, 3136 cm^{-1}. Found: C, 77.72%; H, 4.78%; N, 5.39%. Calcd for $C_{17}H_{13}NO_2$: C, 77.55%; H, 4.98%; N, 5.32%.

2.2. Determination of equilibrium constant

An aqueous solution (3 cm^3) containing metal salts ([$CuCl_2$] or [$FeCl_3$]/mol dm^{-3} = 0–0.1) was shaken with a chloroform solution (3 cm^3) of BPA or **3** (5×10^{-5} mol dm^{-3}) for 5 min. The chloroform layer was measured spectrophotometrically (Cu(II): λ = 330 nm, Fe(III): 430 nm) and

the equilibrium constants were estimated by using the Benesi–Hildebrand approximation equation [8].

2.3. Transport of Cu(II) with *3a* and *3b*

Transport experiments were performed using a liquid membrane system which consists of source phase (10 cm^3, 5×10^{-3} mol dm^{-3} $CuCl_2$), chloroform layer (10 cm^3, 5×10^{-3} mol dm^{-3} carrier), and a receiving phase (10 cm^3, 2.0 mol dm^{-3} hydrochloric acid). A single apparatus and a constant stirring at 25°C were used. As described [9], to measure Cu(II), 0.5 cm^3 was also taken from aq I and aq II and was diluted with water to 5 cm^3. To the diluted solution (0.5 cm^3) aqueous citric acid solution (2.00 g, in 10 cm^3) was added to acidify the solution, and then aqueous EDTA solution (500 mg of EDTA hydrate in 10 cm^3) was added. The mixture was adjusted to pH = 9.0 by adding NH_3. After 20 min the mixture was transferred into a separate funnel and was diluted with water to 50 cm^3. A sodium diethyldithiocarbamate (DDTC) solution (1×10^{-2} mol dm^{-3}, 5 cm^3) was added and was shaken with $CHCl_3$ (10 cm^3). The organic layer was dried onto a filter paper and was measured spectrophotometrically ($\lambda = 440$ nm).

3. Result and discussion

N-Hydroxy-*N*-naphthylbenzamides (**3**) were prepared from nitronaphthalenes in two steps, as shown in Scheme 1 [10]. Reduction of **1** with raney-nickel and hydrazine furnished the hydroxylamines (**2**), which were converted to the corresponding *N*-hydroxy-*N*-naphthylbenzamides by benzoylation. The structure and purity of **3a** and **3b** were ascertained by NMR spectroscopy and elemental analyses.

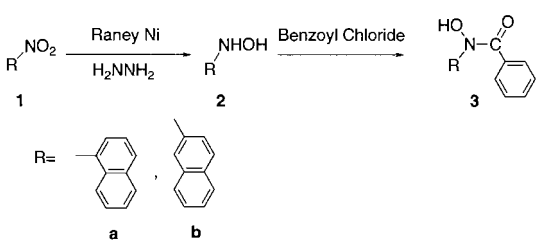

Scheme 1.

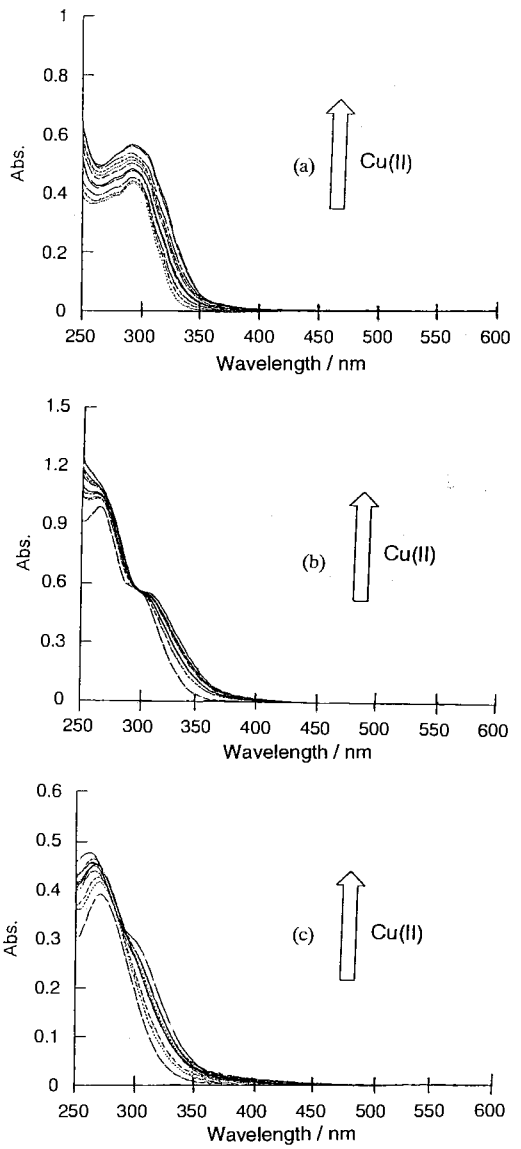

Fig. 1. The absorption spectral changes of (a) **3a**, (b) **3b** and (c) BPA (5×10^{-5} mol dm^{-3}) in chloroform that was equilibrated with aqueous $CuCl_2$ (0–0.1 mol dm^{-3}).

Extraction of various metal ions (1.0×10^{-2} mol dm^{-3}) into the chloroform solutions containing **3** (5.0×10^{-5} mol dm^{-3}) was checked by UV

spectroscopy; lithium, sodium, potassium, magnesium, calcium, barium, cobalt, nickel, and zinc ions revealed no indication of UV spectral change, but Cu(II) and Fe(III) showed a spectral change. In Figs. 1 and 2 are shown the absorption spectra of **3** and BPA obtained in the presence of varying concentrations of Cu(II) or Fe(III). The complexation of **3** and BPA with Cu(II) (Fig. 1) and Fe(III) (Fig. 2) showed an enhancement of the absorption, while the Fe(III) complex gave a new band at 430 nm. The composition of the complexes was determined as 1 (metal):2 (ligand) for the Cu(II)–**3** system and 1:3 for the Fe(III)–**3** system by the molar ratio method. Fig. 3 shows

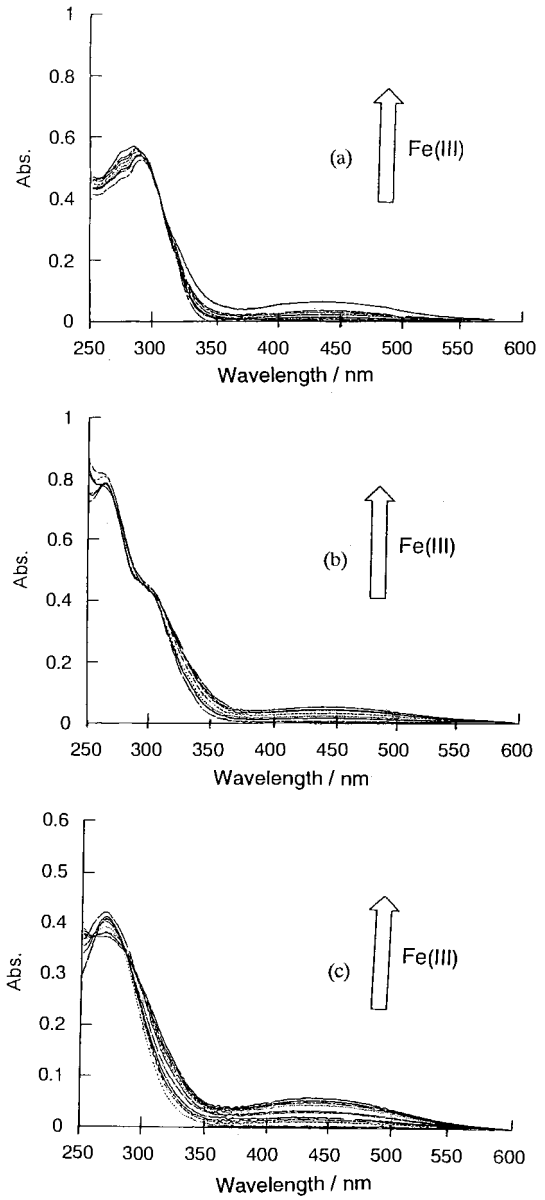

Fig. 2. The absorption spectral changes of (a) **3a**, (b) **3b** and (c) BPA (5×10^{-5} mol dm^{-3}) in chloroform that was equilibrated with aqueous $FeCl_3$ (0–0.1 mol dm^{-3}).

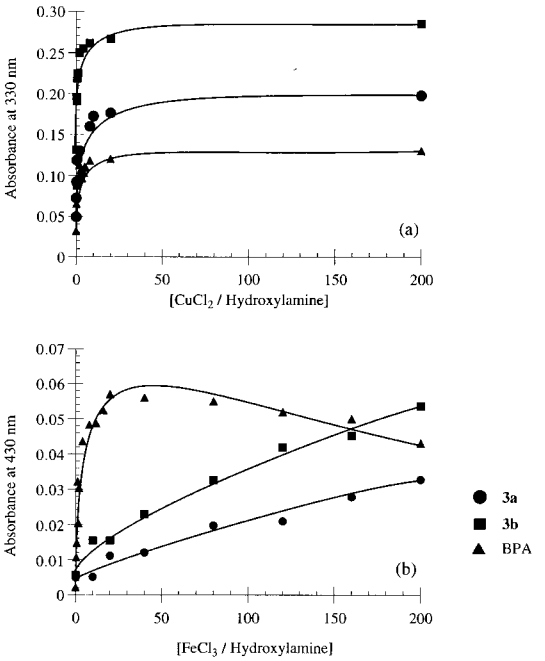

Fig. 3. The absorption spectral changes (Cu(II): $\lambda = 330$ nm, Fe(III): 430 nm) of **3a**, **3b** and BPA induced by (a) Cu(II) and (b) Fe(III).

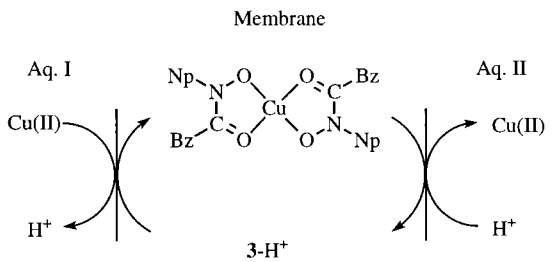

Fig. 4. Schematic representation of the reactions taking place at the boundary of the source phase and the chloroform and at the boundary of the chloroform and the receiving phase.

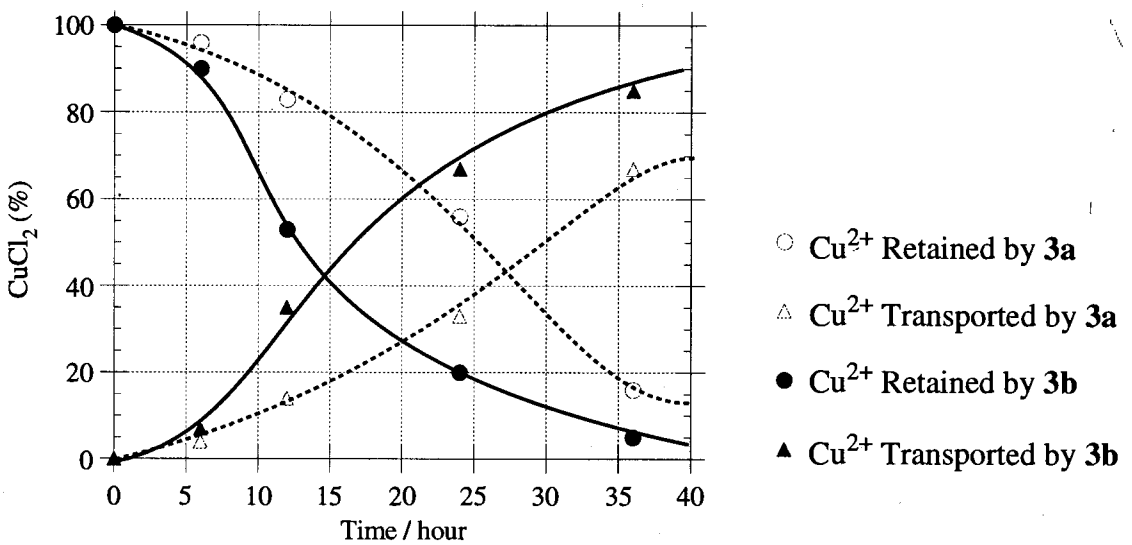

Fig. 5. Percent of copper in the source phase ($CuCl_2$, 5×10^{-3} mol dm^{-3}, 10 cm^3) and the receiving phase (2 mol dm^{-3} HCl, 10 cm^3) as a function of time (h) using the chloroform phase (10 cm^3) for carrier **3a** and **3b** (5×10^{-3} mol dm^{-3}).

the Cu(II) and Fe(III)-induced changes in the UV spectra for **3** and BPA. The extraction equilibrium constants were determined by the Benesi–Hildebrand method [8]. The equilibrium constants of Cu(II) complex were larger than those of Fe(III) complex and the increasing order of equilibrium constants was **3a** (Cu(II): 25 400; Fe(III): 70) < **3b** (Cu(II): 73 300; Fe(III): 200) < BPA (Cu(II): 95 500; Fe(III): 10 000). Interestingly, the Fe(III)–BPA complex was distributed into the water with excess Fe(III). The hydroxylamine **3** captures Cu(II) ion under neutral conditions and liberates it upon acidification with hydrochloric acid as detected by UV spectroscopy. This means that **3a** and **3b** can serve as a transporting agent of Cu(II) through the liquid membrane.

Transport experiments were performed using a liquid membrane system (see experimental Section 2). The Cu(II) concentrations in the aqueous compartments were monitored as a function of time by means of the colorimetric method. The transport data are an average of at least three runs whose experimental error is less than 5%. No movement of Cu(II) through the chloroform was observed unless a carrier was used. Cu(II) transport with **3a** and **3b** was promoted by the counterflow of protons from the receiving to the source phase, although proton concentration was not quantitatively investigated. Fig. 4 shows that the reaction takes place at both interfaces. It is worth noting that the Cu(II) transport rate data in Fig. 5 correlates with the equilibrium constant data.

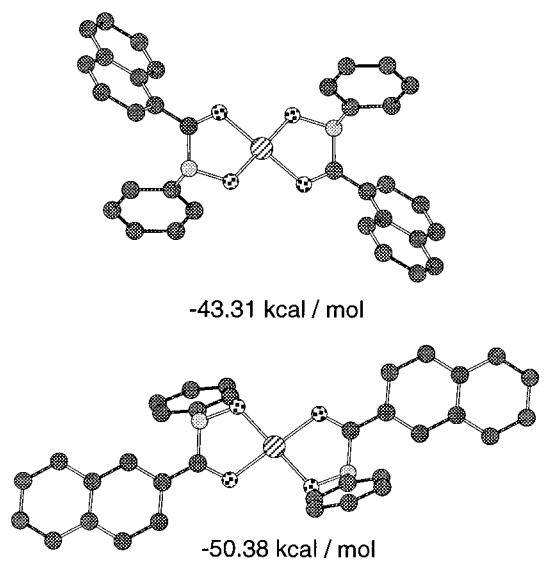

Fig. 6. The structures of copper(II) complexes of **3a** and **3b** as calculated by MM2.

This suggests that Cu(II) transport in the liquid membrane system is controlled by the thermodynamic stability of the Cu(II)–**3** complexes in the membrane solvent. A comparison of the equilibrium constants confirms that extraction of Cu(II) from source phase into chloroform actually favors **3b** over **3a**. The hydroxylamine **3b** is a better carrier in a liquid membrane system. It is likely that the 2-naphthyl group of **3b** exerts less steric effects on the stability of Cu(II)–**3** complexes than the 1-naphthyl. These results suggest that the contribution of the naphthyl group position, on Cu(II) uptake by means of hydroxamic acid is large.

The MM2 calculations [11] were applied to the Cu(II) complexes of **3a** and **3b**. The geometries were optimized so as to give minimum energy (Fig. 6). Thus, we are led to the complex with **3a** being sterically less stable than **3b**. This conclusion is consistent with lower equilibrium constant and slower transport rate for the Cu(II)–**3a** system.

In summary, hydroxamic acid derivatives with naphthyl substituents were effective for Cu(II) transport through a liquid membrane and indicates that slight structural changes affect the extraction and transport rate of Cu(II) to a greater extent. This makes it possible to design an effective carrier for Cu(II) separation.

References

[1] E. Lipczynska-Kochany, Chem. Rev. 91 (1991) 477.
[2] S. Mizukami, K. Nagata, Coord. Chem. Rev. 3 (1968) 267.
[3] T.J. King, P.G. Harrison, J. Chem. Soc. Chem. Comm. (1972) 815.
[4] R.D. Noble, J.D. Way (Eds.), Liquid Membaranes: Theory and Applications, American Chemical Society, Washington, DC, 1987.
[5] T. Araki, H. Tsukube (Eds.), Liquid Membaranes: Chemical Applications, CRC Press, Boca Raton, FL, 1990.
[6] A. Mori, K. Kubo, H. Takeshita, Coord. Chem. Rev. 148 (1996) 71.
[7] L.K. Shpigun, E.N. Abanina, Zh. Anal. Khim. 39 (1984) 1829.
[8] H.A. Benesi, J.H. Hildebrand, J. Am. Chem. Soc. 71 (1949) 2703.
[9] Shin Jikken Kagaku Koza vol. 9, Chemical Society of Japan, Maruzen, Tokyo, 1975, p. 382.
[10] N.R. Ayyanger, K.C. Brahme, U.R. Kalkote, K.V. Srinivasan, Synthesis (1984) 938.
[11] Computer calculations were performed with the CAChe-MM2 program from Sony-Tektronics.

.

ELSEVIER

Talanta 45 (1998) 969–976

Talanta

Simultaneous determination of propranolol and pindolol by synchronous spectrofluorimetry

Tomás Pérez Ruiz *, Carmen Martínez-Lozano, Virginia Tomás, José Carpena

Department of Analytical Chemistry, Faculty of Chemistry, University of Murcia, 30071, Murcia, Spain

Received 27 November 1996; received in revised form 11 March 1997; accepted 30 June 1997

Abstract

The simultaneous determination of propranolol and pindolol using synchronous fluorescence spectrometric techniques is described. The method involves measuring the natural fluorescence of these drugs in a 50% (v/v) ethanol–water medium using zero and first derivative synchronous spectrofluorimetry. Under the optimum conditions, the linear determination ranges of propanolol and pindolol are ca. 0.02–1.0 and 0.04–1.2 μg ml^{-1}, respectively. The results showed that propranolol and pindolol can be determined simultaneously when the concentration ratio of propranolol to pindolol varies from 1:100 to 50:1 in the mixed sample. The method has been satisfactorily applied to the determination of propranolol and pindolol in urine samples and propranolol in pharmaceutical preparations.

Keywords: Propranolol; Pindolol; Synchronous fluorescence spectrometry

1. Introduction

Propranolol (PRO: 1-[isopropylamino-3-[1-naphthyloxy]-2-propanol) and pindolol (PIN: [1-(isopropylamino)-3 (4-indolyloxy) 2-propanol]) are members of a heterogeneous group of drugs classified as beta-adrenergic receptor blockers and are generally prescribed in the treatment of hypertension, angina pectoris, cardiac arrhythmias and hypertrophic subaortic stenosis [1,2], but are also sometimes used as doping agents in sport.

Because of their similar spectral features, the determination of these compounds in mixtures has so far been carried out by using gas chromatography [3–5] and liquid chromatography [6–9].

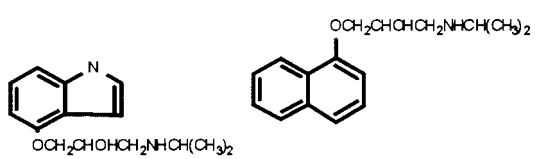

Pindolol Propranolol

Several fluorimetric methods have been applied to the individual determination of PIN [10,11] and PRO [12–14] based on their native fluorescence or on derivative reactions. Because the fluorescence spectra of PRO and PIN overlap, conventional spectrofluorimetry does not permit simultaneous determination of these compounds.

* Corresponding author. Fax: +34 68 364148.

PII S0039-9140(97)00203-8

Synchronous luminescence spectrometry involves the simultaneous scanning of both the excitation and emission monochromators, which are synchronised in such a way that a well-defined relationship is maintained between their wavelengths. Conventionally, this relationship is a constant wavelength difference. The advantages of the synchronous technique are a reduction in spectral complexity, peak bandwidth, Rayleigh scattering and Raman scattering [15]

The combination of synchronous scanning fluorimetry and derivatives is more advantageous than differentiation of the conventional emission spectrum in terms of sensitivity, because the amplitude of the derivative signal is inversely proportional to the band width of the original spectrum [16,17]

The aim of the present work was to find a new fluorimetric method that is simple, time-saving and accurate for the determination of PRO and PIN. The paper describes two methods to resolve the mixture of these drugs by employing synchronous fluorescence spectrometry, and first derivative synchronous spectrofluorimetry when the molar ratio PRO/PIN is higher than ten or lower than 0.04.

2. Experimental

2.1. Reagents

All reagents were of analytical grade and doubly distilled water was used in all experiments. PRO and PIN (both $>99.6\%$ pure) were obtained from Sigma (St. Louis, MO) and used for preparing 300 μg ml^{-1} stock standard solutions by dissolving the drugs in 50% v/v ethanol–water mixture. Working solutions of lower concentration were freshly prepared by appropriate dilution of the stock standard solution.

Britton–Robinson buffer solutions of different pH values were prepared by the addition of 1 M sodium hydroxide solution to a 0.2 M solution of phosphoric, boric and acetic acids. The final pH was checked with a glass electrode.

2.2. Apparatus

An Aminco Bowman Series 2 spectrofluorimeter equipped with a xenon lamp and interfaced to an DTK computer was used for fluorescence measurements. The software provides mathematical manipulation of the spectra and calculates first and second derivatives by the simplified least-squares procedure of Savitzky and Golay [18]. In addition, tridimensional spectra presented in the form of isometric projection may be obtained. The contour plots were calculated using the 'Galactic' application program from the data in ASCII format obtained with the spectrofluorimeter.

Further, a Colora thermostatic water-bath circulator was used for temperature control of the cell compartment and a Radiometer digital pH-meter with a combined glass-saturated calomel electrode was used to check the pH values.

2.3. Procedures

2.3.1. Determination of PRO and PIN by constant wavelength synchronous spectrofluorimetry

To a 10 ml volumetric flask was added an adequate volume of the PRO/PIN sample to give final concentrations in the range 1.0–0.02 μg ml^{-1} PRO and 1.2–0.04 μg ml^{-1} PIN. Then 5 ml of ethanol was added and the mixture was diluted to the mark with distilled water. Synchronous spectra were recorded (at 25 ± 0.5°C) by scanning both monochromators at a constant wavelength difference $\Delta\lambda = 18$ nm ($\lambda_{ex} = 200$–280 nm, $\lambda_{em} = 218$–298 nm) and a scan speed of 240 nm min^{-1}. Hereafter all wavelengths referring to synchronous spectra are taken as equal to those of the corresponding emission wavelengths. The fluorescence intensities measured at 305 and 323 nm were directly proportional to PIN and PRO concentrations, respectively. Each analyte in the mixture was evaluated from the corresponding calibration graph, obtained previously under the same conditions as those for the mixture. The synchronous spectrum of the 50% (v/v) ethanol–water was stored in memory as a 'background spectrum' and was subtracted from all subsequently obtained spectra.

2.3.2. Determination of PRO and PIN by first derivative constant wavelength synchronous spectra

This technique allows the simultaneous determination of PRO and PIN by recording only one synchronous spectrum when drugs are found in the molar ratio PRO/PIN from 1/100 to 50/1. First-derivative measurements were made as the vertical distance from the first-derivative synchronous spectrum at 291 nm to the baseline for PIN and at 341 nm to the base line for PRO.

2.3.3. Determination of PIN and PRO in urine

The urine sample was filtered. A suitable aliquot (5 ml) was placed into 25 ml stopped glass tubes in ice. To each tube were added 0.5 ml 2 mol l^{-1} sodium hydroxide and 10 ml diethyl ether. PRO and PIN were extracted into the ethereal layer by mechanically vortexing the phases for 2 min. The phases were separated by centrifugation (3 min at 1000 g) and 8 ml of the ethereal extract was transferred to clean 15-ml tapered glass-stoppered tubes containing 2 ml of 0.01 M hydrochloric acid. PRO and PIN were extracted into the aqueous phase by mechanically vortexing the solution for 1 min. After separation of the phases by centrifugation the aqueous phase was frozen by immersion of the tubes in ice and the ethereal phase aspirated. The aqueous phase was then washed with 5 ml of *n*-heptane by mechanically vortexing the solution for 1 min. After centrifugation and freezing of the aqueous phase, the *n*-heptane was aspirated and discarded. Accurate aliquots of the aqueous phase were neutralised with 0.1 M sodium hydroxide and analysed following the procedure described for the first-derivative synchronous fluorescence spectrometry.

2.3.4. Determination of PRO in pharmaceutical preparations

The tablets were finely powdered and weighed. An amount of this powder, equivalent to about 50 mg of PRO was accurately weighed and shaken with 50 ml of distilled water in a water-bath at 60–70°C for 10 min. After cooling, 50 ml of ethanol were added and the solution was sonicated in an ultrasonic bath for 5 min before being filtered through a Millipore filter.

The filtrate was then diluted with distilled water to 100 ml in a calibrated flask. An appropriately diluted aliquot of this solution was analysed following the synchronous fluorescence spectrometric procedure.

The injections were appropriately diluted with 50% (v/v) ethanol–water and analysed following the procedure for tablets.

3. Results and discussion

PRO and PIN are fluorescent in ethanol–water media. The effect of the ethanol content in the medium was investigated. An increase of ethanol content in the medium causes a continuous increase in the fluorescence intensity of PIN while the fluorescence intensity of PRO increases up to a 25% (v/v) ethanol–water, above which it decreases slightly. A 50% (v/v) ethanol–water medium was chosen for further studies.

PRO shows two excitation maxima at 232 and 295 nm and exhibits fluorescence maximum at 324 and 337 nm. PIN has its excitation maxima at 223 and 281 nm and exhibits maximum fluorescence at 308 nm. The fluorescence spectra of these drugs overlap considerably and, as a result, the conventional spectrofluorimetric method does not permit the simultaneous determination of both compounds.

The extent of the overlap of these compounds was examined by obtaining the total spectrofluorimetric information available in the excitation–emission matrix. In Fig. 1, the three-dimensional spectra of PRO and PIN are represented as an isometric projection, where the emission spectra at stepped increments of the excitation wavelength have been recorded and plotted.

In Fig. 1 (low part) the tree dimensional spectra have been transformed into a contour plot en the excitation–emission plane. The contour representation of the fluorescence profile of PRO and PIN offers an easy way of finding the best trajectory to be followed in order to obtain synchronous fluorescence spectra for the complete resolution of overlapping component peaks. The parallel diagonal lines superimposed on the contour plots represent the scan paths through the

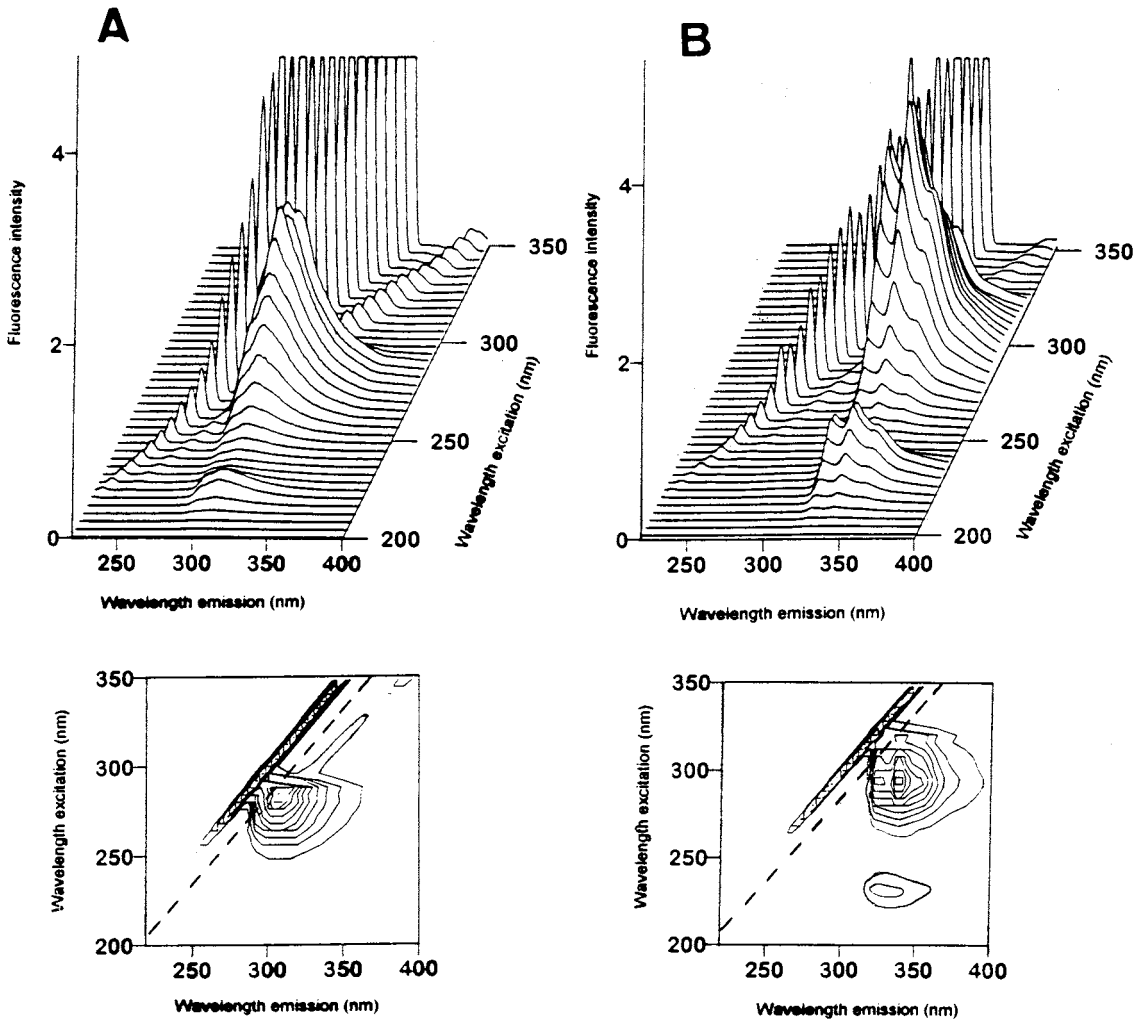

Fig. 1. Three-dimensional and two-dimensional (contour plots) total fluorescence spectra of pindolol (A) and propranolol (B). Other conditions as in figure $C_{PIN} = 10$ μmol l^{-1}, $C_{PRO} = 1$ μmol l^{-1}.

excitation–emission matrix that would be obtained with synchronous scans at the wavelength interval shown. The optimum path for determining PRO and PIN in mixtures seems to be $\Delta\lambda =$ 18 nm; it passes near the maximum for PIN but at some distance from the maximum for PRO; however, the determination of the mixture is sufficiently sensitive because PRO is much more fluorescent than PIN.

3.1. Synchronous fluorescence spectrometry

The synchronous fluorescence spectra of PRO, PIN and that of their mixture taken at a constant wavelength difference $\Delta\lambda = 18$ nm are shown in Fig. 2. The peaks corresponding to PIN (305 nm) and PRO (323 nm) are well resolved and it is thus possible to determine both drugs simultaneously in a mixture.

Chemical variables were studied to obtain the best measurement conditions and maximum fluorescence signals. Thus, the influence of pH on the fluorescence was studied by adding Britton–Robinson buffer solutions of different pH values. Fluorescence intensity of PRO and PIN is not affected by this variable in the range studied (pH between 3.0 and 9.0). A pH value of 6.0 was selected for further fluorescence measurements.

3.2. Analytical characteristics

The concentration of PRO and the fluorescence intensity measured at 323 nm are linearly related over a sample concentration range 0.02–1.0 μg ml^{-1}. PIN concentration and the fluorescence measured at 305 nm are linearly related over the range 0.04–1.2 μg ml^{-1}. The correlation coefficient for the standard calibration graphs were 0.9998 and 0.9994 ($n = 11$) for PRO and PIN, respectively. The detection limits (signal three times the standard deviations of the average blank signal) were 0.003 μg ml^{-1} for PRO and 0.007 μg ml^{-1} for PIN. The relative standard deviation for a mixture of 0.10 and 0.09 μg ml^{-1} PIN ($n = 6$) were 0.29 and 0.36%, respectively.

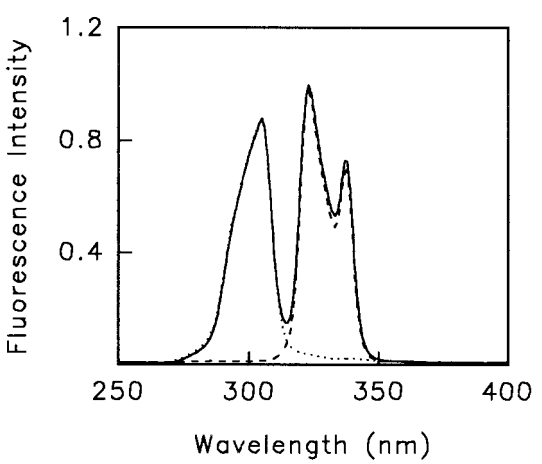

Fig. 2. Synchronous fluorescence spectra of pindolol (dotted line), propranolol (dashed line) and their mixture (solid line). $\Delta\lambda = 18$ nm. Other conditions as Fig. 1.

Table 1
Analysis of synthetic mixtures of pindolol and propranolol

Method used[a]	Added (μg ml^{-1})		Found[b] (μg ml^{-1})	
	PIN	PRO	PIN	PRO
SFS	0.900	0.050	0.898 ± 0.008	0.051 ± 0.003
	0.900	0.100	0.902 ± 0.012	0.099 ± 0.003
	0.800	0.200	0.810 ± 0.001	0.202 ± 0.004
	0.300	0.800	0.305 ± 0.006	0.806 ± 0.009
	0.100	1.00	0.103 ± 0.004	0.990 ± 0.008
	0.100	2.00	0.108 ± 0.003	2.02 ± 0.02
FDSFS	0.02	1.0	0.019 ± 0.001	1.02 ± 0.02
	0.05	1.0	0.048 ± 0.001	0.997 ± 0.01
	0.90	0.02	0.903 ± 0.009	0.022 ± 0.002
	0.90	0.01	0.892 ± 0.020	0.0096 ± 0.003

[a] SFS = Synchronous fluorescence spectrometry, FDSFS = First-derivative synchronous fluorescence spectrometry.
[b] Means ± SD of four determinations.

The proposed method was applied to the simultaneous determination of PRO and PIN in synthetic mixtures containing different ratios of both drugs and the results are given in Table 1. It can be seen that a good recovery was achieved for the two drugs in PRO/PIN ratios between 10 and 0.05.

3.3. First-derivative synchronous fluorescence spectrometry

The resolution of the mixture PRO/PIN at molar ratios higher than 10 is poor because the PIN band partially overlaps that of PRO. This spectral overlapping can be resolved, however, by differentiation of the synchronous spectra. The use of first and second derivatives was tried and, as expected, a degradation of the signal-to-noise ratio occurred with the higher order differentiation.

The most appropriate parameters to register synchronous derivative spectra were selected. A scan speed of 240 nm min^{-1} was selected after verifying that this parameter hardly affect the derivative signal obtained.

Fig. 3 shows first derivative synchronous fluorescence spectra of PRO and PIN and of a mixture of both drugs. By applying the zero-crossing technique to the first derivative synchronous spectrum of the mixture, both analytes can be determined by measuring the vertical distance to the zero line at 291 and 341 nm, which are proportional to PIN and PRO concentrations, respectively. The resolution of the mixture is precise because the heights measured correspond to peaks in the first derivative spectrum.

The determination was carried out in a single scan by using the calibration graphs obtained for each component, which covered concentration ranges from 0.04 to 1.2 μg ml^{-1} for PIN and from 0.02 to 1.0 μg ml^{-1} for PRO. Mixtures of PRO and PIN in ratios up to 1:100 and 50:1 were resolved (see Table 1).

3.4. Interferences

In order to assess the possible analytical applications of the synchronous spectrofluorimetric procedure described above, the effect of concomitant species on the determination of PRO and PIN in real samples was studies by analysing synthetic sample solutions containing 0.3 μg ml^{-1} of each analyte and various excess amounts of the foreign compound up to 120 μg ml^{-1}. The tolerance ratio of each foreign substance was taken as the largest amount yielding an error less than 4% in the analytical signal of PRO or PIN. Glucose, sucrose, maltose, lactose, saccharin, fructose, caffeine, cyclamate, and citrate were tolerated in large amounts (400-fold excess was the maximum tested); a 50-fold excess of acetylsalicylic acid and 20-fold excess of riboflavin and salicylic acid were also tolerated.

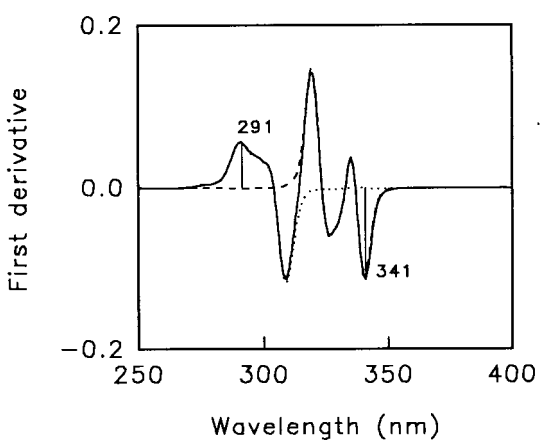

Fig. 3. Fist-derivative synchronous fluorescence spectra of pindolol (dotted line), propranolol (dashed line) and their mixture (solid line). Other conditions as in figure.

3.5. Applications

PRO and PIN are almost completely absorbed from the gastro-intestinal tract. Since they are only partially metabolised and are excreted in the urine both unchanged and in the form of metabolytes, the proposed method appears to be useful for the simultaneous determination of these drugs in urine samples. However, human urine is composed of numerous organic substances, some of which are fluorescent [19] and provide a high background fluorescence, thus interfering with the direct determination of the drugs. In this case a prior extraction step is necessary. The pretreatment and procedure described under Experimental were used in each instance.

Urine samples spiked with PRO and PIN at different concentrations and at different mass ratios were prepared by adding known amounts of PRO and PIN to drug-free urine samples. The mean analytical recoveries were 96 ± 3 and 97 ± 3% for PRO and PIN, respectively as shown in Table 2.

As the dosage forms containing PIN were not available in the local market, we prepared our own according to the literature methods. Commercial pharmaceuticals containing PRO were available and some of them were analysed. The data in Table 3 show that the PRO and PIN contents measured by the proposed method were in good statistical agreement with the amounts added and with the values supplied by the manufacturers. Recovery studies were also carried out on samples to which known amounts of PRO and PIN had been added. In all cases quantitative recoveries between 98.6 and 105% were obtained.

Table 2
Analytical recoveries of pindolol and propranolol added to drug-free urine samples

Concentration added (μg ml^{-1})		Concentration found[a] (μg ml^{-1})		Recovery (%) ± SD[a]	
PIN	PRO	PIN	PRO	PIN	PRO
12.0	50.0	11.5	49.7	96 ± 4	99 ± 2
12.0	5.0	11.7	4.9	98 ± 2	98 ± 3
12.0	0.2	11.8	0.18	98 ± 2	90 ± 6
15.0	2.0	14.5	1.92	97 ± 3	96 ± 4
15.0	0.5	14.6	0.49	97 ± 3	98 ± 2
20.0	1.0	19.8	0.96	99 ± 2	96 ± 3
				Mean	
				97 ± 3	96 ± 3

[a] Average of three determinations.

Table 3
Determination of propranolol in pharmaceutical preparations

Product (laboratory)[a]	Content (mg tab^{-1} or ml^{-1})		Found[b] (mg tab^{-1} or ml^{-1})	
	PIN	PRO	PIN	PRO
Tablets I (Home made)	5	5	5 ± 0.2	4.9 ± 0.3
Tablets II (Home made)	1	10	1 ± 0.1	9.9 ± 0.2
Sumial (Farma)		40		40.6 ± 0.6
Betadipresan-DIU (Fides)		100		100.2 ± 0.2
Betadipresan (Fides)		100		100.1 ± 0.2
Sumial injectable (Farma)		5		4.9 ± 0.3

[a] Composition of samples: Tablets I: pindolol, 5 mg, propranolol, 5 mg, lactose, 50 mg, other excipients upto 100 mg. Tablets II: pindolol, 1 mg, propranolol, 10 mg, methyl cellulose upto 50 mg. Sumial 40: propranolol hydrochloride, 40 mg; lactose,125 mg; other excipients up to 200 mg. Betadipresan-DIU: propranolol hydrochloride, 100 mg; hydralazine hydrochloride, 50 mg; bendroflumethiazide, 5 mg; lactose and other excipients. Betadipresan: propranolol hydrochloride, 100 mg; hydralazine hydrochloride, 50 mg; lactose and other excipients. Sumial injectable: propranolol hydrochloride, 5 mg; citric acid and water up to 5 ml.
[b] Means ± SD of three determinations.

4. Conclusions

Molecular synchronous spectrofluorimetry resolves binary mixtures of PIN and PRO in a 50% (v/v) ethanol–water medium. Better separation of the compounds is achieved by applying the first derivative to the synchronous fluorescence spectra. Mixtures of PRO and PIN in molar ratios up to 1:100 and 50:1 were resolved.

The results obtained in the study of the recovery of these analytes testifies to the usefulness of the proposed method to expedite routine analysis of these two drugs.

Acknowledgements

The authors gratefully acknowledge financial support from the 'Dirección General de Investigación Científica y Técnica' and 'Comunidad Autonoma de Murcia'.

References

[1] O.B. Garfein, Ther. Drug Monit. 4 (1982) 1.
[2] S. Wolfson, R.A. Heinle, M.V. Herman, Am. J. Cardiol. 18 (1966) 345.
[3] M. Guerret, J. Chromatogr. 221 (1980) 387.
[4] H. Maurer, K. Pileger, J. Chromatogr. 382 (1986) 147.
[5] C.L. Davies, J. Chromatogr. A 664 (1995) 341.
[6] L. Ye, Z. Xiangxi, Anal. Chim. Acta 196 (1987) 255.
[7] W.H. Pirkle, J. Chromatogr. 558 (1991) 1.
[8] M.T. Saarinen, H. Siren, M.L. Riekkola, J. Chromatogr. A 664 (1995) 341.
[9] P. Lukkari, H. Siren, J. Chromatogr. A 717 (1995) 211.
[10] M.E. Mohamed, M.S. Tawakkol, H.Y. Aboul-Enein, J. Assoc. Off. Anal. Chem. 66 (1983) 273.
[11] C.L. Jennings, A. Bobick, E.T. Fagan, P.I. Korner, Brit. J. Clin. Pharmacol. 7 (1979) 245.
[12] J.W. Black, W.A.M. Duncan, R.G. Shanks, Brit. J. Pharmacol. 25 (1965) 577.
[13] M. Kraml, W.T. Robinson, Clin. Chim. Acta 24 (1978) 171.
[14] H. Migulla, H. Mack, Pharmacie 36 (1981) 443.
[15] E.L. Wehry, in: G.G. Guilbault (Ed.), Practical Fluorescence, Marcel Dekker, New York, 1990, pp. 378–406.
[16] G.L. Green, T.C. O'Haver, Anal. Chem. 46 (1974) 2191.
[17] P. John, I. Soutar, Anal. Chem. 48 (1976) 520.
[18] A. Savitzky, M.J.E. Golay, Anal. Chem. 36 (1964) 1627.
[19] M.J.P. Leiner, M.R. Hubmann, O.W. Wolfbeis, Anal. Chim. Acta 198 (1987) 13.

.

ELSEVIER

Talanta 45 (1998) 977–988

Talanta

Membrane filtration studies of aquatic humic substances and their metal species: a concise overview Part 1. Analytical fractionation by means of sequential-stage ultrafiltration

P. Burba [a,*], B. Aster [a], T. Nifant'eva [b], V. Shkinev [b], B.Ya. Spivakov [b]

[a] *Institute for Spectrochemistry and Applied Spectroscopy, 44139 Dortmund, Germany*
[b] *Vernadsky Institute of Geochemistry and Analytical Chemistry, Moscow 117975, Russia*

Received 13 February 1997; received in revised form 23 June 1997; accepted 30 June 1997

Abstract

A concise overview (75 references) of the analytical fractionation of aquatic humic substances using sequential-stage ultrafiltration is presented. First, humic substances in aquatic environments and actual problems connected with their fractionation and analysis are briefly considered. The molecular size classification of dissolved humic substances by means of multistage ultrafiltration, with special emphasis on on-line techniques, is the focal point of the discussion. In particular, the capabilities of ultrafiltration for the size fractionation and characterization of species formed between colloidal humic substances and pollutants (e.g. metals) are stressed. © 1998 Elsevier Science B.V.

Keywords: Aquatic humic substances; Fractionation; Metal distribution; Molecular size classification; Sequential-stage ultrafiltration

1. Introduction

The so-called humic substances (HS) are the main contributors to the organic carbon globally distributed in aquatic and terrestrial environments [1]. According to current estimations, more than 50% of the dissolved organic carbon (DOC) in surface, ground and seawater consist of refractory polyelectrolytes of the HS type [2]. They are continuously formed by microbial processes (humification) from plant remainders and other debris, either in aquatic systems (aquagenic HS) or in soils (pedogenic HS) [3]. In general, aquatic HS are complex mixtures of related macromolecules of varying composition, structures, functionalities and molecular masses, strongly influenced by their genesis and the grade of humification [4]. Mostly, they consist of a great variety of aliphatic, aromatic, carbohydrate and amino acid substructures irregularly connected together and substituted by a broad spectrum of functional groups. Due to this structural versatility, HS are involved in many environment processes [5], especially in

* Corresponding author. Fax: +49 231 1392120; e-mail: burba@isas-dortmund.de.

PII S0039-9140(97)00204-X

binding, transport and deposition of inorganic and organic pollutants (e.g. heavy metal ions, pesticides) [6]. In particular, the formation of HS/metal complexes of diverse stability/lability is of increasing interest for the speciation of trace metals in natural waters [7].

A detailed characterization of HS and their manifold processes in the environment requires the application of powerful analytical tools combined from various chemical, spectroscopic and fractionation methods [8,9]. The most serious hindrance in the analysis of HS, however, is the fact that analytical signals observed from HS and their processes generally are sums of numerous slightly different sub-signals, leading to their broadening and, thus, lowering their resolution and specificity. In case of mixtures of definable biotic macromolecules, for instance carbohydrates or proteins, efficient separation procedures can fully overcome this analytical problem. Due to the extreme complexity of HS mixtures and the very small number of identical molecules contained even in highly resolved HS fractions [9], however, so far no 'high-performance' separation procedures exist for HS molecules (high-resolution mass spectrometry for small ones excepted). In practice, instead of 'HP' separations, merely a more or less rough fractionation of dissolved HS can be achieved based on differentiable properties of the contained macromolecules, for example their varying hydrophilic/hydrophobic interaction with RP sorbents in high-performance liquid chromatography (HPLC) systems [10], different affinity to metal-containing sorbents [11], different behaviour in electric fields (e.g. conventional and capillary electrophoresis [12], size-exclusion of non-fitting molecules in gel phases of uniform pore size [13], or their size discrimination on ultramembranes of adequate molecular mass cut-off [14].

Among the separation principles mentioned, the fractionation of dissolved HS by ultrafiltration (UF) on suitable membrane filters is a simple way to differentiate such polydisperse mixtures of macromolecules as a function of their molecular size, hardly influencing or altering their chemical composition. Moreover, UF is one of the few separation methods functioning without additional separation media and auxiliary reagents, for instance gel phases, electrolytes or buffers, respectively, thus avoiding blank substances as interferents. The simple and reliable scale-up of UF from the micro to the macro dimension in commercial UF units (e.g. Millipore–Amicon, Pall Filtron) is another relevant advantage of this separation principle. In the case of aquatic HS, the most valid argument for their fractionation by UF is the fact that many interactions and processes of HS in the environment can be more or less dependent on their molecular size, for instance their binding capability towards pollutants [15] and their sorption behaviour onto mineral surfaces and suspended materials, respectively [16]. Therefore, molecular size fractionation and classification of dissolved HS by UF [14], performed under reproducible and reliable conditions [17], enables such processes to be differentiated as a function of their molecular size. It has to be realized, however, that HS in aquatic environments are only a part of a complex and dynamic colloid system [18]. Thus, in the case of analytical size fractionation of HS in natural waters by UF or other methods, some basic considerations about aquatic colloids are useful.

2. Size fractionation of aquatic colloids

Due to a long-standing convention in water chemistry, for the discrimination between the 'dissolved' phase and the 'particulate' phase in aquatic environments, membrane filters with a pore size of 0.45 μm are applied. This choice is arbitrary, since size distributions of aquatic substances including HS colloids extend continuously from some tens of nanometres (e.g. hydrated metal ions) to hundreds of micrometres (e.g. suspended matter) as schematically indicated in Fig. 1 for a variety of naturally occurring components, which can be fractionated by filtration techniques. Despite the fact that below the 0.45 μm limit, real inorganic and organic particles still exist in natural waters, the term 'particles' is operationally assigned only to components with a size greater than 0.45 μm. The terms macromolecules and/or colloids are preferred for molecular sizes between

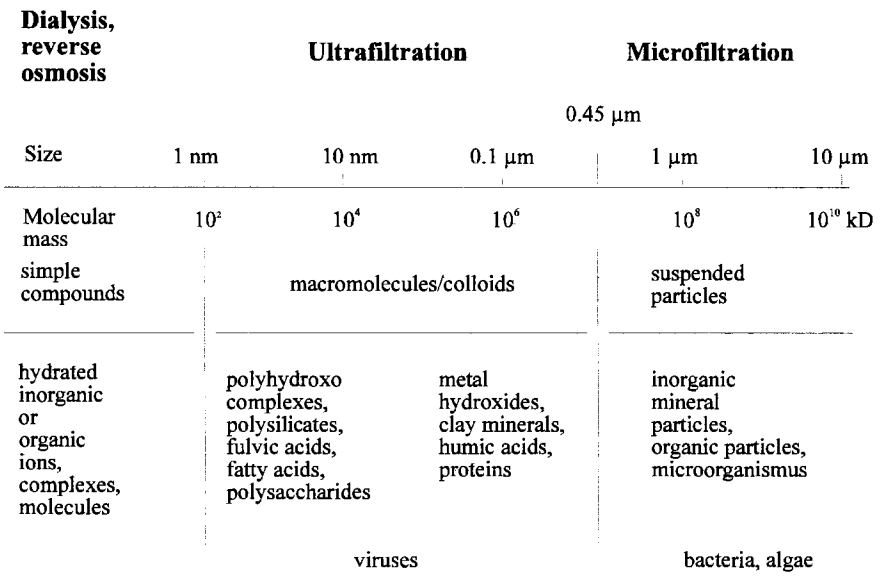

Fig. 1. Size and mass range of natural constituents in aquatic systems.

1 nm and 0.45 μm, which is roughly comparable to a molecular-mass range from <1 to >1000 kDa in the case of HS considered here in aquatic systems.

More detailed information about the molecular size distribution in HS under study can be provided by a conventional size classification procedure, for instance gel permeation chromatography (GPC) in defined gel phases, which has been preferably used for the fractionation of HS in aquatic systems and in soils [13,19–21], respectively, despite a number of serious limitations (e.g. artifacts by HS sorption, calibration problems). According to these and other results [10,22], the molecular-mass distribution of dissolved HS stemming from typical aquatic systems (e.g. surface, ground, bog water) mostly ranges from about 500 to some 10 000 Da, often with maxima in the range of some 1000 Da [23]. In such a case, an average molecular weight, either as number-average molecular weight M_n or as weight-average molecular weight M_w, which can be determined by a variety of methods [24], is an insufficient parameter for the description of colloidal HS.

Using GPC and UF, respectively, for the evaluation of molecular-mass distributions in dissolved HS, however, it is to be realized that in this case, the molecular size and not the molecular mass is the criterion governing the fractionation process. Unfavourably, humic macromolecules dissolved in aqueous solution are suggested to be loosely wound, flexible molecular strands, roughly describable by a random-coil model [25], which are mostly constituents of a complex colloidal system strongly depending on the pH value and the electrolyte concentration [26]. The size of dissolved HS molecules can range from full molecular expansion at small electrolyte concentration to strong shrinking or collapse (precipitation) in salt-rich solutions [26]. Thus, in the case of aquatic HS, both of the methods mentioned merely enable an operationally defined molecular size classification of the contained colloids instead of an accurately evaluated and stable molecular mass distribution. Nevertheless, the size fractionation of dissolved HS is indispensable for their classification and for reducing the polydispersity in HS mixtures to be characterized. For this purpose, advanced multistage UF procedures performed by means of a simple on-line technique are considered here as a promising tool.

Table 1
Commercial membranes used in sequential-stage ultrafiltration of aquatic colloids

Membrane	Fractions	References
UM-2, UM-20, UM-20E, (Amicon Corp.)	>20, 20–10, 10–1, <1 kDa	[27]
8, 0.2, 0.035 μm (Schleicher and Schüll); PM10, DM5, UM2, UM05 (Amicon Corp.)	>0.05 μm, 0.05 μm–100 kDa, 100–10, 10–0.2, <0.2 kDa	[29]
UM05, UM2, (Amicon Corp.)	Estim. of permeation coeff.	[30]
BA83, AC64, AC63, AC62, AC61 (Schleicher and Schüll)	200–35, 35–20, 20–10, 10–5, <5 nm	[31]
8, 3, 1, 0.6, 0.4, 0.2, 0.1, 0.05, 0.03, 0.015 μm (Nucleopore Corp.); 8, 3, 1.2, 0.45, 0.1, 0.05, 0.01 μm, Sartorius GmbH	>8, 8–3, 3–1.2, 1.2–0.45, 0.45–0.1, 0.1–0.05, 0.05–0.01, <0.1 μm	[32]
Filtron NOVA, polyethersulfone (Pall Filtron)	>100, 100–50, 50–10, 10–5, 5–1, <1 kDa	[42]
UM-05, (Amicon Corp.); PSAC, PTGC, PSED, PTHK, (Millipore Corp.) (mixture of cellulose acetate and cellulose nitrate)	0.4 μm–100 kDa, 100–25, 25–10, 10–1, <1 kDa	[58]
YM100, PM10, YM2, 8400 cell, (Amicon Corp.)	>100, 100–10, 3–10, <3 kDa	[59]
H1P 10-8, hollow fiber cartridges	0.1–0.005, <0.005 μm	[66]
H1P100, H1P10-20, H1P1-43, hollow fiber cartridges	>100, 100–10, 10–1, <1 kDa	[67]
YM3, YM10 (regenerated cellulose), PM10, YM30, PM30, XM50, 202 cell, (Amicon Corp.)	>50, 50–30, 30–25, 25–10, 10–3.5, 3.5–3, <3 kDa	[68]

3. UF of aquatic HS

Conventional UF procedures have been studied since the early 1970s with respect of their fractionation performance for naturally occurring colloids such as HS in aquatic systems [27–31]. The main focus of these and other studies [14] was to characterize the size range of aquatic macromolecules and their metal loadings below the arbitrary particle cut-off at 0.45 μm.

3.1. Sequential procedures

For this purpose, different UF membranes and conventional one-stage filtration techniques (e.g. concentration or washing mode, sequential or parallel filtration) summarized in Table 1 were studied, bearing in mind that the molecular size distribution of dissolved HS is strongly dependent on a variety of aquatic and operational parameters (e.g. pH, electrolyte concentration, HS concentration, operational filtration conditions). In most cases, sequential filtration through a series of ultramembranes has been used for HS fractionation. Using this UF technique, each filtrate obtained with an appropriate starting ultramembrane (e.g. 100 kDa) is further fractionated with ultramembranes of decreasing pore sizes down to 1 kDa followed by a washing stage [29]. Afterwards, the HS fractions remaining on the filters can be withdrawn for detailed characterization. In the parallel mode, however, aliquots of the initial water sample to be fractionated are filtered in parallel through filters with pore sizes in the range 1.5–400 nm [32]. Not only organic colloids of the HS type, but also naturally occurring inorganic colloids (e.g. Fe and Mn oxyhydroxides) in the size range 1 nm–1 μm could be size fractionated by means of these UF techniques [33]. It is noteworthy that ultrafiltration by means of the above mentioned washing technique yields relatively reproducible results, minimizing coagulation and aggregation processes in the cell compared to the concentration technique [29]. A considerable disadvantage of all sequential UF procedures, however, is the extended period of time required to filtrate and to wash a HS sample solution step by step through a series of UF membranes. Moreover, continuous transformation processes of HS (e.g. alteration of the molecular size, precipitation) influencing the reliability of the fractionation results can also occur during long operation times. Another potential drawback is the risk of contamination or loss of HS or other

analytes (e.g. metal species) by their sorption on the surface of polymer materials being part of the UF equipment used.

3.2. On-line procedures

Analytical risks of this kind can generally be diminished using an on-line flow procedure for UF instead of a time-consuming process consisting of single stages which are to be performed step by step. In principle, on-line multistage ultrafiltration (MS-UF) applied to the fractionation of dissolved organic macromolecules (including HS) can be realized by two different flow techniques: (1) a series of conventional stirred UF cells connected together and equipped with appropriate membranes or (2) a cascade of suitable membranes of decreasing pore size installed like the stages of a technical separation column.

3.2.1. On-line combinations of stirred cells

Already during the 1960s [34–36], on-line UF by different combinations of stirred cells was being proposed for the advanced fractionation of biotic macromolecules (e.g. proteins). The design of these early 'diafiltration' systems has been described elsewhere [35]. In operation, the solution to be fractionated is placed in the uppermost compartment of the train equipped with the most open filter. Below are water- or buffer-filled compartments with progressively lower cut-off membranes. Sample and washing solution, respectively, are either pumped or gas-driven through the system until the desired throughput is reached. Insofar as the cells are completely fluid-filled and the final ultrafiltrate is at atmospheric pressure, a step pressure drop throughout the system occurs. The resulting filtration rate is mainly governed by the filtration through the membrane of smallest pore size.

A mathematical characterization of such continuous multistage (dia)filtration operations applied to different biopolymers has been described elsewhere [37–40].

Up to now, on-line combinations of stirred UF cells, in contrast to off-line combinations as described above [30,41], have scarcely been applied for the molecular size fractionation of dissolved HS. For example, an on-line three-stage system of stirred UF cells [37], modified from [36] and equipped with membranes of the NMWCO of 1, 10 and 30 kDa, was utilized for the molecular size characterization of the DOC (mainly HS) in some natural waters being used as reservoirs for the production of drinking water.

3.2.2. On-line cascade systems

On-line UF systems consisting of a cascade of membranes (e.g. hollow fibre, flat membrane) are in principle a simple separation technique, being comparable to the stages of a chromatography column. Accordingly, mixtures of dissolved organic macromolecules penetrating the train of the installed membranes (or retained by them) can be fractionated as a function of their molecular size. Increasing concentrations of macromolecules on the membrane surfaces, however, can cause polarization and clogging effects (see Section 3.3), respectively, which might strongly interfere with this on-line filtration process and its reliability. To reduce such undesired concentration effects, a turbulent circulation of the solution over the membrane surface is required. It can be realized by a fast tangential flow of the introduced sample over the membrane. For the collection of the sample fractions obtained, a small-volume reservoir on every stage of such an UF system can serve.

The on-line fractionation of aquatic HS by a multistage (MS)-UF system arranged as a filtration cascade has recently been described [42,43]. The flow scheme of this analytical-scale MS-UF device equipped with membranes of decreasing pore size (M_1: 100, M_2: 50, M_3: 10, M_4: 5 and M_5: 1 kDa) and processed by a multichannel peristaltic pump is shown in Fig. 2. Accordingly, the HS solution (e.g. 10 ml) to be size-classified is cycled under pressure (2 bar) over the first membrane M_1. The permeate introduced into the tangential flow over the next membrane M_2 and through the reservoir R_2 is processed in an analogous way, reaching successively the membranes M_3, M_4 and M_5. Finally, the molecules or ions able to penetrate all installed membranes are contained in the filtrate F_6 of the last membrane. Afterwards, the HS fractions contained in the reservoirs R_2–R_5 are further fractionated by an

additional washing stage with water (10 ml). Then, the HS fractions F_1–F_6 obtained by this MS-UF procedure can be characterized by conventional spectroscopic and chemical methods.

3.3. Interferences, artifacts and limitations

Despite its simple methodology, one- and multistage UF of dissolved aquatic macromolecules such as HS or other natural colloids can be connected with the risk of interferences, considerably influencing the reliability of the separation results obtained.

First of all, the quality of UF fractionations of macromolecules depends on the quality of the membranes provided by their manufacturers (e.g. Millipore, Amicon, Pall Filtron). An optimal membrane, for instance, should have a well-defined average and narrow pore size distribution, its retention curve should be characterized thoroughly by the fractionation of a number of well-tried globular macromolecules (and/or polyelectrolytes) and its sorption capability towards the macromolecules to be fractionated should be low. Moreover, a number of artifacts may result from the UF process and are to be considered in choosing the optimal filtration conditions for HS fractionation. Unfavourably, the concentration polarization which is caused by the increasing surface concentration of macromolecules retained as thin layer on the surface of the membrane can more or less decrease the flow rate through the membrane. Fast stirring or a turbulent tangential flow of the sample solution over the membrane enables this effect to be reduced. However, when the surface concentration of macromolecules, for instance HS, on the membrane is too high, clogging and then surface coagulation on the membrane by the retained macromolecules or colloids can occur, falsifying its separation cut-off [42]. Another systematic artifact of the UF process scarcely studied up to now is the potential aggregation of HS molecules produced by an intermediate loss of their hydrate layer during the penetration of small membrane pores [14].

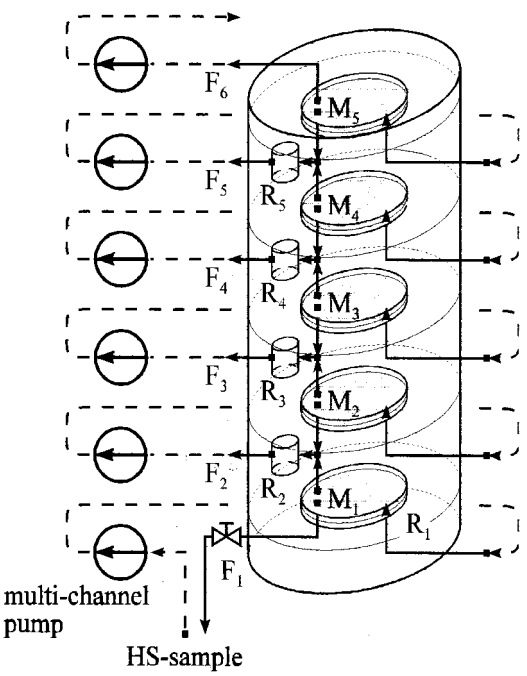

Fig. 2. Multistage ultrafiltration system (MS-UF) arranged as a filtration cascade.

Other limitations of UF in the case of multistage fractionation of HS can occur from their natural diversity and polydispersity. Accordingly, molecular size distribution obtained from HS through UF might be operationally influenced by different interactions of the HS fractions (for instance, variation in partial structures or functional groups) towards the membranes used. In particular, it should be borne in mind that the molecular size distribution of HS assessed by MS-UF is strongly dependent on the electrolyte, but less on the HS concentration (at < 1 mg ml^{-1} HS) and the pH value (at pH > 4) [42]. In such a case, a supplementary size classification by a reference method (e.g. GPC) is recommended.

4. Molecular size distribution of HS

As already discussed, the molecular size distribution (MSD) of dissolved HS is an important parameter for the characterization of the grade of their polydispersity. A series of recent studies has exhibited that the MSDs of aquatic and soil HS

Table 2
Aquatic HS and methods used for their molecular size classification

Source of HS	Fractions	Method	References
Ground water (Bocholt; Fuhrberg, Germany)	>100, 50–100, 10–50, 5–10, 1–5, <1 kDa	Ultrafiltration	[42]
Suwannee River: HA, FA	>10 kDa	Small-angle X-ray scattering	[44]
Bog water (Brunnenseemoor, Germany)	Continuous fractionation (from <1 to <5000 kDa)	Gel permeation chromatography	[46]
Bog water (Hohlohsee, Germany)	Continuous fractionation (from <1 to <5000 kDa)	Gel permeation chromatography	[46]
Leachate (Braunschweig, Germany)	Continuous fractionation (from <1 to <5000 kDa)	Gel permeation chromatography	[46]
Soil extract (Munich gravel plain, Germany)	Continuous fractionation (from <1 to <5000 kDa)	Gel permeation chromatography	[46]
32 Samples of different origin	0.2 μm–300 kDa, 300–10, 10–5, <5 kDa	Ultrafiltration	[50]
River (Rio Negro, Rio Solimoes, Brasil)	>100, 10–100, 3–10, <3 kDa	Ultrafiltration	[59]
Ground water (Kise, Norway)	>0.45, 0.1–0.45, 0.005–0.1, <0.005 μm)	Ultrafiltration	[66]
Lake water (Lake Tyrifjorden, Lake Kjellingtjenn, Norway)	>0.45, 0.1–0.45, 0.005–0.1, <0.005 μm)	Centrifugation	[66]
Surface water (Lake Tjeukemeer, Netherland)	>50, 50–30, 30–25, 25–10, 10–3.5, 3.5–3, <3 kDa	Gel permeation chromatography, Ultrafiltration	[68]
IHSS standard from Suwannee river	>300, 100–300, 50–100, 10–50, 1–10, <1 kDa	Ultrafiltration	[69]
Dam reservoir: drinking water reservoir (Apremont, France)	>1.5, 1.5–0.5, 0.5–0.2, <0.2 kDa	Ultrafiltration	[70]

are for the most part different, as are those of FA and HA from the same source [44–46]. In particular, in aquatic environments the transport, deposition and processes of the contained HS can be influenced considerably by their MSD.

4.1. Molecular size classification of aquatic HS

The organic constituents of the colloidal phase in natural waters, typically distributed in the diameter range of 1 nm–1 μm, consist predominantly of HS [47]. In general, organic and inorganic constituents of natural aquatic colloids are irregularly linked together forming 'macromolecules' of high intrinsic heterogeneity and dynamics (e.g. coagulation) [48,49]. Thus, it should be realized that the MSD of 'macromolecules' in humic-rich water samples is strongly dependent on unavoidable transformation processes, shifting its value considerably to high-molecular-mass fractions. In the case of isolated and redissolved HS pre-purified by well-tried separation procedures (e.g. XAD 8), the molecular size classification seems to be less problematic and results mostly in a well-reproducible characteristic MSD. Table 2 summarizes typical examples of aquatic HS studied with respect to their MSD by using different procedures. In most cases, the major fractions of the investigated HS stemming from various aquatic sources were found in the range below 10 kDa, with considerable parts at less than 1 kDa presumably to be attributed to the class of FA. In other cases, however, when HS in electrolyte-poor water samples were fractionated under nearly 'in situ' conditions, considerable HS fractions were found in the colloidal phase above 50 kDa [42]. This observation might indicate that HS in untreated natural waters of low conductivity are a major constituent of the colloidal phase, rapidly and strongly changing (e.g. coagulation, precipitation) by alteration of physical and chemical parameters (e.g. salt concentration, pH, addition of buffer).

4.2. Molecular size of HS: transformations and dynamics

HS dissolved in aquatic systems are mostly regarded as stable organic polyelectrolytes which are widely refractory against further alteration or decomposition. The 'stability' of HS often proved with respect to their structural properties (e.g. partial structures, capacity for H^+ and metal ions) cannot be expected in the case of their molecular size. Due to their colloidal character in solution, HS do not form a stable mixture of defined macromolecules but a complex system of high dynamics and transformation. Such a behaviour could be observed in the case of isolated fractions of HS obtained from their molecular size assessment (e.g. by GPC or UF; [45,50]). Accordingly, GPC fractions of typical soil HS refractionated after short periods of time under the same separation conditions exhibited their transformation into smaller and bigger 'molecules'. This effect can be explained by continuous association and dissociation of colloidal HS 'particles' in aqueous systems, particularly influenced by the pH value, electrolyte concentration and metal ions [51–53]. Using MS-UF for the fractionation of aquatic HS pre-isolated by XAD 8, a marked transformation of their molecular size as a function of the NaCl concentration could also be observed [42]: even small NaCl concentrations of less than 0.5 g l^{-1} NaCl caused significant alteration of the MSD of the studied HS, resulting in a strong increase of their small molecular size fractions of less than 1000 Da. This effect is presumably due to shrinking of hydrated HS colloids as a function of the osmotic pressure which arises from dissolved NaCl. Moreover, it could be shown by MS-UF that dissolved HS partially loaded with heavy metal ions intermediately form aggregates of larger molecular size which, however, were continuously reduced after a period of some days [43]. Significant differences of the MSD shown for the same aquatic HS which had been preconcentrated by both XAD 8 and preparative UF were probably due to their strongly denaturing hydrolysis during the XAD 8 procedure (e.g. sorption at $pH < 2$, elution at pH 13).

4.3. Distribution of metals and organic pollutants

Conventional one-stage UF is an appropriate method to study the distribution of metal ions and organic pollutants, respectively, between colloidal HS and the solution phase. A series of recent papers has stressed the capabilities of UF with respect to the differentiation of free and HS-bound species of various environmental analytes [54–57]. Using sequential UF through a series of appropriate membranes, it was possible to characterize the distribution of HS and their metal species as a function of their molecular size. Table 3 summarizes previous UF studies concerning the fractionation of macromolecular metal species in different water environments. Accordingly, many trace metals in natural waters (e.g. lake, river, bog, groundwater) fractionated by UF in the range from < 0.45 μm to < 1000 Da were found to be associated preferably with aquatic macromolecules of the humic type. Moreover, it could be shown that in humic-rich natural waters, many heavy metals were predominantly bound to high-molecular-mass colloids (> 10 kDa) mainly consisting of HS [43,58,59]. A similar observation was made in the case of HS-bound mercury species distributed in organic-rich floodplains of a river estuary (Elbe, Germany) [60]. In an analogous way, conventional UF cells can be used to differentiate between free and HS-bound fractions of pesticides (e.g. atrazine) [61] in aquatic systems.

Using MS-UF for the fractionation of dissolved HS and their metal species, the molecular size distribution of both the HS and the species formed can be assessed. Accordingly, it could be shown (see Fig. 3) [42] that in a slightly acidic humic-rich surface water (pH 3.8, 75 mg l^{-1} DOC), only the species of Al and Fe (referred to as the HS mass) were relatively evenly distributed between low- and high-molecular-mass fractions (from < 1 to > 100 kDa) whereas Cu, Mn, Ni and Zn widely dissociated from HS were preferably found in the fraction below 1 kDa. In contrast to these results, however, parallel studies using MS-UF for HS fractionation and atomic

Table 3
Ultrafiltration of aquatic humic substances: metal and DOC distribution patterns

Water sample	Fractions	Trace metals and DOC	pH	References
Bog water	0.45 μm–10 kDa, 10–1, 1–0.5, <0.5kDa	Cd, DOC	5, 6, 7	[15]
Surface waters (two samples)	>20, 20–10, 10–1, <1 kDa	Ca, Fe, DOC	Natural	[27]
River, bog water	0.45 μm–100 kDa, 100–50, 50–10, 10–5, 5–1, <1 kDa	Al, Cu, Fe, Mn, Zn, DOC	3, 4, 6, 8, 9	[42]
River water (five samples)	0.4 μm–100 kDa, 100–25, 25–10, 10–1, <1 kDa	Ca, Cd, Fe, Pb, DOC	Natural	[58]
Ground and lake water	0.1–0.005, <0.005 μm	Al, Ba, Ca, Cd, Ce, Co, Cr, Cu, Eu, Fe, K, La, Mg, Mn, Na, Sc, Sr, Zn	Natural: 7.6, 6.8, 5.3	[66]
Ground, bog, river water (five samples)	>100, 100–10, 10–1, <1 kDa	Co, Mn, Zn	Natural	[67]
River water (three samples)	0.45 μm–10 kDa, 10–0.5, <0.5 kDa	Al, Ag, As, Ba, Ca, Ce, Co, Cr, Fe, K, Lu, Mg, Mn, Na, Ni, Rb, Sb, Sc, Se, Sr, Tb, Tm, U, V, W, Zn, DOC	Natural: 8.2, 7.0, 6.9	[71]
Lysimeter waters from soils	NMWCO: 10 and 1 kDa	Al, Fe, Mn, Na, DOC	Natural: 3–4	[72]
Ground water (three samples)	0.45–0.002, <0.002 μm	Ac, Al, Cs, Pb, Sr, Th	Natural: 6.6–7.8	[73]
Solution of Laurentian humic acid (extracted from soil)	>1, <1 kD	Ca, Mg	5	[74]
Surface water (from some bogs and lakes)	0.45–0.1 μm, 0.1 μm–100 kDa, 100–30, 30–3, <3 kDa	Ba, Ca, Fe, Mg, Mn, Sr, DOC	Natural: 4–5, 7, 5–6	[75]

absorption spectrometry (AAS) or total-reflection X-ray fluorescence spectrometry (TXRF) for metal determination showed that in other aquatic environments, Al and Fe were predominantly contained in the macromolecular fractions of more than 50 kDa [43,62].

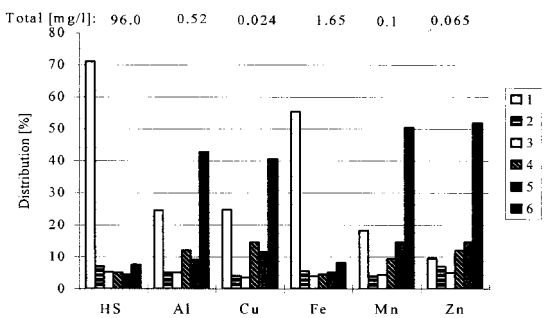

Fig. 3. Molecular size distribution of selected aquatic HS (VM4-Original) and their metal species.

4.4. Speciation using MS-UF

Besides the molecular size fractionation of HS colloids, MS-UF also permits the analytical discrimination of labile/inert metal species bound to HS. For this purpose a combined procedure, consisting of EDTA exchange of labile metal fractions in solution, a subsequent MS-UF fractionation (NMWCO at 1, 5, 10, 50 and 100 kDa) of the inert HS species and the low-molecular EDTA/metal complexes formed and, finally, metal determinations by TXRF (Al by AAS), has been proposed [62]. Using this three-step procedure, it could be shown (see Fig. 4(a) and (b)) that not only natural Al and Fe species preferably occurring in the macromolecular fractions F_1 and F_2 (>50 kDa) of aquatic HS are highly inert against EDTA, but also Cu, Mn and Zn species (Fig. 4(a): HS HO10-UF, preconcentrated from a

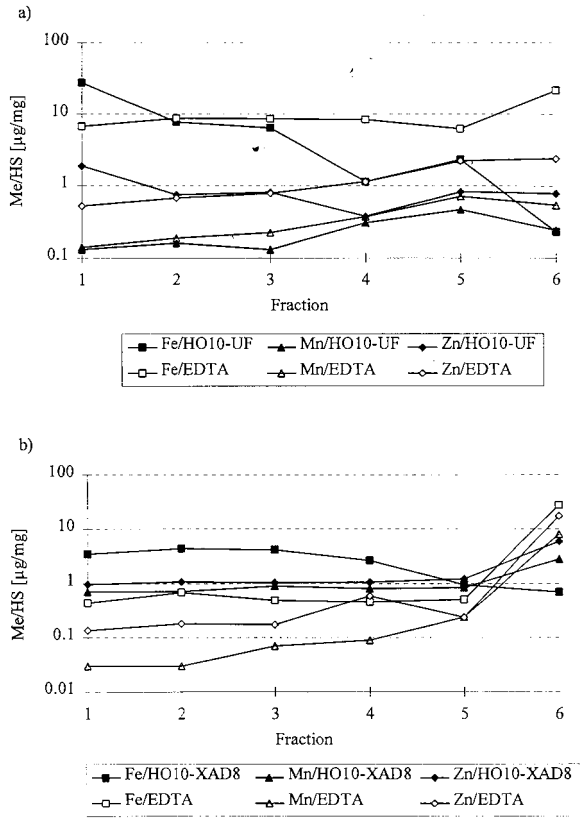

Fig. 4. EDTA lability of HS/metal species and their distribution in molecular size fractions obtained by MS-UF: (a) natural metal loading (HO10-UF); (b) synthetic metal loading (HO10-XAD8 loaded with 1.0 µg mg^{-1} each of Fe(III), Mn(II) and Zn(II)).

brown water by UF). Thus, reaction periods of more than 24 h are required to exchange the EDTA-labile metal fractions in dissolved HS. In contrast to this behaviour, 'synthetic' metal species freshly formed between dissolved HS (Fig. 4(b): HS HO10-XAD8, isolated by XAD8) and spiked metal ions exhibited a high lability (70–95%) towards EDTA. It is noteworthy that choosing EDTA as discriminator and TXRF as the determination method enables a very sensitive multi-element speciation in HS-rich aquatic systems, even at the lower µg l^{-1} level.

The above mentioned studies and the preceding ones using immobilized chelators [63–65] for the discrimination of labile/inert HS/metal species clearly exhibit strong differences between 'natural' and 'synthetic' species. Accordingly, the lability ('reactivity') of 'natural' metal species, operationally described by the kinetics and the yield of such exchange reactions, is by one or more orders of magnitude lower than that of 'synthetic' ones. These findings show that colloidal HS/metal species and their 'reactivity' in natural aquatic systems can hardly be modelled by simple complexation between isolated HS and metal ions in synthetic solutions.

5. Conclusions

HS and their metal loadings are the main components of many colloidal systems existing in aquatic environments. Ideally, their characterization by physical or chemical methods should be performed under in situ or at least nature-like conditions [48]. For the molecular size classification of colloidal HS, soft fractionation procedures hardly changing their natural properties are needed. UF performed as a sequential-stage or on-line cascade technique through appropriate high-performance membranes can largely meet such requirements.

UF with respect to size classification in colloidal aquatic systems, however, is to be considered generally with a number of critical reservations: (a) its reliability depends heavily on the quality of the applied membranes (e.g. their pore size classification and calibration); (b) in the case of increased HS concentrations, polarization or coagulation of the colloids on the membrane surface can systematically falsify the results; (c) undesired sorption of HS molecules on polymer surfaces of the UF device might occur; (d) in the case of membranes of low NMWCO (< 5 kDa) and small surface, UF is a slow separation process; (e) size classifications of HS using UF are strongly dependent on the chosen operation parameters and, therefore, not easily comparable to those obtained with other systems.

MS-UF performed through high-performance membranes arranged as a cascade system can minimize the above mentioned limitations. The diafiltration mode combined with the tangential

flow principle decreases the concentration polarization, coagulation and sorption of the fractionated HS. Moreover, due to small and defined reservoir volumes within the single stages, preconcentration of the HS fractions under study is obtained. Lastly, the on-line principle significantly reduces the period of time required for UF.

To summarize, the MS-UF has been shown to be a promising method for the size classification of HS in natural water samples not altered by any reagents, buffers or electrolytes. MS-UF performed at the sampling site can also be a promising tool for the in situ size classification of sensitive colloidal systems such as HS and their metal species in natural waters. By combining EDTA exchange with MS-UF, the lability of natural HS/metal species, which strongly governs their environmental processes in aquatic systems, can be differentiated meaningfully as a function of their molecular size.

Acknowledgements

This work was financially supported by the Deutsche Forschungsgemeinschaft (DFG-Schwerpunktprogramm ROSIG), the 'Bundesministerium für Bildung, Wissenschaft, Forschung und Technologie' and the 'Ministerium für Wissenschaft und Forschung des Landes Nordrhein-Westfalen'. We thank Dr Gudrun Abbt-Braun, Engler-Bunte-Institut (Karlsruhe, Germany), for providing appropriate reference HS from aquatic environments.

References

[1] B. Allard, H. Boren, A. Grimvall (Eds.), Humic Substances in the Aquatic and Terrestrial Environment, Springer-Verlag, Berlin, 1991.
[2] G.R. Aiken, D.M. McKnight, R.L. Wershaw, P. MacCarthy (Eds.), Humic Substances in Soil, Sediment and Water, Wiley, New York, 1985.
[3] F.J. Stevenson, Humus Chemistry, Wiley, New York, 1996, pp. 1–23.
[4] C.E. Clapp, M.H.B. Hayes, N. Senesi, S.M. Griffith (Eds.), Humic Substances and Organic Matter in Soil and Water Environments: Characterization, Transformations and Interactions, IHSS, St. Paul, MN, 1996.
[5] G. Matthess, Scope, in: G. Matthess, F.H. Frimmel, P. Hirsch, H.D. Schulz, E. Usdowski (Eds.), Progress in Hydrogeochemistry, Springer-Verlag, Berlin, 1992, pp. 1–6.
[6] J.H. Weber, in: F.H. Frimmel, R.F. Christmann (Eds.), Humic Substances and their Role in the Environment, Wiley, Chichester, 1988, pp. 165–178.
[7] J. Buffle, Complexation Reactions in Aquatic Systems—An Analytical Approach, E. Horwood, Chichester, 1988, pp. 304–371.
[8] M.H.B. Hayes, P. MacCarthy, R.C. Malcolm, R.S. Swift (Eds.), Humic Substances II: In Search of Structure, Part II, Wiley, New York, 1989, pp. 3–764.
[9] P. MacCarthy, J.A. Rice, in: G.R. Aiken, D.M. McKnight, R.L. Wershaw, P. MacCarthy (Eds.), Humic Substances in Soil, Sediment and Water, Wiley, New York, 1985, pp. 527–559.
[10] F.H. Frimmel, in: G. Matthess, F.H. Frimmel, P. Hirsch, H.D. Schulz, E. Usdowski (Eds.), Progress in Hydrogeochemistry, Springer-Verlag, Berlin, 1992, pp. 24–28.
[11] P. Burba, A. Abbatepaulo, Vom Wasser 75 (1990) 201.
[12] J.M. Duxbury, in: M.H.B. Hayes, P. MacCarthy, R.C. Malcolm, R.S. Swift (Eds.), Humic Substances II: In Search of Structure, Wiley, Chichester, 1989, pp. 257–409.
[13] J.A. Leenheer, in: G.R. Aiken, D.M. McKnight, R.L. Wershaw, P. MacCarthy (Eds.), Humic Substances in Soil, Sediment and Water (Geochemistry, Isolation and Characterization), Wiley, New York, 1985, pp. 409–429.
[14] J. Buffle, D. Perret, M. Newman, in: J.Buffle, H.P. van Leeuwen (Eds.), Environmental Particles, vol. 1, Lewis, Boca Raton, FL, 1992, pp. 171–220.
[15] J. John, B. Salbu, E. Gjessing, H. Bjoerrstad, Water Res. 22 (1988) 1381.
[16] T. Tanaka, M. Senoo, Mater. Res. Soc. Symp. Proc. 353 (1995) 1013.
[17] J. Buffle, Complexation Reactions in Aquatic Systems—An Analytical Approach, E. Horwood, Chichester, 1988, pp. 570–591.
[18] J. Buffle, G.G. Leppard, Environ. Sci. Technol. 29 (1995) 2176.
[19] W. Finger, B. Post, H. Klamberg, Z. Pflanzenern. Bod. 154 (1991) 287.
[20] M. De Nobili, E. Gjessing, P. Sequi, in: M.H.B. Hayes, P. MacCarthy, R.C. Malcolm, R.S. Swift (Eds.), Humic Substances II: In Search of Structure, Wiley, Chichester, 1989, pp. 561–592.
[21] F. Fuchs, Vom Wasser 64 (1985) 129.
[22] P.J. Shaw, H. de Haan, R.I. Jones, Environ. Technol. 15 (1994) 753.
[23] D. Hongve, J. Baann, G. Becher, S. Lomo, Environ. Int. 22 (1996) 489.
[24] M.H.B. Hayes, P. MacCarthy, R.C. Malcolm, R.S. Swift (Eds.), Humic Substances II: In Search of Structure, Part III, Wiley, Chichester, 1989, pp. 450–638.

[25] R.S. Swift, in: M.H.B. Hayes, P. MacCarthy, R.C. Malcolm, R.S. Swift (Eds.), Humic Substances II: In Search of Structure, Wiley, Chichester, 1989, pp. 450–466.
[26] J. Kilduff, W.J. Weber Jr., Environ. Sci. Technol. 26 (1992) 569.
[27] E.T. Gjessing, Environ. Sci. Technol. 4 (1970) 437.
[28] R.G. Smith Jr., Anal. Chem. 48 (1976) 74.
[29] J. Buffle, P. Deladoey, W. Haerdi, Anal. Chim. Acta 101 (1978) 339.
[30] S.H. Eberle, K.-P. Knobel, S. von Hodenberg, Vom Wasser 53 (1979) 53.
[31] H. de Haan, T. de Boer, J. Voerman, H.A. Kramer, J.R. Moed, Verh. Int. Verei. Limnol. 22 (1984) 876.
[32] D.P.H. Laxen, I.M. Chandler, Anal. Chem. 54 (1982) 1350.
[33] D.P.H. Laxen, I.M. Chandler, Geochim. Cosmochim. Acta 47 (1993) 731.
[34] W.F. Blatt, B.G. Hudson, S.M. Robinson, E.M. Zipilivan, Nature 216 (1967) 511.
[35] G.F. Fallick, Proc. Biochem. 9 (1969) 29.
[36] W.F. Blatt, J. Agr. Food Chem. 19 (1971) 589.
[37] O. Hoyer, Z. Wasser–Abwasserforsch. 16 (1983) 191.
[38] N.C. Beaton, P.R. Klinkowski, J. Separ. Technol 4 (1983) 1.
[39] P.E. Barker, A. Till, J. Membrane Sci. 72 (1992) 1.
[40] H. Niemi, S. Palosaari, J. Membrane Sci. 91 (1994) 111.
[41] J. Buffle, P. Deladoey, J. Zumstein, W. Haerdi, Schweiz. Z. Hydrol. 44 (2) (1982) 325.
[42] P. Burba, V. Shkinev, B.Ya. Spivakov, Fresenius J. Anal. Chem. 351 (1995) 74.
[43] B. Aster, P. Burba, J.A.C. Broekaert, Fresenius J. Anal. Chem. 354 (1996) 722.
[44] E.M. Thurman, R.L. Wershaw, R.L. Malcolm, D.J. Pinckney, Org. Geochem. 4 (1982) 27.
[45] B. Post, H. Klamberg, in: G. Matthes, F.H. Frimmel, P. Hirsch, H.D. Schulz, E. Usdowski, Progress in Hydrogeochemistry, Springer-Verlag, Berlin, 1992, pp. 56–60.
[46] F.H. Frimmel, G. Abbt-Braun, in: B. Allard, H. Boren, A. Grimvall (Eds.), Humic Substances in the Aquatic and Terrestrial Environment, Springer-Verlag, Berlin, 1991, pp. 37–46.
[47] E.M. Thurman, Organic Geochemistry of Natural Waters, Nighoff-Junk, Dordrecht, 1985, pp. 1–497.
[48] J. Buffle, G.G. Leppard, Environ. Sci. Technol. 29 (1995) 2176.
[49] DFG Deutsche Forschungsgemeinschaft, F.H. Frimmel, G. Abbt-Braun (Eds.), Refraktäre organische Säuren in Gewässern, Mitteilung XII der Senatskommission für Wasserforschung, VCH, Weinheim, Germany, 1993, pp. 79–135.
[50] A. Krüger, Eigenschaften und Dynamik von umweltrelevanten Metallen in Böden und Fließgewässern unter dem Einfluß von Huminstoffen, Thesis, University of Leipzig, Germany, 1995.
[51] G.G. Leppard, J. Buffle, R. Bandat, Water Res. 20 (1985) 185.
[52] H. Kipton, J. Powell, R.M. Town, Anal. Chim. Acta 267 (1992) 47.
[53] B. Ceccanti, M. Calcinai, M. Bonmati-Pont, C. Ciardi, R. Tarsitano, Sci. Total Environ. 81/82 (1989) 471.
[54] J.H. Ephraim, Anal. Chim. Acta 267 (1992) 39.
[55] J.R. Tuschall Jr., P.L. Brezonik, Anal. Chim. Acta 149 (1983) 47.
[56] J. Buffle, C. Staub, Anal. Chem. 56 (1984) 2837.
[57] Z.D. Wang, D.S. Gamble, C.H. Langford, Anal. Chim. Acta 232 (1990) 181.
[58] M.R. Hoffman, E.C. Yost, S.J. Eisenreich, W.J. Maier, Environ. Sci. Technol. 15 (1981) 655.
[59] I.L. Küchler, N. Miekeley, B.R. Forsberg, Sci. Total Environ. 156 (1994) 207.
[60] D. Wallschläger, M.V.M. Desai, R.D. Wilken, Water, Air, Soil Pollut. 89 (1996) 1.
[61] D.S. Gamble, M.I. Haniff, R.H. Zienius, Anal. Chem. 58 (1986) 727.
[62] B. Aster, A. von Bohlen, P. Burba, Spectrochim. Acta B 52 (1997) 1009.
[63] P. Burba, J. Rocha, D. Klockow, Fresenius J. Anal. Chem. 349 (1994) 800.
[64] P. Burba, Fresenius J. Anal. Chem. 348 (1994) 301.
[65] K. Hirose, Y. Dokiya, Y. Sugimura, Mar. Chem. 11 (1982) 343.
[66] B. Salbu, H.E. Bjornstad, N.S. Lindstrom, E. Lydersen, Talanta 32 (1985) 907.
[67] B. Salbu, J. Radioanal. Nucl. Chem. 112 (1) (1987) 169.
[68] P.J. Shaw, R.I. Jones, H. de Haan, Environ. Technol. 15 (1994) 765.
[69] R.S. Summers, P.K. Cornel, P.V. Roberts, Sci. Total. Environ. 62 (1987) 27.
[70] C. Belin, C. Quellec, M. Lamotte, M. Ewald, Ph. Simon, Environ. Technol. 14 (1993) 1131.
[71] Y. Tanizaki, M. Yamazaki, T. Shimokawa, Kogai 24 (1989) 405.
[72] M. Spiteller, Sci. Total Environ. 62 (1987) 47.
[73] K.H. Lieser, A. Ament, R. Hill, R.N. Singh, U. Stingl, B. Thybusch, Radiochim. Acta 49 (1990) 83.
[74] L.E. Sojo, Anal. Chim. Acta 258 (1992) 219.
[75] N.A. Marley, J.S. Gaffney, K.H. Orlandini, K.C. Picel, G.R. Choppin, Sci. Total Environ. 113 (1992) 159.

.

ELSEVIER

Talanta 45 (1998) 989–1000

Talanta

Influence of mixture design on multivariate prediction of PAHs in mixture spectra

Dragan A. Cirovic

University of Bristol, Lyndhurst, Alexandra Park, Bristol BS6 6QB, UK

Received 3 April 1997; received in revised form 18 June 1997; accepted 30 June 1997

Abstract

This work describes a simulation study aimed at establishing the impact of mixture design on the prediction ability of PLS regression models. Data sets are formed by multiplying UV absorbance spectra of 12 PAHs by their concentration profiles. In these case studies, either all possible mixtures of 1–12 components are used or randomly chosen selections of the mixtures. The effects of the number of samples and the number of concentration levels in the mixture designs on the results of the calibration are assessed. Comparisons are made between models formed using orthogonal fractional factorial mixture designs and those based on random designs. The applicability limits of the orthogonal designs are analysed in terms of actual concentration ranges of individual components in the mixtures.

Keywords: Multi-level mixture design; Multivariate regression; Plackett–Burman mixture design; PLS

1. Introduction

The prediction ability of a regression model is affected by a number of factors. They can be divided into two main groups: (i) noise and (ii) experimental design [1–11]. The impact of the former group is defined by means of analysis of variance of experimental error (σ^2). The main sources of errors are: sampling procedure, instrument, environment (measurement conditions), the operator, and so on. The latter group is often called the controllable factors, because in many cases the experimenter is able to plan the experiments. In this study we consider the mixture design in terms of its effects on the prediction ability of latent variable regression methods.

1.1. Orthogonal fractional factorial experimental design

The orthogonal mixture design is characterised by the fact that all combinations of concentration levels of the mixture components occur the same number of times for all pairs of components. The full factorial design of the mixtures implies that all combinations of the levels for all factors are present. However, in practice such an elaborate design is rarely needed, and only a fraction of it is used instead. The minimal required size of a fractional design (the minimal number of samples) depends on the type and the intensity of interactions between variables. The higher the number of interactions, the more complex the design needed.

0039-9140/98/$19.00
PII S0039-9140(97)00205-1

1.2. Latin square design

Probably the most straightforward way of constructing orthogonal arrays is to superimpose orthogonal Latin squares [1–4,12–19]. Latin squares are matrices in which every level of each factor is combined only once with every level of other factors. From a combinatorial point of view, this means that the same element does not occur more than once in any row or any column.

There exist up to two mutually orthogonal three-level Latin squares. The squares in Table 1 are formed by rotating the first row (the sequence: −1 0 1) to the left by one and two places, respectively. The initial displacement of the elements in the first row and the order of the rows are arbitrary. The superposition of these two Latin squares gives an orthogonal design (Table 2). The bold italic columns are the row and column indices of the Latin squares from Table 1 and the elements in columns 3 and 4 are their corresponding elements.

The issue of the existence of mutually orthogonal Latin squares is a problem of discrete mathematics which has been a subject of various misinterpretations for a long time. Euler postulated in the 18th century a theorem [20] according to which the pairs of orthogonal squares exist only if the number of design levels is a prime number or a power of a prime number. Numerous and diverse proofs of this theorem were reported over the course of the following centuries. However, in the late 1950s, it was shown that Euler's conjecture was wrong [21–25].

In order for an experimental design matrix to be orthogonal, the number of rows (I) has to be an integer multiple ($k = 1, 2, \ldots$) of the power ($r = 2, 3, \ldots$) of a number of layers ($Q = 2, 3, \ldots$):

$$I = kQ^r$$

Table 1
Two mutually orthogonal three-level Latin squares

	−1	***0***	***1***		***−1***	***0***	***1***
−1	−1	0	1	***−1***	−1	0	1
0	0	1	−1	***0***	1	−1	0
1	1	−1	0	***1***	0	1	−1

The row and column indices are bold italic.

Table 2
Three-level Latin squares design

−1	***−1***	−1	−1
−1	***0***	0	0
−1	***1***	1	1
0	***−1***	0	1
0	***0***	1	−1
0	***1***	−1	0
1	***−1***	1	0
1	***0***	−1	1
1	***1***	0	−1

The bold italic columns are indices of the Latin squares.

It can be shown that the maximal number of mutually orthogonal factors (n) in a design matrix with I rows, or the number of components in the mixture set, is

$$n = \frac{I-1}{Q-1}$$

If we consider the case of a 3-level design from Table 2, the above equations imply that the addition of another column (the fifth one), e.g. a column consisting of elements of some third three-level Latin square, would lead to the loss of orthogonality of the design, regardless of the fact that the new column would be orthogonal to the majority of the existing ones. For the case where $r = 2$, and under the assumption of no interactions between the components, up to $Q + 1$ factors can be modelled. A method of building designs with $r > 2$ is a somewhat more complex procedure, a detailed description of which is available in the literature [1].

1.3. Plackett–Burman design

The design commonly referred in the literature as the Plackett and Burman design is actually only one of a number of designs which are described in their original paper [26]. All designs analysed by Plackett and Burman are based on Latin squares. The one which is most often associated with their name is a so-called cyclic orthogonal design. This design was reported earlier by Stevens [13] (Placket and Burman did not claim that they invented that design). Their main contribution was that they systematically evaluated properties of the orthogonal experimental designs.

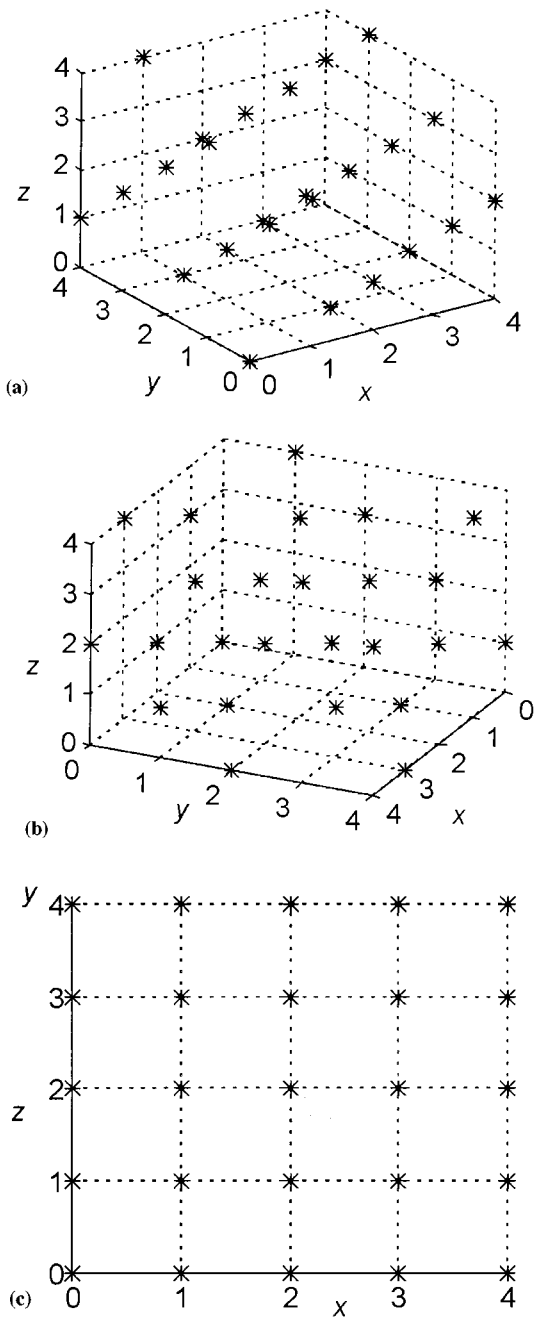

Fig. 1. Five-level Plackett–Burman design with 25 samples from the three different perspectives defined with the following (azimuth, elevation) pairs [27]: (a) (− 35°, 30°); (b) (115°, 30°); and (c) (0°, 0°).

The cyclic solution design is formed by a circular rotation of a single design column. Whilst the first element is always kept in place, the remaining elements are rotated (the elements from the second to the last one in Tables 5–8; see Appendix A). The disposition of the levels in the column to be rotated is essential, as only certain permutations of levels are allowed. The comprehensive theoretical studies of this topic can be found in the discrete mathematics literature (it is commonly addressed within the scope of Galois fields [12,26]). A more complete overview of these designs is available elsewhere [1,26]. The two-level designs are particularly flexible in respect to the number of samples. Nearly all of the two-level designs (Hadamard matrices), with the number of rows an integer multiple of 4, exist.

It is quite common to use the Plackett–Burman design primarily for screening purposes. This is because it allows modelling of only a very limited number of interactions between the variables. Nevertheless, if it is known that the modelled factors are mutually independent, or that the given design is sufficiently large to model the interactions, it is reasonable to employ this design for calibration purposes. In the analysis of UV/VIS data, it is commonly assumed that Beers law applies, according to which the absorbance profiles of the chemical components are independent and additive. For this reason, UV spectra of PAH solutions are well suited for the assessment of the advantages and shortcomings of the application of Plackett–Burman designs in calibration.

One of the most important tools in experimental design analysis is visualisation of experimental points. The graph of a two-level Plackett–Burman design is quite simple; the experimental points are at the corners of a hyper-cube. The disposition of the experimental points is less obvious for the case of a multilevel design. This is illustrated for the case of a five-level Plackett–Burman design with three factors (Fig. 1). The first two views (Fig. 1(a) and (b)) show that the experimental points form a set of roughly parallel planes (they are displayed in their side and front perspective). The third view, which is the

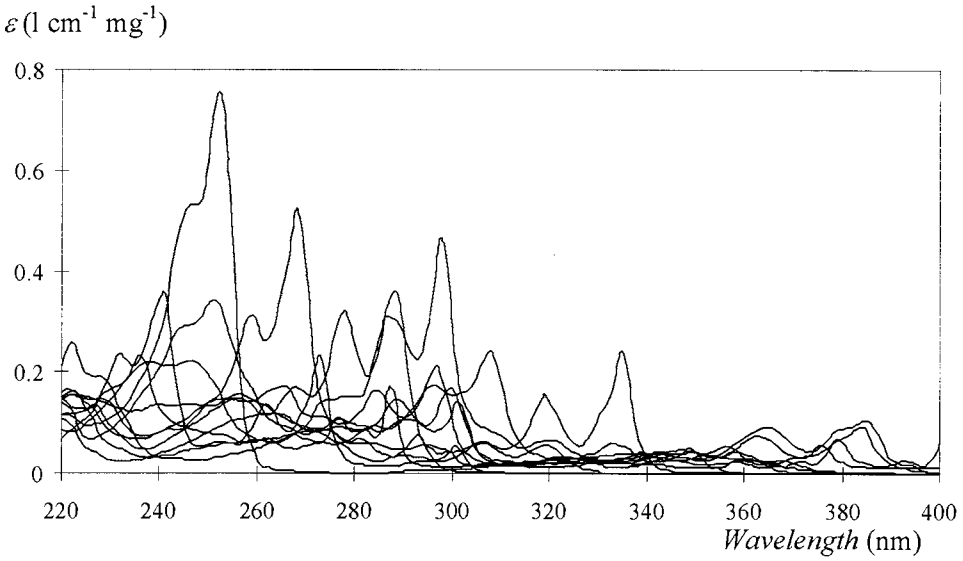

Fig. 2. Absorption coefficients of 12 PAHs in the spectral region 220–400 nm.

projection along the y-axis, confirms what was said earlier about the orthogonal designs, that all combinations of layers are present an equal number of times, only once in this case. Similar projections are obtainable for the remaining combinations of axes.

Table 3
The top-level concentration of the scaled two-level Plackett–Burman design

N	Compound	Concentration (ng ml^{-1})
1	Anthracene	190
2	Benzo(*a*)anthracene	430
3	Benzo(*a*)pyrene	310
4	Benzo(*b*)fluoranthene	500
5	Benzo(*g*,*h*,*i*)perylene	60
6	Benzo(*k*)fluoranthene	330
7	Chrysene	400
8	Dibenzo(*a*,*h*)anthracene	170
9	Fluorene	780
10	Fluoranthene	90
11	Phenanthrene	560
12	Pyrene	520

1.4. Simulation conditions and data sets

This study is concerned with the calibration of the UV absorbance data block (X) against the concentration profiles of the mixture (y_i, $i = 1, \ldots, n$). A set of absorption coefficients in the spectral range 220–400 nm for a selection of 12 PAHs is used. Their UV spectra are overlaid in Fig. 2. A single simulation run takes into account all possible mixtures containing 1–12 components. The total number of the mixtures is a sum of binomial coefficients (C_n^{12}, $n = 1, \ldots, 12$). The absorbance data sets are generated by multiplying concentration profiles of the mixtures with the absorption coefficients ($X = CS'$). The simulations utilise PLS1 calibration models only. The calibration results are presented in a form of the averaged root mean square error ($\mathrm{RMSE} = (M^{-1} \Sigma_{i=1}^{M} (\hat{y}_i - y_i)^2)^{1/2}$) of the M samples, which are the averages over the C_n^{12} mixtures of n-th order ($\mathrm{ARMSE}_n = \mathrm{RMSE}_n / C_n^{12}$). The predicted concentration values are denoted with the 'hat'.

A series of case studies is performed using data sets based on two-, three-, five- and seven-level Plackett–Burman designs. The concentrations of the individual chemical components in the designed mixtures are in the range 0–800 (805) ng

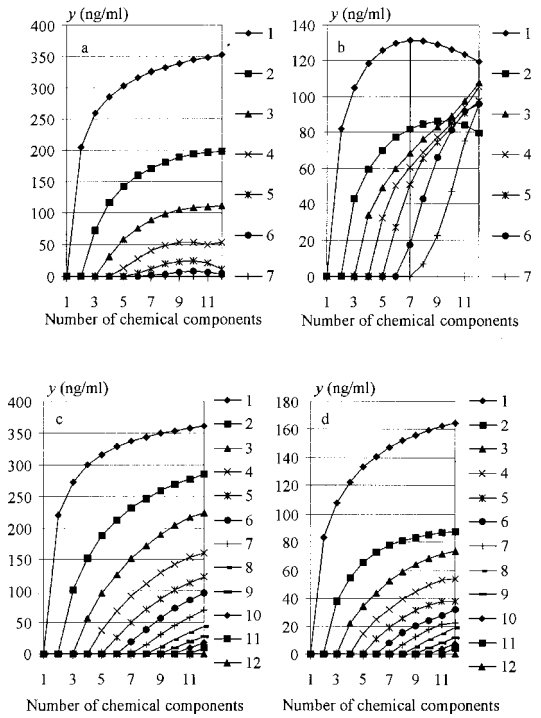

Fig. 3. RMSE of PLS1 regression models with up to 12 latent variables applied to the calibration data sets based on the two-level Plackett–Burman design, without added noise. Validation data sets are based on the SET 1 concentration profiles. Calibration data set contained eight samples: (a) calibration and (b) validation; and 16 samples: (c) calibration and (d) validation.

ml^{-1}. The values of the concentration levels for different designs are therefore respectively 800, 400, 200 and 135 ng ml^{-1}. This selection of concentration ranges is large enough to incorporate the experimentally observed PAH concentration.

For validation purposes, two sets of concentration profiles are used. They are denoted as SET 1 and SET 2. The former is obtained by sampling the air at the vicinity of an industrial source of PAH pollution. The concentration ranges of this data set are not uniform (Table 3). The latter one (SET 2) is a set of random concentration profiles with uniform concentration ranges (0–800 ng ml^{-1}) for all chemical components.

2. Results and discussion

The abundance of the PAHs in the air in diverse industrial conditions is effected by many factors. The contents of mixtures may vary within a single pollution source and over a period of time. Variations are even more probable between different types of industries. Calibration models aimed at simultaneous modelling of samples collected at diverse pollution sources have to be more general than the models intended to describe some narrowly defined data sets.

In the majority of the simulations described in this work, we use the uniform concentration ranges (0–800 ng ml^{-1}) for the calibration data set. Such a choice of concentration ranges is likely to be a rather unrealistic constraint. Nevertheless, it is the preferred one because we wish to look into the possibility of using general (inter-industry) calibration models. The selection of the set of oversized concentration ranges as a basis of the calibration data set allow us to gain an insight into regression characteristics of calibration models with a generalised concentration domain. It should be noted that our aim in this work is to outline the main trends of the impact of the experimental design on the multivariate calibration, rather than to advocate use of artificially generated mixtures in the modelling of real data sets.

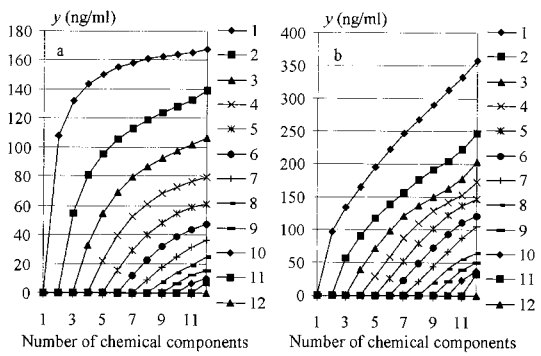

Fig. 4. RMSE of PLS1 regression models with 1–12 latent variables applied to the random calibration data sets (first 16 samples from SET 2), without added noise. Validation data sets are based on the two-level Plackett–Burman design (SET 1). The graphs refer to: (a) calibration and (b) validation.

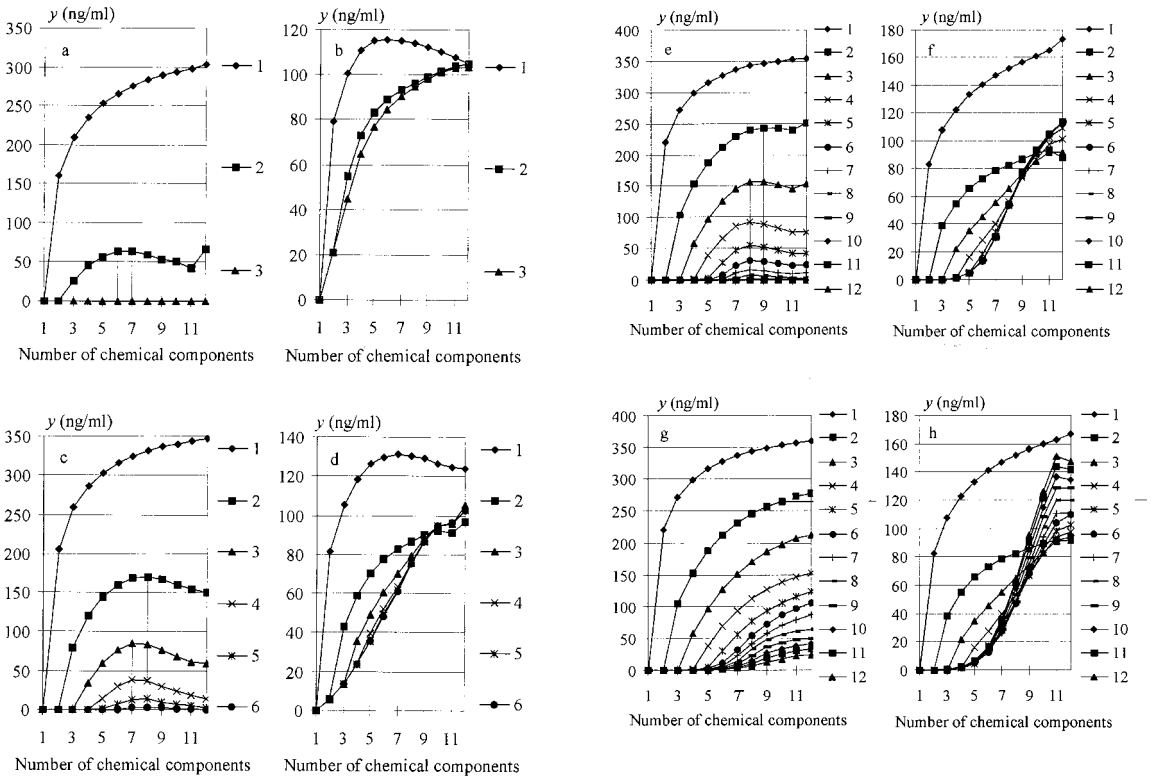

Fig. 5. RMSE of PLS1 regression models with up to 12 latent variables applied to the calibration data set based on the two-level Plackett–Burman design. Normally distributed noise with standard deviation of 0.05 AU is added to the absorbance blocks. Concentration data sets contained: (a) 4, (c) 8, (e) 16 and (g) 96 samples. Validation data sets with corresponding numbers of samples, (b), (d), (f) and (h) respectively, are based on the random concentration profiles (SET 1).

2.1. Two-level experimental designs

2.1.1. Noise-free simulations

Simulations with noise-free data are performed as a reference to simulations with noisy data. As little as 16 noise-free samples generated using the two-level design (Table 5; see Appendix A) provide a sufficient information basis for the PLS1 calibration models to fully describe the contents of the individual components in the mixtures (Fig. 3), i.e. whenever the number of latent variables exactly matches the complexity of the mixtures, prediction error equals zero. The number of samples in the two-level experimental design should exceed the number of chemical components (variables) in the mixtures in order for a design to be orthogonal. In addition to that, the data sets with fewer samples than chemical components are underdetermined in a mathematical sense, i.e. it is impossible to uniquely solve these systems of equations. The orthogonal noise-free data consisting of eight samples allow extraction of only up to seven latent variables (see Fig. 3(a)). The eighth principal component is indistinguishable from the seventh one: both are zero. In respect to the validation data (Fig. 3(b)), it is

Table 4
Maximal numbers of latent variable needed to achieve minimal errors in the calibration models based on the two-level Plackett–Burman designs

N samples	4	8	12	16	20	24	32	36	96
Calibration	2	6	8	8	8	9	10	10	12
Validation	3	5	5	6	6	6	6	6	6

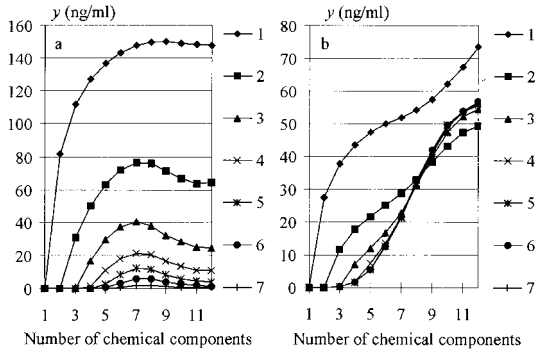

Fig. 6. RMSE of PLS1 regression models with up to seven latent variables. Calibration data sets are based on the two-level Plackett–Burman design with concentration ranges given in Table 4 and with 16 samples. Validation data sets are based on random concentration profiles from SET 2. Normally distributed noise with standard deviation of 0.05 AU is added to the absorbance data. The graphs refer to: (a) calibration and (b) validation.

apparent that the complexity of the calibration models and the complexity of the mixtures are proportional in a one-to-one ratio up to the level of seven-component mixtures. The remaining more complex mixtures cannot be fully modelled in this case. Extraction of the eighth and the higher latent variables is pointless, as they account for 0% of variance. The calibration models for the mixtures with 8–12 components are underdetermined for a given sample size.

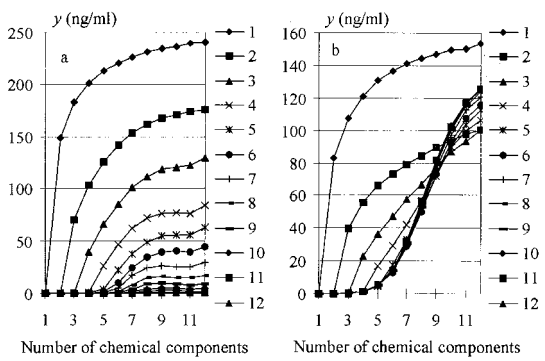

Fig. 7. RMSE of PLS1 regression models with 1–12 latent variables. Calibration data sets are formed using the Plackett–Burman design with 49 samples and seven concentration levels. Normally distributed noise with standard deviation of 0.05 AU is added to the absorbance: (a) calibration and (b) validation data sets.

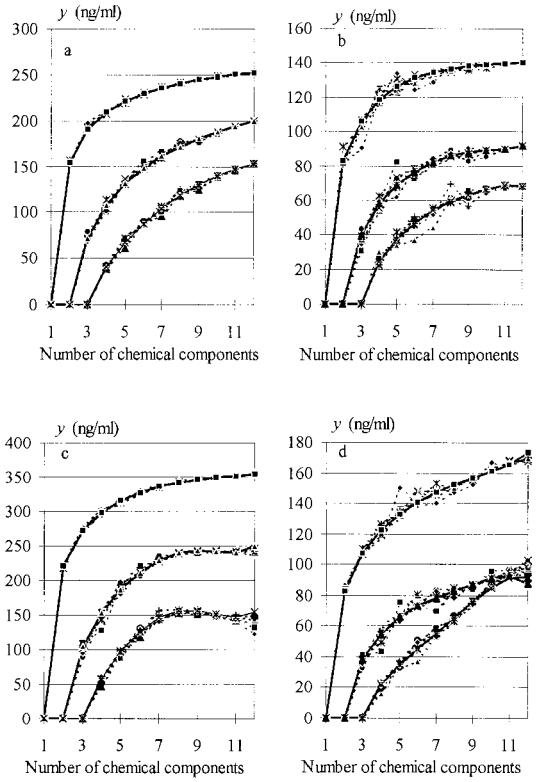

Fig. 8. Partial simulations. RMSE of PLS1 regression models using one to four latent variables. Dashed lines refer to the partial simulations with up to: 10, 25, 50, 75, 100, 125 and 150 mixtures. The full lines refer to the simulation with all possible mixtures. Noise-free simulations with five levels and 25 samples: (a) calibration and (b) validation. Simulations with added noise to absorbance data (0.05 AU) with two levels and 16 samples: (c) calibration and (d) validation.

The nine-component mixtures are significant for the fact that they mark the level of mixture complexity at which error curves cross each other (Fig. 3(b)), i.e. the extraction of the third latent variable causes an increase in validation error. This is important because these simulations are noise free. At this level of mixture complexity, for a given selection of PAHs, the multivariate calibration models are unable to distinguish the individual chemical components to the extent that the increase in the number of PCs above two has to be labelled as modelling of noise. If it were not known how many chemical components were in

Table 5
Two-level experimental design

4	***−1***	−1	1	1																					
8	***−1***	1	1	1	−1	1	−1	−1																	
12	***−1***	1	1	−1	1	1	1	−1	−1	−1	1	−1													
16	***−1***	1	1	1	1	−1	1	−1	1	1	−1	−1	1	−1	−1	−1									
20	***−1***	1	1	−1	−1	1	1	1	1	−1	1	−1	1	−1	−1	−1	−1	1	1	−1					
24	***−1***	1	1	1	1	1	−1	1	−1	1	1	−1	−1	1	1	−1	−1	1	−1	1	−1	−1	−1	−1	
32	***−1***	−1	−1	−1	−1	1	−1	1	−1	1	1	1	−1	1	1	−1	−1	−1	1	1	1	1	1	−1	
	−1	1	1	−1	1	−1	−1	1																	
36	***−1***	−1	1	−1	1	1	1	−1	−1	−1	1	1	1	1	1	−1	1	1	1	−1	−1	1	−1	−1	
	−1	−1	1	−1	1	−1	1	1	−1	−1	1	−1													
48	***−1***	1	1	1	1	1	−1	1	1	1	1	−1	−1	1	−1	1	−1	1	1	1	−1	−1	1	−1	
	−1	1	1	−1	1	1	−1	−1	−1	1	−1	1	−1	1	1	−1	−1	−1	−1	1	−1	−1	−1	−1	

96 Double design for $N = 48$

This table contains the selection of ten experimental designs. The maximal numbers of the orthogonal columns equals the numbers of rows minus one.

Table 6
Three-level experimental design

9	***−1***	−1	0	1	1	−1	1	0	0																
27	***−1***	−1	−1	0	−1	0	1	0	0	1	−1	0	0	0	−1	−1	1	−1	1	0	1	1	0	−1	1	1	1
81	***−1***	−1	0	0	0	0	1	−1	0	1	0	0	1	0	1	−1	1	−1	1	1	0	0	−1	1	−1	0	0
	−1	−1	0	1	1	1	−1	1	0	−1	−1	1	−1	−1	−1	1	1	1	1	0	−1	1	0	1	1	0	1
	0	−1	0	−1	0	0	1	1	−1	0	−1	1	1	−1	−1	1	0	0	0	−1	0	1	−1	−1	0	−1	−1

This table contains the selection of three experimental designs with 9, 27 and 81 samples, respectively. The maximal numbers of orthogonal columns are 4, 13 and 40.

Table 7
Five-level experimental design

25	***−2***	−2	2	−1	−1	0	−1	−2	1	0	0	2	0	−2	−1	2	2	1	2	−2	0	1	1	−1	1
125	***−2***	−2	0	0	0	−1	−2	2	−1	−1	2	−1	1	−1	1	2	−1	0	−2	0	−1	−1	−2	0	2
	2	1	−1	2	−2	0	−2	−2	2	2	2	0	−2	1	0	0	1	0	−1	0	−1	1	0	2	−2
	2	0	0	−2	2	1	1	−1	0	1	−2	2	−2	−2	1	1	1	2	−2	−1	2	2	−1	2	0
	2	0	−1	2	1	−2	1	2	2	−2	1	−1	−1	0	2	−1	−2	1	−2	−2	−1	−1	−1	1	−2
	0	1	1	0	1	2	1	2	0	1	−1	−2	−1	1	1	−2	−1	0	0	2	1	0	−2	−1	−2

This table contains the selection of two experimental designs with 5 and 125 samples, respectively. The maximal numbers of orthogonal columns are 6 and 31.

Table 8
Seven-level experimental design

49	***−3***	−3	−2	−1	3	−1	−1	−2	3	−3	2	0	−1	0
	0	2	−1	−3	1	−2	0	−2	−2	1	0	−3	3	2
	−2	2	2	3	−2	−3	−1	1	2	1	1	−1	2	−3
	0	3	1	3	3	0	1							

The maximal number of the orthogonal columns is 8.

the mixtures, all calibration models on the far right-hand side of Fig. 3(b) would have been declared as the two PC models. This would be a quite adequate assumption, as that would be the best prediction that those models could offer. Besides, the more complex mixtures (i.e. 12 components) appear to be better modelled than the simpler ones, or the messier the data set, the better the prediction results (see the two-PC error curve). This thread of logic may be quite deceptive because calibration models are applied to the random and underdetermined data. In other words, the multivariate calibration algorithms are faced with a virtually impossible task of determining the latent variables from a very scarce information basis. They produce the best possible solutions, but they are still purely circumstantial. When the data contain a sufficient information content (Fig. 3(c)–(d)), the main difference between the calibration and prediction is manifested in terms of the uniformity of decrease in the amount of variance explained by the subsequent latent variables. The random validation set is characterised by a disproportionately big gap between the one- and two-component models.

In all the cases analysed so far, the calibration errors substantially exceed the validation ones (Fig. 3). This anomaly is due to relative ratios of the concentration ranges of two data sets. The calibration data spans a much wider mixture domain and, consequently, the errors referring to the validation data are much smaller. The prediction performances of the calibration models containing insufficient numbers of latent variables are sensitive to the size of the concentration space of the mixtures. The computational confirmation of this statement is given in Fig. 4, in which SET 2 is used as a test set and SET 1 as validation set. Although both sets span the same concentration ranges, very few points from SET 2 can be found at the edges or at the corners of the mixture domain. Consequently, these models have relatively low calibration errors, but they under-perform when used for validation of an orthogonal data set.

The above simulations can be regarded as examples of: (i) calibration in which data come from several different sources (a wide mixture domain) but models are validated against data from a single source (Fig. 3); and (ii) calibration and validation which are based on the data which span the equally wide concentration domain, but where the two data sets are based on different experimental designs (Fig. 4). The prediction errors in either case are quite high. The way to improve prediction performance while using data which is analogous to the simulations presented in Fig. 3 is to scale calibration experimental domain. If this is done in accordance with Table 3, the prediction results retain the above described trends (Fig. 3) and the ratio of calibration versus validation errors are preserved, but the absolute values of the errors become dramatically smaller.

2.1.2. Simulations with added noise

The regularities which apply to the noise-free data are the ideal case. The presence of noise forces calibration models to deviate from their ideal state. It can be speculated that the larger the calibration data set, the better the models. A similar logic can be used with respect to the number of levels of the experimental design. In the first instance, we focus on the size of sample sets. All simulations are performed using absorbance data which contains normally distributed noise with the standard deviation of 0.05 AU, while the concentration profiles are noise free.

The results of simulations which utilise calibration data based on the two-level Plackett–Burman design are given in Fig. 5. The simulations with only four samples are given as an extreme case of the calibration with underdetermined data (Fig. 5(a) and (b)). These results are quite deceiving in the sense that it looks as if the three latent variables are sufficient to fully model all mixtures with 3–12 components. It should be noted that, however limited these models are, their prediction ability does not lag far behind the more elaborate ones (Fig. 5(c)–(h)). Some of the simulations with noisy data could be coupled with those based on the noise-free data (Fig. 5(c) and (d) and Fig. 3(a) and (b), and Fig. 5(e) and (f) and Fig. 3(c) and (d) are counterparts). The models based on eight noisy samples cannot provide errorless predictions even for the binary mixtures (Fig. 5(d)). Although the models based on 16 samples are considerably better, they are still far from their noise-free counterparts. At this noise level (16 sample set), the effect of noise is negligible for the mixtures with four or less chemical components. Our simulations show that the increase in data size after a certain point has hardly any effect on the prediction ability of the calibration models. This can be seen from Table 4 which contains a summary of the maximal numbers of latent variables used in the calibration models over all considered mixtures, given as a function of sample size. This comparison is intended for illustrative purposes only and, for that reason, the numbers of latent variables are determined by visual inspection. The actual positions of the maxima vary. In the validation case, these numbers refer to the models before the first point of interception of the error curves. After that point the additional PCs are not counted because they are counterproductive.

Comparison of the calibration error curves in Fig. 5 reveals that their shape slowly approaches the ideal case, i.e. their maxima, which are marked by vertical lines, are being shifted towards the right-hand side and they are becoming flatter. However, calibration models based on noisy data cannot produce the quality of predictions of the noise-free models even when a substantial number of samples is used. Simulations with 96 samples (Fig. 5(g) and (h)) show that the presence of noise sets limits to the best performance of the calibration models. The validation error curves are virtually unresponsive to the further increase in the number of samples. These error curves are in the vicinity of a horizontal axis only for the mixtures with up to four components. The major effect of having a huge calibration data set is the increases in sensitivity of the more complex mixtures to over-fitting. A sharp rise in the value of prediction errors occurs when these mixtures are modelled with more than two latent variables.

It is of interest to make a comparison between the calibration models based on data with the uniform concentration profiles (0–800 ng ml^{-1}) and the models with the scaled ranges in the presence of noise. As in the noise-free simulations, the 16-sample data sets are used. The results (Fig. 6) imply that while the absolute values of errors correspond to their noise-free counterparts, the error curves do not preserve their shape.

2.2. Multilevel experimental designs

A series of simulations is performed using orthogonal designs with three, five and seven concentration levels (see Tables 6–8). They are aimed at assessing the impact of the number of concentration levels in the orthogonal mixture design on the results of calibration. The results show that the main effect of the increase in the number of concentration levels on the prediction ability of the calibration models is a steady decrease of the absolute values of errors. The pattern of error curves is independent of the number of mixture design levels (Fig. 7).

For the five- and seven-level mixtures, the amount of added noise is varied in order to obtain an account of the effect of various noise levels on the calibration results. Simulations with different noise levels outlined the limits of the multivariate regression models. The increase in the amount of added noise transforms the models from ones with nearly perfect prediction ability into models with well defined error limits. There is a noise level which marks the point of a qualitative change in the type of noise impact on the prediction ability of regression models. Whenever data contain noise, calibration models can

provide errorless prediction for the simple mixtures only. The value of average prediction error for the more complex mixture depends on a standard deviation of the noise and on the mixture complexity. The high noise levels not only set prediction error limits but they cause the calibration models of the complex mixtures to become sensitive to over-fitting, and the error curves start to intercept.

2.3. Partial simulations

If only a subset of all possible mixtures is modelled and the regression errors are then averaged, the averages do not form a smooth function of the number of mixture components. The variations around a full simulation error line are dependent on the actual selections of the mixtures within the subsets. This is illustrated by performing simulations on the data with and without added noise (Fig. 8). The oscillations are the consequence of the actual selection of the mixtures within the subset. This tells us that the quality of the prediction is a function of mixture composition, because it depends on the properties of the mixture constituents. If for a moment we return to Fig. 2, we can see that only a few of the absorption curves have strong characteristic peaks, and that there is a number of compounds whose spectra are likely to be completely in the shadow of the other components. The mixtures for which it is possible to either uniquely assign some of the wavelengths to the individual components, or to combinations of the components, are likely to be more amenable to the multivariate calibration than those in which one or more components are completely masked by the others.

3. Conclusions

One of the basic assumptions in the regression analysis is that for a given calibration method and a noise pattern, the prediction results are only as good as the analysed data. The quality of the data set is defined in terms of the actual selection of the mixture components (their physical properties) and their experimental design. The former factor should be understood in terms of overlapping of the PAH spectra. The actual selection of components in the mixture limits the prediction ability of the calibration models. The noise-free simulations have shown that the problem of not having uniquely represented mixture components does not occur for the group of 12 PAH used in this study; providing that there is a sufficient number of samples, the complexity of the calibration model is directly proportional to the number of components in the mixture.

It is shown that when the experimental domain is adjusted to the specific data set, prediction results are good, as long the test samples fall within the training domain. This condition is unlikely to be satisfied for the samples of diverse origins (i.e. samples which originate from different industrial sources of PAH pollution). Simulations where the validation experimental domain does not match the calibration one show a significant decrease in prediction ability. The more general calibration models, those with the training experimental domain wide enough to accounts for several types of industries, allow equally good prediction for all samples. However, the overall level of prediction errors associated with these models is well above the levels of the specific calibration models. The conclusion is that, although a general calibration model is readily feasible, there is little advantage in using it.

Noisy data sets cannot be modelled without prediction errors, regardless of the number of samples. The noise masks the fine differences between the mixture components, and for this reason they cannot be accounted for by the multivariate regression algorithm in the more complex mixtures. The actual value of the lowest prediction error for a given set of PAHs is a function of the noise level and mixture complexity.

Acknowledgements

The author gratefully acknowledges the Health and Safety Executives (HSE) of the United Kingdom for providing financial support for this work. None of the statements made in this paper imply any HSE acceptance or approval.

Appendix A. Plackett–Burman experimental designs

Tables 5–8 contain an overview of the Plackett–Burman experimental designs with two, three, five and seven levels. Only the first columns of the corresponding designs are given. For each design, the first element (the one which should not be rotated) is bold italic. Only the designs used in this work are listed. The designs levels are presented in their centred form.

References

[1] N. Logothetis, H.P. Wynn, Quality Through Design: Experimental Design, Off-line Quality Control, and Taguchi's Contribution, Clarendon Press, Oxford, 1989.
[2] G.E.P. Box, W.G. Hunter, J.S. Hunter, Statistics for Experimenters, An Introduction to Design, Data Analysis and Model Building, Wiley, New York, 1978.
[3] S.N. Deming, S.L. Morgan, Experimental Design: A Chemometrics Approach, Elsevier, Amsterdam, 1993.
[4] C. Daniel, Applications of Statistics to Industrial Experimentation, Wiley, New York, 1976.
[5] G.E.P. Box, Technometrics 8 (1966) 184.
[6] P.W. Araujo, R.G. Brereton, Trends Anal. Chem. 15 (1996) 26.
[7] P.W. Araujo, R.G. Brereton, Trends Anal. Chem. 15 (1996) 63.
[8] P.W. Araujo, R.G. Brereton, Trends Anal. Chem. 15 (1996) 156.
[9] M. Sergent, D. Mathieu, R. Phan-Tan-Luu, G. Drava, Chemom. Intell. Lab. Syst. 27 (1995) 153.
[10] J.A. Van Leeuwen, L.M.C. Buydens, B.G.M. Vandeginste, G. Kateman, P.J. Schoenmakers, M. Mulholland, Chemom. Intell. Lab. Syst. 10 (1991) 337.
[11] D.J. Wheeler, Understanding Statistical Process Control, Statistical Process Control, Knoxville, TN, 1987.
[12] J. Dénes, A.D. Keedwell, Latin Squares and Their Applications, English University Press, Budapest, 1974.
[13] W.L. Stevens, Ann. Eugenics 9 (1939) 82.
[14] A. Dey, Orthogonal Fractional Factorial Designs, Wiley Eastern, New Delhi, 1985.
[15] L.D. Baumert, S.W. Golumb, M.J. Hall, Bull. Am. Math. Soc. 68 (1962) 237.
[16] O.J. Dunn, V.A. Clark, Applied Statistics: Analysis of Variance and Regression, Wiley, New York, 1987.
[17] J.S. Hunter, Qual. Eng. 1 (1989) 453.
[18] F. Yates, The Design and Analysis of Factorial Experiments, Imperial Bureau of Soil Science, Harperdon, 1937.
[19] R.A. Brualdi, Introductory Combinatorics, North-Holland, New York, 1977.
[20] L. Euler, Memoir presented to Academy of Science of St. Petersburg on 8 March 1779, published as: Leonardi Euleri Opera Omnia, Série 1, vol. 7, 1932, p. 291.
[21] R.C. Bose, S.S. Shrikhande, Proc. Natl. Acad. Sci. USA 45 (1958) 734.
[22] R.C. Bose, S.S. Shrikhande, Am. Math. Soc. 95 (1960) 191.
[23] E.T. Parker, Proc. Am. Math. Soc. 10 (1959) 946.
[24] E.T. Parker, Proc. Natl. Acad. Sci. USA 45 (1959) 859.
[25] R.C. Bose, S.S. Shrikhande, E.T. Parker, Can. J. Math. 12 (1960) 189.
[26] R.L. Plackett, J.P. Burman, Biometrica 33 (1946) 305.
[27] Matlab, Reference Guide, The Math Works, Natick, 1992.

.

ELSEVIER

Talanta 45 (1998) 1001–1006

Talanta

A rapid method for the clean-up of chlorinated biphenyls (CBs) isolated from environmental samples

Anu Thompson [a,*], Paul McMorn [b], George A. Wolff [a]

[a] *Environmental Organic Chemistry and Geochemistry Group, Oceanography Laboratories, Department of Earth Sciences, University of Liverpool, Liverpool, L69 3BX, UK*

[b] *Leverhulme Centre for Innovative Catalysis, Department of Chemistry, University of Liverpool, Liverpool, L69 3BX, UK*

Received 12 May 1997; received in revised form 27 June 1997; accepted 30 June 1997

Abstract

The use of silicalite, a zeolitic form of silica, is suggested as a means of purifying samples prior to the determination of chlorinated biphenyls (CBs), particularly those which are heavily contaminated with petroleum derived *n*-alkanes. Experiments using mussel, fish and sediment extracts show that CBs are recovered quantitatively after silicalite treatment of lipid extracts. © 1998 Elsevier Science B.V.

Keywords: Chlorinated biphenyls (CBs); GC–MS; *n*-alkanes; Silicalite

1. Introduction

The determination of CBs in environmental samples usually involves solvent extraction of the sample matrix followed by adsorption chromatography prior to analysis by GC–ECD or GC–MS. Chromatography columns containing alumina, [1], silica [2], or Fluorisil [3] are widely used to separate CBs from interfering compounds prior to analysis.

The two-column clean-up and separation technique developed by Holden and Marsden [1] has been used routinely in this laboratory, with some modifications. Briefly, the sample is extracted in *n*-hexane or *n*-hexane/acetone (4–24 h) and the concentrated extract is first applied to an alumina column (3 g, 5% deactivated) which is eluted with *n*-hexane, this eluent then being applied to a silica column (3 g, 3% deactivated). The alumina retains most of the co-extracted lipid material, whilst the silica column retains any residual lipid material and also separates CBs from other organochlorine compounds. This work-up is suitable for most environmental samples. For example, CB levels have been readily determined using this procedure in mussel and fish tissue, shag eggs, and marine sediments [4,5]. However, the method is not adequate for the determination of CBs in samples which also contain high concentrations of *n*-alkanes (See Section 3—Results and discussion).

Urea adduction and zeolite-based molecular sieves are routinely used to separate *n*-alkanes from other saturated hydrocarbon components of

* Corresponding author. Fax: +44 151 7944099; e-mail: anu@liverpool.ac.uk

PII S0039-9140(97)00206-3

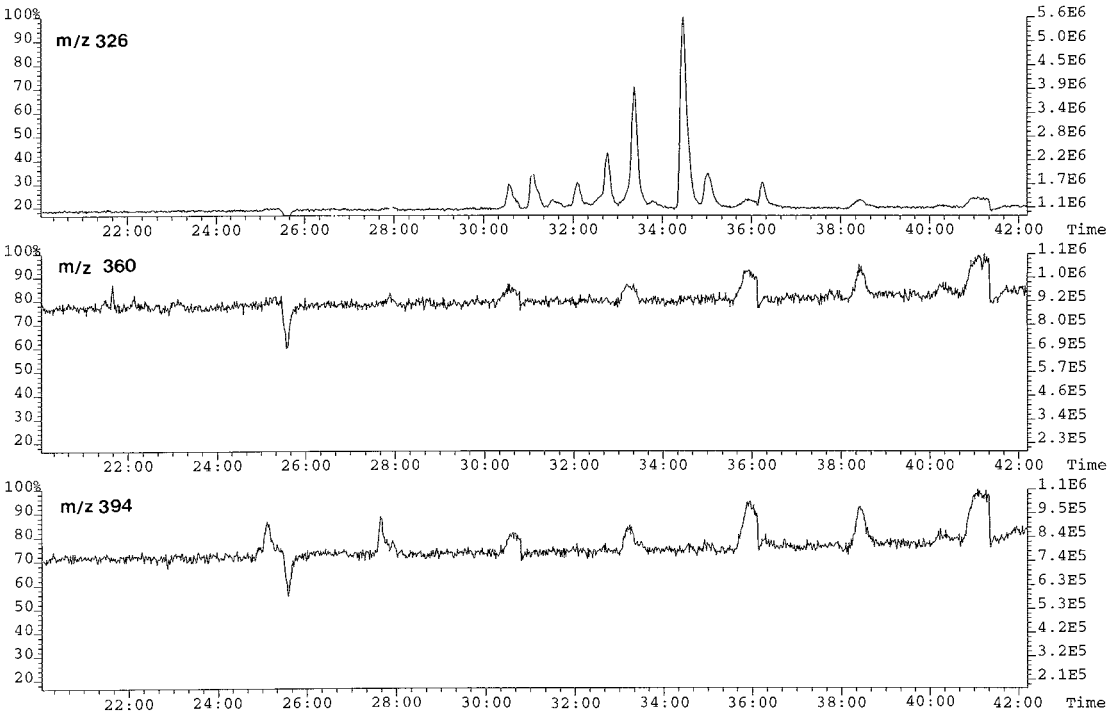

Fig. 1. NICI–GC–MS (single-ion monitoring) mass chromatograms ($m/z = 326$, 360 and 394, molecular ions for penta, hexa and hepta-chlorinated biphenyl, respectively) of the Loch Ness sediment sample after standard clean-up (see text). x-axis: retention time in minutes; y-axis: peak intensity.

petroleum [6]. Urea adduction requires stringent experimental conditions and the adduction often has to be repeated several times if an excess of interfering *n*-alkanes is present. The use of zeolitic-based molecular sieves to remove *n*-alkanes usually involves reflux of the sample extract in benzene, toluene or iso-octane (12–24 h). The sieves, which retain the *n*-alkanes, are then removed and the solvent is evaporated to leave the branched and cyclic fraction.

Recently, West et al. [7] used silicalite, a synthetic zeolitic form of silica, to isolate branched and cyclic alkane fractions from *n*-alkanes for analysis of biological markers in a rapid, convenient and simple clean-up. The channels of silicalite consist of two pore sizes; circular pores that have diameters of about 6 Å and elliptical pores with 5.1–5.7 Å diameter. These offer a slightly larger zeolitic pore size than the Linde 5 Å molecular sieve [8] and silicalite, therefore, sorbs *n*-alkanes, isomeric monomethyl alkanes and a limited number of single-ring compounds [9].

In this note, we report the use of silicalite to separate CBs from co-occurring *n*-alkanes in hydrocarbon contaminated environmental samples, following the method used by West et al. [7]. A mussel sample, fish reference standard and a sediment reference standard were also analysed in order to compare recoveries of CBs using alumina/silicalite and alumina/silica/silicalite. The aliphatic fraction of a Columbian crude oil was treated with silicalite in order to determine the sample loading at which *n*-alkane breakthrough occurs.

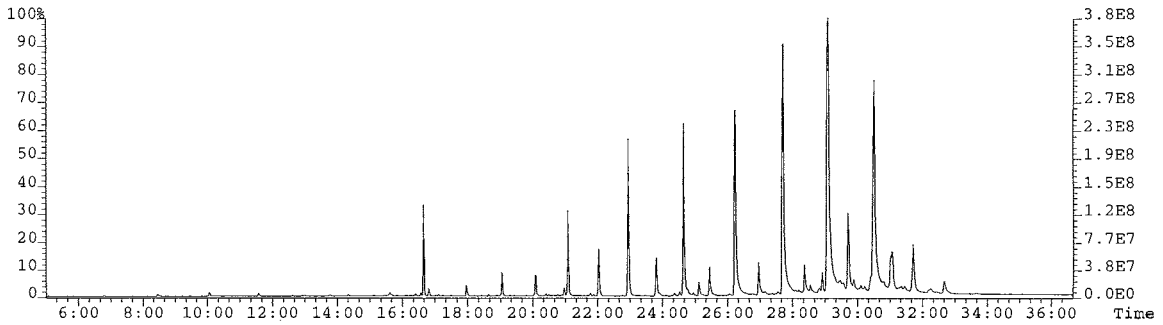

Fig. 2. Total ion chromatogram of the Loch Ness sediment sample analysed in full scan electron impact mode, showing a typical higher plant *n*-alkane distribution. *x*-axis: retention time in minutes; *y*-axis: peak intensity.

2. Experimental

2.1. Materials and methods

Details of the materials and procedures involved in the extraction, clean-up and analysis of CBs have been described previously [5]. Silica (containing 0.1 wt% Na_2O and 1.0 wt% water) for the synthesis of silicalite was obtained from BDH (Poole, UK). Tetrapropylammonium bromide (TPABr) and sodium hydroxide pellets were obtained from Fluka, Poole, UK).

Silicalite was synthesised by a standard procedure [10] with some modifications. Briefly, a solution of sodium hydroxide and tetrapropylammonium bromide (TPABr) in doubly-distilled water was added to silica and the resulting mixture was placed in an autoclave and heated to 175°C for 48 h. The resulting white solids were filtered and dried at 100°C. The silicalite was then activated at 550°C overnight, prior to use.

Silicalite columns were prepared by plugging a Pasteur pipette with a small piece of pre-extracted cotton wool and adding activated silicalite powder (1.4 g). Typically, the sample extract was made up to 2 ml with *n*-hexane and applied to the column, which was then eluted with *n*-hexane (8 ml). The solvent was then removed under a gentle stream of nitrogen. (The *n*-alkanes can be recovered from the silicalite by treating the latter with 30% hydrofluoric acid followed by *n*-hexane extraction. [7]).

2.2. Sample treatment

Sections from a sediment core from Loch Ness (provided by Professor S Rowland, University of Plymouth, UK) were extracted and cleaned-up as previously described [5]. The extracts were further passed through silicalite columns after initial NICI–GC–MS analysis showed the presence of large amounts of interfering compounds.

A mussel sample, a fish reference standard (MA-B-3/OC), and a sediment reference standard (Canadian reference marine sediment HS-2) were extracted as previously described [5]. Each extract was then divided into three equal portions (by volume) and each was treated as follows:

1. Alumina (5% deactivated)/silica (3% deactivated) clean-up.
2. Alumina (5% deactivated) followed by silicalite clean-up.
3. Alumina (5% deactivated)/silica (3% deactivated) followed by silicalite clean-up.

The saturated components of a Columbian crude oil ($\approx$ 70% saturates) were isolated by chromatography on silica using *n*-hexane as the eluent. Portions of 10, 25, 60, 90, 141 and 190 mg of the saturates fraction were then made up to 2 ml and transferred onto silicalite columns, as above (see Section 2.1—Materials and methods).

2.3. Gas chromatography–mass spectrometry

CBs were determined using negative ion chemical ionisation gas chromatography–mass spectroscopy (NICI–GC–MS). Full details for the

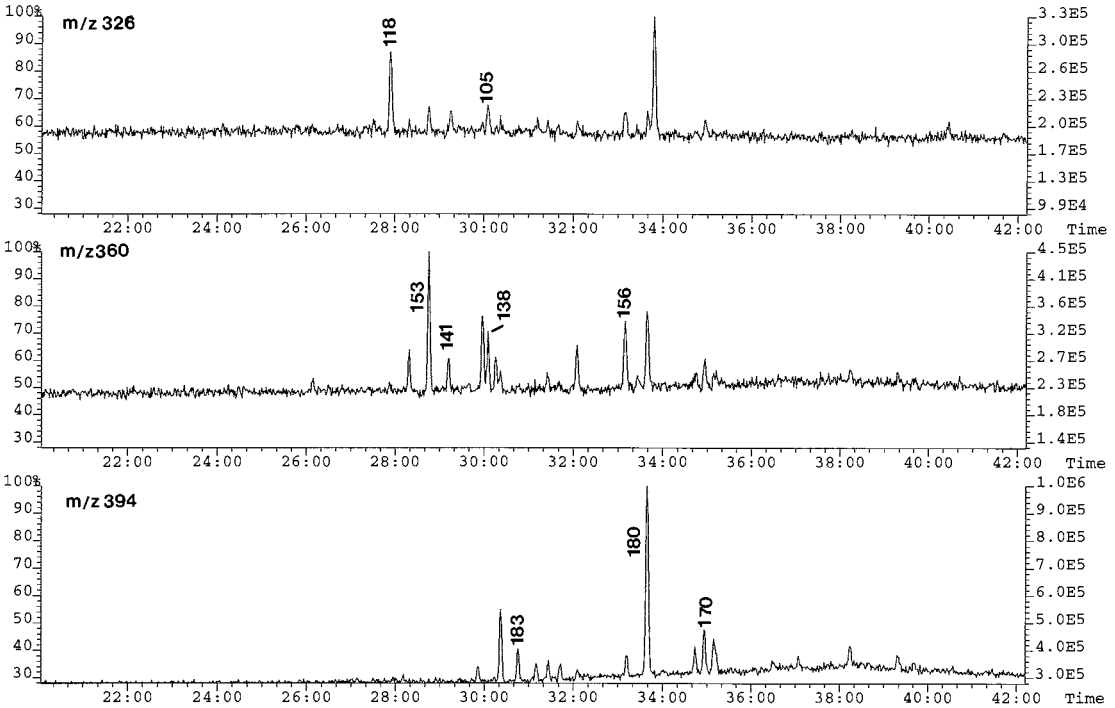

Fig. 3. NICI-GCMS mass chromatograms ($m/z = 326$, 360 and 394) of the Loch Ness sediment section after silicalite clean-up. ΣCB (22 congeners) = 1.4 ng g^{-1} dry weight. Peak numbering identifies congeners. x-axis: retention time in minutes; y-axis: peak intensity.

operating conditions have been described previously [5]. Briefly, a fused silica capillary column (25 m, 0.2 mm id, HT-5 0.1 μm film thickness J&W or a 25 m × 0.2 mm, 0.25 μm film thickness, BPX-5, SGE) with a deactivated retention gap was introduced directly into the chemical ionisation source of a VG-TS250 magnetic sector mass spectrometer. Samples were introduced by on-column injection; helium was used as a carrier gas (ca. 2 ml min^{-1}) and methane (source pressure ca. 8×10^{-5} mbar) as reagent gas for negative ionisation. Perflurobutylamine was used to calibrate the mass axis (m/z 264, 414, 452 and 633) at the same source pressures as those used during analysis. CBs were identified from their full scan spectra when possible and by comparison of their relative retention times with those of the authentic standards.

Saturate fractions from the Columbian crude oil were analysed using electron-impact GC–MS under conditions described previously [11].

2.4. Quantification

Five standard mixtures (between 0.05 and 0.2 μg ml^{-1}) of individual CB congeners [5] were used for calibration purposes and for the determination of response factors in selected ion monitoring (SIM) mode, relative to the internal standard, octachloronaphthalene. Quantification was carried out by comparison of the areas of the internal standard peak to CB peaks and correction with the appropriate relative retention indices.

3. Results and discussion

GC–MS analysis of a lacustrine sediment sample (Loch Ness, Scotland), that had been extracted and treated according to the method described above [1] showed that the CBs were poorly resolved and difficult to identify due to the

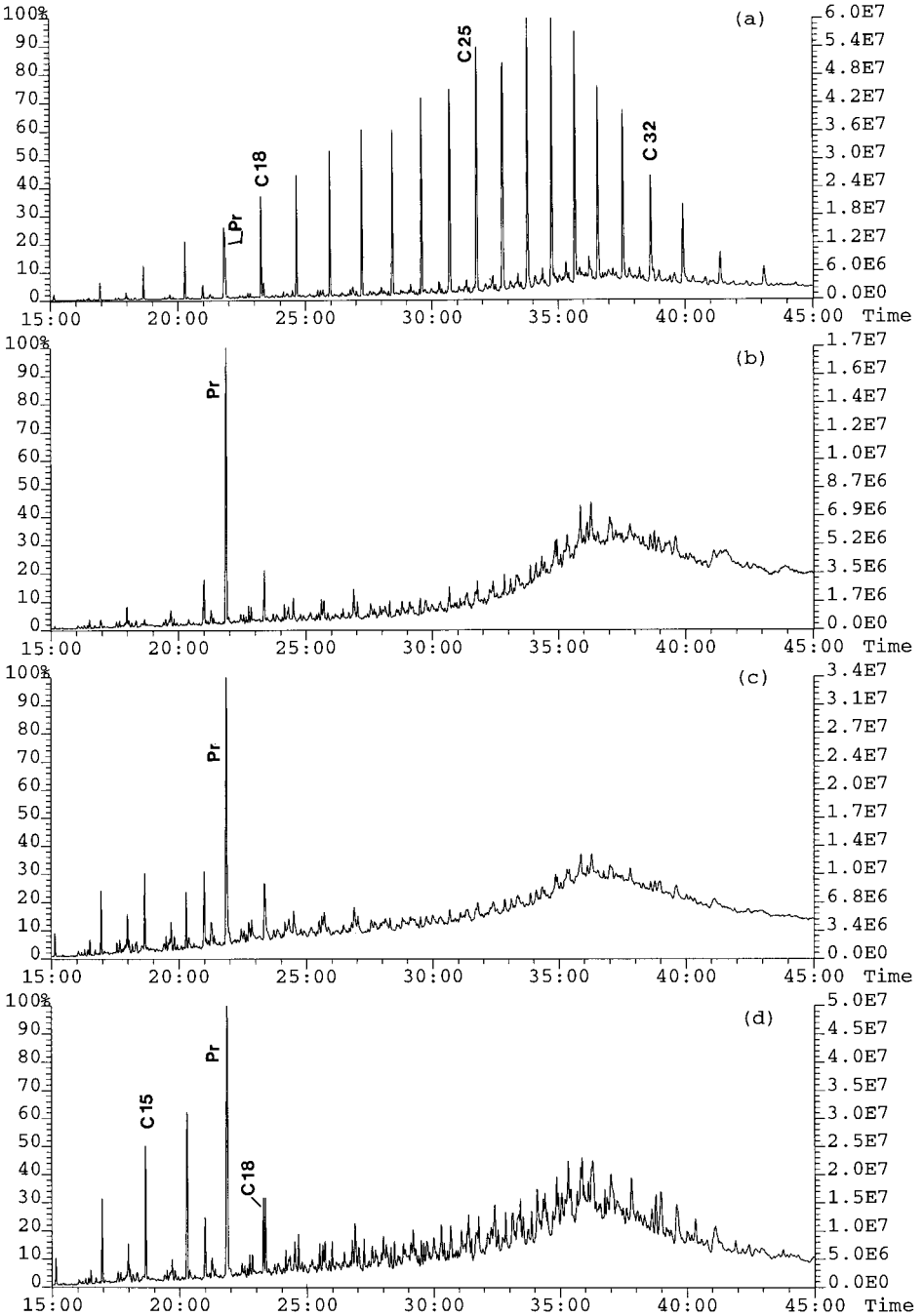

Fig. 4. Total ion chromatograms of (a): Columbian crude oil saturates fraction prior to silicalite treatment; (b), (c), (d): 10, 60 and 190 mg saturates fraction after silicalite treatment, analysed in full scan electron impact mode. *x*-axis: retention time in minutes; *y*-axis: peak intensity. (Pr = Pristane)

.

interference of co-eluting compounds (Fig. 1). Repeated alumina/silica clean-up did not improve the chromatographic resolution. When the sample was analysed in electron impact mode, it was shown to contain a relatively high concentration of *n*-alkanes (Fig. 2). The sample was subsequently treated with silicalite in order to remove the *n*-alkanes and then re-analysed. This clearly improved the chromatographic resolution of the CBs (Fig. 3.) and allowed the determination of the CBs, despite their relatively low concentration ($\Sigma CB = 1.4$ ng g^{-1} dry weight).

The recoveries of individual CBs in the mussel, fish standard and sediment standard using alumina/silicalite and alumina/silica/silicalite were in the range 96–103% indicating that no CBs were retained on the silicalite. Furthermore, there were no distributional differences between samples before and after silicalite clean-up.

Treatment of the Columbian crude oil aliphatic hydrocarbons with silicalite showed that *n*-alkanes higher than C19 were retained on the silicalite for all sample loadings (Fig. 4.). However, there was some break-through of the lower ($<$C16) chain alkanes at sample loadings of 60 mg and above. The highest sample load used in this experiment was 190 mg, but it may be possible to use even larger sample loadings if only higher chain *n*-alkanes are to be removed.

4. Conclusion

Sample clean-up using alumina and silicalite provides a rapid and convenient route for the analysis of CBs and is particularly useful for those environmental samples which contain a high relative concentration of *n*-alkanes. The break-through of *n*-alkanes is minimal, even where sample loadings are very high.

Acknowledgements

The authors would like to thank G. Harriman (GHGeochemical services) for his interest in this work and gift of the Columbian crude oil. This is EOCGG contribution No. 24.

References

[1] A.V. Holden, K. Marsden, J. Chromatogr. 44 (1969) 481.
[2] V. Contardi, R. Capelli, G. Zanicchi, M. Drago, Analyst (London) 108 (1983) 510.
[3] M. Camps, J. Planas, M. Gomez-Catalan, M. Sabroso, J. To-Figueras, J. Corbella, Bull. Environ. Contam. Toxicol. 42 (1989) 195.
[4] J.A. Allen, A. Thompson, Mar. Pollut. Bull. 32 (1996) 890.
[5] A. Thompson, J.A. Allen, D. Dodoo, J. Hunter, S. Hawkins, G.A. Wolff, Mar. Pollut. Bull. 32 (1996) 232.
[6] M.T. Murphy, Analytical methods, in, Organic Geochemistry, Springer, Berlin, 1969, p. 74.
[7] N. West, R. Alexander, R. Kagi, Org. Geochem. 15 (1990) 499.
[8] T.M. Hoering, D.H. Freeman, J. Chromatogr. 316 (1984) 333.
[9] R.M. Dessau, Absorption and Ion Exchange with Synthetic Zeolites, ACS Symposium Series No. 135, Washington, 1980, p. 123.
[10] D.T. Hayhurst, A. Nastro, R. Aiello, F. Crea, G. Giordano, Zeolites 8 (1988) 416.
[11] G.A. Wolff, M.R. Preston, G. Harriman, S.J. Rowland, Mar. Pollut. Bull. 26 (1993) 567.

.

ELSEVIER

Talanta 45 (1998) 1007–1014

Talanta

Potentiometric study of the protonation and distribution equilibria of D-gluconic-δ-lactone acid in sodium perchlorate solutions at 25°C and construction of a thermodynamic model

J. Zubiaur *, R. Castaño, N. Etxebarria, L.A. Fernández, J.M. Madariaga

Kimika Analitikoaren Saila, Euskal Herriko Unibertsitatea, 644 PK, E-48080 Bilbao, Spain

Received 3 April 1997; received in revised form 30 June 1997; accepted 4 July 1997

Abstract

The protolytic behavior of D-gluconic-δ-lactone acid has been studied by means of automated potentiometric titrations at different ionic strengths in the range $0.1 \leq I \leq 3.0$ mol dm^{-3} in $NaClO_4$ at 25°C. This study reveals a protolytic equilibrium of gluconic acid as well as a distribution equilibrium between gluconic acid (HG) and its lactone form (L). The values of the stoichiometric constants obtained have been correlated by means of the modified Bromley methodology. The thermodynamic constants obtained were $\log \beta^0 = 3.92 \pm 0.10$ for the protolytic equilibrium $H^+ + G^- \rightleftharpoons HG$ and $\log K_r^0 = -0.81 \pm 0.09$ for the distribution equilibrium $HG \rightleftharpoons L$. © 1998 Elsevier Science B.V.

Keywords: Potentiometry; Gluconic acid; Thermodynamic model

1. Introduction

Many of the organic protolytes are often used in the pharmacology, chemical and electrochemical industry. Some of them are relevant in different environmental systems or play a key role in biochemical processes [1,2]. Therefore, the use of validated thermodynamic models can be very valuable in order to predict the behavior of these systems or in the design of new chemical processes [3].

The hydrolysis of organic acids and bases has been extensively studied and the results are reported in the literature [4–6]. In the same way many experiments have been performed in order to develop thermodynamic models. These models are mainly based on variations of the activity coefficients, temperature, etc. of the species involved, which try to explain the variability of the chemical equilibria [7]. These models can also be very useful for simulation and prediction purposes in many different fields. However, it is very difficult to construct robust thermodynamic models in many simple chemical systems due to a lack of critical and systematical studies at different ionic media, strengths and at different temperatures.

* Corresponding author. Tel.: + 34 4 4647700; fax: + 34 4 4648500; e-mail: qaazucoj@lg.ehu.es

PII S0039-9140(97)00207-5

One of the industrial activities in which different substituted carboxylic acids can be found together with other organic and inorganic substances is metal electroplating and finishing. Moreover, these processes are responsible for spills with high a content of metallic waste in streams or rivers. Thus, the development of processes related with the recovery of raw materials and the minimisation of wastes has a key importance. Nevertheless, due to the high complexity of the chemical speciation of these systems the development of thermodynamic models of the main equilibria involved could be helpful before tackling the design of any new process.

Among the organic ligands, gluconic acid and its salts are widely used as alkaline cleaner agents and as masking or sequestering agents forming metal complexes. Although metal gluconates are not as stable as other carboxylate complexes (citrate, tartrate) they are stable enough to avoid the removal of metals to established levels before being spilled out [8,9].

Gluconic acid hydrolyzes in water according with the general scheme shown in Fig. 1. It is generally established that one to four aldono lactones (γ-lactones) are much more stable and resistant toward hydrolysis than their corresponding six ring member isomers (δ-lactones) [10,11]. This behavior can be attributed to the presence of the exo-double bond which stabilizes the five-membered rings [12].

Many works have been undertaken in order to evaluate the kinetics and the values of the rate constants of the lactone hydrolysis as well as to establish the existence or not of interconversion equilibria between D-glucono-δ and γ-lactones. Although in the 1960s some authors postulated the existence of this kind of interconversion equilibria [13,14]. Later works have shown that the δ-lactone-gluconic acid equilibrium is established before sensible amounts of γ-lactone can be formed [15,16] and only at high pH values the interconversion equilibria can be appreciated [17].

As it has been pointed out before, in the different compilations of stability constants [4–6,18] only few data concerning the protolysis equilibrium of gluconic acid are available. Most of these data are calculated at only one ionic strength in chloride or nitrate media [16,18–25] which makes the development of a thermodynamic model impossible. Due to this lack of information the determination of the protolytic constants of gluconic acid at different ionic strengths in the range $0.1 \leq I \leq 3.0$ mol dm^{-3} has been considered necessary. In these experimental conditions and $NaClO_4$ as the inert electrolyte, only the δ-lactone form will be considered present in solution.

2. Experimental

2.1. Reagents and solutions

All reagents were used without further purification. The stock solution of D-gluconic-δ-lactone acid (Sigma > 99%) was standardized adding an excess of standard sodium hydroxide solution. This was followed by a back-titration with standard hydrochloric acid solution using phenolphthalein as indicator. The solutions of D-gluconic-δ-lactone acid are prone to form colonies of micro-organisms, therefore all the solutions were prepared ready to use.

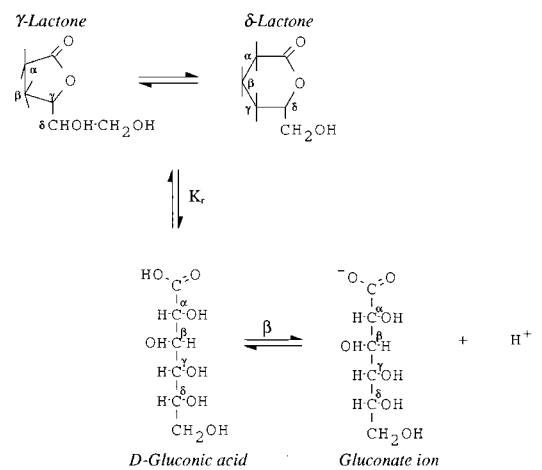

Fig. 1. Lactonitation and dissociation process of D-gluconic acid. β denotes the protolysis constant and K_r is the distribution constant.

Stock solutions of sodium hydroxide (Merck) and perchloric acid (Fluka) were standardised against potassium hydrogenphthalate (Merck) and tris-(hydroxymethyl)aminomethane (Merck), respectively using phenolphthalein and bromocresol green as indicators [26]. The ionic medium used was sodium perchlorate monohydrate (Fluka). The concentration of the stock solution was tested gravimetrically after evaporation of known aliquots at 110°C.

All these solutions were prepared at the corresponding ionic strengths used in this work (0.1, 0.5, 1.0, 2.0 and 3.0 mol dm^{-3}) and the analytical concentration of all of them showed a mean relative standard deviation $< 0.2\%$.

2.2. Apparatus

The experiments were carried out with an automatic potentiometric titration system developed in our laboratory [27] which can control up to three titrations at the same time. The titration system is composed of a five mouth glass cell in which the double-liquid junction Ag–AgCl(s) reference electrode (Metrohm 6.0726.100 RC) and the glass electrode (Metrohm 6.0101.00 PE) were introduced. The potentiometric measurements were made with the following cell where I is the ionic strength of the solution.

$$Ag/AgCl(s)/NaClO_4 I \text{ (mol dm}^{-3}) \text{ AgCl(sat)}$$

$$//NaClO_4 I \text{ (mol dm}^{-3})//\text{Test solution/G.E.} \quad (1)$$

Both electrodes were connected to a preamplifier in order to adapt the electrical signal to the voltmeter. The electromotive force measurement was carried out with a Hewlett–Packard HP 3421 A voltmeter with a resolution of 5.5 digits, connected to a computer (PC.286). The titrant additions were performed with a Metrohm Dosimat 725 burette with a precision of ± 5 μl. The temperature was kept constant at 25.0 ± 0.1°C with a thermostated oil-bath and the experimentation was conducted under N_2 atmosphere in order to avoid the dissolution of the atmospheric CO_2. Additionally magnetic stirring was employed during the titration.

2.3. Procedure

Each titration of D-gluconic-δ-lactone acid splitted off in two parts: the determination of the standard potential (E^0) of the cell (Eq. (1)) and the titration of the organic acid. In the first part a suitable volume of $NaClO_4$ stock solution was taken and diluted with Milli Q water to the desired ionic strength of the solution reaching a final volume of 75 cm^3. This solution was titrated with standard $HClO_4$ solution (at the same ionic strength under study) and from the (E, V) data, within $2 \leq pH \leq 4$, the E^0 value was determined for each titration. E^0 values at different titrations showed a high repeteability so it can be considered that the stability in each titration was assured. Once this titration ended a known volume of standardized D-gluconic-δ-lactone acid solution was added to the titration vessel and the resulting solution was titrated with standard NaOH solution, at the same ionic strength, up to $pH \approx 8$. The concentrations of D-gluconic-δ-lactone acid titrated in this work were 0.005 and 0.010 mol dm^{-3} and each titration was repeated twice.

Initially, the D-gluconic-δ-lactone was titrated using the same conditions for the E^0 determination. Therefore a waiting time of 5 min after each addition, followed by a maximum of 15 readings every 1 min was programmed, considering that the equilibrium was reached when a standard deviation of the last three readings was $< \pm 0.05$ mV.

The titration curves were graphically treated by means of the Z function (average number of protons bound to gluconate), which will be explained later. It was observed that the Z values in these conditions were different from the theoretical curve expected for a monoprotic acid as can be seen in Fig. 2.

Since the deviation from the expected Z values can be attributed to slow equilibration processes, several titrations were performed at $I = 0.5$ mol dm^{-3} just altering the waiting times after each addition. The results of these experiments are summarized in Fig. 2 and it can be seen how the experimental and the expected Z values get closer at increasing waiting times. When the waiting

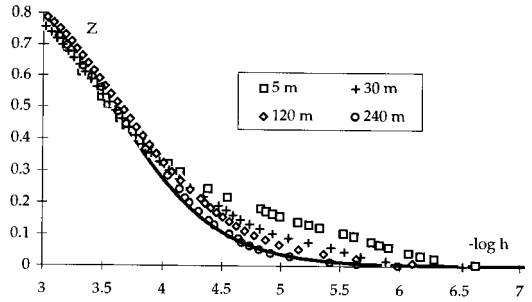

Fig. 2. Representation of Z vs. $-\log h$, at different waiting times for $I=0.5$ mol dm^{-3}. (——) denotes the theoretical curve considering a monoprotic system with $\log \beta \approx 3.6$.

time is 240 min both the continuous line and the experimental Z values are superimposed so this time is the minimum at which these titrations could be performed.

This fact was only observed in the interval $3.8 \leq pH \leq 6.5$ as can be seen in Fig. 3, which agreed with previous kinetic measurements of this system [28]. Therefore, each titration lasted 2 weeks approximately opposite to 12 h necessary to realize another type of acid-base titrations.

2.4. Determination of h

The measured potential can be expressed by the Nernst equation

$$E = E_0 + g \log h + E_j(h) \quad (2)$$

where the liquid junction potential, $E_j(h)$, can be expressed as in Eq. (3)

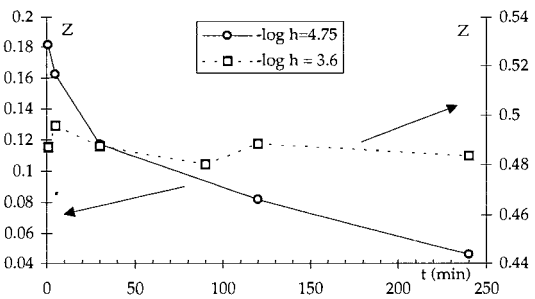

Fig. 3. Representation of Z as a function of time for the different values of $-\log h$.

$$E_j(h) = j_a h + j_b K_w h^{-1} \quad (3)$$

The values of the liquid junction coefficients (j_a and j_b) and the autoprotolysis constant of water (K_w) for the ionic strengths 0.5, 1.0, 2.0 and 3.0 mol dm^{-3} in $NaClO_4$ were calculated in a previous work [29]. The values for the 0.1 mol dm^{-3} ionic strength had to be calculated in this work. In this sense, several ionic media titrations were performed to determine the acid liquid junction coefficient. The results where treated by means of Gran's method [30] and numerically refined with the MODEL FUNCTION version [31] of the LETAGROP program [32] concluding that $j_a = -565 \pm 6$ mV mol^{-1} dm^3. Since the pH of the titration never reached values higher than eight it was not necessary to calculate the basic liquid junction coefficient. Finally, the value of K_w was estimated applying the Modified Bromley Methodology to the water autoprotolysis equilibrium ([33]; R. Castaño, unpublished data).

3. Results and discussion

Taking into account the considerations pointed out before, the equilibria that take place in solution can be written as follows:

$$H^+ + G^- \rightleftharpoons HG \quad (4)$$

$$HG \rightleftharpoons L \quad (5)$$

where G^- denotes the gluconate ion, HG the gluconic acid and L the δ-lactone form of gluconic acid. The corresponding formation equilibrium constants can be expressed as follows:

$${}^I\beta = \frac{[HG]}{[H^+][G^-]} \quad (6)$$

$${}^IK_r = \frac{[L]}{[HG]} \quad (7)$$

where ${}^I\beta$ is the stoichiometric protonation constant and ${}^IK_r$ is the corresponding stoichiometric distribution constant at I ionic strength.

All the titrations were initially treated graphically plotting the Z function against $-\log(h)$ [34]. The Z function is defined in this case as the average number of protons bound to gluconate and it can be directly calculated as follows:

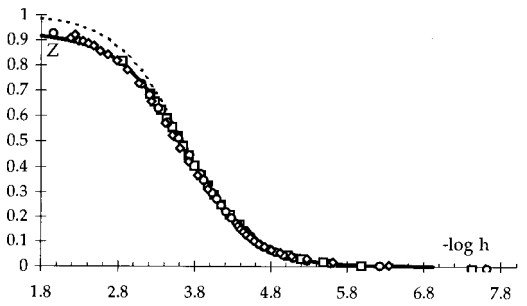

Fig. 4. Representation of Z vs. $-\log h$, for $I = 1.0$ mol dm^{-3} in $NaClO_4$. (○), (◇) $G_{tot} = 0.01$ mol dm^{-3}, (□) $G_{tot} = 0.005$ mol dm^{-3}, (——) theoretic considering the β and the K_r values, (– – –) theoretic considering the β value.

$$Z = \frac{H_{tot} - h + K_w h^{-1}}{G_{tot}} \quad (8)$$

where H_{tot} is the total concentration of protons, h is the free concentration of protons, K_w is the water autoprotolysis constant and G_{tot} is the total concentration of D-gluconic-δ-lactone acid.

Taking into account the equilibria involved in this system (Eqs. (6) and (7)) the Z function can be also written as the following expression:

$$Z = \frac{{}^{I}\beta h}{1 + {}^{I}\beta h + {}^{I}\beta\, {}^{I}K_r h} \quad (9)$$

Since both functions (Eqs. (8) and (9)) should have the same shape a normalized curve can be built by means of a normalized variable (U) and one parameter (p) defined as follows:

$$U = {}^{I}\beta h \quad (10)$$

$$p = {}^{I}K_r \quad (11)$$

Thus, Eq. (9) can be rewritten as:

$$Z = \frac{U}{1 + U + pU} \quad (12)$$

The experimental curves were plotted using Eq. (8) while the theoretical curves were constructed from Eq. (12). Both curves can be compared and from the position of the best fit it is possible to calculate the value of the protonation and distribution constants.

In Fig. 4 there is good agreement between experimental Z curves for different total concentrations of D-gluconic-δ-lactone acid and the theoretical curve at 1.0 mol dm^{-3} in $NaClO_4$. It can be stressed that the fitting needs the use of both constants to reproduce the experimental behavior. When only the protonation equilibrium is considered the theoretical curve (dashed line) fits the lower part of the experimental data but not the whole curve. On the contrary, when both constants are used (continuous line) the experimental Z values can be fitted in the whole experimental range, which is the distribution of gluconic acid responsible for having Z values < 1. From the graphical treatment it can also be concluded that the values of Z are completely independent of the total concentration of D-gluconic-δ-lactone, which confirms the absence of aggregation phenomena.

The results obtained graphically were refined by numerical treatment. There are several programs for the general treatment of the potentiometric titrations, BSTAC [35], the NYTIT [36] version of LETAGROP program [32], STACO [37], HYPERQUAD (S. Sammartano, personal communication, 1995). None of these are valid in this case because they do not consider the distribution equilibria between species with equal stoichiometry and in the same phase.

In order to avoid that problem a multipurpose regression program was used to fit the parameters of Eq. (9). The program used was NLREG (Nonlinear Regression Analysis Program) [38], which minimizes the square sum of absolute error in Z values:

$$W = \sum (Z_{exp} - Z_{cal})^2 \quad (13)$$

where Z_{cal} is defined as in Eq. (9). From the fit at each ionic strength it is possible to determine the best values of ${}^{I}\beta$ and ${}^{I}K_r$. The values of the graphical and numerical treatments are collected in Table 1.

From these results it was observed that the distribution constant (K_r) decreases with increasing I values, reaching to very low values almost close to the experimental uncertainty of Z values, at 3.0 mol dm^{-3}. This means that the formation curves reach Z values closer to one with increasing ionic strength . This fact can also be observed in the distribution diagrams at 0.1 and 3.0 mol

Table 1
Values of the protonation and distribution constant for D-gluconic-δ-lactone acid at different ionic strengths in $NaClO_4$

I (mol dm^{-3})	Graphical method		Numerical method	
	Log β	Log K_r	Log $\beta \pm 3\sigma$	Log K_r $\pm 3\sigma$
0.1	3.70	−0.91	3.70 ± 0.01	−0.91 ± 0.06
0.5	3.59	−0.93	3.60 ± 0.02	−0.93 ± 0.10
1.0	3.60	−1.09	3.63 ± 0.01	−1.15 ± 0.06
2.0	3.71	−1.44	3.71 ± 0.02	−1.35 ± 0.12
3.0	3.84	−1.92	3.85 ± 0.01	−1.90 ± 0.33

dm^{-3} represented in Fig. 5. This behavior seems to be contradictory with that proposed by Mitchell et al., who concluded that the distribution constants between the gluconic acid and its lactone forms were independent of the ionic strength [15]. However, the ionic strength range employed by these authors was $0.1 \leq I \leq 0.4$ mol dm^{-3} and in those conditions the variation of the K_r values can be considered negligible as can be seen from the data collected in Table 1.

Some works have been found in the literature, in which the protolysis and the distribution constants have been calculated [15,16,28]. However the ionic media and strengths, if stated, were different, so in the best case it was possible to estimate the stoichimetric values of the constants in the $NaClO_4$ media. Generally speaking, the values given by Pocker and Green [16] in NaCl 0.5 mol dm^{-3} are very similar to the values proposed in this paper.

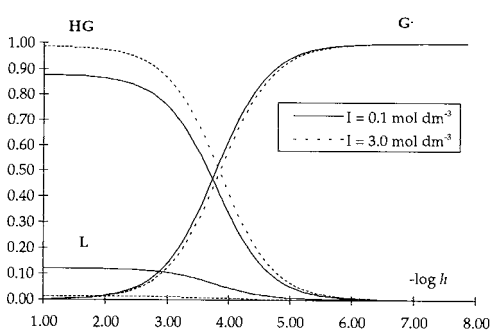

Fig. 5. Distribution diagram of D-gluconic-δ-lactone acid for $I = 0.1$ and 3.0 mol dm^{-3} $NaClO_4$.

As was stressed in the introduction, one of the main aims of this paper was the development of a thermodynamic model for the protolytic equilibria of D-gluconic-δ-lactone acid. This model has been developed computing the activity coefficients of the different species by means of the Modified Bromley Methodology (MBM) [33,39] which has been successfully used to explain this kind of equilibria in other chemical systems [29,40–42].

If the activities of all the species are taken into account, Eq. (6) and Eq. (7) can be rewritten as follows:

$$\beta^0 = \frac{\{HG\}}{\{H^+\}\{G^-\}} = {}^I\beta \frac{\gamma_{HG}}{\gamma_{H^+}\gamma_{G^-}} \quad (14)$$

$$K_r^0 = \frac{\{L\}}{\{HG\}} = {}^IK_r \frac{\gamma_L}{\gamma_{HG}} \quad (15)$$

where β^0 and K_r^0 are the thermodynamic constants (or the infinite dilution constants) and γ denotes the activity coefficient in molar scale. According to the MBM [33] the dependence of the protolysis and the distribution equilibria with the ionic strength can be expressed as follows:

$$\log {}^I\beta = \log \beta^0 + 2D + \left(\frac{(0.06 + 0.6B_{H^+,ClO_4^-})}{(1+1.5I)^2} + B_{H^+,ClO_4^-}\right)I + \left(\frac{(0.06 + 0.6B_{G^-,Na^+})}{(1+1.5I)^2} + B_{G^-,Na^+}\right)I - S_{HG,NaClO_4}I \quad (16)$$

$$\log {}^IK_r = \log K_r^0 + (S_{L,NaClO_4} - S_{HG,NaClO_4})I \quad (17)$$

where $D = -0.511I^{1/2}/(1+I^{1/2})$ dm$^{3/2}$ mol$^{-1/2}$, $B_{H^+,ClO_4^-} = 0.182$ dm^3 mol^{-1} [33], I is the ionic strength and S is the salt coefficient of a neutral species in a molar scale [43]. From these two equations and using all the formation constants

Table 2
Thermodynamic constants and interaction parameters for the D-gluconic-δ-lactone acid[a]

Log β^0	3.92 ± 0.10
Log K_r^0	-0.81 ± 0.09
$B_{G-,Na+}$	-0.23 ± 0.09
$S_{HG,NaClO_4}$	-0.24 ± 0.06
$S_{L,NaClO_4}$	0.11 ± 0.09

[a] Standard deviation is given as $\pm 3\sigma$.

experimentally determined, the values of the thermodynamic constants, interaction parameters and salt coefficients can be calculated. This calculation was carried out making use of the Excel spreadsheet [44] and the NLREG program [38].

As can be seen in Eq. (17), the distribution constant shows a linear dependence with the ionic strength. Therefore, both salt coefficients can not be determined simultaneously due to the high covariance even if both Eq. (16) and Eq. (17) are used together. If both equations are used separately, from Eq. (17) only their difference can be estimated instead of their salt coefficients. From the value of $S_{HG,NaClO_4}$, estimated from Eq. (16) and the difference it is possible to calculate the value of $S_{L,NaClO_4}$ without the covariance. The values of the thermodynamic constants and interaction parameters are shown in Table 2. In Fig. 6 and Fig. 7 the good fit of the experimental data and the theoretical curves are shown.

Once the values of the thermodynamic constants and interaction parameters are known it is possible to estimate the values of the stoichiometric constants in any other ionic strength and in some cases in other ionic media as well. This is due to the relationships that the interaction parameters show with the charge and ionic radii of the ions [39].

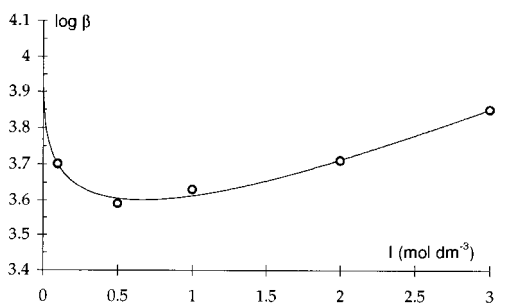

Fig. 6. Values of log β as a function of the ionic strength. (○) experimental, (——) theoretic using Eq. (16) and the values collected in Table 2.

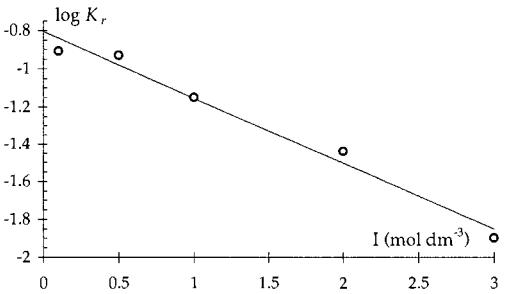

Fig. 7. Values of log K_r as a function of ionic strength. (○) experimental, (——) theoretic using Eq. (17) and the values collected in Table 2.

The thermodynamical model of the protonation and distribution of D-gluconic-δ-lactone acid, together with the complexation of this ligand with Ni(II) (R. Castaño, unpublished data) and the systems already studied [29,40] are actually being used to develop a thermodynamical model of Ni(II) in an electrochemical plating solution.

Acknowledgements

Rosario Castaño wishes to thank the scholarship granted to her by the Basque Government. This work was financially supported by the Basque Government through the project no. PGV 9230.

References

[1] R.L. Bassett, D.C. Melchior, Chemical Modeling of Aqueous Systems II, (ACS Symposium Series No. 416), American Chemical Society, Washington DC, 1990.
[2] M.L. Apel, J. Bridges, M.F. Szabo, S.H. Ambekar, in: J.W. Patterson, R. Passino (Eds.), Metals Speciation and Recovery, vol. 2, Lewis, MI, 1990, p. 516.
[3] J.M. Madariaga, in: H. Hendstrom, H. Skrog (Eds.), Advances in Recycling Technologies, vol. 2, Hutchis, Copenhagen, 1993.

[4] IUPAC, Dissociation Constants of Organic Acids in Aqueous Solution, (reprinted from Pure Appl. Chem. 1 (2–3)), Butterworth, London, 1961.
[5] D.D. Perrin, Dissociation Constants of Organic Bases in Aqueous Solution, IUPAC, Butterworth, London, 1965.
[6] E.P. Serjeant, B. Dempsey, Ionisation Constants of Organic Acids in Aqueous Solution, (IUPAC Chemical Data Series No. 23), Pergamon, Oxford, 1979.
[7] K.S. Pitzer, Activity Coefficients in Electrolyte Solutions, 2nd ed., CRC Press, Boca Raton, FL, 1991.
[8] D.T. Sawyer, Chem. Rev. 64 (1964) 633.
[9] B. Srinivasan, Plat. Surf. Finish. 57 (1984).
[10] H.C. Brown, J.H. Brewster, H. Shecter, J. Am. Chem. Soc. 76 (1954) 467.
[11] F. Shafizadeh, Adv. Carbohydr. Chem. 13 (1958) 10.
[12] C.R. Nelson, Carbohydr. Res. 68 (1979) 55.
[13] M.A. Jermyn, Biochim. Biophys. Acta 37 (1960) 78.
[14] T. Takahashi, M. Mitsumoto, Nature 199 (1963) 765.
[15] R.E. Mitchell, F.R. Duke, Ann. New York Acad. Sci. 172 (1970) 129.
[16] Y. Pocker, E. Green, J. Am. Chem. Soc. 95 (1) (1973) 113.
[17] K. Shimahara, T. Takahashi, Biochim. Biophys. Acta 201 (1970) 410.
[18] IUPAC, Stability Constants Database, 2nd Release, Academic Software, UK, 1993.
[19] R.K. Cannan, A. Kibrick, J. Am. Chem. Soc. 60 (1938) 2314.
[20] F. Coccioli, M. Vicedomini, J. Inorg. Nucl. Chem. 40 (1978) 2103.
[21] R.J. Motekaitis, A.E. Martell, Inorg. Chem. 23 (1984) 18.
[22] Y.D. Fridman, N.V. Dolgashova, G.A. Rustemova, Russ. J. Inorg. Chem. 26 (10) (1981) 1485.
[23] K. Blomqvist, E.R. Still, Anal. Chem. 57 (1985) 749.
[24] T.N. Maksin, B.Z. Zmbova, D.S. Veselinovic, J. Serb. Chem. Soc. 56 (1991) 337.
[25] G.M. Escandar, L.F. Sala, Can. J. Chem. 70 (1992) 2053.
[26] G.H. Jeffery, J. Basset, J. Mendham, R.C. Denney, Vogel's Textbook of Quantitative Chemical Analysis, Longman, London, 1989.
[27] R. Cazallas, M.J. Citores, N. Etxebarria, L.A. Fernández, J.M. Madariaga, Talanta 41 (1994) 1637.
[28] D.T. Sawyer, J.B. Bagger, J. Am. Chem. Soc. 81 (1959) 5302.
[29] A. Lopategi, R. Castaño, N. Etxebarria, J.M. Madariaga, J. Chem. Soc., Dalton Trans., (1995) 3843.
[30] G. Gran, Analyst 77 (1952) 661.
[31] J.L. Fonseca, Bs.C Thesis, University of the Basque Country, Bilbao, Spain, 1989.
[32] N. Ingri, L.G. Sillén, Acta Chem. Scand. 16 (1962) 173.
[33] G. Borge, R. Castaño, M.P. Carril, M.S. Corbillón, J.M. Madariaga, Fluid Phase Equilibria 121 (1996) 85.
[34] F.J.C. Rossotti, H. Rossotti, The Determination of Stability Constants, McGraw-Hill, New York, 1961.
[35] C. De Stefano, P. Mineo, C. Rigano, S. Sammartano, Ann. Chim. 83 (1993) 243.
[36] P. Browner, L.G. Sillén, R. Whitaker, Ark. Kemi. 31 (1969) 365.
[37] P. Gans, A. Sabatini, Hyperquad, Protonic Software, 1992.
[38] P.H. Sherrod, NLREG-Nonlinear Regression Analysis Program, Nashville, TN, 1995.
[39] G. Borge, N. Etxebarria, L.A. Fernández, M.A. Olazabal, J.M. Madariaga, Fluid Phase Equilibria 121 (1996) 99.
[40] R. Castaño, N. Etxebarria, J.M. Madariaga, J. Chem. Soc., Dalton Trans., (1994) 2729.
[41] A. Rios, G. Arana, N. Etxebarria, L.A. Fernández, Talanta 43 (1996) 11.
[42] R. Gil, M.S. Corbillón, M.A. Olazabal, J.M. Madariaga, Talanta 44 (1997) 891.
[43] F.A. Long, W.F. McDevit, Chem Rev. 51 (1952) 119.
[44] Excel 4.0, Microsoft Corporation, Redmound, WA, 1992.

.

ELSEVIER

Talanta 45 (1998) 1015–1021

Talanta

Enzymatic methods for the determination of α-glycerophosphate and α-glycerophosphate oxidase with an automated FIA system

Efstratios R. Kiranas, Miltiades I. Karayannis, Stella M. Tzouwara-Karayanni *

Department of Chemistry, University of Ioannina, Ioannina 45110, Greece

Received 23 April 1997; received in revised form 7 July 1997; accepted 7 July 1997

Abstract

A procedure for the enzymatic determination of α-glycerophosphate (α-GP) has been developed, using an automated in-house FIA system, with immobilized glycerol-3-phosphate oxidase (GPO) on non-porous glass beads, following optimization of the immobilization and analytical parameters. Fabricated single bead string reactors (SBSR) were used in connection with the FIA system, following optimization of its parameters. The half-life of GPO-SBSR regarding reduction of the enzyme activity was found to be 110 days for its use in 20 triplicate measurements daily and storage at 4°C in the appropriate buffer. The regression equation of the calibration graph for the determination of α-GP was: $A_{max} = (10 \pm 2) \times 10^{-4} + (22\,134 \pm 12) \times 10^{-4}$ (mmol l^{-1} α-GP). The lower limit of quantitation was 0.74 μmol l^{-1} α-GP and the RSD of the method 0.05% ($r = 0.9999$). The same FIA system and procedure can be also used for the determination of the GPO activity, with the α-GP as substrate. The regression equation for this calibration graph was: $A_{max} = (23 \pm 18) \times 10^{-4} + (190 \pm 1) \times 10^{-4}$ (μg ml^{-1} GPO), the lower limit of quantitation was 0.782×10^{-3} mg ml^{-1} (0.782 ppm) GPO and the RSD of the method 0.53% ($r = 0.9999$). Serum samples obtained from hospitalized patients were deproteinized by gel filtration and analyzed under pseudo-first order conditions, at various concentrations of α-GP. A kinetic study of the reduction of α-GP in serum versus time is given and an observed reaction rate constant $k_{ob} = 106.5 \times 10^{-4}$ min^{-1} was determined. © 1998 Elsevier Science B.V.

Keywords: Glycerol-3-phosphate oxidase; Peroxidase; α-Glycerophosphate; Immobilization; FIA

1. Introduction

Glycerol-3-phosphate oxidase (GPO; EC 1.1.3.21) from *Aerococcus viridans*, catalyzes the oxidation of α-glycerophosphate (α-GP) to dihydroxyacetone phosphate, according to the reaction:

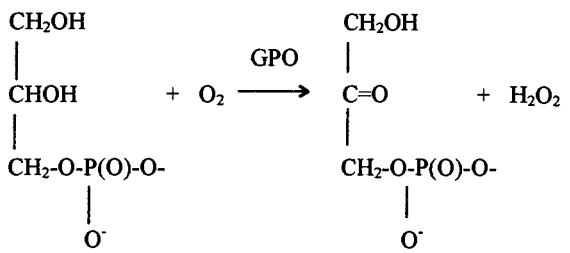

GPO does not appear in human's body. GPO from microorganisms was used for α-GP determi-

* Corresponding author.

PII S0039-9140(97)00210-5

nation in amniotic fluid [1], Mg in serum [2], serum triglycerides [3,4] and glycerol in wines [5].

α-GP is also an intermediate metabolite in a number of major metabolic pathways, as the anabolic and catabolic pathways of lipids. Its generation in mitochondria of diabetic rats [6] and in animal lenses due to 'sugar' cataracts [7], is apparently related to the activation of different pathways. A large-scale synthesis of α-GP has been developed using immobilized alkaline phosphatase [8]. It is usually determined spectrophotometrically or fluorometrically in conventional batch experiments [9,10]. So, it is important to develop a fast, reproducible and reliable procedure for the analytical determinations of this metabolite, useful in bioanalytical laboratories or during its biotechnological production in industries.

In the present work, GPO was immobilized on non-porous glass beads, following optimization of the immobilization conditions. Teflon tubing was filled with the non-porous glass beads to fabricate Single Bead String Reactors (SBSR), which were linked to a home-made FIA-system, for the determinations of α-GP in synthetic and real samples (human serum), following optimization of its parameters. The method is based on the enzymic oxidation of α-GP and the determination of the H_2O_2 generated by Trinder's reagent measuring the absorbance at 510 nm [14]. The stability of the SBSR with the immobilized GPO has been also investigated. A manifold of an automated FIA set-up for the determination of soluble GPO, has also been elaborated.

2. Experimental procedures

2.1. Reagents

All chemicals were of analytical-reagent grade.

2.1.1. Tris–HCl buffer solutions, 0.05 mol l^{-1}, (pH 7.0–9.0)

Prepared by mixing in a 100 ml calibrated flask 50 ml of 100 mmol l^{-1} tris(hydroxymethyl)-methylamine (tris; Sigma), the appropriate volumes of 100 mmol l^{-1} HCl and diluting to volume with water.

2.1.2. Reagent (R)

In a 10 ml calibrated flask dissolve 0.8 mg horseradish Peroxidase (PO; EC 1.11.1.7; 250 U mg^{-1} solid with Pyrogallol as substrate; Sigma, St. Louis, MO), 1 ml of 10 mmol l^{-1} 4-aminoantipyrine (AAP; Sigma) and 1 ml of 10 mmol l^{-1} 3,5-dichloro-2-hydroxyphenyl sulfonic acid (DCPS; Sigma) in Tris–HCl 50 mmol l^{-1} buffer (pH 7.0) and dilute to volume.

2.1.3. Reagent R_1

Weigh 3.704 mg α-GP (di-monocyclohexylammonium salt; approx. 95%; FW 370.4 Da; Sigma) into a 10 ml calibrated flask and dilute to volume with Tris–HCl buffer (pH 7.8).

2.1.4. Standard GPO solution 0.03 mg ml^{-1}

It was prepared by weighing 1.50 mg GPO from *A. viridans* (70% protein; 120 U mg^{-1} solid; Sigma) into a 50 ml calibrated flask and diluting to volume with Tris–HCl buffer (pH 7.8).

2.1.5. Human serum

The pre-analysed human serum samples from patients were obtained fresh from the University of Ioannina Hospital and were kept under freezing conditions. Deproteinization of the samples was necessary due to the low diffusion velocities and the Tyndall effect of protein macromolecules, which resulted in high blanks and double-peak shapes during the flow injection (FI) measurements.

2.1.6. SBSR

The non-porous glass beads were 0.5 mm in diameter (Proper Mfg, New York, NY). After the immobilization of GPO on these surfaces, the glass beads were inserted into the teflon reactor tubes (0.8 mm i.d.; Gilson) by suction with a glass syringe. The SBSR's were filled with the buffer of immobilization and stored in a refrigerator (4°C), when not in use. A reactor containing untreated glass beads, was fabricated in a similar way to the enzyme reactors (plain reactor). Its function was to control the completion of the reaction and improve the value of the dispersion coefficient. The detailed description of the immobilization procedure is described below.

2.2. Apparatus

The FIA measurements were performed with an automated in-house built unit, consisting of an eight-channel peristaltic pump (Ismatec, IPN/S), a four-way pneumatic rotary-injection valve (Rheodyne, type 50 Teflon), and a filter spectrophotometer (miniature continuous flow analyzer [11]) with a 2.0 μl microcell, equipped with an optical fibre.

The unit also included a series of 2 SBSRs: one 5 cm long bearing glass beads with immobilized GPO and a second 40 cm bearing plain beads. The first SBSR was replaced by a 15 cm plain reactor when measuring soluble GPO. An interface unit RTI-800/815 multi-function input-output board was used for the collection of data points and for the activation of the injection valve, by an IBM-compatible PC. The experimental set-up is shown in Fig. 1.

2.3. Procedures

2.3.1. Immobilization

The procedure for the immobilization of GPO was the same as elsewhere described [12] and improved [13]. The optimum time for glutaraldehyde attachments was a 1 h period at room temperature, followed by additional 24 h period at 4°C. The maximum efficiency of immobilization was found at pH 7.3, with optimum soluble GPO

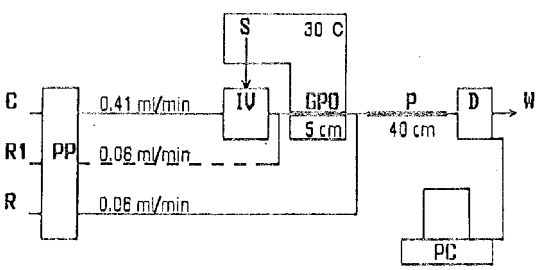

Fig. 1. Experimental set-up and FIA manifold. PP, peristaltic pump; W, waste; IV, injection valve; GPO, SBSR with immobilized GPO; D, detector; P, SBSR with plain beads; PC, personal computer; C, carrier (Tris–HCl 50 mmol l^{-1}); S, sample (α-GP or GPO in Tris–HCl 50 mmol l^{-1}); *R*, reagent (AAP + DCPS + PO in Tris–HCl 50 mmol l^{-1}, pH 7.0); *R*1, reagent 1 (α-GP 30 mmol l^{-1} in Tris–HCl 50 mmol l^{-1}, pH 7.8).

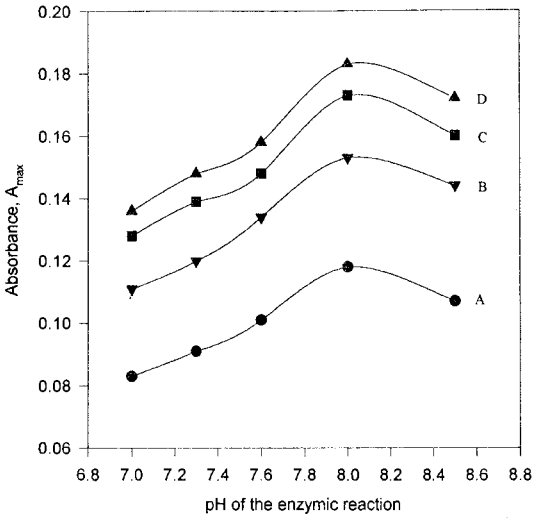

Fig. 2. Dependence of the efficiency of the enzymic system 'Immobilized GPO-soluble PO', from the pH, at varius concentrations of α-GP: $A = 0.010$ mmol l^{-1}, $B = 0.020$ mmol l^{-1}, $C = 0.030$ mmol l^{-1} and $D = 0.040$ mmol l^{-1} α-GP.

concentration corresponding to 0.75 mg per gram of glass beads. The beads were then transferred in the enzyme solution and remained for 24 h at 4°C in order to achieve the highest efficiency for immobilisation.

2.3.2. Deproteinization of serum samples

A Sephadex G-25 superfine column (Pharmacia; Uppsala; Sweden) was used for the deproteinization of the serum samples. The dimensions of the column were 1.5 cm i.d. and 4.8 cm in length. The fractionation range for peptides and globular proteins was 1000–5000 Da. Each serum sample (400 μl) with 1.5 mmol l^{-1} added α-GP was applied to the column and elution effected with 8 ml of Tris–HCl buffer 50 mmol l^{-1} (pH 8.1). Determination of α-GP in the eluate fractions showed that 100% of the analyte appeared between 2.5 and 6.5 ml of the elution volume. This procedure guarantees an almost undetectable absorbance blank (0.0005–0.0020 A) during the FI measurements.

2.3.3. Measurements

Each run starts automatically by initiating the injection valve with the PC. The standard sample

S (α-GP in Tris–HCl buffer, pH 8.1) or the unknown sample (30 μl) is injected into the carrier *C* stream (Tris–HCl buffer, pH 8.1) and proceeds through the GPO reactor, where the α-GP is oxidized to dihydroxyacetone phosphate while H_2O_2 is produced. At the output of this reactor the Trinder's reagent *R* merges with the new mixture, then proceeds through the plain *P* reactor and finally reaches the cell of the spectrophotometer *D*, where absorbance against time is recorded at 510 nm and the peak maximum A_{max}, marked [14].

In the case of soluble GPO determination, GPO solutions (in Tris–HCl buffer pH 7.8; 30 μl) are injected as sample S into the carrier stream *C* and the Reagent R_1 meets the sample at the output of the valve. The mixture proceeds through the first plain reactor GPO (10 cm length) and then the procedure continues as in the case of immobilized GPO.

3. Results and discussion

3.1. Optimum parameters and specifications of the FIA-system

The optimum operational conditions of FIA mode with the immobilized GPO were the following: A 'sample loop' of 30 μl ensures analytically acceptable values of A_{max} and economy in the use of the reagents for a single run. The optimum lengths of the SBS-Reactors are 5 cm for GPO in the case of immobilized enzyme (10 cm in the case of soluble GPO determinations) and 40 cm for *P* reactor.

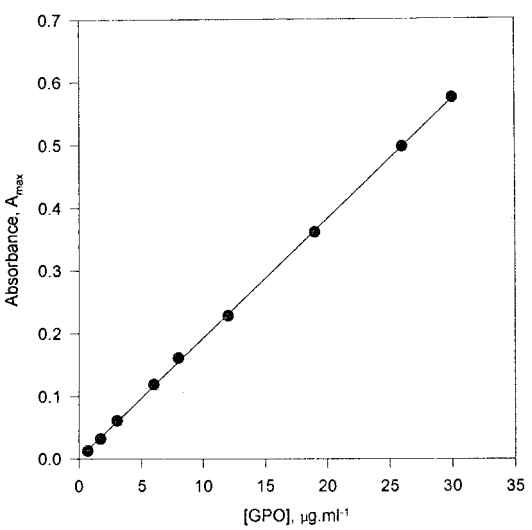

Fig. 3. Calibration graph for the determination or soluble GPO, using α-GP as substrate.

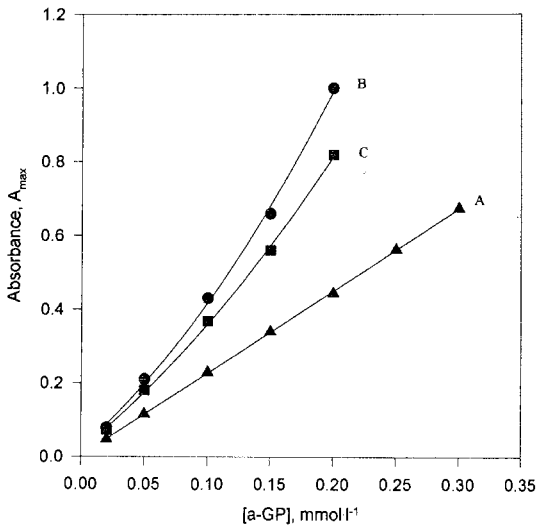

Fig. 4. Calibration graphs for α-GP determination using GPO SBSR of different lengths: A = 5 cm, B = 10 cm and C = 20 cm.

The optimum flow rates in the FI manifold were: 0.41 ml min^{-1} and 0.06 ml min^{-1} for the carrier *C* and reagent *R*, respectively. The optimum flow rate of the α-GP reagent (R_1) in the FIA mode for the determination of GPO activity was 0.06 ml min^{-1}.

The dispersion coefficient ($D = A_0/A_{max}$) of both FIA modes were determined by applying the Ruzicka-Hansen empirical method [15], which is based on the absorbance measurements with and without dispersion of alizarin red solution at 510 nm. The values $D = 5.4$ and 4.6 for soluble GPO and α-GP determinations respectively were found. The corresponding FIA systems allows the performance of 80 and 84 measurements per h. Univariable optimization procedure was used for this study.

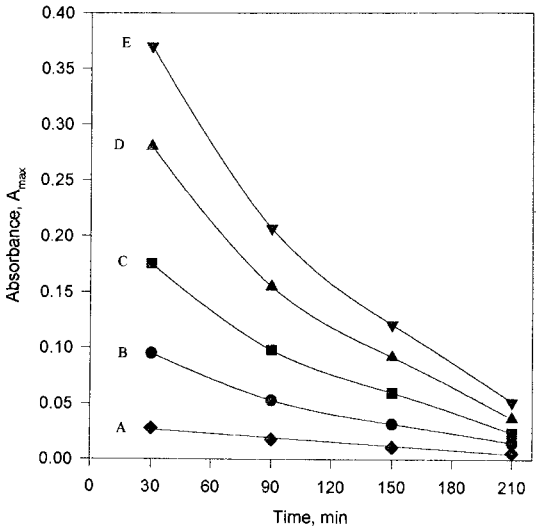

Fig. 5. Reaction curves for the destruction of α-GP in serum, for five different initial concentrations. A = 0.016 mmol l^{-1}, B = 0.060 mmol l^{-1}, C = 0.108 mmol l^{-1}, D = 0.170 mmol l^{-1} and E = 0.230 mmol l^{-1} α-GP.

3.2. Optimum pH values for the enzymic reactions

The optimum pH values for the enzymic system immobilized GPO-soluble PO, are in the range 7.9–8.3, as shown in Fig. 2. The measurements were performed in Tris–HCl buffer of pH 8.1. The optimum pH value in the case of the enzymic system soluble GPO-soluble PO was found to be 7.8.

3.3. Optimum temperature for the enzymic reactions

In both cases the optimum temperature of the enzymic systems was 30°C. Higher or lower values showed a negative influence on the activity of both enzymic systems.

3.4. Half-life ($t_{1/2}$) of the GPO reactor

The experiments for the half-life determination of the GPO reactor were performed every day, with about twenty measurements per day. After daily use the SBSR was filled with Tris–HCl buffer (pH 7.3) and stored in a refrigerator at 4°C. The half-life of the reactor was 110 days, time which allows 2200 measurements, without change of the linear dynamic range of the working curve. The amount of GPO which was immobilized on the SBSR allows only 21 measurements of the substrate in conventional batch experiments.

3.5. Determination of soluble GPO

The linear dynamic range of the calibration curve for soluble GPO determination, with α-GP at saturation concentration (30 mmol l^{-1}) as substrate was found to be from 1×10^{-3} to 30×10^{-3} mg ml^{-1}, as shown in Fig. 3. The regression equation of this straight line was:

$$A_{max} = (23 \pm 18) \times 10^{-4} + (190 \pm 1) \times 10^{-7}\ [\text{mg ml}^{-1}\ \text{GPO}], \quad (r = 0.9999) \tag{1}$$

The lower limit of quantitation was found to be 0.782×10^{-3} mg ml^{-1} GPO and the accuracy of the method, RSD = 0.53%, $n = 6$.

Table 1
Experimental and theoretical values of absorbance A_0 and calculated k_{ob} for the kinetics of the destruction of α-GP in serum, at varius concentrations

[α-GP] mmol l^{-1}	k_{ob} (10^{-4} min^{-1})	r	$(A_{max})_0$	
			Experimental	Theoretical
0.016	85 ± 4	0.9974	0.038	0.038
0.060	101 ± 6	0.9964	0.132	0.136
0.108	108 ± 11	0.9902	0.256	0.245
0.170	110 ± 10	0.9918	0.412	0.391
0.230	107 ± 8	0.9943	0.535	0.522

Table 2
Correction factor for times t after sampling

t	5	10	15	20	30	40	60
$(A_{max})_0/(A_{max})_t$	1.06	1.11	1.17	1.24	1.38	1.53	1.89

3.6. Determination of α-GP

Fig. 4 shows the calibration graphs for the determination of α-GP with different lengths of reactors bearing immobilized GPO. A positive deviation from linearity of the working curves was observed, for SBSR lengths greater than 5 cm. This can be attributed to the high concentrations of α-dihydroxyacetone phosphate produced during the oxidation of α-GP. This product probably takes part in the nucleophilic addition reactions with Trinder's reagent (AAP = 4-aminoantipyrine + DCPS = 3,5-dichloro-2-hydroxyphenylsulphonic acid + peroxidase) or with the products of Trinder's reaction:

$$H_2O_2 + AAP + DCPS \xrightarrow{\text{peroxidase}} \text{red dye} + H_2SO_4$$

thus, forming compounds which also absorb at 510 nm. This explanation is strengthened by the observed decrease of the slope in the calibration curve (C) for lengths greater than 10 cm.

The use of a GPO reactor of 5 cm length, provides a large linear range and constant sensitivity. The regression equation of this straight line is:

$$A_{max} = (10 \pm 2) \times 10^{-4} + (22\,134 \pm 12) \times 10^{-4}\ [\text{mmol}\,l^{-1}\alpha - \text{GP}] \quad (2)$$

with correlation coefficient of $r = 0.9999$. The lower limit of quantitation was 0.74×10^{-3} mmol l^{-1} α-GP, and the accuracy of the method RSD = 0.05%.

The proposed procedure offers many significant advantages. It is fast (requiring 43 s including injection and run), very simple (at least in the stage of the measurements), sensitive and accurate.

3.7. Determination of α-GP in human serum

Trying to apply the above mentioned procedure for the determination of α-GP in human serum we noticed a continuous decrease in its concentration probably due to its destruction in the serum environment.

It means that substantial delay of the determination, after sampling of blood, will have an erroneous result. To overcome this drawback and make the appropriate corrections it is necessary to know the rate of the destruction of α-GP in order to extrapolate to the original concentration at the time of sampling. To achieve this the following procedure was followed.

To five different equal portions of the serum from hospitalized patients, known amounts of α-GP were added before deproteinization by gel filtration. Each deproteinized serum sample was diluted about ten times during the procedure to avoid double peaks and high blank values due to physical interferences. The calibration graph of the standard additions method for the serum samples showed a continuous decrease in its slope versus time, although the serum samples were stored in the refrigerator (5°C) after each measurement (Fig. 5). The decrease of α-GP concentration in the serum samples follows the kinetics of a pseudo-first order reaction, which can mathematically be described by the following equation:

$$(A_{max})_t = (A_{max})_0 \cdot e^{-k_{ob} \cdot t} \quad (3)$$

where $(A_{max})_0$ is the absorbance of the original concentration of α-GP in the serum samples and k_{ob} the observed reaction rate constant of the disappearance of α-GP in the serum samples. From the slope of the logarithmic form of the above equation,

$$\ln(A_{max})_t = \ln(A_{max})_0 - k_{ob} \cdot t \quad (4)$$

the observed reaction rate constant k_{ob} may be evaluated.

As shown in Table 1, the calculated values for A_{max} are in good agreement with the theoretical

ones, for the five experiments. The disappearance of α-GP in serum could be explained by its oxidation by serum constituents since its reducing properties are well known. Excluding the value 85×10^{-4} min^{-1} (which refers to a very low concentration of α-GP and is therefore probably affected by high relative experimental error) a mean value of $k_{ob} = 106.5 \times 10^{-4}$ min^{-1} can be calculated from the remaining four k_{ob} values.

In summary the procedure for the determination of α-GP in human serum includes the following steps: (1) sampling at time t_1; (2) preparation of the blood sample to obtain serum; (3) deproteinization and dilution; (4) measurement of (A_{max}) at time t_2; (5) calculation of $(A_{max})_0$ applying Eq. (3) for $t = t_2 - t_1$; and (6) calculation of [α-GP] from the regression Eq. (2).

A 5% error is introduced into the assay of α-GP in human serum if the elapsed time between sampling and measurement of A_{max} is 4.8 min. After 1 h the sample is loosing about 50% of its original concentration.

Table 2 gives the correction factors for delay times (t): 5, 10, 15, 20, 30, 40, 60 min after sampling.

.

References

[1] D.J. Artiss, W.M. McGowan, R.T. Strandberg, E. Epstein, B. Zak, Clin. Chem. 30 (4) (1984) 534–537.
[2] C.M. Wimmer, D.J. Artiss, B. Zak, Clin. Chem. 32 (4) (1986) 629–632.
[3] P. Fossati, L. Prencipe, Clin. Chem. 28 (10) (1982) 2077–2080.
[4] M.Y. Le Dain, R. Ferrat, T. Hartmann, J. Clin. Chem. Clin. Biochem. 26 (11) (1988) 756–757.
[5] R. Puchades, L. Lemieux, E.R. Simard, J. Food Sci. 56 (4) (1991) 1097–1100.
[6] M.-H. Giroix, J. Passchaert, D. Baible, Y. Leclerq-Meyer, A. Sener, B. Portha, J.W. Malaisse, Diabetes 40 (2) (1991) 227–232.
[7] H.M. Cheng, H. Xiong, K. Hirose, Exp. Eye Res. 43 (1989) 281–285.
[8] A. Pradines, A. Klaebe, J. Perie, F. Paul, P. Monsan, Enzyme Microb. Technol. 13 (1991) 19–23.
[9] G.D. Mc CoY, K.A. Doeg, Anal. Biochem. 64 (1975) 115–120.
[10] M.R. Lilley, K.P. Gragame, M.S.R. Ali, Anal. Biochem. 148 (1985) 282–287.
[11] J.C. Patton, S.R. Crouch, Anal. Chim. Acta 179 (1986) 189–201.
[12] C.L.M. Stults, Practical considerations for the use of immobilized enzymes in flow injection analysis, Ph.D. Dissertation, Michigan State Univ., East Lansing, MI, 1987.
[13] R.E. Kiranas, M.S. Tzouwara-Karayanni, M.I. Karayannis, Acta Chim. Hung. 129 (1992) 461–468.
[14] P. Trinder, Ann. Clin. Biochem. 6 (1969) 24–27.
[15] J. Ruzicka, E.H. Hansen, Flow Injection Analysis, 2nd edn., Wiley, New York, 1988, pp. 23–26.

ELSEVIER

Talanta 45 (1998) 1023–1029

Talanta

Short Communication

Microwave assisted reduction of Se^{VI} to Se^{IV} and determination by HG/FI-ICP/MS for inorganic selenium speciation

Riansares Muñoz Olivas, O.F.X. Donard *

Laboratoire de Chimie Bio-Inorganique et Environement, CNRS 132, Université de Pau et des Pays de l'Adour, Pau et des Pays de l'Adour, 64000, Pau, France

Received 12 July 1996; received in revised form 26 May 1997; accepted 29 May 1997

Abstract

Speciation of inorganic selenium using hydride generation method is a widespread analytical method nowadays. However, a reduction step of Se^{VI} to Se^{IV} is necessary as the hydride-forming species is $HSeO_3^-$ (oxydation state + IV). This paper describes the development of a batch assisted microwave system allowing a rapid (< 5 min) conversion of Se^{VI} to Se^{IV}. Hydride generation is performed by a flow injection system and detection by ICP/MS. Detection limits of 6 and 8 pg for Se^{IV} and for Se^{VI} (by using a sample loop of 200 μl) respectively have been achieved. This method has been validated by participating in a European certification exercise for inorganic Se speciation in aqueous solutions. © 1998 Elsevier Science B.V.

Keywords: Selenium speciation; Microwave reduction; ICP/MS

1. Introduction

The toxicity of selenium depends on the chemical form in which this element is present in the environment [1]. It is generally accepted that the inorganic species are more toxic than the organic ones. Inorganic species for selenium identified in the environment are Se^{IV} and Se^{VI}. The development of reliable techniques to determine the different species is necessary. The most common method used to differentiate between the inorganic forms of selenium makes use of hydride generation hyphenated to different atomic spectrometry detectors: AAS, ICP/AES, ICP/MS etc.[2,3]. Hydride generation processes the sample with sodium tetrahydroborate in an acidic medium (usually HCl) in order to obtain the selenium hydride.

The hydride formed will be swept to the detector by a stream of an inert gas. However, selenium hydride can only be formed initially from Se^{IV}. Se^{VI} requires to be reduced to Se^{IV} prior to the formation of the hydride. Several reducing agents have been used to perform this reduction. Boiling HCl solution is the preferred reducing

* Corresponding author.

PII S0039-9140(97)00172-0

media [4–6]. This reduction step has been most often performed in open beakers on a hot plate. This approach led to some losses of Se by evaporation and to a long reaction time required for total reduction of Se^{VI} to Se^{IV} (30–40 min). These problems have recently been overcome by performing an on-line reduction system with a graphite bath at 140°C [7] and by using microwaves assisted sample preparation procedures [8,9].

In this paper, we report a simple approach using an open vessel focused monomode system to report the quick reduction of Se^{VI} to Se^{IV} in an HCl medium. Selenium was then determined by FIA-hydride generation and detection by ICP/MS. This simple method has been validated during the certification exercise of the Measurement and Testing Program (formerly BCR) of the EC on inorganic selenium speciation.

2. Experimental

2.1. Instrumentation

The analytical system used for the determination of the selenium hydride was a Perkin-Elmer FIAS 200 fitted with a gas–liquid separator and coupled to a Perkin-Elmer Model Elan 5000 ICP/MS. The interface between ICP/MS and flow injection manifold was made of Teflon and allowed direct linking between the flow injection manifold to the injector of the ICP/MS. Argon flow rates were controlled by mass flow controllers. Data processing was performed with the ELAN graphics software and the CHROMAFILE software. Quantitation was based on peak area. Three Se isotopes (^{77}Se, ^{78}Se, ^{82}Se) were simultaneously monitored to evaluate possible isobaric interferences. The isotope ^{78}Se provided best signal to noise ratio. Then it has been selected for data presentation in the Figs. 1–4. Operational routine conditions have been fully described elsewhere [10].

An open focused monomode microwave oven Microdigest A-301 (2450 MHz, maximum power 200 W) (Prolabo, France) was used for the microwave reduction of Se^{VI} to Se^{IV}. With this system, the sample is placed in the wave-guide were microwave energy is focused with maximum intensity.

The microwave power delivered by the magnetron is very reproducible and is controlled by a TX32 programmer. This control allows power to be incremented from 20 to 200 W by steps of 10 W. The time of exposure of the sample can be set by steps of 1 min. The samples are placed in 50 ml open vessels system made of borosilicate glass. A refluxing unit on top of the sample holder prevents possible losses of the analytes by volatilisation.

The temperature of the sample is continuously measured by a Megal 500 thermometer (Prolabo, France) introduced in the sample solution. This thermometer is connected to a microcomputer which can continuously record the temperature evolution of the sample when submitted to the microwave field.

Advantages presented by this open focused microwave system included: (i) the use of small quantities of reagent; (ii) the use of a refluxing unit minimising the loss of volatile species formed during the reduction step; (iii) the high power energy focused and delivered to the sample; and (iv) the quality and reproducibility of the energy delivered to the sample. All of the above reasons translate into considerable decreases in the sample preparation time.

2.2. Reagents

All reagents used were of highest purity grade. Stock solutions of Se^{IV} and Se^{VI} at 100 mg l^{-1} concentration level were prepared by dissolving appropriate amounts of SeO_3Na_2 and SeO_4Na_2 (Aldrich $>99\%$) and weakly acidified with HCl acid (pH 2). These solutions were stored in glass bottles at 4°C in the dark. Working solutions were prepared daily by dilution of the 100 mg l^{-1} stock solutions.

Hydrochloric acid (Suprapur grade from Merck) was used as carrier solution to facilitate hydride generation and as reducing agent for Se^{VI}.

Sodium borohydride solutions of 2 g l^{-1} $NaBH_4$ (Fluka min. 97%) were prepared daily and were stabilised by addition of 0.5 g l^{-1} of NaOH (Prolabo min. 97%) to prevent a possible reagent decomposition by hydration.

2.3. Analytical procedure

2.3.1. Determination of Se^{IV}

It was performed by forming the volatile hydride by reaction with $NaBH_4$ with a flow injection/hydride generation device and detected by ICP/MS. The optimisation of the hydride generation by flow injection has been described in detail [10]. Optimal operating conditions are summarised in Table 1.

2.3.2. Determination of total inorganic Se

A solution containing the two inorganic species was mixed with HCl for a final volume of 10 ml and heated in the microwave oven to convert all Se^{VI} present into the reduced Se^{IV} form. The selenium hydride is then generated in the flow injection/hydride generation unit and detected by ICP/MS. Se^{VI} concentrations correspond to the difference obtained between the total Se and Se^{IV} fractions. A scheme of the speciation procedure is shown in Fig. 1. After microwave reduction of the sample, the solution is cooled at room temperature prior to hydride generation in order to avoid any bias via temperature effects during the hydride generation procedure [11].

Table 1
Optimal operating conditions for speciation of Se^{VI} and Se^{IV}

FIA/HG	Sample loop volume	200 µl
	Reagent flow rate	
	HCl	10 ml min^{-1}
	$NaBH_4$	6 ml min^{-1}
	Sample	3 ml min^{-1}
	Reagent concentration	
	HCl	1.3 mol l^{-1}
	$NaBH_4$	2 g l^{-1} +0.5 g l^{-1} NaOH
MW	Reaction time	2 min
	Power setting	140 W
	HCl concentration	6 mol l^{-1}
ICP/MS	Power supply	1100 W
	Gas flow rate	
	Plasma	15 l min^{-1}
	Auxiliary	0.80 l min^{-1}
	Nebulization	1.10 l min^{-1}
	Acquisition parameters	
	Dwell time	35 ms
	Sweeps	2
	Readings	130
	Replicates	3
	Scan mode	Peak hopping

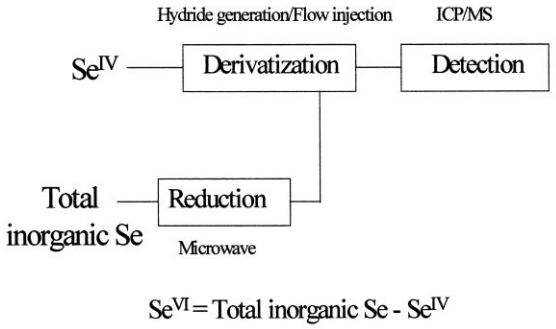

Fig. 1. Scheme of the speciation procedure between Se^{VI} and Se^{IV}.

3. Results and discussion

3.1. Influence of HCL concentration

The reaction occurring can be written as follows:

$$HSeO_4^- + 3H^+ + 2Cl^- \rightarrow H_2SeO_3 + Cl_2 + H_2O$$

Previous works [4–6] have established the optimum HCl concentration for a quantitative reduction of Se^{VI} to Se^{IV} in the 5–6 mol l^{-1} range. The high concentration of H^+ and Cl^- with the 5–6 mol l^{-1} solutions combined to the low concentration of Cl_2, (most of the chlorine formed is lost by evaporation) will shift the reaction to the right. A concentration of 6 mol l^{-1} allows a recovery of 100% of the analyte. This concentration was retained and further used in our microwave reduction procedure.

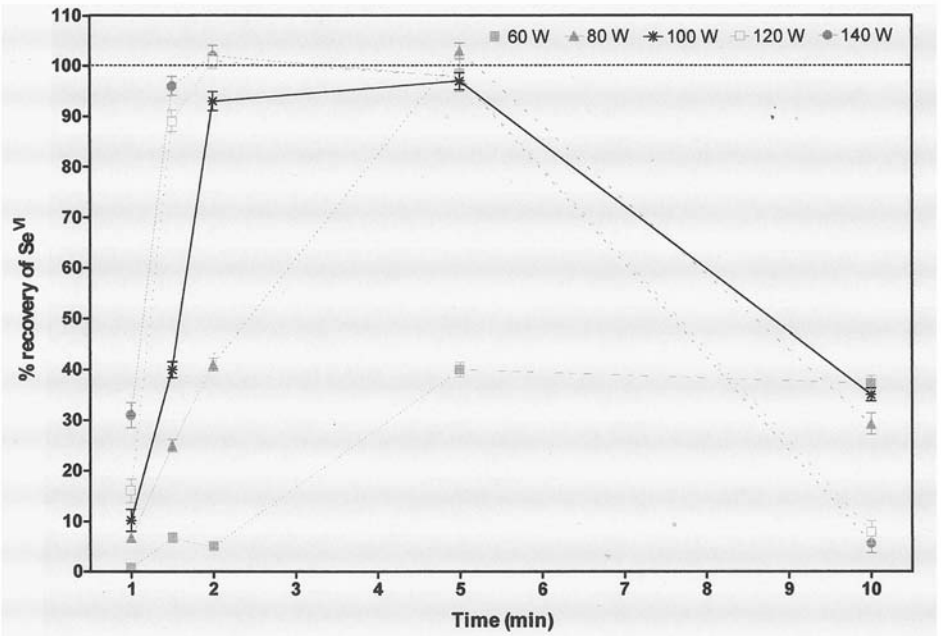

Fig. 2. Se^{VI} recovery obtained in a focused microwave device (Working concentration 1 μg l^{-1} as Se content; HCl concentration 6 mol l^{-1}).

3.2. Influence of the reaction time and power applied in the microwave device

Parameters studied during the microwaves assisted reduction of selenium were the reaction time (from 1 to 10 min) and the power delivered (ranging from 60 to 140 W). All these parameters were studied for a fixed HCl solution of 6 mol l^{-1}. The results obtained expressed as yield of the conversion of a 1 μg l^{-1} Se^{VI} to Se^{IV} with respect to the reaction time and for different power settings are presented in Fig. 2. Recoveries obtained for the reduction of Se^{VI} appear to be strongly dependent on both the time and the power applied. If severe difference between the kinetics of conversion is obtained for 60 and 80 W power applied thus resulting in slow conversion of Se^{VI} to Se^{IV}, very rapid conversion rates can be observed for 100–140 W power applied. In this case the reaction is completed within <2 min. Reaction times higher than 5 min presented poor recoveries due to losses of the analytes by evaporation of the solution; by volatilisation of selenium chloride formed during the reaction; or by back-oxidation of the Se^{IV} by free chlorine formed as secondary product during the reduction [9]. The best compromise between the irradiation time and the power setting applied to achieve a quantitative reduction retained for further routine work was performed in a 6 mol l^{-1} HCl reduction media irradiated for 2 min with a 120–140 W power setting.

Fig. 3 gives the temperature rise recorded during the reducing kinetics obtained under the microwave field. The initial temperature slopes at $t=0$ are quite similar for the three higher power settings (100 W, 120 W, 140 W). This fact may translate the rapid absorption rate of the reaction media for these three high power settings (heating is very fast and reaches 118°C within <2 min). The temperature then remains stable over time. The temperature rises above the boiling point of the azeotropic solution. The highest temperature reached in our experiments was close to 120°C and was then 10°C higher than the normal boiling point of this azeotrope (109°C). This effect is not

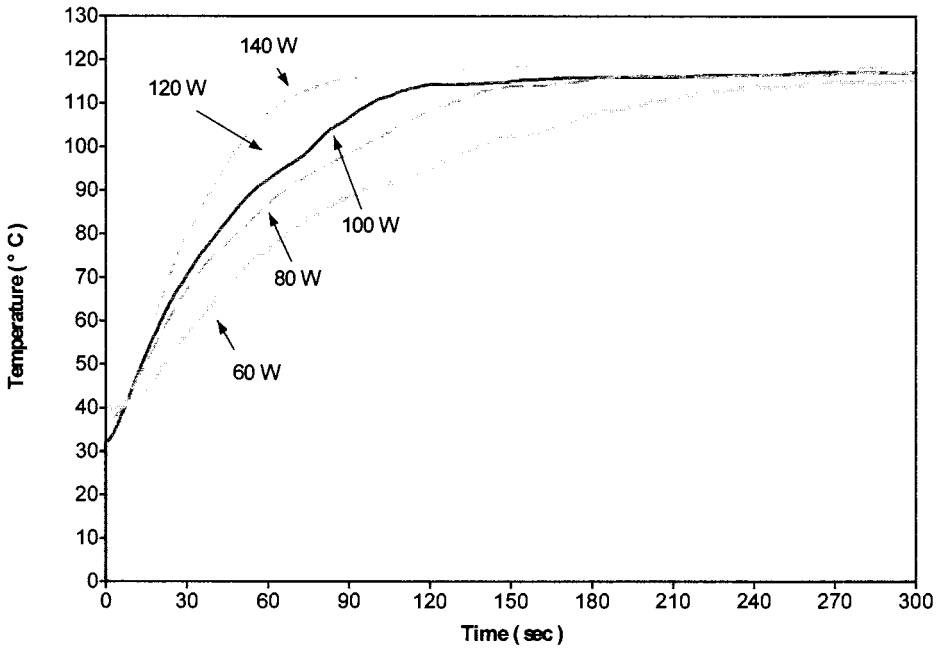

Fig. 3. Temperature curve in function of heating time in a focused microwave device (Working concentration 1 μg l^{-1} Se^{VI}; HCl concentration 6 mol l^{-1}).

unusual under microwave irradiation since superheating can be observed in samples submitted to microwave irradiation.

3.3. Analytical performances and validation of the method

The best compromise between the irradiation time and the power setting applied to achieve a quantitative reduction retained for further routine work was performed in a 6 mol l^{-1} HCl reduction media irradiated for 2 min with a 120 W power setting.

The resulting transient signal obtained in our HG/FI-ICP/MS system for a solution of 1 μg l^{-1} of Se^{IV} and Se^{VI} after microwave treatment is presented in Fig. 4. A quantitative yield for the reduction of Se^{VI} to Se^{IV} and very good repeatability and precision were obtained for the two Se species under our working conditions. Under these experimental conditions, the precision obtained expressed as the relative deviation of five replicates was 3.0% for Se^{IV} and 3.2% for Se^{VI}. Overall detection limits obtained then were 6 pg for Se^{IV} and 8 pg for Se^{VI} for a FIA sample loop of 200 μl.

This method was validated in an intercalibration exercise for the certification of inorganic selenium species in synthetic chloride aqueous media. The addition of Cl^- in the synthetic samples is based in two main reasons: (1) in order to simulate a seawater matrix, and (2) because of its stabilising effect for these species was proven during a longterm stability study [12]. In this study, inorganic selenium species were shown to be stable for more than 1 year in an aqueous and chloride matrix. This certification campaign was organised by the Measurements and Testing Program. The results we have obtained with the microwave assisted reduction techniques for the speciation of inorganic selenium are presented in Table 2 with the mean of all participating laboratories.

These results demonstrate the efficiency and validity of microwaves assisted reduction procedures. The high Cl^- concentration added to the sample has shown not to interfere in our method.

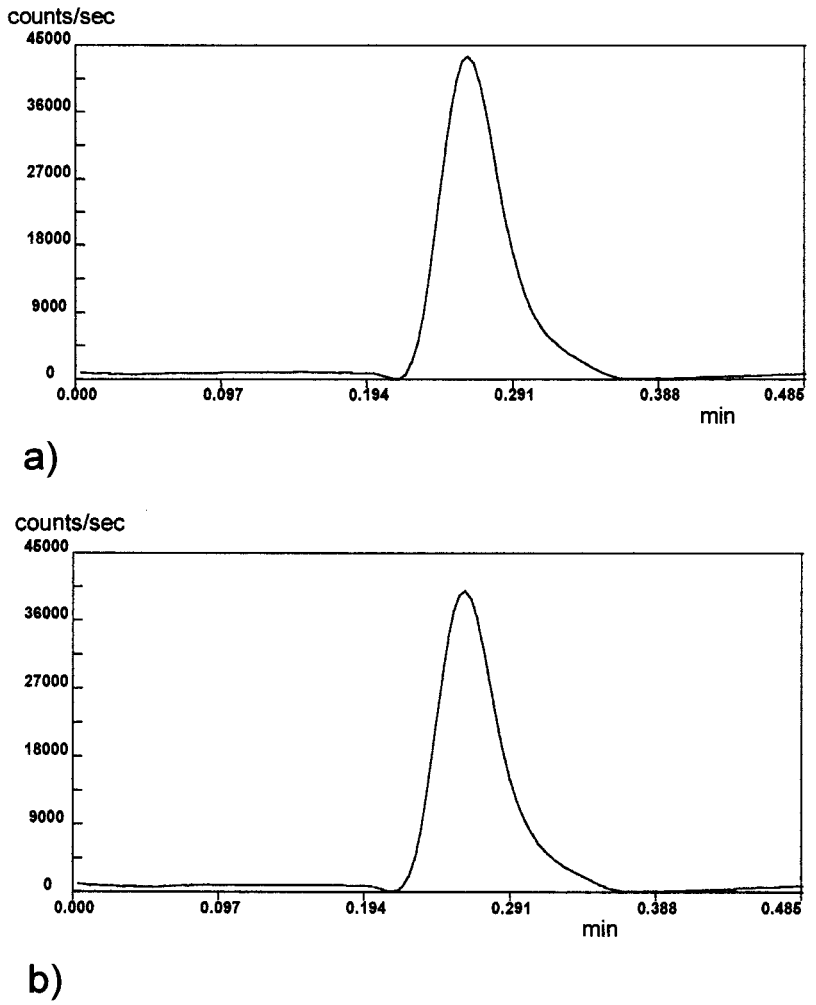

Fig. 4. Transient signal obtained by HG/FI – ICP/MS for a solution containing 1 μg l^{-1} of Se^{IV} and 1 μg l^{-1} of total inorganic Se with: (a) before microwave treatment and (b) after microwave treatment.

Table 2
Results from the intercomparison and from the certification exercices for Se^{IV} and Se^{IV}

Solution	Species	Intercalibration exercise		Certification exercise	
		Amount (μg l^{-1})[a]	Average (μg l^{-1})[b]	Amount (μg l^{-1})[a]	Average (μg l^{-1})[b]
A	Se^{IV}	52 ± 1	49 ± 8	34 ± 1	35 ± 2
High content	Se^{VI}	45 ± 2	49 ± 14	48 ± 3	45 ± 4
B	Se^{IV}	5.2 ± 0.1	5 ± 1	5.8 ± 0.2	5.8 ± 0.4
Low content	Se^{VI}	6.6 ± 0.3	6 ± 2	8.2 ± 0.5	7.7 ± 0.7

[a] Value measured by our MW/HG/FI-ICP/MS system (average from 5 replicates).
[b] Mean of the laboratory means.

Acknowledgements

The authors want to acknowledge the Prolabo France company for supplying the A301 microwave device. We would like to thank the Measurements and Testing Programme from the EC for supporting this work.

References

[1] S.E. Raptis, G. Kaiser, G. Tolg, Fresenius J. Anal. Chem. 316 (1983) 105.
[2] R. Muñoz Olivas, O.F.X. Donard, C. Camara, Ph. Quevauviller, Anal. Chim. Acta. 286 (1994) 357–370.
[3] X. Dauchy, M. Potin-Gautier, A. Astruc, M. Astruc, Fresenius J. Anal. Chem. 348 (1994) 792–805.
[4] G.A. Cutter, Anal. Chim. Acta. 98 (1978) 59.
[5] S.C. Apte, A.G. Howard, J. Anal. At. Spectr. 1 (1986) 379.
[6] J.L. Fio, R. Fujii, Soil Sci. Am. J. 54 (1990) 363–369.
[7] G. Cobo Fernandez, M.A. Palacios, C. Camara, Anal. Chim. Acta. 283 (1993) 386–392.
[8] G. Cobo Fernandez, M.A. Palacios, D. Chakraborti, Ph. Quevauviller, C. Camara, Fresenius J. Anal. Chem. 351 (1995) 438.
[9] L. Pitts, P.J. Worsfold, S.J. Hill, Analyst 119 (1994) 2785.
[10] R. Muñoz Olivas, C.R. Quétel, O.F.X. Donard, J. Anal. At. Spect. 10 (1995) 865–870.
[11] D.L. Tsalev, M. Sperling, B. Welz, Analyst 117 (1992) 1729.
[12] G. Cobo, M.A. Palacios, C. Camara, F. Reis, Ph. Quevauviller, Anal. Chim. Acta 286 (1994) 371.

ELSEVIER

Talanta 45 (1998) 1031–1033

Talanta

Letter to the editor

About the voltammetric determination of the stability constants for some metal ions complexes with the hydrogen sulfide anion

Florinel Gabriel Bănică *, Ana Ion

Norwegian University of Science and Technology (NTNU), Department of Chemistry, N-7034, Trondheim, Norway

Received 30 May 1997; accepted 13 June 1997

Recently Luther, III et al. used square wave voltammetry on the mercury drop electrode to measure the stability constants of some metal ion-hydrogen sulfide complexes at a very low concentration level [1]. The stability constants are defined as $\beta_j = [M_j(HS^-)^{2j-1}]/[M^{2+}]^j[HS^-]$. It was assumed that the potential of the anodic peak due to mercury oxidation is a function of SH^- concentration according to the Nernst equation. It was also presumed that the binding of SH^- to a metal ion induces a shift in the peak potential which is dependent on both the combining ratio and the stability of the soluble complexes. Taking into account these postulates, the formalism of DeFord and Hume [2,3] was employed to calculate the stability constants in several metal ion-SH^- systems. It is noteworthy that this formalism was originally developed for the case of the reversible polarographic reduction of a metal ion in the presence of a high excess of ligand giving a series of successive labile complexes. Under these conditions it is possible to compute the formation constants as the coefficients of a polynomial relating the ligand concentration to the values of the shift in the half-wave potential (Eq. 5 and 6 in [1]). A graphical method was used initially to this end, but dedicated computer programs were subsequently developed [4,5]. The graphical method consists in the sequential determination of the formation constants β_j using the extrapolation of non-linear curves.

In the commented paper [1] the curves were fitted by empirical interpolation functions and then extrapolated to zero in order to find the values of the formation constants. Apparently this allows a better accuracy as compared with the graphical procedure, although the main drawback of the non-linear extrapolation cannot be completely removed. An example of calculation is provided in Fig. 1 [1] for the nickel ion and also the experimental data used in this case are available (Table 1 in [1]).

A summary examination of Fig. 1 in [1] reveals however a high scatter of the points on the third and fourth graphs as well as a marked deviation of the line in the fourth graph from the horizontal, which is at variance with the theory [2,3]. Another reason for scepticism is the discrepancy between the huge values of the reported constants and the minute shift in the peak potential.

These findings prompted us to recalculate the values of the formation constants by means of the multiparametric curve fitting procedure. The

* Corresponding author.

PII S0039-9140(97)00190-2

solver tool of the Microsoft Excel 5 spreadsheet program was used to this end according to the recommendations in [6]. Accordingly, the values of the parameters β_j were adjusted as to get the minimum value of the sum of squares of the residuals, $\Sigma(F_{0,calc}\text{-}F_{0,exp})^2$, where $F_{0,exp}$ represents the values of the function F_0 in Table 1 [1] and $F_{0,calc}$ the values calculated by Eq. 5 in the same reference. This procedure is similar to that previously used by Meites [4]. It was tested with the data of Heath and Hefter [7] and gave results in excellent agreement with that obtained in the quoted paper by the graphical method.

The following values of the β constants were found in this way for the Ni^{2+}–SH^- system by means of the experimental data in [1]: $\beta_3 = 1.06 \times 10^{16}$; $\beta_2 = -1.15 \times 10^{11}$; $\beta_1 = 6.16 \times 10^5$; $\beta_0 = 0.118$. It is very important to note that the results obtained by an accurate numerical computation are in conflict with two strong physical restrictions: (i) one of the constant gets a negative value and (ii) β_0 strongly differs from 1, the value expected on theoretical ground [2,3]. Since it could be presumed that this failure is due to an inappropriate complexation model the same procedure was applied by assuming that the maximum co-ordination number, n is either 4 or 2 instead of 3 (a linear model with $n = 1$ is clearly not appropriate). The results in both these cases shows the same kind of disagreement with the theoretical prerequisite. In addition the residuals obtained with the values in [1] shows a clear deterministic trend and monotonously increase with the rise of Ni^{2+} concentration reaching anomalously high values whereas the residuals computed with the above given β values are very small and randomly distributed around zero (Fig. 1). However, in view of the inconsistency above mentioned under (i) and (ii) the β values reported in the present paper should be considered only as empirical coefficient of a fitting polynomial without any physico-chemical meaning.

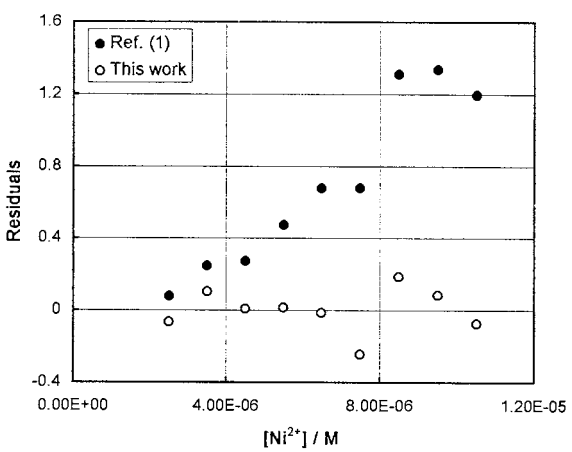

Fig. 1. Residuals distribution. β values from [1] (●) or calculated in this paper (○).

It is easy to prove that the theoretical ground of the method in [1] is formally correct. It results therefore that the experimental data in Table 1 [1] do not fulfil the conditions for the application of DeFord and Hume method and any attempt to calculate some stability constant in this way leads to erroneous results. This is not due to some computing errors but to an intrinsic inconsistency of the above procedure with the chemistry of the investigated system. Presumably the actual combination scheme is completely different from that assumed in [1] and the formation of solid phases should also be taken into account. The adsorption of sulfide ion or its metal ion compounds is another source for deviation from the requirements of the DeFord and Hume method. There is still at least one methodological fault in [1] in connection with the prerequisite of a high excess of ligand [2,3]. This condition secures the absence of any significant ligand concentration gradient near the electrode surface. The ligand (in a broader sense) is in [1] the metal ion and the concentration ratio Ni^{2+}/HS^- for the data in Fig. 1 and Table 1 ranges between only about 1 and 5. For comparison, the ligand/metal ratio in the Cd^{2+}-Cl^- system investigated in [7] extends from about 10 to 2.5×10^4.

Some uncertainty also arises from the composition of the background electrolyte (half-diluted sea water). The complex ionic composition as well as the presence of natural surface active compounds may contribute to the deviation form the expected behavior. In this connection it is

important to point out that any method for the determination of physico-chemical constants in natural water samples should be previously tested using synthetic samples with a well known composition.

It results therefore that the stability constants for the species $[Ni_j(HS^-)]2^{j-1}$ reported in [1] are at least dubious. In view of the previous comments it is also questionable how reliable are the stability constants determined in [1] by the same method for other metal ions (Mn^{2+}, Fe^{2+}, Co^{2+}).

References

[1] G.W. Luther III, D.T. Rikhard, S. Theberge, A. Olroyd, Environ. Sci. Technol. 30 (1996) 671–679.
[2] D.D. DeFord, D.N. Hume, J. Am. Chem. Soc. 73 (1951) 5321–5322.
[3] Z. Galus, Fundamentals of Electrochemical Analysis, Ch. 14, Ellis Horwood, New York, 1994.
[4] L. Meites, Talanta 22 (1975) 561–572.
[5] D.J. Leggett, Talanta (1980) 787–793.
[6] S. Walsh, D. Diamond, Talanta 42 (1995) 561–572.
[7] G.A. Heath, G. Hefter, J. Electroanal. Chem. 84 (1977) 295–302.

.

ELSEVIER

Talanta 45 (1998) 1035–1038

Talanta

Book reviews

Pharmaceuticals and Thermal Analysis—special issue of thermochimica acta
J.L. Ford (Editor), Elsevier, Amsterdam; 1995, x + 360 pp.; £155; Softback; ISSN: 0040-6031

This special issue is the complete volume 248 of the journal 'Thermochimica acta' and its theme is the thermal analysis of pharmaceutically relevant materials. The editor, James Ford, is well known for his 1989 publication with Peter Timmins, of 'Pharmaceutical Thermal Analysis'. There are 20 contributions—mainly review articles—from authors in industry and academia and a wide range of topics are covered.

It is fitting that the first and largest article deals with the characterization of polymorphs and solvates—a most relevant topic for the pharmaceutical industry. The review by D. Giron, which contains much background information, is well presented and the list of drug substances with polymorphic or pseudo-polymorphic behaviour is the most comprehensive that I have seen. Excipients commonly found in drug formulations are also treated similarly in a separate Table. The thermodynamic and kinetics aspects are covered, DSC and TGA curves are presented and microcalorimetric techniques are discussed. A total of 301 references are included. Polymorphism is also dealt more specifically in other articles of this publication, e.g. with reference to polyethylene glycols, ibopamin and terfenadine. Related to polymorphism is the second article in this volume which deals with the characterization of pharmaceutical hydrates. This includes background information and pharmaceutical implications of crystalline stoichiometric hydrates. Details of complementary spectroscopic techniques are also presented.

Other articles are each 10–20 pages long and deal with techniques (e.g., isothermal microcalorimetry and dynamic mechanical thermal analysis), excipients (e.g., lactose, magnesium stearate and fatty suppository bases), and dosage forms (e.g., microspheres, hydrogels and tablets). Other contributions include thermal analysis of glassy pharmaceuticals, spray dried products, proteins, liposomes, skin and chiral drug mixtures. Crystal disruption is also examined. I can understand why no attempt was made to arrange the presentations into any common group headings as there would be much overlap. Author and subject indexes are appended.

Overall this volume will be useful to both the student and the experienced practitioner and is a recommended purchase for the library.

P.J. Cox
The Robert Gordon University
Aberdeen
UK

PII S0039-9140(97)00161-6

Molecular Modelling—Principles and Applications
A.R. Leach (Editor), Addison Wesley Longman, Harlow; 1996, xvi + 595 pp.; £35.00; Softback; ISBN: 0-582-23933-8

I had just been asked to prepare lectures on molecular modelling for final year Pharmacy students when this book arrived on my desk. What a

ELSEVIER

Talanta 45 (1998) 1035–1038

Talanta

Book reviews

Pharmaceuticals and Thermal Analysis—special issue of thermochimica acta
J.L. Ford (Editor), Elsevier, Amsterdam; 1995, x + 360 pp.; £155; Softback; ISSN: 0040-6031

This special issue is the complete volume 248 of the journal 'Thermochimica acta' and its theme is the thermal analysis of pharmaceutically relevant materials. The editor, James Ford, is well known for his 1989 publication with Peter Timmins, of 'Pharmaceutical Thermal Analysis'. There are 20 contributions—mainly review articles—from authors in industry and academia and a wide range of topics are covered.

It is fitting that the first and largest article deals with the characterization of polymorphs and solvates—a most relevant topic for the pharmaceutical industry. The review by D. Giron, which contains much background information, is well presented and the list of drug substances with polymorphic or pseudo-polymorphic behaviour is the most comprehensive that I have seen. Excipients commonly found in drug formulations are also treated similarly in a separate Table. The thermodynamic and kinetics aspects are covered, DSC and TGA curves are presented and microcalorimetric techniques are discussed. A total of 301 references are included. Polymorphism is also dealt more specifically in other articles of this publication, e.g. with reference to polyethylene glycols, ibopamin and terfenadine. Related to polymorphism is the second article in this volume which deals with the characterization of pharmaceutical hydrates. This includes background information and pharmaceutical implications of crystalline stoichiometric hydrates. Details of complementary spectroscopic techniques are also presented.

Other articles are each 10–20 pages long and deal with techniques (e.g., isothermal microcalorimetry and dynamic mechanical thermal analysis), excipients (e.g., lactose, magnesium stearate and fatty suppository bases), and dosage forms (e.g., microspheres, hydrogels and tablets). Other contributions include thermal analysis of glassy pharmaceuticals, spray dried products, proteins, liposomes, skin and chiral drug mixtures. Crystal disruption is also examined. I can understand why no attempt was made to arrange the presentations into any common group headings as there would be much overlap. Author and subject indexes are appended.

Overall this volume will be useful to both the student and the experienced practitioner and is a recommended purchase for the library.

P.J. Cox
The Robert Gordon University
Aberdeen
UK

PII S0039-9140(97)00161-6

Molecular Modelling—Principles and Applications
A.R. Leach (Editor), Addison Wesley Longman, Harlow; 1996, xvi + 595 pp.; £35.00; Softback; ISBN: 0-582-23933-8

I had just been asked to prepare lectures on molecular modelling for final year Pharmacy students when this book arrived on my desk. What a

stroke of luck. The author of the book is based in the pharmaceutical industry and the subject matter is covered very comprehensively. All the major techniques are included and although some assumptions of prior knowledge are made the first chapter deals with some useful elementary concepts and details of further reading are given. Some web sites are also included but, as warned, some of these addresses have now changed.

For computer-based molecular modelling extensive calculations are performed and these are based on either quantum mechanics or molecular mechanics. The mathematics associated with quantum mechanics is covered extensively in chapter 2—far too extensively for undergraduates but suitable for the research worker. A chapter is then devoted to the empirical technique of molecular mechanics which is less mathematical demanding. These first 3 chapters are just over 200 pages long and 7 chapters remain. Energy minimisation and related methods for exploring the energy surface are then covered—in particular first and second order derivative methods. General principle involved in the two most common simulation techniques—molecular dynamics and the Monte Carlo methods—are mentioned in chapter 5. These methods are then dealt with in detail in separate chapters.

The chapter on conformational analysis concentrates on the numerous methods used for exploring conformational space, e.g., model-building, random search, genetic algorithms, distance geometry, searching structural databases, clustering algorithms, pattern recognition, etc. Chapter 9 discusses three important problems in molecular modelling: the calculation of free energies, the effect of the solvent and the simulation of chemical reactions. Potential pitfalls are mentioned and interesting case studies are used to illustrate the different ways of approaching these problems.

The final chapter 'The use of molecular modelling to discover and design new molecules' uses examples drawn primarily from the pharmaceutical industry. It contains information on three-dimensional pharmacophores, molecular docking, De novo ligand design, lead compound identification, molecular similarity and QSAR relationships.

Colour plates 16, are included in the centre of the book to show the magnificent molecular graphics representations of molecules and many diagrams are included throughout. Further reading lists and references are extensive. Highly recommended.

P.J. Cox
The Robert Gordon University
Aberdeen
UK

PII S0039-9140(97)00162-8

Applications of Synchrotron Radiation to Materials Analysis
H. Saisho, Y. Gonshi (Editors), Elsevier, Amsterdam; 1996, vii + 501 pp. US$343.75; ISBN: 0-444-88857-8

Synchrotron radiation has a lot to offer to chemists and this book, which is a welcome, if expensive, addition to the literature, forms part of the Elsevier Analytical Spectroscopy Library. It is a review of synchrotron radiation applications in chemistry and provides a scholarly approach to the subject, in some depth, despite its obvious parochialism. In fact the title of the book may have been better as 'As Review of Japanese Applications of …'.

The editors have set out to provide a source for the users of Synchrotron Radiation and the first chapter is a good introduction to storage rings and the basic instrumentation. It concentrates on the facilities at the Photon Factory and SPring8 but the basic principles apply to all Synchrotron Radiation sources.

Different techniques are covered in the subsequent chapters. In chapter 2 X-ray fluorescence is discussed; this quantitative chemical analysis technique has been around for a long time and the chapter concentrates on the benefits that Synchrotron Radiation can bring in terms of resolution; there is also a useful review of the theory for thin layers.

For large scale structures, 2-dimensional imaging techniques, via microbeams and chemical state analysis, are covered in chapter 3 which contains a good section on source sizes and chemical imag-

stroke of luck. The author of the book is based in the pharmaceutical industry and the subject matter is covered very comprehensively. All the major techniques are included and although some assumptions of prior knowledge are made the first chapter deals with some useful elementary concepts and details of further reading are given. Some web sites are also included but, as warned, some of these addresses have now changed.

For computer-based molecular modelling extensive calculations are performed and these are based on either quantum mechanics or molecular mechanics. The mathematics associated with quantum mechanics is covered extensively in chapter 2—far too extensively for undergraduates but suitable for the research worker. A chapter is then devoted to the empirical technique of molecular mechanics which is less mathematical demanding. These first 3 chapters are just over 200 pages long and 7 chapters remain. Energy minimisation and related methods for exploring the energy surface are then covered—in particular first and second order derivative methods. General principle involved in the two most common simulation techniques—molecular dynamics and the Monte Carlo methods—are mentioned in chapter 5. These methods are then dealt with in detail in separate chapters.

The chapter on conformational analysis concentrates on the numerous methods used for exploring conformational space, e.g., model-building, random search, genetic algorithms, distance geometry, searching structural databases, clustering algorithms, pattern recognition, etc. Chapter 9 discusses three important problems in molecular modelling: the calculation of free energies, the effect of the solvent and the simulation of chemical reactions. Potential pitfalls are mentioned and interesting case studies are used to illustrate the different ways of approaching these problems.

The final chapter 'The use of molecular modelling to discover and design new molecules' uses examples drawn primarily from the pharmaceutical industry. It contains information on three-dimensional pharmacophores, molecular docking, De novo ligand design, lead compound identification, molecular similarity and QSAR relationships.

Colour plates 16, are included in the centre of the book to show the magnificent molecular graphics representations of molecules and many diagrams are included throughout. Further reading lists and references are extensive. Highly recommended.

P.J. Cox
The Robert Gordon University
Aberdeen
UK

PII S0039-9140(97)00162-8

Applications of Synchrotron Radiation to Materials Analysis
H. Saisho, Y. Gonshi (Editors), Elsevier, Amsterdam; 1996, vii + 501 pp. US$343.75; ISBN: 0-444-88857-8

Synchrotron radiation has a lot to offer to chemists and this book, which is a welcome, if expensive, addition to the literature, forms part of the Elsevier Analytical Spectroscopy Library. It is a review of synchrotron radiation applications in chemistry and provides a scholarly approach to the subject, in some depth, despite its obvious parochialism. In fact the title of the book may have been better as 'As Review of Japanese Applications of …'.

The editors have set out to provide a source for the users of Synchrotron Radiation and the first chapter is a good introduction to storage rings and the basic instrumentation. It concentrates on the facilities at the Photon Factory and SPring8 but the basic principles apply to all Synchrotron Radiation sources.

Different techniques are covered in the subsequent chapters. In chapter 2 X-ray fluorescence is discussed; this quantitative chemical analysis technique has been around for a long time and the chapter concentrates on the benefits that Synchrotron Radiation can bring in terms of resolution; there is also a useful review of the theory for thin layers.

For large scale structures, 2-dimensional imaging techniques, via microbeams and chemical state analysis, are covered in chapter 3 which contains a good section on source sizes and chemical imag-

ing and then a review of applications to a wide range of materials. The theory and practice of 3-D imaging by X-ray microtomography is discussed in the final chapter where examples of structural studies in the μm region on composites, minerals and food are presented. The fifth chapter on small angle X-ray scattering covers instrumentation, theory and applications of reciprocal space studies on materials in the 1000–10 Å region and concentrates on polymers and biology.

The family of local structure techniques based around X-ray absorption spectroscopy (XAS) are covered in the 4th, and longest, chapter. The differences between XANES, XAFS, EXAFS are carefully explained and the theory and practice of the various techniques reviewed. There is a detailed discussion of data analysis which is supported by a multitude of examples from inorganic materials. As an example of the scholarly style chapter 4 contains 66 diagrams and 244 references.

Surface structure analyses are covered in chapter 5 which includes a table explaining all the acronyms. This chapter covers a lot of ground including surface sensitive EXAFS, photoelectron spectroscopy and surface X-ray diffraction.

Powder diffraction, and the applications of Rietveld refinement to crystal structure determination, are covered in chapter 7 where angle and energy dispersive techniques are compared with high resolution powder diffraction by neutrons.

This book is excellent (if biased) on the limited subjects it covers, there are few typographical errors and the text is well illustrated. A more comprehensive coverage would have included the techniques of protein and molecular crystallography and more on VUV spectroscopy. This book is one for the specialist, unless you are a very wealthy collector of scientific tomes, and I could only recommend it for an institutional library.

A.J. Ryan

PII S0039-9140(97)00170-7

Modern Aspects of Electrochemistry no. 30
R.E. White, B.E. Conway, J.O'M. Bockris (Editors), Plenum, New York; 1996, xii + 541 pp.; US$125; ISBN: 0-306-45450-5

This text is Volume 30 in a long running series on topics of current interest in electrochemistry. It is very much a research oriented book which would be rather complex for undergraduates or non-specialists to follow. Readers will require a strong background knowledge in electrochemistry in order to have a reasonable understanding of the text. It does however provide detailed information on the subject areas described which would be of great value to researchers in these areas. Plenty of detailed references are provided in each chapter and all diagrams are well laid out and clearly presented. A cumulative author index for the whole series is also provided.

There are a total of 5 chapters covering several aspects of electrochemistry including photoelectrochemistry, electrodeposition of metals, metal oxide electrodes and hydrogen sorption on electrode materials. The first chapter describes surface techniques for analysis of semiconductor/electrolyte interfaces. This is achieved in a comprehensive manner with a good development of the processes occurring at the semiconductor/electrolyte interface. The application of several ultra high vacuum surface science techniques (e.g., photoelectron spectroscopic methods, LEED and LEISS) for the examination of the interface are subsequently detailed. This includes case studies for materials such as silicon, gallium arsenide and tungsten selenide. Chapter 2 provides a description of Schottky barrier photoelectrodes. The chapter begins with a development of intrinsic and extrinsic semiconductors, photovoltaic junction and photoelectrochemical devices. Schottky barrier cells are subsequently discussed together with the photoelectrochemical process involved in solar energy conversion and types of cell used in such applications. The use of oxide films as low cost photoelectrodes is described with particular reference to titanium and tin dioxides. Information on preparation, examination of film homogeneity, conductivity, and techniques for enhancement of the photoelectrochemical characteristics of such electrodes are also detailed. The information on the preparation and characterisation of the metal oxide films was of particular interest with useful detail and references provided. The mechanisms of electrodeposition are covered in

ing and then a review of applications to a wide range of materials. The theory and practice of 3-D imaging by X-ray microtomography is discussed in the final chapter where examples of structural studies in the μm region on composites, minerals and food are presented. The fifth chapter on small angle X-ray scattering covers instrumentation, theory and applications of reciprocal space studies on materials in the 1000–10 Å region and concentrates on polymers and biology.

The family of local structure techniques based around X-ray absorption spectroscopy (XAS) are covered in the 4th, and longest, chapter. The differences between XANES, XAFS, EXAFS are carefully explained and the theory and practice of the various techniques reviewed. There is a detailed discussion of data analysis which is supported by a multitude of examples from inorganic materials. As an example of the scholarly style chapter 4 contains 66 diagrams and 244 references.

Surface structure analyses are covered in chapter 5 which includes a table explaining all the acronyms. This chapter covers a lot of ground including surface sensitive EXAFS, photoelectron spectroscopy and surface X-ray diffraction.

Powder diffraction, and the applications of Rietveld refinement to crystal structure determination, are covered in chapter 7 where angle and energy dispersive techniques are compared with high resolution powder diffraction by neutrons.

This book is excellent (if biased) on the limited subjects it covers, there are few typographical errors and the text is well illustrated. A more comprehensive coverage would have included the techniques of protein and molecular crystallography and more on VUV spectroscopy. This book is one for the specialist, unless you are a very wealthy collector of scientific tomes, and I could only recommend it for an institutional library.

A.J. Ryan

PII S0039-9140(97)00170-7

Modern Aspects of Electrochemistry no. 30
R.E. White, B.E. Conway, J.O'M. Bockris (Editors), Plenum, New York; 1996, xii + 541 pp.; US$125; ISBN: 0-306-45450-5

This text is Volume 30 in a long running series on topics of current interest in electrochemistry. It is very much a research oriented book which would be rather complex for undergraduates or non-specialists to follow. Readers will require a strong background knowledge in electrochemistry in order to have a reasonable understanding of the text. It does however provide detailed information on the subject areas described which would be of great value to researchers in these areas. Plenty of detailed references are provided in each chapter and all diagrams are well laid out and clearly presented. A cumulative author index for the whole series is also provided.

There are a total of 5 chapters covering several aspects of electrochemistry including photoelectrochemistry, electrodeposition of metals, metal oxide electrodes and hydrogen sorption on electrode materials. The first chapter describes surface techniques for analysis of semiconductor/electrolyte interfaces. This is achieved in a comprehensive manner with a good development of the processes occurring at the semiconductor/electrolyte interface. The application of several ultra high vacuum surface science techniques (e.g., photoelectron spectroscopic methods, LEED and LEISS) for the examination of the interface are subsequently detailed. This includes case studies for materials such as silicon, gallium arsenide and tungsten selenide. Chapter 2 provides a description of Schottky barrier photoelectrodes. The chapter begins with a development of intrinsic and extrinsic semiconductors, photovoltaic junction and photoelectrochemical devices. Schottky barrier cells are subsequently discussed together with the photoelectrochemical process involved in solar energy conversion and types of cell used in such applications. The use of oxide films as low cost photoelectrodes is described with particular reference to titanium and tin dioxides. Information on preparation, examination of film homogeneity, conductivity, and techniques for enhancement of the photoelectrochemical characteristics of such electrodes are also detailed. The information on the preparation and characterisation of the metal oxide films was of particular interest with useful detail and references provided. The mechanisms of electrodeposition are covered in

Chapter 3. This includes mathematical models of deposition, simulations of the models and real systems for coarse and spongy coatings as well as for dendritic growth. The authors have made good use of micrographic illustrations for various deposits discussed. The information provides good background for researchers in this area with well developed, easy to follow, equations. Chapter 4 is devoted to manganese dioxide electrodes in aqueous solution, particularly their use in batteries. The background discussed includes a description of previous literature on this topic. The mechanism of discharge of MnO_2 electrodes in alkaline media is outlined together with the experimental methods used to confirm these mechanisms such as XRD, microscopy and equilibrium potential studies. The discharge of MnO_2 in Leclanche and $ZnCl_2$ electrolytes is covered in detail together with a section on the recharging of MnO_2 electrodes. The final topic discussed is the mechanisms for the deposition of MnO_2. The sorption of hydrogen is detailed in chapter 5. This includes a discussion of both absorption and adsorption of hydrogen which includes some useful detail on experimental methods. Palladium is used as a case study for discussion of such processes with detail on the absorption of hydrogen on iron, nickel, titanium and zirconium also described. The chapter subsequently develops models of hydrogen entry on hydrogen evolving electrodes and the permeation of hydrogen in various metals.

To conclude this book is a useful further development of an important reference series in electrochemistry which maintains the high standard set in the previous volumes.

P.K.J. Robertson

PII S0039-9140(97)00166-5

ELSEVIER

Talanta 45 (1998) 1039–1047

Talanta

Studies about the adsorption on lichen *Evernia prunastri* by enthalpimetric measurements

Marta Letizia Antonelli, Patrizia Ercole, Luigi Campanella *

Department of Chemistry, University 'La Sapienza', P. le Aldo Moro, 5-00185 Rome, Italy

Received 10 June 1996; received in revised form 22 May 1997; accepted 23 May 1997

Abstract

Lichens are bioaccumulators of divalent metal ions and the interaction between the lichens and five heavy metals was studied. In order to have a better understanding of the metal-uptake process by the lichens, data from atomic absorption spectroscopy were used to calculate the apparent coordination constants of the lichen–metal ion interactions by means of the Langmuir elaboration and microcalorimetric measurements to obtain enthalpimetric information. The results showed a correlation between the Langmuir constants and enthalpimetric measurements. © 1998 Elsevier Science B.V.

Keywords: Lichens; Metal uptake; Microcalorimetry; Langmuir plot

1. Introduction

The lichens are dual organisms [1], an association between an alga and a fungus. Many lichens live in stressed environmental conditions, where few other organisms survive. Because of their great capacity for adsorption and resistance to environmental stress, they are good pollution indicators [2], exhibiting a slow growth and longevity. Lichens have been used to monitor environmental quality [3] since 1926, when Sernander [4] published a map of Stockholm. He established concentric bands, characterized by different lichen floras, reflecting a gradient of the pollution. Since, then numerous studies have established pollution maps based on the distribution of epiphytic lichens, for example, the methods of Hawksworth and Rose [5], Le Blanc and De Sloover [6], Wanner and Amman [7], and Nimis [8,9].

Lichens act as bioaccumulators [10] via their capacity to adsorb pollutants from the environment and pollutant concentrations in the lichen's thalli can be measured. Metal ions are very rapidly adsorbed by the lichens [11]. Thus metal levels in lichens represent a measure of the accumulation and deposition over a defined period of time. The remarkable ability of the lichens to accumulate many elements [12], from the alkali metals to the heaviest of the transition metals such as lead, has been established unequivocally in the last 20 years. Recently Richardson published a review of the metal uptake in lichens and

* Corresponding author. Fax: +39 6 49913725.

PII S0039-9140(97)00226-9

fungi [13]. Three mechanisms have been proposed: (1) an intracellular uptake via an exchange process, (2) intracellular accumulation, and (3) trapping of metal-rich particulates. Various researchers have attempted to understand the binding process by using techniques such as nuclear magnetic resonance (NMR), electron paramagnetic resonance (EPR) and luminescence; but there is still some lack in understanding the overall process responsible for the metal uptake and accumulation in lichens. In order to improve this understanding a new approach was taken, in this study, to investigate metal–lichen interactions based upon the microcalorimetric technique [14], which provides useful informations on the energetics of the process. Moreover, in order to quantify the capacity of the lichens for coordinating different metal-ions, a sort of apparent interaction constant (in particular a so-called complexing capacity) between the lichen (considered as an overall ligand) and five different metal ions was calculated by means of the Langmuir plot [15]. Such plots have been obtained in other research for a wide variety of microorganism and substances [16] which bind metal ions. In this work, the Langmuir plots have been used to compare the amount of the metal ion adsorbed with the heat of reaction evolved. By relating the enthalpimetric results with the interaction capacities, useful informations on the bioaccumulation mechanism can be obtained which confirms the value of using the lichens as bioindicators.

2. Materials and methods

2.1. Materials

Lichen samples belonging to the species *Evernia prunastri*, a common epiphytic and fruticose lichen in Europe, were collected from an unpolluted location on Monteluco (L'Aquila) on *Prunus spinosa* and *Quercus pubescens*. Only the thallus was collected eliminating the bark. After collection, the lichens, before the experimentation, were held at 4°C for 24 h and were sprayed with water. After drying, they were cut to obtain sample weights. All the measurements were made using living lichens, because our interest was focused on the interactions of the living plant with the metal ions. We made some preliminary experiments with non-living lichens in order to observe the isothermal curves and also the calorimetric response in the basal conditions. The obtained results showed that the accumulation processes is not influenced by the viability of the lichen, whereas the calorimetric response was zero with non-living species as expected. Some samples were not treated with the heavy metal solutions in order to determinate the initial heavy metal level by means of microwaves mineralizer and AAS. When the initial heavy metal level was ≥ 2.0 mg kg^{-1} (of lichen) it was subtracted in the computation of the metal ion uptake. All chemicals used for the calorimetric experiments were analytical grade: lead nitrate, cadmium nitrate, copper nitrate, chromium nitrate, zinc nitrate were from Merck. Standard titrated solutions of metals were prepared from the salts and the working solutions were obtained by dilution, using NaOH and HCl to provide the optimum pH of 4.5, coincident with the lichen's physiological pH of 4.5–6.0. For the isotherms of adsorption using AAS, the corresponding solutions BDH-Spectrosol Standard for AAS, at pH 4.5, were used. The water was deionized and distilled on $KMnO_4$.

2.2. Instrumentation

All pH measurements were performed by a pH-meter Amel, model 329; metal ion determinations by an atomic adsorption spectrophotometer Thermo Jarrel ASH Smith-HIEFTJE 11; microweighing by a Mettler PM 460 analytical balance; usual weighing by a Gibertini TM 5600 balance were pointed out. The enthalpimetric measurements were carried out by means of a batch microcalorimeter of the heat conduction type (LKB 2107) [17] equipped with two gold vessels of about 7 ml total volume, a multitemp cooling circulator (LKB 2209), a control unit (LKB 2107-350) and a potentiometric recorder (LKB 2210). Each vessel consists of a chamber partially divided into two compartments of 2.5 and 4.5 ml, respectively, by an interior wall. The reactants are introduced in the two compartments separately.

When the experiment begins the calorimetric unit is rotated: thereby the reactants will be mixed and the reaction takes place. All the instrumentation was housed in a thermostated room at 25 ± 1°C, all the measurements were performed at 25.00 ± 0.01°C. The calorimetric accuracy was checked by measuring the sucrose dilution heat [17] and our results were in agreement with the literature values within 0.5%.

2.3. Methods

2.3.1. Atomic absorption spectrophotometry

In order to plot isothermal curves relative to the metal uptake from the lichens many batch experiments have been performed. Weighed quantities of living lichen were incubated with titrated metal solutions at varying concentrations. The experiments were performed for different periods of time up to a maximum of 1440 min. Replicates were shaking in the solutions which were analysed by AAS [18] in order to find the residual concentration of each metal ion. Instrumental conditions were optimized for each metal and the appropriate hollow cathode lamp was used with a lamp current of 5 mA. The calibration curve method was used by means of standard solutions prepared for each metal ion within the right concentration range. To apply the Langmuir plot necessary to compute the apparent coordination constants relative to the overall lichen–metal ion interaction, many experiments were performed at fixed time periods. By examining the uptake isothermal curves, it is evident that for all the metal ions the reaction kinetics is quite rapid and that the maximum uptake is reached in the first 4 min. Sampling from the batch ampoules was therefore made at 5 min from the starting of the contact between the weighed quantity of the lichen and the titrated ion solutions. The metal concentration of solutions varied from 10 to 40 ppm while the lichen dry weight was fixed equal to 0.25 g.

2.3.2. Microcalorimetry

The measurements of the heat evolved during the binding process seems to be non-specific, but the values of the real heat obtained of interaction in every experiment is calculated by considering each contribute ion: basal heat, dilution effects and/or other heat effects due to some collateral reactions. When a living system is under examination it is, firstly necessary to know the basal heat quantity [19] associated with a quantity of the lichen sample, i.e. the calorimetric effect due to the life of the lichen in water solution without the presence of the metal ion must be determined. After that it is possible to determine the heat effect due to the metal–lichen interaction when the living system comes into contact with the ion solution. It is necessary to know if an undesirable heat quantity due to the metal ion dilution develops, so that the measurements of the lichen–metal interaction are made in a differential way. In the first case the calorimeter was filled as it follows:

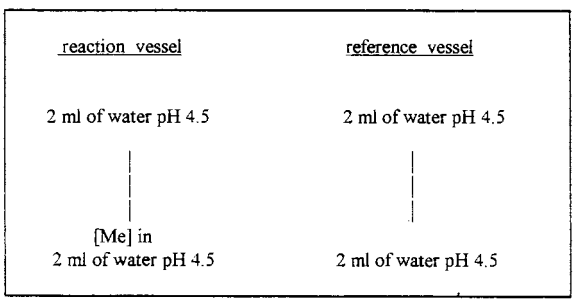

In order to avoid possible heat effects of neutralization, it is very important that all the solutions in the calorimeter should be at the same pH value. In the case of lichens the optimum pH value is about 4.5, so that all the solutions (water or metal ion in water) were maintained at that pH by the appropriate addition of acid or alkali as necessary. The instrument baseline was recorded before loading the calorimetric vessels. To measure the basal heat production, the measuring vessels were filled as in the following schema:

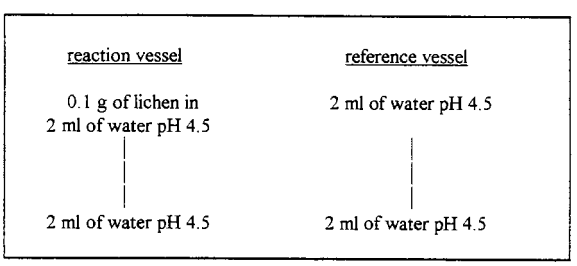

After 30 min of thermal equilibration, the calorimetric unit was rotated and the heat output was recorded and monitored for at least 30 min. During the trace recording, the calorimeter drum was rotated at a 10-min interval to minimize lichen sedimentation inside the calorimetric vessel. The lichen-derived heat production was calculated by considering that the instrument output is directly related to the heat evolved inside the calorimeter:

$$V = k\delta q/\delta t \quad (1)$$

where V is the thermopile voltage, k is an instrumental constant and q represents the heat evolved during the period of time t. By integrating the experimental curve (V versus t), it is possible to calculate the overall heat quantity, Q_{lichen}, which is directly proportional to the area (A_{lichen}) subtended by the curve:

$$Q_{\text{lichen}} = \epsilon A_{\text{lichen}} \quad (2)$$

The ϵ constant, (expressed in calories per cm^2) determined by a series of electrical calibration depends on the physical characteristics of the calorimeter in different experimental condition of temperature, sensibility and record scale and it is not correlated with the chemical system studied. During the calorimetric recordings the viability of the lichens did not vary significantly. The measurements of the metal–lichen interaction were performed as in the following schema:

reaction vessel	reference vessel
0.1 g of lichen in 2 ml of water pH 4.5	2 ml of water pH 4.5
2 ml [Me] in water pH 4.5	2 ml [Me] in water pH 4.5

After filling, the calorimeter was left to equilibrate for about 30 min, then the recorder was switched on and the thermopile voltage vs time curve recorded. When the curve reached a steady state, relative to the lichen basal heat, the calorimetric drum was rotated and therefore the lichen came in contact with the ion solution: so that the heat effect due to the metal–lichen interaction was recorded. The heat quantities associated with the specific interaction between the lichens and each metal ion have been determined by measuring the area subtended by the curve V versus time from the baseline, referring to the steady state of the basal heat effect, in an interval of 40 min and then the value has been normalized to 1 h and per gram of lichenic sample.

2.4. Data processing

2.4.1. Langmuir elaboration

In order to find out the overall apparent interaction constant relative to the metal–lichen coordination, for each different metal ion the Langmuir equation was used:

$$1/[\text{Me}]_{\text{ads.}} = 1/[\text{Me}]_{\text{ads. max}} + 1/K[\text{Me}]_{\text{ads. max}} \cdot 1/[\text{Me}]_{\text{sol.}} \quad (3)$$

where $[\text{Me}]_{\text{ads.}}$ represents the difference between the initial analytical metal ion concentration and the $[\text{Me}]_{\text{sol}}$. measured by AAS in the solution after contact with the lichen for 5 min; $[\text{Me}]_{\text{ads. max}}$ represents the maximum uptake of the metal ion. This value is obtained graphically from the intercept in the plot $1/[\text{Me}]_{\text{ads.}}$ versus $1/[\text{Me}]_{\text{sol.}}$; K is the value of the apparent interaction constant obtained from the angular coefficient of the straight line [20].

2.4.2. Thermodynamic data

After setting the instrumental conditions of the amplifier and the recorder, the appropriate calorimetric constant ϵ was determined which allowed the Q_{lichen} value to be calculated:

$$Q_{\text{lichen}} = \epsilon A_{\text{lichen}} \quad (4)$$

Because $-\Delta H_{\text{lichen}} = Q_{\text{lichen}}/\text{g}$ lichen, it is possible to evaluate the enthalpy variation associated with the overall lichen metabolism during one hour. The value of A_{lichen} was calculated by measuring the area subtended by the experimental curve (V versus t) during 10 min and then extrapolating it to 1 h.

So we finally obtained an overall enthalpy variation value ΔH_{lichen} expressed in calories per gram per hour (cal g^{-1} h^{-1}). The A_{lichen} values are the average of three different measures of the same calorimetric curve (V versus t); the ΔH_{lichen} value is obtained by the average of at least three different experiments performed in the same experimental conditions, i.e. at the same lichen quantity and at the same metal concentration level if present. All the concentration values refer to the solutions in the calorimetric vessel during the interaction with the lichens. It is to be noticed that the $\Delta H_{\text{Me-lichen}}$ normalized value does not correspond to a classic thermodynamic enthalpy of reaction, because it is not expressed in calories per mol. In fact it is impossible to say which molecule in the lichen could be responsible, or the only one responsible, for the metal coordination, so we considered the lichen 'in toto' as an overall coordinating agent in the calorimetric data processing as in the Langmuir elaboration. Hence the $\Delta H_{\text{Me-lichen}}$ values reported represent the total heat effect due to the reaction which takes into account the overall interaction between each metal ion and the lichen (chemical coordination, eventual intracellular metabolism).

3. Results

3.1. Metal ion-uptake

In Fig. 1, the behaviour relative to the uptake of each metal ion by the lichens are reported. It is firstly noticed that the maximum metal quantity is adsorbed in a few minutes: in particular for all the metals the maximum concentration adsorbed is 100%, except for Cu for which the maximum is 80%, using metal concentration equivalent to 10 mg l^{-1}. Therefore, the samples to which the Langmuir equation was applied were assessed 5 min after the contact between the lichen and the metal ion. It was noticed that the variability of the results on different samples of the same type of lichen is so low that the observed behaviour did not depend upon the intersample biological variation.

3.2. Determination of the apparent coordination constants relative to the metal–lichen interaction

The Langmuir plot relative to the uptake of all the metal ions under study are reported in Fig. 2. The straight lines have been obtained by means of the Eq. (3), which represents the linearized equation of Langmuir. In fact, the $K'_{\text{Me-lichen}}$ is defined as follows:

$$H_xL + Me^{x+} \leftrightarrow MeL + xH^+$$

$$K'_{\text{Me-lichen}} = \frac{[\text{MeL}][\text{H}^+]^x}{[\text{H}_x\text{L}][\text{Me}^{x+}]}$$

It is possible to insert $[H^+]$ in the $K'_{\text{Me-lichen}}$ value if $[H^+]^x$ is constant, therefore, the conditional coordination constant is obtained at constant pH and temperature values:

$$K_{\text{Me-lichen}} = \frac{[\text{MeL}]}{[\text{H}_x\text{L}][\text{Me}^{x+}]}$$

pH = const. and T = const.

The greater the $K_{\text{Me-lichen}}$ value, the greater is the capacity of the ligand (the lichen in our case) of adsorbing metal ion. It is to be noticed that the conditional constant calculated in the examined systems does not represent a thermodynamic coordination constant but, only an apparent complexing capacity. This is for two reasons: (1) because L in the examined systems is the lichen 'in toto' and not a single ligand molecule; (2) because these constants strongly depend upon the considered concentration range.

By examining tables, it is possible to know the $K_{\text{Me-lichen}}$ calculated for each examined ion and this trend is observed: $\text{Pb} \gg \text{Zn} > \text{Cd} \approx \text{Cu} \approx \text{Cr}$. Moreover, in this work, it has been possible to insert $[H^+]$ increases accordingly, but this increment is so low that the pH measurement of the solutions before and after the uptake of all the metal ions was unchanged. These pH controls were performed for each considered metal ion.

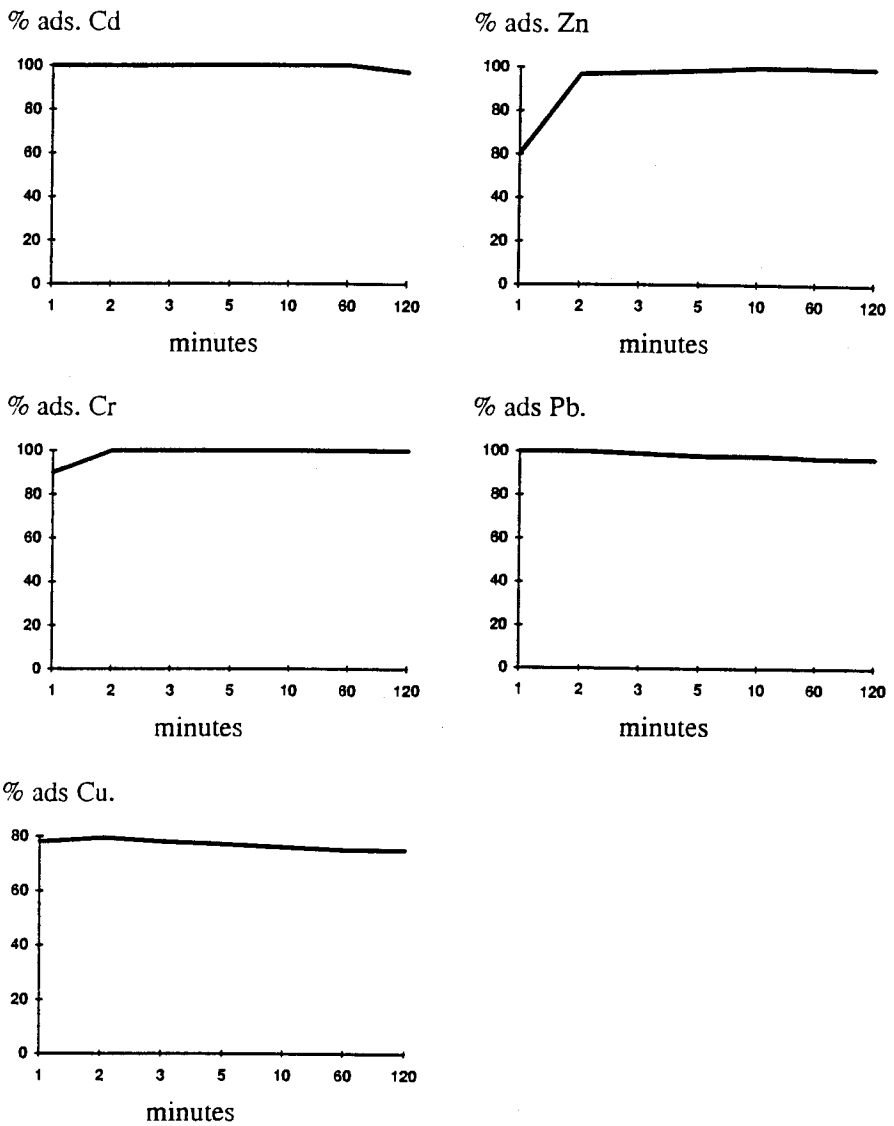

Fig. 1. Isothermal curves relative to the metal ion-uptake by the lichens at pH 4,5, [Me] = 10 mg l^{-1}.

3.3. Thermodynamic results

First of all it must be underlined that all the enthalpy variations observed are exothermic. From the thermogram reported in Fig. 3 the enthalpy variation (ΔH_{lichen}), relative to the lichen in the basal conditions (living lichen at physiological pH and in the absence of metal ions) has been calculated and it is equal to 5.08 cal g^{-1} h^{-1}. With respect to each considered metal ion the $\Delta H_{\text{Me-lichen}}$ (i.e. the enthalpy variation related to the metal ion–lichen interaction) has been obtained from the relative thermogram, by measuring the area subtended by the curves V versus time in a period of time and normalized to 1 h and by subtracting the basal heat quantity. In Fig. 4, two thermograms relative to Pb–lichen and Cr–lichen interactions are reported as an exam-

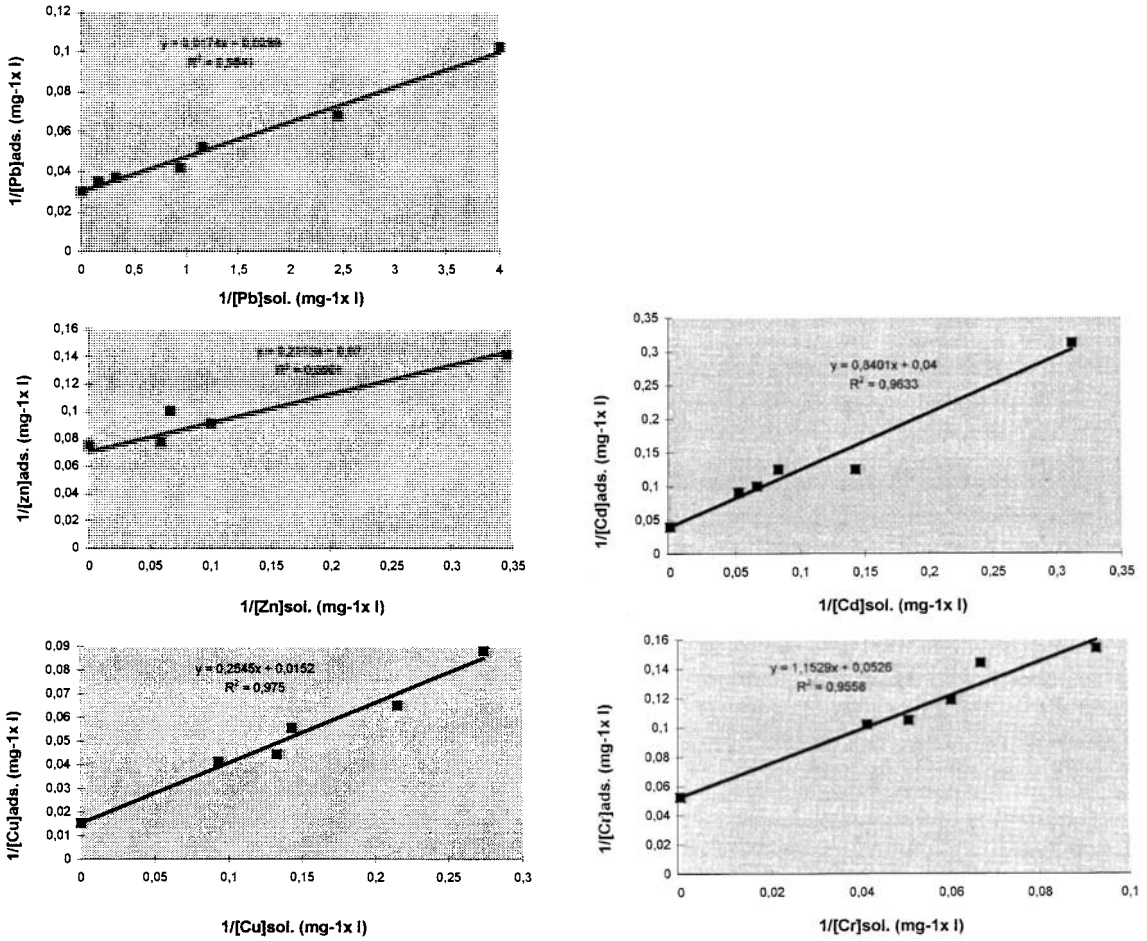

Fig. 2. (a) and (b) Interpolation curves relative to the Langmuir plot for each considered metal ion.

ple. As it can be seen in all cases the calorimetric response, relative to the basal condition of the lichen (i.e. before the drum rotation and therefore in the absence of metal ion), is shown; after that the metal–lichen interaction by the new steady state voltage line is indicated. The initial part of the curve does not represent the rotation peaks because, in this case, we cannot rotate the drum before the steady state relative to the basal heat has been reached. After that the calorimetric drum is rotated to mix the lichen solution together with the metal ion one. In Table 1, the $\Delta H_{\text{Me-lichen}}$ are listed and each value corresponds to a mean value of at least three different calorimetric measurements. The trend of ΔH values is in agreement with that showed by the interaction constants ($K_{\text{Me-lichen}}$).

4. Discussion and conclusions

The apparent complexing capacity values ($K_{\text{Me-lichen}}$), the enthalpy variations ($\Delta H_{\text{Me-lichen}}$) and the maximum concentration values of adsorbed metal ions ($[\text{Me}]_{\text{ads. max}}$) are shown in Tables 1 and 2. By comparing the complexing capacities with the enthalpimetric data, a similar trend comes out for the considered metal ions and also it seems that the lead adsorption on the lichen is stronger with respect to the other metal ions. In particular

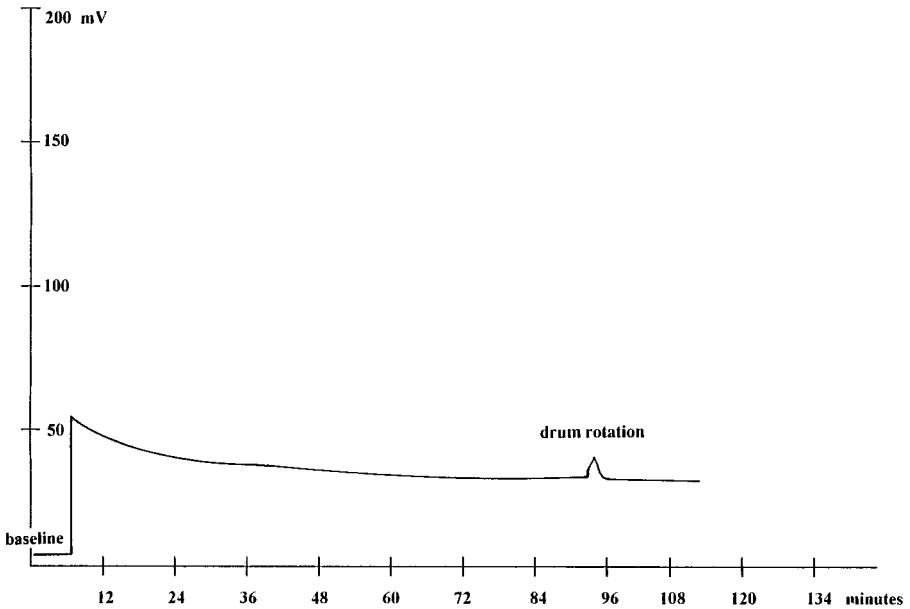

Fig. 3. Thermogram relative to the living lichen in the basal conditions.

it can be seen that the $K_{\text{Pb-lichen}}$ and also the $\Delta H_{\text{Pb-lichen}}$ are one order of magnitude greater than the respective ones relative to zinc ion and more than two orders of magnitude greater with respect to the other metals. With respect to chromium, cadmium and copper ions, a comparable and weak interaction with the lichen is observed.

By considering the equilibrium constant and the enthalpy trends the sequence $Pb \gg Zn > Cd \approx Cu \approx Cr$ is obtained. These results confirm that an useful correlation exists between the metal binding and the enthalpimetric evidence in metal uptake for the lichen *Evernia prunastri*. In contrast, if the maximum concentration of adsorbed metal is considered, the trend is different: $Cu \gg Pb > Cd > Cr > Zn$. In Nieboer and Richardson [21], a toxicity sequence for the same metal ions is reported with respect to algae and fungi, which confirms our trend of the maximum concentration of adsorbed metal. The authors suppose that these metal ions, being able to bind to non-oxygen centres in membrane proteins, are likely to induce serious membrane structural changes. The toxicity trend reported could explain our $[Me]_{\text{ads. max}}$ sequence, because the global metal uptake is a parameter which reflects a not equilibrium state. It takes account of many different processes such as the physical trapping of metals on the lichen surface and other chemical processes such as intracellular accumulation and ligand bindings. All these physico-chemical events contribute to the toxic effects of such metal ions on the lichens.

It is also well known [13] that some of the considered metal ions are involved in the intracellular uptake by the lichens. In particular, their accumulation is correlated with the presence of other ions such as calcium [22].

With respect to all the metal ions examined the same trend is observed for the constants and the enthalpy variations of interaction, whereas $[Me]_{\text{ads. max}}$ values are all of the same magnitude and they show a very different trend. This strange behaviour could be explained by considering that constants and enthalpies take account of chemical processes at equilibrium: such as the complexation interaction. The maximum metal concentrations adsorbed, on the contrary, reflect a more complicated process of interaction. The physical absorption phenomenon is involved in addition to chemical complexation (here evidenced). A further confirmation of some possible inversion of trend

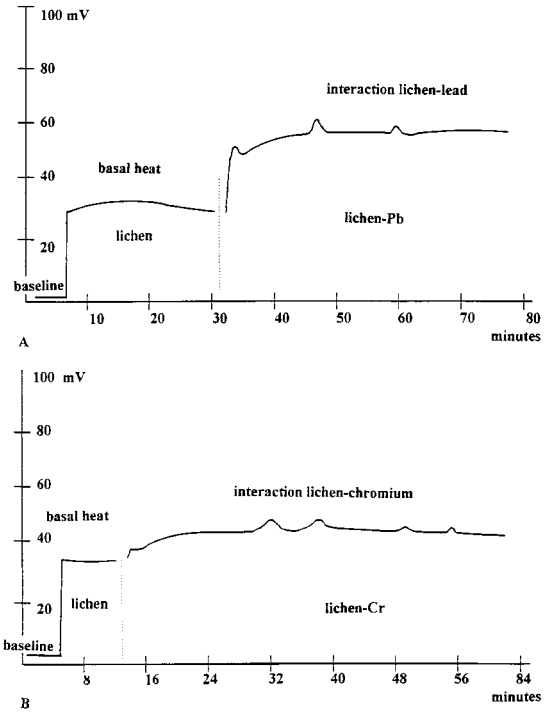

Fig. 4. (a) Thermogram relative to the Pb–lichen interaction. (b) Thermogram relative to the Cr–lichen interaction.

between $K_{\text{Me-lichen}}$ and $[\text{Me}]_{\text{ads. max}}$ is shown by the data reported by Davila and Millero [16] concerning the interactions of other ligands and algae with the same metal ions. The results of our experiments are more pertinent to wet deposition metal uptake than to air particulate metal uptake, the two main mechanisms of metal bioaccumulation. Our results, confirm a correlation between the apparent complexing capacity values and the enthalpimetric measurements in the metal uptake of the lichen *Evernia prunastri*. The calorimetric measurements during the binding process seem to be a novel and useful approach to ascertain that lichens are suitable bioaccumulators for soluble heavy metals around metal emitting pollution sources.

Table 1
Comparison between enthalpimetric measurements and Langmuir elaboration relative to each examined metal ion

Metal	$K_{\text{Me-lichen}}$ (mg l^{-1})	$-\Delta H_{\text{Me-lichen}}$ (cal g^{-1} h^{-1})
Pb	2.12	3.2
Zn	0.37	1.4
Cd	0.05	0.7
Cu	0.06	0.4
Cr	0.04	0.3

Table 2
$[\text{Me}]_{\text{ads. max}}$ relative to each examined metal ion

Metal	$[\text{Me}]_{\text{ads. max}}$ (mg l^{-1})
Pb	31.9
Zn	14.3
Cd	25.0
Cu	65.8
Cr	19

References

[1] B. Anzalone, Botanica Farmaceutica II, 1989.
[2] R. Herzig, et al., Int. J. Environ. Anal. Chem. 35 (1989) 43–57.
[3] W.A. Feder, W.J. Manning, Air Pollut. Control Assoc. Inf. Rep. 3, Pittsburg, Pennsylvania, 1979, p. 380.
[4] D.L. Hawksworth, Air pollution and lichens, in: B.W. Ferry, M.S. Baddley, D.L. Hawksworth (Eds.) London, 1973.
[5] D.L. Hawksworth, F. Rose, Nature 227 (1970) 145–148.
[6] B. Le Blanc, S. De Sloover, Can. J. Bot. 48 (1970) 1485–1496.
[7] H. Wanner, K. Amman, P. Berlincourt, P. Fillinger, Int. Symp. Climat. Freib. Geogr. Hefte., 1986 (in press).
[8] P.L. Nimis, Stud. Geobot. 5 (1985) 49–74.
[9] P.L. Nimis, Gortania 7 (1986) 147–172.
[10] L. Campanella, E. Cardarelli, M. Achilli, A. Bartoli, G. Massari, Ann. Bot. 52 (11) (1994) 239–266.
[11] E. Nieboer, et al., Can. J. Bot. 54 (1976) 724–733.
[12] D.H.S. Richardson, Pollution Monitoring with Lichens, Richmond, Slough, 1992.
[13] D.H.S. Richardson, Symbiosis 18 (1995) 119–127.
[14] M.A.V. Ribeiro da Silva, NATO ASI Ser., ser. C, vol. 119, 1982, pp. 439–488.
[15] P.W. Atkins, Chimica Fisica, Nicola Zanichelli, Bologna, 1986, pp. 814–818.
[16] M. Gonzalez-Davila, F.J. Millero, Geochim. Cosmochim. Acta 54 (1990) 761–768.
[17] I. Wadso, Acta Chem. Scand. 22 (1968) 927.
[18] L. Campanella, E. Cardarelli, M. Achilli, A. Bartoli, Inquinamento 6 (1993) 56–63.
[19] M.L. Antonelli, M. Luciani, L. Silvestroni, Thermochim. Acta 180 (1991) 107–115.
[20] M. Gonzalez-Davila, J. Colloid Interface Sci. 137 (1) (1990) 102–110.
[21] E. Nieboer, D.H.S. Richardson, Environ. Pollut. (Ser. B) 1 (1980) 3–26.
[22] D.H. Brown, A. Avalos, Ann. Bot. 71 (1993) 467–473.

ELSEVIER

Talanta 45 (1998) 1049–1060

Talanta

Scattering dilution method in Fourier transform infrared spectrometry[1]

Dedicated to: Professor Baiulescu

Mikio Kaihara [a,*], Yohichi Gohshi [b]

[a] *Department of Chemical Engineering, Ichinoseki National College of Technology, Aza-Takanashi, Hagisho, Ichinoseki, Iwate 021, Japan*

[b] *Department of Applied Chemistry, School of Engineering, The University of Tokyo, 7-3-1, Hongo, Bunkyo-ku, Tokyo 113, Japan*

Received 21 November 1996; received in revised form 21 May 1997; accepted 23 May 1997

Abstract

For the measurement methods of powder samples or muddy samples using infrared spectrometry, we proposed the scattering dilution method and scattering filter method. In our methods, the fabricating pellets are made by pressing mixed alkali halide powders (KBr/CsI). That is why the dilution powder's (KBr/CsI powders') packing ratio becomes almost 100%, thus giving the pellets a sufficient scattering effect. These methods have novel advantages versus transmission or diffuse reflectance methods although our proposal has much criticism and negative comments. © 1998 Elsevier Science B.V.

Keywords: IR; Scattering dilution method; Scattering filter method; Diffuse reflection method

* Corresponding author.

[1] This manuscript is based on one of the author's (Y.Gohshi's) invited lectures at the 13th Romania National Conference on Analytical Chemistry in May, 1996. This lecture was the last part of a three part lecture series (1992, 1994, 1996) in Romania.

In the last lecture (1996), he cited the 'scattering dilution method (SDM)' and the 'scattering filter method (SFM)' and pointed out that some of these novel methods are not easily accepted as V.A. Fassel (I.C.P.) [15,16] said that acceptance by the analytical community needs time.

Gohshi already insisted that Innovation needs three large elements [17]. These efforts in SDM or SFM are supported by a sustained need (measurement methods for highly scattering samples) and fundamental approach (theory, microscopic (Kubelka-Mumk) and macroscopic (Shibata)). Information (the opal glass method in VIS region) initiated and helped the research and progress. And, technologies (FT-IR on spherical mirrors) made actual breakthrough.

PII S0039-9140(97)00225-7

1. Introduction Hitherto, an ultimate analysis or a proximate analysis (carbon content, water content, etc.) are done as the analysis or evaluation methods for pitches or coals. According to the development of analytical instruments, gas chromatography or NMR were used for the analysis of the dissolved portion of pitches or coals samples. However, we gave much attention to infrared (IR) spectrometry because we could characterize pitches or coals in nature, which were seldom divided into each chemical component.

As a popular IR measurement method of powders or solid samples, the KBr pellet method has been used in many laboratories. Recently, the diffuse reflectance method (DRM) has been also widely used. The IR analysis of pitches or coals has been studied by Frederick [1], Osawa [2] Solomon [3] and many other researchers. In particular, Solomon examined the functional group type analysis of coals using the KBr pellet method [2].

We also thought that the KBr pellet method could be better for obtaining detailed information from the spectra of such samples because this method would give well reproducible spectra. In Fig. 1, the IR spectrum of a coal tar pitch is shown. We separately crushed the specimen and KBr well and prepared minute particles of less than 50 μm in diameter, and mixed 1 mg of the sample with 99 mg of KBr, then formed the specimen pellet and the reference pellet with a diameter of 10 mm ϕ using a vacuum press at a pressure of 7 t cm^{-2} [2]. Generally, we draw the so-called base line and remove the spectrum background from the raw spectrum and analyze the remainder as the absorption spectrum. But in comparing the absorption peak to the background of the raw data (Fig. 1), we had a suspicion as to whether or not the absorption peak could be correct. Solomon [3] and Osawa [2] already pointed out that this high spectral background would be caused by the scattering due to samples. So, we started our research to develop a new IR spectral measurement method that had high analytical precision.

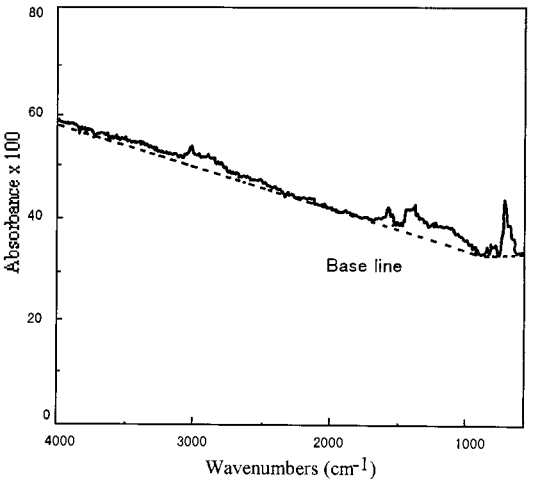

Fig. 1. Transmission spectrum of a coal tar pitch by KBr pellet method.

2. Scattering dilution method and the criticism

2.1. Background of the scattering dilution method

First, we examined methods which could get rid of most of the scattering. The relationships between scattering and refractive indices of the samples or matrix, scattering and wavelength or particle diameter are shown in Fig. 2. Refractive indices of samples and matrix are different in (A). When the wavelength is longer than the particle size, little scattering occurs. But it becomes significantly strong when the wavelength is almost comparable with the particle size. The refraction becomes dominant when the wavelength is smaller

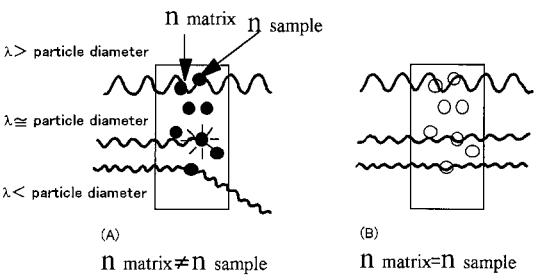

Fig. 2. Relationship between scattering and refractive indices (sample, matrix), scattering and wavelength or particle diameter.

Table 1
Refractive index (n) and carbon content of coals

	Tenhoku	Taiheiyo	Kashima	Akabira	Miike	Yubari	Moura	New River	Itmann
n	1.7	1.7	1.7	1.8	1.8	1.8	1.8	1.8	2.0
C% (d.a.f.)	72.7	77.8	78.1	83.4	84.5	86.2	87.6	89.0	90.2

than the particle size. The refractive index of the matrix is similar to those of the sample powders in (B). In this case, the incident light goes straight regardless of the sample grain sizes or the wavelength. So, the most straightforward way to suppress any background is to adopt a material with the same refractive index of the sample as the matrix. The relation of refractive index and carbon content of some major coals are summarized in Table 1. From this table, we understand that the refractive index of some major coals is distributed over a range of 1.66–1.96. The optical properties of major infrared transmission materials are compiled in Table 2. There are two groups with refractive indices that range from 1.5 to 1.7 and approximately 2.4. This table shows that appropriate transmission materials of infrared rays for the pellet method hardly exist in the range of the refractive index of coals. Only CsI ($n = 1.7$) is near those of coals.

So, we made the pellets of the same coal using KBr ($n = 1.5$) and CsI ($n = 1.7$). The measured IR absorption spectra are shown in Fig. 3. We understood that the background spectrum was substantially reduced. In other words, for the dilution matrix (the pellet method) having a refraction index near that of the sample, we could reduce the scattering caused by the sample particles and get good quality spectra. However, it is difficult to find a dilution matrix having a refractive index, n, similar to the sample's n. Thus, controlling the refractive index of the dilution matrix is useful for reducing the scattering, but there will be a limit. Even if the dilution material has an equal average refraction index such as pitches or coals, such samples are composed of particles with a different refraction index and have a refractive index distribution.

So, crushing such samples as much as possible has been a more popular method for reducing scattering than matching the refractive index [2]. However, powdering samples to small particles often needs a large effort and it sometimes changes the properties of the samples. Especially, in the case of pitch samples, we found crushing was not very useful. We suggested the reason to be that pitches were viscous and composed of quite minute heterogeneous grains of different chemical components.

Secondly, we examined methods that utilize scattering. We first tried DRM. In recent years, this method is widely used because sample preparation is relatively simple and the obtained spectra are similar to those from the KBr transmission method. The optics for DRM are shown in Fig. 4.

However, we found that DRM for pitches or coals is less reproducible than the KBr pellet method. The linearity of the calibration curve, in general, is not very good. The calibration curve becomes linear in the log–log graph [4], thus, there remains some difficulty [4,5]. Additionally, spectra are distorted by unstable scattering efficiency and distribution of the absorbing light path length. Enormous efforts have been done to improve the DRM quantification characteristics. A barrier metal plate to remove the specular reflectance light caused by the first powder layer has recently been proposed as shown in Fig. 4. Additionally, a specimen preparation tool [6], which makes improvement in spectra reproducibility, is proposed, but one of the most important merits of DRM, easy specimen preparation, could be sacrificed.

Finally, we studied the positive utilization of the scattering effect, i.e. achieving complete optical compensation between the specimen path and the reference path. This method was proposed by Shibata, as an opal glass method [7,8] in the visible region using opal glass as the diffuser in 1954. In Fig. 5, the concept of this method is

Table 2
Optical properties of IR transparent materials

Material	Refractive n	Reflectivity (%)	Solubility (g ml^{-1})	Density (g cm^{-3})	Melting point (°C)
NaCl	1.5	8.3	35.7	2.16	801
KBr	1.5	8.8	53.5	2.75	730
CsI	1.7	14.3	44	4.53	621
KRS-5	2.4	28.4	0.05	7.2	414
ZnSe	2.4	31	0	31	1100

illustrated. Setting the scattering plates (opal glass) on the front side of both the sample cuvette and the reference cuvette is necessary. In this case, from Eq. (1), we can get the true absorption spectra [7,8].

$$\log \frac{\alpha I_0}{\alpha I_p + \alpha I_d} = \log \frac{I_0}{I_p + I_d} = \log \frac{I_0}{I_t} = pE_t \quad (1)$$

where α is the scattering coefficient; I_0 is the incident light; I_t is the transmitted light; I_p is the pararell transmission light; I_d is the scattered light; pE_t is the semi-integral attenuance.

Shibata measured some biological liquid (suspension) samples, for example, chlorophyll, leaves and so on and obtained high quality spectra. He developed a detailed theory of the macroscopic optical meanings [7,8].

To our knowledge, this method has not been applied to IR spectrometry due to the lack of opal glass for IR work. An idea, then came to us, which is to use rough surface KBr pellets as opal glass. The spectrum is shown in Fig. 6, where (A) was taken using the KBr pellet method and (B) was done by this method. Comparing both results, it is clear that using a rough surface KBr pellet could be valid for reducing the spectral background to some extent. For further improvement, we sandwiched KBr powders between KBr pellets for generating more scattering and used this sandwich filter as the scattering plate. This method is roughly equal to a diffuse transmission method. The spectrum obtained by this method had significantly reduced the spectral background (Fig. 7). That is why we found that the opal glass method concept could be applied to deleting the large spectral background of pitches or coals (optically dark, solid powder samples) in the infrared region. However, a rough surface plate and fine powders were not very ideal for reducing the background. The rough surface pellet had an incomplete scattering capability. Using powder materials would give some problems, for example, low spectra reproducibility, low calibration curve linearity and so on (the same problems as the DRM), because powders do not have a stable packing efficiency or constant scattering effi-

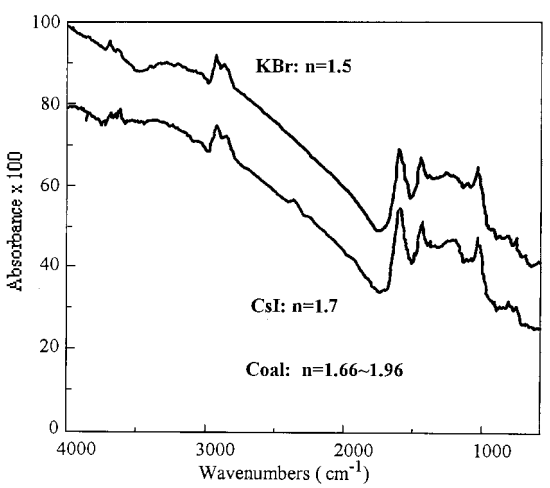

Fig. 3. Refractive indices of dilution materials and the profiles of transmission spectra of a coal.

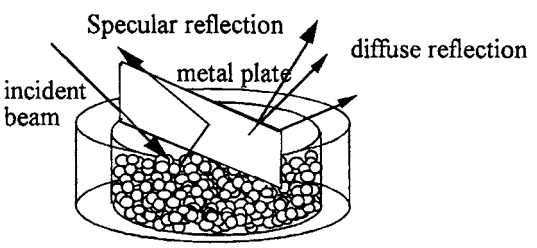

Fig. 4. Optics of diffuse reflection method (DRM).

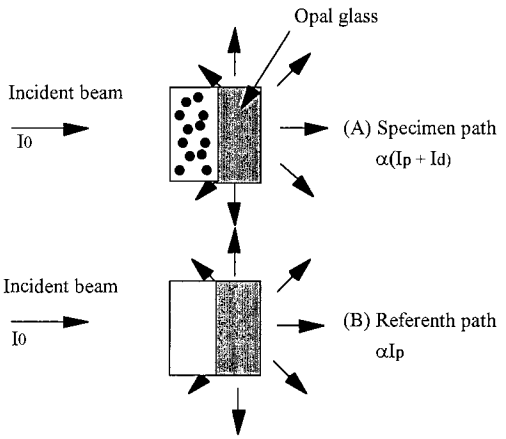

Fig. 5. Concept of opal glass method in visible region by Shibata.

ciency. Realizing the complete scattering with a perfect stable packing ratio of powders became our target. We needed some innovations to solve this contradiction in this field.

2.2. Scattering filter method and scattering dilution method

Therefore, we pursued methods to prepare a scattering plate which let infrared rays fully scatter, aiming at the resolution of the above-mentioned subject. As a result, we found that the plate which

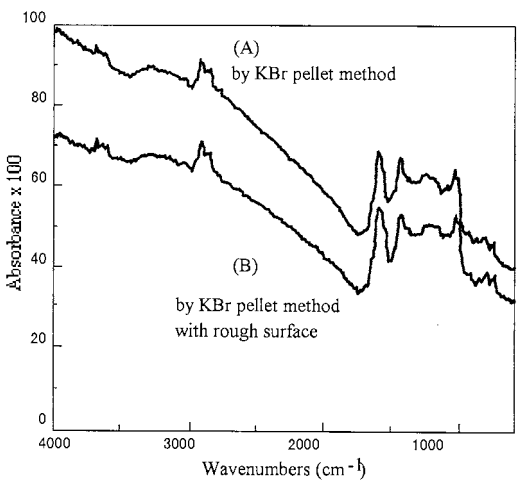

Fig. 6. The effect by using a rough surface KBr pellet to the spectral profile.

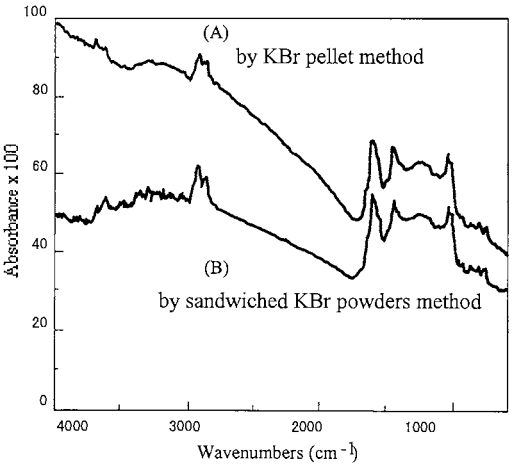

Fig. 7. The effect by sandwiched KBr powders to the spectral profile.

was composed of two types of powders having different refractive indices and was pressed under vacuum conditions gave a good scattering effect [9]. We show the general idea in Fig. 8. The scattering media as used before did not consider mixing different materials and press-forming them into a pellet. That is to say, to our knowledge, there was no idea for infrared spectrometry to use mixed nonhomogeneous alkali halide dilution materials.

In selection of these dilution materials, we referred to the optical properties of the major infrared transmission materials listed in Table 2.

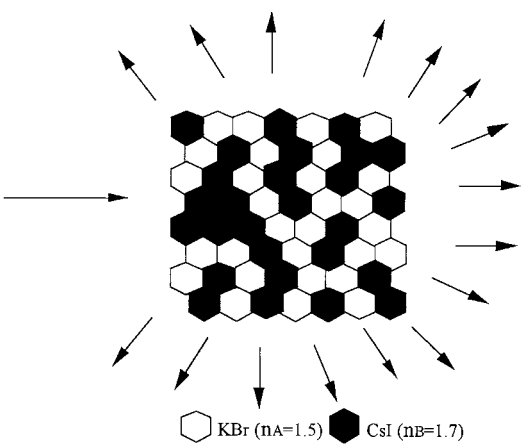

Fig. 8. Idea of mixed powders' pellet having different n components (nA, nB) for scattering media.

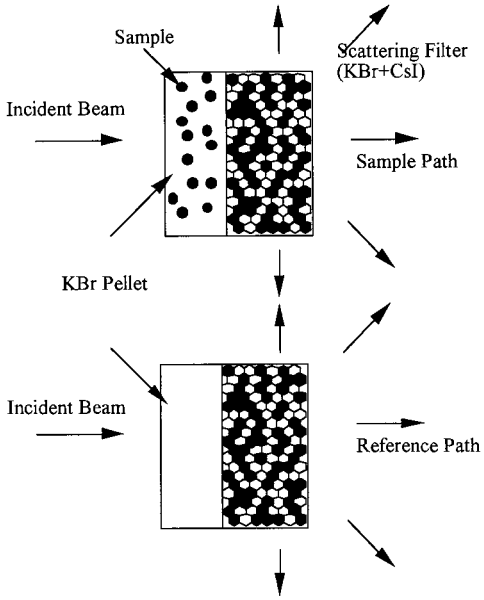

Fig. 9. Opal glass method with mixed alkalihalide pellet [scattering filter method (SFM)].

Among these, we adopted KBr and CsI which had different refractive indices and low reflection indices. When the reflection index was high, specular reflectance could be dominant and that could give a distorted spectra. In Fig. 9, we explained the concept of using the scattering plate, which we called the scattering filter method (SFM), that is

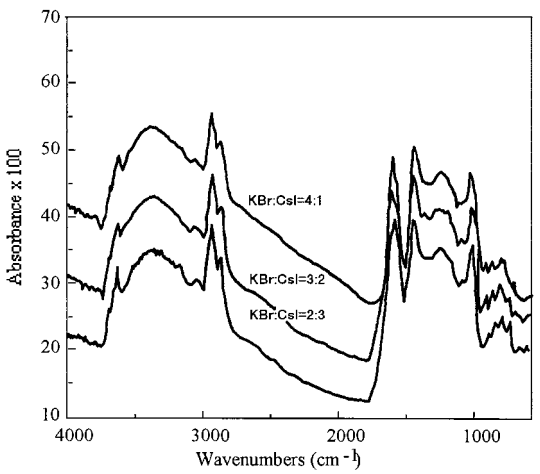

Fig. 10. Relation between KBr/CsI ratios and the background reduction effect of coal spectra.

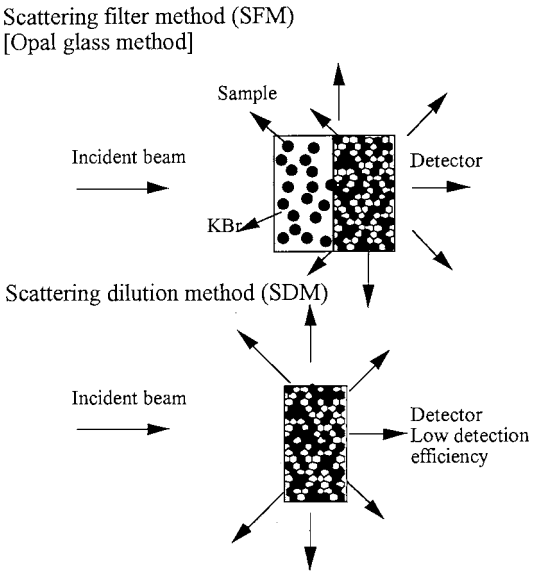

Fig. 11. Concepts of SFM and SDM.

essentially the same as the concept of the opal glass method. In Fig. 10, the influence of the CsI and KBr mixture ratio is shown. The optimum mixing ratio of KBr/CsI was 2/3 [10]. When the weight ratio of KBr and CsI is 2:3, if the size distributions could be the same, the capacity ratio becomes almost 1:1 as the density of KBr and CsI are 2.75 and 4.53, respectively. If the scattering effect mostly occurred at the powdery boundaries

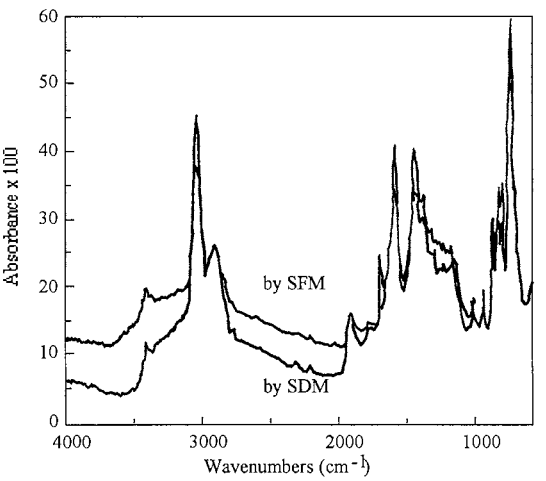

Fig. 12. Comparison of SFM and SDM.

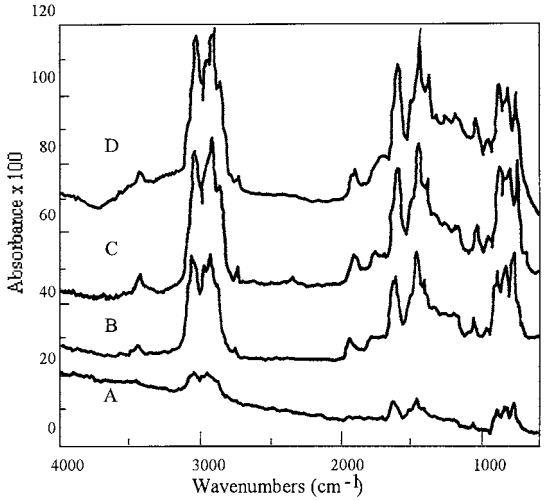

Fig. 13. Relation between spectral profiles and the sample powder size in SDM. A, <100 μm; B, <76 μm; C, <53 μm; D, <20 μm.

of KBr and CsI, each powder should mutually contact quite well after press forming. That is why, we estimated, this mixing ratio could be best for generating good scattering.

At this stage, though the improvement was large, there still remained a high background and our method (SFM) is not very different from the opal glass method. So, we pursued a more effective method for high quality spectra, and a theoretical explanation from a microscopic point of

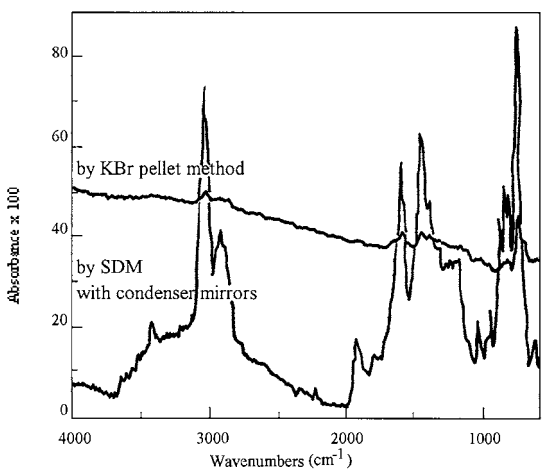

Fig. 14. Comparison of the spectra by KBr pellet method and SDM with condenser mirrors.

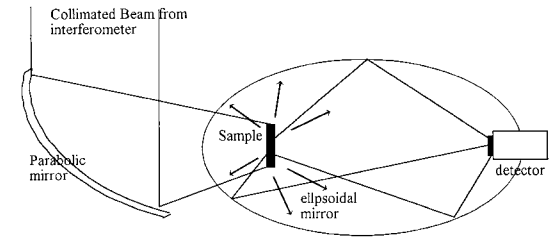

Fig. 15. Block diagram and profiles of light paths of a new accessory in FT-IR spectroscopy.

view. We proposed a new method which used mixed alkali halide powders as new dilution materials [11]. If any theory could exactly explain this new method, we could advance to the stage of an ideal spectroscopic method. A theoretical discussion will be given later. In Fig. 11, the macroscopic model concept of SFM and the scattering dilution method (SDM) are shown. Both methods are explained by Eq. (1) from a macroscopic point of view. Fig. 12 shows a comparison of the spectra of coal tar pitches taken by SFM and by SDM. The concentration of sample pellet was 1.0%. We crushed and then well mixed 1 mg of the sample and 99 mg of the mixed alkali halide, formed a sample pellet and a reference pellet of 10 mm ϕ diameter using a vacuum press at a pressure of 7 t cm^{-1} [2]. The grain size distribution

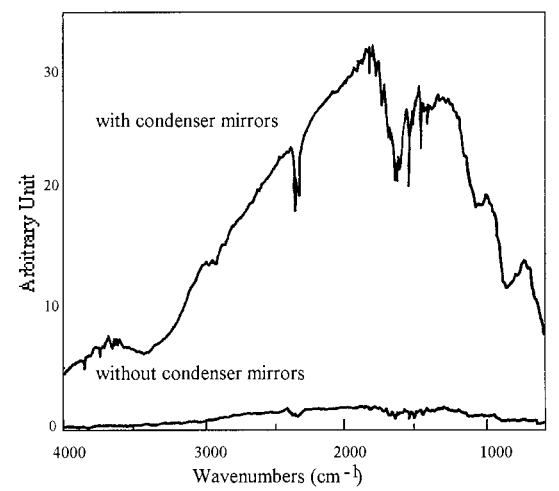

Fig. 16. Improvement in detection efficiency of lights transmitted and scattered.

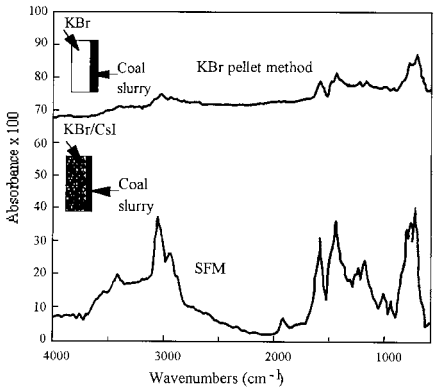

Fig. 17. IR spectra of a coal slurry (very viscous liquid) by KBr pellet method and SFM.

was under 120 μm in diameter. SDM is superior to SFM in sharpness or intensity of the absorption peaks, especially in the higher wave number region.

In the case of SDM, the optimized mixing ratio of KBr and CsI was also 2:3. In Fig. 13, the grain size effect of the mixed alkali halide powders is shown. When the distribution of the grain sizes of the mixed alkali halide is both under 20 and 50 μm, the obtained spectra have almost the same profiles. However, when the distribution of the grain size of the mixed alkali halides is under 106 μm, the obtained spectra have few small absorption peaks. We suppose that the size distributions of particles should be under 20–50 μm, which was almost the same as those of the DRM.

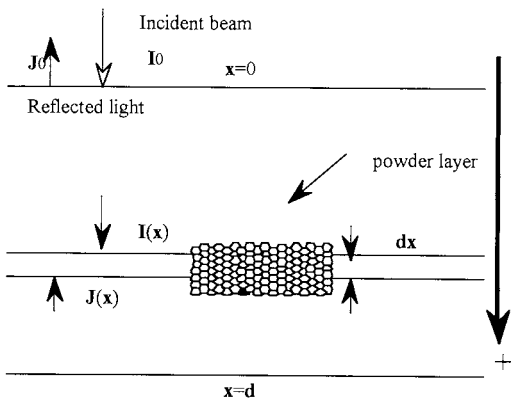

Fig. 18. Kubelka–Munk's model of different powder's layer.

2.3. Criticism of SDM and the subject

We submitted the results mentioned above with a title 'New dilution materials for sensitivity enhancement in the FT-IR spectroscopy of pitches as typical highly scattering samples,' which was published [10] in 1989. However, M.L.E. Tevruch and P.R. Griffiths criticized our paper [12]. They insisted that our conclusion was incorrect because our mixed alkali halide powders did not have a sensitivity enhancement effect in DRM. They applied the mixed alkali halide to DRM and the new dilution materials were not useful.

The scattering in DRM was caused by the refractive index difference between the air and the alkali halide, but the scattering in SDM was caused by the difference in the refractive indices between the CsI and the KBr. That is why the number of alkali halide species have no specular meanings in DRM. Their experimental results proved that their experiments and our experiments were both correct at the same time.

We felt that the second most important subject of SDM or SFM would be improvement of the detection efficiency of the scattered light. So, we compared the KBr pellet method with SDM using our new light collection accessories in Fig. 14. Without using the light collection accessories, the signal to noise (SN) ratio of the original (not corrected by the reference spectrum) spectrum is low, but with the condenser mirrors, absorptions are strong, and high quality spectra are provided with sharp absorption peaks even under a high scattering condition.

This optical system made from a combination of parabolic and oval mirrors is shown in Fig. 15 [13]. We show the improvement in the detection efficiency using this light collection optics in Fig. 16. The improvement of the collection efficiency of light energy became approximately 10–20 times.

In Fig. 17, we also compared a spectrum by SFM with condenser mirrors to a spectrum using the usual KBr pellet method of a coal slurry (high grade viscosity). The coated coal slurry on the surface of a mixed halide pellet was measured. As for a spectrum by SFM, the effectiveness was demonstrated by being an extremely sharp spectrum.

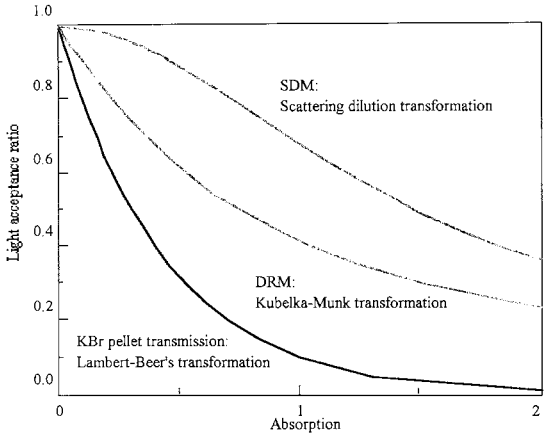

Fig. 19. Comparison of the transformation curve of SDM, DRM and transmission method.

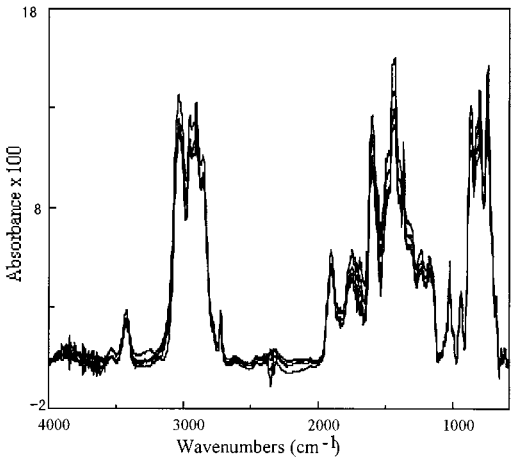

Fig. 21. Comparison of five spectra by DRM.

Because the preparation of alkali halide powders is a little troublesome, we developed a powder preparation method, the so-called recrystallization method [14]. Easier preparation makes the SDM/SFM more practical.

2.4. Theory of SDM and SFM

The macroscopic theory of SDM or SFM is based on Shibata's opal glass method. The incident light, which was impinged on the mixed alkali halide sample pellet or the reference pellet, was scattered quite well. That is to say, the scattered light by sample particles and the parallel transmission light will be scattered uniformly and completely and the constant part of such light will be detected. That is why we can obtain pE_t (Eq. (1)). We postuate that the Eq. (1) should be applied to SDM.

Next, as a microscopic theory, we applied the Kubeluka–Munk (K–M) theory to SDM as shown in Fig. 18. In the case of SDM, the impinged light should be quite well scattered shortly after the light enters the pellet. Therefore, we assumed that the completely scattered light would

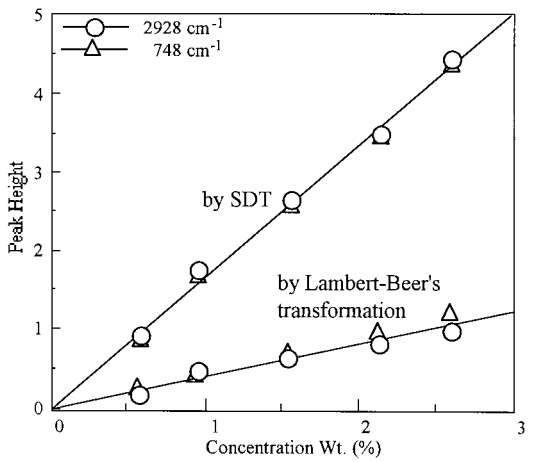

Fig. 20. Comparison of carribration curves by SDT and by Lambert–Beer's transformation.

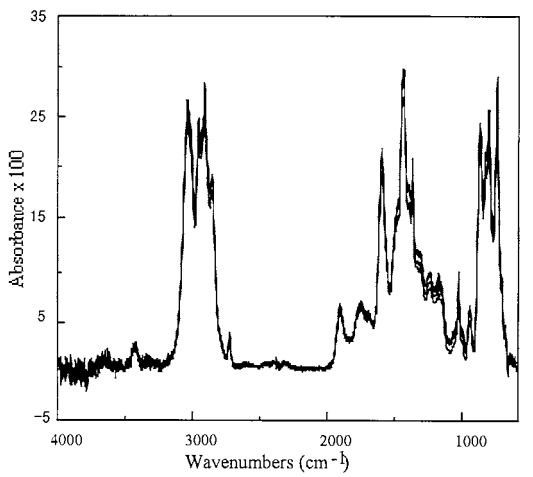

Fig. 22. Comparison of five spectra by SDM.

be impinged on the sample particles. This condition is also the supposition of the K–M theory. In the case of SDM with condenser mirrors, both front (T) and back (R) scattered light will be gathered. That is the reason why the relation between all the light acceptance ratios ($T+R$) and absorptions should be expressed as Eq. (2).

$$T+R=\frac{4\sqrt{\frac{k}{(k+2)}}+\frac{2}{k+2)}\left(e\sqrt{[k(k+2s)]}-e^{-}\sqrt{[k(k+2s)]}\right)}{\left(1+\sqrt{\frac{k}{(k+2)}}\right)^{2}e\sqrt{[k(k+2s)]}-\left(1-\sqrt{\frac{k}{(k+2)}}\right)^{2}e^{-}\sqrt{[k(+2s)]}} \quad (2)$$

where T is the transmission light; R is the reflectance light; s is the scattering efficiency; k is the absorption efficiency.

If we could suppose $s=1.0$, we can measure the light acceptance ratio and solve the above non-linear equation and obtain the absorption spectrum. This transformation, from the light acceptance ratio to k, we call scattering dilution transformation (SDT). From a microscopic point of view, we compared the three methods of transformation to absorption, i.e. Lambert–Beer's transformation, Kubeluka–Munk transformation, and SDT in Fig. 19.

Lambert–Beer's transformation: $k=\log(1/T)$

Kubeluka–Munk transformation: $k=s(1-R)^2/2R$

$$\text{SDT: } T+R=\frac{4\sqrt{\frac{k}{(k+2)}}+\frac{2}{(k+2)}\left(e\sqrt{[k(k+2)]}-e^{-}\sqrt{[k(k+2)]}\right)}{\left(1+\sqrt{\frac{k}{(k+2)}}\right)^{2}e\sqrt{[k(k+2)]}-\left(1-\sqrt{\frac{k}{(k+2)}}\right)^{2}e^{-}\sqrt{[k(k+2)]}}$$

In the case of DRM, the scattering coefficient, s, is not always constant because a powders' packing ratio is not always stable. We usually then, compensate the unstableness of s by dividing the detected intensity for the specimen by the detected intensity for the reference. But, in the case of SDM, s is quite stable, because the powder packing ratio is almost 100%. Judging from Fig. 19, a small change in the light acceptance ratio means a large change in the absorption in SDM. This tendency is remarkable in the range of the higher light acceptance region compared with DRM or the KBr pellet transmission method. This could mean that SDM is quite sensitive.

The calibration curve of a coal tar pitch is drawn in Fig. 20. Judging from the result, SDM is several times more sensitive than that of the transmission method and the linearity was the same as that of the transmission method. These results mean that SDM should be well explained by the K–M theory.

By the way, in the case of DRM, the reproducibility of spectra was sometimes said to be slightly poor [4,5]. We then, compared the reproducibility of spectra in the case of SDM and DRM. In Figs. 21 and 22, we overwrote five obtained spectra by DRM and SDM, respectively. In the case of DRM, we separately crushed the sample and KBr and prepared minute particles of less than 50 μm, then a 1 mg sample and 99 mg of KBr were mixed quite well. In the case of SDM, the prepared sample powder (1 mg) and the halides (99 mg) were mixed. We formed the sample pellet and the reference pellet having a diameter of 10 mm ϕ using a vacuum press at a pressure of 7 t cm^{-1} [2]. As a result, the largest difference in peak heights of DRM was roughly 5–10%, but the largest difference in peak heights of SDM was roughly 5% or less. SDM has a better repeatability of spectra than DRM.

2.5. Future of SDM

Characteristic points of each method, the transmission method, DRM and SDM/SFM, are expressed in Table 3. The level of scattering by

Table 3
Comparison of the measurement methods depending on the scattering level by powders

	Scattering by specimen	Transmission	DRM	SDM/SFM
Qualitative				
Background	Low	○	○	○
	High	x	○	○
Sharpness of absorption band	Low	○	○	○
	High	x	○	○
Specular reflection	Low	○	○	○
	High	○	△	△
Effect of $\bar{d}$	Low	○	△	○
	High	○	△	○
Quantitative				
Repeatability	Low	○	△	○
	High	△	△	○
Linearity of calibration	Low	○	△	○
	High	x	△	○
Sensitivity	Low	△	○	○
	High	x	○	○

samples and the qualitative and quantitative spectral qualities were compared. An ideal measurement method was defined as the method which is background free, specular reflectance free and has a sharp spectra without concerning the scattering level caused by the samples.

In the case of transmission, low scattering samples have high quality spectra without a large background, but highly scattering samples such as coal tar pitches or coals, have a large background, winding baseline and small absorption peaks with poor analytical precision. In the case of DRM, even scattering samples have relatively good spectra, but the quantitative precision is not very good. In the case of SDM, even samples of high scattering give good spectra, and the quantitative precision is also good. Fig. 23 is an illustration between the relative position of each measurement method based on Table 3. The theory of SDM is well explained by SDT and this means SDM is the opposite of the transmission method. The proposed expression for SDT is well suited to the Kubeluka–Munk differential equations and has a general feature. Still more, almost every powder sample (pitches, coals, organic materials polymers, metal oxide and so on) should have a scattering effect, more or less. That is why SDM could be a standard measurement method in the future.

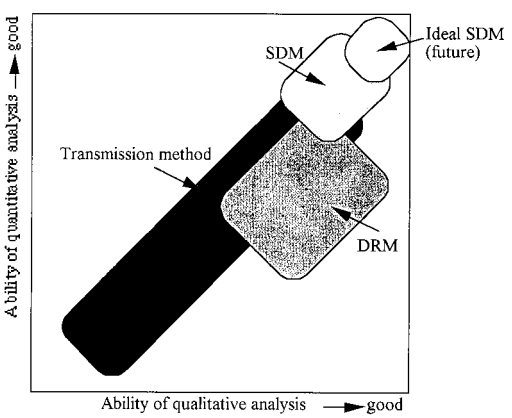

Fig. 23. Comparison of measuring methods for nonhomogeneous powder samples.

3. Conclusion

SDM could be a standard measurement method in the future. We could use DRM as a method characterized by its simple preparation, and use SDM as a method characterized by its analytical reliability.

Acknowledgements

We are grateful to the NKK corp for the sample preparations and back-up. Further more, we give our thanks for the preparation of this paper by Yasunori Ohoka, Tomoko Kumagai, and Noemi Cristina Murakami (students of Ichinoseki National College of Technology).

References

[1] P. Fredericks, Appl. Spectrosc. 39 (1985) 303.
[2] Y. Osawa, H. Muramatsu, S. Fujii, J. Fuel, Soc. Jpn. 48 (1969) 703.
[3] P. Solomon, R. Carangelo, Fuel 61 (1982) 663.
[4] Hattori, Murakami, Jasco, IR Report 2 (1984) 1.
[5] T. Suzuki, S. Nishizawa, Tanso 141 (1990) 45.
[6] M.L.E. Tevruch, P.R. Griffins, Appl. Spectrosc. 43 (1989) 1492.
[7] K. Shibata, J. Spectrosc, Soc. Jpn. 15 (1966) 86.
[8] K. Shibata, K. Benson, A.A. Calvin, M. Calvin, Biophys. Acta. 15 (1954) 461.
[9] M. Kaihara, H. Mametsuka, H. Iwata, Y. Gohshi, Anal. Lett. 21 (1988) 681.
[10] M. Kaihara, H. Mametsuka, H. Iwata, Y. Gohshi, Appl. Spectrosc. 43 (1989) 154.
[11] M. Kaihara, H. Mametsuka, H. Iwata, Y. Gohshi, Appl. Spectrosc. 43 (1989) 477.
[12] M.L.E. Tevruch, P.R. Griffins, Appl. Spectrosc. 43 (1989) 1293.
[13] M. Kaihara, H. Mametsuka, N. Gunji, Y. Gohshi, Rev. Sci. Instrum. 60 (1989) 1015.
[14] M. Kaihara, H. Mametsuka, N. Gunji, Y. Gohshi, Appl. Spectrosc. 44 (1990) 111.
[15] H.S. Robert, F.A. Velmer, G.D. Flesch, H.J. Svec, Anal. Chem. 52 (1980) 2283.
[16] V.A. Fassel, Spectrochim. Acta Part A 40A (1985) 1281.
[17] Y. Gohshi, Bunseki (1987) 772.

ELSEVIER

Talanta 45 (1998) 1061–1071

Talanta

Mechanistic study and kinetic determination of vitamin C employing the sequential injection technique

Salah M. Sultan *, Nabeel I. Desai

The Chemistry Department, King Fahd University of Petroleum and minerals, KFUPM PO Box # 2026, Dhahran, 31261, Saudi Arabia

Received 7 May 1997; received in revised form 1 July 1997; accepted 2 July 1997

Abstract

For the first time, the robust sequential injection (SI) technique has been employed for full kinetic investigation of the oxidation reaction of vitamin C. Iron(III) in sulphuric acid media was used as an oxidant and 1,10-phenanthroline as an indicator and the resulting solution of tris 1,10-phenanthroline-iron(II) complex was monitored spectrophotometrically at 510 nm. The reaction orders with respect to each reagent were determined by the SI-technique and were found to be 1, 1, and -1 for vitamin C, iron(III) and hydrogen ions respectively. On the basis of these values a rate law was developed and a plausible mechanism was established. A kinetic method for the analysis of vitamin C in drug formulations based on the results obtained above was thus validated. The drug in the range 20–300 ppm was determined by the kinetic method using 1.6×10^{-3} mol dm^{-3} ammonium ferric sulphate in 0.02 mol dm^{-3} sulphuric acid with the aspiration volume of 944 μl and the fixed-time of 180 s. The results thus obtained by the SI-kinetic method were statistically compared with those obtained by the British Pharmacoebia standard method and found to be accurate, precise and fast. © 1998 Elsevier Science B.V.

Keywords: Sequential injection analysis; Kinetics; Mechanism; Fixed-time method; Vitamin C; 1:10-phenanthroline-iron(II) complex; Iron(III) oxidant

1. Introduction

Vitamin C (1-keto-1-threo-hexono-*g*-lactone-2,3-enediol) is commonly known as l-ascorbic acid. It is the enediol-group [–C(OH)=C(OH)–] which is responsible for the molecule's acidic and reducing properties. It has received the attention of various researchers in different fields and many analytical methods have been described so far [1–3].

Determination of vitamin C using flow injection analysis (FIA) has been applied, but they are complex and subject to numerous interferences [2].

In the British Pharmacopoeia (BP) monograph [4], a titrimetric method involving the use of Cerium(IV) as a titrant and ferroin sulphate as an indicator in sulphuric acid media, is the one described for the determination of vitamin C in drug formulations.

* Corresponding author. Tel.: +966 3 8604277.

PII S0039-9140(97)00217-8

Apart from the original papers describing the principles of sequential injection analysis (SIA) [5–11], few publications have appeared in the literature so far. It is apparent that the sequential injection SI technique is still infant and its full versatility and capacity is yet to be explored. The remarkable development of SI technique allows mechanistic scientists to use simple, computer controlled instrument that has been lacking for decades, which will replace the time consuming manual dilution procedures that are currently being performed. In SIA, reaction times and mutual zone dispersion can be altered directly from the computer keyboard. Therefore an attempt will be made to exploit the capabilities of this technique in studying the chemical kinetics of the system. The methods developed so far by SI were aimed to satisfy some desirable features required for routine analysis. These features include, simplicity, short time of analysis where no sacrifice should be made with respect to precision and accuracy. Tolerance of the methods to uncontrolled factors, known as ruggedness, is also considered. The research in the exploration of the capability of this technique led to publish a first ever paper in kinetic studies by Sultan [12]. As was observed from the literature, most if not all of the kinetic methods of analysis reported so far by SI-technique lack a full investigation of the kinetics and mechanism of the chemical reactions involved. Therefore, it can be inferred that with the emergence of a robust technique such as the SI-technique there is a excellent chance to reshape the kinetic methods of analysis in order to include a full investigation of the kinetics and mechanism of the chemical reaction. In addition the computer controlled SI-technique could lead to a vast resurgence in the activity in this field and other related ones.

The utilization of SI-technique for the first time in the full kinetic studies of vitamin C, the oxidation reaction mechanism of which still remains unexplored, is expected to be a new addition to literature not only to the analytical chemist and FIA world but also to the kineticists and mechanistic researchers. Reaction rate constants as well as other kinetic parameters will be determined and a plausible mechanism for the reaction will be proposed.

2. Experimental

2.1. Apparatus

2.1.1. Sequential injection analyzer

The sequential injection analyzer was constructed from the following components:

1. A high quality peristaltic pump (C4V, Alitea, Medina, WA) is used. It features eight stainless steel rollers on individual bearings.
2. A Valco-10 port selector valve (cheminert, Valco, Houston, TX) is used to select the flows. Upchurch fittings (Upchurch, Oak Harbor, WA) were used to lock unused ports.
3. The holding coil and the reaction coil tubings as well as the tubings connecting the different units were made of PTFE (0.8 mm i.d.). Teflon nuts and ferrules (Upchurch, Oak Harbor, WA) were used to fit these tubes into the different parts of the apparatus. Pump tubings were Phar Med™ 1.02 mm i.d. (Upchurch, Oak Harbor, WA) held on the pump rollers by FIA peristaltic pump tubing adapters (Upchurch, Oak Harbor, WA).
4. Mixing chamber of 20 mm i.d. is connected at position ten of the multi-port selector valve, which is used for kinetic studies.
5. A Spectronic Mini-20 spectrophotometer (Milton Roy, Rochester, NY), with a grating monochromator detector, a Unovic ultra-micro-flow-through cell (Unovic instruments, NY) of 20 μl size and with a pathlength of 1.0 mm is used.
6. A personal computer (Austin computers system, Austin, TX) working at 33 MHz, and equipped with a 120 MB hard disk, 4 MB RAM and VGA Graphics, is used to monitor digitally the pump and the valve. The communication between the computer and the external devices was expanded by a general purpose I/O board (Model ADA-110, Real Time Devices (RTD), State Collage, PA). The computer is also used to collect the data, alternatively the data is recorded by Model 0555 single channel strip-chart recorder (Cole Parmer, Chicago, IL).
7. In addition to the personal computer a Recorder Model 0555 single channel-strip-

chart recorder (Cole Parmer, Chicago, USA) was used for peak absorbance-time recording.

Perkin Elmer Lambda 5 UV/Visible spectrophotometer equipped with 10.00 mm cells was used for preliminary investigations.

2.1.2. Software packages

Microsoft windows 3.10 with DOS 6.20 was utilized to run the following softwares for research work.

FIA Lab 2.0 (beta release), Alitea USA, Inc. is used to program the sequential injection system for analysis under predefined specific conditions.

Sigmaplot, version 1.02, Jandel Scientific Corporation, for data handling calculations and forming graphs.

Microsoft Word, version 6.0, Microsoft Corporation, for building tables and text writing.

2.2. Reagents

2.2.0.1. Iron(III) solution. An equimolar stock solution of 0.05 mol dm^{-3} iron(III) solution was prepared in 0.05 mol dm^{-3} sulphuric acid by dissolving exactly about 6.0412 g of dried ammonium ferric sulphate $NH_4Fe(SO_4)_2.12H_2O$ (99% BDH, Poole, UK) in 0.05 mol dm^{-3} sulphuric acid in a 250 ml calibrated flask. The solution was heated for one hour with frequent stirring, then kept in dark and used after 24 h to guarantee complete dissolution into a clear green transparent solution.

Solutions of ammonium ferric sulphate (AFS) in which the concentration of acid is lower than the concentration of AFS could not be prepared as in such solutions partial dissolution takes place due to hydrolyzation. Therefore equimolar stock solution was prepared.

The working solutions were 0.01 mol dm^{-3} ammonium ferric sulphate (AFS) in 0.01 mol dm^{-3} sulphuric acid, and 2.5×10^{-3} mol dm^{-3} (AFS) in 2.5×10^{-3} mol dm^{-3} sulphuric acid. The former was used to determine order of reaction with respect to sulphuric acid and vitamin C also this was used to find the activation energy at different temperatures and calibration curve, and the latter was used to determine the order of reaction with respect to AFS.

Solutions of AFS having concentrations more than 0.01 mol dm^{-3} were not used in the experiments as AFS solutions have their own colour and interferes with the colour of tris-1,10-phenanthroline iron(II) complex. Moreover very dilute equimolar solutions, that is 5.0×10^{-4} mol dm^{-3} AFS in 5.0×10^{-4} mol dm^{-3} H_2SO_4 were not used either since the acid concentration is very low and such AFS solutions hydrolyze or degrade into a turbid solution.

2.2.0.2. 1,10-phenanthroline monohydrate solution. 0.01 mol dm^{-3} solution of this indicator (Fisher Scientific, ACS reagent) $C_{12}H_8N_2.H_2O$ was prepared by adding the required amount in 100 ml flask. The solution was made up to the volume and then heated in a water bath for one hour with shaking at different times. It was used only when freshly prepared.

2.2.0.3. Sulphuric acid solution. A stock solution of 10 mol dm^{-3} H_2SO_4 (95–98%, Specific gravity 1.84 kg l^{-1}, Merck, UK) was prepared.

A series of working solutions were prepared from 0.001 mol dm^{-3} to 4.0 mol dm^{-3}. Among these 1.0 mol dm^{-3} solution was used to determine the order of reaction with respect to acid, activation energy and the calibration curve, 0.5 mol dm^{-3} was used for order of reaction with respect to ammonium ferric sulphate. For the order of reaction with respect to vitamin C the same acid present in 0.01 mol dm^{-3} ammonium ferric sulphate was utilized which was 0.01 mol dm^{-3}, so acid was not introduced from a separate port through the selector valve in the method.

2.2.0.4. Vitamin C solution. This was always freshly prepared $C_6H_8O_6$ (99.5% Fluka AG, Switzerland, batch No. 238304 883). Therefore, after repeated experimental trials, the working solution were proved to be 4.0×10^{-2} mol dm^{-3}, because at this concentration, the change of colour with respect to time was slow enough to be measured spectrophotometrically, and this concentration was used for determining order of reaction with respect to ammonium ferric sulphate. Similarly working solutions of 1.13×10^{-3} mol dm^{-3} (200 ppm) was used when determining or-

der of reaction with respect to vitamin C, and 8×10^{-3} mol dm^{-3} when determining order of reaction with respect to sulphuric acid and the activation energy. The calibration curve was determined by exactly about 5.68×10^{-3} mol dm^{-3} (1000 ppm) stock solution and from this 1.1355×10^{-4}, 2.8388×10^{-4}, 5.678×10^{-4}, 8.5164×10^{-4}, 1.1355×10^{-3}, 1.4194×10^{-3}, 1.7033×10^{-3} mol dm^{-3}, or respectively 20, 50, 100, 150, 200, 250, 300 ppm solutions were prepared.

2.2.0.5. Tablets formulations of proprietary drugs. The stock solutions of 1000 ppm (m/V) for each proprietary drug were prepared by crushing five to ten tablets priorly weighed out, and dissolving an amount of the powder equivalent to a certain mass of the tested drug in water or dilute acid solution.

The proprietary drug 'Beminal C' capsules were not crushed, only the casing of the capsules were removed to obtain the active ingredients.

The proprietary effervescent tablets (Redoxon, Upsa and Cal-C-Vita) were weighed as mentioned above and dissolved directly to give a stock solution of 1000 ppm (m/V) without further treatment. The stock solution of 1000 ppm (m/V) for Octovit and Beminal C proprietary drugs were prepared by heating the mixture at 50°C for 15–30 min in a water bath, shaken for five minutes, filtered through an ordinary filter paper, washed with the hot water or hot acid solution several times and finally the filtrate plus washings were completed to the mark in a calibrated flask. The temperature was not raised above 50°C when preparing stock solutions of Octovit and Beminal C as vitamin C dissociates at higher temperatures. Appropriate dilutions were made from these stock solutions.

2.3. Method

2.3.1. Determination of flow-rate

The pump speed is altered by changing the revolution per minute-meter (rmp) on the instrument. The rate of flow of the reagent inside the pump tubes was found out by withdrawing liquid (distilled water) at one end of the tube and collecting at the other end in a measuring cylinder. The volume of the liquid collected at a certain time gives the flow-rate in ml min^{-1} at that particular rpm value. This process was repeated for different rpm values giving different amount of flow-rate, thus a graph between flow-rate and rpm is formed to obtain a straight line giving slope and intercept as follows: Flow-rate $= 0.73644 + 0.05726$ rpm

Therefore, for pump speed of 500 rpm, which was used in this work, flow-rate will be 1.77 ml min^{-1} or 29.5 μl s^{-1}.

2.3.2. Procedure

The SIA manifold is represented by Fig. 1 with the pump operable at a flow rate of 29.5 μl s^{-1}, volumes from standard solutions could be withdrawn for certain time precisely adjustable by the pump stroke through the computer board and the following steps were performed:

1. Iron(III), sulphuric acid, 1,10-phenanthroline and the drug (vitamin C) were connected to the selector valve through ports 2, 3, 4 and 9 respectively. Whereas the mixing chamber was connected at port 10. Water (deionized) is pumped as a carrier solution through valve 1 in the forward mode to the detector then waste for 25.0 s (737.5 μl).
2. About 80 μl each of the above reagents around the selector valve were introduced sequentially into the holding coil in the reverse mode for 3.0 s (88.5 μl), then transferring the excess together with some carrier to auxiliary waste through valve 7 in the forward mode for 8.0 s (236 μl).

   In the analysis method, Iron(III) and sulphuric acid concentrations are kept constant by transferring fixed volumes by fixing the time of withdrawal of reagents with the help of a computer program. The fixed volume being transferred is previously calculated from known concentrations of these reagents. Iron(III) is aspirated into the holding coil in a reverse mode for 8.0 s (236 μl) and transferred to the mixing chamber by forward motion of the pump for 10 s (295 μl). Sulphuric acid is taken in the holding coil for 1.0 s (29.5 μl) which is then pushed into the mixing chamber together with the carrier for 12.0 s (354 μl). 1,10-phenanthroline is also withdrawn for 8.0

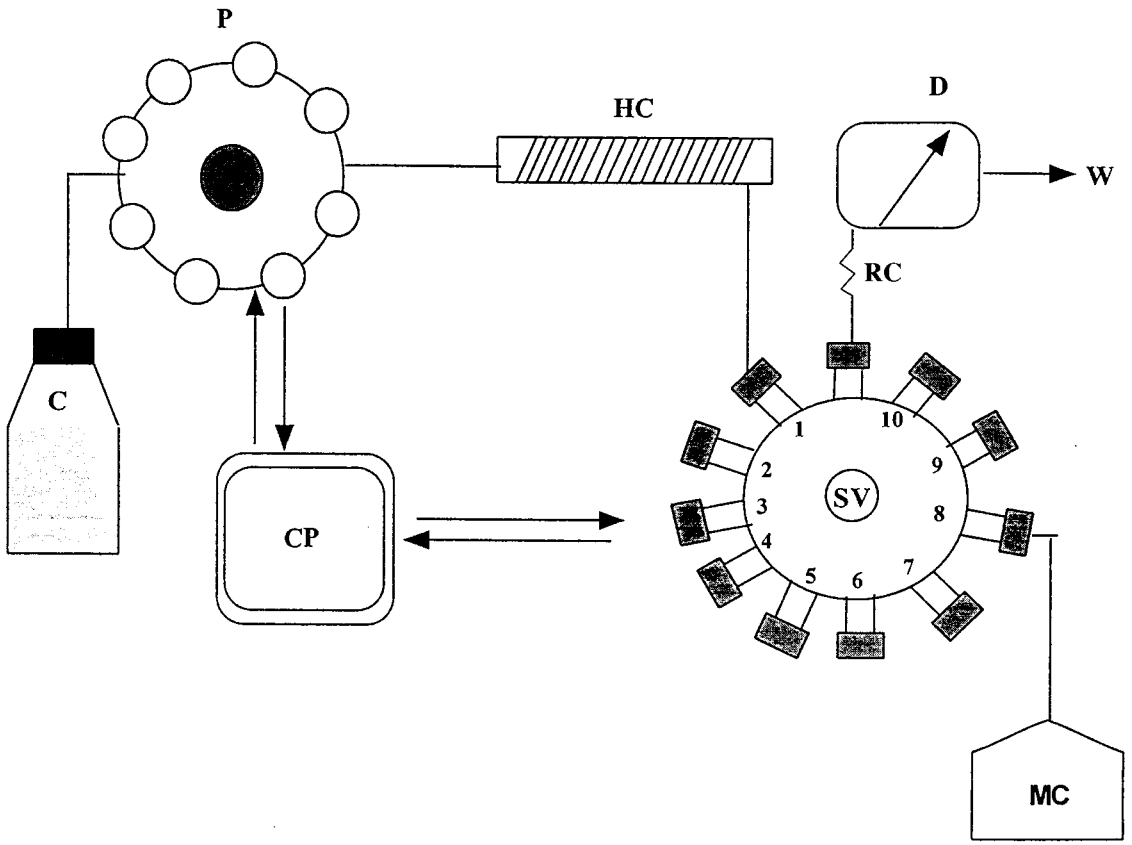

Fig. 1. SIA-manifold; C, carrier; P, peristaltic pump; HC, holding coil; SV, selector valve; RC, reaction coil; D, detector; CP, computer; MC, mixing chamber and W, waste.

s (236 μl) then pushed to the mixing chamber for 12.0 s (354 μl). This phase is referred to as the transfer volume (V_T).

3. A certain known volume of the test solution is withdrawn into the holding coil then pushed into the mixing chamber together with some carrier solution for 16.0 s (472 μl) in a separate step referred to as the sample volume (V_S). Note that both V_T and V_S were always pushed to the mixing chamber for 50.0 s (1475 μl) to keep its volume constant throughout the experiment. Moreover the concentration of test solution was kept at least ten times diluted as compared to the other reagents in the mixing chamber.
4. A known volume of the aliquot solution is withdrawn from the mixing chamber and transferred to the holding coil in a reverse mode for 3.0 s (88.5 μl), then pushed in the forward direction for 28.0 s (826 μl) to the detector for signal monitoring. This phase is referred to as the analysis volume (V_A).
5. For kinetic measurements at variable times, reagents and drug solutions are arrested for the predetermined time in the mixing chamber prior to the analysis volume is withdrawn.

For determining reaction orders with respect to one reactant, all other components are kept constant and treated as V_T. The one varied is considered the V_S and the process is repeated by taking different volumes for V_S from a single standard

solution, so that the kinetics monitored corresponds to different required solutions i.e. having different concentrations.

3. Results and discussion

3.1. Kinetic determination of vitamin C

The present SIA method was based on the oxidation of vitamin C with iron(III) in sulphuric acid media [12], using 1,10-phenanthroline indicator. The kinetics of this reaction was thoroughly investigated by monitoring the increase of absorbance of tris-1,10-phenanthroline iron(II) red complex at the wavelength of maximum absorbance which is 510 nm. The intense absorption of tris-1,10-phenanthroline iron(II) complex is due to charge transfer from iron(II) to 1,10-phenanthroline ligand [13]. The reaction order with respect to each reactant, the activation energy were determined and the mechanism was postulated. Finally a kinetic method for the determination of vitamin C was adopted.

The partial orders with respect to the different variables, assumed to have an influence on the rate equation, was carried out by considering the differential form of the rate equation involving the pseudo zero order reactions; when the rate of formation of the products and other reactants are virtually negligible. In this method [14] all reactants, except the one under investigation [A], are kept constant at higher concentrations and the rates are measured for the reactant being investigated by varying its concentration. From the plot between absorbance and time, rates were calculated by applying the fixed-time method which involves measuring the absorbance as 'ΔA' of the product at a predetermined time 'Δt' from the start of the reaction, $\text{Rate} = \Delta A/\Delta t = k'[\text{A}]n$ where k' is the pseudo rate constant and n is the order of the reaction.

3.2. Reaction order with respect to $[H^+]$

The complexation reaction was found to be reasonably slow in sulphuric acid concentration in the range of 6.6×10^{-3} and 3.66×10^{-2} mol dm^{-3} allowing for possible kinetic investigations to be followed spectrophotometrically. It was observed that the reaction rate decreases as the acid concentration is increased as represented in Fig. 2. The change in the absorbance with respect to time for each aliquot drawn from the mixing chamber was monitored to find the order of reaction with respect to sulphuric acid. The concentration of ammonium ferric sulphate and ascorbic acid were kept constant at 1.6×10^{-3} and 6.4×10^{-4} mol dm^{-3} respectively while the concentration of the acid in the mixing chamber was varied by withdrawing the acid from the mixing chamber through valve # 3 at different fixed times of 32 s. The rate of the reaction is then dependent on the change of the concentration of sulphuric acid, and hence:

$$\text{Rate} = k'[\text{H}^+]n$$

The plot of log $(\Delta A/\Delta t)$ versus log$[H_2SO_4]$, values for which are to be found in Table 1, for the determination of the order of reaction and rate constant with respect to hydrogen ions resulted in a straight the slope of which was -1.04 with a correlation coefficient (r^2) of 0.977. The

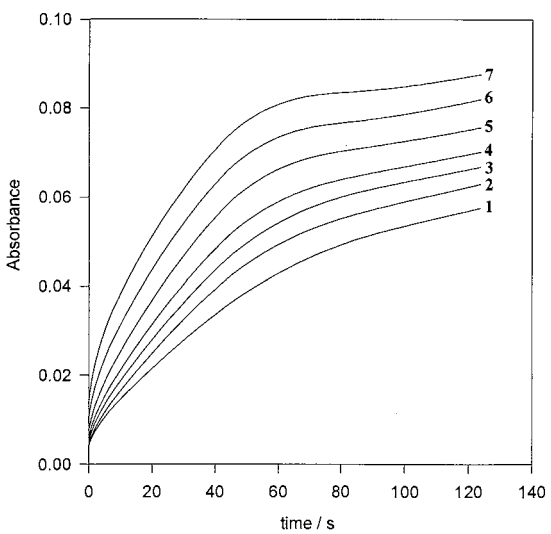

Fig. 2. Absorbance–time curves for the determination of the order of reaction with respect to hydrogen ions. $[Fe^{3+}] = 1.6 \times 10^{-3}$ mol dm^{-3}; [vitamin C] $= 6.4 \times 10^{-4}$ mol dm^{-3}; $[H_2SO_4]$ = (1) 0.0366; (2) 0.0316; (3) 0.0266; (4) 0.0216; (5) 0.0166; (6) 0.0066 mol dm^{-3}; delay time, $d_t = 12.0$ s.

Table 1
Calculated rates of the reaction at 25°C for different sulphuric acid concentrations at constant concentrations of ammonium ferric sulphate (1.6×10^{-3} mol dm^{-3}) and ascorbic acid (6.4×10^{-4} mol dm^{-3})

No.	[H$^+$] in mol dm^{-3}	log[H$^+$]	ΔA	$\Delta A/\Delta t$	log $\Delta A/\Delta t$
1	0.0066	−2.1805	0.01530	4.8920×10^{-3}	−2.3105
2	0.0116	−1.9355	0.01370	4.3638×10^{-3}	−2.3601
3	0.0166	−1.7799	0.01120	3.5687×10^{-3}	−2.4475
4	0.0216	−1.6655	0.00714	2.2812×10^{-3}	−2.6418
5	0.0266	−1.5751	0.00644	2.0585×10^{-3}	−2.6864
6	0.0316	−1.5003	0.00443	1.4151×10^{-3}	−2.8492
7	0.0366	−1.4365	0.00427	1.3642×10^{-3}	−2.8651

order of the reaction with respect to hydrogen ion concentration is therefore equal to inverse one (-1), indicating that hydrogen ions are generated as a product. From the slope, the value of the pseudo rate constant k' was found to be equal 4.34×10^{-5} s^{-1}.

3.3. Reaction order with respect to ammonium ferric sulphate

The order of reaction with respect to ammonium ferric sulphate was determined by observing the change in the absorbance with respect to time (Fig. 3) for each aliquot drawn from the mixing chamber. The concentration of sulphuric acid and ascorbic acid were kept constant at 1.79×10^{-2} and 5.6×10^{-3} mol dm^{-3} while the concentration of ammonium ferric sulphate (AFS) in the mixing chamber was varied between 2.75×10^{-4} to 3.75×10^{-4} mol dm^{-3} by withdrawing the AFS from valve #2 at different times. The rate of the reaction is then dependent on the change of the concentration of (AFS) as follows:

$$\text{Rate} = k'[\text{Fe(III)}]n$$

Rates were calculated from the absorbance–time plots by measuring the absorbance as 'ΔA' of the product at a predetermined time 'Δt' from the start of the reaction.

The plot of log($\Delta A/\Delta t$) versus log[Fe^{3+}] for the determination of order of reaction and rate constant with respect to ammonium ferric sulphate (Table 2) resulted in a straight line the slope of which was 0.937 with a correlation coefficient (r^2) of 0.962 indicating that the order of reaction with respect to ammonium ferric sulphate concentration is equal to one. From the intercept the rate constant k' equals to 4.29×10^{-5} s^{-1}.

3.4. Reaction order with respect to ascorbic acid (vitamin C)

Absorbance–time curves were run (Fig. 4) and the order of reaction with respect to vitamin C was determined. The concentration of sulphuric acid and ammonium ferric sulphate were kept constant at 2.162×10^{-3} mol dm^{-3} each, while

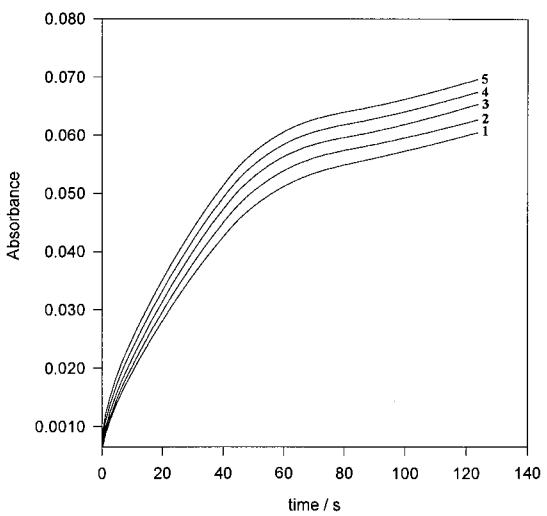

Fig. 3. Absorbance–time curves for the determination of the order of reaction with respect to ammonium ferric sulphate. [vitamin C] = 5.6×10^{-3} mol dm^{-3}; [H_2SO_4] = 1.79×10^{-2} mol dm^{-3}; [Fe^{3+}] = (1) 2.75×10^{-4}; (2) 3.00×10^{-4}; (3) 3.25×10^{-4}; (4) 3.50×10^{-4}; (5) 3.75×10^{-4} mol dm^{-3}; delay time, d_t = 12.0 s.

Table 2
Calculated rates of the reaction at 25°C for different ammonium ferric sulphate concentrations at constant concentrations of sulphuric acid (0.0179 mol dm^{-3}) and ascorbic acid (5.6×10^{-3} mol dm^{-3})

No.	$[Fe^{3+}]$ in mol dm^{-3}	$\log[Fe^{3+}]$	ΔA	$\Delta A/\Delta t$	$\log \Delta A/\Delta t$
1	3.75×10^{-4}	−3.4260	0.0136	2.598×10^{-3}	−2.5853
2	3.50×10^{-4}	−3.4559	0.0134	2.564×10^{-3}	−2.5911
3	3.25×10^{-4}	−3.4881	0.0118	2.266×10^{-3}	−2.6448
4	3.00×10^{-4}	−3.5229	0.0114	2.175×10^{-3}	−2.6626
5	2.75×10^{-4}	−3.5607	0.0103	1.965×10^{-3}	−2.7067

the concentration of vitamin C was varied between 1.38×10^{-4} and 2.148×10^{-4} mol dm^{-3}. This was achieved by withdrawing the vitamin C at different times from the mixing chamber through valve # 9. The rate of the reaction is therefor dependent on the change of the concentration of vitamin C as under:

$$\text{Rate} = k'[(\text{vitamin C})]n$$

Again by applying the fixed-time method rates were calculated from the plot of Fig. 4 by measuring the absorbance as 'ΔA' of the product at a predetermined time 'Δt' from the start of the reaction the values of which are introduced in Table 3.

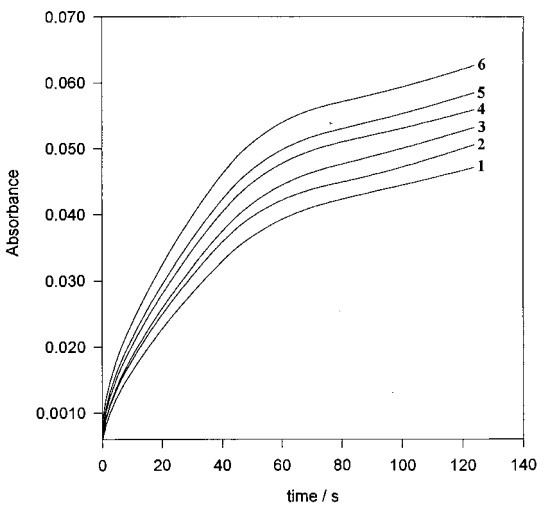

Fig. 4. Absorbance–time curves for the determination of the order of reaction with respect to vitamin C. $[Fe^{3+}] = [H_2SO_4] = 2.162 \times 10^{-3}$ mol dm^{-3}; [vitamin C] = (1) 1.3810×10^{-4}; (2) 1.5345×10^{-4}; (3) 1.6879×10^{-4}; (4) 1.8414×10^{-4}; (5) 1.9948×10^{-4}; (6) 2.1483×10^{-4} mol dm^{-3}; delay time, $d_t = 12.0$ s.

The plot of $\log(\Delta A/\Delta t)$ versus log[vitamin C] resulted in a straight line the slope of which was 1.05 with a correlation coefficient (r^2) of 0.987 indicating that the order of reaction with respect to vitamin C concentration is therefore equal to one. From the intercept value, the rate constant k' was found to be equal to 48.98×10^{-5} s^{-1}.

3.5. Activation energy

Experiments were conducted at varied temperatures between 20.0–45.0°C keeping the concentration of the solutions in the mixing chamber (m.c.) constant that is 1.6×10^{-3} mol dm^{-3} iron(III), 0.03 mol dm^{-3} sulphuric acid, 3.2×10^{-4} mol dm^{-3} vitamin C and 1.6×10^{-3} mol dm^{-3} 1,10-phenanthroline. This was done by fixing the time of withdrawal of each reagent from their respective ports. Runs were repeated at different temperatures. The pseudo-first order rate constants were calculated for each kinetic curve at different temperatures as given in Table 4.

Regression analysis of the plot of $\log k'$ verses $1/T$ (Table 4) was carried out using the following Arrhenius (R) equation

$$\log k' = -\frac{E_a}{2.303R}\frac{1}{T} + \log[A]$$

where E_a is the activation energy; R is the gas constant ($R = 8.314$ J K^{-1} mol^{-1}); T is the temperature in Kelvin and A is the pre-exponential factor. The activation energy (E_a) is calculated from the intercept of the plot of $\log k'$ and inverse of temperature in kelvin and was found to be = 146.72 kJ mol^{-1}. This value is similar to the previously reported value [12] which was reported to be 145 kJ mol^{-1}.

Table 3
Calculated rates of the reaction at 25°C for different ascorbic acid concentrations at constant concentrations of sulphuric acid (0.0179 mol dm^{-3}) and ammonium ferric sulphate (5.6×10^{-3} mol dm^{-3})

No.	[Vitamin C] in mol dm^{-3}	log[Vitamin C]	ΔA	$\Delta A/\Delta t$	$\log \Delta A/\Delta t$
1	2.148×10^{-4}	−3.6679	0.0153	7.328×10^{-3}	−2.1350
2	1.995×10^{-4}	−3.7001	0.0137	6.558×10^{-3}	−2.1833
3	1.841×10^{-4}	−3.7349	0.0126	6.041×10^{-3}	−2.2189
4	1.688×10^{-4}	−3.7727	0.0118	5.643×10^{-3}	−2.2485
5	1.535×10^{-4}	−3.8140	0.0103	4.924×10^{-3}	−2.3077
6	1.381×10^{-4}	−3.8598	0.00965	4.617×10^{-3}	−2.3356

4. Reaction mechanism

The rate law, as can be derived from the partial orders of the reaction, that is one with respect to ammonium ferric sulphate or iron(III), one with respect to ascorbic acid and minus one with respect to hydrogen ions. The rate law thus has the following form:

$$\text{Rate} = k\frac{[Fe^{3+}][\text{ascorbic acid}]}{[H^+]}$$

It was also found that it is a two step reaction with a molecularity of 1:2 ascorbic acid to iron(III) respectively.

The fact that, the rate of the oxidation is retarded at higher acid concentrations, would certainly indicate that it is the ascorbate anion (HA^-) and not the ascorbic acid molecular form is the reacting species. This is confirmed by the fact that the reaction stops at pH lower than 0.5 where the anions associate in the reversible step of the following typical weak acid reaction:

Table 4
Calculated values of rate constants for the reaction mixture containing 1.6×10^{-3} mol dm^{-3} ammonium ferric sulphate, 0.0316 mol dm^{-3} sulphuric acid and 3.2×10^{-4} mol dm^{-3} vitamin C at variable temperatures

No.	T (°C)	$1/T\times10^3$ (K)	k' (10^{-3})	$\log k'$
1	20.0	3.41297	0.058631	−4.23187
2	25.0	3.35570	0.187253	−3.72757
3	30.0	3.30033	1.199140	−2.92113
4	35.0	3.24675	1.774557	−2.75091
5	40.0	3.19489	3.823448	−2.41754
6	45.0	3.14465	6.503393	−2.18686

$$H_2Asc \Leftrightarrow 2H^+ + Asc^{2-}$$

It is necessary to report that the ascorbic acid second dissociation constant was found to be 1.7×10^{-5}. The protons shifting between the enol and keto forms are the ones possible to initiate the reaction as they are susceptible to electrophilic species.

The following plausible mechanism is suggested and proved to be consistent with the above rate law:

$$H_2Asc \Leftrightarrow H^+ + HAsc^- \quad (1)$$

$$HAsc^- + Fe^{3+} \Leftrightarrow Fe^{2+} + HAs\dot{c} \quad (2)$$

$$HAs\dot{c} + Fe^{3+} \Leftrightarrow Fe^{2+} + Asc^{2-} + H^+ \quad (3)$$

$$H_2Asc + 2Fe^{3+} \Leftrightarrow 2Fe^{2+} + 2H^+ \quad (4)$$

Table 5
Calibration equations at different fixed times using 1.6×10^{-3} mol dm^{-3} ammonium ferric sulphate 0.02 mol dm^{-3} sulphuric acid

Time (s)	Calibration equation	Correlation coefficient (r^2)
60	$A = 0.0047 + 0.00007C$	0.9978
180	$A = 0.0104 + 0.000171C$	0.9992
300	$A = 0.0151 + 0.000190C$	0.9938
480	$A = 0.0191 + 0.000207C$	0.9892

Table 6
Statistical comparison of the results obtained by the SIA method and those obtained by the BP method for the analysis of vitamin C in proprietary drugs

Drug	Supplier	Contents (mg)	Mean recovery +SD%*		t**
			SIA method	BP method	
Redoxon	Roche, Switzerland	Vitamin C (1000)	99.22 ± 0.8	99.53 ± 0.9	0.87
Upsa	Lab. Upsa, France	Vitamin C (1000)	99.57 ± 0.6	99.41 ± 0.3	0.60
Cal-C-Vita	Roche, Swizerland	Vitamin C (1000) Calcium (250) Vitamin D (300 i.u.) Citric acid (1350) Vitamin B6 (15) Carbohydrates (881) Sodium (170)	99.76 ± 0.8	100.2 ± 0.8	1.23
Octovit	SK and F, England	Vitamin C (30) Vitamin A (2500 i.u.) Vitamin B1 (1) Vitamin B2 (1.5) Vitamin B6 (2) Vitamin B12 (2μg) Nicotinamide (20) Vitamin D (100 i.u.) Vitamin E (10) Calcium (100) Iron (10)	100.1 ± 0.5	99.86 ± 0.7	1.07
Beminal with C Fortis	Wyeth-Ayerst, Canada	Vitamin C (300) Vitamin B12 (mcg) Thiamine (35) Riboflavin (15) Niaciamide (50) Pyridoxine (5) Pantothenic Acid (18.4)	98.93 ± 1.0	98.77 ± 0.9	0.36

* Standard deviation (SD) for five determinations based on label claim, $n = 5$.
** Theoretical value at 95% confidence level = 2.13.

It is now apparent that the ascorbate anion is generated in a preequilibrium reversible step thus reacting with one mole of iron(III) in the slow rate determining step giving ascorbate anion radical which in turn reacts with another molecule of iron(III) to give final products. The overall reaction equation thus obtained is also consistent with the experimental molecularity. It is interesting to emphasize that the assumption of the ascorbate anion radical being the active reacting species is not acceptable simply because, if so considered, the mechanism steps would not be consistent with the rate law experimentally deduced.

5. Analytical Appraisals

The calibration curves were obtained by plotting absorbance versus time for a wide range of vitamin C concentration keeping other reactants constant at 1.6×10^{-3} mol dm^{-3} ammonium ferric sulphate in 0.02 mol dm^{-3} sulphuric acid. Measurements for absorbance values were taken at different fixed times of 60, 180, 300, 480 s. The calibration plot showed excellent linearity for the determination of vitamin C concentration in the range 20–300 ppm. It is apparent from Table 5 that the fixed time of 180 s gives the best correla-

tion coefficient. Hence for the determination of vitamin C in proprietary drugs the best calibration chosen for analysis of the drug in pharmaceutical preparations is as follows:

$$A = 0.0104 + 0.000171C$$

6. Application

The sequential injection fixed-time method was applied to the determination of vitamin C in the proprietary drugs. The analysis was repeated six times and the results obtained were found to be highly precise with the standard deviation of less than 1.2% and a recovery of not less than 99.89% of the claimed content in the drugs. The method suffered no interferences from excipients usually added to the drug formulations such as calcium, citric acid, carbohydrates and vitamins B, and D. The accuracy was judged by comparing the results obtained for the same batch of samples with those obtained by the British Pharmacopeia method [3].

It has been found that sequential injection fixed-time method [14] is simple, accurate, more sensitive than the spectrophotometric methods and the electrochemical methods of this compound. The present method is not elaborate and time consuming as compared to the chromatographic or even the manual spectrophotometric methods. The results for the analysis of proprietary drugs with both the SI method and the BP method introduced in Table 6 shows the percentage recovery, the standard deviation and the Student's t-test values. The calculated Student t-test proves that the present SIA kinetic method is accurate and precise.

7. Conclusion

It can be seen that with the emergence of robust techniques such as the SI-technique there is a excellent chance to reshape the kinetic methods of analysis in order to include a full investigation of the kinetics and mechanism of chemical reactions. The reaction of vitamin C with iron(III) as an oxidant in sulphuric acid media using 1,10-phenanthroline indicator was studied. Kinetic parameters, such as the order of the reaction with respect to each reactant and the activation energy, were all determined, and accordingly the mechanism is postulated thus validating a method for the determination of vitamin C. The kinetics thus validated, led to the exploration of an accurate, precise and reliable kinetic method for the determination of this compound in its pharmaceutical preparations.

Acknowledgements

Mr. Nabeel Ibrahim Desai wishes to thank KFUPM for the award of scholarship to study for M.S. degree.

References

[1] S.M. Sultan, E. Bishop, J. Pharm. Biomed. Anal. 8 (4) (1990) 345.
[2] S.M. Sultan, A.M. Abdennabi, F.O. Suliman, Talanta 41 (1) (1994) 125.
[3] S.M. Sultan, Talanta 40 (5) (1993) 593.
[4] British Pharmacopoeia, 5th ed., vol. II, HM Stationary Office, London, 1988, pp. 47–48.
[5] J. Ruzicka, T. Gubeli, Anal. Chem. 63 (1991) 1680.
[6] T. Gubeli, G.D. Christian, J. Ruzicka, Anal. Chem. 63 (1991) 2407.
[7] A. Baron, M. Guzman, J. Ruzicka, G.D. Christian, Analyst 117 (1992) 1839.
[8] J. Ruzicka, E.H. Hansen, Flow Injection Analysis, 2nd ed., Wiley, New York, 1988.
[9] A. Ivaska, J. Ruzicka, Analyst 118 (1993) 885.
[10] J. Ruzicka, G.D. Marshall, Anal. Chim. Acta. 237 (1990) 329.
[11] G.D. Christian, J. Ruzicka, Anal. Chim. Acta. 261 (1992) 11.
[12] S.M. Sultan, F.E.O. Suliman, Analyst 111 (1996) 617.
[13] E. Bishop, Indicators, Pergamon Oxford, 1973.
[14] S.M. Sultan, Analyst 113 (1988) 149.

ELSEVIER

Talanta 45 (1998) 1073–1080

Talanta

Multivariate calibration applied to synchronous fluorescence spectrometry. Simultaneous determination of polycyclic aromatic hydrocarbons in water samples

R. Ferrer, J.L. Beltrán, J. Guiteras *

Departament de Química Analítica. Universitat de Barcelona, Diagonal, 647. Barcelona, E-08028, Spain

Received 28 April 1997; received in revised form 7 July 1997; accepted 7 July 1997

Abstract

Synchronous fluorescence spectra of mixtures containing ten polycyclic aromatic hydrocarbons (anthracene, benz[a]anthracene, benzo[a]pyrene, chrysene, fluoranthene, fluorene, naphthalene, perylene, phenanthrene and pyrene) have been used for the determination of these compounds by Partial Least Squares Regression (PLSR), using both PLS-1 and PLS-2. Different procedures have been used for the pretreatment of the data in order to obtain better models, and the size of the calibration matrix has also been studied. The best models have been used for the determination of the above mentioned PAHs in spiked natural water samples at concentration levels between 4 and 20 ng ml^{-1}. Recoveries ranged from 80 to 120% in most cases, although fluorene gave significantly lower results. © 1998 Elsevier Science B.V.

Keywords: PAHs; Synchronous spectrofluorimetry; Multivariate calibration; PLS

1. Introduction

The determination of several compounds in a mixture can be a difficult problem, especially when their analytical characteristics are not very different. In this case, the use of a separation method is normally required, and chromatographic methods are frequently used.

Another approach, however, is to try to avoid the separation step. In some cases, new procedures can be developed, which, making full use of the possibilities offered by chemometrics and by the wide availability of powerful and relatively inexpensive computers, may become an alternative for chromatographic methods.

Among the available multivariate calibration procedures, Partial Least Squares Regression (PLSR) and Principal Component Regression (PCR) are the most suited for multicomponent spectral analysis. PLSR is based on the regression of chemical concentrations on latent variables (factors) and, therefore, it differs from other calibration procedures (such as PCR) in that it uses the concentration data from the training set and the spectral data for modeling, whereas PCR only

* Corresponding author. Tel.: + 34 3 4021276; fax: + 34 3 4021233; e-mail: jacinto@zeus.qui.ub.es

PII S0039-9140(97)00212-9

uses the spectral data [1]. This enables PLS to reduce the influence of dominant, but irrelevant, factors and to yield models of lower dimensionality. Two different algorithms of PLS are available: PLS-1, which builds a calibration model for each analyte, and PLS-2, which has the advantage of being able to model several analytes simultaneously.

Multivariate calibration methods, particularly PLS, have been used for quantitative analysis in combination with several spectroscopic techniques, such as UV-Visible spectroscopy [2,3], fluorescence spectroscopy [4,5] and infrared spectroscopy [6,7]. The main advantage of multicomponent analysis lies in the speed with which results can be obtained, because the previous separation step, usually a lengthy process, can be avoided.

Of all spectroscopic techniques, spectrofluorimetry is well suited to be used in combination with multicomponent analysis, because there are relatively few compounds having intrinsic fluorescence. This fact, combined with the possibility of changing either the excitation wavelength or the emission wavelength, or both simultaneously, greatly increases the selectivity of spectrofluorimetric methods. Additionally, detection limits can often be improved by simply increasing the intensity of the radiation used for excitation.

Among the compounds having intrinsic fluorescence, polycyclic aromatic hydrocarbons (PAHs) are particularly important. These substances, whose mutagenic and/or carcinogenic effects are well known, can be originated by natural and anthropogenic processes, and they can be found in many different kinds of samples, such as biological (meat, fish) [8–10] or environmental (soils, sediments, airborne particulates, water) [11–16]. For this reason, their detection and monitoring has become an important problem and this has led to the development of new and faster analytical methods, offering improved selectivity and sensitivity [8,9,17].

In this paper, the PLS multivariate calibration method (PLS-1 and PLS-2) has been applied for the determination of ten PAHs (anthracene, benz[a]anthracene, benzo[a]pyrene, chrysene, fluoranthene, fluorene, naphthalene, perylene, phenanthrene and pyrene) from the synchronous fluorescence spectra of the samples, recorded at three different wavelength increments. Both PLS-1 and PLS-2 were tested. The difference between these two procedures lies in the fact that PLS-1 can only model a single compound at a time, because all the other components of the sample are considered to be interferences, while PLS-2 can model several compounds simultaneously. The synchronous spectra from 70 mixtures of the compounds to be determined were used as calibration set in order to build the model, and a further 15 mixtures were used as external validation set to test the predictive ability of the method. An aqueous micellar medium was used as solvent, in order to increase the fluorescence of the compounds.

The proposed method was used to determine the concentration of PAHs in spiked natural waters, and the results were in good agreement with the added amounts.

2. Experimental

2.1. Reagents

Stock standard solutions (about 200 μg ml^{-1}) of PAHs were prepared by dissolving the pure solid (Supelco) in either methanol (benzo[a]pyrene, fluoranthene, fluorene, naphthalene, phenanthrene and pyrene) or acetonitrile (anthracene, benz[a]anthracene, chrysene and perylene), depending on its solubility.

Acetonitrile and methanol were of analytical reagent quality (Merck). Doubly distilled water (Milli-Q +, Millipore) and Brij-35 (Polyoxyethylenlaurylether, Merck) were used in the surfactant solutions.

3. Apparatus

Synchronous fluorescence spectra were recorded on an Aminco Bowman Series 2 spectrofluorimeter, equipped with a quartz cell (1-cm pathlength) and slits width of 16 nm.

All calculations were performed in an IBM RS/6000 computer, using algorithms from the PLS-Toolbox [18], written in MATLAB (MathWorks).

4. Procedures

Standards were prepared by addition of known amounts of the stock solutions to 25 ml of $3.6 \cdot 10^{-3}$ mol l^{-1} solution of Brij-35 (40 times its critical micellar concentration). The synchronous spectra of each solution were recorded at increments ($\Delta\lambda$) of 10, 50 and 100 nm. The excitation range was from 200 to 550 nm, so the emission range varied with $\Delta\lambda$ (e.g. for $\Delta\lambda = 10$ nm, the emission scan range was from 210 to 560 nm). In all cases, emission readings were taken each nanometer (351 data points for each spectrum).

Before being used in the calculations, the three synchronous spectra recorded for each standard or sample were linked together to obtain a global spectrum. In Fig. 1 the synchronous spectra for each PAH are shown.

5. Results and discussion

A preliminary study indicated that better results were obtained with spectra recorded at wavelength increments of 50 or 100 nm, and therefore they were used in all further calculations. The synchronous spectra obtained at $\Delta\lambda = 10$ nm were rejected because the information they provided was insufficient to discriminate between different compounds.

A calibration set of 70 standards and an independent validation set of 15 standards, containing PAHs at concentrations ranging from 2 to 20 ng ml^{-1}, were used. The optimum dimensionality of the PLS methods was obtained from the PRESS function (Prediction Error Sum of Squares), defined as:

$$\text{PRESS} = \sum_{i=1}^{N} (\hat{y}_i - y_i)^2$$

where N is the number of samples, y_i is the true concentration and $\hat{y}_i$ is the predicted concentration of sample i. In both PLS methods (PLS-1 and PLS-2), PRESS was calculated by cross-validation [19,20], leaving out one sample at a time, to model the system. The concentration of the sample left out was, therefore, predicted by means of a model obtained with the $N-1$ remaining samples. The number of factors chosen to build the model was the lowest for which the PRESS had no significative differences with the value of PRESS for the next number of factors.

The independent validation set (15 samples) was then used to test the selected models. The prediction ability of the model for each PAH was expressed as the RMSD (Root Mean Square Difference):

$$\text{RMSD} = \left[\frac{1}{N} \sum_{i=1}^{N} (\hat{y}_i - y_i)^2 \right]^{0.5}$$

In the PLS-1 modelling, the covariance between the spectral scores and a single compound is maximized, while in the PLS-2 modelling it is the covariance between the spectral scores and a linear combination of several variables what is maximized. A minimum of ten factors, or latent variables, must be chosen, as ten PAHs are to be determined. There are, in addition, sources of non-linearities, such as chemical interactions or non-linear responses of the detector, whose influence can also be modelled by the inclusion of additional factors in the regression model. Consequently, more than ten factors were required to build the models.

5.1. Data preprocessing

Several procedures were used to preprocess the data, in order to obtain the best possible resolution of the system.

When the data were centered against the mean, the mean of each column (wavelengths) was subtracted from all data in it (**mean centering**). When scaling was performed against the mean and the standard deviation, the mean of each column (wavelengths) was subtracted from all data in it and the result was divided by the standard deviation of the column, thus obtaining a matrix where

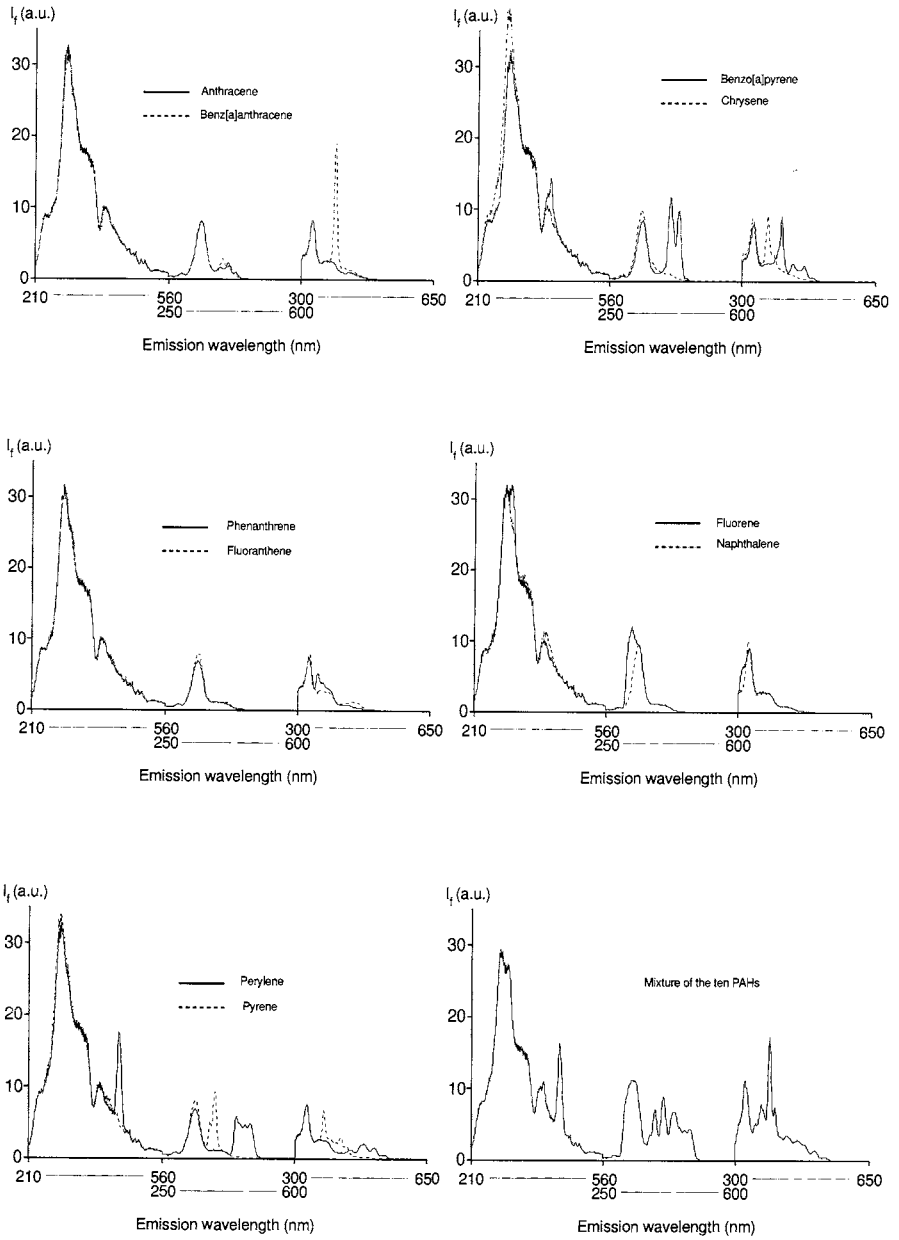

Fig. 1. Synchronous spectra (at wavelength increases of 10, 50 and 100 nm) for each of the PAHs studied.

each column had zero mean and a variance equal to the unity (**scaled data**).

The results of these pretreatments are given, in terms of RMSD, in Table 1 for PLS-1 and in Table 2 for PLS-2. In Fig. 2 the cumulative PRESS for the PLS-2 modelling is plotted versus the number of factors. In both PLS-1 and PLS-2 the best overall results were obtained for unpro-

Table 1
Effect (RMSD values) of the different preprocessing algorithms on the modelling with PLS-1 (in parentheses the number of factors used for the modelling)

Compound	Preprocessing algorithm		
	None	MC	ScMS
Anthracene	0.40 (14)	0.49 (14)	2.49 (14)
Benz[a]anthracene	0.36 (10)	0.39 (11)	0.43 (10)
Benzo[a]pyrene	0.27 (11)	0.26 (13)	0.22 (10)
Chrysene	0.39 (14)	0.34 (13)	0.34 (11)
Fluoranthene	0.55 (13)	0.54 (13)	1.00 (13)
Fluorene	0.58 (13)	0.42 (14)	0.61 (11)
Naphthalene	0.48 (13)	0.47 (13)	0.77 (11)
Perylene	0.23 (10)	0.21 (10)	0.23 (10)
Phenanthrene	0.61 (10)	0.58 (11)	0.66 (11)
Pyrene	0.28 (14)	0.27 (14)	0.34 (10)

None: Raw data.
MC: Raw data mean centered.
ScMS: Raw data scaled against the mean and the standard deviation.

cessed data and when only mean centering was applied.

In PLS-1, the best individual results were obtained from centered data for chrysene, phenanthrene, fluoranthene, fluorene, naphthalene, perylene and pyrene, while no preprocessing was best for anthracene and benz[a]anthracene. Only for benzo[a]pyrene the best results were obtained from scaled data. Anyway, results obtained by mean centering were quite good in all cases, and this procedure could be considered to be a good compromise for all compounds.

Table 2
Effect (RMSD values) of the different preprocessing algorithms on the modelling with PLS-2 (in parentheses the number of factors used for the modelling)

Compound	Preprocessing algorithm		
	None (15)	MC (15)	ScMS (17)
Anthracene	0.52	0.57	2.67
Benz[a]anthracene	0.38	0.33	0.46
Benzo[a]pyrene	0.30	0.28	4.04
Chrysene	0.52	0.36	0.39
Fluoranthene	0.50	0.55	1.28
Fluorene	0.64	0.65	0.66
Naphthalene	0.44	0.46	0.69
Perylene	0.21	0.20	0.24
Phenanthrene	0.51	0.48	0.83
Pyrene	0.51	0.43	0.30

None: Raw data.
MC: Raw data mean centered.
ScMS: Raw data scaled against the mean and the standard deviation.

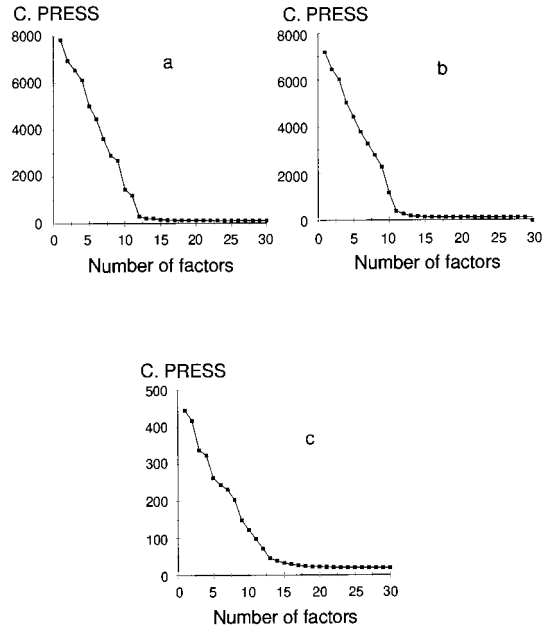

Fig. 2. Representation of the cumulative PRESS vs. the number of principal components for the PLS-1 modelling. a) With no preprocessing of the raw data, b) the raw data were scaled against the mean, and, c) the raw data were scaled against the mean and the standard deviation.

In PLS-2, the best results were obtained from raw data for anthracene, fluoranthene, fluorene and naphthalene, and from mean centered data for benz[a]anthracene, benzo[a]pyrene, chrysene, phenanthrene and perylene. Although the lowest RMSD is obtained from raw data in some cases, and from centered data in others, there are no significant differences in RMSD for both results. Consequently, and to avoid the manipulation of the raw data, these were used without any preprocessing.

5.2. Effect of the size of the data matrix

Considering that the initial calibration set consisted of 70 samples, and that two consecutive spectra (at $\Delta\lambda$ of 50 and 100 nm) with 351 data

Table 3
Effect (RMSD values) of the number of points of the spectra taken for the calibration (PLS-2, in parentheses the number of factors used for the modelling)

Compound	All points (15)	1 each 3 (15)	1 each 5 (13)	1 each 7 (13)	1 each 10 (12)
Anthracene	0.52	0.48	0.54	0.61	0.84
Benz[a]anthracene	0.38	0.36	0.32	0.27	0.31
Benzo[a]pyrene	0.30	0.30	0.30	0.32	0.29
Chrysene	0.52	0.54	0.56	0.60	0.72
Fluoranthene	0.50	0.54	0.90	0.86	0.75
Fluorene	0.64	0.68	0.74	0.81	0.75
Naphthalene	0.44	0.53	0.52	0.93	0.88
Perylene	0.21	0.20	0.22	0.21	0.22
Phenanthrene	0.51	0.54	0.59	0.65	0.72
Pyrene	0.51	0.49	0.46	0.45	0.48

Table 4
Effect (RMSD values) of the number of samples of the calibration set taken for the calibration (PLS-2, in parentheses the number of factors used for the modelling)

Compound	70 (15)	60 (15)	50 (15)	40 (14)	30 (13)
Anthracene	0.52	0.60	0.76	1.27	0.93
Benz[a]anthracene	0.38	0.34	0.24	0.25	0.30
Benzo[a]pyrene	0.30	0.29	0.23	0.35	0.36
Chrysene	0.52	0.53	0.54	0.47	0.51
Fluoranthene	0.50	0.58	0.41	0.44	0.69
Fluorene	0.64	0.66	0.52	0.52	0.81
Naphthalene	0.44	0.65	0.66	0.85	0.82
Perylene	0.21	0.20	0.23	0.26	0.28
Phenanthrene	0.51	0.51	0.57	0.55	0.58
Pyrene	0.51	0.47	0.36	0.48	1.02

points were recorded for each one, the calibration matrix contained about 50 000 data points. Thus, the building of the calibration matrix is a lengthy procedure, and any reduction in its size will shorten the time required to obtain the raw data and to process them.

In order to optimize the number of samples required for a correct calibration, and the number of data points that each spectrum should contain, the RMSD was calculated by PLS-2 (using the raw data) at different reductions of spectral data points (taking one out of every one, three, four, seven or ten points) and with different numbers of samples used for calibration (30, 40, 50, 60 and 70).

Results, shown in Table 3, indicated that the number of data points taken in each spectrum influenced most of the compounds in a similar way (up to one of each five or seven points could be taken without significant increases of their RMSD values). The possibility to reduce the number of points taken for the calculations can be attributed to the intense and well-differentiated bands that each compound shows. Only fluoranthene and naphthalene had a different behaviour, which could be attributed to the fact that their spectra were closely overlapped with those of phenanthrene and fluorene, respectively. The number of samples used for the calibration set,

Table 5
Results obtained in natural spiked water samples for PLS-1 and PLS-2 models (with no preprocessing of the raw data).

Compound	Added (ng ml^{-1})	PLS-1		PLS-2	
		Found ± std (ng ml^{-1})[a]	Recovery ± std (%)	Found ± std (ng ml^{-1})[a]	Recovery ± std (%)
Anthracene	4.2	5.2 ± 0.3	123.6 ± 7.3	4.5 ± 0.4	106.1 ± 9.9
	8.9	8.4 ± 0.7	93.5 ± 7.9	6.6 ± 1.0	74.3 ± 11.5
	12.9	10.2 ± 0.8	79.3 ± 6.6	8.2 ± 0.9	63.7 ± 7.2
	17.9	14.2 ± 0.4	79.4 ± 7.6	11.0 ± 1.6	61.6 ± 9.2
Benz[a]anthracene	3.9	3.8 ± 0.1	97.2 ± 1.5	4.2 ± 0.1	108.5 ± 1.7
	8.2	8.0 ± 0.2	99.6 ± 2.1	8.4 ± 0.1	102.2 ± 0.2
	11.9	10.6 ± 0.3	89.0 ± 2.2	11.3 ± 0.5	93.8 ± 0.9
	16.4	16.0 ± 0.4	97.1 ± 2.7	16.5 ± 0.3	100.4 ± 1.8
Benzo[a]pyrene	4.7	4.9 ± 0.2	104.3 ± 4.0	4.9 ± 0.2	103.8 ± 3.7
	10.0	10.2 ± 0.6	102.2 ± 5.6	10.1 ± 0.6	101.7 ± 5.6
	14.3	13.2 ± 0.5	92.3 ± 3.5	13.2 ± 0.5	92.1 ± 3.6
	19.3	20.1 ± 0.9	103.7 ± 4.9	20.1 ± 0.9	103.7 ± 4.9
Chrysene	3.8	4.5 ± 0.3	116.9 ± 7.2	4.1 ± 0.4	106.4 ± 11.1
	8.1	9.1 ± 0.3	111.2 ± 2.9	7.1 ± 0.4	87.9 ± 5.2
	11.7	11.7 ± 0.1	100.3 ± 0.6	9.2 ± 0.6	78.8 ± 5.1
	16.2	17.7 ± 0.3	109.2 ± 2.0	13.4 ± 0.7	82.9 ± 4.6
Fluoranthene	4.7	7.0 ± 0.1	147.8 ± 2.4	6.7 ± 0.1	143.2 ± 2.3
	10.0	11.9 ± 0.2	118.6 ± 2.4	11.1 ± 0.5	110.9 ± 5.4
	13.1	14.5 ± 0.3	100.9 ± 2.0	13.5 ± 0.6	93.4 ± 4.1
	20.0	21.8 ± 0.2	109.8 ± 0.8	20.2 ± 0.7	101.3 ± 3.4
Fluorene	4.5	0.3 ± 0.2	7.3 ± 3.8	0.3 ± 0.2	7.5 ± 3.5
	9.7	3.3 ± 0.2	33.8 ± 1.6	1.63 ± 0.1	16.8 ± 0.9
	13.9	5.6 ± 0.1	40.4 ± 0.8	3.5 ± 0.1	25.4 ± 0.7
	19.3	9.0 ± 0.1	46.6 ± 0.3	5.4 ± 0.1	28.0 ± 0.6
Naphthalene	5.2	3.5 ± 0.3	68.5 ± 5.8	3.8 ± 0.3	74.6 ± 5.8
	11.0	7.9 ± 0.5	71.9 ± 5.0	8.1 ± 0.6	73.4 ± 5.1
	13.9	10.9 ± 0.8	68.7 ± 5.6	10.9 ± 1.1	68.7 ± 6.8
	21.9	17.8 ± 0.9	81.0 ± 4.0	17.8 ± 1.0	81.2 ± 4.7
Perylene	3.8	4.5 ± 0.1	120.4 ± 3.0	4.7 ± 0.1	123.8 ± 1.8
	8.0	9.11 ± 0.3	113.6 ± 4.2	8.7 ± 0.1	108.2 ± 0.6
	11.5	11.8 ± 0.3	102.7 ± 8.6	11.2 ± 0.1	96.8 ± 0.4
	16.0	18.2 ± 0.5	114.0 ± 3.1	16.7 ± 0.1	104.5 ± 0.9
Phenanthrene	4.3	4.7 ± 0.3	111.1 ± 7.0	4.8 ± 0.2	113.0 ± 5.7
	9.1	8.5 ± 0.3	94.0 ± 3.1	8.6 ± 0.2	95.1 ± 2.5
	13.1	10.3 ± 0.5	78.9 ± 3.9	10.5 ± 0.4	80.6 ± 3.0
	18.1	15.2 ± 0.6	83.7 ± 3.61	15.5 ± 0.5	85.4 ± 2.5
Pyrene	4.1	4.2 ± 0.1	102.3 ± 3.5	4.2 ± 0.2	103.4 ± 3.7
	8.7	9.2 ± 0.6	104.8 ± 6.9	8.4 ± 0.1	96.6 ± 1.2
	12.6	12.0 ± 0.3	95.4 ± 2.7	11.0 ± 0.1	87.7 ± 0.8
	17.4	18.1 ± 0.1	103.7 ± 6.4	16.2 ± 0.4	93.1 ± 2.6

[a] Mean of three independent samples.

however, had a stronger influence. From results in Table 4 it was evident that the RMSD for anthracene and naphthalene increased as the number of samples was decreased, while no tendency could be detected in the remaining compounds. It could be concluded that an important factor was the number of standards used for calibration, and that the number of data points taken in each spectrum had a minor influence.

5.3. Analysis of spiked natural water samples

The models obtained with PLS-1 and PLS-2 from the raw data of the calibration matrix were applied to the resolution of mixtures of PAHs in spiked natural water samples. For this purpose, 25 ml samples of natural water were spiked with PAHs, at four concentration levels (4, 9, 12 and 20 ng ml^{-1}), with all PAHS in a sample having similar concentrations, and enough Brij-35 solution was added to reach a concentration equivalent to 40 cmc. The synchronous fluorescence spectra, recorded at wavelength increments of 50 and 100 nm, were used to calculate the concentrations. The results, shown in Table 5, indicated a good agreement between the amounts added and found, and only fluorene had recoveries (ratio amount found/amount added) lower than 30%, which can probably be attributed to interferences from the sample matrix, concretely to fluorescence from Brij-35.

6. Conclusions

The use of the data provided by synchronous spectra in combination with multivariate calibration (Partial Least Squares Regression, in this case) is a powerful analytical tool, which can be used for the resolution of complex mixtures. In this paper it has been used for the determination of ten PAHs in spiked water samples, with satisfactory results.

The overall results show that, as could be expected, PLS-1 is generally more effective than PLS-2 to model the system, because each compound is treated individually. Of course this has the drawback that the analysis of a sample containing several analytes requires a longer amount of time. In the case of compounds whose synchronous spectra are similar, or closely overlapped, PLS-2 gives usually better results than PLS-1, because the model is built for all compounds simultaneously.

.

Acknowledgements

The authors thank the Comisión Interministerial de Ciencia y Tecnología (CICYT) for supporting this study.

References

[1] D.M. Haaland, E.V. Thomas, Anal. Chem. 60 (1988) 1193.
[2] P.X. Zhang, D. Littlejohn, Chemometr. Intell. Lab. Syst. 34 (1996) 203.
[3] A. Espinosa Mansilla, F. Salinas, M. Del Olmo, I.P. Paya, Appl. Spec. 50 (1996) 449.
[4] R.D.B. Jimenez, A.I.J. Abizanda, F.J. Moreno, J.J.A. Leon, Clin. Chim. Acta 249 (1996) 21.
[5] R. Bro, J. Chemometr. 10 (1996) 47.
[6] F.R. Vandevoort, K.P. Memon, J. Sedman, A.A. Ismail, J. Am. Oil Chem. Soc. 73 (1996) 411.
[7] J. Dubois, F.R. Vandevoort, J. Sedman, A.A. Ismail, H.R. Ramaswamy, J. Am. Oil Chem. Soc. 73 (1996) 787.
[8] A. Bjorseth, Handbook of Polycyclic Aromatic Hydrocarbons, Marcel Dekker, New York. 1983.
[9] C.A. Menzie, B.B. Potocki, J. Santodonato, Environ. Sci. Technol. 26 (1992) 1278.
[10] S.A. Wise, B.A. Benner Jr., R.G. Christensen, B.J. Koster, J. Kurz, M.M. Schantz, R. Zeizier, Environ. Sci. Technol. 25 (1991) 1695.
[11] A.I. Krilov, I.O. Kostyuk, N.F. Volynets, J. Anal. Chem. 50 (1995) 494.
[12] H.G. Kicinski, S. Adamek, A. Kettrup, Chromatographia 28 (1989) 203.
[13] E.R. Brouwer, A.N.J. Hermans, H. Lingeman, U.A.Th. Brinkman, J. Chromatogr. A 669 (1994) 45.
[14] G. Codina, M.T. Vaquero, L. Comellas, F.B. Puig, J. Chromatogr. A 673 (1994) 21.
[15] S.A. Wise, M.M. Schantz, B.A. Benner Jr., M.J. Hays, S.B. Schiller, Anal. Chem. 67 (1995) 1171.
[16] C. Escrivá, E. Viana, J.C. Moltó, Y. Picó, J. Mañes, J. Chromatogr. 676 (1994) 375.
[17] T. Vo-Dinh (Ed.), Chemical Analysis of Polycyclic Aromatic Compounds, Wiley, New York, 1989.
[18] B.M. Wise, PLS Toolbox for Use With MATLAB™, CPAC, Washington, 1992.
[19] S. Wold, Technometrics 20 (1978) 397.
[20] P. Geladi, B.R. Kowalski, Anal. Chim. Acta 185 (1986) 19.

ELSEVIER

Talanta 45 (1998) 1081–1087

Talanta

Solid-Phase microextraction with Whatman 1PS paper and direct room-temperature solid-matrix luminescence analysis

Jie Chen, Robert J. Hurtubise *

Department of Chemistry, University of Wyoming, Laramie, WY 82071, USA

Received 4 June 1997; received in revised form 2 July 1997; accepted 7 July 1997

Abstract

Solid-phase microextraction has been combined with solid-matrix luminescence for the detection of a variety of compounds at sub-nanogram levels for the first time. Whatman 1PS paper was placed in water solutions of polar and nonpolar compounds for the selective removal of the nonpolar compounds such as benzo(a)pyrene. Distribution constants were obtained for 4-phenylphenol, benzo(f)quinoline, benzo(h)quinoline, phenanthrene, and benzo(a)pyrene. The distribution constants showed that phenanthrene and benzo(a)pyrene in water had a very strong affinity for the 1PS paper. Once the solutes were extracted for a fixed period of time, the 1PS paper was dried, and either the solid-matrix fluorescence or solid-matrix phosphorescence was detected from the adsorbed lumiphors by using the appropriate excitation wavelengths. It was a simple matter to detect at least three adsorbed compounds on the 1PS paper by solid-matrix luminescence. Benzo(a)pyrene was easily detected at a level of 0.02 ng ml^{-1} in water.

Keywords: Solid-Phase; Microextraction; Luminescence analysis

Considerable attention has been given to the trace analysis of organic pollutants in water [1–6]. Analytical methods with lower detection levels are needed for water samples compared to other types of environmental samples because greater purity is demanded, for example, for drinking water. Sophisticated analytical methods, such as gas chromatography–mass spectrometry (GC–MS) and liquid chromatography–mass spectrometry (LC–MS), are routinely used for the trace determination of organics in environmental samples [7,8]. However, these analytical procedures are costly, time-consuming, and labor intensive. Currently, interest has turned to the development of simple and economical analytical techniques for rapid on-site detection and determinations of water contaminants. It is preferable to carry out the analysis in the field because the preservation of a water sample after its collection is critical to ensure accurate results. It is expensive and difficult to store and transport the sample from the field to the laboratory before analysis, and in the case of an emergency, such as chemical spills, speed of analysis is required.

* Corresponding author. Tel.: +1 307 7662434; fax: +1 307 7662807; Hurtubis@uwyo.edu

0039-9140/98/$19.00
PII S0039-9140(97)00214-2

Solid matrix room-temperature luminescence is the technique whereby room-temperature fluorescence (RTF) and room-temperature phosphorescence (RTP) are measured from compounds adsorbed on solid materials such as filter paper or cyclodextrin powders [9–11]. In this study, a solid-phase microextraction (SPME) technique was combined with solid-matrix room-temperature luminescence (SMRTL). Whatman 1PS filter paper was used as a solid-phase extracting material and the solid medium for obtaining the solid-matrix luminescence data. This approach eliminates the sample pre-concentration step and combines the advantages of SPE and solid-matrix luminescence. Another benefit of coupling the SPME with SMRTL is that this approach avoids the desorption of the sample components. With SPME, the analyte adsorbed on the solid phase usually must be desorbed, which may cause problems in the reproducibility and reliability of the analysis [12–16]. When SPME is combined with solid-matrix luminescence, the adsorbed analyte is transferred into the sample compartment of the luminescence spectrometer for analysis without the need for desorption of the analyte.

1. Experimental

1.1. Instruments

The RTF and RTP intensity measurements and spectra were obtained with either a Perkin-Elmer LS-50B spectrofluorometer or a Photon (PTI) LS-100 spectrofluorometer. For room-temperature luminescence measurements, the filter paper samples were placed in a sample holder, which had a 0.64 cm diameter.

1.2. Reagents

All the filter paper samples (Whatman 1PS) were obtained from Whatman, Clifton, NJ, and they were developed in distilled ethanol at least three times to minimize luminescence impurities in the paper. Benzo(f)quinoline (99 + %, TCI, Tokyo, Japan) was used as received. Benzo(a)pyrene was Aldrich Gold Label reagent and used as received. 4-Phenylphenol and phenanthrene were purchased from Aldrich and recrystallized from distilled ethanol. Tetrol I-1 was purchased from the Midwest Research Institute (NCI Chemical Carcinogen Repository, Kansas City, MO) and used as received. The methanol employed was HPLC grade and purchased from J.T. Baker. Absolute ethanol (Midwest Grain, Pekin, IL) was distilled prior to use.

1.3. Sample preparations and SPME experiments

All glassware used in the SPME experiments were first cleaned with 1:1 nitric acid:water solution to remove any possible organic contaminants. After thorough rinsing the glassware was allowed to dry at room temperature. The stock solutions were prepared by dissolving the sample compounds in methanol solution with the help of sonication. To prepare standard solutions, an aliquot of the stock solution was diluted to a desired volume with pure water. The percentage of the methanol in solution never exceeded 1% of the total volume. All standard solutions were freshly prepared to diminish the possible adsorption of sample compounds on the container wall.

For SPME an immersion approach was employed. In the immersion approach, a circular piece of Whatman 1PS filter paper, which was held by a tweezers, was immersed into the test solution in a vial for a fixed period of time. During this period of time, the solution was stirred. The stirring time was normally 15 min. After immersion, the filter paper sample was dried at 105°C for 30 min. Then, the filter paper sample was put in the sample holder and placed inside of sample compartment of the luminescence spectrometer. The appropriate excitation and emission wavelengths were used to obtain the RTF and RTP data.

1.4. Determination the amount of solute adsorbed on 1PS filter paper

In order to determine the amount of compound adsorbed on the filter paper by SPME, first the immersion step with 1PS paper was carried out. Then, the 1PS filter paper with the sample ad-

sorbed on it was treated with 2.0 ml of methanol by lightly sonicating the paper for 10 min to remove the adsorbed compound from 1PS filter paper. The concentration of lumiphor in the methanol was determined by using a solution fluorescence calibration curve. The amount of sample adsorbed on 1PS filter paper was employed to calculate the distribution constants. See Eq. (1).

2. Results and discussion

Filter paper is the most widely used solid substrate in solid-matrix RTF and RTP. In this work, Whatman 1PS filter paper was used. It has been impregnated with silicone oil, and thus it is a hydrophobic material. Recently, it has been used as a substrate for RTP measurements [17]. The 1PS paper can induce strong RTP without the addition of a heavy atom [18]. This can be accomplished because 1PS paper contains a tin complex which gives stability to the paper, and, most likely, the tin complex enhances the RTP of adsorbed phosphors by the heavy-atom effect [18].

Several compounds with different structural features were investigated: benzo(f)quinoline (B(f)Q), benzo(a)pyrene (B(a)P), phenanthrene, benzo(a)pyrene-r-7,t-8,9,c-10-tetrahydrotetrol (tetrol I-1), and 4-phenylphenol (4-PP). B(a)P and phenanthrene are polycyclic aromatic hydrocarbons and are very hydrophobic. Tetrol I-1 is a hydrolysis product of B(a)P-DNA adducts, and it is important in cancer research [17]. B(f)Q and 4-PP are important environmental compounds, and they are more polar compounds than B(a)P and phenanthrene.

The solid-matrix RTF excitation and emission spectra obtained from the SPE of 10 ml of a 10 ng ml^{-1} B(a)P solution with Whatman 1PS filter paper are shown in Fig. 1. The spectra obtained by the SPME approach showed essentially no differences in their spectra compared to solution spectra and the solid-matrix RTF spectra obtained by spotting the sample solution onto filter paper. The solid-matrix RTF spectra of the other model compounds examined gave similar results as B(a)P.

Complete removal of the dissolved solutes does not occur in SPME with 1PS filter paper. Instead, an equilibrium is reached between the solutes in the aqueous phase and the solutes adsorbed on the solid phase. The efficiency of the adsorption is controlled by many factors such as the time of extraction, the concentration of analytes, the viscosity of the solution, and the adsorption nature of the analytes.

Fig. 2 gives the solid-matrix RTF relative intensity of several model compounds adsorbed on 1PS filter paper after the sample solutions (10 ng ml^{-1}) were extracted with 1PS filter paper for different time periods. As indicated in the Figure, there is a break in the plot for each of the compounds. The intensity increased rapidly in the beginning of the extraction, and after about 20 min, the slope became smaller which indicated that the filter paper was approaching saturation. The average relative standard deviation for the RTF data in Fig. 2 was about 7.3%. The solid-matrix RTP data of B(f)Q, tetrol I-1, and phenanthrene gave similar plots. B(a)P did not give a strong RTP signal on 1PS paper; thus its RTP was not investigated. It would be necessary to add an external heavy-atom salt to enhance the RTP of B(a)P.

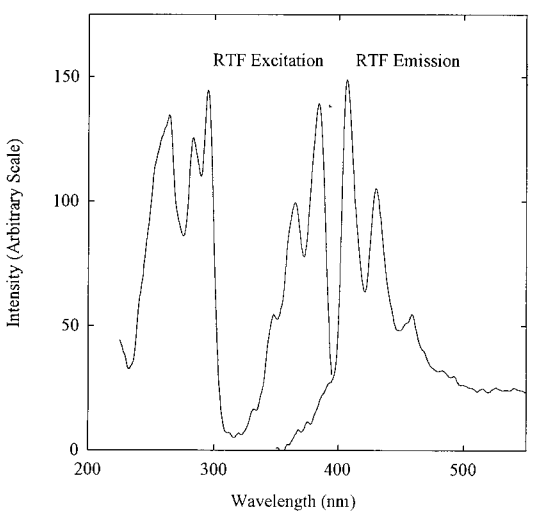

Fig. 1. Solid-Matrix RTF excitation and emission spectra of B(a)P adsorbed on Whatman 1PS filter paper after SPME for 15 min.

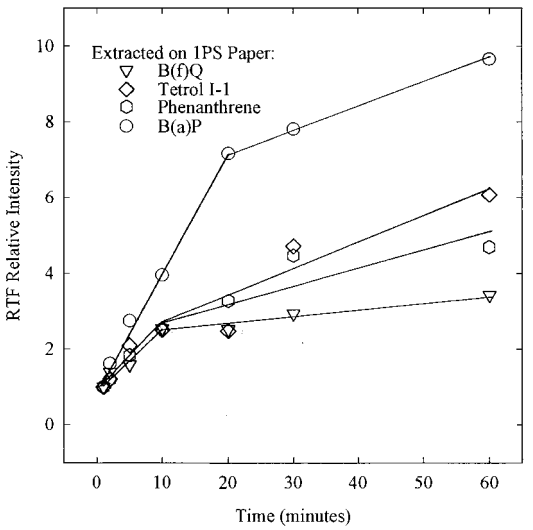

Fig. 2. Time profiles for SPME on Whatman 1PS filter paper for the immersion approach.

For the four compounds studied, the solid-matrix RTF of B(a)P increased rapidly as the extraction time increased, while the B(f)Q gave the smallest increase. The extraction behavior of these compounds show that the molecular structure of compounds will have a major effect on extraction efficiency. For the compounds studied, the number of aromatic rings and the polarity of the compound are major factors in determining the extraction efficiency. The greater the number of aromatic rings in nonpolar compounds the greater the amount of the compound extracted onto 1PS filter paper. An increase in the polarity of a compound would decrease the extraction efficiency. The RTP intensity of tetrol I-1 increased more rapidly than its RTF. This showed that RTP would be a more sensitive approach for detecting tetrol I-1 than RTF.

2.1. The relationship between the sample concentration in solution and the solid-matrix luminescence

In SPME with 1PS filter paper, the amount of the analyte extracted onto 1PS filter paper would be a function of the concentration of analyte in solution. Calibration curves were obtained by plotting the solid-matrix RTF and/or RTP intensity of the analyte adsorbed versus the concentration of the sample solution. B(f)Q showed linear relationships for the entire concentration range studied for both the RTF and RTP measurements, up to 1000 ng ml^{-1}. The linear correlation coefficients for the plot were 0.997 for RTF and 0.994 for RTP. Table 1 lists the limits of detection and linear ranges for B(f)Q, phenanthrene, and B(a)P. The different linear ranges are related to relative magnitude of RTF and RTP signals. Because B(a)P gives a strong solid-matrix RTF signal, its linear range would be the less. It can be seen that the LODs are lower for RTP than for RTF for B(f)Q and phenanthrene. For RTF, B(a)P has the lowest LOD, which was 0.02 ng ml^{-1}. The magnitude of the LODs are generally related to the order of polarity of the compounds. The LODs will be the lowest for low polarity compounds because they would be more strongly attracted to the 1PS paper. However, other factors would be involved such as the quantum yield of a lumiphor on 1PS paper. The data for the calibration curves and LODs in Table 1 were obtained with 15 min extraction times.

2.2. The effects of stirring of the solution in SPE of model compounds with 1PS filter paper

Stirring of the solution will allow the analyte in the bulk solution to partition more effectively. Some experiments were carried out to determine how effective stirring would be in speeding the partition process. The test analyte was B(f)Q in water, and three sample concentrations (0.02 μg ml^{-1}. 0.1 μg ml^{-1}, and 1.0 μg ml^{-1}) were tested with Whatman 1PS filter paper. The extraction time was 15 min. For the three concentrations tested, the solid-matrix RTF intensities were significantly affected by stirring. The intensities were about 50% stronger with stirring than without stirring. These results shows that the stirring is very important for improving the extraction efficiency. Further studies are needed to determine the optimum conditions for stirring.

Table 1
Limits of detection and linear ranges for several compounds[a,b]

Sample	RTF		RTP	
	Linear range (ng ml^{-1})	LOD (ng ml^{-1})	Linear range (ng ml^{-1})	LOD (ng ml^{-1})
B(f)Q	0–1000	2.2	0–1000	0.9
Phenanthrene	0–100	0.7	0–200	0.1
B(a)P	0–10	0.02	—	—

[a] The limits of detection (LOD) were calculated by:

$$\mathrm{LOD} = \frac{3s_B}{m}$$

where s_B is the standard deviation of the blank measurements and m is the slope of the RTF or RTP intensities versus concentration plot.
[b] Extraction time 15 min.

2.3. Determination of the distribution constants of model compounds between 1PS filter paper and water

In an equilibrium system between the solid and aqueous phases, the amount of analyte adsorbed by the solid phase is primarily affected by three factors: the distribution constant, the volume of the solid phase, and the concentration of analyte in water. The number of moles of analyte adsorbed on the surface of the extraction material can be described by Eq. (1) [16,19]:

$$n_s = KV_sC_{aq} \quad (1)$$

where n_s is the number of moles of analyte absorbed on the solid phase, K is the distribution constant, V_s is the volume of the solid phase, and the C_{aq} is the equilibrium concentration of analyte in water. Eq. (1) shows that an increase in the volume of the solid phase (V_s) would increase the amount of analyte adsorbed. The distribution constant K is the measure of the affinity of the extraction material toward the analyte, and it is characteristic of the extraction material and analyte. Large K values mean high affinity between the extraction material and analyte. In this study, the distribution constants of several model compounds on 1PS filter paper were obtained by using Eq. (1). The average V_s value was calculated from the average area of the 1PS filter paper and the average thickness of the paper used in the extraction experiments [19]. The C_{aq} value was obtained after the sample solution was extracted with 1PS filter paper for a set time period, and n_s was experimentally determined. Once these parameters were acquired, the distribution constant was calculated with Eq. (1).

The distribution constants were obtained for B(a)P, B(f)Q, B(h)Q, 4-PP and phenanthrene. Fig. 3 gives the results of the experiments with the appropriate error bars. By comparing the K values with the molecular characteristics of the model compounds, it is clear that larger nonpolar

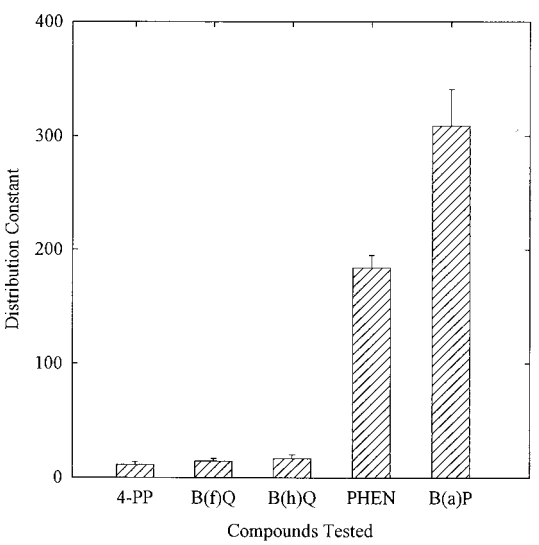

Fig. 3. The distribution constants for several model compounds with Whatman 1PS filter paper and water.

molecules have much higher K values than smaller polar molecules. B(a)P had the greatest affinity for the 1PS paper with phenanthrene showing the next strongest affinity. The results in Fig. 3 indicate that the 1PS paper is very selective for polycyclic aromatic hydrocarbons. Thus, it would be possible to selectively remove a much greater fraction of the polycyclic aromatic hydrocarbons from water relative to polar compounds.

2.4. SPME and solid-matrix luminescence of mixtures of compounds with 1PS filter paper

From the magnitude of the K values obtained, it was shown that polycyclic aromatic hydrocarbons will have a greater tendency to adsorb on 1PS filter paper than polar compounds. In this part of the study, SPME was used in conjunction with solid-matrix luminescence to explore the detection of the isolated components. Several binary and ternary model compounds systems (4-PP, B(f)Q, B(a)P, and phenanthrene) were investigated with Whatman 1PS filter paper for the extraction of compounds from water and the detection by solid-matrix RTF and RTP.

As an example of the removal PAH from water by 1PS paper, and characterization of isolated components by solid-matrix RTF and RTP, Fig. 4 shows the solid-matrix luminescence spectra obtained from a water solution of B(a)P (10 ng ml^{-1}) and phenanthrene (10 ng ml^{-1}) that was extracted for 15 min. The three solid-matrix RTF bands at 350, 367, and 392 nm are from phenanthrene, whereas the three solid-matrix RTF bands at 40, 432, and 458 nm are from B(a)P. Obviously these two compounds are easily distinguished by their RTF spectra. In addition, the solid-matrix RTP of phenanthrene can be readily obtained. Phenanthrene gave major RTP bands at 470 and 502 nm. Thus, the presence of phenanthrene was readily confirmed by RTP. B(a)P does not give an RTP signal on 1PS paper.

Fig. 5 shows the solid-matrix RTF spectra acquired from 1PS paper by exciting the different lumiphors at their appropriate excitation wavelengths. The 1PS paper was in a solution of B(f)Q (100 ng ml^{-1}), 4-PP (100 ng ml^{-1}), and B(a)P (20 ng ml^{-1}) for 15 min, dried, and then the solid-

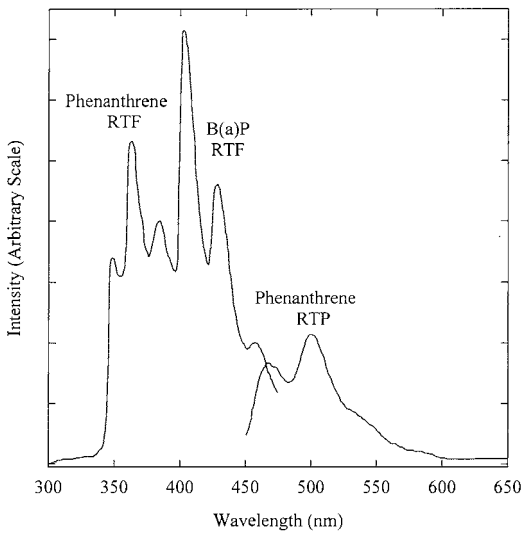

Fig. 4. Solid-matrix RTF spectra of B(a)P and solid-matrix RTF and RTP spectra of phenanthrene on Whatman 1PS filter paper after extraction of a water solution with 1PS filter paper.

matrix RTF spectra obtained. The band centered around 334 nm is from 4-PP, the two peaks at 351 and 366 nm are for B(f)Q, and the bands at 407, 430, and 456 nm are from B(a)P. Obviously the

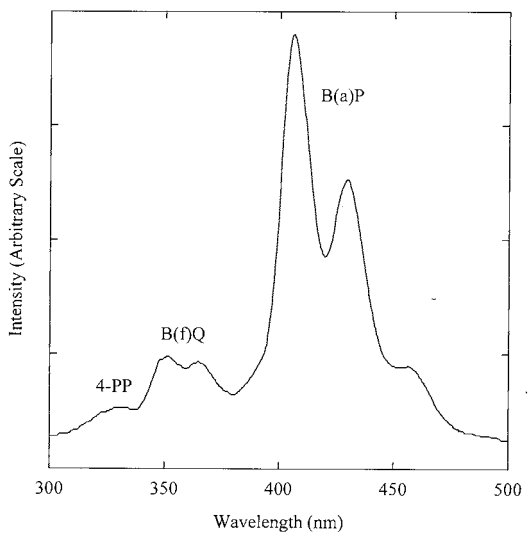

Fig. 5. Solid-matrix RTF spectra of 4-PP, B(f)Q, and B(a)P on Whatman 1PS paper after extraction of a water solution with 1PS filter paper.

B(a)P was very easily detected because it was readily removed from water, and its solid-matrix RTF emission bands were at longer wavelengths than the solid-matrix RTF of 4-PP and B(f)Q. As indicated in the Figure, 4-PP and B(f)Q gave weaker signals because their extraction efficiencies are much less. However, Fig. 5 shows that it is possible to detect all three compounds by solid-matrix RTF. With solid-matrix RTP, it was possible to confirm the presence of B(f)Q by selective excitation. However, both 4-PP and B(f)Q emit RTP in the same general spectral region. By exciting at 243 nm, the RTP emission of from 4-PP and B(f)P appeared, and it was not possible to distinguish the two compounds. With an excitation wavelength of 263 nm, the solid-matrix RTP emission band for B(f)Q at 495 nm was enhanced considerably, thus indicating the presence of B(f)Q.

The examples presented in Figs. 4 and 5 show the potential of using solid-matrix luminescence to detect lumiphors isolated by SPME with 1PS paper. B(a)P is one of the most important compounds in the environment, and it was readily removed from water and detected by solid-matrix RTF at the sub-nanogram level.

Acknowledgements

Financial support for this project was provided by the Department of Energy, Division of Chemical Sciences, Grant DE-FG-06-95 ER14551.

References

[1] D.J. Futoma, S.R. Smith, T.E. Smith, J. Tanaka, Polycyclic Aromatic Hydrocarbons in Water Systems, CRC Press, Boca Raton, FL, 1981.
[2] F.I. Onuska, in: B.K. Afghan, A.S.Y. Chau (Eds.), Analysis of Trace Organics in the Aquatic Environment, CRC Press, Boca Raton, FL, 1989.
[3] C.J. Koester, R.E. Clement, Crit. Rev. Anal. Chem. 24 (1993) 263.
[4] E.R. Brouwer, A.N.J. Hermans, H. Lingeman, U.A.Th. Brinkman, J. Chromatogr. 669 (1994) 45.
[5] J. Saxena, J. Kozuchowski, D.K. Basu, Environ. Sci. Tech. 11 (1977) 682.
[6] L.F. Capitan, R. Avidad Castaneda, M. De Olmo Iruela, J.L. Vichez Quero, Mikrochim. Acta 112 (1993) 55.
[7] J.W. Eichelberger, W.L. Behymer, W.L. Budde, EPA Method 525.1 Determination of Organic Compounds in Drinking Water by Liquid–Solid Extraction ans Capillary Column Gas Chromatography/Mass Spectrometry, Revision 2.2, USEPA, Cincinnati, OH, 1991.
[8] L.S. Clesceri, A.E. Greenberg, R.R. Trussell (Eds.), Standard Methods for the Examination of Water and Wastewater, 17th ed., American Public Health Association, Washington, DC, 1989.
[9] T. Vo-Dinh, Room Temperature Phosphorimetry for Chemical Analysis, Wiley, New York, 1984.
[10] R.J. Hurtubise, Phosphorimetry: Theory, Instrumentation, and Applications, VCH, New York, 1990.
[11] R.J. Hurtubise in S.J. Schulman (Ed.), Molecular Luminescence Spectrometry: Methods and Applications, Part II, Wiley, New York, 1988, chap. 1.
[12] D. Louch, S. Motlagh, J. Pawliszyn, Anal. Chem. 64 (1992) 1187.
[13] D.W. Potter, J. Pawliszyn, Environ. Sci. Tech. 28 (1994) 298.
[14] K.D. Bucholz, J. Pawliszyn, Anal. Chem. 66 (1994) 160.
[15] H.B. Wan, H. Chi, M.K. Wong, C.Y. Mok, Anal. Chim. Acta 298 (1994) 219.
[16] C.L. Arthur, J. Pawliszyn, Anal. Chem. 62 (1990) 2145.
[17] S.W. Tjoie, R.J. Hurtubise, Anal. Lett. 26 (1993) 572.
[18] S.W. Tjioe, R.J. Hurtubise, Talanta 41 (1994) 595.
[19] C.L. Arthur, L.M. Killam, S. Motlagh, M. Lim, D.W. Potter, J. Pawliszyn, Environ. Sci. Technol. 26 (1992) 979.

ELSEVIER

Talanta 45 (1998) 1089–1096

Talanta

Chelating resin containing s-bonded dithizone for the separation of copper(II), nickel(II) and zinc(II)

Rupal Shah, Surekha Devi *

Department of Chemistry, M.S. University, Baroda, 390002, India

Received 12 February 1997; received in revised form 7 July 1997; accepted 8 July 1997

Abstract

Analytical and physicochemical properties of a crosslinked poly (vinyl pyridine) based resin containing dithizone were examined. The resin was further used for the preconcentration of copper, nickel and zinc at batch and column level. Various conditions such as pH, equilibration time, temperature were optimised for the maximum loading of copper, nickel and zinc. The loading capacities of the resin for copper, nickel and zinc were observed to be 0.51, 0.59 and 0.65 mmol g^{-1} of dry resin respectively. Elution of loaded copper, nickel and zinc from the resin was done by using 0.1 M HCl, 0.1 M H_2SO_4 and 0.1 M HNO_3 respectively. Separation of copper, nickel and zinc in binary and ternary mixtures was achieved without any cross contamination. © 1998 Elsevier Science B.V.

Keywords: Copper(II); Nickel(II); Zinc(II); Separation; s-bonded dithizone

1. Introduction

Chelating resins have found wide spread applications in the preconcentration of trace metals from waste water. The resins containing macroporous cross-linked polystyrene, polyacrylonitrile, poly methacrylic acid esters, cellulose and other polymeric matrices as ion exchangers have been reported by Warshawsky [1–3]. For the purpose a polystyrene divinylbenzene based resin containing *N*-hydroxy ethylene thylene diamine group for the preconcentration of copper, nickel and zinc has been reported by Dev and Rao [4]. An adsorbent prepared by reacting high molecular weight polyethylene imine with a cross linked and activated agarose gel was reported by Steinmann et al. [5] for the preconcentration of copper, nickel, cadmium and zinc. The preconcentration of copper, nickel and zinc from the matrix by a column containing 8-quinolinol immobilised on porous glass was reported by Malamas et al. [6]. A series of terpolymeric chelating resins containing 8-hydroxyquinoline and resorcinol/hydroquinone were prepared and used for the preconcentration of copper, nickel and zinc by Purohit and Devi [7–9].

Chelating resins containing dithizone have also been reported [10–13] for the preconcentration of Hg(II), As(III), Sb(III) and Cu(II). A polystyrene divinylbenzene resin anchored with a chelating regent dithizone was reported by Grote and Ket-

* Corresponding author. Tel.: +91 265 328122/331130; fax: +91 265 339594/331130.

PII S0039-9140(97)00215-4

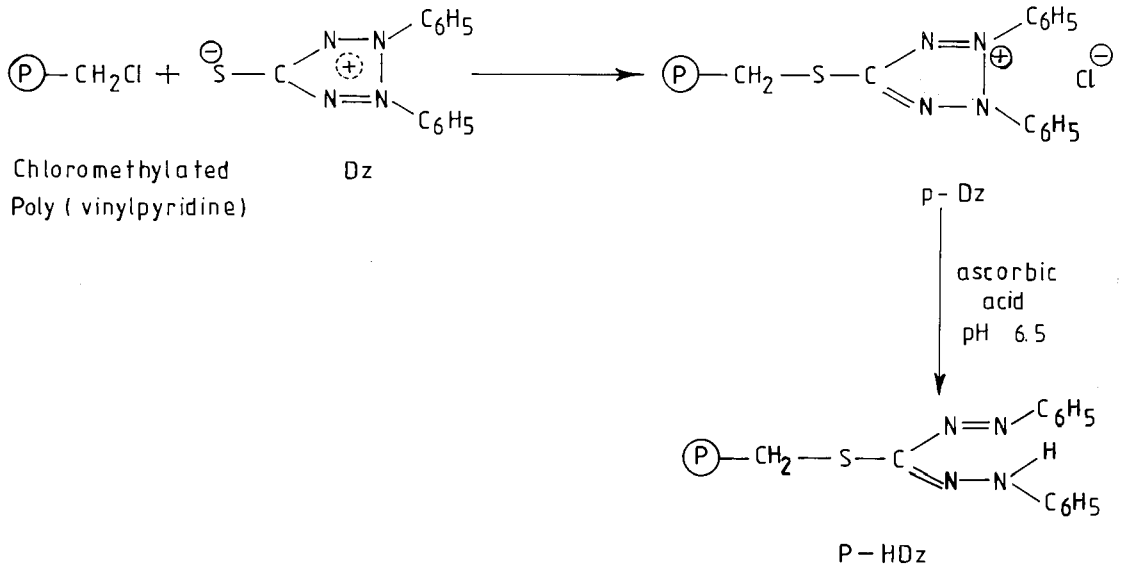

Fig. 1. Synthesis of the resin. D_z = dehydrodithizone, HD_z = dithizone.

trup [14]. They have used this support for the sorption of gold and platinum group metals and base metals like copper, nickel and zinc. But they have not reported the sorption capacities for these metal ions. Chwatowska and Kosiarska [15] have reported anchoring of dithizone to the diazotised styrene-divinyl benzone support. This chelating resin was further used for the sorption of Ag(I), Cd(II), Cu(II), Pb(II), Ni(II), Co(II) and Zn(II) at static and dynamic conditions.

We are reporting here anchoring of dithizone on crosslinked 4-vinylpyridine-divinyl benzene copolymer. The chelating polymeric matrix is further used for the preconcentration and separation of copper, nickel and zinc. Due to the presence of vinyl pyridine group the overall chelating ability of the resin is expected to improve considerably.

2. Experimental

2.1. Reagents

All reagents used were of AR grade. Doubly distilled deionised water was used throughout the work.

2.2. Metal solutions

Stock solutions of 10 mg cm^{-3} concentration of Cu(II), Ni(II) and Zn(II) metal ions were prepared by dissolving required quantity of the corresponding salts into deionised water. Standardisation of the solutions was done volumetrically following the literature methods [16]. The solutions were diluted whenever required using doubly distilled deionised water.

2.3. Synthesis of the chelating resin

A copolymer of 4-vinylpyridine-divinylbenzene was synthesised by suspension polymerisation. The crosslinked poly (vinyl pyridine) was chloromethylated and dithizone was coupled to it following the method reported by Grote and Kettrup [14]. The physicochemical properties of the chelating resin were studied, according to the literature methods reported earlier [17].

The separation of copper, nickel and zinc was studied under static and dynamic conditions. To determine the chelating capacity and stability of the sorbent, conditions such as pH, metal ion

Table 1
Physicochemical properties of the resin

Property	
Moisture content (g g^{-1})	0.047
True density (g cm^{-3})	1.24
Void volume (cm^3 g^{-1})	0.72
Metal exchange capacity at pH 5 (mmol g^{-1})	
Cu(II)	0.51
Ni(II)	0.59
Zn(II)	0.65

concentration, equilibration time and eluting agent were optimised at static conditions. The extent of copper, nickel and zinc exchange was determined volumetrically from the supernatant liquid as well as after eluting copper, nickel and zinc from the resin.

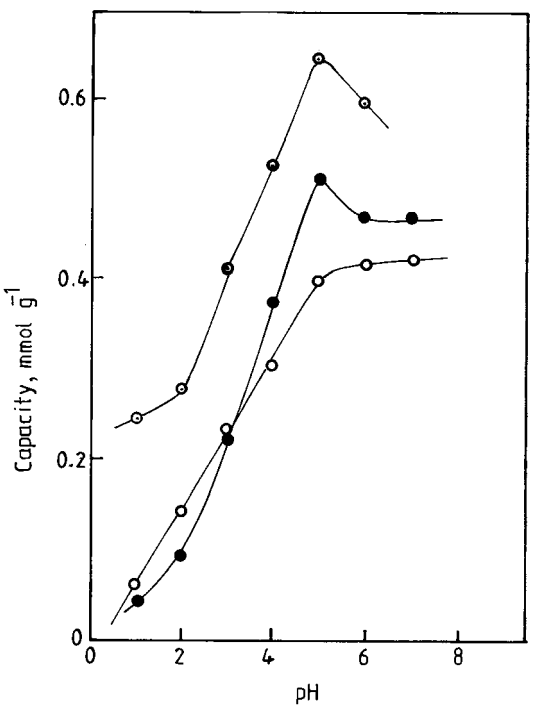

Fig. 2. Effect of pH on metal exchange. 0.1 g resin, 25 cm^3 reaction volume, equilibration time 24 h, copper, nickel and zinc concentration 200, 400, 400 μg cm^{-3} respectively. ● Copper, ○ nickel, ⊙ zinc.

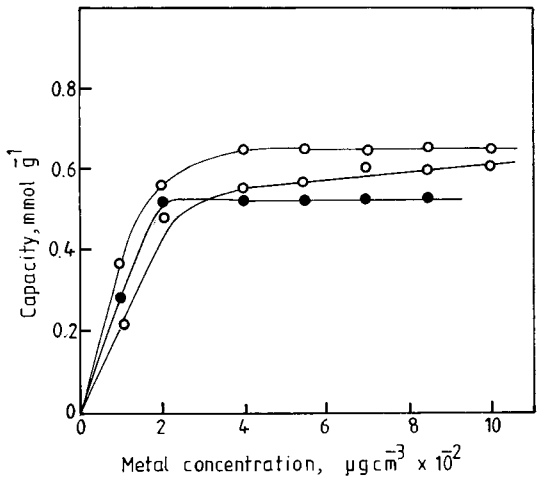

Fig. 3. Effect of metal ion concentration on % exchange. 0.1 g resin, pH 5, equilibration time 24 h, 25 cm^3 reaction volume. ● Copper, ○ nickel, ⊙ zinc.

3. Metal exchange capacities

The copper, nickel and zinc exchange capacity of the resin was determined by a batch process

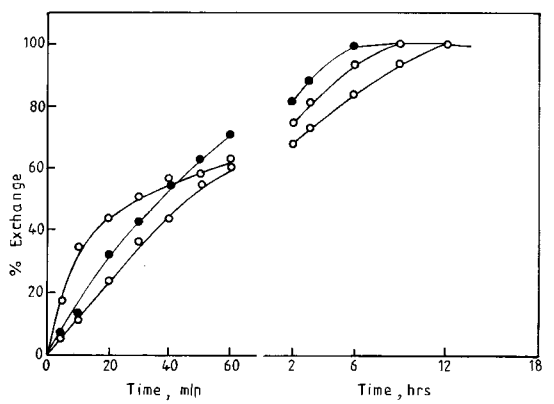

Fig. 4. Kinetics of metal exchange. 0.1 g resin, pH 5, 25 cm^3 reaction volume, equilibration time 24 h, copper, nickel and zinc concentration 200, 800, 400 μg cm^{-3} respectively. ● Copper, ○ nickel, ⊙ zinc.

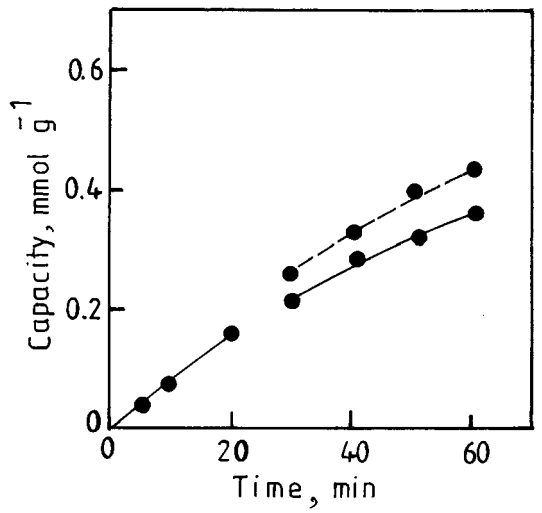

Fig. 5. Interruption test. 0.1 g resin, pH 5, 25 cm^3 reaction volume, equilibration time 24 h, copper, concentration 200 μg cm^{-3}.

equilibrating 0.1 g of the dry resin sample with 0.2 M acetate/citrate-phosphate buffer of pH 5.0 for 24 h. The resin was further equilibrated with 25.0 cm^3 of 200, 800 and 400 μg cm^{-3} of copper, nickel and zinc solution respectively for 24 h.

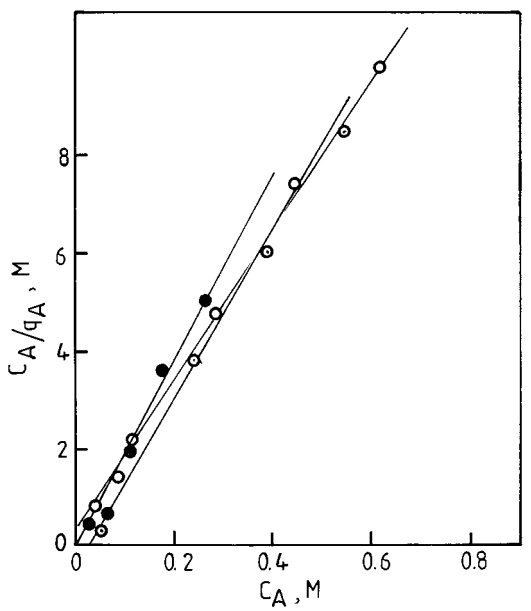

Fig. 6. Extended Langmuir adsoption isotherm. ● Copper, ○ nickel, ⊙ zinc.

Total exchange capacity and distribution coefficient of copper, nickel and zinc were calculated as:

$$\text{Total exchange capacity (mmol g}^{-1}) = \frac{(C_0 - C_A)V}{W}$$

where C_0 = initial concentration of metal ion in mmol, C_A = equilibrium concentration of metal ion in mmol, V = volume of the solution and W = weight of the dry resin.

3.1. Exchange kinetics

The rate of exchange of metal in 0.2 M acetate buffer of pH 5.0 was determined by equilibrating 0.1 g of the sorbent with 25.0 cm^3 solution of 200, 800 and 400 μg cm^{-3} copper, nickel and zinc for various time intervals. The time required for 50% exchange was calculated from the % exchange vs time plots. The mode of diffusion of metal ion through solution towards the resin was determined by the interruption test [17] and was confirmed by the method reported by Nativ et al. [18].

3.2. Thermodynamics and exchange process

The rate of exchange of metal at pH 5.0 in 0.2 M acetate buffer was determined by equilibrating 0.1 g sorbent with 50.0 cm^3 of 400 μg cm^{-3} copper, nickel and zinc solution. The kinetics of exchange of copper, nickel and zinc was studied at 30, 40 and 50°C. From the results obtained, exchange rate constant K and activation energy ΔE were calculated.

3.3. Desorption studies

Quantitative stripping of copper, nickel and zinc from the dithizone loaded sorbent was carried out by using various acids of different strengths.

Table 2
Data for extended Langmuir adsorption hypothesis for ion exchange M concentration of metals

C_0	C_A	q_A	C_A/q_A	α	Q (calculated mmol g^{-1})	Q (experimental mmol g^{-1})
Copper(II)						
0.039	0.011	0.028	0.404	9.62	0.42	0.28
0.079	0.027	0.051	0.530	17.39	0.47	0.51
0.157	0.105	0.052	2.002	32.73	0.47	0.51
0.236	0.185	0.051	3.590	48.19	0.47	0.51
0.314	0.262	0.052	5.004	63.46	0.47	0.51
Nickel(II)						
0.085	0.038	0.047	0.83	5.81	0.42	0.47
0.170	0.117	0.054	2.18	9.64	0.51	0.54
0.340	0.282	0.058	4.83	17.24	0.57	0.59
0.511	0.450	0.061	7.43	24.90	0.59	0.60
0.681	0.618	0.063	9.81	32.52	0.60	0.60
Zinc(II)						
0.076	0.021	0.054	0.390	28.36	0.60	0.55
0.153	0.089	0.064	1.38	55.03	0.62	0.65
0.306	0.242	0.063	3.83	108.00	0.64	0.65
0.459	0.393	0.065	6.02	161.14	0.64	0.65
0.611	0.547	0.064	8.50	213.93	0.64	0.65

3.4. Chromatographic separations

Compact column of ~15.0 cm length and 1.0 cm i.d. was prepared with 3.0 g of the resin. The column was equilibrated at pH 5.0 using 0.2 M acetate buffer solution. The breakthrough and column capacities and interstitial volume were determined according to the literature methods [17,19].

The separations of binary mixtures of Cu(II) and Zn(II), Zn(II) and Ni(II) and Ni(II) and Cu(II) and ternary mixture of Cu(II), Ni(II) and Zn(II) were attempted at optimised conditions.

4. Results and discussion

The resin beads of 20–60 mesh size were used throughout the work. The resin was thoroughly analysed by various techniques. The intermediate chloromethylated poly (vinyl pyridine) was analysed for chlorine content by fusing it with sodium peroxide and estimating the chlorine content by Volhard's method [16]. It was observed that the product contains 1.4 mmol g^{-1} chloride, where as the extent of dithizone anchored on chloromethylated intermediate was found to be ~1.1 mmol g^{-1}. This was confirmed through the elemental analysis of the chloromethylated 4-vinyl pyridine-divinyl benzene copolymer and the copolymer loaded with dithizone. The difference in the extent of chloride in chloromethylated poly (vinyl pyridine) and the dithizone anchored support is due to the chemical binding of dithizone to the support through chloride. This was further confirmed through FTIR analysis of the copolymer and copolymer loaded with dithizone. The appearance of the characteristic i.r. absorption band of C=S groups linked to nitrogen at 1400–1450 cm^{-1} in the ir spectrum of copolymer loaded with dithozone, is taken as the proof for the presence of the dithizone in the support. The reactions involved in the anchoring of dithizone on poly (vinyl pyridine) are given in Fig. 1 The resin showed good thermal and chemical stability up to 200°C and 6 M acids. In the presence of alkalies, colour of the resin became intense. The physicochemical properties of the dithizone loaded support are given in Table 1 The sorbent used for more than 20 times in succession under static conditions did not show any decrease in sorption efficiency. Chwastowska and Kosiarska

Table 3
Rate constant (k) and activation energy (ΔE) for copper, nickel and zinc exchange

Metal	Rate constant $k \times 10^4$ s at °C			Activation energy ΔE J mol$^{-1} \times 10^{-4}$
	30	40	50	
Cu(II)	8.25	9.91	10.48	1.04
Ni(II)	1.70	2.02	3.32	2.72
Zn(II)	9.32	9.50	10.12	0.33

[15] have also reported no decrease in sorption efficiency up to 25 succession under static conditions for dithizone loaded on St-DVB support.

The effect of pH on copper, nickel and zinc exchange is illustrated in Fig. 2. It was observed that in acetate buffer exchange of copper and nickel was quantitative but zinc was not exchanged with the resin. Hence, zinc exchange was carried out in citrate–phosphate buffer. The optimum pH for all the metal ions exchange was observed to be five. Earlier report [15] gives pH range 5–6.5 for these metal exchanges.

In the study of effect of copper, nickel and zinc ion concentration on the exchange capacity, it was observed that resin shows saturation at 200, 800 and 400 μg cm^{-3} copper, nickel and zinc ion concentration respectively (Fig. 3).

From the kinetics of copper, nickel and zinc exchange (Fig. 4), it was observed that 6, 9 and 12 h contacting time is required for the 100% exchange of copper, zinc and nickel respectively. However, the time required for the 50% exchange ($t_{1/2}$) of zinc, copper and nickel was observed to be 45.5, 35.5 and 30.0 min respectively. From the interruption test, it was observed that copper, nickel and zinc exchange is a particle diffusion process. The 10.0 min interruption pause during the test gives time for the concentration gradients developed in the beads to level out resulting in the increase in exchange rate after reimmersion. The representative plot of percent exchange vs time with interruption and without interruption for copper, exchange is given in Fig. 5. In film diffusion no concentration gradient exists in the beads and hence the interruption does not affect the concentration gradients across the beads resulting into no effect on exchange rate. The particle diffusion is also confirmed with the mathematical model proposed by Nativ et al. [18]. A plot of time vs $[1-3(1-X)^{2/3}+2(1-X)]$ was constructed where 'X' is the fraction conversion of the resin which is a ratio between the measured and maximum exchange capacity. According to this model straight line passing through origin confirms the shell progression mechanism controlled by film diffusion through the reacted layer. The Nativ plot for copper, nickel and zinc exchange gave intercept on X axis eliminating film diffusion and confirming the diffusion of copper, nickel and zinc by particle diffusion process.

The reaction for the exchange process can be written as

$$y\overline{RA} + B^{y+} = \overline{Ry}B + yA^{x+}$$

where RA indicates solid phase having yA^{x+} exchangeable ions and B^{y+} as exchangeable counter ion in the solution phase. In the present study charges on A and B are 1 and 2, i.e. $x=1$ and $y=2$. Adsorption of ions from solution to solid is governed by Langmuir adsorption isotherm. This can be applied to ion exchange process with specific assumptions.

1. The first assumption is that the selectivity coefficient or separation factor remains unchanged or little changed over the exchange involved.
2. Secondly, for homovalent and heterovalent exchange, the concentration of one of the ions or of the total solution is constant, and
3. Unlike selectivity coefficient, the separation factor obtained for the Langmuir plot can not be regarded as a constant depending on site adsorption energy.

Table 4
Column characterisation

Sr. No.	Metal	Column length (cm)	Interstitial volume (V_0) (cm^3)	Break through capacity BTC (mM g^{-1})	Total column capacity TC (mM g^{-1})	Degree of utilization BTC/TC
1	Cu(II)	15.0	2.1	0.61	1.16	0.53
2	Ni(II)	15.0	2.1	0.12	0.89	0.13
3	Zn(II)	15.0	2.1	0.16	0.91	0.18

Based on these assumptions Misak [20] has modified Langmuir adsorption isotherm for the ion exchange process. Accordingly exchange process can be governed by

$$\frac{C_A}{q_A}=\frac{C_A}{Q}\left[1-\frac{x}{\alpha y}\right]+\frac{C_0}{\alpha y Q}$$

where q_A is the amount of metal 'A' sorbed (mmol g^{-1}), C_A is equilibrium concentration of metal A in solution, C_0 is initial concentration of metal ion in the solution. Q is the maximum exchange capacity x and y are charges on A and B and α is a separation factor. From the above equation, a plot of C_A/q_A vs C_A was constructed (Fig. 6). α and Q were calculated from the slope and intercept respectively. The theoretically calculated Q values (Table 2) for copper, nickel and zinc are observed to be in good agreement with the experimental values.

4.1. Thermodynamics and rate of exchange

The reaction rates for the exchange of copper, nickel and zinc on the resin were determined at different temperatures. The initial rate constant k was calculated using equation for the first order exchange reaction:

$$-\frac{dc}{dt}=k_c \quad \text{and} \quad -\log(a-f)=\frac{kt}{2.303}$$

where 'a' is the initial concentration of metal ion and 'f' is the concentration of metal ion exchanged on the resin. It was observed that the plot of $-\log(a-f)$ vs t is not a straight line. Hence mirror method [21] was used to calculate the rate constant from the initial rate of the exchange where the plot is a straight line. From the $\log k$ vs $1/T$ plot, the activation energy required for complex formation was calculated. The calculated activation energy ΔE and rate constants are given in Table 3.

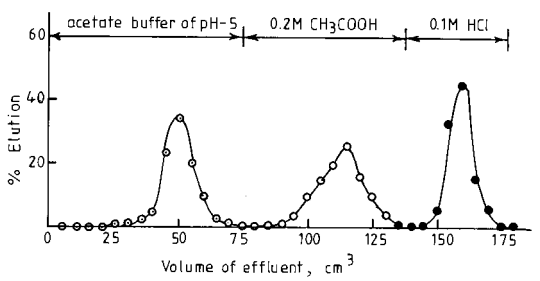

Fig. 7. Separation of copper, nickel and zinc. ● Copper, ○ nickel, ⊙ zinc.

4.2. Desorption of copper, nickel and zinc from the resin

Desorption of copper, nickel and zinc from the resin was tried with various acids of different strengths. It was observed that 0.1 M HCL could elute copper, nickel and zinc quantitatively where as 0.1 M HNO_3 and 0.1 M H_2SO_4 could elute copper and zinc quantitatively but even with higher concentration of HNO_3 and H_2SO_4, only 44% and 55% of nickel was eluted. Nickel was eluted quantitatively with 2.0 M CH_3COOH. Where as copper and zinc were not at all eluted with CH_3COOH. With 1.0% thiourea incomplete elution of copper and nickel was achieved whereas zinc was eluted quantitatively. Chwastowska and Kosiarska [15] have reported quantitative stripping of copper, nickel and Zinc by 4 M HCl.

4.3. Chromatographic separations

The column characteristics for copper, nickel and zinc are given in Table 4. From the results obtained for the effect of pH on the metal ex-

change and elution study, it was observed that copper, nickel and zinc can be separated from each other due to difference in eluting reagents. Hence synthetic mixtures of (i) copper and nickel, (ii) nickel and zinc, (iii) zinc and copper and (iv) copper, nickel and zinc were passed through the column at a flow rate of 1 cm^3 min^{-1}. The column effluents were analysed for every metal ion in the mixture.

For the separation of binary mixtures of copper(II) and nickel(II) 30 ml of 1:1 mixtures of 10 mg concentration were passed through the column at pH 5.0 using 0.2 M acetate buffer at a flow rate of 1 cm^3 min^{-1}. The column was washed with deionised water to remove unexchanged metal ions. However, no metal was observed in the column effluent, indicating complete exchange of metal ions on the resin. Separation of metal ions was achieved with the help of selective elution technique by passing first 60 cm^3 of 0.2 M acetic acid as an eluent for nickel followed by 70 cm^3 of 0.1 M HCl for elution of copper.

In the separation of nickel(II) and zinc(II), and zinc(II) and copper(II), 30 ml of 1:1 mixtures of 10 mg concentration were passed through the column at a flow rate of 1 cm^3 min^{-1}. The pH of the mixtures was maintained at five using 0.2 M acetate buffer. At this condition exchange of zinc did not take place and hence first few fractions of column effluent showed complete leaching of zinc. The column was further washed with deionised water and copper and nickel were eluted as described earlier.

In the separation of ternary mixtures of copper, nickel and zinc, 30 ml of 1:1:1 mixtures of 10 mg strength were passed through the column at pH 5.0 using 0.2 M acetate buffer. Zinc was not exchanged at this condition and was obtained in the first few fractions of column effluent. Copper and nickel were quantitatively exchanged on the column and were eluted and estimated as described earlier. The representative separation pattern for copper(II), nickel(II) and zinc(II) is given in Fig. 7. The separations of copper(II)–Au(III)–Pt(IV) [22], Zn(II)–Cd(II)–Hg(II) [23], Ni(II)–Pt(IV) and Ni(II)–Pt(II) [24] are reported else where.

In the similar study by using dithizone loaded on St-DVB polymer Chwastowska and Kosiarska [15] have shown effect of flow rate on dynamic exchange of metal ions. Optimum flow rate is reported to be 2 ml min^{-1}. However, no separations have been reported. The metal exchange capacities for copper, nickel and zinc were reported to be 0.08, 0.04 and 0.04 mmol g^{-1} respectively which are almost ten times less than those observed in the present study.

References

[1] A. Warshawsky, Ion Exchange Sci. Technol. (1984) 604.
[2] A. Warshawsky, Ion Exchange Sci. Technol. (1986) 67.
[3] A. Warshawsky, Crit. Rep. Appl. Chem. 19 (1987) 127 and 166.
[4] K. Dev, G.N. Rao, Analyst 20 (1995) 2509.
[5] L. Steinmann, J. Porath, P. Hashemi, A. Olin, Talanta 41 (1994) 10.
[6] F. Malamas, M. Bengtsson, G. Johansson, Anal. Chim. Acta 160 (1984) 1.
[7] R. Purohit, S. Devi, Talanta 38 (1991) 753.
[8] R. Purohit, S. Devi, Analyst 120 (1995) 555.
[9] R. Purohit, S. Devi, Analyst 116 (1991) 825.
[10] Y.K. Lee, K.J. Whang, K. Veho, Talanta 22 (1975) 535.
[11] M.F. Garcia, R.P. Qarcia, N.B. Garcia, A.S. Medel, Talanta 41 (1994) 1833.
[12] T. Braun, A.B. Farag, Anal. Chim. Acta 69 (1974) 85.
[13] M. Grieshbach, K.H. Leiser, (Riedlde Haen A.G.), Eur. Pat. Appl. 14, 222 (cl.08 F8/30), 1979.
[14] M. Grote, A. Kettrup, Anal. Chim. Acta 172 (1985) 223.
[15] J. Chwastowska, E. Kosiarska, Talanta 35 (1988) 439.
[16] A.I. Vogel, Handbook of Quantitative Inorganic Analysis, Longman, London, 1978.
[17] F. Helfferich, Ion Exchange, McGraw-Hill, New York, 1962.
[18] M. Nativ, S. Goldstein, G. Schmuchler, J. Inorg. Nucl. Chem. 1975 (1951) 37.
[19] J. Inczedy, Analytical Applications of Ion Exchangers, Pergamon Press, Oxford, 1966.
[20] N.Z. Misak, React. Polym 21 (1993) 53.
[21] A.A. Forst, R.G. Pearson, Kinetics and Mechanism, New York, 1961. p.46.
[22] R. Shah, S. Devi, Analyst 121 (1996) 807.
[23] R. Shah, S. Devi, React. Func. Polymers 31 (1996) 1.
[24] R. Shah, S. Devi, Anal. Chim. Acta 17869 (1997) 1.

.

ELSEVIER

Talanta 45 (1998) 1097–1102

Talanta

A sensitive spectrophotometric method for the determination of dithiocarbamate fungicide and its application in environmental samples

Ritu Kesari, V.K. Gupta *

School of Studies in Chemistry, Pt. Ravishankar Shukla University, Raipur, 492 010, M.P., India

Received 11 March 1997; received in revised form 7 July 1997; accepted 8 July 1997

Abstract

A sensitive spectrophotometric method based on the evolution of CS_2 and colour development by leuco crystal violet is described for the determination of dithiocarbamate fungicides, e.g. thiram, ziram and zineb. Dithiocarbamate fungicides release CS_2 on acid hydrolysis. This CS_2 is absorbed in ethanolic sodium hydroxide and forms xanthate. The xanthate formed is subsequently treated with potassium iodate and *N*-chlorosuccinimide, during which free iodine is liberated. Crystal violet dye was formed through selective oxidation of leuco crystal violet by liberated iodine, which has an absorbance maxima at 595 nm. The colour systems obey Beer's law in the range of 0.02–0.20, 0.02–0.24 and 0.04–0.32 ppm for thiram, ziram and zineb respectively. The molar absorptivity of the colour system were found to be 9.6×10^5, 1.1×10^6 and $6.8 \times 10^5 \pm 100$ l mol^{-1} cm^{-1} for thiram, ziram and zineb respectively. The method has been successfully applied to the determination of these dithiocarbamate fungicides in various environmental samples. © 1998 Elsevier Science B.V.

Keywords: Spectrophotometric; Dithiocarbamate fungicides; *N*-chlorosuccinimide; Leuco crystal violet

1. Introduction

Thiram (bis-dimethyl thiocarbanoyl disulphide), ziram (zinc-dimethyl dithiocarbamate) and zineb (Zinc ethylene-1,2-bis-dithiocarbamate) are important and widely used fungicides. These are protective fungicides for use on seeds foliages, fruits and vegetable crops. These fungicides have chronic toxicity causing allergic infections to skin and asthmatic phenomena. Exposure to zineb can also cause functional changes in the cardiovascular system. The acute oral LD_{50} value of thiram, ziram and zineb are 375, 1400 and 5200 mg kg^{-1} respectively for rats [1–3].

Various instrumental methods have been reported for the determination of dithiocarbamate fungicides such as TLC [4], HPLC [5], GC [6], Polarography [7] etc. A few spectrophotometric methods are based on Clark's method [8] where dithiocarbamates are decomposed under acidic conditions to give carbon disulphide which is trapped in methyl potassium hydroxide to give

* Corresponding author.

PII S0039-9140(97)00208-7

potassium methyl xanthate, which is then titrated iodometrically. Petrascu [9,10] and Rosenthal et al. [11] have modified Clark's method. Other methods [12–14], use toxic benzylmercaptan and metallic compounds and are less sensitive.

In the present communication a simple and sensitive method is proposed for the determination of thiram, ziram and zineb. The methodology involves the evolution of CS_2 from the above fungicides on acid hydrolysis. This CS_2 was absorbed in ethanolic NaOH and formed a pale yellow coloured xanthate. This xanthate is subsequently treated with potassium iodate and the iodine liberated is reacted with leuco crystal violet in the presence of *N*-chlorosuccinimide. The crystal violet dye formed showed maximum absorbance at 595 nm. This method has been applied to different environmental samples and its analytical parameters have been optimised. The method has been found to be more sensitive than other reported methods and is fairly reproducible.

2. Experimental

2.1. Apparatus

A Systronics UV-vis spectrophotometer 108 with 2 cm matched silica cells was used for all spectral measurements. Systronics pH meter model 331 was used for pH measurements. The digestion–absorption apparatus is the same as described by Lowen and Pease [15].

2.2. Reagents

All reagents were of analytical reagent grade and double distilled deionised water was used throughout the experiment.

2.3. Stock solution of zineb (Indofil), ziram (Hindustan CIBA–Geigy) and thiram (Swarup)

1 mg ml^{-1} solution of zineb in EDTA (0.1 mol l^{-1}), ziram in chloroform and of thiram in acetone were prepared. The required working standard solutions were prepared by appropriate dilution of the stock.

2.4. Absorbing solution

5% solution of ethanolic sodium hydroxide solution was prepared as an absorbing solution for CS_2.

2.5. Potassium iodate (Merck)

0.1 M solution was prepared by dissolving 0.713 g of KIO_3 in 1 l water.

2.6. N-chlorosuccinimide solution (Aldrich)

250 mg of *N*-chlorosuccinimide was added to 250 ml volumetric flask containing 2.5 g of succinimide and volume was made up to the mark with water. The solution was stable for six months. Succinimide increases the stability of the *N*-chlorosuccinimide as reported [16].

2.7. Leuco crystal violet (LCV) (Eastman Kodak)

To a 1 l volumetric flask, 200 ml water, 3 ml of 85% phosphoric acid and 250 mg of LCV [4,4′,4″ methyldynitric (*N*,*N*-dimethyl aniline)] were added and shaken gently until the dye dissolved and then diluted to 1 l with water. The solution was colourless when prepared and stable for several months.

2.8. Buffer solution

Buffer solution of pH 4.0 ± 0.1 was prepared in a 500 ml volumetric flask by dissolving 17.01 g of potassium hydrogen phosphate in 490 ml water. 85% phosphoric acid was added dropwise until the pH becomes 4.0 ± 0.1 the solution was then diluted to the mark with water.

2.9. Procedure

A known amount of working standard solution of thiram, ziram and zineb prepared in suitable solvent was introduced in the digestion flask of digestion–absorption apparatus. Chloroform was evaporated in the case of ziram. Then hot 9 M H_2SO_4 was added dropwise to the above solution for hydrolysis during which CS_2 was released. 5

ml of ethanolic sodium hydroxide solution was taken as an absorbing solution. Aspiration was carried out for about 30–40 min. The pale yellow xanthate obtained was diluted with water as required. Aliquots of this solution (0.5–5 μg for thiram, 0.5–7 μg for ziram and 1–8 μg for zineb) were taken in a 25 ml calibrated test tube. To it 2 ml phosphate buffer solution, 1 ml of potassium iodate, 1 ml of *N*-chlorosuccinimide were added and gently shaken for a few seconds. 1 ml of LCV solution was added to the solution and it was kept for 25 min for complete colour development. The crystal violet dye liberated shows maximum absorbance at 595 nm. The blank value was subtracted from the value obtained from that of the standard.

3. Results and discussion

3.1. Effect of temperature

Under the optimum conditions 30–35°C was the most suitable temperature for colour development.

3.2. Effect of time

It was found that 25 min. were necessary for complete colour development which was stable for several days.

3.3. Effect of pH

The pH of 4.0 ± 0.1 was found to be the best for the formation of CV from LCV under optimum conditions. It was observed that pH above 5 severely affected the stability and sensitivity of the dye. Colour did not develop below pH 3.2. The pH was maintained at 4.0 ± 0.1 by using phosphate buffer solution.

3.4. Effect of the reagent concentration

Under the proposed condition 2 ml of phosphate buffer solution, 1 ml of 0.1 M KIO_3 solution, 1 ml of 0.1% *N*-chlorosuccinimide solution and 1 ml of LCV were necessary for complete colour development and maximum sensitivity. The absorbance was found to decrease on lowering the reagent concentration, while there was no significant increase in the absorbance on an increase in concentration of the reagent.

Beer's law is obeyed in the range of 0.02–2, 0.02–0.24 and 0.04–0.32 ppm of thiram, ziram and zineb respectively. (i.e. 0.5–5, 0.5–7 and 1–8 μg per 25 ml of the final solution). The coloured system showed the maximum absorbance at 595 nm. The molar absorptivity were 9.6×10^5, 1.1×10^6 and $6.8 \times 10^5 \pm 100$ l mol^{-1} cm^{-1} and Sandell's sensitivity were found to be 0.0002, 0.0002 and 0.0004 μg cm^{-1} for thiram, ziram and zineb respectively.

3.5. Effect of reproducibility

Reproducibility of the method has been checked by analysing 4 μg per 25 ml of thiram, ziram and zineb. The standard deviation was 0.005, 0.006 and 0.006 and relative standard deviation was ± 0.78, 1.07 and 1.5% for thiram, ziram and zineb respectively when replicate analysis done over a period of seven days.

3.6. Effect of possible interference

The tolerance limit for various diverse ions and pesticides likely to be present with these fungicides was evaluated and are shown in Table 1. Most of the common ions did not interfere in the procedure. Only compounds which evolve carbon disulphide during acid hydrolysis interfere in this method and such contaminations are unlikely or rare. Hydrogen sulphide interferes and is eliminated by its absorption in lead acetate prior to the passing of carbon disulphide in the absorbing solution. Nitrogen dioxide, formaldehyde, Cu^{2+} and Fe^{2+} did not interfere under the optimum conditions. Hg^{2+} and Mn^{4+} had a positive catalysing effect on this reaction.

3.7. Colour reaction

The colour reaction involves the following steps as described in Scheme 1. The probable reactions involved are as follows.

Table 1
Effect of possible interferents in the determination of zineb, ziram and thiram

Possible interferents (Pesticides)	Tolerance limit[a] μg per 25 ml	Possible interferents (Ions)	Tolerance limit[a] μg per 25 ml
Mancozeb	1200	Sb^{3+}	700
Propoxure, Carbaryl	1000	Fe^{2+}, Fe^{3+}	600
Ethyl parathion	950	Cd^{2+}, Cu^{2+}, Co^{2+}	350
DDT, BHC	800	Po_4^{3-}	200
Phorate	500	Mg^{2+}, Zn^{2+}	100
Kelthane	450	Ca^{2+}	80
Malathion	300	Br^-, Cl^-	75

Concentration of dithiocarbamate—4 μg per 25 ml.
[a] Tolerance limit may vary the absorbance value by $\pm 2\%$.

1. Liberation of carbon disulphide from zineb, ziram and thiram by acid hydrolysis at higher temperature.
2. Formation of xanthate with the treatment of carbon disulphide with alcohlic sodium hydroxide.
3. Iodine is liberated as a result of reaction between potassium iodate and the xanthate formed, in the presence of *N*-chlorosuccinimide.
4. Formation of crystal violet dye through selective oxidation of leuco crystal violet by liberated iodine.

3.8. Application

The proposed method has been satisfactorily applied to the determination of thiram, ziram, zineb in various samples of polluted water, vegetables, grains and biological samples. The results obtained were in good agreement with the reported method.

3.9. Determination of dithiocarbamate fungicides in polluted water

250 ml agricultural waste water samples were taken from the fields where thiram, ziram, or zineb had been sprayed as fungicide. These samples were filtered through a Whatman No. 40 filter paper. Sample with zineb was taken in the impinger without any further treatment. Ziram and thiram containing, water samples were extracted with 2×15 ml portions of chloroform. The washing was collected. Aliquots of the above solution were taken in an impinger. The details of digestion and absorption are the same as given earlier. Samples were analysed for zineb, ziram and thiram by proposed as well as reported method [14]. Results are given in the Table 2.

3.10. Determination of zineb, ziram and thiram in vegetable and grain samples

Various samples of vegetables, potato tubers, lettuce and wheat were collected from agricultural fields where thiram, ziram or zineb had been used. Samples were weighed and ground in the mixer. The ground pulp of zineb containing samples were washed with 2×15 ml portions of 0.1 mol l^{-1} EDTA solution [17]. Ziram and thiram samples were washed with 2×15 ml portions of chloroform. The washings were collected. Aliquots of these washings were taken in an impinger and analysed by the proposed as well as reported method [14] (Table 2). To check the recoveries known amount of zineb, ziram or thiram were added to various samples of water, vegetables and grain and then analysed by the proposed method with a recovery of 93–98%. The results are also compared with the values obtained by the reported method [14] and are found to be in good agreement.

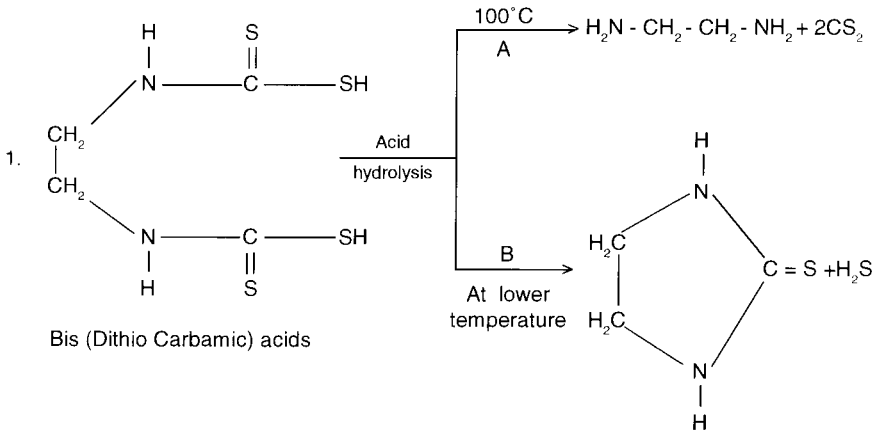
1.
Bis (Dithio Carbamic) acids
Acid hydrolysis
100°C
A
$H_2N - CH_2 - CH_2 - NH_2 + 2CS_2$
B
At lower temperature
$C = S + H_2S$

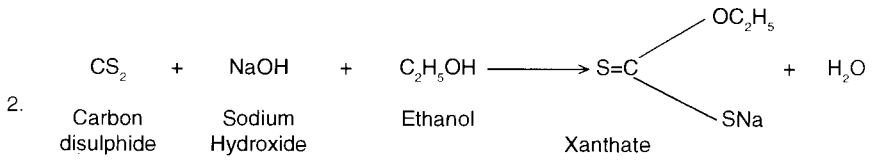
2.
CS_2 + NaOH + C_2H_5OH → $S=C$ + H_2O
Carbon disulphide
Sodium Hydroxide
Ethanol
Xanthate
OC_2H_5
SNa

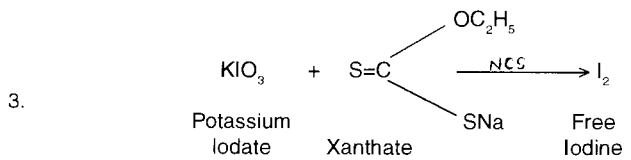
3.
KIO_3 + $S=C$ → I_2
NCS
Potassium Iodate
Xanthate
Free Iodine
OC_2H_5
SNa

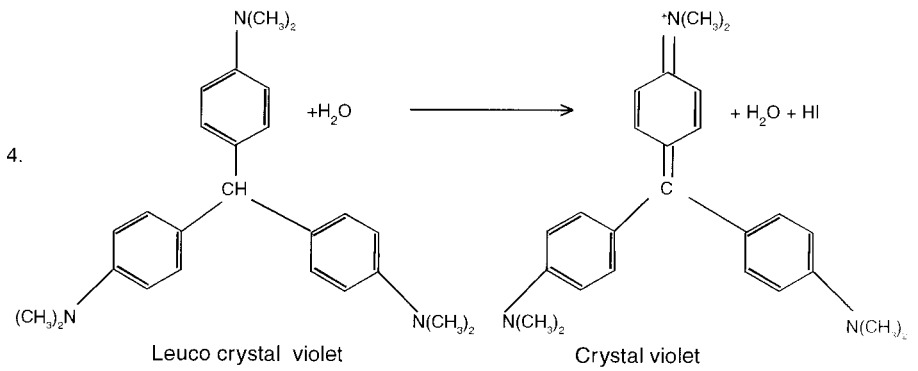
4.
$N(CH_3)_2$
$+H_2O$
CH
$(CH_3)_2N$
$N(CH_3)_2$
Leuco crystal violet
$+H_2O + HI$
C
Crystal violet

Scheme 1.

Table 2
Application of the method to the determination of dithiocarbamates in various samples

Sample[a]	Fungicides found[b] in μg	
	Proposed method	Reported method [14]
Polluted water	3.27	3.20
(zineb)	6.20	6.15
Potato tubers	4.50	4.40
(zineb)	7.50	7.21
Lettuce	2.75	2.70
(thiram)	4.55	4.35
Cucumber	3.50	3.27
(thiram)	4.60	4.45
Wheat	6.00	5.89
(ziram)	6.50	6.48

[a] Amount of samples: Water sample, 250 ml, Veg. and grain sample, 100 g.
[b] Mean of three replicate analysis.

3.11. Determination of thiram, ziram and zineb in blood and urine samples

Since the presence of these fungicides has been reported in blood and urine, the method has applied for their determination in biological samples. Known amounts of thiram, ziram or zineb solution was added to blood and urine samples and later determined by the proposed method with the recovery of 95–99% which is in agreement with the reported method [14].

4. Conclusion

The present method for the determination of dithiocarbamates via CS_2 evaluation is simple, sensitive and fairly reproducible. The method is compared with the method reported by Verma et al. [14] using tetra-acetonitrilocopper(I) perchlorate and found to be more sensitive and selective and avoids the use of hazardous chemicals. This method is successfully applied to the determination of dithiocarbamate fungicides in the environmental and biological samples.

Acknowledgements

The authors are grateful to the Head, Department of Chemistry, Pt. Ravishankar Shukla University, Raipur for providing facilities. One of them (R.K.) is thankful to Pt. Ravishankar Shukla University for providing research scholarship.

References

[1] I.F. Kolpakov, L.P. Soboleva, Gig. Tr. Prof. Zabol 6 (1987) 35 (Chem. Abstr. 107 (1987) 182617q).
[2] G.S. Gruzdyev, The Chemical Protection of Plants, Mir, Moscow, 1983, p. 284.
[3] H. Martin, Pesticide Manual, Basic Information on the Chemicals Used as Active Components of Pesticides, 1st ed. British Crop Protection Council, UK, 1968.
[4] E.B. Muzhanovskii, A.F. Fartushnyi, A.I. Sedov, Sub-Med. Ekspert 25 (1982) 42 (Russia) (Anal. Abstr. 45 (1983) 587.)
[5] H. Irth, G.J. Jong De, U.A.T. Brinkman, R.W. Frei, J. Chromatogr. 370 (3) (1986) 439.
[6] M. Uno, T. Okado, M. Nozawa, K. Tanigawa, Shokuhim Eiseigabu Zasshi 23 (6) (1982) 474 (Japan) (Anal. Abstr. 46 (1984) 221).
[7] D. Karageogiev, Gradinar. Lozar. Nauka 18 (1981) 33 (Bulgaria) (Chem. Abstr. 96 (1982) 17594z).
[8] D.G. Clark, H. Baum, E.L. Stanley, W.F. Hester, Anal. Chem. 23 (1951) 1842.
[9] S. Petrascu, Rev. Chem. (Bucharest) 17 (1986) 687.
[10] A.L.J. Rao, N. Verma, Talanta 36 (1989) 1041.
[11] J. Rosenthal, R.L. Carlson, F.L. Stanley, J. Assoc. Off. Agric. Chem. 36 (1953) 1170.
[12] B.C. Verma, R.V. Sood, M.S. Sindhu, Talanta 30 (1983) 787.
[13] A.K. Malik, A.L.J. Rao, Talanta 37 (1990) 1205.
[14] B.C. Verma, R.K. Sood, S. Chauhan, A. Sood, N.K. Sharma, D.K. Shrama, Proc. Indian Nat. Sci. Acad. 52 (1986) 1420.
[15] W.K. Lowen, H.L. Pease, in: G. Zweig (Ed.), Analytical Methods for Pesticides, Plant Growth Regulators and Food Additives vol. 3, Academic press, New York, 1964 p. 69.
[16] D.L. Lambert, G.L. Hatch, B. Mosier, Anal. Chem. 47 (1975) 915.
[17] J.V. Das, V.K. Gupta, Chem. Anal. 40 (1995) 85.

ELSEVIER

Talanta 45 (1998) 1103–1109

Talanta

Determination of absorptivity and formation constant of a chalcone association complex

Sonia E. Blanco, Ferdinando H. Ferretti *

Departamento de Química, Facultad de Química, Bioquímica y Farmacia, Universidad Nacional de San Luis, Chacabuco y Pedernera, 5700 San Luis, Argentina

Received 13 March 1997; received in revised form 7 July 1997; accepted 8 July 1997

Abstract

A UV spectrometric method was developed to determine the molar absorptivity (ε_C) and formation constant (K_c) of the association complex of unsubstituted chalcone in cyclohexane, in the concentration range from $4.00 \cdot 10^{-4}$ to $2.00 \cdot 10^{-2}$ mol dm^{-3}. The thermodynamic and spectroscopic magnitudes such as K_c and ε_C contribute to the understanding of the physicochemical behavior of several α,β-unsaturated carbonylic compounds, of low solubility in water, as it is the case of numerous flavonoids of chemical and biological importance. The studied association complex, formed by two chalcone molecules, is characterized by the constants ε_C (300.8 nm) $= 4.98 \cdot 10^4$ dm^3 mol^{-1} cm^{-1} and $K_c = 5.58 \cdot 10^3$. The method proposed is convenient for the study of solute–solute molecular associations particularly those due to dipole–dipole interactions. © 1998 Elsevier Science B.V.

Keywords: Absorptivity constant; Formation constant; UV spectrometric method

1. Introduction

The biological actions exerted by numerous flavonoids are varied and important. In particular, chalcones and flavanones arouse scientific interest due to their antimicrobial [1–3] and fungicide [4] activity, their enzyme inhibiting and inducing capacity [5,6], and other therapeutic applications [7–9]. In chemical and pharmaceutical laboratories a wide array of analytical methods (chromatographic [10,11], electrochemical [12,13], and spectroscopic [14,15], among others) is available for the study of these compounds in natural or synthetic products, in drugs [16] or biological fluids. However, UV/VIS spectroscopic methods, which have greatly improved in the latest years [17], are those of most frequent use due to their simplicity and accuracy.

It is well known that Beer's Law is of great importance in UV/VIS spectroscopy. Very few exceptions can be found for the direct relation existing between absorbance and optical path longitude. However, deviations from the direct proportionality between the absorbance of a substance and its concentration can sometimes be observed [18]. Beer's Law clearly accounts for the absorption of a compound and its concentration only in diluted solutions, this is, when molecular interactions are not significant.

* Corresponding author. Fax: + 54 652 31301.

PII S0039-9140(97)00209-9

By analyzing the physicochemical properties of flavonoids with relatively simple structures, it could be proved that unsubstituted chalcone complies with Beer's Law in concentrations lower than $1.00 \cdot 10^{-4}$ mol dm^{-3}. For higher concentrations, the measured absorbances were higher than those expected according to its analytical concentration. This phenomenon led us to further investigate the UV spectroscopic behavior of this substance in high concentrations. A method was developed which allows the determination of the molar absorptivity, stoichiometry, and formation constant of solute–solute association complexes. The method was particularly used to reveal and characterize the formation of association complexes of chalcone dissolved in cyclohexane, in the concentration range between $4.00 \cdot 10^{-4}$ and $2.00 \cdot 10^{-2}$ mol dm^{-3}.

2. Experimental

2.1. Reagents

The structure of unsubstituted chalcone (S) is shown in Fig. 1. This substance was obtained by Claisen–Schmidt condensation [19] and was purified by repeated crystallization from methanol–water. The purity control was performed by TLC with aluminum sheets polyamide 11 F_{254} (Merck) using methanol as eluant, and by UV spectroscopy (methanol).

Cyclohexane and methanol (Merck, spectroscopic grade) were used to prepare all the solutions.

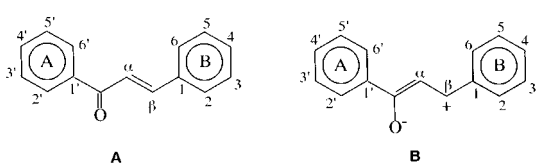

Fig. 1. (a) Structure of unsubstituted chalcone; (b) Most likely resonant form of the molecular resonance hybrid.

2.2. Apparatus

Absorption spectra were performed on a Shimadzu UV 160 A double beam spectrophotometer with 1 cm thermostatically controlled cells, between 200 and 350 nm. The temperature (25.0 ± 0.1°C) and stirring (450 rpm) conditions for the experiments of chalcone solubility in cyclohexane were kept constant by using a Variomag Electronicrührer Einhängethermostat MR equipped with a Telemodul 40 S stirrer.

2.3. Procedure

All the solutions were prepared by weighing with an accuracy of ± 0.0001 g and kept at the same temperature.

To determine molar absorptivity ε_S (dm^3 mol^{-1} cm^{-1}), solutions of S in cyclohexane were prepared varying the concentration between $1.40 \cdot 10^{-5}$ and $7.50 \cdot 10^{-5}$ mol dm^{-3}, the range within which Beer's Law applies. The solutions were stabilized at 25.0 ± 0.1°C for 15 min, and their spectra were recorded.

To determine the solubility in cyclohexane $C_{S_{sat}}$ (mol dm^{-3}), two saturated solutions of the pure substance were prepared and maintained at 25.0 ± 0.1°C, with permanent stirring (450 rpm) for 1 h. After letting the solutions stand for 10 min at the same temperature, four samples were taken from the saturated solutions (0.1577, 0.3299, 0.7903 and 0.7758 g) and were mixed with cyclohexane (1.2742, 0.9010, 0.7809 and 0.4706 g). Then 6.00 ± 0.01 μl of each of the four standard solutions were conveniently diluted with cyclohexane (3.8959, 7.6750, 16.1638 and 21.0398 g) and their absorbance was read at the chalcone maximum absorption wavelengths: 300.8 nm (0.575, 0.718, 0.644 and 0.608) and 225.2 nm (0.304, 0.380, 0.340 and 0.321).

To analyze the possible formation of solute–solute association complexes at 25.0 ± 0.1°C, a stock solution of chalcone $2.072 \cdot 10^{-2}$ mol dm^{-3} (density = 0.7828 g ml^{-1}) was prepared in cyclohexane (density = 0.7785 g ml^{-1}). Then, variable amounts of the stock solution (0.1575–3.2488 g, column 2, Table 1) were mixed with adequate amounts of cyclohexane (7.4980–0.5745 g,

Table 1
Obtained data for a typical experiment of formation of unsubstituted chalcone in cyclohexane association complex ($n=2$) at 25.0 ± 0.1°C

Cy (g)	Solution 1 (g)	Solutions $J \cdot 10^3$	Cy (g)	Solution J (g)	A	$(A-A_i)_j$	$H_j \cdot 10^2$	$X_j \cdot 10^2$
			Dilution J			Solution J		
7.4980	0.1575	0.4240	2.3150	0.1954	0.799	0.536	0.145	0.028
7.6441	0.2590	0.6754	2.5614	0.1581	0.956	0.946	0.256	0.049
7.2888	0.3277	0.8868	2.6300	0.1195	0.939	1.257	0.341	0.064
3.6640	0.1909	1.0210	2.7058	0.0981	0.872	1.502	0.407	0.077
3.4816	0.3840	2.0480	5.3882	0.0983	0.901	3.293	0.892	0.169
3.3023	0.5870	3.1130	5.3799	0.0607	0.854	5.124	1.389	0.263
3.1555	0.7645	4.0230	4.6442	0.0383	0.810	6.718	1.820	0.344
2.9079	0.8844	4.8120	5.3805	0.0376	0.823	8.184	2.218	0.420
2.6823	1.1475	6.1840	6.5256	0.0384	0.893	10.74	2.912	0.552
2.5392	1.3183	7.0550	7.6534	0.0382	0.865	12.28	3.327	0.630
2.4551	1.5231	7.9060	7.5863	0.0187	0.480	13.80	3.740	0.707
2.1429	1.7028	9.1460	4.9431	0.0181	0.825	16.26	4.408	0.836
1.8833	1.9042	10.390	5.7369	0.0183	0.817	18.56	5.031	0.954
1.3318	2.5077	13.510	7.1179	0.0181	0.848	24.40	6.612	1.255
0.9781	2.9245	15.510	7.6335	0.0188	0.943	28.05	7.602	1.440
0.5745	3.2488	17.590	9.6000	0.0189	0.856	31.99	8.669	1.643
		194[a]				369[b]		

n, number of chalcone molecules associated in solution (Eq. (5)); Cy, cyclohexane; Solution 1, solution of chalcone $2.072 \cdot 10^{-2}$ mol dm^{-3}; Solutions J, solutions of chalcone of concentrations C_{S_j} (mol dm^{-3}); A, measured absorbance of the dilution of the corresponding solution J; A_i, ideal absorbance of the corresponding solution J (Eq. (20)); $(A-A_i)_j$, real difference between experimental A and A_i of the corresponding solution J (Eq. (19)); $H_j = X_j/X_{sat}$ (Eq. (21)); X_j, molar concentration of converted chalcone in solution J (Eq. (17)); X_{sat}, molar concentration of converted chalcone in the saturated solution.
[a] Molar concentration of chalcone in saturated solution (solubility) at 25.0 ± 0.1°C = 0.194 mol dm^{-3}.
[b] Real difference between experimental A and A_i of the chalcone saturated solution at 25.0 ± 0.1°C.

column 1, Table 1). This series of standard solutions (16 in total), were maintained at 25.0 ± 0.1°C for 10 min. The analytic concentrations C_S (mol dm^{-3}) of these standard solutions, covered the range between $4.240 \cdot 10^{-4}$ and $1.759 \cdot 10^{-2}$ mol dm^{-3} (column 3, Table 1). To measure the corresponding absorbance at 300.8 nm, samples were taken of these 16 solutions (0.1954–0.0181 g, column 5, Table 1) and diluted with cyclohexane (2.3150–9.6000 g, column 4, Table 1). In this manner, errors in the spectrometric reading were minimized, with absorbance measurements ranging between 0.500 and 1.000 (column 6, Table 1). All of these experiences were carried out in duplicate.

3. Method

It is known that a reversible transformation in a closed system, isothermic and at constant pressure, reaches equilibrium with a minimum content of free energy [20]. Thus, in a saturated solution of chalcone in cyclohexane in contact with a solid solute, at a given temperature, the following equilibrium is reached

$$\text{Chalcone}_{(\text{solid phase})} \Leftrightarrow \text{Chalcone}_{(\text{organic phase})}$$

The composition of this equilibrium state is defined by the thermodynamic equilibrium constant K_a. This means that chalcone dissolves in cyclohexane at a certain temperature, up to a magnitude determined by K_a. In our case, this constant is expressed as:

$$K_a = a_{\text{chalcone(organic)}}/a_{\text{chalcone(solid)}} \quad (1)$$

with a being the activity. Since by convention $a_{(\text{solids})} = 1$, it follows that:

$$K_a = a_{\text{chalcone(organic)}} \quad (2)$$

Since the a of a solute is linked to its molar concentration C (mol dm^{-3}), in the form $a = C\gamma$ (γ = molar activity coefficient), Eq. (2) can be written as:

$$K_a = C_{\text{chalcone(organic)}}\gamma_{\text{chalcone(organic)}} \quad (3)$$

Assuming that $\gamma \cong 1$ ($\gamma \to 1$, when $C \to 0$), [21a] the activities of the component (a) can be substituted for the pertinent molar concentrations to calculate the approximate equilibrium constant K_s. This is:

$$K_a \cong K_s = C_{\text{chalcone(organic)}} \quad (4)$$

For low or moderately soluble substances it is reasonable to accept that $\gamma \cong 1$. Therefore, in our case K_s represents the maximum solubility (mol dm^{-3}) of chalcone in cyclohexane.

The formation reaction of an association complex (C_c) in solution, with n molecules of any solute S, can be represented as

$$nS \Leftrightarrow C_c \quad (5)$$

If C_{complex} is the molar concentration of the complex, C_S is the analytical molar concentration of S and X is the molar concentration of S involved in the complex formation, it follows that:

$$C_{Ac} = X/n \quad (6)$$

Then, the equilibrium constant (K_c) of the complex formation can be expressed as:

$$K_c = X/n(C_S - X)^n \quad (7)$$

For a series of j solutions with different C_{S_j}, it is clear that:

$$K_c = X_j/n(C_{S_j} - X_j)^n = X_{sat}/n(C_{Ssat} - X_{sat})^n \quad (8)$$

Subscripts j ($j = 1, 2, 3$, etc.) and sat, indicate solutions of S of concentration C_{S_j} and saturated, respectively. From the following equality,

$$X_j/n(C_{S_j} - X_j)^n = X_{sat}/n(C_{Ssat} - X_{sat})^n \quad (9)$$

the following is obtained:

$$X_j(C_{Ssat} - X_{sat})^n = X_{sat}(C_{S_j} - X_j)^n \quad (10)$$

This equation can be rewritten as:

$$(X_j/X_{sat}) = [(C_{S_j} - X_j)/(C_{Ssat} - X_{sat})]^n \quad (11)$$

If H_j is used to represent the quantity (X_j/X_{sat}), this is,

$$H_j = (X_j/X_{sat}) \quad (12)$$

Eq. (11) can be written as,

$$H_j = [(C_{S_j} - X_j)/(C_{Ssat} - X_{sat})]^n \quad (13)$$

Solving $(C_{S_j} - X_j)^n$ and taking both terms of the equation to the power $1/n$, the following relation is obtained:

$$H_j^{1/n}(C_{Ssat} - X_{sat}) = (C_{S_j} - X_j) \quad (14)$$

from which,

$$H_j^{1/n}C_{Ssat} - H_j^{1/n}X_{sat} = C_{S_j} - X_j \quad (15)$$

From Eq. (12) it can be inferred that:

$$X_{sat} = X_j/H_j = X_jH_j^{-1} \quad (16)$$

By inserting this result into Eq. (15) and then solving X_j, the following expression is obtained,

$$X_j = (C_{Ssat}H_j^{1/n} - C_{S_j})/[H_j^{(1-n)/n} - 1] \quad (17)$$

On the other hand and taking into account Beer's Law (with a 1 cm optical path) and that $C_c = X/n$ (Eq. (6)), it can be stated that:

$$A = \varepsilon_S(C_S - X) + \varepsilon_C X/n \quad (18)$$

A being measured absorbance of the solution, and ε_S and ε_C are the corresponding molar absorptivities (dm^3 mol^{-1} cm^{-1}) of S and C_{Ac}. By operating and reordering terms, the following expression is obtained:

$$A - A_i = X(\varepsilon_C/n - \varepsilon_S) \quad (19)$$

where A_i, defined by equation

$$A_i = \varepsilon_S C_S \quad (20)$$

is the solution ideal absorbance, i.e. the absorbance of S in absence of interaction ($X = 0$). By using Eq. (12) and Eq. (19) the following relationship is obtained:

$$H_j = (X_j/X_{sat}) = (A - A_i)_j/(A - A_i)X_{sat} \quad (21)$$

which calculates H_j by measuring the pertinent absorbance. Then, once the substance solubility ($C_{S_{sat}}$) and the C_{S_j} concentrations of a series of

standard solutions are known, the values of X_j for a given n can be calculated by means of Eq. (17). Obviously, the value proposed for n is correct when the following linear relation is satisfied:

$$\ln X_j = \ln (nK_c) + n \ln (C_{S_j} - X_j) \quad (22)$$

The above equation is obtained by applying logarithms to Eq. (7) and reordering terms. Eq. (22) indicates that by plotting $\ln X_j$ versus $\ln (C_{S_j} - X_j)$, the value for K_c can be calculated from the straight line intersection. On the other hand from Eq. (19) it can be inferred that

$$\varepsilon_C = n[\varepsilon_S + (A - A_i)_j / X_j] \quad (23)$$

Therefore, the complex molar absorptivity can be obtained by calculating the mean of the ε_C values obtained with this equation.

4. Results and discussion

The main characteristics of an α,β-unsaturated carbonylic compound such as chalcone (Fig. 1) can be obtained from its UV absorption spectrum (Fig. 2).

In these compounds, both the benzoyl and the cinnamoyl groups interact with the carbonylic group through σ and π bonds. Such interactions favor the delocalization of π electrons, and the carbonylic group loses part of its characteristic properties. The partial integration of the carbonyl

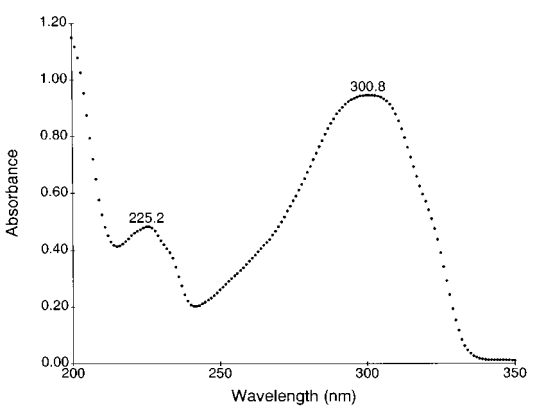

Fig. 2. UV absorption spectrum of chalcone in cyclohexane at 25.0 ± 0.1°C.

to the adjacent olefinic group causes a transference of electronic deficiency from the $C_{carbonylic}$ atom to the atom C of position β. The UV spectrum of chalcone in cyclohexane (Fig. 2), is characterized by two major absorption bands with maxima at 300.8 nm and 225.2 nm, originated by the cinnamoyl and benzoyl groups, respectively, and a valley at 241.4 nm.

4.1. Solubility and molar absorptivities

The solubility and molar absorptivities determined at 25.0 ± 0.1°C for unsubstituted chalcone in cyclohexane were:

$K_s = C_{S_{sat}} = \text{Solubility} = 0.194 \text{ mol dm}^{-3}$
$\varepsilon_S(300.8 \text{ nm}) = 2.30 \cdot 10^4 \text{ dm}^3 \text{ mol}^{-1} \text{ cm}^{-1}$
$\varepsilon_S(225.2 \text{ nm}) = 1.21 \cdot 10^4 \text{ dm}^3 \text{ mol}^{-1} \text{ cm}^{-1}$

4.2. Data of a typical experiment

The results obtained in an experiment of formation of the chalcone association complex ($n = 2$) in cyclohexane are given in Table 1. Even though the calculations for the data in this Table are not complicated, they are given as an example and for the sake of clarity for the first solution ($j = 1$) only.

4.2.1. Calculation of C_{S_1}

Composition: 7.4980 g of cyclohexane (density = 0.7785 g ml^{-1}) + 0.1575 g of chalcone solution in cyclohexane $2.072 \cdot 10^{-2}$ mol dm^{-3} (density = 0.7828 g ml^{-1}). $C_{S_1} = [(0.1575/0.7828) \times 2.072 \cdot 10^{-2})]$

$/[(0.1575/0.7828) + (7.4980/0.7785)]$

$C_{S_1} = 4.240 \cdot 10^{-4} \text{ mol dm}^{-3}$.

4.2.2. Calculation of the solution density

Density = 0.7785 × fraction (w/w) cyclohexane + 0.7828 × fraction (w/w) chalcone solution.

Density = $0.7785 \times 7.4980/(7.4980 + 0.1575)$

$+ 0.7828 \times 0.1575/(7.4980 + 0.1575)$

Density = $0.77859 \cong 0.7786 \text{ g ml}^{-1}$.

4.2.3. Concentration of the dilution (C_{D_1}) performed to measure absorbance

Composition: 2.3150 g of cyclohexane + 0.1954 g of chalcone solution $4.240 \cdot 10^{-4}$ mol dm^{-3} (density = 0.7786 g ml^{-1}). $C_{D_1} = [(0.1954/0.7786) \times 4.240 \cdot 10^{-4}]$

$/[(0.1954/0.7786) + (2.3150/0.7785)]$

$C_{D_1} = 3.300 \cdot 10^{-5}$ mol dm^{-3}

Absorbance measured for this dilution = 0.799.

4.2.4. Calculation of $(A - A_i)_1$.

(a) Absorbance of the solution: $A = A$ dilution $\times C_{S_1}/C_{D_1} = 0.799 \times 4.240 \cdot 10^{-4}/3.300 \cdot 10^{-5}$

$= 10.266.$

(b) Ideal absorbance of the solution: $A_i = \varepsilon_S C_S$ (Eq. (20)); $A_i = 2.295 \cdot 10^4 \times 4.240 \cdot 10^{-4} = 9.731$; therefore, $(A - A_i)_1 = 10.266 - 9.731 = 0.535$.

4.2.5. Calculation of H_1 (Eq. (21)).

$C_{S_{sat}} = 0.194$ mol dm^{-3}; $(A - A_i)_{sat} = 369$; $(A - A_i)_1 = 0.535$

$H_1 = 0.535/369 = 1.450 \cdot 10^{-3}$.

4.2.6. Calculation of X_1 (Eq. (17)).

$X_1 = [0.194 \times (1.450 \cdot 10^{-3})^{1/2} - 4.240 \cdot 10^{-4})]$

$/[(1.450\ 10^{-3})^{-1/2} - 1]$

$X_1 = 2.757 \cdot 10^{-4} \cong 2.8 \cdot 10^{-4}$.

According to Eq. (22), the data of $\ln X_j$ versus $\ln (C_{S_j} - X_j)$ were adjusted by the least square method, obtaining the following values:

Slope = $n = 1.988$ (S.D. = 0.0376); $n \cong 2$

Intersection = $\ln (nK_c) = 9.314$ (S.D. = 0.285)

$R = 0.997$; S.D. = 0.0943; $N = 16$

From the straight line intersection value, it was obtained that:

$K_c = 5.58 \cdot 10^3$

Also, with Eq. (23) it was obtained that:

$\varepsilon_C(300.8\ nm) = 4.98 \cdot 10^4\ dm^3\ mol^{-1}\ cm^{-1}$

The unsubstituted chalcone is a simple flavonoid practically insoluble in water and having a considerable dipolar moment (2.99 D, benzene) [22]. It is clear that when two polar molecules approximate an interaction force originates between them. In general, if molecules were able to take all the possible relative orientations with the same probability, the total net energy of interactions would be zero. This is to say that the attractive forces of the dipoles when they take the positive pole–negative pole orientation are compensated with their repulsive forces when they are positive–positive or negative–negative oriented [21b]. In a solution, however, since the energies involved in the attractive interactions are lower than those in repulsive ones, it is very likely that the former dominate over the latter.

As can be observed in Fig. 1, the studied substance does not have ionizable groups in its structure. The group of highest reactivity is the carbonyl, which sometimes presents acid–base properties in hydroxylic solvents. This means that unsubstituted chalcone dissolved in cyclohexane behaves as a true non electrolyte. According to its dipolar moment, it is reasonable to assume that chalcone forms association complexes in high concentrations. In this case, the solute–solute intermolecular distances are greatly reduced, and therefore, the interactions between them are increased. The high value obtained for the complex molar absorptivity matches data reported in the literature for solute molecular associations [23].

Calculations with X_j (Eq. (17)) data obtained with values of $n \neq 2$ were also performed. In these cases, the deviation of experimental data with respect to the adjusting straight line gradually increased with the values proposed for n (3, 4, 5, etc.) The slopes calculated deviated over 100% from those established by Eq. (22). The most satisfactory results were obtained with $n = 2$ and are those previously presented.

In this paper, the method proposed has only been exemplified by the association complex ($n = 2$) of chalcone in cyclohexane. However, the possible values for n (Eq. (5)) are not theoretically constrained, which implies that the method could be applicable to complexes with $n > 2$. At present, similar experiments are being carried out in our laboratories with other flavonoids (flavones and flavonols) in organic solvents and hydroalcoholic

mixtures, in order to confirm our previous statement. The method here proposed is useful and reliable for the study of solute–solute molecular interactions involving dipole–dipole interactions. Obviously, these interactions are favored by elevated solute concentrations. It is therefore reasonable that Beer's Law, which establishes a direct proportionality between the solution absorbance and the analytic molar concentration of the solute, does not hold for this case. This is explained by the fact that the solution measured absorbance is the sum of the absorbance of the uncomplexated solute plus the absorbance of the formed association complex. Finally, it must be noted that the obtainment of thermodynamic and spectroscopic magnitudes such as K_c and ε_C is of great importance to know the physicochemical behavior of several α,β-unsaturated carbonylic compounds of low solubility in water.

References

[1] H. Tsuchiya, M. Sato, T. Miyazaki, A. Fujiwara, S. Tanigaki, M. Ohyama, T. Tanaka, M. Linuma, J. Ethnopharm. 50 (1996) 27–34.

[2] A. Mori, C. Nishino, N. Enoki, S. Tawata, Phytochemistry 26 (1987) 2231–2234.

[3] H. Fukui, K. Goto, M. Tabata, Chem. Pharm. Bull. 36 (1988) 4174–4176.

[4] M. Maillard, M. Hamburger, M.P. Gupta, K. Hostettmann, Planta Med. 55 (1989) 281–282.

[5] C. Bohmont, L. Aaronson, K. Mann, R.S. Pardini, J. Nat. Prod. 50 (1987) 427–433.

[6] M.H. Siess, M. Guillermic, A.M. LeBon, M. Suschetet, Xenobiotica 19 (1989) 1379–1386.

[7] S.R. Husain, J. Cillard, P. Cillard, Phytochemistry 26 (1987) 2489–2491.

[8] T. Hatano, H. Kagawa, T. Yasuhara, T. Okuda, Chem. Pharm. Bull. 36 (1988) 2090–2097.

[9] V.A. Belyakov, V.A. Roginsky, W. Bors, J. Chem. Soc., Perkin Trans. II (1995) 2319–2326.

[10] I. Rustan, N. Michel, M. Segent, G. Lesgards, R.P. Tan Luu, Analusis 23 (1995) 398–402.

[11] M.L. Bieganowska, A. Petruczynik, A.M. Zobel, J. Planar Chromatogr. 9 (1996) 273–279.

[12] D. Obendorf, E. Reichart, Electroanalysis 7 (1995) 1075–1081.

[13] M. Born, P.A. Carrupt, R. Zini, Helv. Chim. Acta 79 (1996) 1147–1158.

[14] B. Botta, G.D. Monache, Heteroccycles 43 (1996) 1415–1421.

[15] C.E. Ardanaz, P. Traldi, U. Vettori, J. Kavka, F. Guidugli, Rapid Commun. Mass Spectrom. 5 (1991) 5–10.

[16] U.S. Pharmacopeia 23, N.F. 18; United States Pharmacopeial Convention, Rockville, MD, 1995.

[17] C. Altesor, P. Corbi, I. Dol, M. Knochen, Analyst 118 (1993) 1549–1553.

[18] D.A. Skoog, J.J. Leary, Análisis Instrumental, 4th ed., McGraw-Hill, New York, 1994, pp. 145–149.

[19] H. Wagner, L. Farkas, Synthesis of flavonoids, in: J.B. Harborne, T.J. Mabry, H. Mabry (Eds.), The Flavonoids, Part I, Academic Press, New York, 1975, p. 131.

[20] R.S. Treptow, J. Chem. Educ. 73 (1996) 51–54.

[21a] P.W. Atkins, Physical Chemistry, 5th ed., Oxford University Press, USA, 1995, pp. 230–232; 343–344.

[21b] P.W Atkins, Physical Chemistry, 5th ed., Oxford University Press, USA, 1995 pp. 763–764.

[22] S.V. Tsukerman, Y.N. Surov, V.F. Lavrushin, Zh.Obshch. Khim. 38 (1967) 524–529.

[23] C.N. Rao, Espectroscopia Ultravioleta y Visible, Alhambra, Madrid, 1970, p. 4

ELSEVIER

Talanta 45 (1998) 1111–1114

Talanta

A new spray reagent for the detection of synthetic pyrethroids containing a nitrile group on thin-layer plates

Suman Gupta, Swadesh Kumar Handa *, Krishan Kumar Sharma

Division of Agricultural Chemicals, Indian Agricultural, Research Institute, New Delhi, 110 012, India

Received 9 April 1997; received in revised form 8 July 1997; accepted 9 July 1997

Abstract

This paper describes a new spray reagent for selective detection of synthetic pyrethroids containing α-cyano group i.e. lambda-cyhalothrin, deltamethrin, cyfluthrin and fluvalinate by thin layer chromatography. These synthetic pyrethroids on alkaline hydrolysis, yield a cynohydrin derivative which degrades to give HCN and a corresponding aldehyde. This liberated HCN reduces 2-(4-iodophenyl)-3-(4-nitrophenyl)-5-phenyl tetrazolium chloride (INT) to formazan, a pink product in the presence of phenazonium methosulfate (PMS). The pink colour formed remain stable for more than 24 h. Other group of insecticides like organophosphorus, organochlorine and carbamate do not interfere in the determination. Pyrethroid insecticides not containing hydrolysable nitrile group also do not interfere. The limit of detection is from 0.5 to 1 μg. © 1998 Elsevier Science B.V.

Keywords: Spray reagent; Detection; Synthetic pyrethroids; Thin-layer plates; Nitrile

Several gas–liquid and high performance liquid chromatographic procedures are available in the literature for the analysis of synthetic pyrethroids [1–7], but these analytical methods involve very costly equipments. Thin layer chromatographic (TLC) detection using chromogenic reagent has also been reported, for example, phosphomolybdic acid for the detection of permethrin, cypermethrin and deltamethrin [8], palladium chloride for the detection of deltamethrin [9], silver nitrate impregnated alumina G plates followed by irradiation with UV light for the detection of halogenated synthetic pyrethroids [10], copper acetate and *o*-tolidine for the detection of fenvalerate, cypermethrin and deltamethrin [11], *o*-dinitrobenzene and *p*-nitrobenzaldehyde for the detection of fenpropathrin, flucythrinate, fluvalinate and PP-321 [12]. We report here the use of 2-(4-iodophenyl)-3-(4-nitrophenyl) 5-phenyl tetrazolium chloride (INT) and phenazonium methosulfate (PMS), a sensitive chromogenic reagent for the detection of lambda-cyhalothrin (1:1 mixture of (S)-α-cyano-3-phenoxybenzyl (Z)-(1R,3R)-3-(2-chloro-3,3,3-trifluoropropenyl)-2,2-dimethyl cyclopropanecarboxylate and (R)-α-cyano-3-phenoxybenzyl (Z)-(1S, 3S)-3-(2-chloro-3,3,3-trifluoropropenyl)-2,2-dimethyl cyclopropanecarboxylate, **1**), deltamethrin ((S)-α-cyano-3-phenoxy benzyl(1R,3R)-3-(2,2-dibromovinyl)-2,2-dimethyl cyclopropanecarboxy-

* Corresponding author. Fax: +91 11 5766420.

PII S0039-9140(97)00211-7

Table 1
Mean Rf values (X100) of lambda-cyhalothrin, fluvalinate, deltamethrin and cyfluthrin

Solvent system	Lambda-cyhalothrin	Fluvalinate	Delta-methrin	Cyfluthrin
Toluene:hexane (1:1)	48	41	45	43
Chloroform:hexane (1:4)	17	12	12	12
Chloroform:hexane (1:1)	42	42	43	42
Diethylether:hexane (1:9)	44	29	43	39
Diethylether:hexane (1:19)	31	21	32	28
Acetone:hexane (1:9)	45	41	47	47
Acetone:hexane (1:4)	50	43	47	46
Ethyl acetate:hexane (1:19)	37	29	33	30
Carbon tetrachloride	22	22	24	25

late, **2**), cyfluthrin ((RS)-α-cyano-4-fluoro-3-phenoxybenzyl(1RS,3RS;1RS,3SR)-3-(2,2-dichlorovinyl)-2,2-dimethyl cyclopropanecarboxylate, **3**) and fluvalinate((RS)-α-cyano-3-phenoxybenzyl *N*-(2-chloro-α,α,α-trifluoro-*p*-tolyl)-*D*-valinate, **4**) on TLC plates. The reagent gives stable pink spot on blue background for pyrethroid insecticides containing an α-cyano group.

1. Experimental

1.1. Materials

Fluvalinate (Tech. 88.1%), lambda-cyhalothrin (Tech. 83.2%), deltamethrin (Anal. 99%) and cyfluthrin (Tech. 93.52%) were supplied by Sandoz, Bombay, India; ICI Madras; Institute of Organic Industrial Chemistry, Poland and Bayer, Bombay, India respectively. Standard solution of these pyrethroids were prepared in acetone (each 1 mg ml^{-1}). 20% Methanolic potassium hydroxide solution was prepared by dissolving 20 g of potassium hydroxide in 10 ml of distilled water and diluting to 100 ml with methanol.

1.2. Thin-layer chromatography

Silica gel G coated thin layer chromatographic plates were made by spreading a slurry of silica gel in water (1:2) to a thickness of 0.5 mm with the help of an applicator. The plates were air-dried and then activated for 1 h at 100°C in oven. These activated plates were stored in desiccator over calcium chloride until used. 1 μl sample of standard solution of each synthetic pyrethroid (1 mg ml^{-1}) was quantitatively transferred to a TLC plate with the help of Hamilton Microliter Syringe. After introducing the last sample, the plate was air-dried and subsequently developed in the solvent system hexane–acetone (9:1). The development was carried out in a presaturated tank with an elution time of 25–30 min and an elution distance of 20 cm. The developed plate was air-dried and sprayed with 20% Methanolic KOH solution in a fume cupboard; after 10 min it was evenly sprayed with chromogenic reagent which was always freshly prepared by dissolving 0.4 g of INT and 0.1 g of PMS in 100 ml of distilled water separately and mixing the aqueous solutions of INT and PMS in the ratio of 10:2. The synthetic pyrethroids containing a cyanide group appeared as pink spots on blue background on the TLC plates. The Rf values of four synthetic pyrethroid insecticides, used in the study, in different solvent systems are given in Table 1.

1.3. Extraction of samples

Fortified sample (25 g) was chopped and transferred into Waring blender and churned for 2 min. with 100 ml of acetone. The sample was filtered through Whatman filter paper No. 1 in Buchner funnel under suction. The residue was re-extracted with additional 100 ml of acetone and again filtered under suction. Acetone layers

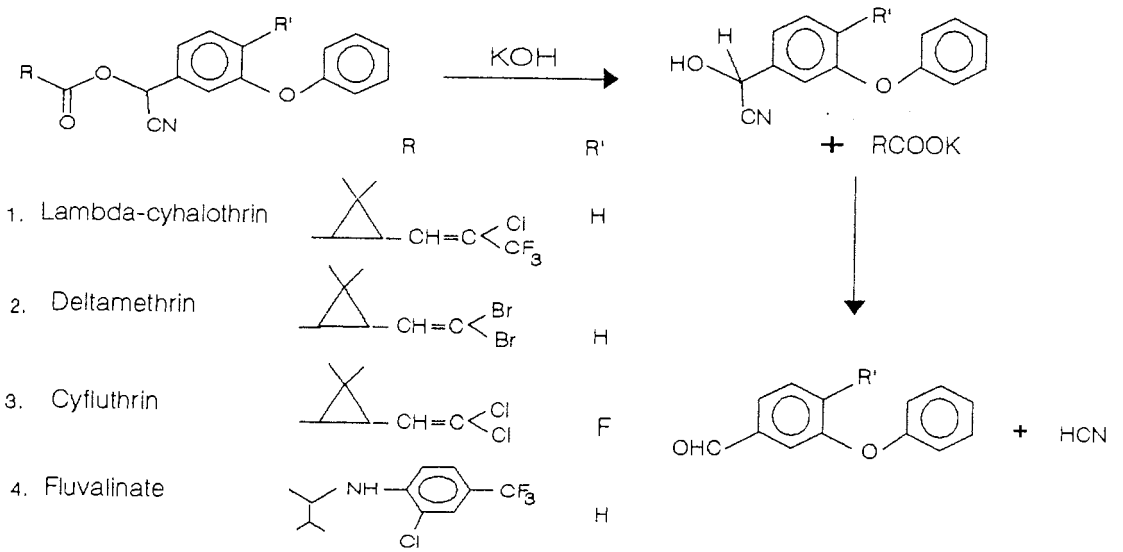

Fig. 1. Alkaline hydrolysis of synthetic pyrethroids.

were combined and concentrated in Kuderna–Danish evaporator and then diluted with 100 ml water. The pyrethroid was extracted from aqueous phase with *n*-hexane (3×50 ml). The combined hexane layers were dried over sodium sulfate and concentrated to small volume again using Kuderna–Danish evaporator. A known volume of solution was spotted on to activated TLC plate together with the standard solution of pyrethroid insecticide. The plate was developed and the spots were located as described in the previous section.

2. Results and discussion

Under alkaline condition the hydrolysis of α-cyanoester pyrethroids has been shown to proceed by the nucleophilic attack of hydroxyl ion, resulting in the formation of cyanohydrin derivative, which degrades to give HCN and the corresponding aldehyde [13]. This liberated HCN reduces INT to formazan, a pink product, in the presence of PMS, which quickly transfers the reducing equivalents ($2H^-$) from HCN to INT. [14,15] A schematic representation of the reactions involved has been depicted in Figs. 1 and 2. An advantage of the proposed chromogenic reagent for detecting synthetic pyrethroids over others is the excellent colour stability. The pink colour formed remain stable for more than 24 h. INT is a highly sensitive tetrazolium salt and was earlier used by Bhagyalakshmi and Nandakumar [16] to detect cyanide in medicinal drugs and confectionery. We have used this reagent to detect the cyanide liberated from synthetic pyrethroids on treatment with alkaline potassium hydroxide. Pink chromatogram was not obtained with the pyrethroids

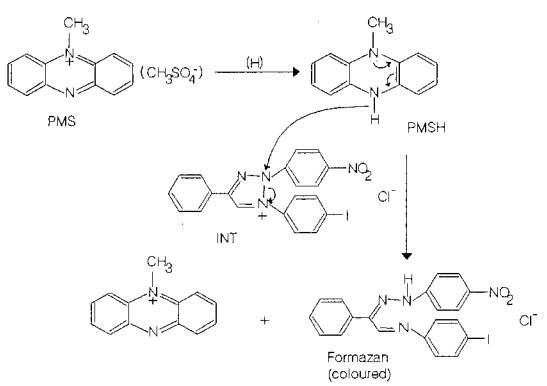

Fig. 2. Formation of coloured fomazan from INT.

that did not contain a hydrolysable nitrile group like permethrin, resmethrin and allethrin. Other group of insecticides like organophosphorus, organochlorine and carbamate do not interfere in the analysis. Different concentrations of pyrethroid insecticides are applied to TLC plates and the limit of detection by chromogenic analysis is found to be around 0.5 μg for cyfluthrin, deltamethrin and lambda-cyhalothrin and 1.0 μg for fluvalinate.

The method is applied to determine these synthetic pyrethroids in the fortified samples of cabbage, cauliflower and tomatoes without elaborate clean-up. Recoveries were found to be in the range 80–90% based on minimum detection limit.

Different concentrations of methanolic potassium hydroxide viz 5, 10, 15 and 20% were tried and it was found that the spray with 20% MeOH–KOH gave the best spot. Different time intervals, 10, 15, 20 and 30 min, between the spray of methanolic potassium hydroxide and chromogenic reagent were studied for the colour formation and the colour intensity of the four TLC plates were matched after 30 min. of the spray of last plate and it was found that there is no visible difference in the colour intensity of the spots in four plates. All the spots were equally bright.

Effect of temperature on colour intensity was also studied. Two plates were developed as previously and after spraying with 20% MeOH–KOH, one plate was kept at room temperature (20°C) and the other at 50°C in an oven. After 10 min both the plates were sprayed with chromogenic reagent and it was found that initially the plate kept at 50°C gave more bright spot but after 30 min the intensities of the colour became almost equal. Further, it is observed that cyfluthrin and fluvalinate gave more intense spots as compared to deltamethrin and lambda-cyhalothrin.

The reagent described here is sensitive and selective for synthetic pyrethroids cyfluthrin, fluvalinate, deltamethrin and lambda-cyhalothrin, containing an α-nitrile group and the method can be used routinely for the instant testing of these pyrethroids as residues or as formulation. The method can be extended to include other pyrethroid insecticides like fenvalerate, fenpropathrin and cypermethrin also containing an α-nitrile group.

Acknowledgements

CAS Registry No.: Lambda-Cyhalothrin [91465-08-6], fluvalinate [69409-94-5], deltamethrin [52918-63-5], cyfluthrin [68359-37-5].

References

[1] P.G. Baker, P. Bottomley, Analyst 107 (1982) 206.
[2] R.A. Chapman, H.S. Simmons, J. Assoc. Off. Anal. Chem. 60 (1977) 977.
[3] E. Bolygo, F. Zakar, J. Assoc. Off. Anal. Chem. 66 (1983) 1013.
[4] S. Sakaue, T. Nara, M. Horiba, S. Yamamoto, Agric. Biol. Chem. 46 (1982) 2165.
[5] A. Jacques, H.L. Ong, G.W. Sheehan, in: G. Zweig, J. Sherma (Eds.), Analytical Methods for Pesticides and Plant Growth Regulators, Vol. XIII, Academic Press, FL, 1984, p. 9.
[6] Y.W. Lee, N.D. Westcolt, R.A. Reichle, J. Assoc. Off. Anal. Chem. 61 (1978) 869.
[7] C. Meinard, P. Bruneau, J. Perronnet, J. Chromatogr. 349 (1985) 109.
[8] T. Shomo, K. Ohsawa, J.E. Casida, J. Agric. Food Chem. 27 (1979) 316.
[9] L.O. Ruzo, J.L. Engel, J.E. Casida, J. Agric. Food Chem. 27 (1979) 725.
[10] R. Sundarajan, R.P. Chawla, J. Assoc. Off. Anal. Chem. 66 (1983) 1009.
[11] V.B. Patil, M.T. Sevalkar, S.V. Padalikar, Analyst 117 (1992) 75.
[12] R. Khazanchi, S.K. Handa, J. Assoc. Off. Anal. Chem. 72 (1989) 512.
[13] P. Ommilleri, J. Agric. Food Chem. 32 (1984) 1122.
[14] B. Henderson, N. Loveridge, Histochemistry 72 (1981) 617.
[15] T.E. King, J. Biol. Chem. 238 (1963) 4032.
[16] K. Bhagyalakshmi, N.V. Nanda Kumar, J. Assoc. Off. Anal. Chem. 72 (1989) 429.

ELSEVIER

Talanta 45 (1998) 1115–1122

Talanta

Indirect determination of cyclamate by an on-line continuous precipitation-dissolution flow system

M.C. Yebra *, P. Bermejo

Department of Analytical Chemistry, Nutrition and Bromatology, Chemistry Faculty, University of Santiago, 15706-Santiago de Compostela, Spain

Received 14 April 1997; received in revised form 8 July 1997; accepted 9 July 1997

Abstract

A continuous-flow procedure is proposed for the indirect determination of sodium cyclamate by an atomic absorption spectrometric method in artificial sweeteners mixtures and soft drinks. Sulfamic group is oxidized to sulfate and it is continuously precipited with lead ion in a flow manifold. The lead sulfate formed is retained on a filter, washed with diluted ethanol and dissolved in ammonium acetate for on-line atomic absorption determination of lead, the amount of which in the precipitate is proportional to that of cyclamate in the sample. The proposed method allows the determination of sodium cyclamate in the range 1–90 μg ml^{-1} with a relative standard deviation of 3.1% at a rate of ca. 35 samples per h. The 3σ detection limit is 0.25 μg ml^{-1}. The method is very selective, no compounds normally found in the analysed samples and other artificial sweeteners had any effect on the determination of cyclamate. © 1998 Elsevier Science B.V.

Keywords: Flame atomic absorption spectrometry; Flow injection; Continuous precipitation-dissolution; Cyclamate; Sweeteners; Soft drinks

1. Introduction

Sodium cyclamate (sodium *N*-cyclohexylsulfamate or sodium cyclohexanesulfamate) is an intense sweetening agent. Sodium cyclamate has been used as a substitute for sucrose by diabetics and others needing to restrict their intake of carbohydrates. It is permitted in several countries, however, it is banned in the USA and UK after controversial toxicity studies because of concern about its metabolite cyclohexylamine and its carcinogenicity effects [1].

The oxidation of sulfamate group to sulfate in the presence of sodium nitrite is used for their detection and determination by precipitation with barium chloride (official method for the determination of sodium cyclamate in soft drinks) [2] or spectrometric measuring of the excess of nitrite in the visible region [3] and in the UV region [4]. Some analyses for cyclamate in soft drinks, and artificial sweetening tablets involve spectrophotometric detection [5], electrochemical methods [6,7], and chromatographic methods (liquid chro-

* Corresponding author. Tel.: + 34 81 591079; fax: + 34 81 595012.

PII S0039-9140(97)00219-1

matography and capillary zone electrophoresis) for the separation and determination of sweeteners have been proposed using UV [8,9] or visible [10] detectors. Gas chromatography has been employed for the determination of sodium cyclamate in beverages [11]. Flow-injection methods allow the determination of sodium cyclamate by chemiluminometric determination [12]; by spectrophotometric determination [13]; and by titration with biamperometric detection [14]. No atomic absorption procedures for the determination of sodium cyclamate have been reported.

Continuous precipitation systems [15–19] coupled to an atomic absorption spectrometer has been used for the direct [20] and the indirect determination of inorganic anions [21–26] and indirect determinations of organic compounds [27–32].

The proposed method for the indirect determination of cyclamate in presence of other sweeteners is based on the oxidation of sulfamic group to sulfate by use sodium nitrite in acid medium. After, sulfate is precipitated with lead nitrate. The procedure is adapted to a flow system with precipitate dissolution. The precipitate is dissolved in ammonium acetate (owing to the formation of soluble lead acetate) and dissolved lead is measured by flame atomic absorption spectrometry. The method was applied to the determination of cyclamate in artificial sweetening tablets and soft drinks.

2. Experimental

2.1. Apparatus

A Perkin Elmer 5000 atomic absorption spectrometer equipped with a bead impact system in the burner chamber and a hollow cathode lead lamp was used. The wavelength and lamp current used were 217 nm and 12 mA, respectively. The acetylene flow-rate was 2.0 l min^{-1} and an air flow-rate of 21.5 l min^{-1} was employed to obtain a clear blue flame. The aspiration flow-rate of the nebuliser was adjusted to the same as the flow-rate of the dissolving solution of the precipitate (3.8 ml min^{-1}). The spectrometer output was connected to a Perkin Elmer 50 Servograph recorder with a range of 5 mV. The signals measured were the heights of the absorbance peaks. A Crison standard pH-meter with Ingold U 455 electrode was used for measurement.

The flow system consisted of a Gilson Minipuls-3 peristaltic pump, fitted with PVC tubing, four Reodyne (Model 5041 and 5301) four-way or switching valves and PTFE tubing (0.5 mm i.d.) for the coils. A home-made filtration device (Fig. 1) was made of a teflon tubing (4 cm long, 2 cm internal long and 3 mm i.d.) packed with a cotton pulp and the ends of the filter column were plugged with filter paper (Whatman N°1), chamber inner volume 141 μl. This precipitate collector was effective in retaining the precipitate and did not produce excessive back pressure if the precipitate was dissolved following each precipitation cycle.

2.2. Reagents

A lead solution (1.000 g l^{-1}) was prepared by dissolving 1.5985 g of lead nitrate (Merck) in 1 l of 0.5% v/v nitric acid. A 1000 mg l^{-1} sodium cyclamate (Sigma) standard was prepared in ultrapure water. Sodium nitritre (Merck) 0.3 M solution was prepared by dissolving 2.07 g in water and diluted to 100 ml. Ammonium acetate (Merck) 2 M solution was prepared by dissolving 15.416 g in water and diluted to 100 ml ethanol (Merck). Glacial acetic acid (Merck). Ultrapure water of 18.3 M Ω cm^{-1} resistivity obtained from a Milli-Q water purification system (Millipore) served for sample dilutions.

All chemicals were of analytical-reagent grade.

2.3. Sample preparation

2.3.1. Solid samples

Commercially available tablets were placed in a mortar and ground to a fine powder. An amount equivalent to 3–10 mg of cyclamate was dissolved in water with electromagnetic stirring and diluted to 50 ml in a calibrated flask. For continuous flow analyses, different aliquots of the sample solution (2.5–8 ml) and 1.25 ml of concentrated acetic acid were placed in 25 ml volumetric flask and dilutes to the mark with water.

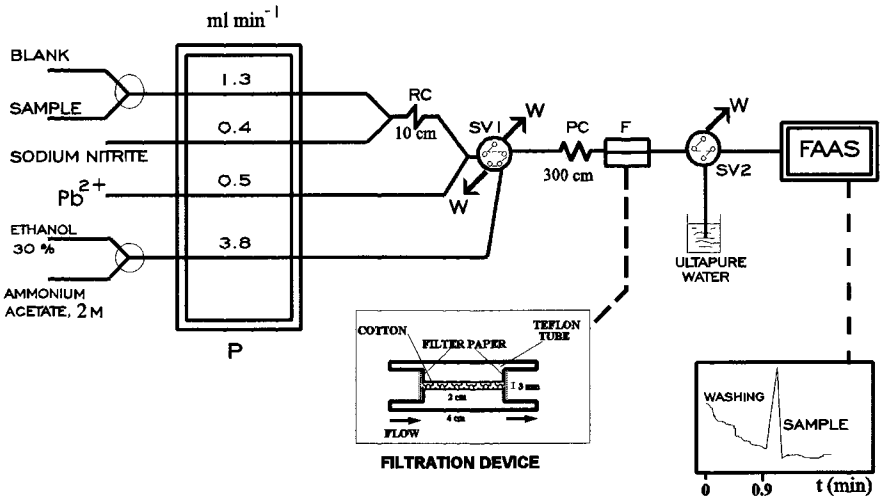

Fig. 1. Continuous precipitation-dissolution manifold for the indirect determination of sodium cyclamate. SV, switching valves; P, peristaltic pump; RC, reaction coil; PC, precipitation coil; W, waste lines; F, filter; FAAS, flame atomic absorption spectrometer.

2.3.2. Liquid samples

Carbonated beverages were descarbonated by repeated shaking. Aliquots of the sample solution (4–6 ml) were placed in 25 ml volumetric flask containing 1.25 ml of concentrated acetic acid and diluted to the mark with water.

2.4. Procedure

The sample or standard solutions containing between 1 and 90 μg ml^{-1} cyclamate, in 5% v/v acetic acid (pH 2.5), the 0.3 M sodium nitrite solution and the precipitating reagent (375 μg ml^{-1} lead solution in 30% v/v ethanol, pH 1.4) are passed through the flow system using the continuous-flow manifold shown in Fig. 1 for 15 s. In the reaction-precipitation step, the sodium nitrite solution and the sample solution were mixed in the reaction coil, where oxidation of the sulfamate group takes place. After, the sulfate formed merged with the precipitating reagent stream, and were mixed in the precipitation coil, where the precipitation occurs. The lead sulfate precipitate was retained on the filter device. The reagent stream was sent to waste via switching valve 2 and ultrapure water was aspirated by the nebuliser in order to flush it after each measurement. Then, in the second step (washing step), switching valve 1 was actuated to introduce a 30% ethanol stream for about 50 s (until zero response was obtained). Then, in the third step, the dissolving solution (2 M ammonium acetate) is allowed to pass which dissolves the precipitated lead sulfate retained on the filter and carries it to the nebuliser to be determined. The AAS signal obtained is proportional to the lead concentration, which is in turn proportional to the cyclamate concentration in the aspirated sample volume. A blank (5% acetic acid) was run in parallel, the absorbance of which ranged between 0.003 and 0.005.

3. Results and discussion

A preliminary study involving a reversed-flow injection system through which the sample was circulated and into which the precipitating reagent (400 μg ml^{-1} lead) was injected, was initially performed because the system was the simplest possible; the results were unsatisfactory as cyclamate concentrations below a few g l^{-1} were undetectable and cyclamate as a sodium salt, was aspirated continuously by the instrument, which disrupted the flame and affected the precision of the results.

3.1. Selection of the washing and dissolving solutions

Lead is adsorbed on the precipitate surface as a result of the continuous passage of its solution through it. Therefore, it is necessary to remove adsorbed Pb(II) prior to dissolving the precipitate in order to avoid systematic errors. With this purpose various washing solutions were tried: water, ethanol and diluted nitric acid. Prior to dissolution, a water stream was passed to remove Pb(II) adsorbed on the precipitate from the lead stream (350 μg ml^{-1}). When the precipitate was washed with water or diluted nitric acid, the signal obtained for Pb(II) is virtually negligible when the dissolving solution (ammonium acetate) was passed. These two washing solutions were consequently discarded for use. As can be seen in Fig. 2, three calibration curves by using ethanol at different concentrations as a washing solution and ammonium acetate as a dissolving solution have been run.

The use of 10 and 20% ethanol ensured complete washing, but also dissolved lead sulfate at concentrations below 17 and 6 μg ml^{-1} completely, and higher concentrations partly, therefore yields no signal or minor signal after the subsequent dissolution with ammonium acetate. A 30% ethanol concentration ensured complete

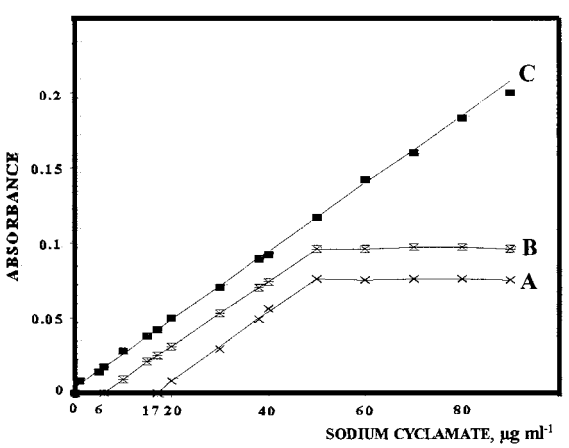

Fig. 2. Calibration curves for cyclamate obtained with different concentrations of ethanol as washing solution: A, 10%; B, 20%; C, 30%. Dissolving solution: 0.5 M ammonium acetate.

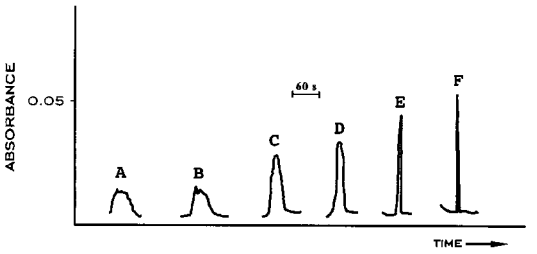

Fig. 3. Effect of various reagents on the precipitate dissolution: A, 0.5 M EDTA; B, 0.5 M sodium chloride; C, 1 M nitric acid; D, 1 M hydrochloric acid; E, 0.1 M ammonia; F, 0.5 M ammonium acetate. Washing solution: 30% ethanol.

washing with no partial precipitate dissolution. According to the above considerations, an ethanol concentration of 30% was chosen in order to achieve the best possible results in the washing step and to avoid the precipitate dissolution.

Small amounts of the lead sulfate precipitate (obtained from sodium cyclamate) were subjected to the possible dissolving action of various reagents including sodium chloride, ammonium acetate, ammonia, EDTA, nitric acid, and hydrochloric acid at different concentrations in test tubes. The results were satisfactory in all instances, but ammonium acetate dissolved the precipitate more rapidly than the other reagents tested, which required a longer shaking time to provide complete dissolution. The above mentioned dissolving reagents were tested in a continuous flow system similar to that shown in Fig. 1 by using 0.325 ml of sample solutions containing 20 μg ml^{-1} cyclamate in acidic medium, in order to select the fastest dissolution. As is shown in Fig. 3, the best results were obtained for 0.3 M ammonium acetate. The other solutions acted more slowly and the sodium salts (sodium chloride and EDTA disodium salt) destabilized the burner flame. In order to determine the optimal concentration of the ammonium acetate dissolving reagent, concentrations between 0.1 and 3 M were studied. Dissolution of the precipitate was complete above 0.5 M ammonium acetate, since absorbance remained constant up to a concentration of 3 M. An 2 M ammonium acetate solution was chosen because it dissolved the precipitate very rapidly (about 20 s) and ensured dissolution

of larger amounts of precipitate (up to 90 μg ml^{-1} cyclamate).

3.2. Optimization of chemical and FIA variables

This study was performed by continuously introducing 0.325 ml of a sample containing 20 μg ml^{-1} sodium cyclamate. Chemical parameters were varied while keeping the FI variables constant. First, the reaction between sodium cyclamate and sodium nitrite was studied. This reaction takes place in acidic medium, therefore, sample pH was optimized. The sample pH was varied from 2 to 5 adjusting the solution with diluted hydrochloric acid. The results obtained were compared with those obtained using acetic acid to adjust pH. In all instances, the signal increased when acetic acid was used, because the lead sulfate precipitate was partly or completely dissolved in diluted hydrochloric acid. The absorbance versus pH graph shows a plateau from 2.1 to 2.7. A pH of 2.5, which was obtained by preparing the cyclamate samples in 5% acetic acid was selected. The effect of the sodium nitrite concentration was studied in the range 0–0.5 M. The signal increased with increasing sodium nitrite concentration up to 0.3 M. In these conditions, sodium nitrite concentration was in excess to form sulfate, therefore, the signal increase can be explained by the effect of the ionic strength, which favoured the lead sulfate precipitation. The effect of the pH of the lead solution over the range 0.5–6.0 was studied in order to obtain the best precipitation conditions. The absorbance remained constant over the pH range of 1.2–5. The concentration of the lead solution was varied between 50 and 600 μg ml^{-1}, the analytical signal increased with increasing concentration of lead up to 100 μg ml^{-1}, above which a steady state was reached as a result of precipitation of the lead sulfate being favoured. Concentrations above 400 μg ml^{-1} required a longer washing step owing to increased adsorption of lead on the precipitate. The influence of the ethanol concentration on the solubility of lead sulfate was studied. The absorbance increased with increasing ethanol concentration in the lead solution up to 30%. Thus, was verified that this solvent favored the precipitation of lead sulfate. Therefore, a lead solution of 375 μg ml^{-1} in 30% v/v ethanol at pH 1.4, obtained directly from the stock solutions with no pH adjustment, was thus chosen.

The length of the reaction and precipitation coils and the flow-rates were studied.

The influence of the reaction coil (RC) length was investigated between 10 and 300 cm (0.5 mm i.d.). This length showed no relevant influence, which confirmed the high rate of the oxidation reaction. Therefore, a short RC (10 cm) was chosen. The effect of the precipitation coil (PC) length was studied between 50 and 500 cm (0.5 mm i.d.). Short PC (less than 250 cm) resulted in residence times that were too short for the reaction to be complete, while PC longer than 400 cm increased the residence time of the precipitate in the coil and caused it to be partly adsorbed on the inner walls of the PTFE tubing, thereby, the dissolved precipitate solution was diffused over a large area and the peak height signal decreased as a result. A PC that was 300 cm long and 0.5 mm in i.d. (residence time 16 s) was selected for further experiments.

Sample flow-rate (0.325 ml of a solution containing 20 μg cyclamate ml^{-1}) was changed between 0.5 and 2.5 ml min^{-1} at a constant lead flow-rate of 0.5 ml min^{-1}, the analytical signal increased up to 1.5 ml min^{-1}, because the sample was less markadly diluted at the higher flow-rates and the residence time of the precipitate in the PC was more short, which entailed incomplete precipitation. The sodium nitrite flow-rate was studied between 0.2 and 2.0 ml min^{-1}. Absorbance was constant up to 0.5 ml min^{-1}, flow-rate above 0.5 ml min^{-1} entailed short residence time in the reaction and precipitation coils. Increasing the precipitating reagent flow-rate (375 μg ml^{-1}) was equivalent to increasing the lead concentration, this flow-rate presented a plateau from 0.2 to 0.7 ml min^{-1}, although flow-rate above 0.5 ml min^{-1} required a longer washing step. A sample flow-rate of 1.3 ml min^{-1}, a sodium nitrite flow-rate of 0.4 ml min^{-1}, and a lead flow-rate of 0.5 ml min^{-1} were thus chosen as a compromise.

The flow-rates of the washing and dissolving reagent must be higher than 3.0 ml min^{-1} in order not to lengthen the washing step overly and

because lower dissolving stream flow-rates resulted in broader lower peaks. A flow-rate of 3.8 ml min^{-1} was thus selected for both reagents.

3.3. Calibration

The calibration graph obtained under the optimum conditions stated in Fig. 1 and as described under Section 2.4 was linear over the range 1–90 μg cyclamate ml^{-1}. The graph equation is $A = 3.4 \times 10^{-3} + 2.3 \times 10^{-3}\ C$; $r = 0.996$ $(N = 7)$ where A is absorbance and C the sodium cyclamate concentration in μg ml^{-1}.

The detection limit (0.25 μg ml^{-1}) was calculated as three-fold the standard deviation of the peak height for 30 injections of the same blank (5% acetic acid). The relative standard deviation obtained for 11 samples containing 20 μg ml^{-1} of sodium cyclamate was 3.1%. The sample throughput was about 35 samples h^{-1}.

3.4. Study of interferences

A study of interferents was performed with samples containing 20 μg ml^{-1} of sodium cyclamate and 50-fold excesses of potential interferents. No interference ($< 5\%$) was caused from the presence of large amounts of common substances present in soft drinks and artificial sweeteners mixtures: saccharin, fructose, aspartame, lactose, dextrose, glucose, sodium citrate, sodium bicarbonate, sodium benzoate and caffeine.

3.5. Analyses of artificial sweeteners and soft drinks

Sodium cyclamate in four samples of solid artificial sweeteners and four samples of soft drinks was determined by the proposed method. These results obtained in five individual determinations and their standard deviations are shown in Table 1. Because the cyclamate content was not stated on the packing, recovery tests were done. So, the standard addition method was used to determine sodium cyclamate in the samples. Therefore, different amounts of sample were analysed by using the flow system in order to obtain the cyclamate concentration. Then, aliquots of dilute solid sample (0.63–2 ml) from 50 ml volumetric flasks and dissolved as described under Experimental, and aliquots of liquid samples (8–10 ml) were placed in 25 ml volumetric flasks and supplied with different concentrations of sodium cyclamate (1–70 μg ml^{-1}). Accuracy of the method was checked by the AOAC standard method based on barium sulfate precipitation [2]. Results obtained with both methods were compared by the paired t-test. As shown in Table 1, since the calculated $|t|$

Table 1
Determination of sodium cyclamate in artificial sweeteners and soft drinks

Sample[a]	Concentration of sodium cyclamate[b] (mg g^{-1})	
	Present method	Official method
(1) Artificial sweetener	137 ± 3	133 ± 7
(2) Artificial sweetener	140 ± 2	136 ± 6
(3) Artificial sweetener	195 ± 4	197 ± 8
(4) Artificial sweetener	165 ± 4	163 ± 7
Soft drinks	Concentration of sodium cyclamate[b] (mg l^{-1})	
(5) Orange soda	125 ± 2	119 ± 5
(6) Lemon soda	160 ± 3	154 ± 6
(7) Lemon tea	174 ± 5	167 ± 7
(8) Cola	147 ± 2	150 ± 5

X (mean difference), 3; standard deviation (S.D.), 3.7; $n = 8$. $t = X\sqrt{n}/\text{S.D.} = 2.26$; critical value of $|t|$ $(P = 0.05)$, 2.37.

[a] Sample composition: (1) sodium cyclamate, sodium saccharin, monosodium citrate and sodium bicarbonate; (2) sodium cyclamate, sodium saccharin and fructose; (3) sodium cyclamate, sodium saccharin and lactose; (4) sodium cyclamate, sodium saccharin and dextrose; (5) orange juice, carbonated water, citric acid, sugars, gum arabic, sodium benzoate, orange yellow S, tartrazine, sodium saccharin and sodium cyclamate; (6) lemon juice, carbonated water, citric acid, sugars, gum arabic, sodium benzoate, orange yellow S, quinoline yellow, sodium saccharin and sodium cyclamate; (7) water, concentrated lemon juice, citric acid, sodium citrate, tea extract, sodium saccharin and sodium cyclamate; (8) caffeine, carbonated water, sugars, caramel, sodium benzoate, sodium saccharin and sodium cyclamate. Samples were analysed by the standard- addition method.

[b] Average of five individual determinations $\pm$S.D.

Table 2
Recoveries of sodium cyclamate added to samples

Sample[a]	Addition (μg ml^{-1})	Recovery (%)
1	5	97.2
	10	100.5
2	5	95.7
	10	97.5
3	5	96.1
	10	98.2
4	5	95.7
	10	98.3
5	5	98.5
	10	100.3
6	5	95.7
	10	97.2
7	5	96.1
	10	98.8
8	5	95.7
	10	98.5

[a] Identified in Table 1.

value is smaller than that obtained from the t-distribution table, the null hypothesis is retained: both methods do not give significantly different values for the cyclamate concentration and thus, the agreement between the two methods is satisfactory.

Finally, in order to test the reliability of the proposed method, cyclamate spikes (5 and 10 μg ml^{-1}) were added to each sample after dilution. Table 2 gives the results obtained, the recovery values better than 95% indicate the values obtained to be reliable and demonstrates the applicability of the method.

4. Conclusions

The present method allows the indirect determination of sodium cyclamate by means of a continuous precipitation-dissolution system by flame atomic absorption spectrometric detection. It is simple, rapid, and selective. Moreover, lower detection limit, reduction of sample and reagent consumption are achieved. It provides several advantages over the AOAC precipitation method, including higher sensitivity, lower sample consumption, higher precision and higher sampling frequency. Chromatographic methods allowed determination of cyclamate in a higher concentration range, which involves higher detection limits. Thus, Zhang et al. [11] determined cyclamate at a concentration range of 216–754 μg ml^{-1} by gas chromatography. Cyclamate is difficult to determine by liquid chromatography, because it is not easily detectable by ultraviolet or refractive index methods except in high concentrations (50–500 μg ml^{-1}). No atomic absorption procedures for the determination of sodium cyclamate have been reported, and with other works involving FIA higher detection limit were obtained. Gouveia et al. [13] by a spectrophotometric detection based on the reaction between nitrite and cyclamate and determining the excess of sodium nitrite by the Griess reaction, achieved a detection limit of 6 μg ml^{-1}, and Fatibello-Filho et al. [14] by a biamperometric titration achieved a detection limit of 262 μg ml^{-1}. The chemiluminometric method proposed Psarellis et al. [12] required a liquid chromatographic separation of cyclamate from other sweeteners, which interfered its determination. This method is suitable for the determination of cyclamate in artificial sweetening tablets and soft drinks, without interference of common substances present in these samples.

References

[1] R. Kham, P.A. Konowicz, Encyclopedia of Analytical Science, in: A. Townshend (Ed.), Academic Press, London, Vol 9, 1995, 5085 pp.
[2] Official Methods of Analysis of the Association of Official Analytical Chemists, AOAC, Washington, DC., 1995, 44.
[3] C.S.P. Sastry, K.R. Srinivas, K.M.M.K. Prasad, Anal. Lett. 29 (1996) 1329.
[4] M.M. Amer, I.A. Haroun, M.I. Walash, F.M. Ashour, Pharmazie 33 (1978) 435.
[5] C.S.P. Sastry, K.R. Srinivas, K.M.M.K. Prasad, A.G. Krishnamacharyulu, Analyst 120 (1995) 1793.
[6] M. Geissler, B. Schiffel, C. Kuhnhardt, Anal. Chim. Acta 124 (1982) 237.
[7] W. Hollack, B. Krinitz, J. Assoc. Off. Anal. Chem. 63 (1980) 163.
[8] J.F. Lawrence, Charbonneanu, J. Assoc. Off. Anal. Chem. 71 (1988) 934.
[9] C.O. Thomspson, V.C. Trenerry, B. Kemmery, J. Chromatogr. A. 704 (1995) 203.

[10] J.F. Lawrence, Int. J. Environ. Anal. Chem. 38 (1990) 115.
[11] N. Zhang, L. Liang, Y. Liu, Shipin Kexue 150 (1992) 47.
[12] I.M. Psarellis, E.G. Sarantonis, A.C. Calokerinos, Anal. Chim. Acta 272 (1993) 265.
[13] S.T. Gouveia, O. Fatibello-Filho, J. de Araujo Nobrega, Analyst 120 (1995) 2009.
[14] O. Fatibello-Filho, M.D. Capelato, S.A. Calafatti, Analyst 120 (1995) 2407.
[15] M. Valcárcel, M. Gallego, TrAC trends, Anal. Chem. 8 (1980) 34.
[16] M. Valcárcel, M. Gallego, in: J.L. Burguera (Ed.), Flow Injection Atomic Spectroscopy, Dekker, New York, 1989, Ch. 5.
[17] M. Valcárcel, M.D. Luque de Castro, Non-Chromatographic Continuous Separation Techniques, The Royal Society of Chemistry, Cambridge, 1991.
[18] Z. Fang, Flow injection Separation and Preconcentration, VCH, Weinheim, 1993.
[19] V. Kuban, Fresenius J. Anal. Chem. 346 (1993) 873.
[20] Z. Fang, M. Sperling, J. Anal. At. Spectrom. 6 (1991) 301.
[21] P. Martínez-Jiménez, M. Gallego, M. Valcárcel, J. Anal. At. Spectrom. 2 (1987) 2111.
[22] P. Martínez-Jiménez, M. Gallego, M. Valcárcel, Anal. Chem. 59 (1987) 69.
[23] J. Zorro, M. Gallego, M. Valcárcel, Microchem. J. 39 (1989) 71.
[24] M. Gallego, M. Valcárcel, Mikrochim. Acta III (1991) 163.
[25] F.T. Esmadi, M.A. Kharoaf, A.S. Attiyat, Analyst 116 (1991) 353.
[26] F.T. Esmadi, M.A. Kharoaf, A.S. Attiyat, Talanta 12 (1990) 1123.
[27] R. Montero, M. Gallego, M. Valcárcel, J. Anal. At. Spectrom. 3 (1988) 725.
[28] R. Montero, M. Gallego, M. Valcárcel, Anal. Chim. Acta 215 (1988) 241.
[29] M.C. Yebra, M. Gallego, M. Valcárcel, Anal. Chim. Acta 276 (1993) 385.
[30] M. Eisman, M. Gallego, M. Valcárcel, J. Anal. At. Spectrom. 8 (1993) 1117.
[31] M.C. Yebra, M. Gallego, M. Valcárcel, Anal. Chim. Acta 308 (1995) 275.
[32] M.C. Yebra, M. Gallego, M. Valcárcel, Anal. Chim. Acta 308 (1995) 357.

ELSEVIER

Talanta 45 (1998) 1123–1129

Talanta

Catalytic kinetic simultaneous determination of iron, silver and manganese with the Kalman filter by using flow injection analysis stopped-flow spectrophotometry

Ying-Zhi Ye *, Hong-Yan Mao, Ya-Hua Chen

Chemistry Department of Zhengzhou University, Zhengzhou 450052, People's Republic of China

Received 25 November 1996; received in revised form 2 July 1997; accepted 10 July 1997

Abstract

A catalytic differential kinetic method with Kalman filter for the simultaneous determination of multi-component is described. The oxidization of Rhodamine B (RB) by potassium periodate in a slightly acid solution is a slow reaction. But iron(III), silver(I) or manganese(II) has a differential catalytic effect on the oxidation reaction of RB in the presence of 1,10-phenanthroline as the activator. So iron, silver and manganese can be simultaneously determined by measuring the decreasing absorbance of the dye (RB) at 555 nm. A flow injection analysis stopped-flow spectrophotometric system with a microcomputer performs the determinations. This method has been applied to determining iron, silver and manganese of alloy samples with satisfactory results. © 1998 Elsevier Science B.V.

Keywords: Kalman filter; Catalytic differential kinetic spectrophotometry; Simultaneous determination

1. Introduction

Rhodamine B is widely used as a complexing agent for the determination of numerous metal ions by spectrophotometric method [1]. But only a few reports concerning the oxidization of Rhodamine B by periodate have been found, which is catalysed by manganese(II) in the presence of nitrilotriacetic acid as activator [2,3]. Although catalytic reactions offer good sensitivity [4], most of them have poor selectivity, because usually several transition metal ions show similar catalytic effects. Many methods have been developed for the catalytic kinetic analysis [5–7], but not all are suitable for the simultaneous determination with a single kinetic run. A new method for the simultaneous determination of iron(III), silver(I) and manganese(II) is proposed here, based on the kinetic differences of the three catalysts on this redox indicator reaction by using 1,10-phenanthroline as activator.

The Kalman filter has several advantages, such as simplicity, speed and recursive nature. It has been successfully applied to the processing of data for differential kinetic determinations in recent years [8–10]. But no application of the Kalman filter to the study of catalytic differential kinetics has been described previously. In this work, the

* Corresponding author. Fax: +86 371 7973895.

PII S0039-9140(97)00235-X

data were acquired and treated with Kalman filter for the simultaneous determination of multi-component. The stopped-flow technique was also exploited as a means of accomplishing automation and rapid handling.

2. Theory

2.1. Principles of the method

Suppose a reaction between A and B is a pseudo-first-order reaction under the condition of excess B.

$$A + B \underset{k_R, T_1}{\rightarrow} X + Y \quad (1)$$

If there is no catalyst in the system, the uncatalysed reaction's rate equation at temperature T_1 can be expressed as [11]:

$$dx/dt = k'_R \cdot (a - x) \quad (2)$$

where a is the initial concentration of A, $(a-x)$ and x are the concentration of A and X at any time t respectively, k_R is the rate constant of the uncatalysed reaction at T_1, which is the initial temperature of the reaction solution. The k'_R is equal to $k_R \cdot b$, b is the concentration of B. Taking the Integral, Eq. (2) becomes:

$$\log [a/(a-x)] = k'_R \cdot t \quad (3)$$

In spectrophotometry, if substance A has maximum absorptivity at λ^* nm, based on Beer's Law, the absorbances, A_0 and A_R, are used in Eq. (3) instead of concentrations, a and $(a-x)$. Then at any time t Eq. (3) may be simplified as:

$$\log (A_0/A_R) = k'_R \cdot t \quad (4)$$

where A_0 is the absorbance of the solution before reaction, A_R is the absorbance of the uncatalysed reaction at any time t. If this reaction is catalysed by M_1:

$$A + B \overset{M_1}{\underset{k_1, T_1}{\rightarrow}} X + Y \quad (5)$$

The rate equation of the reaction can be obtained as:

$$dx/dt = k'_1 \cdot (a - x) \cdot C_1 \quad (6)$$

Taking the integral, Eq. (6) becomes:

$$\log [a/(a-x)] = k'_1 \cdot t \cdot C_1 \quad (7)$$

If there are three catalysts M_1, M_2 and M_3, which catalyze the above same indicator reaction, when the behaviors of the catalysts are independent, the overall reaction rate is given by following equation:

$$V_{total} = dx/dt = (k'_1 \cdot C_1 + k'_2 \cdot C_2 + k'_3 \cdot C_3) \cdot (a - x) \quad (8)$$

Taking the uncatalysed reaction into account and integral of Eq. (8), we obtain:

$$\log [a/(a-x)] = (k'_R + k'_1 \cdot C_1 + k'_2 \cdot C_2 + k'_3 \cdot C_3) \cdot t = k'_R \cdot t + (k'_1 \cdot C_1 + k'_2 \cdot C_2 + k'_3 \cdot C_3) \cdot t \quad (9)$$

Substituting Eq. (4) into Eq. (9), and using the absorbances, A_0 and A_t, instead of concentrations, a and $(a-x)$ in Eq. (9) yields:

$$\log (A_R/A_t) = (k'_1 \cdot C_1 + k'_2 \cdot C_2 + k'_3 \cdot C_3) \cdot t \quad (10)$$

where A_t is the absorbance of the catalysed reactions at any time t, k_i $(i = 1, 2, 3)$ is the rate constant of the catalysed reaction by M_i $(i = 1, 2, 3)$ at time t and temperature T_1.

Under certain conditions, we can obtain an Eq. (10), which can not be used to simultaneously determine multi-component because k'_i is constant. To solve the problem, we must gain a set of independent equations by changing the operating conditions such as acidity, temperature, but the operations of these methods have caused trouble. In this work, the nature of the temperature gradient is used as a solution to address this difficulty. Because the initial temperature T_1 of the reaction solution is higher than the temperature T_2 of the sample compartment (e.g. T_2 is the temperature of air-conditioned room), and the amount of reaction solution stopped in the flow cell is small, so the temperature of the reaction solution falls with rising reaction time, then the reaction results at a certain time t_j $(j = 1, 2, \ldots, m)$ is the summation of the individual reaction results at many different temperature T, and it can be regarded approximately as the reaction result at a certain temperature T_k. That is to say, an empirical relationship in the form of Eq. (11) will be assumed in this

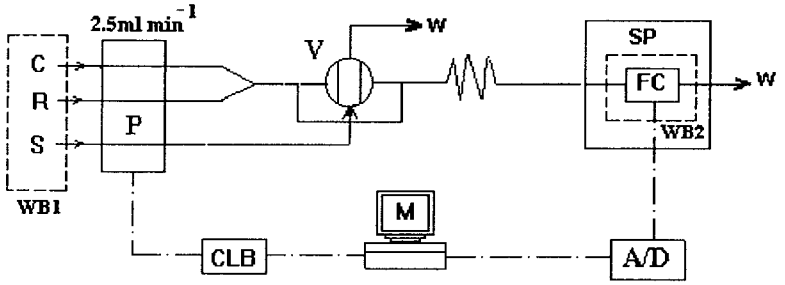

Fig. 1. Schematic flow diagram of the system. C, carrier; R, potassium periodate solution; S, sample; WB1, thermostatic water bath (30°C); WB2, sample compartment (15°C); P, peoristaltic pump; V, injection valve; FC, flow cell; W, waste; M, microcomputer; SP, spectrophotometer; CLB, the control circuit boad of the pump.

work, where K_{ij} have different values at different T_k (different t).Based on the characteristics of the apparatus in this work, the method is easy to operate.

$$\log (A_{Rj}/A_j) = K_{1j} \cdot C_1 + K_{2j} \cdot C_2 + K_{3j} \cdot C_3 \qquad (11)$$

where K_{ij} is the contributions of catalysts M_i to the overall reaction rate (it is named as the coefficient of catalytic reaction in this paper), and the K_{ij} values can be evaluated from the plot of the $\log(A_R/A_t)$ vs. C_i by calibration with standard solutions of different C_i at a series of time t_j ($j = 1, 2,..., m$) (namely at a series of temperature T_k) respectively. C_i is the concentration of catalyst M_i.

Measuring the absorbance values of the uncatalysed reaction A_{Rj} and the overall catalysed reaction A_j at the fixed wavelength λ* nm and at different time t_j , the concentration C_i of every catalyst in the mixture can be calculated from Eq. (11).

2.2. Data processing

Various methods can be proposed for data processing such as traditional multivariate calibration methods, principal components regression, Kalman filter and so on. The Kalman filter has strong analytical functions for the complex data. It is fast, low internal storage capacity, and suited for computerization or automation. In addition, the calculated results are tending towards stability with the filtering proceeding, the value of the error covariance matrix is tending toward the minimum and it is meaningless to go on, then we can stop this testing and data processing immediately, which will raise the efficiency. So we use the Kalman filter to work out the concentration of every catalyst. If both the model noise and the measurement noise are Gaussian white-noise, the state transition model and the measurement model can be formulated as:

$$C(t+1) = I \cdot C(t) \qquad (12)$$

$$Y(t) = \log(A_R/A_t) = K(t) \cdot C(t) \qquad (13)$$

where $C(t)$ is the state vector (n), which is what one wishes to determine, and I is the identity matrix; $K(t)$ is called the observation matrix ($m \times n$) referring to the reaction coefficient matrix K_{ij} in Eq. (11); and $Y(t)$ is the vector of measurables.

The algorithm for the Kalman filter describes the optimal estimation of the state vector by a recursive procedure. When no prior information is available, the filter is generally initiated with $C(0) = 0$. The inital value of the error covariance matrix $P(0)$ is equal to $I \cdot \delta^2$ (δ^2 was in the range of 10^{-4}–10^{-1}) and the measurement noise variance R was chosen as 1×10^{-6}. Based on the above-mentioned theory and the Kalman filtering algorithm equations, a computer BASIC program was written in our laboratory for data acquisition and processing.

3. Experimental

3.1. Reagents and solutions

Iron, silver and manganese standard stock solutions (1.000, 1.000 and 0.702 mg ml^{-1}) were prepared by dissolving the high purity metals in a suitable portion of purified 'GR' grade nitric acid (1 + 1). Working solutions were made by appropriate dilution of the stock solutions just before use. Rhodamine B (0.1 mg ml^{-1}), 1,10-phenanthroline (0.2%, w/v) and potassium periodate (0.01 mol l^{-1}) solutions were also prepared. Buffer solutions of 1 mol l^{-1} sodium acetate-acetic acid of different pHs were used. Other reagents were of analytical grade and all solutions were prepared with doubly distilled water.

3.2. Apparatus

The absorbance spectra were obtained with a Shimadzu UV-3000 recording spectrophotometer (Japan).

The flow injection system (Fig. 1) consisted of a Model 53W UV/Vis spectrophotometer (Shanghai Opitical Instrument Factory, China) equipped with a 1-cm flow cell (Yixing Qiting Experimental Glassware Factory, Jiangsu, China), a Model LZ-1010 multi-channel peristaltic pump and a LZ-1020 rotary injection valve (Shenyang Zhaofa Research Institute of Automation, Shenyang, China). The solutions were thermostatized by means of a Model WC/09-05 thermostatic bath. The spectrophotometer was interfaced to an Apple II microcomputer equipped with A/D card (developed by ourselves). The operation of the pump is controlled by Apple II microcomputer.

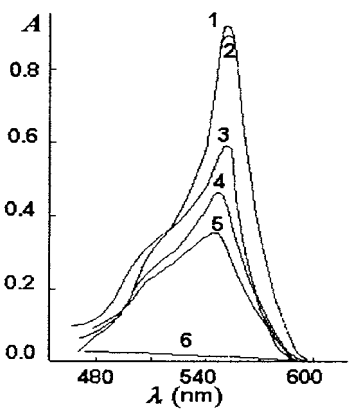

Fig. 2. Absorption spectra of a 4 μg ml^{-1} solution of Rhodamine B (in 0.12 M pH 3.6 acetate buffer) in the presence of (1) phen, (2) phen + KIO_4, (3) phen. + KIO_4 + Mn, (4) phen + KIO_4 + Ag, (5) phen + KIO_4 + Fe, (6) the finished product (2 h), where phen = 0.24 mg ml^{-1} 1,10-phenanthroline, $KIO_4 = 8 \times 10^{-5}$mol l^{-1} potassium periodate, Fe = 30 ng ml^{-1}iron(III), Ag = 30 ng ml^{-1} silver(I), Mn = 30 ng ml^{-1} manganese(II), 30°C.

3.3. General procedure

The FIA experimental series (Fig. 1) required three separate reagent solutions (C, R and S). Solution C was prepared by mixing 6 ml of 1,10-phenanthroline and 2 ml of Rhodamine B in 4 ml of acetate buffer (pH 3.6) and diluting with water to 25 ml; R consisted of 1 ml of potassium periodate in 25 ml of water, and S was obtained by adding between 0.5 and 5 μg iron(III) (or silver(I), manganese(II)) or sample solution in 2 ml of acetate buffer (pH 3.6) and diluting with water to 25 ml. The reagent blank solution was prepared in the same way but without ions determined. Reagent solutions were pumped through the system at 2.5 ml min^{-1} and about 200 μl sample solution was injected by the LZ-1020 rotary injection valve. The solutions were mixed in the tubing in each run. After 7 s from the start of injection, the pump stopped, and the absorbance values at 555 nm (against water) were collected every 0.7 s in about 1 min. The $A-t$ curve was displayed on CRT screen, then the concentration of the analytes were automatically calculated by the microcomputer.

3.4. Preparation of samples

About 0.05 g aluminium or copper alloy was accurately weighed and dissolved in 4 ml of nitric acid (1 + 1) by gentle heating. After complete dissolution of the sample, the solution was evaporated to eliminate nitrogen oxides. After cooling and filtering the solution, the filtrate was transferred quantitatively into a 100-ml volumetric flask, finally diluted with water to the mark. Then a suitable portion of this solution was analysed.

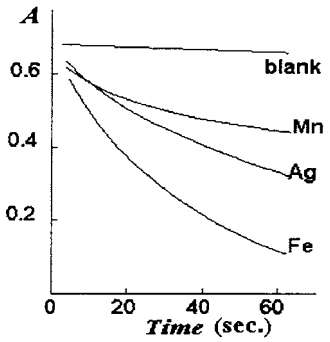

Fig. 3. Absorbance-time curves: 2×10^{-4}mol l^{-1} KIO_4, 0.2 μg ml^{-1}Mn(II), 0.2 μg ml^{-1}Ag(I), 0.2 μg ml^{-1}Fe(III), Other experimental conditions, as in Fig. 2.

4. Results and discussion

4.1. Spectral characteristics

Fig. 2 shows the absorption spectra obtained in the absence (curve 2) and presence (curves 3, 4 and 5) of metal ions with a pH 3.6 buffer 3 min after the reaction. The decrease of the absorbance values in the maximum absorbance peak (555 nm) can be observed in the presence of metal ions. All results show that the absorbance value differences were maximum at 555 nm, and the finished product did not present any absorbance in the range 400–800 nm (curve 6). Therefore, 555 nm was selected as operating parameters during all laboratory work.

4.2. Dynamic characteristics

The absorbance-time curves of the reactions are shown in Fig. 3. The oxidation of Rhodamine B by periodate is a slow process (uncatalysed reaction). Iron(III), silver(I) and manganese(II) can catalyze the oxidized reaction in the presence of 1,10-phenanthroline as activator. The differential catalytic effects of them are suitable for the simultaneous determination of the three catalysts.

4.3. Choice of activator

The activators most widely used have been nitrilotriacetic acid [2,3], 2,2′-bipyridyl and 1,10-phenanthroline. Preliminary experiments show that 1,10-phenanthroline has an activating effect on the Rhodamine B-periodate reaction which is catalysed by Fe(III), Ag(I) and Mn(II), respectively. Whereas nitrilotriacetic acid only accelerates the reaction with manganese, and 2,2′-bipyridyl affects none of them. Therefore, 1,10-phenanthroline is chosen as the activator.

4.4. Optimization of system variables

To decrease the effect of the blank reaction (uncatalysed reaction), mix the solution C and R just before sample injection (Fig. 1). From preliminary investigations and previous experience, the optimization of the system variables yielded the following values: coil length, 35 cm and i.d. 1.2 mm; flow-rate of each channel, 2.5 ml min^{-1}; sample volume, 200 μl and delaytime, 7 s. Under these conditions, there was no significant variation of signal.

4.5. Effects of reaction variables

In this study of the effect of variables, all concentrations indicated are the initial concentrations for the carrier solutions in the tubing.

The acidity of the test solution has a significant effect on the reaction rates. Preliminary experiments show that acetate buffer is a optimal medium. The reaction rate increases with decreasing pH over the range 3.0–5.2 and does not depend on pH in the range 3.3–3.6 for both the catalysed and uncatalysed reactions. A pH of 3.6 was recommended because it leads to the maxi-

Table 1
The additivity of catalytic effect

Added amount (μg ml^{-1})			$\log(A_R/A_t)$		
Fe	Ag	Mn	16 s	30 s	44 s
0.04	0.00	0.00	0.119	0.185	0.236
0.00	0.04	0.00	0.101	0.150	0.211
0.00	0.00	0.08	0.094	0.111	0.137
0.04	0.04	0.08	0.298	0.447	0.602
The sum of individual catalytic effects			0.314	0.446	0.584

Table 2
Analytical results of synthetic samples

Added (μg)			Found (μg) ($n = 5$, average)			Recovery (%)			Ratio		
Fe	Ag	Mn	Fe	Ag	Mn	Fe	Ag	Mn	Fe	Ag	Mn
0.50	2.00	1.50	0.48	1.81	1.53	96.0	90.5	102.0	1:	4:	3
1.00	2.00	2.00	0.90	2.16	1.89	90.0	108.0	94.5	1:	2:	2
1.00	2.00	1.00	1.08	2.17	1.07	108.0	108.5	107.0	1:	2:	1
1.50	1.50	1.50	1.35	1.52	1.43	90.0	101.3	95.3	1:	1:	1
1.50	1.00	1.50	1.38	1.05	1.51	92.0	105.0	100.7	3:	2:	3
1.50	2.50	0.50	1.62	2.30	0.49	108.0	92.0	98.0	3:	5:	1

mum difference between the two rates. The former were found to increase with the acetate buffer concentration up to 0.24 mol l^{-1}, above which it remained constant.The uncatalysed reaction rate did not change with the buffer concentrations. A 0.24 mol l^{-1} acetate buffer concentration was chosen.

The influence of Rhodamine B concentration was evaluated over the range 4–16 μg ml^{-1}, the sensitivity of the reactions was found to increase with dye concentration up to 8 μg ml^{-1} and remain constant above it. So a 8 μg ml^{-1} Rhodamine B concentration, which provides an adequate absorbance at 555 nm, was selected.

The effect of varying potassium periodate concentration in the range 1×10^{-4}–6×10^{-4} mol l^{-1} was studied. The values of $\log(A_R/A_t)$ increase with periodate concentration up to 4×10^{-4} mol l^{-1} and then become constant. A 4×10^{-4} mol l^{-1} concentration was chosen because it gave maximum sensitivity of the reaction.

The variation of the reaction rate with 1,10-phenanthroline concentration was also studied. Only the rates of catalysed reactions increase with 1,10-phenanthroline concentration up to 0.48 mg ml^{-1}. Increasing the activator concentration above 0.48 mg ml^{-1} does not affect the rates of the catalysed reactions. The maximum differences between the catalysed and uncatalysed reaction rates are obtained with 0.48 mg ml^{-1} 1,10-phenanthroline, so this was the concentration advocated in the procedure.

The dependence of the reaction rates on temperature was examined between 25 and 40°C with thermostatic water bath. The temperature effect is more pronounced for the catalysed reaction, while the uncatalysed reaction rate increases slightly with temperature. An initial reaction temperature of 30°C was selected for further studies. When the reaction began, the temperature of the solution in the cell will not steady until it falls in with the cell's temperature (approximately 15°C).

4.6. Calibration graph and effect of foreign ions

Under the above operating conditions, there was a satisfactory linear relationship between $\log(A_R/A_t)$ and the concentration of each analyte in the range 20–160 ng ml^{-1} at any time t. Based on the slopes of these lines at a series of time t_j ($j = 1, 2, \ldots, 20$), The catalytic reaction coefficient matrix $K_{20 \times 3}$ was obtained and then fed into the microcomputer and kept for the future use.

No matter which method we use to work out the concentration of the analytes, the catalytic effect of every catalyst must accord with additivity. As can be seen in Table 1, the total catalytic effect of the three catalyst mixtures is equivalent to the sum of the individual catalytic effects with a average relative error of $\pm 4.7\%$, which is in accordance with Eq. (11). So we can use it for data processing.

The study of interference ions was performed by injecting a standard mixture containing 40 ng ml^{-1} of each cation (Fe, Ag and Mn) and a certain amount of foreign ions into the system. It was assumed that this amount did not interfere,

Table 3
Determination results of alloy samples

Sample	Certified (%)		Added (%)	Found[a] (%)			RSD (%)		
	Fe	Mn	Ag	Fe	Mn	Ag	Fe	Mn	Ag
Aluminium alloy ZL8(BY 2204-1)	0.24	0.68	0.40	0.25	0.71	0.39	4.4	5.3	3.9
Aluminium alloy ZL11(BY 2206-1)	0.56	0.31	0.40	0.57	0.32	0.42	5.7	8.1	5.1
Copper alloy By 2005-1	0.75	0.95	1.00	0.70	0.92	1.05	5.5	5.1	6.3

[a] Average of six separate determinations.

if it caused a relative error of less than 5%. According to this criterion, the following excesses of ions do not interfere: more than 1000-fold amount of NO_3^-, SO_4^{2-}, Mg^{2+}, Ca^{2+}, Al^{3+} and Cd^{2+}; at least 200-fold of Hg^{2+}, Pb^{2+}, Ni^{2+}, Cu^{2+}, Cr^{6+}, Zn^{2+}, Cr^{3+}, Cl^- and PO_4^{3-}; 50-fold of Mo^{6+}, Sb^{3+}, Bi^{3+}, V^{5+} and F^- and 10-fold of Sn^{4+}, W^{6+}, Ti^{4+}. Moreover, it should be pointed out that these ions do not exceed the tolerance ratio in samples. Therefore the samples can be determined directly free from prior separation or masking.

4.7. Accuracy and precision

First, the proposed method was applied to the analysis of synthetic samples, and the recovery factors of each element were calculated. The synthetic samples were prepared by adding a given amount of each ion determined. The subsequent procedure for analysis was described as above. The results calculated by using the matrix $K_{20\times3}$ and Kalman filter are summarized in Table 2. The recoveries ranged from 90.0 to 108.5% and the relative standard deviation (RSD) was better than 10%.

4.8. Applications

The procedure has been applied to the simultaneous determination of iron, silver and manganese in alloy samples. The results are given in Table 3 and show to be in good agreement with the certified values, thus confirming the reliability of the proposed method.

5. Conclusion

The computer-based FIA system makes it easy to control the testing conditions of the proposed method. Using Rhodamine B-periodate indicator reaction catalysed by Fe^{3+}, Ag^+ and Mn^{2+}, the simultaneous determination of these catalysts by means of catalytic differential kinetic method with the Kalman filter is rapid, simple, accurate and precise.

Acknowledgements

The authors gratefully acknowledge financial support from the Natural Science Foundation of Henan Province, China.

References

[1] Z. Marczenko, Spectrophotometric Determination of Elements, Wydawnictwa Naukowo-Techniczne 1976.
[2] X.K. Zhang, T.Y. Tian, Fenxi Huaxue (China) 19 (1991) 789.
[3] Z.L. Jiang, Yankuang Ceshi (China) 9 (1990) 189.
[4] D. Pèrez-Bendito, M. silva, Kinetic Methods in Analytical Chemistry, Horwood, Chichester 1988.
[5] D. Pèrez-Bendito, Analyst 109 (1984) 891.
[6] D. Pèrez-Bendito, Analyst 115 (1990) 699.
[7] G.Z. Fang, Z.X. Guo, Fenxi Huaxue (China) 21 (1993) 1347.
[8] P.D. Wentzell, M.I. Karayannis, S.R. Crouch, Anal. Chim. Acta 224 (1989) 263.
[9] B.M. Quencer, S.R. Crouch, Analyst 118 (1993) 695.
[10] Y.Z. Ye, H.Y. Han, Y.H. Chen, Fenxi Huaxue (China) 23 (1995) 1126.
[11] S.J. Chen, S.Q. Wu, Applied Kinetic Analysis (in Chinese), Geology Press, Beijing, 1989, pp. 25.

ELSEVIER

Talanta 45 (1998) 1131–1138

Talanta

Chemiluminescent determination of pyridoxine hydrochloride in pharmaceutical samples using flow injection

Abdulrahman A. Alwarthan [a,*], Fatima A. Aly [b]

[a] *Department of Chemistry, College of Science, King Saud University, P.O. Box 2455, Riyadh-11451, Saudi Arabia*
[b] *Department of Chemistry, College of Science, Women Student-Medical Studies, Sciences Sections, King Saud University, P.O. Box 22452, Riyadh-11495, Saudi Arabia*

Received 11 March 1997; received in revised form 15 July 1997; accepted 15 July 1997

Abstract

A chemiluminescent method using flow injection is described for the determination of pyridoxine hydrochloride. Its detection limit, linearity and reproducibility were examined. The method is based on the enhancing effect of pyridoxine hydrochloride on the chemiluminescence generated by the oxidation of luminol with hydrogen peroxide in aqueous potassium hydroxide and sodium oxalate. The proposed method is simple and inexpensive. The chemiluminescence intensity is a linear function of pyridoxine hydrochloride concentration over the range 10–250 μg ml^{-1} with a detection limit of 6 μg ml^{-1}. The applicability of the method was demonstrated by the determination of pyridoxine hydrochloride in different tablet formulations and some dietary sources. © 1998 Elsevier Science B.V.

Keywords: Chemiluminescence determination; Dietary sources; Flow injection; Luminol; Pyridoxine·HCl; Tablet formulation

1. Introduction

Accurate determination of water-soluble vitamins is very important in the food and pharmaceutical industries. Pyridoxine hydrochloride (pyridoxine·HCl) was the first of the B_6 group of vitamins to be isolated and it is essential in the diet for the metabolism of amino acids and the maintenance of body cells [1].

A deficiency of vitamin B_6 may dispose a patient towards nerve or blood disorders, and in children might eventually cause convulsions. Therapeutically, it is administered to make up a vitamin deficiency, especially if that deficiency has resulted in neuritis or anemia, to treat premenstrual syndrome. An increased dietary intake may be required during pregnancy or breast-feeding, or during growth in childhood [2].

A variety of methods for the determination of pyridoxine·HCl have been developed and subsequently reviewed by Hashmi [3]. Liquid chromatography with electrochemical detection [4–7] has been reported. A highly sensitive spectrophotometric procedure based on the formation of an azo dye by the reaction between pyridoxine and diazotised *p*-nitroaniline, followed by reaction of

* Corresponding author. Fax: +966 4674253.

PII S0039-9140(97)00223-3

this azo dye with mercury(II) to form a stable complex, has been reported [1]. Other reported methods include spectrofluorimetry [8], polarography [9], high-performance liquid chromatography [10], thin-layer chromatography [11], and laser desorption mass spectroscopy [12].

Chemiluminescence (CL) analysis has some advantages such as sensitivity, ease of use and simple instrumentation, and has been actively investigated for the highly sensitive detection of small amounts of chemical species at ultra-trace levels [13,14]. Since many CL reactions are very fast, they give rise to imprecise measurements as a result of irreproducible mixing of sample and reagents, but the reproducibility and selectivity of the CL analysis can be improved by combination with a flow injection (FI) method.

In aqueous solutions, the most commonly used chemiluminescent species is luminol (5-amino-2,3-dihydrophthalazine-1,4-dione), which reacts with hydrogen peroxide in the presence of a catalyst (generally a metal or metal-containing compound) in alkaline solution to yield 3-aminophthalate in an excited electronic state which returns to ground state with the production of light [15–18]. The light intensity can easily be monitored with a photomultiplier tube with no wavelength discrimination.

In clinical samples, luminol is used frequently as a chemiluminescent reagent. A typical clinical CL reaction uses luminol with horseradish peroxidase (POD) as catalyst:

$$2H_2O_2 + \text{luminol} + OH^- \xrightarrow{POD} 3-\text{aminophthalate} + N_2 + 3H_2O + h\nu \ (425\ \text{nm})$$

An increase in CL emission from luminol oxidation by hydrogen peroxide in alkaline solution was found when it was mixed with a solution of pyridoxine·HCl in the presence of sodium oxalate solution. If pyridoxine·HCl is arranged to be the rate-limiting reagent, then the amount of enhanced emission is proportional to the concentration of pyridoxine; thus the amount of pyridoxine can be determined by measuring the increase in CL. Based on these findings, a new FI-CL method was developed for the determination of pyridoxine·HCl. A review of the literature showed that this is the first method for pyridoxine·HCl determination based on enhancement of the CL reaction.

2. Experimental

2.1. Instruments and flow system

The flow system used for determination and CL detection of pyridoxine·HCl, shown schematically in Fig. 1, was the same as reported earlier [14]. A Gilson Minipuls 3MP4 peristaltic pump was used to drive the carrier and CL reagent streams through the flow system. Each stream was pumped at a constant flow rate of 3.8 ml min^{-1}, using PTFE tubing (0.8 mm i.d.). Pyridoxine·HCl solution was inserted into the carrier stream of luminol using an injection valve from Rheodyne (Luton, UK). The emitted light was measured by a photomultiplier tube (Thorn EMI, 9789QB). The signal was recorded by a Yokogawa Model 3021 recorder (Yokogawa, Japan). Peak heights were measured.

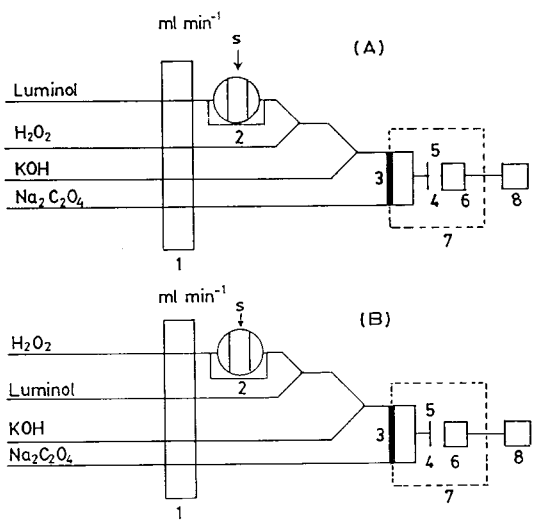

Fig. 1. Schematic diagram showing two configurations (A and B) of the flow-injection system used for the determination of pyridoxine hydrochloride and some of its pharmaceutical preparations; (1) peristaltic pump; (2) sample injection; (3) perspex T-piece; (4) waste; (5) coiled flow cell; (6) PMT; (7) housing; (8) recorder.

2.2. Reagents

Analytical reagent grade chemicals and doubly distilled water were used throughout.

Pyridoxine standard solution, 1000 μg ml^{-1}, was prepared from pyridoxine·HCl (BDH Biochemicals, Poole, UK) and dissolved in distilled water. Working standard solutions were prepared by appropriate dilution immediately before use.

Luminol (5-amino-2,3-dihydrophthalazine-1,4-dione) was obtained from Aldrich (Milwauke, WI). Luminol stock solution, 1×10^{-2} M, was made by dissolving 0.1772 g of luminol in 100 ml of 0.1 M sodium carbonate buffer (pH 10). This solution was a stable for a few months.

Hydrogen peroxide solution was prepared just before use by diluting a measured amount of 30% (w/v) standard solution (BDH, UK) with degassed water.

Oxalate standard solution, 0.20 M, was prepared from sodium oxalate (BDH, UK; previously dried at 100°C and stored in a desiccator over calcium chloride) dissolved in distilled water. Solutions of lower concentrations were prepared by dilution of the standard solution with distilled water.

2.3. Procedure for tablets

Two types of tablets containing pyridoxine·HCl were analysed: Benadon 300 mg per tablet (Roche, Switzerland), and Tri-B 125 mg per tablet (Nile, Egypt).

Three tablets of Benadon were individually weighed, crushed and pulverized. A representative weight equivalent to 300 mg as per label was weighed and dissolved in distilled water and then diluted to a volume of 100 ml in a calibrated flask. No filtration was done.

For Tri-B, five tablets were individually weighed, crushed and pulverized. A representative weight equivalent to 125 mg as per label was weighed and dissolved in distilled water. The dissolution of pyridoxine·HCl from the tablets was facilitated by an ultrasonic generator. Then the solution was filtered into a 50 ml calibrated flask. The insoluble residue was washed several times with distilled water, the filtrates were transferred to a 100 ml calibrated flask and the solution was made up to volume with distilled water.

Recovery computation was based on the standard calibration graph.

2.4. Procedure for dietary sources extracts

Five different dietary sources of pyridoxine·HCl (i.e. peanut, yeast, lemon, tomato and apple) were prepared for recovery analysis. After cutting each sample into small pieces, extraction was done solely with water; the extraction solutions were clarified by double centrifugation and filtration.

The extracted materials were strongly acidic, in the pH range 2.0–4.5. Preliminary results showed that acidic sample solutions greatly inhibit the intensity signal. Thus, the pH of each extracted material was adjusted to 9.0–9.5 before the total volume was made up to 100 ml. A 5.0 ml aliquot was pipetted from the above solution and made up to 100 ml with distilled water, thus giving a dilution factor of 20.

3. Results and discussion

3.1. Configuration designs

The FI configuration used for the determination of pyridoxine was so designed to provide different reaction conditions for magnifying its enhancing effect on the CL generated by the reaction of luminol and hydrogen peroxide. Two different configurations (A and B) were tested for this purpose (Fig. 1).

In configuration A, the sample was mixed with the luminol solution, after which it started to mix with the hydrogen peroxide, potassium hydroxide and oxalate solutions before it reached the detector, as shown in Fig. 1.

In configuration B, the sample was mixed with the hydrogen peroxide solution, then mixed with the luminol, potassium hydroxide and oxalate solutions before it reached the detector.

Configuration A was found to give greater CL signal, approximately 40 times greater than the signal height obtained using configuration B.

Configuration A was therefore chosen for the determination of pyridoxine·HCl as it provided the greatest sensitivity and the fastest restoration of the baseline.

3.2. Optimization of manifold parameters

The variables studied were the volume injected and the flow rate. The concentrations used in these experiments were: luminol, 5×10^{-3} mol l^{-1}; hydrogen peroxide, 5×10^{-3} mol l^{-1}; potassium hydroxide, 0.10 mol l^{-1}; oxalate, 0.10 mol l^{-1}; sample, 250 μg ml^{-1}.

The volume injected was varied between 10 and 400 μl. The difference in peak heights between blank and the sample increased with increasing volumes injected up to 250 μl, above which it started to decrease continuously. The volume chosen was 250 μl.

The flow rates of the luminol, hydrogen peroxide, potassium hydroxide and sodium oxalate streams were varied over the range 4.8–21 ml min^{-1}. The signal was maximal and virtually constant between 15.2 and 21 ml min^{-1}. The total flow rate chosen was 15.2 ml min^{-1} (3.8 ml min^{-1} for each channel). The peak height obviously depended on the residence time of the sample in the flow system. The best results were obtained at a total flow rate of 15.2 ml min^{-1}.

3.3. Optimization of reagent concentrations

The effect of varying the concentrations of luminol, hydrogen peroxide, potassium hydroxide and sodium oxalate was tested in the optimized flow system.

The effect of luminol concentration was studied in the range 1.0×10^{-5} to 1.0×10^{-2} mol l^{-1}. As can be seen from Fig. 2A, the difference in peak heights for the uncatalysed and catalysed reactions increased with increasing reagent concentration up to 5.0×10^{-3} mol l^{-1}, but it decreased at higher concentrations. A 5.0×10^{-3} mol l^{-1} luminol solution was selected.

The difference in peak heights for the blank and for pyridoxine increased with increasing hydrogen peroxide concentrations up to 5.0×10^{-3} mol l^{-1}, above which it decreased, as shown in Fig. 2B. The working solution chosen was 5.0×10^{-3} mol l^{-1}.

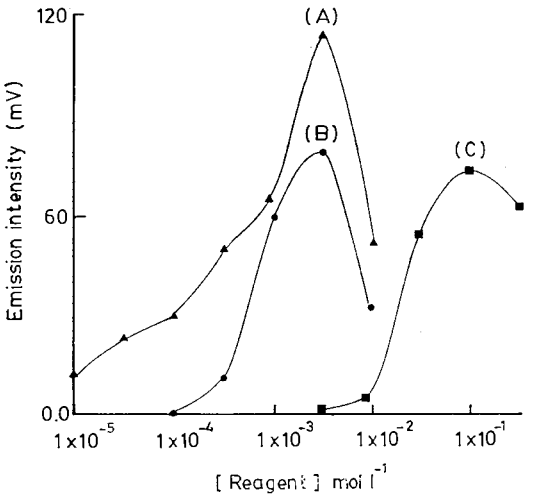

Fig. 2. Effect of reaction variables on pyridoxine catalysed reaction between luminol and H_2O_2. Variables: (A) luminol concentration; (B) hydrogen peroxide concentration; and (C) potassium hydroxide.

The effect of potassium hydroxide on the CL reaction is shown in Fig. 2C; as can be seen, a strongly basic solution was required for maximum development of the CL reaction.

Luminol shows CL in an alkaline environment only [19]. To determine the pH dependence of the light emission during luminol oxidation, several experiments were carried out in various buffer solutions covering the region pH 7–12. Using the manifold shown in Fig. 1A, the effect of buffer addition was examined in the CL-FI procedure. Buffer solutions, 0.1 M, were prepared from $NaC_2H_3O_2$, Na_2CO_3, $Na_2B_4O_7$, $Na_2H_2PO_4 \cdot 2H_2O$ and $Na_2C_2O_4$ media (all media were sodium salts). The results showed that the CL emission intensity obtained in a medium of $Na_2C_2O_4$ (pH 12) is stronger than that obtained in the other media (Table 1). Not only is the CL emission intensity obtained in oxalate medium stronger, but also the effect of pyridoxine in enhancing the CL is the greatest. Buffers with a final pH higher than 12 (borate) or with a pH lower than 8 (phosphate) gave negligible emission.

The effects of variations in oxalate buffer concentration were then investigated over the range 1.0×10^{-3} to 2.0×10^{-1} mol l^{-1}. Maximum CL emission intensity was obtained with 0.15 M buffer, which was used in subsequent studies. The enhancement of the CL signal by oxalate might be interpreted on the basis of formation of a highly energetic peroxylic group between the excited species, aminophthalate and the oxalate anion. The CL reaction mechanism can be briefly expressed by the following reaction [20–22]:

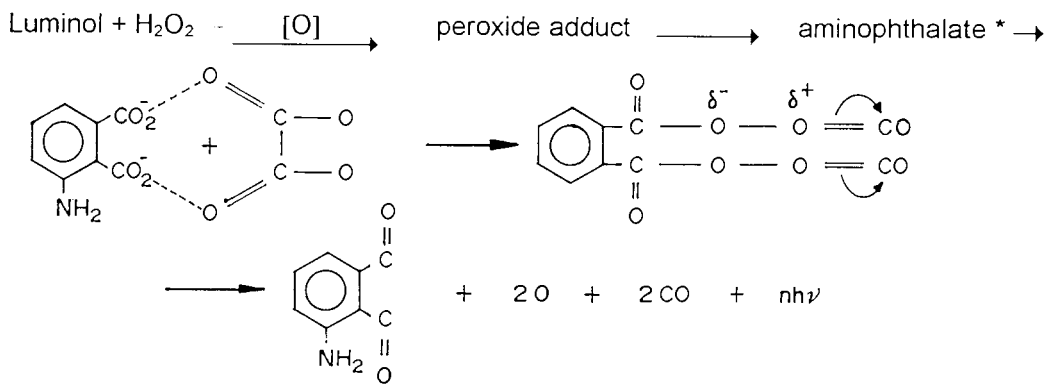

The peroxylic species then breaks to give singlet oxygen, CO, and aminophthalate. The singlet oxygen ($^1\Delta_g$) reverts to the ground state ($^3\Sigma_9$) emitting light, while triplet carbonyls are known to have a heterogeneous spectrum. Such a postulation is now under investigation.

Table 1
The influence of different buffers (all 0.1 M) on the CL emission intensity for pyridoxine determination

Buffer	Average intensity (mV)	pH of final solution (collected from the waste)
No buffer	80	–
$NaC_2H_3O_2$	140	11.92
Na_2CO_3	4	11.99
$Na_2B_4O_7$	2	12.95
$Na_2H_2PO_4 \cdot 2H_2O$	0	7.87
$Na_2C_2O_4$	304	11.98

3.4. Calibration characteristics

Under the optimum operating conditions, analytical characteristics such as reproducibility and detection limit were investigated for pyridoxine·HCl.

A calibration graph of pyridoxine·HCl was constructed between the CL intensity (voltage intensity, Y, mV) and the concentration range 10–250 μg ml^{-1} in which the graph was linear. This linear range allows the determination of 10 μg ml^{-1} levels of pyridoxine. The regression line of emission intensity (I) on pyridoxine concentration (C) was $I = 18.657 + 1.001C$ ($r = 0.999$, $n = 10$) with a detection limit (2 × noise) of 6 μg ml^{-1}. The relative standard deviation was less than 5% for eight determinations of 100 μg ml^{-1} pyridoxine. The sample throughput was 124 samples h^{-1}.

The method was tested for several synthetic samples of pyridoxine·HCl. Some of the analytical results are given in Table 2.

Table 2
Determination of pyridoxine·HCl in synthetic samples

Sample	Taken (μg ml^{-1})	Found[a] (μg ml^{-1})	Error (%)
1	25.0	25.0	0.0
2	40.0	40.5	+1.3
3	70.0	69.7	−0.4
4	100.0	98.8	−1.2
5	140.0	140.3	+0.2

[a] Average of four determinations.

Table 3
Interference study

Interfering species	Concentration ($\mu g\ ml^{-1}$)	Remarks
No interferent		
Arabinose Fructose Glucose Sucrose Nicotinamide Carbowax	100	No interference
Alanine Glucosamine L-Methionine Thymine Starch	10	$>10\ \mu g\ ml^{-1}$ interferes by decreasing the emission
Mercaptoethanol	1	$>1\ \mu g\ ml^{-1}$ strong interference occurs
Cysteine Histidine		Interference occurs strongly even at $1\ \mu g\ ml^{-1}$

Amount of pyridoxine·HCl used, $100\ \mu g\ ml^{-1}$.

3.5. Interferences

The interference of various organic compounds usually associated with pyridoxine was studied and the results are given in Table 3. No interference was observed from the presence of arabinose, fructose, glucose, sucrose, nicotinamide and carbowax. Alanine, glucosamine, methionine, thymine and starch interfered when present at a concentration higher than $10\ \mu g\ ml^{-1}$. Cysteine and histidine interfered strongly even at the $1\ \mu g\ ml^{-1}$ level.

Therefore, it should be noted that the method cannot be applied to samples containing alanine, glucosamine, methionine, thymine, starch, mercaptoethanol, cysteine and histidine. However, the CL detector might be used for the analysis of such interferents after liquid chromatographic separation.

3.6. Application of the method

The method was applied to the determination of pyridoxine hydrochloride in two multi-vitamin formulations. The accuracy of this CL procedure was tested by performing recovery experiments on solutions prepared from two different pyridoxine·HCl formulations, as shown in Table 4. Poor recovery was obtained in the case of Tri-B tablets, because this formulation is considered combined vitamins for B_1, B_6, B_{12} and folic acid, and contains metal ions as well as other organic compounds which greatly affect the CL intensity due to the formation of stable complexes or insoluble compounds.

The proposed method was also evaluated by analysing a pharmaceutical formulation of pyridoxine·HCl (Benadon; Roche, Switzerland). It was considered of interest to compare the results from the proposed procedure with those from a spectrophotometric assay for pyridoxine·HCl [1], which involves the formation of an azo dye by

Table 4
Recovery of pyridoxine·HCl in sample solutions of multi-vitamin formulations

Formulation	Pyridoxine·HCl ($\mu g\ ml^{-1}$)			Recovery (%)
	Present	Added	Recovered[a]	
Benadon (300 mg) (Roche, Switzerland)	100	30	31	103.3
	100	40	40.5	101.3
	100	50	51.5	103
Tri-B (125 mg) (Nile, Egypt)	100	40	8.5	21.3
	100	50	12	24
	100	60	15.8	26.3

[a] Average of four determinations per sample.

Table 5
Determination of pyridoxine·HCl (PN) in a commercial formulation with CL and Nirmalchandar and Balasubramanian (N&B) methods

Formulation	Amount of PN (mg)			Recovery (%)	
	Claimed	Found[a]		CL	N&B
		CL	N&B		
Benadon tablets (300 mg) (Roche, Switzerland)					
Sample 1	300	305	301	101.7	100.3
Sample 2	300	299	299	99.7	99.7
Sample 3	300	300	297	100.0	99.0

[a] Average of four determinations per sample.

reaction between pyridoxine and diazotised *p*-nitroaniline followed by reaction of the azo dye with mercury(II) to form a stable complex. Statistical analysis of the results reveals that there is no significant difference between the two methods (see Table 5).

The results obtained using the proposed method in the analysis of Benadon were also compared with those obtained by the official method, in which a quantity of powdered tablets containing 20 mg of pyridoxine·HCl was shaken in 50 ml of 0.025 M standard phosphate buffer for 15 min and diluted to 100 ml with the same solvent. The suspension was mixed and filtered; 5 ml of the filtrate was diluted to 100 ml with the same solvent. The absorbance of the final solution was measured in the range 230–350 nm [23]. As can be seen from Table 6, there was good agreement between the two methods.

The method was also applied to the assay of pyridoxine·HCl in some fresh dietary sources, namely peanut, yeast, lemon, tomato and apple. The results obtained are shown in Table 7 and agree with published results for the occurrence of vitamin B_6 in dietary sources [24].

4. Conclusion

The results presented in this paper clearly demonstrate that the enhancing effect of pyridoxine·HCl on the oxidation of luminol by hydrogen peroxide can be used for the determination of pyridoxine·HCl in a flow system. The versatility and simplicity of this method permits the analysis of a large number of samples.

Table 6
Determination of pyridoxine·HCl in Benadon tablet (300 mg, Roche, Switzerland) with the proposed CL procedure and the official BP method

Sample	Pyridoxine·HCl found[a] (μg ml^{-1})			Recovery (%)	
	Claimed	CL	BP	CL	BP
1	15	14.9	15	99.3	100
2	25	25.3	24.8	101.2	99.2
3	45	45.1	45.3	100.2	100.7
4	60	60	60.6	100	101

[a] Average of four determinations per sample.

Table 7
Determination of pyridoxine·HCl in some dietary sources such as peanut, yeast, lemon, tomato and apple

Sample	Recovery[a] (μg 100 g^{-1})	Reported recovery[b] (μg 100 g^{-1})
Peanut	2720	10^3–10^4
Yeast	5480	10^3–10^4
Lemon	83	10–100
Tomato	221	100–1000
Apple	37	10–100

[a] Average of three determinations.
[b] Data from [24].

Acknowledgements

The authors are very grateful to Dr. M.I. Khalil for useful discussions.

References

[1] V. Nirmalchandar, N. Balasubramanian, Analyst 113 (1988) 1097.
[2] I.K.M. Morton, J.M. Hall, J. Halliday, H. Graham, H. Shapiro, Medicines, The Comprehensive Guide, 2nd ed. Bloomsbury, London, 1991, p. 479.
[3] M.V.H. Hashmi, Assay of Vitamins in Pharmaceutical Preparations, Wiley, London, 1973, pp. 188–212.
[4] W. Hou, E. Wang, Talanta 37 (1990) 841.
[5] W.A. Behrens, R. Madere, Anal. Biochem. 165 (1987) 102.
[6] K. Kamata, T. Hagiwara, M. Takahashi, S. Uehara, K. Nakayama, K. Akiyama, J. Chromatogr. 356 (1986) 326.
[7] J. Martinez Calatayud, S. Sagrado Vives, F. Sanmiguel Roche, Pharmazie 44 (1989) 351.
[8] Y. Liang, Y. Lin, Yaowu Fenxi Zazhi 1989, 9(1), 32(Ch) (Anal. Abstr. 3E28, 1990, p. 139).
[9] G.W. Chase Jr., A.M. Soliman, J. Micronutr. Anal. 7 (1990) 15.
[10] H. Wei, Y. Cheng, Yaowu Fenxi Zazhi 1990, 10(6), 371(Ch) (Anal. Abstr. 5G101, 1991, 53(5), p. 508).
[11] J.M. McMahon, Anal. Biochem. 147 (1985) 535.
[12] A.A. Alwarthan, Analyst 118 (1993) 639.
[13] A.A. Alwarthan, Anal. Chim. Acta 317 (1995) 233.
[14] A.A. Alwarthan, S.A. Al-Tamrah, A.A. Akel, Anal. Chim. Acta 292 (1991) 201.
[15] W.R. Seitz, W.W. Suydam, D.M. Hercules, Anal. Chem. 44 (1972) 957.
[16] L.L. Klopf, T.A. Nieman, Anal. Chem. 55 (1983) 1080.
[17] D.B. Paul, Talanta 25 (1978) 377.
[18] L.J. Kricka, G.H.G. Thorpe, Analyst 108 (1983) 1274.
[19] U. Isacsson, G. Wettermrk, Anal. Chim. Acta 83 (1976) 227.
[20] M.I. Khalil, J.A.M. Al- Sharqaui, Inorg. Chim. Acta 121 (1986) 27.
[21] J.A.M. Al-Sharqaui, M.I. Khalil, H.A. Daban, Inorg. Chim. Acta 132 (1987) 95.
[22] M.E. Murphy, H.H. Sies, Anal. Proc. 27 (1990) 217.
[23] British Pharmacopeia, International Edition, Vol. II, HMSO, London, 1988, p. 999.
[24] R.J. Kutsky, Handbook of Vitamins and Hormones, Van Nostrand Reinhold, New York, 1973, pp. 54–61.

ELSEVIER

Talanta 45 (1998) 1139–1146

Talanta

Biomass-modified carbon paste electrodes for monitoring dissolved metal ions

Hua Yao, Gerald J. Ramelow *

Department of Chemistry, P.O. Box 90455, McNeese State University, Lake Charles, LA 70609, USA

Received 4 April 1997; received in revised form 11 July 1997; accepted 15 July 1997

Abstract

Electrodes were prepared by incorporating dried, nonliving biomass of a common lichen, *Ramalina stenospora*, and *Sphagnum* (peat) moss in carbon paste. The electrodes were tested on solutions containing Pb(II) and Cu(II) ions by immersing the electrode in the solution for selected periods of time to accumulate ions. Following this the electrode was connected to a potentiostat and the applied voltage scanned from -1.0 to $+0.5$ V vs. SCE. Any adsorbed metal ions were stripped back into solution at the appropriate oxidizing voltage. The ratio of biomass to mineral oil to graphite has been found to be crucial to electrode performance. Different ratios of the three components using the lichen *Ramalina stenospora* were evaluated for maximum electrode performance. Only two electrode compositions gave a good electrode response for lead. Electrodes containing peat moss were superior in performance to lichen-containing electrodes for lead. Electrodes based on the lichens *Cladina evansii* and *Letharia vulpina*, the marine algae *Ulva lactuca* and *Sargassum fluitans*, the blue-green alga *Spirulina platensis*, and the aquatic plant *Eichhornia crassipes* did not respond to lead at all. All functioning electrodes studies showed a poor response toward copper(II) ions. © 1998 Elsevier Science B.V.

Keywords: Carbon paste electrodes; Peat moss; Lichens

1. Introduction

Microorganisms such as bacteria, algae, fungi and mosses, and aquatic plants possess mechanisms to remove metal ions from solution through metabolic pathways and passive adsorption [1–11]. The latter are rapid and highly pH-dependent. The binding is thought to involve mainly carboxylate groups on cell wall surfaces [12]. Cellular material thus has the properties of an ion exchanger in which hydrogen ions compete with metal ions for binding sites.

The uptake of metal ions by lichens has been extensively studied because of their use as air pollution monitors [13,14] Lichens, composed of two organisms, a fungus and an alga, living in a symbiotic relationship, rapidly remove metal ions metals from aqueous solution in a pH-dependent manner similar to algae and fungi [15–17]. Nonliving biomass accumulates metal ions more rapidly and more effectively than live tissue.

* Corresponding author. Fax: +1 318 4755950.

PII S0039-9140(97)00239-7

Sphagnum moss is another biomass type which has a particularly strong ability to bind metal ions [18,19]. *Sphagnum* moss is widely sold in a partially decomposed form as peat moss which is used as a soil conditioner by gardeners. Peat moss has been found to be an extremely effective metal ion sorber for certain metals [20,21].

The metal ion accumulating properties of certain types of nonliving biomass has been combined with anodic stripping voltammetry to produce metal ion sensors [22–27]. Biomass was incorporated in carbon paste electrodes in weight percentages from 11 to 20 to accumulate metal ions from solution through passive adsorption. The sorbed metals were subsequently stripped from the electrode by applying an oxidation potential. The height of the stripping current peak is then used as a measure of the initial ion concentration in solution The present study was undertaken to investigate the factors affecting the performance of carbon paste electrodes incorporating biomass derived from a lichen and peat moss.

2. Experimental

2.1. Preparation of carbon paste electrodes

Powdered biomass was mixed with graphite powder and mineral oil at selected ratios of all three components. For most experiments with peat moss and other biomass-based electrodes, 0.2 g of biomass was first mixed with 0.4 g of mineral oil and then mixed with 0.4 g of graphite powder to give 20% biomass by weight. The mixture was then packed solidly into a glass tube and a polished copper wire (20 gauge) was inserted into the mixture. For *Ramalina stenospora* electrodes, in order to identify the best biomass/graphite powder/mineral oil ratio, different ratios of biomass (usually 115–250 mesh sized) to graphite and mineral oil were investigated. Electrodes were tested in both the anodic stripping voltammetric (ASV) and sorption mode (SM) measurements. A 5-ppm Pb, Cd, and Cu solution was used for the ASV measurements and a 5-ppm Pb standard solution was used for the SM measurements.

2.2. Anodic stripping voltammetric experiments

A polarographic analyzer (Princeton Applied Research Model PAR 174A) with an X-Y Plotter (Schlumberger) was used for all electrode experiments. To determine the electrical conductivity of electrodes prepared with biomass, the electrode was placed in the voltammetric cell containing a 5-ppm, mixed-metal standard solution of Pb, Cu, and Cd. A negative potential (-1.0 V relative to the SCE) was applied to the electrode for a selected period of time to reduce the metal ions and plate them onto the electrode surface. The potential was then scanned in a positive direction from -1.0 to $+0.5$ V at 10 mV s^{-1}. A voltammogram (current vs. applied voltage) was recorded and the electrical conductivity of the electrode was identified by presence of current peaks for the oxidation of each metal.

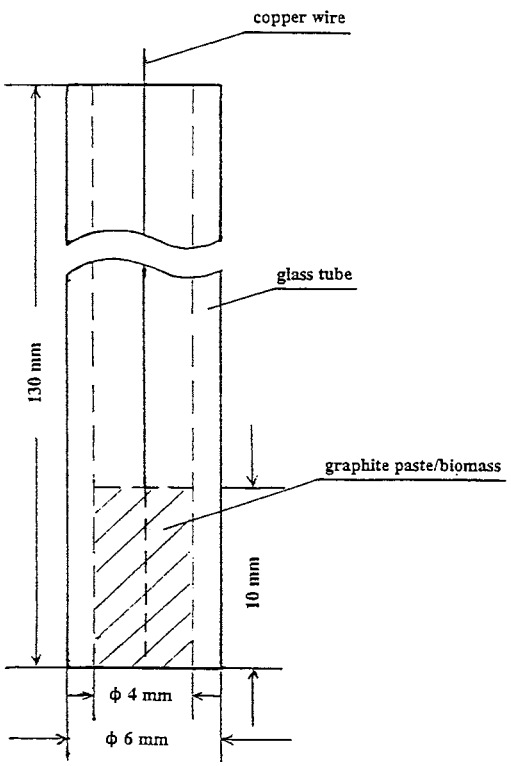

Fig. 1. Schematic of carbon paste/biomass electrode.

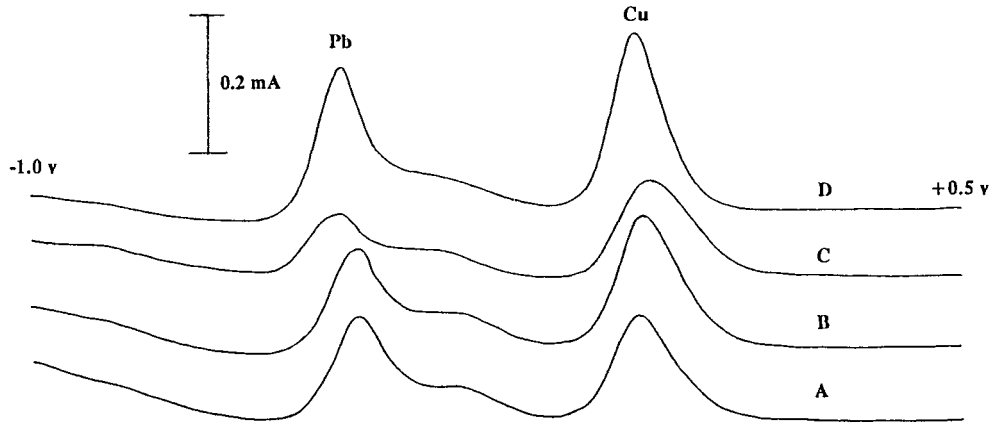

Fig. 2. Anodic stripping voltammograms of Pb(II) and Cu(II) measured by four peat moss electrodes incorporating different mesh-sized biomass. (A) 30–60 mesh; (B) 60–115 mesh; (C) 115–250 mesh; (D) >250 mesh.

The polarographic analyzer was also used to determine the metal ion uptake by carbon paste electrodes prepared with biomass. An electrode was dipped in a 0.1 M HCl solution for 2 min, followed by a rinse with doubly deionized water to remove any bound metals. The electrode was then placed in a 0.05 M sodium acetate solution at pH 7.2 for 30 s. After rinsing with doubly deionized water, the electrode was dipped in a standard metal solution for a selected period time at open circuit to accumulate metal ions. The electrode was then removed from the standard solution rinsed with water, blotted dry, and placed in pure electrolyte in the voltammetric cell. An applied potential was scanned then from -1.0 to $+0.5$ V at a rate of 10 mV s^{-1}. The voltammogram of the electrode was recorded and metal uptake was identified by the presence of current peaks.

To study the effect of pH on electrode performance, a series of 5-ppm Pb standard solutions was prepared in 0.05 M KH_2PO_4 and the pH adjusted to values from 2 to 6 with nitric acid or ammonium hydroxide. Sorption-mode measurements of a peat moss electrode were carried out in each pH-adjusted standard using a 2-min deposition time.

The effect of deposition time on subsequent current peak height was studied by running sorption-mode measurements of a peat moss electrode with different deposition times from 1 to 8 min in a 5-ppm Pb standard at pH 2.9.

To study the effect of metal concentration, a series of Pb standards from 1 to 15 ppm was prepared in doubly deionized water and adjusted to pH 4.0 with ammonium hydroxide. Sorption-mode measurements with a peat moss electrode were carried out on the Pb standards using a 3-min deposition time.

A water sample was collected from a local polluted waterway, Contraband Bayou, and filtered immediately in the laboratory. After the natural pH of the water was measured, a 100-ml aliquot of the sample was analyzed for Pb content by using a peat moss electrode in the SM mode. The sample was then spiked with a standard solution of Pb (1000 mg l^{-1}) to give a final concentration of 5 ppm and the pH adjusted to different values in the range 2–8. Each sample at a different pH was measured in the SM mode with a 3-min deposition time.

3. Results and discussion

3.1. Anodic stripping voltammetric measurements (ASV)

The primary aim of the study was to develop electrodes for use as dissolved metal ion sensors.

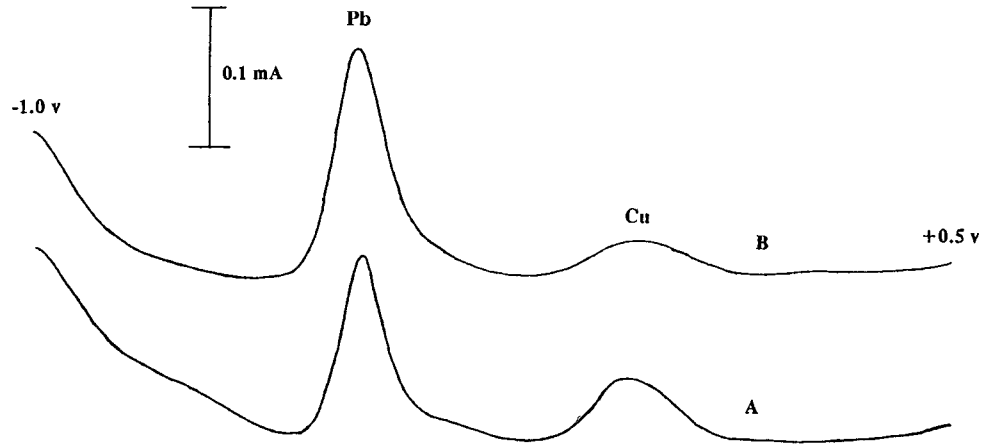

Fig. 3. Anodic stripping voltammograms of Pb(II) and Cu(II) measured by two *Ramalina stenospora* electrodes.

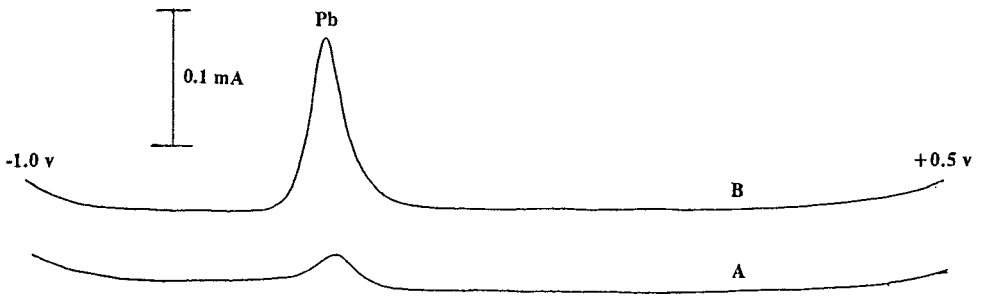

Fig. 4. Comparison of sorption-mode voltammograms of Pb(II) measured by (A) *Ramalina stenospora* and (B) peat moss electrodes.

Many types of biomass, including the seaweeds *Sargassum fluitans* and *Ulva lactuca*, the lichens *Ramalina stenospora* and *Cladina evansii*, the blue green alga, *Spirulina platensis*, and peat moss were tested. A schematic of the type of carbon paste/biomass electrode used in this work is shown in Fig. 1. If the electrode is electrically conductive, metal ions should be reduced and plated onto the electrode when the electrode is given a negative potential relative to the SCE and dipped in a mixed-metal standard solution for a selected period of time. The plated metals can be stripped off by scanning the potential to the electrode in a positive direction. By recording the voltammogram, different metals will be identified by the presence of current peaks at characteristic potentials. The presence of these characteristic peaks demonstrates the electrical conductivity of the electrode.

Fig. 2 shows the voltammogram of electrodes prepared with peat moss. Fig. 3 shows the voltammogram of two electrodes prepared with *Ramalina stenospora*. Lead and copper peaks appear at -0.53 and -0.05 V vs. SCE, respectively. It is apparent that electrodes prepared with both *Ramalina stenospora* and peat moss were electrically conductive. The electrodes prepared with the seaweeds *Sargassum fluitans* and *Ulva lactuca*, the lichen *Cladina evansii*, and the blue-green alga, *Spirulina platensis*, did not function in

Table 1
Component ratios for electrodes prepared with a lichen, *Ramalina stenospora*[a]

Electrode no.	Treatment	Biomass wt. (g)	Oil wt. (g)	Graphite wt. (g)	Biomass %	ASV	SM
1	None	0.20	0.40	0.40	20.0	+	−
2	Washed, 60°C	0.20	0.40	0.40	0.20	+	−
3	Washed, 60°C	0.20	0.30	0.40	22.2	+	+
4	Washed, 60°C	0.20	0.35	0.40	21.0	+	−
5	Washed, 60°C	0.20	0.33	0.40	21.5	+	−
6(I)	Washed, 60°C	0.20	0.30	0.40	22.2	+	+
6(II)	Washed, 60°C	0.20	0.30	0.40	22.2	+	+
7	Washed, 60°C	0.20	0.28	0.40	22.7	+	−
8	Washed, 60°C	0.20	0.30	0.35	23.5	+	−
9	Washed, 60°C	0.20	0.30	0.30	25.0	+	−
10	Washed, 60°C	0.20	0.25	0.30	26.7	+	−
11	Washed, 60°C	0.20	0.30	0.25	26.7	+ (low)	−
12	Washed, 60°C	0.20	0.25	0.25	28.6	+ (low)	+ (low)
13	None	0.20	0.30	0.40	22.2	+	−
14	None	0.20	0.28	0.30	25.6	+	−
15	None	0.20	0.24	0.30	27.0	+	−
16	None	0.20	0.30	0.40	22.2	+	−
17	None	0.20	0.40	0.40	20.0	+	−

[a] 115–250 mesh biomass used in all cases except for electrode numbers 16 and 17 in which <250 mesh was used.

the ASV mode and thus were not investigated further.

3.2. Sorption mode measurements (SM)

All electrodes prepared were most sensitive to Pb(II) ions. Electrodes previously shown to be electrically conductive were used to measure lead ions in aqueous solutions. Lead ions were adsorbed by the biomass component of the electrodes upon immersion in a 5-ppm standard solution for a selected period of time. The sorbed metals are reduced to the zero valence state upon application of a negative potential. The sorbed and reduced metals were stripped off by scanning the applied potential from −1.0 to +0.5 V. Fig. 4 shows the voltammograms of sorbed lead stripped off from *Ramalina* and peat moss electrodes. The lead peaks are observed at −0.53 V vs. SCE. Comparison of peak heights indicates

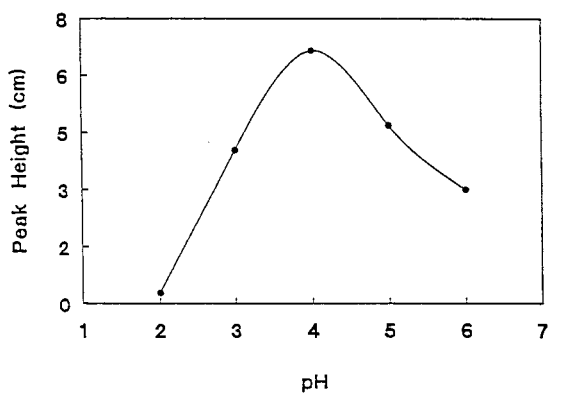

Fig. 5. Stripping peak heights of Pb(II) sorbed by a peat moss electrode at pH 2–6.

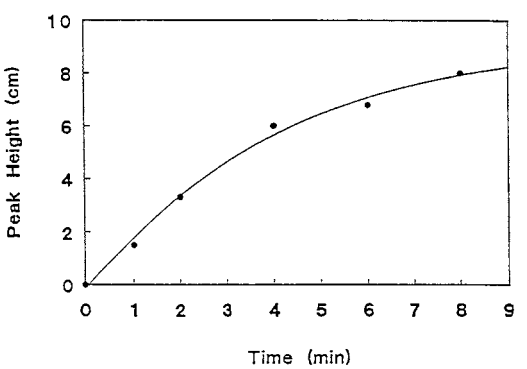

Fig. 6. Stripping peak heights of Pb(II) measured by a peat moss electrode after different deposition times.

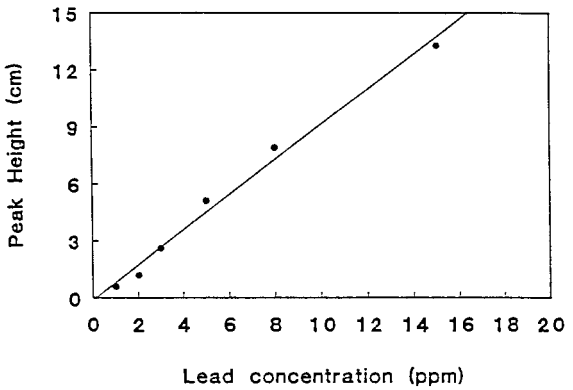

Fig. 7. Stripping peak heights of Pb(II) measured by a peat moss electrode for different Pb(II) concentrations.

that the peat moss electrode was more sensitive to Pb(II) ions than the *Ramalina stensospora* electrode.

The sorption of Cu(II) ions by peat moss electrodes was also studied but the results were inconsistent. One electrode responded well to copper ions but the electrode surface seemed to become saturated quickly and the response was much less than for Pb(II) ions. Subsequent experiments with Cu(II) ions were inconclusive. The factors affecting copper accumulation need to be studied further.

3.3. Electrode compositions (optimum ratios of biomass to graphite to mineral oil)

In order to provide optimum electrode performance in both ASV and SM modes, it was necessary to determine the optimum ratio of biomass/graphite powder/mineral oil. *Ramalina stenospora* was the biomass type used to study the effect of electrode composition. The results obtained are presented in Table 1. It is interesting that although all electrodes prepared with *Ramalina stenospora* worked well in the ASV mode, only two electrodes (composition ratios) out of 17 tested functioned in the SM mode. And furthermore, none of the *Ramalina* electrodes performed as well as the peat moss electrodes which all had a fixed gram ratio of biomass/graphite/mineral oil of 0.2/0.4/0.4, as recommended by Conner et al. [22]. The capability of metal ion uptake depends on percentage of biomass, while electrical conductivity of electrodes depends on the percentage of graphite. It is apparent that the effects of graphite and biomass being somewhat opposite to each other, the ratio of all three components must be adjusted carefully.

3.4. pH-Dependence of metal uptake by electrodes

Since previous studies have shown a strong pH-dependence of metal binding in aqueous solution by nonliving biomass for many microorganisms, there was concern that uptake of metal ions by biomass-based electrodes could be affected by the pH of the testing solutions. An electrode prepared with peat moss was used to study the effect of pH. Peak heights, which represent uptake of Pb(II) by electrode at different pH values, are plotted in Fig. 5. It is apparent from the plot that the effect of pH was great. Maximum peak height was observed at pH 4.0. As a result, electrodes can be cleaned of residual metal in a low pH solution such as 0.1 M HCl solution. To test the effectiveness of acid cleaning, a lichen and a peat moss electrode were first immersed in a 5-ppm Pb(II) solution for 2 and 8 min, respectively. Then a voltage scan from -1.0 to $+0.5$ V was obtained for each. Finally, each was dipped in a 0.1 M HCl solution for 2 min and the voltammogram run again. The absence of a lead peak in the second scan confirms the complete removal of lead from the electrode by the acid rinse.

3.5. Deposition time studies

One of the aims the study was to investigate the effect on metal uptake by variations in deposition time. Deposition times ranging from 1 to 8 min in a 5-ppm Pb standard solution were studied. The peak heights of Pb are plotted vs. deposition time in Fig. 6. It is seen that peak height obtained for Pb was linear with deposition time up to 3 min.

3.6. Metal concentration studies

If the sorption mode is to be used as a method for measuring lead, the linearity between Pb con-

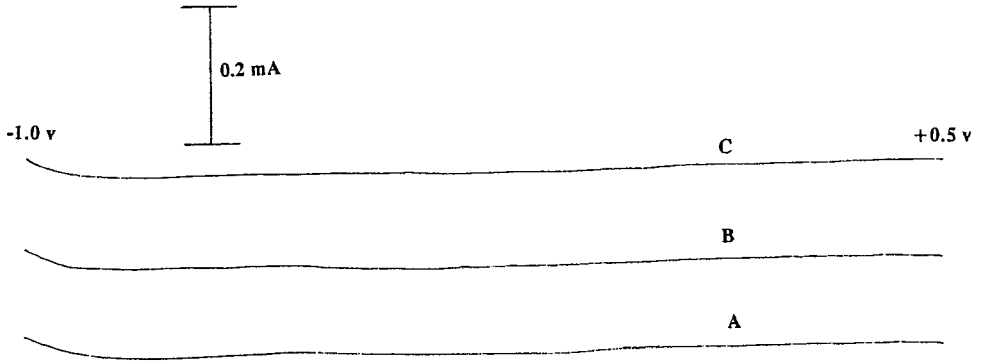

Fig. 8. Stripping-mode voltammograms of Pb(II) in a water sample from Contraband Bayou measured by a peat moss electrode.

centration and voltammogram peak height needs to be studied. Voltammograms were obtained for concentrations from 1 to 15 ppm with an electrode prepared with peat moss using with a 2-min deposition time. The peak heights, which represent the uptakes obtained in different concentration of Pb standards, are plotted in Fig. 7. It is apparent from the plot that the relationship between peak height and Pb concentration is linear.

3.7. Monitoring dissolved metal ions in water samples

The strong response of certain biomass-based carbon paste electrodes to Pb(II) ions makes them promising for measuring dissolved lead ions in water samples, both in the laboratory and in the field. In the final phase of this study an attempt was made to investigate the practicality of using carbon paste/biomass electrodes for measuring dissolved Pb (II) ions in a natural water sample. A sample from a local waterway, Contraband Bayou, was tested for dissolved lead with the results shown in Fig. 8. No significant Pb in the sample could be detected since no Pb peak was observed for deposition times from 3 to 8 min, The absence of Pb was confirmed by flame atomic absorption analysis of the sample. To demonstrate that Pb measurements of natural waters are feasible, the same sample was spiked with a Pb(II)

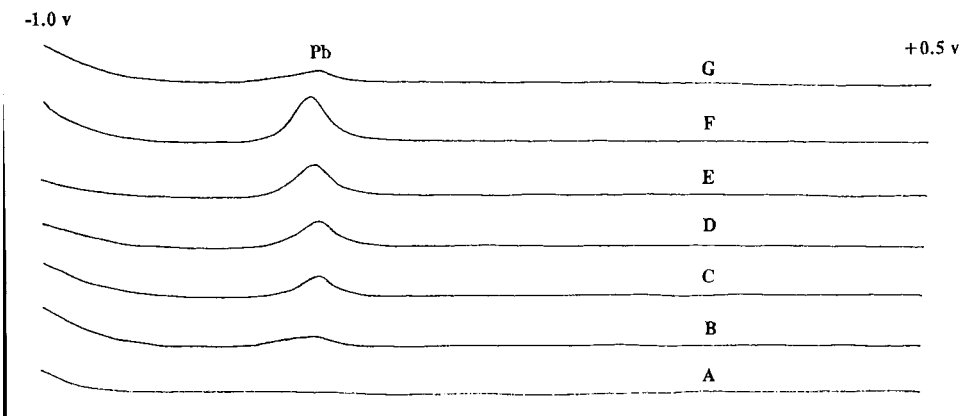

Fig. 9. Sorption-mode voltammograms of Pb(II) in a spiked water sample from Contraband Bayou measured by a peat moss electrode at different pH values. (A) blank; (B) pH 3.0; (C) pH 3.9; (D) pH 5.1; (E) pH 6.0; (F) pH 7.3; (G) pH 8.1.

standard solution to give a 5-ppm Pb concentration. The results obtained are presented in Fig. 9. It is observed that the peak heights of Pb obtained by the electrode in the spiked sample are much lower than those obtained for standards. The results also indicate that the maximum peak height for the natural water sample is at about pH 7. This is much greater that the maximum obtained for aqueous standards at pH 4. The great difference between sample and standard is believed to be due to matrix effects in the sample.

References

[1] L.R. Drake, G.D. Rayson, Anal. Chem. 68 (1996) 22A.
[2] T.J. Beveridge, R.G.E. Murray, J. Bacteriol. 127 (1976) 1502.
[3] A. Nakajima, T. Horokoshi, T. Sakaguchi, Eur. J. Microbiol. Biotechnol. 12 (1981) 76.
[4] P. Harris, G. Ramelow, Environ. Sci. Technol. 24 (1990) 220.
[5] J.M. Tobin, D.G. Cooper, R.J. Neufeld, Appl. Environ. Microbiol. 47 (1984) 821.
[6] M. Tsezsos, B. Volesky, Biotechnol. Bioeng. 23 (1981) 583.
[7] D. Khummongkol, G.S. Canterford, C. Fryer, Biotechnol. Bioeng. 24 (1982) 2643.
[8] A. Les, R.W. Walker, Water Air Soil Pollut. 23 (1984) 129.
[9] D.W. Darnall, B. Greene, M. Hosea, R.M. McPherson, M. Henzi, M.D. Alexander, Trace metal removal from aqueous solution, in: R. Thompson (Ed.), Special Publication No. 61, Royal Society of Chemistry, 1986, pp. 1–25.
[10] B. Greene, M. Hosea, R. McPherson, M. Henzi, M.D. Alexander, D. Darnall, Environ. Sci. Technol. 20 (1986) 627.
[11] K. Breuer, A. Melzer, Oecologia 82 (1990) 461.
[12] R.H. Crist, K. Oberholser, D. Schwartz, J. Marzoff, D. Ryder, D.R. Crist, Environ. Sci. Technol. 22 (1988) 755.
[13] K.J. Puckett, E. Nieboer, M.J. Gorzynski, D.H.S. Richardson, New Phytol. 72 (1973) 329.
[14] E. Nieboer, D.H.S. Richardson, F.D. Tomassini, Bryologist 8 (1978) 226.
[15] G.J. Ramelow, Y. Zhang, L. Liu, Microbios 66 (1991) 95.
[16] D.H.S. Richardson, E. Nieboer, Endeavor 5 (1981) 127.
[17] E. Nieboer, K.J. Puckett, B. Grace, Can. J. Bot. 54 (1976) 724.
[18] P. Pakarinen, K. Tolonen, Oikos 28 (1977) 69.
[19] P. Pakarinen, Ann. Bot. Fenn. 15 (1978) 287.
[20] K. Aulio, Bull. Environ. Contam. Toxicol. 35 (1985) 439.
[21] Y. Hao, A.L. Roach, G.J. Ramelow, J. Environ. Sci. Health A28 (1993) 2333.
[22] M. Conner, E. Dempsey, M.R. Smyth, D.H.S. Richardson, Electroanalysis 3 (1991) 331.
[23] E. Dempsey, M.R. Smyth, D.H.S. Richardson, Analyst 117 (1992) 1467.
[24] J.L. Gardea-Torresdey, D. Darnall, J. Wang, Anal. Chem. 60 (1988) 72.
[25] J.L. Gardea-Torresdey, D. Darnall, J. Wang, J. Electroanal. Chem. 252 (1988) 197.
[26] J. Wang, N. Naser, D. Darnall, J. Gardea-Torresdey, Electroanalysis 4 (1992) 71.
[27] J. Wang, B. Tian, G.D. Rayson, Talanta 39 (1992) 1637.

ELSEVIER

Talanta 45 (1998) 1147–1154

Talanta

Determination of aluminium and manganese in human scalp hair by electrothermal atomic absorption spectrometry using slurry sampling

Pilar Bermejo-Barrera *, Antonio Moreda-Piñeiro, Jorge Moreda-Piñeiro, Adela Bermejo-Barrera

Department of Analytical Chemistry, Nutrition and Bromatology, Faculty of Chemistry, University of Santiago de Compostela, E-15706 Santiago de Compostela, Spain

Received 4 April 1997; received in revised form 15 July 1997; accepted 15 July 1997

Abstract

Methods for the determination of aluminium and manganese in human scalp hair samples by electrothermal atomic absorption spectrometry using the slurry sampling technique were developed. Palladium and magnesium nitrate were used as chemical modifiers. Hair samples were pulverized using a zirconia vibrational mill ball, and were prepared as aqueous slurries. Determinations can be performed in the linear ranges of 1.9–150 μg l^{-1} Al^{3+} and 0.03–10.0 μg l^{-1} Mn^{2+}. Limits of detection of 0.9 mg kg^{-1} and 27.6 μg kg^{-1} were obtained for aluminium and manganese, respectively. The analytical recoveries were between 99.6 and 101.8% for aluminium and in the 98.3–101.3% range for manganese. The repeatability of the methods ($n = 11$), slurry preparation procedure and ETAAS measurement, was 16.0 and 7.9% for aluminium and manganese, respectively. The methods were finally applied to the aluminium and manganese determination in 25 scalp hair samples from healthy adults. The levels for aluminium were between 8.21 and 74.08 mg kg^{-1}, while concentrations between 0.03 and 1.20 mg kg^{-1} were found for manganese. © 1998 Elsevier Science B.V.

Keywords: Aluminium; Electrothermal atomic absorption spectrometry; Human scalp hair; Manganese; Slurry sampling

1. Introduction

Inorganic constituents in living organisms, such as metallic species, have been usually assessed through their determination in blood and urine [1,2]. Thus, it is well stabilized different relationships between the levels of certain metals in these clinical samples and certain pathologies. Although the determination of elements in human hair presents several advantages, such a greater concentration of the different metals in this sample than in blood or urine [2,3], the diagnostic potential of human hair has still to be fully exploited [4]. This can be attributed to the unclear relationship between trace elements and certain pathologies and

* Corresponding author.

PII S0039-9140(97)00230-0

Table 1
Graphite furnace temperature programmes and spectrophotometer operating conditions

Step	Temperature (°C)	Ramp time (s)	Hold time (s)	Ar flow (ml min^{-1})
Drying	150	20	15	300
Pyrolysis	1500[a]	10	15	300
Atomization	2500[b]	0	3	200[c] (Read)
Cleaning	2600	2	2	300

Operating conditions: Al and Mn hollow cathode lamps; wavelenghts, 309.3 (Al) and 279.5 (Mn) nm; spectral bandwidth 0.7 (Al) and 0.2 (Mn) nm; integration time, 3 s; peak-area measurements; D_2 lamp background corrector, injection volume, 20 ml; pyrolytic graphite tubes and L'vov platform.
[a] 1200°C for manganese.
[b] 2200°C for manganese.
[c] Gas stop for manganese.

the complexity of the preanalytical and analytical procedures.

Aluminium is considered a nonessential trace element of low toxicity while manganese is assumed as essential to men but toxic at high concentrations [1]. As the occurrence of these metals in the industrial exposure, the development of analytical methods for the determination of them in human samples are necessary. Moreover, the toxicology of aluminium is linked to the Alzheimer's disease.

However, there are certain problems when elements analysis is performed using hair samples, as the variation in element concentration along the hair and with the sampling site [5]. According to Bencze [5] the first drawback can be overcome if the segments of the hair follicles, that are biologically active, are sampled, hair length to 2–3 cm. To overcome the second difficulty, hair sample must be collected from the occipital region of the head, near as possible to the scalp [5].

As hair is a solid material, a previous sample pretreatment is required. Usually, acid [6–8] and alkali [9] digestions procedures have been proposed to prepare the hair sample prior to analysis. These solid sample pretreatments present certain problems such as the long time required to destroy the samples, the consumption of acids and the possibility of sample contamination or analyte losses. To overcome these problems the use of the introduction of the solid samples as slurries is an attractive alternative and thus the electrothermal atomization atomic absorption spectrometry (ETAAS) combined with the slurry sampling technique has been recognized as adequate to determine metallic species in several matrices [10]. In this sense, the use of ultrasonic autosamplers, described by Miller-Ihli [11–13] offers the best conditions for the application of slurry sampling—ETAAS methods for routine analysis.

The atomization of slurries prepared from biological materials can presents as aim problem a high background signal as a consequence of the undestroyed matrix sample, which can not be corrected by the deuterium lamp corrector. In addition, the built-up of carbonaceous residues inside the graphite tube are usually occurred [14–16]. These problems can be solved using chemical modification [17–19] and air/oxygen ashing stages [14–16,20,21].

In this paper, methods for the aluminium and manganese determination in human scalp hair by ETAAS using the slurry sampling technique are proposed. Chemical modifiers such as palladium, magnesium nitrate and palladium–magnesium nitrate, were investigated for both metals. Finally, the methods were applied to several human scalp hair samples from healthy adults and to different reference materials.

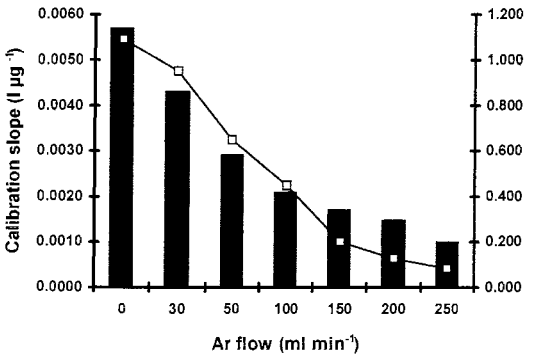

Fig. 1. Effect of different argon flow rates during the atomization step on the slope of aluminium calibration graph (bars) and aluminium absorbance from a hair slurry diluted 1:1 (line).

2. Experimental

2.1. Apparatus

A Perkin-Elmer 1100B atomic absorption spectrometer equipped with a Perkin-Elmer HGA 700 graphite furnace and a Perkin-Elmer AS 70 autosampler was used for aluminium measurements. A Perkin-Elmer 1100B atomic absorption spectrometer equipped with a Perkin-Elmer HGA 400 graphite furnace and a Perkin-Elmer AS 40 autosampler was used for manganese determination. A deuterium lamp was used as background correction system in both cases. Operating conditions for both metals are given in Table 1. A Laser Coulter series LS100 Fraunhofer Optical Model

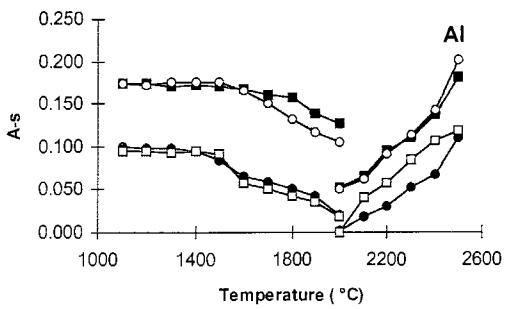

Fig. 2. Aluminium: Pyrolysis (left) and atomization (right) curves for hair slurries corresponding to the use of Pd (□), Mg (■) and Pd–Mg (○) as chemical modifiers, and without chemical modification (•).

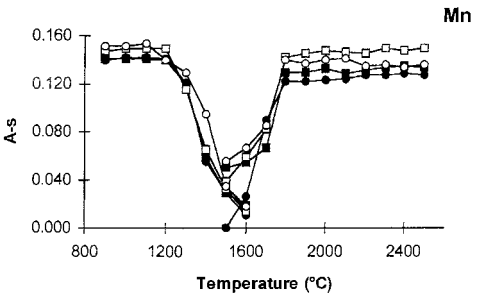

Fig. 3. Manganese: pyrolisis (left) and atomization (right) curves for hair slurries corresponding to the use of Pd (□), Mg (■) and Pd–Mg (○) as chemical modifiers, and without chemical modification (•).

particle sizer (Coulter Electronics, Hialeach, FL) was used to obtain the particle size distribution. A vibrational mill ball, Retsch, equipped with zirconia cups (15 ml in size) and zirconia balls (7 mm diameter) was used to pulverize samples and to reduce the particle size. An Agimatic magnetic agitator from Selecta (Barcelona, Spain) was used to suspend the slurry particles prior to the measurements.

2.2. Reagents

Acetone, 99.7% (Carlo Erba Analytical, Milan, Italy). Aluminium nitrate stock standard solution, 1.000 g l^{-1} (Merck, Darmstadt, Germany). Glycerol 99.4% (Sigma, St. Louis, MO) Magnesium nitrate (BDH, Poole, UK). Manganese nitrate stock standard solution, 1.000 g l^{-1} (Roimil,

Table 2
Extraction of aluminium and manganese from human scalp hair slurries by addition of nitric acid

Nitric acid concentration (%), v/v	% Extraction	
	Aluminium	Manganese
0.0	27.4	30.4
0.5	68.3	74.2
1.0	90.2	95.6
1.5	97.5	99.3
2.0	99.7	99.5
3.0	99.4	99.4
4.0	99.6	99.5

Table 3
Within-run precision, expressed as RSD(%) for 11 injections, corresponding to nitric acid, at a concentration of 2.0% (v/v), and wetting agents (Triton X-10O, Viscaiex HV30 and glycerol) at cocentrations of 0.2% (m/v)

	Aluminium	Manganese
Without agent	15.5	6.8
HNO_3	13.2	5.5
Triton X-100	4.2	1.6
Viscalex HV30	12.6	6.0
Glycerol	4.5	1.4

Cambridge, UK) Nitric acid AnalaR nitric acid (69.0–70.5% with maximum aluminium and manganese contents of 0.02 and 0.005 mg l^{-1}, respectively, BDH). Palladium (99.999%, Aldrich Chemicals, Milwaukee, WI). Reference material CRM 397 Human Hair (Commission of the European Communities Community Bureau of Reference, BCR). Reference materials DOLT-1 and DORM-1 Dogfish Liver and Dogfish Muscle (National Research Council of Canada). Triton X-100 (Merck). Viscalex HV30 (Allied Coloids, Bradford, UK).

2.3. Procedures

Hair samples were collected from the scalp region of the head with stainless scissors. The hair length was oscillated between 2 and 3 cm. A hair washing step is needed to remove exogenous trace elements from the hair surface. The washing procedure carried out was the recommended by the International Atomic Energy Agency [22], and thus, hair samples were washed with ultrapure water (three times), then with acetone (three times) and finally, again with ultrapure water. Then, the hair samples were oven dried at 100°C.

Hair samples were then pulverized in a zirconia vibrational mill ball. A time of 20 min was required to obtain an adequate pulverization of hair and also an effective particle size reduction. Therefore, a mean particle diameter of 0.8 μm was obtained. For times lower than 20 min, although mean particle diameter lower than 10 μm were obtained, a great portion of the hair results unpowdered and thus sieving was necessary. Finally, 0.1 g of the hair powder was suspended in a few ml of ultrapure water, and then the slurry was diluted to 25 ml. This gives a slurry concentration of 0.4% (m/v) and offers a mass volume/liquid volume ratio in according to Miller-Ihli [23].

For measurements, volumes between 0.25 and 0.60 ml of the hair slurries were transferred to autosampler cups, adding adequate volumes of palladium or magnesium nitrate, used as chemical modifier for manganese and aluminium, respectively, to get concentrations of 25 mg l^{-1} of palladium and 10 mg l^{-1} of magnesium nitrate after dilution to 1 ml. Glycerol, at a concentration of 0.4% (m/v) was added as a wetting agent. Calibration graphs were performed over the 1.9–150.0 and 0.03–10.00 μg l^{-1} ranges, for aluminium and manganese, respectively.

3. Results and discussion

Due to the relative high aluminium concentration in human scalp hair, between 8.2 and 74.08 mg kg^{-1} as results of this work, it was necessary dilute the hair slurries in order to obtain aluminium absorbances in the work range of the conventional spectrometers. The dilution carried out to obtain aluminium absorbances lower than 0.300 A.s, was between 1:75 and 1:100. This high dilution of hair slurries brings problems on the representivity of the portion of the slurry which is introduced into the atomizer. Therefore, a decrease on the sensitivity of conventional ETAAS determination of aluminium is required. In this sense, the use of less sensitive resonance lines is an adequate possibility [24]. However, the use of resonance lines below 400, as 396.2 [25] and 394.4 nm [24], offers problems on signal/noise ratio, obtaining a poor precision. According to Hernández-Córdoba et al. [16] the use of Ar flow during the atomization step offers a satisfactory sensitivity reduction, avoiding the problems related to the use of less sensitive resonance lines. By this way, different Ar flows during the atomization step, between 20 and 250 ml min^{-1}, were tested, recording the aluminium absorbance for each case and also studying the variation of the slope of a calibration graph. The results are plotted in Fig. 1

Table 4
Linear range and calibration and standard addition graphs

	Linear range (μg l^{-1})	Calibration graph	Standard addition graph
Aluminium	1.9–150.0	$A_i = 0.002 + 0.0014$ [Al]; $r = 0.999$	$A_i = 0.044 + 0.0019$ [Al]; r = 0.999
Manganese	0.03–10.00	$A_i = 0.005 + 0.036$ [Mn]; $r = 0.999$	$A_i = 0.065 + 0.033$ [Mn]; r = 0.999

A_i means integrated absorbance and [Al] and [Mn] are in μg l^{-1}.

for the slope of the calibration graph and the aluminium absorbance. As it can be seen, both parameters gradually decrease, and an adequate reduction of the sensitivity is reached for Ar flows higher than 150 ml min^{-1}. Therefore, an Ar flow rate of 200 ml min^{-1} was chosen, and the calibration graph was performed over the 0–150 μg l^{-1} Al^{3+} range.

3.1. Graphite furnace temperature programmes

Chemical modifiers such as palladium, magnesium nitrate and palladium–magnesium nitrate, were investigated for both aluminium and manganese. In Fig. 2 and Fig. 3 are shown the pyrolysis and atomization curves obtained for aluminium and manganese, respectively, corresponding to different chemical modifiers and also in absence of chemical modification. As it can be seen in Fig. 2, a little increase in the pyrolysis temperature is observed for aluminium when the chemical modifiers used are present. In the same way, a soft increase in the manganese stabilization is obtained for the use of palladium or palladium–magnesium nitrate (Fig. 3). This can mean that chemical modification are not necessary, however, an important reduction on the background signal is obtained when the chemical modifiers tested are added, and thus for manganese, the background signal decreases from 0.350 in absence of chemical modification to 0.040–0.100 A.s for the use of the different chemical modifiers. The determination of the optimum atomization temperatures showed that 2500°C can be attained for aluminium for the presence or absence of chemical modification. For manganese, atomization temperatures between 2100 and 2200°C can be selected.

From studies on the effect of different amounts of palladium and magnesium nitrate on the aluminium and manganese absorbances it can be said that important decreases on the aluminium and manganese absorbances in presence of palladium or magnesium nitrate, respectively, were observed. Therefore, and due to the fact that similar pyrolysis and atomization temperatures are reached for the use of palladium, magnesium nitrate and palladium–magnesium nitrate, magnesium nitrate and palladium were chosen for aluminium and manganese, respectively, at optimum concentration of 10 and 25 mg l^{-1} for magnesium nitrate and palladium, respectively.

3.2. Effect of an acid predigestion of the slurry: stability of the slurries

Several authors nave proposed the use of slurries acidified with nitric acid [11–13,15,16, 20,21,23]. The effect of the acid medium involves that the analyses are mobilized from the solid particles to the liquid media, which gives an significative improvement in the precision of the methods. In the present work, it was observed that a total extraction of the aluminium and manganese is reached with a nitric acid concentration of 2 0% (v/v), as it can be seen in Table 2 where different percentages of the analyses extractions are shown. The percentages were obtained recording the analyte (aluminium and manganese) absorbance from the slurry and from the liquid phase, after the deposition of the slurry particles. It can be seen that in absence of acid medium a significative partitioning of aluminium and manganese between the solid and the liquid phase is obtained, about 27.4 and 30.4% for aluminium and manganese, respectively.

The effect of the acid medium on the precision was evaluated studying the within-run precision

Table 5
Sensitivity of the methods

	LOD (μg kg^{-1})	LOQ (μg kg^{-1})	m_0 (pg)[a]	Blank value (A.s.)[b]
Aluminium	0.9[c]	3.1[c]	86.7 ± 3.5	0.004 ± 0.001
Manganese	27.6	92.1	2.3 ± 0.2	0.002 ± 0.001

[a] $n = 4$.
[b] $n = 11$.
[c] mg kg^{-1}.

for eleven replicate injections of hair slurries with and without nitric acid. As can be seen in Table 3, any improvement in the precision was obtained when nitric acid is present. Therefore, the use of aqueous slurries was chosen.

The stability of the slurries was also studied using different wetting agents reported in literature as Triton X-10O, Viscalex HV40 and glycerol. In Table 3 are also shown the within-run precision corresponding to 11 replicate injections of different hair slurries with the different agents. As it can be seen, a significative improvement in the precision, lowest RSD values, are obtained when Triton X-100 and glycerol are used as wetting agents. Due to problems related to the volumetric measurement of Triton X-100 solutions, glycerol was selected as most adequate agent. The optimum glycerol concentration found was 0.4% (w/v).

3.3. Analytical performances

In Table 4 are given the linear ranges obtained for each case moreover the equations of calibration and standard addition graphs. The *t*-test, confidence level of 95.0%, [26] was applied to compare both graphs, obtaining that slopes of calibration and standard addition graphs are statistically similar for aluminium and manganese determination. Therefore, matrix effects can be assumed as not important.

The limit of detection (LOD) and the limit of quantification (LOQ), defined as 3 and 10 SD m^{-1}, respectively, where SD is the standard deviation of 11 measurements of a blank and m is the slope of the aqueous calibration graph, referred to 0.1 g of hair sample are given in Table 5. The characteristic mass (m_O) defined as

$$m_0 = \frac{0.0044\ CV}{A_{i_c} - A_{i_b}}$$

where C is the analyte concentration, V is the injection volume, and A_{i_c} and A_{i_b} are the analyte absorbances of the sample and blank, respectively, are also shown in Table 5 for each case.

The within-batch precision and the analytical recovery are given in Table 6 and it can be seen that good aluminium and manganese recoveries and precision are reached. For manganese, the precision and the analytical recovery was also studied with hair slurries prepared from different amounts of hair sample, between 0.05 and 0.4 g, which, after dilution to 25 ml (procedure section) offer slurry concentrations in the 0.2–1.6% (m/v) range. To study the effect of the sample concentration on the precision, different volumes of Mn^{2+} aqueous standard solution were added to the hair slurries prepared from small amount of sample, obtaining similar analyse absorbances. Results are shown in Table 7, where the RSD (%) values are related to 11 replicate injections of each hair slurry. The analytical recoveries ($n = 11$) obtained for concentration levels of 5.0 and 10.0 μg l^{-1} of Mn^{2+}, are also shown in Table 7. As can be seen the slurry concentration can be increased until 0.4 g without loss of the analytical performances. Therefore, it can be concluded that an amount of hair sample of 0.1 g is adequate and representative mass to develop the analysis.

On the other hand, the accuracy of the method for manganese determination was studied by analysis of three different reference materials, CRM 397 (human hair) with indicative value 11.2 ± 0.3 mg kg^{-1}, and DOLT-1 (dogfish liver) and DORM-1 (dogfish muscle) with manganese certified contents of 8.72 ± 0.53 and 1.32 ± 0.26 mg

Table 6
Within-batch precision ($n = 11$) and analytical recovery ($n = 11$) obtained for hair slurries spiked with 50, 75, 100 and 150 1 μg l^{-1} Al^{3+}, and 1.0, 2.0, 3.0 and 5.0 μg l^{-1} Mn^{2+}

Aluminium			Manganese		
[Al] (μg l^{-1})	RSD (%)	Analytical recovery (%)	[Mn] μg l^{-1}	RSD (%)	Analytical recovery (%)
0.0	9.0	—	0.0	3.3	—
50.0	3.6	98.8 ± 3.6	1.0	1.1	103.3 ± 1.2
75.0	3.0	97.0 ± 3.8	2.0	0.8	102.1 ± 1.0
100.0	2.3	101.5 ± 3.4	3.0	0.6	102.3 ± 0.8
150.0	1.9	103.4 ± 2.8	5.0	0.5	99.5 ± 0.8

kg^{-1}, respectively. The results obtained, 11.6 ± 0.3, 8.76 ± 0.15 and 1.24 ± 0.12 mg kg^{-1}, for CRM 397, DOLT-1 and DORM-1, respectively, show that good accuracy is reached.

Finally, the repeatability of the method, slurry preparation and aluminium and manganese determination, was stabilized by determining the aluminium and manganese contents in 11 slurries prepared from a same hair sample. The results, expressed as RSD(%), were 16.0 and 7.9 for aluminium and manganese, respectively.

3.4. Interferences study

The effects of different anionic and cationic species on the aluminium and manganese absorbances were evaluated. The species were added to a hair slurry at concentrations twice as high as that found in human hair [4]. It was considered that a species presents interfering behaviour at a certain concentration when an increase or decrease in the absorbance higher than the within-batch precision of the method (9.0 and 3.3%, for Al and Mn, respectively) is observed. In base of this, it can be said that cations as Ag^{+}, Ca^{2+}, Cd^{2+}, Cu^{2+}, Cr^{3+}, Fe^{2+}, K^{+}, Na^{+}, Ni^{2+}, Pb^{2+}, Sn^{2+} and Zn^{2+}, and anions as Cl^{-}, PO_4^{3-}, SiO_3^{2-} and SO_4^{2-}, at the concentrations tested, do not produce interfering effects.

3.5. Application

The methods were applied to 25 scalp hair samples from healthy adults. Fig. 4(a, b) show the aluminium and manganese distribution in scalp hair, respectively. As shown, the aluminium concentration is varied between 8.19 and 74.08 mg kg^{-1}. The mean aluminium concentration is 30.15 mg kg^{-1} with a standard deviation of 18.53 mg kg^{-1} and a variance of 343.46 mg kg^{-1}. The manganese concentration falls between 0.03 and 1.20 mg kg^{-1}, with a mean manganese concentration of 0.35 mg kg^{-1} (standard deviation of 0.31 mg kg^{-1} and variance of 0.098 mg kg^{-1}).

Table 7
Within-run precision and analytical recovery obtained for different slurry concentrations

Slurry concentration (%) (m/v)	RSD (%)	Analytical recovery (%)	
		+2.5 μg l^{-1} Mn^{2+}	+5.0 μg l^{-1} Mn^{2+}
0.2	2.3	103.2 ± 1.7	99.2 ± 0.6
0.3	1.7	101.9 ± 1.5	100.4 ± 0.8
0.4	1.4	98.3 ± 1.3	101.3 ± 0.6
0.8	2.6	101.4 ± 1.9	98.6 ± 1.1
1.6	3.3	98.0 ± 2.4	99.3 ± 1.2

$n = 11$.

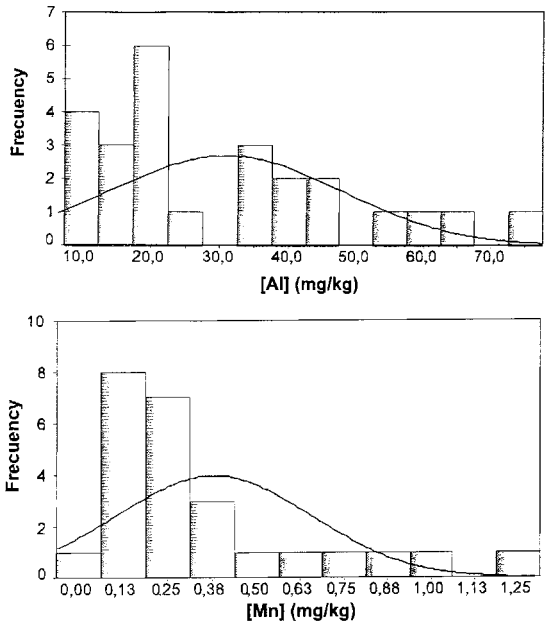

Fig. 4. Frequency distribution of aluminium (a) and manganese (b) in 25 human scalp hair from healthy adults.

As it can be seen, the aluminium concentrations found in scalp hair samples from healthy adults from Galicia (north-west Spain) are higher than the reported in literature [4], between 0.1 and 36.0 mg kg^{-1}. However, the manganese concentrations are lower than the reported in hair from people of other countries, between 0.04 and 24 mg kg^{-1} in accordance with Caroli et al. [4] and similar than the given by Iyengar [27], between 0.5 and 1.5 mg kg^{-1}. As it can be seen, there is important differences in the elements hair levels in function to each research group. The differences can be due, between other factors, to the different analytical methodology employed. Finally, for aluminium, some link between the relatively high aluminium hair levels and the elevated aluminium content in soil and waters of Galicia can be stabilized. In this sense and according to Iyengar [27], there appears to be some relationship between the relatively high levels of certain elements in biological samples from a country and the levels of those elements in soils of those countries.

References

[1] D.L. Tsalev, Atomic Absorption Spectrometry: Occupational and Environmental Health Practise, vol. II, CRC Press, Boca Raton, FL, 1984.
[2] J.L. Burguera, M. Burguera, C.E. Rondón, C. Rivas, J. A Burguera, O.M. Alarcón, J. Trace Elem. Electrolytes Health Dis. 1 (1987) 21.
[3] I.D. Capel, M.H. Pinnok, H.M. Donell, D.C. Williams, E.C.G. Grant, Clin. Chem. 27 (1981) 879.
[4] S. Caroli, A. Alimonti, E. Coni, F. Petrucci, O. Senofonte, N. Violante, Crit. Rev. Anal. Chem. 24 (1994) 363.
[5] K. Bencze, Fresenius J. Anal. Chem. 338 (1990) 58.
[6] U. Voellkopt, Z. Grobenski, At. Spectrosc. 5 (1984) 115.
[7] J.R. Castillo, A. Fernández, Microchem. J. 39 (1989) 224.
[8] T.S. Srikumar, A. Källgard, S. Lindeberg, P.A. Öckerman, B. Akesson, J. Trace Elem. Electrolytes Health Dis. 8 (1994) 21.
[9] T. Uchida, H. Isoyama, K. Yarnada, K. Oguchi, G. Nakagawa, H. Sugie, C. Iida, Anal. Chim. Acta 256 (1992) 277.
[10] C. Bendicho, M. De Loos-Vollebrect, J. Anal. At. Spectrom. 6 (1991) 353.
[11] N. Miller-Ihli, Fresenius J. Anal. Chem. 345 (1993) 482.
[12] N. Miller-Ihli, Spectrochim. Acta 44 (Part B) (1989) 1221.
[13] N. Miller-Ihli, Fresenius J. Anal. Chem. 337 (1990) 271.
[14] L. Ebdon, H G.M. Perry, J. Anal. At. Spectrom. 3 (1988) 131.
[15] P. Viñas, N. Campillo, I. López-García, M. Hernández-Córdoba, Fresenius J. Anal. Chem. 349 (1994) 306.
[16] P. Viñas, N. Campillo, I. López-García, M. Hernández-Cordoba, Talanta 42 (1995) 527.
[17] P. Bermejo-Barrera, A. Moreda-Piñeiro, T. Romero-Barbeito, J. Moreda-Piñeiro, A. Bermejo-Barrera, Talanta 43 (1996) 1099.
[18] P. Bermejo-Barrera, A. Moreda-Piñeiro, T. Romero-Barbeito, J. Moreda-Piñeiro, A. Bermejo-Barrera, Clin. Chem. 42 (1996) 1287.
[19] P. Bermejo-Barrera, A. Moreda-Piñeiro, J. Moreda-Piñeiro, A. Bermejo-Barrera, J. Anal. At. Spectrom. 12 (1997) 301.
[20] P. Viñas, N. Campillo, I. López-García, M. Hernández-Cordoba, Food Chem. 50 (1994) 317.
[21] P. Viñas, N. Campillo, I. López-García, M. Hernández-Cordoba, Analyst 119 (1994) 1119.
[22] Report on the Second Research Co-ordination Meeting of IAEA, Neuherberg, 1985.
[23] N. Miller-Ihli, At. Spectrosc. 13 (1992) 1.
[24] M. Hoenig, P. Regnier, L. Chou, J. Anal. At. Spectrom. 6 (1991) 273.
[25] P.E. Gardiner, M. Stoeppler, H.W. Nurnberg, Analyst 110 (1985) 611.
[26] J.C. Miller, J.N. Miller, Statistics for Analytical Chemistry, ch. 3, Wiley, New York, 1984.
[27] G.V. Iyengar, Element analysis of biological systems, in: Biomedical, Environmental, Compositional, and Methodological Aspects of Trace Elements, vol. 1, ch. 8, CRC Press, Boca Raton, FL, 1989.

ELSEVIER

Talanta 45 (1998) 1155–1165

Talanta

Fluorescence quenching of anthropogenic fulvic acids by Cu(II), Fe(III) and UO_2^{2+}

Joaquim C.G. Esteves da Silva, Adélio A.S.C. Machado *, César J.S. Oliveira, Marta S.S.D.S. Pinto

LAQUIPAI, Faculdade de Ciências, R. Campo Alegre 687, P4150 Porto, Portugal

Received 30 July 1996; received in revised form 14 July 1997; accepted 15 July 1997

Abstract

The quenching of the fluorescence of three anthropogenic fulvic acids (FA) provoked by Cu(II) (pH 6.0), Fe(III) (pH 4.0) and UO_2^{2+} (pH 3.5), was analyzed by a non-linear method and by Stern-Volmer plots. The FA samples were extracted from composted sewage sludges (csFA), composted municipal wastes (mwFA) and composted livestock wastes (lsFA). Synchronous-scan fluorescence (SyF) spectra were collected as a function of metal ion concentration. Spectral data were treated by a self-modeling mixture analysis method (SIMPLISMA) to detect the SyF spectral band with the strongest quenching and to calculate the corresponding quenching profile. The analysis of these profiles by a non-linear method allowed the estimation of conditional stability constants (K) and of the percentage of non-complexing fluorophores. The same quantitative information was obtained by the modified Stern-Volmer equation taking into account the existence of fluorophores that do not participate in the complexation. Good agreement was found between the results of the two procedures. The log K calculated by the non-linear method were (standard deviation in parenthesis): csFA, Cu(II), 4.22 (5); Fe(III), 5.0 (1); UO_2^{2+}, 5.2 (2); mwFA, Cu(II), 4.21 (3); Fe(III), 5.6 (2); UO_2^{2+}, 4.7 (3); lsFA, Cu(II), 4.51 (8); Fe(III), 5.5 (2); UO_2^{2+}, 3.6 (2). © 1998 Elsevier Science B.V.

Keywords: Anthropogenic fulvic acids; Fluorescence quenching; Cu(II); Fe(III); UO_2^{2+}; Complexation; Stability constants

1. Introduction

The quenching of the intrinsic fluorescence of humic substances (HS) by paramagnetic metal ions is a well known phenomenon that has often been used for acquiring qualitative and quantitative information on the effect of these substances on the environmental fate of metal ions [1–19]. The sensitivity, non-destructivity and simplicity of molecular fluorescence make it a suitable technique for the analysis of the interactions between HS and metal ions that cause quenching. However, several factors may affect the quantitative interpretation of quenching interactions. These include: (i) the quenching may result from the formation of stable non-fluorescence complexes between the fluorescent binding sites of HS and

* Corresponding author. Tel.: +351 2 6082874; fax: +351 2 6082959.

PII S0039-9140(97)00224-5

the metal ions (static quenching), or from collisional quenching; (ii) due to the intrinsic chemical heterogeneity of HS (different chemical structures and/or similar chemical structures in different chemical environments) only part of their fluorescent structures in their molecules complex metal ions; (iii) the HS macromolecules contain different moieties with different physico-chemical properties (for example, with respect to charge accumulation and hydrophobicity) and this may affect the macroscopic fluorescence of FA.

Since its introduction in 1982, the method of Ryan and Weber [2,3] has been often used for the macroscopic interpretation of the quenching of HS fluorescence by metal ions. This method assumes that the quenching is only due to the formation of 1:1 stoichiometry complexes. Although the method was tested with simple fluorescent ligands with well defined structure [2,12] and its results were shown to be compatible with those from other techniques [2], its validity has been questioned [6,10,17,18]. Considering the complexity of the chemical nature of HS and of the effects of metal complexation on their fluorescence, it is desirable to devise alternative procedures for the analysis of the quenching which allow mutual assessment of results. This is the background idea underlying the present work.

This paper describes a study of the quenching of fluorescence by Cu(II), Fe(III) and UO_2^{2+} of three fulvic acids (FA) of anthropogenic origin. These three metal ions were selected because of their relatively high quenching efficiencies [2,3,5,13,15–20] and their interest in environmental studies. FA are the most soluble fraction of HS and therefore are thought to have a special role in the environmental mobility of metal ions. The characterization of anthropogenic FA and of their association with metal ions deserves at present much attention, due to the increasing practice of recycling organic wastes [21–25]. The present samples were extracted from composted sewage sludges (csFA), composted municipal wastes (mwFA) and composted livestock wastes (lsFA).

The experimental methodology of the work was based on the use of the synchronous-scan excitation mode of molecular fluorescence (SyF) to follow the quenching in the FA spectra upon addition of metal ions. One of the advantages of the quenching technique for the study of the interaction of FA with metal ions is the direct monitorization of the ligand status. This advantage cannot be achieved by methods that involve electrochemical and separation techniques to measure the free metal concentration. In the case of complex substances like FA, the use of direct information about the ligand status is more robust than that of indirect information, because in this case the experimental data usually can fit different models. The spectral data were preprocessed by a self-modeling mixture analysis method, i.e. SIMPLISMA [26,27], to detect the SyF spectral range or, more precisely, the wavelength where the strongest relative quenching occurs. The use of self-modeling mixture analysis methods in the preprocessing of SyF spectral data proved to be a useful tool to obtain intensity fluorescence profiles in previous studies [15–18,20,28–32].

The objectives of the work were: (i) to characterize the effect of the metal ions on the fluorescence properties of anthropogenic FA at pH values where there occurs no extensive hydrolysis [pH 6.0 for Cu(II) and 3.5 for UO_2^{2+}] or formation of insoluble hydrolysis products [4.0 for Fe(III)] which could affect the fluorescence measurements due to colloid formation; (ii) to obtain quantitative information about the association of the anthropogenic FA with metal ions from the analysis of the quenching profiles by the method of Ryan and Weber [2,3] (here called the non-linear method); (iii) to analyze the quenching profiles by graphical methods (Stern-Volmer plots [33–35]) to compare results and to obtain further information about the observed steady-state quenching.

2. Theory

The procedure used in this work and other similar procedures were developed by our group [15–17,20,28–32] for the study of the acid-base and metal complexation of HS. The present procedure is based on the collection of two-dimen-

sional sets of spectral data and their treatment by self-modeling chemometric techniques to find the number of types of binding sites and to obtain separate spectral data on the main ones. Therefore, the chemical heterogeneity of the HS [36–38] is partially reduced by the chemometric calculations. However, in practice, due to the complexity of humic ligands, the resolution is not absolute and conditional stability constants are obtained.

The complexation reaction between the main binding sites of FA (represented by L) and a metal ion (M) can be represented by (charges omitted)

$$M + L \leftrightarrow ML \tag{1}$$

and the corresponding average conditional equilibrium constant (K) at a constant pH is given by

$$K = [ML]/([L][M]) \tag{2}$$

If the ligands L are fluorescent and have similar SyF properties, the fraction of free ligand (α) can be calculated from the measurements of the initial fluorescence of the ligand solution without (I_0) and with (I) metal ion present (for dilute solutions, the fluorescence intensity is proportional to the analyte concentration)

$$\alpha = (I - I_{ML})/(I_0 - I_{ML}) \tag{3}$$

where I_{ML} is the lower limit of fluorescence intensity due to the fluorescence of the complex [ML] or fluorophores that do not participate in the complexation reaction.

According to Ryan and Weber [2,3], the following relationship between the fluorescence intensity (I) and the total metal ion concentration (C_M) is obtained

$$\begin{aligned} I = {} & [I_{ML} - 100/(2KC_L)] \\ & \{(KC_L + KC_M + 1) \\ & - [(KC_L + KC_M + 1)^2 - 4K^2C_LC_M]^{1/2}\} + 100 \end{aligned} \tag{4}$$

where C_L is the total ligand concentration. This equation can be solved for K, C_L and I_{ML} by nonlinear regression analysis. The quality of its adjustment to the quenching profiles is assessed by the analysis of two error functions, the sum of the squares of the residuals (SSR) and the average deviation (AD),

$$SSR = \Sigma(I_{exp} - I_{cal})^2 \tag{5a}$$

$$AD = (\Sigma\,|I_{exp} - I_{cal}|)/N_p \tag{5b}$$

where the summations are over the total number of points used in the calculations (N_p), I_{exp} is the experimental fluorescence intensity and I_{cal} the calculated fluorescence intensity.

As stable complexes between the binding sites of FA and the paramagnetic metal ions are expected, the observed decrease of fluorescence as a function of the metal ion concentration is primarily due to static quenching. If only the ligand contributes to I_o ($I_{ML} = 0$), the following Stern-Volmer law can be obtained by combining Eq. (2) and Eq. (3) [33]

$$I_0/I = 1 + K[M] \tag{6}$$

The representation of I_0/I as a function of [M] (total concentration of metal ion not complexed with L) allows an estimation of K (the previously defined conditional stability constant or static quenching constant) from the slope of the plot, if a straight line is obtained. However, only C_M is known experimentally and its use instead of [M] in Eq. (6) requires that $C_M \cong [M]$. This condition can only be fulfilled for values of C_M enough higher than the total ligand concentration and/or for relatively low K.

An upward curvature of the Stern-Volmer plot may suggest the existence of collisional besides static quenching [33]. A modification of Eq. (6) to account for the existence of both quenching mechanisms originates [33,34]

$$(I_0/I - 1)/[M] = (K_d + K) + K_dK[M] \tag{7}$$

where K_d is the constant for collisional quenching. From the plot of $(I_0/I - 1)/[M]$ versus [M], both static and collisional quenching constants can be estimated [26,27].

The existence in the FA molecules of fluorophores that have no metal ion complexation properties, but make a constant contribution to the overall quenching profiles, provokes deviations from linearity of Eq. (6)) towards the x-axis. If f is the fraction of the initial fluorescence that corresponds to the binding fluorophores, the following equation can be obtained [33,35]

$$I_0/\Delta I = 1/(fK[M]) + 1/f \quad (8)$$

where $\Delta I = I_0 - I$. If the plot of $I_0/\Delta I$ versus $1/[M]$ is linear, K and f can be estimated ($1/(fK)$ = slope; $1/f$ = intercept).

The parameter f of Eq. (8) gives information similar to that provided by the parameter I_{ML} of Eq. (4), although the two equations are derived by different approaches. Indeed, as the maximum initial fluorescence is adjusted to 100 fluorescence units in the non-linear method, I_{ML} gives the percentage of fluorophores that do not participate in the complexation, and the following relationship between f (expressed as percentage) and I_{ML} must hold

$$I_{ML} = 100 - f \quad (9)$$

3. Experimental

3.1. Reagents

The three samples of composted solid wastes are commercialized under the names Agronat (Câmara Municipal da Maia, Maia), Fertor (Lipor, Porto) and Guano Sansão (Húmica, Setúbal). The raw materials from which these composts derive are sewage sludge, municipal solid wastes and livestock waste (mixed with vegetable residues), respectively.

FA were isolated by a procedure recommended by the International Humic Substances Society (IHSS) for the extraction of these materials from soils [39]. Briefly, this procedure consists of the acidification of the raw materials to pH 1 with hydrogen chloride, followed by adsorption of the organic solute by XAD-8 resin in a column, elution with sodium hydroxide, acidification with a cation exchanger in the acid form and freeze-drying.

About 120 mg l^{-1} FA solutions were prepared in 0.1 mol l^{-1} potassium nitrate. A solution of decarbonated potassium hydroxide was used to adjust the pH to a constant value: Cu(II), pH 6.0; Fe(III), pH 4.0; UO_2^{2+}, pH 3.5. Standard Cu(II), Fe(III) and UO_2^{2+} solutions prepared from the corresponding nitrates were used as titrants. The range of metal ion concentration covered in the titrations were: all samples of FA + Cu(II)—between 0 and 0.4 mmol l^{-1}; all samples of FA + Fe(III)—between 0 and 0.07 mmol l^{-1}; csFA + UO_2^{2+}—between 0 and 0.07 mmol l^{-1}; mwFA + UO_2^{2+} and lsFA + UO_2^{2+}—between 0 and 0.2 mmol l^{-1}.

3.2. Equipment

Potentiometric measurements were made as described previously [15–17]. The experiments were carried out under nitrogen at 25.0 ± 0.2°C. The potentiometric cell was calibrated with two buffer solutions (pH_1 6.784 and pH_2 3.883) with the ionic strength adjusted to 0.1 M.

SyF measurements were made with a Perkin-Elmer (Norwalk, CT, USA) LS-50 luminescence spectrometer with a flow cell. A peristaltic pump forced the displacement of the titrated solution into the flow cell. SyF spectra were recorded with excitation between 250–550 nm, with the following settings: 7.5 nm excitation and emission slit width; wavelength difference between the excitation and emission monochromators of 25 nm; scan rate of 200 nm min^{-1}; the spectra were digitized at every 0.5 nm throughout the spectral range. Because the objective was to measure the spectral variations provoked by the metal ions, and not any qualitative comparison of them, no correction was made on the raw spectra

3.3. Data analysis

After the subtraction of the background spectrum (solution of 0.1 M potassium nitrate), spectral data were stored on disk, converted to ASCII format with LAB CALC software (Galactic Industries Co. USA) and reduced to a version with 5 nm resolution to be used in the calculations. SIMPLISMA was implemented as described by Windig et al. [26,27] and, for the present application, in [16,28]. Equilibrium parameters calculations by the non-linear method were described in [16,17].

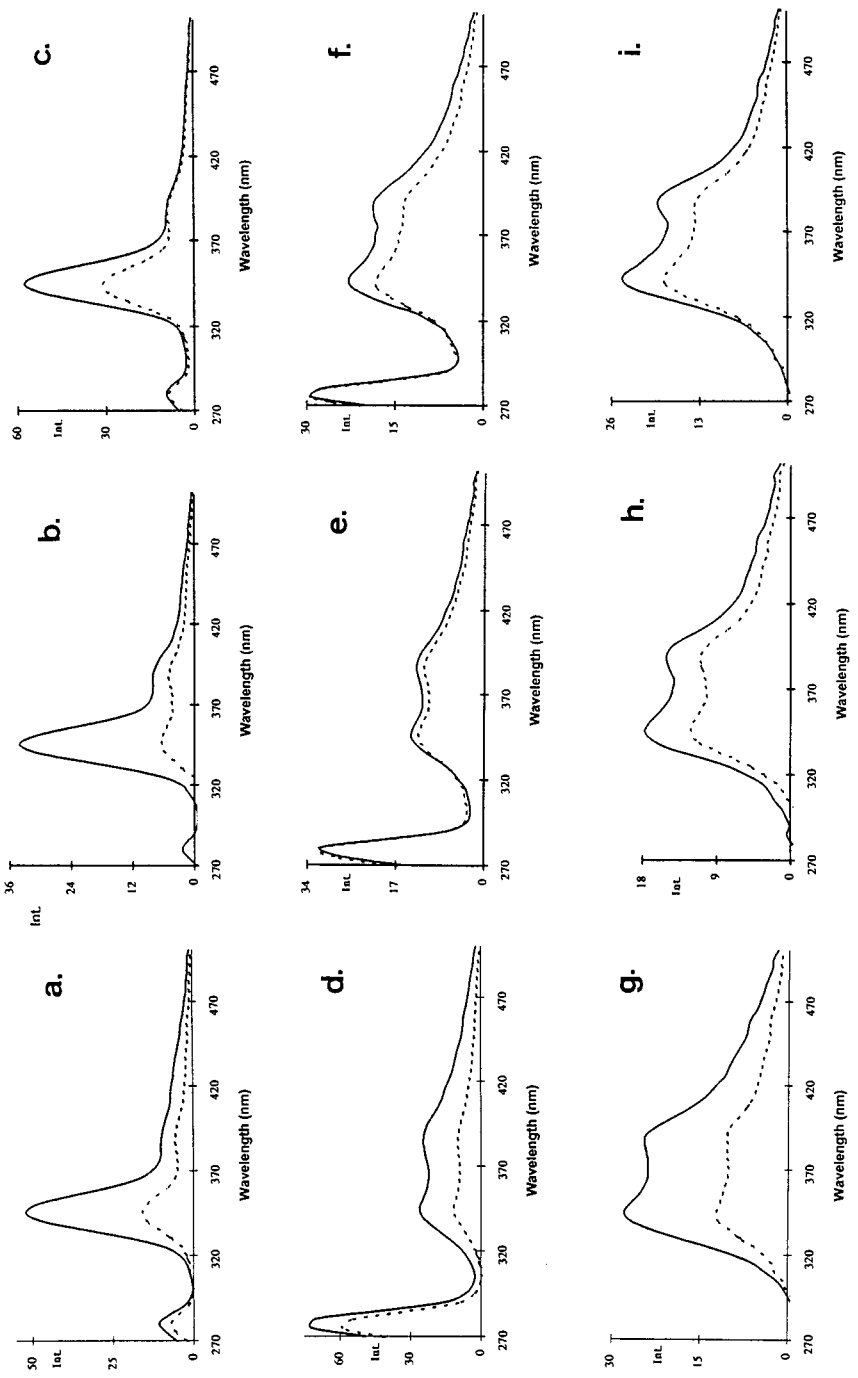

Fig. 1. Synchronous-scan fluorescence spectra of (a, b, c) csFA, (d, e, f) mwFA and (g, h, i) lsFA in the absence (full line spectra) and in the presence (dot line spectra) of excess of (a, d, g) Cu(II) (pH 6.0), (b, e, h) Fe(III) (pH 4.0) and (c, f, i) UO_2^{2+} (pH 3.5).

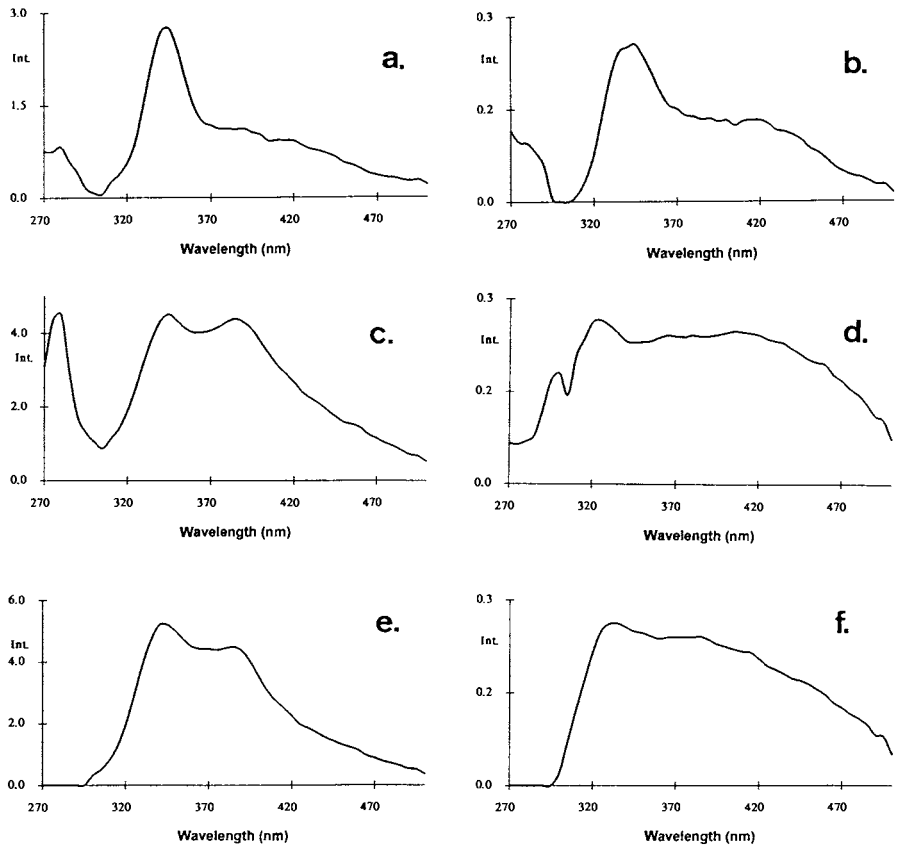

Fig. 2. Standard deviation (a, c, e) and purity (b, d, f) spectra corresponding to the Cu(II) experiments with (a, b) csFA, (c, d) mwFA and (e, f) lsFA.

4. Results and discussion

4.1. Selection of the wavelength to monitor the quenching

Fig. 1 shows the SyF spectra of the three anthropogenic FA in the absence and in the presence of Cu(II) (pH 6.0), Fe(III) (pH 4.0) or UO_2^{2+} (pH 3.5). The shapes of the SyF spectra of the three samples are quite different. Indeed, the SyF spectra of csFA and mwFA have well defined and relatively strong bands at about 350 and 280 nm, respectively, while that of lsFA is characterized by two partially overlapping bands centered at about 250 and 290 nm. These SyF spectral singularities of the FA extracted from the three composted materials suggest differences in the fluorescent structures and reveal the fingerprinting potential of the SyF spectroscopy for this type of compounds as recently discussed [40].

A detailed analysis of the 320–420 nm wavelength range of the spectra in Fig. 1 shows that the bands present in the lsFA sample (350 and 390 nm) occur also in the other two samples but with different relative intensities. This reveals the existence of common fluorescent structural units in the three FA samples, although in different proportions.

Fig. 1 shows quenching of the fluorescence in the whole spectrum or in some bands of the SyF spectra by all the three metal ions. For the csFA sample, the main SyF band at 350 nm is the most quenched. For the mwFA and lsFA samples, the strongest quenching occurs also in the 320–420

nm range, whereas the band at 280 nm of the mwFA sample is not affected.

SIMPLISMA provides a suitable criterion to identify the band with the strongest quenching. Indeed, its first step is the selection of the wavelength with the strongest relative variation, which is made upon analysis of the standard deviation (S.D.) and purity spectra [16,29–31]. Fig. 2 shows typical S.D. and purity spectra for the experiments with Cu(II).

The S.D. spectra (Fig. 2a, c, e) are approximately similar to the raw spectra (Fig. 1a, d, g) except for mwFA. This similarity shows that the quenching is proportional to the intensity of the bands. For mwFA, the three bands that constitute the S.D. spectrum have equal intensities, while in the original SyF spectrum the band at 280 nm is much more intense than the others. These differences arise because the quenching is mainly observed in the 320–420 nm range, which shows a relatively high S.D., while it is weaker for the 280 nm band, and consequently its S.D. is relatively small. The purity spectra (Fig. 2b, d, f), which are the ratio of the S.D. to the average spectra, confirm this effect, showing that the relative quenching is approximately constant in the 320–420 nm range for the three samples, with a slight maximum between 320–350 nm. Indeed, the purity spectra are characterized by a very broad band which extends from about 300 nm to 450 nm. Owing to these characteristics of the S.D. and purity spectra, and because all the raw spectra have a SyF band located at 350 nm, this wavelength was chosen to monitor the quenching of fluorescence in all experiments. As the quenching was always detected in the same wavelength range, at about 350 nm, the nature of the fluorescent binding sites is suggested to be similar in the three samples.

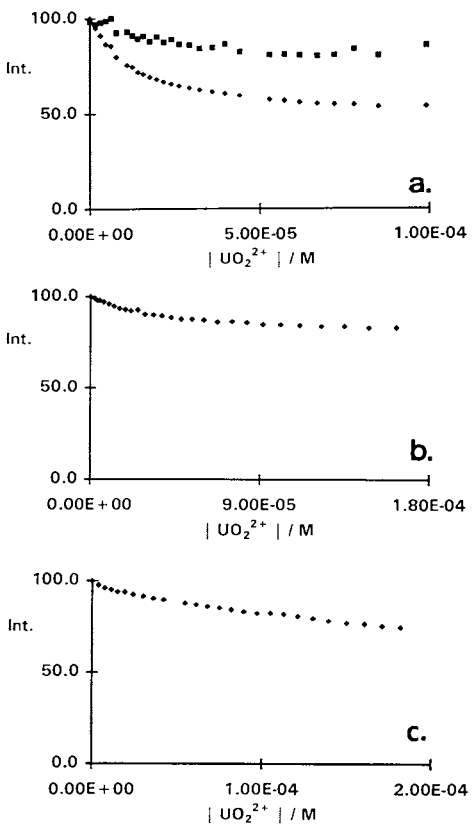

Fig. 3. Typical quenching profiles for the experiments of (a) csFA, (b) mwFA and (c) lsFA with UO_2^{2+}.

After the selection of the wavelengths where different quenchings were detected, the quenching profiles were obtained. As example, those for the UO_2^{2+} ion are shown in Fig. 3. To proceed to the analysis of the quenching profiles, they were scaled to a maximum intensity of 100.

4.2. Analysis of the quenching by the non-linear method

Table 1 shows the results obtained by non-linear adjustment of the quenching profiles to Eq. (4) to calculate K, C_L and I_{ML}. The values of the SSR and AD functions show that the quality of the adjustment was good, particularly because the AD is always less than 1.

The analysis of the logarithm of the calculated conditional stability constants [log K] shows that for Cu(II) and Fe(III), the stability of the complexes is almost independent of the FA sample, ranging from 4.2 to 4.5 and 5.0 to 5.6, respectively. For UO_2^{2+} different log K values were obtained for the three FA samples, ranging from about 5.0, for the csFA, to about 3.7 for the lsFA (mwFA has an intermediate value of about 4.7). This result may be due to two factors: (i) at pH 3.5 the complexation equilibrium is disturbed by

Table 1
Equilibrium parameters calculated by the non-linear analysis

Sample	N_e	Log K	C_L	I_{ML}	N_p	SSR	AD	Δ|M|
Cu(II) (pH 6.0)								
csFA	4	4.22 (5)	*	20 (1)	16	1.6	0.2	0.05–0.3
mwFA	3	4.21 (3)	*	38 (5)	18	3.2	0.4	0.003–0.3
lsFA	3	4.51 (8)	0.042 (6)	33 (5)	21	2.4	0.2	0.003–0.3
Fe(III) (pH 4.0)								
csFA	3	5.0 (1)	*	16 (8)	16	1.6	0.8	0.001–0.05
mwFA	4	5.6 (2)	0.021 (2)	87 (3)	15	4.4	0.5	0.001–0.04
lsFA	3	5.5 (2)	0.018 (9)	75 (8)	22	5.6	0.4	0.001–0.05
UO_2^{2+} (pH 3.5)								
csFA	5	5.2 (2)	*	53 (7)	17	2.1	0.3	0.003–0.04
mwFA	3	4.7 (3)	*	82 (2)	25	2.6	0.3	0.01–0.2
lsFA	2	3.6 (2)	*	37 (11)	18	6.3	0.5	0.02–0.2

N_e, number of independent experiments used in calculations; Log K, logarithm of the conditional stability constant; C_L, concentration of the ligand (mmol l^{-1}); I_{ML}, fluorescence intensity due to the bound ligand; N_p, number of points used in calculations; SSR, sum of squares of residuals; AD, average deviation of the estimates; Δ|M|, concentration range used in calculations (mmol l^{-1}).
Average and standard deviations in brackets for Log K, C_L and I_{ML}, and typical values for the other parameters.
* No reasonable values were obtained, but fixed concentration values between 10^{-9} and 10^{-3} mol l^{-1} showed no influence on the other calculated parameters.

the protonation of the binding sites; (ii) the UO_2^{2+} ion has complex photochemical properties [41], which may affect the quenching due to complex formation. The comparison of the values of log K shows that Fe(III) forms a complex more stable than Cu(II), although this comparison is limited because values of pH are different. This higher stability of the Fe(III) complex is similar to that observed for simple ligands with the same type of binding sites as FA, like salicylic acid and catechol [42,43].

Only a few C_L values could be obtained from the analysis of the quenching profiles, namely for the lsFA sample with Cu(II) [0.042 (8) mM] and with Fe(III) [0.018 (9) mM] and for the mwFA sample with Fe(III) [0.021 (2) mM]. This problem, i.e. the relatively high imprecision on the estimated C_L value, is a limitation of the non-linear method, particularly when the concentration of the binding sites and/or the conditional stability constants are relatively low [16,17,20]. However, even when C_L is fixed to markedly different values, both the values of log K and I_{ML}, and the quality of the final overall adjustment, are not affected.

A relatively high variability is observed in the I_{ML} values, which were usually higher for UO_2^{2+} and Fe(III) than for Cu(II) for all FA samples. This may be a consequence of the reduction of the background fluorescence due to non binding structures when the pH is raised and, probably, to the different quenching efficiencies of the three metal ions. Moreover, the decreasing trend in I_{ML} values,

$$\text{mwFA} > \text{lsFA} > \text{csFA}$$

observed independently of the metal ion, corresponds to a decrease on the amount of non-binding fluorescence structures.

A brief comparison of the log K and I_{ML} results with those obtained for soil FA samples by a similar experimental and data analysis procedure [16,17,20], showed that: (i) for Cu(II) and UO_2^{2+} the log K calculated for the anthropogenic and soil FA samples are of similar magnitude; and (ii) an higher percentage of fluorescent structures with non-binding ability for metal ions occurs in the anthropogenic FA.

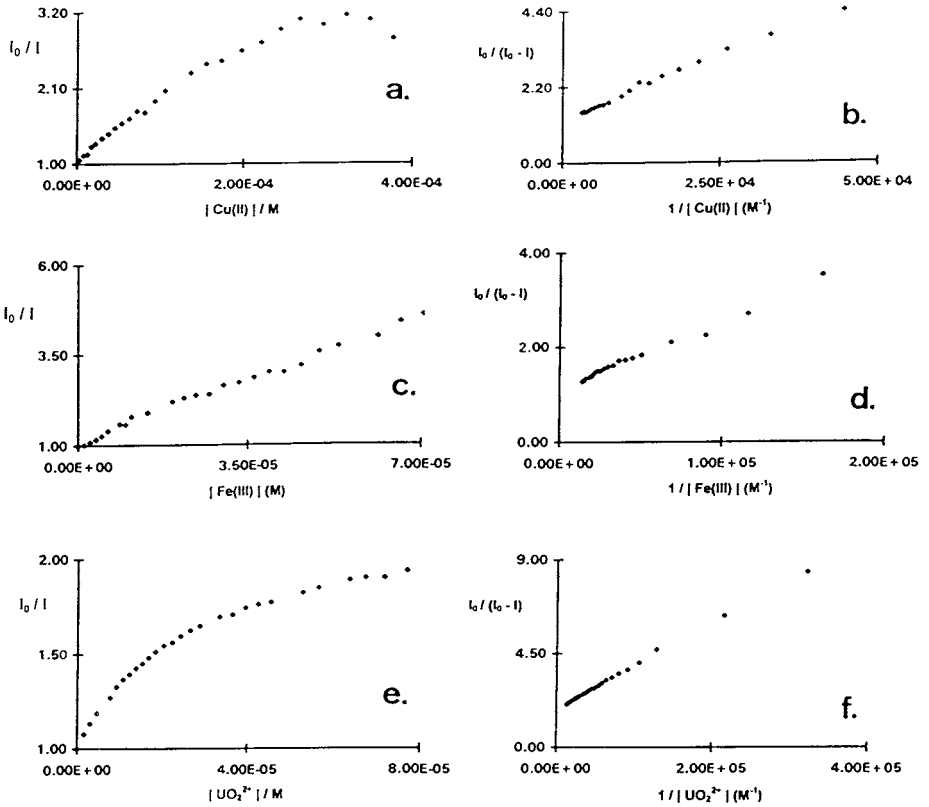

Fig. 4. Typical Stern-Volmer plots for the experiments with csFA and (a, b) Cu(II), (c, d) Fe(III) and (e, f) UO_2^{2+}: (a, c, e) original Stern-Volmer plots; and (b, d, f) modified Stern-Volmer plots.

4.3. Analysis of the quenching by Stern-Volmer plots

The Stern-Volmer plots Eq. (6) of the quenching profiles have all similar shapes (Fig. 3). These representation are approximately linear for the lower concentration range of metal ion, but progressively deviate towards the x-axis, in a more or less marked way, at higher concentrations. Fig. 4a, c, e show typical Stern-Volmer plots for the csFA sample and the three metal ions.

As discussed in the theory section, the deviations towards the x-axis suggest the existence of a contribution to the quenching of fluorophores that do not participate in the complexation reaction, because either they are not accessible for complexation or have no structural complexing properties. When data are treated by the modified Stern-Volmer equation that accommodates this type of deviation Eq. (8) (Fig. 4b, d, f show the plots that correspond to Fig. 4a, c, e, respectively), linear plots were obtained for the Cu(II) and UO_2^{2+} quenching data. For the case of Fe(III), the linear correlation was poorer, which may be due to two factors: (i) an experimental disturbance of the acquisition of the fluorescence intensity signal owing to, for instance, the precipitation of Fe(III) oxo-hydroxide colloids and their interaction with FA; (ii) an oversimplification of the model used. The quantitative information obtained from these plots is shown in Table 2.

4.4. Comparison of the two methods

The comparison of the values of f [or rather $(100-f)$ in Table 2; Eq. (9)] with those of I_{ML}

Table 2
Equilibrium parameters calculated by the modified Stern-Volmer equation[a]

Sample	N_e	Log K	f	$(100-f)$	N_p	R	$\Delta\|M\|$
Cu(II) (pH 6.0)							
csFA	4	4.32 (1)	76 (2)	24	20	0.9992	0.03–0.3
mwFA	2	4.22 (3)	61 (6)	39	19	0.9995	0.02–0.4
lsFA	3	4.21 (2)	67 (8)	33	13	0.9989	0.03–0.3
Fe(III) (pH 4.0)							
csFA	3	4.87 (7)	90 (2)	10	25	0.9969	0.001–0.07
mwFA	3	4.66 (3)	22 (3)	78	10	0.9922	0.006–0.02
lsFA	2	4.5 (1)	34 (8)	66	19	0.9980	0.002–0.05
UO_2^{2+} (pH 3.5)							
csFA	5	5.1 (2)	50 (10)	50	21	0.9995	0.003–0.08
mwFA	3	4.4 (1)	21 (1)	79	14	0.9982	0.01–0.15
lsFA	3	3.8 (3)	41 (13)	59	18	0.9956	0.02–0.2

[a] See footnote to Table 1. f, fraction of the initial fluorescence that corresponds to binding sites (expressed as percentage); R, correlation coefficient. Average and standard deviations in brackets for Log K and f, and typical values for the other parameters.

(Table 1) shows that they are similar, as well as the log K calculated by the two methods for Cu(II) and UO_2^{2+}. The modified Stern-Volmer estimated smaller log K values than the non-linear method for the case of Fe(III)—the larger deviations are observed for the mwFA and lsFA samples [about one log K unit]. As discussed previously, these two FA samples have higher percentage of fluorescent structures that do not participate in the metal ion complexation. A possible explanation for the observed deviation is that a fraction of the fluorescence due to these structures is deactivated by collisional quenching and the interpretation of the measured quenching profiles as only static quenching results in its overestimation.

The overall agreement observed between the results obtained by the non linear method and by the Stern-Volmer plots supports that the quenching provoked by Cu(II), Fe(III) or UO_2^{2+} is mainly static, due to the formation of 1:1 complexes, and that the three FA samples have all a relatively high percentage of fluorophores that do not participate in the complexation reaction.

5. Conclusions

This work showed that the Cu(II), Fe(III) and UO_2^{2+} provoke marked quenching of the fluorescence of anthropogenic FA samples extracted from composted materials (sewage sludges and municipal and livestock wastes). The results suggest that the three FA contain qualitatively similar fluorophores that interact with the metal ions.

The results of the non-linear method of Ryan and Weber and of the modified Stern-Volmer plots were quantitatively similar, suggesting that the simple 1:1 complexation model is a valid approximation for the FA under study. Both methods of quenching profile analysis provided close values for the conditional stability constants and the percentage of fluorescent binding sites accessible for the complexation of the metal ions.

Acknowledgements

An MSc grant (to CJSO) is acknowledged to the Project PRAXIS XXI. A PBIC C QUI 2177 95 project grant is acknowledged to JNICT (Lisbon). The samples were obtained in research under contract 30/96 with DGQA. W. Windig, Eastman Kodak Company, New York (USA), is acknowledged for providing a copy of the SIMPLISMA package.

References

[1] R.A. Saar, J.H. Weber, Anal. Chem. 52 (1980) 2095.
[2] D.K. Ryan, J.H. Weber, Anal. Chem. 54 (1982) 986.
[3] D.K. Ryan, J.H. Weber, Environ. Sci. Technol. 16 (1982) 866.
[4] D.K. Ryan, C.P. Thompson, J.H. Weber, Can. J. Chem. 61 (1983) 1505.
[5] T.D. Waite, F.M.M. Morel, Anal. Chim. Acta 162 (1984) 263.
[6] F.H. Frimmel, W. Hopp, F. Z. Anal. Chem. 352 (1986) 68.
[7] S.E. Cabaniss, M.S. Shuman, Anal. Chem. 58 (1986) 398.
[8] P. Blaser, G. Sposito, Soil Sci. Soc. Am. J. 51 (1987) 612.
[9] G. Sposito, N. Senesi, K.M. Holtzclaw, Soil Sci. Soc. Am. J. 52 (1988) 632.
[10] W. Shotyk, G. Sposito, Soil Sci. Soc. Am. J. 52 (1988) 1293.
[11] S.E. Cabaniss, M.S. Shuman, Anal. Chem. 60 (1988) 2418.
[12] N. Senesi, Anal. Chim. Acta 232 (1990) 77.
[13] L.S. Ventry, D.K. Ryan, T.R. Gilbert, Microchem. J. 44 (1991) 201.
[14] S.E. Cabaniss, Environ. Sci. Technol. 26 (1992) 1133.
[15] A.A.S.C. Machado, J.C.G. Esteves da Silva, Chemom. Intell. Lab. Syst. 19 (1993) 155.
[16] A.A.S.C. Machado, J.C.G. Esteves da Silva, J.A.C. Maia, Anal. Chim. Acta 292 (1994) 121.
[17] J.C.G. Esteves da Silva, A.A.S.C. Machado, Chemom. Intell. Lab. Syst. 27 (1995) 115.
[18] R.L. Cook, C.H. Langford, Anal. Chem. 67 (1995) 174.
[19] J. Luster, T. LLoyd, G. Sposito, Environ. Sci. Technol. 30 (1996) 1565.
[20] J.C.G. Esteves da Silva, A.A.S.C. Machado, C.J.S. Oliveira, Analyst 121 (1996) 1373.
[21] G. Sposito, K.N. Holtzclaw, J. Baham, Soil Sci. Soc. Am. J. 40 (1976) 691.
[22] G. Sposito, K.N. Holtzclaw, C.S. LeVesque-Madore, Soil Sci. Soc. Am. J. 43 (1979) 1148.
[23] N. Senesi, D.F. Bocian, G. Sposito, Soil Sci. Soc. Am. J. 49 (1985) 119.
[24] N. Senesi, G. Sposito, K.N. Holtzclaw, G.R. Bradford, J.Environ. Qual. 18 (1989) 186.
[25] P.L. Giusquiani, G. Gigliotti, D. Businelli, J. Environ. Qual. 21 (1992) 330.
[26] W. Windig, J. Guilment, Anal. Chem. 63 (1991) 1425.
[27] W. Windig, C.E. Heckler, F.A. Agblevor, R.J. Evans, Chemom. Intell. Lab. Syst. 14 (1992) 195.
[28] J.C.G. Esteves da Silva, A.A.S.C. Machado, Talanta 41 (1994) 2095.
[29] C.S.P.C.O. Silva, J.C.G. Esteves da Silva, A.A.S.C. Machado, Appl. Spectrosc. 48 (1994) 363.
[30] J.C.G. Esteves da Silva, A.A.S.C. Machado, T.M.O. Garcia, Appl. Spectrosc. 49 (1995) 1500.
[31] J.C.G. Esteves da Silva, A.A.S.C. Machado, Appl. Spectrosc. 50 (1996) 436.
[32] J.C.G. Esteves da Silva, A.A.S.C. Machado, M. Angeles Ramos, F. Arce, F. Rey, Environ. Sci. Technol. 30 (1996) 3155.
[33] J.R. Lakowicz, Principles of Fluorescence Spectroscopy, ch. 9, Plenum Press, New York, 1983.
[34] E.R. Carraway, J.N. Demas, B.A. DeGraff, Anal. Chem. 63 (1991) 332.
[35] S.S. Leher, Biochemistry 10 (1971) 3254.
[36] J. Buffle, Complexation Reactions in Aquatic Systems: An Analytical Approach, ch. 5, 6, Ellis Horwood, Chichester, 1988.
[37] J.C.M. de Vit, W.H. van Riemsdijk, M.M. Nederlof, D.G. Kinniburgh, L.K. Koopal, Anal. Chim. Acta 232 (1990) 189.
[38] D.G. Kinniburgh, C.J. Milne, M.F. Benedetti, J.P. Pinheiro, J. Filius, L.K. Koopal, W.H. van Riemsdijk, Environ. Sci. Technol. 30 (1996) 1687.
[39] E.M. Thurman (Rapporteur), Isolation of soil and aquatic humic substances (Group Report), in: F.H. Frimmel, R.F. Christman (Eds.), Humic Substances and their Role in the Environment, Wiley-Interscience, New York, 1988, pp. 31–43.
[40] N. Senesi, T.M. Miano, M.R. Provenzano, Fluorescence spectroscopy as a mean of distinguishing fulvic and humic acids from dissolved and sedimentary aquatic sources and terrestrial sources, in: B. Allerd, H. Bóren, A. Grimvall (Eds.), Humic Substances in the Aquatic and Terrestral Environment, Springer-Verlag, New York, 1991, pp. 63–73.
[41] S.F. Formosinho, M.G.M. Miguel, J. Chem. Soc. Faraday Trans. 80 (1984) 1717.
[42] L.G. Sillen, A.E. Martell, Stability Constants, The Chemical Society, London, 1965.
[43] L.G. Sillen, A.E. Martell, Stability Constants: Suppl. 1, The Chemical Society, London, 1971.

ELSEVIER

Talanta 45 (1998) 1167–1175

Talanta

Determination of arsenic(III) and arsenic(V) by electrothermal atomic absorption spectrometry after complexation and sorption on a C-18 bonded silica column

Dirce Pozebon, Valderi L. Dressler, José A. Gomes Neto [1], Adilson J. Curtius *

Departamento de Química, Universidade Federal de Santa Catarina (UFSC), Campus Universitário Trindade, 88040-900 Florianópolis, Brazil

Received 29 April 1997; received in revised form 14 July 1997; accepted 16 July 1997

Abstract

A flow injection procedure for the separation and pre-concentration of inorganic arsenic based on the complexation with ammonium diethyl dithiophosphate (DDTP) and sorption on a C-18 bonded silica gel minicolumn is proposed. During the sample injection by a time-based fashion, the As^{3+}-DDTP complex is stripped from the solution and retained in the column. Arsenic(V) and other ions that do not form complexes are discarded. After reduction to the trivalent state by using potassium iodide plus ascorbic acid, total arsenic is determined by electrothermal atomic absorption spectrometry (ETAAS). Arsenic(V) concentration can be calculated by difference. After processing 6 ml sample volume, the As^{3+}-DDTP complexes were eluted directly into the autosampler cup (120 μl). Ethanol was used for column rinsing. Influence of pH, reagent concentration, pre-concentration and elution time and column size were investigated. When 30 μl of eluate plus 10 μl of 0.1% (w/v) $Pd(NO_3)_2$ were dispensed into the graphite tube, analytical curve in the 0.3–3 μg As l^{-1} range was obtained ($r = 0.9991$). The accuracy was checked for arsenic determination in a certified water, spiked tap water and synthetic mixtures of arsenite and arsenate. Good recoveries (97–108%) of spiked samples were found. Results are precise (RSD 7.5 and 6% for 0.5 and 2.5 μg l^{-1}, $n = 10$) and in agreement with the certified value of reference material at 95% confidence level. © 1998 Elsevier Science B.V.

Keywords: Arsenic; C-18 bonded silica; Diethyl dithiophosphate; Flow injection analysis; Electrothermal atomic absorption spectrometry

1. Introduction

Accurate determination of arsenic in environmental, biological and food samples is of importance due to the toxicity of this heavy metal and its related compounds [1,2]. The deleterious effects of arsenic in humans depends on the ingested or inhaled species. Regarding inorganic arsenic,

* Corresponding author. Fax: + 55 48 2319711.

[1] On leave from the Departamento de Química Analítica, Instituto de Química, Universidade Estadual Paulista, Araraquara, SP, Brazil.

PII S0039-9140(97)00234-8

trivalent species are considered to be more toxic [3,4] and generally are found at ultra-trace levels. In this context, the development of methods for separation and pre-concentration of arsenic are necessary.

Several hyphenated techniques have been used for these purposes [5–9]. For example, ion-exchange chromatography has been used for separating different arsenic compounds. In a subsequent step, atomic absorption spectrometry [5], atomic fluorescence spectrometry [6], hydride generation [7], inductively coupled plasma mass spectrometry [8] or emission spectrometry [9] are usually used as detection techniques.

Reactions involving complexating agents such as dithiocarbamates (DTC) and dithiophosphates (DTP) are simple and alternative ways to perform separations of different oxidation states of arsenic [10–12]. Spectrophotometric methods exploiting these ligands are based on the extraction of As(III), complexed with DTP or DTC, from aqueous medium to an organic phase [11,13] or by sorption on solid supports [10]. While DTC reagents are very unstable in acidic media [14], DTP's are unique being highly stable in these media [11,14]. This is a very important advantage of the use of DTP's as complexing agents, since the media resulting from sample preservation and/or dissolution are usually acidic.

With regards to liquid–liquid extraction, trivalent arsenic in fresh and sea water was determined after metal complexation with ammonium *sec*-buthyl dithiophosphate and extraction with hexane. The arsenic content in the organic phase was determined by ETAAS [12]. Diethyl dithiocarbamate was also used to determine arsenic in water and slurry of marine sediment: after extraction of the metallic complex with methyl isobuthyl ketone or sorption on a C-18 reversed-phase column, arsenic present in the extracts or in the eluate was determined by electrothermal atomic absorption spectrometry [10,13]. Although diethyl dithiophosphate (DDTP) has good selectivity and remarkable stability in acidic medium for several metals at different oxidation states, little attention has been given to its reactions concerning the development of spectrometric procedures for preconcentration of arsenic.

In this work, the reaction between arsenic and DDTP and sorption of the metallic complex on a C-18 bonded silica gel minicolumn is proposed for determination of inorganic arsenic. The on-line separation or pre-concentration step was carried out in a flow-injection system. The performance of the proposed procedure was checked after analysis of natural waters and standard reference material by ETAAS.

2. Experimental

2.1. Reagents, analytical solutions and samples

All solutions were prepared with analytical grade chemicals. The water was distilled and deionized employing a Milli-Q system (Millipore). Argon (White Martins, Brazil) was 99.996% purity and the ammonium diethyl dithiophosphate (Aldrich) was used without further purification. The ethanol used as washing solution was purchased at the local market and purified using active coal.

The autosampler washing solution was 0.1% (v/v) of Triton X-100 in 0.2% (v/v) Suprapur nitric acid (Merck).

A 1.0% (w/v) ammonium diethyl dithiophosphate solution was prepared weekly by dissolving 1.0 g DDTP in ≈ 5 ml of ethanol and diluting up to 100 ml with water. This solution was kept in a refrigerator.

Arsenic(III) stock standard solution (1000 mg l^{-1}) was prepared by dissolving 0.1320 g As_2O_3 (Merck) in 2.0 ml of 1.0 mol l^{-1} NaOH [12]. To this solution 5 ml of 0.5 mol l^{-1} HCl were added and the volume was completed to 100 ml with water. Arsenic(V) stock standard solution (1000 mg l^{-1}) was prepared by diluting the Merck Titrisol ampoule with water.

The trivalent arsenic analytical solutions (0.3–3 μg l^{-1}) were prepared daily by appropriate dilution of stock in 5% (v/v) Suprapur HCl (Merck) and 0.1% (w/v) DDTP in the presence of 500 mg of ascorbic acid and 500 mg KI. Analytical solutions without reducing agents were also made up.

The pentavalent arsenic analytical solutions (0.3–3 μg l^{-1}) were prepared daily by adding

arsenic solution, 5 ml concentrated HCl, 500 mg of ascorbic acid and 500 mg KI and dissolved in ≈ 50 ml water. After 30 min, 10 ml of 1% (w/v) DDTP solution was added and the volume was made up to 100 ml with water. Analytical solutions without reducing agents were also prepared.

A 0.1% (w/v) chemical modifier solution was prepared diluting palladium stock solution (10 g l^{-1}, Merck) in water.

The sorbent minicolumn was built up by packing C-18 bonded silica gel (Waters Division of Millipore, Part. No. 51910, 50–100 μm) into a 10 × 3 mm i.d. Tygon tube. Plugs of polyurethane foam were placed at both ends of the packed column in order to avoid sorbent losses during system operation.

Tap water was collected at the Chemistry Department of Santa Catarina Federal University. This water was used without previous treatment. The standard reference material from the National Institute of Standards and Technology (SRM 1643d) with a certified value for total arsenic was used. This water was diluted 1:25 before the separation procedure.

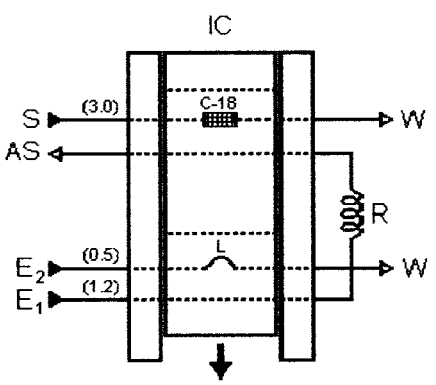

Fig. 1. Flow diagram of the system for arsenic determination. IC, injector-commutator; S, sample; E_1, water; E_2, ethanol; W, waste; L, ethanol sampling loop (150 μl); C-18, minicolumn; AS, autosampler cup; R, homogenization coil (25 cm, i.d. = 0.7 mm) Numbers in brackets equal flow rates in ml min^{-1}. Arrows to the right show the directions of the solution flows. The arrow downwards indicates the movement of the central part of the injector-commutator.

2.2. The flow system

The flow system depicted in Fig. 1 employed a peristaltic pump, Model B332II, from Micronal (São Paulo, Brazil), furnished with Tygon pumping tubes, a homemade injector-commutator (IC) electronically operated, polyethylene tubing (i.d. 0.7 mm) and accessories.

The system operation comprises two steps: preconcentration in the position specified in Fig. 1 and elution in the next position. Samples or the analytical solutions (S) flowed through the sorbent minicolumn (C-18) where the As^{3+}-DDTP complex is retained. Pentavalent arsenic and others potential interferents, if present, pass through the column and are discharged (W). When the injector-commutator is switched, the minicolumn is inserted into the eluant E_1 which, in reverse flow, washes the column and displaces the arsenic ions. It should be stressed that in this position the first 13 s of eluate are discharged. Only the fraction volume between 14 and 21 s is collected into the autosampler cup for further measurements. The ethanol volume (E_2; pumped by gravity) selected by loop L, is inserted into the E_1 carrier stream in order to leach the free ligand from the minicolumn. When the injector-commutator was switched back to the position specified in Fig. 1, another cycle started. In this way, determination of arsenic was always performed off-line.

2.3. Procedure

The system in Fig. 1 was used to study the main parameters related to the minicolumn operation. Influence of acidity, acid composition, ligand and reducing reagents concentrations, sorbent column size, flow rates of sample and eluant, timing and ethanol loop length were studied.

Arsenic complexation was investigated by varying ligand concentration [0.01–1.0% (w/v) DDTP], the nature and concentration of acid [0.10–10% (v/v) HNO_3 or HCl] and the interaction time between arsenic and DDTP in the 1–120 min time interval.

The concentration of the reducing mixture (potassium iodide plus ascorbic acid, 1 + 1, w/w) was investigated in the 0.1–5% (w/v) interval. For

each particular concentration, the solution was prepared in 0.012–1.2 mol l^{-1} HCl and different reduction times (1–60 min) were tested.

Influence of column loading time was studied within 30 and 600 s. Different column length (5–20 mm, i.d. = 3 mm) were tested. Elution conditions were investigated by changing the flow rate of E_1 (0.5–3.0 ml min^{-1}), the loop length of ethanol (25–100 cm) and eluant composition.

The analytical measurements at the spectrometer were optimized by varying the amount of chemical modifier (Pd: 0–15 μg; Mg: 0–30 μg), sample volume (10–30 μl), order of addition of the modifier and atomization and pyrolysis temperatures.

2.4. Instrumentation

A Perkin-Elmer 3110 atomic absorption spectrometer equipped with an AS-60 autosampler, an HGA-600 graphite furnace atomizer, pyrolytic graphite coated graphite tubes (Perkin-Elmer Part No. B0109 322) with pyrolytic graphite L'vov platforms (Perkin-Elmer Part No. B0109 324) were used. The monochromator was adjusted to 193.7 nm and the slit-width to low 0.7 nm. Atomic signal was measured in peak area mode. An arsenic hollow cathode lamp (Hitachi) was used at a current of 14 mA. The measurements were carried out using the stabilized temperature platform furnace (STPF) conditions [15], which minimizes the interferences in the vapor phase. These conditions included the use of tubes with platforms, internal gas stop during atomization, integrated absorbance, chemical modifier and background correction (with a deuterium arc lamp).

3. Results and discussion

3.1. Optimization of the furnace conditions

All measurements were initially performed according to the manufacturers' conditions and a preliminary furnace temperature program (1200°C for the pyrolysis and 2300°C for the atomization) for 20 μl of 50.0 μg As^{3+} l^{-1} analytical solution and addition of Pd (10 μg) was tested. When Pd was not added, arsenic loss for pyrolysis temperatures higher than 200°C was observed.

High background signals were observed (Fig. 2) when arsenic analytical solutions were processed in the flow system due to impurities in the ligand solutions. The contamination from DDTP was eliminated by passing the DDTP solutions through a 50 × 5 mm C-18 column. In order to minimize these background levels, higher pyrolysis temperature combined with the addition of chemical modifiers was also necessary.

The influence of the palladium on the background level and atomic signal was of utmost relevance. Addition of a 0.1% (m/v) $Pd(NO_3)_2$ solution, allowed the extension of the pyrolysis temperature up to 1400°C with notable background level reduction without losses of arsenic (Fig. 3). The atomic signals enhanced by ≈40% when Pd injected volume varied from 5 to 10 μl; for aliquots larger than 10 μl, the signals were not improved. The volume of modifier was then elected as 10 μl.

Besides the addition of palladium, the presence of magnesium was also investigated. Since magnesium nitrate increased the background level without enhancing the atomic signals, only Pd was used as chemical modifier. It is important to comment that the autosampler pipette became brownish-colored probably due to the adsorption of metallic palladium or Pd-DDTP complexes, increasing the background levels and measurement instability. This drawback was circumvented by injecting both modifier and sample solutions in separated steps, according to the temperature program developed for this study (Table 1). Pd(II) has high tendency to be reduced to the metallic state in the presence of DDTP because this ligand is a powerful reducing agent for some ions. With that procedure, higher sample volume could be injected into the graphite tube. For higher sensitivity, 30 μl of eluate was selected.

3.2. Optimization of the FIA system

The flow system depicted in Fig. 1 was designed to obtain high sensitivity since low levels of arsenic have usually been found in natural waters.

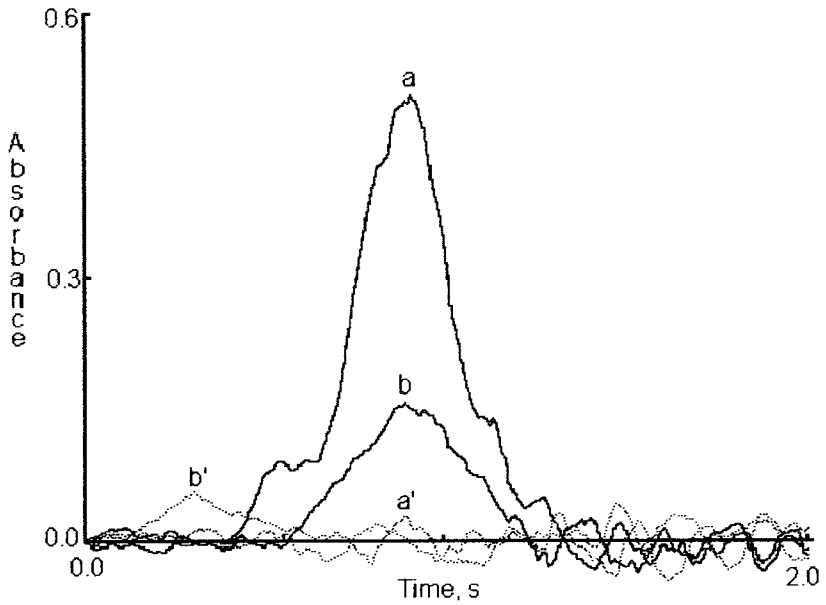

Fig. 2. Influence of palladium on the background and atomic pulses. after processing the solution in the flow system. Initial arsenic concentration: 2.00 μg As l^{-1} (b) Without modifier (pyrolysis temperature of 200°C) and (a) with modifier (pyrolysis temperature of 1400°C); (- - -) Background signal, (—) atomic signal. Eluate collection in the 14–21 s interval and 120 s preconcentration time.

The first experiments were carried out by setting 120 s pre-concentration time and the arsenic (III) analytical solutions were prepared in 0.1% (w/v) DDTP.

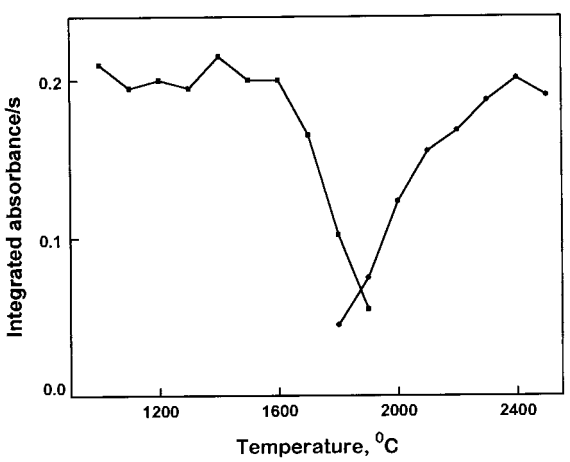

Fig. 3. Pyrolysis and atomization temperature curves after reduction and preconcentration. Initial arsenic concentration: 2.00 μg l^{-1}.

The nature and concentration of the acid have an important role in the complexation efficiency. Oxidizing acids, e.g. nitric and sulfuric acid, must be avoided since arsenic may be converted to the pentavalent state. Since these species are not complexed by DDTP, they are not retained in the minicolumn. To maintain the original As(III)/As(V) concentration ratio in the samples, the complexation step was carried out with hydrochloric acid. The complex formation is dependent on the HCl concentration (Fig. 4). The atomic signals were in the blank level for acid concentrations lower than 0.01% HCl (v/v). Without reducing agents (Curve a of Fig. 4), the signals increase up to 0.5% HCl (v/v). Higher acid concentrations, apparently do not change the signals. According to Bode and Arnswald [11], the complex composition is $As(DDTP)_3$. An excess of ligand is used in order to promote the formation of the complex. The signal obtained with 0.05% (w/v) DDTP is 80% lower than that obtained with 0.5% (w/v). Higher DDTP concentrations were not investigated due to difficulties in the solubi-

Table 1
Temperature programme for the arsenic determination[a]

Step	Temperature (°C)	Ramp (s)	Hold (s)	Flow rate (ml min^{-1})
1	90	10	15	300
2	200	20	10	300
3	1400	15	15	300
4[b]	2400	0	4	0
5	2650	3	8	300
6	20	1	8	300

[a] Conditions of pipetting sequence and running program: (I) Pipetting modifier; (II) Run step one to two; (III) Extra wash; (IV) Pipetting sample; and (V) Run step one to end.
[b] Read in this step.

lization of the ligand. Further experiments were then conducted with samples or analytical solutions prepared in 0.1% (w/v) DDTP.

As the complex formation between As(III) and DDTP was only slightly affected by the reaction time, samples could be processed in the FIA system, immediately after ligand addition and solution homogenization.

The hydrochloric acid, potassium iodide plus ascorbic acid concentrations and reduction time were important parameters to be considered at the reduction step. Preliminary tests were carried out using 0.5% (w/v) KI, 0.5% (w/v) ascorbic acid and 60 min as the reducing time. The acid concentration was varied in the 0.01–10% (v/v) range. As higher signals were obtained for 5% (v/v) or higher HCl concentration (Fig. 4, Curve b), this one was elected for further experiments. A flow rate of water through the minicolumn was adequate to remove the majority of the remaining chloride ions before the arsenic elution. In order to define the amount of reducing agent, when potassium iodide plus ascorbic acid (1 + 1, w/w) concentration was increased up to 5% (w/v), better signal was observed for 3% (w/v), the concentration selected in this work (Fig. 5a). The reducing time was studied and the best condition was attained at 30 min (Fig. 5b). It should be stressed that this waiting time was extremely long for on-line reduction in the flow system. As the decisive query was the analytical demonstration for arsenic determination at trace levels after complexation with DDTP and sorption on a C-18

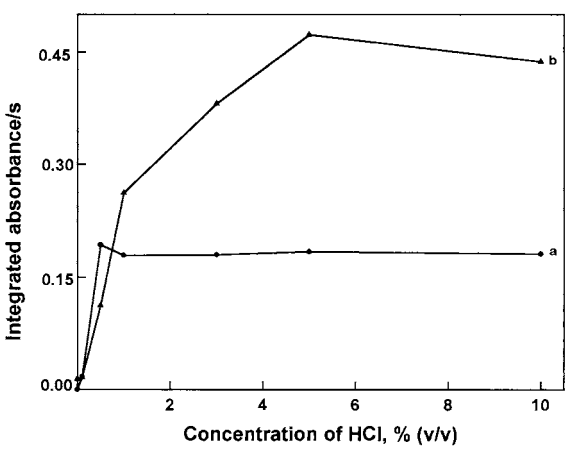

Fig. 4. Influence of HCl concentration on reduction and complexation of As(V). (a) 1.00 μg l^{-1} As^{3+} analytical solution in 0.1% (w/v) DDTP without reducing agents; (b) 2.50 μg l^{-1} As^{5+} analytical solution in 0.1% (w/v) DDTP plus 0.5% (w/v) KI and 0.5% (w/v) ascorbic acid. Reaction time: 30 min.

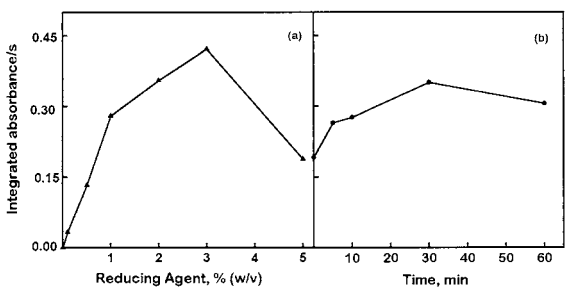

Fig. 5. Influence of KI-ascorbic acid addition (a) and reduction time (b) on As(V). The analytical solution was 2.00 μg l^{-1} As^{5+} in 0.1% (w/v) DDTP and 5% (v/v) HCl. The reduction time studies were carried out with 2.5% (w/v) KI and 2.5% (w/v) ascorbic acid.

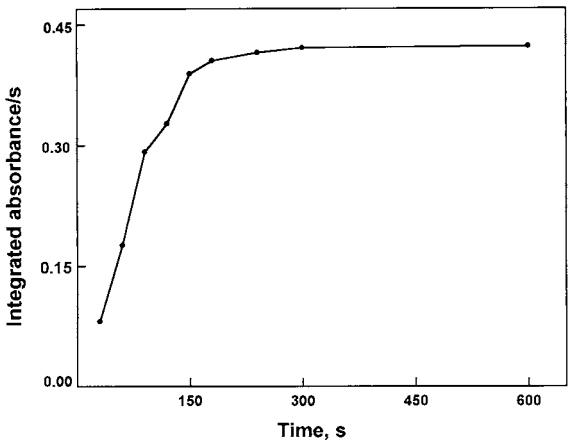

Fig. 6. Influence of the column loading time on the arsenic signal. Pre-concentration of 2.50 μg l^{-1} As^{3+} initial analytical solution in 0.1% (w/v) DDTP plus 5% (w/v) HCl.

column, the reduction was then carried out off-line.

The minicolumn length cannot be increased at will because high hydrodynamic pressure may cause leakage of the flowing solutions. In fact, for the flow rates selected in this work, when the column was longer than 20 mm, leakage of the sample and eluate solutions was observed. Columns shorter than 10 mm length were not tested due to the distance between the two connecting points located at the main part of the injector-commutator. As a compromise between sorption capacities and hydrodynamic pressure, a column of 10×3 mm was chosen.

Commutation time is a relevant parameter since it is related to both pre-concentration and washing steps. The signal increased steeply up to 150 s, but for longer times was almost independent of the commutation time due to the breakthrough of the column (Fig. 6). Good sensitivity was attained for times higher than 300 s, but the loading efficiency was poor and fewer samples could be processed per hour. A time of 120 s was set, since the choice was sensitivity, preconcentration efficiency and sample processing frequency. In this situation, a enrichment factor of ≈ 30 times was obtained.

Flow rates of S and E_1 are important parameters since they determine the sensitivity, hydrodynamic pressure, elution efficiency, sample consumption and column washing. Although higher analytical signals were observed with sample flow rates higher than 3.0 ml min^{-1}, solution leakage at the inlet of the column was observed. On the other hand, when flow rates were lower than 1.0 ml min^{-1}, the analytical signals decreased about 82% of those obtained at 3.0 ml min^{-1}. As a compromise between system stability, sensitivity and time, a flow rate of 3.0 ml min^{-1} was then selected. When E_1 flow rate was lower than 0.5 ml min^{-1}, both elution and washing time were too long. A good elution and column rinsing, were achieved for 1.2 ml min^{-1}; the flow rate selected for further experiments. In order to avoid problems related to the analyte transportation through the minicolumn, elution in a reverse flow was adopted. Considering that the As-DDTP complex was eluted with water, a second eluant was used as a guarantee to wash out the adsorbed ligand. A 30 cm long ethanol loop (150 μl) was inserted into the water carrier stream (Fig. 1). With the injector-commutator in the elution position, the eluate fraction collected between 14 and 21 s showed the highest arsenic concentration (Fig. 7) and was the time interval selected for subsequent measurements. An additional time of 50 s was necessary to permit the

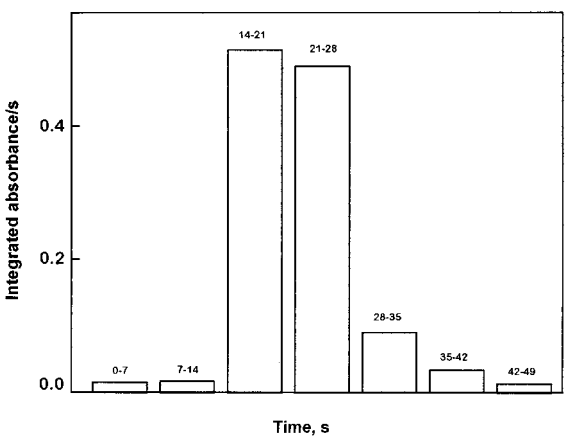

Fig. 7. Influence of time collection on eluate fraction. Numbers above the bars correspond to the time interval for collecting 3.00 μg l^{-1} As^{3+} initial analytical solution in 0.1% (w/v) DDTP plus 5% (w/v) HCl. The time the injector-commutator is switched to the elution position corresponds to $t = 0$.

Table 2
Results for arsenic in spiked tap water and in a certified water ($n = 3$)

Sample	Spiked (μg l^{-1})		Found (μg l^{-1})		Certified value (μg l^{-1})
	As(III)	As(V)	As(III)	As(V)	
1	2.00	0.50	2.05 ± 0.13	0.46 ± 0.05	—
2	0.50	2.00	0.56 ± 0.04	2.20 ± 0.14	—
3	0.00	2.50	0.00 ± 0.06	2.43 ± 0.13	—
SRM	—	—	12.11 ± 1.33	41.11 ± 2.45	56.02 ± 0.73

passage of the ethanol plug through the mini-column before starting another preconcentration cycle. It should be pointed out that, variations in E_1 flow rates can change the collected fraction. In fact, if the time interval for eluate collection was taken outside the 14–28 s range, a drastic reduction of the atomic signals can occur. As the ternary complex is unstable in pH higher than 5, a flow of water inside the column during the elution step was necessary to destroy the complex and elute the analyte. To avoid problems arising from the peristaltic pump fluctuations, it is a good practice to monitor the pH at the outlet column as an indicator of the time to select the optimum eluate fraction.

3.3. Arsenic determination

After system optimization, the applicability and accuracy of the proposed procedure for arsenic determination were investigated in three spiked tap water samples and one certified reference water. Each tap water sample was spiked with arsenic(III) and arsenic(V) to obtain two different [As(III)]/[As(V)] ratios. Good recoveries (97–108%) of spiked samples were found as shown in Table 2. Results are precise (RSD 7.5 and 6% for 0.5 and 2.5 μg l^{-1}, $n = 10$) and the total arsenic concentration is in agreement with the certified value of the reference material at 95% confidence level.

For a 120 s pre-concentration time and 30 μl of eluate volume, analytical curves in the 0.3–3 μg l^{-1} range were always attained with good linearity ($r = 0.9991$). In this situation, 20 samples could be processed per hour. The detection limit (3 s/a, where 's' is the S.D. of 10 measurements of the blank and 'a' is the slope of the analytical curve) was calculated as 0.15 μg l^{-1} for As(III). This proposal is a novel and rapid method for determining total arsenic and also inorganic arsenic species. Although the quoted limit of detection of 0.15 μg l^{-1} would be insufficient to determine As(III) in most reducing, or biologically-active waters, the sensitivity can be improved by appropriate selection of pre-concentration time or sample flow-rate.

In view of the relatively high amounts of reducing agents in the processed samples, it is a good practice to change the C-18 bonded silica after ≈ 200 pre-concentration cycles to avoid signal deterioration. The use of a mixture of sodium hydrogensulphite, sodium thiosulphate and potassium iodide, as a reducing agent, is an alternative to the mixture of KI and ascorbic acid, but the lifetime of the column was shorter (≈ 100 cycles) with the former.

In conclusion, this work presents an alternative procedure for the determination of total inorganic arsenic and inorganic arsenic species at trace levels in waters, after complexation with DDTP and on-line sorption on C-18 with good efficiency. In case organoarsenicals are present in the real sample, they should be extracted before the determination of the inorganic species by the proposed method.

Acknowledgements

The authors thank the FINEP (Financiadora de Estudos e Projetos) and CNPq (Conselho Nacional de Desenvolvimento Científico e Tecnológico) for financially supporting this work. The

authors thank also Marcia M. Silva for supplying the C-18 silica gel.

References

[1] G.F. Vandergrift, D.T. Reed, I.R. Tasker (Eds.), Environmental Remediation. Removing Organic and Metal Ion Pollutants. American Chemical Society, Washington, DC, 1992, 275 pp.
[2] J.K. Irgolic, A.E. Marttel, Environmental Inorganic Chemistry. VCH, New York, 1985, 654 pp.
[3] G.E. Batley, Trace Elements Speciation: Analytical Methods and Problems. CRC Press, Boca Raton, FL, 1989, 350 pp.
[4] A. Vercruyse (Ed.), Hazardous Metals in Human Toxicology. Elsevier, New York, 1984, 337 pp.
[5] B.S. Chana, J.N. Smith, Anal. Chim. Acta 197 (1987) 177.
[6] Á. Woller, Z. Mester, P. Fodor, J. Anal. At. Spectrom. 10 (1995) 609.
[7] S. Nielsen, J.J. Sloth, E.H. Hansen, Talanta 43 (1996) 867.
[8] J. Wang, M.J. Tomlinson, J.A. Caruso, J. Anal. At. Spectrom. 10 (1995) 601.
[9] J.M. Costa-Fernández, F. Junzer, R. Pereiro-García, A. Sanz-Medel, J. Anal. At. Spectrom., 10 (1995) 1019.
[10] M. Sperling, X. Yin, B. Welz, Spectrochim. Acta 46B (1991) 1798.
[11] H. Bode, W. Arnswald, Fresenius Z. Anal. Chem. 185 (1962) 179.
[12] D. Chakrabarti, W. De Jonghe, F. Adams, Anal. Chim. Acta. 120 (1980) 121.
[13] P. Bermejo-Barrera, M.C. Barciela-Alonso, M. Ferrón-Novais, A. Bermejo-Barrera, J. Anal. At. Spectrom. 10 (1995) 247.
[14] R. Ma, F. Adams, Spectrochim. Acta 1996 (1917) 51B.
[15] B. Welz, Atomic Absorption Spectrometry, 2nd ed., VCH, Weinheim, 1985, 506 pp.

ELSEVIER

Talanta 45 (1998) 1177–1188

Talanta

Potentiometric study of Cu(II) and Ni(II) complexation with two high molecular weight poly(acrylic acids)

Catherine Morlay *, Monique Cromer, Yolande Mouginot, Olivier Vittori

Laboratoire d'Electrochimie Analytique, Laboratoire d'Instrumentation et de Chimie Analytique en Solution, Université Claude Bernard Lyon 1, CPE, 43 Bvd du 11 novembre 1918, 69622 Villeurbanne Cedex, France

Received 3 December 1996; received in revised form 19 June 1997; accepted 17 July 1997

Abstract

The copper (II) or nickel (II) complex formation with two poly(acrylic acids) of high molecular weight ($Mw = 2.5 \times 10^5$ and 3×10^6) was investigated in aqueous dilute solution ($NaNO_3$ 0.1 mol l^{-1}; 25°C). Potentiometric titrations were carried out, first to precise the acid-base properties of the two polymers, and secondly to determine the stability constants of the MA and MA_2 complex species formed. The Bjerrum's method, modified by Gregor et al. (J. Phys. Chem., 59 (1955) 34–39), for the study of polymeric acids was used. The results obtained showed that both polymers present very similar properties. As expected, copper (II) is more readily bound to poly(acrylic acids). CuA_2 was the predominant observed species; the global stability constant $\log \beta_{102}$ was found to be close to 6.6. With nickel (II), none of the complex species MA or MA_2 becomes predominant ($\log \beta_{102} = 5.5$). Finally, the PAA complexes present a greater stability compared with that of monomeric analogs. © 1998 Elsevier Science B.V.

Keywords: High molecular weight poly(acrylic acids); Copper (II); Nickel (II); Complexation; Potentiometry

1. Introduction

Acrylic acid derivatives are involved in the elaboration of numerous products employed in a variety of domains. In particular, linear hydrosoluble poly(acrylic acids) (PAAs) of high molecular weight are used in the water treatment field (as flocculants, dispersants) and for sludge conditioning (as sludge thickeners). Furthermore, PAAs are commonly chosen as models to study the complexation by natural organic macromolecules such as humic substances for example [1–5].

Effluents or natural waters that contain or receive metal ions are generally very complex media. As a consequence, the fate and the elimination of metal ions present in these aqueous media at very low concentrations depend on the interactions existing between these metal ions and the other organic or inorganic substances also naturally present in the bulk water and/or introduced during a water treatment process; in particular, this is the case of the flocculants employed for the drinking water production or for the physicochemical treatment of wastewaters.

The aim of this study was to assess the capability of industrial flocculants used in the water

* Corresponding author. Fax: + 33 04 72448479.

PII S0039-9140(97)00229-4

treatment field to trap heavy metal ions present at low concentrations in water. This work deals with the metal binding properties of two high molecular weight hydrosoluble PAAs as they constitute the base of the elaboration of a variety of industrial flocculants.

Some previous work dealt with the complexation properties of PAAs [6–10]. However, the PAAs studied were not always fully described and, in particular, their molecular weight was not always mentioned. We chose to study commercial, well defined PAAs. One of the PAAs we considered has an average molecular weight comparable to those commonly studied in previous work ($Mw = 2.5 \times 10^5$) [6–10] whereas the second one has a very high molecular weight ($Mw = 3 \times 10^6$) and thus typically represents synthetic organic polymers used as cationic flocculants in the water treatment field.

Several studies have dealt with hydrosoluble PAAs and more especially with their metal binding properties in aqueous solution using potentiometric titrations [6–10]. However, almost all of these studies only considered copper (II) which is an interesting ion as it leads to electrochemically reversible systems. In this paper, the metal ions examined are copper (II) and nickel (II) cations. We chose to study PAAs complexation properties towards copper (II) to be able to compare our results with the largest literature data in that field of research; this validation of our experimental procedure and data treatment would then allow us to go forward with nickel (II) ion and discuss the results obtained. By contrast, very little attention has been paid to nickel (II) [7]. It is probably because nickel (II) leads to electrochemically irreversible systems. Nevertheless, the European Community, the USA-EPA (Environmental Protection Agency) and the World Health Organization have mentioned either maximal concentrations or guideline values for nickel in drinking water and that limits are much lower than those cited for copper.

The acid-base properties of the PAAs under study were examined because they directly influence the complexation behaviour of the polymers. Furthermore, it had to be done in exactly the same operational conditions than those later used for the complexation study.

This work was carried out in dilute aqueous solution using protometry as an investigation mean. In the present paper, we have chosen to preferentially present the curves obtained with the higher molecular weight PAA ($Mw = 3 \times 10^6$) and nickel (II), first because this metal ion has been less studied and secondly because our results differ from those previously reported in the literature [7].

2. Theoretical considerations

2.1. Ligand concentration

For polymer compounds, the first problem that arises is the definition of the ligand concentration. Indeed, the polymer nature of the compound makes the assignation of a definite molecular weight difficult and consequently a molar concentration has little significance. In the case of PAAs, carboxylic groups are the only functional groups present in the polymer structure and hence they are the reactive sites of the ligand. However, these carboxyl groups are expected to exhibit different acid strengths [1,11]. Thus, rather than a ligand concentration, we shall define the total (weak) titratable acidity content C_A expressed in eq l^{-1}. C_A corresponds to the total reactive site concentration of the polymer as used next for the complexation study.

2.2. Metal complexation

For a binary system involving only one metal ion M and one type of complexing sites which can be protonated (HA) or not (A), the general complexation equilibrium may be written as follow (electrical charges are omitted for simplification):

$$pM + qH + rA \rightleftarrows M_pH_qA_r \quad (1)$$

In this study, we chose to examine concentration ratios of complexing sites (carboxylate groups) to metal ions ($R = C_A/C_M$) in aqueous solution higher than unity; thus, the formation of mononuclear complexes (i.e. $p = 1$; simple binary system) was only considered and Eq. (1) may be simplified as:

$$M + qH + rA \rightleftarrows MH_qA_r \quad (2)$$

Equilibria in Eqs. (1) and (2) point out the existence of a possible competition between the protons and the metal ions for the complexing sites of the ligand. When metal ions are introduced in a solution containing the protonated ligand (HA), the complexation phenomenon may occur as:

$$M + HA \rightleftarrows MA + H \quad (3)$$

$$MA + HA \rightleftarrows MA_2 + H \quad (4)$$

$$MA_{r-1} + HA \rightleftarrows MA_r + H \quad (5)$$

and therefore a release of protons from the ligand is expected (q value other than null is not significant). The ability of a protonated ligand to complex metal ions thus not only depends on the stability constant of the resulting metal-ligand complexes but also depends on the dissociation constant of the ligand which is important to know with accuracy.

2.2.1. Acid-base properties of polymer compounds: determination of the ligand dissociation constant

The characterization of the acid-base behaviour of a polyelectrolyte is somewhat difficult as the acid strength of its functional groups (and thus its apparent dissociation constant K_A^H) varies with its degree of dissociation which depends on the pH of the medium [1,11,12]. During the alkali titration of the protonated polyelectrolyte (HA), its dissociation is characterized by an α_A coefficient calculated from the titration plots (volume of titrant; pH) according to a procedure derived from the Irving-Rossotti's method [13]:

$$\alpha_A = a/C_A = ([B] + h - oh)/C_A \quad (6)$$

with a: concentration of the dissociated form of the polymer functional groups A (in eq l^{-1}); [B]: concentration of the alkali solution once poured in the analysis cell; h: concentration of free protons; oh: concentration of free hydroxide ions (deduced from the ionic product of water).

The apparent dissociation constant of the ligand (K_A^H) is obtained at every pH value by Eq. (4):

$$K_A^H = a \cdot h/[HA] \quad (7)$$

with

$$[HA] = C_A - a = C_A \cdot (1 - \alpha_A) \quad (8)$$

The polymer weak acidity is then usually characterized by the features of the so-called extended Henderson-Hasselbalch equation [14]:

$$pH = pK_m^H + n \cdot \log(\alpha_A/(1 - \alpha_A)) \quad (9)$$

where pK_m^H is the apparent dissociation constant at half-dissociation ($\alpha_A = 0.5$) and n is an empirical constant representative of the important intramolecular electrostatic forces characteristic of a polyelectrolyte and which influence its protonic dissociation. The representation of the extended Henderson-Hasselbalch equation leads to the determination of pK_m^H and n.

2.2.2. Metal complexation by polymer compounds: determination of the stability constants of the metal–polymer complexes

During the alkali titration of the polyelectrolyte (HA) in the presence of metal ions (M), its dissociation is characterized by an α_M coefficient calculated from the titration plots:

$$\alpha_M = (a + \Sigma(r \cdot [MA_r]))/C_A = ([B] + h - oh)/C_A \quad (10)$$

where MA_r represents any metal-ligand complex formed.

The Bjerrum approach [15], modified by Gregor et al. [6] for the analysis of complexes formed with macromolecules, has been used; a competition reaction is supposed to take place between the metal ions and the protons for the reactive sites of the polymer. The expression of the successive complexation constants b_r (see Eq. (5)) is:

$$b_r = ([MA_r] \cdot h)/([MA_{r-1}] \cdot [HA]) \quad (11)$$

The average number of complexing sites bound to one metal ion (average coordination number), $\bar{r}$, is expressed as follows:

$$\bar{r} = (\Sigma\, r \cdot [MA_r])/C_M = (C_A - [HA] - a)/C_M \quad (12)$$

where C_M represents the total concentration of the metal ion and with:

$$[HA] = C_A \cdot (1 - \alpha_M) \quad (13)$$

and

$$a = K_A^H \cdot [HA]/h \quad (14)$$

K_A^H is the apparent dissociation constant of the ligand at the considered pH and is determined from the experimental values of pH and alkali volume. It is assumed that, at a fixed pH, the dissociation of the polyelectrolyte is the same in the presence as well as in the absence of metal ion (i.e. K_A^H unchanged; Eqs. (7) and (8)).

During the alkali titration of the ligand in the presence of metal ions, $\bar{r}$ can be calculated for every titration plot. The formation curve $\bar{r}$ versus $-\log([HA]/h)$ (or $p([HA]/h)$) allows the estimation of the successive complexation constants b_r at the half integral values of $\bar{r}$. The 'classical' successive complexation constants $K_r = [MA_r]/([MA_{r-1}] \cdot a)$ are then calculated using the general relation:

$$K_r = b_r/K_A^H \quad (15)$$

where K_A^H is considered at the pH of determination of $\log b_r$. As Gregor et al. [6] did, in the present work, we limited our investigations to the MA and MA_2 complexes. We can define a global stability constant β_{102} for the formation of the MA_2 species as:

$$\beta_{102} = K_1 \cdot K_2 \quad (16)$$

K_1 and K_2 being calculated from Eq. (15).

3. Experimental

3.1. Chemical and reagents

All the reagents were of analytical grade. PAA 2.5×10^5 or PAA 3×10^6 stock solutions (1 g l^{-1}) were prepared from commercial products (Aldrich, Germany) without further purification and stored in glass bottles at room temperature (≈ 20°C) in the dark and less than 15 days. Dilute solutions for analysis were prepared daily. Metal ion stock solutions (2×10^{-2} mol l^{-1}) were prepared from copper nitrate (Prolabo, France) and nickel nitrate (Fluka Chemika, Switzerland) and standardized using an EDTA disodium salt solution (Merck, Germany). The stock solution of supporting electrolyte, $NaNO_3$ (Fluka Chemika), was 1 mol l^{-1}. For potentiometric titrations, a 0.1 mol l^{-1} sodium hydroxide (Prolabo) solution was prepared and standardized with a 5×10^{-2} mol l^{-1} (weighted amount) potassium monohydrogenophthalate (Fluka Chemika) solution. Two pH buffers, pH 4.008 and 9.196, were prepared daily with potassium monohydrogenophthalate and sodium tetraborate decahydrate 0.05 mol l^{-1}, respectively (Fluka Chemika products). All the solutions were prepared with freshly distilled water.

3.2. Apparatus

Potentiometric analyses (protometric titrations) were carried out with a TT-Processeur 2 (Tacussel, France) automatic titrator equipped with an electronic burette (Tacussel, Model EBX3) and fitted with a glass combined electrode (Tacussel, Model XC 100; silver/silver chloride/solution of KCl + AgCl saturated in the two elements reference electrode). The electrode response is calibrated daily and checked after every titration using the two pH buffers. The processing software allows the automatic detection of inflexion points by the calculation of the titration derivative curve (dpH/dV). Titration data and curves were recorded using an Epson LX 800 printer.

3.3. Analytical procedure

All the samples were treated in exactly the same way. All the solutions to be analyzed contained $NaNO_3$ as supporting electrolyte at a 0.1 mol l^{-1} final concentration. The measurements were performed at 25.0 ± 0.1°C under a nitrogen atmosphere and with a 50 ml total volume of solution in the analysis cell. Oxygen was carefully removed from the samples containing PAA by an initial nitrogen bubbling of 20 min.

Samples containing known constant volumes of one of the two stock solutions of the studied PAAs were titrated with the carbonate-free 0.1 mol l^{-1} NaOH solution either in the absence or in the presence of metal ions Cu(II) or Ni(II). NaOH solutions were kept free of carbonate using a carbon dioxide trap containing NaOH beads and fitted on the flask cap. The stirring of the

samples was vigorous enough to ensure a rapid homogenization. Two or three different concentration ratios $R = C_A/C_M$ (C_A: total complexing site concentration, C_M: total metal ion concentration; $3.1 < R < 13.2$) were examined for each PAA with each metal ion. To avoid waiting too long and to be able to carry out the whole titration on a reasonable delay, we set a maximum waiting time (called 'maximum increment delay') of 120 s (the same for all experiments) between two additions of the sodium hydroxide solution when the stability criterion could not be respected (0.01 pH unit min^{-1}). The titration of PAA samples either in the absence or in the presence of metal ions then lasted 4–5 h. The operative conditions are listed in Table 1. Direct and derivative titration curves were recorded. The reproducibility of both copper (II) and nickel (II) complexation has been examined by multiple measurements. In order to determine the ionic product of water, the carbonate-free 0.1 mol l^{-1} NaOH solution was poured in 50 ml of the 0.1 mol l^{-1} $NaNO_3$ solution at 25°C and under a stream of nitrogen. The proton concentration was measured after each addition of the NaOH solution and the concentration of hydroxide ions was calculated. The ionic product of water calculated from the experimental data was found to be $pK_w = 13.83$.

4. Results and discussion

4.1. Acid-base properties of the studied PAAs

4.1.1. Ligand total concentration

Only one equivalence point, around pH 9.0–9.3, was detectable on the titration curves of the dilute PAA samples. The transformation of the titration curves to linear plots with the Gran function [16,17] later derived by McCallum and Midgley [18] revealed the presence of only one type of weak acidity for both PAA 2.5×10^5 and PAA 3×10^6. This method was also used to estimate the total acidity content of the stock solutions (C_{A0}) prepared for this study. For PAA 2.5×10^5 and PAA 3×10^6 stock solutions, the values were, respectively: $C_{A0} = 13.1$ meq l^{-1} and $C_{A0} = 12.7$ meq l^{-1}. In the following, C_A represents the actual complexing site total concentration in the analysis cell (i.e. taking into account the dilution of the stock solution).

Table 1
Operative conditions for the potentiometric study

Slope of the glass combination electrode	-58.3 ± 0.3 mV/pH
Volume increments	
Minimum	50 μl
Maximum	150 μl
Stability criterion	0.01 pH unit min^{-1}
or maximum increment delay	120 s
Inflexion detection	Incremental

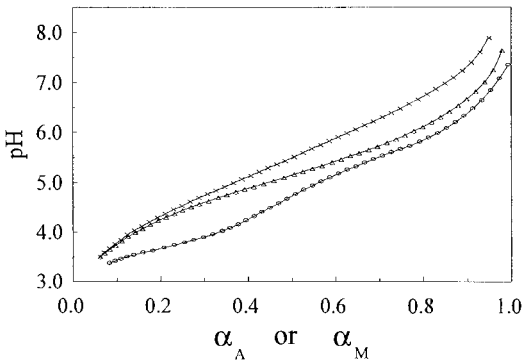

Fig. 1. Plot of pH versus the dissociation coefficient of PAA 3×10^6 in the absence (α_A; X) or in the presence (α_M) of metal ion (○, Cu(II); △, Ni(II)) for very close values of $R = C_A/C_M$ ($R = 6.1$ and 6.4, respectively; $C_A = 5.1$ meq l^{-1}).

4.1.2. PAA dissociation constant

Fig. 1 gives the variation of pH versus the dissociation coefficient α_A for PAA 3×10^6. Fig. 2 illustrates the variation of the apparent dissociation constant pK_A^H versus pH (pK_A^H was calculated for every titration plot using the relation $pK_A^H = pH - \log(\alpha_A/(1-\alpha_A))$; see Eq. (7)). As expected with a polyelectrolyte, the acid strength of the PAA carboxyl groups varies with pH.

The main problem of a theoretical interpretation of potentiometric titration curves of polyelectrolytes is the quantitative description of the

dependence of the apparent pK_A^H value on the degree of dissociation α_A. No linear variation of pK_A^H with α_A can be observed. According to Breuer [19], during the dissociation of PAA, the ionized carboxylic groups of the polyacid induce electrostatic attraction forces towards the protons. As a consequence, the deprotonation of a functional group depends on the degree of dissociation of all the other functional groups of the macromolecule and pK_A^H varies with α_A and thus with pH. As α_A increases, the protons remaining on the polyacid become less and less mobile, which leads to a continuous decrease in the acid strength of the polymer. This has been discussed for PAAs in different papers on the subject [1,11]. Furthermore, the pK_A^H value should also be affected by a conformational change due to intramolecular interactions [20]. Models have been proposed for the interpretation of the dissociation behaviour of poly(vinyl carboxylic acids) such as poly(acrylic acids) [21,22], but we did not consider this particular aspect in our present work.

The representation of pH versus $\log(\alpha_A/(1-\alpha_A))$ for PAA 3×10^6 (Fig. 3) shows that the extended Henderson-Hasselbalch equation is reasonably applicable for α_A in the 0.25–0.75 range (i.e. $\log(\alpha_A/(1-\alpha_A))$ in the -0.48 to $+0.48$ range), which corresponds to a pH range of 4.5–6.5 (Fig. 3). The values of pK_m^H (pK_A^H for $\alpha_A=0.5$; pK_m^H corresponds to the pH value read for $\log(\alpha_A/(1-\alpha_A))=0$ on Fig. 3) and n (slope of the linear portion of the curve, determined by least square regression) can be estimated from this curve: $pK_m^H=5.50$ and $n=2.05$. Very similar results were obtained with PAA 2.5×10^5 ($pK_m^H=5.42$ and $n=2.07$). The error on the pK_A^H, pK_m^H and n values was estimated by titrating twice the same stock solution of PAA. This error was estimated to be ±0.01 for pK_A^H and pK_m^H values and ±0.01 for n value.

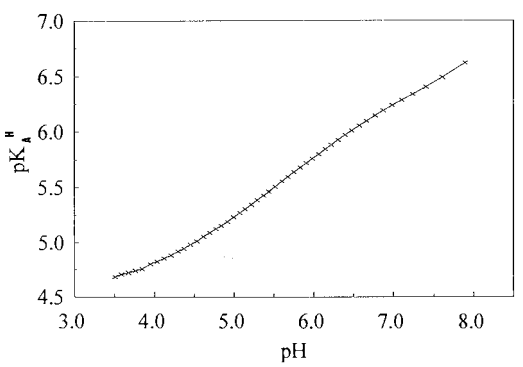

Fig. 2. Variation of pK_A^H versus pH for PAA 3×10^6 ($C_A=5.1$ meq l^{-1}).

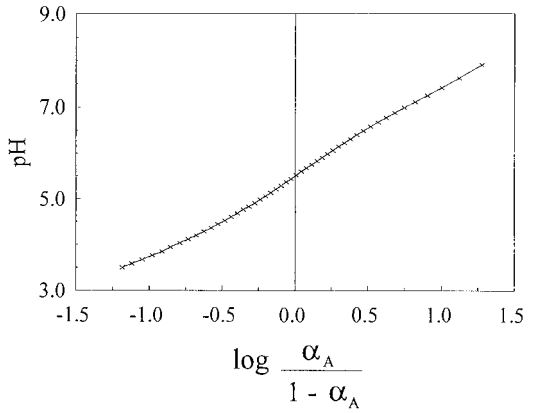

Fig. 3. Henderson-Hasselbalch plots for the determination of the acid-base properties of PAA 3×10^6 ($C_A=5.1$ meq l^{-1}).

Although pK_m^H and n are often constants over a relatively large neutralization range [12], in most cases they should be considered as empirical parameters [1]. Indeed, it has been observed that, for the same polymer, pK_m^H and n are constants only for a given set of conditions; they both vary with the ionic composition of the solution (nature and concentration of the salts present in the solution) and they both decrease with an increase in the ionic strength of the solution [6,7].

The value of n is unity for a simple weak acid (as acetic acid for example) [6]. For polyelectrolytes, the value of n depends on the electric field present around the macromolecule and is always greater than 1; it varies from a value somewhat above 1 to about 2 and is often close to 2 [1,6]. Considering previous work, Gregor et al. [6] reported that pK_m^H and n were independent of the degree of polymerization of the PAA (above a certain minimum not specified). McLaren et al. [7] nuanced this statement by taking into account the influence of the PAA concentration; carrying out potentiometric titrations on a sample of very high

Table 2
Values of pK_m^H and n found in the literature for PAAs

Average molecular weight	PAA concentration (eq l^{-1})	$NaNO_3$ concentration (mol l^{-1})	pK_m^H	n	Reference
3×10^4–10^5	10^{-2}	None	5.92	2.0	[6]
	10^{-2}	None	6.17	2.0	
	10^{-2}	0.2	4.91	1.69	
	10^{-2}	1	4.48	–	
	10^{-2}	2	4.30	1.39	
	10^{-2}	3	4.23	–	[7]
3.52×10^5	10^{-2}	None	6,17	–	
	10^{-2}	0.25	4.9[a]	–	
	10^{-2}	1.0	4.80	–	
	10^{-3}	None	7.1[a]	–	
	10^{-3}	0.25	4.9[a]	–	
1.92×10^6	10^{-2}	None	7.23	–	[7]
	10^{-2}	0.25	5.3[a]	–	
	10^{-2}	1.0	5.15	–	
	10^{-3}	None	7.7[a]	–	
	10^{-3}	0.25	5.4[a]	–	
2.5×10^5	5.2×10^{-3}	0.1	5.42[b]	2.07[c]	This study
3×10^6	5.1×10^{-3}	0.1	5.50[b]	2.05[c]	This study

[a] Graphical determination from [7].
[b] The error on pK_m^H value was estimated to be ±0.01.
[c] The error on n value was estimated to be ±0.01.

average molecular weight PAA ($Mw = 1.92\times10^6$) in the 10^{-4}–10^{-2} eq l^{-1} concentration range, they found that, for polymer concentrations greater than about 10^{-4} eq l^{-1}, this material behaved as a weaker acid, under given conditions, than a lower molecular weight sample ($Mw = 3.52\times10^5$). Only at very high dilutions (close to 10^{-4} eq l^{-1}) the two materials seemed to have practically the same pK_m^H values. Most of the work reported in the literature has been carried out with PAA concentrations in the 10^{-3}–10^{-1} eq l^{-1} range and, according to McLaren et al. [7], this is the region where there is relatively little change in pK_m^H. Their results showed that this variation was almost non-existent (±0.1) in the presence of 0.25 mol l^{-1} $NaNO_3$ for the two PAAs, of, respectively, 3.52×10^5 and 1.92×10^6 average molecular weight they examined. It has also been reported that n depends on the ligand concentration [23].

In the light of these remarks, we can now compare our results to those mentioned in the literature. We only considered studies carried out with linear PAAs, with $NaNO_3$ as supporting electrolyte and at 25°C. Table 2 presents our results and the values of pK_m^H and n found in the literature. We took into account the concentration of $NaNO_3$, the average molecular weight and the concentration of the PAA. Keeping in mind the variation factors mentioned above, it appears that our results are in good agreement with those reported by other authors for PAAs. We did not observe a stronger acidity for the lower molecular weight PAA as McLaren et al. [7] did. From our results, we can conclude that no significant difference seems to exist in the acid-base properties of the two PAAs under study and the values obtained for the empirical constant n shows the importance of intramolecular electrostatic forces on the polymer dissociation.

4.2. Metal complexation

4.2.1. Qualitative study

Calculations were made, using the formula provided by Baes and Mesmer [24], to assess the possible existence of metal hydroxides. Taking into account the value of C_M, we checked that

neither soluble nor insoluble metal hydroxides were significantly formed during the alkali titration, even in the higher pH region.

By comparison with the curve obtained with the ligand alone, the 'ligand + metal ion' titration curves show a supplementary release of protons which is attributed to the formation of metal complexes. For any pH located in the pH range where complexation takes place, the dissociation coefficient of the PAA 3×10^6 in the presence of metal ions, α_M, is higher than the corresponding α_A obtained in the absence of metal ions (Fig. 1). Interactions of copper (II) or nickel (II) with the PAA during alkali titration correspond to the competition between metal ions and protons for the reactive sites of the ligand. The two metal ions show different behaviours. For $R = C_A/C_M$ around 6, the complexation occurs significantly in the 3.5–7.5 pH range for copper (II) and in the 4.5–7.5 pH range for nickel (II) (Fig. 1). Moreover, for a given ratio $R = C_A/C_M$ and at every pH, complexation appears to be more significant with copper (II) than with nickel (II). Similar results were obtained with PAA 2.5×10^5.

4.2.2. Quantitative study

Two or three different ligand to metal ratios, $R = C_A/C_M$, were studied for each PAA with each of the metal ions (R around 3.1, 6.3 and 12.6 with $C_A \approx 5.1$ meq l^{-1} and $4.0.10^{-4} < C_M < 16.6 \times 10^{-4}$ mol l^{-1}). The exact values of C_A/C_M used in each case are given in Tables 3 and 4.

Table 3
Stability constants $\log K_1$ and $\log K_2$ and corresponding pH and pK_A^H values obtained for the Cu(II)/PAA 2.5×10^5 and Ni(II)/PAA 2.5×10^5 systems with different values of $R = C_A/C_M$ ($C_A = 5.2$ meq l^{-1})

R	Cu(II)		Ni(II)	
	6.3	12.6	6.6	13.2
$\log K_1^a$ ($\bar{r} = 0.5$)	3.4	3.3	2.8	2.7
pH	3.60	3.70	4.87	5.10
pK_A^{Hb}	4.64	4.68	5.12	5.24
$\log K_2^a$ ($\bar{r} = 1.5$)	3.2	3.0	2.7	2.6
pH	4.15	4.30	5.57	5.60
pK_A^{Hb}	4.81	4.87	5.49	5.51
$\log \beta_{102}^c$	6.6	6.3	5.5	5.3

[a] The error on $\log K_1$ and $\log K_2$ was estimated to be ± 0.1.
[b] The error on pK_A^H was estimated to be ± 0.01.
[c] The error on $\log \beta_{102}$ was estimated to be ± 0.2.

Fig. 4 shows the evolution of pH versus α_M for PAA 3×10^6 in the presence of nickel (II) for the three different ratios C_A/C_M examined. It appears that the extent of the complexation phenomenon depends on the concentration ratio considered; for a constant reactive site total concentration C_A and for a fixed pH, α_M increases as C_M increases (or with a decreasing C_A/C_M ratio) showing an enhanced complexation phenomenon. Further-

Table 4
Stability constants $\log K_1$ and $\log K_2$ and corresponding pH and pK_A^H values obtained for the Cu(II)/PAA 3×10^6 and Ni(II)/PAA 3×10^6 systems with different values of $R = C_A/C_M$ ($C_A = 5.1$ meq l^{-1})

R	Cu(II)			Ni(II)		
	3.1	6.1	12.2	3.2	6.4	12.7
$\log K_1^a$ ($\bar{r} = 0.5$)	3.6	3.5	3.5	2.9	2.8	2.8
pH	3.47	3.55	3.58	4.79	4.84	4.75
pK_A^{Hb}	4.69	4.70	4.78	5.13	5.15	5.11
$\log K_2^a$ ($\bar{r} = 1.5$)	3.3	3.2	3.1	2.9	2.7	2.7
pH	4.37	4.10	4.12	5.55	5.47	5.34
pK_A^{Hb}	4.95	4.86	4.85	5.53	5.48	5.41
$\log \beta_{102}^c$	6.9	6.7	6.6	5.8	5.5	5.5

[a] The error on $\log K_1$ and $\log K_2$ was estimated to be ± 0.1.
[b] The error on pK_A^H was estimated to be ± 0.01.
[c] The error on $\log \beta_{102}$ was estimated to be ± 0.2.

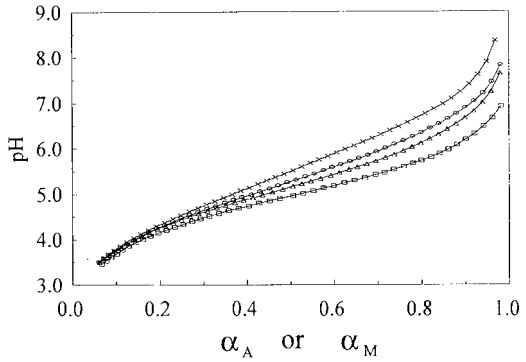

Fig. 4. Plot of pH versus the dissociation coefficient of PAA 3×10^6 in the absence (α_A, X) or in the presence (α_M) of Ni(II) for different values of R ($R = 3.2$ □; 6.4 △; 12.7 ○) ($C_A = 5.1$ meq l^{-1}).

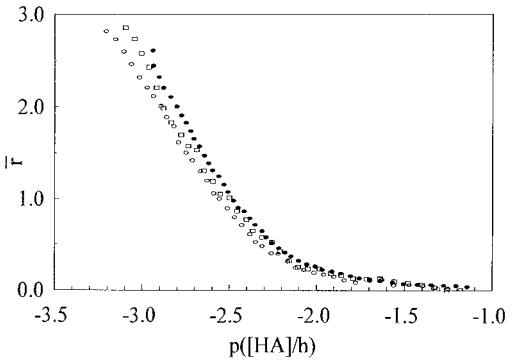

Fig. 5. Formation curves obtained for the Ni(II)/PAA 3×10^6 system with different values of R: ●, 3.2; ○, 6.4; □, 12.7 ($C_A = 5.1$ meq l^{-1}).

more, when C_A/C_M decreases, complexation occurs in a lower pH range. Similar results were obtained with copper (II). The behaviour of PAA 2.5×10^5 was similar to that of PAA 3×10^6.

The corresponding formation curves $\bar{r}$ versus $p([HA]/h)$ were calculated from the experimental data. The K_A^H values needed to study PAA complexation (see Eq. (14)) were obtained from a graphical interpolation of the curve pK_A^H versus pH (Fig. 2). Indeed, as it is not possible to point out a change in the acidity of the polymer due to metal complexation during the alkali titration, we have to make the fundamental assumption that the acid-base properties of the polymers remain the same either in the absence or in the presence of metal ions (this assumption was mentioned in Section 2.2.2) to be able to carry out the study of metal complexation of PAAs. Otherwise, the supplementary dissociation of the polymer in the presence of metal ions ($\alpha_M > \alpha_A$) could not be estimated. As an example, Fig. 5 shows the formation curves obtained with PAA 3×10^6 in the presence of nickel (II) and for the three ratios C_A/C_M examined; it is seen that all plots are very close one from another, attesting to the general validity of the approach used (the same fact was observed in the other cases, i.e. PAA 2.5×10^5 and/or copper (II)). Fig. 6 presents the formation curves obtained in the presence of nickel (II) for PAA 2.5×10^5 or PAA 3×10^6 with the intermediate concentration ratio ($C_A/C_M = 6.4$ or 6.6, respectively) (solid lines were not drawn on Figs. 5 and 6 because the experimental points were too close one from the others). Fig. 7 shows the formation curves obtained with PAA 3×10^6 in the presence of copper (II) or nickel (II) for the intermediate values of C_A/C_M ($C_A/C_M = 6.1$ or 6.4, respectively). The values of $-\log b_r$ correspond to the values of $p([HA]/h)$ read for $\bar{r} = 0.5$ or 1.5 and they were obtained by a graphical interpolation of the formation curve. The values of the complexation constants K_1, K_2 and β_{102}, as well as the pH and pK_A^H values for which K_1 and K_2 were determined are presented in Tables 3 and 4, for PAA 2.5×10^5 and PAA 3×10^6, respectively. The reproducibility of both copper (II) and

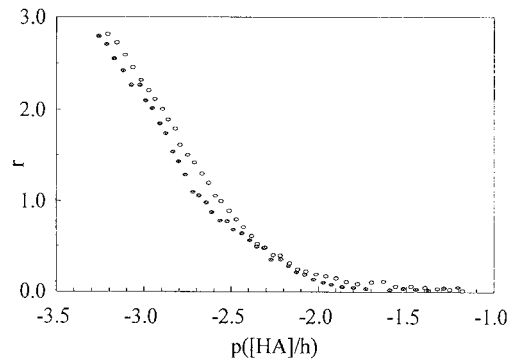

Fig. 6. Formation curves obtained for the Ni(II)/PAA 2.5×10^5 system (●; $R = 6.6$; $C_A = 5.2$ meq l^{-1}) and for the Ni(II)/PAA 3×10^6 system (○; $R = 6.4$; $C_A = 5.1$ meq l^{-1}).

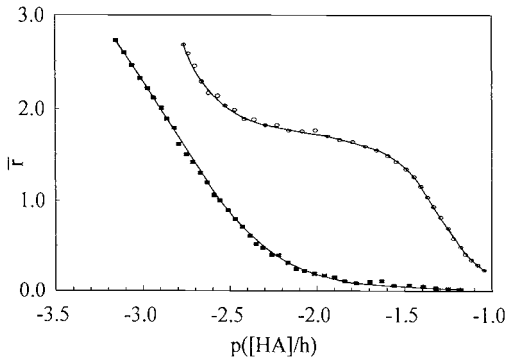

Fig. 7. Formation curves obtained for the Cu(II)/PAA 3×10^6 system (○; $R = 6.1$) and for the Ni(II)/PAA 3×10^6 system (■; $R = 6.4$) ($C_A = 5.1$ meq l^{-1}).

nickel (II) complexation were examined by multiple measurements (three determinations in each case). The experimental error on the values of $\log K$ ($\log K_1$ or $\log K_2$) and $\log \beta_{102}$ were estimated to be ± 0.1 and ± 0.2, respectively.

The formation of the MA_3 species was not considered for several reasons. For the calculations we made, the experimental pH value corresponding to $\bar{r} = 3.0$ would be around 6.0. The representation of pH versus α_A or α_M (Fig. 1) shows that α_M would be 0.85 or 0.80 for PAA 3×10^6 in the presence of Cu(II) or Ni(II), respectively, and with $R = C_A/C_M \approx 6$. This implies that the dissociation of the initially protonated PAA is well advanced and that electrostatic forces may occur which gradually lead to an extended form of the PAA chain; it is then highly improbable that sites that are not vicinal on the polymer chain could form complexes of the MA_3 type. However, even with three vicinal complexing sites (carboxylate groups) on the polymer chain, it is not seen how these items could link to the same metal ion. The formation of MA_3 complex species can be considered in the case of simple ligands by contrast with polymer ligands. But even in that case, ligand to metal ratios have to be important and much higher than those we considered with the PAAs. Moreover, in the case of high molecular weight polymers, steric effects due to the macromolecule hinder the formation of metal complexes having high coordination numbers. Finally, interpolymer chains bridging by metal ions is highly improbable at the low PAA concentrations we considered here ($C_A \approx 5 \times 10^{-3}$ eq l^{-1}) [7].

These results (Tables 3 and 4) show that:

1. When three parameters are selected: molecular weight of the PAA, nature of the metal ion and concentration ratio C_A/C_M, the values of $\log K_1$ and $\log K_2$ for MA and MA_2 species, respectively, are very close, $\log K_2$ being hardly lower than $\log K_1$; $\log K_2$ is systematically estimated at a higher pH than $\log K_1$
2. When two parameters are selected: molecular weight of the PAA and nature of the metal ion, a decrease in the concentration ratio C_A/C_M leads to a slight increase of $\log K_1$ and $\log K_2$ values
3. Whatever the PAA considered and whatever the concentration ratio examined, MA or MA_2 complexes formed with copper (II) present a higher stability and are formed at a lower pH than the corresponding complexes formed with nickel (II)
4. Complexes formed with PAA 2.5×10^5 or PAA 3×10^6 exhibit very similar stabilities and are also formed at very close pH values.

The formation curves obtained for copper (II)–PAA systems present a marked decrease of their slope for the average coordination number $\bar{r}$ in the 1.5–2.0 range, approaching $\bar{r} = 2.0$ ($4.2 < pH < 5.2$; $0.3 < \alpha_M < 0.6$; Fig. 7). This plateau means that the corresponding CuA_2 complex species is thus the predominant species formed in that region compared to the CuA species. This has also been reported in previous work [6–9]. Remembering the definition of $\bar{r}$, it means that two reactive sites (carboxylate groups) of the ligand are involved in the complexation of one metal ion Cu (II) [7,8]. It is strongly believed that these two carboxylate groups are vicinal on the polymer chain which implies the formation of eight membered rings [8].

Elsewhere, the formation curves $\bar{r}$ versus $p([HA]/h)$ for copper (II)–PAA systems present an important slope for $\bar{r}$ about 1 ($3.7 < pH < 3.8$; $0.2 < \alpha_M < 0.4$; Fig. 7). This has also been observed by other authors [6,8]. One may conclude that the stability constants of the CuA and CuA_2

Table 5
Values of log K_1 and log β_{102} found in the literature for copper (II)–PAA complexes and obtained by potentiometric measurements

Average molecular weight	$NaNO_3$ or KNO_3 concentration (mol l^{-1})	C_A (eq l^{-1})	C_M (mol l^{-1})	$R = C_A/C_M$	log K_1	log β_{102}	Reference
3×10^4–10^5	$NaNO_3$ 0.2	10^{-2}	2.46×10^{-3} or 9.85×10^{-3}	4.1 or 1.0	–	7.5	[6]
$\approx5\times10^3$	KNO_3 0.15	1.4×10^{-2}	–[a]	–[a]	3	5.8	[10]
–[b]	KNO_3 0.1	9.9×10^{-3}	10^{-3}	9.9	–	≈6[c]	[9]

[a] Value not clearly specified.
[b] Value not mentioned.
[c] Order of magnitude according to the authors.

species are quite close [6,8] and that, as a consequence, both species exist with comparable concentrations in that domain.

Finally, the value of $\bar{r}$ increases in a very important manner above $\bar{r} = 2$ (pH > 5.2; $\alpha_M > 0.6$; Fig. 7). This suggests that in that region some other complexes may then possibly be formed besides the CuA_2 complex species but their precise nature cannot be found from the formation curves [7–9].

Concerning the nickel (II)–PAA systems, the formation curves do not present any plateau for $\bar{r}$ in the 0–2 range ($3.5 < pH < 6.0$; $0.06 < \alpha_M < 0.86$; Fig. 7), which means that none of the two complex species MA and MA_2 becomes predominant in that domain of $\bar{r}$. This observation does not agree with the work of McLaren et al. [7] who observed a flattening of the formation curve for $\bar{r}$ close to 2.

In order to compare the stability constants we obtained to those cited in the literature, some precisions have to be given at this point of the discussion. In particular, it was found that the stability 'constants' vary with the composition of the solution (nature and concentration of neutral salts) but also with the PAA concentration, the dissociation coefficient α_M of the polymer (which is linked to the pH and to the potential at the surface of the polyion) and with a possible conformational transition of the PAA in the course of its potentiometric titration in the presence of metal ion [6,7,9,10]. It has been shown previously that charge effects induced by the polymer dissociation during the titration in the presence of metal ions may lead to molecular interactions which considerably affect complexation reactions and which even are the cause of conformational transition of the polymer between an extended and a compact form [7,9]. Furthermore, it has been suggested that high PAA concentrations (2.5×10^{-3} eq l^{-1}; [7]) could lead to intermolecular interactions between PAA chains which may induce a rather gel like behaviour; this phenomenon is more pronounced when the macromolecule is branched [7]. Thus, it was thought that only orders of magnitude of these constants could be given and compared [9]. However, no mention was found on the effect of the molecular weight of the PAA on its binding properties.

To compare our results to those mentioned in previous work, as we did before for pK_m^H and n, we only considered studies carried out with linear PAAs, with $NaNO_3$ (or KNO_3) as supporting electrolyte and at 25°C. Table 5 presents the values of log K_1 and log β_{102} found in the literature for copper (II)–PAA complexes and obtained by potentiometric measurements. The experimental conditions used by the different authors cited are also mentioned in Table 5: the concentration of $NaNO_3$ (or KNO_3), the average molecular weight and the concentration of the PAA as well as the total concentration of the metal ion and the concentration ratio $R = C_A/C_M$. Unfortunately, no work was directly comparable to our data for nickel (II)–PAA complexes [7].

For copper (II)–PAA system, even for various molecular weights of the complexing polymer, it appears that the stability constants we determined are in quite good agreement with those cited in the literature.

Moreover, the comparison of our results with those obtained for metal complexes of simple carboxylic acids, such as, for example, the analogous monomer glutaric acid ($\log K_1 = 2.4$ and 1.6 with copper (II) and nickel (II), respectively; [25]), reveals an increased stability for the complexes of polymeric acids.

5. Conclusion

The aim of this study was, first, to precise the acid-base properties of two poly(acrylic acids) of 2.5×10^5 and 3×10^6 average molecular weight and, secondly, to assess their binding properties towards copper (II) and nickel (II) ions in dilute aqueous solution. The results obtained showed that the two PAAs present both similarities for acid strengths and metal binding properties towards the ions under study. Furthermore, compared to the monomer analog glutaric acid, it appears that PAAs are better complexing agents. As expected, copper (II) ions are more readily bound by both PAAs than nickel(II) ions. However, the values of $\log \beta_{102}$ obtained for nickel (II) complex species ($\log \beta_{102} \approx 5.5$) suggest that the PAAs of high molecular weight studied here could contribute to the elimination of nickel (II) ions during the flocculation step of contaminated water treatment.

References

[1] J. Buffle, Complexation Reactions in Aquatic Systems: An Analytical Approach, Ellis Horwood, Chichester, 1988.
[2] M. Vasconcelos, A. Machado, F. Rey, Ann. Quim. Int. Ed. 92 (4) (1996) 243–248.
[3] H. Powell, E. Fenton, Anal. Chim. Acta 334 (1-2) (1996) 27–28.
[4] M. Ricart, I. Villaescusa, F. de la Torre, React. Funct. Polym. 28 (2) (1996) 159–165.
[5] E. Tipping, Binding models concerning natural organic substance performance assessment, Proc. NEA Workshop 1994 (1995), pp. 163–168.
[6] H.P. Gregor, L.B. Luttinger, E.M. Loebl, J. Phys. Chem. 59 (1955) 34–39.
[7] J.V. McLaren, J.D. Watts, A. Gilbert, J. Polym. Sci. 16C (1967) 1900–1915.
[8] P. Monjol, Bull. Soc. Chim. 4 (1972) 1319–1323.
[9] F. Yamashita, T. Komatsu, T. Nakagawa, Bull. Chem. Soc. Jpn. 52 (1) (1979) 30–33.
[10] J.A. Marinsky, N. Imai, M.C. Lim, Isr. J. Chem. 11 (5) (1973) 601–622.
[11] H. Dautzenber, W. Jaeger, J. Köt, B. Philipp, C. Seidel, D. Stscherbina, Polyelectrolytes: Formation, Characterization and Application, Hanser, Munich, 1994.
[12] A. Katchalsky, P. Spitnik, J. Polymer. Sci. 2 (1947) 432–446.
[13] H.M. Irving, H.S. Rossotti, J. Chem. Soc. (1954) 2904–2910.
[14] A. Katchalsky, J. Gillis, Rec. Trav. Chim. 68 (1949) 879–897.
[15] J. Bjerrum, Metal Ammine Formation in Aqueous Solution, Haase, Copenhagen, 1941.
[16] G. Gran, Acta Chem. Scand. 4 (1950) 559–577.
[17] G. Gran, Analyst 77 (1952) 661–671.
[18] C. McCallum, D. Midgley, Anal. Chim. Acta 78 (1975) 171–181.
[19] M.M. Breuer, Polyelectrolytes, in: A.D. Jenkins (Ed.), Polymer Science, North-Holland, Amsterdam, 1972, pp. 1135–1185.
[20] J.C. Fenyo, J. Beaumais, E. Selegny, J. Polym. Sci. 12C (11) (1974) 2659–2670.
[21] M. Nagasawa, T. Murase, K. Kondo, J. Phys. Chem. 69 (11) (1965) 4005–4012.
[22] Y. Kawaguchi, M. Nagasawa, J. Phys. Chem. 73 (12) (1969) 4382–4384.
[23] F.J. Stevenson, Humus Chemistry, Genesis, Composition, Reactions, Wiley, New York, 1982.
[24] C.F. Baes, R.E. Mesmer, The Hydrolysis of Cations, Wiley, New York, 1976.
[25] A.E. Martell, R.M. Smith, Critical Stability Constants, vol. 3, Other Organic Ligands, Plenum Press, New York, 1977.

ELSEVIER

Talanta 45 (1998) 1189–1199

Talanta

Bonded stationary phases for reversed phase liquid chromatography with a water mobile phase: application to subcritical water extraction

Toby E. Young [a], Scott T. Ecker [a], Robert E. Synovec [a,*], Nathan T. Hawley [b], Jonathan P. Lomber [b], Chien M. Wai [b]

[a] *Department of Chemistry, Box 351700, University of Washington, Seattle, WA 98195-1700, USA*
[b] *Department of Chemistry, Renfrew Hall, University of Idaho, Moscow, ID 83844-2343, USA*

Received 14 May 1997; accepted 17 July 1997

Abstract

Reversed phase high-performance liquid chromatography (RP-HPLC) is demonstrated for hydrophobic analytes such as aromatic hydrocarbons on a chemically bonded stationary phase and a mobile phase consisting of only water. Reversed phase liquid chromatography separations using a water-only mobile phase has been termed WRP-LC for water-only reversed phase LC. Reasonable capacity factors are achieved through the use of a non-porous silica substrate resulting in a chromatographic phase volume ratio much lower than usually found in RP-HPLC. Two types of bonded WRP-LC columns have been developed and applied. A brush phase was synthesized from an organochlorosilane. The other phase, synthesized from an organodichlorosilane, is termed a branch phase and results in a polymeric structure of greater thickness than the brush phase. A baseline separation of a mixture containing benzaldehyde, benzene, toluene, and ethyl benzene in less than 5 min is demonstrated using a water mobile phase with 12 000 plates generated for the unretained benzaldehyde peak. The theoretically predicted minimum reduced plate height is also shown to be approached for the unretained analyte using the brush phase. As an application, subcritical water extraction (SWE) at 200°C is combined with WRP-LC. This combination allows for the extraction of organic compounds from solid matrices immediately followed by liquid chromatographic separation of those extracted compounds all using a solvent of 100% water. We demonstrate SWE/WRP-LC by spiking benzene, ethyl benzene, and naphthalene onto sand then extracting the analytes with SWE followed by chromatographic separation on a WRP column. A sand sample contaminated with gasoline was also analyzed using SWE/WRP-LC. This extraction process also provides kinetic information about the rate of analyte extraction from the sand matrix. Under the conditions employed, analytes were extracted at different rates, providing additional selectivity in addition to the WRP-LC separation. © 1998 Elsevier Science S.A.

Keywords: Reverse phase liquid chromatography; Water mobile phase; Subcritical water extraction

* Corresponding author. Fax: +1 206 6858665; e-mail: synovec@gibbs.chem.washington.edu

PII S0039-9140(97)00233-6

1. Introduction

Traditionally, the extensive use of reversed phase liquid chromatography (RP-LC) for the chemical analysis of hydrophobic compounds requires 50–100% of an organic solvent in the mobile phase [1]. The need for a high percentage of organic solvent in the mobile phase is due to the stationary phase composition, often a highly porous silica derivatized with octadecylsilane, i.e. C18. Porous silica leads to a high surface area per gram of stationary phase [2] which in turn produces a phase volume ratio (volume of stationary phase to volume of mobile phase) requiring an organic solvent modifier in the mobile phase to achieve a good separation [3].

Recently we reported that RP-LC separations of hydrophobic compounds are possible with a mobile phase comprised of only water [4] which we have termed WRP-LC for water-only reversed phase liquid chromatography. The stationary phase for WRP-LC was based upon a non-porous silica substrate with an absorbed layer of hydrophobic polymer and illustrated the feasibility of using a water-only mobile phase. The adsorbed stationary phase, however, was susceptible to continuous degradation, bringing into question long term stability. Furthermore, it was desired to improve the chromatographic performance of the WRP-LC columns to a level on par with commercially available columns.

The objective of this work was to construct a bonded WRP-LC stationary phase which would address the two issues of column stability and separation efficiency. Two different bonded phases were constructed though both utilized the same mono-dispersed, non-porous silica substrate. The first stationary phase was synthesized from (tetradecafluoro-1,1,2,2-hydrooctyl)

dimethylchlorosilane monomers, an eight carbon chain with carbons three through eight fully fluorinated. A stationary phase made from a monochlorosilane is termed a brush phase [5] and will be referred to as such in this paper. The second bonded phase was synthesized from a dichlorosilane containing a (3,3,3)-trifluoropropyl carbon chain. Dichlorosilanes by virtue of having two reactive sites (the two chlorine atoms) can form polymeric chains when bonding to the silica surface [5] with the result being a bonded stationary phase that tends to be thicker than a brush phase. Stationary phases synthesized from dichlorosilanes are termed oligomeric or branched phases.

The vast majority of reversed phase stationary phases are of the brush type. Syntheses involving di- and trichlorosilanes are considerably more complicated and consequently are less commonly practiced. Akapo et al., however, have investigated the properties of stationary phases made from dichlorosilanes [6–9]. These phases were made by the stepwise silanization of hydroxyl groups on silica with an *n*-octymethyldichlorosilane monomer followed by subsequent hydroloysis of the unreacted chlorine atom to form a silanol. This silanol can now react with another monomer. Each silanization step adds another layer of stationary phase resulting in an increase in the percentage carbon load. It was found that beyond three silanization steps (corresponding to a carbon loading of 11%) retention time remained constant with only a slight increase in retention time up to three silanization steps [6].

Oligomeric stationary phases have been shown to be more stable than conventional brush phases, particularly below pH 3 [7] or above pH 9 [8]. For this reason, an oligomeric, branched phase was synthesized and its chromatographic performance reported here. Surface erosion progressively takes place on a stationary phase containing a single oligomer as more mobile phase passes through the column. What effect this has on retention depends on the nature of the analyte. Lewis bases increase their retention due to increased interaction with exposed silanol groups. Analytes without ionic or polar groups tend to decrease their retention due to the loss of stationary phase material. As the layers of a oligomeric phase become thicker due to more chains being bonded to the silica, the erosion becomes progressively less. It was also found that a phase comprised of multiple oligomeric chains will exhibit a retention mechanism controlled almost exclusively by dispersive interactions [9]. It follows that in contrast to other types of bonded phases, residual silanol groups do

not appear to be present or at least are not readily available.

Akapo found that as the number of layers increases, a decrease in specific surface area and pore volume of the silica substrate followed. This effect becomes significant when a purely microporous substrate is used and can lead to total blockage of the pores when exhaustively silanized, effectively resulting in a non-porous packing [6]. This has important consequences for RP-LC. A stationary phase bound to a non-porous substrate will have a lower phase volume ratio (volume of stationary phase to the volume of mobile phase) than the same stationary phase bound to a porous substrate. This is due strictly to the decreased surface area available on the substrate.

Analyte retention factor is dictated by and is directly proportional to two terms, the phase volume ratio and the distribution coefficient, K_D, the concentration of analyte in the stationary phase divided by the concentration in the mobile phase. When separating hydrophobic analytes in a mobile phase of 100% water, as we did in this work, the distribution coefficient is significantly large enough that to achieve reasonable retention factors, the phase volume ratio needs to be decreased. A stationary phase bound to a porous substrate will not meet this criteria due to its high surface area and consequently high phase volume ratio. A non-porous substrate will, on the other hand. A more detailed explanation can be found elsewhere [4].

In addition to the results of the bonded WRP-LC phases, we also report on the interfacing of subcritical water extraction (SWE) with WRP-LC and apply the SWE/WRP-LC instrument to the analysis of hydrophobic organic compounds extracted from sand. In this combination, subcritical water is passed through an extraction cell containing sand spiked with organic compounds such as benzene, ethyl benzene, and naphthalene. A sample containing sand spiked with gasoline is also examined. Analytes are extracted into subcritical water which flows through the extraction cell, normally at 200°C and 750 psi of pressure. Monitoring of the extraction process is accomplished by taking heartcuts of the extract with respect to time and injecting them onto a WRP column for chromatographic separation. Both the extraction and separation are done using a mobile phase of 100% water.

Water-only separations have also been evolving in the field of sample preparation by solvent-extraction for chemical analysis [10–12]. Subcritical water extraction (SWE), i.e. water extraction at high temperature, was found to extract organic pollutants such as polynuclear aromatic hydrocarbons (PAHs) and polychlorinated biphenyls PCBs from soil, reducing the use of organic solvents in chemical analysis [13–15]. The vast majority of analytical supercritical fluid extraction (SFE) applications utilized supercritical CO_2 due to its low toxicity and excellent extraction properties for many non-polar organics [16–28]. At the same time, the polarity of CO_2 is low and efficient extractions are not always possible. In such cases CO_2 is usually modified by adding an organic solvent, such as methanol, or a selective ligand [21–33]. Hawthorne recently demonstrated that water is a strong enough mobile phase to elute alcohols, hydroxy-substituted benzenes, and amino acids from a reversed phase polystyrene stationary phase when heated above 40°C [34]. Improved separations were obtained as the temperature was raised up to 175°C. In the work reported here, the chromatographic separations with the novel stationary phases were done with the water mobile phase at room temperature, though the extractions were done using hot, subcritical water.

The dielectric constant of water is primarily an inverse function of temperature and only mildly dependent on pressure [35] and extractions are effective using water without the need to go to the supercritical state [10–12]. At room temperature, the dielectic constant, ϵ, of water is near 80 making it much too polar to solvate hydrophobic organic compounds, such as hydrocarbons, PAHs and PCBs [35]. By raising the temperature to 300°C and the pressure to just 500 psi, the dielectric constant of water drops to approximately 20, making it similar to ethanol ($\epsilon = 24$) and methanol ($\epsilon = 33$). This significant drop in dielectric constant allows hydrophobic compounds, which have a limited water solubility at room temperature, to more readily dissolve in water. An

illustrative example of how effectively high temperature water can increase solubility is found with benzo[e]pyrene. At 350°C and 100 bar, the solubility of benzo[e]pyrene increased from 4 ng/ml under ambient conditions [36] to approximately 10% (w/w), an increase of 25 million-fold [37]. Also, since the dielectric constant of water does gradually decrease with increasing temperature, and the dielectric constant is a measure the solvating power of a solvent, considerable selectivity is gained through the use of water. This may be contrasted with supercritical CO_2 having a dielectric constant range of 1–1.6 [38].

2. Experimental

2.1. Reagents

Non-porous spherical silica (Powder Technologies, Burnsville, MN) was used as the substrate in the WRP stationary phases. The silica has a mean diameter of 6.7 ± 0.2 μm and a specific surface area of 0.37 $m^2\ g^{-1}$ of silica. The stationary phase was synthesized by functionalizing the silica with either the monochlorosilane, (tridecafluoro-1,1,2,2-tetrahydrooctyl)dimethychlorosilane (98%, Gelest, Tullytown, PA), or the dichlorosilane, (3,3,3-trifluororpropyl)methyldichlorosilane (98%, Gelest, Tullytown, PA). End-capping was accomplished using hexamethyldisilazane (98%, Gelest, Tullytown, PA). Reagent grade pyridine (Burdick and Jackson, Muskegon, MI) was used as an acid scavenger. The synthesis was carried out in a solvent of anhydrous toluene (99.8%, Aldrich, Milwaukee, WI) under an atmosphere of dry nitrogen. THF, methylene chloride, methanol, and acetone were used as wash solvents and were all of analytical grade quality (J.T. Baker, Phillipsburg, NJ). Water was deionized to 18 MΩ resistance with a Millipore water system (Millipore, Bedford, MA).

2.2. Synthesis of brush and branched WRP stationary phases

The synthesis procedure for the WRP phases was modified from a generalized method given by Scott [5] and is designed to produce 10 g of stationary phase, enough to fill a 4.6 mm I.D. × 250 mm in length chromatography column. Ten grams of the non-porous spherical silica are first dried at 225°C in a vacuum oven for 24 h then placed in a three neck reaction flask. The flask is fitted with a condensing column in the center neck and rubber septums in the two remaining necks. A purge line of dry nitrogen was placed through one septum with a thermometer fitted through the remaining septum. The flask and condensing column had been previously dried overnight at 125°C, then purged with dry nitrogen for 12 h to ensure a dry atmosphere. Anhydrous toluene (100 ml) is pumped into the flask via a stainless steel canula by placing the toluene bottle under a positive pressure of dry N_2. A volume of 100 μl of the chlorosilane reagent (dichlorosilane if a branched phase is being made) is placed in the three-neck flask using a nitrogen purged micro syringe (Hamilton, Reno, NV). Pyridine (10 μl) is added as an acid scavenger. The slurry of 10 g of silica, 100 ml anhydrous toluene, 100 μl chlorosilane, and 10 μl pyridine were mixed with a mechanical stir bar and refluxed at 110°C for 12 h. After refluxing, the slurry is poured into a Buchner funnel fitted with filter paper of 2 μm porosity (Whatman # 5, Hillsboro, OR). The newly synthesized stationary phase is now washed with 25 ml aliquots of THF, toluene, methylene chloride, methanol, 50% methanol/water, and acetone in that order.

End-capping of the brush phase is done by placing the newly washed phase back into the reaction flask, adding more anhydrous toluene in the manner described previously, followed by the addition of the end-capping reagent hexamethyldisilazane (50 μl). This mixture is stirred and heated at 80°C for 1 h then filtered and washed as done previously. Finally, the stationary phase is dried at 125°C for 18 h. If, however, a branched phase is being made, then the stationary phase is first dried at 220°C for 12 h before being placed back in the reaction flask. The synthesis is now repeated using fresh toluene and another 100 μl of the dichlorosilane reagent. The filter/wash steps are then repeated followed by another 12 h of drying at 220°C before commencing with end-cap-

ping and a final washing and drying step. The synthesis step can be repeated as many times as desired with each repetition adding another layer of stationary phase. In this work, however, a maximum of two repetitions was done.

The volumes of reagents used were calculated to provide a large molar excess. Silanol coverage on the surface of silica has been estimated at 9.0 ± 1.0 μmol m^{-2} of silica [39]. Due to steric shielding of silanol groups by bonded material the concentration of accessible silanols has been calculated at approximately 4 μmol m^{-2} [5]. Combining this value with a specific surface area of 0.37 m^2 g^{-1} for the non-porous silica and the use of 10 g of silica in the synthesis it is found that there are a total of 15 μmol of silanols available for coverage. In the synthesis a volume of 100 μl chlorosilane reagent is used which translates into 334 μmol, providing for a ratio of 22 μmol of reagent per μmol of silanol.

2.3. Packing of the water-only reversed phase column

The synthesized WRP stationary phases were packed in stainless steel chromatography columns (Alltech, Deerfield, IL) measuring 4.6 mm I.D. × 250 mm in length and fitted with 0.5 μm frits. To ensure the highest level of cleanliness, each column is first washed with a series of solvents as suggested by Karger [40]. At a flow rate of 1.0 ml/min, 30 ml of hexane are flushed through the column which is followed with methanol, acetone, 50% phosphoric acid, 10% (v/v) nitric acid, water (till neutral), then lastly with acetone. This procedure is designed to remove grease, detergents, surface oxides, and other contaminants from the inside of the columns before packing.

A slurry packing technique [5] was used to pack the columns used in this work. The slurry consisting of the surfactant sodium dodecyl sulfate (SDS) (Aldrich, Milwaukee, WI), water and the stationary phase, was thoroughly sonicated to ensure a homogenous mixture. Next, the slurry is placed in a reservoir chamber situated between a single piston solvent pump (Beckman Instruments, Model 114M, Berkley, CA) and the column to be packed. The pump pushed the slurry into the column, the stationary phase becoming trapped by the 0.5 μm frit placed in the output end-cap, while the SDS solution passed through. The packed column was then removed from the reservoir, the Swaglok union connecting the column to the reservoir replaced with an end-cap, and the stationary phase compressed further under 5000 psi of water using a high pressure solvent pump (Ranin, HPXL Solvent Delivery Pump, Woburn, MA).

2.4. Construction of subcritical water extraction device

The subcritical water extraction (SWE) device used in our system is shown in Fig. 1. This device consists of a syringe pump (Isco, model 2600), a Varian GC oven, a supercritical water extraction cell, two needle valves and a temperature controller (Omega Scientific Model CN9000A, Stanford, CT) for the oven. Stainless steel tubing measuring 1/16 in. O.D. × 0.020 in. I.D. was used throughout the SWE. The extraction cell measures 5 mm I.D. × 100 mm in length (2 ml in volume) and was purchased from Keystone Scientific (Bellefonte, PA). Five feet of coiled tubing (labeled HC in Fig. 1) in the GC oven allows water to reach the necessary temperature before entering the extraction cell. After passing through the extraction cell, effluent leaves the oven passing through a needle valve used as a pressure regulator before entering three feet of coiled tubing (CC). This tubing is immersed in an ice bath and

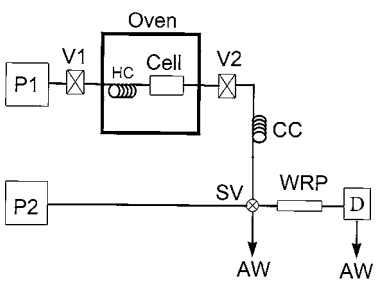

Fig. 1. Schematic of SWE/WRP-LC instrument. P1 and P2, water pump for SWE and WRP-LC systems, respectively; V1 and V2, needle valves; HC, heating coil; CC, cooling coil; Cell, SWE extraction cell; SV, switching valve; WRP, WRP-LC column; D, UV/VIS absorbance detector; AW, aqueous waste.

serves to cool the effluent before entering the switching valve, SV (Rheodyne 7010, Cotati, CA).

2.5. Operation of the SWE/WRP-LC instrument

Washed sea sand (Fischer Scientific, Pittsburgh, PA) is first placed in the SFE cell with a small amount of glass wool placed at both ends to keep sand particles from clogging the frits. Analytes were spiked onto the sand from a micro pipette. The SFE cell is positioned vertically inside the oven and the entire system filled with water from pump P1. The downstream needle valve V2 is now closed and P1 allowed to run, until the extraction cell is pressurized to 50 atmospheres (735 psi). At this point, valve V1 is closed, pump P1 shut off and the oven heated to 200°C, unless otherwise stated. While the oven is heating, water from pump P2 is continuously flowed through the Rheodyne switching valve, SV, the attached WRP column and subsequently the UV/VIS absorbance detector (Linear Instruments Model 205, Fremont, CA).

The operating pressure of the WRP-LC separation is 1200 psi at a flow rate of 1.0 ml min^{-1}. Once the oven has reach the desired temperature, pump P1 is turned back on with the flow rate set to 1 ml min^{-1} followed immediately by the opening of valves V1 and V2, resulting in the back pressure stabilizing at around 900 psi. Prior to injecting analyte onto the WRP-LC, the SWE effluent is cooled to approximately room temperature via the cooling coil, CC in Fig. 1. Effluent immediately begins to flow through the 10 μl sample loop fitted on SV, which is in the Load position, before continuing onto an aqueous waste collection vial. The experiment is conducted such that in the first 60 s, all of the flow is sent to aqueous waste (AW). After 60 s SV is turned to the Inject position and a 10 μl is injected onto the WRP column. The components of the injected plug are separated and then detected as a series of peaks via the UV/VIS absorbance detector. The switching valve is left in the Inject position for 30 s then switched back to Load. Heartcuts of the SWE effluent stream are then made every 2 min unless otherwise noted.

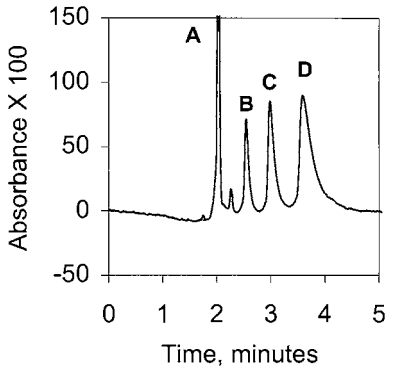

Fig. 2. WRP-LC separation of 10 μl sample containing 10 ppm benzaldehyde (A), 5 ppm benzene (B), 5 ppm toluene (C), 10 ppm ethyl benzene (D) with a water mobile phase at a flow rate of 0.75 ml/min on a 4.6 mm × 250 mm branched WRP column. Detection was done with UV absorbance at 200 nm.

All data collection was done on a Dell 486/66 computer using Dionex chromatography software and a Dionex data acquisition board. All tubing in the SWE was 1/16 in. O.D. × 0.020 in. I.D. stainless steel while tubing for the LC portion was made of poly(etheretherketone) (PEEK) measuring 1/16 in. O.D. × 0.010 in. I.D. (Upchurch, Oak Harbor, WA).

3. Results and discussion

The two bonded stationary phases for WRP-LC were evaluated with regard to separation efficiency and retention of hydrophobic analytes. Fig. 2 illustrates a separation of four hydrophobic analytes using the branch WRP phase. This baseline separation was obtained using a mobile phase of 100% water, a flow rate of 0.75 ml min^{-1} and UV absorbance detection at 200 nm. Benzaldehyde, labeled A in Fig. 2, achieves an efficiency of 12 000 plates at a $k = 0$. Ethyl benzene ($k = 1$) elutes with 1300 plates. Furthermore, chromatographic efficiency data for the brush WRP phase was calculated for benzoic acid and ethyl benzene, and are reported in Fig. 3. The reduced plate height for the unretained benzoic acid approaches two over the linear flow velocity range covered which is near the theoretically predicted minimum for columns operating in the high performance

region [41] while the reduced plate height for ethyl benzene was much higher. What this suggests is that this particular WRP column is operating near its optimum limit with respect to an unretained analyte. With this brush phase and a flow rate of 0.75 ml min^{-1}, the unretained ($k=0$) benzoic acid peak had an efficiency of 16 000 plates, similar to that obtained with the branched phase. At the same flow rate and a $k=1$, the efficiency as given by ethyl benzene is 500 plates. Both the brush and branch phases provided useful separations, but the branch phase appeared to be more stable over time, as anticipated.

The high plate count for an unretained peak suggests both the brush and branched columns are packed fairly well. The loss of efficiency for retained peaks, however, raises concern over the stationary phase. While a complete explanation of the problem is not possible without further work, it is believed that either a varying stationary phase thickness, a wide particle distribution, or slow mass transfer kinetics into and out of the stationary phase may play a role. All of these effects would manifest themselves as a multipath effect [4,42,43]. While a wide particle size distribution can also cause a multipath effect, the high plate count as well as the absence of a significant y-intercept in Fig. 3 for the unretained benzoic acid peak would indicate that the size distribution is sufficiently narrow. Moreover, the flow resistance parameter for the packed column was reasonable for the specified particle size, suggesting a narrow particle size distribution. The presence, on the other hand, of a significant y-intercept in Fig. 3 for the retained ethyl benzene peak is indicative of an abnormally high multipath term. If this term is not due to the particle size distribution then we would be led to believe that it is due to either non-uniform coverage of the silica by the stationary phase or the kinetics of the partitioning process. As stated previously, however, more work is needed to fully understand the reasons behind the loss in efficiency for retained analytes in water-only reversed phase separations. None the less, at higher linear flow velocities, retained analytes have band broadening that is approaching that of commercial columns, as is in evidence in Fig. 2.

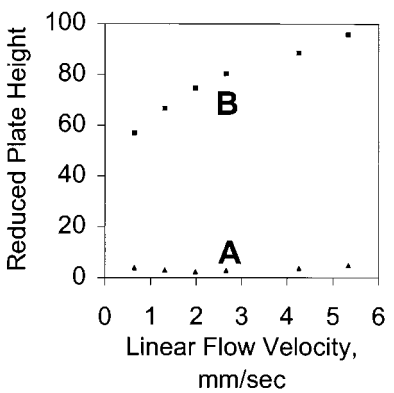

Fig. 3. Reduced plate height, h, as a function of linear flow velocity, u, on a brush-type WRP column for the unretained analyte benzoic acid (A) and a retained analyte ethyl benzene, $k=1$ (B). A linear flow velocity of 2.7 mm s^{-1} corresponds to a volumetric flow rate of 1.0 ml min^{-1}. The column dimensions and detection were the same as in Fig. 2.

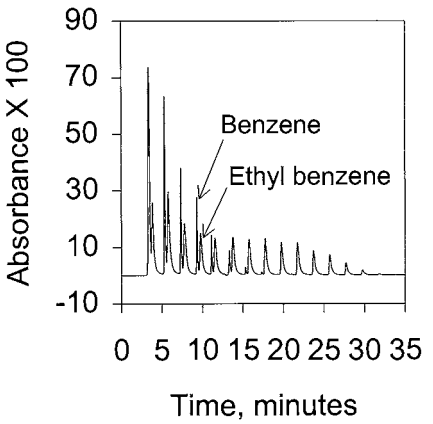

Fig. 4. SWE/WRP-LC of benzene and ethyl benzene from sand. A mass of 10 mg of each analyte was spiked onto 2 ml of sand and the experiment conducted as described in the Section 2. WRP-LC separation was performed using the brush-type phase with the column measuring 4.6 mm × 250 mm and a heartcut sample volume of 10 μl. The flow rate through both the SWE and the WRP were 1.0 ml min^{-1}. A total of 15 heartcuts were analyzed with the benzene and ethyl benzene peaks in the fourth heartcut labeled.

As an example of where water-only RP-LC could be applied, we focused on the interfacing of WRP-LC and SWE. An example of the data obtained with the SWE/WRP-LC device is provided in Fig. 4. Here, the extraction cell (volume

2.2 ml) was filled with sea sand followed by the spiking of 10 mg each of benzene and ethyl benzene onto the sand. The sample cell was placed inside the SWE oven and the experiment run as described in the Section 2. Heartcuts were taken 2 min apart with the first injection taken at 1.5 min on the time axis of Fig. 4. The first 1.5 min of SWE effluent was allowed to run to waste before making the first injection in order for the flow and pressure to stabilize. Chromatographic separations were obtained with a column packed with the brush WRP stationary phase.

Fig. 4 demonstrates that use of a water-only solvent system for both the extraction and chromatographic separation of hydrophobic analytes was successful. Each pair of peaks represents a separate heartcut of extract at a different point in time during the extraction process and provides some insight into the dynamics of the SWE extraction process. Based on the differences in peak height it is clear that the relative concentrations of benzene and ethyl benzene are not the same with each heartcut. This means the analytes are not being removed from the sand at the same rate. The concentration of benzene, proportional to peak height, starts out at a maximum then gradually decreases with each subsequent heartcut injection until completely removed after 17 min. Ethyl benzene, on the other hand, does not reach a maximum concentration until the second heartcut then gradually decreases in concentration until disappearing after 30 min.

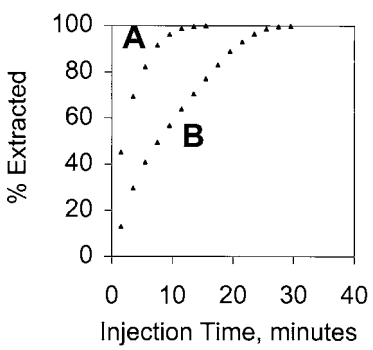

Fig. 5. Running-sum percentage of benzene (A) and ethyl benzene (B) extracted as a function of injection time for the extraction data (peak areas) presented in Fig. 4.

To quantitate this behavior, Fig. 5 shows the total percentage of analyte extracted as a function of the injection time for each heartcut. Quantification was done by first integrating the area under each peak for each heartcut. The area under any one peak expressed as a percentage is then calculated by dividing the area under that one peak by the total area. From Fig. 5 one sees that the first heartcut at 1.5 min contains approximately 45% of the total benzene extracted and detected. The percent extracted continues to increase sharply with total extraction occurring with the heartcut made at 17 min. At the same time, the first heartcut only contains roughly 15% of the ethyl benzene total extracted and detected. Moreover, the rate of extraction of ethyl benzene is not as fast as benzene. The observation of different extraction rates may be used to gain additional chemical selectivity. The source of this selectivity in SWE is due to a combination of differential extraction rates and relative solubility of each analyte passing through the cooling coil prior to the separation step.

Chemical analysis by SWE/WRP-LC was repeated again using benzene and ethyl benzene in the sample cell along with the addition of naphthalene. Sea sand placed in the extraction cell was spiked with 40 mg each of benzene and ethyl benzene and 5 mg of naphthalene. Extraction and separation conditions were the same as those used in Fig. 3 except heartcuts were made every 5 min instead of every 2 min in order to allow for the elution of naphthalene by WRP-LC. The complete extraction data set is not shown for brevity. Naphthalene was not detected in the first heartcut though a substantial majority of the benzene and ethyl benzene were extracted. Naphthalene began to show in the second heartcut as are small amounts of the benzene and ethyl benzene. Fig. 6 shows the separation of benzene, ethyl benzene, and naphthalene made from the eighth heartcut injected onto the WRP-LC at 37.5 min. Detectable amounts of these analytes continued to elute from the extraction cell for 50 min.

The SWE/WRP-LC instrument was also applied for the characterization of a complex sample (gasoline) spiked into the sand matrix. Fig. 7(a) illustrates what is seen when unleaded gasoline is

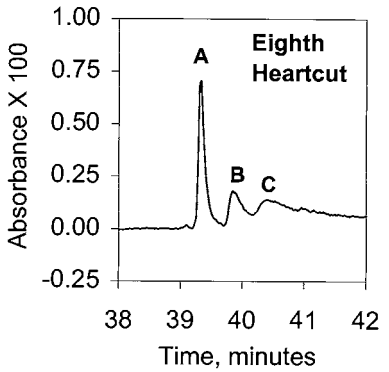

Fig. 6. The eighth heartcut from a SWE/WRP-LC of a mixture of benzene (A), ethyl benzene (B) and naphthalene (C) from sand. The injection was made at 37.5 min after beginning the extraction. A quantity of 40 mg benzene, and 40 mg ethyl benzene, and 5 mg naphthalene were spiked onto 2 ml of sand. The WRP-LC column and other experimental conditions were the same as in Fig. 4 except that heartcuts were taken 5 min apart. As a percentage, peak (A) and peak (B) represents approximately 0.5% of the total benzene and ethyl benzene detected, respectively, while peak (C) contains roughly 1% of the naphthalene.

spiked onto sand followed by extraction with subcritical water and injection onto a WRP column. A 20 mg quantity of gasoline was placed onto the sand, although no quantification of the results was attempted. The idea was to gain some insight into the chromatographic pattern that was obtained, which could possibly be used in rapid characterization. The first heartcut made at 1.5 min contains the largest fraction of analyte overall and while none of the components are well resolved, five peaks are apparent in the chromatogram, probably small aromatic compounds. Fewer peaks are seen in subsequent heartcuts along with decreasing peak heights (i.e. concentration) for those observed peaks. To emphasize the chemical selectivity gained in the SWE procedure, heartcuts 1 and 6 were normalized to the same area and overlaid in Fig. 7(b) for comparison. From this figure the presence of differential extraction rates for analytes becomes more apparent. Indeed, a few analytes present in heartcut 1 are not present in heartcut 6, while a broad, pronounced peak in heartcut 6 is not seen in heartcut 1. Based on retention time, past experience with separating small aromatics on WRP columns, and the nature of the sample (gasoline), the early eluting analytes seen in heartcut 1 are most likely small aromatic compounds possibly containing polar groups (aldehydes, carboxylic acids, etc.) and as such are slightly more water soluble. These early eluting peaks in heartcut 1 are not seen in heartcut 6 as by that time they had been fully extracted. Likewise, only a small amount of the analyte(s) in the third peak of heartcut 6 had been extracted in the first heartcut due to lower solubility in water.

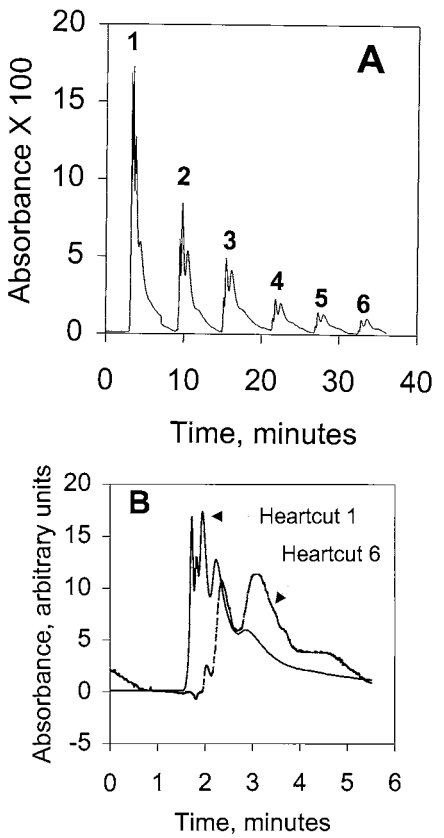

Fig. 7. SWE/WRP-LC of a 20 mg sample of unleaded gasoline on 2 ml of sand. All experimental conditions were the same as in Fig. 4 except that heartcuts were taken 5 min apart. (A) Depicts all six of the heartcuts taken while (B) illustrates the data for heartcuts one and six normalized to the same area and overlaid.

4. Conclusions

Two different chemically bonded stationary phases which can operate in a reversed phase mode using a mobile phase of 100% water have been synthesized and their chromatographic performance demonstrated. The branch stationary phase synthesized produced an efficient separation of four hydrophobic analytes with the unretained analyte producing 12 000 plates while the unretained analyte on the brush phase eluted with an efficiency of 16 000 plates. At a retention factor of one, however, the branch phase produced slightly more than 2.5 times as many plates as the brush phase. The optimum reduced plate height value of two was also approached on the brush phase indicating the column was operating in the high performance region. These results work toward the goal of developing robust and efficient stationary phases capable of performing reversed phase separations without the need for organic solvents in the mobile phase.

We also demonstrated an application of WRP-LC by interfacing it with subcritical water extraction. Hydrophobic organic compounds were repeatedly extracted from a solid matrix using a solvent system of 100% water with the extracted analytes then separated on a WRP-LC column, in order to characterize the data obtained by SWE/WRP-LC.

Acknowledgements

We thank the Center for Process Analytical Chemistry (CPAC), a National Science Foundation University/Industry Cooperative Research Center at the University of Washington, for financial support.

References

[1] J.L. Glajch, J.J. Kirkland, L.R. Snyder, J. Chromatogr. 238 (1982) 269.
[2] S.D. Fazio, S.A. Tomellini, H. Shih-Hsien, J.B. Crowther, T.V. Raglione, T.R. Floyd, R.A. Hartwick, Anal. Chem. 57 (1985) 1559.
[3] B.L. Karger, L.R. Snyder, C. Horvath, An Introduction to Separation Science, Ch. 5, Wiley Interscience, New York, 1973.
[4] M.D. Foster, R.E. Synovec, Anal. Chem. 68 (1996) 2838.
[5] R.P.W. Scott, Silica Gel and Bonded Phases, Wiley, New York, 1993.
[6] S.O. Akapo, A. Furst, T.M. Khong, C.F. Simpson, J. Chromatogr. 471 (1989) 283.
[7] S.O. Akapo, R.P.W. Scott, C.F. Simpson, J. Liq. Chromatogr. 14 (2) (1991) 217.
[8] G. Buamah, M.Sc. Thesis, Birkbeck College, University of London, 1996.
[9] S.O. Akapo, R.P.W. Scott, C.F. Simpson, J. Chromatogr. Sci. 14 (1991) 217.
[10] S.B. Hawthorne, Y. Yang, D.J. Miller, Anal. Chem. 66 (1994) 2912.
[11] Y. Yang, S. Bøwadt, S.B. Hawthorne, D.J. Miller, Anal. Chem. 67 (1995) 4571.
[12] K.J. Hageman, L. Mazeas, C.B. Grabanski, D.J. Miller, S.B. Hawthorne, Anal. Chem. 68 (1996) 3892.
[13] S.B. Hawthorne, Anal. Chem. 62 (1990) 633A.
[14] R.W. Vannoorl, J.-P. Chervet, H. Lingeman, G.J. DeJong, U.A.TH. Brinkman, J. Chromatogr. 505 (1990) 45.
[15] T.L. Chester, J.D. Pinkston, D.E. Raynie, Anal. Chem. 68 (1996) 487R.
[16] J.J. Langenfeld, S.B. Hawthorne, D.J. Miller, J. Pawliszyn, Anal. Chem. 65 (1993) 338.
[17] J.J. Langenfeld, S.B. Hawthorne, D.J. Miller, M.D. Burford, Anal. Chem. 64 (1992) 1614.
[18] N. Alexandrou, J. Pawliszyn, Anal. Chem. 61 (1989) 2770.
[19] N. Alexandrou, J. Pawliszyn, Anal. Chem. 64 (1992) 301.
[20] T. Paschke, S.B. Hawthorne, D.J. Miller, B.J. Wenclawiak, J. Chromatogr. 609 (1992) 333.
[21] F.I. Onuska, K.A. Terry, J. High Resolut. Chromatogr. 12 (1989) 357.
[22] B.W. Wright, C.W. Wright, R.W. Gale, R.D. Smith, Anal. Chem. 59 (1987) 38.
[23] J.R. Wheeler, M.E. McNally, J. Chromatogr. Sci. 27 (1989) 534.
[24] J.J. Langenfeld, S.B. Hawthorne, D.J. Miller, J. Pawliszyn, Anal. Chem. 66 (1994) 909.
[25] J. Pawliszyn, J. Chromatogr. Sci. 31 (1993) 31.
[26] J.R. Dean (Ed.), Applications of Supercritical Fluids in Industrial Analysis, Blackie Academic, Glasgow, 1993.
[27] L.T. Taylor, Supercritical Fluid Extraction, Wiley, New York, 1996.
[28] S.A. Westwood (Ed.), Supercritical Fluid Extraction and its use in Chromatographic Sample Preparation, Blackie Academic, Glasgow, 1993.
[29] J.W. Hill, H.H. Hill, J. Chromatogr. Sci. 31 (1993) 6.
[30] I.J. Barnabas, J.R. Dean, W.R. Tomlinson, S.P. Owen, Anal. Chem. 67 (1995) 2064.
[31] C.M. Wai, Y. Lin, R.D. Brauer, S. Wang, W.F. Beckert, Talanta 40 (1993) 1325.
[32] Y. Lin, C.M. Wai, F.M. Jean, R.D. Brauer, Environ. Sci. Technol. 28 (1994) 1190.

[33] S. Wang, C.M. Wai, J. Chromatogr. A (1997) in press.
[34] D.J. Miller, S.B. Hawthorne, Anal. Chem. 69 (1997) 623.
[35] L. Haar, J.S. Gallagher, G.S. Kell, National Bureau of Standards/National Research Council Steam Tables, Hemisphere, Bristol, PA, 1984.
[36] D. Mackay, W.Y. Shiu, J. Chem. Eng. Data 22 (1977) 399.
[37] N.D. Sanders, Ind. Eng. Chem. Fundam. 25 (1986) 171.
[38] B.D. Drakes, R.L Smith Jr., J. Supercrit. Fluids 3 (1990) 162.
[39] K.K. Unger, In porous silica, Elsevier, J. Chromatogr. Lib. 16 (1976) 66.
[40] B.L. Karger, K. Conroe, H. Engelhardt, J Chromatogr. 8 (1970) 242.
[41] J.C. Giddings, Unified Separation Science, Ch. 10–12, Wiley-Interscience, New York, 1991.
[42] J.H. Knox, M. Saleem, J. Chromatogr. Sci. 10 (1972) 80.
[43] C. Horvath, H.J. Lin, J. Chromatogr. 149 (1978) 43–70.

ELSEVIER

Talanta 45 (1998) 1201–1210

Talanta

Use of zirconium oxychloride to neutralize HF in the microwave-assisted acid dissolution of ceramic glazes for their chemical analysis by ICP-OES

M. Dondi, B. Fabbri *, C. Mingazzini

CNR-IRTEC, Research Institute for Ceramic Technology, via Granarolo 64, 48018 Faenza (RA), Italy

Received 22 May 1997; received in revised form 16 July 1997; accepted 17 July 1997

Abstract

The use of a zirconium compound ($ZrOCl_2$) to neutralize HF in the microwave-assisted acid dissolution of ceramic glazes for their chemical analysis was tested. Zr is a strong complexing agent for the fluorine ion and permits the determination of those elements which would form insoluble fluorides. The use of Zr implies strong spectral interferences and a high salt content; however, we found that at least 27 elements can be measured with low detection limits, and satisfactory precision and accuracy. In addition, the use of $ZrOCl_2$ would permit the complete analysis of a ceramic glaze with a single attack when acid-resistant mineral phases are not present. For potassium determinations in acid matrix, the addition of an ionization buffer was studied in order to increase sensitivity, avoiding ionization interferences and non-linear calibration curves. © 1998 Elsevier Science B.V.

Keywords: Ceramic glazes; Microwave-assisted sample preparation; ICP-OES; HF complexation; Chemical analysis

1. Introduction

Ceramic glazes are produced starting from many different synthetic and natural materials (Table 1). Part of the raw materials are mixed into a rotary kiln, fused and poured into water to obtain glasses (the so-called 'frits'). Various frits and unfritted raw materials are then mixed to obtain the desired glazes. There is in fact a wide composition range for ceramic frits and glazes, depending on the required characteristics of fusibility, brightness, colour, etc. Because the composition of frits can vary significantly during the processing, due to volatilization and/or incomplete fusion, routine analysis is needed.

Of the different instrumental techniques today available for elemental analysis, ICP-OES is the most suitable for ceramic materials, but methodologies for sample decomposition must be applied. A scheme for the total chemical analysis by ICP-OES of ceramic glazes must comprise at least two attacks. Boric alkaline fusion is necessary to determine those elements which are present in acid-resistant mineral phases while the constituents of the flux and the volatile elements must

* Corresponding author. Tel: +39 546 699718; fax: +39 546 46381; e-mail: fabbri@irtec1.irtec.bo.cnr.it

PII S0039-9140(97)00227-0

Table 1
Principal raw materials and elements of interest in industrial ceramic frits and glazes

Raw material	Elements
Feldspars; kaolin; lead oxide; borates; dolomite; Ba, Ca and K carbonates; Na and K nitrates; zinc oxide; alumina	Network forming and modifying cations: Al, B, Ca, K, Li, Mg, Na, Si, Pb, Zn
Zircon ($ZrSiO_4$) and cassiterite (SnO_2), used to give the white-opaque colour	Minor elements (colour): As, Ba, Bi, Cd, Co, Cr, Cu, Fe, Mn, Ni, P, S, Sb, Sr, Ti, V, etc.
	Elements contained in acid resistant mineral phases: Zr, Hf, Sn

be determined subsequently [1]. We tested possible methodologies of acid attack to couple with fusion with $Li_2B_4O_7$. The use of fluoridic acid in a sealed vessel (Fig. 1) allows the dissolution of the sample without loss of volatile species (particularly SiF_4 and BF_3), but complexing HF after the attack is necessary to dissolve insoluble fluorides. To this purpose boric acid is normally used [2]. Alternatively many metallic cations which form very stable complexes with F^- could be theoretically used [3], but practically only Al^{3+} has been proposed for the determination of boron in geological materials [4,5]. The use of aluminium for the complete analysis of ceramic glazes is not possible because of the precipitation of some insoluble fluorides and the impossibility of determining Al itself, so zirconium oxychloride seems the best choice.

2. Experimental

2.1. Instrumentation and reagents

Microwave-assisted digestions were performed with the Milestone® MLS 1200 microwave oven, equipped with the HPV 80 TFM® digestion vessels (resisting up to 10 MPa and 330°C) and internal TFM® liners.

The solutions were analysed with the Varian® Liberty 200 sequential ICP-OES, equipped with a 1800 grooves mm^{-1} holographic grating, a 0.75-m focal length Czerny-Turner optical system, a V-groove nebulizer, a Sturman-Master inert nebulization chamber and a demountable torch with an alumina injector. The RF generator is based on a 40.68 MHz crystal-controlled oscillator. For measuring emission lines below 190 nm, the monochromator is evacuated and the optical path between the plasma and the entrance slit purged with argon.

Bidistilled water, reagent grade salts and acids (HNO_3 16 M, HCl 12 M, HF 29 M) were used throughout. Three multielemental calibrating solutions (Table 2) were prepared starting from 23 Titrisol® standard solutions and one multielemental standard solution (Merck®, multi-element solution IV). All the reagents used for the

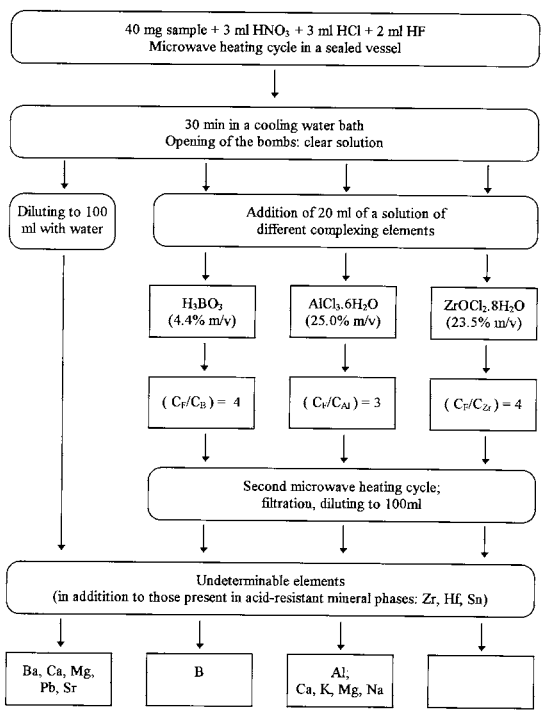

Fig. 1. Comparison of different methodologies of acid attack for the analysis of ceramic glazes.

Table 2
Elemental concentration of the multielemental calibrating solutions

Element ($mg\,l^{-1}$)	Solution		
	S1	S2	S3
Al	11	106	40
As	2	20	
B	1	6	50
Ba	1	6	10
Bi	1	6	
Ca	11	106	40
Cd	1	6	
Co	1	6	10
Cr	1	6	10
Cu	1	6	10
Fe	11	6	40
Ga	1	6	
In	1	6	
K	41	6	20
Li	1	6	20
Mg	11	6	40
Mn	1	6	10
Na	41	6	20
Ni	1	6	20
PO_4	2	20	
Pb	1	6	100
Sb	2	20	
Si	200	100	50
Sn	2	20	50
Sr	1	6	10
Ti	2	20	
V	2	20	
Zn	1	6	100

dissolution of the samples were added to the standard solutions; the blank solution was prepared in the same way.

Reagent grade $ZrOCl_2 \cdot 8\ H_2O$ was purchased from Fluka®. This salt contains $\leq 0.005\%$ Ca, Na, K, SO_4 and Ti; $\leq 0.001\%$ Cr, Fe and Pb; $\leq 0.0005\%$ Cd, Co, Cu, Mg, Mn, Ni and Zn; in addition we determined about 0.43% of hafnium. First, 235 g of salt were dissolved in some 700 ml of water prior adding 165 ml of HCl as stabilizer. The solution was then filtrated and diluted to one litre to obtain a 0.72 M Zr solution.

2.2. Procedure for microwave-assisted decomposition

A fraction of 40 mg of sample is weighed in the TFM® liner and this is introduced in the HPV 80 bomb. Then 3 ml HNO_3, 3 ml HCl and 2 ml HF are added in this order, taking care to wet the solid homogeneously; then the cap is screwed up. Three vessels are introduced into the oven and the microwave program is started. A heating cycle of 250 W for 10 min, 0 W for 10 min, 250 W for 10 min, 0 W for 10 min is suitable to prevent an excessive heating and the opening of the containers during the treatment. Then the bombs are cooled in a water bath at least for 30 min; the caps are unscrewed and 20 ml of the 0.72 M Zr solution are added before a second short heating cycle (250 W for 10 min). Then the solution is transferred into a plastic calibrated flask and diluted to 100 ml with distilled water. This solution is used for the determination of all the elements except K. For the determination of K, 25 ml of solution are pipetted into a plastic bottle and 0.5 ml of 9.7% m/v CsCl solution are added, to obtain a final solution containing 1.5 $g\,l^{-1}$ Cs.

2.3. Analysis of solutions by ICP-OES

Because of the high concentration of Zr and Hf in the sample solutions (13.2 and 0.2 $g\,l^{-1}$, respectively) also very weak non-tabulated emission lines of these elements can cause relevant spectral interferences [6]. The analytical lines chosen, together with the interferences detected on the usually adopted analytical lines, are reported in Table 3.

Due to the high salt content of solutions, the best sensitivity together with good reproducibility were generally obtained adopting high power and low nebulizer pressure (Table 4). The optimum viewing height was 8 mm for most elements; 18 mm were adopted for Na and Mg, to reduce the background intensity and to avoid the detection saturation respectively. For the lower energy lines (Li, K) the power was reduced while for the higher energy lines (S, P) it was increased to the maximum value allowed.

Table 3
Analytical lines and interferences detected in $HF-ZrOCl_2$ solutions

Element	Analytical lines (nm)		
	Chosen	Alternative	Interfered (by Ar, Hf or Zr)
Al	309.27(I)	394.40(I); 236.71(I); 308.22(I)	396.15(I); 237.31(I); 167.08(II)
As	188.98(I)		193.70(I)
B	249.68(I)	249.77(I)	
Ba	493.41(II)	614.17(II); 649.69(II)	455.40(II)
Bi	223.06(I)		306.77(I); 222.83(I)
Ca	317.93(II)	393.36(II); 396.85(II)	
Cd	214.44(II)	226.50(II)	
Co	238.89(II)		228.62(II); 237.86(II)
Cr	205.55(II)		267.72(II); 206.15(II)
Cu	223.01(II)	224.70(II)	324.75(I); 327.40(I)
Fe	238.20(II)	259.94(II)	
K	769.90(I)	766.49(I)	
Ga	294.36(I)	Line not suitable for traces	
In	410.18(I)	Line not suitable for traces	
Li	610.36(I)		670.78(I)
Mg	279.55(II)		
Mn	293.93(II)	257.61(II); 259.37(II)	
Na	588.90(I)		589.59(I)
Ni	231.60(II)	232.00(I)	221.65(II)
P	177.50(I) 185.94(I)	213.62(I); 178.77(I)	214.91(I); 253.57(I)
Pb	217.00(I)		All other principal lines
S	182.03(I)		180.73(I)
Sb	217.92(I)	206.83(I)	217.58(I); 231.15(I)
Si	251.61(I)	288.16(I)	
Sn	189.93(II)	235.48(I)	All other principal lines
Sr	407.77(II)		216.57(II); 421.55(II)
Ti	334.94(II)		
V	311.84(II)		All other principal lines
Zn	213.86(I)		

The ratio Mg(II) 280 nm to Mg(I) 285 nm is reported as a parameter of excitation condition, independent of the instrumentation. The high values relative to all the elements, except potassium, are high enough to indicate low matrix effects [7,8]. In contrast the low value relative to K is associated to strong ionization interferences and an ionization buffer is necessary.

3. Results and discussion

3.1. Reactions for complexing fluorine ion

Boric alkaline fusion is an essential part of a general scheme of analysis of ceramic glazes because acid-resistant phase minerals are often present. A suitable methodology of acid attack should permit at least the determination of the constituents of the alkaline flux (Li and B) and of elements which form volatile compounds (As, Cd, Pb, S, Sb and Zn, in particular). In our experience, losses of tin during fusion with $Li_2B_4O_7$ were negligible: this is very important because this element is normally present as acid-resistant cassiterite (SnO_2).

The block diagram in Fig. 1 shows that complexing of HF is necessary in order to determine those elements which otherwise would form insoluble fluorides (column 1), in particular Ba, Ca, Mg, Pb and Sr. The most classical procedure of HF complexation with boric acid is not useful in

Table 4
Operating parameters for measures by ICP-OES

Elements	Power (kW)	Ar flow rate ($l\,min^{-1}$)		Nebulizer pressure (kPa)	Viewing height (mm)	Mg(II)/Mg(I)
		Outer	Intermediate			
Al, As, B, Ba, Bi, Ca, Cd, Co, Cr, Cu, Fe, Mn, Ni, Pb, Sb, Si, Sn, Sr, Ti, V, Zn	1.5	16.5	2.25	150	8	9.50
Na, Mg	1.5	16.5	2.25	150	18	7.35
S, P	1.7	22.5	2.25	170	8	8.75
Li	1.2	15.0	2.25	150	8	7.60
K	0.8	10.5	2.25	300	6	0.65

Table 5
Calculated F^- concentrations in the sample solution for various composition of the attack mixture[a]

HF in the attack mixture (ml)	C_F/C_{Zr}	[F] in the final solution	Prediction	Observation
1.8	3.6	$2.0*10^{-6}$ M	Clear solution	Clear solution
2.0	4.0	$9.5*10^{-6}$ M	Clear solution	Clear solution
2.2	4.4	$3.3*10^{-5}$ M	Clear solution	Clear solution
2.4	4.8	$6.2*10^{-5}$ M	Clear solution	Clear solution
2.6	5.2	$9.3*10^{-5}$ M	Clear solution	Low losses of Ca
2.8	5.4	$1.2*10^{-4}$ M	$CaF_2\downarrow$	Losses of Ca

[a] Observations and predictions for the attack on the standard BCS 174/2 (43.2% CaO; 4.63% MgO; 11.90% P_2O_5).

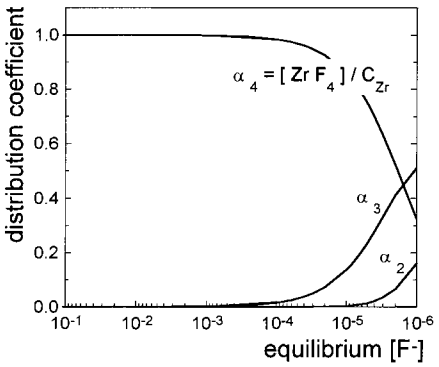

Fig. 2. Distribution diagram for zirconium (IV)–fluoride complexes.

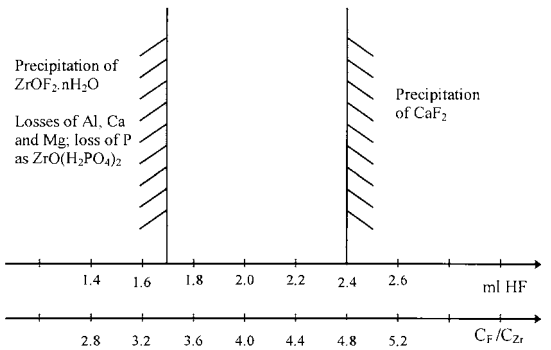

Fig. 3. Experimental results obtained by changing the amount of HF in the proposed dissolution procedure.

our case because of the impossibility of determining boron (column 2). The usage of $AlCl_3$ (column 3) was successfully tested in order to determine B, Li, Pb and Zn in ceramic glazes [9], but the precipitation of aluminium fluoride, probably in a hydrated form, and of many fluoroaluminates (Ca, K, Mg and Na) is a serious disadvantage.

The use of $ZrOCl_2$ is a possible alternative. The formation of a very stable complex between Zr^{4+} and F^- prevents the precipitation of insoluble fluorides. In addition no information from acid attack is lost, because Zr in glazes is generally

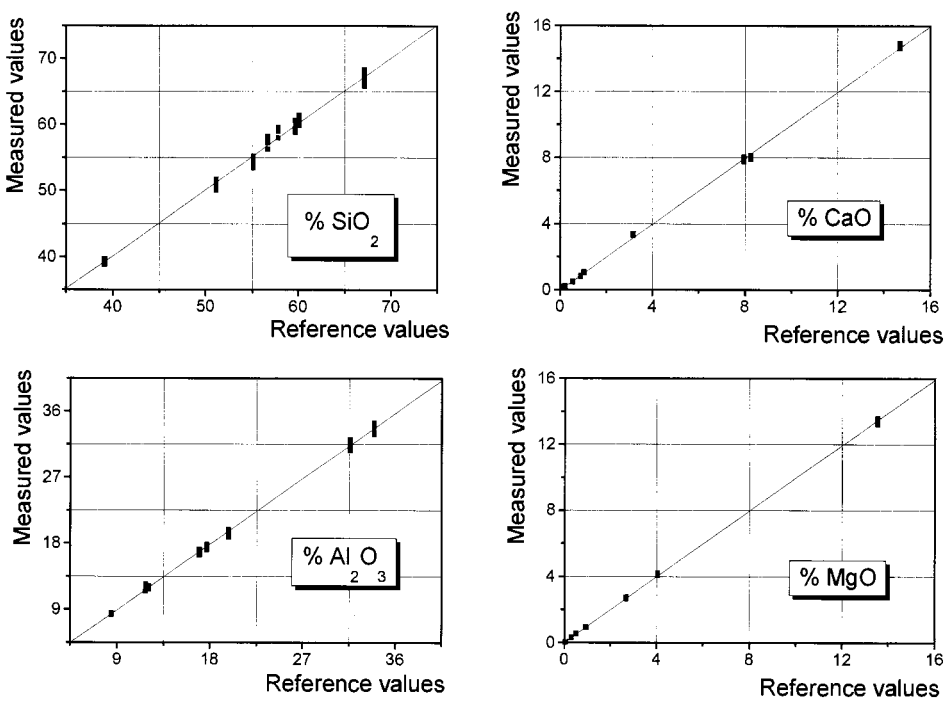

Fig. 4. Examples of plots of measured versus reference values for standard samples: the results of the different measures on the same solution are reported.

Table 6
Weighted regression parameters (and confidence interval with $P = 95\%$) for experimental versus reference plots

	Concentration range (wt%)	Correlation coefficient	Intercept (a)	Slope (b)
SiO_2	39.1–67.1	0.9960	0.035 ± 1.658	1.002 ± 0.029
Al_2O_3	0.1–33.9	0.9998	0.004 ± 0.026	0.991 ± 0.006
CaO	0.2–14.7	0.9994	-0.020 ± 0.016	0.997 ± 0.010
Fe_2O_3	0.1–17.9	0.9997	0.004 ± 0.004	1.001 ± 0.007
MgO	0.3–13.6	0.9998	0.002 ± 0.012	0.999 ± 0.006
Na_2O	0.3–10.4	0.9993	-0.005 ± 0.019	1.004 ± 0.013
TiO_2	0.1–3.8	0.9968	-0.004 ± 0.002	0.996 ± 0.026
K_2O[a]	0.8–11.2	0.9998	-0.061 ± 0.030	1.025 ± 0.006

[a] Cs added as ionization buffer.

present as acid resistant $ZrSiO_4$ and determined in the solution obtained by alkaline fusion.

The equilibrium concentration of free F^- in the sample solution was calculated by solving the system:

1. Acidity constant of HF: $[H^+][F^-]/[HF] = 6.6*10^{-4}$ M
2. Mass balance: $C_{Zr} = [ZrF_4] + [ZrF_3^+] = 0.15$ M
3. Mass balance: $C_F = 4[ZrF_4] + 3[ZrF_3^+] + [F^-] + [HF] = 0.52$ M
4. Complexation reaction: $\beta_4/\beta_3 = [ZrF_4]/[ZrF_3^+][F^-] = 10^{5.8}$ M^{-1}

Because the acidity constant of HF is very low, it can be assumed that:

$$[H^+] = C_{NO_3} + C_{Cl} + [F^-] \sim C_{NO_3} + C_{Cl} = 1.24 \text{ M}$$

Therefore, the F^- concentration can be calculated and results $9.5*10^{-6}$ M.

It should be noted that only the reaction $ZrF_3^+ + F^- \rightarrow ZrF_4$ was considered. The opportunity of this simplification can be deduced from the examination of the distribution diagram of the complexes between Zr and F in the concentration range of interest (Fig. 2), calculated from the stability constants [3].

Now it is possible to foresee if the masking of F with Zr prevents or not the precipitation of fluorides, in particular calcium fluoride, which is the most insoluble ($K_{sp} = 3.9*10^{-11}$ M^3). To this purpose we took into consideration a sample containing a very high quantity of calcium (international standard BCS 174/2, 43.2% CaO). In this case the threshold F^- concentration for precipitation would be $1.1*10^{-4}$ M, that is much higher than the calculated one. So calcium fluoride precipitation should not occur.

Because this approach is somewhat approxi-

Table 7
Experimental values (mean and confidence interval with $P = 95\%$) for B, Ba, Li, Pb and Zn in some reference materials

		Percentage				
		B_2O_3	BaO	Li_2O	PbO	ZnO
BCR 126A	ICP		1.05 ± 0.03	0.50 ± 0.01	24.0 ± 0.3	1.02 ± 0.06
	REF		1.04	0.50	24.0	1.02
MPC 08	ICP	11.28 ± 0.20	2.16 ± 0.05			
	REF	11.50 ± 0.30	2.05 ± 0.11			
MPC 12	ICP	10.30 ± 0.20	0.92 ± 0.02			1.49 ± 0.04
	REF	10.50 ± 0.20	0.92 ± 0.07			1.53 ± 0.04
NBS 181	ICP			6.20 ± 0.20		
	REF			6.39		

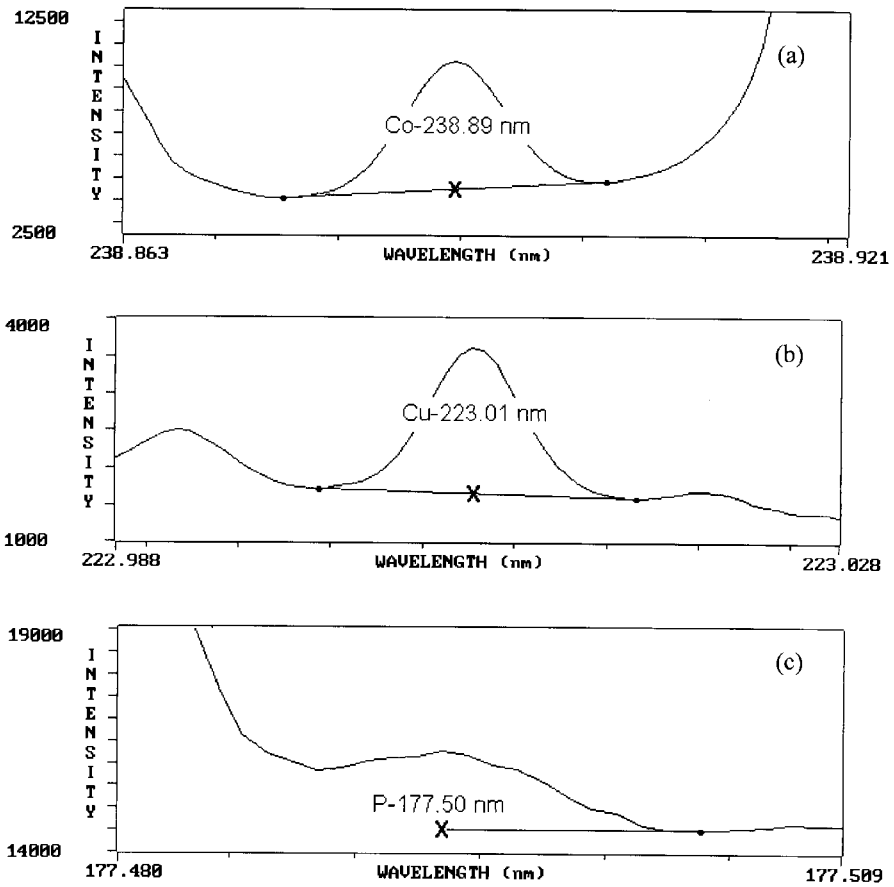

Fig. 5. ICP optical emission spectrum registered aspirating 1 mg l^{-1} of Co (a), Cu (b) and P (c).

mate, empirical observations were made by attacking the standard BCS 174/2. In order to determine the variation range of the quantity of HF which gives a clear solution, different amounts of HF were used (Table 5). A clear solution was obtained up to a maximum quantity of 2.4 ml of HF, so the empirical results and the theoretical values are in good accordance.

However, another important phenomenon should be considered: the precipitation of insoluble oxyfluorides when C_F/C_{Zr} is too low [10]. We found that precipitation of $ZrOF_2 \cdot n\ H_2O$ (with n around 5) occurs when the C_F/C_{Zr} molar ratio is below 3.4, which corresponds to 1.7 ml HF in the experimental conditions (Fig. 3). This phenomenon is independent of the sample because it occurs also during the preparation of the operational blank. In addition, if a sample is attacked, all the P and part of Al, Ca and Mg are lost. In conclusion, the range for HF volumes in order to inhibit precipitation of fluorides (1.7–2.4 ml) is large enough to prevent inaccuracy due to errors in pipetting HF.

3.2. Accuracy and precision for the proposed methodology

Certified reference materials (CCMET MRG1, SY2, SY3; BCS 269, 348, 375, 376; BCR 126A, NBS 181) and in-house standards (MPC) were dissolved by microwave-assisted decomposition and analysed. Al, Ca, Fe, Mg, Mn, Na, Ti and Si

Table 8
Results (mean and confidence interval with $P = 95\%$) obtained with and without ionization buffer

% K_2O	Reference values	Without Cs	1.5 g l^{-1} Cs
BCS 375	0.79	0.60 ± 0.02	0.75 ± 0.01
BCS 269	2.62	1.91 ± 0.04	2.56 ± 0.05
CCMET SY3	4.23	3.50 ± 0.05	4.29 ± 0.03
CCMET SY2	4.45	3.72 ± 0.02	4.53 ± 0.03
BCR 126A	10.00	9.13 ± 0.07	10.09 ± 0.08
BCS 376	11.20	10.27 ± 0.11	11.25 ± 0.07

were determined in an unique sequential program, repeated five times; a calibration was performed every hour. The results were plotted versus the reference data and the linear regressions were calculated for each analyte. Some examples are reported in Fig. 4. To account for the increasing standard deviation of the results with increasing concentration, a weight was attributed to each measured value, inversely proportional to the theoretical concentration of each reference material [11]. Calculated slopes and intercepts do not differ from the theoretical values, 1 and 0, respectively, with a significance level of 95% (Table 6), so accuracy can be considered satisfactory. In addition precision is very good because relative standard deviations are generally below 2%.

Bias of the results was checked also for B, Li, Pb, Zn and Ba by analysing some reference materials. The results obtained are reported in Table 7. The comparison between reference and obtained concentrations allows to affirm that accuracy and precision are good also for these elements.

The complexity of the emission spectra of Zr and Hf influences the detection limits in the HF–$ZrOCl_2$ matrix and a great care is necessary in the choice of the positions used for background corrections. Some scans are reported to show how critical this choice is in the worst cases (Fig. 5). In these cases only an accurate matrix matching of standards and samples and the use of a high resolution spectrometer can ensure accuracy at low concentration levels. However, estimated detection limits are generally below 0.01% of oxide in the sample (0.05% for P_2O_5 and SO_3); these limits are satisfactory for the chemical analysis of ceramic glazes.

3.3. Potassium determinations

In ICP-OES the sensitivity of potassium atomic lines is low and spectral interferences are important (Mg on K-766.49 and Zr on K-769.90), unless plasma power is reduced and the nebulization pressure of the sample increased. But such operating conditions (sometimes called 'cold plasma') decrease both the electron number density and the efficiency of the atomization processes.

In Table 8, the results obtained for potassium with and without ionization buffer are reported; the multielemental solution 1 (Table 2) and the blank solution were used for calibration. In this case, the data obtained without Cs addition are lower than the reference values. On the other hand, calibration curves performed with monoelemental standards are slightly non-linear (upward curvature) and the results obtained on the samples are higher than the real concentrations. Both effects are attributable to the low electron density corresponding to the 'cold plasma' conditions, while the influence of an incomplete atomization can be neglected.

A lot of experimental evaluations of electron density in normal plasma conditions can be found in the literature [12–14] while measured values in the 'cold plasma' conditions have not been reported [15]. Probably at low power the electronic concentration in the plasma decreases so much that the ionization equilibrium of potassium shifts depending on matrix concentration, a situation which resembles what happens in flames [16]. The addition of an Easy Ionized Element (EIE) as ionization buffer increases electron density and restores accuracy and linearity.

4. Conclusions

By complexing the fluorine ion with Zr^{4+}, instead of H_3BO_3 or Al^{3+}, the number of elements of a glaze which are determinable from a single acid attack was increased. Experiments and theoretical considerations demonstrated the robustness of the adopted dissolution procedure. Accuracy and precision of measures by ICP-OES were satisfactory, but an ionization buffer was necessary for K determinations. Limits of detection are compara-

tively high due to spectral overlaps with Zr and Hf emission spectra, however below the normal needs of the specific application, that is the chemical analysis of ceramic glazes. For the analysis of samples containing cassiterite, zircon and other acid-resistant mineral phases a second attack is necessary.

The complexation of HF with Zr^{4+} could be very useful for the analysis of vitreous coatings on finished ceramic articles. In fact, it would be possible to obtain quantitative results from controlled HF treatment of small areas (approximately 1 cm^2). Due to the fact that all the elements would be determined, it would be possible to take advantage of a final mass balance.

References

[1] B. Fabbri, F. Donati, Ceramurgia 12 (1983) 75.
[2] F.E. Smith, E.A. Arsenault, Talanta 43 (1996) 1207.
[3] A.E. Martell, R.M. Smith, Critical Stability Constants, vol. IV, Inorganic Complexes, Plenum Press, New York, 1976, p. 99.
[4] J.C. Mills, Anal. Chim. Acta 183 (1986) 231.
[5] B.A. Zarcinas, B. Cartwright, Analyst 112 (1987) 1107.
[6] E. Mentasti, C. Sarzanini, O. Abollino, G. Cocito, E. Modone, J. Anal. Atom. Spectrom. 4 (1989) 17.
[7] M. Mermet, Anal. Chim. Acta 250 (1991) 85.
[8] I. Novotny, J.C. Farinas, Jia-liang Wan, E. Poussel, J.-M. Mermet, Spectrochim. Acta 51B (1996) 1517.
[9] G. Guarini, C. Mingazzini, Intern. Rep. no. 6, IRTEC-CNR, Faenza, Italy, 1996.
[10] W.F. Linke, Solubilities of Inorganic and Organic Compounds, 4th ed., vol. II, Am. Chem. Soc., 1965.
[11] J.C. Miller, J.N. Miller, Statistics for Analytical Chemistry, Ellis Horwood, Chichester, 1984.
[12] D.S. Hanselman, N.N. Sesi, M. Huang, G.M. Hieftje, Spectrochim. Acta 49B (1994) 495.
[13] M.R. Tripkovic, I.D. Holclajtner-Antunovic, J. Anal. Atom. Spectrom. 8 (1993) 349.
[14] F. Fernandez, M. Murillo, N. Carrion, J.M. Mermet, J. Anal. Atom. Spectrom. 9 (1994) 217.
[15] S. Scott, D. Tanner, J. Anal. Atom. Spectrom. 10 (1995) 905.
[16] C.T.J. Alkemade, R. Herrmann, Fundamentals of Analytical Flame Spectroscopy, Adam Hilger, Bristol, 1979.

ELSEVIER

Talanta 45 (1998) 1211–1217

Talanta

Silicon determination by inductively coupled plasma atomic emission spectrometry after generation of volatile silicon tetrafluoride

A. Lopez Molinero *, L. Martinez, A. Villareal, J.R. Castillo

Department of Analytical Chemistry, Faculty of Sciences, University of Zaragoza, 50009 Zaragoza, Spain

Received 12 November 1996; received in revised form 10 July 1997; accepted 22 July 1997

Abstract

A method for the determination of silicon by inductively coupled plasma atomic emission spectrometry (ICP-AES) is described. The procedure is based on a discontinuous generation of volatile silicon tetrafluoride in concentrated sulphuric acid medium after injecting 125 μl of 0.1%, w/v sodium fluoride solution into 100 μl of the sample. The gaseous silicon tetrafluoride is fed directly into the ICP torch by a flow of 250 ml min^{-1} Ar carrier gas. The calibration curve was linear up to at least 100 μg ml^{-1} of Si(IV) and the absolute detection limit was 9.8 ng working with a solution volume of 100 μl. The relative standard deviation for six measurements of 10 μg ml^{-1} of Si(IV) was 2.32%. The method was applied to the determination of silicon in water and iron ores. © 1998 Elsevier Science B.V.

Keywords: Silicon determination; Volatile silicon tetrafluoride; Inductively coupled plasma atomic emission spectrometry

1. Introduction

Silicon is an important element and its determination is of analytical interest for different sample types [1]. There have been several reports concerning the determination of silicon in biological media by electrothermal atomic absorption spectrometry (ETAAS) and inductively coupled plasma atomic emission spectrometry (ICP-AES) [2–4]. Silicon is an essential trace element in humans and its determination in food has been carried out by ICP-AES [5]. In the semiconductor industry ultra-pure water is of the utmost importance and silicon is determined by ICP mass spectrometry (ICP-MS) [6]. Silicon is an important element in the steel industry and has been determined by ICP-MS in this type of matrix [7].

The interest in sensitive methods of silicon determination is evident but many of the methods reported have drawbacks or interferences, in ICP-MS from the polyatomic ions produced by nitrogen, oxygen, hydrogen and carbon or in ICP-AES due to the influence of the acid digestion mixtures when Si and other silicate-bound elements have to be dissolved.

* Corresponding author. Tel.: + 34 76 761290; fax: + 34 76 761292; e-mail: Qanal@msf.unizar.es

PII S0039-9140(97)00231-2

In atomic spectrometry the conversion of elements to volatile compounds as a method for sample introduction into the atomizer or vaporizer has been adopted in order to overcome problems of poor sensitivity and interferences. In particular, it has been applied to hydride forming elements [8].

The formation of volatile species of silicon as a possible way of increasing the sensitivity of its determinations has been studied. Two principal volatile species of silicon have been used in analytical literature: SiH_4 and SiF_4. The hydride generation of silane for the determination of silicate by ICP-AES has recently been reported [9]. The method involves adding a $LiAlH_4$ solution and heating at 700°C in order to generate the SiH_4 volatile phase prior to its introduction to an ICP. Silicon tetrafluoride is a gaseous compound of silicon, well known in classical analysis [10] but has hardly ever been used in instrumental silicon determination. Recently the generation of volatile SiF_4 was used in atomic spectrometry for the indirect determination of fluorine by direct current plasma atomic emission spectrometry [11].

In this paper silicon determination by means of the discontinuous generation of volatile silicon tetrafluoride and its direct introduction to an inductively coupled plasma spectrometer has been carried out.

2. Experimental

2.1. Instrumentation

A Perkin-Elmer (P-E) model Plasma-40 ICP-AES (Norwalk, CT) was used with the standard operating conditions as shown in Table 1. The system is equipped with an IBM XT 10 Mb Hard Disk computer and has P-40 software on memory. Signals were obtained with an analogic Omniscribe recorder series D5000 Recorder Mod. D5117-2.

Omnifit flow injection analysis equipment (injection valves, reaction coils, loops and connectors) was used for the mountings and a four channel Gilson Minipuls peristaltic pump. Tygon, nylon and PTFE tubes and conductions were also used. For gas conductions quick-connectors of different shapes and sizes were used.

2.2. Reagents and standards

A 1000 μg ml^{-1} standard silicon solution was prepared by fusing 0.2139 g of silicon dioxide (Sigma) with 2 g of sodium carbonate (Merck) in a platinum crucible. The melt was then dissolved in 100 ml of deionized water. This solution and its dilutions were stored in polyethylene flasks.

Sodium fluoride (Merck) and sulphuric acid (Panreac) were also used. The water was deionized, Milli-Q quality. All the chemicals used were of analytical grade.

2.3. Silicon tetrafluoride generation assembly

The flow chart for the generation of silicon tetrafluoride is shown in Fig. 1. The apparatus consists of a 3 ml reaction vessel made of PTFE. A rubber stopper, pierced and fitted to the reaction vessel is used. Sodium fluoride is injected with a FIA injection valve (Omnifit) equipped with a loop of 125 μl. A two-way key is used to lead the Ar carrier gas either to the reaction vessel or to the plasma. Nylon tubes of 2 mm i.d. are used and joined with quick connectors (Clifco series PM).

Table 1
Instumental parameters for ICP-AES (P-E plasma 40)

R.f. frequency (MHz)	40
Incident power (kW)	1
Torch	Demountable type P-E.
Injector tube	Alumina
Ar gas (99.995%) flow rates (dm^3 min^{-1})	
Outer	12
Intermediate	0.6
Nebulizer	1.0
Observation height (mm)	15
Spray chamber	Ryton
Silicon emission line (nm)	254.611

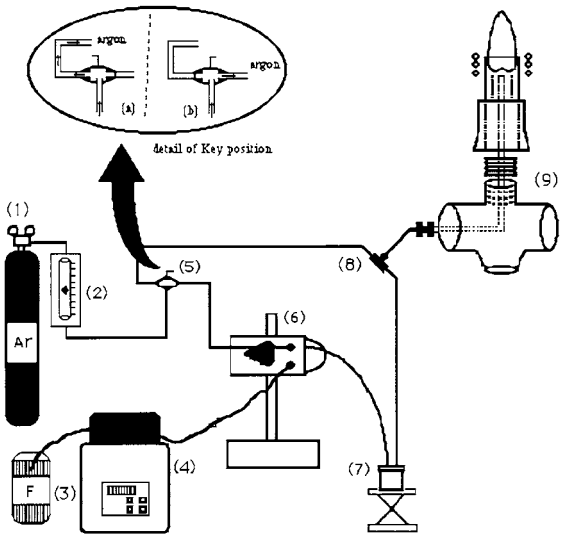

Fig. 1. Schematic diagram of the instrument assembly used. (1) Tank of argon; (2) carrier gas flow regulator; (3) fluoride ion solution; (4) peristaltic pump; (5) two-way key; (6) injection valve for fluoride solution; (7) reaction vessel; (8) three-port quick connector; (9) ICP torch.

2.4. Procedure of silicon tetrafluoride generation

Concentrated sulphuric acid (350 μl) and the sample solution containing silicon (100 μl) are placed in the reaction vessel. After stoppering the vessel, the Ar carrier gas (a steady flow of 250 ml min^{-1} is maintained) can be channelled throughout it. By setting the key (5) to position (b)(Fig. 1) the gas is first passed through the FIA valve, then through the reaction vessel and finally directed to the torch. A short period of time is needed to stabilize the plasma (30 s) prior to the injection of sodium fluoride (125 μl) via the FIA valve.

The atomic line of silicon at 251.611 nm is chosen to measure the emission intensity, which is continuously recorded and thus transient peaks are obtained. Once the recording of silicon emission has finished, the flow of Ar carrier gas through the FIA valve and the reaction vessel is interrupted by means of the key (5), which is rotated to its position (a), re-directing the flow of gas to the torch. In the latter position a stable plasma is maintained while a new sample is being prepared for analysis.

3. Results

3.1. Experimental assembly

Gaseous silicon tetrafluoride has never been introduced into an ICP spectrometer because when SiF_4 is generated, hydrofluoric acid must be in excess and it may produce corrosion of the glass or quartz nebulizer and plasma torch. Consequently it results in high values of blank silicon signals.

In this paper a new method for silicon determination has been used consisting of the discontinuous generation of silicon tetrafluoride by the classical reaction, and its direct introduction to the ICP spectrometer. In our experimental set-up the nebulizer and the nebulization chamber are not used, the nebulizer gas acts as a carrier gas and is channelled to the torch via the injector tube. The tube is made of alumina. This assembly is HF resistant and significantly reduces the blank signals.

3.2. Optimization of variables

The variables studied can be divided into three types.

- variables of the reaction vessel: size, volume.
- variables of the reaction, i.e. volume and concentration of the sample (silicon), fluoride ion and sulphuric acid. The order of the addition of reagents has also been studied.
- instrumental parameters of detection, i.e. injection gas flow and observation height.

A cylindrical shape for the reaction vessel was chosen and different sizes were tested (varying in section and height). The optimized vessel is the same as in a previous work [12].

Reaction and detection variables were optimized by means of the Simplex MSM [13] and Univariant methods. The following optimum values were adopted: 350 μl of concentrated sulphuric acid are first placed in the vessel: 100 ml of silicon solution are then added. The vessel is closed and shaken in order to obtain a homogeneous solution. Finally 125 μl of 0.1% (w/v) sodium fluoride solution are injected via a FIA manual injection valve. The Ar carrier gas was set

Table 2
Effect of the NaF solution concentration on both the blank emission and the Si emission intensity

% w/v NaF	Blank signal[a] (u.r.)	Silicon signal[b] (u.r.)	Net silicon signal (u.r.)
0.01	0.1	1.2	1.1
0.1	3.7	10.5	6.8
0.3	11.7	12.9	1.2
0.5	22.6	24.0	1.4

[a] Blank signal corresponds to the injection of 100 μl of deionized water, Milli Q.
[b] Silicon signal corresponds to the injection of 100 μl of 10 μg ml^{-1} of Si(IV).

to 250 ml min^{-1} and the observation height above the coil was set to 15 mm.

The order of the addition of reagents was studied. The best results were obtained when the generation of the exothermic dilution heat of sulphuric acid is favored. So this acid was placed into the vessel first and the sample or silicon solution was then added. Fluoride solution was injected last.

A range of sodium fluoride concentration from 0.01 to 1.0% (w/v) was studied. The highest values of concentration produced the highest value of silicon signals but with high values of blank signal. The results of Table 2 show the influence of NaF concentration on the blank emission.

As can be seen the best net signal (silicon signal–blank signal) was obtained for 0.1%, w/v. For 1.0% NaF the signals were over readings. The effect of the transport length between the reaction vessel and the ICP torch was studied. We worked with the shortest distance possible, which in our mounting was 15 cm.

3.3. Temperature in the reaction vessel

Silicon tetrafluoride has a boiling temperature of −86°C. It is low and allows its volatilization at ambient temperature, however it is favored by increasing the temperature of the solution. This is attained by the heat generated in the exothermic reaction between water and sulphuric acid. We determined the temperature in the reaction mixture experimentally by means of a Thermistor Thermometer Digitec model 704(type LN HB 1977) sounding line. In this way a temperature value of sulphuric acid prior to reaction of 26°C is obtained and after the addition of silicon solution and the injection of fluoride solution the temperature rose to 76°C. After 3 min the measured temperature was 49°C.

3.4. Performance of the method

The values of merit of this method were found when working in optimum conditions. A linear calibration graph $Y = 8.7643 + 2.7094X$ between 0.5 and 100 μg ml^{-1} of Si(IV) was found with a regression coefficient of 0.998. Y is the intensity of the silicon emission in relative units measured at 251.611 nm and X is the concentration of silicon in solution in μg ml^{-1}. Typical peak shapes obtained in this experiment are shown in Fig. 2. From this experiment, an instrumental detection limit (3 s) of 0.098 μg ml^{-1} can be derived. This detection limit, obtained with 100 μl of sample, corresponds to an absolute limit of detection of 9.8 ng. The reproducibility of the method is 2.32% r.s.d. based on six measurements of 10 μg ml^{-1} of Si. The blank control is also important data in this method. Previously, the influence of fluoride concentration on the blank emission has been shown. In the calibration experience typical blank signals were obtained with emission signals in the order of 0.3 u.r. and reproducibility in the order of 3%. From this blank signal a low blank concentration equivalent (less than 0.5 μg ml^{-1} of silicon) can be derived.

3.5. Interference

The effects of various cations and anions on the Si emission intensity were investigated. Permissible concentrations causing errors of less than 10% are given in Table 3. Alkaline elements in the

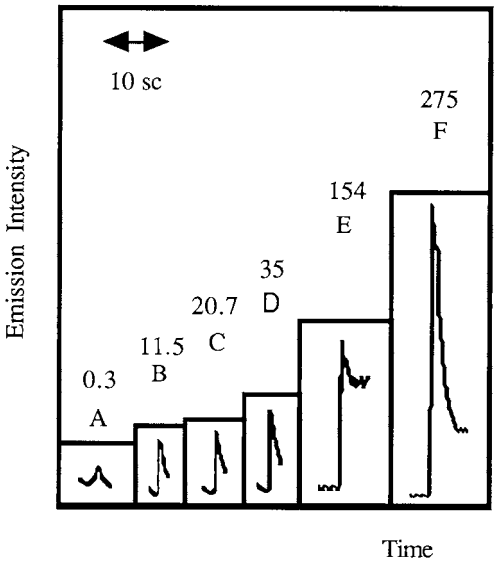

Fig. 2. Typical emission signals at silicon 251.611 nm produced by standard silicon solution: A, blank; B, 1; C, 5; D, 10; E, 50; F, 100 μg ml^{-1} silicon. The numbers next to the peaks are peak-height measurements in cm.

tested range did not interfere with the determination. However metalloid elements such as As(III) and B(III) might react with fluoride ions and generate their fluorides. Iron reacts in the same form with fluoride by formation of its complexes. Anions such as PO_4^{3-} and NO_3^- slightly interfered. The interference of chlorides produced an enhancement of the silicon signal. The interference of alkaline earth elements Ca^{2+}, Mg^{2+} and lead is produced by sulphate precipitation.

3.6. Application

The proposed method was applied to the determination of silicon in liquid and solid samples that is in water and iron ores. These two types of samples were not certified but their contents were compared with those obtained using standard or reference methods.

3.6.1. Silicon determination in water

Silicon determination was carried out in two different types of waters. Water sample number 1 was purchased mineral water and water sample number 2 was obtained from the city water net. When the new proposed method was applied only 100 μl of sample were injected. The results of this method were compared with those obtained with an alternative standard method by ICP-AES. This standard method was performed in the P-E ICP/plasma 40 working at standard conditions, given in Table 1, but with continuous nebulization of liquid samples using a cross-flow nebulizer. The results obtained are gathered in Table 4.

It can be seen that there is not a great difference between the values given by the standard ICP-AES method and the new proposed method.

3.6.2. Silicon in iron ores

Silicon content in iron ores which are used in iron oxide pigments for paints was determined using a reference gravimetric method [14] and the results compared with the results obtained with the new method.

Table 3
Tolerance limits of foreign ions for the determination of Si(IV) (results within 10% error)

Ion	Concentration ratio foreign ion/Si(IV)	Ion	Concentration ratio foreign ion/Si(IV)
Na^+	>800[a]	As(III)	>10
K^+	>800[a]	Sb(III)	>50
Ca^{2+}	>80	B(III)	>10
Mg^{2+}	>100	NH_4^+	>100
Pb^{2+}	>200[a]	PO_4^{3-}	>30 000[a]
Bi^{3+}	>400[a]	Cl^-	>8000
Fe^{3+}	>10	$CO_3^=$	>8000[a]
Al^{3+}	>400[a]	NO_3^-	>20 000[a]

Si(IV) as $NASiO_3$, 100 μl of 5 μg ml^{-1} of silicon were added. The foreign ions, 100 μl of the studied concentration (μg ml^{-1}) were added.

[a] Maximum concentration tested.

Table 4
Silicon content in water samples found by the standard method and the new proposed method

Method	Replicates	Water sample	
		No. 1 ($\mu g\ ml^{-1}$)	No. 2 ($\mu g\ ml^{-1}$)
Standard ICP-AES	5	5.3 ± 0.1	6.8 ± 0.4
ICP, volatile SiF_4	5	5.1 ± 0.6	6.5 ± 0.5

Results are expressed as the mean value $\pm$ S.D.

The gravimetric method was as follows: solid sample was dried, homogenized and ground under 20 μm. The sample (1–2 g) was decomposed by hydrochloric and nitric acid and evaporated to fumes. The residue was fused with sodium carbonate. Then the melt was dissolved with hydrochloric acid and the residues were removed by filtration. The silicon was then determined from the loss in weight resulting from treatment of the residue with hydrofluoric acid.

The new method was applied to the analysis of silicon in the same iron ores as the gravimetric method but with much more reduced amounts of the sample. It was evaluated using two different procedures of sample preparation.

Procedure 1: alkaline fusion. The sample (0.02 g) was decomposed by alkaline fusion with sodium carbonate. Then the solidified melt was dissolved with diluted hydrochloric acid. The new method was applied to this solution for the silicon determination. With this procedure the standard solutions for the calibration graph were prepared with the same concentration of Fe(III) and hydrochloric acid as the sample.

Procedure 2: insoluble residue. The sample (0.02 g) was decomposed by hydrochloric and nitric acid. The insoluble residue was filtered off and fused with sodium carbonate. The melt was dissolved with diluted hydrochloric acid. Silicon was determined in this solution by the new method. In this case the standard solutions for the calibration graph were prepared with the same concentration of hydrochloric acid as the sample. The results obtained are gathered in Table 5.

It can be seen that the procedure 1 of sample preparation gave higher contents of silicon than procedure 2 (exception sample number 3) however the difference is not important. From a practical point of view procedure 1 is more recommended (less laborious) than procedure 2. On the other hand the differences between the results found with gravimetric method and the results of the new method were not significant. It can be said that the analytical results obtained by the proposed method gave good agreement with those obtained by the gravimetric method.

4. Conclusion

The generation of silicon tetrafluoride in a batch mode allows the introduction of silicon in a ICP as volatile phase. This procedure is the basis of a new method to determine silicon by atomic

Table 5
Results obtained for determination of silicon in iron ores by a reference graviemetric and the new proposed method after the application of two different procedures for sample preparation

Method	Replicates	Iron ore		
		No. 1 $\%SiO_2$ (w/w)	No. 2 $\%SiO_2$ (w/w)	No.3 $\%SiO_2$ (w/w)
Gravimetric	1	7.4	7.8	7.7
ICP, volatile SiF_4 after alkaline fusion procedure 1	4	9.6 ± 1.3	7.6 ± 0.4	7.6 ± 0.2
ICP, volatile SiF_4, after insoluble residue procedure 2	4	7.4 ± 0.2	7.0 ± 0.7	8.0 ± 0.6

Results are expressed as the mean value $\pm$ S.D.

emission spectrometry. The use of a FIA assembly reduces the size of the sample to 100 μl and a low absolute detection limit of 9.8 ng is obtained. The proposed method can be applied to the determination of Si in liquid and solid samples such as water and iron ores.

Acknowledgements

This work was financed by project 93/0306 of the Spanish DGICYT.

References

[1] A.P. Krushevska, R.M. Barnes, J. Anal. At. Spectrosc. 9 (1994) 981.
[2] R. Kobayasahi, K. Imaizumi, M. Kudo, Anal. Sci. 11 (1995) 267.
[3] Z. Huang, Spectrochim. Acta 50B (1995) 1383.
[4] K. Wrobel, E. Blanco, A. Sanz-Medel, J. Anal. At. Spectrom. 8 (1993) 915.
[5] A.P. Krushevska, R.M. Barnes, Analyst 119 (1994) 131.
[6] Y. Takaku, K. Masuda, T. Takahashi, T. Shimamura, J. Anal. At. Spectrom. 9 (1994) 1385.
[7] H.M. Kuss, D. Bossmann, M. Muller, At. Spectroc. 15 (1994) 148.
[8] M. Thompson, B. Pahlavanpour, S.J. Walton, G.F. Kirkbright, Analyst 103 (1978) 705.
[9] T. Kumamaru, M. Uchida, K. Fujiwara, Y. Okasmoto, K. Fujiwara, Appl. Spectrosc. 49 (1995) 76.
[10] J.A. Stobart, Analyst 94 (1969) 1142.
[11] N. Barnett, H. Beere, L. Ebdon, B. Fairman, J. Anal. At. Spectrom. 4 (1989) 805.
[12] A. Lopez Molinero, A. Ferrer, J.R. Castillo, Talanta 40 (1993) 1397.
[13] J.A. Nelder, R. Mead, Comput. J. 7 (1965) 308.
[14] British Standard Institution, Method for the determination of silicion in iron ores (gravimetric method), BS 4158: part 3, London, UK, 1972.

ELSEVIER

Talanta 45 (1998) 1219–1225

Talanta

Potentiometric study of the mixed-metal complex formation of tetracarboxylate-18-crown-6 with aluminum and alkali and alkaline earth cations

Nahid Tavakkoli [a], Mojtaba Shamsipur [b,*]

[a] *Department of Chemistry, Shiraz University, Shiraz, Iran*
[b] *Department of Chemistry, Razi University, Kermanshah, Iran*

Received 15 January 1997; received in revised form 7 July 1997; accepted 22 July 1997

Abstract

We give evidence for the formation of mixed-metal complexes of tetracarboxylate-18-crown-6 in the form of Al^{3+}-macrocycle-M^{Z+}, with M^{Z+} being an alkali or an alkaline earth cation. These binuclear systems are characterized by potentiometric p[H] titrations and the equilibrium constants for all major complexes formed are described. The results are presented in the form of distribution diagrams revealing the concentrations of individual complex species as a function of p[H]. The stability of the resulting mixed-metal complexes with Al^{3+} and alkali and alkaline earth cations vary in the order $Na^+ > K^+ > Cs^+$ and $Ca^{2+} > Sr^{2+} > Ba^{2+}$. The complex behavior can be rationalized in terms of electrostatic interactions and direct coordination of the cations by the carboxylate groups from the crown ether periphery. © 1998 Elsevier Science B.V.

Keywords: Tetracarboxylate-18-crown-6; Mixed-metal complex; Al^{3+}; Alkali; Alkaline earth; p[H]-metry

1. Introduction

Although the formation and characteristics of mixed-ligand ternary complexes are frequently reported [1–4], the study of mixed-metal complexes in solution has received much less attention. Martell and co-workers have recently shown some interesting results on the solution study of homobinucleating macrocyclic and macrobicyclic ligands with transition metal ions and the ability of these complexes to combine with various anions as bridging groups. [5–9]. However, in comparison, the study in solution of mixed-metal complexes having one ligand and two different metal ions is quite sparse [10,11].

Among different parameters influencing the complexation of crown ethers with metal ions [12,13], substitution on the macrocyclic ring has found to play an important role [14–21]. The polycarboxylate-18-crown-6 ethers derived from tartaric acid in particular possess very interesting features [19–21]. The tartrate derived units impart some rigidity to the 18-crown-6 ring which leads to well defined conformations. In addition, the

* Corresponding author.

PII S0039-9140(97)00236-1

ionized carboxylate groups result in a strong electrostatic field which can greatly enhance the complex stability for alkali and alkaline earth cations [19]. Thus, the carboxylate groups may act as additional ligating sites as was observed in the case of lariat ethers [22,23]. There is some spectroscopic evidence which strongly suggest the direct and cooperative carboxylate-cation interactions, especially in the case of small cations of high charge density [24–26].

Further to our research work on the thermodynamics [14–18,27–31] and kinetics [32–36] of complexation of macrocyclic ligands with different metal ions, we have recently studied mixed-ligand [37] and mixed-metal complexes with some cyclic and acyclic ligands [38,39]. The possibility of formation of homo- and heterobinuclear complexes is attributed to a series of factors, among which are the presence of two complexing sites of well separated coordinating centers [40]. In this paper we used tetracarboxylate-18-crown-6 (TC18C6, I) as a potential candidate to study its heteronuclear complexes MM′TC18C6 (where $M = Al^{3+}$ and $M' =$ alkali and alkaline earth cations) in aqueous solution at 25°C and ionic strength of 0.05 M by a p[H] metric method. It is well known that the Al^{3+} ion possesses a high tendency to interact with the carboxylate groups [41] of TC18C6 rather than the donating oxygen atoms in its macrocyclic cavity [42], while an opposite behavior has been reported for the alkali and alkaline earth cations [19,20,42]. Thus, the ionic species selected were expected to form some mixed-metal complexes Al^{3+}-TC18C6-M^{Z+} with the ligand.

2. Experimental

Reagent grade crown ether TC18C6 (Merck) was of the highest purity available and used without any further purification except for vacuum drying over P_2O_5 for 72 h. All other reagents used were of analytical grade and vacuum dried before use. All of the metal nitrate (Merck and Fluka) stock solutions were made up with triply distilled deionized water. The base used for potentiometric p[H] titrations was carbonate free tetrabutyl-ammonium hydroxide (Merck), which was standardized against primary standard ovendried potassium hydrogen phthalate (Merck). A CO_2-free atmosphere for the base was ensured throughout.

The potentiometric apparatus used consisted of a 100-ml glass jacketed cell, a constant temperature bath (Lo-Temprol 154 thermostat, 25.0 ± 0.1°C), glass and reference (Calomel) electrodes and a 10 ml capacity Metrohm piston burette, for which the tip was sealed in the cap of the titration cell with a clamp and O-rings. Atmospheric CO_2 was excluded from the titration cell with a purging stream of purified nitrogen gas. The electrodes were calibrated in the thermostated cell with standard acid base to read p[H] directly ($p[H] = -\log [H^+]$). The value of $K_W = [H^+][OH^-]$ used in the computations was $10^{-13.78}$ [40]. In all experiments, a 5.0×10^{-4} M solution of the ligand was used. The ionic strength was adjusted to 0.05 M with tetraethylammonium perchlorate (TEAP, Merck). Before an experimental point (p[H]) was measured, sufficient time was allowed for establishment of equilibrium.

Ligand protonation constants and metal-macrocycle complexes' protonation, stability and hydrolysis constants were calculated using the program BEST methods described by Martell with Motekaitis [43].

3. Results and discussion

Daly et al. [44], previously reported the crystal and molecular structure of the 1:1 complex between enthylenediammonium cation and TC18C6. It was shown that the macrocycle is roughly planar and the carboxy groups of each tartaric acid residue are in diaxial relationship extending above and below the macrocycle's plane, so that their lateral interactions with bound species would be possible. In the crystalline form, the substrate dication was clearly found to locate between two macrocycles, with one $-NH_3^+$ site anchored to the top of a ligand core and the other $-NH_3^+$ group is in contact with the two carboxy groups at the bottom of a neighbouring complex molecule. These results led us to investigate the

possibility of the formation of mixed-metal complexes (with two different metal cations instead of a diammonium cation for each ligand molecule) of TC18C6 in aqueous solution. It should be noted that the 1:1 complexation of this macrocycle with some alkali and alkaline earth cations has already been reported by Dalton et al.[19].

We employed potentiometric titrations to investigate the mixed-metal complexes of TC18C6 with Al^{3+} and Na^+, K^+, Cs^+, Ca^{2+}, Sr^{2+} and Ba^{2+} ions in aqueous solution. The equilibrium potentiometric p[H] titration profiles of the free ligand appear with 1:1 and 1:2 molar ratio to Al^{3+} ion in Fig. 1. The protonation constants ($K_n^H = [H_nL]/[LH_{(n-1)}][H]^n$) were calculated by fitting the potentiometric p[H] data to the program BEST [41]. The results are listed in Table 1, together with the previous results, for comparison. The species distribution of TC18C6 in the absence of metal ions is shown in Fig. 2. It is seen that the ligand exists solely in completely deprotonated form at p[H] > 6.

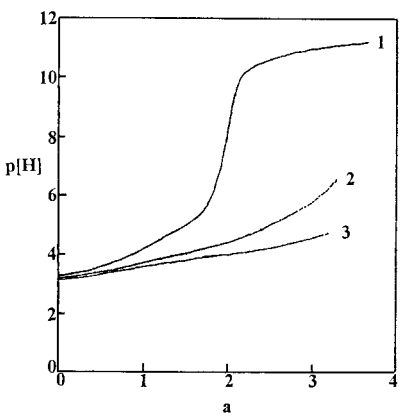

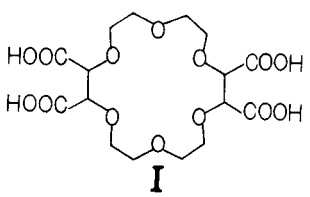

I

Fig. 1. Potentionetric equilibrium curves of TC18C6 (1), TC18C6.Al^{3+} (2) and TC18C6. $2Al^{3+}$ (3) at 25°C and ionic strength of 0.05 M. a = moles of base added per mole of ligand.

As it is seen from Fig. 1, the potentiometric titration curve of TC18C6 is depressed considerably in the presence of Al^{3+} ion at the ligand to metal mole rations of 1:1 and, especially, 1:2. The extent of depression depends both on the stoichiometries of the resulting complexes and the ability of the metal ion to bind to the ligand. The cumulative stability constants, β_{lmh}, are defined by Eq. (1) (charges are omitted for simplicity).

$$1L + mM + hH \overset{\beta_{lmh}}{=} L_lM_mH_h$$

$$\beta_{lmh} = \frac{[L_lM_mH_n]}{[L^l][M]^m[H]^h} \quad (1)$$

where L = ligand, M = metal ion, H = proton, and l, m and h are the respective stoichiometric coefficients. Since the ligand and complex activity coefficients are unknown, the β_{lmh} values are defined in terms of concentrations. The errors introduced are minimized by use of a high constant ionic strength and low ligand concentration.

The potentiometric p[H] titration curves of TC18C6 in the presence of different amounts of the metal ions were fitted to the program BEST, in order to calculate the cumulative stability constants of likely complexed species in solution. The results are also included in Table 1 and the species distribution diagram of TC18C6 in the presence of Al^{3+} ion at a ligand to metal mole ratio of 1:2 is shown in Fig. 3. From Fig. 3 it is obvious that the TC18C6-Al_2 complex is formed to the extent of 32% of the total ligand at p[H] 3.8 and decreases in concentration at lower and higher p[H] values by converting to its protonated and deprotonated forms, respectively. At this mole ratio, only negligible concentration of the 1:1 complex is formed at the p[H] range studied.

In order to investigate the formation of heterogeneous complexes of TC18C6-Al^{3+} with Na^+, K^+, Cs^+, Ca^{2+}, Sr^{2+} and Ba^{2+} ions in aqueous solution, the potentiometric p[H] titrations were performed in solutions containing 1:1:1 mole ratios of the macrocycle: Al^{3+}:M^{Z+} system. The cumulative stability constants of the resulting $L_lM_mM'_mH_h$ complexes (where L = ligand, M = Al^{3+}, M′ = M^{Z+} and H = proton) were evaluated by the computer fitting of the corresponding titration curves to the program BEST and the results are

Table 1
Logarithm of cumalative stability constants of the ordinary (l,m,h) and mixed-metal (l,m,m′,h) complexes with TC18C6 at 25°C and ionic strength of 0.05 M

Metal ion	Stoichiometry[b]			log β[a]	Metal ion	Stoichiometry[c]				log β[a]
	l	m	h			l	m	m′	h	
H^+	1	0	1	4.88	Al^{3+}	1	1	1	0	16.7
	1	0	2	8.78		1	1	1	1	20.4
	1	0	3	11.53		1	1	1	2	24.1
	1	0	4	13.66		1	1	1	−1	12.3
						1	1	1	−2	8.8
H^{+d}	1	0	1	4.88	Na^+	1	1	1	0	17.7
	1	0	2	9.17		1	1	1	1	20.9
	1	0	3	12.01		1	1	1	2	24.6
	1	0	4	14.14		1	1	1	−1	13.3
						1	1	1	−2	8.3
Na^+	1	1	0	4.4	K^+	1	1	1	0	16.9
	1	1	1	9.2		1	1	1	1	20.3
	1	1	2	12.7		1	1	1	2	22.9
						1	1	1	−1	12.2
						1	1	1	−2	6.5
Na^{+d}	1	1	0	4.5						
	1	1	1	9.0						
	1	1	2	11.1						
K^{+d}	1	1	0	4.8	Cs^+	1	1	1	0	16.6
	1	1	1	9.6		1	1	1	1	20.8
	1	1	2	12.6		1	1	1	2	24.6
						1	1	1	−1	12.6
						1	1	1	−2	−0.8
Ca^{2+d}	1	1	0	8.6	Ca^{2+}	1	1	1	0	20.2
	1	1	1	11.9		1	1	1	1	23.1
	1	1	2	—		1	1	1	2	18.3
						1	1	1	−1	8.6
						1	1	1	−2	10.5
Sr^{2+d}	1	1	0	8.0	Sr^{2+}	1	1	1	0	19.5
	1	1	1	10.9		1	1	1	1	22.3
	1	1	2	—		1	1	1	2	17.4
						1	1	1	−1	8.23
						1	1	1	−2	10.33
Ba^{2+d}	1	1	0	7.2	Ba^{2+}	1	1	1	0	18.9
	1	1	1	11.0		1	1	1	1	23.6
	1	1	2	—		1	1	1	2	19.1
						1	1	1	−1	14.9
						1	1	1	−2	9.5
Al^{3+}	1	1	0	9.0						
	1	1	1	13.1						
	1	1	2	17.3						

[a] Uncertainties in the cumulative stability constants are estimated as ± 0.5 of the last significant digit.
[b] l, TC18C6; m, cation; h, proton.
[c] l, TC18C6; m, $A1^{3+}$; m′, second metal ion; h, proton.
[d] Data taken from [19].

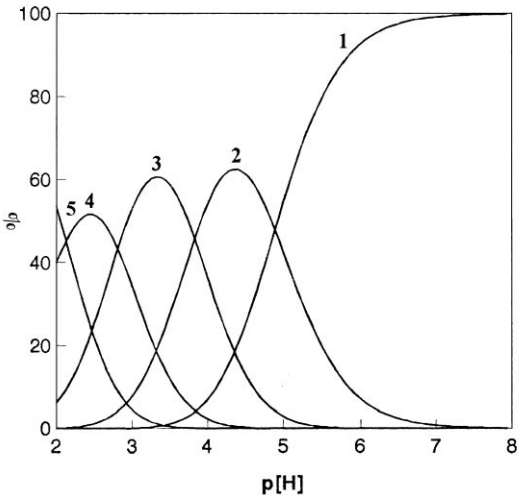

Fig. 2. Distribution of TC18C6 in the absence of metal ions. 1, L; 2, HL; 3, H_2L; 4, H_3L; 5, H_4L.

summarized in Table 1. Since the Al^{3+} ion hydrolyzes even at low pH values, the following equilibria were also considered calculating the cumulative stability constants [45]

$$Al^{3+} + 3OH^- = Al(OH)_3 \qquad K_{sp} = 3.5 \times 10^{-34}$$

$$Al(OH)_3 + OH^- = Al(OH)_4^- \qquad K_f \cong 10$$

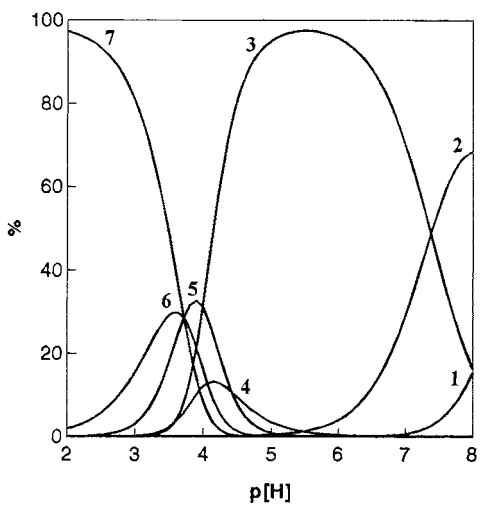

Fig. 3. Distribution curves for the 1:2 TC18C6-$2Al^{3+}$ system. 1, $Al_2L(OH)_4$; 2, $Al_2L(OH)_3$; 3, $Al_2L(OH)_2$; 4, $Al_2L(OH)$; 5, Al_2L; 6, Al_2HL; 7, Al_2H_2L.

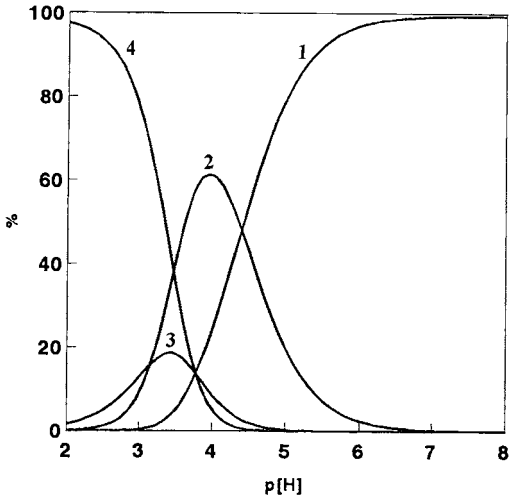

Fig. 4. Distribution curves for the 1:1:1 TC18C6-Al^{3+}-Na^+ system. 1, AlNaLOH; 2, AlNaL; 3, AlNaHL; 4, $AlNaH_2L$.

A sample species distribution diagram for TC18C6-Al^{3+}-Na^+ system is also shown in Fig. 4. It is clear that the diprotonated form of the mixed-metal complex, is formed to the extent of 98% at p[H] 2. The diprotonated form is gradually converted to the monoprotonated complex at around p[H] 3.5, which in turn is converted at about p[H] 4.0 to the deprotonated form. The mixed-metal complex is then converted to its monohydroxo form at about p[H] 4.8. Above p[H] 6 the dihydroxo mixed-metal complex is the predominant species in aqueous solution. It is interesting to note that, in all 1:1:1 TC18C6-Al^3-M^{2+} systems studied, the corresponding potentiometric p[H] titration curves can only be fitted to a model considering the formation of a heteronuclear 1:2 (ligand-to-metal) complex in solution. Any attempt to fit these data to the models neglecting the presence of such mixed-metal complexes was completely unsuccessful.

Comparing the stability data given in Table 1 with that obtained with the parent unsubstituted macrocycle 18C6 in aqueous solution [12,13] revealed that the affinity of TC18C6 for the cations indicated is at least three orders of magnitude higher than that of 18C6. That is, the stability constants of TC18C6-metal ion complexes fall within the stability range associated with the cor-

responding cryptates of C221 and C222. This could be mainly due to a favourable electrostatic interaction between the anionic ligand an the complexed cations.

As expected, in the course of complexation of metal ions with TC18C6, not only the size of cation, but also, and to a greater extent, the cationic charge density will be of vital importance. While the stability of Ca^{2+} complex with 18C6 in aqueous is only one order of magnitude higher than that of Na^{+} ion (with the same ionic size of Ca^{2+} ion) [12], TC18C6 forms a 1:1 complex with the former cation which is some four orders of magnitude more stable than that with the latter one. This is a clear indication for the fundamental role of the cationic charge in the complexation reactions with anionic macrocycles such as TC18C6. It is interesting to note that, Al^{3+} ion with an ionic size much smaller than that of Ca^{2+} ion and, consequently, much less suitable for the cavity of the macrocycle, forms an even more stable 1:1 complex than Ca^{2+} ion with TC18C6. It may be concluded that, in the case of very small cations possessing a high charge density such as Al^{3+} ion, the cation is mainly involved in rather strong interactions with the negatively charged carboxylate groups on the macrocyclic ring rather than ion-dipole interactions with the donating oxygen atoms of the macrocycles cavity. To the best of our knowledge, there is no research cited on the complexation of Al^{3+} ion with the parent macrocycle 18C6, which supports the above mentioned conclusion.

The reported stability order of the 1:1 complexes of alkaline earth cations with 18C6 in both aqueous and nonaqueous solutions is $Ba^{2+} > Sr^{2+} > Ca^{2+}$ [12–15], which is mainly based on the best fitting condition of Ba^{2+} ion inside the macrocycle's cavity. While, in the case of both 1:1 and 1:2 heteronuclear complexes of TC18C6 with these cations (Table 1), the stability order is reversed, i.e. $Ca^{2+} > Sr^{2+} > Ba^{2+}$. A similar reversed stability order is also observed for the mixed-metal complexes of alkali ions, i.e. $Na^{+} > K^{+} > Cs^{+}$. Despite their least favourable ionic sizes for the cavity of TC18C6, Ca^{2+} and Na^{+} ions form the most stable complexes with the ligand in their series, respectively, indicating the dominant role of the charged groups on the macrocycle's periphery which leads to an even strong electrostatic interaction with Ca^{2+} and Na^{+} ions with the highest charge densities in their series.

It should be noted that, the reported crystalline structure for the 1:1 complexes between Ca^{2+} [46] and K^{+} [47] ions with tetrafunctional 18C6 derivatives similar to TC18C6 clearly revealed that the complexed cations are located inside the macrocyclic cavity, as for the most cation complexes of macrocyclic polyethers [48], so that the six ring ether oxygens are in close contact with the included cations. The short cation-carboxylate distances indicated strong electrostatic interaction with one or two carboxylate groups. Thus, in solution, the alkali and alkaline earth cations used are also expected to penetrate, to some extent, inside the TC18C6 macrocyclic cavity and bind to the six oxygen atoms of the ring, while they have a more or less strong lateral electrostatic interaction with at least one of the carboxylate groups of the ring. However, based on the above discussions it seems reasonable to assume that Al^{3+} ion with an ionic size too small for the ligand's cavity in one hand, and a very high charged density (compared with alkali and alkaline earth cations), in the other, is located above the plane of crown ether's cavity so that it can have strong interactions with the two anionic carboxylate groups being in a diaxial situation and extending above the macrocycle's plane. Finally, the 18C6 ring of the ligand is expected to choose a kind of boat shape configuration [44] to minimize the possible electrostatic repulsions between the two complexed cations which are located above and below its structural plane. As discussed, the formation of such mixed-metal complexes in solution is another good example of the principle that 'the guest organizes the host' [23,49].

References

[1] M. Tabata, M. Tanaka, J. Inorg. Nucl. Chem. 38 (1976) 1529.
[2] G. Arena, R.P. Bonomo, S. Musumeci, R. Purrello, E. Rizzarelli, S. Sammartano, J. Chem. Soc. Dalton Trans., (1983) 1279.

[3] V.K. Patel, U.V. Chudasama, P.K. Bhattacharya, J. Chem. Soc. Dalfon Trans., (1983) 1901.
[4] M.S. Nair, P.T. Arasu, M.S. Pillai, C. Natarajan, Talanta 43 (1993) 1411.
[5] R.J. Motekaitis, A.E. Martell, J. Am. Chem. Soc. 110 (1988) 7715.
[6] A.E. Martell, J. Inclus. Phenom. 7 (1989) 99.
[7] R. Menif, A.E. Martell, P.J. Squattrito, A. Clearfield, Inorg Chem. 29 (1990) 4723.
[8] B. Szpoganicz, R.J. Motekaitis, A.E. Martell, Inorg. Chem. 29 (1990) 1467.
[9] A.E. Martell, R.J. Motekaitis, D. Chen, I. Murase, Pure Appl. Chem. 65 (1993) 959.
[10] P. Amico, G. Arena, P.G. Daniele, G. Ostacoli, E. Rizzarelli, S. Sammartano, Inorg. Chem. 20 (1981) 772.
[11] G. Arena, V. Cucinotta, E. Rizzarelli, P.G. Daniele, G. Ostacoli, S. Sammartano, J. Chem. Soc. Dalton Trans., (1988) 1267.
[12] R.M. Izatt, J.S. Bradshaw, S.A. Nielsen, J.D. Lamb, J.J. Christensen, D. Sen, Chem. Rev. 85 (1985) 271.
[13] R.M. Izatt, K. Pawlak, J.S. Bradshaw, Chem. Rev. 91 (1991) 1721.
[14] S. Kashanian, M. Shamsipur, Inorg. Chim. Acta 155 (1989) 203.
[15] A. Semnani, M. Shamsipur, J. Electroanal. Chem. 315 (1991) 95.
[16] H. Parham, M. Shamsipur, Talanta 16 (1993) 1353.
[17] A. Jabbari, M. Hasani, M. Shamsipur, J. Inclus. Phenom. 15 (1993) 329.
[18] M. Hasani, M. Shamsipur, J. Solution Chem. 23 (1994) 721.
[19] P.J. Dulton, T.M. Fyles, S.J. McDermid, Can. J. Chem. 66 (1988) 1097.
[20] P.J. Dulton, T.M. Fyles, S.P. Hansen, J. Inclus. Phenom. 17 (1989) 173.
[21] A. Anantanarayan, T.M. Fyles, Can. J. Chem. 68 (1990) 1338.
[22] D.M. Dishong, C.J. Diamond, M.I. Cinomann, G.W. Gokel, J. Am. Chem. Soc. 105 (1983) 586.
[23] R.D. Gandour, F.R. Franczeck, V.J. Gatto, C. Minganti, R.A. Schultz, B.D. White, K.A. Arnold, D. Mazzocchi, S.R. Miller, G.W. Gokel, J. Am. Chem. Soc. 108 (1986) 4078.
[24] H. Dugas, P. Veroack, M. Ptak, Can. J. Chem. 62 (1984) 489.
[25] T.M. Fyles, D.M. Whifield, Can. J. Chem. 62 (1984) 507.
[26] R.J. Adamic, E.M. Eyring, S. Petrucci, R.A. Bartsch, J. Phys. Chem. 89 (1985) 3752.
[27] J. Ghasemi, M. Shamsipur, J. Coord. Chem. 31 (1994) 265.
[28] H. Khajesharifi, M. Shamsipur, J. Coord Chem. 35 (1995) 289.
[29] J. Ghasemi, M. Shamsipur, J. Solution Chem. 25 (1996) 485.
[30] E. Karkhaneei, A. Afkhami, M. Shamsipur, Polyhedron 15 (1996) 1989.
[31] M.R. Ganjali, H. Eshghi, H. Sharghi, M. Shamsipur, J. Electroanal. Chem. 405 (1996) 177.
[32] M. Shamsipur, A.I. Popov, J. Phys. Chem. 92 (1988) 147.
[33] M.K. Amini, M. Shamsipur, J. Phys. Chem. 95 (1991) 9601.
[34] A. Rouhollahi, M.K. Amini, M. Shamsipur, J. Solution Chem. 23 (1994) 63.
[35] J. Ghasemi, M. Shamsipur, Polyhedron 15 (1996) 923.
[36] N. Alizadeh, M. Shamsipur, J. Chem. Soc. Faraday Trans., (1996) 4391.
[37] M. Hasani, M. Shamsipur, unpublished results.
[38] H. Abdollahi, M.S. Thesis, Shiraz University, Shiraz, Iran, 1995.
[39] T. Madrakian, J. Zolgharnein, M. Shamsipur, J. Coord Chem. 40 (1996) 121.
[40] G. Schwarzenbach, H. Flaschka, Complexetric Titrations, Methuen, London, 1969.
[41] R.J. Motekaitis, A.E. Martell, Inorg. Chem. 28 (1989) 3499.
[42] R.M. Izatt, J.S. Bradshaw, S.A. Nielsen, J.D. Lamb, J.J. Christensen, D. Sen, Chem. Rev. 85 (1985) 271.
[43] A.E. Martell, R.J. Motekaitis, Determination and Use of Stability Constants, 2nd ed., VCH, New York, 1992.
[44] J.J. Daly, P. Schonholzer, J.P. Behr, J.M. Lehn, Helv. Chim. Acta 64 (1981) 1444.
[45] L.G. Sillen, A.E. Martell, Stability Constants of Metal-Ion Complexes, The Chemical Society, London, 1971.
[46] J.P. Behr, J.M. Lehn, D. Moras, J.C. Thierry, J. Am. Chem. Soc. 103 (1981) 701.
[47] J.P. Behr, J.M. Lehn, A.C. Dock, D. Moras, Nature 293 (1982) 526.
[48] M.R. Truter, Struct. Bonding (Berlin) 16 (1973) 71.
[49] D.C. Cram, V.N. Trueblood, Top. Curr. Chem. 98 (1981) 43.

ELSEVIER

Talanta 45 (1998) 1227–1234

Talanta

New spectrophotometric method for the determination of some drugs with iodine and wool fast blue BL

Chilukuri S.P. Sastry *, Sankuratripati G. Rao, Petla Y. Naidu, Kommula R. Srinivas

Foods and Drugs Laboratories, Department of Organic Chemistry, Foods, Drugs and Water, Andhra University, Visakhapatnam 530 003, India

Received 14 April 1997; received in revised form 21 July 1997; accepted 22 July 1997

Abstract

A simple, sensitive and selective method is proposed for the spectrophotometric determination of drugs, viz. ampicillin, penicillin V, amoxycillin, cloxacillin, cefadroxil, ceftezoxime, griseofulvin, streptomycin, nicoumalone and acebutolol HCl, based on their reactivity with iodine. The method involves the addition of excess iodine of known concentration to the drug in the presence of NaOH and the unreacted iodine is determined by the measurement of the decrease in the absorbance of the dye wool fast blue BL ($\lambda_{max} = 540$ nm) which was found to be the most suitable of several dyes tested. This method was applied for the determination of drug contents in pharmaceutical formulations and enabled the determination of the drugs in microgram quantities (0.8–9.6 μg ml^{-1}). No interferences were observed from excipients and the validity of the method was tested against reference methods. © 1998 Elsevier Science B.V.

Keywords: Iodine in alkaline medium; Wool fast blue BL; Spectrophotometry

1. Introduction

In recent years there has been growing interest in the role of iodine in alkaline medium as an analytical reagent in the determination of organic compounds. Its more important application is as a reagent for a number of interesting oxidation reactions because of its selectivity towards aldehydes [1,6], methyl ketones [2], reducing sugars [3,4], β-lactum antibiotics [5] and few others under a variety of experimental conditions. Generally an excess of standard iodine is added to the analyte in alkaline medium (exists as hypoiodite) and is allowed to react for a given time. The released iodine after acidifying the unreacted hypoiodite is estimated either by titration with sodium thiosulphate (or sodium arsenite) or colorimetrically by using chromogenic reagents such as metol-INH [2] or sulphanilamide [5]. As there is no direct method for the determination of iodine in alkaline medium (hypoiodite) straightaway avoiding one step (acidifying the solution for the release of free iodine), efforts have been made to develop such a method. Even though the

* Corresponding author. Fax: +91 891 555547.

PII S0039-9140(97)00237-3

coloured azine and oxazine dyes are well known for their high absorptivity, they have not been utilised for estimating excess hypoiodite in the indirect determination of drugs. Although a few methods are available for the visible spectrophotometric estimation of AMP [7–12], PEN V [7–12], AMX [7–12], CLX [7–12], CFL [13,14], CFT [15,16], GRF [17–19], STP [20–24], NIC [25,26] and ACH [25,26], they suffer one or the other disadvantage such as low sensitivity, lack of selectivity and simplicity.

The present investigation proposes a selective and sensitive indirect spectrophotometric method for the determination of ampicillin (AMP) (4-thia-1-azobicyclo[3.2.0]heptane-2-carboxylic acid, 6-[(aminophenyl acetyl) amino]-3,3-dimethyl-7-oxo[2S-2α,5α,6β (S*)], an antibiotic), penicillin V (PEN V) (4-thia-1-azobicyclo[3.2.0])haptane-2-carboxylic-3,3-dimethyl-7-oxo-6-[(phenoxy acetyl) amino]-[2S-(2α,5α,6β)], an antibiotic), amoxycillin (AMX) (4-thia-1-azobicyclo[3.2.0]haptane-2-carboxylic acid, 6-{[amino-(4-hydroxyphenyl) acetyl] amino}-3,3-dimethyl-7-oxo-[2S-(2α,5α,6β) (S*)], an antibiotic), cloxacillin (CLX) (4-thia-1-azobicyclo[3.2.0]-heptane-carboxylic acid, 6-{[[3-(2-chlorophenyl)-5-methyl-4-oxozolyl] carbonyl] amino}-3,3-dimethyl-7-oxo-[2S-(2α,5α,6β)], an antibiotic), cefdroxyl (CFL) (5-thia-1-azabicyclo[4.2.0]octa-2-ene-2-carboxylic acid, 7-{[amino(4-hydroxyphenyl) acetyl] amino]-3-methyl-8-oxo-[6R-(6α,7β) (R*)], an antibacterial agent), ceftezoxime (CFT) (5-thia-1-azabicyclo[4.2.0]oct-2-ene-2-carboxylic acid, 7-[(2-amino-4-thiazolyl methoxyimino) acetyl]amino]-8-oxo-, an antibiotic), griseofulvin (GRF) (Spiro [benzofuran-2(3H),1^1-[2-cyclohexene]-3,4^1 dione, 7-chloro-2^1,4,6-trimethoxy-6^1-methyl (1^{1}s-*trans*)-, an antifungal agent), streptomycin (STP) (D-streptamine, *O*-2-deoxy-2-(methylamino)-α-2-glucopyranosyl-(1$\rightarrow$2)-*O*-5-deoxy-3-*c*-formyl-α-2-lyxofuranasyl-(1$\rightarrow$4)-*N*,*N*′-bis (amino imino methyl)-, an antibiotic), nicoumalone (NIC) (2H-1-benzopyran-2-one 4-hydroxy-3-[1-[4-nitrophenyl]-3-oxobutyl]-, an anticoagulant), and acebutolol HCl (ACH) (butanamide, *N*-[3-acetyl-4-[2-hydroxy-3-[(1-methyl) amino] propoxy] phenyl]-, an antiarrhythmic agent), in bulk form and pharmaceutical formulations. Any one of the drugs mentioned above is made to react with an excess of iodine under alkaline conditions, and the unreacted hypoiodite quantitatively reduces the intensity of wool fast blue BL (WFB) colour, an oxidizable phenazine dye (5,9-dianilo-7-phenyl 4,10-disulph benzo[α]phenazinium hydroxide inner salt, C.I. No. 50316) through the disruption of chromophore in it.

2. Experimental

2.1. Apparatus

A Milton Roy Spectronic 1201 UV-visible spectrophotometer with matched quartz cells and an Elico LI-120 model digital pH meter were used for absorbance and pH measurements, respectively.

2.2. Reagents

All chemicals were of analytical grade and all solutions were prepared in triply distilled water.

An aqueous solution of wool fast blue BL (chroma, 1 mg ml^{-1}) was prepared and was further diluted to 200 μg ml^{-1}. Aqueous solution of iodine was prepared by dissolving 100 mg each of iodine (E. Merck) and potassium iodide (E. Merck) in 100 ml of distilled water and standardized iodimetrically. This solution was further diluted to 200 μg ml^{-1}. Aqueous solution of sodium hydroxide (E. Merck, 1 M) was prepared.

2.3. Preparation of standard drug solutions

A 1-mg ml^{-1} solution of each drug was prepared by dissolving initially 100 mg in 10 ml of distilled water (for AMP, PEN V, AMX, CLX, CFL, CFT, STP, NIC and ACH) or in 10 ml of methanol (for GRF) followed by dilution to 100 ml with distilled water. These stock solutions were further diluted stepwise with distilled water to give working standard solutions (AMP, PEN V, AMX, CLX, CFL, CFT, and STP, 20 μg ml^{-1}; NIC and ACH, 40 μg ml^{-1}).

2.4. Preparation of sample solutions

An amount of tablet, or capsule powder equivalent to 100 mg of active ingredient was dissolved in 4 × 15 ml portions of distilled water (MeOH in case of GRF) and filtered if any insoluble portion was left. The combined filtrate was diluted to 100 ml with distilled water to give the concentration of 1 mg ml^{-1}. In the case of injections, a volume of injection equivalent to 100 mg of drug, was diluted directly to 100 ml with distilled water (1 mg ml^{-1}). The stock solutions of each drug in various kinds of formulations were further diluted with distilled water as described under the preparation of standard solutions to obtain working standard solutions.

2.5. Recommended procedure for bulk samples and pharmaceutical formulations

To each 25-ml graduated test tube containing aliquots of standard drug solution (AMP, PEN V, AMX, CLX, CFL, CFT, STP, 1.0–5.0 ml, 20 μg ml^{-1}; GRF, 1.0–6.0 ml, 20 μg ml^{-1}; NIC, ACH, 1.0–5.0 ml, 40 μg ml^{-1}), 2.0 ml of 1.0 M NaOH solution was added and the volume was made up to 10 ml with distilled water. The contents were allowed to stand for 10 min at room temperature (for AMP, PEN V, AMX, CLX, CFL and CFT) or at boiling water temperature (for GRF and STP) or 5 min at 45–50°C (for NIC and ACH), cooled to room temperature, then 3.0 ml of iodine solution (200 μg.ml^{-1}) added, and diluted to 19 ml with distilled water. After 5 min, 6.0 ml of dye solution was added and the absorbance measured 5 min later at 540 nm against distilled water. In the same way corresponding blank (omitting drug) and dye (omitting drug and iodine) solutions were prepared and their absorbances were measured against distilled water. The decrease in absorbance corresponding to consumed iodine, which in turn corresponded to the drug quantity, was obtained by subtracting the decrease in absorbance of the test solution (dye-test), from that of the blank solution (dye-blank). The calibration graph was drawn by plotting the decrease in the absorbance of the dye (WFB) against the concentration of the drug. The amount of drug in any sample was computed from its calibration graph.

3. Results and discussion

In preliminary experiments, several phenazine and oxazine dyes such as neutral violet (NV, CA, 3562-46-7), neutral red (NR, CA, 553-24-2), wool fast blue BL (WFB, CA, 6378-88-7), azocarmine G (AG, CA, 25641-18-3), lissamine blue BF (LBBF, CA, 6448-97-1), gallocyanine (GC, CA, 1562-85-2), gallamine blue (GB, CA, 1563-02-06), solocrome prune AS (SPAS, CA, 6416-51-9) and cresyl fast violet acetate (CFVA, CA, 10510-54-0) were tested for reaction with iodine in alkaline medium. These investigations revealed that NV, WFB, GB, SPAS and CFVA exhibit quantitative reactions, with iodine in alkaline medium by a definitive decrease in absorbance for a specific concentration of iodine in alkaline medium. As the difference in the absorbance was found to be higher in the case of WFB, it was preferred over others in further investigation.

The spectra of WFB, WFB–iodine and drug–iodine–WFB in NaOH medium are presented in Figs. 1 and 2. The similarity in the nature of the spectra indicates that the products formed by interaction of drug–iodine and iodine–dye in alkaline medium do not effect the accuracy of the determination.

The method involves two steps, namely reaction of the drug with an excess of iodine in alkaline medium giving products involving oxidation and the estimation of excess hypoiodite using a known excess of WFB. The excess dye remaining is then measured with a spectrophotometer at 540 nm. The effect of iodine concentration and alkali at different temperatures for different time intervals in the first step, and the effect of a wool fast blue BL at ambient temperature in the second step, the waiting period in each step with respect to maximum sensitivity, minimum blank, adherence to Beer's law, reproducibility and stability of final colour were studied by means of controlled experiments varying one parameter at a time [27].

3.1. Effect of alkali, iodine concentration, time and temperature

The studies on the variation of alkali concentration indicated that a constant absorbance is

obtained in final concentration of 0.06–0.1 M NaOH or 0.07–0.15 M Na_2CO_3 at an iodine concentration of 600 μg. As the difference in absorbance between the sample and the blank was found to be highest for the NaOH medium, subsequent studies were carried out in 0.08 M NaOH medium.

In order to ascertain the linear relationship between the concentration of added iodine and the corresponding decrease in the absorbance of WFB (1200 μg), experiments were carried out in 0.08 M NaOH medium, varying amounts of iodine. As the decrease in absorbance was found to be linear up to an amount of 600 μg of iodine, subsequent studies were carried out with 1200 μg of WFB and 600 μg of iodine in 25 ml of 0.08 M NaOH medium.

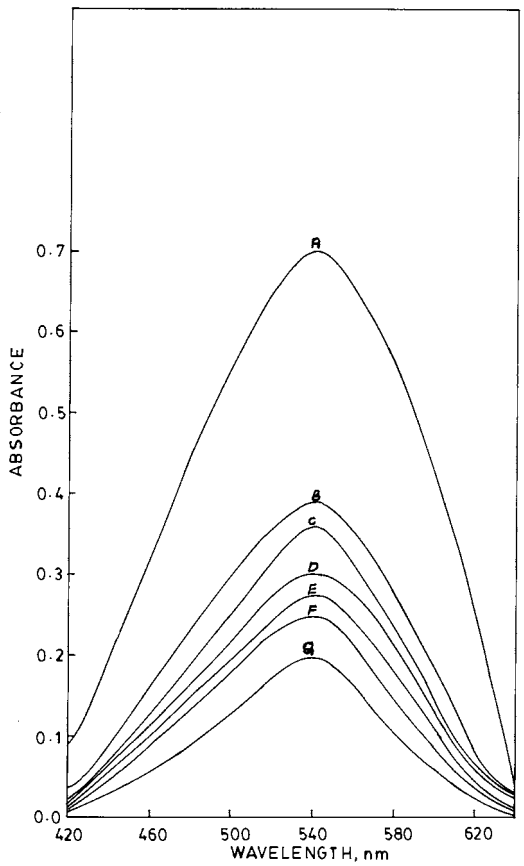

Fig. 1. Absorption spectra of (A) WFB against distilled water; (B) ampicillin–I_2–WFB; (C) amoxycillin–I_2–WFB; (D) cefadroxil–I_2–WFB; (E) cloxacillin–I_2–WFB; (F) penicillin V–I_2–WFB; (G) WFB–I_2 system (blank) against distilled water. Concentrations: NaOH, 8.0×10^{-2} M; WFB, 7.82×10^{-5} M; I_2, 9.45×10^{-5} M; AMP, 9.15×10^{-6} M; AMX, 7.63×10^{-6} M; CFL, 8.39×10^{-6} M; CLX, 6.72×10^{-6} M; PEN V, 9.13×10^{-6} M.

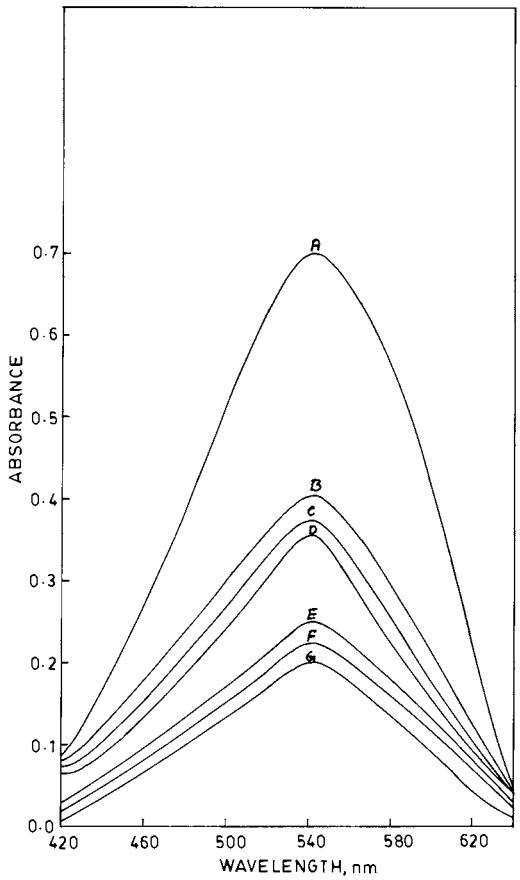

Fig. 2. Absorption spectra of (A) WFB against distilled water; (B) ceftizoxime–I_2–WFB; (C) acebutolol HCl–I_2–WFB; (D) griseofulvin–I_2–WFB; (E) nicoumalone–I_2–WFB; (F) streptomycin–I_2–WFB; (G) WFB–I_2 system (blank) against distilled water. Concentrations: NaOH, 8.0×10^{-2} M; WFB, 7.82×10^{-5} M; I_2, 9.45×10^{-5} M; CFT, 7.89×10^{-6} M; ACH, 2.27×10^{-5} M; GRF, 9.07×10^{-6} M; NIC, 2.26×10^{-5} M; STP, 2.19×10^{-6} M.

Fixed amount of iodine (3.0 ml, 200 μg ml^{-1}), WFB (6.0 ml, 200 μg ml^{-1}) and NaOH (2.0 ml, 1.0 M) were used in a total volume of 25 ml in further investigation.

The optimum conditions established for the first step include alkaline hydrolysis of drug (28 ±

3°C, 10 min for AMP, PEN V, AMX, CLX, CFL, CFT; 45–50°C, 5 min for NIC and ACH; boiling water temperature, 10 min for GRF and STP) followed by oxidation of hydrolysed product of drug with hypoiodite (5 min, 28 ± 3°C). The reaction between excess hypoiodite and WFB in the second step proceeds at ambient temperature within 5 min.

The above optimum conditions were incorporated in the recommended procedure.

3.2. Analytical data

The optical characteristics such as Beer's law limits (Figs. 3 and 4), molar absorptivity and Sandell's sensitivity of different drugs in the method are given in Table 1. The precision of the method was found by measuring the absorbances of six separate samples containing known amounts of drug, (AMX, PEN V, AMX, CLX, CFL, CFT and STP, 80 μg; GRF, 100 μg; NIC, 200 μg; ACH, 160 mg), and the results obtained are incorporated in Table 1. Regression analysis using the method of least squares was made to evaluate the slope (b), intercept (a), correlation coefficient (r) and standard error of estimation (S_e) [28,29] for each system and are presented in Table 1.

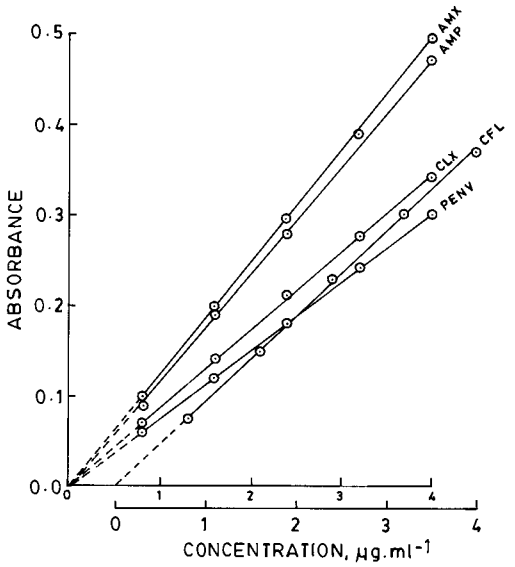

Fig. 3. Beer's law plots of amoxycillin (AMX), ampicillin (AMP), cloxacillin (CLX), cefadroxil (CFL) and penicillin V (PEN V) with I_2–WFB system. [I_2], 9.45×10^{-5} M; [WFB], 7.82×10^{-5} M; [NaOH], 8.0×10^{-2} M.

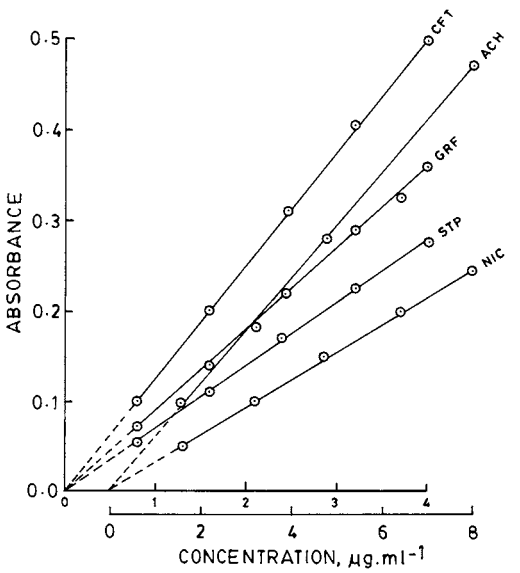

Fig. 4. Beer's law plots of ceftizoxime (CFT), acebutolol HCl (ACH), griseofulvin (GRF), streptomycin (STP) and nicoumalone (NIC) with I_2–WFB system. [I_2], 9.45×10^{-5} M; [WFB], 7.82×10^{-5} M; [NaOH], 8.0×10^{-2} M.

The interference studies in the determination of drugs in pharmaceutical formulations revealed that the normally existing excipients and additives were found not to interfere, even when present in large excess than they usually exist. The method was applied for the estimation of drugs in pharmaceutical formulations and compared with appropriate reference methods (AMP [30], PEN V [30], AMX [30], CLX [30], CFL [13], CFT [15], GRF [31], STP [21], NIC [30] and ACH [25]) by means of the F- and t-tests. Results presented in Table 2, show that the proposed method does not differ significantly from the reference method for each drug. As an additional check of accuracy, recovery experiments were performed by adding a fixed amount of the drug to the pre-analysed formulation. These results are also summarized in Table 2.

The drugs (acebutolol, nicoumalone) or their alkaline hydrolysis products (maltol from strepto-

Table 1
Optical and regression characteristics, precision, accuracy of the proposed procedure with iodine/WFB

Parameters	AMP	PEN V	AMX	CLX	CFL	CFT	GRF	STP	NIC	ACH
Beer's Law Limits (mg ml^{-1})	0.8–4.0	0.8–4.0	0.8–4.0	0.8–4.0	0.8–4.0	0.8–4.0	0.8–4.0	0.8–4.0	1.6–9.6	1.6–8.0
Molar absorptivity (l mol^{-1} cm^{-1})	4.12×10^{4}	2.62×10^{4}	4.85×10^{4}	4.10×10^{4}	3.56×10^{4}	5.15×10^{4}	3.18×10^{4}	1.00×10^{5}	1.09×10^{4}	1.96×10^{4}
Sandell's sensitivity (μg cm^{-2}/0.001 absorbance unit)	8.47×10^{-3}	1.33×10^{-2}	8.64×10^{-3}	1.15×10^{-2}	1.07×10^{-2}	7.87×10^{-3}	1.10×10^{-2}	1.41×10^{-2}	3.22×10^{-2}	1.72×10^{-2}
Regression equation (Y)[a]										
Slope (b)	1.19×10^{-1}	7.46×10^{-2}	1.13×10^{-1}	8.58×10^{-2}	9.28×10^{-2}	1.27×10^{-1}	9.22×10^{-2}	6.92×10^{-2}	3.12×10^{-2}	5.90×10^{-2}
Standard deviation on slope (S_b)	3.77×10^{-3}	6.57×10^{-4}	2.52×10^{-3}	3.14×10^{-4}	6.41×10^{-4}	1.07×10^{-3}	2.01×10^{-3}	1.10×10^{-3}	2.95×10^{-4}	4.50×10^{-4}
Intercept (a)	-7.0×10^{-4}	1.30×10^{-3}	1.12×10^{-2}	7.0×10^{-4}	2.30×10^{-3}	-5.0×10^{-4}	-6.8×10^{-3}	1.0×10^{-3}	-1.33×10^{-4}	-1.80×10^{-3}
Standard deviation on intercept (S_a)	1.00×10^{-2}	1.74×10^{-3}	6.71×10^{-3}	8.34×10^{-4}	1.70×10^{-3}	2.86×10^{-3}	5.32×10^{-3}	2.91×10^{-3}	1.56×10^{-3}	2.38×10^{-3}
Standard error of estimation (S_e)	9.55×10^{-3}	1.66×10^{-3}	6.39×10^{-3}	7.95×10^{-4}	1.62×10^{-3}	2.72×10^{-3}	5.07×10^{-3}	2.78×10^{-3}	1.49×10^{-3}	2.28×10^{-3}
Correlation coefficient (r)	0.9995	0.9998	0.9992	0.9999	0.9998	0.9994	0.9996	0.9998	0.9998	0.9999
Relative standard deviation (%)[b]	0.53	0.72	0.34	0.63	0.74	0.53	0.42	0.57	0.22	0.66
% range of error (confidence limits)[b]										
0.05 level	0.56	0.76	0.35	0.66	0.78	0.56	0.44	0.59	0.23	0.70
0.01 level	0.87	1.18	0.55	1.03	1.21	0.87	0.69	0.93	0.36	1.08

[a] $Y = a \pm bC$, where C is the concentration in μg ml^{-1} and Y in absorbance units.
[b] Six replicate samples of 80 μg (AMP, PEN V, AMX, CLX, CFL, CFT, STP), 100 μg (GRF), 200 μg (NIC), and 160 μg (ACH).

Table 2
Analysis of pharmaceutical formulations by proposed (I_2/WFB) and reference method

Formulations	Labelled amount (mg)	Amount found[a] (mg)		% recovery in proposed method[b]
		Proposed method	Reference method	
AMP				
Capsules	250	247.7 ± 1.02 ($F = 1.12$; $t = 1.08$)	249.2 ± 0.96	99.4 ± 0.61
Capsules	500	499.2 ± 1.21 ($F = 1.03$; $t = 1.22$)	495.3 ± 1.19	98.2 ± 0.57
PEN V				
Tablets	30	29.6 ± 0.13 ($F = 1.33$; $t = 1.07$)	30.1 ± 0.15	100.0 ± 0.65
Tablets	65	64.1 ± 0.34 ($F = 1.67$; $t = 1.25$)	65.0 ± 0.44	99.7 ± 0.21
AMX				
Tablets	250	245.6 ± 0.44 ($F = 2.82$; $t = 1.02$)	248.3 ± 0.74	100.1 ± 0.34
Capsules	500	495.7 ± 0.42 ($F = 4.69$; $t = 1.72$)	497.2 ± 0.91	99.5 ± 0.45
CLX				
Capsules	250	248.7 ± 0.84 ($F = 2.77$; $t = 1.92$)	250.3 ± 1.40	99.7 ± 0.74
CFL				
Tablets	500	493.5 ± 0.93 ($F = 2.56$; $t = 0.35$)	495.2 ± 1.49	98.2 ± 0.12
Capsules	500	501.6 ± 0.86 ($F = 1.33$; $t = 0.66$)	500.0 ± 0.99	98.4 ± 0.39
CFT				
Injection	250	250.1 ± 1.25 ($F = 2.63$; $t = 1.91$)	248.7 ± 0.77	98.7 ± 0.34
Injection	500	495.8 ± 0.32 ($F = 1.35$; $t = 0.43$)	497.1 ± 0.37	99.2 ± 0.71
GRF				
Tablets	125	123.9 ± 0.71 ($F = 1.05$; $t = 0.74$)	124.7 ± 0.69	99.3 ± 0.47
Tablets	250	247.2 ± 1.02 ($F = 2.46$; $t = 1.25$)	248.1 ± 0.65	98.7 ± 0.34
STP				
Injection, I	500	502.5 ± 0.68 ($F = 2.6$; $t = 1.87$)	498.7 ± 1.1	98.9 ± 0.24
Injection, II	500	497.3 ± 1.02 ($F = 1.22$; $t = 1.74$)	496.1 ± 0.42	100.0 ± 1.21
NIC				
Tablets, I	4	3.98 ± 0.058 ($F = 1.14$; $t = 0.82$)	4.01 ± 0.062	100.2 ± 0.74
Tablets, II	4	3.92 ± 0.091 ($F = 4.47$; $t = 2.01$)	3.99 ± 0.043	99.2 ± 0.11
ACH				
Tablets	400	397.6 ± 0.75 ($F = 1.31$; $t = 1.80$)	398.1 ± 0.86	99.6 ± 0.48
Tablets	200	201.6 ± 0.38 ($F = 1.87$; $t = 0.50$)	200.2 ± 0.052	99.8 ± 0.51

[a] Average ± standard deviation ($n = 6$). The t and F values refer to comparison of the proposed method with the reference method theoretical values at 95% confidence limit = 2.57, $F = 5.05$.
[b] Recovery of 10 mg added to the pre-analysed pharmaceutical formulations (average of three determinations).

mycin, corresponding penicilloic acid from ampicillin, amoxycillin, penicillin V and cloxacillin and cephalosphoric acid from cefadroxil and ceftezoxime through cleavage of β-lactum ring, and grisefuvinic acid from griseofulvin) [5,6], undergo oxidation rapidly and quantitatively on treatment with iodine in alkaline medium due to the participation of functional groups present in them. The further slow over oxidation that is observed has been ascribed to further oxidation of the products. Wool fast blue BL is coloured but its oxidation product(s) are colourless as the chromophoric groups existing originally in the dye undergo oxidative destruction. Although the iodine oxidation of each drug or dye under experimental conditions is not stoichiometric, reproducible values are attained.

4. Conclusions

A new indirect spectrophotometric method is proposed for the determination of drugs, viz. ampicillin, penicillin V, amoxycillin, cloxacillin,

cefadroxil, ceftezoxime, griseofulvin, streptomycin, nicoumalone and acebutolol HCl, in bulk and pharmaceutical formulations, based on their reactivity with iodine. This method is advantageous over many of the reported spectrophotometric methods for these drugs with respect to λ_{max}, stability of coloured species, sensitivity, precision, and accuracy. Hence, the method can be used as an alternative for rapid and routine determination of bulk samples and various pharmaceutical formulations in microgram quantities (0.8–9.6 μg ml^{-1}).

References

[1] Z. Romijn, Anal. Chem. 36 (1897) 349.
[2] C.S.P. Sastry, T.T. Rao, A. Sailaja, J.V. Rao, Talanta 38 (1991) 1107.
[3] K. Myrback, E. Gyllensvard, Suensk Kem. Tid. 54 (1942) 17.
[4] C.A. Lobry de Bruyn, W.A.V. Ekenstein, Rev. Trav. Chim. 14 (1895) 203.
[5] C.S.P. Sastry, T.E. Divakar, U.V. Prasad, Talanta 33 (2) (1986) 164.
[6] T. Higuchi, H.E. Brochman, Pharmaceutical Analysis, Interscience, London, 1961.
[7] L. Mazor, M.K. Papay, Z. Anal. Chim. 171 (1959) 98.
[8] M.M. Ellaithy, M.G. El Bardicy, M.W. Ibrahim, Indian J. Pharm. Sci. 47 (1985) 174.
[9] J. Emmanuel, M. Ray, East. Pharm. 27 (1984) 235.
[10] R. Prabhat Pal, J. Biol. Chem. 234 (1959) 618.
[11] D.M. Shingbal, R.R. Naik, Indian Drugs 22 (1985) 271.
[12] R.G. Bhatkar, L. Almeida, Indian Drugs 21 (1983) 70.
[13] P.B. Issopoulos, Acta Pharm. Hung. 61 (1991) 205.
[14] D. Marini, M.E. Dicoceo, Rass. Chim. 32 (1980) 231.
[15] V.U. Joseph, T.C. Jain, J. Antibiot. 39 (1986) 669.
[16] B. Pospisilova, J. Pharmazie 43 (1988) 246.
[17] H.W. Unterman, A. Duca, Chim. Anal. 2 (1971) 197.
[18] A. Mizsei, A. Squabo, Nature 196 (1962) 1199.
[19] M.M. Amer, A.A. Habeeb, J. Drug Res. 7 (1975) 123.
[20] N.M. Alykov, Antibiotic 29 (1984) 336.
[21] E.M. Barilari, M. Katz, An. Asoc. Quim. Argentina 75 (1958) 310.
[22] K.C. Agarwal, B.N. Dutta, Sci. Cult. 27 (1961) 450.
[23] W.M. Alykov, Zh. Anal. Chim. 36 (1981) 1606.
[24] E.M. Sawitskaya, V.D. Kartseva, Zh. Anal. Khim. 8 (1953) 46.
[25] C.S.P. Sastry, T.E. Divakar, M.K. Tummuru, Indian Drugs 22 (1984) 28.
[26] C.S.P. Sastry, T.T. Rao, A. Sailaja, Talanta 38 (1991) 1057.
[27] D.L. Massart, B.G.M. Yandeginste, S.N. Deming, Y. Michotle, L. Kaufman, Chemometrics, A Text Book, Elsevier, Amsterdam, 1988, p. 293.
[28] M.D. Patergill, D.E. Sands, J. Chem. Educ. 58 (1979) 244.
[29] R.B. Davies, J.E. Thompson, H.L. Pardue, Clin. Chem. 24 (1978) 611.
[30] British Pharmacopoeia, vol. I and II, HMSO, London, 1988.
[31] Pharmacopoeia of India, 3rd ed., MOHAFW, Government of India, 1985.

ELSEVIER

Talanta 45 (1998) 1235–1245

Talanta

The separation of platinum and palladium by selective extraction of $H_2Pt(SCN)_6$ and $H_2Pd(SCN)_4$ using a polyTHF-impregnated filter

R.D. Oleschuk, A. Chow *

Department of Chemistry, University of Manitoba, Manitoba R3T 2N2, Canada

Received 5 May 1997; received in revised form 21 July 1997; accepted 22 July 1997

Abstract

Platinum and palladium are known to form complexes with the thiocyanate ion in solution. The isolation and separation of both platinum and palladium as thiocyanate complexes is demonstrated by passing them through an organic-impregnated filter (OIF) prepared with polyTHF. Simultaneous extraction is performed by converting both metals into the extractable form. Sequential extraction is achieved by exploiting the difference in the rates of formation for the extractable complexes of the two metals. The extraction of both metals is rapid with quantitative recoveries of platinum with flow rates as high as 600 ml min^{-1} in small samples, while recoveries from larger volume samples were considerably lower. Once extracted, the metals can be removed from the OIF by conversion to a non-extractable form with a high pH eluting solution. The rapid separation, isolation and preconcentration of both platinum and palladium from aqueous samples is demonstrated. © 1998 Elsevier Science B.V.

Keywords: Platinum; Palladium; Selective extraction

1. Introduction

The value of platinum and palladium as precious metals has prompted several investigations into their separation and preconcentration. Most methods involve the complexation of the metals followed by either solvent extraction or ion exchange of the complexes[1–13]. Solvent extraction is one of the most widely used methods for the separation of platinum and palladium from aqueous solutions because of its inherent simplicity. Platinum(IV) and palladium(II) form a number of complexes that are soluble in organic solvents because of the labile character of their chloro complexes, $PtCl_6^{2-}$ and $PdCl_4^{2-}$ towards several hydrophobic ligands. This leads to the formation of several highly extractable complexes at room temperature.

Although both metals undergo substitution reactions, the rates of the reactions for palladium are faster by a factor of 10^5–10^6 than those for platinum [14]. Both metals prefer to coordinate most strongly with polarizable atoms which has focussed the development of extracting agents on

* Corresponding author. Fax: +1 204 2750905.

PII S0039-9140(97)00232-4

those with donor atoms such as sulphur, phosphorous and nitrogen. Such ligands are termed 'soft' by the empirical Pearson classification.

Thiocyanate (SCN^-) has long been known to form extractable complexes with both platinum and palladium. The SCN^- ligand can coordinate with either the 'hard' nitrogen atom, or 'softer' sulphur atom. Both platinum(IV) and palladium(II) form complexes coordinating with the sulphur atom, leading to the formation of $Pt(SCN)_6^{2-}$ and $Pd(SCN)_4^{2-}$ complexes under appropriate solution conditions. Both complexes have been shown to be extractable into oxygen-containing organic solvents [15–18]. The relative rates of complex formation for each of these metals are quite different. Palladium(II) in the presence of SCN^-, undergoes a substitution reaction almost instantaneously while the formation of the platinum(IV) thiocyanate complex is highly dependant on SCN^- and acid concentrations, although formation can be accelerated photochemically or with heating [19,20]. The difference in the formation of the platinum(IV) and palladium(II) thiocyanate complexes was first exploited for the separation of the metals by Ishida et al. [21] on an anion exchanger and then by Al-Bazi et al. [16] on polyurethane foam.

In this paper we describe the rapid extraction and isolation of platinum(IV) and palladium(II) from acidic thiocyanate solutions using a fluorocarbon filter impregnated with α-hydro-ω hydroxypoly(oxy-1,4-butanediyl), (polyTHF), shown in Fig. 1. Although linear polyethers such as polyTHF are weaker cation chelators than their cyclic analogues, they are effective extractants for some metal complexes. By impregnating a porous polytetrafluoroethylene filter with polyTHF, the platinum(IV) and palladium(II) thiocyanate complexes can be rapidly extracted from a solution as it passes through the impregnated filter. This device is termed an organic-impregnated filter (OIF) [22]. This extraction is highly dependent on the flow rate, thiocyanate concentration and acidity, as well as the length of time allowed for the development of the extractable complexes.

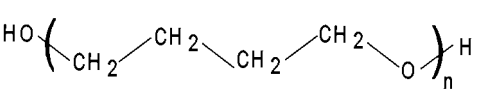

Fig. 1. The structure of polyTHF.

2. Experimental

2.1. Chemicals and instrumentation

A sample of PolyTHF of nominal molecular weight 1000 ± 50 g mol^{-1} was provided by BASF, USA. Potassium chloride and ammonium hydroxide were supplied by Mallinkrodt and hydrochloric acid by Fisher Scientific. A stock 1000 μg ml^{-1} palladium solution was prepared from palladium(II) chloride in 0.1 M hydrochloric acid. A stock 1000 μg ml^{-1} platinum solution was prepared from sodium hexachloroplatinate(IV) in hydrochloric acid. Confirmation of the formation of the $[Pd(SCN)_4]^{2-}$ and $[Pt(SCN)_6]^{2-}$ complexes was performed on a Hewlett Packard 8452A Diode Array Spectrophotometer. Atomic absorption was done using a Varian SpectrAA-20 atomic absorption spectrometer equipped with Pd and Pt Cathodean hollow cathode lamps and an air-acetylene flame. Polytetrafluoroethylene filters were used to prepare the OIF. Filters were supplied by Millipore with the following specifications: pore size 3.0 μm, 47 mm diameter, 85% porosity and thickness 200 μm, (catalogue # FGLP04700).

2.2. Preparation of the OIF

The OIF was prepared by first liquefying the polyTHF at 65°C in an oven for approximately 10 min. PolyTHF is a waxy solid at room temperature requiring softening to facilitate impregnation. The filter to be impregnated was first weighed and placed in a standard Millipore high performance liquid chromatography (HPLC) filtration device. Then 3–5 ml of polyTHF was poured into the filtering receptacle and a vacuum applied to pull polymer through the filter until it had been either all passed through, or coated on the filter. The filter was then removed from the filtering apparatus and any excess polyTHF beaded on the sur-

face was gently removed from the polytetrafluoroethylene filter by pressing with a Kimwipe™. The organic-impregnated filter was weighed and was then ready to be used for extraction. The impregnation process yielded a filter with an active area of 9.6 cm^2 and requires less than 10 min of preparation time.

PolyTHF forms the active layer of the OIF in the platinum/palladium extraction. The preparation process leads to an average loading of 100 mg of polyTHF on the filter. PolyTHF coats the entire surface of the filter, penetrates into the pores of the filter and then solidifies. Scanning electron microscopy revealed that there are still holes visible on the surface of the OIF facilitating the passage of liquid through the filter. The presence of holes after the impregnation is essential for adequate flow through the filter because otherwise the filter would be clogged and unusable.

Once the OIF had been prepared it was clamped in a standard HPLC filtration apparatus. The platinum/palladium-containing solution was then transferred to the filtering receptacle and a vacuum applied to the bottom filter flask to obtain the desired flow rate of the solution. The average flow rate was then calculated by dividing the volume of solution filtered by the time required for filtration. After the solution had passed through the OIF, an aliquot of the filtrate was taken for further analysis and the solution was transferred back to the filtering receptacle and the filtration/extraction process repeated until the desired number of passes through the OIF had been completed. Once extracted the platinum or palladium complex was recovered from the filter by passing the eluting solvent through the filter and collecting the filtrate for analysis.

3. Results and discussion

3.1. Extraction of $H_2Pd(SCN)_4$ with an OIF

Palladium in the presence of suitable HCl and NH_4SCN concentrations forms the $[Pd(SCN)_4]^{2-}$ complex. This complex is a weak acid and at a low pH becomes protonated to form the neutral species $H_2Pd(SCN)_4$ as shown in Fig. 2. This

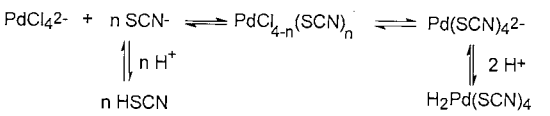

Fig. 2. The formation of the neutral palladium(II) thiocyanate complex.

complex has been shown to be extracted into organic solvents possessing ether linkages in their structure. The formation of the orange/brown $[Pd(SCN)_4]^{2-}$ complex occurs almost instantaneously upon the addition of sufficient amounts of thiocyanate ligand.

Several different solutions were prepared with varying concentrations of ammonium thiocyanate while maintaining a constant HCl concentration. Solutions of 4.7×10^{-5} M Pd and 0.73 M HCl were prepared with ammonium thiocyanate concentrations ranging from 1×10^{-4} to 0.1 M. The formation of the $[Pd(SCN)_4]^{2-}$ was observed at 308 nm [23].

The results of passing each of these solutions through an OIF at 40 ml min^{-1} are shown in Fig. 3. The extraction of the $H_2Pd(SCN)_4$ complex could be monitored visually by the development of an orange/brown hue on the surface of the OIF due to the sorption of the complex into the active layer of the filter.

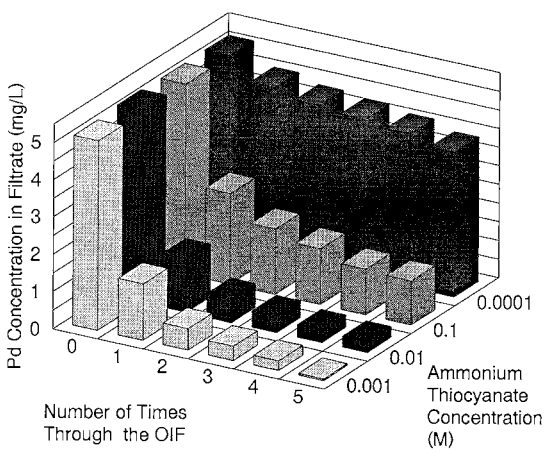

Fig. 3. The extraction of Pd(II) from solutions containing different NH_4SCN concentrations and 0.73 M HCl. Experiment was performed on 100 ml of solution at 40 ml min^{-1}.

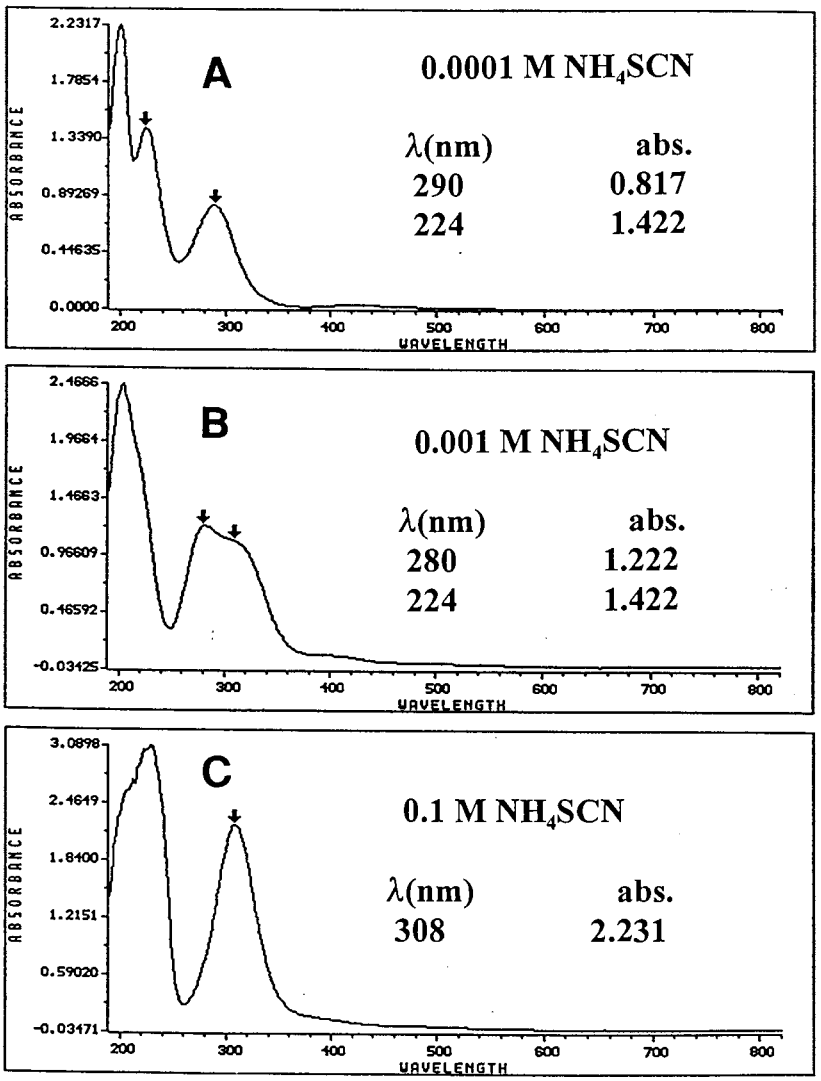

Fig. 4. The UV/Vis spectra of solutions containing 5 μg ml^{-1} Pd and 0.73 M HCl and various concentrations of NH_4SCN. A, 1×10^{-4} M NH_4SCN; B, 1×10^{-3} NH_4SCN; C, 0.1 M NH_4SCN.

At a concentration of 1.0×10^{-4} M NH_4SCN only 20% of the initial Pd is removed even after five passes through the OIF. The stoichiometric amount of thiocyanate ligand needed to form the complex is 1.9×10^{-4} M. By increasing the NH_4SCN concentration to 0.001 M and 0.01 M the amount of the $H_2Pd(SCN)_4$ complex extracted is increased. In these cases there is an adequate SCN^- concentration to form the $Pd(SCN)_4^{2-}$ complex and subsequently $>96\%$ of the Pd is extracted after five passes through the OIF.

A further increase in the NH_4SCN concentration to 0.1 M decreases the amount of Pd extracted from 99 to 70%. Fig. 4 shows the spectra of three solutions containing 5 μg ml^{-1} Pd concentrations and NH_4SCN concentrations ranging from 1×10^{-4} to 0.1 M. In spectra 'A' there is no significant peak at 308 nm indicating that very

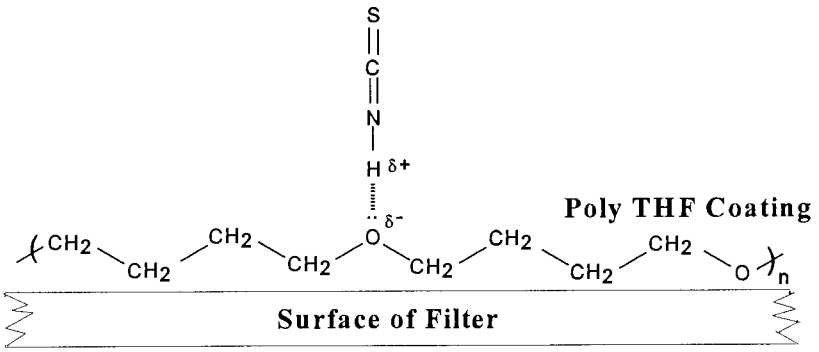

Fig. 5. Hydrogen bonding of thiocyanic acid (HSCN) to polyTHF.

little of the $Pd(SCN)_4^{2-}$ complex has formed. Increasing the NH_4SCN concentration to 0.001 M produces a peak at 308 nm in addition to a peak at 280 nm. The peak at 280 nm is presumed to be mixed Pd complexes with the general formula, $PdCl_{4-n}(SCN)_n^{2-}$ $(n = 1, 2, 3)$. Further increasing the NH_4SCN to > 0.01 M produces solely the $Pd(SCN)_4^{2-}$ complex. Experimental results suggest optimum extraction takes place when sufficient ligand is available to form the extractable complex. Although this resolves the lack of extraction at low thiocyanate concentrations it does not explain the poorer extraction at higher thiocyanate concentrations. The smaller extraction at higher complexing agent concentrations can be attributed to an increase in the amount of free SCN^- ion present in solution. In sufficiently acidic solutions the free thiocyanate becomes protonated to form thiocyanic acid(HSCN) with a $pK_a \approx -1.0$ to -2.0 [26,27]. It has been suggested [28] that HSCN is also extracted from solution into organic solvents. The thiocyanic acid forms hydrogen bonds [29] with the ether oxygens present in the active layer shown in Fig. 5. Hydrogen bonding with the ether oxygen, blocks the possible sorption sites on the surface of the OIF preventing the metal complex from being sorbed by the active layer of the OIF. The effects of the thiocyanic acid can be controlled by minimizing the amount of free acid and free thiocyanate that is present in solution. For the extraction of platinum and palladium complexes this is best achieved by controlling the thiocyanate concentration because a relatively high acid concentration is required to produce the extractable metal complexes.

The effect of solution flow rate on the extraction of $H_2Pd(SCN)_4$ was examined using the best extraction conditions from Fig. 3 consisting of 100 ml of 5 μg ml^{-1} Pd in 0.001 M NH_4SCN/0.73 M HCl. Several different flow rates were tested ranging from 2 to 600 ml min^{-1} and the results are shown in Fig. 6. At a relatively low flow rate of 2 ml min^{-1}, the palladium complex is 98% removed from solution after only one pass through the OIF. In comparison, only 32% of the palladium complex is removed at a flow rate of 600 ml min^{-1} after one pass. The poor extraction

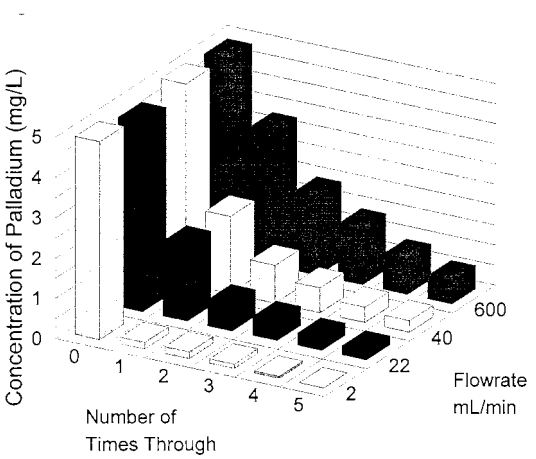

Fig. 6. The extraction of Pd(II) from solutions containing 0.001 M NH_4SCN/0.73 M HCl using different flow rates.

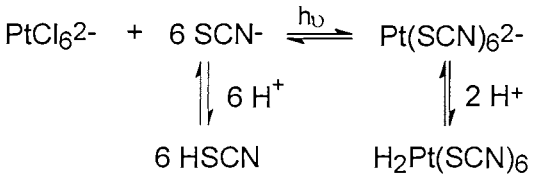

Fig. 7. The formation of the neutral platinum(IV) thiocyanate complex.

can be improved by passing the solution through the OIF several times. Five passes through the OIF at 20, 40 and 600 ml min^{-1} led to recoveries of 96, 95 and 84% respectively.

The flow rate required for quantitative recovery can be increased using a 'stacked' OIF consisting of two OIF's placed on top of one another. This doubles the amount of material available to sorb the metal complexes and allows flow rates of up to 10 ml min^{-1} while still quantitatively removing the $H_2Pd(SCN)_4$ from solution in one pass through the OIF.

3.2. Extraction of $H_2Pt(SCN)_6$ with an OIF

Platinum(IV) also forms an extractable complex in the presence of suitable concentrations of NH_4SCN and HCl (Fig. 7), although at a much slower rate than palladium(II). Platinum forms the complex $Pt(SCN)_6^{2-}$, which like $Pd(SCN)_4^{2-}$, is a relatively weak acid that can become protonated at a sufficiently low pH. The protonated neutral complex has been shown to be responsible for the extraction of platinum from aqueous solutions into various organic solvents. The substitution reaction of $PtCl_6^{2-}$ and SCN^- to develop $Pt(SCN)_6^{2-}$ is slow requiring several hours to form at room temperature and in the absence of strong light. The rate of formation of the $Pt(SCN)_6^{2-}$ complex can be accelerated by exposing the solution to either UV light or heat. The formation of the $[Pt(SCN)_6]^{2-}$ was observed at 286 and 360 nm [24,25].

Fig. 8 shows the passage of two solutions, identical in composition, through the OIF. One solution was passed through the OIF 5 min after being prepared while the other was exposed to sunlight for 1 h and then passed through the filter. Analysis of the freshly prepared solution showed only one peak ($\lambda_{max} = 262$ nm) due to the presence of the $PtCl_6^{2-}$ complex. The freshly prepared solution showed very little extraction even after five passes through the OIF at a flow rate of 100 ml min^{-1}. Conversely, the solution that was exposed to UV light for 1 h showed $>99\%$ extraction after only one pass through the OIF with the same flow rate. The spectrum of this solution prior to passing it through the OIF revealed a large peak at 286 nm indicating the presence of the $Pt(SCN)_6^{2-}$ complex. The platinum extraction can be followed visually by the appearance of a yellow hue on the surface of the OIF that becomes darker with increasing amounts of $H_2Pt(SCN)_6$ sorbed into the active layer of the OIF.

The effect of flow rates from 15 to 600 ml min^{-1} on the extraction of the $H_2Pt(SCN)_6$ was tested. Even at a flow rate of 600 ml min^{-1} $>99\%$ of the $H_2Pt(SCN)_6$ is removed from solution. These results are markedly different from those for $H_2Pd(SCN)_4$ which showed a much

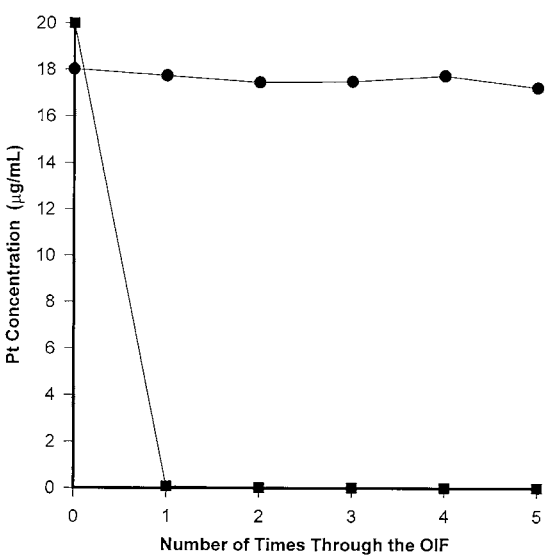

Fig. 8. The extraction of two solutions of 15 μg ml^{-1} Pt(IV)/ 1×10^{-3} M NH_4SCN/ 0.73 M HCl at a flow rate of 100 ml min^{-1}: ●, Pt (IV) concentration present in the filtrate for a freshly prepared solution; ■, Pt (IV) concentration in the filtrate for a solution exposed to UV light to form the extractable complex.

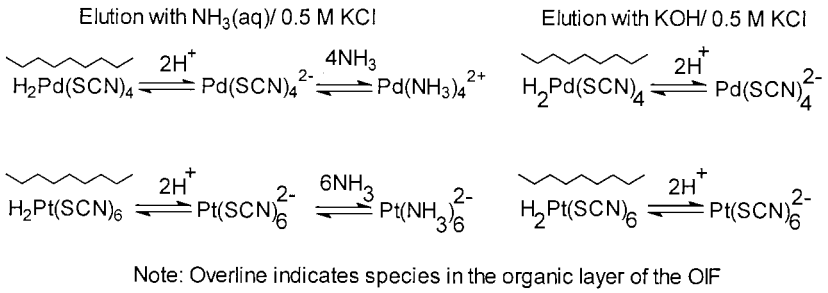

Fig. 9. Elution of palladium from the OIF with different eluting solutions.

poorer extraction at a flow rate of 600 ml min^{-1}. The difference in the relative rates of extraction for each of the metal complexes is probably due to two reasons. Platinum(IV) has a larger ionic radius and a higher oxidation state than palladium(II). Both factors contribute to the formation of a stable six coordinate platinum thiocyanate complex compared to a four coordinate complex for palladium(II). The increased number of hydrophobic ligands and larger size of the complex makes the platinum species much more hydrophobic than that of the palladium. Consequently, the extraction into the hydrophobic layer of the OIF is much faster for $H_2Pt(SCN)_6$ than for $H_2Pd(SCN)_4$. The second factor effecting the rate of extraction concerns the equilibria of the complexes. Analysis of optimum solution conditions shows that all of the platinum is in the form of the extractable complex while palladium is an equilibrium between several complexes

3.3. Recovery of platinum(IV) and palladium(II) from the OIF

Once the platinum(IV) or palladium(II) complexes have been extracted onto the filter they can be removed by converting either of the complexes from an extractable to a non-extractable form. Al-Bazi et al. [16] have shown that by converting both the $H_2Pt(SCN)_6$ and $H_2Pd(SCN)_4$ complexes to their ammonia analogues allows the recovery of these metals from polyurethane foam. Also we have shown [22] that a metal complex can be eluted from an OIF by simply using conditions that favour deprotonation of the metal complex as shown in Fig. 9.

The recovery of each of the metals from the OIF was attempted using eluting solutions composed of 0.1 M NH_3(aq)/0.5 M KCl. As the eluting solution is added to the OIF for both the recovery of platinum and palladium, the filter changes from coloured to colourless because the thiocyanate complexes undergo a substitution reaction to form their ammonia analogues. Consequently each of the metals is removed from the OIF into the eluting solution with recoveries of between 95 and 100%. The eluting process is rapid requiring only 20 s of contact time for the conversion of the complexes and their removal from the filter.

The elution of the metals from the OIF may be due to either the deprotonation of the complexes or the change to the ammonia complex. To determine which process is responsible for elution, a different eluting solution was used composed of 0.1 M KOH/0.5 M KCl. Potassium hydroxide was chosen because it does not develop an alternative complex with either platinum(IV) or palladium(II) but maintains a high pH favoring the deprotonation of the thiocyanate complexes. Eluting the platinum and palladium complexes with KOH solution showed that both are removed from the OIF with $>95\%$ recoveries. The high recovery indicates that the deprotonation step is responsible for the elution of the complexes from the filter, rather than conversion to another complex. Although both eluting solutions lead to excellent recoveries, their stabilities on standing are quite different. The metals are stable in the ammonium hydroxide eluting solution indefinitely, while those in the potassium hydroxide solution precipitate in a matter of hours.

3.4. Simultaneous extraction of $H_2Pd(SCN)_4$ and $H_2Pt(SCN)_6$ with an OIF

In the previous two sections we have described the extraction of platinum(IV) and palladium(II) individually. To determine the ability of the OIF to simultaneously extract both $H_2Pt(SCN)_6$ and $H_2Pd(SCN)_4$ a solution containing both metals in their extractable forms was passed through the OIF. A solution containing both 15 μg ml^{-1} Pd(II) and 15 μg ml^{-1} Pt(IV) in 0.01 M NH_4SCN/0.73 M HCl was prepared and exposed to sunlight for 5 h. The thiocyanate concentration was increased by an order of magnitude to provide sufficient ligand for the formation of the extractable complexes for both metals. In cases where inadequate amounts of thiocyanate were present both metals suffered poor extraction. The solution containing the two metals was passed through an OIF and fractions collected after each pass for analysis. The results of the experiment are shown in Fig. 10. The platinum and palladium complexes are both extracted into the OIF simultaneously. The platinum complex is quantitatively extracted from the solution after two passes through the OIF at 70 ml min^{-1} while the Pd is 95% removed from solution after the third pass through the OIF. The results show that both metals can be simultaneously removed from solution as their thiocyanate complexes if both are in an extractable form.

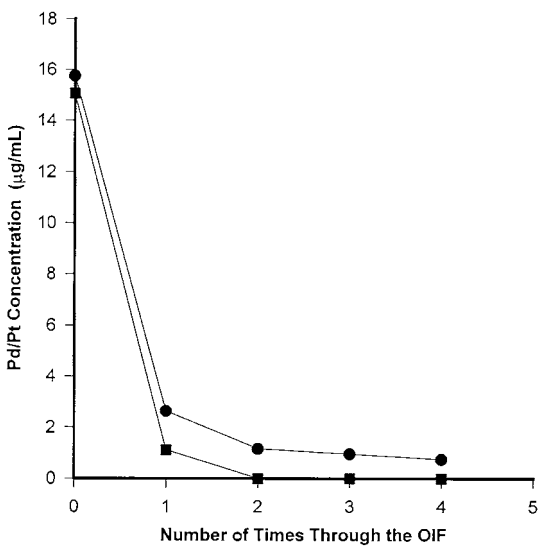

Fig. 10. Simultaneous extraction of both Pt(IV) and Pd(II) from a solution of 0.01 M NH_4SCN/0.73 M HCl at a flow rate of 70 ml min^{-1}: ●, Pd (II) concentration in filtrate; ■, Pt (IV) concentration in filtrate.

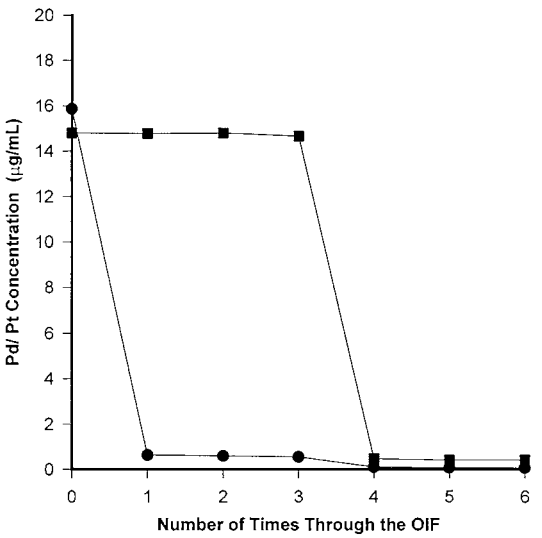

Fig. 11. Separation of Pt(IV) and Pd(II) using an OIF from a solution of 0.01 M NH_4SCN/0.73 M HCl at a flow rate of 20 ml min^{-1}. After the third pass through the filter the filtrate was exposed to UV light: ●, Pd(II) concentration in filtrate; ■, Pt(IV) concentration in filtrate.

3.5. Separation of $H_2Pd(SCN)_4$ and $H_2Pt(SCN)_6$ with an OIF

We have shown that both the platinum(IV) and the palladium(II) thiocyanate complexes can be extracted either individually or simultaneously. The separation of these two complexes can be achieved using the same solution chemistry and conditions as described. The $H_2Pd(SCN)_4$ complex is formed at a much faster rate than that of the $H_2Pt(SCN)_6$ and therefore the palladium(II) complex can be removed prior to the development of the extractable platinum(IV) complex separating the two metal complexes from one another. A solution containing 15 μg ml^{-1} palladium(II) and 15 μg ml^{-1} platinum(IV) in 0.01 M NH_4SCN/0.726 M HCl was freshly prepared and passed

through the OIF three times at a flow rate of 20 ml min^{-1}. The results are shown in Fig. 11.

After only one pass, 98% of the palladium was removed from solution while the platinum concentration remained at 15 μg ml^{-1} throughout. After the third pass through the OIF the remaining filtrate was exposed to sunlight for 3 h to allow the extractable platinum complex to develop. The irradiated solution was then passed through the OIF at 20 ml min^{-1}. After one pass through the filter 98% of the platinum was extracted from the irradiated solution and remained on the filter throughout the final two passes. This demonstrates that these two metals can be separated with high recoveries and excellent selectivity using the OIF process.

3.6. Preconcentration of platinum and palladium using the OIF

Platinum and palladium are often present a low levels below the 5 ng l^{-1} level [30] in marine and natural waters. At low concentrations platinum and palladium are difficult to separate, recover and determine. Several tests were performed to determine the suitability of the OIF for use as a preconcentration device. One litre solutions were prepared containing various concentration levels of palladium ranging from 1 to 100 ng ml^{-1} in 0.001 M NH_4SCN/0.73 M HCl. Each of the solutions was passed through a freshly prepared OIF at a flow rate of 20 ml min^{-1}. The palladium complex was then washed from the filter using 10 ml of an eluting solution of 0.1 M NH_3(aq)/0.5 M KCl. The amount of palladium recovered did not exceed 20% of what was present in solution even though favourable extraction conditions were used. The poor extraction suggests that either the increased amount of thiocyanic acid coming in contact with the OIF from the larger sample size or the lower concentration of palladium is interfering with the extraction process. To determine which factor was responsible for the poor recoveries a smaller volume of sample with the same palladium concentration was passed through the OIF. A solution consisting of 100 ng ml^{-1} was passed through the OIF three times at a flow rate of 20 ml min^{-1}. After eluting the palladium with 10 ml of the ammonium hydroxide eluting solution, a 98% palladium recovery was obtained producing a ten-fold increase in concentration in the eluting solution compared to the initial sample. This result shows that even at low palladium concentrations the extraction is effective and that the poor recoveries can again be attributed to the presence of thiocyanic acid in solution. The lower palladium concentrations and larger sample volume contributes to increased amounts of total thiocyanic acid in the sample interfering with the extraction of the palladium complex. The overall extraction is limited by the exchange capacity of the OIF for the thiocyanic acid present in solution. Once the available sorption sites are blocked by the thiocyanic acid the metal complexes are no longer extracted from solution.

To eliminate the problem of excess thiocyanic acid two routes can be taken. The first method involves changing the concentration of NH_4SCN present in solution. The results of changing the SCN^- concentrations are shown in Table 1 where 10 ml of eluting solution were used to recover the palladium. If quantitative recovery was obtained a concentration factor of 100 would result.

The results show that the optimum NH_4SCN concentration for the recovery of palladium from 1 l solutions is approximately 1.9×10^{-4} M, although the recovery is still quite low. The recovery of palladium in 10 ml of eluting solution results in an increase in concentration of 20–30 × from the original 1 l starting solution.

The amount of acid present in solution can also be varied to try to minimize the effect of HSCN in the solution although sufficient acid is required to protonate the metal thiocyanate complexes. Hydrochloric acid concentrations ranging from 0.73 to 0.073 M were tested with resulting recoveries ranging from 32 to 40% for one pass through the filter.

The interference caused by the presence of HSCN is a considerable problem when trying to obtain large preconcentration factors with the OIF. By carefully controlling the ammonium thiocyanate and hydrochloric acid concentration the effects of the interference can be somewhat minimized. The OIF process has been shown to be unsuitable for large volume preconcentration (i.e.

Table 1
The effect of varying NH_4SCN concentration on the recovery of palladium

Concentration			Solution volume (ml)	% Recovery
Pd (ng ml^{-1})	NH_4SCN (M)	HCI (M)		
100	1.0×10^{-2}	0.73	1000	20
100	1.0×10^{-3}	0.73	1000	17
100	1.9×10^{-4}	0.73	1000	32

$$\% \text{ Recovery} = \frac{\text{Mass of metal in eluting solution}}{\text{Mass of metal in original sample}}$$

>1 l) because of the relatively poor recoveries, but is suitable for smaller volume preconcentration where the effect of thiocyanic acid is not as prevalent.

4. Conclusions

A polytetrafluoroethylene filter impregnated with poly(tetramethylene) ether glycol can selectively extract platinum and palladium from NH_4SCN/HCl solutions that flow through it. The extraction is due to the formation of the $H_2Pd(SCN)_4$ and $H_2Pt(SCN)_6$ complexes and their subsequent extraction into the polyTHF layer on the OIF. The rate of extraction was found to be optimum in solutions containing between 0.01 and 0.001 M NH_4SCN. Extraction efficiencies decreased with increasing amounts of thiocyanic acid present in the sample.

Once extracted, the protonated complexes, $H_2Pd(SCN)_4$ and $H_2Pt(SCN)_6$, can be eluted from the filter by converting them to the anionic, $Pd(SCN)_4^{2-}$ and $Pt(SCN)_6^{2-}$ complexes using a basic solution. The deprotonated forms of the complexes are no longer soluble in polyTHF layer and are eluted.

Platinum(IV) and palladium(II) can be extracted individually or simultaneously depending on the different solution conditions used for the extraction. Separation of the two metals can be achieved by exploiting the difference in the rate of formation of their thiocyanate complexes. Palladium develops the extractable complex almost instantaneously in the presence of the SCN^- ligand, while platinum requires several hours under 'normal' conditions to develop the extractable complex. The separation of palladium from platinum demonstrates the ability of the OIF to separate metals from one another in solution but interferences from HSCN limit analytical applications.

Acknowledgements

This work is supported by the Natural Science and Engineering Research Council of Canada and a University of Manitoba scholarship.

References

[1] M.L. Lee, G. Tölg, Anal. Chim. Acta 272 (1993) 193.
[2] R. Gaita, S.J. Al-Bazi, Talanta 42 (1995) 249.
[3] P. Di, D.E. Davey, Talanta 42 (1995) 685.
[4] J. Enzweiler, P.J. Potts, Talanta 42 (1995) 1411.
[5] Y. Baba, T. Fukumoto, Chem. Lett. 5 (1992) 727.
[6] G. Lee, K. Chung, Analyst 115 (1990) 965.
[7] E.M. Basova, V.M. Ivanov, T.A. Bol'shova, N.A. Babkova, Zh. Anal. Khim. 45 (1990) 671.
[8] S. Kumar, R. Verma, B. Venkataramani, V.S. Raju, S. Gangadhara, Solvent Extraction Ion Exchange 13 (1995) 1097.
[9] Z. Su, Q. Pu, X. Luo, X. Chang, G. Zhan, F. Ren, Talanta 42 (1995) 1127.
[10] J. Fu, S. Nakamura, K. Akiba, Anal. Sci. 11 (1995) 149.
[11] C. Gavino, G. Marangoni, B. Pitteri, N. Stevanato, A. Vavasori, React. Polym. 14 (1991) 143.

[12] G.E.M. Hall, J.C. Pelchat, Anal. At. Spectrom. 8 (1993) 1059.
[13] S.J. Al-Bazi, A. Chow, Talanta 31 (1984) 815.
[14] A.T. Yordanov, J.T. Mague, D.M. Maxhill, Inorg. Chim. Acta. 240 (1995) 441.
[15] J.H. Forsythe, R.J. Magee, C.L. Wilson, Talanta 3 (1960) 330.
[16] S.J. Al-Bazi, A. Chow, Anal. Chem. 55 (1983) 1094.
[17] S.J. Al-Bazi, A. Chow, Talanta 29 (1982) 507.
[18] S.J. Al-Bazi, A. Chow, Talanta 30 (1983) 487.
[19] J.H.W. Forsythe, R.J. Magee, C.L. Wilson, Talanta 3 (1960) 330.
[20] P. Senise, L.R.M. Pitombo, Talanta 11 (1964) 1185.
[21] K. Ishida, T. Kiriyama, R. Kuroda, Anal. Chim. Acta. 41 (1968) 537.
[22] R.D. Oleschuk, A. Chow, Talanta 44 (1997) 1371.
[23] R.J. Magee, M.A. Khattak, Microchem. J. 8 (1964) 285.
[24] P. Senise, L.R.M. Pitombo, Talanta 11 (1964) 1185.
[25] D.L. Swihart, W.R. Mason, Inorg. Chem. 9 (1970) 1749.
[26] T.D.B. Morgan, G. Stedman, P.A.E. Whincup, J. Chem. Soc. (1965) 4813.
[27] T.I. Crowell, M.G. Hankins, J. Phys. Chem. 73 (1969) 1380.
[28] A. Jurriaanse, D.M. Kemp, Talanta 15 (1968) 1287.
[29] T.M. Barakat, N. Legge, A.D.E. Pullin, Trans. Faraday Soc. 5 (1963) 1773.
[30] G.E.M. Hall, J.C. Pelchat, J. Anal. At. Spectrom. 8 (1993) 1059.

ELSEVIER

Talanta 45 (1998) 1247–1253

Talanta

A sensitive flow-injection method for determination of trace amounts of nitrite

M.F. Mousavi [a,*], A. Jabbari [b], S. Nouroozi [a]

[a] *Department of Chemistry, Tarbiat Modarres University, P.O. Box 14155-4838, Tehran, Iran*
[b] *Department of Chemistry, Razi University, Kermanshah, Iran*

Received 23 October 1996; received in revised form 23 July 1997; accepted 23 July 1997

Abstract

A new sensitive colour reaction for nitrite determination is presented. In acidic medium, nitrite was reacted with safranine to form a diazonium salt which caused the reddish-orange dye colour of the solution to change to blue. The carrier stream, into which the sample solution was injected, was doubly distilled water. The reagent solution stream, which contained safranine dye, hydrochloric acid and potassium chloride, was mixed with the carrier in a 3-m length of silicon tubing (bore 0.5 mm) maintained at 30°C in a thermostatic bath. The absorbance intensity was measured at 520 nm. The detection limit was 20 ng ml^{-1} and the RSD% of 20 injections of 1 μg ml^{-1} of nitrite was 0.65%. Analysis can be done at a rate of up to 30 h^{-1}. Under the optimum conditions in the concentration range of 30–4000 ng ml^{-1} of nitrite ion, a linear calibration graph was obtained ($r = 0.9999$). The method was applied successfully to the determination of nitrite in sausages. © 1998 Elsevier Science B.V.

Keywords: Nitrite determination; FIA; Safranine; Spectrophotometry

1. Introduction

Because of the important role of nitrite ion in producing nitrosamine, a potent carcinogenic material, in the human body and the increasing use of nitrite and nitrate as a preservative in the food industry at permissible concentrations [1], its determination at trace level is of special interest. Nitrite is also undesirable in water owing to its toxicity [2,3]. Many spectrophotometric [4–6], kinetic [7–9], fluorimetric [10–13], Chromatoghraphic [14–16] and FIA [17–19] methods have been developed for the determination of nitrite. Some of the methods give good sensitivity and selectivity, but require very expensive reagents, close control of pH and some are time consuming.

This work describes a simple, rapid and sensitive FIA method for the determination of trace amounts of nitrite based on the reduction reaction of safranine by nitrite ions. Since the reduced form of the dyestuff is blue, the reaction can be easily monitored spectrophotometrically. To the best of our knowledge there is no published report on the uses of this reagent for the determination of nitrite ions.

* Corresponding author. Fax: +98 21 8006544; e-mail: mousavim@net1cs.modares.ac.ir.

PII S0039-9140(97)00240-3

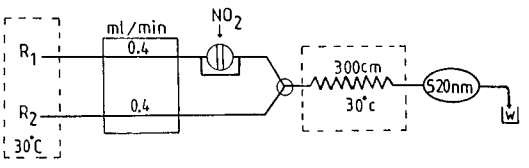

Fig. 1. FIA manifold for the determination of nitrite. R_1, water; R_2, (safranine + HCl + KCl).

2. Experimental

2.1. Reagents

All chemicals used were of the highest purity available and used without any further purification. Doubly distilled water was used throughout.

Nitrite stock standard solution (1000 μg ml^{-1}) was prepared by dissolving 0.1500 g of sodium nitrite (Aldrich, dried at 110°C for 4 h, cooled in a desiccator) in water containing a pellet of sodium hydroxide to prevent liberation of nitrous acid, and 1 ml of chloroform (HPLC, grade) to inhibit bacterial growth [20], and diluting to 100 ml in a calibrated volumetric flask. Working solutions were prepared by appropriate dilution of the stock solution with water.

Safranine stock solution (300 μg ml^{-1}) was prepared by directly dissolving 0.1500 g of the dyestuff (Aldrich) in water and dilution to the

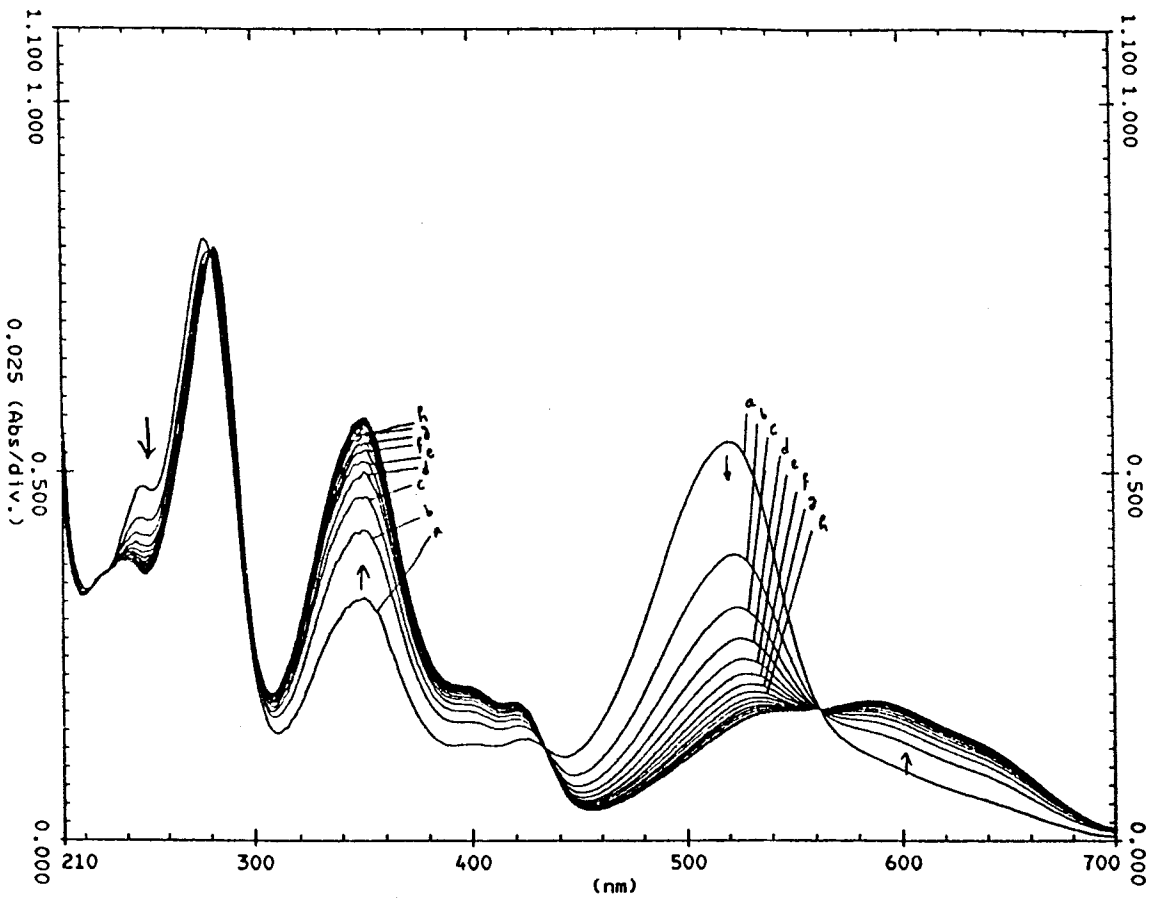

Fig. 2. Absorption spectra of safranine in the presence of 2 μg ml^{-1} of nitrite after (a) 30 s; (b) 100 s; (c) 170 s; (d) 240 s; (e) 310 s; (f) 380 s; (g) 450 s; and (h) 520 s from iniatiation of the reaction.

mark in a 500-ml standard flask. Hydrochloric acid (2 M) was prepared from concentrated HCl (Aldrich, 37% W/V).

The carrier stream was doubly distilled water.

2.2. Apparatus

For the spectrophotometric determination of nitrite, the flow injection manifold shown in Fig. 1 was used. Silicon tubing of 0.5 mm i.d. was used for the manifold and the mixing tees were made of glass. Samples were injected using a rotary Rheodyne valve with a sample loop of 110 μl. A 12-channel peristaltic pump (Desaga) was used for propelling the carrier and reagents. A Shimadzu UV-Vis 2100 double-beam Spectrophotometer with a thermostated flow cell was used to record the absorbance of safranine at 520 nm. All reagents were placed in a 30°C thermostated bath. The reaction coil was placed in a 30°C water bath. The cell compartment was also maintained at 30°C by circulation of thermostated water. A Shimadzu TB-85 thermobath and a GFL water bath were used.

After washing the flow injection manifold with water for about 5 min, samples and standards were examined using the flow system used, under the following optimized conditions: length of reaction coil, 300 cm; flow rate of different streams, 0.4 ml min^{-1}; sample injection volume, 110 μl; hydrochloric acid concentration, 0.5 M; safranine concentration, 17 μg ml^{-1}; temperature 30°C. In order to avoid the adsorption of safranine into the inner walls of silicon tubing, at the end of each working day the manifolds were washed by pumping water for 30 min, followed by 50% acetone–water for 10 min and finally by pure acetone for 5 min.

2.3. Sausage preparation

Mix 5.000 g of finely comminuted sausage with 40 ml of water. Heat to 80°C and transfer quantitatively to a 250-ml volumetric flask. Add 200 ml of hot water. Place the flask on a stream bath and let stand for 2 h, with occasional shaking. Then add 5 ml saturated mercuric chloride solution, dilute to mark with nitrite-free water, and mix. Filter and determine the nitrite on a suitable aliquot of filtrate [22].

3. Results and discussion

3.1. Batchwise study

Safranine is used as a new reagent for nitrite determination. It reacts with nitrite as follows:

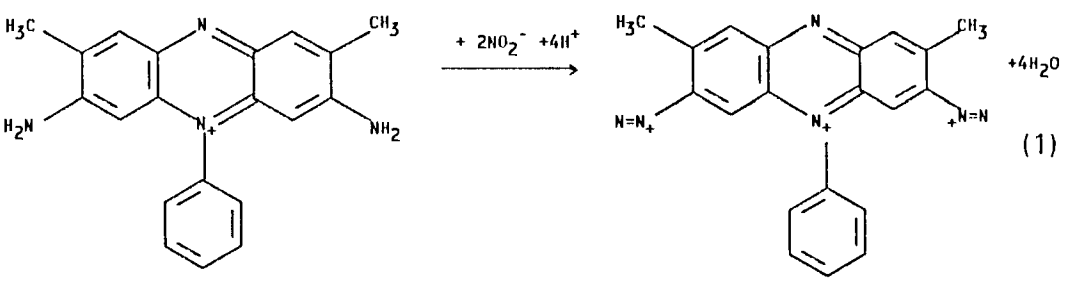

The tetra-azotized compound formed on reaction with nitrite is blue but has poor molar absorptivity (Fig. 2), so a decrease in colour intensity of reddish-orange dye (520 nm) is followed in the proposed work for better sensitivity.

It was found that, at constant concentration of safranine, the rate of diozonium production (Eq. (1)) is proportional to the nitrite concentration. The absorbance signal of the dyestuff at 520 nm was found to have a linear decrease by raising nitrite concentration.

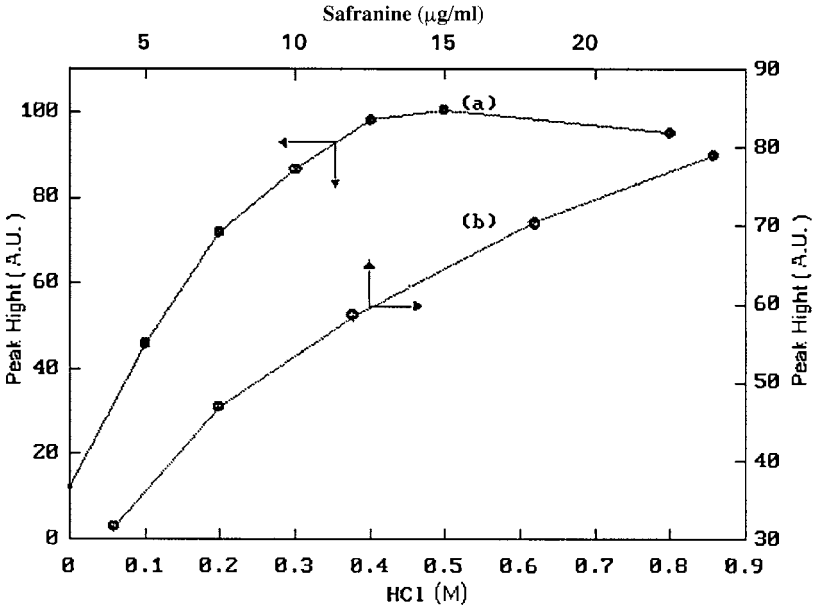

Fig. 3. Effect of safranine and HCl concentration on the peak height. Conditions: nitrite, 0.8 μg ml^{-1}; sample loop volume, 110 μl; reaction coil length, 300 cm; flow-rate, 0.4 ml min^{-1}; $T = 25°C$; safranine 17 μg ml^{-1} (a); HCl 0.16 M (b).

3.2. Chemical and flow optimization

The flow-injection manifold depicted in Fig. 1 was investigated in relation to chemical and flow variables, in order to obtain optimum conditions for the system. They were optimized by making all variables constant and varying one each at a time.

Effect of acidic media on the peak height was investigated up to 0.80 M of hydrochloric acid, and the results are shown in Fig. 3, curve a. It is seen that there is an increase in the peak height when the concentration of HCl was varied up to 0.4 M, while at higher acid concentrations no considerable change in the response was observed; 0.5 M HCl was used for this study.

The influence of safranine concentration on the peak height was studied (Fig. 3, curve b) in the range of 4–24 μg ml^{-1} and the best results were obtained at about 17 μg ml^{-1} of the dye, although higher sensitivities can be achieved at higher safranine concentration, the base line would be noisy and the signal measurement will be less accurate.

In FIA systems, the height of response peak depends on the residence time of the sample zone in the system, i.e., on the flow rate, the tube length and sample loop volume. Fig. 4 shows the influences of flow rate and reaction coil length on the peak height. The best response was achieved at a flow rate of 0.4 ml min^{-1}; the lower flow rates gave higher peaks, but their reproducibility was weak and the peaks broadened, which results in increased response times (Fig. 4, curve a).

From Fig. 4, curve b, it can also be seen that there is a gradual increase in the response peak with increasing the length of the reaction coil from 80 to 300 cm, while a further increase did not result in any significant change in the sensitivity. A reaction coil length of 300 cm was then selected.

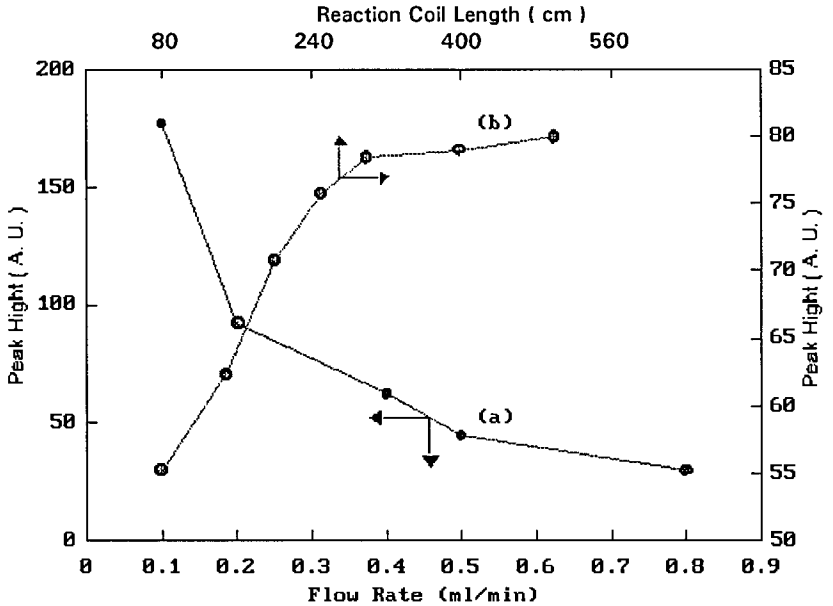

Fig. 4. Effects of flow rate (a), and reaction coil length (b), on the peak height. Conditions: safranine 12 μg ml^{-1}; KCl, 0.06 M; nitrite, 0.8 μg ml^{-1}; HCl 0.16 M; $T = 25$°C; sample loop volume, 110 μl; and flow-rate, 0.4 ml min^{-1} for curve a; reaction coil length, 150 cm for curve b.

The effect of sample volume was also investigated in the range of 20–150 μl to obtain the best overall response. A sample volume of 110 μl gave the highest response. The effect of temperature on the peak height was studied between 25 and 55°C (Fig. 5). A temperature of 30°C was used as the most suitable, although at higher temperatures (45°C) higher sensitivities could be obtained.

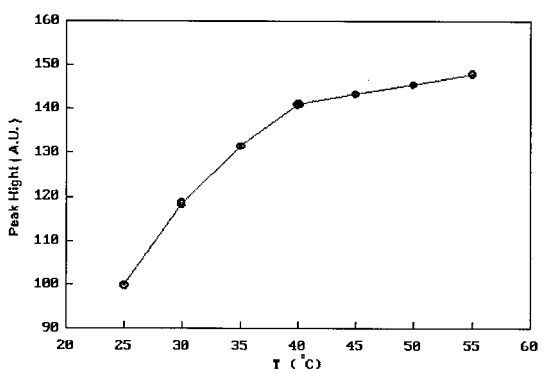

Fig. 5. Effect of temperature on the peak height. Conditions: nitrite, 0.8 μg ml^{-1}; sample loop volume, 110 μl; reaction coil length, 300 cm; flow-rate, 0.4 ml min^{-1}; safranine, 17 μg ml^{-1}; HCl, 0.5 M; KCl, 0.105 M.

The influence of ionic strength on the peak height was studied by using KCl salt. The results indicated that change in ionic strength of the solution has no considerable effect on the response up to 0.3 M of KCl concentration in final solution.

3.3. Calibration curve and statistical data

Under the optimum conditions described above, in the concentration range of 30–4000 ng ml^{-1} of nitrite a quite linear calibration curve was obtained: $H_{mm} = -1.6 + 550.2C_{ppm}$ ($r = 0.9999$, $n = 37$). Some typical peaks obtained at different concentrations of nitrite given in Fig. 6.

By using the signal to noise ratio equal to 3 as a limiting requirement, the experimental detection limit was found to be 30 ng ml^{-1}. The sampling rate was 25–30 h^{-1}. The relative standard deviation of 20 replicate measurements is 0.65% for 1.0 μg ml^{-1} of nitrite.

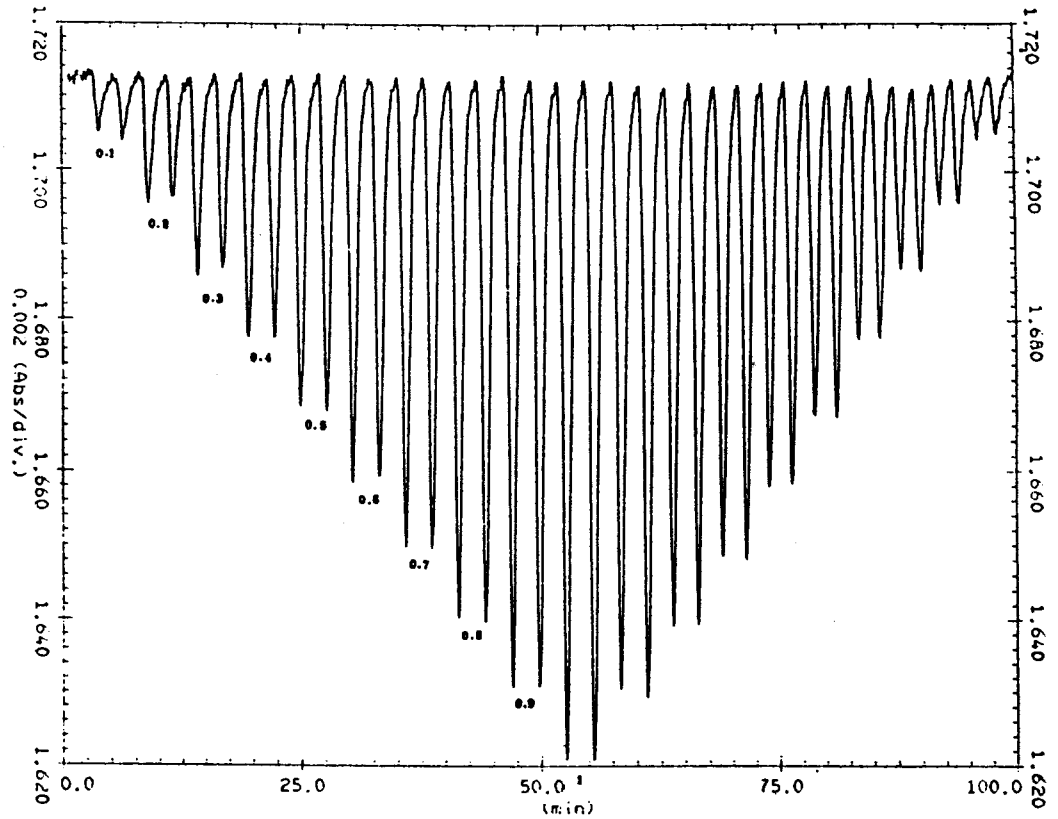

Fig. 6. FIA signals obtained at varing nitrite concentration. The numbers on the peaks show the concentration of nitrite in μg ml^{-1}.

3.4. Interference study

The effects of various anions and cations on the determination of 1.0 μg ml^{-1} nitrite ion were investigated and the results are summarized in Table 1. The tolerance limit was taken as the concentration of diverse ion causing less than a 3% relative error. As can be seen, many anions and cations have no considerable effect on the determination of nitrite. However, the presence of sulphite ion causes serious interference. The interfering effect of this anion was removed by the use of formaldehyde [21]. It should be noted that excess amount of formaldehyde (up to 5.0×10^{-3} M) does not interfere with safranine.

Table 1
Tolerance limits of diverse ions on the determination of (1 μg ml^{-1}) nitrite

Ion	Tolerated ratio of foreign ion to nitrite
Pb^{2+}, OCN^-, K^+, Cl^-	1000[a]
SO_4^{2-}	600
Mn^{2+}, Zn^{2+}, Cu^{2+}, Ni^{2+}, Co^{2+}, Mg^{2+}, Ba^{2+}	500
Cd^{2+}, Li^+, Ce^{3+}, Fe^{3+}, NO_3^-, CO_3^{2-}, Br^-	
CN^-, $H_2PO_4^-$, HPO_4^{2-}, $C_2O_4^{2-}$, IO_3^-, CH_3COO^-, F^-	
Hg^{2+}, Na^+	250
SO_3^{2-}	130[b]
Ag^+, SCN^-, I^-	40
$S_2O_5^{2-}$	7
BrO_3^-	5

[a] Above of which was not tested.
[b] After masking with formaldehyde [21].

Table 2
Determination of nitrite in sausage

Nitrite added (μg ml^{-1})	Nitrite found (μg ml^{-1})	Nitrite recovered (μg ml^{-1})	% Recovery (μg ml^{-1})
None	0.198	—	—
0.4	0.584	0.386	96.5
0.6	0.766	0.568	94.6
0.8	0.955	0.757	94.6

3.5. Determination of nitrite in real sample

The method was applied to determination of nitrite in a sausage sample. The results are given in Table 2. As can be seen, the recovery of added nitrite at different levels in the sample is quantitative. In order to validate the accuracy of the proposed method, it was applied to the determination of nitrite in different sausage samples and the results were compared with those obtained by the Griess standard method [22]. The nitrite concentration obtained by the proposed method was 0.138 μg ml^{-1}, which is in excellent agreement with 0.141 μg ml^{-1}, obtained from the standard method (relative error −1.84%).

4. Conclusion

The method described is significant with respect to the development of a simple manifold for determining traces of nitrite at levels between 30 and 4000 ng ml^{-1}. Its simplicity, excellent reproducibility, freedom from pH effect and broad range of nitrite determination are coupled with the high speed of the FIA technique.

Acknowledgements

This work was supported by the Tarbiat Modarres University Research Council.

References

[1] W. Lijinsky, S.S. Epstein, Nature 21 (1970) 225.
[2] F.A. Patty, Industrial Hygience and Toxicology, vol. II, Interscience, New York, 1963, p. 917.
[3] E.J. Calabrese, Pollutants and High-Risk Groups, Wily-Interscience, New York, 1978, pp. 99–187.
[4] V. Raman, M.S. Dabbas, Microchem. J. 40 (1989) 242.
[5] K. Rachana, C. Lata, V.K. Gupta, Analyst 116 (1991) 667.
[6] S.S. Naik, Int. J. Environ. Anal. Chem. 44 (1991) 153.
[7] A.A. Ensafi, M. Keyvanfard, Anal. Lett. 27 (1) (1994) 169.
[8] A. Afkhami, A.A. Mogharnesband, Anal. Lett. 27 (5) (1994) 991.
[9] A.A. Ensafi, M. Samimfar, Talanta 40 (1993) 1375.
[10] S. Motomizu, H. Mikass, K. Toei, Talanta 33 (1986) 725.
[11] H.D. Axelrod, N.A. Engel, Anal. Chem. 47 (1975) 922.
[12] J.H. Wiersma, Anal. Lett 3 (1970) 123.
[13] N.Q. Jie, J.H. Yang, F.Q. Meng, Talanta 40 (1993) 1009.
[14] R.G. Girse, J. Chromatogr. 171 (1979) 523.
[15] H.J. Cortes, J. Chromatogr. 243 (1982) 5117.
[16] M. Gennaro, P.L. Bertolo, A. Cordero, Anal. Chim. Acta 239 (1990) 203.
[17] L. Anderson, Anal. Chim. Acta 110 (1979) 123.
[18] S. Motomizu, H. Mikasa, K. Toei, Talanta 33 (1986) 729.
[19] A. Chaurasia, K.K. Verma, Talanta 41 (1994) 1275.
[20] R.B. Lew, Analyst 102 (1977) 477.
[21] M.F. Mousavi, M. Shamsipur, Bull. Chem. Soc. Jpn. 65 (1992) 2770.
[22] F.J. Welcher (Ed.), Standard Methods of Chemical Analysis, 6th ed., vol. 3, part B, Robert E. Krieger, Malabar, FL, 1975, p. 1127.

ELSEVIER

Talanta 45 (1998) 1255–1266

Talanta

The application of flow programming with pulsed amperometric detection for liquid chromatography

Rosa L. Earley, Jennifer S. Miller, Lawrence E. Welch *

Department of Chemistry, Knox College, Galesburg, IL 61401, USA

Received 19 November 1996; received in revised form 21 July 1997; accepted 23 July 1997

Abstract

A mixture of seven penicillins was separated on a C-8 column and detected using pulsed amperometric detection (PAD). Due to the polarity range of the penicillin mixture, a gradient program was necessary to produce a reasonable separation, causing some baseline shifting. Application of a flow program, where the solvent flow rate is varied within the separation, was also examined, and found to cause only a small shift in baseline response for PAD. Further examination of a variety of different flow programs was undertaken to characterize the baseline and analyte response under these conditions. Notable was that the shift in baseline from the flow program could be altered to give a shift toward either increased or decreased current, depending on the waveform and solvent combination in use. By manipulating these two parameters, one can customize the PAD response to a flow program, which may allow flow programs to be designed that only produce a minimal impact on the detector response. © 1998 Elsevier Science B.V.

1. Introduction

The penicillins are a class of β-lactam antibiotics that are important for both human and veterinary medicine. Veterinary applications include use as a surgical prophylactic and as therapy for a number of bacterial infections, notably for treatment of mastitis in ruminant animals [1,2]. Despite regulations banning milking during antibiotic therapy, detectable amounts of penicillins have been found in the milk supply, leading to mandates for screening procedures [3]. Due to the severe reactions that accidental exposure can cause for those with penicillin allergies, these screening strategies are important for public health.

Although various biochemical assays [4] have been investigated for penicillin screening, the most popular methodology has incorporated HPLC with UV detection in the 200–230 nm range [5–7]. Due to the complexity of the milk sample matrix, the selectivity of HPLC is necessary to isolate the penicillins, most commonly with reversed phase procedures on C-18 and C-8 columns [4,6,8–10]. The detection is sensitive in the UV range used, although selectivity is poor. Many assays that have been developed use extra-column extraction and concentration steps to improve detectability and sensitivity [4,7,9]. Other strategies tested involve chemical reactions to produce a better chromophore [11–13], and derivatizing the penicillins to allow introduction of a more sensitive detector [14,15].

* Corresponding author. Fax: +1 309 3417718.

PII S0039-9140(97)00238-5

An alternative strategy for detection of the underivatized penicillins following HPLC is pulsed electrochemical detection (PED) [16,17]. This typically involves anodic oxidation of the analyte molecules within a pulsing potential waveform that continually cleans and rejuvenates the working electrode. The most common form of PED is pulsed amperometric detection (PAD), which employs a three-step potential waveform [18]. This manner of detection has been demonstrated for penicillins [19], as well as various methods of indirect PAD which do not involve actual oxidation of the sample [20,21]. A screening assay was developed to apply HPLC-PAD to milk samples containing a mixture of penicillins using a C-18 column [22].

PAD presents a challenge to select a solvent mixture that will serve satisfactorily as a chromatographic mobile phase and as a residual electrolyte solution. Incorporation of common gradient elution methods can pose compatibility problems for electrochemical detectors. PAD is known to respond to changes in pH due to the role of H^+ in the detection process [23,24]. Use of a glass reference electrode [25,26] and of some alternative PAD waveforms [27] have allowed some degree of tolerance to pH shifts. Alterations in solution polarity also look to be problematic, as they promise to alter the kinetics of the detection electrochemistry, changing the output current. As with pH alterations, those willing to tolerate small shifts in the baseline response can undertake modest polarity changes during a separation [20,28].

Alterations of solvent flow rate were known to cause some alteration in PAD peak characteristics [27,29] and to cause baseline shifts. Alteration of solvent flow rate during a separation is known as flow programming, which is considered to be a little-used solution to the chromatographic general elution problem [30]. Flow programming is most commonly used to increase the resolution in the small k' region with a low early rate of flow, followed by an increase that sacrifices later resolution but shortens the total analysis time [31]. An advantage of flow programming is that it can be done with lower cost solvent delivery equipment compared with performing gradient elution. Electrochemical detectors in general are known to be quite responsive to flow and pressure changes within the detection cell, so it has been a general practice to avoid procedures such as flow rate variation in the midst of data collection, making this type of change only between trials.

The goal of this work was to develop a penicillin separation for milk screening applications that used PAD with a C-8 stationary phase. During the course of these studies the subject of flow programs became of interest, and an effort was made to assess their compatibility with the penicillin separation and for PAD in general.

2. Experimental

All penicillins were purchased from Sigma Chemical Co. (St. Louis, MO). Methanol and acetonitrile were reagent grade from Fisher (Pittsburgh, PA). All other solutions were made from reagent grade chemicals from Aldrich (Milwaukee, WI), Baker (Phillipsburg, NJ), Fisher, or Sigma. Water was distilled and deionized before use as a solvent.

Cyclic voltammetry (CV) studies were conducted using a RDE4 potentiostat from Pine Instrument Co. (Grove City, PA). The working electrode was the gold disk on an AFDT07 from Pine, which had a diameter of 5.0 mm. A PIR rotator from Pine was used for rotating disc experiments. A Ag/AgCl reference electrode (BAS, West Lafayette, IN) and a platinum wire counter electrode were standard for CV experiments. A N_2 sparge was utilized when noted. A BAS MF-2060 Polishing Kit was used to polish the working electrode; in addition potential cycling to the voltage limits of the system, as defined by the onset of solvent breakdown, was helpful to restore electrode activity following temporary losses of sensitivity.

Most flow injection analysis and HPLC trials were done with a Waters 625 LC system (Milford, MA) and a Waters 464 Pulsed Electrochemical Detector. A 75-μl sample injection loop was employed for all flow injection trials and a 50-μl loop was used for chromatographic trials.

Injected penicillin solutions during flow injection analysis trials were all solvent matched with the mobile phase to avoid having a system peak overlapping with the analytical peak. To improve the flow stability during flow injection analysis, an Upchurch (Oak Harbor, WA) U-469 back pressure regulator was placed in-line following the pump. All mobile phases were vacuum filtered through an Alltech (Deerfield, IL) 0.20-μm nylon filter. The mobile phase mixtures were degassed further using a 30-ml min^{-1} helium sparge during the flow injection trials. Some trials utilized a Hewlett Packard 1050 series (Palo Alto, CA) gradient pump in place of the Waters pump. A Novapak C-8 (4-μm) Radial-Pak cartridge (Waters) was employed as the chromatographic stationary phase. The cartridge had an internal diameter of 8 mm and a length of 100 mm. The cartridge was housed in a Waters 8×10 Radial-Pak compression module.

Flowing stream work utilized a thin-layer cell with a single gold working electrode having a diameter of 2.5 mm. The counter electrode was a stainless steel block mounted opposing the thin-layer cell, with the flow channel created by a teflon spacer between the two. The reference electrode was a Ag/AgCl. The BAS MF-2060 Polishing Kit was used to polish the working electrode.

Current integration was always during the final 16.7 ms of the detection step, as required by the detector. Detector signal polarity was inverted so that increased anodic response would produce peaks rather than troughs on the output plots. Output data was collected by a PC using LabCalc software (Galactic Industries, Salem, NH). The collection interval was synchronized with the potentiostat, such that a single data point was collected per PAD cycle. Quoted detection limits represent $S/N = 3$. Determination of peak asymmetry factors was done using measurements at 20% of the peak height rather than the standard 10%, as prior work had found better precision under these conditions [29]. The chromatographic data was smoothed by application of a Savitsky–Golay algorithm [32].

3. Results and discussion

Initial work focused on resolving and speciating a mixture of seven penicillins placed within a milk sample, and it was hoped to design a separation such that the system peak, known to be large from previous milk separations, would not obliterate the early-eluting peaks. Due to the wide variety of side chain groups on the various penicillins, it was clear that a broad range of k' values would be encountered for the mixture. Any isocratic elution scheme that provided sufficient retention for the first peak (ampicillin), forced the later peaks (cloxacillin, nafcillin, and dicloxacillin), to be retained for unacceptably long periods of much greater than 30 min. Thus, solvent programming was undertaken to allow a change in solvent strength during the separation.

In this case, an aqueous electrolyte solution was too polar for proper chromatographic retention, so it was diluted with an organic modifier. To produce significant retention for ampicillin, the initial solvent mixture should contain only a low percentage of organic modifier. To push the later peaks off the column, the fraction of organic modifier was increased. This typically caused a significant shift in baseline detector response. One way to lessen the shift was to change to a ternary solvent, incorporating both acetonitrile and methanol as modifiers. The acetonitrile has greater elution strength for the penicillins than the methanol, so exchanging methanol for acetonitrile could push analytes off the column faster without creating a large polarity shift.

Fig. 1A shows an early attempt to separate the seven penicillins, with the gradient program in use portrayed in Table 1A and the waveform given in Table 2A. Under these conditions the detection mode is indirect PAD, with a current change toward the top of the page representing a decrease in anodic signal [21,33]. The initial weak 12/8/80 (vol.% methanol/% acetonitrile/% 0.02 M acetate buffer (pH 4.7)) solvent is altered to the stronger 10/25/65 to push the later peaks off the column. Despite doing this over a period of 10 min, it can be seen that a large baseline shift takes place. The reasoning for the shift in detector response can be derived from the cyclic voltammograms shown in

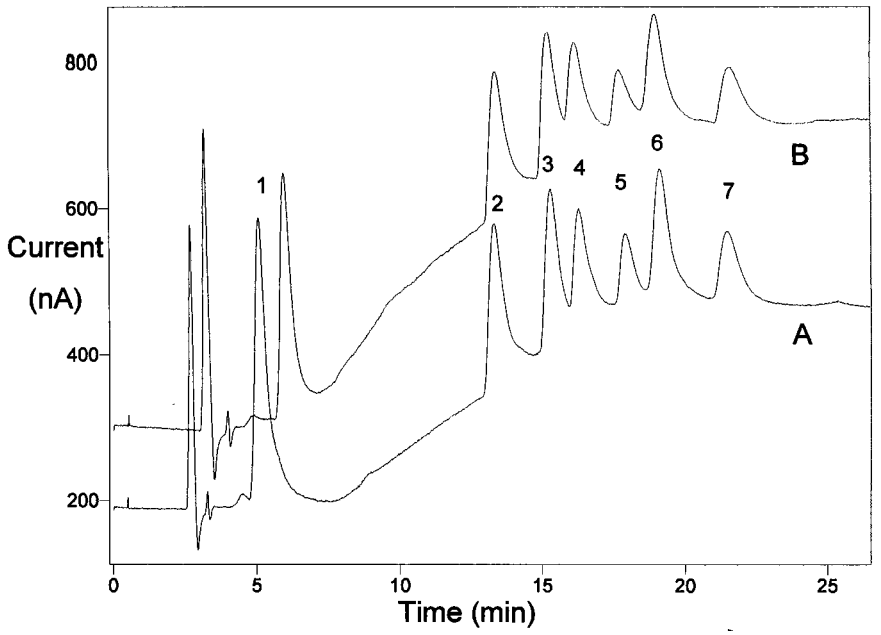

Fig. 1. Elution of seven penicillins with and without flow programming using identical solvent gradients. NovaPak C-8 column. Waveform: given in Table 2A. Penicillins all present at 1×10^{-3} M: (1) ampicillin, (2) penicillin G, (3) penicillin V, (4) oxacillin, (5) cloxacillin, (6) nafcillin, (7) dicloxacillin. Traces: (A) constant flow, 1.2 ml/min, complete solvent program given in Table 1A; (B) flow rate increase from 1.0 to 1.5 ml min^{-1} between 3 and 4 min, complete solvent program given in Table 1B.

Fig. 2. A trace of the Au residual in the initial 12/8/80 solvent is shown in A, with the corresponding residual of 10/25/65 given as trace B. It can be seen that in the positive potential region correlating with the E1 value utilized in Fig. 1A, that trace B yields less anodic current than trace A. Given that the 10/25/65 solvent is less polar and contains less electrolyte than the initial solution, one would expect slower electron transport and the need for greater overpotential to grow surface oxide. Lacking this, the current is depressed as shown in Fig. 2, and as portrayed by the baseline rise in Fig. 1A.

Various attempts were made to minimize the baseline perturbation. Running the gradient between the two eluents over a longer period of time surely would have lessened the impact, but was not desirable in light of the already significant retention time of the later peaks. One strategy that was attempted was flow programming, incorporating an increase in the flow rate during the regular solvent program, going from 1.0 to 1.5 ml min^{-1} (the entire program is given in Table 1B). Shown in Fig. 1B, it can be seen that this in fact made the baseline shift even worse. Still, the modest nature of the shift was somewhat of a surprise; past experience had associated flow rate changes within a separation with large, unacceptable baseline surges. It was clear that the minor impact observed in Fig. 1B opened up the door to considering flow programming during the optimization of the penicillin separation.

Various flow programs using 12/8/80 or 10/25/65 consistently showed that an increase in flow rate caused a corresponding reduction in the anodic baseline current. A preponderance of the background current in this potential region is due to the growth of a surface oxide layer on the working electrode. Voltammetric studies using a rotating disc electrode showed that there was no significant mass transport dependence for the output current from this process, leaving no obvious explanation for the baseline shift.

Table 1
Solvent programs for separation of the penicillins

Time (min)	Composition (volume % methanol/acetonitrile/0.02 M acetate buffer (pH 4.7))	Flow rate (ml min^{-1})
A		
0–4	12/8/80	1.2
4–14	12/8/80–10/25/65 (linear ramp)	1.2
14 to end	10/25/65	1.2
B		
0–3	12/8/80	1.0
3–4	12/8/80	1.0–1.5
4–14	12/8/80–10/25/65 (linear ramp)	1.5
14 to end	10/25/65	1.5
C		
0–6	12/8/80	1.0
6–7	12/8/80–11.8/10.0/78.2 (linear ramp)	1.0–1.5
7–12	11.8/10.0/78.2–10.6/20.2/69.2 (linear ramp)	1.5–1.9
12–14	10.6/20.2/69.2–10/25/65 (linear ramp)	1.9
14 to end	10/25/65	1.9

To gain a more detailed understanding of the changes seen during flow programming, a structured series of trials were undertaken. Since the point of interest was detector response rather than any kind of chromatographic parameter, the experiments were run as flow injection analysis (FIA) trials with constant solvent composition throughout. The 12/8/80 methanol/acetonitrile/0.02 M acetate buffer mixture used as the initial solvent in Fig. 1 was selected for use with the various flow programs. The PAD waveform given in Table 2A was used for all of these trials. After an initial period pumping this solvent at a constant rate, an injection of 1.00×10^{-3} M penicillin G was made prior to any change in flow rate. After completion of the penicillin G peak, the flow rate program was undertaken. Six minutes after program completion, a second injection of the same penicillin G solution was made using the terminal conditions of the flow program. Fig. 3 shows the output of a typical trial. Each set of conditions was performed in triplicate to insure reproducibility.

Table 2
PAD waveforms

Potential (mV)	Time (s)
A	
1350	0.167
1500	0.167
−200	0.333
B	
1450	0.333
1550	0.333
−300	0.416

Tabulated for each of the trials in Table 3 is the relative change ((peak 1 − peak 2)/peak 1) in peak height, relative change in peak area, the relative change in peak tailing by measurement of peak asymmetry factors (PAF) [29], the total change in current during the period of flow rate change, and the maximum slope that occurred in the region of perturbation. The direction of the shift in baseline was consistent, mirroring that seen in Fig. 1. The observed parameter that correlated the strongest with the change in flow program was the maximum slope. For all initial/final flow settings, the slope decreased as the transition period was extended to longer times. As the ratio of final to initial flow rate increased, the magnitude of the slope increased. Most of the measured parameters were altered when new initial/final rate settings were introduced, but the slope was clearly the best indicator of the period over which the transition took place.

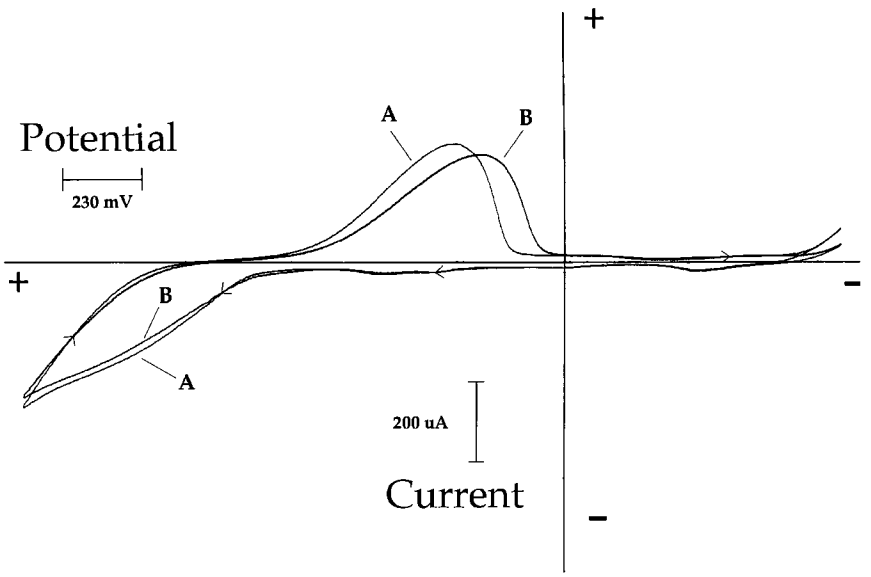

Fig. 2. Residual cyclic voltammograms of two different chromatographic solvents on gold. Solution deoxygenated with N_2. Scan rate: 100 mV s^{-1} (arrows denote scan direction). Rotation speed: 900 rpm. Traces: (A) 12% methanol/8% acetonitrile/80% 0.02 M acetate buffer (pH 4.7) (v/v); (B) 10% methanol/25% acetonitrile/65% 0.02 M acetate buffer (pH 4.7) (v/v).

The amount of shift in the baseline signal was proportional to the amount of flow rate change, although the correlation was not as strong as with the slope. The final baseline measurement was always delayed until 5 min after the completion of the solvent program to ensure complete equilibration. The baseline shifts were small; when coupled with the potential for small slopes in the residual baseline, greater uncertainty and a weaker correlation with the flow rate change resulted. The baseline shift looked to be independent of the transition time in the flow program.

As would be expected, the peak areas got much smaller as the flow rate was increased due to the temporal compression of the sample plug. Varying the transition period of the flow change did not alter the relative change in the peak area, which was solely a function of the initial and final flow rates in use. Unlike the baseline shift, the peak area change was constant for a given increment in flow rate, regardless of the proportion of the change as compared to the initial conditions.

The peak height trends mirror those seen for peak area, although the data is not as precise. This is largely due to the fact that the FIA peak profiles were only being defined by data collection at 0.666 Hz. with the PAD waveform in use. For the trials utilizing very high flow rates, insufficient data points were collected to trace out the peak profile with great accuracy, resulting in uncertainty determining the actual signal maximum for each peak. Whereas the compression of the time axis would obviously cause a reduction in peak area, this would not be the case for peak height. As has been noted [27], for a kinetically slow electrochemical reaction, an increase in flow rate and the corresponding shorter residence time of the sample in the detector flow cell is enough to observe a drop in faradaic efficiency. The drop in peak height shows that a smaller fraction of the penicillin sample adsorbs to the working electrode as the flow rate is increased, reducing the degree of oxide suppression.

Despite being even less precise than the peak height data, the PAF values for an identical penicillin G injection increase proportionally with flow rate. The high flow rate narrows the time profile of the sample plug, but the rate of sample desorption from the electrode surface due to surface electrochemistry does not change. This causes a

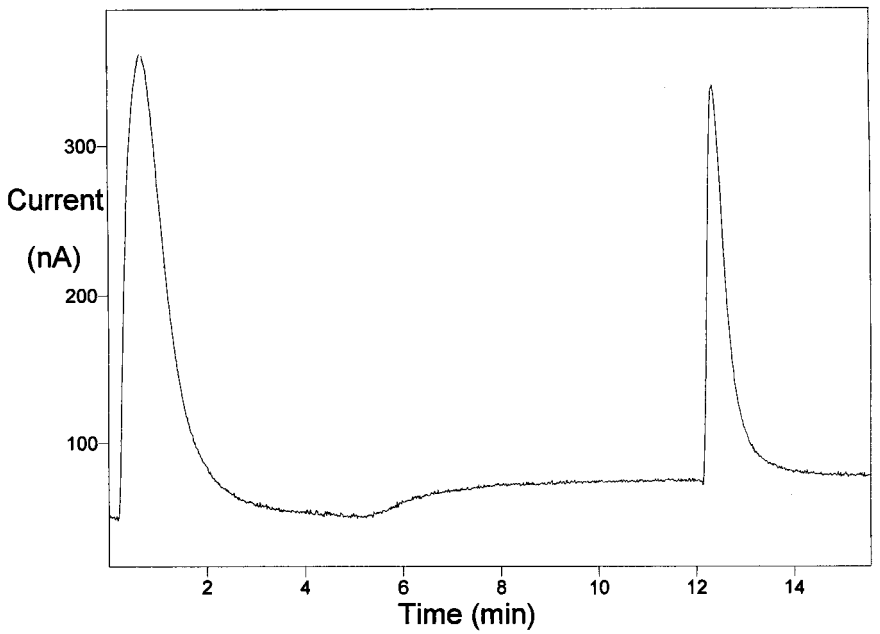

Fig. 3. Typical output data from the flow programming variation used to produce the data in Table 3. Flow injection analysis, both injections 1×10^{-3} M penicillin G. Solvent: 12% methanol/8% acetonitrile/80% 0.02 M acetate buffer (pH 4.7) (v/v). Flow program: initial flow, 0.5 ml min^{-1}; final flow, 1.5 ml min^{-1}; transition period, linear ramp between 5 and 6 min.

shift in mass toward the tail end of the peak relative to the narrower profile, which ultimately leads to greater tailing and a higher PAF value. There is a strong resemblance between the trends for PAF change and baseline shift.

Although the parameters measured in Table 3 characterized how different flow programs would affect the penicillin separation in development, the direction of the baseline shift remained a mystery. Subsequent trials using the 12/8/80 solvent with flow programming were studied using a wide variety of PAD waveforms (including both direct and indirect PAD). As expected, the magnitude of the baseline shift could be altered, but the direction of the shift remained the same for all (i.e. less anodic current as flow rate was increased).

An examination of flow programming with different solvent compositions yielded further information of interest. Incorporating the same waveform used with the Table 3 trials (given in Table 2A) with an unmodified 0.02 M acetate buffer (pH 4.7) solvent produced opposing response to flow rate changes as compared to 12/8/80. In other words, anodic current increased as the flow rate was increased. A comparison of these two solvents utilizing identical waveforms and flow programs can be seen in Fig. 4, along with an additional trial using the 10/25/65 solvent. The baseline shift has a strong dependence on the polarity of the solvent, suggesting that the shift is due to kinetic alterations of the residual electrochemical processes taking place.

This behavior mimics that seen when electroinactive adsorbates are introduced into an amperometric detector, thoroughly detailed by Polta and Johnson [33]. At the lowest potentials in the oxide region, the presence of the adsorbate was shown to reduce the anodic residual current, but when much greater overpotential was applied, the signal underwent a crossover to produce greater signal with adsorbate present. Polta and Johnson used this behavior to indirectly detect these electroinactive adsorbates in either a 'positive' or a 'negative' manner, depending on which side of the crossover potential they were operating. Like introduction

Table 3
Flow programming data

Program description	Relative Δ peak height	Relative Δ peak area	Relative Δ PAF	Baseline shift (nA)	Maximum slope (nA min^{-1})
0.5–1.0 ml, over 1 min	0.101	0.30	−0.13	13.9	−6.0
0.5–1.0 ml, over 3 min	0.0581	0.32	−0.31	16.3	−4.8
0.5–1.0 ml, over 5 min	0.0795	0.32	−0.20	13.6	−3.2
1.0–1.5 ml, over 1 min	0.0803	0.31	−0.098	9.45	−4.6
1.0–1.5 ml, over 3 min	0.0793	0.32	−0.17	9.42	−2.4
1.0–1.5 ml, over 5 min	0.0632	0.29	−0.12	7.72	−1.6
0.5–1.5 ml, over 1 min	0.157	0.458	−0.40	21.9	−12
0.5–1.5 ml, over 3 min	0.147	0.454	−0.37	24.4	−7.7
0.5–1.5 ml, over 5 min	0.146	0.441	−0.27	25.5	−5.2
1.0–2.0 ml, over 1 min	0.151	0.439	−0.18	15.9	−7.5
1.0–2.0 ml, over 3 min	0.144	0.43	−0.17	13.8	−4.6
1.0–2.0 ml, over 5 min	0.155	0.454	−0.19	21.5	−3.2
1.5–2.5 ml, over 1 min	0.132	0.47	−0.18	8.74	−5.3
1.5–2.5 ml, over 3 min	0.143	0.47	−0.17	7.70	−2.6
1.5–2.5 ml, over 5 min	0.139	0.47	−0.18	6.88	−1.5
1.0–2.5 ml, over 1 min	0.1987	0.512	−0.23	14.6	−8.9
1.0–2.5 ml, over 3 min	0.2096	0.522	−0.26	14.2	−4.3
1.0–2.5 ml, over 5 min	0.2147	0.542	−0.360	21.1	−4.0

of adsorbate, increasing the flow rate through the detector cell slows the kinetics of the electrochemical reactions in the detector cell. The lower potential region of the residual oxide process will be suppressed, but with sufficient overpotential a crossover can be reached to yield a current enhancement at larger voltages. The kinetic effect of the flow program is relative, as the three solvents tested in Fig. 4 already have significant kinetic differences due to their varying polarity and efficiency as electrolyte. For the high ionic strength of the acetate buffer solvent, the electrode surface oxide is grown at smaller potentials than for the solvents containing organic modifier. As organic modifier content is increased, the oxide formation region is pushed to more and more positive values. This will also push the suppression/enhancement crossover point for a flow rate increase to more positive potentials. The behavior observed in Fig. 4 results from the detection conditions being more positive of the crossover point for the acetate buffer solvent, yet less positive of the crossover in both of the less polar solvents.

Given this behavior, two expected conclusions could be sought. First, the addition of sufficient overpotential to the waveform should allow a crossover to be observed for the 12/8/80 solvent. As noted previously, all of the different waveforms tested, even those with increased detection overpotential, yielded a decrease in anodic signal with increased flow rate. Even at the highest E1 value that produced stable response, 1850 mV, the response to the flow increase could not be inverted. It was apparent that even though the crossover was not reached, it was being approached; the baseline shift got smaller at the higher detection potentials tested. Even though inversion with the 12/8/80 proved impossible, a second conclusion would be that the 0.02 M acetate solvent could be inverted. Given that a flow rate increase caused an enhancement of the anodic current in Fig. 4 for this solvent, one would expect that a decrease in detection potential should push the response toward the crossover point and eventually invert the response to the flow increase. This behavior was possible to induce, as is shown in Fig. 5. Holding all other waveform parameters constant, an E1 of 1350 mV and one of 1050 mV gave opposing responses to an increase in solvent flow, clearly illustrating that they are on opposite sides of the crossover point. The trace with an E1 of 1200 mV was in the

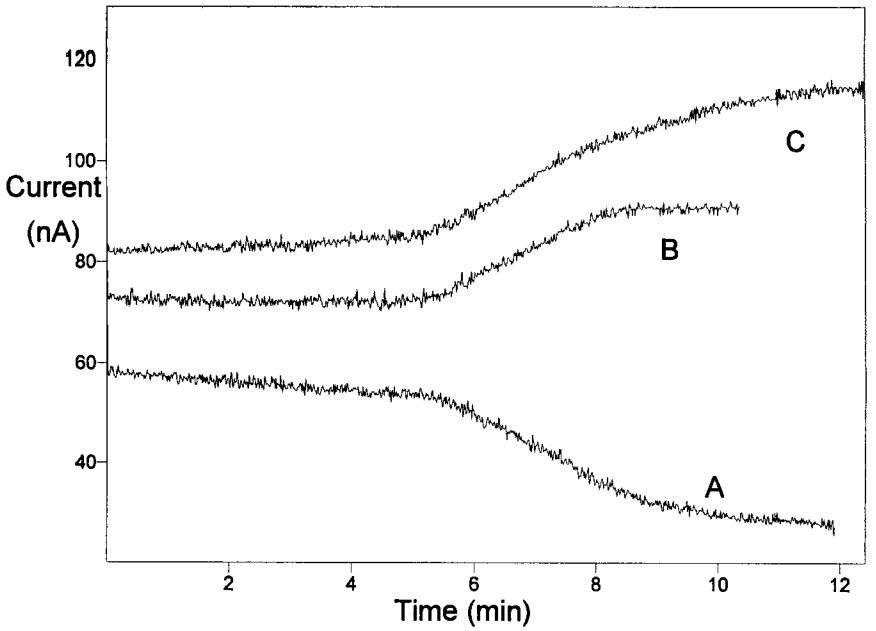

Fig. 4. Differing responses to an identical flow program for three different solvents using the same PAD waveform. Flow injection analysis. Flow program: initial flow, 1.0 ml min^{-1}; final flow, 2.5 ml min^{-1}; transition period, linear ramp between 5 and 8 min. PAD waveform: given in Table 2A. Traces: (A) solvent, 0.02 M acetate buffer (pH 4.7); (B) solvent, 12% methanol/8% acetonitrile/80% 0.02 M acetate buffer (pH 4.7) (v/v); (C) solvent, 10% methanol/25% acetonitrile/65% 0.02 M acetate buffer (pH 4.7) (v/v).

region of the crossover; this response was not completely unperturbed, but rather showed only a very small net baseline shift.

Interpreting from these trials, flow programming looked to be an attractive way to speed up the elution of later, well-resolved peaks. Despite the observation of sloping and shifting baselines caused by these gradients, actual applications seemed likely to utilize much less severe programs than those tested in Table 3, minimizing the baseline alterations. Along with the perturbation being much smaller than expected, the presence of a suppression/enhancement crossover potential allows many interesting possibilities. If the solvent allows incorporation of a waveform at the crossover point, the impact of flow rate changes on the PAD response can be minimized. Whether these conditions will also provide sensitive response to the analyte is, of course, also an important concern. For the penicillin separation under development, the flow program (increase rate with time) and solvent program (decrease polarity with time) that improved the chromatograph both decreased the anodic baseline current. Although this is envisioned as being fairly typical of reversed-phase HPLC-PAD applications, it may be possible in future work to design a separation whereby the flow program and the solvent program produce opposing behavior, potentially done in a manner to balance the baseline perturbation from each.

The observed alteration of peak heights, areas, and shapes with flow rate would be of concern to those performing quantitative studies, but proper calibration would still permit accurate concentration determinations. Some sacrifice in detectability would result from shifting to higher flow rates, but this would be only a minor effect. Another notable feature of the flow program was that it was not unusual for the baseline perturbation to extend several minutes past the end of the transition period within the program; this should be kept in mind when designing a program.

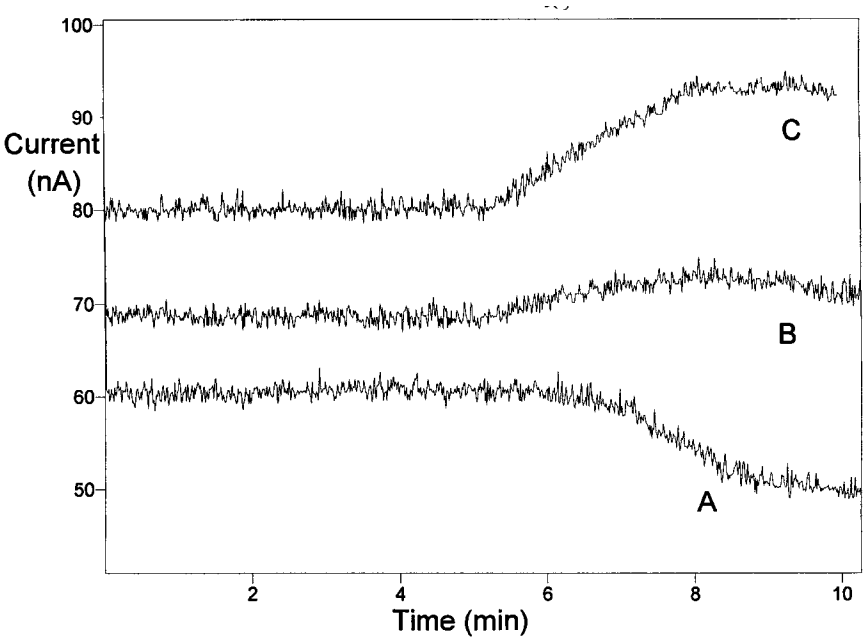

Fig. 5. Differing responses to an identical flow program for three different waveforms using the same solvent. Flow injection analysis. Flow program: initial flow, 1.0 ml min^{-1}; final flow, 2.5 ml min^{-1}; transition period, linear ramp between 5 and 8 min. Solvent: 0.02 M acetate buffer (pH 4.7). PAD waveform: given in Table 2A, except for E1 which was varied for each trace. Traces: (A) E1, 1350 mV, (B) E1, 1200 mV, (C) E1, 1050 mV.

For the penicillin separation, the benefits of the flow program looked to outweigh the shortcomings. A small increase in the baseline shift was to be expected, but the separation was greatly improved by reducing the analysis time without compromising resolution. Another factor minimizing perturbation was that the penicillin separation featured a wide gap between ampicillin and the later eluting peaks. If the baseline were shifted by imposition of a flow program in this time span, it was unlikely to interfere with the response from any of the eluted analytes.

Making full use of flow programming, a final separation was designed for use separating the seven penicillins. The solvent program is given in Table 1C and the accompanying PAD waveform detailed in Table 2B. After spiking a milk sample with the seven penicillins, they were separated as shown in Fig. 6. As expected, a very large void response was observed; the ampicillin peak overlapped a little bit, but not enough to cause any serious problems. The flow program appeared to contribute somewhat to the sloping baseline seen between 5 and 10 min, yet the affect was minor compared to the composition gradient and it blended well with void peak response. The program in use allowed ampicillin to be retained longer than the early trials to minimize void overlap, yet the later peaks were still pushed off in a reasonable time. The PAD waveform was altered in a manner that pushed the detector closer to the suppression/enhancement crossover point, minimizing the amount of baseline shift observed. Moving the waveform even closer to the crossover was not beneficial, as this attenuated peak size as the transition from indirect PAD to direct PAD was approached [19]. Detection limits for each of the penicillins using this separation are listed in Table 4. All are detectable to less than 1×10^{-5} M without derivatization. It can be noted that the detection limits are higher for the later-eluting species. This can be attributed partially to the loss in sensitivity that was expected at these higher flow rates, although the reduction in solvent polarity was a factor as well [20,22].

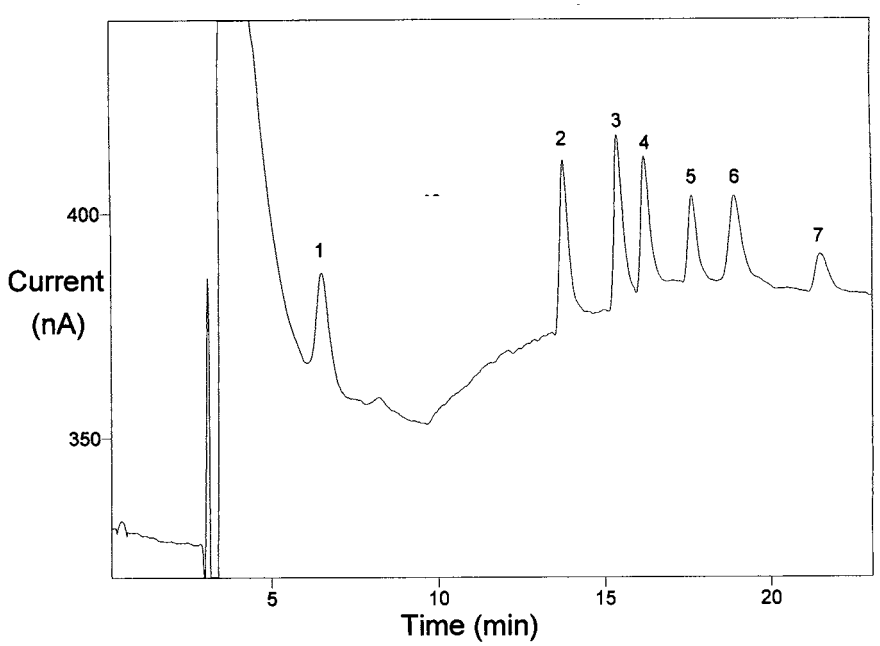

Fig. 6. Optimized determination of seven penicillins within a milk sample. NovaPak C-8 column. Waveform: given in Table 2B. Solvent program: given in Table 1C. All penicillins present prior to sample workup at 1×10^{-4} M: (1) ampicillin, (2) penicillin G, (3) penicillin V, (4) oxacillin, (5) cloxacillin, (6) nafcillin, (7) dicloxacillin.

4. Conclusion

Flow programming will produce a baseline offset for a PAD detector under most conditions, although the observed changes were less than expected. The slope produced during the region of change is proportional to the degree of flow rate change and the speed with which it is undertaken. The amount of baseline shift is proportional to the magnitude of the rate change, but is not greatly affected by the length of the transition period. Using the typical strategy of increasing the flow rate during a trial, one may get a baseline shift in either direction depending on the solvent composition and the waveform in use. Low polarity and low detection potentials favor a decrease in the anodic current as flow is increased, high polarity and high detection potentials tend toward the opposite. Customization of the solvent composition and the waveform will allow alteration of the baseline shift, potentially to produce minimal response to flow shifts or to produce a response opposing that produced by a concurrent solvent program. If these alterations can be made without compromising detector sensitivity, flow programming should prove valuable for other HPLC-PAD assays.

Table 4
Detection limits of the penicillins in milk from the optimized separation

Penicillin	Detection limit (M)
Ampicillin	3×10^{-6}
Penicillin G	1×10^{-6}
Penicillin V	1×10^{-6}
Oxacillin	2×10^{-6}
Cloxacillin	3×10^{-6}
Nafcillin	3×10^{-6}
Dicloxacillin	6×10^{-6}

Acknowledgements

Financial support for RLE was the result of a grant to the college from the US Department of

Education's Ronald E. McNair Post-Baccalaureate Achievement Program. Financial support for JSM was from a Ford Undergraduate Research Fellowship from Knox College, partially supported by The Ford Foundation. Additional support came from Knox College via the Faculty Research Program and the College Honors Program. The generous donation of equipment from the Waters Chromatography Division of the Millipore Corporation and from the Hewlett-Packard Corporation via a University Instructional Equipment Grant is acknowledged with gratitude. Thanks to Selen Altunata, Dan Mossman, and Mark Lehmann for programming assistance, and to John Polta and Bob Kooser for helpful discussions.

References

[1] I.P. Kaniou, G.A. Zachariadis, J.A. Stratis, J. Liq. Chromatogr. 16 (1993) 2891.
[2] R.R. Leder, V.M. Lane, D.P. Barrett, J. Am. Vet. Med. Assoc. 192 (1988) 1299.
[3] K. Schneider, Chicago Tribune, Dec. 28, 1990, Section 1, p. 5.
[4] W.A. Moats, J. Chromatogr. 507 (1990) 177.
[5] F. Jehl, P. Birckel, H. Monteil, J. Chromatogr. 413 (1987) 109.
[6] A. Marzo, N. Monti, M. Ripamonti, E.A. Martelli, M. Picari, J. Chromatogr. 507 (1990) 235.
[7] W.A. Moats, R. Malisch, J. Assoc. Off. Anal. Chem. 75 (1992) 257.
[8] F.W. Teare, R.H. Kwan, M. Spino, S.M. Macleod, J. Pharm. Sci. 71 (1982) 938.
[9] H. Terada, Y. Sakabe, J. Chromatogr. 348 (1985) 379.
[10] J.O. Miners, J. Liq. Chromatogr. 8 (1985) 2827.
[11] A. Besada, N. Tadros, Mikrochim. Acta 2 (1987) 225.
[12] W.T. Kok, J.J. Havax, W.H. Voogt, U.A.T. Brinkman, R.W. Frei, Anal. Chem. 57 (1985) 2580.
[13] B. Morelli, Anal. Lett. 20 (1987) 141.
[14] M.E. Rogers, M.W. Adlard, G. Saunders, G. Holt, J. Chromatogr. 257 (1983) 91.
[15] M.E. Rogers, M.W. Adlard, G. Saunders, G. Holt, J. Chromatogr. 297 (1984) 385.
[16] D.C. Johnson, W.R. LaCourse, Anal. Chem. 62 (1990) 589A.
[17] D.C. Johnson, W.R. LaCourse, Electroanalysis 4 (1992) 367.
[18] S. Hughes, D.C. Johnson, Anal. Chim. Acta 132 (1981) 11.
[19] L. Koprowski, E. Kirchmann, L.E. Welch, Electroanalysis 5 (1993) 473.
[20] E. Kirchmann, L.E. Welch, J. Chromatogr. 633 (1993) 111.
[21] S. Altunata, R.L. Earley, D.M. Mossman, L.E. Welch, Talanta 42 (1995) 17.
[22] E. Kirchmann, R.L. Earley, L.E. Welch, J. Liq. Chromatogr. 17 (1994) 1755.
[23] J.D. Olechno, S.R. Carter, W.T. Edwards, D.G. Gillen, Am. Biotech. Lab. 5 (1985) 38.
[24] J.A. Polta, I. Yeo, D.C. Johnson, Anal. Chem. 57 (1985) 563.
[25] W.R. LaCourse, D.A. Mead Jr., D.C. Johnson, Anal. Chem. 62 (1990) 220.
[26] L.E. Welch, W.R. LaCourse, D.A. Mead Jr., D.C. Johnson, Anal. Chem. 61 (1989) 555.
[27] M.A. Doscotch, J.A. Jones, L.E. Welch, Anal. Chim. Acta 55 (1997) 344.
[28] L.E. Welch, D.C. Johnson, J. Liq. Chromatogr. 13 (1990) 1387.
[29] M.W. Lehmann, M.R. Fahr, L.E. Welch, Talanta 44 (1997) 1231.
[30] L.R. Snyder, J.J. Kirkland, Introduction to Modern Liquid Chromatography, 2nd ed., Wiley-Interscience, New York, 1979.
[31] B. Ravindranath, Principles and Practice of Chromatography, Halsted Press/John Wiley and Sons, New York, 1989.
[32] A. Savitzky, M.J.E. Golay, Anal. Chem. 36 (1964) 1627.
[33] J.A. Polta, D.C. Johnson, Anal. Chem. 57 (1985) 1373.

ELSEVIER

Talanta 45 (1998) 1267–1279

Talanta

A software for the estimation of binding parameters of biochemical equilibria based on statistical probability model

E. Fisicaro [a], A. Braibanti [a,*], R. Sambasiva Rao [1,a], C. Compari [a], A. Ghiozzi [a], G. Nageswara Rao [b]

[a] *Institute of Applied Physical Chemistry, University of Parma, Parma, Italy*
[b] *Bioinorganic Chemistry Laboratories, Andhra University, Visakhapatnam, India*

Received 28 October 1996; received in revised form 16 July 1997; accepted 28 July 1997

Abstract

An algorithm is proposed for the estimation of binding parameters for the interaction of biologically important macromolecules with smaller ones from electrometric titration data. The mathematical model is based on the representation of equilibria in terms of probability concepts of statistical molecular thermodynamics. The refinement of equilibrium concentrations of the components and estimation of binding parameters (log site constant and cooperativity factor) is performed using singular value decomposition, a chemometric technique which overcomes the general obstacles due to near singularity. The present software is validated with a number of biochemical systems of varying number of sites and cooperativity factors. The effect of random errors of realistic magnitude in experimental data is studied using the simulated primary data for some typical systems. The safe area within which approximate binding parameters ensure convergence has been reported for the non-self starting optimization algorithms. © 1998 Elsevier Science B.V.

Keywords: Algorithms; Parameters; Electrometric

1. Introduction

Many of the biological processes—food cycle, functioning of drugs, effect of pollutants—are controlled by solution processes involving macromolecules and small molecules (oxygen) and ions (like proton and metal ions). A comprehensive knowledge of kinetics of formation, thermodynamic equilibria and kinetic stability of the products has vital applications. If the rate of interaction is diffusion controlled and the resulting species are sufficiently stable, the solution equilibria are investigated by equilibrium methods. The tertiary structure of macromolecules and enzyme catalysis involve metal ions while denaturation and renaturation associate with hydrogen ions.

The concept of binding sites and number of classes is in vogue [1–6] for the interaction of the

* Corresponding author. Tel.: +39 521 905024; fax: +39 521 905006.

[1] On leave from School of Chemistry, Andhra University, Visakhapatnam, India

PII S0039-9140(97)00242-7

macromolecules with small molecules. For example, an oxygen molecule interacts with myoglobin, a monomer, whose binding site (active site or the prosthetic group) is the heme group. It represents a system with one class and single binding site. Inosine and GDP have phosphate groups with two and three binding sites of the same class. Ribonuclease, on the other hand, has four classes, viz., carboxyl, imidazole, phenoxy and ϵ-amino groups. The number of binding sites are two in carboxyl class while one each in the remaining classes. Thus chemometric investigation of multiple equilibria in the presence of micelles, inert electrolytes and water miscible cosolvents at different temperatures generates complementary information useful in understanding bioprocesses.

In continuation of our efforts to apply statistical thermodynamic models [7,8] for macroscopic processes and developing software [9], we report in this communication, the algorithm and the results of binding parameters from electrometric titration data.

2. Chemometric model for the interaction of a macromolecule with small ligands

The formation thermodynamics of biologically important processes involving contact interactions between a protein (macromolecule, MM) and proton/metal ion (ligand, L) is considered. A mathematical model of these interactions can be developed based on thermodynamic/statistical mechanical/quantum mechanical postulates. A generalized model [10] consisting of a set of submodels has become popular as a natural methodology appropriate to deal with very complex biochemical processes. The binding of a macromolecule to a ligand can be represented by a quantized energy level model (Fig. 1). The binding of L to MM is equivalent to increasing the number of accessible cells or to dilute L which contributes to the entropy of the system. The site constant or the partition function is equal to the total change in entropy which contains both an enthalpy equivalent entropy ($\Delta H/T$) and intrinsic entropy contribution (ΔS) [7]. Thus the extent of binding equilibria is related to the partition function of the ingredients. The monitoring of equilibria by potentiometric and spectrophotometric procedures involves measurement of concentration (reciprocal of dilution) or entropy while that of calorimetric technique involves enthalpy [11]. As there is no chemical reaction amongst macromolecules, the state of either MM or L is represented separately each by a non-reacting ensemble. The whole reaction mixture is represented by a reacting ensemble. The joint probability of transition between the levels is given by the free energy probability (Eq. (1)).

$$\exp(-\Delta G_i/RT) = \exp(-\Delta H_i/RT)\exp(\Delta S_i/R) \quad (1)$$

The change in the concentration of any of these species varies the hydrogen ion concentration or emf and thus they are termed as macrospecies. If two ligands are bound to MM and the binding sites are similar, then they are considered to belong to a single class with a unique site constant. The statistically indistinguishable species which contribute to the mass-balance but cannot be monitored with an experimental probe are known as microspecies.

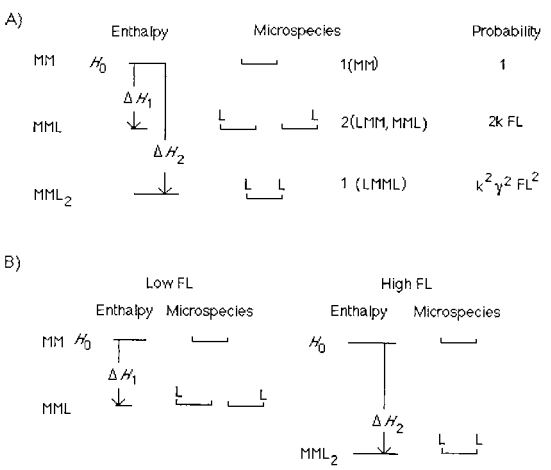

Fig. 1. Molecular thermodynamic diagram for complexes MML and MML_2. A) Enthalpy levels, number of microspecie (multiplicity), and probability. If $\gamma = 1$, then $\Delta H_2 = 2\Delta H_1$. B) Effect of cooperativity. If $\gamma < 1$, then $\Delta H_2 < 2\Delta H_1$.

3. Algorithm

For a macromolecule, with a number of classes (n-class) the group parameters to be estimated (NPAR) for each class are site constant and cooperativity factor. The column vectors contain number of sites and their parameters in each class (notation of tensor algebra is given in Appendix A).

[sites(1) sites(2). . .sites(n-class)]′

[ks(1) ks(2). . . .ks(n-class)]′

[b(1) b(2). . . .b(n-class)]′

The number of mass-balance equations (NMBE) at each point is two and if the total number of points in different experiments (NEXP) is NP then it results in $2 * \mathrm{NP}$ equations. Confining to monitoring hydrogen ion concentration (NEMF) the number of free concentrations (NC) at each experimental point is (NMBE-NEMF) $*$ NP. Then the total number of parameters to be estimated from $2 * \mathrm{NP}$ non-linear equations is $2 * (\mathrm{NP} + n\text{-class})$.

4. Estimation of free concentrations

The sum of residuals in total concentration of macromolecule (RMM) is a non-linear continuous function of FMM and FL (Eqs. (2) and (3))

$$\mathrm{RMM} = \mathrm{TMMC} - \mathrm{TMME} \tag{2}$$

$$= \mathrm{FMM} + [\mathrm{MML}] + [\mathrm{MML2}] + \cdots + [\mathrm{MML}n] - \mathrm{TMME} \tag{3}$$

It is linearized by truncating all the terms of its Taylor series beyond first degree (Eq. (4))

$$\mathrm{RMM}(\mathrm{FMM} + s\mathrm{FMM}, \mathrm{FL} + s\mathrm{FL}) = \mathrm{RMM} + (\delta\mathrm{RMM}/\delta\mathrm{FMM}) * s\mathrm{FMM} + (\delta\mathrm{RMM}/\delta\mathrm{FL}) * s\mathrm{FL} = 0 \quad \text{or}$$

$$[\mathrm{gRMM}][s\mathrm{FX}] = -\mathrm{RMM} \tag{4}$$

where gRMM is the gradient vector. This equation has no unique solution as two free concentrations are to be calculated from a single equation. The residual in ligand concentration results in Eq. (5). Now the estimation of the shift in free concentrations is a deterministic problem

$$[\mathrm{gRL}][s\mathrm{FX}] = -\mathrm{RL} \tag{5}$$

as the number of equations are equal to the number of parameters (FMM, FL)

$$s\mathrm{FX} = \left[\frac{g\mathrm{RL}'}{\mathrm{gRMM}'}\right] * \left[\frac{\mathrm{RM}}{\mathrm{RL}}\right] \tag{6}$$

Since the free concentrations at a point are independent of those at other titre values, FX are estimated NP times using a highly sparse matrix of size $2 * \mathrm{NP}$ by $2 * \mathrm{NP}$.

5. Molecular thermodynamic model for the equilibrium concentrations of macrospecies

The purpose of the present paper is to develop a computer algorithm based on the representation of the solution equilibria in terms of probability concepts of statistical molecular thermodynamics. For the non-competitive binding of a ligand to the macromolecule, the total concentrations of the species in equilibrium are obtained as the product of probabilities of microequilibria for different classes of sites.

As the site constant for a class is identical for different sites, the concentrations of macrospecies should be identical which is contradictory to the experience. The statistical factor (SF) which depends on the number of free sites partially takes into account of the differences in the concentrations of microspecies. It is given by the binomial expansion or Pascal triangle. A column vector, ind-space, containing number of sites in that class plus one is defined.

A cooperativity factor b is introduced to consider the effect of inter-class difference not accounted for by the simple statistical factor. However, inter-class cooperativity also plays a role in the case of molecules with heteroatoms. Then the cooperativity factors are represented by a symmetric matrix of size n-class by n-class. In the present case, the diagonal elements representing the cooperativity between the sites in a class alone are tested.

ZMM = SUM [SUM(CBGF)]
ZL = [SUM(SUM(CBGF) -1)]*FMM/FL + 1
If self association of macromolecules &
polymeric form of the complexes are present
Then
TMM = FMM*{ZMM + FMM(∂ZMM/∂FMM)}
Else
TMM = FMM*ZMM as ∂ZMM/∂FMM = 0
Endif
TL = FL*[ZL + FL(∂ZL/∂FL)]

(*) : X=MM, M, or L
ZX : Partition function with respect to X
: [Sum of the ratios of concentrations of micro species containing X to concentration of free X(FX)]
TX : Total concentration
BGF(X) : Binding generating function with X as receptor vector defined in equation (10)
CBGF(X) : Cumulative binding generating function with X as receptor ; a rectangular matrix for more than one class obtained as tensor product of coresponding BGFs

Fig. 2. The partition functions (*).

The binary generating function (BGF) for a class expresses the probability of occupation of ligand on the macromolecule and is obtained by the expansion of the binomial expression $(1 + ks(j) * \mathrm{FL})$ which is equal to

$$_{\mathrm{site}(j)+1}\boxed{\mathrm{BGF}}^{1} = \mathrm{SF} * (ks * \mathrm{FL})\text{^ind-space} \quad (7)$$

where ind-space is represented by the indexes of the elements of the vector BGF, each element defining one species. Here each element of the vector is multiplied by the corresponding element in the other. And the process is illustrated by a system with one class and two sites. Then the ind-space becomes [0 1 2]′

$$_{\mathrm{sites}(j)+1}\boxed{\mathrm{BGF}}1 = \begin{bmatrix} \mathrm{SF1} \\ \mathrm{SF2} \\ \mathrm{SF3} \end{bmatrix} * (ks(1) * \mathrm{FL})\text{^} \begin{bmatrix} 0 \\ 1 \\ 2 \end{bmatrix} \quad (8)$$

$$= \begin{bmatrix} \mathrm{SF1} \\ \mathrm{SF2} \\ \mathrm{SF3} \end{bmatrix} * \begin{bmatrix} (ks(1) * \mathrm{FL})^0 \\ (ks(1) * \mathrm{FL})^1 \\ (ks(1) * \mathrm{FL})^2 \end{bmatrix} \quad (9)$$

$$= \begin{bmatrix} \mathrm{SF1} * 1 \\ \mathrm{SF2} * (ks(1) * \mathrm{FL}) \\ \mathrm{SF3} * (ks(1) * \mathrm{FL})^2 \end{bmatrix} \quad (10)$$

The elements of BGF correspond to the terms of the partition functions for MM (or ratio of concentration of macrospecies to FMM) and thus ZMM is equal to the sum (SUM) of the elements of BGF (Fig. 2)

$$_{1}\boxed{\mathrm{ZMM}}^{1} = \mathrm{SUM(BGF)} \quad (11)$$

The total concentration calculated at ith point (TMMCi) is the product of FMMi with the corresponding partition function given by Eq. (12).

$$_{1}\boxed{\mathrm{TMMC}i}^{1} = {}_{1}\boxed{\mathrm{FMM}i}^{1} * {}_{1}\boxed{\mathrm{ZMM}i}^{1} \quad (12)$$

An illustration of algorithm for the calculation of cumulative generating function of MM and L for two classes of sites is given in Fig. 3.

The probability of occupation for the binding process of more than one class of sites is proportional to the product of probabilities of occupation in each class. The BGF for each class is obtained by the above algorithm and tensorial product is used to obtain the cumulative BGF

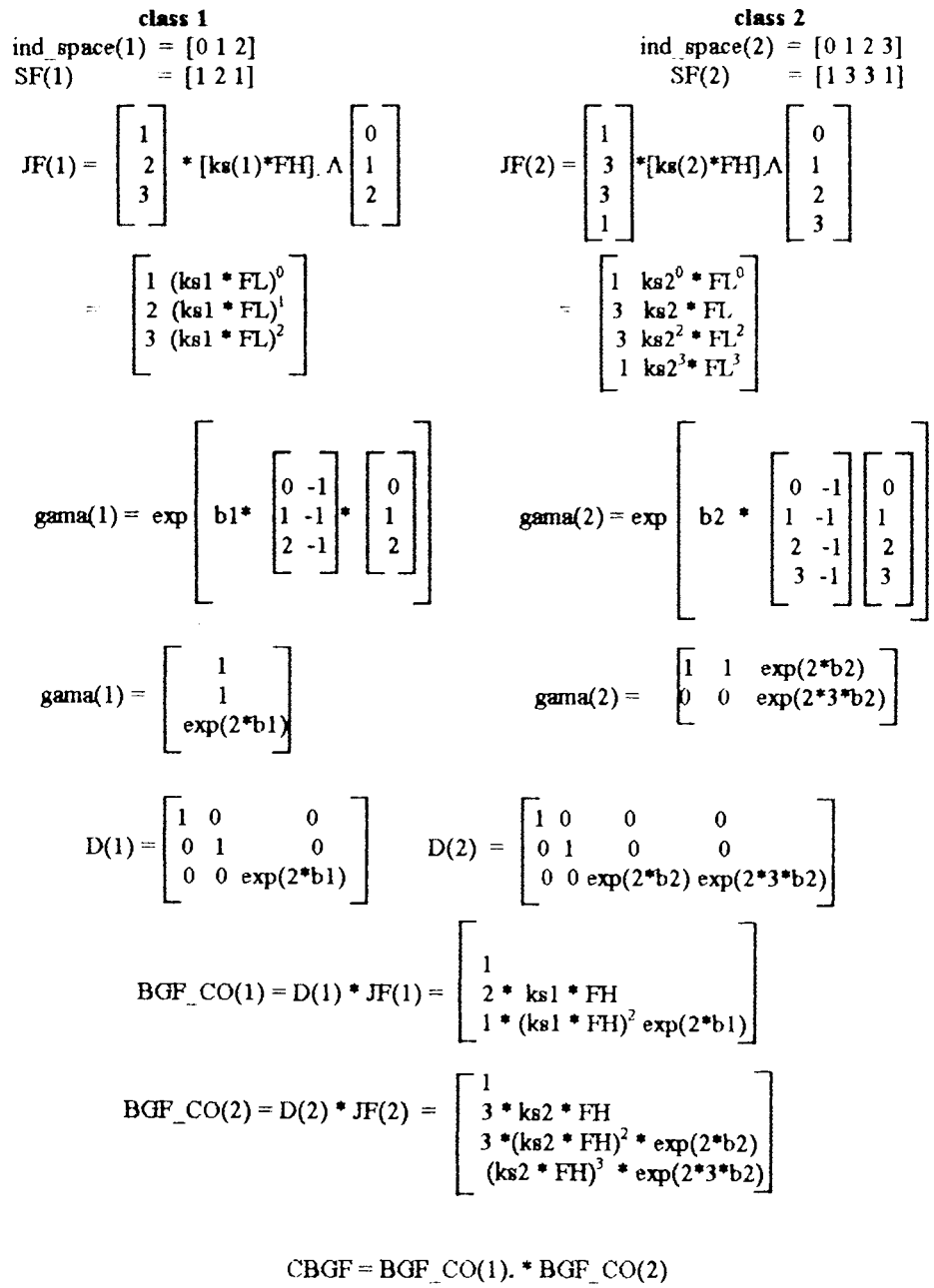

Fig. 3. Calculation of cumulative binary generating function of a macro molecule of two classes with two and three sites, respectively.

(CBGF). When cooperativity factor is introduced BGF is modified to BGFCO. It is obtained by premultiplying BGF with the diagonal matrix (D).

6. Estimation of binding parameters

Unlike free concentrations, site constants and cooperativity factors are group parameters (p).

∂TX/∂p	Algebraic form	Matrix form
Kj * ∂TMMi/∂Kj	$\sum_{i=1}^{NMS} CMS$	oner′ * CMS. * onec
∂TMMi/∂bj	$\sum CMS_i * (i_j-1) * i_j$	oner′ *(CBGF. * COE)*onec
FMMi*∂TMMi/∂FMMi	$\sum CMS_i$	oner′ *CMS. * onec
FLi *∂TMMi/∂FLi	$\sum CMS_i *(i_j-1)*i_j$	oner′ *(CMS.*COE) *onec
FMMi*∂TLi/∂FMMi	$\sum CMS_i*(i_j-1)*i_j$	oner′ *(CMS.*COE)*onec
FLi*∂TLi/∂FLi	$\sum CMS_i*\{(i_j-1)*i_j\}$	oner′ *(CMS.*COE)*onec

$_r[CMS]^c$: concentration of microspecies matrix = FMMi * CBGF

oner = oner(r,1); onec = (c,1)

oner′ * CBGF * onec = sum(sum(CBGF))

$_r[COE]^c$ = coefficient matrix

Fig. 4. Derivatives of mass-balance equations with respect to free concentrations and parameters.

The estimation of *ks* and *b* (NPAR $\geq 2 * n$-class) from $2 *$ NMBE equations is a over-determined situation. The principle of least squares is adopted accepting that best linear unbiased estimators (BLUE) can be obtained even for the case of non-linear problem. Although residuals in several quantities (emf, $\bar{n}$, moles of alkali per mole of metal ion) have been used in the object function, the sum of residuals in all mass-balance equations (R) is used in this package.

The calculation of shift vector in the refinement of binding parameters ($J * sp = R$) and free concentrations of components ($JRX * sFX = RX$) involves finding the inverse of a real matrix. The derivatives of mass-balance equations with respect to free concentrations and parameters are given in Fig. 4. Least squares method is generally employed as it gives maximum likelihood or minimum variance of the fit. However, the method fails or yields absurd values when $J^T * J$ is singular or nearly singular. This difficulty, which arises during the iterative process, is overcome by rotating the direction of the shift vector (obtained from the first order approximations of the Taylor series) towards the maximum. Twist matrix of Sillen, Marquardt parameter, Steene-Byrne vector and dog-leg procedures are noteworthy attempts [12,13] to move towards the steepest descent method.

It is indicated in some software packages [14] that matrix of normal equations is not positive definite. The singularity problem is a consequence of cumulative errors of different sources like model errors (due to introduction of spurious species, species with linear dependent stoichiometry), experimental errors (data, intermediate parameters), truncation error (as a result of omission of terms in the Taylor's expansion) and

$$s \quad J * R$$
$$J * s = R$$

$$s = J^{-} * R = J^{+} * R$$

SVD decomposition $s = (U*S*V')^{+} * R = (V*S^{-1}*U') * R$

IF truncated U,V, and S are used instead of U,S,V
Then $sp = Jp^{+} * Rp$
for binding parameters $sp = (Vp * Sp^{-1} * Up') * Rp$
for free concentrations $sFX = J^{+}*FX * RX$
$= (V*FX * sFX^{-1} * U*FX') * RX$
$sFX = JFX^{+} * RX$
$= JFX^{-1} * RX$ (for free concentration as J is square matrix)
$sp = (Jp' * Jp)^{-1} * Jp' * R$ (for shifts in parameters as J is a rectangular matrix)

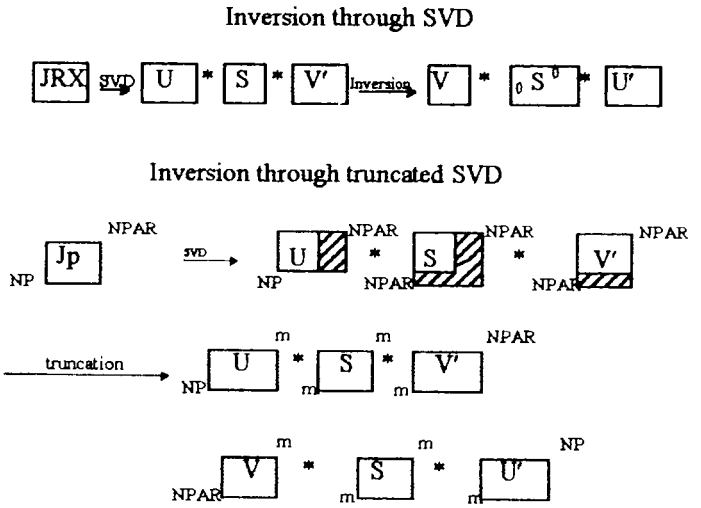

Fig. 5. SVD in the refinement of free concentration and binding parameters.

round off errors in numerical calculations. Another significant source is the approximate parameter values which are far away from the local optima [15] or beyond the safe area limits [16]. So the pseudo inverse is introduced.

Any orthogonal transformation takes care of the inversion of a nearly singular Jacobian (J) but singular value decomposition (SVD) is the best choice [17] in view of it's unique advantages. SVD of a matrix or second order tensor is a linear mathematical decomposition into influence of row designees (U), the importance of each influence (diagonal elements of S) and the corresponding influence of column designees (V). U and V are orthogonal matrices (Fig. 5). The power of SVD is best used by selecting the statistically significant positive singular values. Truncated SVD obtained by deleting all zeros and insignificant singular values together with their corresponding vectors is used in obtaining the inverse.

We have taken the SVD of J avoiding the complications arising in dealing with $J^{T} * J$. The truncated U, V and S are used to get the inverse of J. As U and V are orthogonal matrices, the

transpose of each corresponds to its inverse. S being a diagonal matrix, reciprocal of the diagonal elements results in inverse of S. Thus this hybrid procedure not only avoids the conventional inversion but combines the advantages of eigen vector projection and least squares principle using all the information in the J matrix.

Since the magnitudes of FX differ by several orders of magnitude from the binding parameters, a two stage optimization is implemented. With the initial set of site constants and cooperativity factors, FMM and FL at each experimental point are refined. If the value of the object function in the current iteration is different from the previous one, binding parameters are refined. This cycle is terminated only when multiple convergence criteria are satisfied [14]. Further over-ambitious modelling is avoided taking into account of the precision of primary data and cumulative errors from other sources.

7. Experimental

The molecular thermodynamic model to calculate the concentrations of macrospecies in biochemical equilibria and the algorithm to estimate the binding parameters are tested for several systems. The choice of the biomolecules is based on the increasing number of classes and sites in each class (Table 1). Primary experimental data obtainable from electrometric titration using a glass electrode are simulated with SOPHD [18] and the numerical values are rounded off to third decimal place for both pH and volume. The values of binding parameters are estimated using SITECON. Fig. 6 depicts the subroutines used in SITECON which can be executed on a microcomputer under DOS environment. The package is based on the concept of cooperativity and a unique site constant for each class is applicable to macromolecular equilibria. Most of the algorithm is developed in tensor algebra making it amenable for parallel processing. The mode of input of primary experimental data, guess values of *ks* and *b* is described in Fig. 7. Real life electrometric titration data sets were generated by the addition of normally distributed random noise of zero mean and fixed S.D. to the primary data. The effect of different magnitudes of S.D. was implemented through central composite design [19].

8. Results and discussion

A perusal of Table 1 indicates the applicability of the statistical thermodynamic model for the estimation of site constants and cooperativity factor. The advantage of the concept of binding parameters is a drastic decrease in the number of parameters as compared to the Adair (overall) or step-wise stability constants. A detailed account of the systems investigated follows.

9. Systems with one class

Four macromolecules—Keratine, Cytochrome C, lactic dehydrogenase and Thymine—each of

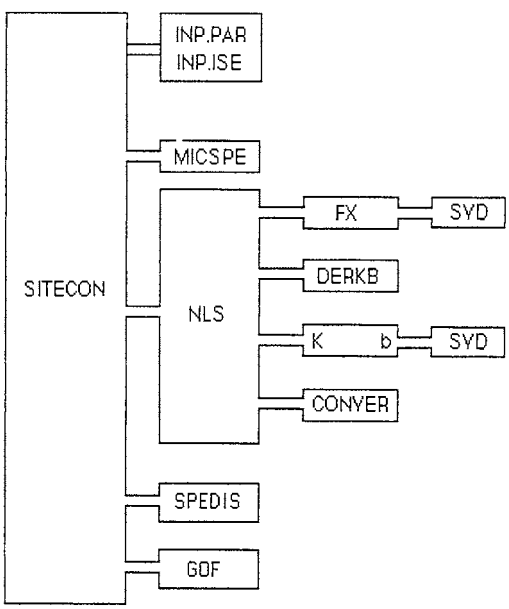

Fig. 6. A snapshot of the computer program SITECON. INP.PAR = Input Parameters; INP.ISE = Input Experimental Data; NLS = Non Linear Least Squares; MICSPE = Microspecies; CONVER = Convergence; FX = Free Concentrations; SVD = Single Value Decomposition; GOF = Goodness of Fit; SPEDIS = Species Distribution; DERKB = Derivatives of K, b; K = Site Constant; b = Cooperativity coefficient.

Table 1
Refinement of site constants and cooperativity using SITECON program

System	Class no.	No. of sites	Stepwise stability[a] const.	Refined		Reproduced stepwise st. const.[a]	Error sum of squares	Correlation coefficient
				Site const.	Coop. factor			
Cytochrome C	1	1 (imidazole)	6.60	6.60 (0.61e−4)	0.0	6.600	0.158e−10	—
Inosine	1	2 (phosphate)	6.16 5.28	5.859 (0.11e−3)	0.320 (0.26e−3)	6.160 5.280	0.977e−10	0.835
GDP	1	3 (phosphate)	9.60 6.30 2.90 4.40	9.130 (0.003)	3.297 (0.004)	9.607 6.267 2.926	0.184e−6	0.613
Nuclease	1	4 (imidazole)	5.60 5.90 6.10 6.60	6.157 (0.035)	−0.435 (−0.030)	6.689 6.736 6.713 6.579	0.119e−4	−0.972
Cytosine	1 2	1(pyridyl) 1(amino)	4.40 11.71	11.409 (0.11e−3)	7.723 11.710	4.400	0.116e−10	0.580
Clupeine	1 2	1(carboxyl) 1(amino)	5.05 8.30	5.050 8.299 (0.43e−4)	0.0 0.0	5.050 8.299	0.280e−10	−0.001
Lysozyme	1 2	2(carboxyl) 1(phenoxy)	6.80 5.80 10.40	5.498 (0.65e−3) 10.400 (0.11e−3)	−1.846 (−0.15e−2) 0.0	6.801 5.799 10.400	0.580e−10	2–0.998 3–0.001 0.001 1 2
Collagen	1 2 3	1(carboxyl) 1(imidazole) 1(phenoxy)	3.95 7.10 10.50	3.950 (0.23e−3) 7.100 (0.16e−3) 10.499 (0.95e−4)	0.0 0.0 0.0	3.950 7.100 10.499	0.320e−10	2 0.000 3 − 0.008 -0.005 1 2

[a] In log units.

```
      Clupeine                TITLE
      1                       IPRIN = 0 (FINAL RESULTS);1:CYCLES2:ALL
      2                       NMBE
      2     2                 n_class, n_classv
      100                     MAXIT
L                             NAME OF MACROMOLECULE
H                             NAME OF LIGAND
  30.0   0.01  0.1            Temp, SD in volume, SD in EMF/pH
   0.0   0.0  0  1  1  0      logks, b, n_site
-14.    0.0 -1  2  2  0
   8.0   0.0  1  2  1  2
   5.    0.0  1  2  1  2
   0.5   1.0                  CON of L, CON of H  (IN MILLIMOLES)
0.0   -0.2                   TITRANT L, ALKALI  (-ve VALUE)
100                           E0(STANDARD POTENTIAL)
50.                           INITIAL VOLUME (milli litres)
0  .000  3.531                V pH
0  .100  3.817
0  .200  4.041
    -     -
    -     -
    -     -
0   4.700   9.159
0   4.800   9.347
-1  4.900   9.630
_____________________
n_class  : NO OF CLASSES
n_classv : NO OF CLASSES TO BE VARIED
logks    : LOG OF SITE CONSTANT
b        : CO OPERATIVITY
n_site   : NO OF SITES IN THE CLASS
key      : 0 = FIXED, 1 = REFINE logk & b, 2 = REFINE logk, 3= REFINE b
```

Fig. 7. The mode of input for the program SITECON.

which contains only one site for the interaction are popular biochemical equilibria. The carboxyl, imidazole, phenolic and amino groups of these compounds however spanned the interesting pH region 4–10 for many bioprocesses. The estimated values of log *ks* agree well with those reported in literature (true values). Even very different initial input value converged to the optimum as it is a single equilibrium.

Inosine and GDP with two and three phosphate moieties, respectively, represent systems with multiple sites. Even in the presence of random noise the binding parameters refined with the present program coincide with those reported in literature [20]. Fig. 8 depicts the effect of guess values of log *ks* and *b* in the refinement process. It is instructive that the safe area decreases as compared to that with one equilibrium and from time to time several attempts have been made in literature to arrive at reasonable initial input values [14].

1,2,3,4-Butane tetracarboxylic acid has four sites and the system has a negative cooperativity for successive binding of protons. The formation of Ni(II)-ammonia complexes represents the interaction of ammonia with a receptor [nickel(II)] with six sites all belonging to the same class. The formation of species of higher stoichiometry i.e. those with greater than three ligand molecules requires not only higher amount of ammonia but also higher ratio of ligand to receptor. The refined binding parameters are in very nice agreement with the reported values.

10. Systems with two classes

The primary data for solution equilibria of two classes each with one and two sites with and without cooperativity are analyzed. In EDTA, the four carboxylic groups belong to one class with negligible cooperativity and the two amino groups form another class with appreciable anticooperativity. The slight differences in the binding parameters from those estimated earlier is a consequence of increasing complexity of the systems and increasing number of overlapping equilibria in the region where signal-to-noise ratio is high.

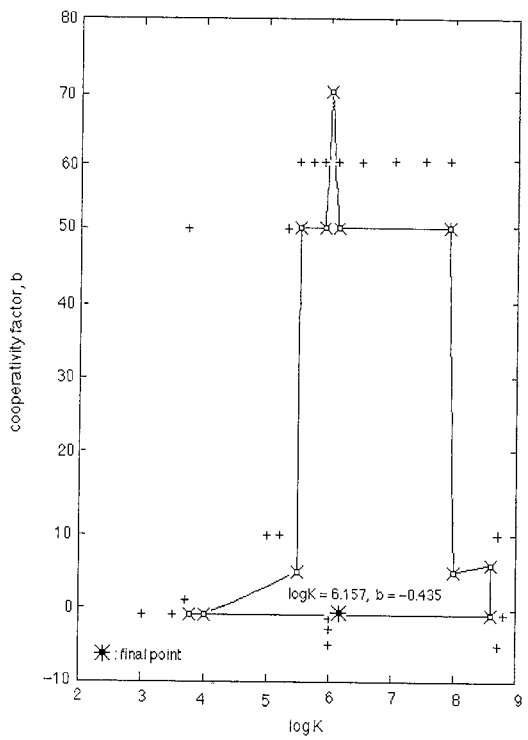

Fig. 8. Effect of initial (guess) estimates of log ks and b of Nuclease in the refinement by SITECON program. Solid line indicates the safe area limit of guess values within which the parameters are refined. (the empty circles indicate the guess values for which the algorithm failed, + indicates failure)

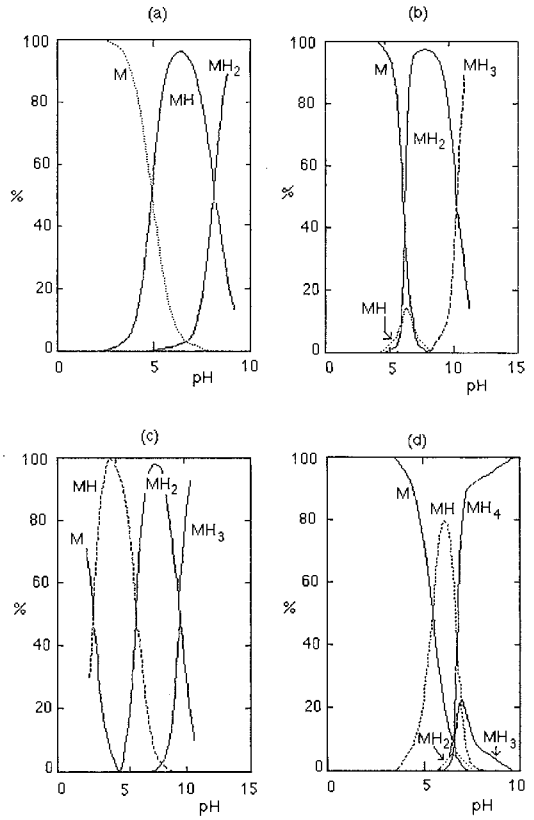

Fig. 9. Distribution diagrams of some typical systems: (a) Clupeine; (b) Lysozyme; (c) GDP; and (d) Nuclease.

11. Systems with three or more classes

Although the number of classes and sites increases, the parameters estimated by the present method are far less than the number of equilibria. Here also we considered the system with no cooperativity and studied the effect of keeping one or two parameters fixed. Conventional 2-dimensional distribution of the species of the proton interaction with some typical macromolecules as a function of pH is depicted in Fig. 9.

12. Effect of random errors in primary data

The confidence interval of the species distribution over a pH range throws light in understanding biochemical equilibria, drug action, lethal

Table 2
The effect of random errors in primary data on the binding parameters. The random errors are chosen by central composite design

Mean of random error		Refined parameters		log βs	ESS × e10
pH	Volume	Log ks	b		
0.0500	0.0100	5.868 (0.015)	0.349 (0.037)	6.169 11.433	190
0.0020	0.0100	5.867 (0.015)	0.349 (0.037)	6.169 11.433	190
0.0020	0.0010	5.858 (0.0006)	0.317 (0.001)	6.159 11.440	0.32
0.0599	0.0055	5.874 (0.0189)	0.329 (0.044)	6.152 11.454	260
0.0260	0.0119	5.851 (0.008)	0.329 (0.019)	6.152 11.416	51

dose for poisons and optimal concentrations of antidotes. In order to gain insight into this aspect a central composite design is adopted to introduce random errors in pH and volume of titrant. Two different series of random numbers were generated with MATLAB software and added to the simulated primary data for Inosine system. A perusal of the refined binding parameters (Table 2) with the data sets indicates that a deviation of around 0.02 in logarithm of site constant is observed for experiments 5 and 6. The results of Monte-Carlo experiments to estimate realistic confidence intervals of stability constants with normal and non-normal noise will be reported elsewhere.

13. Significance of initial estimates of binding parameters

During a search for new species, improvement of chemical model or reinvestigation with more accurate/sophisticated equipment, the binding parameters of biochemical/chemical equilibria corresponding to almost all species are known apriori. Many newly developed computer programs were validated for complicated equilibria with initial parameters slightly different from the best values. In order to avoid the mishap of arriving at a wrong chemical model with species that are unlikely to exist or that with genuine species being rejected, an indepth study of the effect of initial constants that are far away from the best ones was performed for protonation of nuclease.

From Fig. 8 it is clear that the data are fitted into the same chemical model when the log site constant is 2 units on either side of the best value. Even a very high value (≈ 170) for the initial input of the cooperativity factor converges to the same chemical model. However, when initial b value is -1.5, refinement was terminated as a consequence of the matrix of normal equations being not positive. It shows that the different parameters have varied influence which depends upon the object function surface as a function of binding parameters and the way of navigating on it (optimization algorithm).

Appendix A. Conventions and Notations

1. Bold face lower case letters represent a column vector and it is an n tuple of real numbers.

$$\mathbf{x} = [\mathbf{x}1 \ \ \mathbf{x}2 \ldots \mathbf{x}np]'$$

2. The row vector, a transpose of the column vector $\mathbf{x}$ is represented as $\mathbf{x}'$.

3. The matrices or second order tensors are represented by bold face capital letters **A**.

4. The terms rows and columns will be extended to tubes (planes) for third and higher orders.

5. Open face or shadowed bold face capital letters correspond to three-way (stack of matrices, data cube) or higher way tensors.

6. The terms order, ways and mode are synonyms but different from the conventional order of the matrix.

7. $\|X\|$ = Frobenius or Euclidian norm.

8. SUM(SUM(A)): Double summation over the indices of the matrix.

Matrix And Tensor Operators (implementable in MATLAB)

*: Conventional vector or matrix multiplication

$\otimes$: tensor, Kronecker or outer product

$x \otimes y$ is a dyad and is equivalent to the matrix product $\mathbf{x} * \mathbf{y}'$

$$\mathbf{x}.*\mathbf{y} = \begin{bmatrix} \mathbf{x}1 \\ \mathbf{x}2 \\ \mathbf{x}3 \end{bmatrix} * \begin{bmatrix} \mathbf{y}1 \\ \mathbf{y}2 \\ \mathbf{y}3 \end{bmatrix} = \begin{bmatrix} \mathbf{x}1 * \mathbf{y}1 \\ \mathbf{x}2 * \mathbf{y}2 \\ \mathbf{x}3 * \mathbf{y}3 \end{bmatrix}$$

Similarly

$$\mathbf{x}./\mathbf{y} = \begin{bmatrix} \mathbf{x}1/\mathbf{y}1 \\ \mathbf{x}2/\mathbf{y}2 \\ \mathbf{x}3/\mathbf{y}3 \end{bmatrix} \begin{bmatrix} \mathbf{y}1 & \mathbf{y}2 & \mathbf{y}3 \\ \mathbf{X}1 & \mathbf{X}2 & \mathbf{X}3 \end{bmatrix}$$

Kronecker product $\mathbf{X} \otimes \mathbf{Y}$ gives

$$\begin{bmatrix} \mathbf{X}(1,1) & \mathbf{X}(1,2) & \mathbf{X}(1,3) \\ \mathbf{X}(2,1) & \mathbf{X}(2,2) & \mathbf{X}(2,3) \end{bmatrix} \begin{bmatrix} \mathbf{y}1 \\ \mathbf{y}2 \end{bmatrix}$$

$$= \begin{bmatrix} \mathbf{X}(1,1) * \mathbf{y}1 & \mathbf{X}(1,2) * \mathbf{y}1 & \mathbf{X}(1,3) * \mathbf{y}1 \\ \mathbf{X}(2,1) * \mathbf{y}2 & \mathbf{X}(2,2) * \mathbf{y}2 & \mathbf{X}(2,3) * \mathbf{y}2 \end{bmatrix}$$

Kronecker addition is defined as

$$\mathbf{X} \oplus \mathbf{Y} = \begin{bmatrix} \mathbf{X}(1,1) + \mathbf{y}1 & \mathbf{X}(1,1) + \mathbf{y}2 & \mathbf{X}(1,2) + \mathbf{y}1 \\ \mathbf{X}(2,1) + \mathbf{y}1 & \mathbf{X}(2,1) + \mathbf{y}2 & \mathbf{X}(2,2) + \mathbf{y}1 \end{bmatrix}$$

$$\begin{bmatrix} \mathbf{X}(1,2) + \mathbf{y}2 & \mathbf{X}(1,3) + \mathbf{y}1 & \mathbf{X}(1,3) + \mathbf{y}2 \\ \mathbf{X}(2,2) + \mathbf{y}2 & \mathbf{X}(2,3) + \mathbf{y}1 & \mathbf{X}(2,3) + \mathbf{y}2 \end{bmatrix}$$

References

[1] J. Wyman, Adv. Prot. Chem. 19 (1964) 223.

[2] E. Di Cera, S.J. Gill, A. Wyman, Proc. Natl. Acad. Sci, USA 85 (1988) 449.

[3] J. Wyman, S.J. Gill, Binding and Linkage, University Science Books, Mill Valley, CA, 1990.

[4] F. Rusling, T.F. Kumosinski, Non-linear Computer Modelling of Chemical and Biochemical Data, Academic Press, CA, 1996.

[5] M. Brunori, M. Coletta, E. Dicera, Biophys. Chem. 23 (1986) 215–222.

[6] C. Rivetti, A. Mozzarelli, G.L. Rossi, E.R. Henry, W.A. Eaton, Oxygen binding by single crystals of hemoglobin, Biochemistry 32 (1993) 2888–2906.

[7] A. Braibanti, E. Fisicaro, F. Dallavalle, J.D. Lamb, J. Phys. Chem. 97 (1993) 8054–8061.

[8] A. Braibanti, E. Fisicaro, F. Dallavalle, J.D. Lamb, J.L. Oscarson, R. Sambasiva Rao, J. Phys. Chem. 98 (1994) 626–634.

[9] A. Braibanti, R. Sambasiva Rao, A. Ravindrababu, G. Nageswara Rao, Ann. Chim 85 (1995) 17–29.

[10] E. Clementi, R.H. Sarma (Eds.), Structure and Dynamics: Nucleic Acids and Proteins, Adenine Press, NY, 1983, p. 321.

[11] A. Braibanti, E. Fisicaro, F. Dallavalle, F.X. Ughi, Ann. Chim. 80 (1990) 303–339.

[12] W.H. Press, B.P. Flannery, S.A. Teukolsky, W.T. Vetterling, Numerical Recipes, 2nd ed., Cambridge University Press, Cambridge, 1992.

[13] J. Militsky, M. Meloun, Talanta 40 (1993) 269–277.

[14] G. Nageswara Rao, R. Sambasiva Rao, J. Ind. Council Chem. 8 (1992) 12–28.

[15] A. Ravindrababu, R. Sambasiva Rao, J. Chem. Eng. Data 37 (1992) 526–531.

[16] A. Ravindrababu, D. MuraliKrishna, R. Sambasiva Rao, Talanta 40 (1993) 1873–1882.

[17] G.H. Golub, C.F. Van Loan, Matrix Computations, North Oxford Academic, Oxford, 1983.

[18] R. Sambasiva Rao, A. Satyanarayana, P.V. Krishna Rao, Proceedings of the Summer Simulation Conference, The Society for Computer Simulation, 1984, 563–568.

[19] S.N. Deming, S.L. Morgan, Experimental Design: A Chemometric Approach, Elsevier, Amsterdam, 1987.

[20] J. Steinhardt, J.A. Reynolds, Multible Equilibria in Proteins, Academic Press, New York, 1969.

ELSEVIER

Talanta 45 (1998) 1281–1284

Talanta

Short communication

Determination of sulphur and total sulphur dioxide in wines by an ICP-AES method

I. Sarudi *, J. Kelemen

Department of Chemistry, Faculty of Animal Science, Pannon Agricultural University, Kaposvár, Hungary

Received 27 November 1996; received in revised form 6 June 1997; accepted 17 July 1997

Abstract

Sulphur contents of the original sample and the sample free from sulphur dioxide were determined by ICP-AES following nitric acid digestion under high pressure (using PAAR HPA equipment), and the total sulphur content was calculated from the difference between the results obtained. With the aim of preparing a sample free from sulphur dioxide, bound sulphur dioxide was released by sodium hydroxide, then after acidifying by phosphoric acid, boiling was carried out. Relative standard deviations of the results obtained for total sulphur, the sulphur without S(IV) and total sulphur dioxide were lower than 2.5, 3.5 and 5% respectively. Various amounts of sulphur (in the form of Na_2SO_4), added to wine samples, were successfully recovered between 95.5 and 104.9%. Based on comparative analyses performed by a widely accepted classic method, the indirect method developed was found to be adequate for the determination of total sulphur dioxide. The procedure is suitable for serial tests. © 1998 Elsevier Science B.V.

Keywords: Sulphur; Sulphur dioxide; ICP

1. Introduction

Sulphur dioxide is generally used as an antioxidant and disinfectant in winemaking. In consequence of sulphurization, wine sulphur consists predominantly of various S(IV) formations and the sulphate ions formed from a part of the sulphur dioxide used. In addition to these, wine sulphur contents usually also contains some sulphate originating from the grape, and traces of hydrogen sulphide. The quantity of S(II) is negligible in comparison with that of S(IV) or S(VI).

With respect to sulphur dioxide, three collective terms are accepted in wine chemistry: free SO_2, which is defined as the sum of unreacted forms (SO_2, H_2SO_3, HSO_3^- and SO_3^{2-}), and bound SO_2 which is combined with different aldehydes or ketones and can be released by hydrolysis [1,2], as well as total SO_2, which is the sum of the free and bound forms of SO_2. The free and total SO_2 contents are important analytical parameters in the quality control of wines. The determination of these can be achieved in a number of ways.

* Corresponding author.

PII S0039-9140(97)00228-2

The Rankine method [1–3], generally accepted as a reference method, involves distillation followed by alkalimetric titration, this being laborious and time consuming. In this respect, the other classic procedure referred to as the Ripper method [2,4] and its improved variation [5] are more advantageous than the Rankine method, since these involve merely iodometric titration. However, both have the drawback that several reducing compounds and colouring materials in red wines interfere in the determination of SO_2.

It appears that the voltametric methods are the most accurate ones for the determination of wine SO_2 [6,7]. These are still not widespread, perhaps because their sampling rate is quite low. The other electrochemical procedures generally performed, such as non-automated potentiometric determination [8] or coulometric titration [9], are also not frequently encountered in practice. In contrast with these, conventional spectrophotometric determination using *p*-rosaniline [10] is rather widely applied, even today. The application of GC [11–13] or HPLC [13] is also relatively frequent in this field. In the last two decades several automated procedures have been developed for SO_2 determination applying different potentiometric [4,14–17], spectrophotometric [18–24], chemiluminescent [25] or so-termed molecular-emission-cavity [26] techniques.The present paper demonstrates that total SO_2 in wine samples can also be determined by means of ICP-AES.

2. Experimental

2.1. Chemicals and reagents

All chemicals used were of analytical reagent grade. Distilled water was prepared from a 0.05% sodium hydroxide solution in glass apparatus. Prior to the digestion of the sample, 3 M NaOH and 4 M H_3PO_4 were used, and the digestion was performed with 65% nitric acid. Aqueous standard solutions containing 0.5, 1, 2, 3, 4 and 5 mg l^{-1} sulphur resp. were prepared by dilution from a 100 mg l^{-1} sulphur stock solution which in turn was made up from sodium sulphate dried at 110°C. The standard solutions (and the blank) in each case always contained those chemicals which had also been used for the preparation of the samples (practical matrix matching).

2.2. Instrumentation and operating parameters

The digestion of the sample was carried out in PAAR HPA (High Pressure Asher) equipment. This was heated from 50°C and then to 160°C with a heating rate of 2.5°C min^{-1}. A temperature of 160°C having been reached, this was maintained for 2 h.

Sulphur concentration was measured with a TJA Atomscan 25 type ICP-AES spectrometer. The operating parameters are listed in Table 1.

2.3. Procedures

For the determination of wine sulphur without S(IV), 10 ml of the NaOH solution and 25 ml of the wine sample were measured into a 100 ml Kohlrausch flask, then after 3 min 10 ml of the H_3PO_4 solution was added. Subsequently, the mixture was gently boiled for 15 min while nitrogen was bubbled through it and the evaporated water was occasionally replaced. The SO_2 having been removed in this way, the flask was cooled to room temperature and filled up with water. In the HPA equipment 0.5 ml of the sample pretreated in the way described above was digested with 3 ml of concentrated HNO_3 and after cooling the volume of the solution obtained was made up to 10 ml with water. Finally, the sulphur concentration of the solution obtained was measured by ICP-AES.

Table 1
Operating conditions for ICP-AES measurements

R.f. generator frequency	27.12 MHz
Forward power	1150 W
Plasma gas flow rate	12 l min^{-1}
Auxiliary gas flow rate	1 l min^{-1}
Nebulizer	Babbington cross-flow type
Nebulizer gas pressure	30.1 psi
Peristaltic pump flow rate	1 l min^{-1}
Plasma viewing position	15 mm above top of torch
Entrance slit height	2 mm
Integration time	30 ms
Wavelength (sulphur)	182.037 nm

Table 2
Results of sulphur determinations by ICP method and comparative SO_2 determinations in wine samples (mg l^{-1})

No.	Wine sample	Sulphur				Total sulphur dioxide			
		Total		Without S(IV)		Calculated[a]	Rankine method [3]		Difference
		$\bar{X}$	S.D.	$\bar{X}$	S.D.		$\bar{X}$	S.D.	
1	Dry white I	172.3	2.3	150.1	2.8	44.4	47.0	3.1	−2.6
2	Dry white II	268.7	5.4	152.4	4.6	232.4	224.9	7.8	7.5
3	Sweet white I	184.2	4.5	129.0	4.4	110.3	104.6	4.5	5.7
4	Sweet white II	211.6	4.9	134.2	3.1	154.6	159.1	7.2	−4.5
5.	Dry red	153.8	2.7	118.5	2.3	70.5	74.6	4.0	−4.1
6	Sweet red	190.4	3.8	126.7	4.2	127.3	122.5	5.6	4.8
7	Rosê	183.1	2.6	135.3	3.2	95.5	94.7	4.2	0.8

[a]From the results obtained for total sulphur and sulphur without S(IV)
Each time the number of determinations made was five.

With the exception of the boiling of the sample acidified by H_3PO_4, the method described above was also applied for the determination of total wine sulphur.

3. Results and discussion

The regression equation of a typical standard curve was $y = 3.32 + 47.89x$, where x is the sulphur concentration in mg l^{-1} and y is the analytical signal in arbitrary units. The standard deviation of intercept and the slope were 1.97 and 0.55, respectively. It was found by t-test that the intercept is also significant from zero ($p < 0.01$). It appears that the intercept is due to the impurities existing in the reagents.

To establish the limit of detection (LOD), eight blank solutions were prepared (using NaOH and H_3PO_4 solutions, nitric acid and distilled water). The mean and the standard deviation of the blank signals obtained were 2.95 and 1.59, respectively, in arbitrary units. The LOD for sulphur in the sample diluted 80-fold was calculated from the standard deviation of the blank signals (noise, N) and the slope of the standard curve (S) as follows: $LOD = 3N/S = 0.1$ mg l^{-1}.

In a red wine containing 11.5 v/v% alcohol, 9.2 g l^{-1} sugar and 21.8 g l^{-1} extract free from sugar, 158.3 mg l^{-1} sulphur was found (R.S.D. = 1.8%, $n = 5$). Subsequently, the sulphur content of the original sample was increased by the addition of dried Na_2SO_4 and sulphur determinations ($n = 5$) were repeatedly performed. For artificial concentration enhancements of 37.0, 51.6, 76.4 and 109.3 mg l^{-1}, recovery rates of 96.4, 101.7, 95.5 and 104.9%, respectively, were calculated from the differences between the corresponding average values.

To check the day-to-day reproducibilities of the sulphur and total SO_2 determinations, a white wine containing 12.4 v/v% alcohol, 49.8 g l^{-1} sugar and 22.3 g l^{-1} extract free from sugar was subjected to the complete procedure described above, once a day for 5 consecutive days. The values were found as follows: for total sulphur 206.4 mg l^{-1} with 2.4% R.S.D., for sulphur in the sample free from SO_2 115.9 mg l^{-1} with 3.3% R.S.D., and for the calculated total SO_2 180.8 mg l^{-1} with 4.7% R.S.D. (On the third day total SO_2 was also determined by the distillation method recommended by Rankine [3]. The mean and the R.S.D. of the four results obtained in this manner were 178.7 mg l^{-1} and 4.4%, respectively.)

Several further wine samples were also analysed by the method described in the present paper as well as by the above-mentioned classic method [3]. As shown in Table 2, the results obtained by the two methods are in fairly close agreement. Besides, it can be proved that the relative standard deviations for total sulphur and the sulphur without S(IV) were less than 2.5 and 3.5%, respectively.

4. Conclusion

On the basis of our results it may be safely concluded that the ICP-AES methods developed by us are adequate for the determinations of the total sulphur and the sulphur without S(IV) in wine, and these facts provide a possibility for the indirect determination of total SO_2. The reliability of this indirect method is acceptable for practical work, and the procedure is suitable for serial tests.

Acknowledgements

Financial support from the National Fund for Scientific Research (OTKA T014427) is gratefully acknowledged.

References

[1] M.A. Amerine, C.S. Ough, Methods for Analysis of Musts and Wines, Wiley, New York, 1980, pp. 201, 341.
[2] C.S. Ough, J. Assoc. Off. Anal. Chem. 69 (1986) 5.
[3] B.C. Rankine, K.F. Pocock, Aust. Wine Brew. Spirit Rev. 88 (1970) 40.
[4] G. Etherington, Lab. Pract. 39 (1990) 127.
[5] J. Schneyder, G. Vlcek, Mitt. Klosterneuburg Rebe Wein Obst. Frucheverwert 27 (1977) 87.
[6] P. Bruno, M. Caseli, A. DiFano, A. Traini, Analyst 104 (1979) 1083.
[7] T.J. Cardwell, R.W. Cattrall, G.N. Chen, G.R. Scollary, Analyst 116 (1991) 253.
[8] J.M. Vahl, J.E. Converse, J. Assoc. Off. Anal. Chem. 63 (1980) 194.
[9] J.P. Villeton-Pachot, M. Persin, J.Y. Gal, Analysis 8 (1980) 422.
[10] E. Hieke, A. Krisel, Fresenius' Z. Anal. Chem. 285 (1977) 39.
[11] D. Barnett, E.G. Davis, J. Chromatogr. Sci. 21 (1983) 205.
[12] E.G. Davis, D. Barnett, P.M. Moy, J. Food Technol. 18 (1983) 233.
[13] M. Dyson, Anal. Proc. (Lond.) 30 (1993) 79.
[14] M. LGranados, S. Maspoch, M. Blanco, Anal. Chim. Acta 179 (1986) 445.
[15] C.S. duPlessis, A. Tromp, Agrochemophysica 6 (1974) 1.
[16] N. Grekas, A.C. Galokerinos, Analyst (Lond.) 110 (1985) 335.
[17] K. Matsumoto, H. Matsubara, H. Ukeda, Y. Osajima, Agric. Biol. Chem. 53 (1989) 2347.
[18] E. Roure, J.J. Fombon, C. Dasmaris, Bios (Nancy) 20 (1989) 45.
[19] J. Ruzicka, E.H. Hansen, Anal. Chim. Acta 114 (1980) 19.
[20] J. Moller, B. Winter, Fresenius' Z. Anal. Chem. 320 (1985) 451.
[21] F. Lazaro, M.D. Luque de Castro, M. Valcarcel, Anal. Chem. 59 (1987) 950.
[22] P. Linares, M.D. Luque de Castro, M. Valcarcel, Anal. Chim. Acta 225 (1989) 443.
[23] J. Krausova, J. Jedlickova, Prum. Potravin 41 (1990) 40.
[24] J. Bartroli, M. Escalada, C.J. Jorquere, J. Alonso, Anal. Chem. 63 (1991) 2352.
[25] J.L. Burguera, M. Burguera, Anal. Chim. Acta 214 (1988) 429.
[26] M. Grekas, A.C. Calokerinos, Analyst (Lond.) 110 (1985) 335.

ELSEVIER

Talanta 45 (1998) 1285–1286

Talanta

Book reviews

From Chemical Topology to Three-Dimensional Geometry
A.T. Balaban (editor), Plenum, New York; 1997, xviii + 420 pp.; US$125; ISBN: 0-306-45462-9

Chemical topology (or chemical graph theory) traditionally encompasses only chemical constitution and thus ignores 3D molecular features. This book attempts to present mathematical procedures, including topological methods, which consider the 3D aspects of molecular chemistry. It brings together mathematics and the shape of molecules. Ten chapters are presented by several different authors.

Chapters 1–4 and 6 are concerned with procedures for 2D–3D conversion and the subsequent uses for Quantitative Structure Analysis Relationships and molecular similarity studies. Many such procedures are mathematically intensive and are invariably incorporated into computer software but the book is not overtly mathematical. The application of these techniques is most relevant in the Pharmaceutical industry.

Chapter 5 deals with recognition of membrane protein structure from amino acid sequence. It addresses the correlation between the primary structure of proteins (i.e. the sequence of amino acids) and the 3D structure which related to activity.

Chapters 7–9 discuss topological methods applied to fullerenes and congeneric structures—some of these 'exotic fullerenes' do not yet exist but certain toroidal structures might have reasonable stability. The last chapter by R. Bruce King is an excellent introduction to the application of graph theory and topology to inorganic clusters and congeners. Many carefully produced diagrams are included, each chapter is appended with numerous references and an index is included.

Overall a book for the graduate with an interest in molecular modelling. Very useful for those in the Pharmaceutical industry and for all those with an interest in modern mathematical chemistry.

P.J. Cox
The Robert Gordon University
Aberdeen
UK

PII S0039-9140(97)00163-X

Modern Methods for Trace Element Determination
C. Vandecasteele, C.B. Block, Wiley, Chichester, 3rd reprint; 1997, xi + 330 pp.; £24.95; Softback; ISBN: 0-471-97445-5

This book is excellent for anyone wishing to learn how to successfully carry out trace element analysis. It brings together information about nearly all the analytical techniques available and also includes lots of useful information about sample preparation. The theories of techniques are covered, but in a very concise manner and techniques are continuously compared and criticised. The book skips over out of date techniques and concentrates on those methods currently in use and being developed. The chapter on the comparison of atomic spectrometric methods is particularly useful.

Chapter one is a brief introduction and a detailed chapter follows this on sample preparation, including microwave digestion and matrix separa-

ELSEVIER

Talanta 45 (1998) 1285–1286

Talanta

Book reviews

From Chemical Topology to Three-Dimensional Geometry
A.T. Balaban (editor), Plenum, New York; 1997, xviii + 420 pp.; US$125; ISBN: 0-306-45462-9

Chemical topology (or chemical graph theory) traditionally encompasses only chemical constitution and thus ignores 3D molecular features. This book attempts to present mathematical procedures, including topological methods, which consider the 3D aspects of molecular chemistry. It brings together mathematics and the shape of molecules. Ten chapters are presented by several different authors.

Chapters 1–4 and 6 are concerned with procedures for 2D–3D conversion and the subsequent uses for Quantitative Structure Analysis Relationships and molecular similarity studies. Many such procedures are mathematically intensive and are invariably incorporated into computer software but the book is not overtly mathematical. The application of these techniques is most relevant in the Pharmaceutical industry.

Chapter 5 deals with recognition of membrane protein structure from amino acid sequence. It addresses the correlation between the primary structure of proteins (i.e. the sequence of amino acids) and the 3D structure which related to activity.

Chapters 7–9 discuss topological methods applied to fullerenes and congeneric structures—some of these 'exotic fullerenes' do not yet exist but certain toroidal structures might have reasonable stability. The last chapter by R. Bruce King is an excellent introduction to the application of graph theory and topology to inorganic clusters and congeners. Many carefully produced diagrams are included, each chapter is appended with numerous references and an index is included.

Overall a book for the graduate with an interest in molecular modelling. Very useful for those in the Pharmaceutical industry and for all those with an interest in modern mathematical chemistry.

P.J. Cox
The Robert Gordon University
Aberdeen
UK

PII S0039-9140(97)00163-X

Modern Methods for Trace Element Determination
C. Vandecasteele, C.B. Block, Wiley, Chichester, 3rd reprint; 1997, xi + 330 pp.; £24.95; Softback; ISBN: 0-471-97445-5

This book is excellent for anyone wishing to learn how to successfully carry out trace element analysis. It brings together information about nearly all the analytical techniques available and also includes lots of useful information about sample preparation. The theories of techniques are covered, but in a very concise manner and techniques are continuously compared and criticised. The book skips over out of date techniques and concentrates on those methods currently in use and being developed. The chapter on the comparison of atomic spectrometric methods is particularly useful.

Chapter one is a brief introduction and a detailed chapter follows this on sample preparation, including microwave digestion and matrix separa-

tion methods. It may have been useful to briefly mention about sample preparation techniques for speciation studies, but of course not everything can be covered. Chapter three provides the information needed to make the measurement and check they are properly validated and this is followed by a short theoretical chapter on spectrochemical theory and instrumentation. Atomic absorption, emission and fluorescence are then covered in separate chapters with details of performance characteristics and interferences. Chapter eight compares these methods and then chapter nine covers mass spectrometry including ICP MS with comparisons and practical details again playing an important part. A chapter on X-ray methods follows, including the less well known techniques of total-reflection X-ray fluorescence spectrometry and particle induced X-ray emission analysis (PIXE). The last technique to be covered is activation analysis and the book ends with a very brief mention of metal speciation. Throughout the book there are useful examples of applications for environmental, medical and materials applications. The main omission of the book is the electroanalytical techniques of adsorptive and anodic stripping voltammetry. Although I realise that every technique cannot be included these techniques are used widely for the environmental analysis of water samples. The speciation chapter is also a bit of an afterthought considering it is so important these days, however, it could rapidly become a very large topic.

I would recommend this book to anybody who has to carry out trace analysis of industrial, environmental and biological samples and especially to anybody just starting off on this track. The book is very easy to read and quite self-contained.

G. Greenway

PII S0039-9140(97)00164-1

Wilson & Wilson's Comprehensive Analytical Chemistry

S.G. Weber (Editor); volume XXX; *Spectrochemical Trace Analysis for Metals and Metalloids* by R. Lobinski and Z. Marczenko, Elsevier, Amsterdam; 1996, xxix + 808 pp.; Dfl475.00; ISBN 0-444-82368-9

The description 'Comprehensive' in the title of this long-established series is reflected in both the broad scope and the abundance of detail of this latest volume. The experience of the second author in writing an encyclopedic account of spectrophotometric methods for the elements is evident in the approach to dealing with each individual element—54 chapters varying in length from three pages (Sr, or Na&K) to 20 pages each for Se and for Hg. But just in these longer chapters, the active research interests of the first author concerning the speciation of organometallic forms of the elements provide the special slant which makes this book so valuable. Extensive tabulations of papers from the literature make possible the mention of a large number of references, many of them from the mid 1990s. This broad survey of the recent literature on speciation of those elements which can form organometallic compounds is a particularly important feature of this book.

The first section of the book—Chapters 1–8—serves as an introduction to the techniques of modern trace analysis, and while it is well written and not too long, it is questionable as to whether it need have been incorporated in what is anyway rather a large book. However, I am happy to find here compilations of realistic limits of detection for atomic spectroscopic techniques, rather than the usually quoted optimistic but unattainable limits so often taken from instrument manufacturers' brochures. The second part of the book deals with multi-element trace analysis of real samples, and offers much useful information on sampling and handling of geological materials, biological materials, and industrial materials.

I have enjoyed reading this book, and have been happy to discover valuable references which I had previously missed. I can recommend it strongly for all groups active in the area of environmental analysis, especially of speciation of trace heavy metals.

I.L. Marr

PII S0039-9140(97)00165-3

tion methods. It may have been useful to briefly mention about sample preparation techniques for speciation studies, but of course not everything can be covered. Chapter three provides the information needed to make the measurement and check they are properly validated and this is followed by a short theoretical chapter on spectrochemical theory and instrumentation. Atomic absorption, emission and fluorescence are then covered in separate chapters with details of performance characteristics and interferences. Chapter eight compares these methods and then chapter nine covers mass spectrometry including ICP MS with comparisons and practical details again playing an important part. A chapter on X-ray methods follows, including the less well known techniques of total-reflection X-ray fluorescence spectrometry and particle induced X-ray emission analysis (PIXE). The last technique to be covered is activation analysis and the book ends with a very brief mention of metal speciation. Throughout the book there are useful examples of applications for environmental, medical and materials applications. The main omission of the book is the electroanalytical techniques of adsorptive and anodic stripping voltammetry. Although I realise that every technique cannot be included these techniques are used widely for the environmental analysis of water samples. The speciation chapter is also a bit of an afterthought considering it is so important these days, however, it could rapidly become a very large topic.

I would recommend this book to anybody who has to carry out trace analysis of industrial, environmental and biological samples and especially to anybody just starting off on this track. The book is very easy to read and quite self-contained.

G. Greenway

PII S0039-9140(97)00164-1

Wilson & Wilson's Comprehensive Analytical Chemistry

S.G. Weber (Editor); volume XXX; *Spectrochemical Trace Analysis for Metals and Metalloids* by R. Lobinski and Z. Marczenko, Elsevier, Amsterdam; 1996, xxix + 808 pp.; Dfl475.00; ISBN 0-444-82368-9

The description 'Comprehensive' in the title of this long-established series is reflected in both the broad scope and the abundance of detail of this latest volume. The experience of the second author in writing an encyclopedic account of spectrophotometric methods for the elements is evident in the approach to dealing with each individual element—54 chapters varying in length from three pages (Sr, or Na&K) to 20 pages each for Se and for Hg. But just in these longer chapters, the active research interests of the first author concerning the speciation of organometallic forms of the elements provide the special slant which makes this book so valuable. Extensive tabulations of papers from the literature make possible the mention of a large number of references, many of them from the mid 1990s. This broad survey of the recent literature on speciation of those elements which can form organometallic compounds is a particularly important feature of this book.

The first section of the book—Chapters 1–8—serves as an introduction to the techniques of modern trace analysis, and while it is well written and not too long, it is questionable as to whether it need have been incorporated in what is anyway rather a large book. However, I am happy to find here compilations of realistic limits of detection for atomic spectroscopic techniques, rather than the usually quoted optimistic but unattainable limits so often taken from instrument manufacturers' brochures. The second part of the book deals with multi-element trace analysis of real samples, and offers much useful information on sampling and handling of geological materials, biological materials, and industrial materials.

I have enjoyed reading this book, and have been happy to discover valuable references which I had previously missed. I can recommend it strongly for all groups active in the area of environmental analysis, especially of speciation of trace heavy metals.

I.L. Marr

PII S0039-9140(97)00165-3

ELSEVIER

Talanta 45 (1998) 1287–1288

Talanta

Erratum

Erratum to "Use of dichloromethane with dithizone as an alternative solvent to carbon tetrachloride restricted by Montreal Protocol" [Talanta 44 (1997) 947][1]

A.M. Kiwan

Department of Chemistry, Faculty of Science, United Arab Emirates University, P.O. Box 17551, Al-Ain United Arab Emirates

The publisher regrets the omission of Table 1 from the above article. The table is printed overleaf.

[1] PII of original article: S0039-9140(96)02135-2

PII S0039-9140(97)00230-0

Table 1
Characteristic absorption and extraction data for dithizone and its metal complexes in dichloromethane and carbon tetrachloride.

Compound	Solvent[a]	λ_{max}, 1 nm	ε_{max}, 1×10^{-3} l.mol^{-1}.cm^{-1}	λ_{max}, 2 nm	ε_{max}, 2×10^{-3} l.mol^{-1}.cm^{-1}	$pH_{1/2}$	log K_{ext}
H_2Dz	CH_2Cl_2	609, 609[b]	41.6, 38.79[b]	445, 445[b]	18.4, 17.53[b]	10.3, 10.13[b]	
	CCl_4	620	34.6	450	20.0	8.7, 8.94	
	$CHCl_3$	605	41.5	442	16.0	10.58, 10.8[c]	
$Cd(HDz)_2$	CH_2Cl_2	514	90.0	—	—	3.74	0.51 ± 0.02 (5)
	CCl_4	520	88.0	—	—	2.9	2.14
$Co(HDz)_2$	CH_2Cl_2	538	74.9	—	—	5.55	-3.1 ± 0.1 (4)
	CCl_4	542	59.2	—	—	3.2	1.53
$Cu(HDz)_2$	CH_2Cl_2	543	51.2	—	—	1.1	5.8 ± 0.1 (6)
	CCl_4	550	45.2	—	—	−1.3	10.53
$Hg(HDz)_2$	CH_2Cl_2	488	74.8	—	—	−9.0	26.0 ± 0.2 (5)
	CCl_4	485	72.2	—	—	−9.4	26.85
$Pb(HDz)_2$	CH_2Cl_2	520, 520[d]	78.3, 65[d]	—	—	3.97	0.6 ± 0.01 (5)
	CCl_4	520	67.0–72.0	—	—	3.8	0.4
$Zn(HDz)_2$	CH_2Cl_2	528	97.7	—	—	4.45	-0.90 ± 0.02 (5)
	CCl_4	535	92.6	—	—	2.8	2.3
Ag(HDz)	CH_2Cl_2	465	35.3	—	—	−2.0	6.0[e]
	CCl_4	463	27.2	—	—	−2.5	6.5
Tl(HDz)	CH_2Cl_2	524	43.5	—	—	7.8	-3.8 ± 0.1 (4)
	CCl_4	510	27.0	—	—	7.3	−3.3
$Bi(HDz)_3$	CH_2Cl_2	497, 498[d]	88.2, 75[d]	—	—	0.9	9.3 ± 0.2 (5)
	CCl_4	490	84.6	—	—	0.7	9.98
$In(HDz)_3$	CH_2Cl_2	527	126.6	—	—	0.6	2.15 ± 0.05 (5)
	CCl_4	510	87.0	—	—	2.4	4.84
$Ni(HDz)_2$	CH_2Cl_2	667	19.9	545	30.0	6.5	-4.87 ± 0.1 (5)
				492	33.3		
	CCl_4	665	19.2	670	20.0	3.4	1.18

[a] Absorption and extraction data in CCl_4 are from Refs. [6,8,9]. Values in parentheses are the number of measurements. Aqueous phase: 0.5 M $NaClO_4$–0.02 M Sodium Acetate.
[b] Ref. [20], [c] Ref. [6], [d] Ref. [21], [e] Ref. 9

ELSEVIER

Talanta 45 (1998) 1303–1306

Talanta

Author Index

Volume 45 (1998)

Abuo Ali, S.B., 865
Acree, W.E., Jr., 39
Adell, A., 777
Agrawal, Y.K., 397
Akaiwa, H., 549
Akinbo, O.T., 137
Alatorre Ordaz, A., 875
Aldhaheri, S.M., 203
Alexander, P.W., 155
Alwarthan, A.A., 1131
Aly, F.A., 1131
Amagai, T., 113
Amira, M.F., 189
Ang, H.G., 739
Ang, K.C., 663
Ang, S.G., 693
Antonelli, M.L., 1039
Argekar, A.P., 909
Arranz, A., 417
Arranz, J.F., 417
Asano, Y., 565, 575
Aster, B., 977
Atanasova, D., 857
Author, A., 227, 473
Avila Rodríguez, M., 875
Aw, T.C., 673

Baldini, E., 91
Baldwin, D.P., 229
Bănică, F.G., 1031
Bansal, R.K., 411
Bao, G.W., 727, 751
Barbosa, J., 817
Bari, V.R., 297
Barrón, D., 817
Barrón Zambrano, J.A., 875
Beltrán, J.L., 817, 1073
Bermejo, A., 325
Bermejo-Barrera, A., 807, 1147
Bermejo-Barrera, P., 807, 1147
Bermejo, P., 325, 1115
Bessière, J., 357
Bhajan Singh, H., 331
Blanco-González, E., 25
Blanco, S.E., 1103
Blanc, R., 105
Borge, G., 463
Braibanti, A., 1267
Burba, P., 977
Burguera, J.L., 531
Burguera, M., 531
Butí, S., 817

Cai, X., 273
Cameán, A.M., 379
Campanella, L., 1039
Cannata-Andía, J.B., 25
Carnahan, J.W., 137
Carpena, J., 969
Carrero, P., 531
Casero, I., 167
Castaño, R., 1007
Castillo, J.R., 1211
Celso Moreira, J., 317
Cesar Rocha, J., 317
Chalk, S.J., 591
Chan, H., 721
Chen, H.-Y., 851
Chen, J., 1081
Chen, Y.-H., 1123
Chen, Z.K., 727
Chew, C.H., 735, 767
Chiswell, B., 85
Chong, P.S., 693
Choong, M.L., 673
Chow, A., 257, 1235
Chuah, G.K., 739
Cirovic, D.A., 989
Compari, C., 1267
Cromer, M., 1177
Cross, J.H., 19
Cucca, L., 91
Curtius, A.J., 1167
Daniele, P.G., 425
Danielsson, B., 557
da Silva, M.P., 883
Delgado, R., 451
de Magalhães Padilha, P., 317
Desai, N.I., 1061
de Souza Teixeira, M.F., 249
Despas, C., 357
De Stefano, C., 425
Devi, S., 1089
Dhorda, U.J., 297
Dieckmann, C., 85
do Carmo Federici, C., 317
Domagala, S., 91
Dominguez, R., 325
Donard, O.F., 1023
Dondi, M., 1201
Doretti, L., 891
Doumenq, P., 1
Dressler, V.L., 1167
Du, B., 957
D'Ulivo, A., 801
Durán Merás, I., 899

Earley, R.L., 1255
Ecker, S.T., 1189
Eiceman, G.A., 57
El-Naggar, G.A., 189, 865
El-Shahawi, M.S., 203
El-Shazly, S.A., 189
Ercole, P., 1039
Esteves da Silva, J.C., 1155
Etxebarria, N., 1007

Fabbri, B., 1201
Fang, H.-Q., 851
Faraci, D., 801
Fatibello-Filho, O., 249
Fdez de Betoño, S., 417
Fell, N.F., Jr, 279
Fernandes, J.R., 273
Fernández, L.A., 1007

PII S0039-9140(98)00010-1

Ferrara, D., 891
Ferrer, R., 1073
Ferretti, F.H., 1103
Fetzer, J.C., 39
Figueira, M.C., 451
Filipović-Kovačević, Ž., 843
Fisicaro, E., 1267
Fleet, B., 703
Fung, Y.-S., 619, 641
Fushinuki, Y., 575

Gan, L.M., 735, 767
Gao, J., 303
Gascón, J.L., 181
Gattolin, P., 891
George, A., 285
Gesser, H.D., 257
Ghiozzi, A., 1267
Gohshi, Y., 1049
Gomes Neto, J.A., 1167
Gómez-Hens, A., 829
González, A.G., 379
Grant, D.H., 273
Guerrero, M.I., 379
Guiliano, M., 1
Guiteras, J., 1073
Gunasingham, H., 703
Gupta, N., 279
Gupta, S., 1111
Gupta, V.K., 343, 1097

Hachiya, H., 575
Hamilton, B., 85
Handa, S.K., 1111
Han, M.Y., 735
Han, S., 127
Han, S.H., 437
Harada, H., 543
Hattingh, C.J., 485
Hawley, N.T., 1189
Haygarth, P.M., 47
Hefter, G.T., 931
Hemmi, A., 575
Herce-Pagliai, C., 379
Hibbert, D.B., 155
Higuchi, K., 445
Hillard, S.W., 493, 507, 513
Horng, C.-J., 75
Huang, W., 735
Huang, X., 127
Hurtubise, R.J., 1081

Imato, T., 565, 575
Ion, A., 1031
Ishizuki, T., 349
Itabashi, H., 549
Ito, S., 575

Jabbari, A., 1247
Jacquot, F., 1
Jaenicke, S., 703, 739
Jain, V.K., 397
Jiang, Y.-Y., 787
Jiménez-Carmona, M.M., 883
Ji, W., 735
Johansson, G., 557

Kaihara, M., 1049
Kaminaga, C., 963
Kang, J., 303
Kang, T.-F., 291
Karayannis, M.I., 1015
Karlberg, B., 477
Katragadda, S., 257
Kawamoto, H., 549
Kawi, S., 759
Kelemen, J., 1281
Kesari, R., 1097
Khaw, M.C., 673
Khayyami, M., 557
Khor, E., 713
Kim, J.S., 437
Kiranas, E.R., 1015
Kiwan, A.M., 203
Koay, E.S., 673
Kobayashi, F., 575
Kong, X., 13
Korenaga, T., 445
Kuban, P., 477
Kubo, J., 963
Kubo, K., 963
Kumar, A., 387
Kumar Agnihotri, N., 331
Kumar Singh, V., 331

Lampugnani, L., 801
Lane, J.L., 19
Larsson, P.-O., 557
Lau, K.-M., 619, 641
Lee, C.H., 437
Lee, H.K., 613, 631, 657, 683
Li, G.-J., 759
Li, K., 119
Limero, T.F., 19
Li, N.-Q., 787
Lin, S.-R., 75
Li, S.F., 613, 657, 663, 683, 721, 727, 751, 767
Liu, D., 405
Liu, F., 119
Liu, J., 663, 767
Liu, R., 405
Liu, T., 13
Liu, W., 631
Liu, X., 543

Loh, W.L., 739
Lomber, J.P., 1189
Lopez Molinero, A., 1211
Lora, S., 891
Lu, H., 119
Luque de Castro, M.D., 371, 883

Machado, A.A., 1155
Madariaga, J.M., 463, 1007
Mahmoud, M.E., 309
Manchanda, V.K., 387
Manclús, J.J., 371
Mao, H.-Y., 1123
Markey, R., 935
Martinez, L., 1211
Martínez-Lozano, C., 969
Mathur, P.K., 433
Matsushita, H., 113
Matthews, G.P., 47
May, P.M., 931
McKelvie, I.D., 47
McMorn, P., 1001
Medina-Hernández, M.J., 835
Menéndez-Fraga, P., 25
Mille, G., 1
Miller, J.S., 1255
Mingazzini, C., 1201
Miyamae, Y., 519
Moalla, S.M., 213
Mohapatra, P.K., 387
Montoya, A., 371
Moreda, J.M., 417
Moreda-Piñeiro, A., 807, 1147
Moreda-Piñeiro, J., 807, 1147
Morgan, J., 935
Morlay, C., 1177
Mouginot, Y., 1177
Mou, S., 119
Mousavi, M.F., 1247
Munoz, D., 1
Muñoz de la Peña, A., 899
Muñoz Olivas, R., 1023
Murthy, A.S., 951

Nageswara Rao, G., 1267
Naidu, P.Y., 795, 1227
Nakahara, T., 917
Narusawa, Y., 519
Navalón, A., 105
Navarro Mendoza, R., 875
Naylor, S., 603
Ng, S.C., 735
Nifant'eva, T., 977
Nishino, H., 917
Niwa, H., 349
Nóbrega, J.A., 265
Nouroozi, S., 1247

O'Halloran, K., 85
Ohura, H., 565
Oleschuk, R.D., 1235
Oliveira, C.J., 1155
Osada, Y., 583
Ozsoz, M., 273

Paama, L., 35
Palrecha, M.M., 433
Panadero, S., 829
Pandey, S., 39
Parmeter, J.E., 57
Pathak, P.N., 387
Patonay, G., 285
Peat, D.M., 47
Peña Garcia, N., 557
Perämäki, P., 35
Pérez-Bendito, D., 167, 829
Pérez Pita, M.T., 557
Pérez Ruiz, T., 969
Pesavento, M., 91
Petrissans, J., 777
Pinto, A.Z., 249
Pinto, M.S., 1155
Pozebon, D., 1167
Prenesti, E., 425
Preston, D., 57
Puri, B.K., 411
Puri, S., 411

Quek, C.H., 735
Qu, F., 787
Quintino, S., 451

Rai, M.K., 343
Ramelow, G.J., 1139
Rao, S.G., 1227
Richter, P., 147
Rivas, C., 531
Riviello, J.M., 119
Rocha, F.R., 265
Rodríguez, C., 147
Rodríguez, M., 181
Rodriguez Cáceres, M.I., 899
Rodriguez, I., 683
Rodriguez, J., 57
Rönkkömäki, H., 35
Rubio, S., 167
Russeva, E., 857

Sabarathinam, R.M., 703
Sagrado, S., 835
Sait, S.S., 397
Sakai, A., 575
Sakai, T., 543
Sakurai, T., 963
Saleh, M.H., 203
Salinas López, F., 899
Sambasiva Rao, R., 1267
Sammartano, S., 425
Sanchez-Ramos, S., 835
Sanz-Medel, A., 25
Sarudi, I., 1281
Sastry, C.S., 795, 1227
Saucedo Medina, T.I., 875
Scherrer, P., 1
Schiavon, F., 891
Sethi, S.K., 673
Shah, R., 1089
Shamsipur, M., 1219
Sharma, J., 951
Sharma, K.K., 1111
Shen, G.-L., 291
Shetty, A.K., 909
Shinde, V.M., 925
Shkinev, V., 977
Shrivastav, P., 397
Sicilia, D., 167
Sipos, L., 843
Spivakov, B.Y., 977
Srinivas, K.R., 1227
Stefanova, V., 857
Stein, H., 935
Stewart, K.K., 493, 507, 513
Suárez, J.A., 181
Sugimoto, K., 543
Suh, M.Y., 437
Sultan, S.M., 1061
Sun, A., 405
Sundaresan, M., 297
Sun, J.-J., 851
Suzuki, M., 583
Suzuki, S., 917
Synovec, R.E., 1189

Taher, M.A., 411
Takahashi, Y., 113
Takahata, M., 549
Takeyoshi, K., 543
Tang, H., 291
Taniguchi, I., 575
Tan, S.C., 713
Tan, T.K., 713
Tavakkoli, N., 1219
Theodoro de Sousa Campos, J., 317
Thompson, A., 1001
Tiano, G., 57
Tomás, V., 969
Tomlinson, A.J., 603
Tong, S., 119
Toral, M.I., 147
Tran, C.D., 237
Troncoso, A.M., 379
Tsalev, D.L., 801
Tung, H.-S., 619
Turonek, M.L., 931
Tzouwara-Karayanni, S.M., 1015

Ura, N., 543

Vanisha Das, J., 343
van Staden, J.F., 485
Vartak, S.V., 925
Velasco-Arjona, A., 371
Veronese, F.M., 891
Vilchez, J.L., 105
Villareal, A., 1211
Vittori, O., 1177

Wada, H., 349
Wai, C.M., 1189
Walcarius, A., 357
Wall, J., 85
Wang, F., 19
Wang, H., 405
Wang, J., 273
Wang, P., 657
Wang, X., 127
Wan, H.B., 663
Wehr, T., 673
Wei, Q., 957
Welch, L.E., 1255
Wolff, G.A., 1001
Wong, S.M., 713
Worsfold, P.J., 47

Xia, X., 13
Xie, Z.-Y., 291
Xu, G., 127
Xu, G.Q., 735

Yamada, H., 349
Yamane, T., 583
Yamasaki, S., 565
Yang, J.-Z., 947
Yang, W., 303
Yang, X., 155
Yang, Y., 445
Yan, Y., 119
Yao, H., 1139
Yao, T., 917
Yasui, T., 349
Yebra, M.C., 1115
Ye, Y.-Z., 1123
Yin, Y., 127
Young, T.E., 1189
Yuchi, A., 349
Yu, R.-Q., 291

Zaghloul, A.A., 189, 865
Zamboni, R., 801
Zamzow, D.S., 229
Zhang, P.-C., 767
Zhang, S., 727
Zhang, W., 127
Zhang, X.J., 735
Zhang, X.-X., 445
Zhang, Y., 613
Zhang, Z.-F., 947
Zhao, G., 303, 721
Zhao, S., 13, 303
Zhou, D.-M., 851
Zhu, L., 113
Zhu, M., 673
Zou, B.S., 735
Zubiaur, J., 1007

ELSEVIER

Talanta 45 (1998) 1307–1316

Talanta

Subject Index

Volume 45 (1998)

Absorption spectra . . . 947
Absorptivity constant . . . 1103
Accelerated leaching . . . 883
Acetonitrile–water mixtures . . . 817
Acetylcholine esterase . . . 557
Acetylthiocholine . . . 557
Acid rain . . . 641
Acousto-optic tunable-filter . . . 279
Adsorptive . . . 433
Adsorptive preconcentration . . . 417
Adsorptive stripping voltammetry . . . 273
Affinity constant . . . 91
Aflatoxin B_1 . . . 91
Air particulate matters . . . 619
Al^{3+} . . . 1219
Algorithms . . . 1267
Alkali . . . 1219
Alkaline earth . . . 1219
Alkaline fusion . . . 935
Alkyltrimethylammonium surfactants . . . 167
Al-TBP . . . 35
Aluminium . . . 1147
Aluminoxamine . . . 25
Ammonia . . . 19
Ammonia determination . . . 405
Ammonia oxidation . . . 405
Amperometric . . . 557
Amperometric detection . . . 917
Amperometric determination . . . 851
Amylase activity . . . 565
Analysis . . . 19
Analyte . . . 493
Analyte transport . . . 137
Aniline . . . 851
Anion analysis . . . 641
Anionic surfactants . . . 543
Anions . . . 477
Anodic stripping voltammetry . . . 703
Anthropogenic fulvic acids . . . 1155
Antimony determination . . . 801
Antimony speciation . . . 127
Apolipoprotein E . . . 673

PII S0039-9140(98)00011-3

Aquatic humic substances . . . 977
Aqueous ammonia. . . . 357
Aqueous solution . . . 425
Arsenic . . . 1167
Arsenic speciation . . . 531
Ascorbic acid. . . . 851, 951
Astemizole . . . 795
ATM imaging . . . 767
Atomic absorption spectrometry. . . . 75, 531
Atomic absorption spectrophotometry . . . 397
Atomic emission spectrometry . . . 137
Atomic emission spectroscopy . . . 229
Atomic force microscopy . . . 751
Automated analysis . . . 531
Automatic analysis . . . 113
Axial dispersion coefficient . . . 519

Benzene-1,3,5-tricarboxylic acid . . . 303
Benzoquinone . . . 951
Benzothiaxolyldiazoaminoazobenzene . . . 13
Biologically derived peptides . . . 603
Biosensor . . . 557
Biosensors . . . 891
Bismuth(III) . . . 249
Blackfoot disease . . . 75
Blood analysis . . . 703
Boron . . . 835
Bromopyrogallol red . . . 127
Butanol–octanol mixture . . . 387
ByT-FAS . . . 507

Capillary column . . . 631
Capillary electrophoresis 477, 613, 619, 641, 673
Capillary electrophoresis separation . . . 683
Capillary zone electrophoresis . . . 657
Carbon paste electrodes. . . . 1139
Catalysis . . . 851
Catalytic determination . . . 549
Catalytic differential kinetic spectrophotometry . . . 1123
Catalytic photometric detection . . . 583
Cation analysis. . . . 619
C-18 bonded silica. . . . 1167
Cellulose phosphate . . . 317
Ceramic glazes . . . 1201
Ceramic materials . . . 835
Cetylpyridinium chloride . . . 39
Chelating resin matrix . . . 397
Chelation ion chromatography. . . . 119
Chemical analysis . . . 1201
Chemically modified electrode . . . 291
Chemiluminescence determination . . . 1131
Chemiluminescent whole *E. Coli* transcription assay . . . 513
Chip . . . 613
Chitosan . . . 713
Chlorate. . . . 657
Chloride. . . . 485
Chlorinated biphenyls (CBs) . . . 1001

Chlorpyrifos . . . 371
Chronopotentiometry . . . 273
Coated graphite-epoxy ion-selective electrode . . . 249
Complexation . . . 437, 1155, 1177
Complexes of trivalent metal ions . . . 451
Complex matrix . . . 119
Continuous precipitation-dissolution . . . 1115
Copolymerization . . . 767, 851
Copper . . . 147, 843
Copper (II) . . . 1177
Copper(II) . . . 397, 425, 1089
Crude oil . . . 1
Cryogenic trapping . . . 531
Cu(II) . . . 963, 1155
Cyclamate . . . 1115
Cyclic voltammetry . . . 951
β-Cyclodextrin . . . 303

Database . . . 591
Degree of deacetylation . . . 713
Derivative spectrophotometry . . . 411
Desferrioxamine . . . 25
Detection . . . 19, 1111
Detection cell . . . 493
Detection of organic vapors . . . 727
Determination . . . 19, 433
Diaza-18-crown-6-diisopropionic acid . . . 437
Dicarboxylate ligands . . . 865
Dicarboxylic acids . . . 189
Dicyclohexano 18 crown 6 . . . 387
Dielectric sensors . . . 357
Dietary sources . . . 1131
Diethyl dithiophosphate . . . 1167
Diffuse reflection method . . . 1049
1,5-Di-(2-fluorophenyl)-3-mercaptoformazan . . . 203
Digestive medicine . . . 565
3,4-Dihydroxybenzoic acid . . . 851
Dissociation constant . . . 947
Dissociation constants . . . 189
Dithiocarbamate fungicides . . . 1097
Diuretics . . . 817
Divalent cations . . . 683
DNA . . . 787
Dosage forms . . . 297

Electrochemical . . . 787
Electrodialysis . . . 485
Electrometric . . . 1267
Electrothermal atomic absorption spectrometry . . . 1147, 1167
ELISA . . . 91, 371
Elution peak profile . . . 777
EMF Method . . . 189
Environmental markers . . . 1
Enzyme kinetics . . . 507
Enzyme reactor . . . 917
Epi-fluorescence microscope . . . 613
Eriochrome black-T . . . 309

ETAAS . . . 807
Ethyl alcohol . . . 865
Ethylene . . . 19
Extractant . . . 909
Extraction . . . 925
Extraction chromatography . . . 181

FAAS . . . 325
Fe . . . 325
$[Fe(CN)_6]^{3-}$–$[Fe(CN)_6]^{4-}$ potential buffer . . . 565
Fe(III) . . . 1155
Ferrioxamine . . . 25
FIA . . . 445, 507, 1015, 1247
First derivative UV-spectrophotometry . . . 713
Fixed-time method . . . 1061
Flame atomic absorption spectrometry . . . 1115
Flat sheet membrane desolvator . . . 137
Flow analysis . . . 591
Flow injection . . . 1115, 1131
Flow-injection . . . 565
Flow injection . . . 47, 531
Flow injection analysis . . . 485, 549, 575, 1167
Flow injection cytometry . . . 513
Flow injection spectrophotometric determination . . . 835
Flow injection spectrophotometry . . . 265
Flow injection system . . . 583
Flow system . . . 155
Flow-through cell . . . 357
Fluorescence . . . 113
Fluorescence quenching . . . 39, 1155
Fluoresence . . . 303
Fluorometry . . . 899
Formation constant . . . 1103
Fractionation . . . 213, 977
Fruit . . . 371

Gallium metal . . . 433
Gas chromatography . . . 777
Gas diffusion . . . 477
Gasoline . . . 957
Gas sensor . . . 759
GC–MS . . . 1, 1001
Glass electrode . . . 931
Glassy carbon electrode . . . 273
Gluconic acid . . . 1007
Glucose oxidase . . . 891
Glycerol-3-phosphate oxidase . . . 1015
α-Glycerophosphate . . . 1015

Heavy metal analysis . . . 155
Heavy metals . . . 317
Herbicide . . . 417
HF complexation . . . 1201
High molecular weight poly(acrylic acids) . . . 1177
High performance nebulizer . . . 325
High-precision potentiometric titrations . . . 931
High-resolution spectroscopy . . . 229

Hot injection . . . 807
HPLC . . . 113, 631
Human scalp hair . . . 1147
Hydride generation . . . 531, 801
Hydrofluoric acid interference . . . 801
Hydrogen electrode . . . 931
Hydrogen sulfide . . . 85
Hydrophobic interaction chromatography . . . 693
Hydroxamic acid . . . 963
7-Hydroxymethylnalidixic acid . . . 899

ICP . . . 1281
ICP-AES . . . 35
ICP-AES analysis . . . 857
ICP/MS . . . 1023
ICP-OES . . . 1201
Immobilization . . . 309, 1015
Immunodetermination . . . 91
Indoor pollution . . . 113
Inductively coupled plasma atomic emission spectrometry . . . 1211
In-line reaction column . . . 445
Instrumentation . . . 507
Integrated retention–detection . . . 883
Iodine in alkaline medium . . . 1227
Ion-exchange . . . 721
Ion-exchange chromatography . . . 693
Ion exchange equilibrium constants . . . 463
Ionic strength . . . 463
Ionisation . . . 357
Ion mobility spectrometry (IMS) . . . 19
Ionophore . . . 155
Ion-pair . . . 865
Ion selective electrode . . . 155
IR . . . 1049
Iridium . . . 411
Iron . . . 147, 883
Iron(III) oxidant . . . 1061
Isoforms . . . 693
Isosbestic point . . . 947

Kalman filter . . . 1123
Kinetic method . . . 829
Kinetics . . . 1061

Langmuir plot . . . 1039
Lanthanide . . . 119
Lanthanides . . . 437
Lanthanide-sensitized luminescence . . . 829
Latex particles . . . 767
LB films . . . 727
L-cysteine and boric acid effect . . . 801
Lead . . . 703, 909
Lead–acid batteries . . . 265
Lead(II) . . . 397
Lead(II) detection . . . 203
Leuco crystal violet . . . 1097
L-Glutamate . . . 917

Lichens . . . 1039, 1139
Ligands . . . 147
Limit of quantitation . . . 297
Linear dynamic range . . . 297
Linear solvation energy relationship . . . 817
Liquid–liquid . . . 875
Liquid membrane . . . 963
L-tyrosine . . . 947
Luminescence analysis . . . 1081
Luminol . . . 1131

Malachite Green . . . 543
Manganese . . . 1147
MCM-41 . . . 759
Mechanism . . . 1061
Mediator . . . 557
Membrane electrode . . . 155
Mercury film electrode . . . 703
Mercury(II) . . . 203
Mesoporous SnO_2 . . . 759
Metal determination . . . 379
Metal distribution . . . 977
Metal ions . . . 349
Metallothioneins . . . 693
Metal tetraaminophthalocyanine . . . 291
Metal uptake . . . 1039
Methods . . . 795
Methods of calculation . . . 463
Micellar liquid chromatography . . . 25
Micellar medium . . . 331
Microcalorimetry . . . 1039
Microcrystalline naphthalene . . . 411
Microdialysis probe . . . 917
Microelectrode . . . 851
Microemulsion . . . 957
Microextraction . . . 1081
Microwave-assisted sample preparation . . . 1201
Microwave heating . . . 531
Microwave mineralisation . . . 35
Microwave reduction . . . 1023
Milk components . . . 325
Mixed-metal complex . . . 1219
Mixed micellar media . . . 127
Mixed micelle-based methodology . . . 167
Mixed solvent . . . 543
$[Mo(CO)_6]$ . . . 739
Molecular size classification . . . 977
Molybdenite . . . 935
mPC–CE–MS/MS . . . 603
Multi-level mixture design . . . 989
Multiple injection . . . 807
Multivariate calibration . . . 1073
Multivariate regression . . . 989

NADH . . . 951
Nafion . . . 721
Nalidixic acid . . . 899

n-alkanes . . . 1001
Nanoparticles. . . . 735
1-Naphthalenacetamide (NAD) . . . 105
1-Naphthylacetic acid (NAA) . . . 105
N-chlorosuccinimide. . . . 1097
Negative thermal ion mass spectrometry . . . 935
New phase separator . . . 543
Nickel . . . 13, 807
Nickel (II). . . . 1177
Nickel(II) . . . 1089
Nickel naphthenate . . . 957
NiTMpyP. . . . 787
Nitralin . . . 417
Nitrate . . . 265, 657
Nitrile . . . 1111
Nitrite determination . . . 1247

On-line sample pretreatment . . . 119
Optical nonlinearities . . . 735
Organic anion analysis . . . 641
Organic energetic materials. . . . 279
Ozone . . . 843

PAHs . . . 1073
Palladium. . . . 1235
p-Aminobenzoic acid . . . 829
Parameters . . . 1267
Paraquat . . . 343
Partial least squares . . . 899
Passive neutral membranes . . . 485
Passive sampler . . . 445
Pattern recognition . . . 379
Pb(II) ion-selective electrode detector . . . 575
Peak height. . . . 331
Peat moss. . . . 1139
PEG-modified glucose oxidase . . . 891
Peroxidase . . . 1015
Pesticides . . . 631
PETN . . . 57
Pharmaceutical samples. . . . 829
1:10-phenanthroline-iron(II) complex . . . 1061
p[H]-metry . . . 1219
Phosphorus speciation . . . 47
Photo-oxidation . . . 47
pH-Potentiometric methods . . . 451
pH response . . . 291
Physical steady state. . . . 493
Phytohormone analysis . . . 105
Pindolol. . . . 969
Pitzer's equation . . . 947
p*K* values. . . . 817
Plackett–Burman mixture design . . . 989
Platinum . . . 1235
PLS . . . 989, 1073
Polyaminopolycarboxymethylated ligands . . . 451
Polycyclic aromatic hydrocarbons . . . 39, 113
Poly(ethylene oxide) . . . 767

Polyurethane foam . . . 203
Portunus pelagicus . . . 693
Potentiometry . . . 249, 291, 463, 1007, 1177
Preconcentration . . . 137, 317, 397, 857
Preferential solvation . . . 817
Premicellar aggregates . . . 167
Propranolol . . . 969
p-sulfonated calix[*n*]arenes . . . 683
PVA cryogel . . . 891
Pyridoxine·HCl . . . 1131
1-(2-pyridylazo)-2-naphthol . . . 331, 411

Quartz crystal microbalance sensor . . . 721, 727
Quinolylazo compounds . . . 349

Radioactive waste and liquid scintillation counting . . . 181
Raman spectra . . . 279
RDX . . . 57
Redox method . . . 451
Refractive index . . . 265
Residual chlorine . . . 575
Restriction fragment length polymorphisms . . . 673
Reversed flow injection analysis . . . 405
Reversed-phase high-performance liquid chromotography . . . 349
Reversed phase liquid chromatography . . . 25
Reverse phase liquid chromatography . . . 1189
River water and seawater . . . 583
Robot . . . 371
RVC-electrode . . . 557

Safranine . . . 1247
Sample digestion . . . 843
Sample introduction . . . 137
s-bonded dithizone . . . 1089
Scattering dilution method . . . 1049
Scattering filter method . . . 1049
Schlieren effect . . . 265
Sea water . . . 807
Sediment . . . 213
Sediment analysis . . . 801
Selective extraction . . . 1235
Selective quenching agents . . . 39
Selenium speciation . . . 1023
Sensitivity AFM . . . 727
Sensors . . . 951
Separation . . . 925, 1089
Sephadex gel . . . 583
Sequence analysis . . . 603
Sequential injection analysis . . . 1061
Sequential-stage ultrafiltration . . . 977
Short capillary . . . 613
Silica–ERT . . . 309
Silica gel . . . 357
Silicalite . . . 1001
Silicon determination . . . 1211
Silver(I) . . . 549
Simultaneous determination . . . 1123

Single-line manifold flow injection analysis. . . . 519
Slurry sampling . . . 1147
Sodium borohydride. . . . 343
Sodium diethyldithiocarbamate . . . 857
Sodium perchlorate . . . 931
Soft drinks . . . 1115
Soil . . . 371, 883
Soil analysis . . . 105
Soil leachate . . . 47
Solid adsorption thermal machines . . . 777
Solid-Phase . . . 1081
Solid-phase extraction. . . . 631
Solid-phase spectrofluorimetry . . . 105
Solvent effect on. . . . 189
Solvent extraction . . . 437, 543, 549
Spectrometer . . . 229
α-spectrometry . . . 181
Spectrophotometric . . . 795, 1097
Spectrophotometry . . . 13, 127, 147, 343, 405, 425, 909, 957, 1227, 1247
Spray reagent . . . 1111
Sr(II) . . . 387
Stability constants . . . 1155
Stability constants determination . . . 451
Stöber silica . . . 357
Stopped-flow technique . . . 829
Stripping . . . 433
Stripping voltammetry . . . 417
Styrene . . . 767
Subcritical water extraction . . . 1189
Substrate recycling. . . . 917
Sulfur . . . 85
Sulphur . . . 1281
Sulphur dioxide . . . 1281
Sulphur dioxide in air. . . . 445
Sulphuric acid . . . 875
Superporous agarose gel . . . 557
Surface acidity . . . 739
Surface reactions. . . . 739
Surfactant. . . . 331
Surfactant template . . . 759
Sweeteners . . . 1115
Synchronous fluorescence spectrometry . . . 969
Synchronous spectrofluorimetry . . . 1073
Synthetic pyrethroids . . . 1111
Synthetic samples . . . 411

Tablet formulation . . . 1131
Tamoxifen . . . 273
Tap water. . . . 575
TBPA . . . 35
Temperature programmed decomposition . . . 739
Tetracarboxylate-18-crown-6 . . . 1219
Thermal analysis. . . . 35
Thermodynamic . . . 875
Thermodynamic model . . . 1007
Thermodynamic parameters . . . 189
Thin-layer plates. . . . 1111

Thiocholine . . . 557
Tip shapes . . . 751
TNT . . . 57
TPASO . . . 925
Trace analysis . . . 619, 641
Trace elements . . . 75, 213
Trace vanadium . . . 583
Transport . . . 963
3,5,6-Trichloro-2-pyridinol . . . 371
Trough depth . . . 331

UO_2^{2+} . . . 1155
Uremic serum . . . 25
Urine analysis . . . 75
UV spectrometric method . . . 1103

Vapor generator . . . 57
Vitamin C . . . 1061
Volatile silicon tetrafluoride . . . 1211
Voltammetry . . . 433, 843

Wall-jet cell . . . 703
Water . . . 857
Water analysis . . . 317, 657
Water mobile phase . . . 1189
Weathering . . . 1
Wine vinegars . . . 379
Wool fast blue BL . . . 1227
World Wide Web . . . 591

Zeeman correction . . . 807
Zinc(II) . . . 397, 1089
Zirconia . . . 85
Zn . . . 325
ZnO thin films . . . 751
Zone-circulating flow injection analysis . . . 519
Z-scan technique . . . 735

Talanta

The International Journal of Pure and Applied Analytical Chemistry

Volume 45 (1997)

ELSEVIER

Amsterdam–Lausanne–New York–Oxford–Shannon–Tokyo